SRR-CWDA-2019-00001
Revision 0

PERFORMANCE ASSESSMENT

for the Saltstone Disposal Facility at the Savannah River Site

Prepared by: Savannah River Remediation LLC
Waste Disposal Authority
Aiken, SC 29808

Savannah River Remediation
AMENTUM | BECHTEL | JACOBS | BWXT

Prepared for the U.S. Department of Energy under Contract No. DE-AC09-09SR22505

Revision Summary

Revision Number	Description	Date of Issue
A	Initial issue for DOE-SR Review	May 2019
B	Issue for DOE LFRG Review	August 2019
0	Initial issue to address DOE LFRG Review Comments	March 2020

TABLE OF CONTENTS

APPENDICES

TABLE OF FIGURES

TABLE OF TABLES

Acronyms

ACI	American Concrete Institute
ACM	Alternative Conceptual Model
AEA	Air-Entraining Admixture
ALARA	As Low As Reasonably Achievable
APR	Air Pathway Release
ARP	Actinide Removal Process
ASTM	American Society for Testing and Materials
BE	Best Estimate
BFS	Blast Furnace Slag
CA	Composite Analysis
CAB	Citizens Advisory Board
CBP	Cementitious Barrier Partnership
CD-ROM	Compact Disk – Read Only Memory
CE	Conservative Estimate
CERCLA	Comprehensive Environmental Response, Compensation, and Liability Act
CFR	Code of Federal Regulations
Ci	Curie
CLM	Central Climatology
CLSM	Controlled Low Strength Material
CPT	Cone Penetration Test
CSH	Calcium-Silicate-Hydrate
CV	Compliance Value
CY	Calendar Year
DAS	Disposal Authorization Statement
DBE	Design Basis Earthquake
DCF	Dose Conversion Factor
DDA	Deliquification, Dissolution, and Adjustment
D_e	Effective Diffusion coefficient
DF	Decontamination Factor

DLL	Dynamic Link Library
DLM	Dynamic Leaching Method
DM	Design Margin
DOE	Department of Energy
DOE-HQ	DOE-Headquarters
DOE-SR	DOE-Savannah River
DRF	Dose Release Factor
DSA	Documented Safety Analysis
DSS	Decontaminated Salt Solution
DWPF	Defense Waste Processing Facility
ECC	Engineered Closure Cap
EDE	Effective Dose Equivalent
EDF	Effective Dose Factor
E_h	Oxidation Potential
EIS	Environmental Impact Statement
EPA	Environmental Protection Agency
ET	Evapotranspiration
ETF	Effluent Treatment Facility
FEPs	Features, Events, and Processes
FF	Fast Flow
FFA	Federal Facility Agreement
FMB	Fourmile Branch
FMF	Fuel Material Facility
ft	foot
FTF	F-Area Tank Farm
FY	Fiscal Year
GAU	Gordon Aquifer Unit
GCL	Geosynthetic Clay Liner
GCU	Gordon Confining Unit
GSA	General Separations Area
GTG	GoldSim Technology Group

GWB	The Geochemist's Workbench
HDPE	High-Density Polyethylene
HELP	Hydrologic Evaluation of Landfill Performance
HLW	High-Level Waste
HPC	High Performance Concrete
HRWRA	High-Range Water-Reducing Admixture
HRR	Highly Radioactive Radionuclide
HTF	H-Area Tank Farm
HWMF	Hazardous Waste Management Facility
ID	Identifier
IHI	Inadvertent Human Intruder
IM	Interaction Matrix
ISDP	Interim Salt Disposition Project
ITP	In-Tank Precipitation Facility
K_d	Partition (or Distribution) Coefficient
K_{sat}	Saturated Hydraulic Conductivity
LAZ	Lower Aquifer Zone of the Upper Three Runs Aquifer
LDE	Leading Diagonal Element
LFRG	Low-Level Waste Disposal Facility Federal Review Group
LHS	Latin Hypercube Sampling
LLC	Limited Liability Company
LLW	Low-Level Waste
LVZ	Lower Vadose Zone
MEP	Maximum Extent Practical
meq e^-/g	milliequivalents of electrons per gram
MCC	Moisture Characteristic Curve
MCL	Maximum Contaminant Level
MCU	Modular Caustic Side Solvent Extraction Unit
MOP	Member of the Public
MPAD	Most Probable and Defensible
MQB	McQueen Branch

MSL	Mean Sea Level
mtyp	Material Type
N/A	Not Applicable
NBS	National Bureau of Standards
NCRP	National Council on Radiation Protection and Measurements
ND	Not Detected
NDAA	National Defense Authorization Act
NPDES	National Pollutant Discharge Elimination System
NRC	Nuclear Regulatory Commission
ODE	Off-Diagonal Element
ORCHESTRA	Objects Representing Chemical Speciation and Transport
PA	Performance Assessment
PC	Performance Category or Personal Computer
PEST	Parametric Estimation
PGA	Peak Ground Acceleration
pH	Potential of Hydrogen
PMP	Probable Maximum Precipitation
PNNL	Pacific Northwest National Laboratory
PODD	Performance Objective Demonstration Document
PRCC	Partially Ranked Correlation Coefficient
PRG	Preliminary Remediation Goal
PVC	Polyvinyl Chloride
QA	Quality Assurance
QAMP	Quality Assurance Management Plan
RAI	Requests for Additional Information
RCRA	Resource Conservation and Recovery Act
RFI	RCRA Facility Invesitgations
RH	Relative Humidity
RM	River Mile
RS	Random Seed
RUSLE	Revised Universal Soil Loss Equation

SA	Special Analysis
SCDHEC	South Carolina Department of Health and Environmental Control
SCR	Stress Crack Resistance
SDF	Saltstone Disposal Facility
SDF APR	SDF Air Pathway Release Model
SDF-WIDE	Saltstone Disposal Facility – Waste Inventory Disposed Estimator
SDI	Salt Disposition Integration
SDU	Saltstone Disposal Unit
SL	Seepline
SPF	Saltstone Production Facility
SQAP	Software Quality Assurance Plan
SREL	Savannah River Ecology Laboratory
SRNL	Savannah River National Laboratory
SRR	Savannah River Remediation LLC
SRRC	Standardized Rank Regression Coefficient
SRS	Savannah River Site
SWCC	Soil Water Characteristic Curve
SWMU	Solid Waste Management Unit
SWPF	Salt Waste Processing Facility
SZ	Saturated Zone
TBD	To Be Determined
TCCZ	Tan Clay Confining Zone
TCCR	Tank Closure Cesium Removal System
TEDE	Total Effective Dose Equivalent
TER	Technical Evaluation Report
TRR	Technical Review Reports
TSR	Technical Safety Requirement
TZ	Transmissive Zone
UAZ	Upper Aquifer Zone of the Upper Three Runs Aquifer
UDQE	Unreviewed Disposal Question Evaluation
USDA	United States Department of Agriculture

USGS	United States Geological Survey
UTM	Universal Transverse Mercator
UTR	Upper Three Runs
UV	Ultraviolet
UVA	University of Virginia
UWMQ	Unreviewed Waste Management Question
UZ	Unsaturated Zone
VCO	Vault Concrete One (SDU 1/4)
VCT	Vault Concrete Two (SDU 2/6/7)
VU	Vanderbilt University
WAC	Waste Acceptance Criteria
WCS	Waste Characterization System
WDA	Waste Disposal Authority
WRA	Water-Reducing Admixture
WWTF	Waste Water Treatment Facility
XRD	X-Ray Diffraction

1 EXECUTIVE SUMMARY

This Performance Assessment (PA) was prepared to support the continued operations and eventual final closure of the Saltstone Disposal Facility (SDF) at the Savannah River Site (SRS). This PA has been developed consistent with the requirements of the United States Department of Energy (DOE) Order 435.1, Change 1, *Radioactive Waste Management*, and the DOE Standard, DOE-STD-5002-2017, *Disposal Authorization Statement and Tank Closure Documentation*.

The timing of this PA revision is associated with four main drivers:

1. The design and layout of the SDF Saltstone Disposal Units (SDUs) have undergone major changes since the last PA revision.
2. The breadth of Savannah River Remediation LLC (SRR)-targeted research and development activities in recent years has provided new information and increased the confidence in key transport modeling inputs and assumptions.
3. Three significant SDF PA Special Analyses have been conducted since the last PA revision and this information needs to be consolidated into the new PA revision.
4. DOE-STD-5002-2017 states that PAs should be revised at a minimum every ten years and the previous SDF PA was completed in 2009.

DOE must demonstrate that a reasonable expectation (assurance) exists that the design, operation, and eventual closure of the SDF will meet the following requirements:

- DOE Manual 435.1-1, *Radioactive Waste Management Manual*, Chapter IV.P.;
- Title 10 of the Code of Federal Regulations (CFR) Part 61, Subpart C performance objectives as required by the *Ronald W. Reagan National Defense Authorization Act for Fiscal Year 2005* (NDAA), Section 3116; and
- Ground water protection standards pursuant to South Carolina Department of Health and Environmental Control (SCDHEC) Regulation 61-58, *State Primary Drinking Water Regulations*.

When reviewed in aggregate, the results of all SDF PA modeling and analyses, including extensive deterministic and probabilistic uncertainty and sensitivities analyses, provide a reasonable expectation that all performance objectives and required standards will be met and the operation of the SDF can continue and will be protective of human health and the environment.

1.1 Description of Performance Objectives

Requirements in both DOE M 435.1-1 and 10 CFR 61 stipulate that a PA should provide reasonable expectation that low-level waste (LLW) disposal will comply with specified performance objectives. DOE M 435.1-1 and 10 CFR 61 both require assessments of impacts to hypothetical receptors, including future members of the public (MOPs) and inadvertent human intruders (IHIs). DOE M 435.1-1 also requires assessments for impacts to water resources. These assessments were performed to address a 1,000-year Compliance Period after facility closure (per DOE M 435.1-1), as well as informational 10,000-year Performance and Long-Term Exploratory (greater than 10,000-year) Periods to identify potential peak doses occurring beyond the regulatory Compliance Period.

Consistent with DOE M 435.1-1, the performance objectives for the SDF are (1) doses to the MOP "shall not exceed 25 [millirem] mrem … in a year total effective dose equivalent from all exposure pathways, excluding the dose from radon and its progeny in air;" (2) doses to the MOP "via the air pathway shall not exceed 10 mrem … in a year total effective dose equivalent, excluding the dose from radon and its progeny in air;" and (3) the "[r]elease of radon shall be less than an average flux of 20 pCi/m^2/s at the surface of the disposal facility." To put these SDF PA radiological doses into perspective, it should be noted that an individual flying on a roundtrip transcontinental trip in the United States will receive approximately 5 mrem during the course of these flights. The average United States citizen receives 620 mrem in a year (NCRP-160) and individuals living in Denver, Colorado will receive greater than 1,000 mrem each year due to the higher natural, terrestrial, and cosmic radiation levels in that area.

For the MOP, the point of compliance for the performance objectives and for determining the impacts on water resources is the location of highest projected dose or concentration at or beyond a 100-meter buffer zone surrounding the disposal units. For the IHI, the point of compliance is adjacent to the disposal units corresponding to a reasonable intruder scenario; for the SDF, the assumed intruder drills a well into contaminated soils adjacent to the disposal units. For the performance objective relevant to radon, the point of compliance is the surface of the disposal facility.

Additionally, the protection of water resources is achieved through the requirement that water concentrations not exceed the Maximum Contaminant Levels (MCLs) specified in the South Carolina State Primary Drinking Water Regulations. [SCDHEC R.61-58] The MCLs for radionuclides are based on a 4 mrem/yr dose for beta- and gamma-emitting nuclides, 15 pCi/L for alpha-emitting nuclides, and 5 pCi/L for radium.

1.2 SDF Facility Overview

The SRS is located in south-central South Carolina, approximately 100 miles from the Atlantic coast. The SDF is located in Z-Area, which is in the central region of SRS. Z-Area consists of approximately 161 acres. The Saltstone facility consists of two components: one is the Saltstone Production Facility (SPF) which receives and treats LLW salt solution to produce a grout slurry; and the second is the SDF which consists of SDUs that receive the grout slurry from the SPF. "Saltstone" refers to the solidified (cured) grout slurry and is a cementitious waste form made by mixing LLW salt solution with a dry mix containing blast furnace slag, fly ash, and cement.

This SDF PA assumes that the final SDF configuration will include two existing rectangular SDUs (SDUs 1 and 4), six existing 150-foot diameter SDUs (SDUs 2A, 2B, 3A, 3B, 5A, and 5B), one existing 375-foot diameter SDU (SDU 6), one 375-foot diameter SDU that is currently being constructed (SDU 7), and five future 375-foot diameter SDUs (SDUs 8, 9, 10, 11, and 12), resulting in a total of 15 disposal structures. The relative layout for the SDF as modeled for this PA is depicted in Figure 1.2-1; the shapes with brown outlines indicate the locations of the SDUs.

Planning and construction of additional SDUs to meet future waste volume demands is ongoing and SDUs will be constructed as needed to coordinate with salt processing rates.

Figure 1.2-1: SDF Layout

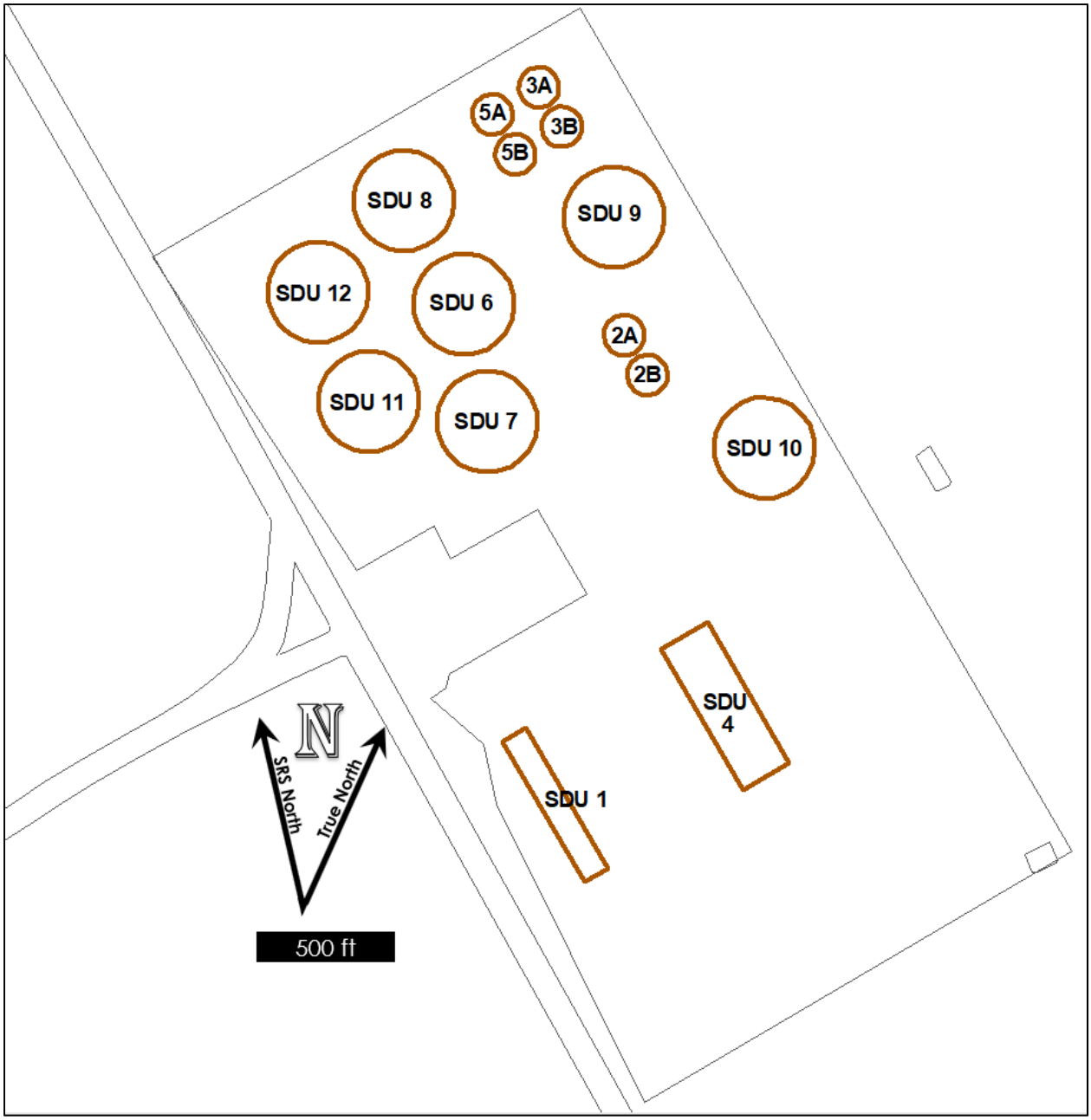

Each SDU is permitted as part of the Class 3 Landfill (Landfill Permit No. 025500-1603) per SCDHEC regulations, enabling waste disposal in compliance with state regulations:

- SDUs 1 and 4 were permitted via the initial permit (Landfill Permit No. 025500-1603 [DHEC_02-28-1995; DHEC_04-16-1996; DHEC_01-23-2007]);
- SDUs 2A and 2B were permitted via modification DHEC_09-09-2008;
- SDUs 3A, 3B, 5A, and 5B were permitted via modification DHEC_05-12-2011; and
- SDU 6 was permitted via modification DHEC_12-17-2012.
- Other SDUs will be permitted via future modifications.

The subsurface environment beneath the SDF is made up of varying layers of predominantly sandy or predominantly clayey sediments. As a result of the varying texture layers, the subsurface consists of two aquifer units, the Upper Three Runs Aquifer and the Gordon Aquifer, which are separated by the Gordon Confining Unit (or "Green Clay"). The Upper Three Runs Aquifer may be subdivided into two zones, an Upper Aquifer Zone and a Lower Aquifer Zone, separated by the Tan Clay Confining Zone. Relative to the Gordon Confining Unit, the Tan Clay Confining Zone is generally not as effective a barrier to contaminant transport (i.e., it is expected that the Upper Aquifer Zone and the Lower Aquifer Zone would exhibit similar contaminant concentrations, while the Gordon Confining Unit would limit transport such that the Gordon Aquifer is expected to show lower contaminant concentrations).

1.3 PA Model Development Process

In the most general terms, this PA relies on modeling projections to provide reasonable expectation that performance objectives will be met. The models used in this PA were developed using the relevant features, events, and processes (FEPs) identified during the FEPs screening process described in Section 4.1.1. The FEPs process identifies those system features, events, and physical processes that may have a significant impact on the performance of the SDF disposal system. This process was performed by a team of subject matter experts from SRR Savannah River National Laboratory (SRNL), the DOE Hanford Site, and academia who determined which FEPs to consider during the development of SDF PA models. The identified FEPs provide the basis for understanding the physical systems and features represented within the PA models, including considerations for how the modeled features interact collectively and considerations for how they will evolve over time.

After identifying the relevant FEPs, a "Central Scenario" was developed from a range of potential future scenarios using an "interaction matrix," on the *Guidance for Conducting Technical Analyses for 10 CFR Part 61* (draft NUREG-2175) from the U.S. Nuclear Regulatory Commission (NRC) (ML14357A072), as described in Section 4.1.2. With the interaction matrix approach, primary components of the system (i.e., safety-significant features) are identified along with the various interactions between those primary model components (i.e., processes). The system components and interactions between them were used to develop the conceptual model for the Central Scenario (SRR-CWDA-2018-00006), which is summarized in Section 1.4.

Using the conceptual model for the Central Scenario, a reasonable but defensible Compliance Case was developed for evaluating the long-term performance of the SDF. This conceptual model was also used to develop sensitivity cases for evaluating specific inputs to the Compliance Case, and a probabilistic model to evaluate uncertainties around combinations of values or conditions. In addition to the Central Scenario conceptual model, alternative conceptual models were also developed to evaluate the conditions that are different from the Central Scenario. From these alternative conceptual models, additional sensitivity cases were developed. Collectively, these models provide the basis for establishing that performance objectives will be met and provide insights relative to potential risks or uncertainties that may impact long-term performance.

Note that none these modeling cases are developed from a single, comprehensive mathematical model; rather the system has been subdivided into multiple, manageable submodels. These submodels are each run independently, and then integrated to produce the PA results. Figure 1.3-1 provides a high-level overview of these submodels along with key inputs and outputs are interconnected. These are discussed in more detail throughout Section 4.

Figure 1.3-1: Overview of Submodel Integration for the SDF PA

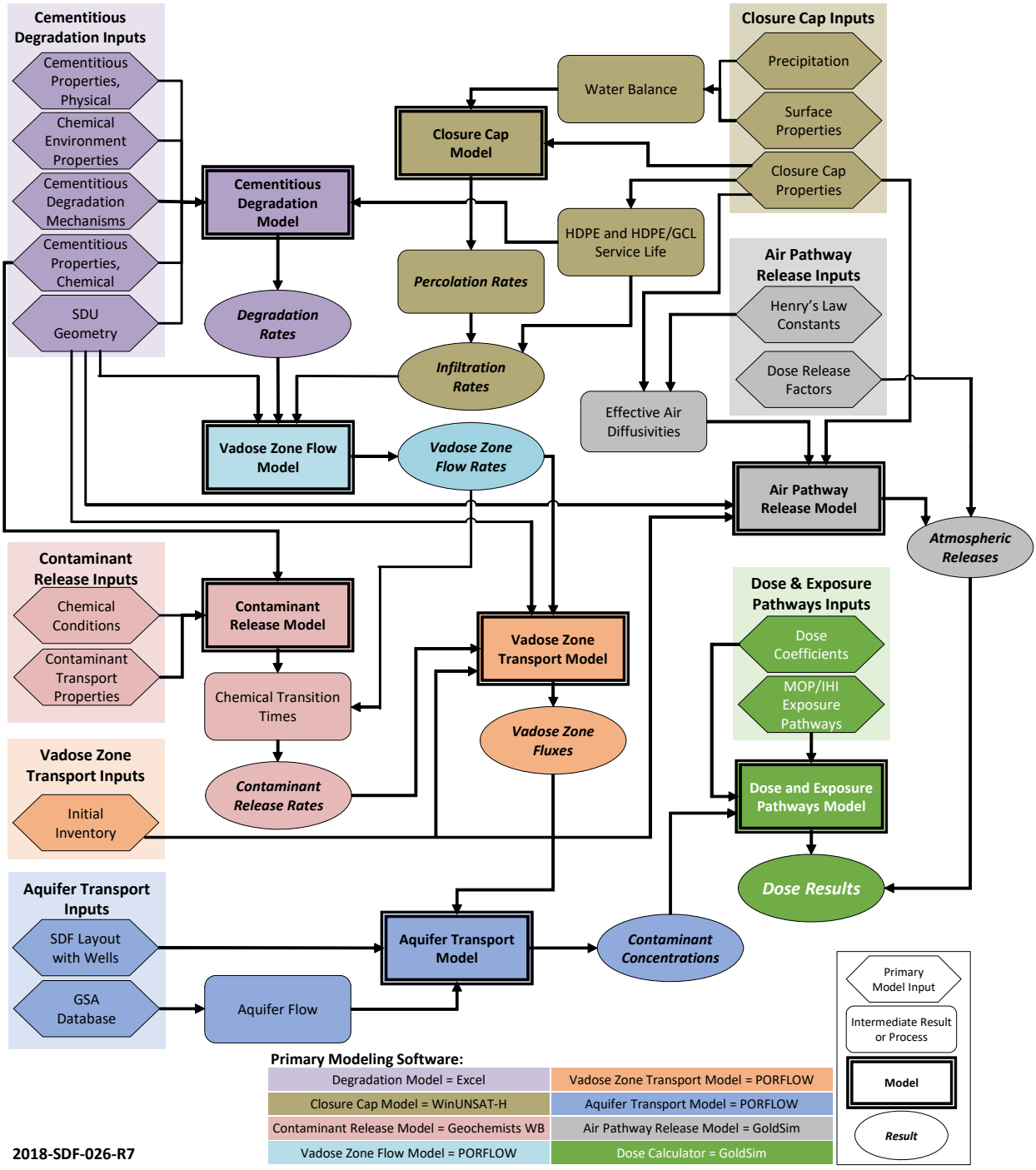

The flow and transport processes simulated within this SDF PA relies on complex PORFLOW and GoldSim models (see Section 4.4). PORFLOW is a deterministic, three-dimensional flow and transport modeling software. As a deterministic modeling software, the models designed in PORFLOW use a single value for each input parameter. Alternatively, GoldSim is a one-dimensional flow and transport modeling software that can be used for both deterministic and probabilistic simulations. In probabilistic mode, GoldSim can be used to evaluate multiple parameter values in a computationally-efficient manner.

The probabilistic model developed within GoldSim uses data that was abstracted from the PORFLOW models (see Section 4.5). The probabilistic model randomly samples values for selected parameters within the Central Scenario to provide insights relative to the influence that parameter uncertainty may exhibit on the overall performance of the system. Section 5.7.1 provides a listing of each of the modeling distributions that were considered within the probabilistic model. Additional discussion of the development of the probabilistic model is provided in Sections 4.5 and 5.6.

1.4 Conceptual Model for the Central Scenario

The following provides an overview of the conceptual model for the Central Scenario. As described in Section 1.3, the Central Scenario describes the system components and interactions between them. To generate modeling cases, such as the Compliance Case, the Central Scenario is appled to mathematical models with appropriate modeling inputs (see Section 4).

1.4.1 Pre-Closure SDF Conditions

Liquid waste from the tank farms is mixed with dry grout feeds to create a waste form called saltstone. After mixing, the wet saltstone slurry is poured into large concrete structures known as SDUs at the SDF. Once the slurry cures within the SDUs, saltstone becomes a solid, low-permeability waste form. Saltstone is designed to immobilize waste, minimize water transport, provide long-term site stability, and prevent future inadvertent intrusion into the waste form. The SDUs are designed to be leak-tight during disposal operation, preventing contaminants from escaping into the environment and to limit any infiltrating water from contacting the waste form. When waste disposal operations end, all remaining void spaces within the SDUs will be grouted, the SDUs will be surrounded with backfill material, and the entire facility will be placed under an engineered multi-layered closure cap. The layers are designed to control surface erosion, prevent human and animal intrusion, and particularly to channel any infiltrating water away from the SDUs.

1.4.2 Initial Post-Closure SDF Conditions

The conceptual closure cap layers are described in detail in Section 3.2.6. One of the most important closure cap layers is the "composite barrier" beneath the upper sand drainage layer. The composite barrier will consist of seam-welded sheets of impermeable, high density polyethylene (HDPE) placed on top of a geosynthetic clay liner (GCL). The HDPE material is both dense and impermeable and is designed to intercept 100% of all incoming water. The

drainage layers above the HDPE layers will have a very high hydraulic conductivity to expedite lateral drainage away from the SDUs and towards the edges of the closure cap.

Despite the expectation that all water will be stopped by intact HDPE material because of quality control measures, this SDF PA assumes that there will be initial defects of the HDPE in the form of small diameter holes. Due to the importance of the HDPE in preventing water infiltration, prior to use the HDPE sheets will be inspected for holes and defects and will not be placed unless adequate repairs can be implemented. After HDPE installation, the leak-tight seams (where the HDPE sheets will be welded together) will be inspected for defects, followed by any necessary repairs. Nonetheless, a few potential defects are assumed to survive the quality control measures. The defects are assumed to be 2 mm in diameter based on design recommendations. Five defects per hectare are assumed.

Any water that leaks through the seam defects will next contact the GCL. GCLs are a fabric material with interwoven clay (e.g., bentonite). The GCL serves two purposes. First, when GCLs are used beneath HDPE layers, they have been proven to provide very good contact with the HDPE, which can limit the lateral flow extent for any water leaking through the HDPE. Next, the bentonite clay within the GCL swells when in contact with water. This swelling significantly reduces the hydraulic conductivity of the GCL, thus slowing the rate at which water can leak through any HDPE defects. Collectively, the initial conditions of the closure cap reduce the natural infiltration rate by nearly five orders of magnitude (from approximately 400 mm/yr to less than 0.01 mm/yr).

In addition to the upper sand drainage layer in the closure cap, there will also be a lower sand drainage layer, which will be placed over another composite barrier directly atop each SDU roof. This provides a redundancy that significantly limits the amount of water that can contact the SDUs.

Any water that leaks through the composite barriers could eventually contact the SDU concrete (i.e., the roof or walls). Because the SDU concrete has a low initial hydraulic conductivity, it is expected to function as an additional barrier to any flow. Water penetrating through the SDU concrete will reach the saltstone waste form, contact contaminants, and initiate releases to the environment by displacing contaminated saltstone pore water. Contaminant release by diffusion through the SDU concrete barriers and waste form constitutes a second release mechanism. Contaminants released from the SDUs will migrate through the partially saturated vadose zone soils and then pass into the local aquifer system (or saturated zone). Once in the saturated zone, contaminants will be transported along the predominant direction(s) of ground water flow, and eventually reach the designated points of assessment (e.g., water wells used for drinking water and irrigation).

Because only a limited amount of water is estimated to pass through the engineered barriers, and due to the low hydraulic conductivities of the materials throughout the system, it is expected that only the most mobile contaminants and/or those with very high inventories will pose any potential risk to a member of the public within the first 1,000 to 10,000 years or more after the closure cap is installed. Of the contaminants considered in this SDF PA, Cs-137, I-129, Sr-90, and Tc-99 are the most likely to pose a dose risk. However, because Cs-137 and Sr-90 have relatively

short half-lives (approximately 30 years), they are expected to undergo significant decay before reaching any point(s) of assessment. Therefore, only I-129 and Tc-99 are predicted to produce a long-term dose risk for a member of the public.

1.4.3 Closure Cap Performance and Assumptions

This SDF PA makes four major assumptions about the performance of the closure cap:

1) It is assumed that the side slopes and the erosion control barrier of the cap will be constructed with sufficient engineering controls (e.g., large riprap) to minimize the influence of erosion. Further, credit is taken for 100 years of institutional control. During this time, it is assumed that cap maintenance would identify and remediate any onset of rills or gullying. After 100 years, any potential erosion to the closure cap is expected to be localized such that the overall impacts to closure cap performance would be minimal. Regardless, some sensitivity cases have been evaluated for the potential impacts should the closure cap fail to perform as designed.

2) The Compliance Case of this SDF PA assumes that after 500 years, rooting structures will penetrate into the upper sand drainage layer and then follow the interface between the sand and the underlying HDPE layer (where water is expected to be most accessible). As such, the saturated hydraulic conductivity of the upper sand drainage layer is assumed to decrease by a factor of five (from 5.0E-04 m/s to 1.0E-04 m/s). This assumption results in an increase to the estimated infiltration rate by more than a factor of 15 (from 0.006 mm/yr to 0.091 mm/yr).

3) Based on recent studies conducted on HDPE materials under extreme conditions, the HDPE layer in the closure cap is expected to have a service life of at least 2,000 years. This service life estimate is based on pessimistic conditions that are not representative of the SDF (i.e., based on exposure to municipal solid waste leachates that have higher metal concentrations and higher ionic strength than would be expected at the SDF). It is expected that as long as the HDPE remains under pressure (i.e., buried beneath the upper layers of the closure cap) and therefore not subject to tensile loading, stress cracks will not form, and the material will continue to perform well throughout the 10,000-year Performance Period. However, this SDF PA assumes that at 2,000 years the HDPE material will become partially degraded, resulting in a general increase to size of the existing defects. At 2,000 years the assumed initial defects are modeled as increasing from 2 mm to 10 mm in diameter. This assumption results in an approximate 40% increase in the estimated infiltration rate (from 0.091 mm/yr to 0.13 mm/yr).

4) Finally, it is assumed that the climatic conditions at SRS will remain approximately the same as the current conditions. Environmental studies in the region show evidence that the climatic conditions have remained steady for the past 8,000 years. Therefore, assuming continued climate conditions is reasonable. It is noted that some climate change models show that slightly wetter climate conditions could result from climate change; however, these models also show that the local annual precipitation would only increase by approximately 10% to 15%. Regardless, this SDF PA includes a sensitivity case to

evaluate the potential impacts for both wetter and drier future climatic conditions. These sensitivity cases demonstrate that the performance of the system is not strongly sensitive to potential changes in climatic conditions.

For the Compliance Case, the end state of the closure cap retains a significant degree of functionality. Even after degradation assumptions are applied, the closure cap reduces the infiltration rate from a natural impingement rate of 400 mm/yr to a steady state infiltration rate of 0.13 mm/yr. Due to the relative importance of the closure cap, this SDF PA also includes multiple sensitivity cases that examine the impacts of unexpected or unrealistic closure cap performance assumptions. For example, one sensitivity case assumes that the closure cap is only made of soil and does not include the HDPE or GCL barriers. While such cases do not reflect the expected future conditions, they provide insights on the importance of the closure cap and demonstrate that should the closure cap completely fail, the other engineered barriers within the system provide sufficient controls to meet performance objectives by mitigating the release and transport of contaminants.

1.4.4 Long-Term Cementitious Materials Performance and Assumptions

Along with the closure cap, other major components of the closure system include the SDU concrete and the saltstone waste form. Both materials have initially low saturated hydraulic conductivities and provide reducing (anaerobic) conditions, which will limit the release of Tc-99 (as discussed in Section 4.4.3.3.4).

The SDU concrete and saltstone are susceptible to various cementitious degradation mechanisms. This degradation is simulated by increasing the saturated hydraulic conductivity and the diffusion coefficient of the SDU concrete over time (i.e., hydraulic degradation) and by changing the chemistry of the pore solution over time. The assumed end state for the SDU concrete and saltstone is a final hydraulic conductivity and diffusion coefficient that are equivalent to the surrounding soil materials (e.g., backfill). This assumption is expected to overestimate the final hydraulic conductivity of these cementitious materials.

The SDU concrete is reinforced with steel rebar which makes it a structurally stable material. Because carbon dioxide is assumed to be dissolved within the infiltrating water, as this water interacts with the pore solution in the SDU concrete, the carbon dioxide will become carbonic acid that accelerates corrosion of the steel rebar. The corrosion products (rust) have more volume than the concrete; as they expand, hydraulic degradation will occur. Note that the exterior of the SDU walls will be coated in shotcrete which would slow the ingress of water and the resulting rate of carbonation; however, this barrier is not credited within this SDF PA.

Additionally, the high sulfate content of the saltstone waste form is expected to result in sulfate attack on the SDU concrete. As sulfates in the saltstone dissolve into pore solution and interact with the SDU concrete, it will react with the concrete mineralogy to form expansive minerals such as ettringite. As these minerals precipitate within the SDU concrete, they will create internal pressure that is assumed to damage the concrete resulting in hydraulic degradation. Note that most SDUs are expected to include an interior liner, which would significantly delay and/or

prevent sulfate attack. As with the shotcrete on the SDU walls, the interior liners are not credited in this SDF PA beyond the period of disposal operations.

Because carbonation occurs from the outside in and sulfate attack occurs from the inside out, these are simulated as simultaneous advancing fronts. When the two fronts meet, complete degradation is assumed. While other degradation mechanisms were considered, aggressive assumptions are applied to estimate the rates of carbonation and sulfate attack, such that these two phenomena are expected to drive the degradation rates of the SDU concrete. Given these aggressive assumptions, the SDU concrete is modeled to undergo complete hydraulic degradation after roughly 1,000 years, depending on the thickness of the component.

Because the SDU concrete degrades over this timescale, various modeling cases considered within this SDF PA show that it is not a significant protective barrier with respect to peak doses beyond 1,000 years. However, if less aggressive assumptions were applied to the degradation calculations, or if a different end state were assumed, and if higher infiltration rates are assumed, the performance of the SDU concrete could become significant.

Conversely, the saltstone waste form is expected to last much longer than the SDU concrete. It is not subject to significant damage via carbonation or sulfate attack. Further, because it is enclosed within the SDU concrete, it is expected to be protected from various other degradation mechanisms. This SDF PA assumes that hydraulic degradation of the saltstone will be driven by decalcification (i.e., the gradual leaching of calcium-bearing binders) as a function of pore solution exchanges. Given the very low infiltration rates and the low permeability of saltstone, significant decalcification is expected to take millions of years. As such, for the first 1,000 to 10,000 years the hydraulic conductivity of saltstone undergoes very little change. Sensitivity cases within this PA that assume extremely high (albeit unrealistic) infiltration rates still meet performance objectives because of the persistence of the low hydraulic conductivity of the saltstone, which limits flow rates through the waste form.

1.4.5 Long-Term Chemical Conditions within Cementitious Materials

The changing chemical conditions of the cementitious materials also play an important role in the performance of the system. Different radionuclides have different transport properties depending on the chemical environment. The slag-bearing SDU concrete and saltstone are assumed to provide initially reduced (i.e., anaerobic) chemical environments. Initially, these materials have a low Eh (a measurement of reduction potential) and a high pH (a measurement of basicity and acidity). As infiltrating water enters the cementitious materials, it is assumed to fill the available pore space and displace the existing pore solution. As such, flow through the cementitious materials results in continuous exchanges of the pore solution. Incoming water carries in oxygen, which will eventually increase the Eh. To maximize the rate of oxidation, all infiltrating water is assumed to have a dissolved oxygen content that is in equilibrium with atmospheric oxygen, although it is expected that subsurface water will have a lower oxygen content. The infiltrate also contains dissolved CO_2 which reacts with calcium minerals (e.g., calcium-silicate-hydrate) to form calcite. As these minerals are reacted, the pH of the system decreases.

During disposal operations, the SDUs are completely exposed and some oxidation is expected to occur prior to the closure cap being constructed. However, due to various lines of evidence (see Appendix A), this pre-closure oxidation of the system is expected to be limited and to have a negligible impact on the overall performance of the system.

1.4.6 Inventory and Contaminant Releases

Although this SDF PA evaluates the release and transport of dozens of contaminants, previous SDF modeling has consistently shown that only three radionuclides are risk-significant for long-term doses: I-129, Ra-226, and Tc-99. The results of this SDF PA show that I-129 and Tc-99 continue to be major dose contributors, but Ra-226 is no longer a major contributor.

The reasons for the reduced importance of Ra-226 are that earlier inventory assumptions significantly overestimated the assumed inventory for most radionuclides, including Ra-226 and its parents (e.g., Th-230). This SDF PA applies much more realistic inventory assumptions than earlier modeling efforts, which reduced the estimated inventory for Ra-226 and its parents by an order of magnitude. Next, the transport properties for radium in saltstone have also been updated. For simulating transport, this SDF PA uses updated K_d values (i.e., partition coefficients) for radium based on recommendations developed from saltstone-specific studies. The K_ds applied for radium in saltstone are significantly higher in this SDF PA than in previous modeling. For example, the previous K_d for initial reducing conditions was 100 mL/g while this SDF PA uses updated recommendations with an initial value of 6,000 mL/g. Note that for transport modeling, lower K_ds indicate greater mobility and higher K_ds indicate less mobility.

The estimated inventories and the transport properties for I-129 and Tc-99 have also been updated for this SDF PA. The inventory updates are based on extensive quantitative analyses of tank farm waste characterization data to reduce the uncertainties around the estimated disposal inventories for I-129 and Tc-99. While the updated estimates are more realistic, assumptions were built into the estimation approaches to ensure that these inventory estimates continue to overpredict the inventories, thus maintaining a reasonable degree of defensibility.

The updated transport properties for I-129 and Tc-99 are based on measured releases from SDU 2A cores and from simulant samples using Dynamic Leaching Method (DLM) tests. Using DLM test data, these radionuclides are shown to be more mobile than previously assumed under some conditions. These values are shown in Table 1.4-1.

Very low infiltration rates in the Compliance Case lead to a diffusion dominated system at early times. Both I-129 and Tc-99 diffuse in all directions from the SDUs, then migrate downward through the vadose zone towards the water table. Because vadose zone transport is diffusion dominated, as opposed to being advection dominated, discrete features such as potential cracks in the saltstone are not expected to significantly alter the performance of the system. Sensitivity cases confirm this behavior (see Section 5.8.8.2).

Due to the low K_d values for I-129, all available I-129 is expected to be completely flushed from the SDUs within three to four pore volume exchanges. However, because of the low flow rates, this release of I-129 is expected to take tens of thousands of years. Tc-99 has a shorter half-life

(211,000 years), larger inventory, and slower release rate. As such, most of the Tc-99 inventory is expected to decay away prior to being released under Compliance Case conditions.

Table 1.4-1: Summary of Controlling Transport Properties for I-129 and Tc-99

Radio-nuclide	Saltstone Pore Solution Chemistry	Controlling Transport Property	Previous Model Value	Updated Model Value
I-129	Initial Condition (Eh < 0 mV, pH > 11.5)	K_d (mL/g)	9	0.07
	pH Transition (Eh < 0 mV, pH < 11.5)	K_d (mL/g)	9	0.71
	EH Transition (Eh > 0 mV, pH < 11.5)	K_d (mL/g)	4	4
Tc-99	Initial Condition (Eh < 0 mV, pH > 11)	Solubility (mol/L)	1.0E-08*	9.7E-07*
	pH Transition (Eh < 0 mV, pH < 11)	Solubility (mol/L)	1.0E-08*	4.5E-07*
	EH Transition (Eh > 0 mV, pH < 11)	K_d (mL/g)	0.5	0.5

Note: * Within the transport model, these solubility controls are applied as effective K_ds, where:
1.0E-08 mol/L is equivalent to approximately 2,000 mL/g,
9.7E-07 mol/L is equivalent to approximately 20 mL/g, and
4.5E-07 mol/L is equivalent to approximately 43 mL/g.

1.4.7 Ground Water Transport and Well Depths

For compliance purposes, ground water concentrations are estimated along an assumed boundary 100 meters from the SDUs (for the MOP doses) or closer (for the IHI doses). Because this 100-meter boundary is defined by the locations of the SDUs, the SDUs constructed along the outer perimeter of the facility are closer to this boundary and are, therefore, more likely to contribute higher concentrations to the dose results. The distances from the SDUs to the 100-meter boundary are measured as straight lines along the ground surface; however, subsurface ground water transport often follows more tortuous travel paths. As a result, the travel distances for contaminant transport from the SDUs to the 100-meter boundary is always greater than 100 meters.

Given that the 375-foot diameter SDUs contain more than 10 times the volume of the 150-foot diameter SDUs, these larger SDUs are estimated to have much more inventory. Therefore, releases from the larger SDUs dominate the dose results. For most SDUs, the thickness of the vadose zone (i.e., the vertical distance from the bottom of the SDU to the top of the water table) is estimated to be more than 35 feet; however, due to field conditions, SDU 9 is modeled to be constructed at a lower elevation resulting in a thinner vadose zone (23 feet), such that contaminants released from SDU 9 take less time to be transported to the water table compared to other SDUs. Because of this shorter transport time, SDU 9 is the primary SDU controlling doses over the first few thousand years. However, the plume that emanates from SDU 9 is relatively isolated, whereas the plumes emanating from other SDUs show significant overlaps. Because of this, the importance of SDU 9 as a dominant dose driver will eventually be overwhelmed by the releases from other SDUs as these overlapping plumes reach the points of assessment.

Beneath the SDF, the water table is generally at an elevation of 215 feet to 235 feet above mean sea level (MSL). This water table defines the top of the most shallow aquifer: Upper Three Runs Aquifer. This aquifer has been subdivided into two zones, an Upper Aquifer Zone and a Lower Aquifer Zone, separated by the Tan Clay Confining Zone. Beneath the Lower Aquifer Zone is the Gordon Confining Unit (or "Green Clay") and beneath that is the Gordon Aquifer. The top of

the Gordon Aquifer is approximately 160 feet to 170 feet above MSL (or approximately 65 to 70 feet below the SDUs).

Relative to the Gordon Confining Unit, the Tan Clay Confining Zone is not as effective a barrier to contaminant transport. It is expected that contaminants that migrate to the Upper Three Runs Aquifer would exhibit similar concentrations regardless of the aquifer zone, while contaminants that migrate to the Gordon Aquifer would have concentrations that are less than 5% of the concentrations in the Upper Three Runs Aquifer. In general, the ground water within the Upper Three Runs Aquifer beneath the SDF travels towards the nearby streams: either northwest towards Upper Three Runs or east towards Fourmile Branch, while ground water within the Gordon Aquifer only travels towards the northwest.

In the vicinity of SRS, the average well depth is drilled to approximately 160 feet from the surface. This means that most water wells are drilled into the Gordon Aquifer or deeper. Despite this, the doses used for establishing compliance to performance objectives always assume the highest ground water concentrations regardless of depth. This is equivalent to assuming that the water wells are less than 100 feet from the surface.

The contaminated well water is assumed to be the primary source of drinking water and will be used for bathing, irrigation of crops, and for watering livestock, thus exposing future individuals to potential doses.

1.4.8 Conceptual Model Summary

The multi-layered closure cap will be designed to effectively channel water away from the SDUs and to mitigate potential erosion. Infiltration rates through the closure cap are estimated by assuming initial defects in the HDPE to allow leakage. Initially water that leaks through these defects will be deflected by the SDU concrete, but the SDU concrete is assumed to degrade quickly. Water that flows through the SDU concrete will reach relatively impermeable saltstone and initiate slow contaminant releases. Once released, the contaminants will migrate through the more than 35 feet of vadose zone soils (or 23 feet if released from SDU 9), down to the water table, where ground water will transport the contaminants to an assumed well. Concentrations from the assumed well will be used to estimate doses to future individuals.

1.5 PA Analysis Summary

A broad set of analyses have been performed to evaluate SDF performance considering uncertainties in the future evolution of the facility. These analyses include:

- A Central Scenario, which has been evaluated for three sets of input parameters as an indicator of parameter uncertainty (Section 5.8.1).
- A probabilistic parameter uncertainty analysis of the Central Scenario, which supplements and augments the understanding of parameter uncertainties (Section 5.7.3).

- A set of deterministic sensitivity cases to further explore parametric uncertainties, including evaluations of:
  - infiltration rates (Section 5.8.2),
  - material properties (Section 5.8.3),
  - contaminant release and transport rates (Section 5.8.4),
  - future disposal inventories (Section 5.8.5),
  - dose parameters (Section 5.8.6), and
  - vadose zone flow and transport conditions (Section 5.8.8).
- Additional deterministic sensitivity cases developed based on Alternative Conceptual Models (ACMs), which explore conceptual and mathematical model uncertainties, including:
  - soil-only closure cap scenario (Section 5.8.2.4),
  - climate condition scenarios (Section 5.8.2.6),
  - cementitious degradation analyses (Section 5.8.3.6),
  - early release scenarios (Section 5.8.9.1),
  - fast flow path scenarios (Sections 5.8.8.2 and 5.8.9.5), and
  - colloid transport scenario (Section 5.8.9.6).
- A set of special deterministic sensitivity cases designed to support facility operations and management decisions related to SDF disposal, including:
  - a design margin analysis (Section 5.8.7.1),
  - an analysis that assumes soil disposal in SDU 1 (Section 5.8.7.2),
  - an analysis that addresses the waste bags in SDU 4 (Section 5.8.7.3), and
  - an analysis that assumes SDU 4 will be filled with controlled low strength material (CLSM) instead of grout (Section 5.8.7.4).

Each of these analyses supports a different type of understanding of the system. The case for the postclosure safety of the facility comes from the broad understanding of the behavior of the facility under this wide set of potential conditions. Collectively, these analyses support risk-informed decisions for the SDF and show that the system complies with performance objectives presented in Section 1.7.

Radiological doses to human receptors are analyzed in this PA for the MOP all-pathways analysis, the MOP air pathway analysis, the Chronic IHI analysis, and the Acute IHI analysis for comparison to the relevant performance objectives. For these analyses, 52 radioactive isotopes and 27 chemicals were modeled (or considered). Radon fluxes were also evaluated. The release pathways identified that result in potential dose contributions were:

- leaching from the saltstone waste form resulting in contamination of the local subsurface ground water and streams, and
- gaseous diffusion into the atmosphere above the SDUs.

This SDF PA uses a hybrid modeling approach. In this hybrid approach, two primary modeling programs were used to simulate releases and to estimate the concentrations at the points of assessment (e.g., the 1-meter or 100-meter boundaries):

1. **PORFLOW:** A deterministic flow and transport simulation software, which was used to simulate ground water flow and transport and to demonstrate compliance with the performance objectives.
2. **GoldSim:** A dual-mode (deterministic and probabilistic) simulation software, which used flow data abstracted from PORFLOW to facilitate sensitivity and uncertainty analyses and to provide additional insights into the relative importance of various parameters.

The modeling results in this SDF PA provide technical information at different points of assessment that can be used in the subsequent regulatory decision documents. This SDF PA provides ground water concentrations for radionuclides at 1 meter from selected SDUs, at 1-meter from the SDF, at 100 meters from the SDF, and at the two seeplines impacted by the SDF: Upper Three Runs (UTR) and McQueen Branch (MQB). The ground water concentrations are provided for each of three potentially impacted aquifers under the SDF, as applicable.

The SDF PA also provides ground water concentrations for chemical contaminants at 1 meter from selected SDUs, at 1 meter from the SDF, and at 100 meters from the SDF. The MOP doses are provided based on the 100-meter concentrations, consistent with the requirements of DOE M 435.1-1, as well as at the UTR and MQB seeplines. All ground water concentrations were calculated using the PORFLOW Aquifer Transport Model, as described in Section 4.4.6. In addition, this PA provides IHI doses, air pathway doses, and radon ground-surface fluxes consistent with the requirements of DOE M 435.1-1 and 10 CFR 61.42.

Figure 1.5-1 presents various points of assessment used for evaluating SDF performance. The 100-meter boundary around the SDUs (used to evaluate doses to the MOP) is divided into eight sectors, each shown as colored diamonds around the facility perimeter (Sectors A through H). The sectors were organized to be approximately the same length along the 100-meter boundary because each sector has an equal probability of representing the location that a future MOP might select for drilling a well for water. The dashed pink outline indicates the 1-meter boundary around the SDUs (used to evaluate doses to the IHI). Colored diamonds with the black outlines indicate the locations for selected IHI well positions adjacent to specific SDUs inside the facility boundary and used for further evaluation of IHI doses.

For the Compliance Case, the peak all-pathways annual dose for the MOP at 100 meters is calculated using the highest 100-meter ground water pathway dose results in combination with the peak air pathway results. However, as described in Section 5.3, dose contributions from the air pathway are negligible. As such, the all-pathways dose is effectively the same as the ground water pathway dose.

For Compliance Case modeling, the peak 100-meter ground water pathway dose within 1,000 years occurs along Sector D (9.4E-03 mrem/yr), with the next highest peak doses occurring along Sector C (5.7E-03 mrem/yr). The most significant contaminants contributing to this dose are I-129 and Tc-99 released from SDU 9. Over time, the location of the peak dose shifts to Sector B as the contaminant plumes of I-129 and Tc-99 released from SDUs 8 and 6 overlap.

Figure 1.5-1: SDF Layout with Points of Assessment

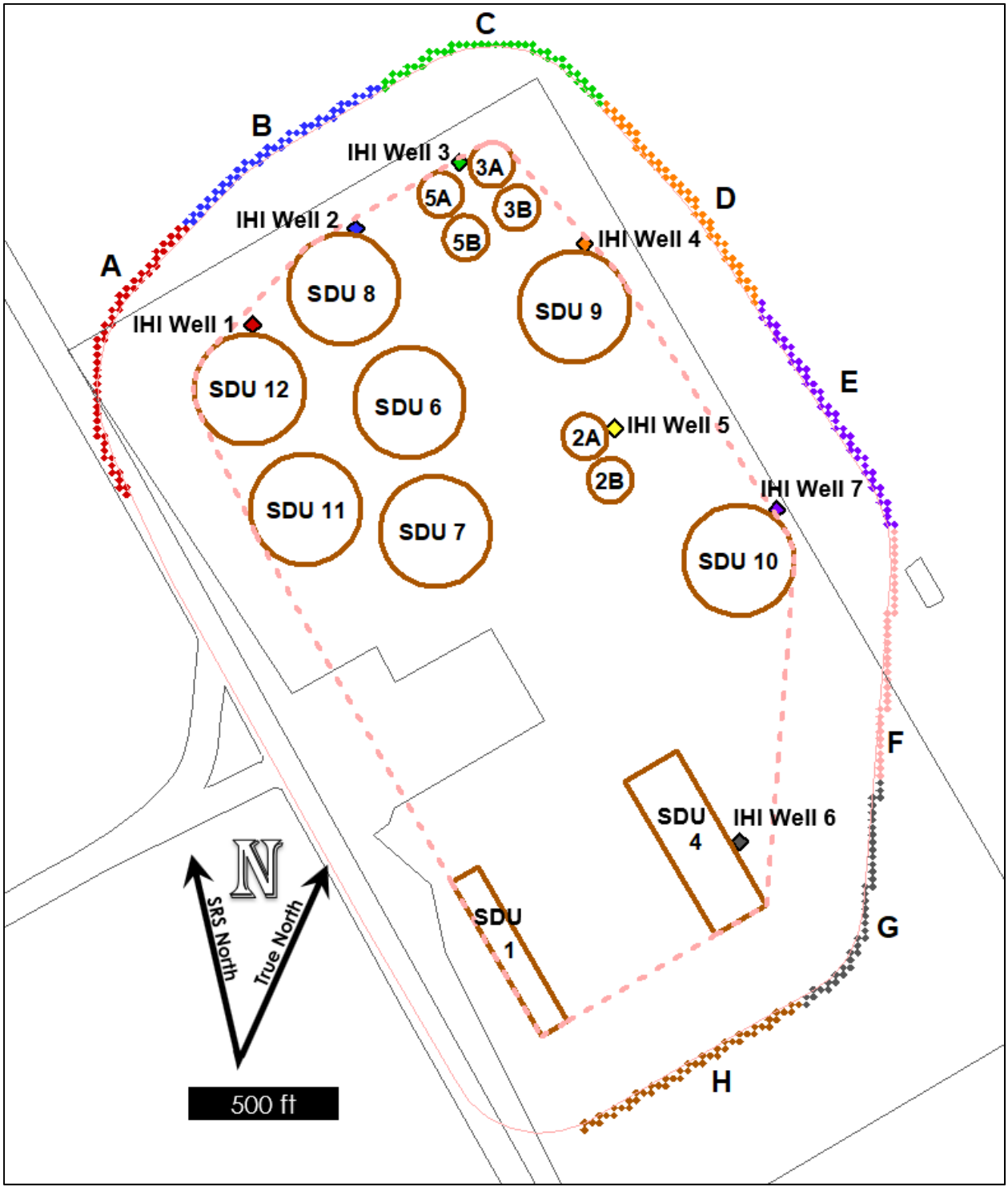

Note: The 1-meter facility boundary is indicated by pink dashed line. IHI wells are placed adjacent to and downgradient of SDUs in transport modeling.

When interpreting PA results, it is important to recognize that the peak doses are associated with specific locations and times. Since there are 15 unique SDUs and multiple contaminants with varying release and transport rates, there is significant temporal and spatial complexity inherent in the modeling system. Artificially removing an SDU from the model may reduce the doses associated with that SDU, but the overall SDF PA peak dose will not necessarily be reduced by a corresponding amount; the overall SDF PA peak dose may merely shift to a different location and/or time. For example, reducing the inventories assigned to SDUs 6 and 8 might not significantly reduce the peak dose along Sector B because SDUs 11 and 12 provide a similar contribution to doses along Sector B, albeit at a different location along the sector.

The Compliance Case dose results are dominated by contributions from I-129 and Tc-99 because both radionuclides are highly mobile throughout the entire system and both have very long half-lives (~15M years and ~211,000 years, respectively). Additionally, I-129 has a relatively high dose conversion factor when ingested and Tc-99 is relatively abundant within the inventory. The dose contributions from I-129 and Tc-99 for the Compliance Case are shown for the Compliance Period (Figure 1.5-2) and the Performance Period (Figure 1.5-3). Note that none of these doses challenge the 25 mrem/yr performance objective within either the Compliance Period or the Performance Period.

In addition to the Central Scenario deterministic cases, numerous alternative models and sensitivity cases were developed. Section 5.8 presents dose results for the alternative models and sensitivity cases. These cases were developed to provide insights relative to specific assumptions, configurations, or input values, such as those listed at the beginning of Section 1.5.

As described in Section 5.7, a series of probabilistic analyses were also developed for further understanding of the model and its associated input parameters, and to support risk-informed decisions for the SDF. These probabilistic results can be used to place the deterministic analyses results into context (i.e., to risk inform the deterministic results). The peak of the mean of the all-pathways doses within 10,000 years using the probabilistic model was approximately 4.8 mrem/yr. The median (50^{th} percentile) and 95^{th} percentile values were approximately 3.1 mrem/yr and 15 mrem/yr, respectively. Figure 1.5-4 provides the statistical time history of the doses from the probabilistic MOP analysis.

Of the 3,000 realizations, none have doses that exceed the 25 mrem/yr performance objective within the Compliance Period, although 32 of the realizations (approximately 1%) do exceed 25 mrem/yr within the Performance Period, with highest realization showing 37 mrem/yr at 10,000 years. However, it should be noted that these probabilistic results are based on the SDF GoldSim Model which is abstracted from the more complex PORFLOW models. As demonstrated in Sections 5.6 and 5.8.1, when equivalent modeling conditions are assumed in both GoldSim and PORFLOW, the simplified SDF GoldSim Model yields higher dose results relative to PORFLOW. Consistent with this observation, the dose results presented in Figure 1.5-4 are generally higher than what might be expected had each realization been simulated using PORFLOW. Therefore, although a small number of realizations exceed the 25 mrem/yr performance objective, these doses are overstating risk.

Figure 1.5-2: Radionuclide Dose Contributors to Sector D for the 100-Meter MOP Peak Ground Water Pathways Dose within 1,000 Years

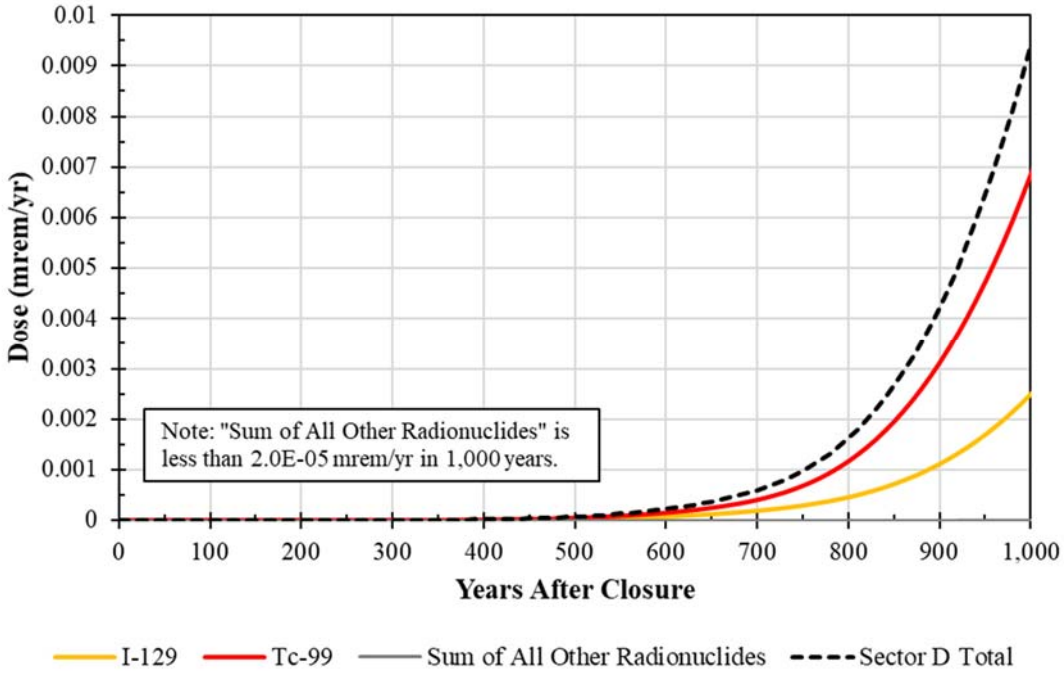

Figure 1.5-3: Radionuclide Dose Contributors to Sector B for the 100-Meter MOP Peak Ground Water Pathways Dose within 10,000 Years

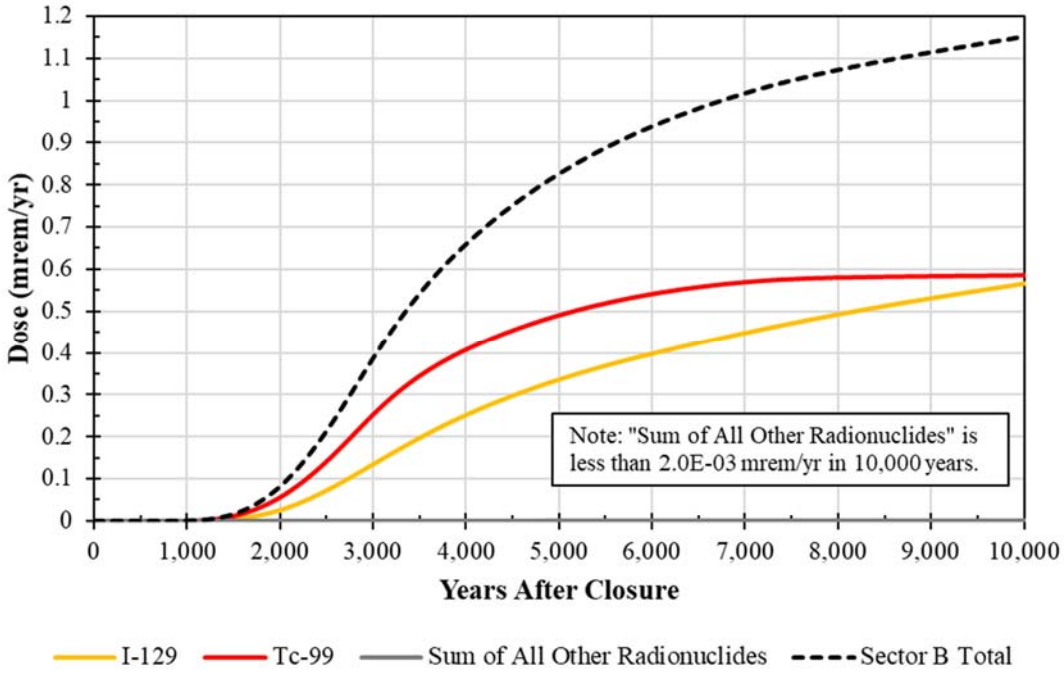

Figure 1.5-4: Statistical Time History of the Probabilistic MOP Doses (0 to 10,000 Years)

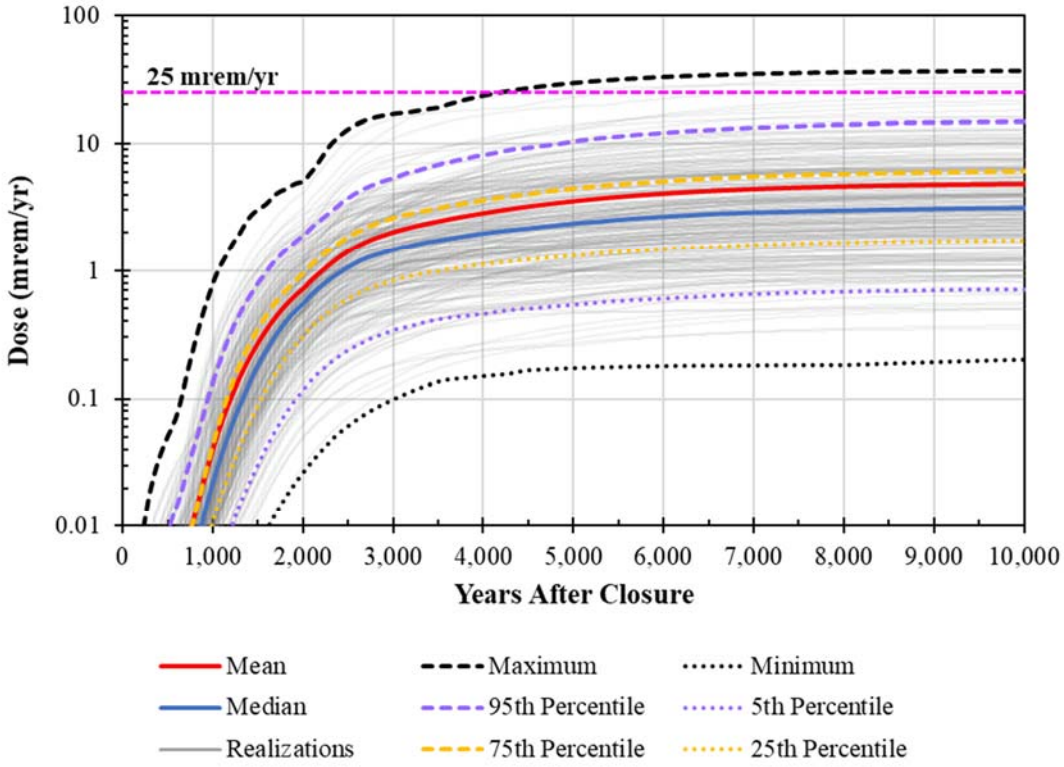

Note: For the individual realizations, only the first 245 realizations are displayed. The statistical values (e.g., Mean and Maximum) are determined using data from 3,000 individual realizations.

The peak projected ground water concentrations were also calculated for evaluation against the SCDHEC ground water protection standards (see Section 5.2). All chemical concentrations were less than the MCL or Preliminary Remediation Goal (PRG) at a distance of 1 meter from the SDF within 1,000 years. For the radiological MCLs, all concentrations were less than the respective MCL at a distance of 1 meter from the SDF within 1,000 years.

Similarly, the peak radon flux was determined to be 1.6E-05 pCi/m²/sec within the Compliance Period and 7.4E-04 pCi/m²/s within the Performance Period (see Section 5.3). Both values are well below the 20 pCi/m²/s performance objective.

1.6 Key Modeling Changes Compared to the 2009 SDF PA

This PA is a revision of the 2009 SDF PA (SRR-CWDA-2009-00017). While some aspects of the PA modeling approach and input values remain the same, there are many key changes that are impactful to the results. In general, the intent of these changes was to incorporate new information, including data from ongoing research and development activities, and to reflect current and planned designs and locations of the SDUs. Some of the more impactful changes include:

- The 2009 SDF PA assumed a different SDF configuration which included 64 of the 150-foot diameter SDUs. This PA incorporates the current plans which makes use of significantly fewer (but much larger) 375-foot diameter SDUs.

- The ground water model for the General Separations Area (GSA) has been updated using more recent characterization and monitoring well data, including additional wells in Z-Area. With this update, the calibration of the ground water model in the vicinity of the SDF went from relying on data from eight wells to nineteen wells. In addition to incorporating recent well data, the updated GSA Model includes changes to reflect various facilities throughout the GSA (e.g., closure of the H-Area Ash Basin), and includes an additional calibration zone to improve the agreement between the well data and the simulation data. The flow fields from this updated GSA Model are used to simulate the ground water transport.
- The "Base Case" (equivalent to the Compliance Case) of the 2009 SDF PA did not degrade saltstone over time. This PA incorporates the latest modeling approaches using recommendations developed by the Cementitious Barriers Partnership and material science experts at Vanderbilt University. The degradation modeling uses physical and chemical properties based on recent laboratory testing performed by the Savannah River Ecology Laboratory (SREL) and SIMCO.
- The initial physical properties of saltstone have been updated to reflect new data from field-emplaced saltstone that was cored out of SDU 2A and studied. Most significantly, the initial saturated hydraulic conductivity is lower than previously assumed.
- The closure cap model used to estimate infiltration rates has been revised to incorporate updated assumptions and to use WinUNSAT-H software instead of HELP (Hydrologic Evaluation of Landfill Performance). The 2009 SDF PA assumed that pine trees growing atop the closure cap would have roots that would penetrate into the HDPE layers of the closure cap, degrading the overall performance of the HDPE over time. Based on consultation with cover system experts at the University of Virginia (UVA) School of Engineering, it has been determined that this was an unrealistic and overly pessimistic assumption. Vegetation is opportunistic: rooting structures develop by seeking out water sources that require the least amount of energy to extract. Further, recent laboratory studies and data analsyses at UVA have been used to improve predictions for the service life of HDPE under extreme conditions. A revised closure cap model applies this improved understanding of the HDPE material and uses realistic modeling assumptions to improve the estimated infiltration rates.
- The 2009 SDF PA assumed that cementitious materials would quickly transition from "young-aged" (pH Region I) to "moderate-aged" (pH Region II) material; for modeling purposes the initial condition of the material was assumed to be "moderate-aged." However, it has been determined that with the low flow rates that are expected, this chemical transition is not expected to occur until thousands of years after facility closure; therefore, the new model now includes "young-aged" material as the initial condition.
- The release model for Tc-99 has been updated to reflect data from the latest available studies. Specifically, a "shrinking core" modeling approach has been adopted using data collected from Dynamic Leaching Method (DLM) laboratory testing performed on cores extracted from SDU 2A as well as laboratory-prepared simulant samples. The shrinking

core approach is described in Section 4.4.5.2. The DLM tests demonstrated that under adverse (high flow) conditions, the solubility limit for technetium can be as high as 9.7E-07 mol/L when the pH is greater than or equal to 11 and 4.5E-07 mol/L when the pH is less than 11. While the SDF Special Analyses previously assumed a reasonable technetium solubility limit of 1.0E-08 mol/L, the Compliance Case within this PA uses the higher values from the DLM tests to ensure greater defensibility.

- The iodine partition coefficient (K_d) in saltstone has also been updated to reflect the results of the DLM testing of a simulated saltstone core. In the 2009 SDF PA, iodine in saltstone had a K_d of 9 mL/g for Reducing Region II and a K_d of 15 mL/g in Oxidizing Region II based on concrete K_d data. For this PA, the initial saltstone K_d is 0.07 mL/g which is lower than previously assumed. However, this low value is only expected to persist during the first pore volume, after which the saltstone K_d is modeled to increase to 0.71 mL/g. Additionally, due to the dose significance of I-129, the release of iodine is now simulated using the more realistic "shrinking core" modeling approach.
- For SDUs that have been constructed and put into service, the actual disposal inventories have been incorporated into the SDF modeling to replace earlier inventory projections.
- The date of facility closure has been updated. In the 2009 SDF PA, it was expected that the SDF would be closed on October 1, 2030. Now, based on current SRS plans for liquid waste operations, it is expected that the facility will be closed seven years later (October 1, 2037).
- Dose calculations have been updated to reflect new dose conversion factors from DOE and the U.S. Environmental Protection Agency (EPA). [DOE-STD-1196-2011 and EPA-402-R-18-001].
- The definition of the human receptor has been updated to reflect newer exposure factor data from the EPA. [EPA-600-R-090-052F]. For example, it was previously assumed in the 2009 SDF PA that the human receptor drank contaminated water at a rate of 0.92 L/day; it is now assumed that they drink 1.38 L/day.

There are significant differences between this SDF PA and other PAs at SRS. One of the greatest differences is that the SDF is the only facility that has saltstone as the waste form. For the F-Tank Farm and H-Tank Farm PAs (SRS-REG-2007-00002; SRR-CWDA-2010-00128), the waste form is residual waste remaining in waste tanks and ancillary structures following cleaning activities, while the E-Area Low-Level Waste Facility PA (WSRC-STI-2007-00306) considers the disposal of other (non-saltstone) low-level solid waste.

Aside from the waste form and the associated containment structures, most of the more general differences between this SDF PA and the other SRS PAs are due to this SDF PA implementing improvements developed subsequent to the development and approval of the other PAs. The SDF PA uses updated inputs in many areas that were not available to the previous PAs, such as soil adsorption (i.e., K_d values), which were updated based on the 2016 revision of the *Geochemical Data Package for Performance Assessment Calculations Related to the Savannah River Site*. [SRNL-STI-2009-00473]

All SRS PAs simulate the long-term performance of facilities that are in close proximity to one another at SRS. Accordingly, they all share similar environmental conditions (e.g., precipitation, soil properties, hydrologic stratigraphy, bounding streams, etc.). Due to these shared conditions, all SRS PAs simulate subsurface groundwater flow using the GSA Model, although it should be noted that the other PAs used earlier versions of the GSA Model. Also, each PA modifies the GSA Model to provide increased resolution within the localized area being simulated. Despite all the SRS PAs using the GSA Model, this SDF PA uses the most recent version of the model, as informed by more recent well data. [SRNL-STI-2018-00643] Incorporation of newer well and characterization data and more sophisticated calibration procedures resulted in slightly different flow conditions being used in this SDF PA relative to the other SRS PAs (i.e., the F-Tank Farm PA, H-Tank Farm PA, and the E-Area Low-Level Waste Facility PA). [SRS-REG-2007-00002; SRR-CWDA-2010-00128; WSRC-STI-2007-00306] Potential impacts from the update to the GSA Model, relative to each of the other facilities, have been evaluated. [SRR-CWDA-2017-00068; SRNL-STI-2018-00624]

In addition to the environmental conditions, another notable similarity between this SDF PA and the other SRS PAs is the preliminary closure cap design. While the slope angle and slope lengths of the planned closure caps vary by facility, they all incorporate the same or similar material layers and material thicknesses. [WSRC-STI-2007-00184; WSRC-STI-2007-00306; WSRC-STI-2008-00244] However, like the 2009 SDF PA, the other SRS PAs assume that roots will aggressively penetrate through the HDPE of the closure caps, while this updated SDF PA assumes that root structures will advance in pursuit of water along the top of the HDPE where the supply is expected to be more abundant. As a result, after a few decades of closure cap degradation, the other SRS closure cap simulations yield greater vadose zone flow rates relative to this SDF PA. The closure cap modeling for the E-Area Low-Level Waste Facility PA is more unique than the other SRS PAs because it also considers the potential for waste subsidence; this is not expected in the other PAs because any void spaces within the waste containment structures (i.e., waste tanks and SDUs) will be grouted.

The dose calculation methodology used within this SDF PA, based on the *Dose Calculation Methodology for Liquid Waste Performance Assessments at the Savannah River Site* (SRR-CWDA-2013-00058), updated the definition of the human receptor. This dose calculation report was developed and revised after the other SRS PAs were issued. Further, the dose conversion factors and exposure parameters used within the dose calculations reflect newer data from the DOE (DOE-STD-1196-2011) and the EPA (EPA-402-R-18-001; EPA-600-R-090-052F). This data was not yet available when the other SRS PAs were issued.

Finally, this SDF PA also implements improved techniques for modeling, such as including a "shrinking core model" to better simulate bulk chemistry changes in the cementitious materials and to better simulate the releases of technetium and iodine over time.

1.7 PA Conclusion

Table 1.7-1 provides a summary of the Compliance Case results, demonstrating that each of the performance objectives shall be met by the SDF. Note that DOE M 435.1-1 results reflect a 1,000-year Compliance Period and 10 CFR 61 results reflect a 10,000-year Performance Period.

Since the MCLs are specific to various radiological and chemical concentrations, they are listed in separate tables, as provided in Section 5.2. The projected SDF concentrations in these tables are below the MCLs throughout the 1,000-year Compliance Period.

The results of all SDF PA modeling, including the three Central Scenario cases, the ACMs, the other sensitivity cases, and the probabilistic results provide a reasonable expectation that all performance objectives will be met and that operation of the SDF can continue and will be protective of human health and the environment.

Table 1.7-1: Comparison of Peak Dose, Release, or Concentration Results versus Performance Objectives

Performance Objectives			PA Results
DOE M 435.1-1	All Pathway MOP Dose	25 mrem/yr in 1,000 years	9.4E-03 mrem/yr
	Air Pathway MOP Dose	10 mrem/yr in 1,000 years	5.2E-09 mrem/yr
	Chronic IHI Dose	100 mrem/yr in 1,000 years	0.30 mrem/yr
	Acute IHI Dose	500 mrem/yr in 1,000 years	4.1E-05 mrem/yr
	Radon Release	20 pCi/m^2/sec in 1,000 years	1.6E-05 pCi/m^2/sec
10 CFR 61.41*	All-Pathways MOP Dose	25 mrem/yr	1.2 mrem/yr
10 CFR 61.42*	Intruder Dose	500 mrem/yr **	2.2 mrem/yr
SCDHEC R.61-58	South Carolina Ground Water Protection Standard	Concentrations below the maximum contaminant levels (MCLs) in 1,000 years	< MCLs

Notes: (a) Unlike the performance objectives described in DOE M 435.1-1, the performance objectives for 10 CFR 61 are not associated with a prescribed period for compliance. The doses provided for these performance objectives are based on the 10,000-year Performance Period.
(b) A quantitative limit is not specified. The SDF must ensure the protection of the IHI after a 100-year active institutional control period. Based on NUREG-1854 guidance, 500 mrem/yr is assumed for the performance objective. [ML072360184]

This page intentionally left blank.

2 INTRODUCTION

PA models are typically used for evaluating the potential exposure to human receptors for thousands of years into the future. PA models simulate (1) the release of radionuclides (and chemical contaminants) from the disposal site, (2) transport of contaminants through the environment, and (3) exposure/ impacts to potential receptors. The PA process provides the technical basis for subsequent decision documents to demonstrate compliance with the performance objectives of DOE M 435.1-1 and 10 CFR 61. [DOE M 435.1-1, 10 CFR 61]

2.1 History of Performance Assessment-Related Documents

This SDF PA assesses the long-term fate and transport of DOE LLW disposed of at the SDF. The PA must provide a reasonable expectation that the facility design and method of disposal will comply with the performance objectives of DOE M 435.1-1 and Subpart C of Part 61 of Title 10 Code of Federal Regulation (10 CFR 61), which ensures protection of public health and safety in limiting doses to a hypothetical member of the public (MOP) or an inadvertent human intruder (IHI). [DOE M 435.1-1, 10 CFR 61]

2.1.1 Previous Performance Assessments and Analyses

This PA is a revision to the 2009 SDF PA. The purpose of this revision is: (1) to consolidate updated information that has been evaluated via Special Analyses (SAs) since the 2009 SDF PA was issued, (2) to incorporate new inputs developed through research, and (3) to address lessons learned. [SRR-CWDA-2009-00017, SRR-CWDA-2013-00062, SRR-CWDA-2014-00006, SRR-CWDA-2016-00072] This PA shall also address, to the extent possible, issues that have been documented by technical staff at the U.S. Nuclear Regulatory Commission (NRC) via the Technical Evaluation Report (TER) (ML121170309) that was issued in response to the 2009 SDF PA, as well as Requests for Additional Information (RAIs) (ML100820097, ML103400571, ML14148A153, ML15161A541). In addition, consideration was given to Technical Review Reports (TRRs) issued by the NRC. The following sections provide a summary of historical documentation leading up to the development of this PA, beginning with the 1992 Radiological PA for the Saltstone Facility. [WSRC-RP-92-1360]

Figure 2.1-1 and Figure 2.1-2 provide an overview of the more recent PA-related documentation, beginning with the 2009 SDF PA. Documents in blue were developed by SRR on behalf of DOE. Documents in orange were developed by technical staff at the NRC. Arrows indicate relationships between documents. In addition to the PA and SAs, these figures show the related RAIs and RAI Response documents. Figure 2.1-2 also shows the NRC's Monitoring Plan for the SDF (ML13100A113) as well as DOE's *Crosswalk to the NRC Monitoring Plan for SDF* (SRR-CWDA-2014-00002), which provided a comprehensive listing of documents related to the Monitoring Factors identified by the NRC.

Figure 2.1-1: SDF PA-Related and NRC Documentation Timeline: 2009 to 2012

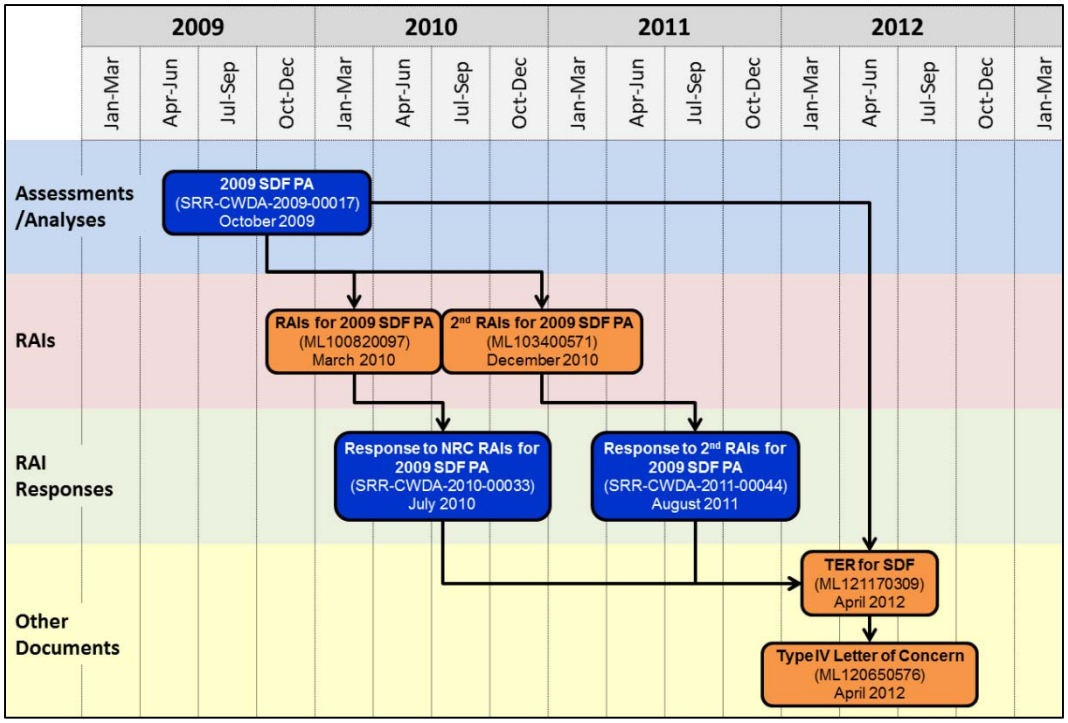

Figure 2.1-2: SDF PA-Related and NRC Documentation Timeline: 2013 to 2016

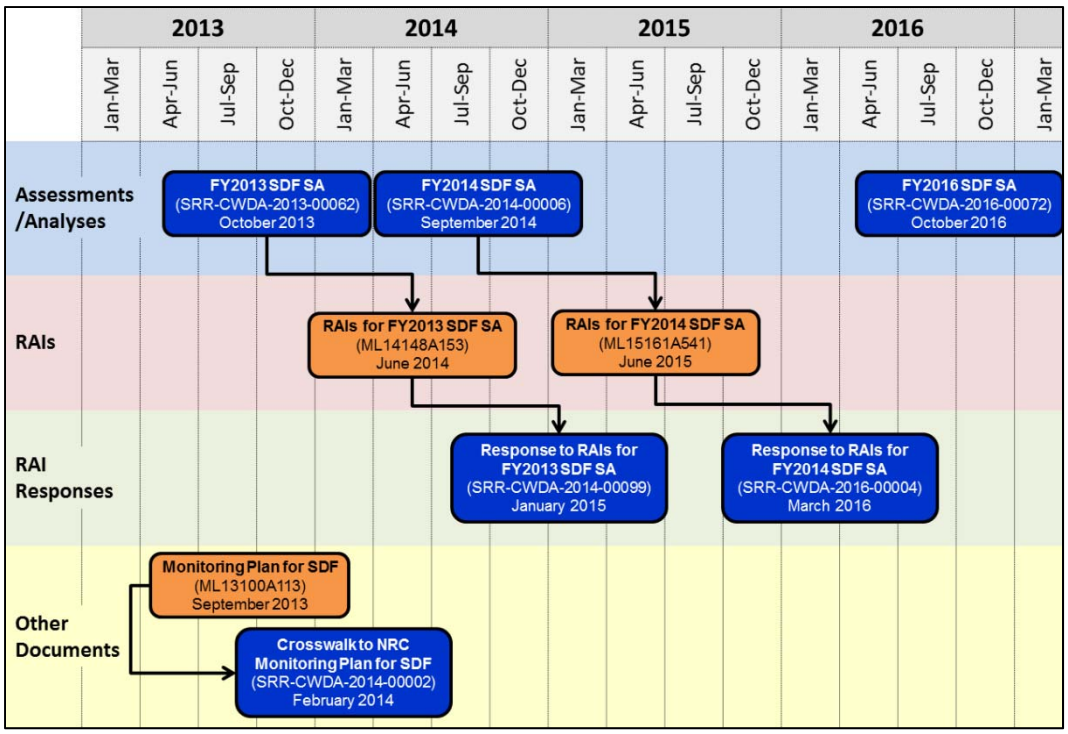

2.1.1.1 1992 Radiological Performance Assessment

A radiological PA was issued in 1992 following the design and construction of the Saltstone Production Facility (hereafter referred to as the 1992 PA). [WSRC-RP-92-1360] The 1992 PA was written in accordance with the requirements contained in DOE O 5820.2A (the PA requirements for this order have been superseded by the issuance of DOE O 435.1, Chg. 1, and its associated manual and guidance). The inventory assumptions in this initial evaluation were based on the decontaminated salt solution stream from the In-Tank Precipitation Facility (ITP) and the concentrate stream from the Effluent Treatment Facility (ETF). The 1992 PA evaluated waste material in SDUs 1 and 4 and projected the results for future SDUs, assuming rectangular disposal units referred to as "vaults." The ground water evaluation point for this and future performance objective compliance reviews was a hypothetical ground water well at a point 100 meters (m) from the disposal units. The ground water pathways performance objective assumed in the 1992 PA was a dose of 4 mrem/yr from direct water ingestion for all radionuclides combined. The ground water pathways analysis was quantitative in nature, while the air pathways analysis was a qualitative evaluation, which concluded that the air pathways were insignificant relative to the ground water pathways. The intruder scenarios were also evaluated in a qualitative fashion. The dose calculations in the 1992 PA were based on the anticipated inventory and determined to be within performance limits. In 1998, an addendum was developed for the 1992 PA in order to address comments from the DOE PA Peer Review Panel and DOE Headquarters (DOE-HQ). [WSRC-RP-98-00156] There was no change in the conclusions of the 1992 PA based upon the 1998 Addendum. [WSRC-RP-92-1360, WSRC-RP-98-00156]

2.1.1.2 2002 Special Analysis: Reevaluation of the Inadvertent Human Intruder, Ground Water, Air, and Radon Analyses for the SDF

In 2002, a Special Analysis (SA) (2002 SA) was performed in response to updated facility inventory information as a result of suspended ITP operations and replacing that waste stream with an expected low activity salt solution feed. [WSRC-TR-2002-00456] DOE O 435.1, Chg. 1, and its associated manual and guidance had also been issued and the 2002 SA used this order for determining compliance. Rather than using a specific radionuclide list for evaluation, like used in the 1992 PA, a radionuclide screening evaluation was performed using a methodology introduced by the National Council on Radiation Protection and Measurements (NCRP). [NCRP-123, Vol. 1] Relative to the list of radionuclides listed in the 1992 PA, the NCRP screening yielded one new radionuclide of interest: Np-237. Rather than calculating specific doses from a fixed radionuclide inventory, the 2002 SA calculated radionuclide inventory limits against specific objectives of 25 mrem/yr from all-pathways, 10 mrem/yr from the air pathways, and the EPA MCLs for the ground water pathways. [WSRC-TR-2002-00456, SCDHEC R.61-58] The 1992 PA doses for a specific radionuclide inventory were used to determine the individual radionuclide limits. For beta-gamma radionuclides, the MCL limit is 4 mrem/yr from the direct ingestion ground water pathways and 15 pCi/L for alpha-emitting radionuclides. Since Np-237 was not included in the 1992 PA, the limit for this radionuclide was

calculated in the 2002 SA. The air pathways analysis was quantitative in the 2002 SA. The results of the intruder and ground water and air pathways analyses demonstrated compliance with DOE M 435.1-1. [WSRC-TR-2002-00456, WSRC-RP-92-1360]

2.1.1.3 2005 Special Analysis: Revision of Saltstone SDU 4 Disposal Limits

The 2005 Special Analysis (2005 SA) updated information on the SDF feed solutions, modeling methods, and closure cap design. [WSRC-TR-2005-00074] The 2005 SA supplemented the analyses in the 1992 PA and superseded the analyses in the 2002 SA. The 2005 SA evaluated the SDF against the specific performance objectives of DOE M 435.1-1 and 10 CFR 61. [WSRC-TR-2005-00074, WSRC-RP-92-1360, WSRC-TR-2002-00456]

The salt waste inventory was updated to reflect new estimates of the total inventory expected to be disposed of in SDU 4 (referred to as Vault 4), including Deliquification, Dissolution, and Adjustment (DDA) feed, as well as the anticipated decontaminated solution from the future Salt Waste Processing Facility (SWPF). The 2005 SA recalculated the ground water transport and air transport doses. An all-pathways analysis was performed, which included residential and agricultural pathways. The radionuclide limits were calculated for specific exposure pathways and a limit determined for each pathway at the most restrictive exposure period between 100 and 10,000 years after facility closure. The most restrictive limit for any pathway for each radionuclide was chosen as the limit, and thus a sum-of-fractions for any waste inventory would over estimate the impacts. The 2005 SA included many sensitivity evaluations, but it only included limits for SDU 4. [WSRC-TR-2005-00074] The intruder scenarios were also recalculated and determined to be in compliance with the DOE M 435.1-1 requirements.

2.1.1.4 2005 Performance Objective Demonstration Document

Removal and disposal of low-activity salt waste is critical in order to establish empty tank space for future tank waste processing operations, including the Actinide Removal Process (ARP), Modular Caustic Side Solvent Extraction Unit (MCU), and the SWPF. It will also ensure that vitrification of the high-activity waste will be able to continue uninterrupted.

The ability to dispose of the low-activity salt waste in the SDF required determination of compliance with NDAA Section 3116. One requirement of NDAA Section 3116 is to demonstrate compliance with the performance objectives set out in 10 CFR 61. [NDAA_3116, 10 CFR 61] The Performance Objective Demonstration Document (PODD) was developed to demonstrate compliance with 10 CFR 61 Subpart C and was presented in a format that would meet the requirements of NDAA Section 3116. [CBU-PIT-2005-00146]

The PODD addressed the disposal of solidified low-activity salt waste streams into the SDF as saltstone and its compliance with performance objectives for near-surface disposal of radioactive waste. Specifically, the PODD demonstrated and documented that the solidified low-activity salt waste from SRS salt processing activities would meet the

performance objectives set out in 10 CFR 61 Subpart C by assuming all future salt solution inventory was placed in SDU 4. [10 CFR 61, CBU-PIT-2005-00146]

2.1.1.5 2009 SDF Performance Assessment and Technical Evaluation

The 2009 SDF PA was prepared and issued in October 2009 to support the operation and eventual closure of the SDF. [SRR-CWDA-2009-00017] The 2009 SDF PA was prepared to demonstrate compliance with the performance objectives of DOE M 435.1-1 and 10 CFR 61. [DOE M 435.1-1, 10 CFR 61] The 2009 SDF PA incorporated lessons learned between 1992 and 2009.

After approval by DOE and upon initial review of the 2009 SDF PA, the NRC issued RAIs in March 2010 (ML100820097) for which DOE provided a response (SRR-CWDA-2010-00033) in July 2010. In December 2010, the NRC provided a second set of RAIs (ML103400571), to which DOE responded (SRR-CWDA-2011-00044) in August 2011.

Subsequent to the review of the second set of RAI responses, the NRC issued a TER for the 2009 SDF PA. [ML121170309] The NRC TER concluded that the proposed disposal activities for salt waste may result in releases that exceed the performance objective in §61.41 of 10 CFR Part 61, for the protection of the general population at a time much greater than 1,000 years, but within 10,000 years. Based on the results of this TER, in April 2012, the NRC issued a Type IV letter of concern (ML120650576) indicating that the performance objective in §61.41 may not be met.

Multiple information exchanges between DOE and NRC technical staff have occurred since the issuance of the Type IV letter of concern. This 2019 update to the PA incorporates the results of research and development activities designed to address a number of the higher priority concerns raised by the NRC.

2.1.1.6 SDF Disposal Authorization

DOE issued a Disposal Authorization Statement (DAS) transmittal letter, dated May 22, 2012, for the SDF with a stipulation that a sensitivity analysis be performed to ensure that the performance objective in §61.41 of 10 CFR Part 61 is met. [WDPD-12-49] In response to the DAS, a sensitivity analysis (SRR-CWDA-2012-00103) was prepared that assumed an inventory of Tc-99 approximately four times less than modeled in the 2009 SDF PA in the six newly constructed 150-foot (ft) diameter, cylindrical SDUs, based on anticipated salt waste processing and disposal activities. The sensitivity analysis also assumed a Tc-99 inventory in SDU 1 that was twice the then current inventory to account for future potential disposal activities. The Tc-99 inventory in SDU 4 was assumed to be limited to the then current Tc-99 inventories. DOE considered the actions defined in the DAS complete as documented in the *Disposal Authorization Statement for the Savannah River Site Saltstone Disposal Facility - Prestart Corrective Actions Complete* letter dated July 31, 2012. [WDPD-12-66]

2.1.1.7 FY2013 SDF Special Analysis: Updated Cementitious Degradation

In October 2013, a SA was performed to take advantage of new information developed since the issuance of the 2009 SDF PA. [SRR-CWDA-2013-00062] Hereinafter, this SA is referred to as the Fiscal Year (FY) 2013 SDF SA. The FY2013 SDF SA was developed to evaluate new information not previously considered in analyses conducted to support the 2009 SDF PA, and in the responses to RAIs issued by the NRC. [SRR-CWDA-2010-00033; SRR-CWDA-2011-00044] Information considered in the FY2013 SDF SA included SDU design features not previously considered, new information relating to the degradation of cementitious materials, new information relating to the release of technetium from reducing environments within cementitious materials, and updated parameters relating to the dose pathway methodology.

After approval by DOE and upon review of the FY2013 SDF SA, the NRC issued RAIs in June 2014 (ML14148A153), to which DOE provided a response (SRR-CWDA-2014-00099) in January 2015.

2.1.1.8 FY2014 SDF Special Analysis: 375-Foot Diameter SDUs

In September 2014, another SA (hereinafter referred to as the FY2014 SDF SA) was performed. [SRR-CWDA-2014-00006] This FY2014 SDF SA applied four major changes relative to the FY2013 SDF SA: (1) introduced a new SDU design (from 150-foot diameter to 375-foot diameter); (2) updated the modeled inventory; (3) increased the fill height (i.e., no clean cap) for the SDUs; and (4) addressed secondary issues from the Low-Level Waste Disposal Facility Federal Review Group (LFRG) as presented in the *Low Level Waste Disposal Facility Federal Review Group Review Report on the Savannah River Site Salt Waste Disposal Special Analysis to the 2009 Performance Assessment* (DOE-OS-2013-10-15-01).

After approval by DOE and upon review of the FY2014 SDF SA, the NRC issued RAIs in June 2015 (ML15161A541), to which DOE responded (SRR-CWDA-2016-00004) in March 2016.

2.1.1.9 FY2016 SDF Special Analysis: Observed SDU 6 Conditions

In October 2016, another SA (hereinafter referred to as the FY2016 SDF SA) was performed; this SA evaluated the impacts from: (1) revising the SDF layout; (2) observed field conditions of SDU 6; and (3) modifications to future SDUs that were implemented to provide construction margin based on the observed field conditions and construction experience from SDU 6. [SRR-CWDA-2016-00072]

Prior to beginning construction of SDU 7, it was determined that various obstacles in the field created challenges with the original siting location for the SDU. [SRR-SDU-2011-00002] The FY2016 SDF SA was initiated to evaluate a proposed change to the location of SDU 7. Specifically, SDU 7 was moved approximately 190 ft to the west of the initial site (from a center point of N77239.33, E66539.26 to a center point of N77230.51, E66390.28). [G-TAR-Z-00004] The FY2016 SDF SA also noted that the FY2014 SDF SA used approximate SDU locations for the modeling of transport from future SDUs. Updated

center point locations, informed by recent planning decisions, were available for SDUs 6, 8, and 9, based on the *Saltstone Disposal Site Cylindrical Disposal Cells General Arrangement Plan*. [C-CX-Z-00003] This SA incorporated these SDU locations.

In addition, the FY2016 SDF SA reflected the observed field conditions of SDU 6. Specifically, cracking was observed in both the roof and the floor during construction operations. Prior to making SDU 6 available for disposal operations, these cracks were repaired through epoxy injection and a liner was installed to mitigate the impacts from such cracks. [C-SPP-Z-00008, G-ESR-Z-00019] However, for greater defensibility, this SA did not credit these repairs. Instead, this SA assumed a higher initial hydraulic conductivity for the roof and floor to simulate conditions observed during initial leak-tightness testing in November 2015. [G-ESR-Z-00019]

Based on the observed conditions of SDU 6, additional changes were also made to the future 375-foot diameter SDUs. Although the application of lessons learned is expected to reduce the extent of the cracking, SDUs 8 through 12 were modeled with additional joints through the roof and floor. These additional joints were included to provide additional design margin or as explicit through-cracks. Alternatively, because SDU 7 is the next SDU to be constructed, proof-of-concept was not available to credit lessons learned with mitigating cracking through the roof and floor. Therefore, no credit was taken for the application of the lessons learned; as such, SDU 7 was modeled with the same properties as SDU 6 (i.e., a higher initial hydraulic conductivity for the roof and floor is assumed).

2.1.2 Modeling Process Overview

In the development of this updated SDF PA, a more systematic model development approach was applied relative to the approaches applied in previous SDF modeling efforts. Specifically, this approach followed these five steps:

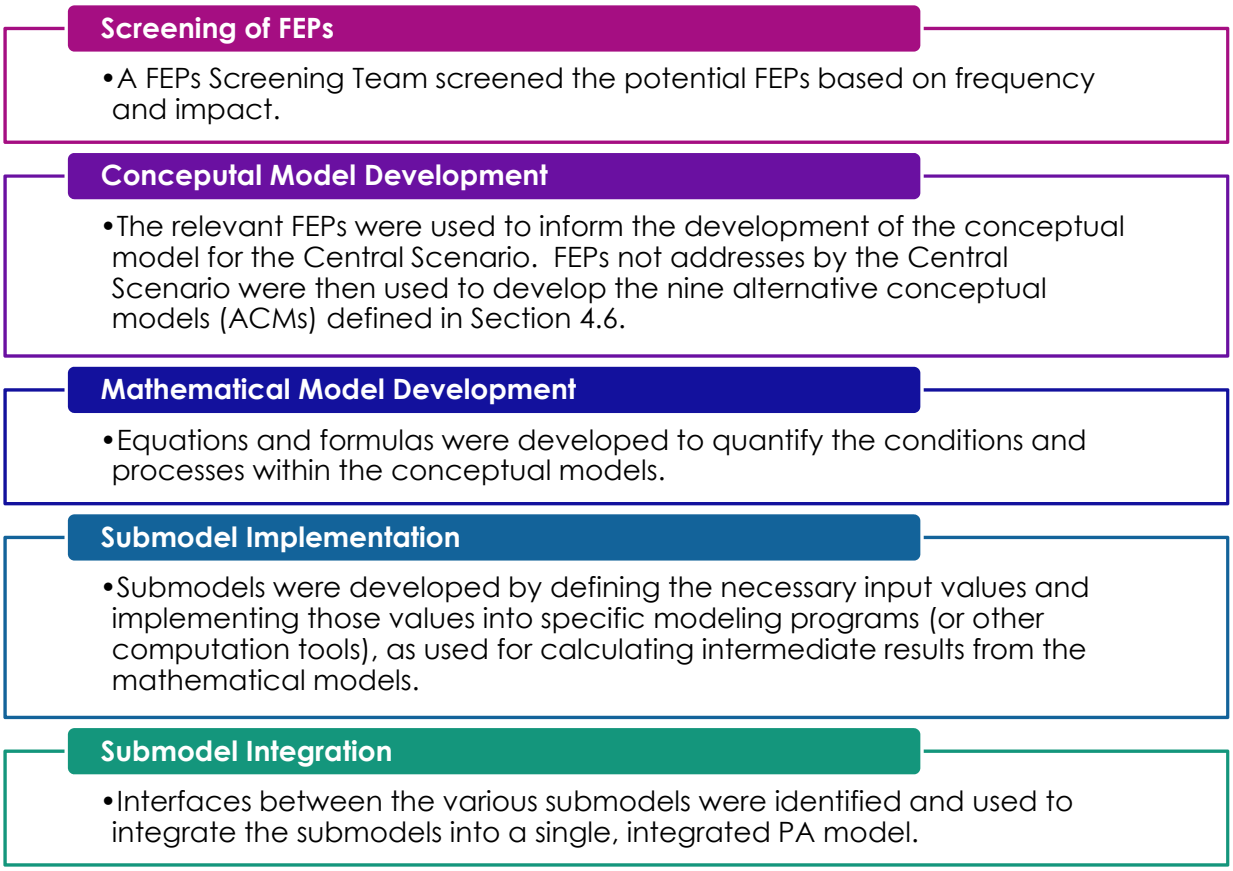

Each of these steps are described in greater detail throughout Section 4.4.

2.2 General Facility Description

2.2.1 Savannah River Site

The Savannah River Site (SRS) is located along the Savannah River in south-central South Carolina, approximately 100 miles inland from the Atlantic Coast. The Savannah River serves as a portion of the southwestern site boundary. SRS occupies approximately 310 square miles (198,000 acres), and includes portions of Aiken, Barnwell, and Allendale counties in South Carolina (Figure 2.2-1). SRS contains numerous developed areas related to past and current site operations. The developed areas occupy less than 10% of the site footprint while the remainder of the site is undeveloped forest or wetlands. Section 3.1 provides additional details about SRS.

Figure 2.2-1: General Location Map of the Savannah River Site

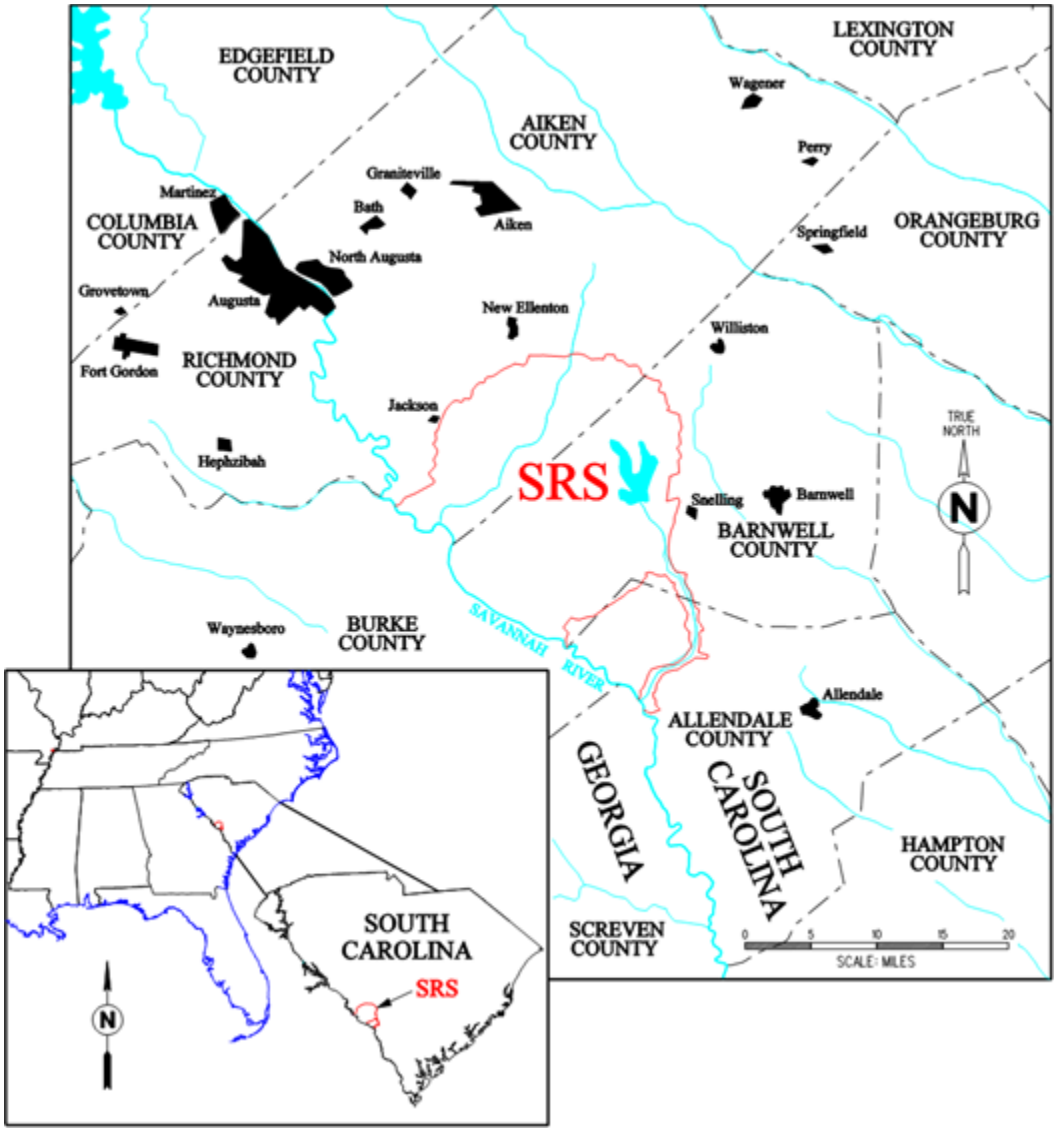

2.2.2 Saltstone Facility

The Saltstone Facility is in Z Area near the center of SRS and contains two integrated waste treatment units, the Saltstone Production Facility (SPF) and the Saltstone Disposal Facility (SDF) (Figure 2.2-2). The SPF receives and processes decontaminated salt solution (DSS) to produce saltstone that is in turn sent to the SDF for final disposal inside SDUs. The SPF is permitted as a waste water treatment facility per South Carolina Department of Health and Environmental Control (SCDHEC) Standards for Wastewater Facility Construction. [SCDHEC R.61-67] The SDF is permitted as a Class 3 Landfill per SCDHEC R.61-107.19, *SWM*: *Solid Waste Landfills and Structural Fill*. [SCDHEC R.61-107.19] SPF and SDF operations are also covered by the SRS Air Quality Permit. [TV-0080-0041]

The radiological requirements for the SDF saltstone waste form are contained in the landfill permit. The permit concentrations are consistent with the estimated inventory presented in

Section 3.3. The SDF Waste Acceptance Criteria (WAC) reflects the most restrictive limit either from the permit, Documented Safety Analysis (DSA), or the PA. [WSRC-SA-2003-00001, X-SD-Z-00004] Additional SDF details are provided in Section 3.2.

Figure 2.2-2: General Separations Area at SRS (Including Z Area)

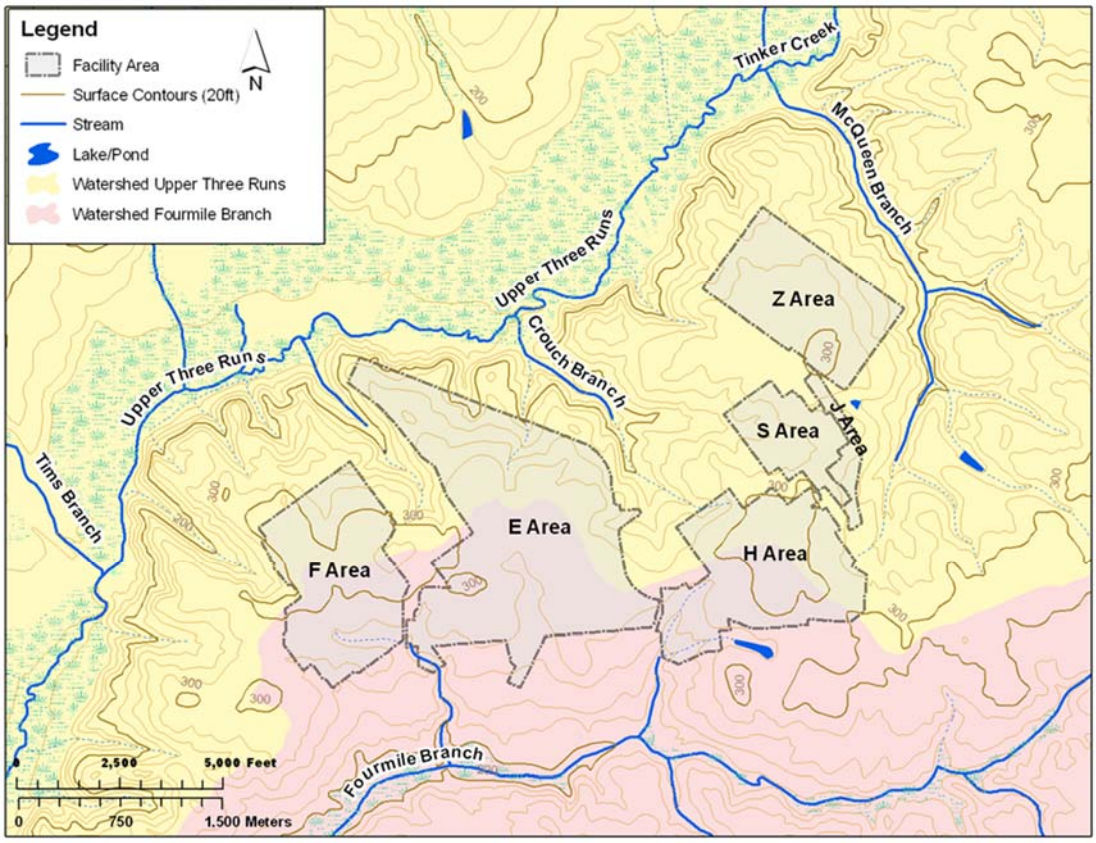

2.2.3 Waste Treatment

Liquid waste from the SRS Tank Farms currently undergoes a decontamination process at the Actinide Removal Process (ARP) and Modular Caustic Side Solvent Extraction Unit (MCU). ARP/MCU work as an integrated system to remove a significant amount of the radioactivity from salt waste solutions. A smaller volume of salt solution is also processed by the Tank Closure Cesium Removal System (TCCR) which uses a different process than ARP/MCU but generates both concentrated radionuclide and DSS products. After treatment, the stripped radionuclides are sent to the Defense Waste Processing Facility (DWPF) for mixing with molten glass and solidification in stainless steel cylinders, while the DSS is transferred to the SPF where it is mixed with dry solids to form the cement-like, saltstone slurry. The saltstone slurry is then transferred to the SDF and placed into the appropriate SDU where it cures and hardens into the final solid waste form. The composition of the stabilized solid waste form will limit the future release of radionuclides and chemical contaminants. The ARP/MCU will eventually be replaced by higher capacity decontamination processing systems in the SWPF currently under construction, but with similar system products.

2.3 Design Features

The key features, including design features, considered in this SDF PA are those that have the most potential impact on the modeling results. At a very high level, the functions of the design features may be summarized as follows:

- **Inventory**: The SDF WAC shall limit concentrations of radionuclides and chemical contaminants within saltstone (discussed in Section 3.3).
- **Waste form stability**: By solidifying the DSS into a solid saltstone waste form, radionuclides and chemical contaminants will be immobilized and the influx of water shall be limited.
- **Waste form chemistry**: The chemistry of the saltstone waste form is designed to delay or limit releases of some constituents (e.g., Tc-99).
- **Closure cap**: The closure cap is designed to limit the infiltration of water from the ground surface to the roof of the SDUs.
- **Backfill**: The backfill surrounding the SDUs will provide structural support to the overlying closure cap and protect the SDU concrete from mechanical damage.
- **HDPE and GCL Layers**: The HDPE and GCL layers within the closure cap and below the SDUs are layers designed to mitigate water flow through the SDUs.
- **SDU roof slope**: The roof of the SDUs are sloped to divert water away from the waste form.
- **SDU concrete**: The roof, walls, and floors of the SDU have a low saturated hydraulic conductivity to limit the influx of water and to retard the release of radionuclides and chemical contaminants.

With the exceptions of the inventory, the backfill, and the roof slope, each of these functions are expected to degrade over time. The waste form is expected to undergo decalcification, which will increase the saturated hydraulic conductivity and oxidation, and ultimately mitigate the waste form's ability to delay or limit releases. Over time, the materials of the closure cap are expected to degrade such that water infiltration rates into the system would increase. The HDPE layers will be subject to antioxidant depletion, and eventually reduced stress crack resistance, which may increase the average size of defects in the HDPE. Finally, the SDU concrete is expected to be susceptible to sulfate attack and carbonation, which will increase the saturated hydraulic conductivity.

Additional details regarding the functionality of the design features may be found in Section 3 of the *Conceptual Model Development for the Saltstone Disposal Facility Performance Assessment*. [SRR-CWDA-2018-00006]

2.4 SDF Lifecycle and Closure Plan

2.4.1 Disposal Operations

There are currently nine SDUs at the SDF: SDUs 1, 2A, 2B, 3A, 3B, 4, 5A, 5B, and 6. The first SDUs were constructed between 1986 and 1988. These units, known then as Vaults 1 and 4, are rectangular structures that are divided internally into smaller cells. A cylindrical water tank-type design was used for SDUs 2, 3, 5 and 6, although the cylinder size was greatly increased for SDU

6 to reflect cost savings and future disposal capacity needs. The SDU 6 design is currently planned for future SDUs 7 through 12. SDU construction and operation details are summarized in Table 2.4-1.

The SPF started operations in June 1990 and the first saltstone disposal was into SDU 1. SDU 1 received waste intermittently from 1990 to 1996. Disposal into SDU 4 began in 1997 and ended in 2011. There are no plans for additional disposal into SDUs 1 and 4. [SRR-CWDA-2017-00078] SDUs 2A and 2B received saltstone between 2012 and 2014 and there are no plans for additional disposal operations into these SDUs. [SRR-CWDA-2017-00078] SDUs 5A and 5B received saltstone between 2013 to 2017 and there are no plans for additional disposal operations into these SDUs. [SRR-CWDA-2017-00078] Disposal to SDUs 3A began in 2017 and is currently underway. At the time the modeling inventory was established (i.e., as of March 31, 2018), SDUs 3B and 6 had not received any waste (Table 2.4-1).

Additional SDUs beyond SDU 7 will be constructed, as needed, in coordination with salt waste processing production rates. Based on projected waste streams and capacities, five additional 375-foot diameter SDUs will be needed beyond SDU 7. [SRR-LWP-2009-00001]

Table 2.4-1: Saltstone Disposal Unit Design, Construction, and Operations Details

SDU Number	SDU Design Parameters (Note: SDU height is for the sidewall)	Construction Period	Saltstone Receipt Period	Approximate Capacity (Mgal)
1[a]	Rectangular Vault – 100 ft wide, 600 ft long, 25 ft high, divided into 6 cells	1986-1988	1990-1996[b]	11
4[a]	Rectangular Vault – 200 ft wide, 600 ft long, 26 ft high, divided into 12 cells	1986-1988	1997-2011[b]	22
2A	Cylindrical Tanks – 150 ft diameter, 22 ft high	2008-2009	2012-2014[b]	2.8
2B		2008-2009	2012-2014[b]	2.8
3A		2011-2013	2017-	2.8
3B		2011-2013	TBD	2.8
5A		2011-2013	2013-2017[b]	2.8
5B		2011-2013	2013-2017[b]	2.8
6	Cylindrical Tanks – 375 ft diameter, 43 ft high	2014-2017	TBD	32.8
7		2018-	TBD	32.8
8		TBD	TBD	32.8
9		TBD	TBD	32.8
10		TBD	TBD	32.8
11		TBD	TBD	32.8
12		TBD	TBD	32.8

a Historically referred to as Vaults 1 and 4.
b No further saltstone additions are planned.
TBD – To Be Determined

2.4.2 Facility Closure

Operation of the SPF and SDF is expected to continue until an assumed SDF closure date of October 1, 2037. After disposal operations are complete, an engineered closure cap will be constructed over the SDF. The final closure cap, along with the inherent SDU construction features (roof, walls, etc.), will restrict vertical water infiltration. The U.S. federal government will own and maintain control of SRS, including the SDF, in perpetuity.

2.5 Related Documents

The FY2019 SDF PA was prepared within the regulatory context of LLW management per DOE O 435.1, Chg. 1, and the associated implementation manual (DOE M 435.1-1). Additional context has been added to address National Defense Authorization Act (NDAA) for FY2005 Section 3116, SCDHEC wastewater construction and operations permit regulations, and the SRS Federal Facility Agreement (FFA) pursuant to Section 120 of the Comprehensive Environmental Response, Compensation, and Liability Act (CERCLA) and Sections 3008(h) and 6001 of the Resource Conservation and Recovery Act (RCRA). [SCDHEC R.61-67, SCDHEC R.61-82, DHEC_01-25-1993, DHEC_02-28-1995, WSRC-OS-94-42] The *DOE Standard Disposal Authorization Statement and Tank Closure Documentation* was also relied on for guidance. [DOE-STD-5002-2017] This PA was influenced by, and has an influence on, other documents that are discussed in this section.

2.5.1 Ground Water Protection Management Program

The SDF Closure Plan (SRR-CWDA-2013-00037) documents requirements for protection of water resources. The appropriate measures for protection of water resources have been determined to be the EPA Safe Drinking Water Act MCLs (https://www.epa.gov/ground-water-and-drinking-water/national-primary-drinking-water-regulations). The MCLs for the radionuclides are based on 4 mrem/yr for beta-gamma emitting nuclides, 15 pCi/L for alpha emitting nuclides, and 5 pCi/L for radium. The MCLs are listed with the 100m results for the SDF in Section 5.2.

The plan for protection of ground water at SRS is documented in the *SRS Groundwater Protection Program*. [SRNS-TR-2009-00076] The hydrogeology information used in this SDF PA is consistent with that in the ground water protection program. The *SRS Groundwater Protection Program* is focused on those activities regulated by external agencies (i.e., the State of South Carolina and the EPA). [SRNS-TR-2009-00076] Consistent with guidance for preparing the FY2019 SDF PA, the requirement of DOE O 435.1, Chg.1 to identify impacts to water resources has been addressed by assessing the concentrations of radioactive or chemical contaminants against standards for public drinking water supplies established by EPA and SCDHEC. [SRNS-TR-2009-00076, DOE O 435.1, Chg. 1]

2.5.2 Savannah River Site End State Vision

The *SRS End State Vision* focuses on site facilities and areas that are the responsibility of the DOE Office of Environmental Management, which includes SDF and SPF. [PIT-MISC-0089]

SRS End State Vision

- The entire site will be owned and controlled by the federal government in perpetuity.
- The property will be used only for industrial purposes.
- Site boundaries will remain unchanged.
- Residential use will not be allowed on-site.

The DOE solicited public input into the *SRS End State Vision*. The document contains an appendix that addresses public comments received, including recommendations and endorsement from the SRS Citizens Advisory Board (CAB). [PIT-MISC-0089]

2.5.3 Savannah River Site Land Use Plan

The *Savannah River Site Land Use Plan* (SRNS-RP-2014-00537) provides the framework for integrating the SRS mission and vision with ecological, economic, cultural, and social factors in a regional context and to support decision-making for near-term and long-term use of the site, including the SDF. The *Savannah River Site Land Use Plan* describes the current site conditions, defines a vision for the evolution of the site, outlines actions to achieve the vision, and guides the allocation of resources toward attainment of that vision. This plan provides guidance and direction for the future physical development of the site and a framework within which detailed analyses will be conducted to determine the courses of action required to reach optimum site configuration. The plan is based on specific assumptions. If these assumptions were to change, the plan would be updated to reflect the changed conditions. Guidelines on which the SRS land use is based include:

- Giving priority to protection of workers and the public;
- Maintaining site security;
- Maintaining other appropriate institutional controls;
- Considering worker, public, and environmental risks, benefits, and costs;
- Restricted use programs for units regulated under CERCLA or under RCRA;
- Maintaining existing SRS boundaries;
- Continuing federal ownership of the land; and
- Prohibiting residential use of any SRS land.

2.5.4 Federal Facility Agreement for the Savannah River Site

The FFA entered into by SCDHEC, the DOE, and the EPA "governs the corrective/remedial action process from site investigation through site remediation and describes procedures… for that process." [WSRC-OS-94-42] It contains requirements for (1) site investigation and remediation of releases and potential releases of hazardous substances, and (2) interim status corrective actions for releases of hazardous wastes or hazardous constituents.

The SDF SDUs are considered Solid Waste Management Units (SWMUs) in the FFA, Appendix H. Per the FFA, "SWMUs shall mean those units subject to applicable RCRA corrective action requirements, identified by EPA and SCDHEC, either presently or in the future, as requiring further investigation." [WSRC-OS-94-42]

The FFA delineates the relationship between its requirements and the requirements for corrective measures being conducted under Sections 3004(u) and 3004(v) according to the conditions of the SRS's Federal RCRA permit and the South Carolina State Hazardous Waste permit. All proposed remediation plans under the FFA are subject to review and comment by the EPA, SCDHEC, stakeholders, and the public and approval by both the EPA and SCDHEC. A formal dispute resolution process is set forth in the FFA in case of disagreement on any actions to be taken.

2.6 Regulatory Context

The PA performance objectives are identified in DOE M 435.1-1 and 10 CFR 61 which are referenced by the NDAA for FY2005. Section 3116 of the NDAA specifies the criteria for DOE to classify residual waste as non-high-level waste (HLW) for purposes of onsite disposition. The NDAA is applicable only to South Carolina and Idaho.

2.6.1 DOE M 435.1-1 Performance Objectives and Requirements

The DOE LLW disposal performance objectives are defined in DOE M 435.1-1 IV.P (1). DOE-Headquarters (DOE-HQ) issued a letter *Compliance with DOE M 435.1-1 Waste Incidental to Reprocessing Requirements and Implementation of Section 3116(a) of the National Defense Authorization Act for Fiscal Year 2005 (NDAA)*, from Mr. Rispoli to Mr. Allison, which offers guidance and clarification concerning the requirements in DOE O 435.1, Chg.1, when the requirements of NDAA Section 3116 are also applicable to avoid duplication of efforts. [DOE_02-09-2006]

The DOE LLW disposal performance objectives (DOE M 435.1-1 IV.P (1)) are:

> *"Low-level waste disposal facilities shall be sited, designed, operated, maintained, and closed so that a reasonable expectation exists that the following performance objectives will be met for waste disposed of after September 26, 1988:*
>
> *(a) Dose to representative members of the public shall not exceed 25 mrem (0.25 mSv) in a year Total Effective Dose Equivalent (TEDE) from all exposure pathways, excluding the dose from radon and its progeny in air.*
>
> *(b) Dose to representative members of the public via the air pathway shall not exceed 10 mrem (0.10 mSv) in a year TEDE, excluding the dose from radon and its progeny.*
>
> *(c) Release of radon shall be less than an average flux of 20 pCi/m^2/s (0.74 Bq/m^2/s) at the surface of the disposal facility. Alternatively, a limit of 0.5 pCi/l (0.0185 Bq/l) of air may be applied at the boundary of the facility."*

Item *(a)* is similar to 10 CFR 61.41, and this PA provides the information relative to items *(b)* and *(c)* for completeness.

In addition to the DOE LLW disposal performance objectives cited above, the following information from DOE M 435.1-1 IV.P (2) is considered:

"(g) For purposes of establishing limits on radionuclides that may be disposed of near-surface, the performance assessment shall include an assessment of impacts to water resources.

(h) For purposes of establishing limits on the concentration of radionuclides that may be disposed of near-surface, the performance assessment shall include an assessment of impacts calculated for a hypothetical person assumed to inadvertently intrude for a temporary period into the low-level waste disposal facility. For intruder analyses, institutional controls shall be assumed to be effective in deterring intrusion for at least 100 years following closure. The intruder analyses shall use performance measures for chronic and acute exposure scenarios, respectively, of 100 mrem in a year and 500 mrem total effective dose equivalent excluding radon in air."

Item *(g)* is similar to the SCDHEC ground water protection requirement and 10 CFR 61.42, and the exposure performance measures for the inadverdent human intruder from item *(h)* is similar to 10 CFR 61.42.

2.6.2 10 CFR 61 Performance Objectives

Subpart C of 10 CFR 61 lists the five performance objectives, which are reproduced below:

Section 61.40 General Requirement

"Land disposal facilities must be sited, designed, operated, closed, and controlled after closure so that reasonable assurance exists that exposures to humans are within the limits established in the performance objectives in Sections 61.41 through 61.44."

Section 61.41 Protection of the General Population from Releases of Radioactivity

"Concentrations of radioactive material, which may be released to the general environment in ground water, surface water, air, soil, plants, or animals, must not result in an annual dose exceeding an equivalent of 25 millirems to the whole body, 75 millirems to the thyroid, and 25 millirems to any other organ of any member of the public. Reasonable effort should be made to maintain releases of radioactivity in effluents to the general environment as low as is reasonably achievable."

Section 61.42 Protection of Individuals from Inadvertent Intrusion

"Design, operation, and closure of the land disposal facility must ensure protection of any individual inadvertently intruding into the disposal site and occupying the site or contacting the waste at any time after active institutional controls over the disposal site are removed."

Section 61.43 Protection of Individuals During Operations

"Operations at the land disposal facility must be conducted in compliance with the standards for radiation protection set out in part 20 of this chapter, except for releases of radioactivity in effluents from the land disposal facility, which shall be governed by Section 61.41 of this part. Every reasonable effort shall be made to maintain radiation exposures as low as is reasonably achievable."

The NRC acknowledged that using a performance objective of 25 mrem/yr effective dose is acceptable versus considering individual organ doses, as well as using a whole-body

dose-equivalent limit of 500 mrem/yr effective dose is appropriate to assess intruder scenarios. [ML072360184 (NUREG-1854)]

Section 61.44 Stability of the Disposal Site After Closure
"The disposal facility must be sited, designed, used, operated, and closed to achieve long-term stability of the disposal site and to eliminate to the extent practicable the need for ongoing active maintenance of the disposal site following closure so that only surveillance, monitoring, or minor custodial care are required."

2.6.3 Point of Assessment and Timing Assumptions

The point of assessment for the SDF PA is the point of highest concentration at least 100 meters from the footprint of the SDUs. Based on current ground water modeling, the point of highest concentration occurs at a point that is 100 meters from the SDUs (as opposed to some point further away). Because the location of this point of highest concentration changes over time (due to time-dependent plume interactions), the point of assessment is assumed to move along a hypothetical 100-meter boundary such that the point of assessment always reflects the point of the highest possible concentration along this boundary.

Numerous assumptions and predictions were made in assessing the performance of the SDF over the 1,000-year Compliance Period and the 10,000-year Performance Period. A summary of the key assumptions supporting the SDF PA analyses are discussed in this section.

2.6.3.1 Institutional Controls

As noted in Section 2.5.3, the *Savannah River Site Land Use Plan* assumes that the entire site will be owned and controlled by the federal government in perpetuity. [SRNS-RP-2014-00537] However, for the purpose of this PA only, no federal protection of the SDF is assumed beyond the 100-year period of institutional control. A 100-year period of institutional control is assumed to begin in year 2037. The Compliance Period will span 1,000 years following closure. The Performance Period will span 10,000 years following closure.

2.6.3.2 Site Characteristics Assumptions

The characterization and monitoring data for the GSA is extensive and provided an understanding of hydrogeology of the SDF and a reasonable data set to represent long term conditions.

2.6.3.3 Facility Design Assumptions

A low-infiltration closure cap will be placed above the SDF disposal units and is expected to perform as described in Section 3.2.6. The Closure Cap Model (Section 4.4.1) used available data to simulate a future precipitation rate and the resulting infiltration rate is expected to change over time.

2.6.3.4 Stabilized Contaminants Characteristic Assumptions

2.6.3.4.1 Inventory

The inventory estimate for the SDF disposal units at closure is expected to sufficiently bound the actual inventory as described in Section 3.3. An initial radionuclide screening process was developed and performed to support characterization efforts and is applicable to SDF PA modeling as described in Section 4.4.

2.6.3.4.2 Waste Form

Saltstone is a cementitious waste form created through the mixing of a low-level waste salt solution, which originates in the SRS F-and H-Area liquid waste storage tanks, with a dry mix containing blast furnace slag, fly ash, and cement. The SPF currently uses operating procedures to control the formulation of the saltstone. A review of a number of premix feed batches indicated that the variability of the dry materials is within approximately 3% of the nominal formulation at the 95% confidence interval. The results of the ongoing research (e.g., DLM testing) will be used in conjunction with the operational information to evaluate any impacts as part of PA maintenance.

Over the course of time, the mobile contaminants in the closed SDF disposal units are expected to be released and gradually migrate downward through unsaturated soil to the hydrogeologic units comprised of the shallow aquifers underlying the SDF.

2.6.3.5 Integrated Site Conceptual Model Assumptions

2.6.3.5.1 Degradation and Contaminant Movement

The mechanism generally controlling the release of contaminants from SDF is the adsorption characteristic of the saltstone expressed by the K_d (partition coefficient), which is element dependent and differs as the saltstone Eh (oxidation potential or measure of reduction potential) and pH (measure of acidity or basicity) conditions change over time. Contaminant concentrations in saltstone are not generally expected to be limited by solubility. The degradation of the disposal unit concrete (walls, roof, and floor) is dominated by internal sulfate attack from the saltstone as described in Section 4.4.2. The rates of contaminant release and movement from saltstone are principally controlled by these factors:

- Chemical and physical properties (e.g., K_d) of the saltstone, disposal unit, and soil;
- Physical properties (e.g., void structure and hydraulic conductivity, etc.) and state (e.g., integrity) of the waste form and disposal unit concrete and soil;

- Chemical properties (e.g., reduction capacity) and state (e.g., Eh and pH) of the waste form and disposal unit concrete; and
- Infiltration to the saltstone through the disposal unit from the overlying soil.

The SDUs are designed for a dual role that limits releases of contaminants out of the disposal unit and limits the migration of water and oxygen into the disposal unit via dissolved oxygen in water, thus delaying movement of contaminants and oxidation of the saltstone. The SDF is designed to retain Tc-99 through the use of slag-bearing saltstone and disposal unit concrete formulations, which create a low Eh environment. The ground water concentrations are assumed to be the highest concentration in the area at 100m or farther from the SDF.

2.6.3.5.2 Infiltration and Erosion Control

Section 3.2.6 describes the preliminary design for the engineered, multi-layered closure cap. This closure cap provides a a minimum 10 feet (ft) of clean material above each SDU to minimize infiltration and to act as an intruder deterrent. The erosion control barrier within the closure cap is expected to limit surface erosion while rip rap material along the side slopes will be sized to limit erosion at the edges of the closure cap. The closure cap is expected to perform as designed; the estimated infiltration rates are provided in Section 4.4.1.

2.7 Summary of Key Assumptions

Since the Compliance Case is used to support the demonstration of compliance, the key assumptions provided below all describe Compliance Case assumption, unless specifically noted otherwise. These assumptions generally pertain to the other modeling cases, except where the purpose or definition of the modeling case requires an alternative assumption.

2.7.1 Land Use Assumptions

After the institutional control period, the members of the public (MOPs) and inadvertent human intruders (IHIs) are assumed to drill wells for water in the vicinity of the Saltstone Disposal Units (SDUs).

The *Savannah River Site Land Use Plan* assumes that the entire site will be owned and controlled by the federal government for periods of time longer than the assessment period. [SRNS-RP-2014-00537] However, for the purpose of this SDF PA, no federal protection is assumed beyond a 100-year period of institutional control. The 100-year period of institutional control is assumed to begin in the year 2037. It is assumed that after this institutional control period (during year 2137), MOPs will have no prior knowledge of SRS and will live on the land and place water wells 100-meters from the SDUs. Similarly, IHIs will place water wells adjacent to the SDUs (i.e., one meter from the SDUs).

2.7.2 Climate Assumptions

The long-term climate is assumed to reflect current conditions.

The modeling parameters that are most likely to be influenced by changes to climate are infiltration and ground water flow/aquifer depth. These parameters are expected to exhibit natural variation over long periods as a function of the prevailing climate conditions. Leigh (2008) describes a study of the long-term climate of the Atlantic Coastal Plain of the Southeastern United States based on pollen and paleochannel records. [DOI:10.1016/j.geomorph.2008.05.024] Leigh (2008) determined approximately 8,200 years ago, the local climate transitioned from a cooler, dryer period to the current state, which has remained relatively unchanged ever since. Based on this long period (8,200 years) of relatively steady climate conditions, this SDF PA assumes that the local climate conditions will continue to remain unchanged throughout the Performance Period (i.e., at least 10,000 years). Infiltration rates and ground water conditions associated with alternative climate conditions will be evaluated as part of alternative conceptual models or as sensitivity models.

Short-term climate variability is ignored.

Short-term changes (e.g., seasonal, annual fluctuations, etc.) in infiltration or aquifer depth are not considered in the model due to the extended time ranges involved. Instead, steady-state modeling was used to approximate the infiltration rates into the system and the long-term ground water conditions.

2.7.3 Closure Cap Assumptions

The closure cap is assumed to be covered by natural perennial grass.

Three forms of vegetation have been considered for a vegetative cover atop the engineered closure cap: pine, bamboo, and grass. Of these, pine and bamboo both generate more above ground biomass than grass, which would result in greater transpiration than a grass cover. Accordingly, assuming a grass cover permits more water to become deep drainage. [SRRA107772-000009]

Erosion of the closure cap is ignored in the infiltration estimates because the erosion barrier and the riprap along the side slopes of the closure cap will be designed and/or sized to minimize the influences of erosion.

While limited erosion is expected to occur over the time periods considered in this SDF PA, it is not expected to significantly impact the infiltration estimates. The erosion barrier will be designed to prevent riprap movement during a probable maximum precipitation (PMP) event and form a barrier to erosion and gully formation (i.e., provide closure cap physical stability). It will be used to maintain a minimum 10 feet of clean material above the disposal units to act as an

intruder deterrent. It will also act to preclude burrowing animals from access to underlying closure cap layers. [WSRC-STI-2008-00244]

The intention of the riprap is to: (1) stabilize the underlying layer, (2) provide erosion protection to the toe, (3) transition flow from the side slope to adjacent areas, and (4) provide gully intrusion protection to the embankment. [WSRC-STI-2008-00244]

Preliminary estimates of potential surface erosion is estimated to be less than 2 inches over 1,000 years and between 3 inches and 18 inches over 10,000 years (see Section 4.4.1.5). Because this is expected to be a slow process, as the topsoil is eroded at the surface, deposition of biomass from the vegetation and other environmental conditions would influence the underlying backfill soil such that the backfill soil directly beneath the eroded topsoil is assumed to evolve into topsoil and replace any surface mass that is lost to erosion. As such, the topsoil layer is assumed to remain 6 inches thick into perpetuity, while the underlying upper backfill layer would become thinner over time as a response to soil loss.

It should also be noted that the closure cap modeling did evaluate the influence of the thickness of the middle backfill layer. This layer is expected to have a minimum thickness at the apex of the closure cap (1 foot) and a maximum thickness (more than 20 feet) at the perimeter of the cap. Despite the difference of more than 19 feet between the minimum and maximum thicknesses, the resulting deep drainage estimates only varied by a few mm per year (from about 405 mm/yr at the apex to 413 mm/yr at the perimeter of the cap). [SRRA107772-000009] This indicates that the infiltration estimates may not be strongly sensitive to variations in the thicknesses of the backfill layers.

Additionally, as a modeling simplification, the 12-inch foundation layer is not credited in either the Closure Cap Model or the Vadose Zone Flow Model, thus the closure cap has an additional 12 inches of material that has not been considered.

The hydraulic properties of the near-surface earthen layers are assumed to have undergone pedogenesis.

The closure cap is designed with various layers with varying material properties for various functions (e.g., erosion prevention, infiltration barrier, lateral drainage, water storage, etc.). [WSRC-STI-2008-00244] The upper backfill layer, middle backfill layer, and lower backfill layer are expected to be comprised of clayey sands sourced from local quarries. Similarly, the erosion barrier will be comprised of angular stone infilled with sands and sourced from local quarries. While these earthen layers will be control-compacted during emplacement, this compaction will only be credited for the lower backfill layer, but will not be credited when modeling the upper backfill layer, erosion barrier, and middle backfill layers. As such, the initial saturated hydraulic conductivities for these three layers, as well as the top soil layer, are all assumed to be 1.0E-04 cm/s. [SRRA107772-000009] Earlier modeling assumed a value of 4.1E-05 cm/s for the backfill layers (based on compaction) and 1.3E-04 cm/s for the erosion barrier. [WSRC-STI-2008-00244]

The interfaces between closure cap layers are assumed to remain stable, without significant mixing between the grains of fine and coarse layers.

Previous closure cap modeling for the SDF assumed that fine-grained clay colloids from the clayey backfill layers would migrate over time into the underlying sand drainage layers. [WSRC-STI-2008-00244] This migration was assumed to result in the sand drainage layers becoming "silted up," which would decrease the saturated hydraulic conductivity and retard lateral flow. Natural analogs, such as the Tu-Dun tombs in south-central China and a Japanese burial mound in northern Kyushu prefecture, showed that even in humid environments such mixing of layers was not observed. [SRRA107772-000009] Therefore, it is now considered reasonable to assume that the interfaces between these layers will remain stable for the duration of the simulations.

The high-density polyethylene (HDPE) layers are assumed to be installed with five circular defects (2 mm diameter each) per hectare.

This assumption is consistent with a high level of quality control. [SRRA107772-000009]

HDPE layers have a service life of approximately 2,000 years.

Recent studies of HDPE performance have provided a more in-depth understanding of conditions under which this material will degrade. Based on Tian, *et. al.* (2017), antioxidant depletion is expected to take approximately 730 years (Stage I), followed by an induction period of approximately 25 years (Stage II), after which degradation begins. For this SDF PA, it is assumed that the HDPE no longer performs as designed once the stress crack resistance (SCR) of the material reaches 50%, which is estimated to take approximately 1,220 years after the end of the induction period (Stage III). So, 730 years for Stage I, 25 years for Stage II, and 1,220 years for Stage III gives an estimated service life of 1,975 years. Note that this is the shortest estimated service life based on data presented in Tian, et.al. (2017); given a different set of assumptions, the service life could be as long as 3,550 years. [DOI: 10.1061/(ASCE)GT.1943-5606.0001643] As such, it is reasonable to round the 1,975-year value to 2,000 years for modeling purposes.

Once the HDPE service life is reached, the closure cap model assumes that all the 2 mm diameter defects instantly expand to 10 mm diameter defects.

Once the HDPE reaches the end of the assumed service life (2,000 years), it will still be present within the closure cap and it will continue to act as a barrier to flow. As such, it is not reasonable to assume that the material completely stops performing as a barrier to flow. Instead, as described in *Predicting Long-Term Percolation from the SDF Closure Cap* (SRRA107772-000009), it is reasonable to assume that in the degraded state, existing defects will enlarge from 2 mm diameter defects to 10 mm diameter defects as it is expected that edges of the existing defects would be susceptible to damage. [SRRA107772-000009]

2.7.4 Inventory Assumptions

The entire soluble inventory for the Tank Farms is assumed to be destined for disposal at the SDF.

This is expected to overestimate inventory because some of the soluble Tank Farm waste is likely to remain in the tanks and transfer lines as residual waste after waste removal activities are complete. [SRR-CWDA-2018-00041] Some of the soluble Tank Farm waste may also be mixed into sludge and disposed of as vitreous waste via DWPF.

The inventories for future disposal to the SDF assume that the H-Canyon will transfer 300,000 gallons of waste into the Tank Farms each year from FY2018 to FY2025. [SRR-CWDA-2018-00041]

This is expected to be an overestimate. From 2007 to 2017, less than 1,600,000 gallons of waste were transferred from H-Canyon to the Tank Farms. On average, approximately 143,000 gallons per year were transferred. [SRR-CWDA-2018-00049]

The inventories for future disposal to the SDF will be distributed evenly, based on available space in the SDUs. [SRR-CWDA-2018-00041]

DOE has begun developing plans to ensure higher-activity wastes are disposed of into SDUs 6 and 7. Based on model results, disposing more inventory into these SDUs will reduce dose risk, as SDUs 6 and 7 are further from the 100-meter boundary and are more impacted by the influences of a ground water divide. If more waste is disposed of into these SDUs, less will be available for disposal in the later SDUs. While these plans are still in an incipient stage, once they are enacted, it is expected that the current assumption of distributed waste allocation will be biased towards overestimating dose. Further, within each SDU, the distribution of contaminants is assumed to be homogenous.

A salt processing decontamination factor (DF) of 200 is assumed for cesium.

It has been demonstrated that the historic decontamination approach exhibits a DF that is typically between 200 and 400 (SRR-SPT-2016-00009), so a DF of 200 is reasonable based on historic application. However, advances in solvent technology have significantly improved this DF to a value of 10,000 to 100,000 after initial facility start-ups (SRR-SPT-2016-00009), such that the assumed DF of 200 overestimates that cesium inventories.

For the Compliance Case the future disposal inventories were increased by 50%.

While a "realistic" inventory was determined based on the best available information, there is still uncertainty in the future inventory estimates. As such, the realistic estimates were increased by 50% (for most of the radionuclides and chemicals) to support the demonstration of compliance for use in the Compliance Case. [SRR-CWDA-2018-00041] The exception is the I-129 inventory,

which assumed the total Tank Farm inventory (soluble plus insoluble), rather than applying a full 50% increase to the realistic values. [SRR-CWDA-2018-00041, SRR-CWDA-2015-00077] Due to recent tank sampling and analysis activities to better characterize the inventory of I-129, this assumption is appropriate.

2.7.5 SDU Assumptions

The walls of SDUs 1 and 4 are assumed to be initially degraded.

Based on observed field conditions for SDUs 1 and 4, the concrete walls of these two SDUs are assumed to be initially degraded (i.e., initial saturated hydraulic conductivity and effective diffusion coefficient of compacted backfill: 4.1E-05 cm/s and 5.3E-06 cm^2/sec, respectively). [SRR-CWDA-2018-00004] After SDUs 1 and 4, the design of the SDUs was modified to withstand hydrostatic head equivalent to the SDU fill height thus mitigating the risk of potential cracking on the walls. [CBU-ENG-2003-00103, LWO-SSF-2009-00001]

The roof and floor of SDU 6 are assumed to be partially degraded.

Cracks were observed in the concrete roof and floor of SDU 6, likely due to insufficient moisture during curing. While remediation efforts included epoxy injection into cracks and an interior liner over the floor and up the walls of the SDU, the concrete roof and floor of this SDU are assumed to be partially degraded (i.e., initial saturated hydraulic conductivity of 6.2E-06 cm/s). [SRR-CWDA-2016-00072, SRR-CWDA-2018-00004, SRNL-STI-2018-00077] The SDU concrete formulation and the concrete pouring and curing strategy was modified for future SDUs (SDUs 7 through 12) to mitigate the risks of future crack formation. [SRR-SDU-2016-00027, SRR-SDU-2017-00013]

Interior liners or coatings are not credited.

Most of the SDUs have some form of interior coating or liner to prevent, or slow, the rate of sulfate attack (i.e., an important mechanism for concrete degradation). However, the effectiveness of these coatings and layers has not been rigorously tested for the periods of time considered in this PA; therefore, these are not credited in the modeling that supports the SDF PA.

Exterior barriers are not credited.

Most of the SDUs will be wrapped in pre-stressing wire and/or coated with a layer of shotcrete (a type of sprayed-on mortar). It is expected that the shotcrete layer will likely slow or delay carbonation of the SDU walls and mitigate some of the ingress of water, as well as retarding the transport of contaminants (via cementitious K_d values). However, such layers are not credited in the modeling that supports the SDF PA.

Once the SDUs are backfilled, it is assumed they will not be subject to mechanical damage.

This SDF PA assumes that no significant structural changes or mechanical damages will affect the SDUs during the closure process. Any significant changes to the SDU features that are observed prior to backfilling and closure shall be addressed through SDU-specific assumptions (e.g., the SDU 1 and 4 walls and the SDU 6 floor and roof). Once the SDUs are backfilled, it is assumed that the backfill will provide structural support to the SDU to prevent any additional mechanical damage from occurring.

The primary mechanisms for SDU concrete degradation are assumed to be sulfate attack and carbonation.

SDU concrete degradation is expected to be dominated by internal sulfate attack from the saltstone, and, to a lesser extent, carbonation-induced rebar corrosion; however, the concrete may be susceptible to other degradation mechanisms including cracking from seismic events, settlement, and external static loading, chloride ingress induced rebar corrosion, alkali-silica reactions, calcium leaching, freeze-thaw cycling, and microbial degradation. These other mechanisms are not expected to exceed the effect of sulfate attack. [SRR-CWDA-2011-00044] Therefore, although they may contribute to the degradation of the concrete and embedded steel of the SDUs, they will not result in a large-scale difference in degradation rate from the current degradation model of the structure.

The walls of the 375-foot diameter SDUs are assumed to undergo sulfate attack prior to facility closure.

As part of degradation modeling, the walls of 375-foot diameter SDUs are assumed to experience desiccation due to atmospheric exposure to a depth of 1 cm. [SRNL-STI-2018-00077] This assumption only applies to the 375-foot diameter SDUs because (1) the walls of the rectangular SDUs (SDUs 1 and 4) are already assumed to be degraded and (2) the walls of the 150-foot diameter SDUs are treated with a water-proof coating. (Note that while this water-proofing will likely delay sulfate attack after closure, this function is not credited as indicated in a previous assumption.)

An exponential degradation curve is assumed for representing the hydraulic degradation of the SDU concrete.

The saturated hydraulic conductivity of SDU concrete will be based on the geometric mean of the saturated hydraulic conductivity in (1) the non-degraded portion of the concrete and (2) the degraded portion of the concrete. [SRRA110110-000004, SRNL-STI-2018-00077] While changes to the depth of degradation are expected to occur at a linear rate, there is a non-linear relationship between the combined properties of non-degraded and degraded materials. This non-linear relationship is assumed to be best represented by using the geometric mean to blend the non-degraded and degraded material properties into a uniform material to simplify modeling.

Applying the geometric mean provides a exponential degradation curve. This assumption is supported extensively in the relevant literature as evaluated in *Predicting the Hydraulic Conductivity Over Time for Degrading Saltstone Vault Concrete - Task 5 (Subcontract Number SRRA110110)*. [SRRA110110-000004]

The final degraded condition of SDU concrete is assumed to be hydraulically equivalent to the surrounding control compacted backfill or vadose zone soil.

It is expected that fully degraded SDU concrete will retain some of its barrier performance properties for periods of time longer than the assessment period; however, the final degraded state of SDU concrete is unknown. As a simplifying assumption, it is assumed that SDU concrete will degrade until its hydraulic properties are in equilibrium with the surrounding soils.

2.7.6 Saltstone Assumptions

Data from SDU 2A Core analyses are assumed to be the best representation of saltstone material properties.

While data from laboratory-prepared simulant samples provide useful insights to inform input assumptions, the best representation of field-emplaced, cured saltstone are the core samples that that were taken directly from SDU 2A. [SRR-CWDA-2015-00066, SRR-CWDA-2018-00004]

Clean cap grout is not credited.

After filling operations are complete, but prior to emplacement of the closure cap, void spaces within the SDUs will be filled in with a "clean cap" (i.e., non-radioactive grout) to provide physical stability for the SDU roof to support the weight of the closure cap. While this clean cap material is expected to delay or retard sulfate attack on the SDU concrete and to mitigate the flow into the saltstone waste form, it is ignored. Instead, the saltstone waste form is modeled as filling the entire interior of the SDUs, such that sulfate attack is modeled to begin at the time of closure (or, for the 375-foot diameter SDUs, prior to closure, as described in Section 4.4.2). If the clean cap grout material were credited, the timing of peak doses could be delayed, but the magnitude would not be significantly affected.

Saltstone is assumed to be initially fully saturated.

It is expected that cured saltstone will be partially saturated when the closure cap is installed over the SDUs; however, as a simplifying assumption, the material is assumed to be initially fully saturated. When a porous material is only partially saturated, flow through that media is slowed by the matric potential of the open pores. Conversely, a fully saturated media is unable to retain additional fluid, such that any fluid that enters the system must displace the existing fluid with in the pores via outward flow. By assuming that the saltstone is initially fully saturated, all incoming flow will translate into outward flow.

The primary mechanism for saltstone degradation is assumed to be decalcification.

The saltstone will be completely encapsulated within the concrete SDUs. As such, no significant mechanical degradation is expected to influence the performance of saltstone. Similarly, due to the chemical characteristics of saltstone, it is not subject to sulfate attack or microbial induced degradation, and because saltstone has no rebar or steel embedded within it, it is also not subject to carbonation. Therefore, it is reasonable to assume that decalcification (i.e., dissolution and chemical leaching of calcium) is the primary mechanism of saltstone degradation.

An exponential degradation curve is assumed for representing the hydraulic degradation of the saltstone waste form.

The saturated hydraulic conductivity of saltstone will be based on the geometric mean of the saturated hydraulic conductivity in (1) the non-degraded portion of the saltstone and (2) the degraded portion of the saltstone. [SRRA110110-000004, SRNL-STI-2018-00077] While changes to the depth of degradation are expected to occur at a linear rate, there is a non-linear relationship between the combined properties of non-degraded and degraded materials. This non-linear relationship is assumed to be best represented by using the geometric mean to blend the non-degraded and degraded material properties into a uniform material to simplify modeling. Applying the geometric mean provides a exponential degradation curve. This assumption is supported extensively in the relevant literature as evaluated in *Predicting the Hydraulic Conductivity Over Time for Degrading Saltstone Vault Concrete - Task 5 (Subcontract Number SRRA110110)*. [SRRA110110-000004]

The final degraded condition of saltstone is assumed to be hydraulically equivalent to the surrounding control compacted backfill or vadose zone soil.

It is expected that fully degraded saltstone will retain some of its barrier-performance properties for periods of time longer than the assessment period; however, the final degraded state of saltstone is unknown. As a simplifying assumption, it is assumed that saltstone will (eventually) degrade until its hydraulic properties are in equilibrium with the surrounding soils. Note that this end state is not achieved in the any of the time-frames considered for flow and transport modeling.

2.7.7 Contaminant Release and Transport Assumptions

The evolution for the pore chemistry of saltstone is assumed to be driven by pore volume "flushes" (or exchanges).

Within SDF PA modeling, the release rates of contaminants are controlled by the chemical environment. The assumed chemical evolution is as follows:

Reducing Region I → Reducing Region III → Oxidizing Region III → Oxidizing Region IV

This progression is based on geochemical modeling. [SRNL-STI-2018-00586] The first transition, Reducing Region I to Reducing Region III, is both an Eh and pH transition as the highly soluble minerals are flushed from the material. The next transition, from Reducing Region III to Oxidizing Region III, is an Eh transition based on the reducing capacity of the material; the transition occurs once the incoming dissolved oxygen consumes the chemical reductants. Finally, the transition from Oxidizing Region III to Oxidizing Region IV is a pH transition driven by changes in the pore solution chemistry as various chemicals are leached from the saltstone (i.e., calcium silicate hydrate (CSH) and/or calcium hydroxide ($Ca(OH)_2$)). With geochemical modeling, these transitions are simulated as occurring based on pore-volume flushes (i.e., as a function of pore solution exchanges).

Infiltrating water is assumed to be in equilibrium with atmospheric oxygen.

It is expected that dissolved oxygen within infiltrating waters will have lower concentrations than surface waters that are in equilibrium with the atmosphere. Regardless, it is assumed that all infiltrating water contains oxygen at levels that are in equilibrium with atmospheric oxygen. With the higher oxygen concentrations, the reductants within reducing chemical environments will be consumed more quickly, thus this assumption is biased towards producing accelerated rates of oxidation.

Technetium release is solubility controlled under reducing conditions and is simulated with a shrinking core modeling approach.

For the expected Tc-99 disposal activities, the aqueous concentration of Tc-99 in saltstone under reducing conditions will be limited by solubility. Under solubility control, nearly all Tc-99 partitions to an immobile solid phase (effective $K_d \approx 20$ mL/g). In contrast, under oxidizing conditions most Tc-99 will partition to the mobile liquid phase ($K_d = 0.5$ mL/g).

Saltstone is assumed to be a reducing monolith initially, but gradually become oxidizing as dissolved oxygen infiltrates and reacts with slag. Oxidation is assumed to take the form of a sharp front, moving inward from exposure surfaces, such that apart from the reaction front consuming reduction capacity, saltstone is locally either fully reducing or fully oxidizing. The oxidizing zone takes the form of a growing rind around a shrinking core of reducing saltstone. Under this set of assumptions Tc-99 will be relatively immobile in the reduced core and relatively mobile in the oxidized rind. Because Tc-99 is expected to be a significant dose driver, and its mobility varies significantly between reducing and oxidizing conditions, a more accurate spatial-temporal simulation of the slag oxidation process and its effects on Tc-99 mobility is warranted.

Thus, a "shrinking core" modeling approach is applied to Tc-99 in both saltstone and slag-bearing concrete. The shrinking core model simulates oxidation and Tc-99 transport on a cell-by-cell basis, in contrast to the general modeling approach which varies chemical conditions and transport parameters on a much coarser zone-by-zone basis based on pore volume exchanges. Furthermore,

the solubility limit of Tc-99 is pH dependent: 9.7E-07 mol/L for pH > 11 and 4.5E-07 mol/L for pH < 11.

Analogous to the reduction-oxidation (Eh) state, the saltstone monolith is assumed to have an initially high pH (> 11) but gradually transition to a lower pH (< 11) as buffering capacity is consumed by infiltrating soil moisture and diffusion. To capture the pH dependence of Tc-99 solubility in cementitious materials, the Tc-99 transport model simulates two shrinking cores: low Eh and high pH. An effective K_d for Tc-99 is assigned to each grid cell based on its local Eh and pH conditions. The pH front advances faster than the Eh front, so the observed combinations of Eh and pH are low Eh + high pH, low Eh + low pH, and high Eh + low pH. The corresponding Tc-99 transport modes are solubility control at 9.7E-07 mol/L, solubility control at 4.5E-07 mol/L, and sorption control with K_d = 0.5 mL/g, respectively.

Iodine release is also simulated with a shrinking core modeling approach.

As with Tc-99, previous SDF modeling efforts have indicated that I-129 is also expected to be a potentially significant dose driver. While I-129 is not expected to be solubility controlled, its transport properties are Eh and pH dependent. Thus a "shrinking core" modeling approach is also applied to I-129 transport, unlike other non-Tc-99 species. The I-129 and Tc-99 transport models both simulate reduction capacity consumption by dissolved oxygen and buffering capacity consumption by a tracer on a cell-by-cell basis, so their spatial-temporal Eh and pH variations in cementitious materials are the same. For I-129, the K_d value is assigned to each grid cell based on its local Eh and pH conditions: 0.07 mL/g for low Eh + high pH, 0.71 mL/g for low Eh + low pH, and 4.0 mL/g for high Eh + low pH.

No solubility controls are assumed for other radionuclides.

Except for Tc-99, the contaminant concentrations in saltstone are assumed to be K_d-controlled, with no solubility limitations. While the contaminants within the saltstone are expected to come from soluble waste streams, it is possible that there may be some insoluble contaminants within the waste which may be influenced by solubility controls (e.g., uranium). If so, the release and transport rates for such contaminants would likely be slowed as the contaminants would precipitate. As a simplifying modeling assumption, these potential interactions are ignored.

2.7.8 Dose Assumptions

The point of assessment for compliance assumes the highest concentration for each contaminant anywhere along a sector.

The Aquifer Transport Model simulates three-dimensional plumes for each contaminant. Concentrations are determined along the 100-meter boundary and at various depths, including the Upper Aquifer Zone of the Upper Three Runs Aquifer, the Lower Aquifer Zone of the Upper Three Runs Aquifer, and the Gordon Aquifer. Due to contaminant-specific transport factors,

different contaminants may reach the 100-meter boundary at different times and at different points and depths along the boundary. For compliance concentrations, each contaminant is assumed to be the maximum concentration at the sector boundary, regardless of location. For example, at Sector A, Tc-99 may have a higher concentration near the east end of the Sector, while Pu-239 may have a higher concentration near the west end, but doses to the MOP at Sector A shall be determined using these highest concentrations despite being taken from different locations along the Sector boundary. This approach is assumed for both the 100-meter and 1-meter boundary concentrations.

The human receptor is assumed to be a gender-weighted, age-weighted adult with the average habits of a subsistence farmer in the approximate vicinity of SRS.

As described in the *Dose Calculation Methodology for Liquid Waste Performance Assessments at the Savannah River Site* (SRR-CWDA-2013-00058), for the purposes of the applied dose methodology, the average subsistence farmer is assumed to grow crops, raise livestock, and participate in water recreation (i.e., boating, swimming, and fishing).

The human receptor is assumed to consume food and water at the rate of an adult but is susceptible to dose risk based on an age-averaged "reference person."

While the intake and exposure rates of the human receptor shall be based on adult behaviors, the dose conversion factors shall be based on "reference person" values, which were calculated by averaging derived dose coefficients across all age groups. Although this is an inherently unrealistic approach, the net effect is slightly higher dose results. This artificial, yet reasonable, approach is intended to mitigate some of the uncertainties that are inherent in human behavior and human physiology, thus improving the general defensibility of the dose results. [SRR-CWDA-2013-00058]

3 SITE AND FACILITY CHARACTERISTICS

Section 3.1 discusses the general site characteristics and presents details for those characteristics influencing the contaminant transport modeling inputs and assumptions developed and explained in Section 4.4.

- Section 3.1.1 provides a general description and layout of SRS and the SDF and includes the population distribution in the surrounding area and future SRS land use planning.
- Section 3.1.2 describes meteorological and climatological data collection at SRS. This data determines appropriate modeling assumptions related to rainfall and temperature to assess the performance of the SDF closure cap. Dose Release Factors (DRFs) are developed from atmospheric dispersion conditions based on the meteorological and climatological data and are used to model the dispersion of gaseous contaminants emanating from the surface of the closed SDF described in Section 5.3.
- Section 3.1.3 provides a general description of SRS ecology.
- Section 3.1.4 provides information regarding SRS geology, seismology, and volcanology.
- Section 3.1.5 provides information regarding SRS hydrology that informs the modeling inputs related to the flow of surface water and ground water.
- Section 3.1.6 identifies the information sources available concerning the geochemistry of the soils and cementitious material that are used to inform the modeling inputs related to radionuclide migration in the environment.
- Sections 3.1.7 and 3.1.8 address natural resource management of the site and general information on sources of natural and background radiation exposure.

Section 3.2 describes the design of existing and anticipated SDF disposal units and the SDF closure cap concept.

- Sections 3.2.1 through 3.2.4 discuss the design and construction of the SDUs.
- Section 3.2.5 provides the saltstone waste form specifications.
- Section 3.2.6 provides the design performance requirements and constructability requirements for the conceptual SDF closure cap and the results of the closure cap infiltration analysis presented in SRRA107772-000009.

Section 3.3 presents the known and estimated inventories of the radionuclides and chemicals remaining in the disposal units at the time of SDF closure.

3.1 Site Characteristics

Evaluation of radionuclide transport and human exposure resulting from radionuclide release from the SDF to the environment requires careful consideration of factors affecting transport processes and exposure potential. Topographic features and hydrogeologic characteristics strongly affect the direction and flow of water and thus radionuclides potentially released from the closure site. Projected land use and population distributions affect the estimation of human exposure. This section discusses the relevant natural and demographic characteristics of Z-Area and the surrounding vicinity.

3.1.1 Geography, Demographics, Populations, and Use of Adjacent Lands

3.1.1.1 SRS Site Description

Savannah River Site is a federal facility owned and managed by the DOE. The site was constructed in the early 1950s to produce nuclear materials for national defense and deep space missions. The site lies along the Savannah River in south-central South Carolina, approximately 100 miles inland from the Atlantic Coast, approximately 12 miles south of Aiken, South Carolina, and 15 miles southeast of Augusta, Georgia (Figure 3.1-1). [SRNS-RP-2018-00470] The site occupies approximately 310 square miles (198,000 acres) and includes portions of Aiken, Barnwell, and Allendale counties in South Carolina (Figure 3.1-1). SRS contains numerous developed areas related to past and current site operations. About 10% of the SRS land is industrial; the remaining 90% consists of natural and managed forests. [SRNS-RP-2018-00470]

Prominent geographic features within 30 miles of SRS include the Savannah River, which forms a portion of the southwest site boundary, and Clarks Hill Lake, also known as Thurmond Lake (Figure 3.1-1). Clarks Hill Lake is the largest nearby reservoir and public recreational area. It lies on the Savannah River approximately 40 miles upstream of the center of SRS.

Within the site boundary, prominent water features include PAR Pond and L Lake that were constructed as cooling water impoundments for former reactors. PAR Pond covers approximately 2,700 acres in the eastern sector of SRS and L Lake covers approximately 1,000 acres in the southern sector of SRS. [WSRC-IM-2004-00008]

The major SRS operational areas are listed in Table 3.1-1 and shown on Figure 3.1-2.

Table 3.1-1: SRS Operational Areas and Functions

SRS Area	Operational Function
A	Includes the SRNL and SREL and support services
B	Administrative offices, support services, and laboratories
C, K, L, P[a], R[a]	Reactor areas (K and L material storage)
D[a]	Heavy water, power, and steam production
E	Solid LLW disposal
F, H	Tank Farms (F-Tank Farm and H-Tank Farm) and material separations (F- and H-Canyon)
J	SWPF
M[a]	Fuel and target fabrication
N	Construction administration and activities
S	DWPF
TNX[a]	Semi-works-scale separations equipment and development and testing
Z	SPF and SDF

[a] Facilities in these areas have been deactivated and decommissioned.

Figure 3.1-1: Location of the SRS and Adjacent Areas

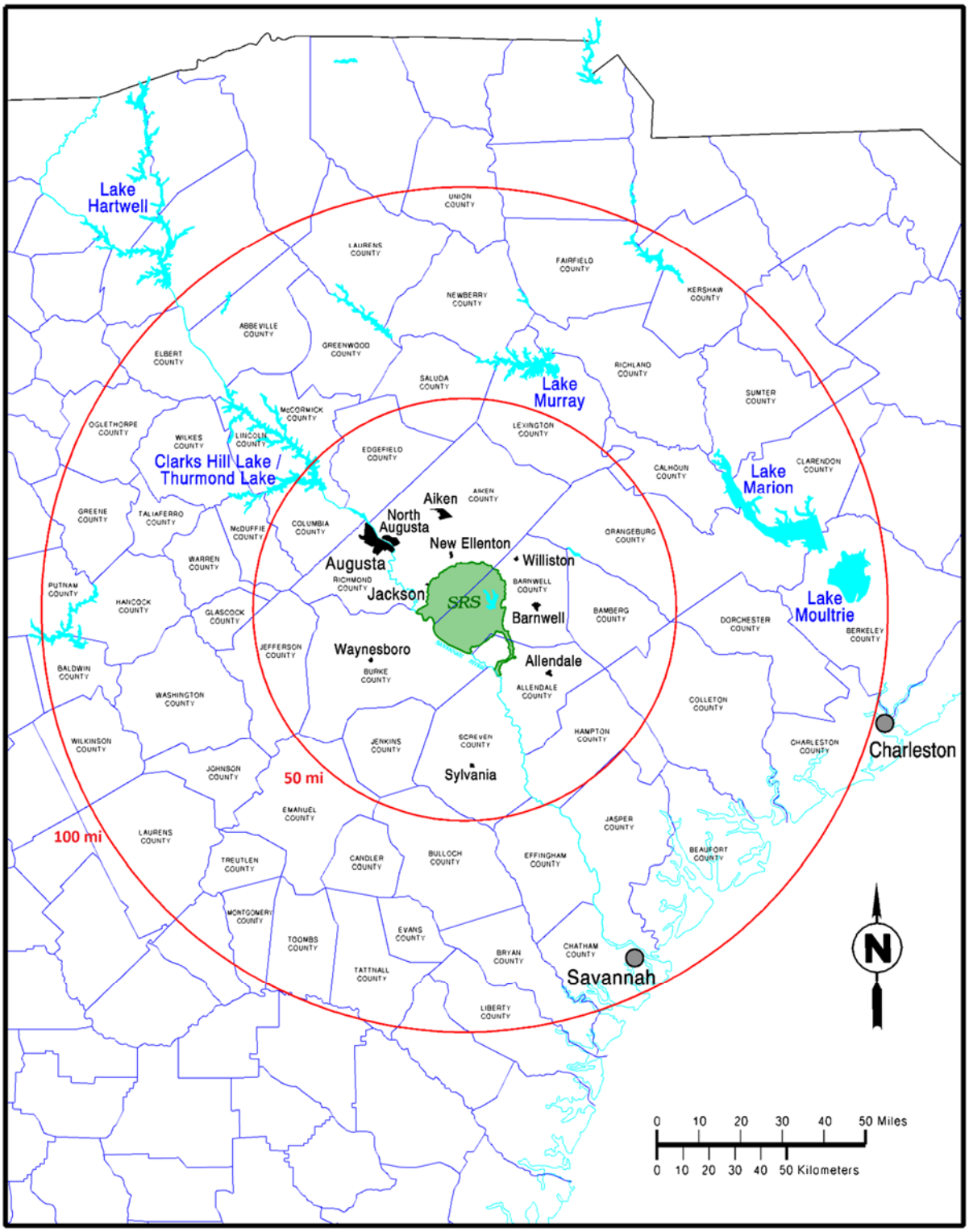

Figure 3.1-2: SRS Operational Areas Location Map

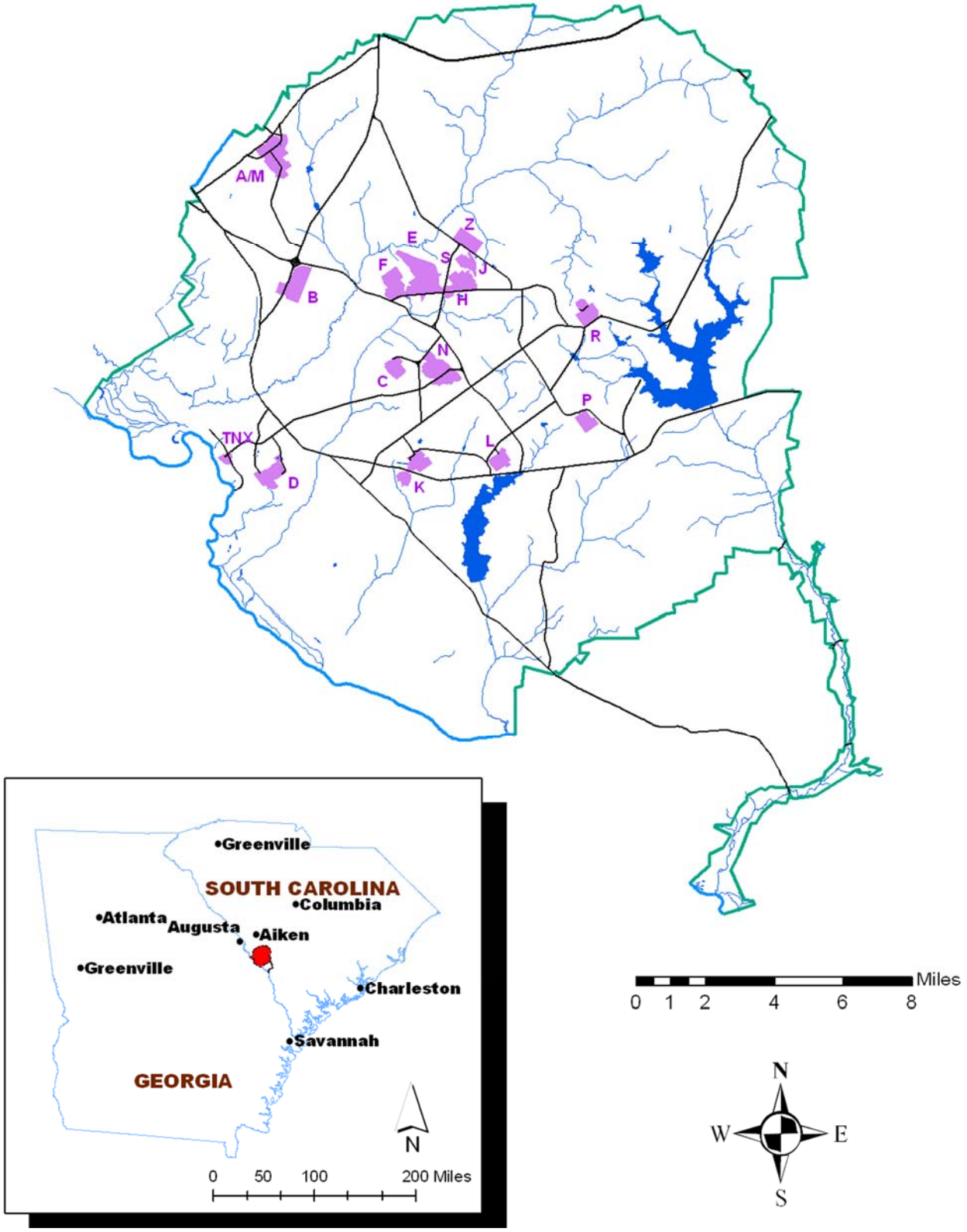

3.1.1.1.1 General Separations Area and Z-Area Descriptions

The SDF is located in Z-Area, which is in the central region of the SRS referred to as the General Separations Area (GSA) (Figure 3.1-3). The GSA is located atop a ridge running southwest to northeast that forms the drainage divide between two watersheds, Upper Three Runs (UTR) to the north and Fourmile Branch (FMB) to the south. Surface drainage in Z-Area is northwest to north toward UTR and northeast and southeast toward McQueen Branch. Z-Area was chosen for the SDF site based on considerations of depth to the water table, distance to surface water and the public, available surface area, surface topography, and its proximity to the waste generation sites. [WSRC-RP-92-1360] Z-Area is approximately 161 acres in size and is situated northeast of the DWPF, which is in S-Area.

Figure 3.1-3: Layout and Topography of the GSA

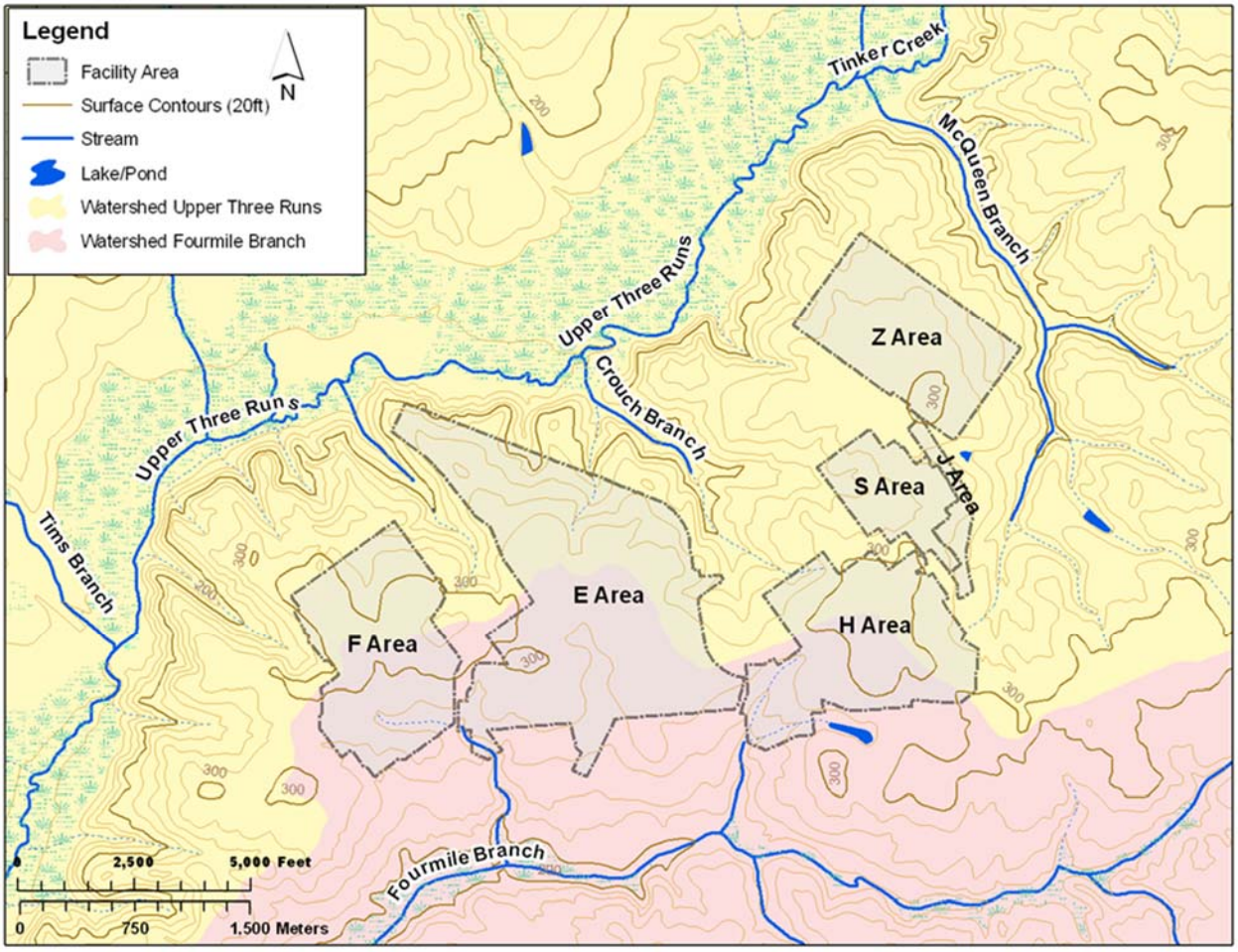

The GSA also contains the F-Area and H-Area Separations and associated Tank Farm Facilities, the DWPF, the E-Area Low-Level Waste Disposal Facilities, and the SWPF.

Above grade structures, utilities, and equipment will be removed from the SDF and SPF area prior to installation of the closure cap; thus, no ancillary equipment

that will impact the modeling will remain prior to final closure. Figure 3.1-4 provides an anticipated layout of the SDF current and future SDUs based on *Future Saltstone Disposal Units Siting – Systems Engineering Evaluation* (G-AES-S-00004).

Figure 3.1-4: Anticipated Layout of the SDF

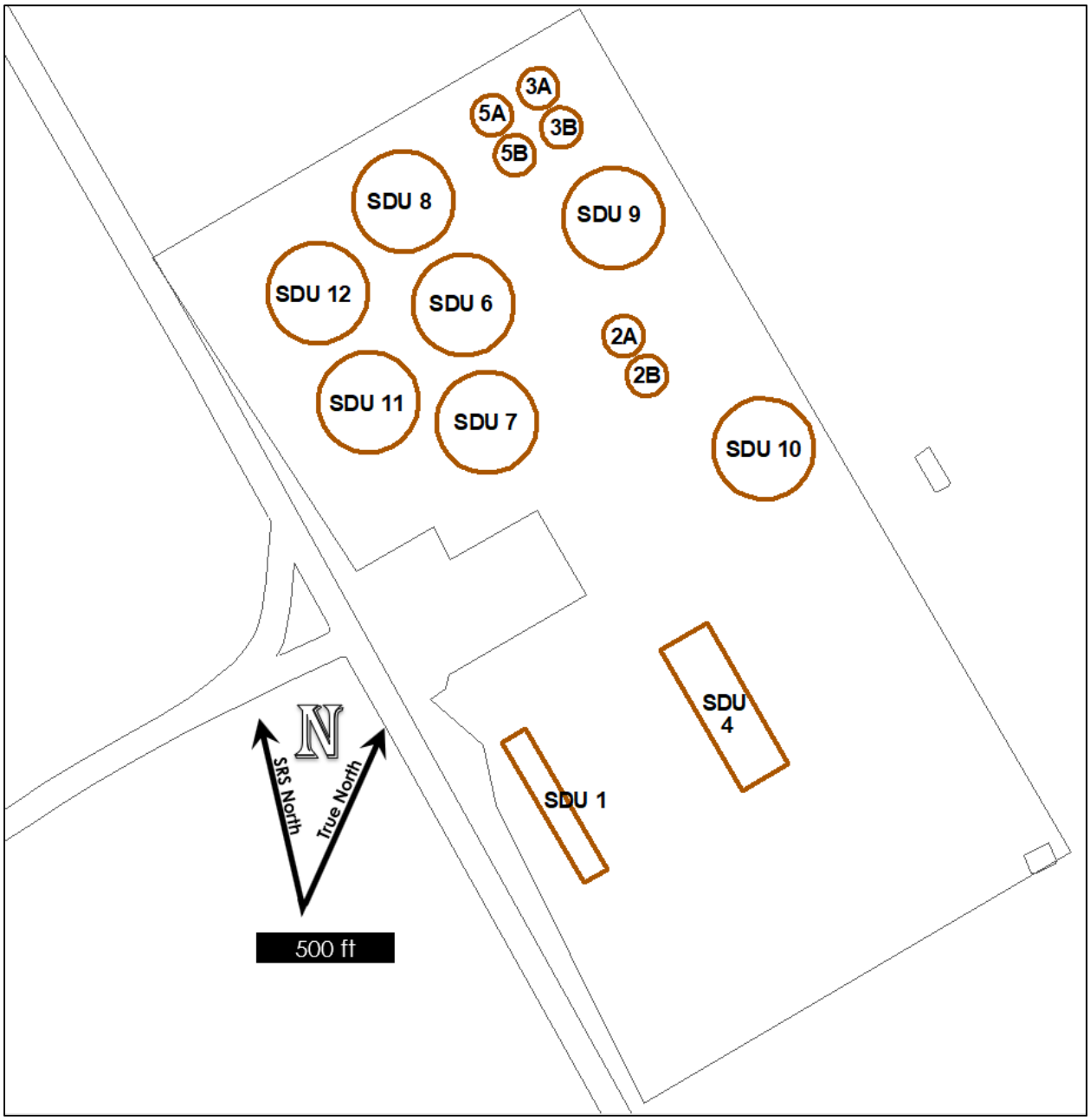

3.1.1.2 Population Distribution

According to U.S. Census Bureau data, the estimated 2017 population in the eight-county region of influence was 602,761. Four of the counties lie in South Carolina and include Aiken, Allendale, Bamberg, and Barnwell. The other four counties lie in Georgia and

include Burke, Columbia, Richmond, and Screven (Figure 3.1-1). The region includes the counties immediately adjacent to SRS and where the majority of SRS workers reside. Approximately 86.5% of the region live in the following three counties: Aiken (27.9%), Richmond (33.5%), and Columbia (25.1%). Only approximately 13.5% of this region population lives in the remaining counties as shown in Table 3.1-2. [www.factfinder.census.gov]

Table 3.1-2: Population Distribution and Percent of Region for Counties and Selected Communities

Jurisdiction	2010 Population Estimate	2017 Population Estimate[a]	2017 % Region
SOUTH CAROLINA			
Aiken County	160,099	168,179	27.9%
Allendale County	10,419	9,002	1.5%
Bamberg County	15,987	14,381	2.4%
Barnwell County	22,621	21,345	3.5%
GEORGIA			
Burke County	23,316	22,522	3.7%
Columbia County	124,053	151,579	25.1%
Richmond County	200,549	201,800	33.5%
Screven County	14,593	13,953	2.3%
Eight-County Total	**571,637**	**602,761**	

a 2017 Population estimates as of July 1, 2017 are based on 2010 population census and are provided by the U.S. Census Bureau, Population Estimates Program, www.factfinder.census.gov; data for births, deaths, and domestic and international migration were used by the U.S. Census Bureau to update the 2010 base counts.

From 2010 to 2017, the population in the eight-county region grew an estimated 5.4%. Columbia County had the highest estimated growth at approximately 22.2%, followed by Aiken County with an estimated growth of approximately 5.0%, and Richmond County with an estimated growth of 0.6%. Allendale, Bamberg, Barnwell, Burke, and Screven Counties experienced a net population loss. Calculations are based on information obtained from the U.S. Census Bureau website (www.factfinder.census.gov).

Further information regarding the eight-county region around SRS can be found in the *High-Level Waste Tank Closure Final Environmental Impact Statement*. [DOE-EIS-0303]

3.1.1.3 Land Use – Present and Planned

The SRS is predominantly contained within Aiken and Barnwell counties in South Carolina. Each county within the state is required to maintain a comprehensive plan outlining the framework and guidance for county planning. *Aiken County South Carolina Comprehensive Plan 2014-2024* is the latest plan available for Aiken County. For Barnwell County, the latest plan is the *Barnwell County Comprehensive Plan*, dated June 2007. Within Aiken County, approximately 22% of the land is used for crops and pastures, approximately 70% is forested, and less than 10% is built up (residential, commercial, or industrial). Within Barnwell County, less than 35% of the land is used for crops and pastures, approximately 65% is forested, and less than 1% is built up (residential,

commercial, or industrial). Both of county plans include information on Future Land Use for the counties. [PIT-MISC-0200; PIT-MISC-0201]

Land within a 5-mile radius of the SDF is entirely within SRS boundaries and is currently used either for industrial purposes or for cultivating pine forests. Although SRS is heavily forested, the current land use within the entire GSA is classified as heavy nuclear industrial. Plans for the future of SRS are addressed in the two planning documents identified below and described in Sections 2.5.2 and 2.5.3, indicating SRS will be federally-controlled land in perpetuity:

- *SRS End State Vision* (PIT-MISC-0089) and
- *Savannah River Site Land Use Plan* (SRNS-RP-2014-00537).

3.1.2 Meteorology and Climatology

3.1.2.1 General SRS Climate

The SRS region has a humid subtropical climate characterized by relatively short, mild winters and long, warm, humid summers.

Summer-like conditions typically last from May through September, when the area is frequently under the influence of a western extension in the semi-permanent Atlantic subtropical anticyclone (i.e., the 'Bermuda' high). In summer, winds are light and cold fronts generally remain well north of the area. Daily high temperatures during the summer months exceed 90°F on more than half of all days on average. Scattered afternoon and evening thunderstorms are common throughout this period. The influence of the Bermuda high begins to diminish during the fall and continental air masses become more prevalent, resulting in lower humidity and more moderate temperatures. Average rainfall during the fall is usually the least of the four seasons.

In the winter months, mid-latitude low pressure systems and associated fronts often migrate through the region. As a result, conditions frequently alternate between warm, moist, subtropical air from the Gulf of Mexico region and cool, dry, Arctic air. The Appalachian Mountains to the north and northwest of SRS help to moderate the extremely cold temperatures that are associated with occasional outbreaks of Arctic air. Consequently, less than one-third of winter days have minimum temperatures below freezing on average and days with temperatures below 20°F are rare. Measurable snowfall occurs on average once every four years.

Tornadoes over the region occur more frequently in spring than the other seasons of the year. Although spring weather is somewhat windy, temperatures are usually mild and humidity is relatively low. [SRNL-RP-2017-00424]

3.1.2.2 Meteorological Data Collection

SRS meteorological data is collected from a network of nine primary monitoring stations located adjacent to eight operational areas (A-, C-, D-, F-, H-, K-, L-, and P-Areas) and are equipped to measure wind direction, wind speed, temperature, and dew point at a height

of 61 meters (m) above ground. Temperature is also measured at 2m on these towers. A ninth tower near N-Area, known as the Central Climatology (CLM) site, is instrumented with wind, temperature, and relative humidity (RH) sensors at the following four levels above ground: 2m (4m for wind), 18m, 36m, and 61m. The CLM site is also equipped with an automated tipping bucket rain gauge, a barometric pressure sensor, and a solar radiometer near the tower at ground level.

Data acquisition units at each station record wind speed and direction from a sonic anemometer at a rate of 10 measurements per second. Measurements from the temperature and humidity instruments and the ground-level instruments at CLM are recorded at 1-second intervals. Every 15 minutes, the 9,000-wind speed and direction and 900-temperature and humidity data points are processed to generate statistical summaries for each variable, including averages and instantaneous maxima, and the results are uploaded to a relational database for permanent archiving. [SRNL-RP-2017-00424]

A cloud height sensor, known as a ceilometer, is in B-Area and gives information about cloud coverage, as well as fog or smoke. All aspects of the meteorological data collection program meet applicable regulatory criteria.

Additional precipitation measurements are collected from a network of 10 plastic wedge rain gauges across SRS (Figure 3.1-5). These gauges are read manually by security or operations personnel once per day, usually around 6:00 am. The daily data is reported to the SRNL Atmospheric Technologies Center, reviewed for any obvious flaws, and manually entered into a permanent electronic database. Twelve rain gauges were used until 2013 when monitoring of the gauges at Barricade 5 and F-Area was stopped.

Measurements of temperature and RH are also recorded from a weather station located in A-Area adjacent to SRNL. This station consists of a standard National Weather Service "cotton region" instrument shelter. Data collected from this station is manually tabulated for archiving of daily high and low values of temperature and RH.

In addition, the Tall Tower facility near Beech Island, South Carolina, provides a set of high-quality meteorological measurements that are unique to the Southeastern United States. This facility utilizes fast-response sonic anemometers, water vapor sensors, barometric pressure sensors, slow-response temperature sensors, and RH sensors. The data are collected at 30m, 61m, and 304m above ground level. Spread-spectrum modems at each measurement level transmit raw data to a redundant set of computers at SRNL. Data processing software determines mean values and other statistical quantities every 15 minutes and the results are uploaded to a relational database. [WSRC-TR-2007-00118]

Quality assurance of the data is conducted in two phases: an initial screening of recent data, followed by an in-depth review and final quality classification. The initial screening, performed twice daily by qualified instrument technicians, consists of a thorough examination of 15-minute data retrieved from the database in conjunction with a summary of instrument diagnostics obtained from the local data acquisition units. Potential problems are noted in a daily check sheet and, as needed, data acquisition unit

software is configured to assign a quality control tag to data collected from the questionable instruments. Quality flags are also set during periods of calibration and maintenance

Figure 3.1-5: SRS Meteorological Monitoring Network

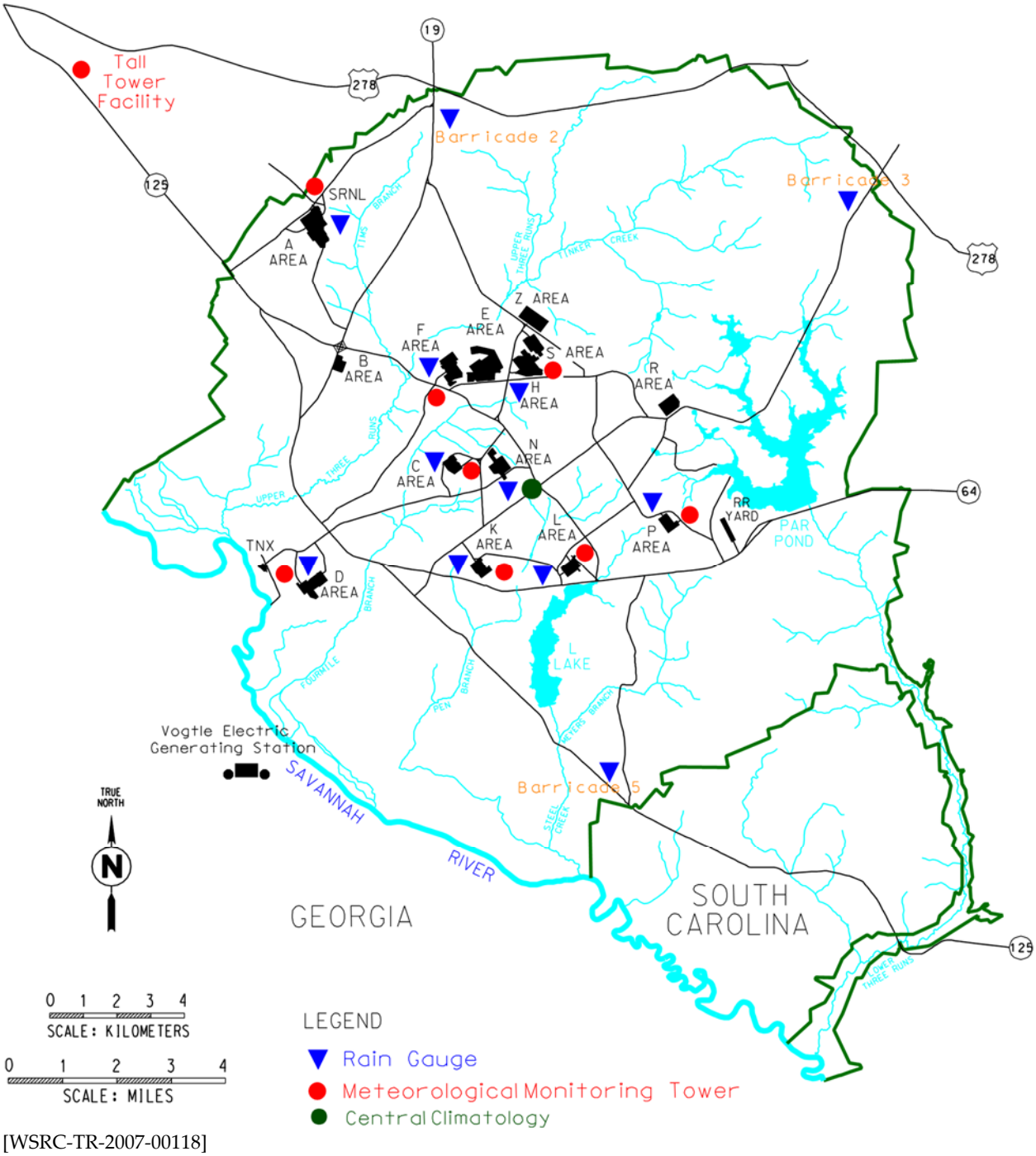

[WSRC-TR-2007-00118]

Long-term climatological records are available for precipitation starting in 1964 and for temperature starting in 1968. Statistics generated from these data are used for comparisons with the annual summaries. From 1985 through 1995, the temperature

values used were based on the average of daily maxima and minima recorded at the SRNL instrument shelter. Since 1995, temperature measurements are taken from the 2m level of the CLM. Likewise, precipitation values reported prior to 1995 are based on daily observations from the SRNL rain gauge; then after 1995, precipitation data began to be continuously collected with the CLM tipping bucket rain gauge. [SRNL-RP-2017-00424]

3.1.2.2.1 Atmospheric Dispersion

Since the mid-1970s, a 5-year database of meteorological conditions at SRS has been updated to support dose calculations for release scenarios affecting onsite and offsite populations. The meteorological database includes wind speed, wind direction, temperature, dew point, and horizontal and vertical turbulence intensities. The most recent database is for the period January 1, 2007, through December 31, 2011, and consists of one-hour time averages of temperature and dewpoint, wind speed, direction, and turbulence. [SRNL-STI-2013-00268] This data is used to determine dose release factors (DRFs) in the air pathways dose modeling evaluation described in Section 5.3.

3.1.2.3 Data Pertinent to the Performance Assessment Modeling

Weather data pertinent to the PA modeling are atmospheric dispersion, precipitation, and air temperature.

3.1.2.3.1 Precipitation

Compilations of rainfall data obtained from meteorological data collection described above for years 1964 through 2016 for the site are compiled by SRNL Atmospheric Technology Services and provided in an attachment to SRRA107772-000009. An average precipitation of 47.1 inches per year results from the 53-year overall SRS monitoring period.

For estimating infiltration rates through the closure cap (see Section 4.4.1), the years 2002 (40.6 inches/yr or 1030 mm/yr) and 2004 (47.1 inches/yr or 1191 mm/yr) were selected as the "typical years." Typical years are different from long-term average conditions because a typical year is an actual data set that exhibits natural variability and is not affected by the smoothing inherent in long-term averages. [SRRA107772-000009] Meteorological data from these years were used to establish long-term expected climate conditions.

Similarly, the wettest 10-year period (from 1989 to 1998) was used to determine conditions based on an assumed wetter climate condition, with an annual average rainfall of 52.4 inches/yr (1330 mm/yr), or 11.2% more than average. Note that an increase in precipitation will likely be accompanied by an increase in average temperature and a reduction in the frequency of sub-freezing conditions. Greater precipitation and higher temperatures promote additional biomass growth, longer growing seasons, and higher evapotranspiration. Thus, elevated evapo-

transpiration from these factors reduces deep percolation of water; however, this was not incorporated into the analysis for estimating infiltration rates. In addition, the topsoil layer to be used in the closure cap will be sourced on site and will generally be sandy loam to loamy sand. The topsoil is sufficiently permeable to maintain runoff <15% of the total annual water balance. [SRRA107772-000009]

3.1.2.3.2 Air Temperature

A compilation of air temperature data obtained from meteorological data collection described above for years 1968 through 2005 is provided in WSRC-STI-2008-00244 and supplemented with more recent on-site data from SRNL Atmospheric Technology Services monitoring point 700-A, located in A-Area. This monitoring point had the most complete data set for the time period in question. For the 37-year period from 1968 through 2005, the annual average air temperature was approximately 64°F with an average monthly air temperature ranging from a low of approximately 46°F to a high of approximately 81°F.

For estimating infiltration rates through the closure cap (see Section 4.4.1), temperature data from the years 2002 and 2004 were selected as the "typical years," while air temperature data from the wettest 10-year period (from 1989 to 1998) was used to determine conditions based on an assumed wetter climate condition.

3.1.3 Ecology

SRS ecological resources and wildlife are briefly discussed in this section. Comprehensive descriptions and details are in SRS Ecology: Environmental Information Document (WSRC-TR-2005-00201).

The site supports abundant terrestrial, semi-aquatic, and aquatic wildlife, as well as several species considered threatened or endangered. Since the early 1950s, the site has changed from 67% forest and 33% agriculture to 94% forest, with the remainder in aquatic habitats and developed areas. Wildlife populations correspondingly shifted from forest-farm edge utilizing species to a predominance of forest-dwelling species. The site currently supports 44 species of amphibians, 60 species of reptiles, 255 species of birds, and 55 species of mammals. These populations include urban wildlife, several commercially and recreationally important species, and a few threatened or endangered species. Protection and restoration of all flora and fauna to a point where their existence is not jeopardized are principal goals of federal and state environmental programs. Those species of plants and animals afforded governmental protection are referred to collectively as "species of concern." [WSRC-TR-2005-00201]

Note that vegetation on the SDF closure cap is assumed to be natural perennial grass cover during the institutional control period (100 years), as exists at other locations at SRS. [SRRA107772-000009] Because pine forestation is common across the sandy South Carolina Coastal Plain, ingress of pine is postulated as the most likely vegetative succession to occur over the long term. Variables such as climate change or invasive or exotic species are possible; however, there are

significant uncertainties associated with such conditions. Despite this, infiltration estimates for this SDF PA assume that the grass cover will persist indefinitely because pine forestation reduces infiltration relative to grasses and therefore grass is a pessimistic assumption relative to closure cap infiltration.

SRS has extensive, widely distributed wetlands and most are associated with floodplains, creeks, or impoundments. Additionally, approximately 200 Carolina bays are present on the site. Carolina bays are unique wetland features of the Southeastern United States. They are isolated wetland habitats dispersed throughout the uplands of SRS. The Carolina bays at SRS exhibit extremely variable hydrogeology and a range of plant communities from herbaceous marsh to forested wetland. [DOE-EIS-0303]

The Savannah River bounds SRS to the southwest for approximately 20 miles. The river floodplain supports an extensive swamp, covering approximately 15 square miles of SRS and a natural levee separates the swamp from the river. Timber was cut in the swamp from the turn of the century until 1951, when the Atomic Energy Commission assumed control of the area. Presently, the swamp forest is comprised of two kinds of forested wetland communities: areas that are slightly elevated and well-drained are characterized by a mixture of oak species, as well as red maple, sweet gum, and other hardwood species; and low-lying areas that are continuously flooded and dominated by second-growth bald cypress and water tupelo. [DOE-EIS-0303]

The site supports abundant herpetofauna because of its temperate climate and diverse habitats. The herpetofauna species include 17 salamanders, 27 frogs and toads, 1 crocodilian, 13 turtles, 9 lizards, and 36 snakes. The class Amphibia is represented on-site by 2 orders, 11 families, 16 genera, and 44 species. The class Reptilia are represented by 3 orders, 12 families, 41 genera, and 59 species. [WSRC-TR-2005-00201]

More than 255 species of birds can be found at SRS. Waterfowl and wading birds, as well as many upland species, use the SRS aquatic habitats year-round. The site's Carolina bays and emergent marshes are used by 67% of these birds. This type of habitat is used by 68% of the upland species. Edge or shoreline areas account for high numbers of upland birds at the Carolina bays and emergent marshes, stream, and small drainage corridors, and river swamp habitats. The aquatic birds are most common in open water habitats. [WSRC-TR-2005-00201] Other common birds at SRS include the mourning dove and the eastern wild turkey.

Large mammals inhabiting the site include white-tailed deer and feral hogs. Raccoon, beaver, and otter are relatively common throughout the SRS wetlands. In addition, the gray fox, opossum, bobcat, gray squirrel, fox squirrel, eastern cottontail, northern bobwhite, and coyote are common at SRS.

In recent years, non-native armadillos have been migrating into the area. Armadillos dig long, shallow burrows that can extend laterally for tens of feet and downward for up to five feet. Other small mammals, such as moles, voles, and shrews, can also create shallow borrows. However, it is expected that the erosion barrier of the SDF closure cap (see Section 3.2.6), would prevent burrowing animals from penetrating to depths that would disrupt the performance of the closure cap.

There are three dominant species of ants in South Carolina and across the SRS: fire ants, carpenter ants, and pavement ants. Of these three, fire ants tend to be the most prevalent at SRS. They have been shown to burrow as deep as 10 feet below ground surface, but typically, tunnels are much shallower. Colonies in clayey soils tend to have deeper burrows than those in sandy soils. Surficial soils at SRS consist of sand to clayey sand. In addition, ants tend to not borrow across saturated horizons, such as would be expected at the interface between the sand drainage layers and the HDPE layers of the designed closure cap (see Section 3.2.6). Given the current SDF closure cap design, it is unlikely that ants would penetrate to depths that would disrupt the performance of the closure cap.

Threatened or endangered plant and animal species known to exist or that might be found on the overall site include the smooth purple coneflower, wood stork, red-cockaded woodpecker, and short-nose sturgeon. [WSRC-TR-2005-00201]

The SDF is located within a densely developed, industrialized area of SRS. The immediate area provides habitat for only those animal species typically classified as urban wildlife. Species commonly encountered in this type of urban landscape include the Southern toad, green anole, rat snake, rock dove, European starling, house mouse, opossum, and feral cats and dogs. Grasses and landscaped areas within SDF also provide some marginal terrestrial wildlife habitat. Several ground-foraging bird species (e.g., American robin, killdeer, and mourning dove) and small mammals (e.g., cotton mouse, cotton rat, and Eastern cottontail) that use lawns and landscaped areas around buildings may be present at certain times of the year, depending on the level of human activity (e.g., frequency of mowing). Pine plantations managed for timber production by the U.S. Forest Service (under an interagency agreement with DOE) occupy surrounding areas.

The UTR seepline area is in a bottomland hardwood forest community. The canopy layer of this bottomland forest is dominated by sweet gum, red maple, and red bay. Sweet bay is also common. The understory consists largely of saplings of these same species, as well as an herbaceous layer of smilax, dog hobble, giant cane, poison ivy, chain fern, and hepatica. At the upland edge of the seepline, scattered American holly and white oak occur. Dominant along FMB in this area are tag alder, willow, sweet gum, and wax myrtle. [DOE-EIS-0303]

No endangered or threatened fish or wildlife species have been recorded near the UTR seepline. The seepline and associated bottomland community do not provide habitat favored by endangered or threatened fish and wildlife species known to occur at SRS. The American alligator is the only federally-protected species that could potentially occur in the seepline area. [DOE-EIS-0303]

According to summaries of studies on UTR documented in the SRS Ecology: Environmental Information Document (WSRC-TR-2005-00201), the macro invertebrate communities of UTR drainage are unusual. They include many rare species and contain species not often found living together in the same freshwater system. Since UTR is a spring-fed stream and is colder and generally clearer than most surface water at its low elevation, species typical of unpolluted streams in northern North America or the southern Appalachian Mountains are found here, along with lowland (Atlantic Coastal Plain) species.

The fish community of UTR is typical of third- and higher-order streams on SRS that have not been greatly affected by industrial operations, with shiners and sunfish dominating collections. The smaller tributaries of UTR are dominated by shiners and other small-bodied species (e.g., pirate perch, madtoms, and darters) indicative of un-impacted streams in the Atlantic Coastal Plain. In the 1970s, the United States Geological Survey (USGS) designated UTR as a National Hydrological Benchmark Stream due to its high water-quality and rich fauna. However, this designation was rescinded in 1992 due to increased development of the UTR watershed north of SRS site boundaries. [DOE-EIS-0303]

3.1.4 Geology, Seismology, and Volcanology

Regional and local information on the geologic and seismic characteristics at the SDF are presented in this section. Since SRS is not located within a region of active plate tectonics characterized by volcanism, volcanism is not an issue of concern and it is omitted from the discussion in this PA. [WSRC-IM-2004-00008]

3.1.4.1 Regional and Site-Specific Topography

Figure 3.1-6 shows the relationship of SRS to the overall regional geological provinces of the eastern United States. Figure 3.1-7 shows the regional physiographic provinces in South Carolina. As shown on Figure 3.1-7, much of SRS lies within the Aiken Plateau, which has an approximate 5% slope to the southeast. The Savannah and Congaree Rivers bound the plateau, which extends from the Fall Line to the Orangeburg escarpment. The highly dissected surface of the Aiken Plateau is characterized by broad interfluvial areas with narrow, steep-sided valleys. Local relief can be as much as 300 feet. Figure 3.1-3 shows the local topography of the GSA. [WSRC-TR-95-0046]

SRS is on the Atlantic Coastal Plain Physiographic Province approximately 25 miles southeast of the Fall Line that separates the relatively unconsolidated Coastal Plain sediments to the east from the underlying Piedmont Physiographic Province to the west (Figure 3.1-6 and Figure 3.1-7). Beneath the Coastal Plain sediments two geologic terrains are present. One is the Dunbarton Basin, a Triassic-Jurassic rift basin filled with lithified terrigenous and lacustrine sediments, and the other is a crystalline terrain of metamorphosed sedimentary and igneous rock that may range in age from Precambrian to late Paleozoic. Early to middle Mesozoic (Triassic to Jurassic) rocks occur in isolated fault-bounded valleys either exposed within the crystalline belts or buried beneath the Coastal Plain sediments. The Coastal Plain sediments were derived from erosion of the crystalline rocks during the late Mesozoic (Cretaceous). The Cretaceous and younger sediments are not significantly indurated. The total thickness of the sediment package at SRS varies from approximately 700 feet at the northwest site boundary to 1,400 feet at the southeast boundary. [WSRC-STI-2006-00198, WSRC-TR-95-0046]

Figure 3.1-6: Regional Geological Provinces of the Eastern United States

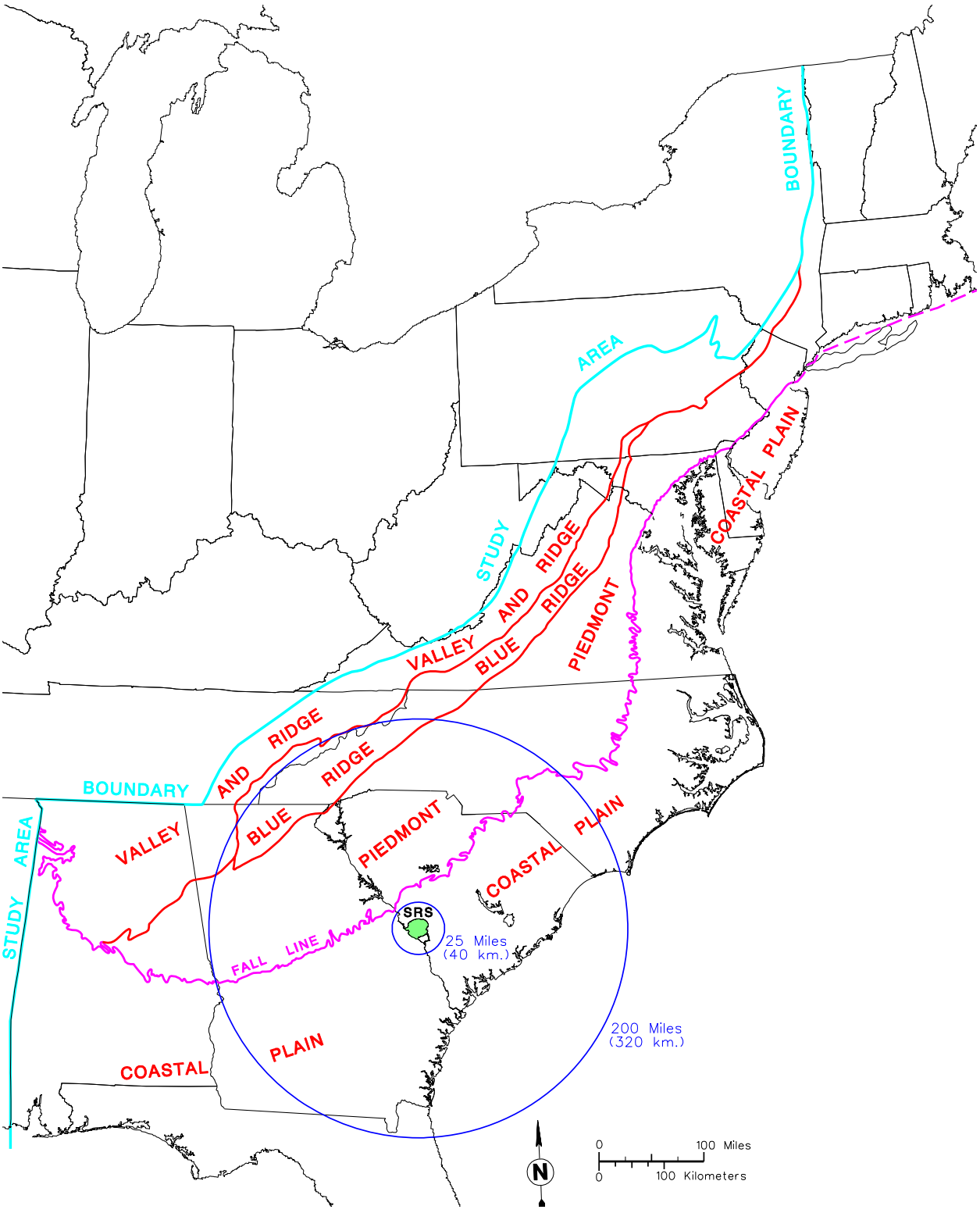

[WSRC-TR-95-0046, Figure 2-1]

Figure 3.1-7: Regional Physiographic Provinces of South Carolina

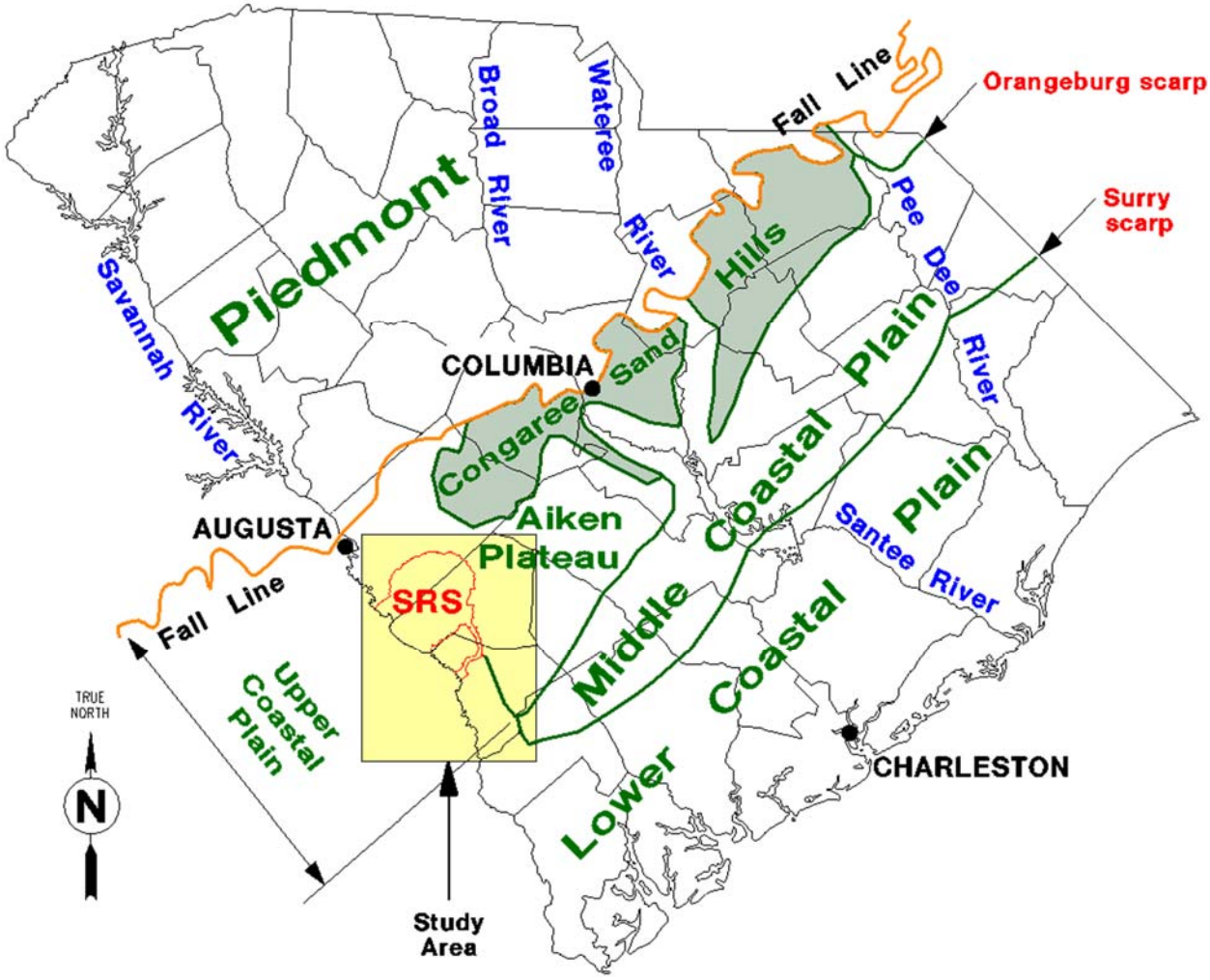

[WSRC-TR-95-0046, Figure 2-3]

3.1.4.2 Site Soils

SRS contains seven major soil associations: Chastain-Tawcaw-Shellbluff, Rembert-Hornsville, Blanton-Lakeland, Fuquay-Blanton-Dothan, Orangeburg, Vaucluse-Ailey, and Troup-Pinkney-Lucy. Figure 3.1-8 delineates the general soil associations at SRS.

The overall general soil association for the SDF is the Fuquay-Blanton-Dothan. The predominant soil type is the Blanton Sand, with minor amounts of Fuquay, Dothan, and Lucy Sands. These soils are all well-drained, with the Blanton Sand being somewhat excessively-drained. They all support 0% to 6% slopes. The Blanton Sand has a thick, sandy surface layer and subsurface layer, and a loamy subsoil. Dothan Sand is well-drained and has a loamy subsoil. Lucy Sand is well-drained and has a moderately thick, sandy surface layer and subsurface layer, and a loamy subsoil at a depth of 20 to 40 inches. Since these soils have a low available water capacity, low organic matter content, rapid leaching, and low fertility, they are best suited for timber production. At the SDF, a small area of Udorthent soil consisting of well-drained sandy to clayey soils formed in

the spoils from localized construction operations, are present near the southwest border of Z-Area (Figure 3.1-8).

Additional details for these associations are in the *Soil Survey of the Savannah River Plant Area, Parts of Aiken, Barnwell, and Allendale Counties, South Carolina* (PIT-MISC-0104).

Figure 3.1-8: General Soil Associations for SRS

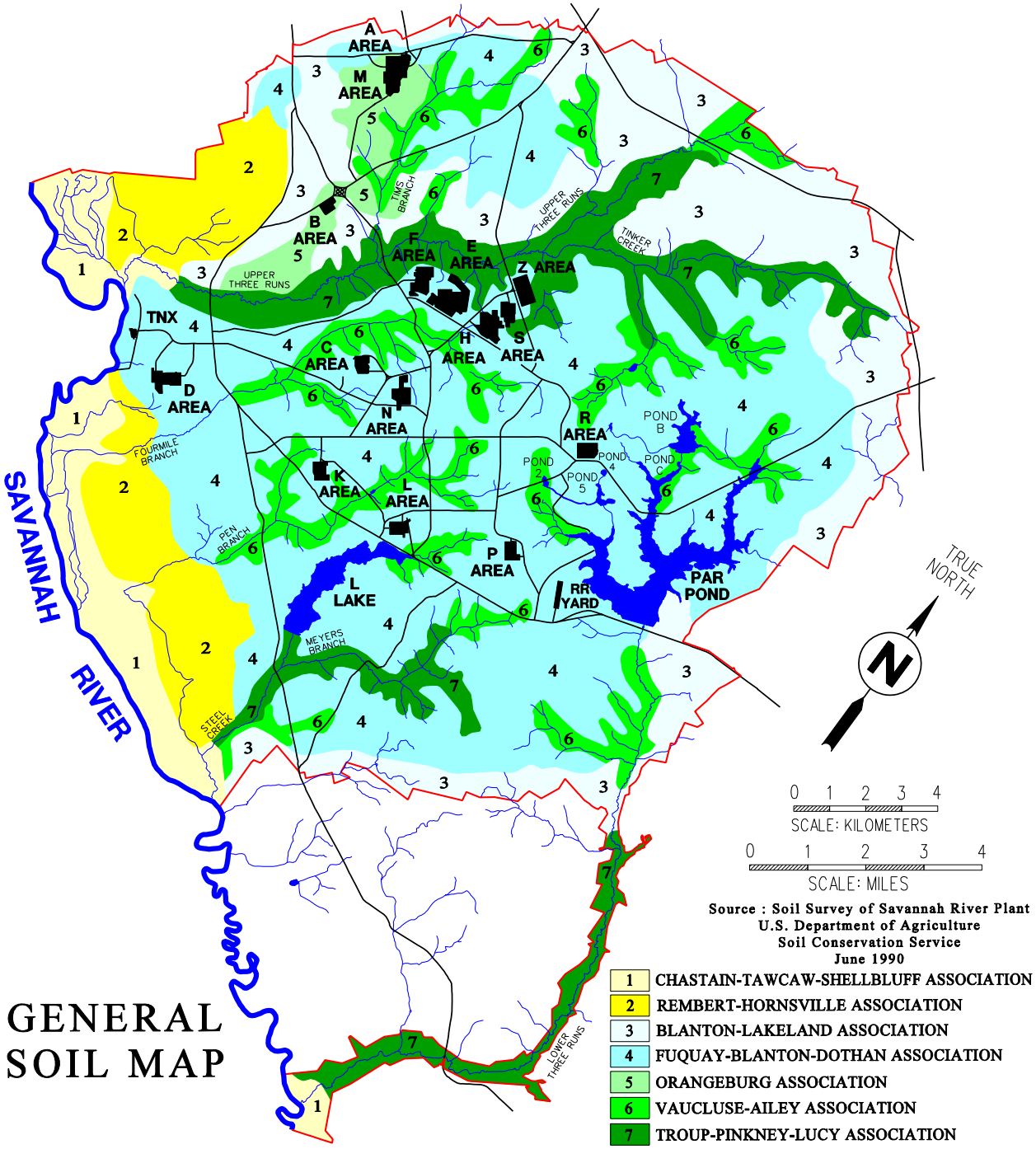

Note: Udorthent soils are present as disturbed soils in industrial areas and are not shown on map.

The Z-Area soils have also been characterized using the "textural triangle" (Figure 3.1-9) according to the U.S. Department of Agriculture (USDA) system. [WSRC-STI-2006-00198] While this approach only focused on the upper 12 feet of vadose zone soil, the results indicate that the texture of the soil is low in silt and high in sand with varying amounts of clay.

Figure 3.1-9: Textural Triangle for E-Area and Z-Area Vadose Zone Soils

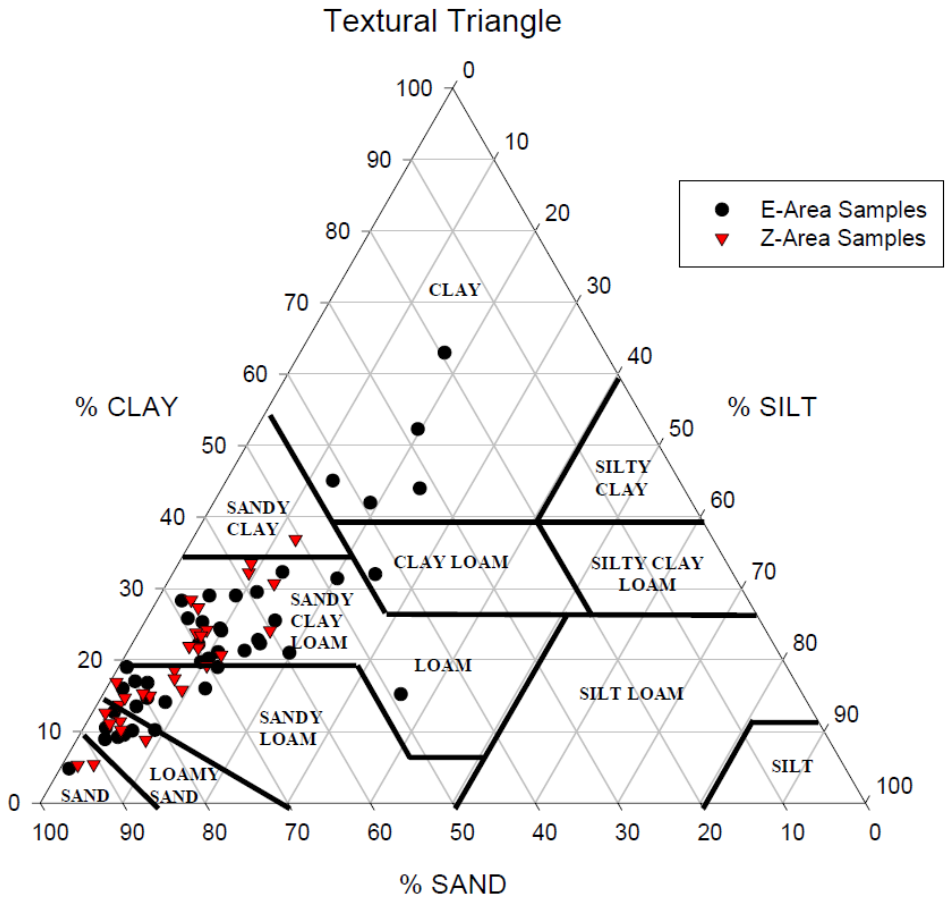

[WSRC-STI-2006-00198]

3.1.4.3 Site Geology

The uppermost geologic unit in the SDF is comprised of the middle to late Miocene-age Upland Unit, which extends over much of SRS. The term "Upland Unit" is an informal name used to describe sediments at higher elevations located in the Upper Coastal Plain in southwestern South Carolina. This area has also been referred to as the Aiken Plateau. The Upland Unit includes the vadose zone and a portion of the Upper Aquifer Zone (UAZ) of the UTR Aquifer. The occurrence of cross-bedded, poorly sorted sands with clay lenses in the Aiken Plateau indicates fluvial deposition (high-energy channel deposits to channel-fill deposits) with occasional transitional marine influence. This depositional environment results in wide differences in lithology and presents a very complex system

of transmissive and confining beds or zones. The lower surface of the Upland Unit is very irregular due to the erosional contact with the underlying formations. [DOE-EIS-0303]

A notable feature of the Upland Unit is its compositional variability. This formation predominantly consists of red-brown to yellow-orange, gray, and tan colored, coarse to fine grained sand, pebbly sand with lenses and beds of sandy clay, and clay. In general, going vertically upward through the unit, grain sorting becomes poorer, clay beds become more abundant and thicker, and sands become more clay-rich and indurated. In some areas, small-scale joints and fractures, both of which are commonly filled with sand or silt, traverse the unit. The mineralogy of the sands and pebbles is primarily quartz with some feldspar. In areas to the east-southeast, sediments may become more phosphatic and dolomitic. The soils in the Upland Unit may contain as much as 20% to 40% clay. [DOE-EIS-0303]

Below the Upland Unit lies the Tobacco Road Formation, consisting of red, brown, tan, purple, and orange quartz sands and clayey quartz sands. These sands are fine to coarse grained and moderately to poorly sorted with minor clay laminae. In general, the Tobacco Road Formation sands are muddier, more micaceous, and more highly colored than the sands of the underlying Dry Branch Formation. The base of the Tobacco Road Formation is marked in places by a coarse layer that contains flat quartz pebbles. Clay laminae in the upper part of the formation suggest that some of the unit was deposited in a transitional, low-energy environment, such as a tidal flat. The Tobacco Road Formation is approximately 20-foot thick and is part of the UAZ. [SRNL-STI-2010-00148]

Underlying the Tobacco Road Formation is the Dry Branch Formation, consisting of variably colored, poorly sorted to well-sorted sand with an interbedded tan to gray clay. The upper portion of the Dry Branch Formation is within the UAZ. The middle to lower portion of the Dry Branch Formation includes the Twiggs Clay – a semi-confining clay layer also designated as the Tan Clay Confining Zone (TCCZ), which separates the UAZ from the Lower Aquifer Zone (LAZ) of the UTR Aquifer.

Below the Twiggs Clay are the Clinchfield and Santee Formations. At the SDF, the Santee Formation is composed of mixed clastic and carbonate materials, with clastic material being dominant; the interpreted depositional scenario is a moderate energy, middle shelf environment with input of both clastic and carbonate sediments. Lithologic and petrographic studies have divided the Santee Formation in the GSA into eight microfacies: quartz sand (stone), terrigenous mud (stone), skeletal lime mudstone, skeletal wackestone, skeletal packstone, skeletal grainstone, microsparite, and siliceous mudstone. [WSRC-RP-94-54] None of these depositional environments contains significant amounts of limestone that would be conducive to the formation of karst features such as large subsurface voids or caves within the vicinity of the SDF.

The calcareous intervals within the Santee Formation at SRS contain “soft zones” related to the dissolution of carbonate material. As reported in early site characterization documents, potential voids were recognized while drilling into the Santee Formation by drilling rod “drops,” and anomalous drilling fluid and grout losses. Soft zones have been

encountered beneath most of the SRS, but they become more prevalent in the southeastern portion of the site. The distribution correlates with the well-documented pattern of increasing carbonate content in the Santee Formation to the southeast area of SRS. This lateral variation in carbonate content reflects the depositional environments of the Santee Formation at the site, changing from nearshore and inner shelf environments with primarily terrigenous input in the northwest, to quiet water outer shelf conditions of carbonate accumulation in the southeast. [WSRC-RP-94-54, WSRC-TR-99-4083]

For more than 60 years, the SRS soft zones have been the subject of many general and facility-specific investigations. These studies have shown that the soft zones are isolated, discrete, poorly connected, non-uniformly distributed features filled with loose, fine-grained, water-saturated sediment within the LAZ. [SRNL-TR-2012-00160] Although their size and shape vary greatly, their average thickness is generally only a few feet with a postulated maximum lateral dimension approximately 10 to 20 feet or less. [K-ESR-G-00013]

In the GSA, which includes the SDF, there is no evidence of actual subsurface karst features such as voids or caves that would act as open ground water flow conduits. In historical and recent literature, no documentation was found of void spaces or other geologic phenomena that would influence contaminant migration in a manner not already captured in the GSA ground water model.

Underlying the Santee Formation is the Warley Hill Formation, often referred to as "Green Clay" or Gordon Confining Unit, which forms a hydrologic barrier separating the LAZ from the underlying Gordon Aquifer of the Congaree Formation.

A more detailed description of the geology and soils of the GSA, which includes the SDF, is in the *Hydrogeologic Framework of West-Central South Carolina* (PIT-MISC-0112).

3.1.4.4 Seismology

The seismic history of the Southeastern United States spans a period of nearly three centuries and is dominated by the estimated magnitude 7.0 Charleston earthquake of August 31, 1886. The historical database for the region is essentially composed of two data sets extending back to 1698. The first set consists of pre-network, mostly qualitative data from 1698 to 1974, and the second set covers the period of instrumentally recorded, or post-network seismicity data, from 1974 through the present. Figure 3.1-10 shows the locations of historic seismic events in the Southeast through 2009 and Figure 3.1-11 shows the epicenters for seismic events within a 50-mile radius of SRS through 2003. [WSRC-MS-2003-00617, USGS OFR 2010-1059]

Figure 3.1-10: Historic Seismic Events in the Southeast United States

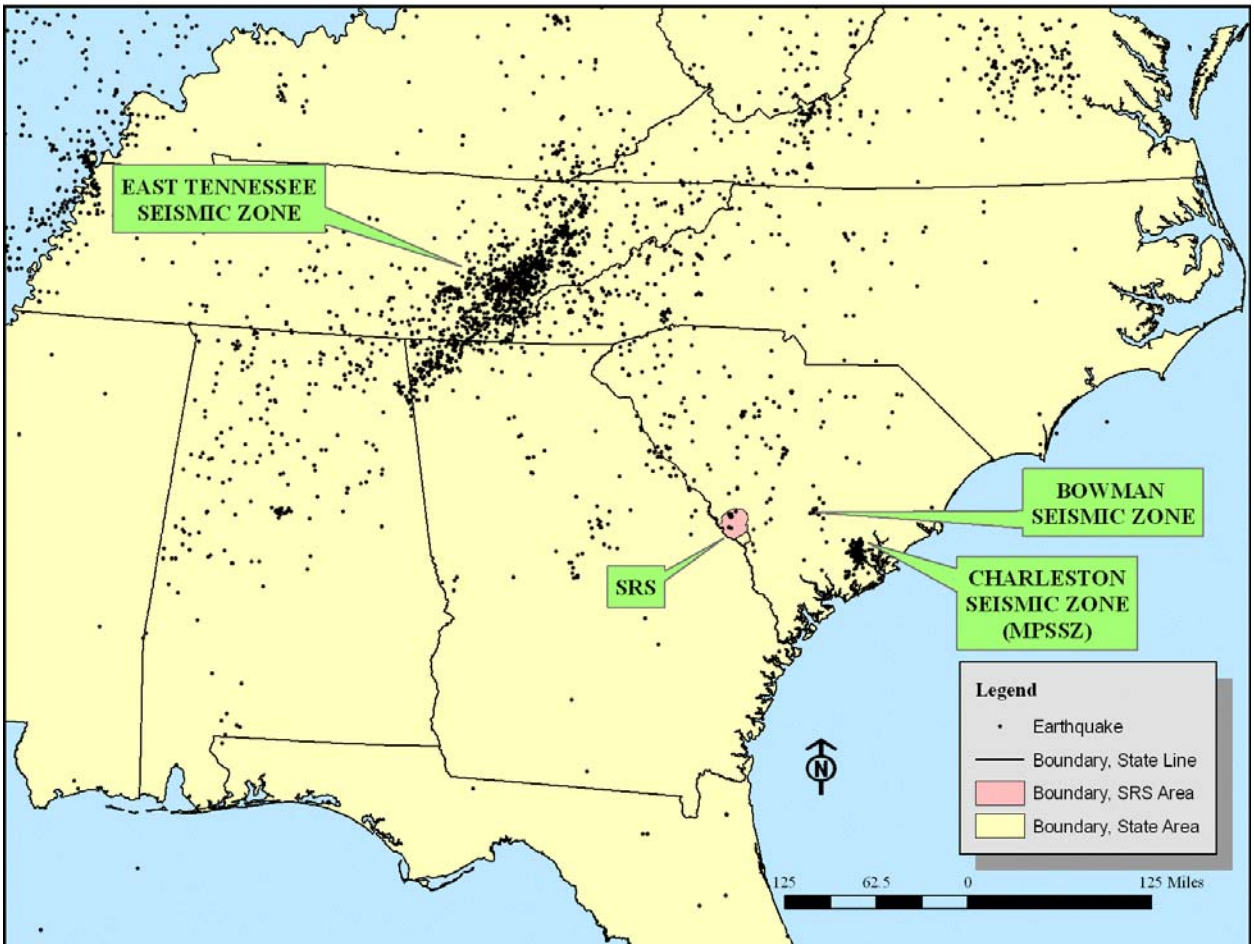

[USGS OFR 2010-1059]

Figure 3.1-11: Seismic Events within a 50-Mile Radius of SRS

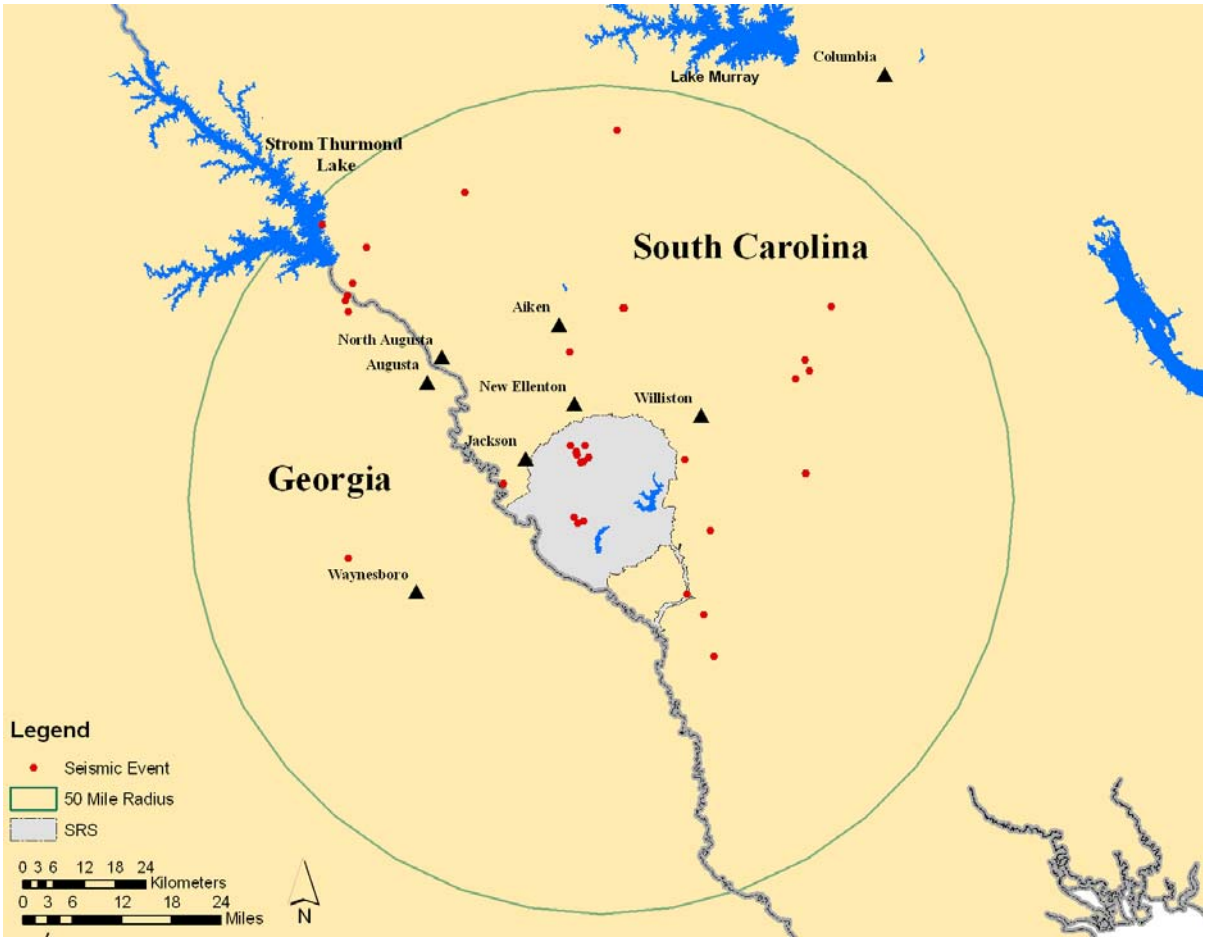

[WSRC-MS-2003-00617]

The most recent seismic event reported by the USGS within a 50-mile radius of SRS was a magnitude 3.2 earthquake on June 20, 2017. The epicenter was approximately 6 kilometers southwest of downtown Augusta, Georgia. It was followed by a magnitude 2.1 aftershock the next day. [https://earthquake.usgs.gov] No damage at SRS was recorded.

Four earthquakes with epicenters within the SRS boundary have occurred since the installation of the SRS seismic monitoring network in 1976:

- June 9, 1985 – Magnitude 2.6,
- August 5, 1988 – Magnitude 2.0,
- May 17, 1997 – Magnitude 2.5, and
- October 8, 2001 – Magnitude 2.6.

No strong motion accelerometers were triggered because of these events. Seven additional aftershocks occurred in the October 2001 epicentral area. These events were attributed to localized small-scale faults associated with pockets of relatively high stress

concentration and were not related to any large-scale regional features. [WSRC-MS-2003-00617]

The regional faults within SRS and vicinity are shown in Figure 3.1-12. A study entitled *Comparison of Cenozoic Faulting at the Savannah River Site to Fault Characteristics of the Atlantic Coast Fault Province: Implications for Fault Capability* (WSRC-TR-2000-00310) provides additional information. Based on strong similarities in both geometry and movement histories, the study concluded that the major regional scale Cretaceous to Tertiary faulting at SRS is closely associated with and may be included in the Atlantic Coastal Fault Province. The Atlantic Coastal Fault Province faults have been well studied and several specific faults have been investigated in detail by the regulatory agencies. In all documented cases, these faults have been declared "not capable" in terms of Appendix A 10 CFR 100 and 10 CFR 100.23 criteria. A "capable fault" is defined as having had a movement at or near the ground surface at least once within the past 35,000 years or movement of a recurring nature within the past 500,000 years. By application of the association clause in Appendix A 10 CFR 100, the faults at SRS were also considered "not capable." [WSRC-TR-2000-00310]

In 1976, a three-station short-period seismic network was established at SRS. A fourth station consisting of one vertical and two horizontal movement measuring instruments was added in 1986. In 1999, a total of 13 strong motion accelerographs were installed in selected mission-critical structures and remote field locations. Detailed information regarding seismic characteristics at SRS is in the Documented Safety Analysis (DSA), *DSA Support Document – Site Characteristics and Program Descriptions Chapter* 1 (WSRC-IM-2004-00008).

Considering the proximity to the Tinker Creek Fault, Z-Area could be impacted by activity on the Tinker Creek Fault. The liquefaction potential for SDU 4 was investigated using the Design Basis Earthquake (DBE) parameters. The investigation determined that the soils beneath SDU 4 were not susceptible to significant liquefaction for earthquakes, having a peak ground acceleration (PGA) ≤17% of the force of gravity (g) and ≤6.5 magnitude. The worst-case settlement was estimated to be about 1.25 inches. [K-CLC-Z-00001]

A geotechnical evaluation of the potential for settlement of the 375-foot diameter SDUs (SDU 6) was performed in 2012. Settlement due to liquefaction ranged from ¼ inch to 2 ¼ inches for a magnitude 7.5 DBE (2,500-year event) with a PGA of 0.18 g (force of gravity). The weighted average settlement due to liquefaction for SDU 6 is ¼ inch for the DBE earthquake. [K-ESR-Z-00005] A similar geotechnical evaluation was performed for SDU 7 in 2017. The weighted average settlement due to liquefaction for SDU 7 is ¾ inch for the DBE earthquake. [K-ESR-Z-00008]

Figure 3.1-12: Regional Scale Faults for SRS and Vicinity

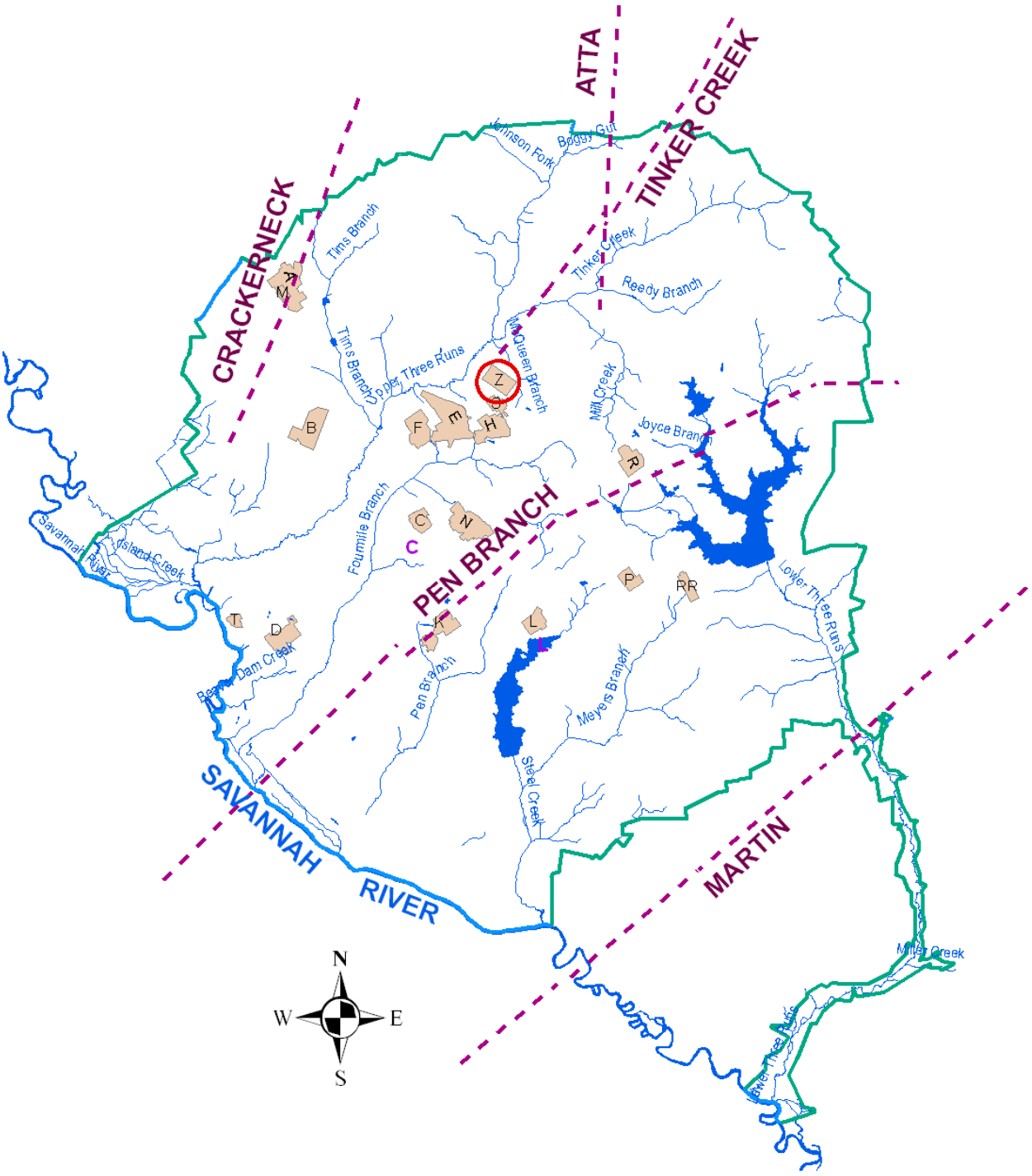

[WSRC-TR-2000-00310, Figure 10]

3.1.4.5 Soft Zone Response

Soft zones are often areas of under-consolidated material in a stronger matrix material that essentially forms an arch that allows the soft zone to remain under-consolidated. A

large seismic event could cause the soil arch to fail, resulting in settlement as the soft zone material compacts and becomes consolidated. [K-ESR-Z-00005]

Soft zones have been documented in early SRS subsurface investigations. The soft zones were identified by drilling rod "drops" associated with voids and anomalous drilling fluid losses and grout "takes" (losses). Soft zones are associated with the Santee Formation beneath SRS and may be susceptible to seismic activity. However, despite their under-consolidated nature, soft zones have remained structurally competent in the presence of significant overburden stresses for a long time. [SRNL-TR-2012-00160]

The predicted behavior of soft zones under both static and dynamic conditions has been modeled for numerous SRS facilities. These calculations show soft zones to be stable under static conditions and dynamic analyses predict that soft zones will not collapse in response to a DBE. [WSRC-TR-99-4083] The DBE and associated ground motion, measured in peak ground acceleration equaling 0.2 g (force of gravity) for SRS facility construction, is based on historic seismic events in the region, the geologic literature, and attenuation relationships. [WSRC-TR-90-0284]

As a conservative approach, the design for some SRS facilities assumes that soft zones will collapse (compact) in response to applied stress. An analysis for the proposed Actinide Packaging and Storage Facility within the GSA calculated the collapse of an approximately 8-foot thick, two-layer soft zone would cause a ground surface settlement of approximately 4 inches. [K-CLC-F-00034]

Soft zones were identified in three Cone Penetration Tests (CPTs) during the subsurface investigation at the SDU 6 site. No soft zone samples were obtained. Two CPTs had total soft zone thicknesses of less than 1.5 feet and the third measured 5.8 feet of soft zone material. Soft zone settlements were assumed to occur because of their potential compression during a seismic event. The settlement was computed by applying consolidation theory to the soft zone and an empirical analysis using soft ground tunneling analogy to propagate the settlement to the surface. [K-ESR-Z-00005]

Surface settlements for wide areas underlain by soft zones were calculated by superimposing settlement profiles for multiple narrow soft zones to simulate the desired area width. For SDU 6, a series of 5-feet wide soft zones were utilized to represent an area underlain by soft zones ranging in width from 25 feet to 150 feet. The analysis results indicated a maximum soft zone induced settlement of 0.5 inches and the maximum differential settlement of 0.5 inches. [K-ESR-Z-00005]

In addition, for the E-Area vaults in the GSA, a structural degradation study was prepared. This study included an evaluation of ground motion effects on the vaults. Ground motion magnitudes were extrapolated from SRS performance categories (PCs) PC-1 to PC-4 site-specific seismic criteria. For horizontal acceleration, a 0.45 force of gravity value was obtained by extrapolating the zero period accelerations (i.e., peak ground acceleration) of the SRS design response for PC-1 to PC-4. [T-CLC-E-00018]

For vertical acceleration (2.0 force of gravity), a bounding approach was taken by extrapolating the peak of the SRS horizontal design response spectra for PC-1 to PC-4. This approach results in the large discrepancy between horizontal and vertical acceleration. This bounding approach for vertical acceleration was used in the structural degradation study because the item of concern was a buried roof slab with voids below. Therefore, the E-Area vault roof could respond differently than the ground (i.e., not peak ground acceleration). As the SDUs will have no significant voids after grouting, this issue is not a concern. [T-CLC-E-00018]

Due to the lack of vertical/horizontal studies for low probability of exceedance events at SRS, the same bounding criteria used in the E-Area study were used for the structural assessment for the SDUs; however, it is recognized that 2.0 force of gravity is a bounding number. [T-CLC-F-00421] This is not a realistic number for ground acceleration at SRS. At the nearby Vogtle Electric Generating Plant, the vertical/horizontal ratio for the maximum considered event was 1.0, so a similar ratio should be considered acceptable for the SDF. [ML092290639 (NUREG-1923)] Based on a vertical/horizontal ratio of 1.0, the maximum vertical acceleration would be 0.45 force of gravity, much less than 2.0 assumed.

The PC-3 period of occurrence (or return period) is 2,500 years (probability of exceedance 4.0E-04) and the PC-4 period of occurrence is 10,000 years (probability of exceedance is 1.0E-04). In the E-Area analysis, soil analyses indicated the differential lateral displacement between the top and bottom elevations of the E-Area vault (approximately 28 feet in height) were 0.05 inches for a PC-3 event and 0.09 inches for a PC-4 event. The height differential in the E-Area vaults is similar to the height differential of the SDUs. Extrapolating to a probability of exceedance of 1.0E-06, a very low probability event, gives a maximum lateral differential displacement of 0.22 inches. For this small amount of deformation, the soil would deform locally at the boundaries of the SDU and stresses induced in the SDU structure will be minimal. [T-CLC-E-00018]

Although such calculations are an important aspect of nuclear safety evaluations, it is noteworthy that soft zones in the Eocene age Santee Formation have survived without collapsing for tens of millions of years and have presumably persisted through many earthquakes, including the magnitude 7.5 DBE with a 2,500-year return interval and less frequent events of even greater magnitude. [SRR-CWDA-2011-00054, RAI-SS-3]

3.1.4.6 SDU Structural Response and Settlement

A structural assessment was prepared for the SDUs. The latest available structural settlement analysis is for the 375-foot diameter SDU 7. [K-ESR-Z-00008] SDU settlement can occur due to two loads – static load and seismic loads. Static settlement is likely to occur due to the large overburden load from the closure cap. This settlement is expected to be relatively uniform. Any static differential settlement would be small in magnitude and cause an SDU to rotate as a rigid body. However, small magnitudes of rigid body rotation will induce only small lateral forces that can be considered negligible. [K-ESR-Z-00008]

As discussed earlier, seismic differential settlement can occur due to liquefaction and soft zone settlement. Calculations for settlement due to liquefaction for SDU 7 range from 0.4 to 2.1 inches for the magnitude 7.5 DBE. The magnitude weighted average using the SRS hazard deaggregation is less than 0.75 inches for the DBE. [K-ESR-Z-00008]

To ensure seismic induced degradation mechanisms were addressed, seismic considerations were included in the design of the conceptual closure cap.

3.1.5 Hydrology

As described in Section 3.1.5.2, the database used for the 2018 update to the GSA ground water model developed in PORFLOW (hereafter referred to as the GSA Model) is a subset of the site-wide lithology and ground water data sets. It was developed using soil and ground water characterization and monitoring data collected for the GSA and vicinity. The database is used as the basis for hydrogeologic input values into the computational model for ground water flow and contaminant transport for the SDF as described in Section 4.4.6. [SRNL-STI-2018-00643]

3.1.5.1 Regional Hydrogeology

The SRS lies in the Atlantic Coastal Plain, a southeast-dipping wedge of unconsolidated and semi-consolidated sediment, which extends from its contact with the Piedmont Province at the Fall Line to the continental shelf edge. Sediments range in geologic age from late Cretaceous to Recent and include sands, clays, limestones, and gravels. This sedimentary sequence increases in thickness from essentially zero at the Fall Line to more than 4,000 feet at the Atlantic Coast. At SRS, coastal plain sediments thicken from approximately 700 feet at the northwestern site boundary to approximately 1,400 feet at the southeastern site boundary and form a series of aquifers and confining or semi-confining units. [WSRC-STI-2006-00198]

Figure 3.1-13 shows a generalized cross section of sedimentary strata and their corresponding depositional environments for the Upper Coastal Plain down-dip through the SRS into the Lower Coastal Plain. Figure 3.1-14 shows the regional lithologic units discussed in Section 3.1.4.2 and their corresponding hydrostratigraphic units at SRS. This classification system is consistent with the established regional system and is now widely used as the SRS standard. [SRNL-STI-2010-00148]

Figure 3.1-13: Regional Northwest to Southeast Cross Section

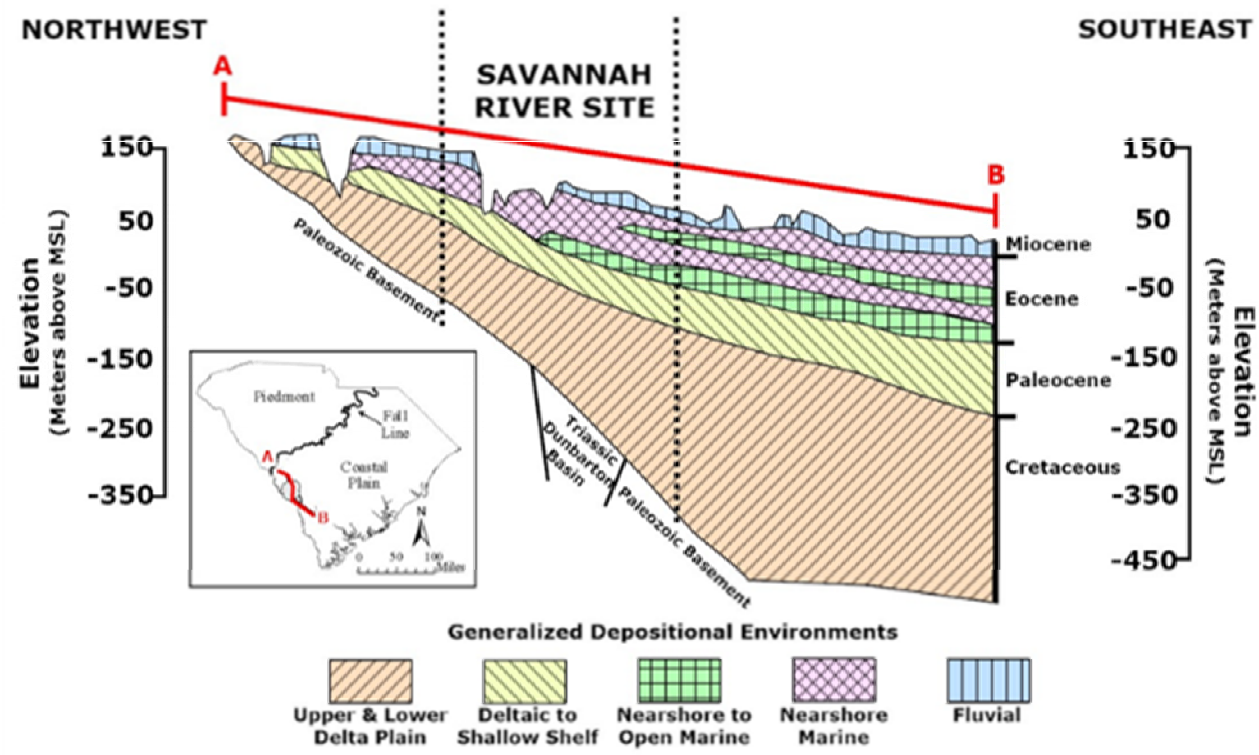

[WSRC-STI-2006-00198, Figure 4-6]

Figure 3.1-14: Comparison of Chronostratigraphic, Lithostratigraphic, and Hydrostratigraphic Units in the SRS Region

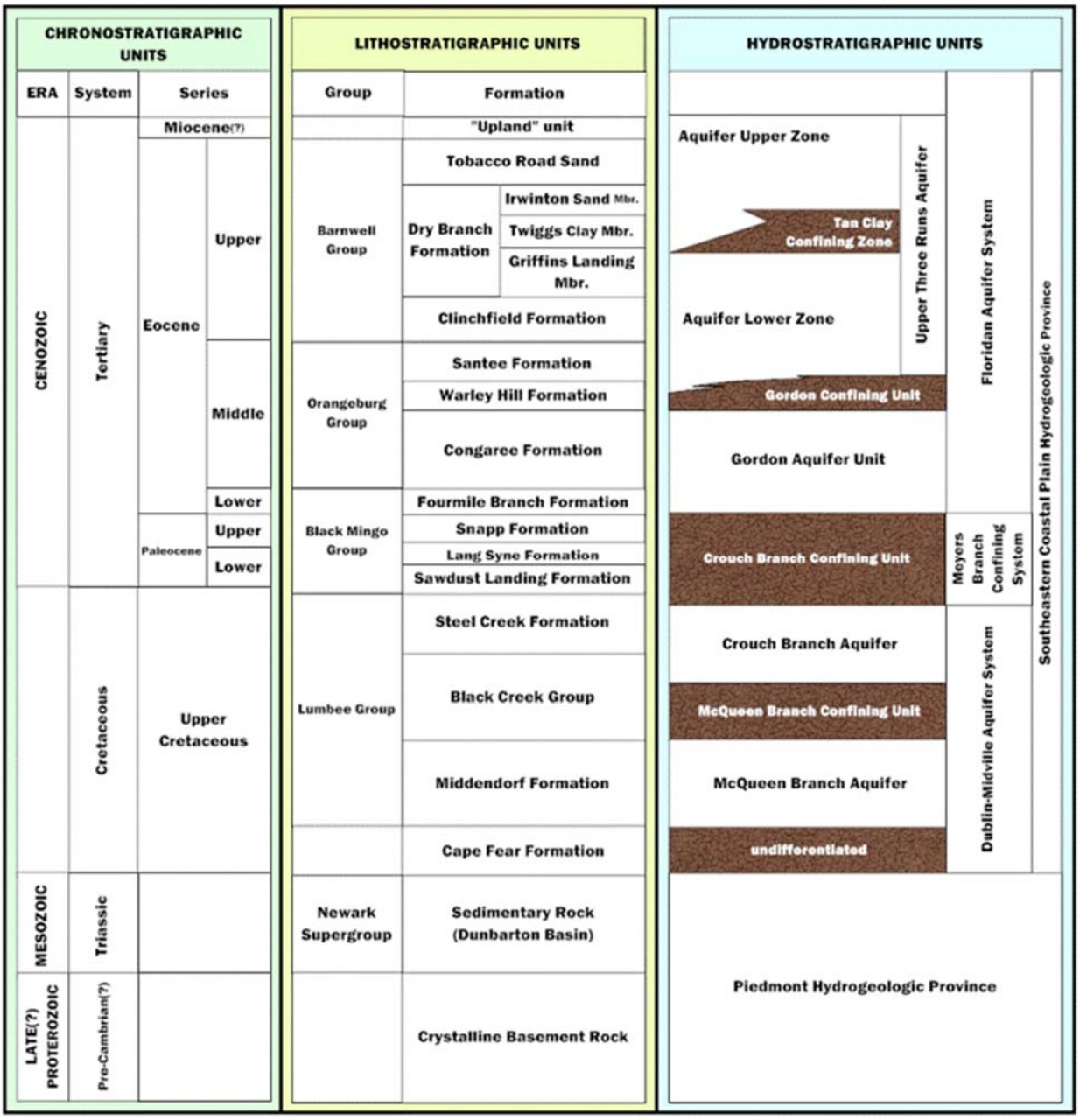

[SRNL-STI-2010-00148, Figure 2]

Ground water within the Floridan Aquifer system flows toward streams and swamps and into the Savannah River at rates ranging from inches to several hundred feet per year. The depth to which nearby streams cut into sediments, the lithology of the sediments, and the orientation of the sediment formations control the horizontal and vertical movement of the ground water. The valleys of smaller perennial streams in the GSA, such as Fourmile Branch (FMB), McQueen Branch (MQB), and Crouch Branch, allow surface discharge from the shallow saturated geologic formations. The valleys of major tributaries to the

Savannah River (e.g., UTR) drain formations at greater depth. With water discharge to the streams, the hydraulic head in the discharging unit can become less than the underlying unit. If this occurs, ground water has the potential to migrate upward from the lower unit to the overlying unit. [DOE-EIS-0303] Figure 3.1-15 and Figure 3.1-16 are potentiometric maps of the UTR Aquifer and Gordon Aquifer, respectively from the *Environmental Report for 2011*. [SRNS-STI-2012-00200]

Figure 3.1-15: Potentiometric Surface of the Upper Three Runs Aquifer

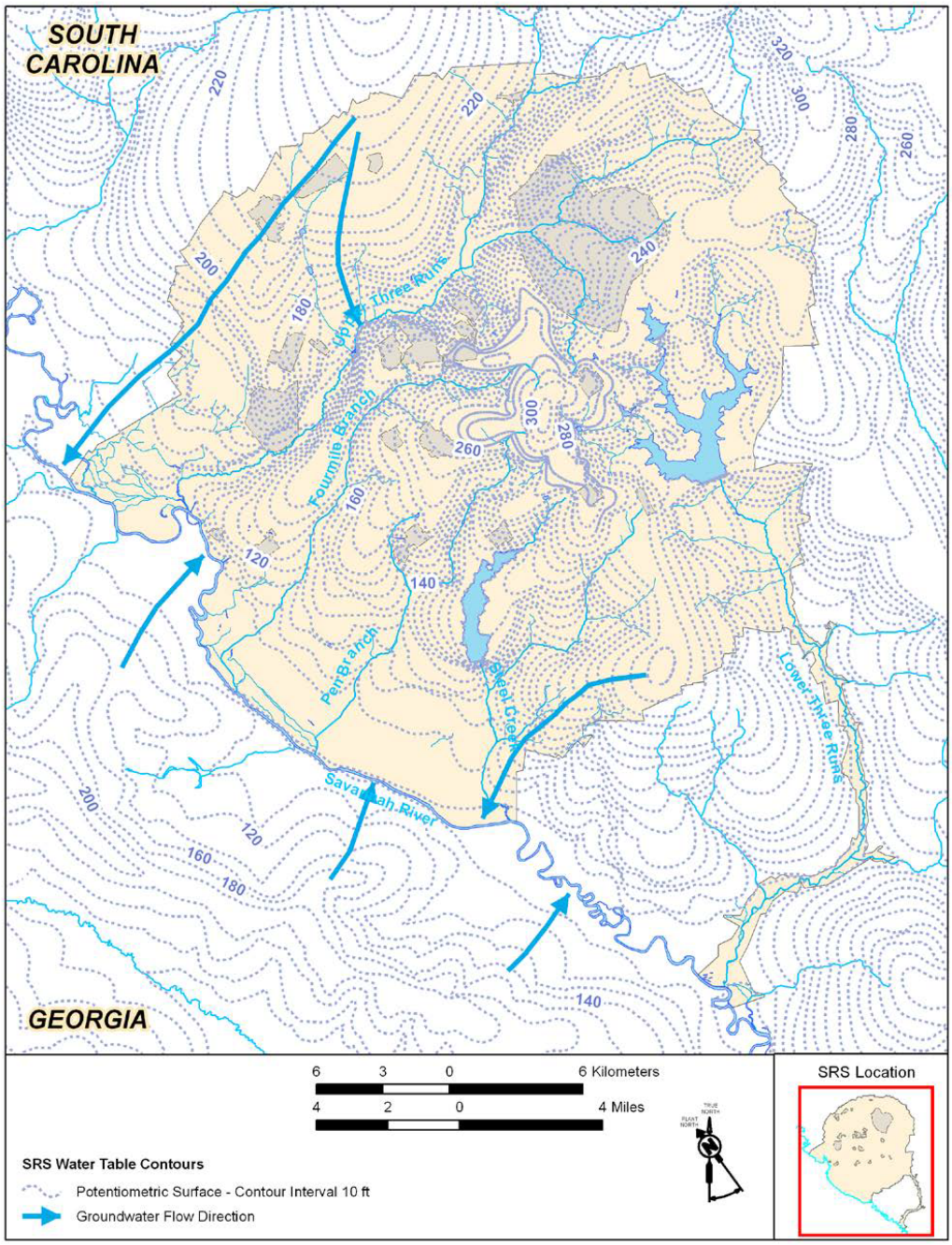

[SRNS-STI-2012-00200]

Figure 3.1-16: Potentiometric Surface of the Gordon Aquifer

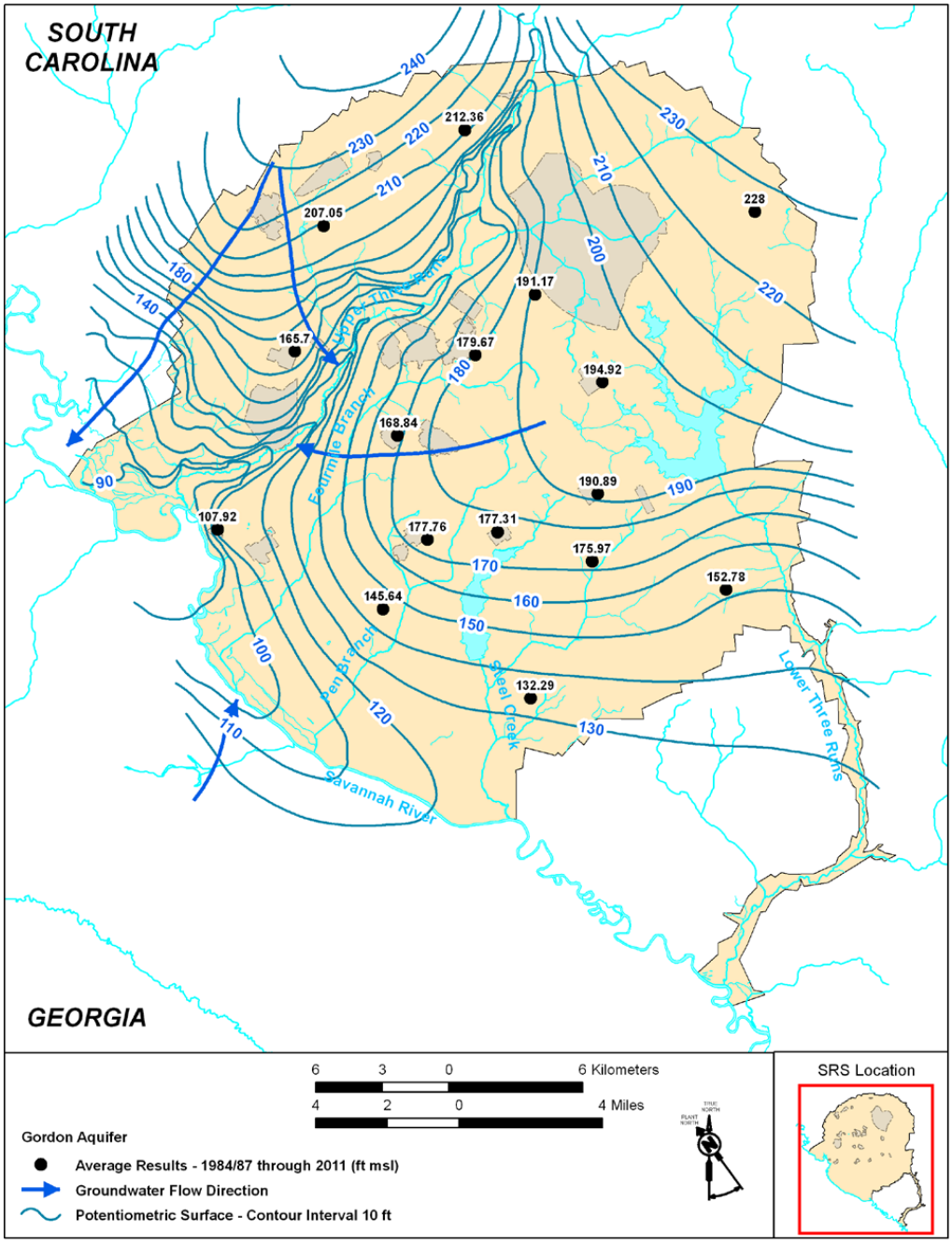

[SRNS-STI-2012-00200]

3.1.5.2 Characterization of Local Hydrogeology

The GSA has been the focus of numerous geological and hydrogeological investigations. Early work in the 1950s and 1960s included ground water monitor well installations. Further characterization and monitoring have been conducted in the area from the 1970s through the present, mainly to support ground water characterization and site

decommissioning activities. A GSA Model for simulating ground water has been established using field data and hydrogeological interpretations for the GSA and vicinity. As new information becomes available, it is added to the GSA Model. Although characterization and monitoring have been ongoing, the additional data has not altered the fundamental understanding of ground water flow patterns and gradients in the GSA. The *Integrated Hydrogeological Model of the General Separations Area, Volume 1: Hydrogeologic Framework* (WSRC-TR-96-0399) Volumes 1 and 2, contains a comprehensive discussion of the early data set.

A database used for creating the 2016 version of the GSA Model, containing the SRS characterization and monitoring data and interpretations, was used as the basis for the 2018 update. The GSA Model uses hydrogeologic input values to generate the computational model for ground water flow and is used for the contaminant transport modeling described in Section 4.4.6.

Since the issuance of *Integrated Hydrogeological Model of the General Separations Area,* (WSRC-TR-96-0399), additional CPTs and boreholes have been completed in the GSA, including Z-Area. In 2016, as part of the effort to update and calibrate the GSA 2016 PORFLOW model, the hydrogeologic data elements of the existing model were reviewed, new borehole data interpreted, and a new, larger dataset created to support the updated model.

As part of this model update, CPT curves, geophysical logs, and lithologic core descriptions throughout the model area were reviewed, down-selected, and incorporated into the hydrostratigraphic model. The goal of down-selection was to add two-dimensional and three-dimensional detail to the existing geologic model, especially in areas where borehole control points were originally sparse. New borehole data were selected primarily based on two-dimensional spatial distribution and on the length, depth, and continuity of borehole records available for interpretation; longer, deeper, and more continuous borehole data were preferentially selected over shorter, shallower, and less continuous data.

To improve model resolution, more than 200 new borehole control points and more than 600 new hydrostratigraphic picks (through 2015) were added to the 2016 version of the GSA Model. [SRNL-STI-2016-00516]

The merged and interpreted dataset currently includes more than 600 borehole locations and more than 1,900 hydrostratigraphic picks, including 611 picks for the TCCZ, 576 for the Lower Aquifer Zone (LAZ), 378 for the Gordon Confining Unit (GCU), and 303 for the Gordon Aquifer Unit (GAU).

In 2018, further refinement of the GSA Model was performed to incorporate updates to model calibration targets, closure of the H-Area Ash Basin, construction of E-Area Slit Trench operational covers, and plume information from the Mixed Waste Management Facility and Low-Level Radioactive Waste Disposal Facility. Another objective was to

lower hydraulic head residuals by adding another calibration zone. [SRNL-STI-2018-00643]

Figure 3.1-17 shows all the locations used to determine the hydrostratigraphic unit boundaries (i.e., "picks") used prior to the 2016 version of the GSA Model. Picks were made based on a combination of geophysical logs, CPT logs, and core descriptions. Figure 3.1-18 through Figure 3.1-21 show the locations where laboratory determined permeability data, multiple well pump tests, single well pump tests, and slug test data used in the 2018 GSA Model was collected. These data were used to interpret the local hydrogeology beneath the SDF.

Figure 3.1-22 shows the locations of the previously evaluated CPTs and boreholes (solid light green dots with small black center dots) in addition to the new CPTs and boreholes interpreted for the GSA 2016 re-evaluation (solid light green dots). Results from this examination revealed the TCCZ is present in most of the boreholes and CPTs evaluated at the SDF. [SRNL-STI-2016-00516]

Figure 3.1-17: Hydrostratigraphic Pick Locations Prior to the 2016 GSA Model

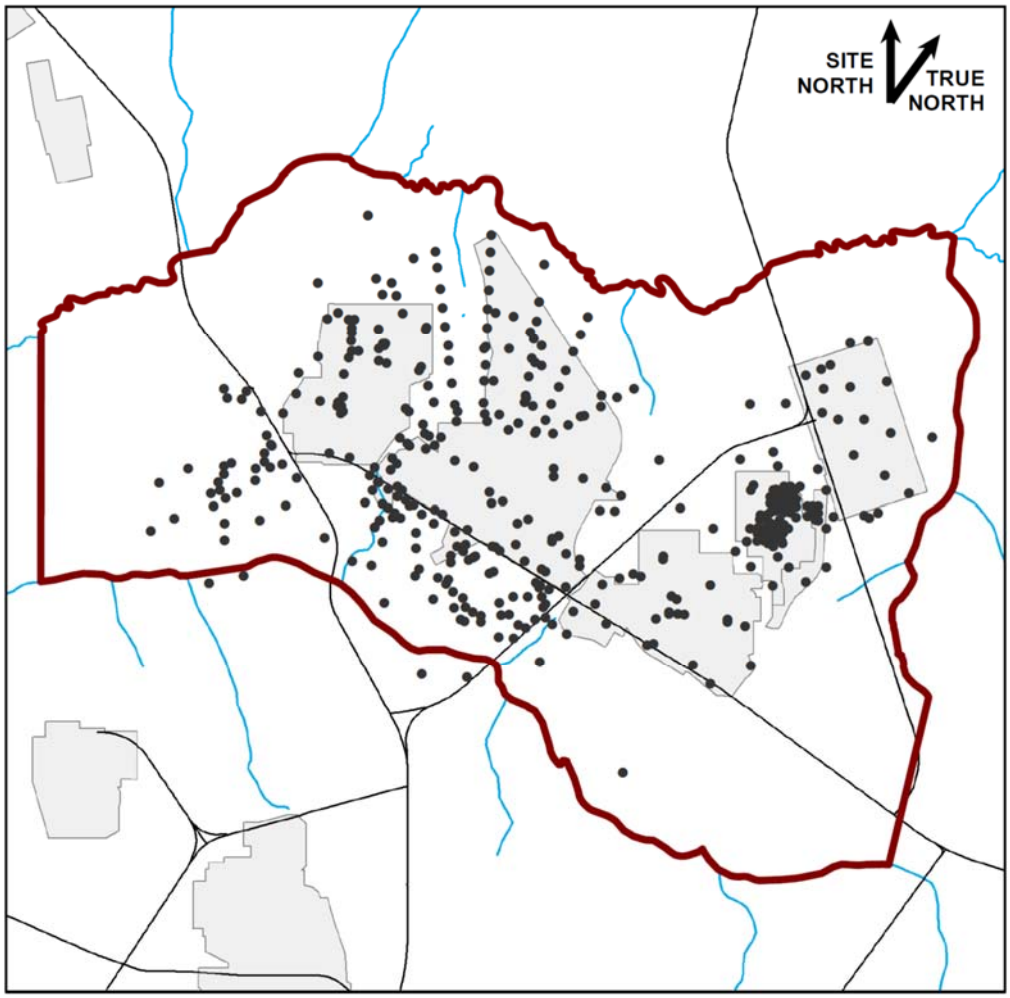

[SRNL-STI-2016-00516]

Figure 3.1-18: Locations for Laboratory Determined Permeabilities Used for the 2016 GSA Model

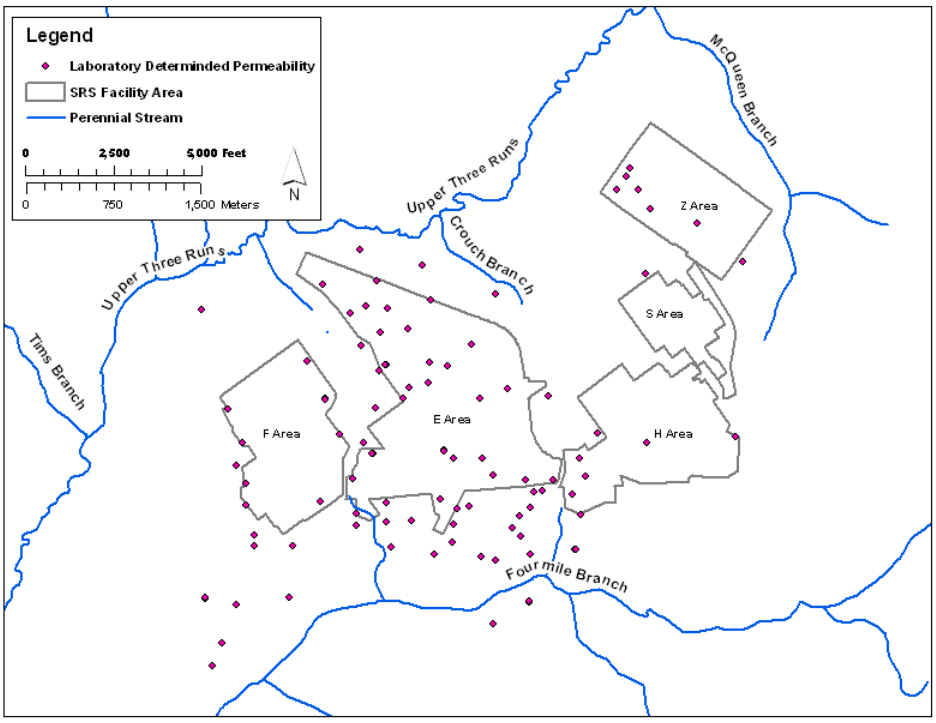

[SRNL-ESB-2007-00035]

Figure 3.1-19: Multiple Well Pump Test Locations Used for the 2016 GSA Model

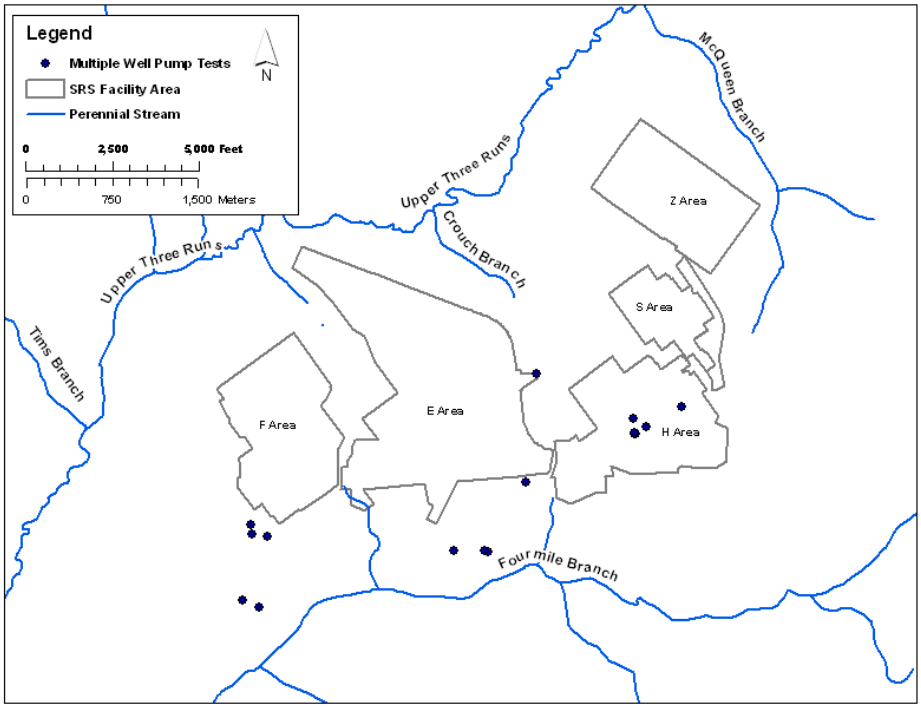

[WSRC-TR-96-0399, Vol. 2]

Figure 3.1-20: Single Well Pump Test Locations Used for the 2016 GSA Model

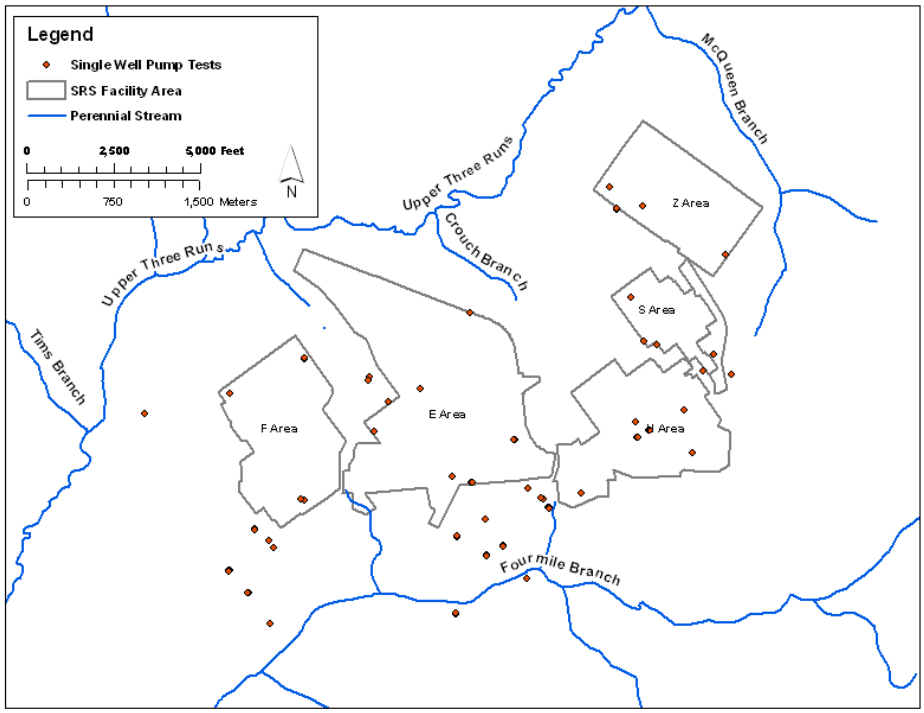

[WSRC-TR-96-0399, Vol. 2]

Figure 3.1-21: Slug Test Well Locations Used for the 2016 GSA Model

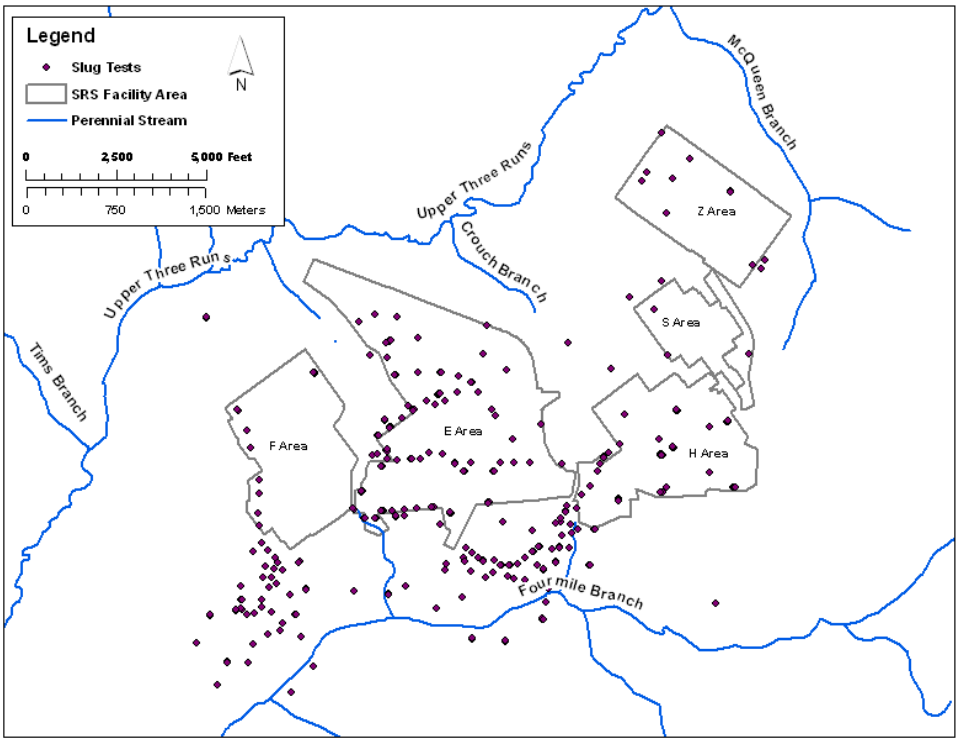

[WSRC-TR-96-0399, Vol. 2]

Figure 3.1-22: Locations of CPT and Well Boreholes for the 2016 GSA Model

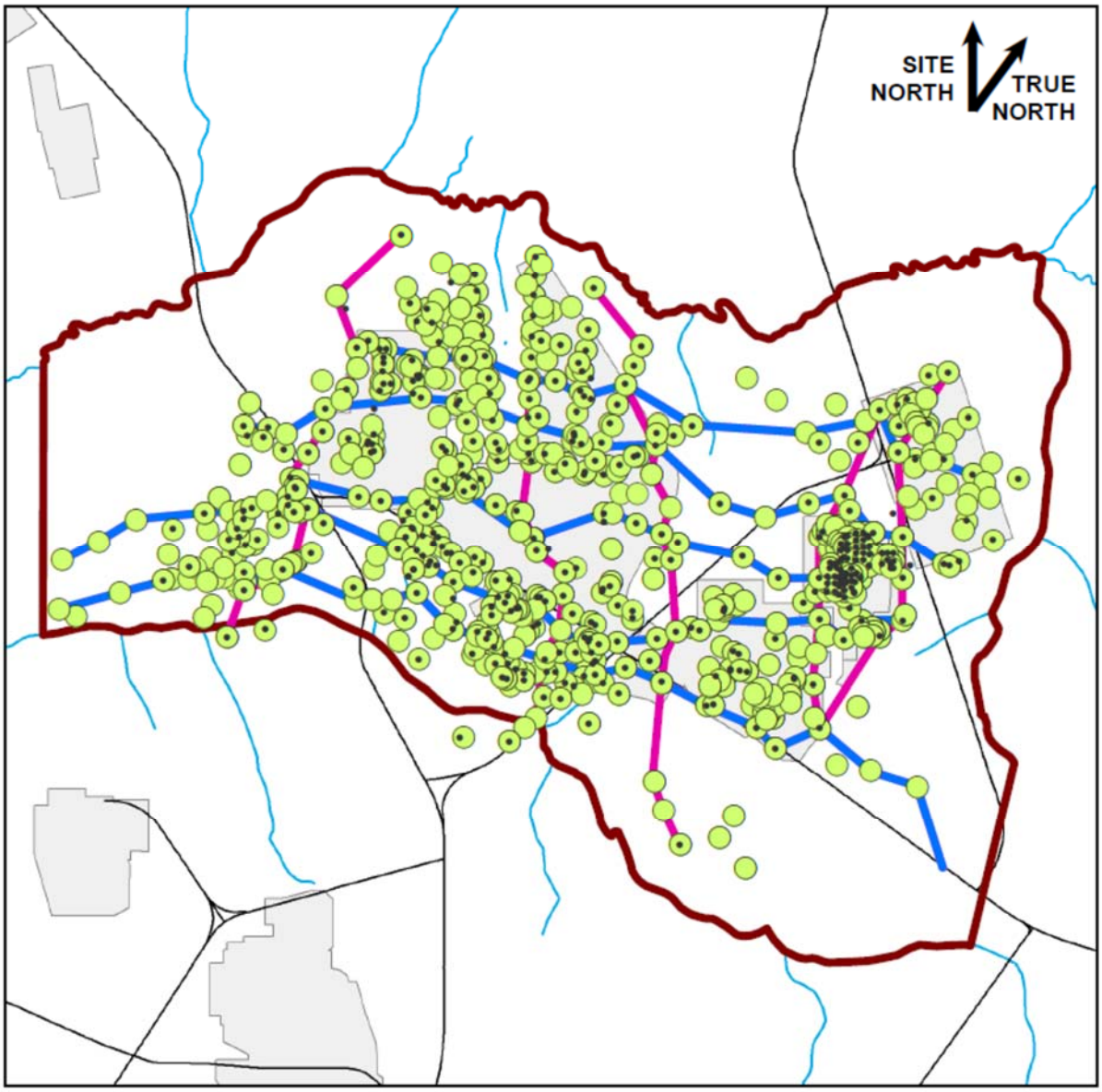

Note: Light green dots with no small black center dot represent data points added for the GSA 2016 update. [SRNL-STI-2016-00516]

Using the RockWorks software, the picks for hydrostratigraphic surfaces – TCCZ, LAZ, GCU, and GAU – were gridded to produce altitude-contour maps. Figure 3.1-23 shows a topographic color contour map of the TCCZ as interpreted for the GSA. The cell size for each square grid was 20 meters by 20 meters. Note that for more localized transport modeling, as described in Section 4.4.6, smaller discretization is used to reduce the effects of numerical dispersion. Each hydrostratigraphic surface was krigged using the RockWorks high-fidelity option. [SRNL-STI-2016-00516] The hydrostratigraphic surfaces were then used for creating the 2016 GSA Model, and the subsequently updated for the 2018 GSA Model.

Figure 3.1-23: Altitude-Contour Map of the TCCZ in the GSA

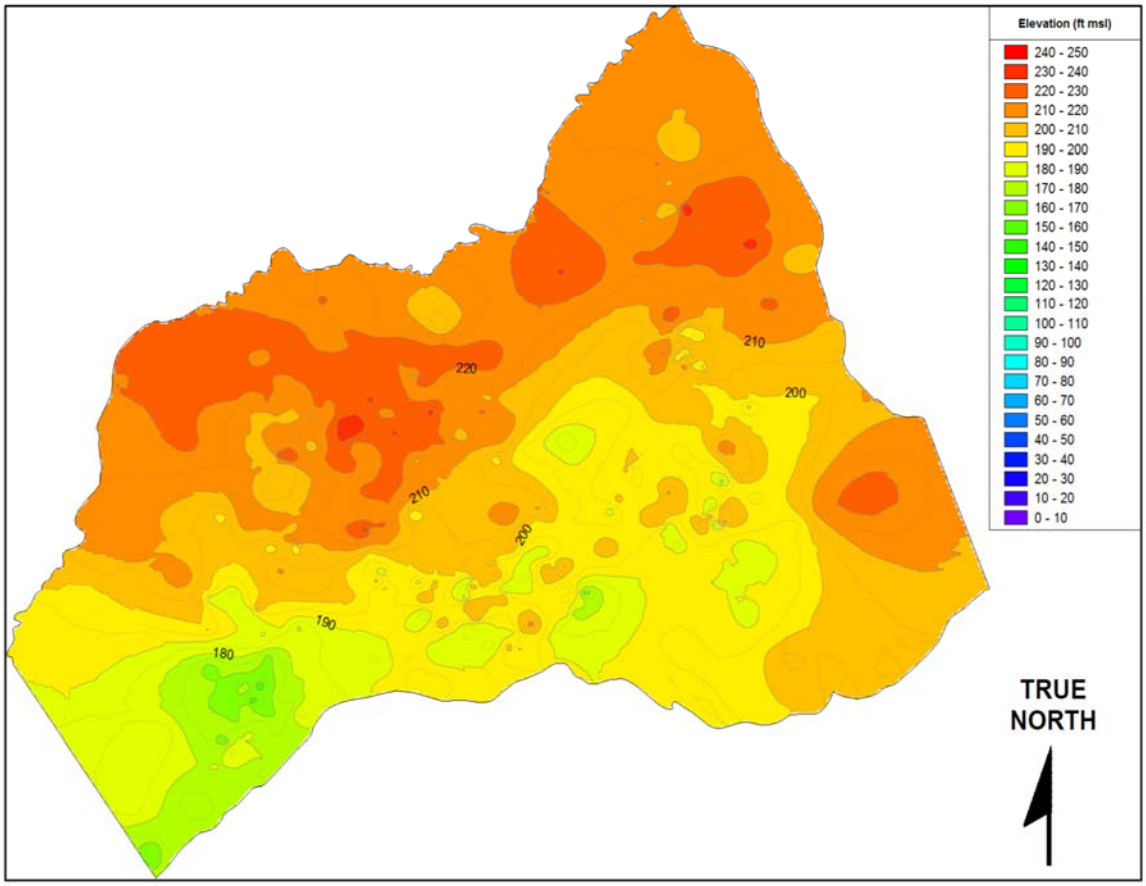

[SRNL-STI-2016-00516]

In reviewing the 2016 GSA Model, several additional Z-Area monitoring wells were identified that had been recently installed at the SDF but were not picked up during the 2016 update because there were not enough monitoring data points available at the end of 2015. In addition, the 2016 GSA Model needed to be calibrated to account for flow of known releases and plumes within the GSA and additional rainfall data for more recent periods.

The SRNL was tasked with providing a 2018 update to the GSA Model to address these issues. The report, entitled *Updated General Separations Areas (GSA) Groundwater Model Calibration Targets*, SRNL-STI-2018-00336, addressed the following issues:

- Import new well measurement data for B, F, H, UTR, Z, and GSA site groupings,
- Analyze individual well hydrographs and eliminate measurements thought to be in error or to reflect anthropogenic perturbations,
- Calculate the water level statistical quantities associated with each target well,
- Identify the hydrostratigraphic unit associated with each well based on the position of the well screen in the subsurface and the configuration of the interfaces between hydrostratigraphic units, and
- Calculate weighting factors for each calibration target.

These revisions were used to create the updated GSA Model to support area PAs and the Composite Analysis (CA).

To establish a steady state period for rainfall infiltration, data were imported from the Atmospheric Technologies Group climate data for the two weather stations located within the GSA Model footprint (based on meteorological data from F-Area and H-Area). [https://weather.srs.gov/weather/climate_data/] Daily precipitation was totaled for each month; where both F- and H-Area measurements existed for a collection date, they were averaged. The updated rainfall data is illustrated in Figure 3.1-24. The Base period was set to run from January 1, 2004, through April 1, 2018, and is relatively free from transient adjustments in ground water levels, which therefore provides optimal calibration targets.

Figure 3.1-24: Rainfall Data from F- and H-Area Climate Data

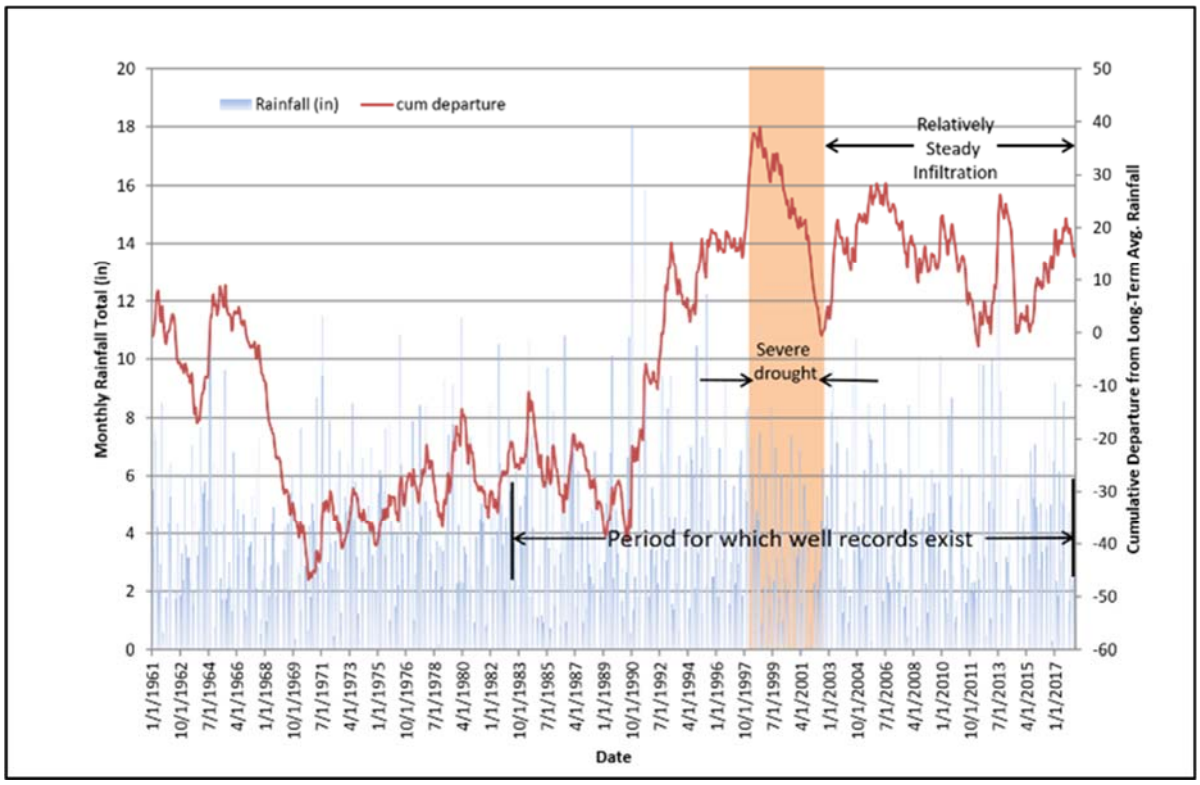

[SRNL-STI-2018-00336]

To prepare Base Period hydrographs and statistical quantities, water level measurements were downloaded from the Records Management database for various SRS areas and site groupings, including B, F, H, UTR, Z, and GSA. The data was downloaded using an initial date (January 1, 2004) as the "Base Period" time slice through to the present (May 2, 2018); this yielded 55,386 data points. The measured depths were converted to water level elevations based on the reference elevation for the well. Initially, the data included multiple types of wells; only those described as monitoring wells, wells, and piezometric wells were kept for further analysis, which left 48,657 data points. It was found that several measurement records were missing the measured depths. These were removed, leaving 48,155 data points and 946 wells.

Each well is required to have a hydrostratigraphic aquifer designation to indicate which wells are in hydraulic communication with each other. It was found that additional imported wells did not have documented hydrostratigraphic aquifer designations. The additional wells were further analyzed to ensure they existed within the GSA Model footprint – 85 of the 946 wells were outside of the footprint, leaving 861 wells, and 59 wells required hydrostratigraphic aquifer designations. To designate the remaining wells with a certain hydrostratigraphic aquifer designation, the elevations of the screen top and a point 5-feet below the bottom of the well screen was compared to the elevation of the interfaces between adjacent hydrostratigraphic aquifer designations at each well location. A schematic of this process is shown in Figure 3.1-25. [SRNL-STI-2018-00336]

Figure 3.1-25: Schematic of Well Screens and Hydrostratigraphic Designations

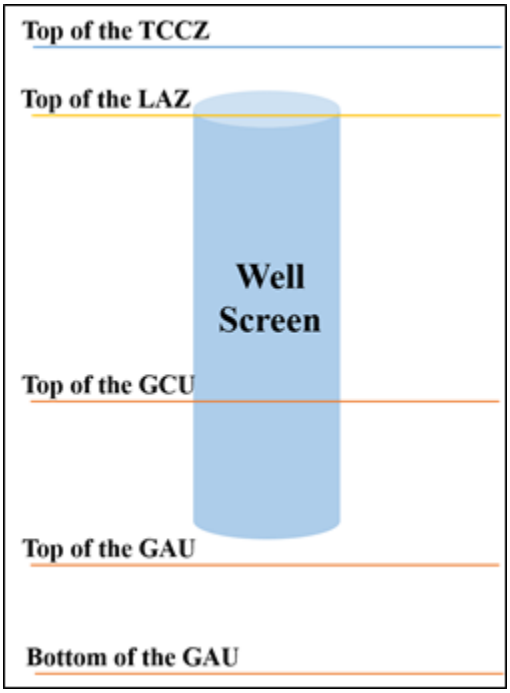

[SRNL-STI-2018-00336]

The water level calibration targets were then assigned a geographic weight that captures the density of wells on a spatial basis using the polygonal de-clustering approach. The polygon areas for the UAZ, LAZ, and GAU are shown in Figure 3.1-26, Figure 3.1-27, and Figure 3.1-28, respectively. Note these figures use Universal Transverse Mercator (UTM) coordinates.

Figure 3.1-26: Polygonal Areas for Inverse Distance Weighting for the UAZ

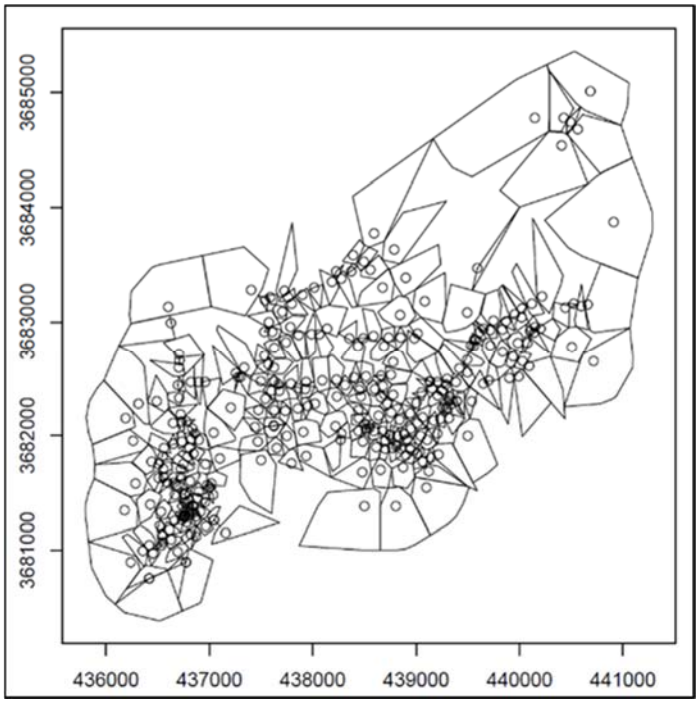

[SRNL-STI-2018-00336]

Figure 3.1-27: Polygonal Areas for Inverse Distance Weighting for the LAZ

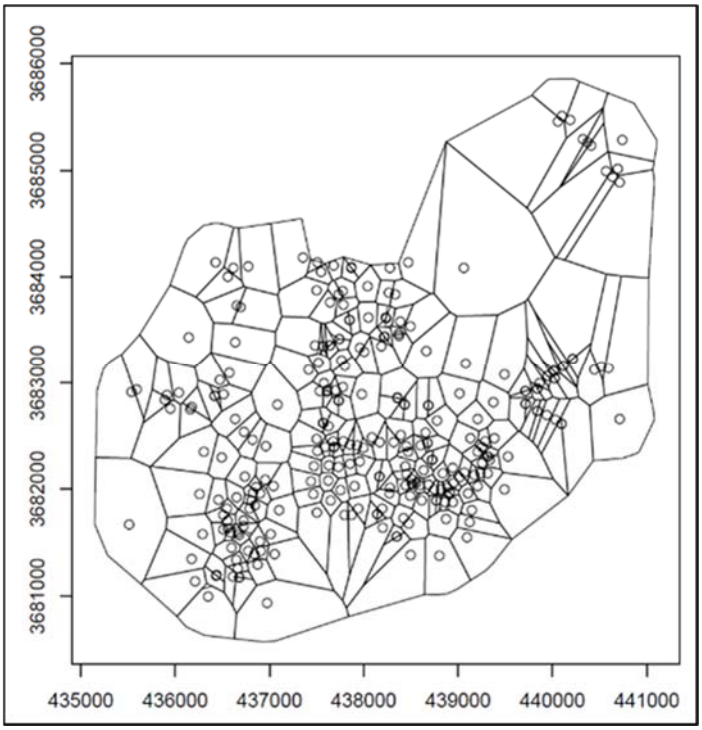

[SRNL-STI-2018-00336]

Figure 3.1-28: Polygonal Areas for Inverse Distance Weighting for the GAU

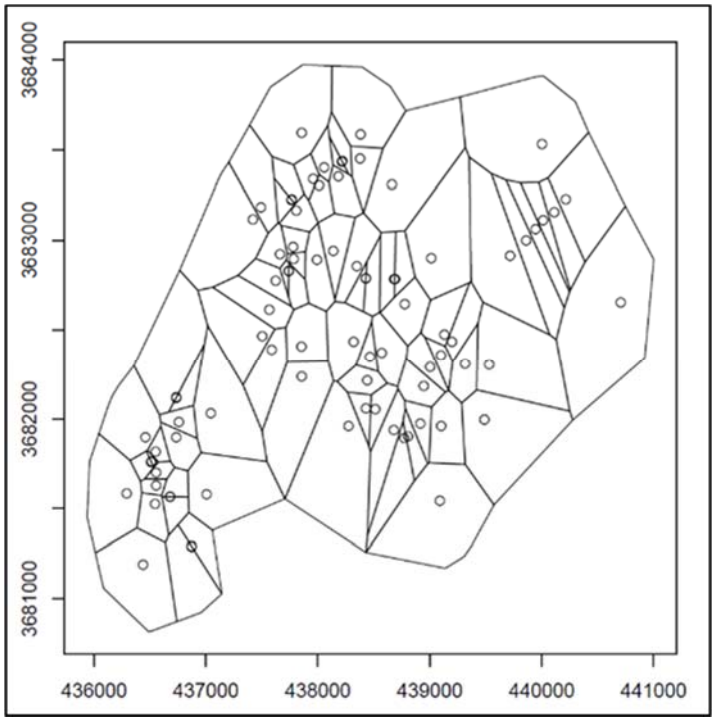

[SRNL-STI-2018-00336]

A total of 45,668 depth to water measurements obtained from 731 wells were evaluated and used to generate new Base Period target well hydrographs presented in SRNL-STI-2018-00336. An exercise was conducted to identify and remove any spurious measurements from the hydrographs and the water level statistical quantities were then computed for each well. These data were used to update the GSA Model in 2018.

3.1.5.3 Ground Water Flow in the GSA

Near Z-Area, the Aiken Plateau is dissected by numerous streams that greatly influence the local ground water system. Z-Area is on a local topographic high, approximately 300 feet above mean sea level (MSL) with a local relief of approximately 160 feet. Z-Area is bound by McQueen Branch to the northeast, UTR to the northwest, and Crouch Branch to the southwest (Figure 3.1-3). McQueen Branch is a tributary of UTR, which drains into the Savannah River approximately 10 miles southwest of Z-Area.

UTR lies approximately 3,000 feet from the northwest corner of Z-Area. The east corner of Z-Area is located approximately 500 feet from McQueen Branch. McQueen Branch and Crouch Branch are incised into the topographic high southeast and southwest of Z-Area such that their headwaters come within approximately 3,300 feet of each other approximately 4,600 feet south of Z-Area (Figure 3.1-3). The elevation changes in both tributaries range from approximately 150 to 250 feet. [WSRC-RP-92-1360]

The UTR watershed drains approximately 190 square miles of the Upper Coastal Plain northeast of the Savannah River. Significant tributaries to UTR are Tinker Creek, which

is a headwaters branch that comes in north of Z-Area, and Tims Branch, which connects south of Z-Area (Figure 3.1-3). There are no lakes or flow control structures on UTR or its tributaries. The stream channel has a low gradient and is meandering. Its floodplain ranges in width from 0.25 to 1 mile and is heavily forested with hardwoods. [WSRC-RP-92-1360]

Two smaller tributaries of UTR, the McQueen Branch and Crouch Branch, are located northeast to southeast and west of Z-Area, respectively, and both tributaries receive runoff from Z-Area. McQueen Branch has a drainage area of approximately 4.25 square miles and Crouch Branch has a drainage area of approximately 1.1 square miles. [WSRC-RP-92-1360]

The average water table elevation beneath the SDF is approximately 215 to 235 feet above MSL. [WSRC-TR-2005-00131, SRNS-TR-2018-00149, SRNS-TR-2018-00292] Based on the 1Q2018 well measurements (SRNS-TR-2018-00292) and the planned locations for each SDU, the depth to the water table varies from a maximum of 45.5 ft (beneath SDU 1) to a minimum of 30 feet (beneath the planned location of SDU 9). See Section 4.3.1.

The horizontal ground water gradient in the vicinity of SDU 4 is 0.009 feet/foot. [SRNS-TR-2018-00149]

Figure 3.1-29 is a generalized east-west cross section through the center of the GSA showing the conceptual ground water flow patterns in the UTR Aquifer and the Gordon Aquifer.

Figure 3.1-29: Conceptual Diagram of Ground Water Flow Beneath the GSA

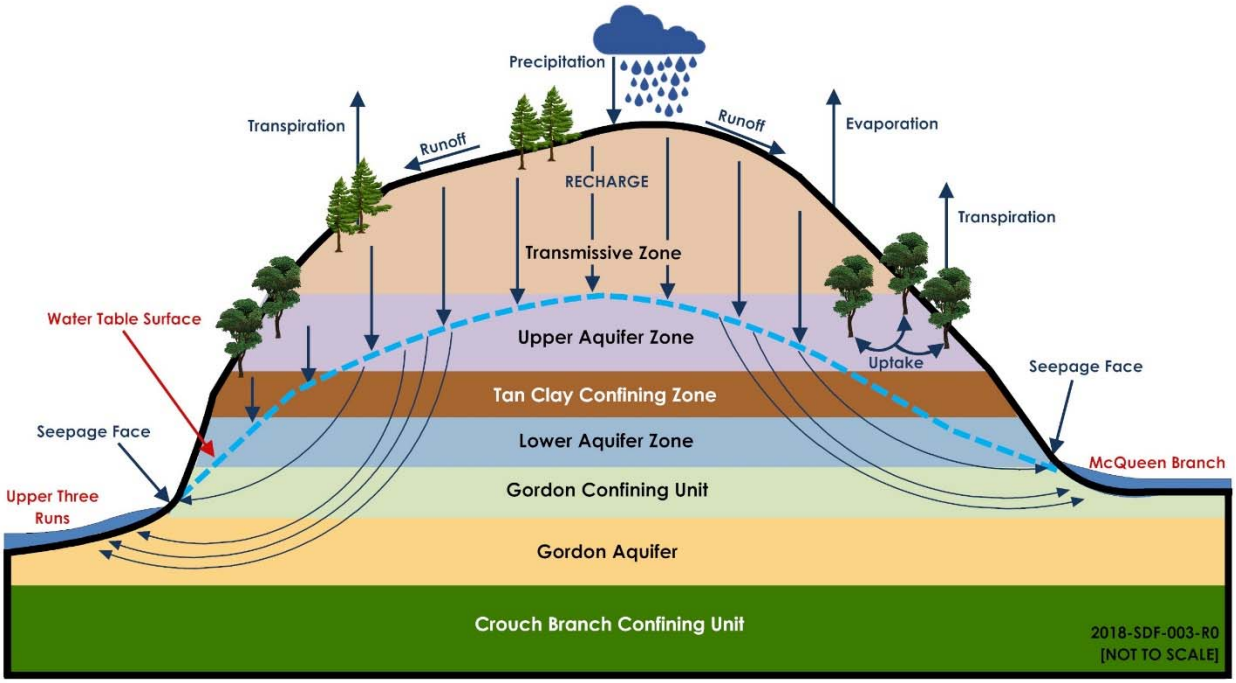

The aquifers of primary interest for SDF modeling are the UAZ, LAZ, and the Gordon Aquifer. Potential contamination from the SDF is not expected to enter the deeper Crouch Branch Aquifer because an upward gradient exists between the Crouch Branch and Gordon Aquifers near UTR. Plate 17 of the *Hydrogeological Framework of West-Central South Carolina* (PIT-MISC-0112) gives the leakance coefficient of the Crouch Branch Confining Unit, of the Meyers Branch Confining System, as roughly 3E-06 per day, which corresponds to 0.13 in/yr for every 10 feet of head difference. The measurement of head difference across the Crouch Branch Confining Unit is zero to 20 feet causing an upward flow averaging 0.13 in/yr. [PIT-MISC-0112] Flow across the unit is therefore a small fraction of total recharge, and is negligible in the SDF modeling.

Calcareous intervals and the associated soft zones are not treated separately in the ground water flow model because they are isolated and discontinuous in the GSA, representing only a small fraction of the LAZ. These features occur near the base of the LAZ in the GSA and do not extend through the entire thickness of the aquifer. [WSRC-TR-99-4083] A further evaluation of more than 60 years of onsite investigation and research into soft zone occurrence, origin, and properties concludes that soft zones at the SRS appear not to be a critical influence on either ground water flow or contaminant transport. [SRNL-TR-2012-00160]

3.1.5.4 Surface Water Flow in the GSA

The Savannah River, which forms the boundary between Georgia and South Carolina, is the principal surface-water system near SRS. The river constitutes most of the SRS southwestern boundary from about River Mile (RM)-142 to RM-160. Five upstream reservoirs (Lake Jocassee, Lake Keowee, Lake Hartwell, Richard B. Russell Lake, and Lake Strom Thurmond) minimize the effects from droughts and the impacts of low river flow on downstream water quality and fish and wildlife resources. Figure 3.1-30 shows the Savannah River Basin dams. The long-term yearly Savannah River flow at SRS estimated by the USGS averages 10,000 ft^3/s. [SRNS-RP-2018-00470] For 2017, the USGS measured flow rate at RM-118.8 was 5,698 ft^3/s. This value reflects a downward trend in the data with an average measure flow rate of 7,530 ft^3/s during the past 10 years. [SRNS-RP-2018-00470]

The major tributaries to the Savannah River that occur on SRS are UTR, FMB, Pen Branch, Steel Creek, and Lower Three Runs (Figure 3.1-31). These tributaries drain all of SRS except for a small area on the northeast side of the site, which drains to a tributary of the Salkehatchie River. Each of these streams originates on the Aiken Plateau in the Coastal Plain and drop 50 to 200 feet in elevation before discharging into the Savannah River. The source for most surface water on SRS is either rainfall (Section 3.1.2), water pumped from the Savannah River used for cooling site facilities, or ground water discharging to surface streams. The streams, which historically have received varying amounts of effluent from SRS operations, are not commercial sources of water. Downstream of SRS, the Savannah River is used as a domestic water supply source and for commercial and sport fishing, boating, and other recreational activities. [DOE-EIS-0303]

Figure 3.1-30: Savannah River Basin Dams

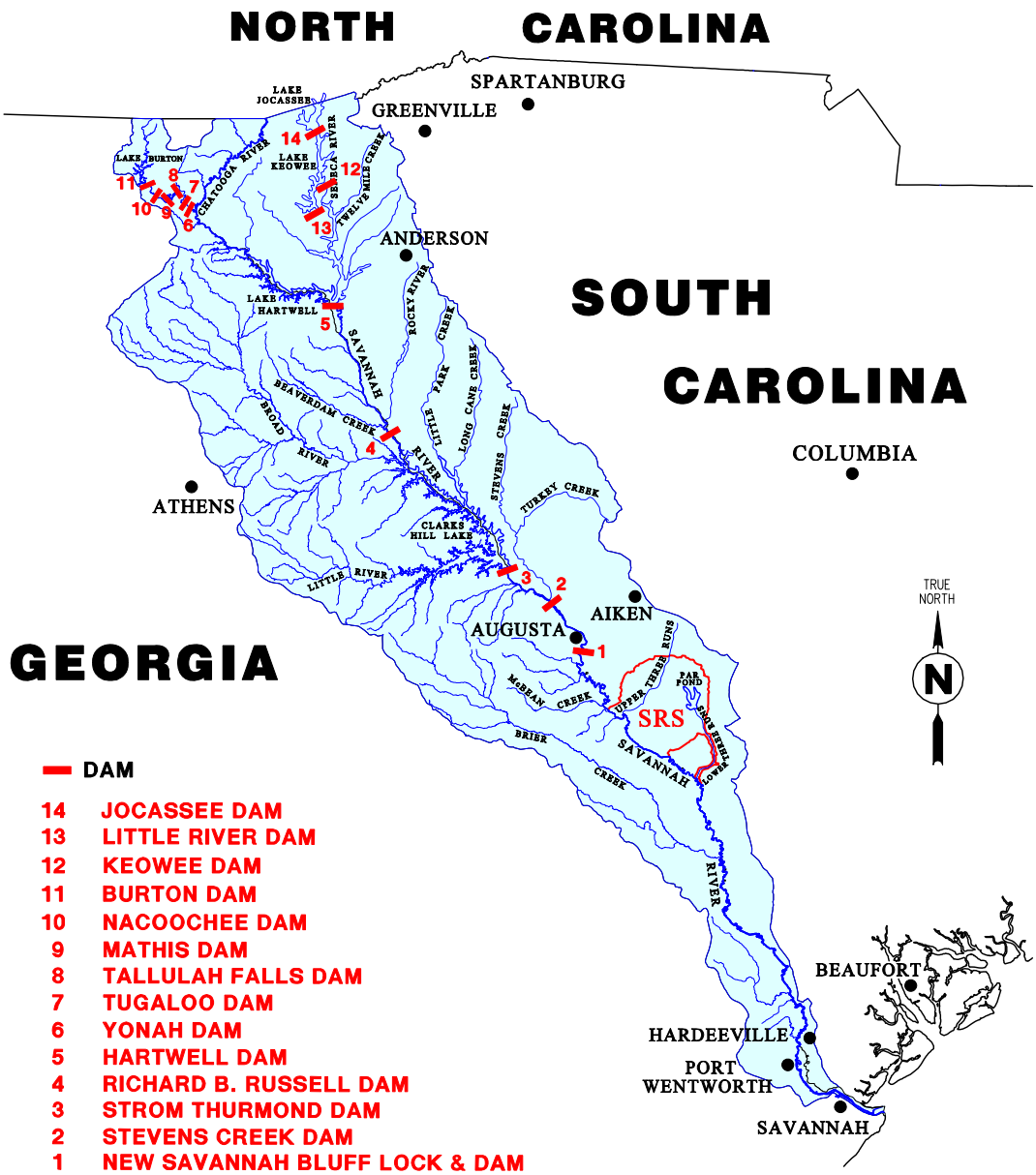

Figure 3.1-31: SRS Watershed Boundaries and Major Tributaries

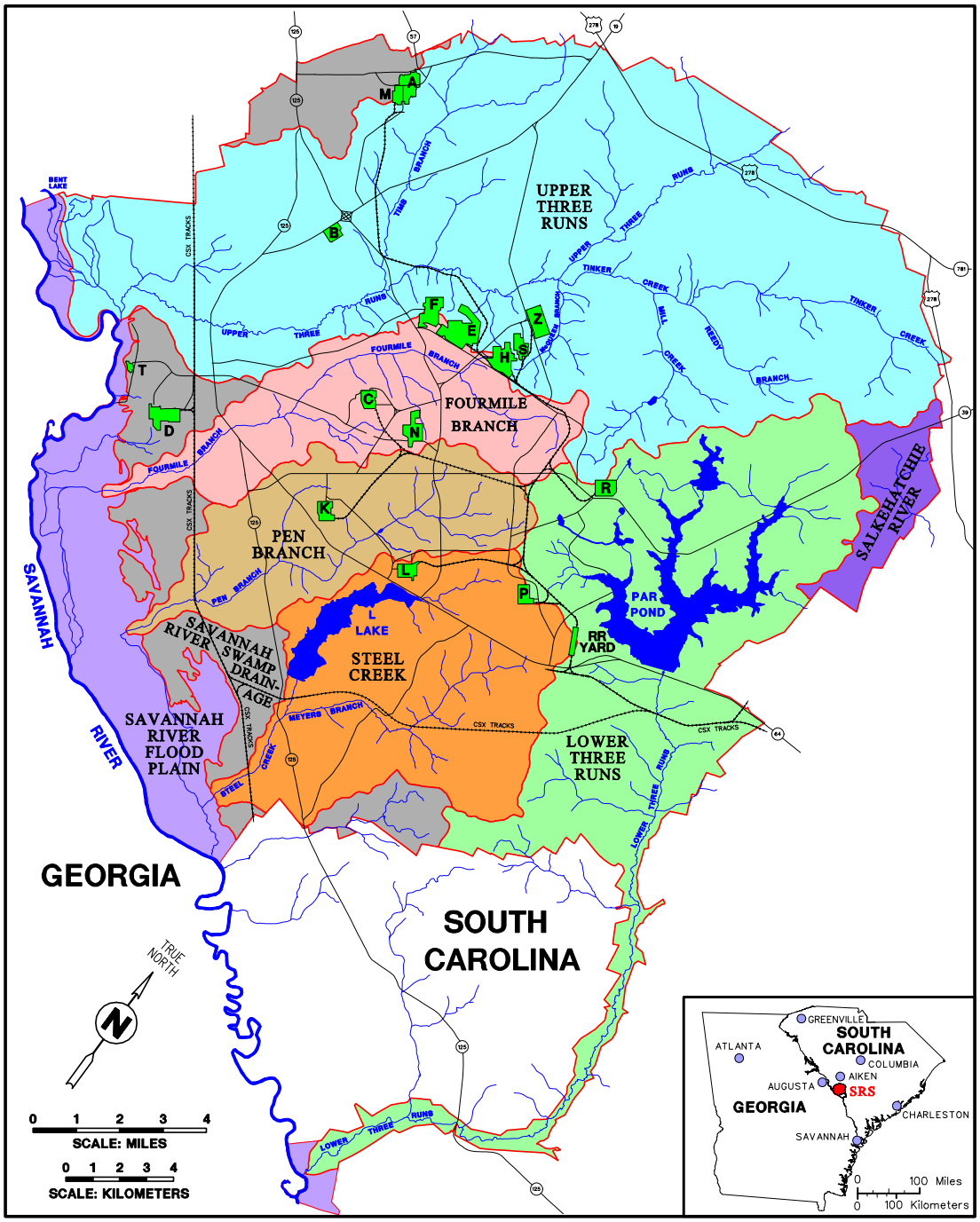

The natural flow of SRS streams ranges from 8 ft^3/s in smaller streams to 245 ft^3/s in UTR. [WSRC-IM-2004-00008] Gauging stations in the GSA (Figure 3.1-32) monitor flows for UTR and FMB. Both FMB and UTR are measured monthly for water flow, temperature, and quality. The annual *Savannah River Site Environmental Report for 2017* contains detailed information on flow rates and water quality of the Savannah River and the SRS streams. [SRNS-RP-2018-00470]

Figure 3.1-32: GSA Stream Gauging Stations

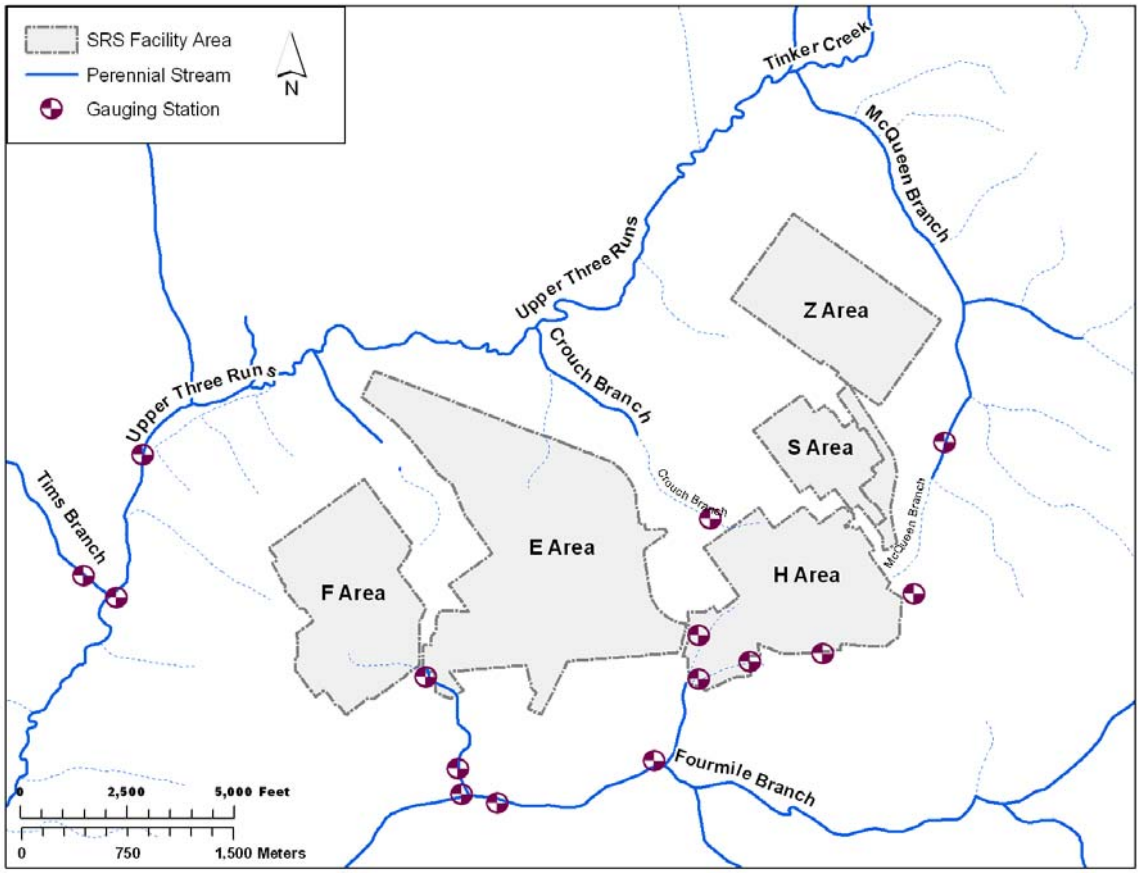

The South Carolina Department of Health and Environmental Control (SCDHEC) regulates the physical properties and concentrations of chemicals and metals in SRS effluents under the National Pollutant Discharge Elimination System (NPDES) program.

SCDHEC, which also regulates biological water quality standards for SRS waters, has classified the Savannah River and SRS streams as "Freshwaters." [DOE-EIS-0303] Freshwaters are defined as suitable for primary and secondary contact recreation and a source for drinking water supply after conventional treatment in accordance with SCDHEC requirements. Freshwaters are suitable for fishing, the survival and propagation of a balanced indigenous aquatic community of fauna and flora, and industrial and agricultural uses. [SCDHEC R.61-68]

The longest SRS stream, UTR, is a large blackwater stream in the northern part of the SRS that discharges to the Savannah River. It drains an area of over 195 square miles and is approximately 25 miles long, with its lower 17 miles within the SRS boundary. This stream receives more water from underground sources than other SRS streams and is the only stream with headwaters arising outside the site. The UTR is the only major tributary at SRS that has not received thermal discharges. [DOE-EIS-0303] The UTR stream valley has meandering channels, especially in the lower reaches, and its floodplain ranges in width from 0.25 to 1 mile. Its stream valley has a steep southeastern side and gently sloping northwestern side.

The FMB is a blackwater stream that originates near the center of SRS and flows southwest for 15 miles before joining the Savannah River. It drains an area of approximately 22 square miles inside SRS including much of F-, H-, and C-Areas. In its lower reaches, the FMB broadens and flows via braided channels through a delta formed during periods of high flow. Downstream of the delta, the channels rejoin into one main channel confined by natural levees that flow parallel to the Savannah River. The FMB joins the Savannah River through a breach in the levees downriver from Beaver Dam Creek. Most of the flow discharges in the Savannah River, while a small portion flows west and enters Beaver Dam Creek. [DOE-EIS-0303]

Probabilistic flood height elevation curves were calculated for seven SRS site areas for various runoff-discharge events from the UTR and FMB basins. For UTR near Z-Area, the mean flood water levels for the 100-, 1,000-, 10,000-, and 100,000-year events were approximately 152, 154, 156, and 160 feet above MSL, respectively. [WSRC-TR-99-00369] These elevations are well below the lowest SDF disposal unit elevation of 260 feet above MSL. The flood water levels are also well below the lowest elevation of the lower conceptual closure cap foundation layer, at the bottom of the side slope, and approximately 257 feet above MSL. [WSRC-STI-2008-00244] There was no flood threat to Z Area from the FMB, and therefore, flooding was not considered to be a concern for this PA.

Currently, SDF storm water drainage is diverted indirectly to McQueen Branch, which drains into Tinker Creek near its junction with UTR. Tinker Creek will be unaffected by SDF operations and closure activities. The installation of the SDF closure cap may necessitate changes to the SDF drainage system, which will be designed later as part of the overall closure of SDF.

3.1.5.5 Hydrologic Properties Specific to SDF

As noted previously, the geology below the SDF (from the surface down) consists of the partially saturated vadose zone, followed by the UTR Aquifer (which contains the Tan Clay Confining Unit), the Gordon Confining Unit and the Gordon Aquifer. The UTR Aquifer begins at the water table below the SDF. Various hydrologic parameters used for SDF modeling were taken from *Hydraulic Property Data Package for the E-Area and Z-Area Soils, Cementitious Materials, and Waste Zones*, WSRC-STI-2006-00198, and are discussed in more detail later in Section 4.3.1.

Porosity values for the SDF soils reflect laboratory measurements of the total volume of pore space in the soil samples. Since samples were collected from the vadose zone, where flow primarily occurs in the vertical direction perpendicular to strata, the total porosity was assumed to be roughly equivalent to the effective porosity. Bulk density corresponds to the dry bulk density or the total mass of dry soil per unit volume of material (including pore spaces). Particle density reflects the mass of dry soil particles per unit volume of soil particles (not including pore space). Porosity measurements ranged from 29% to 48%, averaging 39%; dry bulk density ranged from 1.37 g/cm^3 to 1.90 g/cm^3, averaging 1.6 g/cm^3; and particle density varied from 2.61 g/cm^3 to 2.81 g/cm^3, averaging 2.7 g/cm^3.

Saturated hydraulic conductivity values reflect an asymmetric relationship within the vadose zone, aquifer units, and confining units. Within the Vadose Zone, the horizontal hydraulic conductivity values range from 6.2E-05 cm/s to 3.3E-04 cm/s, while vertical hydraulic conductivity values range from 8.7E-06 cm/s to 9.1E-05 cm/s. For the UTR Aquifer, horizontal hydraulic conductivity values range from 5.3E-03 cm/s to 1.9E-03 cm/s, while vertical hydraulic conductivity values range from 1.7E-04 cm/s to 6.4E-05 cm/s. For the Gordon Aquifer Unit, the horizontal hydraulic conductivity values average 1.3E-02 cm/s, while vertical hydraulic conductivity values average 1.3E-04 cm/s.

Where it is present, the Tan Clay Confining Zone (which is not considered an effective barrier to the vertical migration of contaminants) has horizontal hydraulic conductivity values that average 2.1E-05 cm/s, while the vertical hydraulic conductivity values average 7.0E-07 cm/s. In contrast, the Gordon Confining Unit is considered an effective barrier to the vertical migration of contaminants. For the Gordon Confining Unit, the horizontal hydraulic conductivity values average 3.5E-08 cm/s, while vertical hydraulic conductivity values average 3.5E-09 cm/s. Additional details are presented in Section 4.4.6.

Values for soil water retention curves for various materials, including clay and clayey sand, are taken from *Hydraulic Property Data Package for the E-Area and Z-Area Soils, Cementitious Materials, and Waste Zones*, WSRC-STI-2006-00198.

3.1.6 Geochemistry

Migration of contaminants through the vadose zone and ground water can be greatly influenced by the geochemical conditions of the subsurface system. *Geochemical Data Package for Performance Assessment Calculations Related to the Savannah River Site*, SRNL-STI-2009-00473, contains geochemical data for SRS soils and includes recommendations for transport properties to use in contaminant transport modeling (K_d values). Properties are provided for various chemical conditions (e.g., oxidizing versus reducing environments, different pH conditions, etc.). The geochemical data used for transport modeling are described throughout Sections 4.3 and 4.4, and are not reproduced here.

Ground water monitoring is performed twice a year at the SDF at 22 monitoring wells, which includes 2 background wells. Ground water monitoring results are presented in *Z-Area Saltstone Disposal Facility Groundwater Monitoring Report for 2018*, SRNS-TR-2018-00292 and provides analytical data for a suite of contaminants, and well water data such as water level, pH, specific

conductance, total alkalinity, water temperature, and turbidity. For the 22 monitoring wells at the SDF in 2018, the average ground water pH reading was 5.7. [SRNS-TR-2018-00292] As part of the ground water monitoring report, the current geochemical characteristics are compared to historical values for the SDF to look for trends in changes that may indicate the potential for historical releases from the SDUs and to establish baselines for modeling.

3.1.7 Natural Resources

Natural resources at SRS are managed under the *Natural Resources Management Plan for the Savannah River Site*, prepared for DOE by the USDA Forest Service-Savannah River. [NRMP-2005] This plan, which governs SRS natural resource management, was updated in May 2005 and fosters the following principles:

- All work will be done in accordance with integrated safety management components found in DOE Policy 450.4A, *Integrated Safety Management Policy*;
- Environmental stewardship activities will be compatible with future SRS missions;
- SRS will continue to protect and manage SRS natural resources;
- Sustainable resource management will be applied to SRS natural resources;
- Close cooperation will be maintained among organizations when managing and protecting SRS natural resources;
- The results of research, monitoring and operational findings will be used in the management of SRS natural resources;
- Restoration of native communities and species will continue;
- Employees, customers, stakeholders, state natural resource officials, and regulators will be invited to participate in the natural resource planning process; and
- SRS will maintain the area as a National Environmental Research Park.

3.1.7.1 Water Resources

SRS monitors non-radioactive liquid discharges to surface waters through the NPDES permit program, as mandated by the Clean Water Act. As required by the EPA and SCDHEC, SRS has NPDES permits in place for discharges to the waters of the United States and South Carolina. These permits establish the specific sites to be monitored, water parameters to be tested and monitoring frequency, as well as collection, analytical, and reporting methods. Continuous surveillance monitoring of site streams occurs downstream of several process areas to detect and quantify levels of radioactivity in effluents transported to the Savannah River. General summaries of the monitoring are available to the public in the SRS annual Environmental Report for 2017. [SRNS-RP-2018-00470] Table 3.1-3 characterizes Savannah River water quality both upstream and downstream of SRS. Table 3.1-4 characterizes water quality in UTR and FMB downstream of the GSA and Z-Area.

Table 3.1-3: Water Quality in the Savannah River Upstream and Downstream from SRS (CY2017)

Parameter	Unit of Measure	Upstream[b]		Downstream[c]	
		Minimum	Maximum[a]	Minimum	Maximum[a]
Aluminum	mg/L	<0.040	0.609	0.0671	0.711
Cadmium	mg/L	<0.0005	0.00127	<0.0005	0.00433
Chromium	mg/L	<0.0020	<0.0020	<0.0020	0.00318
Copper	mg/L	<0.0002	0.00724	<0.0020	0.00338
Dissolved Oxygen	mg/L	7.23	10.23	6.22	10.66
Gross Alpha Radioactivity	pCi/L	ND	0.457	ND	0.543
Lead	mg/L	<0.0100	<0.0100	<0.0100	<0.0100
Mercury	µg/L	<0.0200	<0.0200	<0.0200	<0.0200
Nickel	mg/L	<0.0030	0.00337	<0.0030	<0.0030
Nitrate (as N)	mg/L	0.159	0.624	0.199	0.786
pH	pH units	5.27	7.92	6.42	7.65
Phosphorous	mg/L	0.086	0.210	0.086	0.380
Suspended Solids	mg/L	3	15	6	17
Temperature	°C	9.4	26.2	8.7	28.0
Tritium	pCi/L	ND	263	148	1,930
Zinc	mg/L	0.00271	0.0231	0.00331	0.0188

Notes: All data from SRNS-TR-2018-00099, which accompanies the annual SRS Environmental Report SRNS-RP-2018-00470. Parameters are those the DOE routinely measures as a regulatory requirement or as part of ongoing monitoring programs.

ND Not Detected

[a] The maximum listed concentration is the highest single result found during the 12-month sampling period

[b] Data from sampling location RM-160

[c] Data from sampling location RM-118.8

Table 3.1-4: Water Quality in Selected SRS Streams (CY2017)

	Temperature (°C)	pH	Dissolved Oxygen (mg/L)	Total Suspended Solids (mg/L)
Sampling Location: FMB (Downstream from GSA)[a]				
Mean	17.5	7.23	8.89	7.33
Range	6.4 – 25.6	6.27 – 8.11	7.08 – 11.78	1 – 35
Sampling Location: UTR (Downstream from GSA)[b]				
Mean	17.4	7.30	8.70	9.17
Range	8.8 – 25.8	6.73 – 7.96	6.92 – 11.50	2 – 25

Notes: All data from SRNS-TR-2018-00099, which accompanies the annual SRS Environmental Report SRNS-RP-2018-00470.

[a] Stream sample location FMC-6

[b] Stream sample location U3R-4

3.1.7.1.1 Ground Water

The Federal Safe Drinking Water Act was enacted in 1974 to protect public drinking water supplies. The SRS domestic water is supplied by 17 separate systems, all of which use ground water sources. The A-Area drinking water system supplies most site areas. Remote facilities, such as field laboratories, barricades, and pump houses, use small drinking water systems or bottled water.

The SCDHEC requires SRS to collect 10 bacteriological samples each month from the domestic system that supplies most areas at SRS. SRS exceeds this requirement by collecting 15 samples per month from various areas. SRS also samples the domestic water systems for lead and copper on a three-year rotating cycle. [SRNS-RP-2018-00470]

Table 3.1-5 provides a summary of the most recent maximum ground water monitoring results for those areas that most likely discharge to UTR. The *Savannah River Site Environmental Report for 2017,* (SRNS-RP-2018-00470), contains the latest annual summary of monitoring well ground water sampling results summarized by area. The ground water in these areas is not being consumed and active remediation projects are in progress to address ground water contamination conditions.

Table 3.1-5: Monitoring Well Results for Major Areas within SRS (2017)

Location	Major Contaminants	Units	2017 Maximum Concentration	Maximum Contaminant Level (MCL)	Likely Stream Endpoint
E-Area	Trichloroethylene	µg/L	500	5	UTR/Crouch Branch in North; FMB in South
	1,4-Dioxane	µg/L	690	6.1[a]	
	Tritium	pCi/L	20,600,000	20,000	
	Gross Alpha	pCi/L	17.9	15	
	Nonvolatile Beta	pCi/L	45.8	50	
F-Area	Trichloroethylene	µg/L	29.4	5	UTR/Crouch Branch in North; FMB in South
	Tritium	pCi/L	70,500	20,000	
	Gross Alpha	pCi/L	1,160	15	
	Nonvolatile Beta	pCi/L	844	50[b]	
F-Area Hazardous Waste Management Facility (HWMF)	Trichloroethylene	µg/L	17	5	FMB
	Tritium	pCi/L	1,460,000	20,000	
	Gross Alpha	pCi/L	479	15	
	Nonvolatile Beta	pCi/L	921	50[b]	
H-Area	Trichloroethylene	µg/L	4.92		UTR/Crouch Branch in North; FMB in South
	Tritium	pCi/L	28900	20,000	
	Gross Alpha	pCi/L	56.5	15	
	Nonvolatile Beta	pCi/L	99.1	50[b]	
H-Area HWMF	Trichloroethylene	µg/L	134	5	FMB
	Tritium	pCi/L	1,460,000	20,000	
	Gross Alpha	pCi/L	56.5	15	
	Nonvolatile Beta	pCi/L	99.1	50[b]	
Z-Area	Technetium-99	pCi/L	126	50[b]	UTR
	Nonvolatile Beta	pCi/L	51.9	50[b]	

[SRNS-RP-2018-00470]

[a] The 1,4 Dioxane MCL is a RCRA Permitted Ground Water Protection Standard.

[b] The MCL for nonvolatile beta activity (pCi/L) equivalent to 4 mrem/yr varies according to the specific beta emitters present in the sample. At SRS, this value equates to 50 pCi/L.

It should be noted that these are maximum values generally associated with wells very close to the contaminant source areas and not stream concentrations. By the time the ground water reaches a stream it has lower contaminant concentrations because of natural attenuation processes.

Continued environmental monitoring, one of the required conditions in the modified Class 3 landfill permit for the SDF, ensures the timely response to any potential impacts to the ground water. [DHEC_09-09-2008] Environmental monitoring requirement include:

- Maintaining a ground water detection monitoring system,
- Collecting and analyzing ground water samples in accordance with an approved ground water monitoring plan,
- Assessing and implementing corrective actions for any ground water impact, and
- Providing semi-annual, annual, and biennial reports on the results of the ground water monitoring analyses. [DHEC_09-09-2008]

3.1.7.2 Geologic Resources

The SRS is located on the Atlantic Coastal Plain where economical geologic resources are limited to depositional materials such as sand, gravel, clay, carbonate, and phosphate. Economic geologic resources at the SRS are limited to sand from borrow pits. No economic deposits of clay, usually in the form of kaolinite, have been identified within the SRS boundary. [ISBN: 1-59726-010X] The nearest deposits of mineable kaolinite are restricted to the area of the Atlantic Coastal Plain adjacent to the Fall Line, approximately 15 miles northwest of the SRS.

Based on hundreds of geologic borings throughout SRS, local carbonate horizons do exist; however, there are no economically viable carbonate horizons located below the SDF. [ISBN: 1-59726-010X] Within the SRS, these horizons are limited to the southeastern portion of the site, at depths of 200 feet or more below ground the surface. [PIT-MISC-0112] The nearest economical deposits of carbonate are located approximately 50 miles southeast of the SRS, near Eutawville, SC at the Martin-Marietta Berkeley Quarry.

Although phosphates are common in Coastal Plain sediments, extractable quantities are restricted to areas of the South Carolina Low Country, near Charleston, SC, approximately 100 miles to the southeast of the SRS. [ISBN: 1-59726-010X]

3.1.8 Natural and Background Radiation

All human beings are exposed to ionizing radiation that includes naturally occurring and man-made sources. An individual's average dose contribution estimates from various sources were obtained from the review information presented in NCRP Report 160 and are shown in Figure 3.1-33. A person living in the United States receives an annual radiation dose, on average, of approximately of 620 mrem/yr. [NCRP-160] The dose from SRS operations to the representative person during calendar year 2017 was estimated to be 0.25 millirem. [SRNS-RP-2018-00470]

Figure 3.1-33: Major Sources of Radiation Exposure near SRS

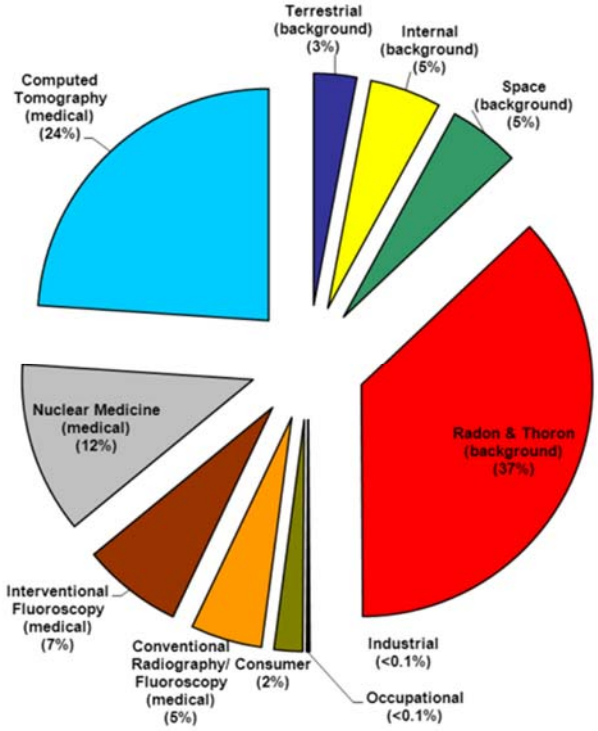

The major sources of radiation exposure to an average MOP are attributed to naturally occurring radiation (311 mrem/year) and medical exposure (300 mrem/year). This naturally occurring radiation is often referred to as natural background radiation and includes dose from background radon and its decay products (37%), space (cosmic) radiation (5%), internal radionuclides occurring naturally in the body (5%), and natural radioactive material in the ground (3%). The dominant medical sources include dose from computed tomography (24%), nuclear medicine (12%), and interventional and conventional radiography/fluoroscopy (12%). The remainder of the dose is from consumer products (2%), industrial/educational/research activities (0.1%), and occupational exposure (0.1%). [NCRP-160]

3.2 Principal Facility Design and Operational Features

The principal design features described herein provide nominal or approximate values for the design dimensions relevant to modeling and should not be used as a basis for construction or quality-related activities. The appropriate engineering documents and design drawings should be consulted for more detail (e.g., design tolerances) of the actual construction of the SDUs.

The Saltstone Facility consists of two facility segments located in Z-Area; (1) the SPF, which receives and mixes the salt solution and dry feeds to produce saltstone, and (2) the SDF, which consists of disposal units used for the final disposition of the saltstone.

The SDF currently consists of existing SDUs 1, 2, 3, 4, 5, and 6 and is modeled to include six additional 375-foot diameter SDUs. In the 2009 SDF PA, the SDUs are identified as Vault 1 for SDU 1, Vault 4 for SDU 4, and Future Disposal Cells for the 150-foot diameter cylindrical SDUs

(SDUs 2, 3, and 5). SDU 6 and future SDUs 7 through 12 consist of 375-foot diameter cylindrical SDUs. Figure 3.2-1 provides an aerial view of the SDF, including the locations of SDUs 1, 2, 3, 4, 5, and 6. SDU 7 construction activities began in 2018.

Figure 3.2-1: SDF Aerial View

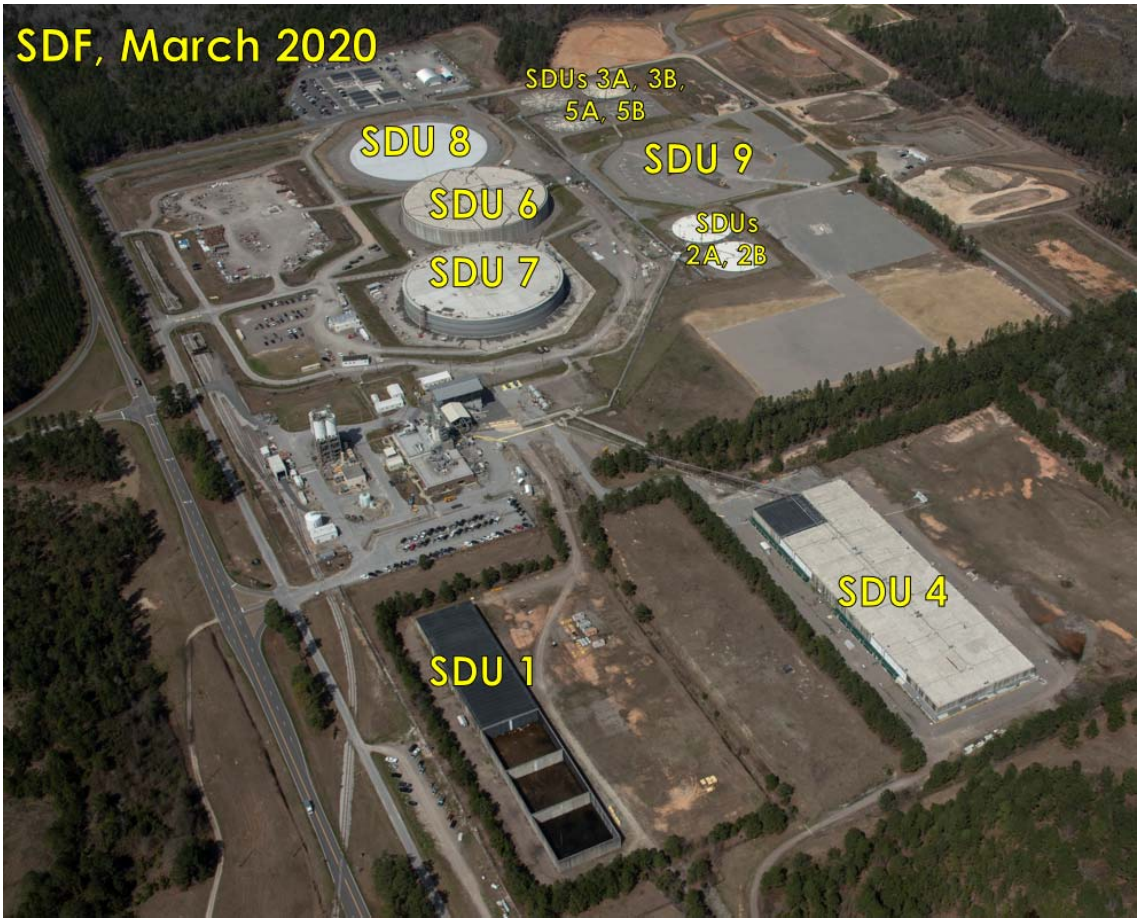

Above grade support structures, utilities, and equipment will be removed from the SDF and SPF prior to installation of the closure cap. Thus, no ancillary equipment or material inventory that would impact the PA modeling will remain prior to final closure. Figure 1.5-1 provided an anticipated layout of the SDF current and future SDUs placement as modified from *Future Saltstone Disposal Units Siting – Systems Engineering Evaluation*, G-AES-S-00004. The light pink dotted line around the SDUs represents the 1-meter boundary to be used for PA modeling. The solid thin red line around the SDUs represents the 100-meter boundary to be used for PA modeling.

3.2.1 SDU 1

SDU 1 is an above-grade, rectangular, reinforced concrete disposal unit divided into six equal individual cells. The walls and floor of the SDU are reinforced concrete and designed for gravity loads. A rolling roof was originally installed on SDU 1, but has since been removed (see Figure 3.2-2 and Figure 3.2-3). Cells A, B, and C have been filled with saltstone, clean capped with grout,

and the permanent roof sealed. Figure 3.2-2 shows SDU 1 prior to the construction of the permanent roof. Figure 3.2-3 shows SDU 1 current conditions.

3.2.1.1 SDU 1 History

SDU 1 was constructed between 1986 and 1988 in two phases; (1) the working slab, foundation, interior walls, and exterior walls, and (2) the permanent roof (only on cells that contain waste, Cells A, B and C). SDU 1 experienced cracks from construction and operational events dating back to 1988. The report ESH-WPG-2006-00132, *Z-Area Industrial Solid Waste Landfill Vault Cracking*, provides a history of the cracking experienced with SDU 1 and the repairs and remediation actions conducted to limit future weeping from the SDU. The general mechanism for water weeping from the cracks in the SDU 1 walls stems from construction cracks and/or that of hydrostatic forces on the wall from the accumulation of water in the gap that formed between the saltstone monolith and the SDU wall. The sources of water within the gap were from rainwater intrusion, bleed water from the saltstone curing process, and flush water from cleaning the transfer lines after a saltstone transfer into the SDU. To limit further accumulation of rainwater in the gap between the saltstone monolith and the SDU walls, a foam sealant was installed in the gap between the SDU roof and the wall, flashing was installed over the edge of the SDU roof and wall, and an ethylene propylene diene monomer membrane was applied over the entire roof surface. In addition, a polymer sealant was applied to the inside surface of the outside walls of the remaining cells to seal any shrinkage cracks developed during the saltstone curing process. [ESH-WPG-2006-00132]

Environmental monitoring, discussed in Section 3.1.7, ensures the timely response to any potential impacts to the ground water resulting from SDU 1 weepage.

3.2.1.2 SDU 1 Dimensions

SDU 1 is approximately 600 feet long, 100 feet wide, and 27 feet high. The SDU is divided into two units, each 100 feet by 300 feet, with a 3-inch separation gap between the units. Each unit is further divided into three cells of approximately 100 feet by 100 feet. The 100-foot dimension is taken from the centerline of 18-inch thick concrete walls; thus, the interior dimensions of the cells are 98 feet, 6 inches. [ESH-WPG-2006-00132] Figure 3.2-3 provides an exterior photograph of SDU 1, Figure 3.2-4 and Figure 3.2-5 provide plan and elevation view design drawing information for the disposal unit, and Figure 3.2-6 provides a conceptual model cross section of the disposal unit model input, including the saltstone and clean cap grout.

The SDU 1 system filled with saltstone consists of the following from lowest elevation to highest elevation:

- Controlled compacted backfill soil base,
- 4-inch thick concrete working slab,
- 24-inch thick reinforced concrete floor slab,
- 18-inch thick reinforced concrete walls,

- 24 feet of saltstone poured into the cell from above,
- Minimum 6-inch thick clean cap grout, and
- Poured-in-place concrete roof with approximately 2% slope. [W780625, C-CC-Z-0010, WSRC-STI-2006-00198]

Figure 3.2-2: SDU 1 and SDU 4 Arrangement after Initial Construction

[LWO-CES-2006-00010]

Figure 3.2-3: SDU 1 Exterior View

[SRR-CWDA-2009-00050]

Figure 3.2-4: SDU 1 Plan View

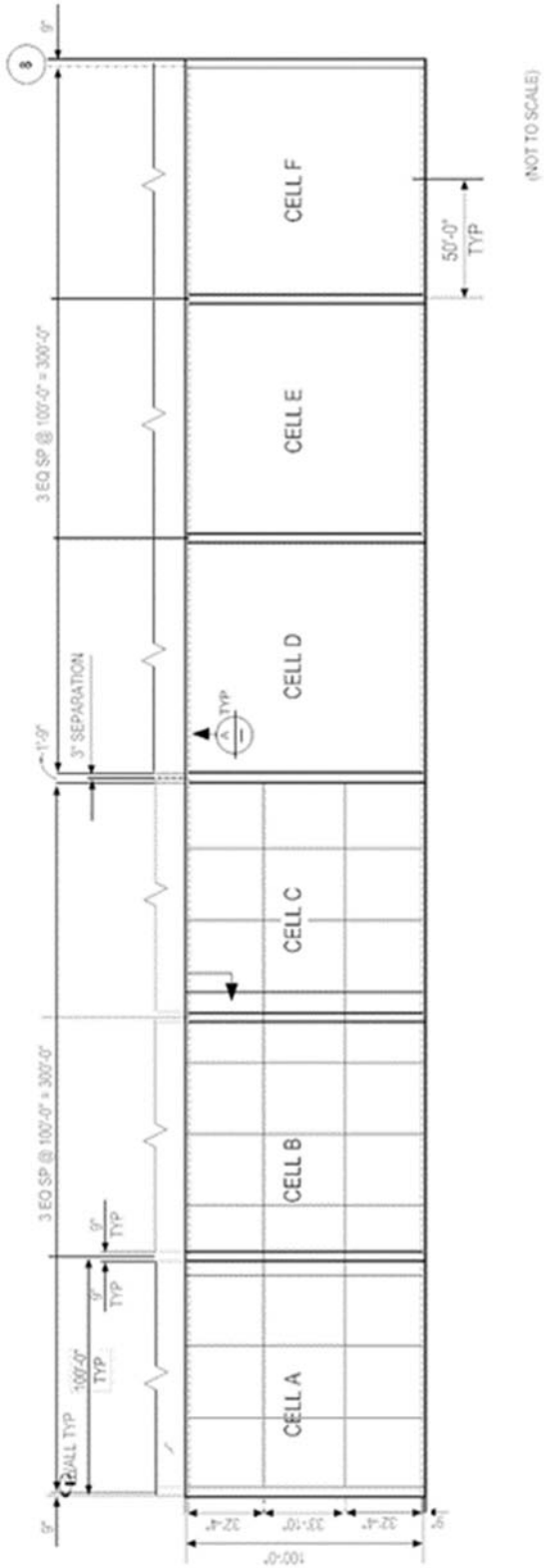

[W780625]

Figure 3.2-5: SDU 1 Interior Elevation Marks

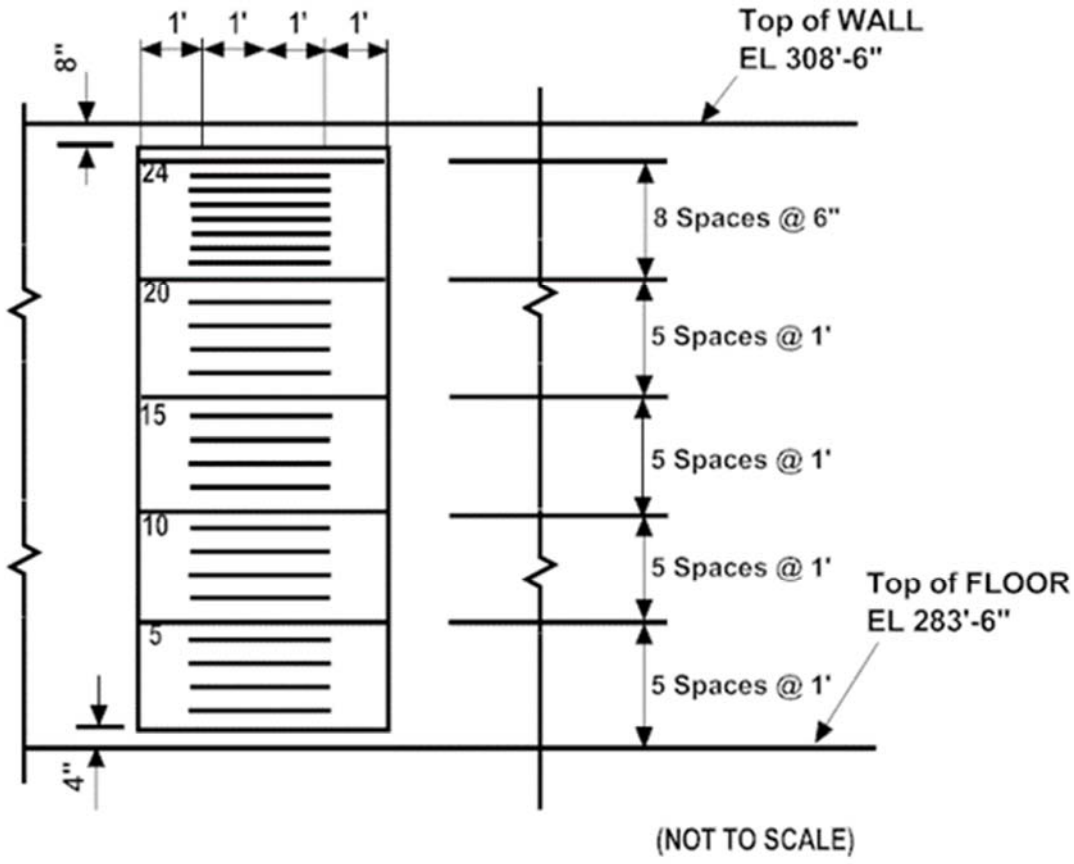

[W780625]

Figure 3.2-6: SDU 1 Conceptual Model Cross Section

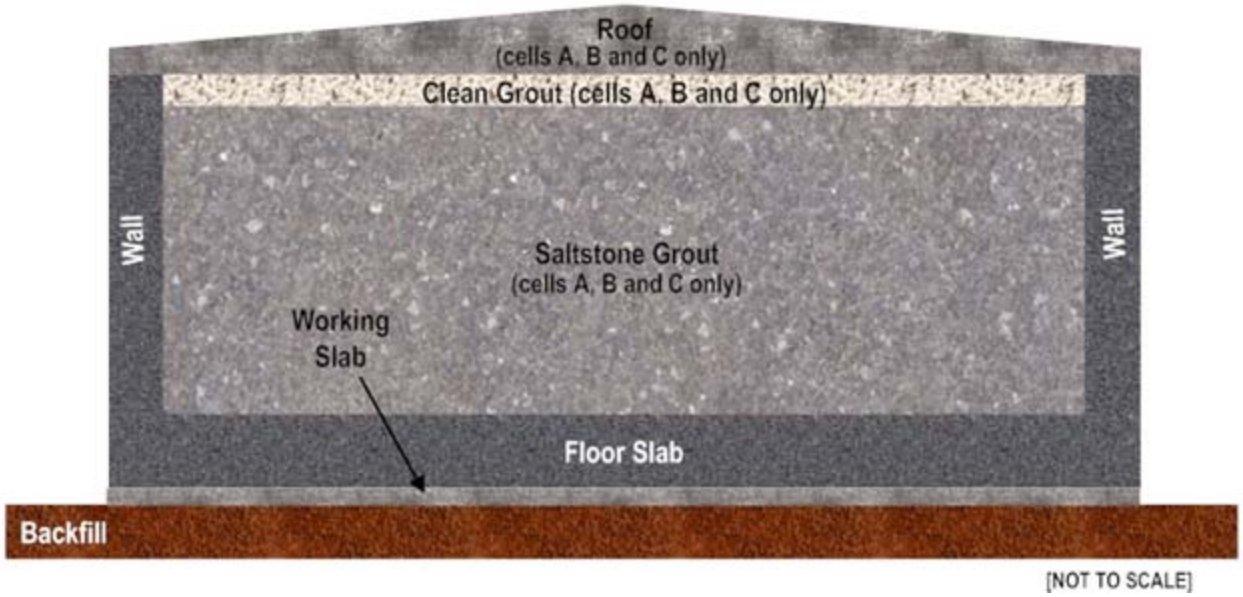

[SRR-CWDA-2013-00037]

3.2.1.3 SDU 1 Concrete Specification

The concrete formulations used in the foundation and walls of SDU 1 are presented in Table 3.2-1.

Table 3.2-1: SDU 1 Concrete Formulations

Ingredient	Working Slab Quantity (lbs/yd^3)	Floor Slab and Walls Quantity (lbs/yd^3)	Roof Quantity (lbs/yd^3)
Type II ASTM C 150 Cement	413	419	400
Grade 120 ASTM C 989 Blast Furnace Slag	0	278	0
Type F ASTM C 618 Fly Ash	73	0	70
Sand ASTM C 33	1,356	1,133	1,149
No. 67 ASTM C 33 Aggregate (maximum 0.75 inches)	1,698	1,798	1,900
Water (maximum)	272 (32.6 gal/yd^3)	268 (32.1 gal/yd^3)	292 (35.0 gal/yd^3)
Water to Cementitious Material Ratio	0.56	0.385	0.62
Minimum Compressive Strength at 28 days	2,000 psi	4,000 psi	3,000 psi

[WSRC-STI-2006-00198]
ASTM = American Society for Testing and Materials

3.2.1.4 SDU 1 Roof, Wall, and Base

The SDU 1 roof has a minimum thickness of 6 inches and is poured-in-place concrete with approximately 2% slope. Cells A, B, and C have been filled and the permanent roof installed. Cells D, E, and F contain no saltstone and have no roof (see Figure 3.2-3). The 18-inch thick wall, and 24-inch thick floor slab are reinforced concrete with a minimum compressive strength of 4,000 psi. The working slab, with a thickness of 4 inches, has a minimum compressive strength of 2,000 psi. [W780625] Water stops were used during the construction of the floors and the wall-to-floor interface.

Figure 3.2-4 presents a portion of the floor design for SDU 1. The grid shows half of the 60 constructed concrete floor sections. The total length of the floor construction joints in SDU 1 is approximately 3,000 feet. [W780625] Water stops are also included along the interface of all interior and exterior wall-to-floor joints for a total of 2,000 linear feet. The total length of these construction joints is 5,000 feet. [SRR-CWDA-2013-00064] The construction joints are modeled as fast-flow zones within the SDU 1 floor and wall-to-floor interface. [SRR-CWDA-2013-00062]

3.2.2 SDU 4

3.2.2.1 SDU 4 History

The original construction of SDU 4 was performed between 1986 and 1988, and at that time SDU 4 was referred to as Vaults 6 and 7. Construction of SDU 4 includes 12 cells consisting of the working slab, floor slab, exterior walls, and interior walls. The walls and

floor slab of the SDU are constructed of reinforced concrete. In 1996, prior to starting waste disposal operations into SDU 4, a rolling roof (similar to that on SDU 1) was replaced with a permanent roof to provide operational flexibility. This allowed for more than two partially filled cells at any one time and reduced potential rainwater intrusion. The permanent concrete roof was painted with a dura-cool coating for heat dissipation/reflection, not as a waterproof coating. However, the roof joints allowed small amounts of rainwater to enter the SDU cells and the addition of bleedwater from disposal operations continued to occur. This resulted in wall cracking similar to that experienced in SDU 1. Therefore, roof joint sealing and cell draining was instituted to remediate the liquid accumulation. Figure 3.2-2 shows SDU 4 prior to the construction of permanent roof. [LWO-CES-2006-00010]

Cell A contains 10,000 drums of Fuel Material Facility (FMF) non-hazardous saltcrete generated from the operation of the Waste Water Treatment Facility (WWTF) at FMF. [OPS-DTZ-90-0027] This inventory has been included in the SDU 4 inventory accounting in Section 3.3. The metal 55-gallon drums were completely filled with contaminated waste by combining the liquid FMF WWTF waste with a dry concrete mix in a batch mixer and pouring into the drums. The void space in Cell A surrounding the drums is filled with clean grout.

Eight cells in SDU 4 have been modified with a drain water management system designed to relieve the hydrostatic head on the SDU walls. This drain water management system, detailed in Section 3.2.2.5, collects any liquid that may appear between the solidified saltstone and the SDU wall, returning the liquid through pipes to the SPF to be used in the production of saltstone. [CBU-ENG-2003-00103]

Environmental monitoring, discussed in Section 3.1.7.1, ensures the timely response to any potential impacts to the ground water resulting from SDU weepage.

3.2.2.2 SDU 4 Dimensions

SDU 4 is an above-grade, rectangular, reinforced concrete SDU. It is approximately 600 feet long, 200 feet wide, and 27 feet high at the exterior wall. SDU 4 is divided into two units each, 200 feet by 300 feet, with a 3-inch separation gap between the units. Each unit is further divided into six cells with a footprint of approximately 100 feet by 100 feet. Thus, SDU 4 is comprised of twelve 100 feet by 100 feet cells. The 100-foot dimension is taken from the centerline of 18-inch thick concrete walls; the interior dimensions of the cells are 98 feet, 6 inches. Figure 3.2-7 provides an exterior view of SDU 4, Figure 3.2-8 provides a roof plan design drawing view, and Figure 3.2-9 provides a cross section view (the saltstone and clean cap grout are not shown for clarity). [W828992, C-CC-Z-0013, WSRC-STI-2006-00198]

The SDU 4 system, when filled with saltstone, consists of the following from lowest elevation to highest:

- Controlled compacted backfill soil base,
- 4-inch thick concrete working slab,

- 2-foot thick reinforced concrete floor slab,
- 18-inch thick reinforced concrete walls,
- 10-inch diameter carbon steel roof support columns filled with lean concrete (except in Cell A),
- Drain water management system (except in Cells A, C, G, and I),
- 24 feet, 9 inches (maximum) of saltstone poured in from the center of the cell roof (except Cell A),
- Drums of low-activity waste encapsulated by clean cap grout (Cell A only),
- Minimum 15-inch thick clean cap grout (all cells),
- Poured-in-place concrete over steel decking roof with approximately 2% slope (except Cell A), and
- Concrete encased wire mesh roof with approximately 2% slope (Cell A only). [C-CC-Z-0013, C-CS-Z-0002, WSRC-STI-2006-00198, W828992, W828993]

Figure 3.2-7: SDU 4 Exterior View

[SRR-CWDA-2013-00037]

Figure 3.2-8: SDU 4 Roof Plan View

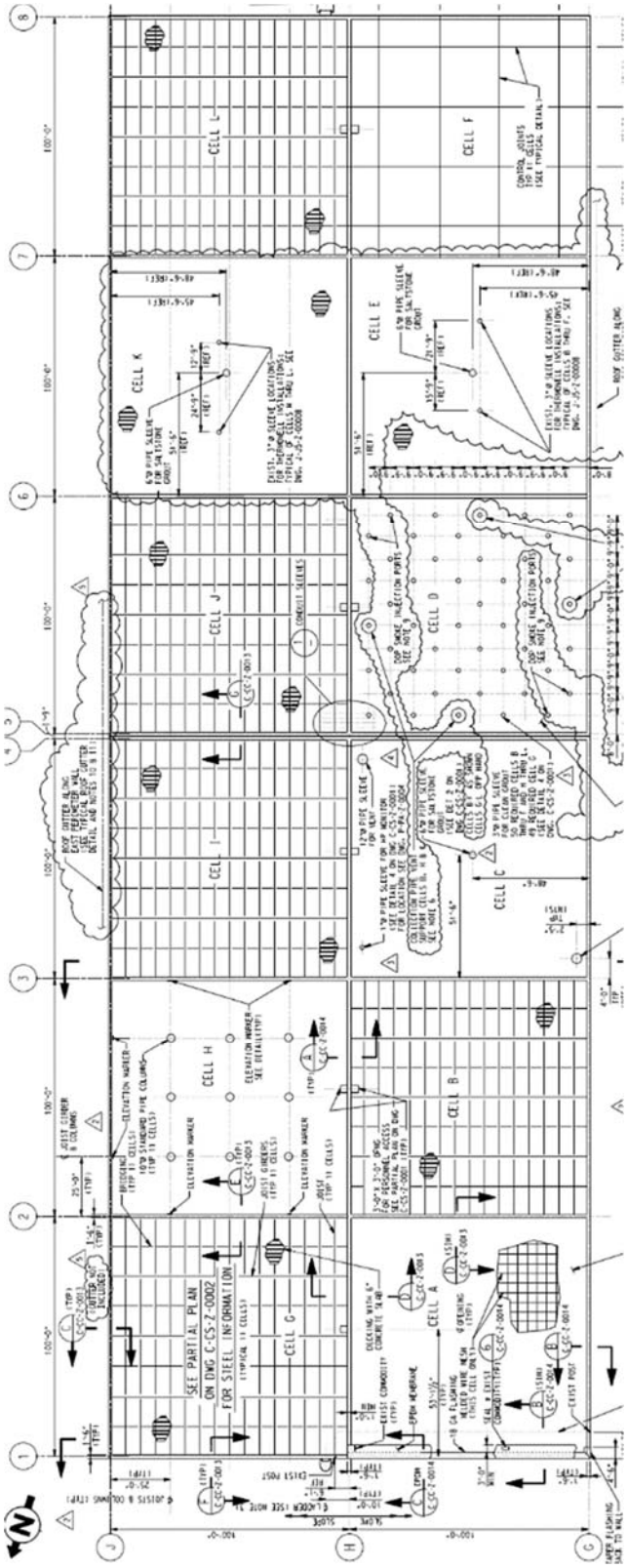

[Cropped from C-CC-Z-0012. For full notes and details, refer to the referenced design drawing.]

Figure 3.2-9: SDU 4 Cross Section

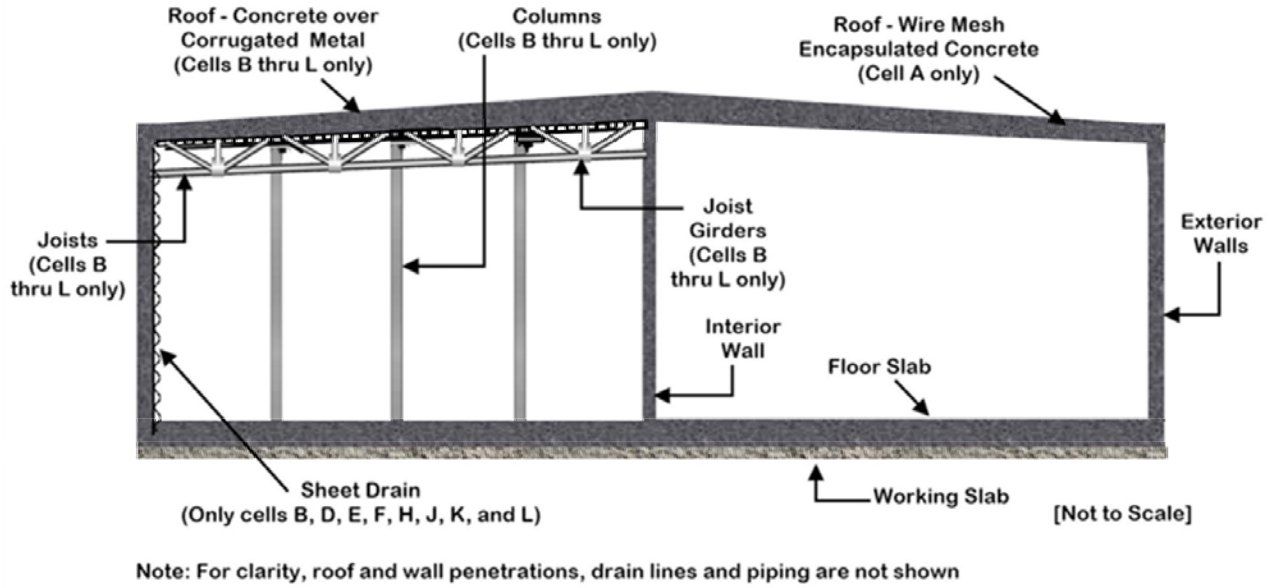

[W828993, C-CC-Z-0012, C-CS-Z-0002]

3.2.2.3 SDU 4 Concrete Specifications

The concrete formulations used in the working slab, floor slab, walls, and roof of SDU 4 are presented in Table 3.2-2.

Table 3.2-2: SDU 4 Concrete Formulations

Ingredient	Working Slab Quantity (lbs/yd³)	Floor Slab and Walls to 25 feet Quantity (lbs/yd³)	Walls above 25 feet and Roof (lbs/yd³)
Type II, ASTM C150 Cement	413	419	466
Grade 120, ASTM C 989 Blast Furnace Slag	0	278	0
Type F, ASTM C 618 Fly Ash	73	0	62
ASTM C 33 Sand	1,356	1,133	1,190
No. 67, ASTM C 33 Aggregate (maximum 0.75 inches)	1,698	1,798	1,800
Water (maximum)	273 (32.7 gal/yd³)	254 (30.4 gal/yd³)	296 (35.5 gal/yd³)
Water to Cementitious Material Ratio	0.56	0.36	0.56
Minimum Compressive Strength at 28 days	2,000 psi	4,000 psi	4,000 psi

[WSRC-STI-2006-00198]
ASTM = American Society for Testing and Materials

3.2.2.4 SDU 4 Walls, Columns, and Floor

The initial walls and floor slab of the SDU are made of reinforced concrete construction with the walls designed for gravity loads plus the hydrostatic head associated with the saltstone. The original wall height for SDU 4 was 25 feet. In 1996, the walls of the SDU

(exterior and interior) were extended 1 foot, 6 inches in height to allow for the installation of a concrete roof. The exterior and interior SDU walls are 18 inches thick. [WSRC-STI-2006-00198]

Each SDU 4 cell contains two or three 1-inch diameter through-wall drain lines in the bottom of an exterior wall. A 2-inch diameter through-wall, schedule 40 stainless steel pipe penetrates the exterior wall of Cells B, D, E, F, H, J, K, and L in order to transfer the collected liquids in the sheet drain system from inside the cell to the SPF. Finally, partial penetrations exist in SDU 4 exterior walls from anchor bolts used for ladders and pipe supports. [WSRC-STI-2006-00198]

Cells B through L each contain nine equally spaced roof support columns comprised of concrete filled 10-inch diameter schedule 40 carbon steel pipes (Figure 3.2-8 and Figure 3.2-11). [C-CS-Z-0002, C-CC-Z-0012] The floor is a 2 foot reinforced concrete slab, which was placed on top of a separate 4 inch concrete working slab (see Table 3.2-2 for concrete formulations). [WSRC-STI-2006-00198]

Similar to the construction of SDU 1, SDU 4 also included water stops as part of the construction of the floor and the wall-to-floor interface. Figure 3.2-10 presents a portion of the floor design, showing the floor for six of the 12 cells within SDU 4. The grid shows half of the 120 constructed concrete floor sections. The total length of the floor construction joints in SDU 4 is 6,012 linear feet ((8 × 301.5 feet) + (18 × 200 feet)). [W828992] Water stops are also included along the interface of all interior and exterior wall-to-floor joints for a total of 2,806 linear feet. In total, there are 8,818 linear feet of construction joints in SDU 4. [SRR-CWDA-2013-00064] The construction joints are modeled as fast-flow zones within the SDU 4 floor and wall-to-floor interface. [SRR-CWDA-2013-00062]

3.2.2.5 SDU 4 Drain Water Management System

The drain water management system consists of the sheet drains placed against the SDU walls (both interior and exterior) and a polyvinyl chloride (PVC) piping system that collects the water for transfer back to SPF to be re-fed into the dry feeds mix used for saltstone.

Cells B, D, E, F, H, J, K, and L have sheet drains (polystyrene sheet with 0.437-inch dimples covered on one side and a non-woven, needle-punched polypropylene filter fabric on the other side) installed on the walls to limit the buildup of hydrostatic head by collecting drain water and condensate from the cells. [WSRC-STI-2006-00198]

The sheet drains were installed to mitigate potential cracking of the SDU walls due to hydrostatic head created by drain water. The sheet drain collects free water that accumulates in the narrow gap between the SDU wall and the saltstone waste form. The sheet drain also acts as a barrier to keep water away from the wall. [WSRC-STI-2006-00198]

The drain water collection system will be emptied, filled with grout to the extent practical, and will permanently remain in place within the SDU after the operational period. The

external drain water collection system valve assemblies will be removed, and the holes plugged. [CBU-ENG-2003-00103]

Figure 3.2-10: SDU 4 Floor Construction Sections

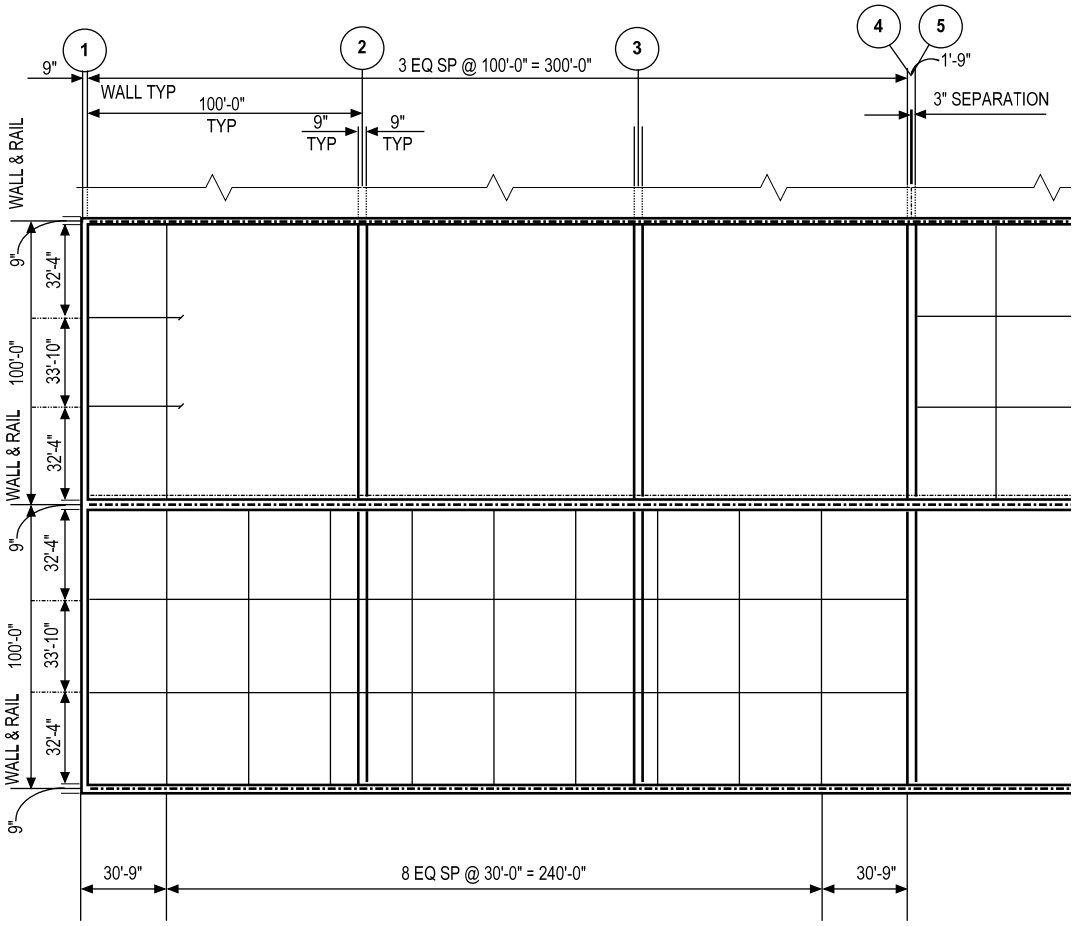

[W828992]

3.2.2.6 SDU 4 Roof

Cell A of SDU 4 contains drums of low-activity U.S. Naval fuel waste that have been filled with concrete. The cell was filled with grout, and covered with a roof comprised of wire mesh and a 3-inch concrete topping. [C-CC-Z-0013] At least 15 inches of clean cap grout exists between the waste drums and the concrete topping below the top of the cell. [C-CC-Z-0012]

The remaining cells in SDU 4 are covered with a sloped (approximately 2%) permanent roof consisting of a minimum 6-inch thick poured-in-place concrete slab over 20-gauge corrugated metal decking. The roof is supported by steel joists and 10-inch diameter standard pipe columns filled with lean concrete. The roof is painted with a dura-cool coating to help heat dissipation/reflection. [C-CS-Z-0002, WSRC-STI-2006-00198]

SDU 4 contains the following roof penetrations in the roof of each cell (except for Cell A whose roof contains no penetrations):

- 50, 3-inch diameter pipe sleeves per cell for the clean cap pour (49 in Cell G),
- Two, 12-inch diameter pipe sleeves per cell for venting,
- One, 6-inch diameter pipe sleeve per cell for pouring saltstone,
- One, 3-foot by 3-foot personnel/camera access opening per cell, and
- One, 1-inch diameter pipe sleeve per cell for radiological monitoring. [C-CS-Z-0002, C-CC-Z-0012, WSRC-STI-2006-00198]

The design includes 50, 3-inch pipes that penetrate the roof of each cell, except Cell A. These pipes provide capped ports for pouring clean grout into the cell. The pipes are evenly spaced across the roof, allowing complete coverage of the cell. Each pipe will be filled or capped with grout when the cell is closed. The grouting and capping process will be designed and installed to prevent these 50 penetrations from becoming a potential flow path in the future. Figure 3.2-8 and Figure 3.2-11 show details related to the SDU 4 roof. Figure 3.2-12 is a photograph of the interior of the SDU 4 roof. [C-CS-Z-0002, C-CC-Z-0012, WSRC-STI-2006-00198]

The roof girder system was considered as a means of degradation of the saltstone and clean cap via carbonation. The columns were also considered separate from the saltstone as they experience degradation via carbonation.

Figure 3.2-11: SDU 4 Permanent Roof Plan Details (Cells B through L)

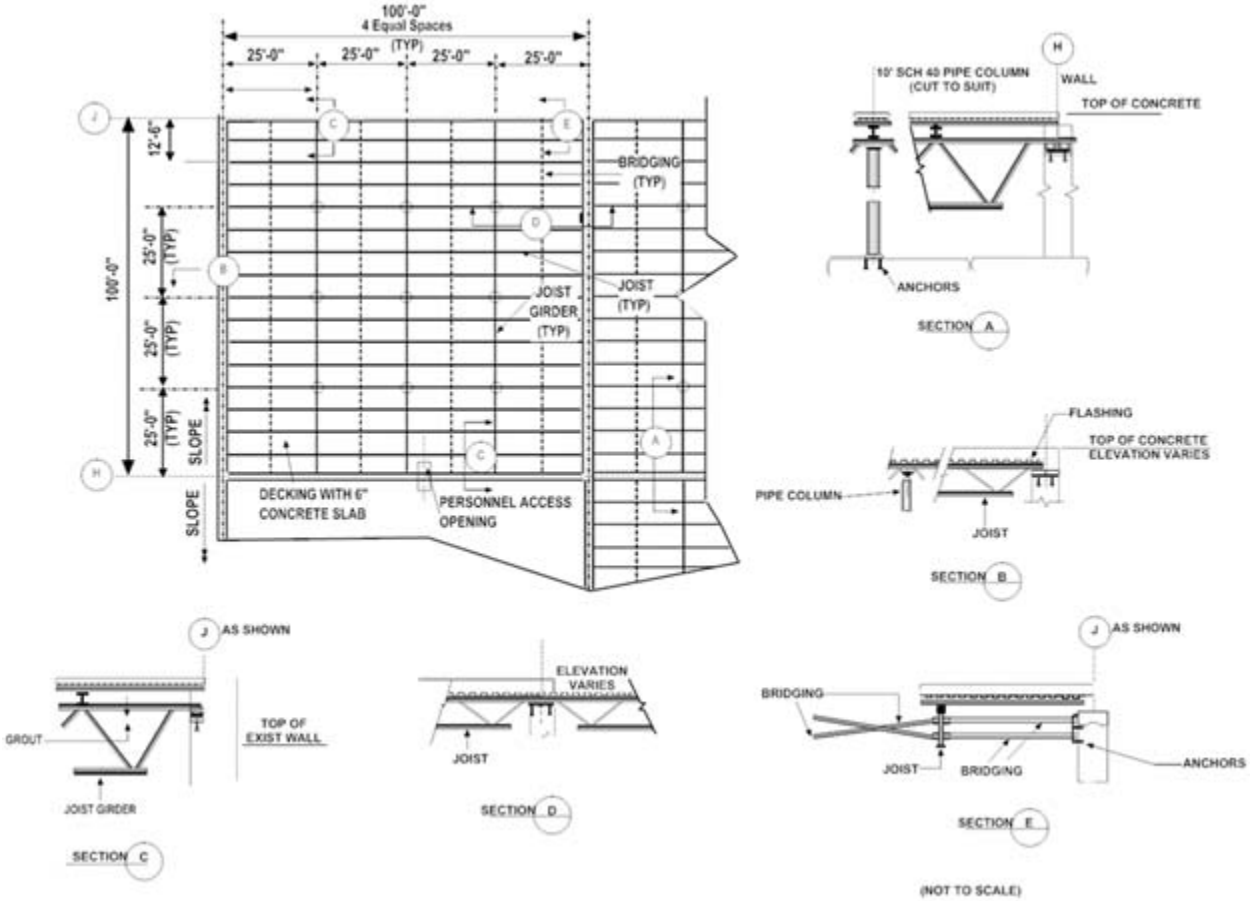

[C-CS-Z-0002]

Figure 3.2-12: Interior View of SDU 4 Roof (Cells B through L)

[SRR-CWDA-2009-00017]

3.2.3 150-Foot Diameter SDUs

The 150-foot diameter cylindrical SDUs were an upgrade to the SDU 1 and 4 designs to account for the potential hydrostatic head and associated damage experienced in the SDUs 1 and 4. The design of the 150-foot diameter SDU is a commercial water tank design that has been upgraded for waste disposal purposes. The cylindrcal 150-foot diameter SDUs consist of pairs of cells designated as "A" and "B" for SDUs 2, 3, and 5. The layout of the 150-foot diameter SDUs constructed in Z-Area is presented in Figure 3.1-4. SDU cells 2A/2B were constructed between 2008 and 2009. SDU cells 3A/3B and 5A/5B were constructed between 2011 and 2013.

Cone penetration tests and geotechnical boreholes to a depth of over 100 feet below the surface, and laboratory testing of soils removed from under the footprint of the 150-foot diameter SDUs were performed. Subsurface conditions were characterized and soil properties were determined using site-specific data, as well as existing data from surrounding areas. [WSP-SSF-2005-00023] Seismic stability analyses have been conducted for the 150-foot diameter SDUs and documented in K-ESR-Z-00001 and K-ESR-Z-00002.

Figure 3.2-13 is a photograph of a typical 150-foot diameter SDU under construction. Construction of SDU 2A/2B disposal cells began in November 2008. Project construction efforts for SDU 2A/2B concluded in November 2009. [SRR-CWDA-2009-00050] Construction of the

SDU 3A/3B and 5A/5B disposal cells began in February 2011. Project construction efforts for SDU 3A/3B and 5A/5B concluded June 2013. [SRR-CWDA-2013-00050]

Figure 3.2-13: Typical 150-Foot Diameter SDU Under Construction

[SRR-CWDA-2013-00050]

The 150-foot diameter SDU design consists of a Type V (sulfate-resistant) concrete floor slab, upper mud mat, a Type V concrete roof, and pre-stressed Type V concrete walls. The walls consist of pre-cast panels of Type V reinforced concrete cast on a 26-gauge (0.179 inch) steel diaphragm. Cured wall panels are lifted and set on the perimeter footer of the base slab, leaving approximately 12 inches between wall panels. A steel diaphragm closure strip is secured to the exterior of the walls, interlocking with the exterior steel diaphragm of each adjacent wall panel. A wooden form is installed on the interior, opposite the closure strip, creating a channel from the base of the SDU to the top of the walls. Type V concrete is poured in each channel to complete the exterior wall. The interlocking sections of the steel diaphragm are filled with epoxy to complete the water-tight barrier. This water-tight feature is an improvement in the design relative to the SDU 1 and SDU 4 designs. The steel diaphragm has no horizontal joints. [WB00001K-004-G]

Vertical reinforcing bars were installed to resist bending moments, shrinkage, and temperature stresses. High strength pre-stressing wires were installed around the disposal unit under tension as specified in the design. The SDU wall pre-stressing is designed to carry the hydraulic load and help facilitate the walls being in compression. Shotcrete was used during various stages of the SDU construction to secure the pre-stressing wires. The reinforcing steel, pre-stressing wire, and steel shell diaphragm were all of carbon steel construction. [WB00001K-004-G]

3.2.3.1 150-Foot Diameter SDU Dimensions

Design of SDUs 2, 3, and 5 consists of two identical cells designated as "Cell A" and "Cell B" (e.g., SDU Cell 2A and SDU Cell 2B). The diameter of each cell is 150 feet and the roof slopes from an elevation of 23.5 feet at the center to 22 feet at the walls. [WB00001K-004-G] The reinforced cylindrical concrete cell is constructed below grade to the roof. The location of the cell was prepared by excavating and then stockpiling the native soil to be used as backfill around the completed cell. [C-CG-Z-00030] Each cell has a nominal capacity of 2.9 million gallons.

Each SDU consists of the following:

- Controlled compacted backfill soil base;
- 4-inch thick lower concrete mud mat [WB00001K-004-G];
- GCL consisting of a minimum 0.75 lbs/ft^2 sodium bentonite covered by a 100 mil HDPE liner above the lower mud mat [WB00001K-004-G, C-SPP-Z-00006, WSP-SSF-2005-00023];
- 6-inch thick upper mud mat of Type V (sulfate-resistant) concrete [WB00001K-004-G, WSP-SSF-2005-00023];
- Minimum 8-inch thick cast-in-place floor slab of Type V concrete [WB00001K-004-G, WSP-SSF-2005-00023];
- Minimum 8-inch thick pre-cast walls of Type V concrete [WB00001K-004-G, WSP-SSF-2005-00023];
- Shotcrete (minimum thickness of 1 inch) placed on the exterior of the walls to cover the reinforcing bar and the layers of prestressing wire [WB00001K-004-G];
- Exterior side of the walls covered with a 100 mil HDPE geomembrane [WB00001K-004-G, WSP-SSF-2005-00023];
- 48 roof support columns of 14-inch diameter Type V concrete with a typical spacing of approximately 20-foot centers [WB00001K-004-G];
- Maximum 21.5 feet of saltstone or other cementitious waste form poured into the disposal unit through a roof penetration at the center of the SDU [WSRC-STI-2006-00198];
- Minimum 8-inch thick roof of Type V concrete with a nominal 2% slope in place prior to the saltstone pour [WB00001K-004-G, WSP-SSF-2005-00023]; and
- Roof penetrations will exist for personnel access, ventilation, drain water removal, thermocouple trees, cameras, and saltstone. [WB00001K-004-G, C-CH-Z-00014]

Figure 3.2-14 provides the conceptual model cross section of a 150-foot diameter SDU cell. [WB00001K-004-G]

Figure 3.2-14: 150-Foot Diameter SDU Cell Conceptual Model Cross Section

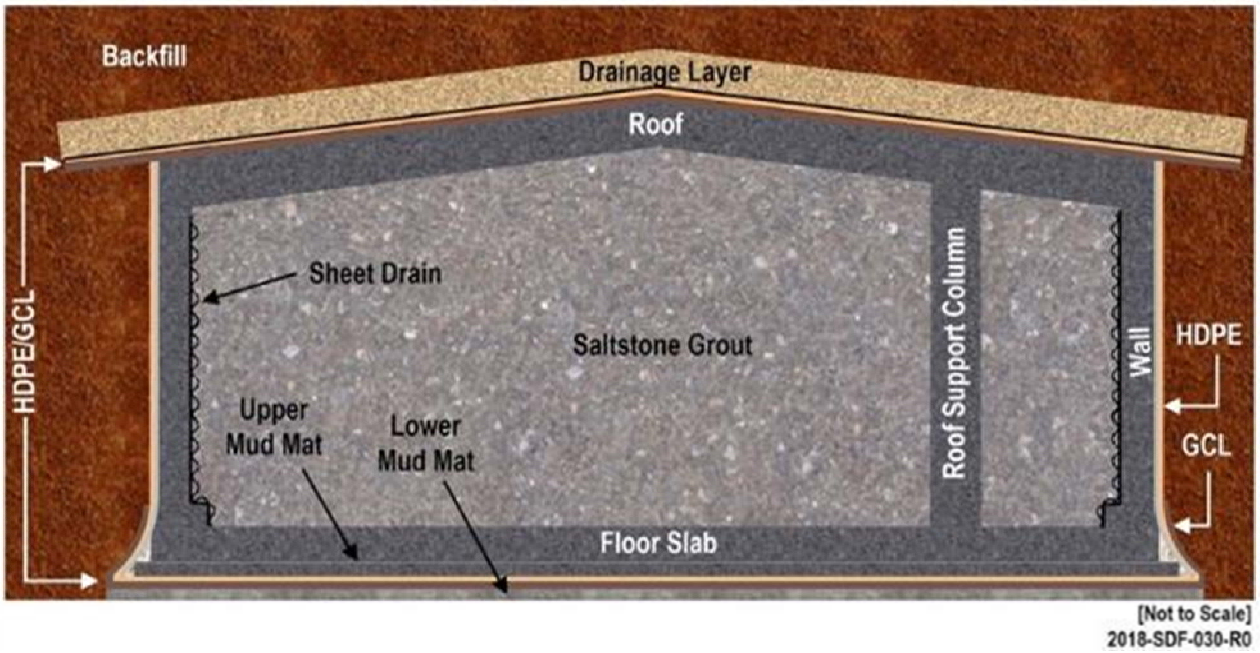

[SRR-CWDA-2013-00037] Note: For clarity, roof penetrations are not shown; see Figure 3.2-16 for the roof plan.

3.2.3.2 150-Foot Diameter SDU Concrete Specifications

The waste stream disposed of in the 150-foot diameter SDUs was high in sulfates, which can attack hardened concrete. Due to this high sulfate nature, the SDUs upper mud mat, floor slab, walls, and roof are constructed with a Type V (sulfate-resistant) concrete mix. This formulation is also designed to retard the ingress and movement of water. Pozzolans and slag were added to the cement to reduce the water to cementitious materials ratio. This also helps reduce the saturated hydraulic conductivity of the concrete. In addition, the walls were constructed with wire pre-stressing and the exterior is backfilled with soil allowing for the walls to be under compression, further minimizing water penetration into the walls. Table 3.2-3 presents the 150-foot diameter SDU concrete mix formula. [SRNL-STI-2008-00421]

The concrete attributes important to the SDF SDUs are:

- Low hydraulic conductivity,
- High pH,
- Low Eh,
- High degradation resistance, and
- High sulfate attack resistance.

Table 3.2-3: 150-Foot Diameter SDU Concrete Formulation

Ingredient	Material Quantity (lbs/yd^3)
Type V Cement (Lehigh T-V #2; ASTM C 150)	213
Grade 100 Blast furnace slag (Holcim Grade 100 Slag; ASTM C 989)	284
Silica Fume (W. R. Grace Silica Fume; ASTM C 1240)	47.3
Type F Fly ash (SEFA Group, Class "F" Fly Ash; ASTM C 618)	165.7
Sand (Natural Washed Sand; ASTM C 33)	911
Aggregate (#67 Granite; ASTM C 33)	1,850
Water (maximum)	270 (32.3 gal/yd^3)
Maximum water to cementitious material ratio	0.38
Grace WRDA 35 (oz/cwt c+p)	5
Grace Darex II (oz/cwt c+p)	0.4 to 0.5
Grace Adva 380 (oz/cwt c+p)	3 to 4

[SRNL-STI-2008-00421]
ASTM = American Society for Testing and Materials

3.2.3.3 150-Foot Diameter SDU Roof

The SDU roof was formed and poured in place using Type V (sulfate-resistant) concrete with a minimum thickness of 8 inches. The roof was constructed with a nominal slope of 2%. [WSP-SSF-2005-00023] Figure 3.2-15 and Figure 3.2-16 depict additional details regarding the roof.

Roof penetrations are available for ventilation, drain water removal, thermocouple trees, closed circuit television, personnel access during construction, and saltstone and grout pouring. The penetrations include steel pipes, except for the drain water line, which will be PVC. Figure 3.2-16 depicts a typical roof plan for the SDUs showing many of the penetrations (for details, see WB00001K-004-G). The roof penetrations are sealed in a manner to prevent rain infiltration using neoprene gasket material. Once the SDUs are filled, the roof mounted support equipment will be removed and the penetrations will be filled/capped in a manner that makes them equivalent to the rest of the roof specifications. The HDPE/GCL liner system will be extended over the roof prior to installation of the closure cap. [WSP-SSF-2005-00023]

Figure 3.2-15: 150-Foot Diameter SDU Roof-Column Detail

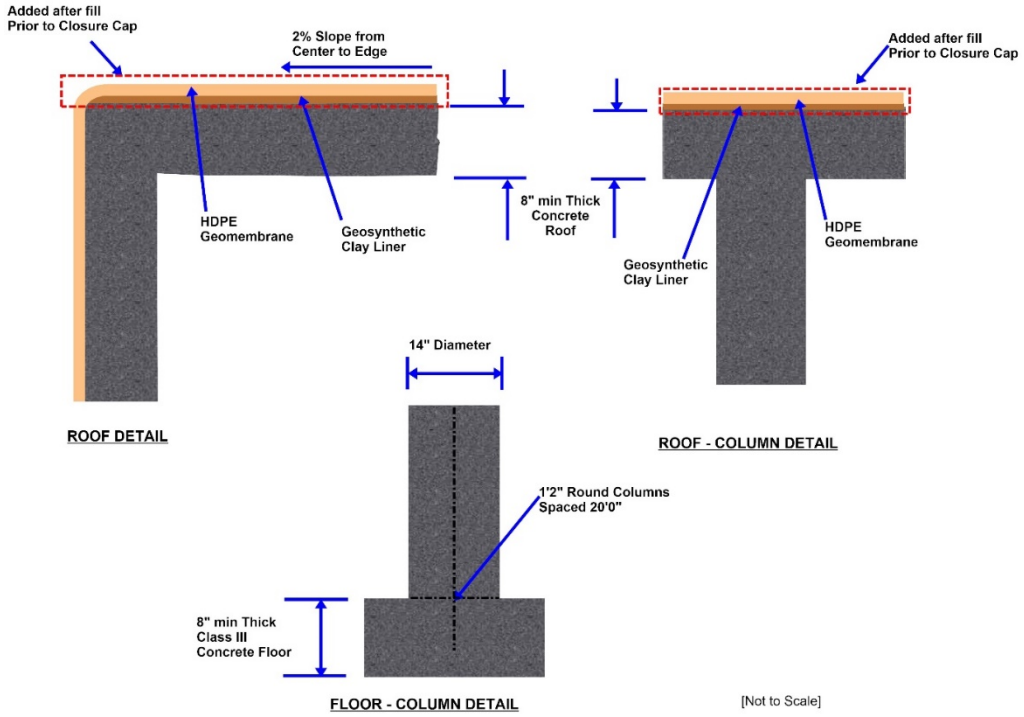

[WB00001K-004-G, WSRC-STI-2008-00244, C-SPP-Z-00006]

Figure 3.2-16: 150-Foot Diameter SDU Roof Plan (Typical)

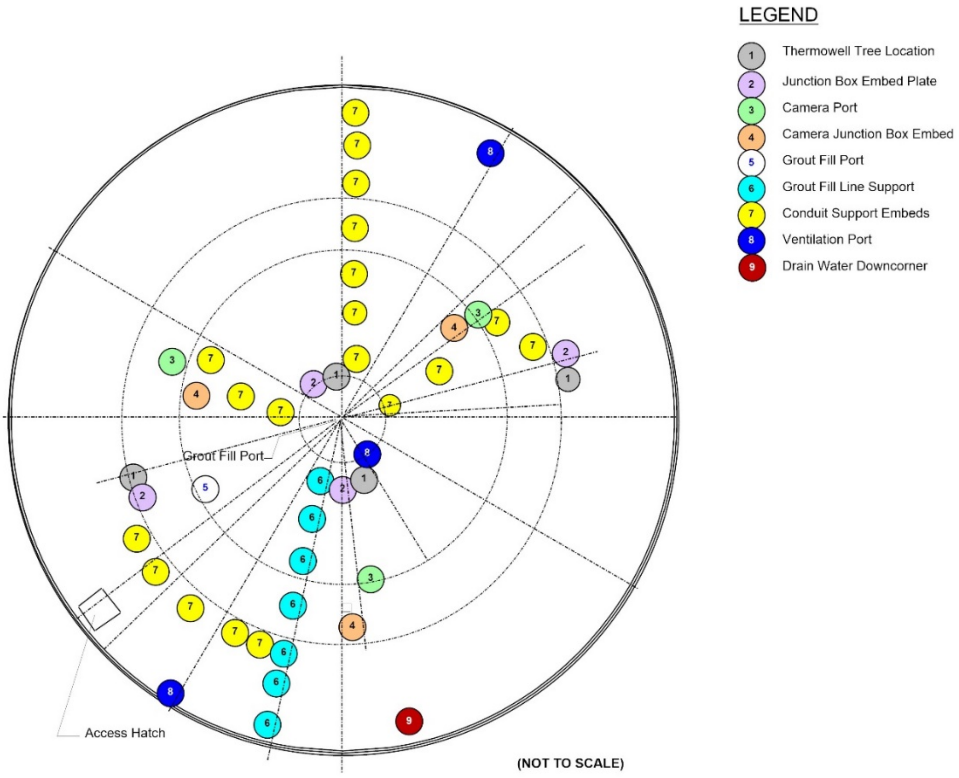

[WB00001K-004-G, C-CH-Z-00014] Note: Not all penetrations are shown.

3.2.3.1 150-Foot Diameter SDU Walls and Columns

The walls are constructed of pre-cast Type V (sulfate-resistant) concrete panels with a minimum thickness of 8 inches. The panels are tilted up onto the poured concrete floor. Wall joints were sealed using Type V concrete mix poured between each panel. The only wall penetrations that exist are anchors to attach sheet drain material to the walls. In addition, SDU's 2A and 2B contain anchors that penetrate into the floor to secure the drain water header to the floor. Figure 3.2-17 depicts the wall design details and Figure 3.2-18 shows wall panels under construction. [WSP-SSF-2005-00023, WB00001K-004-G]

Figure 3.2-17: 150-Foot Diameter SDU Wall Detail

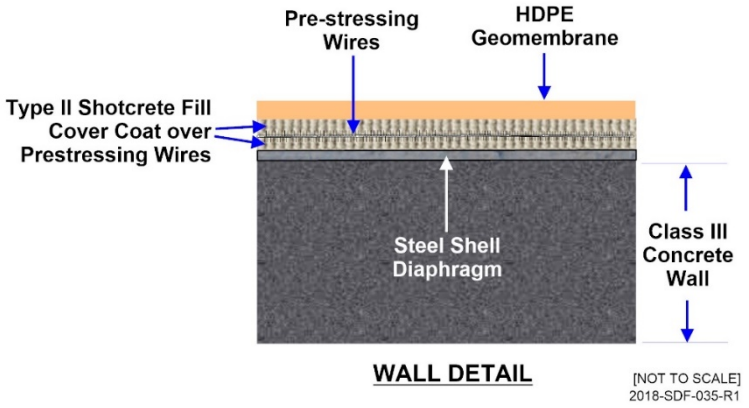

[WB00001K-004-G]

Figure 3.2-18: 150-Foot Diameter SDU Wall Panels Under Construction

[SRR-CWDA-2013-00050]

A steel shell diaphragm was installed incorporated in the pre-cast concrete panels. The steel shell wall joints were sealed watertight by injecting with a polysulfide epoxy material from the bottom to the top. Pre-stressing wires were installed around the circumference of the disposal unit wall. The pre-stressing wires were covered with shotcrete for protection as described in Section 3.2.3. [WSP-SSF-2005-00023, WB00001K-004-G]

The HDPE/GCL liner system beneath the SDUs upper mud mat is welded to an identical liner system surrounding the walls (see Section 3.2.3.2 for addition details on floor design). [WSP-SSF-2005-00023] This HDPE liner design extends the entire height of the disposal unit, while the GCL extends to a height of approximately 2 feet above the upper mud mat. The HDPE/GCL installation will resume on the roof at closure. Figure 3.2-15 and Figure 3.2-17 depict the liner system on the walls and the roof. [C-SPP-Z-00006]

Each 150-foot diameter SDU is designed with 48 Type V (sulfate-resistant) concrete columns to support the roof. Typical column spacing is approximately 20-feet between centers. The typical construction is shown on Figure 3.2-15. [WB00001K-004-G]

The drain water management system consists of the sheet drains and a PVC header system that collects the water for transfer back to the process via a roof penetration (shown in Figure 3.2-16) to be re-fed into the dry feeds mix to form grout. The drain water collection system will be emptied, filled with grout to the extent practical, and will permanently remain in place within the SDU after the operational period. The external drain water collection system valve assemblies will be removed, and the holes plugged. [CBU-ENG-2003-00103]

All 150-foot diameter SDUs are designed to have sheet drains (polystyrene sheet with 0.437-inch dimples covered on one side with a non-woven, needle-punched polypropylene filter fabric) installed on the walls. These were installed to collect free water that accumulates in the SDU. Additionally, it acts as a barrier to keep water away from the wall. [WSRC-STI-2006-00198]

3.2.3.2 150-Foot Diameter SDU Floor

The existing grade was excavated for the base layers. The base layers consist of the components as shown in Figure 3.2-19. There are two circular concrete mud mats, upper and lower, each with a thickness of 6 inches. [WB00001K-004-G]

The lower mud mat was constructed on the excavated compacted grade. A GCL was installed over the lower mud mat. The GCL consists of bentonite sandwiched between two geotextiles. Bentonite, the hydraulically functional portion of a GCL, is the general term given to swelling type montmorillonite clay, which formed as the stable alteration product of volcanic ash. [WSP-SSF-2005-00023]

A 100 mil HDPE liner with welded joints was installed above of the GCL. The upper mud mat, with a minimum thickness of 6 inches consisting of Type V concrete, was poured on top of the HDPE/GCL in order to protect the HDPE/GCL during construction. A circular

Type V concrete floor slab was poured in place with a minimum thickness of 8 inches. [WB00001K-004-G, WSP-SSF-2005-00023]

Figure 3.2-19: 150-Foot Diameter SDU Base Details

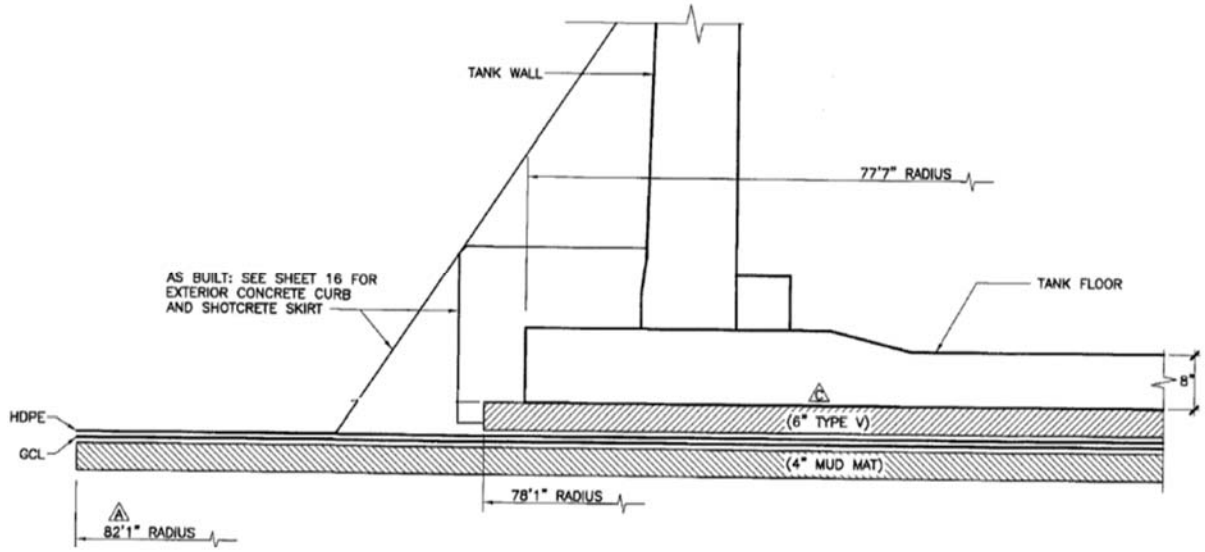

[WB00001K-004-G]

The SDU concrete, in conjunction with the encasing HDPE geomembrane, form a composite barrier that limits both advective and diffusive contaminant transport. [WB00001K-004-G, WSP-SSF-2005-00023, C-SPP-Z-00006]

Figure 3.2-20 is a photograph of the placement of the lower mud mat prior to the installation of the GCL.

Figure 3.2-20: Placement of Lower Mud Mat for 150-Foot Diameter SDU Construction

[SRR-CWDA-2013-00050]

3.2.3.3 150-Foot Diameter Disposal Cell Interior Coating

An interior coating consisting of a mat-reinforced epoxy-novolac thermosetting lining was applied to the walls and floor of the 150-foot diameter SDUs to mitigate sulfate attack from short-term exposure saltstone bleed water by capillary suction and diffusion of sulfate from the pore fluid of the cured saltstone. The sulfates are inherent in the salt solution waste stream used to form saltstone by the SPF. Mat-reinforced thermosetting polymer linings are expected to maintain high integrity during initial disposal unit operations, after which protection is not assumed in PA modeling. This is based on several assumptions, including limited oxidation, gradual temperature decline, tolerable radiation dose with minimal dose rate effects, minimal differential settlement, and proper installation. [WSRC-TR-2008-00090]

3.2.4 375-Foot Diameter SDUs

In 2011, the geometry of the SDU design was increased from the 150-foot diameter to the 375-foot diameter design to provide additional capacity to support the increased feed rate associated with SWPF and to enhance the economy of scale in construction. A total of seven 375-foot diameter SDUs will be constructed in Z-Area and the projected locations are presented in Figure 3.2-21. SDU 6 was constructed between 2014 and 2017. Currently, the six future 375-foot diameter SDUs are to be designed, constructed, and modeled similarly to the existing SDU 6. Lessons learned from construction of each SDU will be incorporated into future designs and modeling parameters will be adjusted accordingly. Cone penetration tests and geotechnical boreholes to a depth of over 100 feet below the surface, and laboratory testing of soils removed from under the footprint of the 150-foot diameter SDUs were performed. [K-CLC-Z-00023] Subsurface conditions were characterized and soil properties were determined using site-specific data, as well as existing data from surrounding areas. Seismic stability analyses have been conducted for the sites of SDU 6 and SDU 7 and documented in the *Saltstone Disposal Unit 6 Geotechnical Investigation Report*, K-ESR-Z-00005 and *Saltstone Disposal Unit 7 Geotechnical Investigation Report*, K-ESR-Z-00008, respectively. Figure 3.2-21 provides a conceptual design of the layout for the future 375-foot diameter SDUs 7 through 12, all similar in design to the existing SDU 6. SDU 7 is currently under construction, but the final location of SDUs 8 through 12, and any additional SDUs required, are subject to change.

SDU 6 basic construction includes Type V (sulfate-resistant) concrete floor slab and roof and pre-stressed Type V concrete walls. The pre-stressed walls are cast-in-place panels of Type V concrete, reinforcing bars, vertical tensioning cables, and horizontal pre-stressing wires and covered with shotcrete. [C-SPP-Z-00008, C-SPP-Z-00015] The roof is supported by 208 concrete columns. [C-CC-Z-00039] The disposal unit includes an HDPE geomembrane between the upper and lower mud mats. Another HDPE geomembrane layer will be installed over the roof and beneath a sand drainage layer after disposal operations are complete. [C-SPP-Z-00008]

Figure 3.2-21: Artist Depiction of the Proposed 375-Foot Diameter SDU Layout

[G-AES-S-00004]

3.2.4.1 Dimensions of the 375-Foot Diameter SDUs

The nominal interior diameter of the unit is 375 feet with a minimum interior height of 43 feet. The floor and roof of SDU 6 both have a 1.5% downward slope from the center of the unit. For future 375-foot diameter SDUs, the floor will be designed with no slope, but the roof will remain 1.5%. [C-CC-Z-00042, C-CC-Z-00063]

Each of these SDUs shall consist of the following:

- Controlled compacted backfill soil base [C-CY-Z-00006];
- 4-inch thick lower concrete mud mat (minimum) [C-CY-Z-00006];
- GCL consisting of a minimum 0.75 lbs/ft^2 sodium bentonite covered by a 100 mil HDPE liner above the lower mud mat for SDU 6 (future SDUs 7 through 12 will be constructed with a minimum 60 mil HDPE liner) [C-SPP-Z-00008, SRR-CWDA-2018-00012];
- 6-inch thick upper concrete mud mat [C-CY-Z-00006];
- 12-inch thick cast-in-place floor slab of Type V (sulfate-resistant) concrete for SDU 6 (for future SDUs 7 through 12, the floor will consist of a 24-inch thick cast-in-place floor slab of Type V concrete) [C-SPP-Z-00008, C-CC-Z-00044, C-SPP-Z-00015, C-CC-Z-00059];
- Cast-in-place walls of Type V concrete for SDU 6 have a minimum 10-inch thickness at the roof and 24-inch thickness at the floor [C-SPP-Z-00008, C-SPP-Z-00015, C-CC-Z-00042], for future SDUs 7 through 12 the cast-in-place walls,

constructed of Type V concrete, shall have a minimum 12-inch thickness at the roof and 24-inch thickness at the floor (SRR-CWDA-2018-00012);

- Shotcrete is placed on the exterior of the walls to cover the layers of prestressing wire [C-SPP-Z-00008, C-SPP-Z-00015];
- 208 roof support columns of Type II cement, 24-inch diameter, with a typical spacing of 23-foot centers (each column has a 5-foot square footing for SDU 6, the footing has been removed for future SDUs 7 through 12 due to the increase in floor thickness) [C-SPP-Z-00008, C-SPP-Z-00015, C-CC-Z-00039, C-CC-Z-00042];
- Maximum of 43 feet of saltstone or other cementitious waste form poured into the disposal unit through a roof penetration [C-CC-Z-00063, C-CC-Z-00042];
- 12-inch thick roof of Type V concrete with a 1.5% slope in place prior to the saltstone pour [C-SPP-Z-00008, C-CC-Z-00042, C-CC-Z-00063];
- Wall-to-floor and wall-to-roof joints made of neoprene or sponge rubber bearing pads will be 1 inch thick between the wall and the roof and 2 inches thick between the floor and the wall prior to compression by the weight of the wall and roof [C-SPP-Z-00008, C-SPP-Z-00015, C-CC-Z-00063, C-CC-Z-00042, C-CC-Z-00066];
- Additional construction joints with water stops will exist in both the floor and the roof [C-CC-Z-00044, C-CC-Z-00066]; and
- Roof penetrations will exist for ventilation, drain water management system, thermocouple trees, cameras, and saltstone pouring. [C-CC-Z-00049]

Figure 3.2-22 (A) provides a conceptual model cross section of 375-foot diameter SDU 6. Figure 3.2-22 (B) provides a conceptual model cross section of 375-foot diameter SDUs 7 through 12. [C-CC-Z-00039, C-CC-Z-00042, HLW-SSF-TTR-2013-0021]

Figure 3.2-22: Conceptual Model Cross Sections for 375-Foot Diameter SDUs

(A) SDU 6

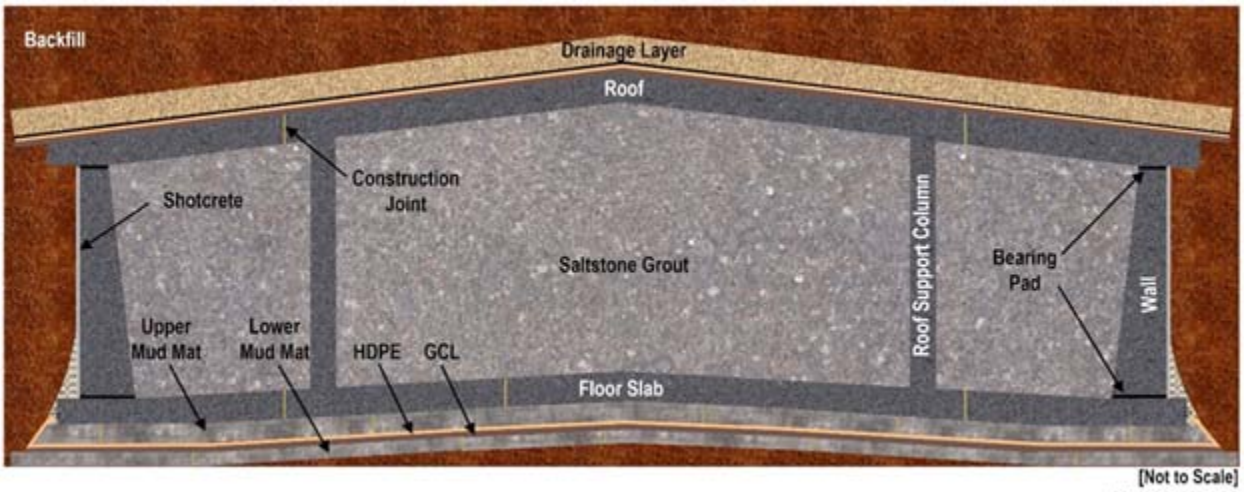

(B) SDUs 7 through 12

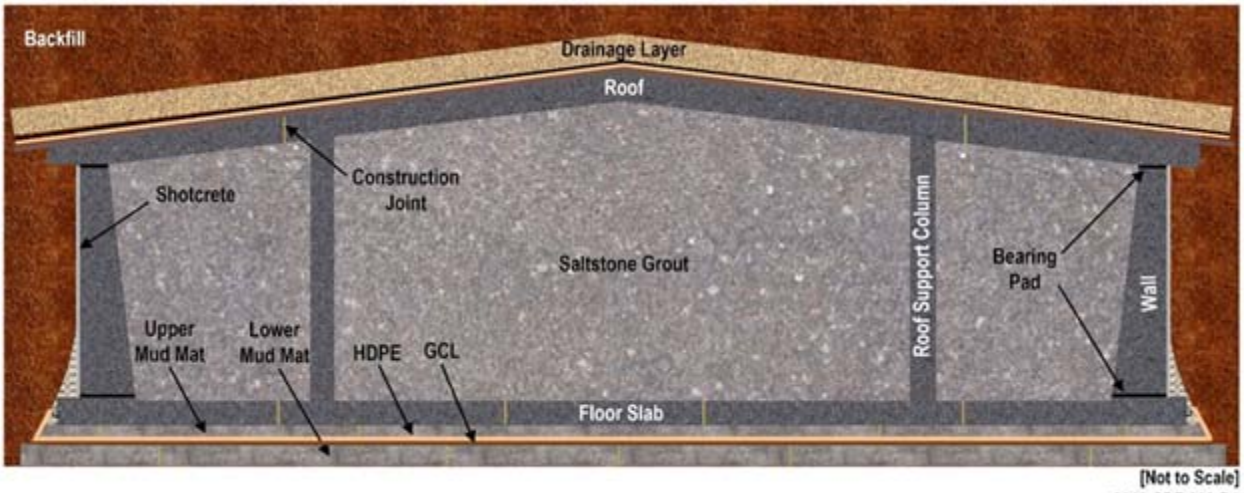

[SRR-CWDA-2013-00037] Note: For clarity, roof penetrations are not shown.

3.2.4.2 375-Foot Diameter SDU Concrete Specifications

The waste stream to be disposed of in the 375-foot diameter SDUs is expected to be high in sulfates, which can attack hardened concrete. Due to this high sulfate nature the 375-foot diameter SDUs floor slab, walls, and roof are constructed with a Type V (sulfate-resistant) concrete. This concrete formulation is designed to retard the ingress and movement of water. A pozzolan (fly ash and/or silica fume) and slag are to be added to the cement to reduce the water to cementitious material ratio. This will also help reduce the saturated hydraulic conductivity of the concrete. In addition, the walls will be constructed with wire pre-stressing. At closure, the exterior is to be backfilled allowing for the walls to be under compression, further minimizing water penetration into the walls. Table 3.2-4 presents the concrete mix formula used for the construction of SDU 6. [C-SPP-Z-00008]

The concrete attributes important to the 375-foot diameter SDUs are:

- Low hydraulic conductivity,
- High pH,
- Low Eh,
- High degradation resistance, and
- High sulfate attack resistance.

Table 3.2-4: SDU 6 Concrete Formulation

Ingredient	Material Quantity
Cement: Lehigh - Leeds, Alabama, Type V	213 lbs/yd^3
Slag: Holcim, Grade 100	284 lbs/yd^3
Fly Ash: Southeastern Fly Ash Co, Class F	163 lbs/yd^3
Silica Fume: Force 10,000, W.R. Grace & Co.	50 lbs/yd^3
Sand: Foster Dixiana #33, Clearwater Sand Plant	991 lbs/yd^3
Stone: Rinker Aggregates #67, Dogwood Quarry	1,850 lbs/yd^3
Water: City/County (Potable)	269 lbs/yd^3 (32.2 gal/yd^3)
Design Air	4.5%
Air-Entraining Admixture (AEA): Darex II, W.R. Grace & Co.	3.91 oz/yd^3
Water-Reducing Admixture (WRA): WRDA 35, W.R. Grace & Co.	42.6 oz/yd^3
High-Range Water-Reducing Admixture (HRWRA): ADVA 380, W.R. Grace & Co.	34.1 oz/yd^3

[C-SPP-Z-00008]

After the construction of SDU 6, a new concrete formula was designed for the construction of future SDUs 7 through 12. The future 375-foot diameter SDU concrete formulation specifications are presented in Table 3.2-5. [C-SPP-Z-00015]

Table 3.2-5: SDU 7 through 12 Concrete Formulation

Ingredient	Material Quantity
Cement: Holcim, Alabama, Type V	213 lbs/yd^3
Slag: Lehigh, Grade 120	284 lbs/yd^3
Fly Ash: Southeastern Fly Ash Co, Class F	163 lbs/yd^3
Silica Fume: Force 10,000, GCP Applies Technology, Inc.	50 lbs/yd^3
Sand: Tank Bottom Slab: South Carolina Minerals, Inc., Beech Island, SC	1,046 lbs/yd^3
Sand: Walls, Columns, Roof: South Carolina Minerals, Inc., Beech Island, SC	1,091 lbs/yd^3
Stone: Tank Bottom Slab: #467, Dogwood Quarry (Blend of 24.2% #4, 75.8% #67 stone)	1,795 lbs/yd^3
Stone: Walls, Columns, Roof: #67 stone, Dogwood Quarry	1,750 lbs/yd^3
Water: City/County (Potable)	264 lbs/yd^3 (31.6 gal/ yd^3)
Design Air	3% to 6%
Shrinkage-Reducing Admixture: Type S, Eclipse 4500, GCP Applied Technologies, Inc.	0.75 gal/yd^3
AEA: Darex II, GCP Applied Technologies, Inc.	5.5 oz/yd^3
HRWRA: Tank Bottom Slab: Type F, ADVA 455, GCP Applied Technologies, Inc.	63.9 oz/yd^3
HRWRA: Walls, Columns, Roof: Type F, ADVA 455, GCP Applied Technologies, Inc.	56.8 oz/yd^3

[C-SPP-Z-00015]

3.2.4.3 375-Foot Diameter SDU Roof

The 12-inch thick roof is formed and poured in place using Type V (sulfate-resistant) concrete. The roof is constructed with a slope of 1.5%. The roof is constructed on bearing pads atop the wall. Construction joints in the roof are sealed with water stops. Figure 3.2-23 depicts additional salient features regarding the roof, walls, and support columns for the 375-foot diameter SDUs. [C-SPP-Z-00008, C-CC-Z-00042]

Figure 3.2-23: 375-Foot Diameter Roof-Wall-Column Details for SDUs

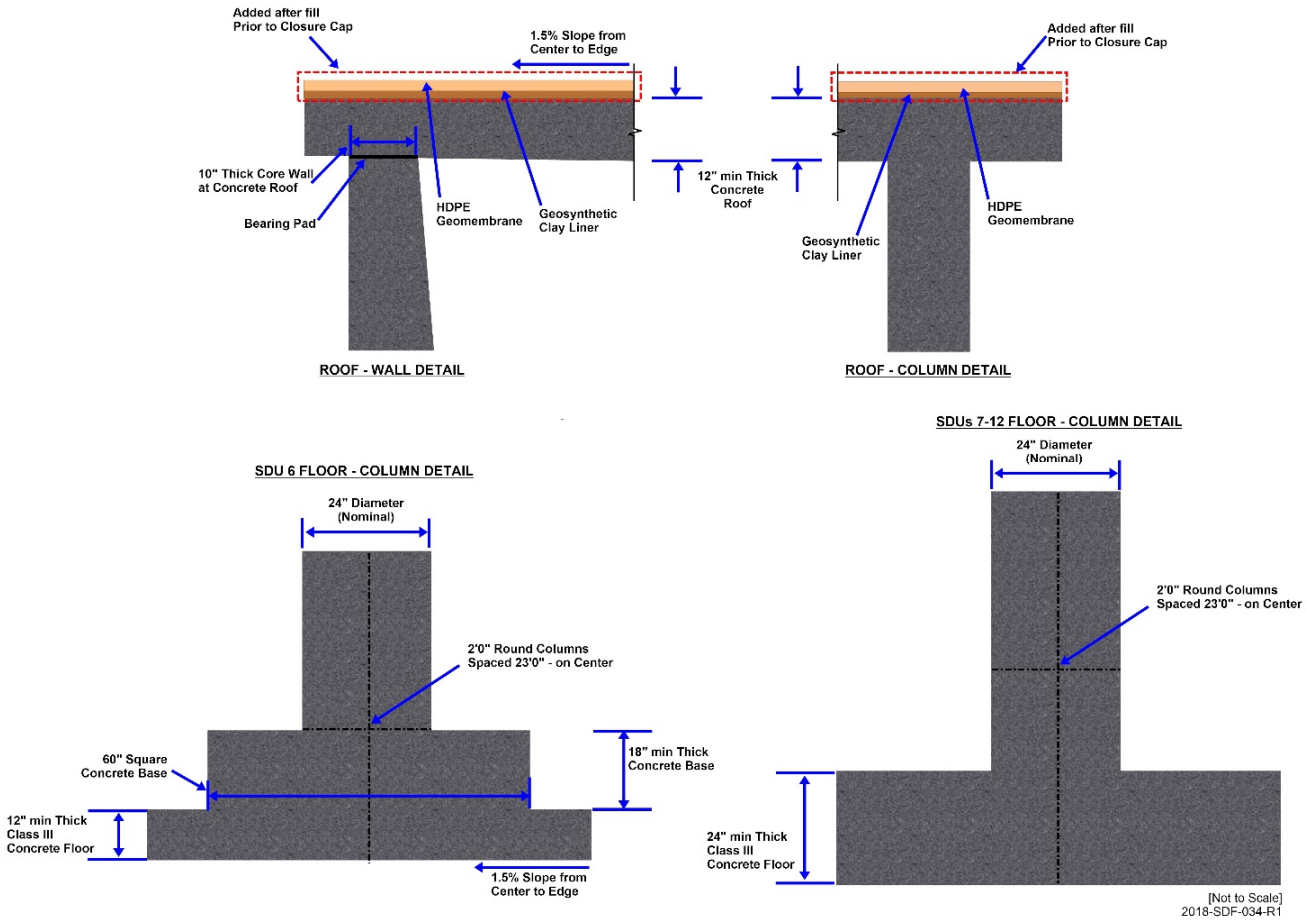

[C-CC-Z-00042 and C-CC-Z-00063]

Roof penetrations will exist for ventilation, drain water system, thermocouple trees, cameras, and saltstone pouring. [C-CC-Z-00049] Prior to closure, the roof-mounted items will be removed and the penetrations will be filled according to roof specifications. The HDPE/GCL liner system will be installed over the roof prior to installation of the closure cap. [C-SPP-Z-00008]

3.2.4.4 375-Foot Diameter SDU Walls and Support Columns

The walls are designed to be constructed of cast-in-place Type V (sulfate-resistant) concrete panels. Figure 3.2-24 shows an individual wall segment for SDU 6 as the wall form is being removed. For SDU 6, the walls were constructed with a minimum thickness

of 10 inches at the roof (Figure 3.2-25) and increasing in thickness to a minimum of 24 inches at the floor. [C-SPP-Z-00008, C-CC-Z-00042] For future SDUs 7 through 12, the walls shall be constructed of cast-in-place Type V concrete panels with a minimum thickness of 12 inches at the roof and a minimum of 24 inches at the floor. The walls are constructed to rest on bearing pads atop the floor slab. Figure 3.2-25 depicts the wall and floor design details for SDU 6 and the typical wall and floor design for future SDUs 7 through 12.

Figure 3.2-24: 375-Foot Diameter SDU Wall Section Cast in Place

[SRR-SDU-2017-00044]

Figure 3.2-25: 375-Foot Diameter Base Details for SDUs

(A) SDU 6

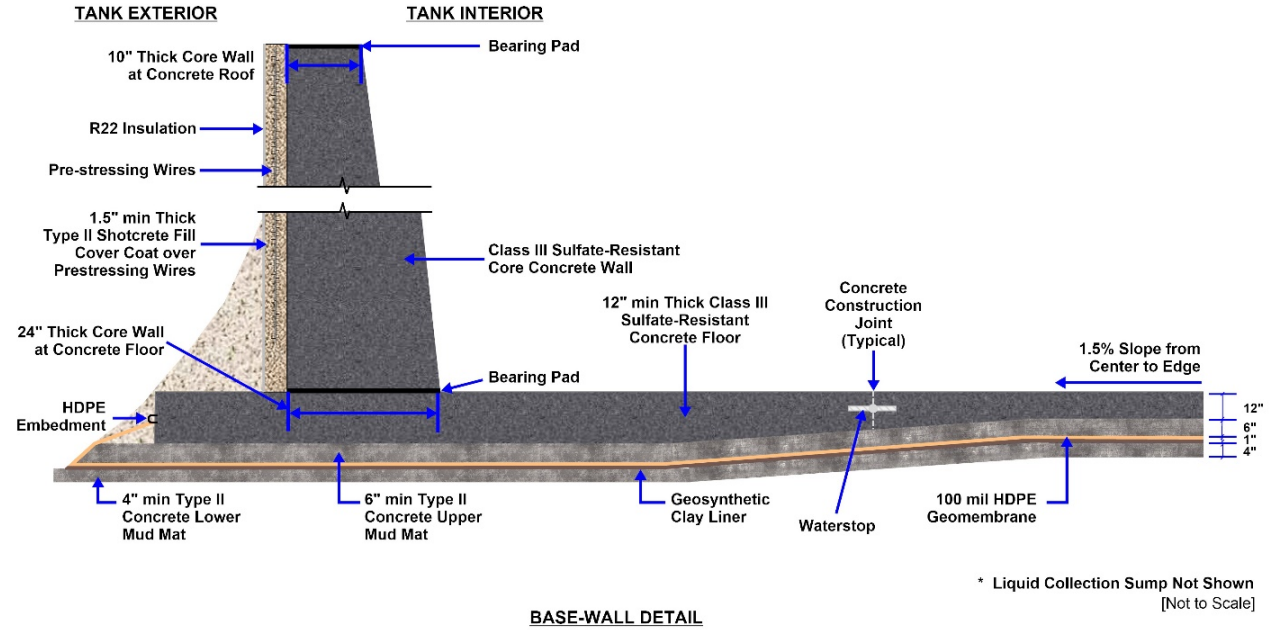

(B) SDUs 7 through 12

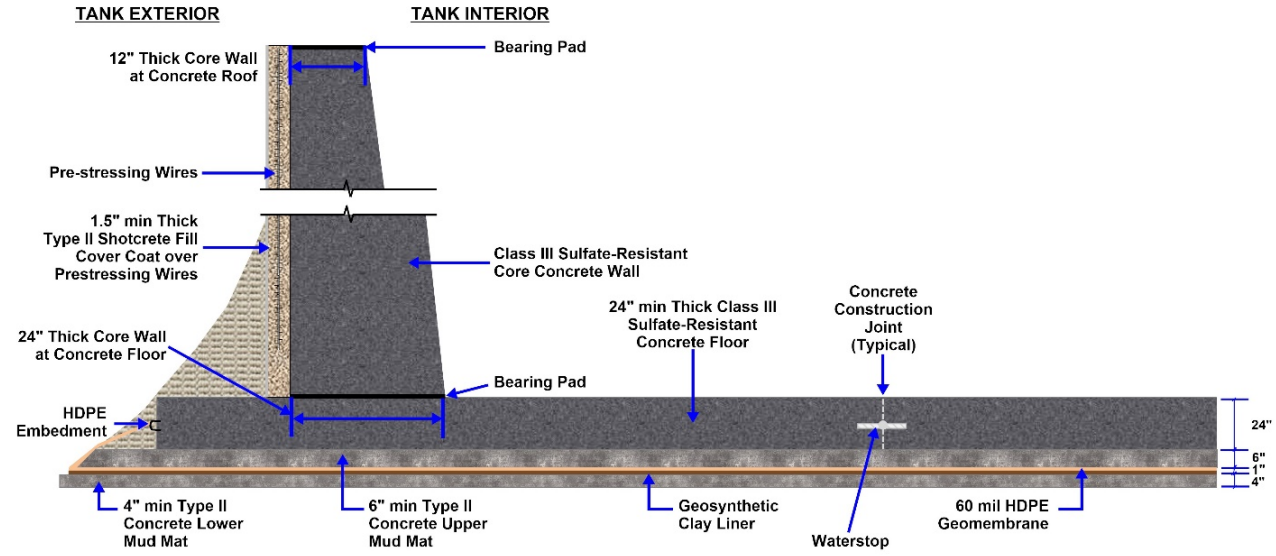

[C-CC-Z-00042] Note: The 100-mil thick HDPE geomembrane shown below the upper mud mat applies only to SDU 6. HDPE liners below the upper mud mat on future SDUs will be 60-mil thick. In addition, the floor slope of 1.5% only applies to SDU 6; future SDUs 7 through 12 will have level floors.

Pre-stressing wires are installed around the circumference of the pre-cast concrete panels that make the disposal unit wall. The pre-stressing wires are covered with shotcrete (Figure 3.2-26). The fresh shotcrete is wet down and covered with plastic wrapping to help retain moisture during the curing period. [SRR-SDU-2017-00044]

Figure 3.2-26: 375-Foot Diameter SDU with Pre-Stress Wire Wrapping Covered with Shotcrete

[SRR-SDU-2017-00044]

Each 375-foot diameter SDU is designed with 208 24-inch diameter columns to support the roof. Typical column spacing is approximately 23 feet. Each SDU 6 column rests on a 5-foot square, 18-inch thick concrete pedestal. [C-SPP-Z-00008, C-CC-Z-00039, C-CC-Z-00042] Figure 3.2-27 shows the columns as constructed within SDU 6 and their relationship to the roof and floor. Note that for future SDUs (SDU 7 through 12), the pedestal has been removed from the design and column capitals have been added at the roof. [C-CC-Z-00063]

Figure 3.2-27: 375-Foot Diameter SDU Columns as Installed in SDU 6

[SRR-SDU-2017-00044]

3.2.4.5 375-Foot Diameter SDU Floor

The existing grade is excavated for the base layers. The base layers consist of the components as shown in Figure 3.2-25.

There are two circular concrete mud mats, upper and lower, with 6-inch and 4-inch thicknesses, respectively. The lower mud mat is constructed on the excavated compacted grade using Type II cement. [C-CY-Z-00006] A GCL is installed over the lower mud mat. The GCL consists of bentonite sandwiched between two geotextiles. Bentonite, the hydraulically functional portion of a GCL, is the general term given to swelling type montmorillonite clay, which formed as the stable alteration product of volcanic ash.

A 100 mil-thick HDPE liner welded at the joints is installed above the GCL on SDU 6. [C-SPP-Z-00008] Future SDUs 7 through SDU 12 will be designed with a minimum 60-mil thick HDPE liners above the GCL. [SRR-CWDA-2018-00012] The 6-inch upper mud mat consisting of Type II cement, is poured on top of the HDPE/GCL in order to protect the

HDPE/GCL during construction. [C-SPP-Z-00008, C-CY-Z-00006, C-CY-Z-00011, C-SPP-Z-00015]

For SDU 6, a circular minimum 12-inch thick Type V concrete floor slab was poured in place with a 1.5% slope, from the center to the outer edge. [C-SPP-Z-00008, C-CC-Z-00044] For future SDUs 7 through 12, the thickness of the floor has been increased to 24 inches and the floor will have no slope. Construction joints in the floor slab are sealed with water stops. The disposal unit concrete, in conjunction with the encasing HDPE geomembrane, form a composite advective and diffusive barrier to contaminant migration. [C-SPP-Z-00008, C-SPP-Z-00015] Figure 3.2-28 presents a graphical representation of the design for the installed water stops (indicated in blue) along the floor and walls.

Figure 3.2-28: 375-Foot Diameter SDU 6 Design with Water Stops in Floor and Walls

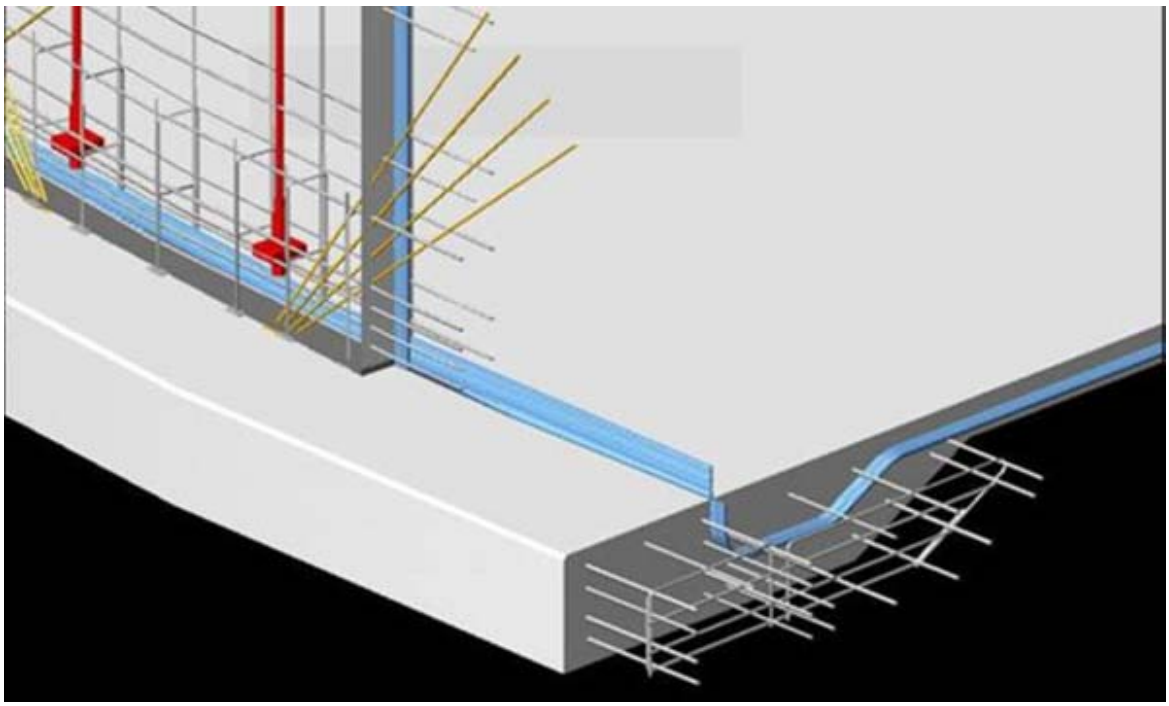

[SRR-SDU-2017-00044]

3.2.4.6 375-Foot Diameter Disposal Cell Interior Coating

SCDHEC's expectation, before issuance of an approval to commence SDU disposal operations, is zero leakage, as no release of radioactive or hazardous material to the environment during operations is acceptable. The concept of zero leakage has been conveyed to SCDHEC during meetings by DOE, SRR, and the tank vendor from the start of circular SDU construction, beginning with SDU 2.

SRR has maintained the stance that a request will not be made to put any SDU into operation until zero leakage is demonstrated by evidence of a successful water tightness test.

SDU 6 was required to demonstrate a water tight design in accordance with American Concrete Institute (ACI) 350.1-2010 *Specification for Tightness Testing of Environmental Engineering Concrete Containment Structures*, (ACI 350.1-2010). The ACI 350.1 acceptance criteria consist of Part 1, which is a qualitative test, and Part 2, which is a quantitative test. Part 1 includes observation of the exterior surfaces of the containment structure including joints, repaired honeycombed areas, and cracks which shall not have moisture that can picked up on a dry hand. Part 1 allows for wet areas on top of the wall footing, but does not allow for observation of flowing water. Part 2 criteria is the measurement of loss of water height for a 72-hour period measured within 1/16 inch and compensated for temperature and evaporation. The acceptable loss of height for SDU 6 was 1/8 inch measured over the 72-hour. A loss of an 1/8 inch in SDU 6 equates to approximately 8,600 gallons. [SRR-SDU-2015-00016]

Additionally, a dye/tracer test with no observation of dye by the naked eye or evidence of dye fluorescence at any location up to the wetted level exterior of the tank was required by the design input (M-TC-Z-00008). Procurement Specification C-SPP-Z-00008 along with ACI 350.1 provide the acceptance criteria for the tests.

SDU 6 was filled using a combination of domestic water and well water from three production wells installed at the SDF. SDU 6 subsequently failed the initial dye/tracer test. SDU6 was suspected to be leaking through the foundation through either cracks in the floor slab or leak paths in the floor slab construction joints. Shrinkage cracks in the floor slab were repaired with flowable epoxy prior to the initial leak test. Post leak testing, the floor slab was inspected and additional cracks were identified and some existing cracks had propagated. The possibility was raised that the construction joints may be feeding water to the adjacent cracks and allowing migration around the water stops in the joints. [SRR-SDU-2015-00016]

After the initial leak test, to mitigate leakage from SDU 6, an adhered elastomer liner system was selected and installed on the walls and floor of the SDU to chemically protect the concrete from the high-pH, high-sulfate saltstone solutions and to achieve leak tightness. After liner installation, a second full-height hydrostatic water test was conducted in 2016 with no signs of leakage. [SRR-SDU-2017-00001]

Although the liner has been installed and leak-tested for SDU 6 and is planned for SDU 7, no credit is taken for these liners in the PA models. Additionally, for modeling purposes the roof and floor of SDU 6 are assumed to be initially degraded with an initial saturated hydraulic conductivity of 6.2E-06 cm/s based on an assumed bounding leak rate, as described in the *Evaluation of Revised Future Saltstone Disposal Unit Locations by PORFLOW Simulations*. [SRNL-STI-2016-00534]

3.2.5 Saltstone Waste Form Specifications

Section 4.3.1.2 describes the material properties of saltstone. The measured data used to develop the recommended values (SRR-CWDA-2018-00004) were based on laboratory tests performed by SRNL (SRNL-STI-2008-00421) and SREL (SRRA099188-000005) using SDU 2A cores and simulant

samples. Based on these studies, a formula for mixing saltstone has been proceduralized through the *Premix Blending & Conveying System Operating Manual* (SW24.5, Section 2.11: Premix Blending Panel Keypad and Display Operation). Table 3.2-6 presents the formula for mixing saltstone. [SRNL-STI-2008-00421] These dry feeds are mixed with decontaminated salt solution (or water for making clean cap grout), using a nominal water-to-premix ratio of 0.60. This mix creates a pumpable slurry that cures into the saltstone waste form which immobilizes contaminants.

Table 3.2-6: Saltstone and Clean Cap Grout Formulation

Ingredient	Dry Feed Weight Percent
Blast furnace slag (grade 100 or 120)	45
Fly ash (Class F)	45
Ordinary Portland cement (Type II)	10

[SRNL-STI-2008-00421]

3.2.6 Closure Cap Design

An engineered closure cap will be installed over the SDF following the end of the operational period. The layers of the current preliminary closure cap design are based on an SRNL report (WSRC-STI-2008-00244), but with an increased slope at the surface (i.e., 3% slope instead of 1.5% slope) to meet closure requirements specified in the *New Consolidated Solid Waste Landfill Regulation*. [SCDHEC R.61-107.19] The closure cap design is preliminary and conceptual in nature, being consistent with a scoping level concept. However, it does provide sufficient information for planning purposes, evaluating the closure cap configuration relative to its constructability and functionality, and for estimating infiltration rates over time through modeling. Regardless, this closure cap design is not intended to constitute the final design. Final design and a re-evaluation of infiltration will be performed near the end of the operational period. Technological advances, increased knowledge, and improved modeling capabilities are all likely prior to closure and will result in improvements in both the final closure cap design and infiltration estimates. Any major changes to the design of the closure cap will require an updated evaluation via the appropriate change control processes (e.g., Unreviewed Waste Management Question (UWMQ) Evaluation, Special Analysis, PA revision, or equivalent process).

3.2.6.1 Closure Cap Background

The SDF closure cap is primarily intended to provide physical stabilization of the site, minimize infiltration, and provide an intruder deterrent. Two closure caps are anticipated to be constructed over the SDF disposal units at the end of the operational period: one large closure cap for the cylindrical SDUs and one smaller closure cap for the rectangular SDUs (see Figure 3.2-29). Cross sections from this preliminary closure cap design are also provided (see Figure 3.2-30 and Figure 3.2-31). [SRR-CWDA-2018-00087] During the operational period, active SDF facility maintenance sufficient to prevent both infiltration of rainwater into the disposal units and subsurface discharge out of the disposal units is assumed. Closure of the facility is assumed to begin with the installation of the closure cap (currently assumed to be October 1, 2037).

After installation of the closure cap, the 100-year institutional control period is assumed to begin, during which active SDF maintenance will be conducted to repair any significant erosion or closure cap defects and to prevent pine forest succession. Note that Section 4.4.1.3.2 indicates that the succession of pine forest would result in lower infiltration rates due to the abundance of above ground biomass and leaf area, relative to grass. [SRRA107772-000009] Despite this, during the institutional control period, the closure cap surface will be kept clear of any vegetation that might obstruct inspection of the closure cap surface.

Beyond the 100-year institutional control period, the performance of the closure cap throughout the remainder of the 1,000-year Compliance Period and the 10,000-year Performance Period (respectively) assume no active SDF maintenance will be conducted. [WSRC-STI-2008-00244]

3.2.6.2 Closure Cap Slope Length

The larger, northern area over the cylindrical SDUs was used to determine the most bounding approach for finding the maximum slope length. This larger cap has the longest slope, running to the northwest from an apex above SDU 6. This longest cap surface-slope is estimated to be 1,020 feet. [SRR-CWDA-2018-00087] The *Saltstone Disposal Facility Closure Cap Concept Update for Large-Scale Disposal Units* also includes an alternative closure cap design which assumes the previous 1.5% slope and includes the 375-foot diameter SDUs. This alternative design results in a maximum surface-slope of 1,170 feet, from an apex above SDU 6 towards the southeast. [SRR-CWDA-2018-00087] This longer slope length shall be assumed for estimating infiltration as it results in slightly higher values. The cap for the southern area over the rectangular SDUs is smaller than the cap for the northern area, so infiltration for the smaller cap is expected to be less than that of the larger closure cap. [WSRC-STI-2008-00244, SRRA107772-000009]

3.2.6.3 Closure Cap Physical Stability Requirements

Physical stability requirements for the final closure cap design shall be established according to stability calculations equivalent to those presented in Appendix A of *Saltstone Disposal Facility Closure Cap Concept and Infiltration Estimates*. [WSRC-STI-2008-00244] Stability calculations for the following key components of the closure cap will be developed in detail to support final closure cap designs:

- Vegetative soil cover,
- Erosion barrier,
- Side slope, and
- Toe of the side slope.

Figure 3.2-29: SDF Closure Cap Design Configuration

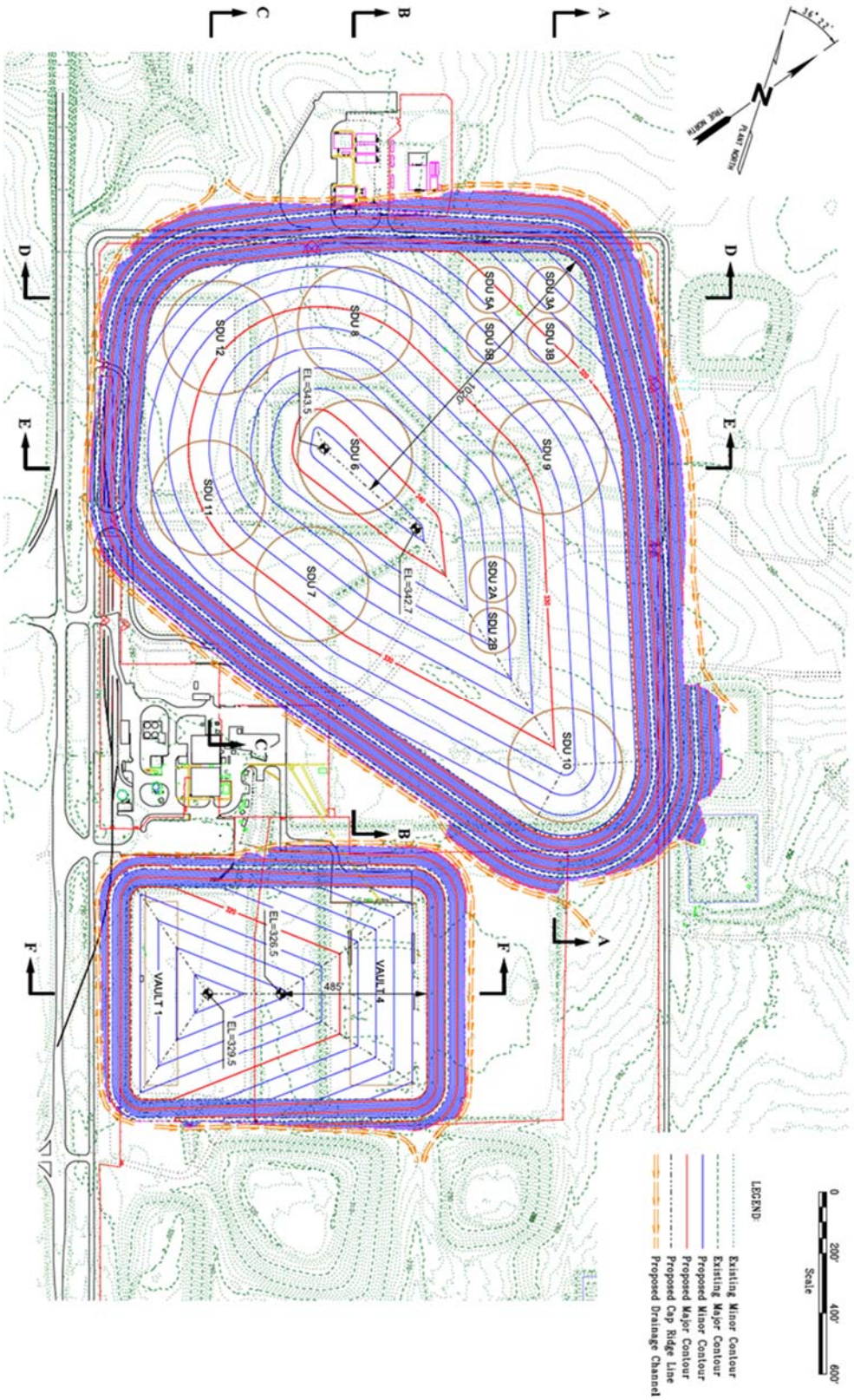

[SRR-CWDA-2018-00087]

Figure 3.2-30: SDF Closure Cap Design Configuration (Cross Sections 1 of 2)

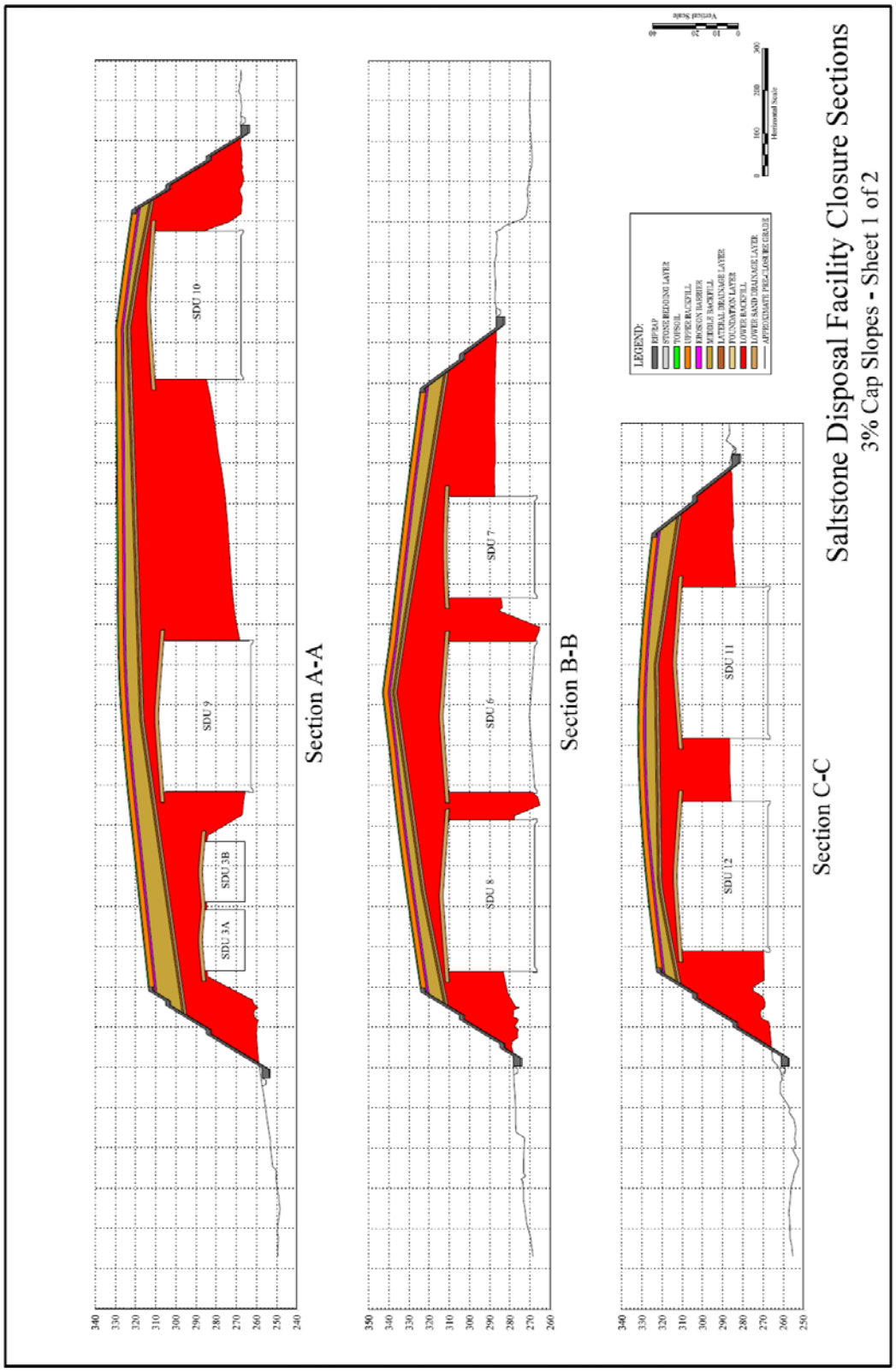

[SRR-CWDA-2018-00087]

Figure 3.2-31: SDF Closure Cap Design Configuration (Cross Sections 2 of 2)

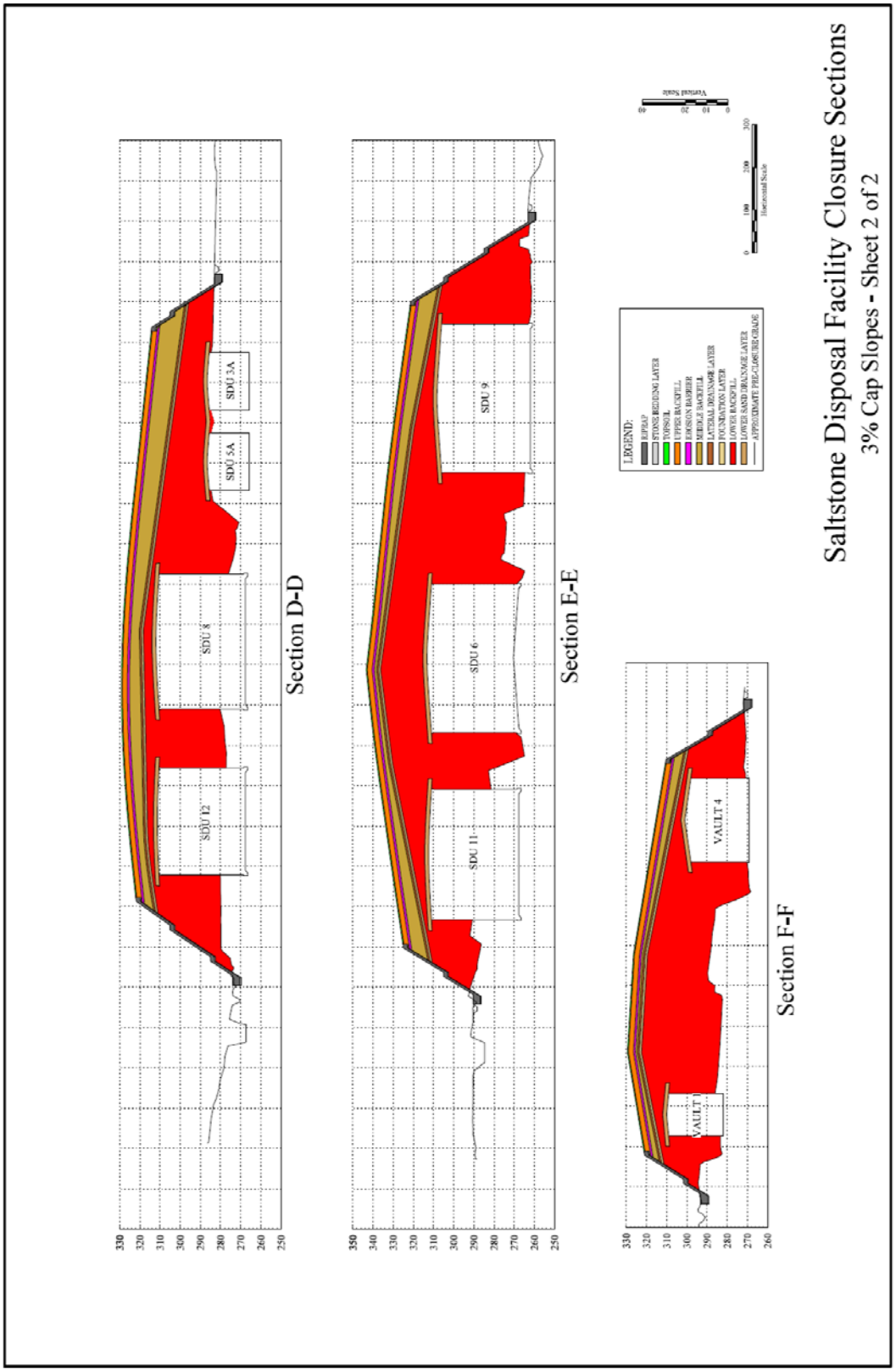

[SRR-CWDA-2018-00087]

3.2.6.4 Conceptual Closure Cap General Design Features

It is anticipated that the SDF closure cap will consist of the layers outlined in Table 3.2-7 and depicted from top to bottom in Figure 3.2-32 and Figure 3.2-33.

Table 3.2-7: Generic SDF Closure Cap Design Layers

Layer [a]	Layer Thickness (in)
Vegetative Cover	N/A
Topsoil	6
Upper Backfill	30
Erosion Barrier	12
Geotextile Fabric	Not specified.
Middle Backfill	12 (minimum, will increase from cap apex to toe due to difference between surface slope and the slope of the upper lateral sand drainage layer)
Geotextile Filter Fabric	0.1 (minimum)
Upper Lateral Sand Drainage Layer	12
Geotextile Fabric	Not specified.
High Density Polyethylene (HDPE) Geomembrane	0.06 (60 mil)
Geosynthetic Clay Liner (GCL)	0.2
Foundation Layer (backfill with bentonite admix)	12
Lower Backfill	12 (minimum, will increase from cap toe to apex due to slope of the upper lateral sand drainage layer)
Geotextile Filter Fabric [b]	Not specified.
Lower Lateral Sand Drainage Layer, extends approximately 25 feet from disposal unit [b]	24
Geotextile Fabric [b]	Not specified.
HDPE Geomembrane [b]	0.1
GCL [b]	0.2

[WSRC-STI-2008-00244, Table 4]

(a) The layers are arranged in the table to reflect their order from top to bottom in the SDF closure cap.

(b) Layer is above each disposal unit and does not cover the entire SDF area.

Note: Detailed explanations and functions of the layers are provided in Table 3.2-8.

Figure 3.2-32: SDF Conceptual Closure Cap Configuration

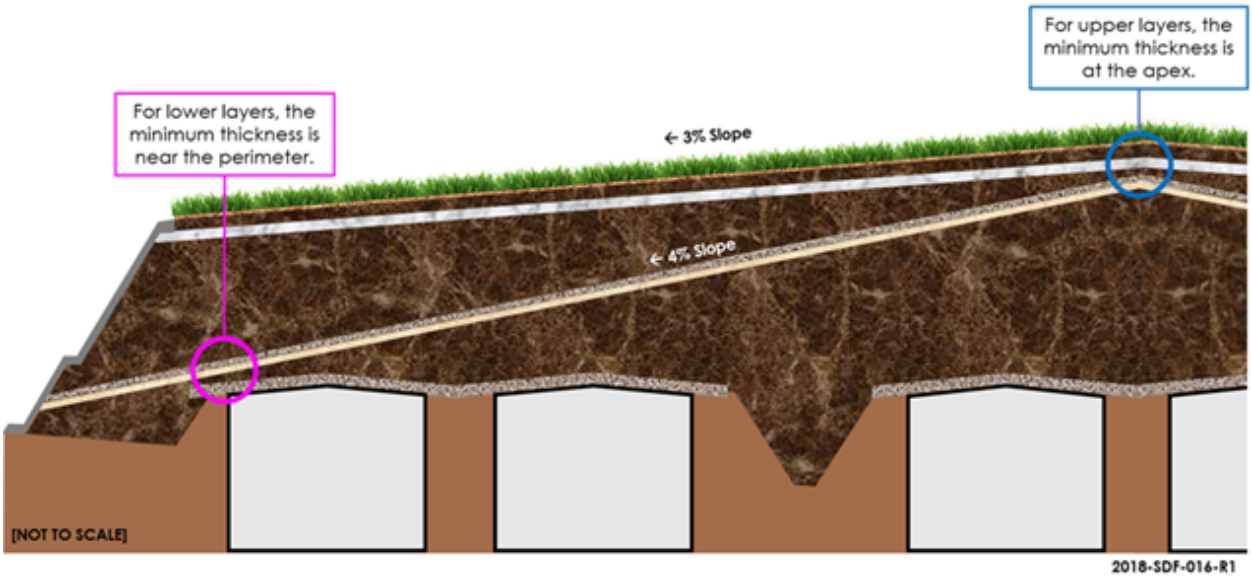

[SRR-CWDA-2018-00006]

Figure 3.2-33: SDF Conceptual Closure Cap Layers

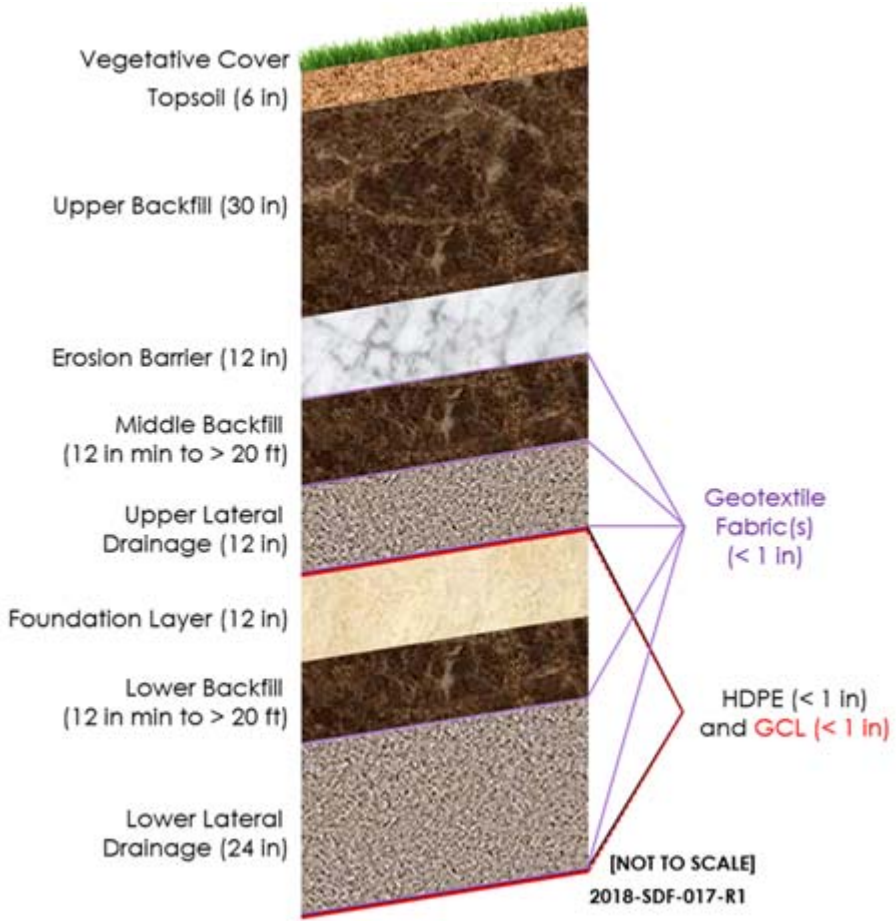

[SRR-CWDA-2018-00006]

Table 3.2-8 provides an overview of the function of each of these layers. Figure 3.2-34 illustrates the significant features associated with the conceptual design of the side slope and toe of the SDF closure cap.

Note that while the design of the closure cap shows the lower backfill and lower lateral sand drainage layers, these lower features are not explicitly included in the Closure Cap Model (as described in Section 4.4.1). Instead the Closure Cap Model provides percolation rates through the composite barrier (the combined HDPE and GCL layers) beneath the upper lateral sand drainage layer. These percolation rates are used as infiltration rates in the Vadose Zone Flow Model (described in Section 4.4.4). The Vadose Zone Flow Model does include these lower features. As a simplification, the Foundation Layer is not included in either model.

Table 3.2-8: Function of the SDF Closure Cap Design Layers

Layer	Function
Vegetative Cover	The vegetative cover will be established to promote runoff, minimize erosion, and promote evapotranspiration. The initial vegetative cover will be a persistent grass such as bahia. Other vegetation may be considered for the final closure cap design and may be planted at any point during the institutional control period.
Topsoil	The topsoil will be designed to support a vegetative cover, promote runoff, prevent the initiation of gullying, and provide water storage for the promotion of evapotranspiration.
Upper Backfill	The upper backfill will be designed to increase the elevation of the closure cap to that necessary for placement of the topsoil and to provide water storage for the promotion of evapotranspiration.
Erosion Barrier	The erosion barrier will be designed to prevent riprap movement during a probable maximum precipitation (PMP) event and therefore form a barrier to further erosion and gully formation (i.e., provide closure cap physical stability). It will be used to maintain a minimum 10 feet of clean material above the disposal units to act as an intruder deterrent. It will also act to preclude burrowing animals from access to underlying closure cap layers. It also provides minimal water storage for the promotion of evapotranspiration.
Geotextile Fabric	This geotextile fabric will be designed to prevent the penetration of erosion barrier stone into the underlying middle backfill and to prevent piping of the middle backfill through the erosion barrier voids.
Middle Backfill	The middle backfill will provide water storage for the promotion of evapotranspiration in the event that the topsoil and upper backfill are eroded away; the overlying erosion barrier provides only minimal water storage.
Geotextile Filter Fabric	This geotextile filter fabric will be designed to provide filtration between the overlying middle backfill and the underlying upper lateral sand drainage layer. This filtration will allow water to freely flow from the middle backfill to the upper lateral sand drainage layer, while preventing the migration of soil from the middle backfill to the upper lateral sand drainage layer.
Upper Lateral Sand Drainage Layer	The upper lateral sand drainage layer will be a 1-foot thick coarse sand layer designed to: ▪ Divert infiltrating water away from the underlying disposal units and transport the water to the perimeter drainage system, in conjunction with the underlying composite hydraulic barrier (i.e., HDPE and GCL), and

Layer	Function
	▪ Provide the necessary confining pressures to allow the underlying GCL to hydrate properly.
Geotextile Fabric	This geotextile fabric will protect the underlying HDPE from puncture or tear during placement of the overlying upper lateral sand drainage layer.
HDPE Geomembrane	The HDPE geomembrane will form a composite hydraulic barrier in conjunction with the GCL. The composite hydraulic barrier will be designed to promote lateral drainage through the overlying upper lateral sand drainage layer and minimize infiltration to the disposal units.
GCL	The GCL will form a composite hydraulic barrier described above in conjunction with the HDPE. As part of the composite hydraulic barrier, the GCL is designed to hydraulically plug any holes that may develop in the HDPE.
Foundation Layer	Provide structural support and required contours for slope of 4% for overlying layers. Provide relatively low-permeability layer directly above lower backfill.
Lower Backfill	The lower backfill will be designed to: ▪ Provide structural support for the rest of the overlying closure cap ▪ Produce the required contours and produce a slope of 4% for the overlying layers ▪ Produce the maximum 3:1 side slopes of the closure cap ▪ Promote drainage of infiltrating water away from and around the disposal units
Layers Above Each SDU	
Geotextile Filter Fabric	This geotextile filter fabric will be designed to provide filtration between the overlying lower backfill and the underlying lower lateral sand drainage layer. This filtration will allow water to freely flow from the lower backfill to the lower lateral sand drainage layer, while preventing the migration of soil from the lower backfill to the lower lateral sand drainage layer.
Lower Lateral Sand Drainage Layer	The lower lateral sand drainage layer will extend approximately 25 feet from each disposal unit and is designed primarily to prevent buildup of hydraulic head on top of the disposal units. The portion of this drainage layer extending beyond each disposal unit roof edge will be constructed atop backfill soils around the SDUs.
Geotextile Fabric	This geotextile fabric will be designed to protect the underlying HDPE from puncture or tear during placement of the overlying lower lateral sand drainage layer.
HDPE Geomembrane	The HDPE will be designed to form a composite hydraulic barrier in conjunction with the GCL. The composite hydraulic barrier will be designed to promote lateral drainage through the overlying lower lateral sand drainage layer and minimize infiltration to the disposal units.
GCL	The GCL will form a composite hydraulic barrier in conjunction with the HDPE as described above. As part of the composite hydraulic barrier, the GCL is designed to hydraulically plug any holes that may develop through the HDPE.

[WSRC-STI-2008-00244, Table 5]

Figure 3.2-34: SDF Conceptual Closure Cap: Side Slope and Toe Detail

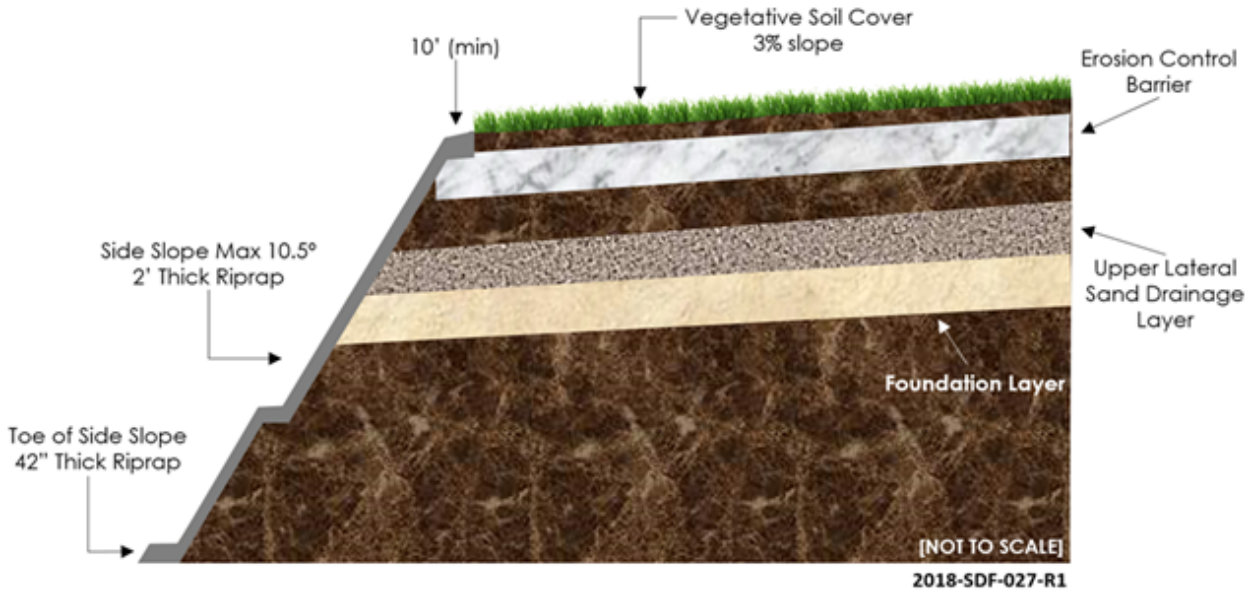

[WSRC-STI-2008-00244]

3.2.6.5 Site Preparation

Site preparation will be required to ready the SDF area for installation of the closure cap. The exact nature of such site preparation has not yet been determined. However, it will need to address the following:

- Above grade structures, utilities, and other interferences that could interfere with closure cap construction;
- Existing surfaces (surface soils, backfill soils placed around the SDUs, asphalt, riprap, disposal unit, etc.) over which the closure cap will be constructed; and
- Placement of GCL, HDPE, and geotextile fabric layers on each disposal unit prior to placement of lower lateral sand drainage layer above each disposal unit (e.g., if SDUs have HDPE along the outer walls, the HDPE above each disposal unit will be welded to the HDPE on the SDU sides).

The SPF, along with any other above-grade structures, utilities, etc. that could interfere with closure cap construction, will be removed from the SDF area prior to closure cap installation. The existing surfaces (i.e., surface soils, backfill soils placed around the SDUs, and riprap) over which the closure cap is to be constructed will be prepared prior to closure cap construction. Preparation includes removing three to six inches of existing surface soil to eliminate any topsoil and vegetation present, rough grading to establish a base elevation, and compaction. Additionally, existing riprap will be removed or voids within the existing riprap surfaces will be filled in to eliminate the potential for subsidence. [WSRC-STI-2008-00244]

Detailed information regarding the purpose, design, and constructability of each of the SDF closure cap layers listed in Table 3.2-8 are provided in WSRC-STI-2008-00244.

3.2.6.5.1 Closure Cap Preparation Above Each Disposal Unit

As described in WSRC-STI-2008-00244, a GCL will overlay each SDU. An HDPE layer will be placed over the GCL, followed by a geotextile fabric. Finally, the lower lateral sand drainage layer will be placed on top of the geotextile fabric. Because the lower lateral sand drainage layer, the geotextile fabric, GCL, and HDPE layers are placed directly above each disposal unit and are not contiguous across the closure cap, they are not considered part of the SDF closure cap for modeling purposes (instead, these features are included in the Vadose Zone Flow Model, described in Section 4.4.4). Further details regarding the lower lateral sand drainage layer, the geotextile fabric, GCL, and HDPE layers are provided in WSRC-STI-2008-00244.

3.2.6.5.2 Vegetative Cover

A vegetative cover will be established to promote runoff, minimize erosion, and promote evapotranspiration (ET). The topsoil will be fertilized, seeded, and mulched to provide a vegetative cover. The initial vegetative cover is assumed to be a persistent grass such as bahia. During seeding and establishment of the initial grass, appropriate mulch, erosion control fabric, or similar substances will be used to protect the surface. [WSRC-STI-2008-00244]

The area will be repaired through transplanting or replanting to ensure that a self-maintaining cover is developed. If it is determined that other vegetative species are more desirable for ensuring the long-term performance of the closure cap (e.g., bamboo), the other vegetative species will be planted as the final vegetative cover prior to the end of the 100-year institutional control period.

3.2.6.5.3 Closure Cap Side Slopes and Toe

The toe (along the perimeter) of closure cap side slopes will consist of a riprap layer. The intention of this riprap is to: (1) stabilize the underlying layer, (2) provide erosion protection to the toe, (3) transition flow from the side slope to adjacent areas, and (4) provide gully intrusion protection to the embankment. This riprap layer will extend at least 20 feet from the toe of the side slope as shown in Figure 3.2-34.

The closure cap side slopes will be placed at a maximum 10.5° slope and have a riprap surface with an underlying gravel bedding layer to prevent gully formation on the side slopes and to provide long-term slope stability. The side-slope riprap and underlying gravel bedding layer will extend from the toe of the side slope, up the side slope, and onto the top slope for at least 10 feet, as shown in Figure 3.2-34.

An integrated drainage system will be designed and built to handle the runoff from the closure cap and drainage from the lateral sand drainage layers. The runoff and lateral drainage will be directed to a system of riprap-lined ditches, which will be designed in accordance with current guidance (equivalent to

NUREG-1623). [ML022530043,] The riprap-lined ditches will direct the water away from the SDF closure cap as a whole and will be constructed around the perimeter of the SDF closure cap. The ditches will discharge into sedimentation basins, as necessary for sediment control. [WSRC-STI-2008-00244]

3.2.6.6 Closure Cap Performance without Degradation

Figure 3.2-35 depicts a summary of intermediate results (water balance) from intact closure cap modeling described in *Predicting Long-Term Percolation from the SDF Closure Cap* (SRRA107772-000009). This closure cap model was developed using WinUNSAT-H software. The material properties used in this assessment of the closure cap configuration are provided in SRRA107772-000009.

Figure 3.2-35: SDF Closure Cap: Year 0 (intact) Water Balance

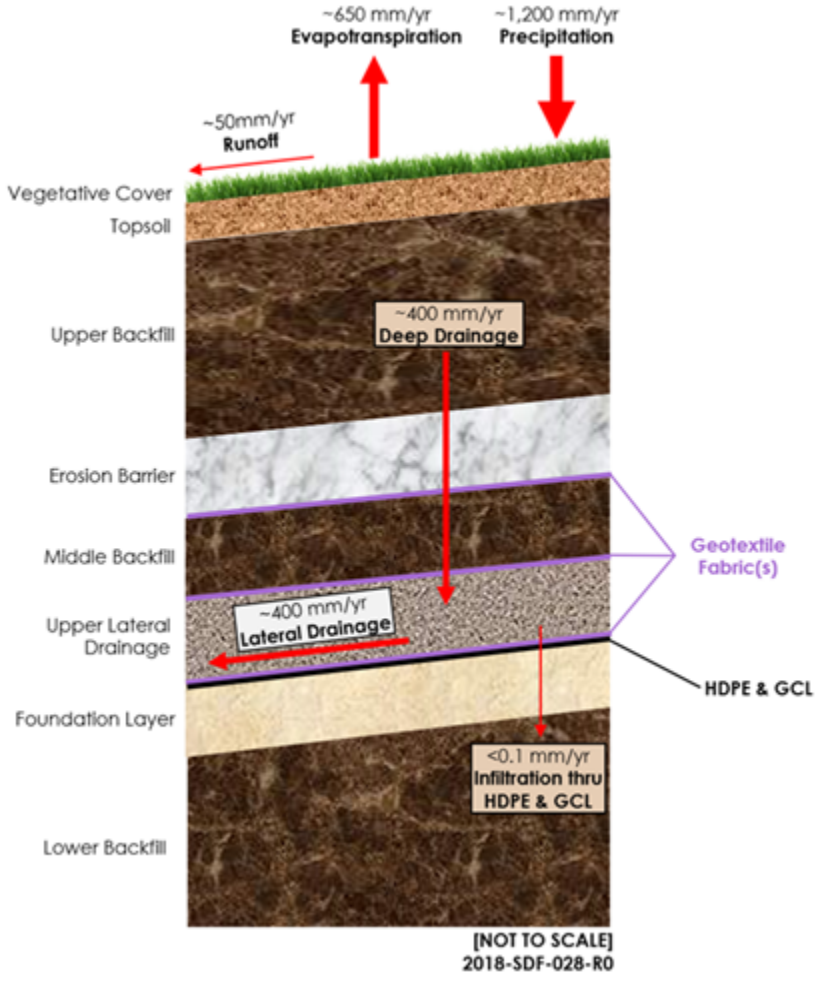

[Developed based on SRRA107772-000009]

3.2.6.7 Closure Cap Degradation Mechanisms

Potential SDF closure cap degradation mechanisms presented in this section are discussed in context of the Central Scenario. This scenario assumes that climate conditions remain

the same as current conditions throughout the 10,000-year Performance Period, and that the vegetative cover remains as grass. [SRRA107772-000009]

Table 3.2-9 provides a list of potential SDF closure cap degradation mechanisms that were considered during the development of the closure cap design or for the development of the closure cap model. [WSRC-STI-2008-00244, SRRA107772-000009] The table lists the potential degradation mechanisms associated with the various SDF closure cap layers.

Table 3.2-9: SDF Closure Cap, Potential Degradation Mechanisms

Affected Layer	Potential Degradation Mechanism
All	Static loading induced settlement Seismic induced liquefaction and subsequent settlement Seismic induced slope instability Seismic induced lateral spread Seismic induced direct rupture due to faulting SDU or saltstone subsidence
Vegetative Cover	Succession Stressors (droughts, disease, fire, and biological)
Soil above the Erosion Barrier	Erosion Loss of compaction Desiccation (wet-dry cycles) Biological (root penetration, burrowing animals)
Erosion Barrier	Weathering (Dissolution) Biological (root penetration only) Chemical (waste leachate)
Lateral Sand Drainage Layers	Silting-in Biological (root penetration for upper sand drainage layer only) Mineral precipitation and microbial growth
HDPE Geomembrane	Ultraviolet (UV) radiation Antioxidant depletion Thermal oxidation High energy irradiation Tensile stress cracking Biological (microbial, root penetration) Chemical (waste leachate)
GCL	Slope stability Freeze-thaw cycles Dissolution Divalent cations (Ca^{+2}, Mg^{+2}, etc.) Desiccation (wet-dry cycles) Biological (root penetration, burrowing animals) Chemical (waste leachate)

3.2.6.7.1 Seismicity, Settlement, or Subsidence

As described in Section 6.1 of *Saltstone Disposal Facility Closure Cap Concept and Infiltration Estimates* (WSRC-STI-2008-00244):

> *Settlement will occur due to two phenomena: first settlement due to the static load of the cap system itself, and second settlement due to seismic shaking (liquefaction or partial liquefaction). The current SDF closure cap concept indicates that the thickness of the cover system will be on the order of 25-ft to 45-ft over the disposal cell tops. It is expected that static settlement due to this load … would be less than*

2 to 3 inches, based on previous analyses in nearby F-Area. This amount of settlement would be expected to occur uniformly over the entire area of the cap, thus differential settlement would be negligible assuming the subsurface conditions are relatively uniform.

Further, seismic-induced lateral spread and seismic-induced direct rupture due to faulting are both considered to be of no consequence as the location of the SDF is not conducive to lateral spreading or surface faulting. [WSRC-STI-2008-00244]

With respect to the stability of each SDU, prior to construction each site undergoes a rigorous geotechnical investigation to confirm the suitability of the site, as indicated by Table 3.2-10.

Table 3.2-10: Site-Specific Geotechnical Investigations for the SDF

Investigation	Geotechnical Reports
Site Stability, General	K-CLC-Z-00002 K-CLC-Z-00027
Site Stability, SDU 1	K-ESR-Z-00003 K-CLC-Z-00018 K-CLC-Z-00019 K-CLC-Z-00020 K-CLC-Z-00021
Site Stability, SDU 2	K-ESR-Z-00001 K-CLC-Z-00005 K-CLC-Z-00007 K-CLC-Z-00008 K-CLC-Z-00009 K-CLC-Z-00010 K-CLC-Z-00011
Site Stability, SDU 4	K-CLC-Z-00001 K-CLC-Z-00003 K-CLC-Z-00004
Site Stability, SDU 3 & 5	K-ESR-Z-00002 K-CLC-Z-00012 K-CLC-Z-00013 K-CLC-Z-00014 K-CLC-Z-00015 K-CLC-Z-00016
Site Stability, SDU 6	K-ESR-Z-00005 K-CLC-Z-00022 K-CLC-Z-00024 K-CLC-Z-00025 K-CLC-Z-00026 K-ESR-Z-00004 K-ESR-Z-00006
Site Stability, SDU 7	K-ESR-Z-00008 K-CLC-Z-00029 K-CLC-Z-00031 K-CLC-Z-00032 K-CLC-Z-00033

Of these site-specific geotechnical investigations, only one indicated that there may be some risk of settlement requiring additional evaluation: *Evaluation on the*

Stability of Saltstone Disposal Facility Closure Cap System over SDU 4 with Cells C and I Containing Stacked Waste Bags. [K-CLC-Z-00028] This investigation looked at piles of waste bags that were placed into SDU 4 Cells C and I, and postulated that once they are grouted in place there is a possibility that air may become trapped, leaving void spaces subject to potential collapse.

Subsidence of the saltstone waste form or collapse of the SDU roof is not considered a credible degradation mechanism to the SDF closure cap because the disposal units will be filled with saltstone or "clean" grout (i.e., uncontaminated grout) to eliminate void spaces. See additional discussion in Section 5.8.7.3.

3.2.6.7.2 Vegetation: Succession or Stressors

As described earlier, the initial vegetative cover is assumed to be a persistent grass such as bahia. It is noted that "Bahia [grass] is a very hardy species in this region and will continue to be a dominant ground cover for many years after active maintenance has ceased." [WSRC-STI-2008-00244] While grass is assumed for the duration of the PA models, it is expected that over time pine forestation will advance and overtake the grass as the primary vegetative cover atop the closure cap.

As explained in Section 4.4.1, three vegetative covers were considered: specifically, grass, bamboo, and pine. The "abundance of above ground biomass and leaf area for both species [i.e., bamboo and pine] relative to grass will transpire more than a grass cover because transpiration is proportional to leaf area … Thus, assuming grass cover permits more water to become deep drainage that enters the lateral drainage layer than would occur with pine or bamboo cover." [SRRA107772-000009] As such, a simplifying assumption is made that the bahia grass cover will persist indefinitely.

If it is determined that a vegetative species other than grass is more desirable for ensuring the long-term performance of the closure cap, then the more desirable vegetative species will be planted as the final vegetative cover prior to the end of the 100-year institutional control period. Appropriate evaluations will be performed to confirm that performance objectives will continue to be met.

With respect to stressors, Section 6.2 of *Saltstone Disposal Facility Closure Cap Concept and Infiltration Estimates* (WSRC-STI-2008-00244) states:

> *Vegetative stressors (droughts, disease, fire, and biological) primarily impact the SDF closure cap in terms of the rate of succession rather than as any long term degradation mechanism on their own. Therefore these vegetative stressors will not be considered as a SDF closure cap degradation mechanism for modeling purposes.*

3.2.6.7.3 Loss of Compaction

In previous closure cap modeling, loss of soil compaction was not considered. Accordingly, *Saltstone Disposal Facility Closure Cap Concept and Infiltration Estimates*

(WSRC-STI-2008-00244) recommended the use of backfill properties which were based on studies of control-compacted backfill. For the upper and middle backfill layers, the assumed material properties have been updated to represent soils that have undergone pedogenesis and are in equilibrium with their surroundings. [SRRA107772-000009] For example the saturated hydraulic conductivity has been increased from a previous value of 4.1E-05 cm/s to 1.0E-04 cm/s. The revised properties are consistent with recommendations for the hydraulic properties of earthen covers in NUREG/CR-7028. [ML12005A110]

Note that for the lower backfill layer, this SDF PA still assumes compaction (e.g., 4.1E-05 cm/s) on the basis that pressure from the overlying layers is expected to maintain the compaction in perpetuity.

3.2.6.7.4 Erosion and Gullying

As a requirement for an acceptable final closure cap design, physical stability requirements will be established based on a stability analysis equivalent to that presented in Appendix A of *Saltstone Disposal Facility Closure Cap Concept and Infiltration Estimates* (WSRC-STI-2008-00244). Such an analysis will ensure that the closure cap will be engineered in a manner that mitigates risks associated with potential erosion or gullying events.

Section 6.3.1 of *Saltstone Disposal Facility Closure Cap Concept and Infiltration Estimates* (WSRC-STI-2008-00244) states:

> *[T]he SDF closure cap vegetative soil cover (i.e., topsoil and upper backfill), erosion barrier, side slope, and toe of the side slope have been designed to be physically stable relative to erosion potential resulting from a SRS-specific PMP event … While the slope and slope length of topsoil and upper backfill layers have been specified to prevent the initiation of gullying during a PMP event, these layers are subject to erosion, since they are located above the erosion barrier. The erosion barrier has been designed to preclude further erosion into the SDF closure cap profile … Therefore layers located below the erosion barrier are not subject to erosion. Since the soil layers located above the erosion barrier are subject to erosion, erosion of these layers will be considered as a SDF closure cap degradation mechanism for modeling purposes.*

Any physical stability requirements established by the stability analysis will be documented in a revision to *Unreviewed Waste Management Question Requirements Document for Saltstone Facility* (SRR-CWDA-2011-00196). This document is issued to provide Unreviewed Waste Management Question (UWMQ) screening criteria used to ensure that salt waste disposal activities will not invalidate the results or conclusions of the SDF PA (per S4-ENG.46).

3.2.6.7.5 Desiccation (Wet-Dry Cycles) and Freeze-Thaw Cycles

Section 6.3.2 of *Saltstone Disposal Facility Closure Cap Concept and Infiltration Estimates* (WSRC-STI-2008-00244) indicates that the soil properties for soils assumed for the closure cap materials are highly unlikely to undergo significant cracking related to wet-dry cycles and therefore will not be considered a viable SDF closure cap degradation mechanism. Similarly, Section 6.3.2 of *Saltstone Disposal Facility Closure Cap Concept and Infiltration Estimates* (WSRC-STI-2008-00244) indicates that the local climate is such that the depth of any freeze-thaw cycle is not sufficient to significantly impact the closure cap and will also not be considered as a viable SDF closure cap degradation mechanism.

3.2.6.7.6 Biological Intrusion

Section 6.7.7 of *Saltstone Disposal Facility Closure Cap Concept and Infiltration Estimates* (WSRC-STI-2008-00244) states:

> *Plant roots can freely penetrate unprotected GCLs and results in increases in the hydraulic conductivity of the GCL… but not HDPE geomembranes except in locations of existing holes within the HDPE geomembrane.*

and:

> *While burrowing animals can potentially damage unprotected GCLs in general, damage of the SDF Closure Cap GCL is not considered a threat due to the presence of the overlying erosion barrier, which will be designed to preclude burrowing animals … from reaching the GCL. Therefore burrowing animals will not be considered as a SDF Closure Cap GCL degradation mechanism for modeling purposes.*

However, the *Saltstone Disposal Facility Closure Cap Concept and Infiltration Estimates* (WSRC-STI-2008-00244) relied on assumptions about the propagation of holes through the HDPE, asserting that root penetration through these holes could become significant over time. This assumption has been discounted as unreasonable in *Predicting Long-Term Percolation from the SDF Closure Cap* (SRRA107772-000009), which states:

> *Jones and Phifer (2008)* [WSRC-STI-2008-00244] *assumed that the hydraulic conductivity of the GCL would increase in response to penetration of tree roots if the surface of the cover ultimately was covered with pine or bamboo. Studies conducted since 2008 suggest this is not a reasonable scenario. Vegetation is opportunistic, seeking out sources of water that require the least amount of energy to extract. Roots accumulate in regions where water is more plentiful and readily extracted, and do not grow towards regions where water is less plentiful and more difficult to extract. For example, when covers are exhumed, roots are observed on the surface of textural contrasts where water accumulates (e.g., on the upper surface of fine-over-coarse arrangement of soil layers). The composite barrier,*

> *drainage layer, and overlying soils in the ECC* [engineered closure cap] *promote accumulation of water above the composite barrier, and drying of soils below the composite barrier... Thus, root systems accumulate above composite barriers rather than below them. No root systems were observed below the composite barrier at any of the covers evaluated in NUREG/CR-7028* (ML12005A110).

As a result of this recent characterization of root penetrations (relative to the SDF closure cap), damage due to tree roots was not considered a viable degradation mechanism for the closure cap as long as the GCL remains intact from other degradation mechanisms. Note that this conclusion is also consistent with the assumed vegetative cover of bahia grass.

3.2.6.7.7 Chemical Degradation and Weathering

For the SDF closure cap, chemical degradation from contact with waste leachate (a potential by-product from weathering) is generally not applicable to the closure cap layers because these layers are all located above the SDUs and the predominant direction of flow is expected to be from the top down. Further, the saltstone waste form is contained within the SDUs and located multiple feet below any closure cap layer that could potentially be affected by leachate (i.e., erosion barrier, HDPE, and the GCL). Therefore, chemical degradation of the SDF closure cap by leachate is not considered applicable. [WSRC-STI-2008-00244]

3.2.6.7.8 Cation Exchange

Section 6.7.4 of *Saltstone Disposal Facility Closure Cap Concept and Infiltration Estimates* (WSRC-STI-2008-00244) states:

> *The bentonite used in GCLs is generally sodium or calcium bentonite. Sodium bentonite is used more frequently than calcium bentonite because of its superior swelling capacity and lower initial permeability … However within closure caps, sodium bentonite GCLs that are not protected by an overlying geomembrane are susceptible to exchange of sodium with divalent cations such as calcium and magnesium particularly when calcium and magnesium rich soils overly* [sic] *the GCL … The conversion of hydrated sodium bentonite to calcium bentonite results in a decrease in the swell potential or potential volume of water bound to the mineral surface (i.e., immobile water) and a subsequent increase in the saturated hydraulic conductivity of the GCL particularly under conditions of low confining or overburden stress such as found in closure caps.*

However, this interpretation of the process has been superseded based on more recent observations. As described in *Predicting Long-Term Percolation from the SDF Closure Cap* (SRRA107772-000009):

> *Recent studies have shown … that GCLs hydrate and rapidly swell osmotically in humid climates, and that the water associated with this swelling process is strongly bound to the bentonite surface. Consequently, even if cation exchange occurs, the*

> *hydraulic conductivity remains unchanged provided that the GCL does not dehydrate.*

Consistent with these observations, the SDF closure cap modeling described in *Predicting Long-Term Percolation from the SDF Closure Cap* (SRRA107772-000009) indicates that:

> *The saturated hydraulic conductivity of the GCL was assumed to be 1×10^{-10} m/s (as recommended in NUREG/CR-7028* (ML12005A110) *for conditions without specific data) or 1×10^{-11} m/s (based on recent exhumations of GCLs in composite barriers at sites in humid climates).*

3.2.6.7.9 Mineral Precipitation and Microbial Growth

Degradation due to mineral precipitation and microbial growth are primarily degradation mechanisms associated with leachate collection layers rather than closure cap layers. Leachate collection layers receive leachate containing both organic and inorganic degradation products from waste; whereas, closure cap layers only receive non-contaminated water from infiltration. Since infiltrating SRS water is very low in both mineral and organic content and the layers will not contact waste leachate, mineral precipitation and microbial growth within the lateral sand drainage layers is not considered applicable to the SDF closure cap.

3.2.6.7.10 Slope Stability

The geotechnical investigations identified in Table 3.2-10 include considerations of slope stability specific to the construction of each SDU. A similar analysis will be performed to consider the slope stability of the final design of the SDF closure cap prior to emplacement. Additional analysis and discussion with respect to slope stability is provided in Section 4.4.1.

3.2.6.7.11 HDPE Degradation

As described in the *Conceptual Model Development for the Saltstone Disposal Facility Performance Assessment* (SRR-CWDA-2018-00006), HDPE layers are expected to degrade as a result of antioxidant depletion. For estimating the service life of an HDPE, three stages of chemical aging are considered (see Figure 3.2-36): antioxidant depletion (T_A), induction time (T_B), and polymer degradation (T_C). During the first stage (T_A), two processes occur which deplete antioxidants: oxygen diffuses into the geomembrane and the physical loss of the antioxidants from the geomembrane. Once the antioxidants have been depleted, oxidation of the HDPE begins (T_B); however, this process is initially very slow with negligible impacts. Finally, the oxidation process accelerates (T_C), resulting in decomposition in the material as free radicals attack the polymer chains. [DOI: 10.1061/(ASCE)1090-0241(1998)124:6(532)] It is assumed that this chemical decomposition process will be localized, attacking the edges of the material (i.e.,

pre-existing defects or holes), which will result in an increase of the diameter of the existing holes.

Figure 3.2-36: Conceptual Stages of Chemical Aging of HDPE Geomembranes

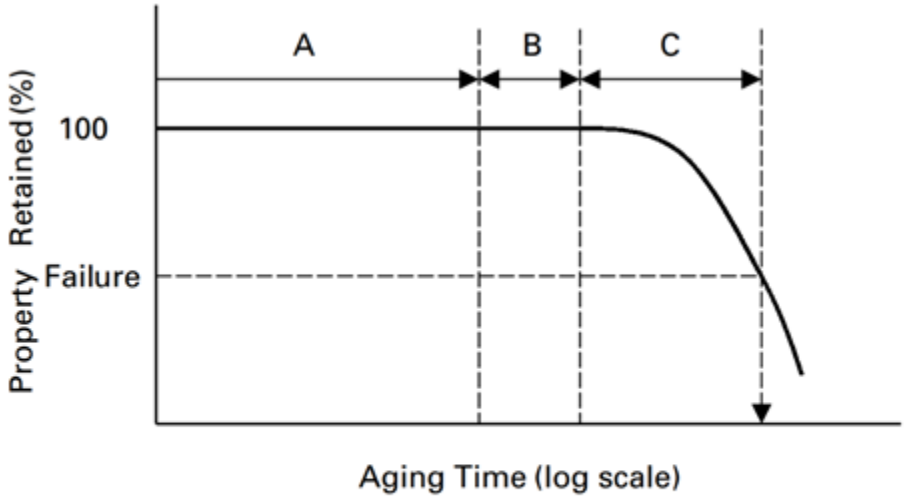

A = Period during which depletion of antioxidants occurs
B = Induction time to onset of polymer degradation
C = Time to reach the failure level of degradation of a particular property

Service Life $T = T_A + T_B + T_C$

[DOI: 10.1061/(ASCE)1090-0241(1998)124:6(532)]

The assumed timing for each degradation stage is primarily based on Tian, et.al. (2017), *Antioxidant Depletion and Service Life Prediction for HDPE Geomembranes Exposed to Low-Level Radioactive Waste Leachate*. [DOI: 10.1061/(ASCE)GT.1943-5606.0001643] For HDPE in a low-level waste disposal facility, the predicted antioxidant depletion time (T_A) is 730 years. For the second and third stages, Tian, et.al. (2017) considered three properties: break strength, break strain, and stress crack resistance. For Stage II (T_B), the shortest duration is 25 years and for Stage III (T_C) the shortest duration is 1,220 years. Thus, the total service life is estimated to be 1,975 years. It should be noted that this is estimate is biased towards a shorter service life. Based on other information provided in Tian, et.al. (2017), the HDPE service life could extend to as long as 3,550 years.

The remaining HDPE degradation processes identified in Table 3.2-9 (which are not otherwise discussed) include: ultraviolet radiation, thermal oxidation, and high energy irradiation. Section 6.6 of *Saltstone Disposal Facility Closure Cap Concept and Infiltration Estimates* (WSRC-STI-2008-00244) describes each of these processes and provides a basis for excluding them from further consideration.

3.2.6.7.12 Silting-In

"Silting-in" is a process in which it is assumed that the lateral sand drainage layers silt up over time as colloidal clay migrates from the overlying backfill. [WSRC-STI-2008-00244] However, as described in *Predicting Long-Term Percolation from the SDF Closure Cap*, this phenomenon "has not [been] observed during exhumation of modern final covers or in historic sites that are analogs." [SRRA107772-000009] This can be seen in photographs of the layered soils analogues (see Figure 3.2-37, Figure 3.2-38, and Figure 3.2-39).

These photographs provide evidence that layered soils remain well-structured and that any silting-in processes are unlikely to occur. Therefore, this process will not be considered a viable degradation mechanism for modeling purposes.

Figure 3.2-37: Analog Site: 8-Year-Old Engineered Cover in Omaha, NE

[ML12005A110, SRRA107772-000009]

Figure 3.2-38: Analog Site: 3,000-Year-Old Tu-Dun Tombs in South-Central China

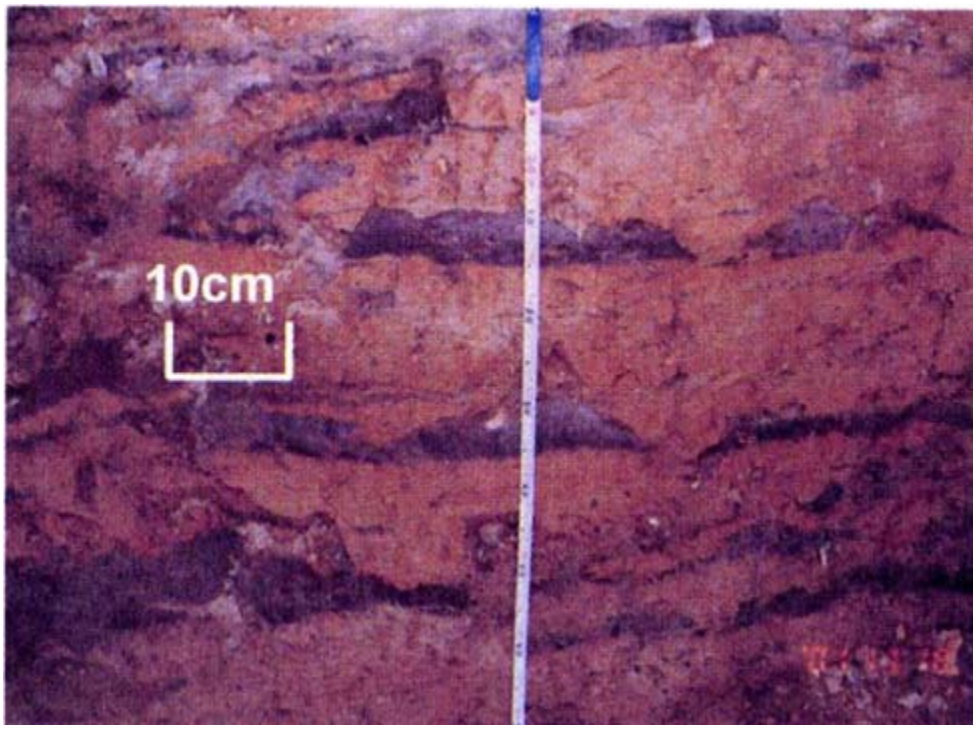

[Onitsuka, et.al. (2006), SRRA107772-000009]

Figure 3.2-39: Analog Site: 2,000-Year-Old Burial Mound in Northern Kyushu Prefecture, Japan

[Hudson and Barnes (1991), SRRA107772-000009]

3.2.6.7.13 Summary of Degradation Mechanisms

Nearly all of the degradation mechanisms identified in Table 3.2-9 are not applicable to the SDF closure cap and will not receive further consideration. Notable exceptions are considerations of erosion, gullying, and slope stability, which will be addressed to support final closure cap design, and HDPE degradation from anti-oxidant depletion which is incorporated in closure cap modeling as well as the cementitious degradation modeling (see Sections 4.4.1 and 4.4.2). In addition, differential settlement of the closure cap above Cells C and I of SDU 4 is also analyzed to address any risks associated with the potential of void spaces associated with waste bags (see Section 5.8.7.3).

Section 4.4.1 describes the closure cap modeling based on this closure cap design and the identified degradation mechanisms.

3.2.6.8 Open Issues for Further Design

Listed below are open issues related to the SDF closure cap concept, particularly in regard to degradation issues, which will be addressed as the design concept matures in the future.

- Are other vegetative species more desirable for improving or enhancing the overall performance of the closure cap?
- What are the requirements for the lower backfill particularly in terms of its ability to drain water away from and around the disposal units?
- What is the estimated weathering rate of the erosion barrier, toe of side slopes, and side slopes stone (assumed granite) based upon natural or archaeological analogs and available literature?
- What material should be used to fill the stone voids of the erosion barrier to prevent loss of overlying material into the erosion barrier?
- Should a sodium bentonite or calcium bentonite GCL be used?
- Is the 50-foot extension of the closure cap beyond the sides of the disposal units sufficient to prevent infiltration at the side slopes, the perimeter drainage system, or the natural surrounding land surface from impacting contaminant transport out of the disposal units?

The final design must allow the free transport of water out of the lateral sand drainage layers and into the side slope riprap, while at the same time preventing sand movement from the lateral sand drainage layers into the side slope riprap.

3.3 Development of PA Waste Inventory

The following approach was used for estimating radiological and chemical inventories for use in the SDF PA modeling for those contaminants listed in Table 3.3-1 and Table 3.3-2.

- The current SDF inventory (as of March 31, 2018), current Tank Farm total inventory, and the projected H-Canyon to Tank Farm influent inventory were used to develop initial inventory estimates.

- Adjustments were made to the initial inventory estimates to account for some uncertainty in the final inventory estimates. These adjustments included developing an inventory for those radionuclides not reported and recommendations for PA modeling were applied to potential dose drivers.
- The contaminant screening process discussed in Section 3.3.2 consisted of several steps to arrive at a risk-informed list of radionuclides and chemicals to be included in the SDF closure inventory estimates.

Specific details of the inventory methodology can be found in SRR-CWDA-2018-00041, Rev. 3, and of the screening methodology in SRR-CWDA-2018-00044, Rev. 3.

Table 3.3-1: Radionuclides Considered for SDF Inventory Development

H-3	Nb-94	Pr-144	Th-229	Pu-242
C-14	Tc-99	Ce-144	Th-230	Am-242m
Na-22	Ru-106	Pm-147	Pa-231	Am-242
Al-26	Rh-106	Sm-147	Th-232	Cm-242
Cl-36	Pd-107	Sm-151	U-232	Cm-243
K-40	Ag-108m	Eu-152	U-233	Am-243
Ca-41	Te-125m	Gd-152	U-234	Pu-244
Ni-59	Sb-125	Eu-154	U-235	Cm-244
Co-60	Sb-126	Eu-155	U-236	Cm-245
Ni-63	Sb-126m	Lu-174	Np-237	Cm-246
Se-79	Sn-126	Pt-193	Pu-238	Cm-247
Y-90	I-129	Bi-210m	U-238	Cm-248
Sr-90	Cs-134	Pb-210	Pu-239	Bk-249
Zr-93	Cs-135	Ra-226	Pu-240	Cf-249
Nb-93m	Ba-137m	Ac-227	Pu-241	Cf-251
Mo-93	Cs-137	Ra-228	Am-241	Cf-252

Table 3.3-2: Chemicals Considered for SDF Inventory Development

Ag	Cd	F^-	Mo	PO_4	U
Al	Cl^-	Fe	Ni	Sb	Zn
As	Co	Hg	NO_2	Se	
B	Cr	I	NO_3	SO_4	
Ba	Cu	Mn	Pb	Sr	

It should be noted that all waste transferred to SPF is required to be in compliance with the Waste Acceptance Criteria (WAC) of SDF, thus all inventory currently disposed of at SDF and all future inventory is/will be compliant with the SDF WAC. No waste processed for final disposal in SDF shall exceed WAC limits set forth in X-SD-Z-00004 and compliance with the SDF WAC is demonstrated using the *Tank 50 Waste Compliance Plan for Transfers to Saltstone During Salt Disposition Integration (SDI)*, X-WCP-H-00043. If the WAC cannot be met, a deviation may be granted if justified by the generator and determined by the Saltstone Facility Engineering to be within the safety basis and permit condition for waste treatment and disposal in Z-Area. Additionally, as Decontaminated Salt Solution (DSS) is transferred from the SPF feed tank (Tank 50) to SDF for on-site disposition, the material is routinely sampled for chemical and radionuclide constituents.

3.3.1 Inventory Methodology

To estimate the future material to be disposed of within the SDF, the starting point material currently stored in the Tank Farm waste tanks and additional material received to the Tank Farm from the H-Canyon were identified as the source of the disposed of material. Then the radionuclides were adjusted based on their expected treatment processes. The remaining inventory was assumed to be sent to Saltstone and was distributed among the certain disposal units with remaining space and future disposal units.

3.3.1.1 Initial SDF Inventory

The initial SDF inventory was estimated by using the SDF - Waste Inventory Disposed Estimator (SDF-WIDE) model (SRR-CWDA-2015-00003) which uses waste sample analysis results from the SDF feed tank and transfer volumes into the SDUs to estimate of disposal inventories. Saltstone Engineering issues a quarterly report to provide data required by Section III.7 of the Consent Order of Dismissal (07-ALJ-07-121-CC), including cumulative process volume of salt waste, cumulative process volume of saltstone, and cumulative inventory of radioactivity (in curies). Tank 50 sample analysis results are also used to update the SDF-WIDE model disposed of and current inventory on an annual basis.

In order to update the current SDF radiological and chemical inventory for those constituents listed in Table 3.3-1 and Table 3.3-2, historical Tank 50 sample information described above was compiled from the beginning of SPF processing. Where historical data was not available, information was either calculated based on documented special methods or estimated based on process knowledge. Transfer volume data was also compiled using the Saltstone Engineering quarterly reports from the beginning of processing using the volumes reported transferred from Tank 50 to the SPF. The radionuclide inventory resulting from the combination of these transfers and corresponding representative samples was decayed to March 31, 2018, to develop the "current inventory" for SDF using the SDF-WIDE model Version 1.7 as described in SRR-CWDA-2018-00041, Rev. 3.

3.3.1.2 Initial Tank Farm Inventory Estimates

The majority of the radionuclide concentrations and the entire inventory of chemical constituents in the Tank Farm are estimated using data from the SRS Waste Characterization System (WCS).

3.3.1.2.1 The Waste Characterization System

WCS is an electronic information system that tracks waste tank data, including radiological and chemical inventories, based on sample analyses, process histories, composition studies, and theoretical relationships. [CMT-HTF-2017-00069] The system (initially developed in 1995) tracks the dry sludge concentrations of 40 radiological and 37 chemical waste compounds in each of the SRS waste tanks. The 40 radionuclides tracked in WCS were selected primarily based on their

impact on waste tank safety basis source term, inhalation dose potential, or on the E-Area Vault WAC.

Currently, WCS tracks total supernate (free liquid, salt interstitial liquid and sludge interstitial liquid) inventories of Cs-137, Ba-137m, Th-232, U-232, U-234, U-235, U-236, U-238, Np-237, Pu-238, Pu-239, Pu-240, Pu-241, Am-241, Am-242m, Cm-244, and Cm-245. Within WCS, H-3, C-14, Co-60, Ni-63, Sr-90, Yr-90, Tc-99, and I-129 liquid supernate phase inventories are estimated with algorithms. Concentrations of C-14, Sr-90, Y-90, Cs-137, Ba-137m, U-235, U-238, Pu-238, and Pu-239 of the entrained sludge solids in the saltcake as reported in WCS are multiplied by the total salt volume in each tank to obtain salt radioactive inventories. Total supernate inventories of Ag, Al, As, B, Ba, Benzene, Ca, Cd, Co, Cr, Cs, Cu, Fe, Hg, Mg, Mn, Mo, Nd, Ni, Pb, Pu, Ru, Se, Si, Sr, Ti, TPB, U, Zn, Zr, $AlOH_4^-$, Cl^-, CO_3^-, $C_2O_4^-$, F^-, Na, NO_2^-, NO_3^-, OH^-, PO_4^{-3}, and SO_4^- for each waste tank are taken from WCS.

Further information concerning the use of the WCS and its maintenance is provided in SRR-CWDA-2018-00041, Rev. 3. The applicable Computer Program Modification Tracker for WCS at the time data was accessed (January 8, 2018) is CMT-HTF-2017-00069.

3.3.1.2.2 Constituents Not Addressed in the WCS

Additional estimating was required where no input from WCS was available for a particular radiological or chemical constituent. In addition, updated special analysis methods provided estimates for additional isotopes.

Supernate phase inventories of Ni-59, Nb-94, Ru-106, Rh-106, Sb-125, Sn-126, Cs-134, Cs-135, Ce-144, Pr-144, Pm-147, Eu-154, Cm-244, and Cm-245 were determined based on reported solubility factors in and/or ratios of the supernate and sludge inventories of similar elements. Additional sludge inventories were identified for Se-79, Sm-151, Eu-152, Eu-155, Am-243, Cm-243, Cm-246, Cm-247, Cm-248, Bk-249, Cf-249, Cf-251, and Cf-252. Inventories of Na-22, Al-26, Te-125, Sb-126, Sb-126m, Ra-226, Ra-228, Ac-227, Th-229, Th-230, and Pa-231 were determined based on additional special methods. Crystalized salt solids phase chemical inventory was determined using WCS inventory outputs of Na_2SO_4, Na_3PO_4, $NaAlO_2*2H_2O$, NaCl, NaF, $NaNO_2$, and $NaNO_3$. WCS total salt chemical inventories were multiplied by the respective weight percent fractions of chemicals of concern SO_4, PO_4, Al, Cl-, F-, NO_2, and NO_3 in order to estimate the mass of the chemicals of interest after dissolution of the crystalline salt.

Affected constituents and the methods used to estimate their inventories are detailed in SRR-CWDA-2018-00041, Rev. 3.

3.3.1.2.3 Initial Inventory Adjustments

There are several radionuclides not reported in the 2018 Tank Farm Inventory which required further evaluation to develop an inventory. Those radionuclides requiring further estimating for the purpose of the PA model include Cl-36, K-40, Zr-93, Nb-93m, Pd-107, and Pt-193. Concentrations for these radionuclides were assigned as described in SRR-CWDA-2018-00041, Rev. 3.

Initial inventory adjustments to dose driving radionuclides, Tc-99 and I-129, reduced future uncertainty. An updated approach was recommended for projecting I-129 and Tc-99 inventories based on characterization of previous Tank Farm samples in SRR-CWDA-2015-00077 and SRR-CWDA-2015-00123, respectively. The updated approaches and the methods used to apply them are detailed in SRR-CWDA-2018-00041, Rev. 3.

3.3.1.3 Tank Farm Additions

H-Canyon will continue to transfer material to the Tank Farm. This material will add to the current inventory of the Tank Farm. To account for this, projected volumes and concentrations were used to estimate the added material from the future canyon transfers. Neither the Effluent Treatment Facility (ETF) nor DWPF recycle feeds were considered as they were accounted for in the initial Tank Farm inventory estimate. Further information on the determination of Tank Farm additions is provided in SRR-CWDA-2018-00041, Rev. 3.

3.3.1.4 Liquid Waste Treatments

For the purpose of the SRR-CWDA-2018-00041, Rev. 3, inventory estimate, the treatments that were considered included sludge removal, Deliquification, Dissolution and Adjustment (DDA), Actinide Removal Process / Modular Caustic Side Solvent Extraction Unit (ARP/MCU), and Salt Waste Processing Facility (SWPF). The insoluble sludge inventory was not included in the inventory estimates due to the sludge removal treatment process. The sludge removal treatment was assumed to have no effect on the supernate, salt, and interstitial liquid inventories. No effect of DDA processing was applied to the Tank Farm Inventory. Decontamination factors (DFs) for Cesium (200 DF) and solids filtering ratios (0%) were assumed for ARP/MCU and SWPF in SRR-CWDA-2018-00041, Rev. 3.

3.3.1.5 Saltstone Disposal Units

As of March 31, 2018, inventories of waste were within SDUs 1, 2A, 2B, 3A, 4, 5A, and 5B. SDUs 1, 2A, 2B, 4, 5A, and 5B are considered completely filled and inventories at closure were decayed to January 1, 2037, and used exclusively with no additional material assumed to be disposed of within these units whose inventories are reported in SRR-CWDA-2018-00041, Rev. 3.

In addition to emplaced saltstone, SDU 4 has United States Naval fuel waste contained within 10,032 55-gallon drums and emplaced in Cell A. [OPS-DTZ-90-0027] The material in the drums has also been decayed to January 1, 2037.

It should also be noted that although considered operationally filled, remaining space in SDUs 1, 2A, 2B, 3A, 4, 5A, and 5B will be filled with clean cap grout. However, SDU 1 cells D, E, and F are considered viable options for disposal of failed saltstone equipment at closure rather than transporting the used equipment to another repository as SDU 1 Cell D though F have no permanent roof installed as shown in Figure 3.2-3. The inventory contribution from future saltstone equipment is unknown; however, the equipment would be from saltstone facilities only, and therefore, residual waste remaining on the equipment would not exceed the SDF WAC. If used for equipment disposal, Cells D through F will be filled, like other SDU cells, with clean cap grout to design capacity prior to closure. SDU 1 inventory at closure reported in Section 3.3.3 does not incorporate inventory contributions from failed equipment.

SDU Cell 3A is approximately 15% full. The current contents formed the starting point for the SDU 3A inventory. The remaining space within this unit was assumed to be completely filled with saltstone to the operational fill limit. To estimate the inventory of the remaining space, a ratio of the empty volume to the total SDF available volume was multiplied by the current total Tank Farm inventory. This inventory was then added to SDU 3A's disposed of inventory.

Existing SDUs 3B and 6 have not received any saltstone as of March 31, 2018, and future SDUs 7 through 12 each have a grout capacity of 32.8 Mgal (SRR-SDU-2017-00003). For all radionuclide and chemical constituents, an inventory estimate was developed in SRR-CWDA-2018-00041, Rev. 3. It was assumed that the entire soluble and insoluble (salt) inventory present in both Tank Farms was divided evenly across all remaining SDU space (including the remaining volume in SDU 3A) volumetrically.

3.3.1.6 SDF Estimated Inventories at Closure

Three inventories were developed for SDF modeling purposes in SRR-CWDA-2018-00041, Rev. 3 for each SDU: (1) Realistic, (2) Most Probable and Defensible (MPAD), and (3) Pessimistic. The realistic modeling methods added the disposed of inventory to the estimated Tank Farm inventory (i.e., total soluble Tank Farm inventories) and evenly distributed the inventory based on the remaining available SDU volumes.

MPAD inventory values were generated to support Compliance Case modeling (i.e., models used to demonstrate compliance to performance objectives). The MPAD values for I-129 and Tc-99 were scaled up to address a reasonable degree of uncertainty based on the recommendations provided in SRR-CWDA-2015-00077 and SRR-CWDA-2015-00123, respectively. The MPAD values for all other radionuclides and chemicals were based on the realistic inventories increased by approximately 50%, plus the inventories already disposed of in the SDF; this scaling was based on the recommended scaling for the MPAD values of I-129 (SRR-CWDA-2015-00077).

The pessimistic inventory values for I-129 and Tc-99 were scaled up further to address a more defensible degree of uncertainty based on the recommendations provided in SRR-CWDA-2015-00077 and SRR-CWDA-2015-00123, respectively. The pessimistic values for all other radionuclides and chemicals were based on the realistic inventories increased by approximately 60%, plus the inventories already disposed of in the SDF; this scaling was based on the recommended scaling for the pessimistic values of Tc-99 (SRR-CWDA-2015-00123).

In addition to the three deterministic inventory sets, sampling distributions are also considered for probabilistic simulations. The sampling distributions are provided in Section 5.7.1.2. Because significant work has gone into collecting and analyzing data for the concentrations of I-129 and Tc-99 (SRR-CWDA-2015-00077, SRR-CWDA-2015-00123), these radionuclides have less variability applied to their distributions relative to the other radionuclides (SRR-CWDA-2018-00076).

The remaining radionuclides are treated more generically, with a single sampling distribution applied to all of the radionuclides. This approach is appropriate because these other radionuclides exhibit very little risk-significance (SRR-CWDA-2019-00055). When running the SDF GoldSim Model in probabilistic mode, each realization samples a value along a log-normal distribution ranging from a minimum of 0.10 to a maximum of 14.4; this sampled value was then multiplied by the realistic inventories for all radionuclides, except for I-129 and Tc-99 (which have their own unique distributions), thus generating a randomly sampled inventory set.

It is important to consider the applicability of the data used to inform uncertainty. For example, SRR-CWDA-2018-00076 relied on waste tank samples from the Tank Farms to generate uncertainty distributions to use in probabilistic modeling. While the characterization data may show that from tank-to-tank there can be significant variability in concentrations of specific radionuclides, using this waste tank variability as a surrogate for SDF inventory uncertainty is likely to over-estimate the ranges of uncertainty. This is because waste from tanks that are identified as having relatively high concentrations are generally expected to be mixed with waste from tanks with relatively low concentrations during the salt batching process, such that the range of concentration variability would be significantly reduced during waste processing. Additionally, as these salt batches are processed through SPF, they will be disposed of into multimillion-gallon disposal units. Because each salt batch will represent only a fraction of the total waste disposed of into each SDU, it is unlikely any single SDU would receive all of its waste from only higher-concentration or lower-concentration salt batches. As disposal operations continue, the feeds from the salt batches will continue to be characterized and this data will continue to be used to update disposal inventories, thus reducing uncertainty over time.

3.3.2 Waste Characteristics Screening

Table 3.3-1 and Table 3.3-2 list all of the radionuclides and chemicals, respectively that were considered during the development of the SDF inventories. While this list is comprehensive, a screening process was applied to the radionuclides to ensure that PA modeling would focus on

radionuclides with the most dose significance. This screening process is described within SRR-CWDA-2018-00044, Rev. 3, and summarized herein.

3.3.2.1 Evaluation of Radionuclides

Figure 3.3-1 provides an overview of the screening logic. The steps for screening were applied as follows:

Step 1: Identify the current projected SDF inventory at closure. As described in Section 3.3.1 the inventories are based on a combination of the waste that has already been disposed of into SDUs and projected future disposals based on existing tank farm inventories.

Step 2: Identify radionuclides with half-lives less than 5 years as presented in SRR-CWDA-2018-00018. Those with half-lives less than 5 years can be screened out provided they do not decay to significant daughters, as defined in NCRP-123 Vol. II, Table 3-1. Any short-lived radionuclides with significant long-lived daughters required further evaluation.

Step 3: For short-lived radionuclides with significant long-lived daughters, the parent-to-daughter ratios were evaluated (i.e., dividing the inventory at closure of the parent by the inventory at closure of the daughter radionuclide). If the current inventory (Ci) of the parent is significantly less than that of the daughter (i.e., less than two orders of magnitude or more), then it is unlikely the decay and ingrowth would significantly alter the inventory of the longer-lived daughter. Therefore, it is reasonable to exclude the short-lived parent, despite having significant longer-lived daughters. Any short-lived radionuclides with parent-to-daughter ratios greater than 0.01 were screened back in and those with ratios less than 0.01 were screened out.

Step 4: Apply Work Sheets for Ground Burial Screening Calculations from NCRP-123 Vol. II for each radionuclide. These work sheets were developed by the National Council on Radiation Protection and Measurements (NCRP) as a simplified screening approach to determine compliance for ground burial of radionuclides.

Step 5: Radionuclides with screening values developed from Ground Burial Screening Calculations from NCRP-123 Vol. II greater than 0.1 are screened in, except for those whose dose is calculated with an assumed secular equilibrium. Radionuclides with screening values less than 0.1 require further evaluation.

Step 6: Ingestion and inhalation pathways dose potentials are calculated for each radionuclide. This approach assumes that a member of the public (MOP) drinks two liters (L) of saltstone grout per day and inhales 8,000 cubic meters (m^3) of saltstone grout per year (yr). These assumptions are judged to be an extremely protective screening criteria since both assumptions non-mechanistically (and unrealistically) assume the medium of ingestion or inhalation is hardened saltstone.

Step 7: Maximum water exposure and soil exposure dose potentials for each radionuclide is determined following the process described in SRR-CWDA-2018-00044, Rev. 3.

Figure 3.3-1: Radionuclide Screening Flowchart

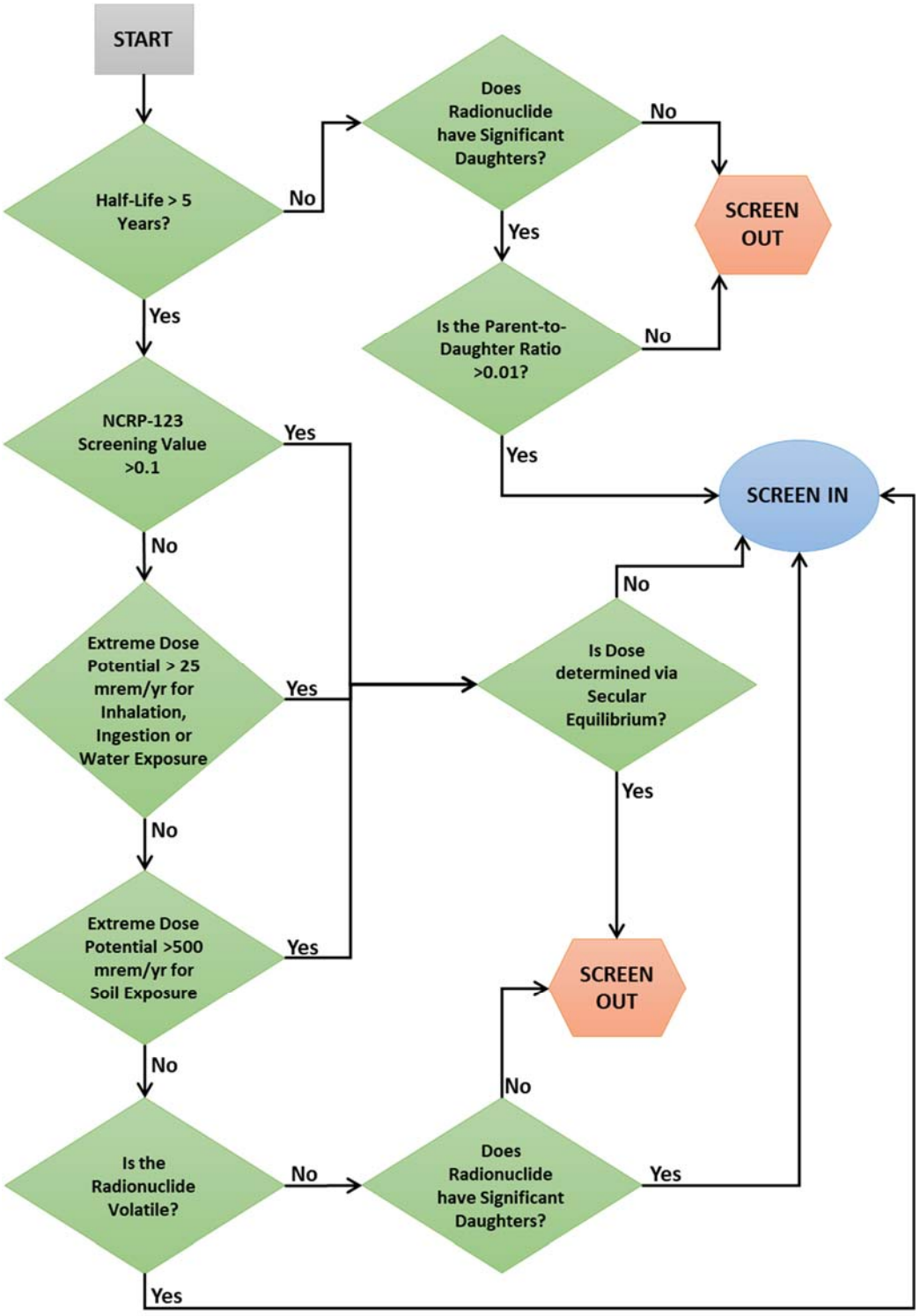

[SRR-CWDA-2018-00044, Rev. 3]

Step 8: The dose potentials calculated in Steps 6 and 7 for ingestion, inhalation, water exposure and soil exposure are compared to performance objective-based values (10 CFR 61, DOE M 435.1-1). If any of the dose potentials for inhalation, ingestion or water exposure are greater than 25 mrem/yr, or if the dose potential for soil exposure is greater than 500 mrem/yr for an individual radionuclide, the radionuclide was screened in (except in cases where the radionuclide dose was determined based on secular equilibrium). Radionuclides exceeding performance objectives whose dose was determined via assumed secular equilibrium are screened out. If a radionuclide's dose potential did not exceed the respective performance objective-based maximum values, further evaluation is required.

Step 9: For those radionuclides that did not exceed any performance objective, the radionuclide is compared to the list of volatile radionuclides as defined in SRR-CWDA-2018-00025. If the radionuclide was listed as volatile it was screened in.

Step 10: For the remaining radionuclides that are found to not be volatile, those with significant long-lived daughters are identified. Per NCRP-123 Vol. II radionuclides with significant daughters are screened in, while those with no significant daughters are screened out.

The resulting list of screened-in radionuclides is provided in Table 3.3-3.

Table 3.3-3: Radionuclides of Concern

H-3	Nb-94	Pb-210	U-235	Am-243
C-14	Tc-99	Ra-226	U-236	Cm-243
Al-26	Pd-107	Ac-227	Np-237	Cm-244
Cl-36	Sn-126	Ra-228	Pu-238	Cm-245
K-40	I-129	Th-229	U-238	Pu-244
Co-60	Cs-135	Th-230	Pu-239	Cm-247
Ni-63	Cs-137	Pa-231	Pu-240	Cf-249
Se-79	Sm-151	Th-232	Pu-241	Cf-251
Sr-90	Eu-152	U-232	Am-241	
Zr-93	Eu-154	U-233	Pu-242	
Nb-93m	Pt-193	U-234	Am-242m	

The SDF PA models use these species and their decay products as source material. The major decay chains are shown in Figure 3.3-2. The figure only includes radionuclides with half-lives greater than one year.

Figure 3.3-2: Major Decay Chains Included in GoldSim Model

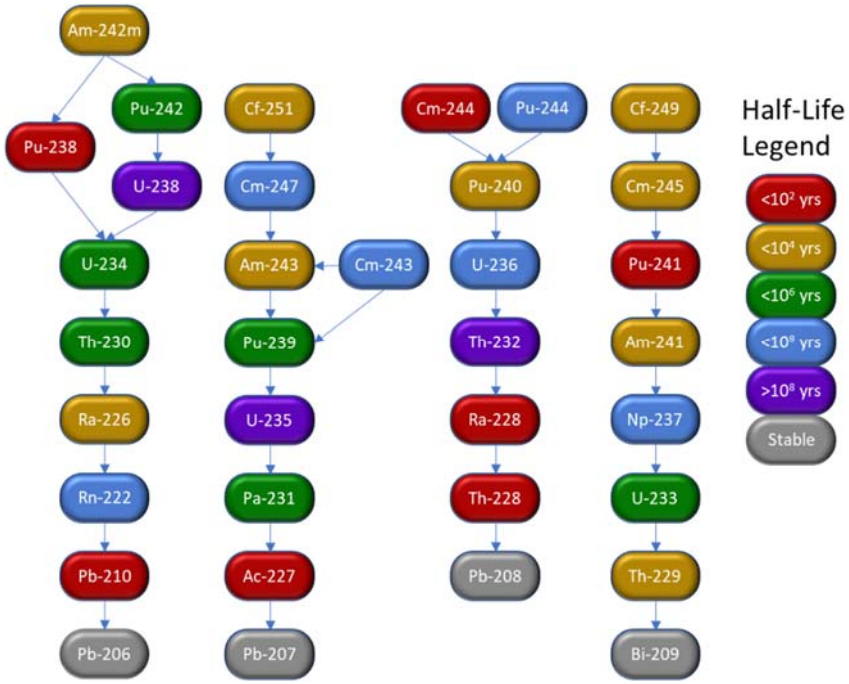

3.3.2.2 Evaluation of Chemicals

As waste tank inventories of saltcake, supernate, interstitial salt, and interstitial sludge will be processed, and a portion will be disposed of in SDF, the chemical constituents used in the H-Area Tank Farm (HTF) PA (SRR-CWDA-2010-00023, Rev. 6) were also consider for the SDF PA. The list of chemical constituents that were included in the PA modeling was derived from a screening process consisting of several steps to arrive at an appropriate list of constituents to be included in the HTF and SDF closure inventory estimates. The approach was developed for use in screening the chemicals of interest in Tanks 18 and 19; since the chemical constituents for F-Area Tank Farm (FTF) and HTF are assumed the same, using the developed list was appropriate. Table 3.3-4 lists the chemical constituents of concern for the SDF PA.

Table 3.3-4: Chemical Inventory of Concern

Ag	Cd	F^-	Mo	PO_4	U
Al	Cl^-	Fe	Ni	Sb	Zn
As	Co	Hg	NO_2	Se	
B	Cr	I	NO_3	SO_4	
Ba	Cu	Mn	Pb	Sr	

Further information can be found on evaluation of the radiological and chemical constituents in the SDF inventory screening and closure inventory documents. [SRR-CWDA-2018-00041, Rev. 3; SRR-CWDA-2018-00044, Rev. 3]

3.3.3 Final SDF Inventory Estimates at Closure

As the system plan calls for SPF flushing in fiscal year 2036 and in liquid waste closure in fiscal year 2037 (SRR-LWP-2009-00001, Rev. 21), all the radiological and chemical inventories have been decay corrected to 2037. After all waste inventory adjustments, the final recommended radionuclide inventory estimates are provided in Table 3.3-5 through Table 3.3-7 (SRR-CWDA-2018-00044, Rev. 3). The recommended chemical constituent estimated inventories are provided in Table 3.3-8 through Table 3.3-10 (SRR-CWDA-2018-00041, Rev. 3).

Estimated conservatism and uncertainty are addressed in Section 5.8.5. In addition, further details can be found in SRR-CWDA-2018-00041, Rev. 3.

Note that although a more recent revision of *Determination of Inventory for FY2019 Performance Assessment Modeling* (SRR-CWDA-2018-00041) is available (Revision 3), the values presented in the following tables reflect the recommended values from Revision 2, as these are the values used for PA-related modeling activities. During the document review of this PA, it was determined that the previously recommended special method for Sr-90 (from SRR-CWDA-2018-00041, Rev. 2) may underestimate the concentration of Sr-90 relative to Cs-137 concentrations. In response to this review comment, *Determination of Inventory for FY2019 Performance Assessment Modeling* (SRR-CWDA-2018-00041) was updated, from Revision 2 to Revision 3, to modify the Sr-90 special method approach. While special methods are only used for a limited number of samples, the estimated inventory values for Cl-36, K-40, and Sr-90 disposed of into SDU 1 increased. No other SDU inventories were impacted by this change. An evaluation was performed and documented in *Addendum to FY2019 SDF PA QA Report, SRR-CWDA-2018-00068* (SRR-CWDA-2019-00046). This evaluation demonstrated that the dose impact from this change was negligible. As a result, while Revision 3 of SRR-CWDA-2018-00041 reflects a more recent inventory estimate, the modeling performed within this PA used the inventory as reported in Revision 2 of SRR-CWDA-2018-00041.

Table 3.3-5: Realistic SDF Radionuclide Inventory Estimate (Ci) at Closure

Radionuclide	SDU 1	SDU 2A	SDU 2B	SDU 3A	SDU 3B	SDU 4	SDU 5A	SDU 5B
H-3	4.61E+00	7.97E-01	6.76E-01	3.10E+01	3.65E+01	1.23E+01	1.94E+00	1.19E+00
C-14	1.31E+00	2.40E+00	2.44E+00	5.76E+00	6.21E+00	6.50E+00	3.17E+00	3.77E+00
Al-26	2.62E-01	8.98E-04	8.56E-04	2.41E-01	2.87E-01	9.75E-01	1.02E-03	8.59E-04
Cl-36	7.02E-08	1.06E-04	1.30E-04	9.09E-03	1.06E-02	1.49E-02	3.10E-03	7.71E-04
K-40	7.02E-08	1.06E-04	1.30E-04	9.09E-03	1.06E-02	1.49E-02	3.10E-03	1.72E-03
Co-60	3.52E-05	7.50E-05	8.41E-05	7.56E-02	9.02E-02	5.75E-03	1.98E-03	9.13E-05
Ni-63	1.05E-01	3.90E-02	3.11E-02	1.97E+00	2.34E+00	2.75E+00	5.45E-02	2.22E-02
Se-79	3.44E-01	1.34E-01	1.23E-01	9.30E-01	1.07E+00	9.75E+00	2.72E-01	1.68E-01
Sr-90	6.97E-03	1.06E+01	1.30E+01	3.61E+04	4.31E+04	1.50E+03	3.11E+02	7.74E+01
Zr-93	7.69E-01	2.64E-01	3.83E-01	9.36E-01	1.06E+00	8.15E+00	3.05E-01	2.86E-01
Nb-93m	7.52E-01	2.67E-01	3.96E-01	9.44E-01	1.04E+00	1.93E+03	4.05E-01	2.95E-01
Nb-94	2.03E-03	1.89E-03	1.63E-03	1.70E-03	1.61E-03	8.93E-02	2.65E-03	2.06E-03
Tc-99	4.93E+01	1.14E+02	1.37E+02	2.57E+02	2.53E+02	6.34E+02	1.75E+02	1.20E+02
Pd-107	8.38E-03	6.03E-03	6.06E-03	9.93E-03	1.06E-02	3.75E-02	6.46E-03	6.42E-03
Sn-126	1.22E+00	7.62E-01	6.83E-01	3.94E+00	4.17E+00	2.22E+00	1.65E+00	9.47E-01
I-129	2.01E-01	7.31E-02	6.83E-02	1.85E-01	1.80E-01	2.77E-01	1.39E-01	8.68E-02
Cs-135	4.95E-02	3.36E-02	3.38E-02	1.79E-02	1.42E-02	1.73E+00	3.60E-02	3.58E-02
Cs-137	4.07E+00	3.99E+03	4.91E+03	2.67E+03	2.61E+03	1.09E+05	2.47E+03	5.10E+03
Sm-151	4.78E-03	1.44E-01	1.26E-01	3.86E+01	4.60E+01	1.70E+01	2.22E-01	1.84E-01
Eu-152	5.81E-04	9.77E-05	9.82E-05	7.88E-02	9.39E-02	2.77E-02	1.05E-04	1.04E-04
Eu-154	1.13E-04	1.77E-03	3.18E-03	7.28E-01	8.68E-01	6.73E-01	9.18E-04	9.57E-04
Pt-193	1.26E+00	1.20E+00	1.20E+00	9.07E-01	8.13E-01	6.84E+00	1.34E+00	1.31E+00
Pb-210	4.22E-07	2.47E-06	1.42E-06	2.86E-07	2.71E-07	3.24E-05	5.88E-07	5.73E-07
Ra-226	9.53E-07	8.56E-06	4.93E-06	8.78E-07	7.60E-07	8.27E-05	2.30E-06	2.18E-06
Ac-227	2.55E-06	1.01E-06	1.30E-06	1.39E-05	1.33E-06	9.55E-05	2.48E-05	4.02E-05
Ra-228	7.68E-06	1.26E-05	1.92E-05	2.57E-03	3.07E-03	2.10E-04	1.35E-05	2.26E-05
Th-229	5.33E-04	4.28E-03	8.24E-03	8.51E-04	6.15E-04	3.64E+00	2.30E-03	2.11E-03
Th-230	6.48E-05	9.00E-04	5.55E-04	8.01E-05	5.35E-05	6.32E-03	3.13E-04	2.87E-04
Pa-231	4.08E-06	1.62E-06	2.07E-06	3.20E-06	3.42E-06	1.52E-04	2.49E-06	2.06E-06
Th-232	7.69E-06	1.26E-05	1.92E-05	2.57E-03	3.07E-03	2.10E-04	1.35E-05	2.26E-05
U-232	5.40E-04	1.13E-02	1.10E-02	2.56E-03	4.23E-04	9.72E-02	1.19E-02	1.63E-02
U-233	7.76E-02	9.51E-01	1.32E+00	2.70E-01	1.38E-01	8.86E+00	1.17E+00	1.07E+00
U-234	9.93E-02	6.16E-01	8.54E-01	2.93E-01	2.28E-01	8.98E+00	7.60E-01	6.88E-01
U-235	2.51E-03	9.93E-04	1.27E-03	4.88E-03	5.57E-03	9.37E-02	1.53E-03	1.27E-03
U-236	6.49E-03	6.37E-03	8.85E-03	1.16E-02	1.25E-02	8.35E-02	7.82E-03	7.18E-03
Np-237	3.94E-03	1.60E-01	9.61E-02	1.25E-01	1.36E-01	5.76E-01	8.51E-02	7.76E-02
Pu-238	6.18E-03	4.92E+00	4.67E+00	1.45E+03	1.71E+03	2.69E+02	6.52E+01	2.25E+01
U-238	1.07E-02	2.24E-02	2.65E-02	1.55E-01	1.81E-01	7.93E-02	3.28E-02	2.85E-02
Pu-239	1.43E-02	5.28E-01	5.19E-01	8.91E+01	1.06E+02	5.86E+01	1.86E+00	7.39E-01
Pu-240	1.35E-02	5.27E-01	5.18E-01	1.90E+01	2.20E+01	7.27E+01	1.85E+00	7.38E-01
Pu-241	8.25E-03	6.71E-01	6.39E-01	1.71E+02	2.00E+02	3.61E+01	1.05E+01	3.48E+00
Am-241	2.30E-03	9.08E-02	1.03E-01	1.40E+02	1.67E+02	2.16E+01	6.04E-01	2.11E-01
Pu-242	1.57E-03	3.76E-01	5.21E-01	9.09E-02	3.56E-02	4.12E+00	4.61E-01	4.21E-01
Am-242m	6.20E-05	9.09E-03	5.78E-03	6.80E-02	8.11E-02	1.74E-02	9.18E-04	7.57E-04
Cm-243	2.94E-04	3.42E-04	3.40E-04	3.26E-04	3.09E-04	5.28E-03	3.91E-04	3.80E-04
Am-243	1.42E-03	4.23E-03	4.90E-03	5.68E-02	6.74E-02	5.17E-01	3.94E-03	9.23E-03
Pu-244	1.01E-05	1.74E-03	2.42E-03	4.21E-04	1.64E-04	1.68E-02	2.14E-03	1.95E-03
Cm-244	1.45E-03	9.44E-02	1.07E-01	1.01E+00	1.20E+00	1.56E+01	4.67E-02	5.30E-02
Cm-245	2.71E-04	1.46E-02	2.22E-02	2.38E-03	9.09E-04	7.78E-01	1.50E-02	1.31E-02
Cm-247	1.59E-13	1.67E-02	1.41E-02	8.39E-04	9.37E-14	1.06E-01	2.13E-02	1.77E-02
Cf-249	8.46E-13	1.72E-02	1.42E-02	8.50E-04	5.21E-13	2.67E-01	2.15E-02	1.77E-02
Cf-251	3.04E-14	1.32E-02	1.07E-02	6.01E-04	1.83E-14	9.17E-02	1.66E-02	1.49E-02

Table 3.3-5: Realistic SDF Radionuclide Inventory Estimate (Ci) at Closure (Continued)

Radionuclide	SDU 6	SDU 7	SDU 8	SDU 9	SDU 10	SDU 11	SDU 12	Total
H-3	4.26E+02	4.26E+02	4.26E+02	4.26E+02	4.26E+02	4.26E+02	4.26E+02	3.07E+03
C-14	7.25E+01	7.25E+01	7.25E+01	7.25E+01	7.25E+01	7.25E+01	7.25E+01	5.39E+02
Al-26	3.35E+00	3.35E+00	3.35E+00	3.35E+00	3.35E+00	3.35E+00	3.35E+00	2.52E+01
Cl-36	1.23E-01	1.23E-01	1.23E-01	1.23E-01	1.23E-01	1.23E-01	1.23E-01	9.02E-01
K-40	1.23E-01	1.23E-01	1.23E-01	1.23E-01	1.23E-01	1.23E-01	1.23E-01	9.03E-01
Co-60	1.05E+00	1.05E+00	1.05E+00	1.05E+00	1.05E+00	1.05E+00	1.05E+00	7.54E+00
Ni-63	2.73E+01	2.73E+01	2.73E+01	2.73E+01	2.73E+01	2.73E+01	2.73E+01	1.99E+02
Se-79	1.25E+01	1.25E+01	1.25E+01	1.25E+01	1.25E+01	1.25E+01	1.25E+01	1.00E+02
Sr-90	5.03E+05	5.03E+05	5.03E+05	5.03E+05	5.03E+05	5.03E+05	5.03E+05	3.60E+06
Zr-93	1.23E+01	1.23E+01	1.23E+01	1.23E+01	1.23E+01	1.23E+01	1.23E+01	9.85E+01
Nb-93m	1.22E+01	1.22E+01	1.22E+01	1.22E+01	1.22E+01	1.22E+01	1.22E+01	2.02E+03
Nb-94	1.88E-02	1.88E-02	1.88E-02	1.88E-02	1.88E-02	1.88E-02	1.88E-02	2.34E-01
Tc-99	2.96E+03	2.96E+03	2.96E+03	2.96E+03	2.96E+03	2.96E+03	2.96E+03	2.24E+04
Pd-107	1.23E-01	1.23E-01	1.23E-01	1.23E-01	1.23E-01	1.23E-01	1.23E-01	9.55E-01
Sn-126	4.86E+01	4.86E+01	4.86E+01	4.86E+01	4.86E+01	4.86E+01	4.86E+01	3.56E+02
I-129	2.10E+00	2.10E+00	2.10E+00	2.10E+00	2.10E+00	2.10E+00	2.10E+00	1.59E+01
Cs-135	1.66E-01	1.66E-01	1.66E-01	1.66E-01	1.66E-01	1.66E-01	1.66E-01	3.12E+00
Cs-137	3.05E+04	3.05E+04	3.05E+04	3.05E+04	3.05E+04	3.05E+04	3.05E+04	3.44E+05
Sm-151	5.37E+02	5.37E+02	5.37E+02	5.37E+02	5.37E+02	5.37E+02	5.37E+02	3.86E+03
Eu-152	1.10E+00	1.10E+00	1.10E+00	1.10E+00	1.10E+00	1.10E+00	1.10E+00	7.88E+00
Eu-154	1.01E+01	1.01E+01	1.01E+01	1.01E+01	1.01E+01	1.01E+01	1.01E+01	7.32E+01
Pt-193	9.49E+00	9.49E+00	9.49E+00	9.49E+00	9.49E+00	9.49E+00	9.49E+00	8.13E+01
Pb-210	3.16E-06	3.16E-06	3.16E-06	3.16E-06	3.16E-06	3.16E-06	3.16E-06	6.06E-05
Ra-226	8.87E-06	8.87E-06	8.87E-06	8.87E-06	8.87E-06	8.87E-06	8.87E-06	1.65E-04
Ac-227	1.55E-05	1.55E-05	1.55E-05	1.55E-05	1.55E-05	1.55E-05	1.55E-05	2.89E-04
Ra-228	3.58E-02	3.58E-02	3.58E-02	3.58E-02	3.58E-02	3.58E-02	3.58E-02	2.56E-01
Th-229	7.18E-03	7.18E-03	7.18E-03	7.18E-03	7.18E-03	7.18E-03	7.18E-03	3.71E+00
Th-230	6.24E-04	6.24E-04	6.24E-04	6.24E-04	6.24E-04	6.24E-04	6.24E-04	1.29E-02
Pa-231	3.99E-05	3.99E-05	3.99E-05	3.99E-05	3.99E-05	3.99E-05	3.99E-05	4.51E-04
Th-232	3.58E-02	3.58E-02	3.58E-02	3.58E-02	3.58E-02	3.58E-02	3.58E-02	2.56E-01
U-232	4.93E-03	4.93E-03	4.93E-03	4.93E-03	4.93E-03	4.93E-03	4.93E-03	1.86E-01
U-233	1.61E+00	1.61E+00	1.61E+00	1.61E+00	1.61E+00	1.61E+00	1.61E+00	2.51E+01
U-234	2.67E+00	2.67E+00	2.67E+00	2.67E+00	2.67E+00	2.67E+00	2.67E+00	3.12E+01
U-235	6.51E-02	6.51E-02	6.51E-02	6.51E-02	6.51E-02	6.51E-02	6.51E-02	5.67E-01
U-236	1.46E-01	1.46E-01	1.46E-01	1.46E-01	1.46E-01	1.46E-01	1.46E-01	1.16E+00
Np-237	1.58E+00	1.58E+00	1.58E+00	1.58E+00	1.58E+00	1.58E+00	1.58E+00	1.23E+01
Pu-238	1.99E+04	1.99E+04	1.99E+04	1.99E+04	1.99E+04	1.99E+04	1.99E+04	1.43E+05
U-238	2.11E+00	2.11E+00	2.11E+00	2.11E+00	2.11E+00	2.11E+00	2.11E+00	1.53E+01
Pu-239	1.23E+03	1.23E+03	1.23E+03	1.23E+03	1.23E+03	1.23E+03	1.23E+03	8.88E+03
Pu-240	2.57E+02	2.57E+02	2.57E+02	2.57E+02	2.57E+02	2.57E+02	2.57E+02	1.91E+03
Pu-241	2.34E+03	2.34E+03	2.34E+03	2.34E+03	2.34E+03	2.34E+03	2.34E+03	1.68E+04
Am-241	1.95E+03	1.95E+03	1.95E+03	1.95E+03	1.95E+03	1.95E+03	1.95E+03	1.40E+04
Pu-242	4.15E-01	4.15E-01	4.15E-01	4.15E-01	4.15E-01	4.15E-01	4.15E-01	8.94E+00
Am-242m	9.47E-01	9.47E-01	9.47E-01	9.47E-01	9.47E-01	9.47E-01	9.47E-01	6.81E+00
Cm-243	3.61E-03	3.61E-03	3.61E-03	3.61E-03	3.61E-03	3.61E-03	3.61E-03	3.29E-02
Am-243	7.87E-01	7.87E-01	7.87E-01	7.87E-01	7.87E-01	7.87E-01	7.87E-01	6.17E+00
Pu-244	1.92E-03	1.92E-03	1.92E-03	1.92E-03	1.92E-03	1.92E-03	1.92E-03	3.91E-02
Cm-244	1.40E+01	1.40E+01	1.40E+01	1.40E+01	1.40E+01	1.40E+01	1.40E+01	1.16E+02
Cm-245	1.06E-02	1.06E-02	1.06E-02	1.06E-02	1.06E-02	1.06E-02	1.06E-02	9.20E-01
Cm-247	1.09E-12	1.09E-12	1.09E-12	1.09E-12	1.09E-12	1.09E-12	1.09E-12	1.77E-01
Cf-249	6.08E-12	6.08E-12	6.08E-12	6.08E-12	6.08E-12	6.08E-12	6.08E-12	3.38E-01
Cf-251	2.14E-13	2.14E-13	2.14E-13	2.14E-13	2.14E-13	2.14E-13	2.14E-13	1.48E-01

Table 3.3-6: MPAD SDF Radionuclide Inventory Estimate (Ci) at Closure

Radionuclide	SDU 1	SDU 2A	SDU 2B	SDU 3A	SDU 3B	SDU 4	SDU 5A	SDU 5B
H-3	4.61E+00	7.97E-01	6.76E-01	4.54E+01	5.36E+01	1.23E+01	1.94E+00	1.19E+00
C-14	1.31E+00	2.40E+00	2.44E+00	8.21E+00	9.14E+00	6.50E+00	3.17E+00	3.77E+00
Al-26	2.62E-01	8.98E-04	8.56E-04	3.54E-01	4.22E-01	9.75E-01	1.02E-03	8.59E-04
Cl-36	7.02E-08	1.06E-04	1.30E-04	1.33E-02	1.55E-02	1.49E-02	3.10E-03	7.71E-04
K-40	7.02E-08	1.06E-04	1.30E-04	1.33E-02	1.55E-02	1.49E-02	3.10E-03	1.72E-03
Co-60	3.52E-05	7.50E-05	8.41E-05	1.11E-01	1.33E-01	5.75E-03	1.98E-03	9.13E-05
Ni-63	1.05E-01	3.90E-02	3.11E-02	2.90E+00	3.44E+00	2.75E+00	5.45E-02	2.22E-02
Se-79	3.44E-01	1.34E-01	1.23E-01	1.35E+00	1.58E+00	9.75E+00	2.72E-01	1.68E-01
Sr-90	6.97E-03	1.06E+01	1.30E+01	5.31E+04	6.34E+04	1.50E+03	3.11E+02	7.74E+01
Zr-93	7.69E-01	2.64E-01	3.83E-01	1.35E+00	1.55E+00	8.15E+00	3.05E-01	2.86E-01
Nb-93m	7.52E-01	2.67E-01	3.96E-01	1.36E+00	1.53E+00	1.93E+03	4.05E-01	2.95E-01
Nb-94	2.03E-03	1.89E-03	1.63E-03	2.33E-03	2.37E-03	8.93E-02	2.65E-03	2.06E-03
Tc-99	4.93E+01	1.14E+02	1.37E+02	3.63E+02	3.80E+02	6.34E+02	1.75E+02	1.20E+02
Pd-107	8.38E-03	6.03E-03	6.06E-03	1.41E-02	1.55E-02	3.75E-02	6.46E-03	6.42E-03
Sn-126	1.22E+00	7.62E-01	6.83E-01	5.58E+00	6.13E+00	2.22E+00	1.65E+00	9.47E-01
I-129	2.01E-01	7.31E-02	6.83E-02	1.92E-01	1.88E-01	2.77E-01	1.39E-01	8.68E-02
Cs-135	4.95E-02	3.36E-02	3.38E-02	2.35E-02	2.09E-02	1.73E+00	3.60E-02	3.58E-02
Cs-137	4.07E+00	3.99E+03	4.91E+03	3.70E+03	3.84E+03	1.09E+05	2.47E+03	5.10E+03
Sm-151	4.78E-03	1.44E-01	1.26E-01	5.67E+01	6.76E+01	1.70E+01	2.22E-01	1.84E-01
Eu-152	5.81E-04	9.77E-05	9.82E-05	1.16E-01	1.38E-01	2.77E-02	1.05E-04	1.04E-04
Eu-154	1.13E-04	1.77E-03	3.18E-03	1.07E+00	1.28E+00	6.73E-01	9.18E-04	9.57E-04
Pt-193	1.26E+00	1.20E+00	1.20E+00	1.23E+00	1.20E+00	6.84E+00	1.34E+00	1.31E+00
Pb-210	4.22E-07	2.47E-06	1.42E-06	3.93E-07	3.99E-07	3.24E-05	5.88E-07	5.73E-07
Ra-226	9.53E-07	8.56E-06	4.93E-06	1.18E-06	1.12E-06	8.27E-05	2.30E-06	2.18E-06
Ac-227	2.55E-06	1.01E-06	1.30E-06	1.45E-05	1.95E-06	9.55E-05	2.48E-05	4.02E-05
Ra-228	7.68E-06	1.26E-05	1.92E-05	3.78E-03	4.51E-03	2.10E-04	1.35E-05	2.26E-05
Th-229	5.33E-04	4.28E-03	8.24E-03	1.09E-03	9.05E-04	3.64E+00	2.30E-03	2.11E-03
Th-230	6.48E-05	9.00E-04	5.55E-04	1.01E-04	7.86E-05	6.32E-03	3.13E-04	2.87E-04
Pa-231	4.08E-06	1.62E-06	2.07E-06	4.55E-06	5.03E-06	1.52E-04	2.49E-06	2.06E-06
Th-232	7.69E-06	1.26E-05	1.92E-05	3.78E-03	4.51E-03	2.10E-04	1.35E-05	2.26E-05
U-232	5.40E-04	1.13E-02	1.10E-02	2.73E-03	6.21E-04	9.72E-02	1.19E-02	1.63E-02
U-233	7.76E-02	9.51E-01	1.32E+00	3.24E-01	2.02E-01	8.86E+00	1.17E+00	1.07E+00
U-234	9.93E-02	6.16E-01	8.54E-01	3.83E-01	3.36E-01	8.98E+00	7.60E-01	6.88E-01
U-235	2.51E-03	9.93E-04	1.27E-03	7.08E-03	8.20E-03	9.37E-02	1.53E-03	1.27E-03
U-236	6.49E-03	6.37E-03	8.85E-03	1.65E-02	1.83E-02	8.35E-02	7.82E-03	7.18E-03
Np-237	3.94E-03	1.60E-01	9.61E-02	1.79E-01	2.00E-01	5.76E-01	8.51E-02	7.76E-02
Pu-238	6.18E-03	4.92E+00	4.67E+00	2.12E+03	2.51E+03	2.69E+02	6.52E+01	2.25E+01
U-238	1.07E-02	2.24E-02	2.65E-02	2.27E-01	2.66E-01	7.93E-02	3.28E-02	2.85E-02
Pu-239	1.43E-02	5.28E-01	5.19E-01	1.31E+02	1.55E+02	5.86E+01	1.86E+00	7.39E-01
Pu-240	1.35E-02	5.27E-01	5.18E-01	2.77E+01	3.23E+01	7.27E+01	1.85E+00	7.38E-01
Pu-241	8.25E-03	6.71E-01	6.39E-01	2.51E+02	2.95E+02	3.61E+01	1.05E+01	3.48E+00
Am-241	2.30E-03	9.08E-02	1.03E-01	2.06E+02	2.46E+02	2.16E+01	6.04E-01	2.11E-01
Pu-242	1.57E-03	3.76E-01	5.21E-01	1.05E-01	5.23E-02	4.12E+00	4.61E-01	4.21E-01
Am-242m	6.20E-05	9.09E-03	5.78E-03	1.00E-01	1.19E-01	1.74E-02	9.18E-04	7.57E-04
Cm-243	2.94E-04	3.42E-04	3.40E-04	4.48E-04	4.55E-04	5.28E-03	3.91E-04	3.80E-04
Am-243	1.42E-03	4.23E-03	4.90E-03	8.34E-02	9.92E-02	5.17E-01	3.94E-03	9.23E-03
Pu-244	1.01E-05	1.74E-03	2.42E-03	4.86E-04	2.42E-04	1.68E-02	2.14E-03	1.95E-03
Cm-244	1.45E-03	9.44E-02	1.07E-01	1.48E+00	1.77E+00	1.56E+01	4.67E-02	5.30E-02
Cm-245	2.71E-04	1.46E-02	2.22E-02	2.74E-03	1.34E-03	7.78E-01	1.50E-02	1.31E-02
Cm-247	1.59E-13	1.67E-02	1.41E-02	8.39E-04	1.38E-13	1.06E-01	2.13E-02	1.77E-02
Cf-249	8.46E-13	1.72E-02	1.42E-02	8.50E-04	7.66E-13	2.67E-01	2.15E-02	1.77E-02
Cf-251	3.04E-14	1.32E-02	1.07E-02	6.01E-04	2.69E-14	9.17E-02	1.66E-02	1.49E-02

Table 3.3-6: MPAD SDF Radionuclide Inventory Estimate (Ci) at Closure (Continued)

Radionuclide	SDU 6	SDU 7	SDU 8	SDU 9	SDU 10	SDU 11	SDU 12	Total
H-3	6.26E+02	6.26E+02	6.26E+02	6.26E+02	6.26E+02	6.26E+02	6.26E+02	4.50E+03
C-14	1.07E+02	1.07E+02	1.07E+02	1.07E+02	1.07E+02	1.07E+02	1.07E+02	7.83E+02
Al-26	4.92E+00	4.92E+00	4.92E+00	4.92E+00	4.92E+00	4.92E+00	4.92E+00	3.65E+01
Cl-36	1.81E-01	1.81E-01	1.81E-01	1.81E-01	1.81E-01	1.81E-01	1.81E-01	1.32E+00
K-40	1.81E-01	1.81E-01	1.81E-01	1.81E-01	1.81E-01	1.81E-01	1.81E-01	1.32E+00
Co-60	1.55E+00	1.55E+00	1.55E+00	1.55E+00	1.55E+00	1.55E+00	1.55E+00	1.11E+01
Ni-63	4.02E+01	4.02E+01	4.02E+01	4.02E+01	4.02E+01	4.02E+01	4.02E+01	2.91E+02
Se-79	1.84E+01	1.84E+01	1.84E+01	1.84E+01	1.84E+01	1.84E+01	1.84E+01	1.42E+02
Sr-90	7.40E+05	7.40E+05	7.40E+05	7.40E+05	7.40E+05	7.40E+05	7.40E+05	5.30E+06
Zr-93	1.81E+01	1.81E+01	1.81E+01	1.81E+01	1.81E+01	1.81E+01	1.81E+01	1.40E+02
Nb-93m	1.79E+01	1.79E+01	1.79E+01	1.79E+01	1.79E+01	1.79E+01	1.79E+01	2.06E+03
Nb-94	2.76E-02	2.76E-02	2.76E-02	2.76E-02	2.76E-02	2.76E-02	2.76E-02	2.98E-01
Tc-99	4.43E+03	4.43E+03	4.43E+03	4.43E+03	4.43E+03	4.43E+03	4.43E+03	3.30E+04
Pd-107	1.81E-01	1.81E-01	1.81E-01	1.81E-01	1.81E-01	1.81E-01	1.81E-01	1.37E+00
Sn-126	7.15E+01	7.15E+01	7.15E+01	7.15E+01	7.15E+01	7.15E+01	7.15E+01	5.20E+02
I-129	2.20E+00	2.20E+00	2.20E+00	2.20E+00	2.20E+00	2.20E+00	2.20E+00	1.66E+01
Cs-135	2.44E-01	2.44E-01	2.44E-01	2.44E-01	2.44E-01	2.44E-01	2.44E-01	3.68E+00
Cs-137	4.48E+04	4.48E+04	4.48E+04	4.48E+04	4.48E+04	4.48E+04	4.48E+04	4.47E+05
Sm-151	7.89E+02	7.89E+02	7.89E+02	7.89E+02	7.89E+02	7.89E+02	7.89E+02	5.67E+03
Eu-152	1.61E+00	1.61E+00	1.61E+00	1.61E+00	1.61E+00	1.61E+00	1.61E+00	1.16E+01
Eu-154	1.49E+01	1.49E+01	1.49E+01	1.49E+01	1.49E+01	1.49E+01	1.49E+01	1.07E+02
Pt-193	1.40E+01	1.40E+01	1.40E+01	1.40E+01	1.40E+01	1.40E+01	1.40E+01	1.13E+02
Pb-210	4.65E-06	4.65E-06	4.65E-06	4.65E-06	4.65E-06	4.65E-06	4.65E-06	7.12E-05
Ra-226	1.30E-05	1.30E-05	1.30E-05	1.30E-05	1.30E-05	1.30E-05	1.30E-05	1.95E-04
Ac-227	2.28E-05	2.28E-05	2.28E-05	2.28E-05	2.28E-05	2.28E-05	2.28E-05	3.41E-04
Ra-228	5.26E-02	5.26E-02	5.26E-02	5.26E-02	5.26E-02	5.26E-02	5.26E-02	3.77E-01
Th-229	1.06E-02	1.06E-02	1.06E-02	1.06E-02	1.06E-02	1.06E-02	1.06E-02	3.73E+00
Th-230	9.18E-04	9.18E-04	9.18E-04	9.18E-04	9.18E-04	9.18E-04	9.18E-04	1.50E-02
Pa-231	5.87E-05	5.87E-05	5.87E-05	5.87E-05	5.87E-05	5.87E-05	5.87E-05	5.85E-04
Th-232	5.26E-02	5.26E-02	5.26E-02	5.26E-02	5.26E-02	5.26E-02	5.26E-02	3.77E-01
U-232	7.25E-03	7.25E-03	7.25E-03	7.25E-03	7.25E-03	7.25E-03	7.25E-03	2.02E-01
U-233	2.36E+00	2.36E+00	2.36E+00	2.36E+00	2.36E+00	2.36E+00	2.36E+00	3.05E+01
U-234	3.92E+00	3.92E+00	3.92E+00	3.92E+00	3.92E+00	3.92E+00	3.92E+00	4.02E+01
U-235	9.57E-02	9.57E-02	9.57E-02	9.57E-02	9.57E-02	9.57E-02	9.57E-02	7.86E-01
U-236	2.14E-01	2.14E-01	2.14E-01	2.14E-01	2.14E-01	2.14E-01	2.14E-01	1.65E+00
Np-237	2.33E+00	2.33E+00	2.33E+00	2.33E+00	2.33E+00	2.33E+00	2.33E+00	1.77E+01
Pu-238	2.93E+04	2.93E+04	2.93E+04	2.93E+04	2.93E+04	2.93E+04	2.93E+04	2.10E+05
U-238	3.10E+00	3.10E+00	3.10E+00	3.10E+00	3.10E+00	3.10E+00	3.10E+00	2.24E+01
Pu-239	1.81E+03	1.81E+03	1.81E+03	1.81E+03	1.81E+03	1.81E+03	1.81E+03	1.30E+04
Pu-240	3.77E+02	3.77E+02	3.77E+02	3.77E+02	3.77E+02	3.77E+02	3.77E+02	2.78E+03
Pu-241	3.44E+03	3.44E+03	3.44E+03	3.44E+03	3.44E+03	3.44E+03	3.44E+03	2.47E+04
Am-241	2.87E+03	2.87E+03	2.87E+03	2.87E+03	2.87E+03	2.87E+03	2.87E+03	2.06E+04
Pu-242	6.11E-01	6.11E-01	6.11E-01	6.11E-01	6.11E-01	6.11E-01	6.11E-01	1.03E+01
Am-242m	1.39E+00	1.39E+00	1.39E+00	1.39E+00	1.39E+00	1.39E+00	1.39E+00	1.00E+01
Cm-243	5.31E-03	5.31E-03	5.31E-03	5.31E-03	5.31E-03	5.31E-03	5.31E-03	4.51E-02
Am-243	1.16E+00	1.16E+00	1.16E+00	1.16E+00	1.16E+00	1.16E+00	1.16E+00	8.82E+00
Pu-244	2.82E-03	2.82E-03	2.82E-03	2.82E-03	2.82E-03	2.82E-03	2.82E-03	4.55E-02
Cm-244	2.06E+01	2.06E+01	2.06E+01	2.06E+01	2.06E+01	2.06E+01	2.06E+01	1.64E+02
Cm-245	1.56E-02	1.56E-02	1.56E-02	1.56E-02	1.56E-02	1.56E-02	1.56E-02	9.56E-01
Cm-247	1.61E-12	1.61E-12	1.61E-12	1.61E-12	1.61E-12	1.61E-12	1.61E-12	1.77E-01
Cf-249	8.95E-12	8.95E-12	8.95E-12	8.95E-12	8.95E-12	8.95E-12	8.95E-12	3.38E-01
Cf-251	3.14E-13	3.14E-13	3.14E-13	3.14E-13	3.14E-13	3.14E-13	3.14E-13	1.48E-01

Table 3.3-7: Pessimistic SDF Radionuclide Inventory Estimate (Ci) at Closure

Radionuclide	SDU 1	SDU 2A	SDU 2B	SDU 3A	SDU 3B	SDU 4	SDU 5A	SDU 5B
H-3	4.61E+00	7.97E-01	6.76E-01	4.88E+01	5.77E+01	1.23E+01	1.94E+00	1.19E+00
C-14	1.31E+00	2.40E+00	2.44E+00	8.79E+00	9.83E+00	6.50E+00	3.17E+00	3.77E+00
Al-26	2.62E-01	8.98E-04	8.56E-04	3.81E-01	4.54E-01	9.75E-01	1.02E-03	8.59E-04
Cl-36	7.02E-08	1.06E-04	1.30E-04	1.42E-02	1.67E-02	1.49E-02	3.10E-03	7.71E-04
K-40	7.02E-08	1.06E-04	1.30E-04	1.42E-02	1.67E-02	1.49E-02	3.10E-03	1.72E-03
Co-60	3.52E-05	7.50E-05	8.41E-05	1.20E-01	1.43E-01	5.75E-03	1.98E-03	9.13E-05
Ni-63	1.05E-01	3.90E-02	3.11E-02	3.11E+00	3.70E+00	2.75E+00	5.45E-02	2.22E-02
Se-79	3.44E-01	1.34E-01	1.23E-01	1.45E+00	1.69E+00	9.75E+00	2.72E-01	1.68E-01
Sr-90	6.97E-03	1.06E+01	1.30E+01	5.72E+04	6.82E+04	1.50E+03	3.11E+02	7.74E+01
Zr-93	7.69E-01	2.64E-01	3.83E-01	1.45E+00	1.67E+00	8.15E+00	3.05E-01	2.86E-01
Nb-93m	7.52E-01	2.67E-01	3.96E-01	1.45E+00	1.65E+00	1.93E+03	4.05E-01	2.95E-01
Nb-94	2.03E-03	1.89E-03	1.63E-03	2.48E-03	2.54E-03	8.93E-02	2.65E-03	2.06E-03
Tc-99	4.93E+01	1.14E+02	1.37E+02	3.88E+02	4.10E+02	6.34E+02	1.75E+02	1.20E+02
Pd-107	8.38E-03	6.03E-03	6.06E-03	1.51E-02	1.67E-02	3.75E-02	6.46E-03	6.42E-03
Sn-126	1.22E+00	7.62E-01	6.83E-01	5.97E+00	6.59E+00	2.22E+00	1.65E+00	9.47E-01
I-129	2.01E-01	7.31E-02	6.83E-02	2.70E-01	2.82E-01	2.77E-01	1.39E-01	8.68E-02
Cs-135	4.95E-02	3.36E-02	3.38E-02	2.48E-02	2.25E-02	1.73E+00	3.60E-02	3.58E-02
Cs-137	4.07E+00	3.99E+03	4.91E+03	3.95E+03	4.13E+03	1.09E+05	2.47E+03	5.10E+03
Sm-151	4.78E-03	1.44E-01	1.26E-01	6.10E+01	7.27E+01	1.70E+01	2.22E-01	1.84E-01
Eu-152	5.81E-04	9.77E-05	9.82E-05	1.25E-01	1.49E-01	2.77E-02	1.05E-04	1.04E-04
Eu-154	1.13E-04	1.77E-03	3.18E-03	1.15E+00	1.37E+00	6.73E-01	9.18E-04	9.57E-04
Pt-193	1.26E+00	1.20E+00	1.20E+00	1.30E+00	1.29E+00	6.84E+00	1.34E+00	1.31E+00
Pb-210	4.22E-07	2.47E-06	1.42E-06	4.19E-07	4.29E-07	3.24E-05	5.88E-07	5.73E-07
Ra-226	9.53E-07	8.56E-06	4.93E-06	1.25E-06	1.20E-06	8.27E-05	2.30E-06	2.18E-06
Ac-227	2.55E-06	1.01E-06	1.30E-06	1.46E-05	2.10E-06	9.55E-05	2.48E-05	4.02E-05
Ra-228	7.68E-06	1.26E-05	1.92E-05	4.07E-03	4.85E-03	2.10E-04	1.35E-05	2.26E-05
Th-229	5.33E-04	4.28E-03	8.24E-03	1.15E-03	9.73E-04	3.64E+00	2.30E-03	2.11E-03
Th-230	6.48E-05	9.00E-04	5.55E-04	1.06E-04	8.46E-05	6.32E-03	3.13E-04	2.87E-04
Pa-231	4.08E-06	1.62E-06	2.07E-06	4.87E-06	5.41E-06	1.52E-04	2.49E-06	2.06E-06
Th-232	7.69E-06	1.26E-05	1.92E-05	4.07E-03	4.85E-03	2.10E-04	1.35E-05	2.26E-05
U-232	5.40E-04	1.13E-02	1.10E-02	2.77E-03	6.68E-04	9.72E-02	1.19E-02	1.63E-02
U-233	7.76E-02	9.51E-01	1.32E+00	3.37E-01	2.18E-01	8.86E+00	1.17E+00	1.07E+00
U-234	9.93E-02	6.16E-01	8.54E-01	4.04E-01	3.61E-01	8.98E+00	7.60E-01	6.88E-01
U-235	2.51E-03	9.93E-04	1.27E-03	7.60E-03	8.82E-03	9.37E-02	1.53E-03	1.27E-03
U-236	6.49E-03	6.37E-03	8.85E-03	1.76E-02	1.97E-02	8.35E-02	7.82E-03	7.18E-03
Np-237	3.94E-03	1.60E-01	9.61E-02	1.91E-01	2.15E-01	5.76E-01	8.51E-02	7.76E-02
Pu-238	6.18E-03	4.92E+00	4.67E+00	2.28E+03	2.70E+03	2.69E+02	6.52E+01	2.25E+01
U-238	1.07E-02	2.24E-02	2.65E-02	2.44E-01	2.86E-01	7.93E-02	3.28E-02	2.85E-02
Pu-239	1.43E-02	5.28E-01	5.19E-01	1.41E+02	1.67E+02	5.86E+01	1.86E+00	7.39E-01
Pu-240	1.35E-02	5.27E-01	5.18E-01	2.98E+01	3.48E+01	7.27E+01	1.85E+00	7.38E-01
Pu-241	8.25E-03	6.71E-01	6.39E-01	2.69E+02	3.17E+02	3.61E+01	1.05E+01	3.48E+00
Am-241	2.30E-03	9.08E-02	1.03E-01	2.22E+02	2.64E+02	2.16E+01	6.04E-01	2.11E-01
Pu-242	1.57E-03	3.76E-01	5.21E-01	1.08E-01	5.63E-02	4.12E+00	4.61E-01	4.21E-01
Am-242m	6.20E-05	9.09E-03	5.78E-03	1.08E-01	1.28E-01	1.74E-02	9.18E-04	7.57E-04
Cm-243	2.94E-04	3.42E-04	3.40E-04	4.77E-04	4.89E-04	5.28E-03	3.91E-04	3.80E-04
Am-243	1.42E-03	4.23E-03	4.90E-03	8.97E-02	1.07E-01	5.17E-01	3.94E-03	9.23E-03
Pu-244	1.01E-05	1.74E-03	2.42E-03	5.02E-04	2.60E-04	1.68E-02	2.14E-03	1.95E-03
Cm-244	1.45E-03	9.44E-02	1.07E-01	1.60E+00	1.90E+00	1.56E+01	4.67E-02	5.30E-02
Cm-245	2.71E-04	1.46E-02	2.22E-02	2.83E-03	1.44E-03	7.78E-01	1.50E-02	1.31E-02
Cm-247	1.59E-13	1.67E-02	1.41E-02	8.39E-04	1.48E-13	1.06E-01	2.13E-02	1.77E-02
Cf-249	8.46E-13	1.72E-02	1.42E-02	8.50E-04	8.24E-13	2.67E-01	2.15E-02	1.77E-02
Cf-251	3.04E-14	1.32E-02	1.07E-02	6.01E-04	2.90E-14	9.17E-02	1.66E-02	1.49E-02

Table 3.3-7: Pessimistic SDF Radionuclide Inventory Estimate (Ci) at Closure (Continued)

Radionuclide	SDU 6	SDU 7	SDU 8	SDU 9	SDU 10	SDU 11	SDU 12	Total
H-3	6.73E+02	6.73E+02	6.73E+02	6.73E+02	6.73E+02	6.73E+02	6.73E+02	4.84E+03
C-14	1.15E+02	1.15E+02	1.15E+02	1.15E+02	1.15E+02	1.15E+02	1.15E+02	8.41E+02
Al-26	5.30E+00	5.30E+00	5.30E+00	5.30E+00	5.30E+00	5.30E+00	5.30E+00	3.92E+01
Cl-36	1.95E-01	1.95E-01	1.95E-01	1.95E-01	1.95E-01	1.95E-01	1.95E-01	1.42E+00
K-40	1.95E-01	1.95E-01	1.95E-01	1.95E-01	1.95E-01	1.95E-01	1.95E-01	1.42E+00
Co-60	1.66E+00	1.66E+00	1.66E+00	1.66E+00	1.66E+00	1.66E+00	1.66E+00	1.19E+01
Ni-63	4.32E+01	4.32E+01	4.32E+01	4.32E+01	4.32E+01	4.32E+01	4.32E+01	3.12E+02
Se-79	1.98E+01	1.98E+01	1.98E+01	1.98E+01	1.98E+01	1.98E+01	1.98E+01	1.52E+02
Sr-90	7.96E+05	7.96E+05	7.96E+05	7.96E+05	7.96E+05	7.96E+05	7.96E+05	5.70E+06
Zr-93	1.95E+01	1.95E+01	1.95E+01	1.95E+01	1.95E+01	1.95E+01	1.95E+01	1.50E+02
Nb-93m	1.92E+01	1.92E+01	1.92E+01	1.92E+01	1.92E+01	1.92E+01	1.92E+01	2.07E+03
Nb-94	2.97E-02	2.97E-02	2.97E-02	2.97E-02	2.97E-02	2.97E-02	2.97E-02	3.12E-01
Tc-99	4.78E+03	4.78E+03	4.78E+03	4.78E+03	4.78E+03	4.78E+03	4.78E+03	3.55E+04
Pd-107	1.95E-01	1.95E-01	1.95E-01	1.95E-01	1.95E-01	1.95E-01	1.95E-01	1.47E+00
Sn-126	7.70E+01	7.70E+01	7.70E+01	7.70E+01	7.70E+01	7.70E+01	7.70E+01	5.59E+02
I-129	3.29E+00	3.29E+00	3.29E+00	3.29E+00	3.29E+00	3.29E+00	3.29E+00	2.44E+01
Cs-135	2.63E-01	2.63E-01	2.63E-01	2.63E-01	2.63E-01	2.63E-01	2.63E-01	3.81E+00
Cs-137	4.82E+04	4.82E+04	4.82E+04	4.82E+04	4.82E+04	4.82E+04	4.82E+04	4.71E+05
Sm-151	8.49E+02	8.49E+02	8.49E+02	8.49E+02	8.49E+02	8.49E+02	8.49E+02	6.09E+03
Eu-152	1.73E+00	1.73E+00	1.73E+00	1.73E+00	1.73E+00	1.73E+00	1.73E+00	1.24E+01
Eu-154	1.60E+01	1.60E+01	1.60E+01	1.60E+01	1.60E+01	1.60E+01	1.60E+01	1.15E+02
Pt-193	1.50E+01	1.50E+01	1.50E+01	1.50E+01	1.50E+01	1.50E+01	1.50E+01	1.21E+02
Pb-210	5.01E-06	5.01E-06	5.01E-06	5.01E-06	5.01E-06	5.01E-06	5.01E-06	7.38E-05
Ra-226	1.40E-05	1.40E-05	1.40E-05	1.40E-05	1.40E-05	1.40E-05	1.40E-05	2.02E-04
Ac-227	2.45E-05	2.45E-05	2.45E-05	2.45E-05	2.45E-05	2.45E-05	2.45E-05	3.53E-04
Ra-228	5.66E-02	5.66E-02	5.66E-02	5.66E-02	5.66E-02	5.66E-02	5.66E-02	4.05E-01
Th-229	1.14E-02	1.14E-02	1.14E-02	1.14E-02	1.14E-02	1.14E-02	1.14E-02	3.74E+00
Th-230	9.87E-04	9.87E-04	9.87E-04	9.87E-04	9.87E-04	9.87E-04	9.87E-04	1.55E-02
Pa-231	6.32E-05	6.32E-05	6.32E-05	6.32E-05	6.32E-05	6.32E-05	6.32E-05	6.17E-04
Th-232	5.66E-02	5.66E-02	5.66E-02	5.66E-02	5.66E-02	5.66E-02	5.66E-02	4.06E-01
U-232	7.80E-03	7.80E-03	7.80E-03	7.80E-03	7.80E-03	7.80E-03	7.80E-03	2.06E-01
U-233	2.54E+00	2.54E+00	2.54E+00	2.54E+00	2.54E+00	2.54E+00	2.54E+00	3.18E+01
U-234	4.22E+00	4.22E+00	4.22E+00	4.22E+00	4.22E+00	4.22E+00	4.22E+00	4.23E+01
U-235	1.03E-01	1.03E-01	1.03E-01	1.03E-01	1.03E-01	1.03E-01	1.03E-01	8.38E-01
U-236	2.30E-01	2.30E-01	2.30E-01	2.30E-01	2.30E-01	2.30E-01	2.30E-01	1.77E+00
Np-237	2.51E+00	2.51E+00	2.51E+00	2.51E+00	2.51E+00	2.51E+00	2.51E+00	1.89E+01
Pu-238	3.15E+04	3.15E+04	3.15E+04	3.15E+04	3.15E+04	3.15E+04	3.15E+04	2.26E+05
U-238	3.34E+00	3.34E+00	3.34E+00	3.34E+00	3.34E+00	3.34E+00	3.34E+00	2.41E+01
Pu-239	1.95E+03	1.95E+03	1.95E+03	1.95E+03	1.95E+03	1.95E+03	1.95E+03	1.40E+04
Pu-240	4.06E+02	4.06E+02	4.06E+02	4.06E+02	4.06E+02	4.06E+02	4.06E+02	2.98E+03
Pu-241	3.70E+03	3.70E+03	3.70E+03	3.70E+03	3.70E+03	3.70E+03	3.70E+03	2.65E+04
Am-241	3.09E+03	3.09E+03	3.09E+03	3.09E+03	3.09E+03	3.09E+03	3.09E+03	2.21E+04
Pu-242	6.57E-01	6.57E-01	6.57E-01	6.57E-01	6.57E-01	6.57E-01	6.57E-01	1.07E+01
Am-242m	1.50E+00	1.50E+00	1.50E+00	1.50E+00	1.50E+00	1.50E+00	1.50E+00	1.08E+01
Cm-243	5.71E-03	5.71E-03	5.71E-03	5.71E-03	5.71E-03	5.71E-03	5.71E-03	4.80E-02
Am-243	1.25E+00	1.25E+00	1.25E+00	1.25E+00	1.25E+00	1.25E+00	1.25E+00	9.45E+00
Pu-244	3.03E-03	3.03E-03	3.03E-03	3.03E-03	3.03E-03	3.03E-03	3.03E-03	4.71E-02
Cm-244	2.22E+01	2.22E+01	2.22E+01	2.22E+01	2.22E+01	2.22E+01	2.22E+01	1.75E+02
Cm-245	1.68E-02	1.68E-02	1.68E-02	1.68E-02	1.68E-02	1.68E-02	1.68E-02	9.65E-01
Cm-247	1.73E-12	1.73E-12	1.73E-12	1.73E-12	1.73E-12	1.73E-12	1.73E-12	1.77E-01
Cf-249	9.62E-12	9.62E-12	9.62E-12	9.62E-12	9.62E-12	9.62E-12	9.62E-12	3.38E-01
Cf-251	3.38E-13	3.38E-13	3.38E-13	3.38E-13	3.38E-13	3.38E-13	3.38E-13	1.48E-01

Table 3.3-8: Realistic SDF Chemical Inventory Estimate (kg) at Closure

Chemical	SDU 1	SDU 2A	SDU 2B	SDU 3A	SDU 3B	SDU 4	SDU 5A	SDU 5B
Cl^-	2.72E+03	1.99E+03	7.64E+02	8.80E+02	4.87E+02	1.02E+04	1.77E+03	1.22E+03
F^-	1.54E+02	1.86E+03	5.82E+02	9.17E+02	9.78E+02	6.33E+03	5.93E+02	3.58E+02
NO_3	7.69E+05	7.06E+05	6.28E+05	7.81E+05	7.98E+05	4.75E+06	6.94E+05	7.41E+05
NO_2	7.69E+03	1.07E+05	1.10E+05	8.49E+04	7.07E+04	2.41E+05	1.61E+05	1.34E+05
PO_4	7.68E+02	2.41E+03	2.15E+03	4.60E+03	5.24E+03	1.47E+04	2.47E+03	2.63E+03
SO_4	2.31E+03	2.58E+04	2.13E+04	2.39E+04	2.39E+04	1.13E+05	3.10E+04	3.19E+04
Al	7.69E+03	2.18E+04	1.85E+04	1.23E+04	9.39E+03	1.10E+05	2.03E+04	2.16E+04
Ag	3.01E+00	6.67E+00	8.20E+00	4.28E+00	5.41E-01	5.52E+01	1.52E+01	1.07E+01
As	7.69E-01	2.16E+01	2.71E+00	7.53E+01	8.95E+01	2.55E+02	6.65E-01	6.15E-01
B	7.68E+01	2.75E+02	3.86E+02	1.27E+02	9.84E+01	1.64E+03	2.95E+02	2.51E+02
Ba	7.69E+00	8.77E+01	4.51E+00	1.74E+00	1.15E+00	3.44E+01	3.17E+00	4.52E+00
Cd	1.71E+00	6.90E+00	6.84E+00	6.98E+00	4.46E+00	2.30E+01	2.09E+01	9.94E+00
Co	7.69E-01	1.80E+00	4.56E-01	5.36E-01	6.08E-01	5.20E+00	1.21E-01	1.11E-01
Cr	1.64E+01	2.01E+02	2.19E+02	2.11E+02	1.91E+02	1.28E+03	2.63E+02	2.10E+02
Cu	1.18E+01	1.63E+01	5.87E+00	1.25E+02	1.35E+02	2.22E+02	2.40E+01	1.27E+01
Fe	7.68E+01	3.72E+01	5.92E+01	3.04E+01	1.88E+01	3.95E+03	3.74E+01	4.69E+01
Hg	7.69E+00	3.40E+02	2.23E+02	1.40E+02	8.56E+01	6.59E+02	5.64E+02	4.93E+02
I	2.80E-01	4.14E-01	3.86E-01	1.96E-01	2.68E-03	8.01E-01	7.87E-01	4.91E-01
Mn	2.75E+01	9.87E+00	1.65E+01	4.04E+01	4.67E+01	2.60E+03	9.84E+00	6.61E+00
Mo	7.68E+01	4.65E+01	4.28E+01	2.59E+01	8.36E+00	7.32E+02	6.38E+01	3.59E+01
Ni	1.11E+01	2.73E+01	1.83E+01	2.84E+01	1.09E+01	3.32E+02	1.03E+02	4.16E+01
Pb	7.69E+00	4.68E+00	1.78E+00	4.40E+01	4.56E+01	2.08E+02	1.88E+00	4.49E+00
Se	7.69E-01	7.82E+00	5.24E+00	2.66E+02	3.17E+02	8.38E+00	7.92E-01	1.09E+00
Sb	7.69E+00	1.78E+02	1.86E+02	2.31E+00	1.59E+00	1.54E+02	5.26E+00	9.15E+01
Sr	7.00E+01	4.18E+00	6.97E-01	6.80E+00	7.87E+00	1.31E+02	1.01E+00	1.12E+00
U	4.54E+00	6.75E+01	7.97E+01	1.59E+01	5.54E+00	1.78E+02	9.87E+01	8.58E+01
Zn	2.04E+02	4.33E+01	4.07E+01	1.60E+02	1.83E+02	4.51E+02	5.95E+01	4.53E+01

Table 3.3-8: Realistic SDF Chemical Inventory Estimate (kg) at Closure (Continued)

Chemical	SDU 6	SDU 7	SDU 8	SDU 9	SDU 10	SDU 11	SDU 12	Total
Cl^-	5.68E+03	5.68E+03	5.68E+03	5.68E+03	5.68E+03	5.68E+03	5.68E+03	5.98E+04
F^-	1.14E+04	1.14E+04	1.14E+04	1.14E+04	1.14E+04	1.14E+04	1.14E+04	9.17E+04
NO_3	9.31E+06	9.31E+06	9.31E+06	9.31E+06	9.31E+06	9.31E+06	9.31E+06	7.50E+07
NO_2	8.26E+05	8.26E+05	8.26E+05	8.26E+05	8.26E+05	8.26E+05	8.26E+05	6.70E+06
PO_4	6.12E+04	6.12E+04	6.12E+04	6.12E+04	6.12E+04	6.12E+04	6.12E+04	4.63E+05
SO_4	2.79E+05	2.79E+05	2.79E+05	2.79E+05	2.79E+05	2.79E+05	2.79E+05	2.23E+06
Al	1.10E+05	1.10E+05	1.10E+05	1.10E+05	1.10E+05	1.10E+05	1.10E+05	9.89E+05
Ag	6.31E+00	6.31E+00	6.31E+00	6.31E+00	6.31E+00	6.31E+00	6.31E+00	1.48E+02
As	1.05E+03	1.05E+03	1.05E+03	1.05E+03	1.05E+03	1.05E+03	1.05E+03	7.76E+03
B	1.15E+03	1.15E+03	1.15E+03	1.15E+03	1.15E+03	1.15E+03	1.15E+03	1.12E+04
Ba	1.35E+01	1.35E+01	1.35E+01	1.35E+01	1.35E+01	1.35E+01	1.35E+01	2.39E+02
Cd	5.21E+01	5.21E+01	5.21E+01	5.21E+01	5.21E+01	5.21E+01	5.21E+01	4.46E+02
Co	7.09E+00	7.09E+00	7.09E+00	7.09E+00	7.09E+00	7.09E+00	7.09E+00	5.92E+01
Cr	2.24E+03	2.24E+03	2.24E+03	2.24E+03	2.24E+03	2.24E+03	2.24E+03	1.82E+04
Cu	1.58E+03	1.58E+03	1.58E+03	1.58E+03	1.58E+03	1.58E+03	1.58E+03	1.16E+04
Fe	2.19E+02	2.19E+02	2.19E+02	2.19E+02	2.19E+02	2.19E+02	2.19E+02	5.79E+03
Hg	9.99E+02	9.99E+02	9.99E+02	9.99E+02	9.99E+02	9.99E+02	9.99E+02	9.50E+03
I	3.13E-02	3.13E-02	3.13E-02	3.13E-02	3.13E-02	3.13E-02	3.13E-02	3.58E+00
Mn	5.45E+02	5.45E+02	5.45E+02	5.45E+02	5.45E+02	5.45E+02	5.45E+02	6.57E+03
Mo	9.76E+01	9.76E+01	9.76E+01	9.76E+01	9.76E+01	9.76E+01	9.76E+01	1.72E+03
Ni	1.27E+02	1.27E+02	1.27E+02	1.27E+02	1.27E+02	1.27E+02	1.27E+02	1.46E+03
Pb	5.32E+02	5.32E+02	5.32E+02	5.32E+02	5.32E+02	5.32E+02	5.32E+02	4.04E+03
Se	3.70E+03	3.70E+03	3.70E+03	3.70E+03	3.70E+03	3.70E+03	3.70E+03	2.65E+04
Sb	1.85E+01	1.85E+01	1.85E+01	1.85E+01	1.85E+01	1.85E+01	1.85E+01	7.56E+02
Sr	9.19E+01	9.19E+01	9.19E+01	9.19E+01	9.19E+01	9.19E+01	9.19E+01	8.65E+02
U	6.47E+01	6.47E+01	6.47E+01	6.47E+01	6.47E+01	6.47E+01	6.47E+01	9.89E+02
Zn	2.13E+03	2.13E+03	2.13E+03	2.13E+03	2.13E+03	2.13E+03	2.13E+03	1.61E+04

Table 3.3-9: MPAD SDF Chemical Inventory Estimate (kg) at Closure

Chemical	SDU 1	SDU2A	SDU 2B	SDU 3A	SDU 3B	SDU 4	SDU 5A	SDU 5B
Cl^-	2.72E+03	1.99E+03	7.64E+02	1.07E+03	7.16E+02	1.02E+04	1.77E+03	1.22E+03
F^-	1.54E+02	1.86E+03	5.82E+02	1.30E+03	1.44E+03	6.33E+03	5.93E+02	3.58E+02
NO_3	7.69E+05	7.06E+05	6.28E+05	1.10E+06	1.17E+06	4.75E+06	6.94E+05	7.41E+05
NO_2	7.69E+03	1.07E+05	1.10E+05	1.13E+05	1.04E+05	2.41E+05	1.61E+05	1.34E+05
PO_4	7.68E+02	2.41E+03	2.15E+03	6.67E+03	7.71E+03	1.47E+04	2.47E+03	2.63E+03
SO_4	2.31E+03	2.58E+04	2.13E+04	3.33E+04	3.51E+04	1.13E+05	3.10E+04	3.19E+04
Al	7.69E+03	2.18E+04	1.85E+04	1.60E+04	1.38E+04	1.10E+05	2.03E+04	2.16E+04
Ag	3.01E+00	6.67E+00	8.20E+00	4.49E+00	7.95E-01	5.52E+01	1.52E+01	1.07E+01
As	7.69E-01	2.16E+01	2.71E+00	1.11E+02	1.32E+02	2.55E+02	6.65E-01	6.15E-01
B	7.68E+01	2.75E+02	3.86E+02	1.66E+02	1.45E+02	1.64E+03	2.95E+02	2.51E+02
Ba	7.69E+00	8.77E+01	4.51E+00	2.19E+00	1.70E+00	3.44E+01	3.17E+00	4.52E+00
Cd	1.71E+00	6.90E+00	6.84E+00	8.74E+00	6.57E+00	2.30E+01	2.09E+01	9.94E+00
Co	7.69E-01	1.80E+00	4.56E-01	7.75E-01	8.93E-01	5.20E+00	1.21E-01	1.11E-01
Cr	1.64E+01	2.01E+02	2.19E+02	2.86E+02	2.82E+02	1.28E+03	2.63E+02	2.10E+02
Cu	1.18E+01	1.63E+01	5.87E+00	1.79E+02	1.99E+02	2.22E+02	2.40E+01	1.27E+01
Fe	7.68E+01	3.72E+01	5.92E+01	3.78E+01	2.76E+01	3.95E+03	3.74E+01	4.69E+01
Hg	7.69E+00	3.40E+02	2.23E+02	1.74E+02	1.26E+02	6.59E+02	5.64E+02	4.93E+02
I	2.80E-01	4.14E-01	3.86E-01	1.97E-01	3.95E-03	8.01E-01	7.87E-01	4.91E-01
Mn	2.75E+01	9.87E+00	1.65E+01	5.89E+01	6.86E+01	2.60E+03	9.84E+00	6.61E+00
Mo	7.68E+01	4.65E+01	4.28E+01	2.92E+01	1.23E+01	7.32E+02	6.38E+01	3.59E+01
Ni	1.11E+01	2.73E+01	1.83E+01	3.27E+01	1.61E+01	3.32E+02	1.03E+02	4.16E+01
Pb	7.69E+00	4.68E+00	1.78E+00	6.20E+01	6.70E+01	2.08E+02	1.88E+00	4.49E+00
Se	7.69E-01	7.82E+00	5.24E+00	3.91E+02	4.66E+02	8.38E+00	7.92E-01	1.09E+00
Sb	7.69E+00	1.78E+02	1.86E+02	2.94E+00	2.34E+00	1.54E+02	5.26E+00	9.15E+01
Sr	7.00E+01	4.18E+00	6.97E-01	9.91E+00	1.16E+01	1.31E+02	1.01E+00	1.12E+00
U	4.54E+00	6.75E+01	7.97E+01	1.81E+01	8.15E+00	1.78E+02	9.87E+01	8.58E+01
Zn	2.04E+02	4.33E+01	4.07E+01	2.32E+02	2.69E+02	4.51E+02	5.95E+01	4.53E+01

Table 3.3-9: MPAD SDF Chemical Inventory Estimate (kg) at Closure (Continued)

Chemical	SDU 6	SDU 7	SDU 8	SDU 9	SDU 10	SDU 11	SDU 12	Total
Cl^-	8.36E+03	8.36E+03	8.36E+03	8.36E+03	8.36E+03	8.36E+03	8.36E+03	7.89E+04
F^-	1.68E+04	1.68E+04	1.68E+04	1.68E+04	1.68E+04	1.68E+04	1.68E+04	1.30E+05
NO_3	1.37E+07	1.37E+07	1.37E+07	1.37E+07	1.37E+07	1.37E+07	1.37E+07	1.06E+08
NO_2	1.21E+06	1.21E+06	1.21E+06	1.21E+06	1.21E+06	1.21E+06	1.21E+06	9.48E+06
PO_4	8.99E+04	8.99E+04	8.99E+04	8.99E+04	8.99E+04	8.99E+04	8.99E+04	6.69E+05
SO_4	4.10E+05	4.10E+05	4.10E+05	4.10E+05	4.10E+05	4.10E+05	4.10E+05	3.16E+06
Al	1.61E+05	1.61E+05	1.61E+05	1.61E+05	1.61E+05	1.61E+05	1.61E+05	1.36E+06
Ag	9.28E+00	9.28E+00	9.28E+00	9.28E+00	9.28E+00	9.28E+00	9.28E+00	1.69E+02
As	1.54E+03	1.54E+03	1.54E+03	1.54E+03	1.54E+03	1.54E+03	1.54E+03	1.13E+04
B	1.69E+03	1.69E+03	1.69E+03	1.69E+03	1.69E+03	1.69E+03	1.69E+03	1.51E+04
Ba	1.98E+01	1.98E+01	1.98E+01	1.98E+01	1.98E+01	1.98E+01	1.98E+01	2.84E+02
Cd	7.66E+01	7.66E+01	7.66E+01	7.66E+01	7.66E+01	7.66E+01	7.66E+01	6.21E+02
Co	1.04E+01	1.04E+01	1.04E+01	1.04E+01	1.04E+01	1.04E+01	1.04E+01	8.31E+01
Cr	3.29E+03	3.29E+03	3.29E+03	3.29E+03	3.29E+03	3.29E+03	3.29E+03	2.58E+04
Cu	2.33E+03	2.33E+03	2.33E+03	2.33E+03	2.33E+03	2.33E+03	2.33E+03	1.69E+04
Fe	3.23E+02	3.23E+02	3.23E+02	3.23E+02	3.23E+02	3.23E+02	3.23E+02	6.53E+03
Hg	1.47E+03	1.47E+03	1.47E+03	1.47E+03	1.47E+03	1.47E+03	1.47E+03	1.29E+04
I	4.61E-02	4.61E-02	4.61E-02	4.61E-02	4.61E-02	4.61E-02	4.61E-02	3.68E+00
Mn	8.01E+02	8.01E+02	8.01E+02	8.01E+02	8.01E+02	8.01E+02	8.01E+02	8.41E+03
Mo	1.44E+02	1.44E+02	1.44E+02	1.44E+02	1.44E+02	1.44E+02	1.44E+02	2.04E+03
Ni	1.87E+02	1.87E+02	1.87E+02	1.87E+02	1.87E+02	1.87E+02	1.87E+02	1.89E+03
Pb	7.82E+02	7.82E+02	7.82E+02	7.82E+02	7.82E+02	7.82E+02	7.82E+02	5.83E+03
Se	5.44E+03	5.44E+03	5.44E+03	5.44E+03	5.44E+03	5.44E+03	5.44E+03	3.90E+04
Sb	2.73E+01	2.73E+01	2.73E+01	2.73E+01	2.73E+01	2.73E+01	2.73E+01	8.18E+02
Sr	1.35E+02	1.35E+02	1.35E+02	1.35E+02	1.35E+02	1.35E+02	1.35E+02	1.17E+03
U	9.51E+01	9.51E+01	9.51E+01	9.51E+01	9.51E+01	9.51E+01	9.51E+01	1.21E+03
Zn	3.13E+03	3.13E+03	3.13E+03	3.13E+03	3.13E+03	3.13E+03	3.13E+03	2.33E+04

Table 3.3-10: Pessimistic SDF Chemical Inventory Estimate (kg) at Closure

Chemical	SDU 1	SDU 2A	SDU 2B	SDU 3A	SDU 3B	SDU 4	SDU 5A	SDU 5B
Cl^-	2.72E+03	1.99E+03	7.64E+02	1.12E+03	7.70E+02	1.02E+04	1.77E+03	1.22E+03
F^-	1.54E+02	1.86E+03	5.82E+02	1.39E+03	1.55E+03	6.33E+03	5.93E+02	3.58E+02
NO_3	7.69E+05	7.06E+05	6.28E+05	1.17E+06	1.26E+06	4.75E+06	6.94E+05	7.41E+05
NO_2	7.69E+03	1.07E+05	1.10E+05	1.19E+05	1.12E+05	2.41E+05	1.61E+05	1.34E+05
PO_4	7.68E+02	2.41E+03	2.15E+03	7.15E+03	8.29E+03	1.47E+04	2.47E+03	2.63E+03
SO_4	2.31E+03	2.58E+04	2.13E+04	3.55E+04	3.78E+04	1.13E+05	3.10E+04	3.19E+04
Al	7.69E+03	2.18E+04	1.85E+04	1.69E+04	1.49E+04	1.10E+05	2.03E+04	2.16E+04
Ag	3.01E+00	6.67E+00	8.20E+00	4.54E+00	8.55E-01	5.52E+01	1.52E+01	1.07E+01
As	7.69E-01	2.16E+01	2.71E+00	1.19E+02	1.42E+02	2.55E+02	6.65E-01	6.15E-01
B	7.68E+01	2.75E+02	3.86E+02	1.75E+02	1.56E+02	1.64E+03	2.95E+02	2.51E+02
Ba	7.69E+00	8.77E+01	4.51E+00	2.30E+00	1.82E+00	3.44E+01	3.17E+00	4.52E+00
Cd	1.71E+00	6.90E+00	6.84E+00	9.16E+00	7.06E+00	2.30E+01	2.09E+01	9.94E+00
Co	7.69E-01	1.80E+00	4.56E-01	8.32E-01	9.61E-01	5.20E+00	1.21E-01	1.11E-01
Cr	1.64E+01	2.01E+02	2.19E+02	3.04E+02	3.03E+02	1.28E+03	2.63E+02	2.10E+02
Cu	1.18E+01	1.63E+01	5.87E+00	1.91E+02	2.14E+02	2.22E+02	2.40E+01	1.27E+01
Fe	7.68E+01	3.72E+01	5.92E+01	3.96E+01	2.97E+01	3.95E+03	3.74E+01	4.69E+01
Hg	7.69E+00	3.40E+02	2.23E+02	1.82E+02	1.35E+02	6.59E+02	5.64E+02	4.93E+02
I	2.80E-01	4.14E-01	3.86E-01	1.98E-01	4.25E-03	8.01E-01	7.87E-01	4.91E-01
Mn	2.75E+01	9.87E+00	1.65E+01	6.32E+01	7.38E+01	2.60E+03	9.84E+00	6.61E+00
Mo	7.68E+01	4.65E+01	4.28E+01	3.00E+01	1.32E+01	7.32E+02	6.38E+01	3.59E+01
Ni	1.11E+01	2.73E+01	1.83E+01	3.37E+01	1.73E+01	3.32E+02	1.03E+02	4.16E+01
Pb	7.69E+00	4.68E+00	1.78E+00	6.62E+01	7.21E+01	2.08E+02	1.88E+00	4.49E+00
Se	7.69E-01	7.82E+00	5.24E+00	4.21E+02	5.02E+02	8.38E+00	7.92E-01	1.09E+00
Sb	7.69E+00	1.78E+02	1.86E+02	3.08E+00	2.51E+00	1.54E+02	5.26E+00	9.15E+01
Sr	7.00E+01	4.18E+00	6.97E-01	1.06E+01	1.25E+01	1.31E+02	1.01E+00	1.12E+00
U	4.54E+00	6.75E+01	7.97E+01	1.86E+01	8.77E+00	1.78E+02	9.87E+01	8.58E+01
Zn	2.04E+02	4.33E+01	4.07E+01	2.49E+02	2.89E+02	4.51E+02	5.95E+01	4.53E+01

Table 3.3-10: Pessimistic SDF Chemical Inventory Estimate (kg) at Closure (Continued)

Chemical	SDU 6	SDU 7	SDU 8	SDU 9	SDU 10	SDU 11	SDU 12	Total
Cl^-	8.99E+03	8.99E+03	8.99E+03	8.99E+03	8.99E+03	8.99E+03	8.99E+03	8.35E+04
F^-	1.81E+04	1.81E+04	1.81E+04	1.81E+04	1.81E+04	1.81E+04	1.81E+04	1.39E+05
NO_3	1.47E+07	1.47E+07	1.47E+07	1.47E+07	1.47E+07	1.47E+07	1.47E+07	1.14E+08
NO_2	1.31E+06	1.31E+06	1.31E+06	1.31E+06	1.31E+06	1.31E+06	1.31E+06	1.01E+07
PO_4	9.68E+04	9.68E+04	9.68E+04	9.68E+04	9.68E+04	9.68E+04	9.68E+04	7.18E+05
SO_4	4.41E+05	4.41E+05	4.41E+05	4.41E+05	4.41E+05	4.41E+05	4.41E+05	3.39E+06
Al	1.73E+05	1.73E+05	1.73E+05	1.73E+05	1.73E+05	1.73E+05	1.73E+05	1.45E+06
Ag	9.98E+00	9.98E+00	9.98E+00	9.98E+00	9.98E+00	9.98E+00	9.98E+00	1.74E+02
As	1.65E+03	1.65E+03	1.65E+03	1.65E+03	1.65E+03	1.65E+03	1.65E+03	1.21E+04
B	1.82E+03	1.82E+03	1.82E+03	1.82E+03	1.82E+03	1.82E+03	1.82E+03	1.60E+04
Ba	2.13E+01	2.13E+01	2.13E+01	2.13E+01	2.13E+01	2.13E+01	2.13E+01	2.95E+02
Cd	8.24E+01	8.24E+01	8.24E+01	8.24E+01	8.24E+01	8.24E+01	8.24E+01	6.63E+02
Co	1.12E+01	1.12E+01	1.12E+01	1.12E+01	1.12E+01	1.12E+01	1.12E+01	8.88E+01
Cr	3.54E+03	3.54E+03	3.54E+03	3.54E+03	3.54E+03	3.54E+03	3.54E+03	2.75E+04
Cu	2.50E+03	2.50E+03	2.50E+03	2.50E+03	2.50E+03	2.50E+03	2.50E+03	1.82E+04
Fe	3.47E+02	3.47E+02	3.47E+02	3.47E+02	3.47E+02	3.47E+02	3.47E+02	6.70E+03
Hg	1.58E+03	1.58E+03	1.58E+03	1.58E+03	1.58E+03	1.58E+03	1.58E+03	1.37E+04
I	4.96E-02	4.96E-02	4.96E-02	4.96E-02	4.96E-02	4.96E-02	4.96E-02	3.71E+00
Mn	8.62E+02	8.62E+02	8.62E+02	8.62E+02	8.62E+02	8.62E+02	8.62E+02	8.84E+03
Mo	1.54E+02	1.54E+02	1.54E+02	1.54E+02	1.54E+02	1.54E+02	1.54E+02	2.12E+03
Ni	2.02E+02	2.02E+02	2.02E+02	2.02E+02	2.02E+02	2.02E+02	2.02E+02	2.00E+03
Pb	8.41E+02	8.41E+02	8.41E+02	8.41E+02	8.41E+02	8.41E+02	8.41E+02	6.26E+03
Se	5.85E+03	5.85E+03	5.85E+03	5.85E+03	5.85E+03	5.85E+03	5.85E+03	4.19E+04
Sb	2.93E+01	2.93E+01	2.93E+01	2.93E+01	2.93E+01	2.93E+01	2.93E+01	8.33E+02
Sr	1.45E+02	1.45E+02	1.45E+02	1.45E+02	1.45E+02	1.45E+02	1.45E+02	1.25E+03
U	1.02E+02	1.02E+02	1.02E+02	1.02E+02	1.02E+02	1.02E+02	1.02E+02	1.26E+03
Zn	3.37E+03	3.37E+03	3.37E+03	3.37E+03	3.37E+03	3.37E+03	3.37E+03	2.50E+04

3.3.4 SDU 1 and SDU 4 Individual Cell Inventory Estimates at Closure

As a modeling simplification, the individual cells within SDU 1 and SDU 4 are simulated as having uniform waste concentrations distributed into each cell (based on the total SDU inventories), as this facilitates greater computational efficiency with a minimal impact on the total dose results. However, in some cases it is useful to evaluate the individual cell inventories of SDU 1 and SDU 4. Estimates of the individual cell inventory were developed for SDU 1 Cells A through C and SDU 4 Cells A through L and are presented here as Table 3.3-11 and Table 3.3-12 (for radionuclides) and Table 3.3-13 and Table 3.3-14 (for chemicals). [SRR-CWDA-2018-00062] It should be noted that there are slight differences between the SDU 1 and SDU 4 total inventory estimates in Section 3.3.3 and those presented here. These differences are due to the number of significant figures used during intermediate calculations and are always less than 1% of the total values (i.e., the differences are minor and do not affect conclusions drawn from either set of inventory estimates).

Table 3.3-11: SDU 1 Cells Radionuclide Inventory Estimate (Ci) at Closure

Radionuclide	A	B	C	SDU 1 Total
H-3	1.41E+00	1.97E+00	1.23E+00	4.61E+00
C-14	4.68E-01	4.29E-01	4.14E-01	1.31E+00
Al-26	6.99E-02	7.15E-02	1.21E-01	2.62E-01
Cl-36	2.79E-09	9.68E-09	5.77E-08	7.02E-08
K-40	2.79E-09	9.68E-09	5.77E-08	7.02E-08
Co-60	6.56E-06	1.31E-05	1.55E-05	3.52E-05
Ni-63	1.44E-03	6.71E-03	9.66E-02	1.05E-01
Se-79	9.29E-02	6.97E-02	1.81E-01	3.44E-01
Sr-90	1.97E-04	9.75E-04	5.80E-03	6.97E-03
Zr-93	2.05E-01	2.10E-01	3.54E-01	7.68E-01
Nb-93m	2.00E-01	2.05E-01	3.47E-01	7.52E-01
Nb-94	7.85E-04	6.02E-04	6.41E-04	2.03E-03
Tc-99	3.81E-01	2.95E+01	1.94E+01	4.93E+01
Pd-107	2.23E-03	2.29E-03	3.86E-03	8.38E-03
Sn-126	2.99E-01	1.90E-01	7.34E-01	1.22E+00
I-129	1.17E-02	1.65E-02	1.73E-01	2.01E-01
Cs-135	1.54E-02	1.27E-02	2.15E-02	4.95E-02
Cs-137	7.90E-01	8.98E-01	2.39E+00	4.07E+00
Sm-151	8.50E-04	2.66E-03	1.27E-03	4.78E-03
Eu-152	3.64E-05	3.90E-05	5.05E-04	5.81E-04
Eu-154	1.88E-05	1.95E-05	7.46E-05	1.13E-04
Pt-193	3.24E-01	3.38E-01	6.01E-01	1.26E+00
Pb-210	1.06E-07	1.02E-07	2.15E-07	4.22E-07
Ra-226	2.31E-07	2.25E-07	4.98E-07	9.53E-07
Ra-228	2.05E-06	2.10E-06	3.54E-06	7.68E-06
Ac-227	6.72E-07	6.83E-07	1.20E-06	2.55E-06
Th-229	1.06E-04	1.08E-04	3.19E-04	5.33E-04
Th-230	1.52E-05	1.51E-05	3.45E-05	6.48E-05
Th-232	2.05E-06	2.10E-06	3.54E-06	7.68E-06
Pa-231	1.07E-06	1.09E-06	1.91E-06	4.08E-06
U-232	1.40E-04	1.45E-04	2.54E-04	5.39E-04
U-233	1.56E-02	1.60E-02	4.60E-02	7.76E-02
U-234	2.40E-02	2.45E-02	5.08E-02	9.93E-02
U-235	6.60E-04	6.75E-04	1.18E-03	2.51E-03
U-236	2.19E-03	2.24E-03	2.05E-03	6.49E-03
U-238	2.05E-03	2.10E-03	6.60E-03	1.07E-02
Np-237	2.89E-05	1.16E-04	3.80E-03	3.94E-03
Pu-238	2.77E-04	1.76E-04	5.73E-03	6.18E-03
Pu-239	3.94E-04	6.25E-04	1.33E-02	1.43E-02
Pu-240	3.96E-04	4.77E-04	1.26E-02	1.35E-02
Pu-241	1.07E-04	5.65E-04	7.58E-03	8.25E-03
Pu-242	2.05E-04	2.10E-04	1.15E-03	1.57E-03
Pu-244	2.05E-06	2.10E-06	5.99E-06	1.01E-05
Am-241	2.04E-04	3.12E-04	1.79E-03	2.30E-03
Am-242m	1.63E-05	1.68E-05	2.89E-05	6.20E-05
Am-243	3.77E-04	3.86E-04	6.53E-04	1.42E-03
Cm-243	7.34E-05	7.73E-05	1.43E-04	2.94E-04
Cm-244	3.48E-04	3.73E-04	7.27E-04	1.45E-03
Cm-245	7.22E-05	7.40E-05	1.25E-04	2.71E-04
Cm-247	4.24E-14	4.34E-14	7.33E-14	1.59E-13
Cf-249	2.25E-13	2.30E-13	3.92E-13	8.46E-13
Cf-251	8.09E-15	8.28E-15	1.40E-14	3.04E-14

Table 3.3-12: SDU 4 Cells, Radionuclide Inventory Estimate (Ci) at Closure

Radionuclide	A	B	C	D	E	F
H-3	3.89E+00	3.58E-01	1.02E+00	7.00E-01	1.30E+00	3.76E-01
C-14	0.00E+00	8.49E-01	7.67E-02	1.24E+00	1.93E-01	1.06E+00
Al-26	7.12E-02	3.51E-04	8.77E-02	4.14E-01	1.19E-01	4.23E-04
Cl-36	0.00E+00	4.00E-04	2.55E-08	4.37E-03	3.96E-03	9.09E-04
K-40	0.00E+00	4.00E-04	2.55E-08	4.37E-03	3.96E-03	9.09E-04
Co-60	1.08E-03	1.73E-04	2.35E-05	8.45E-04	1.33E-03	4.54E-04
Ni-63	0.00E+00	7.79E-02	7.15E-03	5.05E-01	8.51E-01	2.11E-01
Se-79	0.00E+00	5.36E-02	8.78E-03	2.29E+00	4.44E+00	6.24E-01
Sr-90	0.00E+00	4.01E+01	2.79E-03	4.40E+02	3.98E+02	9.13E+01
Zr-93	2.09E-01	2.80E-01	2.57E-01	1.27E+00	1.43E+00	6.96E-01
Nb-93m	2.04E-01	7.30E+01	2.52E-01	3.45E+02	3.92E+02	1.88E+02
Nb-94	0.00E+00	9.83E-04	5.45E-04	2.53E-02	3.38E-02	1.67E-03
Tc-99	0.00E+00	1.24E+02	1.20E+01	6.58E+01	1.46E+00	9.04E+01
Pd-107	2.28E-03	3.89E-03	2.80E-03	3.49E-03	3.80E-03	3.31E-03
Sn-126	0.00E+00	4.93E-01	6.25E-04	2.05E-01	2.67E-01	2.74E-01
I-129	0.00E+00	1.96E-02	7.31E-02	1.70E-02	1.12E-02	1.74E-02
Cs-135	1.27E-02	1.64E-01	1.56E-02	4.62E-01	1.95E-01	2.02E-01
Cs-137	0.00E+00	4.51E+03	2.66E+00	3.42E+04	7.68E+02	1.52E+04
Sm-151	1.46E-03	2.76E+00	9.24E-04	3.87E+00	2.94E+00	1.55E+00
Eu-152	3.66E-05	6.31E-05	1.08E-03	6.26E-03	6.19E-05	9.21E-04
Eu-154	0.00E+00	2.53E-02	6.91E-05	1.32E-01	2.05E-01	6.70E-02
Pt-193	3.31E-01	7.59E-01	4.83E-01	6.50E-01	7.00E-01	6.31E-01
Pb-210	1.33E-05	1.02E-06	3.44E-07	3.15E-06	2.64E-06	1.45E-06
Ra-226	3.15E-05	3.45E-06	9.34E-07	7.06E-06	5.54E-06	4.73E-06
Ra-228	2.09E-06	1.33E-05	2.57E-06	3.63E-05	4.13E-05	1.90E-05
Ac-227	6.13E-05	1.02E-06	1.60E-06	9.19E-07	2.61E-06	1.07E-06
Th-229	1.09E-04	3.58E+00	7.81E-04	7.93E-03	3.65E-03	5.17E-03
Th-230	2.26E-03	3.71E-04	7.88E-05	3.75E-04	2.44E-04	4.90E-04
Th-232	2.09E-06	1.33E-05	2.57E-06	3.64E-05	4.13E-05	1.90E-05
Pa-231	9.78E-05	1.62E-06	2.59E-06	1.47E-06	4.17E-06	1.70E-06
U-232	1.43E-04	7.48E-03	1.99E-04	2.34E-03	2.43E-03	3.58E-02
U-233	1.59E-02	7.23E-01	1.17E-01	1.12E+00	5.18E-01	7.31E-01
U-234	3.20E+00	5.26E-01	1.17E-01	5.37E-01	3.48E-01	6.96E-01
U-235	5.99E-02	9.97E-04	1.64E-03	9.05E-04	2.57E-03	1.05E-03
U-236	2.24E-03	5.31E-03	1.64E-03	1.27E-02	1.72E-02	6.28E-03
U-238	1.00E-04	1.47E-02	7.82E-03	3.54E-03	8.47E-03	4.04E-03
Np-237	3.04E-09	8.74E-02	3.04E-04	7.07E-02	1.05E-01	3.95E-02
Pu-238	6.35E-07	1.24E+01	4.16E-03	7.31E+01	3.17E+01	2.74E+01
Pu-239	6.96E-07	1.49E+00	6.19E-04	3.29E+00	2.75E+00	4.44E+01
Pu-240	2.08E-03	1.49E+00	6.20E-04	3.30E+00	3.43E+00	4.49E+01
Pu-241	6.59E-05	1.56E+00	9.74E-04	1.41E+01	3.50E+00	2.30E+00
Pu-242	2.09E-04	1.90E-01	1.50E-04	3.32E-01	5.01E-01	3.33E-01
Pu-244	2.09E-06	8.83E-04	6.95E-07	1.22E-03	9.39E-04	1.41E-03
Am-241	1.97E-04	9.10E-01	1.73E-04	4.73E+00	5.24E+00	1.93E+00
Am-242m	1.66E-05	7.71E-04	2.17E-05	4.07E-03	5.34E-03	7.93E-04
Am-243	3.85E-04	2.29E-02	4.74E-04	5.73E-02	7.20E-02	3.71E-02
Cm-243	7.46E-05	2.12E-04	1.61E-04	1.76E-04	2.03E-03	1.73E-04
Cm-244	3.52E-04	8.86E-01	4.79E-04	3.19E+00	4.36E+00	1.71E+00
Cm-245	7.37E-05	2.14E-02	9.07E-05	1.18E-01	2.16E-01	2.05E-02
Cm-247	4.32E-14	3.22E-02	5.32E-14	6.63E-14	1.56E-08	1.57E-02
Cf-249	2.29E-13	1.57E-02	2.88E-13	3.64E-13	3.95E-13	1.57E-02
Cf-251	8.24E-15	2.35E-02	1.02E-14	1.28E-14	1.04E-02	1.05E-02

Table 3.3-12: SDU 4 Cells, Radionuclide Inventory Estimate (Ci) at Closure (Continued)

Radionuclide	G	H	I	J	K	L	SDU 4 Total
H-3	1.77E+00	1.42E-01	1.31E+00	4.23E-01	5.49E-01	4.39E-01	1.23E+01
C-14	1.36E-01	4.80E-01	6.76E-02	4.98E-01	1.04E+00	8.23E-01	6.46E+00
Al-26	1.09E-01	1.19E-04	7.07E-02	8.61E-03	8.37E-02	1.05E-02	9.75E-01
Cl-36	3.05E-08	2.17E-04	1.19E-08	9.24E-04	2.99E-03	1.13E-03	1.49E-02
K-40	3.05E-08	2.17E-04	1.19E-08	9.24E-04	2.99E-03	1.13E-03	1.49E-02
Co-60	1.29E-05	1.05E-04	2.06E-05	5.18E-04	6.48E-04	5.21E-04	5.73E-03
Ni-63	1.52E-02	3.83E-02	3.40E-03	4.79E-01	2.92E-01	2.63E-01	2.74E+00
Se-79	1.74E-02	9.79E-02	7.57E-03	5.42E-01	9.57E-01	6.88E-01	9.73E+00
Sr-90	3.23E-03	2.18E+01	1.30E-03	9.28E+01	3.01E+02	1.13E+02	1.50E+03
Zr-93	3.21E-01	2.13E-01	2.07E-01	1.11E+00	1.37E+00	7.69E-01	8.13E+00
Nb-93m	3.14E-01	5.59E+01	2.03E-01	2.97E+02	3.67E+02	2.07E+02	1.93E+03
Nb-94	6.72E-04	3.77E-04	3.52E-04	1.97E-03	2.20E-02	1.60E-03	8.92E-02
Tc-99	2.66E+01	4.68E+01	6.83E+00	9.80E+01	9.19E+01	6.80E+01	6.32E+02
Pd-107	3.50E-03	1.66E-03	2.26E-03	3.75E-03	3.65E-03	2.99E-03	3.74E-02
Sn-126	8.64E-02	1.73E-01	3.76E-04	3.68E-01	9.72E-02	2.48E-01	2.21E+00
I-129	5.54E-02	7.20E-03	3.49E-02	2.01E-02	7.09E-03	1.37E-02	2.77E-01
Cs-135	1.95E-02	2.95E-02	1.26E-02	5.78E-02	4.01E-01	1.54E-01	1.73E+00
Cs-137	1.45E+00	2.77E+03	2.54E+00	7.50E+03	3.14E+04	1.24E+04	1.09E+05
Sm-151	1.25E-03	2.47E-01	1.16E-03	1.06E+00	2.96E+00	1.58E+00	1.70E+01
Eu-152	1.28E-03	2.35E-04	4.56E-04	5.21E-04	1.62E-02	5.89E-04	2.77E-02
Eu-154	6.41E-05	1.43E-02	4.14E-05	7.31E-02	7.86E-02	7.63E-02	6.71E-01
Pt-193	5.75E-01	3.21E-01	3.91E-01	7.21E-01	6.88E-01	5.67E-01	6.82E+00
Pb-210	1.23E-06	2.86E-07	1.91E-07	3.89E-06	2.82E-06	2.03E-06	3.23E-05
Ra-226	3.19E-06	9.46E-07	5.08E-07	1.31E-05	6.02E-06	5.49E-06	8.25E-05
Ra-228	3.21E-06	4.95E-06	2.07E-06	3.31E-05	3.26E-05	1.88E-05	2.09E-04
Ac-227	6.60E-06	4.95E-07	1.34E-06	1.64E-05	7.86E-07	1.34E-06	9.55E-05
Th-229	2.53E-03	1.18E-03	4.14E-04	2.70E-02	1.39E-03	7.17E-03	3.64E+00
Th-230	2.55E-04	9.96E-05	4.17E-05	1.40E-03	2.56E-04	4.37E-04	6.31E-03
Th-232	3.21E-06	4.95E-06	2.07E-06	3.31E-05	3.26E-05	1.88E-05	2.09E-04
Pa-231	1.06E-05	7.90E-07	2.15E-06	2.62E-05	1.25E-06	2.14E-06	1.52E-04
U-232	2.40E-04	3.91E-03	1.61E-04	1.25E-02	1.66E-02	1.49E-02	9.67E-02
U-233	3.66E-01	1.67E-01	6.12E-02	3.82E+00	1.97E-01	1.01E+00	8.85E+00
U-234	3.66E-01	1.42E-01	6.12E-02	1.99E+00	3.66E-01	6.20E-01	8.96E+00
U-235	6.55E-03	4.86E-04	1.35E-03	1.61E-02	7.72E-04	1.31E-03	9.37E-02
U-236	6.55E-03	1.85E-03	1.35E-03	1.82E-02	3.87E-03	6.15E-03	8.33E-02
U-238	1.22E-02	4.77E-03	7.35E-03	8.92E-03	2.38E-03	4.87E-03	7.92E-02
Np-237	1.14E-03	1.61E-02	1.43E-04	1.23E-01	3.78E-02	9.40E-02	5.75E-01
Pu-238	3.54E-03	9.27E+00	5.55E-03	4.03E+01	4.83E+01	2.59E+01	2.68E+02
Pu-239	3.44E-03	5.97E-01	5.75E-04	2.55E+00	2.05E+00	1.42E+00	5.86E+01
Pu-240	3.44E-03	5.97E-01	5.74E-04	1.37E+01	2.05E+00	3.24E+00	7.27E+01
Pu-241	2.11E-03	1.55E+00	6.49E-04	5.93E+00	4.45E+00	2.66E+00	3.61E+01
Pu-242	3.13E-04	1.10E-01	8.09E-05	2.07E+00	1.35E-01	4.52E-01	4.12E+00
Pu-244	1.45E-06	5.09E-04	3.76E-07	9.56E-03	3.61E-04	1.87E-03	1.68E-02
Am-241	1.42E-03	5.80E-01	1.33E-04	2.89E+00	2.93E+00	2.37E+00	2.16E+01
Am-242m	2.67E-05	5.12E-04	1.76E-05	1.31E-03	3.51E-03	9.37E-04	1.73E-02
Am-243	5.91E-04	3.59E-03	3.82E-04	1.74E-01	9.89E-02	4.87E-02	5.16E-01
Cm-243	1.42E-04	8.93E-05	1.54E-04	1.71E-03	1.87E-04	1.55E-04	5.27E-03
Cm-244	7.67E-04	2.69E-01	2.51E-04	1.58E+00	2.05E+00	1.51E+00	1.56E+01
Cm-245	1.13E-04	1.07E-02	7.32E-05	3.18E-02	3.43E-01	1.61E-02	7.77E-01
Cm-247	6.64E-14	1.23E-02	4.29E-14	3.13E-02	6.93E-14	1.44E-02	1.06E-01
Cf-249	3.58E-13	1.24E-01	2.33E-13	9.72E-02	3.81E-13	1.44E-02	2.67E-01
Cf-251	1.27E-14	1.07E-02	8.26E-15	2.57E-02	1.34E-14	1.06E-02	9.14E-02

Table 3.3-13: SDU 1 Cells, Chemical Inventory Estimate (kg) at Closure

Chemical	A	B	C	SDU 1 Total
Cl^-	7.24E+02	7.42E+02	1.25E+03	2.72E+03
F^-	4.09E+01	4.19E+01	7.08E+01	1.54E+02
NO_3	2.05E+05	2.10E+05	3.54E+05	7.68E+05
NO_2	2.05E+03	2.10E+03	3.54E+03	7.68E+03
PO_4	2.05E+02	2.10E+02	3.54E+02	7.68E+02
SO_4	6.14E+02	6.29E+02	1.06E+03	2.30E+03
Al	2.05E+03	2.10E+03	3.54E+03	7.68E+03
Ag	8.02E-01	8.22E-01	1.39E+00	3.01E+00
As	2.05E-01	2.10E-01	3.54E-01	7.68E-01
B	2.05E+01	2.10E+01	3.54E+01	7.68E+01
Ba	2.05E+00	2.10E+00	3.54E+00	7.69E+00
Cd	4.56E-01	4.68E-01	7.90E-01	1.71E+00
Co	2.05E-01	2.10E-01	3.54E-01	7.68E-01
Cr	4.38E+00	4.49E+00	7.58E+00	1.64E+01
Cu	3.13E+00	3.21E+00	5.42E+00	1.18E+01
Fe	2.05E+01	2.10E+01	3.54E+01	7.68E+01
Hg	2.05E+00	2.10E+00	3.54E+00	7.68E+00
I	9.82E-02	6.76E-02	1.14E-01	2.80E-01
Mn	7.33E+00	7.51E+00	1.27E+01	2.75E+01
Mo	2.05E+01	2.10E+01	3.54E+01	7.68E+01
Ni	2.95E+00	3.02E+00	5.10E+00	1.11E+01
Pb	2.05E+00	2.10E+00	3.54E+00	7.68E+00
Se	2.05E-01	2.10E-01	3.54E-01	7.68E-01
Sb	2.05E+00	2.10E+00	3.54E+00	7.68E+00
Sr	1.86E+01	1.91E+01	3.23E+01	7.00E+01
U	1.21E+00	1.24E+00	2.09E+00	4.54E+00
Zn	5.42E+01	5.56E+01	9.38E+01	2.04E+02

Table 3.3-14: SDU 4 Cells, Chemical Inventory Estimate (kg) at Closure

Chemical	A	B	C	D	E	F
Cl^-	0.00E+00	6.96E+02	9.10E+02	2.30E+03	1.63E+03	7.01E+02
F^-	0.00E+00	3.57E+02	5.14E+01	2.03E+03	1.50E+03	6.80E+02
NO_3	6.04E+05	4.99E+05	2.57E+05	4.01E+05	6.08E+05	3.84E+05
NO_2	0.00E+00	7.70E+04	2.57E+03	2.27E+04	4.80E+03	2.16E+04
PO_4	0.00E+00	1.83E+03	2.57E+02	2.42E+03	9.21E+02	2.32E+03
SO_4	0.00E+00	1.65E+04	7.71E+02	1.35E+04	2.20E+03	2.05E+04
Al	0.00E+00	1.09E+04	2.57E+03	1.57E+04	2.47E+04	9.92E+03
Ag	1.34E-08	5.38E+00	1.01E+00	4.83E+00	1.85E+01	3.96E+00
As	2.51E+02	6.28E-01	2.57E-01	3.32E-01	4.27E-01	3.52E-01
B	0.00E+00	4.31E+02	2.57E+01	5.72E+01	2.17E+02	9.98E+01
Ba	9.51E-08	1.93E+00	2.57E+00	3.04E+00	9.42E+00	1.60E+00
Cd	0.00E+00	2.58E+00	5.73E-01	1.78E+00	5.83E+00	1.69E+00
Co	0.00E+00	1.82E+00	2.57E-01	3.92E-01	7.41E-01	3.24E-01
Cr	3.38E+02	1.62E+02	5.50E+00	1.04E+02	5.01E+01	1.26E+02
Cu	1.71E+02	2.33E+00	3.93E+00	6.84E+00	1.61E+01	1.99E+00
Fe	0.00E+00	1.86E+02	2.57E+01	6.12E+02	1.21E+03	3.83E+02
Hg	7.10E+00	7.74E+01	2.57E+00	1.29E+02	2.52E+02	3.17E+01
I	0.00E+00	1.11E-01	8.29E-02	5.71E-02	2.37E-02	9.84E-02
Mn	0.00E+00	2.25E+01	9.20E+00	3.75E+02	8.15E+02	2.45E+02
Mo	0.00E+00	6.13E+01	2.57E+01	1.59E+01	5.93E+01	9.33E+01
Ni	4.10E-07	1.39E+01	3.70E+00	5.43E+01	1.08E+02	1.71E+01
Pb	2.59E-09	9.69E-01	2.57E+00	3.25E+00	1.01E+02	6.91E-01
Se	0.00E+00	1.26E+00	2.57E-01	6.61E-01	8.41E-01	7.06E-01
Sb	2.09E+00	3.94E+01	2.57E+00	1.15E+01	1.75E+00	3.07E+01
Sr	0.00E+00	1.95E-01	2.34E+01	6.81E+00	3.68E+01	3.16E-01
U	3.55E+01	4.45E+01	1.52E+00	3.63E+00	7.25E+00	1.28E+01
Zn	0.00E+00	2.05E+01	6.81E+01	4.05E+01	8.31E+01	1.46E+01

Table 3.3-14: SDU 4 Cells, Chemical Inventory Estimate (kg) at Closure (Continued)

Chemical	G	H	I	J	K	L	SDU 4 Total
Cl^-	1.14E+03	2.54E+02	7.34E+02	5.40E+02	6.41E+02	6.18E+02	1.02E+04
F^-	6.41E+01	1.52E+02	4.15E+01	3.24E+02	5.82E+02	5.30E+02	6.31E+03
NO_3	3.21E+05	2.11E+05	2.07E+05	5.13E+05	3.71E+05	3.63E+05	4.74E+06
NO_2	3.21E+03	2.28E+04	2.07E+03	4.36E+04	2.23E+04	1.81E+04	2.41E+05
PO_4	3.21E+02	7.28E+02	2.07E+02	1.68E+03	2.15E+03	1.79E+03	1.46E+04
SO_4	9.62E+02	6.52E+03	6.22E+02	1.66E+04	1.86E+04	1.57E+04	1.12E+05
Al	3.21E+03	4.44E+03	2.07E+03	1.19E+04	1.34E+04	1.06E+04	1.09E+05
Ag	1.26E+00	2.08E+00	8.13E-01	6.78E+00	3.16E+00	7.22E+00	5.50E+01
As	3.21E-01	1.58E-01	2.07E-01	5.61E-01	4.93E-01	6.02E-01	2.55E+02
B	3.21E+01	1.94E+02	2.07E+01	3.86E+02	2.08E+01	1.50E+02	1.63E+03
Ba	3.21E+00	7.53E-01	2.07E+00	2.61E+00	1.70E+00	4.85E+00	3.37E+01
Cd	7.15E-01	1.00E+00	4.62E-01	4.10E+00	1.53E+00	2.72E+00	2.30E+01
Co	3.21E-01	4.76E-02	2.07E-01	5.91E-01	1.98E-01	2.87E-01	5.19E+00
Cr	6.86E+00	6.91E+01	4.44E+00	1.53E+02	1.44E+02	1.10E+02	1.27E+03
Cu	4.91E+00	9.04E-01	3.17E+00	4.77E+00	3.49E+00	3.20E+00	2.22E+02
Fe	3.21E+01	1.28E+02	2.07E+01	3.90E+02	5.62E+02	3.88E+02	3.93E+03
Hg	3.21E+00	2.86E+01	2.07E+00	5.26E+01	4.09E+01	3.02E+01	6.57E+02
I	1.03E-01	4.07E-02	6.69E-02	1.14E-01	2.26E-02	7.76E-02	7.98E-01
Mn	1.15E+01	1.41E+02	7.42E+00	3.42E+02	3.60E+02	2.65E+02	2.59E+03
Mo	3.21E+01	3.22E+01	2.07E+01	8.45E+01	1.83E+02	1.21E+02	7.28E+02
Ni	4.62E+00	9.16E+00	2.99E+00	3.13E+01	5.03E+01	3.48E+01	3.30E+02
Pb	3.21E+00	1.93E-01	2.07E+00	1.56E+01	1.63E+00	7.66E+01	2.08E+02
Se	3.21E-01	6.32E-01	2.07E-01	1.27E+00	9.89E-01	1.21E+00	8.35E+00
Sb	3.21E+00	1.54E+00	2.07E+00	1.76E+01	1.81E+01	2.23E+01	1.53E+02
Sr	2.92E+01	7.17E-02	1.89E+01	1.29E+00	1.72E+00	1.18E+01	1.31E+02
U	1.90E+00	1.45E+01	1.23E+00	3.50E+01	4.58E+00	1.54E+01	1.78E+02
Zn	8.50E+01	8.62E+00	5.50E+01	2.09E+01	3.35E+01	2.07E+01	4.51E+02

4 ANALYSIS OF PERFORMANCE

This section provides a detailed description of model development.

- Section 4.1 provides an overview of the process from the Features, Event, and Process (FEPs) Screening and Conceptual Model Development to the Submodel Implementation and Submodel Integration.
- Section 4.2 describes the software used for each of the primary submodels.
- Section 4.3 describes the key inputs.
- Section 4.4 describes the development of each specific submodel.
- Sections 4.5 and 4.6 describes alternative models, sensitivity models, and probabilistic models.

4.1 Modeling Process

As described in Section 2.1.2, the development of this updated SDF PA applied a more systematic approach than was used for previous SDF modeling efforts. Figure 4.1-1 provides a high-level overview of the general process followed for this systematic approach to PA development, followed by additional discussion of the various steps in this process.

Figure 4.1-1: SDF PA Modeling Process Overview

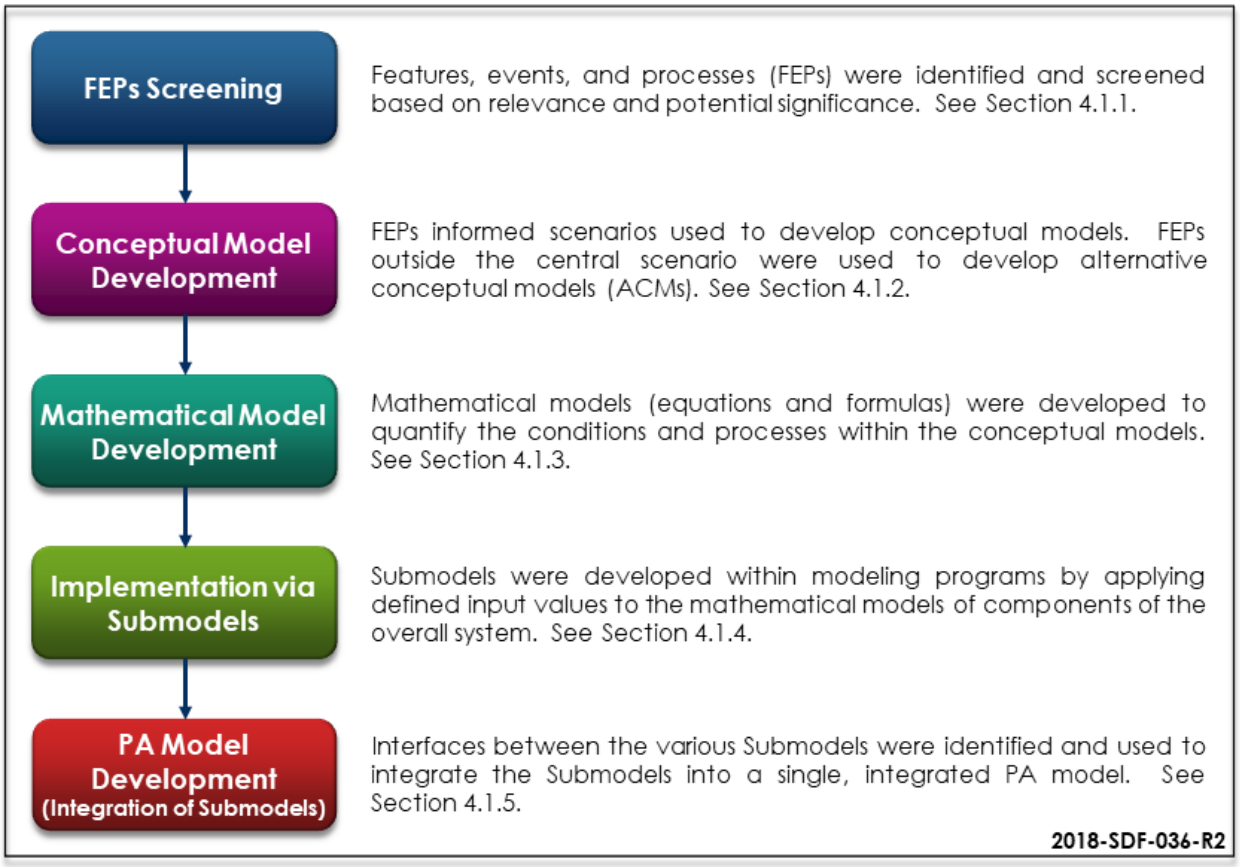

4.1.1 FEPs Screening

An overview of the FEPs Screening process is provided in Figure 4.1-2 and the complete process is detailed in *Features, Events, and Processes for the Saltstone Disposal Facility Performance Assessment* (SRR-CWDA-2017-00057). The first step in the development of this SDF PA was the identification of the relevant FEPs. An initial list of 345 potential FEPs was developed based on a literature review of other United States and international FEPs documents and a review of the 2009 SDF PA and other PA-related documents. [SRR-CWDA-2017-00057] The collected FEPs were then organized and assigned numbers based on the FEPs Groups and Sub-Groups shown in Table 4.1-1.

Figure 4.1-2: SDF PA Modeling Process – FEPs Screening Process

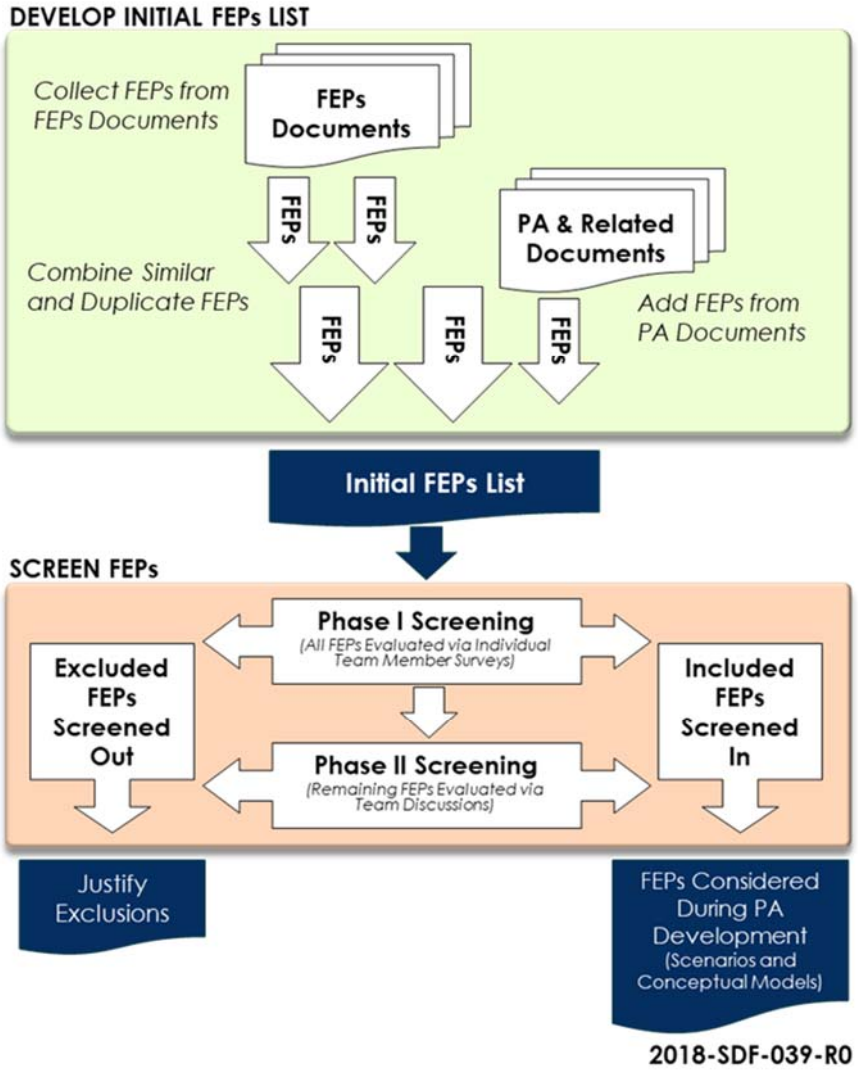

Table 4.1-1: FEPs Groups and Sub-Groups

Group	Sub-Group
1.0 Assessment Basis	1.1 General
1.0 Assessment Basis	1.2 Regulations and Controls
1.0 Assessment Basis	1.3 Models and Calculations
1.0 Assessment Basis	1.4 Other Assessment Factors
2.0 External Factors	2.1 Human Characteristics
2.0 External Factors	2.2 Land and Water Management
2.0 External Factors	2.3 Future Human Activity
2.0 External Factors	2.4 Biological Factors
2.0 External Factors	2.5 Geologic Features
2.0 External Factors	2.6 Geologic Processes
2.0 External Factors	2.7 Climate
2.0 External Factors	2.8 Water Cycle
3.0 Closure System	3.1 General Closure System
3.0 Closure System	3.2 Pre-Closure Activities
3.0 Closure System	3.3 Closure System Components
3.0 Closure System	3.4 Closure System Hydrology
3.0 Closure System	3.5 Chemical Processes
3.0 Closure System	3.6 Thermal Processes
3.0 Closure System	3.7 Material Degradation
3.0 Closure System	3.8 Other Closure System Factors
4.0 Contaminant Factors	4.1 Contaminant Description
4.0 Contaminant Factors	4.2 Contaminant Properties
4.0 Contaminant Factors	4.3 Concentrations
4.0 Contaminant Factors	4.4 Exposure Factors
4.0 Contaminant Factors	4.5 Other Contaminant Factors
5.0 Flow and Transport	5.1 Flow Factors
5.0 Flow and Transport	5.2 Flow Processes
5.0 Flow and Transport	5.3 Release and Transport
5.0 Flow and Transport	5.4 Other Flow and Transport Factors
6.0 Disruptive Events	6.1 Intrusion
6.0 Disruptive Events	6.2 Seismic Events
6.0 Disruptive Events	6.3 Igneous Events
6.0 Disruptive Events	6.4 Other Events

Next, a "FEPs Screening Team" was assembled to include subject matter experts in various disciplines including PA modeling, materials sciences, geology, chemistry, environmental engineering, and nuclear engineering. This team of nine individuals reviewed the 345 FEPs from the initial FEPs list and performed a subjective screening based on perceived frequency and perceived impact. [SRR-CWDA-2017-00057] The screening criteria used by the FEPs Screening Team, and the associated screening matrix, are shown in Table 4.1-2, Table 4.1-3, and Table 4.1-4. These tables include ordinal values for each criterion.

Table 4.1-2: FEPs Screening Criterion for Perceived Frequency

Description	Perceived Frequency	Score
Anticipated, Expected, or Already Known to Exist or Occur	Will Occur in 10,000 Years	2
Unlikely or Extremely Unlikely	May Occur in 10,000 Years	1
Beyond Extremely Unlikely	Not Expected to Occur in 10,000 Years	0

Table 4.1-3: FEPs Screening Criterion for Perceived Impact

Description	Perceived Impact to Member of Public	Score
High	Significant Impact on Release or Dose	2
Moderate	Moderate Impact on Release or Dose	1
Negligible	No or Negligible Impact on Release or Dose	0

Table 4.1-4: FEPs Screening Criteria Matrix

Frequency / Impact		Beyond Extremely Unlikely	Unlikely or Extremely Unlikely	Anticipated, Expected, or Already Known to Exist or Occur
		0	1	2
High	**2**	*Considered*	Screened In	Screened In
Moderate	**1**	Screened Out	*Considered*	*Considered*
Negligible	**0**	Screened Out	Screened Out	Screened Out

Each member of the FEPs Screening Team was provided with an Initial FEPs List and instructed to use their professional judgment to assign the most appropriate ordinal values for each FEP, much like completing a survey. The values were then mapped to the screening matrix (shown in Table 4.1-4). If the team members unanimously agreed to screen a FEP in or out, prior to any discussion, then it was assumed that the FEP is well understood and further discussion or evaluation of the FEP was unnecessary. FEPs that were not initially screened in or out during Phase I advanced to Phase II. For Phase II, the FEPs Screening Team discussed the remaining FEPs to determine the final recommended disposition of each FEP. [SRR-CWDA-2017-00057]

For FEPs that were screened out, the FEPs Screening Team developed and documented justifications for their exclusions. Of the 345 initial FEPs, 61 were screened out and 284 were screened in (i.e., determined to be potentially relevant to the SDF PA). Table 4.1-5 provides a complete listing of the FEPs that were considered and provides the justification for excluding the 61 FEPs that were screened out. The remaining FEPs were then used as a basis to inform decisions related to conceptual model development (see Section 4.1.2). For more information on the development and organization of the initial FEPs list, see *Features, Events, and Processes for the Saltstone Disposal Facility Performance Assessment*. [SRR-CWDA-2017-00057]

While Table 4.1-5 indicates the screening decisions, not every FEP that was screened in is explicitly analyzed in the SDF PA. These FEPs were given appropriate consideration during PA development; however, many are addressed external to the PA or do not directly translate to explicit modeling activities. For example, while the Waste Acceptance Criteria (WAC) (X-SD-Z-00004) may inform inventory development, they are not explicitly considered or modeled within this PA. More discussion of this topic is provided in Section 4.1.2.

Table 4.1-5: FEPs Screening Results

FEP ID	FEP Name (Short)	FEP Description	Final Deter-mination	Comments and/or Screen Out Justification
1.1.01	Assessment Purpose	Consideration for the purpose of the performance assessment of a waste closure facility.	Screen In	Programmatically screened in by WDA prior to screening evaluations.
1.1.02	Assessment Context Factors	Factors related to determining the scope or boundary conditions for the performance assessment of a waste closure facility. These include: a) factors related to the purpose for which the assessment is being performed, b) the regulatory requirements and criteria, c) the assessment philosophy that will be followed, and d) the overall framework within which the assessment will be performed.	Screen In	Programmatically screened in by WDA prior to screening evaluations.
1.1.03	Assessment Conditions	Factors related to the conditions (or framework) under which the performance assessment of the waste closure facility and closure system will be performed.	Screen In	Programmatically screened in by WDA prior to screening evaluations.
1.1.04	Assessment Timeframe (Phases of Disposal)	Factors related to the timeframe over which the waste closure facility may present human health or environmental hazards and be considered for the performance assessment. Examples of time periods to consider include: from closure to the end of institutional control; institutional control to 10,000 years; beyond 10,000 years; and the timing of the peak impact.	Screen In	Programmatically screened in by WDA prior to screening evaluations.
1.1.05	Safety Effects Beyond Periods of Control	Consideration for the effects of waste releases beyond the periods of facility controls. The continued isolation of the contaminants should not depend on actions by future generations to maintain the integrity of the closure system. The assessment should consider impacts on the health of future generations with respect to the relevant levels of impact that are acceptable today.	Screen In	Programmatically screened in by WDA prior to screening evaluations.
1.1.06	Spatial Domain of Concern	Factors related to the spatial domain over which the contaminants and the waste closure facility may present significant human health or environmental hazard and that will be considered in the post-closure performance assessment. This includes consideration for the level of discretization to apply to the spatial domain.	Screen In	Programmatically screened in by WDA prior to screening evaluations.
1.1.07	Assessment Endpoints	Concentration, flux, or health impact (risk/dose) criteria used to quantify the impact of the contaminants released from the waste closure facility. The endpoints may include: a) the concentration in disposed material, b) the contaminant flux from the waste closure facility, c) contaminant concentration in environmental media (e.g., soil, sediment, ground water, surface water, fauna and flora, and the atmosphere), and d) risks to human health.	Screen In	Programmatically screened in by WDA prior to screening evaluations.
1.1.08	Transparency of Assessment Approach	A transparent assessment approach ensures that all assumptions, constraints, and conditions imposed on the assessment and made within the assessment, are communicated or documented to all stakeholders. Such documentation includes scenario development and handling of expert judgment; model development decisions and justifications; input parameter values; and approaches with respect to the treatment of subjective uncertainties.	Screen In	Programmatically screened in by WDA prior to screening evaluations.
1.1.09	Documentation and Presentation of Results	The effective documentation, presentation and communication of the performance assessment using a variety of techniques (such as written material, videos, presentations, CD-ROM, web pages) tailored to the needs of the various stakeholders.	Screen In	Programmatically screened in by WDA prior to screening evaluations.

Table 4.1-5: FEPs Screening Results (Continued)

FEP ID	FEP Name (Short)	FEP Description	Final Deter-mination	Comments and/or Screen Out Justification
1.2.01	Regulatory Compliance	Factors related to the compliance of regulatory requirements, conditions, and criteria associated with all stages of the development, operation, and closure of the facility with respect to influences on the post-closure performance assessment or the permitting and/or licensing of the closure facility. This includes consideration for Resource Conservation and Recovery Act (RCRA) and Comprehensive Environmental Response, Compensation, and Liability Act (CERCLA) requirements.	Screen In	Programmatically screened in by WDA prior to screening evaluations.
1.2.02	Administrative Control of the Waste Closure Facility	Factors related to failure of administrative control measures and responsibilities for these measures during the pre-operational, operational, and post-closure (institutional control) periods. Measures applicable for the institutional control period can be divided into: active institutional control measures (such as monitoring, surveillance and remedial work) and passive institutional control measures (such as land use controls, site markers, and record keeping).	Screen In	Programmatically screened in by WDA prior to screening evaluations.
1.2.03	Functional and Technical Requirements and Criteria	Factors related to functional and technical requirements to be considered in the development of a safety case for the waste closure facility. Examples of such factors include: a) minimizing infiltration of water into disposal units, b) ensuring the integrity of disposal unit covers, c) providing the structural stability of system components, d) minimizing contact of waste with standing water, e) providing adequate drainage, minimizing the need for long-term maintenance, and f) providing barriers against intrusion.	Screen In	Programmatically screened in by WDA prior to screening evaluations.
1.2.04	Performance Requirements and Criteria	Factors related to performance requirements and criteria to be considered in the development of waste closure facility and the associated performance assessment. Closure systems are designed to satisfy a number of requirements to ensure the long-term safety of the closure facility. Criteria specific to closure system design can be performance driven (derived from site and facility-specific models) or prescriptive (i.e., regulatory criteria that apply to an entire class of facility).	Screen In	Programmatically screened in by WDA prior to screening evaluations.
1.2.05	Protection of Human Health and the Environment	Factors related to the regulatory requirements, criteria, and standards for the protection of human health and the environment during the lifetime of the waste closure facility and that would have an influence on the post-closure performance assessment and the assessment endpoints.	Screen In	Programmatically screened in by WDA prior to screening evaluations.
1.2.06	SDF Performance Period	The SDF permit states that as part of the U.S. Nuclear Regulatory Commission's (NRC) consultation with DOE's Waste Determination, the NRC has reviewed the anticipated performance of the SDF over the next 10,000 years.	Screen In	Programmatically screened in by WDA prior to screening evaluations.
1.2.07	Permitted Influent Waste Stream Compositions	The SDF permit specifies the physical composition of the waste streams entering the SPF.	Screen In	Programmatically screened in by WDA prior to screening evaluations.
1.2.08	Waste Classification and Characterization for Regulatory Compliance	Factors related to classifying waste and ensuring that waste(s) accepted for disposal or closure meet specific requirements and criteria, such that the waste(s) is/are consistent with the operational and long-term safety cases for the waste closure facility.	Screen In	Programmatically screened in by WDA prior to screening evaluations.
1.2.09	Waste Acceptance Requirements and Criteria	Factors related to defining waste acceptance requirements and criteria and ensuring that waste(s) accepted for disposal or closure meet specific requirements and criteria, such that the waste(s) is/are consistent with the operational and long-term safety cases for the waste closure facility.	Screen In	Programmatically screened in by WDA prior to screening evaluations.
1.2.10	Technical Safety Requirements for Operating the Saltstone Facility	Factors related to the self-imposed Technical Safety Requirements (TSRs) developed to address safe operations in the Saltstone Facility (Z-Area). [S-TSR-Z-00002]	Screen In	Programmatically screened in by WDA prior to screening evaluations.

Table 4.1-5: FEPs Screening Results (Continued)

FEP ID	FEP Name (Short)	FEP Description	Final Deter-mination	Comments and/or Screen Out Justification
1.2.11	ALARA	Factors related to "As Low As Reasonably Achievable" (ALARA) requirements and goals. This is a requirement to ensure risks are minimized with respect to the radiological detriment to members of the public that may result from the disposal of wastes. Social, economic, and public policy considerations should be included in the ALARA analysis, as well as a discussion of "dose savings" and the economic costs of those dose savings, as well as any other costs, such as potential increases in the dose to site workers.	Screen In	Programmatically screened in by WDA prior to screening evaluations.
1.3.01	Model and Data Issues	Factors related to modeling of the disposal system. Model and data issues are general (i.e., methodological) issues affecting the modeling process and data usage. Model issues include: a) the approach and assumptions associated with the selection of conceptual models, b) the mathematical implementation of conceptual models, c) spatial and temporal discretization, d) models of coupled processes, and e) boundary and initial conditions. Data issues include the derivation of data values, correlations, and dependence of parameter selection on model scale.	Screen In	Programmatically screened in by WDA prior to screening evaluations.
1.3.02	Conceptual Model Description	A clear, integrated description of the conceptual model(s) is needed to ensure adequate representation of the physical system and whether the mathematical model adequately represents the conceptual model.	Screen In	Programmatically screened in by WDA prior to screening evaluations.
1.3.03	Model Confidence	Factors related to activities that build confidence in the performance assessment modeling. Activities include verification of performance, calibration of performance, and validation of performance.	Screen In	Programmatically screened in by WDA prior to screening evaluations.
1.3.04	Model Calibration with SDU 4 Data	Observed, advective releases from SDU 4 should be used to calibrate transport modeling.	Screen In	
1.3.05	Points of Assessment	Assumed points (locations) for measuring the calculated concentrations or dose to demonstrate compliance or performance.	Screen In	Programmatically screened in by WDA prior to screening evaluations.
1.3.06	Evaluate Multiple Endpoints	The use of multiple lines of reasoning and the calculation of multiple endpoints helps ensure that the varied interests of stakeholders are addressed and understood. Demonstration of the performance of individual system components and their expected time evolution increases confidence in the performance of the whole system. Presentation of a number of safety indicators over a range of timeframes allows stakeholders to focus attention on indicators and timeframes of the greatest interest.	Screen In	Programmatically screened in by WDA prior to screening evaluations.
1.3.07	Model Approaches	Factors related to the modeling approaches applied in the performance assessment. Some examples include: a) simple scoping calculations that can be computed using a hand calculator or spreadsheet, b) worst case (or bounding) calculations that deal with uncertainty, and c) conceptual and mathematical models. This also includes consideration for deterministic modeling versus probabilistic modeling approaches.	Screen In	Programmatically screened in by WDA prior to screening evaluations.
1.3.08	Model Abstraction	Evaluation or justification for modeling simplification or abstraction methods. For example the use of a radial model to define flow fields and column influence on flow fields when the columns are dispersed throughout the SDUs should be evaluated.	Screen In	Programmatically screened in by WDA prior to screening evaluations.
1.3.09	Conservative Assessment Approach	Using a conservative, or cautious, approach applies assumptions that will not result in the end-point(s) being underestimated. In applying this approach, there is a danger that aggregation of conservative assumptions, each of which may be appropriate in its own right, may result in an unrealistic estimate of potential impacts. Therefore, it is necessary to document and justify the nature of each assumption in the assessment.	Screen In	Programmatically screened in by WDA prior to screening evaluations.

Table 4.1-5: FEPs Screening Results (Continued)

FEP ID	FEP Name (Short)	FEP Description	Final Deter-mination	Comments and/or Screen Out Justification
1.3.10	Realistic Assessment Approach	A realistic, or equitable, approach applies assumptions with respect to physical reality (including what is possible and likely to occur). This approach is typically used when some knowledge of the actual system or conditions are available. The disadvantage of applying realistic assumptions in the assessment is that results might be underestimated. Therefore, it is necessary to document and justify the nature of each assumption in the assessment.	Screen In	Programmatically screened in by WDA prior to screening evaluations.
1.3.11	Prospective Evaluation Assessment Approach	A prospective evaluation approach emphasizes that the intent of the performance assessment is not to predict actual system behavior but to improve system understanding such that appropriate emphasis may be directed towards specific system components (i.e., those with the greatest potential impact on regulatory compliance).	Screen Out	Screened Out Prior to Phase I: The intent of this FEP is to develop a model which focuses on the impacts of specific model features or processes. Given that the impact of specific system components cannot be fully understood without first understanding realistic expected conditions, this FEP speaks to a modeling approach that may not be useful except under very specific conditions. As the recommended approach is to develop a conservative model, a realistic model, and a compliance model, the "prospective evaluation" approach is not needed.
1.3.12	Reasonable Assurance Assessment Approach	The reasonable assurance approach emphasizes that performance assessments are not exact reflections of reality. As such, the goal of a performance assessment is to determine the conditions for which reasonable assurance of regulatory compliance can be achieved. This approach is more of a decision tool, rather than a method to predict the actual behavior of a disposal system into the future. The results are a function of the data, design, and assumptions used in the analysis.	Screen In	Programmatically screened in by WDA prior to screening evaluations.
1.3.13	Systematic Assessment Approach	Different systematic or structured approaches can be followed to perform performance assessments of waste closure facilities, all aimed at improving the confidence in the assessment results. Factors to be considered in a systematic approach include: a) the necessary level of appropriate documentation, b) rigor and technical justification for decisions and methods used, c) use of multiple lines of reasoning to broaden result sets, d) use of iterations, e) development of system understanding and expertise, and f) demonstration of performance.	Screen In	Programmatically screened in by WDA prior to screening evaluations.
1.3.14	Iterative Assessment Approach	Performance Assessments, by their nature, require an iterative approach, aiming at continual improvement of the safety case. This implies that a performance assessment process will have to go through two or more consecutive iterations. The advantage of such an approach is that it allows one to use information from the previous assessment to refine the design of the system and the collection of additional data.	Screen In	Programmatically screened in by WDA prior to screening evaluations.

Table 4.1-5: FEPs Screening Results (Continued)

FEP ID	FEP Name (Short)	FEP Description	Final Deter-mination	Comments and/or Screen Out Justification
1.3.15	Alternative Simplified Modeling Approach	Supplement the sophisticated model with a less complex model for explanatory purposes and as a confidence-building tool. A well-designed simplified model may help foster public understanding and acceptance of the waste closure facility. While simplification may cause loss of detail, demonstration of equivalence of simple and complex methods may be possible if it can be shown that the simplifications focus on the critical factors related to system performance and safety.	Screen In	Programmatically screened in by WDA prior to screening evaluations.
1.3.16	Sensitivity Analyses	Factors related to the performance of sensitivity analyses of the post-closure performance assessment. Sensitivity analyses help to establish a comprehensive and defensible safety case and provide insights into system behavior that may lead to design improvements.	Screen In	Programmatically screened in by WDA prior to screening evaluations.
1.3.17	Uncertainties	Factors related to the identification and treatment of model/future uncertainties in the performance assessment. Such factors include: a) conceptual model uncertainty, b) mathematical model uncertainty, c) computer model uncertainty d) parameter/data uncertainty, and e) subjective uncertainties.	Screen In	Programmatically screened in by WDA prior to screening evaluations.
1.3.18	Processing Limitations to Modeling	Factors related to the processing (computing) limitations to running the performance assessment models.	Screen In	Programmatically screened in by WDA prior to screening evaluations.
1.3.19	Software Codes	Factors related to software selection and software quality assurance practices for codes important to the performance and safety of the waste closure facility as they apply to modeling, model validation, calibration, and benchmarking.	Screen In	Programmatically screened in by WDA prior to screening evaluations.
1.4.01	Target Audience (Stakeholder Involvement)	Factors related to the definition of the target audience and their involvement in the post-closure safety assessment process of the waste closure facility.	Screen In	Programmatically screened in by WDA prior to screening evaluations.
1.4.02	Confidence Building (External to Modeling)	Activities, other than modeling, to address the concerns of stakeholders, such as validation and analogue studies, as well as public hearings to maintain an open dialogue.	Screen In	Programmatically screened in by WDA prior to screening evaluations.
1.4.03	Development of Expertise	Develop expertise and understanding of the performance assessment process and determination of related strategic issues.	Screen In	Programmatically screened in by WDA prior to screening evaluations.
1.4.04	Regulatory and Peer Reviews	A requirement that the performance assessment should be subject to rigorous regulatory and peer review processes as part of developing a comprehensive and defensible safety case for a waste closure facility. Reviewers should be satisfied that good engineering practices are used in design, construction, operation, and closure of the facility and that good science has been applied in investigating and researching the site and related FEPS, and in evaluating and interpreting the resulting data and methodologies used.	Screen In	Programmatically screened in by WDA prior to screening evaluations.
1.4.05	Monitoring and Surveillance	Factors related to the monitoring and surveillance that is carried out during operations or following closure of individual disposal units or total the waste closure facility. This includes monitoring and surveillance for operational safety and parameters related to long-term safety and performance. Regulations, confidence building activities, or public pressure may determine the extent and requirement for such a monitoring and surveillance program.	Screen In	Programmatically screened in by WDA prior to screening evaluations.
1.4.06	Retrievability	Factors related to any design, emplacement, operational or administrative measures that might be applied or considered in order to enable or ease retrieval of radioactive wastes from the waste closure facility. An interim period might be planned between waste emplacement and final Tank Farm closure, during which time retrieval is possible.	Screen Out	Screened Out Prior to Phase I: Waste retrievability is not considered an option for the SDF PA. This FEP should be excluded.

Table 4.1-5: FEPs Screening Results (Continued)

FEP ID	FEP Name (Short)	FEP Description	Final Deter-mination	Comments and/or Screen Out Justification
2.1.01	Definition of the Exposed Member of the Public	Factors related to the determination of the "Member of the Public" (MOP), the representative and reasonably or conservatively exposed individual for whom doses and results shall be evaluated, or the inadvertent human intruder (IHI). Defining the MOP/IHI shall consider regulatory stipulations, conservatisms, and group homogeneity (in terms of diet and habits, location). Definitions should consider behaviors that impact exposure and the differences between a "maximally exposed individual", a "reference person", or an "average member of the critical group."	Screen In	Programmatically screened in by WDA prior to screening evaluations.
2.1.02	Human Physiology (Metabolism, Diet, and Fluid Intake)	Factors related to intake human consumption and ingestion. Human diets can vary greatly, both qualitatively and quantitatively. In addition to food and fluid intake, humans may also consume other things such as medicines, drugs, soils, and minerals. Consideration could also be given to vegetarian and other special diets, and to changes in diet due to external factors.	Screen In	
2.1.03	Demographics and Community	Factors related to demographic features and assumed urban development in the vicinity of the waste closure facility. In addition to population density and location, consideration should be given to the types of communities: hunter-gatherer/nomadic communities; agricultural communities; self-sufficient rural communities; other rural communities; and urban communities. Changes in any of these conditions may influence the performance of the facility.	Screen In	
2.1.04	Human Behavior and Habits (Non-Diet Related)	Factors related to non-diet related behavior and habits of humans to whom exposures from the waste closure facility are calculated. These factors include time spent in various environments, activities, and uses of materials and may be influenced by agricultural practices, technology, and societal factors (e.g., culture, religion, economics). Examples include: a) outdoor activities (e.g., fishing, logging, swimming, etc.), b) keeping of pets that could become contaminated, and c) agricultural practices (e.g., plowing, cultivation, harvesting, etc.).	Screen In	
2.1.05	Anthropogenic Features	Exclusion /inclusion of anthropogenic features such as abandoned wells that could form discrete transport pathways.	Screen In	
2.1.06	Human Dwellings	The characteristics of the houses or other structures or shelters in which humans spend time. The dwelling location, materials used in construction, design elements (e.g., for improved energy efficiency and air tightness), dwelling size, heating sources, the likelihood of infiltration of water or gases, and the introduction of other contaminants into the dwelling may all affect human exposure to contaminants.	Screen In	
2.2.01	Natural and Geological Resources and Land Use	Factors related to natural resources and land use, particularly those that might encourage investigation or excavation at or near the waste closure facility. Examples of natural resources include: water, lumber, oil and gas (such as methane), minerals, and geothermal energy. Examples of land use include: reclamation/extension, logging, agricultural activity, urbanization, and waste disposal.	Screen In	
2.2.02	Water Management	Factors related to ground water and surface water management. Water management is accomplished through a combination of dams, reservoirs, canals, pipelines, and collection and storage facilities. Water management activities could have a major influence on the behavior and transport of contaminants.	Screen In	

Table 4.1-5: FEPs Screening Results (Continued)

FEP ID	FEP Name (Short)	FEP Description	Final Deter-mination	Comments and/or Screen Out Justification
2.2.03	Natural/Semi-Natural Land and Water Use	The use of natural or semi-natural tracts of land and water such as forest, bush and lakes. Uses include the gathering of special foodstuffs and resources (e.g., picking wild blueberries and gathering of peat and wood for household heating).	Screen Out	Screened Out - The FEPs Screening Team identified this FEP as being very broad in scope. Other more discrete FEPs have been identified which more accurately capture the relevant features, events, or processes which should be considered within the PA; as such, this FEP is screened out.
2.2.04	Rural and Agricultural Land and Water Use	The use of land and water for agriculture, fisheries, game ranching and similar practices. Practices include: a) fish hatcheries and fish farming, b) ranching of indigenous and imported animals, c) draining of wetlands for farming use, d) gardening, e) irrigation, f) plowing, g) other farming practices such as greenhouses or hydroponics, fertilization, and the use of herbicides, pesticides, fungicides and related products, h) recycling and composting, i) crop storage, and j) outdoor spraying of water to cool buildings and control dust. Consideration for the duration of land use may need to be considered.	Screen In	
2.2.05	Urban and Industrial Land and Water Use	The use of land and water for urban or industrial purposes. Water has a variety of industrial uses: mining, the pulp and paper industry, food preparation, and electricity generation. Establishment of large water-use systems could influence the behavior and transport of contaminants in the environment and introduce remote sources of contaminants to a large community (such as the concentration of effluent sewage at a single point of discharge). Additionally, produce from hobby gardens in urban areas might be more contaminated than agricultural crops because the amateur gardener might over-irrigate.	Screen In	
2.2.06	Leisure and Other Uses of the Environment	Leisure activities, their effects on the surface environment, and implications for contaminant exposure pathways. Examples include: a) swimming and boating, b) hiking, c) camping, d) skiing, and e) sports activities. Many of these activities might influence which exposure pathways have significant impacts.	Screen In	
2.2.07	Pollution (Soil, Ground Water, Air, etc.)	Factors related to any type of human activities associated with pollution of the surface environment at or near waste closure facility site that can potentially affect the performance of the system, or the exposure pathways at or near the waste closure facility. Pollution (air, soil, and ground water) is possible from various sources (e.g., agricultural, industrial, and urban development). These pollution conditions may alter a) the chemical composition of the soil or ground water, b) the contaminant migration properties, c) vegetation, and d) human health.	Screen Out	Screened Out - The FEPs Screening Team identified this FEP as being very broad in scope. Other more discrete FEPs have been identified which more accurately capture the relevant features, events, or processes which should be considered within the PA; as such, this FEP is screened out.

Table 4.1-5: FEPs Screening Results (Continued)

FEP ID	FEP Name (Short)	FEP Description	Final Deter-mination	Comments and/or Screen Out Justification
2.2.08	Ozone Layer Failure	Human actions (i.e., the use of certain industrial chemicals) may lead to destruction or damage to the earth's ozone layer. This may lead to significant changes to the climate locally and globally, affecting properties of the geosphere such as ground water flow patterns.	Screen Out	Screened Out - While it is acknowledged that this FEP cannot be screened out based on frequency and/or impact, the FEPs Screening Team has determined that any approach to address this FEP within a PA would rely heavily upon unjustifiable assumptions and would be highly speculative. As such, the FEPs Screening Team recommends excluding this FEP from consideration in the PA.
2.3.01	Future Knowledge of the Facility	Factors related to the degree of knowledge of the existence, location and/or nature of the waste closure facility, including the retention of related records and the construction of markers to inform future humans of the location and contents of the facility. The loss of such records and markers may increase the likelihood of inadvertent intrusion.	Screen In	
2.3.02	Future Human Actions (Active)	Factors related to human actions and regional practices associated with the post-closure period (future), which may affect the performance of the natural (geological) and/or engineered barriers, and consequently the waste closure facility.	Screen In	
2.3.03	Social and Institutional Developments	Factors related to changes in future social patterns and degree of local government, planning and regulation. Specific factors include: a) changes in planning controls and environmental legislation, b) demographic change and urban development, c) changes in land use, and d) loss of records or societal memory of the waste closure facility location and hazards.	Screen In	
2.3.04	Technological Developments	Factors related to future developments in human technology and changes in the capacity and motivation to implement technologies (i.e., research and development). Technological developments may affect the long-term performance of the waste closure facility. These include changes in the ability of humans to intrude the site, and changes that might affect contaminant exposure and its health implications. For example: Scientific and technological advances may lead to a total cure for cancer, thereby reducing the risks from radiation exposure.	Screen Out	Screened Out - While it is acknowledged that this FEP cannot be screened out based on frequency and/or impact, the FEPs Screening Team has determined that any approach to address this FEP within a PA would rely heavily upon unjustifiable assumptions and would be highly speculative. As such, the FEPs Screening Team recommends excluding this FEP from consideration in the PA.
2.3.05	No Technological Development	The conservative assumption that technological development will not occur, on the basis of uncertainty as to what types of developments may or may not occur. In these cases it is assumed that the past and present technological developments are a sufficient indication for future developments.	Screen In	This is the assumed condition for the SDF PA.

Table 4.1-5: FEPs Screening Results (Continued)

FEP ID	FEP Name (Short)	FEP Description	Final Deter-mination	Comments and/or Screen Out Justification
2.3.06	Retrograde Developments	The conservative assumption that technological capacities may be lost due to degradation of society or failure to pass on generational expertise.	Screen Out	Screened Out - While it is acknowledged that this FEP cannot be screened out based on frequency and/or impact, the FEPs Screening Team has determined that any approach to address this FEP within a PA would rely heavily upon unjustifiable assumptions and would be highly speculative. As such, the FEPs Screening Team recommends excluding this FEP from consideration in the PA.
2.4.01	Biomes	Factors related to the characteristics of biomes found on earth, and their evolution. A biome is a mixed community of plants and animals (a biotic community) occupying a major geographical area on a continental scale. Usually applied to terrestrial environments, each biome is characterized by similarity of structure or physiology rather than by species composition. Within a particular biome, plants and animals are regarded as being well adapted to each other and to broadly similar environmental conditions, especially climate. Important factors influencing biomes (excluding human activity) include temperature, precipitation, latitude, and altitude.	Screen Out	Screened Out - The FEPs Screening Team identified this FEP as being very broad in scope. Other more discrete FEPs have been identified which more accurately capture the relevant features, events, or processes which should be considered within the PA; as such, this FEP is screened out.
2.4.02	Vegetation	Factors related to the characteristics of terrestrial and aquatic vegetation both as individual plants and in mass, and their evolution.	Screen Out	Screened Out - The FEPs Screening Team identified this FEP as being very broad in scope. Other more discrete FEPs have been identified which more accurately capture the relevant features, events, or processes which should be considered within the PA; as such, this FEP is screened out.
2.4.03	Animal Populations	Factors related to the characteristics of the terrestrial and aquatic animals both as individual animals and as populations, and their evolution.	Screen Out	Screened Out - The FEPs Screening Team identified this FEP as being very broad in scope. Other more discrete FEPs have been identified which more accurately capture the relevant features, events, or processes which should be considered within the PA; as such, this FEP is screened out.

Table 4.1-5: FEPs Screening Results (Continued)

FEP ID	FEP Name (Short)	FEP Description	Final Deter-mination	Comments and/or Screen Out Justification
2.4.04	Species Evolution	Factors related to the possibility of biological evolution or genetic manipulation of humans, microbial, animal and plant species, and related consequences. Over the times scales considered natural evolution may be possible. The rate varies between organisms. Humans are subject to biological evolution, although perhaps to a lesser degree. Evolution may affect anatomical features and physiological processes and the effects of contaminant exposure.	Screen Out	Screened Out - While it is acknowledged that this FEP cannot be screened out based on frequency and/or impact, the FEPs Screening Team has determined that any approach to address this FEP within a PA would rely heavily upon unjustifiable assumptions and would be highly speculative. As such, the FEPs Screening Team recommends excluding this FEP from consideration in the PA.
2.4.05	Microbial Activity	Microbes exist naturally in soils and ground water. Other microbes may be introduced on construction materials and in the air during excavation, operation and closure procedures. These microbes may affect chemical conditions and can affect the rates of some reactions. They may also directly affect contaminant transport by acting as organic colloids or by affecting redox potential and pH.	Screen In	
2.4.06	Biological Uptake	Consumption factors and transfer factors (including uncertainty).	Screen In	
2.4.07	Bioaccumulation	Buildup of radionuclides in soils and influence on plant and animal products.	Screen In	
2.5.01	Topography and Landforms	Factors related to the topography and surface morphology (relief and shape of the surface) of the waste closure facility region and its evolution over time. Topographical features include outcrops and hills, water-filled depressions, wetlands, recharge areas and discharge areas. Topography, precipitation, and surficial permeability distribution in the system will determine the flow boundary conditions (i.e., location and amount of recharge and discharge in the system).	Screen In	
2.5.02	Geological Environment and Processes	Factors related to features and processes of the geological environment surrounding the waste closure facility.	Screen In	
2.5.03	Stratigraphy and Host Lithology	Factors related to the properties and evolution of the local stratigraphy and lithology. Stratigraphy is the succession of geological formations and rock structures and types that make up the region. The various units may help isolate the waste and influence where surface water infiltrates and where ground-waters eventually discharge. Lithology describes the relevant properties of the geological units, including: thermal and hydraulic conductivity, compressive and shear strength, porosity, tortuosity, thickness, etc. The inhomogeneity and uncertainty of these properties is also part of their characterization. These properties could change with time and temperature.	Screen In	
2.5.04	Near-Surface Aquifers and Water-Bearing Features	Factors related to the characteristics and formation of aquifers and water-bearing features within a few meters of the land surface and their evolution. Aquifers are formed by the gathering of water between alternating layering of permeable and impermeable rock on a local or regional scale.	Screen In	
2.5.05	Hydraulic Properties	Properties of the host rock and other rock units that affect the migration of fluids, including a) hydraulic conductivity in the context of flow through a porous medium, b) the presence of open fractures, c) capillary suction, and d) the gas-entry pressure. Changes of hydraulic properties due to changes in rock stress or fault movements.	Screen In	

Table 4.1-5: FEPs Screening Results (Continued)

FEP ID	FEP Name (Short)	FEP Description	Final Deter-mination	Comments and/or Screen Out Justification
2.5.06	Depositional Environments and Landforms	Factors related to landforms formed from the deposition of weathered and eroded surface materials. On occasion, these deposits can be compressed and/or altered by pressure, heat and chemical processes to become sedimentary rocks. This includes landforms with some of the following geomorphic features: beaches, deltas, flood plains, and glacial moraines.	Screen Out	Low Impact - The SDF is generally higher than surrounding areas. As such, deposition would primarily be attributed to dust accumulation. Further, any deposits above the system would likely improve barrier performance.
2.5.07	Soils and Sediment	The soils and sediments that overlie the rock of the geosphere, including their evolution in time. Soil type is determined by many different factors (e.g., formative process, geology, climate, vegetation, land use). The physical and chemical attributes of the surficial soils (such as organic matter content and pH) may influence the mobility of radionuclides. Feature includes overburden and aquatic and marine sediments.	Screen In	
2.5.08	Geologic Discontinuities and Boundary Conditions (Fractures, Faults, and Cracks)	Factors related to the properties and characteristics of large scale discontinuities in the geosphere, such as faults, fractures, dikes, and folds. These geological discontinuities often form the boundaries of an aquifer.	Screen In	
2.5.09	Stress Regimes	Geological media deforms according to the acting stress field and its inherent strength. Changes in the ground water flow and changes in the temperature field will change the active stress acting on the rock, which in turn will change fracture properties and ground water flow. Stress regimes can change due to: coupled thermal-hydro-mechanical effects; swelling of materials; isostatic rebound (such as when glaciers recede); and salt creep.	Screen Out	Low Frequency: Based on strong similarities in both geometry and movement histories, studies have shown that the major regional scale faulting on the Savannah River Site and vicinity is closely associated with and maybe included in the Atlantic Coastal Fault Province. The faults in the Atlantic Coastal Fault Province have been well-studied. In all documented cases, these faults have been declared “not capable” in terms of Appendix A of 10 CFR 100. [WSRC-TR-2000-00310; WSRC-RP-94-0136]
2.5.10	Unconsolidated Soft Zones	The presence of soft zones (e.g., the calcareous zone in the Santee Formation of the SRS) may influence stability of the waste closure facility and have an effect on flow.	Screen In	
2.5.11	Undetected Geologic Features	Natural or man-made features that are not detected during site investigation, or even during excavation, construction, or operation. Examples of possible features are a) faults, b) fracture zones, c) induced fractures caused by excavation, and d) other discontinuities. These features could play a significant role in the transport of ground water to and from the waste closure facility.	Screen In	

Table 4.1-5: FEPs Screening Results (Continued)

FEP ID	FEP Name (Short)	FEP Description	Final Deter-mination	Comments and/or Screen Out Justification
2.6.01	Tectonic Activity and Processes	Factors related to tectonic movement at plate boundaries, the potential for tectonic movement, and its effects on the performance of the waste closure facility. Large-scale tectonic activity, such as regional uplift, subsidence, folding, mountain building, or other processes related to plate movements, could affect performance by altering the physical and thermohydrologic properties of the geosphere.	Screen Out	Screened Out - While it is acknowledged that this FEP cannot be screened out based on frequency and/or impact, the FEPs Screening Team has determined that any approach to address this FEP within a PA would rely heavily upon unjustifiable assumptions and would be highly speculative. As such, the FEPs Screening Team recommends excluding this FEP from consideration in the PA.
2.6.02	Orogeny	Factors related to the formation of mountains (orogeny), the potential for orogeny and its effects on the performance of the waste closure facility.	Screen Out	Screened Out - While it is acknowledged that this FEP cannot be screened out based on frequency and/or impact, the FEPs Screening Team has determined that any approach to address this FEP within a PA would rely heavily upon unjustifiable assumptions and would be highly speculative. As such, the FEPs Screening Team recommends excluding this FEP from consideration in the PA.
2.6.03	Diagenesis and Pedogenesis	Diagenesis refers to processes that take place in rocks after formation but before eventual metamorphism or weathering. Pedogenesis is the conversion of rock materials into soils. These processes may affect biosphere uptake and near-surface system evolution as it involves geohydrologic, atmospheric and biological processes (burrowing animals, plant roots activity/invasion) at or near the surface on time scales of a few hundred to thousands of years.	Screen Out	Low Impact - The SDF is generally dominated by the presence of sands and clays; rocks are not dominantly present. As such, any rocks which may be present and form into soil would have a limited impact on overall system performance.
2.6.04	Deformation and Metamorphism	Factors related to the physical deformation (elastic, plastic, or brittle) or metamorphism of geological structures in response to geological forces such as tectonic movement and orogeny or in response to stress fields generated either at plate margins or in regions of anomalous stress. This includes a) faulting, b) fracturing, c) extrusion and, d) compression and folding of rocks. A fault is a large-scale discontinuity or fracture in the Earth's crust accompanied by displacement of one side of the fracture relative to the other. Fractures may be caused by compressional or tensional forces in the Earth's crust.	Screen Out	Low Frequency - As a part of the Atlantic Plain Province, the SRS is a passive tectonic margin wherein significant events, relevant to this FEP, are highly unlikely.

Table 4.1-5: FEPs Screening Results (Continued)

FEP ID	FEP Name (Short)	FEP Description	Final Deter-mination	Comments and/or Screen Out Justification
2.6.05	Mechanical Effects on Geologic Features	Factors related to the mechanical processes and conditions that affect the geosphere and the overall evolution of conditions of the natural system with time. This includes the effects of changes due to the seismicity, excavation, and the long-term presence of the closure system.	Screen In	
2.6.06	Sedimentation	The processes by which deposited sediments at or near the Earth's surface are formed into rocks by compaction, cementation and crystallization, i.e., under conditions of temperature and pressure normal to the upper few kilometers of the Earth's crust.	Screen Out	Low Impact - The SDF is generally higher than surrounding areas. As such, deposits of sediments would be primarily attributed to dust accumulation. Further, any deposits above the system would likely improve barrier performance.
2.6.07	Erosion and Weathering	Erosion and weathering are processes which lead to the denudation of the land surface and a reduction in topography. Erosion and weathering may cause changes to the present day topography through denudation and are thus capable of affecting both local and regional hydrology. Weathering refers to physical and chemical processes that alter and degrade rocks and soil at and near the land surface. Erosion involves the transport of surficial material away from the site by various mechanisms including glacial, fluvial, eolian (involving wind), and chemical processes. Surficial materials, including weathering products, are also subject to gravity, and erosion can take place by mass wastage processes (e.g., landslides). The extent of denudation depends to a large extent on climate and the rate of local uplift.	Screen In	
2.6.08	Deposition	Deposition is the geological process by which material is added to a landform or land mass. The process may change topography and thus affects local and regional hydrology. Deposition of surficial materials can occur by a variety of means, including fluvial, eolian, and lacustrine deposition and redistribution of soil through weathering and mass wasting processes.	Screen Out	Low Impact - The SDF is generally higher than surrounding areas. As such, deposition would primarily be attributed to dust accumulation. Further, any deposits above the system would likely improve barrier performance.
2.6.09	Creeping of the Rock Mass	Creeping of the rock mass is the slow movement of the rock along pre-existing discontinuities or in the rock matrix due to differential stress fields at a very slow rate. Creep of the rock mass may affect the hydraulic properties of the rock and may have a mechanical impact on the backfill.	Screen Out	This FEP is not applicable to the SDF system or is outside the scope of an SDF PA.
2.6.10	Large Scale Salt Processes (Diapirism, Dissolution, and Creep)	Salt diapirism is the intrusion or upwelling of a salt formation into overlying strata (such as salt domes). Salt dissolution can occur when any soluble mineral is removed by flowing water. Large-scale dissolution is a potentially important process in rocks that are composed predominantly of water-soluble evaporite minerals. Salt creep is the continuous deformation of a salt formation as a response to an applied stress such as overburden pressure.	Screen Out	This FEP is not applicable to the SDF system or is outside the scope of an SDF PA.

Table 4.1-5: FEPs Screening Results (Continued)

FEP ID	FEP Name (Short)	FEP Description	Final Deter-mination	Comments and/or Screen Out Justification
2.6.11	Mass Wasting	Mass wasting is the geomorphic process by which materials move downslope under the force of gravity. Types of mass wasting include creep, slides, flow, topples, and falls, each with its own characteristic features, and taking place over timescales from seconds to years. Mass wasting occurs on both terrestrial and submarine slopes, and the largest and most disastrous mass wasting events may be related to some extraordinary activity or occurrences, including: a) earthquakes, b) slope modification (e.g., human activity), c) undercutting (typically along stream banks or by surf action along the coast), d) exceptional precipitation, and e) volcanic eruptions.	Screen In	
2.6.12	Hydrogeological Processes and Conditions	Factors related to the hydraulic and hydrogeological processes that affect the geosphere and the overall evolution of conditions due to the excavation, construction, and long-term presence of the closure facility. During hydrogeological investigations, efforts should describe the existing and projected water uses; location, extent and interrelationship of the important hydrogeological units in the region; recharge and discharge of the major hydrogeological units; regional and local water tables and their gradients and seasonal fluctuations; an estimate of ground water flow velocities and direction; radionuclides travel times along most likely flow paths from the closure facility to the biosphere.	Screen In	
2.6.13	Impact of the Engineered System on Geologic Processes	Factors related to interactions between the engineered systems and the natural system. For example, the effects of head buildup within different closure cap layers, or the effect of layer slope stability, etc.	Screen In	
2.6.14	Closure Cap Performance (Differential Settlement)	Differential settlement could occur due to the presence of the relatively rigid disposal cells within the lower backfill and non-uniform thickness of the backfill. This could affect the drainage efficiency of the upper drainage layer and the integrity of the geomembrane layer.	Screen In	
2.7.01	Climate and Weather	The characteristics of climate and weather including precipitation, temperature, pressure, and wind speed and direction, and their evolution. Climate and weather may have a major influence on transport of contaminants in the environment through recharging of surface-water bodies and leaching of soils, and affect human behavior of irrigation requirements for agricultural crops and the source of drinking water. The variability in the climate and weather (such as drought, flooding, storms, and duration of snow melt and their potential effects) can influence erosion, the accumulation and release of contaminants, and potential human exposure.	Screen In	
2.7.02	Atmosphere	The transport of radionuclides and chemical contaminants in the atmosphere as gas, vapor, or suspended fine particulate or aerosol. Contaminants may enter the atmosphere as a result of water evaporation, degassing from soils or water, transpiration from plants, suspension due to wind erosion, plowing, or fires. The atmosphere may provide a significant mechanism to transport, dilute, or remove these contaminants by advection and dispersion. This category provides for specific human and animal exposure pathways.	Screen In	

Table 4.1-5: FEPs Screening Results (Continued)

FEP ID	FEP Name (Short)	FEP Description	Final Deter-mination	Comments and/or Screen Out Justification
2.7.03	Cold Weather Effects	Factors related to cold weather effects (i.e., physical processes) and associated landforms. Permafrost and seasonal freeze/thaw cycles are characteristic of periglacial environments that may impact erosional processes. This FEP includes the effects of glaciers and ice sheets within the region of the waste closure facility. For example, frost heaving pushes the ground surface up and causes a downslope movement of rocks. Gelifluction occurs when the thawed layer becomes saturated with melt water and slowly moves downslope forming distinctive lobes and sheets of debris. Rock glaciers form as a tongue or lobe of ice-cemented rock debris that moves slowly downslope in a manner similar to glaciers.	Screen In	
2.7.04	Warm Weather Effects	Factors related to warm tropical and desert climates and their effect on the performance of the waste closure facility. For example, warm weather may increase evapotranspiration thus reducing infiltration and eventual transport.	Screen In	
2.7.05	Solar Radiation	Solar radiation is used in ecosystems to heat the atmosphere and to evaporate and transpire water into the atmosphere. Sunlight is also necessary for photosynthesis, which provides the energy for plant growth and metabolism, and the organic food for other forms of life.	Screen In	
2.7.06	Acid Rain	Acid rain refers to precipitation on a local to regional scale containing higher than normal amounts of nitric and sulfuric acids. This can result from man-made sources such as emissions produced from the burning of fossil fuels. Acid rain can influence the behavior and transport of contaminants in the biosphere by affecting surface water and soil chemistry and detrimentally affect aquatic and terrestrial life by interfering with the growth, reproduction, and thus survival of affected organisms.	Screen In	
2.7.07	Precipitation	Precipitation depends on climate and is an important control on the amount of runoff and infiltration, flow in the unsaturated zone, and ground water recharge. It transports solutes with it as it flows downward through the subsurface or escapes as runoff. Precipitation influences agricultural practices of the receptor.	Screen In	
2.7.08	Climate Change	Climate change includes the effects of long-term change in global climate (e.g., glacial/interglacial cycles) and shorter-term change in regional and local climate. Climate is typically characterized by temporal variations in precipitation and temperature and may affect the long-term performance of the waste closure facility. This includes the effects of greenhouse gases and potential for global warming.	Screen Out	Screened Out - The FEPs Screening Team identified this FEP as being very broad in scope. Other more discrete FEPs have been identified which more accurately capture the relevant features, events, or processes which should be considered within the PA; as such, this FEP is screened out.
2.7.09	Response to Climate Change	Hydrological/hydrogeological, ecological, human, and geomorphological responses to climate change.	Screen Out	Screened Out - The FEPs Screening Team identified this FEP as being very broad in scope. Other more discrete FEPs have been identified which more accurately capture the relevant features, events, or processes which should be considered within the PA; as such, this FEP is screened out.

Table 4.1-5: FEPs Screening Results (Continued)

FEP ID	FEP Name (Short)	FEP Description	Final Deter-mination	Comments and/or Screen Out Justification
2.8.01	Water	The characteristics of water, and its evolution. Water is the medium by which mineral nutrients enter and are translocated in plants and is required for photosynthetic chemical reactions. The original source of this water is precipitation from the atmosphere and plants and animals receive their water from the Earth's surface and soil.	Screen In	
2.8.02	Hydrological Regime and Water Balance (Near-Surface)	Factors related to near-surface hydrology at a catchment scale and also soil water balance, runoff, the flushing rate of surface-water bodies, and their evolution. Extremes such as drought, flooding, storms and snow melt may be relevant. Changes to the hydrological regime could also induce changes in the behavior of the critical group.	Screen In	
2.8.03	Evapotranspiration	Evapotranspiration removes water from soil and rock by evaporation and transpiration via plant root water uptake. Surface water runoff and evapotranspiration are components in the water balance, together with precipitation, infiltration, and change in soil water storage.	Screen In	
2.8.04	Infiltration and Recharge	Infiltration into the subsurface provides a boundary condition for ground water flow in the unsaturated zone. The amount and location of the infiltration influences the amount of seepage through the closure cap, and the amount and location of recharge influences the height of the water table, the hydraulic gradient, and the specific discharge. Mixing of these waters could result in mineral precipitation, dissolution, and altered chemical gradients in the subsurface.	Screen In	
2.8.05	Focused Infiltration	An engineered closure cap may create focused infiltration along surface channels. Such focused infiltration can influence ground water flow.	Screen In	
2.8.06	Surface Runoff	Surface runoff produces erosion, and can feed washes, arroyos, and impoundments, where flooding may lead to increased recharge. Surface water runoff and evapotranspiration are components in the water balance, together with precipitation, infiltration, and change in soil water storage.	Screen In	
2.8.07	Surface-Water Bodies	The characteristics of surface-water bodies such as rivers, lakes, wetlands and springs, and their evolution in time. These water bodies can indicate watershed boundaries and act as recharge zones for ground water and, as such, can influence ground water chemistry and contaminant transport. Contaminant transport and mixing can occur within the surface water bodies (such as dilution, sedimentation, aeration, stream flow, and river meander).	Screen In	
2.8.08	Capillary Rise	Capillary rise, or wicking, involves the drawing up of water, above the water table or above locally saturated zones through continuous pores, due to a net upward force produced by the attraction of the water molecules to a solid surface until the suction gradient is balanced by the gravitational pull downward.	Screen In	
2.8.09	Discharge Zones Outside the Assessment Domain	Some contaminants could be released and discharged to the surface environment at locations beyond the assessment domain (or the reference biosphere). Radionuclides transported in ground water as solutes or solid materials (colloids) from the far-field may discharge at specific "outcrops" that are outside the reference biosphere.	Screen Out	Low Impact - Releases outside the modeling domain are not expected to exceed the concentrations within the modeling domain.
2.8.10	Discharge Zones Within the Assessment Domain	Locations (within the assessment domain) where the water table intersects the surface allow ground waters to flow out onto the surface as springs, seepage lines, streams, wetlands or lakes. Discharge zones are often low-lying areas such as at the margin or bottoms of lakes and wetlands. Springs may also be found at various elevations depending on factors such as the lithology and stratigraphy of the geosphere and the location of outcropping geological units.	Screen In	

Table 4.1-5: FEPs Screening Results (Continued)

FEP ID	FEP Name (Short)	FEP Description	Final Deter-mination	Comments and/or Screen Out Justification
3.1.01	Site Characterization and Investigations	Factors related to site characterization. Such factors include: a) determining which site investigations are needed (both prior and during construction and operation), b) evaluations of related assessments, c) defining the level of detail required (to support both a general understanding of the site, its past evolution, and likely future natural evolution over a period of time), and d) a specific understanding of the impact on safety of associated FEPs. These activities establish baseline conditions and data.	Screen In	Programmatically screened in by WDA prior to screening evaluations.
3.1.02	Site Development	Factors related to any type of human activities during site development that can potentially affect the performance of the waste closure facility or the exposure pathways after closure. Examples of site development include the following: construction of roads, residential buildings (urban), or industries. This includes earthmoving works such as leveling of the site, modifications of natural site drainage, and construction of dams).	Screen Out	Screened Out Prior to Phase I: While it is acknowledged that this FEP cannot be screened out based on frequency and/or impact, any approach to address this FEP within a PA would rely heavily upon unjustifiable assumptions and would be highly speculative. As such, the FEPs Screening Team recommends excluding this FEP from consideration in the PA.
3.1.03	Facility Factors	Factors related to decisions taken and events occurring during the life cycle of the waste closure facility that may influence the performance of the facility. These include those features, events, and processes occurring during pre-operational, operational, and post-closure periods of the waste closure facility whose principal effect is to determine the evolution of the physical, chemical, biological, and human conditions of the waste closure facility with the purpose to estimate the release and migration of contaminants and the consequent exposure to human beings and the environment.	Screen In	Programmatically screened in by WDA prior to screening evaluations.
3.1.04	Multi-Barrier Safety Function	Consideration for applying a multi-barrier closure system (using both natural and engineered barriers) that is designed to ensure long-term safety by means of multiple safety functions.	Screen In	Programmatically screened in by WDA prior to screening evaluations.
3.2.01	Design Basis for Engineered Components	Factors related to the design of the waste closure facility and facility components (and associated design documentation) and the ways in which the design contributes to long-term performance. The performance assessment must account for design features, material characteristics, design influences on the environment, and assumptions regarding the design of the waste closure facility (i.e., the safety concept and the engineering specifications for excavation, construction, operation and closure). Design should ensure that the functional requirements and criteria are met.	Screen In	Programmatically screened in by WDA prior to screening evaluations.
3.2.02	Schedule and Planning	A detailed description of the major activities associated with the construction, the operation, the closure of the waste closure facility, and the schedule and resources required for that purpose. Relevant events may include monitoring activities to provide data on the transient behavior of the system or to provide input to the final assessment. The sequence of events and time between events may have implications for long-term performance.	Screen In	Programmatically screened in by WDA prior to screening evaluations.

Table 4.1-5: FEPs Screening Results (Continued)

FEP ID	FEP Name (Short)	FEP Description	Final Deter-mination	Comments and/or Screen Out Justification
3.2.03	Procurement of Items and Services	Factors related to quality assurance that will be applied during the procurement of items and services important to the safety of the waste closure facility.	Screen Out	Any activities which may occur prior to the emplacement of a closure cap would be addressed and evaluated via the UDQE process - then impacts would either be mitigated or the SDF PA would be revised to reflect the new conditions. As such, this FEP is outside the scope of the current SDF PA.
3.2.04	Manufacturing and Commissioning of Components	Factors related to the commissioning and manufacturing of components and subcomponents activities important to the safety of a waste closure facility (such as the possibility and impacts of manufacturing defects).	Screen In	
3.2.05	Construction	Factors related to the excavation, stabilization, and the installation and assembly of structural elements according to the assessed design and approved schedule and planning. The major tasks of construction of waste closure facility include: a) excavation, testing, and preparation of soil material, b) placement of monitoring systems, c) placement of engineered barrier systems, d) installation of drainage control features, e) revegetation, and f) quality control.	Screen In	
3.2.06	Costs of Construction, Operation, Closure	Factors related to the costs of constructing, operating, and closing the waste closure facility.	Screen Out	This FEP is not applicable to the SDF system or is outside the scope of an SDF PA.
3.2.07	Alternate Container Design and Construction	Factors related to alternate container design and construction, including the physical, chemical and mechanical characteristics of the container; and factors related to excavation, stabilization, and the installation and assembly of structural elements of a new/alternate design container according to the assessed design and approved schedule and planning.	Screen In	
3.2.08	Discrete Capping of Disposal Units	Consideration of factors related to the impacts of capping each disposal unit as they are filled, as opposed to a single closure cap over the entire disposal facility.	Screen In	
3.2.09	Repairs of Construction Defects	Factors related to construction defects and repairs. This includes cracks during curing and epoxy injection of cracks. This may also include nail holes (e.g., to install temporary rails for construction safety), and other temporary penetrations that may occur during construction activities.	Screen In	
3.2.10	Preparation of Cementitious Materials	Factors related to the conditions under which cementitious materials are poured and cured and how those conditions affect the material properties. This includes the water-to-premix ratio, ad mixtures, pouring into standing water, pour height, curing temperatures, curing humidities, the influence of curing on leachability (analogue to active sheet drain system), influences on density, etc.	Screen In	
3.2.11	Operation	Factors related to the operation (waste emplacement, backfilling, monitoring and surveillance, remedial activities) of the waste closure facility, according to the approved schedule and planning for the facility.	Screen In	
3.2.12	Removal or Stabilization of Waste	Factors related to the waste storage, removal, and stabilization of waste tanks and disposal units at the waste closure facility. Distinction can be made between qualitative and quantitative requirements for the removal and stabilization of radioactive waste from waste tanks at the waste closure facility.	Screen In	

Table 4.1-5: FEPs Screening Results (Continued)

FEP ID	FEP Name (Short)	FEP Description	Final Deter-mination	Comments and/or Screen Out Justification
3.2.13	Disposal Unit and/or Facility Closure	Factors related to the end of waste disposal operations and the closure of individual waste tanks. These closure activities are undertaken mainly to prevent human access into and limit the migration of contaminants from the individual waste tanks. This includes planning, preparation, decommissioning of components, and confirmation activities.	Screen In	
3.3.01	Closure System Features and Materials	Features related to the closure operations of the waste closure facility and the materials used for that purpose, according to the approved schedule and planning for the facility. A wide variety of materials can be used in combination to provide the overall system with the required properties to prevent human access into and limit the migration of contaminants from the waste closure facility.	Screen In	
3.3.02	Geometry of the Waste Tank, Container, or Package	The geometry of the disposal container or waste tanks may influence performance. For example, changes to the roof slope of disposal units can influence flow rates. The thickness of the wall or roof can influence material performance.	Screen In	
3.3.03	Consolidation of System Components	Factors related to the consolidation of engineered barrier system components. Such consolidation may affect the development of the chemical environment and, therefore, the radionuclide transport out of the closure system.	Screen In	
3.3.04	Closure System Buffer (Closure Cap, Backfill, and Near-Field Soil) Properties	The backfill and other soil mineralogy will affect the buffering of geochemical conditions in response to perturbation by the cementitious materials and residual wastes, and provide a substrate for sorption of contaminants. Used to inform the selection of distribution [partition] coefficients that describe contaminant mobility. Mineralogical dehydration reactions release water affecting hydrologic conditions. Dehydration of zeolites may lead to large-scale volume changes affecting flow and/or waste tank stability. The likelihood of geothermal fluids might cause changes in mineralogical composition.	Screen In	
3.3.05	Clay (Bentonite and Vermiculite) Effects	Clay layers (such as Bentonite/Vermiculite) provide a barrier to ground water flow and act as a mechanical barrier to protect the waste tank. The material will degrade over time by physical and chemical processes and thus its barrier functions will diminish. This will have an impact on radionuclide release processes and rate. For example, in a ground or pore water containing suspended bentonite/vermiculite clay particles, there is sometimes a tendency for the bentonite/vermiculite clay particles to coagulate and form larger aggregates, and may settle to form clay-rich sediment. This process is promoted by an increase in the salinity of the solution.	Screen In	
3.3.06	Integrity of Non-cementitious Materials	There is uncertainty associated with long term performance of novel components (e.g., epoxy, and neoprene seals). If radionuclides flow through fast pathways created by degradation of such component (e.g., joint material) instead of through the disposal unit cementitious material, radionuclides may not be effectively retained in the disposal unit concrete.	Screen In	
3.3.07	Ancillary Equipment and Piping/Transfer Lines	Factors related to ancillary equipment and transfer lines (including evaporators, mixers, robotics, cooling coils, etc.) and their effects on other system components and processes.	Screen In	
3.3.08	Closure Cap Performance (Side Slopes)	The physical stability of the closure cap side slopes is important for the long-term stability and performance of the closure cap as a whole. The following physical mechanisms that could degrade the closure cover: Static-loading induced settlement, seismic-induced liquefaction and subsequent settlement, seismic-induced slope instability, seismic-induced lateral spread, seismic-induced direct rupture due to faulting, Slumping of the side slope, Downslope creep of the riprap, and Vegetation growth on side slopes.	Screen In	

Table 4.1-5: FEPs Screening Results (Continued)

FEP ID	FEP Name (Short)	FEP Description	Final Deter-mination	Comments and/or Screen Out Justification
3.3.09	Closure Cap Thickness and Material Properties	The vertical distance between the top of the closure cap and the top of the waste closure facility.	Screen In	
3.3.10	Closure Cap Performance (Hydraulic Properties)	Support or justification needed for assumed hydraulic properties (including hydraulic conductivity) for the various layers within the closure cap.	Screen In	
3.3.11	Performance of Disposal Structure Roofs and HDPE/GCL Layers	The lower lateral drainage layer above each disposal unit diverts nearly all of the infiltrating water around the disposal units. This diversion of infiltrating water is due to the large difference in the hydraulic conductivity between the lower lateral drainage layer and the disposal unit roofs (for Vaults 1 and 4) and the HDPE/GCL layer (for the SDUs) An increase in the amount of infiltrating water will increase the amount of leaching from and the rate of degradation of the waste form, impacting dose.	Screen In	
3.3.12	Waste Tank, Container, or Package: Physical Characteristics	Physical characteristics of the container include: a) dimensions and geometry, b) permeability and porosity, c) density, d) void space, e) surface finish and level of cleanliness, and f) external or internal coatings or linings.	Screen In	
3.3.13	Waste Tank, Container, or Package: Chemical Characteristics	Chemical characteristics of the container include: a) chemical composition of container, b) chemical stability and confinement in the near-field, c) reactivity, and d) gas generation.	Screen In	
3.3.14	Waste Tank, Container, or Package: Mechanical Characteristics	Mechanical characteristics of the container include: a) tensile and compressive strengths, b) abrasion resistance, and c) ductility. Considers materials that may have been used, such as: a) carbon steel, b) stainless steel, c) polymers and polymer impregnated concrete, d) asbestos cement, e) reinforced concrete, f) cast steel, g) modular cast iron, h) spheroidal graphite cast iron, i) polyethylene, j) lead, k) titanium, l) ceramics, m) stainless steel, and n) HDPE. Considers function (the role of the waste container) and repackaging capabilities.	Screen In	
3.3.15	Disposal Unit Drainage System	Physical characteristics of the container include: a) dimensions and geometry, b) permeability and porosity, c) density, d) void space, e) surface finish and level of cleanliness, and f) external or internal coatings or linings.	Screen In	
3.3.16	Pore Space Interconnectivity	While pore volume is important, the interconnectivity and tortuosity of pore spaces also requires consideration. Contaminants exposed to interconnected pores are more likely to undergo release and transport than contaminants exposed to non-connected pores.	Screen In	
3.3.17	Variability of Field Emplaced Saltstone	Variations in the composition of saltstone grout produced at the SPF and emplaced in the disposal units (e.g., variations in the water-to-cementitious material ratio, aluminate concentration, presence of admixtures, pour conditions) may affect hydraulic properties of saltstone grout.	Screen In	
3.3.18	Leak Tightness of System	Factors related to the degree to which the disposal units are "sealed" (e.g., air tight versus water tight). Do the bearing pads between the wall and floor or waterstops through the roof or floor provide baths for oxygen or water ingress? Does the application of "sealants" affect performances?	Screen In	
3.3.19	Discrete Engineering Features	Discrete engineering features such as material interfaces, the vault liner coating, anchor bolts, pre-stressing wires, waterstops, and the extent of the roof and floor and mud mats beyond the wall can unexpectedly influence system performance.	Screen In	

Table 4.1-5: FEPs Screening Results (Continued)

FEP ID	FEP Name (Short)	FEP Description	Final Deter-mination	Comments and/or Screen Out Justification
3.3.20	Saltstone Formula	Factors related to the saltstone formula. This includes the influence of slag versus fly-ash content on saltstone properties, as well as impacts from waste chemistry or admixtures.	Screen In	
3.4.01	Hydrological Processes and Conditions	The hydrological and hydrogeological processes (including coupled effects) that affect the interactions between infiltrating water and engineered features, and the overall hydrological evolution of the closure system with time.	Screen In	
3.4.02	Hydraulic Conductivity of Concrete and Saltstone	Factors related to the hydraulic performance of field-emplaced saltstone and disposal unit concrete, including mechanical degradation, chemical degradation, and hydraulic degradations, and the interactions between the various degradation mechanisms. Assumptions regarding timing, rates of change, and final conditions should be considered and addressed.	Screen In	
3.4.03	Hydraulic Performance of the Waste Form	Factors that influence the hydraulic performance of the saltstone waste form. This may include the composition of the waste form, the heterogeneity, the interconnectedness of pore spaces, etc.	Screen In	
3.4.04	Hydraulic Performance of the Closure Cap	Combined influence of lateral drainage layer HDPE/GCL, and roof on infiltration, waste storage, and flow diversion.	Screen In	
3.4.05	Saturation of Fractures	Factors related to fracturing and the influence to water movement and saturation of the fractures.	Screen In	
3.4.06	Moisture Characteristic Curves	Moisture Characteristic Curves (or Water Retention Curves) is the relationship between water content and water potential which can be used to predict water storage within a specified volume of defined material.	Screen In	
3.4.07	Hydrostatic Pressure on the Closure System	Waste and system components within the saturated zone will be subjected to hydrostatic pressure (or suction head) in addition to stresses associated with the evolution of the waste and cementitious materials.	Screen In	
3.4.08	Dispersivity Inside SDUs	Factors related to the dispersion of contaminants within the SDUs and how such dispersion may impact release rates and peak concentrations.	Screen In	
3.4.09	Dispersivity In the Saturated Zone	Factors related to the dispersion of contaminants within the saturated zone after release from the SDUs and how such dispersion may influence time of dose peaks, magnitude of dose peaks, and overall performance of the system.	Screen In	
3.4.10	Osmotic Pressure	Osmosis is the flow of water through a semi-permeable membrane so that the molecular concentration solutions on either side of the membrane become equal. Osmotic pressure effects the flow within the saltstone monolith and potential changes to the internal structure of the saltstone (e.g., swelling), and hyper-filtration of dissolved constituents.	Screen In	
3.4.11	Water Table Variability	Influence of water table fluctuations on oxidation of cementitious materials and radionuclide release from the SDUs.	Screen Out	Low Probability - While variability in the water table is expected, the vadose zone thickness in the vicinity of the SDF is such that the water table variability is unlikely to impact system performance.

Table 4.1-5: FEPs Screening Results (Continued)

FEP ID	FEP Name (Short)	FEP Description	Final Deter-mination	Comments and/or Screen Out Justification
3.4.12	Resaturation and Desaturation	After closure, ground water may flow from the near-field into the engineered system and from far-field materials into near-field materials causing these environments to hydraulically saturate or resaturate. Ground water may cause materials to expand, resulting in a general homogenization of physical and chemical characteristics. This resaturation will impact thermal, hydraulic, mechanical, and chemical properties. For example, metals may corrode and temperatures may cool.	Screen In	
3.4.13	Condensation on Closure System Surfaces	Condensation of water on engineered system components may affect the hydrologic and chemical environment. Emplacement of waste can create thermal gradients that can lead to cold traps (locations characterized by transferal of latent heat). This can create condensation, leading to enhanced moisture at the site of engineered system components. Waste emplacement geometry and thermal loading may affect the scale at which condensation occurs.	Screen In	
3.5.01	Chemical Degradation	Factors related to the chemical degradation rates (i.e., delays before onsets of processes, rates of change, steps changes, etc.) and how different features or materials are impacted (e.g., walls, roof, floor, saltstone, joint material, columns, etc.)	Screen In	
3.5.02	Evolving Water Chemistry in the Near-Field	Factors related to the chemical properties of water in the backfill and near-field environment. The water chemistry in the near-field materials is controlled by the composition of the ambient natural ground water and the composition of waters leaving the engineered system. The water chemistry in the near-field controls transport and retardation processes related to contaminants released from the engineered system.	Screen In	
3.5.03	Evolving Water Chemistry in the Engineered System and Waste Form	Factors related to the chemical properties of water in the engineered system components and the waste form. Chemistry of water flowing into the engineered system components and the waste form is affected by initial water chemistry in the rock, mineral and gas composition in the rock, and thermal-hydrological-chemical processes in the rock. Chemical effects on the engineered system components and the waste form (e.g., dissolution) may be enhanced or altered in a system where metals, waste, rock minerals, and water are all in physical contact with one another. This water will react with the various metals and cementitious materials (e.g., grout) causing considerable changes to the chemistry of the intruding water. When radionuclides are released, this will result in further changes to the water chemistry.	Screen In	
3.5.04	Evolving Water Chemistry in the Far-Field	Factors related to the chemical properties of water in the backfill and far-field environment. The initial chemistry of the far-field environment reflects the natural, present-day system. This far-field ground water chemistry is controlled largely by rock- and soil-water interactions and by mixing with waters from the near-field and from the surface. However, perturbations can occur due to climate change which can cause infiltration of sea-water or glacial melt waters.	Screen In	
3.5.05	Chemical Effects of Waste-Rock Contact	Waste and rock may be placed in direct contact by mechanical failure of the waste packages. Chemical effects on the waste (e.g., dissolution) may be enhanced or altered in a system where waste, rock minerals, and water are all in physical contact with one another, relative to a system where only waste and water are in physical contact.	Screen Out	This FEP is not applicable to the SDF system or is outside the scope of an SDF PA.

Table 4.1-5: FEPs Screening Results (Continued)

FEP ID	FEP Name (Short)	FEP Description	Final Deter-mination	Comments and/or Screen Out Justification
3.5.06	Chemical/Geochemical Processes and Conditions	The chemical and longer-term geochemical processes that affect the system and the overall chemical evolution over time. This includes the effects of chemical and geochemical influences on and degradation of a) wastes, b) containers and engineered components, c) backfill, and d) host material by ground water entering from the surrounding geology. Properties that may be affected include permeability and sorption.	Screen In	
3.5.07	Chemical Condition Transitions	Factors related to the timing of and the number of chemical condition transitions considered in the model, and the basis for such assumptions. More transitions may result in better reflection of expected conditions over time, but could significantly increase the complexity of the model and the time needed to run simulations. An example of this is the inclusion or exclusion of a "young" concrete chemical environment.	Screen In	
3.5.08	pH Conditions	The pH conditions in water owing to interactions between the water and the cementitious materials. pH (along with E_h and chloride and sulfate conditions) is an important determinant in the chemical behavior, which in turn affects the release and transport of contaminants in ground water and gas.	Screen In	
3.5.09	E_h Conditions	The E_h conditions in water owing to interactions between the water and the cementitious materials. E_h (along with pH and chloride and sulfate conditions) is an important determinant in the chemical behavior of any waste closure facility, which in turn affects the release and transport of contaminants in ground water and gas. An oxygen-deficient environment (anaerobic) promotes the formation of lower, and often less soluble, oxidation states of radioelements, promotes relatively slow corrosion and microbial processes, and minimizes the rate of gas generation.	Screen In	
3.5.10	Sulfate Attack	Independent analysis used to validate sulfate attack model used to evaluate degradation of cementitious material (see SRNL-STI-2013-00118 Rev. 2)	Screen In	
3.5.11	Carbon Dioxide Influx	Cementitious degradation from carbonation is dependent on the availability of carbon dioxide. The rate of carbon dioxide influx into the system will affect this rate of degradation.	Screen In	
3.5.12	Oxidation Influx	Air-phase oxygen transport influences reduction capacity. Factors related to the pathway of oxidation from top of roof or outer surface of the wall through floor (via unsaturated fractures and/or interconnected pores), and how these pathways may evolve over time and influence the rate of oxidation over time should be considered.	Screen In	
3.5.13	Dispersion of the Oxidation Front	Stagnant zones (or dead end pore space) may allow oxygen to leave elements or mixing cells before the reducing capacity in the elements or mixing cells is exhausted, therefore dispersing the dissolution front.	Screen In	
3.5.14	Reduction Capacity	As Tc-99 is released is can be re-reduced when it comes into contact with reducing material. Further, it may be possible that the slag (or other reductive components) within the cementitious materials could be less than 100% effective as a reducing agent, resulting in premature releases.	Screen In	
3.5.15	Shrinking Core Model Applicability	Consider using the shrinking core model for addition contaminants (in addition to Tc-99) and what those impacts may be.	Screen In	
3.5.16	Re-Reduction and Re-Concentration	Factors related to processes related to re-reduction and re-concentration on Tc-99 release concerning transient nature of the of release.	Screen In	
3.5.17	Diffusion control on chemical reactions	Stagnant zones (dead end pore space) may decrease the apparent rate of chemical reactions, such as radionuclide dissolution/precipitation reactions and reactions controlling the reduction-oxidation state.	Screen In	

Table 4.1-5: FEPs Screening Results (Continued)

FEP ID	FEP Name (Short)	FEP Description	Final Deter-mination	Comments and/or Screen Out Justification
3.5.18	Complexation in the Natural System	Effects on the physical and chemical environment due to complexing agents such as carbonate, fluoride, and humic and fulvic acids present in natural ground waters could affect radionuclide transport in the natural system (e.g., correlations between reducing capacity and Tc-99 release).	Screen In	
3.5.19	Leaching	Leaching is the removal by water of minerals from the solid materials (i.e., concrete, bentonite and asphalt) that could affect waste closure facility performance.	Screen In	
3.5.20	Reaction Kinetics	Chemical reactions, such as radionuclide dissolution/precipitation reactions and reactions controlling the reduction-oxidation state, may not be at equilibrium within the closure system.	Screen In	
3.5.21	Pooling Water above SDUs	Pooling water above an SDU could increase residence time and alter the chemistry of infiltrating water. It could also indicate a preferential flow path into the SDU.	Screen In	
3.5.22	Rind (Chemically Altered Zone) Forms in the Near-Field	Thermal-chemical processes involving precipitation, condensation, and re-dissolution could alter the properties of the adjacent materials. These alterations may form a rind, or altered zone with hydrological, thermal, and mineralogical properties different from the initial conditions.	Screen Out	Screened Out - The FEPs Screening Team identified this FEP as being very broad in scope. Other more discrete FEPs have been identified which more accurately capture the relevant features, events, or processes which should be considered within the PA; as such, this FEP is screened out.
3.5.23	Osmotic Effects on Chemistry	Osmosis is the flow of water through a semi-permeable membrane such that a pressure differential occurs in response to unequal solute concentrations. Water deposited on the surface of concrete (by condensation or through incoming ground water) and the pore water would eventually have the same ionic compositions, with osmosis playing a role in achieving this if the pore structure of the concrete acted like a semi-permeable membrane.	Screen Out	This FEP is screened out. Osmotic effects are not expected to occur under SDF conditions.
3.5.24	Colloid Generation	Colloids may be generated by chemical, physical, and microbiological processes. Contaminants can sorb onto these colloids which may affect their subsequent transport through the system.	Screen In	
3.5.25	Chelating Agent Effects	The effect of chelating agents derived from the pore water on the performance of a closure system. Chelating agents are organic compounds, usually carboxylic acids, which have a number of locations in each molecule that can bind metal ions to form soluble species. The resulting complexes are usually highly stable, a factor that can increase can increase (or decrease) the solubility of the complexed element significantly. The chief concern is that these complexing agents can chemically bond with a radionuclide, metallic elements, or other contaminant to form another stable species.	Screen In	
3.5.26	Validation of Chemical Properties	Independent analysis should be used to validate chemical properties (e.g., distribution ratio and solubility limits) used in SDU models.	Screen In	
3.6.01	Thermal Processes and Conditions the Engineered System	Factors related to the thermal processes that affect the wastes, packaging and engineering features in the closure system and the overall evolution of the thermal conditions over time. A range of processes could potentially give off heat including: a) concrete hydration, and radioactive decay, b) chemical reactions (such as corrosion and uranium oxidation), and c) microbiological processes. Thermal processes affect the integrity of the engineered system components and the release and transport of contaminants in ground water and gases.	Screen In	

Table 4.1-5: FEPs Screening Results (Continued)

FEP ID	FEP Name (Short)	FEP Description	Final Deter-mination	Comments and/or Screen Out Justification
3.6.02	Thermal Processes and Conditions on the Natural System	Factors related to the thermal processes that affect the backfill and the near-field and far-field natural environments and the overall evolution of the thermal conditions over time. A range of processes could potentially give off heat including: a) the effects of seasonal and global climate change, b) excavation activities, c) geothermal activity, d) convective heat transport, and e) the long-term presence of the waste closure facility. The thermal properties of the soils and host rock affect the migration of contaminants from the disposal system.	Screen In	
3.6.03	Temperature and Thermal Gradient Effects on the Geosphere	Factors related to the thermal processes that affect the geosphere and the overall evolution of conditions with time due to the long-term presence of the closure facility. The variety of materials in the near-field barriers will have different thermal expansion coefficients. Thus, if the temperature of the near-field changes, the barriers may expand or contract at different rates, causing changes to the stresses acting on them, and may cause minor physical effects on some barriers. The temperature of the far-field is largely controlled by the natural geothermal gradient, although it may be influenced by changing climate at the surface. The temperature in the far-field will be a control on the rates of chemical and microbiological processes, and can influence the stress field, ground water flow, diffusion rates, and radionuclide transport.	Screen Out	Given the local geologic conditions, igneous or geothermal events at Z-Area are highly unlikely. As such, this FEP is screened out.
3.6.04	Effects of System Heat on the Biosphere	Heat released from radioactive decay of the waste may increase the temperatures at the surface above the system. This could result in local or extensive changes in the ecological characteristics.	Screen Out	Low probability - Given the effects of dilution and the low activity of the SDF waste, significant heating after emplacement of the closure cap is considered to be extremely unlikely and is excluded from consideration in the PA.
3.6.05	Thermo-Chemical Alteration, Near-Field	Thermal effects may influence chemical alterations and radionuclide transport directly (such as radionuclide speciation and solubility in the natural system) or indirectly (such as changes in the mineralogy along the flow path). Relevant processes include: a) volume effects associated with silica phase changes, b) precipitation and dissolution of fracture-filling minerals (such as silica and calcite), and c) alteration of zeolites and other minerals to clays.	Screen In	
3.6.06	Thermo-Mechanical Stresses Alter Characteristics of Engineered Barrier System Components	Heat from the waste causes thermal expansion of the surrounding materials, generating changes to the stress field that may change the properties (both hydrologic and mechanical) in and along faults, fractures, and solid materials (such as the grouted monolith). Cooling as the radioactive material decays will also change the stress field, further affecting material properties.	Screen Out	Low probability - Given the effects of dilution and the low activity of the SDF waste, significant heating after emplacement of the closure cap is considered to be extremely unlikely and is excluded from consideration in the PA.
3.6.07	Recrystallization of Vitrified Wastes	Recrystallization is a slow process and typically occurs only if a high glass temperature is maintained over a prolonged period. Recrystallization of vitrified (glass) wastes could occur under high heat and/or pressure, leading to a less corrosion-resistant waste form.	Screen Out	This FEP is not applicable to the SDF system or is outside the scope of an SDF PA.

Table 4.1-5: FEPs Screening Results (Continued)

FEP ID	FEP Name (Short)	FEP Description	Final Deter-mination	Comments and/or Screen Out Justification
3.7.01	Rate and Mode of Degradation	Describe criteria for inclusion/exclusion for all degradation processes (i.e., sulfate attack, alkali-silica reaction, carbonation, chloride-induced corrosion, calcium leaching, microbial degradation, freeze-thaw cycles, cracking from seismic events, settlement, external static loading, etc.). Consideration should be given for coupled processes as well.	Screen In	
3.7.02	Mechanical Degradation Mechanisms	Consideration of: 1) cracking due to seismic events, 2) settlement due to overburden, 3) subsidence due to calcareous zones, 4) cracking due to static loading, 5) cracking due to expansive chemical reactions with ions in the soil, 6) increased porosity and/or cracking due soil corrodents in the soil, 7) cracking due to freeze thaw processes	Screen In	
3.7.03	Creep of Metallic Materials in the Engineered System	As a result of exposure to high temperatures (>400°C) and pressures for long periods of time, metal components of the engineered system may experience 'creep', a slow but continuous plastic deformation, often in response to stresses or internal void space. In extreme cases creep may lead to a breach in the metals, releasing waste.	Screen Out	This FEP is not applicable to the SDF system or is outside the scope of an SDF PA.
3.7.04	Degradation of Non-Metal Solids: Backfill, Rock, Grout, Cement, etc.	Factors related to the degradation of non-metal solids within the engineered closure system (e.g., backfill, rock, grout, cementitious materials, etc.). These will be affected by physical and chemical degradation processes. These processes will affect the pore water chemistry, the solubility and sorption of radionuclides, and the mechanical stability of the waste tanks. Degradation of backfill by flowing ground water, either by erosion of particulate matter or by dissolution, may occur by a combination of physical and chemical processes, and their degradation may impact on other parts of the closure system.	Screen In	
3.7.05	Degradation of Waste Form (Saltstone) Matrix	The SDF performance is sensitive to the rate of water flow through saltstone. Also, increased saltstone diffusivity is expected to increase the release of redox sensitive radionuclides by increasing saltstone oxidation. SDF performance is also sensitive to the rate of increase of saltstone hydraulic conductivity and diffusivity because sudden degradation of saltstone can result in pulse-like releases that would cause a higher annual dose than a more gradual release. Sudden hydraulic degradation may be particularly detrimental if it occurs many thousands of years after site closure, after significant oxidation has occurred.	Screen In	
3.7.06	Concrete Shrinkage/Expansion	Concrete shows volume changes during the curing phase and during aging which can impact the integrity and hydraulic properties of the material. Shrinkage and expansion may result in fracturing and/or the generation of flow paths.	Screen In	
3.7.07	Corrosion	The corrosive effect of water on metals in the engineered barrier system. Corrosion includes generalized, localized, and galvanic processes. This also includes chemical interactions related to corrosion products and processes related to corrosion enhanced by microbial influences and radiolysis.	Screen In	
3.7.08	Swelling of Backfill and Emplacement Materials	The backfill may be a mixture of partially dried bentonite and an inert filler material. The bentonite or vermiculite will take-up water during the resaturation phase and swell as the clay minerals adsorb water into their lattice structure. Swelling of the bentonite will affect properties which are important for water and gas transport through the backfill and for radionuclide transport and release.	Screen In	
3.7.09	Localized Degradation	Discuss impacts of localized degradation or degradation occurring within material zones.	Screen In	

Table 4.1-5: FEPs Screening Results (Continued)

FEP ID	FEP Name (Short)	FEP Description	Final Deter-mination	Comments and/or Screen Out Justification
3.7.10	Coupled Degradation Processes	Hydraulic degradation may increase flow which can increase other degradation mechanisms (e.g., decalcification), which can further increase hydraulic degradation; thus, creating a degradation feedback loop.	Screen In	
3.7.11	Surface and Closure Cap Degradation	Discuss hydraulic performance and design of erosion protection (vegetative cover, erosion barrier, side slopes, and toe of side slopes, etc.) to assure physical stability of the closure cap.	Screen In	
3.7.12	HDPE Degradation	Discuss individual processes that break down HDPE (UV Radiation, antioxidant depletion by leaching and associated oxidation, thermal oxidation, tensile stress cracking, high-energy irradiation, attack from saltstone leachate, biological degradation, including microbial action, root penetration, and burrowing animals, etc.). Consideration could also be given to the impact of insufficient bonding of materials.	Screen In	
3.7.13	GCL Degradation	Discuss individual processes that break down GCL (divalent cations, slope-stability, freeze-thaw cycles, dissolution, desiccation due to wet/dry cycles and biological degradation including root penetration, and burrowing animals, etc.)	Screen In	
3.7.14	Joint and Polymer Degradation	Effects of the degradation of polymeric materials, epoxy, joint rubber, etc.	Screen In	
3.7.15	Waste Form (Saltstone) and Concrete (SDU) Macroscopic Fracturing	Radionuclides that flow through fast-pathways created by fractures in the disposal unit floors or walls are not expected to experience as much sorption as radionuclides moving through an unfractured cementitious matrix.	Screen In	
3.7.16	Waste Form Chemical Degradation	Waste form degradation processes and effects on sorption and solubility. Chemical reduction of Tc by saltstone (see discussion of presence of sodium thiosulfate in experiments). Reducing capacity of saltstone.	Screen In	
3.7.17	Carbonation	The carbonate conditions and chemical processes owing to interactions between the water and the cementitious materials and engineered features. Carbonate and carbon dioxide concentrations, along with pH and E_h, are important in affecting the chemical behavior of any cementitious material, which in turn affects the release and transport of contaminants in ground water and gas.	Screen In	
3.7.18	Sulfate Attack	Importance of sulfate degradation and updated conceptual model for internal degradation of columns on influence on flow and transport simulations	Screen In	
3.7.19	Site Stability	Inventory and material cracking, settlement effects on overburden, compression due to overburden, dissolution of underlying calcareous settlement	Screen In	
3.7.20	Stress-Corrosion Cracking and Hydride Cracking of Engineered System Metals	Stress-corrosion cracking, or hydride embrittlement and cracking, may mechanically weaken the container and promote subsequent failure or other corrosion mechanisms. The process might be accelerated if hydrogen is attracted to and accumulates at a defect or crack site, forming metal hydrides that promote degradation.	Screen Out	This FEP is not applicable to the SDF system or is outside the scope of an SDF PA.
3.7.21	Oxygen Embrittlement of Engineered System Metals	A potential failure mechanism for engineered system metals is oxygen embrittlement, resulting from the diffusion of interstitial oxygen in the metals at high temperatures.	Screen Out	This FEP is not applicable to the SDF system or is outside the scope of an SDF PA.
3.7.22	Chemical Degradation of Engineered System Metals	Degradation of the metal materials used in the engineered system may occur by chemical or microbial processes, and may affect long-term system performance.	Screen In	

Table 4.1-5: FEPs Screening Results (Continued)

FEP ID	FEP Name (Short)	FEP Description	Final Deter-mination	Comments and/or Screen Out Justification
3.8.01	Alternatives to Pre-Closure Activities	Factors related to alternative waste closure facility design, construction, operation, and closure conditions rather than those in the approved schedule and planning. Included are the poor design, construction, operation, and closure conditions and the effects on long-term safety and performance.	Screen Out	Any activities which may occur prior to the emplacement of a closure cap would be addressed and evaluated via the UDQE process - then impacts would either be mitigated or the SDF PA would be revised to reflect the new conditions. As such, this FEP is outside the scope of the current SDF PA.
3.8.02	Void Space Formation	If waste packages and/or canisters are not completely filled, then the unfilled inert gas or air-filled volume could influence water-chemistry calculations. Diffusion-controlled cavity growth is a possible creep rupture mechanism that could occur under the temperature and pressure conditions that prevail during dry storage of spent fuel. It might also occur during disposal.	Screen In	
3.8.03	Electrochemical Effects in the Closure System (Including Anion Exclusion)	Electrochemical effects (or gradients) may establish an electric potential within or between closure system materials, particularly where two different metals occur close together in saturated conditions or in response to natural electrical currents in far-field rock. Migration of ions within such an electric field could affect corrosion of metals and could also have a direct effect on the dissolution and transport of radionuclides as charged ions. Anion exclusion refers to the overlapping of electrical double layers within a pore and the subsequent exclusion (full or partial) of anions and cations from the pore. Neutral species and water itself may migrate through such a pore unimpeded.	Screen Out	This FEP is not applicable to the SDF system or is outside the scope of an SDF PA.
3.8.04	Error in Waste Removal and Stabilization	Deviations from the design and/or errors in waste removal and stabilization that could affect long-term performance of the waste closure facility.	Screen Out	Any activities which may occur prior to the emplacement of a closure cap would be addressed and evaluated via the UDQE process - then impacts would either be mitigated or the SDF PA would be revised to reflect the new conditions. As such, this FEP is outside the scope of the current SDF PA.
3.8.05	Inadequate Quality Assurance/Control and Deviations from Design	Quality assurance and control procedures and tests during the design, construction, operation, and closure of the waste closure facility. Factors related to the failure or poor implementation of quality assurance and quality control procedures during the life cycle of the waste closure facility.	Screen In	
3.8.06	Incomplete Closure	Factors related to incomplete filling, construction, and/or closure (premature abandonment) of the waste closure facility.	Screen In	

Table 4.1-5: FEPs Screening Results (Continued)

FEP ID	FEP Name (Short)	FEP Description	Final Deter-mination	Comments and/or Screen Out Justification
3.8.07	Mechanical Effects at Engineered Barrier System Component Interfaces	Factors related to the mechanical effects that occur at the interfaces between the engineered components of the closure system and the near-field environment. These factors include: a) the physical effects of steady-state contact (such as mechanical and static loading) at these interfaces, b) the effects of backfill and grouting for resisting to rockfall and structure collapse, c) the effects of physical impacts to the backfill and grout itself, and d) the effects of drilling and excavating at or near the closure facility. These factors may also be caused by forces such as rockfall and seismic-induced impacts, and internal and external stresses. These stresses will act on the engineered components and can be partially responsible for failure of the engineered barriers.	Screen In	
3.8.08	Remedial Actions	Factors related to actions taken to remediate problems or issues related to the performance of the waste closure facility. This FEP addresses the concern that remedial actions may worsen the situation, possibly because it was incorrectly determined that performance was impaired, or because remedial actions are improperly undertaken or unknowingly defeat important barriers. Another possibility is that contaminated materials from remedial activities may not be adequately stored or disposed.	Screen In	
4.1.01	Highly Radioactive Radionuclides (HRRs)	Identification of HRRs, selection of radionuclides characterized in residual waste, selection of treatment technologies to remove HRRs to the Maximum Extent Practicable (MEP), and screening of radionuclides for the purpose of performance assessment calculations.	Screen In	
4.1.02	Metallic Wastes	The physical, chemical, and biological characteristics of the metallic wastes and any conditioning material at the time of disposal are important for the definition of contaminant release rates (source term); gas generation rate; and geochemical conditions in the waste closure facility.	Screen In	
4.1.03	Non-Metallic, Inorganic Wastes	The physical, chemical and biological characteristics of non-metallic, inorganic wastes and solutes at the time of disposal are important for the definition of: contaminant release rates (source term); gas generation rate; and geochemical conditions in the waste closure facility.	Screen In	
4.1.04	Organic Wastes	Factors related to the characteristics of radionuclides or chemical contaminants that are organic or have the potential to form organics under prevailing waste closure facility and environmental conditions. Organic compounds may include stable organic complexes which may form compounds with other contaminants (usually metals). The resulting organic forms may be more or less mobile or toxic than the original form. Conditioning material at the time of disposal is important for defining contaminant release rates (source term), gas generation rates, and geochemical conditions in the waste closure facility	Screen In	
4.1.05	Volatiles and Potential for Volatility	Factors related to the characteristics of radiotoxic and chemotoxic species that are volatile or have the potential for volatility under prevailing waste closure facility and environmental conditions.	Screen In	
4.1.06	Waste Allocation and Emplacement	Describes the assumptions regarding the distribution or allocation of wastes (i.e., variance between waste tanks), including waste type(s) and amount(s). Some waste types and inventories may require special waste emplacement arrangements to simplify the disposal practice, to ensure safety, or to ensure structure stability in the disposal zone.	Screen In	
4.1.07	Tank Farm Waste Acceptance Criteria	F/H Tank Waste Acceptance Criteria for liquid waste indicating that individual transfers or waste streams to the Tank Farm do not need to meet downstream Saltstone (others listed) acceptance criteria (except for influents to Tank 50), but a given stream must not prevent the Tank Farm from meeting downstream criteria. Exception - Saltstone WAC Targets may be exceeded by an influent to Tank 50 given the downstream impact analysis evaluates the stream as ultimately acceptable.	Screen Out	This FEP is not applicable to the SDF system or is outside the scope of an SDF PA. (The SDF Waste Acceptance Criteria is the only relevant Waste Acceptance Criteria.)

Table 4.1-5: FEPs Screening Results (Continued)

FEP ID	FEP Name (Short)	FEP Description	Final Deter-mination	Comments and/or Screen Out Justification
4.1.08	SDF Waste Acceptance Criteria	Waste Acceptance Criteria for Aqueous Waste Sent to the Z-Area Saltstone Production Facility. This document contains the criteria for aqueous waste transferred from Tank 50H to the Saltstone Facility though an interarea transfer line that connects Tank 50H to the Salt Feed Tank in Z-Area during Interim Salt Disposition Project (ISDP) operations. Low level waste meeting the criteria in this document can be safely transferred, stored, and treated in the SPF for subsequent disposal as saltstone in the SDF.	Screen In	
4.1.09	Waste Type Classification	Classification of the radioactive waste into exempt waste, low and intermediate level waste (short lived and long lived) or any other country-specific waste classification scheme. A variety of waste forms and waste types may be disposed of within the closure system. Some of types may have initial degradation characteristics. Therefore, the effectiveness of each waste form as a barrier to radionuclide mobilization should be considered.	Screen In	
4.2.01	Waste Form Characteristics	Contaminant characteristics are related to the physical, chemical (organic and inorganic) and radiological properties of the contaminant(s) contained in the residual waste of the closure facility. Chemical characteristics of the waste form include: a) chemical composition, b) chemical stability and confinement in the near-field, c) reactivity, d) gas generation, e) toxicity, and f) decomposition of organic wastes. Physical characteristics of the waste form include: a) permeability and porosity, b) homogeneity (distribution of waste and matrix constituents within the waste form, c) density, d) voids, e) preferential pathways in waste form.	Screen In	
4.2.02	Radioactive Decay and In-Growth	Radioactive decay is a fundamental process that affects all radioactive (unstable) nuclides. Radioactive decay will change the inventory of radionuclides in the waste, and the heat generation will affect the temperature in the near-field and the stability of the waste form and other cementitious materials.	Screen In	
4.2.03	Waste Homogeneity	A description of the homogeneity of the waste in the closure facility. Different categories of heterogeneity are possible in a waste closure facility: a) heterogeneity in the disposal concepts, b) heterogeneity in the waste stream, and c) heterogeneity in the distribution of the radionuclides in the waste or waste form.	Screen In	
4.2.04	Contaminant Solubility, Solubility Limits, and Speciation	Speciation and solubility processes, including their evolution in time, occurring in the accessible environment that effect the dissolution/precipitation of contaminants. Large solubility limits increase the mobility of contaminants, but low solubility limits may lead to larger exposures when precipitation occurs. Small concentrations of complexing agents could form stable dissolved species, enhancing the dissolution of contaminants from the waste form and increasing their solubility. Conversely, solubility limits will be smaller when complexing agents have low concentrations or where the chemical environment decreases the stability of dissolved species or enhances the stability of a solid phase.	Screen In	
4.2.05	Degradation of the Inorganic Waste	Degradation and failure processes: The waste form type and associated characteristics will determine the dominant waste form degradation processes including: a) physical degradation processes (e.g., physical stress), b) chemical degradation processes (e.g., sulfate attack), and c) biological degradation processes (e.g., notifying bacteria and heterotrophic organisms), together with the physical, chemical, hydrological and biological conditions in the waste closure facility and environment. Consequently, degradation of inorganic wastes may impact on the release and transport of radionuclides from the near-field.	Screen In	

Table 4.1-5: FEPs Screening Results (Continued)

FEP ID	FEP Name (Short)	FEP Description	Final Deter-mination	Comments and/or Screen Out Justification
4.2.06	Degradation of the Organic Waste	Degradation and failure processes: The waste form type and associated characteristics will determine the dominant waste form degradation processes including: a) physical degradation processes (e.g., physical stress), b) chemical degradation processes (e.g., sulfate attack), and c) biological degradation processes (e.g., notifying bacteria and heterotrophic organisms), together with the physical, chemical, hydrological and biological conditions in the waste closure facility and environment. Consequently, degradation of organic wastes may impact on the release and transport of radionuclides from the near-field.	Screen In	
4.2.07	Localized Interactions Between Emplaced Wastes	Co-location refers to the disposal of various types of wastes in close proximity. Co-disposal refers to the disposal of different waste types within the same waste package. Co-location and co-disposal might affect thermal outputs, chemical interactions, or radionuclide mobilization.	Screen In	
4.2.08	Radiation Effects	Relative importance of (for exclusion/inclusion discussion) alpha recoil on the dissolution of alpha emitter daughter products, especially radon.	Screen In	
4.2.09	Solubility and Sorption Changes From Chemical and Temperature Interactions	Factors related to release of the various contaminants, by desorption and solubility influences, into the invading pore waters. For example, radionuclides in secondary uranium mineral phases, such as neptunium in schoepite and uranium silicates, could affect radionuclide concentrations (during radionuclide alteration, the radionuclides could be chemically bound to immobile compounds and result in a reduction of available radionuclides for mobilization).	Screen In	
4.2.10	Dissolution and Precipitation	Dissolution and precipitation processes, including their evolution in time. Most contaminants are released from the residual waste when they dissolve into the ground water that has entered the waste tank, and many contaminants could re-precipitate as different compounds. Precipitation could also occur if there is an abrupt change in the chemical environment (including ground water composition and pH) or if ingrowth from radioactive decay produces a local increase in concentration.	Screen In	
4.3.01	Waste Inventory	A description of the total radionuclide content in the waste (total activity in units of curies, or mass in grams) and a description of the content of individual radionuclides (radionuclide composition) and chemicals (chemical composition, typically in units of density or concentration) in the waste. A description of the physical content of the waste material in its untreated form (i.e., as generated). A description of the physical size of the waste and/or waste containers used to dispose the waste material in its untreated or treated (stabilized) form.	Screen In	
4.3.02	Waste Inventory (Alternate Waste Locations)	Account for inventory expected to remain in the sheet drain systems and the inventory expected to remain in the transfer lines at the time of closure.	Screen In	
4.3.03	Waste Inventory (Disposal Configuration)	Waste should be processed in a deliberate way such that disposal configurations support risk reduction.	Screen In	
4.3.04	Contaminant Concentrations in Water and Other Media	Factors related to the concentrations of contaminants in: a) environmental media; b) drinking water, foodstuffs or drugs that may be consumed by humans; c) environmental media other than drinking water, foodstuffs or drugs; and d) human manufactured materials or environmental materials used by humans for special uses, e.g., clothing, building materials, peat. This includes ground water concentrations.	Screen In	

Table 4.1-5: FEPs Screening Results (Continued)

FEP ID	FEP Name (Short)	FEP Description	Final Deter-mination	Comments and/or Screen Out Justification
4.3.05	Dilution of Radionuclides in Ground Water	Dilution due to mixing of contaminated and uncontaminated water may affect radionuclide concentrations in ground water during transport in the saturated zone and during pumping at a withdrawal well. For example: Mixing or dilution of the radioactive species from the waste with species of the same element from other sources (i.e., stable and/or naturally occurring isotopes of the same element) could lead to a reduction of the radiological consequences.	Screen In	
4.3.06	Radionuclide Accumulation (Recycling) in Soils	Radionuclide accumulation in soils may occur as a result of upwelling of contaminated ground water (leaching, evaporation at discharge location), deposition of contaminated water or particulates (irrigation water, runoff), and/or atmospheric deposition. Radionuclides that have accumulated in soils (e.g., from deposition of contaminated irrigation water) may leach out of the soil and be recycled back into the ground water as a result of recharge (either from natural or agriculturally induced infiltration). The recycled radionuclides may lead to enhanced radionuclide exposure at the receptor.	Screen In	
4.3.07	Waste Inventory (Unexpected Sources)	Previously unexpected waste streams sent to SDF.	Screen Out	Screened Out - While it is acknowledged that this FEP cannot be screened out based on frequency and/or impact, the FEPs Screening Team has determined that any approach to address this FEP within a PA would rely heavily upon unjustifiable assumptions and would be highly speculative. As such, the FEPs Screening Team recommends excluding this FEP from consideration in the PA.
4.4.01	Human Exposure Pathways	Ingestion, inhalation, and external exposure pathways.	Screen In	
4.4.02	Food Preparation and Water Processing	Factors related to human diet and fluid intake of dietary foodstuffs and water between its original (raw) form and consumption by human beings and animals. Other influences include water filtration, diet of uncontaminated food, and food preparation techniques.	Screen In	
4.4.03	Animal, Plant, and Microbe Uptake and Migration of Contaminants	Factors related to migration of radionuclides and chemical contaminants as a result of animal, plant and microbial activity. Radionuclides may be transported and transferred through and between different compartments of the biosphere. Temporally and spatially dependent physical and chemical environments in the biosphere may lead to alteration of both the physical and chemical properties of the radionuclides as they move through or between the different compartments of the biosphere. Uptake and accumulation of contaminants by plants could affect potential exposure pathways. Uptake and bioaccumulation of contaminants in aquatic organisms could affect potential exposure pathways. These plants and aquatic organisms may be used as feed for livestock and/or consumed directly by humans.	Screen In	

Table 4.1-5: FEPs Screening Results (Continued)

FEP ID	FEP Name (Short)	FEP Description	Final Deter-mination	Comments and/or Screen Out Justification
4.4.04	Radiological and Chemical Toxicity/Effects	A description of the total toxic content in the waste (organic, inorganic, chemical), and a description of the content of individual toxic elements in the waste. The effects of radiation and chemical contaminants on man and other organisms can be classified in several different ways: somatic or genetic, occurring in the exposed individual or in the offspring of the exposed individual, respectively; and stochastic or non-stochastic, where the probability of the effect is a function of dose received, or the severity of the effect is a function of dose received and no effect may be observed below some threshold, respectively.	Screen In	
4.4.05	Radiological Dose Effects/Risks	The radiation dose is calculated from exposure rates (external, inhalation, and ingestion) and dose coefficients. The latter are based upon radiation type, human metabolism, metabolism of the element of concern in the human body, and duration of exposure. Includes consideration of annual, lifetime, individual, and collective doses. Also includes sensitization to radiation so that its effects are more severe.	Screen In	
4.4.06	Radon and Radon Daughter Exposure (Noble Gas Contamination)	Radon and radon progeny exposure is considered separately from exposure to other radionuclides because the behavior of radon and its progeny, and their modes of exposure, are somewhat different. Radon is mobile and readily enters different components of the biosphere. Exposure to radon almost always implies exposure to its progeny which are relatively immobile and reactive. The principal mode of exposure to humans is inhalation of radon progeny attached to dust particles.	Screen In	
4.5.01	Contaminant Concentrations Pre-Closure	Account for contaminant concentrations found in ground water monitoring wells and surface water and sediments of sedimentation basins in Z-Area and the impacts the concentrations will have on area closure.	Screen In	
4.5.02	Contaminants from Other Man-Made Sources or Facilities	Factors related to radiation exposure and risks due to interactions or cumulative effects from man-made sources (such as other burial grounds or waste closure facilities) in the vicinity of the waste closure facility.	Screen In	
4.5.03	Natural or Background Radiation	Factors related to radiation exposure and risks due to naturally occurring or background radiation.	Screen In	
4.5.04	Nuclear Criticality	Factors related to possibility and effects of spontaneous nuclear chain reactions within the system (e.g., near-field, far-field, within the waste form, etc.) A chain reaction is the self-sustaining process of nuclear fission in which each neutron released from fission triggers, on average, at least one other nuclear fission. Nuclear criticality requires a sufficient concentration and localized mass (critical mass) of fissile isotopes and also presence of neutron moderating materials in a suitable geometry; a chain reaction will be damped by the presence of neutron absorbing isotopes.	Screen Out	Low probability - Given the effects of dilution and the low activity of the SDF waste, a nuclear ciriticality event is considered extremely unlikely and is excluded from consideration in the PA.
4.5.05	Radiation Effects on the Waste Closure System	When radionuclides decay, the emitted high-energy particle could result in the production of radicals in the water or air and they may then enhance the degradation/corrosion rate of the cementitious materials. Strong radiation fields could lead to radiation damage to the residual waste and surrounding waste tank. This effect would increase the dissolution rate and transport of radionuclides from the residual waste into the ground water.	Screen In	

Table 4.1-5: FEPs Screening Results (Continued)

FEP ID	FEP Name (Short)	FEP Description	Final Deter-mination	Comments and/or Screen Out Justification
4.5.06	Radiolysis Effects	Alpha, beta, gamma, and neutron irradiation of water can cause disassociation of molecules, leading to gas production and changes in chemical conditions (potential, pH, and concentration of reactive radicals). Radiation emitted during radioactive decay of unstable nuclides can cause radiolysis of the ground water and of water-bearing solid materials. This radiolysis can lead to the formation of oxidants and free hydrogen gas which will impact on the redox conditions in the near-field, leading to a change in radionuclide solubilities.	Screen In	
4.5.07	Radionuclide Interaction with Corrosion Products	Corrosion of materials will generate a range of possible solid secondary alteration products which depend on the ground water chemistry. Radionuclides released from the source term may interact with these alteration products by a range of processes such as sorption/desorption or (co-)precipitation/dissolution reactions. These interactions have the potential for significantly controlling radionuclide release rates from the near-field.	Screen In	
4.5.08	Medical Radiation	Factors related to radiation exposure and risks due to medical procedures.	Screen Out	This FEP is not applicable to the SDF system or is outside the scope of an SDF PA.
5.1.01	Ground Water Flow and Movement (Near-Field)	Unsaturated and saturated flow may occur along preferential pathways in and surrounding the waste tanks. Physical and chemical properties of the cementitious materials, in both intact and degraded states, should be considered in evaluating pathways. Preferential pathways for ground water flow and diffusion may exist within the transfer lines. Backfill, plugs, and seals may not preclude hydrological, chemical, and thermal interactions between the various system components. Water outflows are responsible for the transport of dissolved radionuclides away from the waste tanks and ancillary equipment.	Screen In	
5.1.02	Ground Water Flow and Movement (Far-Field)	Ground water flow in the saturated zone below the water table may affect long-term performance of the closure system. The location, magnitude, and direction of flow under present and future conditions and the hydraulic properties of the rock are all relevant.	Screen In	
5.1.03	Focusing of Flow Along Preferred Flow Paths (Fingers, Weeps, Faults, Fractures, etc.)	Development of preferential flow paths and/or the alteration of preferential flow paths. Heterogeneities in rock properties, including fractures and faults, may contribute to focusing of unsaturated flow into zones of greater and lower saturation that may persist as preferential flow paths. Fractures or other analogous channels may act as conduits for fluids to move into the subsurface to interact with the waste tanks and as conduits for fluids to leave the vicinity of the waste tanks and be conducted to the saturated zone. Water may flow through only a portion of the fracture network, including flow through a restricted portion of a given fracture plane.	Screen In	
5.1.04	External Flow Boundaries	The external flow boundary conditions of the hydrogeological system control the location and amount of recharge and discharge, and are a control on the geometry of the flow system. The external flow boundary conditions are, thus, important to define for modeling ground water flow and radionuclide transport in the far-field.	Screen In	
5.1.05	Unsaturated Zone Properties	Moisture characteristic curves (van Genuchten)	Screen In	

Table 4.1-5: FEPs Screening Results (Continued)

FEP ID	FEP Name (Short)	FEP Description	Final Deter-mination	Comments and/or Screen Out Justification
5.1.06	Thickness of the Saturated Zone and the Vadose Zone	Transport (and contaminant concentrations) can be influenced by the thicknesses of these zones.	Screen In	
5.1.07	Episodic Or Pulse Flow and Release	Episodic flow could occur as a result of episodic infiltration. Episodic or pulse release of radionuclides from the waste tanks and radionuclide transport in the ground water may occur both because of episodic flow into the waste tanks, and because of pulse releases from failed waste tanks.	Screen In	
5.1.08	Water Influx at the Closure Facility	An increase in the water flux may affect thermal, hydrologic, chemical, and mechanical behavior of the system.	Screen In	
5.1.09	Flow Diversion and Bypass Flow	Flow in unsaturated rock tends to be diverted by the closure cap. The resulting diversion of flow could have an effect on seepage into the waste tanks. Flow diversion could also lead to the development of a zone of lower flow rates and low saturation beneath the closure cap. The movement of water through the soil along a pathway other than that provided by the microscopic pore spaces within the soil matrix (such as shrinkage cracks, faunal burrows, and voids left following the decay of plant roots). Bypass flow can transmit water through soils whose matrix is not saturated faster than under laminar flow.	Screen In	
5.1.10	Alteration and Chemical Weathering Along Flow Paths	Chemical (water-rock) reactions between ground water and the rock and any fracture minerals will lead to progressive changes to the solid phases along the flow path and to its hydraulic properties. Ongoing chemical reactions (precipitation and dissolution) between ground water and rock and fracture minerals lead to weathering of the migration path resulting in increased ground water flow and channeling. Weathering may alter the mineral composition and physical composition of the fractures and pores, as well as the ground water chemistry and generation of colloids. These water-rock reactions can impede or enhance radionuclide transport depending on their nature.	Screen In	
5.1.11	Chemically-Induced Density Effects on Ground Water Flow	Chemically-induced spatial variation in ground water density may affect ground water flow.	Screen Out	Low Impact - relative to other FEPs, the impacts from chemically-induced density effects on ground water are expected to be negligible.
5.1.12	Film/Laminar Flow	Water may enter the waste tanks by a film flow process. This differs from the traditional view of flow in a capillary network where the wetting phase exclusively occupies capillaries with apertures smaller than some level defined by the capillary pressure. A film flow process could allow water to enter a waste tank at non-zero capillary pressure.	Screen In	
5.1.13	Calcareous Zone Flow	Impacts on flow from calcareous zones.	Screen In	
5.1.14	Deformation at Flow Interfaces	Deformation and associated influence on flow systems at joints and material interfaces	Screen In	
5.1.15	Vadose Zone Depth	The vertical distance between the bottom of the floor of the disposal unit or closure facility and the top of the saturated zone.	Screen In	
5.1.16	Saturated Zone Depth	The vertical distance between the top of the saturated zone and the bottom point (or intake) of the assessment well.	Screen In	
5.1.17	Depth of Assessment Well	The depth from which the assessment well draws water.	Screen In	

Table 4.1-5: FEPs Screening Results (Continued)

FEP ID	FEP Name (Short)	FEP Description	Final Deter-mination	Comments and/or Screen Out Justification
5.1.18	Horizontal Distance to Points of Assessment	The horizontal distance between the waste closure facility and the assessment well or stream.	Screen In	
5.1.19	Minimum Buffer Zone	The SDF permit specifies that there should be a minimum buffer zone of 3 feet between the seasonal high water table and/or bedrock and the lowest elevation of the disposal area.	Screen In	
5.1.20	Chemical Composition of Infiltrating Rainwater	Chemical composition of rainwater may vary over time. Additionally, as the rainwater infiltrates through the top soil and closure cap to reach the SDUs, its chemical composition may change over time as different mineral phases are dissolved/depleted.	Screen In	
5.2.01	Diffusion (Molecular Diffusion and Matric)	Diffusion is the process whereby chemical species move through water-filled cracks and voids under the influence of a chemical potential gradient (usually a concentration gradient). Radionuclides can migrate by diffusion from inside the tank to the backfill, after the tank has been breached. In addition, dissolved species in the ground waters outside the tank can be transported into the tank by diffusion. Both inward and outward diffusion of species will affect the ground water chemistry and the release of solubility controlled species. Matrix diffusion is the process by which radionuclides and other species in the water flowing along fractures migrate into the non-flowing micro-fractures and into the micro-porosity of the surrounding rock mass. Matrix diffusion can provide an efficient retardation mechanism for both sorbing and non-sorbing contaminants.	Screen In	
5.2.02	Advection	Transport of fluids and dissolved contaminants by advection with the flowing ground water may occur. Physical and chemical properties of the system and system components, in both intact and degraded states, should be considered in evaluating advective transport.	Screen In	
5.2.03	Dispersion and Imbibition	Dispersion is the collective name for the consequences of a number of processes that cause 'spreading-out' of a contaminant plume in all directions, superimposed on the bulk movement predicted by a simple advection model. It results in a spatially distributed contaminant plume. Water flowing in fractures or other channels in the unsaturated zone may be imbibed into the surrounding rock matrix. This may occur during steady flow, episodic flow, or into matrix pores that have been dried out during the thermal period.	Screen In	
5.2.04	Hydraulic Conductivities in the Natural Barrier	Hydraulic conductivity is the ease with which a fluid (usually water) can move through pore spaces or fractures. The natural barriers through which water may flow include sandy soils, clayey soils, gravels and (if deep enough) bedrock.	Screen In	
5.2.05	Hydrological Response to Geological Changes	Effects on regional ground water flow and pressures arising from large-scale geological changes. Effects include changes in ground water flow and pressures caused by erosion, and changes to hydraulic properties of geological units caused by changes in rock stress or fault movements. Within and underlying low-permeability geological formations, the hydrogeological conditions may have characteristics that reflect past geological conditions and are in a state of disequilibrium.	Screen Out	Screened Out - The FEPs Screening Team identified this FEP as being very broad in scope. Other more discrete FEPs have been identified which more accurately capture the relevant features, events, or processes which should be considered within the PA; as such, this FEP is screened out.

Table 4.1-5: FEPs Screening Results (Continued)

FEP ID	FEP Name (Short)	FEP Description	Final Deter-mination	Comments and/or Screen Out Justification
5.2.06	Hydraulic Potentials and Gradients	Hydraulic gradients drive fluid flow through the host rock and other rock units. The near-surface hydraulic gradients are topographically controlled and are in equilibrium with the current surface conditions. Hydraulic gradients will evolve with time due to changes in climate and landform, but more significantly due to glacial cycles.	Screen In	
5.2.07	Hydrothermal Activity	Naturally occurring high-temperature ground water may induce hydrothermal alteration of minerals in the rocks through which the high-temperature ground water flows. Factors related to hydrothermal activity, the potential for hydrothermal activity and its effects on the performance of the waste closure facility.	Screen Out	Given the local geologic conditions, igneous or geothermal events at Z-Area are highly unlikely. As such, this FEP is screened out.
5.2.08	Interfaces Between Different Waters	There is potential for the development of interfaces between ground waters of different composition in the near and far-field rock. At these interfaces, changes may occur in radionuclide solubilities and ground water flow which could affect radionuclide transport and release.	Screen In	
5.2.09	Perched Water Develops	Zones of perched water may develop above the water table which may affect flow between the surface and the waste tanks. If these zones develop within the disposal units, a "bath tub" effect may occur (i.e., water "pooling" and possibly filling the unit prior to degradation of the disposal unit walls and/or liner). If they develop below the waste tanks, they may affect flow pathways and radionuclide transport between the waste tanks and the saturated zone.	Screen In	
5.2.10	Drainage Channel Influx	Effects of water entering the perimeter drainage channels	Screen In	
5.2.11	Effects Related to Air and Vapor Flow and Evaporation within the System	FEP addresses the effects of dry-out within the rocks. Natural convective air circulation transfers energy between a hot and a cold region (source and sink, respectively) using the heat of vaporization and movement of the vapor as the transfer mechanism. Two phase circulation continues until the heat source is too weak to provide the thermal gradients required to drive it. Alteration of the rock may include dissolution that maintains the permeability necessary to support the circulation.	Screen In	
5.3.01	Contaminant Release and Migration Factors	The Contaminant Release and Migration category is related to the physical, chemical, and radiological processes that directly affect the release (i.e., that will result in the contaminants being available for migration into the environment) and migration of contaminants in the disposal system domain that will result in a contaminant concentration in environmental media.	Screen In	Programmatically screened in by WDA prior to screening evaluations.
5.3.02	Contaminant Release from the Waste Form and Engineered Barrier System	Radionuclides will be released from the waste forms by a variety of mechanisms either into solution, to secondary solid alteration phases, as colloids, or in the gaseous phase. The nature and abundance of the released species will depend on the chemistry of the near-field pore-waters and the degradation rate of the waste form. Radionuclides in the form of solutes or colloids released from the residual waste can migrate by diffusion or by water exchange from inside the waste tank to the ground water, after the waste tank has been breached. Radionuclides can also migrate in the gas phase. Release and transport of radionuclides and other solute species from the waste tank will affect the ground water chemistry (radionuclide content) inside the waste tank and in the surrounding soil. Radionuclides released from the waste tank can be transported through the backfill in solution or as a gas, and possibly also in colloidal form. The mechanisms and rate of radionuclide transport through the backfill are determined largely by the physical properties of the backfill materials. Transport through the backfill controls the release rate to the near-field environment.	Screen In	

Table 4.1-5: FEPs Screening Results (Continued)

FEP ID	FEP Name (Short)	FEP Description	Final Deter-mination	Comments and/or Screen Out Justification
5.3.03	Contaminant Release Pathways	Factors related to the pathways as well as the associated processes and conditions for the release of radiotoxic and chemotoxic species from its physical state of the waste closure facility. Factors related to the properties and characteristics of smaller discontinuities and features within the geosphere (saturated and unsaturated) that are expected to be the main paths for contaminant migration, and as they may evolve after closure.	Screen In	Programmatically screened in by WDA prior to screening evaluations.
5.3.04	Long-Term Release of Radionuclides	The release of radionuclides to the environment may occur over a long period of time, as a result of the timing and magnitude of the waste tanks/waste packages degradation, and radionuclide transport.	Screen In	
5.3.05	Water-Mediated Migration of Contaminants	Transport of radionuclides and chemical contaminants in ground water and surface water. Water-mediated transport processes include: a) advection or movement with the bulk movement of the fluid, b) percolation or convection, where the movement of the fluid is driven by gravity and heat, respectively, c) dispersion, or the spread in the spatial distribution of contaminants with time because of differential rates of advective or convective transport, d) molecular diffusion, or the random movement of individual atoms or molecules within the fluid; matrix diffusion or diffusion into stagnant pores, and e) multiphase transport processes including unsaturated flow.	Screen In	
5.3.06	Colloid Facilitated Transport	When contaminants precipitate out of solution or sorb to a solid phase they are generally regarded as immobile; however, precipitation of a contaminant on or sorption to a mobile solid phase such as colloids can facilitate contaminant transport in the subsurface. Colloidal particles are thought to exist in glass and cement leachates. Stabilization (colloid particles suspended in solution) is dependent on the colloid and ground water composition as well as the water flow forces. Transport of colloids through the porous media is dependent on physical mechanisms (e.g., straining, diffusion, gravitational settling) as well as physicochemical attraction to the matrix itself.	Screen In	
5.3.07	Cementitious Leachate Impacts on Underlying Sediment	Cementitious porewater contains moderate levels of dissolved solids. When the cementitious porewater enters the underlying/surrounding sediment, it alters the porewater chemistry of the sediment which can impact contaminant transport.	Screen In	
5.3.08	Reduction-Oxidation Potential (Redox Fronts)	The generation and propagation of a redox front influence contaminant transport due to variations in solubilities and concentrations at the interfaces between waters with varying redox potentials. This geochemical instability may also result in the generation of colloids.	Screen In	
5.3.09	Fast Transport Pathways	Fast pathways for water and radionuclide transport between the surface and depth can occur in the form of highly transmissive natural features (such as large fractures) or as poorly sealed shafts and boreholes. The presence of such fast pathways could potentially bypass large regions of the far-field rock and lead to early and large releases to the surface.	Screen In	

Table 4.1-5: FEPs Screening Results (Continued)

FEP ID	FEP Name (Short)	FEP Description	Final Deter-mination	Comments and/or Screen Out Justification
5.3.10	Gas-Mediated Migration of Contaminants	The transport of radionuclides and chemical contaminants in gas or vapor phase, or as fine particulate or aerosols suspended in gas or vapor. Radioactive and chemically toxic gases may be generated by degradation of waste closure facility components, generated from the wastes, microbial degradation of organic material, or naturally occurring, and transported in the gas phase into the geosphere. The gas generated may form a free gas phase that could impact on the transport and release of radionuclides. In some cases, radionuclides may be directly associated with the gas molecules whilst, in other cases, the gas phase will impact on the movement of ground waters containing dissolved radionuclides. Pressure variations due to gas generation may affect flow patterns and contaminant transport in the natural system. Issues such as dwelling location, which could affect seepage of gases such as radon into basements, and heating source, could involve biogas production.	Screen In	
5.3.11	Solid-Mediated Migration of Contaminants	The transport of radionuclides and chemical contaminants in large-scale solid phase movement (such as large-scale erosion processes) or smaller-scale processes (such as rinse mechanisms or colloidal transport) can also occur, leading to movement of contaminants.	Screen In	
5.3.12	Multiphase Transport Processes	Contaminant migration in the disturbed zone could be influenced by: a) the development of a fractured/cracked system caused by the construction of the waste closure facility, b) an alteration of the flow regime caused by a changes in porosity or permeability, c) changes in the sorption properties of the disturbed zone, or d) gaseous (or diffusive) release of contaminants generated in the near-field. Porewater may flow into, and gas out of, the waste tanks in a complex process governed by hydraulic gradients, geosphere gas and liquid flow parameters, gas pressure, and relative saturations in the geosphere.	Screen In	
5.3.13	Radionuclide Fluxes to the Biosphere	Radionuclide fluxes from the closure facility into environmental media as an indicator of barrier performance. Care should be taken to define appropriate areas and volumes over which the fluxes are to be defined in order to make comparisons between those derived from the waste closure facility and fluxes of naturally occurring radionuclides.	Screen In	
5.3.14	Radionuclide Release Outside The Reference Biosphere	Radionuclide releases and accumulations outside the reference biosphere can occur. This could include: a) areas surrounding distant springs and surface water bodies, b) remote natural outfalls, and c) discharge areas such as playas, forests, grasslands, or wetlands that occur in isolated areas in the region. This might also include withdrawal from wells in remote areas. Sediment transport and redistribution may cause concentration or dilution of radionuclides. Flora and fauna in these areas may be exposed and radionuclides be bioaccumulated and enter the food chain. Intermittent use of these areas by humans may also lead to exposure.	Screen Out	Low Impact - Releases outside the modeling domain are not expected to exceed the concentrations within the modeling domain.
5.4.01	K_d Retardation: Sorption and Desorption of Dissolved Contaminants	Sorption and desorption of radionuclides and chemical contaminants describes the physicochemical interactions of a dissolved species with a solid phase to remove the species from solution. Desorption is the opposite process. Sorption and desorption are often described by a simple partition coefficient (K_d), also called the distribution [partition] coefficient. Sorption of radionuclides from the waste occurring on the cementitious materials, their degradation products, and on surfaces of fractures and matrix in rock or soil will retard the migration of those species. Sorption may be reversible or irreversible, and it may occur as a linear or nonlinear process.	Screen In	

Table 4.1-5: FEPs Screening Results (Continued)

FEP ID	FEP Name (Short)	FEP Description	Final Deter-mination	Comments and/or Screen Out Justification
5.4.02	K_d Retardation: Correlations	Due to similarities in chemical properties, groups of radionuclide specific partition coefficients (K_ds) will tend to be correlated. This feature should be considered in sampling of sorption coefficients in stochastic simulations.	Screen In	
5.4.03	K_d Retardation: Leachate Impacts	Factors related to the use of "leachate factors" and other modifiers to K_ds to reflect changes to K_ds driven by changes to the chemical environment.	Screen In	
5.4.04	Organic Matter Impacts on Sorption	Cellulosic materials (e.g., wood, paper) are readily degradable in the environment which leads to the formation of both solid and dissolved cellulose degradation products. The presence of natural organic matter (e.g., humic acid, fulvic acid, etc.) in the subsurface can greatly influence a contaminant's speciation and mobility.	Screen In	
5.4.05	Oxidation along Fractures	Oxidation may occur along saturated fractures (via oxidized pore water) or along unsaturated fractures (via gas transport). Changes to fracture saturation as a function of time may also influence oxidation.	Screen In	
5.4.06	Rinse Release	Studies of Tc release from saltstone samples often demonstrate an initial relatively rapid release of Tc that is characterized as a “rinse-release” phenomenon and excluded from calculated release rates.	Screen In	
5.4.07	Solubility Limits	Factors related to solubility controls and precipitation of contaminants.	Screen In	
6.1.01	Inadvertent Human Intrusion	Humans without knowledge or awareness of the existence of the waste closure facility could accidentally intrude into the system and experience exposures to contaminants. In addition, activities may result in damage to containment, increasing contaminant release rates. An example of an inadvertent action includes an archeological or scientific study of the site. Note: other intrusions (such as meteorite impacts, drilling, and excavating) are discussed in other FEPs.	Screen In	
6.1.02	Deliberate Human Intrusion	Humans could deliberately intrude into the waste closure facility although without appropriate precautions, and experience exposures to contaminants. In addition, activities may result in damage to containment, increasing contaminant release rates. Motivation for deliberate human intrusion includes: a) mining and waste retrieval, b) site remediation/improvement activities, c) facility sabotage, and d) acts of war. Note that other intrusions (such as meteorite impacts, drilling, and excavating) are discussed in other FEPs.	Screen Out	This FEP is not applicable to the SDF system or is outside the scope of an SDF PA.
6.1.03	Drilling Activities	Factors related to any drilling activities in the vicinity of the waste closure facility. This includes: a) exploratory boreholes (for minerals or natural gas and oil), b) boreholes drilled for water-supply wells, c) boreholes drilled before construction of the facility, and d) boreholes drilled after the existence or the purpose of the closure facility has been forgotten. Other drilling activities might include: a) the production of geothermal energy, b) the injection of liquid wastes, and c) other scientific studies.	Screen In	
6.1.04	Excavating and Mining Activities	Factors related to any excavation and mining activities in the vicinity of the waste closure facility (excluding drilling). This includes: a) mining for natural resources (ore, oil, gas, etc.), b) mining to retrieve or extract components of the waste or of the closure facility, c) tunneling for the purpose of constructing subterranean dwellings, and d) tunneling for the purpose of additional waste storage or disposal. Activities may include: a) open excavation, b) tunneling, c) solution mining, d) digging, e) blasting, f) breaking, and g) loading and hauling of material. Some of these activating may result in the production of tailings, which may subsequently release contaminants.	Screen In	

Table 4.1-5: FEPs Screening Results (Continued)

FEP ID	FEP Name (Short)	FEP Description	Final Deter-mination	Comments and/or Screen Out Justification
6.1.05	Igneous or Seismic Event Precedes Human Intrusion	An igneous or seismic event (e.g., a dike) could intersect the waste closure facility and alter the material and structural properties of the closure system (engineered and natural barriers). Because of the change in properties of these materials resulting from an igneous intrusion, an intruder using ground water exploration drilling techniques may not be able to recognize that something other than naturally-occurring material has been encountered.	Screen Out	Given the local geologic conditions, igneous or geothermal events at Z-Area are highly unlikely. Further, seismic events are explicilty considered in other, screened in FEPs. As such, this FEP is screened out.
6.1.06	Animal/Plant Intrusion	Factors related to the intrusion of animal and plant into the waste closure facility, leading to the disruption in performance. For example, pine trees are typically assumed to be the most deeply rooted naturally occurring climax plant species at SRS, which may degrade the closure cap barriers through root penetration.	Screen In	
6.1.07	Invertebrate (e.g., Ant Colonies) Induced Transport	Factors related to the intrusion of invertebrate animals (e.g., ant colonies) and potential transport of contaminated soils resulting in disruption of performance.	Not Screened	Note: This FEP has not undergone formal screening. It was not explicitly considered as part of the FEPs analysis documented in SRR-CWDA-2017-00057. It has been added here for completeness. See additional discussion in Section 6.7.
6.2.01	Seismicity	Factors related to the effects of seismic events on the closure system. Such factors include: a) liquefaction of the backfill materials and soils, b) shaking and damage to the waste form or engineered components, c) rockfalls, and d) extension or creation of fractures or faults. External effects also include: a) tidal waves (tsunamis), b) liquefaction of soil, c) formation of new discharge areas, d) alteration of river courses, and e) destruction of dams. Multiple events occurring close together in time might have effects that are not simply additive.	Screen In	
6.2.02	Seismicity Associated with Igneous Activity	Seismicity associated with future igneous activity that may affect disposal and closure system performance.	Screen Out	Given the local geologic conditions, igneous events at Z-Area are highly unlikely. As such, this FEP is screened out.
6.2.03	Seismic-Induced Damage or Changes to System Components	Factors related to physical damage or property changes to components of the waste closure system due to seismic events. Types of damage include: a) damage from repeated vibration, b) damage from physical contact between components, c) damage from rockfall, d) damage from stress resulting in dynamic or static loading, and e) damages related to movement or displacement of components or materials. Such damage mechanisms could lead to degraded performance. This includes changes to system chemistry, hydrology, and thermo-hydrology. Consider effects on porosity and permeability, fault and fractures, and effects to perched water and aquifers.	Screen In	
6.2.04	Effects of Subsidence	Subsidence at or near the closure facility may affect the properties of the natural system materials and surface topography. Changes in rock and soil properties, such as enhanced permeability, may alter flow paths from the surface to the waste closure facility. Changes in surface topography may alter run-off and infiltration, and may create impoundments.	Screen In	

Table 4.1-5: FEPs Screening Results (Continued)

FEP ID	FEP Name (Short)	FEP Description	Final Deter-mination	Comments and/or Screen Out Justification
6.3.01	Volcanic Eruptions and Magmatic Activity	Factors related to volcanic eruptions and magmatic activities, including changes to topography or surface drainage patterns (via effusive lava flows or development of a volcanic cone). Specifically, magmatic vents could pass directly through the waste closure system, interacting with the waste. Some of the waste (entrained, dissolved, or volatized) could then be transported away from the waste closure facility. Of most concern is transport directly along the land surface to the MOP. Additionally, large-scale volcanic activity has the potential to influence short-term climatic change that could alter rainfall and infiltration.	Screen Out	Given the local geologic conditions, igneous or geothermal events at Z-Area are highly unlikely. As such, this FEP is screened out.
6.3.02	Igneous Intrusion Into the Closure Facility	Igneous activity at or near the waste closure facility may cause change the backfill and rock and soil properties (e.g., stress fields, thermal regimes, permeabilities, etc.). This may alter the hydrology, mineralogy, or the overall integrity of the waste closure facility. Magma from an igneous intrusion may flow into the facility, forming a sill, dike, or dike swarm. This could result in magma, pyroclastic debris, and volcanic gases entering the facility and interacting with the engineered components and the waste forms. This could lead to accelerated system failure (e.g., attack by magmatic volatiles, damage by flowing or fragmented magma, thermal effects) and dissolution or volatilization of waste. Igneous activity may change the infiltration rates, ground water flow directions, water level, water chemistry, and temperature.	Screen Out	Given the local geologic conditions, igneous or geothermal events at Z-Area are highly unlikely. As such, this FEP is screened out.
6.3.03	Ashfall	Following a volcanic event, finely divided waste particles may be carried up a volcanic vent and deposited on the land surface from an ash cloud. Deposited contaminants may leach out of the ash and be transported through the subsurface or redistributed on the surface via aeolian and fluvial processes.	Screen Out	Given the local geologic conditions, igneous or geothermal events at Z-Area are highly unlikely. As such, this FEP is screened out.
6.4.01	Accidents and Unplanned Events	Factors related to accidents and unplanned events, which might have an impact on long-term performance or safety of the waste closure facility.	Screen Out	Screened Out - While it is acknowledged that this FEP cannot be screened out based on frequency and/or impact, the FEPs Screening Team has determined that any approach to address this FEP within a PA would rely heavily upon unjustifiable assumptions and would be highly speculative. As such, the FEPs Screening Team recommends excluding this FEP from consideration in the PA.
6.4.02	Flooding or Drainage System Failure	Factors related to flooding (or drainage system failures) of the site or facilities during construction, operation, or post-closure that could introduce additional water into the system, which could affect the long-term performance of the waste closure facility.	Screen In	
6.4.03	Releases Prior to Closure	Factors related to release of contaminants after waste emplacement but prior to closure of the waste closure facility.	Screen In	
6.4.04	Forest/Brush Fire	Fire prior to closure cap emplacement resulting in accidental release of radionuclides.	Screen In	

Table 4.1-5: FEPs Screening Results (Continued)

FEP ID	FEP Name (Short)	FEP Description	Final Deter-mination	Comments and/or Screen Out Justification
6.4.05	Explosions and Crashes	Factors related to deliberate or accidental explosions and crashes that might impact the waste closure facility. Examples include: a) underground nuclear testing, b) aircraft crash on the site, c) acts of war or sabotage, and d) accidental equipment or chemical explosions.	Screen Out	Screened Out - While it is acknowledged that this FEP cannot be screened out based on frequency and/or impact, the FEPs Screening Team has determined that any approach to address this FEP within a PA would rely heavily upon unjustifiable assumptions and would be highly speculative. As such, the FEPs Screening Team recommends excluding this FEP from consideration in the PA.
6.4.06	Movement of the Waste Form	Backfill provides a stable physical and chemical environment for the waste form, and isolates the engineered system components from the near-field natural environment and flowing ground waters. The effectiveness may be diminished if the waste moves within the backfill. This could occur as a result of sinking, uneven swelling of clays and backfill materials, expansion of engineered system materials, or movement of the near-field geosphere via slumping or stresses.	Screen In	
6.4.07	Cave-In, Collapse, or Rockfall	Partial or complete collapse or cave-in of the engineered components or discrete rockfall could occur as a result of thermal effects, stresses related to excavation, or other mechanisms (including seismic activity). Cave-ins and rockfalls could affect the stability of the engineered components or result in static loading from rock overburden, as well as altering flow paths.	Screen In	
6.4.08	Extraterrestrial Events	Factors related to extraterrestrial events (e.g., supernova, solar flare, gamma-ray burster, and events associated with alien life forms) may affect long-term performance of the disposal system.	Screen Out	Screened Out - While it is acknowledged that this FEP cannot be screened out based on frequency and/or impact, the FEPs Screening Team has determined that any approach to address this FEP within a PA would rely heavily upon unjustifiable assumptions and would be highly speculative. As such, the FEPs Screening Team recommends excluding this FEP from consideration in the PA.

Table 4.1-5: FEPs Screening Results (Continued)

FEP ID	FEP Name (Short)	FEP Description	Final Deter-mination	Comments and/or Screen Out Justification
6.4.09	Impacts from Meteorites or Space Debris	Factors related to impacts from meteorites or space debris (natural or man-made) occurring at or near the waste closure system. Such impacts could create a crater, damage system components, or cause physical and chemical changes in materials.	Screen Out	Screened Out - While it is acknowledged that this FEP cannot be screened out based on frequency and/or impact, the FEPs Screening Team has determined that any approach to address this FEP within a PA would rely heavily upon unjustifiable assumptions and would be highly speculative. As such, the FEPs Screening Team recommends excluding this FEP from consideration in the PA.
6.4.10	Changes to Earth's Tidal Processes	Earth tides are small pressure variations in the ground water flow system caused by changes to the gravitational field due to the relative movements of the Earth, the Sun and the Moon. Earth tides may have an influence on the transport and retardation of radionuclides in the far field.	Screen Out	Screened out during Phase I: Based on proximity to coast lines, this FEP is not expected to have a significant impact on system performance.
6.4.11	Changes in the Earth's Magnetic Field	Changes in the earth's magnetic field could affect the long-term performance of the waste closure facility.	Screen Out	Screened out during Phase I: Changes to the earth's magnetic field are not expected to have a significant impact on system performance.

[SRR-CWDA-2017-00057]

4.1.2 Conceptual Model Development

After completing the FEPs screening process, the included FEPs were used in the development of the conceptual models for the Central Scenario and to develop sensitivity cases based on alternative conceptual models (ACMs). In the context of the SDF PA, a scenario is a subset of FEPs used to identify conditions or processes that may influence the evolution of the disposal facility, while a conceptual model is a description of the evolution of the system that includes or addresses the FEPs within a given subset.

The first scenario developed was the Central Scenario. This is the scenario that reflects the most likely or expected future evolution of the disposal site (i.e., the most probable and defensible scenario). The FEPs list was used to develop the conceptual model for the Central Scenario as follows:

- Selected FEPs were used to define the assessment context (e.g., performance objectives and time periods to consider). While the assessment context does not typically address specific physical features, it does define the purpose and scope of the performance assessment, which should be considered continuously during PA development.
- Next, a system description was developed from the FEPs list to ensure the key features of the SDF disposal system were identified and defined (see Sections 2.2, 2.3, and 3). The system description includes the geologic features and the natural environment, engineered features including the barriers designed to mitigate contaminant releases, and contaminant properties that are relevant to release and transport, but it does not explicitly consider the evolution of these features over time or the interactions between these features.

Note that FEPs addressed within these first two bullets are applicable to every conceptual model.

- Next, an "Interaction Matrix" (IM) was developed to help define the conceptual model for the Central Scenario. The IM approach was based on the *Guidance for Conducting Technical Analyses for 10 CFR Part 61* (draft NUREG-2175) from the NRC. [ML14357A072] With the interaction matrix approach, primary components of the system (i.e., safety-significant features) are identified along with the various interactions between those primary model components (i.e., processes). Within the interactions matrix, these primary components of the system are identified as "leading diagonal elements" (LDEs) and "off-diagonal elements" (ODEs) based on the way the interaction matrix is organized. In addition, the expected (most likely) evolution of the LDEs is postulated based on the ODEs. All of the LDEs and ODEs identified within the interaction matrix were mapped to specific FEPs. [SRR-CWDA-2018-00006]

From this approach, the set of FEPs that were used to define the assessment context, the system description, and the LDEs and ODEs represent the Central Scenario and a description of how all these FEPs fit together represents the conceptual model of the Central Scenario.

The IM for the Conceptual Description of the Central Scnario is a two-dimensional matrix that provides a graphical depiction of the key features of a system and the interactions between those key features. The LDEs for the Central Scenario IM are listed in Table 4.1-6 and graphically

depicted in Figure 4.1-3 and Figure 4.1-4. Each of these LDEs are discussed in greater detail within the *Conceptual Model Development for the Saltstone Disposal Facility Performance Assessment*. [SRR-CWDA-2018-00006]

Table 4.1-6: Leading Diagonal Elements for SDF PA Central Scenario

IM ID	Leading Diagonal Element	Associated Figure(s)
01	Precipitation	Figure 4.1-3
02	Closure Cap	Figure 4.1-3
03	SDU Roof	Figure 4.1-3
04	Waste (Decontaminanted Salt Solution)	Figure 4.1-3
05	Saltstone Hydraulic Conductivity	Figure 4.1-3
06	Saltstone Reducing Capacity	Figure 4.1-3
07	Pore Water Chemistry	Figure 4.1-3
08	Gaseous Phases	Figure 4.1-3
09	SDU Columns	Figure 4.1-3
10	SDU Joints/ Waterstops	Figure 4.1-3
11	SDU Interior Liner	Figure 4.1-3
12	SDU Walls and Floor	Figure 4.1-3
13	Upper Mud Mat	Figure 4.1-3
14	Liner Between Mud Mats	Figure 4.1-3
15	Lower Mud Mat	Figure 4.1-3
16	Backfill	Figure 4.1-3
17	Ground Water Chemistry	Figure 4.1-3
18	Vadose Zone	Figure 4.1-3 and Figure 4.1-4
19	Saturated Zone	Figure 4.1-3 and Figure 4.1-4
20	1-Meter or 100-Meter Well	Figure 4.1-4
21	Surface Streams	Figure 4.1-4
22	Soil	Figure 4.1-4
23	Vegetation	Figure 4.1-4
24	Livestock	Figure 4.1-4
25	Human	Figure 4.1-4
26	Exposure/ Risk	Not pictured

It is noted that Figure 4.1-3 provides a simplistic depiction of the closure cap. While the closure cap design features multiple discrete layers, each with explicit functionality, for PA modeling the purpose of the closure cap is to limit the infiltration into the system. As such, the conceptualization step of the model development process did not require a fully detailed closure cap. Model implementation does consider the various closure cap layers with respect to determining how those layers ultimately impacted infiltration rates.

The Conceptual Model IM is depicted in Figure 4.1-5.

Figure 4.1-3: Depiction of the Leading Diagonal Elements for SDF PA IM: SDUs and Near Field Environment

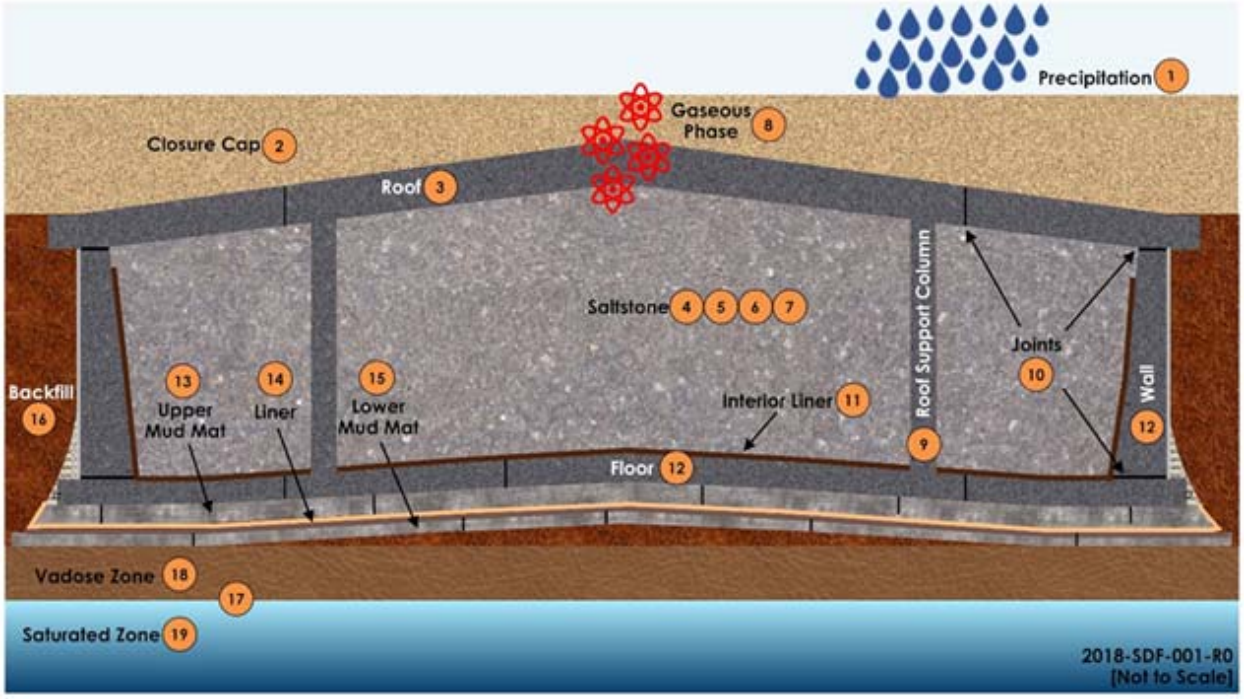

Note: Not all LDEs are depicted in this figure. See Table 4.1-6 for a complete listing of LDEs.

Figure 4.1-4: Depiction of the Leading Diagonal Elements for SDF PA IM: Human Exposure and Uptake

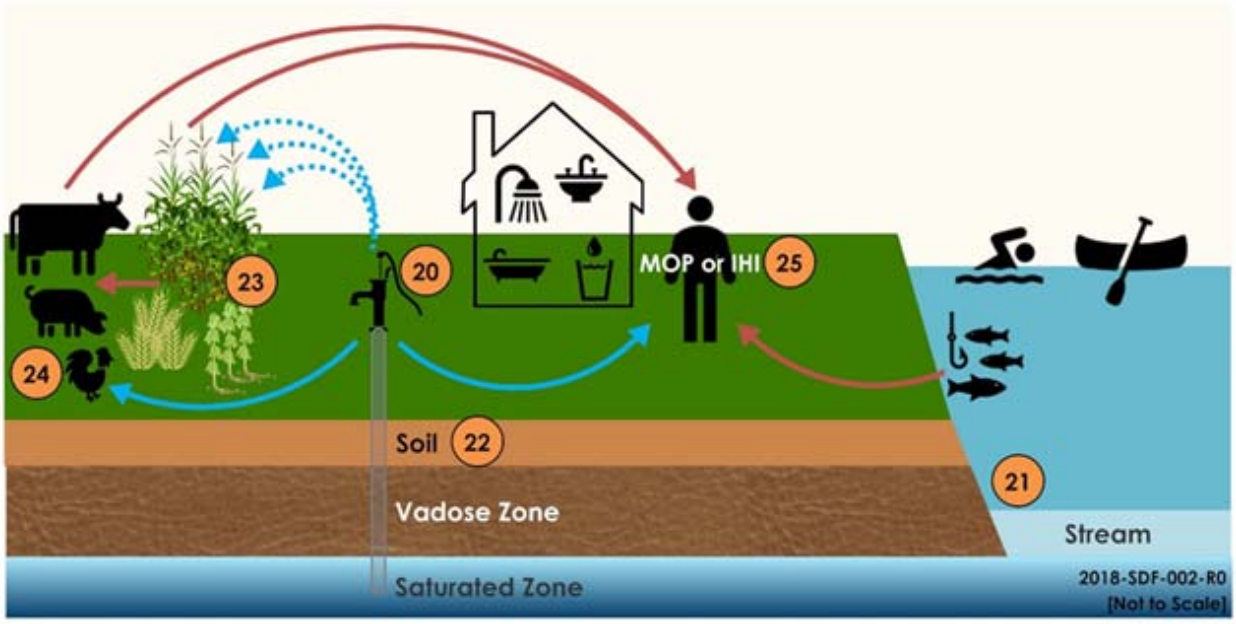

Note: Not all LDEs are depicted in this figure. See Table 4.1-6 for a complete listing of LDEs.

Figure 4.1-5: Central Scenario, Completed Interaction Matrix

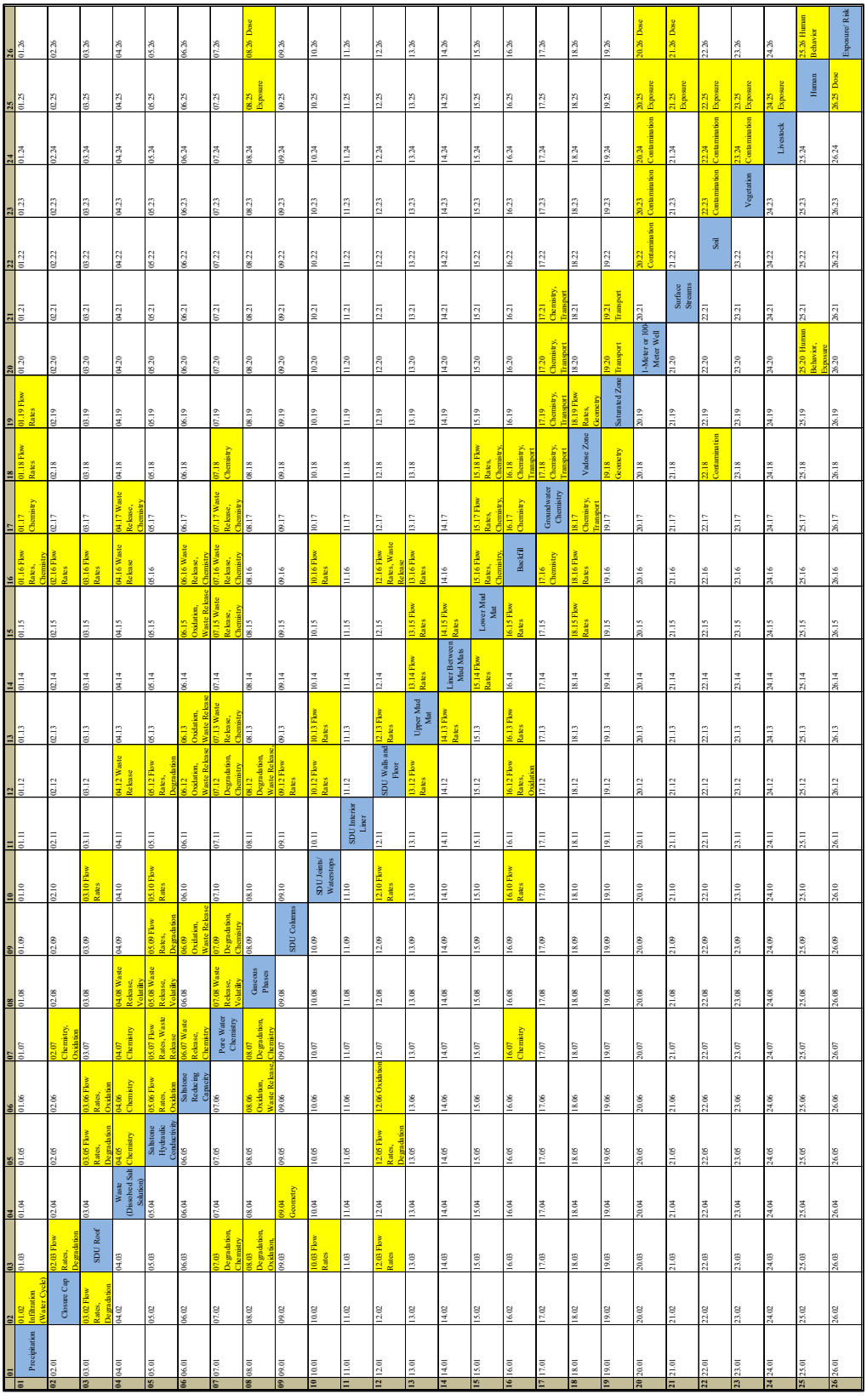

	01	02	03	04	05	06	07	08	09	10	11	12	13	14	15	16	17	18	19	20	21	22	23	24	25	26
01	Precipitation	01.02 Infiltration (Water Cycle)	01.03	01.04	01.05	01.06	01.07	01.08	01.09	01.10	01.11	01.12	01.13	01.14	01.15	01.16 Flow Rates, Chemistry	01.17 Chemistry	01.18 Flow Rates	01.19 Flow Rates	01.20	01.21	01.22	01.23	01.24	01.25	01.26
02	02.01	Closure Cap	02.03 Flow Rates, Degradation	02.04	02.05	02.06	02.07 Chemistry, Oxidation	02.08	02.09	02.10	02.11	02.12	02.13	02.14	02.15	02.16 Flow Rates	02.17	02.18	02.19	02.20	02.21	02.22	02.23	02.24	02.25	02.26
03	03.01	03.02 Flow Rates, Degradation	SDU Roof	03.04	03.05 Flow Rates, Degradation	03.06 Flow Rates, Oxidation	03.07	03.08	03.09	03.10 Flow Rates	03.11	03.12	03.13	03.14	03.15	03.16 Flow Rates	03.17	03.18	03.19	03.20	03.21	03.22	03.23	03.24	03.25	03.26
04	04.01	04.02	04.03	Waste (Dissolved Salt Solution)	04.05 Chemistry	04.06 Chemistry	04.07 Chemistry	04.08 Waste Release, Volatility	04.09	04.10	04.11	04.12 Waste Release	04.13	04.14	04.15	04.16 Waste Release	04.17 Waste Release, Chemistry	04.18	04.19	04.20	04.21	04.22	04.23	04.24	04.25	04.26
05	05.01	05.02	05.03	05.04	Saltstone Hydraulic Conductivity	05.06 Flow Rates, Oxidation	05.07 Flow Rates, Waste Release	05.08 Waste Release, Volatility	05.09 Flow Rates, Degradation	05.10 Flow Rates	05.11	05.12 Flow Rates, Degradation	05.13	05.14	05.15	05.16	05.17	05.18	05.19	05.20	05.21	05.22	05.23	05.24	05.25	05.26
06	06.01	06.02	06.03	06.04	06.05	Saltstone Reducing Capacity	06.07 Waste Release, Chemistry	06.08	06.09 Oxidation, Waste Release	06.10	06.11	06.12 Oxidation, Waste Release	06.13 Oxidation, Waste Release	06.14	06.15 Oxidation, Waste Release	06.16 Waste Release, Chemistry	06.17	06.18	06.19	06.20	06.21	06.22	06.23	06.24	06.25	06.26
07	07.01	07.02	07.03 Degradation, Oxidation	07.04	07.05	07.06	Pore Water Chemistry	07.08 Waste Release, Volatility	07.09 Degradation, Chemistry	07.10	07.11	07.12 Degradation, Chemistry	07.13 Waste Release, Chemistry	07.14	07.15 Waste Release, Chemistry	07.16 Waste Release, Chemistry	07.17 Waste Release, Chemistry	07.18 Chemistry	07.19	07.20	07.21	07.22	07.23	07.24	07.25	07.26
08	08.01	08.02	08.03 Degradation, Oxidation	08.04	08.05	08.06 Oxidation, Waste Release	08.07 Degradation, Chemistry	Gaseous Phases	08.09	08.10	08.11	08.12 Degradation, Waste Release	08.13	08.14	08.15	08.16	08.17	08.18	08.19	08.20	08.21	08.22	08.23	08.24	08.25 Exposure	08.26 Dose
09	09.01	09.02	09.03	09.04 Geometry	09.05	09.06	09.07	09.08	SDU Columns	09.10	09.11	09.12 Flow Rates	09.13	09.14	09.15	09.16	09.17	09.18	09.19	09.20	09.21	09.22	09.23	09.24	09.25	09.26
10	10.01	10.02	10.03 Flow Rates	10.04	10.05	10.06	10.07	10.08	10.09	SDU Joints/ Waterstops	10.11	10.12 Flow Rates	10.13 Flow Rates	10.14	10.15	10.16 Flow Rates	10.17	10.18	10.19	10.20	10.21	10.22	10.23	10.24	10.25	10.26
11	11.01	11.02	11.03	11.04	11.05	11.06	11.07	11.08	11.09	11.10	SDU Interior Liner	11.12	11.13	11.14	11.15	11.16	11.17	11.18	11.19	11.20	11.21	11.22	11.23	11.24	11.25	11.26
12	12.01	12.02	12.03 Flow Rates	12.04	12.05 Flow Rates, Degradation	12.06 Oxidation	12.07	12.08	12.09	12.10 Flow Rates	12.11	SDU Walls and Floor	12.13 Flow Rates	12.14	12.15	12.16 Flow Rates, Waste Release	12.17	12.18	12.19	12.20	12.21	12.22	12.23	12.24	12.25	12.26
13	13.01	13.02	13.03	13.04	13.05	13.06	13.07	13.08	13.09	13.10	13.11	13.12 Flow Rates	Upper Mud Mat	13.14 Flow Rates	13.15 Flow Rates	13.16 Flow Rates	13.17	13.18	13.19	13.20	13.21	13.22	13.23	13.24	13.25	13.26
14	14.01	14.02	14.03	14.04	14.05	14.06	14.07	14.08	14.09	14.10	14.11	14.12	14.13 Flow Rates	Liner Between Mud Mats	14.15 Flow Rates	14.16	14.17		14.19	14.20	14.21	14.22	14.23	14.24	14.25	14.26
15	15.01	15.02	15.03	15.04	15.05	15.06	15.07	15.08	15.09	15.10	15.11	15.12	15.13	15.14 Flow Rates	Lower Mud Mat	15.16 Flow Rates, Chemistry	15.17 Flow Rates, Chemistry,	15.18 Flow Rates, Chemistry,	15.19	15.20	15.21	15.22	15.23	15.24	15.25	15.26
16	16.01	16.02	16.03	16.04	16.05	16.06	16.07 Chemistry	16.08	16.09	16.10 Flow Rates	16.11	16.12 Flow Rates, Oxidation	16.13 Flow Rates	16.14	16.15 Flow Rates	Backfill	16.17 Chemistry	16.18 Chemistry, Transport	16.19	16.20	16.21	16.22	16.23	16.24	16.25	16.26
17	17.01	17.02	17.03	17.04	17.05	17.06	17.07	17.08	17.09	17.10	17.11	17.12	17.13	17.14	17.15	17.16 Chemistry	Groundwater Chemistry	17.18 Chemistry, Transport	17.19 Chemistry, Transport	17.20 Chemistry, Transport	17.21 Chemistry, Transport	17.22	17.23	17.24	17.25	17.26
18	18.01	18.02	18.03	18.04	18.05	18.06	18.07	18.08	18.09	18.10	18.11	18.12	18.13	18.14	18.15 Flow Rates	18.16 Flow Rates	18.17 Chemistry, Transport	Vadose Zone	18.19 Flow Rates, Geometry	18.20	18.21	18.22	18.23	18.24	18.25	18.26
19	19.01	19.02	19.03	19.04	19.05	19.06	19.07	19.08	19.09	19.10	19.11	19.12	19.13	19.14	19.15	19.16	19.17	19.18 Geometry	Saturated Zone	19.20 Transport	19.21 Transport	19.22	19.23	19.24	19.25	19.26
20	20.01	20.02	20.03	20.04	20.05	20.06	20.07	20.08	20.09	20.10	20.11	20.12	20.13	20.14	20.15	20.16	20.17	20.18	20.19	1-Meter or 100-Meter Well	20.21	20.22 Contamination	20.23 Contamination	20.24 Contamination	20.25 Exposure	20.26 Dose
21	21.01	21.02	21.03	21.04	21.05	21.06	21.07	21.08	21.09	21.10	21.11	21.12	21.13	21.14	21.15	21.16	21.17	21.18	21.19	21.20	Surface Streams	21.22	21.23	21.24	21.25 Exposure	21.26 Dose
22	22.01	22.02	22.03	22.04	22.05	22.06	22.07	22.08	22.09	22.10	22.11	22.12	22.13	22.14	22.15	22.16	22.17	22.18 Contamination	22.19	22.20	22.21	Soil	22.23 Contamination	22.24 Contamination	22.25 Exposure	22.26
23	23.01	23.02	23.03	23.04	23.05	23.06	23.07	23.08	23.09	23.10	23.11	23.12	23.13	23.14	23.15	23.16	23.17	23.18	23.19	23.20	23.21	23.22	Vegetation	23.24 Contamination	23.25 Exposure	23.26
24	24.01	24.02	24.03	24.04	24.05	24.06	24.07	24.08	24.09	24.10	24.11	24.12	24.13	24.14	24.15	24.16	24.17	24.18	24.19	24.20	24.21	24.22	24.23	Livestock	24.25 Exposure	24.26
25	25.01	25.02	25.03	25.04	25.05	25.06	25.07	25.08	25.09	25.10	25.11	25.12	25.13	25.14	25.15	25.16	25.17	25.18	25.19	25.20 Human Behavior, Exposure	25.21	25.22	25.23	25.24	Human Behavior	25.26 Human Behavior
26	26.01	26.02	26.03	26.04	26.05	26.06	26.07	26.08	26.09	26.10	26.11	26.12	26.13	26.14	26.15	26.16	26.17	26.18	26.19	26.20	26.21	26.22	26.23	26.24	26.25 Dose	Exposure/ Risk

After identifying the LDEs and placing them diagonally within the IM (blue cells in Figure 4.1-5), interactions and relationships between the LDEs were identified. These interactions and relationships are the ODEs and were also entered into the IM (yellow cells in Figure 4.1-5). Descriptions for each of the LDEs and ODEs are available within the *Conceptual Model Development for the Saltstone Disposal Facility Performance Assessment* report. [SRR-CWDA-2018-00006]

This IM served as a tool for ensuring that all of the relevant FEPs identified during the screening process are addressed. To ensure this, a "FEPs Audit" was performed. The elements and interactions within the IM were compared against the screened-in FEPs (see Table 4.1-5). Figure 4.1-6 provides an overview of the FEPs auditing process.

Essentially, FEPs that were outside the context of the Central Scenario were organized into Alternative Scenarios. These Alternative Scenarios were then used to inform the development of ACMs. Nine ACMs were developed based on nine Alternative Scenarios, as described in Section 4.6:

- Early Releases Scenario,
- Infiltration Scenario,
- Fast Flow Paths through SDUs Scenario,
- Fast Flow Paths through Ground Water Scenario,
- No Closure Cap Scenario,
- Stratified Saltstone Scenario,
- Perched Water Scenario,
- Colloid Transport Scenario, and
- Inadvertent Human Intruder (IHI) Scenario.

The conceptual models from the Central Scenario and each of the Alternative Scenarios were then used to develop individual modeling cases as depicted within Figure 4.1-7. For example, within the context of the Central Scenario, three modeling cases were developed:

- The Realistic Case which makes input assumptions based on best estimate values regardless of defensibility;
- The Pessimistic Case which makes input assumptions that are biased towards increasing the dose results to maximize defensibility; and
- The Compliance Case which assumes a combination of the most probable and defensible (MPAD) input values and is used for demonstrating compliance to performance objectives.

Figure 4.1-6: FEPs Auditing Process for Conceptual Model Development

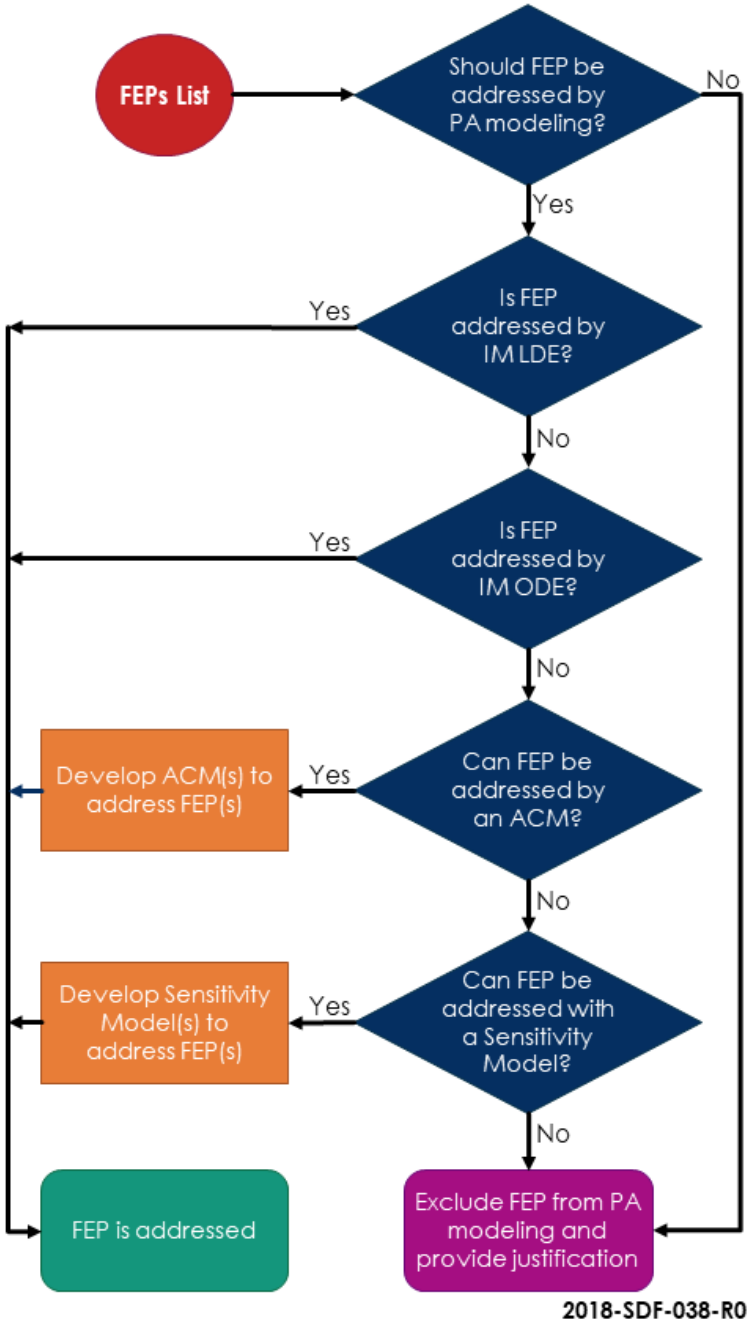

Figure 4.1-7: Overview of Modeling Case Development

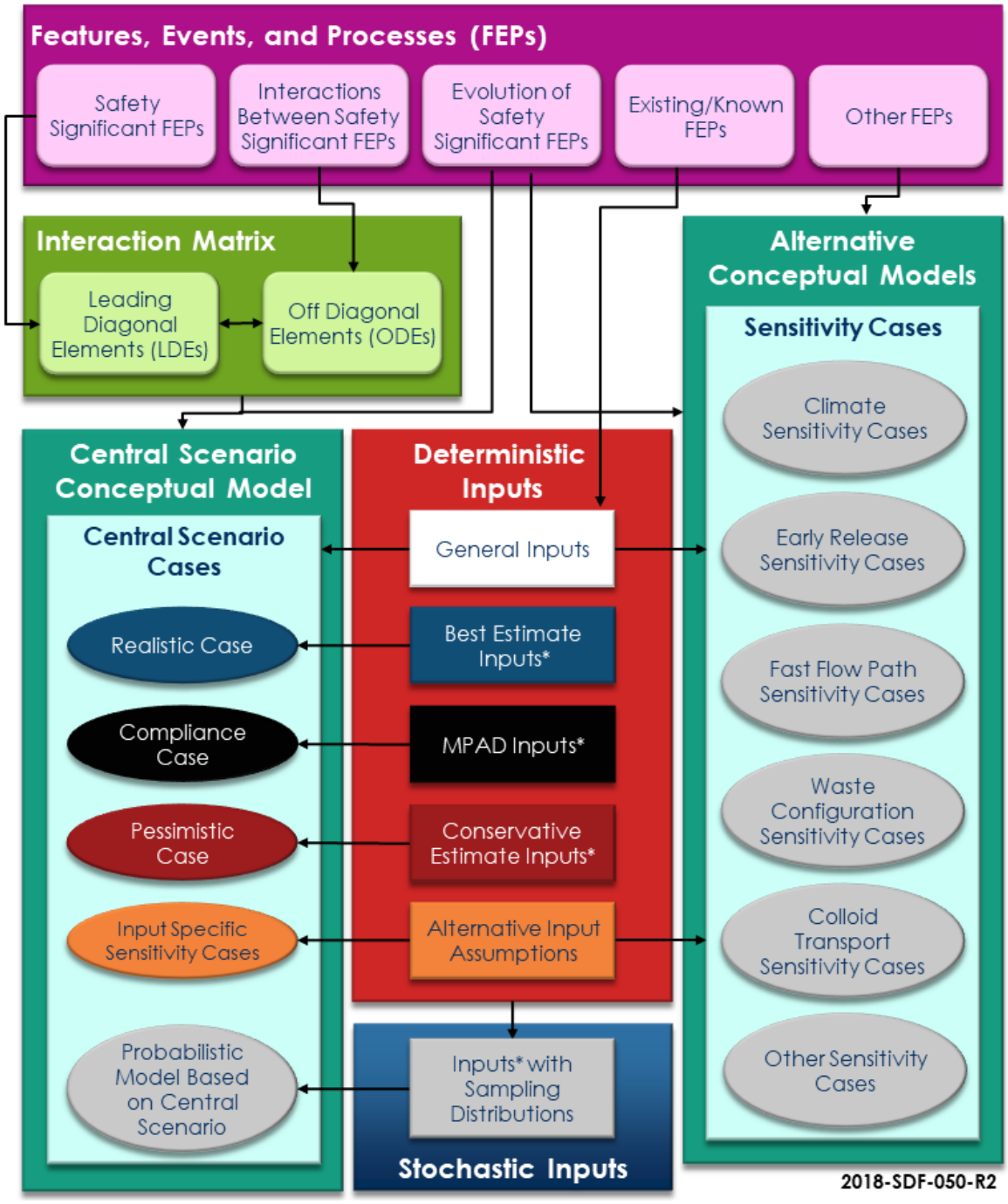

Note: * For selected inputs to the Central Scenario cases, see Section 5.8.1. For the inputs with sampling distributions, see Section 5.7.1. All other inputs are considered general inputs and are defined throughout Sections 4.3 and 4.4.

A selection of the remaining FEPs (i.e., those not addressed within the either the Conceptual Model for the Central Scenario or the ACMs) were then used to develop additional sensitivity cases:

- A sensitivity case was developed to consider potential dose impacts from the SDU 4 releases described in SRNL-L3200-2017-00107 and SRNL-STI-2018-00643 (to address FEP 6.4.03), see the "Early Release Case 2" in Section 5.8.9.1.
- A sensitivity case was developed to evaluate the impacts from a collapsed roof due to potential void space within the SDU (to address FEP 3.8.02 and FEP 6.4.07), see Section 5.8.9.3.

Finally, a few sensitivity cases were recommended within *Conceptual Model Development for the Saltstone Disposal Facility Performance Assessment*. (SRR-CWDA-2018-00006), but did not end up being explicitly modeled. Regardless of whether or not they were modeled, these were each given consideration to address the respective FEPs:

- A sensitivity case was recommended to evaluate the potential impacts from the discrete capping of specific SDUs (to address FEP 3.2.08), as is discussed in Section 5.8.2.4.
- A sensitivity case was recommended to evaluate alternative SDU designs and/or SDF layouts (to address FEP 3.2.07 and FEP 4.1.06). Any significant changes to SDU designs or the planned SDF layout would require additional evaluation via appropriate change control processes (e.g., Unreviewed Waste Management Question (UWMQ) Evaluation, Special Analysis, PA revision, or equivalent process) to disposition such changes. Therefore, because this PA reflects the most current SDU designs and SDF layout, consideration of alternatives is not necessary.
- An evaluation of the potential impacts of acid rain (to address FEP 2.7.06) was considered as discussed in Section 5.8.9.8.
- A sensitivity case was recommended to evaluate the impacts from leaving grout transfer lines in place within the SDF (to address FEP 3.3.07). This will be addressed by disposal operations as future closure plans are developed. If necessary, once details are available, a Special Analysis or future PA revision may be developed to better disposition this possibility.

For more information and additional details related to conceptual model development, see the *Conceptual Model Development for the Saltstone Disposal Facility Performance Assessment*. [SRR-CWDA-2018-00006]

4.1.3 Mathematical Model Development

Mathematical models define the governing equations and formulas used to translate (or abstract) the conceptual models from qualitative descriptions into quantifiable calculations. Development of each mathematical model is explicit to respective submodels which represent components of the overall system. As such, readers should refer to the discussions for each submodel for the respective details as provided in Section 4.4. An overview of each submodel supporting the SDF PA is provided in Section 4.1.5.

4.1.4 Implementation Via Submodels

Once the mathematical models are defined, subject matter experts and/or modelers implement those mathematical models into various modeling software (or equivalent computational platform). Each set of implemented mathematical models represents a submodel. The primary submodels used for this SDF PA are:

- Closure Cap Model (see Section 4.4.1)
  - Used to estimate infiltration rates through the closure cap based on surface conditions and closure cap properties.
  - Developed using WinUNSAT-H software and Excel.
- Cementitious Degradation Model (see Section 4.4.2)
  - Used to estimate degradation rates for SDU concrete and saltstone, based on cementitious material properties and the chemical environmental conditions.
  - Developed using literature models via Excel.
- Contaminant Release Model (see Section 4.4.3)
  - Used to predict chemical transitions (e.g., pH, Eh) in SDU concrete and saltstone, and corresponding release rates for contaminants.
  - Developed using The Geochemist's Workbench (GWB) software.
- Vadose Zone Flow Model (see Section 4.4.4)
  - Used to develop flow rates through SDU concrete, saltstone, backfill, and vadose zone soil based on infiltration rates and cementitious degradation rates.
  - Developed using PORFLOW software.
- Vadose Zone Transport Model (see Section 4.4.5)
  - Used to estimate contaminant fluxes from the SDUs into the natural environment based on flow rates, contaminant release rates, and contaminant transport properties.
  - Developed using PORFLOW software for Central Scenario cases and selected deterministic sensitivity models.
  - Developed using GoldSim software for probabilistic modeling and selected deterministic sensitivity models.
- Aquifer Transport Model (see Section 4.4.6)
  - Used to simulate saturated zone transport and to estimate contaminant concentrations at the points of assessment based on ground water flow conditions and contaminant fluxes.
  - Developed using PORFLOW software for Central Scenario cases and selected deterministic sensitivity models.
  - Developed using GoldSim software for probabilistic modeling and selected deterministic sensitivity models.
- Air Pathway Release Model (see Section 4.4.7)
  - Used to estimate gaseous ground surface fluxes for volatile radionuclides.
  - Developed using GoldSim software.
- Dose and Exposure Pathways Model (see Section 4.4.8)

- Used to convert concentrations at the points of assessment into dose estimates based on the assumed behaviors of a hypothetical human receptor.
- Developed using GoldSim software.

As with the development of the mathematical models, the implementation via submodels is explicit to each submodel. As such, readers should refer to the discussions for each submodel for the respective details as provided in Section 4.4.

4.1.5 PA Model Development (Integration of Submodels)

Each submodel will require explicit inputs and provide explicit outputs. Many submodels use the same or similar inputs, such that consistent assumptions are necessary. In order to fully integrate these submodels into a comprehensive SDF PA Model, these explicit inputs and outputs must be identified. Figure 4.1-8 provides a high-level overview of the key inputs and outputs from each submodel, and how they interconnect.

More discussion on the key assumptions is provided in Section 2.7.

Figure 4.1-8: Overview of Submodel Integration for the SDF PA

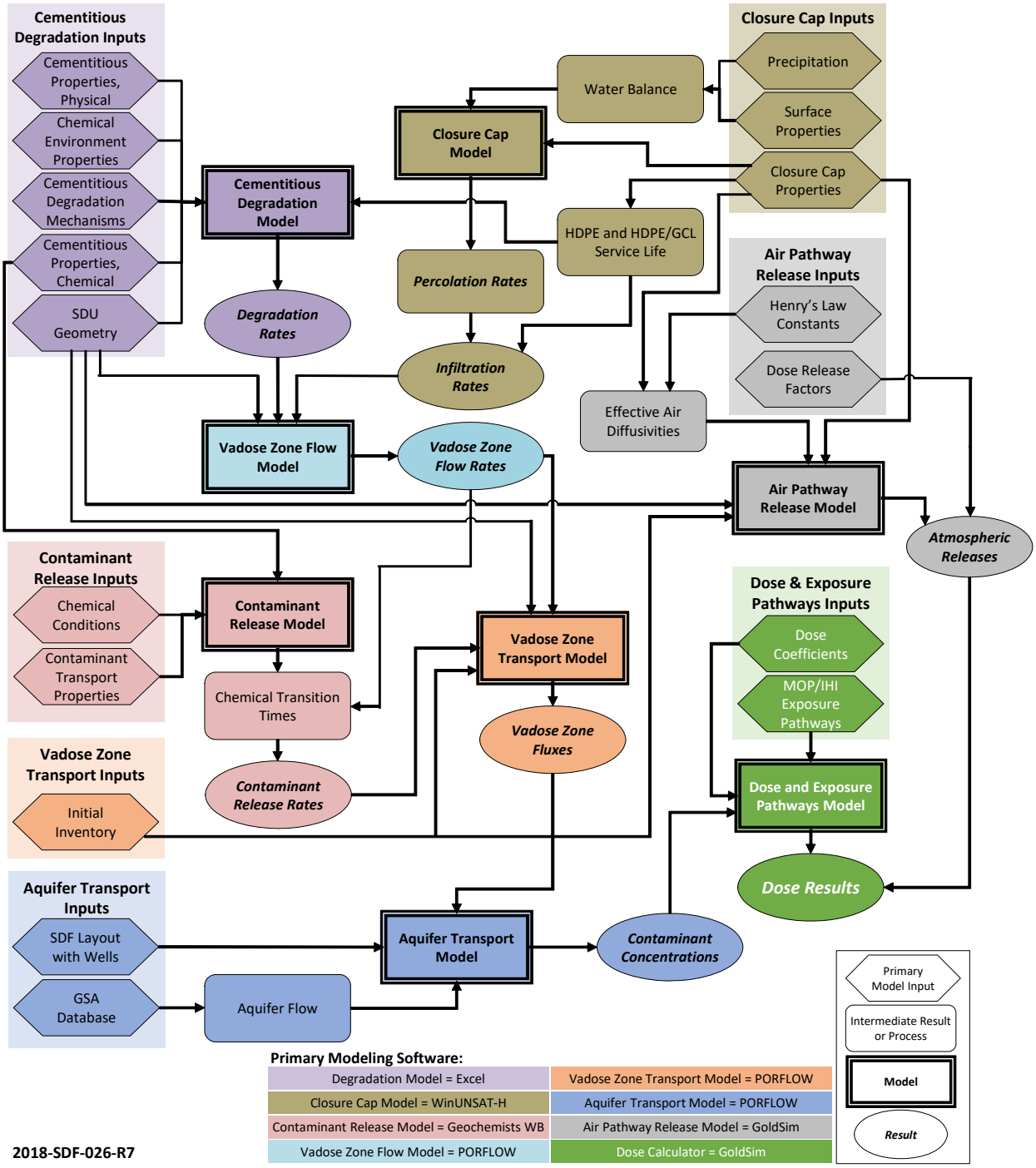

4.2 Modeling Codes

In the process of completing the SDF PA, a variety of modeling codes were used to perform various media transport, radiological dose, and ground water concentration calculations to demonstrate compliance with performance objectives and risk evaluations. The purpose of this

section is to provide a brief description for each modeling code and to identify the relevant software quality assurance documents. These descriptions include the function of the code and the associated manuals or technical documents.

4.2.1 Software Quality Assurance

The hierarchy of the SRS Quality Assurance (QA) documents is described in this section.

4.2.1.1 QA Overview

The *Quality Assurance Manual* 1Q provides the structure and procedures for achieving and verifying the SRS requirements for quality. The manual consists of a series of QA procedures that describe applicable QA requirements. 1Q Manual, Procedure 2-1, *Quality Assurance Program*, Section 5.2 states that the QA program has been developed to be responsive to the requirements of DOE O 414.1D and DOE *Nuclear Safety Management*, Title 10 CFR 830, Subpart A, *Quality Assurance Requirements*. [1Q Manual, Procedure 2-1]

Due to the size and complexity of SRS and its varied products, services, and missions, the QA program has been defined in a standard framework of company policy, procedures, and instructions to be used by the implementing organizations to perform quality-related activities. [1Q Manual, Procedure 2-1]

4.2.1.2 Software QA

Software QA is conducted in accordance with the requirements of the 1Q Manual, Procedure 20-1 (*Software Quality Assurance*). All software developed onsite at SRS is qualified through the development and execution of the Software Quality Assurance Plans (SQAPs). Due to the graded approach for software QA, some software codes which were developed offsite also have SQAPs associated with them while some do not. Regardless, verification testing was performed to verify the functionality of each software code. The discussion of each modeling code used (see Section 4.2.2) includes references to the appropriate SQAP or verification testing documents.

4.2.1.3 Model Checking

The E7 Manual, *Conduct of Engineering Manual*, Procedure 2.60, *Technical Reviews,* is the QA implementing procedure for performing technical reviews of SRS models developed for the SDF PA. This procedure defines the processes used at SRS to verify the inputs and outputs for the different modeling codes. The end use of data drives the level of review required. Design Verification, the highest-level review, must be performed for work affecting Safety Significant/Safety Class systems. Design Check is the next lower level of review and is required for all Production Support and General Service design output documents. Since the work associated with the PA and associated documents are not related to Safety Significant or Safety Class systems, the Design Check represents the appropriate level of rigor.

During a Design Check, the technical accuracy of the design document is assured by performing the following activities:

- A mathematical check, if appropriate;
- A review for correct use of technical input, including quality requirements;
- A check for appropriate use of methods, computer programs, etc.;
- A review of the approach used and reasonableness of the output; and
- An administrative check (e.g., page numbers, format).

To perform a Design Check, the checker must meet the following criteria:

- Cannot be a participant in the development of the portion of the document being checked (e.g., sufficiently independent of the document section preparation),
- Must be knowledgeable in the area of the design or analysis for which they review, and
- Must be capable of performing similar design or analysis activities.

4.2.2 Modeling Codes Used

Six primary modeling codes were used to support the SDF PA, as discussed below. These are WinUNSAT-H, The Geochemist's Workbench, PORFLOW, GoldSim, and CAP88-PC. In addition to these modeling codes, Microsoft Excel is also used extensively for performing selected analytical calculations. The following discussions provide a high-level overview of how these modeling codes were used in the PA. More detailed discussions of specific formulas, calculations, or equations performed by this software are provided within the modeling discussions throughout Section 4.4.

4.2.2.1 WinUNSAT-H (Closure Cap Modeling)

WinUNSAT-H is a Windows implementation of the UNSAT-H code. The UNSAT-H code was developed by Pacific Northwest National Laboratory (PNNL) using FORTRAN (coding language). [SRNL-STI-2009-00572] UNSAT-H is a variably saturated flow code that is used to predict unsaturated flow, water redistribution, and atmospheric interactions for the design of landfill and burial covers (i.e., closure caps). WinUNSAT-H requires as inputs weather information, soil properties, and closure cap design data. It provides water balance estimates for surface runoff, evapotranspiration, lateral drainage, vertical percolation (i.e., infiltration), hydraulic head, and water storage for the evaluation of various landfill designs. [SRRA107772-000009]

WinUNSAT-H has been used extensively over the past two decades for predicting the hydrology of covers for waste containment systems and is a widely used model for design of water balance final covers. WinUNSAT-H has been used for a diverse range of climates and has been verified using data sets from large-scale field experiments. [SRRA107772-000009]

For the PA, WinUNSAT-H was used to determine the percolation rate, or deep annual drainage rate, for two climate conditions for the closure cap – average climate conditions based on typical weather conditions over the past 50 years and wetter climate conditions based the wettest 10-year period over the past 50 years. The percolation rate for the typical climate conditions was approximately 400 mm/yr, while the wetter climate conditions

yielded a rate of approximately 650 mm/yr (see Section 4.4.1). These intermediate results from WinUNSAT-H were then coupled with the Giroud-Houlihan analytical solution (see Section 4.4.1) to estimate infiltration rates through the engineered closure cap. [SRRA107772-000009] These infiltration estimates are used as inputs to the subsequent flow and contaminant transport models (i.e., PORFLOW models).

Verification testing of this software is documented in *UNSAT-H Version 3.0: Unsaturated Soil Water and Heat Flow Model - Theory, User Manual, and Examples*. [PNNL-13249] As the closure cap model was developed offsite by a third-party vendor, the approach for peer reviews and software quality assurance controls are described in the vendor-prepared document *UVA Quality Assurance Document for Research Conducted in Support of SRR* (SRRA107772-000005).

4.2.2.2 CBP Software Toolbox (Cementitious Degradation Model)

The DOE Cementitious Barriers Partnership (CBP) Software Toolbox was not explicitly used in the PA, but this is worth noting because it has been used for cementitious degradation modeling in earlier iterations of SDF modeling, specifically, the FY2013, FY2014, and FY2016 SDF SAs. However, for this SDF PA cementitious degradation was simulated using analytic solutions, as documented in *Degradation of Saltstone Disposal Unit Cementitious Materials* (SRNL-STI-2018-00077). These analytical solutions were calculated within Microsoft Excel.

While this approach did not explicitly rely on the CBP Software Toolbox, the analytical solutions were supported by characterization data developed for the CBP Software Toolbox. Further, several intermediate results (e.g., degradation rates) were compared to earlier analyses which did use the CBP Software Toolbox. These comparisons were favorable, showing that the analytic solutions from the Microsoft Excel file produced degradatuib rates were either equivalent to or higher than the respective values from the CBP Software Toolbox. [SRNL-STI-2018-00077, SRNL-STI-2015-00236] This Cementitious Degradation Model is described in Section 4.4.2.

Independent design checking of these cementitious degradation calculations (i.e., technical checking of the Microsoft Excel file) was performed in accordance with SRS Manual E7, *Conduct of Engineering*, Procedure 2.60, *Technical Reviews* as indicated on the signature page of SRNL-STI-2018-00077 and documented in the *Performance Assessment for the Saltstone Disposal Facility at the Savannah River Site: Quality Assurance Report* (SRR-CWDA-2018-00068).

4.2.2.3 The Geochemist's Workbench (Contaminant Release Model)

The Geochemist's Workbench (GWB), Release 10.0, is a geochemical modeling software originally developed by the University of Illinois and is now maintained by Aqueous Solutions, LLC (Bethke and Yeakel, 2015). This software is used for manipulating chemical reactions, calculating stability diagrams and the equilibrium states of natural waters, tracing reaction processes, modeling reactive transport, plotting the results of

these calculations, and storing the related data. The software contains tools for balancing reactions, calculating activity diagrams, computing speciation in aqueous solutions, plotting the results of these calculations, and storing the related data (Bethke and Yeakel, 2015). The SQAP for GWB Release 10.0 is covered by the *Software Quality Assurance Plan for The Geochemist's Workbench®*. [Q-SQP-A-00007] Previous SQAPs were also prepared for earlier releases (SRR-CWDA-2010-00154, B-SQP-A-00068); tests from each release shows the same results, demonstrating that this is a matured software package that produces consistent results.

As described in Section 4.4.3, this code was used to estimate chemical conditions, such as the transition times associated with oxidation. These calculations supported the conceptual model of contaminant releases from the saltstone waste form. [SRNL-STI-2018-00586]

4.2.2.4 PORFLOW (Deterministic Flow and Transport Modeling)

PORFLOW is a commercial computational fluid dynamics tool developed by Analytic & Computational Research, Inc. PORFLOW numerically solves problems involving transient or steady state fluid flow, heat, salinity, and mass transport in multi-phase, variably saturated, porous, or fractured media with dynamic phase change. PORFLOW was used in the SDF PA modeling to calculate fluid flow and contaminant transport in the vadose and saturated zones. PORFLOW transport results were used in subsequent models to calculate radiological doses and perform human health and ecological risk evaluations. PORFLOW flow results were also used to conduct probabilistic simulations of contaminant transport via GoldSim, another computational tool.

PORFLOW accommodates alternate fluid and media property relations and complex and arbitrary boundary conditions. The geometry may be two-dimensional or three-dimensional, Cartesian, or cylindrical, and the mesh may be structured or unstructured, giving maximum flexibility to the user. Version 6.42.9 of PORFLOW was used to accomplish SDF PA simulations. Version 6.42.9 is the latest site version of PORFLOW and contains the "STRAtified" aquifer dispersion model and the greater limit on the number of "STATistics" files, which were identified as necessary for the prior work. PORFLOW was used at SRS for calculations supporting the FTF and HTF PAs and by Idaho National Laboratory for analyses supporting operational closure of the Tank Farm facility and for previous SDF PA and SA modeling work. [SRS-REG-2007-00002, SRR-CWDA-2010-00128, DOE/ID-10966, SRR-CWDA-2009-00017, SRR-CWDA-2013-00062, SRR-CWDA-2014-00006, SRR-CWDA-2016-00072]

For the SDF PA, PORFLOW is an appropriate code because it can accommodate calculations in both the saturated and unsaturated zones and has the ability to simulate first-order decay and progeny in-growth associated with radionuclide chains, which is necessary for calculations involving radioactive stabilized contaminant disposal.

The following provides documentation of testing for the current version for use: *PORFLOW 6.42.9 Testing and Verification Document* (SRNL-STI-2018-00275). The SQAP for

PORFLOW is covered by the *PORFLOW Software Quality Assurance Plan* (G-SQP-A-00012). [G-SQP-A-00012]

Accompanying PORFLOW is MESH3D: a grid refinement tool developed by SRNL for extracting a portion of a PORFLOW model grid and flow solution and optionally refining the cutout grid by subdividing cells. [Q-SQP-G-00003] The velocity and saturation fields are refined using a mass-conserving interpolation method. MESH3D is used to extract and refine a portion of the GSA Model in the vicinity of SDF for performing higher resolution transport simulations of plume migration from SDU sources out to 100 meters. Software design, use, testing, and QA plan for MESH3D are addressed by Q-SQP-G-00003.

The design check of the data used to perform the PORFLOW modeling is documented in SRNL-L3200-2018-00177 and additional QA reviews are described in Section 9, and all technical findings have been satisfactorily resolved. The scope of the design check includes:

- Vadose Zone Flow Model (see Section 4.4.4) setup and inputs,
- Vadose Zone Transport Model (see Section 4.4.5) setup and inputs, and
- Aquifer Transport Model (see Section 4.4.6) setup and inputs.

4.2.2.5 GoldSim (Probabilistic and Deterministic Sensitivity Transport Modeling and Dose Modeling)

GoldSim is a commercial program developed by GoldSim Technology Group LLC (GTG). It is a user-friendly, graphical, Windows-based program designed for carrying out dynamic probabilistic simulations of complex systems to support management and decision-making in engineering, science, and business. In addition to the probabilistic capabilities, it also has deterministic capabilities that are used for performing dose calculations and deterministic sensitivity modeling.

GoldSim was used to assist in developing uncertainty analyses for the SDF PA. The parameters modeled in GoldSim identified important input parameters in the ground water transport model. GoldSim used the flow field outputs from PORFLOW to perform transport calculations and for evaluating the importance of input parameters. GoldSim was also used to calculate the air pathway releases (see Section 4.4.7). [SRR-CWDA-2018-00025] Finally, GoldSim was also used to estimate doses using the contaminant transport results from either PORFLOW or GoldSim (see Section 4.4.8).

GoldSim was designed to facilitate the construction of large, complex models. The user can build a model of a system in a hierarchical, modular manner, such that the model can evolve and add detail as more knowledge regarding the system is obtained. Other features, such as the ability to manipulate arrays, the ability to "localize" parts of a model, and the ability to assign version numbers to a model that is constantly being modified and improved, further facilitate the construction and management of large models. GoldSim has an extensive internal database of units and conversion factors allowing the user to enter data and display results in any units and/or define customized units. GoldSim

ensures dimensional consistency in models and carries out all the unit conversions internally, eliminating the need to carry out error-prone unit conversions. The user can dynamically link external programs or spreadsheets directly into a SDF GoldSim Model. In addition, GoldSim was specifically designed to support the addition of customized modules (program extensions) to address specialized applications, such as contaminant transport.

GoldSim Version 12.1 is used for the PA porous medium transport and dose analyses because: 1) its capabilities meet program needs, 2) it allows for ease of input changes and output visualization, and 3) it is used by other DOE sites (e.g., Nevada Test Site, Yucca Mountain Project, and Hanford PAs) and the NRC.

The GTG provides a user's guide (GTG-2018a) and a separate guide for contaminant transport calculations (GTG-2017b). The SQAP for the GoldSim software is covered by B-SQP-C-00002. Data verification for the SDF GoldSim model is covered under SRR-CWDA-2018-00068.

A dynamic link library, *ReadFlowFields.DLL*, was also developed for use in conjunction with the area-specific GoldSim models. [B-SQP-C-00003] Functionally, this software is used to read data into a GoldSim model file from an external input file. For the SDF GoldSim Model, the dynamic link library is used to read in flow data from files generated using the Vadose Zone Flow Model (see Section 4.4.4). The SQAP for the *ReadFlowFields.DLL* is covered by B-SQP-C-00003.

4.2.2.6 CAP88-PC (Air Pathway Release Modeling)

The CAP88-PC computer software is a set of computer programs, databases, and associated utility programs developed by the EPA for estimating dose and risk from radionuclide emissions to air. CAP88-PC modeling was used in the SDF PA to estimate annual dose to human receptors based on atmospheric plume data using the radionuclide diffusion to the surface results from the air pathway release modeling performed with GoldSim (see Section 4.4.7). [SRR-CWDA-2018-00025, SRNL-STI-2008-00415]

The CAP88-PC software was developed by the EPA and used to demonstrate compliance with 40 CFR 61 *National Emissions Standards for Hazardous Air Pollutants*, Subpart H. CAP88-PC uses a modified Gaussian plume equation to estimate the average dispersion of radionuclides released from up to six sources at the same release location with different release heights. Assessments are done for a circular grid with a radius up to 50 miles.

A user's guide for CAP88-PC is available. [CAP88-PC_3.0] The SQAP for CAP88-PC used for the SDF PA calculations is covered by Q-SQP-A-00002. Validation testing for the latest version of the code is documented in *CAP88-PC Version 4 Testing Report*. [CAP88-PC_4.0]

4.3 General Model Inputs

As described in Section 4.1.5, various mathematical models were used to perform the calculations that are necessary for developing the PA. These submodels include:

- Closure Cap Model (Section 4.4.1),
- Cementitious Degradation Model (Section 4.4.2),
- Contaminant Release Model (Section 4.4.3),
- Vadose Zone Flow Model (Section 4.4.4),
- Vadose Zone Transport Model (Section 4.4.5),
- Aquifer Transport Model (Section 4.4.6),
- Airborne Pathway Release Model (Section 4.4.7), and
- Dose and Exposure Pathways Model (Section 4.4.8).

Each of these submodels and their specific inputs are discussed in detail throughout Section 4.4. Because many of these models use the same or similar inputs, Figure 4.1-8 provides an overview of model integration into the SDF PA.

The various modeling inputs used in these models are divided into three categories:

- Material Property Inputs (Section 4.3.1),
- Release and Transport Property Inputs (Section 4.3.2), and
- SDU-Specific Model Inputs (Section 4.3.3).

When developing inputs for PAs, there is often a trade-off between defensibility and realism, especially for parameters that may have more potential uncertainty. Where a range of values are presented, the general tendency of PA analysts is to err on the side of caution, thus selecting more defensible values. However, applying this approach for multiple parameter selections may have a compounding effect, providing model results which may be far removed from expected future conditions. While this approach may provide robust defensibility for establishing compliance, if PA models are too far removed from realistic or expected future conditions, they may become inappropriate to use in assessing actual risk.

Previous efforts to develop input parameters for the 2009 SDF PA (SRR-CWDA-2009-00017) and subsequent SDF SAs (SRR-CWDA-2013-00062, SRR-CWDA-2014-00006, and SRR-CWDA-2016-00072) have generally fallen into this approach of assigning values that were biased toward pessimistic or defensible assumptions. For the purposes of this PA, an alternative philosophy was adopted for the development of many key model inputs. Rather than recommending a single input value, a set of input values was recommended. The general philosophy was to develop three sets of recommended values:

- Best Estimate Values (i.e., the most realistic or expected) to reflect expected future conditions regardless of the level of defensibility and used to create a Realistic Case,
- Conservative Estimate Values (i.e., biased towards pessimistic results) to represent highly defensible modeling assumptions and used to develop a Pessimistic Case, and
- Compliance Values (i.e., using a reasonable combination of the most probable and defensible (MPAD) inputs), blending the Best Estimate approach with the Conservative Estimate approach to provide values recommended for the Compliance Case.

Note that most inputs used within these three modeling cases are the same for all three cases; the inputs that were varied between these cases focused only on those which were expected to have the greatest influence on the resulting long-term doses. For example, the thickness of the SDU

walls was not varied, because any uncertainty associated with SDU wall thicknesses is expected to be negligible and therefore would have a minimal impact on the resulting doses. The selection of the inputs to vary and the assignment of the specific values used within each set of inputs is generally based on engineering judgement, as informed by appropriate literature reviews, field observations, or laboratory data.

4.3.1 Material Property Inputs

Two types of materials are defined by the material property inputs within this section: soil materials (including the vadose zone) and cementitious materials.

4.3.1.1 Soil Property Inputs

As a modeling simplification, only a single set of input values are considered for these soil properties (i.e., there are not separate input values recommended for the Realistic Case, the Compliance Case, and the Pessimistic Case). The recommended values described below are equivalent to the best estimate values as informed by field observations and laboratory studies. Uncertainty associated with select soil properties is evaluated via the probabilistic modeling (see Section 5.7.1).

The vadose zone at the SDF can be divided into two regions, an Upper Vadose Zone and a Lower Vadose Zone. The Upper Vadose Zone (over 264 feet above MSL) consists of finer-grained sediments and typically displays a higher gamma ray, cone penetration test (CPT) friction ratio, and pore pressure response. The Lower Vadose Zone (below 264 feet above MSL) has a higher sand content and generally exhibits a lower gamma ray, CPT friction ratio, and pore pressure response.

For modeling, the depth of the vadose zone is defined as the distance from the base of the disposal unit to the water table and is presented in Table 4.3-1. As shown, the modeled values are generally as informed (For additional discussion of the model definition for the "base of the disposal unit" see Section 4.3.1.2.5.) The estimated water table elevations for individual SDUs are extracted from the GSA Model, using the "GSA_2018.LW" modeling case described in the *GSA from the Updated Groundwater Flow Simulations of the Savannah River Site General Separations Area* (SRNL-STI-2018-00643).

It should be noted that for SDUs 7, 8, 10, 11, and 12, the modeled depth of the vadose zone was assumed to be the same, based on an average depth from earlier estimates. Due to the equivalent designs, construction materials, and very similar depths, modeling efficiency within the vadose zone models was derived by simulating these as identical SDUs (see Sections 4.4.4 and 4.4.5). These differences in the vadose zone depths are expected to have a negligible impact to overall system performance.

Table 4.3-1: Estimated Depth of Vadose Zone for SDF Disposal Units for PORFLOW Modeling

SDF Disposal Unit	Disposal Unit Base Elevation (Feet above MSL) [d]	Estimated Elevation of Water Table (Feet above MSL)		Depth to Water Table (or Vadose Zone Thickness) (Feet)	
		Measured Well Data [e]	Based on GSA Model [d]	Based on Measured Well Data	As Modeled in PORFLOW
SDU 1 [a]	281.5	236	234.5	45.5	48
SDU 4 [a]	269	230	232.3	39	38.4
SDU Cell 2A	268	223	229	45	42
SDU Cell 2B	268	224	229.6	44	42
SDU Cell 3A	261	217	224.9	44	42
SDU Cell 3B	261	218	225.5	43	42
SDU Cell 5A	261	218	225.5	43	42
SDU Cell 5B	261	219	226.3	42	42
SDU 6	265	223	229	45	42
SDU 7 (future) [c]	265	228	231	37	36
SDU 8 (future) [c]	265	220	227.4	45	36
SDU 9 (future)[b]	250	220	227	30	23
SDU 10 (future) [c]	265	223	228.2	42	36
SDU 11 (future) [c]	265	226	230.7	39	36
SDU 12 (future) [c]	265	223	229	42	36

[W828993, C-CX-Z-0001, C-CG-Z-00027, C-CG-Z-00028, K-CLC-Z-00013, K-ESR-Z-00002, C-CG-Z-00048, G-AES-S-00004]

(a) Base elevation for SDUs 1 and 4 is at the bottom of the disposal unit floor slab and for the remaining SDUs at the bottom of the lower mud mat.

(b) Base elevation for SDU 9 is 15 feet lower than the other SDU 7 Type SDUs due to additional excavation requirements noted during the geotechnical evaluation for SDU 9. [K-ESR-Z-00010]

(c) SDUs 7, 8, and 10-12 used an average vadose thickness of 36 feet for PORFLOW modeling.

(d) Estimated water table elevations extracted from the GSA Model. [SRNL-STI-2018-00336, SRNL-STI-2018-00643]

(e) Measured well data based on 1Q 2018 measurments. [SRNS-TR-2018-00292]

The hydraulic properties of the soils surrounding and below the SDUs are required for the PA. Soil material properties required for modeling include:

- Saturated effective diffusion coefficient (D_e),
- Average total porosity,
- Average dry bulk density,
- Average particle density,
- Saturated horizontal hydraulic conductivity
- Saturated vertical hydraulic conductivity, and
- Moisture characteristic curves (MCCs).

Aside from the MCCs, these hydraulic properties are modeled as not changing over time because the relative stability of the soil grains and structure. Table 4.3-2 provides the hydraulic properties for the soil materials. Most of these material properties come directly from *Hydraulic Property Data Package for the E-Area and Z-Area Soils, Cementitious Materials, and Waste Zones* (WSRC-STI-2006-00198).

Table 4.3-2: Hydraulic Properties of Soils

Parameter	Sand Drain	Backfill	Upper Vadose	Lower Vadose	Gravel
Saturated Effective Diffusion Coefficient D_e (cm^2/sec)	8.0E-06	5.3E-06	5.3E-06	5.3E-06	9.4E-06
Average Total Porosity (%)	41.7	35	39	39	39
Average Dry Bulk Density (g/cm^3)	1.55	1.71	1.65	1.62	1.82
Average Particle Density (g/cm^3)	2.66	2.63	2.70	2.66	2.60
Saturated Horizontal Hydraulic Conductivity (cm/s)	5.0E-02	7.6E-05	6.2E-05	3.3E-04	1.5E-01
Saturated Vertical Hydraulic Conductivity (cm/s)	5.0E-02	4.1E-05	8.7E-06	9.1E-05	1.5E-01

[WSRC-STI-2006-00198, Table 5-18 and WSRC-STI-2008-00244, Section 5.4.4 (for the sand drain)]
Note: Within PORFLOW Vadose Zone modeling (Sections 4.4.4 and 4.4.5), the Lower Vadose Zone properties are assumed for properties defined as "Native Soils."

The saturated hydraulic conductivities and porosity of the sand drainage layer (see Sand Drain in Table 4.3-2) are based on the design specification for procured sands rather than on site-specific sand materials. [WSRC-STI-2008-00244] This material is used as a layer within the closure cap and as a layer above the SDU roofs for purposes of promoting lateral flow away from the SDUs.

Backfill surrounding the SDUs will be composed mostly of excavated soil from the Upper Vadose Zone that has been disturbed and compacted upon placement around the constructed SDUs. Rather than assuming properties based on the Upper Vadose Zone properties, backfill-specific properties were developed for modeling purposes. These properties were based on an analysis of E-Area and Z-Area soils, then applied an upscaling methodology to account for compaction. [WSRC-STI-2006-00198]

When materials are not fully saturated, the unsaturated portion of the material behaves like a sponge, pulling the available moisture into it. This is referred to as suction head or water potential. MCCs are used to define the relationships between water content (θ) and suction head (ψ). Under drier conditions, this suction head reduces the effective hydraulic conductivity. The characteristic curves for each of the soil materials are presented in Figure 4.3-1. These curves were developed using the van Genuchten function and parameters, as defined for the modeling described in *PORFLOW Simulations Supporting the Saltstone Performance Assessment Revision*. [SRNL-STI-2018-00652]

Figure 4.3-1: MCCs for Soil Materials

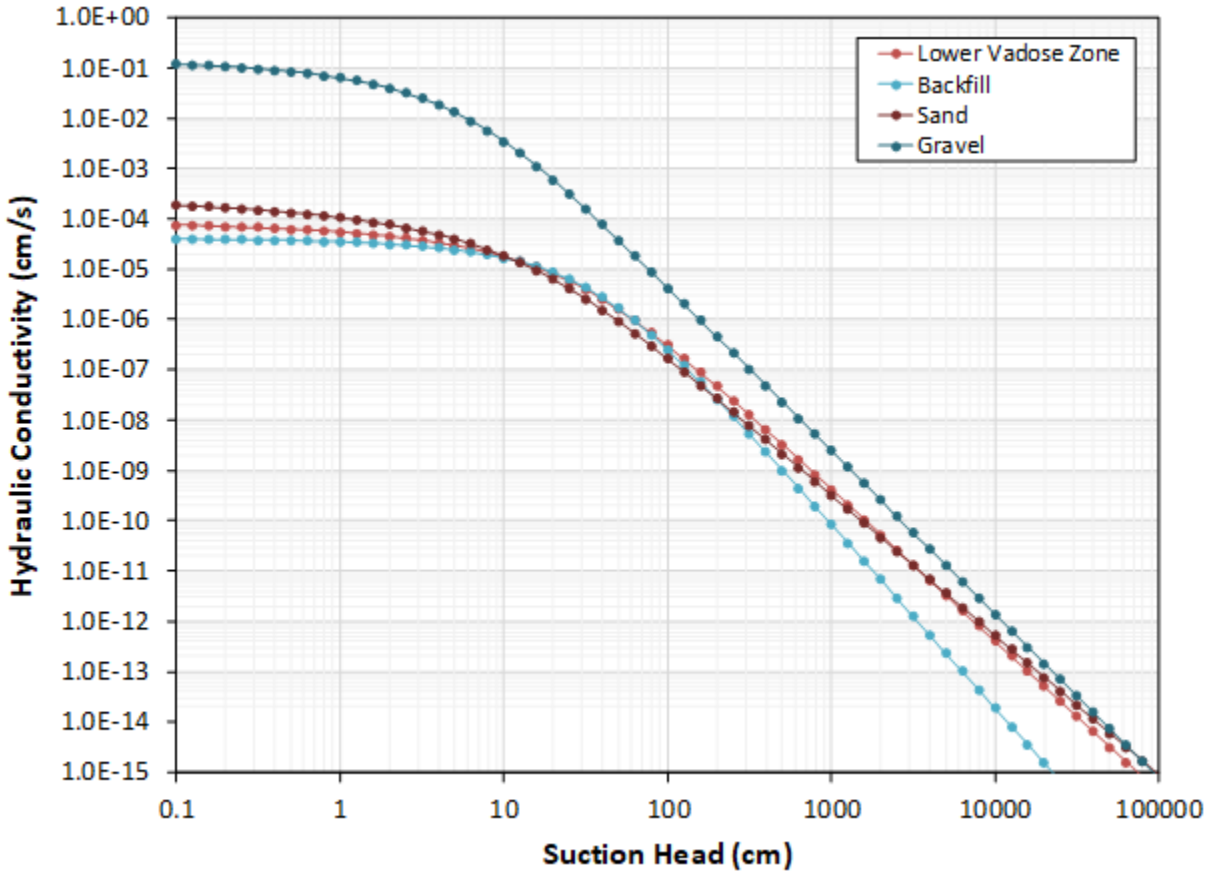

[SRNL-STI-2018-00652]

4.3.1.2 Cementitious Material Property Inputs

This subsection focuses on the following hydraulic properties of cementitious materials (i.e., the saltstone waste form and SDU concrete):

- Dry bulk density,
- Solid phase (or particle) density,
- Total porosity,
- Initial saturated hydraulic conductivity,
- Initial effective diffusion coefficient, and
- MCCs.

Previous modeling efforts used one set of assumptions for these parameters, regardless of the modeling approach. Since these parameters were not varied to reflect alternative modeling assumptions, all previous models applied one relatively pessimistic set of inputs, regardless of the assumed modeling conditions. As such, all resulting degradation calculations were biased towards faster degradation rates, regardless of any other variables. To establish a better baseline, ranges of potential input values were considered to better reflect the potnential for uncertainty.

The initial saturated hydraulic conductivity and the initial effective diffusion coefficient parameters both exhibit behaviors that can vary over relatively wide ranges (i.e., orders of magnitude), the other parameters considered (dry bulk density, solid phase density, and porosity) typically vary over relatively small ranges (i.e., less than a factor of 10).

The various material property inputs used, and their various justifications are presented in *Recommended Values for Cementitious Degradation Modeling to Support Future SDF Modeling* (SRR-CWDA-2018-00004). Table 4.3-3 provides a summary of the recommended material property inputs for compliance modeling, realistic modeling, and pessimistic modeling.

As an example for how these inputs were developed, the saturated hydraulic conductivities for the saltstone were developed based on recent the Dynamic Leaching Method (DLM) testing of saltstone core samples that were extracted from SDU 2A as well as laboratory-prepared simulant samples, developed using the formulation provided in Table 3.2-6. The DLM test is designed to force leachate through the interior of a saltstone monolith sample to mimic the eventual ingress of water into saltstone and establish the dynamic leaching behavior of saltstone contaminants. The empirical leaching data gathered from these studies is used to improve and supplement the contaminant release model discussed in Section 4.4.3.

In addition to providing empirical leaching data for saltstone samples, the DLM also allows for the saturated hydraulic conductivity of the sample to be measured throughout the duration of the experiment (on the order of months to years). This permits researchers to observe how a saltstone sample's saturated hydraulic conductivity changes over time as the monolith ages (i.e., as the chemistry of the pore solution and solid phase evolve with subsequent pore flushes). Examination of the test results indicated that aside from the saltstone simulant made with Holcim blast furnace slag (BFS), nearly all of the measured saturated hydraulic conductivity values were less than 1E-09 cm/s. On average, the saltstone simulants made with Lehigh BFS demonstrated the lowest saturated hydraulic conductivity value, and the field-emplaced saltstone cores from SDU 2A (which were made with Holicm BFS) decreased dramatically within two pore volume exchanges (Figure 4.3-2).

The *Property Data for Core Samples Extracted from SDU Cell 2A* (SRR-CWDA-2016-00051) reported saturated hydraulic conductivities for saltstone that were greater than 1.0E-09 cm/s. It is important to note these earlier tests used a method that had a minimum detection limit of 1.0E-09 cm/s. While nearly all the measurements were below this detection limit, mean values were calculated for each sample set by assuming a minimum value of 1.0E-09 cm/s; as such, the reported mean values for the sample sets were skewed high. The DLM test method developed by SREL was specifically designed to measure saturated hydraulic conductivities lower than 1.0E-09 cm/s.

While DLM data was collected from both radionuclide-spiked saltstone simulant samples and actual saltstone cores from SDU 2A, additional credence is placed on the latter data source given its pedigree. Therefore, given that both the saltstone simulant made with

Holcim BFS and the SDU 2A cores were produced with the same dry feed composition and BFS source, the saturated hydraulic conductivties measured from the SDU 2A cores are considered more definitive. Of the two SDU 2A core samples, the one with the higher saturated hydraulic conductivity values (Sample 2A - Core A in Figure 4.3-2) was selected to represent the MPAD value, while the sample with the lower saturated hydraulic conductivity (Sample 2A - Core B in Figure 4.3-2) was selected to represent the best estimate values. Note that Lehigh Samples A and C have similar values to the best estimate. Finally, the saltstone simulant sample made with the Holcim BFS, which showed the highest saturated hydraulic conductivity (Holcim in Figure 4.3-2), was selected for use in pessimistic modeling. [SRR-CWDA-2018-00004]

Figure 4.3-2: DLM-Measured Saturated Hydraulic Conductivity of Saltstone

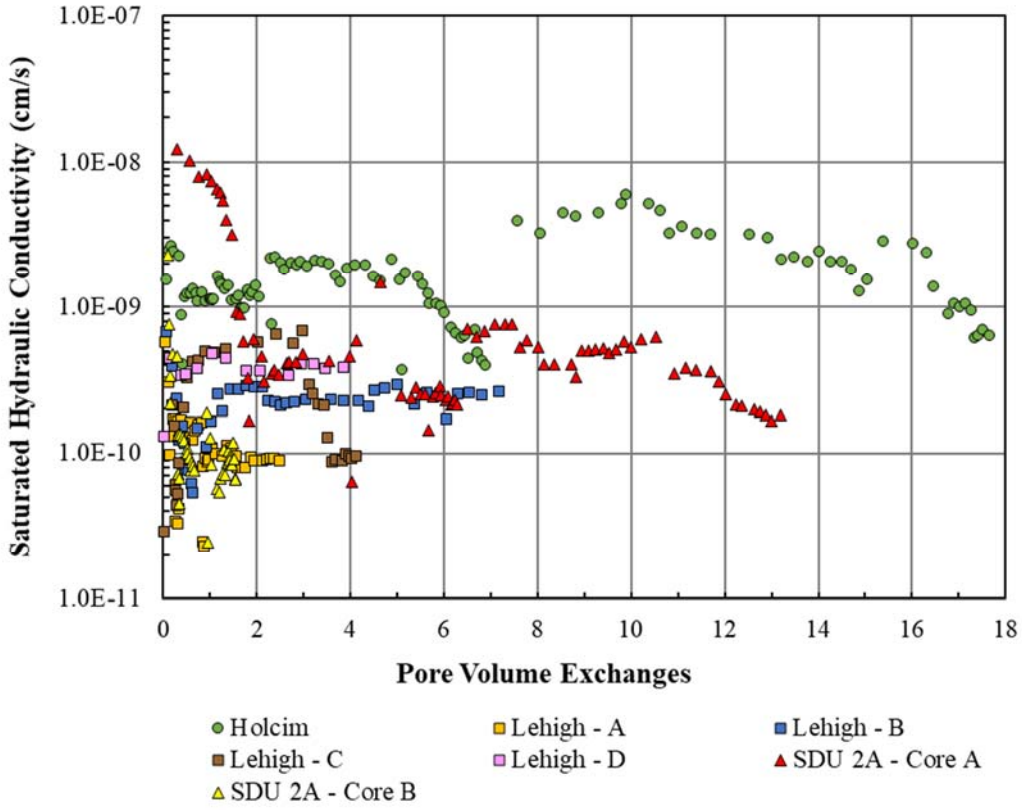

Similarly, the saturated hydraulic conductivities for the SDU concrete for future SDUs is based on recent testing performed on the new SDU concrete formulation from Table 3.2-5. [0000138886-000024] From these these tests, the Best Estimate value represents the average of the last measurement from each sample, the Conservative Estimate value represents the single highest measurement, and the MPAD value represents the average of the Best Estimate and the Conservative Estimate values. [SRR-CWDA-2018-00004] A similar approach was applied for the selection of the other values.

Table 4.3-3: Recommended Input Values for Cementitious Material Properties

Parameter	Unit	Saltstone	SDU 1/4 Concrete Floor	SDU 1/4 Concrete Walls	SDU 1/4 Concrete Roof	SDU Concrete for Existing* Cylindrical SDUs (Roof, Floor, Walls)	SDU Concrete for Future* Cylindrical SDUs (Roof, Floor, Walls)	SDU Concrete for Mud Mats and Columns
Global Values - For All Modeling								
Dry Bulk Density	g/cm^3	0.932	2.28	2.21	2.28	2.18	2.18	2.06
Solid Phase Density	g/cm^3	2.72	2.55	2.70	2.55	2.45	2.45	2.61
Total Porosity	unitless	0.656	0.106	0.181	0.106	0.110	0.110	0.211
MPAD Values - For Compliance Modeling								
Initial Saturated Hydraulic Conductivity	cm/s	5.00E-10	7.80E-10	4.10E-05	7.80E-10	1.40E-10	7.80E-10	5.00E-09
Initial Effective Diffusion Coefficient	cm^2/sec	1.30E-08	5.30E-08	5.30E-06	9.70E-08	5.30E-08	5.30E-08	3.90E-07
Moisture Characteristic Curve**	Not applicable	"Saltstone CV"	"High Qualtiy Concrete"	"High Qualtiy Concrete"	"Ordinary Qualtiy Concrete"	"High Qualtiy Concrete"	"High Qualtiy Concrete"	"Low Quality Concrete"
Best Estimate Values - For Realistic Modeling								
Initial Saturated Hydraulic Conductivity	cm/s	1.00E-10	3.10E-10	1.00E-08	3.10E-10	1.00E-10	6.40E-10	5.00E-09
Initial Effective Diffusion Coefficient	cm^2/sec	6.80E-09	3.50E-08	5.00E-07	6.00E-08	3.50E-08	3.50E-08	1.20E-07
Moisture Characteristic Curve**	Not applicable	"Saltstone BE"	"High Qualtiy Concrete"	"High Qualtiy Concrete"	"Ordinary Qualtiy Concrete"	"High Qualtiy Concrete"	"High Qualtiy Concrete"	"Low Quality Concrete"
Conservative Estimate Values - For Pessimistic Modeling								
Initial Saturated Hydraulic Conductivity	cm/s	2.00E-09	2.10E-09	4.10E-05	2.10E-09	3.20E-10	9.10E-10	1.00E-08
Initial Effective Diffusion Coefficient	cm^2/sec	3.40E-08	6.00E-08	5.30E-06	1.20E-07	6.00E-08	6.00E-08	5.00E-07
Moisture Characteristic Curve**	Not applicable	"Saltstone CE"	"High Qualtiy Concrete"	"High Qualtiy Concrete"	"Ordinary Qualtiy Concrete"	"High Qualtiy Concrete"	"High Qualtiy Concrete"	"Low Quality Concrete"

Note: Some exceptions may apply to address observed field conditions or other considerations.

*Existing Cylindrical SDUs include 2A, 2B, 3A, 3B, 5A, 5B and 6. SDUs 7 and greater are Future Cylindrical SDUs.

** For moisture characteristic curves, see Figure 4.3-3. CV = Compliance Value, BE = Best Estimate, and CE = Conservative Estimate as discussed in Section 4.4.2.

The MCCs for each of the cementitious materials are presented in Figure 4.3-3.

Figure 4.3-3: MCCs for Cementitious Materials

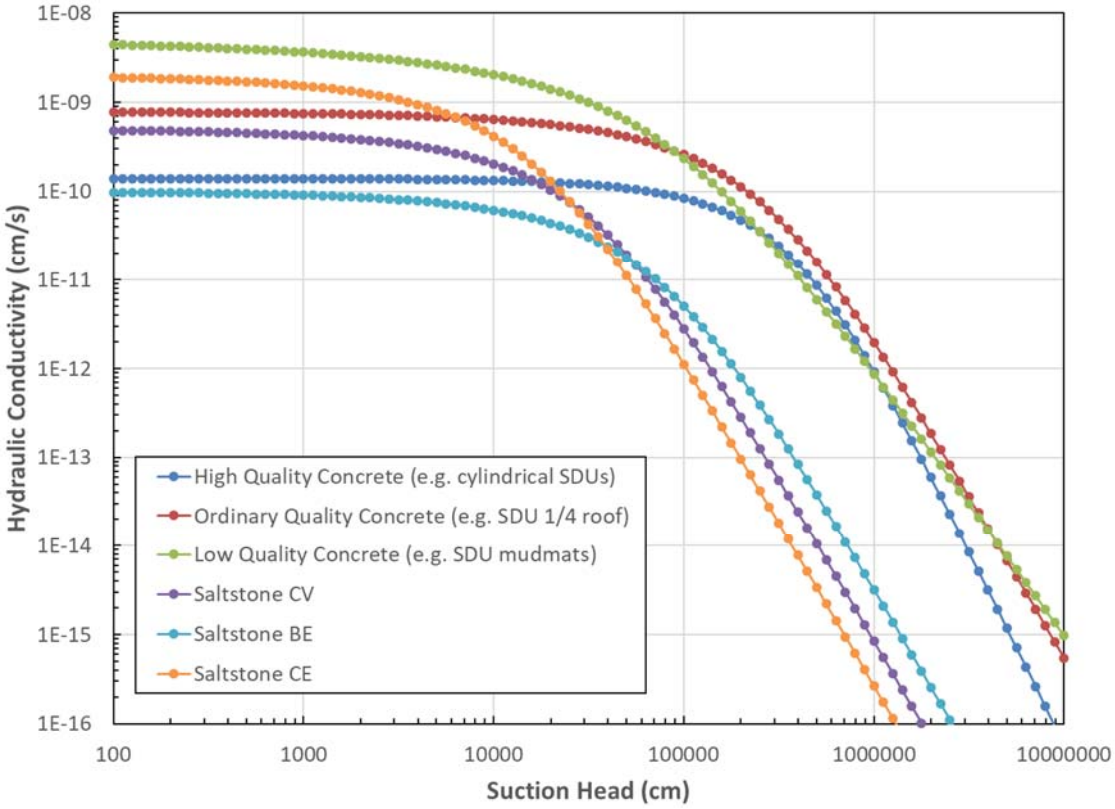

Note: CV = Compliance Value, BE = Best Estimate, and CE = Conservative Estimate as discussed in Section 4.4.2. [SRNL-STI-2018-00652]

In addition to the cementitious material properties listed above, the following cementitious material properties and conditions are also applied to modeling for this PA.

4.3.1.2.1 As-Built Conditions

Post-construction observations in the field have shown that some SDU materials might not perform as designed. Based on these observed field conditions, various assumptions are imposed to ensure greater defensibility of the models.

For SDUs 1 and 4, the walls are assumed to have the hydraulic conductivities of the surrounding backfill material. This is based on observed weep sites along the walls. [SRR-CWDA-2018-00036] The extent of the damage is not known, so the walls are assumed to provide no protection as a potential hydraulic barrier.

Similarly, after observing cracks in the roof and floor of SDU 6 post-construction, the FY2016 SDF SA was developed based on the observed "as-built" conditions of SDU 6. [SRR-CWDA-2016-00072] These "as-built" conditions assumed an initially degraded floor and roof for SDU 6 based on a bounding assumption for a leak rate as described in the *Evaluation of Revised Future Saltstone Disposal Unit Locations by*

PORFLOW Simulations. [SRNL-STI-2016-00534] For the PA, these "as-built" conditions shall continue to be applied to the modeling of SDU 6.

4.3.1.2.2 SDU 7 Roof and Floor Joints

For the construction of SDU 7, the arrangement of the roof and floor joints (from C-CC-Z-00060 and C-CC-Z-00059) were based on an evaluation to mitigate the risk for potential future cracking. [SRR-SDU-2017-00013] This report provided recommendations for the construction of SDU 7, based on lessons learned from the construction of SDU 6. For the PA, the recommendations for SDU 7 will be applied to all future SDUs. [SRR-CWDA-2018-00012]

4.3.1.2.3 Concrete Formulation Specifications for Future SDUs and SDU Columns

Procurement specification C-SPP-Z-00015, Attachments 03300-A and 03300-C, contains the concrete specifications for SDU 7 and other future SDUs. While this reference would indicate that the columns will be made with a "high quality" concrete (same as walls and roof), it is still appropriate to assign the columns the properties of "low quality" concrete. This is based on the lessons learned from construction of SDU 6 where "pock marks," or divots, in the external surfaces of the columns were identified. [SRR-CWDA-2018-00012]

4.3.1.2.4 Clean Cap Materials

In previous modeling, a layer of clean cap material (i.e., grout with similar properties to saltstone, but with no contaminant inventory) was assumed to be poured between the saltstone waste form and the SDU roofs. This assumption used to apply to SDUs 1 and 4 and the 150-foot diameter SDUs. Since there are currently no plans to add any more saltstone to SDUs 1 and 4, it is appropriate to continue including a layer of clean cap for these units. However, for the 150-foot diameter and the 375-foot diameter SDUs, no clean cap shall be assumed. These SDUs will be assumed to be filled to capacity with the saltstone waste form.

4.3.1.2.5 Mud Mat Properties

The modeled "base elevations" for SDUs 1 and 4 are defined as the bottom of the floor slab, which rests on top of the disposal unit's four-inch-thick working slab (i.e., as a modeling simplification, the working slab is not modeled for SDUs 1 and 4).

The modeled "base elevations" for the cylindrical SDUs are defined as the bottom of the lower mud mat. While the mud mats for the cylindrical SDUs are explicitly modeled in the PA, it should be noted that their hydraulic properties (for all mud mats except for the upper mud mats of the 150-foot diameter SDUs) are assumed to be the same as the backfill material. However, the material does retain the chemical properties of concrete.

When the mud mats were poured for the 150-foot diameter SDUs, quality inspections of the upper mud mats were performed, but these inspections were not performed for the lower mud mats. As such, only the upper mud mats are credited for passing quality inspections. [SRR-CWDA-2018-00012]

For the 375-foot diameter SDUs, there were no such mud mat inspections. It is assumed that when these larger SDUs are constructed, the heavier construction equipment has the potential to damage the mud mats. As such, assuming that these mud mats have the hydraulic properties of soil provides a bias for higher-than-expected flow rates.

4.3.2 Release and Transport Property Inputs

The release and transport of contaminants within PA models are typically controlled by partition coefficients (K_ds) and solubility limits.

4.3.2.1 Soil and Cementitious Material K_ds

Nearly all of the recommended K_d values were taken from *Geochemical Data Package for Performance Assessment Calculations Related to the Savannah River Site*. [SRNL-STI-2009-00473] The values within this report were developed based on an extensive literature review and recent SRS site-specific studies.

It is expected that the pore solution passing through the cementitious materials (SDU concrete and saltstone) will alter the chemistry of the soils beneath the SDUs. Table 4.3-4 provides the recommended K_ds for modeling transport through soils for most elements and provides recommendations for the altered K_d values based on these leachate impacts. For modeling purposes, the leachate-impacted soil K_ds are assumed to be applicable to soils/sediments between the SDUs and the water table until the saltstone waste form is oxidized.

Table 4.3-5 provides the recommended K_ds for modeling transport through cementitious materials (SDU concrete and saltstone) for most elements. The redox state of the material (i.e., reducing versus oxidizing) is defined by the Eh of the pore solution within the material. Initially, the cementitious materials with significant amounts of BFS, such as saltstone, are assumed to be reducing, but as water passes though the pores, the dissolved oxygen will consume the reducing agents within the materials until the reducing capacity is consumed and the material becomes oxidizing. Similarly, the chemical region (Region I, Region II, or Region III) is defined the pH of the pore solution within the material. As water passes though the pores, it is chemically buffered by the material. Over time, the pH of the pore solution will decrease and approach equilibrium with the natural infiltrating water. As this happens, the chemical region will transition. These processes are described in greater detail in Section 4.4.3.1.

Uncertainty associated with these K_d values is evaluated via the probabilistic modeling (see Section 5.7.1). In addition, a set of sensitivity cases was developed to evaluate risks associated with this uncertainty (see Section 5.8.4.3).

Table 4.3-4: Recommended K_d Values for Soils

Element or Ion	Backfill or Clayey Soils (mL/g)	Leachate-Impacted Clayey Soils (mL/g)	Vadose Zone or Sandy Soils (mL/g)	Leachate-Impacted Sandy Soils (mL/g)
Ac	9,000	10,000	1,000	2,000
Ag	30	100	10	30
Al	1,000	2,000	1,000	2,000
Am	9,000	10,000	1,000	2,000
As	200	300	100	100
B *	0	0	0	0
Ba	100	300	20	50
C	400	2,000	10	50
Cd	30	90	20	50
Cf	9,000	10,000	1,000	2,000
Cl	8	0.8	1	0.1
Cm	9,000	10,000	1,000	2,000
Co	100	300	40	100
Cr	1,000	1,000	400	600
Cs	50	50	10	10
Cu	70	200	50	200
Eu	9,000	10,000	1,000	2,000
F	8	0.8	1	0.1
Fe	400	600	200	300
H	0	0	0	0
Hg	1,000	3,000	800	3,000
I	3	0.3	1	0.1
K	30	30	5	5
Mn	200	300	20	20
Mo	1,000	1,000	1,000	1,000
N	8	0.8	1	0.1
NO_2 *	0	0	0	0
NO_3 *	0	0	0	0
Nb	1,000	1,000	1,000	1,000
Ni	30	100	7	20
Np	9	10	3	5
Pa	9	10	3	5
Pb	5,000	20,000	2,000	6,000
PO_4 *	0	0	0	0
Pt	30	100	7	20
Pu	6,000	10,000	650	1,000
Ra	200	500	30	80
Rn	0	0	0	0
Sb	3,000	4,000	3,000	4,000
Se	1,000	1,000	1,000	1,000
Sm	9,000	10,000	1,000	2,000
Sn	5,000	20,000	2,000	6,000
SO_4 *	0	0	0	0
Sr	20	50	5	20
Tc	1.8	0.2	0.6	0.06
Th	2,000	4,000	900	2,000
U	400	1,000	300	900
Zn	30	90	20	50
Zr	2,000	4,000	900	2,000

[SRNL-STI-2009-00473, SRR-CWDA-2017-00019]

Note: Values with asterisks (*) assume zero values (i.e., no retardation) in PA modeling.

Table 4.3-5: Recommended K_d Values for Cementitious Materials

Element or Ion	Reducing Environment (Eh < 0 mV)			Oxidizing Environment (Eh > 0 mV)		
	Region I (mL/g)	Region II (mL/g)	Region III (mL/g)	Region I (mL/g)	Region II (mL/g)	Region III (mL/g)
Ac	7,000	7,000	1,000	6,000	6,000	600
Ag	5,000	5,000	1,000	4,000	4,000	400
Al	7,000	7,000	1,000	6,000	6,000	600
Am	7,000	7,000	1,000	6,000	6,000	600
As	200	200	100	300	300	100
B *	0	0	0	0	0	0
Ba	6,000	6,000	600	200	100	200
C	2,000	5,000	50	2,000	5,000	50
Cd	5,000	5,000	1,000	4,000	4,000	400
Cf	7,000	7,000	1,000	6,000	6,000	600
Cl	0	10	1	0	10	1
Cm	7,000	7,000	1,000	6,000	6,000	600
Co	5,000	5,000	1,000	4,000	4,000	400
Cr	1,000	1,000	1,000	10	10	1
Cs	2	20	10	2	20	10
Cu	5,000	5,000	1,000	4,000	4,000	400
Eu	7,000	7,000	1,000	6,000	6,000	600
F	0	10	1	0	10	1
Fe	7,000	7,000	1,000	6,000	6,000	600
H	0	0	0	0	0	0
Hg	500	500	100	300	300	100
I	0	2	0	8	10	4
K	2	20	10	2	20	10
Mn	100	100	10	100	100	10
Mo	300	300	200	3	3	3
N	0	0	0	0	0	0
NO_2 *	0	0	0	0	0	0
NO_3 *	0	0	0	0	0	0
Nb	1,000	1,000	500	1,000	1,000	500
Ni	70	400	400	70	400	400
Np	10,000	10,000	5,000	10,000	10,000	5,000
Pa	10,000	10,000	5,000	10,000	10,000	5,000
Pb	5,000	5,000	1,000	300	300	100
PO_4 *	0	0	0	0	0	0
Pt	5,000	5,000	1,000	4,000	4,000	400
Pu	10,000	10,000	2,000	10,000	10,000	2,000
Ra	6,000	6,000	600	200	100	200
Rn	0	0	0	0	0	0
Sb	200	200	100	200	200	100
Se	300	300	200	3	3	3
Sm	7,000	7,000	1,000	6,000	6,000	600
Sn	4,000	4,000	2,000	4,000	4,000	2,000
SO_4 *	0	0	0	0	0	0
Sr	1,000	1,000	100	90	20	90
Tc	1,000	1,000	1,000	0.8	0.8	0.5
Th	10,000	10,000	2,000	10,000	10,000	2,000
U	5,000	5,000	5,000	1,000	5,000	5,000
Zn	5,000	5,000	1,000	4,000	4,000	400
Zr	10,000	10,000	2,000	10,000	10,000	2,000

[SRNL-STI-2009-00473, SRR-CWDA-2017-00019]

Note: Values with asterisks (*) assume zero values (i.e., no retardation) in PA modeling.

For selected elements, there are saltstone-specific K_d recommendations. Because saltstone has significant amounts of BFS in its formula, relative to typical concrete, the transport properties for some elements exhibit different transport properties within saltstone. Specifically, barium (Ba), radium (Ra), and strontium (Sr) have relatively large K_d values when BFS is a major component in the material formulation (e.g., saltstone), irrespective of the redox status because they form a strong bond to the sulfur in BFS regardless of whether the sulfur is oxidizing or reducing. The recommended saltstone-specific K_d values are provided in Table 4.3-6. For elements or species not included in Table 4.3-6, the cementitious K_ds in Table 4.3-5 should be used for simulating transport through saltstone. [SRNL-STI-2009-00473] Iodine (I) also has a saltstone-specific K_d, as discussed below.

Table 4.3-6: Recommended Saltstone Specific K_d Values

Element	Reducing Environment (Eh < 0 mV)			Oxidizing Environment (Eh > 0 mV)		
	Region I (mL/g)	Region II (mL/g)	Region III (mL/g)	Region I (mL/g)	Region II (mL/g)	Region III (mL/g)
Ba	6,000	6,000	600	6,000	6,000	600
I	0.07	0.71	0.71	8	10	4
Ra	6,000	6,000	600	6,000	6,000	600
Sr	1,000	1,000	100	1,000	1,000	100

Note: Ba, Ra, and Sr values are from SRNL-STI-2009-00473, I values in reducing environment are from SRR-CWDA-2018-00045, and I values in oxidizing environment are from SRNL-STI-2009-00473.

The iodine K_d values for simulating I-129 releases from the saltstone waste form were derived from recent experimental test data as documented in *Iodine K_ds for Simulating I-129 Releases from Saltstone SDUs*. [SRR-CWDA-2018-00045] A GoldSim-based optimization model was developed to determine appropriate values based on experimental results from DLM testing of saltstone simulant samples. In addition to the Compliance Case, additional specific inputs sets have been derived to be used in alternative modeling cases. The recommended I-129 K_d values for reducing saltstone for the Compliance Case and alternative cases are provided in Table 4.3-7.

Table 4.3-7: I-129 K_d Values for Reducing Saltstone Based on Results of Simulant Sample Releases for use in Specific Input Sets

Modeling Value	<1.0 Pore Volumes Exchanged	>1.0 Pore Volumes Exchanged
Best Estimate (Realistic)	0.16 mL/g	2.77 mL/g
Compliance (MPAD)	0.07 mL/g	0.71 mL/g
Conservative Estimate (Pessimistic)	0.07 mL/g	0.71 mL/g

[SRR-CWDA-2018-00045]

4.3.2.2 Solubility Limits for Simulating Tc-99 Releases from SDUs

As a modeling assumption, contaminant concentrations in saltstone are not generally limited by solubility. This assumption is expected to bias modeling results to faster-than-expected release rates because applying solubility controls is expected to mitigate release rates. The one exception to this assumption is the release of technetium under reducing conditions.

The technetium solubility limits for simulating Tc-99 releases from the reducing saltstone waste form were derived from recent experimental test data (SRRA099188-000003) documented in *Technetium Solubility for Simulating Tc-99 Releases from Saltstone SDUs*. [SRR-CWDA-2018-00046] A GoldSim-based optimization model was developed to determine appropriate values based on actual experimental results from DLM testing of SDU 2A cores and simulant samples. In addition to the Compliance Case, additional specific inputs sets have been derived to be used in alternative modeling cases. The recommended Tc-99 solubility limits for reducing saltstone for the SDF PA are presented in Table 4.3-8.

Table 4.3-8: Tc-99 Solubility Limit Values for Reducing Saltstone Based on Results of SREL Tc-99 DLM Simulant Sample Releases for use in Specific Input Sets

Modeling Value	Saltstone pH >=11	Saltstone pH <11
Best Estimate (Realistic)	2.0E-07 mol/L	7.4E-08 mol/L
Compliance (MPAD)	9.7E-07 mol/L	4.5E-07 mol/L
Conservative Estimate (Pessimistic)	9.7E-07 mol/L	4.5E-07 mol/L

[SRR-CWDA-2018-00046]

4.3.2.3 Saltstone Reducing Capacity

The saltstone formula includes BFS as a reducing agent to slow the release of technetium. Dissolved oxygen will consume this reducing agent as it enters the system. As such, the saltstone waste form will have relatively low dissolved oxygen content until the cumulative oxygen ingress exceeds the reducing capacity of the saltstone. Therefore, the reducing capacity of saltstone is important as Tc-99 is relatively immobile within reducing environments.

The recommended reducing capacity of saltstone (given in milliequivalents of electrons per gram (meq e^-/g)) is documented in *Recommended Reducing Capacity for Saltstone for the SDF PA*. [SRR-CWDA-2018-00048] Studies have been performed in which the Ce(IV) and Cr(VI) testing methods were both evaluated in an effort to develop a standard method for quantifying reducing capacity of saltstone samples (SREL-R-14-0006 and SREL-R-16-0003). The results of these studies were taken into consideration as part of the recommendation for saltstone reducing capacity values. Table 4.3-9 summarizes the recommendations for the reducing capacity of saltstone.

Table 4.3-9: Summary of Recommended Reducing Capacities for Cementitious Materials

Modeling Value	Recommended Saltstone Value (meq e^-/g)	Recommended SDU Concrete Value (meq e^-/g)
Best Estimate (Realistic)	0.65	0.239
Compliance (MPAD)	0.50	0.209
Conservative Estimate (Pessimistic)	0.35	0.178

[SRR-CWDA-2018-00048, SRNL-STI-2018-00586]

4.3.3 SDU-Specific Model Inputs

In general, the modeling inputs for the SDUs are based on various design drawings with some modification to reflect observed (or "as-built") conditions. Section 3.2 provides most of these details. For the future 375-foot diameter SDUs (i.e., SDUs 7 through 12), the dimensions and other specifications are based on the design drawings for the construction of SDU 7 and are summarized in Table 4.3-10. The design specifications for SDU 7 reflect the intended design for SDU 7 and are applied for the Compliance Case modeling of SDU 7 and all subsequent SDUs to be constructed. Similarly, the as-built conditions for SDU 6 (also provided in Table 4.3-10) are based on field observations and are used for the Compliance Case modeling of SDU 6 only.

In addition to the design specifications for SDU 7, inputs for modeling a "Design Margin" (DM) Case for SDU 7 are also provided in Table 4.3-10. The design margin case is an alternative modeling scenario that considers construction margin to ensure that potential deviations from the design, which may occur during construction, will not significantly impact the expected performance of the SDU. The design margin case is described in Section 5.8.7.1.

In addition, SRR-SDU-2017-00003 indicates the minimum grout capacity for the 375-foot diameter SDUs is 32.8 Mgal, assuming a 41-foot fill height. While this is the operational fill height, modeling assumes that the saltstone waste form will fill the entire SDU (i.e., 43 feet) to ensure that future operational capacity will not be limited by the PA.

Table 4.3-10: Summary of Design Specifications for Modeling 375-Foot Diameter SDUs

Dimension or Specification	SDU 7 Design	SDU 7 Design Margin	SDU 6 As-Built Conditions
Roof Thickness	12 inches	9 inches	12 inches
Roof Slope (from center)	1.5%	1.0%	1.5%
Linear Joint Length in Roof (e.g., water stops)	1,220 linear feet	3,200 linear feet	1,231 linear feet
Roof Overhang	9 inches	9 inches	9 inches
Roof to Wall Interface Rubber Pad	1 inch	1 inch	1 inch
Wall Average Inner Diameter	375 feet	375 feet	375 feet
Wall Top Thickness	12 inches	7 inches	10 inches
Wall Base Thickness	24 inches	20 inches	24 inches
Wall Panels Count	25 individual	25 individual	25 individual
Wall Height	43 feet	43 feet	43 feet
Wall Thermocouple Tree Number	1 tree	1 tree	Not applicable
Wall Thermocouple Tree Void Space	1 cubic foot	1 cubic foot	Not applicable
Wall Thermocouple Tree Casing	2-inch diameter pipe that penetrates vertically through roof and into wall	2-inch diameter pipe that penetrates vertically through roof and into wall	Not applicable
Wall Form Penetration Depth	Penetrations will be repaired.	7.25 inches	Penetrations will be repaired.
Wall Form Penetrations Cumulative Surface Area Impact	Penetrations will be repaired.	16 square feet	Penetrations will be repaired.
Floor Thickness	24 inches	12 inches	Variable, Assumed min. 12 inches
Floor Slope (from center)	None	None	1.5%
Floor Extends Beyond Wall	2.25 feet	2.25 feet	2.25 feet
Linear Joint Length in Floor (e.g., water stops)	1,980 feet	3,200 feet	1,974 feet
Wall/Floor Interface Rubber Pad	2 inches thick	2 inches thick	2 inches thick
Support Column Number	208 Columns	208 Columns	208 Columns
Support Column Diameter	24 inches	20 inches	24 inches
Support Column Bases	None	None	5-foot square and 18-inches tall
HDPE Thickness	60 mils	None	100 mils
Combined Mud Mat Thickness	10 inches	8 inches	10 inches
SO_4 Concentration in Pore Water (molarity)	0.1M	0.1M	0.1M
Clean Cap	None	None	None

[SRR-CWDA-2018-00012]

4.4 Integrated Modeling Approach

This section describes each of the submodels used in the development of this PA. Figure 4.1-8 provided a general overview of each of these submodels. This figure also indicated the software used for each submodel, and selected high-level inputs and outputs, and identified how each submodel related to the others. However, it should be noted that Figure 4.1-8 only illustrates the integration of submodels as they apply to the deterministic modeling approach used for the demonstration of compliance (i.e., the Compliance Case).

Each of the respective submodels are described in greater detail throughout Section 4.4:

- Section 4.4.1 describes the **Closure Cap Model** which is used to estimate infiltration rates based on environmental conditions and closure cap design;
- Section 4.4.2 describes the **Cementitious Degradation Model** which is used to estimate the rates of hydraulic degradation for both the SDU concrete and the saltstone waste form;
- Section 4.4.3 describes the **Contaminant Release Model** which is used to estimate the chemical conditions and transitions that influence release and transport rates;
- Section 4.4.4 describes the **Vadose Zone Flow Model** which uses the infiltration rates from the Closure Cap Model and the hydraulic degradation rates from the Cementitious Degradation Model to estimate flow rates through the vadose zone;
- Section 4.4.5 describes the **Vadose Zone Transport Model** which uses the flow rates from the Vadose Zone Flow Model and the chemical transitions from the Contaminant Release Model to estimate fluxes for contaminants released from the saltstone waste form, through the SDU concrete, and into the soils;
- Section 4.4.6 describes the **Aquifer Transport Model** which uses the contaminant fluxes from the Vadose Zone Transport Model and flow modeling from the GSA Model, as updated in 2018 (SRNL-STI-2018-00643) and modified to apply greater spatial discretization, to estimate contaminant concentrations at selected points of compliance (e.g., wells along the 100-meter boundary);
- Section 4.4.7 describes the **Airborne Pathway Release Model** which uses inventory values, volatility data, and the closure cap design to estimate airborne releases for selected contaminants; and
- Section 4.4.8 describes the **Dose and Exposure Pathways Model** which uses contaminant concentrations from the Aquifer Transport Model along with dose coefficients and an assumed definition of the human receptor to estimate doses to the MOP and IHI.

This deterministic modeling approach relies on well-discretized, two-dimensional and three-dimensional PORFLOW models (see Sections 4.4.4, 4.4.5, and 4.4.6) to establish compliance with performance objectives (i.e., the Compliance Case model). Additionally, a probabilistic model has been developed within GoldSim using simplified, one-dimensional and pseudo- two-dimensional modeling approaches (see Section 4.5). This probabilistic model was developed by partially abstracting flow information from PORFLOW and reading the abstracted data into GoldSim. Figure 4.4-1 provides an additional overview of how information from PORFLOW is integrated into the probabilistic GoldSim model.

A comparison of various PORFLOW-based results and the respective GoldSim-based results was used to validate the use of the probabilistic modeling approach. This comparison is described as "benchmarking" (see Section 5.6). The probabilistic model is used to randomly sample values for select parameters to provide insights relative to the influence that parameter uncertainty may exhibit on the overall performance of the system.

Figure 4.4-1: Integration Between Deterministic (PORFLOW) Modeling and Probabilistic (GoldSim) Modeling Approaches

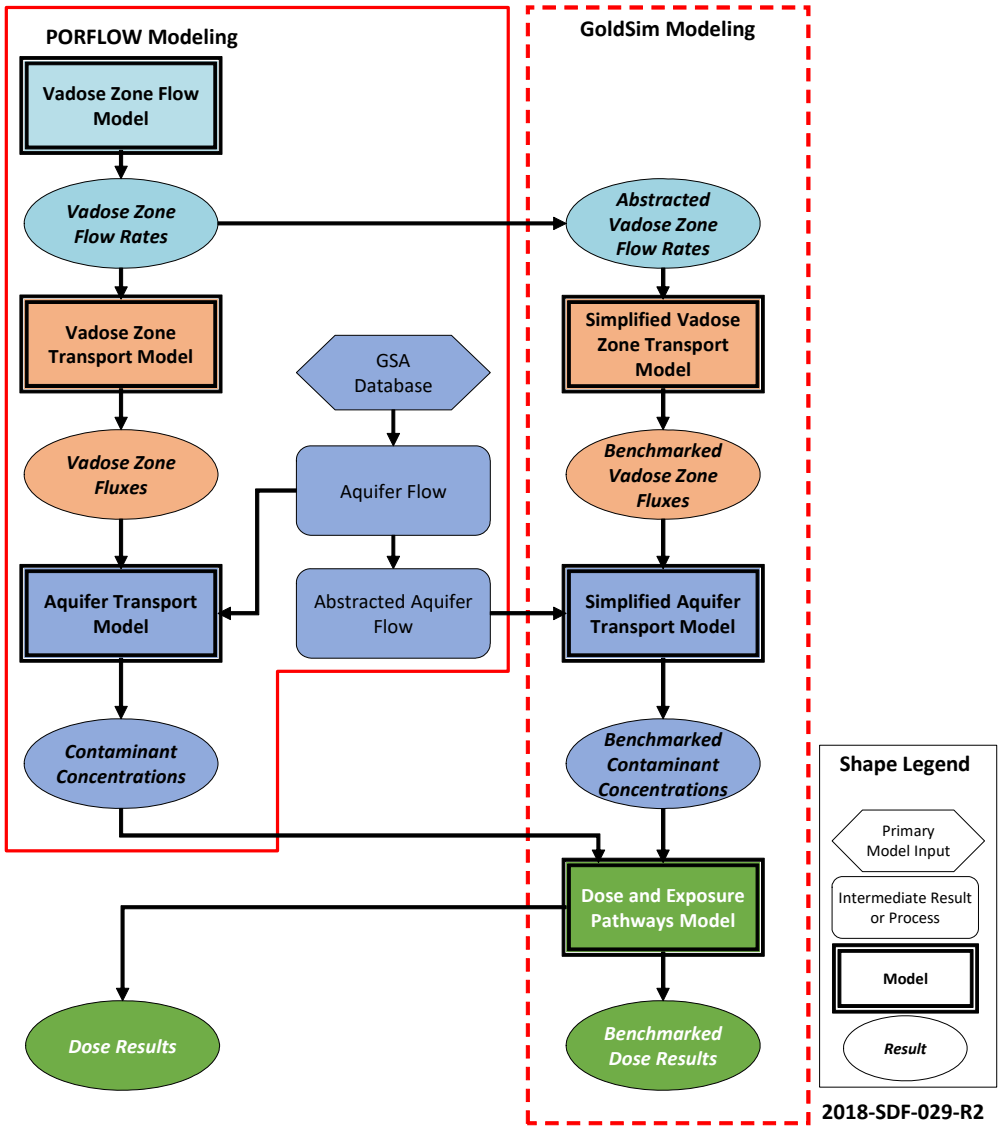

4.4.1 Closure Cap Model

The closure cap, as described in Section 3.2.6, is an engineered cover system designed to limit infiltration into the SDF. The following provides a description of the modeling approach used to estimate the performance of the closure cap. Section 4.4.1.4.4 provides the resulting infiltration rates.

Prior to reading the following subsections it is important to clarify the terminology used herein. In hydrology, "infiltration" is typically defined as water that is absorbed by the soil at the surface, passing through the interface between the atmosphere and the ground surface. Alternatively, the term "percolation" is the descending motion of water as it moves through the soil profile. As discussed below, the term "percolation" is only used to describe the combined infiltration and percolation through the upper portion of the closure cap, while "leakage" is used to describe water that passes through the composite barrier. The calculated leakage rate is assumed to be equal to the percolation rate, at depth. However, throughout this PA the term "infiltration" is used in the place of "percolation." In other words, instead of using "infiltration" to describe water passing through the surface interface, it is used to describe water at the model interface (i.e., where it passes from the Closure Cap Model and into the Vadose Zone Model (see Section 4.4.1.4.5 and 4.4.4)). When actual surface infiltration is being described, it is modified with the word "surface" to clarify the distinction (i.e., "surface infiltration"). The choice to use the term "infiltration" rather than updating the text to use "percolation" is intended to maintain consistent terminology with other modeling sections, which refer to the water entering the Vadose Zone Model as "infiltration."

4.4.1.1 Conceptual Model of the Closure Cap

The original conceptual design for the closure cap was based on *Saltstone Disposal Facility Closure Cap Concept and Infiltration Estimates*. [WSRC-STI-2008-00244] Relative to the design described in this 2008 document, the closure cap design has recently been modified to accommodate the updated SDF layout which includes the larger, 375-foot diameter SDUs and incorporates a 3% surface slope (instead of 1.5%) to meet closure requirements specified in the *New Consolidated Solid Waste Landfill Regulation*. [SCDHEC R.61-107.19] These changes are described in Section 3.2.6. The updated design is documented in the *Saltstone Disposal Facility Closure Cap Concept Update for Large-Scale Disposal Units* (SRR-CWDA-2018-00087) and is described in Section 3.2.6.1. Figure 4.4-2 shows a typical cross section.

The development of the closure cap model, as described in *Predicting Long-Term Percolation from the SDF Closure Cap* (SRRA107772-000009), was based on the original conceptual design drawings (see Figures 5 through 8 in WSRC-STI-2008-00244). Since the new design maintains all of the original layers and the minimum thicknesses for each layer, it is expected that the increased surface slope (from 1.5% to 3%) will increase surface runoff relative to the original design. With increased runoff, less water will be available for infiltration. As such, the Closure Cap Model for the SDF is expected to overestimate infiltration rates.

Figure 4.4-2: SDF Closure Cap, Typical Features

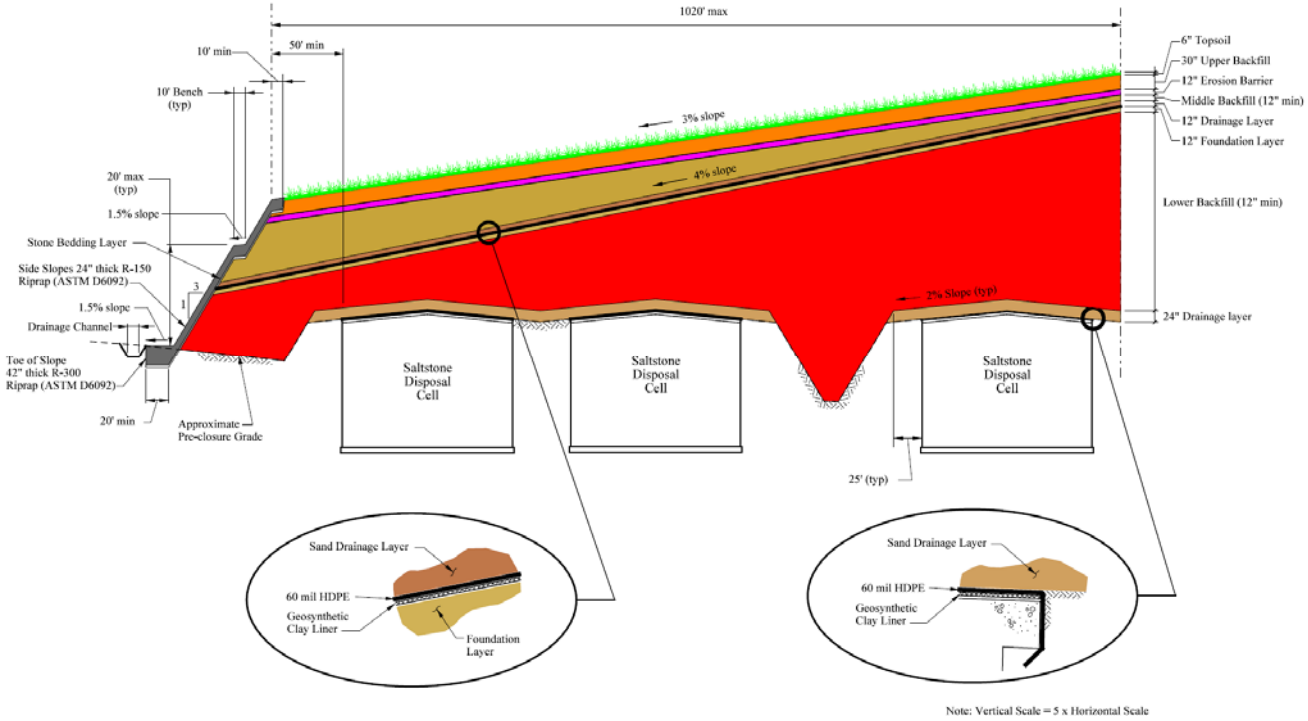

[SRR-CWDA-2018-00087]

Conceptually, the Closure Cap Model is organized into two parts. The first part addresses the percolation through the upper layers of the closure cap down to the upper lateral sand drainage layer (see Figure 3.2-33), while the second part considers the leakage rate based on the combined performance of the lateral sand drainage layer and the "composite barrier" (i.e., the combined HDPE and GCL layers). Note that the lower layers (i.e., the foundation layer, the lower backfill layer, the lower lateral sand drainage layer, and the composite barrier (HDPE and GCL layers) directly above each SDU) are not included in the Closure Cap Model. With respect to hydrological processes, the SDF PA models do not include the foundation layer, while the other lower layers are addressed as part of the Vadose Zone Flow Model (see Section 4.4.4).

Figure 4.4-3 shows the conceptual model for the first part of the Closure Cap Model. This part of the model addresses how meteorological/environmental conditions and material properties influence percolation through to the upper lateral sand drainage layer. As shown, water is introduced into the system as precipitation (P). Solar radiation and vegetation removes water from the system via evaporation (E) and transpiration (T). Surface runoff (R) also removes water from the system. The remaining water is then expected to penetrate through the surface and percolate downward. The rate of percolation (P_r) is then determined based on the hydraulic properties of each layer of the closure cap.

Figure 4.4-3: Conceptual Model for Percolation Through the Upper Closure Cap

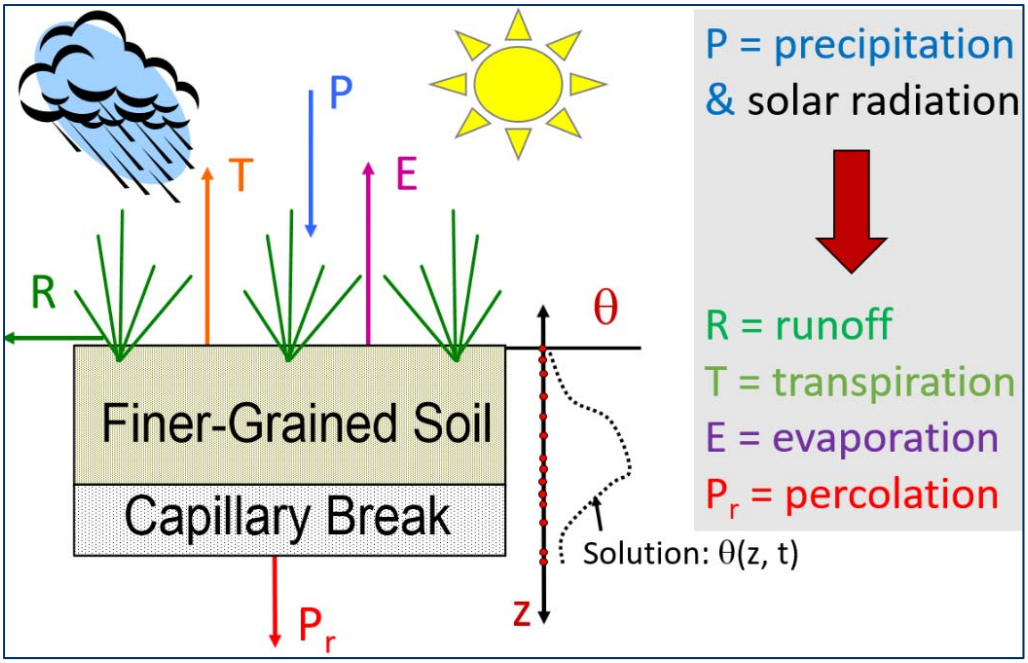

[SRR-CWDA-2018-00035]

Figure 4.4-4 shows the conceptual model for the second part of the Closure Cap Model. Water percolating from above will enter the upper lateral sand drainage layer. Within the sand, downward flow is expected to be significantly impeded by the composite barrier. As such, most of the percolating water is expected to follow the slope of the closure cap and shed laterally to the edges of the SDF closure cap. However, due to assumed holes through the HDPE some of the water will leak through the composite barrier. Infiltration into the lower backfill for the Vadose Zone Model is assumed to be equal to the leakage rate through the composite barrier.

Figure 4.4-4: Conceptual Model for Leakage Through the Composite Barrier

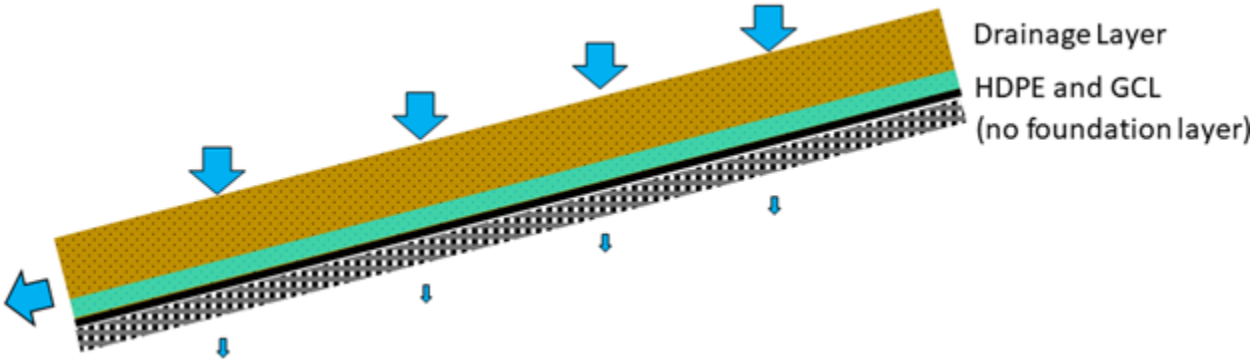

[SRR-CWDA-2018-00035]

4.4.1.2 Implementation of the Closure Cap Model

To address the two-part conceptual model, implementation of the model was also setup in two parts. The variably saturated flow code WinUNSAT-H was used to predict

percolation rates using unsaturated flow, water redistribution, and surface or near-surface interactions for the portion of the cover profile overlying the upper lateral sand drainage layer. A combination of analytical and semi-analytical equations was used to predict the leakage rates using the percolation rates predicted by WinUNSAT-H, lateral flow in the drainage layer, and assumptions about the performance of the composite barrier (see Figure 4.4-5). [SRRA107772-000009]

Figure 4.4-5: Overview of Closure Cap Model Implementation

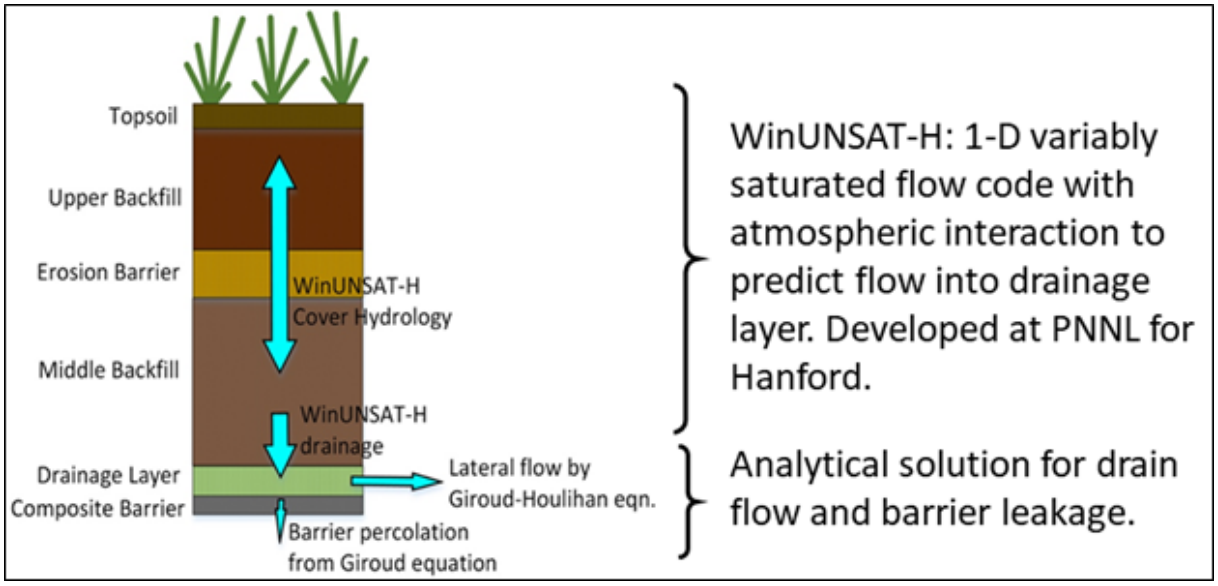

[SRR-CWDA-2018-00035]

4.4.1.2.1 Percolation Calculations

As described by Benson and Benavides (SRRA107772-000009), WinUNSAT-H employs an atmospheric boundary condition consisting of evaporation and surface infiltration, where runoff is computed as the difference between applied precipitation and the surface infiltration. The surface infiltration rate is controlled by the rate at which precipitation is applied and by the moisture capacity of the cover, the latter defined by the hydrologic conditions in the cover during surface infiltration. WinUNSAT-H also simulates vegetative water uptake by distributing the potential transpiration throughout the root zone in proportion to the relative root density. Collectively, the potential transpiration and the potential evaporation are computed from the potential evapotranspiration (ET) based on a leaf area index. Finally, a unit head gradient boundary condition was used to simulate percolation from the base of the middle backfill layer into the lower lateral sand drainage layer. [SRRA107772-000009]

For determining variably saturated flow, Richards equation (Eq. 4.4-1) is used. [SRRA107772-000009] This equation serves as the primary differential equation solved by WinUNSAT-H; it describes changes in water storage, isothermal redistribution of liquid water, and water uptake by plants (PNNL-13249):

$$\frac{\partial \theta}{\partial \Psi}\frac{\partial \Psi}{\partial t} = -\frac{\partial}{\partial z}\left[K_c \frac{\partial \Psi}{\partial z} + K_\Psi\right] - S(z,t) \quad \text{Eq. 4.4-1}$$

where:

θ = volumetric water content (m^3/m^3),

Ψ = matric suction (m),

K_c = combined hydraulic conductivity (for liquid and vapor flows) in m/s,

K_Ψ = unsaturated hydraulic conductivity (m/s),

z = vertical distance in m (z = 0 at ground surface),

t = time (s), and

$S(z,t)$ = sink term for root water uptake ($\frac{m^3/s}{m^3}$).

Note that this approach is one-dimensional. As described in Section 4.4.8.1, the Closure Cap Model is based on the original SDF closure cap design which only assumed a shallow 1.5% slope at the surface. As such, the two-dimensional influences from lateral flow were assumed to be negligible. However, the new closure cap design includes a 3% surface slope. This is not included in the model; therefore, the model may be underestimating the influence of runoff.

Within WinUNSAT-H, a modified form of Richards equation (Eq. 4.4-2) is used to focus on the terms used to define the percolation rate (q):

$$q = -\left[K_c \frac{\partial \Psi}{\partial z} + K_\Psi\right] \quad \text{Eq. 4.4-2}$$

where:

q = percolation rate in m/s,

Ψ = matric suction (m),

K_c= combined hydraulic conductivity (for liquid and vapor flows) in m/s,

K_Ψ = unsaturated hydraulic conductivity (m/s), and

z = vertical distance in m (z = 0 at ground surface).

4.4.1.2.2 Leakage Rate (Infiltration) Calculations

As previously indicated, SDF modeling assumes that infiltration into the lower backfill is equivalent to the leakage rate through the composite barrier. An analytical approach is used to predict this leakage rate. [SRRA107772-000009] This approach combines the Giroud-Houlihan analytical solution for predicting the average depth of flow within a drainage barrier with Giroud's empirical solution for calculating leak rates for composite barriers. [DOI: 10.1680/gein.2004.11.1.43, ISSN 1072-6349]

The average depth of flow within a drainage barrier is determined as:

$$d = \frac{qL}{K_d \sin \beta} \quad \text{Eq. 4.4-3}$$

where:

d = depth (i.e., maximum liquid thickness) in m,

q = percolation rate from middle backfill into the upper lateral sand drainage layer in m/s,

L = horizontal slope length in m,

K_d = hydraulic conductivity of the upper lateral sand drainage layer in m/s, and

β = angle in radians, which is effectively the slope (rise over run).

This analytical solution was developed based on Darcy's Law and mass balance principles. [SRRA107772-000009; DOI: 10.1680/gein.2004.11.1.43] To maximize the calculated value of d, this equation assumes that the composite barrier beneath the sand drainage layer is free of holes and defects. Although Benson and Benavides describe this as the formula for the *average* depth of flow (SRRA107772-000009), the source reference (Giroud *et al.* 2004, DOI: 10.1680/gein.2004.11.1.43) indicates that this is a bounding formula for the *maximum* liquid thickness. As such, the application of this formula as the *average* depth is intentionally biased towards a larger value. This is important because a larger depth value results in a higher estimate of the leakage rate.

Also note that Giroud *et al. (*2004) use the term "thickness" instead of the more familiar "depth" because thickness is measured perpendicular to the angle of the drainage slope while depth is typically measured vertically. [DOI: 10.1680/gein.2004.11.1.43]

As a final note, while the "Notations" section at the end of Giroud *et al. (*2004) specifies that the angle of the slope (β) has units in degrees (°), the example calculations throughout the reference paper clearly show that the value of the slope is being input as the rise over run (i.e., the change in the vertical distance over the change in the horizontal distance). [DOI: 10.1680/gein.2004.11.1.43] For small angles, this value is nearly equal to the angle β expressed in radians. [DOI: 10.1680/gein.2004.11.1.43] For the purposes of this PA, it is assumed that the input for this formula is the rise over run of the slope.

Next, as described in Giroud 1997 (ISSN 1072-6349), the formula for calculating the leakage rate through a single defect is determined as:

$$Q = C_{qo}\left[1 + 0.1\left(\frac{d}{t_b}\right)^{0.95}\right] a^{0.1}(d)^{0.9} K_b^{0.74} \quad \text{Eq. 4.4-4}$$

where:

Q = leakage rate per HDPE hole (or defect) in m^3/s,

C_{qo} = contact factor (unitless),

d = depth (i.e., maximum liquid thickness) in m,

a = area (in m^2) of the average defect,

t_b = thickness of the GCL barrier in m, and

K_b = hydraulic conductivity in m/s of the GCL barrier.

Foose *et al.* (2001) have shown that this equation tends to overestimate the leakage rate. [DOI: 10.1061/(ASCE)1090-0241(2001)127:6(510)] Given that this equation tends to overestimate the leakage rate and because the estimate for depth (d) uses a bounding value, it is expected that the estimated leakage rate from Eq. 4.4-4 will be biased high.

Combined, these formulas (Eq. 4.4-3 and Eq. 4.4-4) give the leakage rate (Q) from a single defect in the composite barrier based on an average depth of flow (Eq. 4.4-5). [ISSN 1072-6349]

$$Q = 0.976 C_{qo} \left[1 + 0.1 \left(\frac{qL}{t_b K_d \sin\beta}\right)^{0.95}\right] d^{0.2} \left(\frac{qL}{K_d \sin\beta}\right)^{0.9} K_b^{0.74} \qquad \text{Eq. 4.4-5}$$

where:

Q = leakage rate per HDPE hole (or defect) in m^3/s,

C_{qo} = contact factor (unitless),

q = percolation rate from middle backfill into the upper lateral sand drainage layer in m/s,

L = horizontal slope length in m,

t_b = thickness of the GCL barrier in m,

K_d = hydraulic conductivity of the upper lateral sand drainage layer in m/s,

β = angle in radians, which is effectively the slope (rise over run),

d = diameter of HDPE hole (or defect) in m, and

K_b = hydraulic conductivity in m/s of the GCL barrier.

Eq. 4.4-5 shows that the estimated leakage rate is a function of the slope and the slope-length of the closure cap, the hydraulic properties of the upper lateral sand drainage layer and the GCL, and assumptions about HDPE performance (size of the defects).

Implicit to Eq. 4.4-5 is the limitation of the wetted area beneath the hole or defect. Given the limited size of the assumed defect, the impact on flow into the lower backfill underlying the composite barrier is expected to be localized (i.e., the spreading of water after passing through the hole or defect would be limited). As such, only a limited area within proximity to the footprint of the defect would be

wetted by the water passing through the defect, and the edge of this limited wetted area would be bounded by a phreatic surface beyond which the backfill would not be saturated.

As a modeling simplification, this wetted area is assumed to encompass the entire area beneath the closure cap. This is imposed by multiplying the leakage rate per defect (m^3/s) by the number of assumed defects per unit area and then dividing that value by the unit area (m^2). The resulting value is the average leakage rate (m/s) per unit area. While this modeling simplification underestimates localized effects within the wetted area, it overestimates saturation and flow for all areas beyond the limited wetted area. Given uncertainties in the potential locations for these assumed defects and given that localized flow would result in localized releases (thus reducing the overall impacts on the SDUs and the waste form), this simplifying assumption is expected to result in an overestimate of potential releases and transport.

4.4.1.3 Inputs and Assumptions for the Closure Cap Model

The following sections describe the key inputs and assumptions used in the Closure Cap Model for the SDF PA.

4.4.1.3.1 Meteorological Data

It is assumed that meteorological conditions will remain approximately the same as current conditions. This assumption is based on Leigh's 2008 study: *Late Quaternary Climates and River Channels of the Atlantic Coastal Plain, Southeastern USA*. [DOI:10.1016/j.geomorph.2008.05.024] This article examined the paleoclimate record along river channels in eastern Georgia and in the Carolinas. The study showed that river networks in the area exhibited four distinct morphological phases over the past 30,000 years "that closely correspond to major climatic and paleoenvironmental episodes." Of the significant climate-changing events, the most recent was a warming event which occurred during the last half of the Holocene (approximately 8,000 years ago). Since then, records indicate the regional environment "demonstrates climatic similarity to modern conditions." [DOI:10.1016/j.geomorph.2008.05.024]

While future climate conditions remain a source of modeling uncertainty, because the local environment has not shown significant changes over the past 8,000 years, it is reasonable to expect conditions will continue to be similar. As a simplification, this assumption is extrapolated into perpetuity for modeling purposes; however, wetter climate conditions will also be considered as an alternative modeling scenario to provide insights into how the assumed climate conditions may influence the performance of the system.

Meteorological conditions used for the WinUNSAT-H modeling were based on SRS precipitation data from 1964 to 2016 (Figure 4.4-6). In the more than 50 years

examined, the maximum annual rainfall occurred in 1964 with 72 inches/yr (1830 mm/yr), and the minimum occurred in 2010 with 29 inches/yr (724 mm/yr). Mean and median precipitation over this period were 47.1 inches/yr (1196 mm/yr) and 45.6 inches/yr (1158 mm/yr), respectively.

Figure 4.4-6: SRS Annual Precipitation Record: 1964 to 2016

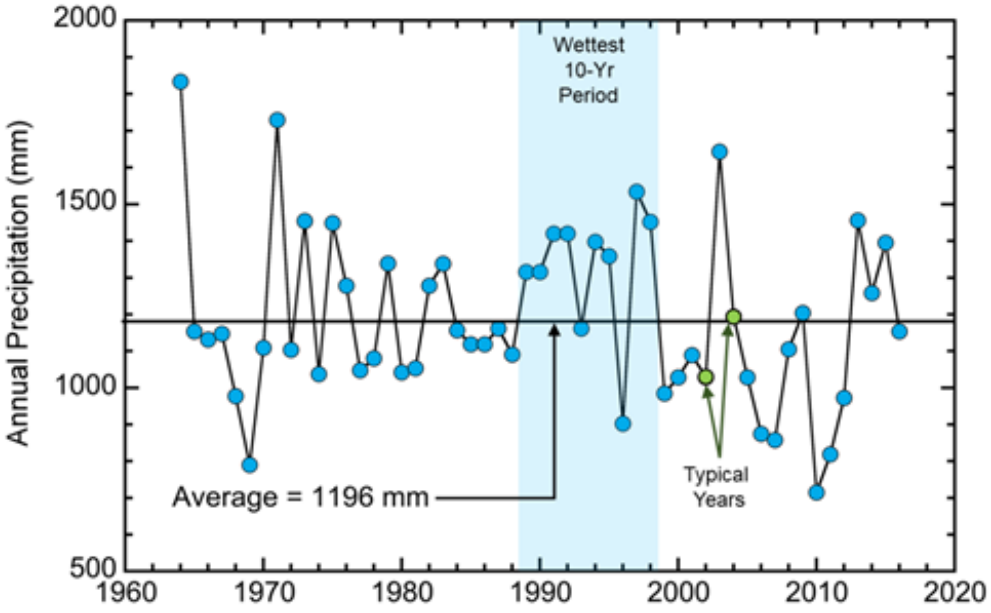

[SRRA107772-000009]

Given these values, "typical years" were selected. Years with highly unusual meteorological events were not considered. The years 2002 (40.6 inches/yr or 1030 mm/yr) and 2004 (47.1 inches/yr or 1191 mm/yr) were selected as the "typical years." Typical years are different from long-term average conditions because a typical year is an actual data set that exhibits natural variability and is not affected by the smoothing inherent in long-term averages. [SRRA107772-000009] Meteorological data from these years were used to establish long-term expected climate conditions.

Similarly, the wettest 10-year period (from 1989 to 1998) was used to determine conditions based on an assumed wetter climate condition, with an annual average rainfall of 52.4 inches/yr (1330 mm/yr), or 11.2% more than average.

4.4.1.3.2 Vegetation

Three types of vegetation were considered for vegetative cover atop the closure cap: bamboo, pine, and grass. Bamboo and pine both have abundant above ground biomass and leaf area, relative to grass, such that these would be expected to transpire more than grass. [SRRA107772-000009] Therefore, grass was selected to ensure greater defensibility in the estimated infiltration rates.

4.4.1.3.3 Layer Thicknesses for the SDF Closure Cap

Table 3.2-7 provided a summary of the designed thicknesses for each layer of the SDF closure cap. Table 4.4-1 provides the modeled thicknesses for each layer.

Table 4.4-1: Modeled Thicknesses for SDF Closure Cap Layers

Layer [a]	Layer Thickness
Vegetative Cover	N/A
Topsoil	150 mm (6 in)
Upper Backfill	760 mm (30 in)
Erosion Barrier	305 mm (12 in)
Geotextile Fabric	0 (not included in modeling)
Middle Backfill	305 mm (12 in)
Geotextile Filter Fabric	0 (not included in modeling)
Upper Lateral Sand Drainage Layer	305 mm (12 in)
Geotextile Fabric	0 (not included in modeling)
HDPE and GCL (Composite Barrier)[b]	8 mm (0.3 in)
Foundation Layer (backfill with bentonite admix)	0 (not included in modeling)

[SRRA107772-000009]

(a) The layers are arranged in the table to reflect their order from top to bottom in the SDF closure cap.

(b) The composite barrier thickness was revised from 10 mm (as described in SRRA107772-000009) to a more defensible 8 mm.

As indicated in Figure 4.4-2, the middle backfill and lower backfill layers of the designed closure cap have thicknesses that vary based on the location relative to the apex and the perimeter of the closure cap. During development of the WinUNSAT-H model, an evaluation was performed that considered the impacts of the thickness of the middle backfill layer. For the entire range of thicknesses considered, the annual percolation rates differed by less than 2%. Thus, all subsequent simulations were conducted with the middle backfill layer set at a thickness of 12 inches (305 mm). [SRRA107772-000009] Since the lower backfill is simulated as part of the vadose zone flow model, the assumed thickness of the middle backfill does not affect the estimated infiltration rates.

According to *Predicting Long-Term Percolation from the SDF Closure Cap* (SRRA107772-000009), the thickness of the composite barrier (i.e., the HDPE and the GCL, combined) was assumed to be 10 mm based on the design specifications described in *Saltstone Disposal Facility Closure Cap Concept and Infiltration Estimates*. (WSRC-STI-2008-00244). While infiltration rates are not strongly sensitive to this 10-mm thickness, this PA assumed a thickness of 8 mm to ensure greater defensibility because there is uncertainty in the final closure cap design specifications.

The geotextile fabric and geotextile filter fabric layers are not credited for any hydraulic performance. Therefore, as a model simplification, these layers are not included in the closure cap modeling.

4.4.1.3.4 Hydraulic Properties for the SDF Closure Cap

The assumed hydraulic properties for each modeled layer of the SDF closure cap are provided in Table 4.4-2.

Table 4.4-2: Hydraulic Properties for Select SDF Closure Cap Layers

Layer [a]	Saturated Hydraulic Conductivity, K_s (cm/s)	Porosity (%)	α (1/kPa)	*n* (unitless)
Topsoil	3.0E-03	40	0.17	1.3
Upper Backfill	1.0E-04	40	0.02	1.3
Erosion Barrier	1.0E-04	15	0.02	1.3
Middle Backfill	1.0E-04	40	0.02	1.3
Upper Lateral Sand Drainage Layer	5.0E-02 (realistic) or 1.0E-02 (bounding)	N/A	N/A	N/A
GCL	1.0E-09 (expected) or 1.0E-08 (bounding)	N/A	N/A	N/A
HDPE	Impervious except for assumed holes (or defects)	N/A	N/A	N/A

[SRRA107772-000009]

(a) The layers are arranged in the table to reflect their order from top to bottom in the SDF closure cap.
N/A = Not Applicable.

For the backfill layers, the saturated hydraulic conductivities are slightly higher than the recommended values assumed for the lower backfill material as modeled in the Vadose Zone Flow Model (see Section 4.4.4). The higher values for the closure cap material assumes that the soil layers have undergone pedogenesis and lost compaction.

For the upper lateral sand drainage layer, performance is expected to improve with increased hydraulic conductivity. The procurement requirement for the sand material shall specify a minimum saturated hydraulic conductivity of 5.0E-02 cm/s. [WSRC-STI-2008-00244] As such, this value is the basis for the expected (or realistic) input value. However, a lower value (1.0E-02 cm/s) may also be assumed to address potential uncertainties related to the long-term performance of the material.

For the GCL, two conditions may be assumed for the saturated hydraulic conductivity: 1.0E-09 cm/s (for expected conditions) or 1.0E-08 cm/s (for bounding conditions). These values were informed by NUREG/CR-7028 (ML12005A110), which indicated that GCLs placed on a moist subgrade and covered with HDPE and soil show very low saturated hydraulic conductivities (i.e., less than 5.0E-09 cm/s).

The assumed porosity values for the topsoil and backfill layers are consistent with site-specific data reported in Table 5-18 of *Hydraulic Property Data Package for the E-Area and Z-Area Soils, Cementitious Materials, and Waste Zones* (WSRC-STI-2006-00198). The erosion barrier porosity is from *Saltstone Disposal Facility Closure Cap and Infiltration Estimates* (WSRC-STI-2008-00244).

The final two properties (α and n) are shape parameters for the soil moisture characteristic curves (also known as soil water characteristic curves (SWCCs) or water retention curves), as discussed in Section 4.4.1.3.5. The shape parameters describe the rate at which the water content changes with suction head (or matric potential, ψ). The values for the α and n parameters are consistent with and near the upper bound of the recommendations on hydraulic properties for earthen covers as provided in NUREG/CR-7028 for simulating long-term naturalized conditions in PAs. [ML12005A110, SRRA107772-000009]. These values are recommended in Section 10.2 of NUREG/CR-7028, based on an analysis of data from multiple sites as presented in Table 6.3 of NUREG/CR-7028. [ML12005A110]

4.4.1.3.5 Moisture Characteristic Curves

Moisture characteristic curves are used to define the relationship between water content (or saturation levels) and matric suction. For the SDF Closure Cap Model, this relationship is characterized with a van Genuchten model (SRRA107772-000009):

$$\theta = \theta_r + (\theta_s - \theta_r)\left[\frac{1}{1 + (\alpha\psi)^n}\right]^m \qquad \text{Eq. 4.4-6}$$

where:

θ = volumetric water content (m^3/m^3),

θ_r = residual volumetric water content (m^3/m^3) determined for each node during each timestep,

θ_s = saturated volumetric water content (m^3/m^3) determined for each node during each timestep,

ψ = matric suction (m), which is determined based on a simulation using typical year meteorological data (SRRA107772-000009),

α = shape parameter (m^{-1}) (see Table 4.4-2),

n = a dimensionless shape parameter (see Table 4.4-2), and

$m = 1 - n^{-1}$ (unitless)

Note the WinUNSAT-H modeling for typical years uses initial conditions such that initial matric suction (ψ) is assumed to be 1000 kPa throughout the profile on the first day of the first year. The simulation was carried forward for five years using very discrete timesteps; at each timestep, the matric potential changes based on the changing saturation conditions. The WinUNSAT-H modeling for wetter years assumes an initial matric potential (ψ) based on the final value from the typical conditions simulation. This approach provides a realistic initial condition that reflects hydrologic processes occurring within the cover profile. In this study, the end-of-year heads reached an equilibrium state after the third year of the 5-year simulation. [SRRA107772-000009]

The moisture characteristic curves are then used to determine the unsaturated hydraulic conductivity for materials that are not fully saturated, using the van Genuchten-Mualem model (SRRA107772-000009):

$$K_\theta = K_s \Theta^\ell \left[1 - \left(1 - \Theta^{1/m}\right)^m\right]^2 \qquad \text{Eq. 4.4-7}$$

where:

K_θ = unsaturated hydraulic conductivity,

K_s = saturated hydraulic conductivity (see Table 4.4-2),

Θ = effective saturation (see Eq. 4.4-8),

ℓ = pore interaction term assumed to be -1.5 (SRRA107772-000009), and

$m = 1 - n^{-1}$ (see Eq. 4.4-6).

The effective saturation term (Θ) is defined by:

$$\Theta = \frac{\theta - \theta_r}{\theta_s - \theta_r} \qquad \text{Eq. 4.4-8}$$

where:

Θ = effective saturation,

θ = volumetric water content (bounded by porosity in Table 4.4-113),

θ_r = residual volumetric water content (see Eq. 4.4-6), and

θ_s = saturated volumetric water content (see Eq. 4.4-6).

4.4.1.3.6 HDPE Performance

The HDPE is an extremely important barrier relative to the performance of the SDF. It is expected to be an impervious and relatively long-lasting material. The HDPE performance relies on three key assumptions:

1. The assumed service life of the HDPE,
2. The assumed diameter of each defect, and
3. The assumed number of initial defects per area.

The following discusses each of these assumptions.

HDPE Service Life

As described in Section 3.2.6.7, the assumed service life of the HDPE is based on a three-staged chemical aging process (see Figure 3.2-36): antioxidant depletion (T_A), induction time (T_B), and polymer degradation (T_C). During the first stage (T_A), two processes occur which deplete antioxidants: oxygen diffuses into the geomembrane and the physical loss of the antioxidants from the geomembrane. Once the antioxidants are depleted, oxidation of the HDPE begins (T_B); however, this process is initially very slow with negligible impacts. Finally, the oxidation

process accelerates (T_C), resulting in decomposition in the material as free radicals attack the polymer chains. [Hsuan and Koerner, 1998 (DOI: 10.1061/(ASCE)1090-0241(1998)124:6(532))] It is assumed that this chemical decomposition process is localized, attacking the edges of the material (i.e., pre-existing defects or holes), which results in an increase of the diameter of the existing holes.

The assumed timing for each degradation stage is based on *Antioxidant Depletion and Service Life Prediction for HDPE Geomembranes Exposed to Low-Level Radioactive Waste Leachate*. [Tian, *et.al*., 2017 (DOI: 10.1061/(ASCE)GT.1943-5606.0001643)] For HDPE in a low-level waste disposal facility, the predicted antioxidant depletion time (T_A) is 730 years. For the second and third stages, Tian, et.al. (2017) considered three properties: break strength, break strain, and stress crack resistance. For Stage II (T_B), the shortest duration is 25 years and for Stage III (T_C) the shortest duration is 1,220 years. Thus, the minimum total service life is estimated to be 1,975 years. Note that if the longest durations for Stages II and III had been applied, the service life of the HDPE could be as long as 3,550 years. For modeling purposes, a service life of 2,000 years is assumed.

It should be noted that the service life estimates from Tian, *et.al*., 2017 (DOI: 10.1061/(ASCE)GT.1943-5606.0001643) are likely to underestimate the life span of HDPE. This is because the estimates for Stage II and Stage III degradation were developed based on data for HDPE exposed to leachates from municipal solid waste. Antioxidant depletion HDPE occurs more quickly when it is exposed to leachate from municipal solid waste relative to low-level waste or mixed waste leachate because municipal solid waste leachates have higher metal concentrations (i.e., catalysts to oxidation) and higher ionic strength than other leachates. [DOI: 10.1061/(ASCE)GT.1943-5606.0001643] Because the HDPE in the composite barrier of the SDF closure cap is placed above the waste, it is not expected to be exposed to any leachates other than those based on the natural environment.

Defect Diameter

Two diameters are assumed for each defect. As an initial condition, all initially assumed defects are assumed to have a relatively small diameter (2 mm). Giroud and Bonaparte (DOI: 10.1016/0266-1144(89)90009-5) indicate that this is the size of holes due to defective seams "that might escape detection by a construction quality assurance program."

Once the HDPE reaches the end of its service life, it is assumed that antioxidant depletion and flow along the perimeter of the existing defects would enlarge the holes. It is assumed that the diameter of the existing defects will increase by a factor of 5 (from 2 mm to 10 mm). This hole size was recommended by Benson and Benavides (SRRA107772-000009) to represent the expected effects of antioxidant depletion.

Number of Initial Defects

Giroud and Bonaparte (DOI: 10.1016/0266-1144(89)90009-5) provide an extensive analysis of geomembrane (i.e., HDPE) installations, detection of defects as part of quality assurance programs, and the effectiveness of defect repairs. Their study examined multiple sites of various sizes and functions and found general consistency in their findings. During initial inspections, one defect was identified for every 30 to 50 feet of seams. There was one outlier site in which one defect was identified for every 23 feet of seams; however, this site was not representative of a typical reservoir or liner system because this was a liner installed within a small acid holding tank with more complex geometry (i.e., angles and piping). For the sites described by Giroud and Bonaparte, after initial inspection and identification of the defects, repairs were made to reduce the number of defects. Based on follow up inspections, it is estimated that these repairs reduced the number of defects by a factor of 30 or more. [DOI: 10.1016/0266-1144(89)90009-5]

Based on their analysis, Giroud and Bonaparte (DOI: 10.1016/0266-1144(89)90009-5) conclude that "An average of one defect per 300 m (1,000 ft) of field seam can be expected with reasonably good installation, adequate quality assurance (which implies adequate quality control), and repair of noted defects. (Quality assurance followed by adequate repair drastically decreases the number of seam defects but does not totally eliminate them.)" The purpose of quality assurance inspections is to identify deficiencies. This implies that adequate quality control is necessary to support the recommendations from Giroud and Bonaparte. They also indicate that if HDPE geomembrane panels 6 to 10 meters wide are used, then one defect per 300 m (1000 ft) of seam is equivalent to a frequency of 3 to 5 seam defects per hectare. [DOI: 10.1016/0266-1144(89)90009-5]

Based on this discussion, the assumed number of initial defects is "five circular holes per hectare, which is consistent with a high level of quality control." [SRRA107772-000009] It should be acknowledged that Giroud and Bonaparte (DOI: 10.1016/0266-1144(89)90009-5) have indicated that a "frequency of 25 holes/ha (10 holes/acre) or more is possible when quality assurance is limited to an engineer spot-checking the work done by the geomembrane installer." However, it is appropriate to assume a high level of quality control for the construction of the SDF closure cap because HDPE installation is already being performed in support of SDU construction (i.e., HDPE between the upper and lower mud mats), and this work applies a rigorous quality control program that includes modern techniques for leak detection and repairs. [C-SPP-Z-00019] As part of closure cap construction, the HDPE installation, detection of defects, and repairs of defects shall all be performed according to standards established by the American Society for Testing and Materials (ASTM). Depending on the seam welding method used, each seam will be tested for defects and repaired using vacuum testing device, spark testing device, or air channel pressure test for double wedge welded seams, or shear and peel testing. [C-SPP-Z-00019]

4.4.1.3.7 Other Inputs and Assumptions in Support of the Closure Cap Model

The slope of the composite barrier and the drainage layer, the maximum slope length, and the contact factor are all required inputs for the leakage rate calculation (Eq. 4.4-5) which have not yet been discussed herein.

The slope (β) is the change in the vertical distance over the change in the horizontal distance, or the rise over run. The leakage rate is based on the slope of the underlying lower backfill layer and foundation layer. As defined in Table 3.2-8, the lower backfill layer has a 4% slope (or 4:100 = 0.04).

As described in Section 3.2.6.2, the *Saltstone Disposal Facility Closure Cap Concept Update for Large-Scale Disposal Units* (SRR-CWDA-2018-00087) included an alternative closure cap design which assumes a shallow 1.5% surface-slope. This design results in a maximum surface-slope of 1,170 feet (356.6 m). Although the assumed design (i.e., the closure cap with the 4% slope for the composite barrier and drainage system, as shown in Figure 4.4-2) has a maximum surface slope length of 1,020 feet (311 m), the higher value of 1,170 feet was assumed for the horizontal slope length (L) in Eq. 4.4-5 because this longer length results in a higher leakage rate estimate. This assumed input ensures that the infiltration values will be overestimated.

Finally, the unitless contact factor (C_{qo}) is assumed to be 0.21. This value assumes good contact conditions between the GCL and the overlying HDPE per Giroud (1997). [ISSN 1072-6349] There are three reasons that good contact is expected:

1) The lower backfill and foundation layers of the closure cap are expected to undergo grading and compaction to create a relatively smooth surface upon which to place the GCL.
2) The GCL placement will be performed according to quality control standards to minimize the occurrence of wrinkles and surface irregularities.
3) The HDPE will be under constant pressure because it will be buried beneath a minimum of six feet of material and a hydraulic head is expected to form over it as water percolates through the overlying materials. This assumption is consistent with discussions by Giroud and Bonaparte (DOI: 10.1016/0266-1144(89)90022-8).

4.4.1.3.8 Summary of Assumptions

The key assumptions for the Closure Cap Model are summarized as follows. These assumptions are used for compliance modeling; however, some sensitivity cases or alternative models are provided in Section 5.8.2 to provide additional insights into the significance of some of these assumptions.

- Impacts of erosion are assumed to have a negligible impact on infiltration rates. See Section 4.4.1.5 for erosion estimates.
- Future meteorological conditions will reflect current conditions.
- The vegetative cover over the closure cap will be grass.
- The geotextile fabric and geotextile filter fabric layers and the foundation layer are not credited for any hydraulic performance.
- Closure Cap layers with thicknesses that vary are assumed to be the minimum thickness.
- The hydraulic conductivities of the topsoil and upper and middle backfill layers are based on the assumptions that the soils have undergone pedogenesis and lost compaction.
- The hydraulic conductivity of the upper lateral sand drainage layer assumes that minimum procurement specifications (i.e., 5.0E-02 cm/s) will be met.
- The assumed service life of the HDPE is 2,000 years.
- The assumed diameter of each HDPE defect is 2 mm (initially) and 10 mm (after the end of service life).
- The assumed number of initial defects is 5 holes per hectare.
- The composite barrier and drainage layer have a 4% slope.
- The maximum slope length is assumed to be 1,170 feet (356.6 m).
- The contact factor 0.21 is based on assuming good contact between the HDPE and GCL layers.

4.4.1.4 Intermediate Results and Interfaces for the Closure Cap Model

The following sections present intermediate results from the closure cap model and specify interfaces between the closure cap model and other models used in the SDF PA.

4.4.1.4.1 Volumetric Water Content

As indicated in Section 4.4.1.3.3, an evaluation was performed that considered the impacts of the thickness of the middle backfill layer. This evaluation determined that the thickness of the middle backfill layer is insignificant hydraulically because the erosion barrier acts as a "choke" in the cover profile, forcing water redistribution to occur almost exclusively in the upper backfill layer and the topsoil. [SRRA107772-000009]

The erosion barrier has the same saturated hydraulic conductivity as the upper and middle backfill layers, but has much lower porosity (Table 4.4-2). Consequently, the erosion barrier remains saturated or nearly saturated at all times, such that the rate at which water can flow through the erosion barrier is limited by its saturated hydraulic conductivity. As a result, little redistribution of water occurs in the middle backfill layer, and flow occurs through the erosion barrier and middle backfill layer under nearly unit gradient conditions.

This behavior is illustrated by the following figures, which show water content versus node number (effectively depth) in the profile for a typical year (2002) via Figure 4.4-7 and the wettest year from the wettest ten-year period (1997) via Figure 4.4-8.

Figure 4.4-7: Volumetric Water Content Profile of a Typical Year (2002)

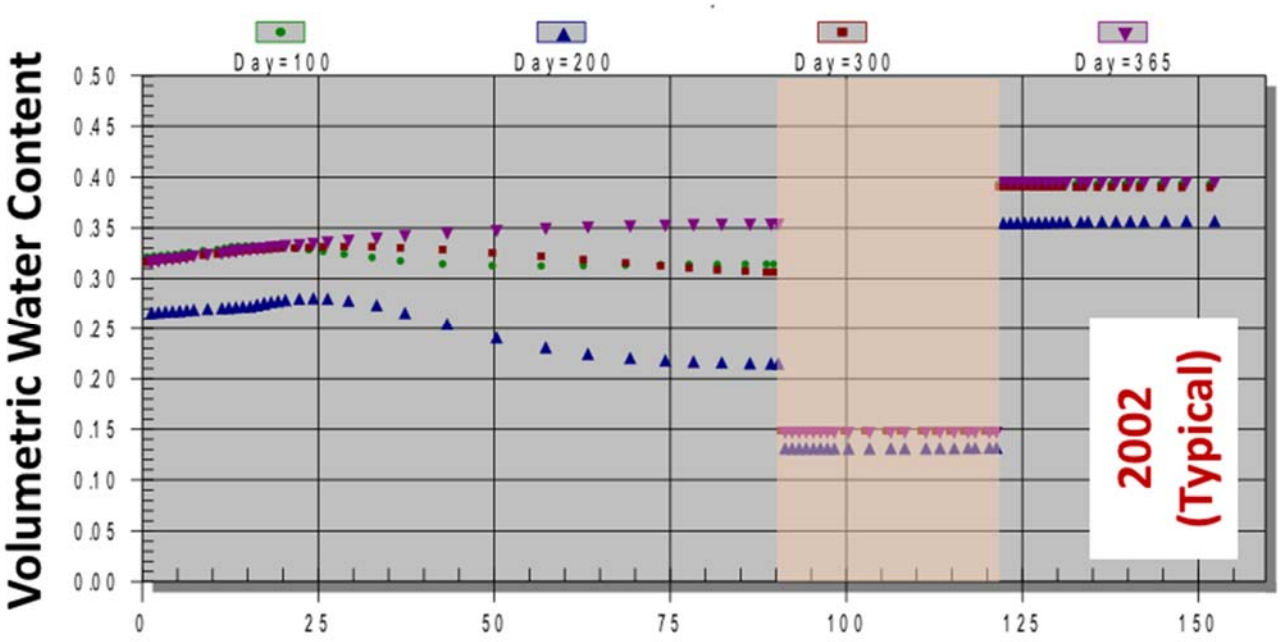

[SRRA107772-000009]

Figure 4.4-8: Volumetric Water Content Profile of a Wetter Year (1997)

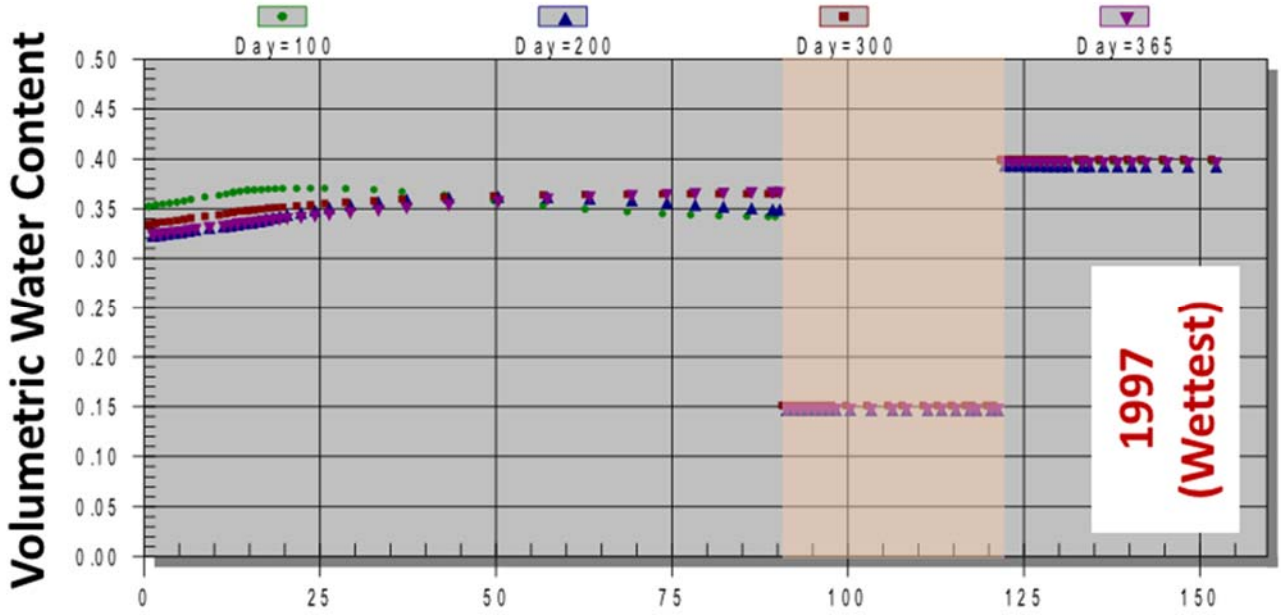

[SRRA107772-000009]

Note that the nodal spacing (or thickness) was set to 1 mm near the boundaries and as large as 60 mm away from the boundaries to achieve a mass balance error < 1 mm/yr. [SRRA107772-000009] These figures indicate the nodal position of the erosion barrier as a tan block. These results show four different times during the year (Julian day = 100, 200, 300, and 365). For both profile years, the water content profile is relatively uniform with depth and near saturation in the erosion barrier and the middle backfill layer. In contrast, a significant variation in water content can occur with depth and time above the erosion barrier due to seasonal water redistribution caused by atmospheric forcing at the surface (e.g., see typical year profile in Figure 4.4-7).

4.4.1.4.2 Water Balance and Percolation Rates

The next intermediate result from the Closure Cap Model is the water balance summary for the typical years and from the years from the 10-year wettest period (1989 to 1998) (Figure 4.4-9).

Figure 4.4-9: Water Balance for Simulated Years

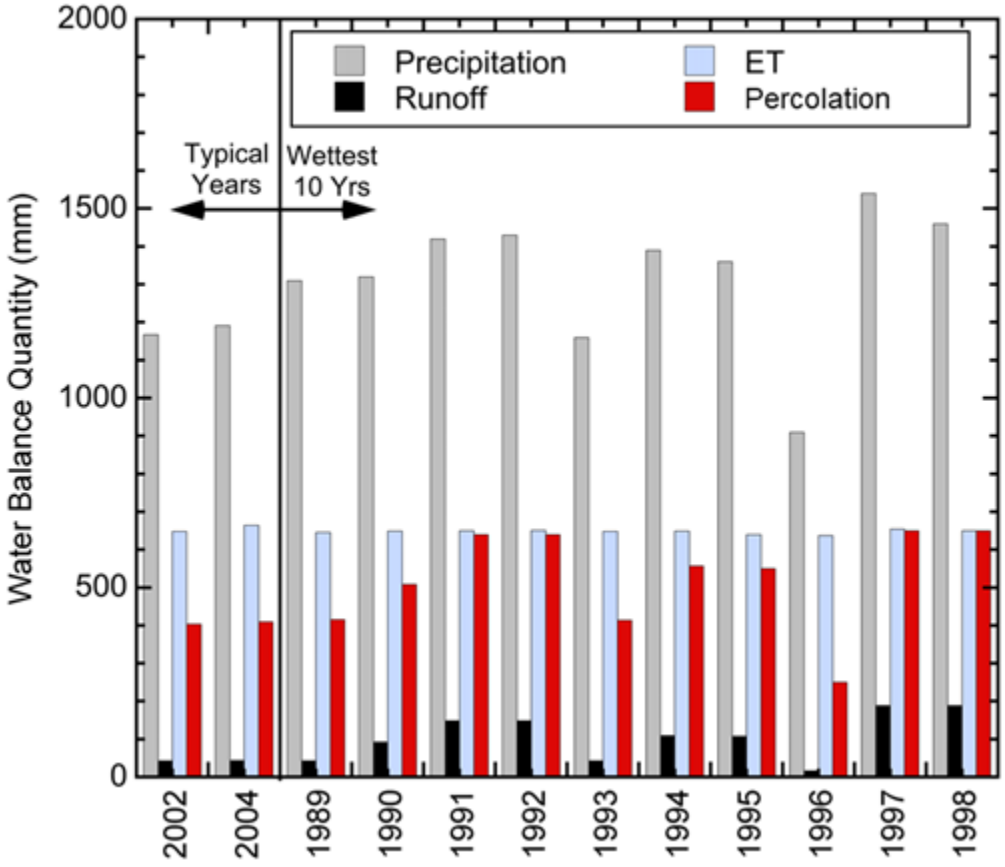

[SRRA107772-000009]

As shown, the evapotranspiration (ET) shows relatively little variability (near 650 mm/yr). This is due to the humid climate with conditions near the maximum

potential ET. As such, the calculated percolation rate varies mainly as a function of the precipitation and runoff.

Figure 4.4-10 provides a more direct comparison of the deep drainage rates versus the annual precipitation. This figure shows that percolation is closely (but not perfectly) correlated to the precipitation rate; for the two typical years (2002 and 2004) and two of the other years evaluated from the 10-wettest year period (1989 and 1993), percolation was estimated to be approximately 400 mm/yr.

Figure 4.4-10: Percolation versus Annual Precipitation

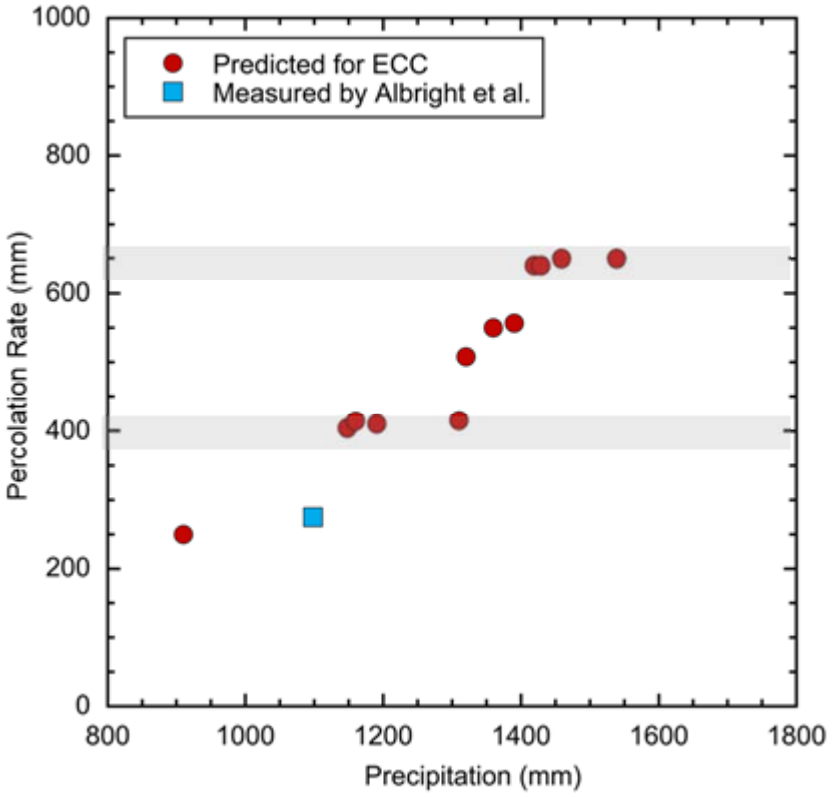

[SRRA107772-000009]
ECC = Engineered Closure Cap

Also, in the wettest 10-year period, the year 1996 showed relatively little precipitation, resulting in a relatively low percolation rate (approximately 250 mm/yr). The four highest precipitation years (1991, 1992, 1997 and 1998) all resulted in approximately 650 mm/yr. Therefore, 400 mm/yr was selected as a representative percolation rate for expected climate conditions and 650 mm/yr was selected as a representative percolation rate for wetter climate conditions (Table 4.4-3). [SRRA107772-000009]

Table 4.4-3: Summary of Percolation Estimates

Climate Condition	Percolation Rate (mm/yr)
Current and Expected Climate Condition	400
Wetter Climate Condition	650

Note that the percolation rate of 400 mm/yr is consistent with earlier modeling efforts. In 2008, similar modeling was performed which included an estimate of infiltration for an equivalent closure cap but excluded the composite barrier and lateral sand drainage layer; the resulting estimate was 16.45 in/yr (or 417.8 mm/yr). [WSRC-STI-2008-00244] Similarly, a large scale estimate of the average recharge rate for the entire General Separations Area was estimated to be an approximately 15 in/yr (380 mm/yr). This estimate applies to the natural system with no closure cap. For this latter estimate, a range of uncertainty was specified as being between 10 in/yr (250 mm/yr) and 16 in/yr (410 mm/yr), as summarized in *Groundwater Flow Simulation of the Savannah River Site General Separations Area*. [SRNL-STI-2017-00008, Rev. 1] The similarity of these results provides confidence in the recommended percolation rate of 400 mm/yr.

While the percolation rate correlates closely to the precipitation rates, this correlation is not perfectly linear. The temporal variability and durations of individual rainfall events within each simulated year influenced the resulting runoff and percolation rates, resulting in the non-linearity of this comparison.

Figure 4.4-10 also shows an actual field-measured value (blue square) from an analogue site in Albany, GA. This site is approximately 200 miles southwest of the Savannah River Site and has a similar cap design and very similar meteorological conditions. Since the Albany, GA, data point is at the lower-end of the values shown, it may indicate that the WinUNSAT-H model may slightly over-estimate percolation under the SRS-like conditions.

4.4.1.4.3 Leakage Rates (Infiltration)

The leakage rates through the composite barrier (HDPE and GCL layers) were calculated using Eq. 4.4-5. These leakage rates serve as the basis for the infiltration rates assumed in the Vadose Zone Flow Model (see Section 4.4.4). The calculations were repeated a number of times to evaluate the system over a range of varying conditions. To summarize, the following inputs were used: the two percolation rates (Table 4.4-3), the two saturated hydraulic conductivities for the upper lateral sand drainage layer (Table 4.4-2), and the two HDPE defect diameters (2 mm and 10 mm, per Section 4.4.1.3.6). In addition to these parameters, one calculation was also performed which assumed the more bounding saturated hydraulic conductivity for the GCL (i.e., 1.0E-08 cm/s instead of 1.0E-09 cm/s per Table 4.4-2). Table 4.4-4 shows the resulting infiltration rates.

Table 4.4-4: Summary of Infiltration Rate Estimates

Percolation Rate (mm/yr)	Drainage Layer Saturated Conductivity (cm/s)	HDPE Defect Diameter (mm)	Calculated Infiltration Rate (mm/yr)
400	5.0E-02	2	0.0060
400	5.0E-02	10	0.0083
400	1.0E-02	2	0.091
400	1.0E-02	10	0.13
400	1.0E-02	10	0.69 [a]
650	5.0E-02	2	0.013
650	5.0E-02	10	0.018
650	1.0E-02	2	0.22
650	1.0E-02	10	0.30

[Modified from SRRA107772-000009; colors added to assist in comparison to Table 4.4-5]
(a) This calculation assumed the saturated hydraulic conductivity of the GCL was 1.0E-08 cm/s. All others assumed 1.0E-09 cm/s.

4.4.1.4.4 Recommended Infiltration Rates

An evaluation of the leakage rates shown in Table 4.4-4 was performed to select recommended infiltration rates as would be appropriate for various modeling conditions or scenarios. [SRR-CWDA-2018-00030] Table 4.4-5 provides the recommended infiltration rates based on this evaluation. Note that the coloring of the text in Table 4.4-5 maps to the depiction of these recommendations, as shown in Figure 4.4-11. In addition to the recommended infiltration rates, historical results from the previous Hydrologic Evaluation of Landfill Performance (HELP) modeling (WSRC-STI-2008-00244) are also depicted. These earlier infiltration recommendations from HELP modeling relied on assumptions which are now deemed to be unrealistic based an improved understanding of closure system performance (i.e., "silting in" of the upper lateral sand drainage layer and the assumptions that tree roots will puncture holes through the composite barrier). [SRRA107772-000009]

Table 4.4-5: Recommended Infiltration Rates for SDF PA Modeling

Year	Current and Expected Climate Condition			Wetter Climate Condition	
	Best Estimate (Realistic) (mm/yr)	Compliance (MPAD) (mm/yr)	Pessimistic (Conservative) (mm/yr)	Best Estimate (mm/yr)	MPAD (mm/yr)
0	0.0060	0.0060	0.0060	0.013	0.013
500	0.0060	0.0060	0.0060	0.013	0.013
500	0.0060	0.091	0.091	0.013	0.22
2000	0.0060	0.091	0.091	0.013	0.22
>2000	0.0083	0.13	0.69	0.018	0.30

[SRR-CWDA-2018-00030]

Figure 4.4-11: Recommended Infiltration Rates Based on the Calculated Leakage Rates from the Closure Cap Model

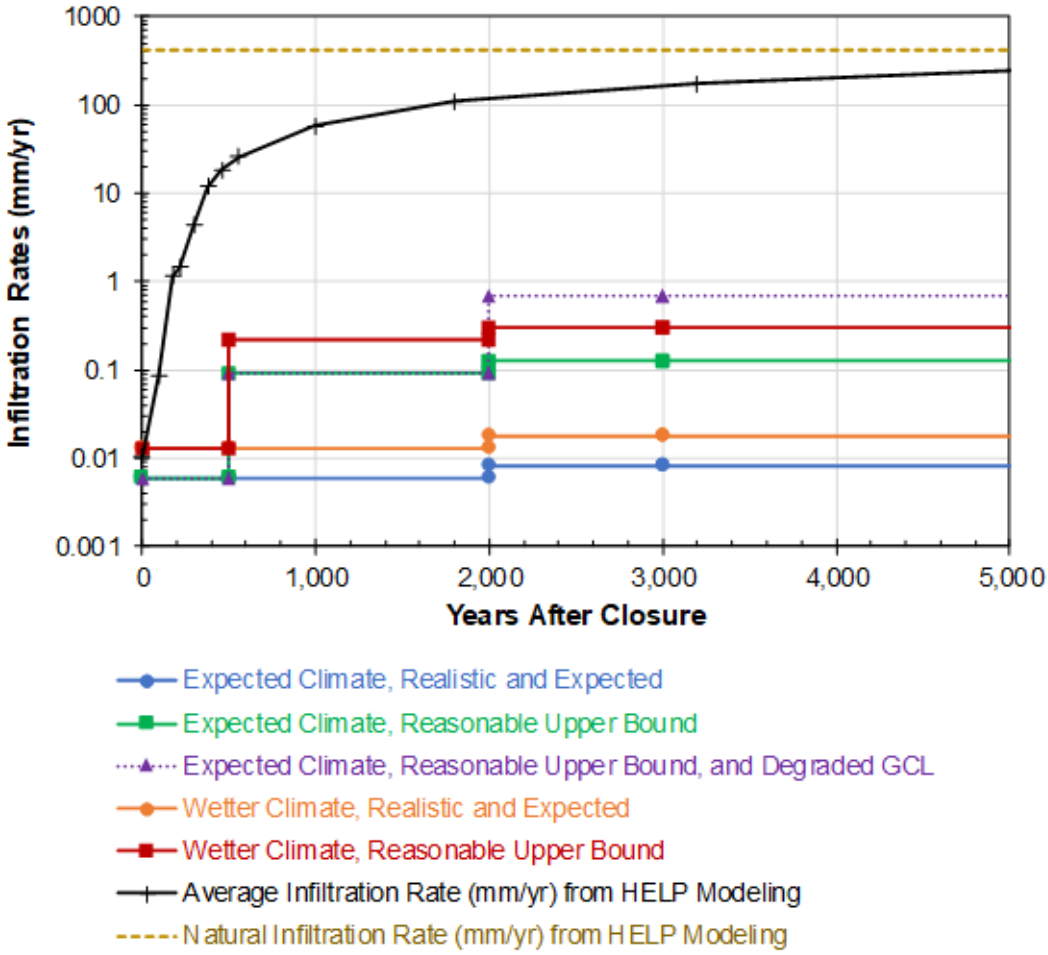

Note: The Average Infiltration Rate from HELP Modeling and the Natural Infiltration Rate from HELP Modeling come from earlier (2008) modeling, described in WSRC-STI-2008-00244, which relied on different assumptions.

Within each climate condition, the values are identical for the first 500 years. This is because the three materials which are expected to have the greatest influence on the infiltrations rates (i.e., the sand drainage layer, the HDPE, and the GCL) are all expected to perform as designed for the first 500 years. At 500 years, the Compliance Case and the Pessimistic Cases assume that the sand drainage layer becomes modestly less permeable. Based on the observations of the analog sites described near the end of Section 3.2.6.7, this is a pessimistic assumption; as such, it is applied to the Compliance Case for enhanced defensibility, and applied to the Pessimistic Case because it is appropriate, given the purpose of these modeling cases. Then at 2,000 years, the Compliance Case and the Pessimistic Cases both assume that holes in the HDPE increase in size as a result of antioxidant depletion. Also at 2,000 years, the Pessimistic Case represents an unlikely scenario in which

the GCL becomes more 10 times more permeable as the result of assumed cation exchange.

Note the values presented here are not identical to those reported by the University of Virginia (UVA) (SRRA107772-000009). This is due to a correction that was implemented to the infiltration calculation, as discussed in SRR-CWDA-2018-00030.

4.4.1.4.5 Modeling Interfaces for the Closure Cap Model

As described earlier, the Closure Cap Model does not include the foundation layer, lower backfill layer, lower lateral sand drainage layer, or the composite barrier (HDPE and GCL layers) above each SDU. The SDF PA ignores the foundation layer. Therefore, the Closure Cap Model interfaces with the Vadose Zone Flow Model where the composite barrier (between the upper lateral sand drainage layer and the ignored foundation layer) contacts the top of the lower backfill. At this interface, the estimated infiltration rates from the closure cap model are used as a primary input for the Vadose Zone Flow Model (see Section 4.4.4).

In addition to the modeling interface, there are a few inputs and assumptions made within the Closure Cap Model that influence other models. Specifically, the closure cap design and physical properties that are used as inputs to the Closure Cap Model are also used as inputs to the Airborne Pathway Release Model (Section 4.4.7).

Finally, it should be noted that while both the Closure Cap Model and the Cementitious Degradation Model (Section 4.4.2) evaluate the service life for the HDPE and HDPE/GCL layers based on research from Tian, et.al., 2017 (DOI: 10.1061/(ASCE)GT.1943-5606.0001643), different approaches were used to simulate the degradation of the material. Specifically, the HDPE within the closure cap model is simulated as degrading as a step change that initiates at 2,000 years. Alternatively, within the Cementitious Degradation Model the composite barrier above the roof of each SDU (which includes HDPE) is simulated to degrade over time, with a service life of approximately 1,600 to 1,900 years.

4.4.1.5 Evaluation of Potential Long-Term Erosion

As indicated in 2.7.3, this PA assumes that erosion will not significantly impact the estimated infiltration rates. The estimates for the percolation rates ignored the potential impacts from surface erosion. Regardless, Section 5.8.2 includes a number of sensitivity cases developed to provide insights relative to the potential risks associated with erosion. Also as indicated in Section 3.2.6.7, erosion, gullying, and slope stability will all be addressed as part of the final closure cap design. Additionally, the following provides a preliminary evaluation of long-term sheet erosion.

While erosion is expected to increase the percolation rate over time, such an increase is not expected to be significant within the Compliance Period (i.e., within the first

1,000 years). To support this assertion, the rate of erosion is estimated below using the Revised Universal Soil Loss Equation (RUSLE) from the United States Department of Agriculture's Handbook: *Predicting Soil Erosion by Water: A Guide to Conservation Planning With the Revised Universal Soil Loss Equation (RUSLE)* (USDA-HDBK-703).

The formula for the RUSLE (USDA-HDBK-703) is given as:

$$A = R \times K \times L \times S \times C \times P \qquad \text{Eq. 4.4-9}$$

where:

A = Computed spatial average soil loss and temporal average soil loss per unit of area, expressed in the units selected for K and for the period selected for R. In practice, these are usually selected so that A is expressed in ton/acre/year.

R = Rainfall-runoff erosivity factor: the rainfall erosion index plus a factor for any significant runoff from snowmelt.

K = Soil erodibility factor: the soil-loss rate per erosion index unit for a specified soil as measured on a standard plot, which is defined as a 72.6-ft (22.1-m) length of uniform 9% slope in continuous clean-tilled fallow.

L = Slope length factor: the ratio of soil loss from the field slope length to soil loss from a 72.6-ft length under identical conditions.

S = Slope steepness factor: the ratio of soil loss from the field slope gradient to soil loss from a 9% slope under otherwise identical conditions.

C = Cover-management factor: the ratio of soil loss from an area with specified cover and management to soil loss from an identical area in tilled continuous fallow.

P = Erosion Control Practice Factor: the ratio of soil loss with a support practice like contouring, strip-cropping, or terracing to soil loss with straight-row farming up and down the slope.

Table 4.4-6 provides the recommended values for each of these RUSLE parameters. With the exception of the "cover management factor" (more commonly referred to as a "vegetative cover factor"), each of these parameters has a single value assigned to it. Therefore, Eq. 4.4-9 can be shortened to:

$$A = 49.4 \times C \qquad \text{Eq. 4.4-10}$$

where:

A = average soil loss (ton/acre/year),

49.4 = constant (in units of ton/acre/year) based on parameter values in Table 4.4-6, and

C = vegetative cover factor (dimensionless).

For the vegetative cover factor, three scenarios are considered: pinewood forest, bahia grass, and "unmanaged undergrowth," wherein the latter is based on a discussion provided in the NRC's *Technical Review: Hydraulic Performance and Erosion Control of the*

Planned Saltstone Disposal Facility Closure Cap and Adjacent Area (Docket No. PROJ0734) [ML18002A545]. Note that the Closure Cap Model assumes grass cover as this vegetation is expected to provide the highest estimate for infiltration rates. However, given the environmental conditions at SRS, it is very likely that after the institutional control period the vegetative cover may be overcome by advancing pinewood.

Table 4.4-6: Erosion Estimate Parameters for RUSLE

Parameter	Short Description	Assumed Value(s)	Basis for Assumed Value(s)
R	Erosion Index	300 (100 ft • ton/acre per in/yr)	Based on interpretation of Figure 2-1 from USDA-HDBK-703, which shows that Aiken County (i.e., the location of the SDF) is between the erosion index values of 275 and 300 (in units of 100 ft • ton/acre per in/yr). Because the location of the SDF is nearer the 300 value, and because the higher value will bias results towards higher rates of erosion, this value is assumed.
K	Soil Erodibility Factor	0.28 (tons/acre per unit of R)	Appendix I of WSRC-STI-2008-00244 provides a soil erodibility factor of 0.28 for typical SRS topsoil and 0.2 for SRS control compacted backfill. These values were based on an analysis of the soil textural classifications. The higher of the two values (0.28) is assumed as this will bias the results toward a higher erosion estimate.
L	Length Factor	0.59	The length and slope factors are combined into a single parameter. The value of 0.59 was extrapolated based on the data in Table 4-1 from USDA-HDBK-703, based on a 3% surface slope and maximum slope length of 1,170 feet. Note that for the closure cap design with the 3% slope the maximum slope is 1,020 feet (per SRR-CWDA-2018-00087), but for greater defensibility, the higher slope length (based on an alternative design with a 1.5% surface slope) is assumed.
S	Slope Factor		
C	Vegetative Cover Factor	0.001	Factor for pinewood forest, as assumed in Appendix I of WSRC-STI-2008-00244.
		0.004	Factor for bahia grass, as assumed in Appendix I of WSRC-STI-2008-00244.
		0.007	Factor for unmanaged undergrowth, assumed based on the discussion provided in the NRC's *Technical Review: Hydraulic Performance and Erosion Control of the Planned Saltstone Disposal Facility Closure Cap and Adjacent Area (Docket No. PROJ0734)*. [ML18002A545]
P	Erosion Control Practice Factor	1	Chapter 6 of USDA-HDBK-703 provides a quantitative approach for estimating the support practice factor for contouring; however, for the SDF PA the maximum value of 1 is assumed for simplicity as this will bias the results toward a higher erosion estimate.

Given an assumed dry bulk density for SRS topsoil of 1.67 g/cm^3 (or 104.25 lbs/ft^3) (per Appendix I of WSRC-STI-2008-00244), the average soil loss is converted into an erosional loss rate (in/yr) as follows:

$$Erosional\ Loss = \frac{A \times 2000\frac{lbs}{ton} \times 12\frac{in}{ft}}{43560\frac{ft^2}{acre} \times 104.25\frac{lbs}{ft^3}} \qquad \text{Eq. 4.4-11}$$

where:

A = average soil loss (ton/acre/year) as calculated in Eq. 4.4-10.

Table 4.4-7 provides the estimated erosional loss rates for each assumed vegetative cover.

Table 4.4-7: Estimated Erosional Loss Rates

Assumed Vegetative Cover	Estimated Soil Loss (tons/acre/year)	Estimated Erosional Loss Rate (in/yr)
Pinewood Forest	0.049	2.6E-04
Bahia Grass	0.20	1.0E-03
Unmanaged Undergrowth	0.35	1.8E-03

To apply these estimated erosional loss rates, it is reasonable to assume that vegetation would persist at the surface, despite erosion: the SRS environment is such that growth of vegetation is relatively stable. As the topsoil is eroded at the surface, deposition of biomass from the vegetation and other environmental conditions would influence the underlying backfill soil such that the backfill soil directly beneath the topsoil would evolve into topsoil and replace any surface mass that is lost to erosion. As such, the topsoil layer is assumed to remain 6 inches thick into perpetuity, while the underlying upper backfill layer would become thinner over time as a response to soil loss.

Table 4.4-8 provides an overview of the potential change to the thickness of the upper backfill layer over time, based on the assumed vegetative covers. These changes are also depicted graphically in Figure 4.4-12. These results show that within 10,000 years none of the conditions fully depleted the upper backfill layer.

Table 4.4-8: Estimated Thickness (in) of the Upper Backfill Layer Over Time, Based on Assumed Vegetative Covers

Year	Upper Backfill Thickness (in)		
	Pinewood Forest	Bahia Grass	Unmanaged Undergrowth
0	30.0	30.0	30.0
50	30.0	29.9	29.9
100	30.0	29.9	29.8
200	29.9	29.8	29.6
500	29.9	29.5	29.1
800	29.8	29.2	28.5
1,000	29.7	29.0	28.2
1,200	29.7	28.7	27.8
1,600	29.6	28.3	27.1
2,000	29.5	27.9	26.3
4,000	29.0	25.8	22.7
6,000	28.4	23.7	19.0
8,000	27.9	21.6	15.4
10,000	27.4	19.6	11.7

Figure 4.4-12: Estimated Erosional Profiles for the Upper Backfill Layer

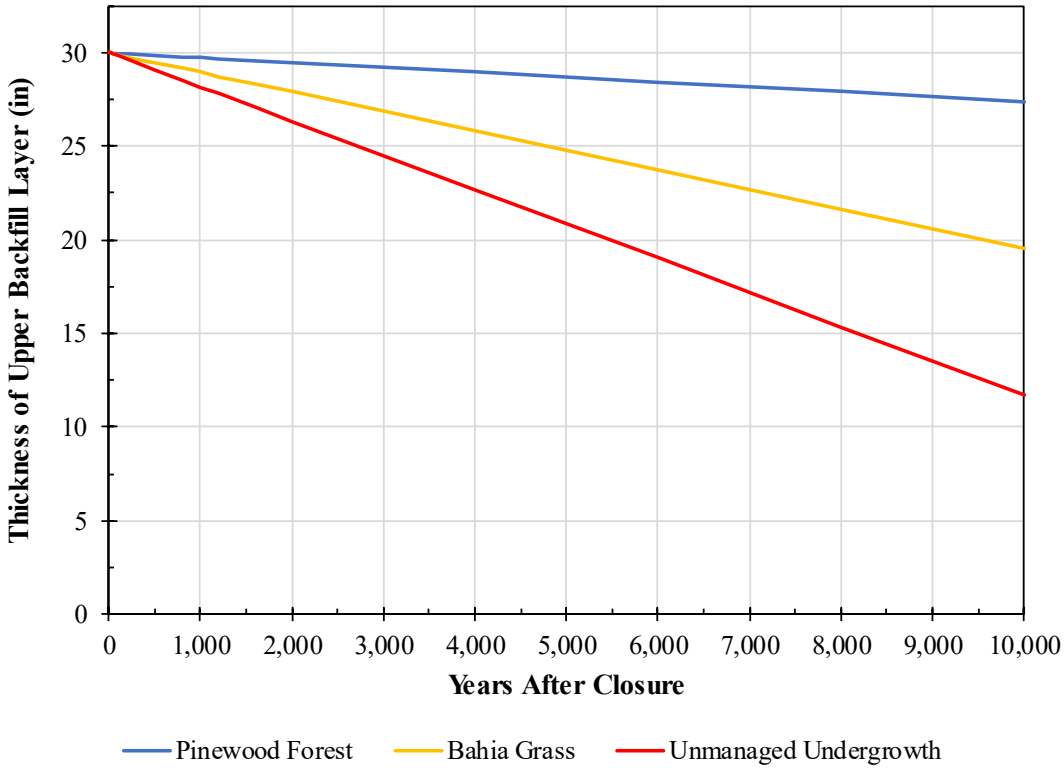

As described in Section 4.4.1.3.3, an evaluation was performed during the development of the WinUNSAT-H model to consider the impacts of the thickness of the middle backfill layer, which can vary significantly between the apex of the closure cap and the edge of the side slope. Over the entire range of thicknesses considered, the annual percolation rates differed by less than 2%, indicating that the middle backfill thickness will have a negligible influence on the infiltration rates, relative to other parameters.

While the upper backfill layer and the middle backfill layer are separate and discrete features within the current closure cap design, they both have identical material properties and serve similar functions. Given that the thickness of the middle backfill layer does not have a strong influence over infiltration rates, it is reasonable to expect that changes to the thickness of the upper backfill layer would also exhibit a minimal influence. Therefore, given this evaluation of potential long-term erosion, the assumption that erosion will not significantly influence the SDF performance is reasonable.

Regardless, a number of sensitivity cases have been developed to evaluate infiltration rates under extremely different (i.e., less reasonable) modeling assumptions (see Section 5.8.2). Because a number of these sensitivity cases assume much higher infiltration rates, the dose results are higher than the Compliance Case; however, all of the doses meet performance objectives.

4.4.2 Cementitious Degradation Model

The SDF is designed to contain salt waste through: (1) immobilization of initially liquid salt feedwater in the form of a monolithic, low permeability, low Eh, saltstone; and (2) encapsulation of the saltstone within SDUs, which are comprised of barriers to advective and diffusive release to the environment, as well as slowing the ingress of oxygen from outside the disposal unit to the saltstone monolith. The design intent is to limit contaminant release to a controlled and low rate. Cementitious materials play a prominent role in the design and long-term performance of the SDF. Saltstone exhibits low permeability and diffusivity, and thus represents a physical barrier to waste release. The waste form is also reducing, which creates a chemical barrier to waste release for certain key radionuclides, notably Tc-99. Similarly, the concrete shell of a SDU provides an additional physical and chemical barrier to radionuclide release to the environment. [SRNL-STI-2018-00077]

Over time, disposal unit materials are expected to degrade through a variety of mechanisms, leading to higher contaminant releases. The physical and chemical state of cementitious materials will evolve over time through a variety of processes, leading to degraded barrier performance over PA timescales of thousands to tens of thousands of years. Previous studies of cementitious material degradation in the context of low-level waste disposal have identified sulfate attack, carbonation-influenced steel corrosion, and decalcification (primary constituent leaching) as the chemical degradation phenomena of most relevance to SRS exposure conditions. [ML121240822, WSRC-STI-2007-00607, SRNL-STI-2010-00035, CBP-TR-2009-002, SRNL-STI-2013-00118, SRNL-STI-2015-00236]

This section discusses the cementitious degradation analyses used to develop degradation time scales in support of the SDF PA flow and transport modeling efforts as fully documented in SRNL-STI-2018-00077. The analyses were performed for each of the three degradation phenomena (sulfate attack, carbonation-influenced steel corrosion, and decalcification) with degradation time scales estimated for saltstone and SDU concrete associated with each SDU design under "conservative estimate" (CE), "compliance value" (CV), and "best estimate" (BE) assumptions. Note that the three assumptions referred to as CE, CV, and BE, reflect the values used for the Pessimistic Case, the Compliance Case, and the Realistic Case, respectively. The combined effects of multiple phenomena were then considered to determine the most limiting degradation time scale for each cementitious material. Degradation times were estimated using analytic solutions, supported by numerical simulation codes provided through the DOE Cementitious Barriers Partnership (CBP) Software Toolbox (http://cementbarriers.org). Also considered in the development of the degradation times were the added influences of processes occurring during facility construction and/or operations, such as anchor penetrations and exposure to bleed water.

The specific SDU designs evaluated are SDU 1, SDU 4, SDU 2-types (SDU 2A, SDU 2B, SDU 3A, SDU 3B, SDU 5A, SDU 5B), SDU 6, and SDU 7-types (SDU 7, SDU 8, SDU 9, SDU 10, SDU 11, SDU 12). Only one scenario is geometric configuration is considered from each of the SDU 1, 4, 2 and 6 designs. This analysis reflects as-built dimensions and construction quality. For the SDU 7-type design, both "Design" and "Design Margin" (DM) configurations are considered. The expected Design scenario represents as-designed dimensions and construction quality for SDUs

7 through 12. The hypothetical DM scenario reflects postulated thinner as-built concrete barriers and unrepaired physical damage from various construction techniques (e.g., wall form wire anchors). For each of the SDU 1, 4, 2, 6 and 7 designs, material degradation is defined for BE, CV, and CE input values.

4.4.2.1 General Moving Reaction Front

The three main degradation mechanisms under consideration share the same basic functional form, wherein a chemical reaction zone moves slowly as a sharp front across the porous medium, and diffusion (except for decalcification of the saltstone monolith at later times) is the dominant transport mode for the fluid (gas or liquid) phase reactant, as shown in Figure 4.4-13.

Figure 4.4-13: Generic Moving Front Controlled by Diffusion

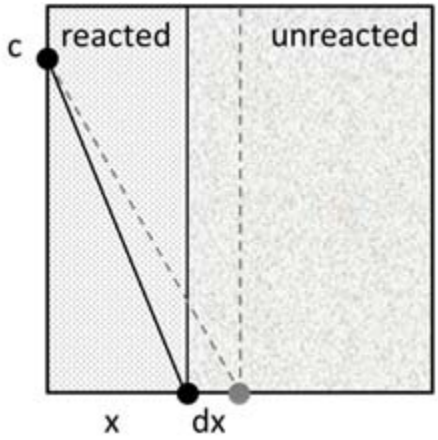

The differential molar balance for the diffusion-controlled moving front system depicted in Figure 4.4-13 can be expressed as:

$$Sn\tau D_m \frac{c}{x} dt = R(1-n)\rho_s dx \qquad \text{Eq. 4.4-12}$$

where:

S = saturation of fluid phase delivering reactant to moving front [L^3 liquid-phase / L^3 void-space],

n = porosity [L^3 void-space / L^3 total],

τ = tortuosity, defined here as the ratio of effective to molecular diffusion coefficient (< 1) [-],

D_m = molecular diffusion coefficient for fluid phase [L^2/T],

x = penetration depth [L],

t = elapsed time [T],

c = concentration of fluid phase reactant [mol / L^3],

R = reaction capacity of solid [mol / M solid], i.e., moles of fluid phase reactant consumed per mass of solid, and

ρ_s = solid / mineral density [M/L^3 solid].

Assuming the fluid phase molecular diffusion coefficient is a constant, integrating Eq. 4.4-12 yields the analytical expression for penetration depth (front position):

$$x = \left[\frac{2Sn\tau D_m ct}{(1-n)\rho_s R}\right]^{1/2} \quad \text{Eq. 4.4-13}$$

which can be rewritten as:

$$x = At^{1/2} \quad \text{Eq. 4.4-14}$$

and A is a rate constant defined as:

$$A = \left[\frac{Sn\tau D_m c}{(1-n)\rho_s R}\right]^{1/2} = \left[\frac{SnD_{eff}c}{\rho_b R}\right]^{1/2} \quad \text{Eq. 4.4-15}$$

where:

D_{eff} = effective diffusion coefficient for fluid phase [L^2/T], and

ρ_b = bulk density [M/L^3].

The time, t_0, it takes for the moving front to reach a specific penetration depth of x_0 can be defined as:

$$t_0 = \frac{{x_0}^2}{A^2} \quad \text{Eq. 4.4-16}$$

Eq. 4.4-13 through Eq. 4.4-16 are generalized equations that based on different reaction parameters can be applied to the three degradation mechanisms. In the case of sulfate attack, sulfate dissolved in the liquid phase diffuses into the porous medium and reacts with the solid to form ettringite or gypsum). In the case of carbonation, carbon dioxide in the gas phase diffuses into the porous medium and reacts with the solid, forming calcite and lowering the pH. In the case of decalcification, the reactive process is calcium in the solid dissolving into the liquid phase; the dissolved calcium then diffusing out of the porous medium (before advection becomes a dominant process). The following sections address the specifics of the analyses performed to evaluate sulfate attack (Section 4.4.2.2), carbonation (Section 4.4.2.3), steel corrosion (Section 4.4.2.4), and decalcification (Section 4.4.2.5).

Although, Eq. 4.4-13, Eq. 4.4-14, and Eq. 4.4-15 assume that the diffusion coefficient is fixed in time and space, if physical damage to the pore structure occurs behind the front, then the effective diffusion coefficient may increase allowing the front to penetrate deeper than assumed based on the $t^{1/2}$ dependence reflected in Eq. 4.4-14. If damage occurs around the reaction front, then the diffusion distance may effectively not increase beyond some maximum distance, δ [L], and penetration depth will be proportional to time t, instead of $t^{1/2}$ at later times. Assuming penetration initially follows Eq. 4.4-14, this alternative relationship is described by:

$$x = \frac{\delta}{t_\delta} t = \frac{\delta}{\delta^2/A^2} t = \frac{A^2}{\delta} t \qquad \text{Eq. 4.4-17}$$

where:

δ = penetration through time t_δ [L], and

t_δ = time at which penetration reaches δ [T].

Eq. 4.4-14 and Eq. 4.4-17 are depicted in Figure 4.4-14.

Figure 4.4-14: Linear Penetration Rate Beyond Distance δ

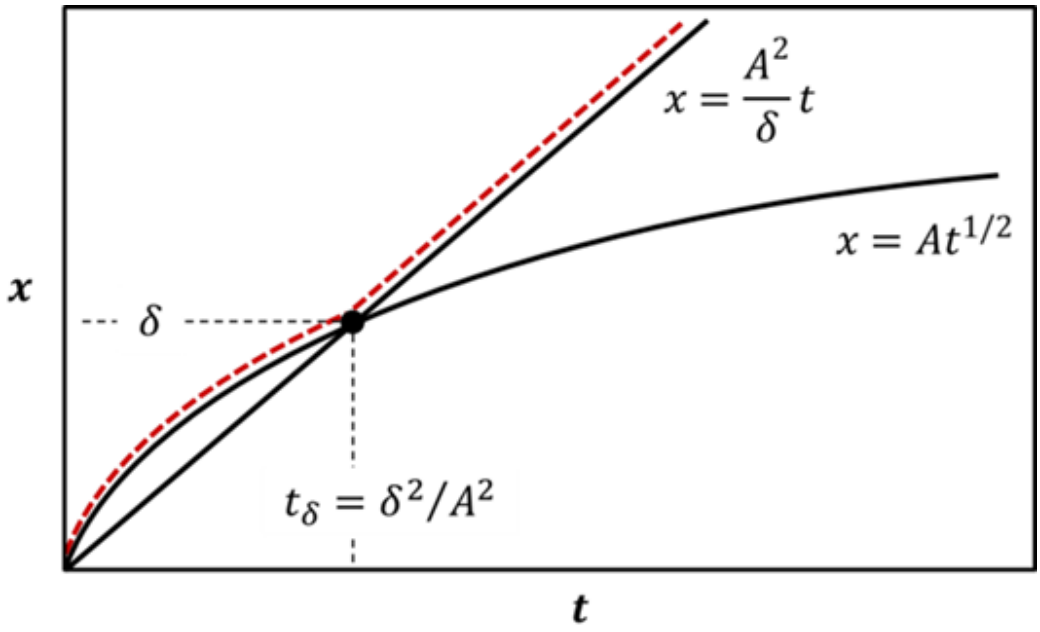

Solving Eq. 4.4-17 for the time it takes for the front to penetrate a depth of x, yields:

$$t = \frac{\delta x}{A^2} \qquad \text{Eq. 4.4-18}$$

which compared to:

$$t = \frac{x^2}{A^2} \qquad \text{Eq. 4.4-19}$$

or the case for the case without localized damage, is a function of penetration depth as opposed to penetration depth squared as reflected in Eq. 4.4-19.

To account for the feedback effects of physical damage on diffusion rates, the minimum of Eq. 4.4-18 and Eq. 4.4-19 may be taken as the estimated degradation time t_0 for a specified material thickness x_0:

$$t_0 = min\left[\frac{{x_0}^2}{A^2}, \frac{\delta x_0}{A^2}\right] \qquad \text{Eq. 4.4-20}$$

The minimum time curve is shown in Figure 4.4-14 as a dashed red line. Selection of δ for Eq. 4.4-20 is discussed later in the context of specific degradation phenomena: sulfate attack, carbonation, steel corrosion, and decalcification.

4.4.2.2 Sulfate Attack

Sulfate attack involves ingress of sulfate ions through concrete pore water and reactions with calcium bearing minerals, including calcium hydroxide and calcium-silicate-hydrate gel ($C\text{-}S\text{-}H$), that produce expansive products, principally ettringite and gypsum. Physical degradation occurs when sufficient ettringite and/or gypsum form to cause internal cracking.

4.4.2.2.1 Ettringite Formation

Calcium sulfate reacts with calcium/aluminum oxide minerals to form calcium aluminum sulfates such as ettringite according to the overall reaction:

$$3CaO \bullet Al_2O_3 \bullet 6H_2O + 3CaSO_4 + 26H_2O = 3CaO \bullet Al_2O_3 \bullet 3CaSO_4 \bullet 32H_2O \quad \text{Eq. 4.4-21}$$

where in cement chemist notation ettringite can be written in the form:

$$C_6A\bar{S}_3H_{32} \quad \text{Eq. 4.4-22}$$

Cement paste is calcium-rich relative to aluminum, so aluminum is the limiting solid-phase reactant. The reaction capacity for ettringite formation based on aluminum availability can be estimated from laboratory characterization of concrete.

SIMCO_03-01-2012 deduced mineral compositions for hydrated SDU concretes based on characterization of the dry mix components in context with thermodynamic considerations; these data summarized in Table 9 of SIMCO_03-01-2012 are reproduced in Table 4.4-9. The only aluminum-bearing phase listed in Table 4.4-9 is monosulfoaluminate (AFm). Equivalent chemical formulas for AFm written in conventional and cement chemist notations include (Matschei, et.al., 2007):

$$Ca_4Al_2(SO_4)(OH)_{12} \cdot 6H_2O = 4CaO \cdot Al_2O_3 \cdot SO_3 \cdot 12H_2O \quad \text{Eq. 4.4-23}$$

and

$$C_4A\bar{S}H_{12} \quad \text{Eq. 4.4-24}$$

Table 4.4-10 presents SDU 1/4 and SDU 2/6/7 reaction capacities calculated based on the dry mix components listed in Table 4.4-9 and the stoichiometry indicated by Eq. 4.4-21 through Eq. 4.4-24. The availability of AFm for reaction is assumed to be 100% on the basis that formation of ettringite from AFm is thermodynamically favorable when additional sulfate enters the system (Matschei, et.al., 2007).

Table 4.4-9: SIMCO_03-01-2012 Characterization of SDU Concretes

Mineral Phase	SDU 1/4 (g/kg)	SDU 2/6/7 (g/kg)
$C\check{S}\check{S}\check{G}H$	118.8	81.2
CH (Portlandite)	7.2	-
AFm	18.4	10.0
C_4FH_{13}	9.9	-

Table 4.4-10: Ettringite Reaction Capacity of AFm Based on SIMCO_03-01-2012

Parameter	SDU 1/4	SDU 2/6/7	Units	Comments
Mass concentration of AFm	18.4	10.0	g/kg solid	SIMCO_03-01-2012 Table 9
Molecular weight of AFm	622	622	g/mol	Approximate value calculated from chemical formula using round numbers for element molecular weights
Molar concentration of AFm	2.96E-02 2.96E-05	1.61E-02 1.61E-05	mol/kg solid mol/g solid	Calculated
Moles Al per mole AFm	2	2	mol Al/ mol AFm	See Eq. 4.4-23
Molar concentration of Al	5.92E-05	3.22E-05	mol/g solid	Calculated
Moles SO_4 reacted per mol Al	1.5	1.5	mol SO_4 / mol Al	See Eq. 4.4-21
Reaction capacity, R	**8.87E-05**	**4.82E-05**	mol SO_4 / g solid	Calculated

Ettringite reaction capacity was similarly estimated based on a concrete characterization performed independently by Vanderbilt University (VU) on different concrete samples (CBP-TR-2010-012-1), as summarized by input to the CBP LeachXS/Objects Representing Chemical Speciation and Transport (ORCHESTRA) sulfate attack module (SRNL-STI-2015-00236) These calculations are presented in Table 4.4-11. The VU characterization is expressed on an elemental basis, thus the mass concentration of Al is directly specified.

Table 4.4-11: Ettringite Reaction Capacity Based on VU Characterization of Total Aluminum

Parameter	SDU 1/4	SDU 2/6/7	Units	Comments
Mass concentration of Al	5,373 5.373	6,108 6.108	mg/kg solid g/kg solid	VU characterization
Molecular weight of Al	27	27	g/mol	
Molar concentration of Al	1.99E-01 1.99E-04	2.26E-01 2.26E-04	mol/kg solid mol/g solid	Calculated
Moles SO_4 reacted per mol Al	1.5	1.5	mol SO_4 / mol Al	See Eq. 4.4-21
Reaction capacity, R	**2.99E-04**	**3.39E-04**	mol SO_4 / g solid	Calculated

The Al reaction capacities in Table 4.4-10 and Table 4.4-11 differ because different samples were tested by SIMCO and VU, and more significantly, because SIMCO and VU assumed different availability of aluminum for reaction due to their independent model calibration/validation efforts.

4.4.2.2.2 Gypsum Formation

The chemical formula for gypsum can be expressed as:

$$CaSO_4 \cdot 2H_2O = CaO \cdot SO_3 \cdot 2H_2O \quad \text{Eq. 4.4-25}$$

or in cement chemist notation as:

$$C\bar{S}H_2 \quad \text{Eq. 4.4-26}$$

Unlike ettringite, calcium availability defines the reaction capacity for gypsum formation. The availability of calcium for gypsum formation is assumed to be less than 100% and limited to that present as calcium hydroxide (Portlandite) following the sulfate attack model of Tixier and Mobasher (2003a, b).

SIMCO Technologies Inc. models CSH gel as a mixture of calcium hydroxide and the calcium silicate hydrate (CSH) mineral (CBP-TR-2010-007-C3, Table 7):

$$C\text{-}S\text{-}H = 1.65CaO \cdot SiO_2 \cdot 1.65H_2O = 0.65Ca(OH)_2 + CaH_2SiO_4 \quad \text{Eq. 4.4-27}$$

In cement chemist notation, Eq. 4.4-27 becomes:

$$C\text{-}S\text{-}H = 0.65CH + CSH \quad \text{Eq. 4.4-28}$$

Table 4.4-12 presents a calculation of the reaction capacity for gypsum formation based on Ca available explicitly as $Ca(OH)_2 = CH$ and implicitly as the CH portion of $C\text{-}S\text{-}H$.

A similar calculation can be performed based on VU characterization of VCO ("Vault Concrete One", SDU 1/4) and VCT ("Vault Concrete Two", SDU 2/6/7) concretes (CBP-TR-2010-012-1), and the resulting initial mineral assemblage in CBP LeachXS/ORCHESTRA sulfate attack module simulations. Inspection of LeachXS/ORCHESTRA simulation output listed in the Appendix of SRNL-STI-2015-00236 indicates that both Portlandite and siliceous hydrogarnet are consumed during sulfate ingress, so both minerals are assumed to contribute to gypsum reaction capacity. Chemical formulas for siliceous hydrogarnet include:

$$C_3AS_{0.8}H_{4.4} = 3CaO \cdot Al_2O_3 \cdot 0.8SiO_2 \cdot 4.4H_2O \quad \text{Eq. 4.4-29}$$

Table 4.4-12: Gypsum Reaction Capacity Based on SIMCO_03-01-2012

Parameter	SDU 1/4	SDU 2/6/7	Units	Comments
Mass concentration of CH	7.2	-	g/kg solid	SIMCO_03-01-2012 Table 9
Molecular weight of CH	74	74	g/mol	$Ca(OH)_2$
Molar concentration of CH	9.73E-02 9.73E-05	-	mol/kg solid mol/g solid	Calculated
Moles of Ca per mole of CH	1	1	mol Ca / mol CH	$CH = Ca(OH)_2$
Molar concentration of Ca as CH	9.73E-05	-	mol/g solid	Calculated
Mass conc. of SIMCO $C\text{-}S\text{-}H$	118.8	81.2	g/kg solid	SIMCO_03-01-2012 Table 9
Molecular weight of SIMCO $C\text{-}S\text{-}H$	182.1	182.1	g/mol	$1.65CaO \cdot SiO_2 \cdot 1.65H_2O$
Molar conc. of SIMCO $C\text{-}S\text{-}H$	6.52E-01 6.52E-04	4.46E-01 4.46E-04	mol/kg solid mol/g solid	Calculated
Moles of Ca as CH per mole of $C\text{-}S\text{-}H$	0.65	0.65	mol Ca / mol $C\text{-}S\text{-}H$	$0.65CH + CSH$
Molar conc. of Ca as $C\text{-}S\text{-}H$	4.24E-04	2.90E-04	mol/g solid	Calculated
Total molar concentration of Ca	5.21E-04	2.90E-04	mol/g solid	Calculated
Moles SO_4 reacted per mol Ca	1	1	mol SO_4 / mol Al	See Eq. 4.4-25
Reaction capacity, R	**5.21E-04**	**2.90E-04**	mol SO_4 / g solid	Calculated

Table 4.4-13 presents a calculation of gypsum reaction capacity based on Ca being available in calcium hydroxide and siliceous hydrogarnet.

As with Al reaction capacity, Ca reaction capacity differs between Table 4.4-12 and Table 4.4-13 due to differing assumptions for mineral availability. The LeachXS/ORCHESTRA output file "output_profiles.dat" did not list the concentrations of $C\text{-}S\text{-}H$ components *C-S-H*_tobermorite and *C-S-H*_jennite. Presumably these minerals provided additional reaction capacity for gypsum formation. An upper bound on reaction capacity can be calculated by assuming all Ca present in the system is available for reaction. This calculation is presented in Table 4.4-14. The increases in reaction capacity for this bounding calculation are modest at +16% for SDU 1/4 concrete and +29% for SDU 2/6/7 concrete.

Table 4.4-13: Gypsum Reaction Capacity Based on VU Characterization and LeachXS Initialization

Parameter	SDU 1/4	SDU 2/6/7	Units	Comments
Porosity	0.115	0.11	cm^3 void/ m^3 total	VU characterization
Saturation	1	1	cm^3 liq./cm^3 void	Saturated exposure conditions
Solid density	2,400	2,310	kg/m^3 solid	VU characterization
Bulk density	2,124 2.124	2,056 2.056	kg/m^3 total g/cm^3 total	Calculated
Molar conc. of CH on a liquid basis	18.7	12.4	mol/L liquid	LeachXS initialization from "output_profiles.dat" (Appendix of SRNL-STI-2015-00236; unreacted concrete at depth)
Molar conc. of CH on a total volume basis	2.15 2.15E-03	1.36 1.36E-03	mol/L total mol/cm^3 total	Calculated
Molar conc. of CH on a solid basis	1.01E-03	6.63E-04	mol/g solid	Calculated
Moles of Ca per mole CH	1	1	mol Ca / mol CH	$CH = Ca(OH)_2$
Molar conc. of Ca in CH on a solid basis	1.01E-03	6.63E-04	mol/g solid	Calculated
Molar conc. of $C_3AS_{0.8}H_{4.4}$ on a liquid basis	1.15	1.09	mol/L liquid	LeachXS initialization from "output_profiles.dat" (Appendix of SRNL-STI-2015-00236; unreacted concrete at depth)
Molar conc. of $C_3AS_{0.8}H_{4.4}$ on a total volume basis	1.32E-01 1.32E-04	1.20E-01 1.20E-04	mol/L total mol/cm^3 total	Calculated
Molar conc. of $C_3AS_{0.8}H_{4.4}$ on a solid basis	6.23E-05	5.83E-05	mol/g solid	Calculated
Moles of Ca per mole $C_3AS_{0.8}H_{4.4}$	3	3	mol Ca / mol $C_3AS_{0.8}H_{4.4}$	$3CaO \cdot Al_2O_3 \cdot 0.8SiO_2 \cdot 4.4H_2O$
Molar conc. of Ca in $C_3AS_{0.8}H_{4.4}$ on a solid basis	1.87E-04	1.75E-04	mol/g solid	Calculated
Total molar conc. of Ca	1.20E-03	8.38E-04	mol/g solid	Calculated
Moles SO_4 reacted per mol Ca	1	1	mol SO_4 / mol Al	See Eq. 4.4-25
Reaction capacity, R	**1.20E-03**	**8.38E-04**	mol SO_4 / g solid	Calculated

Table 4.4-14: Gypsum Reaction Capacity Based on VU Characterization of Total Calcium

Parameter	SDU 1/4	SDU 2/6/7	Units	Comments
Mass concentration of Ca	55,579 55.579	43,193 43.193	mg/kg solid g/kg solid	VU characterization
Molecular weight of Ca	40	40	g/mol	
Molar concentration of Ca	1.39 1.39E-03	1.08 1.08E-03	mol/kg solid mol/g solid	Calculated
Moles SO_4 reacted per mol Ca	1	1	mol SO_4 / mol Al	See Eq. 4.4-25
Reaction capacity, R	**1.39E-03**	**1.08E-03**	mol SO_4 / g solid	Calculated

4.4.2.2.3 Total Reaction Capacity

The total capacity of the solid to react with infiltrating sulfate is taken to be the sum of the capacities for reaction with AFm and any other aluminum phases (to form ettringite) and Portlandite (to form gypsum). Table 4.4-15 summarizes total reaction capacities based on independent material characterizations performed by SIMCO Technologies and VU. The actual total reaction capacity based on VU characterization is expected to lie between the lower ("Portlandite calcium") and upper ("total calcium") estimates.

Table 4.4-15: Total Reaction Capacities

Reaction capacity, R (mol SO_4 reacted / g solid**)**	**SDU 1/4**	**SDU 2/6/7**	**Comments**
SIMCO characterization			
Ettringite formation	8.87E-05	4.82E-05	Table 4.4-10
Gypsum formation	5.21E-04	2.90E-04	Table 4.4-12
Ettringite+gypsum formation	**6.10E-04**	**3.38E-04**	Total capacity
VU characterization			
Ettringite formation	2.99E-04	3.39E-04	Table 4.4-11
Gypsum formation, Portlandite calcium	1.20E-03	8.38E-04	Table 4.4-13
Gypsum formation, total calcium	1.39E-03	1.08E-03	Table 4.4-14
Ettringite+gypsum formation, Portlandite calcium	**1.50E-03**	**1.18E-03**	Lower estimate of total capacity
Ettringite+gypsum formation, total calcium	**1.69E-03**	**1.42E-03**	Upper estimate of total capacity

4.4.2.2.4 Penetration Rate Coefficients

Table 4.4-16 and Table 4.4-17 present sulfate attack rate coefficients calculated using Eq. 4.4-15 for SDU 1 and 4 and SDU 2, 6, and 7 concretes, respectively. Because SDU 1 and 4 wall concretes are assumed to be fully degraded at PA time zero for the CV and CE cases, obviating the need for degradation estimates except for the BE case, penetration rate coefficient calculations are not shown in Table 4.4-16 for these components. However, the rate coefficients for the SDU 1 and SDU 4 walls BE, CV and CE values were calculated to be 0.651 cm/√yr, 2.118 cm/√yr, and 2.118 cm/√yr, respectively.

Note that a higher reaction capacity is associated with a lower rate coefficient, because more time is required to consume more solid-phase reactant for a given fluid-phase reactant transport rate. Thus, the rate coefficients based on SIMCO characterization are higher than those based on VU characterization. The SIMCO rate coefficients (bolded in Table 4.4-16 and Table 4.4-17) are adopted for further analysis as a pessimistic assumption. SRNL-STI-2015-00236 compared sulfate penetration depths based on Eq. 4.4-13 to those simulated by the CBP Software Toolbox version 1.0 sulfate attack module and concluded that the two methods produced similar results.

Table 4.4-16: Penetration Rate Coefficients for Sulfate Attack on SDU 1 and 4 Concrete

Parameter	SDU 1/4 Floor			SDU 1/4 Roof			Units
	BE	CV	CE	BE	CV	CE	
Porosity (a)	0.106	0.106	0.106	0.106	0.106	0.106	cm^3 void / cm^3 total
Bulk density (a)	2.28	2.28	2.28	2.28	2.28	2.28	g solid / cm^3 total
Saturation	1	1	1	1	1	1	cm^3 liquid / cm^3 void
Effective diffusion coefficient (a)	3.5E-08	5.3E-08	6.0E-08	6.0E-08	9.7E-08	1.2E-07	cm^2/s
	1.1	1.7	1.9	1.9	3.1	3.8	cm^2/yr
Exposure concentration (b)	0.1	0.1	0.1	0.1	0.1	0.1	mol / L
	1.0E-04	1.0E-04	1.0E-04	1.0E-04	1.0E-04	1.0E-04	mol / cm^3
SIMCO Technologies, Inc. characterization							
Reaction capacity	6.10E-04	6.10E-04	6.10E-04	6.10E-04	6.10E-04	6.10E-04	mol SO_4 reacted / g solid
Rate coefficient	**0.130**	**0.160**	**0.170**	**0.170**	**0.216**	**0.240**	cm / √yr
Vanderbilt University characterization							
Reaction capacity, lower estimate	1.50E-03	1.50E-03	1.50E-03	1.50E-03	1.50E-03	1.50E-03	mol SO_4 reacted / g solid
Rate coefficient, lower estimate	0.083	0.102	0.108	0.108	0.138	0.153	cm / √yr
Reaction capacity, upper estimate	1.69E-03	1.69E-03	1.69E-03	1.69E-03	1.69E-03	1.69E-03	mol SO_4 reacted / g solid
Rate coefficient, upper estimate	0.078	0.096	0.102	0.102	0.130	0.144	cm / √yr

(a) SRR-CWDA-2018-00004, Table 1.

(b) Average SO_4 concentration of Tank 50 salt solution from 2007 to 2014 is 0.05M (G-ESR-Z-00018). Pore water concentration in cured saltstone is 2x higher than in mixing fluid concentration (SIMCO_06-16-2010, Tables 3 and 8).

Table 4.4-17: Penetration Rate Coefficients for Sulfate Attach on SDU 2, 6, and 7 Concrete

Parameter	SDU 2/6/7 Concrete			SDU 2/6/7 Column			Units
	BE	CV	CE	BE	CV	CE	
Porosity (a)	0.11	0.11	0.11	0.211	0.211	0.211	cm^3 void / cm^3 total
Bulk density (a)	2.18	2.18	2.18	2.06	2.06	2.06	g solid / cm^3 total
Saturation	1	1	1	1	1	1	cm^3 liquid / cm^3 void
Effective diffusion coefficient (a)	3.5E-08	5.3E-08	6.0E-08	1.2E-07	3.9E-07	5.0E-07	cm^2/s
	1.1	1.7	1.9	3.8	12.3	15.8	cm^2/yr
Exposure concentration (b)	0.1	0.1	0.1	0.1	0.1	0.1	mol / L
	1.0E-04	1.0E-04	1.0E-04	1.0E-04	1.0E-04	1.0E-04	mol / cm^3
SIMCO Technologies, Inc. characterization							
Reaction capacity	3.38E-04	3.38E-04	3.38E-04	3.38E-04	3.38E-04	3.38E-04	mol SO_4 reacted / g solid
Rate coefficient	**0.182**	**0.223**	**0.238**	**0.479**	**0.863**	**0.977**	cm / √yr
Vanderbilt University characterization							
Reaction capacity, lower estimate	1.18E-03	1.18E-03	1.18E-03	1.18E-03	1.18E-03	1.18E-03	mol SO_4 reacted / g solid
Rate coefficient, lower estimate	0.097	0.120	0.127	0.257	0.463	0.524	cm / √yr
Reaction capacity, upper estimate	1.42E-03	1.42E-03	1.42E-03	1.42E-03	1.42E-03	1.42E-03	mol SO_4 reacted / g solid
Rate coefficient, upper estimate	0.089	0.109	0.116	0.234	0.421	0.477	cm / √yr

(a) SRR-CWDA-2018-00004, Table 1.

(b) Average SO_4 concentration of Tank 50 salt solution from 2007 to 2014 is 0.05M (G-ESR-Z-00018). Pore water concentration in cured saltstone is 2x higher than in mixing fluid concentration (SIMCO_06-16-2010, Tables 3 and 8).

4.4.2.2.5 Sulfate Attack Prior to Facility Closure

Between construction and disposal unit closure, SDU wall concrete may experience significant desiccation from exposure to the atmosphere. When subsequently exposed to grout slurry and bleed water, sulfate may rapidly penetrate the dry concrete due to strong capillary suction, causing early and accelerated sulfate attack prior to facility closure (SRNL-ESB-2007-00007). Wall sections adjoining sheet drains may be exposed to bleed water multiple times. Drying could also potentially lead to fine-scale shrinkage cracking at wall surfaces and provide a means for accelerated sulfate intrusion (SRNL-ESB-2007-00007).

However, a waterproof coating was applied to the inside wall of SDUs 2/3/5. This coating is assumed to fully protect SDUs 2/3/5 wall concrete from sulfate attack during operations, but not delay the onset of post-closure sulfate attack (SRNL-

STI-2018-00077). Also, SDU 1 and 4 wall concretes are assumed to be already fully degraded, consistent with recent PA modeling (SRNL-STI-2013-00118), obviating further consideration of these components.

Floor concrete is much less likely to dry out because the bottom contacts the damp subsurface, initial saltstone placement will cover the top surface, and its initial saturation may be higher due to more conducive curing conditions (e.g., horizontal surface for holding external moisture). For SDU 1 and 4 roof concrete will generally be protected by clean grout, which may be credited for delaying the onset of sulfate attack after facility closure (Section 4.4.2.6). Also, high humidity conditions inside an SDU during operations will tend to re-saturate roof concrete over time. Therefore, the potential for sulfate attack on SDU floor and roof concrete during operations is considered relatively insignificant.

The components remaining to be considered are the SDUs 6 and 7 through 12 walls. Even though SDU 6 has an extensive liner system installed, the PA modeling ignores it. Installation of liner systems for future SDUs 7 through 12 will be evaluated prior to the start of disposal into these SDUs. Following the approach of SRNL-L3200-2013-00028, initial degradation depth from accelerated sulfate attack is estimated by considering surface cracking and capillary suction. The extent of presumed sulfate attack damage depends on the timescales of chemical reaction and diffusive transport. If the chemical reaction rate is relatively slow (compared to transport), then sulfate entering the system by capillary suction will penetrate to the same depth as the bleed water intrusion before reacting. If the reaction rate is fast, then sulfate will be consumed at a reaction front at a shallower depth.

For the slow reaction scenario, bleed water is assumed to displace all pore water in its path in a plug-flow manner. With this simple model, the penetration depth is:

$$\delta_s = (S_f - S_i)L \qquad \text{Eq. 4.4-30}$$

where S_i and S_f are the initial and final saturations, and L is the wall thickness. The final saturation is assumed to be 100%. WSRC-TR-2005-00054 analyzed concrete rubble exposed to atmospheric conditions (uncovered) at the SRS and observed an average saturation of 73%, which is adopted as a representative initial saturation.

For the fast reaction scenario, the penetration depth depends on the reaction capacity of the solid. Based on SIMCO_03-01-2012 characterization, the reaction capacity for conversion of AFm to ettringite, ignoring potential reaction of sulfate with calcium-bearing phases to form gypsum, is given in Table 4.4-10 as 4.82E-05 mol SO_4 / g solid. The penetration depth is:

$$\delta_f = \frac{(S_f - S_i)nc}{\rho_b R} L \qquad \text{Eq. 4.4-31}$$

where n is porosity, c is sulfate concentration, ρ_b is bulk density, and R is reaction capacity.

Reality is assumed to lie between the slow and fast end-members and coincide with their geometric mean, including hypothetical drying shrinkage cracks to depth δ_c:

$$\delta = \sqrt{(\delta_c + \delta_s)(\delta_c + \delta_f)} \qquad \text{Eq. 4.4-32}$$

By using the geometric mean, the ranges of values for the fast and slow end-members are normalized, keeping an end-member range from dominating the weighting of the members. For example, differences in the ranges of fast and slow end-members would obscure the influence of changes in the reaction capacity of the solid.

Levitt (2003, p. 5) states that the drying shrinkage "has typical crack apertures in the range 0.1-0.5 mm, tapering to zero at depths of about 10 mm." Thus, interior walls are assumed to have surface cracks to a depth of δ_c = 1.0 cm (10 mm) and be physically degraded to at least this depth prior to any sulfate exposure.

As-built dimensions are used for SDU 6. For future SDUs 7 through 12, two scenarios are considered (SRR-CWDA-2018-00012) The SDU 7 "Design" case reflects the current design. The SDU 7 "Design Margin" case assumes thinner components to accommodate potential design changes and/or construction deviations. Input parameters and results for these three cases are summarized by Table 4.4-18 through Table 4.4-20. Since these SDUs are designed to have tapered walls, each wall is divided into 5 vertical segments consistent with recent PA simulations of these units. The average thickness of each segment is used for the parameter L. Initial damage due to early sulfate attack is estimated to be around 1 to 2 inches based on the calculated results shown in Table 4.4-18 through Table 4.4-20.

Table 4.4-18: Degradation of SDU 6 Wall Concrete Segments due to Early Sulfate Attack

Parameter	Wall 1	Wall 2	Wall 3	Wall 4	Wall 5	Units
Thickness, L	22.37	19.08	15.66	12.28	10.33	in
	56.83	48.45	39.77	31.19	26.23	cm
Initial saturation, S_i (a)	0.73	0.73	0.73	0.73	0.73	mL liquid / mL void
Final saturation, S_f	1	1	1	1	1	mL liquid / mL void
Change in saturation, ΔS	0.27	0.27	0.27	0.27	0.27	mL liquid / mL void
Porosity, n (b)	0.11	0.11	0.11	0.11	0.11	mL void / mL total
Surface crack depth, δ_c (c)	1	1	1	1	1	cm
	0.39	0.39	0.39	0.39	0.39	in
Slow reaction						
Penetration fraction	0.27	0.27	0.27	0.27	0.27	
Penetration distance, δ_s	15.34	13.08	10.74	8.42	7.08	cm
Total degraded thickness	16.34	14.08	11.74	9.42	8.08	cm
$\delta_c + \delta_s$	6.43	5.54	4.62	3.71	3.18	in
Fast reaction						
Bulk density, ρ_b (b)	2.18	2.18	2.18	2.18	2.18	g/mL
Bleed water conc., c (d)	0.075	0.075	0.075	0.075	0.075	mol/L
	7.50E-05	7.50E-05	7.50E-05	7.50E-05	7.50E-05	mol/mL
Reaction capacity, R (e)	4.82E-05	4.82E-05	4.82E-05	4.82E-05	4.82E-05	mol SO4 / g solid
	1.1E-04	1.1E-04	1.1E-04	1.1E-04	1.1E-04	mol/mL
	0.11	0.11	0.11	0.11	0.11	mol/L
Penetration fraction	0.02	0.02	0.02	0.02	0.02	
Penetration distance, δ_f	1.20	1.03	0.84	0.66	0.56	cm
Total degraded thickness	2.20	2.03	1.84	1.66	1.56	cm
$\delta_c + \delta_f$	0.87	0.80	0.73	0.65	0.61	in
Initial damage						
Geometric mean value	6.00	5.34	4.65	3.96	3.55	cm
$\sqrt{(\delta_c + \delta_s)(\delta_c + \delta_f)}$	2.36	2.10	1.83	1.56	1.40	in
Intact wall thickness	50.82	43.11	35.12	27.23	22.68	cm
	20.01	**16.97**	**13.83**	**10.72**	**8.93**	in

(a) WSRC-TR-2005-00054
(b) SRR-CWDA-2018-00004
(c) Levitt (2003), page 5
(d) Bleed water concentration taken as the midpoint between feed water (0.05 mol/L, G-ESR-Z-00018) and porewater (~2x, SIMCO_06-16-2010)
(e) Table 4.4-10 – Reaction capacity for conversion of AFm to ettringite. Potential reaction of sulfate with calcium-bearing phases to form gypsum ignored. Based on SIMCO_03-01-2012 characterization.

Table 4.4-19: Degradation of SDU 7 Design Wall Concrete Segments due to Early Sulfate Attack

Parameter	Wall 1	Wall 2	Wall 3	Wall 4	Wall 5	Units
Thickness, L	22.60	19.78	16.85	13.95	12.28	in
	57.42	50.24	42.80	35.44	31.19	cm
Initial saturation, S_i (a)	0.73	0.73	0.73	0.73	0.73	mL liquid / mL void
Final saturation, S_f	1	1	1	1	1	mL liquid / mL void
Change in saturation, ΔS	0.27	0.27	0.27	0.27	0.27	mL liquid / mL void
Porosity, n (b)	0.11	0.11	0.11	0.11	0.11	mL void / mL total
Surface crack depth, δ_c (c)	1	1	1	1	1	cm
	0.39	0.39	0.39	0.39	0.39	in
Slow reaction						
Penetration fraction	0.27	0.27	0.27	0.27	0.27	
Penetration distance, δ_s	15.50	13.56	11.55	9.57	8.42	cm
Total degraded thickness	16.50	14.56	12.55	10.57	9.42	cm
$\delta_c + \delta_s$	6.50	5.73	4.94	4.16	3.71	in
Fast reaction						
Bulk density, ρ_b (b)	2.18	2.18	2.18	2.18	2.18	g/mL
Bleed water conc., c (d)	0.075	0.075	0.075	0.075	0.075	mol/L
	7.50E-05	7.50E-05	7.50E-05	7.50E-05	7.50E-05	mol/mL
Reaction capacity, R (e)	4.82E-05	4.82E-05	4.82E-05	4.82E-05	4.82E-05	mol SO4 / g solid
	1.1E-04	1.1E-04	1.1E-04	1.1E-04	1.1E-04	mol/mL
	0.11	0.11	0.11	0.11	0.11	mol/L
Penetration fraction	0.02	0.02	0.02	0.02	0.02	
Penetration distance, δ_f	1.22	1.06	0.91	0.75	0.66	cm
Total degraded thickness	2.22	2.06	1.91	1.75	1.66	cm
$\delta_c + \delta_f$	0.87	0.81	0.75	0.69	0.65	in
Initial damage						
Geometric mean value	6.05	5.48	4.89	4.30	3.96	cm
$\sqrt{(\delta_c + \delta_s)(\delta_c + \delta_f)}$	2.38	2.16	1.93	1.69	1.56	in
Intact wall thickness	51.37	44.76	37.90	31.14	27.23	cm
	20.22	**17.62**	**14.92**	**12.26**	**10.72**	in

(a) WSRC-TR-2005-00054
(b) SRR-CWDA-2018-00004
(c) Levitt (2003), page 5
(d) Bleed water concentration taken as the midpoint between feed water (0.05 mol/L, G-ESR-Z-00018) and porewater (~2x, SIMCO_06-16-2010)
(e) Table 4.4-10 – Reaction capacity for conversion of *AFm* to ettringite. Potential reaction of sulfate with calcium-bearing phases to form gypsum ignored. Based on SIMCO_03-01-2012 characterization.

Table 4.4-20: Degradation of SDU 7 DM Wall Concrete Segments due to Early Sulfate Attack

Parameter	Wall 1	Wall 2	Wall 3	Wall 4	Wall 5	Units
Thickness, L	18.49	15.43	12.25	9.12	7.30	in
	46.96	39.19	31.12	23.16	18.55	cm
Initial saturation, S_i (a)	0.73	0.73	0.73	0.73	0.73	mL liquid / mL void
Final saturation, S_f	1	1	1	1	1	mL liquid / mL void
Change in saturation, ΔS	0.27	0.27	0.27	0.27	0.27	mL liquid / mL void
Porosity, n (b)	0.11	0.11	0.11	0.11	0.11	mL void / mL total
Surface crack depth, δ_c (c)	1	1	1	1	1	cm
	0.39	0.39	0.39	0.39	0.39	in
Slow reaction						
Penetration fraction	0.27	0.27	0.27	0.27	0.27	
Penetration distance, δ_s	12.68	10.58	8.40	6.25	5.01	cm
Total degraded thickness	13.68	11.58	9.40	7.25	6.01	cm
$\delta_c + \delta_s$	5.39	4.56	3.70	2.86	2.37	in
Fast reaction						
Bulk density, ρ_b (b)	2.18	2.18	2.18	2.18	2.18	g/mL
Bleed water conc., c (d)	0.075	0.075	0.075	0.075	0.075	mol/L
	7.50E-05	7.50E-05	7.50E-05	7.50E-05	7.50E-05	mol/mL
Reaction capacity, R (e)	4.82E-05	4.82E-05	4.82E-05	4.82E-05	4.82E-05	mol SO4 / g solid
	1.1E-04	1.1E-04	1.1E-04	1.1E-04	1.1E-04	mol/mL
	0.11	0.11	0.11	0.11	0.11	mol/L
Penetration fraction	0.02	0.02	0.02	0.02	0.02	
Penetration distance, δ_f	0.99	0.83	0.66	0.49	0.39	cm
Total degraded thickness	1.99	1.83	1.66	1.49	1.39	cm
$\delta_c + \delta_f$	0.79	0.72	0.65	0.59	0.55	in
Initial damage						
Geometric mean value	5.22	4.60	3.95	3.29	2.89	cm
$\sqrt{(\delta_c + \delta_s)(\delta_c + \delta_f)}$	2.06	1.81	1.56	1.29	1.14	in
Intact wall thickness	41.74	34.58	27.17	19.87	15.66	cm
	16.43	**13.61**	**10.70**	**7.82**	**6.16**	in

(a) WSRC-TR-2005-00054
(b) SRR-CWDA-2018-00004
(c) Levitt (2003), page 5
(d) Bleed water concentration taken as the midpoint between feed water (0.05 mol/L, G-ESR-Z-00018) and porewater (~2x, SIMCO_06-16-2010)
(e) Table 4.4-10 Reaction capacity for conversion of AFm to ettringite. Potential reaction of sulfate with calcium-bearing phases to form gypsum ignored. Based on SIMCO_03-01-2012 characterization.

4.4.2.3 Carbonation

Carbonation commonly refers to the reaction of carbon dioxide with calcium hydroxide (Portlandite) to form calcium carbonate (calcite):

$$Ca(OH)_2 + H_2O + CO_2 \rightarrow CaCO_3 + 2H_2O \qquad \text{Eq. 4.4-33}$$

In cement chemist notation, Eq. 4.4-33 becomes:

$$CH + H + \bar{C} \rightarrow C\bar{C} + 2H \qquad \text{Eq. 4.4-34}$$

Carbonation in the context of concrete may include other reactions of carbon dioxide with calcium-bearing minerals, such as calcium-silicate-hydrate gel (C-S-H). Carbonation increases mechanical strength and decreases alkalinity from pH 13 to pH 8.5 in cementitious materials. While the former is generally beneficial, corrosion of embedded steel accelerates as pH approaches carbonated conditions, approximately pH < 10. The volume of the corrosion products far exceeds that of the uncorroded steel, which typically introduces sufficient internal pressure to cause cracking and spalling of the surrounding concrete. Going forward, in this section the term "carbonation" is used as shorthand for "carbonation-influenced corrosion of steel," with the understanding that carbonation itself does not appreciably degrade the hydraulic and transport properties on cementitious materials. Rather, carbonation only leads to physical damage in the presence of embedded steel (e.g., reinforcing bars). Most concrete components of the various SDUs contain reinforcing steel, notable exceptions including the upper and lower mud mats in the 150-foot diameter SDU design. Saltstone also contains embedded steel in the form of metal support columns and roof trusses for SDU 4. Steel corrosion is discussed further in Section 4.4.2.4.

4.4.2.3.1 Analytic Solution

Papadakis, et.al., (1989) developed an analytical solution for carbonation penetration depth with the same basic form as Eq. 4.4-13. Using the present nomenclature, the analytic solution can be written as:

$$x = \left[\frac{2(1-S)nD_{eff}c_{CO_2}t}{c_{Ca(OH)_2}+3c_{CSH}}\right]^{1/2} \qquad \text{Eq. 4.4-35}$$

where:

x = penetration depth [cm],

c_{CO2} = carbon dioxide concentration [mol / cm^3 gas],

t = elapsed time [yr],

$c_{Ca(OH)2}$ = Portlandite concentration [mol / cm^3 total], and

c_{CSH} = concentration of calcium-silicate-hydrate (CSH), where

$$c_{CSH} \equiv 3CaO \bullet 2SiO_2 \bullet 3H_2O \left[{}^{mol}/_{cm^3}\right] \qquad \text{Eq. 4.4-36}$$

Eq. 4.4-35 represents the carbonation penetration depth based on carbonation from the gaseous phase which is expected to dominate under unsaturated conditions, but under saturated or near-saturated conditions dissolved carbon dioxide becomes important at the reaction front. A generalized form of Eq. 4.4-35 can be rewritten as:

$$x = \left[\frac{2((1-S)nD_{eff,g}c_{CO_{2,g}} + SnD_{eff,l}c_{CO_{2,l}})t}{c_{Ca}}\right]^{1/2} = At^{1/2} \qquad \text{Eq. 4.4-37}$$

where g and l denote the gas and liquid phases, respectively, the rate coefficient is

$$A \equiv \left[\frac{2((1-S)nD_{eff,g}c_{CO_{2,g}} + SnD_{eff,l}c_{CO_{2,l}})}{c_{Ca}}\right]^{1/2} \qquad \text{Eq. 4.4-38}$$

and c_{Ca} is the cumulative molar concentration of Ca in $Ca(OH)_2$ and CSH.

The largest sources of uncertainty and pessimistic bias in calculated carbonation penetration depths are the assumed saturation state (S) in Eq. Eq. 4.4-38 and the assumption of a linear penetration rate after carbonation penetrates to an assumed depth δ in Eq. 4.4-20. Cementitious materials will likely be fully saturated, thus precluding a gas pathway for accelerated CO_2 ingress, but unsaturated states are also possible depending on the actual air-entry pressures of these materials and tensions in the surrounding vadose zone soils. Also, fractures are possible and if present would form a gas-phase transport path. A linear penetration rate for long times is thought to be a pessimistic assumption. Uncertainties in saturation state and material properties are considered through separate BE, CV, and CE calculations. The concentrations of the liquid- and solid-phase reactants are better known and uncertainties in these quantities are not considered in the BE, CV and CE variants.

4.4.2.3.2 Gaseous and Dissolved Carbon Dioxide Concentrations

SRNL-L3200-2012-00017 estimated the average and median partial pressure of CO_2 in the vadose zone at the SRS to be roughly $pCO_2=10^{-2}$ = 0.01 atm, compared to an atmospheric partial pressure of 0.00039 atm. Using the ideal gas law at 20ºC, the molar concentration of carbon dioxide in the vadose zone becomes 4.16E-07 mol/cm^3 gas. The concentration of dissolved CO_2 in cement pore water at the cement-soil interface can be estimated by analyzing a calcium carbonate (calcite) system in equilibrium with gaseous CO_2:

$$\begin{gathered} H_2O \rightleftharpoons \mathrm{H}^+ + \mathrm{OH}^- \\ CO_2(g) + H_2O \rightleftharpoons H_2\,CO_3 \\ CO_2(g) + H_2O \rightleftharpoons {HCO_3}^- + \mathrm{H}^+ \\ H_2\,CO_3 \rightleftharpoons {HCO_3}^- + \mathrm{H}^+ \\ {HCO_3}^- \rightleftharpoons {CO_3}^{2-} + \mathrm{H}^+ \\ CaCO_3(s) \rightleftharpoons \mathrm{Ca}^{2+} + {CO_3}^{2-} \end{gathered} \qquad \text{Eq. 4.4-39}$$

For a partial pressure of 0.01 atm, pH is calculated as 7.3, and the dominant form of dissolved carbon is HCO_3^- at a concentration c_{aq} = 3.07E-06 mol/cm^3 liquid as shown in Table 4.4-21. The total concentration of dissolved carbon is c_{aq} = 3.41E-06 mol/cm^3 (Table 4.4-21). The pCO_2 data reported by SRNL-L3200-2012-00017 range from roughly $10^{-2.5}$ to $10^{-1.5}$ atm. The corresponding total concentration of dissolved carbon based on the calculation shown in Table 4.4-21 ranges from c_{aq} =2.2E-06 to 5.6E-06 mol/cm^3. This variation is relatively small compared to other uncertainties in the calculations of carbonation penetration rates and is therefore ignored.

The transport properties and solid phase concentrations for the SDU 1 and 4 floor and wall concrete and SDU 2, 6, and 7 concrete are available from the SRR-CWDA-2018-00004 and SIMCO_03-01-2012. Similar data for saltstone are provided in SRR-CWDA-2018-00004 and SIMCO_06-16-2010 / SRNL-STI-2010-00515. These input data to Eq. 4.4-37 and Eq. 4.4-38 are summarized in Table 4.4-22, Table 4.4-23, and Table 4.4-24 for the BE, CV and CE cases, respectively. The solid phase concentration of calcium in SDU 1 and 4 roof concrete is approximated by scaling the SDU 1 and 4 floor/wall concrete value using the CaO ratios computed in Table 4.4-25 based on the composition of the unhydrated binders (SIMCO_03-01-2012, Table 3, WSRC-STI-2006-00198, and SRNL-EST-2005-00105).

Table 4.4-21: Chemical Equilibrium for Calcium Carbonate (Calcite) at 0.01 atm CO_2

	Reactions				
1)	$H_2O \leftrightarrow H^+ + OH^-$				
2)	$CO_2(g) + H_2O \leftrightarrow H_2CO_3$				
3)	$CO_2(g) + H_2O \leftrightarrow HCO_3^- + H^+$				
4)	$H_2CO_3 \leftrightarrow HCO_3^- + H^+$				
5)	$HCO_3^- \leftrightarrow CO_3^{2-} + H^+$				
6)	$CaCO_3(s) \leftrightarrow Ca^{2+} + CO_3^{2-}$				
	Specifications	value	units	$-\log_{10}$	Comments
1)	p_{CO2}	0.01	atm	2.00	Millings, M. *Summary of Carbon Dioxide in Water Table Wells and the Vadose Zone at SRS*, SRNL-L3200-2012-00017, May 30, 2012.
	Equations	@25C	units	$-\log_{10}K$	Comments
1)	$K_w = [H^+][OH^-]$	1.00E-14	M^2	14	e.g., Table 3.4 (25C), R. A. Freeze and J. A. Cherry, Groundwater, Prentice-Hall, 1979
2)	$K_{CO2} = [H_2CO_3]/p_{CO2}$	3.39E-02	M/atm	1.47	Table 4-1, J. I. Drever, The Geochemistry of Natural Waters, 2nd edition, Prentice-Hall, 1988
3)	$K_1 = [H^+][HCO_3^-]/[H_2CO_3]$	4.47E-07	M	6.35	Table 4-1, J. I. Drever, The Geochemistry of Natural Waters, 2nd edition, Prentice-Hall, 1988
	$K_1 = [H^+][HCO_3^-]/p_{CO2}$		M^2/atm	7.82	same as Table 5-1, Stumm and Morgan, Aquatic Chemistry, Wiley, 1970
4)	$K_2 = [H^+][CO_3^{2-}]/[HCO_3^-]$	4.68E-11	M	10.33	Table 5-1, Stumm and Morgan (1970)
5)	$K_{s0} = [Ca^{2+}][CO_3^{2-}]$	4.47E-09	M^2	8.35	Table 5-1, Stumm and Morgan (1970)
6)	$2*[Ca^{2+}] + [H^+] = [HCO_3^-] + 2*[CO_3^{2-}] + [OH^-]$				Charge balance
	Variables	value	units	value	units
1)	$[H_2CO_3]$	3.39E-04	M	3.39E-07	mol/cm^3
2)	$[H^+]$	4.93E-08	M	7.31	pH
3)	$[OH^-]$	2.03E-07	M	6.69	pOH
4)	$[HCO_3^-]$	3.07E-03	M	3.07E-06	mol/cm^3
5)	$[CO_3^{2-}]$	2.91E-06	M	2.91E-09	mol/cm^3
6)	$[Ca^{2+}]$	1.54E-03	M	1.54E-06	mol/cm^3
	$[H_2CO_3]+[HCO_3^-]+[CO_3^{2-}]$	**3.41E-03**	M	**3.41E-06**	mol/cm^3

Table 4.4-22: Input Data and Rate Coefficients for BE Carbonation Calculations

Parameter	SDU 2/6/7	SDU 1/4	SDU 4 Roof	SDU 1 Roof	Saltstone	Units
p_{CO_2} (a)	0.01	0.01	0.01	0.01	0.01	atm
$c_{CO_2,g}$ (b)	4.16E-07	4.16E-07	4.16E-07	4.16E-07	4.16E-07	mol/cm³ gas
$c_{CO_2,\ell}$ (c)	3.41E-06	3.41E-06	3.41E-06	3.41E-06	3.41E-06	mol/cm³ liquid
n (d)	0.11	0.106	0.106	0.106	0.656	cm³ void / cm³ total
ρ_b (d)	2.18	2.28	2.28	2.28	0.932	g/cm³ total
$D_{m,g}$ (e)	0.165	0.165	0.165	0.165	0.165	cm²/s
τ (f)	1.52E-03	1.52E-03	2.61E-03	2.61E-03	2.96E-04	-
$D_{e,g}$ (g)	2.51E-04	2.51E-04	4.30E-04	4.30E-04	4.88E-05	cm²/s
$D_{e,\ell}$ (d)	3.5E-08	3.5E-08	6.0E-08	6.0E-08	6.8E-09	cm²/s
$[Ca(OH)_2]$	0 (h)	7.2 (h)	-	-	0 (i)	g/kg
$M_{Ca(OH)_2}$ (j)	74	74	-	-	74	g/mol
$c_{Ca(OH)_2}$ (k)	0	2.22E-04	-	-	0	mol/cm³ total
$[CSH]$	81.2 (h)	118.8 (h)	-	-	147.4 (i)	g/kg
M_{CSH} (l)	182.1	182.1	-	-	182.1	g/mol
c_{CSH} (m)	9.72E-04	1.49E-03	-	-	7.54E-04	mol/cm³ total
c_{Ca}	1.60E-03(n)	2.68E-03(n)	2.15E-03(o)	1.85E-03(o)	1.24E-03(n)	mol/cm³ total
S_g (p)	7.0E-06 (~0)	7.0E-06 (~0)	7.0E-06 (~0)	7.0E-06 (~0)	0.0004	cm³ gas / cm³ void
S_ℓ (q)	1	1	1	1	0.9996	cm³ liquid / cm³ void
θ_g (q)	7.2E-07	7.0E-07	7.0E-07	7.0E-07	2.4E-04	cm³ gas / cm³ total
θ_ℓ (q)	0.110	0.106	0.106	0.106	0.656	cm³ liquid / cm³ total
A (r)	**0.023**	**0.017**	**0.025**	**0.027**	**0.032**	cm/√yr

(a) SRNL-L3200-2012-00017
(b) p_{CO_2} and ideal gas law at 20°C
(c) Sum of H_2CO_3, HCO_3^-, and CO_3^{2-} concentrations from Table 4.4-21
(d) SRR-CWDA-2018-00004, Table 1
(e) Marrero and Mason (1972), Table 20, N_2-CO_2 system
(f) Calculated from liquid-phase effective diffusion coefficients in SRR-CWDA-2018-00004, Table 1, assuming a molecular diffusion coefficient of 2.3E-05 cm²/s (Holz, et.al., 2000)
(g) $D_{e,g} = \tau D_{m,g}$
(h) SIMCO_03-01-2012, Tables 9 and 13, 28 day cure
(i) SIMCO_06-16-2010, Tables 6 and 13, WS-2 grout
(j) $M_{Ca(OH)_2}$= 40 + 2(16+1) g/mol
(k) $c_{Ca(OH)_2} = [Ca(OH)_2]\rho_b / M_{Ca(OH)_2}$
(l) The stoichiometry of CSH in cement paste is variable. SIMCO assumes $CSH \rightarrow 0.65Ca(OH)_2 + CaH_2SiO_4 = 1.65CaO \cdot SiO_2 \cdot 1.65H_2O$ in STADIUM modeling (CBP-TR-2010-007-C3, Table 7). M_{CSH} = 1.65(40) + 3.3(1) + 1(28) + 5.3(16) g/mol
(m) $c_{CSH} = \frac{[CSH]\rho_b}{M_{CSH}}$
(n) $c_{Ca} = c_{Ca(OH)_2} + 1.65 \cdot c_{CSH}$; see note (l)
(o) Scaled from "SDU 1/4" concrete using CaO ratio from Table 4.4-25
(p) Computed from van Genuchten (1980) water retention curve and 1,500 cm suction
(q) $S_g + S_\ell = 1$, $\theta_g = S_g n$, and $\theta_\ell = S_\ell n$
(r) Eq. 4.4-38

Table 4.4-23: Input Data and Rate Coefficients for CV Carbonation Calculations

Parameter	SDU 2/6/7	SDU 1/4	SDU 4 Roof	SDU 1 Roof	Saltstone	Units
p_{CO_2} (a)	0.01	0.01	0.01	0.01	0.01	atm
$c_{CO_2,g}$ (b)	4.16E-07	4.16E-07	4.16E-07	4.16E-07	4.16E-07	mol/cm³ gas
$c_{CO_2,\ell}$ (c)	3.41E-06	3.41E-06	3.41E-06	3.41E-06	3.41E-06	mol/cm³ liquid
n (d)	0.11	0.106	0.106	0.106	0.656	cm³ void / cm³ total
ρ_b (d)	2.18	2.28	2.28	2.28	0.932	g/cm³ total
$D_{m,g}$ (e)	0.165	0.165	0.165	0.165	0.165	cm²/s
τ (f)	2.30E-03	2.30E-03	4.22E-03	4.22E-03	5.65E-04	-
$D_{e,g}$ (g)	3.80E-04	3.80E-04	6.96E-04	6.96E-04	9.33E-05	cm²/s
$D_{e,\ell}$ (d)	5.3E-08	5.3E-08	9.7E-08	9.7E-08	1.3E-08	cm²/s
$[Ca(OH)_2]$	0 (h)	7.2 (h)	-	-	0 (i)	g/kg
$M_{Ca(OH)_2}$ (j)	74	74	-	-	74	g/mol
$c_{Ca(OH)_2}$ (k)	0	2.22E-04	-	-	0	mol/cm³ total
$[CSH]$	81.2 (h)	118.8 (h)	-	-	147.4 (i)	g/kg
M_{CSH} (l)	182.1	182.1	-	-	182.1	g/mol
c_{CSH} (m)	9.72E-04	1.49E-03	-	-	7.54E-04	mol/cm³ total
c_{Ca}	1.60E-03(n)	2.68E-03(n)	2.15E-03(o)	1.85E-03(o)	1.24E-03(n)	mol/cm³ total
S_g (p)	0.02	0.02	0.02	0.02	0.02	cm³ gas / cm³ void
S_ℓ (q)	0.98	0.98	0.98	0.98	0.98	cm³ liquid / cm³ void
θ_g (q)	0.0022	0.00212	0.00212	0.00212	0.0131	cm³ gas / cm³ total
θ_ℓ (q)	0.1078	0.10388	0.10388	0.10388	0.6429	cm³ liquid / cm³ total
A (r)	**0.120**	**0.091**	**0.138**	**0.149**	**0.165**	cm/√yr

(a) SRNL-L3200-2012-00017
(b) p_{CO_2} and ideal gas law at 20ºC
(c) Sum of H_2CO_3, HCO_3^-, and CO_3^{2-} concentrations from Table 4.4-21
(d) SRR-CWDA-2018-00004, Table 1
(e) Marrero and Mason (1972), Table 20, N_2-CO_2 system
(f) Calculated from liquid-phase effective diffusion coefficients in SRR-CWDA-2018-00004, Table 1 assuming a molecular diffusion coefficient of 2.3E-05 cm²/s (Holz, et.al., 2000)
(g) $D_{e,g} = \tau D_{m,g}$
(h) SIMCO_03-01-2012, Tables 9 and 13, 28 day cure
(i) SIMCO_06-16-2010, Tables 6 and 13, WS-2 grout
(j) $M_{Ca(OH)_2}$= 40 + 2(16+1) g/mol
(k) $c_{Ca(OH)_2} = [Ca(OH)_2]\rho_b/M_{Ca(OH)_2}$
(l) The stoichiometry of CSH in cement paste is variable. SIMCO assumes $CSH \rightarrow 0.65Ca(OH)_2 + CaH_2SiO_4 = 1.65CaO \cdot SiO_2 \cdot 1.65H_2O$ in STADIUM modeling (CBP-TR-2010-007-C3, Table 7). M_{CSH} = 1.65(40) + 3.3(1) + 1(28) + 5.3(16) g/mol
(m) $c_{CSH} = \frac{[CSH]\rho_b}{M_{CSH}}$
(n) $c_{Ca} = c_{Ca(OH)_2} + 1.65 \cdot c_{CSH}$; see note (l)
(o) Scaled from "SDU 1/4" concrete using CaO ratio from Table 4.4-25
(p) Postulated condition
(q) $S_g + S_\ell = 1$, $\theta_g = S_g n$ and $\theta_\ell = S_\ell n$
(r) Eq. 4.4-38

Table 4.4-24: Input Data and Rate Coefficients for CE Carbonation Calculations

Parameter	SDU 2/6/7	SDU 1/4	SDU 4 Roof	SDU 1 Roof	Saltstone	Units
p_{CO_2} (a)	0.01	0.01	0.01	0.01	0.01	atm
$c_{CO_2,g}$ (b)	4.16E-07	4.16E-07	4.16E-07	4.16E-07	4.16E-07	mol/cm^3 gas
$c_{CO_2,\ell}$ (c)	3.41E-06	3.41E-06	3.41E-06	3.41E-06	3.41E-06	mol/cm^3 liquid
n (d)	0.11	0.106	0.106	0.106	0.656	cm^3 void / cm^3 total
ρ_b (d)	2.18	2.28	2.28	2.28	0.932	g/cm^3 total
$D_{m,g}$ (e)	0.165	0.165	0.165	0.165	0.165	cm^2/s
τ (f)	2.61E-03	2.61E-03	5.22E-03	5.22E-03	1.48E-03	-
$D_{e,g}$ (g)	4.30E-04	4.30E-04	8.61E-04	8.61E-04	2.44E-04	cm^2/s
$D_{e,\ell}$ (d)	6.0E-08	6.0E-08	1.2E-07	1.2E-07	3.4E-08	cm^2/s
$[Ca(OH)_2]$	0 (h)	7.2 (h)	-	-	0 (i)	g/kg
$M_{Ca(OH)_2}$ (j)	74	74	-	-	74	g/mol
$c_{Ca(OH)_2}$ (k)	0	2.22E-04	-	-	0	mol/cm^3 total
$[CSH]$	81.2 (h)	118.8 (h)	-	-	147.4 (i)	g/kg
M_{CSH} (l)	182.1	182.1	-	-	182.1	g/mol
c_{CSH} (m)	9.72E-04	1.49E-03	-	-	7.54E-04	mol/cm^3 total
c_{Ca}	1.60E-03(n)	2.68E-03(n)	2.15E-03(o)	1.85E-03(o)	1.24E-03(n)	mol/cm^3 total
S_g (p)	0.05	0.05	0.05	0.05	0.05	cm^3 gas / cm^3 void
S_ℓ (q)	0.95	0.95	0.95	0.95	0.95	cm^3 liquid / cm^3 void
θ_g (q)	0.0055	0.0053	0.0053	0.0053	0.033	cm^3 gas / cm^3 total
θ_ℓ (q)	0.1045	0.1007	0.1007	0.1007	0.623	cm^3 liquid / cm^3 total
A (r)	**0.199**	**0.151**	**0.238**	**0.257**	**0.415**	cm/√yr

(a) SRNL-L3200-2012-00017
(b) p_{CO_2} and ideal gas law at 20ºC
(c) Sum of H_2CO_3, HCO_3^-, and CO_3^{2-} concentrations from Table 4.4-21
(d) SRR-CWDA-2018-00004, Table 1
(e) Marrero and Mason (1972), Table 20, N_2-CO_2 system
(f) Calculated from liquid-phase effective diffusion coefficients in SRR-CWDA-2018-00004, Table 1, assuming a molecular diffusion coefficient of 2.3E-05 cm^2/s (Holz, et.al., 2000)
(g) $D_{e,g} = \tau D_{m,g}$
(h) SIMCO_03-01-2012, Tables 9 and 13, 28 day cure
(i) SIMCO_06-16-2010, Tables 6 and 13, WS-2 grout
(j) $M_{Ca(OH)_2}$= 40 + 2(16+1) g/mol
(k) $c_{Ca(OH)_2} = [Ca(OH)_2]\rho_b / M_{Ca(OH)_2}$
(l) The stoichiometry of CSH in cement paste is variable. SIMCO assumes $CSH \rightarrow 0.65Ca(OH)_2 + CaH_2SiO_4 = 1.65CaO \cdot SiO_2 \cdot 1.65H_2O$ in STADIUM modeling (CBP-TR-2010-007-C3, Table 7). M_{CSH} = 1.65(40) + 3.3(1) + 1(28) + 5.3(16) g/mol
(m) $c_{CSH} = \frac{[CSH]\rho_b}{M_{CSH}}$
(n) $c_{Ca} = c_{Ca(OH)_2} + 1.65 \cdot c_{CSH}$; see note (l)
(o) Scaled from "SDU 1/4" concrete using CaO ratio from Table 4.4-25
(p) Postulated condition
(q) $S_g + S_\ell = 1$, $\theta_g = S_g n$ and $\theta_\ell = S_\ell n$
(r) Eq. 4.4-38

Table 4.4-25: Estimated Calcium Content in SDU 1 and 4 Roof Concrete Relative to SDU 1 and 4 Floor Concrete

Binder	CaO (%)	SDU 1/4 Floor (lbs/yd³)	SDU 4 Roof (lbs/yd³)	SDU 1 Roof (lbs/yd³)
Type I/II cement Lafarge	64.8	419	466	400
Type IV cement Lehigh	63.8	0	0	0
Blast Furnace Slag, Holcim	37.8	278	0	0
Force 10000 SF Grace	0.6	0	0	0
Class F Fly Ash SEFA	1.32	0	62	70
CaO_{roof}/CaO_{floor}	-	-	0.80	0.69

The molar concentrations of CO_2 in the gas and liquid phases are observed to be similar (within an order of magnitude), whereas the effective diffusion coefficient for gas phase transport is 4 to 5 orders of magnitude larger than its counterpart for the liquid phase. Therefore, gas phase transport generally controls the carbonation process, and liquid phase transport is commonly neglected in the literature (e.g., Papadakis, et.al., 1989). The exception is saturated conditions, where liquid phase transport is the only mechanism delivering CO_2 to the reaction front. The carbonation rate is very slow under these conditions. As a specific example, Rast and Rinker (2012) reported a carbonation depth of 1-2 mm for a concrete core taken from a 50-year-old Hanford waste tank. The rate of carbonation is also minimal under dry conditions, because water is required to support the aqueous reaction $Ca(OH)_2 + H_2O + CO_2 \rightarrow CaCO_3 + 2H_2O$. The maximum rate of carbonation occurs at intermediate conditions, roughly 50% relative humidity (RH) (e.g., Papadakis, et.al., 1989, NUREG/CR-5542 [ML121240822]). The carbonation rate is very sensitive to liquid saturation near full saturation.

4.4.2.3.3 Saturation State

RH and saturation are related through thermodynamic relationships and a material specific water retention curve. Total suction is related to water vapor pressure through the equilibrium thermodynamic relationship (Richards 1965, cited in Fredlund and Rahardjo 1993, Equations 4.1 and 4.3):

$$\psi = \left(P_g - P_\ell\right)/\rho g + \pi = \psi_c + \pi = -\frac{RT}{gM_w} ln\left(\frac{P_v}{P_0}\right) = -\frac{RT}{gM_w} ln(RH) \qquad \text{Eq. 4.4-40}$$

known as the Kelvin relationship where:

ψ = total suction [m],

P_g = gas pressure [Pa],

P_ℓ = liquid pressure [Pa],

ρ = liquid density [kg/m³],

g = gravitational acceleration [m/s²],

π = osmotic suction [m],

ψ_c = capillary or matric suction [m],

R = universal (molar) gas constant [J/mol-K = m³Pa/mol-K],

T = temperature [K],

M_w = molar mass of water [kg/mol],

P_v = water vapor pressure [Pa],

P_0 = vapor pressure at saturation [Pa], and

RH = relative humidity, P_v/P_0 [-].

Considering this expression, water vapor pressure can be viewed as a master variable defining the pressure state of both the gas and liquid phases (Hall and Hoff 2002). The osmotic suction can be estimated from the Morse equation (Huggins 1935 [DOI: 10.1063/1.1749710]):

$$\rho g \pi = iMRT \qquad \text{Eq. 4.4-41}$$

where:

ρ = liquid density [kg/m³],

g = gravitational acceleration [m/s²],

π = osmotic suction [m],

i = van't Hoff factor [-],

M = molarity of the solution [mol/m³],

R = universal (molar) gas constant [J/mol-K = m³Pa/mol-K], and

T = temperature [K].

Eq. 4.4-41 assumes a dilute solution but can be used with increasing approximation for more concentrated solutions. For the case of a dilute solution, the dimensionless van't Hoff factor is approximately one (Daintith, 2008). [DOI: 10.1093/acref/9780199204632.001.0001] Capillary suction is related to saturation through a water retention curve commonly expressed in the form (van Genuchten 1980):

$$S_e = \frac{S - S_r}{1 - S_r} = \frac{\theta - \theta_r}{\theta_s - \theta_r} = \left[\frac{1}{1 + (\alpha \psi_c)^n}\right]^m \qquad \text{Eq. 4.4-42}$$

where:

S = saturation [m³ liquid / m³ void],

S_r = material specific fitting parameter [m³ liquid / m³ void],

θ = water content [m³ liquid / m³ total],

θ_r = material specific fitting parameters [m³ liquid / m³ total],

θ_s = saturated water content = porosity [m³ liquid / m³ total],

α = material specific fitting parameter [1/m],

ψ_c = capillary or matric suction [m], and

n, m = material specific fitting parameters [-].

The subscripts e and r denote "effective" and "residual". Note that S_r and θ_r are correlated (not independent) parameters. It is commonly assumed that $m = 1 - 1/n$. Figure 4.4-15 illustrates water retention curves characteristic of SDU concrete (WSRC-STI-2006-00198) and 20°C cure temperature ARP/MCU saltstone (SRNL-STI-2011-00661) (Figure 4.4-15).

Figure 4.4-15: Water Retention Curves for SDU Concrete and Saltstone

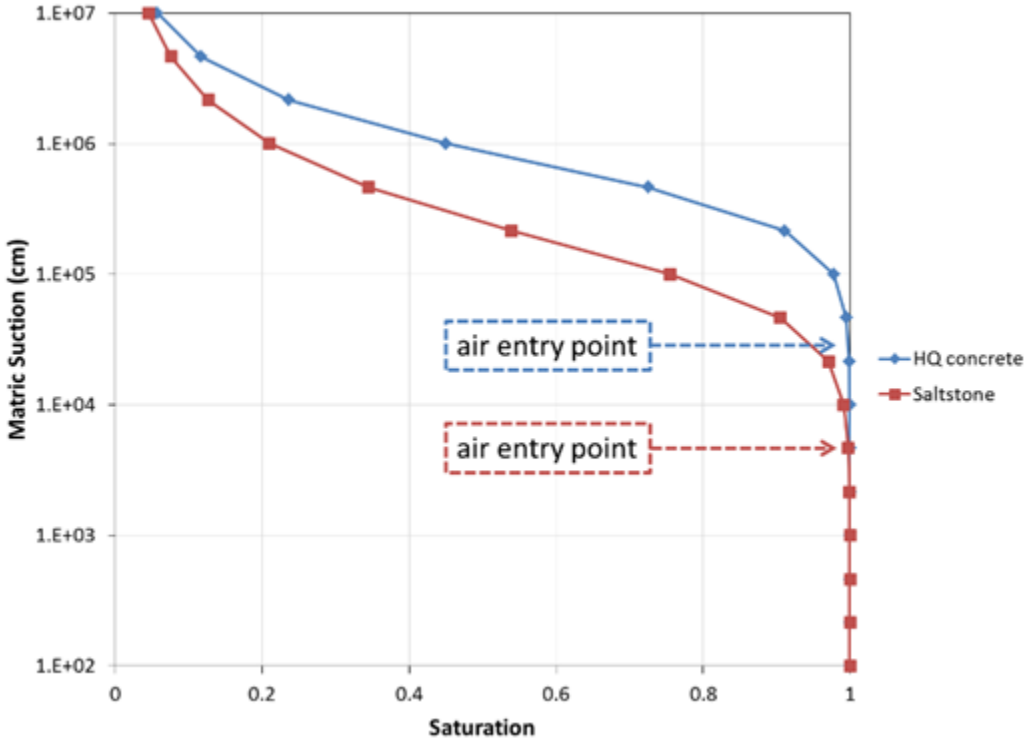

As mentioned previously, the saturation state of a cementitious material strongly affects the rate of carbonation, particularly near full saturation. The anticipated saturation states for SDF cementitious materials can be assessed using Eq. 4.4-40 through Eq. 4.4-42 and estimated soil suction and RH values.

Once buried under a low-permeability cover system, the SDF will initially be exposed to soil conditions approaching gravity equilibrium (no infiltration), where the matric suction head is equal to the height above the water table. Soil moisture contains dissolved solids, but the concentrations are dilute such that osmotic suction is negligible compared to that within cementitious materials. Any infiltration above zero produces capillary suction levels that are lower than under gravity equilibrium. Thus, as the cover system degrades over time, soil suction levels will decrease. With this consideration, the maximum suction head

anticipated for SDUs is roughly 1,500 cm, the approximate height of the SDUs above the water table (15 meters). From Figure 4.4-15, the air entry head is observed to exceed 1,500 cm for saltstone (or clean cap grout) and 10,000 cm for SDU concrete. Thus, SDU concrete is expected to be saturated for all time. Ignoring osmotic effects, saltstone could potentially be slightly unsaturated immediately after cap placement, but if so, would then become saturated by the time the soil suction levels fall below approximately 1,500 cm. Table 4.4-26 shows saturation calculated from the water retention curves depicted in Figure 4.4-15 for the expected maximum capillary suction of approximately 1,500 cm, and 10x higher and lower levels as points of reference (parameter values from WSRC-STI-2006-00198 and SRNL-STI-2011-00661).

Table 4.4-26: Saltstone and Concrete Saturation for Selected Capillary Suctions

Parameter	Saltstone			Concrete		
Saturated water content, θ_s	0.58	0.58	0.58	0.1	0.1	0.1
Residual water content, θ_r	0	0	0	0	0	0
van Genuchten (1980)α (1/cm)	1.008E-05	1.008E-05	1.008E-05	2.086E-06	2.086E-06	2.086E-06
van Genuchten (1980) n	1.67131	1.67131	1.67131	1.9433	1.9433	1.9433
$m = 1 - 1/n$	0.402	0.402	0.402	0.485	0.485	0.485
Capillary suction, ψ_c (cm)	15,000	1,500	150	15,000	1,500	150
Saturation, S	**0.983**	**1.000**	**1.000**	**0.999**	**1.000**	**1.000**

The chemical compositions of pore water in SDU concrete and saltstone have been characterized by SIMCO (SIMCO_06-16-2010, SIMCO_03-01-2012) and are reproduced in Table 4.4-27 through Table 4.4-29. Nitrogen ions, denoted N^-, include NO_2^- and NO_3^- in these tables. The osmotic suctions associated with these molar concentrations are shown in Table 4.4-30 based on Eq. 4.4-41. Over time dissolved species will advect and/or diffuse out of cementitious materials, thus lowering the initial molar concentrations, to levels approaching zero with sufficient time.

Table 4.4-27: Pore Fluid Composition for SDU 2/6/7 Concrete

	28d V2	Molecular Weight	28d V2	28d V2	water
Ion	mmol/L	g/mol	mol/L	g/L	g/L
OH^-	113.9	17	0.114	1.94	
Na^+	26.5	23	0.027	0.61	
K^+	35.8	39	0.036	1.40	
SO_4^{2-}	0	96	0.000	0.00	
Ca^{2+}	2	40	0.002	0.08	
Cl^-	4.2	35	0.004	0.15	
N			0.000	0.00	
CO_3^{2-}			0.000	0.00	
Total			**0.182**	4.2(0.4 wt%)	998

SIMCO_03-01-2012, Table 11

Table 4.4-28: Pore fluid Composition for SDU 1/4 Concrete

	28d V4	Molecular Weight	28d V4	28d V4	water
Ion	mmol/L	g/mol	mol/L	g/L	g/L
OH^-	244.4	17	0.244	4.15	
Na^+	73.9	23	0.074	1.70	
K^+	140.7	39	0.141	5.49	
SO_4^{2-}	0.1	96	0.000	0.01	
Ca^{2+}	1.8	40	0.002	0.07	
Cl^-	4.8	35	0.005	0.17	
N			0.000	0.00	
CO_3^{2-}			0.000	0.00	
Total			**0.466**	11.6(1.1 wt%)	998

SIMCO_03-01-2012, Table 11

Table 4.4-29: Pore Fluid Composition for Saltstone

	28d WS-2	Molecular Weight	28d WS-2	28d WS-2	water
Ion	mmol/L	g/mol	mol/L	g/L	g/L
OH^-	383.9	17	0.384	6.53	
Na^+	4144.2	23	4.144	95.32	
K^+	120.5	39	0.121	4.70	
SO_4^{2-}	111.7	96	0.112	10.72	
Ca^{2+}	0.1	40	0.000	0.00	
Cl^-	11.9	35	0.012	0.42	
N	3552.1	60.4	3.552	214.52	
CO_3^{2-}	46.8	60	0.047	2.81	
Total			**8.371**	335.0(25.1 wt%)	998

SIMCO_06-16-2010, Table 8

Table 4.4-30 includes calculations for two additional concentrations: half the initial values and zero. The total suction is assumed to be 1,500 cm in all cases based on the exposure to soil conditions. The RH corresponding to 1,500 cm is 99.89% from Eq. 4.4-40.

In comparison, carbonation rates reported in the literature are typically focused on 50-70% relative humidity, which is reflective of atmospheric exposure conditions and maximum penetration. For the initial and intermediate molar concentrations, the osmotic suctions exceed the total suction and the capillary suctions are negative-valued (Eq. 4.4-40), total suction is composed of capillary and osmotic suction). The latter implies the pore water pressure is positive, in contrast to pure water that is under tension (negative pressure). Therefore, saturation is 100% when dissolved species are present at these concentrations. The practical implication is that saltstone is expected to be fully saturated at early times, when soil suction levels are the highest, because of osmotic suction. At later times when the molar concentration of the pore fluid drops, soil (total) suction levels will also be lower such that saltstone will remain saturated, even with pure water in its pore space. Thus, the pore spaces of both concrete and grout are

expected to be fully saturated for all time once these materials are in the subsurface.

Table 4.4-30: Relative Humidity and Capillary Suction Corresponding to a Total Suction of 1,500 cm

Parameter	Saltstone			Concrete-V2			Concrete-V4			Units
temperature, T	20	20	20	20	20	20	20	20	20	C
	293.15	293.15	293.15	293.15	293.15	293.15	293.15	293.15	293.15	K
relative humidity, RH	99.89%	99.89%	99.89%	99.89%	99.89%	99.89%	99.89%	99.89%	99.89%	
saturation pressure, P_0	23.46	23.46	23.46	23.46	23.46	23.46	23.46	23.46	23.46	millibar
	2346	2346	2346	2346	2346	2346	2346	2346	2346	Pa
water vapor pressure, P_v	2344	2344	2344	2344	2344	2344	2344	2344	2344	Pa
gas constant, R	8.314	8.314	8.314	8.314	8.314	8.314	8.314	8.314	8.314	J/K-mol
molecular mass of water, M_w	18	18	18	18	18	18	18	18	18	g/mol
gravitational acceleration, g	9.81	9.81	9.81	9.81	9.81	9.81	9.81	9.81	9.81	m/s^2
density of water, ρ	998	998	998	998	998	998	998	998	998	kg/m^3
ρg	9790.38	9790.38	9790.38	9790.38	9790.38	9790.38	9790.38	9790.38	9790.38	Pa/m
total suction, ψ	15	15	15	15	15	15	15	15	15	m
	1500	1500	1500	1500	1500	1500	1500	1500	1500	cm
	146856	146856	146856	146856	146856	146856	146856	146856	146856	Pa
	1.5	1.5	1.5	1.5	1.5	1.5	1.5	1.5	1.5	bar
vant Hoff factor, i	1	1	1	1	1	1	1	1	1	
molarity, M	8.37	4.185	0	0.18	0.09	0	0.47	0.235	0	mol/L
osmotic suction, Π	20399775	10199887	0	438705	219352	0	1145507	572754	0	Pa
	2083.66	1041.83	0.00	44.81	22.40	0.00	117.00	58.50	0.00	m
	208366	104183	0	4481	2240	0	11700	5850	0	cm
	204.0	102.0	0.0	4.4	2.2	0.0	11.5	5.7	0.0	bar
capillary (matric) suction, ψ_c	-2069	-1027	15	-30	-7	15	-102	-44	15	m
	-206866	-102683	1500	-2981	-740	1500	-10200	-4350	1500	cm
	-20252919	-10053032	146856	-291849	-72497	146856	-998651	-425898	146856	Pa
	-202.5	-100.5	1.5	-2.9	-0.7	1.5	-10.0	-4.3	1.5	bar
saturated water content, θ_s	0.58	0.58	0.58	0.1	0.1	0.1	0.1	0.1	0.1	
residual water content, θ_r	0	0	0	0	0	0	0	0	0	
van Genuchten (1980) α	1.008E-05	1.008E-05	1.008E-05	2.086E-06	2.086E-06	2.086E-06	2.086E-06	2.086E-06	2.086E-06	1/cm
van Genuchten (1980) n	1.67131	1.67131	1.67131	1.9433	1.9433	1.9433	1.9433	1.9433	1.9433	
m=1-1/n	0.402	0.402	0.402	0.485	0.485	0.485	0.485	0.485	0.485	
capillary suction, Ψc	-206866	-102683	1500	-2981	-740	1500	-10200	-4350	1500	cm
saturation	1.000	1.000	1.000	1.000	1.000	1.000	1.000	1.000	1.000	

While saturated pores preclude gas-phase CO_2 transport and relatively fast carbonation, these processes may occur should either cementitious material be fractured, depending on matric suction levels and crack aperture. For a perfectly wetting fluid, the capillary rise between two vertical parallel surfaces is:

$$h = \frac{2\sigma}{\rho g b} \quad \text{Eq. 4.4-43}$$

where:

h = capillary rise [m],

σ = surface tension [N/m],

ρ = density [kg/m^3],

g = gravitation acceleration [m/s^2], and

b = aperture [m].

In the context of a vertical fracture subjected to a given pressure head, $P/\rho g$ [m], in the surrounding matrix, the aperture will be liquid-filled under the condition (Wang and Narasimhan 1985):

$$\frac{P}{\rho g} > -\frac{2\sigma}{\rho g b} \quad \text{Eq. 4.4-44}$$

In other words, the fracture will be liquid-filled for positive pressure head and suction (negative pressure) head less than $2\sigma/\rho g b$. Alternatively, the maximum aperture that can be liquid-filled for a given capillary suction head, ψ_c [m], is

$$b = \frac{2\sigma}{\rho g \psi_c} \quad \text{Eq. 4.4-45}$$

For ψ_c = 1,500 cm = 15m, the result is b = 1 μm = 0.04 mil. Hence fractures, if present, are expected to be unsaturated unless very narrow. If these hypothetical fractures were connected, then they would provide a means for gas-phase transport of CO_2 through the porous medium. In the event of gas-phase transport of CO_2, the degradation rate via carbonation would be expected to accelerate. Given that the carbonation rates vary significantly between the BE, CV, and CE calculations, uncertainty associated with this phenomenon is partially addressed through the varying input assumptions used.

4.4.2.3.4 Penetration Rate Coefficients

Returning to Eq. 4.4-37 and Eq. 4.4-38, three conditions are considered for predicting carbonation rates in SDU concrete and saltstone, as shown in Table 4.4-22 through Table 4.4-24. The best-estimate (BE) rate is calculated assuming a capillary suction of 1,500 cm and pure water occupying pore space, i.e., neglecting osmotic effects. Under these conditions SDU concrete is fully liquid saturated and saltstone (or clean cap grout) is liquid saturated at 99.96% (practically saturated). The best-estimate (BE) label is somewhat of a misnomer because suction levels will

be less than 1,500 cm for much of the Performance Period and osmotic effects are present. Thus, saltstone is expected to be liquid saturated. Rather, the label is used in a relative sense compared to the other two scenarios.

The compliance-value and conservative-estimate rates account for uncertainty in water retention curves, and/or the postulation that entrapped air creates a connected pathway for gas-phase transport. Figure 4.4-16 shows water retention curves for a variety of actual and hypothetical materials. The "HQ Concrete" and "Saltstone" curves from Figure 4.4-15 are reproduced in Figure 4.4-16. Three soils, "Clay," "Clay-Sand," and "Backfill" from WSRC-STI-2006-00198, are shown as points of reference. The remaining curves are hypothetical variations on Table 4.4-26 where the α parameter has been increased to lower the air-entry pressures of concrete and saltstone.

At high saturations, the setting $\alpha = 0.0001\ \text{cm}^{-1}$ applied to either concrete or saltstone produces a pessimistic condition in which the matric suction is approximately an order of magnitude lower than that of the saltstone based on Figure 4.4-15.

Figure 4.4-16: Water Retention Curves for Various Reference Materials

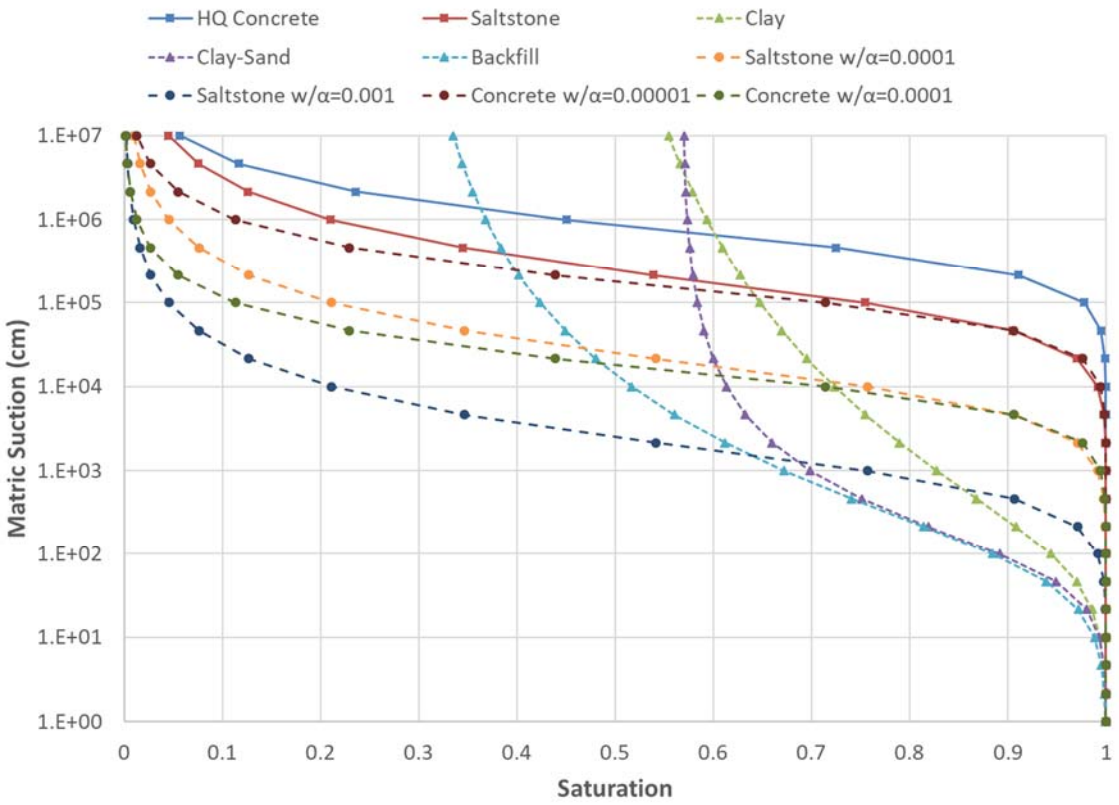

Under the relatively saturated conditions that are expected, saltstone lies midway between the two cementitious materials and the soils, which are surrogates for a

severely degraded state of concrete or saltstone. At a capillary suction of 1,500 cm, liquid saturation for this hypothetical condition is approximately 98% (equivalently 2% gas saturation). Alternatively, saturations of 98% liquid / 2% gas can be tied to pessimistic assumptions about entrapped air. Entrapped air typically occupies 0.5 to 2% of concrete by volume (Daniel and Lobo 2005). [ISBN: 9780803145573] Air pockets are generally expected to be isolated, and thus not connected. A pessimistic assumption is that entrapped air at 2% forms a fully connected pathway for gas-phase transport. The compliance-value calculation assumes 98% liquid saturation / 2% gas saturation due to a much higher than expected α, or connected macro-voids due to entrapped air. The conservative-estimate assumes 95% liquid saturation / 5% gas saturation due to combined effects, or conditions otherwise more pessimistic than the CV case.

Table 4.4-22 through Table 4.4-24 indicate the carbonation rate coefficient A [cm/√yr] from Eq. 4.4-38 for the BE, CV, and CE conditions. The carbonation rate coefficient can be used in Eq. 4.4-16 to predict degradation time t_0 for a specified material thickness x_0.

As a point of reference, Brown, et.al., (2012) performed detailed simulations of carbonation in "VCT" concrete, which is essentially Saltstone SDU 2, 3/5, and 6 concrete, using LeachXS™/ORCHESTRA in a developmental CBP Software Toolbox carbonation module (Brown, et.al., 2013a, b). The carbonation depth was defined as the location where pH < 9. Figure 4.4-17 is a reproduction of simulation results for various CO_2 concentrations based on 30% porosity, 90% liquid saturation, and a diffusion coefficient of 1.E-6 m²/s. These settings produce faster rates of carbonation than any of the cases considered in Table 4.4-22 through Table 4.4-24. Focusing on the 1% CO_2 curve (0.01 atm), the numerical simulations are observed to exhibit an initial time lag before the carbonation front advances from the exposure surface. After √t = 15 √yr (t = 225 yr), the carbonation front stalls at about 1.25 cm. Using t_0 = 225 yr and x_0 = 1.25 cm in Eq. 4.4-16, the equivalent carbonation rate constant is A = 0.083 cm/√yr. The latter is significantly lower than the conservative-estimate value in Table 4.4-24 which indicates that the analytic solution given by Eq. 4.4-37 and other input assumptions are biased in the pessimistic direction. The reason is that the analytic model does not allow calcium to diffuse from the unreacted zone, where concentration is controlled by $Ca(OH)_2$ and $C\text{-}S\text{-}H$ solubility and high, to the reacted zone, where concentration is controlled by $CaCO_3$ solubility and low. Transport of calcium to the reaction front increases the effective reaction capacity at that location (while depleting it deeper), slowing the penetration front.

Because SDU 1 and 4 wall concretes are assumed to be fully degraded at PA time zero for the CV and CE cases, obviating the need for degradation estimates except for the BE case, penetration rate coefficient calculations are not shown in Table 4.4-22 through Table 4.4-24 for these components. However, the rate coefficients

for the SDU 1 and 4 wall BE, CV and CE cases are calculated to be 0.087, 1.212 and 1.886 cm/√yr, respectively.

Figure 4.4-17: Carbonation Simulation Results as a Function of Soil-Gas CO_2 Concentration for 90% Concrete Saturation

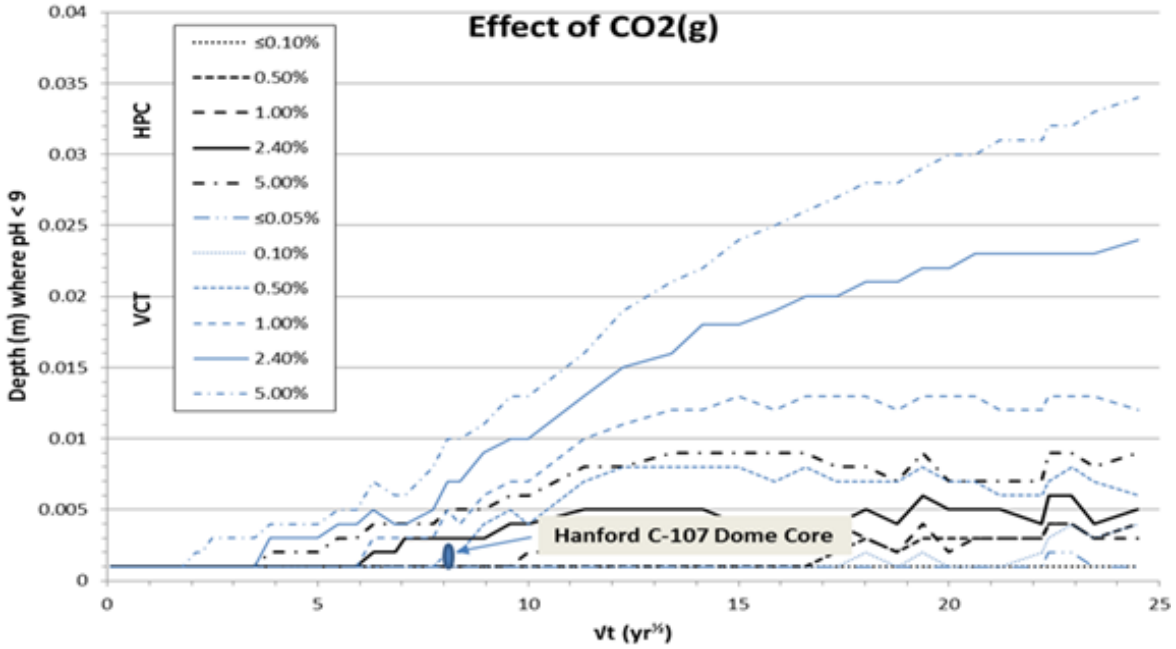

Note: VCT = SDU 2 Concrete and HPC = High Perfromance Concrete
[Source: Brown, et.al., 2013a, b]

4.4.2.4 Steel Corrosion

As noted in the preceding section, steel corrosion products (rust) are expansive and when present inside concrete (e.g., corroded rebar) can exert stresses that cause cracking. Under high pH conditions, such as found in uncarbonated concrete, a passivating layer forms on steel surfaces leading to relatively slow corrosion rates. Specifically, the passive corrosion rate is typically 0.1 μm/yr (ACI 222R-01) and might range between 0.01 and 1 μm/yr (see Ahmad 2003, Equation (14) and surrounding discussion). Much higher corrosion rates, roughly 1,000x (ACI 222R-01, Ahmad 2003), occur at lower pH (<10), found in concrete following the arrival of a carbonation front. Degradation of concrete barriers via corrosion of embedded steel is analyzed for the SDF PA in the manner typical of civil engineering applications focused on structural service life. That is, corrosion is assumed to be negligible prior to carbonation and extensive damage is assumed to coincide with carbonation.

Neglecting passive steel corrosion prior to carbonation is an acceptable simplifying assumption considering the time scale of combined carbonation and external sulfate attack on concrete. In the degradation timing analysis that follows, concrete barriers become fully degraded after roughly a thousand years from a combination of sulfate attack and carbonation. The corrosion depth for passivated steel over this time frame would be nominally 0.1 mm and conservatively 1 mm, which is not expected to cause

significant damage. That is, passive steel corrosion is expected to be a non-limiting degradation phenomenon and is thus not explicitly considered in the degradation calculations that follow.

4.4.2.5 Decalcification

Decalcification in this application refers to leaching of Ca^{2+} in pore water to exterior soil, where the concentration is assumed to be zero. [ML121240822 (NUREG/CR-5542), WSRC-STI-2007-00607, SRNL-STI-2010-00035] Leaching may occur through diffusion and/or advection.

4.4.2.5.1 Penetration Rate Coefficients for Diffusive Decalcification

For diffusion-controlled release between a sharp dissolution front and the soil interface, the penetration depth follows the general Eq. 4.4-13 as:

$$x = \left[\frac{2SnD_{eff}c_{Ca^{2+}}t}{c_{Ca}}\right]^{1/2} = At^{1/2} \qquad \text{Eq. 4.4-46}$$

where:

x = penetration depth [cm],

S = saturation of fluid phase delivering reactant to moving front [cm^3 liquid-phase / cm^3 void-space],

n = porosity [cm^3 void-space / cm^3 total],

D_{eff} = effective diffusion coefficient for fluid phase [cm^2/yr],

t = elapsed time [yr],

$c_{Ca^{2+}}$ = dissolved $c_{Ca^{2+}}$ concentration [mol / cm^3 liquid], and

c_{Ca} = calcium concentration in solid phase [mol / cm^3 total].

Additionally:

$$A \equiv \left[\frac{2SnD_{eff}c_{Ca^{2+}}}{c_{Ca}}\right]^{1/2} \qquad \text{Eq. 4.4-47}$$

where A is the rate coefficient. Table 4.4-31 through Table 4.4-33 present BE, CV and CE input parameters for use in Eq. 4.4-46 and Eq. 4.4-47. Most parameter values come from Table 4.4-22 through Table 4.4-24. The concentration of Ca^{2+} varies through the leaching process; alkali metals leach first, followed by (OH_2), and then *C-S-H*. [ML121240822 (NUREG/CR-5542)] In this analysis, dissolution of *C-S-H* gel is assumed to control the concentration of Ca^{2+} over most of the leaching process, because little or no Portandite $Ca(OH)_2$is expected to occur in SDF cementitious materials (Table 4.4-31 through Table 4.4-33). *C-S-H* dissolves incongruently in that calcites leach preferentially in comparison to silicates. SIMCO (SIMCO_03-01-2012, Table 11) measured $c_{Ca^{2+}}$ in SDU concrete ranging from 1.8 to 2.0 mmol/L, or 1.8E-06 mol/cm^3 to 2.0E-06 mol/cm^3, which is consistent with UCRL-ID-132088, Table 15 (where Ca/Si = 0.9). A value of 2.0E-06 mol/cm^3 is

assumed as an input in Table 4.4-31 through Table 4.4-33. The rate coefficients for decalcification controlled by diffusion are low, indicating a slow process. Because these rate coefficients are small compared to those for other phenomena, uncertainty in $c_{Ca^{2+}}$ is ignored.

Because SDU 1 and 4 wall concretes are assumed to be fully degraded at PA time zero for the CV and CE cases, obviating the need for degradation estimates except for the BE case, penetration rate coefficient calculations are not shown in Table 4.4-31 through Table 4.4-33 for these components. However, the rate coefficients for the SDU 1 and 4 wall BE, CV and CE cases are calculated to be 0.066, 0.216 and 0.216 cm/√yr, respectively.

Table 4.4-31: Input Data and Rate Coefficients for BE Diffusion-Limited Decalcification

Parameter	SDU 2/6/7	SDU 1/4	SDU 4 Roof	SDU 1 Roof	Saltstone	Units
$c_{Ca^{2+}}$ (a)	2.0E-06	2.0E-06	2.0E-06	2.0E-06	2.0E-06	mol/cm³ liquid
n (b)	0.110	0.106	0.106	0.106	0.656	cm³ void / cm³ total
ρ_b (b)	2.18	2.28	2.28	2.28	0.932	g/cm³ total
D_e (b)	3.5E-08	3.5E-08	6.0E-08	6.0E-08	6.8E-09	cm²/s
$[Ca(OH)_2]$	0 (c)	7.2 (c)	-	-	0 (d)	g/kg
$M_{Ca(OH)_2}$ (e)	74	74	-	-	74	g/mol
$c_{Ca(OH)_2}$ (f)	0	2.22E-04	-	-	0	mol/cm³ total
$[CSH]$	81.2 (c)	118.8 (c)	-	-	147.4 (d)	g/kg
M_{CSH} (g)	182.1	182.1	-	-	182.1	g/mol
c_{CSH} (h)	9.72E-04	1.49E-03	-	-	7.54E-04	mol/cm³ total
c_{Ca}	1.60E-03 (i)	2.68E-03 (i)	2.15E-03 (j)	1.85E-03 (j)	1.24E-03 (i)	mol/cm³ total
S_ℓ (k)	1	1	1	1	0.9996	cm³ liquid / cm³ void
θ_ℓ (l)	0.110	0.106	0.106	0.106	0.656	cm³ liquid / cm³ total
A (m)	**0.017**	**0.013**	**0.019**	**0.021**	**0.021**	cm/√yr

(a) Approximate solubility of CSH (SIMCO_03-01-2012, UCRL-ID-132088)
(b) SRR-CWDA-2018-00004, Table 1
(c) SIMCO_03-01-2012, Tables 9 and 13, 28 day cure
(d) SIMCO_06-16-2010, Tables 6 and 13, WS-2 grout
(e) $M_{Ca(OH)_2}$= 40 + 2(16+1) g/mol
(f) $c_{Ca(OH)_2} = [Ca(OH)_2]\rho_b/M_{Ca(OH)_2}$
(g) The stoichiometry of CSH in cement paste is variable. SIMCO assumes $CSH \rightarrow 0.65Ca(OH)_2 + CaH_2SiO_4 = 1.65CaO \cdot SiO_2 \cdot 1.65H_2O$ in STADIUM modeling (CBP-TR-2010-007-C3, Table 7). M_{CSH} = 1.65(40) + 3.3(1) + 1(28) + 5.3(16) g/mol
(h) $c_{CSH} = \frac{[CSH]\rho_b}{M_{CSH}}$
(i) $c_{Ca} = c_{Ca(OH)_2} + 1.65 \cdot c_{CSH}$; see note (g)
(j) Scaled from "SDU 1/4" concrete using CaO ratio from Table 4.4-25
(k) computed from van Genuchten (1980) water retention curve and 1,500 cm suction
(l) $\theta_\ell = S_\ell n$
(m) Eq. 4.4-47

Table 4.4-32: Input Data and Rate Coefficients for CV Diffusion-Limited Decalcification

Parameter	SDU 2/6/7	SDU 1/4	SDU 4 Roof	SDU 1 Roof	Saltstone	Units
$c_{Ca^{2+}}$ (a)	2.0E-06	2.0E-06	2.0E-06	2.0E-06	2.0E-06	mol/cm³ liquid
n (b)	0.11	0.106	0.106	0.106	0.656	cm³ void / cm³ total
ρ_b (b)	2.18	2.28	2.28	2.28	0.932	g/cm³ total
D_e (b)	5.3E-08	5.3E-08	9.7E-08	9.7E-08	1.3E-08	cm²/s
$[Ca(OH)_2]$	0 (c)	7.2 (c)	-	-	0 (d)	g/kg
$M_{Ca(OH)_2}$ (e)	74	74	-	-	74	g/mol
$c_{Ca(OH)_2}$ (f)	0	2.22E-04	-	-	0	mol/cm³ total
$[CSH]$	81.2 (c)	118.8 (c)	-	-	147.4 (d)	g/kg
M_{CSH} (g)	182.1	182.1	-	-	182.1	g/mol
c_{CSH} (h)	9.72E-04	1.49E-03	-	-	7.54E-04	mol/cm³ total
c_{Ca}	1.60E-03 (i)	2.68E-03 (i)	2.15E-03 (j)	1.85E-03 (j)	1.24E-03 (i)	mol/cm³ total
S_ℓ (k)	1	1	1	1	0.9996	cm³ liquid / cm³ void
θ_ℓ (l)	0.110	0.106	0.106	0.106	0.656	cm³ liquid / cm³ total
A (m)	**0.021**	**0.016**	**0.025**	**0.026**	**0.029**	cm/√yr

(a) Approximate solubility of CSH (SIMCO_03-01-2012, UCRL-ID-132088)
(b) SRR-CWDA-2018-00004, Table 1
(c) SIMCO_03-01-2012, Tables 9 and 13, 28 day cure
(d) SIMCO_06-16-2010, Tables 6 and 13, WS-2 grout
(e) $M_{Ca(OH)_2}$= 40 + 2(16+1) g/mol
(f) $c_{Ca(OH)_2} = [Ca(OH)_2]\rho_b / M_{Ca(OH)_2}$
(g) The stoichiometry of CSH in cement paste is variable. SIMCO assumes $CSH \rightarrow 0.65Ca(OH)_2 + CaH_2SiO_4 = 1.65CaO \cdot SiO_2 \cdot 1.65H_2O$ in STADIUM modeling (CBP-TR-2010-007-C3, Table 7). M_{CSH} = 1.65(40) + 3.3(1) + 1(28) + 5.3(16) g/mol
(h) $c_{CSH} = \frac{[CSH]\rho_b}{M_{CSH}}$
(i) $c_{Ca} = c_{Ca(OH)_2} + 1.65 \cdot c_{CSH}$; see note (g)
(j) Scaled from "SDU 1/4" concrete using CaO ratio from Table 4.4-25
(k) computed from van Genuchten (1980) water retention curve and 1,500 cm suction
(l) $\theta_\ell = S_\ell n$
(m) Eq. 4.4-47

Table 4.4-33: Input Data and Rate Coefficients for CE Diffusion-Limited Decalcification

Parameter	SDU 2/6/7	SDU 1/4	SDU 4 Roof	SDU 1 Roof	Saltstone	Units
$c_{Ca^{2+}}$ (a)	2.0E-06	2.0E-06	2.0E-06	2.0E-06	2.0E-06	mol/cm³ liquid
n (b)	0.11	0.106	0.106	0.106	0.656	cm³ void / cm³ total
ρ_b (b)	2.18	2.28	2.28	2.28	0.932	g/cm³ total
D_e (b)	6.0E-08	6.0E-08	1.2E-07	1.2E-07	3.4E-08	cm²/s
$[Ca(OH)_2]$	0 (c)	7.2 (c)	-	-	0 (d)	g/kg
$M_{Ca(OH)_2}$ (e)	74	74	-	-	74	g/mol
$c_{Ca(OH)_2}$ (f)	0	2.22E-04	-	-	0	mol/cm³ total
$[CSH]$	81.2 (c)	118.8 (c)	-	-	147.4 (d)	g/kg
M_{CSH} (g)	182.1	182.1	-	-	182.1	g/mol
c_{CSH} (h)	9.72E-04	1.49E-03	-	-	7.54E-04	mol/cm³ total
c_{Ca}	1.60E-03 (i)	2.68E-03 (i)	2.15E-03 (j)	1.85E-03 (j)	1.24E-03 (i)	mol/cm³ total
S_ℓ (k)	1	1	1	1	0.9996	cm³ liquid / cm³ void
θ_ℓ (l)	0.110	0.106	0.106	0.106	0.656	cm³ liquid / cm³ total
A (m)	**0.023**	**0.017**	**0.027**	**0.029**	**0.048**	cm/√yr

(a) Approximate solubility of CSH (SIMCO_03-01-2012, UCRL-ID-132088)
(b) SRR-CWDA-2018-00004, Table 1
(c) SIMCO_03-01-2012, Tables 9 and 13, 28 day cure
(d) SIMCO_06-16-2010, Tables 6 and 13, WS-2 grout
(e) $M_{Ca(OH)_2}$= 40 + 2(16+1) g/mol
(f) $c_{Ca(OH)_2} = [Ca(OH)_2]\rho_b/M_{Ca(OH)_2}$
(g) The stoichiometry of CSH in cement paste is variable. SIMCO assumes $CSH \rightarrow 0.65Ca(OH)_2 + CaH_2SiO_4 = 1.65CaO \cdot SiO_2 \cdot 1.65H_2O$ in STADIUM modeling (CBP-TR-2010-007-C3, Table 7). M_{CSH} = 1.65(40) + 3.3(1) + 1(28) + 5.3(16) g/mol
(h) $c_{CSH} = \frac{[CSH]\rho_b}{M_{CSH}}$
(i) $c_{Ca} = c_{Ca(OH)_2} + 1.65 \cdot c_{CSH}$; see note (g)
(j) Scaled from "SDU 1/4" concrete using CaO ratio from Table 4.4-25
(k) computed from van Genuchten (1980) water retention curve and 1,500 cm suction
(l) $\theta_\ell = S_\ell n$
(m) Eq. 4.4-47

4.4.2.5.2 Penetration Rate Coefficients for Advective Decalcification

While diffusion may control the decalcification of thinner features at earlier times, specifically in concrete barriers, advection is more likely to control decalcification of the saltstone monolith, considering its greater dimensions and higher hydraulic conductivity. Assuming one-dimensional downward flow, a quasi-steady state advective mass balance for decalcification is:

$$Uc_{Ca^{2+}}t = c_{Ca}h \qquad \text{Eq. 4.4-48}$$

where:

U = Darcy velocity (volumetric water flux) [cm/yr],

t = elapsed time [yr], and

h = saltstone monolith height [cm].

The concentrations are as defined for Eq. 4.4-46. Eq. 4.4-48 assumes that advection occurs uniformly through the entire thickness, the dissolution front advances uniformly, and the exit concentration coincides with Ca^{2+} solubility. Solving for time yields:

$$t = \frac{c_{Ca}}{c_{Ca^{2+}}} \cdot \frac{h}{U} \equiv \left(\frac{1}{A_U}\right) \cdot h \qquad \text{Eq. 4.4-49}$$

where A_U [cm/yr] is the rate coefficient for this advection-based degradation:

$$A_U = \frac{c_{Ca^{2+}}}{c_{Ca}} U \qquad \text{Eq. 4.4-50}$$

Eq. 4.4-49 is more limiting than Eq. 4.4-46 for saltstone based on representative calculations. Note that A_U is inversely proportion to time t, instead of $\sqrt{t}$ for diffusion-limited decalcification.

Table 4.4-34 presents advection-limited decalcification rate coefficients for saltstone. The reaction capacity inputs are taken from Section 4.4.2.5.1. The saturated hydraulic conductivity (K_{sat}) of saltstone is defined by SRR-CWDA-2018-00004.

Table 4.4-34: Input Data and Rate Coefficients for Advection-Limited Decalcification of Saltstone

Parameter	BE Saltstone	CV Saltstone	CE Saltstone	Units
$c_{Ca^{2+}}$ (a)	2.0E-06	2.0E-06	2.0E-06	mol/cm³ liquid
$[Ca(OH)_2]$ (b)	0	0	0	g/kg
$M_{Ca(OH)_2}$ (c)	74	74	74	g/mol
$c_{Ca(OH)_2}$ (d)	0	0	0	mol/cm³ total
$[CSH]$ (b)	147.4	147.4	147.4	g/kg
M_{CSH} (e)	182.1	182.1	182.1	g/mol
c_{CSH} (f)	7.54E-04	7.54E-04	7.54E-04	mol/cm³ total
c_{Ca} (g)	1.24E-03	1.24E-03	1.24E-03	mol/cm³ total
K_{sat} (h)	1.0E-10	5.0E-10	2.0E-09	cm/s
dH/dz (i)	1	3	5	cm/cm
A_U (j)	**5.1E-06**	**7.6E-05**	**5.1E-04**	cm/yr

(a) Approximate solubility of CSH (SIMCO_03-01-2012, UCRL-ID-132088)
(b) SIMCO_06-16-2010, Tables 6 and 13, WS-2 grout
(c) $M_{Ca(OH)_2}$= 40 + 2(16+1) g/mol
(d) $c_{Ca(OH)_2} = [Ca(OH)_2]\rho_b / M_{Ca(OH)_2}$
(e) The stoichiometry of CSH in cement paste is variable. SIMCO assumes $CSH \rightarrow 0.65Ca(OH)_2 + CaH_2SiO_4 = 1.65CaO \cdot SiO_2 \cdot 1.65H_2O$ in STADIUM modeling (CBP-TR-2010-007-C3, Table 7). M_{CSH} = 1.65(40) + 3.3(1) + 1(28) + 5.3(16) g/mol
(f) $c_{CSH} = \frac{[CSH]\rho_b}{M_{CSH}}$
(g) $c_{Ca} = c_{Ca(OH)_2} + 1.65 \cdot c_{CSH}$; see note (e)
(h) SRR-CWDA-2018-00004, Table 1
(i) Postulated values as discussed in Section 4.4.2.5.2
(j) Eq. 4.4-50

The hydraulic head gradient in vadose zone soil tends to be one or less, such that the flowrate is equal to or less than the saturated hydraulic conductivity, per Darcy's law:

$$U \leq -K_{sat} \frac{dH}{dz} \qquad \text{Eq. 4.4-51}$$

For a cementitious monolith placed in the vadose zone, the head gradient can be higher as infiltration flows around the lower permeability obstacle. An upper bound on the gradient can be computed by assuming that water is ponded on the SDU roof up to the ground surface, and the underside of the floor is at gravity equilibrium (Section 4.4.2.3.3) with the water table. Table 4.4-35 shows this calculation using bounding values for all inputs. The result is a gradient of roughly 5 ft/ft. The assumptions for the BE, CV, and CE scenarios are dH/dz = 1, 3, and 5 ft/ft, respectively.

Table 4.4-35: Bounding Hydraulic Head Gradient Calculation

Parameter	Bounding Value	Units	Comments
Maximum distance, roof to ground surface (a)	45	ft	
SDU 1distance, floor to roof (b)	27	ft	
SDU 4 distance, floor to roof (c)	30	ft	
SDU 2 distance, floor to roof (d)	22	ft	
SDU 6/7 distance, floor to roof (e)	43	ft	
Minimum distance, floor to roof	22	ft	SDU 2
Maximum distance, water table to floor (f)	48	ft	SDU 1
Pressure head at roof	45	ft	
Elevation of roof	22	ft	reference is floor
Head at roof	67	ft	
Pressure head at floor	-48	ft	
Elevation of floor	0	ft	reference is floor
Head at floor	-48	ft	
Head difference	115	ft	
Gradient (g)	**5.2**	ft/ft	

(a) WSRC-STI-2008-00244, Figures 6 and 7
(b) SRR-CWDA-2009-00017, Section 3.2.1.1.2
(c) SRR-CWDA-2009-00017, Section 3.2.1.2.2
(d) SRR-CWDA-2009-00017, Section 3.2.1.3.2
(e) SRR-CWDA-2018-00012
(f) SRR-CWDA-2009-00017, Table 4.2-13
(g) Head difference / Floor to roof distance

4.4.2.6 Clean Grout Cap

Saltstone Disposal Units 1 and 4 are expected to be closed with a layer of clean grout between saltstone and the underside of the roof. The potential presence of a clean cap grout in SDU 2, 6, and 7-12 is not credited. The lag time for sulfate in saltstone to effectively reach the roof and initiate sulfate attack is estimated using the analytic solution for diffusion into a semi-infinite medium (Myer 1971, Equation 6.4.29, SRNL-STI-2009-00115, Equation 19b):

$$c = c_0 erfc\left(\frac{x}{2\sqrt{D_e t}}\right) \quad \text{Eq. 4.4-52}$$

where:

c = interior concentration [mol/L],

c_0 = boundary concentration [mol/L],

x = penetration depth [cm],

D_e = effective diffusion coefficient for liquid phase, τD_m [cm²/yr], and

t = elapsed time [yr].

The ratio c/c_0 is assumed to be 10%, 20%, and 50% for the CE, CV, and BE cases to provide an uncertainty range. When these trigger values are reached, sulfate attack is assumed to occur as though the underside of the roof were exposed to the unattenuated sulfate concentration, c_0. The penetration depth is defined to be the minimum thickness of the clean grout: 6 inches and 15 inches for SDU 1 and 4, respectively. Effective diffusion coefficients are defined in SRR-CWDA-2018-00004. The resulting delayed onset times for sulfate attack are shown in Table 4.4-36 and Table 4.4-37.

Table 4.4-36: Delayed Sulfate Attack Onset Times for SDU 1 Roof Concrete

Parameter	BE	CV	CE	Units
Effective diffusion coefficient, D_e	6.0E-08 1.89	9.7E-08 3.06	1.2E-07 3.78	cm2/s cm2/yr
Penetration depth, x	6 15.24	6 15.24	6 15.24	in cm
Relative concentration, c/c_0	0.5	0.2	0.1	-
Penetration time, t	**135**	**23**	**11**	yr

Table 4.4-37: Delayed Sulfate Attack Onset Times for SDU 4 Roof Concrete

Parameter	BE	CV	CE	Units
Effective diffusion coefficient, D_e	6.0E-08 1.89	9.7E-08 3.06	1.2E-07 3.78	cm2/s cm2/yr
Penetration depth, x	15 38.1	15 38.1	15 38.1	in cm
Relative concentration, c/c_0	0.5	0.2	0.1	-
Penetration time, t	**843**	**144**	**71**	yr

4.4.2.7 HDPE/GCL Liners

HDPE and GCL barriers reside between the SDU 2, 6, and 7 upper and lower mud mats beneath reinforced floors, and an HDPE liner resides outside the SDU 2 concrete wall. Initially these barriers have very low permeability and intrinsic diffusion coefficient, and hinder carbonation-influenced steel corrosion. However, these properties gradually increase as HDPE degrades and eventually the HDPE components no longer function as a significant barrier to gaseous and dissolved CO_2 ingress.

SRNL-STI-2015-00236 modeled the influence of HDPE/GCL barriers as a binary effect on carbonation: a liner delayed the onset of carbonation until its effective failure time was reached, after which the liner had no effect on CO_2 ingress. Failure was defined as liner

hydraulic conductivity reaching 100 times its initial value in the PA system model, based on engineering judgement. In this PA analysis, liners are again considered to delay the onset of carbonation, but effective liner failure times are defined using a more rigorous approach. Furthermore, Revision 0 of SRNL-STI-2018-00077 based HDPE degradation on WSRC-TR-2005-00101, WSRC-STI-2008-00244 and SRNL-STI-2009-00115. In this PA analysis (SRNL-STI-2018-00077, Rev. 1), HDPE is assumed to degrade in a similar manner as in the SDF cover system, per SRRA107772-000009 and Tian, et.al., (2017). [DOI: 10.1061/(ASCE)GT.1943-5606.0001643]

Figure 4.4-18 extends Figure 4.4-13 by adding a liner outside the concrete barrier. The liner material may be HDPE, HDPE/GCL or other nonreactive material with respect to solute ingress. Under quasi-steady conditions, the concentration profile across the composite medium will be piecewise linear as depicted in Figure 4.4-18.

Figure 4.4-18: Solute Diffusing Through a Liner and Concrete and Reacting at a Sharp Front

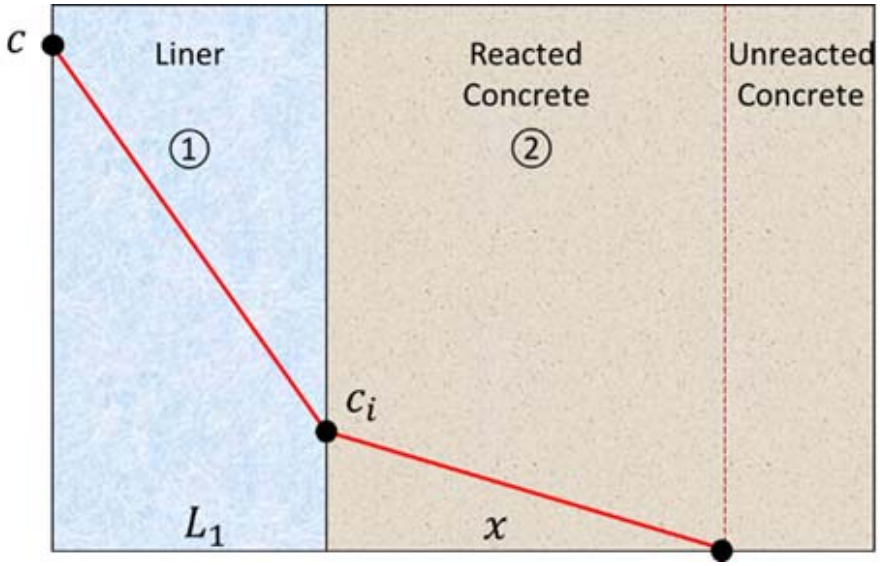

The quasi-steady condition is equivalent to assuming negligible solute mass compared to the reaction capacity of the concrete. For a constant exposure concentration c, the maximum solute mass divided by reaction capacity is:

$$\frac{[(SnL)_1+(Snx)_2]c}{(1-n)\rho_s Rx} \qquad \text{Eq. 4.4-53}$$

where symbols are defined as in Eq. 4.4-12. For a thin or low-porosity liner, the first term in the numerator can be neglected leaving:

$$\frac{Snc}{(1-n)\rho_s R} = \frac{\theta c}{\rho_b R} \qquad \text{Eq. 4.4-54}$$

Applying SDU 2 BE carbonation values from SRNL-STI-2013-00118, Table 3-2, to Eq. 4.4-54 gives:

$$\frac{\left(0.11\frac{\text{cm}^3\text{ liquid}}{\text{cm3}}\right)\left(3.41\text{e-}6\frac{\text{mol}}{\text{cm}^3\text{ liquid}}\right)}{\left(1.63\text{e-}3\frac{\text{mol}}{\text{cm}^3}\right)} = 0.0002 \ll 1 \qquad \text{Eq. 4.4-55}$$

which shows that the quasi-steady assumption is quite good for this representative example.

Fick's law for solute flux can be written in a variety of forms (e.g., SRNL-STI-2016-00175, Section 4.2):

$$F = -Sn\tau D_m \frac{dc}{dx} = -SnD_e \frac{dc}{dx} = -\theta D_e \frac{dc}{dx} = -D_i \frac{dc}{dx} \qquad \text{Eq. 4.4-56}$$

For brevity, the subscript i will be dropped from the intrinsic diffusion coefficient, D_i. At the interface between the liner and concrete, the left and right fluxes must be equal:

$$D_1 \frac{c-c_i}{L_1} = D_2 \frac{c_i}{x} \qquad \text{Eq. 4.4-57}$$

Solving for the interface concentration c_i yields:

$$D_1 \frac{c}{L_1} - D_1 \frac{c_i}{L_1} = D_2 \frac{c_i}{x} \qquad \text{Eq. 4.4-58}$$

$$\frac{D_1}{L_1} c = \left[\frac{D_1}{L_1} + \frac{D_2}{x}\right] c_i \qquad \text{Eq. 4.4-59}$$

$$c_i = \frac{\frac{D_1}{L_1}}{\frac{D_1}{L_1}+\frac{D_2}{x}} c \qquad \text{Eq. 4.4-60}$$

A differential mass balance at reaction front is:

$$D_2 \frac{c_i}{x} dt = \rho_b R dx \qquad \text{Eq. 4.4-61}$$

Substituting the right-hand side of Eq. 4.4-60 for c_i in Eq. 4.4-61 produces:

$$\frac{D_2}{x} \frac{\frac{D_1}{L_1}}{\frac{D_1}{L_1}+\frac{D_2}{x}} c dt = \rho_b R dx \qquad \text{Eq. 4.4-62}$$

$$\frac{D_1 D_2}{D_1 x + D_2 L_1} c dt = \rho_b R dx \qquad \text{Eq. 4.4-63}$$

$$\frac{D_1 D_2 c}{\rho_b R} dt = (D_1 x + D_2 L_1) dx \qquad \text{Eq. 4.4-64}$$

$$\frac{D_2 c}{\rho_b R} dt = \left(x + \frac{D_2}{D_1} L_1\right) dx \qquad \text{Eq. 4.4-65}$$

Assuming the diffusion coefficients are constant through time, differential Eq. 4.4-65 can be readily solved by integration:

$$\frac{D_2 c}{\rho_b R} \int_0^t dt = \int_0^x \left(x + \frac{D_2}{D_1} L_1\right) dx \qquad \text{Eq. 4.4-66}$$

$$\frac{D_2 c t}{\rho_b R} = \left. \frac{\left(x+\frac{D_2}{D_1}L_1\right)^2}{2} \right|_0^x \qquad \text{Eq. 4.4-67}$$

Evaluating the right-hand side of Eq. 4.4-67 and solving for x yields:

$$\frac{D_2 ct}{\rho_b R} = \frac{\left(x+\frac{D_2}{D_1}L_1\right)^2}{2} - \frac{\left(\frac{D_2}{D_1}L_1\right)^2}{2} \quad \text{Eq. 4.4-68}$$

$$\frac{2D_2 ct}{\rho_b R} + \left(\frac{D_2}{D_1}L_1\right)^2 = \left(x+\frac{D_2}{D_1}L_1\right)^2 \quad \text{Eq. 4.4-69}$$

$$x + \frac{D_2}{D_1}L_1 = \left[\frac{2D_2 ct}{\rho_b R} + \left(\frac{D_2}{D_1}L_1\right)^2\right]^{1/2} \quad \text{Eq. 4.4-70}$$

$$x = \left[\frac{2D_2 ct}{\rho_b R} + \left(\frac{D_2}{D_1}L_1\right)^2\right]^{1/2} - \frac{D_2}{D_1}L_1 \quad \text{Eq. 4.4-71}$$

In the more general case, the liner may degrade such that its intrinsic diffusion coefficient is a function of time, $D_1(t)$, and Eq. 4.4-63 becomes:

$$\frac{D_1(t)D_2}{D_1(t)x+D_2L_1} c dt = \rho_b R dx \quad \text{Eq. 4.4-72}$$

$$dx = \frac{D_1(t)D_2}{D_1(t)x+D_2L_1}\frac{c}{\rho_b R}\cdot dt \quad \text{Eq. 4.4-73}$$

The coefficient on the right-hand side of Eq. 4.4-73 is the instantaneous speed of the reaction front, S(x,t):

$$dx = S(x,t)dt \quad \text{Eq. 4.4-74}$$

Eq. 4.4-74 can be solved numerically using a predictor-corrector approach. An initial estimate of the reaction front position at time t^{n+1} (predictor step) is:

$$x^{n+1'} = x^n + S(x^n, t^n)dt \quad \text{Eq. 4.4-75}$$

Using this value, the speed at time t^{n+1} can be estimated as:

$$S(x^{n+1'}, t^{n+1}) \quad \text{Eq. 4.4-76}$$

A refined estimate of the front position at t^{n+1} (corrector step) is:

$$x^{n+1} = x^n + \frac{S\left(x^{n+1'},t^{n+1}\right)+S(x^n,t^n)}{2}dt \quad \text{Eq. 4.4-77}$$

Figure 4.4-19 and Figure 4.4-20 illustrate carbonation penetration depths as a function of time for HDPE/GCL liners wth 100 mil and 60 mil HDPE layers, respectively. [SRR-CWDA-2018-00012] The GCL layer is assumed to be 200 mil (SRNL-STI-2009-00115) based on a minimum 0.75 lbs/ft^2 sodium bentonite (SRR-CWDA-2009-00017, Section 3.2.1.3.2) with a density of approximately 47 lbs/ft^3. [SRNL-STI-2018-00077, Rev. 1] The first (blue) curve is penetration depth for no liner, computed from Eq. 4.4-13. The second (red) curve is computed using Eq. 4.4-77, considering either an HDPE or HDPE + GCL liner. The third (green) curve is Eq. 4.4-13 shifted by the delayed onset time shown in Table 4.4-38. The delayed onset times were manually selected to achieve approximate agreement at intermediate times between the two-layer numerical solution (red curve)

and shifted single-layer analytic solution (green curve). All calculations use SDU 2, 6, and 7 parameter values from Table 4.4-22 through Table 4.4-24. The intrinsic diffusion coefficient for HDPE is based on SRRA107772-000009 and Tian, et.al., (2017). [DOI: 10.1061/(ASCE)GT.1943-5606.0001643] The GCL component is assumed to reduce the gas phase saturation by 50% compared to the HDPE-only case.

At time zero, for the calculations behind Table 4.4-38, HDPE is assumed to have five 10-millimeter diameter holes per hectare (approximately five holes per SDU 6 and 7 roof area), which represents a long-term, fully degraded state (see Section 4.4.1.3.6). No further damage is assumed until antioxidants are depleted around year 750, after which stress crack resistance (SCR) declines from 100% to 50% at year 1,975 or beyond based on 80 mil HDPE (Tian, et.al., 2017). [DOI: 10.1061/(ASCE)GT.1943-5606.0001643] By extrapolation, 0% SCR is projected to occur no sooner than year 3200. In this analysis, HDPE saturated hydraulic conductivity and diffusion coefficient are assumed to increase geometrically between years 750 and 3,200, with the fully-degraded end state being comparable to backfill soil. These assumptions are common to the BE, CV and CE scenarios. Accordingly, the three cases have similar times for HDPE failure and onset of carbonation. However, the rates of carbonation vary significantly between the BE, CV and CE cases.

Table 4.4-38: Delayed Carbonation Onset Times for SDU 2/6/7 Concrete (yr)

Configuration	BE case	CV case	CE case
100 mil HDPE	1,900	1,700	1,600
100 mil HDPE + 200 mil GCL	1,700	1,800	1,750
60 mil HDPE	1,850	1,700	1,600
60 mil HDPE + 200 mil GCL	1,600	1,750	1,700

4.4.2.1 Cementitious Material Degradation Times

Along with sulfate attack, carbonation-influenced steel corrosion, and decalcification, biodegradation was also considered as a potential degradation phenomenon of significance. However, SRNL-STI-2012-00435 concluded that while biodegradation of SDU concrete is likely, it would be concentrated near outer surfaces with penetration limited by the high pH and osmotic pressure of saltstone pore fluid, at least for early times.

Therefore, biodegradation is neglected. The penetration rate coefficients for diffusion-controlled decalcification (Section 4.4.2.5) are smaller than those for sulfate attack (Section 4.4.2.2) and carbonation (Section 4.4.2.3). Thus, decalcification does not drive concrete degradation; nonetheless, penetration depths are computed for information. For saltstone, the sole degradation mechanism is advection-controlled decalcification.

Figure 4.4-19: Carbonation Penetration for SDU2/6/7 Concrete without Liner, with Liner, and Delayed Onset Approximation 100 mil HDPE Cases (scale cm vs. yr)

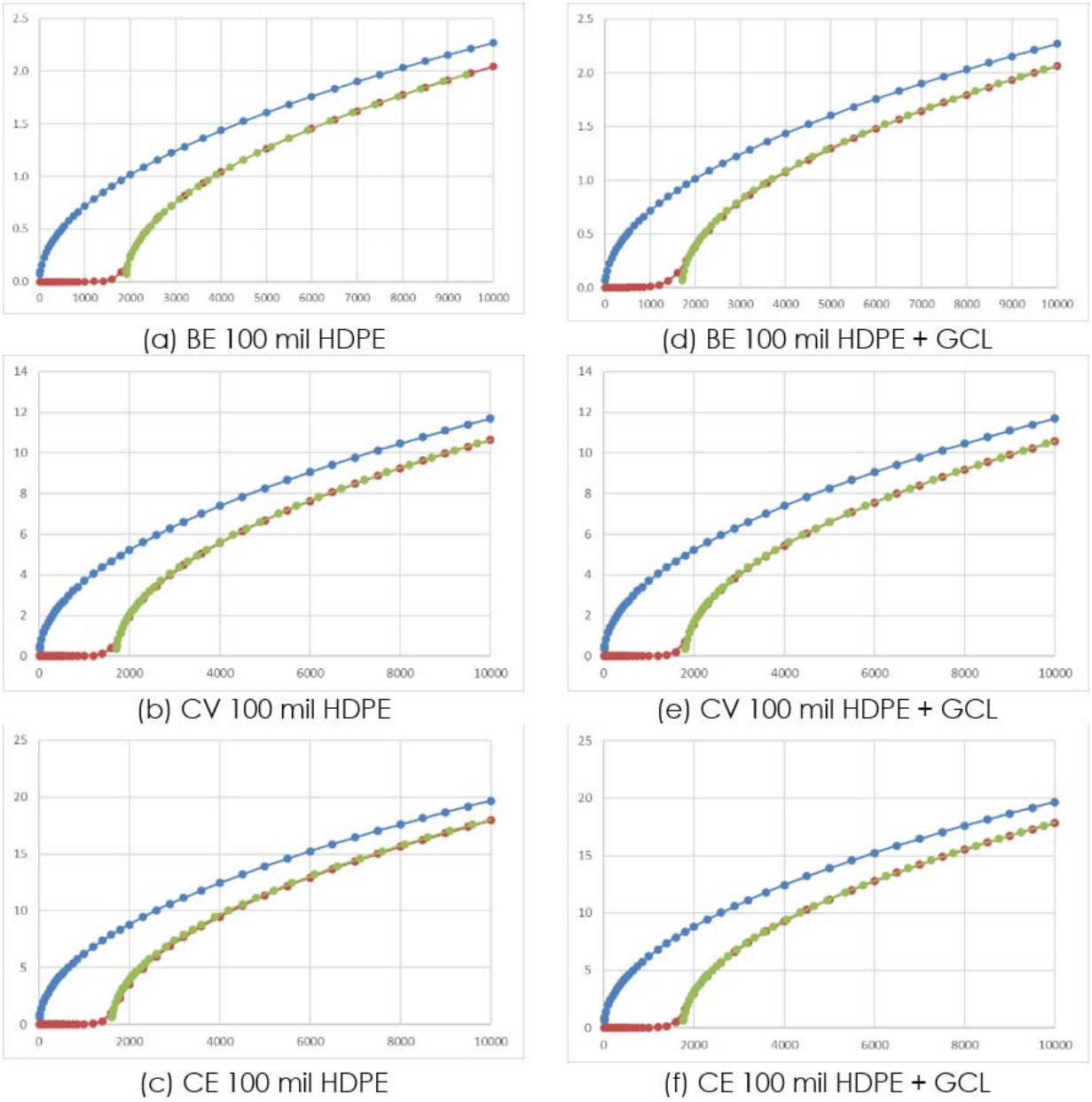

Key: Red curve = numerical simulation of carbonation penetration for a liner + concrete, Blue curve = penetration for concrete alone, Green curve = blue curve with time shift to approximate red curve.

Figure 4.4-20: Carbonation Penetration for SDU2/6/7 Concrete without Liner, with Liner, and Delayed Onset Approximation 60 mil HDPE cases (scale cm vs. yr)

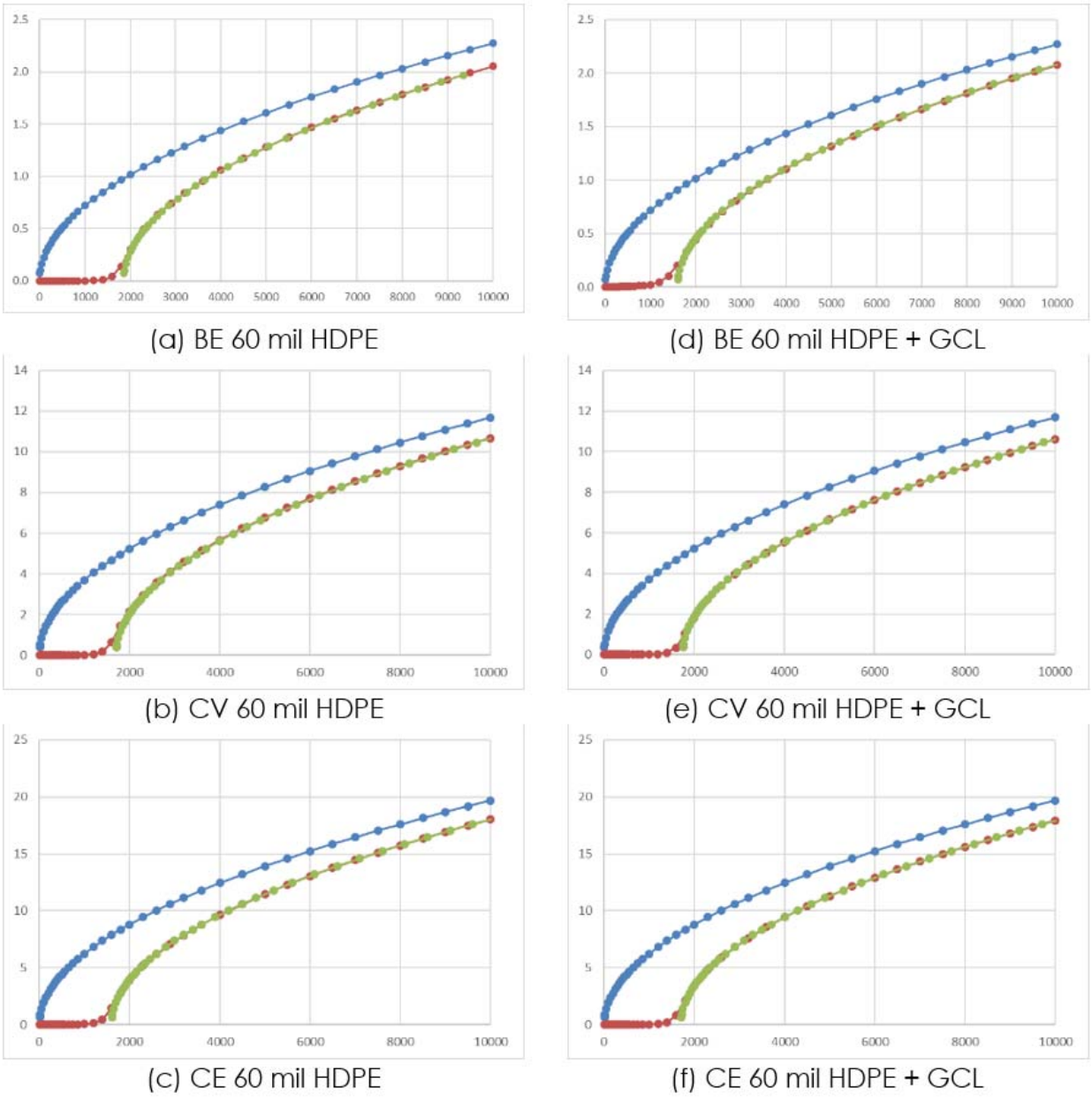

Key: Red curve = numerical simulation of carbonation penetration for a liner + concrete, Blue curve = penetration for concrete alone, Green curve = blue curve with time shift to approximate red curve.

Carbonation advances through concrete from the outside in (triggering fast steel corrosion, Section 4.4.2.4), while sulfate attack, arising from sulfate in saltstone pore water, occurs from the inside moving outward. Complete concrete degradation is assumed to occur when the two reaction fronts meet. In some cases, one or the other degradation mechanism is delayed, due to clean cap grout (Section 4.4.2.6) or an HDPE/GCL liner (Section 4.4.2.7). If the delay is long enough for one process, the other may fully penetrate the thickness in question. Sulfate attack and carbonation are generally assumed to begin

at facility closure, time zero with respect to the PA, on the basis that the operational period is short compared to PA timeframes and can be neglected compared to analysis uncertainties. However, early sulfate attack on SDU 6 and 7 wall concrete is considered in Section 4.4.2.2.5. Although degradation estimates are provided for SDU 1 and 4 wall concretes, these components are assumed to be already fully degraded at PA $t = 0$ for the CV and CE cases, rendering the degradation times irrelevant to system performance.

Penetration times for sulfate attack and carbonation are computed using Eq. 4.4-20. Penetration rate coefficients (A [cm/√yr]) are given in Sections 4.4.2.2.4 and 4.4.2.3.4. The maximum diffusion distance, δ [L], is generally assumed to be 2.54 cm = 1 inch. The choice of δ = 2.54 cm produces sulfate attack results like those generated previously from the Cementitious Barriers Partnership numerical simulations (SRNL-STI-2013-00118, SRNL-STI-2015-00236). With respect to carbonation, the maximum diffusion distance is assumed to be correlated with the spacing of reinforcing steel and thickness of concrete cover. The typical thickness of concrete cover over reinforcing steel is 5 cm, based on American Concrete Institute (ACI) Code 318. The distance δ = 2.54 cm is conservative in comparison. An exception to δ = 1 inch is the SDU 2 floor and upper mud mat system. Because the 4-inch thick upper mud mat does not contain rebar, carbonation is assumed to cause no damage to this material. Therefore, the minimum diffusion distance is 10.16 cm = 4 inches. The SDU 6 and 7 upper mud mat is not credited because this component did/will not undergo quality inspections during construction, unlike SDU 2.

Table 4.4-39 through Table 4.4-44 summarize degradation time calculations for SDUs for three confidence levels: CE, CV, and BE. As noted previously, the compliance value ("MPAD" in SRR-CWDA-2018-00004) is defined to be an intermediate result that is more probable than the conservative estimate and more defensible than the best estimate. The dimensions of the SDU 1, 4, 2, and 6 designs reflect as-built conditions (SDF-IP-05, SDF-IP-07, SRR-CWDA-2018-00012). For future SDU 7, two scenarios are considered (SRR-CWDA-2018-00012). The SDU 7 "Design" case reflects the current design. The SDU 7 "Design Margin" case assumes thinner components to accommodate potential design changes and/or construction deviations. Table 4.4-45 summarizes degradation times for all SDUs.

Table 4.4-39: Degradation Timing for SDU 1 Concrete and Saltstone

Degradation mechanism:			*SA*	*Carb*	*SA*	*Carb*	*SA*	*Carb*	**Sulfate attack**						**Carbonation**						
	Thickness:		CE		CV		BE		**A (cm/√yr)**			**Time (yr)**		**max δ**	**A (cm/√yr)**			**Time (yr)**			**max δ**
Component	(in)	(cm)	(cm)	(cm)	(cm)	(cm)	(cm)	(cm)	CE	CV	BE	CE	CV	BE	(cm)	CE	CV	BE	CE	CV	BE	(cm)
Roof delay										*clean grout:*		11	**23**	135			*HDPE-GCL:*		1750	1800	1700	
Roof degradation	6	15.2	15.2	0	15.2	0	15.2	0	0.240	0.216	0.170	671	830	1342	2.54	0.257	0.149	0.027	0	0	0	2.54
Roof delay+degradation			-1067		-947		-223					683	**853**	1477					1750	**1800**	1700	
Floor delay										*immediate contact:*		0	**0**	0			*no liner:*		0	**0**	0	
Floor degradation	24	61.0	34.0	26.9	45.9	15.0	59.3	1.6	0.170	0.160	0.130	2996	4579	8957	2.54	0.151	0.091	0.017	2996	4579	8957	2.54
Floor delay+degradation			0		0		0					2996	**4579**	8957					2996	**4579**	8957	
Wall delay										*immediate contact:*		0	**0**	0			*no liner:*		0	**0**	0	
Wall degradation	18	45.7	25.5	20.2	34.4	11.3	44.3	1.4	2.118	2.118	0.651	14	19	266	2.54	1.886	1.212	0.087	14	19	266	2.54
Wall delay+degradation			0		0		0					14	**19**	266					14	**19**	266	
Grout delay																						
Grout degradation	294	746.8																				
Grout delay+degradation																						

Degradation mechanism:			**Decalcification**									**Limiting**		
	Thickness:		**A (cm/√yr)**			**Time (yr)**			**max δ**	**CE**	**CV**	**BE**		
Component	(in)	(cm)	CE	CV	BE	CE	CV	BE	(cm)	(yr)	(yr)	(yr)		
Roof delay				*HDPE-GCL:*		1750	1800	1700		**11**	**23**	**135**		
Roof degradation	6	15.24	0.029	0.026	0.021	44594	55168	89189	2.54		Roof			
Roof delay+degradation						46344	56968	90889		**683**	**853**	**1477**		
Floor delay				*no liner:*		0	0	0		**0**	**0**	**0**		
Floor degradation	24	60.96	0.017	0.016	0.013	516493	584709	885416	2.54		Floor			
Floor delay+degradation						516493	584709	885416		**2996**	**4579**	**8957**		
Wall delay				*no liner:*		0	0	0		**0**	**0**	**0**		
Wall degradation	18	45.72	0.216	0.216	0.066	2489	2489	26387	2.54		Wall			
Wall delay+degradation						2489	2489	26387		**14**	**19**	**266**		
Grout delay			A_U **(cm/yr)**			683	853	1477		**683**	**853**	**1477**		
Grout degradation	294	746.8	5.1E-04	7.6E-05	5.1E-06	1473777	9.8E+06	1.5E+08			Grout			
Grout delay+degradation						1.5E+06	**9.8E+06**	1.5E+08		**1.5E+06**	**9.8E+06**	**1.5E+08**		

Table 4.4-40: Degradation Timing for SDU 4 Concrete and Saltstone

Degradation mechanism:	Thickness:		*SA*	*Carb*	*SA*	*Carb*	*SA*	*Carb*	Sulfate attack						Carbonation						
			CE		CV		BE		A (cm/√yr)			Time (yr)			max δ	A (cm/√yr)			Time (yr)			max δ
Component	(in)	(cm)	(cm)	(cm)	(cm)	(cm)	(cm)	(cm)	CE	CV	BE	CE	CV	BE	(cm)	CE	CV	BE	CE	CV	BE	(cm)
Roof delay										*clean grout:*		71	**144**	843			*HDPE-GCL:*		1750	1800	1700	
Roof degradation	4	10.16	10.2	0	10.2	0	10	0.13	0.240	0.216	0.170	447	554	883	2.54	0.238	0.138	0.025	0	0	27	2.54
Roof delay+degradation			-1232		-1102		0					518	**698**	1727					1750	**1800**	1727	
Floor delay										*immediate contact:*		0	**0**	0			*no liner:*		0	**0**	0	
Floor degradation	24	60.96	34	26.9	45.9	15	59.3	1.64	0.170	0.160	0.130	2996	4579	8957	2.54	0.151	0.091	0.017	2996	4579	8957	2.54
Floor delay+degradation			0		0		0					2996	**4579**	8957					2996	**4579**	8957	
Wall delay										*immediate contact:*		0	**0**	0			*no liner:*		0	**0**	0	
Wall degradation	18	45.72	25.5	20.2	34.4	11.3	44.3	1.42	2.118	2.118	0.651	14	19	266	2.54	1.886	1.212	0.087	14	19	266	2.54
Wall delay+degradation			0		0		0					14	**19**	266					14	**19**	266	
Grout - 3.45' delay																						
Grout - 3.45' degradation	273.0	693.4																				
Grout - 3.45' delay+degradation																						
Top saltstone delay																		*Roof:*	518	**698**	1727	
Top saltstone degradation	41.37	105.1							3.45							0.415	0.165	0.032	1549	9801	262774	2.54
Top saltstone delay+degradation																			2068	**10499**	264501	
Column delay																		*Roof or floor min:*	1750	**1800**	1727	
Column degradation*	24	60.96														0.415	0.165	0.032	899	**5686**	152443	2.54
Column delay+degradation																			2649	**7486**	154170	

Degradation mechanism:	Decalcification										Limiting		
	Thickness:		A (cm/√yr)			Time (yr)			max δ		CE	CV	BE
Component	(in)	(cm)	CE	CV	BE	CE	CV	BE	(cm)		(yr)	(yr)	(yr)
Roof delay				*HDPE-GCL:*		1750	1800	1700			**71**	**144**	**843**
Roof degradation	4	10.16	0.027	0.025	0.019	34605	42811	69211	2.54			Roof	
Roof delay+degradation						36355	44611	70911			**518**	**698**	**1727**
Floor delay				*no liner:*		0	0	0			**0**	**0**	**0**
Floor degradation	24	60.96	0.017	0.016	0.013	516493	584709	885416	2.54			Floor	
Floor delay+degradation						516493	584709	885416			**2996**	**4579**	**8957**
Wall delay				*no liner:*		0	0	0			**0**	**0**	**0**
Wall degradation	18	45.72	0.216	0.216	0.066	2489	2489	26387	2.54			Wall	
Wall delay+degradation						2489	2489	26387			**14**	**19**	**266**
Grout - 3.45' delay				A_U (cm/√yr)		2068	10499	264501			**2068**	**10499**	**264501**
Grout - 3.45' degradation	273.0	693.4	5.1E-04	7.6E-05	5.1E-06	1368507	9.1E+06	1.4E+08				Grout-3.45'	
Grout - 3.45' delay+degradation						1.4E+06	**9.1E+06**	1.4E+08			**1.4E+06**	**9.1E+06**	**1.4E+08**
Top saltstone delay											**518**	**698**	**1727**
Top saltstone degradation	41.37	105.1										Top Salt.	
Top saltstone delay+degradation											**2068**	**10499**	**264501**
Column delay											**1750**	**1800**	**1727**
Column degradation*	24	60.96										Column	
Column delay+degradation											**2649**	**7486**	**154170**

segment	start (yr)	end (yr)	segment
grout1	1800	7486	grout12
grout2	7486	13172	grout11
grout3	13172	18858	grout10
grout4	18858	24544	grout9
grout5	24544	30230	grout8
grout6	30230	35916	grout7

Table 4.4-41: Degradation Timing for SDU 2 Concrete and Saltstone

Degradation mechanism:			*SA*	*Carb*	*SA*	*Carb*	*SA*	*Carb*	**Sulfate attack**							**Carbonation**						
	Thickness:		CE		CV		BE		**A (cm/√yr)**			**Time (yr)**			**max δ**	**A (cm/√yr)**			**Time (yr)**			**max δ**
Component	(in)	(cm)	(cm)	(cm)	(cm)	(cm)	(cm)	(cm)	CE	CV	BE	CE	CV	BE	(cm)	CE	CV	BE	CE	CV	BE	(cm)
									no clean grout:								*HDPE-GCL:*					
Roof delay												0	**0**	0					1750	1800	1700	
Roof degradation	8	20.32	20.3	0	20.3	0	20.3	0	0.238	0.223	0.182	914	1034	1566	2.54	0.199	0.120	0.023	0	0	0	2.54
Roof delay+degradation			-836		-766		-134					914	**1034**	1566					1750	**1800**	1700	
									immediate contact:								*HDPE-GCL:*					
FloorUMM delay												0	**0**	0					1750	1800	1700	
FloorUMM degradation	12	30.48	30.5	0	30.5	0	29.9	0.56	0.238	0.223	0.182	1371	1552	2306	2.54	0.199	0.120	0.023	0	0	606	10.16
FloorUMM delay+degradation			-379		-248		0					1371	**1552**	2306					1750	**1800**	2306	
									immediate contact:								*HDPE:*					
Wall delay												0	**0**	0					1600	1700	1900	
Wall degradation	8	20.32	20.3	0	20.3	0	20.3	0	0.238	0.223	0.182	914	1034	1566	2.54	0.199	0.120	0.023	0	0	0	2.54
Wall delay+degradation			-686		-666		-334					914	**1034**	1566					1600	**1700**	1900	
Grout delay																						
Grout degradation	264	670.6																				
Grout delay+degradation																						
									immediate contact:													
Column delay												0	**0**	0								
Column degradation	6.20	15.8	15.8	0	15.8	0	15.8	0	0.977	0.863	0.479	42	54	175	2.54							2.54
Column delay+degradation												42	**54**	175								
UMM delay												0	**0**	0					1750	**1800**	1700	
UMM degradation	4	10.16										from above							from above			
UMM delay+degradation												1371	**1552**	2306					1750	**1800**	2306	

Degradation mechanism:			**Decalcification**								**Limiting**		
	Thickness:		**A (cm/√yr)**			**Time (yr)**			**max δ**		**CE**	**CV**	**BE**
Component	(in)	(cm)	CE	CV	BE	CE	CV	BE	(cm)		(yr)	(yr)	(yr)
					HDPE-GCL:								
Roof delay						1750	1800	1700			**0**	**0**	**0**
Roof degradation	8	20.32	0.023	0.021	0.017	99434	112567	170459	2.54	Roof			
Roof delay+degradation						101184	114367	172159			**914**	**1034**	**1566**
					HDPE-GCL:	1750	1800	1700			**0**	**0**	**0**
FloorUMM delay													
FloorUMM degradation	12	30.48	0.023	0.021	0.017	149151	168851	255688	2.54	FloorUMM			
FloorUMM delay+degradation						150901	170651	257388			**1371**	**1552**	**2306**
					HDPE:	1600	1700	1900			**0**	**0**	**0**
Wall delay													
Wall degradation	8	20.32	0.023	0.021	0.017	99434	112567	170459	2.54	Wall			
Wall delay+degradation						101034	114267	172359			**914**	**1034**	**1566**
			A_U **(cm/yr)**			914	1034	1566			**914**	**1034**	**1566**
Grout delay													
Grout degradation	264	670.6	5.1E-04	7.6E-05	5.1E-06	1323392	8.8E+06	1.3E+08		Grout			
Grout delay+degradation						1.3E+06	**8.8E+06**	1.3E+08			**1.3E+06**	**8.8E+06**	**1.3E+08**
Column delay											**0**	**0**	**0**
Column degradation	6.204	15.8								Column			
Column delay+degradation											**42**	**54**	**175**
											0	**0**	**0**
										UMM			
											1371	**1552**	**2306**

Table 4.4-42: Degradation Timing for SDU 6 Concrete and Saltstone

Degradation mechanism:			*SA*	*Carb*	*SA*	*Carb*	*SA*	*Carb*	**Sulfate attack**							**Carbonation**						
	Thickness:		CE		CV		BE		**A (cm/√yr)**			**Time (yr)**			**max δ**	**A (cm/√yr)**			**Time (yr)**			**max δ**
Component	(in)	(cm)	(cm)	(cm)	(cm)	(cm)	(cm)	(cm)	CE	CV	BE	CE	CV	BE	(cm)	CE	CV	BE	CE	CV	BE	(cm)
Roof delay										*no clean grout:*		0	**0**	0			*HDPE-GCL:*		1750	1800	1700	
Roof degradation	12	30.48	30.5	0	30.5	0	29.9	0.56	0.238	0.223	0.182	1371	1552	2306	2.54	0.199	0.120	0.023	0	0	606	2.54
Roof delay+degradation			-379		-248		0					1371	**1552**	2306					1750	**1800**	2306	
Floor delay										*immediate contact:*		0	**0**	0			*HDPE-GCL:*		1750	1800	1700	
Floor degradation	12	30.48	30.5	0	30.5	0	29.9	0.56	0.238	0.223	0.182	1371	1552	2306	2.54	0.199	0.120	0.023	0	0	606	2.54
Floor delay+degradation			-379		-248		0					1371	**1552**	2306					1750	**1800**	2306	
Wall delay										*immediate contact:*		0	**0**	0			*no liner:*		0	**0**	0	
Wall degradation	8.93	22.68	13.3	9.34	17.6	5.09	21.7	0.93	0.238	0.223	0.182	600	895	1677	2.54	0.199	0.120	0.023	600	895	1677	2.54
Wall delay+degradation			0		0		0					600	**895**	1677					600	**895**	1677	
Wall delay										*immediate contact:*		0	**0**	0			*no liner:*		0	**0**	0	
Wall degradation	10.72	27.23	16	11.2	21.1	6.12	26.2	1.02	0.238	0.223	0.182	720	1075	2020	2.54	0.199	0.120	0.023	720	1075	2020	2.54
Wall delay+degradation			0		0		0					720	**1075**	2020					720	**1075**	2020	
Wall delay										*immediate contact:*		0	**0**	0			*no liner:*		0	**0**	0	
Wall degradation	13.83	35.12	20.7	14.5	27.2	7.89	34	1.17	0.238	0.223	0.182	929	1386	2617	2.54	0.199	0.120	0.023	929	1386	2617	2.54
Wall delay+degradation			0		0		0					929	**1386**	2617					929	**1386**	2617	
Wall delay										*immediate contact:*		0	**0**	0			*no liner:*		0	**0**	0	
Wall degradation	16.97	43.11	25.4	17.8	33.4	9.68	41.8	1.29	0.238	0.223	0.182	1140	1702	3224	2.54	0.199	0.120	0.023	1140	1702	3224	2.54
Wall delay+degradation			0		0		0					1140	**1702**	3224					1140	**1702**	3224	
Wall delay										*immediate contact:*		0	**0**	0			*no liner:*		0	**0**	0	
Wall degradation	20.01	50.82	29.9	20.9	39.4	11.4	49.4	1.41	0.238	0.223	0.182	1344	2006	3810	2.54	0.199	0.120	0.023	1344	2006	3810	2.54
Wall delay+degradation			0		0		0					1344	**2006**	3810					1344	**2006**	3810	
Grout delay																						
Grout degradation	516	1311																				
Grout delay+degradation																						
Column delay										*immediate contact:*		0	**0**	0								
Column degradation	10.63	27.0	27.0	0	27.0	0	27.0	0	0.977	0.863	0.479	72	92	299	2.54							
Column delay+degradation												72	**92**	299								

Table 4.4-42: Degradation Timing for SDU 6 Concrete and Saltstone (Continued)

Degradation mechanism:	Decalcification									Limiting										
	Thickness:		A (cm/yr)			Time (yr)			max δ	CE	CV	BE	Initial thickness		PA t=0 thickness		Times:			
Component	(in)	(cm)	CE	CV	BE	CE	CV	BE	(cm)	(yr)	(yr)	(yr)	(in)	(cm)	(in)	(cm)	CE (yr)	CV (yr)	BE (yr)	
Roof delay				*HDPE-GCL:*		1750	1800	1700		0	0	0								
Roof degradation	12	30.48	0.023	0.021	0.017	149151	168851	255688	2.54		Roof									
Roof delay+degradation						150901	170651	257388		1371	1552	2306								
FloorUMM delay				*HDPE-GCL:*		1750	1800	1700		0	0	0								
FloorUMM degradation	12	30.48	0.023	0.021	0.017	149151	168851	255688	2.54		Floor									
FloorUMM delay+degradation						150901	170651	257388		1371	1552	2306					-94	-140	-262	
Wall delay				*no liner:*		0	0	0		0	0	0								
Wall degradation	8.93	22.68	0.023	0.021	0.017	110989	125648	190268	2.54		Wall ⑤		10.33	26.2	8.93	22.7		Wall ⑤		
Wall delay+degradation						110989	125648	190268		600	895	1677					600	895	1677	
Wall delay				*no liner:*		0	0	0		0	0	0								
Wall degradation	10.72	27.23	0.023	0.021	0.017	133264	150865	228453	2.54		Wall ④		12.28	31.2	10.72	27.2		Wall ④		
Wall delay+degradation						133264	150865	228453		720	1075	2020					-105	-156	-293	
Wall delay				*no liner:*		0	0	0		0	0	0								
Wall degradation	13.83	35.12	0.023	0.021	0.017	171849	194546	294598	2.54		Wall ③		15.66	39.8	13.83	35.1		Wall ③		
Wall delay+degradation						171849	194546	294598		929	1386	2617					720	1075	2020	
Wall delay				*no liner:*		0	0	0		0	0	0								
Wall degradation	16.97	43.11	0.023	0.021	0.017	210956	238818	361638	2.54		Wall ②		19.08	48.5	16.97	43.1		Wall ②		
Wall delay+degradation						210956	238818	361638		1140	1702	3224					-123	-184	-347	
Wall delay				*no liner:*		0	0	0		0	0	0								
Wall degradation	20.01	50.82	0.023	0.021	0.017	248702	281549	426346	2.54		Wall ①		22.37	56.8	20.01	50.8		Wall ①		
Wall delay+degradation						248702	281549	426346		1344	2006	3810					1140	1702	3224	
Grout delay			A_U (cm/yr)			1371	1552	2306		1371	1552	2306								
Grout degradation	516	1311	5.1E-04	7.6E-05	5.1E-06	2586629	1.7E+07	2.6E+08			Grout									
Grout delay+degradation						2.6E+06	**1.7E+07**	2.6E+08		2.6E+06	**1.7E+07**	**2.6E+08**					1344	2006	3810	
Column delay										0	0	0								
Column degradation	10.63	27.0									Column									
Column delay+degradation										72	92	299					-159	-237	-450	

Table 4.4-43: Degradation Timing for SDU 7 Design Concrete and Saltstone

Degradation mechanism:			*SA*	*Carb*	*SA*	*Carb*	*SA*	*Carb*	**Sulfate attack**						**Carbonation**						
	Thickness:		CE	CE	CV	CV	BE	BE	**A (cm/√yr)**			**Time (yr)**		**max δ**	**A (cm/√yr)**			**Time (yr)**		**max δ**
Component	(in)	(cm)	(cm)	(cm)	(cm)	(cm)	(cm)	(cm)	CE	CV	BE	CE	CV	BE	(cm)	CE	CV	BE	CE	CV	BE	(cm)
Roof delay									*no clean grout:*			0	**0**	0		*HDPE-GCL:*			1750	1800	1700	
Roof degradation	12	30.48	30.5	0	30.5	0	29.9	0.56	0.238	0.223	0.182	1371	1552	2306	2.54	0.199	0.120	0.023	0	0	606	2.54
Roof delay+degradation			-379		-248		0					1371	**1552**	2306					1750	**1800**	2306	
Floor delay									*immediate contact:*			0	**0**	0		*HDPE-GCL:*			1700	1750	1600	
Floor degradation	24	60.96	51.4	9.54	55	5.97	59.7	1.25	0.238	0.223	0.182	2312	2800	4603	2.54	0.199	0.120	0.023	612	1050	3003	2.54
Floor delay+degradation			0		0		0					2312	**2800**	4603					2312	**2800**	4603	
Wall delay									*immediate contact:*			0	**0**	0		*no liner:*			0	**0**	0	
Wall degradation	10.72	27.23	16	11.2	21.1	6.12	26.2	1.02	0.238	0.223	0.182	720	1075	2020	2.54	0.199	0.120	0.023	720	1075	2020	2.54
Wall delay+degradation			0		0		0					720	**1075**	2020					720	**1075**	2020	
Wall delay									*immediate contact:*			0	**0**	0		*no liner:*			0	**0**	0	
Wall degradation	12.26	31.14	18.3	12.8	24.1	6.99	30	1.1	0.238	0.223	0.182	824	1229	2316	2.54	0.199	0.120	0.023	824	1229	2316	2.54
Wall delay+degradation			0		0		0					824	**1229**	2316					824	**1229**	2316	
Wall delay									*immediate contact:*			0	**0**	0		*no liner:*			0	**0**	0	
Wall degradation	14.92	37.9	22.3	15.6	29.4	8.51	36.7	1.21	0.238	0.223	0.182	1002	1496	2829	2.54	0.199	0.120	0.023	1002	1496	2829	2.54
Wall delay+degradation			0		0		0					1002	**1496**	2829					1002	**1496**	2829	
Wall delay									*immediate contact:*			0	**0**	0		*no liner:*			0	**0**	0	
Wall degradation	17.62	44.76	26.3	18.4	34.7	10	43.4	1.32	0.238	0.223	0.182	1184	1767	3349	2.54	0.199	0.120	0.023	1184	1767	3349	2.54
Wall delay+degradation			0		0		0					1184	**1767**	3349					1184	**1767**	3349	
Wall delay									*immediate contact:*			0	**0**	0		*no liner:*			0	**0**	0	
Wall degradation	20.22	51.37	30.2	21.2	39.8	11.5	50	1.41	0.238	0.223	0.182	1358	2028	3851	2.54	0.199	0.120	0.023	1358	2028	3851	2.54
Wall delay+degradation			0		0		0					1358	**2028**	3851					1358	**2028**	3851	
Grout delay																						
Grout degradation	516	1311																				
Grout delay+degradation																						
Column delay									*immediate contact:*			0	**0**	0								
Column degradation	10.63	27.0	27.0	0	27.0	0	27.0	0	0.977	0.863	0.479	72	92	299	2.54							
Column delay+degradation												72	**92**	299								

Table 4.4-43: Degradation Timing for SDU 7 Design Concrete and Saltstone (Continued)

Degradation mechanism:	Thickness:		Decalcification A (cm/yr)			Time (yr)			max δ	Limiting			Initial thickness		t=0 thickness		Times:		
Component	(in)	(cm)	CE	CV	BE	CE	CV	BE	(cm)	CE (yr)	CV (yr)	BE (yr)	(in)	(cm)	(in)	(cm)	CE (yr)	CV (yr)	BE (yr)
Roof delay				*HDPE-GCL:*		1750	1800	1700		**0**	**0**	**0**							
Roof degradation	12	30.48	0.023	0.021	0.017	149151	168851	255688	2.54		Roof								
Roof delay+degradation						150901	170651	257388		**1371**	**1552**	**2306**							
FloorUMM delay				*HDPE-GCL:*		1700	1750	1600		**0**	**0**	**0**					**-105**	**-156**	**-293**
FloorUMM degradation	24	60.96	0.023	0.021	0.017	298303	337701	511376	2.54		Floor		12.28	31.2	10.72	27.2		Wall ⑤	
FloorUMM delay+degradation						300003	339451	512976		**2312**	**2800**	**4603**					**720**	**1075**	**2020**
Wall delay				*no liner:*		0	0	0		**0**	**0**	**0**					**-114**	**-170**	**-320**
Wall degradation	10.72	27.23	0.023	0.021	0.017	133264	150865	228453	2.54		Wall ⑤		13.95	35.4	12.26	31.1		Wall ④	
Wall delay+degradation						133264	150865	228453		**720**	**1075**	**2020**					**824**	**1229**	**2316**
Wall delay				*no liner:*		0	0	0		**0**	**0**	**0**					**-129**	**-193**	**-365**
Wall degradation	12.26	31.14	0.023	0.021	0.017	152382	172507	261226	2.54		Wall ④		16.85	42.8	14.92	37.9		Wall ③	
Wall delay+degradation						152382	172507	261226		**824**	**1229**	**2316**					**1002**	**1496**	**2829**
Wall delay				*no liner:*		0	0	0		**0**	**0**	**0**					**-145**	**-216**	**-410**
Wall degradation	14.92	37.9	0.023	0.021	0.017	185477	209975	317961	2.54		Wall ③		19.78	50.2	17.62	44.8		Wall ②	
Wall delay+degradation						185477	209975	317961		**1002**	**1496**	**2829**					**1184**	**1767**	**3349**
Wall delay				*no liner:*		0	0	0		**0**	**0**	**0**					**-160**	**-239**	**-453**
Wall degradation	17.62	44.76	0.023	0.021	0.017	219008	247934	375443	2.54		Wall ②		22.60	57.4	20.22	51.4		Wall ①	
Wall delay+degradation						219008	247934	375443		**1184**	**1767**	**3349**					**1358**	**2028**	**3851**
Wall delay				*no liner:*		0	0	0		**0**	**0**	**0**							
Wall degradation	20.22	51.37	0.023	0.021	0.017	251366	284565	430913	2.54		Wall ①								
Wall delay+degradation						251366	284565	430913		**1358**	**2028**	**3851**							
Grout delay				A_U (cm/yr)		1371	1552	2306		**1371**	**1552**	**2306**							
Grout degradation	516	1311	5.1E-04	7.6E-05	5.1E-06	2586629	1.7E+07	2.6E+08			Grout								
Grout delay+degradation						2.6E+06	**1.7E+07**	2.6E+08		**2.6E+06**	**1.7E+07**	**2.6E+08**							
Column delay										**0**	**0**	**0**							
Column degradation	10.63	27.0									Column								
Column delay+degradation										**72**	**92**	**299**							

Table 4.4-44: Degradation Timing for SDU 7 Design Margin Concrete and Saltstone

Degradation mechanism:			*SA*	*Carb*	*SA*	*Carb*	*SA*	*Carb*	**Sulfate attack**							**Carbonation**						
	Thickness:		CE		CV		BE		**A (cm/√yr)**			**Time (yr)**			**max δ**	**A (cm/√yr)**			**Time (yr)**			**max δ**
Component	(in)	(cm)	(cm)	(cm)	(cm)	(cm)	(cm)	(cm)	CE	CV	BE	CE	CV	BE	(cm)	CE	CV	BE	CE	CV	BE	(cm)
Roof delay										*no clean grout:*		0	**0**	0			*HDPE-GCL:*		1700	1750	1600	
Roof degradation	9	22.86	22.9	0	22.9	0	22.6	0.27	0.238	0.223	0.182	1028	1164	1741	2.54	0.199	0.120	0.023	0	0	141	2.54
Roof delay+degradation			-672		-586		0					1028	**1164**	1741					1700	**1750**	1741	
Floor delay										*immediate contact:*		0	**0**	0			*no liner:*		0	**0**	0	
Floor degradation	12	30.48	17.9	12.6	23.6	6.84	29.4	1.08	0.238	0.223	0.182	806	1203	2266	2.54	0.199	0.120	0.023	806	1203	2266	2.54
Floor delay+degradation			0		0		0					806	**1203**	2266					806	**1203**	2266	
Wall delay										*immediate contact:*		0	**0**	0			*no liner:*		0	**0**	0	
Wall degradation	6.16	15.66	9.21	6.45	12.1	3.52	14.9	0.77	0.238	0.223	0.182	414	618	1147	2.54	0.199	0.120	0.023	414	618	1147	2.54
Wall delay+degradation			0		0		0					414	**618**	1147					414	**618**	1147	
Wall delay										*immediate contact:*		0	**0**	0			*no liner:*		0	**0**	0	
Wall degradation	7.82	19.87	11.7	8.18	15.4	4.46	19	0.87	0.238	0.223	0.182	525	784	1464	2.54	0.199	0.120	0.023	525	784	1464	2.54
Wall delay+degradation			0		0		0					525	**784**	1464					525	**784**	1464	
Wall delay										*immediate contact:*		0	**0**	0			*no liner:*		0	**0**	0	
Wall degradation	10.70	27.17	16	11.2	21.1	6.1	26.1	1.02	0.238	0.223	0.182	719	1073	2016	2.54	0.199	0.120	0.023	719	1073	2016	2.54
Wall delay+degradation			0		0		0					719	**1073**	2016					719	**1073**	2016	
Wall delay										*immediate contact:*		0	**0**	0			*no liner:*		0	**0**	0	
Wall degradation	13.61	34.58	20.3	14.2	26.8	7.77	33.4	1.16	0.238	0.223	0.182	915	1365	2577	2.54	0.199	0.120	0.023	915	1365	2577	2.54
Wall delay+degradation			0		0		0					915	**1365**	2577					915	**1365**	2577	
Wall delay										*immediate contact:*		0	**0**	0			*no liner:*		0	**0**	0	
Wall degradation	16.43	41.74	24.5	17.2	32.4	9.37	40.5	1.27	0.238	0.223	0.182	1104	1648	3119	2.54	0.199	0.120	0.023	1104	1648	3119	2.54
Wall delay+degradation			0		0		0					1104	**1648**	3119					1104	**1648**	3119	
Grout delay																						
Grout degradation	516	1311																				
Grout delay+degradation																						
Column delay										*immediate contact:*		0	**0**	0								
Column degradation	8.86	22.5	22.5	0	22.5	0	22.5	0	0.977	0.863	0.479	60	77	249	2.54							
Column delay+degradation												60	**77**	249								

Table 4.4-44: Degradation Timing for SDU 7 Design Margin Concrete and Saltstone (Continued)

Degradation mechanism:	Thickness:		Decalcification			Time (yr)			max δ	Limiting			Initial thickness		t=0 thickness		Times:		
			A (cm/Yr)							CE	CV	BE					CE	CV	BE
Component	(in)	(cm)	CE	CV	BE	CE	CV	BE	(cm)	(yr)	(yr)	(yr)	(in)	(cm)	(in)	(cm)	(yr)	(yr)	(yr)
Roof delay				*HDPE-GCL:*		1700	1750	1600		**0**	**0**	**0**							
Roof degradation	9	22.86	0.023	0.021	0.017	111864	126638	191766	2.54		Roof								
Roof delay+degradation						113564	128388	193366		**1028**	**1164**	**1741**							
FloorUMM delay				*no liner:*		0	0	0		**0**	**0**	**0**					**-77**	**-114**	**-212**
FloorUMM degradation	12	30.48	0.023	0.021	0.017	149151	168851	255688	2.54		Floor		7.30	18.5	6.16	15.7		Wall ⑤	
FloorUMM delay+degradation						149151	168851	255688		**806**	**1203**	**2266**					**414**	**618**	**1147**
Wall delay				*no liner:*		0	0	0		**0**	**0**	**0**					**-87**	**-130**	**-242**
Wall degradation	6.163	15.66	0.023	0.021	0.017	76607	86725	131326	2.54		Wall ⑤		9.12	23.2	7.82	19.9		Wall ④	
Wall delay+degradation						76607	86725	131326		**414**	**618**	**1147**					**525**	**784**	**1464**
Wall delay				*no liner:*		0	0	0		**0**	**0**	**0**					**-104**	**-156**	**-293**
Wall degradation	7.822	19.87	0.023	0.021	0.017	97220	110061	166664	2.54		Wall ④		12.25	31.1	10.70	27.2		Wall ③	
Wall delay+degradation						97220	110061	166664		**525**	**784**	**1464**					**719**	**1073**	**2016**
Wall delay				*no liner:*		0	0	0		**0**	**0**	**0**					**-122**	**-182**	**-343**
Wall degradation	10.7	27.17	0.023	0.021	0.017	132966	150527	227941	2.54		Wall ③		15.43	39.2	13.61	34.6		Wall ②	
Wall delay+degradation						132966	150527	227941		**719**	**1073**	**2016**					**915**	**1365**	**2577**
Wall delay				*no liner:*		0	0	0		**0**	**0**	**0**					**-138**	**-206**	**-390**
Wall degradation	13.61	34.58	0.023	0.021	0.017	169223	191574	290097	2.54		Wall ②		18.49	47.0	16.43	41.7		Wall ①	
Wall delay+degradation						169223	191574	290097		**915**	**1365**	**2577**					**1104**	**1648**	**3119**
Wall delay				*no liner:*		0	0	0		**0**	**0**	**0**							
Wall degradation	16.43	41.74	0.023	0.021	0.017	204235	231209	350117	2.54		Wall ①								
Wall delay+degradation						204235	231209	350117		**1104**	**1648**	**3119**							
Grout delay				A_U (cm/yr)		1028	1164	1741		**1028**	**1164**	**1741**							
Grout degradation	516	1311	5.1E-04	7.6E-05	5.1E-06	2586629	1.7E+07	2.6E+08			Grout								
Grout delay+degradation						2.6E+06	**1.7E+07**	2.6E+08		**2.6E+06**	**1.7E+07**	**2.6E+08**							
Column delay										**0**	**0**	**0**							
Column degradation	8.862	22.5									Column								
Column delay+degradation										**60**	**77**	**249**							

Table 4.4-45: Summary of Starting and Ending Degradation Times

SDU 1			SDU 4			SDU 2			SDU 6			SDU 7 Design			SDU 7 Design w/Margin		
CE (yr)	CV (yr)	BE (yr)	CE (yr)	CV (yr)	BE (yr)	CE (yr)	CV (yr)	BE (yr)	CE (yr)	CV (yr)	BE (yr)	CE (yr)	CV (yr)	BE (yr)	CE (yr)	CV (yr)	BE (yr)
11	**23**	135	71	**144**	843	0	**0**	0	0	**0**	0	0	**0**	0	0	**0**	0
Roof	6 in		**Roof**	4 in		**Roof**	8 in		**Roof**	12 in		**Roof**	12 in		**Roof**	9 in	
683	**853**	1477	518	**698**	1727	914	**1034**	1566	1371	**1552**	2306	1371	**1552**	2306	1028	**1164**	1741
0	**0**	0	0	**0**	0	0	**0**	0	0	**0**	0	0	**0**	0	0	**0**	0
Floor	24 in		**Floor**	24 in		**FloorUMM**	12 in		**Floor**	12 in		**Floor**	24 in		**Floor**	12 in	
2996	**4579**	8957	2996	**4579**	8957	1371	**1552**	2306	1371	**1552**	2306	2312	**2800**	4603	806	**1203**	2266
0	**0**	0	0	**0**	0	0	**0**	0	0	**0**	0	0	**0**	0	0	**0**	0
Wall	18 in		**Wall**	18 in		**Wall**	8 in		**Wall ⑤**	8.93 in		**Wall ⑤**	10.72 in		**Wall ⑤**	6.16 in	
14	**19**	266	14	**19**	266	914	**1034**	1566	600	**895**	1677	720	**1075**	2020	414	**618**	1147
									0	**0**	0	0	**0**	0	0	**0**	0
									Wall ④	10.72 in		**Wall ④**	12.26 in		**Wall ④**	7.82 in	
									720	**1075**	2020	824	**1229**	2316	525	**784**	1464
									0	**0**	0	0	**0**	0	0	**0**	0
									Wall ③	13.83 in		**Wall ③**	14.92 in		**Wall ③**	10.70 in	
									929	**1386**	2617	1002	**1496**	2829	719	**1073**	2016
									0	**0**	0	0	**0**	0	0	**0**	0
									Wall ②	16.97 in		**Wall ②**	17.62 in		**Wall ②**	13.61 in	
									1140	**1702**	3224	1184	**1767**	3349	915	**1365**	2577
									0	**0**	0	0	**0**	0	0	**0**	0
									Wall ①	20.01 in		**Wall ①**	20.22 in		**Wall ①**	16.43 in	
									1344	**2006**	3810	1358	**2028**	3851	1104	**1648**	3119
683	**853**	1477	2068	**10499**	264501	914	**1034**	1566	1371	**1552**	2306	1371	**1552**	2306	1028	**1164**	1741
Grout	294 in		**Grout-3.4**	273 in		**Grout**	264 in		**Grout**	516 in		**Grout**	516 in		**Grout**	516 in	
1.5E+06	**9.8E+06**	1.5E+08	1.4E+06	**9.1E+06**	1.4E+08	1.3E+06	**8.8E+06**	1.3E+08	2.6E+06	**1.7E+07**	2.6E+08	2.6E+06	**1.7E+07**	2.6E+08	2.6E+06	**1.7E+07**	2.6E+08
			518	**698**	1727												
			Top Salt.	41.37 in													
			2068	**10499**	264501												
			1750	**1800**	1727	0	**0**	0	0	**0**	0	0	**0**	0	0	**0**	0
			Column	24 in		**Column**	6.20 in		**Column**	10.63 in		**Column**	10.63 in		**Column**	8.86 in	
			2649	**7486**	154170	42	**54**	175	72	**92**	299	72	**92**	299	60	**77**	249

4.4.2.2 Calculation Details

The SDU 1 and 4 "Grout" thicknesses include saltstone and clean grout. The 12-inch "FloorUMM" thickness for SDU 2 denotes the combination of an 8-inch floor with rebar and a 4-inch upper mud mat without rebar.

The SDU 4 roof is supported by trusses that will extend into the clean cap grout and upper saltstone when disposal cells are filled. To account for the presence of embedded steel, the upper 3.45 feet of clean grout and saltstone ("Top saltstone") degrades by carbonation-induced steel corrosion. The remaining saltstone thickness, except for the vertical roof support columns, degrades by advection-controlled decalcification.

The SDU 4 trusses are supported by concrete-filled steel pipes. These degrade by carbonation advancing inside the pipe column through concrete and outside the column through grout; both processes lead to accelerated steel corrosion. Carbonation occurs faster through the grout, so only the outer carbonation front is calculated. Carbonation through the column region is assumed to start after the earlier of the roof and floor degradation times, such that columns degrade symmetrically from the top and bottom. PA analysts anticipate discretizing the columns in 2-foot segments for flow and transport simulations; therefore, degradation times are computed for 24-inch increments. The main calculation table indicates the degradation times for the first pair of column segments. Degradation times for all column segments (denoted "grout1", "grout2", etc.) are indicated by a summary list adjoining the main table. Because the carbonation front advances at a constant rate (past 2.54 cm), the elapsed time for the carbonation front to pass through a segment is the same for all segments.

The SDU 2, 6, and 7 roofs are supported by reinforced concrete columns. These degrade immediately by sulfate attack from the outside diameter inward. Because the columns degrade uniformly from top to bottom, they are not subdivided into segments as with SDU 4. Early sulfate attack during operations is ignored because the longevity of the internal columns is already shorter than the roof and floor. Therefore, column degradation does not control waste release.

The SDU 6 and 7 walls are partially degraded at PA time zero, due to early sulfate attack during operations (Section 4.4.2.2.5). After facility closure, the wall segments 1 through 5 degrade at a slower rate (Section 4.4.2.2.4). The degraded thickness Δx is assumed to vary linearly with time for $t_0 < t < t_1$,

$$\Delta x = \frac{t - t_0}{t_1 - t_0} L \qquad \text{Eq. 4.4-78}$$

where L is initial thickness and t_1 is the time of complete degradation. Time t_0 is defined by the constraint:

$$\Delta x_{t=0} = \frac{-t_0}{t_1 - t_0} L \qquad \text{Eq. 4.4-79}$$

The solution is:

$$t_0 = \frac{t_1}{1 - L/\Delta x_{t=0}} < 0 \qquad \text{Eq. 4.4-80}$$

or in terms of undegraded thickness at *t = 0:*

$$t_0 = t_1(1 - L/L_{t=0}) < 0 \qquad \text{Eq. 4.4-81}$$

To support subsequent numerical flow and transport modeling, values for t_0 are included in Table 4.4-42 through Table 4.4-44.

4.4.2.3 Initial Degradation of Cementitious Materials

In addition to early sulfate attack on SDU 6 and 7 wall concrete described in Section 4.4.2.2.5, several features which may be associated with early degradation of concrete components are considered in this section.

Cracks were observed in SDU 6 floor concrete in the field, likely due to insufficient moisture during curing. The equivalent hydraulic conductivity of the field-cured SDU 6 floor concrete was inferred from leak testing by SRNL-STI-2016-00534, Table 2-4 to be approximately 6.2E-06 cm/s, based on calibration to hydraulic leak testing of the disposal unit in the field. This value is adopted for the initial conductivity of both SDU 6 floor and roof concrete, on the basis that the roof was cured in a similar manner to the floor.

Although now superseded by SRNL-STI-2016-00534, SRNL-STI-2016-00511 considered the impact of unrepaired floor penetrations due to nail holes, formwork anchors, center pin, and form brackets on SDU 6 floor concrete. Figure 4.4-21 summarizes the approach for computing an equivalent hydraulic conductivity for the system. "Method 1" is arithmetic averaging followed by harmonic averaging. Alternative "Method 2" is harmonic averaging followed by arithmetic averaging. Equivalent hydraulic conductivity is defined as the geometric average of Methods 1 and 2. This method was reapplied to future SDU 7 (not leak tested) using updated material properties (SRR-CWDA-2018-00004) and dimensions (SRR-CWDA-2018-00012) and extended to BE, CV, and CE confidence levels. Table 4.4-46 summarizes the calculation. [SRNL-STI-2016-00511] Although a calculation of the impact of floor penetrations is performed for the SDU 7 Design case, these results are not carried forward because any floor penetrations will be repaired by design. Conversely, floor penetrations are assumed to remain unrepaired for the SDU 7 Design Margin (DM) case.

SDU 7 wall concrete may likewise be degraded at PA time zero due to penetrations in the form of wire form anchors and thermocouple trees (SRR-CWDA-2018-00012). Because the two types of penetrations differ in depth, the approach of SRNL-STI-2016-00511 is extended from binary to tertiary averaging, as depicted in Figure 4.4-22. Table 4.4-47 through Table 4.4-51 present equivalent hydraulic conductivity estimates for the SDU 7 Design and SDU 7 DM cases. Because wall penetrations for the SDU 7 Design case are assumed to have been repaired at PA time zero or otherwise not compromise the barrier, hydraulic conductivity is unaltered.

Figure 4.4-21: Conceptual Approach for the Equivalent Conductivity of Floor Concrete

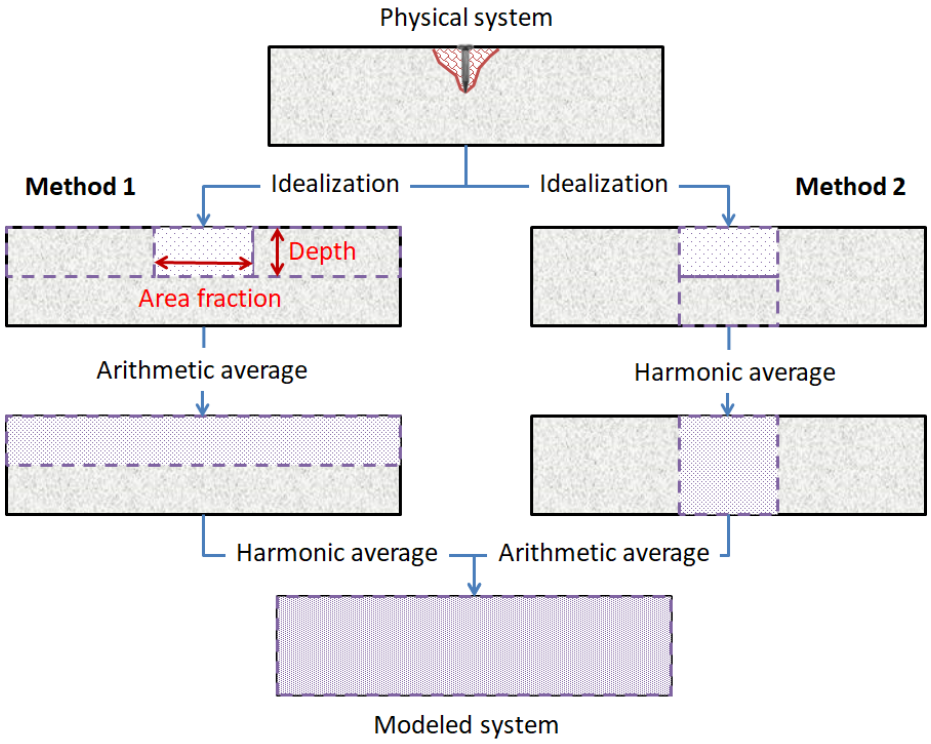

Figure 4.4-22: Conceptual Approach for the Equivalent Conductivity of Wall Concrete

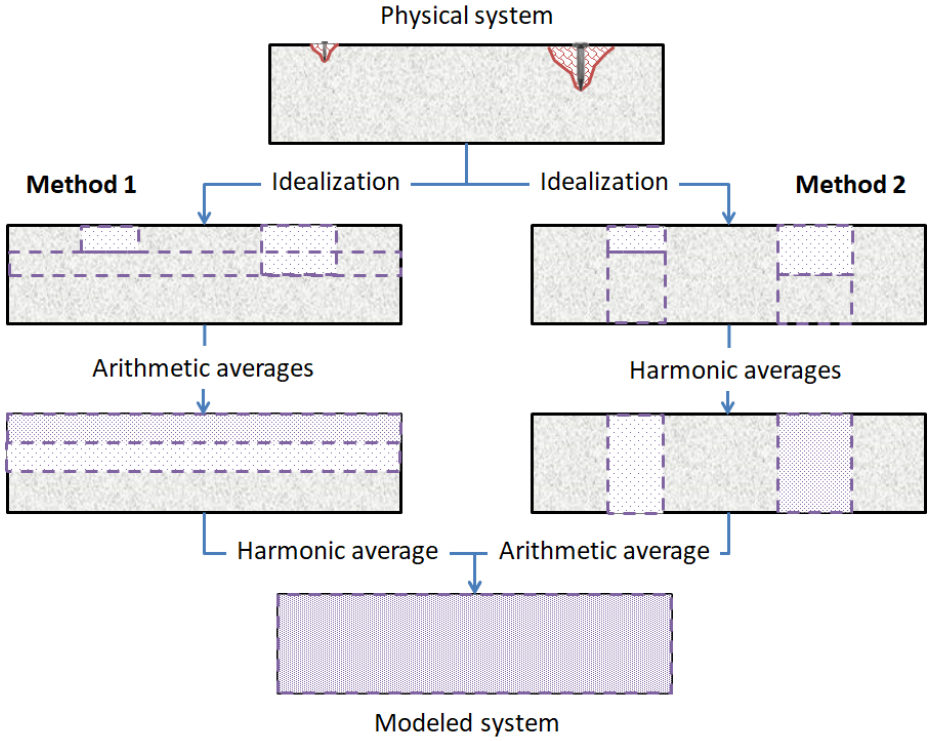

Table 4.4-46: Equivalent Hydraulic Conductivity Considering SDU 7 Floor Penetrations

Case:	BE		CV		CE		Units
	SDU 7	SDU 7 DM	SDU 7	SDU 7 DM	SDU 7	SDU 7 DM	
Floor Thickness	24	12	24	12	24	12	inch
Floor Diameter	375	375	375	375	375	375	ft
Total Floor Area	110447	110447	110447	110447	110447	110447	ft^2
Floor Hydraulic Conductivity	6.4E-10	6.4E-10	7.8E-10	7.8E-10	9.1E-10	9.1E-10	cm/s
Penetration Depth	6	8	6	8	6	8	inch
Impacted Area	16.57	22.09	16.57	22.09	16.57	22.09	ft^2
Impact Area K	1.5E-01	1.5E-01	1.5E-01	1.5E-01	1.5E-01	1.5E-01	cm/s
Impact Area Fraction	0.015%	0.020%	0.015%	0.020%	0.015%	0.020%	
Intact Area Fraction	99.985%	99.980%	99.985%	99.980%	99.985%	99.980%	
Impacted Depth Fraction	25.00%	66.67%	25.00%	66.67%	25.00%	66.67%	
Intact Depth Fraction	75.00%	33.33%	75.00%	33.33%	75.00%	33.33%	
Method 1							
Arithmetic Average	2.25E-05	3.00E-05	2.25E-05	3.00E-05	2.25E-05	3.00E-05	cm/s
Harmonic Average	8.53E-10	1.92E-09	1.04E-09	2.34E-09	1.21E-09	2.73E-09	cm/s
Ratio to intact condition	1.33	3.00	1.33	3.00	1.33	3.00	
Method 2							
Harmonic Average	8.53E-10	1.92E-09	1.04E-09	2.34E-09	1.21E-09	2.73E-09	cm/s
Arithmetic Average	6.40E-10	6.40E-10	7.80E-10	7.80E-10	9.10E-10	9.10E-10	cm/s
Ratio to intact condition	1.00	1.00	1.00	1.00	1.00	1.00	
Modeled System							
Geometric Average	**7.39E-10**	**1.11E-09**	**9.01E-10**	**1.35E-09**	**1.05E-09**	**1.58E-09**	cm/s
Ratio to intact condition	1.15	1.73	1.15	1.73	1.15	1.73	

Table 4.4-47: Equivalent Hydraulic Conductivity Considering SDU 7 Wall Segment 5 Penetrations

	BE		CV		CE		
Case:	**SDU 7**	**SDU 7 DM**	**SDU 7**	**SDU 7 DM**	**SDU 7**	**SDU 7 DM**	**Units**
Wall ⑤ Thickness	12.28	7.30	12.28	7.30	12.28	7.30	inch
Wall Diameter	375	375	375	375	375	375	ft
Wall Height	43	43	43	43	43	43	ft
Total Wall Area	50658	50658	50658	50658	50658	50658	ft^2
K_{sat}, Intact	6.4E-10	6.4E-10	7.8E-10	7.8E-10	9.1E-10	9.1E-10	cm/s
K_{sat}, Penetrations	1.5E-01	1.5E-01	1.5E-01	1.5E-01	1.5E-01	1.5E-01	cm/s
Penetration Depth 1	0	7.25	0	7.25	0	7.25	in
Area 1	0	16	0	16	0	16	ft^2
Penetration Depth 2	0	2	0	2	0	2	in
Area 2	0.00	7.17	0.00	7.17	0.00	7.17	ft^2
Method 1							
Area Fraction 1	0	0.000316	0.000000	0.000316	0.000000	0.000316	
Area Fraction 2	0	0.000141	0.000000	0.000141	0.000000	0.000141	
Arithmetic Average A	6.40E-10	6.86E-05	7.80E-10	6.86E-05	9.10E-10	6.86E-05	cm/s
Arithmetic Average B	6.40E-10	4.74E-05	7.80E-10	4.74E-05	9.10E-10	4.74E-05	cm/s
Arithmetic Average C	6.40E-10	6.40E-10	7.80E-10	7.80E-10	9.10E-10	9.10E-10	cm/s
Thickness Fraction A	0	0.27389	0.00000	0.27389	0.00000	0.27389	
Thickness Fraction B	0	0.71895	0.00000	0.71895	0.00000	0.71895	
Thickness Fraction C	1	0.00717	1.00000	0.00717	1.00000	0.00717	
Harmonic Average	6.40E-10	8.92E-08	7.80E-10	1.09E-07	9.10E-10	1.27E-07	cm/s
Ratio to intact condition	1.00	139.32	1.00	139.26	1.00	139.22	
Method 2							
Thickness Fraction 1	0	0.992834	0.000000	0.992834	0.000000	0.992834	
Thickness Fraction 1	0	0.273885	0.000000	0.273885	0.000000	0.273885	
Harmonic Average A	6.4E-10	8.9E-08	7.8E-10	1.1E-07	9.1E-10	1.3E-07	cm/s
Harmonic Average B	6.4E-10	8.8E-10	7.8E-10	1.1E-09	9.1E-10	1.3E-09	cm/s
Harmonic Average C	6.4E-10	6.4E-10	7.8E-10	7.8E-10	9.1E-10	9.1E-10	cm/s
Area Fraction A	0	0.00032	0.00000	0.00032	0.00000	0.00032	
Area Fraction B	0	0.00014	0.00000	0.00014	0.00000	0.00014	
Area Fraction C	1	0.99954	1.00000	0.99954	1.00000	0.99954	
Arithmetic Average	6.40E-10	6.68E-10	7.80E-10	8.14E-10	9.10E-10	9.50E-10	cm/s
Ratio to intact condition	1.00	1.04	1.00	1.04	1.00	1.04	
Modeled System							
Geometric Average	**6.40E-10**	**7.72E-09**	**7.80E-10**	**9.40E-09**	**9.10E-10**	**1.10E-08**	cm/s
Ratio to intact condition	1.00	12.06	1.00	12.06	1.00	12.05	

Table 4.4-48: Equivalent Hydraulic Conductivity Considering SDU 7 Wall Segment 4 Penetrations

	BE		CV		CE		
Case:	**SDU 7**	**SDU 7 DM**	**SDU 7**	**SDU 7 DM**	**SDU 7**	**SDU 7 DM**	**Units**
Wall ④ Thickness	13.95	9.12	13.95	9.12	13.95	9.12	inch
Wall Diameter	375	375	375	375	375	375	ft
Wall Height	43	43	43	43	43	43	ft
Total Wall Area	50658	50658	50658	50658	50658	50658	ft^2
K_{sat}, Intact	6.4E-10	6.4E-10	7.8E-10	7.8E-10	9.1E-10	9.1E-10	cm/s
K_{sat}, Penetrations	1.5E-01	1.5E-01	1.5E-01	1.5E-01	1.5E-01	1.5E-01	cm/s
Penetration Depth 1	0	7.25	0	7.25	0	7.25	in
Area 1	0	16	0	16	0	16	ft^2
Penetration Depth 2	0	2	0	2	0	2	in
Area 2	0.00	7.17	0.00	7.17	0.00	7.17	ft^2
Method 1							
Area Fraction 1	0	0.000316	0.000000	0.000316	0.000000	0.000316	
Area Fraction 2	0	0.000141	0.000000	0.000141	0.000000	0.000141	
Arithmetic Average A	6.40E-10	6.86E-05	7.80E-10	6.86E-05	9.10E-10	6.86E-05	cm/s
Arithmetic Average B	6.40E-10	4.74E-05	7.80E-10	4.74E-05	9.10E-10	4.74E-05	cm/s
Arithmetic Average C	6.40E-10	6.40E-10	7.80E-10	7.80E-10	9.10E-10	9.10E-10	cm/s
Thickness Fraction A	0	0.21939	0.00000	0.21939	0.00000	0.21939	
Thickness Fraction B	0	0.57589	0.00000	0.57589	0.00000	0.57589	
Thickness Fraction C	1	0.20472	1.00000	0.20472	1.00000	0.20472	
Harmonic Average	6.40E-10	3.13E-09	7.80E-10	3.81E-09	9.10E-10	4.44E-09	cm/s
Ratio to intact condition	1.00	4.88	1.00	4.88	1.00	4.88	
Method 2							
Thickness Fraction 1	0	0.795281	0.000000	0.795281	0.000000	0.795281	
Thickness Fraction 1	0	0.219388	0.000000	0.219388	0.000000	0.219388	
Harmonic Average A	6.4E-10	3.1E-09	7.8E-10	3.8E-09	9.1E-10	4.4E-09	cm/s
Harmonic Average B	6.4E-10	8.2E-10	7.8E-10	1.0E-09	9.1E-10	1.2E-09	cm/s
Harmonic Average C	6.4E-10	6.4E-10	7.8E-10	7.8E-10	9.1E-10	9.1E-10	cm/s
Area Fraction A	0	0.00032	0.00000	0.00032	0.00000	0.00032	
Area Fraction B	0	0.00014	0.00000	0.00014	0.00000	0.00014	
Area Fraction C	1	0.99954	1.00000	0.99954	1.00000	0.99954	
Arithmetic Average	6.40E-10	6.41E-10	7.80E-10	7.81E-10	9.10E-10	9.11E-10	cm/s
Ratio to intact condition	1.00	1.00	1.00	1.00	1.00	1.00	
Modeled System							
Geometric Average	**6.40E-10**	**1.42E-09**	**7.80E-10**	**1.72E-09**	**9.10E-10**	**2.01E-09**	cm/s
Ratio to intact condition	1.00	2.21	1.00	2.21	1.00	2.21	

Table 4.4-49: Equivalent Hydraulic Conductivity Considering SDU 7 Wall Segment 3 Penetrations

	BE		CV		CE		
Case:	**SDU 7**	**SDU 7 DM**	**SDU 7**	**SDU 7 DM**	**SDU 7**	**SDU 7 DM**	**Units**
Wall ③ Thickness	16.85	12.25	16.85	12.25	16.85	12.25	inch
Wall Diameter	375	375	375	375	375	375	ft
Wall Height	43	43	43	43	43	43	ft
Total Wall Area	50658	50658	50658	50658	50658	50658	ft^2
K_{sat}, Intact	6.4E-10	6.4E-10	7.8E-10	7.8E-10	9.1E-10	9.1E-10	cm/s
K_{sat}, Penetrations	1.5E-01	1.5E-01	1.5E-01	1.5E-01	1.5E-01	1.5E-01	cm/s
Penetration Depth 1	0	7.25	0	7.25	0	7.25	in
Area 1	0	16	0	16	0	16	ft^2
Penetration Depth 2	0	2	0	2	0	2	in
Area 2	0.00	7.17	0.00	7.17	0.00	7.17	ft^2
Method 1							
Area Fraction 1	0	0.000316	0.000000	0.000316	0.000000	0.000316	
Area Fraction 2	0	0.000141	0.000000	0.000141	0.000000	0.000141	
Arithmetic Average A	6.40E-10	6.86E-05	7.80E-10	6.86E-05	9.10E-10	6.86E-05	cm/s
Arithmetic Average B	6.40E-10	4.74E-05	7.80E-10	4.74E-05	9.10E-10	4.74E-05	cm/s
Arithmetic Average C	6.40E-10	6.40E-10	7.80E-10	7.80E-10	9.10E-10	9.10E-10	cm/s
Thickness Fraction A	0	0.16323	0.00000	0.16323	0.00000	0.16323	
Thickness Fraction B	0	0.42847	0.00000	0.42847	0.00000	0.42847	
Thickness Fraction C	1	0.40830	1.00000	0.40830	1.00000	0.40830	
Harmonic Average	6.40E-10	1.57E-09	7.80E-10	1.91E-09	9.10E-10	2.23E-09	cm/s
Ratio to intact condition	1.00	2.45	1.00	2.45	1.00	2.45	
Method 2							
Thickness Fraction 1	0	0.591696	0.000000	0.591696	0.000000	0.591696	
Thickness Fraction 1	0	0.163227	0.000000	0.163227	0.000000	0.163227	
Harmonic Average A	6.4E-10	1.6E-09	7.8E-10	1.9E-09	9.1E-10	2.2E-09	cm/s
Harmonic Average B	6.4E-10	7.6E-10	7.8E-10	9.3E-10	9.1E-10	1.1E-09	cm/s
Harmonic Average C	6.4E-10	6.4E-10	7.8E-10	7.8E-10	9.1E-10	9.1E-10	cm/s
Area Fraction A	0	0.00032	0.00000	0.00032	0.00000	0.00032	
Area Fraction B	0	0.00014	0.00000	0.00014	0.00000	0.00014	
Area Fraction C	1	0.99954	1.00000	0.99954	1.00000	0.99954	
Arithmetic Average	6.40E-10	6.40E-10	7.80E-10	7.80E-10	9.10E-10	9.10E-10	cm/s
Ratio to intact condition	1.00	1.00	1.00	1.00	1.00	1.00	
Modeled System							
Geometric Average	**6.40E-10**	**1.00E-09**	**7.80E-10**	**1.22E-09**	**9.10E-10**	**1.42E-09**	cm/s
Ratio to intact condition	1.00	1.57	1.00	1.57	1.00	1.57	

Table 4.4-50: Equivalent Hydraulic Conductivity Considering SDU 7 Wall Segment 2 Penetrations

	BE		CV		CE		
Case:	**SDU 7**	**SDU 7 DM**	**SDU 7**	**SDU 7 DM**	**SDU 7**	**SDU 7 DM**	**Units**
Wall ② Thickness	19.78	15.43	19.78	15.43	19.78	15.43	inch
Wall Diameter	375	375	375	375	375	375	ft
Wall Height	43	43	43	43	43	43	ft
Total Wall Area	50658	50658	50658	50658	50658	50658	ft^2
K_{sat}, Intact	6.4E-10	6.4E-10	7.8E-10	7.8E-10	9.1E-10	9.1E-10	cm/s
K_{sat}, Penetrations	1.5E-01	1.5E-01	1.5E-01	1.5E-01	1.5E-01	1.5E-01	cm/s
Penetration Depth 1	0	7.25	0	7.25	0	7.25	in
Area 1	0	16	0	16	0	16	ft^2
Penetration Depth 2	0	2	0	2	0	2	in
Area 2	0.00	7.17	0.00	7.17	0.00	7.17	ft^2
Method 1							
Area Fraction 1	0	0.000316	0.000000	0.000316	0.000000	0.000316	
Area Fraction 2	0	0.000141	0.000000	0.000141	0.000000	0.000141	
Arithmetic Average A	6.40E-10	6.86E-05	7.80E-10	6.86E-05	9.10E-10	6.86E-05	cm/s
Arithmetic Average B	6.40E-10	4.74E-05	7.80E-10	4.74E-05	9.10E-10	4.74E-05	cm/s
Arithmetic Average C	6.40E-10	6.40E-10	7.80E-10	7.80E-10	9.10E-10	9.10E-10	cm/s
Thickness Fraction A	0	0.12964	0.00000	0.12964	0.00000	0.12964	
Thickness Fraction B	0	0.34031	0.00000	0.34031	0.00000	0.34031	
Thickness Fraction C	1	0.53005	1.00000	0.53005	1.00000	0.53005	
Harmonic Average	6.40E-10	1.21E-09	7.80E-10	1.47E-09	9.10E-10	1.72E-09	cm/s
Ratio to intact condition	1.00	1.89	1.00	1.89	1.00	1.89	
Method 2							
Thickness Fraction 1	0	0.469945	0.000000	0.469945	0.000000	0.469945	
Thickness Fraction 1	0	0.129640	0.000000	0.129640	0.000000	0.129640	
Harmonic Average A	6.4E-10	1.2E-09	7.8E-10	1.5E-09	9.1E-10	1.7E-09	cm/s
Harmonic Average B	6.4E-10	7.4E-10	7.8E-10	9.0E-10	9.1E-10	1.0E-09	cm/s
Harmonic Average C	6.4E-10	6.4E-10	7.8E-10	7.8E-10	9.1E-10	9.1E-10	cm/s
Area Fraction A	0	0.00032	0.00000	0.00032	0.00000	0.00032	
Area Fraction B	0	0.00014	0.00000	0.00014	0.00000	0.00014	
Area Fraction C	1	0.99954	1.00000	0.99954	1.00000	0.99954	
Arithmetic Average	6.40E-10	6.40E-10	7.80E-10	7.80E-10	9.10E-10	9.10E-10	cm/s
Ratio to intact condition	1.00	1.00	1.00	1.00	1.00	1.00	
Modeled System							
Geometric Average	**6.40E-10**	**8.79E-10**	**7.80E-10**	**1.07E-09**	**9.10E-10**	**1.25E-09**	cm/s
Ratio to intact condition	1.00	1.37	1.00	1.37	1.00	1.37	

Table 4.4-51: Equivalent Hydraulic Conductivity Considering SDU 7 Wall Segment 1 Penetrations

	BE		CV		CE		
Case:	SDU 7	SDU 7 DM	SDU 7	SDU 7 DM	SDU 7	SDU 7 DM	Units
Wall ① Thickness	22.60	18.49	22.60	18.49	22.60	18.49	inch
Wall Diameter	375	375	375	375	375	375	ft
Wall Height	43	43	43	43	43	43	ft
Total Wall Area	50658	50658	50658	50658	50658	50658	ft^2
K_{sat}, Intact	6.4E-10	6.4E-10	7.8E-10	7.8E-10	9.1E-10	9.1E-10	cm/s
K_{sat}, Penetrations	1.5E-01	1.5E-01	1.5E-01	1.5E-01	1.5E-01	1.5E-01	cm/s
Penetration Depth 1	0	7.25	0	7.25	0	7.25	in
Area 1	0	16	0	16	0	16	ft^2
Penetration Depth 2	0	2	0	2	0	2	in
Area 2	0.00	7.17	0.00	7.17	0.00	7.17	ft^2
Method 1							
Area Fraction 1	0	0.000316	0.000000	0.000316	0.000000	0.000316	
Area Fraction 2	0	0.000141	0.000000	0.000141	0.000000	0.000141	
Arithmetic Average A	6.40E-10	6.86E-05	7.80E-10	6.86E-05	9.10E-10	6.86E-05	cm/s
Arithmetic Average B	6.40E-10	4.74E-05	7.80E-10	4.74E-05	9.10E-10	4.74E-05	cm/s
Arithmetic Average C	6.40E-10	6.40E-10	7.80E-10	7.80E-10	9.10E-10	9.10E-10	cm/s
Thickness Fraction A	0	0.10818	0.00000	0.10818	0.00000	0.10818	
Thickness Fraction B	0	0.28396	0.00000	0.28396	0.00000	0.28396	
Thickness Fraction C	1	0.60786	1.00000	0.60786	1.00000	0.60786	
Harmonic Average	6.40E-10	1.05E-09	7.80E-10	1.28E-09	9.10E-10	1.50E-09	cm/s
Ratio to intact condition	1.00	1.65	1.00	1.65	1.00	1.65	
Method 2							
Thickness Fraction 1	0	0.392138	0.000000	0.392138	0.000000	0.392138	
Thickness Fraction 1	0	0.108176	0.000000	0.108176	0.000000	0.108176	
Harmonic Average A	6.4E-10	1.1E-09	7.8E-10	1.3E-09	9.1E-10	1.5E-09	cm/s
Harmonic Average B	6.4E-10	7.2E-10	7.8E-10	8.7E-10	9.1E-10	1.0E-09	cm/s
Harmonic Average C	6.4E-10	6.4E-10	7.8E-10	7.8E-10	9.1E-10	9.1E-10	cm/s
Area Fraction A	0	0.00032	0.00000	0.00032	0.00000	0.00032	
Area Fraction B	0	0.00014	0.00000	0.00014	0.00000	0.00014	
Area Fraction C	1	0.99954	1.00000	0.99954	1.00000	0.99954	
Arithmetic Average	6.40E-10	6.40E-10	7.80E-10	7.80E-10	9.10E-10	9.10E-10	cm/s
Ratio to intact condition	1.00	1.00	1.00	1.00	1.00	1.00	
Modeled System							
Geometric Average	**6.40E-10**	**8.21E-10**	**7.80E-10**	**1.00E-09**	**9.10E-10**	**1.17E-09**	cm/s
Ratio to intact condition	1.00x	1.28x	1.00x	1.28x	1.00x	1.28x	

4.4.2.4 Variation of Equivalent Hydraulic Conductivity with Time

Table 4.4-52 summarizes hydraulic conductivity recommendations for each SDU at BE, CV, and CE confidence levels. The initial values are generally drawn from SRR-CWDA-2018-00004 but may also reflect partial degradation at PA time zero due to unrepaired penetrations, suboptimal curing conditions in the field, or early sulfate attack (Sections 4.4.2.2.5 and 4.4.2.3). The final values are those of backfill soil or Lower Vadose Zone native sediment (WSRC-STI-2006-00198, Table 5-18, K_v), depending on which material adjoins a component. With this selection, the fully-degraded cementitious material functions neither as a barrier nor a conduit to flow, relative to its neighboring geologic material.

Table 4.4-52: Summary of Initial and Fully Degraded Hydraulic Conductivities

SDU 1			SDU 4			SDU 2			SDU 6			SDU 7 Design			SDU 7 Design w/Margin		
CE	CV	BE	CE	CV	BE	CE	CV	BE	CE	CV	BE	CE	CV	BE	CE	CV	BE
(cm/s)	(cm/s)	(cm/s)	(cm/s)	(cm/s)	(cm/s)	(cm/s)	(cm/s)	(cm/s)	(cm/s)	(cm/s)	(cm/s)	(cm/s)	(cm/s)	(cm/s)	(cm/s)	(cm/s)	(cm/s)
2.1E-09	**7.8E-10**	3.1E-10	2.1E-09	**7.8E-10**	3.1E-10	3.2E-10	**1.4E-10**	1.0E-10	6.2E-06	**6.2E-06**	6.2E-06	9.1E-10	**7.8E-10**	6.4E-10	1.6E-09	**1.4E-09**	1.1E-09
Roof	6 in		**Roof**	4 in		**Roof**	8 in		**Roof**	12 in		**Roof**	12 in		**Roof**	9 in	
4.1E-05	**4.1E-05**	4.1E-05	4.1E-05	**4.1E-05**	4.1E-05	4.1E-05	**4.1E-05**	4.1E-05	4.1E-05	**4.1E-05**	4.1E-05	4.1E-05	**4.1E-05**	4.1E-05	4.1E-05	**4.1E-05**	4.1E-05
2.1E-09	**7.8E-10**	3.1E-10	2.1E-09	**7.8E-10**	3.1E-10	3.2E-10	**1.4E-10**	1.0E-10	6.2E-06	**6.2E-06**	6.2E-06	9.1E-10	**7.8E-10**	6.4E-10	1.6E-09	**1.4E-09**	1.1E-09
Floor	24 in		**Floor**	24 in		FloorUMM	12 in		**Floor**	12 in		**Floor**	24 in		**Floor**	12 in	
9.1E-05	**9.1E-05**	9.1E-05	9.1E-05	**9.1E-05**	9.1E-05	9.1E-05	**9.1E-05**	9.1E-05	9.1E-05	**9.1E-05**	9.1E-05	9.1E-05	**9.1E-05**	9.1E-05	9.1E-05	**9.1E-05**	9.1E-05
4.1E-05	**4.1E-05**	1.0E-08	4.1E-05	**4.1E-05**	1.0E-08	3.2E-10	**1.4E-10**	1.0E-10	3.2E-10	**1.40E-10**	1.0E-10	9.10E-10	**7.80E-10**	6.40E-10	1.10E-08	**9.40E-09**	7.72E-09
Wall	18 in		**Wall**	18 in		**Wall**	8 in		**Wall ⑤**	8.93 in		**Wall ⑤**	10.72 in		**Wall ⑤**	6.16 in	
4.1E-05	**4.1E-05**	4.1E-05	4.1E-05	**4.1E-05**	4.1E-05	4.1E-05	**4.1E-05**	4.1E-05	4.1E-05	**4.1E-05**	4.1E-05	4.1E-05	**4.1E-05**	4.1E-05	4.1E-05	**4.1E-05**	4.1E-05
									3.2E-10	**1.40E-10**	1.0E-10	9.10E-10	**7.80E-10**	6.40E-10	2.01E-09	**1.72E-09**	1.42E-09
									Wall ④	10.72 in		**Wall ④**	12.26 in		**Wall ④**	7.82 in	
									4.1E-05	**4.1E-05**	4.1E-05	4.1E-05	**4.1E-05**	4.1E-05	4.1E-05	**4.1E-05**	4.1E-05
									3.2E-10	**1.40E-10**	1.0E-10	9.10E-10	**7.80E-10**	6.40E-10	1.42E-09	**1.22E-09**	1.00E-09
Soils:									**Wall ③**	13.83 in		**Wall ③**	14.92 in		**Wall ③**	10.70 in	
Backfill	**4.1E-05**	cm/s							4.1E-05	**4.1E-05**	4.1E-05	4.1E-05	**4.1E-05**	4.1E-05	4.1E-05	**4.1E-05**	4.1E-05
Native soil	**9.1E-05**	cm/s							3.2E-10	**1.40E-10**	1.0E-10	9.10E-10	**7.80E-10**	6.40E-10	1.25E-09	**1.07E-09**	8.79E-10
									Wall ②	16.97 in		**Wall ②**	17.62 in		**Wall ②**	13.61 in	
									4.1E-05	**4.1E-05**	4.1E-05	4.1E-05	**4.1E-05**	4.1E-05	4.1E-05	**4.1E-05**	4.1E-05
									3.2E-10	**1.40E-10**	1.0E-10	9.10E-10	**7.80E-10**	6.40E-10	1.17E-09	**1.00E-09**	8.21E-10
									Wall ①	20.01 in		**Wall ①**	20.22 in		**Wall ①**	16.43 in	
									4.1E-05	**4.1E-05**	4.1E-05	4.1E-05	**4.1E-05**	4.1E-05	4.1E-05	**4.1E-05**	4.1E-05
2.0E-09	**5.0E-10**	1.0E-10	2.0E-09	**5.0E-10**	1.0E-10	2.0E-09	**5.0E-10**	1.0E-10	2.0E-09	**5.0E-10**	1.0E-10	2.0E-09	**5.0E-10**	1.0E-10	2.0E-09	**5.0E-10**	1.0E-10
Grout	294 in		**Grout-3.4**	273 in		**Grout**	264 in		**Grout**	516 in		**Grout**	516 in		**Grout**	516 in	
4.1E-05	**4.1E-05**	4.1E-05	4.1E-05	**4.1E-05**	4.1E-05	4.1E-05	**4.1E-05**	4.1E-05	4.1E-05	**4.1E-05**	4.1E-05	4.1E-05	**4.1E-05**	4.1E-05	4.1E-05	**4.1E-05**	4.1E-05
			2.0E-09	**5.0E-10**	1.0E-10												
			Top Salt.	41.37 in													
			4.1E-05	**4.1E-05**	4.1E-05												
			1.0E-08	**5.0E-09**	5.0E-09	1.0E-08	**5.0E-09**	5.0E-09	1.0E-08	**5.0E-09**	5.0E-09	1.0E-08	**5.0E-09**	5.0E-09	1.0E-08	**5.0E-09**	5.0E-09
			Column	24 in		**Column**	6.20 in		**Column**	10.63 in		**Column**	10.63 in		**Column**	8.86 in	
			4.1E-05	**4.1E-05**	4.1E-05	4.1E-05	**4.1E-05**	4.1E-05	4.1E-05	**4.1E-05**	4.1E-05	4.1E-05	**4.1E-05**	4.1E-05	4.1E-05	**4.1E-05**	4.1E-05

As noted in Section 4.4.2.2 the degraded thickness Δx is assumed to vary linearly with time for t>0, where t_0 and t_1 in Eq. 4.4-78 are summarized in Table 4.4-45 (also see Table 4.4-42 through Table 4.4-44 for SDU 6 and 7 wall segments). A linear variation with time is appropriate for concrete because δ = 2.54 cm for nearly all components, which is small compared to overall thicknesses. Therefore, degradation fronts advance mostly at a constant rate, per Figure 4.4-13 and Eq. 4.4-13. For saltstone, advection-controlled decalcification directly produces a constant penetration rate, or linear variation with time. Eq. 4.4-78 can be rewritten in a form valid for all times as:

$$f(t) \equiv \frac{\Delta x}{L} = \frac{\min[\max(t,t_0),t_1]-t_0}{t_1-t_0} \qquad \text{Eq. 4.4-82}$$

where $0 \le f(t) \le 1$ is the degradation fraction.

PA system modeling will treat each concrete and grout component as a homogeneous material with time-varying hydraulic conductivity. Therefore, the equivalent hydraulic conductivity of each degrading component is needed. Equivalent hydraulic conductivity is generally defined as the uniform hydraulic conductivity value that reproduces some integral behavior of a region, such as spatial average liquid flux for a given hydraulic head gradient. A closely related concept is effective hydraulic, a statistical ensemble average. Sanchez-Vila, et.al., (1995) and Sanchez-Vila, et.al., (2006) provide a comprehensive review of these mathematical concepts, in the context of ground water flow applications. For the level of rigor required in this discussion, the two concepts and terms can be used interchangeably.

A well-known example of equivalent hydraulic conductivity K_e is the arithmetic average K_A for flow parallel to perfect homogeneous layers. For a two-layer system:

$$K_e = K_A = fK_1 + (1-f)K_2 \equiv \overline{K} \qquad \text{Eq. 4.4-83}$$

Another widely-known example is the harmonic average K_H for flow perpendicular to layers. For two perfect layers:

$$K_e = K_H = \frac{1}{\frac{f}{K_1}+\frac{(1-f)}{K_2}} = \left(\overline{K^{-1}}\right)^{-1} \qquad \text{Eq. 4.4-84}$$

or equivalently:

$${K_e}^{-1} = {K_H}^{-1} = f{K_1}^{-1} + (1-f){K_2}^{-1} = \overline{K^{-1}} \qquad \text{Eq. 4.4-85}$$

Matheron (1967) demonstrated that effective hydraulic conductivity is bounded by the arithmetic and harmonic means (Sanchez-Vila, et.al., 2006):

$$\left(\overline{K^{-1}}\right)^{-1} \le K_e \le \overline{K} \qquad \text{Eq. 4.4-86}$$

For an isotropic, log-normal, hydraulic conductivity field in two-dimensions, the effective conductivity is the geometric mean K_G of the point values (Gutjahr, et.al., 1978):

$$K_e = K_G = exp\left[\overline{lnK}\right] \qquad \text{Eq. 4.4-87}$$

An equivalent expression is:

$$lnK_e = lnK_G = \overline{lnK} \qquad \text{Eq. 4.4-88}$$

Arithmetic, harmonic and geometric averaging are special cases of the p-norm (Ababou and Wood 1990) defined by:

$$K_e{}^p \equiv \overline{K^p} \qquad \text{Eq. 4.4-89}$$

where -1 ≤ p ≤ +1 and:

$$\begin{array}{ll} p = -1 & \text{harmonic} \\ p \to 0 & \text{geometric} \\ p = +1 & \text{arithmetic} \end{array} \qquad \text{Eq. 4.4-90}$$

While integer values correspond to well-known averages, p can also take on non-integer values. Many other examples of effective and equivalent conductivity can be found in the literature (e.g., Sanchez-Vila, et.al., 2006, Brown and Garrabrants 2017).

The concept depicted in Figure 4.4-13 is that of a sharp degradation front advancing uniformly and leaving behind fully damaged material, such that the conductivity field is binary and resides in two distinct layers of constant thickness. For this idealized construct, the arithmetic (p = +1) and harmonic (p = -1) averages are the appropriate equivalent hydraulic conductivities for parallel and perpendicular flow, respectively. However, the ideal of perfect layers and a binary conductivity field is not expected in the field. To some extent, the degradation front will advance non-uniformly and conductivity will vary more continuously between intact and fully damaged states. These non-ideal conditions will lead to a deviation from Eq. 4.4-83 and Eq. 4.4-85.

As a more realistic analog to degrading cementitious materials, consider porous-medium flow through an anisotropic, log-normal, unbounded, hydraulic conductivity field in three dimensions. Suppose the spatial correlation length is the same in directions 1 and 2 ($\lambda_1 = \lambda_2 \equiv \lambda_{12}$) and is an order of magnitude lower in direction 3 (λ_3/λ_{12} = 0.1). In the context of an SDU, directions 1 and 2 are those in the plane of a concrete barrier, and direction 3 is normal to the barrier. In terms of a p-norm, the effective conductivities for parallel and perpendicular flow correspond to $p_{12} = +0.86$ and $p_3 = -0.72$ (Gelhar and Axness 1983 [DOI: 10.1029/WR019i001p00161], Ababou and Wood 1990, Sanchez-Vila, et.al., 2006 Equations (46), WSRC-STI-2006-00198 Table 5-6). For a bounded spatial domain with relative extent L/λ = 3, Desbarats (1992) derived equivalent conductivities corresponding to $p_{12} = +0.59$ and $p_3 = -0.33$ (WSRC-STI-2006-00198, Table 5-6). Similarly, Sarris and Paleologos (2004 [DOI: 10.1007/s00477-003-0171-3]) estimated $p_{12} = +0.40$ and $p_3 = +0.05$ for L/λ = 8 (WSRC-STI-2006-00198, Table 5-6). For these examples, note that the equivalent conductivity for parallel flow lies between the arithmetic and geometric means, and closer to the arithmetic average. For perpendicular flow, K_e lies between the geometric and harmonic means, and closer to the geometric average.

Brown and Garrabrants (2017) reviewed effective conductivity literature, in the context of the SDF, and recommended for simplicity that the geometric mean define the equivalent conductivity of heterogeneous cementitious materials. Considering uncertainties, they argue that the geometric mean adequately approximates theoretical results, and data from experimental columns involving layered soils. For perpendicular flow through cementitious barriers, the geometric mean ($p \to 0$) is much higher than the harmonic average ($p = -1$) for idealized layers, and biased high compared to the above set of three analogues ($-0.72 \leq p \leq +0.05$). Based on the recommendation of Brown and Garrabrants (2017) and these additional observations, the geometric mean is adopted for equivalent hydraulic conductivity in this study as a simple and defensible assumption when facility performance is driven by flow perpendicular to barriers.

Thus, the equivalent hydraulic conductivity of a partially-degraded thickness is computed as a function of time using Eq. 4.4-82 and the expression:

$$K_e(t) = exp\left[f(t) \cdot lnK_1 + \left(1 - f(t)\right) \cdot lnK_2\right] \quad \text{Eq. 4.4-91}$$

Where K_1 and K_2 are the initial and fully degraded K values from Table 4.4-52. For simplicity, the conductivity field is assumed to be isotropic:

$$K_h(t) = K_v(t) = K_e(t) \quad \text{Eq. 4.4-92}$$

where the subscripts h and v refer to the horizontal and vertical directions, respectively.

Figure 4.4-23 and Figure 4.4-24 illustrate a hypothetical example of Eq. 4.4-91 ($p \to 0$ or geometric averaging) when $t_0 = 100$ yr, $t_1 = 900$ yr, K_1 = 1.0E-06 cm/s and K_2 = 1.0E-10 cm/s. Also plotted for reference are alternative averages using p = 1 (arithmetic), 0.5, -0.5 and -1 (harmonic).

Figure 4.4-23: Equivalent Hydraulic Conductivity Example (Semi-log)

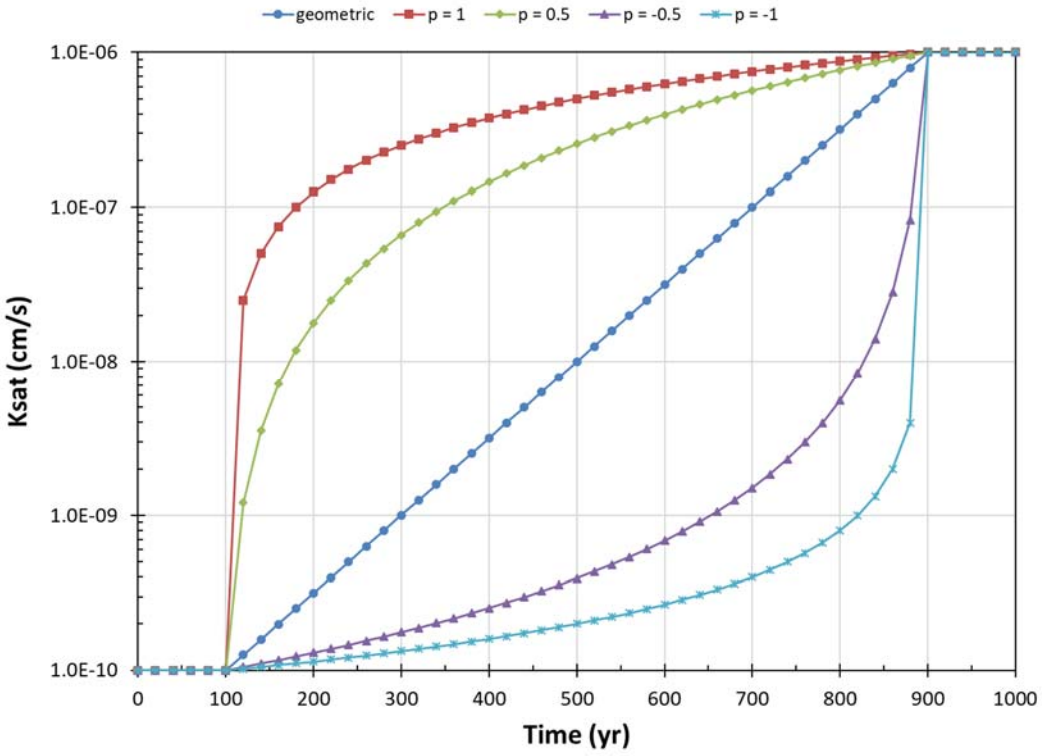

Figure 4.4-24: Equivalent Hydraulic Conductivity Example (Linear)

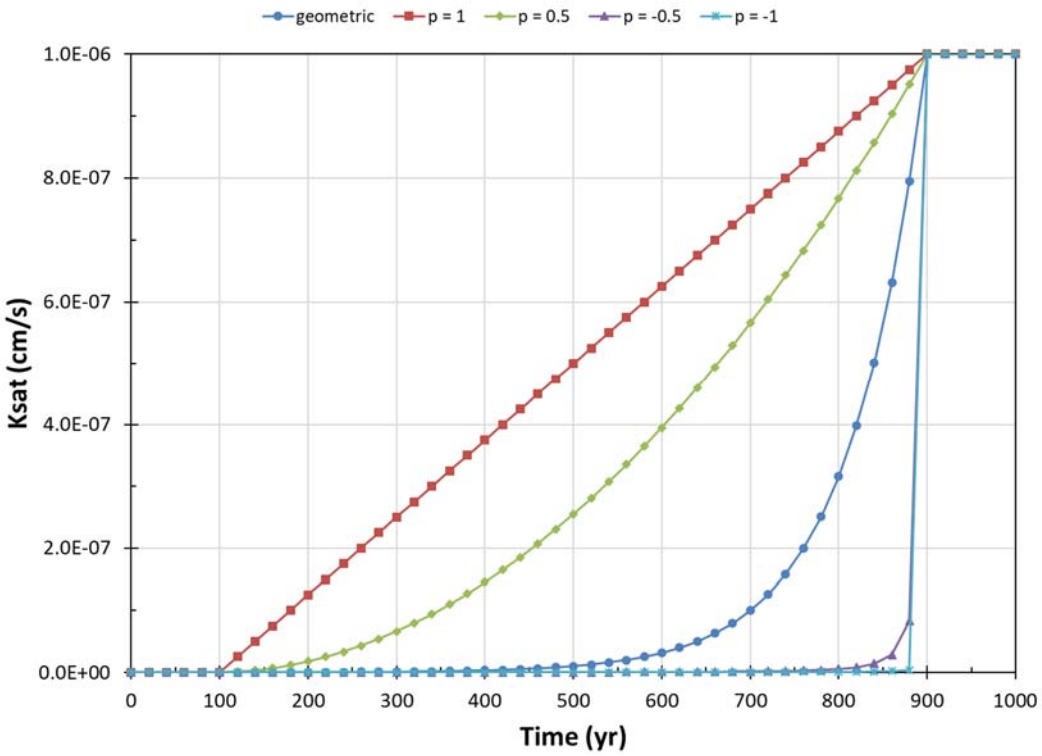

4.4.3 Contaminant Release Model

Radionuclides and chemicals within the SDU concrete and saltstone waste form have specific release and transport properties. The purpose of the Contaminant Release Model is to provide chemical transition times for saltstone and SDU concrete that can be used in the Vadose Zone Transport Model. To generate chemical transition times denoting when specific materials undergo a chemical transition (e.g., reducing to oxidizing), the Contaminant Release Model must be used in conjunction with the Vadose Zone Flow Model.

The following provides a description of the Contaminant Release Model used to develop the data needed to determine these chemical transition times.

4.4.3.1 Conceptual Model for Contaminant Release

Contaminant releases from saltstone and SDU concrete are heavily dependent on the chemical environment of the pore solution (SRNL-TR-2008-00283), wherein "pore solution" is the term that describes any liquid occupying the pore spaces within the cementitious materials. The sum of the total available pore space within the material is referred to as a "pore volume."

The chemical interactions between the pore solution chemistry and the cementitious materials (i.e., the SDU concrete and saltstone), is controlled by the chemical properties of the cementitious materials and the infiltrating water. The mineral composition of saltstone is expected to slowly change as water flows through the pores and reacts with the solid matrices.

Conceptually, this process is simulated using a pore volume exchange model (Figure 4.4-25). This conceptual model assumes that infiltrating water will enter the material (saltstone or SDU concrete) and fill the available pore spaces. Since the pore spaces are completely filled, any incoming infiltrating water will displace the existing pore solution: as flow processes continue, infiltrating water will replace the existing pore volume with a new pore volume.

Figure 4.4-25: Conceptualization of the Pore Volume Exchange Model

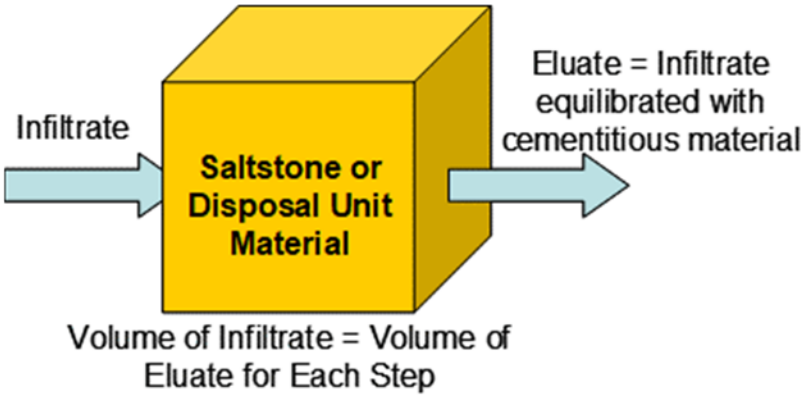

[SRNL-STI-2018-00586]

Flow rates through saltstone and SDU concrete are expected to be low. Therefore, each pore volume of infiltrate is assumed to have a residence time sufficient for the pore solution to equilibrate with the cementitious materials.

Infiltrating water entering the SDU is assumed to be saturated with respect to dissolved oxygen. Reducing agents within the saltstone or the SDU concrete will be consumed by this oxygen as it enters the system. As such, the material will have relatively low oxygen content until the cumulative oxygen ingress exceeds the reducing capacity of the material, defined as the ability of a substance to reduce a given mass of oxidant, expressed in units of reducing equivalents of electrons per mass of a substance (μeq e^-/g). In laboratory studies, the oxidation potential (Eh) is measured in millivolts (mV), which can be positive to indicate an oxidizing chemical environment or negative to indicate a reducing chemical environment. For the PA, this is simulated as a step change from reducing to oxidizing once the reducing capacity has been exceeded (see Section 4.4.3.1.1).

As acidic infiltrate dissolves cementitious minerals present in the saltstone matrix, the pH of the saltstone pore solution will decrease. Transitions from one pH region to the next are a function of the amount of specific constituents, such as calcium silicate hydrate (CSH) and/or calcium hydroxide ($Ca(OH)_2$), available within the material. The availabilities of these constituents are expected to evolve over time as the constituents are leached. As with the Eh transitions, the PA also simulates the pH transitions as step changes from Region I to Region II to Region III to Region IV (see Section 4.4.3.1.2).

Collectively, the chemical evolution of the pore solution in saltstone is expected to be:

Reducing Region I → Reducing Region II → Reducing Region III → Oxidizing Region III → Oxidizing Region IV

However, recent saltstone studies indicate that Reducing Region II may be relatively short-lived (SRRA099188-000005, SRNL-STI-2018-00586), such that skipping this stage yields results that are more representative of the theoretical and laboratory studies. As such, this PA simulates the chemical evolution of saltstone as:

Reducing Region I → Reducing Region III → Oxidizing Region III → Oxidizing Region IV

The basis for this evolution is described in greater detail below.

A similar chemical evolution shall be assumed for SDU concretes that have significant reducing agents:

Reducing Region I → Reducing Region III → Oxidizing Region III → Oxidizing Region IV

For any cementitious material without significant reducing agents, the evolution would assume that the material is initially oxidizing:

Oxidizing Region I → Oxidizing Region III → Oxidizing Region IV

Most radionuclides are relatively immobile within the initially high pH and low Eh environment of the pore water in saltstone. Over time, infiltrating water is expected to change the chemistry of the pore solution, eventually coming to an equilibrium state with the natural environment (lower pH and higher Eh). As the chemical environment transitions, the release rates for specific constituents will also transition (see 4.4.3.1.3).

4.4.3.1.1 Oxidation Potential

The reducing properties of saltstone have been attributed to the sulfide content present in blast furnace slag (BFS). [VSL-14R2890-1, SRNL-TR-2008-00283] This reducing environment allows for immobilization of redox sensitive contaminants such as Tc, which spectroscopic evidence indicates forms a hydrated oxide ($TcO_2 \cdot xH_2O$) and/or sulfide (TcS_x) solid phase (Liu, et.al., 2007, Liu, et.al., 2009, Lukens, et.al., 2005).

Reducing materials will transition to oxidizing with exposure to dissolved oxygen in the infiltrate, thus increasing Eh over time (see Figure 4.4-26). The Eh transitions may be calculated based on the initial reducing capacity of the materials and how that composition changes as a function of pore volume "exchange cycles" as oxidized water moves through the pores (i.e., "pore flushes"). [SRNL-TR-2008-00283, SRR-CWDA-2011-00044]

Figure 4.4-26: Evolution of Pore Solution Eh in Cementitious Materials

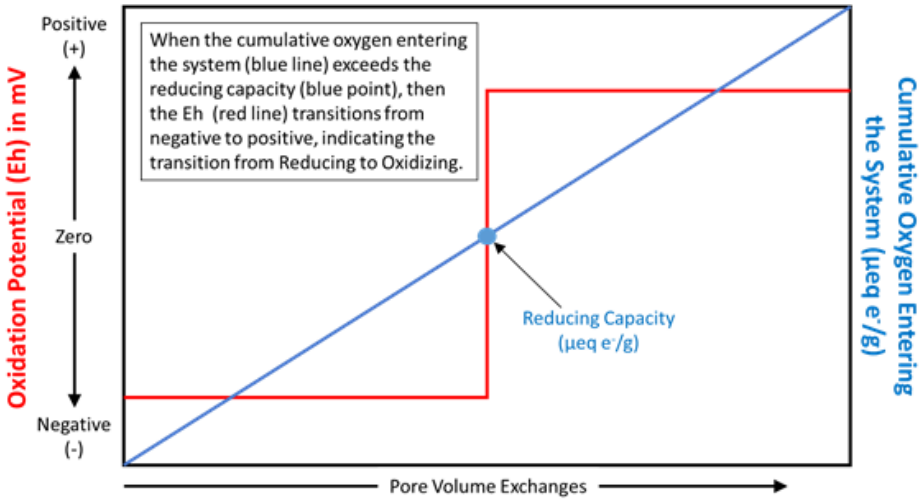

In addition to the saltstone, the high-quality SDU concrete (roof, floor, and walls) also includes BFS for the purposes of improving (decreasing) the hydraulic conductivity of the concrete. This BFS is also credited for functioning as a reducing agent.

The reduction capacity for both saltstone and the SDU concrete is accounted for using the mineral pyrrhotite (FeS) which is consumed by incoming oxygen via Eq. 4.4-93 (SRNL-STI-2018-00586).

$$FeS_{2(s)} + 2O_{2(aq)} \leftrightarrow Fe^{2+} + SO_4^{2-} \quad \text{Eq. 4.4-93}$$

Eight (8) electron equivalents are transferred for every mole of pyrrhotite oxidized, which equates to 91,000 micro equivalents of electrons per gram (μeq e^-/g) of FeS (SRNL-STI-2018-00586).

4.4.3.1.2 pH Environments

Transitions from one pH region to the next are a function of the amount of specific constituents, such as CSH and/or calcium hydroxide ($Ca(OH)_2$), available within the material. The availabilities of these constituents are expected to evolve over time as the constituents are leached from the material.

As acidic infiltrate dissolves cementitious minerals present in the saltstone matrix, the pH of the saltstone pore solution will decrease. This is important because changes in pH can alter the release behavior of contaminants present in saltstone by changing their solubility and sorption properties. Examination of the theoretical solubility curves for technetium (Tc) can be used to demonstrate the effects that changes in pH can have on contaminant solubility (see Section 4.4.3.3.4). Additionally, changes in pH will alter aqueous speciation of contaminants in the pore solution as well as the surface charge of the solid phase (e.g., saltstone), both of which will influence contaminant sorption.

The conceptual model described by Bradbury and Sarott (PIT-MISC-0075), and expanded upon by Ochs, et.al., (2016), has been adopted for this SDF PA to describe how saltstone and SDU concrete pore solution pH evolves over time. For describing the evolution of cementitious materials, the pore solution is categorized into four distinct pH regions (Figure 4.4-27). Each region is described below.

Figure 4.4-27: Evolution of Pore Solution pH in Cementitious Materials

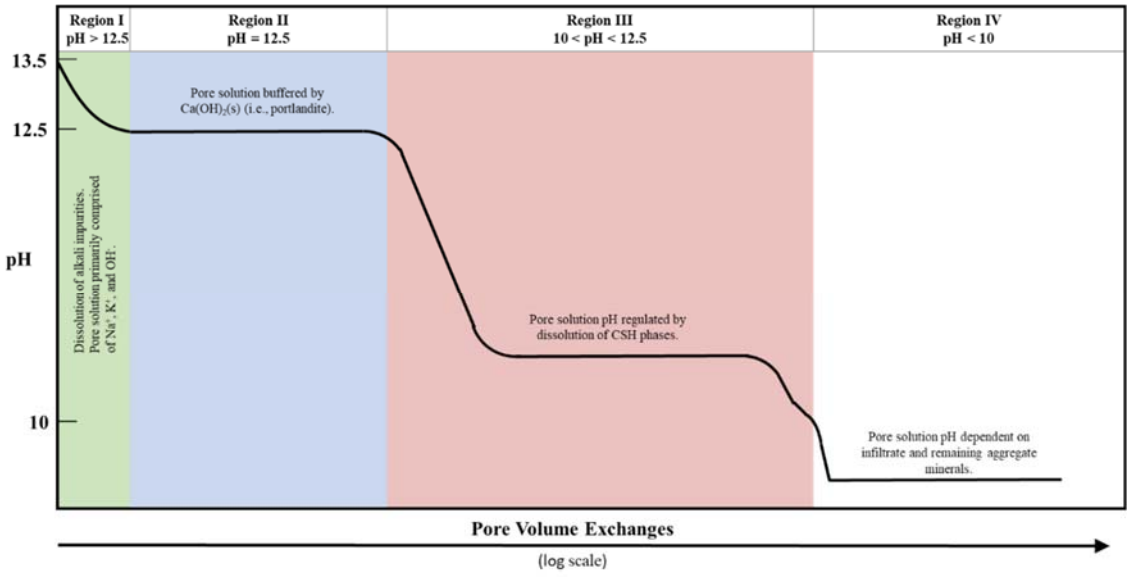

[Figure 2.1 in Ochs, et.al., (2016)]

Region I (pH > 12.5)

Region I is characterized as a high pH (> 12.5), high ionic strength pore solution, comprised primarily of Na^+, K^+, and OH^- ions. [Ochs, et.al., (2016)] The high concentrations of Na^+ and K^+ result from the dissolution of alkali impurities present in the raw ingredients (e.g., Ordinary Portland Cement, BFS, fly ash, and aggregate) that the cementitious material is comprised of. [SRNL-STI-2009-00473] The pH in Region I is controlled by the dissolution of these impurities. [Ochs, et.al., (2016)] Region I is estimated to last between 1 and 100 pore volume exchanges (Berner (1992)) and is sometimes referred to as the "young" stage.

Region II (pH = 12.5)

Once the alkali ions have been flushed from the system (i.e., end of Region I), the pore solution is buffered at a pH of approximately 12.5, controlled by the solubility of $Ca(OH)_2$ (i.e., portlandite). The pore solution composition is analogous to a 0.020 M calcium hydroxide solution. [Ochs, et.al., (2016)] The duration of Region II, colloquially referred to as the "moderately-aged" or "middle-aged" stage, is dependent upon the amount of cement/portlandite present in the structure and has been estimated to last between 100 and 1,000 pore volume exchanges. [Berner (1992)]

Region III (12.5 > pH > 10)

Following the complete dissolution of portlandite (i.e., end of Region II), the pH of the pore solution is controlled by incongruent dissolution of CSH phases. At the start of Region III, referred to as the "aged" stage, the CSH phases present have a Ca/Si ratio of approximately 1.7 (SRNL-STI-2009-00473). Once the CSH begins to dissolve, the Ca/Si ratio of the CSH, as well as the pH of the pore solution, begin to drop. The end of Region III is marked by congruent dissolution of the remaining CSH that results in a pore solution with pH ~10. [Ochs, et.al., (2016)]

Region IV (pH < 10)

Following the complete dissolution of CSH and other hydrated cement components, the pore solution's pH drops below 10 and approaches the pH of the infiltrate. Any further changes to the pore solution chemistry is dependent upon the aggregate minerals still present in the aged cementitious material and the infiltrating water. [Ochs, et.al., (2016)]

4.4.3.1.3 Contaminant Transport Mechanisms

A contaminant's release and transport through the saltstone matrix is controlled via its solubility and sorption properties. With the notable exception of reduced technetium (Tc), all the contaminants present in the saltstone waste form are assumed to be completely soluble (i.e., once contaminants are mobilized they are readily transported and do not precipitate out of solution). Since the contaminants are soluble, their transport is controlled by their sorption properties. For the

purposes of the PA, sorption is a broad term encompassing "all processes that remove solutes from the aqueous phase" (SRNL-STI-2009-00473) such as adsorption, absorption, and co-precipitation.

The K_d construct is used here to quantify all sorption phenomena occurring in the system. The K_d is simply a concentration ratio of contaminant sorbed to the solid phase versus contaminant present in solution (Eq. 4.4-94).

$$K_d = \frac{C_{solid}}{C_{liquid}} \qquad \text{Eq. 4.4-94}$$

where:

K_d = the partition coefficient (volume of aqueous phase per mass of solid phase),

C_{solid} = the concentration of the contaminant sorbed to the solid phase (mass of contaminant per mass of solid phase), and

C_{liquid} = concentration of the contaminant in solution (mass of contaminant per volume of aqueous phase).

4.4.3.2 Implementation of the Contaminant Release Model

To implement the conceptual model for contaminant release from saltstone described in Section 4.4.3.1, a reaction path model capable of simulating aqueous geochemical processes in multiphase environments was developed using The Geochemist's Workbench® (GWB) Professional 10.0.10. [SRNL-STI-2018-00586] Using the software's **React** application, the reaction path model was carried out in "flush" mode. This approach is equivalent to the conceptualization depicted in Figure 4.4-25, "where an entering reactant fluid displaces an equal volume of existing equilibrated fluid from the system. A flush model is traced from the frame of reference of the porous "rock" matrix through which the aqueous fluid migrates." [SRNL-STI-2018-00586]

Figure 4.4-28 illustrates the "Apps" homepage for the GWB Professional 10.0.10 software where the React application is selected as well as several graphical user interfaces where inputs for the model are entered.

For all SDUs, the saltstone waste form is enclosed in a concrete barrier (see Section 4.4.4), hence, contaminants that leach from the saltstone matrix will have to traverse through SDU concrete prior to their release into the environment. Therefore, it is necessary to know the evolving pore solution chemistry of not only the saltstone waste form but also the SDU concrete. Consequently, two different types of porous media were simulated in the GWB reaction path model: saltstone and SDU concrete. Note that the term "SDU concrete" used here is synonymous with "SDU 2/6/7 concrete" used in SRNL-STI-2018-00586.

Figure 4.4-28: GWB Professional 10.0.10 User Interface

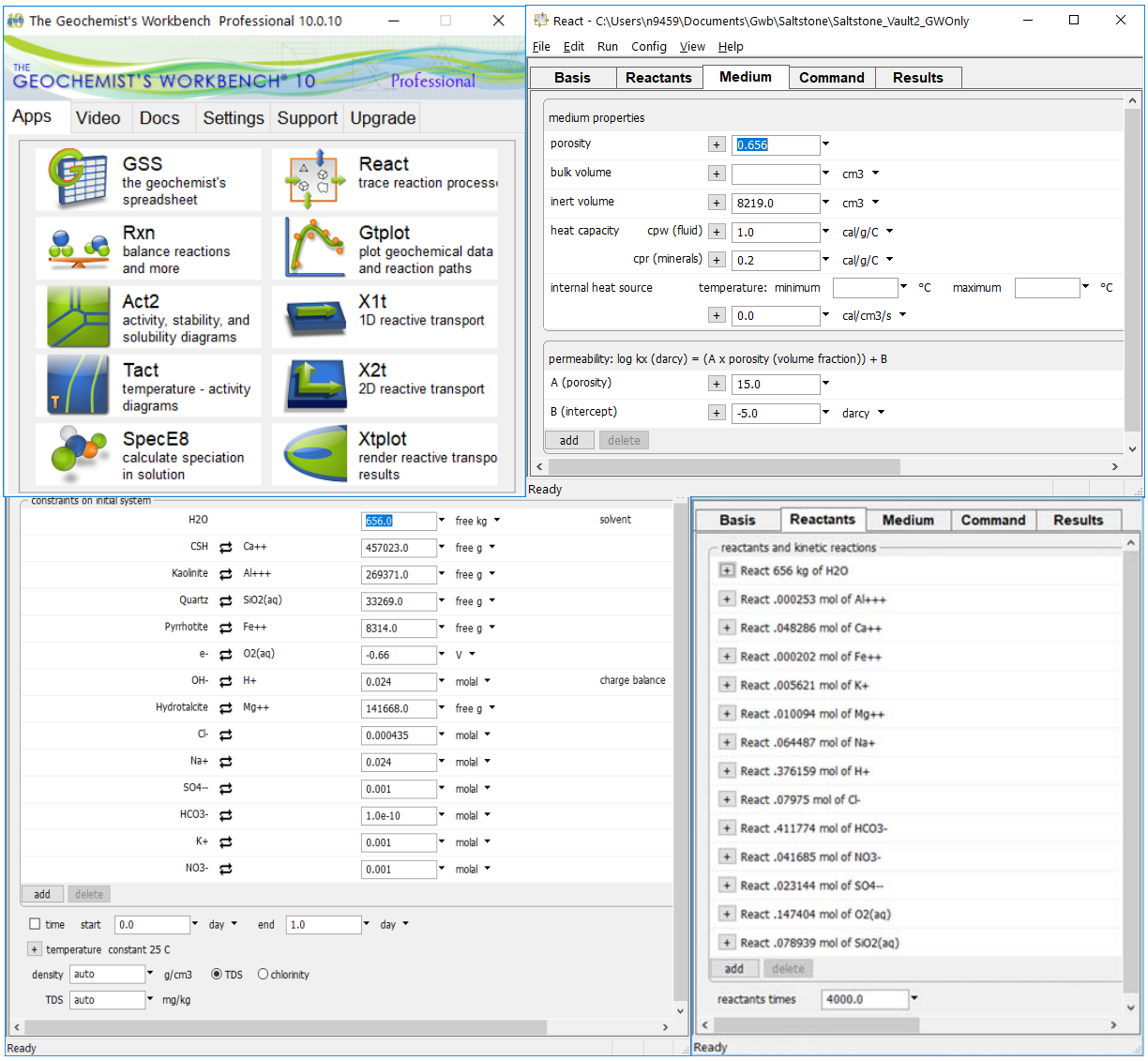

[SRNL-STI-2018-00586]

It is important to note that the GWB reaction path model, herein referred to as the Contaminant Release Model, assumes that each pore volume of infiltrate that enters the cementitious material equilibrates with the porous media prior to its expulsion by an incoming pore volume of infiltrate (Figure 4.4-25). All dissolved ions present in the pore solution after equilibration with the cementitious material are assumed to be carried off with the exiting pore volume. Hence, the readily dissolved salts initially present in the saltstone and SDU concrete are flushed out with the first pore volume, thereby avoiding the need for a less accurate high ionic strength activity coefficient model. [SRNL-STI-2018-00586]

For flush simulations in the Contaminant Release Model, a ground water composition provided in SRNL-L3200-2012-00022 was employed as the baseline infiltrating solution. Infiltrate coming into contact with saltstone will have to first pass through the SDU

concrete. Therefore, two additional infiltrate scenarios were considered for the saltstone reaction path model: ground water equilibrated with excess calcite present in oxidizing Region IV concrete (Figure 4.4-27), and ground water equilibrated with excess CSH present in oxidizing Region II concrete (Figure 4.4-27). Table 4.4-53 provides a summary of the GWB reaction path model scenarios used for PA analysis. It should be noted that all infiltrating solutions used in the Contaminant Release Model are saturated with dissolved oxygen.

Table 4.4-53: Summary of Scenarios Considered for the Contaminant Release Model

Material	Infiltrate		
	Ground Water	Ground Water Equilibrated with Oxidizing Region IV Concrete	Ground Water Equilibrated with Oxidizing Region II Concrete
Saltstone	X	X	X
SDU Concrete	X		

X denotes that the scenario was modeled
All infiltrate solutions are modeled as being saturated with dissolved oxygen.

As a simplifying assumption, the chemical transitions predicted from the "Ground Water Equilibrated with Oxidizing Region II Concrete" scenario presented in Table 4.4-53 were not used (i.e., Eh transition occurs later and there is no pH transition from Region III to Region IV). Additionally, after running the different scenarios, it was noted that the first two saltstone scenarios (i.e., the "Ground Water" infiltrate scenario and the "Ground Water Equilibrated with Oxidizing Region IV Concrete" infiltrate scenario) both yielded the same transition times. [SRNL-STI-2018-00586] As such, the results presented in Section 4.4.3.4.1 are all based on the "Ground Water Equilibrated with Oxidizing Region IV Concrete" infiltrate scenario.

4.4.3.3 Contaminant Release Model Inputs and Assumptions

The following describes the primary inputs and assumptions that apply to the Contaminant Release Model.

4.4.3.3.1 Reducing Capacity

Reductants, or reducing agents, are chemical constituents within a material that can slow or influence the release or transport of contaminants from within the material. As oxygenated infiltrate flows through the material (i.e., SDU concrete or saltstone), the reducing agents will be consumed by oxygen until all of the reducing agents have been exhausted (this threshold is known as the "reducing capacity"). Once the cumulative ingress of oxygen exceeds the reduction capacity, the concrete or saltstone transitions from a reducing chemical environment to an oxidizing chemical environment.

In the previous SDF PA (SRR-CWDA-2009-00017) saltstone was assigned an assumed reducing capacity of 822 μeq e^-/g based on calculations in *Saltstone and Concrete Interactions with Radionuclides: Sorption (K_d), Desorption, and Reduction*

Capacity Measurements (SRNS-STI-2008-00045). Subsequent SDF SAs (SRR-CWDA-2013-00062, SRR-CWDA-2014-00006, and SRR-CWDA-2016-00072) assumed a value for saltstone reduction capacity of 607 μeq e^-/g based on additional experimental measurement. [SRNL-STI-2009-00637]

Since then, an additional study conducted by the Savannah River Ecology Laboratory (SREL) measured the reduction capacity for saltstone simulants using multiple test methods. [SREL-R-14-0006] Consideration of this experimental data in addition to data from two other studies (SRNL-STI-2009-00637, SREL-R-16-0003) led to a new recommended reduction capacity value for saltstone (Table 4.4-54). [SRR-CWDA-2018-00048] Using a similar approach, consideration of reduction capacity values measured on SDU 2 concrete simulant (SRNS-STI-2008-00045, SRNL-STI-2009-00637) led to the recommended values for SDU concrete presented in Table 4.4-54. [SRNL-STI-2018-00586]

Table 4.4-54: Recommended Reducing Capacities for Saltstone and SDU Concrete

Solid Type	Pessimistic Case (μeq e^-/g)	Compliance Case (μeq e^-/g)	Realistic Case (μeq e^-/g)
Saltstone	350	500	650
SDU 2/6/7 Concrete	178	209	239

[SRNL-STI-2018-00586]

4.4.3.3.2 Saltstone and SDU Concrete Mineralogy

Dry mix recipes for saltstone and SDU concrete (i.e., percentage of BFS, fly ash, cement, and inert materials) were used in conjunction with the chemical composition of the dry feed materials to generate a dry mix chemical composition for both saltstone and SDU concrete. [SRNL-STI-2018-00586] Hydration products were assigned to each of the oxide minerals that make up the dry chemical composition of saltstone and SDU concrete. This process resulted in a proposed hydrated mineralogy for both saltstone and SDU concrete (Table 4.4-55).

Table 4.4-55: Mineralogical Compositions of Saltstone and SDU Concrete used in the Contaminant Release Model

Hydrated Mineral	Saltstone Composition (g/m^3)			SDU Concrete Composition(g/m^3)		
	Pessimistic Case	Compliance Case	Realistic Case	Pessimistic Case	Compliance Case	Realistic Case
$CaSiO_3 \cdot H_2O$ (CSH)	458,921	457,972	457,023	347,233	347,114	346,999
$Mg_4Al_2O_7 \cdot 10(H_2O)$ (Hydrotalcite)	142,256	141,962	141,668	66,965	66,942	66,920
$Al_2Si_2O_5(OH)_4$ (Kaolinite)	270,490	269,930	269,371	0	0	0
$Al(OH)_3$ (Gibbsite)	0	0	0	49,546	49,529	49,512
SiO_2 (Quartz)	33,407	33,338	33,269	18,869	18,862	18,856
FeS (Pyrrhotite)	4,477	6,395	8,314	4,264	5,007	5,725
Total GWB Inerts	22,356	22,403	22,449	1,693,124	1,692,546	1,691,987
Total GWB Solids	932,000	932,000	932,000	2,180,000	2,180,000	2,180,000

[SRNL-STI-2018-00586]

The reduction capacity for both saltstone and SDU concrete was accounted for using the mineral pyrrhotite (FeS), which is consumed by incoming oxygen via Eq. 4.4-93. The derived mineralogy for each material was compared to X-ray Diffraction (XRD) data collected for cementitious materials (SRNL-STI-2014-00397) to ensure its validity.

4.4.3.3.3 K_d Assumptions for Vadose Zone Transport Model

As mentioned in Section 4.4.3.1.1, aside from reduced Tc, all contaminants present in the saltstone waste form are assumed to be completely soluble. Therefore, any change in pore solution chemistry will only affect the contaminant's sorption behavior, which is simulated in the Vadose Zone Transport Model using a K_d. The K_d values used in the SDF PA for saltstone and SDU concrete under various chemical environments are presented in Table 4.3-5. As a modeling simplification, cementitious K_d values reported for Region III conditions are also assumed for Region IV (note that there are no cementitious K_d values available in Table 4.3-5 for Region IV conditions).

While the chemical transition from Region III to Region IV does not change the K_d values used to model sorption to cementitious materials, it is assumed to impact the K_d values of the underlying sand and clay regions. Compared to Regions I through III, the cementitious pore water chemistry in Region IV much more closely reflects that of SRS ground water. [WSRC-STI-2007-00544, SRNL-STI-2009-00473] Hence, the chemical transition from Region III to Region IV is thought to signal the end of leachate impacted sand and clay regions present underneath the SDUs. Therefore, once Region IV conditions are reached in the saltstone and SDU concrete, the Vadose Zone Transport Model switches from leachate impacted to non-leachate impacted sand and clay K_ds (Table 4.3-4).

4.4.3.3.4 Technetium Release in Oxidizing Environments

Figure 4.4-29 shows recent experimental data collected using a Dynamic Leaching Method (DLM) to push pore solution through samples of saltstone (both Tc-99 spiked synthetic samples and actual field-emplaced samples from SDU 2A). In addition to the solubility-controlled concentration measurements, this figure also depicts the theoretical solubility curves for solid phases of **$TcO_2 \cdot 1.6(H_2O)$** (in brown) and **$TcO_2 \cdot 2(H_2O)$** (in black) at Eh values of -200 mV (dashed lines) and -400 mV (solid lines). This data suggests that under reducing conditions, Tc release from saltstone is solubility-controlled by one or more hydrated Tc(IV)-oxide solid phases ($TcO_2 \cdot x(H_2O)$). This DLM data (SRRA099188-000005) was considered during the development of the recommended technetium solubility limits (see 4.3.2.3).

Figure 4.4-29: Tc-99 DLM Effluent Data as a Function of pH Compared with Theoretical Solubility Curves

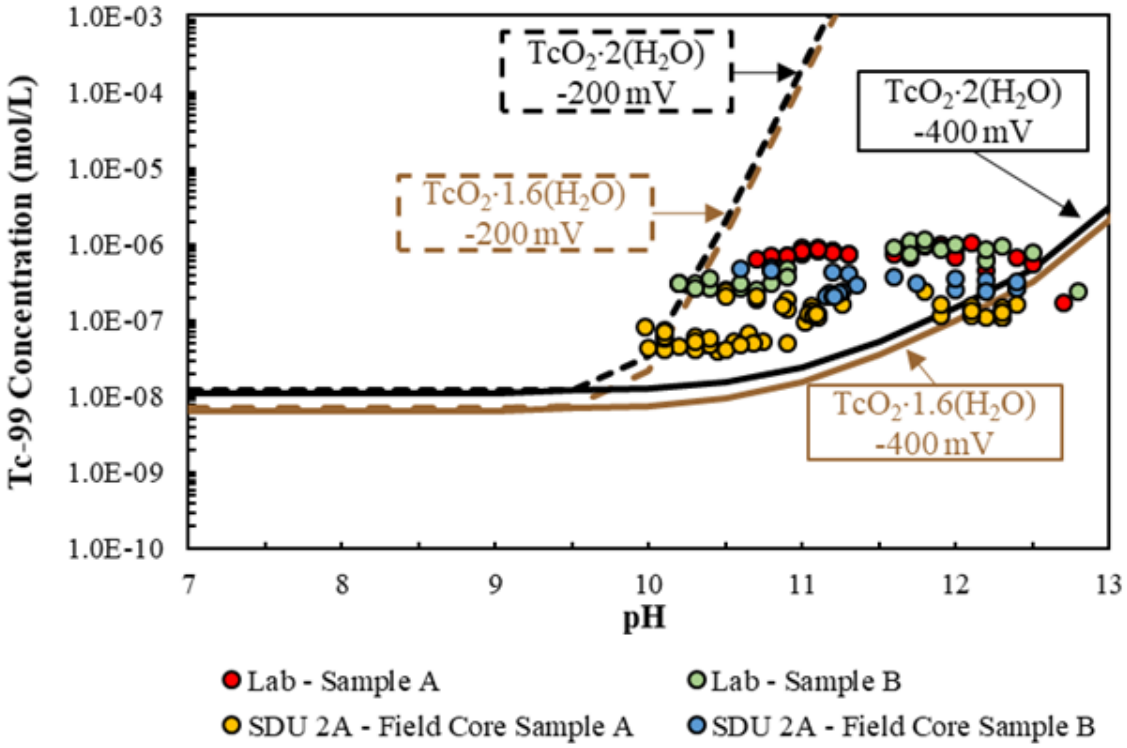

[SRRA099188-000005]

As oxygenated infiltrate flows through the saltstone matrix, the reducing capacity of the saltstone will be exhausted. Once the reducing capacity is exhausted, previously reduced species present in the saltstone will become oxidizing and their transport properties will be altered. This chemical transition drives the Tc release rate within the saltstone. The reduced Tc(IV) species present in Tc-oxide and/or Tc-sulfide solid phase(s) are thought to oxidize to Tc(VII), forming the highly soluble pertechnetate (TcO_4^-) ion. [SRNL-STI-2010-00668] Once oxidized, Tc release from saltstone is K_d controlled.

4.4.3.4 Intermediate Results and Interfaces for the Contaminant Release Model

The Contaminant Release Model estimates the number of pore volume exchanges required for the pore solution chemistry to change. The rates of volumetric flow, as determined in the Vadose Zone Flow Model (Section 4.4.4), are then used to convert the number of pore volume exchanges into time.

The following presents intermediate results from the Contaminant Release Model and specifies interfaces between the Contaminant Release Model and other models used in the SDF PA.

4.4.3.4.1 Contaminant Release Model Results

Based on the derived mineralogy for saltstone and SDU concrete (Table 4.4-55), the different infiltrates considered (Table 4.4-53), and the reduction capacities (Table 4.4-54), the Contaminant Release Model was able to estimate the number of pore volume exchanges necessary to change the pore solution chemistries for saltstone (Table 4.4-56) and SDU concrete (Table 4.4-57). Figure 4.4-30 and Figure 4.4-31 provide visual representations of these saltstone transitions. Similarly, Figure 4.4-33 and Figure 4.4-34 provide a visual representation of these SDU concrete transitions.

Table 4.4-56: Cumulative Pore Volume Exchanges Needed for Saltstone Chemical Transitions in the Contaminant Release Model

Saltstone Chemical Transitions	Cumulative Pore Volume Exchanges		
	Pessimistic Case	Compliance Case	Realistic Case
Eh: Initial Condition* to Oxidizing	600	850	1,100
pH: Initial Condition* to Region III	6**	6**	6**
pH: Initial Condition* to Region IV	1,410	1,400	1,390

[Adapted from Tables 3-1 and 3-2 in SRNL-STI-2018-00586]

*In the Contaminant Release Model, the initial condition of the saltstone pore solution is reducing (Eh = -660 mV) and in Region I (pH 11.8).

** While these results show the saltstone transition from Reducing Region I to Reducing Region III occurs at 6 pore volume exchanges, a simplifying assumption was made in the Vadose Zone Transport Model that this transition occurs after only a single pore volume. The exception to this approach is Tc-99 which transitions at 6 pore volumes, as discussed in Section 4.4.3.4.2.

Table 4.4-57: Cumulative Pore Volume Exchanges Needed for SDU Concrete Chemical Transitions in the Contaminant Release Model

SDU Concrete Chemical Transitions	Cumulative Pore Volume Exchanges		
	Pessimistic Case	Compliance Case	Realistic Case
Eh: Initial Condition* to Oxidizing	3,415	4,000	4,570
pH: Initial Condition* to Region IV	7,610	7,590	7,570

[Adapted from Tables 3-1 and 3-2 in SRNL-STI-2018-00586]

*In the Contaminant Release Model, the initial condition of the SDU Concrete pore solution is reducing (Eh = -660 mV) and in Region III (pH 11.1). For the Vadose Zone Transport Model, a simplifying assumption was made that the SDU concrete starts in Region I and transitions to Region III after one pore volume exchange. The exception to this approach is Tc-99 which transitions at 6 pore volumes, as discussed in Section 4.4.3.4.2.

Note that the early pH transition (from Reducing Region I to Reducing Region III) shown in Figure 4.4-31 happens relatively quickly. Figure 4.4-32 presents this transition at a closer scale to provide additional insight.

Figure 4.4-30: Saltstone Eh Evolution Using the Contaminant Release Model

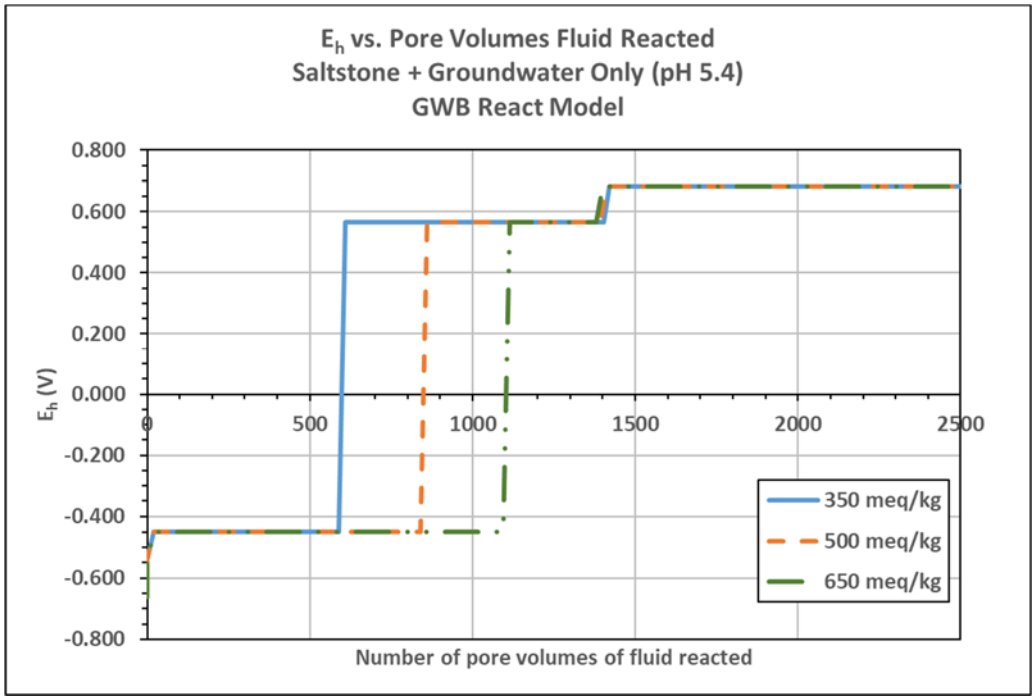

[SRNL-STI-2018-00586]

Figure 4.4-31: Saltstone pH Evolution Using the Contaminant Release Model

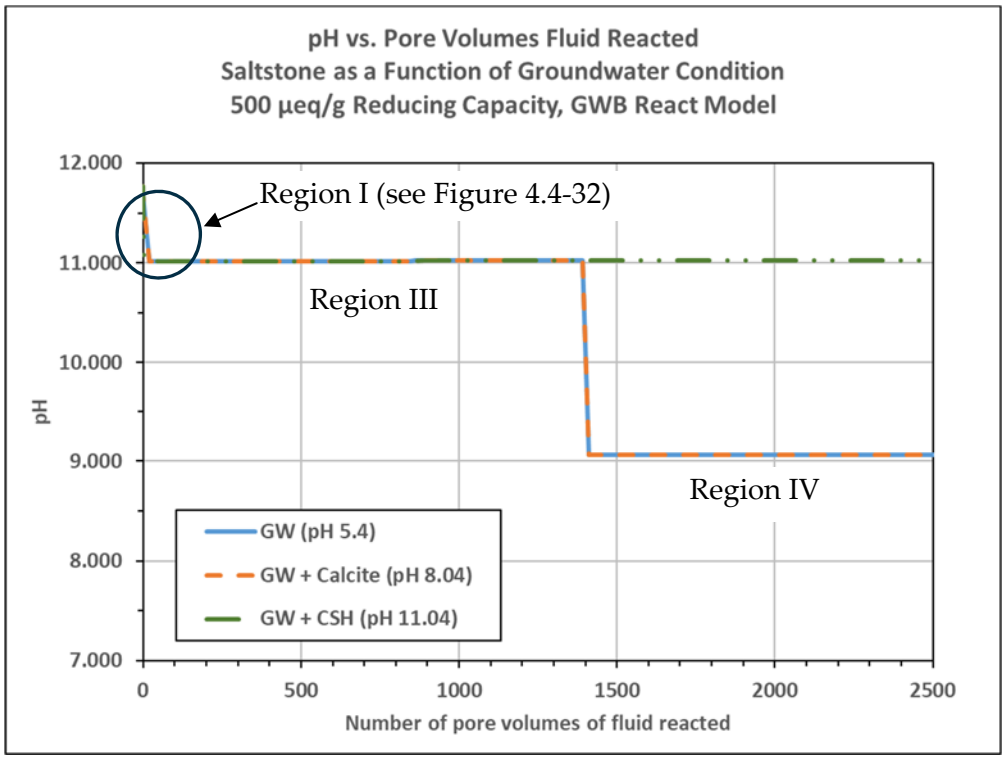

[SRNL-STI-2018-00586]

Figure 4.4-32: Saltstone pH Evolution for the First Ten Pore Volumes Using the Contaminant Release Model

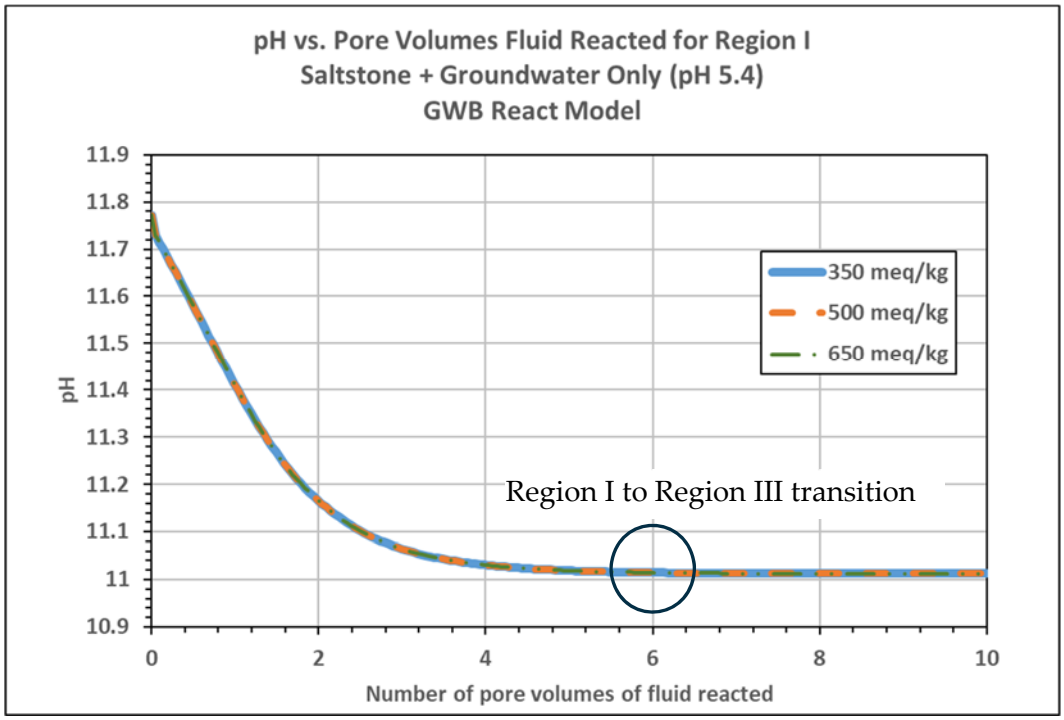

[SRNL-STI-2018-00586]

Figure 4.4-33: SDU Concrete Eh Evolution Using the Contaminant Release Model

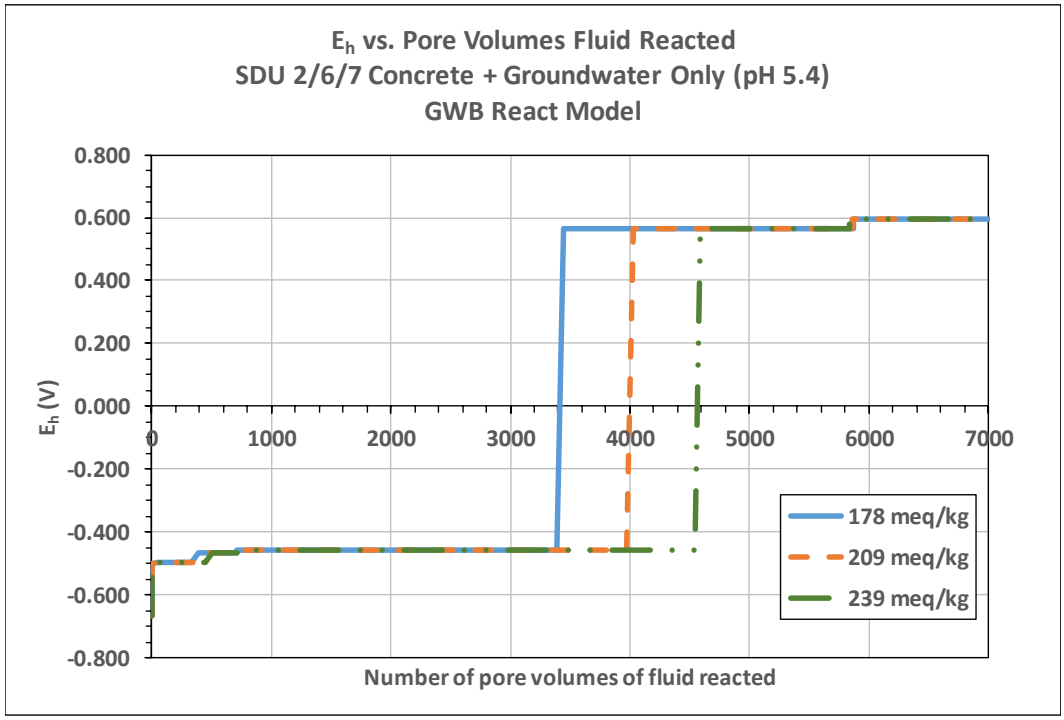

[SRNL-STI-2018-00586]

Figure 4.4-34: SDU Concrete pH Evolution Using the Contaminant Release Model

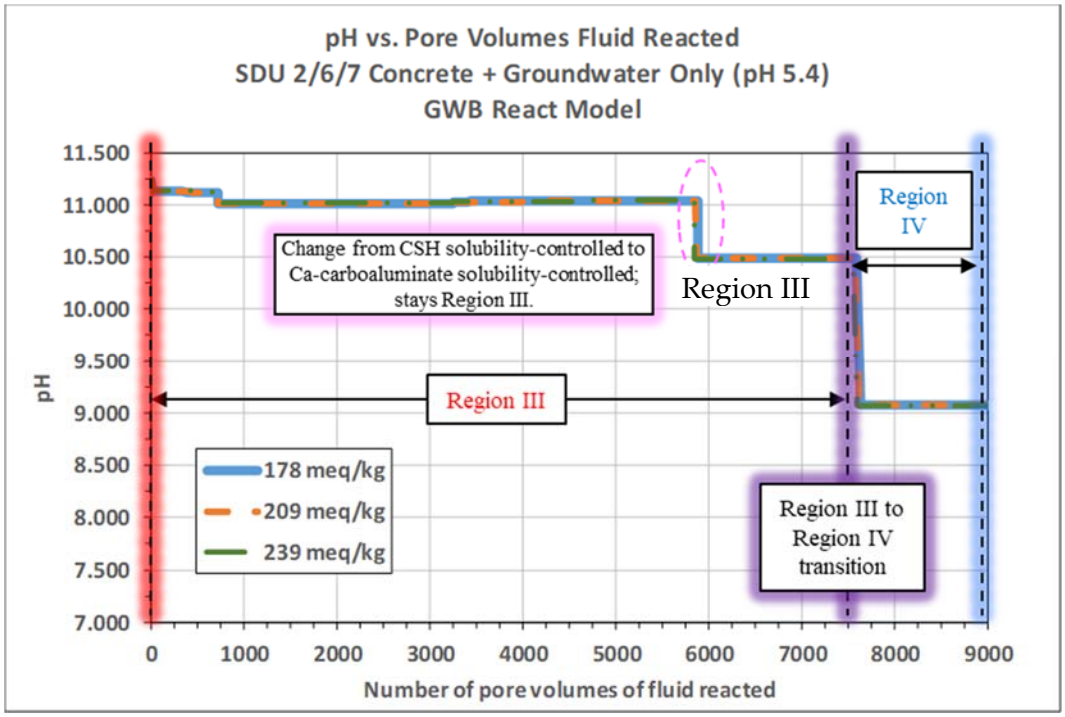

[SRNL-STI-2018-00586]

Validation of Early Saltstone Transitions

Recent leachate data from DLM experiments conducted on simulant and actual saltstone cores (SRRA099188-000005) is presented in Figure 4.4-35. Consistent with the results of the Contaminant Release Model, these DLM experiments demonstrate that the saltstone pore solution starts in Region I before quickly transitioning either briefly to Region II or directly into Region III. The brevity of Region II is expected given that the Ca/Si ratio is less than one. [SRNL-STI-2018-00586] To summarize, the DLM experimental data supports the findings of the Contaminant Release Model (Table 4.4-56).

4.4.3.4.2 Implementation of Contaminant Release Model Results into the SDF PA

In the Vadose Zone Flow Model, the cementitious materials that make up each SDU are modeled as distinct material zones (e.g., lower mud mat, upper mud mat, floor, wall, etc.). While the Vadose Zone Flow Model is running, the number of pore volumes that have passed through a given material zone (i.e., pore volume exchanges) is recorded. As such, the pore volume of each zone is a function of the volume of the given zone and porosity of the material.

For each material zone, the pore volume exchanges are recorded based on the volumetric flow rates from the Vadose Zone Flow Model and then they are compared with the results of the Contaminant Release Model. This comparison

yields chemical transition times for each material zone which can then be used by the Vadose Zone Transport Model to apply appropriate transport properties based on these modeled chemical transitions. Effectively, the chemical transition times function as triggers within the Vadose Zone Transport Model, changing the transport properties of each contaminant in a given material zone to correspond to the predicted pore solution chemistry.

While the Contaminant Release Model shows the saltstone transition from Reducing Region I to Reducing Region III occurs at 6 pore volume exchanges (see Table 4.4-56), a simplifying assumption was made that this transition occurs after only a single pore volume. The exception to this approach is Tc-99, as discussed below.

Since Tc-99 and I-129 releases are modeled in greater detail than the other contaminants, additional discussions on Tc-99 and I-129 releases are included below. For clarity, all species other species will be referred to collectively as "generic" species.

Tc-99 Release Modeling

While in a chemically reducing environment, Tc release from saltstone is solubility controlled. As described in Section 4.3.2.3 and provided in Table 4.3-8, the solubility limit for reduced Tc was developed based on recent DLM experimental data using a GoldSim optimization model. [SRR-CWDA-2018-00046, SRRA099188-000005] The applicability of these Tc solubility values is pH-dependent.

Specifically, technetium's solubility is expected to decrease once the pH of the reducing pore solution drops below 11. Since pH is not explicitly simulated in the Vadose Zone Transport Model, the number of pore volume exchanges necessary to drive the saltstone pH below 11 was determined based on available data from DLM experiments conducted on SDU 2A cores. Consistent with the data presented in Figure 4.4-35, it was estimated that six pore volume exchanges were necessary to drive the saltstone pH below 11. This value was then applied to both saltstone and SDU concrete.

Due to its importance as a dose contributor in the SDF (SRR-CWDA-2009-00017, SRR-CWDA-2013-00062, SRR-CWDA-2014-00006, SRR-CWDA-2016-00072), the release of Tc-99 release is modeled in a more sophisticated manner than the generic species for the Vadose Zone Transport Model. The oxidation state of saltstone is simulated using a shrinking core model of slag oxidation (based on WSRC-RP-2003-00362 and updated in SRNL-STI-2013-00280, SRNL-STI-2014-00083, SRNL-STI-2018-00652, and in Section 4.4.5.2).

Figure 4.4-35: Applied Evolution of Saltstone Pore Solution Chemistry

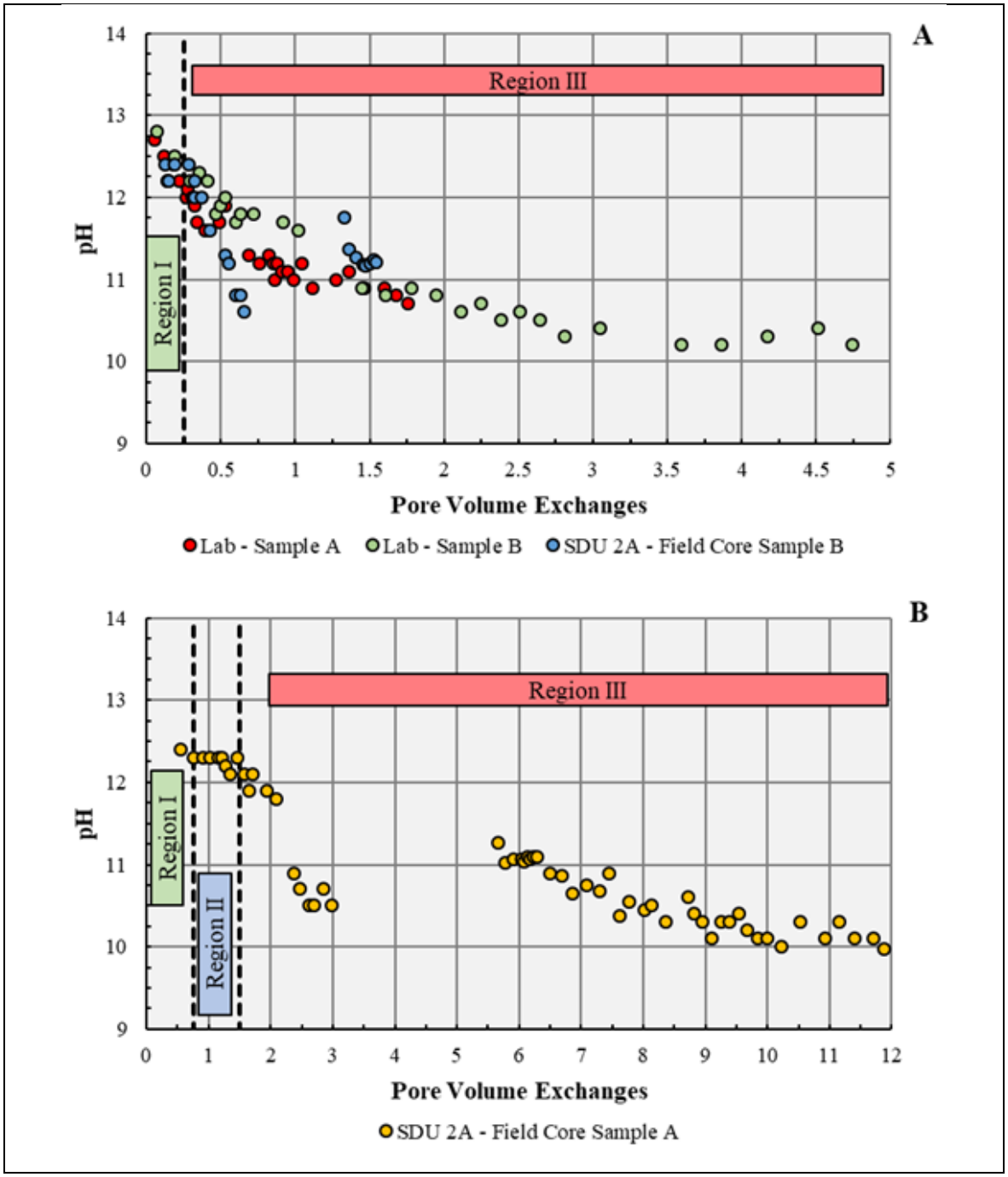

Applies the Conceptual Model from Ochs, et.al., (2016) to the experimental DLM data for (A) laboratory and field samples and (B) second field sample for more pore volume exchanges.

In the shrinking core model, a slag reducing capacity is defined as a solid-phase concentration expressed in units of milliequivalents of electrons per gram (meq e^-/g). Dissolved oxygen at its solubility limit migrates through advection and/or diffusion into saltstone and consumes the slag reducing capacity. The oxidation fraction of each cell, ranging from 0 to 1, is tracked through time. Using

this same shrinking core model, pore volume exchanges can be tracked on a cell-to-cell basis as opposed to a bulk material zone to material zone basis, as used for the generic species. This allows for the Tc solubility transition that occurs after six pore volume exchanges (i.e., once the pH falls below 11) to be modeled with greater discretization.

I-129 Release Modeling

Similar to the Tc solubility limit, the K_d value used to simulate iodine sorption to saltstone under reducing conditions was also developed based on recent DLM experimental data (Figure 4.4-36) using a GoldSim optimization model (Section 4.3.2.1). From this analysis, the recommended K_d value was found to be dependent on the number of pore volume exchanges through the saltstone (Table 4.3-7). Specifically, after one pore volume exchange, the iodine K_d value for saltstone increases approximately one order of magnitude.

Given I-129's importance as a dose contributor in the SDF (SRR-CWDA-2009-00017, SRR-CWDA-2013-00062, SRR-CWDA-2014-00006, SRR-CWDA-2016-00072), the shrinking core model described above was also used to simulate the I-129 releases. [SRNL-STI-2018-00652] Because the shrinking core model is used to track pore volume exchanges on a cell-to-cell basis, this approach allows for the I-129 K_d transition (occurring after the first pore volume exchange) to be more accurately modeled.

Figure 4.4-36: DLM Leachate for I-129 Spiked Saltstone Simulant

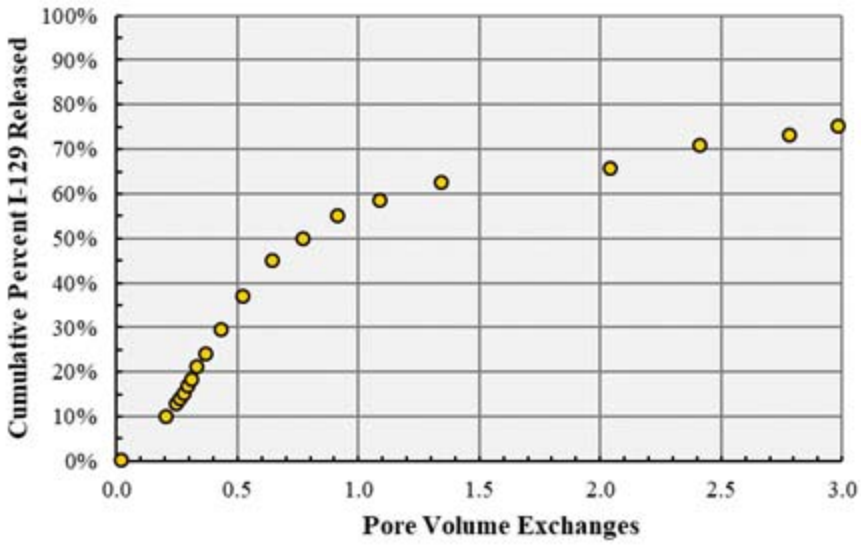

4.4.3.4.3 Chemical Transition Times for Generic Species

As previously mentioned above, the Vadose Zone Flow Model applies the chemical transitions on a bulk material zone (i.e., modeled region) basis. The starting chemical environment assigned to each bulk material zone is presented in Table 4.4-58.

Table 4.4-58: Starting Chemical Environment of Cementitious Modeled Regions

Modeled Region	375-foot diameter SDUs	150-foot diameter SDUs	SDU 1 and SDU 4
Saltstone	Reducing Region I	Reducing Region I	Reducing Region I [a]
Clean Grout	Reducing Region I	Reducing Region I	Reducing Region I
Wall	Reducing Region I [b]	Reducing Region I	Oxidizing Region III [c]
Roof	Reducing Region I	Reducing Region I	Oxidizing Region I
Floor	Reducing Region I	Reducing Region I	Reducing Region I
Upper Mud Mat	Reducing Region I	Reducing Region I	NA
Lower Mud Mat	Oxidizing Region I	Oxidizing Region I	NA

a For SDU 4 the saltstone region is divided between a top portion and a bottom portion as described in the FY2013 SDF SA, Section 3.3.2. Both portions are modeled as starting in Reducing Region I.

b The walls for the 375-foot diameter SDUs are modeled as five distinct segments. Each segment is modeled as starting in Reducing Region I.

c In the shrinking core model, the walls of SDU 1 and SDU 4 are modeled as starting in Reducing Region I. Note that the SDU 1 and 4 walls were constructed with blast furnace slag (Section 3.2.1.1.3 (Table 3.2-1) and Section 3.2.1.2.3 (Table 3.2-2) of SRR-CWDA-2009-00017, respectively).

NA Not applicable

The Vadose Zone Flow Model uses PORFLOW (ACRi, 2010) to evaluate the vadose zone flow fields for individual SDUs. Additional efficiency is derived by modeling only SDU 1, SDU 4, SDU 2, SDU 6, SDU 7, and SDU 9. The "SDU 2" model is used to generate results for all the 150-foot diameter SDUs (i.e., SDU 2A, SDU 2B, SDU 3A, SDU 3B, SDU 5A, and SDU 5B). The "SDU 7" model is used to generate results for all the 375-foot diameter SDUs except for SDUs 6 and 9 (i.e., SDU 7, SDU 8, SDU 10, SDU 11, and SDU 12).

For the generic species (i.e., all species other than I-129 and Tc-99), the chemical transition times for SDU 1, SDU 4, and SDU 2 are presented in Table 4.4-59 through Table 4.4-61 for the Compliance Case, the Realistic Case, and the Pessimistic Case, respectively. Similarly, for all generic species, the chemical transition times for SDU 6, SDU 7, and SDU 9 are presented in Table 4.4-62 through Table 4.4-64 for the Compliance Case, the Realistic Case, and the Pessimistic Case, respectively.

Note that in Table 4.4-59 through Table 4.4-64 the "Clean Grout" designation is used to indicate the top few feet of the SDU fill material. Historically, this material represented a "clean" pour that was used to provide a layer for worker protection. As such this layer was historically assigned no initial inventory but had properties identical to saltstone. While it is still expected that a layer of "clean" material will be poured over the top of the saltstone to complete the filling of each SDU, the exact thickness of this layer is unknown, therefore no credit is taken. Instead, it is now assumed that, aside from SDUs 1 and 4, all the SDUs will be filled to capacity. As such, the "Clean Grout" material property is assumed to have inventory assigned to it thus representing the top-most layer of the saltstone monolith. This

inventory within the Clean Grout material zone is assigned the same concentrations as the saltstone material zone.

Table 4.4-59: "Compliance Case" Transition Times for SDU 1, SDU 4, and 150-ft Diameter SDUs (Years) for Simulating Transport of Generic Species

Modeled Region	SDU 1	SDU 4[a]	SDU 2[b]
Saltstone			
Reducing Region I → Reducing Region III	29,714	Top: 4,323 Bottom: 31,428	25,015
Reducing Region III → Oxidizing Region III	30,535,034	Top: 3,204,494 Bottom: 29,109,040	25,746,312
Oxidizing Region III → Oxidizing Region IV	50,923,364	Top: 5,323,575 Bottom: 48,198,222	43,018,081
Clean Grout			
Reducing Region I → Reducing Region III	1,338	4,103	4,001
Reducing Region III → Oxidizing Region III	556,086	3,024,359	2,969,974
Oxidizing Region III → Oxidizing Region IV	922,467	5,018,419	5,016,542
Wall [c]			
Reducing Region I → Reducing Region III	0	0	1,727
Reducing Region III → Oxidizing Region III	0	0	3,384,605
Oxidizing Region III → Oxidizing Region IV	37,788,764	50,001,928	7,224,429
Roof			
Reducing Region I → Reducing Region III	775	565	675
Reducing Region III → Oxidizing Region III	883,274	319,711	602,832
Oxidizing Region III → Oxidizing Region IV	1,703,833	607,345	1,158,341
Floor			
Reducing Region I → Reducing Region II	29,714	31,428	25,015
Reducing Region III → Oxidizing Region III	30,535,034	29,109,040	25,746,312
Oxidizing Region III → Oxidizing Region IV	50,923,364	48,198,222	43,018,081
Upper Mud Mats			
Reducing Region I → Reducing Region II	NA	NA	25,015
Reducing Region III → Oxidizing Region III	NA	NA	25,746,312
Oxidizing Region III → Oxidizing Region IV	NA	NA	43,018,081
Lower Mud Mats [d]			
Reducing Region I → Reducing Region II	NA	NA	25,015
Reducing Region III → Oxidizing Region III	NA	NA	25,746,312
Oxidizing Region III → Oxidizing Region IV	NA	NA	43,018,081

a For SDU 4 the saltstone region is divided between a top portion and a bottom portion as described in the FY2013 SDF SA (SRR-CWDA-2013-00062), Section 3.3.2.

b For the cylindrical SDUs, only vertical movement of the oxidation front (from the top down) is considered, such that the floor and upper mud mat only transitions from Region I to Region III after the saltstone transition occurs.

c The walls for SDU 1 and SDU 4 are assumed to be in Oxidizing Region III at time 0 years.

d For the shrinking core simulations (i.e., I-129 and Tc-99 transport), these Lower Mud Mat transition times are still applicable.

NA Not applicable

Table 4.4-60: "Realistic Case" Transition Times for SDU 1, SDU 4, and 150-ft Diameter SDUs (Years) for Simulating Transport of Generic Species

Modeled Region	SDU 1	SDU 4[a]	SDU 2[b]
Saltstone			
Reducing Region I → Reducing Region III	384,412	Top: 51,917 Bottom: 453,429	309,400
Reducing Region III → Oxidizing Region III	>100,000,000	Top: 63,140,981 Bottom: >100,000,000	>100,000,000
Oxidizing Region III → Oxidizing Region IV	>100,000,000	Top: 79,870,862 Bottom: >100,000,000	>100,000,000
Clean Grout			
Reducing Region I → Reducing Region III	8,765	47,457	39,948
Reducing Region III → Oxidizing Region III	9,230,170	59,781,776	50,672,003
Oxidizing Region III → Oxidizing Region IV	11,843,903	75,627,252	64,530,421
Wall [c]			
Reducing Region I → Reducing Region III	0	0	11,962
Reducing Region III → Oxidizing Region III	0	0	67,900,092
Oxidizing Region III → Oxidizing Region IV	>100,000,000	>100,000,000	>100,000,000
Roof			
Reducing Region I → Reducing Region III	3,270	1,427	2,198
Reducing Region III → Oxidizing Region III	13,321,370	5,505,887	8,677,263
Oxidizing Region III → Oxidizing Region IV	22,724,952	9,140,221	15,190,127
Floor			
Reducing Region I → Reducing Region II	384,412	453,429	309,400
Reducing Region III → Oxidizing Region III	>100,000,000	>100,000,000	>100,000,000
Oxidizing Region III → Oxidizing Region IV	>100,000,000	>100,000,000	>100,000,000
Upper Mud Mats			
Reducing Region I → Reducing Region II	NA	NA	309,400
Reducing Region III → Oxidizing Region III	NA	NA	>100,000,000
Oxidizing Region III → Oxidizing Region IV	NA	NA	>100,000,000
Lower Mud Mats [d]			
Reducing Region I → Reducing Region II	NA	NA	309,400
Reducing Region III → Oxidizing Region III	NA	NA	>100,000,000
Oxidizing Region III → Oxidizing Region IV	NA	NA	>100,000,000

a For SDU 4 the saltstone region is divided between a top portion and a bottom portion as described in the FY2013 SDF SA (SRR-CWDA-2013-00062), Section 3.3.2.

b For the cylindrical SDUs, only vertical movement of the oxidation front (from the top down) is considered, such that the floor and upper mud mat only transitions from Region I to Region III after the saltstone transition occurs.

c The walls for SDU 1 and SDU 4 are assumed to be in Oxidizing Region III at time 0 years.

d For the shrinking core simulations (i.e., I-129 and Tc-99 transport), these Lower Mud Mat transition times are still applicable.

NA Not applicable

Table 4.4-61: "Pessimistic Case" Transition Times for SDU 1, SDU 4, and 150-ft Diameter SDUs (Years) for Simulating Transport of Generic Species

Modeled Region	SDU 1	SDU 4[a]	SDU 2[b]
Saltstone			
Reducing Region I → Reducing Region III	8,511	Top: 2,499 Bottom: 8,183	7,453
Reducing Region III → Oxidizing Region III	4,263,706	Top: 457,938 Bottom: 3,995,809	3,616,296
Oxidizing Region III → Oxidizing Region IV	10,006,539	Top: 1,071,860 Bottom: 9,403,310	8,484,068
Clean Grout			
Reducing Region I → Reducing Region III	1,221	2,447	2,399
Reducing Region III → Oxidizing Region III	94,752	431,578	484,507
Oxidizing Region III → Oxidizing Region IV	222,030	1,010,390	1,124,527
Wall [c]			
Reducing Region I → Reducing Region III	0	0	1,054
Reducing Region III → Oxidizing Region III	0	0	767,280
Oxidizing Region III → Oxidizing Region IV	8,064,085	10,382,460	2,153,964
Roof			
Reducing Region I → Reducing Region III	728	558	622
Reducing Region III → Oxidizing Region III	177,681	57,284	122,289
Oxidizing Region III → Oxidizing Region IV	396,926	125,785	272,155
Floor			
Reducing Region I → Reducing Region II	8,511	8,183	7,453
Reducing Region III → Oxidizing Region III	4,263,706	3,995,809	3,616,296
Oxidizing Region III → Oxidizing Region IV	10,006,539	9,403,310	8,484,068
Upper Mud Mats			
Reducing Region I → Reducing Region II	NA	NA	7,453
Reducing Region III → Oxidizing Region III	NA	NA	3,616,296
Oxidizing Region III → Oxidizing Region IV	NA	NA	8,484,068
Lower Mud Mats [d]			
Reducing Region I → Reducing Region II	NA	NA	7,453
Reducing Region III → Oxidizing Region III	NA	NA	3,616,296
Oxidizing Region III → Oxidizing Region IV	NA	NA	8,484,068

a For SDU 4 the saltstone region is divided between a top portion and a bottom portion as described in the FY2013 SDF SA (SRR-CWDA-2013-00062), Section 3.3.2.

b For the cylindrical SDUs, only vertical movement of the oxidation front (from the top down) is considered, such that the floor and upper mud mat only transitions from Region I to Region III after the saltstone transition occurs.

C The walls for SDU 1 and SDU 4 are assumed to be in Oxidizing Region III at time 0 years.

D For the shrinking core simulations (i.e., I-129 and Tc-99 transport), these Lower Mud Mat transition times are still applicable.

NA Not applicable

Table 4.4-62: "Compliance Case" Transition Times for 375-ft Diameter SDUs (Years) for Simulating Transport of Generic Species

Modeled Region		SDU 6 [a]	SDU 7 [a]	SDU 9 [a]
Saltstone				
Reducing Region I → Reducing Region III		55,686	56,141	60,387
Reducing Region III → Oxidizing Region III		53,436,202	53,481,733	53,815,475
Oxidizing Region III → Oxidizing Region IV		88,468,636	88,528,787	88,841,393
Clean Grout				
Reducing Region I → Reducing Region III		3,576	4,949	5,141
Reducing Region III → Oxidizing Region III		2,440,153	3,671,369	3,772,002
Oxidizing Region III → Oxidizing Region IV		4,074,559	6,130,520	6,259,691
Wall				
Reducing Region I → Reducing Region III	**Segment 5 (top)**	967	819	794
	Segment 4	2,524	2,440	2,801
	Segment 3	3,109	3,003	3,702
	Segment 2	3,235	3,051	3,162
	Segment 1 (bottom)	3,230	2,727	2,399
Reducing Region III → Oxidizing Region III	**Segment 5 (top)**	1,714,849	1,728,349	1,626,923
	Segment 4	8,819,109	8,788,166	9,412,018
	Segment 3	8,813,991	8,797,247	10,265,686
	Segment 2	7,364,574	7,548,606	9,567,934
	Segment 1 (bottom)	6,196,865	5,835,930	6,408,523
Oxidizing Region III → Oxidizing Region IV	**Segment 5 (top)**	3,153,317	3,180,655	3,037,396
	Segment 4	16,649,560	16,863,432	17,468,535
	Segment 3	17,382,394	17,528,912	19,040,648
	Segment 2	15,305,320	15,635,387	18,072,724
	Segment 1 (bottom)	11,608,499	10,889,675	11,938,223
Roof				
Reducing Region I → Reducing Region III		753	775	793
Reducing Region III → Oxidizing Region III		953,967	962,565	997,438
Oxidizing Region III → Oxidizing Region IV		1,824,855	1,840,227	1,899,740
Floor				
Reducing Region I → Reducing Region III		55,686	56,141	60,387
Reducing Region III → Oxidizing Region III		53,436,202	53,481,733	53,815,475
Oxidizing Region III → Oxidizing Region IV		88,468,636	88,528,787	88,841,393
Upper Mud Mats				
Reducing Region I → Reducing Region III		55,686	56,141	60,387
Reducing Region III → Oxidizing Region III		53,436,202	53,481,733	53,815,475
Oxidizing Region III → Oxidizing Region IV		88,468,636	88,528,787	88,841,393
Lower Mud Mats [b]				
Reducing Region I → Reducing Region III		55,686	56,141	60,387
Reducing Region III → Oxidizing Region III		53,436,202	53,481,733	53,815,475
Oxidizing Region III → Oxidizing Region IV		88,468,636	88,528,787	88,841,393

a For the cylindrical SDUs, only vertical movement of the oxidation front (from the top down) is considered, such that the floor and upper mud mat only transitions from Region I to Region III after the saltstone transition occurs.

B For the shrinking core simulations (i.e., I-129 and Tc-99 transport), these Lower Mud Mat transition times are still applicable.

Table 4.4-63: "Realistic Case" Transition Times for 375-ft Diameter SDUs (Years) for Simulating Transport of Generic Species

Modeled Region		SDU 6 [a]	SDU 7 [a]	SDU 9 [a]
Saltstone				
Reducing Region I → Reducing Region III		734,682	748,481	812,388
Reducing Region III → Oxidizing Region III		>100,000,000	>100,000,000	>100,000,000
Oxidizing Region III → Oxidizing Region IV		>100,000,000	>100,000,000	>100,000,000
Clean Grout				
Reducing Region I → Reducing Region III		37,103	55,405	59,425
Reducing Region III → Oxidizing Region III		41,788,545	62,883,760	67,203,801
Oxidizing Region III → Oxidizing Region IV		52,917,521	79,577,553	85,021,647
Wall				
Reducing Region I → Reducing Region III	**Segment 5 (top)**	8,976	7,177	6,949
	Segment 4	24,946	29,839	40,467
	Segment 3	66,014	69,787	20,256
	Segment 2	53,328	34,054	13,365
	Segment 1 (bottom)	31,104	25,390	14,794
Reducing Region III → Oxidizing Region III	**Segment 5 (top)**	36,981,310	41,032,691	40,150,245
	Segment 4	>100,000,000	>100,000,000	>100,000,000
	Segment 3	>100,000,000	>100,000,000	>100,000,000
	Segment 2	>100,000,000	>100,000,000	77,717,009
	Segment 1 (bottom)	>100,000,000	>100,000,000	80,290,424
Oxidizing Region III → Oxidizing Region IV	**Segment 5 (top)**	61,578,947	67,940,931	65,922,073
	Segment 4	>100,000,000	>100,000,000	>100,000,000
	Segment 3	>100,000,000	>100,000,000	>100,000,000
	Segment 2	>100,000,000	>100,000,000	>100,000,000
	Segment 1 (bottom)	>100,000,000	>100,000,000	>100,000,000
Roof				
Reducing Region I → Reducing Region III		3,411	3,648	3,854
Reducing Region III → Oxidizing Region III		15,040,901	15,211,197	16,124,068
Oxidizing Region III → Oxidizing Region IV		25,062,096	25,373,712	26,889,693
Floor				
Reducing Region I → Reducing Region III		734,682	748,481	812,388
Reducing Region III → Oxidizing Region III		>100,000,000	>100,000,000	>100,000,000
Oxidizing Region III → Oxidizing Region IV		>100,000,000	>100,000,000	>100,000,000
Upper Mud Mats				
Reducing Region I → Reducing Region III		734,682	748,481	812,388
Reducing Region III → Oxidizing Region III		>100,000,000	>100,000,000	>100,000,000
Oxidizing Region III → Oxidizing Region IV		>100,000,000	>100,000,000	>100,000,000
Lower Mud Mats [b]				
Reducing Region I → Reducing Region III		734,682	748,481	812,388
Reducing Region III → Oxidizing Region III		>100,000,000	>100,000,000	>100,000,000
Oxidizing Region III → Oxidizing Region IV		>100,000,000	>100,000,000	>100,000,000

a For the cylindrical SDUs, only vertical movement of the oxidation front (from the top down) is considered, such that the floor and upper mud mat only transitions from Region I to Region III after the saltstone transition occurs.

B For the shrinking core simulations (i.e., I-129 and Tc-99 transport), these Lower Mud Mat transition times are still applicable.

Table 4.4-64: "Pessimistic Case" Transition Times for 375-ft Diameter SDUs (Years) for Simulating Transport of Generic Species

Modeled Region		SDU 6 [a]	SDU 7 [a]	SDU 9 [a]
Saltstone				
Reducing Region I → Reducing Region III		14,370	14,374	14,645
Reducing Region III → Oxidizing Region III		7,311,597	7,327,017	7,340,251
Oxidizing Region III → Oxidizing Region IV		17,086,433	17,127,244	17,142,885
Clean Grout				
Reducing Region I → Reducing Region III		2,335	2,650	2,662
Reducing Region III → Oxidizing Region III		390,857	575,861	578,941
Oxidizing Region III → Oxidizing Region IV		904,988	1,322,372	1,325,675
Wall				
Reducing Region I → Reducing Region III	**Segment 5 (top)**	1,462	1,333	1,266
	Segment 4	2,026	2,035	2,042
	Segment 3	2,148	2,146	2,176
	Segment 2	2,188	2,181	2,210
	Segment 1 (bottom)	2,114	2,086	2,045
Reducing Region III → Oxidizing Region III	**Segment 5 (top)**	171,227	178,287	174,130
	Segment 4	1,042,898	1,127,758	1,110,073
	Segment 3	1,278,557	1,294,067	1,307,988
	Segment 2	1,040,584	1,023,429	1,094,400
	Segment 1 (bottom)	763,326	732,037	763,601
Oxidizing Region III → Oxidizing Region IV	**Segment 5 (top)**	383,000	399,608	392,882
	Segment 4	2,602,627	2,797,301	2,777,337
	Segment 3	3,079,710	3,157,017	3,170,998
	Segment 2	2,780,361	2,773,184	2,866,493
	Segment 1 (bottom)	1,891,363	1,796,962	1,877,773
Roof				
Reducing Region I → Reducing Region III		723	733	738
Reducing Region III → Oxidizing Region III		185,436	185,935	187,568
Oxidizing Region III → Oxidizing Region IV		409,764	410,727	413,214
Floor				
Reducing Region I → Reducing Region III		14,370	14,374	14,645
Reducing Region III → Oxidizing Region III		7,311,597	7,327,017	7,340,251
Oxidizing Region III → Oxidizing Region IV		17,086,433	17,127,244	17,142,885
Upper Mud Mats				
Reducing Region I → Reducing Region III		14,370	14,374	14,645
Reducing Region III → Oxidizing Region III		7,311,597	7,327,017	7,340,251
Oxidizing Region III → Oxidizing Region IV		17,086,433	17,127,244	17,142,885
Lower Mud Mats [b]				
Reducing Region I → Reducing Region III		14,370	14,374	14,645
Reducing Region III → Oxidizing Region III		7,311,597	7,327,017	7,340,251
Oxidizing Region III → Oxidizing Region IV		17,086,433	17,127,244	17,142,885

a For the cylindrical SDUs, only vertical movement of the oxidation front (from the top down) is considered, such that the floor and upper mud mat only transitions from Region I to Region III after the saltstone transition occurs.

B For the shrinking core simulations (i.e., I-129 and Tc-99 transport), these Lower Mud Mat transition times are still applicable.

This page intentionally left blank.

4.4.4 Vadose Zone Flow Model

The Vadose Zone Flow Model simulated vadose zone flow fields for individual SDUs using PORFLOW. For computational efficiency, the SDF disposal units are modeled in two-dimensions. The long, rectangular disposal units, SDUs 1 and 4, are represented in two-dimensional Cartesian coordinates as a cross-sectional slice through the disposal units and surrounding vadose zone soils. End effects on the front and back faces of the two units are not considered. The 150-foot diameter SDUs (2A, 2B, 3A, 3B, 5A, and 5B), and the 375-foot diameter SDUs (6, 7, 8, 9, 10, 11, and 12) are modeled in quasi-two-dimensional cylindrical coordinates by a radial cross section (unit radian pie wedge) that implicitly assumes symmetry about the centerline axis. The simulated flow fields are used as input to the SDF PA Vadose Zone Transport Model simulations in PORFLOW and are also extracted for use in the SDF GoldSim Model.

4.4.4.1 Conceptual Model of the Vadose Zone Flow System

Conceptually, the Vadose Zone Flow Model simulates the evolution of flow through the SDUs and surrounding soils. Due to geometric complexities, each SDU design is simulated independently, such that the Vadose Zone Flow Model is organized into six discrete flow models:

- VadoseSDU1 (for simulating SDU 1),
- VadoseSDU2 (for simulating the 150-foot diameter SDUs),
- VadoseSDU4 (for simulating SDU 4),
- VadoseSDU6 (for simulating SDU 6),
- VadoseSDU7 (for simulating SDUs 7, 8, 10, 11, and 12), and
- VadoseSDU9 (for simulating SDU 9).

Each flow model includes the lower backfill layer of the closure cap, the lower sand drainage layer, a composite barrier (HDPE and GCL) at the roof of the SDUs, the SDUs (including the roof, walls, floors, and mud mats), the saltstone within the SDUs, the backfill surrounding the SDUs, and the vadose zone soils beneath the SDUs.

Section 4.4.1 provides the infiltration rates into the Vadose Zone Flow Model, which change over time in response to the assumed evolution of the closure cap properties. Similarly, as shown in Section 4.4.2, it is expected that the saturated hydraulic conductivity of the cementitious materials (i.e., SDU concrete and saltstone) will also change over time as the material properties degrade. Since the SDU concrete will have an initially low hydraulic conductivity, most infiltrating water will shed off the perimeter of the SDU roof (via the more conductive lower lateral drainage layer) and down the sides of the walls (via the surrounding backfill). The small amount of water that does enter the SDU concrete will eventually flow through the SDU concrete and into the waste form. The initial flow rates through the SDU concrete will be low, but as the concrete degrades over time the flow rates will accelerate. It is assumed that this evolution will continue until the flow rates approach a quasi-equilibrium state in which the hydraulic conductivity through the cementitious materials are assumed to become similar to the surrounding backfill and soil materials (see Figure 4.4-37).

Figure 4.4-37: Conceptualization of SDU Flow Evolution

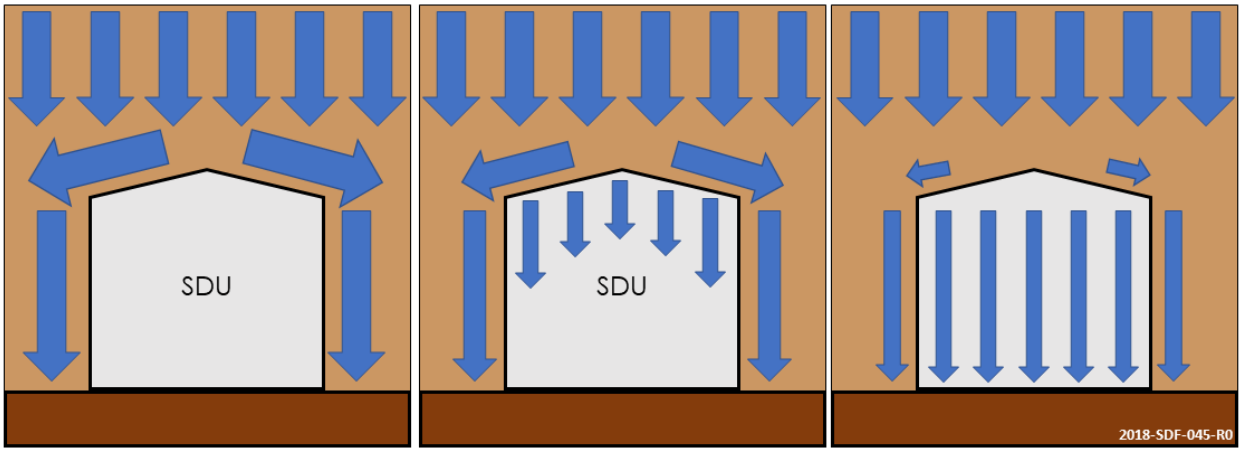

(a) Initially almost all flow will shed from the SDU roof.

(b) As concrete degrades, less flow will shed and more flow will enter into the SDU.

(c) Trend continues until flow through the SDU is similar to flow through backfill.

4.4.4.2 Vadose Zone Flow Model Implementation

The SDF PA uses PORFLOW unsaturated zone flow simulations to generate the flow fields needed to evaluate radionuclide transport from the saltstone waste disposal units, through the underlying unsaturated zone soils, and into the saturated zone at the water table. In addition to defining the advective processes for the subsequent PORFLOW Vadose Zone Transport Model (see Section 4.4.5) to support the Compliance Case and other deterministic modeling cases, the flow results from the Vadose Zone Flow Model are also used as input to the transport simulations in the SDF GoldSim Model that is used to evaluate the influence of parameter uncertainty.

In terms of pressure head, the governing equation for fluid flow as used in PORFLOW and reduced to reflect a single incompressible fluid phase as assumed in the SDF PA PORFLOW flow runs can be rewritten as a modified form of Richards equation (Therrien and Sudicky, 1996) as follows:

$$\frac{\partial(\phi S_w)}{\partial t} = \frac{\partial}{\partial x_i}\left[K_{ij} k_{rw} \frac{\partial(\Psi+z)}{\partial x_j}\right] + Q \qquad \text{Eq. 4.4-95}$$

where:

ϕ = porosity (unitless),

Ψ = pressure head (L),

K_{ij} = the saturated hydraulic conductivity tensor (L/T),

k_{rw} = the relative permeability (unitless),

S_w = the water saturation ($V_{water}/V_{pore\text{-}space}$),

Q = the volumetric rate of fluid injection (> 0) or withdrawal (< 0),

x_i and x_j = vector distances (L) using index notation, and

z = the elevation head (L).

For flow in the i[th] direction, the specific discharge can be written in the form (Therrien and Sudicky, 1996):

$$q_i = -K_i k_{rw} \frac{\partial(\psi+z)}{\partial x_j} \quad \text{Eq. 4.4-96}$$

where:

q_i = the specific discharge (Darcy flux) (L/T).

The boundary conditions used in the SDU-specific Vadose Zone Flow Models include a flux boundary condition defined by a time dependent infiltration rate at the top of the model (Eq. 4.4-97), no flow boundaries at the outer edges of the model for SDUs 1 and 4 and the center and outer edge for the other SDUs (Eq. 4.4-98), and a constant pressure head boundary at the bottom boundary (Eq. 4.4-99). Because the PORFLOW Vadose Zone Flow Model simulates SDUs 1 and 4 as a vertical slice oriented perpendicular to the length of SDUs 1 and 4 and the cylindrical SDUs as 1-radian wedges, the boundary conditions can be posed as follows. Assuming z to be the vertical axis coordinate and x the horizontal axis coordinate for a two-dimensional plane (or radial axis for the cylindrical SDUs), the boundary conditions for the Vadose Zone Flow Model can be represented as:

$$K_{ij} k_{rw} \left[\frac{\partial \psi}{\partial z} + 1\right] = I \quad \text{Eq. 4.4-97}$$

$$\frac{\partial \psi}{\partial x_1} = \frac{\partial \psi}{\partial x_2} = 0 \quad \text{Eq. 4.4-98}$$

$$\psi_{WaterTable} = 0 \quad \text{Eq. 4.4-99}$$

where:

I = infiltration rate (L/T)

z = vertical coordinate taken as positive upwards (L),

x_1 = horizontal (or radial) coordinate at the central plane (or center) of the SDU (L), and

x_2 = horizontal (or radial) coordinate at the end of the modeled backfill around the SDU (L).

Note that each flow field generated by the Vadose Zone Flow Model was created by combining the results from multiple model simulations, where each simulation represents a specific time interval. Within each time interval simulation, results were generated by running a transient flow simulation until a steady-state was approached. Each of these time interval flow simulations were initiated with temporally appropriate input values based on interpolation of time-dependent input values.

4.4.4.2.1 Moisture Characteristic Curves

In unsaturated materials, as simulated in each SDU-specific Vadose Zone Flow Model, pore water is subject to negative pressure head associated with surface

tension generated capillarity within the pore space. The water saturation is a function of these negative pressure heads and the effective hydraulic conductivity controlling the flow rate is a function of the saturation levels. To evaluate flow through an unsaturated system, constitutive relationships of the nature, $\theta = f(\psi)$, must be developed to relate the primary dependent variables: pressure head and moisture content. Additionally, due to the nonlinear nature of hydraulic conductivity where the effective hydraulic conductivity (the product of the saturated hydraulic conductivity and relative permeability, shown in Eq. 4.4-95) decreases with decreased saturation (or water content), a constitutive relationship between saturation and relative permeability of the form $k_{rw} = f(\theta)$ must be defined.

For the materials comprising the SDUs, $\theta = f(\psi)$ is defined with a van Genuchten model (van Genuchten, 1980) where the water content-pressure head relationship is given by:

$$\theta = \theta_r + (\theta_s - \theta_r)\left[\frac{1}{1+(\alpha|\psi|)^n}\right]^m \qquad \psi < 0 \qquad \text{Eq. 4.4-100}$$

$$\theta = \theta_s \qquad \psi \geq 0 \qquad \text{Eq. 4.4-101}$$

and the effective saturation by:

$$S_e = \frac{S-S_r}{1-S_r} = \frac{\theta-\theta_r}{\theta_s-\theta_r} \qquad \text{Eq. 4.4-102}$$

where:

θ = volumetric water content,

θ_r = residual volumetric water content determined for each node during each timestep,

θ_s = saturated volumetric water content determined for each node during each timestep,

ψ = pressure head (L),

α = van Genuchten shape parameter (L^{-1}),

n = van Genuchten shape parameter,

$m = 1 - n^{-1}$, and

S_e = effective saturation.

In addition, for the materials comprising the SDUs, $k_{rw} = f(S_e)$ is defined using the Mualem-van Genuchten model (van Genuchten, 1980) where the relative permeability-effective saturation relationship is given by:

$$k_{rw} = {S_e}^{1/2}\left[1 - \left(1 - {S_e}^{1/m}\right)^m\right]^2 \qquad \text{Eq. 4.4-103}$$

and the effective hydraulic conductivity by:

$$K_{eff} = k_{rw}K_s = K_S S_e^{1/2}\left[1-\left(1-S_e^{1/m}\right)^m\right]^2 \qquad \text{Eq. 4.4-104}$$

where:

k_{rw} = relative permeability,

K_s = saturated hydraulic conductivity, and

K_{eff} = effective hydraulic conductivity.

4.4.4.3 Vadose Zone Flow Model Inputs

The following describes the key inputs and assumptions used in the Vadose Zone Flow Model for the SDF PA.

Because flow is a dimensional process, the geometry of each discrete SDU-specific flow model is important to define; each model has been developed to reflect the geometry of the various SDUs. Up to 27 distinct material types (or mtyp zones) are defined in PORFLOW to represent different materials and to facilitate different flow scenarios (e.g., fast flow paths). The specified discretization for each SDU model is presented in Table 4.4-65 along with the selected coordinate system and the number of mtyp zones that are applicable to each flow model. Following this table are subsections that provide graphic depictions for each of the discrete SDU-specific PORFLOW models. These depictions show the mtyp zones, grids for each model, and include depictions of select corner details. Tables within these subsections provide the modeled dimensions for each SDU. These dimensions are based on the design specifications presented in Section 3.2.

Table 4.4-65: PORFLOW Model Geometry

Disposal Unit	Horizontal Nodes	Vertical Nodes	Total Nodes	Coordinate System	Model Type [a]	Number of mtyp Zones [b]
SDU 1	112	66	7,392	Cartesian	SDU 1	14
SDU 2A	86	109	9,374	Radial	SDU 2	22
SDU 2B	86	109	9,374	Radial	SDU 2	22
SDU 3A	86	109	9,374	Radial	SDU 2	22
SDU 3B	86	109	9,374	Radial	SDU 2	22
SDU 4	193	94	18,142	Cartesian	SDU 4	27
SDU 5A	86	109	9,374	Radial	SDU 2	22
SDU 5B	86	109	9,374	Radial	SDU 2	22
SDU 6	129	154	19,866	Radial	SDU 6	24
SDU 7	129	154	19,866	Radial	SDU 7	24
SDU 8	129	154	19,866	Radial	SDU 7	24
SDU 9	129	154	19,866	Radial	SDU 9	24
SDU 10	129	154	19,866	Radial	SDU 7	24
SDU 11	129	154	19,866	Radial	SDU 7	24
SDU 12	129	154	19,866	Radial	SDU 7	24

Notes: (a) The "SDU 2" model type applies to all 150-foot diameter SDUs. The "SDU 7" model type applies to SDUs 7, 8, 10, 11, and 12. Note that SDU 9 is identical to the SDU 7 model type, but with less thickness for the vadose zone.

(c) mtyp = material type.

4.4.4.3.1 SDU 1 Flow Model Geometry

Figure 4.4-38 shows the modeled mtyp zones for SDU 1. Figure 4.4-39 shows the grid resolution. Figure 4.4-40 and Figure 4.4-41 display additional details at the corners of the SDU. Table 4.4-66 provides the key for the numbered mtyp zones and Table 4.4-67 provides a summary of the modeled dimensions for SDU 1. The material properties for each mtyp zone are defined in Section 4.4.4.3.5.

Figure 4.4-38: SDU 1 Material Zones for PORFLOW Vadose Zone Modeling

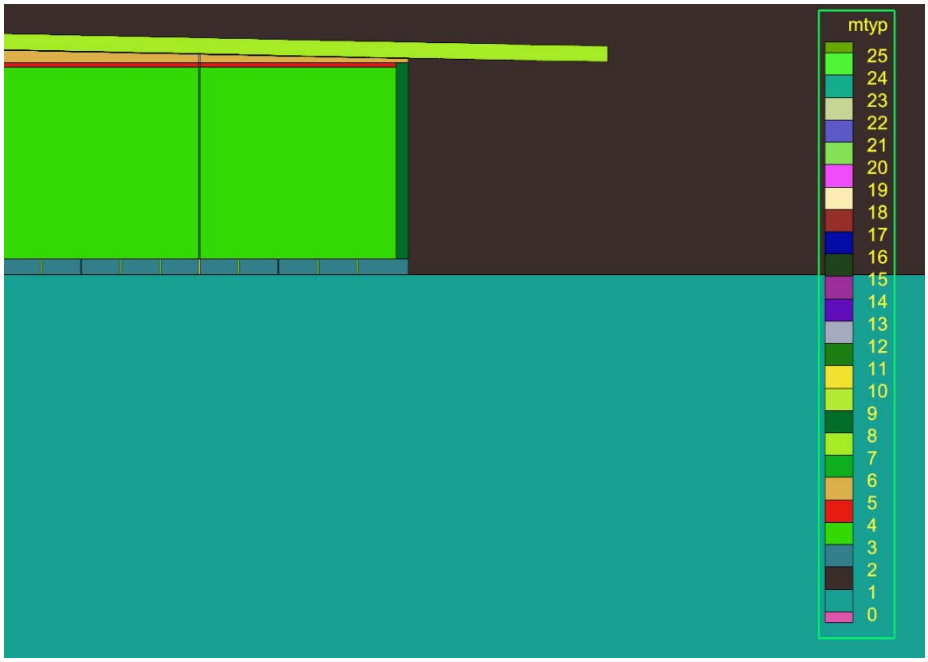

Figure 4.4-39: SDU 1 Gridding for PORFLOW Vadose Zone Modeling

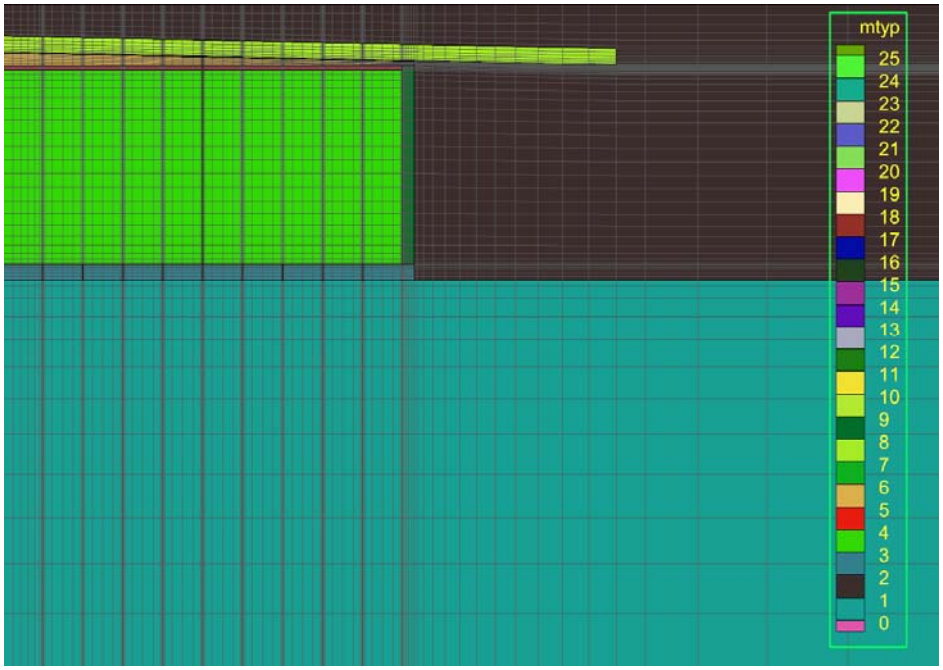

Figure 4.4-40: SDU 1 Upper Corner Detail for PORFLOW Vadose Zone Modeling

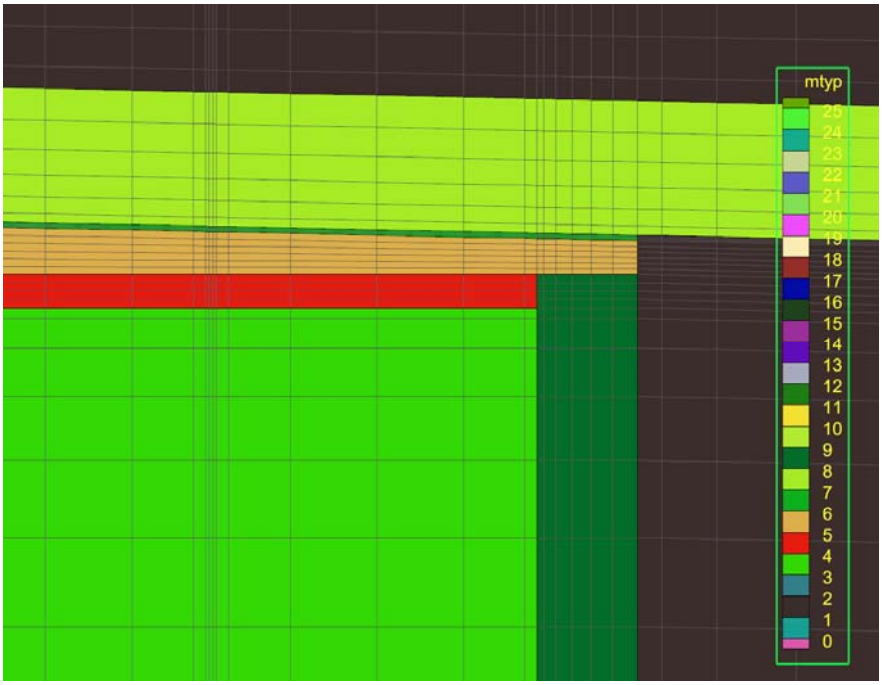

Figure 4.4-41: SDU 1 Lower Corner Detail for PORFLOW Vadose Zone Modeling

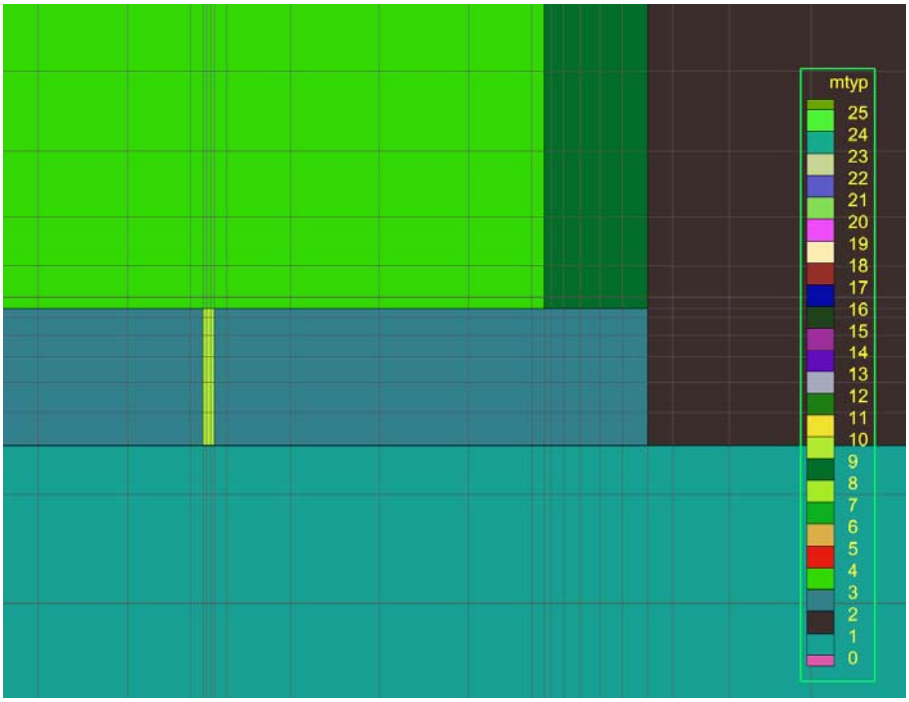

Table 4.4-66: SDU 1 mtyp Zones

Zone	Material Name	Comments
1	NATIVE_SOIL	This mtyp represents the vadose zone soils beneath the SDU. It is assigned the material properties for the Lower Vadose Zone soils.
2	BACKFILL	This mtyp represents the soils surrounding the SDUs and above the SDUs.
3	FLOOR	SDU floor material.
4	SALTSTONE	Saltstone waste form material.
5	CLEAN_GROUT	This mtyp is assigned the same material properties as saltstone but can be simulated with or without an initial inventory for transport modeling.
6	ROOF	SDU roof material.
7	ROOF_HDPE_GCL	This mtyp represents the composite barrier above the SDU roof.
8	SAND_DRAIN	This is the lower sand drainage layer above the SDU.
9	WALL	SDU wall material.
10	JOINT	This mtyp represents the waterstops and other engineered joints at various SDU concrete interfaces. It is assigned the material properties for gravel to promote flow.
11	FF_FLOOR	For the Compliance Case, the "FF" (fast flow) mtyp zones are assigned the same material properties as adjacent materials, but may be modified for sensitivity cases.
12	FF_GROUT	For the Compliance Case, the "FF" (fast flow) mtyp zones are assigned the same material properties as adjacent materials, but may be modified for sensitivity cases.
13	FF_ROOF	For the Compliance Case, the "FF" (fast flow) mtyp zones are assigned the same material properties as adjacent materials, but may be modified for sensitivity cases.
14	FF_ROOF_HDPE	For the Compliance Case, the "FF" (fast flow) mtyp zones are assigned the same material properties as adjacent materials, but may be modified for sensitivity cases.

Table 4.4-67: PORFLOW Model Geometry for SDU 1

Dimension	Units	Modeled Value
Distance to the Water Table	ft	48
Floor Thickness	in	24
Saltstone Thickness	ft	24 – 23.5
Clean Grout Thickness	in	6
Roof Thickness	ft	1.6 – 0.5
Sand Drainage Layer Thickness	ft	2
Minimum Backfill Soil Overburden Thickness Based on Previous Closure Cap Design	ft	4
Roof Slope	%	2.083
Wall Thickness	in	18
Crack Width	in	2
Backfill Width	ft	65 [a]
Sand Drain Extension Length	ft	25

[a] Measured from outside perimeter of SDU to end of model

4.4.4.3.2 SDU 4 Flow Model Geometry

Figure 4.4-42 shows the modeled mtyp zones for SDU 4. Figure 4.4-43 shows the grid resolution. Figure 4.4-44 and Figure 4.4-45 display additional details at the corners of the SDU. Table 4.4-68 provides the key for the numbered mtyp zones

and Table 4.4-69 provides a summary of the modeled dimensions for SDU 4. The material properties for each mtyp zone are defined in Section 4.4.4.3.5.

Figure 4.4-42: SDU 4 Material Zones for PORFLOW Vadose Zone Modeling

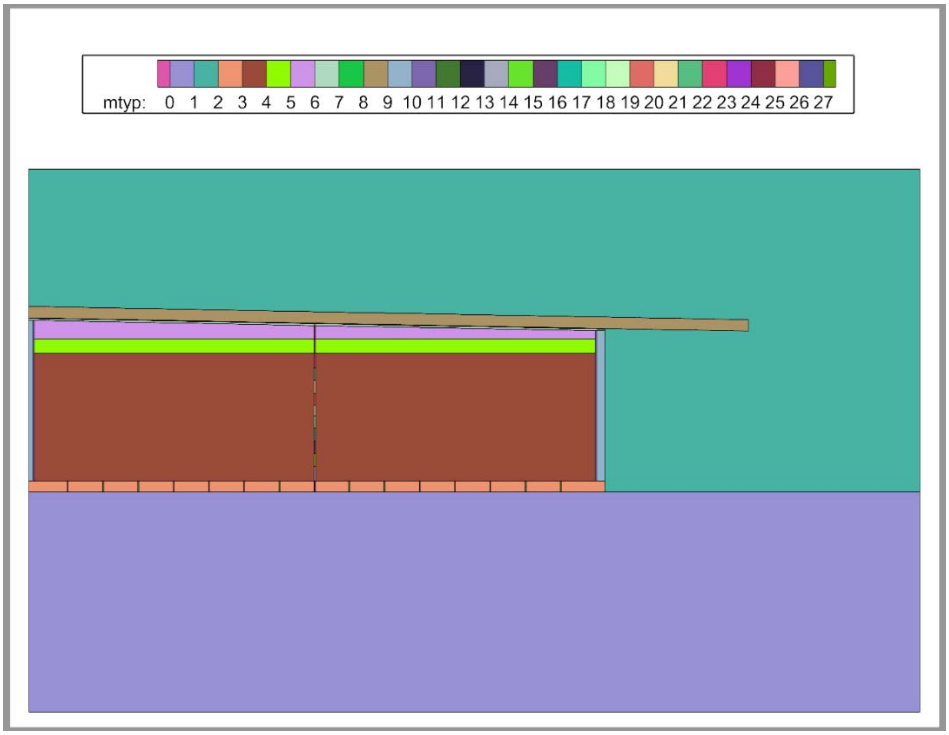

Figure 4.4-43: SDU 4 Gridding for PORFLOW Vadose Zone Modeling

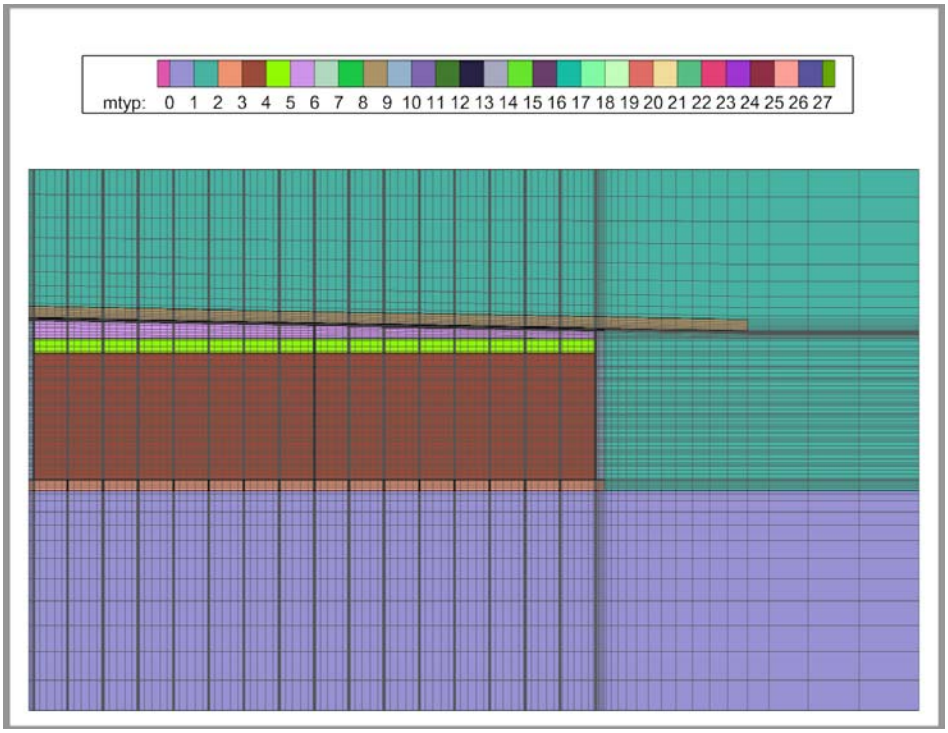

Figure 4.4-44: SDU 4 Upper Corner Detail for PORFLOW Vadose Zone Modeling

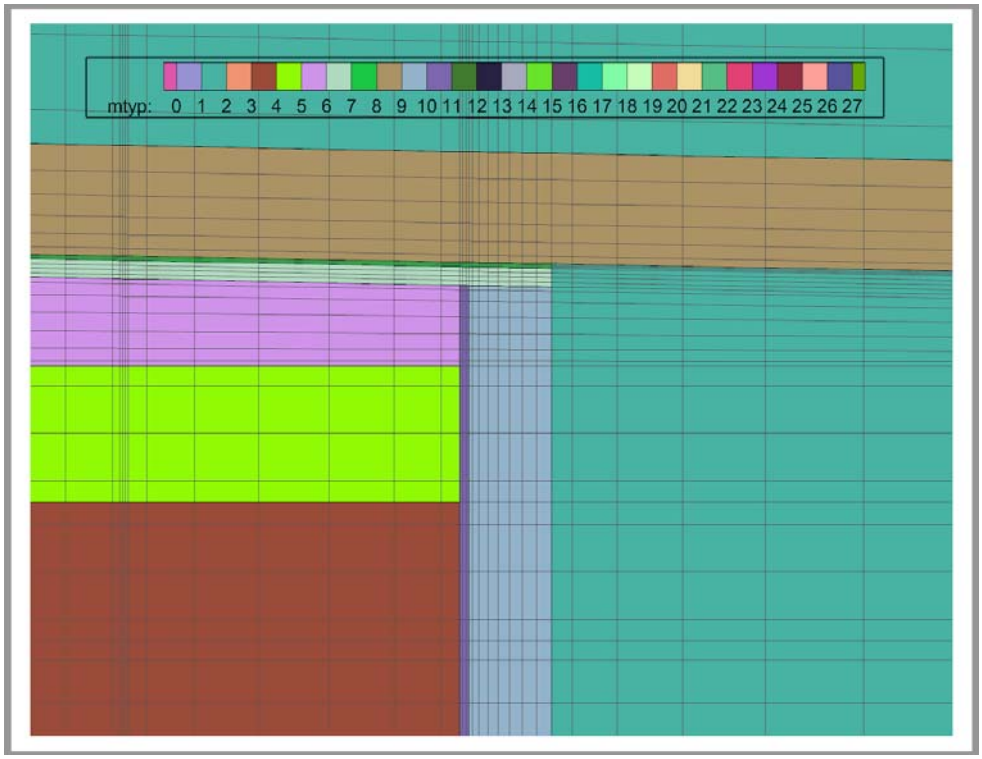

Figure 4.4-45: SDU 4 Lower Corner Detail for PORFLOW Vadose Zone Modeling

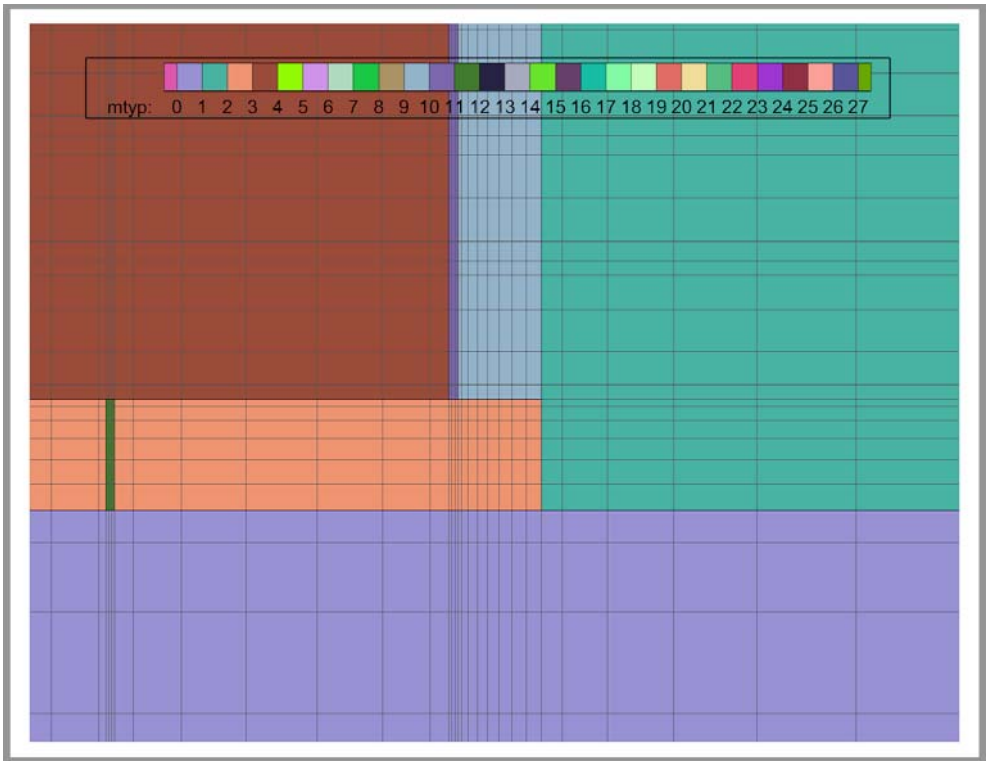

Table 4.4-68: SDU 4 mtyp Zones

Zone	Material Name	Comments
1	NATIVE_SOIL	This mtyp represents the vadose zone soils beneath the SDU. It is assigned the material properties for the Lower Vadose Zone soils.
2	BACKFILL	This mtyp represents the soils surrounding the SDUs and above the SDUs.
3	FLOOR	SDU floor material.
4	SALTSTONE	Saltstone waste form material.
5	SALT_TOP	This mtyp is assigned to the top of the saltstone waste form. Due to the design of the SDU 4 roof, part of the steel structure extends down into the saltstone. While the initial properties are identical to saltstone, this mtyp zone is subject to degradation via carbonation.
6	CLEAN_GROUT	This mtyp is assigned the same material properties as saltstone but can be simulated with or without an initial inventory for transport modeling.
7	ROOF	SDU roof material.
8	ROOF_HDPE_GCL	This mtyp represents the composite barrier above the SDU roof.
9	SAND_DRAIN	This is the lower sand drainage layer above the SDU.
10	WALL	SDU wall material.
11	SHEET_DRAIN	This mtyp represents the sheet drain along the interior of the SDU walls. It is assigned the material properties of saltstone, but the properties can be manipulated to assess potential fast flow path conditions.
12	JOINT	This mtyp represents the waterstops and other engineered joints at various SDU concrete interfaces. It is assigned the material properties for gravel to promote flow.
13	FF_FLOOR	This mtyp represents the floor directly beneath the representative SDU 4 roof-support column.
14-25	FF_GROUTXX (where XX = 1 through 12)	These mtyp segments are used to simulate a representative SDU 4 roof-support column.
26	FF_ROOF	This mtyp represents the roof directly above the representative SDU 4 roof-support column.
27	FF_ROOF_HDPE	This mtyp represents the composite barrier above the representative SDU 4 roof-support column.

Table 4.4-69: PORFLOW Model Geometry for SDU 4

Dimension	Units	Modeled Value
Distance to the Water Table	ft	38.4
Floor Thickness	in	24
Saltstone Thickness	ft	24.75
Clean Grout Thickness	in	39.4 – 17
Roof Thickness	in	4
HDPE/GCL Thickness	in	1
Sand Drainage Layer Thickness	ft	2
Minimum Backfill Soil Overburden Thickness Based on Previous Closure Cap Design	ft	24
Roof Slope	%	1.851
Center Wall Thickness	in	9
Wall Thickness	in	18
Sheet Drain Width	in	2
Crack Width	in	2
Backfill Width	ft	55 [a]
Sand Drain Extension Length	ft	25

[a] Measured from outside perimeter of SDU to end of model

4.4.4.3.3 150-Foot Diameter SDU Flow Model Geometry

Figure 4.4-46 shows the modeled mtyp zones for the 150-foot diameter SDUs. (Note: In PORFLOW the 150-foot diameter SDU model is identified as the "VadoseSDU2" model) Figure 4.4-47 shows the grid resolution. Figure 4.4-48 and Figure 4.4-49 display additional details at the corners of the SDU. Table 4.4-70 provides the key for the numbered mtyp zones and Table 4.4-71 provides a summary of the modeled dimensions for the 150-foot diameter SDUs. The material properties for each mtyp zone are defined in Section 4.4.4.3.5.

Figure 4.4-46: 150-Foot Diameter SDU Material Zones for PORFLOW Vadose Zone Modeling

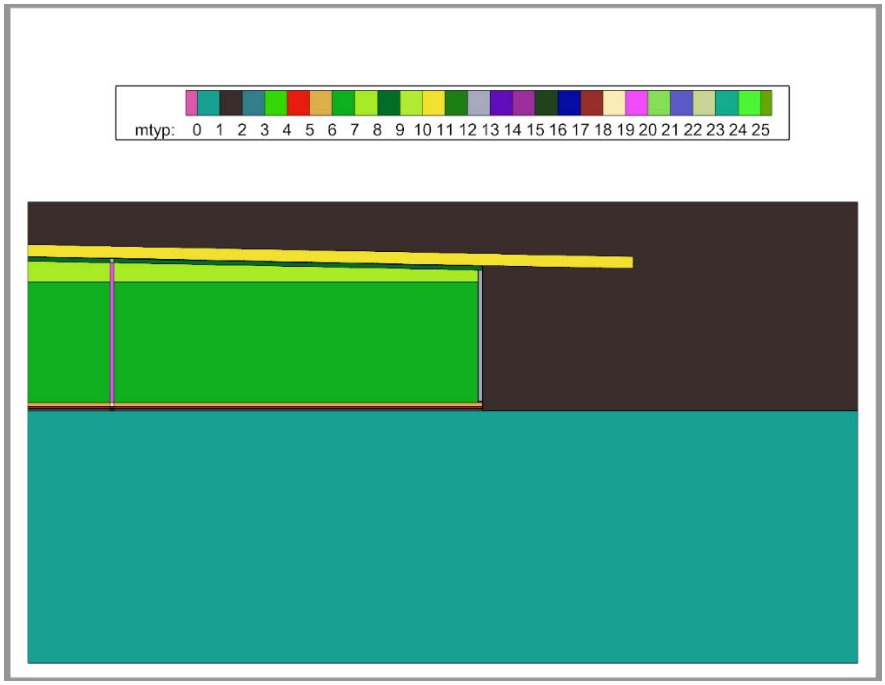

Figure 4.4-47: 150-Foot Diameter SDU Gridding for PORFLOW Vadose Zone Modeling

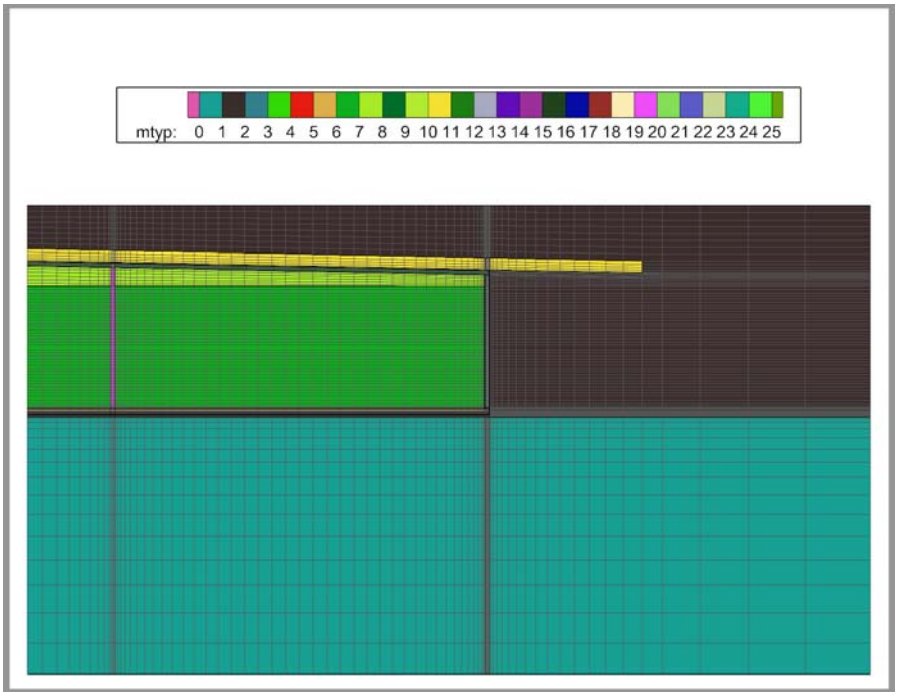

Figure 4.4-48: 150-Foot Diameter SDU Upper Corner Detail for PORFLOW Vadose Zone Modeling

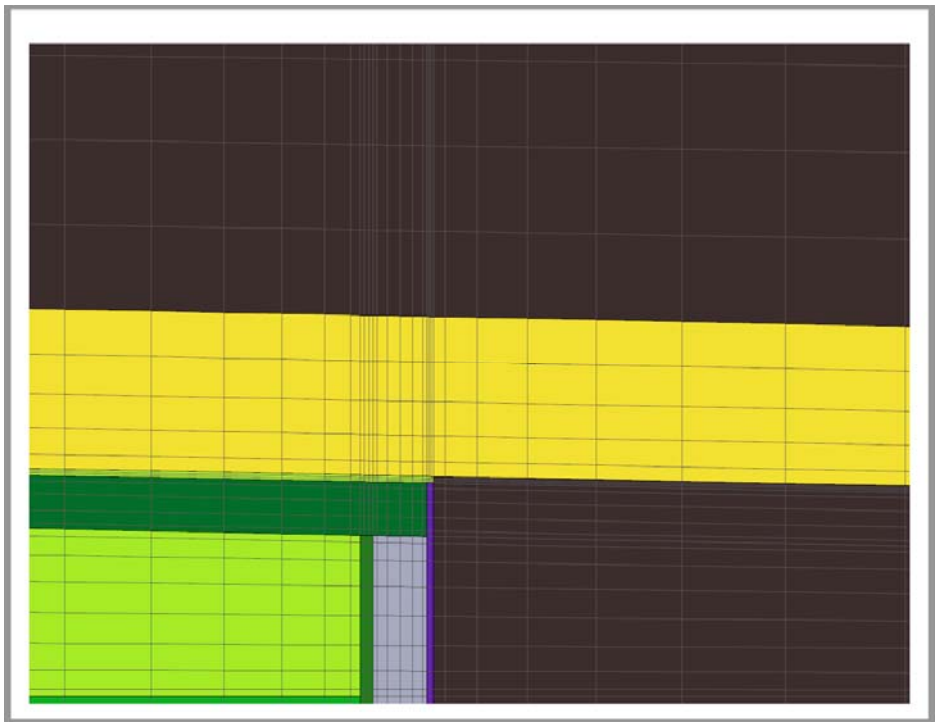

Figure 4.4-49: 150-Foot Diameter SDU Lower Corner Detail for PORFLOW Vadose Zone Modeling

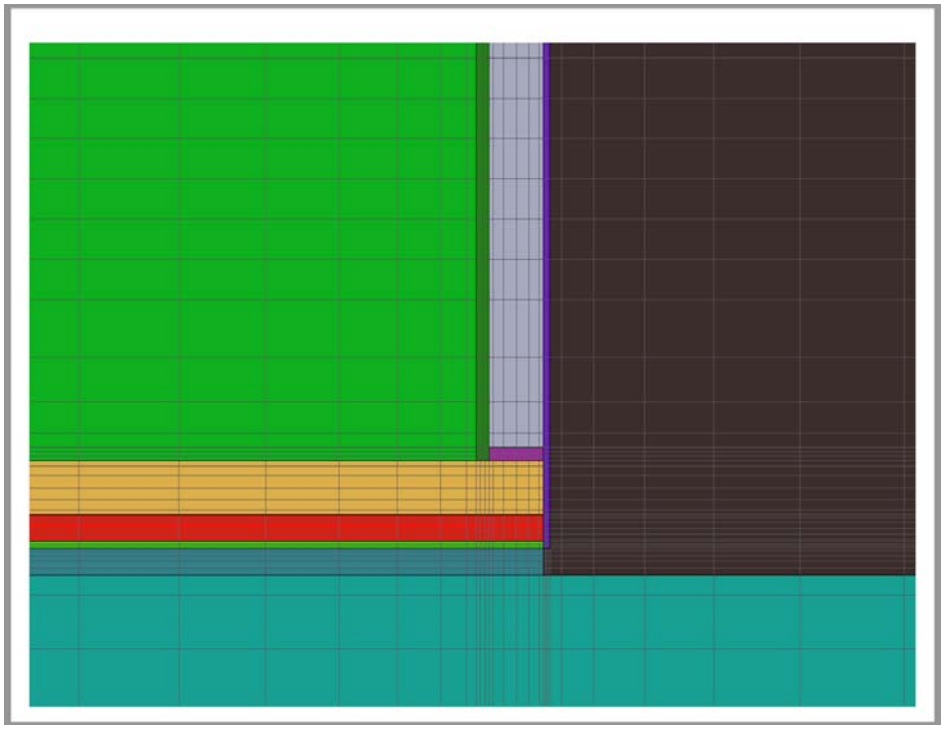

Table 4.4-70: 150-Foot Diameter SDU mtyp Zones

Zone	Material Name	Comments
1	NATIVE_SOIL	This mtyp represents the vadose zone soils beneath the SDU. It is assigned the material properties for the Lower Vadose Zone soils.
2	BACKFILL	This mtyp represents the soils surrounding the SDUs and above the SDUs.
3	LOWER_MUD_MAT	Lower mud mat beneath the SDU.
4	FLOOR_HDPE_GCL	This mtyp represents the composite barrier between the mud mats.
5	UPPER_MUD_MAT	Upper mud mat beneath the SDU.
6	FLOOR	SDU floor material.
7	SALTSTONE	Saltstone waste form material.
8	CLEAN_GROUT	This mtyp is assigned the same material properties as saltstone but can be simulated with or without an initial inventory for transport modeling.
9	ROOF	SDU roof material.
10	ROOF_HDPE_GCL	This mtyp represents the composite barrier above the SDU roof.
11	SAND_DRAIN	This is the lower sand drainage layer above the SDU.
12	SHEET_DRAIN	This mtyp represents the sheet drain along the interior of the SDU walls. It is assigned the material properties of saltstone, but the properties can be manipulated to assess potential fast flow path conditions.
13	WALL	SDU wall material.
14	HDPE	This mtyp represents the HDPE liner along the exterior of the SDU walls.
15	JOINT	This mtyp represents the waterstops and other engineered joints at various SDU concrete interfaces. It is assigned the material properties for gravel to promote flow.
16	FF_LOWER_MUD	This mtyp represents the lower mud mat beneath the representative 150-foot diameter SDU roof-support column.
17	FF_FLOOR_HDPE	This mtyp represents the lower composite barrier beneath the representative 150-foot diameter SDU roof-support column.
18	FF_UPPER_MUD	This mtyp represents the upper mud mat beneath the representative 150-foot diameter SDU roof-support column.
19	FF_FLOOR	This mtyp represents the floor directly beneath the representative 150-foot diameter SDU roof-support column.
20	FF_GROUT	This mtyp zone is used to simulate the representative 150-foot diameter SDU roof-support column.
21	FF_ROOF	This mtyp represents the roof directly above the representative 150-foot diameter SDU roof-support column.
22	FF_ROOF_HDPE	This mtyp represents the composite barrier above the representative 150-foot diameter SDU roof-support column.

Table 4.4-71: PORFLOW Model Geometry for 150-foot Diameter SDUs

Dimension	Units	Modeled Value
Distance to the Water Table	ft	42
Lower Mud Mat Thickness	in	4
HDPE/GCL Thickness	in	1
Upper Mud Mat Thickness	in	4
Floor Thickness	in	8
Saltstone Thickness	ft	20
Clean Grout Thickness	in	42 – 24
Roof Thickness	in	8
HDPE/GCL Thickness	in	1
Sand Drainage Layer Thickness	ft	2
Minimum Backfill Soil Overburden Thickness Based on Previous Closure Cap Design	ft	7
Roof Slope	%	2.00
Inner Saltstone Radius	ft	13.7
Column Width	in	7
Outer Saltstone Thickness	ft	60.5
Sheet Drain Width	in	2
Wall Thickness	in	8
HDPE/GCL Thickness	in	1
Backfill Width	ft	62 [a]
Sand Drain Extension Length	ft	25

[a] Measured from outside perimeter of SDU to end of model

4.4.4.3.4 375-Foot Diameter SDU Flow Model Geometry

Figure 4.4-50 shows the modeled mtyp zones for most of the 375-foot diameter SDUs (i.e., all expect for SDUs 6 and 9, which are described later in Section 4.4.4.3.4, respectively). (Note: In PORFLOW the 375-foot diameter SDU model is identified as the "VadoseSDU7" model.) Figure 4.4-51 shows the grid resolution. Figure 4.4-52 and Figure 4.4-53 display additional details at the corners of the SDU. Table 4.4-72 provides the key for the numbered mtyp zones and Table 4.4-73 provides a summary of the modeled dimensions for the 375-foot diameter SDUs. The material properties for each mtyp zone are defined in Section 4.4.4.3.5.

Figure 4.4-50: SDU 7 Material Zones for PORFLOW Vadose Zone Modeling

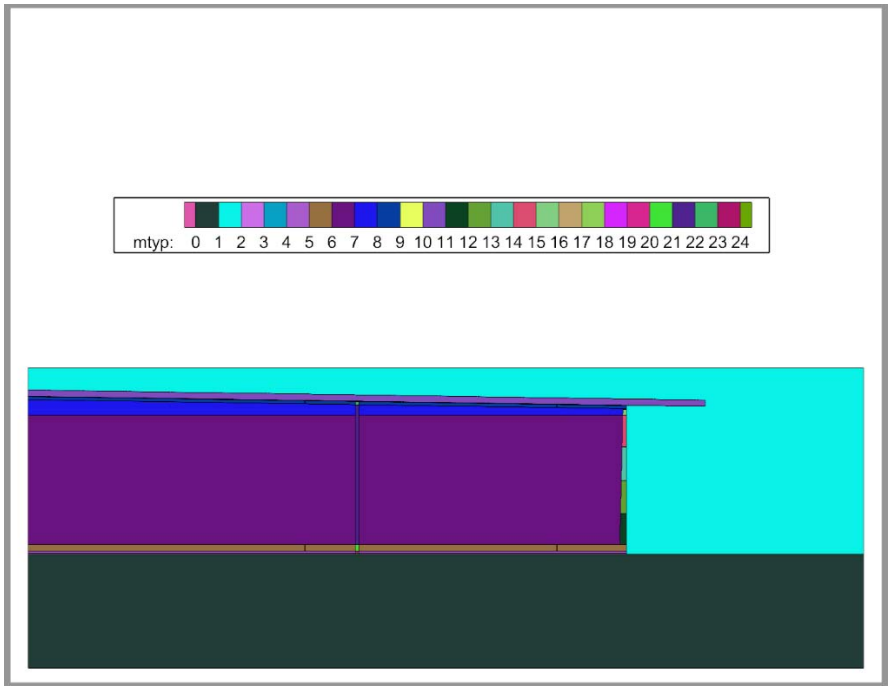

Figure 4.4-51: SDU 7 Gridding for PORFLOW Vadose Zone Modeling

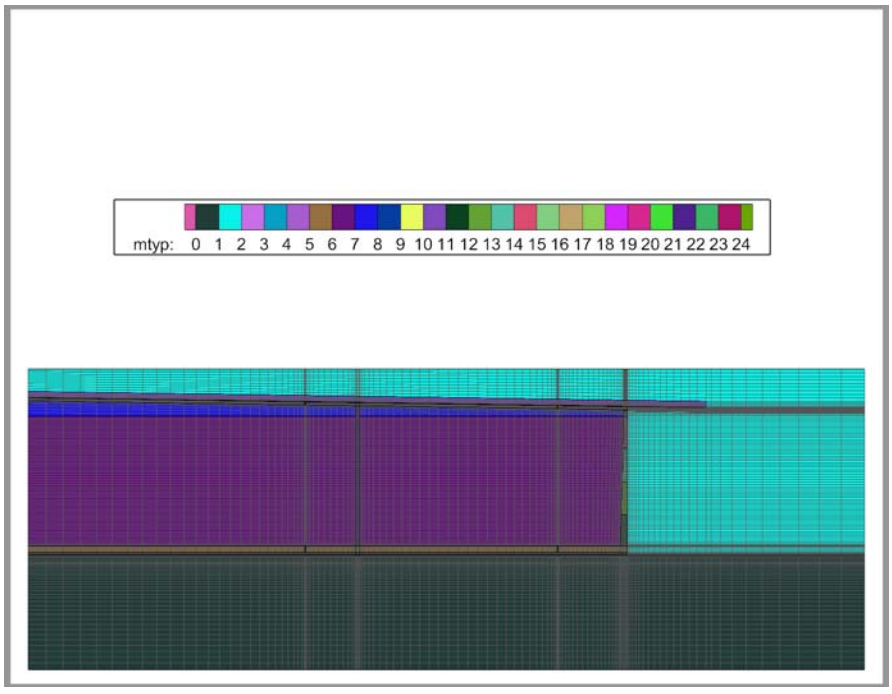

Figure 4.4-52: SDU 7 Upper Corner Detail for PORFLOW Vadose Zone Modeling

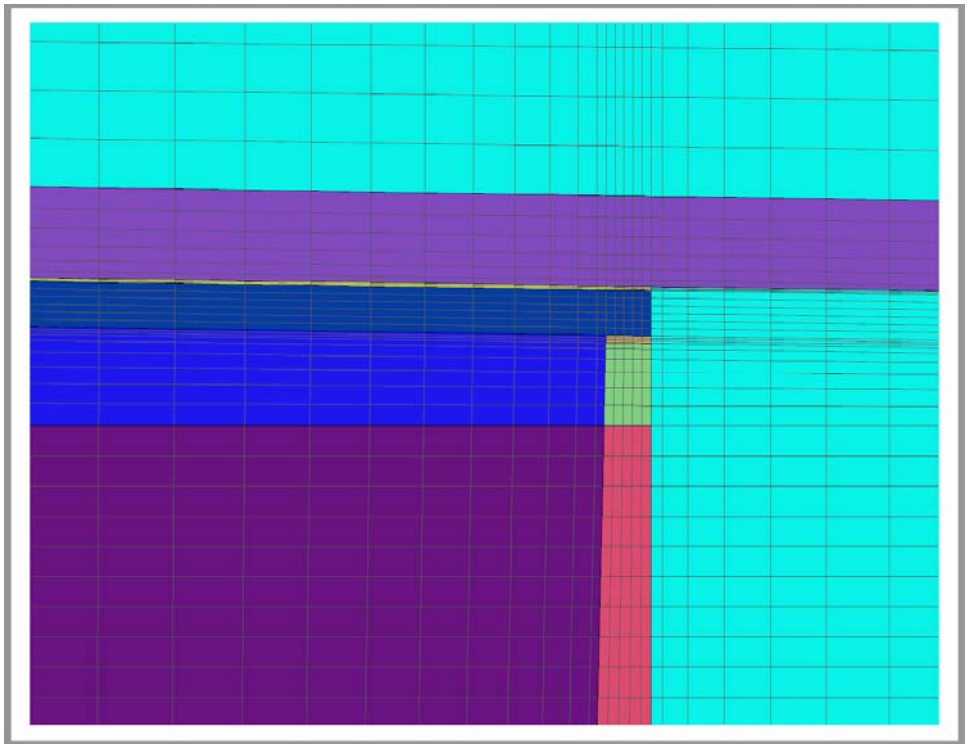

Figure 4.4-53: SDU 7 Lower Corner Detail for PORFLOW Vadose Zone Modeling

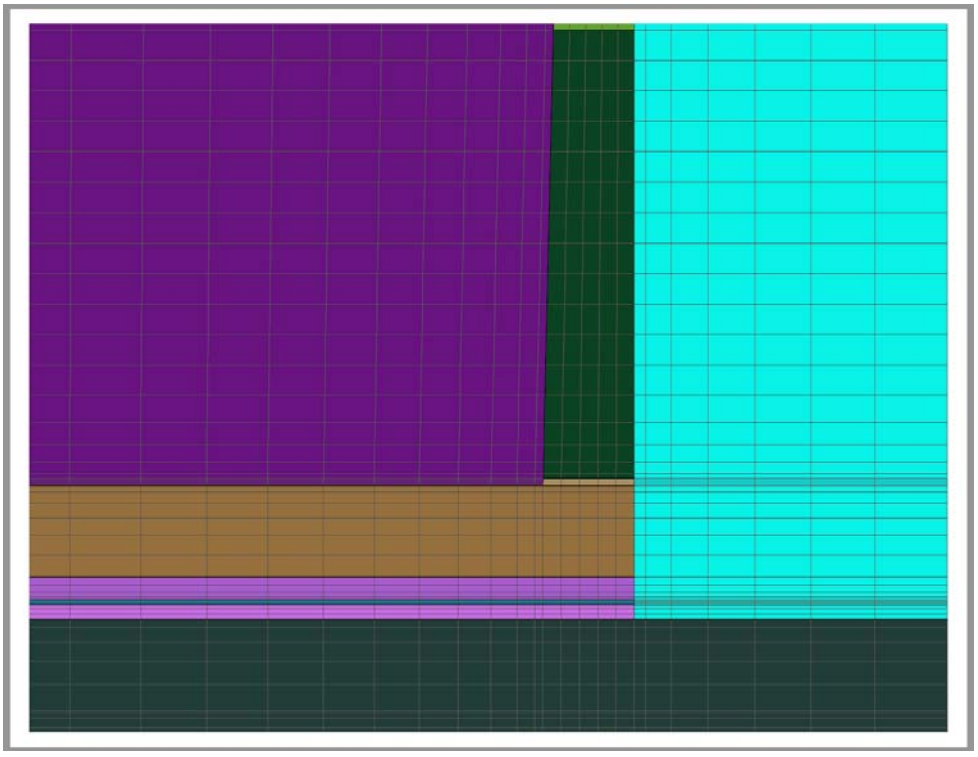

Table 4.4-72: 375-Foot Diameter SDU mtyp Zones

Zone	Material Name	Comments
1	NATIVE_SOIL	This mtyp represents the vadose zone soils beneath the SDU. It is assigned the material properties for the Lower Vadose Zone soils.
2	BACKFILL	This mtyp represents the soils surrounding the SDUs and above the SDUs.
3	LOWER_MUD_MAT	Lower mud mat beneath the SDU.
4	FLOOR_HDPE_GCL	This mtyp represents the composite barrier between the mud mats.
5	UPPER_MUD_MAT	Upper mud mat beneath the SDU.
6	FLOOR	SDU floor material.
7	SALTSTONE	Saltstone waste form material.
8	CLEAN_GROUT	This mtyp is assigned the same material properties as saltstone but can be simulated with or without an initial inventory for transport modeling.
9	ROOF	SDU roof material.
10	ROOF_HDPE_GCL	This mtyp represents the composite barrier above the SDU roof.
11	SAND_DRAIN	This is the lower sand drainage layer above the SDU.
12	WALL_1	SDU wall material (bottom segment).
13	WALL_2	SDU wall material (second segment from the bottom).
14	WALL_3	SDU wall material (middle segment).
15	WALL_4	SDU wall material (second segment from the top).
16	WALL_5	SDU wall material (top segment).
17	JOINT	This mtyp represents the waterstops and other engineered joints at various SDU concrete interfaces. It is assigned the material properties for gravel to promote flow.
18	FF_LOWER_MUD	This mtyp represents the lower mud mat beneath the representative 375-foot diameter SDU roof-support column.
19	FF_FLOOR_HDPE	This mtyp represents the lower composite barrier beneath the representative 375-foot diameter SDU roof-support column.
20	FF_UPPER_MUD	This mtyp represents the upper mud mat beneath the representative 375-foot diameter SDU roof-support column.
21	FF_FLOOR	This mtyp represents the floor directly beneath the representative 375-foot diameter SDU roof-support column.
22	FF_GROUT	This mtyp zone is used to simulate the representative 375-foot diameter SDU roof-support column.
23	FF_ROOF	This mtyp represents the roof directly above the representative 375-foot diameter SDU roof-support column.
24	FF_ROOF_HDPE	This mtyp represents the composite barrier above the representative 375-foot diameter SDU roof-support column.

Table 4.4-73: PORFLOW Model Geometry for 375-Foot Diameter SDUs (Except SDUs 6 and 9)

Dimension	Units	Modeled Value
Distance to the Water Table	ft	36
Lower Mud Mat Thickness	in	4
HDPE/GCL Thickness	in	1
Upper Mud Mat Thickness	in	6
Floor Thickness	in	24
Saltstone Thickness	ft	41
Clean Grout Thickness	ft	1.8 – 4.7
Roof Thickness	in	12
HDPE/GCL Thickness	in	1
Sand Drainage Layer Thickness	ft	2
Minimum Backfill Soil Overburden Thickness Based on Previous Closure Cap Design	ft	7
Wall/Floor Joint Width	in	2
Roof Slope	%	1.50
Floor Slope	%	0.0
Inner Saltstone Width	ft	103.5
Column Width	ft	1
Outer Saltstone Width	ft	83
Vertical Inner/Outer Joint Width	in	2
Wall Thickness, bottom	in	24
Wall Thickness, top	in	12
Backfill Width	ft	75 [a]
Sand Drain Extension Length	ft	25

[a] Measured from outside perimeter of SDU to end of model

SDU 6 Flow Model Geometry

Figure 4.4-54 shows the modeled mtyp zones for SDU 6. Unlike the other 375-foot diameter SDUs, SDU 6 was constructed with a sloped floor. This was due to an earlier design. Figure 4.4-55 shows the grid resolution. Figure 4.4-56 and Figure 4.4-57 display additional details at the corners of the grid. Despite the slightly different geometry, SDU 6 uses the same mtyp zones as the other 375-foot diameter SDUs (see Table 4.4-72). Table 4.4-74 provides a summary of the modeled dimensions for SDU 6. The material properties for each mtyp zone are defined in Section 4.4.4.3.5.

Figure 4.4-54: SDU 6 Material Zones for PORFLOW Vadose Zone Modeling

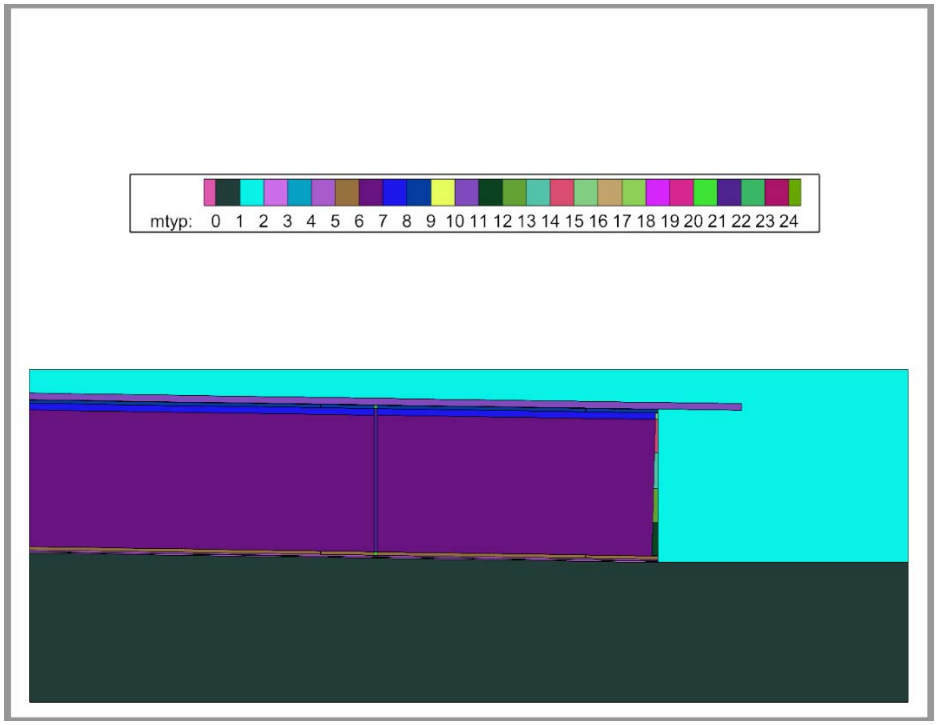

Figure 4.4-55: SDU 6 Gridding for PORFLOW Vadose Zone Modeling

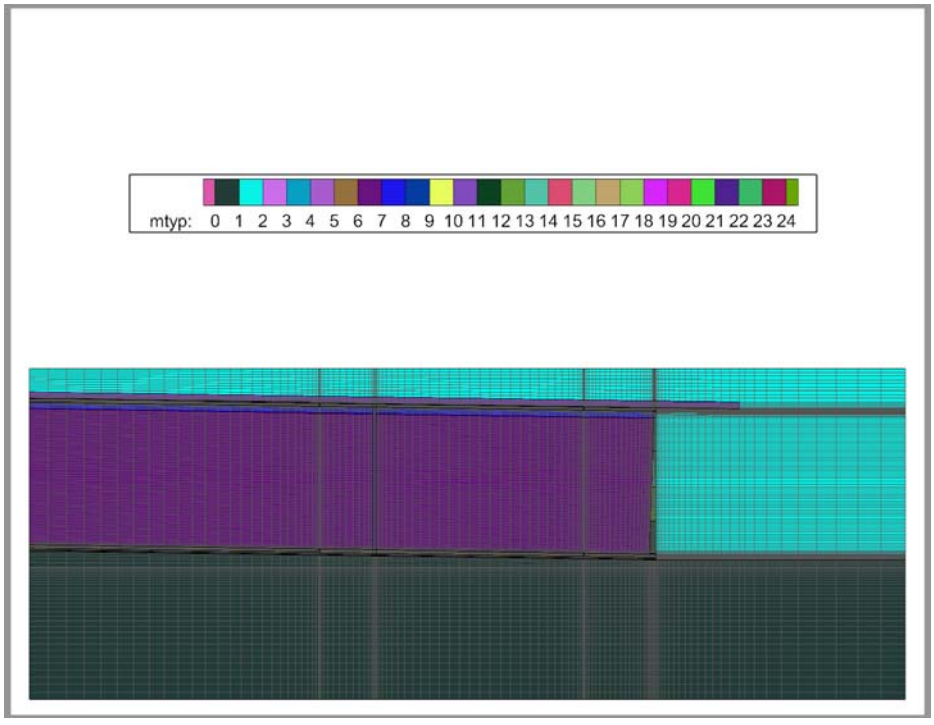

Figure 4.4-56: SDU 6 Upper Corner Detail for PORFLOW Vadose Zone Modeling

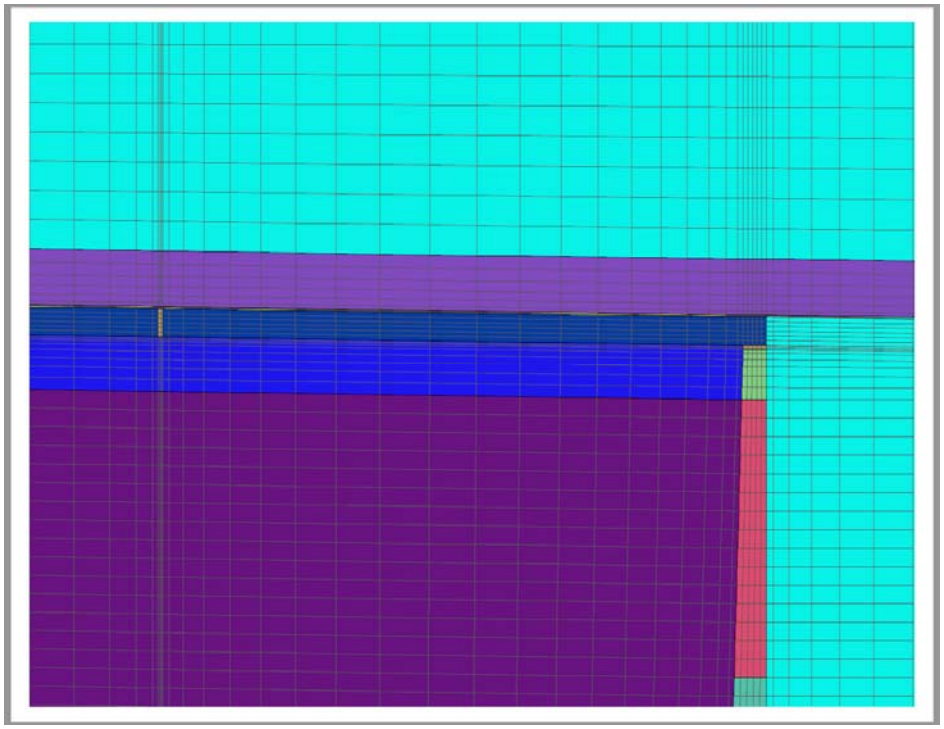

Figure 4.4-57: SDU 6 Lower Corner Detail for PORFLOW Vadose Zone Modeling

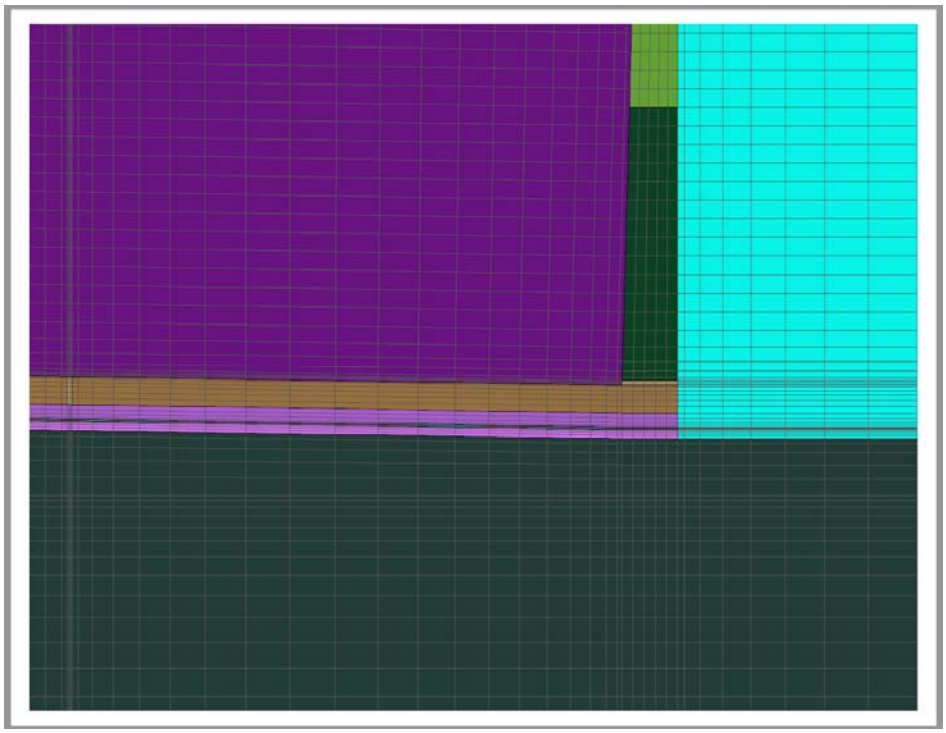

Table 4.4-74: PORFLOW Model Geometry for SDU 6

Dimension	Units	Modeled Value
Distance to the Water Table	ft	42
Lower Mud Mat Thickness	in	4
HDPE/GCL Thickness	in	1
Upper Mud Mat Thickness	in	6
Floor Thickness	in	12
Saltstone Thickness	ft	41
Clean Grout Thickness	ft	1.83 [a]
Roof Thickness	in	12
HDPE/GCL Thickness	in	1
Sand Drainage Layer Thickness	ft	2
Minimum Backfill Soil Overburden Thickness Based on Previous Closure Cap Design	ft	7
Wall/Floor Joint Width	in	2
Roof Slope	%	1.50
Floor Slope	%	1.50
Inner Saltstone Width	ft	103.5
Column Width	ft	1
Outer Saltstone Width	ft	83
Vertical Inner/Outer Joint Width	in	2
Wall Thickness, bottom	in	24
Wall Thickness, top	in	10
Backfill Width	ft	75 [b]
Sand Drain Extension Length	ft	25

[a] For SDU 6 the top of the saltstone waste form is modeled as having a slope that reflects the slope in the roof and the floor. As such, the thickness of the clean grout layer is uniform.

[b] Measured from outside perimeter of SDU to end of model.

SDU 9 Flow Model Geometry

SDU 9 is identical to the other 375-foot diameter SDUs (excluding SDU 6), with one exception: based on the location of SDU 9, it is assumed to be closer to the water table. To simulate this, the vadose zone beneath the SDU is not as thick as modeled for the other SDUs. Figure 4.4-58 shows the modeled mtyp zones for SDU 9. Figure 4.4-59 shows the grid resolution. Figure 4.4-60 and Figure 4.4-61 display additional details at the corners of the SDU. Despite the slightly different geometry, SDU 9 uses the same mtyp zones as the other 375-foot diameter SDUs (see Table 4.4-72). Table 4.4-75 provides a summary of the modeled dimensions for SDU 9. The material properties for each mtyp zone are defined in Section 4.4.4.3.5.

Figure 4.4-58: SDU 9 Material Zones for PORFLOW Vadose Zone Modeling

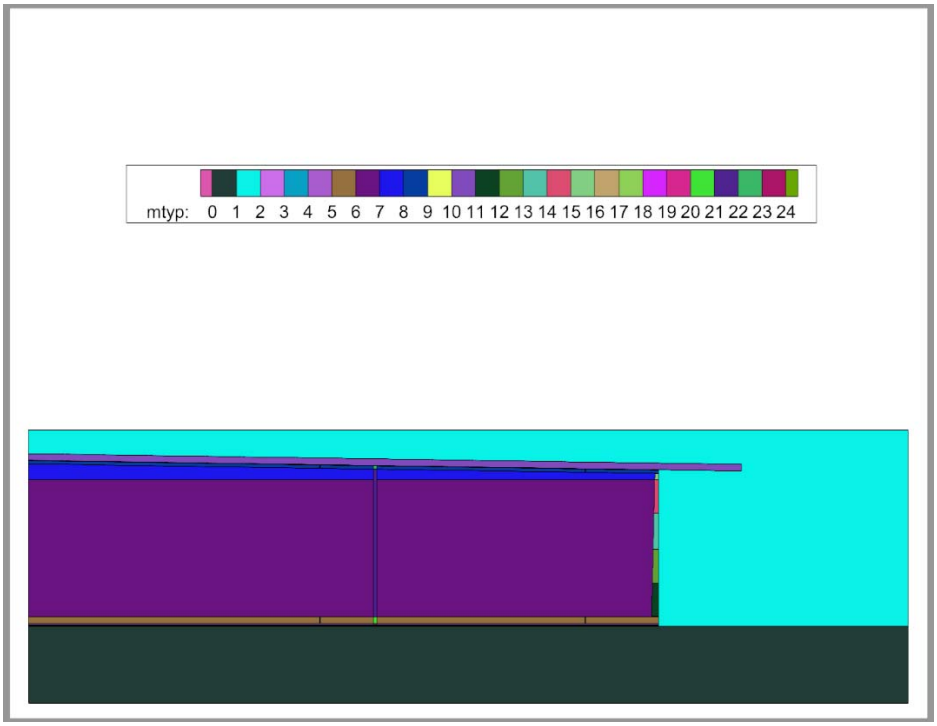

Figure 4.4-59: SDU 9 Gridding for PORFLOW Vadose Zone Modeling

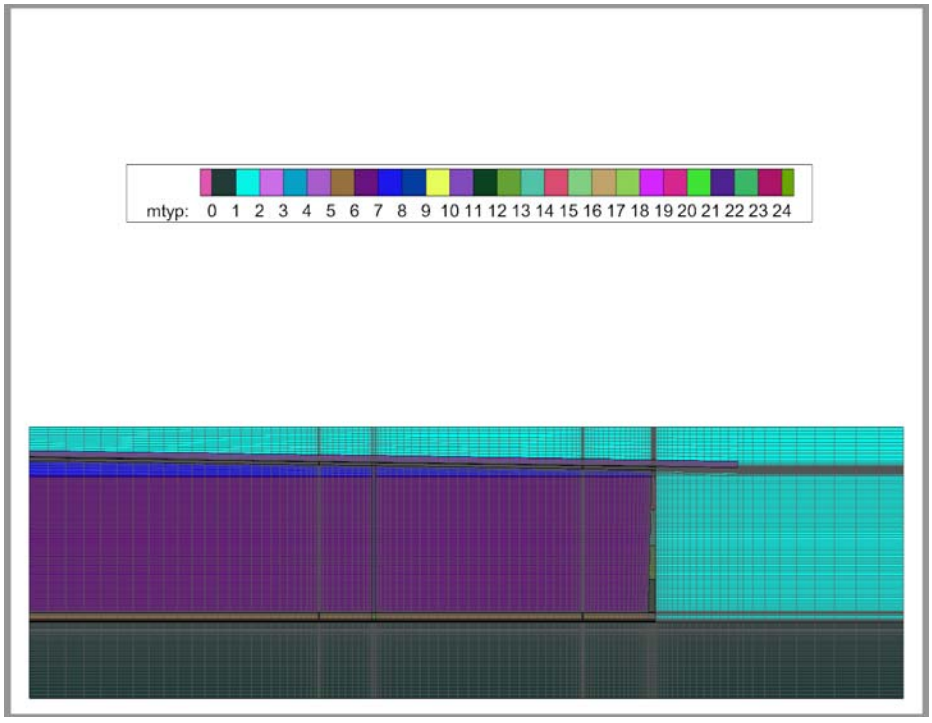

Figure 4.4-60: SDU 9 Upper Corner Detail for PORFLOW Vadose Zone Modeling

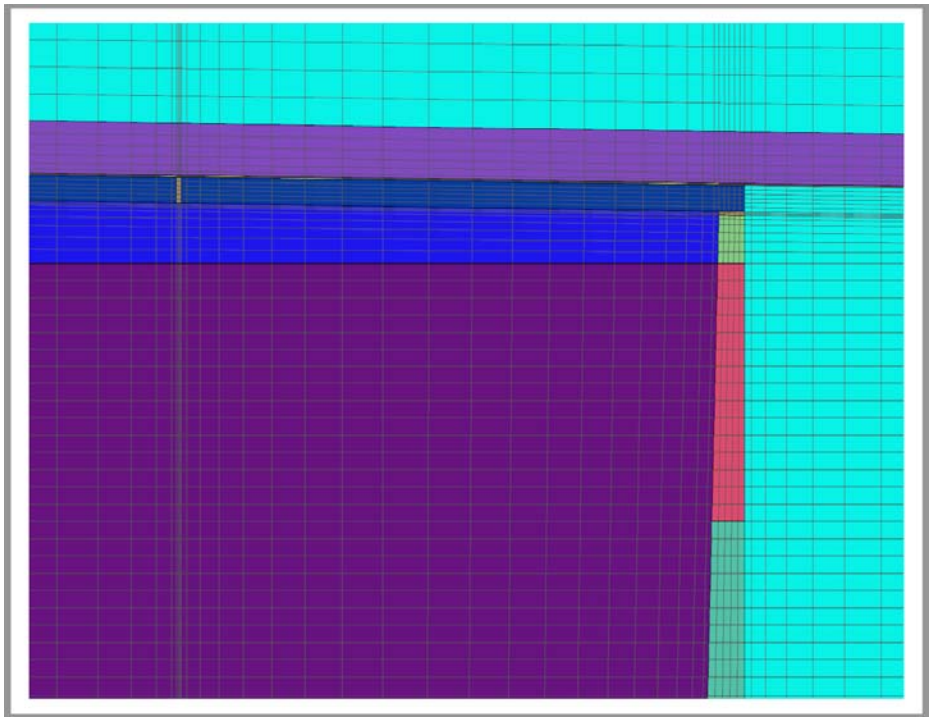

Figure 4.4-61: SDU 9 Lower Corner Detail for PORFLOW Vadose Zone Modeling

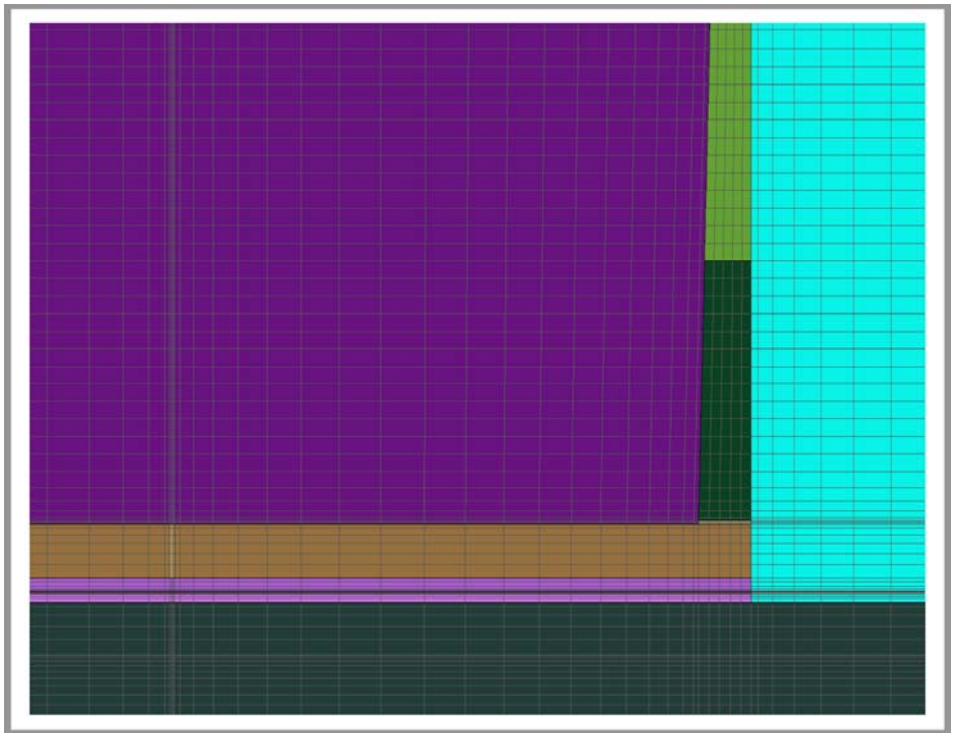

Table 4.4-75: PORFLOW Model Geometry for SDU 9

Dimension	Units	Modeled Value
Distance to the Water Table	ft	23
Lower Mud Mat Thickness	in	4
HDPE/GCL Thickness	in	1
Upper Mud Mat Thickness	in	6
Floor Thickness	in	24
Saltstone Thickness	ft	41
Clean Grout Thickness	ft	1.8 – 4.7
Roof Thickness	in	12
HDPE/GCL Thickness	in	1
Sand Drainage Layer Thickness	ft	2
Minimum Backfill Soil Overburden Thickness Based on Previous Closure Cap Design	ft	7
Wall/Floor Joint Width	in	2
Roof Slope	%	1.50
Floor Slope	%	0.0
Inner Saltstone Width	in	103.5
Column Width	ft	1
Outer Saltstone Width	ft	83
Vertical Inner/Outer Joint Width	in	2
Wall Thickness, bottom	in	24
Wall Thickness, top	in	12
Backfill Width	ft	75 [a]
Sand Drain Extension Length	ft	25

[a] Measured from outside perimeter of SDU to end of model

Design Margin Flow Model Geometry

In addition to the as-designed simulations, a Design Margin (DM) Case has also been developed to evaluate the potential risks associated with construction deviations. For the DM Case, the geometric dimensions of the future SDUs (i.e., SDUs 7 through 12) are modified to assume less roof slope and less thickness of the SDU roof, walls, and floor. Figure 4.4-62 shows the modeled mtyp zones for SDU 7DM. Figure 4.4-63 shows the grid resolution. Figure 4.4-64 and Figure 4.4-65 display additional details at the corners of the SDU. Despite the slightly different geometry, SDU 7DM uses the same mtyp zones as the other 375-foot diameter SDUs (see Table 4.4-72). Table 4.4-76 provides a summary of the modeled dimensions for SDU 7DM. The material properties for each mtyp zone are defined in Section 4.4.4.3.5.

Figure 4.4-62: SDU 7 DM Material Zones for PORFLOW Vadose Zone Modeling

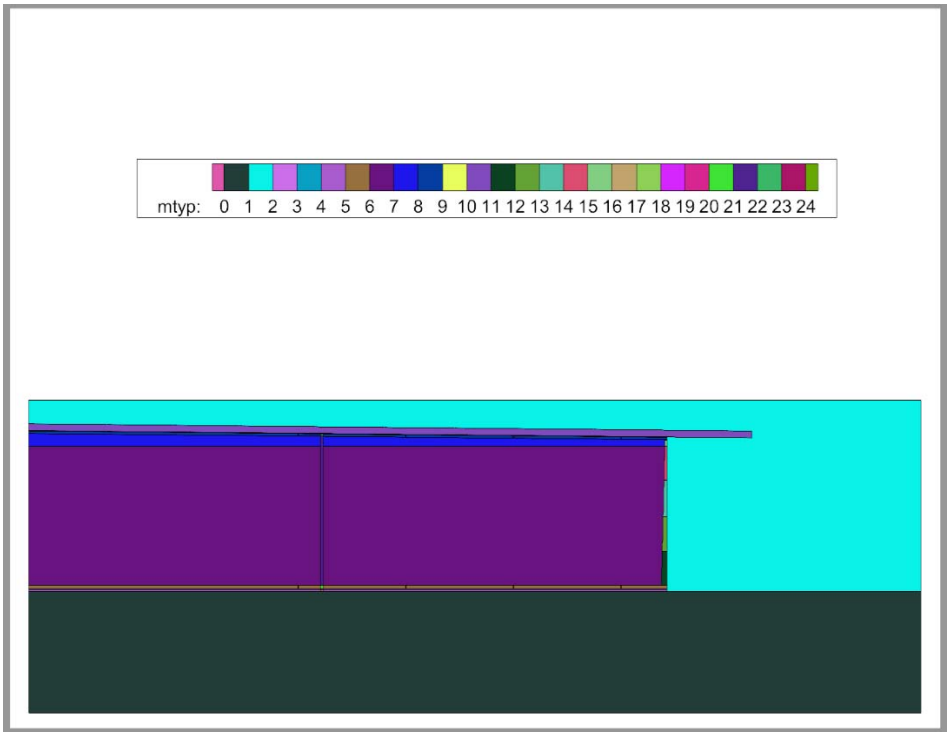

Figure 4.4-63: SDU 7 DM Gridding for PORFLOW Vadose Zone Modeling

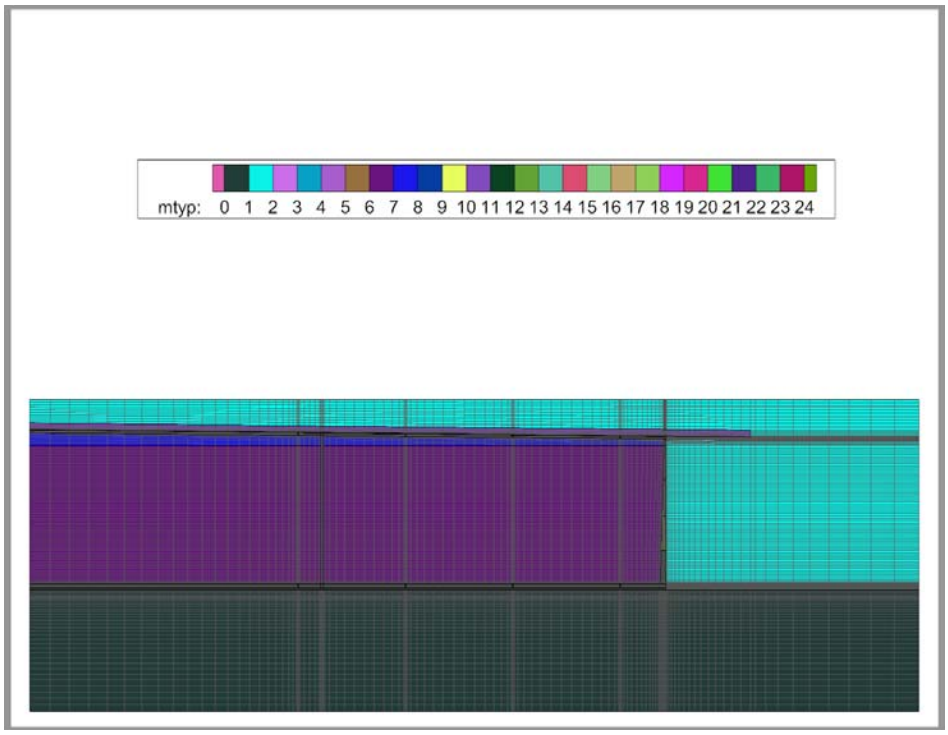

Figure 4.4-64: SDU 7 DM Upper Corner Detail for PORFLOW Vadose Zone Modeling

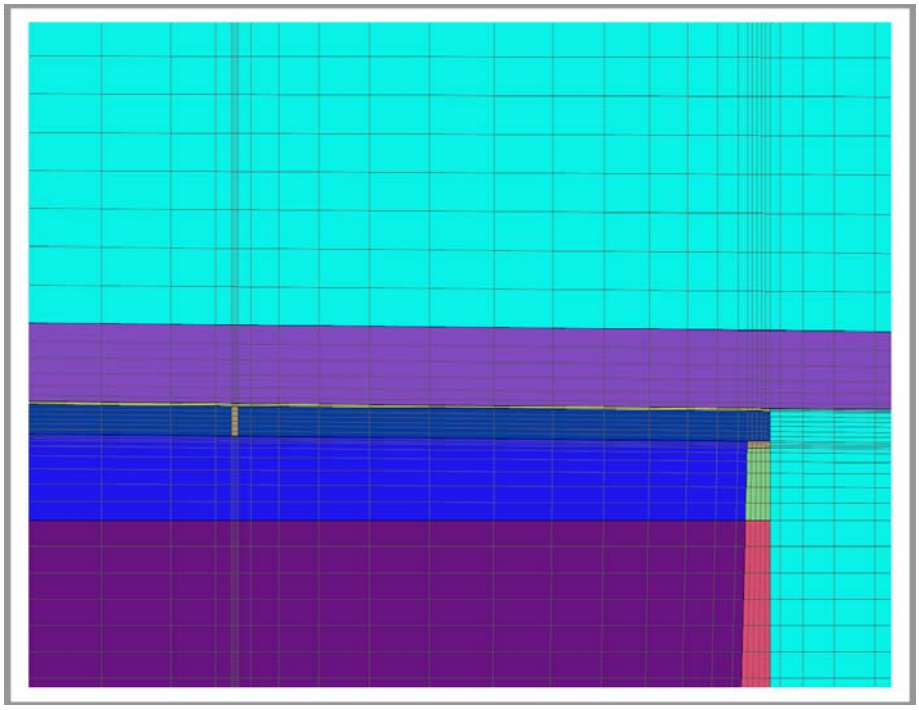

Figure 4.4-65: SDU 7 DM Lower Corner Detail for PORFLOW Vadose Zone Modeling

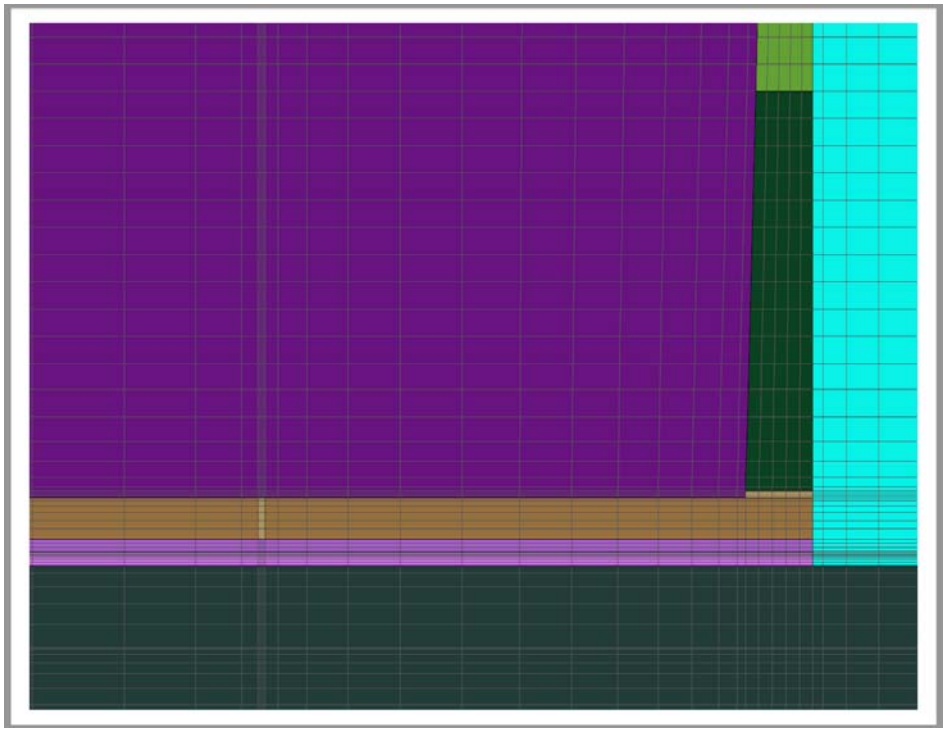

Table 4.4-76: PORFLOW Model Geometry for SDU 7DM

Dimension	Units	Modeled Value
Distance to the Water Table	ft	36
Lower Mud Mat Thickness	in	3
HDPE/GCL Thickness	in	1
Upper Mud Mat Thickness	in	4
Floor Thickness	in	12
Floor/Wall Joint Width	in	2
Saltstone Thickness	ft	41
Clean Grout Thickness	ft	1.8 – 3.7 [a]
Roof Thickness	in	9
Roof/Wall Joint Width	in	2
HDPE/GCL Thickness	in	1
Sand Drainage Layer Thickness	ft	2
Minimum Backfill Soil Overburden Thickness	ft	7
Roof Slope	%	1.00
Floor Slope	%	0
Inner Saltstone Width	ft	86.25
Column Width	ft	0.83
Outer Saltstone Width	ft	100.4
Vertical Inner/Outer Joint Width	in	2
Wall Thickness, bottom	in	20
Wall Thickness, top	in	7
Backfill Width	ft	75 [b]
Sand Drain Extension Length	ft	25

[a] Due to the reduced roof slope (from 1.5% to 1%), the apex of SDU 7DM is not as high as the SDU 7 model. The result is a clean grout layer with less thickness.

[b] Measured from outside perimeter of SDU to end of model.

4.4.4.3.5 Material Properties

The material properties used to define the vadose zone flow system include the hydraulic properties of cementitious materials (i.e., the saltstone waste form and SDU concrete), the sand drain, the backfill, the upper vadose zone (used for "Backfill"), the lower vadose zone (used for "Native Soil"), and gravel (used for joint properties). The controlling PORFLOW flow model input properties include:

- Solid phase (or particle) density,
- Porosity,
- Initial saturated hydraulic conductivity,
- Degraded saturated hydraulic conductivity,
- Saturation-Pressure Head curves, and
- Relative Permeability-Saturation curves.

Except for the saturation-pressure head curves and relative permeability-saturation curves, the hydraulic parameters for the sand drain, lower vadose zone, and gravel are listed in Table 4.3-2. The van Genuchten and Mualem-van Genuchten parameters (van Genuchten, 1980) defining the saturation-pressure head curves and relative permeability-saturation curves for

the sand drain, lower vadose zone, backfill, and gravel can be found in Table 4.4-77.

The "Lower Vadose Zone" material represents undisturbed sediments from SRS E- and Z-Areas below 264 ft-MSL and above the water table. The "Sand" material represents E- and Z-Area vadose zone sediments with less than 25% mud (fines) content. "Control Compacted Backfill" represents backfilled SRS soils that are controlled for grain size / texture and compacted during placement. "Gravel" is a generic material generally representative of gravels and similar very coarse-grained porous media. Site specific data were used to define the properties of Lower Vadose Zone (21 samples), Control Compacted Backfill (19 samples) and Sand (15 samples) shown in Table 4.3-2 and Table 4.4-77. A combination of literature and site-acquired data defined Gravel properties.

Table 4.4-77: van Genuchten Parameters for Soil Materials

Material name	θs	θr	α (1/cm)	n	m
Lower Vadose Zone [a]	0.3905	0.1604	0.0259	1.4048	0.2882
Control Compacted Backfill [b]	0.37	0.224	0.0219	1.659	0.3972
Sand (<25% Mud) [c]	0.3709	0.1074	0.048829	1.312885	0.23832
Gravel [d]	0.2505	0.0189	0.1266	1.5001	0.3334

[Sources: WSRC-STI-2006-00198, SRNL-STI-2018-00652]
a Used for mtyp zone: "Native Soil"
b Used for mtyp zone: "Backfill"
c Used for mtyp zone: "Sand Drain"
d Used for mtyp zone: "Joint"

Except for the saturation-pressure head curves and relative permeability-saturation curves, the hydraulic parameters for the cementitious materials making up the SDU can be found in Table 4.3-3. The van Genuchten and Mualem-van Genuchten parameters (van Genuchten, 1980) defining the saturation-pressure head curves and relative permeability-saturation curves input as tables into the PORFLOW models were developed for non-degraded and degraded media and are presented in Table 4.4-78 through Table 4.4-81. These tables also depict variations in the inputs for each of the three Central Scenario modeling cases (Realistic Case, Compliance Case, Pessimistic Case).

Note that the 150-foot diameter SDUs and SDU 6 have the same cementitious material properties because these have been constructed using nearly identical concrete formulations (see Table 3.2-3 and Table 3.2-4). After lessons learned during the construction of SDU 6, the SDU concrete formulation was modified to reduce the risk of cracking. The new formulation replaces some of the aggregate material with sand and includes a shrinkage-reducing admixture (Table 3.2-5). Based on testing of the new concrete formulation, SDUs 7 through 12 are all modeled as being constructed with a concrete that has a higher initial saturated

hydraulic conductivity relative to the earlier SDUs. The selection of the recommended values is described in SRR-CWDA-2018-00004.

Table 4.4-78: Hydraulic Properties for HDPE and HDPE/GCL

Parameter	HDPE	HDPE/GCL
Initial Saturated Hydraulic Conductivity (cm/s)	2.0E-13	1.8E-12
Saturated Hydraulic Conductivity Once Fully Degraded (cm/s)	4.10E-05	4.10E-05
Porosity, φ	0.3	0.3
van Genuchten Saturated Water Content, θ_s	0.119†	0.119†
van Genuchten Residual Water Content, θ_r	0†	0†
van Genuchten Parameter (1980), α (cm^{-1})	2.8940E-06†	2.8940E-06†
van Genuchten Parameter (1980), n	1.666†	1.666†
m = 1-1/n	0.4	0.4
Blending Averaging	Geometric	Geometric

Notes: † Ordinary/medium quality concrete from WSRC-STI-2006-00198, Table 6-6, Mix M69 is used as a surrogate material for these parameters.
The Closure Cap Model (see Section 4.4.1) also includes a composite HDPE/GCL barrier. Within the Closure Cap Model each component material was explicitly simulated. The HDPE material was assumed to be impervious (except where holes are present), and the GCL material was assigned an initial saturated hydraulic conductivity of 1.0E-08 cm/s. The differences in modeling assumptions between these two models were driven by the different purposes of the two models.

HDPE and composite HDPE/GCL liners are modeled as porous-media and assumed to exhibit water retention and relative permeability behaviors like cementitious materials. Specifically, ordinary/medium quality concrete [WSRC-STI-2006-00198] is the selected surrogate material for assigning van Genuchten / Mualem parameters to HDPE and HDPE/GCL materials. Porosity is arbitrarily set to 30%. Saturated hydraulic conductivities are based on initial HDPE hole size and spatial density. [SRRA107772-000009]

The hydraulic properties of cementitious materials including characteristic curves are defined from a mixture of literature and site-specific data (WSRC-STI-2006-00198, SRNL-STI-2011-00661, SRR-CWDA-2018-00004 Rev. 1), and in a few cases Leverett (1941) scaling. Based on the Leverett J-function, the van Genuchten α parameter for the Compliance Case and Pessimistic Case saltstone materials is defined using:

$$\alpha = \sqrt{\frac{K}{\alpha_{ref}}} K_{ref} \qquad \text{Eq. 4.4-105}$$

where the subscript ref refers to the Realistic Case reference material.

Table 4.4-79: Hydraulic Properties for SDU 1 and SDU 4 Vadose Zone Models

Parameter	Saltstone/ Grout/ Salt Top	Floor	Wall	Roof
Initial Saturated Hydraulic Conductivity (cm/s)	5.00E-10	7.80E-10	4.10E-05	7.80E-10
	1.00E-10	3.10E-10	1.00E-08	3.10E-10
	2.00E-09	2.10E-09	4.10E-05	2.10E-09
Saturated Hydraulic Conductivity Once Fully Degraded (cm/s)	4.10E-05	9.10E-05	4.10E-05	4.10E-05
Porosity, φ	0.656	0.106	0.181	0.106
van Genuchten Saturated Water Content, θ_s	0.58	0.082	0.082	0.119
van Genuchten Residual Water Content, θ_r	0	0	0	0
van Genuchten Parameter (1980), α (cm^{-1})	2.254E-05	2.0856E-06	2.0856E-06	2.894E-06
	1.008E-05			
	4.508E-05			
van Genuchten Parameter (1980), n	1.67131	1.9433	1.9433	1.666
m = 1-1/n	0.402	0.485	0.485	0.4
Blending Averaging	Geometric	Geometric	Geometric	Geometric

[Sources: WSRC-STI-2006-00198, SRNL-STI-2011-00661, SRR-CWDA-2018-00004 Rev. 1]

Notes: Shading indicates the applicable modeling case:

Gray shading indicates Compliance Case inputs,

Blue shading indicates Realistic Case inputs,

Pink shading indicates Pessimistic inputs, and

Inputs that are not shaded are applicable to all modeling cases.

Table 4.4-80: Cementitious Hydraulic Properties for 150-Foot Diameter SDUs and SDU 6 Vadose Zone Models

Parameter	Saltstone/ Grout	Floor	Wall	Roof	Mud Mat	Column
Initial Saturated Hydraulic Conductivity (cm/s)	5.00E-10	1.4E-10 (6.2E-06)	1.40E-10	1.4E-10 (6.2E-06)	(5.00E-09)	5.00E-09
	1.00E-10	1.0E-10 (6.2E-06)	1.00E-10	1.0E-10 (6.2E-06)	(5.00E-09)	5.00E-09
	2.00E-09	3.2E-10 (6.2E-06)	3.20E-10	3.2E-10 (6.2E-06)	(1.00E-08)	1.00E-08
Saturated Hydraulic Conductivity Once Fully Degraded (cm/s)	4.10E-05	9.10E-05	4.10E-05	4.10E-05	(4.10E-05)	4.10E-05
Porosity, φ	0.656	0.11	0.11	0.11	(0.211)	0.211
van Genuchten Saturated Water Content, θ_s	0.58	0.082	0.082	0.082	(0.226)	0.226
van Genuchten Residual Water Content, θ_r	0	0	0	0	(0)	0
van Genuchten Parameter (1980), a (cm^{-1})	2.254E-05	2.0856E-06	2.0856E-06	2.0856E-06	(7.61E-06)	7.61E-06
	1.008E-05					
	4.508E-05					
van Genuchten Parameter (1980), n	1.671	1.943	1.943	1.943	(1.393)	1.393
m = 1-1/n	0.402	0.485	0.485	0.485	(0.282)	0.282
Blending Averaging	Geometric	Geometric	Geometric	Geometric	Geometric	Geometric

[Sources: WSRC-STI-2006-00198, SRNL-STI-2011-00661, SRR-CWDA-2018-00004 Rev. 1]

Notes: Values in parentheses () are applicable to SDU 6 only.

Shading indicates the applicable modeling case:
Gray shading indicates Compliance Case inputs,
Blue shading indicates Realistic Case inputs,
Pink shading indicates Pessimistic inputs, and
Inputs that are not shaded are applicable to all modeling cases.

Table 4.4-81: Cementitious Hydraulic Properties for 375-Foot Diameter SDUs (Except SDU 6) Vadose Zone Models

Parameter	Saltstone/ Grout	Floor	Wall	Roof	Mud Mat	Column
Initial Saturated Hydraulic Conductivity (cm/s)	5.00E-10	7.80E-10	7.80E-10	7.80E-10	5.00E-09	5.00E-09
	1.00E-10	6.40E-10	6.40E-10	6.40E-10	5.00E-09	5.00E-09
	2.00E-09	9.10E-10	9.10E-10	9.10E-10	1.00E-08	1.00E-08
Saturated Hydraulic Conductivity Once Fully Degraded (cm/s)	4.10E-05	9.10E-05	4.10E-05	4.10E-05	4.10E-05	4.10E-05
Porosity, φ	0.656	0.11	0.11	0.11	0.211	0.211
van Genuchten Saturated Water Content, θ_s	0.58	0.082	0.082	0.082	0.226	0.226
van Genuchten Residual Water Content, θ_r	0	0	0	0	0	0
van Genuchten Parameter (1980), α (cm^{-1})	2.254E-05	2.0856E-06	2.0856E-06	2.0856E-06	7.61E-06	7.61E-06
	1.008E-05					
	4.508E-05					
van Genuchten Parameter (1980), n	1.671	1.943	1.943	1.943	1.393	1.393
m = 1-1/n	0.402	0.485	0.485	0.485	0.282	0.282
Blending Averaging	Geometric	Geometric	Geometric	Geometric	Geometric	Geometric

[Sources: WSRC-STI-2006-00198, SRNL-STI-2011-00661, SRR-CWDA-2018-00004 Rev. 1]

Notes: Shading indicates the applicable modeling case:

Gray shading indicates Compliance Case inputs,
Blue shading indicates Realistic Case inputs,
Pink shading indicates Pessimistic inputs, and
Inputs that are not shaded are applicable to all modeling cases.

4.4.4.4 Intermediate Flow Results and Model Interfaces

Volumetric flow rates for each of the flow models are depicted in the following figures (Figure 4.4-66 through Figure 4.4-77). These volumetric flow rates were used in conjunction with the results from the Contaminant Release Model (see Section 4.4.3) to determine the chemical transition times. These chemical transition times are used in the Vadose Zone Transport Model (see Section 4.4.5). The Vadose Zone Transport Model also uses the flow data to simulate the transport of contaminants through the vadose zone.

Two figures are depicted for each of the six Vadose Zone Flow Models. For each pair of figures, the first one shows the Compliance Case results out to 100,000 years after closure (using a logarithmic scale) for select mtyp zones, and the second one shows a comparison of the volumetric flow rates through saltstone, using the three Central Scenario cases.

In general, these figures show that the volumetric flow rates closely resemble the infiltration rates, with significant step changes occurring at 500 years (due to an assumed decrease in the hydraulic conductivity of the sand drainage layer within the closure cap)

and another occurring at 2,000 years (based on the assumed service life of the HDPE within the closure cap). Regardless of the modeling case, nearly all the SDU concrete is simulated to be fully degraded (hydraulically) within the first few thousand years (the only exceptions are the SDU 4 column in the Best Estimate and Compliance Cases, and the SDU 1 and 4 floors in the Best Estimate and Compliance Cases). As such, the overall performance of the disposal system is dominated by the initial saturated hydraulic conductivity of the saltstone waste form.

Typically, there is not much difference in the volumetric flow rates through mtyp zones with significant surface areas: the sand drainage layer, the composite barrier (HDPE and GCL) at the roof, the SDU roof, the saltstone, and the SDU floor. This indicates that flow is predominately downward, as the volume of water entering through the top of a material zone is in equilibrium with the volume of water leaving at the bottom of the material zone.

Comparisons of the volumetric flow rates through saltstone from the three Central Scenario cases show that, regardless of the SDU, for the first 500 years, all three cases show similar results. Between 500 and 2,000 years, the Compliance Case and the Pessimistic Case are both similar and are both approximately an order of magnitude higher than the Realistic Case. After 2,000 years the Pessimistic Case has volumetric flow rates that are approximately four to five times higher than the Compliance Case, while the Compliance Case is slightly more than an order of magnitude higher than the Realistic Case.

Figure 4.4-66: Volumetric Flow Rates Through SDU 1 Materials (Compliance Case)

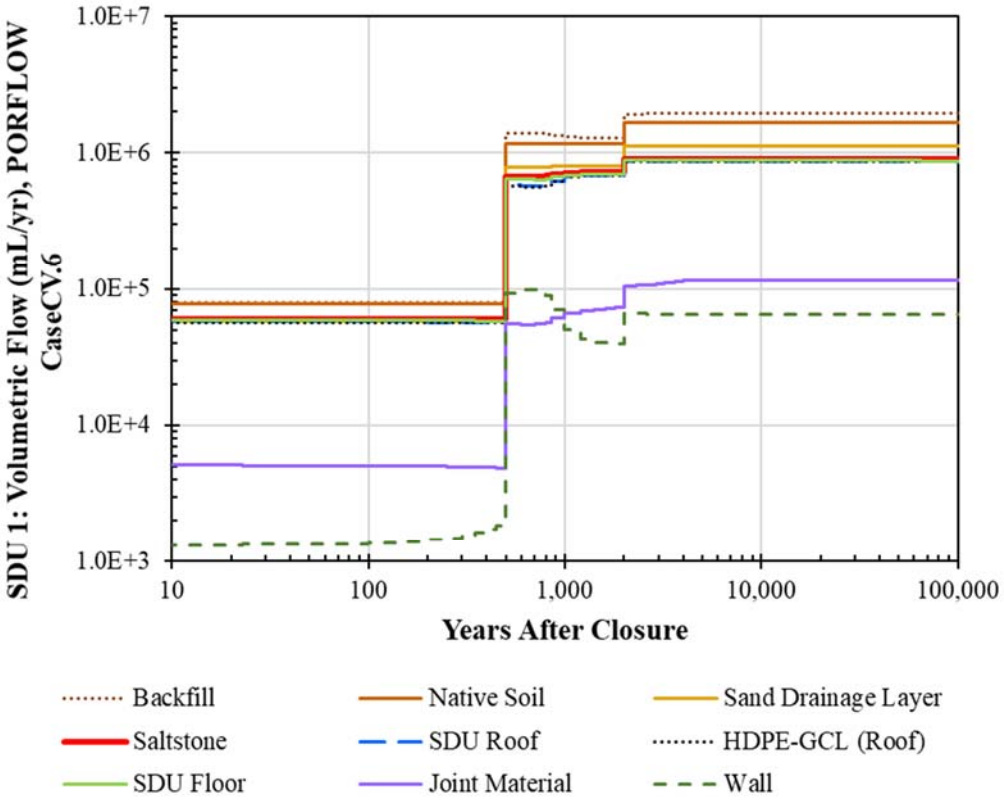

Figure 4.4-67: Comparison of Volumetric Flow Rates Through SDU 1 Saltstone

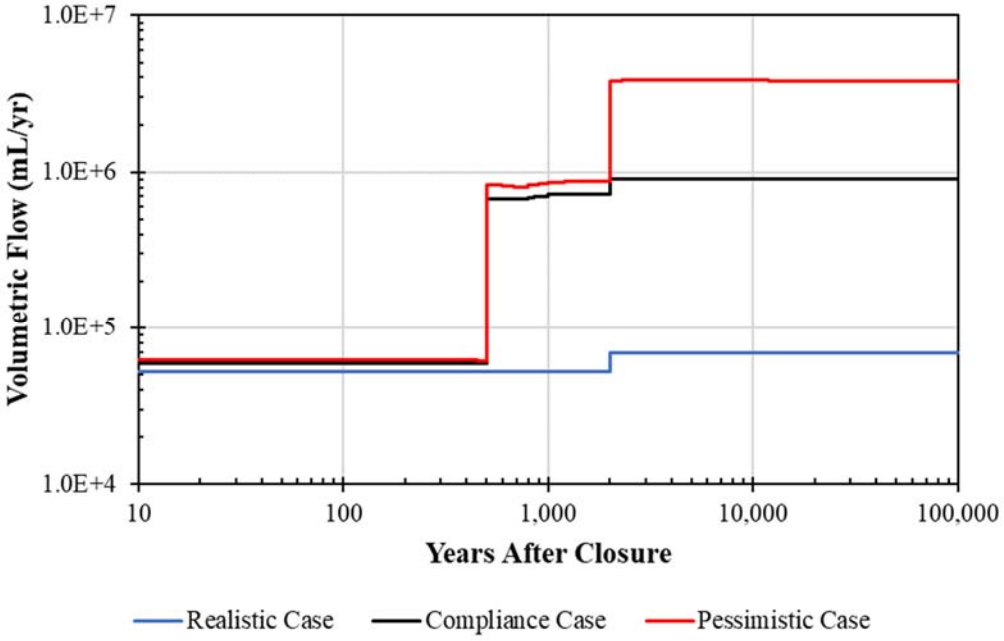

Figure 4.4-68: Volumetric Flow Rates Through SDU 4 Materials (Compliance Case)

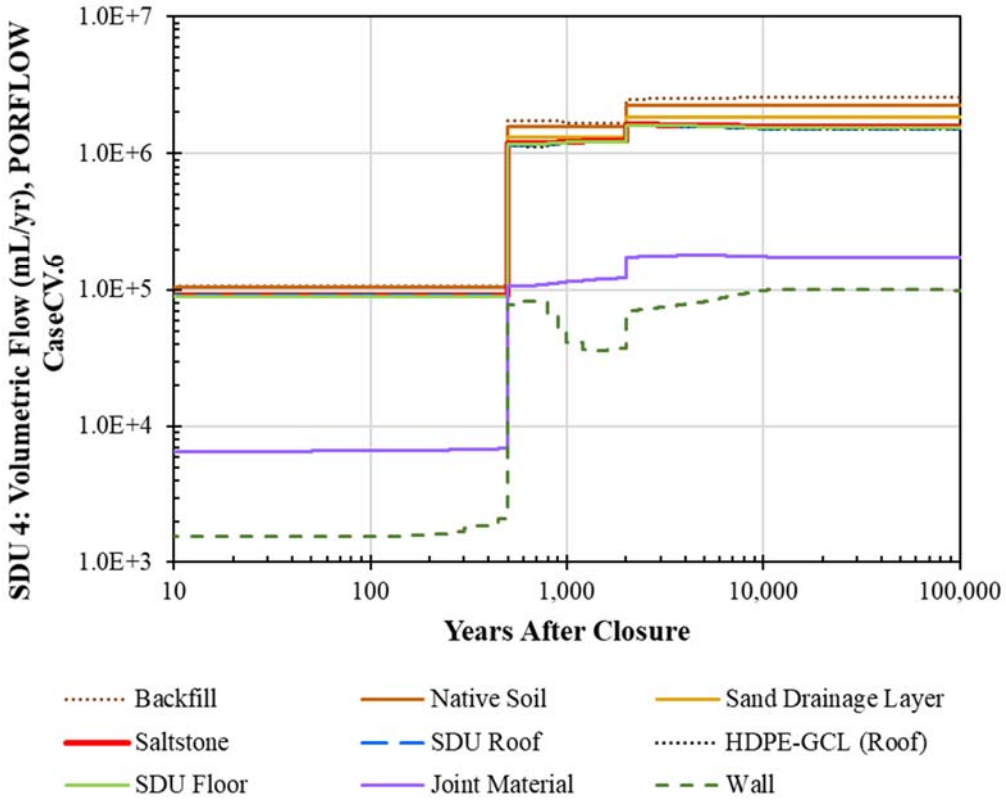

Figure 4.4-69: Comparison of Volumetric Flow Rates Through SDU 4 Saltstone

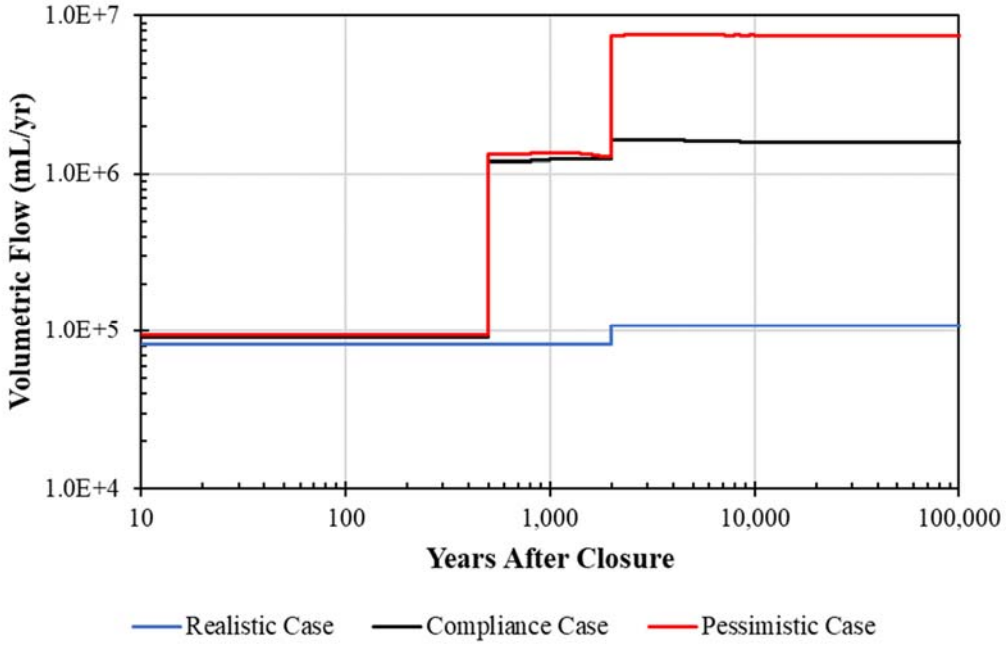

Figure 4.4-70: Volumetric Flow Rates Through 150-Foot Diameter SDU Materials (Compliance Case)

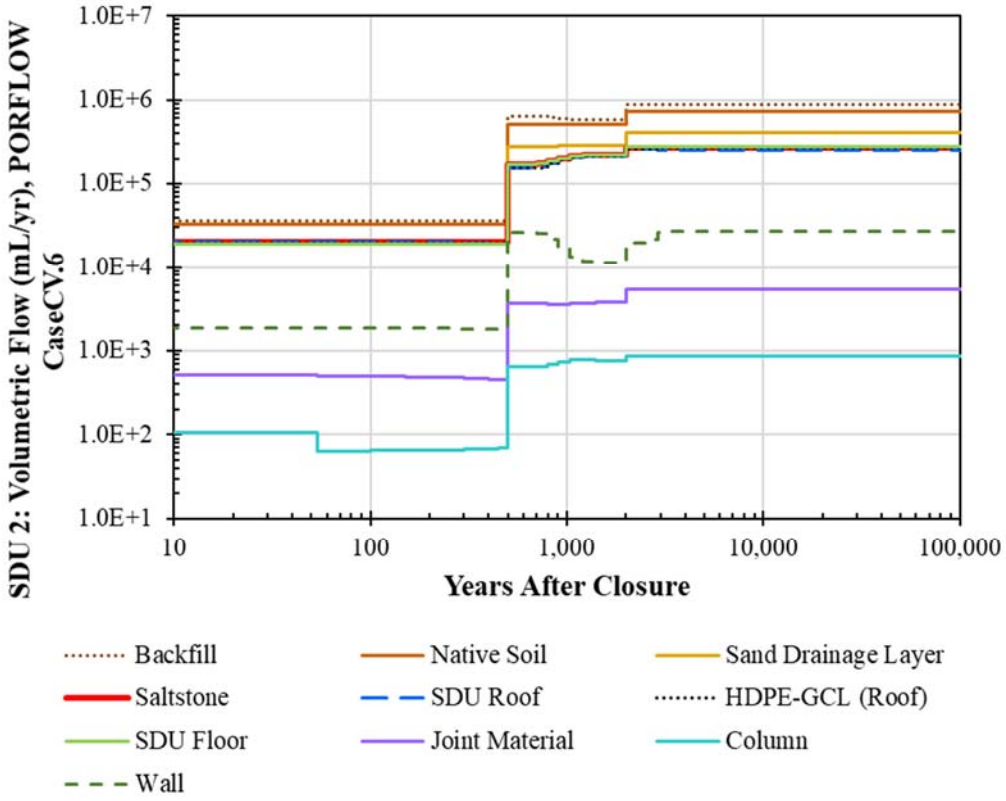

Figure 4.4-71: Comparison of Volumetric Flow Rates Through 150-Foot Diameter SDU Saltstone

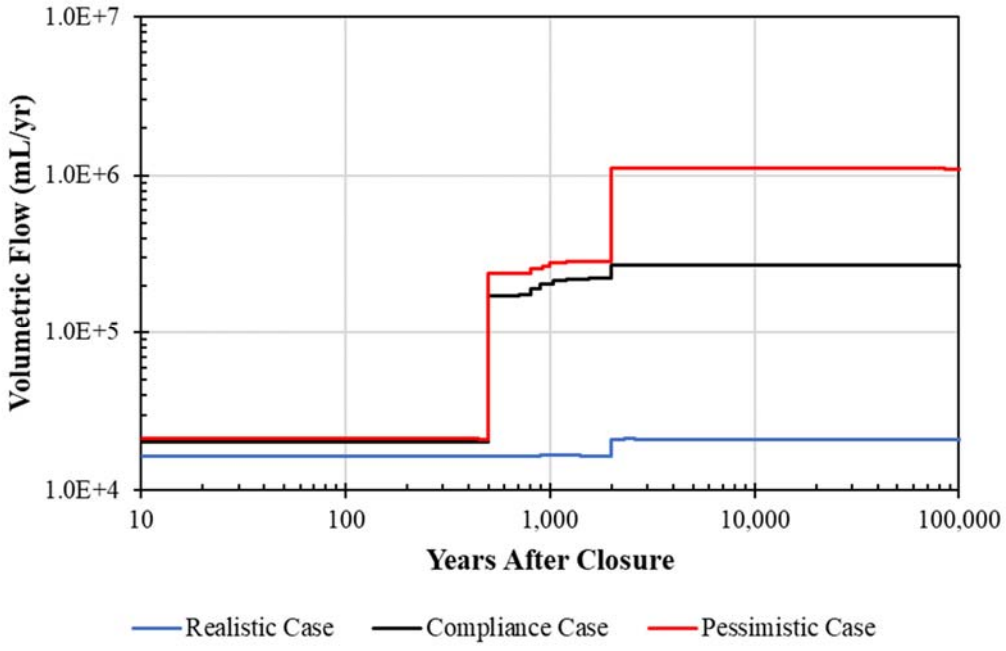

Figure 4.4-72: Volumetric Flow Rates Through 375-Foot Diameter SDU (SDU 7) Materials (Compliance Case)

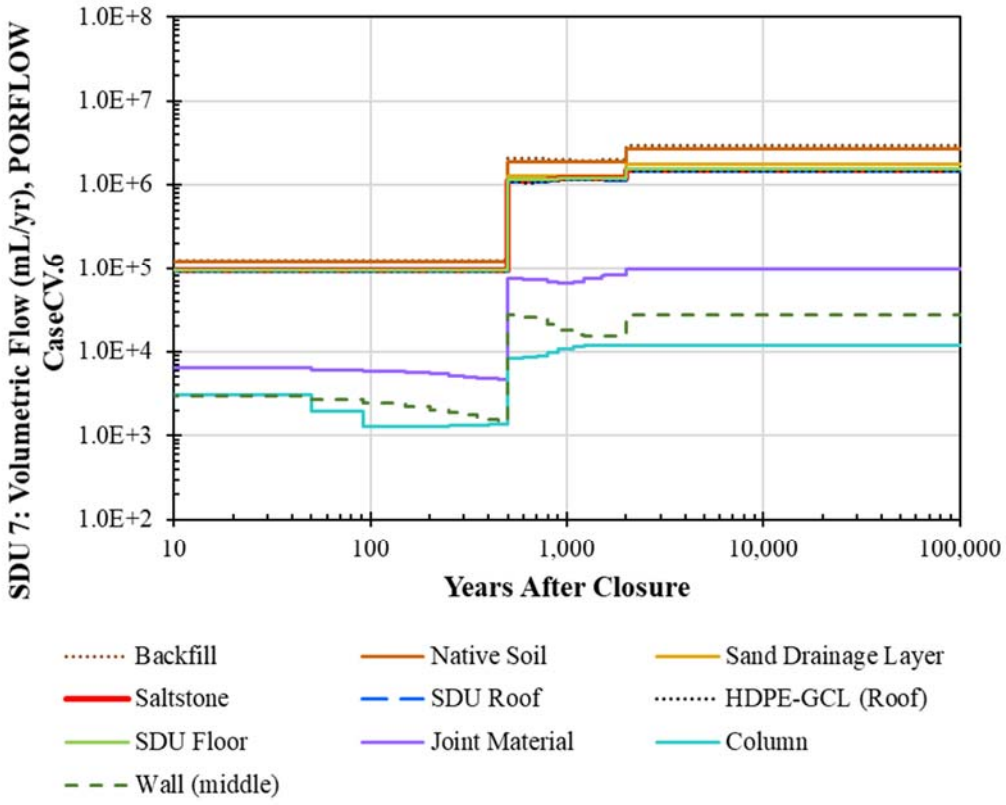

Figure 4.4-73: Comparison of Volumetric Flow Rates Through 375-Foot Diameter SDU (SDU 7) Saltstone

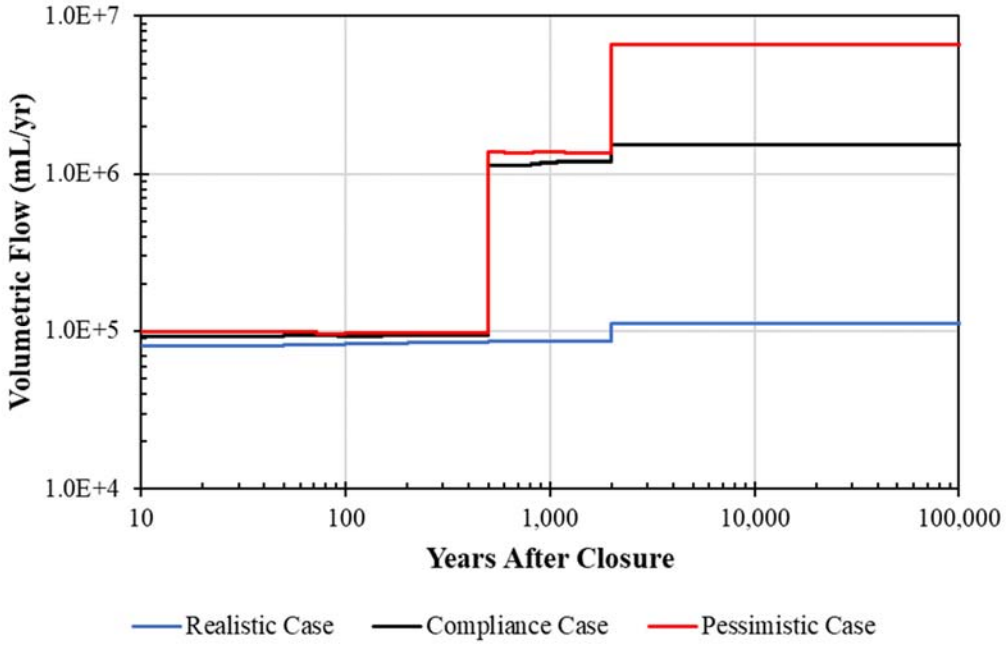

Figure 4.4-74: Volumetric Flow Rates Through SDU 6 Materials (Compliance Case)

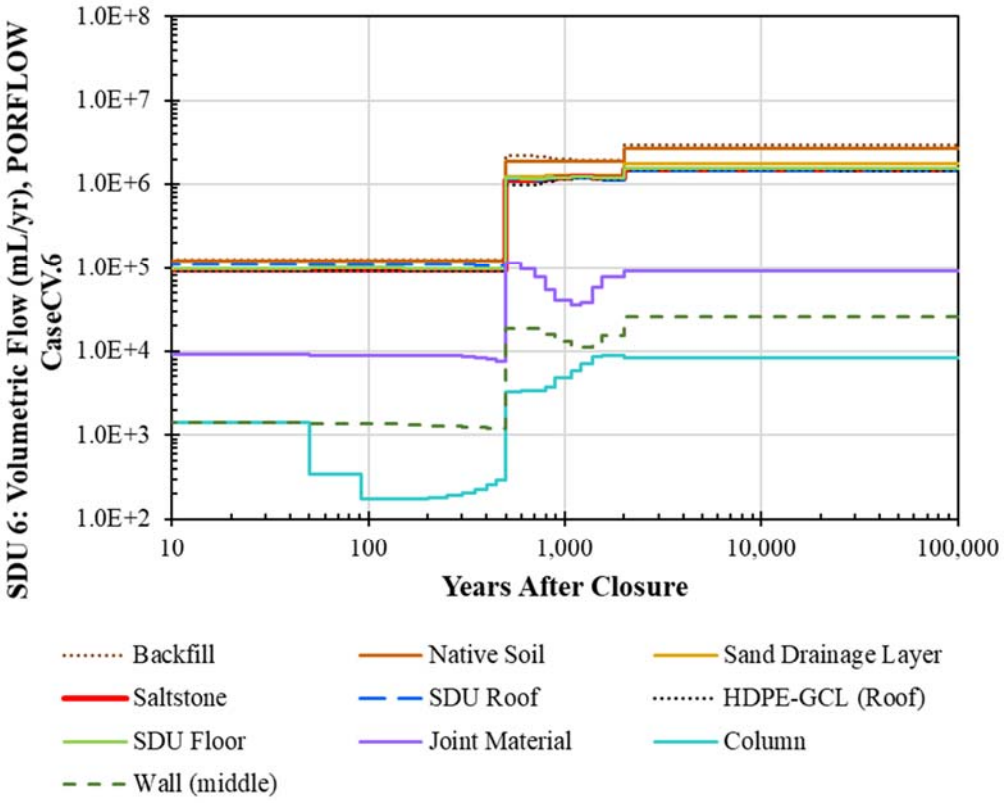

Figure 4.4-75: Comparison of Volumetric Flow Rates Through SDU 6 Saltstone

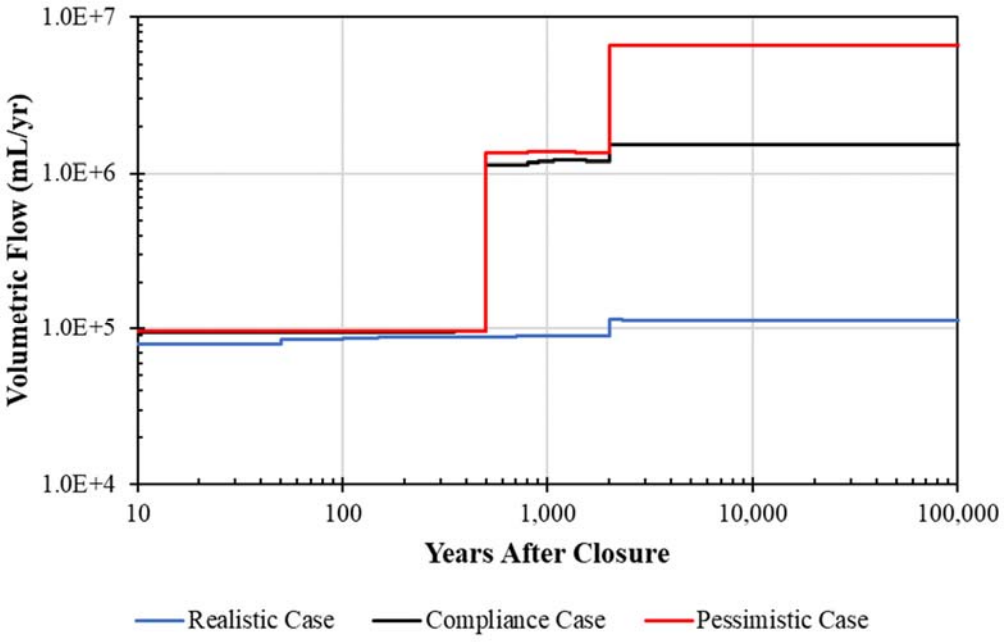

Figure 4.4-76: Volumetric Flow Rates Through SDU 9 Materials (Compliance Case)

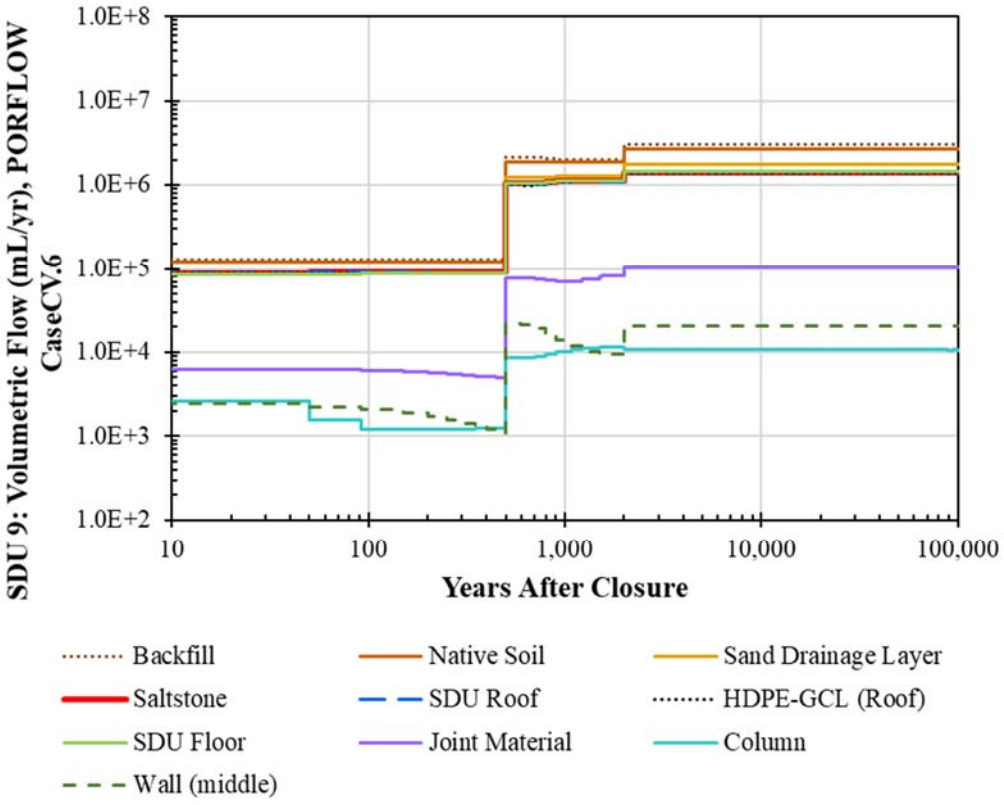

Figure 4.4-77: Comparison of Volumetric Flow Rates Through SDU 9 Saltstone

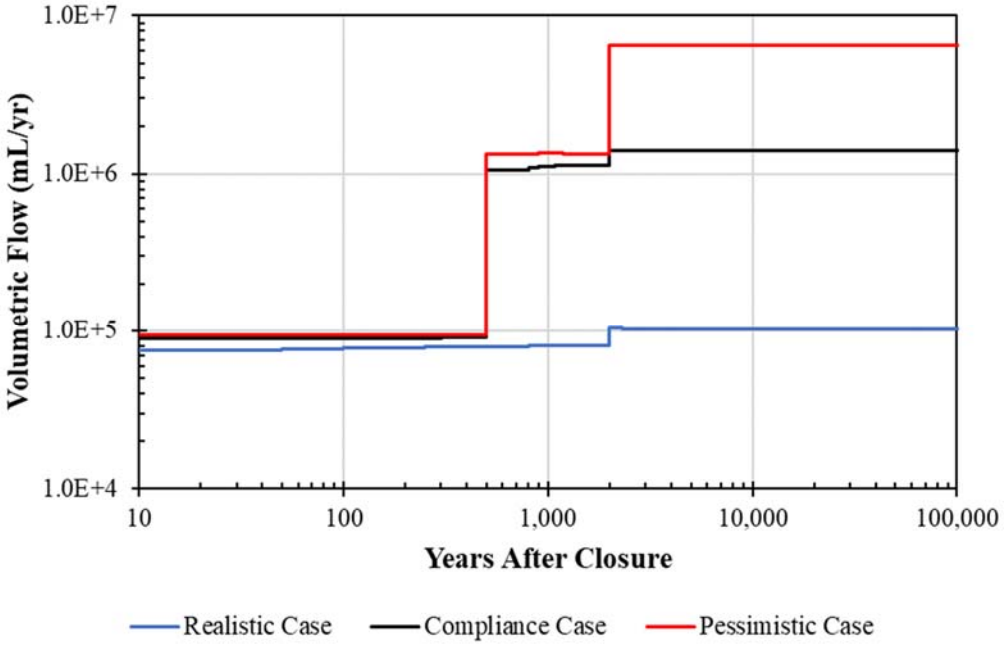

4.4.4.4.1 Flow Field Inputs for the GoldSim Probabilistic Model

In addition to being used in the Vadose Zone Transport Model, the Compliance Case flow fields generated by the Vadose Zone Flow Model are also used to benchmark a SDF GoldSim Model (see Section 5.6), which is an abstraction of the Vadose Zone Transport Model and Aquifer Transport Model. As an abstraction, the SDF GoldSim Model can be efficiently run in a multi-realization (probabilistic) mode to facilitate probabilistic uncertainty analyses or deterministic sensitivity models. The PORFLOW-generated flow fields provide input to the SDF GoldSim Model in the form of time series data of spatially-averaged velocities.

To provide additional insights, a series of alternate sensitivity cases (such as the Realistic Case and the Pessimistic Case) and uncertainty analyses are part of the PA process. The PORFLOW transport models (the Vadose Zone Transport Model and the Aquifer Transport Model) and the SDF GoldSim Model are used for deterministic sensitivity analyses. The SDF GoldSim Model is also used for the probabilistic uncertainty analyses (see Section 5.7). To support this, a set of parametric flow fields was developed using combinations of infiltration rates (Table 4.4-5), cementitious degradation rates, backfill saturated hydraulic conductivities (Table 4.3-2), and initial saltstone hydraulic conductivities (Table 4.3-3). The selection for these parameters is based on SRR-CWDA-2018-00061.

Table 4.4-82 provides a list reflecting the complete recommended spectrum of potential flow fields. Shading has been added to provide a visualization of the parameter options: blue shows the "Best Estimate" options which are equivalent to those used in the Realistic Case, white indicates that the Compliance Case (or MPAD) options were used, and pink shows the "Conservative Estimate" options as used in the Pessimistic Case.

Note, for the saturated hydraulic conductivity of the backfill, all three of the Central Scenario modeling cases used the same values. As such, the higher and lower options for this parameter are shown in orange and green, respectively. In addition to revising the saturated hydraulic conductivities of the backfill, the effective hydraulic conductivities were also revised based on changes to the respective Moisture Characteristic Curves (MCCs) using a technique known as Leverett scaling (see Eq. 4.4-105). Flow Case F27 is printed with a **bold font** to indicate that it represents the conditions used in the Compliance Case.

When used in full probabilistic mode, the SDF GoldSim Model randomly samples from the set of 54 potential flow fields listed in Table 4.4-82, along with all other modeling parameters for which distributions are available in the model. To allow for evaluating the influence of specific flow parameters, an independent stochastic distribution was developed for each of the four flow parameters (see Section 5.7.1). Based on the sampling of these four parameters, the SDF GoldSim Model selects the appropriate flow-field input files associated with the specific selection of parameters.

Table 4.4-82: Summary of Flow Fields for Modeling

Flow (F) Case	Infiltration Rate	Cementitious Degradation Rate	Saturated Hydraulic Conductivity of Backfill (cm/s)	Initial Saturated Hydraulic Conductivity of Saltstone (cm/s)
F01	Best Estimate	Best Estimate	2.0E-05 (vertical) and 3.8E-05 (horizontal)	5.0E-10
F02	Best Estimate	Best Estimate	2.0E-05 (vertical) and 3.8E-05 (horizontal)	2.0E-09
F03	Best Estimate	Best Estimate	4.1E-05 (vertical) and 7.6E-05 (horizontal)	5.0E-10
F04	Best Estimate	Best Estimate	4.1E-05 (vertical) and 7.6E-05 (horizontal)	2.0E-09
F05	Best Estimate	Best Estimate	1.4E-04 (vertical) and 2.7E-04 (horizontal)	5.0E-10
F06	Best Estimate	Best Estimate	1.4E-04 (vertical) and 2.7E-04 (horizontal)	2.0E-09
F07	Best Estimate	Compliance	2.0E-05 (vertical) and 3.8E-05 (horizontal)	5.0E-10
F08	Best Estimate	Compliance	2.0E-05 (vertical) and 3.8E-05 (horizontal)	2.0E-09
F09	Best Estimate	Compliance	4.1E-05 (vertical) and 7.6E-05 (horizontal)	5.0E-10
F10	Best Estimate	Compliance	4.1E-05 (vertical) and 7.6E-05 (horizontal)	2.0E-09
F11	Best Estimate	Compliance	1.4E-04 (vertical) and 2.7E-04 (horizontal)	5.0E-10
F12	Best Estimate	Compliance	1.4E-04 (vertical) and 2.7E-04 (horizontal)	2.0E-09
F13	Best Estimate	Conservative Estimate	2.0E-05 (vertical) and 3.8E-05 (horizontal)	5.0E-10
F14	Best Estimate	Conservative Estimate	2.0E-05 (vertical) and 3.8E-05 (horizontal)	2.0E-09
F15	Best Estimate	Conservative Estimate	4.1E-05 (vertical) and 7.6E-05 (horizontal)	5.0E-10
F16	Best Estimate	Conservative Estimate	4.1E-05 (vertical) and 7.6E-05 (horizontal)	2.0E-09
F17	Best Estimate	Conservative Estimate	1.4E-04 (vertical) and 2.7E-04 (horizontal)	5.0E-10
F18	Best Estimate	Conservative Estimate	1.4E-04 (vertical) and 2.7E-04 (horizontal)	2.0E-09
F19	Compliance	Best Estimate	2.0E-05 (vertical) and 3.8E-05 (horizontal)	5.0E-10
F20	Compliance	Best Estimate	2.0E-05 (vertical) and 3.8E-05 (horizontal)	2.0E-09
F21	Compliance	Best Estimate	4.1E-05 (vertical) and 7.6E-05 (horizontal)	5.0E-10
F22	Compliance	Best Estimate	4.1E-05 (vertical) and 7.6E-05 (horizontal)	2.0E-09
F23	Compliance	Best Estimate	1.4E-04 (vertical) and 2.7E-04 (horizontal)	5.0E-10
F24	Compliance	Best Estimate	1.4E-04 (vertical) and 2.7E-04 (horizontal)	2.0E-09
F25	Compliance	Compliance	2.0E-05 (vertical) and 3.8E-05 (horizontal)	5.0E-10
F26	Compliance	Compliance	2.0E-05 (vertical) and 3.8E-05 (horizontal)	2.0E-09
F27	**Compliance**	**Compliance**	**4.1E-05 (vertical) and 7.6E-05 (horizontal)**	**5.0E-10**
F28	Compliance	Compliance	4.1E-05 (vertical) and 7.6E-05 (horizontal)	2.0E-09
F29	Compliance	Compliance	1.4E-04 (vertical) and 2.7E-04 (horizontal)	5.0E-10
F30	Compliance	Compliance	1.4E-04 (vertical) and 2.7E-04 (horizontal)	2.0E-09
F31	Compliance	Conservative Estimate	2.0E-05 (vertical) and 3.8E-05 (horizontal)	5.0E-10
F32	Compliance	Conservative Estimate	2.0E-05 (vertical) and 3.8E-05 (horizontal)	2.0E-09
F33	Compliance	Conservative Estimate	4.1E-05 (vertical) and 7.6E-05 (horizontal)	5.0E-10
F34	Compliance	Conservative Estimate	4.1E-05 (vertical) and 7.6E-05 (horizontal)	2.0E-09
F35	Compliance	Conservative Estimate	1.4E-04 (vertical) and 2.7E-04 (horizontal)	5.0E-10
F36	Compliance	Conservative Estimate	1.4E-04 (vertical) and 2.7E-04 (horizontal)	2.0E-09
F37	Conservative Estimate	Best Estimate	2.0E-05 (vertical) and 3.8E-05 (horizontal)	5.0E-10
F38	Conservative Estimate	Best Estimate	2.0E-05 (vertical) and 3.8E-05 (horizontal)	2.0E-09
F39	Conservative Estimate	Best Estimate	4.1E-05 (vertical) and 7.6E-05 (horizontal)	5.0E-10
F40	Conservative Estimate	Best Estimate	4.1E-05 (vertical) and 7.6E-05 (horizontal)	2.0E-09
F41	Conservative Estimate	Best Estimate	1.4E-04 (vertical) and 2.7E-04 (horizontal)	5.0E-10
F42	Conservative Estimate	Best Estimate	1.4E-04 (vertical) and 2.7E-04 (horizontal)	2.0E-09
F43	Conservative Estimate	Compliance	2.0E-05 (vertical) and 3.8E-05 (horizontal)	5.0E-10
F44	Conservative Estimate	Compliance	2.0E-05 (vertical) and 3.8E-05 (horizontal)	2.0E-09
F45	Conservative Estimate	Compliance	4.1E-05 (vertical) and 7.6E-05 (horizontal)	5.0E-10
F46	Conservative Estimate	Compliance	4.1E-05 (vertical) and 7.6E-05 (horizontal)	2.0E-09
F47	Conservative Estimate	Compliance	1.4E-04 (vertical) and 2.7E-04 (horizontal)	5.0E-10
F48	Conservative Estimate	Compliance	1.4E-04 (vertical) and 2.7E-04 (horizontal)	2.0E-09
F49	Conservative Estimate	Conservative Estimate	2.0E-05 (vertical) and 3.8E-05 (horizontal)	5.0E-10
F50	Conservative Estimate	Conservative Estimate	2.0E-05 (vertical) and 3.8E-05 (horizontal)	2.0E-09
F51	Conservative Estimate	Conservative Estimate	4.1E-05 (vertical) and 7.6E-05 (horizontal)	5.0E-10
F52	Conservative Estimate	Conservative Estimate	4.1E-05 (vertical) and 7.6E-05 (horizontal)	2.0E-09
F53	Conservative Estimate	Conservative Estimate	1.4E-04 (vertical) and 2.7E-04 (horizontal)	5.0E-10
F54	Conservative Estimate	Conservative Estimate	1.4E-04 (vertical) and 2.7E-04 (horizontal)	2.0E-09

Note that from each of these the flow cases run within the PORFLOW Vadose Zone Flow Model, a set of flow-field specific GoldSim input data files were generated by post-processing PORFLOW output data. The post-processed PORFLOW output files are maintained within a structured folder named *SDF_FY19Data01*, that the SDF GoldSim Model accesses and reads data from while running. Data within this folder includes zone-averaged time histories of Darcy velocities, volumetric flow rates, saturation levels, and diffusion coefficients. This folder also includes other data files generated from PORFLOW and used for running the SDF GoldSim Model including zonal-based scalar data such as the environmental chemical transition times based on changes to Eh and pH.

Figure 4.4-78 provides a comparison of the volumetric flow rates through SDU 7 saltstone based on these parametric flow cases. As shown in the figure, all 54 sets of possible results may be organized into one of five possible groups:

- Low Group assumes the best estimate infiltration rate and either initial saturated hydraulic conductivity of saltstone (5.0E-10 cm/s or 2.0E-09 cm/s)
  - Eighteen cases (F01 through F18)
  - Peak volumetric flow rates within 100,000 years were all approximately 1.3E+05 mL/yr
- Moderate Group assumes the Compliance Case (MPAD) infiltration rate and the more probable initial saturated hydraulic conductivity of saltstone (5.0E-10 cm/s)
  - Nine cases (F19, F21, F23, F25, F27, F29, F31, F33, F35)
  - Peak volumetric flow rates within 100,000 years range between 1.4E+06 mL/yr and 1.6E+06 mL/yr, with an average of 1.5E+06 mL/yr
- Moderate-to-High Group assumes the Compliance Case (MPAD) infiltration rate and the high initial saturated hydraulic conductivity of saltstone (2.0E-09 cm/s)
  - Nine cases (F20, F22, F24, F26, F28, F30, F32, F34, F36)
  - Peak volumetric flow rates within 100,000 years were all approximately 1.9E+06 mL/yr
- High Group assumes the conservative estimate infiltration rate and the more probable initial saturated hydraulic conductivity of saltstone (5.0E-10 cm/s)
  - Nine cases (F37, F39, F41, F43, F45, F47, F49, F51, F53)
  - Peak volumetric flow rates within 100,000 years range between 2.4E+06 mL/yr and 2.6E+06 mL/yr, with an average of 2.5E+06 mL/yr

- Very High Group assumes the conservative estimate infiltration rate and the high initial saturated hydraulic conductivity of saltstone (2.0E-09 cm/s)
  - Nine cases (F38, F40, F42, F44, F46, F48, F50, F52, F54)
  - Peak volumetric flow rates within 100,000 years range between 6.4E+06 mL/yr and 6.9E+06 mL/yr, with an average of 6.6E+06 mL/yr

Note that the results from these modeling cases are presented to 100,000 years after closure. Regardless of the flow case, there were no significant changes to the flow behavior beyond approximately 3,000 years after closure (see Figure 4.4-79). This is because the SDU concrete undergoes complete degradation within the first 3,000 years while the monolithic saltstone material takes much longer than 100,000 years to undergo complete degradation (see Section 4.4.2).

Figure 4.4-78: Volumetric Flow Rates Through SDU 7 Saltstone for Parametric Flow Cases (10,000 Years, Linear Time Scale)

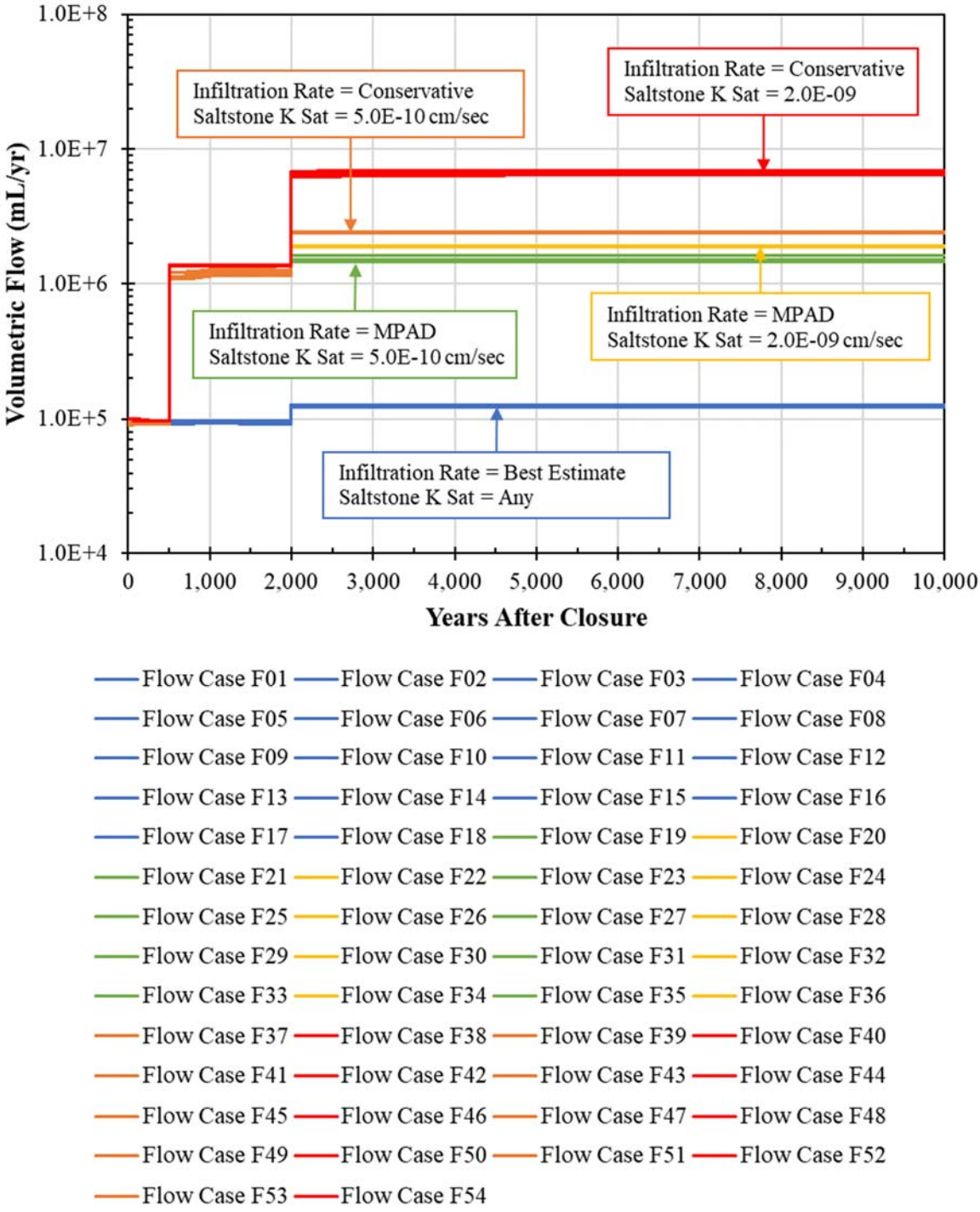

Figure 4.4-79: Volumetric Flow Rates Through SDU 7 Saltstone for Parametric Flow Cases (100,000 Years, Logarithmic Time Scale)

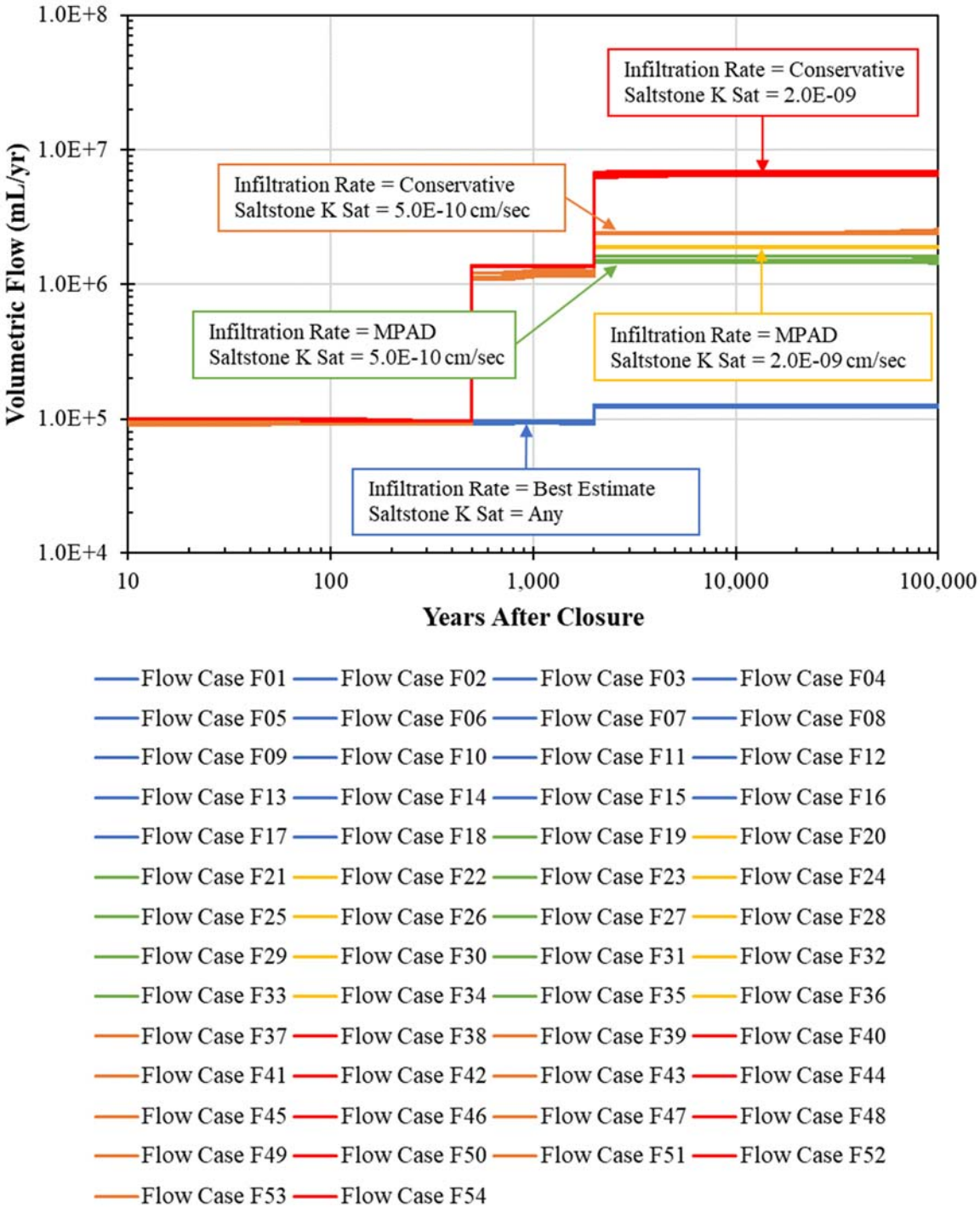

4.4.5 Vadose Zone Transport Model

The deterministic Vadose Zone Transport Model simulates radionuclide releases and transport from the SDF disposal units, through the vadose zone, and down to the water table. The rates of release and transport are based on the flow fields generated for the specific SDUs (see Section 4.4.4) and on the transport properties for the individual contaminants. The Vadose Zone Transport Model was developed using PORFLOW (ACRi, 2010) and assumes the MPAD input values to support the Compliance Case. The model inputs can also be modified to support deterministic sensitivity cases, such as the Realistic Case (which assumes best estimate input values), and the Pessimistic Case (which assumes conservative estimate input values).

For computational efficiency, radionuclide releases from the SDF disposal units are modeled in two-dimensions using PORFLOW. As with the Vadose Zone Flow Model, the rectangular disposal units are represented in two-dimensional Cartesian coordinates and assuming bilateral symmetry as cross-sectional slices from SDU centerline through the disposal units and surrounding vadose zone soils. The cylindrical 150-foot diameter SDUs and 375-foot diameter SDUs are based on radial symmetry and modeled in quasi two-dimensional cylindrical coordinates by a radial cross section (unit radian pie wedge).

As noted in Section 4.4.4, additional efficiency is also derived by modeling only SDUs 1, 2, 4, 6, 7, and 9. The "SDU 2" model is used to generate results for all the 150-foot diameter SDUs (SDUs 2A, 2B, 3A, 3B, 5A, and 5B). The "SDU 7" model is used to generate results for most of the 375-foot diameter SDUs (SDUs 7, 8, 10, 11, and 12). SDU 6, which has a slightly different model geometry, and SDU 9, which is assumed to be built closer to the water table, are modeled individually. To allow for differences in SDU-specific inventories, the modeled inventories for each SDU are set to 1.0 Ci for each radionuclide except Tc-99, with the mass being equally distributed throughout the waste form. For Tc-99, the entire inventory is placed in the Vadose Zone Transport Model to accommodate solubility controls. Note that for SDUs 1 and 4, the inventory is also placed in the walls. The inventory is assigned to the saltstone material zone (see Section 4.4.4) and can also be assigned to the clean grout zone type, depending on the SDU and/or scenario modeled.

4.4.5.1 Conceptual Model of the Vadose Zone Transport System

Conceptually, the Vadose Zone Transport Model simulates the transport of dissolved radionuclides and chemicals in conjunction with the flow of water through the saltstone monolith. The radionuclides and chemicals are transported through the surrounding materials of the engineered barrier (e.g., SDU concrete and surrounding backfill), through the partially saturated or unsaturated part of the natural barrier (i.e., the vadose zone), and out the bottom of the model where they are released at the water table. To simulate transport, the Vadose Zone Transport Model considers three major processes controlling the release and migration of dissolved species in the water phase: diffusive release, advective transport, and partitioning of contaminants between solid and liquid phases. Diffusion is the process by which molecules spread from areas of high concentration to areas of low concentration (Figure 4.4-80). Theoretically, in a closed system without flow, diffusion could continue until the molecules are distributed uniformly throughout the entire system (a condition referred to as equilibrium). In the Vadose Zone Transport

Model, diffusive release is controlled by the effective diffusion coefficients presented in Section 4.3 and is described in Section 4.4.5.2.3.

Figure 4.4-80: Conceptualization of Diffusive Release

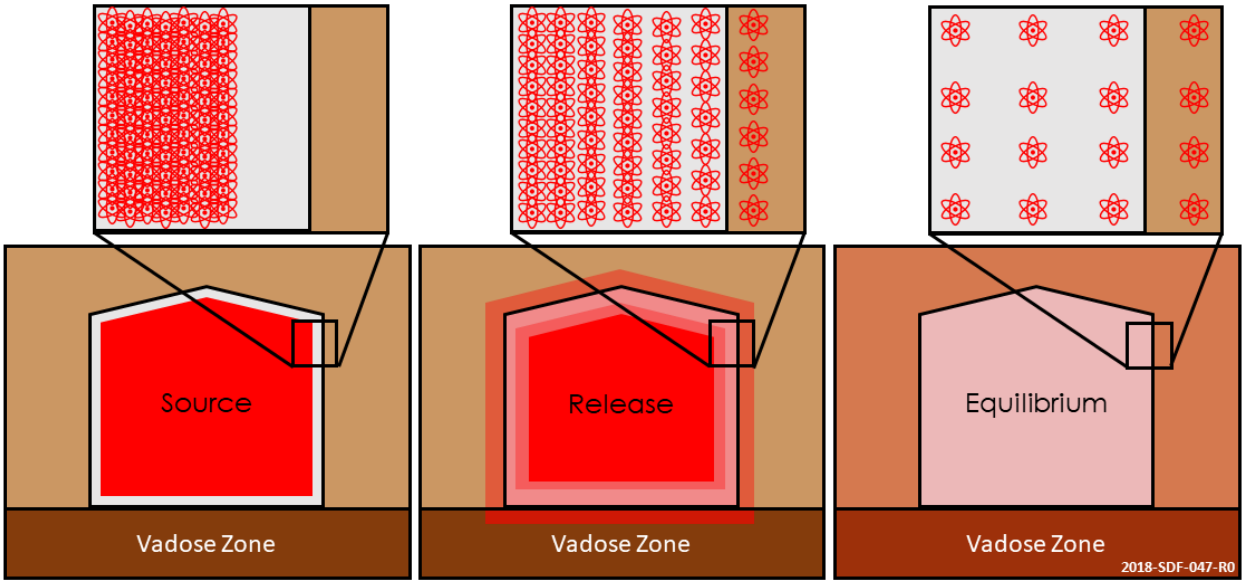

(a) Initially all the source term mass will be contained within the saltstone waste form inside the SDU.

(b) Over time, the contaminants will diffuse from the high concentrations within the SDU into lower concentration materials.

(c) Diffusion will continue until contaminant concentrations are equal through out the simulated materials.

Advective transport is a process in which a dissolved substance is transported by bulk motion of the solvent (Figure 4.4-81). In the Vadose Zone Transport Model, advective transport is simulated as that of the contaminants being carried out of the SDUs via flowing water (Figure 4.4-37), as described in Section 4.4.5.2.2. As such, this process is controlled by the velocity and saturation fields generated by the Vadose Zone Flow Model (Section 4.4.4).

In addition to advection and diffusion, which control the movement of radionuclides within flowing water and the spreading of the dissolved species within the water phase, the migration of the radioactive contaminants is also controlled by the chemical environment. Specifically, processes which influence the liquid and solid phase partitioning, such as sorption (see Section 4.4.5.2.4) and precipitation/dissolution reactions (see Section 4.4.5.2.5), can retard the radionuclide movement within the liquid phase.

These three processes (diffusion, advection, and liquid and solid phase partitioning) collectively define the release and transport of contaminants (Figure 4.4-82). Using these processes, the Vadose Zone Transport Model provides estimated fluxes (i.e., the time-variant rate of mass exchange) of contaminants at the water table.

Figure 4.4-81: Conceptualization of Advective Transport

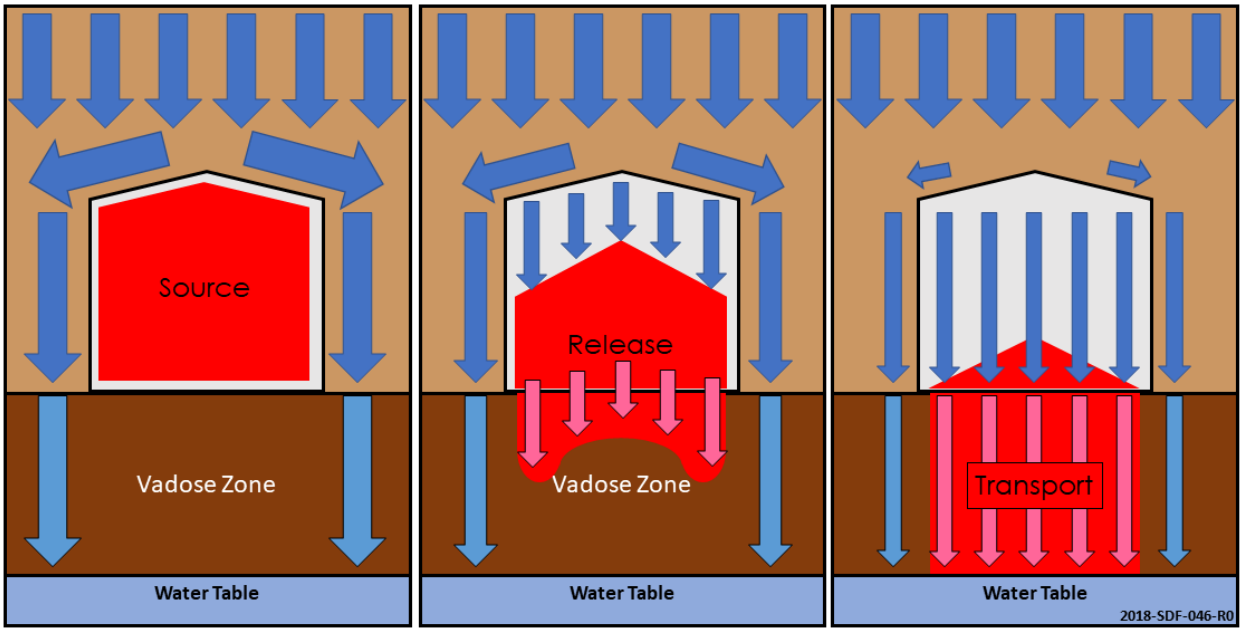

(a) Initially all the source term mass will be contained within the saltstone waste form inside the SDU.

(b) Over time, increasing flow will carry contaminants from the SDU and into the soils.

(c) Advective flow will transport the released contaminants through the vadose zone to the water table.

Figure 4.4-82: Conceptualization of Combined Diffusive and Advective Release and Transport

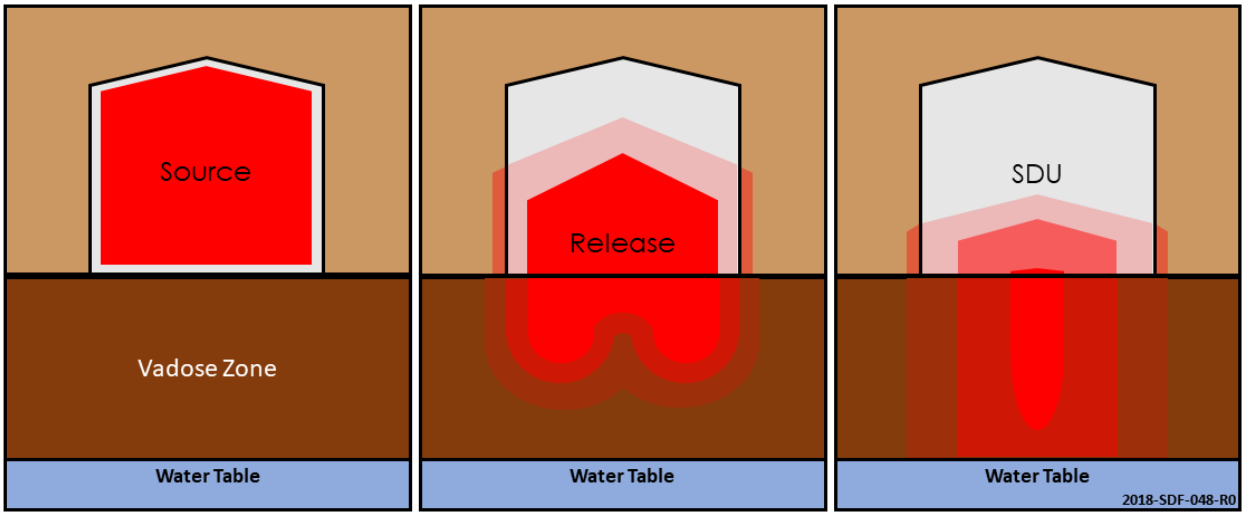

(a) Initially all the source term mass will be contained within the saltstone waste form inside the SDU.

(b) Contaminants will be released via diffusion and advection.

(c) Advective flow will transport the released contaminants through the vadose zone to the water table.

4.4.5.2 Implementation of the Vadose Zone Transport Model

To generate the time-variant radionuclide fluxes at the water table, the Vadose Zone Transport Model uses unsaturated zone transport equations. Within PORFLOW, these

equations are based on the generalized continuity equation for conservation of mass of a compressible fluid in a non-deforming media (see ACRi, 2002). As implemented for the SDF PA using PORFLOW, and assuming the fluid medium, water, is incompressible (and using more standard variable-naming conventions as defined below) the continuity equation can be written as:

$$\frac{\partial(\theta R^k C^k)}{\partial t} = -\frac{\partial}{\partial x_i}\left(q_i C^k\right) + \frac{\partial}{\partial x_i}\left[\theta \mathrm{D}_{ij}\frac{\partial C^k}{\partial x_j}\right] - \theta R^k \lambda^k C^k + \theta \sum_{l=1,NP} \sigma^{lk} R^l \beta^l C^l \qquad \text{Eq. 4.4-106}$$

where:

θ = the moisture content $\left({}^{V_{water}}/_{V_{material}}\right)$,

R^k = the retardation coefficient of the kth species (unitless),

C^k = the concentration of the kth species in the water (M/L^3),

q_i = the specific discharge (Darcy velocity) of water in the ith direction (L/T),

D_{ij} = the hydrodynamic dispersion coefficient tensor (L^2/T),

λ^k = the first-order decay coefficient for the kth species (T^{-1}),

β^k = the first-order production coefficient of the lth species that generates k (T^{-1}),

σ^{lk} = the fraction of decay of the lth species which generates the kth species (unitless),

t = Time (T),

x_i = coordinates in the ith direction (L), and

l = the indices for the parent species (unitless).

The retardation coefficient, which together with the moisture content is used to define the effective storage capacity of the system in terms of C^k, can in turn be written as:

$$R^k = 1 + \frac{\rho_b}{\theta} K_d^k \qquad \text{Eq. 4.4-107}$$

ρ_b = the bulk density of the solid material (M/L^3),

K_d^k = the partitioning coefficient for the kth species (L^3/M), and

θ = the moisture content $\left({}^{V_{water}}/_{V_{material}}\right)$,

where:

$$\rho_b = (1-\phi)\rho_s \qquad \text{Eq. 4.4-108}$$

ρ_s = the solid or particle density (M/L^3), and

ϕ = the total porosity $\left({}^{V_{void}}/_{V_{material}}\right)$.

The hydrodynamic dispersion coefficient, D_{ij}, defined as the sum of the coefficients of molecular diffusion and mechanical dispersion, can be written in the form of:

$$D_{ij} = \tau D_M \delta_{ij} + D_{mech,ij} = D_{eff}\delta_{ij} + D_{mech,ij} \quad \text{Eq. 4.4-109}$$

where:

δ_{ij} = the Kroenecker delta (= 1 for i=j and = 0 for i≠j),

τ = the tortuosity factor (unitless),

D_M = the free-water molecular diffusion coefficient (L^2/T),

$D_{mech,ij}$ = the mechanical dispersion tensor (L^2/T), and

D_{eff} = the effective diffusion coefficient (L^2/T).

4.4.5.2.1 Boundary Conditions for the Vadose Zone Modeling

The boundary conditions used for the SDU-specific Vadose Zone Flow Models and the respective SDU-specific Vadose Zone Transport Models and are depicted in Figure 4.4-83. These boundaries include a zero-flux boundary condition at the top of the model (Eq. 4.4-110), zero gradient boundary condition at the outer edges of the model for SDUs 1 and 4 and the center and outer edge for the cylindrical SDUs (Eq. 4.4-111), and a zero concentration boundary condition at the bottom boundary (Eq. 4.4-112).

Figure 4.4-83: Summary of Boundary Conditions

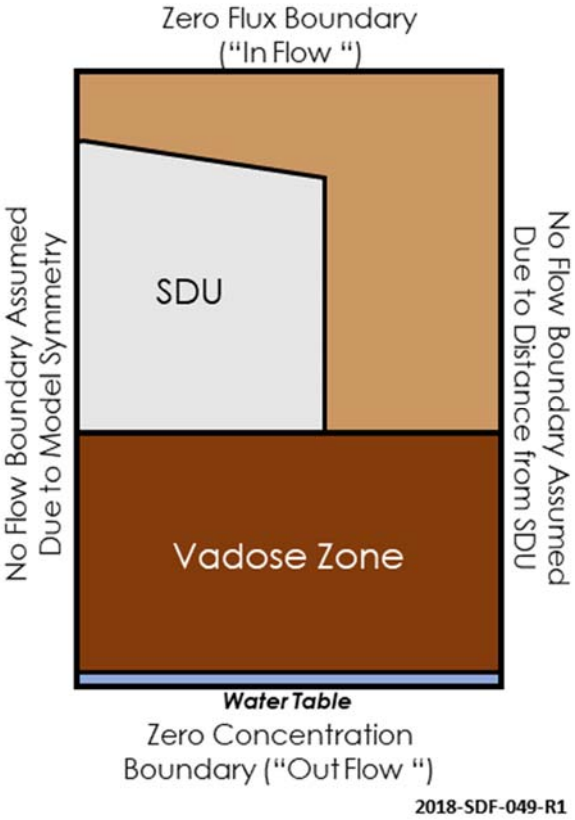

As noted earlier for the Vadose Zone Flow Model, because the PORFLOW Vadose Zone Transport Model simulates SDUs 1 and 4 as a vertical slice oriented perpendicular to the length of SDUs 1 and 4 and the cylindrical SDUs as 1-radian wedges, the boundary conditions can be posed as follows. Assuming z to be the vertical axis coordinate and x the horizontal axis coordinate for a two-dimensional plane (or radial axis for the cylindrical SDUs), the boundary conditions for the Vadose Zone Flow Model can be represented as:

$$I[c^k\ (z = top, t) - c^k_{source}\ (z = top, t)]\text{-}\theta \mathrm{D}_{zz}\ \frac{\partial c^k(z=top,t)}{\partial z} = 0 \qquad \text{Eq. 4.4-110}$$

$$\frac{\partial c^k(x_1,t)}{\partial x} = \frac{\partial c^k(x_2,t)}{\partial x} = 0 \qquad \text{Eq. 4.4-111}$$

$$c^k(z = bottom, t) = 0 \qquad \text{Eq. 4.4-112}$$

where:

I = infiltration rate (L/T),

c^k_{source} = source concentration (L/T),

z = vertical coordinate taken as positive upwards (L),

x_1 = horizontal (or radial) coordinate at the central plane (or center) of the SDU (L), and

x_2 = horizontal (or radial) coordinate at the end of the modeled backfill around the SDU.

Note that the source concentration in Equation Eq. 4.4-109 is presented for completeness, but is set to zero for the PORFLOW Vadose Zone Transport Model making the advective term on the left hand side of the equation effectively a dilution term simulating the influx of fresh water. Because the lateral boundaries are also no-flow boundaries, they become zero-flux boundaries (i.e., no mass leaves the system along the vertical boundaries). The bottom boundary condition in the flow model is a Dirichlet boundary condition (i.e., zero pressure-head) providing a flow exit at the bottom of the system (Eq. 4.4-99). This is coupled with a zero-concentration boundary condition at the bottom of the system creating an advective-diffusive release. Benchmarking exercises presented in Section 5.6 include an analysis comparing the use of the zero-concentration (Dirichlet-type) boundary condition at the bottom of the Vadose Zone Transport Model with a Neumann (zero-gradient) boundary condition.

4.4.5.2.2 Advective Transport through the Vadose Zone Transport Model

Advective transport is the dominant transport process in later time stages as infiltration rates increase (Section 4.4.1) and the SDU materials degrade (Section 4.4.2), thus increasing the flow rates (Section 4.4.4), which ultimately increases the rates of advective transport. Early on, when flow is minimal, diffusion can dominate as the mass spreads faster due to molecular diffusion than the water flows. In the radionuclide transport governing equation (Eq. 4.4-106), the process of advection is defined by the first term on the right-hand side.

The required input used to define advective transport in the Vadose Zone Transport Model are the flow fields generated by the Vadose Zone Flow Model (see Section 4.4.4). Note that each flow field generated by the Vadose Zone Flow Model was created by combining the results from multiple model simulations, where each simulation represents a specific time interval. Within each time interval simulation, results were generated by running a transient flow simulation until a steady-state was approached. Each of these time interval flow simulations were initiated with temporally appropriate input values based on interpolation of time-dependent input values. The Vadose Zone Transport Model uses the resulting flow fields, which include cell-by-cell flow rates and saturations, for each of the steady-state time intervals that occur within the range of time simulated for transport.

4.4.5.2.3 Diffusive Transport through the Vadose Zone Transport Model

Within the Vadose Zone Transport Model, the process of molecular diffusion invokes the spreading of mass independent of the rate of flow. For the SDF PA, during the time range of concern with respect to regulatory compliance, matrix diffusion is the dominant transport process. The process of molecular diffusion is imbedded in the second term on the right-hand side of Eq. 4.4-106, which reflects the composite process of hydrodynamic dispersion. The hydrodynamic tensor in the second term on the right-hand side of Eq. 4.4-106 is expanded in Eq. 4.4-111 with the first term describing the influence of molecular diffusion and the second term the influence of mechanical dispersion.

The SDF PA assumes that the process of mechanical dispersion (spreading out from the center of mass of an advecting plume), as represented by the second term on the right-hand side of Eq. 4.4-111, can be neglected at the scale considered in the Vadose Zone Flow Model because the varying material properties of the cementitious materials are explicitly modeled and dispersion associated with downward flow is expected to be relatively low within the native soils. Note that mechanical dispersion is a function of distance travelled due to advection as defined by the product of flow rate and time.

The tortuosity term found in Eq. 4.4-109 is a scaling factor accounting for the convoluted and constricted pathways that dissolved species travel when diffusing through a porous medium. The Vadose Zone Flow Model assumes that the

tortuosity is isotropic so here it is represented as a scalar value τ, that is multiplied by the Kroenecker delta (an identity matrix) used to assign the values to the diagonal terms of the hydrodynamic dispersion tensor. The initial values for the effective diffusion coefficients are presented in Section 4.3. As the cementitious materials (i.e., saltstone and SDU concrete) degrade over time, the effective diffusion coefficients will increase. Once the cementitious materials are fully degraded the effective diffusion coefficients are assumed to reach the same value as for backfill (5.3E-06 cm^2/s). The other effective diffusion coefficients used throughout the SDF PA models, including those for the sand drainage layer, backfill, vadose zone and joints (joints assume gravel properties), are also provided in Section 4.3 and are assumed to be constant over time.

4.4.5.2.4 Adsorption within the Vadose Zone Transport Model

In addition to the processes of advection and diffusion, which control the movement of radionuclides with the flowing water and the spreading of the dissolved species within the water phase, the migration of the radioactive contaminants within the SDUs is also influenced by the chemical environment through which the water passes.

Processes such as sorption and precipitation/dissolution reactions can retard the radionuclide movement within the water phase. Sorption is the propensity of a dissolved species to sorb onto solid materials (e.g., SDU concrete, soils, etc.). The degree of sorption onto the solid matrix is defined by a species-specific distribution (partition) coefficient, or K_d value. Each material type within the vadose zone models is assigned material-specific K_d values for each contaminant on an elemental basis (as defined in Section 4.3). The applied influence of the K_d values is reflected in Eq. 4.4-106.

Within the Vadose Zone Transport Model, temporal changes to the K_d values are imposed based on changes to the chemical environments as defined using the Contaminant Release Model. Within the Contaminant Release Model, pore-flush exchanges are used to evaluate changes in pore water chemistry as it passes through the pore spaces. At specific, chemistry-defined thresholds the chemical environment (Eh and pH) is assumed to change. The timings for the specific chemical transitions are provided in Section 4.4.3. This approach is applied for all radionuclides and chemicals within the transport models except for I-129 and Tc-99, which are simulated with shrinking core models.

As noted in Section 4.3.2.1, some species may have different sorptive behaviors within cementitious materials that have a significant amount of blast furnace slag (BFS), such as saltstone. Specifically, barium (Ba), radium (Ra), and strontium (Sr) have large K_d values compared to those found in typical concrete formulations without BFS, irrespective of the redox state because they form a strong bond to the sulfur in BFS, regardless of whether the sulfur is oxidizing or reducing. [SRNL-STI-2009-00473] As such, Table 4.3-6 provides saltstone-specific K_d values for

these species. For elements or species not included in this table, the cementitious K_ds in Table 4.3-5 were used for simulating transport through saltstone.

Iodine K_ds are also included in Table 4.3-6, reflecting the derivation of some of the values from a GoldSim optimization model (SRR-CWDA-2018-00045), developed to determine appropriate K_d values and transition times based on experimental results from DLM testing of saltstone simulant samples (SREL-R-17-0004). Because I-129 is expected to be a major dose contributor, its release was simulated in a more rigorous manner than the pore-flush exchange model discussed in Section 4.4.3. I-129 K_d transition times were evaluated on a cell-to-cell basis, implementing cell-specific chemical transitions based on the cell-specific pore-volume exchanges (SRNL-STI-2018-00652 and Section 4.4.5.2.6).

Using this cell-by-cell modeling approach, chemical transitions occur from the outside-in: the chemical transitions occur first at the top and outermost cells of the SDU, then advance downward and inward into the saltstone waste form. The volume of the unimpacted core material shrinks over time, such that this modeling approach is typically referred to as a shrinking core model.

4.4.5.2.5 Technetium Solubility Limits for the Vadose Zone Transport Model

Many of the species within the inventories of the SDUs may exhibit varying degrees of solubility control. As a modeling simplification this process if present is reflected in empirical K_d values for all species except for technetium (i.e., Tc-99).

Tc-99 has the potential to be a major dose contributor. When Tc-99 is in a chemically reducing environment, the releases are expected to be solubility controlled, but when it is in a chemically oxidizing environment, the release is expected to be controlled by a relatively small K_d value. As such a more rigorous modeling approach is warranted to more accurately simulate the release of Tc-99. To achieve this goal, a shrinking core model was used, similar to that used for I-129 (see Section 4.4.5.2.6), but with additional complexity. This complex shrinking core modeling approach can be used to evaluate localized, time-dependent chemical transitions from reducing (solubility control) to oxidizing environments (K_d control) and from reducing higher pH (higher solubility) to reducing lower pH (lower solubility) conditions.

Compared to the Tc-99 solubility controls, the controls imposed by its K_d values are relatively minimal; as such, the transition from a reducing environment to an oxidizing environment represents a significant change in the release behavior of Tc-99 (i.e., once Tc-99 becomes oxidized, the available mass becomes highly mobile, resulting in nearly instantaneous releases of Tc-99 from storage and into the water phase).

Using the shrinking core model, the overall release of Tc-99 from an SDU monolith follows one of two possible modes of release. With the first or early mode, the releases are a function of flow and a constant solubility limit. With the second or

later mode, the releases occur as a pulse from the oxidized cells within the saltstone or SDU. Oxidation occurs in two directions: from the walls inward as oxygen enters the SDU horizontally, and from the roof downward as oxygen enters the SDU vertically. Once the downward moving oxidation front (from the roof down) penetrates all the way through the bottom of the SDU, the second mode of release dominates. This is because Tc-99 that is released from the oxidizing front may transport down into the reducing material (ahead of the moving oxidation front) and become re-reduced, resulting in a buildup of Tc-99 just ahead of the oxidation front. (Note that the second mode of release, as simulated in PORFLOW, assumes total resorption of Tc-99 migrating from an oxidizing environment and into a reducing environment.) This built up mass of Tc-99 would then be available for release when the front reaches the bottom of the SDU. This second mode of release generates the greater risk, but is expected to occur much later in time, while the first release mode will be of lesser risk but will yield continuous releases earlier in time.

PORFLOW Version 6.42.9 does not explicitly provide a built-in means for implementing both solubility control under reducing conditions, and a transition from solubility to sorption control as a function of oxidation. However, both phenomena can be implemented in PORFLOW through a user-defined effective K_d function that varies from cell-to-cell over time.

This cell-to-cell shrinking core model used to simulate the oxidation state of saltstone and the subsequent release of Tc-99, was developed based on a slag-oxidation model first described in the *Estimated Duration of the Subsurface Reducing Environment Produced by the Z-Area Saltstone Disposal Facility* (WSRC-RP-2003-00362) and updated to use the effective K_d solubility modeling approach described in the *PORFLOW Modeling Supporting the FY14 Saltstone Special Analysis* (SRNL-STI-2014-00083) and *PORFLOW Simulations Supporting the Saltstone Performance Assessment Revision* (SRNL-STI-2018-00652).

As implemented for the Vadose Zone Transport Model, infiltrating water is assumed to contain dissolved oxygen. The concentration of dissolved oxygen within the incoming water is assumed to be equal to its solubility limit. The oxygen-rich water then moves into the cementitious materials (via advection and/or diffusion, as shown in Figure 4.4-82). On a cell-by-cell basis, this dissolved oxygen consumes the reducing agents until the cell becomes fully oxidizing. Once Tc-99 begins oxidizing the model uses a modified K_d value (based on the oxidation fraction of the cell) to approximate the processes of precipitation and dissolution (i.e., solubility controls), allowing for a reduction-capacity dependent function to control the dissolution of technetium in the solid phase. The rate of this dissolution (for the modified K_d value) is dependent on the amount of slag remaining in individual model cells. The oxidation fraction of each cell, from 0 to 1, is tracked through time for each computational cell (see Figure 4.4-84). In earlier SDF simulations (i.e., the FY2013 SDF SA (SRR-CWDA-2013-00062)), the

implementation was performed as a step change, where once a cell was fully oxidizing, the release rate of Tc-99 underwent an equivalent step change. With the improved modeling approach using the fractional release rates, the Tc-99 is released from the solid phase to the liquid phase uniformly over the period of cell oxidation, providing a more realistic simulation result (SRNL-STI-2014-00083).

Figure 4.4-84: Comparison of Step Release Rates Versus Fractional Release Rates for Simulation Tc-99 Releases

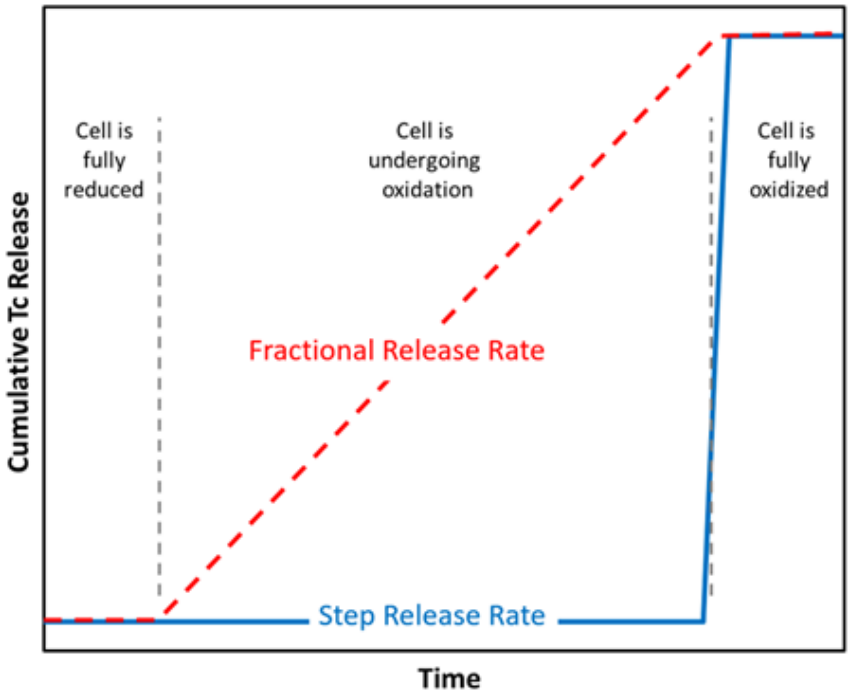

The effective K_d value used to approximate the chemistry-controlled precipitation/ dissolution versus sorption processes, is defined as:

$$K_d = x_{Re}^p K_d^{solubility} + \left(1 - x_{Re}^p\right) min\left[K_d^{redox}, K_d^{ramp}\right] \quad \text{Eq. 4.4-113}$$

where:

$$K_d^{solubility} = max\left[\frac{c_T - Snc_{sol}}{\rho_b c_{sol}}, K_{d,Re}\right] \quad \text{Eq. 4.4-114}$$

$$K_d^{redox} = max\left[\frac{c_{slag,0}}{c_{Ox}} x_{Re} - \frac{Sn}{\rho_b}, K_{d,Ox}\right] \quad \text{Eq. 4.4-115}$$

$$K_d^{ramp} = max\left[K_d^{solubility}, (1 - x_{Re}) K_{d,Ox}\right] \quad \text{Eq. 4.4-116}$$

where:

$c_{slag,0}$ = reducing capacity implemented as initial slag concentration (meq e^-/g),

c_T = total bulk Tc concentration [mol/L] = moles of Tc/Vol (the total mass of technetium in a cell divided by total volume of the cell),

c_{Ox} = dissolved oxygen concentration (1.06E-03 meq e^-/mL),

c_{sol} = Tc solubility limit (mol/L),

x_{Re} = reducing fraction of slag (-) = $(1 - x_{Ox})$ where x_{Ox} is the oxidizing fraction of slag (-),

$K_{d,Ox}$ = partition coefficient under oxidizing conditions (0.5 mL/g),

$K_{d,Re}$ = minimum partition coefficient under reducing conditions (0.01 mL/g),

S = water saturation (unitless),

n = porosity (unitless),

p = User-selected exponent (unitless), and

ρ_b = dry bulk density (g/mL).

Note that prior to this PA, the solubility limit (c_{sol}) was modeled as a constant value, but is now implemented as a calculated value based on the pH of the shrinking core model (see Section 4.3.2.2). As such, the value varies on a cell-by-cell basis as described in the *PORFLOW Simulations Supporting the Saltstone Performance Assessment Revision* (SRNL-STI-2018-00652). Specifically:

$$c_{sol} = x_{pH} c_{sol}^{pH>11} + \left(1 - x_{pH}\right) c_{sol}^{pH<11} \qquad \text{Eq. 4.4-117}$$

where:

x_{pH} = fraction of pH buffer remaining,

$c_{sol}^{pH>11}$= solubility under reducing and higher pH conditions, and

$c_{sol}^{pH<11}$= solubility under reducing and lower pH conditions.

The various K_d expressions embedded in Eq. 4.4-113 and the minimum and maximum value cutoffs ensure a relatively smooth evolution of effective K_d values when a cell transitions from fully reducing to fully oxidizing condition, regardless of the degree of solubility control. Figure 4.4-85 depicts representative K_d evolutions for high, medium, and low Tc total mass.

Figure 4.4-85: Effective K_d Evolution for High, Medium, and Low Tc Total Mass in a Shrinking Core Cell

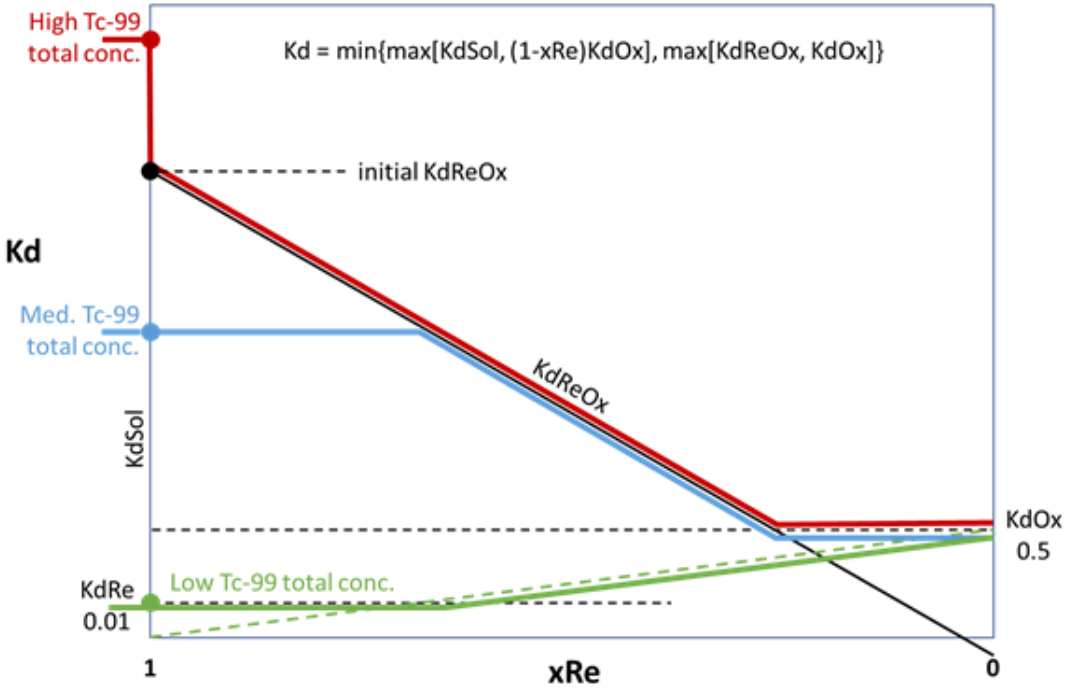

4.4.5.2.6 Iodine Shrinking Core Model for Vadose Zone Transport

The shrinking core model for I-129 transport is similar to that used for Tc-99 transport. Both models simulate the spatial evolution of Eh and pH conditions by modeling the consumption of reduction capacity by dissolved oxygen and the consumption of buffering capacity by a dissolved tracer species. An effective K_d is assigned to I-129 based on the remaining fractions of reducing and buffering capacities on a cell-by-cell basis. Initially an effective K_d value under fully reducing conditions is calculated from

$$K_d^{Re} = x_{pH}K_{d1} + \left(1 - x_{pH}\right)K_{d2} \qquad \text{Eq. 4.4-118}$$

where:

x_{pH} = fraction of pH buffer remaining

K_{d1} = partition coefficient under reducing and higher pH conditions

K_{d2} = partition coefficient under reducing and lower pH conditions

Then, an effective K_d value applicable to fully reducing, mixed, and fully oxidizing conditions is calculated from

$$K_d = x_{Re}K_d^{Re} + (1 - x_{Re})K_d^{Ox} \qquad \text{Eq. 4.4-119}$$

where:

x_{Re} = fraction of reduction capacity remaining,

K_d^{Re} = partition coefficient under reducing conditions (Eq. 4.4-118), and

K_d^{Ox} = partition coefficient under oxidizing conditions.

4.4.5.3 Inputs and Assumptions for the Vadose Zone Transport Model

The inputs to the Vadose Zone Transport Model are already defined in previous sections. For example, the Vadose Zone Transport Model uses the same geometry, material property zones, and model discretization as in the Vadose Zone Flow Model described in Section 4.4.4. Accordingly, the following provides a summary of where readers may find specific input values.

4.4.5.3.1 Inventories

The SDU-specific inventories are provided in Section 3.3.

In the Vadose Zone Transport Model, initial conditions are set by distributing one curie (or kg if not a radionuclide) for each contaminant, as described in Section 4.4.5.2, except for Tc-99 which is modeled using an explicit value to support solubility calculations. Flux results are subsequently post-processed to scale the unit-curie (1.0 Ci) or unit-kilogram (1.0 kg) value based on the actual inventories. This scaling technique is applicable since each radionuclide in the inventory is evaluated in a separate transport simulation, wherein the initial conditions are based on a single species and ingrowth is not influenced by the mixing of ingrowth products from different initial species within the decay chain calculations.

4.4.5.3.2 Vadose Zone Transport Model Geometry

The Vadose Zone Transport Model uses the same model geometry, model discretization, and material zones and properties as used for the Vadose Zone Flow Model (see Section 4.4.4).

4.4.5.3.3 Other Vadose Zone Transport Inputs

Other input values (e.g., effective diffusion coefficients, K_d values, etc.) are provided in Section 4.3.

4.4.5.4 Intermediate Results and Model Interfaces for the Vadose Zone Transport Model

From the Vadose Zone Transport Model, fluxes (or contaminant release rates) at the water table are used as inputs to the Aquifer Transport Model (see Section 4.4.6).

These fluxes are outputted in terms of breakthrough curves at the bottom of the model (i.e., the approximate water table depth). The time-series for each of the contaminant release rates that are based on simulating a unit-curie (1.0 Ci) source term (i.e., all contaminants except for Tc-99) are post-processed to account for SDU dependent inventories (see Section 3.3) and the resultant fluxes are used as inputs to the Aquifer

Transport Model (Section 4.4.6). Note that Tc-99 transport is simulating using the SDU-specific inventory values to account for the solubility control of aqueous concentrations and therefore are not simulated with a unit-curie (1.0 Ci) source term. For radioactive decay chain species, the vadose zone flux outputs for the species and ingrowth calculations from other parents in the decay chain are superimposed at each location.

The following subsections depict the time-dependent breakthrough curves for select radionuclides for each SDU simulation of the Vadose Zone Transport Model using each of the three Central Scenario modeling cases: Realistic Case, Compliance Case, and Pessimistic Case.

4.4.5.4.1 Flux Releases from SDU 1

The Vadose Zone Transport Model breakthrough curves from SDU 1 (for Cl-36, I-129, and Tc-99) are presented in the following figures.

Figure 4.4-86 presents the SDU 1 breakthrough curves for Cl-36 releases at the water table for the Realistic Case (blue), the Compliance Case (black), and the Pessimistic Case (red). Primarily, differences in the breakthrough curve characteristics depicted in Figure 4.4-86 reflect the differences in volumetric flow rates between each of these cases, as presented in Figure 4.4-67.

Figure 4.4-86: Flux Releases of Cl-36 from SDU 1

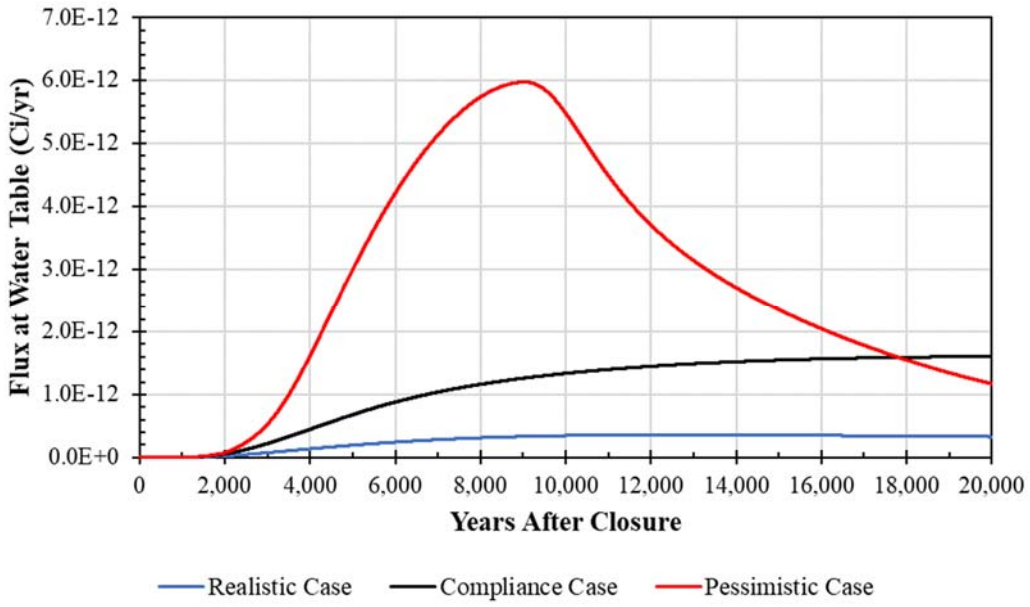

Examining the curve for the Pessimistic Case, a point of inflection is seen that reflects a sudden decrease in release rate at the water table. The sudden decrease is associated with a change in chemical environment throughout the saltstone monolith (and a simultaneous change in cementitious materials beneath the saltstone) from Reduced Region I to Reduced Region III 507ccurring at 8,511 years when the pH drops below 11. Note that the transition from Reduced Region II is

neglected in the transition. The validity of skipping transition Reduced Region I to Reduced Region II is discussed in Section 4.4.3.1.

For Cl-36, the pH transition initiates the onset of the process of adsorption as reflected in a change of chlorine K_d from 0.0 mL/g to 1.0 mL/g during calculations and an associated decrease in dissolved Cl-36 concentrations. Due to the 20,000-year time extent of the SDU 1 Cl-36 simulations, Reduced Region I to Reduced Region III transition effects associated with the Compliance Case and the Realistic Case are not reflected in the breakthrough curves. The pH transition for the Compliance Case occurs 29,714 years after closure and the pH transition for the Realistic Case occurs 384,412 years after closure. Similarly Eh controlled transitions from Reduced Region III to Oxidized Region III associated with each of the three modeling cases are not reflected in their breakthrough curves. The reducing to oxidizing environment transition times based on Eh (Reducing Region III to Oxidizing Region III) occur well beyond the 20,000-year simulation time.

Figure 4.4-87 depicts the breakthrough curves of I-129 releases at the water table for the Realistic Case (blue), the Compliance Case (black), and the Pessimistic Case (red). As with the Cl-36 breakthrough curves (Figure 4.4-86), differences between breakthrough curves for each of these cases in Figure 4.4-87 are dominated by the differences in volumetric flow rates between each of these cases as shown in Figure 4.4-67. The Pessimistic Case curve shows an apparent drop in the I-129 release rate at the water table approximately 10,000 years after closure. The drop in the breakthrough curve reflects the influence of a spatial change in chemical environment over time (starting prior to 8,511 years after closure and continuing after) from Reduced Region I to Reduced Region III in the saltstone monolith and cementitious material below.

The change as depicted in Figure 4.4-87, is based on a shrinking core model (see Section 4.4.3.4.2). Note that the shrinking core model is also used for Tc-99. The shrinking core model used to evaluate I-129 release calculates the transition time based on a more rigorous cell-by-cell evaluation of volume of flow through each cell (see Section 4.4.3.4.2). This means that for the shrinking core model the chemical environments and associated transition times are evaluated based on transport calculations with: (1) the influx of acidic infiltrate reducing the pH of the pore solution causing the gradual transition from one pH region to another and (2) the influx of oxygen consumes the reducing agents until the reducing agents are gradually exhausted from one cell to another and associated transition from one Eh environment to another on a cell-by-cell basis. Because of the more rigorous cell-by-cell analysis of the shrinking core calculations, the chemical transitions within the saltstone monolith and cementitious material below are simulated as occurring gradually (as opposed to instantaneously) releasing the I-129 in a pattern showing a broader (more dispersed) peak, as seen by comparing the Cl-36 (Figure 4.4-86) and the I-129 (Figure 4.4-87) breakthrough curves for the Pessimistic Case.

Figure 4.4-87: Flux Releases of I-129 from SDU 1

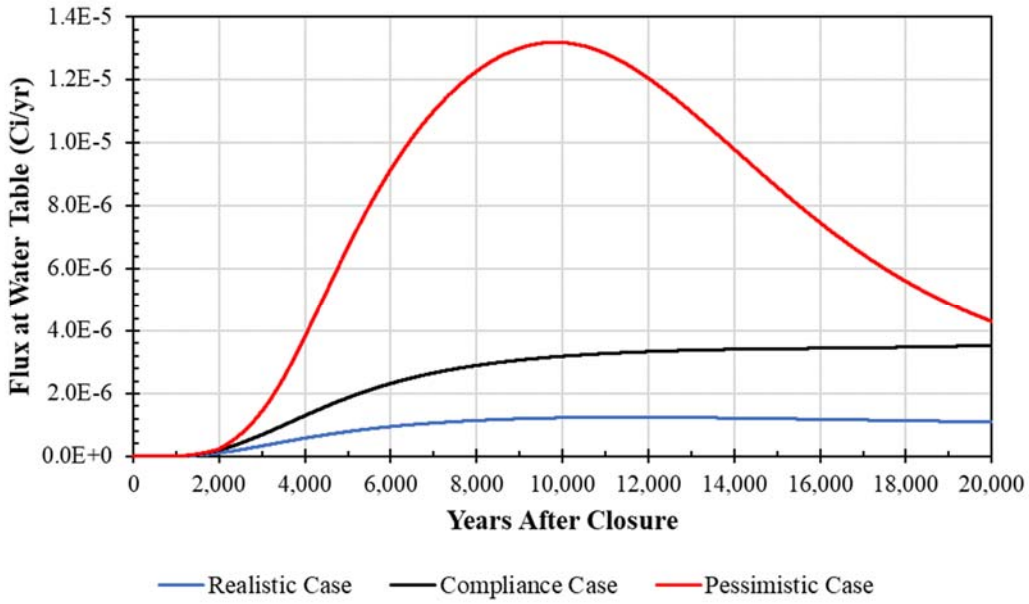

The pH transition initiates an increase in adsorption reflected in a decrease in concentration as driven by a change of iodine K_d. Region I to Region III iodine K_ds transition from 0.07 mL/g to 0.71 mL/g (Table 4.3-6 and Table 4.3-7) for Pessimistic Case and the Compliance Case and from 0.16 mL/g to 2.77 mL/g (Table 4.3-7) for the Realistic Case. Due to the 20,000-year time extent of the simulations, Reduced Region I to Reduced Region III transition times associated with the Compliance Case and the Realistic Case are not perceptively reflected in their associated breakthrough curves. Because the gradual change from reducing to oxidizing environment transitions based on Eh (Reducing Region III to Oxidizing Region III) occurs at a much slower rate, this influence is not perceptible in the curves from the 20,000-year simulations.

Figure 4.4-88 presents the breakthrough curves for Tc-99 releases at the water table for the Realistic Case (blue), the Compliance Case (black), and the Pessimistic Case (red). As with the Cl-36 and I-129 breakthrough curves (Figure 4.4-86 and Figure 4.4-87), the breakthrough curves of Tc-99 release rates presented in Figure 4.4-88 are strongly controlled by the differences in volumetric flow rates between each of the modeling cases as presented in Figure 4.4-67. As discussed above with respect to I-129, the nature of the chemical environment transitioning process associated with the shrinking core model used in the I-129 and Tc-99 simulations is radically different than for the radionuclides evaluated with the simpler (less computationally-intensive) non-shrinking core calculations (i.e., Cl-36). In addition, the Tc-99 transport process differs from that of I-129 because it is based on the solubility control of Tc-99 in the saltstone monolith under reducing conditions, as opposed to adsorption control for I-129.

Figure 4.4-88: Flux Releases of Tc-99 from SDU 1

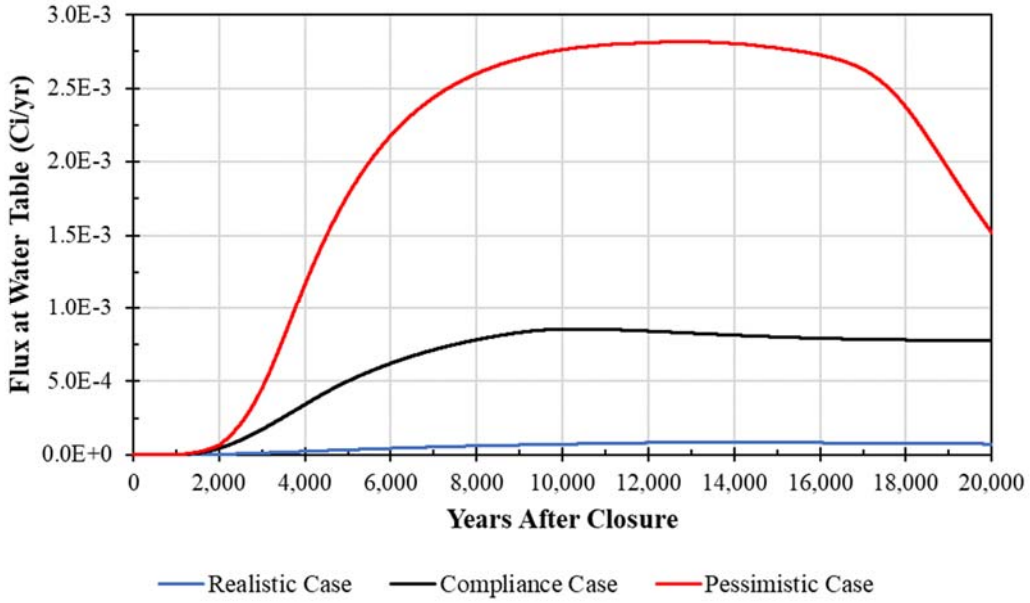

Examining the Pessimistic Case breakthrough curve in Figure 4.4-88, a relatively flat (approximately horizontal) release profile appears between 8,000 and 17,000 years into the simulation. This reflects the influence of solubility control until source concentrations near the bottom of the monolith fall below the solubility limits. The slight deviation from the flatness of the breakthrough curve between 8,000 and 17,000 years reflects the gradual transition of the chemical environment over time within the shrinking-core model. As the Tc-99 in the saltstone monolith is leached out of the monolith, concentrations decrease below the solubility limits from the top of the monolith down over time. Note that the concentrations also decrease horizontally from outside the SDUs inwards but the vertical changes present a strong control over the release. Within most of the bottom half of the monolith, the solubility limit that is imposed by a pH of ≥11 (of 9.7E-07 mol/L) remains after 20,000 years, but enough Tc-99 has been leached out so that the concentrations throughout the monolith have fallen at least one to two orders of magnitude below the solubility limits.

For the Compliance Case, the solubility limit of 9.7E-07 mol/L remains for most of saltstone monolith during the first 20,000 years and the concentrations remain at or slightly below the solubility limit within most of the monolith. For the Realistic Case and its Reduced Region I solubility limit of 2.0E-07 mol/L, the solubility limit remains at 2.0E-07 mol/L over most of the monolith volume with a thin rind of Reduced Region III solubility forming around the perimeter during 20,000 years. For the Realistic Case, except around the perimeter of the Reduced Region I zone, dissolved concentrations remain mainly at the solubility limit of 2.0E-07 mol/L throughout the 20,000-year simulation. In the Reduced Region III rind, outer zone concentrations are mainly below the 7.4E-08 mol/L solubility limit.

Over the time span of 20,000 years, minimal transition from reduced to oxidizing environment occurs within the saltstone with oxygen intrusion into the perimeter cells lowering the concentrations slightly below solubility limits based on partial oxidation of the slag in each of these cases. Within the floor, complete oxidation commonly occurs near the joints and partial oxidation away from the joints. Note that under fully oxidized conditions, the system is K_d-controlled with a K_d of 0.5 mL/g.

4.4.5.4.2 Flux Releases from SDU 4

The Vadose Zone Transport Model breakthrough curves from SDU 4 (for Cl-36, I-129, and Tc-99) are presented in the following figures.

Figure 4.4-89 presents the SDU 4 breakthrough curves for Cl-36 releases at the water table for the Realistic Case (blue), the Compliance Case (black), and the Pessimistic Case (red). Primarily, differences in the breakthrough curve characteristics depicted in Figure 4.4-89 reflect the differences in volumetric flow rates between these three cases as presented in Figure 4.4-69. Additionally, a point of inflection in the curve for the Pessimistic Case reflects a sudden decrease in release rate at the water table, caused by the change in chemical environment in the bottom portion (bottom zone) of the saltstone monolith from Reduced Region I to Reduced Region III 511ccurring 8,183 years after closure. This feature results from the instantaneous change in the chemistry throughout the bottom zone of the saltstone monolith and a simultaneous change in cementitious materials beneath the saltstone. Note that in SDU 4, the upper portion (upper zone) of the saltstone monolith is modeled as a separate zone due to the metal structures it contains which influence degradation rate and transition of chemical environments [SRR-CWDA-2013-00062).

Figure 4.4-89: Flux Releases of Cl-36 from SDU 4

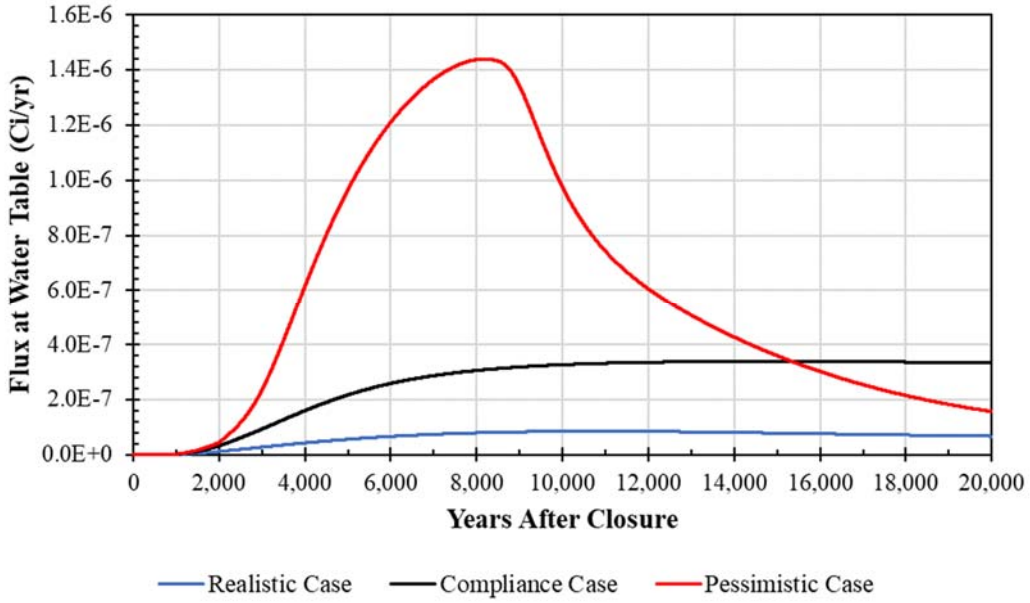

Because of its strong control of the release process at the bottom of the SDU and the associated features in the breakthrough curves, the following discussion will generally reference the bottom zone although top-down processes such as chemical transitions will influence the upper zone first. The monolith bottom zone pH transition initiates the onset of adsorption reflected in a change to the chlorine K_d from 0.0 mL/g to 1.0 mL/g and an associated decrease in the dissolved Cl-36 concentrations. Due to the 20,000-year time extent of the SDU 4 Cl-36 simulations, Reduced Region I to Reduced Region III transition times in the monolith bottom zone associated with the Compliance Case and the Realistic Case are not reflected in their breakthrough curves. The pH transition for the Compliance Case occurs 31,428 years after closure and the pH transition for the bottom of the monolith for the Realistic Case occurs 453,429 years after closure.

Similarly Eh controlled transitions from Reduced Region III to Oxidized Region III associated with all three of these modeling cases are not reflected in their breakthrough curves. The reducing to oxidizing environment transition times based on Eh (Reducing Region III to Oxidizing Region III) occur well beyond the 20,000-year simulation time.

Figure 4.4-90 depicts the breakthrough curves of I-129 releases at the water table for the Realistic Case (blue), the Compliance Case (black), and the Pessimistic Case (red). Like the Cl-36 breakthrough curves (Figure 4.4-89), differences in the I-129 breakthrough curves presented in Figure 4.4-90 are dominated by the differences in volumetric flow rates between each of these modeling cases as shown in Figure 4.4-69 and which directly influence leaching rates. The curve for the Pessimistic Case also depicts a drop in the I-129 release rate at the water table at approximately

9,000 years after closure. This drop in the release rate reflects the influence of the spatially gradual change in the chemical environment from Reduced Region I to Reduced Region III in the bottom zone of the saltstone monolith and the cementitious material below the saltstone, as calculated using a shrinking core model. For the shrinking core model used in I-129 calculations (see Section 4.4.3.4.2) the peak release shows a broader release than seen for Cl-36 (see Figure 4.4-89).

Figure 4.4-90: Flux Releases of I-129 from SDU 4

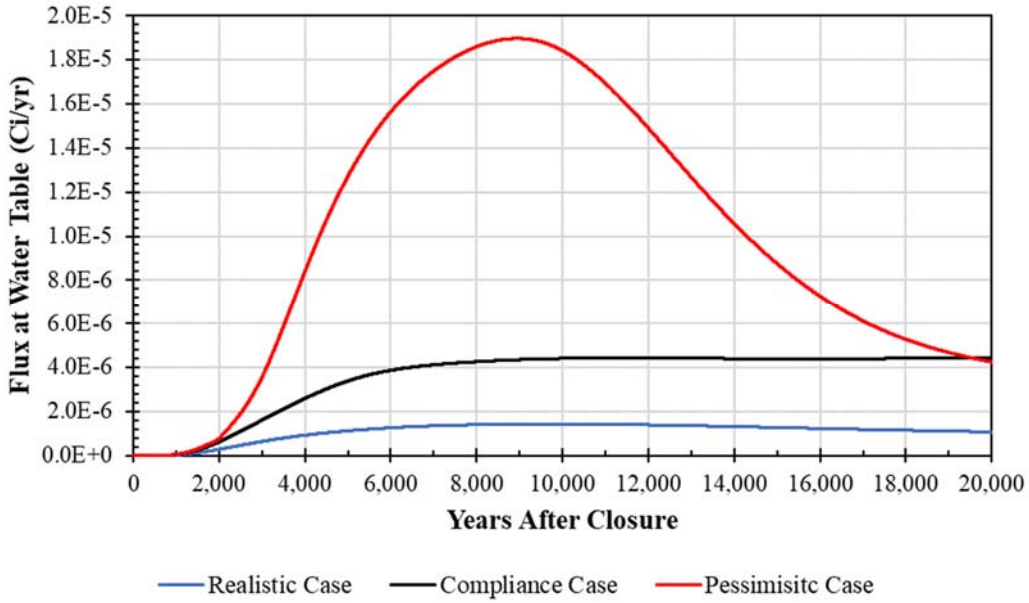

As discussed in Section 4.4.5.4.1, the shrinking core model used to evaluate I-129 release calculates the transition time based on a more rigorous cell-by-cell evaluation of volumetric flow through each cell (see also Section 4.4.3.4.2). A pH transition in a cell initiates an increase in adsorption reflected in a decrease in concentration as driven by a change to the iodine K_d. From Reduced Region I to Reduced Region III the iodine K_ds in saltstone transition from 0.07 mL/g to 0.71 mL/g (Table 4.3-6 and Table 4.3-7) for both the Pessimistic Case and the Compliance Case, and from 0.16 mL/g to 2.77 mL/g (Table 4.3-7) for the Realistic Case.

Due to the 20,000-year time extent of these simulations, the Reduced Region I to Reduced Region III transition times associated with the Compliance Case and the Realistic Case are not reflected in their associated breakthrough curves. Similarly, because the gradual change from reducing to oxidizing environment transitions based on Eh (Reducing Region III to Oxidizing Region III) occurs at a much slower rate, this influence is not perceptible in the curves for each of the 20,000-year simulations.

Figure 4.4-91 presents the breakthrough curves for Tc-99 releases at the water table for the Realistic Case (blue), the Compliance Case (black), and the Pessimistic Case (red). As with the Cl-36 and I-129 breakthrough curves (Figure 4.4-89 and Figure 4.4-90), the breakthrough curves of the release rates presented in Figure 4.4-91 are strongly controlled by the differences in volumetric flow rates between each of these cases as presented in Figure 4.4-69. As discussed above Tc-99 transport simulations utilize the shrinking core model to evaluate chemical environment transitions. In addition, the Tc-99 transport process calculations are based on solubility control of Tc-99 in the saltstone monolith under reducing conditions.

Figure 4.4-91: Flux Releases of Tc-99 from SDU 4

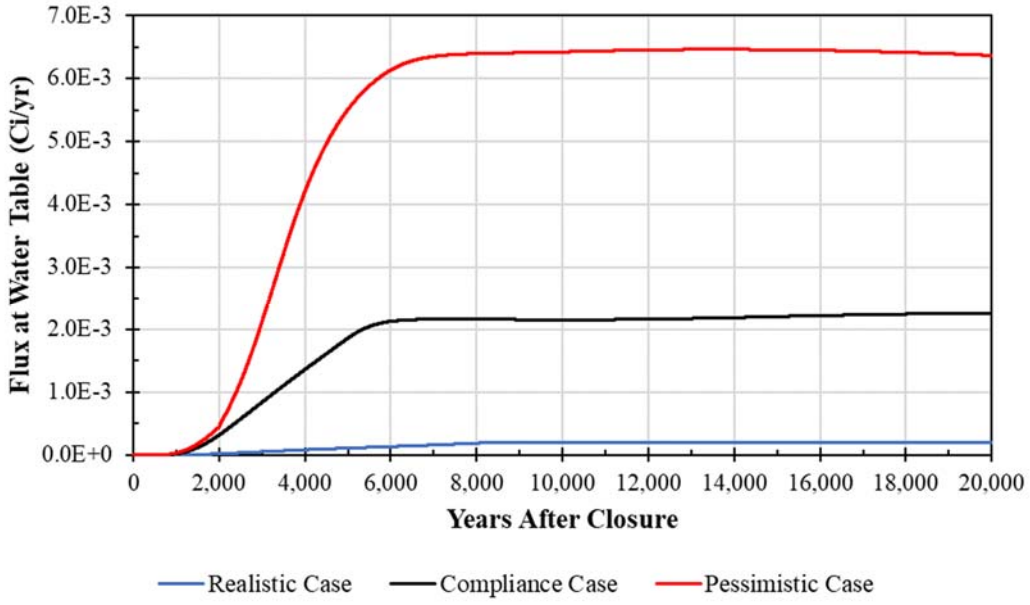

Examining the Pessimistic Case breakthrough curve in Figure 4.4-91, a relatively flat (approximately horizontal) release profile appears after approximately 6,000 years into the simulation extending the influence of the Reduced Region I solubility control in the bottom zone of the saltstone monolith to beyond 20,000 years. This difference between the SDU 4 results (in Figure 4.4-91) and the SDU 1 results (in Figure 4.4-88) where the Pessimistic Case breakthrough curve exhibits a concentration dropoff within the 20,000 year period reflects the large difference in source mass terms (49.3 Ci for SDU 1 and 634 Ci for SDU 4), and what happens in the SDU 1 after the Tc-99 concentrations fall below the solubility limit (Figure 4.4-88).

The slight deviation from flatness of the breakthrough curve after 6,000 years, reflects the gradual transition of chemical environment over time associated with the shrinking-core model. As Tc-99 in the saltstone monolith is leached out of the monolith, concentrations decrease below the solubility limits from the top of the monolith down over time. Within the lower half of the bottom zone of the

monolith a Reduced Region I environment with a solubility limit of 9.7E-07 mol/L remains throughout the 20,000-year simulation. By 20,000 years, this lower zone is overlain by a Reduced Region III zone which has developed over time and has a solubility limit of 4.5E-07 mol/L. Over time, enough Tc-99 has been leached out so that the concentrations in the upper part of this Reduced Region III zone are below solubility limits.

Although pH-driven chemical changes have occurred within the saltstone monolith, it can be seen that the chemical environment at the bottom of the bottom zone of the saltstone monolith dominates the rate at which the Tc-99 is released to the natural system below the SDU. Note that the solubility limit of 9.7E-07 mol/L remains for almost all of saltstone monolith bottom zone for the first 20,000 years of the Compliance Case and the concentrations remain at or slightly below the solubility limit within most of the bottom zone.

For the Realistic Case and its Reduced Region I solubility limit of 2.0E-07 mol/L, the solubility limit remains at 2.0E-07 mol/L over most of the monolith volume and a thin rind of Reduced Region III solubility forms around the perimeter (top, bottom, and along the walls) during 20,000 years. Except for this narrow rind of Reduced Region I material around the outer perimeter and bottom of the bottom monolith section, dissolved concentrations remain mainly at the solubility limit of 2.0E-07 mol/L during the 20,000-year simulation.

For all three cases, over the time span of 20,000 years minimal transition from reduced to oxidizing environment occurs within the saltstone around the perimeter with oxygen intrusion into the perimeter cells lowering the concentrations slightly below solubility limits based on partial oxidation of the slag. Within the floor, complete oxidation commonly occurs near the joints and partial oxidation away from the joints. Note that under fully oxidized conditions, the system is K_d-controlled with a K_d of 0.5 mL/g.

4.4.5.4.3 Flux Releases from 150-Foot Diameter SDUs

The Vadose Zone Transport Model breakthrough curves from 150-foot Diameter SDUs (for Cl-36, I-129, and Tc-99) are presented in the following figures. Note these figures are scaled based on the inventories from SDU 3A.

Figure 4.4-92 presents the SDU 3A breakthrough curves for Cl-36 releases at the water table for the Realistic Case (blue), the Compliance Case (black), and the Pessimistic Case (red). Differences in the breakthrough curve characteristics depicted in Figure 4.4-92 mainly reflect the differences in volumetric flow rates between these three cases as presented in Figure 4.4-71.

Figure 4.4-92: Flux Releases of Cl-36 from 150-Foot Diameter SDUs

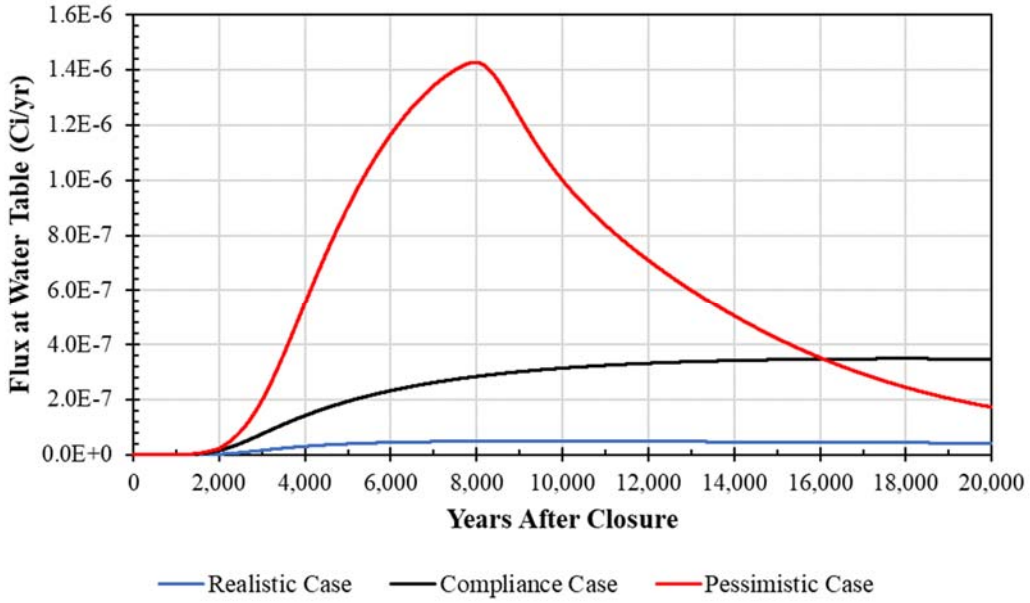

The point of inflection in the Pessimistic Case curve reflects a sudden decrease in the release rate at the water table, showing the influence of the change in chemical environment in the saltstone monolith from Reduced Region I to Reduced Region III 516ccurring 7,453 years after closure (Table 4.4-61). This feature results from the instantaneous change in the chemistry throughout the saltstone monolith and a simultaneous change in cementitious materials beneath the saltstone. The monolith bottom pH transition initiates the onset of adsorption reflected in a change of chlorine K_d from 0.0 mL/g to 1.0 mL/g and associated decrease in dissolved Cl-36 concentrations.

Due to the 20,000-year time extent of these Cl-36 simulations for SDU 3A (and all other 150-foot diameter SDUs), the Reduced Region I to Reduced Region III transition times in the saltstone monolith associated with the Compliance Case and the Realistic Case are not reflected in the presented breakthrough curves. The pH transition for the Compliance Case occurs 25,015 years after closure and the pH transition for the Realistic Case occurs 309,400 years after closure.

Similarly, Eh controlled transitions from Reduced Region III to Oxidized Region III associated with all three of these modeling cases are not reflected in their breakthrough curves. The reducing to oxidizing environment transition times based on Eh (Reducing Region III to Oxidizing Region III) occur well beyond the 20,000-year simulation time.

Figure 4.4-93 depicts the breakthrough curves of I-129 releases at the water table for the Realistic Case (blue), the Compliance Case (black), and the Pessimistic Case (red). As with the Cl-36 breakthrough curves (see Figure 4.4-92), differences in the breakthrough curves presented in Figure 4.4-93 are dominated by the differences

in volumetric flow rates between these modeling cases as presented in Figure 4.4-71 and which directly influence leaching rates. The Pessimistic Case curve also depicts a drop in the I-129 release rate at the water table, this time at approximately 10,000 years after closure.

Figure 4.4-93: Flux Releases of I-129 from 150-Foot Diameter SDUs

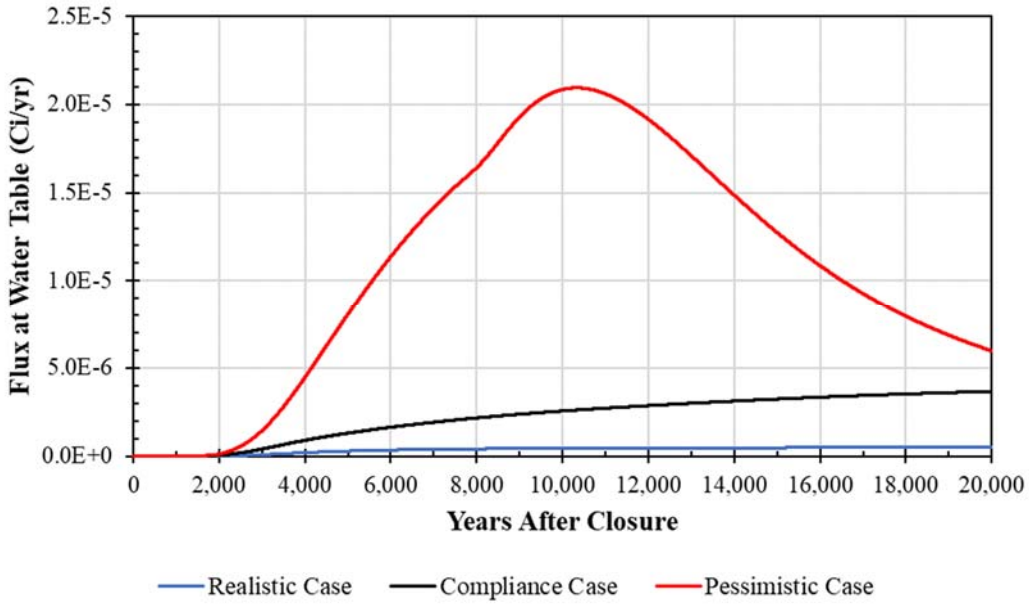

This drop in the release rate reflects the influence of the spatially gradual change in chemical environment from Reduced Region I to Reduced Region III in the saltstone monolith and cementitious material below as calculated using a shrinking core model. Because of the more rigorous cell-by-cell analysis of the shrinking core calculations, the chemical transitions within the saltstone monolith and cementitious material below is simulated as occurring gradually (as opposed to instantaneously), forming a broader release peak for I-129 than seen in the Pessimistic Case breakthrough curve for Cl-36 (see Figure 4.4-92).

The pH transition seen for the Pessimistic Case initiates an increase in adsorption reflected in a decrease in concentration as driven by a change of iodine K_d from 0.07 mL/g to 0.71 mL/g (Table 4.3-6 and Table 4.3-7). Note that for the Compliance Case, the iodine K_d changes when saltstone transitions from Reduced Region I to Reduced Region III, from 0.07 mL/g to 0.71 mL/g (Table 4.3-6 and Table 4.3-7). Similarly, in the Realistic Case the iodine K_d changes from 0.16 mL/g to 2.77 mL/g (Table 4.3-7).

Due to the 20,000-year extent of the SDU 3A I-129 simulations, Reduced Region I to Reduced Region III transition times associated with the Compliance Case and the Realistic Case are not perceptibly reflected in their associated breakthrough curves. Note that there is a slight inflection point at around 8,000 years which is

more pronounced in the 375-foot diameter SDUs and will be discussed with respect to SDU 7 in Section 4.4.5.4.4.

Figure 4.4-94 presents the breakthrough curves for Tc-99 releases at the water table for the Realistic Case (blue), the Compliance Case (black), and the Pessimistic Case (red). As with the Cl-36 and I-129 breakthrough curves (see Figure 4.4-92 and Figure 4.4-93), the breakthrough curves of release rates presented in Figure 4.4-94 are strongly controlled by the differences in volumetric flow rates between the central-case scenarios which are presented in Figure 4.4-71. As discussed above, Tc-99 transport simulations use the shrinking core model to evaluate chemical environment transitions. In addition, the Tc-99 transport process calculations are based on solubility control of Tc-99 in the saltstone monolith when under reducing conditions.

Figure 4.4-94: Flux Releases of Tc-99 from 150-Foot Diameter SDUs

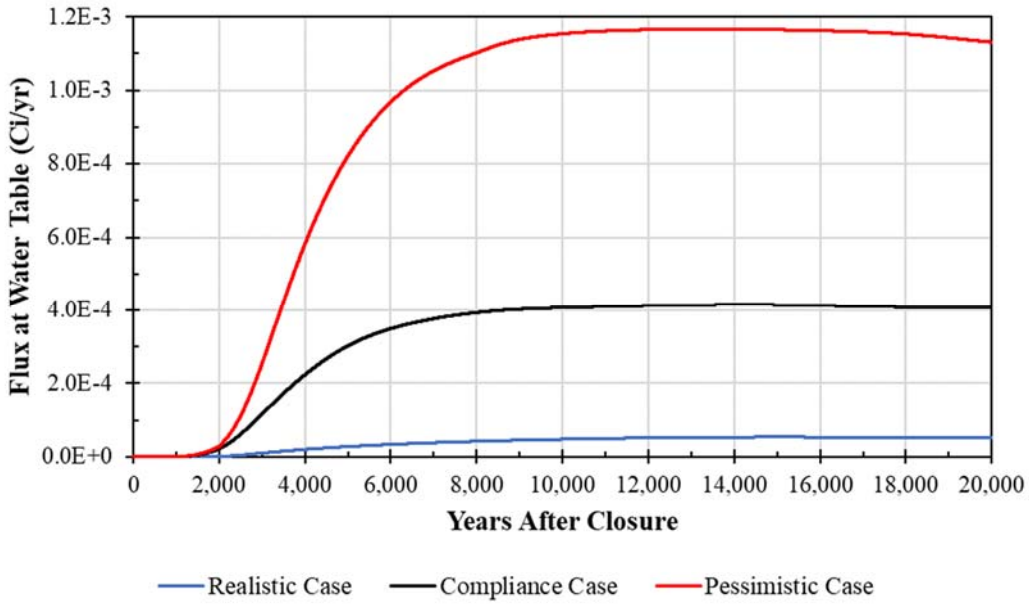

Examining the Pessimistic Case breakthrough curve in Figure 4.4-94, a relatively flat (approximately horizontal) release profile appears after approximately 10,000 years into the simulation and extends beyond 20,000 years, showing the influence of solubility control in the saltstone monolith. The slight deviation from flatness of the breakthrough curve after 10,000 years reflects the gradual transition of chemical environment over time associated with the shrinking-core model. Within the lower half of the saltstone monolith, a Reduced Region I environment with a solubility limit of 9.7E-07 mol/L keeps concentrations mainly at 9.7E-07 mol/L throughout the 20,000-year simulation. By 20,000 years, this lower zone is overlain by a Reduced Region III zone that has developed over 20,000 years and has a solubility limit of 4.5E-07 mol/L with Tc-99 concentrations mainly at the solubility limit of 4.5E-07 mol/L.

Note that for the Compliance Case, the solubility limit of 9.7E-07 mol/L is found in all but a small upper zone of the saltstone monolith and will control most of the release from the saltstone monolith for the first 20,000 years of the Compliance Case. For the Realistic Case and its Reduced Region I solubility limit of 2.0E-07 mol/L, the solubility limit remains at 2.0E-07 mol/L over most of the monolith volume, with only a thin rind of Reduced Region III solubility forming around the perimeter during 20,000 years. For the Realistic Case, except for the rind around the Reduced Region I zone, dissolved concentrations remain mainly at the solubility limit of 2.0E-07 mol/L during the 20,000-year simulation.

Over the time span of 20,000 years minimal transition from reducing to oxidizing environment occurs within the saltstone around the perimeter, with oxygen intrusion into the perimeter cells lowering the concentrations slightly below solubility limits based on partial oxidation of the slag in all three modeling cases. Within the floor, complete oxidation commonly occurs near the joints and partial oxidation away from the joints. Note that under fully oxidized conditions, the system is K_d-controlled with a K_d of 0.5 mL/g.

4.4.5.4.4 Flux Releases from 375-Foot Diameter SDUs

The Vadose Zone Transport Model breakthrough curves from 375-foot diameter SDUs, excluding SDUs 6 and 9, (for Cl-36, I-129, and Tc-99) are presented in the following figures. The 375-foot diameter SDUs, discussed in this section (SDUs 7, 8, 10, 11, and 12) are each simulated as one for Vadose Zone Model releases, except for the Tc-99 releases which were setup to run each SDU separately to allow for potentially different Tc-99 inventories. The following discussion uses SDU 7 to represent all of these 375-foot diameter SDUs.

Figure 4.4-95 presents the SDU 7 breakthrough curves for Cl-36 releases at the water table for the Realistic Case (blue), the Compliance Case (black), and the Pessimistic Case (red). Here again, differences in the breakthrough curve characteristics depicted in Figure 4.4-95 reflect the differences in volumetric flow rates between all three modeling case as presented in Figure 4.4-73.

A point of inflection is only present in the Pessimistic Case curve (for the 20,000-year simulation), representing a sudden decrease in the release rate at the water table due to the influence of the change in chemical environment in the saltstone monolith from Reduced Region I to Reduced Region III occurring 14,374 years after closure (Table 4.4-64). This feature results from the instantaneous change in the chemistry throughout the saltstone monolith and a simultaneous change in cementitious materials beneath the saltstone. The pH transition initiates the onset of adsorption reflected in a change of chlorine K_d from 0.0 mL/g to 1.0 mL/g and associated decrease in dissolved Cl-36 concentrations.

Figure 4.4-95: Flux Releases of Cl-36 from 375-Foot Diameter SDUs

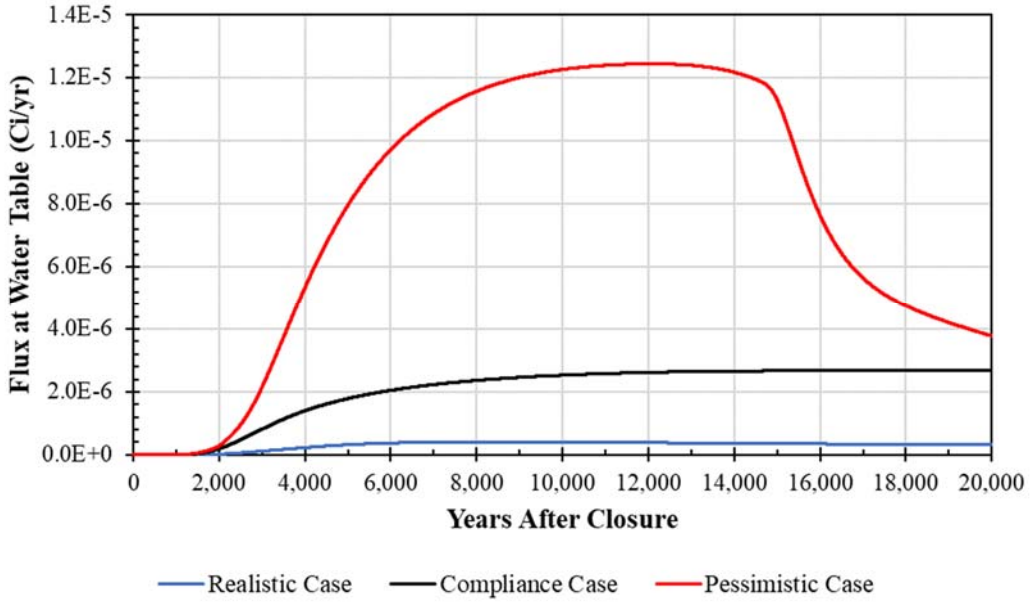

Due to the 20,000-year time extent of the SDU 7 Cl-36 simulations, Reduced Region I to Reduced Region III transition times in the saltstone monolith associated with the Compliance Case and the Realistic Case are not reflected in the presented breakthrough curves (Figure 4.4-95). The pH transition for the Compliance Case occurs 56,141 years after closure (Table 4.4-62), and the pH transition for the Realistic Case occurs 748,481 years after closure (Table 4.4-63).

Eh controlled transitions from Reduced Region III to Oxidized Region III associated with these three modeling cases are not reflected in their associated breakthrough curves (Figure 4.4-95). The reducing to oxidizing environment transition times based on Eh (Reducing Region III to Oxidizing Region III) occur well beyond the 20,000-year simulation time.

Figure 4.4-96 depicts the breakthrough curves of I-129 releases at the water table for the Realistic Case (blue), the Compliance Case (black), and the Pessimistic Case (red). As with the Cl-36 breakthrough curves (see Figure 4.4-95), differences in the breakthrough curves in Figure 4.4-96 are dominated by the differences in volumetric flow rates between these three modeling cases as shown in Figure 4.4-73, and which directly influence leaching rates. The Pessimistic Case curve also depicts a drop in the I-129 release rate at the water table at approximately 16,500 years after closure. This drop in the release rate reflects the influence of the spatially gradual change in chemical environment from Reduced Region I to Reduced Region III in the saltstone monolith and cementitious material below, as calculated using the shrinking core model.

Figure 4.4-96: Flux Releases of I-129 from 375-Foot Diameter SDUs

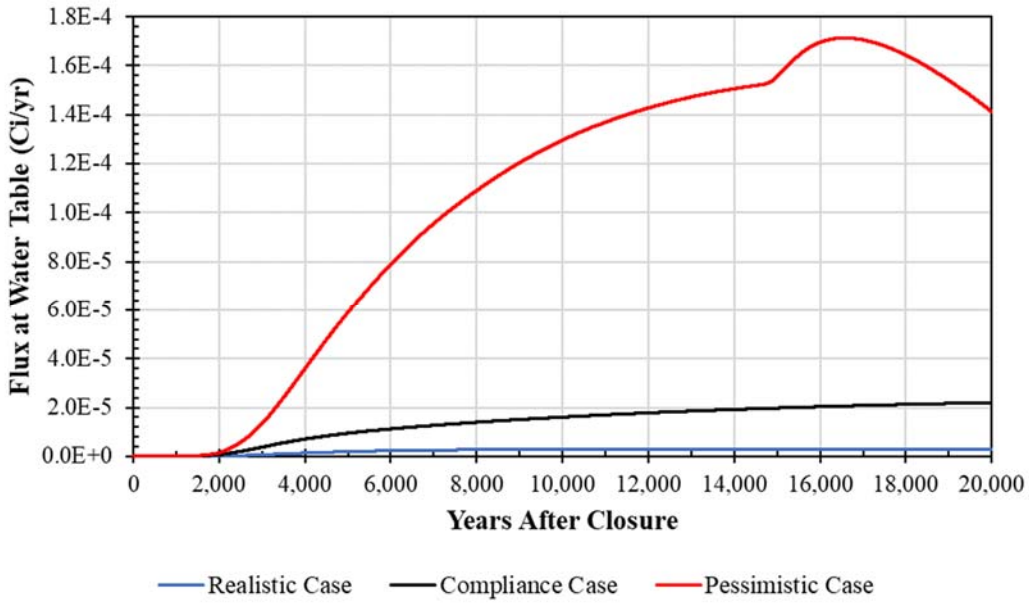

When compared to the Cl-36 curve presented in Figure 4.4-95, an accelerated I-129 release increase occurs at 521ccurring521ely the same time that the decrease occurs for Cl-36. This increase in the I-129 release rate prior to the rate decrease is associated with a decrease in K_d from 8 mL/g to 4 mL/g when the chemical environment throughout the lower mud mat changes from Oxidizing Region I to Oxidizing Region III at 14,374 years after closure (based on the lower mud mat Region I to Region III change presented in Table 4.4-64). Note that since the lower mud mat starts out oxidized it is not influenced by the shrinking core calculations.

Because of the more rigorous cell-to-cell analysis of the shrinking core calculations in the saltstone monolith, the chemical transitions within the saltstone monolith and most of the cementitious material below (all except the lower mud mat that does not use the shrinking core model) are simulated as occuring gradually (as opposed to instantaneously) releasing the I-129 in a manner which forms a broader peak compared to Cl-36 (Figure 4.4-95) as seen after 16,500 years in the Pessimistic Case breakthrough curve (Figure 4.4-96).

The pH transition initiates an increase in adsorption reflected in a decrease in concentration as driven by a change of iodine K_d. Region I to Region III iodine K_ds transition from 0.07 mL/g to 0.71 mL/g (Table 4.3-6 and Table 4.3-7) for the Pessimistic Case and the Compliance Case and from 0.16 mL/g to 2.77 mL/g (Table 4.3-7) for the Realistic Case.

Due to the 20,000-year time extent of the SDU 7 I-129 simulations, Reduced Region I to Reduced Region III transition times associated with the Compliance Case and the Realistic Case are not discernible in their associated breakthrough curves.

Figure 4.4-97 presents the breakthrough curves for SDU 7 Tc-99 releases at the water table for the Realistic Case (blue), the Compliance Case (black), and the Pessimistic Case (red). As with the Cl-36 and I-129 breakthrough curves (see Figure 4.4-95 and Figure 4.4-96), the breakthrough curves of release rates presented in Figure 4.4-97 are strongly controlled by the differences in volumetric flow rates between each of these case as presented in Figure 4.4-73. As discussed above in Section 4.4.5.4.1, Tc-99 transport simulations utilize the shrinking core model to evaluate chemical environment transitions. In addition, the Tc-99 transport process calculations are based on solubility control of Tc-99 in the saltstone monolith when under reducing conditions.

Figure 4.4-97: Flux Releases of Tc-99 from 375-Foot Diameter SDUs

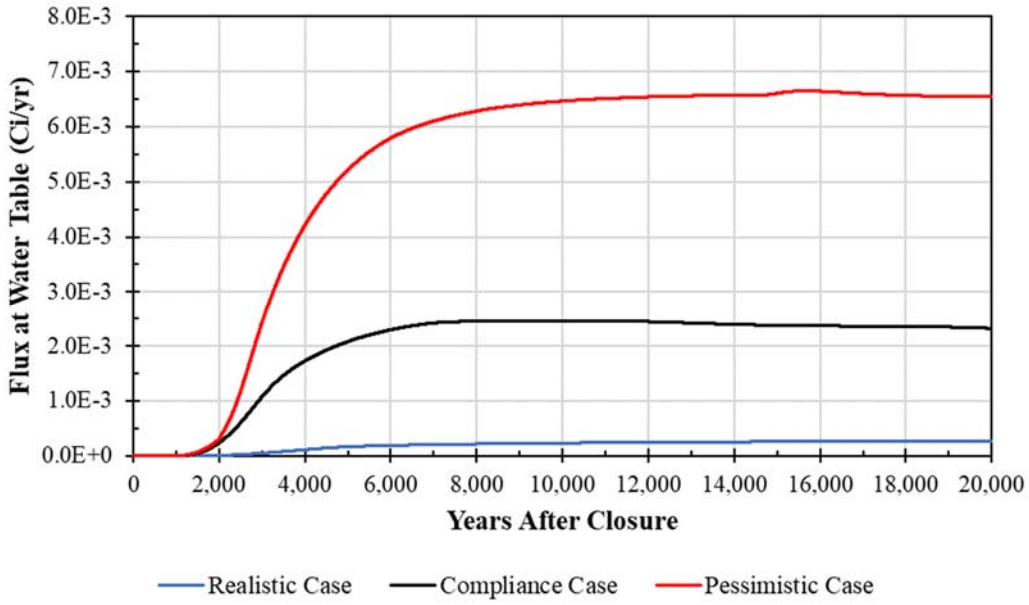

Examining the Pessimistic Case breakthrough curve in Figure 4.4-97, a relatively flat (approximately horizontal) release profile appears after approximately 12,000 years into the simulation showing that the influence of solubility control in the saltstone monolith extends beyond 20,000 years. The slight deviation from flatness of the breakthrough curve after 12,000 years reflects the gradual transition of chemical environment over time associated with the shrinking-core model. Note that the Tc-99 release curve has a slight irregularity in it at around 15,000 years (Figure 4.4-97). The slight irregularity is associated with a decrease in K_d from 0.8 mL/g to 0.5 mL/g in the lower mud mat when the chemical environment in the lower mud mat changes from Oxidized Region I to Oxidized Region III at 14,374 years after closure (Table 4.4-64).

Within the lower 75% (approximately) of the monolith a Reduced Region I environment with a solubility limit of 9.7E-07 mol/L remains throughout the 20,000-year Pessimistic Case simulation. By 20,000 years, this lower zone is

overlain by a Reduced Region III zone which has developed over the 20,000-year simulation time, and has a solubility limit of 4.5E-07 mol/L. A minimal amount of Tc-99 has been leached out, therefore the concentrations in the upper part of this Reduced Region III zone are at the solubility limit of 4.5E-07 mol/L at the end of the simulation.

Note that for the Compliance Case, at the end of the simulation the Reduced Region I solubility limit of 9.7E-07 mol/L is still found in all but a small area of the upper zone, bottom zone, and outer perimeter zone of the saltstone monolith and will control most of the release from the saltstone monolith for the first 20,000 years of the Compliance Case. For the Realistic Case and its Reduced Region I solubility limit of 2.0E-07 mol/L, the solubility limit remains at 2.0E-07 mol/L over most of the monolith volume and a only thin rind of Reduced Region III solubility (7.4E-08 mol/L solubility limit) forms around the perimeter during 20,000 years. Except for this rind, dissolved concentrations remain mainly at the solubility limit of 2.0E-07 mol/L during the 20,000-year simulation.

Over 20,000 years minimal transition occurs from reducing to oxidizing environments within the saltstone. The small volume that does undergo transition occurs only around the perimeter, with oxygen intrusion into the perimeter cells lowering the concentrations slightly below solubility limits based on partial oxidation of the slag in all three of the modeling cases. Within the floor, the top half of the floor has mainly a complete Reduced Region I environment and the bottom half is partially oxidized except near the joints where it is completely oxidized. Note that under fully oxidizing conditions, the system is K_d-controlled with a K_d of 0.5 mL/g.

4.4.5.4.5 Flux Releases from SDU 6

The Vadose Zone Transport Model breakthrough curves from SDU 6 (for Cl-36, I-129, and Tc-99) are presented in the following figures.

Figure 4.4-98 presents the SDU 6 breakthrough curves for Cl-36 releases at the water table for the Realistic Case (blue), the Compliance Case (black), and the Pessimistic Case (red). Differences in the breakthrough curve characteristics depicted in Figure 4.4-98 reflect the differences in volumetric flow rates between each of these modeling cases as presented in Figure 4.4-75. A point of inflection which is only present in the Pessimistic Case curve (for the 20,000-year simulation) represents a sudden decrease in Cl-36 release rate at the water table due to the influence of the change in chemical environment in the saltstone monolith from Reduced Region I to Reduced Region III occurring 14,370 years after closure (Table 4.4-64). This feature results from the instantaneous change in the chemistry throughout the saltstone monolith and a simultaneous change in cementitious materials beneath the saltstone.

Figure 4.4-98: Flux Releases of Cl-36 from SDU 6

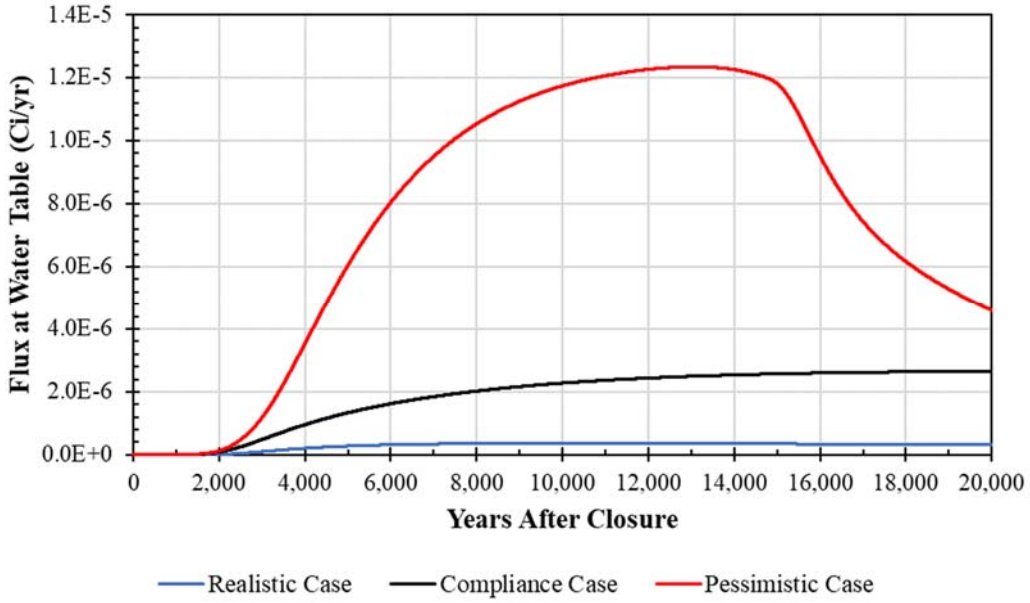

The monolith bottom pH transition initiates the onset of adsorption reflected in a change of chlorine K_d from 0.0 mL/g to 1.0 mL/g and associated decrease in dissolved Cl-36 concentrations. Due to the 20,000-year time extent of the SDU 6 Cl-36 simulations, Reduced Region I to Reduced Region III transition times in the saltstone monolith associated with the Compliance Case and the Realistic Case are not reflected in the presented breakthrough curves. The pH transition for the Compliance Case occurs 55,686 years after closure (Table 4.4-62), and the pH transition for the Realistic Case occurs 734,682 years after closure (Table 4.4-63).

Similarly Eh controlled transitions from Reduced Region III to Oxidized Region III associated with all three of these modeling cases are not reflected in their breakthrough curves. The reducing to oxidizing environment transition times based on Eh (Reducing Region III to Oxidizing Region III) occur well beyond the 20,000-year simulation time.

Figure 4.4-99 depicts the SDU 6 breakthrough curves of I-129 releases at the water table for the Realistic Case (blue), the Compliance Case (black), and the Pessimistic Case (red). As with the Cl-36 breakthrough curves (see Figure 4.4-98), differences in the breakthrough curves in Figure 4.4-99 are dominated by the differences in volumetric flow rates between each of these modeling cases as presented in Figure 4.4-75, which directly influences leaching rates. The Pessimistic Case curve also depicts a drop in the I-129 release rate at the water table this time at about 16,500 years after closure. This drop in the release rate reflects the influence of the spatially gradual change in chemical environment from Reduced Region I to Reduced Region III in the saltstone monolith and cementitious material below as evalulated using the shrinking core model.

Figure 4.4-99: Flux Releases of I-129 from SDU 6

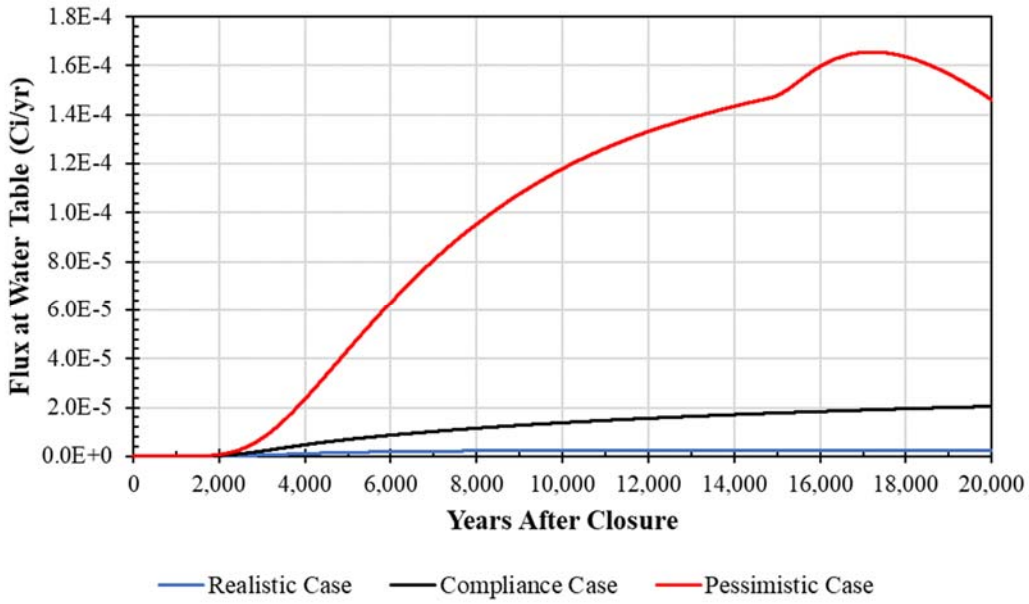

When compared to the Cl-36 curve presented in Figure 4.4-98, an increase in the I-129 release occurs at approximately the same time that the decrease occurs for Cl-36. This increase in the I-129 release rate prior to the rate decrease is associated with a decrease in K_d from 8 mL/g to 4 mL/g when the chemical environment throughout the lower mud mat instantaneously changes from Oxidized Region I to Oxidized Region III at 14,370 years after closure (Table 4.4-64).

Because of the more rigorous cell-to-cell analysis of the shrinking core calculations in the saltstone monolith, the chemical transitions within the saltstone monolith and most of the cementitious material below (all except the lower mud mat that does not use the shrinking core model) are simulated as occurring gradually (as opposed to instantaneously) thus releasing the I-129 in a more dispersed manner than Cl-36 (Figure 4.4-98) as shown after 16,500 years in the Pessimistic Case breakthrough curve. The pH transition initiates an increase in adsorption reflected in a decrease in concentration as driven by a change of iodine K_d. Region I to Region III iodine K_ds transition from 0.07 mL/g to 0.71 mL/g (Table 4.3-6 and Table 4.3-7) for the Pessimistic Case and the Compliance Case and from 0.16 mL/g to 2.77 mL/g (Table 4.3-7) for the Realistic Case.

Due to the 20,000-year time extent of the SDU 6 I-129 simulations, Reduced Region I to Reduced Region III transition times associated with the Compliance Case and the Realistic Case are not discernible in their associated breakthrough curves.

Figure 4.4-100 presents the breakthrough curves for SDU 6 Tc-99 releases at the water table for the Realistic Case (blue), the Compliance Case (black), and the Pessimistic Case (red). As with the Cl-36 and I-129 breakthrough curves (see Figure 4.4-98 and Figure 4.4-99), the breakthrough curves of release rates

presented in Figure 4.4-100 are strongly controlled by the differences in volumetric flow rates between each of these modeling cases as presented in Figure 4.4-75. As discussed above, Tc-99 transport simulations use the shrinking core model to evaluate chemical environment transitions. In addition, the Tc-99 transport process calculations are based on solubility control of Tc-99 in the saltstone monolith when under reducing conditions.

Figure 4.4-100: Flux Releases of Tc-99 from SDU 6

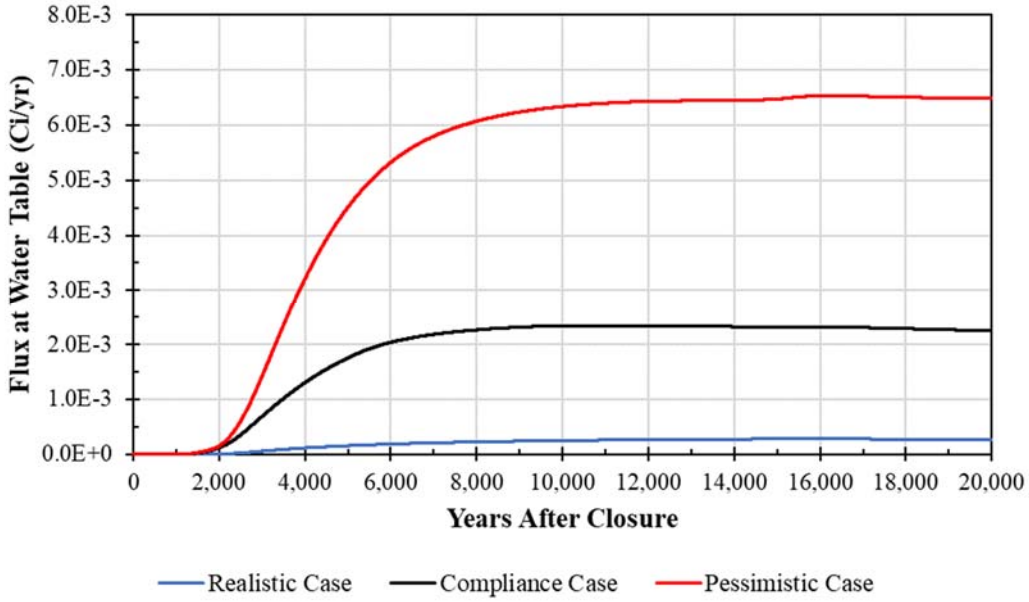

Examining the Pessimistic Case breakthrough curve in Figure 4.4-100, a relatively flat (approximately horizontal) release profile appears after approximately 12,000 years into the simulation showing the influence of solubility control in the saltstone monolith extends beyond 20,000 years. The slight deviation from flatness of the breakthrough curve after 12,000 years reflects the gradual transition of chemical environment over time associated with the shrinking-core model. Note that the Tc-99 release curve has a slight irregularity in it at around 15,000 years (Figure 4.4-100). The slight irregularity is associated with a decrease in K_d from 0.8 mL/g to 0.5 mL/g in the lower mud mat when the chemical environment in the lower mud mat instantaneously changes from Oxidized Region I to Oxidized Region III throughout the mudmat at 14,370 years after closure (Table 4.4-64).

Within the lower 75% the of the monolith a Reduced Region I environment with a solubility limit of 9.7E-07 mol/L remains throughout the 20,000-year simulation for the Pessimistic Case. By 20,000 years, this lower zone is overlain by a Reduced Region III zone which has developed over the 20,000-year simulation time, and has a solubility limit of 4.5E-07 mol/L. A minimal amount of Tc-99 has been leached out, therefore the concentrations in the upper part of this Reduced Region III zone are at the solubility limit of 4.5E-07 mol/L at the end of the simulation.

Note that for the Compliance Case, the solubility limit of 9.7E-07 mol/L is found in all but a small upper zone of the saltstone monolith, at the outside edge of the saltstone monolith and in a thin layer at the bottom of the monolith. The solubility limit will control most of the release from the saltstone monolith for the first 20,000 years of the Compliance Case. For the Realistic Case, with the Reduced Region I solubility limit of 2.0E-07 mol/L, the solubility limit remains at 2.0E-07 mol/L over most of the monolith volume except for a thin rind of Reduced Region III solubility (7.4E-08 mol/L solubility limit) which forms around the perimeter during 20,000 years.

Over the time span of 20,000 years minimal transition from reduced to oxidizing environment occurs within the saltstone around the perimeter with oxygen intrusion into the perimeter cells lowering the concentrations slightly below solubility limits based on partial oxidation of the slag in all three of these modeling cases. Within the floor, the top half of the floor has mainly a complete Reduced Region I environment and the bottom half is partially oxidized except near the joints where it is completely oxidized. Note that under fully oxidizing conditions, the system is K_d-controlled with a K_d of 0.5 mL/g.

4.4.5.4.6 Flux Releases from SDU 9

The Vadose Zone Transport Model breakthrough curves from SDU 9 (for Cl-36, I-129, and Tc-99) are presented in the following figures.

Figure 4.4-101 presents the SDU 9 breakthrough curves for Cl-36 releases at the water table for the Realistic Case (blue), the Compliance Case (black), and the Pessimistic Case (red). The differences in the breakthrough curve characteristics depicted in Figure 4.4-101 reflect the differences in volumetric flow rates between each of these modeling cases as presented in Figure 4.4-77. Additionally, the point of inflection which is only seen in the Pessimistic Case curve represents a sudden decrease in the release rate at the water table, caused by the influence of the change in chemical environment in the saltstone monolith from Reduced Region I to Reduced Region III at 14,645 years after closure (Table 4.4-64).

Figure 4.4-101: Flux Releases of Cl-36 from SDU 9

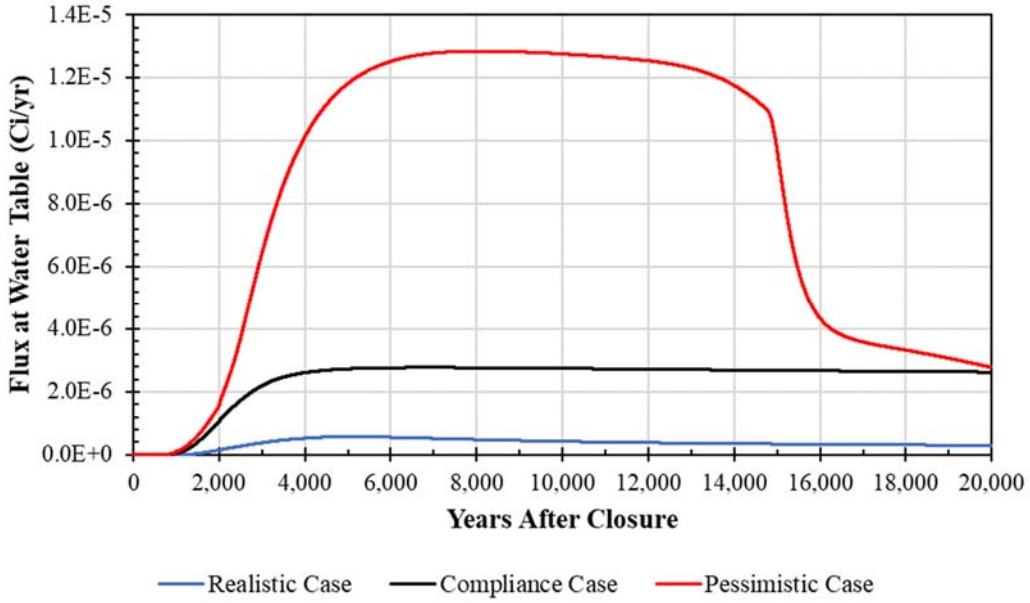

This feature results from the instantaneous change in the chemistry throughout the saltstone monolith and a simultaneous change in cementitious materials beneath the saltstone. The pH transition initiates the onset of adsorption reflected in a change of chlorine K_d from 0.0 mL/g to 1.0 mL/g and associated decrease in dissolved Cl-36 concentrations. Unlike the Cl-36 releases from SDU 6 (Figure 4.4-98) and SDU 7 (Figure 4.4-95), the release from SDU 9, is more representative of a steady pulse release (between 6,000 and 15,000 years after closure), reflecting the shorter transport distance between the bottom of the SDU and the water table.

Due to the 20,000-year time extent of the SDU 9 Cl-36 simulations, Reduced Region I to Reduced Region III transition times in the saltstone monolith associated with the Compliance Case and the Realistic Case are not reflected in the presented breakthrough curves. The pH transition for the Compliance Case occurs 60,387 years after closure (Table 4.4-62), and the pH transition for the Realistic Case occurs 812,388 years after closure (Table 4.4-63).

Similarly Eh controlled transitions from Reduced Region III to Oxidized Region III associated with each of these modeling cases are not reflected in their associated breakthrough curves. The reducing to oxidizing environment transition times based on Eh (Reducing Region III to Oxidizing Region III) occur well beyond the 20,000-year simulation time.

Figure 4.4-102 depicts the breakthrough curves of I-129 releases at the water table for the Realistic Case (blue), the Compliance Case (black), and the Pessimistic Case (red). As with the Cl-36 breakthrough curves (see Figure 4.4-101), differences in the breakthrough curves in Figure 4.4-102 are dominated by the differences in volumetric flow rates between each of these three modeling cases as presented in

Figure 4.4-77, and which directly influence leaching rates. The Pessimistic Case curve depicts a drop in the I-129 release rate at the water table at approximately 15,500 years after closure. The drop in the release rate reflects the influence of the spatially gradual change in chemical environment from Reduced Region I to Reduced Region III in the saltstone monolith and cementitious material below as calculated using the shrinking core model.

Figure 4.4-102: Flux Releases of I-129 from SDU 9

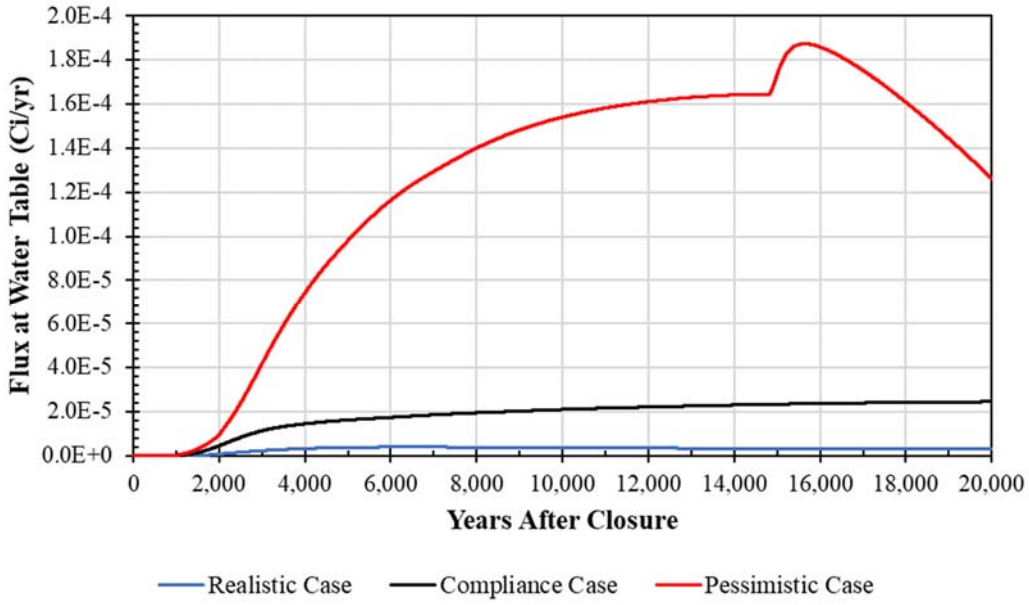

When compared to the Cl-36 curve presented in Figure 4.4-101, an accelerated increase I-129 release occurs at approximately the same time that the decrease occurs for the Cl-36 release (Figure 4.4-101). This increase in the I-129 release rate prior to the rate decrease is associated with a decrease in I-129 K_d in the lower mud mat from 8 mL/g to 4 mL/g when the chemical environment throughout the lower mud mat instantaneously changes from Oxidized Region I to Oxidized Region III at 14,645 years after closure (Table 4.4-64).

Because of the more rigorous cell-to-cell analysis of the shrinking core calculations in the saltstone monolith, the chemical transitions within the saltstone monolith and most of the cementitious material below (all except the lower mud mat that does not use the shrinking core model) are simulated as occurring gradually (as opposed to instantaneously), releasing the I-129 in a more dispersed manner compared to Cl-36 (Figure 4.4-101). Note that compared to releases from SDU 6 (Figure 4.4-99) and SDU 7 (Figure 4.4-96), after the peak is reached, the release rate decrease is steeper (faster) in the SDU 9 simulation because of the shorter transport distance from the bottom of the SDU to the water table (36 ft, 42 ft, and 23 ft for SDU 7, SDU 6, and SDU 9, respectively).

The pH transition initiates an increase in adsorption reflected in a decrease in concentration as driven by a change of iodine K_d. Region I to Region III iodine K_{ds} transition from 0.07 mL/g to 0.71 mL/g (Table 4.3-6 and Table 4.3-7) for the Pessimistic Case and the Compliance Case and from 0.16 mL/g to 2.77 mL/g (Table 4.3-7) for Realistic Case. Due to the 20,000-year time extent of the SDU 9 I-129 simulations, Reduced Region I to Reduced Region III transition times associated with the Compliance Case and the Realistic Case are not discernible in their associated breakthrough curves.

Finally, Figure 4.4-103 presents the breakthrough curves for SDU 9 Tc-99 releases at the water table for the Realistic Case (blue), the Compliance Case (black), and the Pessimistic Case (red). As with the Cl-36 and I-129 breakthrough curves (see Figure 4.4-101 and Figure 4.4-102), the breakthrough curves of release rates presented in Figure 4.4-103 are strongly controlled by the differences in volumetric flow rates between each of these cases as presented in Figure 4.4-77. As previously discussed, Tc-99 transport simulations utilize the shrinking core model to evaluate chemical environment transitions. In addition, the Tc-99 transport process calculations are based on solubility control of Tc-99 in the saltstone monolith when under reducing conditions.

Figure 4.4-103: Flux Releases of Tc-99 from SDU 9

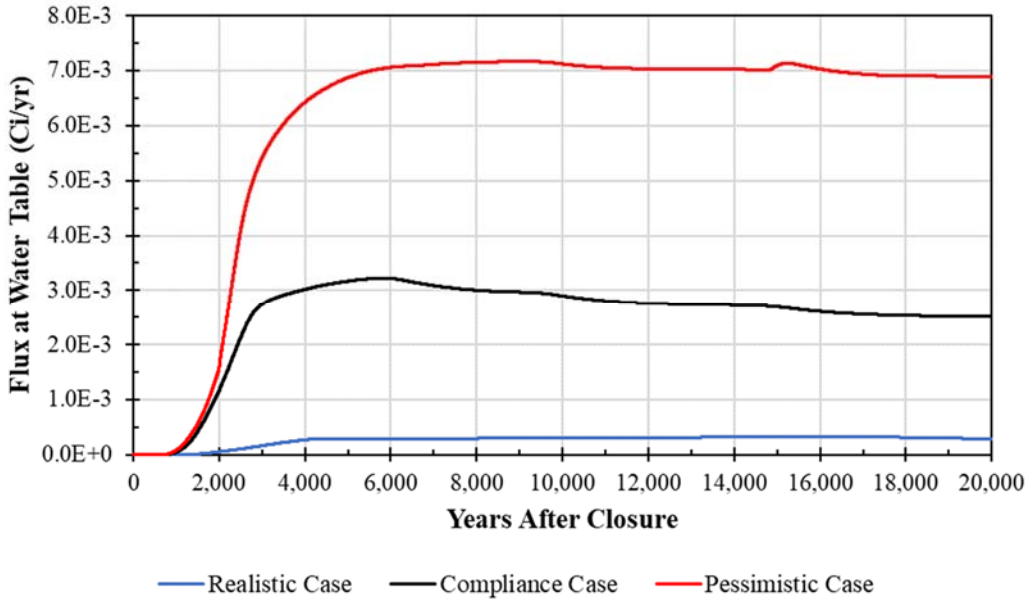

Examining the Pessimistic Case breakthrough curve in Figure 4.4-103, a relatively flat (approximately horizontal) release profile appears after approximately 6,000 years into the simulation showing that the influence of solubility control in the saltstone monolith extends beyond 20,000 years.

Note that the Tc-99 release curve has a slight irregularity in it at around 15,000 years (Figure 4.4-103). The slight irregularity is associated with a decrease

in K_d from 0.8 mL/g to 0.5 mL/g in the lower mud mat when the chemical environment in the lower mud mat instantaneously changes from Oxidized Region I to Oxidized Region III at 14,645 years after closure (Table 4.4-64).

Within the lower 75% of the monolith a Reduced Region I environment with a solubility limit of 9.7E-07 mol/L remains throughout the 20,000-year Pessimistic Case simulation. By 20,000 years, this lower zone is overlain by a Reduced Region III zone which has developed over the 20,000-year simulation time and has a solubility limit of 4.5E-07 mol/L. Not enough Tc-99 has been leached out, therefore the concentrations in the upper part of this Reduced Region III zone are at the solubility limit of 4.5E-07 mol/L at the end of the simulation.

Note that for the Compliance Case, the solubility limit of 9.7E-07 mol/L is found in all but a small upper zone of the saltstone monolith, at the outside edge of the monolith and in a thin layer at the bottom of the monolith, and will control most of the release from the saltstone monolith for the first 20,000 years. For the Realistic Case, with its Reduced Region I solubility limit of 2.0E-07 mol/L, the solubility limit remains at 2.0E-07 mol/L over most of the saltstone monolith volume except where a thin rind of Reduced Region III solubility (7.4E-08 mol/L solubility limit) forms around the perimeter during 20,000 years. Except for this rind, the dissolved concentrations remain mainly at the solubility limit of 2.0E-07 mol/L during the 20,000-year simulation.

Over the time span of 20,000 years, minimal transition from reduced to oxidizing environment occurs only along the saltstone perimeter with oxygen intrusion into the perimeter cells lowering the concentrations to slightly below solubility limits based on partial oxidation of the slag in each of these modeling cases. Within the floor, the top half of the floor has mainly a complete Reduced Region I environment and the bottom half is partially oxidized except near the joints where it is completely oxidized. Note that under fully oxidizing conditions, the system is K_d-controlled with a K_d of 0.5 mL/g.

This page intentionally left blank.

4.4.6 Aquifer Transport Model

The local aquifer system, as described in Section 3.1.5, includes a number of hydrostratigraphic units: The Transmissive Zone (TZ), the Upper Aquifer Zone (UAZ), the Tan Clay Confining Zone (TCCZ), the Lower Aquifer Zone (LAZ), the Gordon Confining Unit (GCU), and the Gordon Aquifer Unit (GAU). Beneath these units is the Crouch Branch Confining Unit, a laterally continuous, dense unit.

The descriptions for these units (shown in Figure 4.4-104) are based on the descriptions from the *Integrated Hydrogeological Model of the General Separations Area* (WSRC-TR-96-0399):

- The **TZ** is a variable sandy region through which precipitated water infiltrates into, facilitating the recharge of underlying aquifers. The TZ is sometimes included as part of the UAZ.
- The **UAZ** is characterized by sand and clayey sand with minor intercalated clay layers.
- The **TCCZ** is characterized by clay and sandy clay interbedded with clayey sand and sand. The clay layers of the TCCZ are not laterally continuous over distances greater than 100 to 200 feet. As such the water table may exist either above or below the TCCZ as a function of location relative to recharge zones.
- The **LAZ** is characterized by fine-grained, well-sorted sand and clayey sand, and includes carbonate sediments and various calcareous components (e.g., calcarenaceous sand).
- The **GCU** separates the GAU from the water table aquifer, which is locally within the UAZ. The GCU is also known as the "green clay" and is characterized as layers of interbedded silty and clayey sand, sandy clay, and clay. Within the GSA, the GCU includes some calcareous sediment.
- The **GAU** is the lowermost unit considered for the PA, as it is bounded by the Crouch Branch Confining Unit. The GAU is characterized as loose sand and clayey sand.

Flow through these layers is modeled in PORFLOW via the GSA Model. This model is used throughout SRS. Considering the GSA Model includes Z-Area, it is applicable to the SDF PA.

The GSA Model simulates ground water under steady-state conditions representing current topography and climate. Potential climate changes affecting infiltration are addressed through sensitivity cases (Section 5.8.2.6). The influence of a future SDF closure cap on ground water flow rates and directions is thought to be minimal and is not explicitly considered in the Aquifer Transport Model simulations. It is expected that the presence of the closure cap will slightly lower the water table beneath Z-Area, increasing the vadose zone transport distance and reducing hydraulic head gradients driving advective transport of waste to exposure points (e.g., 100-meter perimeter). Because perturbations to the water table are expected to be small, the Z-Area cap is expected to have minimal effect on ground water flow directions. For additional information on aquifer flow modeling for the SDF, refer to the *Updated Groundwater Flow Simulations of the Savannah River Site General Separations Area* (SRNL-STI-2018-00643). The following subsections

describe how contaminant transport is modeled through the Z-Area aquifers (or saturated zone), using the flow data from the GSA Model.

Figure 4.4-104: Hydrostratigraphic Units of Concern

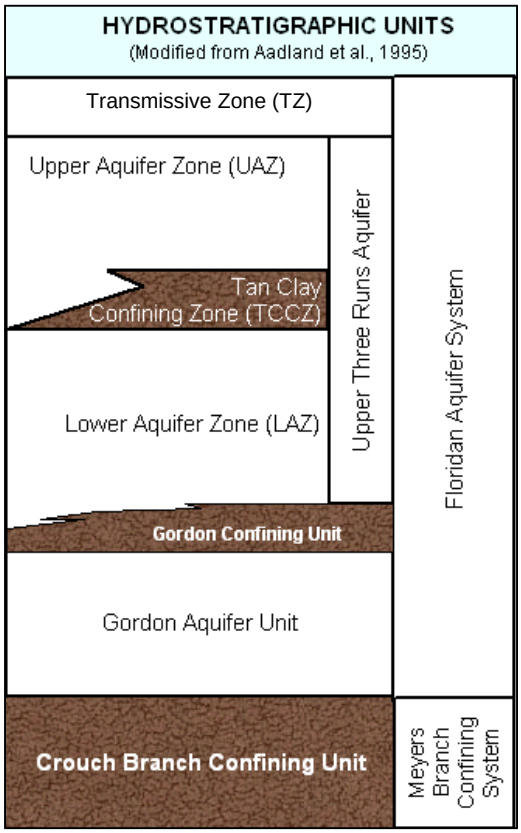

[Modified from PIT-MISC-0112.]

4.4.6.1 Conceptual Model for Aquifer Transport Modeling

Once contaminants released from the SDUs have migrated through the vadose zone, they will breach the water table and enter the saturated zone. Flowing ground water within the saturated zone will then carry the contaminants downgradient, further away from the SDUs. Contaminants within the ground water will form contaminant plumes. Plumes that intercept ground water wells or seepage faces may contribute to contaminant exposures.

Figure 4.4-105 provides a conceptualization of the hydrostratigraphic units through which contaminants will be transported. The blue line in this figure represents the water table. This conceptual model is based on ground water data from hundreds of wells across the GSA that have been collected over several decades (SRNL-STI-2018-00643). For Z-Area, this ground water data is documented via periodic SDF ground water monitoring reports. [SRNS-TR-2018-00149; SRNS-TR-2018-00292] These ground water monitoring reports show the locations for various monitoring wells (e.g., Figure 4.4-106) and include cross sections that depict the water table levels (e.g., Figure 4.4-107).

Figure 4.4-105: Conceptual Diagram of Ground Water Flow Beneath the GSA

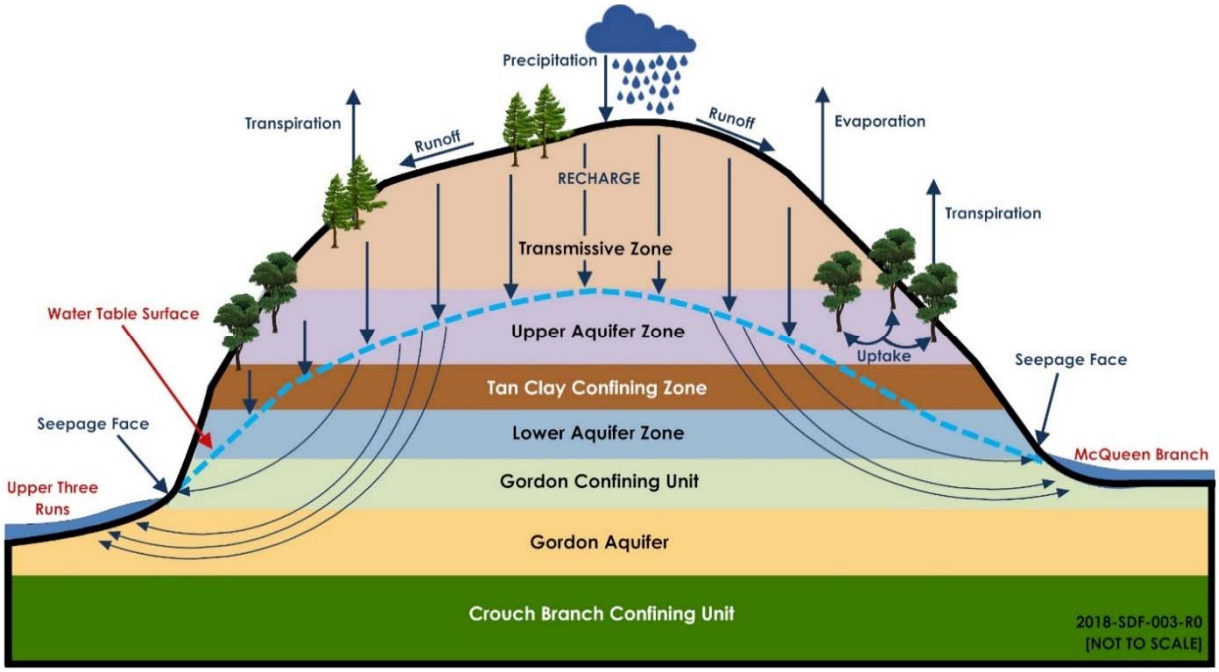

Figure 4.4-106: Montioring Wells for Z-Area

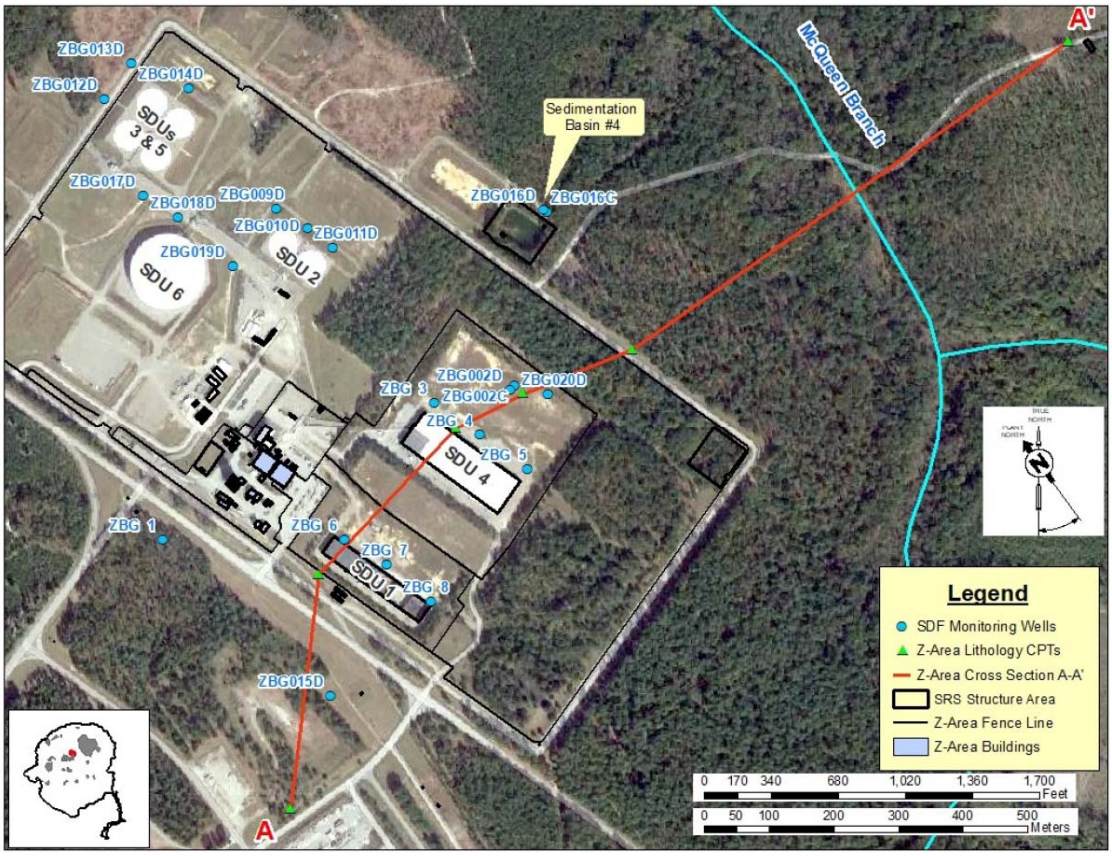

[SRNS-TR-2018-00292]

Figure 4.4-107: Cross Section for Z-Area

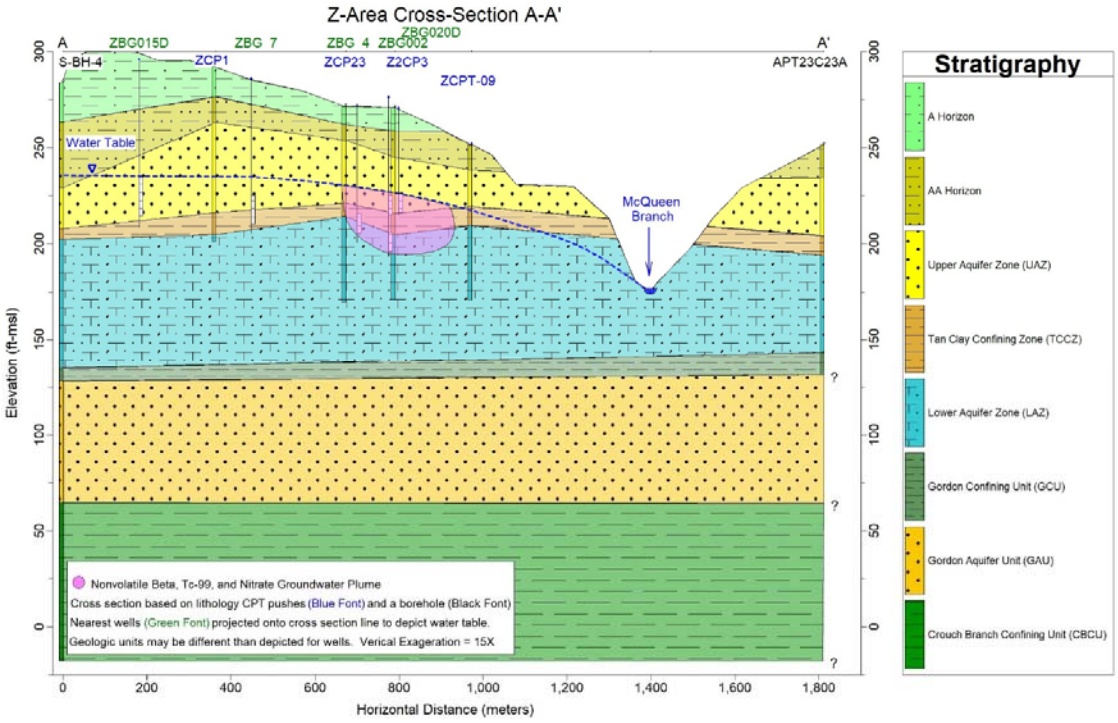

[SRNS-TR-2018-00292]

Table 4.4-83 provides summary water table data available for the Z-Area wells.

Table 4.4-83: Summary of Z-Area Water Table Data Used for the GSA Model

Well Name	Feet Above Mean Sea Level			Range (ft)
	Maximum	Minimum	Mean	
ZBG 1	235.9	230.0	233.1	5.9
ZBG 2	222.7	213.6	218.1	9.1
ZBG002C	225.2	220.3	222.1	4.8
ZBG002D	226.5	223.6	225.4	2.9
ZBG 3	225.7	215.6	220.3	10.1
ZBG 4	225.6	215.1	220.3	10.5
ZBG 5	229.0	210.2	219.7	18.8
ZBG 6	236.4	231.4	233.7	5.0
ZBG 7	236.9	231.8	234.0	5.1
ZBG 8	237.1	231.4	234.2	5.7
ZBG009D	224.3	216.4	220.7	7.9
ZBG010D	222.6	216.2	220.6	6.4
ZBG011D	224.3	209.7	220.3	14.6
ZBG012D	222.4	212.1	216.2	10.2
ZBG013D	224.5	211.6	215.9	12.9
ZBG014D	224.0	212.9	217.7	11.1
ZBG015D	238.1	232.2	235.5	5.9
ZBG016C	216.1	210.8	213.2	5.3
ZBG016D	223.7	222.4	223.4	1.3

Contour maps are generated based on the water table levels. Because ground water flows perpendicular to water table contours, these contour maps indicate the direction of ground water flow (e.g., Figure 4.4-108). These well data, along with additional wells from throughout the GSA, were used in the development of the GSA Model (see Section 3.1.5).

Figure 4.4-108: Z-Area Water Table Contours and Flow Direction

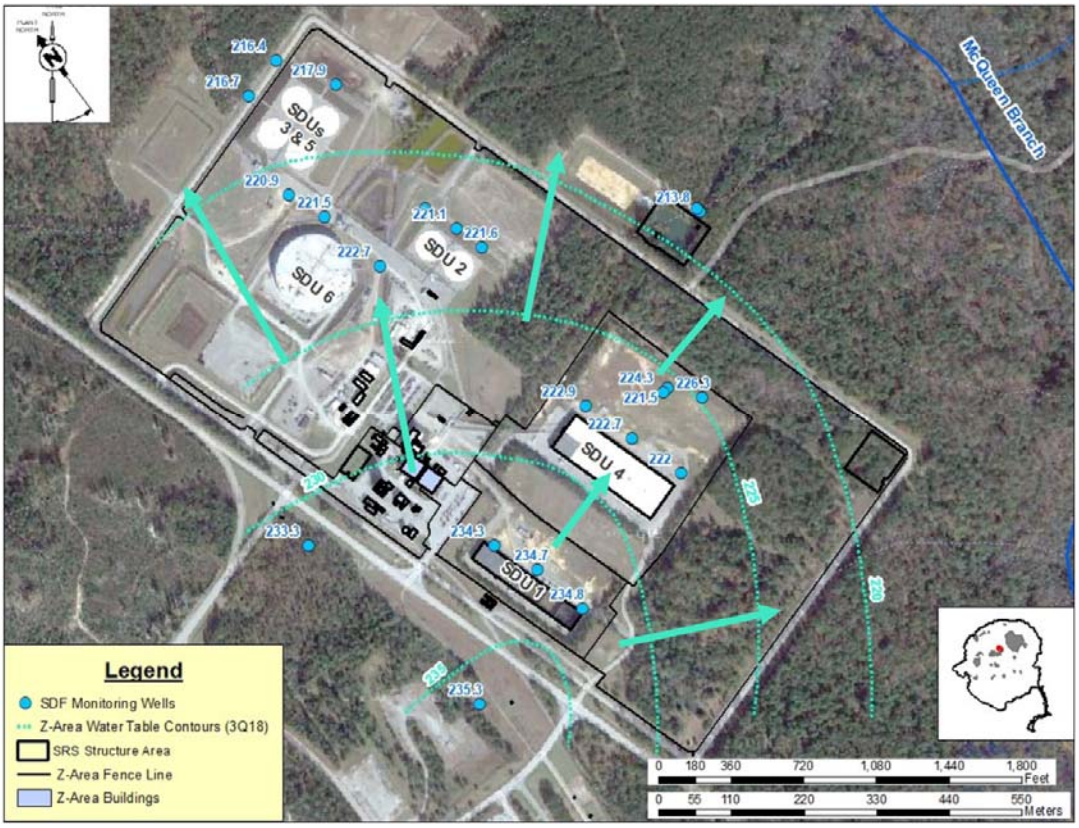

[Modified from SRNS-TR-2018-00292]

Based on the ground water data, the ground water in Z-Area flows in a radial direction from a high point (west of SDU 1) towards McQueen Branch in the east or towards Upper Three Run in the north. No ground water flow is expected to move from the SDUs towards the west or the south.

As indicated by the SDF ground water reports, in addition to measuring the water levels, these wells are also monitored for contaminants. For example, Table 1 of the 2018 ground water monitoring report (SRNS-TR-2018-00292) identifies a number of analytes, including I-129 and Tc-99. These analytes are monitored to ensure ground water protection standards are met. If gross beta (i.e., nonvolatile beta) ever exceeds 30 pCi/mL in a downstream well, then the same well and an applicable background well (ZBG 1 or ZBG015D, see Figure 4.4-106) are resampled within 30 days. If these samples confirm the exceedance results, then a characterization plan will be developed and submitted to SCDHEC. [SRNS-TR-2018-00292] This monitoring program confirms that shallow ground

water within Z-Area migrates towards the nearby streams, either in a north or northwest direction towards the Upper Three Runs or in an easterly direction towards the McQueen Branch.

The water table in the GSA is generally located in the UAZ. Near the SDF, the water table is approximately 40 feet below the surface (see Table 4.3-1). The local surface topography is such that the SDF sits on a hill bounded by two streams: Upper Three Runs to the north and McQueen Branch to the east. At each stream, distance between the ground surface and the water table reduces to zero, terminating at a seepline (or seepage face). For the SDF Aquifer Transport Modeling, the water table provides the upper boundary and the Crouch Branch Confining Unit provides the lower model boundary.

After transport out of the Vadose Zone Transport Model, contaminants will enter the saturated zone beneath the SDUs from which they were released. Then based on flow rates from the GSA Model (SRNL-STI-2018-00643) and based on the transport properties of the soils and the contaminants, will be transported towards the seeplines.

4.4.6.2 Implementation of Aquifer Transport Model

Implementation of the Aquifer Transport Model is organized into two parts. The first, Aquifer Flow Field Refinement, involved refinement of the GSA Model to generate localized flow fields, and the second, Aquifer Transport Implementation, involved the actual contaminant transport modeling.

4.4.6.2.1 Aquifer Flow Field Refinement

The Aquifer Transport Model was developed using the fully three-dimensional GSA Model. As depicted in Figure 4.4-109, the GSA Model encompasses the SDF (in the upper right-hand side of the figure), as well as several other SRS areas. High-level streamline traces are shown in Figure 4.4-109 which emanate from select SRS facilities and generally terminate at the local streams which bound the GSA Model.

Figure 4.4-109: GSA Model with Water Table Contours and Stream Traces from Select SRS Facilities

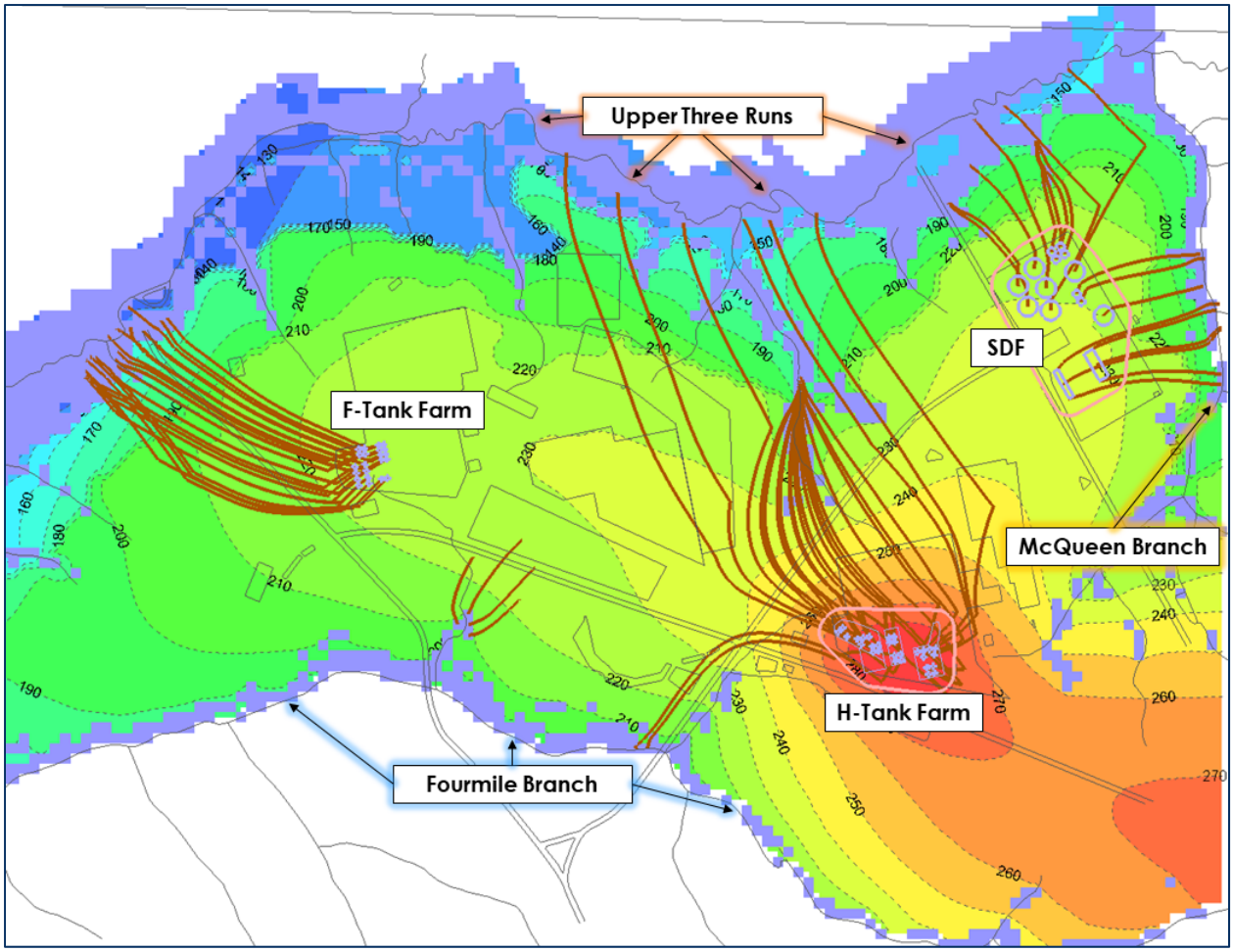

As described in the *Updated Groundwater Flow Simulations of the Savannah River Site General Separations Area*, each subsurface hydrostratigraphic layer has been assigned saturated hydraulic conductivity values based on model calibration performed using a parameter estimation (PEST) calibration code. [SRNL-STI-2018-00643] These values were developed specifically for use in Z-Area modeling based on calibration to local well data. These saturated hydraulic conductivity values for the GSA are shown in Figure 4.4-110 and Figure 4.4-111, and are summarized in Table 4.4-84. These figures also depict red nodes indicating where fluxes (i.e., results from the Vadose Zone Transport Model) are loaded into the Aquifer Transport Model. The depths for these fluxes were selected based on the depth to model nodes that are fully saturated (see Figure 4.4-112) as these nodes provide the simulated representation of the water table.

Figure 4.4-110: GSA at the SDF: Applied Vertical Saturated Hydraulic Conductivities

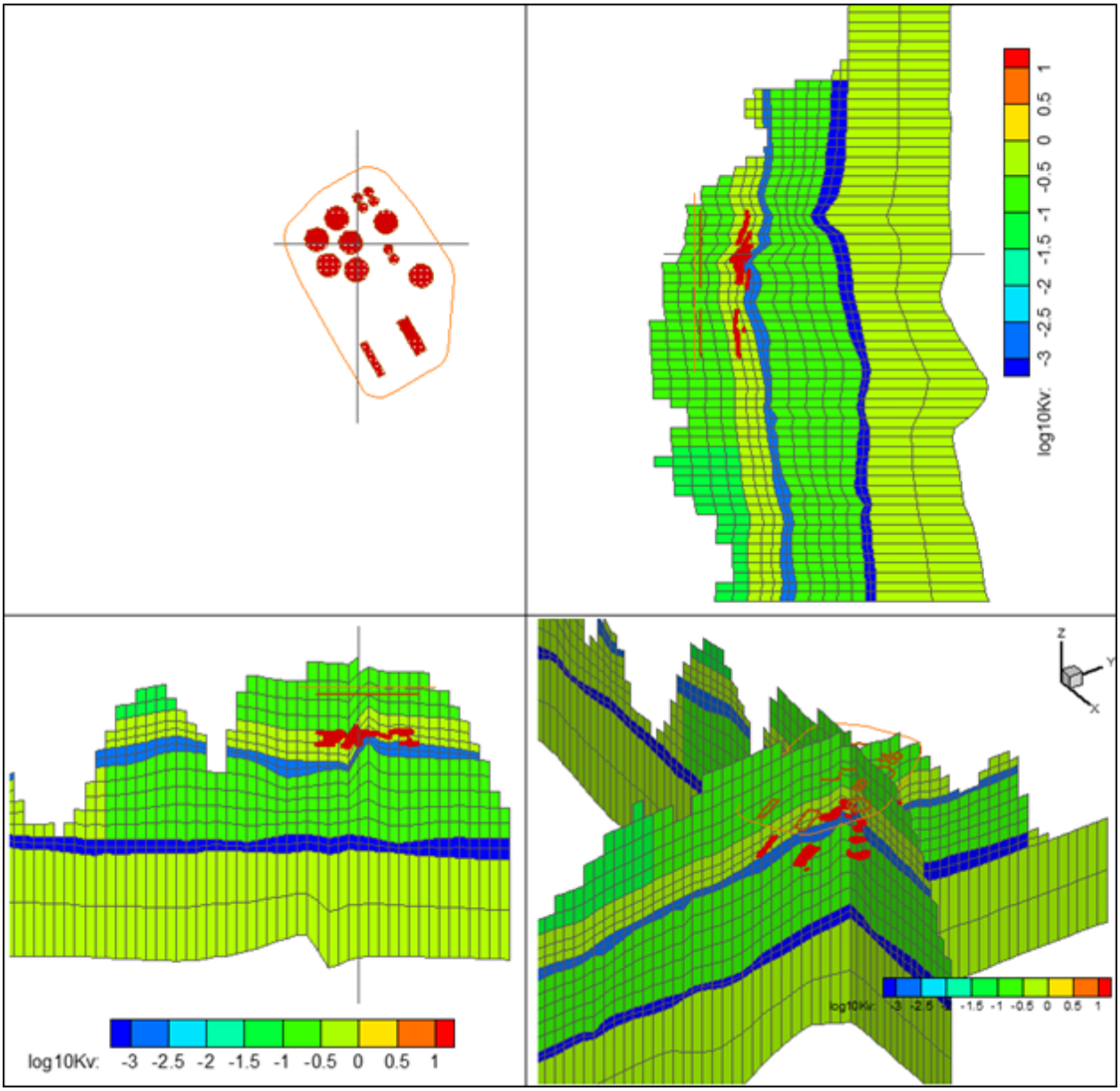

Figure 4.4-111: GSA at the SDF: Applied Horizontal Saturated Hydraulic Conductivities

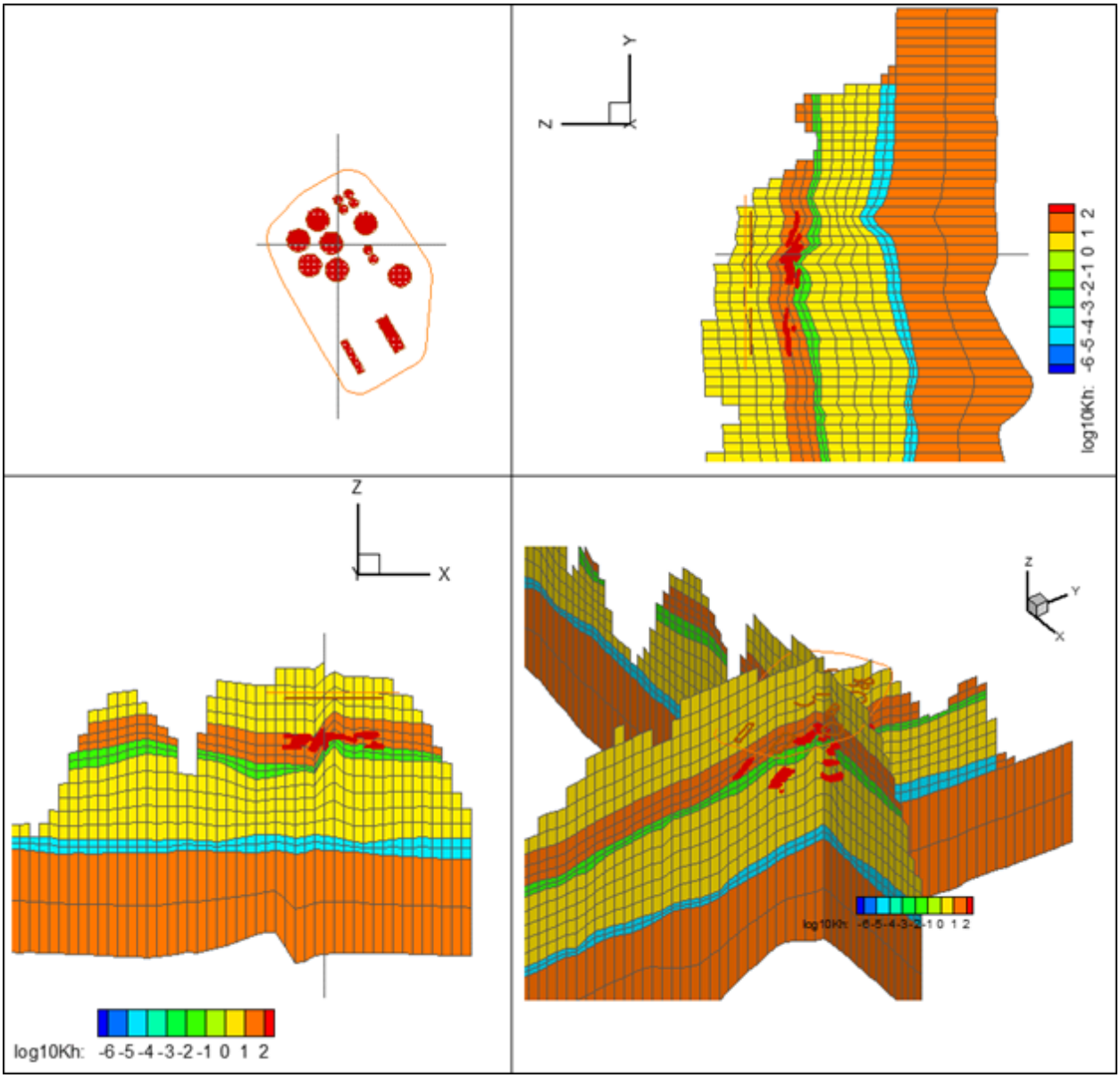

Table 4.4-84: Summary of Applied Saturated Hydraulic Conductivities

GSA Layer	Log10Kv	Vertical Saturated Hydraulic Conductivity		Log10Kh	Horizontal Saturated Hydraulic Conductivity (ft/day)	
		(ft/day)	(cm/s)		(ft/day)	(cm/s)
AAA	-0.866	1.36E-01	4.8E-05	0.616	4.13E+00	1.5E-03
UAZ	-0.308	4.92E-01	1.7E-04	1.17	1.48E+01	5.2E-03
TCCZ	-2.70	1.99E-03	7.0E-07	-1.23	5.96E-02	2.1E-05
LAZ	-0.741	1.82E-01	6.4E-05	0.736	5.44E+00	1.9E-03
GCU	-5	1.00E-05	3.5E-09	-4	1.00E-04	3.5E-08
GAU	-0.420	3.8E-01	1.3E-04	1.58	3.8E+01	1.3E-02

Figure 4.4-112: GSA at the SDF: Fully Saturated Cells

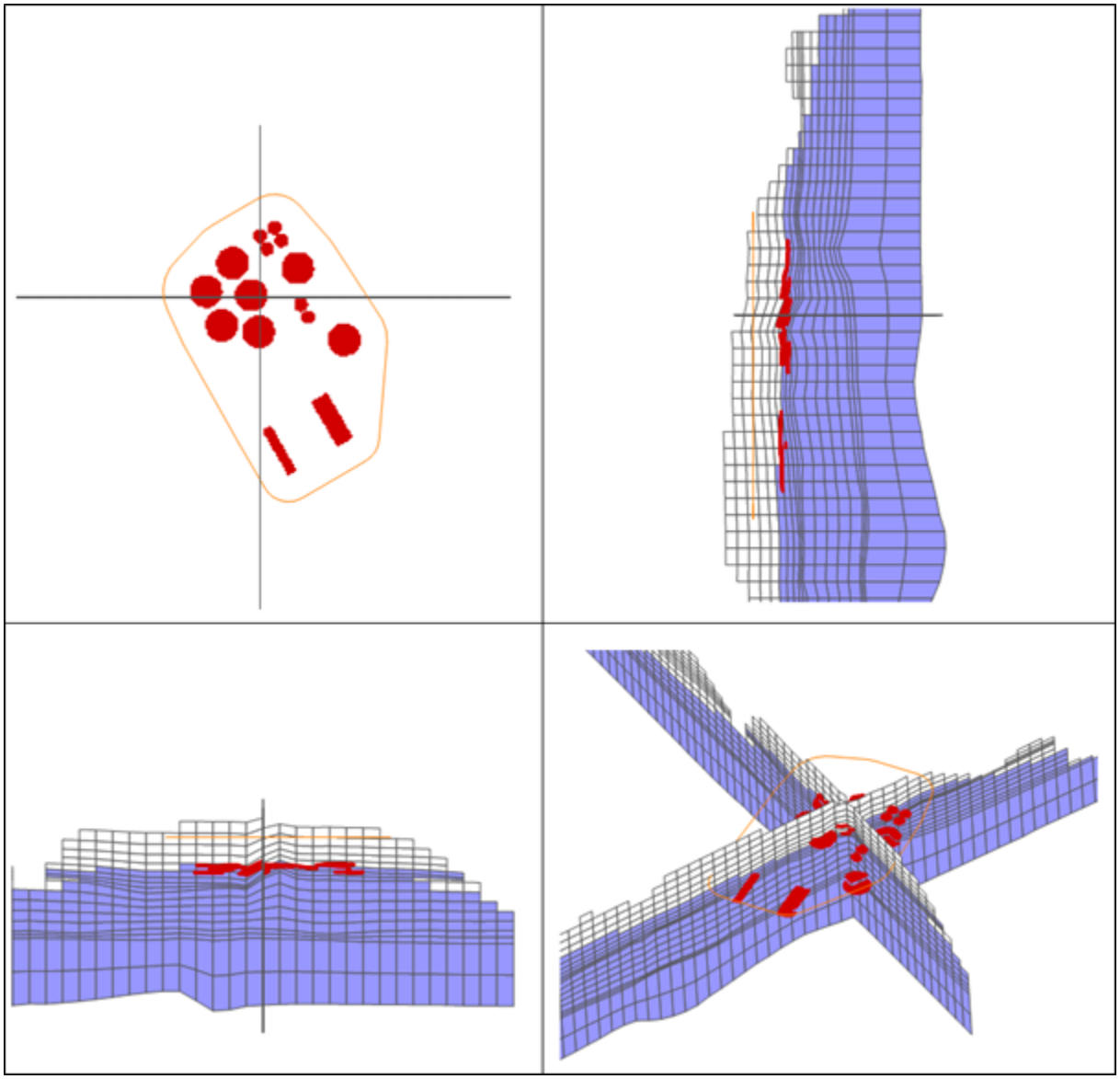

Due to the dimensions of this model, it is computationally inefficient to process flow and transport for the entirety of the GSA. For the purposes of the SDF PA, a smaller grid was extracted from the GSA Model, thus limiting the simulation to the GSA Model nodes that are relevant to the SDF, as shown in Figure 4.4-113. Within this figure, streamline traces are shown from each SDU to the respective seeplines – either at the McQueen Branch (nodes with orange squares) to the east or the Upper Three Runs (nodes with bluish diamonds) to the north.

Note that Figure 4.4-113 also includes vector arrows at the corners of each model cell or element to show the general direction of flow in the Upper Three Runs Aquifer. Both the UAZ and LAZ of the Upper Three Runs Aquifer have relatively similar directions of flow. Two of the streamline traces reached deeper, passing

into the GAU. The GAU is distinct in that all ground water within the GAU beneath the GSA flows in the same direction, towards the northwest.

Figure 4.4-113: SDF-Specific Portion of the GSA Model

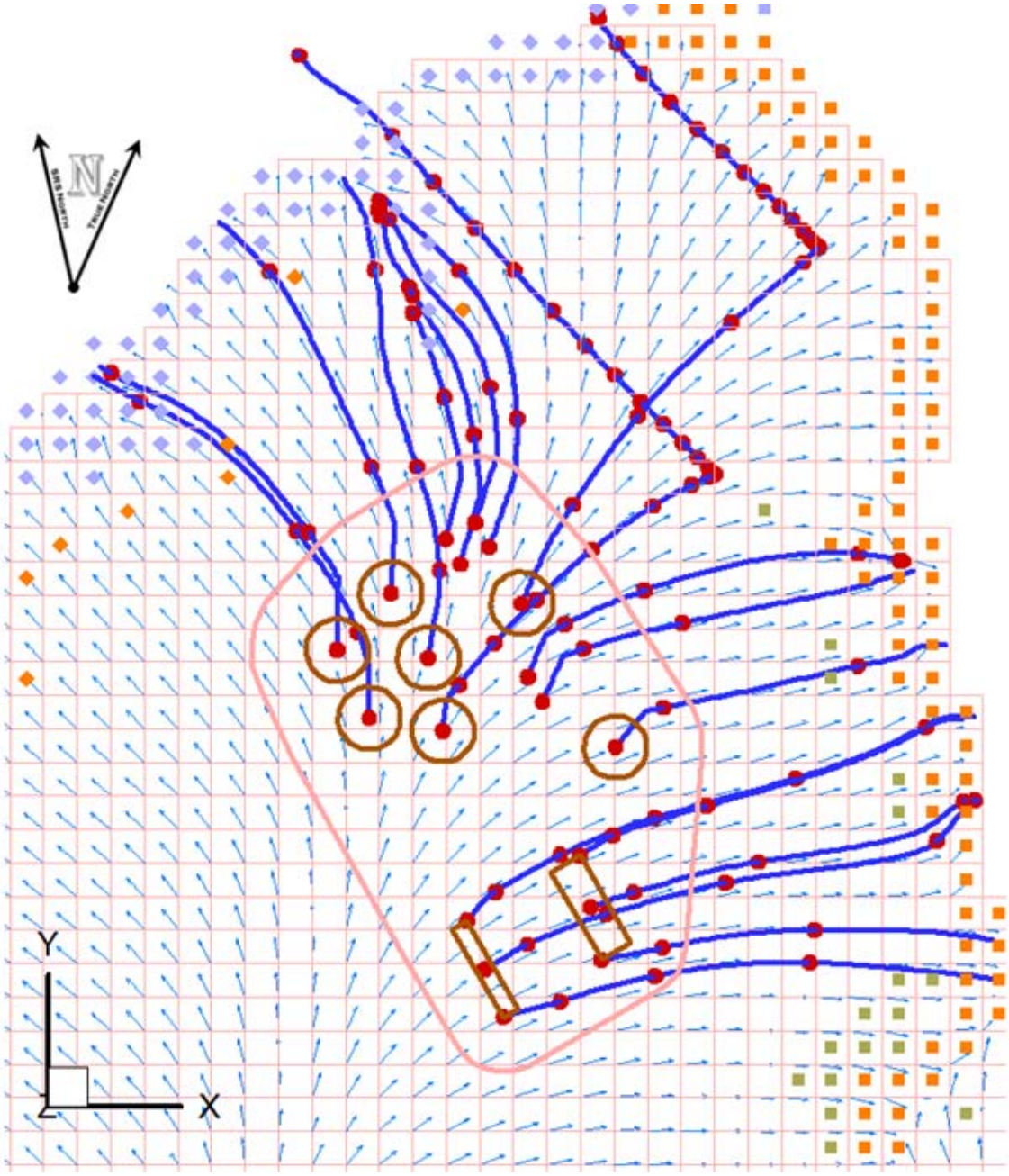

Note: Markers (red dots) are included to indicate ten-year travel times.

The SDF-specific portion of the GSA Model used for Aquifer Transport Modeling has a fairly coarse discretization. While this is appropriate for far-field transport (i.e., from the SDUs to the seeplines), it is not ideal for simulating transport of contaminants closer to the SDUs at this grid resolution (200 feet × 200 feet) and may result in excessive numerical dispersion at the local scale. The SDF flow

velocity field used for aquifer transport modeling was generated directly from the coarser scale GSA Model by subdividing the 200 feet × 200 feet grid cells and using a mass-conserving linear interpolation scheme to assign velocities to the refined 25 feet × 25 feet mesh, rather than a separate flow model requiring its own boundary conditions and properties, as depicted in Figure 4.4-114. [SRNL-STI-2009-00115, SRNL-STI-2018-00643] The grid resolution of 25 feet × 25 feet mesh resolution (and approximately 3 feet vertically near the water table) was chosen to avoid any significant numerical dispersion for longitudinal dispersivities as low as 10 feet. [SRNL-STI-2018-00012]

The SDF velocity field included the entire vertical extent of the GSA Model within the horizontal confines of the SDF domain. This approach ensured strict consistency between the two aquifer flow fields, apart from resolution. As described in Section 3.1.5.2 and in the *Updated Groundwater Flow Simulations of the Savannah River Site General Separations Area* (SRNL-STI-2018-00643), the GSA Model was developed based on measured data from hundreds of ground water wells (i.e., water level calibration targets), including data from 19 wells at the SDF (see Table 4.4-83), to provide a valid representation of ground water flow throughout the GSA. Note that because the SDF velocity flow fields are based on actual ground water data, which does not currently have a closure cap over the SDF, the baseline GSA Model does not account for the potential influence of reduced recharge due to the presence of the closure cap. A sensitivity case in Section 5.8.8.4 is provided to evaluate how the presence of the closure cap may impact doses due the its influence on ground water flow conditions.

4.4.6.2.2 Aquifer Transport Implementation

Upon developing the flow fields for SDF aquifer modeling from the GSA Model, sources and points of assessment were defined. The source nodes were defined as any grid cells with centroids lying within the footprint of each SDU, as based on Figure 4.4-114. Contaminant fluxes from vadose zone beneath each SDU as determined from the Vadose Zone Transport Model in Section 4.4.5, were scaled to reflect SDU-specific inventories and divided proportionally based on the number of SDU source nodes to which they were distributed. These fluxes were then applied to the SDU source nodes.

Also defined are the 1-meter and 100-meter boundary model nodes and cells. The nodes for the 1-meter boundary were defined by creating a convex hull surrounding all SDUs. This convex hull can be thought of as a taut rubber band enveloping the collection of the SDUs. The 1-meter perimeter cells were defined as those grid nodes that adjoin on any side or corner with nodes inside the convex hull of the SDU source nodes. The nodes defining the 100-meter boundary were defined by creating a second convex hull that is based on a buffer zone of 100-meters from each SDU. For diagnostic purposes, the 100-meter boundary was divided into eight sectors labeled A though H (Figure 4.4-114).

Figure 4.4-114: SDF-Scaled GSA Model Used for Aquifer Transport Modeling

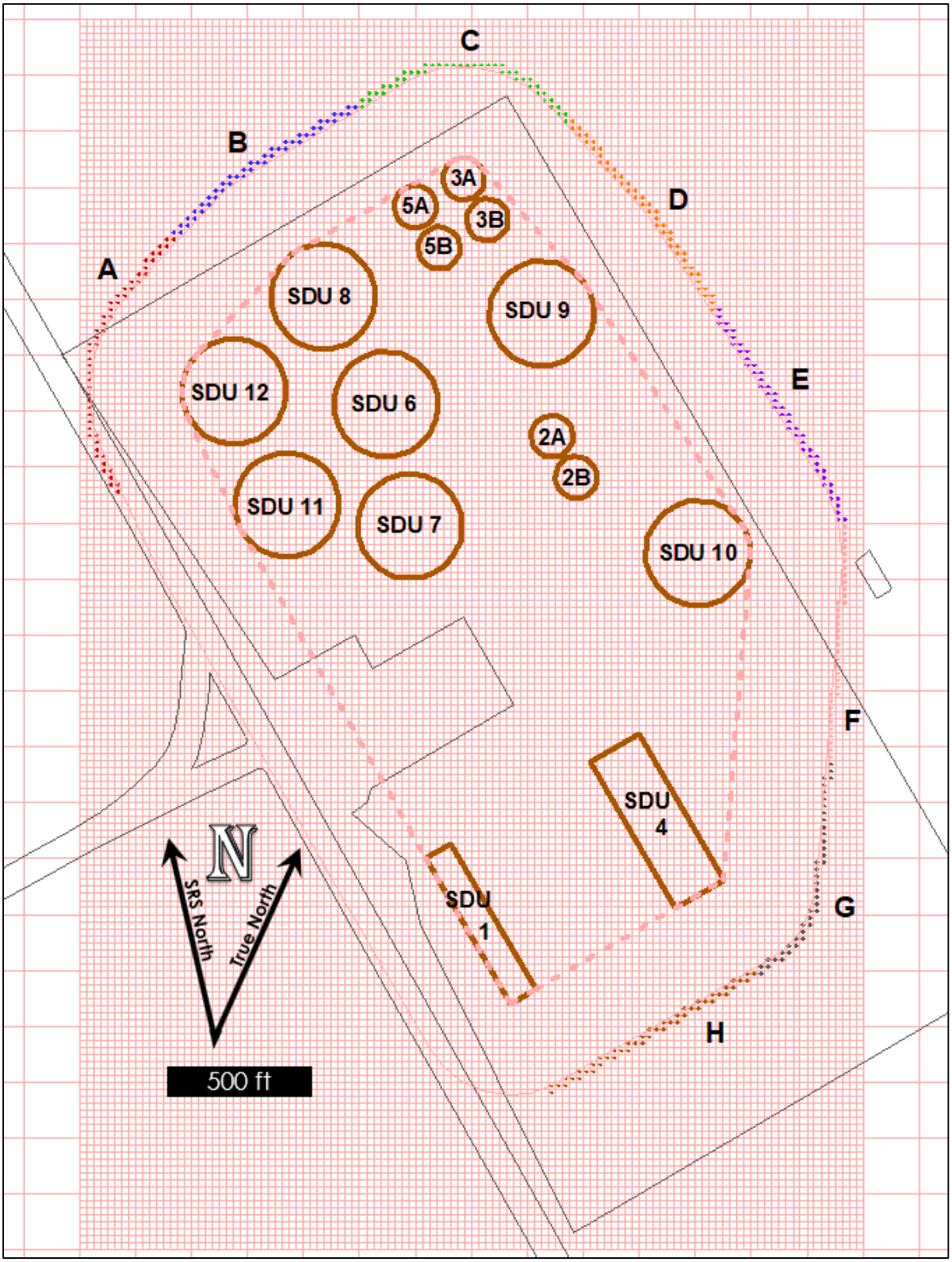

These sectors were organized to be approximately the same length along 100-meter boundary because each sector has an equal probability of representing the location that a future member of the public (MOP) might select for drilling a well for water. For seepline assessments, the GSA Model grid is used (see Figure 4.4-113).

With the flow fields defined as well as the fluxes for the source nodes, transport to the points of assessment is determined using PORFLOW's transport equations, equivalent to those defined in Section 4.4.5 as used in the Vadose Zone Transport Model.

4.4.6.3 Inputs and Assumptions for the Aquifer Transport Model

Inputs to Aquifer Transport Model include the refined SDF velocity field (described in Section 4.4.6.2.1), the contaminant fluxes from the Vadose Transport Model, the soil properties and K_d values in soils (as defined in Section 4.3), and dispersivities (used to define plume spreading).

Mechanical dispersion in the Aquifer Transport Model is based on the dispersion coefficients for vertically stratified anisotropic soils as described in ACRI, 2010:

$$D_{xx} = \alpha_{LH}\frac{V_x^2}{\underline{V}} + \alpha_{TH}\frac{V_y^2}{\underline{V}} + \alpha_{TV}\frac{V_z^2}{\underline{V}} \quad \text{Eq. 4.4-120}$$

$$D_{yy} = \alpha_{TH}\frac{V_x^2}{\underline{V}} + \alpha_{LH}\frac{V_y^2}{\underline{V}} + \alpha_{TV}\frac{V_z^2}{\underline{V}} \quad \text{Eq. 4.4-121}$$

$$D_{zz} = \alpha_{TV}\frac{V_x^2}{\underline{V}} + \alpha_{TV}\frac{V_y^2}{\underline{V}} + \alpha_{LV}\frac{V_z^2}{\underline{V}} \quad \text{Eq. 4.4-122}$$

$$D_{xy} = D_{yx} = (\alpha_{LH-}\alpha_{TH})\frac{V_x V_y}{\underline{V}} \quad \text{Eq. 4.4-123}$$

$$D_{xz} = D_{zx} = \{0.5(\alpha_{LH} + \alpha_{LV}) - \alpha_{TV}\}\frac{V_x V_z}{\underline{V}} \quad \text{Eq. 4.4-124}$$

$$D_{yz} = D_{zy} = \{0.5(\alpha_{LH} + \alpha_{LV}) - \alpha_{TV}\}\frac{V_y V_z}{\underline{V}} \quad \text{Eq. 4.4-125}$$

where:

D_{ij} = the coefficients of mechanical dispersion (m^2/s), wherein the subscripts (i,j) are used to indicate locations based on Cartesian coordinates of x, y, or z,

α_{LH} = the horizontal longitudinal dispersivity (m),

α_{TH} = the horizontal transverse dispersivity (m),

α_{LV} = the vertical longitudinal dispersivity (m),

α_{TV} = the vertical transverse dispersivity (m),

V_i = the component of the particle velocity vector (m/s), wherein the i subscript denotes the direction (x, y, or z), and

$\underline{V}$ = the magnitude of the particle velocity vector (m/s).

The full hydrodynamic dispersion tensor as applied in PORFLOW, which includes the effects of matrix diffusion, is presented in Eq. 4.4-106.

Horizontal plume spreading via mechanical dispersion is determined based on assumed longitudinal and transverse dispersivities of 10 meters and 1 meter, respectively. These values represent 10% and 1% of a nominal 100-meter plume travel distance. Similarly, vertical plume spreading via mechanical dispersion is determined based on assumed vertical longitudinal and transverse dispersivities of 1 meters and 0.1 meters, respectively. These values represent 1% and 0.1% of a nominal 100-meter plume travel distance.

As with the GSA Model (SRNL-STI-2018-00643), ground water flow in the Aquifer Transport Model is controlled by net infiltration or recharge over a broad area surrounding the SDF. While the Vadose Flow Model used lower infiltration rates due to the closure cap system, no credit is taken for the reduced infiltration in the Aquifer Transport Model. That is, flow exiting the Vadose Zone Flow Model (Section 4.4.4) at the water table is not used to define local recharge beneath the SDF within the Aquifer Transport Model. Rather, an average infiltration rate based on field studies is used to define the recharge portion of the combined recharge/drainage boundary condition applied uniformly over the upper boundary of the GSA Model. Despite the difference in the infiltration rates between models, the Aquifer Transport Model assumes that the contaminant flux leaving the bottom of the Vadose Zone Transport Model becomes the source of contamination entering the aquifers.

As described in Section 4.4.6.2.2, for the contaminant source inputs the flux contributions from individual SDUs were assigned to the Aquifer Transport Model grid by uniformly distributing the flux to those water table cells with centroids lying within the footprint of the disposal unit.

4.4.6.4 Intermediate Results and Model Interfaces for the Aquifer Transport Model

The Aquifer Transport Model has two primary model interfaces. First, as an input, it relies on contaminant fluxes at the water table. Since the water table serves as the boundary between the Vadose Zone Transport Model and the Aquifer Transport Model, these fluxes come from the Vadose Zone Transport Model (Section 4.4.5).

Second, as a model output, the Aquifer Transport Model is used to generate contaminant concentrations at various points of assessment (e.g., wells along the 100-meter boundary). These concentration values are then used as input to the Dose and Exposure Pathways Model (Section 4.4.8) to estimate doses to future human receptors.

4.4.6.4.1 Streamline Traces from the Aquifer Transport Model

As an intermediate result, Figure 4.4-115 shows the centerline streamline traces from each SDU based on the refined model gridding described in Section 4.4.6.2.1. Note that Figure 4.4-113 shows equivalent streamline traces, but these streamline traces were based on the less refined gridding used in the GSA Model, thus there are some slight differences in the resulting streamline traces.

4.4.6.4.2 Tracer Plumes from the Aquifer Transport Model

The streamline traces only represent the center of mass along a progressing plume and do not fully capture the three-dimensionality of the contaminant transport. Figure 4.4-116 through Figure 4.4-130 provide the individual plumes emanating from each SDU based on the steady-state release of a hypothetical tracer.

Note that SDU 6 (Figure 4.4-124) and SDU 7 (Figure 4.4-125) both show significant spreading. Figure 4.4-115 fails to adequately illustrate this plume-spreading. This spreading is attributed to a ground water divide that runs between SDUs 7 and 11, through SDU 6 and up into the east-most portion of Sector C. Contaminants released north of the ground water divide are transported in a generally northward direction, while contaminants released south of the ground water divide are transported in a generally eastward direction. However, contaminants released in close proximity to the ground water divide can undergo significant spreading as the plume is transported in both directions.

Figure 4.4-115: Streamline Traces from Each SDU

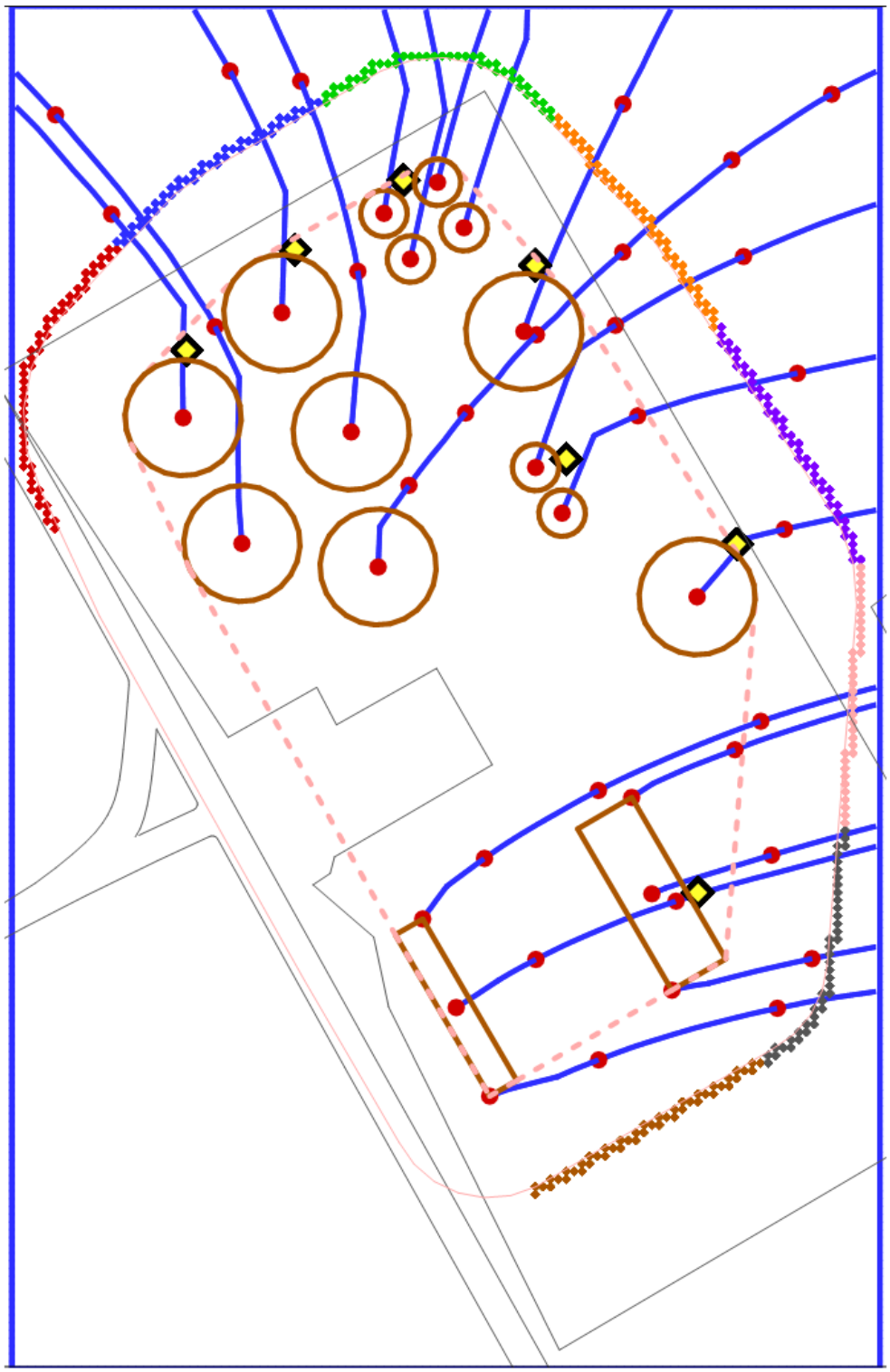

Note: Markers (red dots) are included to indicate ten-year travel times.

Figure 4.4-116: Tracer Plume Simulation for a Steady-State Release from SDU 1

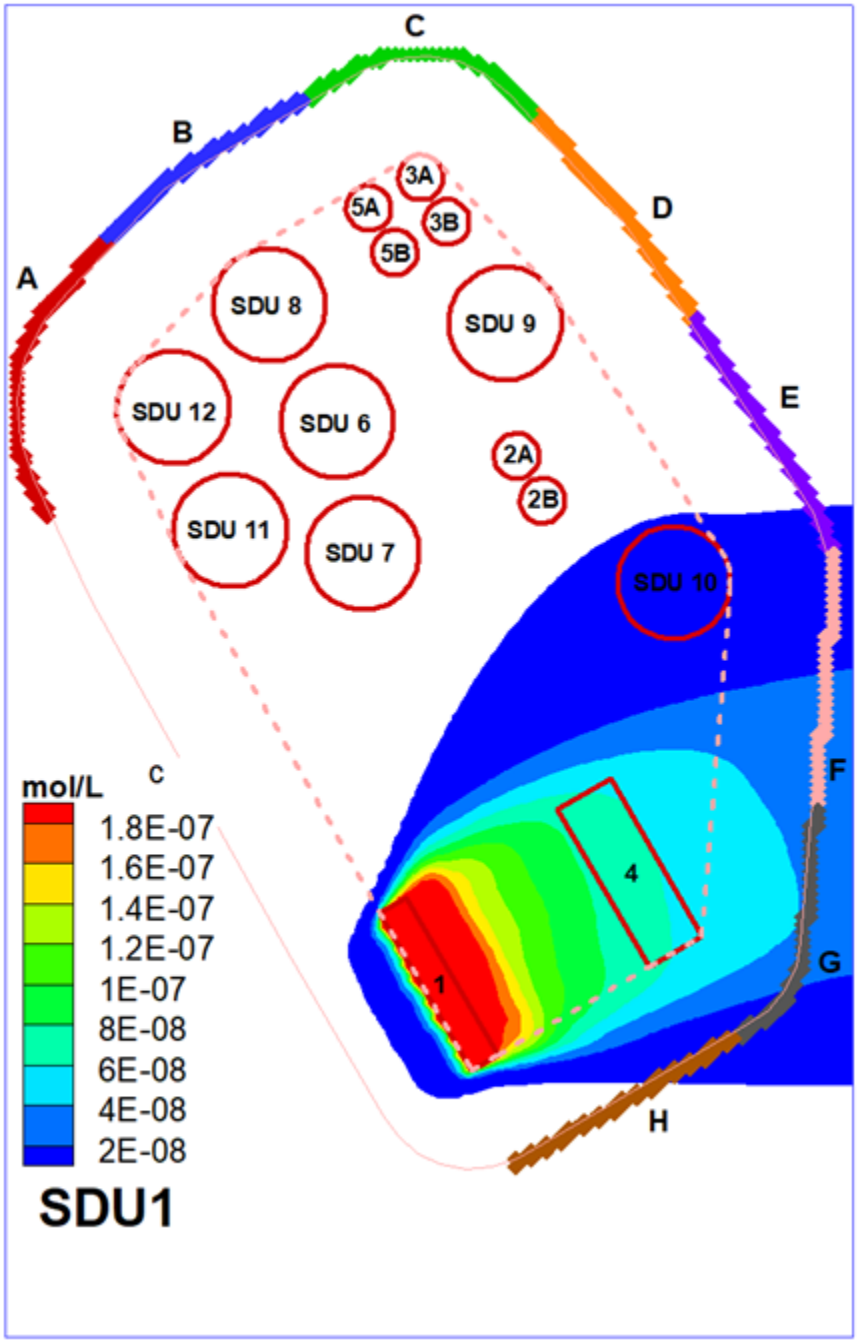

Figure 4.4-117: Tracer Plume Simulation for a Steady-State Release from SDU 4

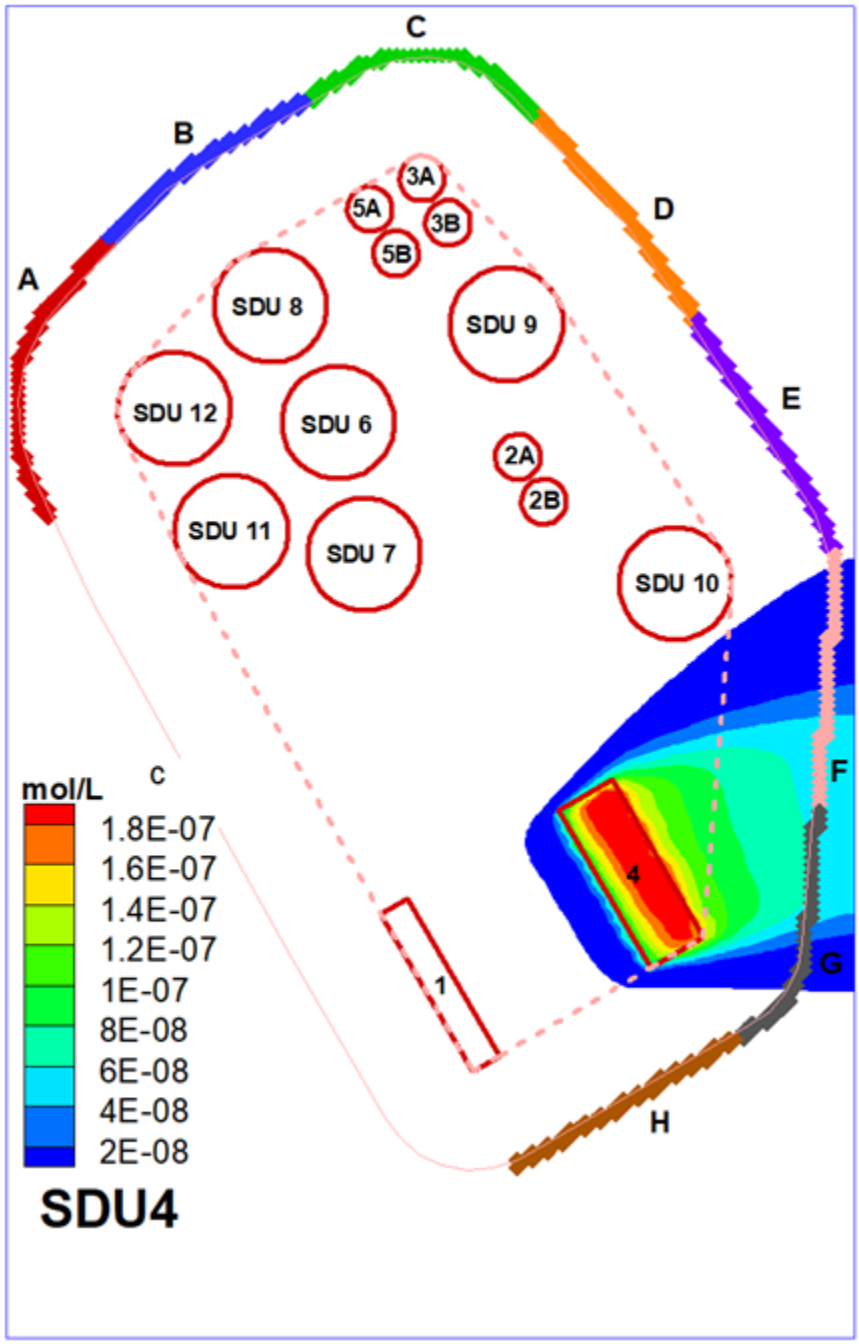

Figure 4.4-118: Tracer Plume Simulation for a Steady-State Release from SDU 2A

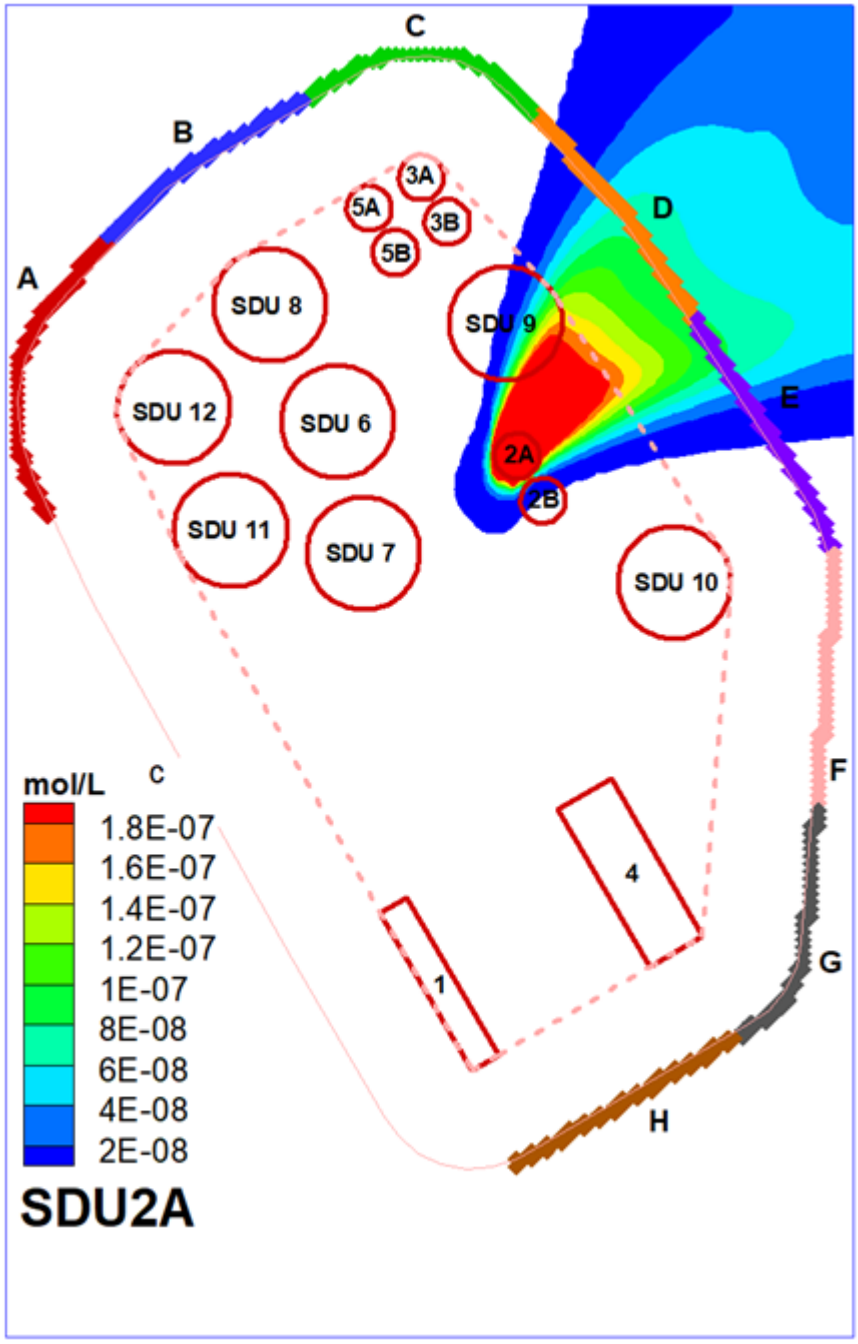

Figure 4.4-119: Tracer Plume Simulation for a Steady-State Release from SDU 2B

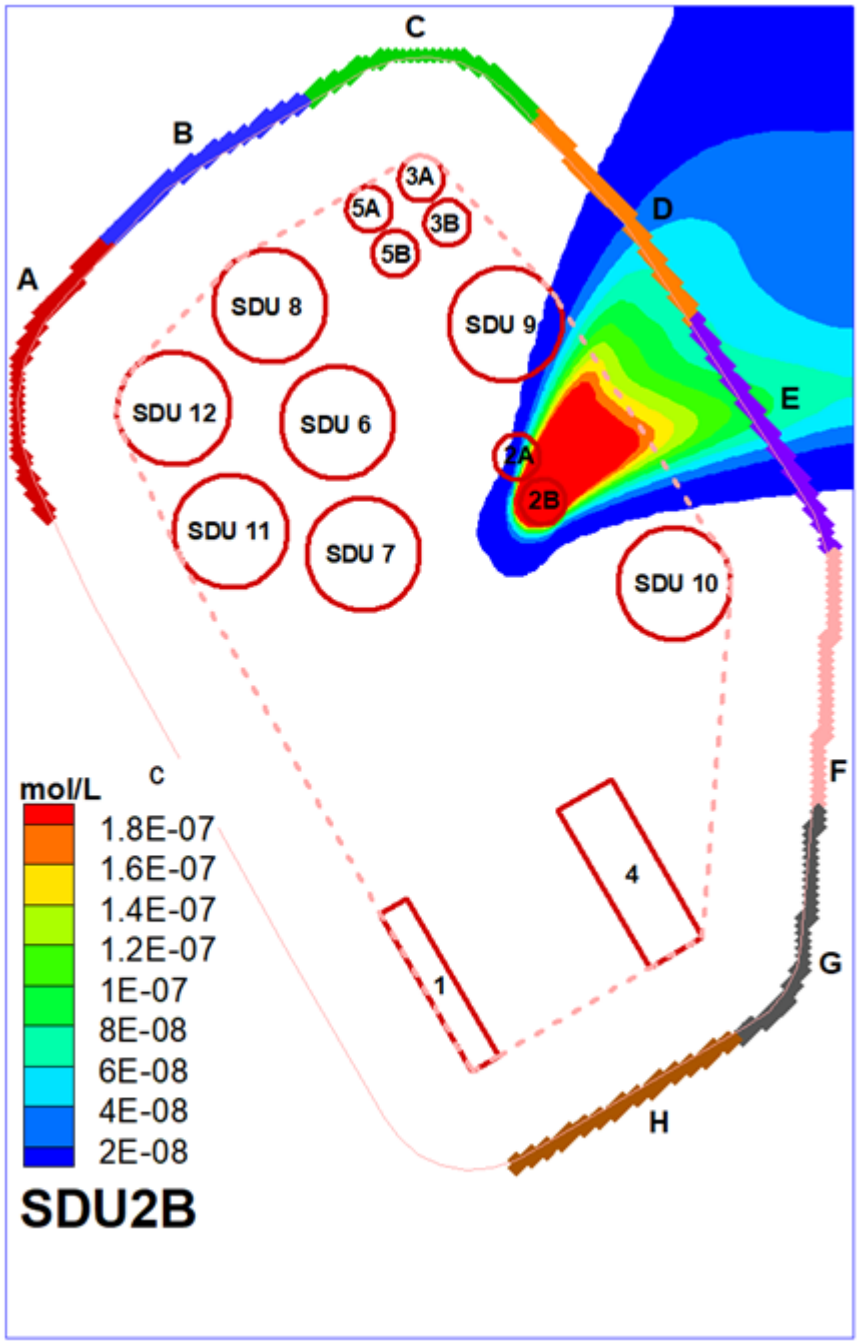

Figure 4.4-120: Tracer Plume Simulation for a Steady-State Release from SDU 3A

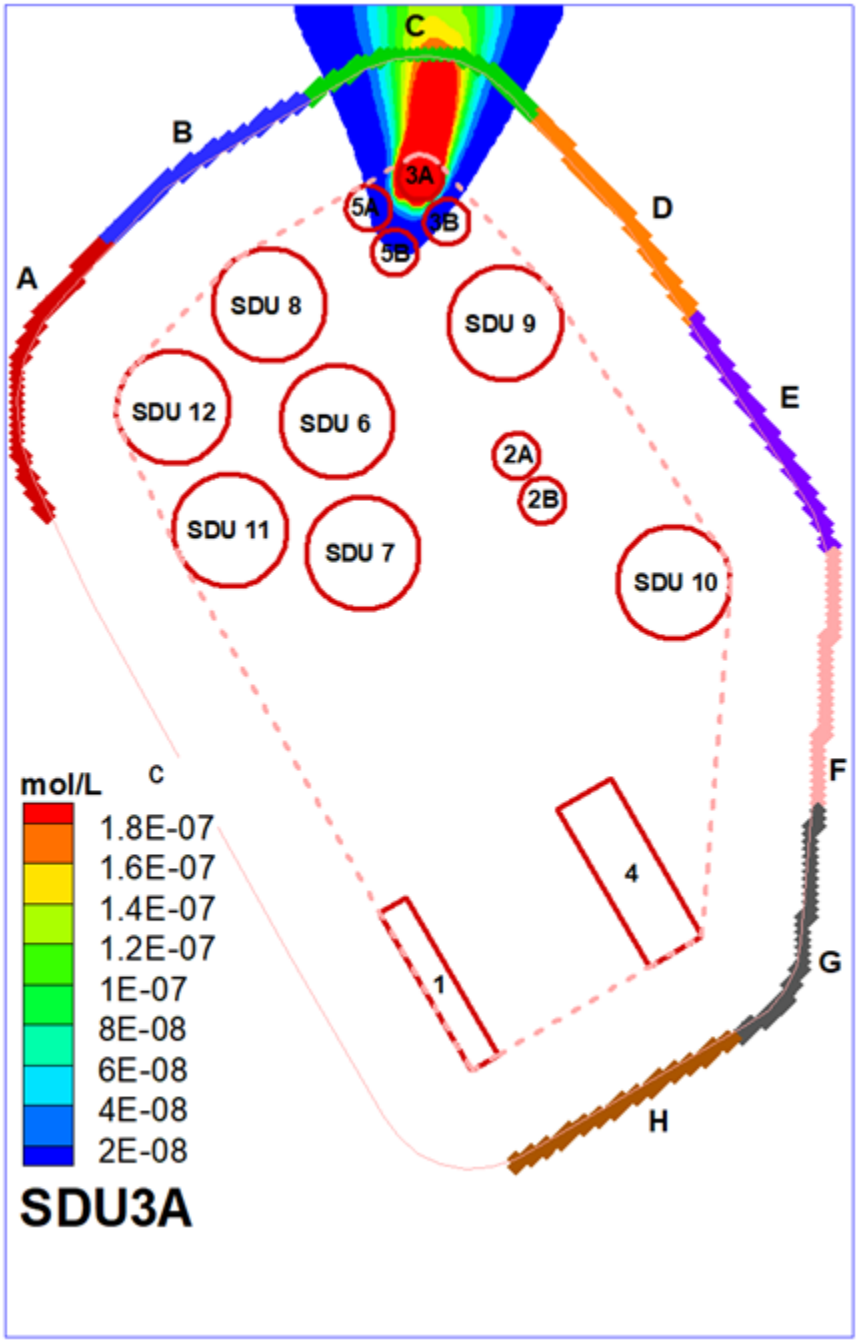

Figure 4.4-121: Tracer Plume Simulation for a Steady-State Release from SDU 3B

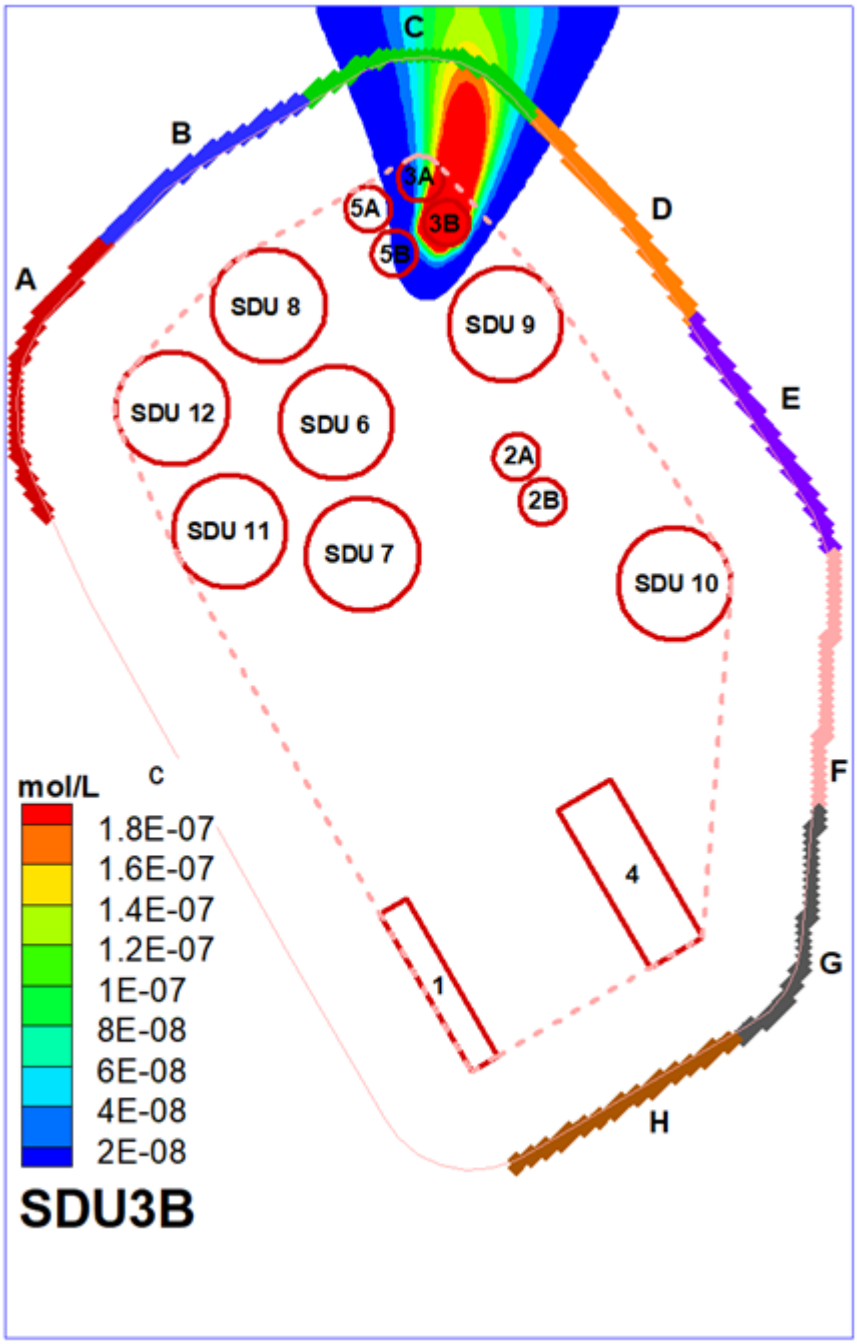

Figure 4.4-122: Tracer Plume Simulation for a Steady-State Release from SDU 5A

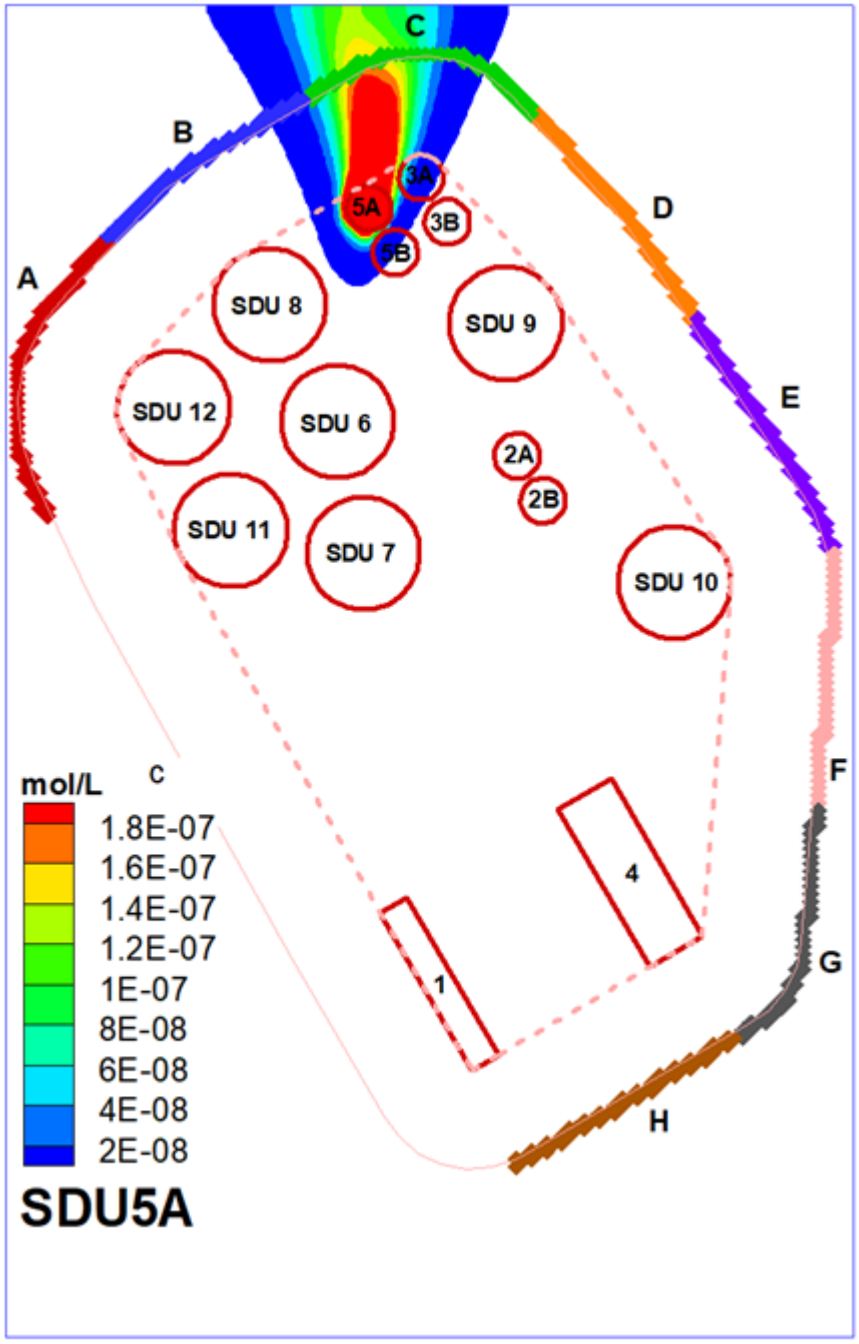

Figure 4.4-123: Tracer Plume Simulation for a Steady-State Release from SDU 5B

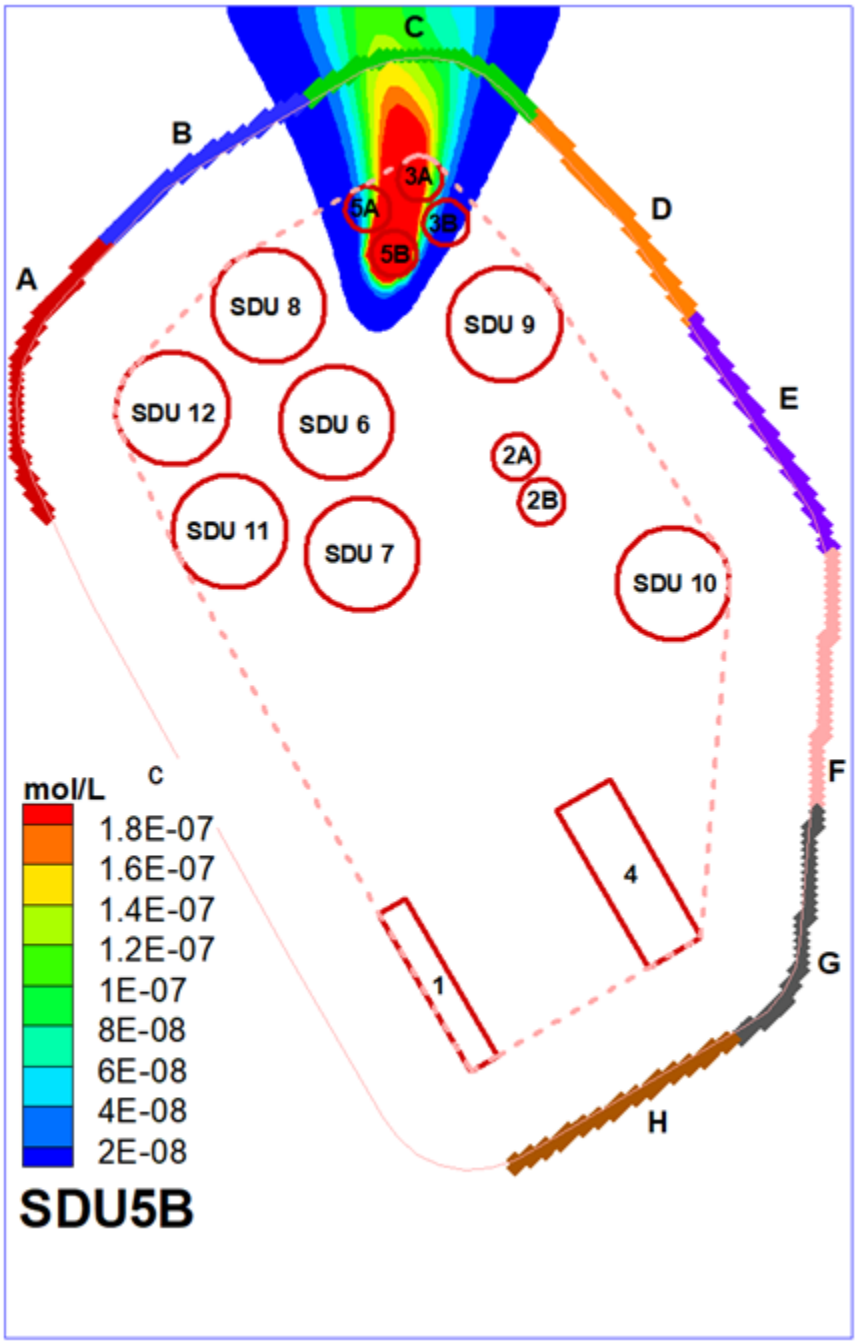

Figure 4.4-124: Tracer Plume Simulation for a Steady-State Release from SDU 6

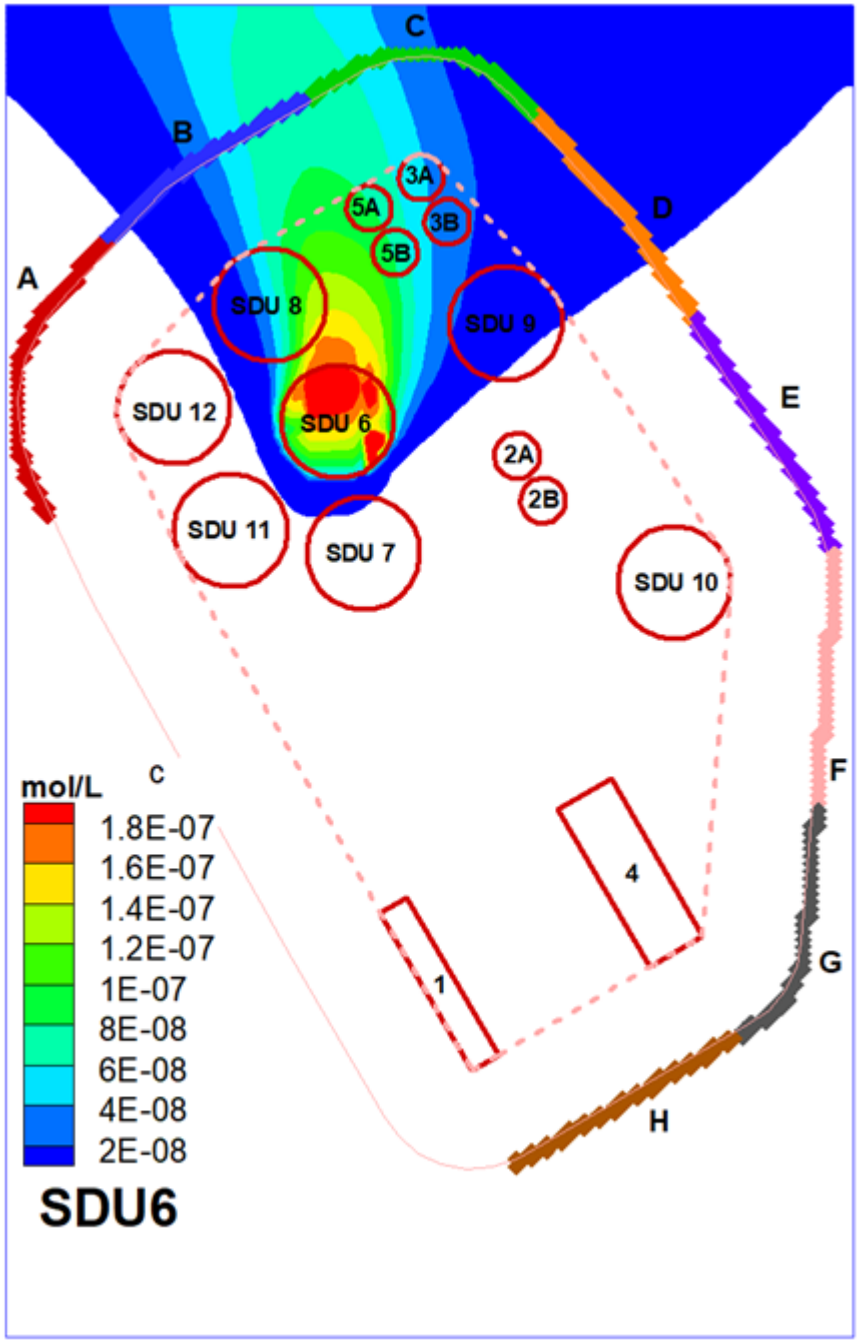

Figure 4.4-125: Tracer Plume Simulation for a Steady-State Release from SDU 7

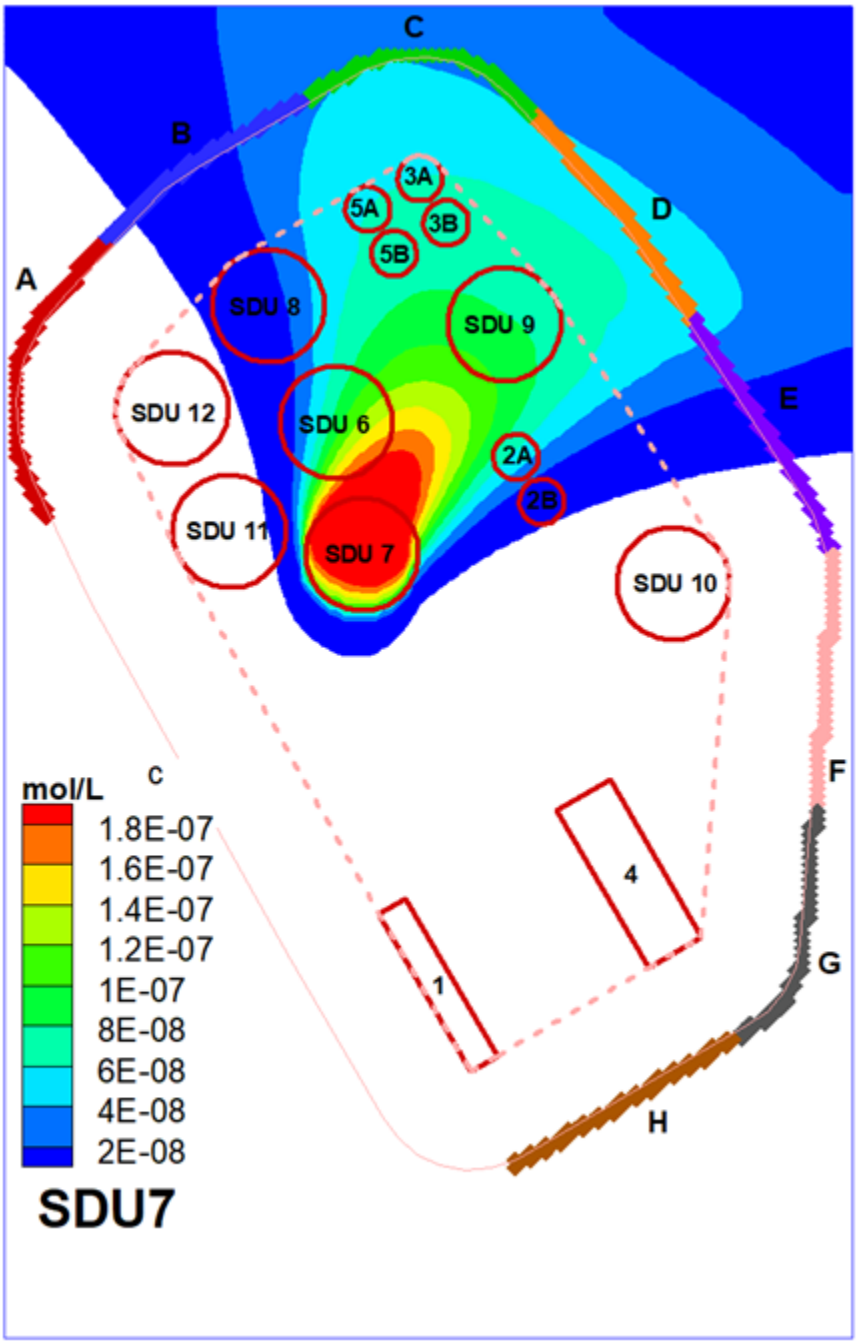

Figure 4.4-126: Tracer Plume Simulation for a Steady-State Release from SDU 8

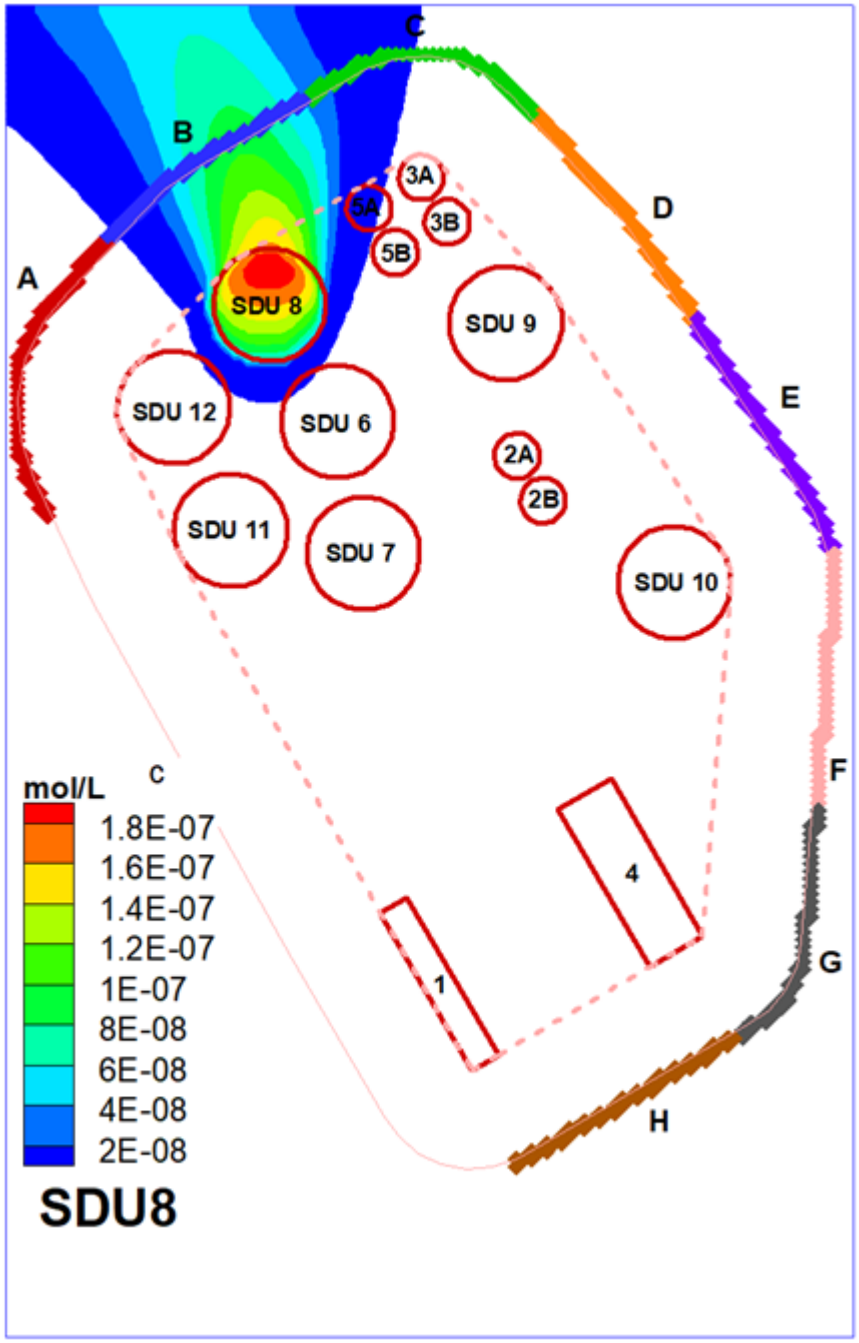

Figure 4.4-127: Tracer Plume Simulation for a Steady-State Release from SDU 9

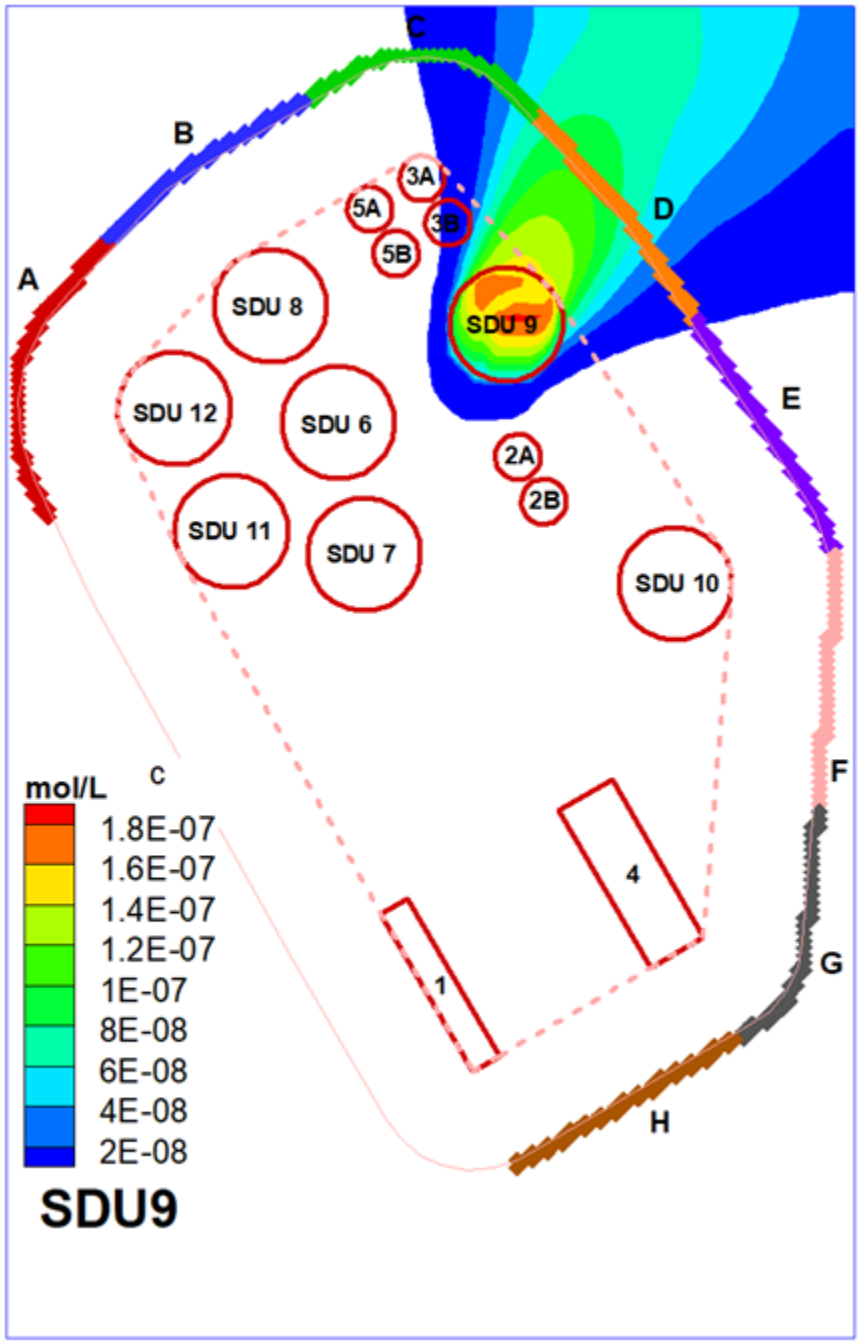

Figure 4.4-128: Tracer Plume Simulation for a Steady-State Release from SDU 10

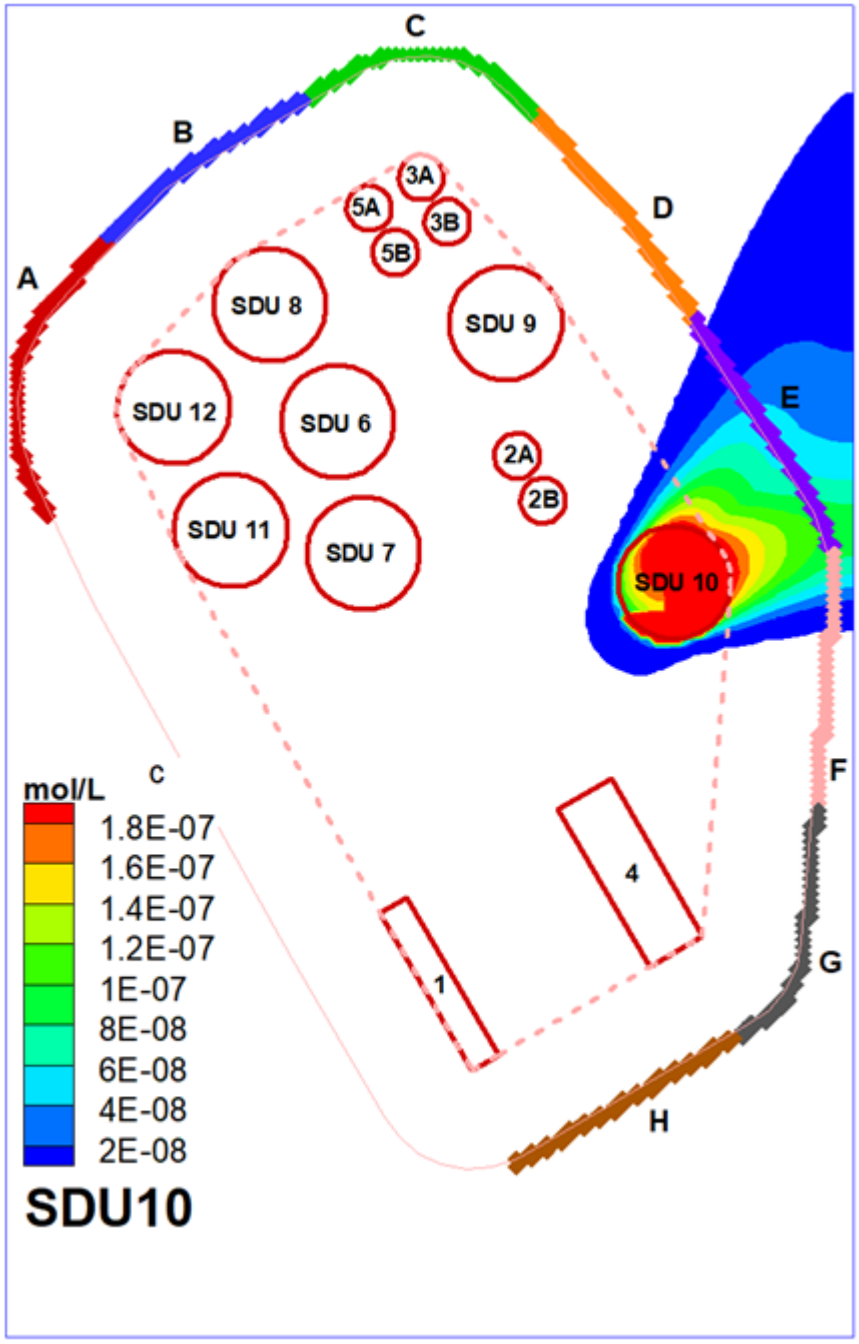

Figure 4.4-129: Tracer Plume Simulation for a Steady-State Release from SDU 11

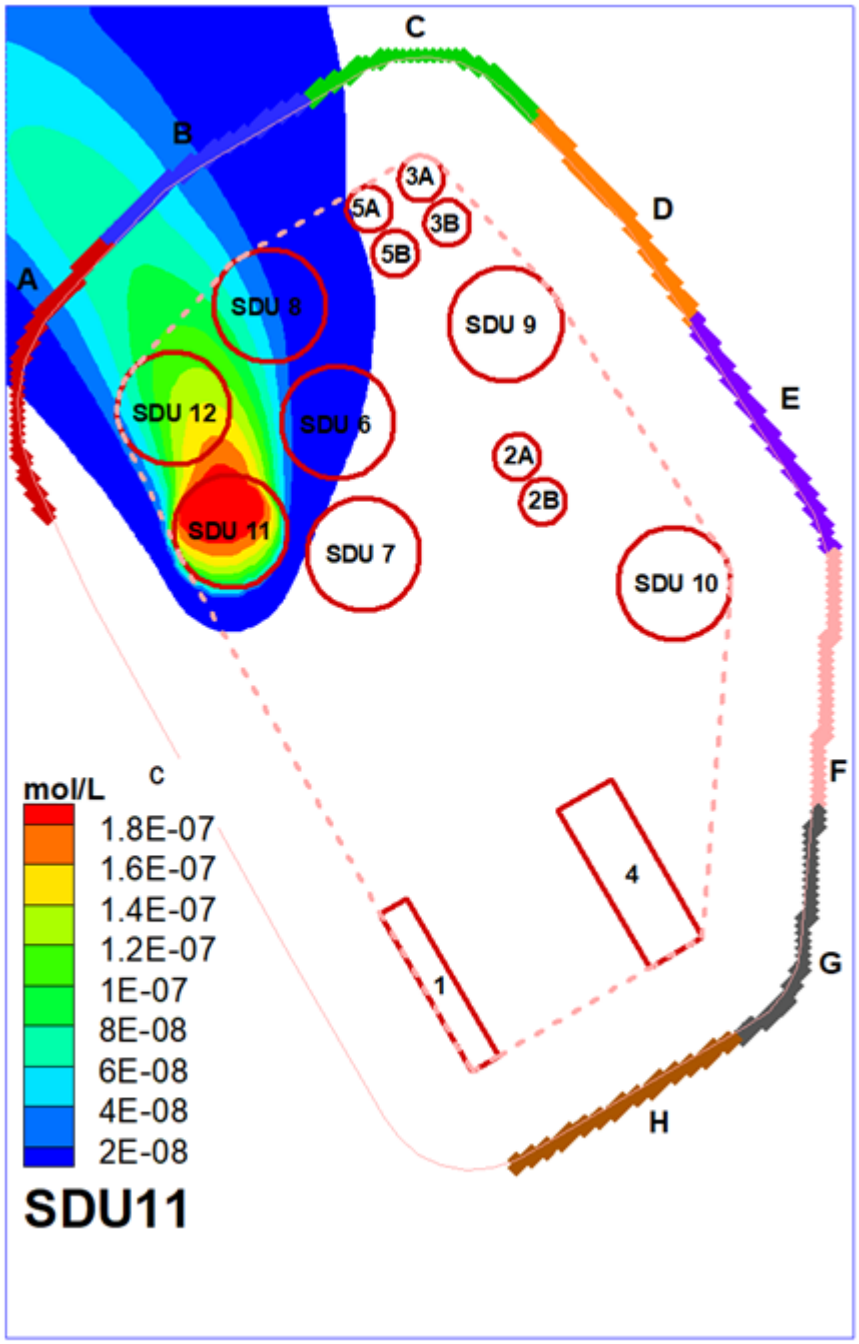

Figure 4.4-130: Tracer Plume Simulation for a Steady-State Release from SDU 12

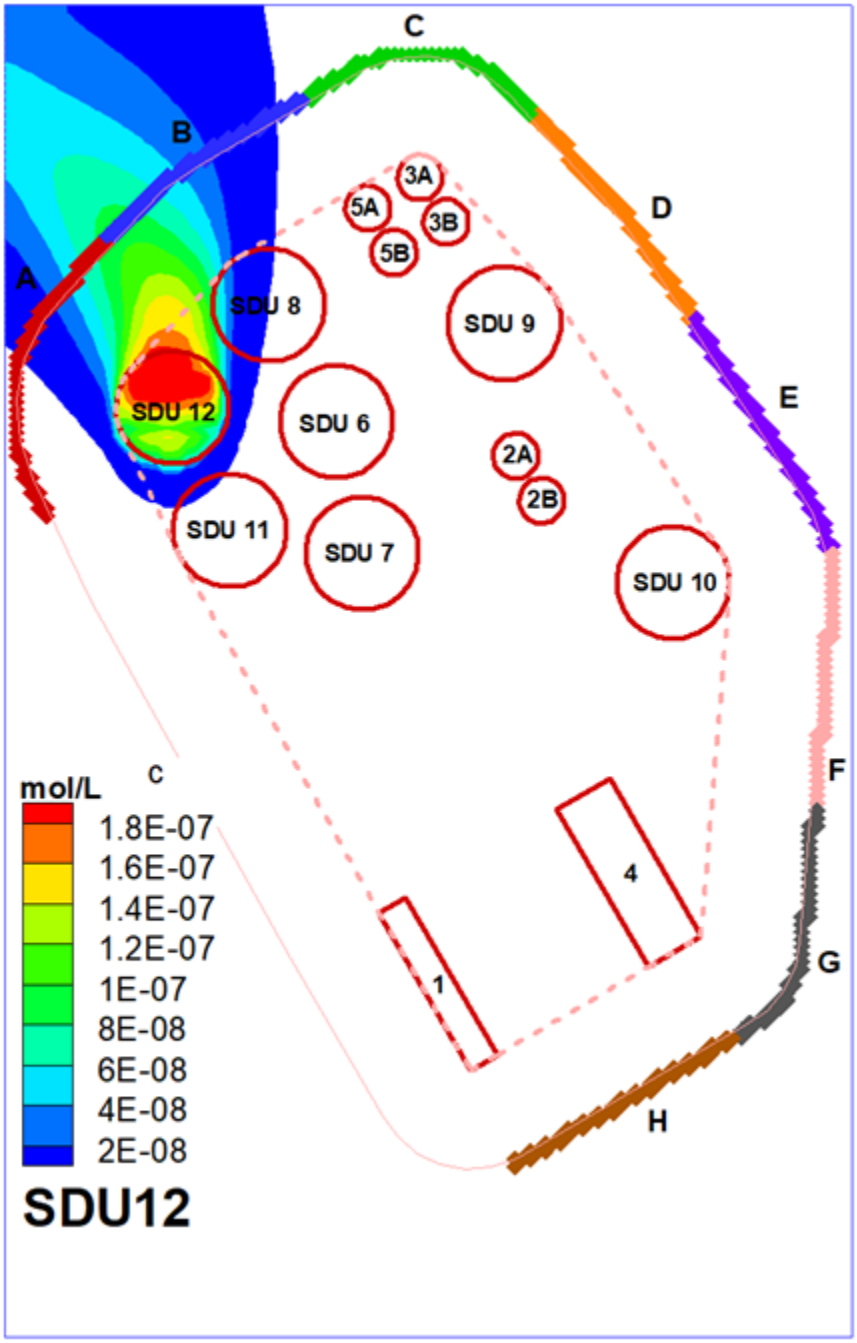

4.4.6.4.3 Breakthrough Curves from the Aquifer Transport Model

From the streamline traces and the plume emanations, additional information about aquifer transport can be determined. First, from the plumes, breakthrough curves may be determined. These breakthrough curves (Figure 4.4-131 to Figure 4.4-145) represent the concentration of a hypothetical tracer at the 100-meter SDF boundary. The peaks in these curves indicate how long it takes for the center of mass of a plume to reach the boundary from the time it is released into the saturated zone beneath the respective SDUs.

As an alternative, the streamline traces (Figure 4.4-115) can also be used to estimate the breakthrough times. For this approach, the coordinate locations and coordinate-specific flow rates were exported from each streamline trace. These values were then used to calculate the centerline distances to the 100-meter boundary and the average rate of flow based on these times and distances. Table 4.4-85 summarizes this information.

Figure 4.4-131: Breakthrough Curve from SDU 1 to the 100-Meter Boundary

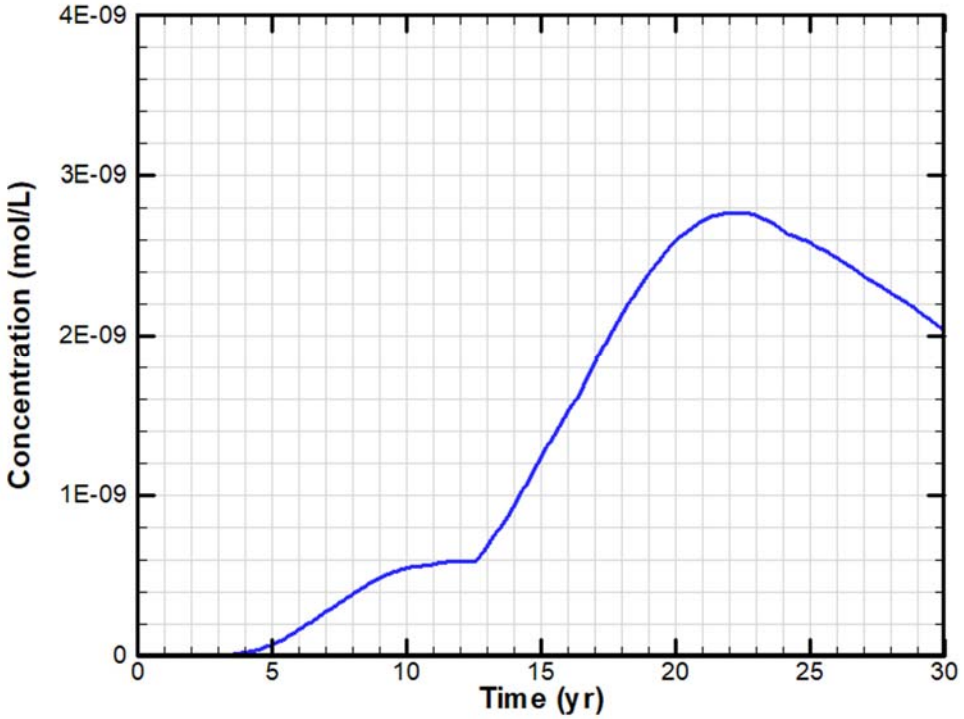

Figure 4.4-132: Breakthrough Curve from SDU 4 to the 100-Meter Boundary

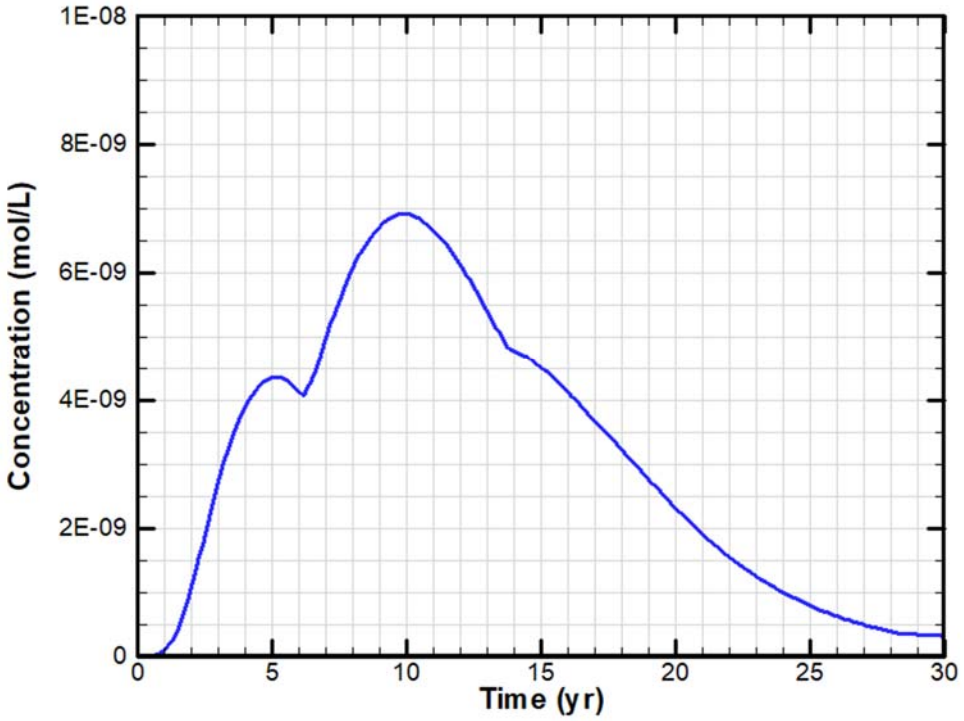

Figure 4.4-133: Breakthrough Curve from SDU 2A to the 100-Meter Boundary

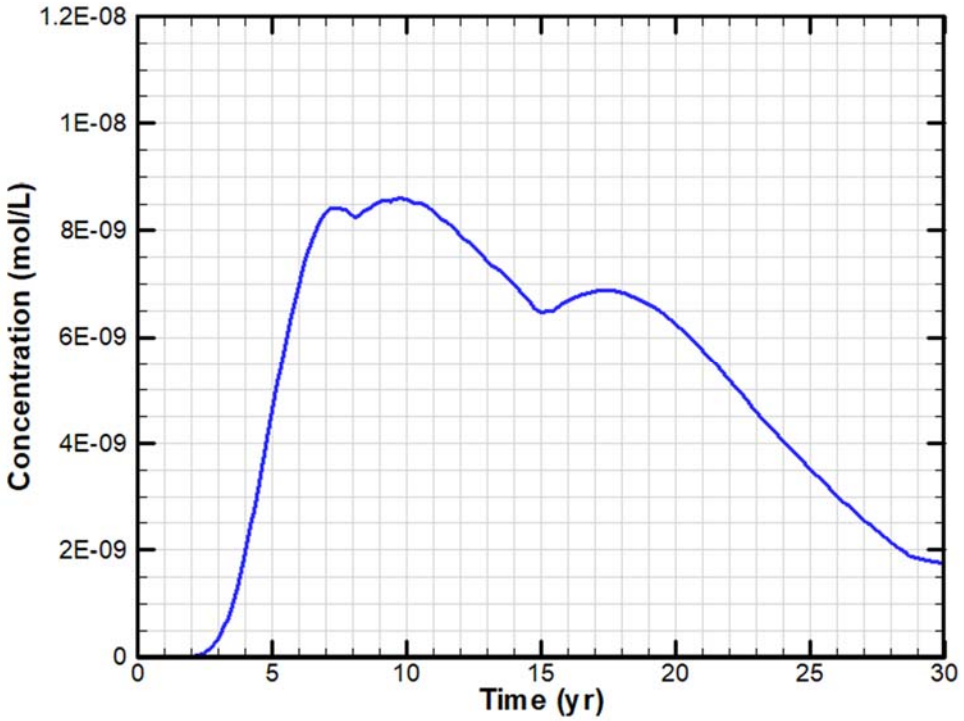

Figure 4.4-134: Breakthrough Curve from SDU 2B to the 100-Meter Boundary

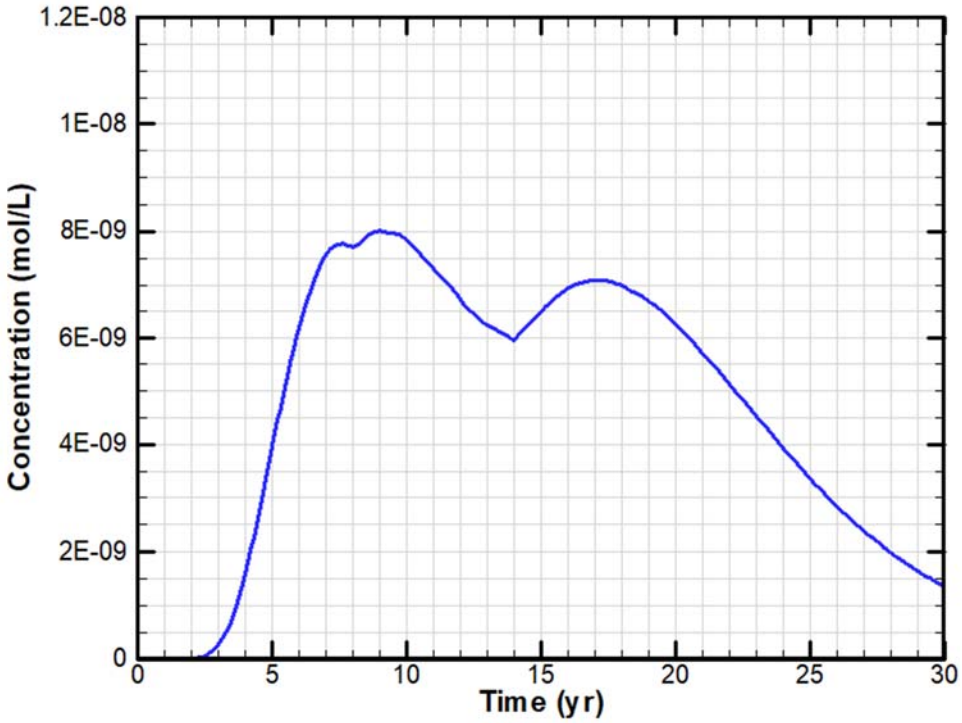

Figure 4.4-135: Breakthrough Curve from SDU 3A to the 100-Meter Boundary

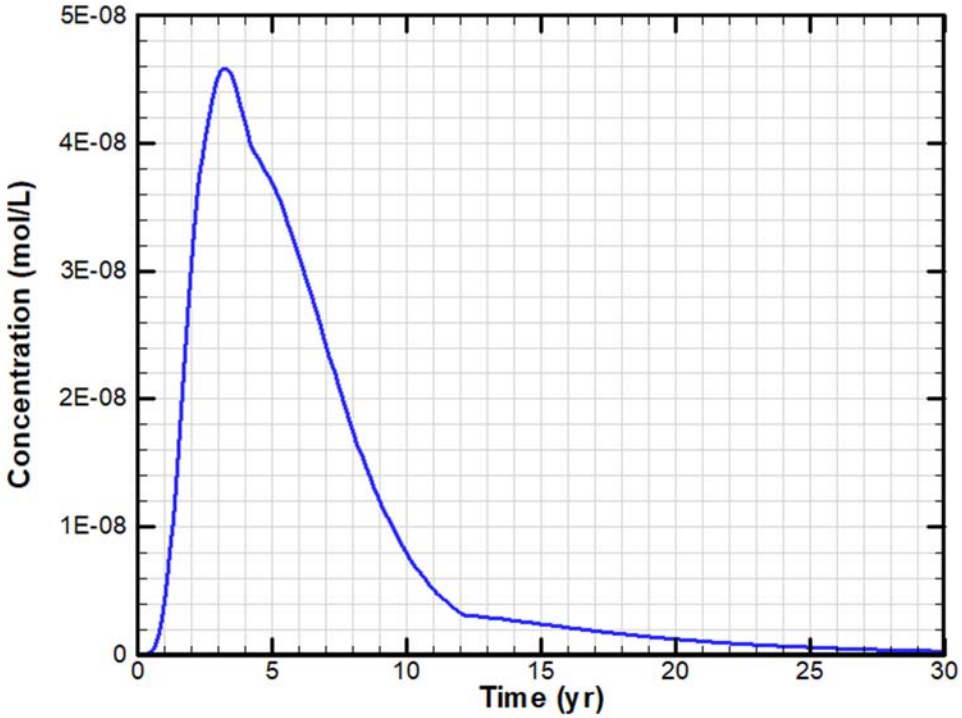

Figure 4.4-136: Breakthrough Curve from SDU 3B to the 100-Meter Boundary

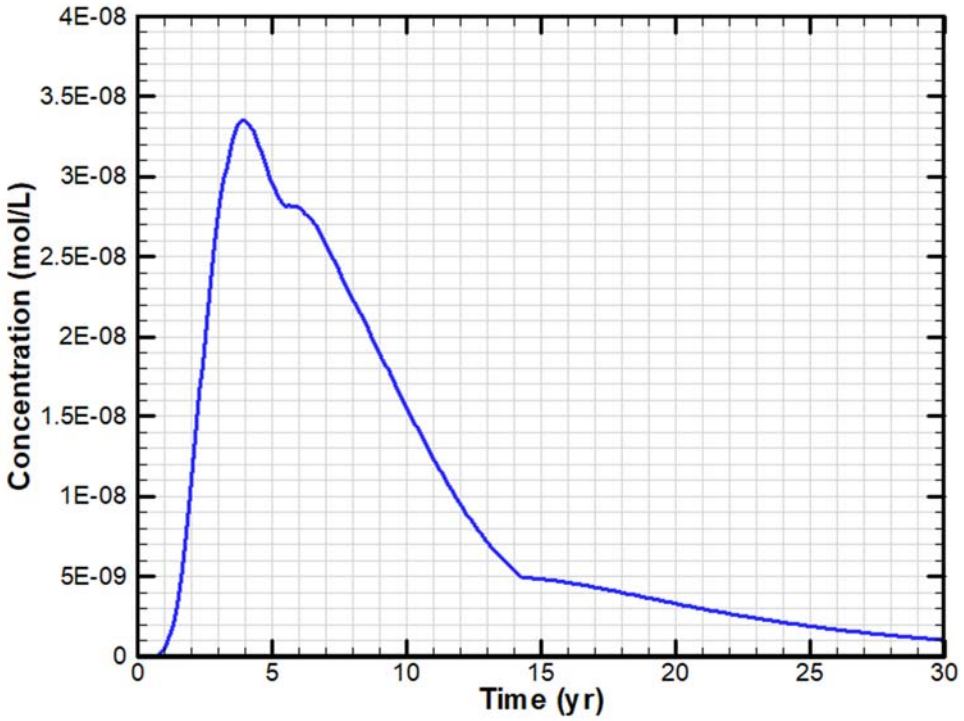

Figure 4.4-137: Breakthrough Curve from SDU 5A to the 100-Meter Boundary

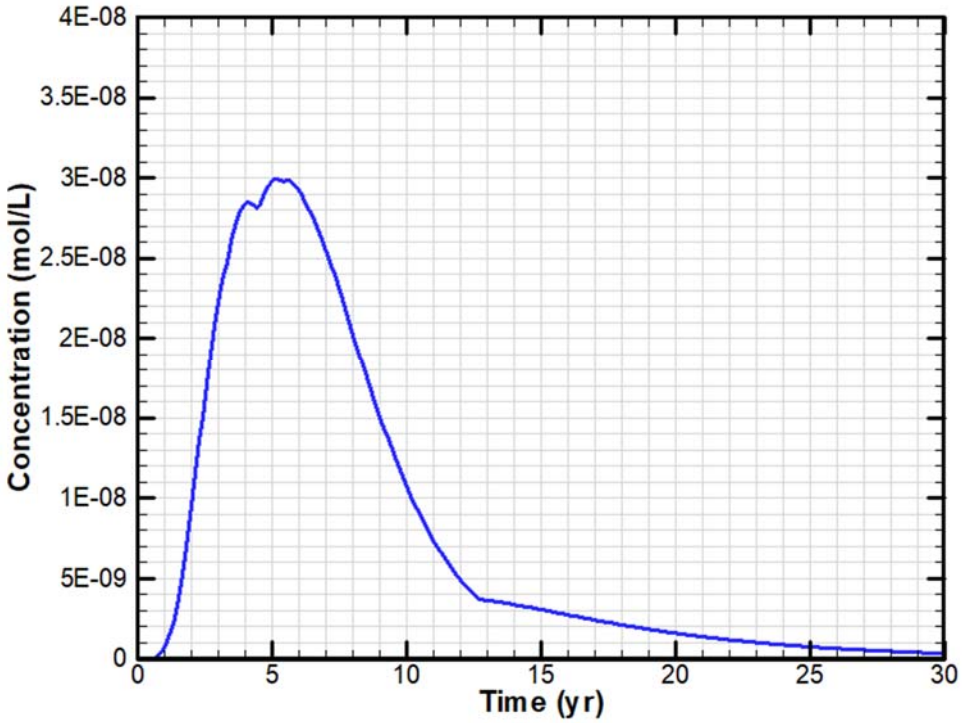

Figure 4.4-138: Breakthrough Curve from SDU 5B to the 100-Meter Boundary

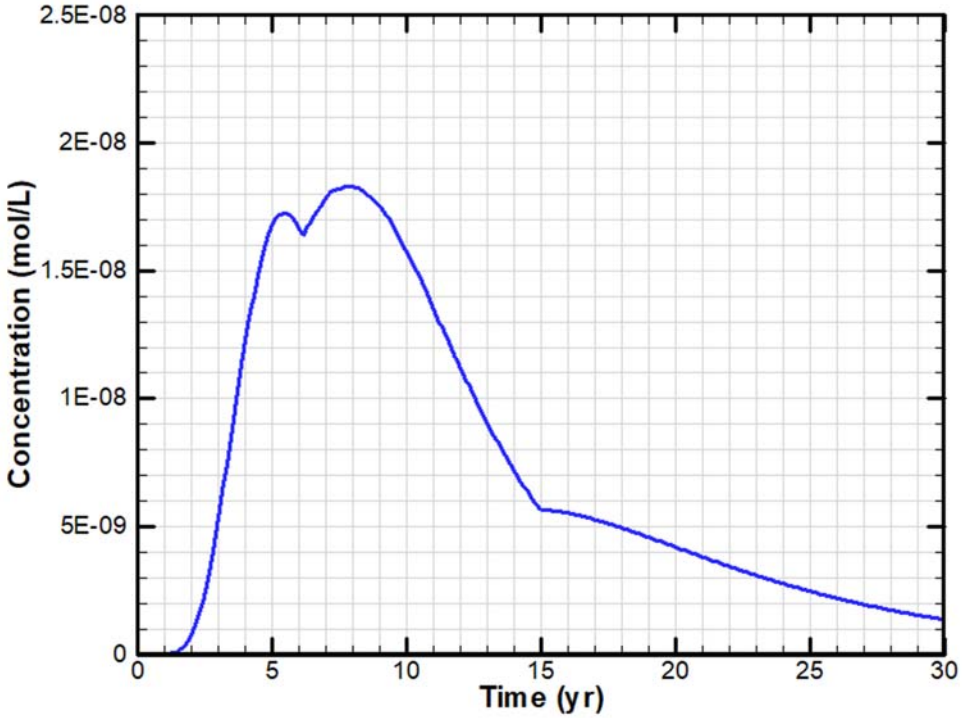

Figure 4.4-139: Breakthrough Curve from SDU 6 to the 100-Meter Boundary

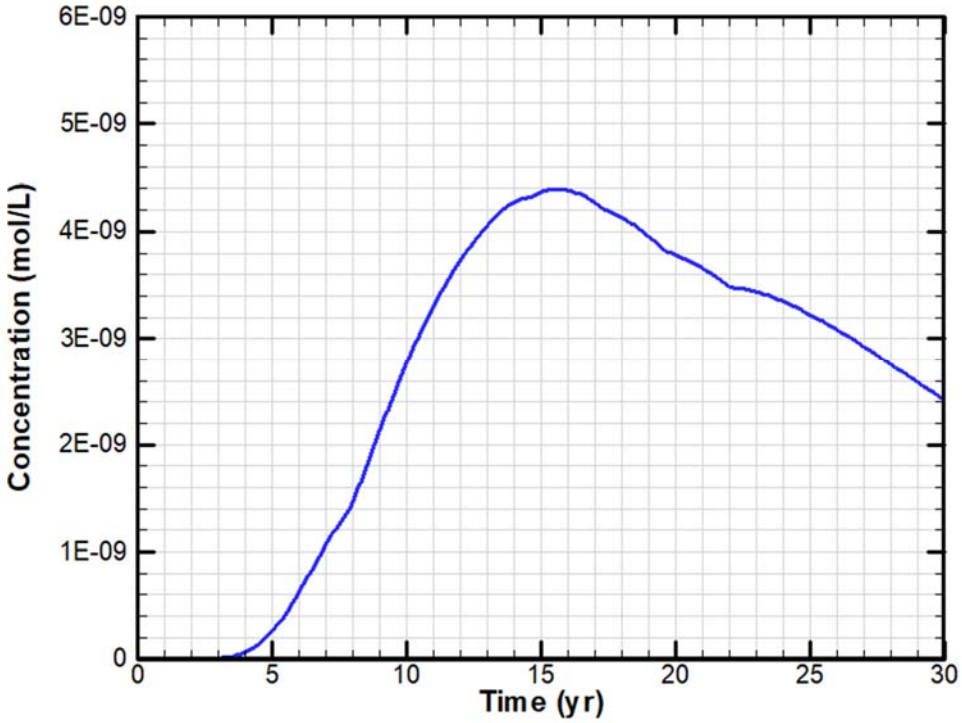

Figure 4.4-140: Breakthrough Curve from SDU 7 to the 100-Meter Boundary

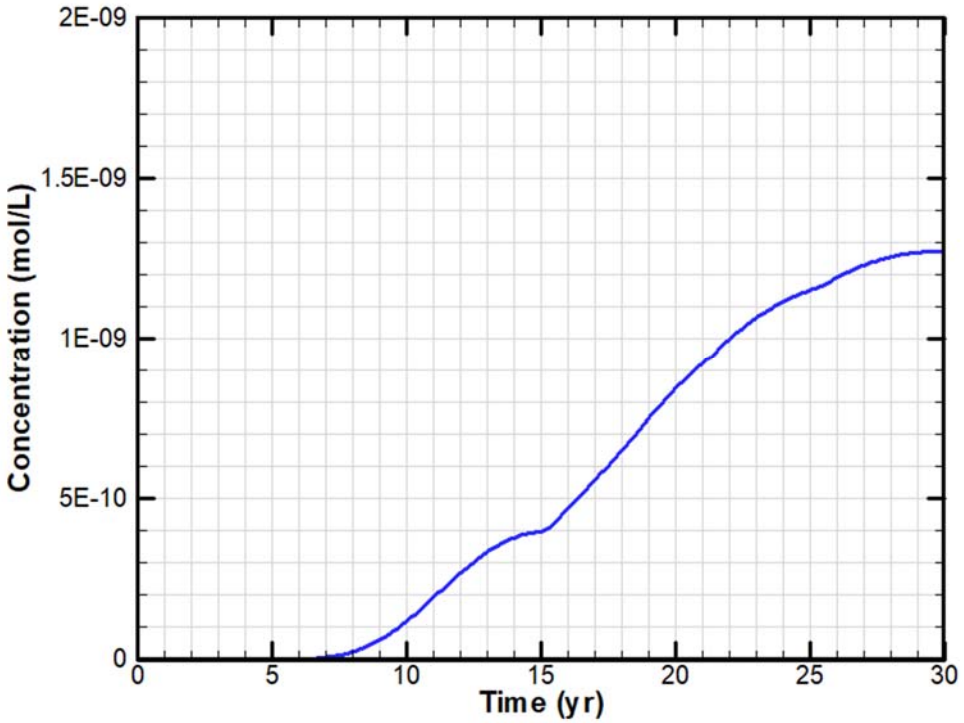

Figure 4.4-141: Breakthrough Curve from SDU 8 to the 100-Meter Boundary

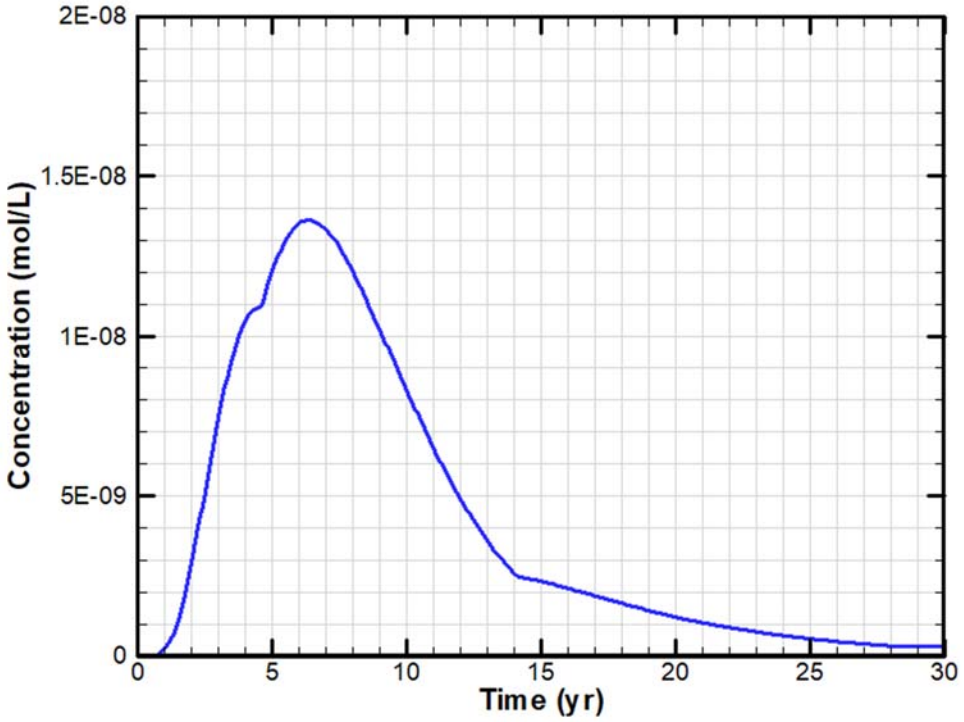

Figure 4.4-142: Breakthrough Curve from SDU 9 to the 100-Meter Boundary

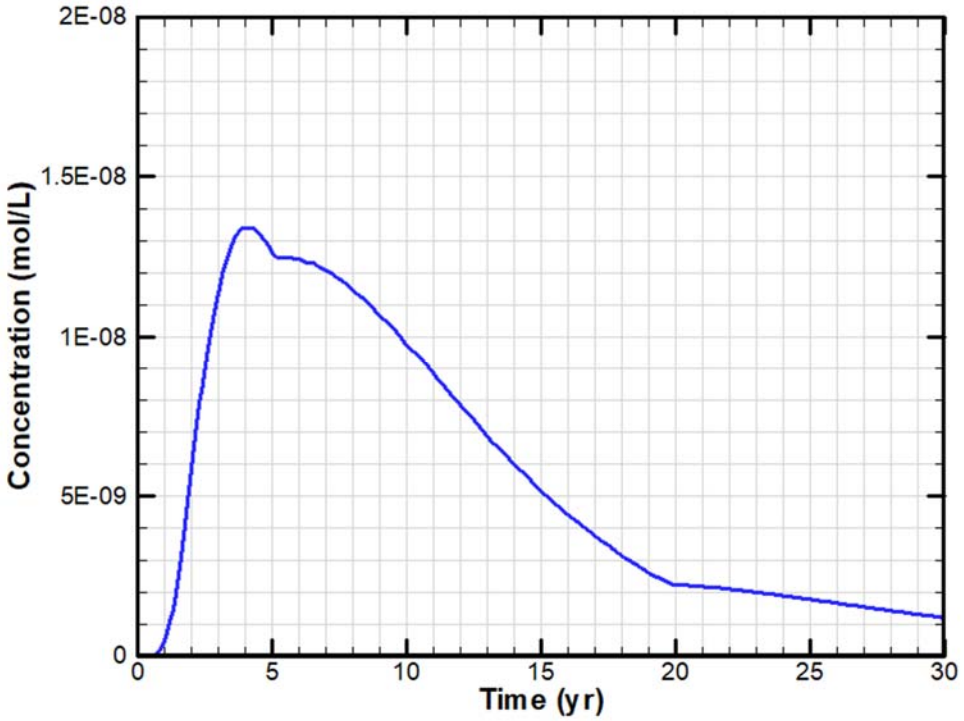

Figure 4.4-143: Breakthrough Curve from SDU 10 to the 100-Meter Boundary

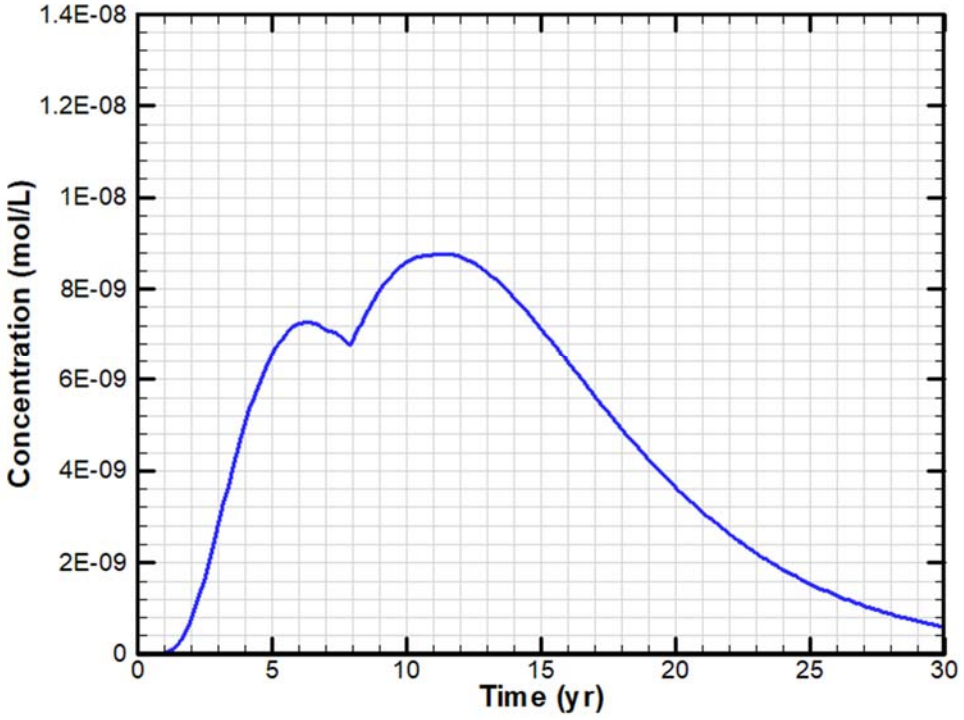

Figure 4.4-144: Breakthrough Curve from SDU 11 to the 100-Meter Boundary

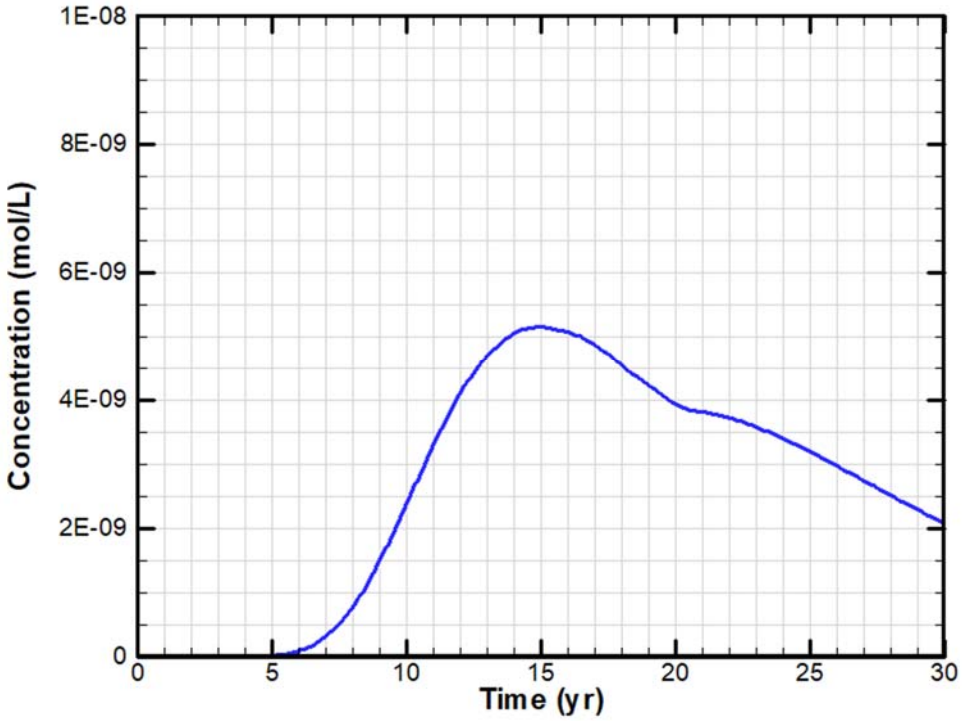

Figure 4.4-145: Breakthrough Curve from SDU 12 to the 100-Meter Boundary

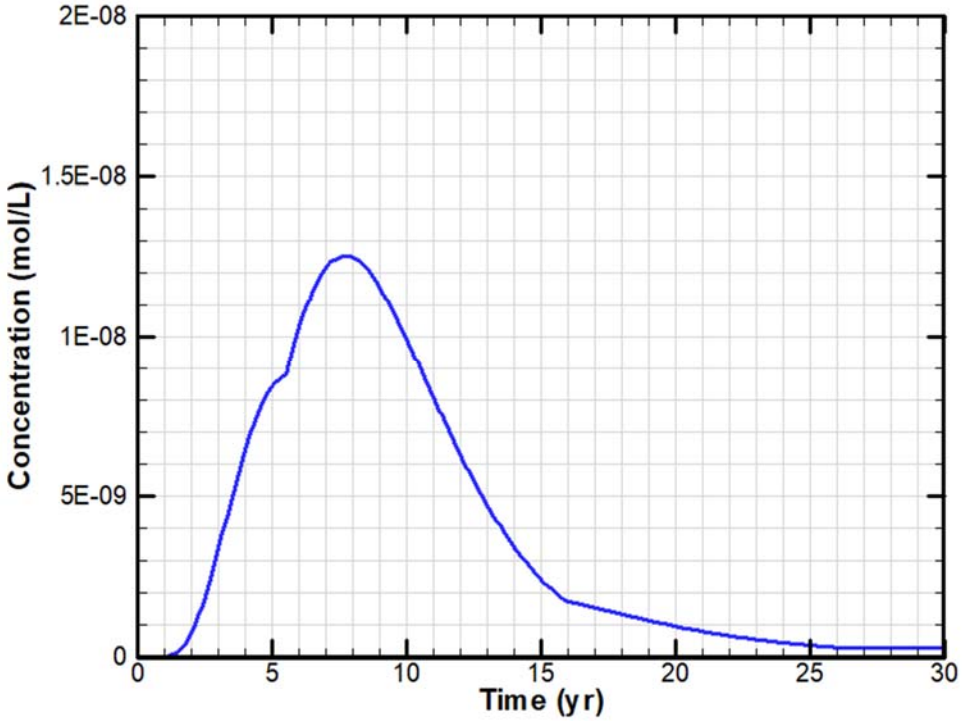

Comparing the average flow rates based on tracer pulses (breakthrough curves) against the average flow rates based on the streamline traces shows that the greatest differences were in the rates estimated for SDUs 2A and 2B, in which the rates based on the breakthrough curves were approximately twice as high as the respective rates based on the streamline traces. Excluding SDUs 2A and 2B, the other SDUs showed a more moderate difference of approximately 20% (i.e., relatively good agreement). While both approaches are valid, the differences in the estimates between these two approaches illustrate the challenges associated with abstracting three-dimensional processes into one- or two-dimensions; a challenge that is addressed in the benchmarking analysis for the SDF GoldSim Model (see Section 5.6).

Table 4.4-85: Summary of Breakthrough Timing to the 100-meter Boundary

SDU	Distance to Boundary (ft)	Based on Tracer Pulses (Figure 4.4-131 through Figure 4.4-145)		Based on Streamline Traces (Figure 4.4-115)	
		Years to Boundary	Average Rate (ft/yr)	Years to Boundary	Average Rate (ft/yr)
SDU 1	1338	22.3	60.0	28.7	46.7
SDU 4	635	9.9	64.2	13.7	46.4
SDU 2A	807	9.8	82.3	16.6	48.6
SDU 2B	803	9.0	89.2	18.1	44.4
SDU 3A	402	3.2	125.5	3.00	134.1
SDU 3B	493	3.9	126.4	3.71	132.9
SDU 5A	494	5.2	95.1	5.92	83.4
SDU 5B	668	7.8	85.6	7.99	83.6
SDU 6	1067	15.6	68.4	19.2	55.5
SDU 7	1424	29.6	48.1	43.0	33.1
SDU 8	578	6.3	91.7	7.59	76.1
SDU 9	572	4.2	136.2	5.90	97.0
SDU 10	545	11.4	47.8	13.3	41.0
SDU 11	1119	14.9	75.1	15.8	70.9
SDU 12	635	7.8	82.0	9.36	67.9

Note: Since transport from SDU 1 and SDU 4 is based on three streamline traces, the values are averaged using: $(0.5\times A_1+A_2+0.5\times A_3)/2$, where A_1 is the northmost streamline trace, A_2, is the central streamline trace, and A_3 is the southmost streamline trace from each SDU.

Also note that the distances to the boundary for each SDU, as presented in Table 4.4-85, indicate that although the straight-line distance from the edges of the SDUs to the boundary is only 100 meters, the streamline traces do not follow direct (straight-line) paths and generally start from the center point of the SDUs (to reflect the center of mass) rather than starting at the edges of the SDUs. The winding, three-dimensional paths (for both the streamline traces and the plumes), along with the added dimensions of the SDUs, result in contaminant travel distances that exceed 100-meters. This phenomenon is further exacerbated by SDUs which are further in from the 100-meter boundary (e.g., SDUs 1 and 7).

This page intentionally left blank.

4.4.7 Airborne Pathway Release and Transport Model

This section describes the details of the SDF Air Pathway Release Model (referred to herein as the SDF APR Model), specifically developed for this revision to the SDF PA. The SDF APR Model is designed to evaluate the air-phase transport of potentially volatile radionuclides. A portion of volatile radionuclides dissolved in interstitial water found within the pores of the saltstone waste form will also partition into the air phase of the pore space. The radionuclides partitioned into the air phase may be released to the accessible environment (the atmosphere) via diffusion through the saltstone monolith, the SDU roof, the sand overlying the SDU roof, and the closure cap barriers.

The SDF APR Model was developed using GoldSim simulation software. GoldSim is an object-oriented, probabilistic modeling software designed to evaluate parameter sensitivity and the influence of parameter uncertainty. The SDF APR Model simulates the migration of radionuclides from SDUs upwards through the overlying closure cap where it is released to the atmosphere and transported down-gradient through the atmosphere. The air and radon pathway analysis performed using the SDF APR Model was conducted for post-closure time periods.

In the GoldSim-based SDF APR Model, the SDUs and overlaying closure cap materials are represented by sets of cell pathway elements (mixing cells) combined in series using diffusive mass flux links between cells to define the diffusive transport of radionuclides from the saltstone monolith upwards through the clean grout (if considered), the concrete roof, and the closure cap comprised of the lower lateral drainage layer, the lower backfill layer, the foundation, the upper lateral drainage layer, the middle backfill layer, and the erosion barrier. At the top of the erosion barrier, the radionuclides are released into the atmosphere.

As a simplifying assumption, the model does not include several layers of the closure cap (topsoil, upper backfill, geotextile fabric, HDPE, and GCL). These layers would be expected to retard the migration of the volatile radionuclides to the surface; thus, by not including them the model results are intentionally biased towards estimating faster-than-expected releases.

For the air pathway analysis, the volatile gaseous-phase radionuclides are evaluated by the SDF APR Model. The radionuclides evaluated by the SDF APR Model for gaseous-phase flow include: C-14, Cl-36, H-3, I-129, Se-79, Sb-125, Sb-126, Sn-126, and Tc-99. The nine radionuclides are the same set as evaluated in the 2009 SDF PA PORFLOW air pathway model and the radionuclide selection is discussed in the PA. [SRR-CWDA-2009-00017] Note that although Sb-125 and Sb-126 are not found in the present inventories included in the Vadose Zone Transport Model, they are included for consistency with earlier airborne release modeling for the SDF. [SRNL-STI-2008-00447 and SRR-CWDA-2009-00017] The ground surface releases of these volatile radionuclides generated by the SDF APR Model are then used in conjunction with dose release factors (DRFs) calculated using CAP88-PC modeling software to evaluate down gradient doses at a 100-meter distance from the SDF and at the site boundary.

In addition to evaluating the ground surface releases for the above volatile radionuclides, the SDF APR model is designed to evaluate radon fluxes at the ground surface. Radon releases are evaluated independently from the other volatile radionuclides. The permissible radon flux for

DOE facilities is addressed in DOE M 435.1-1 IV.P.1(c), stating the radon flux requirement is that the release of radon shall be less than an average yearly flux of 20 pCi/m²/s at the surface of the facility. The performance objective refers only to radon, and the correct species must be analyzed depending on the characteristics of the residual waste stream. For the SDF PA, the instantaneous Rn-222 flux at the land surface was evaluated for 10,000-years. Since the release of radon from the SDUs will be strongly controlled by ingrowth from potential parent radionuclides found in the saltstone, seven parent radionuclides are included in the model. These parent radionuclides include Cm-246, Pu-242, Pu-238, U-238, U-234, Th-230, and Ra-226. The extremely long half-life of U-238 causes its parental radionuclides to be of little concern with respect to their potential contribution to the Rn-222 release at the land surface over the time-period of interest. [SRNL-STI-2008-00447] Rn-222 generated within the waste zone is in the gaseous phase and diffuses outward from this zone into the air-filled soil pores surrounding the disposal units, eventually resulting in some of the radon emanating at the land surface. As such, air is the fluid through which most of the Rn-222 diffuses, although some Rn-222 may dissolve in residual pore water. [SRNL-STI-2008-00447] The parent radionuclides are assumed to exist in the solid phase and therefore do not migrate upward through the air-filled pore space, although they could be leached and transported downward from the waste zone by pore water movement. This potential downward migration of the parent radionuclides is not considered in the radon analysis, as such the model overestimates the radon flux. [SRNL-STI-2008-00447]

4.4.7.1 Air and Radon Pathway Conceptual Model

The SDF APR Model is designed to simulate air-phase diffusive transport of radionuclides from the saltstone monoliths, through the closure cap to the land surface and into the atmosphere for each of the four SDU-types found in the SDF:

- SDU 1, a 100-foot by 600-foot rectangular SDU;
- SDU 4, a 200-foot by 600-foot rectangular SDU;
- 150-foot diameter cylindrical SDUs (representing SDUs 2A, 2B, 3A, 3B, 5A, and 5B); and
- 375-foot diameter cylindrical SDUs (representing SDUs 6, 7, 8, 9, 10, 11, and 12).

The conceptual framework and associated parameters for the air and radon pathway model is designed to be consistent with the Compliance Case (MPAD), where nominal settings for the input parameters are based on a blending between Best Estimate (most realistic) and Pessimistic (conservative) assumptions depending on the parameter uncertainty. The main analysis tool employed is the GoldSim based code, SDF APR, that simulates the diffusive transport of volatile radionuclides and radionuclide chain daughter products in the unsaturated pore-space of porous media. The release of radioactive gases into the atmosphere above the land surface overlying the SDF disposal units was evaluated for the assumed closure scenario. Volatile radionuclides within the air-filled pore space of the saltstone monolith diffuse upwards into and through the air-filled pore space of the overlying materials. Ultimately, some of the radionuclides are released at the land surface. It was assumed that fluctuations in atmospheric pressure at the land surface capable of inducing small pulses of air movement into and out of the

shallow soil profile over relatively short periods would have a net zero effect when averaged over longer periods. Thus, advective transport of radionuclides in air-filled soil pores was not considered a significant process when compared to the rate of air-phase diffusion. [SRNL-STI-2008-00447] In addition, because the magnitude of air-diffusion coefficients is much greater (approximately 5-orders of magnitude greater) than equivalent molecule-specific values for water diffusion coefficients, the model evaluates air-phase transport only.

The components of the closure cap from land surface downwards include a top soil layer, an upper backfill layer, an erosion barrier layer, a geotextile fabric, a middle backfill layer, a geotextile fabric, an upper lateral drainage layer, a geotextile fabric, a HDPE geomembrane, a GCL, a foundation layer (backfill with bentonite admix), a lower backfill layer, a geotextile filter fabric, and a lower lateral sand drainage layer. [WSRC-STI-2008-00244] As a simplifying assumption, the geotextile fabrics, the HDPE, and the GCL are excluded from this analysis. While the geotextile fabrics are not expected to impact gaseous flux, the HDPE and the GCL are both expected to significantly reduce gaseous flux at the land surface, since the HDPE has very low gaseous diffusion coefficients and the GCL would have very little air-filled porosity, since it would be at or near saturation. [SRNL-STI-2008-00447] The top soil layer and the upper backfill layer are also excluded from the analysis since they are located above the erosion barrier and their influence could be negated by erosion. For the purposes of this analysis, it is assumed that SDU and closure-cap modeled structural components situated below the top of the erosion barrier remain intact for the duration of the simulation (10,000 years).

4.4.7.2 Implementation of the Air and Radon Pathway Diffusive Transport Model

In the GoldSim-based SDF APR Model, the SDUs and overlaying closure cap components are represented by sets of GoldSim cell-pathway elements (mixing cells) coupled in series, using diffusive mass flux links to define the diffusive transport of radionuclides from the saltstone monolith upwards through the clean grout, the concrete roof, and the closure cap comprised of the lower lateral drainage layer, the lower backfill layer, the foundation, the upper lateral drainage layer, the middle backfill layer, and the erosion barrier. At the top of the erosion barrier, the radionuclides are released into the atmosphere. As noted above, because of the orders of magnitude difference between water diffusivities and air diffusivities, only the air phase is simulated as a mobile zone. Neglecting the downward process of advection and assuming a one-dimensional upward only process for diffusion maximizes the upwards release at the ground surface. Although the model uses fully coupled diffusive mass flux links, imposing a no-flow/no-diffusion boundary at the bottom of the model, a zero-concentration boundary condition at the top of the model and defining the source zone as mass equally distributed throughout the saltstone monolith at the bottom of the model constrains the model to a vertically upwards concentration gradient and an upwards trend for diffusion. Although simulating the reference fluid and solid phases as immobile zones, with respect to radionuclide transport, the reference fluid (water) and solid phases are still included in the model because of the propensity for most radionuclides to partition between the reference fluid, solid, and air phases with the

reference fluid and solid phases providing storage for dissolved and/or sorbed radionuclides. The partitioning between the three phases is reflected in a retarding influence of the immobile zones on the mobile zone transport. The SDF APR Model also includes an option to allow users to disregarding the storage effects of the water (above the source zone) and the solid phase (throughout the model).

4.4.7.2.1 Implementation of the GoldSim "Top Down" Structure

As discussed in GTG-2018a, the GoldSim software is designed to be amenable to model development using a "top-down" approach, starting from the top (i.e., the ultimate objective of the modeling exercise) and concentrating on the integration and coupling of all system components. At its "top" level (Figure 4.4-146), the SDF APR Model is comprised of four containers used to divide the model into four sections: one for selecting options and setting control parameters (*UserSettings*), a second section containing the input parameters (*GeneralInput*) used to define the system processes controlling the release of volatile radionuclides to the atmosphere, a third section where calculations needed to quantify the release of radionuclides to the atmosphere are performed (*Air_PathwayTransport*), and a fourth section used to capture and organize the results generated in the calculation section (*SDU_Output*).

Figure 4.4-146: "Top" Level of the SDF APR Model

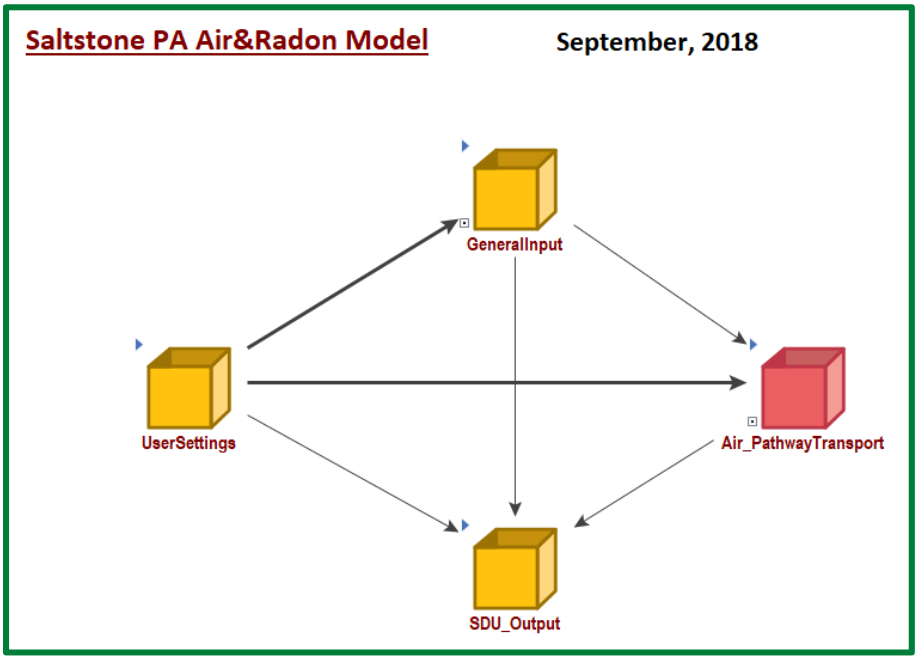

For the release and transport calculations, the model utilizes a GoldSim submodel contained within a set of nested looping containers. GoldSim looping containers behave like Do-Loops in other computer languages (e.g., FORTRAN or C++). This allows the model to run through the complete set of 15 SDUs in looping mode, using the appropriate string of cell-pathway elements for each SDU based on the

SDU-types. The model can also simulate a subset of SDUs or individual SDUs in a simulation based on user defined Model Index Values (Table 4.4-86).

Table 4.4-86: SDU Index Used in the SDF APR Model

Model Index Value	Simulated SDU
1	SDU 2A
2	SDU 2B
3	SDU 3A
4	SDU 3B
5	SDU 5A
6	SDU 5B
7	SDU 6
8	SDU 7
9	SDU 8
10	SDU 9
11	SDU 10
12	SDU 11
13	SDU 12
14	SDU 1
15	SDU 4
0	Loop Through All or a Subset of SDUs

4.4.7.2.2 Implementation of the Air-Phase Transport Calculations in the GoldSim Submodel

This section describes the organization and details of the GoldSim based air-phase transport submodel.

Looping Containers

The upper-level contents of the *Air_PathwayTransport* container controls the repeated processing of the GoldSim SubModel, which contains the radionuclide air-phase release calculation elements for SDU 1, SDU 4, the 150-foot diameter SDUs, and the 375-foot diameter SDUs. A GoldSim SubModel is a specialized container-like element that has the full functionality of a GoldSim Model including time settings and Monte Carlo method and Latin Hypercube Sampling (LHS). The SubModel behaves as a separate "inner" model within an "outer" model. The air-pathway model's transport calculation submodel (*Air_PathwaySubmodel*), hereafter referred to as the "SDU Transport Submodel," is imbedded within two nested GoldSim looping containers (*OuterLoop_SDUs* and *InnerLoop_SDUs*). These looping containers behave like Do-Loops in other computer languages, such as FORTRAN or C++. The SDU Transport Submodel is controlled by the outer loop that loops over the individual SDUs of interest in a simulation (see Figure 4.4-147). Container *NSDU* is the data element that identifies maximum number of SDUs that can be modeled.

Figure 4.4-147: Contents of the *Air_PathwayTransport* Container

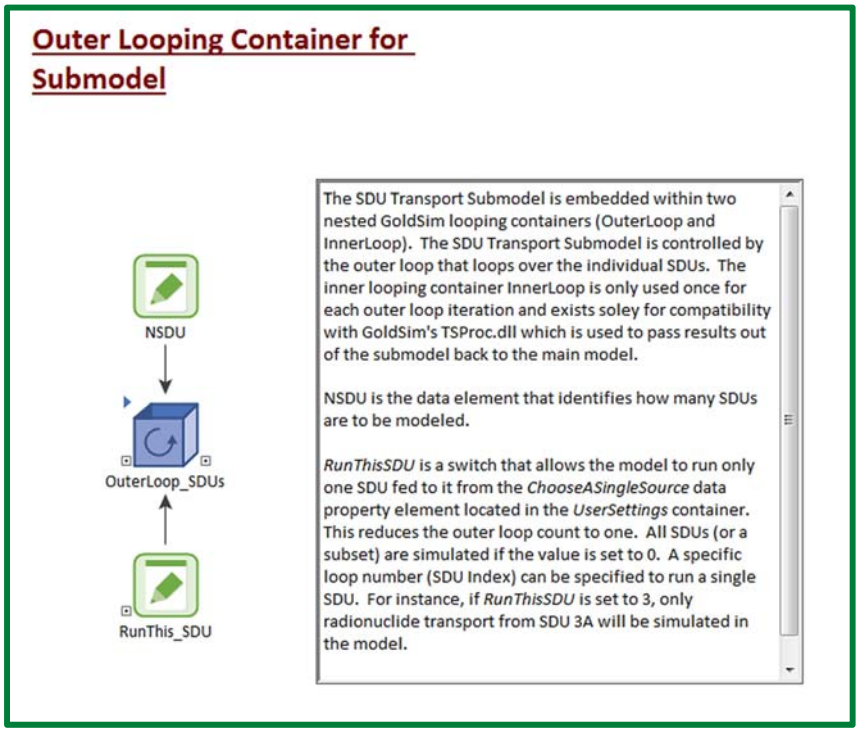

RunThis_SDU is a switch that allows the model to run a single SDU based on the SDU Index (Table 4.4-86) selection fed from the *ChooseASingleSource* data element located in the *UserSettings* container. When users opt to run the model for only a specific SDU, this reduces the outer loop count to one. All SDUs (or a subset of) are simulated if the value is set to 0. A specific loop number (based on the SDU Index in Table 4.4-86) can be specified to run a single SDU. For instance, if *RunThisSDU* is set to 3, only radionuclide transport from SDU 3A will be simulated in the model (see Table 4.4-86).

The inner looping container *InnerLoop_SDUs* (Figure 4.4-148) is used once for each outer loop iteration and exists solely for compatibility with GoldSim's vendor-provided dynamic link library (DLL): *TSProc.dll*. This DLL is used to pass time series results out of the submodel back to the main model. The GoldSim External element *TSProc*, found in the container *TS_Proc_SDUs*, controls the external DLL *TSProc.dll* by calling it as a subroutine.

Figure 4.4-148: Contents of Container *OuterLoop_SDUs*

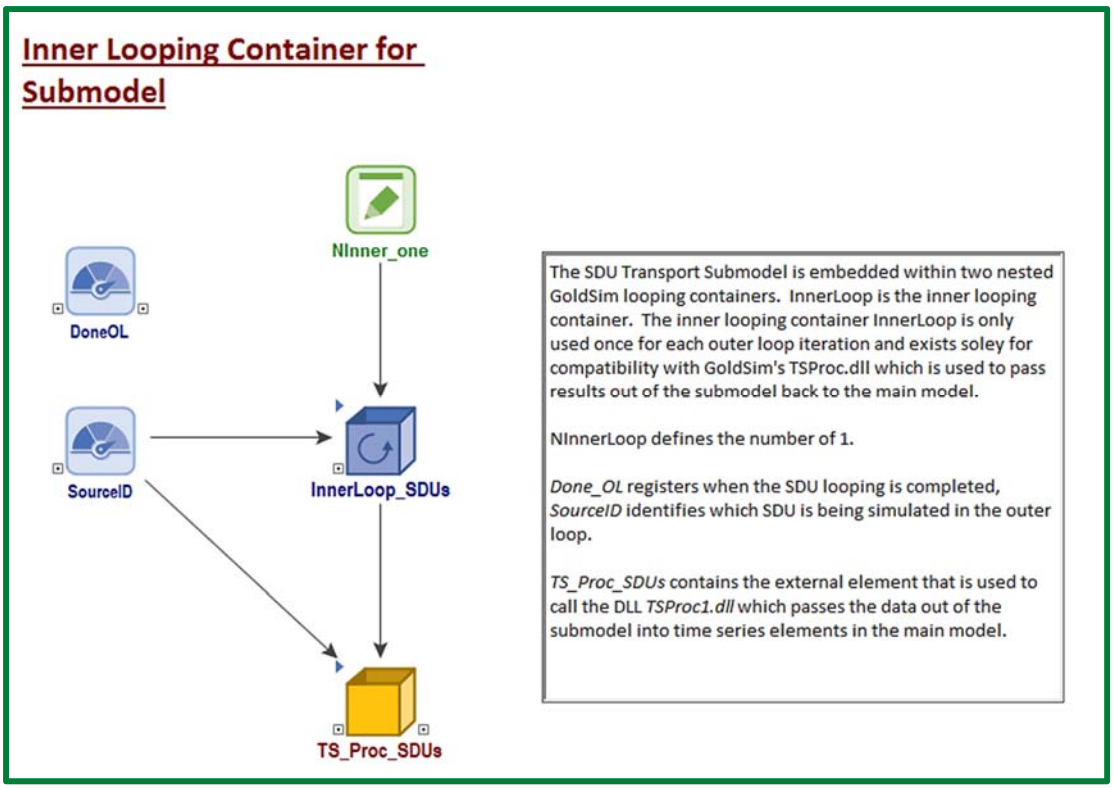

Structure of the GoldSim Submodel

Within the looping container *InnerLoop_SDUs*, resides *SDUTransportSubmodel* (see Figure 4.4-149). This is an independent GoldSim Submodel that is initialized prior to the occurrence of time-stepping within the main model. The GoldSim Submodel calculates the radionuclide releases from the user-selected SDUs and subsequently passes the release values back to the main model in the form of a time series. The time series can then be used as data for calculations in the main model, such as generating input data for models evaluating transport in the atmosphere and/or calculating doses.

Figure 4.4-149: Contents of the Container *InnerLoop_SDUs*

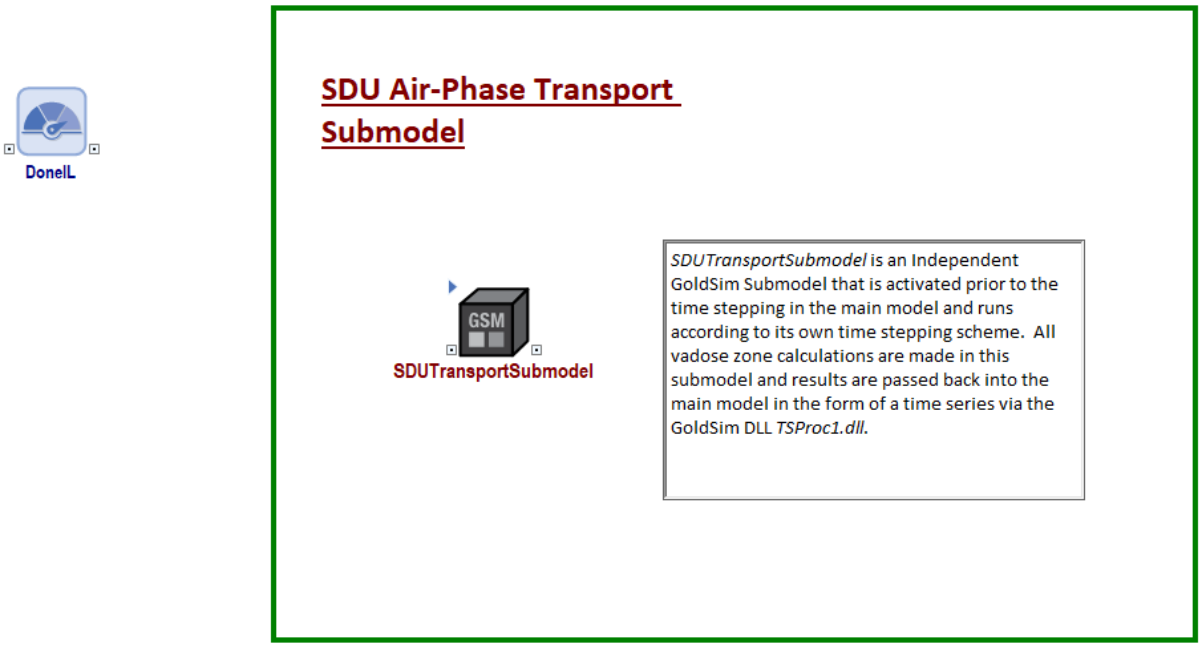

The GoldSim contaminant transport module automatically includes a *Material* container for defining the material properties used in contaminant transport. In addition to the *Material* container, the SDU Transport Submodel is comprised of an *InputData* container, a *SDU_Transport_Results* container, and four SDU-type containers. The *InputData* container contains a set of selector elements used to capture input parameters fed from the main model through the submodel interface into the submodel. The *SDU_Transport_Results* container contains time series elements used to feed the main model through the submodel interface. The air-phase diffusive transport calculation section of the submodel is comprised of four containers, representing the four SDU-types found at the SDF (see Figure 4.4-150):

- SDU 1, a 100-foot by 600-foot rectangular SDU [Container *SDU_V1*];
- SDU 4, a 200-foot by 600-foot rectangular SDU [Container *SDU_V4*];
- 150-foot diameter cylindrical SDUs (i.e., SDUs 2A, 2B, 3A, 3B, 5A, and 5B) [Container *SDU_150ft*]; and
- 375-foot diameter cylindrical SDUs (i.e., SDUs 6, 7, 8, 9, 10, 11, and 12) [Container *SDU_375ft*].

Figure 4.4-150: Submodel Upper Level

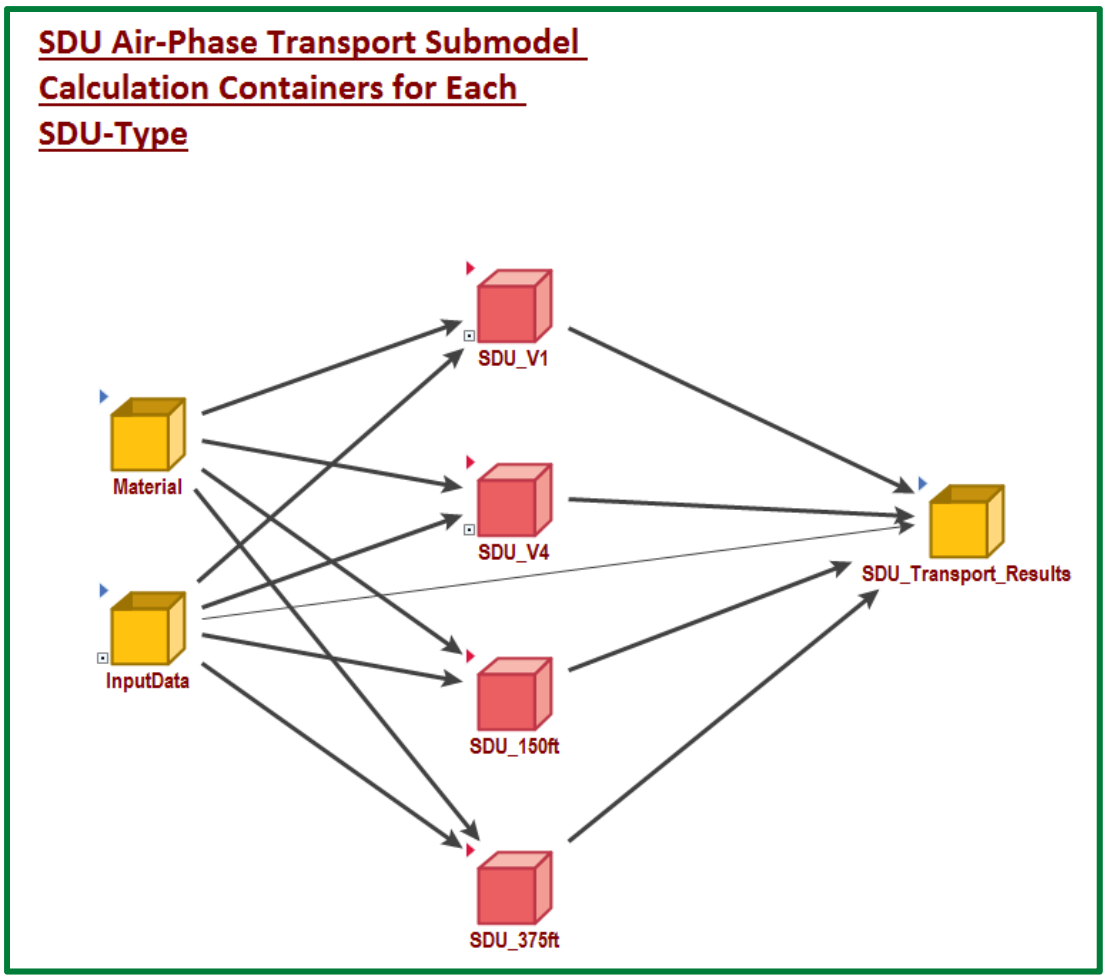

Within each of the four containers, there are SDU-type specific GoldSim cell-pathway networks used to calculate air-phase diffusive transport from the bottom of the saltstone monolith to the top of the erosion barrier, which assumed to be the top surface of the closure cap.

As an example, the container within which the air-phase transport calculations are performed for the 150-foot diameter SDUs, *SDU_150ft*, is described below in more detail. The top-level of *SDU_150ft* container is comprised of an inner container (*SDU_150*) and a set of expression elements used to feed layer-specific parameter vectors to all the layer-specific containers within *SDU_150* (Figure 4.4-151).

Figure 4.4-151: Layer-Based Vector Feeds to 150-Foot Diameter SDU Mixing Cells

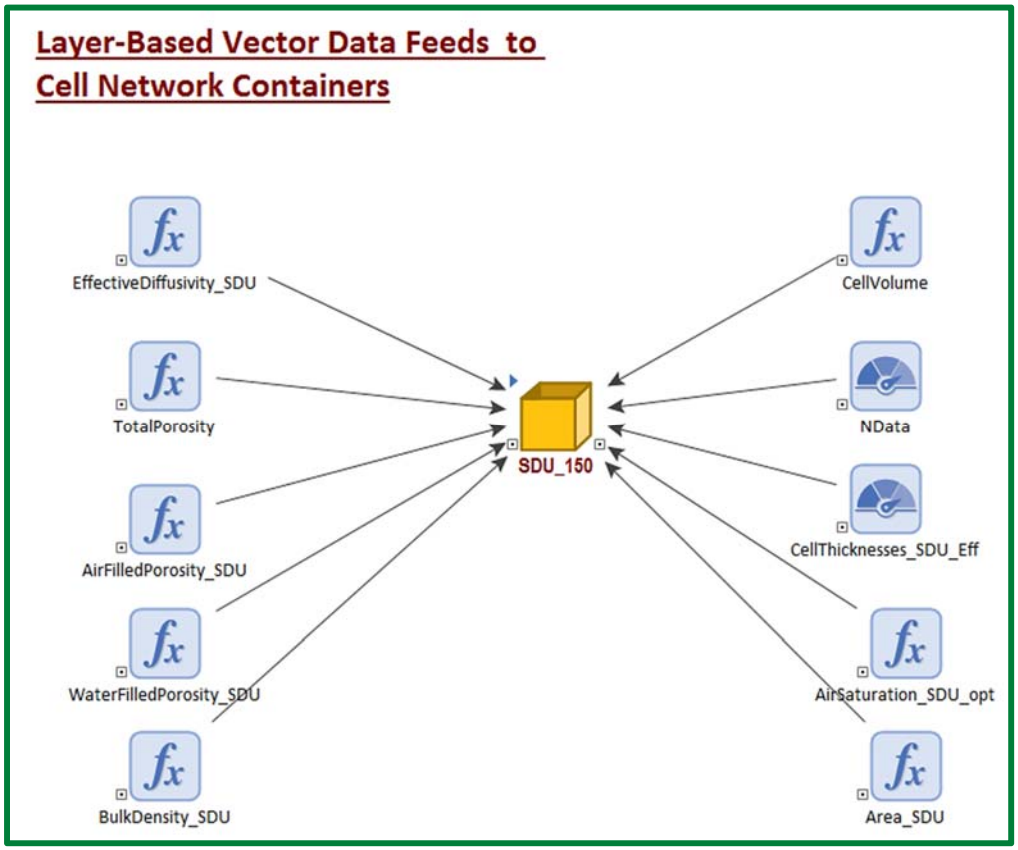

Figure 4.4-152 depicts the layer-specific containers for the 150-foot diameter cylindrical SDUs. Each layer-specific container houses a string of mixing cells linked in series via diffusive-flux links. Figure 4.4-153 illustrates the segment of the linked cell-pathway (mixing-cell) network representing the saltstone monolith. The blue arrows represent the diffusive-flux linkages between the cells. The lack of a linkage at the bottom of the *Salt1* cell pathway (Figure 4.4-153) indicates that the bottom boundary condition has a zero-flux condition, which together with the inventory placement (equally distributed in the saltstone monolith) will force the system to simulate upwards diffusion only. Figure 4.4-154 illustrates the segment of the linked cell-pathway (mixing-cell) network representing the erosion barrier. The diffusive-flux link between the top erosion-barrier cell *EB4* and the container *Sink*, which contains a cell pathway element, *ZeroBC*, controls the release of radionuclide gases. A cell pathway element option in *ZeroBC* is set to approximate a Dirichlet boundary condition of zero-concentration.

For more details on the cell-pathway structure in the other containers depicted in Figure 4.4-152, refer to SRR-CWDA-2018-00025. Details on the air-phase transport calculations performed in SDU Transport Submodel are presented in the following section.

Figure 4.4-152: Example of Zone-Specific GoldSim Containers for Cell Pathway Elements Linked in Series to Simulate Air-Phase Transport through SDUs and Closure Cap Layers for 150-Foot Diameter SDUs

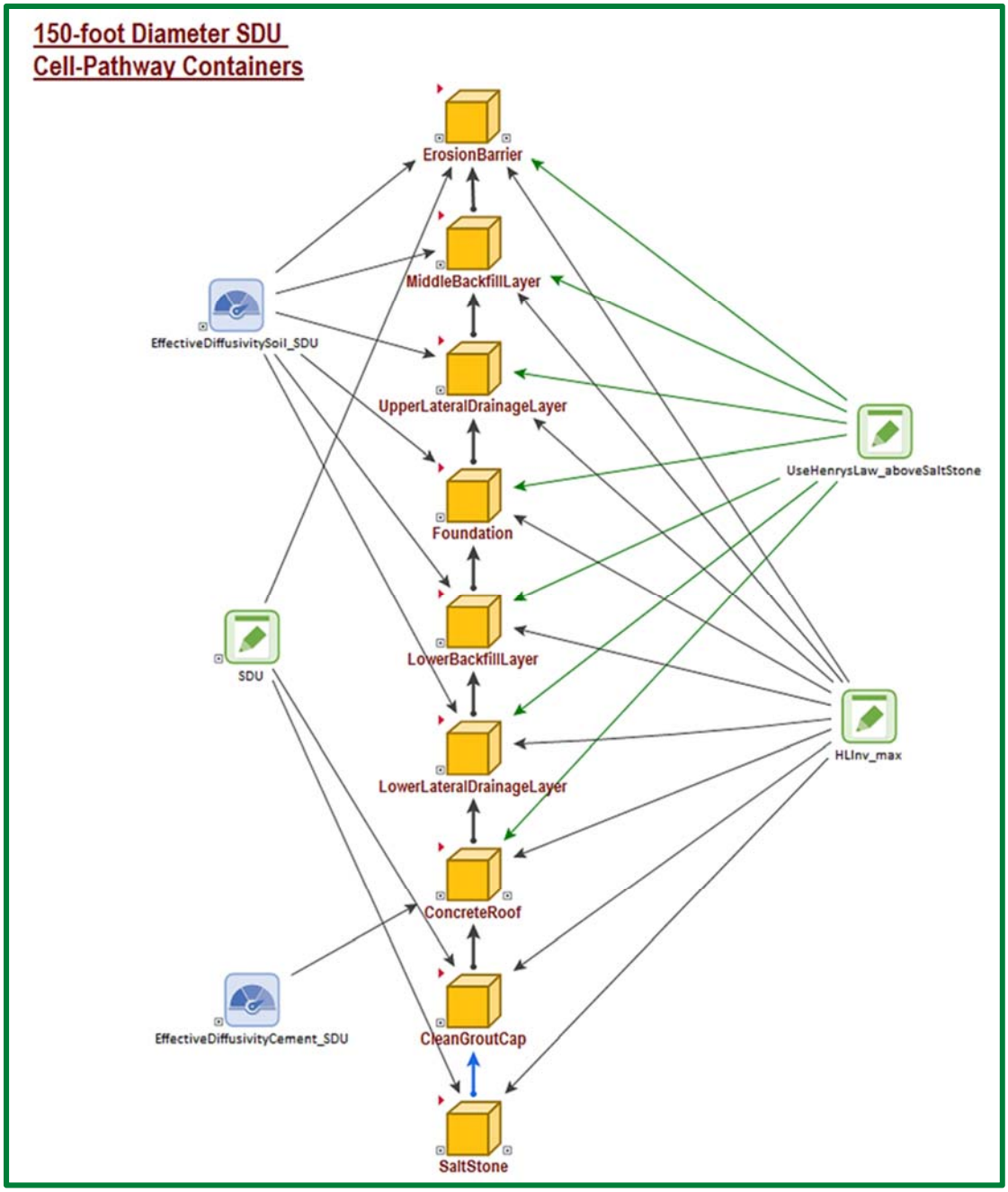

Figure 4.4-153: Example of GoldSim Cell Pathway Elements Linked in Series to Simulate Air-Phase Transport through Saltstone for 150-Foot Diameter SDUs

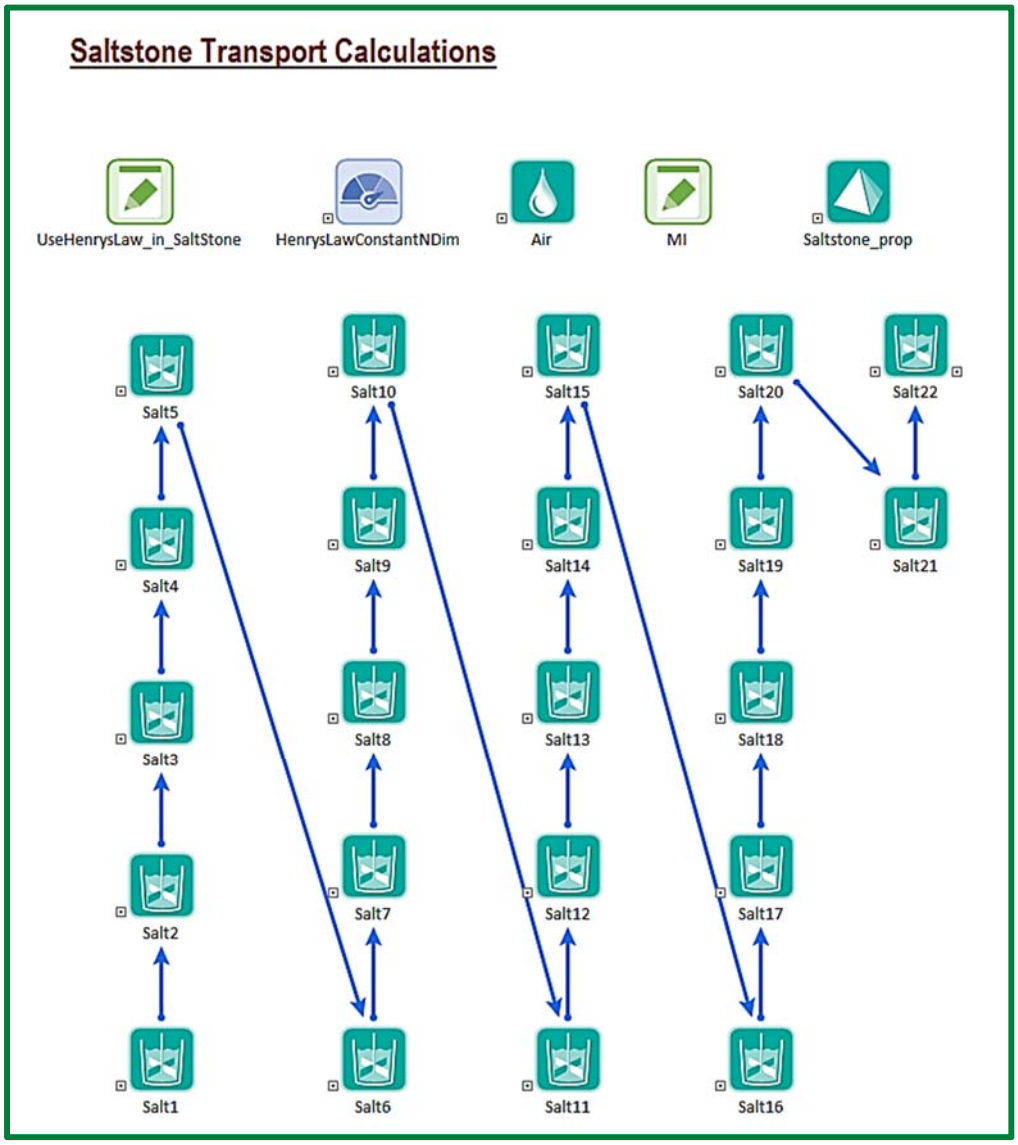

Figure 4.4-154: GoldSim Cell Pathway Elements Linked in Series to Simulate Air-Phase Transport through the Erosion Barrier for 150-Foot Diameter SDUs

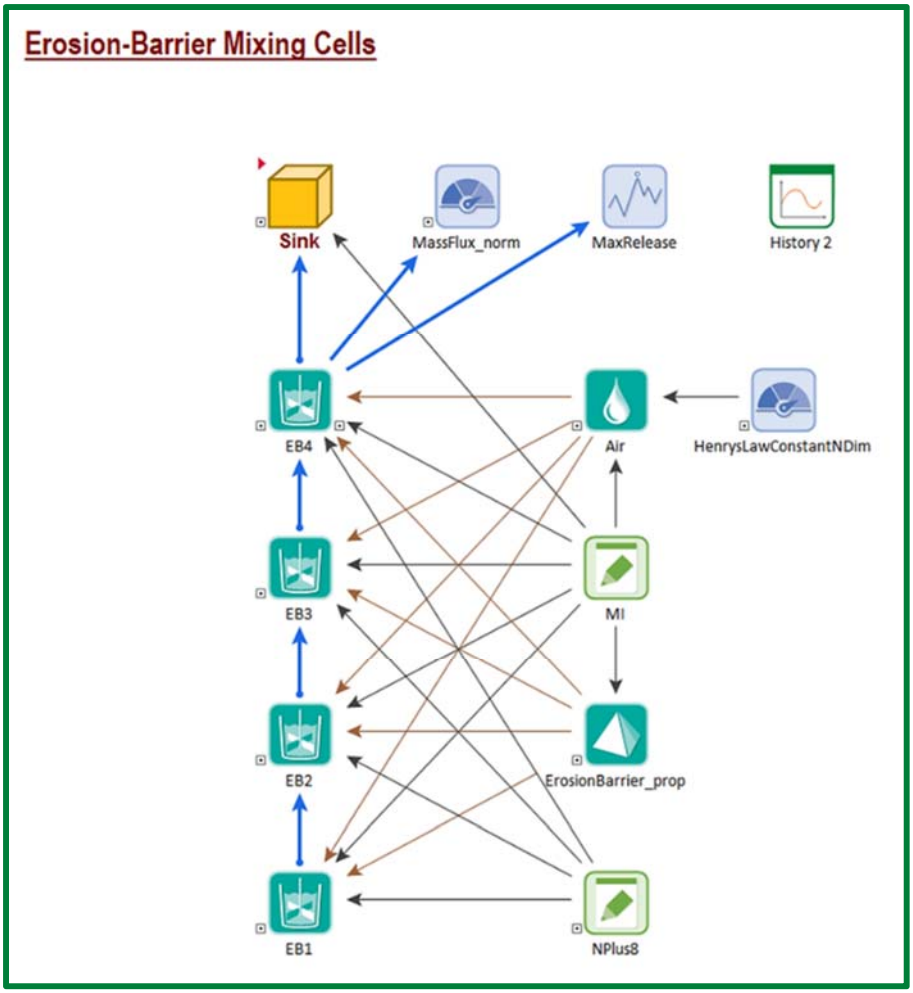

4.4.7.2.3 Air and Radon Model Governing Equations for GoldSim Cell Pathway Networks

The basic mass balance equation for each cell pathway element i, used to develop the four mixing cell networks used in the model implementation, can be written as follows (GTG-2017b):

$$m'_{is} = -m_{is}\lambda_s + \sum_{p=1}^{NP_s} m_{ip}\lambda_p f_p R_{sp}\left(\frac{A_s}{A_p}\right) + \sum_{c=1}^{NF_i} f_{cs} + S_{is} \qquad \text{Eq. 4.4-126}$$

where:

m'_{is} = rate of change of mass of species s in Cell i [M/T],

m_{is} = mass of species s in Cell i [M],

λ_s = decay rate for species s [T^{-1}],

NP_s = number of direct parents for species s,

f_p = fraction of parent p which decays into species s,

R_{sp} = stoichiometric ratio of moles of species s produced per mole of species p decayed,

A_s = molecular (or atomic) weight of species s [M/mol],

A_p = molecular (or atomic) weight of species p [M/mol],

NF_i = number of mass flux links from/to Cell i,

f_{cs} = influx/outflux rate of species s (for Cell i) through mass flux link c [M/T],

S_{is} = rate of direct input of species s to Cell i from "external" sources [M/T], and

p = species index (s) for parent species.

The model's initial condition is set by distributing the total inventory for each SDU at time zero among the mixing zone of the source, using one of two options. The first option is to apportion the total inventory between saltstone-only cells based on the relative cell volume generating equal initial concentrations. The second option is to apportion the inventory among both the saltstone-only and potential clean grout cells, which are designed to allow the user to choose between including a layer of clean grout above the saltstone or filling the SDU with saltstone only. The use of a layer of clean grout is expected to considerably retard the air phase transport.

The initial distribution between solid, water (the reference fluid), and air in each cell is based on the assigned K_ds for the solid/liquid phase partitioning and non-dimensional Henry's Law volatility constants, c_{air}/c_{water} for the air/liquid phase partitioning, where c_{air} [M/L^3] is the air phase concentration and c_{water} [M/L^3] is the water phase concentration. The boundary condition at the bottom of the saltstone monolith is a no-flux boundary condition and the boundary condition at the top of the erosion barrier (representing the atmosphere) is a zero-concentration Dirichlet boundary condition. The use of a zero-concentration boundary condition provides a good approximation of what is seen in the atmosphere where rapid attenuation of the volatiles released to the atmosphere occurs. The lateral boundary conditions are no-flux boundary conditions for each cell. These boundary conditions force all the gas-phase radionuclides to move upward from the saltstone monolith to the land surface. In nature, some lateral and downward diffusion occurs in the air-filled pore space surrounding the stabilized saltstone monolith. Ignoring this lateral and downward movement has the effect of increasing the flux at the land surface, thus overestimating the calculated fluxes.

The transport of air phase (mobile zone) constituents in the model is controlled by the GoldSim diffusive mass flux links used to connect cell-pathway elements in series. The cell-pathway elements linked in series to represent each material zone are found in individual zone-specific closed containers (e.g., see Figure 4.4-153 and Figure 4.4-154) to allow for material-dependent diffusivities. The black arrows between material-zone containers (see Figure 4.4-152) are indicative of the

occurrence of diffusive mass flux links between containers connecting the top mixing cell in the lower zone and the bottom cell in the overlying zone. Figure 4.4-153 presents the contents of the *Saltstone* container depicted at the bottom of Figure 4.4-152. The blue arrows in Figure 4.4-153 are represent the diffusive-flux linkages between the mixing cells making up the saltstone monolith.

The governing equation for the diffusive mass flux link between Cell i and Cell j, can be written in the form:

$$f_{s,i\to j} = D_s\left(c_{ims} - \frac{c_{jns}}{K_{nms}}\right) \qquad \text{Eq. 4.4-127}$$

where:

D_s = diffusive conductance for species s in the mass flux link [L³/T],

c_{ims} = the dissolved concentration of species s in medium m within Cell i [M/L³],

c_{jns} = the dissolved concentration of species s in medium n within Cell j [M/L³], and

K_{nms} = partition coefficient between fluid medium n (in Cell j) and fluid medium m (in Cell i) for species s [L³ medium m / L³ medium n].

The diffusive conductance for species s in the mass flux link as defined in GTG-2018a can be written as:

$$D_s = \frac{A}{\frac{L_i}{f_{ms}d_{ms}\tau_{Pi}r_m(s_m)n_{Pi}} + \frac{L_j}{f_{ns}d_{ns}\tau_{Pj}r_n(s_n)n_{Pj}K_{nms}}} \qquad \text{Eq. 4.4-128}$$

where:

A = the area of the diffusive mass flux link [L²],

L_i = diffusive length for the diffusive mass flux link in Cell i [L],

L_j = diffusive length for the diffusive mass flux link in Cell j [L],

f_{ms} = available porosity for species s in medium m (≤ 1),

f_{ns} = available porosity for species s in medium n (≤ 1),

d_{ms} = fluid diffusivity for species s for fluid m (in Cell i) [L²/T],

d_{ns} = fluid diffusivity for species s for fluid n (in Cell j) [L²/T],

τ_{Pi} = tortuosity for the porous medium defined for the diffusive mass flux link in Cell i (≤ 1),

τ_{Pj} = tortuosity for the porous medium defined for the diffusive mass flux link in Cell j (≤ 1),

$r_m(s_m)$ = diffusive reduction formula for fluid m (in Cell i) to account for saturation level,

$r_n(s_n)$ = diffusive reduction formula for fluid n (in Cell j) to account for saturation level,

s_m = Saturation of fluid m (in Cell i),

s_n = Saturation of fluid n (in Cell j),

n_{Pi} = porosity for the porous medium defined for the diffusive mass flux link in Cell i, and

n_{Pj} = porosity for the porous medium defined for the diffusive mass flux link in Cell j.

The partition coefficient between fluid medium n (in Cell j) and fluid medium m (in Cell i) for species s, K_{nms}, is defined in GTG-2017b as:

$$K_{nms} = \frac{K_{nrs}}{K_{mrs}} \qquad \text{Eq. 4.4-129}$$

where:

K_{mrs} = partition coefficient between fluid medium m and reference fluid r for species s [L³ fluid r/L³ fluid m], and

K_{nrs} = partition coefficient between fluid medium n and reference fluid r for species s [L³ fluid r/L³ fluid n].

Combining Eq. 4.4-127 and Eq. 4.4-129, the governing equation for the diffusive mass flux link between Cell i and Cell j, as used in the SDF APR Model, can be rewritten in the form:

$$f_{s,i\to j} = D_s\left(c_{ims} - \frac{c_{jns}K_{mrs}}{K_{nrs}}\right) \qquad \text{Eq. 4.4-130}$$

As discussed in GTG-2017b, since the flux depends on the concentration on both sides of the link, the GoldSim transport module solves the equations for sets of Cell pathways connected by diffusive mass flux links simultaneously (i.e., treating them as a single coupled system of equations).

$$c_{ims} = \left\{\frac{K_{mrs}}{\sum_{g=1}^{NM_i} K_{grs}VM_{ig}}\right\} m_{is} \qquad \text{Eq. 4.4-131}$$

where:

c_{ims} = concentration of species s in medium m in Cell i [(M/L³) for Fluids or (M/M) for Solids],

m_{is} = mass of species s in Cell i [M],

K_{mrs} = partition coefficient between medium m and reference fluid r for species s [(L³ /L³) for Fluids or (L³/M) for Solids],

K_{grs} = partition coefficient between medium g and reference fluid r for species s [(L³/L³) for Fluids or (L³/M) for Solids],

VM_{ig} = quantity (volume or mass) of medium g in Cell i [L³ for Fluids or M for Solids], and

NM_i = the number of media in Cell i.

As noted in GTG-2017b, for all species, the partition coefficient between the Reference Fluid and itself is 1 (i.e., in the above equation, if m is the Reference Fluid, K_{mrs} = 1).

Within each material zone, the cell-to-cell network numbering system starts at the bottom of the *SaltStone* container, increasing until reaching the top mixing cell in the *ErosionBarrier* container (see Figure 4.4-154) where the air-phase radionuclides are released to a sink cell (called *ZeroBC*) in the container *Sink*. *ZeroBC* is set to have a "Defined Concentration" cell inventory of 0.0 mg/L for each radionuclide creating a zero-concentration boundary condition.

4.4.7.3 Model Input and Assumptions

This section describes the organization and details of the input parameters used to define the system processes controlling the release of volatile radionuclides to the atmosphere. In the *GeneralInput* Container (Figure 4.4-155), the SDF APR Model is comprised of six containers (noted in italics), organizing the data input into groups pertaining to:

1. Model geometries (*Geometry*),
2. SDU-specific inventories (*Inventory*),
3. Physical properties (*PhysicalProperties*),
4. Chemical properties (*ChemicalProperties*),
5. Transport properties (*TransportProperties*), and
6. GoldSim-specific material parameter assembly (*GoldSimMaterialProperties*).

Figure 4.4-155: GoldSim Cell Pathway Elements Linked in Series to Simulate Air-Phase Transport through the Erosion Barrier for 150-Foot Diameter SDUs

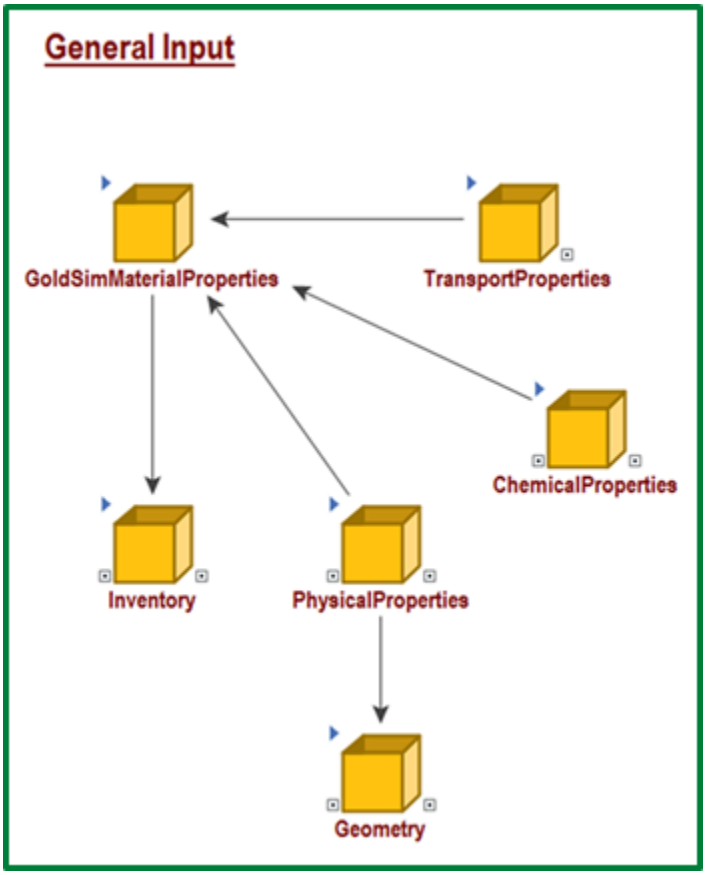

4.4.7.3.1 Model Geometry

The model grid geometry comprised of mixing cells linked in series representing the four SDU types (SDU 1, SDU 4, the 150-foot diameter SDUs, and the 375-foot diameter SDUs) is depicted in Figure 4.4-157 through Figure 4.4-160, and the overlying section of the closure cap is depicted in Figure 4.4-156. The geometric configuration shown in Figure 4.4-156 represents a linked string of 28 three-inch mixing cells comprising the closure cap. The vertical discretization of the string of linked mixing cells representing the closure-cap immediately above the SDU is consistent for each of the SDU types. The mixing cell discretization representing the cementitious materials below the closure cap (saltstone, clean grout, and roof) for SDU 1, SDU 4, the 150-foot diameter SDUs, and the 375-foot diameter SDUs are depicted in Figure 4.4-157, Figure 4.4-158, Figure 4.4-159, and Figure 4.4-160, respectively. The material-zone thicknesses for each of the four different SDU types is presented in Table 4.4-88.

Figure 4.4-156: Schematic of the SDF APR Model Material Zones and Grid for Air and Radon Pathway Analyses for the Closure Cap

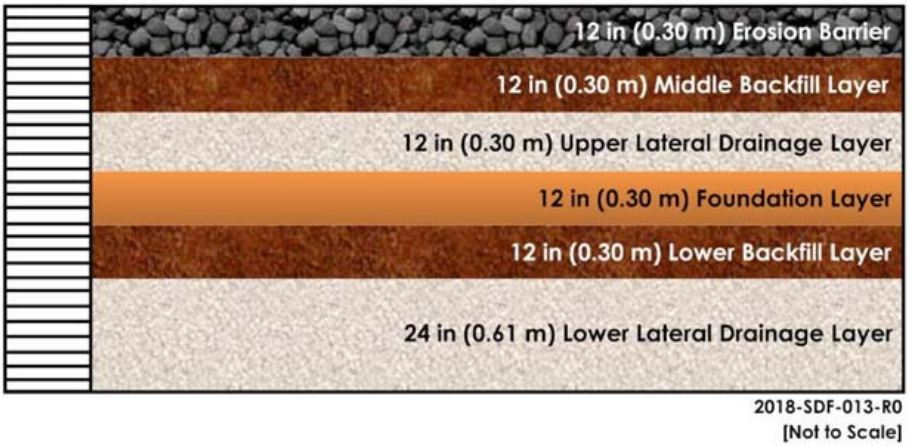

Note: The model grid does not include the following layers: topsoil, upper backfill, geotextile fabric, HDPE, and GCL.

The horizontal cross-sectional areas of the four SDU types are approximately 60,000 ft² (5,570 m²) for SDU 1, 120,000 ft² (11,100 m²) for SDU 4, 17,700 ft² (1,640 m²) for the 150-foot diameter SDUs, and 110,000 ft² (10,200 m²) for the 375-foot diameter SDUs.

The total modeled thickness for closure-cap materials, as depicted in Figure 4.4-156 (excluding the top soil, upper backfill, HDPE, geotextile fabrics, and GCL), is 84 inches (2.1 meters). Table 4.4-87 lists the layer by layer thicknesses of the individual components in the closure cap.

There is a difference between the Closure Cap Model (Section 4.4.1) and the one described here: in the Closure Cap Model, the foundation layer is ignored.

Table 4.4-87: Layer Thicknesses of the Closure Cap

Layer	Layer Thicknesses in Inches (Meters)
Lower Lateral Drainage	24 (0.61)
Lower Backfill	12 (0.30)
Foundation	12 (0.30)
Upper Lateral Drainage	12 (0.30)
Middle Backfill	12 (0.30)
Erosion Barrier	12 (0.30)

[From SRR-CWDA-2018-00025]

Materials comprising the SDU specific models are indicated along with the associated thickness in inches and meters are listed in Table 4.4-88. Total modeled thickness for SDU 1, as depicted in Figure 4.4-157, is 300 inches. Total modeled thickness for SDU 4, as depicted in Figure 4.4-158, is 317 inches. Total modeled thickness for the 150-foot diameter SDUs, as depicted in Figure 4.4-159, is 272 inches. Total modeled thickness for the 375-foot diameter SDUs, as depicted in Figure 4.4-160, is 528 inches.

Table 4.4-88: Layer Thicknesses of SDU 1, SDU 4, the 150-Foot Diameter SDUs, and the 375-Foot Diameter SDUs

Layer	Layer Thicknesses in Inches			
	SDU 1	SDU 4	150-foot Diameter SDUs	375-foot Diameter SDUs
Saltstone	288*	297*	240*	489*
Clean Grout	6*	16*	24*	27*
SDU Roof	6	4	8	12

*The Clean Grout Layer can also be filled with saltstone.
[From SRR-CWDA-2018-00025]

Figure 4.4-157: Schematic of the SDF APR Model Material Zones and Grid for Air and Radon Pathway Analyses for SDU 1

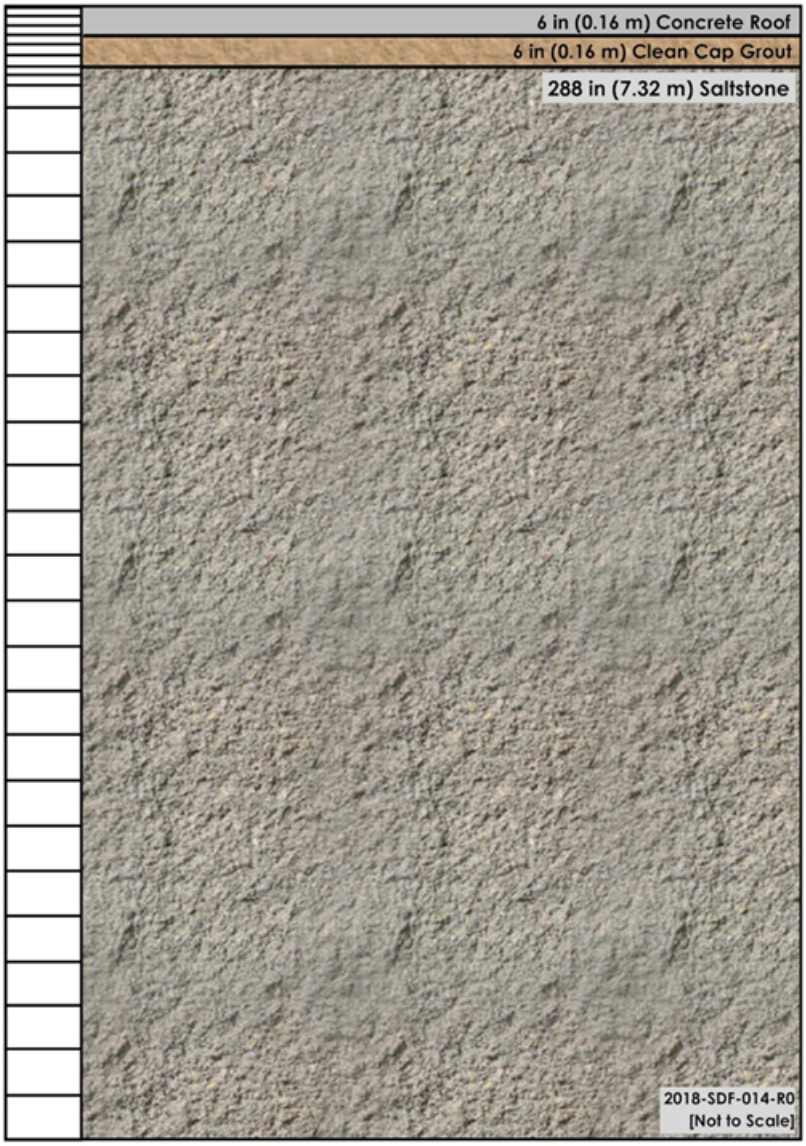

[Modified from SRNL-STI-2008-00447, Figure 3]

Figure 4.4-158: Schematic of the SDF APR Model Material Zones and Grid for Air and Radon Pathway Analyses for SDU 4

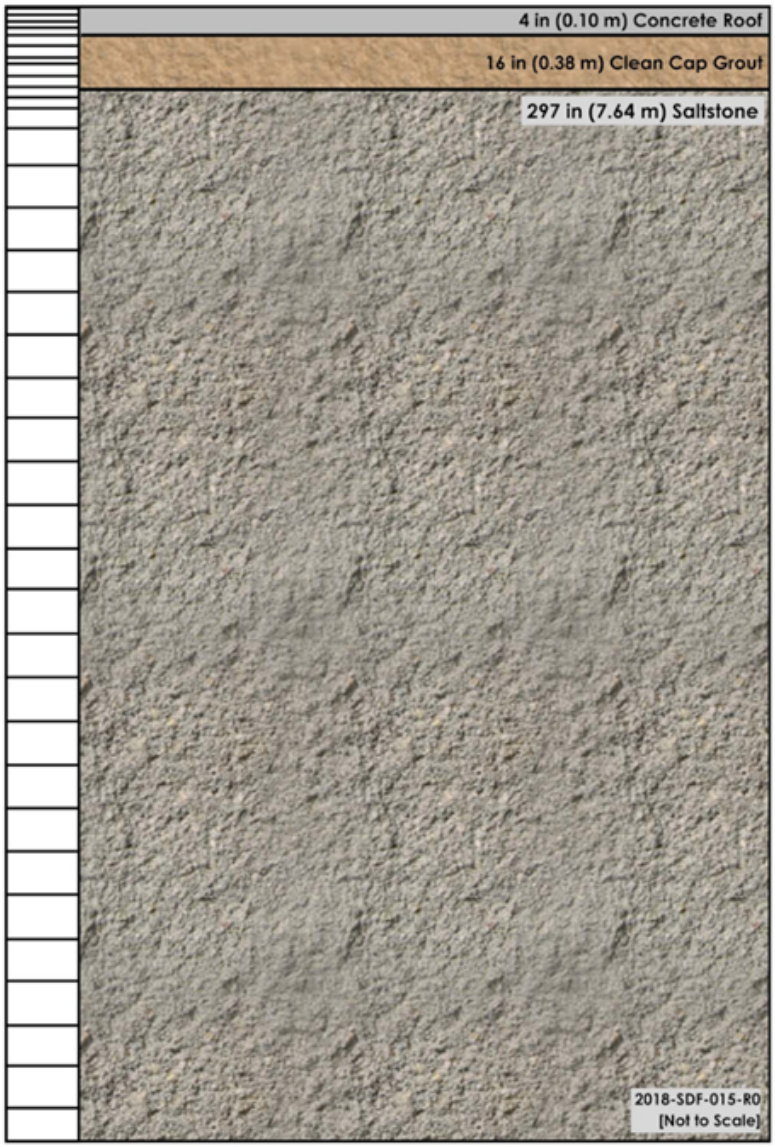

[Modified from SRNL-STI-2008-00447, Figure 5]

Figure 4.4-159: Schematic of the SDF APR Model Material Zones and Grid for Air and Radon Pathway Analyses for 150-Foot Diameter SDUs

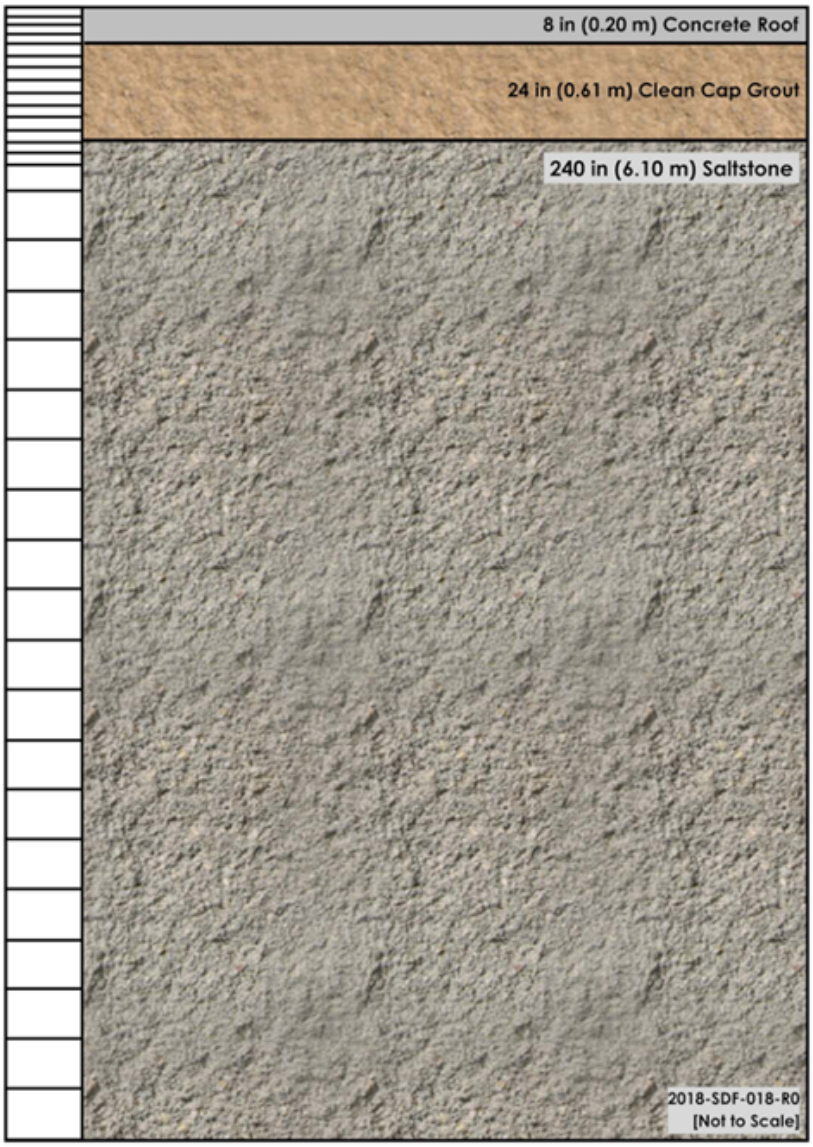

[Modified from SRNL-STI-2008-00447, Figure 4]

Figure 4.4-160: Schematic of the SDF APR Model Material Zones and Grid for Air and Radon Pathway Analyses for 375-Foot Diameter SDUs

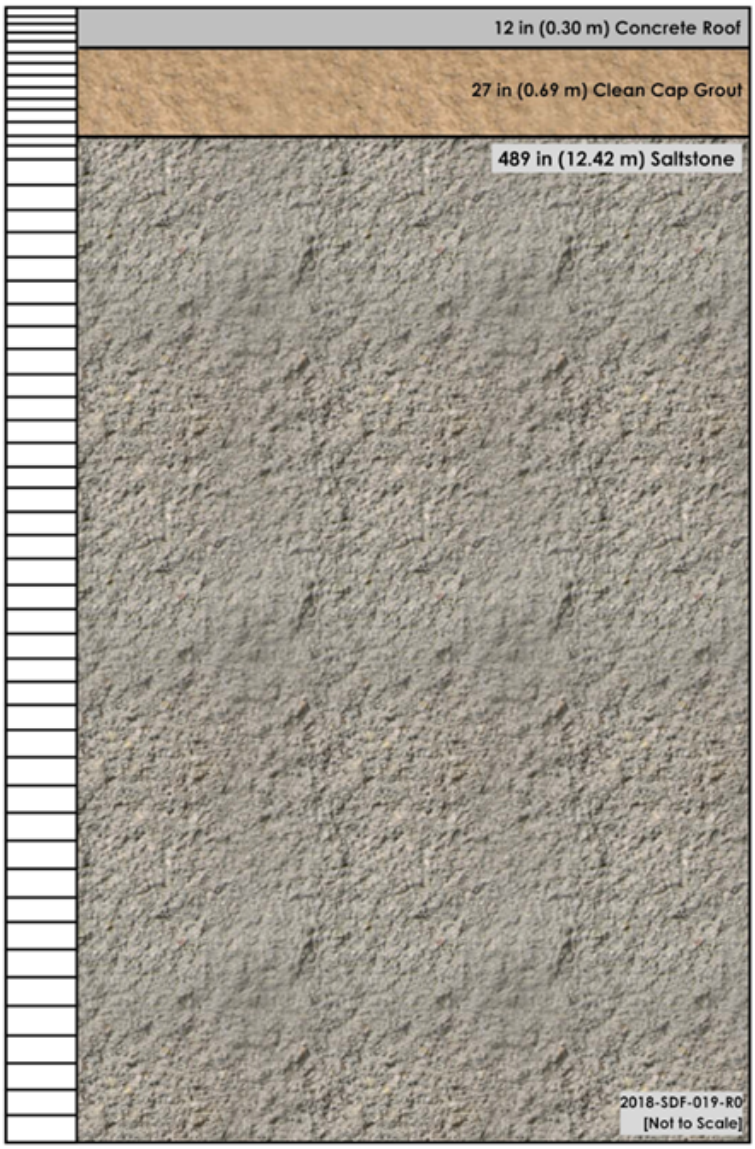

4.4.7.3.2 Physical Properties

The physical material properties important to the air-phase transport of volatile radionuclide elements or radionuclide-based compounds include: 1) the particle density, 2) the total porosity, 3) material-zone specific spatially-averaged saturations, and 4) material-zone specific effective air diffusion coefficient for each radionuclide source element or compound. The effective air diffusion coefficients used for each radionuclide and material-layer are generated by the model, and therefore tortuosity in the GoldSim model was assigned a unit value for each material zone.

Table 4.4-89 provides the values of particle density (ρ) and total porosity (φ_T) for SDU 1 and SDU 4 for the layers appearing in the baseline scenario (i.e., saltstone layer to the erosion barrier) for the simulation period.

Table 4.4-89: Compliance Case Particle Density and Total Porosity (by Layer) for SDU 1 and SDU 4

Layer	SDU 1		SDU 4	
	Particle Density (g/cm³)	Total Porosity (fraction)	Particle Density (g/cm³)	Total Porosity (fraction)
Erosion barrier	2.65	0.150	2.65	0.150
Middle backfill layer	2.63	0.350	2.63	0.350
Upper lateral drainage layer	2.65	0.417	2.65	0.417
Foundation layer	2.63	0.350	2.63	0.350
Lower backfill layer	2.63	0.350	2.63	0.350
Lower drainage layer	2.65	0.417	2.65	0.417
Concrete Roof	2.55	0.106	2.55	0.106
Saltstone, incl. Clean Grout	2.72	0.656	2.72	0.656

SRNL-STI-2008-00447, Table 4, and SRR-CWDA-2018-00004, Table 1

Table 4.4-90 provides the values of particle density (ρ) and total porosity (φ_T) for the 150-foot diameter and the 375-foot diameter SDUs for the layers appearing in the baseline scenario (i.e., saltstone layer to the erosion barrier) for the simulation period.

Note that only the cementitious material values may vary from one SDU-type to another. The dry bulk densities, as required by GoldSim, are generated as follows:

$$\rho_b = (1 - \varphi_T)\rho \qquad \text{Eq. 4.4-132}$$

where:

ρ_b = the bulk density [M/L³],

ρ = the particle density [M/L³], and

φ_T = total porosity [-].

Table 4.4-90: Compliance Case Particle Density and Total Porosity by Layer for 150-Foot Diameter SDUs and 375-Foot Diameter SDUs

Layer	150-Foot Diameter SDUs		375-Foot Diameter SDUs	
	Particle Density (g/cm³)	Total Porosity (fraction)	Particle Density (g/cm³)	Total Porosity (fraction)
Erosion barrier	2.65	0.150	2.65	0.150
Middle backfill layer	2.63	0.350	2.63	0.350
Upper lateral drainage layer	2.65	0.417	2.65	0.417
Foundation layer	2.63	0.350	2.63	0.350
Lower backfill layer	2.63	0.350	2.63	0.350
Lower drainage layer	2.65	0.417	2.65	0.417
Concrete Roof	2.45	0.110	2.45	0.110
Saltstone, incl. Clean Grout	2.72	0.656	2.72	0.656

SRNL-STI-2008-00447, Table 4, and SRR-CWDA-2018-00004, Table 1

The SDU-specific water saturations based on the Compliance Case flow runs are presented in Table 4.4-91 through Table 4.4-94 for SDU 1, SDU 4, the 150-foot diameter SDUs, and the 375-foot diameter SDUs, respectively.

Table 4.4-91: Compliance Case Water Saturation by Layer for SDU 1

Time (yr)	Saltstone	Concrete Roof	Lower Sand Drainage Layer	Foundation and Erosion Barrier	Backfill Layers
0	0.9981	0.9999	0.4575	0.15	0.40
23	0.9981	0.9499	0.4576	0.15	0.40
100	0.9981	0.8856	0.4576	0.15	0.40
150	0.9981	0.8462	0.4576	0.15	0.40
200	0.9981	0.8138	0.4576	0.15	0.40
250	0.9981	0.7867	0.4576	0.15	0.40
300	0.9981	0.7636	0.4576	0.15	0.40
350	0.9981	0.7438	0.4577	0.15	0.40
400	0.9981	0.7267	0.4577	0.15	0.40
450	0.9981	0.7116	0.4577	0.15	0.40
500	0.9992	0.7057	0.5114	0.15	0.40
600	0.9992	0.6855	0.512	0.15	0.40
700	0.9992	0.6692	0.5122	0.15	0.40
800	0.9992	0.6592	0.511	0.15	0.40
853	0.9992	0.6567	0.5081	0.15	0.40
1000	0.9993	0.6576	0.5046	0.15	0.40
1200	0.9993	0.658	0.5031	0.15	0.40
1400	0.9993	0.6581	0.5028	0.15	0.40
1600	0.9993	0.6581	0.5027	0.15	0.40
1800	0.9993	0.6581	0.5027	0.15	0.40
2000	0.9994	0.6666	0.5165	0.15	0.40
2300	0.9994	0.6666	0.5165	0.15	0.40
2600	0.9994	0.6666	0.5165	0.15	0.40
2900	0.9994	0.6666	0.5165	0.15	0.40
3200	0.9994	0.6666	0.5166	0.15	0.40
3600	0.9994	0.6666	0.5166	0.15	0.40
4000	0.9994	0.6667	0.5166	0.15	0.40
4579	0.9994	0.6667	0.5166	0.15	0.40
5000	0.9994	0.6667	0.5166	0.15	0.40
5500	0.9994	0.6667	0.5166	0.15	0.40
6000	0.9993	0.6667	0.5166	0.15	0.40
6500	0.9993	0.6667	0.5166	0.15	0.40
7000	0.9993	0.6667	0.5166	0.15	0.40
7500	0.9993	0.6667	0.5167	0.15	0.40
8000	0.9993	0.6667	0.5167	0.15	0.40
8500	0.9993	0.6667	0.5167	0.15	0.40
9000	0.9993	0.6667	0.5167	0.15	0.40
9500	0.9993	0.6667	0.5167	0.15	0.40
10000	0.9993	0.6667	0.5166	0.15	0.40
11000	0.9993	0.6667	0.5167	0.15	0.40
12000	0.9992	0.6667	0.5167	0.15	0.40
15000	0.9991	0.6667	0.5167	0.15	0.40
20000	0.9991	0.6667	0.5167	0.15	0.40
50000	0.9985	0.6668	0.5167	0.15	0.40
100000	0.9967	0.6669	0.517	0.15	0.40

Table 4.4-92: Compliance Case Water Saturation by Layer for SDU 4

Time (yr)	Saltstone	Concrete Roof	Lower Sand Drainage Layer	Soil–Foundation and Erosion Barrier	Backfill Layers
0	0.9986	0.9999	0.4619	0.15	0.40
50	0.9986	0.9999	0.4619	0.15	0.40
100	0.9986	0.9999	0.4619	0.15	0.40
144	0.9986	0.9999	0.4619	0.15	0.40
200	0.9986	0.9462	0.4619	0.15	0.40
250	0.9986	0.87	0.4619	0.15	0.40
300	0.9986	0.8181	0.4619	0.15	0.40
350	0.9986	0.7785	0.462	0.15	0.40
400	0.9986	0.7472	0.462	0.15	0.40
450	0.9986	0.722	0.462	0.15	0.40
500	0.9986	0.7012	0.462	0.15	0.40
600	0.9993	0.6886	0.5048	0.15	0.40
698	0.9993	0.6643	0.5056	0.15	0.40
800	0.9993	0.6546	0.5055	0.15	0.40
900	0.9993	0.655	0.5024	0.15	0.40
1000	0.9993	0.6553	0.5001	0.15	0.40
1200	0.9993	0.6556	0.4981	0.15	0.40
1400	0.9993	0.6558	0.4974	0.15	0.40
1600	0.9993	0.656	0.4974	0.15	0.40
1800	0.9993	0.6561	0.4975	0.15	0.40
2000	0.9993	0.6562	0.4978	0.15	0.40
2300	0.9994	0.6655	0.514	0.15	0.40
2600	0.9994	0.6657	0.5142	0.15	0.40
2900	0.9994	0.6658	0.5145	0.15	0.40
3200	0.9994	0.666	0.5147	0.15	0.40
3600	0.9994	0.6661	0.515	0.15	0.40
4000	0.9994	0.6663	0.5153	0.15	0.40
4579	0.9994	0.6666	0.5157	0.15	0.40
5000	0.9994	0.6668	0.5161	0.15	0.40
5500	0.9994	0.6671	0.5164	0.15	0.40
6000	0.9994	0.6673	0.5168	0.15	0.40
6500	0.9994	0.6676	0.5172	0.15	0.40
7000	0.9994	0.6679	0.5176	0.15	0.40
7486	0.9994	0.6681	0.5179	0.15	0.40
8000	0.9994	0.6683	0.5183	0.15	0.40
8500	0.9994	0.6686	0.5186	0.15	0.40
9000	0.9994	0.6688	0.519	0.15	0.40
9500	0.9994	0.669	0.5193	0.15	0.40
10499	0.9994	0.6693	0.5198	0.15	0.40
11000	0.9994	0.6695	0.5201	0.15	0.40
12000	0.9994	0.6695	0.5201	0.15	0.40
15000	0.9994	0.6695	0.5201	0.15	0.40
20000	0.9993	0.6695	0.5201	0.15	0.40
50000	0.9987	0.6696	0.5203	0.15	0.40
100000	0.9977	0.6696	0.5203	0.15	0.40

Table 4.4-93: Compliance Case Water Saturation by Layer for 150-Foot Diameter SDUs

Time (yr)	Saltstone	Concrete Roof	Lower Sand Drainage Layer	Soil–Foundation and Erosion Barrier	Backfill Layers
0	0.9986	0.9717	0.4628	0.15	0.40
54	0.9986	0.9266	0.4629	0.15	0.40
100	0.9986	0.8904	0.4629	0.15	0.40
150	0.9986	0.8583	0.4629	0.15	0.40
200	0.9986	0.8309	0.463	0.15	0.40
250	0.9986	0.8071	0.463	0.15	0.40
300	0.9986	0.7863	0.463	0.15	0.40
350	0.9986	0.768	0.4631	0.15	0.40
400	0.9986	0.7517	0.4631	0.15	0.40
450	0.9986	0.7371	0.4632	0.15	0.40
500	0.9994	0.7335	0.5156	0.15	0.40
600	0.9994	0.713	0.5156	0.15	0.40
700	0.9994	0.696	0.5153	0.15	0.40
800	0.9994	0.6821	0.5134	0.15	0.40
900	0.9994	0.6682	0.5113	0.15	0.40
1034	0.9994	0.6612	0.5092	0.15	0.40
1200	0.9994	0.6613	0.508	0.15	0.40
1400	0.9994	0.6612	0.5076	0.15	0.40
1552	0.9994	0.6612	0.5075	0.15	0.40
1800	0.9994	0.6612	0.5075	0.15	0.40
2000	0.9995	0.6686	0.5195	0.15	0.40
2300	0.9995	0.6686	0.5195	0.15	0.40
2600	0.9995	0.6686	0.5195	0.15	0.40
2900	0.9995	0.6685	0.5193	0.15	0.40
3200	0.9994	0.6685	0.5192	0.15	0.40
3600	0.9994	0.6685	0.5192	0.15	0.40
4000	0.9994	0.6685	0.5192	0.15	0.40
4500	0.9994	0.6685	0.5192	0.15	0.40
5000	0.9994	0.6685	0.5192	0.15	0.40
5500	0.9994	0.6685	0.5192	0.15	0.40
6000	0.9994	0.6685	0.5193	0.15	0.40
6500	0.9994	0.6685	0.5192	0.15	0.40
7000	0.9994	0.6685	0.5192	0.15	0.40
7500	0.9994	0.6685	0.5192	0.15	0.40
8000	0.9994	0.6685	0.5192	0.15	0.40
8500	0.9993	0.6685	0.5192	0.15	0.40
9000	0.9993	0.6685	0.5192	0.15	0.40
9500	0.9993	0.6685	0.5192	0.15	0.40
10000	0.9993	0.6685	0.5193	0.15	0.40
11000	0.9993	0.6685	0.5193	0.15	0.40
12000	0.9992	0.6685	0.5193	0.15	0.40
15000	0.9992	0.6685	0.5193	0.15	0.40
20000	0.9991	0.6685	0.5193	0.15	0.40
50000	0.9985	0.6685	0.5193	0.15	0.40
100000	0.9965	0.6687	0.5195	0.15	0.40

Table 4.4-94: Compliance Case Water Saturation by Layer for 375-Foot Diameter SDUs

Time (yr)	Saltstone	Concrete Roof	Lower Sand Drainage Layer	Soil–Foundation and Erosion Barrier	Backfill Layers
0	0.9983	0.9819	0.4493	0.15	0.40
50	0.9983	0.9819	0.4493	0.15	0.40
92	0.9983	0.9516	0.4493	0.15	0.40
150	0.9983	0.9225	0.4493	0.15	0.40
200	0.9983	0.8947	0.4493	0.15	0.40
250	0.9983	0.8719	0.4493	0.15	0.40
300	0.9983	0.8514	0.4494	0.15	0.40
350	0.9983	0.8328	0.4494	0.15	0.40
400	0.9983	0.816	0.4494	0.15	0.40
450	0.9983	0.8006	0.4494	0.15	0.40
500	0.9983	0.7866	0.4494	0.15	0.40
600	0.9994	0.7806	0.5045	0.15	0.40
700	0.9994	0.7598	0.5048	0.15	0.40
800	0.9994	0.7419	0.5045	0.15	0.40
900	0.9993	0.7262	0.5016	0.15	0.40
1075	0.9993	0.7076	0.4987	0.15	0.40
1229	0.9993	0.6892	0.4977	0.15	0.40
1496	0.9993	0.67	0.498	0.15	0.40
1552	0.9993	0.6578	0.4989	0.15	0.40
1767	0.9993	0.6559	0.499	0.15	0.40
2000	0.9993	0.6559	0.499	0.15	0.40
2300	0.9995	0.667	0.5172	0.15	0.40
2600	0.9995	0.667	0.5172	0.15	0.40
2800	0.9995	0.667	0.5172	0.15	0.40
3200	0.9995	0.667	0.5172	0.15	0.40
3600	0.9995	0.667	0.5172	0.15	0.40
4000	0.9995	0.667	0.5172	0.15	0.40
4500	0.9995	0.667	0.5172	0.15	0.40
5000	0.9995	0.667	0.5172	0.15	0.40
5500	0.9995	0.667	0.5172	0.15	0.40
6000	0.9994	0.667	0.5172	0.15	0.40
6500	0.9994	0.667	0.5172	0.15	0.40
7000	0.9994	0.667	0.5172	0.15	0.40
7500	0.9994	0.667	0.5172	0.15	0.40
8000	0.9994	0.667	0.5172	0.15	0.40
8500	0.9994	0.667	0.5172	0.15	0.40
9000	0.9994	0.6671	0.5172	0.15	0.40
9500	0.9994	0.667	0.5172	0.15	0.40
10000	0.9994	0.667	0.5172	0.15	0.40
11000	0.9994	0.6671	0.5172	0.15	0.40
12000	0.9994	0.6671	0.5172	0.15	0.40
15000	0.9994	0.6671	0.5172	0.15	0.40
20000	0.9993	0.6671	0.5172	0.15	0.40
50000	0.999	0.6671	0.5173	0.15	0.40
100000	0.9985	0.6672	0.5174	0.15	0.40

4.4.7.3.3 Chemical Properties

The chemical property data describing the partitioning of volatile radionuclides between the air and liquid phases and between the liquid and solid phases are in the *ChemicalProperties* container (Figure 4.4-155). The container *ChemicalProperties* is subdivided into two containers: one comprised of the data needed to describe

partitioning between the air phase and the liquid phase (water), and the second comprised of the data needed to describe partitioning between the liquid phase (water) and the solid phase.

Partitioning Between Air and Liquid Phases

This section describes the chemical parameters for partitioning between the water and air phases for SDU 1, SDU 4, the 150-foot diameter SDUs, and the 375-foot diameter SDUs in the SDF APR Model. The inputted data includes the inverse of the apparent Henry's Law constants for saltstone, concrete, and soils, the Universal Gas Constant (0.082 atm-L/mol-K), and the temperature (in K) at which the apparent Henry's Law constants are evaluated.

Note that the model input in the form of apparent Henry's Law constants must be transformed to the required input for GoldSim fluid media element air-water partitioning coefficients. The air-water partitioning coefficient is defined in terms of the inverse of the dimensionless Henry's Law solubility constant H^{cc}, which is defined as follows in Sander, 2015:

$$H^{cc} = \frac{c_a}{c_g} \qquad \text{Eq. 4.4-133}$$

where:

c_a = the dissolved concentration of a species in the aqueous phase [M/L^3], and

c_g = the dissolved concentration of a species in a gas phase [M/L^3].

The conversion from the inverse apparent Henry's Law constants to the air-water partitioning coefficient, as used in the GoldSim model, is based on the following equation:

$$K_{aw} = \frac{1}{H^a RT} \qquad \text{Eq. 4.4-134}$$

where:

K_{aw} = the air-water partitioning coefficient,

H^a = the inverse apparent Henry's Law constant [mol/atm-kg or mol/atm-liter assuming that $\varrho_{water} \approx 1$ kg/liter],

R = the Universal Gas Constant (0.082 atm-L/mol-K), and

T = the temperature [K].

All the inverse apparent Henry's Law constants for the radionuclides of concern, except Rn-222, were estimated using The Geochemist's Workbench® based on the potential gases considered for each radionuclide, their reactions with their aqueous components, and associated equilibrium constants for each reaction, as presented in Table 4.4-95. Where multiple gases were evaluated for one radionuclide, the gas with the highest fugacity was selected for use in the model. [SRNL-STI-2008-00447] For Rn-222, the derivation of the inverse apparent Henry's

Law constants was based on the recommended dimensionless value of 4.5 as described in SRNL-STI-2017-00331.

Table 4.4-95: Gases, Reactions with Aqueous Components, and Equilibrium Constants for Each Reaction Used in The Geochemist's Workbench® for Each Radionuclide

Contaminant	Gas Species	Reaction	Log K (25°C)
C-14	CO_2	$CO_{2(g)} + H_2O = HCO_3^- + H^+$	-7.82
Cl-36	Cl_2	$Cl_{2(g)} + H_2O = 2Cl^- + 2H^+ + ½O_2$	3.03
Cl-36	$HClO_4$	$HClO_{4(g)} = Cl^- + 2O_2 + H^+$	33.38
Cl-36	HCl	$HCl_{(g)} = Cl^- + H^+$	6.31
H-3	H_2O	$H_2O(g) = H_2O(l)$	1.50
I-129	I_2	$I_{2(g)} + H_2O = 2I^- + ½O_2 + 2H^+$	-21.53
I-129	HI	$HI_{(g)} = I^- + H^+$	9.31
Sb-125, 126	$SbCl_3$	$SbCl_{3(g)} + 3H_2O = Sb(OH)_3^o + 3Cl^- + 3H^+$	4.83
Sb-125, 126	$SbCl_5$	$SbCl_{5(g)} + 4H_2O = Sb(OH)_3^o + 5Cl^- + ½O_2 + 5H^+$	2.74
Sb-125, 126	SbH_3	$SbH_{3(g)} + 3/2O_2 = Sb(OH)_3^o$	143.11
Se-79	H_2Se	$H_2Se_{(g)} + 3/2O_2 = SeO_3^{-2} + 2H^+$	71.83
Se-79	$SeCl_4$	$SeCl_{4(g)} + 3H_2O = SeO_3^{-2} + 4Cl^- + 6H^+$	13.78
Sn-121m, 126	$SnCl_4$	$SnCl_{4(g)} = Sn^{+4} + 4Cl^-$	15.85
Sn-121m, 126	SnH_4	$SnH_{4(g)} + 4H^+ = 4H_2 + Sn^{+4}$	20.10

SRNL-STI-2008-00447, Table 8 (same as SRNL-TR-2010-00096, Table 1)

Table 4.4-96 provides additional parameters defining the pore-water chemistry used to estimate the inverse apparent Henry's Law constants for saltstone. The different pore water compositions used in the calculations of apparent Henry's Law constants for the roof and closure cap were based on the chemical environments presented in Table 4.4-97. Conditions representing soil (Condition A) and aged concrete (Oxidizing Region III) were used to represent the closure cap and roof, respectively.

Table 4.4-96: Parameters Used in Estimating Apparent Henry's Law Constants for Saltstone

Parameter	Value Used
pH	11.0
Eh	-0.45 V
Na+	0.01 moles/kg
Cl-	0.01 moles/kg
T	25°C

SRNL-STI-2008-00447, Table 9

Table 4.4-97: Pore Water Compositions Under Various Conditions

	pH	Eh (V)	Ca^{+2} (M)	Na^{+} (M)	Cl^{-} (M)	HCO_3^{-} (M)	SO_4^{-2} (M)
Reducing Region II	11.12	-0.48	3.3E-3	4.3E-4	4.3E-4	3.5E-8	1.0E-5
Oxidizing Region II	11.13	0.58	3.2E-3	4.3E-4	4.3E-4	3.5E-8	1.0E-5
Oxidizing Region III	8.23	0.73	4.6E-4	4.3E-4	4.3E-4	1.7E-6	1.0E-5
Condition A[1]	5.4	0.37	6.2E-5	4.4E-5	8.5E-5	9.8E-5	6.3E-6
Condition B[2]	9.3	0.27	2.0E-4	4.3E-5	1.5E-4	2.4E-4	6.2E-6
Condition C[3]	9.8	-0.38	2.1E-4	4.0E-5	2.7E-4	4.2E-5	4.2E-5
Condition D[4]	9.8	0.62	2.1E-4	4.1E-5	2.6E-4	4.2E-5	6.5E-6

From SRNL-TR-2010-00096, Table 2

[1] Condition A = ground water

[2] Condition B = ground water equilibrated with calcite

[3] Condition C = mixture 0.9 ground water + 0.1 Reducing Region II

[4] Condition D = mixture 0.9 ground water + 0.1 Oxidizing Region II

In the SDF APR Model, the species-dependent inverse apparent Henry's Law constants for the radionuclides of concern within the saltstone monolith are assigned, as listed in Table 4.4-98. Note that the inverse Henry's Law constant values listed in Table 4.4-98 are listed in units of mole/atm-kg for consistency with the data source. The SDF APR Model input is in terms of mole/atm-L, which can be approximated from the data in Table 4.4-98 by assuming that $\varrho_{water} \approx 1$kg/liter.

Table 4.4-98: Radionuclides of Interest, the Dominant Gas Under Saltstone Conditions, and the Inverse Apparent Henry's Law Constant for Each Radionuclide

Radionuclide	Gas	H^a (mole/atm-kg)
H-3	Water Vapor	2.1E+03
C-14	CO_2	1.4E+04
Cl-36	HCl	2.3E+17
I-129	HI	2.8E+20
Rn-222	Rn	9.244E-03
Sn-126	SnH_4	2.2E+60
Sb-125, 126	SbH_3	3.3E+34
Se-79	H_2Se	1.1E+06
Tc-99	Tc_2O_7	1.5E+67

From SRNL-STI-2008-00447, Table 10 (except for Rn-222). For Rn-222, the value was derived such that the inverse of the Henry's Law constant would be equal to 4.5 to reflect data from SRNL-STI-2017-00331.

The species-dependent apparent Henry's Law constants for the radionuclides of concern in layers overlying the saltstone are found in Table 4.4-99. For the roof, the chemical environment is assumed to be Oxidizing Region III, and the apparent Henry's Law constants values for the roof are listed in the Oxidizing Region III row of Table 4.4-99. For the closure cap, comprised of backfill and sand, the chemical environment is assumed to be Condition A indicating a ground water chemistry. The apparent Henry's Law constants for the closure cap are listed in Table 4.4-99. Note that the Henry's Law constant values listed in Table 4.4-99 are listed in units of mole/atm-kg for consistency with the data source. The SDF APR

Model input is in terms of mole/atm-L, which can be derived from the data in Table 4.4-99 by assuming that $\rho_{water} \approx 1$kg/liter.

Table 4.4-99: Estimated Apparent Inverse of Henry's Law Constants (moles / atm-kg) for Each Radionuclide in Different Pore Water Compositions

	C-14	Cl-36	H-3	I-129	Rn-222	Sb-125	Se-79	Sn-126	Tc-99
Reducing Region II	8E+04 (CO_2)	3E+17 (HCl)	2.1E+03 (H_2O)	3.6E+20 (HI)		1.8E+35 (SbH_3)	1.8E+06 (H_2Se)	1.3E+61 (Sn)	4.8E+67 (Tc_2O_7)
Oxidizing Region II	8.1E+04 (CO_2)	3.2E+17 (HCl)	2.1E+03 (H_2O)	1.1E+33 (HI)		8.7E+70 ($SbCl_3$)	2.5E+101 (H_2Se)	1.8E+71 ($SnCl_4$)	5.7E+51 (Tc_2O_7)
Oxidizing Region III	2.8E+00 (CO_2)	3.6E+14 (HCl)	2.1E+03 (H_2O)	1.3E+29 (HI)	9.2E-03 (Rn)	4.9E+38 ($SbCl_3$)	3.8E+87 ($SeCl_4$)	6.1E+61 ($SnCl_4$)	7.2E+45 (Tc_2O_7)
Condition A[1]	3.8E-02 (CO_2)	5.2E+11 (HCl)	2.1E+03 (H_2O)	6.3E+14 (HI)	9.2E-03 (Rn)	6.9E+32 ($SbCl_3$)	2.8E+25 (H_2Se)	9.6E+53 ($SnCl_4$)	1.5E+40 (Tc_2O_7)
Condition B[2]	3.6E+01 (CO_2)	4.1E+15 (HCl)	2.1E+03 (H_2O)	5.1E+18 (HI)		4.3E+44 ($SbCl_3$)	2.4E+44 (H_2Se)	5.1E+69 ($SnCl_4$)	9.6E+47 (Tc_2O_7)
Condition C[3]	1.6E+02 (CO_2)	1.4E+16 (HCl)	2.1E+03 (H_2O)	1.7E+19 (HI)		3.5E+34 ($SbCl_3$)	8.5E+04 (H_2Se)	4.7E+60 (Sn)	2.1E+68 (Tc_2O_7)
Condition D[4]	1.6E+02 (CO_2)	1.4E+16 (HCl)	2.1E+03 (H_2O)	7.0E+29 (HI)		9.9E+44 ($SbCl_3$)	1.6E+96 (H_2Se)	4.8E+98 ($SbCl_4$)	1.2E+49 (Tc_2O_7)

Note: Adapted from SRNL-TR-2010-00096, Table 3 (except for Rn-222, which was derived based on SRNL-STI-2017-00331). The dominant gas for each radionuclide is shown in parentheses.

[1] Condition A = ground water

[2] Condition B = ground water equilibrated with calcite

[3] Condition C = mixture 0.9 ground water + 0.1 Reducing Region II

[4] Condition D = mixture 0.9 ground water + 0.1 Oxidizing Region II

Partitioning Between Solid and Liquid Phases

This section describes the chemical parameters describing partitioning between the solid and water phases for SDU 1, SDU 4, the 150-foot diameter SDUs, and the 375-foot diameter SDUs in the SDF APR Model. The elements used to assign the chemical parameters describing partitioning between the solid and water phases for SDU 1, SDU 4, the 150-foot diameter SDUs, and the 375-foot diameter SDUs include linear solid-liquid phase partition coefficients (K_ds) for the cementitious materials (saltstone, clean grout, and the roof), clayey material (backfill), and sandy material (drainage layers).

The linear solid-liquid phase partition coefficient K_ds for cementitious materials are presented in Table 4.4-100. The K_d matrix shown in Table 4.4-100 contains species-specific values for the Reducing Region I, Reducing Region II, Reducing Region III, Oxidizing Region I, Oxidizing Region II, and Oxidizing Region III chemical environments. As a simplifying assumption, the minimum K_d in each row (for each species except for I-129) of Table 4.4-100 is used in the model.

The linear solid-liquid phase partition coefficients K_ds for clayey backfill type materials and for sandy-type materials used in the drainage layers are listed in Table 4.4-101.

Table 4.4-100: Solid-Liquid Phase Partition Coefficients (K_ds) for Cementitious Materials

	Reducing Region I (ml/g)	Reducing Region II (ml/g)	Reducing Region III (ml/g)	Oxidizing Region I (ml/g)	Oxidizing Region II (ml/g)	Oxidizing Region III (ml/g)
C-14	2000	5000	50	2000	5000	50
Cl-36	0	10	1	0	10	1
Cm-246	7000	7000	1000	6000	6000	600
H-3	0	0	0	0	0	0
***I-129**	0	2	0	8	10	4
***I-129**	0.07	0.71	0.71	0.71	0.71	0.71
Pu-238	10000	10000	2000	10000	10000	2000
Pu-242	10000	10000	2000	10000	10000	2000
***Ra-226**	6000	6000	600	200	100	200
***Ra-226**	6000	6000	600	6000	6000	600
Rn-222	0	0	0	0	0	0
Sb-125	200	200	100	200	200	100
Sb-126	200	200	100	200	200	100
Se-79	300	300	200	3	3	3
Sn-126	4000	4000	2000	4000	4000	2000
Tc-99	1000	1000	1000	0.8	0.8	0.5
Th-230	10000	10000	2000	10000	10000	2000
U-234	5000	5000	5000	1000	5000	5000
U-238	5000	5000	5000	1000	5000	5000

Note: *I-129 and Ra-226 each have two sets of K_d values for cementitious materials. The first values listed are specific to the SDU concrete only, while the second values listed (shaded) are specific to the saltstone waste form. Note that the recommended I-129 K_ds for saltstone are based on SRR-CWDA-2018-00045; however, this reference recommends a K_d change after only a single pore volume has infiltrated through the material. While the transition from Reducing Region I to Reducing Region II is expected to take more than a single pore volume, this chemical transition is assumed to trigger the I-129 K_d change. [SRNL-STI-2009-00473, SRR-CWDA-2017-00019, and SRR-CWDA-2018-00045]

Table 4.4-101: Solid-Liquid Phase Partition Coefficients (K_ds) for Soils

	Clayey/ Backfill (ml/g)	Sand (ml/g)
C-14	400	10
Cl-36	8	1
Cm-246	9000	1000
H-3	0	0
I-129	3	1
Pu-238	6000	650
Pu-242	6000	650
Ra-226	200	30
Rn-222	0	0
Sb-125	3000	3000
Sb-126	3000	3000
Se-79	1000	1000
Sn-126	5000	2000
Tc-99	1.8	0.6
Th-230	2000	900
U-234	400	300
U-238	400	300

[SRNL-STI-2009-00473 and SRR-CWDA-2017-00019]

4.4.7.3.4 Other Transport Properties

Other properties affecting air-phase transport in the model include the effective diffusion coefficients, the molecular weights of the molecules containing the radionuclides, the atomic masses of the radionuclides, and the half-lives of the radionuclides. The inputs for the effective diffusion coefficients and the molecular weights of the molecules containing the radionuclides are assembled in the *TransportProperties* container (Figure 4.4-155). The inputs for the radionuclide half-lives and atomic masses are assembled GoldSim data elements found in the *GoldSimMaterialProperties* container (Figure 4.4-155).

The effective air diffusion coefficient of each radionuclide or compound within each material zone was determined based on the derived effective air diffusion coefficient for Rn-222. The zone-specific air diffusion coefficients for Rn-222 in a porous medium are based on a relationship established between pore moisture saturation and the Rn-222 air-diffusion coefficient for pure air. Using this method, a radon effective air-diffusion coefficient was determined for each material type based upon the time-dependent moisture saturation for the material. [Rogers and Nielson, 1991] The model allows the user to choose between two Rn-222 specific relationships correlating the air-phase effective diffusion coefficient and moisture content found in Rogers and Nielson (1991). The first relationship can be written in the form:

$$D_{eff(Rn-222)} = D_{air(Rn-222)} A_0 \varphi_{air}^{b_0} \qquad \text{Eq. 4.4-135}$$

where:

$D_{eff(Rn\text{-}222)}$ = the effective diffusion coefficient for Rn-222 in air,

$D_{air(Rn\text{-}222)}$ = 1.1E-05 m^2/s = the diffusion coefficient for Rn-222 in air,

φ = total porosity,

φ_{air} = (1-S) φ = air-filled porosity,

S = saturation,

A_0 = 0.74 = an empirical constant, and

b_0 = 2.2 = an empirical power term.

The second relationship is written as follows:

$$D_{eff(Rn-222)} = D_{air(Rn-222)} \varphi e^{-(6S\varphi + 6S^{14\varphi})} \qquad \text{Eq. 4.4-136}$$

Subsequently, using Graham's Law, the effective air-diffusion coefficient of each radionuclide or compound evaluated is determined for each material type based on the radon effective air-diffusion coefficient using the following relationship:

$$D_{eff=} D_{eff(Rn-222)} \sqrt{\frac{MWT'}{MWT}} \qquad \text{Eq. 4.4-137}$$

where:

D_{eff} = the effective diffusion coefficient of the radionuclide of interest (m^2/yr) within the material zone of interest,

$D_{eff(Rn\text{-}222)}$ = the effective diffusion coefficient of the reference radionuclide, Rn-222 (m^2/yr) within the material zone of interest,

MWT' = the molecular weight of the reference radionuclide (Rn-222), and

MWT = the molecular weight of the element or compound of interest.

The molecular weights used in the SDF APR Model, are presented in Table 4.4-102. These molecular weights represent volatile gases expected to form in the closure cap, or are based on a molecule of lower molecular weight (for Tc-99). The half-lives and atomic masses of the radionuclides of interest in the air-phase transport model including the volatile radionuclides and their parent species are presented in Table 4.4-103.

Table 4.4-102: Molecular Weights for Expected Gases in Saltstone and Clean Cap Grout Material

	Saltstone and Clean Grout		Roof		Closure Cap	
Radionuclide	Molecular Form in Gaseous State	Molecular Weight	Molecular Form in Gaseous State	Molecular Weight	Molecular Form in Gaseous State	Molecular Weight
C-14	CO_2	46.00	CO_2	46.00	CO_2	46.00
Cl-36	Cl_2	71.94	HCl	36.98	HCl	36.98
H-3	H_2	6.032	H_2O (^3HOH)	20.02	H_2O	20.02
I-129	I_2	257.8	HI	129.9	HI	129.9
Rn-222	Rn	222.0	Rn	222.0	Rn	222.0
Sb-125	Sb	124.9	$SbCl_3$	231.3	$SbCl_3$	231.3
Sb-126	Sb	124.9[a]	$SbCl_3$	231.3	$SbCl_3$	231.3
Se-79	Se	78.92	H_2Se	80.93	$SeCl_4$	220.7
Sn-126	Sn	125.9	$SnCl_4$	267.7	$SnCl_4$	267.7
Tc-99	Tc	98.91	TcO_3	146.9	TcO_3	146.9

[SRR-CWDA-2018-00018]

Note: The molecular weight for Sb-126 is set to 125 for consistency with Sb-125 to avoid warning messages associated with GoldSim's requirement that all diffusion coefficients for isotopes be the same.

Table 4.4-103: Half-Lives and Atomic Mass of Radionuclides of Interest for Air and Radon Pathway Analyses

Radionuclide	Half-Life (yr)	Atomic Mass
C-14	5.70E+03	14.00
Cl-36	3.01E+05	35.97
H-3	1.23E+01	3.016
I-129	1.57E+07	128.9
Sb-125	2.76E+00	124.9
Sb-126	3.39E-02	125.9
Se-79	2.95E+05	78.92
Sn-126	2.30E+05	125.9
Tc-99	2.11E+05	98.91
Rn-222	1.05E-02	222.0
Cm-246	4.72E+03	246.1
Pu-238	8.78E+01	238.0
Pu-242	3.74E+05	242.1
Ra-226	1.60E+03	226.0
Th-230	2.46E+05	230.0
U-234	7.54E+04	234.0
U-238	4.47E+09	238.1

[SRR-CWDA-2018-00018]

4.4.7.3.5 SDU Inventory

The radionuclide inventories (in curies) used to set the initial conditions within the cell pathway elements defining saltstone monoliths for SDU 1, SDU 4, the 150-foot diameter SDUs, and the 375-foot diameter SDUs are presented below in Table 4.4-104, Table 4.4-105, and Table 4.4-106. These inventory values are from Table 3.3-6.

Table 4.4-104: Inventories (Ci) for SDUs 1 and 4

Radionuclide	SDU 1	SDU 4
C-14	1.31E+00	6.50E+00
Cl-36	7.02E-08	1.49E-02
Cm-246	0	0
H-3	4.61E+00	1.23E+01
I-129	2.01E-01	2.77E-01
Pu-238	6.18E-03	2.69E+02
Pu-242	1.57E-03	4.12E+00
Ra-226	9.53E-07	8.27E-05
Rn-222	0	0
Sb-125	1.91E-04	2.30E-01
Sb-126	1.71E-01	3.11E-01
Se-79	3.44E-01	9.75E+00
Sn-126	1.22E+00	2.22E+00
Tc-99	4.93E+01	6.34E+02
Th-230	6.48E-05	6.32E-03
U-234	9.93E-02	8.98E+00
U-238	1.07E-02	7.93E-02

Table 4.4-105: Inventories (Ci) for 150-Foot Diameter SDUs

Radionuclide	SDU 2A	SDU 2B	SDU 3A	SDU 3B	SDU 5A	SDU 5B
C-14	2.40E+00	2.44E+00	8.21E+00	9.14E+00	3.17E+00	3.77E+00
Cl-36	1.06E-04	1.30E-04	1.33E-02	1.55E-02	3.10E-03	7.71E-04
Cm-246	0	0	0	0	0	0
H-3	7.97E-01	6.76E-01	4.54E+01	5.36E+01	1.94E+00	1.19E+00
I-129	7.31E-02	6.83E-02	1.92E-01	1.88E-01	1.39E-01	8.68E-02
Pu-238	4.92E+00	4.67E+00	2.12E+03	2.51E+03	6.52E+01	2.25E+01
Pu-242	3.76E-01	5.21E-01	1.05E-01	5.23E-02	4.61E-01	4.21E-01
Ra-226	8.56E-06	4.93E-06	1.18E-06	1.12E-06	2.30E-06	2.18E-06
Rn-222	0	0	0	0	0	0
Sb-125	7.87E-04	2.49E-03	1.52E-01	1.81E-01	3.58E-04	2.57E-04
Sb-126	1.07E-01	9.56E-02	7.82E-01	8.58E-01	2.31E-01	1.33E-01
Se-79	1.34E-01	1.23E-01	1.35E+00	1.58E+00	2.72E-01	1.68E-01
Sn-126	7.62E-01	6.83E-01	5.58E+00	6.13E+00	1.65E+00	9.47E-01
Tc-99	1.14E+02	1.37E+02	3.63E+02	3.80E+02	1.75E+02	1.20E+02
Th-230	9.00E-04	5.55E-04	1.01E-04	7.86E-05	3.13E-04	2.87E-04
U-234	6.16E-01	8.54E-01	3.83E-01	3.36E-01	7.60E-01	6.88E-01
U-238	2.24E-02	2.65E-02	2.27E-01	2.66E-01	3.28E-02	2.85E-02

Table 4.4-106: Inventories (Ci) for 375-Foot Diameter SDUs

Radionuclide	SDU 6	SDU 7	SDU 8	SDU 9	SDU 10	SDU 11	SDU 12
C-14	1.07E+02	1.07E+02	1.07E+02	1.07E+02	1.07E+02	1.07E+02	1.07E+02
Cl-36	1.81E-01	1.81E-01	1.81E-01	1.81E-01	1.81E-01	1.81E-01	1.81E-01
Cm-246	0	0	0	0	0	0	0
H-3	6.26E+02	6.26E+02	6.26E+02	6.26E+02	6.26E+02	6.26E+02	6.26E+02
I-129	2.20E+00	2.20E+00	2.20E+00	2.20E+00	2.20E+00	2.20E+00	2.20E+00
Pu-238	2.93E+04	2.93E+04	2.93E+04	2.93E+04	2.93E+04	2.93E+04	2.93E+04
Pu-242	6.11E-01	6.11E-01	6.11E-01	6.11E-01	6.11E-01	6.11E-01	6.11E-01
Ra-226	1.30E-05	1.30E-05	1.30E-05	1.30E-05	1.30E-05	1.30E-05	1.30E-05
Rn-222	0	0	0	0	0	0	0
Sb-125	2.12E+00	2.12E+00	2.12E+00	2.12E+00	2.12E+00	2.12E+00	2.12E+00
Sb-126	1.00E+01	1.00E+01	1.00E+01	1.00E+01	1.00E+01	1.00E+01	1.00E+01
Se-79	1.84E+01	1.84E+01	1.84E+01	1.84E+01	1.84E+01	1.84E+01	1.84E+01
Sn-126	7.15E+01	7.15E+01	7.15E+01	7.15E+01	7.15E+01	7.15E+01	7.15E+01
Tc-99	4.43E+03	4.43E+03	4.43E+03	4.43E+03	4.43E+03	4.43E+03	4.43E+03
Th-230	9.18E-04	9.18E-04	9.18E-04	9.18E-04	9.18E-04	9.18E-04	9.18E-04
U-234	3.92E+00	3.92E+00	3.92E+00	3.92E+00	3.92E+00	3.92E+00	3.92E+00
U-238	3.10E+00	3.10E+00	3.10E+00	3.10E+00	3.10E+00	3.10E+00	3.10E+00

4.4.7.3.6 Summary of Key Air and Radon Pathway Assumptions

The following are the key air and radon pathways analysis assumptions associated with each disposal unit simulation (SRR-CWDA-2009-00017, SRNL-STI-2008-00447):

- The waste in all SDUs is represented as saltstone.
- The clean cap grout (i.e., uncontaminated grout used to fill void spaces) within each disposal unit has the same material properties as saltstone.
- Excluding the top soil, upper backfill, HDPE, and GCL layers of the closure cap provides model results that overestimate fluxes.
- Exclusion of all geotextile fabrics has no impact on the model.

- The final closure cap is assumed to remain physically stable below the top of the erosion barrier for the duration of the simulation (10,000 years).
- The dominant process influencing the migration of volatile radionuclides is diffusion upwards to the ground surface.

In addition, several approaches used in support of the 2009 SDF PA (SRR-CWDA-2009-00017, SRNL-STI-2008-00447) continue to be imposed to maintain defensibility. These include:

- The use of boundary conditions that force the volatile radionuclides to move upward from the waste disposal zone to the land surface. This precludes the gaseous radionuclides diffusing sideways and downward in the air-filled pores surrounding the saltstone monolith, effectively increasing the flux released into the atmosphere at the land-surface.
- Not taking credit for the removal of radionuclides via groundwater transport. It is likely that groundwater would remove some dissolved radionuclides; therefore, this results in an overestimate of instantaneous radionuclide flux at the land surface.
- Exclusion of the HDPE and the GCL. Including these materials would significantly reduce gaseous flux at the land surface (i.e., low air-filled porosity and/or low effective gaseous diffusion coefficient).
- Exclusion of the cover materials above the erosion barrier (i.e., top soil and upper backfill layers). Excluding these materials shortens the diffusion pathways and could increase the flux at the land surface.
- Use of the minimum closure cap thicknesses in the model.

An additional conservatism is reflected in the emanation factor used. During the radioactive decay of Ra-226 to Rn-222, enough energy is generated to send a Rn-222 atom an approximate distance of 40 nm by a process known as alpha recoil. As discussed in *The Radon Emanation Coefficient: An Important Tool for Geologic Radon Potential Estimations* (IRC-1993-16), for a radon atom to escape from a soil grain the radium atom needs to reside within the recoil distance of the grain surface (which is dependent on the grain density of the material) and the recoil must send the radon in the direction of the grain surface. The fraction of Rn-222, which winds up in the gas phase divided by the total Rn-222 produced at any time, is referred to as the emanation factor or coefficient. The radon pathway analysis for this PA uses an emanation factor of 1.0 (it basically disregards alpha recoil) to determine the fraction of decayed Rn-222 produced by ingrowth that is released into the gas phase of the saltstone. This value is high relative to the emanation factor of 0.25 used in the previous SDF PA. The values presented in *The Radon Emanation Coefficient: An Important Tool for Geologic Radon Potential Estimations* (IRC-1993-16) provide a range for rocks and soils between 0.05 and 0.7. Also note that based on the National Council on Radiation Protection and Measurements (NCRP), radon pathways through soils have an emanation factor of 0.2 per *NCRP Report No. 103, Control of Radon in House* (NCRP-103).

4.4.8 Dose and Exposure Pathways Model

Dose results are the primary metric for evaluating the performance of the SDF closure system against the performance objectives (as defined in Table 1.7-1). Converting contaminant concentrations into dose results requires assumptions about future human behaviors and an understanding of how those human behaviors influence the risks associated with exposure to contaminants.

4.4.8.1 Conceptual Model for Dose and Exposure Pathways

The conceptualization of the dose and exposure pathways is largely based on the Leading Diagonal Elements (LDEs) depicted in Figure 4.1-4 and identified in Table 4.1-6 as part of the Interaction Matrix (IM). Figure 4.1-4 depicts a water well (IM ID: 20), and a stream (IM ID: 21). Contaminants within these water sources may contaminate soils (IM ID: 22), crops and gardens (IM ID: 23), livestock (IM ID: 24), or be used as a direct water source for the human receptor (IM ID: 25).

4.4.8.1.1 Definition of the Human Receptors

The human receptor (or representative person) is assumed to be the average member of a group of individuals who farms, raises livestock, and participates in water recreation (i.e., boating, swimming, and fishing). It is assumed that all these activities are performed in the vicinity of the SDF. The selection of these activities is intended to ensure that the representative person is equivalent to the concept of the "average member of the critical group." This "average member of the critical group" construct is based on the draft *Guidance for Conducting Technical Analyses for 10 CFR Part 61*, NUREG-2175, from the NRC. [ML14357A072] Specifically, in the context of the recommendations herein, the critical group would be defined as the group of people who meet all of the following criteria:

- People who dwell in the vicinity of the disposal facility or contaminant source,
- People who drink most of their water from wells contaminated by the released contaminants,
- People who bathe or shower in the contaminated water,
- People who grow crops irrigated from the contaminated water,
- People who raise livestock using the contaminated water,
- People whose diets include a significant fraction of locally grown (contaminated) crops,
- People whose diets include a significant fraction of locally raised (contaminated) livestock,
- People whose diets include a significant fraction of fish caught from local (contaminated) streams,
- People who spend some time boating and fishing on local (contaminated) streams,

- People who spend some time swimming in local (contaminated) streams, and
- People who breath contaminated air from down-wind of the disposal facility or contaminant source.

Figure 4.4-161 shows most of these requisite criteria to illustrate the limiting nature of this concept.

Figure 4.4-161: Illustration of the Critical Group Concept

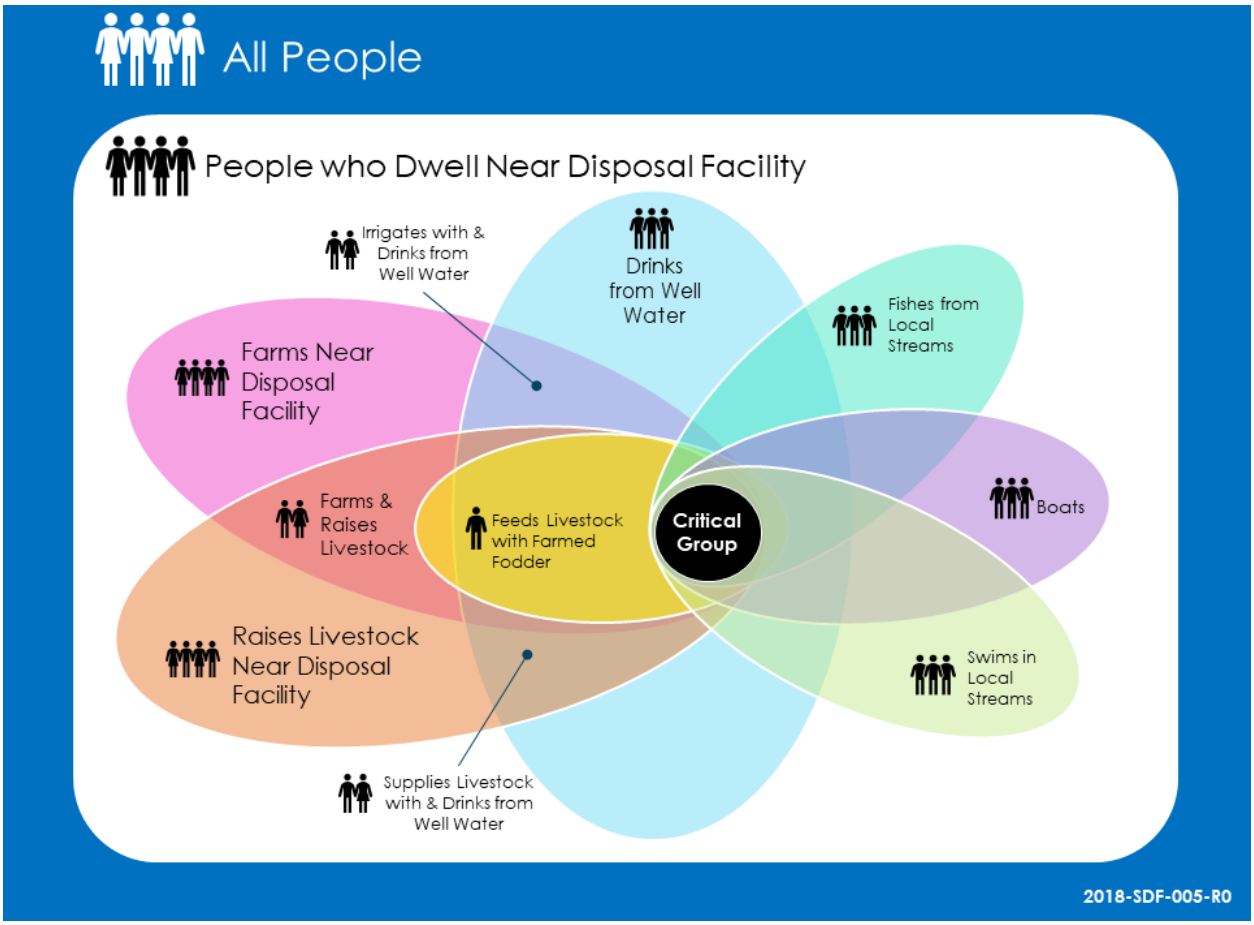

[SRR-CWDA-2013-00058]
Note: The number of people shown within the various segments of the Venn diagram are intended to illustrate that population size diminishes as the number of overlapping segments increases.

The average member of the critical group, then, is an average or typical person within this critical group. Key to this concept is that this is an "average person." As such, it is reasonable to assume that average parameter values would be appropriate for parameters driven by biological needs (as opposed to relying on bounding assumptions for such parameters). Exceptions to the assumed average parameter values shall be imposed for parameters that are influenced by the physical demands imposed by the critical group criteria (e.g., additional water ingestion for physically active adults); however, such exceptions should consider

the principal of reasonableness (i.e., realistic and not outside the range of what people encounter in day-to-day life).

Table 4.4-107 summarizes the definition of the human receptors. Additional discussion of the development of this definition is provided in the *Dose Calculation Methodology for Liquid Waste Performance Assessments at the Savannah River Site*, Rev. 2. [SRR-CWDA-2013-00058]

Table 4.4-107: Definition of Human Receptors

Characteristic	Member of the Public (MOP)	Inadvertent Human Intruder (IHI)
Description of Receptor	Gender-weighted adult farmer	
Occupation of Receptor	Agricultural (Crops and Livestock)	
Recreation of Receptor	Water Activities (Fishing, Boating, and Swimming)	
Region of Receptor	Rural, American South (South Carolina, Georgia)	
Location of Receptor	At the 100-meter boundary - OR – At the nearest downgradient stream	Within the 100-meter boundary (e.g., along a 1-meter boundary)
Behaviors of Receptor	Average (mean) living habits of an adult, with reasonable adjustments to be consistent with influences based on occupation, recreation, and/or region	

[SRR-CWDA-2013-00058]

4.4.8.1.2 Exposure Scenarios

For dose calculations, four exposure scenarios are considered: (1) the MOP at the 100-Meter Well, (2) the MOP at the Stream, (3) the Acute IHI, and (4) the Chronic IHI.

To help define these exposure scenarios, a facility boundary is assumed to surround the SDF. This facility boundary is depicted as straight lines that connect the outer edges of the SDUs. From this facility boundary, another line may be drawn that surrounds the facility boundary at a distance of 100 meters (i.e., the "100-meter boundary"). Figure 1.5-1 provides an illustration of these boundaries. In this figure, the red lines show the locations for each containment structure. The pink dashed-line shows the facility boundary, and the pink solid line shows the 100-meter boundary.

The **MOP at the 100-Meter Well** is an exposure scenario that assumes the MOP uses water from a well that has been drilled somewhere along the 100-meter boundary (i.e., 100 meters away from the contaminated source). The MOP uses the contaminated water in a number of ways (e.g., as a drinking source, for showering, for irrigating crops, etc.).

Note that, as described in Section 4.4.6, the well water concentrations for each sector assume the highest concentrations along the sector boundary for each contaminant, regardless of location. For example, if the highest concentration of Tc-99 occurs at one end of the sector boundary and the highest concentration of I-129 occurs at the opposite end of the sector boundary, these highest

concentrations would be used in combination to find the total dose to the MOP at the 100-meter well for that sector. Additionally, the sector with the highest total dose is used to represent the total dose for compliance. For example, if from 0 years to 1,000 years after closure the highest dose occurs along Sector G, but then after 1,000 years the highest dose occurs along Sector B, then the total dose used for compliance would be first from Sector G then from Sector B.

The **MOP at the Stream** is a similar exposure scenario; however, the contaminated water source is from a stream that is beyond the 100-meter boundary and down-gradient from the contaminated source.

Note that, as with the sector doses, the stream water concentrations for each stream assume the highest concentrations along the seepline for each contaminant, regardless of location. For example, if the highest concentration of Tc-99 occurs at one end of the McQueen Branch and the highest concentration of I-129 occurs at the other end of the McQueen Branch, these highest concentrations would be used in combination to find the total dose to the MOP at the seepline for that stream. Then the higher stream dose (from either McQueen Branch or Upper Three Runs) will be used to represent the total dose for compliance.

Further, the seepline concentrations do not account for any dilution. The concentrations used are based on the contaminant concentrations at the seepline and not the actual stream water concentrations.

The IHI is an assumed future person who lives at or very near the contaminated source and uses water from a well that has been drilled from somewhere *within* the 100-meter boundary. For this PA, this is assumed to be along the 1-meter boundary (dashed line in Figure 1.5-1); however, sensitivities are also performed to evaluate doses at select locations adjacent to specific SDUs, within the 1-meter boundary (see Section 6.4).

The **Acute IHI** exposure scenario assumes that the IHI receptor is a driller who drills a well that is 1-meter from the facility boundary (i.e., the "1-Meter Well"). The Acute IHI receptor comes into direct contact with contaminated drill cuttings for a relatively short amount of time.

Finally, the **Chronic IHI** exposure scenario is similar to the MOP scenarios but includes contributions from the contaminated drill cuttings as well as the higher concentrations of contaminants from the closer 1-meter well (i.e., within the 100-meter boundary).

Note that upon closure of the SDF, the stabilized contaminants will be protected by cementitious materials which are clearly distinguishable from the surrounding soil and make drilling an improbable scenario based on regional drilling practices. Regional drilling conditions are such that a well driller would be likely to stop operations and move their drilling location upon encountering barriers, such as the closure cap erosion barrier or concrete roof. As such, modeling scenarios which

incorporate contaminant concentrations from drill cuttings pulled directly from the waste form do not reflect expected future conditions but are provided as alternative scenarios used to inform decision-making.

4.4.8.1.3 Overview of Contaminant Exposure Process

Figure 4.4-162 illustrates the process through which contaminants may be collected into the biosphere (i.e., received by the MOP or IHI receptors). Once the contaminated media interacts with the environmental collectors (i.e., soil, air, well water, and surface water), the radioactive material then becomes accessible for accumulation and uptake within the biosphere where it becomes a dose risk.

Figure 4.4-162: Contamination Process Overview

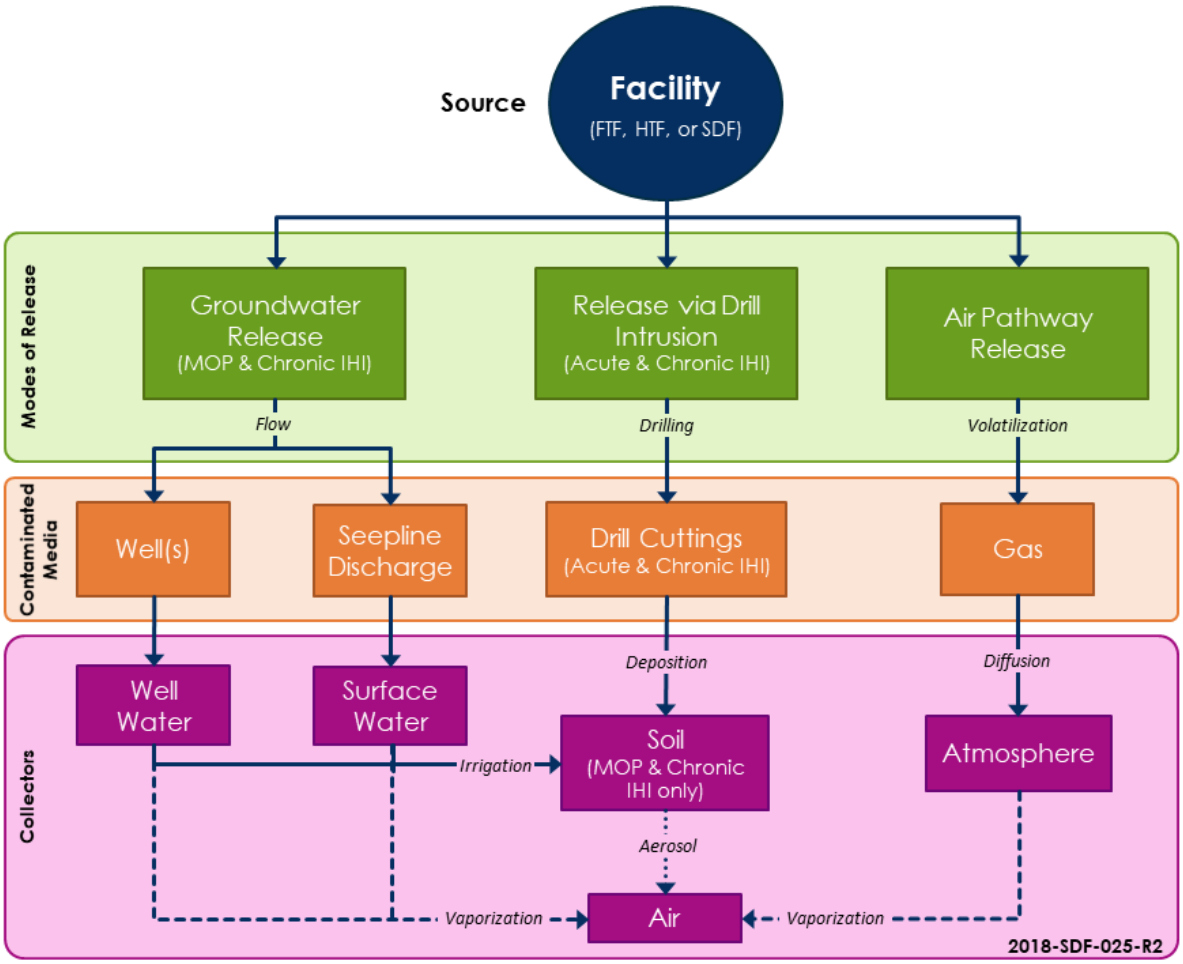

[SRR-CWDA-2013-00058]

The MOP and IHI receptors are assumed to receive doses from various dose pathways. At a high level, all the dose pathways fall into three categories: the ingestion dose pathway, the inhalation dose pathway, and the external exposure dose pathway. The total dose to the MOP or the IHI is the sum of the doses from each of these dose pathway categories. Figure 4.4-163 illustrates the various pathways through which a human receptor receives a dose.

Figure 4.4-163: Dose Pathway Overview

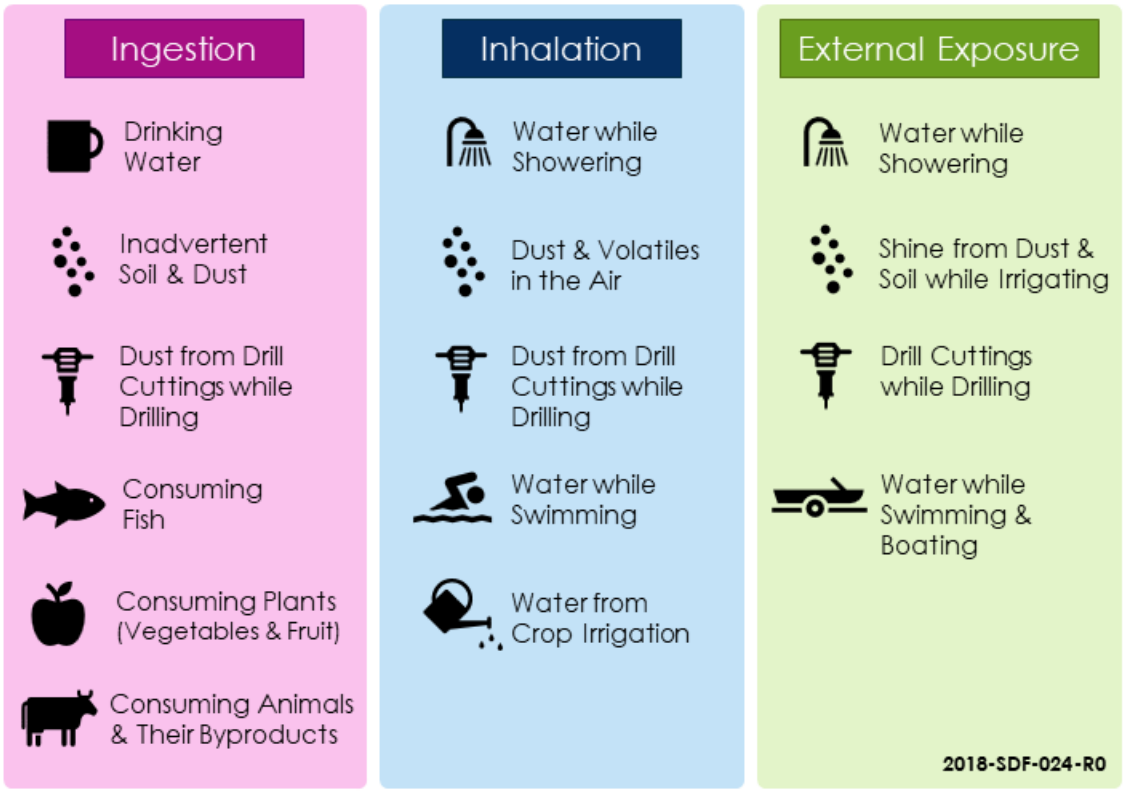

[SRR-CWDA-2013-00058]
Note: Pathways related to drill cuttings only apply to IHI scenarios.

4.4.8.2 Implementation of Dose Calculations

Mathematical implementation of the conceptual model for the dose and exposure pathways is performed as a series of dose calculations within GoldSim. A separate set of dose calculations was developed for each of the four exposure scenarios. Subsections 4.4.8.2.1 through 4.4.8.2.4 present each set of dose calculations. These calculations were all developed in the *Dose Calculation Methodology for Liquid Waste Performance Assessments at the Savannah River Site*, Rev. 2. [SRR-CWDA-2013-00058]

Within GoldSim, all of the dose calculations are implemented within one of two GoldSim containers found at the root of the SDF GoldSim Model file (Figure 4.4-164). The two containers are *Dose_Parameter_Calculations* and *Dose_Results*.

Figure 4.4-164: SDF GoldSim Model: Root Directory

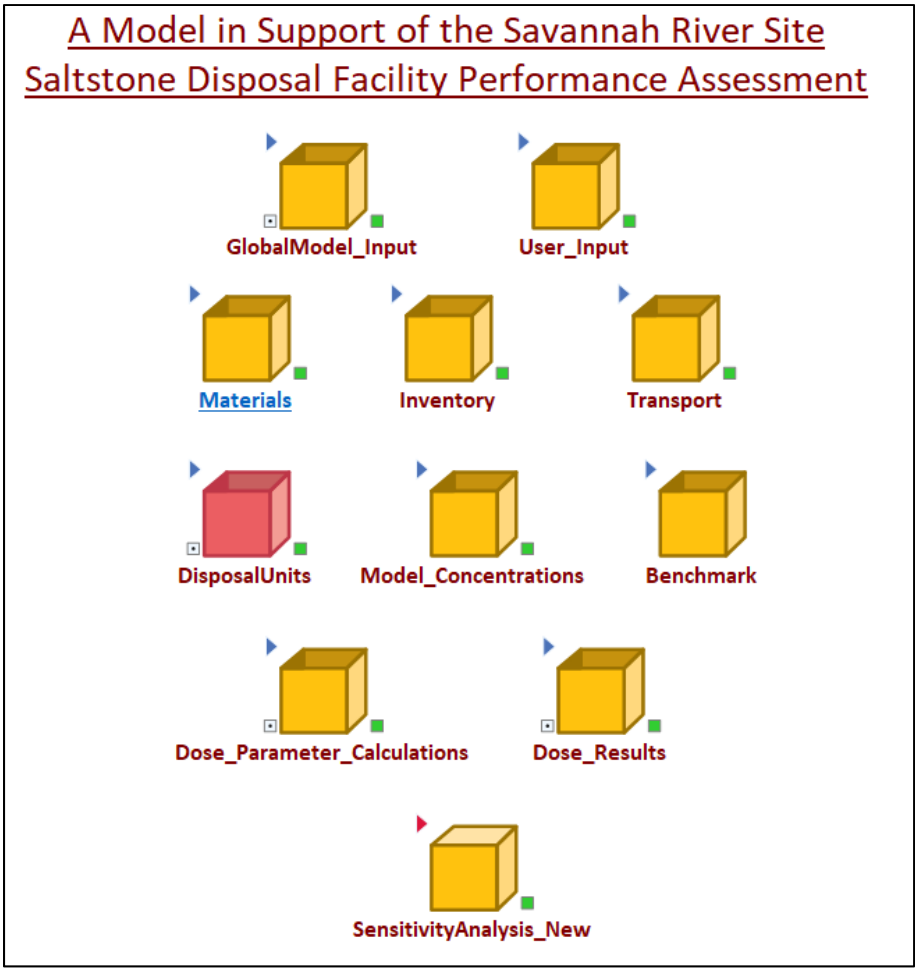

The *Dose_Parameter_Calculations* container includes three additional containers: *DoseParameters* (which holds most of the modeling inputs), *EffectiveDoseFactors* (used to hold calculations for effective dose factors (EDFs)), and *IHI_DrillCutConc_Calc* (used to hold calculations related to drill cuttings). These are shown in Figure 4.4-165.

Figure 4.4-165: Containers within the *Dose_Parameter_Calculations* Container

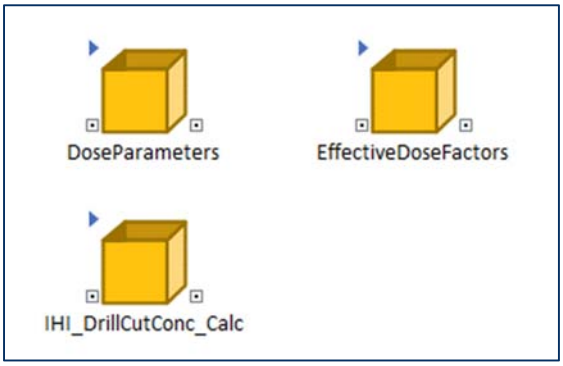

4.4.8.2.1 MOP at the 100-Meter Well Dose Calculations

The following MOP exposure pathways were used in calculating the dose to the MOP receptor with 100-meter well water as a primary water source. The stream is a secondary water source for the pathways involving swimming, boating, and fish ingestion. All transfer times are assumed to be negligible due to the long-term analysis of the PA. Unit conversions are not explicitly stated in the equations, but are implied.

The dose to the MOP at the 100-meter well is determined according to Eq. 4.4-138:

$$D_{MOP,100} = D_{MOP,100,ing} + D_{MOP,100,exp} + D_{MOP,100,inh} \qquad \text{Eq. 4.4-138}$$

where:

$D_{MOP,100}$ = total dose to the MOP at the 100-meter well (mrem/yr),

$D_{MOP,100,ing}$ = dose to the MOP at the 100-meter well (mrem/yr) due to ingestion (see Eq. 4.4-139),

$D_{MOP,100,exp}$ = dose to the MOP at the 100-meter well (mrem/yr) due to exposure (see Eq. 4.4-164), and

$D_{MOP,100,inh}$ = dose to the MOP at the 100-meter well (mrem/yr) due to inhalation (see Eq. 4.4-173).

Within GoldSim, this is implemented within closed containers found within the *Dose_Results* container, wherein each container represents a different SDF Sector (A through H, shown in Figure 4.4-166).

Figure 4.4-166: Dose Result Containers for Each SDF 100-Meter Sector

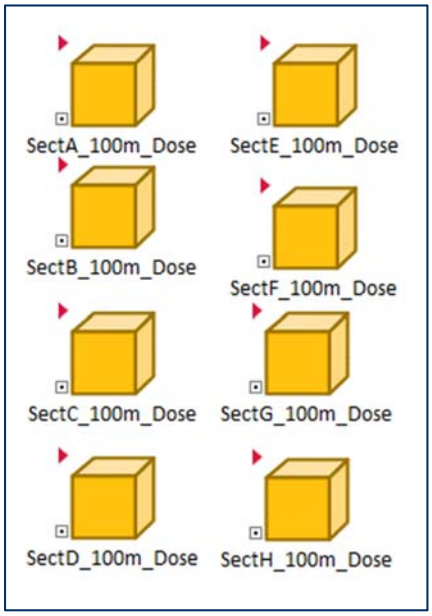

The contents for each of these containers is the same (Figure 4.4-167), except the links to the selector element *Conc_100m* are used to link to the appropriate concentration set. Within each of these containers, a sum element named *Dose_100m_rads* is used to perform Eq. 4.4-138.

Figure 4.4-167: Contents of Each SDF 100-Meter Sector Dose Result Container

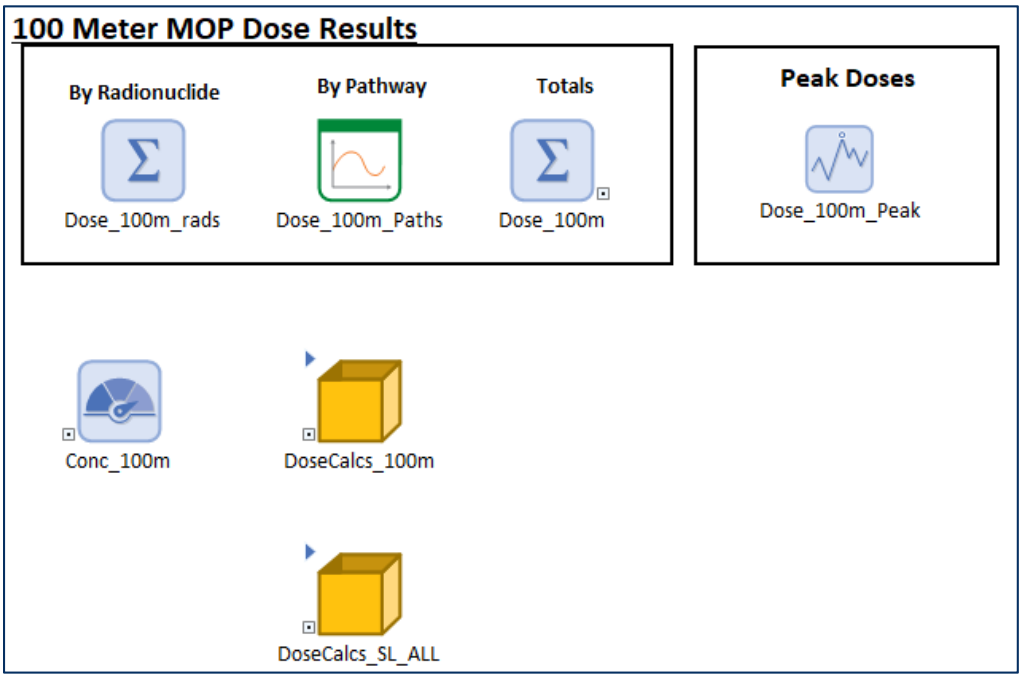

MOP at the 100-Meter Well, Ingestion Dose Pathways

The ingestion dose to the MOP at the 100-meter well is determined according to Eq. 4.4-139:

$$D_{MOP,100,ing} = D_{MOP,100,H2O,ing} + D_{MOP,100,SOIL,ing} + D_{MOP,100,PLANT,ing} + D_{MOP,100,MEAT,ing} + D_{MOP,100,MILK,ing} + D_{MOP,100,POULTRY,ing} + D_{MOP,100,EGG,ing} + D_{SL,FISH,ing} \quad \text{Eq. 4.4-139}$$

where:

$D_{MOP,100,ing}$ = dose to the MOP at the 100-meter well (mrem/yr) due to ingestion,

$D_{MOP,100,H2O,ing}$ = dose to the MOP at the 100-meter well (mrem/yr) due to ingestion of water from the 100-meter well (Eq. 4.4-140),

$D_{MOP,100,SOIL,ing}$ = dose to the MOP at the 100-meter well (mrem/yr) due to ingestion of soil that has been irrigated with water from the 100-meter well (Eq. 4.4-142),

$D_{MOP,100,PLANT,ing}$ = dose to the MOP at the 100-meter well (mrem/yr) due to ingestion of produce (both fruits and vegetables) irrigated from the 100-meter well water (Eq. 4.4-147),

$D_{MOP,100,MEAT,ing}$ = dose to the MOP at the 100-meter well (mrem/yr) due to ingestion of meat (i.e., terrestrial livestock meat such as beef, pork, veal, etc.) that eats fodder watered by and drinks water from the 100-meter well (Eq. 4.4-153),

$D_{MOP,100,MILK,ing}$ = dose to the MOP at the 100-meter well (mrem/yr) due to ingestion of milk that comes from livestock that eats fodder watered by and drinks water from the 100-meter well (Eq. 4.4-156),

$D_{MOP,100,POULTRY,ing}$ = dose to the MOP at the 100-meter well (mrem/yr) due to ingestion of poultry (including chicken, turkey, etc.) that eats fodder watered by and drinks water from the 100-meter well (Eq. 4.4-158),

$D_{MOP,100,EGG,ing}$ = dose to the MOP at the 100-meter well (mrem/yr) due to ingestion of eggs that come from poultry that eats fodder watered by and drinks water from the 100-meter well (Eq. 4.4-160), and

$D_{SL,FISH,ing}$ = dose (mrem/yr) due to ingestion of fish that came from stream water near the contaminated seepline (SL) (Eq. 4.4-162).

The contents of the container *DoseCalcs_100m* (Figure 4.4-168) include another GoldSim sum element: *Dose_100m_Ing_rads*. This element is used to perform Eq. 4.4-139. Similarly, *Dose_100m_Exp_rads* and *Dose_100m_Inh_rads* are used to implement calculations for external exposure pathways and inhalation pathways, respectively.

Figure 4.4-168: Contents of GoldSim Container: *DoseCalcs_100m*

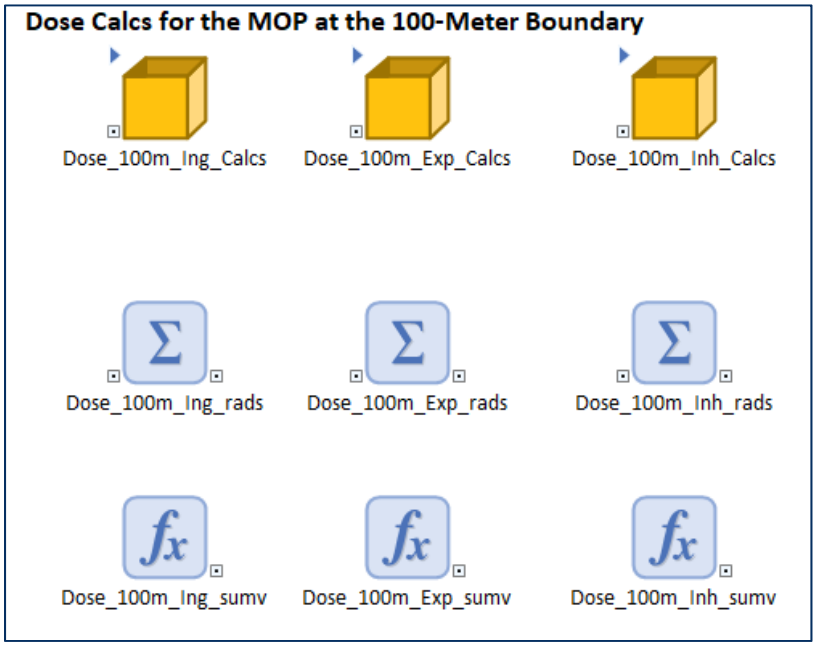

Ingestion of Water (MOP a the 100-Meter Well)

The dose from ingestion of drinking water shall be calculated according to Eq. 4.4-140:

$$D_{MOP,100,H2O,ing} = C_{GW,100} \times EDF_{H2O,ing} \quad \text{Eq. 4.4-140}$$

where:

$D_{MOP,100,H2O,ing}$ = dose to the MOP at the 100-meter well (mrem/yr) due to ingestion of water from the 100-meter well,

$C_{GW,100}$ = radionuclide concentration in ground water from the 100-meter well (pCi/L) as determined from an appropriate contaminant transport model, and

$EDF_{H2O,ing}$ = effective dose factor for ingestion of contaminated ground water (L×mrem)/(pCi×yr), defined in (Eq. 4.4-141), below.

Also within the GoldSim container: *DoseCalcs_100m* is another container named: *Dose_100m_Ing_Calcs* (Figure 4.4-168). Within this container (Figure 4.4-169), Eq. 4.4-140 is implemented via the GoldSim expression element: *WaterIngDose_100m_rads* (for each radionuclide) or *WaterIngDose_100m_sumv* (for a total dose contribution). This implementation approach is the same for each ingestion pathway.

Figure 4.4-169: Contents of GoldSim Container: *Dose_100m_Ing_Calcs*

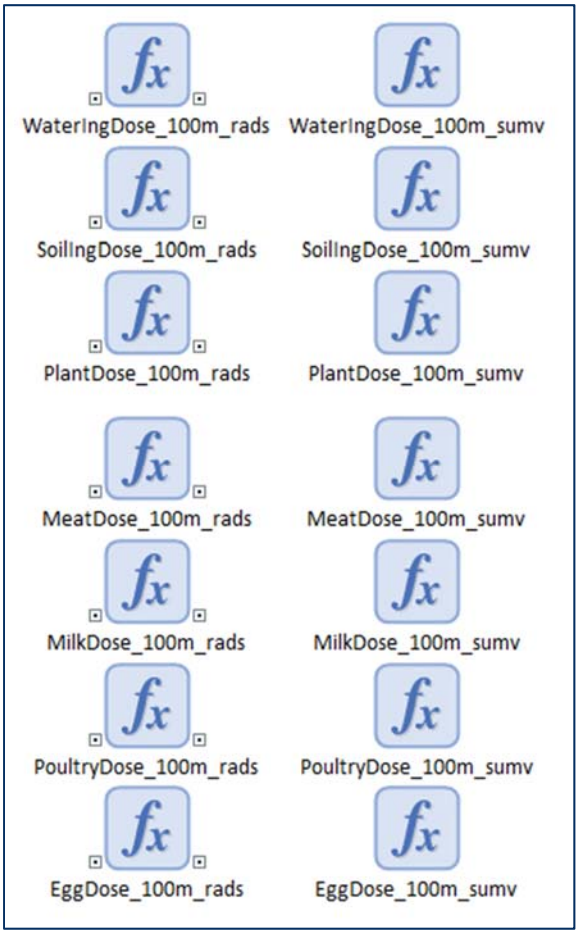

The EDF for ingestion of drinking water shall be calculated as:

$$EDF_{H2O,ing} = U_{H2O} \times DCF_{ing} \quad \text{Eq. 4.4-141}$$

where:

$EDF_{H2O,ing}$ = effective dose factor for ingestion of contaminated ground water (L×mrem)/(pCi×yr),

U_{H2O} = human ingestion rate of water (L/yr) (Table 4.4-110), and

DCF_{ing} = dose conversion factor for ingestion of contaminated ground water (mrem/pCi) (Table 4.4-108).

Within GoldSim the *Dose_Parameter_Calculations* container includes the *EffectiveDoseFactors* container. This *EffectiveDoseFactors* container includes individual GoldSim expression elements for implementing each EDF calculation (Figure 4.4-170).

Ingestion of Soil (MOP at the 100-Meter Well)

The dose from ingestion of soil shall be calculated according to Eq. 4.4-142:

$$D_{MOP,100,SOIL,ing} = C_{GW,100} \times EDF_{SOIL,ing} \quad \text{Eq. 4.4-142}$$

where:

$D_{MOP,100,SOIL,ing}$ = dose to the MOP at the 100-meter well (mrem/yr) due to ingestion of soil that has been irrigated with water from the 100-meter well,

$C_{GW,100}$ = radionuclide concentration in ground water from the 100-meter well (pCi/L) as determined from an appropriate contaminant transport model, and

$EDF_{SOIL,ing}$ = effective dose factor for ingestion of soil contaminated by ground water (L×mrem)/(pCi×yr), defined in Eq. 4.4-143 below.

The EDF for soil ingestion shall be calculated as:

$$EDF_{SOIL,ing} = SOIL \times I_{RF} \times U_{SOIL} \times DCF_{ing} \quad \text{Eq. 4.4-143}$$

where:

$EDF_{SOIL,ing}$ = effective dose factor for ingestion of soil contaminated by ground water (L×mrem)/(pCi×yr),

$SOIL$ = radionuclide deposition and buildup rate in the soil ((m²×yr)/kg) as defined by Eq. 4.4-144 and Eq. 4.4-145 below,

I_{RF} = functional irrigation rate (m/yr) as defined by Eq. 4.4-146 below,

U_{SOIL} = human ingestion rate of soil (kg/yr) (Table 4.4-110), and

DCF_{ing} = dose conversion factor for ingestion of contaminated ground water (mrem/pCi) (Table 4.4-108).

Figure 4.4-170: Contents of GoldSim Container: *EffectiveDoseFactors*

The $SOIL$ parameter from Eq. 4.4-143 (above) is defined as follows:

$$SOIL = \frac{\left(1-e^{-(\lambda_i+\lambda_L)t_b}\right)}{\rho_{ss}\times(\lambda_i+\lambda_L)} \qquad \text{Eq. 4.4-144}$$

where:

$SOIL$ = radionuclide deposition and buildup rate in the soil ((m²×yr)/kg),

λ_i = radiological decay constant (1/yr) (Table 4.4-115),

λ_L = leachate impact on buildup of radionuclides in soil (1/yr) as described in Eq. 4.4-145,

t_b = buildup time of radionuclides in soil (yr) (Table 4.4-115), and

ρ_{ss} = surface soil density (kg/m^2) (Table 4.4-115).

Eq. 4.4-144 uses:

$$\lambda_L = \frac{PR+I_{RF}-ER}{d_{till}\times(MC_{soil}+\rho_{bs}\times Kd_i)} \quad \text{Eq. 4.4-145}$$

where:

λ_L = leachate impact on buildup of radionuclides in soil (1/yr),

PR = precipitation rate (m/yr) (Table 4.4-115),

I_{RF} = functional irrigation rate (m/yr) as defined by Eq. 4.4-146 below,

ER = evapotranspiration rate (m/yr) (Table 4.4-115),

d_{till} = depth of tilling for agriculture or gardening (m) (Table 4.4-116),

MC_{soil} = soil moisture content (unitless) (Table 4.4-115),

ρ_{bs} = dry bulk density of soil (kg/m^3) (Table 4.4-115), and

Kd_i = the sandy soil K_d for radionuclide i (Table 4.3-4).

The functional irrigation rate (I_{RF}) from Eq. 4.4-143 and Eq. 4.4-145 is defined as:

$$I_{RF} = IR \times F_{irr} \quad \text{Eq. 4.4-146}$$

where:

I_{RF} = functional irrigation rate (m/yr),

IR = irrigation rate (m/yr) (Table 4.4-115), and

F_{irr} = fraction of the time produce is irrigated (unitless) (Table 4.4-116).

Within GoldSim, a container named *IntermediateParameterCalcs* can be found within the *DoseParameters* container (Figure 4.4-171). These intermediate parameter calculations (Figure 4.4-172) include GoldSim expression elements: *SOILBuildUp* (used to perform Eq. 4.4-144), *LeachRate* (used to perform Eq. 4.4-145), and *EffIrrigationRate* (used to perform Eq. 4.4-146).

Figure 4.4-171: Contents of Container: *DoseParameters*

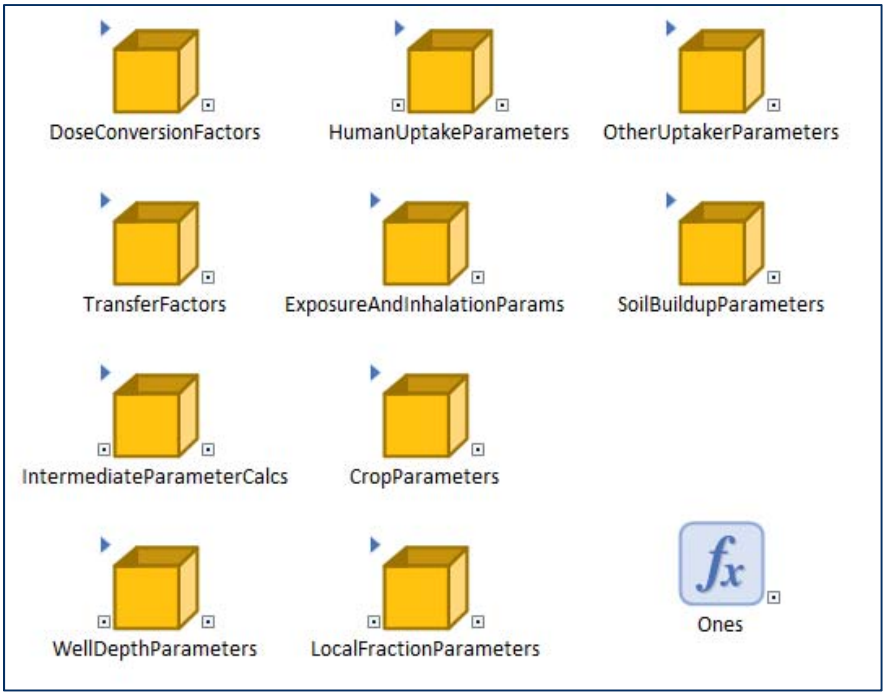

Figure 4.4-172: Contents of Container: *IntermediateParameterCalcs*

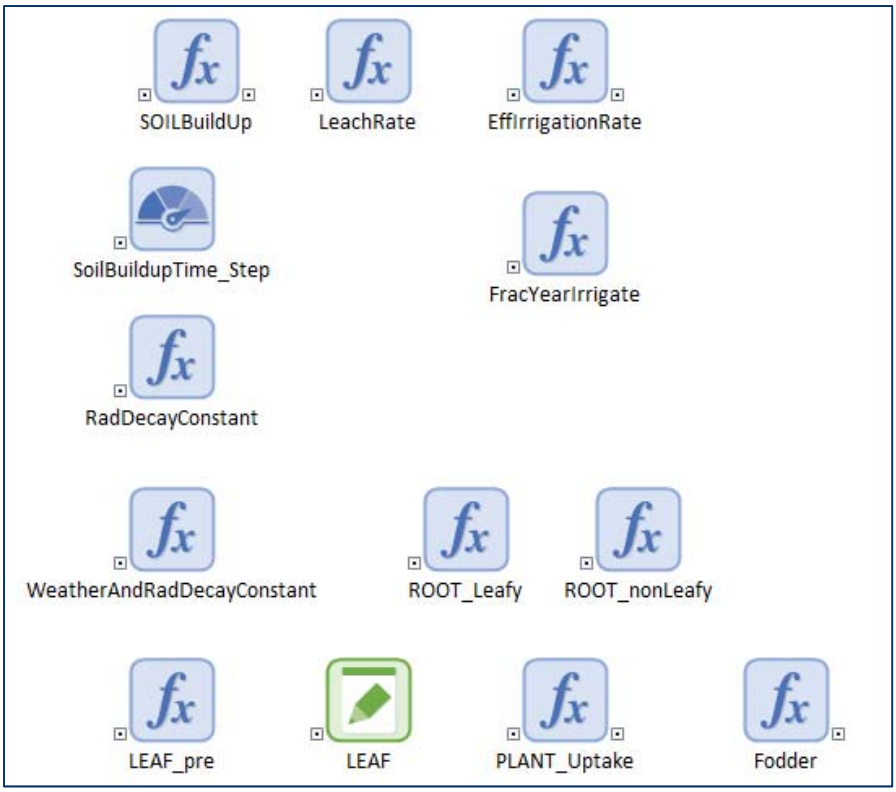

Ingestion of Produce (MOP at the 100-Meter Well)

The dose to the MOP receptor from ingestion of contaminated produce (including leafy vegetables, other vegetables, and fruit) is calculated assuming two contamination exposure pathways: (1) direct deposition of contaminated irrigation water on plants and (2) root uptake of contaminated irrigation water in soil. The irrigation water is from the 100-meter well. The dose is calculated using Eq. 4.4-147:

$$D_{MOP,100,PLANT,ing} = C_{GW,100} \times EDF_{PLANT,ing} \times F_{local,PLANT} \qquad \text{Eq. 4.4-147}$$

where:

$D_{MOP,100,PLANT,ing}$ = dose to the MOP at the 100-meter well (mrem/yr) due to ingestion of produce (both fruits and vegetables) irrigated from the 100-meter well water,

$C_{GW,100}$ = radionuclide concentration in ground water from the 100-meter well (pCi/L) as determined from an appropriate contaminant transport model,

$EDF_{PLANT,ing}$ = effective dose factor for ingestion of plants contaminated by ground water (L×mrem)/(pCi×yr) defined in Eq. 4.4-148 below, and

$F_{local,PLANT}$ = fraction of consumed produce grown locally (unitless) (see Eq. 4.4-247).

The EDF for plant ingestion shall be calculated as:

$$EDF_{PLANT,ing} = I_{RF} \times P_{in} \times U_{PLANT} \times DCF_{ing} \qquad \text{Eq. 4.4-148}$$

where:

$EDF_{PLANT,ing}$ = effective dose factor for ingestion of plants contaminated by ground water (L×mrem)/(pCi×yr),

I_{RF} = functional irrigation rate (m/yr) as defined by Eq. 4.4-146 above,

P_{in} = radionuclide uptake, deposition and retention rate in plants ((m²×yr)/kg) as defined in Eq. 4.4-149 below,

U_{PLANT} = human ingestion rate of plants or produce (kg/yr) (Table 4.4-110), and

DCF_{ing} = dose conversion factor for ingestion (mrem/pCi) (Table 4.4-108).

The plant intake parameter P_{in} from Eq. 4.4-148 is defined as:

$$P_{in} = \left(LEAF \times F_{leaf} \times F_{wash}\right) + ROOT \qquad \text{Eq. 4.4-149}$$

where:

P_{in} = radionuclide uptake, deposition, and retention rate in plants ((m²×yr)/kg),

$LEAF$ = radionuclide deposition and retention rate on produce leaves ((m²×yr)/kg) as defined in Eq. 4.4-150 below,

F_{leaf} = fraction of produce that is leafy (unitless) (Table 4.4-116),

F_{wash} = fraction of material deposited on leaves that is retained after washing (unitless) (Table 4.4-116), and

$ROOT$ = radionuclide uptake through produce roots ((m²×yr)/kg) as defined in Eq. 4.4-151 below.

The $LEAF$ and $ROOT$ parameters from Eq. 4.4-149 are defined by the following equations, where:

$$LEAF = \frac{F_r \times \left(1 - e^{-(\lambda_e t_{irr})}\right)}{Y_g \times \lambda_e} \qquad \text{Eq. 4.4-150}$$

where:

$LEAF$ = radionuclide deposition and retention rate on the produce leaves ((m²×yr)/kg),

F_r = fraction of material deposited on leaves that is retained (unitless) (Table 4.4-116),

λ_e = weathering and radiological decay constant (1/yr) as defined in Eq. 4.4-152 below,

t_{irr} = time produce is exposed to irrigation (yr) (Table 4.4-116), and

Y_g = crop and garden production yield (kg/m²) (Table 4.4-116).

And:

$$ROOT = \left(F_{leaf} \times R_{StoV} \times SOIL\right) + \left(F_{nonleaf} \times R_{StoV} \times SOIL\right) \qquad \text{Eq. 4.4-151}$$

where:

$ROOT$ = radionuclide uptake through produce roots ((m²×yr)/kg),

F_{leaf} = fraction of produce that is leafy (Table 4.4-116),

$F_{nonleaf}$ = fraction of produce that is not leafy (1.0 – F_{leaf}),

R_{StoV} = soil to vegetation ratio (unitless) (Table 4.4-113), and

$SOIL$ = radionuclide deposition ((m²×yr)/kg) as defined in Eq. 4.4-144 above.

Finally, the weathering and radiological decay parameter λ_e from Eq. 4.4-150 is defined as:

$$\lambda_e = \lambda_i + \lambda_w \qquad \text{Eq. 4.4-152}$$

where:

λ_e = weathering and radiological decay constant (1/yr),

λ_i = radiological decay constant (1/yr) [ln(2)/half-life of radionuclide i] (Table 4.4-115), and

λ_w = weathering decay constant (1/yr) (Table 4.4-115).

Within GoldSim, the intermediate calculations are implemented within the container: *IntermediateParameterCalcs* (Figure 4.4-172). These intermediate parameter calculations include GoldSim elements: *PlantUptake* (used to perform Eq. 4.4-149), *LEAF_pre* and *LEAF* (used to perform Eq. 4.4-150), *ROOT_Leafy* and *ROOT_nonLeafy* (used to perform Eq. 4.4-151), and *WeatherAndRadDecayConstant* (used to perform Eq. 4.4-152).

Ingestion of Meat (MOP at the 100-Meter Well)

The meat ingestion pathway assumes that terrestrial livestock consumes contaminated water and fodder irrigated with contaminated water. The water is from the 100-meter well. The fodder is contaminated from direct deposition of contaminated irrigation water on plants and from deposition of contaminated irrigation water in soil followed by root uptake by plants. The buildup of radionuclide concentration in the soil from successive years of irrigation is accounted for. The radionuclide concentration in fodder from deposition and root uptake is calculated as well.

For the purpose of this calculation, meat (or terrestrial livestock) includes all meat that is not classified as poultry or fish. This includes beef, pork, veal, and other game.

After livestock consume contaminated water and fodder, the MOP receptor consumes the contaminated meat. The dose from ingesting contaminated meat is calculated using the following formula:

$$D_{MOP,100,MEAT,ing} = C_{GW,100} \times EDF_{MEAT,ing} \times F_{local,MEAT} \qquad \text{Eq. 4.4-153}$$

where:

$D_{MOP,100,MEAT,ing}$ = dose to the MOP at the 100-meter well (mrem/yr) due to ingestion of meat (i.e., terrestrial livestock meat such as beef, pork, veal, etc.) that eats fodder watered by and drinks water from the 100-meter well,

$C_{GW,100}$ = radionuclide concentration in ground water from the 100-meter well (pCi/L) as determined from an appropriate contaminant transport model,

$EDF_{MEAT,ing}$ = effective dose factor for ingestion of terrestrial livestock meat contaminated by ground water (L×mrem)/(pCi×yr) as defined in Eq. 4.4-154 below, and

$F_{local,MEAT}$ = fraction of terrestrial livestock raised locally (unitless) (Table 4.4-118).

The EDF for meat ingestion shall be calculated as:

$$EDF_{MEAT,ing} = \left(Q_{H2O,MEAT} + \left(Fod \times Q_{fod,MEAT} \times F_{fod,MEAT}\right)\right) \times TC_{MEAT} \times U_{MEAT} \times DCF_{ing} \quad \text{Eq. 4.4-154}$$

where:

$EDF_{MEAT,ing}$ = effective dose factor for ingestion of terrestrial livestock meat contaminated by ground water (L×mrem)/(pCi×yr),

$Q_{H2O,MEAT}$ = ingestion rate of water by terrestrial livestock (L/yr) (Table 4.4-111),

Fod = terrestrial livestock or poultry intake of contaminated feed/fodder (m^3/kg) as defined in Eq. 4.4-155 below,

$Q_{fod,MEAT}$ = ingestion rate of fodder by terrestrial livestock (kg/yr) (Table 4.4-111),

$F_{fod,MEAT}$ = fraction of terrestrial livestock intake from field/pasture that is irrigated with water from the contaminated well (unitless) (Table 4.4-112),

TC_{MEAT} = transfer coefficient for terrestrial livestock (including beef, pork, veal, etc.) (yr/kg) (Table 4.4-113),

U_{MEAT} = human ingestion rate of meat (i.e., terrestrial livestock meat such as beef, pork, veal, etc.) (kg/yr) (Table 4.4-110), and

DCF_{ing} = dose conversion factor for ingestion (mrem/pCi) Table 4.4-108.

The Fod parameter from Eq. 4.4-154 is defined by Eq. 4.4-155. This equation also uses Eq. 4.4-146 and Eq. 4.4-149, as follows:

$$Fod = I_{RF} \times P_{in} \quad \text{Eq. 4.4-155}$$

where:

Fod = terrestrial livestock or poultry intake of contaminated feed/fodder (m^3/kg),

I_{RF} = functional irrigation rate (m/yr) as defined by Eq. 4.4-146 above, and

P_{in} = radionuclide uptake and deposition and retention rate in plants ((m^2×yr)/kg) as defined in Eq. 4.4-149 above.

Within GoldSim, Eq. 4.4-155 is implemented via the expression element: *Fodder* (Figure 4.4-172).

Ingestion of Milk (MOP at the 100-Meter Well)

After milk cows (or other milk-producing livestock) consume contaminated water and fodder, the MOP receptor consumes the contaminated milk. The dose from ingestion of contaminated milk is calculated using the following formula:

$$D_{MOP,100,MILK,ing} = C_{GW,100} \times EDF_{MILK,ing} \times F_{local,MILK} \quad \text{Eq. 4.4-156}$$

where:

$D_{MOP,100,MILK,ing}$ = dose to the MOP at the 100-meter well (mrem/yr) due to ingestion of milk that comes from livestock that eats fodder watered by and drinks water from the 100-meter well,

$C_{GW,100}$ = radionuclide concentration in ground water from the 100-meter well (pCi/L) as determined from an appropriate contaminant transport model,

$EDF_{MILK,ing}$ = effective dose factor for ingestion of milk contaminated by ground water (L×mrem)/(pCi×yr) as defined in Eq. 4.4-157 below, and

$F_{local,MILK}$ = fraction of milk-producing livestock raised locally (unitless) (Table 4.4-118).

The EDF for milk ingestion shall be calculated as:

$$EDF_{MILK,ing} = \left(Q_{H2O,MILK} + \left(Fod \times Q_{fod,MILK} \times F_{fod,MILK}\right)\right) \times TC_{MILK} \times \left(\frac{U_{MILK}}{\rho_{MILK}}\right) \times DCF_{ing} \quad \text{Eq. 4.4-157}$$

where:

$EDF_{MILK,ing}$ = effective dose factor for ingestion of milk contaminated by ground water (L×mrem)/(pCi×yr),

$Q_{H2O,MILK}$ = ingestion rate of water by milk producing livestock (L/yr) (Table 4.4-111),

Fod = terrestrial livestock or poultry intake of contaminated feed/fodder (m^3/kg) as defined in Eq. 4.4-155 above,

$Q_{fod,MILK}$ = ingestion rate of fodder by milk producing livestock (kg/yr) (Table 4.4-111),

$F_{fod,MILK}$ = fraction of milk-producing livestock fodder ingestion from field/pasture that is irrigated with water from the contaminated well (unitless) (Table 4.4-112),

TC_{MILK} = transfer coefficient for milk (yr/L) (Table 4.4-113),

U_{MILK} = human ingestion rate of milk (kg/yr) (Table 4.4-110),

ρ_{MILK} = milk density (kg/L) (Table 4.4-110 – table note), and

DCF_{ing} = dose conversion factor for ingestion (mrem/pCi) (Table 4.4-108).

Ingestion of Poultry (MOP at the 100-Meter Well)

The poultry and egg exposure pathways assume poultry and egg-producing livestock consume contaminated water and fodder irrigated with contaminated water. The contaminated water is from the 100-meter well. The fodder is contaminated from direct deposition of contaminated irrigation water on plants and from deposition of contaminated irrigation water in soil followed by root uptake by plants. It is also assumed that poultry directly ingest contaminated soil

in addition to the water and fodder. The dose from ingestion of contaminated poultry is calculated using the following formula:

$$D_{MOP,100,POULTRY,ing} = C_{GW,100} \times EDF_{POULTRY,ing} \times F_{local,POULTRY} \quad \text{Eq. 4.4-158}$$

where:

$D_{MOP,100,POULTRY,ing}$ = dose to the MOP at the 100-meter well (mrem/yr) due to ingestion of poultry (including chicken, turkey, etc.) that eats fodder watered by and drinks water from the 100-meter well,

$C_{GW,100}$ = radionuclide concentration in ground water from the 100-meter well (pCi/L), as determined from an appropriate contaminant transport model,

$EDF_{POULTRY,ing}$ = effective dose factor for ingestion of poultry contaminated by ground water (L×mrem)/(pCi×yr) as defined in Eq. 4.4-159 below, and

$F_{local,POULTRY}$ = fraction of poultry raised locally (unitless) (Table 4.4-118).

The EDF for poultry ingestion shall be calculated as:

$$EDF_{POULTRY,ing} = \Big(Q_{H2O,POULTRY} + \big(Fod \times Q_{fod,POULTRY} \times F_{fod,POULTRY}\big) + \big(SOIL \times I_{RF} \times Q_{SOIL,POULTRY} \times F_{SOIL,POULTRY}\big)\Big) \times TC_{POULTRY} \times U_{POULTRY} \times DCF_{ing} \quad \text{Eq. 4.4-159}$$

where:

$EDF_{POULTRY,ing}$ = effective dose factor for ingestion of poultry contaminated by ground water (L×mrem)/(pCi×yr),

$Q_{H2O,POULTRY}$ = ingestion rate of water by poultry (L/yr) (Table 4.4-111),

Fod = terrestrial livestock or poultry intake of contaminated feed/fodder (m^3/kg) as defined in Eq. 4.4-155 above,

$Q_{fod,POULTRY}$ = ingestion rate of fodder consumed by poultry (kg/yr) (Table 4.4-111),

$F_{fod,POULTRY}$ = fraction of poultry fodder ingestion from field/pasture that is irrigated with water from the contaminated well (unitless) (Table 4.4-112),

$SOIL$ = radionuclide deposition and buildup rate in the soil ((m^2×yr)/kg) as defined by Eq. 4.4-144,

I_{RF} = functional irrigation rate (m/yr) as defined by Eq. 4.4-146 above,

$Q_{SOIL,POULTRY}$ = ingestion rate of soil by poultry (kg/yr) (Table 4.4-111),

$F_{SOIL,POULTRY}$ = fraction of poultry soil intake from field/pasture that is irrigated with water from the contaminated well (unitless) (Table 4.4-112),

$TC_{POULTRY}$ = transfer coefficient for poultry (yr/kg) (Table 4.4-113),

$U_{POULTRY}$ = human ingestion rate of poultry (kg/yr) (Table 4.4-110), and

DCF_{ing} = dose conversion factor for ingestion (mrem/pCi) (Table 4.4-108).

Ingestion of Egg (MOP at the 100-Meter Well)

After egg-producing livestock consumes the contaminated water and fodder, the MOP consumes the contaminated eggs. The dose from ingestion of contaminated eggs is calculated using the following formula:

$$D_{MOP,100,EGG,ing} = C_{GW,100} \times EDF_{EGG,ing} \times F_{local,EGG} \quad \text{Eq. 4.4-160}$$

where:

$D_{MOP,100,EGG,ing}$ = dose to the MOP at the 100-meter well (mrem/yr) due to ingestion of eggs that come from poultry that eats fodder watered by and drinks water from the 100-meter well,

$C_{GW,100}$ = radionuclide concentration in ground water from the 100-meter well (pCi/L), as determined from an appropriate contaminant transport model,

$EDF_{EGG,ing}$ = effective dose factor for ingestion of eggs contaminated by ground water (L×mrem)/(pCi×yr) as defined in Eq. 4.4-161 below, and

$F_{local,EGG}$ = fraction of eggs raised locally (unitless) (Table 4.4-118).

The EDF for egg ingestion shall be calculated as:

$$EDF_{EGG,ing} = \left(Q_{H2O,EGG} + \left(Fod \times Q_{fod,EGG} \times F_{fod,EGG}\right) + \left(SOIL \times I_{RF} \times Q_{SOIL,EGG} \times F_{SOIL,EGG}\right)\right) \times TC_{EGG} \times U_{EGG} \times DCF_{ing} \quad \text{Eq. 4.4-161}$$

where:

$EDF_{EGG,ing}$ = effective dose factor for ingestion of eggs contaminated by ground water (L×mrem)/(pCi×yr),

$Q_{H2O,EGG}$ = uptake rate of water by egg producers (L/yr) (Table 4.4-111),

Fod = livestock and poultry intake of contaminated feed/fodder (m^3/kg) as defined in Eq. 4.4-155 above,

$Q_{fod,EGG}$ = uptake rate of fodder by egg producers (kg/yr) (Table 4.4-111),

$F_{fod,EGG}$ = fraction of fodder consumed by egg producers from field/pasture that is irrigated with from the contaminated well (unitless) (Table 4.4-112),

$SOIL$ = radionuclide deposition and buildup rate in the soil ((m^2×yr)/kg) as defined by Eq. 4.4-144,

I_{RF} = functional irrigation rate (m/yr) as defined by Eq. 4.4-146 above,

$Q_{SOIL,EGG}$ = uptake rate of soil by eggs (kg/yr) (Table 4.4-111),

$F_{SOIL,EGG}$ = fraction of egg soil intake from field/pasture that is irrigated with from the contaminated well (unitless) (Table 4.4-112),

TC_{EGG} = transfer coefficient for eggs (yr/kg) (Table 4.4-113),

U_{EGG} = human ingestion rate of eggs (kg/yr) (Table 4.4-110), and

DCF_{ing} = dose conversion factor for ingestion (mrem/pCi) (Table 4.4-108).

Ingestion of Fish

The fish ingestion route assumes fish are caught from a contaminated stream at the point of highest concentration, and the MOP receptor in turn consumes the contaminated fish. The dose from ingestion of fish shall be calculated according to Eq. 4.4-162:

$$D_{SL,FISH,ing} = C_{SL} \times EDF_{FISH,ing} \times F_{local,FISH} \quad \text{Eq. 4.4-162}$$

where:

$D_{SL,FISH,ing}$ = dose (mrem/yr) to the MOP or IHI due to ingestion of fish that came from stream water near the contaminated SL,

C_{SL} = radionuclide concentration in stream water at the contaminated SL (pCi/L), as determined from an appropriate contaminant transport model

$EDF_{FISH,ing}$ = effective dose factor for fish ingestion (L×mrem)/(pCi×yr) as defined in Eq. 4.4-163 below, and

$F_{local,FISH}$ = fraction of consumed fish that are fished locally (unitless) (Table 4.4-118).

The EDF for fish ingestion shall be calculated as:

$$EDF_{FISH,ing} = TC_{FISH} \times U_{FISH} \times DCF_{ing} \quad \text{Eq. 4.4-163}$$

where:

$EDF_{FISH,ing}$ = effective dose factor for fish ingestion (L×mrem)/(pCi×yr),

TC_{FISH} = transfer coefficient (or bioaccumulation factor) for fish (L/kg) (Table 4.4-113),

U_{FISH} = human ingestion rate of fish (kg/yr) (Table 4.4-110), and

DCF_{ing} = dose conversion factor for ingestion (mrem/pCi) (Table 4.4-108).

MOP at the 100-Meter Well, Direct Exposure Dose Pathways

The following text defines the parameter $D_{MOP,100,exp}$ from Eq. 4.4-138. The direct exposure dose to the MOP at the 100-meter well is determined according to Eq. 4.4-164:

$$D_{MOP,100,exp} = D_{MOP,100,SOIL,exp} + D_{MOP,100,SHOWER,exp} + D_{SL,SWIM,exp} + D_{SL,BOAT,exp} \quad \text{Eq. 4.4-164}$$

where:

$D_{MOP,100,exp}$ = dose to the MOP at the 100-meter well (mrem/yr) due to exposure,

$D_{MOP,100,SOIL,exp}$ = dose to the MOP at the 100-meter well (mrem/yr) due to direct exposure to soil irrigated from the 100-meter well (Eq. 4.4-165),

$D_{MOP,100,SHOWER,exp}$ = dose to the MOP at the 100-meter well (mrem/yr) due to direct exposure while showering or bathing in water from the 100-meter well (Eq. 4.4-167),

$D_{SL,SWIM,exp}$ = dose (mrem/yr) due to direct exposure from swimming in stream water at the contaminated SL (Eq. 4.4-169), and

$D_{SL,BOAT,exp}$ = dose (mrem/yr) due to direct exposure from boating and fishing in stream water at the contaminated SL (Eq. 4.4-171).

Direct Exposure from Irrigated Soil

The exposure pathway from direct contact with contaminated soil assumes the soil is irrigated with ground water from the 100-meter well and the MOP receptor in turn is exposed during time spent caring for a garden or crop. The radionuclide concentration in the soil and the exposure dose is calculated using the following formula:

$$D_{MOP,100,SOIL,exp} = C_{GW,100} \times EDF_{SOIL,exp} \qquad \text{Eq. 4.4-165}$$

where:

$D_{MOP,100,SOIL,exp}$ = dose to the MOP at the 100-meter well (mrem/yr) due to direct exposure to soil irrigated from the 100-meter well,

$C_{GW,100}$ = radionuclide concentration in ground water from the 100-meter well (pCi/L) as determined from an appropriate contaminant transport model, and

$EDF_{SOIL,exp}$ = effective dose factor for external exposure to soil (L×mrem)/(pCi×yr) as defined in Eq. 4.4-166 below.

The EDF for external exposure to soil shall be calculated as:

$$EDF_{SOIL,exp} = SOIL \times I_{RF} \times DCF_{exp} \times F_{t,g} \times \rho_s \qquad \text{Eq. 4.4-166}$$

where:

$EDF_{SOIL,exp}$ = effective dose factor for external exposure to soil (L×mrem)/(pCi×yr),

$SOIL$ = radionuclide deposition and buildup rate in the soil ((m^2×yr)/kg) as defined by Eq. 4.4-144,

I_{RF} = functional irrigation rate (m/yr) as defined by Eq. 4.4-146 above,

DCF_{exp} = dose conversion factor for external exposure (m^3×mrem)/(pCi×yr) (Table 4.4-108),

$F_{t,g}$ = fraction of the time the MOP spends in the contaminated garden or crop (unitless) (Table 4.4-114), and

ρ_{bs} = dry bulk density of soil (kg/m^3) (Table 4.4-115).

Direct Exposure from Showering (MOP at the 100-Meter Well)

The direct contact exposure pathway from showering and bathing assumes the MOP receptor receives dose from washing in water from the 100-meter well. The dose is calculated using the following formula:

$$D_{MOP,100,SHOWER,exp} = C_{GW,100} \times EDF_{SHOWER,exp} \quad \text{Eq. 4.4-167}$$

where:

$D_{MOP,100,SHOWER,exp}$ = dose to the MOP at the 100-meter well (mrem/yr) due to direct exposure while showering or bathing in water from the 100-meter well,

$C_{GW,100}$ = radionuclide concentration in ground water from the 100-meter well (pCi/L) as determined from an appropriate contaminant transport model, and

$EDF_{SHOWER,exp}$ = effective dose factor for external exposure to water while showering or bathing (L×mrem)/(pCi×yr) as defined in Eq. 4.4-168 below.

The EDF for external exposure to water while showering or bathing shall be calculated as:

$$EDF_{SHOWER,exp} = F_{t,SHOWER} \times GF_{SHOWER} \times DCF_{imm} \quad \text{Eq. 4.4-168}$$

where:

$EDF_{SHOWER,exp}$ = effective dose factor for external exposure to water while showering or bathing (L×mrem)/(pCi×yr),

$F_{t,SHOWER}$ = fraction of time spent showering or bathing (unitless) (Table 4.4-114),

GF_{SHOWER} = geometry factor for showering or bathing (unitless) (Table 4.4-114), and

DCF_{imm} = dose conversion factor for immersion in water (m^3×mrem)/(pCi×yr) (Table 4.4-108).

Note that this calculation assumes full immersion.

Direct Exposure from Swimming

The direct contact exposure pathway from swimming assumes the MOP receptor receives dose from swimming in a contaminated stream at the point of highest concentration. The dose from swimming exposure shall be calculated according to Eq. 4.4-169:

$$D_{SL,SWIM,exp} = C_{SL} \times EDF_{SWIM,exp} \quad \text{Eq. 4.4-169}$$

where:

$D_{SL,SWIM,exp}$ = dose (mrem/yr) due to direct exposure from swimming in stream water at the contaminated SL,

C_{SL} = radionuclide concentration in stream water at the contaminated SL (pCi/L) as determined from an appropriate contaminant transport model, and

$EDF_{SWIM,exp}$ = effective dose factor for external exposure to water while swimming (L×mrem)/(pCi×yr) as defined in Eq. 4.4-170 below.

The EDF for external exposure to water while swimming shall be calculated as:

$$EDF_{SWIM,exp} = F_{t,SWIM} \times GF_{SWIM} \times DCF_{imm} \quad \text{Eq. 4.4-170}$$

where:

$EDF_{SWIM,exp}$ = effective dose factor for external exposure to water while swimming (L×mrem)/(pCi×yr),

$F_{t,SWIM}$ = fraction of time per year spent swimming (unitless) (Table 4.4-114),

GF_{SWIM} = geometry factor for swimming (unitless) (Table 4.4-114), and

DCF_{imm} = dose conversion factor for immersion in water (m^3×mrem)/(pCi×yr) (Table 4.4-108).

Direct Exposure from Boating and Fishing

The direct contact exposure pathway from boating and fishing assumes the MOP receptor receives dose from activities at a contaminated stream. The dose from boating and fishing exposure shall be calculated according to Eq. 4.4-171:

$$D_{SL,BOAT,exp} = C_{SL} \times EDF_{BOAT,exp} \quad \text{Eq. 4.4-171}$$

where:

$D_{SL,BOAT,exp}$ = dose to (mrem/yr) due to direct exposure from boating and fishing in stream water at the contaminated SL,

C_{SL} = radionuclide concentration in stream water at the contaminated SL (pCi/L) as determined from an appropriate contaminant transport model, and

$EDF_{BOAT,exp}$ = effective dose factor for external exposure to water while boating and fishing (L×mrem)/(pCi×yr) as defined in Eq. 4.4-172 below.

The EDF for external exposure to water while boating and fishing shall be calculated as:

$$EDF_{BOAT,exp} = F_{t,BOAT} \times GF_{BOAT} \times DCF_{imm} \quad \text{Eq. 4.4-172}$$

where:

$EDF_{BOAT,exp}$ = effective dose factor for external exposure to water while boating and fishing (L×mrem)/(pCi×yr),

$F_{t,BOAT}$ = fraction of time per year spent boating and fishing (unitless) (Table 4.4-114),

GF_{BOAT} = geometry factor for boating and fishing (unitless) (Table 4.4-114), and

DCF_{imm} = dose conversion factor for immersion in water (m^3×mrem)/(pCi×yr) (Table 4.4-108).

MOP at the 100-Meter Well, Inhalation Dose Pathways

The following text defines the parameter $D_{MOP,100,inh}$ from Eq. 4.4-138. The inhalation dose to the MOP at the 100-meter well is determined according to Eq. 4.4-173:

$$D_{MOP,100,inh} = D_{MOP,100,IRR,inh} + D_{MOP,100,DUST,inh} + D_{MOP,100,SHOWER,inh} + D_{SL,SWIM,inh} \quad \text{Eq. 4.4-173}$$

where:

$D_{MOP,100,inh}$ = dose to the MOP at the 100-meter well (mrem/yr) due to inhalation,

$D_{MOP,100,IRR,inh}$ = dose to the MOP at the 100-meter well (mrem/yr) due to inhalation while irrigating gardens or crops with water from the 100-meter well (Eq. 4.4-174),

$D_{MOP,100,DUST,inh}$ = dose to the MOP at the 100-meter well (mrem/yr) due to inhalation of dust and soil that has been contaminated due to irrigation with water from the 100-meter well (Eq. 4.4-176),

$D_{MOP,100,SHOWER,inh}$ = dose to the MOP at the 100-meter well (mrem/yr) due to inhalation while showering or bathing in water from the 100-meter well (Eq. 4.4-178), and

$D_{SL,SWIM,inh}$ = dose (mrem/yr) due to inhalation while swimming in stream water at the contaminated SL (Eq. 4.4-180).

Inhalation of Water during Irrigation (MOP at the 100-Meter Well)

The exposure pathway from inhalation during irrigation assumes soil is irrigated with ground water from the 100-meter well and the MOP receptor is exposed by breathing while the garden or crop is irrigated but only during time spent caring for a garden or crop. The dose is calculated using the following formula:

$$D_{MOP,100,IRR,inh} = C_{GW,100} \times EDF_{IRR,inh} \quad \text{Eq. 4.4-174}$$

where:

$D_{MOP,100,IRR,inh}$ = dose to the MOP at the 100-meter well (mrem/yr) due to inhalation while irrigating gardens or crops with water from the 100-meter well,

$C_{GW,100}$ = radionuclide concentration in ground water from the 100-meter well (pCi/L) as determined from an appropriate contaminant transport model, and

$EDF_{IRR,inh}$ = effective dose factor for inhalation of water during irrigation (L×mrem)/(pCi×yr) as defined in Eq. 4.4-175 below.

The EDF for inhalation of water during irrigation shall be calculated as:

$$EDF_{IRR,inh} = \frac{U_{AIR} \times F_{t,g} \times MC_{AIR} \times ARF \times DCF_{inh}}{\rho_{H2O}} \quad \text{Eq. 4.4-175}$$

where:

$EDF_{IRR,inh}$ = effective dose factor for inhalation of water during irrigation (L×mrem)/(pCi×yr),

U_{AIR} = air intake (m^3/yr) (Table 4.4-110),

$F_{t,g}$ = fraction of the time the MOP spends in the garden or crop (unitless) (Table 4.4-114),

MC_{AIR} = water contained in air at ambient conditions (kg/m^3) (Table 4.4-114),

ARF = airborne release fraction (unitless) (Table 4.4-114),

DCF_{inh} = dose conversion factor for inhalation (mrem/pCi) (Table 4.4-108), and

ρ_{H2O} = water density (kg/L) (Table 4.4-117).

Inhalation of Dust from Irrigated Soil (MOP at the 100-Meter Well)

The dose pathway associated with inhalation of dust and soil that has been irrigated assumes that dust and soil has been irrigated with ground water from a 100-meter well and that the MOP receptor is exposed by breathing dust during time spent caring for a garden or crop. This formula was derived following the approach of previous pathway calculations. The dose is calculated using the following formula:

$$D_{MOP,100,DUST,inh} = C_{GW,100} \times EDF_{DUST,inh} \quad \text{Eq. 4.4-176}$$

where:

$D_{MOP,100,DUST,inh}$ = dose to the MOP at the 100-meter well (mrem/yr) due to inhalation of dust and soil that has been contaminated due to irrigation with water from the 100-meter well,

$C_{GW,100}$ = radionuclide concentration in ground water from the 100-meter well (pCi/L) as determined from an appropriate contaminant transport model, and

$EDF_{DUST,inh}$ = effective dose factor for inhalation of dust and soil (L×mrem)/(pCi×yr) as defined in Eq. 4.4-177 below.

The EDF for inhalation of dust and soil shall be calculated as:

$$EDF_{DUST,inh} = U_{AIR} \times L_{SOIL} \times SOIL \times I_{RF} \times F_{t,g} \times DCF_{inh} \quad \text{Eq. 4.4-177}$$

where:

$EDF_{DUST,inh}$ = effective dose factor for inhalation of dust and soil (L×mrem)/(pCi×yr),

U_{AIR} = air intake (m^3/yr) (Table 4.4-110),

L_{SOIL} = soil loading in air while working in a garden or crop (kg/m^3) (Table 4.4-114),

$SOIL$ = radionuclide deposition and buildup rate in the soil ((m^2×yr)/kg) as defined by Eq. 4.4-144,

I_{RF} = functional irrigation rate (m/yr) as defined by Eq. 4.4-146 above,

$F_{t,g}$ = fraction of the time the MOP spends in the garden or crop (unitless) (Table 4.4-114), and

DCF_{inh} = dose conversion factor for inhalation (mrem/pCi) (Table 4.4-108).

Inhalation during Showering (MOP at the 100-Meter Well)

The showering inhalation dose pathway assumes the MOP receptor is exposed by breathing humid air within the shower. The source of water for the shower is the 100-meter well. The dose is calculated using the following formula:

$$D_{MOP,100,SHOWER,inh} = C_{GW,100} \times EDF_{SHOWER,inh} \quad \text{Eq. 4.4-178}$$

where:

$D_{MOP,100,SHOWER,inh}$ = dose to the MOP at the 100-meter well (mrem/yr) due to inhalation while showering or bathing in water from the 100-meter well,

$C_{GW,100}$ = radionuclide concentration in ground water from the 100-meter well (pCi/L) as determined from an appropriate contaminant transport model, and

$EDF_{SHOWER,inh}$ = effective dose factor for inhalation of water while showering or bathing (L×mrem)/(pCi×yr) as defined in Eq. 4.4-179 below.

The EDF for inhalation of water while showering or bathing shall be calculated as:

$$EDF_{SHOWER,inh} = \frac{U_{AIR} \times F_{t,SHOWER} \times MC_{SHOWER} \times ARF \times DCF_{inh}}{\rho_{H2O}} \quad \text{Eq. 4.4-179}$$

where:

$EDF_{SHOWER,inh}$ = effective dose factor for inhalation of water while showering or bathing (L×mrem)/(pCi×yr),

U_{AIR} = air intake (m^3/yr) (Table 4.4-110),

$F_{t,SHOWER}$ = fraction of time per year spent showering or bathing (unitless) (Table 4.4-114),

MC_{SHOWER} = water contained in air under shower conditions (kg/m^3) (Table 4.4-114),

ARF = airborne release fraction (unitless) (Table 4.4-114),

DCF_{inh} = dose conversion factor for inhalation (mrem/pCi) (Table 4.4-108), and

ρ_{H2O} = water density (kg/L) (Table 4.4-117).

Inhalation during Swimming

The swimming inhalation pathway assumes that water from a stream has been contaminated by ground water at the SL and that the receptor inhales saturated air. For simplicity, the moisture contained in the inhaled air is assumed to be from stream water at the seepline. The dose is calculated using the following formula:

$$D_{SL,SWIM,inh} = C_{SL} \times EDF_{SWIM,inh} \quad \text{Eq. 4.4-180}$$

where:

$D_{SL,SWIM,inh}$ = dose (mrem/yr) due to inhalation while swimming in stream water at the contaminated SL,

C_{SL} = radionuclide concentration in stream water at the contaminated SL (pCi/L) as determined from an appropriate contaminant transport model, and

$EDF_{SWIM,inh}$ = effective dose factor for inhalation of water while swimming (L×mrem)/(pCi×yr) as defined in Eq. 4.4-181 below.

The EDF for inhalation of water while swimming shall be calculated as:

$$EDF_{SWIM,inh} = \frac{U_{AIR} \times F_{t,SWIM} \times MC_{AIR} \times ARF \times DCF_{inh}}{\rho_{H2O}} \quad \text{Eq. 4.4-181}$$

where:

$EDF_{SWIM,inh}$ = effective dose factor for inhalation of water while swimming (L×mrem)/(pCi×yr),

U_{AIR} = air intake (m^3/yr) (Table 4.4-110),

$F_{t,SWIM}$ = fraction of time per year spent swimming (unitless) (Table 4.4-114),

MC_{AIR} = water contained in air at ambient conditions (kg/m^3) (Table 4.4-114),

ARF = airborne release fraction (unitless) (Table 4.4-114),

DCF_{inh} = dose conversion factor for inhalation (mrem/pCi) (Table 4.4-108), and

ρ_{H2O} = water density (kg/L) (Table 4.4-117).

4.4.8.2.2 MOP at the Stream Dose Calculations

The following MOP exposure pathways were used in calculating the dose to the MOP receptor with stream water near the contaminated SL as a primary water

source. As with the 100-meter well calculations, all transfer times are assumed to be negligible due to the long-term analysis of the PAs.

The dose to the MOP at the SL is determined according to Eq. 4.4-182:

$$D_{MOP,SL} = D_{MOP,SL,ing} + D_{MOP,SL,exp} + D_{MOP,SL,inh} \quad \text{Eq. 4.4-182}$$

where:

$D_{MOP,SL}$ = total dose to the MOP at the SL (mrem/yr),

$D_{MOP,SL,ing}$ = dose to the MOP at the SL (mrem/yr) due to ingestion (see Eq. 4.4-183),

$D_{MOP,SL,exp}$ = dose to the MOP at the SL (mrem/yr) due to exposure (see Eq. 4.4-191), and

$D_{MOP,SL,inh}$ = dose to the MOP at the SL (mrem/yr) due to inhalation (see Eq. 4.4-194).

Within GoldSim, this is implemented within a closed container: *SL_Dose* (found within the *Dose_Results* container), shown in Figure 4.4-173.

The contents of this container (Figure 4.4-174), is similar to that of the 100-meter specific containers except that the concentration element is external to this container because the seepline concentrations are used for multiple exposure scenarios. The sum element named *Dose_SL_rads* is used to perform Eq. 4.4-182.

Figure 4.4-173: Dose Result Container for Seepline (or Stream) Doses

Figure 4.4-174: Contents of Seepline Dose Result Container

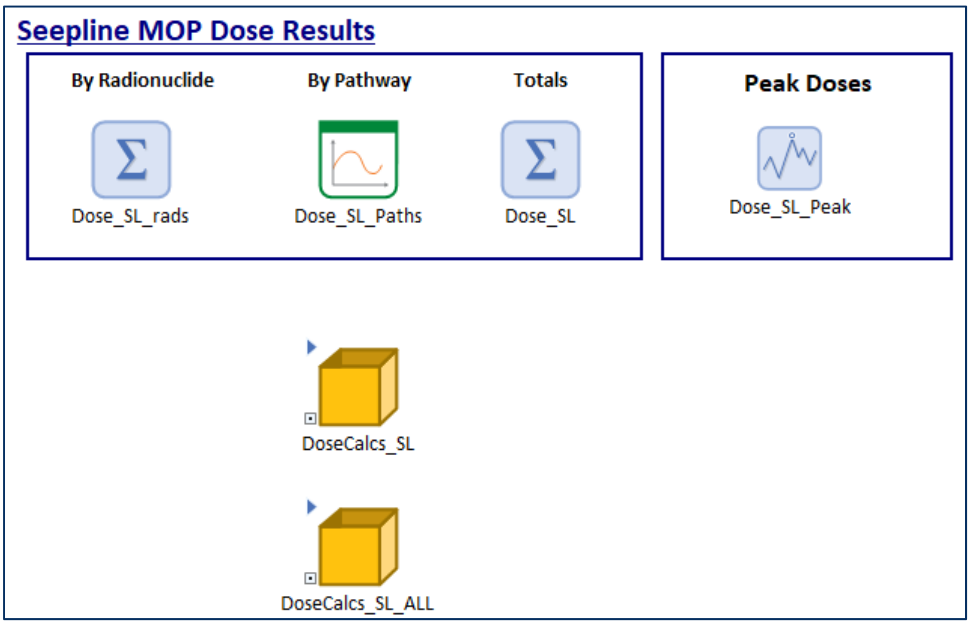

MOP at the SL, Ingestion Dose Pathways

The following text defines the parameter $D_{MOP,SL,ing}$ from Eq. 4.4-182. The ingestion dose to the MOP at the SL is determined according to Eq. 4.4-183:

$$D_{MOP,SL,ing} = D_{MOP,SL,H2O,ing} + D_{MOP,SL,SOIL,ing} + D_{MOP,SL,PLANT,ing} + D_{MOP,SL,MEAT,ing} + D_{MOP,SL,MILK,ing} + D_{MOP,SL,POULTRY,ing} + D_{MOP,SL,EGG,ing} + D_{SL,FISH,ing} \quad \text{Eq. 4.4-183}$$

where:

$D_{MOP,SL,ing}$ = dose to the MOP at the SL (mrem/yr) due to ingestion,

$D_{MOP,SL,H2O,ing}$ = dose to the MOP at the SL (mrem/yr) due to ingestion of water from stream water at the contaminated SL (Eq. 4.4-184),

$D_{MOP,SL,SOIL,ing}$ = dose to the MOP at the SL (mrem/yr) due to ingestion of soil that has been irrigated with water from stream water at the contaminated SL (Eq. 4.4-185),

$D_{MOP,SL,PLANT,ing}$ = dose to the MOP at the SL (mrem/yr) due to ingestion of produce irrigated with water from stream water at the contaminated SL water (Eq. 4.4-186),

$D_{MOP,SL,MEAT,ing}$ = dose to the MOP at the SL (mrem/yr) due to ingestion of meat (i.e., terrestrial livestock meat such as beef, pork, veal, etc.) that eats fodder watered by and drinks water from stream water at the contaminated SL (Eq. 4.4-187),

$D_{MOP,SL,MILK,ing}$ = dose to the MOP at the SL (mrem/yr) due to ingestion of milk that comes from livestock that eats fodder watered by and drinks water from stream water at the contaminated SL (Eq. 4.4-188),

$D_{MOP,SL,POULTRY,ing}$ = dose to the MOP at the SL (mrem/yr) due to ingestion of poultry (including chicken, turkey, etc.) that eats fodder watered by and drinks water from stream water at the contaminated SL (Eq. 4.4-189),

$D_{MOP,SL,EGG,ing}$ = dose to the MOP at the SL (mrem/yr) due to ingestion of eggs that come from poultry that eats fodder watered by and drinks water from stream water at the contaminated SL (Eq. 4.4-190), and

$D_{SL,FISH,ing}$ = dose (mrem/yr) due to ingestion of fish that came from stream water near the contaminated SL, as defined in (Eq. 4.4-162).

Ingestion of Water (MOP at the SL)

The exposure pathway for water ingestion assumes the MOP receptor uses water from the stream at the SL as a drinking source. The incidental ingestion of water from showering and during recreational activities is assumed negligible when compared to ingestion of drinking water. The dose from ingestion of drinking water shall be calculated according to Eq. 4.4-184:

$$D_{MOP,SL,H2O,ing} = C_{SL} \times EDF_{H2O,ing} \qquad \text{Eq. 4.4-184}$$

where:

$D_{MOP,SL,H2O,ing}$ = dose to the MOP at the SL (mrem/yr) due to ingestion of water from stream water at the contaminated SL,

C_{SL} = radionuclide concentration in stream water at the contaminated SL (pCi/L) as determined from an appropriate contaminant transport model, and

$EDF_{H2O,ing}$ = effective dose factor for ingestion of stream water at the contaminated SL (L×mrem)/(pCi×yr) defined in Eq. 4.4-141.

Ingestion of Soil (MOP at the SL)

Exposure pathway from ingestion of soil assumes the soil is irrigated with ground water from the SL and the MOP receptor in turn consumes the contaminated soil. This formula was derived following the approach of the previous pathway calculations. A soil buildup factor was applied to account for the buildup of radionuclide concentration in the soil from successive years of irrigation. The radionuclide concentration in the soil and the dose is calculated using the following formula:

$$D_{MOP,SL,SOIL,ing} = C_{SL} \times EDF_{SOIL,ing} \qquad \text{Eq. 4.4-185}$$

where:

$D_{MOP,SL,SOIL,ing}$ = dose to the MOP at the SL (mrem/yr) due to ingestion of soil that has been irrigated with water from stream water at the contaminated SL,

C_{SL} = radionuclide concentration in stream water at the contaminated SL (pCi/L) as determined from an appropriate contaminant transport model, and

$EDF_{SOIL,ing}$ = effective dose factor for ingestion of soil contaminated by stream water at the SL (L×mrem)/(pCi×yr) defined in Eq. 4.4-143.

Ingestion of Produce (MOP at the SL)

The dose to the MOP receptor from ingestion of contaminated produce (including leafy vegetables, other vegetables, and fruit) is calculated assuming two contamination exposure pathways: (1) direct deposition of contaminated irrigation water on plants and (2) root uptake of contaminated irrigation water in soil. The irrigation water is from the SL. The dose is calculated using Eq. 4.4-186:

$$D_{MOP,SL,PLANT,ing} = C_{SL} \times EDF_{PLANT,ing} \times F_{local,PLANT} \quad \text{Eq. 4.4-186}$$

where:

$D_{MOP,SL,PLANT,ing}$ = dose to the MOP at the SL (mrem/yr) due to ingestion of produce that has been irrigated with stream water from the contaminated SL,

C_{SL} = radionuclide concentration in stream water at the contaminated SL (pCi/L) as determined from an appropriate contaminant transport model,

$EDF_{PLANT,ing}$ = effective dose factor for ingestion of produce contaminated by stream water at the SL (L×mrem)/(pCi×yr) defined in Eq. 4.4-148, and

$F_{local,PLANT}$ = fraction of total produce grown locally (unitless) (Eq. 4.4-247).

Ingestion of Meat (MOP at the SL)

The meat ingestion pathway assumes that terrestrial livestock drinks contaminated stock water and consumes fodder irrigated with contaminated water. The stock water and irrigation water is from the SL. The fodder is contaminated from direct deposition of contaminated irrigation water on plants and from deposition of contaminated irrigation water in soil followed by root uptake by plants. The buildup of radionuclide concentration in the soil from successive years of irrigation is accounted for. The radionuclide concentration in fodder from deposition and root uptake is calculated as well.

For the purpose of this calculation, meat (or terrestrial livestock) includes all meat that is not considered poultry or fish. This includes beef, pork, veal, and other game.

Following the terrestrial livestock ingestion of the contaminated water and fodder, the MOP receptor consumes the contaminated meat. The dose from ingesting contaminated meat is calculated using the following formula:

$$D_{MOP,SL,MEAT,ing} = C_{SL} \times EDF_{MEAT,ing} \times F_{local,MEAT} \quad \text{Eq. 4.4-187}$$

where:

$D_{MOP,SL,MEAT,ing}$ = dose to the MOP at the SL (mrem/yr) due to ingestion of meat (i.e., terrestrial livestock meat such as beef, pork, veal, etc.) that eats fodder watered by and drinks water from stream water at the contaminated SL water,

C_{SL} = radionuclide concentration in stream water at the contaminated SL (pCi/L) as determined from an appropriate contaminant transport model,

$EDF_{MEAT,ing}$ = effective dose factor for ingestion of terrestrial livestock meat contaminated by stream water at the SL (L×mrem)/(pCi×yr) as defined in Eq. 4.4-154, and

$F_{local,MEAT}$ = fraction of terrestrial livestock raised locally (unitless) (Table 4.4-118).

Ingestion of Milk (MOP at the SL)

Following the livestock ingestion of the contaminated water and fodder, the MOP receptor consumes the contaminated milk from the livestock cattle. The dose from ingestion of contaminated milk is calculated using the following formula:

$$D_{MOP,SL,MILK,ing} = C_{SL} \times EDF_{MILK,ing} \times F_{local,MILK} \quad \text{Eq. 4.4-188}$$

where:

$D_{MOP,SL,MILK,ing}$ = dose to the MOP at the SL (mrem/yr) due to ingestion of milk that comes from milk-producing livestock that eats fodder watered by and drinks water from stream water at the contaminated SL,

C_{SL} = radionuclide concentration in stream water at the contaminated SL (pCi/L) as determined from an appropriate contaminant transport model,

$EDF_{MILK,ing}$ = effective dose factor for ingestion of milk contaminated by stream water at the SL (L×mrem)/(pCi×yr) as defined in Eq. 4.4-157, and

$F_{local,MILK}$ = fraction of milk-producing livestock raised locally (unitless) (Table 4.4-118).

Ingestion of Poultry (MOP at the SL)

The poultry and egg ingestion pathways assume poultry drink contaminated stock water and consume fodder irrigated with contaminated water. The stock water and irrigation water are from the SL. The fodder is contaminated from direct deposition of contaminated irrigation water on plants and from deposition of contaminated irrigation water in soil followed by root uptake by plants. It is also assumed that poultry directly ingest contaminated soil in addition to the stock water and fodder. The dose from ingestion of contaminated poultry is calculated using the following formula:

$$D_{MOP,SL,POULTRY,ing} = C_{SL} \times EDF_{POULTRY,ing} \times F_{local,POULTRY} \quad \text{Eq. 4.4-189}$$

where:

$D_{MOP,SL,POULTRY,ing}$ = dose to the MOP at the SL (mrem/yr) due to ingestion of poultry (including chicken, turkey, etc.) that eats fodder watered by and drinks water from stream water at the contaminated SL,

C_{SL} = radionuclide concentration in stream water at the contaminated SL (pCi/L) as determined from an appropriate contaminant transport model,

$EDF_{POULTRY,ing}$ = effective dose factor for ingestion of poultry contaminated by stream water at the SL (L×mrem)/(pCi×yr) as defined in Eq. 4.4-159, and

$F_{local,POULTRY}$ = fraction of poultry raised locally (unitless) (Table 4.4-118).

Ingestion of Egg (MOP at the SL)

Following the poultry ingestion of the contaminated water and fodder, the MOP consumes the contaminated eggs. The dose from ingestion of contaminated eggs is calculated using the following formula:

$$D_{MOP,SL,EGG,ing} = C_{SL} \times EDF_{EGG,ing} \times F_{local,EGG} \quad \text{Eq. 4.4-190}$$

where:

$D_{MOP,SL,EGG,ing}$ = dose to the MOP at the SL (mrem/yr) due to ingestion of eggs that come from poultry that eats fodder watered by and drinks water from stream water at the contaminated SL,

C_{SL} = radionuclide concentration in stream water at the contaminated SL (pCi/L) as determined from an appropriate contaminant transport model,

$EDF_{EGG,ing}$ = effective dose factor for ingestion of eggs contaminated by stream water at the SL (L×mrem)/(pCi×yr) as defined in Eq. 4.4-161, and

$F_{local,EGG}$ = fraction of eggs produced locally (unitless) (Table 4.4-118).

Ingestion of Fish

The fish ingestion route assumes fish are caught from a stream contaminated stream at the point of highest concentration, and the MOP receptor in turn consumes the contaminated fish. The dose from ingestion of fish shall be calculated according to Eq. 4.4-162.

MOP at the SL, Direct Exposure Dose Pathways

The following text defines the parameter $D_{MOP,SL,exp}$ from Eq. 4.4-182. The direct exposure dose to the MOP at the SL is determined according to Eq. 4.4-191:

$$D_{MOP,SL,exp} = D_{MOP,SL,SOIL,exp} + D_{MOP,SL,SHOWER,exp} + D_{SL,SWIM,exp} + D_{SL,BOAT,exp} \quad \text{Eq. 4.4-191}$$

where:

$D_{MOP,SL,exp}$ = dose to the MOP at the SL (mrem/yr) due to exposure,

$D_{MOP,SL,SOIL,exp}$ = dose to the MOP at the SL (mrem/yr) due to direct exposure to soil irrigated from stream water at the SL (Eq. 4.4-192),

$D_{MOP,100,SHOWER,exp}$ = dose to the MOP at the SL (mrem/yr) due to direct exposure while showering or bathing in water from stream water at the SL (Eq. 4.4-193),

$D_{SL,SWIM,exp}$ = dose (mrem/yr) due to direct exposure from swimming in stream water at the contaminated SL as defined in Eq. 4.4-169, and

$D_{SL,BOAT,exp}$ = dose (mrem/yr) due to direct exposure from boating and fishing in stream water at the contaminated SL as defined in Eq. 4.4-171.

Direct Exposure from Irrigated Soil (MOP at the SL)

The exposure pathway from direct contact to contaminated soil assumes the soil is irrigated with water from the SL and the MOP receptor in turn is exposed during time spent caring for a garden or crop. The radionuclide concentration in the soil and the exposure dose is calculated using the following formula:

$$D_{MOP,SL,SOIL,exp} = C_{SL} \times EDF_{SOIL,exp} \qquad \text{Eq. 4.4-192}$$

where:

$D_{MOP,SL,SOIL,exp}$ = dose to the MOP at the SL (mrem/yr) due to direct exposure to soil irrigated from water at the SL,

C_{SL} = radionuclide concentration in stream water at the contaminated SL (pCi/L) as determined from an appropriate contaminant transport model, and

$EDF_{SOIL,exp}$ = effective dose factor for external exposure to soil (L×mrem)/(pCi×yr) as defined in Eq. 4.4-166.

Direct Exposure from Showering (MOP at the SL)

The direct contact exposure pathway from showering and bathing assumes the MOP receptor receives dose from washing in water from the SL. The dose is calculated using the following formula:

$$D_{MOP,SL,SHOWER,exp} = C_{SL} \times EDF_{SHOWER,exp} \qquad \text{Eq. 4.4-193}$$

where:

$D_{MOP,SL,SHOWER,exp}$ = dose to the MOP at the SL (mrem/yr) due to direct exposure while showering or bathing in water from the contaminated SL,

C_{SL} = radionuclide concentration in stream water at the contaminated SL (pCi/L) as determined from an appropriate contaminant transport model, and

$EDF_{SHOWER,exp}$ = effective dose factor for external exposure to water while showering or bathing (L×mrem)/(pCi×yr) as defined in Eq. 4.4-168.

Direct Exposure from Swimming

The direct contact exposure pathway from swimming assumes the MOP receptor receives dose from swimming in a contaminated stream at the point of highest concentration. The dose from swimming exposure shall be calculated according to Eq. 4.4-169.

Direct Exposure from Boating and Fishing

The direct contact exposure pathway from boating and fishing assumes the MOP receptor receives dose from activities in a contaminated stream at the point of highest concentration. The dose from boating and fishing exposure shall be calculated according to Eq. 4.4-171.

MOP at the SL, Inhalation Dose Pathways

The following text defines the parameter $D_{MOP,SL,inh}$ from Eq. 4.4-182. The inhalation dose to the MOP at the SL is determined according to Eq. 4.4-194:

$$D_{MOP,SL,inh} = D_{MOP,SL,IRR,inh} + D_{MOP,SL,DUST,inh} + D_{MOP,SL,SHOWER,inh} + D_{SL,SWIM,inh} \quad \text{Eq. 4.4-194}$$

where:

$D_{MOP,SL,inh}$ = dose to the MOP at the SL (mrem/yr) due to inhalation,

$D_{MOP,SL,IRR,inh}$ = dose to the MOP at the SL (mrem/yr) due to inhalation while irrigating gardens or crops with water from the contaminated SL (Eq. 4.4-195),

$D_{MOP,SL,DUST,inh}$ = dose to the MOP at the SL (mrem/yr) due to inhalation of dust and soil that has been contaminated due to irrigation with water from the contaminated SL (Eq. 4.4-196),

$D_{MOP,SL,SHOWER,inh}$ = dose to the MOP at SL (mrem/yr) due to inhalation while showering or bathing in water from the contaminated SL (Eq. 4.4-197), and

$D_{SL,SWIM,inh}$ = dose (mrem/yr) due to inhalation while swimming in stream water at the contaminated SL as defined in Eq. 4.4-180.

Inhalation of Water During Irrigation (MOP at the SL)

The exposure pathway from inhalation during irrigation assumes soil is irrigated with water from the contaminated SL and the MOP receptor is exposed by breathing while the garden or crop is irrigated but only during time spent caring for a garden or crop. The dose is calculated using the following formula:

$$D_{MOP,SL,IRR,inh} = C_{SL} \times EDF_{IRR,inh} \quad \text{Eq. 4.4-195}$$

where:

$D_{MOP,SL,IRR,inh}$ = dose to the MOP at the SL (mrem/yr) due to inhalation while irrigating gardens or crops with water from the contaminated SL,

C_{SL} = radionuclide concentration in stream water at the contaminated SL (pCi/L) as determined from an appropriate contaminant transport model, and

EDF_{IRRinh} = effective dose factor for inhalation of water during irrigation (L×mrem)/(pCi×yr) as defined in Eq. 4.4-175.

Inhalation of Dust from Irrigated Soil (MOP at the SL)

The dose pathway associated with inhalation of dust and soil that has been irrigated assumes that dust and soil has been irrigated with water from the contaminated SL and that the MOP receptor is exposed by breathing dust during time spent caring for a garden or crop. This formula was derived following the approach of previous pathway calculations. The dose is calculated using the following formula:

$$D_{MOP,SL,DUST,inh} = C_{SL} \times EDF_{DUST,inh} \quad \text{Eq. 4.4-196}$$

where:

$D_{MOP,SL,DUST,inh}$ = dose to the MOP at the SL (mrem/yr) due to inhalation of dust and soil that has been contaminated due to irrigation with water from the contaminated SL,

C_{SL} = radionuclide concentration in stream water at the contaminated SL (pCi/L) as determined from an appropriate contaminant transport model, and

$EDF_{DUSTinh}$ = effective dose factor for inhalation of dust and soil (L×mrem)/(pCi×yr) as defined in Eq. 4.4-177.

Inhalation during Showering (MOP at the SL)

The showering inhalation dose pathway assumes the MOP receptor is exposed by breathing humid air within the shower. The source of water for the shower is the stream at the contaminated SL. The dose is calculated using the following formula:

$$D_{MOP,SL,SHOWER,inh} = C_{SL} \times EDF_{SHOWER,inh} \quad \text{Eq. 4.4-197}$$

where:

$D_{MOP,SL,SHOWER,inh}$ = dose to the MOP at SL (mrem/yr) due to inhalation while showering or bathing in water from the contaminated SL,

C_{SL} = radionuclide concentration in stream water at the contaminated SL (pCi/L) as determined from an appropriate contaminant transport model, and

$EDF_{SHOWER,inh}$ = effective dose factor for inhalation of water while showering or bathing (L×mrem)/(pCi×yr) as defined in Eq. 4.4-179.

Inhalation during Swimming

The swimming inhalation pathway assumes that water from a stream has contamination at the SL and the receptor inhales saturated air. For simplicity, the moisture contained in the inhaled air is assumed to be stream water at the seepline. The dose is calculated using Eq. 4.4-180.

4.4.8.2.3 Acute IHI Dose Calculations

The Acute IHI scenario assumes one of two possible scenarios. In the first scenario, during well installation the drill is assumed to penetrate directly into an SDU. In the second scenario, the drill is assumed to penetrate into soils immediately adjacent to an SDU. Given the material and current drilling practices, the first scenario (directly into an SDU) is not considered a credible scenario and does not represent an expected condition; it is only considered for informational purposes to illustrate bounding conditions. For either scenario, the IHI receptor is exposed to ingestion and inhalation of dust and material from the drill cuttings, and direct exposure through handling the contaminated drill cuttings.

The following IHI exposure pathways were used in calculating the acute dose to the IHI receptor from contaminated drill cuttings. The dose to the Acute IHI is determined according to Eq. 4.4-198:

$$D_{IHIA} = D_{IHIA,ing} + D_{IHIA,exp} + D_{IHIA,inh} \quad \text{Eq. 4.4-198}$$

where:

D_{IHIA} = total dose to the Acute IHI (mrem),

$D_{IHIA,ing}$ = dose to the Acute IHI (mrem) due to ingestion (see Eq. 4.4-199),

$D_{IHIA,exp}$ = dose to the Acute IHI (mrem) due to exposure (see Eq. 4.4-202), and

$D_{IHIA,inh}$ = dose to the Acute IHI (mrem) due to inhalation (see Eq. 4.4-204).

Acute IHI, Ingestion Dose Pathways

The following text defines the parameter $D_{IHIA,ing}$ from Eq. 4.4-198. The Acute IHI ingestion dose is due to the resuspension of material during drilling activities. The Acute IHI ingestion dose is determined according to Eq. 4.4-199:

$$D_{IHIA,ing} = C_{IHIA} \times EDF_{IHIA,ing} \quad \text{Eq. 4.4-199}$$

where:

$D_{IHIA,ing}$ = dose to the Acute IHI (mrem) due to ingestion,

C_{IHIA} = radionuclide concentration in contaminated drill cuttings (pCi/m^3) defined in Eq. 4.4-201 below, and

$EDF_{IHIA,ing}$ = effective dose factor for ingestion of contaminated drill cutting (L×mrem)/(pCi) defined in Eq. 4.4-200 below.

The EDF for ingestion of dust from drill cuttings shall be calculated as:

$$EDF_{IHIA,ing} = \frac{(F_{t,DRILL} \times 1yr) \times U_{SOIL} \times DCF_{ing}}{\rho_s} \quad \text{Eq. 4.4-200}$$

where:

$EDF_{IHIA,ing}$ = effective dose factor for ingestion of contaminated drill cutting (L×mrem)/(pCi),

$F_{t,DRILL}$ = fraction of time exposed to drill cuttings (unitless) (Table 4.4-114),

U_{SOIL} = human ingestion rate of soil (kg/yr) (Table 4.4-110),

DCF_{ing} = ingestion dose conversion factor (mrem/pCi) (Table 4.4-108), and

ρ_{bs} = dry bulk density of soil (kg/m^3) (Table 4.4-115).

The drill cutting concentration can be determined as a function of the maximum drill core activity and the geometry of the drilled well:

$$C_{IHIA} = \frac{Act_{max}}{\pi\left(\frac{well_{diam}}{2}\right)^2 \times well_{dep}} \quad \text{Eq. 4.4-201}$$

where:

C_{IHIA} = radionuclide concentration in contaminated drill cuttings (pCi/m^3),

Act_{max} = maximum drilled core activity or mass (pCi) defined prior to dose calculation based on the inventory from the source of the contaminated drill cuttings,

$well_{diam}$ = well diameter (m) (Table 4.4-117), and

$well_{dep}$ = well depth (m) (Table 4.4-117).

Within GoldSim, the drill cutting concentration is determined within the *IHI_DrillCutConc_Calc* container (shown in Figure 4.4-165). Within *IHI_DrillCutConc_Calc* GoldSim Cell Pathway elements: *DrillCell* (representing the contaminated drill cuttings) and *Garden* (representing the contamination of soil due to drill cuttings) are used for implementing Eq. 4.4-201 (see Figure 4.4-175).

Figure 4.4-175: Contents GoldSim Container: *IHI_DrillCutConc_Calc*

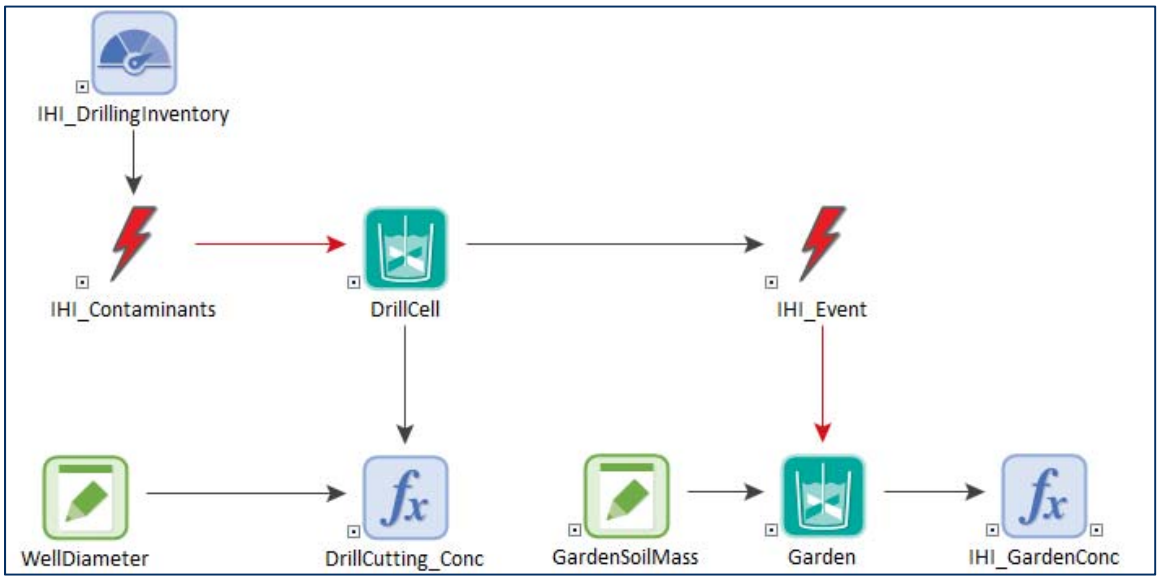

Acute IHI, Direct Exposure Dose Pathways

The following text defines the parameter $D_{IHIA,exp}$ from Eq. 4.4-198. The Acute IHI direct exposure dose is due to direct contact with contaminated material during drilling activities. The Acute IHI exposure dose is determined according to Eq. 4.4-202:

$$D_{IHIA,exp} = C_{IHIA} \times EDF_{IHIA,exp} \qquad \text{Eq. 4.4-202}$$

where:

$D_{IHIA,exp}$ = dose to the Acute IHI (mrem) due to exposure,

C_{IHIA} = radionuclide concentration in contaminated drill cuttings (pCi/m^3) (see Eq. 4.4-201 above), and

$EDF_{IHIA,exp}$ = effective dose factor for direct exposure of contaminated drill cuttings (L×mrem)/(pCi) defined in Eq. 4.4-203 below.

The EDF for direct exposure to drill cuttings shall be calculated as:

$$EDF_{IHIA,exp} = \left(F_{t,DRILL} \times 1yr\right) \times DCF_{exp} \qquad \text{Eq. 4.4-203}$$

where:

$EDF_{IHIA,exp}$ = effective dose factor for direct exposure of contaminated drill cuttings (L×mrem)/(pCi),

$F_{t,DRILL}$ = fraction of time exposed to drill cuttings (unitless) (Table 4.4-114), and

DCF_{exp} = dose conversion factor for external exposure (m^3×mrem)/(pCi×yr) Table 4.4-108.

Acute IHI, Inhalation Dose Pathways

The following text defines the parameter $D_{IHIA,inh}$ from Eq. 4.4-198. The Acute IHI inhalation dose is due to the resuspension of material during drilling activities. The Acute IHI inhalation dose is determined according to Eq. 4.4-204:

$$D_{IHIA,inh} = C_{IHIA} \times EDF_{IHIA,inh} \quad \text{Eq. 4.4-204}$$

where:

$D_{IHIA,inh}$ = dose to the Acute IHI (mrem) due to inhalation,

C_{IHIA} = radionuclide concentration in contaminated drill cuttings (pCi/m^3) (see Eq. 4.4-201 above), and

$EDF_{IHIA,inh}$ = effective dose factor inhalation of dust from contaminated drill cuttings (L×mrem)/(pCi) defined in Eq. 4.4-205 below.

The EDF for inhalation of dust from drill cuttings shall be calculated as:

$$EDF_{IHIA,inh} = \frac{(F_{t,DRILL} \times 1yr) \times L_{SOIL} \times U_{SOIL} \times DCF_{inh}}{\rho_s} \quad \text{Eq. 4.4-205}$$

where:

$EDF_{IHIA,inh}$ = effective dose factor inhalation of dust from contaminated drill cuttings (L×mrem)/(pCi),

$F_{t,DRILL}$ = fraction of time exposed to drill cuttings (unitless) (Table 4.4-114),

L_{SOIL} = soil loading in air while drilling (kg/m^3) (Table 4.4-114),

U_{SOIL} = rate of soil and dust ingestion (m^3/yr) (Table 4.4-110),

DCF_{inh} = dose conversion factor for inhalation (mrem/pCi) (Table 4.4-108), and

ρ_{bs} = dry bulk density of soil (kg/m^3) (Table 4.4-115).

4.4.8.2.4 Chronic IHI Dose Calculations

Provided below are the individual elements of the Chronic IHI pathways. The chronic intruder exposure pathways detailed below are used in calculating the dose to the chronic intruder receptor using a hypothetical well, drilled 1-meter from the facility boundary (i.e., a 1-meter well), as a primary water source. The stream is the secondary water source for the pathways involving swimming, boating, and fish ingestion. All transfer times are assumed negligible due to the long-term analysis of the PA.

The chronic dose to the IHI is determined according to Eq. 4.4-206:

$$D_{IHIC} = D_{IHIC,ing} + D_{IHIC,exp} + D_{IHIC,inh} \quad \text{Eq. 4.4-206}$$

where:

D_{IHIC} = total dose to the Chronic IHI (mrem/yr),

$D_{IHIC,ing}$ = dose to the Chronic IHI (mrem/yr) due to ingestion (see Eq. 4.4-207),

$D_{IHIC,exp}$ = dose to the Chronic IHI (mrem/yr) due to exposure (see Eq. 4.4-234), and

$D_{IHIC,inh}$ = dose to the Chronic IHI (mrem/yr) due to inhalation (see Eq. 4.4-240).

Chronic IHI, Ingestion Dose Pathways

The following text defines the parameter $D_{IHIC,ing}$ from Eq. 4.4-206. The ingestion dose to the Chronic IHI is determined according to Eq. 4.4-207:

$$D_{IHIC,ing} = D_{IHIC,H2O,ing} + D_{IHIC,SOIL,ing} + D_{IHIC,PLANT,ing} + D_{IHIC,MEAT,ing} + D_{IHIC,MILK,ing} + D_{IHIC,POULTRY,ing} + D_{IHIC,EGG,ing} + D_{SL,FISH,ing} \quad \text{Eq. 4.4-207}$$

where:

$D_{IHIC,ing}$ = dose to the Chronic IHI (mrem/yr) due to ingestion,

$D_{IHIC,H2O,ing}$ = dose to the Chronic IHI (mrem/yr) due to ingestion of water from the 1-meter well (Eq. 4.4-208),

$D_{IHIC,SOIL,ing}$ = dose to the Chronic IHI (mrem/yr) due to ingestion of soil that has been irrigated with water from the 1-meter well and contaminated from the deposition of drill cuttings (Eq. 4.4-209),

$D_{IHIC,PLANT,ing}$ = dose to the Chronic IHI (mrem/yr) due to ingestion of produce (both fruits and vegetables) irrigated from the 1-meter well water and contaminated by the deposition of drill cuttings (Eq. 4.4-214),

$D_{IHIC,MEAT,ing}$ = dose to the Chronic IHI (mrem/yr) due to ingestion of meat (i.e., terrestrial livestock meat such as beef, pork, veal, etc.) that drinks water from the 1-meter well and consumes fodder that is grown in soils contaminated by the deposition of drill cuttings and irrigated from the 1-meter well (Eq. 4.4-218),

$D_{IHIC,MILKing}$ = dose to the Chronic IHI (mrem/yr) due to ingestion of milk that comes from milk-producing livestock that drinks water from the 1-meter well and consumes fodder that is grown in soils contaminated by the deposition of drill cuttings and irrigated from the 1-meter well (Eq. 4.4-222),

$D_{IHIC,POULTRYing}$ = dose to the Chronic IHI (mrem/yr) due to ingestion of poultry (including chicken, turkey, etc.) that that drinks water from the 1-meter well and consumes fodder that is grown in soils contaminated by the deposition of drill cuttings and irrigated from the 1-meter well (Eq. 4.4-226),

$D_{IHIC,EGGing}$ = dose to the Chronic IHI (mrem/yr) due to ingestion of eggs that come from poultry that drinks water from the 1-meter well and consumes fodder that is grown in soils contaminated by the deposition of drill cuttings and irrigated from the 1-meter well (Eq. 4.4-230), and

$D_{SL,FISHing}$ = dose to the Chronic IHI (mrem/yr) due to ingestion of fish that came from stream water near the contaminated SL, as defined in Eq. 4.4-162).

Ingestion of Water (Chronic IHI)

The drinking water exposure route assumes a well 1-meter from the facility boundary is used by the IHI receptor as a drinking water source. The incidental ingestion of water from showering and during recreational activities is assumed negligible when compared to ingestion of drinking water. The dose from ingestion of drinking water is calculated using the following formula:

$$D_{IHIC,H2O,ing} = C_{IHIC} \times EDF_{H2O,ing} \quad \text{Eq. 4.4-208}$$

where:

$D_{IHIC,H2O,ing}$ = dose to the Chronic IHI (mrem/yr) due to ingestion of water from the 1-meter well,

C_{IHIC} = radionuclide concentration in ground water from the 1-meter well (pCi/L) as determined from an appropriate contaminant transport model, and

$EDF_{H2O,ing}$ = effective dose factor for ingestion of contaminated ground water (L×mrem)/(pCi×yr) defined in Eq. 4.4-141.

Ingestion of Soil (Chronic IHI)

The soil ingestion exposure pathway assumes soil is contaminated from two contamination sources: (1) the soil is irrigated with ground water from the 1-meter well and (2) deposition of contaminated drill cuttings in the garden or crop soil, as follows:

$$D_{IHIC,SOIL,ing} = D_{IHIC,H2O,SOIL,ing} + D_{IHIC,Drill,SOIL,ing} \quad \text{Eq. 4.4-209}$$

where:

$D_{IHIC,SOIL,ing}$ = dose to the Chronic IHI (mrem/yr) due to ingestion of soil,

$D_{IHIC,H2O,SOIL,ing}$ = dose to the Chronic IHI (mrem/yr) due to ingestion of soil that has been irrigated with water from the 1-meter well, and

$D_{IHIC,Drill,SOIL,ing}$ = dose to the Chronic IHI (mrem/yr) due to ingestion of soil that has been contaminated by drill cuttings.

The dose from ingestion of soil irrigated by 1-meter well water, $D_{IHIC,H2O,SOIL,ing}$, as used in Eq. 4.4-209, is determined according to the following:

$$D_{IHIC,H2O,SOIL,ing} = C_{IHIC} \times EDF_{SOIL,ing} \quad \text{Eq. 4.4-210}$$

where:

$D_{IHIC,H2O,SOIL,ing}$ = dose to the Chronic IHI (mrem/yr) due to ingestion of soil that has been irrigated with water from the 1-meter well (see Eq. 4.4-211),

C_{IHIC} = radionuclide concentration in ground water from the 1-meter well (pCi/L) as determined from an appropriate contaminant transport model (see Eq. 4.4-212), and

$EDF_{SOIL,ing}$ = effective dose factor for ingestion of soil contaminated by ground water (L×mrem)/(pCi×yr) defined in Eq. 4.4-143.

Similarly, dose from ingestion of soil contaminated by drill cuttings, $D_{IHIC,Drill,SOIL,ing}$, is determined according to Eq. 4.4-211:

$$D_{IHIC,Drill,SOIL,ing} = C_{IHI,g} \times EDF_{EDF,SOIL,ing} \quad \text{Eq. 4.4-211}$$

where:

$D_{IHIC,H2O,SOIL,ing}$ = dose to the Chronic IHI (mrem/yr) due to ingestion of soil that has been contaminated by drill cuttings,

$C_{IHIC,g}$ = radionuclide concentration in the garden or crop from contaminated drill cuttings (pCi/m^3) as defined by Eq. 4.4-212 below, and

$EDF_{IHI,SOIL,ing}$ = effective dose factor for ingestion of soil contaminated by drill cuttings (L×mrem)/(pCi×yr) defined in Eq. 4.4-213 below.

The IHI drill cuttings are assumed to be mixed into the volume of the soil:

$$C_{IHIC,g} = \frac{Act_{max}}{A_{garden} \times d_{till}} \quad \text{Eq. 4.4-212}$$

where:

$C_{IHIC,g}$ = radionuclide concentration in the garden or crop soil from contaminated drill cuttings (pCi/m^3),

Act_{max} = maximum drilled core activity or mass (pCi) defined prior to dose calculation based on the inventory from the source of the contaminated drill cuttings,

A_{garden} = garden or crop area (m^2) (Table 4.4-116), and

d_{till} = depth of tilling for agriculture or gardening (m) (Table 4.4-116).

The EDF for ingestion of soil and dust contaminated by drill cuttings shall be calculated as:

$$EDF_{IHIC,SOIL,ing} = \frac{F_{t,g} \times U_{SOIL} \times DCF_{ing}}{\rho_s} \quad \text{Eq. 4.4-213}$$

where:

$EDF_{IHIC,SOILing}$ = effective dose factor for ingestion of soil contaminated by drill cuttings (L×mrem)/(pCi×yr),

$F_{t,g}$ = fraction of the time the IHI spends in the garden or crop (unitless) (Table 4.4-114),

U_{SOIL} = human ingestion rate of soil (kg/yr) (Table 4.4-110),

DCF_{ing} = dose conversion factor for ingestion (mrem/pCi) (Table 4.4-108), and

ρ_{bs} = dry bulk density of soil (kg/m^3) (Table 4.4-115).

Ingestion of Produce (Chronic IHI)

The chronic dose to the IHI receptor from ingestion of contaminated produce (including leafy vegetables, other vegetables, and fruit) is calculated assuming two contamination sources: (1) the soil is irrigated with ground water from the 1-meter well and (2) deposition of contaminated drill cuttings in the garden or crop soil, as follows:

$$D_{IHIC,PLANT,ing} = \left(D_{IHIC,H2O,PLANT,ing} + D_{IHIC,Drill,PLANT,ing}\right) \times F_{local,PLANT} \quad \text{Eq. 4.4-214}$$

where:

$D_{IHIC,PLANT,ing}$ = dose to the Chronic IHI (mrem/yr) due to ingestion of produce,

$D_{IHIC,H2O,PLANT,ing}$ = dose to the Chronic IHI (mrem/yr) due to ingestion of produce that has been irrigated with water from the 1-meter well (Eq. 4.4-215),

$D_{IHIC,Drill,PLANT,ing}$ = dose to the Chronic IHI (mrem/yr) due to ingestion of produce that has been contaminated by drill cuttings (Eq. 4.4-216), and

$F_{local,PLANT}$ = fraction of consumed produce grown locally (unitless) (Eq. 4.4-247).

The dose from ingestion of plants contaminated by ground water $D_{IHIC,H2O,PLANT,ing}$ is calculated using the following formula:

$$D_{IHIC,H2O,PLANT,ing} = C_{IHIC} \times EDF_{PLANT,ing} \quad \text{Eq. 4.4-215}$$

where:

$D_{IHIC,H2O,PLANT,ing}$ = dose to the Chronic IHI (mrem/yr) due to ingestion of produce that has been irrigated with water from the 1-meter well,

C_{IHIC} = radionuclide concentration in ground water from the 1-meter well (pCi/L) as determined from an appropriate contaminant transport model, and

$EDF_{PLANT,ing}$ = effective dose factor for ingestion of plants contaminated by ground water (L×mrem)/(pCi×yr) defined in Eq. 4.4-148.

The dose from ingestion of plants contaminated by drill cuttings $D_{IHIC,Drill,PLANT,ing}$ is calculated using the following formula:

$$D_{IHIC,Drill,PLANT,ing} = C_{IHIC,g} \times EDF_{IHI,PLANT,ing} \quad \text{Eq. 4.4-216}$$

where:

$D_{IHIC,Drill,PLANT,ing}$ = dose to the Chronic IHI (mrem/yr) due to ingestion of produce that has been contaminated by drill cuttings,

$C_{IHIC,g}$ = radionuclide concentration in the garden or crop soil from contaminated drill cuttings (pCi/m^3) as defined by Eq. 4.4-212 (above), and

$EDF_{IHI,PLANT,ing}$ = effective dose factor for ingestion of plants contaminated by drill cuttings (L×mrem)/(pCi×yr) defined in Eq. 4.4-217 below.

The EDF for the dose from ingestion of plants contaminated by drill cuttings shall be calculated as:

$$EDF_{IHIC,PLANT,ing} = \frac{R_{StoV} \times U_{PLANT} \times DCF_{ing}}{\rho_s} \quad \text{Eq. 4.4-217}$$

where:

$EDF_{IHIC,PLANT,ing}$ = effective dose factor for ingestion of plants contaminated by drill cuttings (L×mrem)/(pCi×yr),

R_{StoV} = soil to vegetation ratio (unitless) (Table 4.4-113),

U_{PLANT} = human ingestion rate of plants or produce (kg/yr) (Table 4.4-110),

DCF_{ing} = ingestion dose conversion factor (mrem/pCi) (Table 4.4-108), and

ρ_{bs} = dry bulk density of soil (kg/m^3) (Table 4.4-115).

Ingestion of Meat (Chronic IHI)

The meat ingestion pathway assumes that terrestrial livestock drinks contaminated stock water and consumes fodder irrigated with contaminated water. The stock water and irrigation water are from the 1-meter well. The fodder is contaminated from direct deposition of contaminated irrigation water on plants, from deposition of contaminated irrigation water in soil followed by root uptake by plants, and from drill cuttings. The buildup of radionuclide concentrations in the soil from successive years of irrigation is accounted for. The radionuclide concentration in fodder from deposition and root uptake is calculated as well.

For the purpose of this calculation, meat (or terrestrial livestock) includes all meat that is not considered poultry or fish. This includes beef, pork, veal, and other game.

Following the terrestrial livestock ingestion of the contaminated water and fodder, the IHI receptor consumes the contaminated meat. The dose from ingesting contaminated meat is calculated using the following formula:

$$D_{IHIC,MEAT,ing} = \left(D_{IHIC,H2O,MEAT,ing} + D_{IHIC,Drill,MEAT,ing}\right) \times F_{local,MEAT} \quad \text{Eq. 4.4-218}$$

where:

$D_{IHIC,MEAT,ing}$ = dose to the Chronic IHI (mrem/yr) due to ingestion of meat (i.e., terrestrial livestock meat such as beef, pork, veal, etc.),

$D_{IHIC,H2O,MEAT,ing}$ = dose to the Chronic IHI (mrem/yr) due to ingestion of meat (i.e., terrestrial livestock meat such as beef, pork, veal, etc.) that has been irrigated with water from the 1-meter well (Eq. 4.4-219),

$D_{IHIC,Drill,MEAT,ing}$ = dose to the Chronic IHI (mrem/yr) due to ingestion of meat (i.e., terrestrial livestock meat such as beef, pork, veal, etc.) that drinks water from the 1-meter well and consumes fodder that is grown in soils contaminated by the deposition of drill cuttings and irrigated from the 1-meter well (Eq. 4.4-220), and

$F_{local,MEAT}$ = fraction of consumed terrestrial livestock raised locally (unitless) (Table 4.4-118).

The dose from ingestion of meat that has been contaminated by ground water $D_{IHIC,H2O,MEAT,ing}$ is calculated using the following formula:

$$D_{IHIC,H2O,MEAT,ing} = C_{IHIC} \times EDF_{MEAT,ing} \quad \text{Eq. 4.4-219}$$

where:

$D_{IHIC,H2O,MEAT,ing}$ = dose to the Chronic IHI (mrem/yr) due to ingestion of meat (i.e., terrestrial livestock such as beef, pork, veal, etc.) that has been irrigated with water from the 1-meter well,

C_{IHIC} = radionuclide concentration in ground water from the 1-meter well (pCi/L) as determined from an appropriate contaminant transport model, and

$EDF_{MEAT,ing}$ = effective dose factor for ingestion of terrestrial livestock meat contaminated by ground water (L×mrem)/(pCi×yr) as defined in Eq. 4.4-154.

The dose from ingestion of meat contaminated by drill cuttings $D_{IHIC,Drill,MEAT,ing}$ is calculated using the following formula:

$$D_{IHIC,Drill,MEAT,ing} = C_{IHIC,g} \times EDF_{IHI,MEAT,ing} \quad \text{Eq. 4.4-220}$$

where:

$D_{IHIC,Drill,MEAT,ing}$ = dose to the Chronic IHI (mrem/yr) due to ingestion of meat (i.e., terrestrial livestock meat such as beef, pork, veal, etc.) that drinks water from the 1-meter well and consumes fodder that is grown in soils contaminated by the deposition of drill cuttings and irrigated from the 1-meter well,

$C_{IHIC,g}$ = radionuclide concentration in the garden or crop soil from contaminated drill cuttings (pCi/m^3) as defined by Eq. 4.4-212 (above), and

$EDF_{IHI,MEAT,ing}$ = effective dose factor for ingestion of terrestrial livestock meat contaminated by drill cuttings (L×mrem)/(pCi×yr) as defined in Eq. 4.4-221 (below).

The EDF for the dose from ingestion of meat contaminated by drill cuttings deposited in the soil and used to grow fodder shall be calculated as:

$$EDF_{IHI,MEAT,ing} = \Big(\big(Q_{fod,MEAT} \times (R_{StoV} \times SOIL) \times F_{fod,MEAT}\big) \times (PR + I_{RF} - ER)\Big) \times TC_{MEAT} \times U_{MEAT} \times DCF_{ing} \quad \text{Eq. 4.4-221}$$

where:

$EDF_{IHI,MEAT,ing}$ = effective dose factor for ingestion of terrestrial livestock meat contaminated by drill cuttings (L×mrem)/(pCi×yr),

$Q_{fod,MEAT}$ = ingestion rate of fodder by terrestrial livestock (kg/yr) (Table 4.4-111),

R_{StoV} = soil to vegetation ratio (unitless) (Table 4.4-113),

$SOIL$ = radionuclide deposition and buildup rate in soil ((m²×yr)/kg) as defined in Eq. 4.4-144,

$F_{fod,MEAT}$ = fraction of terrestrial livestock intake from field/pasture that is contaminated by drill cuttings (unitless) (Table 4.4-112),

PR = precipitation rate (m/yr) (Table 4.4-115),

I_{RF} = functional irrigation rate (m/yr) as defined by Eq. 4.4-146,

ER = evapotranspiration rate (m/yr) (Table 4.4-115),

TC_{MEAT} = transfer coefficient for meat (i.e., terrestrial livestock meat such as beef, pork, veal, etc.) (yr/kg) (Table 4.4-113),

U_{MEAT} = human ingestion rate of meat (i.e., terrestrial livestock meat such as beef, pork, veal, etc.) (kg/yr) (Table 4.4-110), and

DCF_{ing} = dose conversion factor for ingestion (mrem/pCi) (Table 4.4-108).

Ingestion of Milk (Chronic IHI)

Following the livestock ingestion of the contaminated water and fodder, the IHI receptor consumes the contaminated milk from milk cows (or other milk-producing livestock) that consumes fodder and water which were contaminated from the 1-meter well. The dose from ingestion of contaminated milk is calculated using the following formula:

$$D_{IHIC,MILK,ing} = \big(D_{IHIC,H2O,MILK,ing} + D_{IHIC,Drill,MILK,ing}\big) \times F_{local,MILK} \quad \text{Eq. 4.4-222}$$

where:

$D_{IHIC,MILK,ing}$ = dose to the Chronic IHI (mrem/yr) due to ingestion of milk,

$D_{IHIC,H2O,MILK,ing}$ = dose to the Chronic IHI (mrem/yr) due to ingestion of milk that comes from milk-producing livestock that consumes fodder and water which were contaminated from the 1-meter well (Eq. 4.4-223),

$D_{IHIC,Drill,MILK,ing}$ = dose to the Chronic IHI (mrem/yr) due to ingestion of milk that has been contaminated by drill cuttings deposited in the soil and used to grow fodder (Eq. 4.4-224), and

$F_{local,MILK}$ = fraction of consumed milk produced locally (unitless) (Table 4.4-118).

The dose from ingestion of milk contaminated by ground water $D_{IHIC,H2O,MILK,ing}$ is calculated using the following formula:

$$D_{IHIC,H2O,MILK,ing} = C_{IHIC} \times EDF_{MILK,ing} \quad \text{Eq. 4.4-223}$$

where:

$D_{IHIC,H2O,MILK,ing}$ = dose to the Chronic IHI (mrem/yr) due to ingestion of milk that comes from milk-producing livestock that consumes fodder and water which were contaminated from the 1-meter well,

C_{IHIC} = radionuclide concentration in ground water from the 1-meter well (pCi/L) as determined from an appropriate contaminant transport model, and

$EDF_{MILK,ing}$ = effective dose factor for ingestion of milk contaminated by ground water (L×mrem)/(pCi×yr) as defined in Eq. 4.4-157.

The dose from ingestion of milk contaminated by milk-producing livestock consuming fodder grown in soils where drill cuttings were deposited $D_{IHIC,Drill,MILK,ing}$ is calculated using the following formula:

$$D_{IHIC,Drill,MILK,ing} = C_{IHIC,g} \times EDF_{IHI,MILK,ing} \quad \text{Eq. 4.4-224}$$

where:

$D_{IHIC,Drill,MILK,ing}$ = dose to the Chronic IHI (mrem/yr) due to ingestion of milk that comes from milk-producing livestock that has been contaminated by consuming fodder grown in soil where drill cuttings were deposited,

$C_{IHIC,g}$ = radionuclide concentration in the garden or crop soil from contaminated drill cuttings (pCi/m^3) as defined by Eq. 4.4-212, and

$EDF_{IHI,MILK,ing}$ = effective dose factor for ingestion of milk that comes from milk-producing livestock contaminated by milk-producing livestock consuming fodder grown in soils where drill cuttings were deposited (L×mrem)/(pCi×yr) as defined in Eq. 4.4-225.

The EDF for the dose from ingestion of milk contaminated by drill cuttings shall be calculated as:

$$EDF_{IHI,MILK,ing} = \Big(\big(Q_{fod,MILK} \times (R_{StoV} \times SOIL) \times F_{fod,MILK}\big) \times (PR + I_{RF} - ER)\Big) \times TC_{MILK} \times \left(\frac{U_{MILK}}{\rho_{milk}}\right) \times DCF_{ing} \quad \text{Eq. 4.4-225}$$

where:

$EDF_{IHI,MILK,ing}$ = effective dose factor for ingestion of milk produced by terrestrial livestock contaminated by drill cuttings (L×mrem)/(pCi×yr),

$Q_{fod,MILK}$ = ingestion rate of fodder by milk-producing livestock (kg/yr) (Table 4.4-111),

R_{StoV} = soil to vegetation ratio (unitless) (Table 4.4-113),

$SOIL$ = radionuclide deposition and buildup rate in soil ((m²×yr)/kg) as defined in Eq. 4.4-144,

$F_{fod,MILK}$ = fraction of milk-producing livestock intake from field/pasture that is contaminated by drill cuttings (unitless) (Table 4.4-112),

PR = precipitation rate (m/yr) (Table 4.4-115),

I_{RF} = functional irrigation rate (m/yr) as defined by Eq. 4.4-146,

ER = evapotranspiration rate (m/yr) (Table 4.4-115),

TC_{MILK} = transfer coefficient for milk-producing livestock (yr/L) (Table 4.4-113),

U_{MILK} = human ingestion rate of milk (kg/yr) (Table 4.4-110),

ρ_{milk} = milk density (kg/L) (Table 4.4-110 – see table note), and

DCF_{ing} = dose conversion factor for ingestion (mrem/pCi) (Table 4.4-108).

Ingestion of Poultry (Chronic IHI)

The poultry and egg ingestion pathways assume poultry drink contaminated stock water and consume fodder irrigated with contaminated water. The stock water and irrigation water is from the 1-meter well. The fodder is contaminated from direct deposition of contaminated irrigation water on plants and from deposition of contaminated irrigation water in soil followed by root uptake by plants and from drill cuttings. It is also assumed that poultry directly ingest contaminated soil in addition to the stock water and fodder. The dose from ingestion of contaminated poultry is calculated using the following formula:

$$D_{IHIC,POULTRY,ing} = \left(D_{IHIC,H2O,POULTRY,ing} + D_{IHIC,Drill,POULTRY,ing}\right) \times F_{local,POULTRY} \quad \text{Eq. 4.4-226}$$

where:

$D_{IHIC,POULTRY,ing}$ = dose to the Chronic IHI (mrem/yr) due to ingestion of poultry,

$D_{IHIC,H2O,POULTRY,ing}$ = dose to the Chronic IHI (mrem/yr) due to ingestion of poultry that consumes fodder and water which were contaminated from the 1-meter well (Eq. 4.4-227),

$D_{IHIC,Drill,POULTRY,ing}$ = dose to the Chronic IHI (mrem/yr) due to ingestion of poultry that has been contaminated by consuming fodder grown in soils where drill cuttings were deposited (Eq. 4.4-228), and

$F_{local,POULTRY}$ = fraction of consumed poultry raised locally (unitless) (Table 4.4-118).

The dose from ingestion of poultry contaminated by ground water $D_{IHIC,H2O,POULTRY,ing}$ is calculated using the following formula:

$$D_{IHIC,H2O,POULTRY,ing} = C_{IHIC} \times EDF_{POULTRY,ing} \quad \text{Eq. 4.4-227}$$

where:

$D_{IHIC,H2O,POULTRY,ing}$ = dose to the Chronic IHI (mrem/yr) due to ingestion of poultry that consumes fodder and water which were contaminated from the 1-meter well,

C_{IHIC} = radionuclide concentration in ground water from the 1-meter well (pCi/L) as determined from an appropriate contaminant transport model, and

$EDF_{POULTRY,ing}$ = effective dose factor for ingestion of poultry contaminated by ground water (L×mrem)/(pCi×yr) as defined in Eq. 4.4-159.

The dose from ingestion of poultry contaminated by drill cuttings $D_{IHIC,Drill,POULTRY,ing}$ is calculated using the following formula:

$$D_{IHIC,Drill,POULTRY,ing} = C_{IHIC,g} \times EDF_{IHI,POULTRY,ing} \quad \text{Eq. 4.4-228}$$

where:

$D_{IHIC,Drill,POULTRY,ing}$ = dose to the Chronic IHI (mrem/yr) due to ingestion of poultry that has been contaminated by drill cuttings,

$C_{IHIC,g}$ = radionuclide concentration in the garden or crop soil from contaminated drill cuttings (pCi/m^3) as defined by Eq. 4.4-212, and

$EDF_{IHI,POULTRY,ing}$ = effective dose factor for ingestion of poultry contaminated by drill cuttings (L×mrem)/(pCi×yr) as defined in Eq. 4.4-229.

The EDF for the dose from ingestion of poultry contaminated by drill cuttings shall be calculated as:

$$EDF_{IHI,POULTRY,ing} = \left(\left[\left(Q_{fod,POULTRY} \times (R_{StoV} \times OIL) \times F_{fod,POULTRY}\right) \times (PR + I_{RF} - ER)\right] + \left[SOIL \times I_{RF} \times Q_{SOIL,POULTRY} \times F_{SOIL,POULTRY}\right]\right) \times TC_{POULTRY} \times U_{POULTRY} \times DCF_{ing} \quad \text{Eq. 4.4-229}$$

where:

$EDF_{IHI,POULTRY,ing}$ = effective dose factor for ingestion of poultry contaminated by drill cuttings (L×mrem)/(pCi×yr),

$Q_{fod,POULTRY}$ = ingestion rate of fodder by poultry (kg/yr) (Table 4.4-111),

R_{StoV} = soil to vegetation ratio (unitless) (Table 4.4-113),

$SOIL$ = radionuclide deposition and buildup rate in soil ((m²×yr)/kg) as defined in Eq. 4.4-144,

$F_{fod,POULTRY}$ = fraction of poultry intake from field/pasture that is contaminated by drill cuttings (unitless) (Table 4.4-112),

PR = precipitation rate (m/yr) (Table 4.4-115),

I_{RF} = functional irrigation rate (m/yr) as defined by Eq. 4.4-146,

ER = evapotranspiration rate (m/yr) (Table 4.4-115),

$Q_{SOIL,POULTRY}$ = ingestion rate of soil by poultry (kg/yr) (Table 4.4-111),

$F_{SOIL,POULTRY}$ = fraction of poultry-soil intake from field/pasture that is contaminated by drill cuttings (unitless) (Table 4.4-112),

$TC_{POULTRY}$ = transfer coefficient for poultry (yr/kg) (Table 4.4-113),

$U_{POULTRY}$ = human ingestion rate of poultry (kg/yr) (Table 4.4-110), and

DCF_{ing} = dose conversion factor for ingestion (mrem/pCi) (Table 4.4-108).

Ingestion of Egg (Chronic IHI)

Following the poultry ingestion of the contaminated water and fodder, the Chronic IHI consumes the contaminated poultry-produced eggs. The dose from ingestion of contaminated eggs is calculated using the following formula:

$$D_{IHIC,EGG,ing} = \left(D_{IHIC,H2O,EGG,ing} + D_{IHIC,Drill,EGG,ing}\right) \times F_{local,EGG} \qquad \text{Eq. 4.4-230}$$

where:

$D_{IHIC,EGG,ing}$ = dose to the Chronic IHI (mrem/yr) due to ingestion of eggs,

$D_{IHIC,H2O,EGG,ing}$ = dose to the Chronic IHI (mrem/yr) due to ingestion of eggs that come from poultry that consumes fodder and water which were contaminated from the 1-meter well (Eq. 4.4-231),

$D_{IHIC,Drill,EGG,ing}$ = dose to the Chronic IHI (mrem/yr) due to ingestion of eggs that come from poultry that consumes fodder grown in soils where drill cuttings were deposited (Eq. 4.4-232), and

$F_{local,EGG}$ = fraction of consumed eggs produced locally (unitless) (Table 4.4-118).

The dose from ingestion of eggs contaminated by ground water $D_{IHIC,H2O,EGG,ing}$ is calculated using the following formula:

$$D_{IHIC,H2O,EGG,ing} = C_{IHIC} \times EDF_{EGG,ing} \qquad \text{Eq. 4.4-231}$$

where:

$D_{IHIC,H2O,EGG,ing}$ = dose to the Chronic IHI (mrem/yr) due to ingestion of eggs that come from poultry that consumes fodder and water which were contaminated from the 1-meter well,

C_{IHIC} = radionuclide concentration in ground water from the 1-meter well (pCi/L) as determined from an appropriate contaminant transport model, and

$EDF_{EGG,ing}$ = effective dose factor for ingestion of eggs contaminated by ground water (L×mrem)/(pCi×yr) as defined in Eq. 4.4-161.

The dose from ingestion of eggs contaminated by drill cuttings $D_{IHIC,Drill,EGG,ing}$ is calculated using the following formula:

$$D_{IHIC,Drill,EGG,ing} = C_{IHIC,g} \times EDF_{IHI,EGG,ing} \quad \text{Eq. 4.4-232}$$

where:

$D_{IHIC,Drill,EGG,ing}$ = dose to the Chronic IHI (mrem/yr) due to ingestion of eggs that have been contaminated by drill cuttings,

$C_{IHIC,g}$ = radionuclide concentration in the garden or crop soil from contaminated drill cuttings (pCi/m^3) as defined by Eq. 4.4-212, and

$EDF_{IHI,EGG,ing}$ = effective dose factor for ingestion of eggs contaminated by drill cuttings (L×mrem)/(pCi×yr) as defined in Eq. 4.4-233.

The EDF for the dose from ingestion of eggs contaminated by drill cuttings shall be calculated as:

$$EDF_{IHI,EGG,ing} = \left(\left[\left(Q_{fod,EGG} \times (R_{StoV} \times SOIL) \times F_{fod,EGG}\right) \times (PR + I_{RF} - ER)\right] + \left[SOIL \times I_{RF} \times Q_{SOIL,EGG} \times F_{SOIL,EGG}\right]\right) \times TC_{EGG} \times U_{EGG} \times DCF_{ing} \quad \text{Eq. 4.4-233}$$

where:

$EDF_{IHI,EGG,ing}$ = effective dose factor for ingestion of eggs contaminated by drill cuttings (L×mrem)/(pCi×yr),

$Q_{fod,EGG}$ = uptake rate of fodder by egg-producers (kg/yr) (Table 4.4-111),

R_{StoV} = soil to vegetation ratio (unitless) (Table 4.4-113),

$SOIL$ = radionuclide deposition and buildup rate in soil ((m^2×yr)/kg) as defined in Eq. 4.4-144,

$F_{fod,EGG}$ = fraction of egg-producer intake from field/pasture that is contaminated by drill cuttings (unitless) (Table 4.4-112),

PR = precipitation rate (m/yr) (Table 4.4-115),

I_{RF} = functional irrigation rate (m/yr) as defined by Eq. 4.4-146,

ER = evapotranspiration rate (m/yr) (Table 4.4-115),

$Q_{SOIL,EGG}$ = uptake rate of soil by egg-producerss (kg/yr) (Table 4.4-111),

$F_{SOIL,EGG}$ = fraction of egg-producer soil intake from field/pasture that is contaminated with drill cuttings (unitless) (Table 4.4-112),

TC_{EGG} = transfer coefficient for eggs (yr/kg) (Table 4.4-113),

U_{EGG} = human ingestion rate of eggs (kg/yr) (Table 4.4-110), and

DCF_{ing} = dose conversion factor for ingestion (mrem/pCi) (Table 4.4-108).

Ingestion of Fish

The fish ingestion route assumes fish are caught from a contaminated stream at the point of highest concentration, and the IHI receptor in turn consumes the contaminated fish. The dose from ingestion of fish shall be calculated according to Eq. 4.4-162.

Chronic IHI, Direct Exposure Dose Pathways

The following text defines the parameter $D_{IHIC,exp}$ from Eq. 4.4-206. The direct exposure dose to the Chronic IHI is determined according to Eq. 4.4-234:

$$D_{IHIC,exp} = D_{IHIC,SOIL,exp} + D_{IHIC,SHOWER,exp} + D_{SL,SWIM,exp} + D_{SL,BOAT,exp} \quad \text{Eq. 4.4-234}$$

where:

$D_{IHIC,exp}$ = dose to the Chronic IHI (mrem/yr) due to exposure,

$D_{IHIC,SOIL,exp}$ = dose to Chronic IHI (mrem/yr) due to direct exposure to soil contaminated by irrigation from the 1-meter well and deposition of drill cuttings (Eq. 4.4-235),

$D_{IHIC,SHOWER,exp}$ = dose to the Chronic IHI (mrem/yr) due to direct exposure while showering or bathing in water from the 1-meter well (Eq. 4.4-239),

$D_{SL,SWIM,exp}$ = dose to the Chronic IHI (mrem/yr) due to direct exposure from swimming in stream water at the contaminated SL as defined in Eq. 4.4-169, and

$D_{SL,BOAT,exp}$ = dose to the Chronic IHI (mrem/yr) due to direct exposure from boating and fishing in stream water at the contaminated SL as defined in Eq. 4.4-171.

Direct Exposure from Irrigated Soil (Chronic IHI)

The exposure pathway from direct contact to contaminated soil assumes the soil is (1) irrigated with ground water from the 1-meter well, and (2) contaminated with drill cuttings. The Chronic IHI receptor is exposed during time spent caring for a garden or crop. The radionuclide concentration in the soil and the exposure dose is calculated using the following formula:

$$D_{IHIC,SOIL,exp} = D_{IHIC,H2O,SOIL,exp} + D_{IHIC,Drill,SOIL,exp} \quad \text{Eq. 4.4-235}$$

where:

$D_{IHIC,SOIL,exp}$ = dose to Chronic IHI (mrem/yr) due to direct exposure to soil contaminated by irrigation from the 1-meter well and deposition of drill cuttings,

$D_{IHIC,H2O,SOIL,exp}$ = dose to Chronic IHI (mrem/yr) due to direct exposure to soil contaminated by irrigation from the 1-meter well (Eq. 4.4-236), and

$D_{IHIC,Drill,SOIL,exp}$ = dose to Chronic IHI (mrem/yr) due to direct exposure to soil contaminated by deposition of drill cuttings (Eq. 4.4-237).

The dose from direct exposure to soil contaminated by ground water $D_{IHIC,H2O,SOIL,exp}$ is calculated using the following formula:

$$D_{IHIC,H2O,SOIL,exp} = C_{IHIC} \times EDF_{SOIL,exp} \quad \text{Eq. 4.4-236}$$

where:

$D_{IHIC,H2O,SOIL,exp}$ = dose to Chronic IHI (mrem/yr) due to direct exposure to soil contaminated by irrigation from the 1-meter well,

C_{IHIC} = radionuclide concentration in ground water from the 1-meter well (pCi/L) as determined from an appropriate contaminant transport model, and

$EDF_{SOIL,exp}$ = effective dose factor for external exposure to soil (L×mrem)/(pCi×yr) as defined in Eq. 4.4-166.

The dose from direct exposure to soil contaminated by drill cuttings $D_{IHIC,Drill,SOIL,exp}$ is calculated using the following formula:

$$D_{IHIC,Drill,SOIL,exp} = C_{IHIC,g} \times EDF_{IHI,SOIL,exp} \quad \text{Eq. 4.4-237}$$

where:

$D_{IHIC,Drill,SOIL,exp}$ = dose to Chronic IHI (mrem/yr) due to direct exposure to soil contaminated by deposition of drill cuttings,

$C_{IHIC,g}$ = radionuclide concentration in the garden or crop soil from contaminated drill cuttings (pCi/m^3) as defined by Eq. 4.4-212, and

$EDF_{IHI,SOIL,exp}$ = effective dose factor for direct exposure to soil contaminated by drill cuttings (L×mrem)/(pCi×yr) as defined in Eq. 4.4-238.

The EDF for IHI soil exposure shall be calculated as:

$$EDF_{IHI,SOIL,exp} = DCF_{exp} \times F_{t,g} \quad \text{Eq. 4.4-238}$$

where:

$EDF_{IHI,SOIL,exp}$ = effective dose factor for direct exposure to soil contaminated by drill cuttings (L×mrem)/(pCi×yr),

DCF_{exp} = dose conversion factor for external exposure (m³×mrem)/(pCi×yr) (Table 4.4-108), and

$F_{t,g}$ = fraction of the time the IHI spends in the garden or crop (unitless) (Table 4.4-114).

Direct Exposure from Showering (Chronic IHI)

The direct contact exposure pathway from showering and bathing assumes the Chronic IHI receptor receives dose from washing in water from the 1-meter well. The dose is calculated using the following formula:

$$D_{IHIC,SHOWER,exp} = C_{IHIC} \times EDF_{SHOWER,exp} \quad \text{Eq. 4.4-239}$$

where:

$D_{IHIC,SHOWER,exp}$ = dose to the Chronic IHI (mrem/yr) due to direct exposure while showering or bathing in water from the 1-meter well,

C_{IHIC} = radionuclide concentration in ground water from the 1-meter well (pCi/L) as determined from an appropriate contaminant transport model, and

$EDF_{SHOWER,exp}$ = effective dose factor for external exposure to water while showering or bathing (L×mrem)/(pCi×yr) as defined in Eq. 4.4-168.

Direct Exposure from Swimming

The direct contact exposure pathway from swimming assumes the Chronic IHI receptor receives dose from swimming in a contaminated stream at the point of highest concentration. The dose from swimming exposure shall be calculated according to Eq. 4.4-169.

Direct Exposure from Boating and Fishing

The direct contact exposure pathway from boating and fishing assumes the Chronic IHI receptor receives dose from activities in a contaminated stream at the point of highest concentration. The dose from boating and fishing exposure shall be calculated according to Eq. 4.4-171.

Chronic Intruder Inhalation Dose Pathways

The following text defines the parameter $D_{IHIC,inh}$ from Eq. 4.4-206. The inhalation dose to the Chronic IHI is determined according to Eq. 4.4-240:

$$D_{IHIC,inh} = D_{IHIC,IRR,inh} + D_{IHIC,DUST,inh} + D_{IHIC,SHOWER,inh} + D_{SL,SWIM,inh} \quad \text{Eq. 4.4-240}$$

where:

$D_{IHIC,inh}$ = dose to the Chronic IHI (mrem/yr) due to inhalation,

$D_{IHIC,IRR,inh}$ = dose to the Chronic IHI (mrem/yr) due to inhalation while irrigating gardens or crops with water from the 1-meter well (Eq. 4.4-241),

$D_{IHIC,DUST,inh}$ = dose to the Chronic IHI (mrem/yr) due to inhalation of dust and soil that has been contaminated due to irrigation with water from the 1-meter well and had drill cuttings deposited in the soil (Eq. 4.4-242),

$D_{IHIC,SHOWER,inh}$ = dose to the Chronic IHI (mrem/yr) due to inhalation while showering or bathing in water from the 1-meter well (Eq. 4.4-246), and

$D_{SL,SWIM,inh}$ = dose to the Chronic IHI (mrem/yr) due to inhalation while swimming in stream water at the contaminated SL as defined in Eq. 4.4-180.

Inhalation of Water during Irrigation (Chronic IHI)

The exposure pathway from inhalation during irrigation assumes soil is irrigated with ground water from the 1-meter well and the Chronic IHI receptor is exposed by breathing while the garden or crop is irrigated but only during time spent caring for a garden or crop. The dose is calculated using the following formula:

$$D_{IHIC,IRR,inh} = C_{IHIC} \times EDF_{IRR,inh} \qquad \text{Eq. 4.4-241}$$

where:

$D_{IHIC,IRR,inh}$ = dose to the Chronic IHI (mrem/yr) due to inhalation while irrigating gardens or crops with water from the 1-meter well,

C_{IHIC} = radionuclide concentration in ground water from the 1-meter well (pCi/L) as determined from an appropriate contaminant transport model, and

$EDF_{IRR,inh}$ = effective dose factor for inhalation of water during irrigation (L×mrem)/(pCi×yr) as defined in Eq. 4.4-175.

Inhalation of Dust from Irrigated Soil (Chronic IHI)

The dose pathway associated with inhalation of dust and soil that has been irrigated assumes that dust and soil has been irrigated with water from the 1-meter well and includes drill cuttings. The Chronic IHI receptor is exposed by breathing dust during time spent caring for a garden or crop. This formula was derived following the approach of previous pathway calculations. The dose is calculated using the following formula:

$$D_{IHIC,DUST,inh} = D_{IHIC,H2O,DUST,inh} + D_{IHIC,Drill,DUST,inh} \qquad \text{Eq. 4.4-242}$$

where:

$D_{IHIC,DUST,inh}$ = dose to the Chronic IHI (mrem/yr) due to inhalation of dust and soil that has been contaminated due to irrigation with water from the 1-meter well and from deposition of drill cuttings,

$D_{IHIC,H2O,DUST,inh}$ = dose to the Chronic IHI (mrem/yr) due to inhalation of dust and soil that has been contaminated due to irrigation with water from the 1-meter well (Eq. 4.4-243), and

$D_{IHIC,Drill,DUST,inh}$ = dose to the Chronic IHI (mrem/yr) due to inhalation of dust and soil that has been contaminated from deposition of drill cuttings (Eq. 4.4-244).

The dose from inhalation of dust and soil contaminated by ground water $D_{IHIC,H2O,DUST,inh}$ is calculated using the following formula:

$$D_{IHIC,H2O,DUST,inh} = C_{IHIC} \times EDF_{DUST,inh} \quad \text{Eq. 4.4-243}$$

where:

$D_{IHIC,H2O,DUST,inh}$ = dose to Chronic IHI (mrem/yr) due to inhalation of dust and soil that has been contaminated due to irrigation with water from the 1-meter well,

C_{IHIC} = radionuclide concentration in ground water from the 1-meter well (pCi/L) as determined from an appropriate contaminant transport model, and

$EDF_{DUST,inh}$ = effective dose factor for inhalation of dust and soil (L×mrem)/(pCi×yr) as defined in Eq. 4.4-177.

The dose from inhalation of dust and soil contaminated by drill cuttings $D_{IHIC,Drill,DUST,inh}$ is calculated using the following formula:

$$D_{IHIC,Drill,DUST,inh} = C_{IHIC,g} \times EDF_{IHIC,DUST,inh} \quad \text{Eq. 4.4-244}$$

where:

$D_{IHIC,Drill,DUST,inh}$ = dose to the Chronic IHI (mrem/yr) due to inhalation of dust and soil that has been contaminated from deposition of drill cuttings,

$C_{IHIC,g}$ = radionuclide concentration in the garden or crop soil from contaminated drill cuttings (pCi/m^3) as defined by Eq. 4.4-212, and

$EDF_{IHIC,DUST,inh}$ = effective dose factor for inhalation of dust from contaminated drill cuttings (L×mrem)/(pCi×yr) as defined in Eq. 4.4-245.

The EDF for inhalation of dust from drill cuttings shall be calculated as:

$$EDF_{IHIC,DUST,inh} = \frac{F_{t,DRILL} \times L_{SOIL} \times U_{AIR} \times DCF_{inh}}{\rho_s} \quad \text{Eq. 4.4-245}$$

where:

$EDF_{IHIC,DUST,inh}$ = effective dose factor for inhalation of dust from contaminated drill cuttings (L×mrem)/(pCi×yr),

$F_{t,DRILL}$ = fraction of time exposed to drill cuttings (unitless) (Table 4.4-114),

L_{SOIL} = soil loading in air while working in a garden or crop (kg/m^3) (Table 4.4-114),

U_{AIR} = air intake (m^3/yr) (Table 4.4-110),

DCF_{inh} = dose conversion factor for inhalation (mrem/pCi) (Table 4.4-108), and

ρ_{bs} = dry bulk density of soil (kg/m^3) (Table 4.4-115).

Inhalation during Showering (Chronic IHI)

The showering inhalation dose pathway assumes the Chronic IHI receptor is exposed by breathing humid air within the shower. The source of water for the shower is a well 1-meter from the contamination source. The dose is calculated using the following formula:

$$D_{IHIC,SHOWER,inh} = C_{IHIC} \times EDF_{SHOWER,inh} \quad \text{Eq. 4.4-246}$$

where:

$D_{IHIC,SHOWER,inh}$ = dose to the Chronic IHI (mrem/yr) due to inhalation while showering or bathing in water from the 1-meter well,

C_{IHIC} = radionuclide concentration in ground water from the 1-meter well (pCi/L) as determined from an appropriate contaminant transport model, and

$EDF_{SHOWER,inh}$ = effective dose factor for inhalation of water while showering or bathing (L×mrem)/(pCi×yr) as defined in Eq. 4.4-179.

Inhalation during Swimming (Chronic IHI)

The swimming inhalation pathway assumes that water from a stream has been contaminated by ground water and that the receptor inhales saturated air. For simplicity, the moisture contained in the inhaled air is assumed to be from stream water at the seepline. The dose is calculated using Eq. 4.4-180.

4.4.8.3 Inputs and Assumptions for the Dose Calculations

The following describes the key inputs and assumptions used in the Dose and Exposure Pathways Model for the SDF PA.

4.4.8.3.1 Dose Conversion Factors

The ingestion and inhalation Dose Conversion Factors (DCFs) were developed from DOE's *Derived Concentration Technical Standard* (DOE-STD-1196-2011, Tables A-1 and A-2, respectively). The values for the external DCFs for both soil and water were developed from the EPA's *Federal Guidance Report 15* (EPA-402-R-18-001, Tables 4-4 and 4-7, respectively). These DCFs are presented in Table 4.4-108. The DCFs for exposure to contaminated air are also included (developed from Table 4-6 of EPA-402-R-18-001). The development of these values is described in the *Dose Calculation Methodology for Liquid Waste Performance Assessments at the Savannah River Site*, Rev. 2. [SRR-CWDA-2013-00058]

The values shaded in gray indicate radionuclides that are assumed to be in secular equilibrium with short-lived daughters, as described below.

Table 4.4-108: Internal and External DCFs for the Reference Person

Radionuclide	Internal DCFs (mrem/pCi)		External DCFs (m^3×mrem)/(pCi×yr)		
	Ingestion DCF_{ing}	Inhalation DCF_{inh}	Soil Exposure (assumes 0.15 m depth) DCF_{exp}	Water Immersion DCF_{imm}	Air Submersion $DCF_{air,sub}$
Ac-227 [a]	1.61E-03	6.42E-01	1.21E-06	4.32E-06	2.20E-03
Al-26	1.29E-05	4.03E-04	8.59E-06	3.16E-05	1.52E-02
Am-241	7.55E-04	1.54E-01	2.56E-08	1.42E-07	6.19E-05
Am-242m [a]	7.34E-04	1.49E-01	2.95E-08	1.30E-07	7.13E-05
Am-243 [a]	7.54E-04	1.52E-01	5.33E-07	2.03E-06	1.03E-03
C-14	2.15E-06	7.51E-06	0.00E+00	3.30E-10	3.00E-07
Cf-249	1.30E-03	6.22E-01	9.75E-07	3.32E-06	1.67E-03
Cf-251	1.32E-03	6.33E-01	2.88E-07	1.06E-06	5.57E-04
Cl-36	3.43E-06	1.40E-04	1.48E-09	2.21E-08	1.93E-05
Cm-243	5.55E-04	1.17E-01	3.27E-07	1.18E-06	6.14E-04
Cm-244	4.55E-04	9.84E-02	9.25E-11	9.53E-10	3.88E-07
Cm-245	7.70E-04	1.57E-01	2.25E-07	8.75E-07	4.58E-04
Cm-247 [a]	7.07E-04	1.43E-01	9.97E-07	3.44E-06	1.73E-03
Co-60	1.27E-05	3.77E-05	8.08E-06	2.97E-05	1.40E-02
Cs-135	9.81E-06	3.39E-06	0.00E+00	2.72E-09	2.52E-06
Cs-137 [a]	5.03E-05	1.73E-05	1.67E-06	5.81E-06	2.84E-03
Eu-152	4.96E-06	3.45E-04	3.63E-06	1.32E-05	6.33E-03
Eu-154	7.29E-06	3.96E-04	3.92E-06	1.42E-05	6.82E-03
H-3	1.55E-07	1.67E-07	0.00E+00	0.00E+00	0.00E+00
I-129	4.00E-04	1.36E-04	5.55E-09	6.14E-08	2.62E-05
K-40	2.28E-05	3.13E-04	5.16E-07	1.94E-06	9.38E-04
Nb-93m	4.77E-07	1.98E-06	1.76E-11	7.33E-10	2.71E-07
Nb-94	6.40E-06	3.96E-05	4.94E-06	1.75E-05	8.42E-03
Ni-63	5.74E-07	1.80E-06	0.00E+00	0.00E+00	0.00E+00
Np-237 [a]	3.99E-04	8.40E-02	6.46E-07	2.29E-06	1.17E-03
Pa-231	1.77E-03	8.51E-01	9.46E-08	3.30E-07	1.67E-04
Pb-210 [a]	7.06E-03	1.67E-02	4.90E-09	4.43E-08	3.46E-05
Pt-193	1.32E-07	2.48E-06	3.19E-13	1.00E-10	3.27E-08
Pu-238	8.44E-04	1.71E-01	4.88E-11	8.03E-10	3.16E-07
Pu-239	9.29E-04	1.86E-01	1.60E-10	8.68E-10	3.99E-07
Pu-240	9.29E-04	1.86E-01	5.11E-11	7.86E-10	3.12E-07
Pu-241	1.75E-05	3.33E-03	3.37E-12	1.34E-11	6.97E-09
Pu-242	8.84E-04	1.76E-01	2.83E-10	1.56E-09	6.92E-07
Pu-244 [a]	8.85E-04	1.73E-01	1.08E-06	3.85E-06	1.90E-03
Ra-226 [a]	1.04E-03	1.29E-02	5.52E-06	2.02E-05	9.73E-03
Ra-228 [a]	3.11E-03	1.68E-01	4.87E-06	1.79E-05	8.65E-03
Se-79	1.01E-05	4.00E-06	0.00E+00	3.86E-10	3.51E-07
Sm-151	3.66E-07	3.43E-05	2.81E-13	5.73E-12	2.24E-09
Sn-126 [a]	1.81E-05	5.89E-04	5.11E-06	1.78E-05	8.76E-03
Sr-90 [a]	1.12E-04	1.37E-04	2.47E-08	1.24E-07	1.03E-04
Tc-99	2.38E-06	1.49E-05	1.14E-12	3.62E-09	3.34E-06
Th-229 [a]	2.36E-03	3.18E-01	7.00E-07	2.57E-06	1.31E-03
Th-230	7.92E-04	5.18E-02	7.16E-10	3.35E-09	1.53E-06
Th-232	8.55E-04	9.18E-02	3.14E-10	1.74E-09	7.62E-07
U-232 [a]	1.76E-03	1.88E-01	2.15E-06	8.10E-06	3.92E-03
U-233	1.89E-04	1.31E-02	5.56E-10	2.37E-09	1.16E-06
U-234	1.83E-04	1.29E-02	2.07E-10	1.39E-09	6.25E-07
U-235 [a]	1.74E-04	1.14E-02	4.55E-07	1.63E-06	8.40E-04
U-236	1.72E-04	1.18E-02	9.85E-11	8.82E-10	3.77E-07
U-238 [a]	1.78E-04	1.06E-02	8.53E-08	3.47E-07	2.00E-04
Zr-93	3.96E-06	3.63E-05	0.00E+00	7.85E-14	7.50E-11

[SRR-CWDA-2013-00058]

(a) Value shows the sum of a parent radionuclide plus daughter products assumed to be in secular equilibrium. See Table 4.4-109 for a summary of which radionuclides were used in this assumption.

DCFs from short-lived progeny are combined with those from the longer-lived parents as a modeling simplification. It is assumed that these daughter products are in secular equilibrium with the parent radionuclides (i.e., decay of the short-lived daughter is equal to ingrowth from the parent). The equilibrium is calculated using the individual DCFs, adjusted by the branching fraction for the daughter products to the parent. Table 4.4-109 provides a summary which radionuclides are assumed to be in secular equilibrium with their daughter products (i.e., those that are shaded in Table 4.4-108).

Table 4.4-109: Radionuclides Assumed to be in Secular Equilibrium

Original Parent Radionuclide	Daughters Assumed at Equilibrium
Ac-227	Th-227
	Fr-223
	Ra-223
	Rn-219
	Po-215
	Pb-211
	Bi-211
	Tl-207
	Po-211
Am-242m	Am-242
	Np-238
	Cm-242
Am-243	Np-239
Bi-210m	Tl-206
Cm-247	Pu-243
Cs-137	Ba-137m
Np-237	Pa-233
Pb-210	Bi-210
	Po-210
Pu-244	U-240
	Np-240m
Ra-226	Rn-222
	Po-218
	Pb-214
	At-218
	Bi-214
	Po-214
Ra-228	Ac-228
	Th-228
	Ra-224
	Rn-220
	Po-216
	Pb-212
	Bi-212
	Po-212
	Tl-208
Sn-126	Sb-126m
	Sb-126
Sr-90	Y-90
Th-229	Ra-225
	Ac-225
	Fr-221
	At-217
	Bi-213
	Po-213
	Tl-209
	Pb-209
U-232	Th-228
	Ra-224
	Rn-220
	Po-216
	Pb-212
	Bi-212
	Po-212
	Tl-208
U-235	Th-231
U-238	Th-234
	Pa-234m
	Pa-234

4.4.8.3.2 Uptake Parameters

The recommendations for human uptake parameters were developed in the *Dose Calculation Methodology for Liquid Waste Performance Assessments at the Savannah River Site*, Rev. 2. [SRR-CWDA-2013-00058] The development of these values was primarily based upon data from the EPA's *Exposure Factors Handbook*. [EPA-600-R-090-052F] The recommended values are summarized in Table 4.4-110. In addition to these recommendations for supporting compliance, the *Dose Calculation Methodology for Liquid Waste Performance Assessments at the Savannah River Site* also includes alternative recommendations based on more realistic (best estimate) assumptions and more conservative (Pessimistic) assumptions.

Table 4.4-110: Human Uptake Parameters

Parameter	Symbol in Equations	Unit	Value [a]	Probabilistic Multiplier				
				Distribution	Mean/ Mode	SD	Min	Max
rate of water ingestion	U_{H2O}	L/yr	505	Gamma	0.92	0.34	0.20	2.22
rate of soil and dust ingestion	U_{SOIL}	kg/yr	1.06	Not applicable				
rate of produce ingestion	U_{PLANT}	kg/yr	207	Log-Normal	0.8 [c]	2.3 [c]	0.01	4.0
rate of meat ingestion	U_{MEAT}	kg/yr	68.7	Log-Normal	0.8 [c]	1.9 [c]	0.02	3.4
rate of milk ingestion	U_{MILK}	kg/yr [b]	75.0	Not applicable				
rate of poultry ingestion	$U_{POULTRY}$	kg/yr	12.1	Not applicable				
rate of egg ingestion	U_{EGG}	kg/yr	11.0	Not applicable				
rate of fish ingestion	U_{FISH}	kg/yr	17.8	Triangular	1.0	N/A	0.78	1.76
human breathing rate	U_{AIR}	m^3/yr	8,000	Not applicable				

[SRR-CWDA-2013-00058]

a This is the recommended value, for use in deterministic modeling to establish compliance to performance objectives.

b For use in dose calculations, this value must be converted to L/yr by assuming a milk density of 1.03 kg/L.

c Use geometric means and standard deviations for these parameters.

SD = standard deviation

N/A = Not Applicable

4.4.8.3.3 Other Uptake Parameters

Table 4.4-111 and Table 4.4-112 provide additional inputs necessary for determining the impacts of biotic uptake (e.g., poultry consuming contaminated feed).

Table 4.4-111: Other Uptake Parameters

Parameter	Symbol in Equations	Unit	Value
ingestion of water by terrestrial livestock	$Q_{H2O,MEAT}$	L/yr	1.02E+04
ingestion of fodder by terrestrial livestock	$Q_{fod,MEAT}$	kg/yr	1.31E+04
ingestion of water by milk-producing livestock	$Q_{H2O,MILK}$	L/yr	1.83E+04
ingestion of fodder by milk-producing livestock	$Q_{fod,MILK}$	kg/yr	1.90E+04
ingestion of water by poultry	$Q_{H2O,POULTRY}$	L/yr	1.10E+02
ingestion of fodder by poultry	$Q_{fod,POULTRY}$	kg/yr	3.65E+01
ingestion of soil by poultry	$Q_{SOIL,POULTRY}$	kg/yr	3.65E+00
ingestion of water by egg-producers	$Q_{H2O,EGG}$	L/yr	1.10E+02
ingestion of fodder by egg-producers	$Q_{fod,EGG}$	kg/yr	3.65E+01
ingestion of soil by egg-producers	$Q_{SOIL,EGG}$	kg/yr	3.65E+00

[SRR-CWDA-2013-00058]

Table 4.4-112: Uptake Fractions for Biotic Receptor Parameters

Parameter	Symbol in Equations	Value
fraction of fodder (consumed by terrestrial livestock) that is contaminated	$F_{fod,MEAT}$	1.0
fraction of fodder (consumed by milk-producing livestock) that is contaminated	$F_{fod,MILK}$	1.0
fraction of fodder (consumed by poultry) that is contaminated	$F_{fod,POULTRY}$	1.0
fraction of soil (consumed by poultry) that is contaminated	$F_{SOIL,POULTRY}$	1.0
fraction of fodder (consumed by egg-producers) that is contaminated	$F_{fod,EGG}$	1.0
fraction of soil (consumed by egg-producers) that is contaminated	$F_{SOIL,EGG}$	1.0

[SRR-CWDA-2013-00058]

4.4.8.3.4 Transfer Coefficients for Biotic Accumulation

Table 4.4-113 provides the transfer coefficients used in the dose calculations. These values are used to determine the biotic accumulation of contaminants in various media. These include soil-to-plant (also known as soil-to-vegetable or soil-to-vegetation ratios), feed-to-meat, feed-to-milk, feed-to-poultry, feed-to-egg, and water-to-fish. The development of each set of values is described in the *Dose Calculation Methodology for Liquid Waste Performance Assessments at the Savannah River Site*, Rev. 2. [SRR-CWDA-2013-00058] Note that the soil-to-plant transfer coefficients were all developed based on the wet weight mass of ingested produce (as opposed to the dry weight); this is because the uptake parameter for the produce ingestion rate (U_{PLANT}) is based on the ingested wet weight of produce.

Also note that previous modeling has shown that total dose results are not particularly sensitive to probabilistic distributions on the transfer coefficients, relative to other dose parameters (see Section 5.6 of SRR-CWDA-2014-00006). Therefore, no probabilistic distributions were recommended for these parameters. [SRR-CWDA-2013-00058]

Table 4.4-113: Summary of Recommended Transfer Coefficients

Element	Soil-to-Plant R_{StoV} (unitless)	Feed-to-Meat TC_{meat} (yr/kg)	Feed-to-Milk TC_{milk} (yr/L)	Feed-to-Poultry $TC_{poultry}$ (yr/kg)	Feed-to-Egg TC_{egg} (yr/kg)	Water-to-Fish TC_{fish} (L/kg)
Ac	5.85E-05	1.10E-06	5.48E-08	1.64E-05	1.10E-05	2.50E+01
Ag	1.48E-04	8.21E-06	1.37E-07	5.48E-03	1.37E-03	1.10E+02
Al	3.04E-04	4.11E-06	5.64E-07	1.00E-20	1.00E-20	5.10E+01
Am	1.08E-04	1.37E-06	1.15E-09	1.64E-05	8.21E-06	2.40E+02
As	3.57E-03	5.48E-06	1.64E-07	2.27E-03	7.12E-04	3.30E+02
B	5.67E-01	2.19E-06	4.23E-06	1.00E-20	1.00E-20	1.00E-20
Ba	9.87E-04	3.83E-07	4.38E-07	5.20E-05	2.38E-03	1.20E+00
Bk	2.40E-04	6.84E-08	5.48E-09	1.00E-20	1.00E-20	2.50E+01
C	2.40E-01	8.49E-05	3.29E-05	1.00E-20	1.00E-20	3.00E+00
Cd	3.19E-01	1.59E-05	5.20E-07	4.65E-03	2.74E-04	2.00E+02
Cf	5.85E-05	1.10E-07	4.11E-09	1.64E-05	1.10E-05	2.50E+01
Cl	1.05E+01	4.65E-05	4.65E-05	8.21E-05	7.39E-03	4.70E+01
Cm	1.72E-04	1.10E-07	5.48E-08	1.64E-05	1.10E-05	3.00E+01
Co	2.18E-02	1.18E-06	3.01E-07	2.66E-03	9.03E-05	7.60E+01
Cr	1.97E-04	2.46E-05	1.18E-06	5.48E-04	2.46E-03	4.00E+01
Cs	1.16E-02	6.02E-05	1.26E-05	7.39E-03	1.10E-03	3.00E+03
Cu	2.53E-01	2.46E-05	5.48E-06	1.37E-03	1.37E-03	2.30E+02
Eu	6.85E-03	5.48E-08	8.21E-08	5.48E-06	1.10E-07	1.30E+02
F	4.46E-03	4.11E-04	2.74E-06	3.83E-05	7.39E-03	1.00E+01
Fe	1.87E-02	3.83E-05	9.58E-08	2.74E-03	4.93E-03	1.70E+02
H	1.15E+00	1.00E-20	4.11E-05	1.00E-20	1.00E-20	1.00E+00
Hg	1.62E-01	6.84E-04	1.29E-06	8.21E-05	1.37E-03	6.10E+03
I	6.39E-03	1.83E-05	1.48E-05	2.38E-05	6.57E-03	3.00E+01
K	5.82E-01	5.48E-05	1.97E-05	1.10E-03	2.74E-03	3.20E+03
Mn	9.75E-02	1.64E-06	1.12E-07	5.20E-06	1.15E-04	2.40E+02
Mo	3.50E-01	2.74E-06	3.01E-06	4.93E-04	1.75E-03	1.90E+00
Nb	4.63E-03	7.12E-10	1.12E-09	8.21E-07	2.74E-06	3.00E+02
Ni	3.16E-02	1.37E-05	2.60E-06	2.74E-06	2.74E-04	2.10E+01
Np	4.39E-03	2.74E-06	1.37E-08	1.64E-05	1.10E-05	2.10E+01
Pa	5.85E-05	1.10E-07	1.37E-08	1.64E-05	1.10E-05	1.00E+01
Pb	6.60E-03	1.92E-06	5.20E-07	2.19E-03	2.74E-03	2.50E+01
Pd	1.86E-02	1.10E-05	2.74E-05	8.21E-07	1.10E-05	1.00E+01
Pt	9.08E-03	1.10E-05	1.41E-05	1.00E-20	1.00E-20	3.50E+01
Pu	2.46E-05	3.01E-09	2.74E-08	8.21E-06	3.29E-06	2.10E+04
Ra	1.03E-02	4.65E-06	1.04E-06	8.21E-05	8.49E-04	4.00E+00
Rn	1.00E-20	1.00E-20	1.00E-20	1.00E-20	1.00E-20	7.55E-10
Sb	6.24E-04	3.29E-06	1.04E-07	1.64E-05	1.92E-04	3.70E+01
Se	6.23E-02	4.11E-05	1.10E-05	2.66E-02	4.38E-02	6.00E+03
Sm	6.85E-03	5.48E-08	8.21E-08	5.48E-06	1.10E-07	3.00E+01
Sn	3.12E-03	2.19E-04	2.74E-06	2.19E-03	2.74E-03	3.00E+03
Sr	1.90E-01	3.56E-06	3.56E-06	5.48E-05	9.58E-04	2.90E+00
Tc	1.17E+01	2.74E-07	3.83E-07	8.21E-05	8.21E-03	2.00E+01
Th	4.31E-04	6.30E-07	1.37E-08	1.64E-05	1.10E-05	6.00E+00
U	4.10E-03	1.07E-06	4.93E-06	2.05E-03	3.01E-03	9.60E-01
Zn	4.27E-01	4.38E-04	7.39E-06	1.29E-03	3.83E-03	3.40E+03
Zr	8.26E-04	3.29E-09	9.86E-09	1.64E-07	5.48E-07	2.20E+01

[SRR-CWDA-2013-00058]

Note: A value of 1.00E-20 is assumed for elements that are expected to have a negligible effect, if any, on dose calculations.

4.4.8.3.5 Exposure and Inhalation Parameters

The amount of exposure and inhalation that a human receptor is subjected to is influenced by human behavior and environmental conditions. For example, in the Acute IHI scenario the human receptor is exposed to drill cuttings because they are assumed to be the driller who is drilling into the contaminated source. Recommendations for these parameters are provided in Table 4.4-114.

Table 4.4-114: Uptake Fractions for Biotic Receptor Parameters

Parameter	Symbol in Equations	Unit	Value
fraction of time spent in a contaminated garden or crop	$F_{t,g}$	none	2.17E-01
fraction of time spent showering or bathing	$F_{tSHOWER}$	none	1.2E-02
geometry factor b for showering or bathing	GF_{SHOWER}	none	1.0
fraction of time spent swimming	F_{tSWIM}	none	4.1E-03
geometry factor b for swimming	GF_{SWIM}	none	1.0
fraction of time spent boating and fishing	F_{tBOAT}	none	7.3E-03
geometry factor b for boating and fishing	GF_{BOAT}	none	0.5
fraction of time spent drilling into contaminated source	F_{tDRILL}	none	2.3E-03
airborne release fraction	ARF	none	1.0E-4
moisture content of ambient air	MC_{AIR}	kg/m3	1.0E-02
moisture content of shower air	MC_{SHOWER}	kg/m3	4.1E-02
mass loading of soil in the air	L_{SOIL}	kg/m3	1.0E-7

[SRR-CWDA-2013-00058]

4.4.8.3.6 Physical Parameters for Dose Calculations

Physical parameters are used to define various environmental factors that influence the movement and accumulation of contaminants prior to uptake by the human receptor. Physical parameters for dose calculations used in Liquid Waste PAs can be organized into three groups: (1) soil parameters, (2) crop and gardening parameters, (3) drilling parameters. Recommended values for each of these sets of physical parameters are defined in Table 4.4-115, Table 4.4-116, and Table 4.4-117, respectively.

Table 4.4-115: Soil Parameters for Dose Calculations

Parameter	Symbol in Equations	Unit	Value	Probabilistic Multiplier				
				Distribution	Mean/ Mode	SD	Min	Max
buildup time of radionuclides in soil	t_b	yr	25	Not applicable				
surface (or areal) density of soil	ρ_{ss}	kg/m^2	240	Normal	1.0	0.07	0.85	1.15
dry bulk density of soil	ρ_{bs}	kg/m^3	1650					
precipitation rate	PR	m/yr	1.25	Not applicable				
evapotranspiration rate	ER	m/yr	0.79	Not applicable				
irrigation rate	IR	m/yr	1.32	Triangular	1.0	N/A	0.5	1.5
radiological decay constant of radionuclide *i*	λ_i	1/yr	Varies [a]	Not applicable				
weathering decay constant	λ_w	1/yr	18.1	Triangular	1.0	N/A	0.6	1.0
soil moisture content	MC_{SOIL}	none	0.2086	Not applicable				

[SRR-CWDA-2013-00058]

a Radiological decay constant of radionuclide i = ln(2)/(half-life (yr) of radionuclide i)

Table 4.4-116: Crop and Gardening Parameters for Dose Calculations

Parameter	Symbol in Equations	Unit	Value	Probabilistic Multiplier				
				Distribution	Mean/ Mode	SD	Min	Max
fraction of material deposited on leaves that is retained	F_r	unitless	0.25 [a]	Triangular	1.0	N/A	0.8	1.0
fraction of material remaining on leaves after washing	F_{wash}	unitless	1	N/A	N/A	N/A	N/A	N/A
time in which crops and gardens are irrigated	t_{irr}	yr	1.92E-01	Normal	1.0	0.1	0.85	1.28
fraction of year in which crops are irrigated	F_{irr}	unitless	t_{irr} per year	N/A	N/A	N/A	N/A	N/A
crop and garden yield (agricultural productivity)	Y_g	kg/m^2	2.2	N/A	N/A	N/A	N/A	N/A
depth of crop garden tilling	d_{till}	m	0.15	Triangular	1.0	N/A	1.0	4.1
fraction of produce that is leafy	F_{leaf}	unitless	0.222	N/A	N/A	N/A	N/A	N/A
Area of garden or crop for family of four	A_{garden}	m^2	100	Triangular	1.0	N/A	1.0	10.0

[SRR-CWDA-2013-00058]

N/A = Not applicable

a Consistent with the footnote in Table 3-2 of the reference document (WSRC-STI-2007-00004, Rev. 4), the retention fraction for Iodine should be multiplied by four (i.e., 0.25 × 4 = 1.0).

Table 4.4-117: Drilling Parameters for Dose Calculations

Parameter	Symbol in Equations	Unit	Value	Probabilistic Multiplier				
				Distribution	Mean/ Mode	SD	Min	Max
well diameter	$well_{diam}$	m	0.203	N/A	N/A	N/A	N/A	N/A
water density	ρ_{H2O}	kg/L	1	N/A	N/A	N/A	N/A	N/A
well depth*	$well_{dep}$	m	30.5	Log-Normal	1.60	1.53	0.32	9.89

[SRR-CWDA-2013-00058]
N/A = Not applicable
* While the sampling distribution for the well depth was developed, as a modeling simplification this PA only uses the recommended value of 30.5 m.

4.4.8.3.7 Local Productivity Parameters for Dose Calculations

The following describes the local fraction (or local productivity) parameters. These parameters are used to define the fraction of food intake that is home-produced, as opposed to coming from other sources. For example, although the MOP is assumed to have a farm (crops or garden), current practices indicate that only a fraction of produce consumed comes directly from home grown sources. As such, only a fraction of the consumed produce would be contaminated. Table 4.4-118 provides a summary of the recommended values.

Table 4.4-118: Recommended Fractional Values for Local Productivity

Parameter Description	Symbol in Equations	Unit	Recommended Value (Mode)	Min	Max
The fraction of consumed water that comes from the contaminated water source.	$F_{local,H2O}$	unitless	1.0	N/A	N/A
The fraction of total produce grown at home.	$F_{local,PLANT}$	unitless	Eq. 4.4-247	N/A	N/A
The fraction of total terrestrial livestock meat produced at home.	$F_{local,MEAT}$	unitless	0.319	0.160	0.638
The fraction of total milk produced at home.	$F_{local,MILK}$	unitless	0.254	0.127	0.508
The fraction of total poultry produced at home.	$F_{local,POULTRY}$	unitless	0.319	0.160	0.638
The fraction of total eggs produced at home.	$F_{local,EGG}$	unitless	0.254	0.127	0.508
The fraction of households that fish.	$F_{local,FISH}$	unitless	0.325	0.163	0.650

[SRR-CWDA-2013-00058]
N/A = Not Applicable

Note: For modeling the local fraction for produce, it is recommended that instead of using an input value, a formula should be applied to ensure that model values are internally consistent. The recommended formula is:

$$F_{local,PLANT} = \frac{(Y_g \times A_{garden})}{U_{PLANT}} \times \frac{1}{(N_{fam} \times 1yr)} \qquad \text{Eq. 4.4-247}$$

where:

$F_{local,PLANT}$ = fraction of consumed produce grown locally (unitless),

Y_g = crop and garden production yield (kg/m^2) (Table 4.4-116),

A_{garden} = garden or crop area (m^2) (Table 4.4-116),

U_{plant} = human ingestion rate of plants or produce (kg/yr) (Table 4.4-110), and

N_{fam} = assumed number of family members = 4.

4.4.8.3.8 Summary of Assumptions

The key assumptions for the Dose and Exposure Pathways calculations are summarized as follows.

- The human receptor is assumed to be a gender-weighted adult farmer who participates in water-related recreational activities.
- Hypothetical future wells used for supplying water to the human receptor are drilled into aquifers with the highest possible concentrations along either the 100-meter boundary or the 1-meter boundary.
- Water recreation, including fishing, is assumed to always occur along a seepline near the SDF and at the point along the stream(s) with the highest possible concentrations.
- Human uptake factors are adjusted to account for occupational, recreational, and regional influences. Note that these adjustments are only applied when they increase the uptake rates. For example, individuals in the South consume fewer fruits and vegetables relative to the national average. Therefore, the national average was assumed without adjusting for this regional influence.
- All water consumed by the human receptor is assumed to be contaminated.
- The human receptor bathes and swims only in contaminated waters.
- The uptake fractions for biotic receptors are all assumed to be 1.0, indicating that 100% of water and fodder consumed by livestock is assumed to be contaminated (i.e., no water or fodder is assumed to come from uncontaminated sources).

4.4.8.4 Interfaces for the Dose and Exposure Pathways

The contaminant concentrations from the Aquifer Transport Model (described in Section 4.4.6) may be applied to these calcualtions to provide dose results. Section 5.5 presents the dose results for the MOP. Sections 6.3, 6.4, and 6.5 present various dose results for the IHI.

4.5 Probabilistic Modeling Overview

The modeling described throughout Section 4.4 was based on the three Central Scenario modeling cases: the Realistic Case, the Compliance Case, and the Pessimistic Case. All three of these Central Scenario modeling cases are "deterministic" modeling cases, meaning each modeling case assumes only a single set of input values and provides only a single set of results. For example, the main focus of the Compliance Case is to establish compliance to the applicable performance objectives, as identified in Table 1.7-1. Given this focus, the input values selected represent a single set of input values which are a combination of both the most probable and most defensible values, thus giving results which serve as a basis for providing reasonable expecation of compliance.

To better address uncertainty and sensitivity of the modeling of the SDF, a probabilistic model was also constructed. This model was necessarily simpler than the PORFLOW ground water model in its environmental transport calculations. GoldSim software is well suited to facilitate probabilistic PA modeling (more information on GoldSim fundamentals is available at the website: www.goldsim.com). This program was developed for PA modeling and includes many features that make it particularly useful, such as integrated solutions of physically-based differential equations from radioactive decay and in-growth, to chemical partitioning and diffusion.

While a deterministic model provides a single set of results, a probabilistic model is a model that incorporates random variables (based on assigned distributions) and provides many sets of results, which may then be described in terms of probability (or likelihood of occurrence). Probabilistic models provide insights with respect to how different combinations of potential values might influence results. The results may then be analyzed to determine which parameters, statistically, exhibit the greatest influence over specific results. The results of the probabilistic uncertainty and sensitivity analyses of this model are discussed in Sections 5.7 and 6.6.

For the SDF PA, the probabilistic SDF model is referred to as the SDF GoldSim Model since it was developed using GoldSim software. This model abstracts the processes simulated in PORFLOW (see Figure 4.4-1). The abstraction approach means that some of the complex processes from the flow and transport modeling in PORFLOW have been simplified into less complex approximations of these processes. For example, rather than using a complex, three-dimensional transport solver to simulate aquifer transport, the probabilistic SDF model uses a one-dimensional "plume function" to estimate concentrations at the points of compliance.

As described at the beginning of Section 4.4, a comparison of various PORFLOW-based results and the respective GoldSim-based results was used to evaluate the appropriateness of the SDF GoldSim Model for use as a surrogate to the more complex PORFLOW models. This comparison is described as "benchmarking" (see Section 5.6). Once the model is benchmarked, it assumed to be appropriate for use in probabilistic modeling, as well as for deterministic sensitivity modeling. Running the SDF GoldSim Model in deterministic mode, rather than in probabilistic mode, allows users to change the values for select parameters to demonstrate the direct impacts of such changes (see Section 5.8).

4.5.1 Probabilistic Modeling Philosophy

The SDF GoldSim Model addresses uncertainty in the input parameters by sampling the values based on defined probability distributions. The collective uncertainty of all stochastic, or probabilistic, inputs is reflected in the range and distribution of the modeled results (e.g., ground water concentrations or doses). If a given input parameter is not treated as an uncertain input, that is, if it is defined deterministically, then it contributes nothing to the overall uncertainty in the results. In reality, few parameters have zero uncertainty. An example of a parameter without a defined range is the half-life of I-129.

In general, the goal is to assign realistic probability distributions to any uncertain parameters which are expected to exhibit significant influence over the dose results. Some parameters, which were previously assigned distributions, are now treated as static (deterministic) input values. For example, within the dose calculations of the FY2014 SDF SA (SRR-CWDA-2014-00006), the rate of soil ingestion was sampled along a defined probability distribution; however, it has been determined that soil ingestion has a negligible impact on the overall dose results, so it has now been assigned a defensible, deterministic value. By reducing the number of these negligible distributions, the probabilistic results are expected to show less statistical "noise" than the results from previous modeling efforts, thus, facilitating more meaningful probabilistic analyses.

Previous versions of the SDF GoldSim Model assigned parameter distributions that typically flanked MPAD values, meaning that the assigned probability distributions would assume minimum values that were less than the MPAD values and maximum values that were greater than the MPAD values. Since the MPAD values are inherently skewed towards a more defensible bias, the central tendencies of the probability distributions skewed towards more conservative results. This previous modeling philosophy was justified because inputs were historically defined based on MPAD assumptions and little effort was made to define inputs in terms of expected values. As such, it made sense to default to the MPAD values as representations of the mean, median, or mode for various distributions. While this approach provided layers of defensibility, it limited the usefulness of the probabilistic modeling results with respect to developing a realistic understanding of which combinations of potential values might exhibit the greatest influence over the results.

For this PA, the probabilistic modeling philosophy is fundamentally different. Given that select parameters within this PA have undergone additional input development to support the three modeling cases of the Central Scenario (i.e., the Realistic Case, the Compliance Case, and the Pessimistic Case), input values are now available that do reflect more realistic or expected conditions. As such, it is now more appropriate to develop distributions which flank these more realistic values.

Adopting a probabilistic approach also allows analysts to determine which model input parameters exhibit the most influence on the results. This is done through sensitivity analysis, which can be used to quantify covariance (i.e., combined variability between random variables) between model inputs and model results (see Section 5.7.4).

Generally speaking, the SDF GoldSim Model includes seven categories of stochastic distributions:

1. Physical Property Uncertainty,
2. Inventory Uncertainty,
3. Parametric Flow Field Sampling,
4. Ground Water Hydrology Uncertainty,
5. K_d Uncertainty,
6. Technetium Solubility Uncertainty, and
7. Dose and Exposure Pathway Uncertainty.

The corresponding stochastic elements and their respective distributions are discussed in greater detail in Section 5.7.1.

4.5.2 GoldSim Modeling as an Abstraction of PORFLOW Modeling

In general, the SDF GoldSim Model may be summarized as three submodels:

1. an abstraction of the PORFLOW Vadose Zone Transport Model,
2. an abstraction of the PORFLOW Aquifer Transport Model, and
3. the Dose and Exposure Pathways Model.

These abstractions are specifically designed to approximate the processes of radionuclide transport from the SDUs to the points of assessment in a manner that also allows for the incorporation of uncertainty. The SDF GoldSim Model, as designed, approximates certain processes less rigorously than the PORFLOW models by using mixing cells for the vadose zone and analytical solutions for the saturated zone. The alternative solution methods used within the SDF GoldSim Model are used in conjunction with abstracted flow data to generate unidirectional and spatially consistent transport, rather than explicitly simulating either two-dimensional processes (as PORFLOW does for release and transport from SDUs 1 and 4), quasi-three-dimensional processes (as PORFLOW does for release and transport from the cylindrical SDUs), or fully three-dimensional processes (as PORFLOW does for aquifer transport). As such, modeling with the SDF GoldSim Model is more time-efficient. This more time-efficient approach allows for the examination of the influences of specific parameters relative to transport. The appropriateness of the abstraction approach as a surrogate for the more complex PORFLOW model is demonstrated in Section 5.6.

Note that the dose calculations included in the SDF GoldSim Model can be used to evaluate doses at the points of assessment using either the concentrations generated within GoldSim (using the transport abstractions) or using the concentrations generated by the Aquifer Transport Model (i.e., PORFLOW). Since implementation of the Dose and Exposure Pathways portion of the SDF GoldSim Model has already been described in Section 4.4.8, the description of this portion of the SDF GoldSim Model is not repeated within this section.

4.5.2.1 Abstraction Summary

As abstractions of the Vadose Zone Transport Model (Section 4.4.5) and the Aquifer Transport Model (Section 4.4.6) as modeled in PORFLOW, the SDF GoldSim Model solves the general equations for transport of dissolved radionuclides and non-radioactive species.

- The abstraction of the Vadose Zone Transport Model (PORFLOW), as applied within the SDF GoldSim Model, is based on zone-averaged flow data derived from PORFLOW model simulation outputs (see Section 4.4.4). The data including Darcy velocities, saturations, volumetric flow rates, etc., are read into the GoldSim model and used to define the advective process for the transport abstraction.
- The abstraction of the Aquifer Transport Model (PORFLOW), as applied within the SDF GoldSim Model, is based on the use of "pipe element" analytic solutions for SDU-specific pathway lengths derived from PORFLOW-generated particle tracking using the GSA Model (as described in the *Updated Groundwater Flow Simulations of the Savannah River Site General Separations Area* (SRNL-STI-2018-00643)). The Darcy velocity along these flow pathways are based on SDU specific particle tracking where the user has the option of choosing between velocities derived; 1) based on the time it takes for a particle released at the center of an SDU to reach the 100-meter boundary in conjunction with the path length from the SDU's center point, or 2) the time for the peak of a breakthrough curve generated from the release of a series of particles filling the SDU to reach the 100-meter boundary and the path length.

The modeling approach for the SDF GoldSim Model relies on the simplifying assumption that one-dimensional vertical flow controls contaminant release and transport through the SDUs and the vadose zone (or unsaturated zone (UZ)), and one-dimensional horizontal flow controls the contaminant transport through the saturated zone (SZ).

At the SDUs, molecular or matrix diffusion in the horizontal direction (e.g., from the saltstone into the SDU walls and from the SDU walls into the surrounding backfill) is also explicitly simulated within the SDF GoldSim Model because this diffusion can be relatively important when flow rates are low.

Note that the PORFLOW Vadose Zone Transport Model automatically outputs Tc-99 fluxes for each SDU. The SDF GoldSim Model automatically reads the outputs from PORFLOW, rather than explicitly modeling Tc-99 releases (as performed for the other radionuclides). The decision to use the Tc-99 releases generated from the PORFLOW Vadose Zone Model as direct inputs to the saturated zone simulation within the SDF GoldSim Model model is based on the application of the shrinking core model to evaluate Tc-99 releases. In this shrinking core model cell-by-cell changes in the chemical environments control the release of potentially large amounts of Tc-99 from localized storage at earlier times than if the releases were based on zone-by-zone changes in chemical environments.

Note that within PORFLOW, the release and transport of I-129 transport is also evaluated using a shrinking core approach. However, the PORFLOW-generated I-129 releases are not used as direct input to the SDF GoldSim Model. The reason that the Tc-99 releases are treated differently than I-129 releases is because the cell-by-cell releases of I-129 associated with the changes to the chemical environment which influences the I-129 K_ds are less likely to generate large pulse-type releases at earlier release times. This is because the small

values for the chemistry-specific K_ds limit the potential magnitude of cell-by-cell I-129 releases from storage.

4.5.2.2 Advective-Dispersive Transport Calculations

Transport calculations within the SDF GoldSim Model are used to simulate the transport of non-conservative species that are subject to sorption. The model also accounts for radioactive decay and/or ingrowth. Other processes controlling the mass releases from saltstone include time-dependent physical and chemical degradation of materials (i.e., saltstone, SDU concrete, and (if applicable) HDPE); however, these other processes are implicitly accounted for by using the flow data collected from the PORFLOW (i.e., the Vadose Zone Flow Model described in Section 4.4.4).

The governing equations for one-dimensional advective-dispersive transport of a dissolved species in a unidirectional flow field can be written as follows:

$$\frac{\partial(\varphi RC)}{\partial t} = D\frac{\partial^2 C}{\partial l^2} - \nu\frac{\partial C}{\partial l} - \varphi R\lambda C + \sum_{i=1}^{N_p} \varphi R\lambda_{pi} C_{pi} \qquad \text{Eq. 4.5-1}$$

where:

φ = effective porosity (unitless),

R = retardation coefficient (unitless),

C = solute concentration (kg/m^3),

t = time (s),

D = dispersion coefficient (m^2/s) (see Eq. 4.5-2 below),

l = distance to point of assessment (m),

ν = Darcy velocity (m/s),

λ = decay coefficient (s^{-1}),

N_p = number of parent species (unitless),

λ_{pi} = decay coefficient of the i^{th} parent (s^{-1}), and

C_{pi} = Solute concentration of the i^{th} parent (kg/m^3).

The hydrodynamic dispersion coefficient (D) used in Eq. 4.5-1 is determined as:

$$D = \nu\alpha + \varphi D_{eff} \qquad \text{Eq. 4.5-2}$$

where:

D = dispersion coefficient (m^2/s),

ν = Darcy velocity (m/s),

α = dispersivity (m),

φ = effective porosity (unitless), and

D_{eff} = effective diffusion coefficient (m^2/s).

The left-hand side term of Eq. 4.5-1 describes the change in mass storage over time, the first term on the right-hand side spreading of mass due to the influence of hydrodynamic dispersion, the second term on the right-hand side describes the influence of advective transport on mass migration, the third term on the right-hand side represents the influence of radionuclide decay of the simulated radionuclide, and the fourth term on the right-hand side represents the influence ingrowth from parent species on the mass balance within the modeled system. In the SDF GoldSim Model the advective-dispersive transport calculations are implemented using a network of GoldSim mixing cell elements to represent transport in the vadose zone and GoldSim pipe elements (analytic solutions) to represent tranpost in the saturated zone (as described in Section 4.5.3).

Note that in the SDF GoldSim Model, the process of hydrodynamic dispersion is handled differently in the vadose zone versus the saturated zone transport (which is also true in the PORFLOW models). The reason can be be seen by examining the first term on the right-hand side of Eq. 4.5-1, which describes the influence of hydrodynamic dispersion, or the spreading of mass dissolved in the liquid phase (Bear, 1972 [ISBN: 9780486656755]). This term is a function of two processes: mechanical dispersion and molecular diffusion as shown in Eq. 4.5-2.

Mechanical dispersion, which is a function of water velocity and the dispersivity, represents the spreading of dissolved mass due to variations in local velocity magnitudes and directions along tortuous flow paths, and between adjacent flow paths (Bear, 1972 [ISBN: 9780486656755]). In terms of an instantaneous point-source release of mass, the degree of spreading associated with mechanical dispersion is a function of the dispersivity and distance traveled by the center of mass of the dissolved species (which is a function of velocity and time). In addition, the dispersivity term used in in advective-dispersive transport simulations is generally considered to be a function of the distance over which the transport takes place (Gelhar, et.al., 1992) reflecting the influence of differences of scales of heterogeneities. The molecular diffusion term describes the random movement of dissolved molecules which has an equilibrating effect reflected in transport of dissolved molecules from areas of high concentration to areas of low concentration and is independent of flow velocity. Because the influence of molecular diffusion depends upon time alone, its influence on hydrodynamic dispersion is generally insignificant relative to mechanical dispersion except under extremely slow velocities.

Mechanical dispersion is not explicitly considered within the either the PORFLOW Vadose Zone Transport Model or in the SDF GoldSim Model. Instead, it is assumed that the influence of mechanical dispersion is negligible in this near-field (small-scale) environment. Therefore, the first term in Eq. 4.5-2 is not considered. (Note that a sensitivity case examining the influence of mechanical dispersion in the PORFLOW Vadose Zone Transport Model is presented in Section 5.8.3.7.) The influence of molecular diffusion on the transport is considered within the vadose zone models, and plays an important role in radionuclide and chemical migration at early times before the

cementitious materials and HDPE liners degrade and the advection term dominates the transport process.

Within the SDF GoldSim Model, saturated zone transport (i.e., the abstraction of the PORFLOW Aquifer Transport Model) explicitly considers longitudinal mechanical dispersion in the pipe elements. In addition, the influence of transverse dispersion perpendicular to the flow direction is superimposed on the pipe-element results using the GoldSim plume function (GTG-2018a). Plume attenuation considers transverse dispersion (for both horizontal and vertical directions) within the SDF GoldSim Model. The GoldSim plume function is a built-in function based on Green's function solutions that can be used to superimpose the influence of transverse (horizontal and vertical) dispersion on the results generated by the one-dimensional advective transport calculations. Applying the plume function to one-dimensional transport results provides quasi-three-dimensional results.

Eq. 4.5-1 can be rewritten to include the effects of horizontal and vertical transverse dispersion:

$$\frac{\partial(\varphi RC)}{\partial t} = D_l \frac{\partial^2 C}{\partial {s_l}^2} + D_{th} \frac{\partial^2 C}{\partial {s_{th}}^2} + D_{tv} \frac{\partial^2 C}{\partial {s_{tv}}^2} - \nu \frac{\partial C}{\partial s_l} - \varphi R \lambda C + \sum_{i=1}^{N_p} \varphi R \lambda_{pi} C_{pi} \qquad \text{Eq. 4.5-3}$$

where:

φ = effective porosity (unitless),

R = retardation coefficient (unitless),

C = solute concentration (kg/m^3),

t = time (s),

D_l = longitudinal dispersion coefficient (m^2/s) (see Eq. 4.5-4 below),

s_l = direction of the flow line,

D_{th} = transverse horizontal dispersion coefficient (m^2/s) (see Eq. 4.5-5 below),

s_{th} = direction normal to the flow line (horizontal),

D_{tv} = transverse vertical dispersion coefficient (m^2/s) (see Eq. 4.5-6 below),

s_{tv} = direction normal to the flow line (vertical),

ν = Darcy velocity (m/s),

λ = decay coefficient (s^{-1}),

N_p = number of parent species (unitless),

λ_{pi} = decay coefficient of the i^{th} parent (s^{-1}), and

C_{pi} = Solute concentration of the i^{th} parent (kg/m^3).

The longitudinal dispersion coefficient (D_l) used in Eq. 4.5-3 is determined as:

$$D_l = \nu_l \alpha_l + \varphi D_{eff} \quad \text{Eq. 4.5-4}$$

where:

D_l = longitudinal dispersion coefficient (m^2/s),

ν_l = Darcy velocity (m/s) in the longitudinal direction,

α_l = longitudinal dispersivity (m),

φ = effective porosity (unitless), and

D_{eff} = effective diffusion coefficient (m^2/s).

Similarly, transverse horizontal dispersion coefficient (D_{th}) used in Eq. 4.5-3 is determined as:

$$D_{th} = \nu_l \alpha_{th} + \varphi D_{eff} \quad \text{Eq. 4.5-5}$$

where:

D_{th} = transverse horizontal dispersion coefficient (m^2/s),

ν_l = Darcy velocity (m/s) in the longitudinal direction,

α_{th} = transverse horizontal dispersivity (m),

φ = effective porosity (unitless), and

D_{eff} = effective diffusion coefficient (m^2/s).

The transverse vertical dispersion coefficient (D_{tv}) used in Eq. 4.5-3 is determined as:

$$D_{tv} = \nu_l \alpha_{tv} + \varphi D_{eff} \quad \text{Eq. 4.5-6}$$

where:

D_{tv} = transverse vertical dispersion coefficient (m^2/s),

ν_l = Darcy velocity (m/s) in the longitudinal direction,

α_{tv} = transverse vertical dispersivity (m),

φ = effective porosity (unitless), and

D_{eff} = effective diffusion coefficient (m^2/s).

4.5.3 GoldSim Layout and Structure

This section presents the model structure and general functionality of model elements in the SDF GoldSim Model. This section only provides a high-level overview of the model implementation; for additional details regarding the development and implementation of the SDF GoldSim Model and the SDF Tc-99 Release Model, refer to the most recent revision of *Updates to the Saltstone Disposal Facility Stochastic Fate and Transport Model* (SRR-CWDA-2013-00073). While many of the

key inputs have been updated to reflect those used in the latest PORFLOW models, the general layout and structure of the GoldSim model files have not significantly changed.

Figure 4.5-1 shows the top level of the SDF GoldSim Model. As shown, there are 11 containers in the root directory (top level) of the model. The GoldSim element names will be referred to in italics:

- *User_Input* – This container holds elements that function as user-defined global modeling parameters. These elements provide functionality to modelers for setting specific inputs and conditions for controlling various modeling runs. For example, one element within this container (*InputSetSelector*) allows users to select between the best estimate input values, the MPAD input values, or the conservative input values.
- *GlobalModel_Input* – This container holds elements that are used to support model indexing, arrays of unit values and zero values, and two of the most important sampling elements: *FlowFieldSampler*, which is used to select a vadose zone flow field, and *Solubility*, which is used to set a value for the technetium solubility. The *GlobalModel_Input* container also includes elements used to read input data from various external files. In addition, the *GlobalModel_Input* container contains file elements that automatically pass Tc-99 release data (from PORFLOW) to the linked containers.
- *Materials* – This container holds many inputs used to define material properties and transport properties. Most notable are the *Species* element, which defines the half-lives and activities for all radionuclides, and the K_d values for each transport media.
- *Inventory* – The elements within this container are used to select, or sample, the inventory values for each SDU.
- *Transport* – This container includes inputs used for performing ground water transport simulations and the plume functions used to estimate the concentrations at various points of assessment within the model.
- *DisposalUnits* – This container includes an *SDU_Data* container, which holds elements used to define the geometry of each SDU: a *Tc99Input* container, which includes elements to read external Tc-99 fluxes from a separate shrinking core model for simulating Tc-99 releases, containers for SDU 1 (*SDU1*) and SDU 4 (*SDU4*), and another container for all other SDUs (*SDUs*). This last container includes a looping structure that is used to simulate the flow and transport of each of the cylindrical SDUs. Each of the SDUs are simulated as a matrix of Cell Pathway elements (often referred to as "mixing cells"), which are organized into columns and rows to approximate the equivalent nodes within the PORFLOW Vadose Zone Transport model (as described in Section 4.4.5). Note the SDF GoldSim Model simulates transport, but relies on the flow data from PORFLOW; as such, the SDU roof is not explicitly modeled in the SDF GoldSim Model.
- *Model_Concentrations* – The elements within this container apply the plume adjustments from the plume functions in the *Transport* container to the contaminant fluxes from the SDUs. These plume functions provide an abstraction of the complex modeling performed by the PORFLOW Aquifer Transport Model (as described in Section 4.4.6).

- *Benchmark* – This container includes results from PORFLOW. These are used to compare GoldSim release and transport results against the equivalent results from PORFLOW to support the Benchmarking analysis.
- *Dose_Parameter_Calculations* – The elements within this container represent the Dose and Exposure Pathways Model (see Section 4.4.8).
- *Dose_Results* – This container collects all the dose results.
- *SensitivityAnalysis_New* – The elements within this container are used to collect sampling distribution data to support the probabilistic sensitivity analyses (see Section 5.7).

Figure 4.5-1: SDF GoldSim Model Root Directory

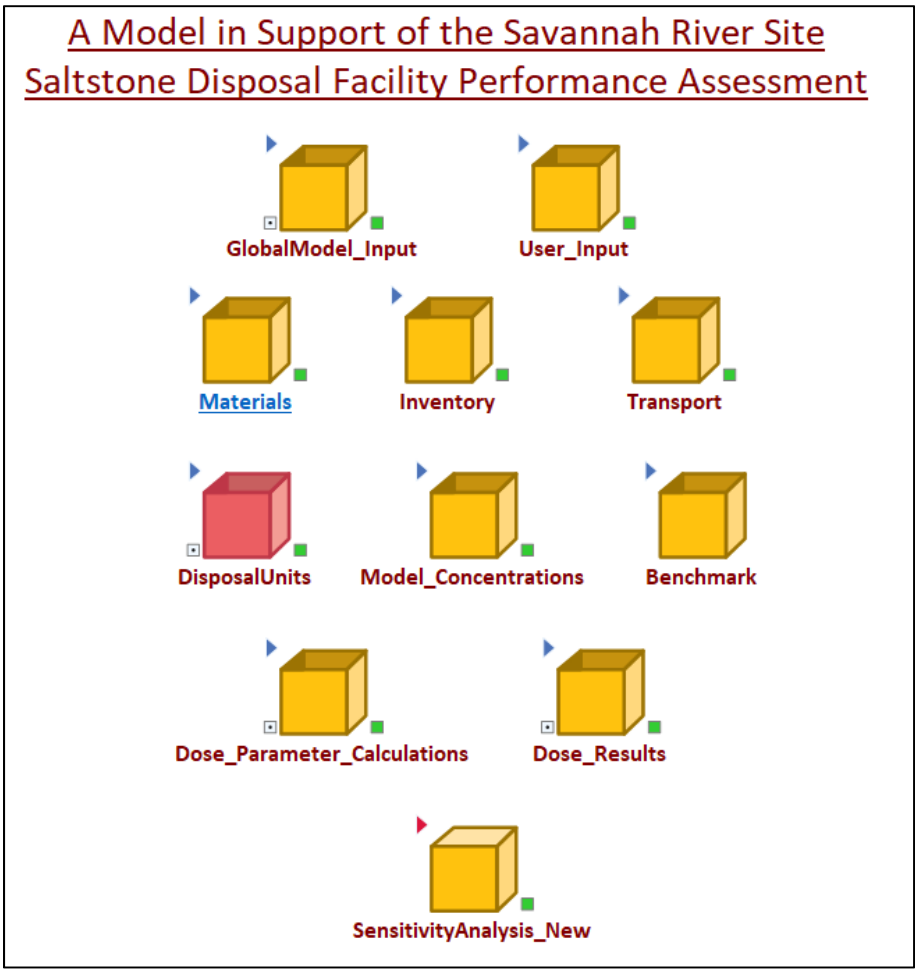

The abstractions of the PORFLOW transport models are primarily contained in the *DisposalUnits* container and the *Transport* container, and the concentration results from these abstractions are saved within the *Model_Concentrations* container. The other containers hold elements which define input values or support the dose calculations or analyses of results.

4.6 Alternative Conceptual Models

The modeling descriptions provided throughout the previous sections have focused on expected conditions (i.e., the Central Scenario). This section discusses specific alternative modeling scenarios developed for this PA. These scenarios require fundamentally different conceptualizations of the system to be fully addressed.

These alternative modeling scenarios were first introduced in the *Conceptual Model Development for the Saltstone Disposal Facility Performance Assessment* (SRR-CWDA-2018-00006) and were designed to address specific FEPs (see Section 4.1.1).

4.6.1 Early Release Scenario

Although it is expected that once backfilled, the SDU concrete will be well protected from mechanical degradation, a concern exists that the SDU concrete will not perform as well as designed with respect to preventing or delaying the release of contaminants. To address this concern, an Early Release Scenario was developed.

This scenario assumes that early releases will occur from the SDUs. The goal of this scenario is not to determine which events or processes could cause the early releases, but rather provide insights as to the potential impacts associated with early releases. As such, the exact mechanisms that cause these releases are not explicitly considered. Instead, this scenario non-mechanistically addresses several events or processes which may result in early releases, including (but not limited to):

- partial oxidation prior to closure,
- construction flaws,
- potential SDU concrete damage from freeze-thaw cycles,
- a significant rainfall event resulting in flooding during disposal operations,
- spilling of contaminants during disposal operations, or
- spalling of the SDU concrete due to a nearby fire.

Accordingly, this scenario provides a non-mechanistic evaluation of multiple FEPs, including the disruptive events identified as FEP 6.4.02 (Flooding or Drainage System Failure), FEP 6.4.03 (Releases Prior to Closure), and FEP 6.4.04 (Forest/Brush Fire). [SRR-CWDA-2017-00057]

Note this scenario also provides insights relative to potential dose impacts from contaminanted soils associated with the weeping of SDU 4. An evaluation of this contamination was developed as "Early Release Case 2" in Section 5.8.9.1. Additional discussion of the development for this alternative conceptual model and the associated results are provided in Section 5.8.9.1.

4.6.2 Climate Uncertainty Scenarios

In the Central Scenario (as described throughout Section 4.4), annual precipitation is assumed to be constant over time based on a long-term average (WSRC-STI-2008-00244, SRRA107772-000009). This simplifying modeling assumption was used to help meet computational demands and was justifiable as short-term variability is expected to be mitigated by the extremely long-time frames considered for PA simulations.

As indicated in Section 4.4.1.3.1, a study of the paleoclimate record along river channels in eastern Georgia and in the Carolinas showed that river networks in the area exhibited four distinct morphological phases over the past 30,000 years "that closely correspond to major climatic and paleoenvironmental episodes." Of the major climate-changing events, the most recent was a warming event which occurred during the last half of the Holocene (approximately 8,000 years ago). Since then, records indicate that the regional environment "demonstrates climatic similarity to modern conditions." [DOI:10.1016/j.geomorph.2008.05.024] Despite this relatively consistent environment over the past 8,000 years, the study also indicated that the availability of moisture "during the first half of the Holocene is the subject of considerable debate." [DOI:10.1016/j.geomorph.2008.05.024] As such, future long-term climate conditions remain a source of potential uncertainty.

Two alternative climate cases were considered as part of the climate uncertainty modeling: a Wetter Climate Case and a Drier Climate Case (see Section 5.8.2.6). If long-term climate change impacts the SDF, it is expected to alter infiltration rates, the depth to the water table, and the rates of ground water flow.

While not specifically an alternative climate change scenario, given that changes to climate may influence infiltration rates, insights may also be gathered from using other alternative infiltration assumptions, as presented in Section 5.8.2. For these evaluations, infiltration rates based on historical Hydrologic Evaluation of Landfill Performance (HELP) modeling (i.e., from the 2008 report *Saltstone Disposal Facility Closure Cap Concept and Infiltration Estimates*, WSRC-STI-2008-00244) were assumed. The assumptions used within this HELP Model are no longer considered appropriate for assessing the performance of the closure cap, because it relied on overly pessimistic assumptions relative to the performance of the HDPE performance and the sand drainage layer. [SRRA107772-000009]

Additional discussion of the development for these alternative conceptual models and the associated results are provided in Section 5.8.2.

4.6.3 Fast Flow Paths Through the SDUs Scenario

As with any cementitious material, cracks are expected to eventually develop within the SDU concrete and within the saltstone. For the Central Scenario, these cracks are expected to be small, with limited depth and width. These cracks are expected to remain relatively small because the SDUs will be surrounded by backfill and will be filled with saltstone (or grout) to ensure that no void spaces remain. With this system design, the SDU concrete (and the saltstone within the SDU concrete) will be supported in all directions, thus relieving many of the stressors that could induce larger cracks. Further, there is also a potential that cracks do form may undergo self-healing as leached minerals precipitate within the cracks.

Accordingly, any cracks that do form are expected to have extremely narrow widths and are unlikely to penetrate completely through the system (from roof to floor). Therefore, for the Central Scenario these cracks are not expected to be significant flow paths. As such, advective flow through the cementitious materials is expected to be dominated by movement through the microstructure (i.e., microcracks or interconnected pores) of the cementitious materials. Despite

this expectation, there is uncertainty as to the prevalence and magnitude of future cracking. To address this uncertainty, a Fast Flow Paths through the SDUs Scenario is considered.

The Fast Flow Paths through the SDUs Scenario is designed to address FEPs related to seismicity, seismic-induced damage or changes to system components, effects of subsidence, and movement of the waste form. Therefore, the recommended scenario assumes that damage is caused by settlement over time from a series of seismic (earthquake) events. Figure 4.6-1 provides a conceptual illustration of this scenario. With this approach, when a major earthquake event occurs, the slope of the initial ground surface (i.e., the ground surface prior to emplacement of the closure cap) will change due to settlement. After settlement, the SDU concrete and saltstone will experience tension due to loading, which can result in the formation of cracks.

Figure 4.6-1: Illustration of the Fast Flow Paths Through the SDUs Scenario

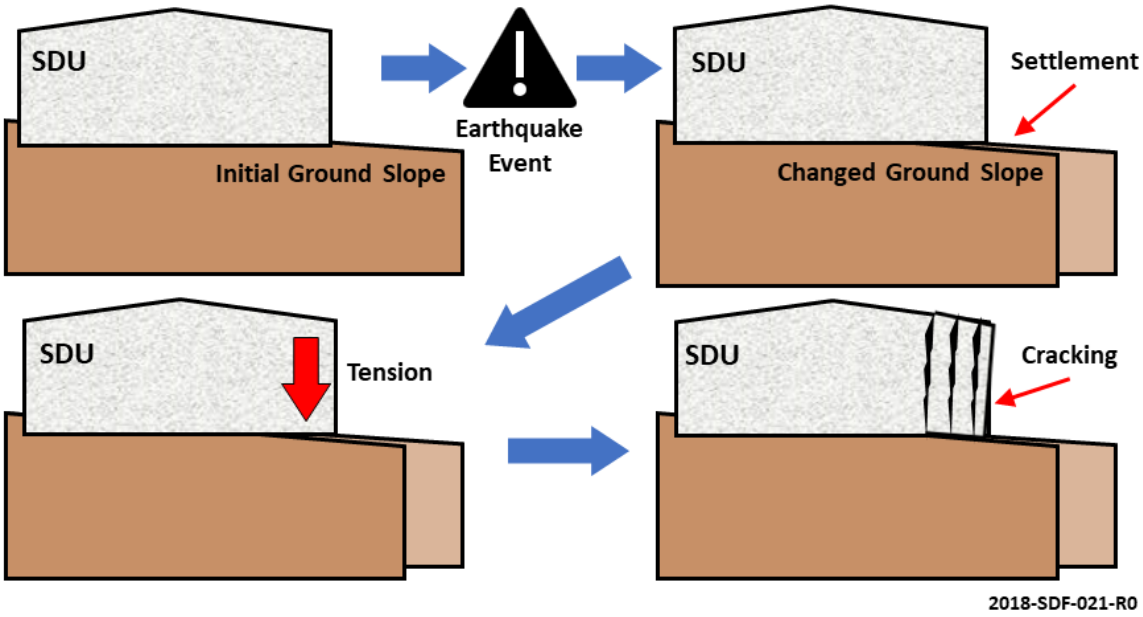

Since crack formation is assumed to occur as a function of earthquake events, it is most likely that the development of such cracks would occur as step changes following major earthquakes. Despite this expectation, this alternative conceptual model assumes that the cracks are initially present at the start of the simulation. This ensures that the simulation is bounding as the full SDU inventory is available at the time of crack formation. This model and the associated results are provided in Section 5.8.8.2.

Note the Compliance Case addresses currently existing cracks. As described in Section 4.3.1.2.1, cracks that have been observed in the existing SDUs are addressed via modeling assumptions for initial conditions. For example, due to the weeping observed through the walls of SDUs 1 and 4, the walls were assigned the material properties of backfill. To address the cracks observed in the roof and floor of SDU 6, the roof and floor of SDU 6 were assigned a higher initial saturated hydraulic conductivity.

4.6.4 Fast Flow Paths Through Ground Water Scenario

For the Central Scenario, the hydraulic properties within specific layers of the vadose zone soils or saturated zone soils (e.g., TCCZ, LAZ, etc.) are assumed to be continuous and, within specific areas of SRS, are also assumed to be homogenous. This assumption in the Central Scenario is consistent with a recent review of "soft zones" performed to support H-Tank Farm activities (see *A Review of Subsurface Soft Zones at Savannah River Site with Emphasis on H Area Tank Farm* (SRNL-TR-2012-00160)). Soft zones are subsurface regions of calcareous or clastic material with distinct material properties, which may or may not promote the formation of caverns, or regions of faster flow. This review of the H-Area soft zones determined that:

- Soft zones beneath SRS are not cavernous voids, but are small, isolated, poorly connected, three-dimensional features filled with loose, fine-grained, water-saturated sediment.
- Despite their under-consolidated nature, soft zones have survived for a very long time and remain structurally competent in the presence of overburden stresses.
- Soft zones appear not to be a critical influence on either ground water flow or contaminant transport.

Given the proximity of Z-Area and the SDF to H-Area, it is reasonable to apply these conclusions to the SDF as well. Despite the conclusions from SRNL-TR-2012-00160, uncertainty regarding the presence of potential soft zone remains. To address this uncertainty, the Fast Flow Paths Through Ground Water Scenario was developed.

For the Fast Flow Paths Through Ground Water Scenario it is assumed that a discrete flow path (i.e., a vertical dike of sand) is present beneath an SDU. It is assumed that this flow path extends from the bottom of an SDU, through the vadose zone, and through the saturated zone (Figure 4.6-2). This flow path can be implemented as a localized area of sand (i.e., soil with higher saturated hydraulic conductivity than the surrounding soils). Within the saturated zone, a similar flow path is assumed in a horizontal direction to channel flow from beneath the SDU to the 100-meter boundary.

Additional discussion of the development for this alternative conceptual model and the associated results are provided in Section 5.8.9.5.

Figure 4.6-2: Illustration of the Proposed Simulations for the Fast Flow Path Through Ground Water Scenario

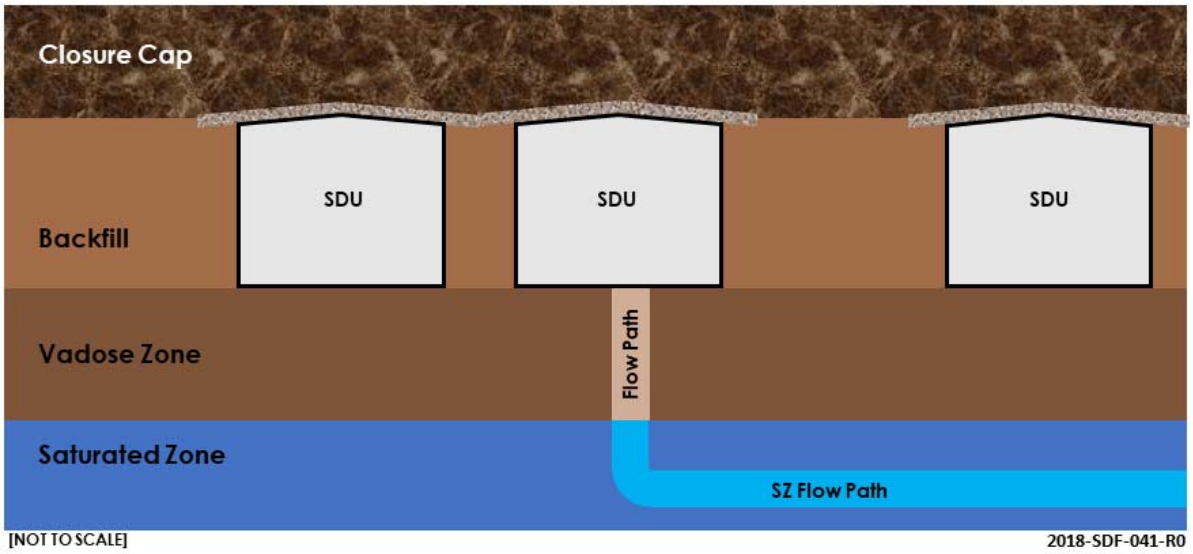

4.6.5 Soil-Only Closure Cap Scenario

The current preliminary closure cap design (as described in Section 3.2.6) specifies a multi-layered engineered closure cap that will significantly limit the influx of water into the system. Any significant deviations from the current design would require additional evaluation via appropriate change control processes (e.g., Unreviewed Waste Management Question (UWMQ) Evaluation, Special Analysis, PA revision, or equivalent process). Regardless, the *Conceptual Model Development for the Saltstone Disposal Facility Performance Assessment* (SRR-CWDA-2018-00006) recommended the development of a "No Closure Cap Scenario" which would assume that no closure cap is placed over any of the SDUs. Such a scenario would still assume that the SDUs are surrounded by backfill such that only the SDU roof would be exposed (Figure 4.6-3).

Figure 4.6-3: Illustration of the No Closure Cap Scenario

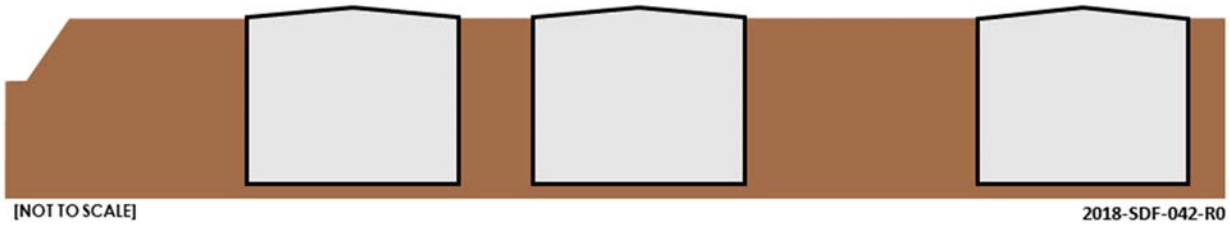

However, because disposal at the SDF is permitted by the state of South Carolina as a Class Three Landfill (Permit #025500-1603), it must meet the requirements for a Class Three Landfill as specified in SCDHEC R.61-107.19, *SWM: Solid Waste Landfills and Structural Fill*. Specifically, Section 258.60 of SCDHEC R.61-107.19 requires that a final cover system be placed over the landfill to minimize infiltration. The cover system is required to have a permeability no greater than 1.0E-05 cm/s, must be at least 18 inches of earthen material, and must include an erosion control barrier. Because this cover system is required, a No Closure Cap Scenario is precluded.

The purpose of the No Closure Cap Scenario was to non-mechanistically examine the impacts from a number of FEPs as identified in Table 4.4-6 of *Conceptual Model Development for the Saltstone Disposal Facility Performance Assessment* (SRR-CWDA-2018-00006). Although state requirements preclude the No Closure Cap Scenario, these FEPs must still be addressed. Therefore, an intermediate conceptual model has been developed: the "Soil-Only Closure Cap Scenario." For this scenario, instead of constructing a highly engineered and robust closure cap, it is assumed that the SDU will simply be buried beneath a layer of native soils. To simulate this, the natural infiltration rate (16.45 in/yr or 417.8 mm/yr) shall be assumed. This simulation and its results are provided in Section 5.8.2.4. Based on the results of this evaluation, a closure cap with engineered layers to reduce water influx into the system is necessary to provide confidence in the long-term performance of the system. As such, the Soil-Only Closure Cap Scenario does not represent a realistic future condition but is included for risk-assessment purposes only.

4.6.6 Stratified Saltstone Scenario

As a model simplification, the Central Scenario assumes that the saltstone within the SDUs is homogenous, with material properties equivalent to assumed nominal values based on the control of conditions during disposal operations. While disposal operations will continue to maintain conditions within specified bounds, the saltstone material properties are expected to exhibit some minor heterogeneity based on variability in the mix, changes in the contaminant concentrations (i.e., differing "salt batches"), and fluctuations in the temperature and humidity during the pouring and curing of fresh saltstone.

Prior to curing, saltstone is highly flowable; as such, it is expected that the heterogeneity will be manifested as stratified layers within the saltstone as each layer is poured (see Figure 4.6-4, where different colors are used to represent differences in the material properties). Each layer is expected to exhibit its own specific material properties, including: initial saturated hydraulic conductivity, initial contaminant concentrations, and initial reducing capacity. Each layer also assumes a unique thickness.

For the Stratified Saltstone Scenario, variable saltstone properties were assigned to the saltstone nodes of the model to create discrete strata. Using the properties of these discrete strata, the degradation rates, flow rates, and release rates were recalculated. It was expected that diffusion and dispersion processes across the strata would mitigate some of the potential effects of these discrete properties.

The Stratified Saltstone Scenario was also used to address FEP 3.8.02 (Void Space Formation) and FEP 6.4.07 (Cave-In, Collapse or Rockfall). To address these FEPs, a sensitivity model assumed that an SDU was not completely filled, leaving a void space between the top of the saltstone and the bottom of the SDU roof. Under the weight of the closure cap, this void space was assumed to result in a collapsed roof. With the Stratified Saltstone Scenario, this was modeled as a relatively high saturated hydraulic conductivity for the SDU roof and the uppermost layers of the saltstone strata, simulating rubble. Note that this does not reflect expected conditions, as the current plan is to completely fill each SDU with saltstone or clean cap grout prior to closure.

Figure 4.6-4: Conceptualization of Stratified Variability in Saltstone

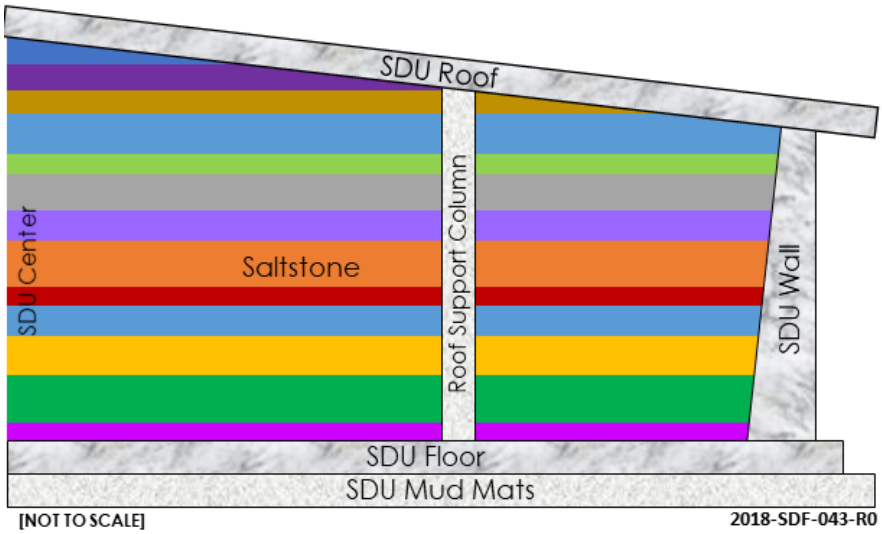

Note: Image depicts half a cross section of a cylindrical SDU, where the left-edge of the depicted SDU represents the center of the SDU (i.e., at the apex of the roof) and the right edge represents the outer edge of the SDU (i.e., the perimeter). Figure is not to scale.

Additional discussion of the development for this alternative conceptual model and the associated results are provided in Section 5.8.3.7.

4.6.7 Perched Water Scenario

The Perched Water Scenario (Figure 4.6-5) assumes the presence of localized perched water. For this scenario two possible conditions were assumed: one wherein the water is perched or pooled above the roof of the SDUs, and the other wherein the water is perched within the vadose zone approximately half way between the bottom of the SDUs and the top of the water table.

Figure 4.6-5: Conceptualization of Perched Water Scenario

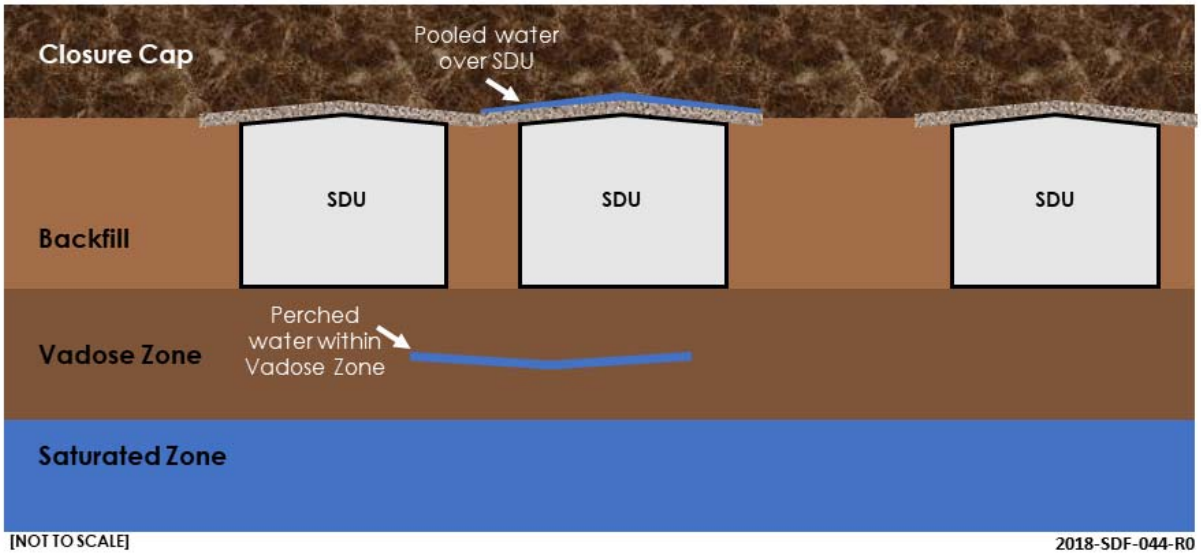

The pooled water over the SDU is expected to generate a pressure head which eventually increases flow into and through the roof. When this occurs, it is likely to increase the rates of contaminant releases as the water flows through the saltstone. Alternatively, the perched water in the vadose zone is likely to dilute the contaminant plume as it passes through the vadose zone.

Additional discussion of the development for this alternative conceptual model and the associated results are provided in Section 5.8.9.4.

4.6.8 Colloid Transport Scenario

The Central Scenario does not explicitly address the potential for colloid formation or transport. Colloids are microscopic particles of a substance within a mixture that do not settle out of suspension. Since colloids do not settle out of suspension, they are readily transported; however, they may also be subject to filtration. It is possible that some slower-moving contaminants (e.g., plutonium or uranium) may sorb to these colloids, resulting in differing transport properties.

The Colloid Transport Scenario assumes that radionuclides will come into contact with and sorb to naturally-occurring clay colloids. Figure 4.6-6 provides an illustration of the potential transport process associated with colloidal migration through clayey soils.

For this scenario, it was assumed that a fraction of contaminants will sorb to these colloids and become mobilized. Effectively, this splits the inventory of said contaminants into two transport groups: slower-moving (K_d-controlled) and faster-moving (colloid-controlled). In reality, it is expected that the colloid-controlled contaminants will undergo cycles of sorbing to mobile colloids and desorbing from mobile colloids. However, as a model simplification this cycle is ignored; instead, it is assumed that once a contaminant becomes attached to a mobile colloid, it will remain attached.

It is noted that within the SDU concrete some colloids may form as a product of corrosion on the structural support metals, such as iron oxides (i.e., rust). These colloids may influence release rates from the saltstone waste form and SDU concrete. However, due to the limited amount of metal available within the system, the impact of these corrosion product colloids is expected to be negligible and were not considered in the Colloid Transport Scenario (i.e., only clay colloids were considered).

Additional discussion of the development for this alternative conceptual model and the associated results are provided in Section 5.8.9.6.

Figure 4.6-6: Illustration of Colloid-Facilitated Transport Processes

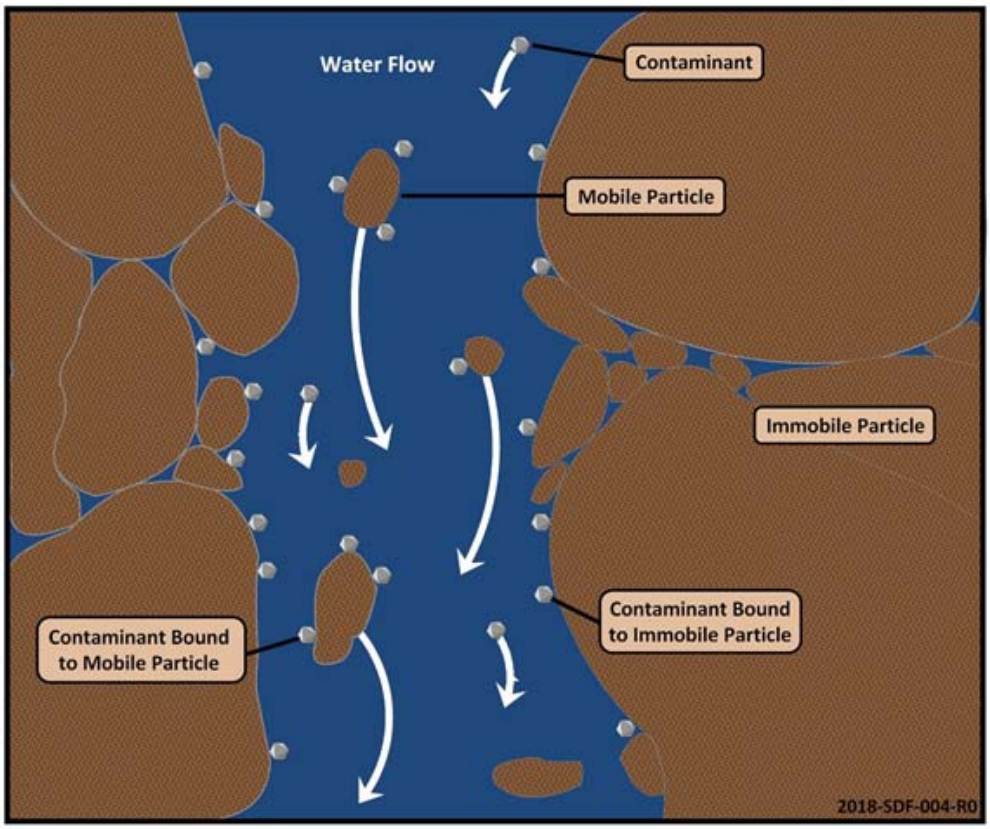

4.6.9 Inadvertent Human Intruder (IHI) Scenario

IHI scenarios are not considered likely. It is expected that DOE will maintain control of the SRS in perpetuity. However, the performance objectives defined in Table 1.7-1 explicitly requires the consideration of an intruder dose, and DOE M 435.1-1, along with NUREG-1854 (ML072360184), provides guidance for assessing system performance relative to these intruder doses.

For the IHI Scenario, the IHI is the human receptor. Like the MOP, the IHI is a gender-weighted, average adult who farms and uses water from a well in the vicinity of the SDUs. Unlike the MOP, instead of drilling a water well 100 meters from the SDUs, the water wells are assumed to be drilled in closer proximity to the SDUs (see Section 4.4.8). Additionally, stylized IHI definitions were also applied for select modeling cases to assess the potential risks associated with disruptive events and processes (FEP 6.1.03). To address FEP 6.1.03 (Drilling Activities), the following Acute IHI and Chronic IHI scenarios are considered:

(1) the Acute IHI who drills a well into the soils adjacent to an SDU (i.e., 1-meter well) (see Section 6.3.1),

(2) the Acute IHI who drills a well that penetrates through the concrete barrier of the SDU roof and into the saltstone waste form (see Section 6.3.2),

(3) the Chronic IHI who uses well water from the 1-meter well *and* mixes the contaminated soil drill cuttings from the 1-meter well into their crops and gardens (see Section 6.4.1),

(4) the Chronic IHI who uses well water from the 1-meter well *and* does not mix drill cuttings into their crops and gardens (see Section 6.4.2),

(5) the Chronic IHI who uses well water from the 1-meter well *and* mixes the contaminated cementitious material drill cuttings (from drilling through an SDU roof and into the saltstone waste form) into their crops and gardens (see Section 6.4.3), and

(6) the Chronic IHI who uses well water from selected IHI well locations *and* mixes the contaminated soil drill cuttings from the 1-meter well into their crops and gardens (see Section 6.5),

All of these IHI scenarios assume complete penetration through the SDF closure cap. For the Chronic IHI scenarios, in addition to mixing the contaminated drill cuttings into their crops and gardens (where the contaminants are taken up by plants and animals), it is also assumed that the Chronic IHI will use contaminated ground water for various purposes (e.g., consumption, irrigation, bathing, etc.). As a simplification, the Chronic IHI scenarios apply the ground water concentrations based on either the 1-meter well (see Section 6.2.2) or on selected located near various SDUs (see Section 6.2.3).

Note that based on current regional practices if drillers strike materials that are relatively impermeable, they will typically move to another drilling site. Additionally, drilling into an SDU would require different equipment (e.g., a diamond core drill bit would be needed in order to be able to penetrate through the steel-reinfored SDU concrete and the saltstone waste form, as opposed using standard mud rotary drills which are typically used for installing wells in the vicinity of SRS). As such, any scenario that assumes a driller will penetrate into an SDU is not considered credible. Therefore, the 1-meter well soil drilling scenarios are used for demonstrating compliance to the Acute IHI and Chronic IHI performance objectives.

FEP 6.1.04 (Excavating and Mining Activities) has been considered for IHI analyses, however due to the local resources and land use (see Section 3.1.7), it is unlikely that any excavation or mining activities would impact the SDF. It is possible that some excavation may occur to develop the land for homes or business, but considering the thicknesses of the closure cap layers, such activity is expected to have a minimal impact. Therefore, excavation and mining scenarios were not explicitly included in this PA. Regardless, the Soil-Only Closure Cap Scenario (introduced in Section 4.6.5) provides a reasonable analogue for how excavation of the top of the closure cap could impact doses. The results of the Soil-Only Closure Cap Scenario are provided in Section 5.8.2.4.

Probabilistic uncertainty associated with the IHI are discussed in Section 6.6 and consideration of other intruder sensitivity cases are described in Section 6.7.

4.6.10 Other Sensitivity Cases

For each of the ACMs listed above, one or more sensitivity cases have been developed to provide insights relative to the risks associated with the given conceptualization. Section 5.8 describes each of the sensitivity cases, as well as additional sensitivity cases. In general, these models provide insights with respect to the influence of the select input values.

5 RESULTS OF ANALYSIS

The purpose of this section is to describe the process of evaluating modeled concentrations and the respective dose-risk at the points of assessment for various pathways and exposure scenarios.

In this PA, the release of radionuclides from the SDUs was controlled, in most cases, by advective movement, which is influenced by the K_d values. These values vary with chemical conditions (e.g., pH and redox potential). The stabilized contaminant release rate is impacted by the water flow through the SDUs and changes over time as the hydraulic properties of the saltstone and SDU concrete degrade. After a contaminant leaves the waste form, concrete retardation and soil retardation impact the contaminant's transport rate into the aquifers.

5.1 Overview of Results Discussion

Results of the environmental transport modeling from the SDUs to the SDF 100-meter boundary are summarized in Section 5.2 for the Compliance Case. These results are provided for each aquifer (Upper Aquifer Zone (UAZ) of the Upper Three Runs Aquifer, the Lower Aquifer Zone (LAZ) of the Upper Three Runs Aquifer, and the Gordon Aquifer Unit (GAU)). For radionuclides, the results are presented in picocurie per liter (pCi/L), while non-radiological chemicals are presented in microgram per liter (μg/L).

In addition to the SDF 100-meter boundary results, contaminant releases were also modeled to determine concentrations at the seeplines of the nearby streams: Upper Three Runs (UTR) and McQueen Branch (MQB). The Compliance Case results are summarized in Section 5.2.2. Collectively, the results from all three Central Scenario cases were used to inform the development of a "100-meter boundary to seepline ratio," hereafter referred to as the seepline ratio (described in Section 5.2.3), which is used to support sensitivity modeling.

Similarly, the results from the three Central Scenario modeling cases were also used to select "sensitivity run radionuclides." These are the radionuclides that were determined to have the largest impact on dose and are defined in Section 5.2.4. Additional scoping analyses have been performed, using the full suite of radionuclides and multiple modeling scenarios with various assumptions to verify that these sensitivity run radionuclides (Cl-36, I-129, and Tc-99) are always the most dominant dose contributors, and that all other radionuclides remain insignificant. Regardless, all of the modeling cases constructed in GoldSim always include the full suite of radionuclides.

The SDF air pathways dose results are calculated and presented in Section 5.3.

Section 5.4 provides a high-level description of the dose scenarios considered for determining the dose results to the MOP. The peak total ground water pathway doses are calculated using the dose calculations defined in Section 4.4.8 for the MOP at 100 meters and for the MOP at the seeplines. The ground water pathway doses are calculated using the peak ground water concentrations defined in Section 5.2. The final dose results are presented in Section 5.5. Similar dose results, as they relate to IHI doses, are described in Sections 6.3 and 6.4.

Section 5.6 describes the benchmarking analysis designed to validate the performance of the SDF GoldSim Model as introduced in Section 4.5.

- Section 5.6.1 provides an overview of the benchmarking process.
- Section 5.6.2 provides benchmarking results of the fluxes (i.e., mass releases) from the SDUs, through the vadose zone, and into the saturated zone.
- Section 5.6.3 provides benchmarking results of the concentrations and doses at the MOP points of assessment. A similar set of benchmarking results, as it relates to the IHI, is described in Section 5.6.4.

Section 5.7 described the probabilistic analyses designed to address uncertainty in the system. The uncertainty analysis was performed using the probabilistic model (i.e., the SDF GoldSim Model) as introduced in Section 4.5.

- Section 5.7.1 summarizes the probabilistic distributions used in the SDF GoldSim Model.
- Section 5.7.2 describes the probabilistic simulations and Section 5.7.3 presents the range of uncertainty exhibited by the probabilistic modeling results.
- Section 5.7.4 provides a quantitative analysis of the probabilistic sensitivity, identifying those parameters which exhibited the greatest influence over the probabilistic modeling results.
- Section 5.7.5 provides additional analyses of the peak doses to the MOP.

Section 6.6 provides a similar probabilistic analysis of the IHI dose results.

Following the probabilistic sensitivity analysis is a series of deterministic sensitivity analyses (Section 5.8), which also addresses the alternative conceptual models, as first presented in Section 4.6. These additional analyses make use of both PORFLOW and GoldSim modeling approaches and provide additional information and insights concerning the conditions and parameters are important to SDF modeling. Similar analyses, as they relate to IHI results are described in Section 6.7.

Finally, Section 5.9 presents an analysis based on the DOE As Low As Reasonably Achievable (ALARA) process.

5.2 Determination of Concentrations at Points of Assessment

The purpose of this section is to present the ground water concentrations for all the radionuclides and chemicals based on the Compliance Case modeling. Ground water concentrations are used for estimating ground water pathway doses to the MOP and the IHI.

5.2.1 Concentrations at the SDF 100-Meter Boundary

The purpose of this section is to present the peak ground water concentrations for each of the radionuclides and chemicals along the SDF 100-meter boundary, within 1,000 years and 10,000 years of SDF closure. The peak ground water concentrations within each sector are presented for each aquifer zone: UAZ, LAZ, and GAU. The results presented here are for the Compliance Case only. The peak radionuclide concentrations in 1,000 years are provided in Table 5.2-1 through Table 5.2-6. The peak chemical concentrations in 1,000 years are provided in Table 5.2-7 through Table 5.2-9.

The peak radionuclide concentrations in 10,000 years are provided in Table 5.2-10 through Table 5.2-15. The peak chemical concentrations in 10,000 years are provided in Table 5.2-16 through Table 5.2-18. These tables also provide the applicable maximum contaminant level (MCL) values from the State Primary Drinking Water Regulation (SCDHEC R.61-58) for comparison against the peak concentrations. The MCL values for beta and photon emitters are calculated in EPA 815-R-02-001 based on a 4 mrem/yr beta-gamma dose. The sum of all the beta-gamma MCL fractions is also provided.

The peak values at 100 meters in 1,000 years, regardless of aquifer, show no radionuclides and no chemicals exceed their respective MCL. Within 1,000 years, the three constituents that are closest to their respective MCLs are I-129, Tc-99, and nitrate (NO_3) in the LAZ. For I-129, the concentration at 1,000 years is 9.6E-03 pCi/L in Sector D (orders of magnitude less than the MCL of 1 pCi/L). For Tc-99, the concentration at 1,000 years is 4.0 pCi/L (orders of magnitude less than the MCL of 900 pCi/L). The sum of the beta-gamma MCL fractions peaked at approximately 1.4E-02, mostly due to the contributions from I-129 and Tc-99. For NO_3, the concentration at 1,000 years is 1.3E+03 μg/L in Sector D (approximately one order of magnitude less than the MCL of 10,000 μg/L).

The peak values at 100 meters in 10,000 years show only I-129 and NO_3 exceed the respective MCLs. I-129 exceeds it respective MCL of 1 pCi/L within 10,000 years at Sectors A through F and the peak concentration is at 10,000 years with a value of 2.3 pCi/L in Sector D (just over twice the MCL of 1 pCi/L). NO_3 exceeds it respective MCL of 10,000 μg/L within 10,000 years at Sectors A through F and the peak concentration is at 10,000 years with a value of 3.2E+04 pCi/L in Sector D (just over three times the MCL of 10,000 μg/L). The only other constituent that approaches its respective MCL is Tc-99. For Tc-99, the concentration at 5,900 years is 350 pCi/L (approximately 39% of the MCL of 900 pCi/L). The sum of the beta-gamma MCL fractions peaked at approximately 2.6, mostly due to the contributions from I-129 and Tc-99.

The peak I-129 dose associated with 2.3 pCi/L is less than the 4 millirem/year drinking water standard (i.e., 0.66 mrem/yr) when calculated using an updated I-129 drinking water dose calculation methodology based on the most current available data. This alternative methodology multiplies the peak concentration by both an updated water ingestion pathway effective dose factor (EDF) and assuming an ingestion rate of 2 liters of water consumed per day (2.3 pCi/L × 0.202 L-mrem/pCi/pCi-yr (EDF) × (2.0 L/day ÷ 1.4 L/day) = 0.66 mrem/yr). This drinking water dose calculation methodology was adapted from the alternative to the basic SCDHEC R.61-58 methodology in the *Industrial Wastewater Closure Module for Liquid Waste Tank 16H H-Area Tank Farm Savannah River Site* (SRR-CWDA-2013-00091), which received SCDHEC approval and EPA concurrence.

The drinking water standard for beta particle and photon radioactivity is specified in the *South Carolina State Primary Drinking Water Regulation* (SCDHEC R.61-58) which states that "The average annual concentration of beta particle and photon radioactivity from man-made radionuclides in drinking water must not produce an annual dose equivalent to the total body or any internal organ greater than 4 millirem/year (mrem/year)." [SCDHEC R.61-58] This total body or organ dose equivalent comparison to the standard is calculated on the basis of two (2) liters per day drinking water intake. The EPA document *Radionuclides in Drinking Water: A Small Entity*

Compliance Guide outlines the requirements for beta particle and photon emitters. [EPA 815-R-02-001] The Compliance Guide contains a table providing the derived concentrations (pCi/L) of beta and photon emitters in drinking water that yield an effective dose equivalent (EDE) of 4 mrem/yr as defined in the *Maximum Permissible Body Burdens and Maximum Permissible Concentrations of Radionuclides in Air and in Water for Occupational Exposure, National Bureau of Standards (NBS) Handbook 69*. [NBS Handbook 69] Rather than using the 168-hour data listed in NBS Handbook 69, the alternative drinking water dose calculation methodology presented in the Tank 16H Industrial Wastewater Closure Module (SRR-CWDA-2013-00091) used the most current water ingestion pathway dose conversion factors from *Dose Calculation Methodology for Liquid Waste Performance Assessments at the Savannah River Site* (SRR-CWDA-2013-00058).

Note that these peak values are from the Compliance Case which incorporates a number of assumptions produce intentionally higher-than-expected doses to ensure greater defensibility. The results from the Realistic Case (i.e., the modeling case based on best estimate assumptions), typically show concentrations for I-129 and Tc-99 that are approximately an order of magnitude lower than the results from the Compliance Case (i.e., less than the applicable MCL values).

It should also be noted that these peak concentrations occurred in the LAZ. While the peak concentrations within the UAZ are typically within an order of magnitude of the peaks in the LAZ, the peak values within the GAU were generally much lower than the LAZ and the UAZ, often by multiple orders of magnitude. Based on current well drilling practices, it is expected that any future wells drilled for drinking water purposes would more likely be drilled into deeper aquifer zones (e.g., the GAU), where concentrations are expected to be much lower.

Appendices B and C show the ground water concentrations for each of these radionuclides for the Realistic Case and the Pessimistic Case, respectively.

Table 5.2-1: Radiological Peak Concentrations along the 100-Meter Boundary for UAZ, Sectors A through D in 1,000 Years

Radionuclide	MCL (pCi/L)	Sector A		Sector B		Sector C		Sector D	
		Conc. (pCi/L)	Year of Peak	Conc. (pCi/L)	Year of Peak	Conc. (pCi/L)	Year of Peak	Conc. (pCi/L)	Year of Peak
Ac-227	N/A	<1E-20	1,000	<1E-20	1,000	<1E-20	1,000	<1E-20	1,000
Al-26	N/A	<1E-20	1,000	<1E-20	1,000	<1E-20	1,000	<1E-20	1,000
Am-241	Total α	<1E-20	1,000	<1E-20	1,000	<1E-20	1,000	<1E-20	1,000
Am-242m	Total α	<1E-20	1,000	<1E-20	1,000	<1E-20	1,000	<1E-20	1,000
Am-243	Total α	<1E-20	1,000	<1E-20	1,000	<1E-20	1,000	<1E-20	1,000
C-14	2,000	<1E-20	1,000	<1E-20	1,000	<1E-20	1,000	<1E-20	1,000
Cf-249	Total α	<1E-20	1,000	<1E-20	1,000	<1E-20	1,000	<1E-20	1,000
Cf-251	Total α	<1E-20	1,000	<1E-20	1,000	<1E-20	1,000	<1E-20	1,000
Cl-36	700	2.3E-05	1,000	6.1E-05	1,000	1.2E-03	1,000	2.7E-03	1,000
Cm-243	Total α	<1E-20	1,000	<1E-20	1,000	<1E-20	1,000	<1E-20	1,000
Cm-244	Total α	<1E-20	1,000	<1E-20	1,000	<1E-20	1,000	<1E-20	1,000
Cm-245	Total α	<1E-20	1,000	<1E-20	1,000	<1E-20	1,000	<1E-20	1,000
Cm-247	Total α	<1E-20	1,000	<1E-20	1,000	<1E-20	1,000	<1E-20	1,000
Co-60	100	<1E-20	460	<1E-20	350	<1E-20	350	<1E-20	330
Cs-135	900	<1E-20	1,000	<1E-20	1,000	<1E-20	1,000	<1E-20	1,000
Cs-137	200	<1E-20	1,000	<1E-20	1,000	<1E-20	1,000	<1E-20	1,000
Eu-152	200	<1E-20	1,000	<1E-20	950	<1E-20	960	<1E-20	970
Eu-154	60	<1E-20	730	<1E-20	630	<1E-20	620	<1E-20	630
H-3	20,000	2.4E-11	210	6.4E-11	210	4.2E-08	150	9.4E-08	150
I-129	1	7.7E-05	1,000	2.0E-04	1,000	3.6E-03	1,000	7.8E-03	1,000
K-40	N/A	<1E-20	1,000	<1E-20	1,000	<1E-20	1,000	<1E-20	1,000
Nb-93m	1,000	<1E-20	1,000	<1E-20	1,000	<1E-20	1,000	<1E-20	1,000
Nb-94	N/A	<1E-20	1,000	<1E-20	1,000	<1E-20	1,000	<1E-20	1,000
Ni-63	50	<1E-20	1,000	<1E-20	960	<1E-20	1,000	<1E-20	1,000
Np-237	Total α	<1E-20	1,000	<1E-20	1,000	<1E-20	1,000	<1E-20	1,000
Pa-231	Total α	<1E-20	1,000	<1E-20	1,000	<1E-20	1,000	<1E-20	1,000
Pb-210	N/A	<1E-20	1,000	<1E-20	1,000	<1E-20	1,000	<1E-20	1,000
Pt-193	3,000	<1E-20	1,000	<1E-20	1,000	<1E-20	1,000	<1E-20	1,000
Pu-238	Total α	<1E-20	1,000	<1E-20	1,000	<1E-20	1,000	<1E-20	1,000
Pu-239	Total α	<1E-20	1,000	<1E-20	1,000	<1E-20	1,000	<1E-20	1,000
Pu-240	Total α	<1E-20	1,000	<1E-20	1,000	<1E-20	1,000	<1E-20	1,000
Pu-241	300	<1E-20	1,000	<1E-20	1,000	<1E-20	1,000	<1E-20	1,000
Pu-242	Total α	<1E-20	1,000	<1E-20	1,000	<1E-20	1,000	<1E-20	1,000
Pu-244	Total α	<1E-20	1,000	<1E-20	1,000	<1E-20	1,000	<1E-20	1,000
Ra-226	Total α /Ra	<1E-20	1,000	<1E-20	1,000	<1E-20	1,000	<1E-20	1,000
Ra-228	Total Ra	<1E-20	1,000	<1E-20	1,000	<1E-20	1,000	<1E-20	1,000
Rn-222	N/A	<1E-20	1,000	<1E-20	1,000	<1E-20	1,000	<1E-20	1,000
Se-79	N/A	<1E-20	1,000	<1E-20	1,000	<1E-20	1,000	<1E-20	1,000
Sm-151	1,000	<1E-20	1,000	<1E-20	1,000	<1E-20	1,000	<1E-20	1,000
Sn-126	N/A	<1E-20	1,000	<1E-20	1,000	<1E-20	1,000	<1E-20	1,000
Sr-90	8	<1E-20	1,000	<1E-20	1,000	<1E-20	1,000	<1E-20	790
Tc-99	900	4.2E-02	1,000	1.1E-01	1,000	1.4E+00	1,000	3.0E+00	1,000
Th-229	Total α	<1E-20	1,000	<1E-20	1,000	<1E-20	1,000	<1E-20	1,000
Th-230	Total α	<1E-20	1,000	<1E-20	1,000	<1E-20	1,000	<1E-20	1,000
Th-232	Total α	<1E-20	1,000	<1E-20	1,000	<1E-20	1,000	<1E-20	1,000
U-232	Total U	<1E-20	1,000	<1E-20	1,000	<1E-20	1,000	<1E-20	1,000
U-233	Total U	<1E-20	1,000	<1E-20	1,000	<1E-20	1,000	<1E-20	1,000
U-234	Total U	<1E-20	1,000	<1E-20	1,000	<1E-20	1,000	<1E-20	1,000
U-235	Total U	<1E-20	1,000	<1E-20	1,000	<1E-20	1,000	<1E-20	1,000
U-236	Total U	<1E-20	1,000	<1E-20	1,000	<1E-20	1,000	<1E-20	1,000
U-238	Total U	<1E-20	1,000	<1E-20	1,000	<1E-20	1,000	<1E-20	1,000
Zr-93	2,000	<1E-20	1,000	<1E-20	1,000	<1E-20	1,000	<1E-20	1,000
Total Alpha	15	<1E-20	1,000	<1E-20	1,000	<1E-20	1,000	<1E-20	1,000
Total Ra	5	<1E-20	1,000	<1E-20	1,000	<1E-20	1,000	<1E-20	1,000
Sum of Beta-Gamma MCL Fractions		1.2E-04	1,000	3.3E-04	1,000	5.2E-03	1,000	1.1E-02	1,000

Table 5.2-2: Radiological Peak Concentrations along the 100-Meter Boundary for UAZ, Sectors E through H in 1,000 Years

Radionuclide	MCL (pCi/L)	Sector E		Sector F		Sector G		Sector H	
		Conc. (pCi/L)	Year of Peak	Conc. (pCi/L)	Year of Peak	Conc. (pCi/L)	Year of Peak	Conc. (pCi/L)	Year of Peak
Ac-227	N/A	<1E-20	1,000	<1E-20	1,000	<1E-20	1,000	<1E-20	1,000
Al-26	N/A	<1E-20	1,000	<1E-20	1,000	<1E-20	1,000	<1E-20	1,000
Am-241	Total α	<1E-20	1,000	<1E-20	1,000	<1E-20	1,000	<1E-20	1,000
Am-242m	Total α	<1E-20	1,000	<1E-20	1,000	<1E-20	1,000	<1E-20	1,000
Am-243	Total α	<1E-20	1,000	<1E-20	1,000	<1E-20	1,000	<1E-20	1,000
C-14	2,000	<1E-20	1,000	<1E-20	1,000	<1E-20	1,000	<1E-20	1,000
Cf-249	Total α	<1E-20	1,000	<1E-20	1,000	<1E-20	1,000	<1E-20	1,000
Cf-251	Total α	<1E-20	1,000	<1E-20	1,000	<1E-20	1,000	<1E-20	1,000
Cl-36	700	4.5E-05	1,000	3.6E-05	1,000	5.8E-05	1,000	1.2E-10	1,000
Cm-243	Total α	<1E-20	1,000	<1E-20	1,000	<1E-20	1,000	<1E-20	1,000
Cm-244	Total α	<1E-20	1,000	<1E-20	870	<1E-20	670	<1E-20	550
Cm-245	Total α	<1E-20	1,000	<1E-20	1,000	<1E-20	1,000	<1E-20	1,000
Cm-247	Total α	<1E-20	1,000	<1E-20	1,000	<1E-20	1,000	<1E-20	1,000
Co-60	100	<1E-20	330	<1E-20	220	<1E-20	170	<1E-20	200
Cs-135	900	<1E-20	1,000	2.1E-20	1,000	1.5E-19	1,000	<1E-20	1,000
Cs-137	200	<1E-20	910	<1E-20	760	<1E-20	690	<1E-20	860
Eu-152	200	<1E-20	950	<1E-20	660	<1E-20	510	<1E-20	450
Eu-154	60	<1E-20	610	<1E-20	420	<1E-20	330	<1E-20	290
H-3	20,000	4.8E-11	210	8.7E-10	160	1.6E-09	150	3.7E-12	170
I-129	1	1.6E-04	1,000	8.9E-04	1,000	1.4E-03	1,000	3.6E-05	1,000
K-40	N/A	<1E-20	1,000	2.4E-18	1,000	8.1E-18	1,000	<1E-20	1,000
Nb-93m	1,000	<1E-20	1,000	<1E-20	1,000	<1E-20	1,000	<1E-20	1,000
Nb-94	N/A	<1E-20	1,000	<1E-20	1,000	<1E-20	1,000	<1E-20	1,000
Ni-63	50	<1E-20	1,000	<1E-20	1,000	<1E-20	1,000	<1E-20	1,000
Np-237	Total α	<1E-20	1,000	7.0E-20	1,000	1.9E-19	1,000	<1E-20	1,000
Pa-231	Total α	<1E-20	1,000	<1E-20	1,000	<1E-20	1,000	<1E-20	1,000
Pb-210	N/A	<1E-20	1,000	<1E-20	1,000	<1E-20	1,000	<1E-20	1,000
Pt-193	3,000	<1E-20	1,000	<1E-20	1,000	<1E-20	980	<1E-20	1,000
Pu-238	Total α	<1E-20	1,000	<1E-20	1,000	<1E-20	1,000	<1E-20	1,000
Pu-239	Total α	<1E-20	1,000	<1E-20	1,000	<1E-20	1,000	<1E-20	1,000
Pu-240	Total α	<1E-20	1,000	<1E-20	1,000	<1E-20	1,000	<1E-20	1,000
Pu-241	300	<1E-20	1,000	<1E-20	1,000	<1E-20	1,000	<1E-20	1,000
Pu-242	Total α	<1E-20	1,000	<1E-20	1,000	<1E-20	1,000	<1E-20	1,000
Pu-244	Total α	<1E-20	1,000	<1E-20	1,000	<1E-20	1,000	<1E-20	1,000
Ra-226	Total α /Ra	<1E-20	1,000	<1E-20	1,000	<1E-20	1,000	<1E-20	1,000
Ra-228	Total Ra	<1E-20	1,000	<1E-20	1,000	<1E-20	1,000	<1E-20	1,000
Rn-222	N/A	<1E-20	1,000	<1E-20	1,000	<1E-20	1,000	<1E-20	1,000
Se-79	N/A	<1E-20	1,000	<1E-20	1,000	<1E-20	1,000	<1E-20	1,000
Sm-151	1,000	<1E-20	1,000	<1E-20	1,000	<1E-20	1,000	<1E-20	1,000
Sn-126	N/A	<1E-20	1,000	<1E-20	1,000	<1E-20	1,000	<1E-20	1,000
Sr-90	8	<1E-20	720	<1E-20	630	<1E-20	590	<1E-20	680
Tc-99	900	8.5E-02	1,000	3.6E-01	1,000	5.7E-01	1,000	6.3E-03	1,000
Th-229	Total α	<1E-20	1,000	<1E-20	1,000	<1E-20	1,000	<1E-20	1,000
Th-230	Total α	<1E-20	1,000	<1E-20	1,000	<1E-20	1,000	<1E-20	1,000
Th-232	Total α	<1E-20	1,000	<1E-20	1,000	<1E-20	1,000	<1E-20	1,000
U-232	Total U	<1E-20	1,000	<1E-20	1,000	<1E-20	1,000	<1E-20	1,000
U-233	Total U	<1E-20	1,000	<1E-20	1,000	<1E-20	1,000	<1E-20	1,000
U-234	Total U	<1E-20	1,000	<1E-20	1,000	<1E-20	1,000	<1E-20	1,000
U-235	Total U	<1E-20	1,000	<1E-20	1,000	<1E-20	1,000	<1E-20	1,000
U-236	Total U	<1E-20	1,000	<1E-20	1,000	<1E-20	1,000	<1E-20	1,000
U-238	Total U	<1E-20	1,000	<1E-20	1,000	<1E-20	1,000	<1E-20	1,000
Zr-93	2,000	<1E-20	1,000	<1E-20	1,000	<1E-20	1,000	<1E-20	1,000
Total Alpha	15	<1E-20	1,000	7.0E-20	1,000	1.9E-19	1,000	<1E-20	1,000
Total Ra	5	<1E-20	1,000	<1E-20	1,000	<1E-20	1,000	<1E-20	1,000
Sum of Beta-Gamma MCL Fractions		2.5E-04	1,000	1.3E-03	1,000	2.1E-03	1,000	4.3E-05	1,000

Table 5.2-3: Radiological Peak Concentrations along the 100-Meter Boundary for LAZ, Sectors A through D in 1,000 Years

Radionuclide	MCL (pCi/L)	Sector A		Sector B		Sector C		Sector D	
		Conc. (pCi/L)	Year of Peak	Conc. (pCi/L)	Year of Peak	Conc. (pCi/L)	Year of Peak	Conc. (pCi/L)	Year of Peak
Ac-227	N/A	<1E-20	1,000	<1E-20	1,000	<1E-20	1,000	<1E-20	1,000
Al-26	N/A	<1E-20	1,000	<1E-20	1,000	<1E-20	1,000	<1E-20	1,000
Am-241	Total α	<1E-20	1,000	<1E-20	1,000	<1E-20	1,000	<1E-20	1,000
Am-242m	Total α	<1E-20	1,000	<1E-20	1,000	<1E-20	1,000	<1E-20	1,000
Am-243	Total α	<1E-20	1,000	<1E-20	1,000	<1E-20	1,000	<1E-20	1,000
C-14	2,000	<1E-20	1,000	<1E-20	1,000	<1E-20	1,000	<1E-20	1,000
Cf-249	Total α	<1E-20	1,000	<1E-20	1,000	<1E-20	1,000	<1E-20	1,000
Cf-251	Total α	<1E-20	1,000	<1E-20	1,000	<1E-20	1,000	<1E-20	1,000
Cl-36	700	8.4E-05	1,000	8.9E-05	1,000	1.9E-03	1,000	3.3E-03	1,000
Cm-243	Total α	<1E-20	1,000	<1E-20	1,000	<1E-20	1,000	<1E-20	1,000
Cm-244	Total α	<1E-20	1,000	<1E-20	1,000	<1E-20	1,000	<1E-20	1,000
Cm-245	Total α	<1E-20	1,000	<1E-20	1,000	<1E-20	1,000	<1E-20	1,000
Cm-247	Total α	<1E-20	1,000	<1E-20	1,000	<1E-20	1,000	<1E-20	1,000
Co-60	100	<1E-20	570	<1E-20	400	<1E-20	370	<1E-20	490
Cs-135	900	<1E-20	1,000	<1E-20	1,000	<1E-20	1,000	<1E-20	1,000
Cs-137	200	<1E-20	1,000	<1E-20	1,000	<1E-20	1,000	<1E-20	1,000
Eu-152	200	<1E-20	1,000	<1E-20	990	<1E-20	1,000	<1E-20	1,000
Eu-154	60	<1E-20	780	<1E-20	650	<1E-20	650	<1E-20	690
H-3	20,000	9.0E-11	220	9.4E-11	220	6.2E-08	160	1.1E-07	160
I-129	1	3.0E-04	1,000	3.1E-04	1,000	5.6E-03	1,000	9.6E-03	1,000
K-40	N/A	<1E-20	1,000	<1E-20	1,000	<1E-20	1,000	<1E-20	1,000
Nb-93m	1,000	<1E-20	1,000	<1E-20	1,000	<1E-20	1,000	<1E-20	1,000
Nb-94	N/A	<1E-20	1,000	<1E-20	1,000	<1E-20	1,000	<1E-20	1,000
Ni-63	50	<1E-20	1,000	<1E-20	1,000	<1E-20	1,000	<1E-20	1,000
Np-237	Total α	<1E-20	1,000	<1E-20	1,000	<1E-20	1,000	<1E-20	1,000
Pa-231	Total α	<1E-20	1,000	<1E-20	1,000	<1E-20	1,000	<1E-20	1,000
Pb-210	N/A	<1E-20	1,000	<1E-20	1,000	<1E-20	1,000	<1E-20	1,000
Pt-193	3,000	<1E-20	1,000	<1E-20	1,000	<1E-20	1,000	<1E-20	1,000
Pu-238	Total α	<1E-20	1,000	<1E-20	1,000	<1E-20	1,000	<1E-20	1,000
Pu-239	Total α	<1E-20	1,000	<1E-20	1,000	<1E-20	1,000	<1E-20	1,000
Pu-240	Total α	<1E-20	1,000	<1E-20	1,000	<1E-20	1,000	<1E-20	1,000
Pu-241	300	<1E-20	1,000	<1E-20	1,000	<1E-20	1,000	<1E-20	1,000
Pu-242	Total α	<1E-20	1,000	<1E-20	1,000	<1E-20	1,000	<1E-20	1,000
Pu-244	Total α	<1E-20	1,000	<1E-20	1,000	<1E-20	1,000	<1E-20	1,000
Ra-226	Total α /Ra	<1E-20	1,000	<1E-20	1,000	<1E-20	1,000	<1E-20	1,000
Ra-228	Total Ra	<1E-20	1,000	<1E-20	1,000	<1E-20	1,000	<1E-20	1,000
Rn-222	N/A	<1E-20	1,000	<1E-20	1,000	<1E-20	1,000	<1E-20	1,000
Se-79	N/A	<1E-20	1,000	<1E-20	1,000	<1E-20	1,000	<1E-20	1,000
Sm-151	1,000	<1E-20	1,000	<1E-20	1,000	<1E-20	1,000	<1E-20	1,000
Sn-126	N/A	<1E-20	1,000	<1E-20	1,000	<1E-20	1,000	<1E-20	1,000
Sr-90	8	<1E-20	1,000	<1E-20	1,000	<1E-20	1,000	<1E-20	820
Tc-99	900	1.7E-01	1,000	1.8E-01	1,000	2.4E+00	1,000	4.0E+00	1,000
Th-229	Total α	<1E-20	1,000	<1E-20	1,000	<1E-20	1,000	<1E-20	1,000
Th-230	Total α	<1E-20	1,000	<1E-20	1,000	<1E-20	1,000	<1E-20	1,000
Th-232	Total α	<1E-20	1,000	<1E-20	1,000	<1E-20	1,000	<1E-20	1,000
U-232	Total U	<1E-20	1,000	<1E-20	1,000	<1E-20	1,000	<1E-20	1,000
U-233	Total U	<1E-20	1,000	<1E-20	1,000	<1E-20	1,000	<1E-20	1,000
U-234	Total U	<1E-20	1,000	<1E-20	1,000	<1E-20	1,000	<1E-20	1,000
U-235	Total U	<1E-20	1,000	<1E-20	1,000	<1E-20	1,000	<1E-20	1,000
U-236	Total U	<1E-20	1,000	<1E-20	1,000	<1E-20	1,000	<1E-20	1,000
U-238	Total U	<1E-20	1,000	<1E-20	1,000	<1E-20	1,000	<1E-20	1,000
Zr-93	2,000	<1E-20	1,000	<1E-20	1,000	<1E-20	1,000	<1E-20	1,000
Total Alpha	15	<1E-20	1,000	<1E-20	1,000	<1E-20	1,000	<1E-20	1,000
Total Ra	5	<1E-20	1,000	<1E-20	1,000	<1E-20	1,000	<1E-20	1,000
Sum of Beta-Gamma MCL Fractions		4.9E-04	1,000	5.1E-04	1,000	8.3E-03	1,000	1.4E-02	1,000

Table 5.2-4: Radiological Peak Concentrations along the 100-Meter Boundary for LAZ, Sectors E through H in 1,000 Years

Radionuclide	MCL (pCi/L)	Sector E		Sector F		Sector G		Sector H	
		Conc. (pCi/L)	Year of Peak	Conc. (pCi/L)	Year of Peak	Conc. (pCi/L)	Year of Peak	Conc. (pCi/L)	Year of Peak
Ac-227	N/A	<1E-20	1,000	<1E-20	1,000	<1E-20	1,000	<1E-20	1,000
Al-26	N/A	<1E-20	1,000	<1E-20	1,000	<1E-20	1,000	<1E-20	1,000
Am-241	Total α	<1E-20	1,000	<1E-20	1,000	<1E-20	1,000	<1E-20	1,000
Am-242m	Total α	<1E-20	1,000	<1E-20	1,000	<1E-20	1,000	<1E-20	1,000
Am-243	Total α	<1E-20	1,000	<1E-20	1,000	<1E-20	1,000	<1E-20	1,000
C-14	2,000	<1E-20	1,000	<1E-20	1,000	<1E-20	1,000	<1E-20	1,000
Cf-249	Total α	<1E-20	1,000	<1E-20	1,000	<1E-20	1,000	<1E-20	1,000
Cf-251	Total α	<1E-20	1,000	<1E-20	1,000	<1E-20	1,000	<1E-20	1,000
Cl-36	700	5.9E-05	1,000	9.0E-05	1,000	1.1E-04	1,000	7.5E-11	1,000
Cm-243	Total α	<1E-20	1,000	<1E-20	1,000	<1E-20	1,000	<1E-20	1,000
Cm-244	Total α	<1E-20	1,000	<1E-20	920	<1E-20	700	<1E-20	640
Cm-245	Total α	<1E-20	1,000	<1E-20	1,000	<1E-20	1,000	<1E-20	1,000
Cm-247	Total α	<1E-20	1,000	<1E-20	1,000	<1E-20	1,000	<1E-20	1,000
Co-60	100	<1E-20	350	<1E-20	240	<1E-20	190	<1E-20	190
Cs-135	900	<1E-20	1,000	<1E-20	1,000	4.7E-20	1,000	<1E-20	1,000
Cs-137	200	<1E-20	970	<1E-20	840	<1E-20	750	<1E-20	930
Eu-152	200	<1E-20	990	<1E-20	690	<1E-20	530	<1E-20	490
Eu-154	60	<1E-20	640	<1E-20	440	<1E-20	340	<1E-20	330
H-3	20,000	3.3E-10	160	1.9E-09	160	2.4E-09	160	3.0E-12	180
I-129	1	2.1E-04	1,000	2.3E-03	1,000	2.7E-03	1,000	3.1E-05	1,000
K-40	N/A	<1E-20	1,000	2.1E-18	1,000	5.5E-18	1,000	<1E-20	1,000
Nb-93m	1,000	<1E-20	1,000	<1E-20	1,000	<1E-20	1,000	<1E-20	1,000
Nb-94	N/A	<1E-20	1,000	<1E-20	1,000	<1E-20	1,000	<1E-20	1,000
Ni-63	50	<1E-20	1,000	<1E-20	1,000	<1E-20	1,000	<1E-20	1,000
Np-237	Total α	<1E-20	1,000	9.2E-20	1,000	1.7E-19	1,000	<1E-20	1,000
Pa-231	Total α	<1E-20	1,000	<1E-20	1,000	<1E-20	1,000	<1E-20	1,000
Pb-210	N/A	<1E-20	1,000	<1E-20	1,000	<1E-20	1,000	<1E-20	1,000
Pt-193	3,000	<1E-20	1,000	<1E-20	1,000	<1E-20	1,000	<1E-20	1,000
Pu-238	Total α	<1E-20	1,000	<1E-20	1,000	<1E-20	1,000	<1E-20	1,000
Pu-239	Total α	<1E-20	1,000	<1E-20	1,000	<1E-20	1,000	<1E-20	1,000
Pu-240	Total α	<1E-20	1,000	<1E-20	1,000	<1E-20	1,000	<1E-20	1,000
Pu-241	300	<1E-20	1,000	<1E-20	1,000	<1E-20	1,000	<1E-20	1,000
Pu-242	Total α	<1E-20	1,000	<1E-20	1,000	<1E-20	1,000	<1E-20	1,000
Pu-244	Total α	<1E-20	1,000	<1E-20	1,000	<1E-20	1,000	<1E-20	1,000
Ra-226	Total α /Ra	<1E-20	1,000	<1E-20	1,000	<1E-20	1,000	<1E-20	1,000
Ra-228	Total Ra	<1E-20	1,000	<1E-20	1,000	<1E-20	1,000	<1E-20	1,000
Rn-222	N/A	<1E-20	1,000	<1E-20	1,000	<1E-20	1,000	<1E-20	1,000
Se-79	N/A	<1E-20	1,000	<1E-20	1,000	<1E-20	1,000	<1E-20	1,000
Sm-151	1,000	<1E-20	1,000	<1E-20	1,000	<1E-20	1,000	<1E-20	1,000
Sn-126	N/A	<1E-20	1,000	<1E-20	1,000	<1E-20	1,000	<1E-20	1,000
Sr-90	8	<1E-20	770	<1E-20	690	<1E-20	630	<1E-20	720
Tc-99	900	1.3E-01	1,000	9.4E-01	1,000	1.1E+00	1,000	5.7E-03	1,000
Th-229	Total α	<1E-20	1,000	<1E-20	1,000	<1E-20	1,000	<1E-20	1,000
Th-230	Total α	<1E-20	1,000	<1E-20	1,000	<1E-20	1,000	<1E-20	1,000
Th-232	Total α	<1E-20	1,000	<1E-20	1,000	<1E-20	1,000	<1E-20	1,000
U-232	Total U	<1E-20	1,000	<1E-20	1,000	<1E-20	1,000	<1E-20	1,000
U-233	Total U	<1E-20	1,000	<1E-20	1,000	<1E-20	1,000	<1E-20	1,000
U-234	Total U	<1E-20	1,000	<1E-20	1,000	<1E-20	1,000	<1E-20	1,000
U-235	Total U	<1E-20	1,000	<1E-20	1,000	<1E-20	1,000	<1E-20	1,000
U-236	Total U	<1E-20	1,000	<1E-20	1,000	<1E-20	1,000	<1E-20	1,000
U-238	Total U	<1E-20	1,000	<1E-20	1,000	<1E-20	1,000	<1E-20	1,000
Zr-93	2,000	<1E-20	1,000	<1E-20	1,000	<1E-20	1,000	<1E-20	1,000
Total Alpha	15	<1E-20	1,000	9.2E-20	1,000	1.7E-19	1,000	<1E-20	1,000
Total Ra	5	<1E-20	1,000	<1E-20	1,000	<1E-20	1,000	<1E-20	1,000
Sum of Beta-Gamma MCL Fractions		3.5E-04	1,000	3.3E-03	1,000	3.9E-03	1,000	3.7E-05	1,000

Table 5.2-5: Radiological Peak Concentrations along the 100-Meter Boundary for GAU, Sectors A through D in 1,000 Years

Radionuclide	MCL (pCi/L)	Sector A		Sector B		Sector C		Sector D	
		Conc. (pCi/L)	Year of Peak	Conc. (pCi/L)	Year of Peak	Conc. (pCi/L)	Year of Peak	Conc. (pCi/L)	Year of Peak
Ac-227	N/A	<1E-20	1,000	<1E-20	1,000	<1E-20	1,000	<1E-20	1,000
Al-26	N/A	<1E-20	1,000	<1E-20	1,000	<1E-20	1,000	<1E-20	1,000
Am-241	Total α	<1E-20	1,000	<1E-20	1,000	<1E-20	1,000	<1E-20	1,000
Am-242m	Total α	<1E-20	1,000	<1E-20	1,000	<1E-20	1,000	<1E-20	1,000
Am-243	Total α	<1E-20	1,000	<1E-20	1,000	<1E-20	1,000	<1E-20	1,000
C-14	2,000	<1E-20	1,000	<1E-20	1,000	<1E-20	1,000	<1E-20	490
Cf-249	Total α	<1E-20	1,000	<1E-20	1,000	<1E-20	1,000	<1E-20	1,000
Cf-251	Total α	<1E-20	1,000	<1E-20	1,000	<1E-20	1,000	<1E-20	1,000
Cl-36	700	3.8E-09	1,000	3.3E-09	1,000	4.5E-08	1,000	2.5E-08	1,000
Cm-243	Total α	<1E-20	1,000	<1E-20	1,000	<1E-20	1,000	<1E-20	1,000
Cm-244	Total α	<1E-20	1,000	<1E-20	1,000	<1E-20	1,000	<1E-20	1,000
Cm-245	Total α	<1E-20	1,000	<1E-20	1,000	<1E-20	1,000	<1E-20	1,000
Cm-247	Total α	<1E-20	1,000	<1E-20	1,000	<1E-20	1,000	<1E-20	1,000
Co-60	100	<1E-20	490	<1E-20	640	<1E-20	450	<1E-20	430
Cs-135	900	<1E-20	1,000	<1E-20	1,000	<1E-20	1,000	<1E-20	1,000
Cs-137	200	<1E-20	1,000	<1E-20	1,000	<1E-20	1,000	<1E-20	1,000
Eu-152	200	<1E-20	1,000	<1E-20	1,000	<1E-20	1,000	<1E-20	1,000
Eu-154	60	<1E-20	1,000	<1E-20	810	<1E-20	810	<1E-20	830
H-3	20,000	4.5E-14	240	1.6E-13	180	1.3E-11	180	7.3E-12	180
I-129	1	7.2E-08	1,000	6.8E-08	1,000	7.0E-07	1,000	3.8E-07	1,000
K-40	N/A	<1E-20	1,000	<1E-20	1,000	<1E-20	1,000	<1E-20	1,000
Nb-93m	1,000	<1E-20	1,000	<1E-20	1,000	<1E-20	1,000	<1E-20	1,000
Nb-94	N/A	<1E-20	1,000	<1E-20	1,000	<1E-20	1,000	<1E-20	1,000
Ni-63	50	<1E-20	1,000	<1E-20	1,000	<1E-20	1,000	<1E-20	440
Np-237	Total α	<1E-20	1,000	<1E-20	1,000	<1E-20	1,000	<1E-20	1,000
Pa-231	Total α	<1E-20	1,000	<1E-20	1,000	<1E-20	1,000	<1E-20	1,000
Pb-210	N/A	<1E-20	1,000	<1E-20	1,000	<1E-20	1,000	<1E-20	1,000
Pt-193	3,000	<1E-20	1,000	<1E-20	1,000	<1E-20	980	<1E-20	410
Pu-238	Total α	<1E-20	1,000	<1E-20	1,000	<1E-20	1,000	<1E-20	1,000
Pu-239	Total α	<1E-20	1,000	<1E-20	1,000	<1E-20	1,000	<1E-20	1,000
Pu-240	Total α	<1E-20	1,000	<1E-20	1,000	<1E-20	1,000	<1E-20	1,000
Pu-241	300	<1E-20	1,000	<1E-20	1,000	<1E-20	1,000	<1E-20	1,000
Pu-242	Total α	<1E-20	1,000	<1E-20	1,000	<1E-20	1,000	<1E-20	1,000
Pu-244	Total α	<1E-20	1,000	<1E-20	1,000	<1E-20	1,000	<1E-20	1,000
Ra-226	Total α /Ra	<1E-20	1,000	<1E-20	1,000	<1E-20	1,000	<1E-20	1,000
Ra-228	Total Ra	<1E-20	1,000	<1E-20	1,000	<1E-20	1,000	<1E-20	1,000
Rn-222	N/A	<1E-20	1,000	<1E-20	1,000	<1E-20	1,000	<1E-20	1,000
Se-79	N/A	<1E-20	1,000	<1E-20	1,000	<1E-20	1,000	<1E-20	1,000
Sm-151	1,000	<1E-20	1,000	<1E-20	1,000	<1E-20	1,000	<1E-20	1,000
Sn-126	N/A	<1E-20	1,000	<1E-20	1,000	<1E-20	1,000	<1E-20	1,000
Sr-90	8	<1E-20	970	<1E-20	980	<1E-20	700	<1E-20	1,000
Tc-99	900	6.8E-05	1,000	7.8E-05	1,000	5.6E-04	1,000	3.0E-04	1,000
Th-229	Total α	<1E-20	1,000	<1E-20	1,000	<1E-20	1,000	<1E-20	1,000
Th-230	Total α	<1E-20	1,000	<1E-20	1,000	<1E-20	1,000	<1E-20	1,000
Th-232	Total α	<1E-20	1,000	<1E-20	1,000	<1E-20	1,000	<1E-20	1,000
U-232	Total U	<1E-20	1,000	<1E-20	1,000	<1E-20	1,000	<1E-20	1,000
U-233	Total U	<1E-20	1,000	<1E-20	1,000	<1E-20	1,000	<1E-20	1,000
U-234	Total U	<1E-20	1,000	<1E-20	1,000	<1E-20	1,000	<1E-20	1,000
U-235	Total U	<1E-20	1,000	<1E-20	1,000	<1E-20	1,000	<1E-20	1,000
U-236	Total U	<1E-20	1,000	<1E-20	1,000	<1E-20	1,000	<1E-20	1,000
U-238	Total U	<1E-20	1,000	<1E-20	1,000	<1E-20	1,000	<1E-20	1,000
Zr-93	2,000	<1E-20	1,000	<1E-20	1,000	<1E-20	1,000	<1E-20	1,000
Total Alpha	15	<1E-20	1,000	<1E-20	1,000	<1E-20	1,000	<1E-20	1,000
Total Ra	5	<1E-20	1,000	<1E-20	1,000	<1E-20	1,000	<1E-20	1,000
Sum of Beta-Gamma MCL Fractions		1.5E-07	1,000	1.5E-07	1,000	1.3E-06	1,000	7.2E-07	1,000

Table 5.2-6: Radiological Peak Concentrations along the 100-Meter Boundary for GAU, Sectors E through H in 1,000 Years

Radionuclide	MCL (pCi/L)	Sector E		Sector F		Sector G		Sector H	
		Conc. (pCi/L)	Year of Peak	Conc. (pCi/L)	Year of Peak	Conc. (pCi/L)	Year of Peak	Conc. (pCi/L)	Year of Peak
Ac-227	N/A	<1E-20	1,000	<1E-20	1,000	<1E-20	1,000	<1E-20	1,000
Al-26	N/A	<1E-20	1,000	<1E-20	1,000	<1E-20	1,000	<1E-20	1,000
Am-241	Total α	<1E-20	1,000	<1E-20	1,000	<1E-20	1,000	<1E-20	1,000
Am-242m	Total α	<1E-20	1,000	<1E-20	1,000	<1E-20	1,000	<1E-20	1,000
Am-243	Total α	<1E-20	1,000	<1E-20	1,000	<1E-20	1,000	<1E-20	1,000
C-14	2,000	<1E-20	1,000	<1E-20	1,000	<1E-20	1,000	<1E-20	1,000
Cf-249	Total α	<1E-20	1,000	<1E-20	1,000	<1E-20	1,000	<1E-20	1,000
Cf-251	Total α	<1E-20	1,000	<1E-20	1,000	<1E-20	1,000	<1E-20	1,000
Cl-36	700	8.1E-11	1,000	1.1E-10	1,000	9.6E-11	1,000	<1E-20	1,000
Cm-243	Total α	<1E-20	1,000	<1E-20	1,000	<1E-20	1,000	<1E-20	1,000
Cm-244	Total α	<1E-20	1,000	<1E-20	1,000	<1E-20	950	<1E-20	990
Cm-245	Total α	<1E-20	1,000	<1E-20	1,000	<1E-20	1,000	<1E-20	1,000
Cm-247	Total α	<1E-20	1,000	<1E-20	1,000	<1E-20	1,000	<1E-20	1,000
Co-60	100	<1E-20	420	<1E-20	340	<1E-20	270	<1E-20	290
Cs-135	900	<1E-20	1,000	<1E-20	1,000	<1E-20	1,000	<1E-20	1,000
Cs-137	200	<1E-20	1,000	<1E-20	1,000	<1E-20	1,000	<1E-20	810
Eu-152	200	<1E-20	900	<1E-20	900	<1E-20	710	<1E-20	740
Eu-154	60	<1E-20	760	<1E-20	690	<1E-20	450	<1E-20	480
H-3	20,000	1.2E-15	240	1.4E-14	190	1.1E-14	190	<1E-20	220
I-129	1	1.7E-09	1,000	1.4E-08	1,000	1.3E-08	1,000	3.8E-18	1,000
K-40	N/A	<1E-20	1,000	<1E-20	1,000	<1E-20	1,000	<1E-20	680
Nb-93m	1,000	<1E-20	1,000	<1E-20	1,000	<1E-20	1,000	<1E-20	1,000
Nb-94	N/A	<1E-20	1,000	<1E-20	1,000	<1E-20	1,000	<1E-20	1,000
Ni-63	50	<1E-20	1,000	<1E-20	1,000	<1E-20	1,000	<1E-20	800
Np-237	Total α	<1E-20	1,000	<1E-20	1,000	<1E-20	1,000	<1E-20	1,000
Pa-231	Total α	<1E-20	1,000	<1E-20	1,000	<1E-20	1,000	<1E-20	1,000
Pb-210	N/A	<1E-20	1,000	<1E-20	1,000	<1E-20	1,000	<1E-20	1,000
Pt-193	3,000	<1E-20	1,000	<1E-20	1,000	<1E-20	1,000	<1E-20	820
Pu-238	Total α	<1E-20	1,000	<1E-20	1,000	<1E-20	1,000	<1E-20	1,000
Pu-239	Total α	<1E-20	1,000	<1E-20	1,000	<1E-20	1,000	<1E-20	1,000
Pu-240	Total α	<1E-20	1,000	<1E-20	1,000	<1E-20	1,000	<1E-20	1,000
Pu-241	300	<1E-20	1,000	<1E-20	1,000	<1E-20	1,000	<1E-20	1,000
Pu-242	Total α	<1E-20	1,000	<1E-20	1,000	<1E-20	1,000	<1E-20	1,000
Pu-244	Total α	<1E-20	1,000	<1E-20	1,000	<1E-20	1,000	<1E-20	1,000
Ra-226	Total α /Ra	<1E-20	1,000	<1E-20	1,000	<1E-20	1,000	<1E-20	1,000
Ra-228	Total Ra	<1E-20	1,000	<1E-20	1,000	<1E-20	1,000	<1E-20	1,000
Rn-222	N/A	<1E-20	1,000	<1E-20	1,000	<1E-20	1,000	<1E-20	1,000
Se-79	N/A	<1E-20	1,000	<1E-20	1,000	<1E-20	1,000	<1E-20	1,000
Sm-151	1,000	<1E-20	1,000	<1E-20	1,000	<1E-20	1,000	<1E-20	1,000
Sn-126	N/A	<1E-20	1,000	<1E-20	1,000	<1E-20	1,000	<1E-20	1,000
Sr-90	8	<1E-20	910	<1E-20	830	<1E-20	810	<1E-20	600
Tc-99	900	1.6E-06	1,000	1.1E-05	1,000	9.3E-06	1,000	9.6E-16	1,000
Th-229	Total α	<1E-20	1,000	<1E-20	1,000	<1E-20	1,000	<1E-20	1,000
Th-230	Total α	<1E-20	1,000	<1E-20	1,000	<1E-20	1,000	<1E-20	1,000
Th-232	Total α	<1E-20	1,000	<1E-20	1,000	<1E-20	1,000	<1E-20	1,000
U-232	Total U	<1E-20	1,000	<1E-20	1,000	<1E-20	1,000	<1E-20	1,000
U-233	Total U	<1E-20	1,000	<1E-20	1,000	<1E-20	1,000	<1E-20	1,000
U-234	Total U	<1E-20	1,000	<1E-20	1,000	<1E-20	1,000	<1E-20	1,000
U-235	Total U	<1E-20	1,000	<1E-20	1,000	<1E-20	1,000	<1E-20	1,000
U-236	Total U	<1E-20	1,000	<1E-20	1,000	<1E-20	1,000	<1E-20	1,000
U-238	Total U	<1E-20	1,000	<1E-20	1,000	<1E-20	1,000	<1E-20	1,000
Zr-93	2,000	<1E-20	1,000	<1E-20	1,000	<1E-20	1,000	<1E-20	1,000
Total Alpha	15	<1E-20	1,000	<1E-20	1,000	<1E-20	1,000	<1E-20	1,000
Total Ra	5	<1E-20	1,000	<1E-20	1,000	<1E-20	1,000	<1E-20	1,000
Sum of Beta-Gamma MCL Fractions		3.4E-09	1,000	2.6E-08	1,000	2.4E-08	1,000	4.8E-18	1,000

Table 5.2-7: Chemical Peak Concentrations along the 100-Meter Boundary for UAZ, Sectors A through H in 1,000 Years

Chemical	MCL (µg/L)	Conc. (µg/L)	Year of Peak	Conc. (µg/L)	Year of Peak	Conc. (µg/L)	Year of Peak	Conc. (µg/L)	Year of Peak
		Sector A		Sector B		Sector C		Sector D	
Cl^-	250,000	1.0E-03	1,000	2.8E-03	1,000	5.7E-02	1,000	1.2E-01	1,000
F^-	4,000	2.1E-03	1,000	5.6E-03	1,000	1.1E-01	1,000	2.5E-01	1,000
NO_3	10,000	3.2E+01	1,000	8.2E+01	1,000	4.3E+02	1,000	8.8E+02	1,000
NO_2	10,000	2.8E+00	1,000	7.2E+00	1,000	3.8E+01	1,000	7.8E+01	1,000
PO_4	N/A	2.1E-01	1,000	5.4E-01	1,000	2.8E+00	1,000	5.8E+00	1,000
SO_4	250,000	9.4E-01	1,000	2.4E+00	1,000	1.3E+01	1,000	2.6E+01	1,000
Al	200	<1E-20	1,000	<1E-20	1,000	<1E-20	1,000	<1E-20	1,000
Ag	100	<1E-20	1,000	<1E-20	1,000	<1E-20	1,000	<1E-20	1,000
As	10	<1E-20	1,000	<1E-20	930	<1E-20	1,000	<1E-20	1,000
B	N/A	3.9E-03	1,000	1.0E-02	1,000	5.3E-02	1,000	1.1E-01	1,000
Ba	2,000	<1E-20	1,000	<1E-20	1,000	<1E-20	1,000	<1E-20	1,000
Cd	5	<1E-20	1,000	<1E-20	1,000	<1E-20	1,000	<1E-20	1,000
Co	N/A	<1E-20	1,000	<1E-20	1,000	<1E-20	1,000	<1E-20	1,000
Cr	100	<1E-20	1,000	<1E-20	1,000	<1E-20	1,000	<1E-20	1,000
Cu	1,300	<1E-20	1,000	<1E-20	1,000	<1E-20	1,000	<1E-20	1,000
Fe	300	<1E-20	1,000	<1E-20	1,000	<1E-20	1,000	<1E-20	1,000
Hg	2	<1E-20	1,000	<1E-20	1,000	<1E-20	1,000	<1E-20	1,000
I	N/A	1.7E-09	1,000	4.4E-09	1,000	2.5E-07	1,000	1.7E-07	1,000
Mn	50	<1E-20	1,000	<1E-20	1,000	<1E-20	1,000	<1E-20	1,000
Mo	N/A	<1E-20	1,000	<1E-20	1,000	<1E-20	1,000	<1E-20	1,000
Ni	N/A	<1E-20	1,000	<1E-20	1,000	<1E-20	1,000	<1E-20	1,000
Pb	15	<1E-20	1,000	<1E-20	1,000	<1E-20	1,000	<1E-20	1,000
Se	50	<1E-20	1,000	<1E-20	1,000	<1E-20	1,000	<1E-20	1,000
Sb	6	<1E-20	1,000	<1E-20	1,000	<1E-20	1,000	<1E-20	1,000
Sr	N/A	<1E-20	1,000	<1E-20	1,000	<1E-20	1,000	<1E-20	1,000
U	30	<1E-20	1,000	<1E-20	1,000	<1E-20	1,000	<1E-20	1,000
Zn	5,000	<1E-20	1,000	<1E-20	1,000	<1E-20	1,000	<1E-20	1,000
Chemical	**MCL**	**Sector E**		**Sector F**		**Sector G**		**Sector H**	
Cl^-	250,000	2.1E-03	1,000	2.5E-02	1,000	4.0E-02	1,000	3.3E-04	1,000
F^-	4,000	4.2E-03	1,000	1.5E-02	1,000	2.5E-02	1,000	1.9E-05	1,000
NO_3	10,000	6.5E+01	1,000	7.3E+01	1,000	1.1E+02	1,000	1.2E+00	1,000
NO_2	10,000	5.7E+00	1,000	3.7E+00	1,000	5.5E+00	1,000	1.2E-02	1,000
PO_4	N/A	4.3E-01	1,000	2.3E-01	1,000	3.4E-01	1,000	1.2E-03	1,000
SO_4	250,000	1.9E+00	1,000	1.7E+00	1,000	2.6E+00	1,000	3.5E-03	1,000
Al	200	<1E-20	1,000	<1E-20	1,000	<1E-20	1,000	<1E-20	1,000
Ag	100	<1E-20	1,000	<1E-20	1,000	<1E-20	1,000	<1E-20	1,000
As	10	<1E-20	1,000	<1E-20	1,000	<1E-20	1,000	<1E-20	1,000
B	N/A	8.0E-03	1,000	2.5E-02	1,000	3.8E-02	1,000	1.2E-04	1,000
Ba	2,000	<1E-20	1,000	<1E-20	1,000	<1E-20	1,000	<1E-20	1,000
Cd	5	<1E-20	1,000	<1E-20	1,000	<1E-20	1,000	<1E-20	1,000
Co	N/A	<1E-20	1,000	<1E-20	1,000	<1E-20	1,000	<1E-20	1,000
Cr	100	<1E-20	1,000	<1E-20	1,000	<1E-20	1,000	<1E-20	1,000
Cu	1,300	<1E-20	1,000	<1E-20	1,000	<1E-20	1,000	<1E-20	1,000
Fe	300	<1E-20	1,000	<1E-20	1,000	<1E-20	1,000	<1E-20	1,000
Hg	2	<1E-20	1,000	<1E-20	1,000	<1E-20	1,000	<1E-20	1,000
I	N/A	1.8E-08	1,000	2.6E-06	1,000	4.2E-06	1,000	5.1E-08	1,000
Mn	50	<1E-20	1,000	<1E-20	1,000	<1E-20	1,000	<1E-20	1,000
Mo	N/A	<1E-20	1,000	<1E-20	1,000	<1E-20	1,000	<1E-20	1,000
Ni	N/A	<1E-20	1,000	<1E-20	1,000	<1E-20	1,000	<1E-20	1,000
Pb	15	<1E-20	1,000	<1E-20	1,000	<1E-20	1,000	<1E-20	1,000
Se	50	<1E-20	1,000	<1E-20	1,000	<1E-20	1,000	<1E-20	1,000
Sb	6	<1E-20	1,000	<1E-20	1,000	<1E-20	1,000	<1E-20	1,000
Sr	N/A	<1E-20	1,000	<1E-20	1,000	<1E-20	1,000	<1E-20	1,000
U	30	<1E-20	1,000	<1E-20	1,000	<1E-20	1,000	<1E-20	1,000
Zn	5,000	<1E-20	1,000	<1E-20	1,000	<1E-20	1,000	<1E-20	1,000

Table 5.2-8: Chemical Peak Concentrations along the 100-Meter Boundary for LAZ, Sectors A through H in 1,000 Years

Chemical	MCL (µg/L)	Conc. (µg/L)	Year of Peak	Conc. (µg/L)	Year of Peak	Conc. (µg/L)	Year of Peak	Conc. (µg/L)	Year of Peak
		Sector A		Sector B		Sector C		Sector D	
Cl^-	250,000	3.9E-03	1,000	4.1E-03	1,000	8.9E-02	1,000	1.5E-01	1,000
F^-	4,000	7.8E-03	1,000	8.2E-03	1,000	1.8E-01	1,000	3.1E-01	1,000
NO_3	10,000	1.5E+02	1,000	1.5E+02	1,000	7.9E+02	1,000	1.3E+03	1,000
NO_2	10,000	1.3E+01	1,000	1.3E+01	1,000	7.0E+01	1,000	1.1E+02	1,000
PO_4	N/A	9.6E-01	1,000	9.9E-01	1,000	5.2E+00	1,000	8.3E+00	1,000
SO_4	250,000	4.4E+00	1,000	4.5E+00	1,000	2.4E+01	1,000	3.8E+01	1,000
Al	200	<1E-20	1,000	<1E-20	1,000	<1E-20	1,000	<1E-20	1,000
Ag	100	<1E-20	1,000	<1E-20	1,000	<1E-20	1,000	<1E-20	1,000
As	10	<1E-20	1,000	<1E-20	1,000	<1E-20	1,000	<1E-20	1,000
B	N/A	1.8E-02	1,000	1.9E-02	1,000	9.7E-02	1,000	1.6E-01	1,000
Ba	2,000	<1E-20	1,000	<1E-20	1,000	<1E-20	1,000	<1E-20	1,000
Cd	5	<1E-20	1,000	<1E-20	1,000	<1E-20	1,000	<1E-20	1,000
Co	N/A	<1E-20	1,000	<1E-20	1,000	<1E-20	1,000	<1E-20	1,000
Cr	100	<1E-20	1,000	<1E-20	1,000	<1E-20	1,000	<1E-20	1,000
Cu	1,300	<1E-20	1,000	<1E-20	1,000	<1E-20	1,000	<1E-20	1,000
Fe	300	<1E-20	1,000	<1E-20	1,000	<1E-20	1,000	<1E-20	1,000
Hg	2	<1E-20	1,000	<1E-20	1,000	<1E-20	1,000	<1E-20	1,000
I	N/A	6.5E-09	1,000	2.2E-08	1,000	3.4E-07	1,000	2.2E-07	1,000
Mn	50	<1E-20	1,000	<1E-20	1,000	<1E-20	1,000	<1E-20	1,000
Mo	N/A	<1E-20	1,000	<1E-20	1,000	<1E-20	1,000	<1E-20	1,000
Ni	N/A	<1E-20	1,000	<1E-20	1,000	<1E-20	1,000	<1E-20	1,000
Pb	15	<1E-20	1,000	<1E-20	1,000	<1E-20	1,000	<1E-20	1,000
Se	50	<1E-20	1,000	<1E-20	1,000	<1E-20	1,000	<1E-20	1,000
Sb	6	<1E-20	1,000	<1E-20	1,000	<1E-20	1,000	<1E-20	1,000
Sr	N/A	<1E-20	1,000	<1E-20	1,000	<1E-20	1,000	<1E-20	1,000
U	30	<1E-20	1,000	<1E-20	1,000	<1E-20	1,000	<1E-20	1,000
Zn	5,000	<1E-20	1,000	<1E-20	1,000	<1E-20	1,000	<1E-20	1,000
Chemical	**MCL**	**Sector E**		**Sector F**		**Sector G**		**Sector H**	
Cl^-	250,000	2.7E-03	1,000	6.2E-02	1,000	7.3E-02	1,000	2.8E-04	1,000
F^-	4,000	5.5E-03	1,000	3.8E-02	1,000	4.5E-02	1,000	1.6E-05	1,000
NO_3	10,000	1.1E+02	1,000	2.0E+02	1,000	2.2E+02	1,000	1.1E+00	1,000
NO_2	10,000	9.9E+00	1,000	1.0E+01	1,000	1.1E+01	1,000	1.1E-02	1,000
PO_4	N/A	7.3E-01	1,000	6.3E-01	1,000	6.8E-01	1,000	1.1E-03	1,000
SO_4	250,000	3.3E+00	1,000	4.7E+00	1,000	5.2E+00	1,000	3.3E-03	1,000
Al	200	<1E-20	1,000	<1E-20	1,000	<1E-20	1,000	<1E-20	1,000
Ag	100	<1E-20	1,000	<1E-20	1,000	<1E-20	1,000	<1E-20	1,000
As	10	<1E-20	1,000	<1E-20	1,000	<1E-20	1,000	<1E-20	1,000
B	N/A	1.4E-02	1,000	6.9E-02	1,000	7.6E-02	1,000	1.1E-04	1,000
Ba	2,000	<1E-20	1,000	<1E-20	1,000	<1E-20	1,000	<1E-20	1,000
Cd	5	<1E-20	1,000	<1E-20	1,000	<1E-20	1,000	<1E-20	1,000
Co	N/A	<1E-20	1,000	<1E-20	1,000	<1E-20	1,000	<1E-20	1,000
Cr	100	<1E-20	1,000	<1E-20	1,000	<1E-20	1,000	<1E-20	1,000
Cu	1,300	<1E-20	1,000	<1E-20	1,000	<1E-20	1,000	<1E-20	1,000
Fe	300	<1E-20	1,000	<1E-20	1,000	<1E-20	1,000	<1E-20	1,000
Hg	2	<1E-20	1,000	<1E-20	1,000	<1E-20	1,000	<1E-20	1,000
I	N/A	7.3E-08	1,000	6.7E-06	1,000	7.8E-06	1,000	4.4E-08	1,000
Mn	50	<1E-20	1,000	<1E-20	1,000	<1E-20	1,000	<1E-20	1,000
Mo	N/A	<1E-20	1,000	<1E-20	1,000	<1E-20	1,000	<1E-20	1,000
Ni	N/A	<1E-20	1,000	<1E-20	1,000	<1E-20	1,000	<1E-20	1,000
Pb	15	<1E-20	1,000	<1E-20	1,000	<1E-20	1,000	<1E-20	1,000
Se	50	<1E-20	1,000	<1E-20	1,000	<1E-20	1,000	<1E-20	1,000
Sb	6	<1E-20	1,000	<1E-20	1,000	<1E-20	1,000	<1E-20	1,000
Sr	N/A	<1E-20	1,000	<1E-20	1,000	<1E-20	1,000	<1E-20	1,000
U	30	<1E-20	1,000	<1E-20	1,000	<1E-20	1,000	<1E-20	1,000
Zn	5,000	<1E-20	1,000	<1E-20	1,000	<1E-20	1,000	<1E-20	1,000

Table 5.2-9: Chemical Peak Concentrations along the 100-Meter Boundary for GAU, Sectors A through H in 1,000 Years

Chemical	MCL (µg/L)	Conc. (µg/L)	Year of Peak	Conc. (µg/L)	Year of Peak	Conc. (µg/L)	Year of Peak	Conc. (µg/L)	Year of Peak
		Sector A		Sector B		Sector C		Sector D	
Cl^-	250,000	1.8E-07	1,000	1.6E-07	1,000	2.1E-06	1,000	1.2E-06	1,000
F^-	4,000	3.6E-07	1,000	3.1E-07	1,000	4.2E-06	1,000	2.4E-06	1,000
NO_3	10,000	3.7E-01	1,000	6.0E-01	1,000	1.7E+00	1,000	8.1E-01	1,000
NO_2	10,000	3.2E-02	1,000	5.3E-02	1,000	1.5E-01	1,000	7.3E-02	1,000
PO_4	N/A	2.4E-03	1,000	3.9E-03	1,000	1.1E-02	1,000	5.3E-03	1,000
SO_4	250,000	1.1E-02	1,000	1.8E-02	1,000	5.0E-02	1,000	2.4E-02	1,000
Al	200	<1E-20	1,000	<1E-20	1,000	<1E-20	1,000	<1E-20	1,000
Ag	100	<1E-20	1,000	<1E-20	1,000	<1E-20	1,000	<1E-20	480
As	10	<1E-20	1,000	<1E-20	1,000	<1E-20	1,000	<1E-20	1,000
B	N/A	4.5E-05	1,000	7.4E-05	1,000	2.1E-04	1,000	1.1E-04	1,000
Ba	2,000	<1E-20	1,000	<1E-20	1,000	<1E-20	1,000	<1E-20	1,000
Cd	5	<1E-20	1,000	<1E-20	1,000	<1E-20	1,000	<1E-20	1,000
Co	N/A	<1E-20	1,000	<1E-20	1,000	<1E-20	1,000	<1E-20	990
Cr	100	<1E-20	1,000	<1E-20	1,000	<1E-20	1,000	<1E-20	1,000
Cu	1,300	<1E-20	1,000	<1E-20	1,000	<1E-20	1,000	<1E-20	1,000
Fe	300	<1E-20	1,000	<1E-20	1,000	<1E-20	1,000	<1E-20	1,000
Hg	2	<1E-20	1,000	<1E-20	1,000	<1E-20	1,000	<1E-20	1,000
I	N/A	8.4E-12	1,000	1.9E-11	1,000	2.5E-11	1,000	1.3E-11	1,000
Mn	50	<1E-20	1,000	<1E-20	1,000	<1E-20	1,000	<1E-20	1,000
Mo	N/A	<1E-20	1,000	<1E-20	1,000	<1E-20	1,000	<1E-20	1,000
Ni	N/A	<1E-20	1,000	<1E-20	1,000	<1E-20	1,000	<1E-20	470
Pb	15	<1E-20	1,000	<1E-20	1,000	<1E-20	1,000	<1E-20	1,000
Se	50	<1E-20	1,000	<1E-20	1,000	<1E-20	1,000	<1E-20	1,000
Sb	6	<1E-20	1,000	<1E-20	1,000	<1E-20	1,000	<1E-20	1,000
Sr	N/A	<1E-20	1,000	<1E-20	1,000	<1E-20	1,000	<1E-20	440
U	30	<1E-20	1,000	<1E-20	1,000	<1E-20	1,000	<1E-20	1,000
Zn	5,000	<1E-20	1,000	<1E-20	1,000	<1E-20	1,000	<1E-20	1,000
Chemical	**MCL**	**Sector E**		**Sector F**		**Sector G**		**Sector H**	
Cl^-	250,000	3.0E-09	1,000	7.6E-08	1,000	7.3E-08	1,000	2.0E-17	1,000
F^-	4,000	6.6E-09	1,000	4.6E-08	1,000	4.1E-08	1,000	1.1E-18	1,000
NO_3	10,000	1.5E-02	1,000	2.5E-02	1,000	1.7E-02	1,000	5.9E-13	1,000
NO_2	10,000	1.2E-03	1,000	1.1E-03	1,000	6.9E-04	1,000	4.2E-15	1,000
PO_4	N/A	9.6E-05	1,000	6.9E-05	1,000	4.3E-05	1,000	4.2E-16	1,000
SO_4	250,000	4.2E-04	1,000	5.1E-04	1,000	3.1E-04	1,000	1.3E-15	1,000
Al	200	<1E-20	1,000	<1E-20	1,000	<1E-20	1,000	<1E-20	1,000
Ag	100	<1E-20	1,000	<1E-20	1,000	<1E-20	1,000	<1E-20	1,000
As	10	<1E-20	1,000	<1E-20	1,000	<1E-20	1,000	<1E-20	1,000
B	N/A	1.5E-06	1,000	7.6E-06	1,000	4.8E-06	1,000	4.2E-17	1,000
Ba	2,000	<1E-20	1,000	<1E-20	1,000	<1E-20	1,000	<1E-20	1,000
Cd	5	<1E-20	1,000	<1E-20	1,000	<1E-20	1,000	<1E-20	1,000
Co	N/A	<1E-20	1,000	<1E-20	1,000	<1E-20	1,000	<1E-20	1,000
Cr	100	<1E-20	1,000	<1E-20	1,000	<1E-20	1,000	<1E-20	1,000
Cu	1,300	<1E-20	1,000	<1E-20	1,000	<1E-20	1,000	<1E-20	1,000
Fe	300	<1E-20	1,000	<1E-20	1,000	<1E-20	1,000	<1E-20	1,000
Hg	2	<1E-20	1,000	<1E-20	1,000	<1E-20	1,000	<1E-20	1,000
I	N/A	3.2E-13	1,000	3.8E-11	1,000	3.4E-11	1,000	<1E-20	1,000
Mn	50	<1E-20	1,000	<1E-20	1,000	<1E-20	1,000	<1E-20	1,000
Mo	N/A	<1E-20	1,000	<1E-20	1,000	<1E-20	1,000	<1E-20	1,000
Ni	N/A	<1E-20	1,000	<1E-20	1,000	<1E-20	1,000	<1E-20	1,000
Pb	15	<1E-20	1,000	<1E-20	1,000	<1E-20	1,000	<1E-20	1,000
Se	50	<1E-20	1,000	<1E-20	1,000	<1E-20	1,000	<1E-20	1,000
Sb	6	<1E-20	1,000	<1E-20	1,000	<1E-20	1,000	<1E-20	1,000
Sr	N/A	<1E-20	1,000	<1E-20	1,000	<1E-20	1,000	<1E-20	1,000
U	30	<1E-20	1,000	<1E-20	1,000	<1E-20	1,000	<1E-20	1,000
Zn	5,000	<1E-20	1,000	<1E-20	1,000	<1E-20	1,000	<1E-20	1,000

Table 5.2-10: Radiological Peak Concentrations along the 100-Meter Boundary for UAZ, Sectors A through D in 10,000 Years

Radionuclide	MCL (pCi/L)	Sector A		Sector B		Sector C		Sector D	
		Conc. (pCi/L)	Year of Peak	Conc. (pCi/L)	Year of Peak	Conc. (pCi/L)	Year of Peak	Conc. (pCi/L)	Year of Peak
Ac-227	N/A	<1E-20	10,000	<1E-20	10,000	9.0E-20	10,000	4.7E-19	10,000
Al-26	N/A	<1E-20	10,000	<1E-20	10,000	<1E-20	10,000	<1E-20	10,000
Am-241	Total α	<1E-20	10,000	<1E-20	10,000	<1E-20	10,000	<1E-20	10,000
Am-242m	Total α	<1E-20	10,000	<1E-20	8,540	<1E-20	8,910	<1E-20	9,180
Am-243	Total α	<1E-20	10,000	<1E-20	10,000	<1E-20	10,000	<1E-20	10,000
C-14	2,000	<1E-20	10,000	<1E-20	10,000	<1E-20	10,000	<1E-20	10,000
Cf-249	Total α	<1E-20	10,000	<1E-20	9,870	<1E-20	10,000	<1E-20	10,000
Cf-251	Total α	<1E-20	10,000	<1E-20	10,000	<1E-20	10,000	<1E-20	10,000
Cl-36	700	6.8E-02	10,000	1.8E-01	9,990	1.3E-01	9,990	1.9E-01	6,860
Cm-243	Total α	<1E-20	2,520	<1E-20	1,730	<1E-20	1,820	<1E-20	1,860
Cm-244	Total α	<1E-20	1,570	<1E-20	1,230	<1E-20	1,250	<1E-20	1,270
Cm-245	Total α	<1E-20	10,000	<1E-20	10,000	<1E-20	10,000	<1E-20	10,000
Cm-247	Total α	<1E-20	10,000	<1E-20	10,000	<1E-20	10,000	<1E-20	10,000
Co-60	100	<1E-20	460	<1E-20	350	<1E-20	350	<1E-20	330
Cs-135	900	5.8E-09	10,000	1.6E-08	10,000	5.3E-05	10,000	1.1E-04	10,000
Cs-137	200	<1E-20	1,570	<1E-20	1,340	<1E-20	1,260	<1E-20	1,320
Eu-152	200	<1E-20	1,180	<1E-20	950	<1E-20	960	<1E-20	970
Eu-154	60	<1E-20	730	<1E-20	630	<1E-20	620	<1E-20	630
H-3	20,000	2.4E-11	210	6.4E-11	210	4.2E-08	150	9.4E-08	150
I-129	1	4.3E-01	10,000	1.1E+00	10,000	8.4E-01	10,000	1.5E+00	9,990
K-40	N/A	5.3E-06	10,000	1.4E-05	10,000	9.4E-04	10,000	2.0E-03	10,000
Nb-93m	1,000	<1E-20	10,000	<1E-20	9,360	<1E-20	10,000	<1E-20	10,000
Nb-94	N/A	<1E-20	10,000	<1E-20	9,340	<1E-20	10,000	<1E-20	10,000
Ni-63	50	<1E-20	5,680	<1E-20	4,220	<1E-20	4,120	<1E-20	4,870
Np-237	Total α	1.8E-16	10,000	4.5E-16	10,000	1.1E-14	10,000	2.2E-14	10,000
Pa-231	Total α	2.4E-19	10,000	6.0E-19	10,000	2.8E-17	10,000	1.5E-16	10,000
Pb-210	N/A	<1E-20	10,000	<1E-20	10,000	<1E-20	10,000	<1E-20	10,000
Pt-193	3,000	<1E-20	1,770	<1E-20	1,660	<1E-20	1,550	<1E-20	1,520
Pu-238	Total α	<1E-20	10,000	<1E-20	7,230	<1E-20	7,480	<1E-20	7,660
Pu-239	Total α	<1E-20	10,000	<1E-20	10,000	<1E-20	10,000	<1E-20	10,000
Pu-240	Total α	<1E-20	10,000	<1E-20	10,000	<1E-20	10,000	<1E-20	10,000
Pu-241	300	<1E-20	10,000	<1E-20	10,000	<1E-20	10,000	<1E-20	10,000
Pu-242	Total α	<1E-20	10,000	<1E-20	10,000	<1E-20	10,000	<1E-20	10,000
Pu-244	Total α	<1E-20	10,000	<1E-20	10,000	<1E-20	10,000	<1E-20	10,000
Ra-226	Total α /Ra	<1E-20	10,000	<1E-20	10,000	<1E-20	10,000	<1E-20	10,000
Ra-228	Total Ra	<1E-20	9,680	<1E-20	10,000	<1E-20	10,000	<1E-20	10,000
Rn-222	N/A	<1E-20	10,000	<1E-20	10,000	<1E-20	10,000	<1E-20	10,000
Se-79	N/A	<1E-20	10,000	<1E-20	10,000	<1E-20	10,000	<1E-20	10,000
Sm-151	1,000	<1E-20	9,210	<1E-20	7,500	<1E-20	6,730	<1E-20	6,900
Sn-126	N/A	<1E-20	10,000	<1E-20	10,000	<1E-20	10,000	<1E-20	10,000
Sr-90	8	<1E-20	1,160	<1E-20	1,190	<1E-20	1,520	<1E-20	790
Tc-99	900	6.6E+01	9,960	1.7E+02	9,650	1.5E+02	10,000	2.2E+02	5,790
Th-229	Total α	<1E-20	10,000	<1E-20	10,000	6.0E-20	10,000	1.2E-19	10,000
Th-230	Total α	<1E-20	9,810	<1E-20	10,000	<1E-20	10,000	<1E-20	10,000
Th-232	Total α	<1E-20	9,800	<1E-20	10,000	<1E-20	10,000	<1E-20	10,000
U-232	Total U	<1E-20	6,590	<1E-20	6,450	<1E-20	5,230	<1E-20	5,340
U-233	Total U	<1E-20	10,000	2.5E-20	10,000	1.2E-18	10,000	2.6E-18	10,000
U-234	Total U	<1E-20	9,630	<1E-20	10,000	<1E-20	10,000	<1E-20	10,000
U-235	Total U	<1E-20	9,630	<1E-20	10,000	<1E-20	10,000	<1E-20	10,000
U-236	Total U	<1E-20	9,630	<1E-20	10,000	<1E-20	10,000	<1E-20	10,000
U-238	Total U	<1E-20	9,630	<1E-20	10,000	<1E-20	10,000	<1E-20	10,000
Zr-93	2,000	<1E-20	10,000	<1E-20	9,360	<1E-20	10,000	<1E-20	10,000
Total Alpha	15	1.8E-16	10,000	4.5E-16	10,000	1.1E-14	10,000	2.2E-14	10,000
Total Ra	5	<1E-20	10,000	<1E-20	10,000	<1E-20	10,000	<1E-20	10,000
Sum of Beta-Gamma MCL Fractions		5.1E-01	10,000	1.3E+00	10,000	1.0E+00	10,000	1.7E+00	9,990

Table 5.2-11: Radiological Peak Concentrations along the 100-Meter Boundary for UAZ, Sectors E through H in 10,000 Years

Radionuclide	MCL (pCi/L)	Sector E		Sector F		Sector G		Sector H	
		Conc. (pCi/L)	Year of Peak	Conc. (pCi/L)	Year of Peak	Conc. (pCi/L)	Year of Peak	Conc. (pCi/L)	Year of Peak
Ac-227	N/A	1.2E-15	10,000	1.7E-13	10,000	2.6E-13	10,000	1.2E-16	10,000
Al-26	N/A	<1E-20	10,000	<1E-20	10,000	<1E-20	10,000	<1E-20	10,000
Am-241	Total α	<1E-20	10,000	<1E-20	10,000	<1E-20	10,000	<1E-20	10,000
Am-242m	Total α	<1E-20	8,660	<1E-20	5,910	<1E-20	4,580	<1E-20	4,950
Am-243	Total α	<1E-20	10,000	<1E-20	10,000	<1E-20	10,000	<1E-20	10,000
C-14	2,000	<1E-20	10,000	1.6E-19	10,000	2.8E-19	10,000	<1E-20	10,000
Cf-249	Total α	<1E-20	10,000	<1E-20	10,000	<1E-20	9,990	<1E-20	10,000
Cf-251	Total α	<1E-20	10,000	<1E-20	10,000	<1E-20	10,000	<1E-20	10,000
Cl-36	700	1.4E-01	9,980	7.3E-03	10,000	9.9E-03	10,000	2.9E-08	10,000
Cm-243	Total α	<1E-20	2,000	<1E-20	1,380	<1E-20	1,050	<1E-20	1,080
Cm-244	Total α	<1E-20	1,260	<1E-20	870	<1E-20	670	<1E-20	550
Cm-245	Total α	<1E-20	10,000	<1E-20	10,000	<1E-20	10,000	<1E-20	10,000
Cm-247	Total α	<1E-20	10,000	<1E-20	10,000	<1E-20	10,000	<1E-20	10,000
Co-60	100	<1E-20	330	<1E-20	220	<1E-20	170	<1E-20	200
Cs-135	900	1.2E-08	10,000	1.9E-07	10,000	3.3E-07	10,000	2.8E-11	10,000
Cs-137	200	<1E-20	910	<1E-20	760	<1E-20	690	<1E-20	860
Eu-152	200	<1E-20	950	<1E-20	660	<1E-20	510	<1E-20	450
Eu-154	60	<1E-20	610	<1E-20	420	<1E-20	330	<1E-20	290
H-3	20,000	4.8E-11	210	8.7E-10	160	1.6E-09	150	3.7E-12	170
I-129	1	9.0E-01	10,000	9.5E-02	10,000	1.4E-01	9,950	1.8E-02	9,990
K-40	N/A	1.1E-05	10,000	5.5E-07	10,000	5.2E-07	10,000	1.0E-12	10,000
Nb-93m	1,000	<1E-20	10,000	<1E-20	10,000	<1E-20	10,000	<1E-20	10,000
Nb-94	N/A	<1E-20	10,000	<1E-20	10,000	<1E-20	10,000	<1E-20	10,000
Ni-63	50	<1E-20	2,220	<1E-20	2,040	<1E-20	1,970	<1E-20	2,060
Np-237	Total α	1.5E-11	10,000	2.2E-09	10,000	3.3E-09	10,000	4.1E-13	10,000
Pa-231	Total α	3.8E-13	10,000	5.4E-11	10,000	8.3E-11	10,000	3.7E-14	10,000
Pb-210	N/A	<1E-20	10,000	<1E-20	10,000	<1E-20	10,000	<1E-20	10,000
Pt-193	3,000	<1E-20	1,180	<1E-20	1,040	<1E-20	980	<1E-20	1,120
Pu-238	Total α	<1E-20	5,410	<1E-20	3,680	<1E-20	2,830	<1E-20	3,130
Pu-239	Total α	<1E-20	10,000	<1E-20	10,000	<1E-20	10,000	<1E-20	10,000
Pu-240	Total α	<1E-20	10,000	<1E-20	10,000	<1E-20	10,000	<1E-20	10,000
Pu-241	300	<1E-20	10,000	<1E-20	10,000	<1E-20	10,000	<1E-20	10,000
Pu-242	Total α	<1E-20	10,000	<1E-20	10,000	<1E-20	10,000	<1E-20	10,000
Pu-244	Total α	<1E-20	10,000	<1E-20	10,000	<1E-20	10,000	<1E-20	10,000
Ra-226	Total α /Ra	<1E-20	10,000	<1E-20	10,000	<1E-20	10,000	<1E-20	10,000
Ra-228	Total Ra	<1E-20	10,000	<1E-20	10,000	<1E-20	10,000	<1E-20	10,000
Rn-222	N/A	<1E-20	10,000	<1E-20	10,000	<1E-20	10,000	<1E-20	10,000
Se-79	N/A	<1E-20	10,000	<1E-20	10,000	<1E-20	10,000	<1E-20	10,000
Sm-151	1,000	<1E-20	5,820	<1E-20	3,950	<1E-20	3,010	<1E-20	4,060
Sn-126	N/A	<1E-20	10,000	<1E-20	10,000	<1E-20	10,000	<1E-20	10,000
Sr-90	8	<1E-20	720	<1E-20	630	<1E-20	590	<1E-20	680
Tc-99	900	1.4E+02	9,630	4.5E+01	7,850	6.8E+01	8,420	4.9E+00	9,990
Th-229	Total α	2.8E-17	10,000	4.1E-15	10,000	6.3E-15	10,000	6.0E-19	10,000
Th-230	Total α	<1E-20	10,000	<1E-20	10,000	<1E-20	10,000	<1E-20	10,000
Th-232	Total α	<1E-20	10,000	<1E-20	10,000	<1E-20	10,000	<1E-20	10,000
U-232	Total U	<1E-20	3,850	<1E-20	2,670	<1E-20	2,080	<1E-20	2,330
U-233	Total U	9.0E-16	10,000	1.3E-13	10,000	2.0E-13	10,000	2.1E-17	10,000
U-234	Total U	<1E-20	10,000	<1E-20	10,000	<1E-20	10,000	<1E-20	10,000
U-235	Total U	<1E-20	10,000	<1E-20	10,000	<1E-20	10,000	<1E-20	10,000
U-236	Total U	<1E-20	10,000	<1E-20	10,000	<1E-20	10,000	<1E-20	10,000
U-238	Total U	<1E-20	10,000	<1E-20	10,000	<1E-20	10,000	<1E-20	10,000
Zr-93	2,000	<1E-20	10,000	<1E-20	10,000	<1E-20	10,000	<1E-20	10,000
Total Alpha	15	1.5E-11	10,000	2.2E-09	10,000	3.4E-09	10,000	4.5E-13	10,000
Total Ra	5	<1E-20	10,000	<1E-20	10,000	<1E-20	10,000	<1E-20	10,000
Sum of Beta-Gamma MCL Fractions		1.1E+00	10,000	1.4E-01	10,000	2.2E-01	10,000	2.4E-02	10,000

Table 5.2-12: Radiological Peak Concentrations along the 100-Meter Boundary for LAZ, Sectors A through D in 10,000 Years

Radionuclide	MCL (pCi/L)	Sector A		Sector B		Sector C		Sector D	
		Conc. (pCi/L)	Year of Peak	Conc. (pCi/L)	Year of Peak	Conc. (pCi/L)	Year of Peak	Conc. (pCi/L)	Year of Peak
Ac-227	N/A	<1E-20	10,000	<1E-20	10,000	1.6E-19	10,000	4.2E-19	10,000
Al-26	N/A	<1E-20	10,000	<1E-20	10,000	<1E-20	10,000	<1E-20	10,000
Am-241	Total α	<1E-20	10,000	<1E-20	10,000	<1E-20	10,000	<1E-20	10,000
Am-242m	Total α	<1E-20	9,510	<1E-20	10,000	<1E-20	9,440	<1E-20	9,750
Am-243	Total α	<1E-20	10,000	<1E-20	10,000	<1E-20	10,000	<1E-20	10,000
C-14	2,000	<1E-20	10,000	<1E-20	10,000	<1E-20	10,000	<1E-20	10,000
Cf-249	Total α	<1E-20	10,000	<1E-20	10,000	<1E-20	10,000	<1E-20	10,000
Cf-251	Total α	<1E-20	10,000	<1E-20	10,000	<1E-20	10,000	<1E-20	10,000
Cl-36	700	3.4E-01	10,000	3.4E-01	10,000	2.8E-01	10,000	3.0E-01	9,160
Cm-243	Total α	<1E-20	2,740	<1E-20	1,850	<1E-20	1,970	<1E-20	2,050
Cm-244	Total α	<1E-20	1,630	<1E-20	1,290	<1E-20	1,330	<1E-20	1,390
Cm-245	Total α	<1E-20	10,000	<1E-20	10,000	<1E-20	10,000	<1E-20	10,000
Cm-247	Total α	<1E-20	10,000	<1E-20	10,000	<1E-20	10,000	<1E-20	10,000
Co-60	100	<1E-20	570	<1E-20	400	<1E-20	370	<1E-20	490
Cs-135	900	2.0E-08	10,000	2.1E-08	10,000	8.3E-05	10,000	1.4E-04	10,000
Cs-137	200	<1E-20	1,620	<1E-20	1,330	<1E-20	1,290	<1E-20	1,350
Eu-152	200	<1E-20	1,230	<1E-20	990	<1E-20	1,010	<1E-20	1,060
Eu-154	60	<1E-20	780	<1E-20	650	<1E-20	650	<1E-20	690
H-3	20,000	9.0E-11	220	9.4E-11	220	6.2E-08	160	1.1E-07	160
I-129	1	2.1E+00	10,000	2.2E+00	10,000	1.7E+00	10,000	2.3E+00	10,000
K-40	N/A	2.3E-05	10,000	2.4E-05	10,000	1.7E-03	10,000	2.8E-03	10,000
Nb-93m	1,000	<1E-20	10,000	<1E-20	10,000	<1E-20	10,000	<1E-20	10,000
Nb-94	N/A	<1E-20	10,000	<1E-20	10,000	<1E-20	10,000	<1E-20	10,000
Ni-63	50	<1E-20	3,000	<1E-20	4,210	<1E-20	4,140	<1E-20	4,900
Np-237	Total α	8.2E-16	10,000	8.4E-16	10,000	2.0E-14	10,000	3.2E-14	10,000
Pa-231	Total α	1.1E-18	10,000	1.1E-18	10,000	5.2E-17	10,000	1.3E-16	10,000
Pb-210	N/A	<1E-20	10,000	<1E-20	10,000	<1E-20	10,000	<1E-20	10,000
Pt-193	3,000	<1E-20	1,710	<1E-20	1,750	<1E-20	1,610	<1E-20	1,550
Pu-238	Total α	<1E-20	10,000	<1E-20	8,270	<1E-20	7,820	<1E-20	8,030
Pu-239	Total α	<1E-20	10,000	<1E-20	10,000	<1E-20	10,000	<1E-20	10,000
Pu-240	Total α	<1E-20	10,000	<1E-20	10,000	<1E-20	10,000	<1E-20	10,000
Pu-241	300	<1E-20	10,000	<1E-20	10,000	<1E-20	10,000	<1E-20	10,000
Pu-242	Total α	<1E-20	10,000	<1E-20	10,000	<1E-20	10,000	<1E-20	10,000
Pu-244	Total α	<1E-20	10,000	<1E-20	10,000	<1E-20	10,000	<1E-20	10,000
Ra-226	Total α /Ra	<1E-20	10,000	<1E-20	10,000	<1E-20	10,000	<1E-20	10,000
Ra-228	Total Ra	<1E-20	10,000	<1E-20	10,000	<1E-20	10,000	<1E-20	10,000
Rn-222	N/A	<1E-20	10,000	<1E-20	10,000	<1E-20	10,000	<1E-20	10,000
Se-79	N/A	<1E-20	10,000	<1E-20	10,000	<1E-20	10,000	<1E-20	10,000
Sm-151	1,000	<1E-20	8,560	<1E-20	7,480	<1E-20	7,100	<1E-20	7,310
Sn-126	N/A	<1E-20	10,000	<1E-20	10,000	<1E-20	10,000	<1E-20	10,000
Sr-90	8	<1E-20	1,060	<1E-20	1,090	<1E-20	1,540	<1E-20	820
Tc-99	900	3.3E+02	9,660	3.4E+02	9,890	2.9E+02	9,920	3.5E+02	5,900
Th-229	Total α	<1E-20	10,000	<1E-20	10,000	1.1E-19	10,000	1.8E-19	10,000
Th-230	Total α	<1E-20	10,000	<1E-20	10,000	<1E-20	10,000	<1E-20	10,000
Th-232	Total α	<1E-20	10,000	<1E-20	10,000	<1E-20	10,000	<1E-20	10,000
U-232	Total U	<1E-20	7,280	<1E-20	5,750	<1E-20	5,450	<1E-20	5,570
U-233	Total U	4.6E-20	10,000	4.7E-20	10,000	2.3E-18	10,000	3.7E-18	10,000
U-234	Total U	<1E-20	10,000	<1E-20	10,000	<1E-20	10,000	<1E-20	10,000
U-235	Total U	<1E-20	10,000	<1E-20	10,000	<1E-20	10,000	<1E-20	10,000
U-236	Total U	<1E-20	10,000	<1E-20	10,000	<1E-20	10,000	<1E-20	10,000
U-238	Total U	<1E-20	10,000	<1E-20	10,000	<1E-20	10,000	<1E-20	10,000
Zr-93	2,000	<1E-20	10,000	<1E-20	10,000	<1E-20	10,000	<1E-20	10,000
Total Alpha	15	8.2E-16	10,000	8.5E-16	10,000	2.0E-14	10,000	3.2E-14	10,000
Total Ra	5	<1E-20	10,000	<1E-20	10,000	<1E-20	10,000	<1E-20	10,000
Sum of Beta-Gamma MCL Fractions		2.5E+00	10,000	2.6E+00	10,000	2.1E+00	10,000	2.6E+00	10,000

Table 5.2-13: Radiological Peak Concentrations along the 100-Meter Boundary for LAZ, Sectors E through H in 10,000 Years

Radionuclide	MCL (pCi/L)	Sector E		Sector F		Sector G		Sector H	
		Conc. (pCi/L)	Year of Peak	Conc. (pCi/L)	Year of Peak	Conc. (pCi/L)	Year of Peak	Conc. (pCi/L)	Year of Peak
Ac-227	N/A	5.2E-16	10,000	4.5E-13	10,000	5.1E-13	10,000	1.1E-16	10,000
Al-26	N/A	<1E-20	10,000	<1E-20	10,000	<1E-20	10,000	<1E-20	10,000
Am-241	Total α	<1E-20	10,000	<1E-20	10,000	<1E-20	10,000	<1E-20	10,000
Am-242m	Total α	<1E-20	9,090	<1E-20	6,410	<1E-20	5,000	<1E-20	4,720
Am-243	Total α	<1E-20	10,000	<1E-20	10,000	<1E-20	10,000	<1E-20	10,000
C-14	2,000	<1E-20	10,000	3.6E-19	10,000	4.5E-19	10,000	<1E-20	10,000
Cf-249	Total α	<1E-20	10,000	<1E-20	10,000	<1E-20	10,000	<1E-20	7,970
Cf-251	Total α	<1E-20	10,000	<1E-20	10,000	<1E-20	10,000	<1E-20	8,800
Cl-36	700	2.5E-01	9,990	2.2E-01	9,990	2.0E-02	10,000	2.1E-08	10,000
Cm-243	Total α	<1E-20	2,100	<1E-20	1,470	<1E-20	1,110	<1E-20	1,010
Cm-244	Total α	<1E-20	1,320	<1E-20	920	<1E-20	700	<1E-20	640
Cm-245	Total α	<1E-20	10,000	<1E-20	10,000	<1E-20	10,000	<1E-20	10,000
Cm-247	Total α	<1E-20	10,000	<1E-20	10,000	<1E-20	10,000	<1E-20	10,000
Co-60	100	<1E-20	350	<1E-20	240	<1E-20	190	<1E-20	190
Cs-135	900	5.2E-07	10,000	4.3E-07	10,000	5.4E-07	10,000	2.3E-11	10,000
Cs-137	200	<1E-20	970	<1E-20	840	<1E-20	750	<1E-20	930
Eu-152	200	<1E-20	990	<1E-20	690	<1E-20	530	<1E-20	490
Eu-154	60	<1E-20	640	<1E-20	440	<1E-20	340	<1E-20	330
H-3	20,000	3.3E-10	160	1.9E-09	160	2.4E-09	160	3.0E-12	180
I-129	1	1.6E+00	10,000	1.4E+00	9,990	3.5E-01	10,000	1.7E-02	9,990
K-40	N/A	1.7E-05	10,000	1.5E-05	10,000	9.6E-07	10,000	6.5E-13	10,000
Nb-93m	1,000	<1E-20	10,000	<1E-20	10,000	<1E-20	10,000	<1E-20	10,000
Nb-94	N/A	<1E-20	10,000	<1E-20	10,000	<1E-20	10,000	<1E-20	10,000
Ni-63	50	<1E-20	2,310	<1E-20	2,150	<1E-20	2,070	<1E-20	2,120
Np-237	Total α	6.6E-12	10,000	5.7E-09	10,000	6.4E-09	10,000	3.8E-13	10,000
Pa-231	Total α	1.6E-13	10,000	1.4E-10	10,000	1.6E-10	10,000	3.4E-14	10,000
Pb-210	N/A	<1E-20	10,000	<1E-20	10,000	<1E-20	10,000	<1E-20	10,000
Pt-193	3,000	<1E-20	1,260	<1E-20	1,130	<1E-20	1,050	<1E-20	1,180
Pu-238	Total α	<1E-20	5,700	<1E-20	3,980	<1E-20	3,110	<1E-20	2,970
Pu-239	Total α	<1E-20	10,000	<1E-20	10,000	<1E-20	10,000	<1E-20	10,000
Pu-240	Total α	<1E-20	10,000	<1E-20	10,000	<1E-20	10,000	<1E-20	10,000
Pu-241	300	<1E-20	10,000	<1E-20	10,000	<1E-20	10,000	<1E-20	10,000
Pu-242	Total α	<1E-20	10,000	<1E-20	10,000	<1E-20	10,000	<1E-20	10,000
Pu-244	Total α	<1E-20	10,000	<1E-20	10,000	<1E-20	10,000	<1E-20	10,000
Ra-226	Total α /Ra	<1E-20	10,000	<1E-20	10,000	<1E-20	10,000	<1E-20	10,000
Ra-228	Total Ra	<1E-20	10,000	<1E-20	10,000	<1E-20	10,000	<1E-20	10,000
Rn-222	N/A	<1E-20	10,000	<1E-20	10,000	<1E-20	10,000	<1E-20	10,000
Se-79	N/A	<1E-20	10,000	<1E-20	10,000	<1E-20	10,000	<1E-20	10,000
Sm-151	1,000	<1E-20	6,110	<1E-20	4,260	<1E-20	3,290	<1E-20	3,740
Sn-126	N/A	<1E-20	10,000	<1E-20	10,000	<1E-20	10,000	<1E-20	10,000
Sr-90	8	<1E-20	770	<1E-20	690	<1E-20	630	<1E-20	720
Tc-99	900	2.5E+02	9,720	2.1E+02	9,660	1.5E+02	9,970	4.7E+00	9,990
Th-229	Total α	1.2E-17	10,000	1.1E-14	10,000	1.2E-14	10,000	5.5E-19	10,000
Th-230	Total α	<1E-20	10,000	<1E-20	10,000	<1E-20	10,000	<1E-20	10,000
Th-232	Total α	<1E-20	10,000	<1E-20	10,000	<1E-20	10,000	<1E-20	10,000
U-232	Total U	<1E-20	4,070	<1E-20	2,900	<1E-20	2,300	<1E-20	1,830
U-233	Total U	3.9E-16	10,000	3.4E-13	10,000	3.9E-13	10,000	2.0E-17	10,000
U-234	Total U	<1E-20	10,000	<1E-20	10,000	<1E-20	10,000	<1E-20	10,000
U-235	Total U	<1E-20	10,000	<1E-20	10,000	<1E-20	10,000	<1E-20	10,000
U-236	Total U	<1E-20	10,000	<1E-20	10,000	<1E-20	10,000	<1E-20	10,000
U-238	Total U	<1E-20	10,000	<1E-20	10,000	<1E-20	10,000	<1E-20	10,000
Zr-93	2,000	<1E-20	10,000	<1E-20	10,000	<1E-20	10,000	<1E-20	10,000
Total Alpha	15	6.7E-12	10,000	5.9E-09	10,000	6.6E-09	10,000	4.1E-13	10,000
Total Ra	5	<1E-20	10,000	<1E-20	10,000	<1E-20	10,000	<1E-20	10,000
Sum of Beta-Gamma MCL Fractions		1.9E+00	10,000	1.6E+00	10,000	5.2E-01	10,000	2.3E-02	10,000

Table 5.2-14: Radiological Peak Concentrations along the 100-Meter Boundary for GAU, Sectors A through D in 10,000 Years

Radionuclide	MCL (pCi/L)	Sector A		Sector B		Sector C		Sector D	
		Conc. (pCi/L)	Year of Peak	Conc. (pCi/L)	Year of Peak	Conc. (pCi/L)	Year of Peak	Conc. (pCi/L)	Year of Peak
Ac-227	N/A	8.5E-19	10,000	4.4E-18	10,000	<1E-20	10,000	<1E-20	10,000
Al-26	N/A	<1E-20	10,000	<1E-20	10,000	<1E-20	10,000	<1E-20	10,000
Am-241	Total α	<1E-20	10,000	<1E-20	10,000	<1E-20	10,000	<1E-20	10,000
Am-242m	Total α	<1E-20	10,000	<1E-20	10,000	<1E-20	10,000	<1E-20	7,940
Am-243	Total α	<1E-20	10,000	<1E-20	10,000	<1E-20	10,000	<1E-20	10,000
C-14	2,000	<1E-20	10,000	<1E-20	10,000	<1E-20	10,000	<1E-20	10,000
Cf-249	Total α	<1E-20	10,000	<1E-20	10,000	<1E-20	9,940	<1E-20	10,000
Cf-251	Total α	<1E-20	10,000	<1E-20	10,000	<1E-20	9,980	<1E-20	10,000
Cl-36	700	1.3E-03	10,000	2.6E-03	10,000	2.4E-03	10,000	7.4E-04	10,000
Cm-243	Total α	<1E-20	3,470	<1E-20	2,180	<1E-20	2,140	<1E-20	2,530
Cm-244	Total α	<1E-20	2,230	<1E-20	1,610	<1E-20	1,600	<1E-20	1,690
Cm-245	Total α	<1E-20	10,000	<1E-20	10,000	<1E-20	10,000	<1E-20	10,000
Cm-247	Total α	<1E-20	10,000	<1E-20	10,000	<1E-20	10,000	<1E-20	10,000
Co-60	100	<1E-20	490	<1E-20	640	<1E-20	450	<1E-20	430
Cs-135	900	8.1E-13	10,000	4.8E-11	10,000	3.3E-09	10,000	1.9E-09	10,000
Cs-137	200	<1E-20	1,280	<1E-20	1,300	<1E-20	1,510	<1E-20	1,600
Eu-152	200	<1E-20	1,690	<1E-20	1,240	<1E-20	1,240	<1E-20	1,290
Eu-154	60	<1E-20	1,100	<1E-20	810	<1E-20	810	<1E-20	830
H-3	20,000	4.5E-14	240	1.6E-13	180	1.3E-11	180	7.3E-12	180
I-129	1	8.9E-03	10,000	1.8E-02	10,000	1.7E-02	10,000	5.8E-03	10,000
K-40	N/A	4.9E-09	10,000	7.3E-09	10,000	3.7E-07	10,000	2.0E-07	10,000
Nb-93m	1,000	<1E-20	10,000	<1E-20	10,000	<1E-20	10,000	<1E-20	10,000
Nb-94	N/A	<1E-20	10,000	<1E-20	10,000	<1E-20	10,000	<1E-20	10,000
Ni-63	50	<1E-20	2,720	<1E-20	2,760	<1E-20	4,580	<1E-20	5,370
Np-237	Total α	1.2E-14	10,000	6.5E-14	10,000	7.5E-17	10,000	1.4E-17	10,000
Pa-231	Total α	2.7E-16	10,000	1.4E-15	10,000	2.0E-18	10,000	1.2E-19	10,000
Pb-210	N/A	<1E-20	10,000	<1E-20	10,000	<1E-20	10,000	<1E-20	5,430
Pt-193	3,000	<1E-20	1,560	<1E-20	1,580	<1E-20	1,710	<1E-20	2,020
Pu-238	Total α	<1E-20	7,940	<1E-20	8,540	<1E-20	9,150	<1E-20	8,300
Pu-239	Total α	<1E-20	10,000	<1E-20	10,000	<1E-20	10,000	<1E-20	10,000
Pu-240	Total α	<1E-20	10,000	<1E-20	10,000	<1E-20	10,000	<1E-20	10,000
Pu-241	300	<1E-20	10,000	<1E-20	10,000	<1E-20	10,000	<1E-20	10,000
Pu-242	Total α	<1E-20	10,000	<1E-20	10,000	<1E-20	10,000	<1E-20	10,000
Pu-244	Total α	<1E-20	10,000	<1E-20	10,000	<1E-20	10,000	<1E-20	10,000
Ra-226	Total α /Ra	<1E-20	10,000	<1E-20	10,000	<1E-20	10,000	<1E-20	5,400
Ra-228	Total Ra	<1E-20	10,000	<1E-20	10,000	<1E-20	10,000	<1E-20	10,000
Rn-222	N/A	<1E-20	10,000	<1E-20	10,000	<1E-20	10,000	<1E-20	5,400
Se-79	N/A	<1E-20	10,000	<1E-20	10,000	<1E-20	10,000	<1E-20	9,830
Sm-151	1,000	<1E-20	8,910	<1E-20	8,320	<1E-20	8,430	<1E-20	7,640
Sn-126	N/A	<1E-20	10,000	<1E-20	10,000	<1E-20	10,000	<1E-20	10,000
Sr-90	8	<1E-20	970	<1E-20	980	<1E-20	700	<1E-20	1,130
Tc-99	900	1.5E+00	9,740	3.2E+00	9,970	3.0E+00	10,000	1.0E+00	9,330
Th-229	Total α	1.6E-20	10,000	8.5E-20	10,000	<1E-20	10,000	<1E-20	10,000
Th-230	Total α	<1E-20	10,000	<1E-20	10,000	<1E-20	10,000	<1E-20	10,000
Th-232	Total α	<1E-20	10,000	<1E-20	10,000	<1E-20	10,000	<1E-20	10,000
U-232	Total U	<1E-20	6,960	<1E-20	6,980	<1E-20	6,350	<1E-20	4,910
U-233	Total U	5.9E-19	10,000	3.2E-18	10,000	<1E-20	10,000	<1E-20	10,000
U-234	Total U	<1E-20	10,000	<1E-20	10,000	<1E-20	10,000	<1E-20	10,000
U-235	Total U	<1E-20	10,000	<1E-20	10,000	<1E-20	10,000	<1E-20	10,000
U-236	Total U	<1E-20	10,000	<1E-20	10,000	<1E-20	10,000	<1E-20	10,000
U-238	Total U	<1E-20	10,000	<1E-20	10,000	<1E-20	10,000	<1E-20	10,000
Zr-93	2,000	<1E-20	10,000	<1E-20	10,000	<1E-20	10,000	<1E-20	10,000
Total Alpha	15	1.2E-14	10,000	6.7E-14	10,000	7.7E-17	10,000	1.4E-17	10,000
Total Ra	5	<1E-20	10,000	<1E-20	10,000	<1E-20	10,000	<1E-20	5,400
Sum of Beta-Gamma MCL Fractions		1.0E-02	10,000	2.2E-02	10,000	2.1E-02	10,000	7.0E-03	10,000

Table 5.2-15: Radiological Peak Concentrations along the 100-Meter Boundary for GAU, Sectors E through H in 10,000 Years

Radionuclide	MCL (pCi/L)	Sector E		Sector F		Sector G		Sector H	
		Conc. (pCi/L)	Year of Peak	Conc. (pCi/L)	Year of Peak	Conc. (pCi/L)	Year of Peak	Conc. (pCi/L)	Year of Peak
Ac-227	N/A	1.2E-20	10,000	8.7E-18	10,000	6.3E-18	10,000	<1E-20	10,000
Al-26	N/A	<1E-20	10,000	<1E-20	10,000	<1E-20	10,000	<1E-20	10,000
Am-241	Total α	<1E-20	10,000	<1E-20	10,000	<1E-20	10,000	<1E-20	10,000
Am-242m	Total α	<1E-20	10,000	<1E-20	8,800	<1E-20	8,110	<1E-20	7,390
Am-243	Total α	<1E-20	10,000	<1E-20	10,000	<1E-20	10,000	<1E-20	10,000
C-14	2,000	<1E-20	10,000	<1E-20	10,000	<1E-20	10,000	<1E-20	10,000
Cf-249	Total α	<1E-20	10,000	<1E-20	10,000	<1E-20	10,000	<1E-20	10,000
Cf-251	Total α	<1E-20	10,000	<1E-20	10,000	<1E-20	10,000	<1E-20	10,000
Cl-36	700	6.0E-05	10,000	5.3E-06	10,000	1.3E-06	10,000	<1E-20	10,000
Cm-243	Total α	<1E-20	2,390	<1E-20	1,940	<1E-20	1,520	<1E-20	1,550
Cm-244	Total α	<1E-20	1,660	<1E-20	1,190	<1E-20	950	<1E-20	990
Cm-245	Total α	<1E-20	10,000	<1E-20	10,000	<1E-20	10,000	<1E-20	10,000
Cm-247	Total α	<1E-20	10,000	<1E-20	10,000	<1E-20	10,000	<1E-20	10,000
Co-60	100	<1E-20	420	<1E-20	340	<1E-20	270	<1E-20	290
Cs-135	900	8.6E-15	10,000	3.9E-13	10,000	3.6E-13	10,000	<1E-20	10,000
Cs-137	200	<1E-20	1,170	<1E-20	1,030	<1E-20	1,000	<1E-20	810
Eu-152	200	<1E-20	1,440	<1E-20	900	<1E-20	710	<1E-20	740
Eu-154	60	<1E-20	760	<1E-20	690	<1E-20	450	<1E-20	480
H-3	20,000	1.2E-15	240	1.4E-14	190	1.1E-14	190	<1E-20	220
I-129	1	4.9E-04	10,000	1.6E-04	10,000	1.4E-04	10,000	1.1E-14	9,990
K-40	N/A	1.2E-10	10,000	3.4E-12	10,000	2.2E-12	10,000	<1E-20	10,000
Nb-93m	1,000	<1E-20	10,000	<1E-20	10,000	<1E-20	10,000	<1E-20	10,000
Nb-94	N/A	<1E-20	10,000	<1E-20	10,000	<1E-20	10,000	<1E-20	10,000
Ni-63	50	<1E-20	2,700	<1E-20	2,520	<1E-20	2,490	<1E-20	2,400
Np-237	Total α	1.1E-16	10,000	1.3E-13	10,000	9.4E-14	10,000	<1E-20	10,000
Pa-231	Total α	3.8E-18	10,000	2.8E-15	10,000	2.0E-15	10,000	<1E-20	10,000
Pb-210	N/A	<1E-20	10,000	<1E-20	10,000	<1E-20	10,000	<1E-20	10,000
Pt-193	3,000	<1E-20	1,500	<1E-20	1,360	<1E-20	1,330	<1E-20	820
Pu-238	Total α	<1E-20	6,830	<1E-20	5,490	<1E-20	4,330	<1E-20	4,620
Pu-239	Total α	<1E-20	10,000	<1E-20	10,000	<1E-20	10,000	<1E-20	10,000
Pu-240	Total α	<1E-20	10,000	<1E-20	10,000	<1E-20	10,000	<1E-20	10,000
Pu-241	300	<1E-20	10,000	<1E-20	10,000	<1E-20	10,000	<1E-20	10,000
Pu-242	Total α	<1E-20	10,000	<1E-20	10,000	<1E-20	10,000	<1E-20	10,000
Pu-244	Total α	<1E-20	10,000	<1E-20	10,000	<1E-20	10,000	<1E-20	10,000
Ra-226	Total α /Ra	<1E-20	10,000	<1E-20	10,000	<1E-20	10,000	<1E-20	10,000
Ra-228	Total Ra	<1E-20	10,000	<1E-20	10,000	<1E-20	10,000	<1E-20	10,000
Rn-222	N/A	<1E-20	10,000	<1E-20	10,000	<1E-20	10,000	<1E-20	10,000
Se-79	N/A	<1E-20	10,000	<1E-20	10,000	<1E-20	10,000	<1E-20	10,000
Sm-151	1,000	<1E-20	7,400	<1E-20	5,890	<1E-20	3,600	<1E-20	4,190
Sn-126	N/A	<1E-20	10,000	<1E-20	10,000	<1E-20	10,000	<1E-20	10,000
Sr-90	8	<1E-20	910	<1E-20	830	<1E-20	810	<1E-20	600
Tc-99	900	8.5E-02	10,000	6.2E-02	10,000	5.0E-02	10,000	3.0E-12	10,000
Th-229	Total α	<1E-20	10,000	2.8E-19	10,000	2.1E-19	10,000	<1E-20	10,000
Th-230	Total α	<1E-20	10,000	<1E-20	10,000	<1E-20	10,000	<1E-20	10,000
Th-232	Total α	<1E-20	10,000	<1E-20	10,000	<1E-20	10,000	<1E-20	10,000
U-232	Total U	<1E-20	4,940	<1E-20	4,000	<1E-20	3,670	<1E-20	3,150
U-233	Total U	<1E-20	10,000	1.2E-17	10,000	8.5E-18	10,000	<1E-20	10,000
U-234	Total U	<1E-20	10,000	<1E-20	10,000	<1E-20	10,000	<1E-20	10,000
U-235	Total U	<1E-20	10,000	<1E-20	10,000	<1E-20	10,000	<1E-20	10,000
U-236	Total U	<1E-20	10,000	<1E-20	10,000	<1E-20	10,000	<1E-20	10,000
U-238	Total U	<1E-20	10,000	<1E-20	10,000	<1E-20	10,000	<1E-20	10,000
Zr-93	2,000	<1E-20	10,000	<1E-20	10,000	<1E-20	10,000	<1E-20	10,000
Total Alpha	15	1.2E-16	10,000	1.3E-13	10,000	9.6E-14	10,000	<1E-20	10,000
Total Ra	5	<1E-20	10,000	<1E-20	10,000	<1E-20	10,000	<1E-20	10,000
Sum of Beta-Gamma MCL Fractions		5.9E-04	10,000	2.2E-04	10,000	2.0E-04	10,000	1.4E-14	10,000

Table 5.2-16: Chemical Peak Concentrations along the 100-Meter Boundary for UAZ, Sectors A through H in 10,000 Years

Chemical	MCL (µg/L)	Conc. (µg/L)	Year of Peak	Conc. (µg/L)	Year of Peak	Conc. (µg/L)	Year of Peak	Conc. (µg/L)	Year of Peak
		Sector A		Sector B		Sector C		Sector D	
Cl^-	250,000	3.2E+00	9,990	8.4E+00	10,000	9.9E+00	10,000	9.3E+00	9,010
F^-	4,000	6.5E+00	10,000	1.7E+01	9,990	1.2E+01	9,980	1.8E+01	8,170
NO_3	10,000	6.2E+03	9,980	1.6E+04	9,970	1.2E+04	9,970	1.7E+04	3,890
NO_2	10,000	5.5E+02	9,980	1.4E+03	9,920	1.4E+03	9,980	1.5E+03	3,990
PO_4	N/A	4.1E+01	9,970	1.1E+02	9,920	7.7E+01	9,970	1.1E+02	4,000
SO_4	250,000	1.9E+02	9,960	4.9E+02	9,960	4.0E+02	10,000	5.0E+02	3,990
Al	200	<1E-20	10,000	<1E-20	10,000	<1E-20	10,000	<1E-20	10,000
Ag	100	<1E-20	10,000	<1E-20	10,000	<1E-20	10,000	<1E-20	10,000
As	10	<1E-20	10,000	<1E-20	10,000	<1E-20	10,000	<1E-20	10,000
B	N/A	7.6E-01	9,980	2.0E+00	9,970	2.3E+00	9,990	2.1E+00	4,160
Ba	2,000	<1E-20	10,000	<1E-20	10,000	<1E-20	10,000	<1E-20	10,000
Cd	5	<1E-20	10,000	<1E-20	10,000	<1E-20	10,000	<1E-20	10,000
Co	N/A	<1E-20	10,000	<1E-20	10,000	<1E-20	10,000	<1E-20	10,000
Cr	100	<1E-20	10,000	<1E-20	10,000	<1E-20	10,000	<1E-20	10,000
Cu	1,300	<1E-20	10,000	<1E-20	10,000	<1E-20	10,000	<1E-20	10,000
Fe	300	<1E-20	10,000	<1E-20	10,000	<1E-20	10,000	<1E-20	10,000
Hg	2	<1E-20	10,000	<1E-20	9,920	<1E-20	10,000	<1E-20	10,000
I	N/A	1.3E-05	10,000	3.5E-05	10,000	2.3E-03	10,000	5.9E-04	10,000
Mn	50	2.6E-20	10,000	3.0E-18	10,000	2.1E-13	10,000	5.2E-13	10,000
Mo	N/A	<1E-20	10,000	<1E-20	10,000	<1E-20	10,000	<1E-20	10,000
Ni	N/A	1.0E-19	10,000	2.3E-16	10,000	6.4E-13	10,000	1.4E-12	10,000
Pb	15	<1E-20	10,000	<1E-20	10,000	<1E-20	10,000	<1E-20	10,000
Se	50	<1E-20	10,000	<1E-20	10,000	<1E-20	10,000	<1E-20	10,000
Sb	6	<1E-20	10,000	<1E-20	10,000	<1E-20	10,000	<1E-20	10,000
Sr	N/A	<1E-20	10,000	<1E-20	10,000	7.7E-18	10,000	1.7E-17	10,000
U	30	<1E-20	9,630	<1E-20	10,000	<1E-20	10,000	<1E-20	10,000
Zn	5,000	<1E-20	10,000	<1E-20	10,000	<1E-20	10,000	<1E-20	10,000
Chemical	**MCL**	**Sector E**		**Sector F**		**Sector G**		**Sector H**	
Cl^-	250,000	6.7E+00	10,000	4.8E+00	10,000	7.1E+00	10,000	3.0E-01	10,000
F^-	4,000	1.3E+01	9,990	2.9E+00	10,000	4.3E+00	10,000	1.7E-02	10,000
NO_3	10,000	1.3E+04	9,980	2.7E+03	9,970	3.9E+03	9,960	1.2E+02	9,990
NO_2	10,000	1.1E+03	9,910	1.3E+02	9,910	2.0E+02	9,910	1.2E+00	9,990
PO_4	N/A	8.4E+01	9,970	8.2E+00	9,960	1.2E+01	9,850	1.2E-01	9,990
SO_4	250,000	3.8E+02	9,970	6.3E+01	9,920	9.2E+01	9,910	3.6E-01	10,000
Al	200	<1E-20	10,000	<1E-20	10,000	<1E-20	10,000	<1E-20	10,000
Ag	100	2.3E-20	10,000	4.7E-18	10,000	8.2E-18	10,000	<1E-20	10,000
As	10	<1E-20	10,000	<1E-20	10,000	<1E-20	10,000	<1E-20	10,000
B	N/A	1.6E+00	9,980	9.1E-01	9,990	1.3E+00	9,980	1.2E-02	9,980
Ba	2,000	<1E-20	10,000	<1E-20	10,000	<1E-20	10,000	<1E-20	10,000
Cd	5	<1E-20	10,000	<1E-20	10,000	1.8E-20	10,000	<1E-20	10,000
Co	N/A	<1E-20	10,000	<1E-20	10,000	<1E-20	10,000	<1E-20	10,000
Cr	100	<1E-20	10,000	<1E-20	10,000	<1E-20	10,000	<1E-20	10,000
Cu	1,300	<1E-20	10,000	<1E-20	10,000	<1E-20	10,000	<1E-20	10,000
Fe	300	<1E-20	10,000	<1E-20	10,000	<1E-20	10,000	<1E-20	10,000
Hg	2	<1E-20	10,000	<1E-20	10,000	<1E-20	10,000	<1E-20	10,000
I	N/A	3.7E-05	10,000	3.4E-04	10,000	5.1E-04	10,000	3.0E-05	10,000
Mn	50	5.6E-16	10,000	1.5E-13	10,000	3.0E-13	10,000	5.6E-18	10,000
Mo	N/A	<1E-20	10,000	<1E-20	10,000	<1E-20	10,000	<1E-20	10,000
Ni	N/A	1.4E-15	10,000	2.5E-13	10,000	4.1E-13	10,000	4.0E-17	10,000
Pb	15	<1E-20	10,000	<1E-20	10,000	<1E-20	10,000	<1E-20	10,000
Se	50	<1E-20	10,000	<1E-20	10,000	<1E-20	10,000	<1E-20	10,000
Sb	6	<1E-20	10,000	<1E-20	10,000	<1E-20	10,000	<1E-20	10,000
Sr	N/A	9.6E-17	10,000	1.5E-14	10,000	2.4E-14	10,000	5.2E-17	10,000
U	30	<1E-20	10,000	<1E-20	10,000	<1E-20	10,000	<1E-20	10,000
Zn	5,000	<1E-20	10,000	1.6E-19	10,000	3.5E-19	10,000	<1E-20	10,000

Table 5.2-17: Chemical Peak Concentrations along the 100-Meter Boundary for LAZ, Sectors A through H in 10,000 Years

Chemical	MCL (µg/L)	Conc. (µg/L)	Year of Peak	Conc. (µg/L)	Year of Peak	Conc. (µg/L)	Year of Peak	Conc. (µg/L)	Year of Peak
		Sector A		Sector B		Sector C		Sector D	
Cl^-	250,000	1.6E+01	10,000	1.6E+01	10,000	1.6E+01	9,990	1.5E+01	9,890
F^-	4,000	3.2E+01	10,000	3.3E+01	10,000	2.7E+01	10,000	2.9E+01	10,000
NO_3	10,000	3.0E+04	9,990	3.2E+04	9,980	2.7E+04	9,990	2.6E+04	4,420
NO_2	10,000	2.7E+03	10,000	2.8E+03	9,980	2.6E+03	10,000	2.3E+03	4,350
PO_4	N/A	2.0E+02	9,980	2.1E+02	9,970	1.8E+02	9,970	1.7E+02	4,200
SO_4	250,000	9.1E+02	9,980	9.6E+02	10,000	8.2E+02	10,000	7.9E+02	4,350
Al	200	<1E-20	10,000	<1E-20	10,000	<1E-20	10,000	<1E-20	10,000
Ag	100	<1E-20	10,000	<1E-20	10,000	<1E-20	10,000	<1E-20	10,000
As	10	<1E-20	10,000	<1E-20	10,000	<1E-20	10,000	<1E-20	10,000
B	N/A	3.8E+00	9,980	3.9E+00	9,990	4.0E+00	9,990	3.3E+00	4,680
Ba	2,000	<1E-20	10,000	<1E-20	10,000	<1E-20	10,000	<1E-20	10,000
Cd	5	<1E-20	10,000	<1E-20	10,000	<1E-20	10,000	<1E-20	10,000
Co	N/A	<1E-20	10,000	<1E-20	10,000	<1E-20	10,000	<1E-20	10,000
Cr	100	<1E-20	10,000	<1E-20	10,000	<1E-20	10,000	<1E-20	10,000
Cu	1,300	<1E-20	10,000	<1E-20	10,000	<1E-20	10,000	<1E-20	10,000
Fe	300	<1E-20	10,000	<1E-20	10,000	<1E-20	10,000	<1E-20	10,000
Hg	2	<1E-20	10,000	<1E-20	10,000	<1E-20	10,000	<1E-20	10,000
I	N/A	6.5E-05	10,000	2.5E-04	10,000	3.3E-03	10,000	1.1E-03	10,000
Mn	50	5.5E-20	10,000	1.1E-16	10,000	2.1E-13	10,000	4.7E-13	10,000
Mo	N/A	<1E-20	10,000	<1E-20	10,000	<1E-20	10,000	<1E-20	10,000
Ni	N/A	3.3E-19	10,000	7.8E-15	10,000	9.0E-13	10,000	1.6E-12	10,000
Pb	15	<1E-20	10,000	<1E-20	10,000	<1E-20	10,000	<1E-20	10,000
Se	50	<1E-20	10,000	<1E-20	10,000	<1E-20	10,000	<1E-20	10,000
Sb	6	<1E-20	10,000	<1E-20	10,000	<1E-20	10,000	<1E-20	10,000
Sr	N/A	<1E-20	10,000	<1E-20	10,000	1.2E-17	10,000	2.0E-17	10,000
U	30	<1E-20	10,000	<1E-20	10,000	<1E-20	10,000	<1E-20	10,000
Zn	5,000	<1E-20	10,000	<1E-20	10,000	<1E-20	10,000	<1E-20	10,000
Chemical	**MCL**	**Sector E**		**Sector F**		**Sector G**		**Sector H**	
Cl^-	250,000	1.2E+01	9,980	1.4E+01	10,000	1.5E+01	10,000	2.9E-01	10,000
F^-	4,000	2.4E+01	10,000	2.1E+01	9,990	8.9E+00	10,000	1.6E-02	10,000
NO_3	10,000	2.3E+04	9,980	2.0E+04	9,980	8.4E+03	9,970	1.2E+02	10,000
NO_2	10,000	2.0E+03	9,980	1.8E+03	9,950	4.1E+02	9,920	1.2E+00	10,000
PO_4	N/A	1.5E+02	9,970	1.3E+02	9,970	2.5E+01	9,960	1.2E-01	10,000
SO_4	250,000	6.9E+02	9,970	5.9E+02	9,980	1.9E+02	9,820	3.5E-01	10,000
Al	200	<1E-20	10,000	<1E-20	10,000	<1E-20	10,000	<1E-20	10,000
Ag	100	<1E-20	10,000	1.0E-17	10,000	1.3E-17	10,000	<1E-20	10,000
As	10	<1E-20	10,000	<1E-20	10,000	<1E-20	10,000	<1E-20	10,000
B	N/A	2.9E+00	10,000	2.6E+00	9,980	2.8E+00	9,980	1.2E-02	9,990
Ba	2,000	<1E-20	10,000	<1E-20	10,000	<1E-20	10,000	<1E-20	10,000
Cd	5	<1E-20	10,000	1.5E-20	10,000	2.2E-20	10,000	<1E-20	10,000
Co	N/A	<1E-20	10,000	<1E-20	10,000	<1E-20	10,000	<1E-20	10,000
Cr	100	<1E-20	10,000	<1E-20	10,000	<1E-20	10,000	<1E-20	10,000
Cu	1,300	<1E-20	10,000	<1E-20	10,000	<1E-20	10,000	<1E-20	10,000
Fe	300	<1E-20	10,000	<1E-20	10,000	<1E-20	10,000	<1E-20	10,000
Hg	2	<1E-20	10,000	<1E-20	10,000	<1E-20	10,000	<1E-20	10,000
I	N/A	1.2E-03	9,990	1.0E-03	9,990	1.1E-03	9,990	2.9E-05	10,000
Mn	50	7.7E-16	10,000	2.8E-13	10,000	4.0E-13	10,000	4.0E-18	10,000
Mo	N/A	<1E-20	10,000	<1E-20	10,000	<1E-20	10,000	<1E-20	10,000
Ni	N/A	1.7E-14	10,000	5.9E-13	10,000	7.1E-13	10,000	3.4E-17	10,000
Pb	15	<1E-20	10,000	<1E-20	10,000	<1E-20	10,000	<1E-20	10,000
Se	50	<1E-20	10,000	<1E-20	10,000	<1E-20	10,000	<1E-20	10,000
Sb	6	<1E-20	10,000	<1E-20	10,000	<1E-20	10,000	<1E-20	10,000
Sr	N/A	4.1E-17	10,000	3.8E-14	10,000	4.4E-14	10,000	4.6E-17	10,000
U	30	<1E-20	10,000	<1E-20	10,000	<1E-20	10,000	<1E-20	10,000
Zn	5,000	<1E-20	10,000	2.9E-19	10,000	4.3E-19	10,000	<1E-20	10,000

Table 5.2-18: Chemical Peak Concentrations along the 100-Meter Boundary for GAU, Sectors A through H in 10,000 Years

Chemical	MCL (µg/L)	Conc. (µg/L)	Year of Peak	Conc. (µg/L)	Year of Peak	Conc. (µg/L)	Year of Peak	Conc. (µg/L)	Year of Peak
		Sector A		Sector B		Sector C		Sector D	
Cl^-	250,000	6.1E-02	10,000	1.3E-01	10,000	1.2E-01	10,000	4.5E-02	10,000
F^-	4,000	1.2E-01	10,000	2.5E-01	10,000	2.3E-01	10,000	7.9E-02	10,000
NO_3	10,000	1.4E+02	9,940	3.1E+02	9,990	2.8E+02	10,000	8.8E+01	9,970
NO_2	10,000	1.2E+01	9,860	2.7E+01	9,990	2.6E+01	10,000	8.4E+00	10,000
PO_4	N/A	8.9E-01	9,990	2.0E+00	9,990	1.9E+00	9,990	5.5E-01	9,940
SO_4	250,000	4.0E+00	9,980	9.2E+00	10,000	8.5E+00	10,000	2.7E+00	9,910
Al	200	<1E-20	10,000	<1E-20	10,000	<1E-20	10,000	<1E-20	10,000
Ag	100	<1E-20	10,000	<1E-20	10,000	<1E-20	10,000	<1E-20	10,000
As	10	<1E-20	10,000	<1E-20	10,000	<1E-20	10,000	<1E-20	10,000
B	N/A	1.7E-02	9,970	3.8E-02	9,990	3.8E-02	9,990	1.4E-02	9,910
Ba	2,000	<1E-20	10,000	<1E-20	10,000	<1E-20	10,000	<1E-20	10,000
Cd	5	<1E-20	10,000	<1E-20	10,000	<1E-20	10,000	<1E-20	10,000
Co	N/A	<1E-20	10,000	<1E-20	10,000	<1E-20	10,000	<1E-20	7,230
Cr	100	<1E-20	10,000	<1E-20	10,000	<1E-20	10,000	<1E-20	10,000
Cu	1,300	<1E-20	10,000	<1E-20	10,000	<1E-20	10,000	<1E-20	9,590
Fe	300	<1E-20	10,000	<1E-20	10,000	<1E-20	10,000	<1E-20	10,000
Hg	2	<1E-20	10,000	<1E-20	10,000	<1E-20	10,000	<1E-20	10,000
I	N/A	3.2E-07	10,000	1.5E-06	10,000	6.1E-06	10,000	2.8E-06	10,000
Mn	50	<1E-20	10,000	<1E-20	10,000	8.7E-20	10,000	5.3E-20	10,000
Mo	N/A	<1E-20	10,000	<1E-20	10,000	<1E-20	10,000	<1E-20	9,850
Ni	N/A	1.1E-19	10,000	9.1E-19	10,000	2.5E-17	10,000	1.4E-17	10,000
Pb	15	<1E-20	10,000	<1E-20	10,000	<1E-20	10,000	<1E-20	10,000
Se	50	<1E-20	10,000	<1E-20	10,000	<1E-20	10,000	<1E-20	9,830
Sb	6	<1E-20	10,000	<1E-20	10,000	<1E-20	10,000	<1E-20	10,000
Sr	N/A	2.1E-20	10,000	8.1E-20	10,000	<1E-20	10,000	<1E-20	10,000
U	30	<1E-20	10,000	<1E-20	10,000	<1E-20	10,000	<1E-20	10,000
Zn	5,000	<1E-20	10,000	<1E-20	10,000	<1E-20	10,000	<1E-20	10,000
Chemical	**MCL**	**Sector E**		**Sector F**		**Sector G**		**Sector H**	
Cl^-	250,000	2.6E-03	10,000	2.3E-03	10,000	2.0E-03	10,000	1.6E-13	10,000
F^-	4,000	5.5E-03	10,000	9.6E-04	10,000	6.3E-04	10,000	8.9E-15	10,000
NO_3	10,000	8.2E+00	10,000	2.8E+00	9,990	1.9E+00	9,980	7.5E-11	10,000
NO_2	10,000	6.9E-01	10,000	1.0E-01	9,870	5.6E-02	10,000	7.5E-13	10,000
PO_4	N/A	5.5E-02	9,990	7.3E-03	10,000	3.8E-03	10,000	7.5E-14	10,000
SO_4	250,000	2.4E-01	9,990	4.7E-02	10,000	2.5E-02	10,000	2.2E-13	9,990
Al	200	<1E-20	10,000	<1E-20	10,000	<1E-20	10,000	<1E-20	10,000
Ag	100	<1E-20	10,000	<1E-20	10,000	<1E-20	10,000	<1E-20	10,000
As	10	<1E-20	10,000	<1E-20	10,000	<1E-20	10,000	<1E-20	10,000
B	N/A	8.6E-04	9,990	7.4E-04	10,000	4.1E-04	9,990	7.5E-15	10,000
Ba	2,000	<1E-20	10,000	<1E-20	10,000	<1E-20	10,000	<1E-20	10,000
Cd	5	<1E-20	10,000	<1E-20	10,000	<1E-20	10,000	<1E-20	10,000
Co	N/A	<1E-20	10,000	<1E-20	10,000	<1E-20	10,000	<1E-20	10,000
Cr	100	<1E-20	10,000	<1E-20	10,000	<1E-20	10,000	<1E-20	10,000
Cu	1,300	<1E-20	10,000	<1E-20	10,000	<1E-20	10,000	<1E-20	10,000
Fe	300	<1E-20	10,000	<1E-20	10,000	<1E-20	10,000	<1E-20	10,000
Hg	2	<1E-20	10,000	<1E-20	10,000	<1E-20	10,000	<1E-20	10,000
I	N/A	2.5E-08	10,000	3.5E-07	10,000	2.9E-07	10,000	1.8E-17	10,000
Mn	50	<1E-20	10,000	1.6E-20	10,000	1.7E-20	10,000	<1E-20	10,000
Mo	N/A	<1E-20	10,000	<1E-20	10,000	<1E-20	10,000	<1E-20	10,000
Ni	N/A	<1E-20	10,000	1.3E-18	10,000	1.1E-18	10,000	<1E-20	10,000
Pb	15	<1E-20	10,000	<1E-20	10,000	<1E-20	10,000	<1E-20	10,000
Se	50	<1E-20	10,000	<1E-20	10,000	<1E-20	10,000	<1E-20	10,000
Sb	6	<1E-20	10,000	<1E-20	10,000	<1E-20	10,000	<1E-20	10,000
Sr	N/A	<1E-20	10,000	1.7E-19	10,000	1.4E-19	10,000	<1E-20	10,000
U	30	<1E-20	10,000	<1E-20	10,000	<1E-20	10,000	<1E-20	10,000
Zn	5,000	<1E-20	10,000	<1E-20	10,000	<1E-20	10,000	<1E-20	10,000

5.2.2 Concentrations at the SDF Seeplines

In addition to the concentrations at the SDF 100-meter boundary, ground water concentrations were also determined along the seeplines for UTR and MQB using the SDF-specific portion of the GSA Model (see Figure 4.4-114). As the only radionuclides of interest at the 100-meter boundary in 10,000 years were Cl-36, I-129, and Tc-99 (see Section 5.2.4 for additional discussion), these were the only radionuclides modeled to the seepline and were subsequently evaluated over a simulation period of 20,000 years. In addition, based on a comparison of the peak chemical concentrations provided in Section 5.2.1, relative to the respective MCLs, the only chemical of interest identified at the 100-meter boundary in 10,000 years was nitrate (NO_3), therefore, this was the only chemical modeled to the seepline. These seepline concentrations were used to derive doses for applicable dose pathways associated with swimming, boating and fishing activities and for the MOP at the seepline dose scenario. For dose calculations, the other radionuclides or chemicals are estimated using the simplified seepline ratio (described in Section 5.2.3).

Table 5.2-19 provides the maximum concentrations for the selected species at the seeplines within 1,000 years, Table 5.2-20 provides the maximum concentrations at the seeplines within 10,000 years, and Table 5.2-21 provides the maximum concentrations at the seeplines within 20,000 years. As would be expected, these maximum seepline concentrations are lower than those along the SDF 100-meter boundary (as provided in Section 5.2.1). While these maximum concentrations are not used to compare against MCLs, the maximum concentrations in 20,000 years from Table 5.2-21 are used in the development of the seepline ratio (see Section 5.2.3).

The peaks within 1,000 years occur at the UTR seepline for Cl-36 and at the MQB seepline for I-129, Tc-99, and NO_3, while the peaks within 10,000 years and 20,000 years all occur at the UTR seepline.

Table 5.2-19: Maximum Concentrations at the SDF Seeplines within 1,000 Years

Radionuclide or Chemical	Max UTR		Max MQB		Maximum of Either Seepline	
	Conc. (pCi/L or µg/L)	Year of Peak	Conc. (pCi/L or µg/L)	Year of Peak	Conc. (pCi/L or µg/L)	Year of Peak
Cl-36	8.8E-05	1,000	8.5E-05	1,000	8.8E-05	1,000
I-129	2.7E-04	1,000	3.1E-04	1,000	3.1E-04	1,000
Tc-99	1.4E-01	1,000	1.4E-01	1,000	1.4E-01	1,000
NO_3	6.7E+01	1,000	7.0E+01	1,000	7.0E+01	1,000

Table 5.2-20: Maximum Concentrations at the SDF Seeplines within 10,000 Years

Radionuclide or Chemical	Max UTR		Max MQB		Maximum of Either Seepline	
	Conc. (pCi/L or µg/L)	Year of Peak	Conc. (pCi/L or µg/L)	Year of Peak	Conc. (pCi/L or µg/L)	Year of Peak
Cl-36	7.7E-02	10,000	4.0E-02	10,000	7.7E-02	10,000
I-129	4.9E-01	10,000	2.9E-01	10,000	4.9E-01	10,000
Tc-99	7.6E+01	9,910	4.9E+01	9,880	7.6E+01	9,910
NO_3	7.1E+03	10,000	4.1E+03	10,000	7.1E+03	10,000

Table 5.2-21: Maximum Concentrations at the SDF Seeplines within 20,000 Years

Radionuclide or Chemical	Max UTR		Max MQB		Maximum of Either Seepline	
	Conc. (pCi/L or µg/L)	Year of Peak	Conc. (pCi/L or µg/L)	Year of Peak	Conc. (pCi/L or µg/L)	Year of Peak
Cl-36	8.3E-02	17,920	4.2E-02	16,900	8.3E-02	17,920
I-129	6.8E-01	20,000	3.8E-01	20,000	6.8E-01	20,000
Tc-99	7.6E+01	10,760	4.9E+01	10,850	7.6E+01	10,760
NO_3	7.1E+03	12,710	4.1E+03	12,870	7.1E+03	12,710

5.2.3 Determination of Seepline Ratio

Dose contributions due to seepline concentrations are needed to calculate total doses. As a modeling simplification, it is assumed that the concentrations along the seeplines may be estimated as a ratio of the 100-meter concentrations.

Three radionuclides were selected for use in determining the seepline ratio: Cl-36, I-129, and Tc-99, plus one chemical: NO_3. These contaminants were selected based on previous SDF modeling efforts which have demonstrated that these are the most likely radionuclides or chemicals to influence the seepline concentrations. [SRR-CWDA-2017-00077] Using results from the Aquifer Transport Model of the Compliance Case, contaminant concentrations were determined along the 100-meter facility boundary for each of eight sectors (Sectors A through H). The maximum values across each of these sectors was then determined to provide a single data set for the highest concentrations at the 100-meter boundary (C_{100m}) over 20,000 years.

Similarly, for each of the contaminants, the highest concentration along the seepline (C_{SL}) was identified (over 20,000 years), regardless of location along the seepline and regardless of the timing of the maximum value within 20,000 years. For each contaminant, the seepline ratio was determined using the following formula:

$$SL = \frac{C_{SL}}{C_{100m}} \qquad \text{Eq. 5.2-1}$$

where:

SL = the seepline ratio (unitless),

C_{SL} = the peak concentration at the seepline (pCi/L or µg/L), and

C_{100m} = the peak concentration at the 100-meter facility boundary (pCi/L or µg/L).

Table 5.2-22 summarizes the seepline ratio values for each contaminant. Based on these ratios, the recommended seepline ratio for use in SDF modeling is a value of 0.22. [SRR-CWDA-2017-00077]

Table 5.2-22: Seepline Ratios Based on Maximum Concentrations Along the SDF Seeplines within 20,000 Years Using Compliance Case Results

Radionuclide or Chemical	C_{100m} (pCi/L or µg/L)	C_{SL} (pCi/L or µg/L)	Seepline Ratio
Cl-36	3.7E-01	8.3E-02	0.22
I-129	3.0E+00	6.8E-01	0.22
Tc-99	3.5E+02	7.6E+01	0.21
NO_3	3.2E+04	7.1E+03	0.22

To validate the use of the seepline ratio, it was applied to maximum 100-meter concentrations of Cl-36, I-129, and Tc-99 (over the simulated period of 20,000 years) and compared to the Aquifer Transport Model concentrations from the final Compliance Case (see Table 5.2-23). These results show that the seepline ratio of 0.22 provides an acceptable value to assume for estimating concentrations along the seepline.

Table 5.2-23: Comparison of Applied Seepline Concentration Ratio to Actual Seepline Concentrations Based on the Compliance Case

Radionuclide or Chemical	Aquifer Transport Result at 100 meters (pCi/L or kg/L)	Result at 100 meters (pCi/L or kg/L) × 0.22	Aquifer Transport Result at Seepline (pCi/L or kg/L)
Cl-36	3.7E-01	8.3E-02	8.3E-02
I-129	3.0E+00	6.7E-01	6.8E-01
Tc-99	3.5E+02	7.8E+01	7.6E+01
NO_3	3.2E+04	7.1E+03	7.1E+03

5.2.4 Determination of Sensitivity Run Radionuclides

The purpose of this section is to present the methodology used to determine which radionuclides were most likely to be major dose contributors, and to identify these radionuclides as "sensitivity run radionuclides." While all radionuclides identified in the SDF inventory (Section 3.3) were included in the Compliance Case modeling efforts, narrowing the catalog of radionuclides down to a smaller list allows sensitivity analyses to concentrate on the few radionuclides that pose the greatest risk to the MOP or IHI such that modeling efforts may focus on the areas of greatest concern.

The sensitivity run radionuclides were determined based on the peak 100-meter ground water concentrations by radionuclide provided in Section 5.2.1; note the peak concentration for each individual radionuclide is not necessarily in the same year. These concentrations were then run through the GoldSim dose calculator to determine dose rates by sector. Any radionuclide in a given sector with greater than 0.25 mrem/yr dose (assuming the Compliance Case pathways and assumptions) anytime within 10,000 years at the 100-meter boundary was considered a sensitivity run radionuclide. The 0.25 mrem/yr screening threshold (100 times less than the 25 mrem/yr performance objective) was considered sufficiently low, such that the contributions of the radionuclides that were screened out would not appreciably affect the peak dose results, even accounting for cumulative pathway effects.

Based on this approach, only two radionuclides met the minimum threshold: I-129 and Tc-99 (see dose results in Section 5.5). Within the Compliance Period (i.e., the first 1,000 years), the next highest dose contributor is Cl-36; this radionuclide was also included in the list of sensitivity run radionuclides to provide a more robust and defensible list.

While the full suite of radionuclides was simulated for the Compliance Case, the sensitivity models only simulate the sensitivity run radionuclides (Cl-36, I-129, and Tc-99) unless there is specific need to evaluate other radionuclides.

5.3 Air Pathways and Radon Flux Analysis

Section 4.4.7 described the method used to determine the airborne concentrations of radionuclides at the 100 m boundary. The full method and total projected inventories used can be found in SRR-CWDA-2018-00025. The modeled inventories are included in Section 4.4.7 in Table 4.4-104 through Table 4.4-106.

5.3.1 Air Pathways Dose

The projected dose for each radionuclide at 100 meters has been determined and presented in Table 5.3-1. The model evaluated the transport of the gaseous-phase radionuclides (C-14, Cl-36, H-3, I-129, Rn-222, Se-79, Sn-126, and Tc-99). As described in Section 4.4.7, the pore space above the SDUs was assumed to be air filled, resulting in the releases shown in Table 5.3-1. While releases were evaluated for every single SDU, the SDU with the highest peak releases occurred from the 375-foot diameter SDUs. Because all of the 375-foot diameter SDUs have the same assumed inventory, these peak releases are the same for all of them (i.e., SDUs 6 through 12). SDUs 1, 2A, 2B, 3A, 3B, 4, 5A, and 5B all exhibited lower releases.

Table 5.3-1: Air Pathway Dose Peak During the Compliance Period

Radionuclides	Release Rate (Ci/yr)	Peak Release Time (year)	100 m DRF (mrem/Ci)	Dose to IHI (mrem/yr)
C-14	4.3E-07	0.34	3.7E-03	1.6E-09
Cl-36	3.6E-23	0.55	7.9E-03	2.8E-25
H-3	4.7E-05	0.08	7.7E-05	3.6E-09
I-129	6.5E-26	1,000	5.5E+00	3.6E-25
			Total Dose	5.2E-09

[SRR-CWDA-2018-00025, SRNL-STI-2008-00415]
Note: All other radionuclides modeled resulted in values less than 1E-30 mrem/yr.

The peak dose during the Performance Period (10,000 years) is effectively the same. Of the radionuclides listed in Table 5.3-1, only I-129 increases after the initial release (by a factor of three within the Performance Period), but because it has a minimal contribution to the air pathway dose total, the increase to I-129 is non-impactful.

Note the timing of the peak releases: these projected doses from the air pathways releases do not take credit for the Institutional Control Period. Figure 5.3-1 shows the air pathways dose contribution over time. The time scale is presented logarithmically to illustrate that the dose peaks within a year, then quickly decreases within 100 years.

The dose release factors (DRFs) are based on air pathway dose modeling using CAP88 software version 3.0. [SRNL-STI-2008-00415] The dose from each radionuclide is calculated by multiplying the release amount by the DRF as shown in Table 5.3-1.

It should be noted that the CAP88 has been updated (version 4.0). Consideration was given to updating the DRFs for this PA. A comparison of the differences between CAP88 versions 3.0 and 4.0 was performed in 2015. [DOI: 10.1097/HP.0000000000000314] Given the low magnitude doses from these modeling results (i.e., total dose peak of 7.2E-10 mrem/yr) relative to the air pathway dose limit (10 mrem/yr), and due to the relatively minor changes to the model between versions

3.0 and 4.0, it was determined that the level of effort necessary to update the DRFs relative to risk significance was unwarranted.

Figure 5.3-1: Air Pathways Dose within 10,000 Years

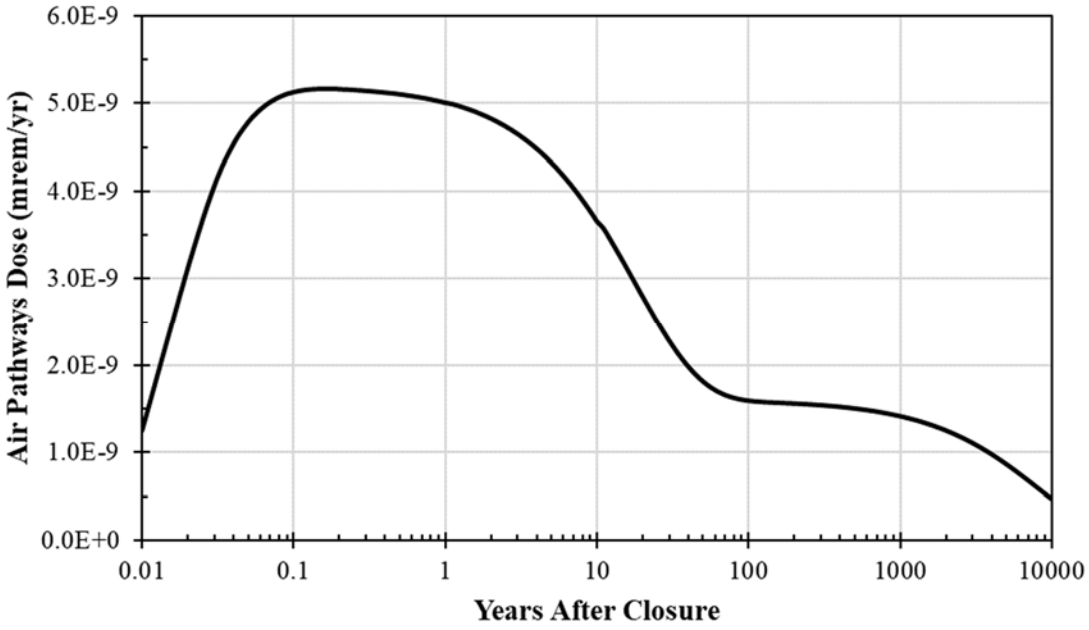

5.3.2 Radon Flux Analysis

For the radon air pathway, the Rn-222 flux was modeled from the decay which resulted from the following radionuclides: Cm-246, Pu-238, Pu-242, Ra-226, Th-230, U-234, and U-238. Table 5.3-2 was developed from the peak release of Rn-222. During the Compliance Period, the peak flux of Rn-222 occurs at the end of the 1,000-year period from the future SDUs. Similarly, during the Performance Period, the peak flux again occurs at the end (at year 10,000). This is due to the in-growth of radon from the long half-lives of the parent radionuclides.

Table 5.3-2: Peak Radon Release

Period	Release (Ci/yr)	Peak Release Time (years)	SDU Area	Peak Flux Averaged over the SDU Area ($pCi/m^2/s$)
Compliance Period	5.2E-06	1,000	110,450 ft^2 (10,260 m^2)	1.6E-05
Performance Period	2.4E-04	10,000		7.4E-04

The peak instantaneous radon flux is found by dividing the maximum yearly release by the surface area of the appropriate SDU, in this case the future SDUs (i.e., 375 ft diameter SDUs).

The permissible radon flux for DOE facilities is addressed in DOE M 435.1-1, Section IV.P.(1) and states the radon flux requirement is that the release of radon shall be less than an average flux of 20 $pCi/m^2/s$ at the surface of the facility. The peak radon flux averaged over the SDU area is below the regulatory limits. This result is an overestimate because it was modeled with a desaturated pore space above the saltstone which promotes faster transport.

5.4 Biotic Pathways and MOP Dose Scenarios

In addition to the air pathways exposure scenario (described in Section 5.3), exposure and doses are also determined based on contaminant concentrations in the ground water. Section 4.4.8 describes how the biotic pathways doses are calculated based on these contaminant concentrations. A complete discussion of the revised biotic pathways and related methodology is provided in *Dose Calculation Methodology for Liquid Waste Performance Assessments at the Savannah River Site*, SRR-CWDA-2013-00058.

The results for these dose calculations are driven by the water sources assumed for exposure. This SDF PA considers doses from two potential MOP exposure scenarios:

- MOP at the 100-Meter Well Scenario (Section 5.4.1),
- MOP at the Seepline Scenario (Section 5.4.2),

The following provides an overview of the applicable exposure pathways for each MOP scenario and describes how the contaminant concentrations at the various points of assessment are determined for each of these exposure scenarios. Note that Section 6.2 describes the IHI exposure scenarios.

5.4.1 MOP at the 100-Meter Well Scenario

For the MOP at the 100-Meter Well Scenario, the human receptor is assumed to be a resident farmer that uses a well at the 100-meter SDF boundary as the primary source of water. For this scenario, two sources of water concentrations are assumed: the 100-meter well and the seepline; these concentrations are determined as described in Sections 5.4.1.1 and 5.4.2.2, respectively. The dose results from this scenario are presented in Section 5.5.

The ingestion pathways are:

- Direct ingestion of contaminated well water,
- Ingestion of soil irrigated with contaminated well water,
- Ingestion of produce irrigated with contaminated well water,
- Ingestion of meat from livestock raised with contaminated well water,
- Ingestion of milk from livestock raised with contaminated well water,
- Ingestion of poultry raised with contaminated well water,
- Ingestion of eggs from poultry raised with contaminated well water, and
- Ingestion of fish from the contaminated seepline (see Section 5.4.2.2).

The direct exposure pathways are:

- Exposure to soil irrigated with contaminated well water,
- Exposure to water during showers using contaminated well water,
- Exposure to water while swimming in the contaminated seepline (see Section 5.4.2.2), and
- Exposure to water while boating in the contaminated seepline (see Section 5.4.2.2).

The inhalation pathways are:

- Inhalation during irrigation using contaminated well water,
- Inhalation of dust from soil irrigated with contaminated well water,

- Inhalation during showers using the contaminated well water, and
- Inhalation while swimming in the contaminated seepline water (see Section 5.4.2.2).

For the MOP at the 100-Meter Well Scenario, the total ground water pathways dose is determined as the sum of the doses from each of these pathways, while the total all pathways dose is determined as the sum of total ground water pathways dose and the total air pathways dose (Section 5.3).

These pathways are defined in Section 4.4.8.

5.4.1.1 Concentrations for Use in the MOP at the 100-Meter Well Scenario

The 100-meter SDF boundary has been organized into eight sectors (labelled A through H as shown in Figure 4.4-114). Dividing the results into sectors was necessary to allow the large amount of concentration data to be stored from PORFLOW and used in the dose calculations, thus making the spatial complexity of the SDF system easier to evaluate.

The boundary length along each sector varies but is typically on the order of approximately 850 to 860 feet. Along these boundary lines, each sector has approximately 40 to 50 nodes. These nodes each represent potential points of assessment (i.e., potential 100-meter wells) for the MOP at the 100-Meter Well Scenario. In addition to the coordinate locations for each well, these wells also have a vertical (or depth) component; the concentrations from each well could be influenced by the aquifer from which water is drawn (UAZ, LAZ, or GAU).

For the SDF dose assessments, the vertical component is simplified by assuming the highest concentration of each contaminant regardless of the depth. For example, if the highest concentration of Ra-226 is at a depth of 50 feet, but the highest concentration of Tc-99 is at a depth of 60 feet, then the Ra-226 concentration at 50 feet will be assumed and the Tc-99 concentration at 60 feet will also be assumed.

Similarly, for each sector, the location of the well, or node, is also simplified by assuming the highest concentration of each contaminant regardless of which node recorded the highest concentration. Conceptually, this is equivalent to assuming that the MOP is changing well locations from year-to-year in order to maximize their exposures.

With this approach, dose results can be assessed for a single set of concentrations (one set recorded for each sector). Each set of concentrations yields the highest possible concentrations along the sector boundary, regardless of the node selection within the sector and regardless of the depth of the aquifer. These concentration results were then applied to the dose calculations, giving time histories for the ground water doses at each sector.

In addition to the concentrations from the 100-meter well water, the MOP exposure pathways also include pathways related to seepline-related activities (e.g., fishing and swimming). The concentrations along the seepline for these exposure pathways are assessed as described in Section 5.4.2.2.

5.4.2 MOP at the Seepline Scenario

For the MOP at the Seepline Scenario, the human receptor is assumed to be a resident farmer that uses water pulled directly from nearby streams as the primary source of water. For this scenario, all water concentrations are based on contamination of water at the seeplines of the streams without any stream dilution, as defined in Section 5.4.2.1. The dose results of this scenario are provided in Section 5.5.2.

The ingestion pathways are:

- Direct ingestion of contaminated seepline water,
- Ingestion of soil irrigated with contaminated seepline water,
- Ingestion of produce irrigated with contaminated seepline water,
- Ingestion of meat from livestock raised with contaminated seepline water,
- Ingestion of milk from livestock raised with contaminated seepline water,
- Ingestion of poultry raised with contaminated seepline water,
- Ingestion of eggs from poultry raised with contaminated seepline water, and
- Ingestion of fish from the contaminated seepline.

The direct exposure pathways are:

- Exposure to soil irrigated with contaminated seepline water,
- Exposure to water during showers using contaminated seepline water,
- Exposure to water while swimming in the contaminated seepline, and
- Exposure to water while boating in the contaminated seepline.

The inhalation pathways are:

- Inhalation during irrigation using contaminated seepline water,
- Inhalation of dust from soil irrigated with contaminated seepline water,
- Inhalation during showers using contaminated seepline water, and
- Inhalation while swimming in the contaminated seepline.

For the MOP at the Seepline Scenario, the total ground water pathways dose is determined as the sum of the doses from each of these pathways, while the total all pathways dose is determined as the sum of total ground water pathways dose and the total air pathways dose (Section 5.3).

These pathways are defined in Section 4.4.8.

5.4.2.1 Seepline Concentrations for Use in the MOP at the Seepline Scenario

Near the SDF are the Upper Three Runs (UTR) and McQueen Branch (MQB). Figure 4.4-113 depicts the nodes used for the UTR points of assessment as blue diamonds and the nodes used for MQB points of assessment as orange squares.

For the dose assessment of the MOP at the Seepline Scenario, the node selection along each seepline is simplified by assuming the highest concentration of each contaminant regardless of which seepline node recorded the highest concentration. Conceptually, this is similar to assuming that the MOP is changing seepline locations from year-to-year in order to maximize their exposures.

With this approach, dose results can be assessed for only two sets of concentrations (i.e., one set is recorded for each seepline), rather than assessing every node. Each set of concentrations yields the highest possible concentrations at the seepline, regardless of the node selection within the given seepline. These concentration results were then applied to the dose calculations, giving time histories for the ground water doses at each seepline.

5.4.2.2 Seepline Concentrations for Use in Other Scenarios

In addition to the MOP at the Seepline Scenario, several other scenarios also include exposure pathways to the human receptor during seepline-related activities (e.g., swimming, fishing, and boating), which are assessed based on the seepline concentrations. To simplify these assessments, the maximum contaminant concentrations between the UTR concentration set and the MQB concentration set is assumed. Note each of these concentration sets, UTR and MQB, were defined in Section 5.4.2.1. This approach provides a single set of concentrations for use in other scenarios.

5.5 Dose Analysis of MOP Exposure

Total ground water release pathways doses were determined based on the ground water concentrations from the Aquifer Transport Model (see Section 4.4.6) and using the calculations defined for the Dose and Exposure Pathways Model (see Section 4.4.8). Peak doses are identified for the Compliance Period (from 0 to 1,000 years after SDF closure) and for the Performance Period (from 0 to 10,000 years after SDF closure). The doses described in this section represent the doses to the MOP for the Compliance Case (i.e., using MPAD assumptions). In some results, the doses are also calculated beyond 10,000 years for the purpose of enhancing the discussion or to explore the risks associate with long-term performance.

Note that as presented in Section 5.3, the contribution to the total dose from the airborne release pathways is negligible. Accordingly, the total dose to the MOP or IHI is, in all cases, effectively equivalent to the associated ground water release pathway dose and will not be discussed independently.

5.5.1 MOP at 100-Meters Ground Water Pathways Dose Results

The peak ground water pathways doses to the MOP along the 100-meter boundary in Sectors A through H (Figure 4.4-114) are calculated using the peak concentration for each radionuclide along the sector (a discussion of how peak concentrations are determined by sector is provided in Section 5.2). These peak ground water pathways doses are the total ground water doses associated with the 100-meter well concentrations.

Section 5.5.1.1 provides an overview of these dose results, by sector. Sections 5.5.1.2, 5.5.1.3, and 5.5.1.4 present these ground water doses according to radionuclide dose contributions, individual ground water pathways dose contributions, and individual SDU dose contributions, respectively. Finally, Section 5.5.1.5 provides a long-term perspective, showing dose results out 100,000 years after SDF closure.

5.5.1.1 MOP at 100-Meters, Sector-Specific Ground Water Pathways Doses

Table 5.5-1 presents the peak ground water pathways doses for the eight sectors along the 100-meter boundary for the 1,000-year Compliance Period and the 10,000-year Performance Period. These results are depicted in Figure 5.5-1 through Figure 5.5-4. Note that most of the dose figures throughout Section 5.5.1 are presenting the same data twice, where the first figure presents the doses on a logarithmic scale to illustrate magnitude and the second figure presents the doses on a linear scale to provide additional perspective.

In the first 1,000 years after SDF closure, the peak MOP ground water dose is estimated to be 9.4E-03 mrem/yr. Approximately 3,000 years after SDF closure, the dose is approximately 0.8 mrem/yr, after which the increases in the ground water dose become more gradual, eventually peaking at approximately 1.2 mrem/yr at 10,000 years after closure. The peak MOP ground water dose remains at least an order of magnitude below the performance objective (25 mrem/yr) throughout both the Compliance Period and the Performance Period.

After the first few thousand years, the doses along the 100-meter boundary in Sectors A through F show very similar magnitudes and behaviors (Figure 5.5-3). This similarity is because the doses along the 100-meter boundary in these sectors are all dominated by the releases from the 375-foot diameter SDUs. For the Compliance Period, the peak dose to the MOP occurs in Sector D (orange curve in Figure 5.5-3). For the Performance Period, the peak dose to the MOP occurs in Sector B (blue curve in Figure 5.5-3). However, it should be noted that at 10,000 years, the doses in Sectors A, B, and D are all very similar in magnitude.

Table 5.5-1: 100-Meter MOP Peak Ground Water Pathways Dose by Sector

Sector	Compliance Period (0 to 1,000 Years)		Performance Period (0 to 10,000 Years)	
	Peak Dose (mrem/yr)	Year of Peak	Peak Dose (mrem/yr)	Year of Peak
Sector A	7.5E-04	1,000	1.1	10,000
Sector B	7.7E-04	1,000	**1.2**	10,000
Sector C	5.7E-03	1,000	0.96	10,000
Sector D	**9.4E-03**	**1,000**	1.1	10,000
Sector E	6.5E-04	1,000	0.86	10,000
Sector F	2.5E-03	1,000	0.75	10,000
Sector G	2.8E-03	1,000	0.40	10,000
Sector H	4.1E-04	1,000	0.069	10,000
Total Dose	**9.4E-03**	**1,000**	**1.2**	**10,000**

Note: Sectors illustrated in Figure 4.4-114.

Figure 5.5-1: 100-Meter MOP Peak Ground Water Pathways Dose within 1,000 Years, Sectors A through H

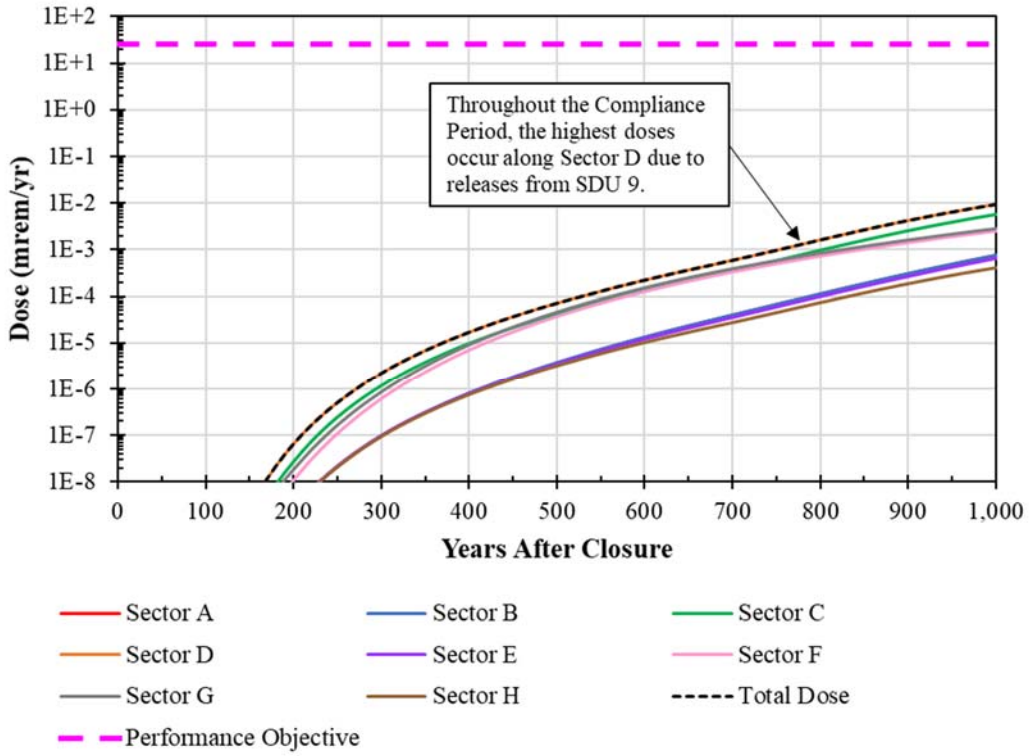

Figure 5.5-2: 100-Meter MOP Peak Ground Water Pathways Dose within 1,000 Years, Sectors A through H (Detail)

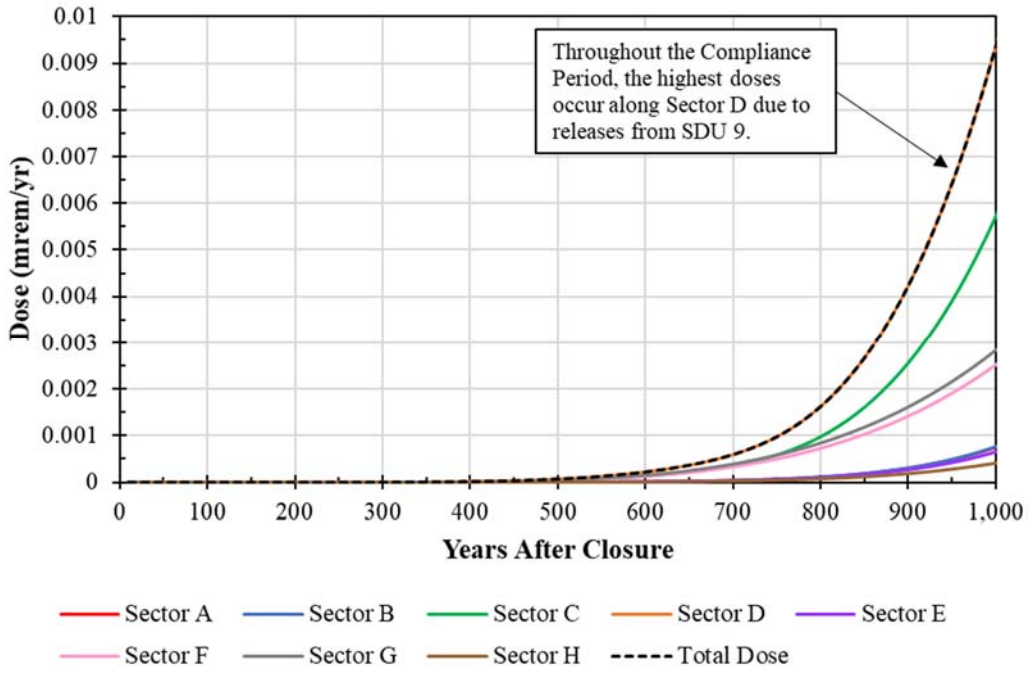

Figure 5.5-3: 100-Meter MOP Peak Ground Water Pathways Dose within 10,000 Years, Sectors A through H

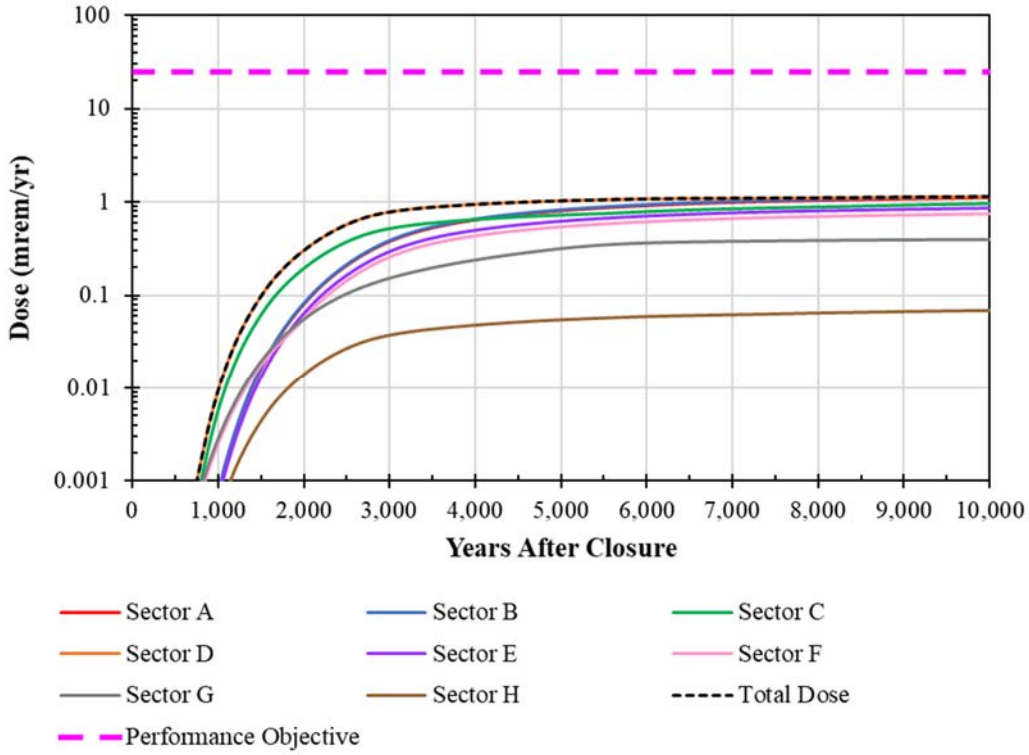

Figure 5.5-4: 100-Meter MOP Peak Ground Water Pathways Dose within 10,000 Years, Sectors A through H (Detail)

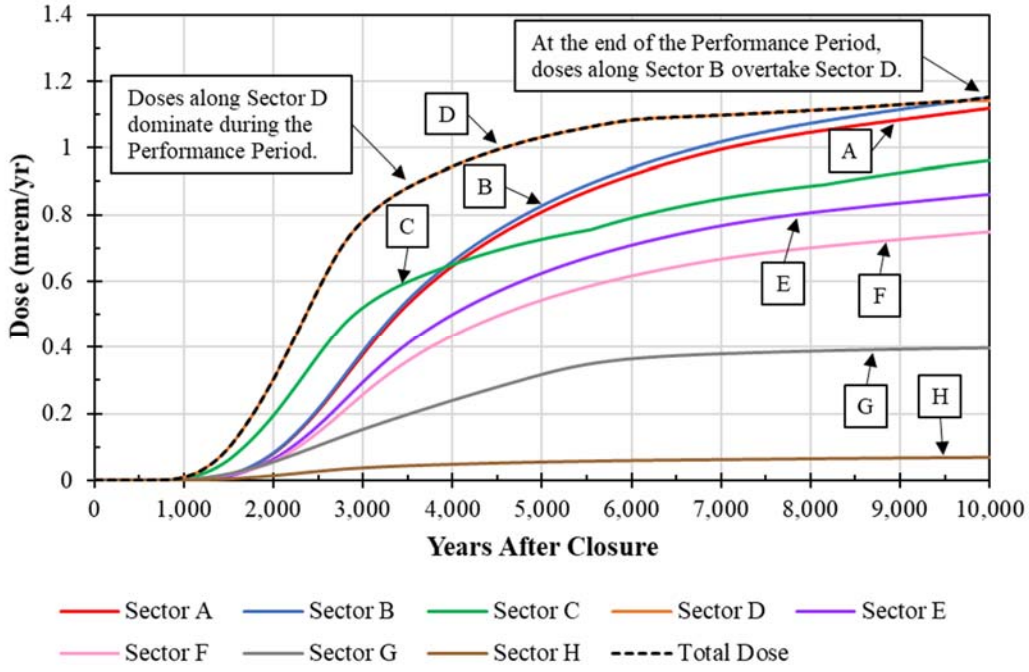

5.5.1.2 MOP at 100-Meters, Individual Radionuclide Contributions to Ground Water Pathways Doses

As previously indicated, the highest doses occur along Sector D until nearly 10,000 years after closure when Sector B becomes the highest dose contributor. As such the following discussion is limited to describing the results along Sectors D and B. Because the doses along Sectors A through F are all heavily influenced by releases from the 375-foot diameter SDUs (i.e., SDUs 6 through 12), the doses along these sectors are all similar to those along Sector D (only at lower magnitudes, with slightly delayed timing). Conversely, the doses along Sectors G and H are influenced by releases from the rectangular SDUs (i.e., SDUs 1 and 4).

During the 1,000-year Compliance Period, the peak ground water pathways dose to the MOP occurs at 1,000 year after closure, along the 100-meter boundary in Sector D and is primarily associated with I-129 (27%) and Tc-99 (73%). These radionuclide dose contributors are graphically depicted in Figure 5.5-5 and Figure 5.5-6. The sum of all other radionuclides only contributed approximately 0.1% of the total dose.

During the 10,000-year Performance Period, the peak ground water pathways dose to the MOP occurs at 10,000 years after closure, along the 100-meter boundary in Sector B and is also primarily associated with I-129 (49%) and Tc-99 (51%). These radionuclide dose contributors are graphically depicted in Figure 5.5-7 and Figure 5.5-8. The sum of all other radionuclides only contributed approximately 0.1% of the total dose.

These results demonstrate that within the Compliance and Performance Periods, I-129 and Tc-99 produce the highest dose contributions relative to the other radionuclides. This is because I-129 and Tc-99 are both highly mobile throughout the entire chemical environment (from the saltstone waste form all the way through the saturate zone), both have very long half-lives (~15M years and ~211,000 years). Additionally, I-129 has a relatively high dose conversion factors when ingested (see Table 4.4-108) and Tc-99 is relatively abundant within the assumed inventory (see Section 3.3.3). The next highest dose contributors are Cl-36, Cs-135, and K-40, but the contributions from these radionuclides are orders of magnitude less than those of I-129 and Tc-99.

These figures also show that the dose contributions from both I-129 and Tc-99 are generally very similar in magnitude. This is coincidental given the relative inventories, modes and rates of release, and dose conversion factors.

Figure 5.5-5: Radionuclide Dose Contributors to Sector D for the 100-Meter MOP Peak Ground Water Pathways Dose within 1,000 Years

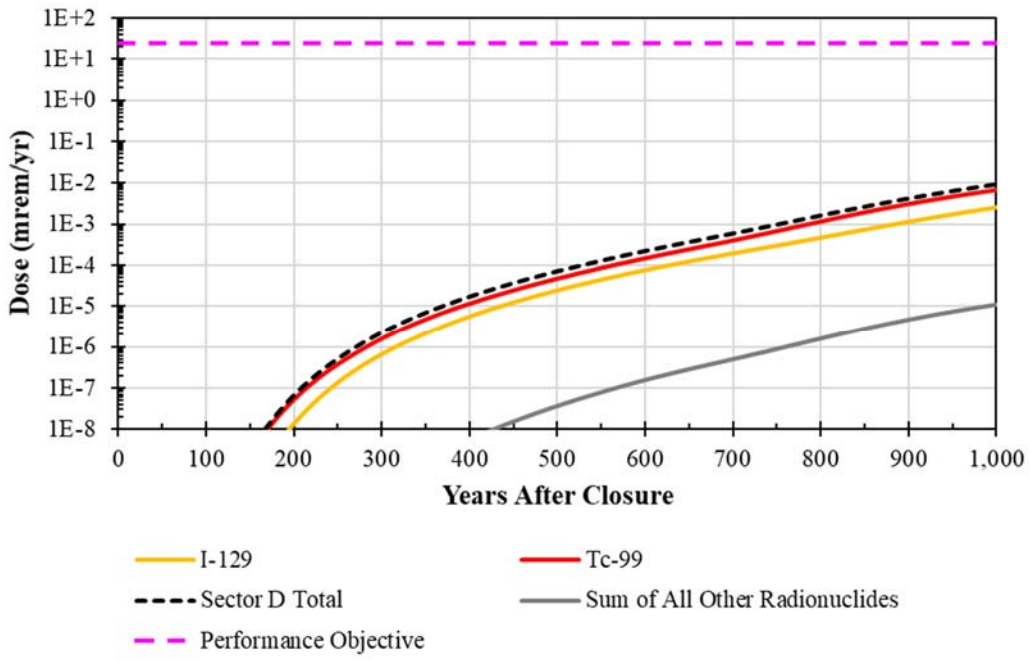

Figure 5.5-6: Radionuclide Dose Contributors to Sector D for the 100-Meter MOP Peak Ground Water Pathways Dose within 1,000 Years (Detail)

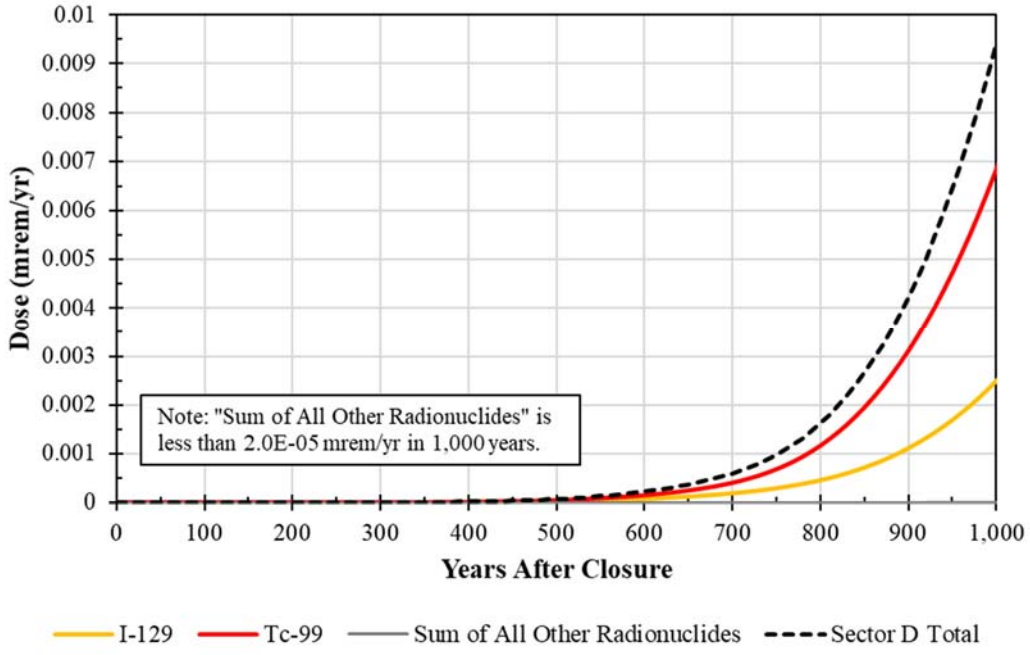

Figure 5.5-7: Radionuclide Dose Contributors to Sector B for the 100-Meter MOP Peak Ground Water Pathways Dose within 10,000 Years

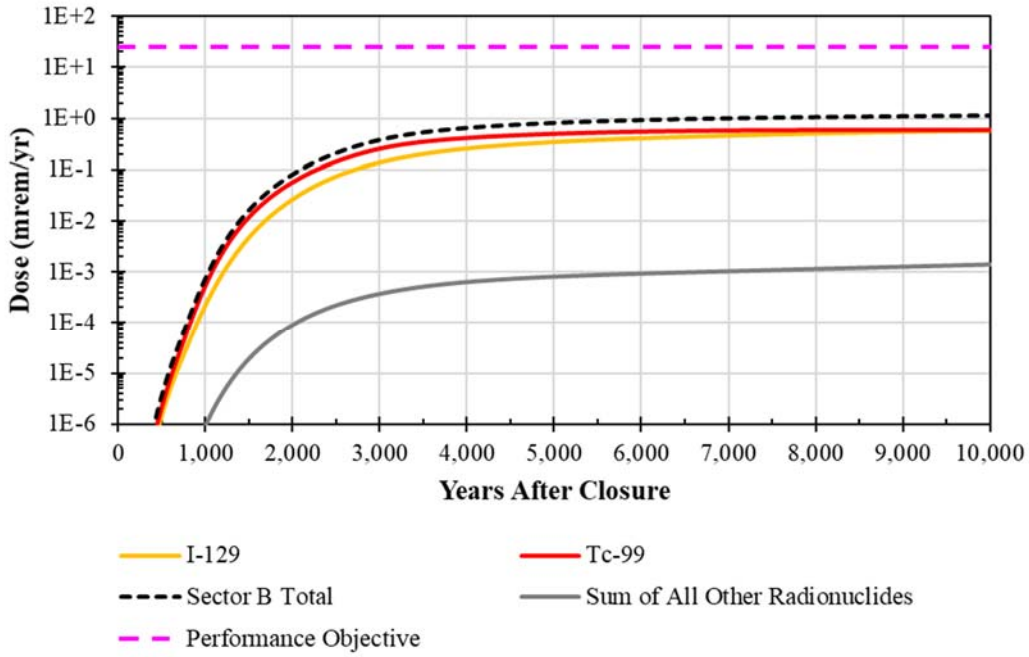

Figure 5.5-8: Radionuclide Dose Contributors to Sector B for the 100-Meter MOP Peak Ground Water Pathways Dose within 10,000 Years (Detail)

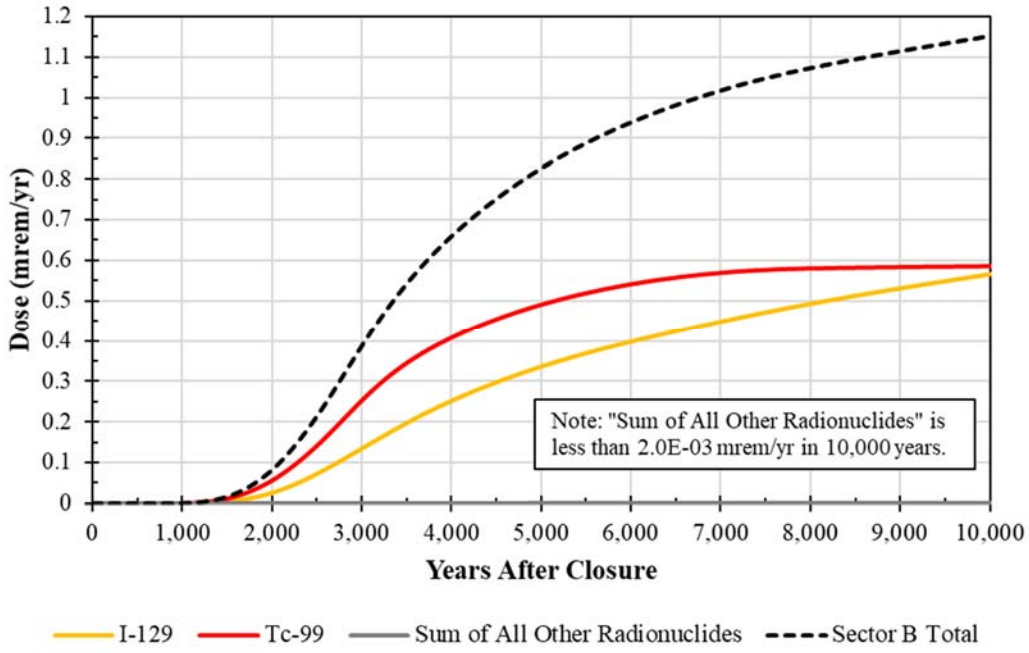

Table 5.5-2 summarizes the relative radionuclide dose contributions to the corresponding to peak doses within the Compliance Period and the Performance Period.

Table 5.5-2: Summary of Radionuclide Dose Contributors for the Peak 100-Meter MOP Peak Ground Water Pathways Doses

Radionuclide	Compliance Period (Peak at Sector D at 1,000 Years)		Performance Period (Peak at Sector B at 10,000 Years)	
	Contribution to Peak Dose (mrem/yr)	Percent of Peak	Contribution to Peak Dose (mrem/yr)	Percent of Peak
I-129	2.5E-03	27%	0.56	49%
Tc-99	6.9E-03	73%	0.59	51%
All Others	1.1E-05	<0.1%	1.4E-03	<0.1%
Total	9.4E-03	100%	1.2	100%

5.5.1.3 MOP at 100-Meters, Individual Pathway Contribtuions to Ground Water Pathways Doses

The total peak ground water pathways dose results are the sum of the doses associated with all the individual 100-meter pathways identified in Section 5.4. Table 5.5-3 shows the relative contributions from the individual ground water pathways to the 100-meter MOP receptor dose at years of the peak doses (i.e., Sector D at 1,000 years after closure for the Compliance Period and Sector B at 10,000 years after closure for the Performance Period). The primary contributors at 1,000 years after closure are water ingestion, plant ingestion, and fish ingestion, which collectively account for 98% of the total dose contributions. The primary contributors at 10,000 years are water ingestion, plant ingestion, and fish ingestion. Collectively these three pathways account for more than 97% of the total dose contributions.

Table 5.5-3: Summary of Ground Water Pathways Dose Contributors for the Peak 100-Meter MOP Doses

Pathway	Compliance Period (Peak at Sector D at 1,000 Years)		Performance Period (Peak at Sector B at 10,000 Years)	
	Contribution to Peak Dose (mrem/yr)	Percent of Peak	Contribution to Peak Dose (mrem/yr)	Percent of Peak
Water Ingestion	6.7E-03	72%	0.85	74%
Plant Ingestion	2.1E-03	22%	0.22	19%
Fish Ingestion	3.9E-04	4%	0.056	5%
All Other Pathways	1.7E-04	2%	0.029	<3%
Total	**9.4E-03**	**100%**	**1.2**	**100%**

These results are graphically depicted over time in Figure 5.5-9 through Figure 5.5-12. In general, water ingestion makes up approximately 74% of the total dose contribution to the 100-meter MOP, while most of the remaining 26% is attributed to contributions from plant or fish ingestion.

Figure 5.5-9: Pathway Contributors to Dose in Sector D within 1,000 Years

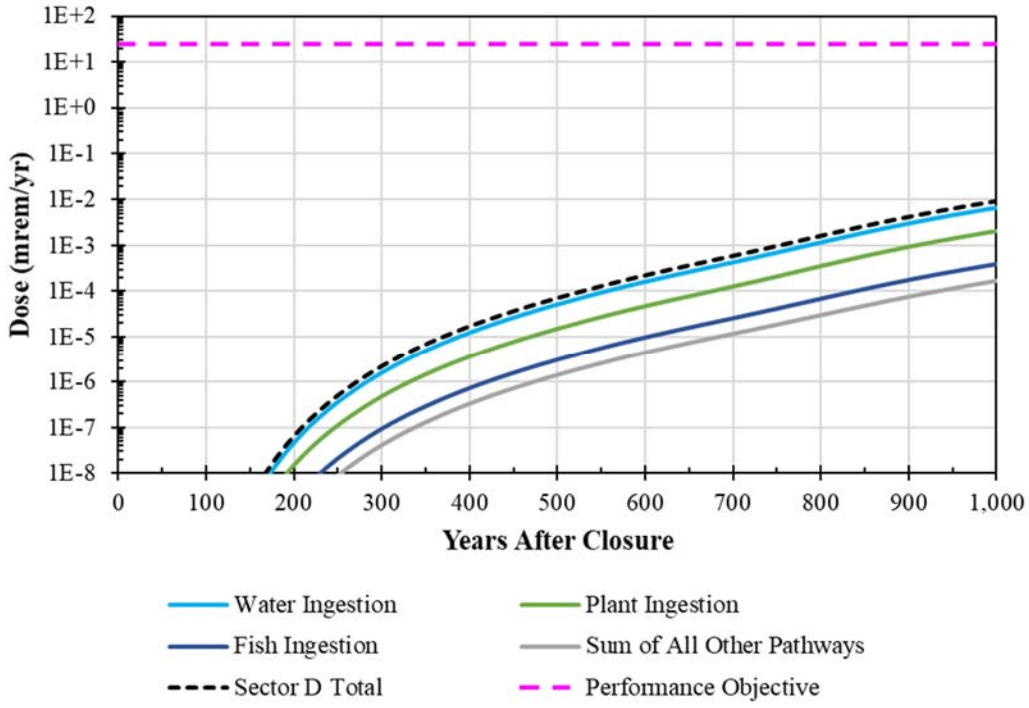

Figure 5.5-10: Pathway Contributors to Dose in Sector D within 1,000 Years (Detail)

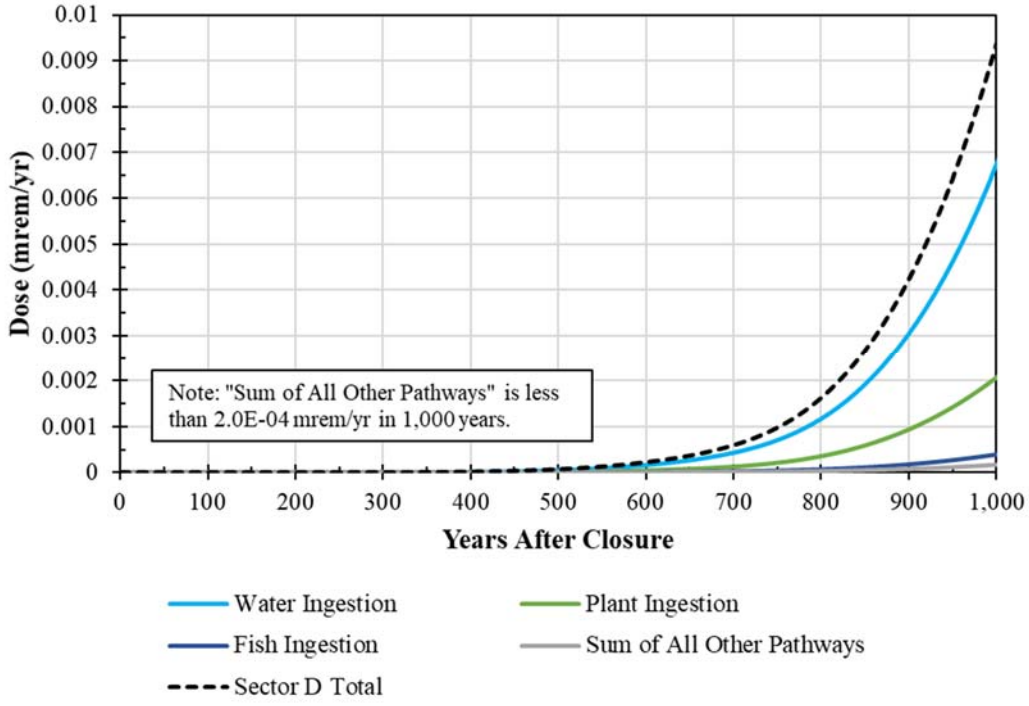

Figure 5.5-11: Pathway Contributors to Dose in Sector B within 10,000 Years

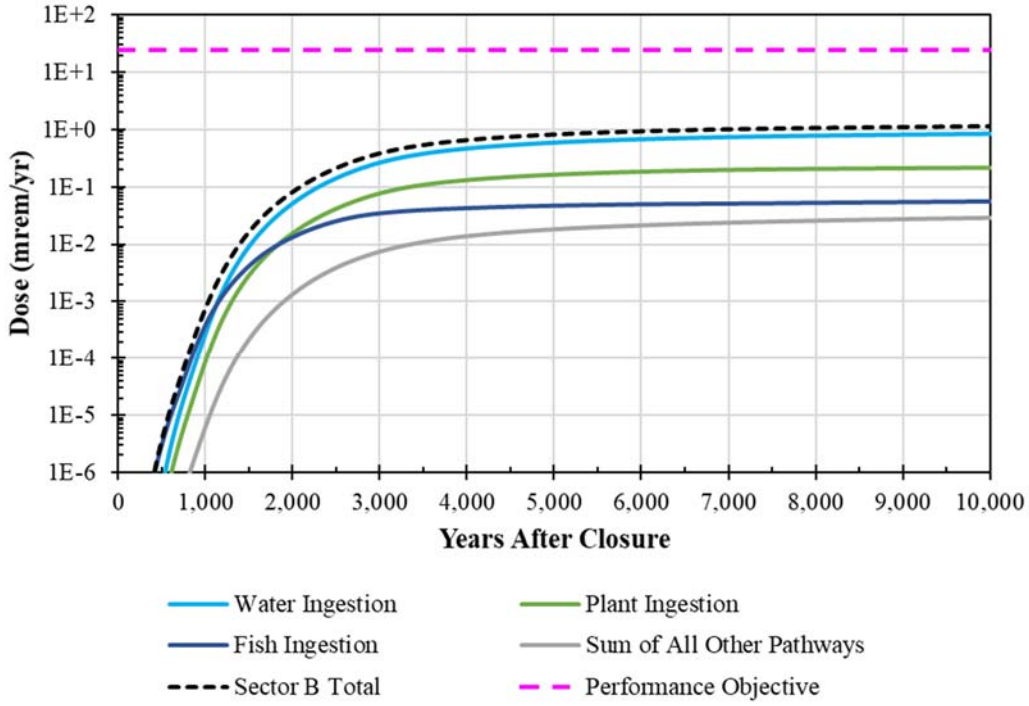

Figure 5.5-12: Pathway Contributors to Dose in Sector B within 10,000 Years (Detail)

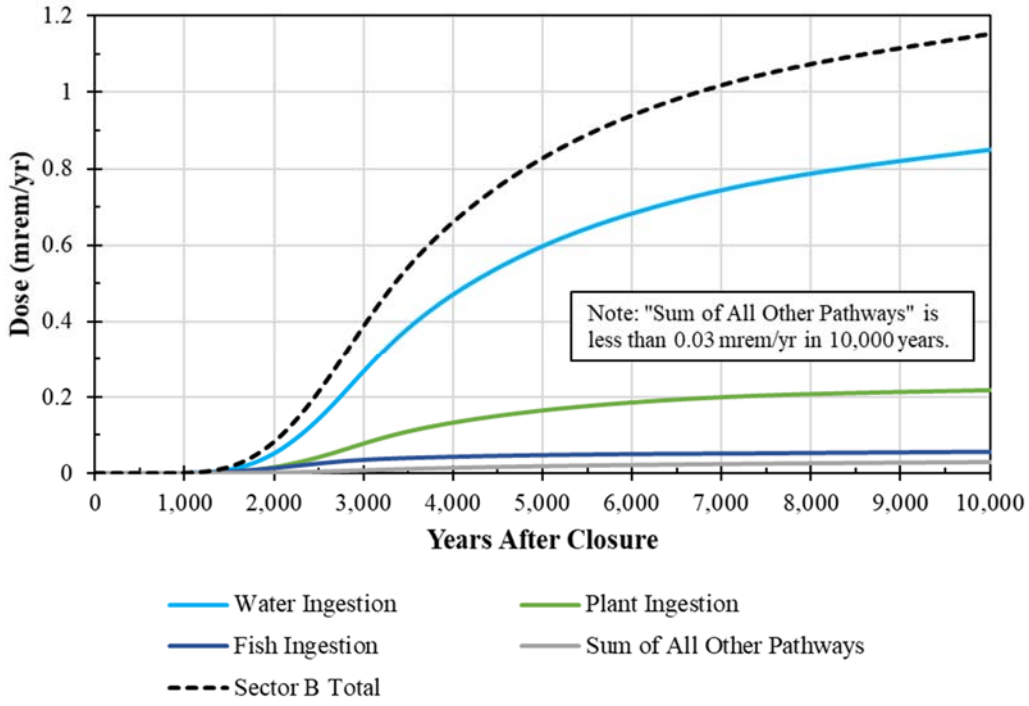

5.5.1.4 MOP at 100-Meters, Individual SDU Contributions to Ground Water Pathways Doses

Table 5.5-4 and Table 5.5-5 show the relative dose contributions from the various distinct SDU sources to each of the sectors (along the 100-meter boundary) for the Compliance Period and for the Performance Period, respectively. These relative percentages are based on relative values at the time of the peak doses for each sector. These results provide valuable insight regarding which disposal units have the most influence on the dose results.

Note that the sum of the relative dose contributions can exceed 100% because the location of the dose contributions from each SDU may not be at the same location as the peak dose when all sources are being considered. For example, during the Performance Period SDU 8 contributes 0.75 mrem/yr at one location along Sector B, but this is a discretely different location along Sector B than the peak dose contribution from SDU 11 (0.59 mrem/yr). In other words, the peak dose along Sector B is not the sum of all the peak SDU dose contributions anywhere along the sector, but rather it is the sum of the dose contributions at one discrete location along the sector.

Figure 5.5-13 shows the individual dose contributions from each SDU to the dose at Sector D during the Compliance Period. Similarly, Figure 5.5-14 shows the individual dose contributions from each SDU to the dose at Sector B during the Performance Period. These figures illustrate the relative importance of specific SDUs.

Table 5.5-4: Relative SDU Source Contributions to 100-Meter MOP Peak Doses During the Compliance Period (0 to 1,000 Years)

	Relative SDU Source Contributions (%) to Each Sector							
Source	**A**	**B**	**C**	**D**	**E**	**F**	**G**	**H**
Year of Peak	*1,000*	*1,000*	*1,000*	*1,000*	*1,000*	*1,000*	*1,000*	*1,000*
SDU 1	<0.1%	<0.1%	<0.1%	<0.1%	0.5%	3.6%	4.0%	100%
SDU 4	<0.1%	<0.1%	<0.1%	<0.1%	2.1%	98%	98%	<0.1%
SDU 2A	<0.1%	<0.1%	<0.1%	0.3%	11.6%	<0.1%	<0.1%	<0.1%
SDU 2B	<0.1%	<0.1%	<0.1%	0.3%	11.9%	<0.1%	<0.1%	<0.1%
SDU 3A	<0.1%	<0.1%	1.9%	<0.1%	<0.1%	<0.1%	<0.1%	<0.1%
SDU 3B	<0.1%	<0.1%	1.6%	<0.1%	<0.1%	<0.1%	<0.1%	<0.1%
SDU 5A	<0.1%	1.6%	1.6%	<0.1%	<0.1%	<0.1%	<0.1%	<0.1%
SDU 5B	<0.1%	0.2%	1.1%	<0.1%	<0.1%	<0.1%	<0.1%	<0.1%
SDU 6	<0.1%	16%	1.1%	<0.1%	<0.1%	<0.1%	<0.1%	<0.1%
SDU 7	<0.1%	9.6%	0.7%	0.4%	13%	<0.1%	<0.1%	<0.1%
SDU 8	<0.1%	81%	2.3%	<0.1%	<0.1%	<0.1%	<0.1%	<0.1%
SDU 9	<0.1%	<0.1%	100%	100%	15%	<0.1%	<0.1%	<0.1%
SDU 10	<0.1%	<0.1%	<0.1%	<0.1%	100%	10.2%	<0.1%	<0.1%
SDU 11	41%	40%	<0.1%	<0.1%	<0.1%	<0.1%	<0.1%	<0.1%
SDU 12	72%	75%	<0.1%	<0.1%	<0.1%	<0.1%	<0.1%	<0.1%

Table 5.5-5: Relative SDU Source Contributions to 100-Meter MOP Peak Doses During the Performance Period (0 to 10,000 Years)

	Relative SDU Source Contributions (%) to Each Sector							
Source	**A**	**B**	**C**	**D**	**E**	**F**	**G**	**H**
Year of Peak	*10,000*	*10,000*	*10,000*	*10,000*	*10,000*	*10,000*	*10,000*	*10,000*
SDU 1	<0.1%	<0.1%	<0.1%	<0.1%	0.2%	11.4%	26%	100%
SDU 4	<0.1%	<0.1%	<0.1%	<0.1%	<0.1%	38%	85%	<0.1%
SDU 2A	<0.1%	<0.1%	<0.1%	6.4%	9.1%	<0.1%	<0.1%	<0.1%
SDU 2B	<0.1%	<0.1%	<0.1%	5.0%	9.3%	<0.1%	<0.1%	<0.1%
SDU 3A	<0.1%	<0.1%	27%	<0.1%	<0.1%	<0.1%	<0.1%	<0.1%
SDU 3B	<0.1%	<0.1%	24%	1.0%	<0.1%	<0.1%	<0.1%	<0.1%
SDU 5A	<0.1%	1.2%	20%	<0.1%	<0.1%	<0.1%	<0.1%	<0.1%
SDU 5B	<0.1%	0.2%	13%	<0.1%	<0.1%	<0.1%	<0.1%	<0.1%
SDU 6	<0.1%	49%	59%	5.1%	<0.1%	<0.1%	<0.1%	<0.1%
SDU 7	<0.1%	27%	36%	39%	45%	<0.1%	<0.1%	<0.1%
SDU 8	<0.1%	69%	33%	<0.1%	<0.1%	<0.1%	<0.1%	<0.1%
SDU 9	<0.1%	<0.1%	68%	92%	0.7%	<0.1%	<0.1%	<0.1%
SDU 10	<0.1%	<0.1%	<0.1%	<0.1%	100%	100%	<0.1%	<0.1%
SDU 11	55%	54%	1.0%	<0.1%	<0.1%	<0.1%	<0.1%	<0.1%
SDU 12	64%	67%	<0.1%	<0.1%	<0.1%	<0.1%	<0.1%	<0.1%

Figure 5.5-13: SDU Source Contributors to Dose in Sector D During the Performance Period

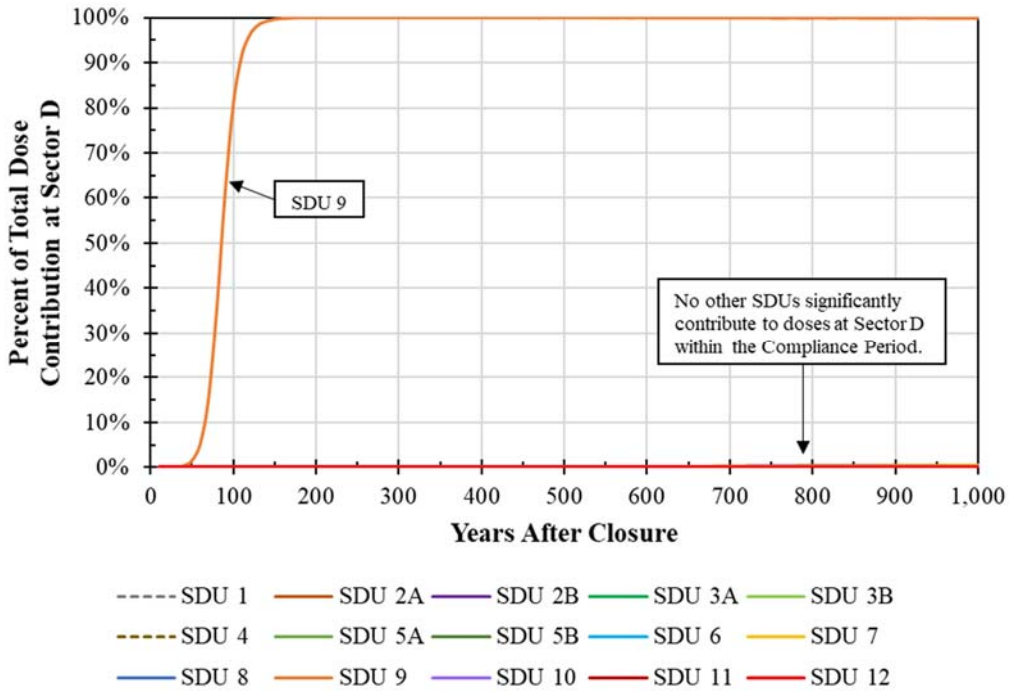

Figure 5.5-14: SDU Source Contributors to Dose in Sector B During the Performance Period

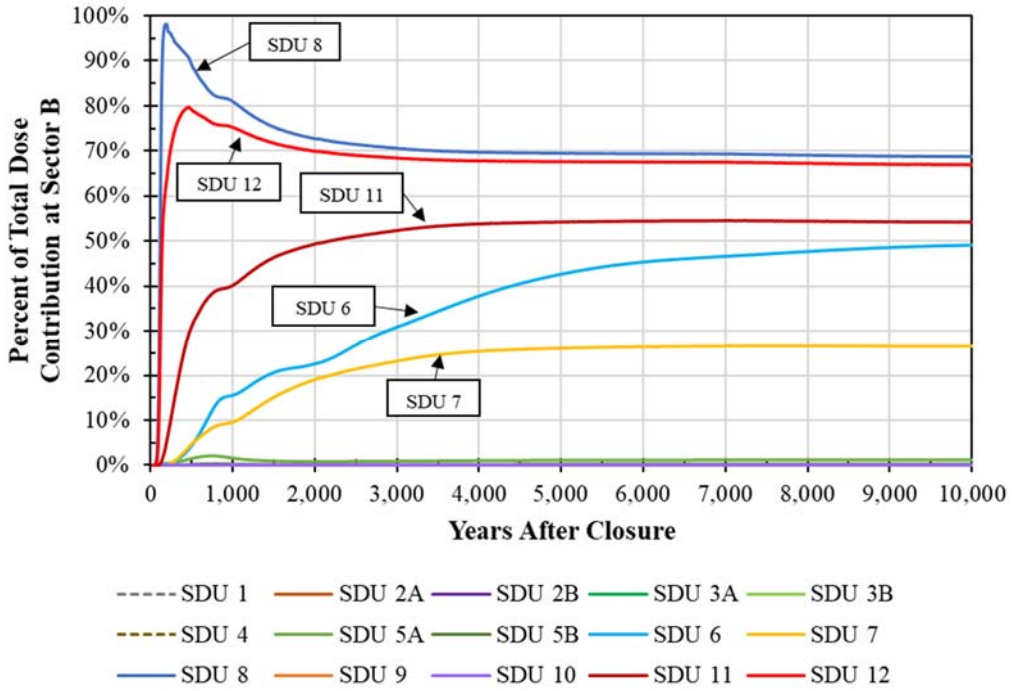

During the Compliance Period and for most of the Performance Period, the highest doses are observed at Sector D. Figure 5.5-15 and Figure 5.5-16 show the transport plumes of I-129 and Tc-99, respectively, from every SDU at three select times: 2,000 years, 5,000 years and 10,000 years after closure. At 1,000 years, no significant plumes were observed.

These figures illustrate how releases from SDU 9 reach the 100-meter boundary (at Sector D) much earlier than other SDUs, and therefore control the doses in early times. SDU 9 remains the primary source for contributing to doses along the 100-meter boundary, until the plumes at Sector B increase in concentration to become higher than the concentrations at Sector D. Due to the distances between the SDUs, this process takes thousands of years. In other words, it is expected that SDU 9 will dominate in early times because this SDU is assumed to be constructed at a lower elevation such that it is in closer proximity to the water table (see Table 4.3-1). While the magnitudes of the doses along the 100-meter boundary in Sectors A through F are similar, the earlier timing for Sector D results in Sector D being the dominant sector throughout most of the Performance Period.

Over time, Sectors A and B increase in importance (see Section 5.5.1.5). Doses to the 100-meter boundary in Sectors A and B are both influenced by the releases from SDUs 11 and 12. Additionally, doses along the 100-meter boundary in Sector B are also strongly influenced by the releases from SDUs 6 and 8. Since the doses for Sectors A and B are driven by plumes from multiple SDUs, when these plumes closely overlap (as shown in Figure 5.5-15 and Figure 5.5-16) the doses at these sectors eventually become higher than at Sector D.

Figure 5.5-15: SDF Plumes for I-129 at 2,000 Years, 5,000 Years, and 10,000 Years After SDF Closure

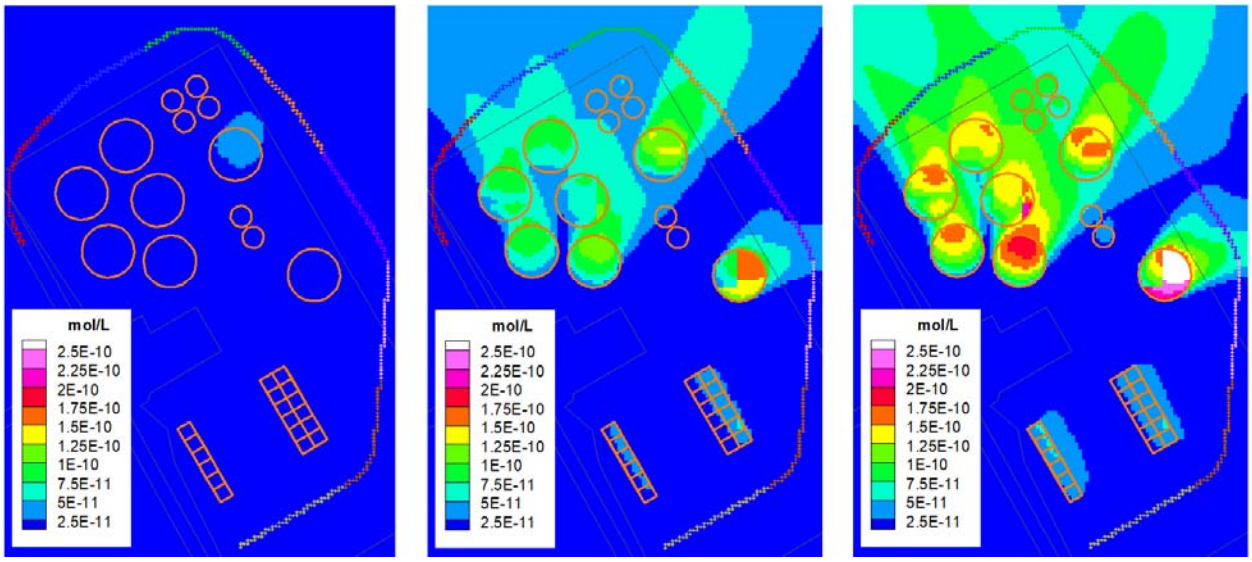

I-129 Plumes at 2,000 Years *I-129 Plumes at 5,000 Years* *I-129 Plumes at 10,000 Years*

Figure 5.5-16: SDF Plumes for Tc-99 at 2,000 Years, 5,000 Years, and 10,000 Years After SDF Closure

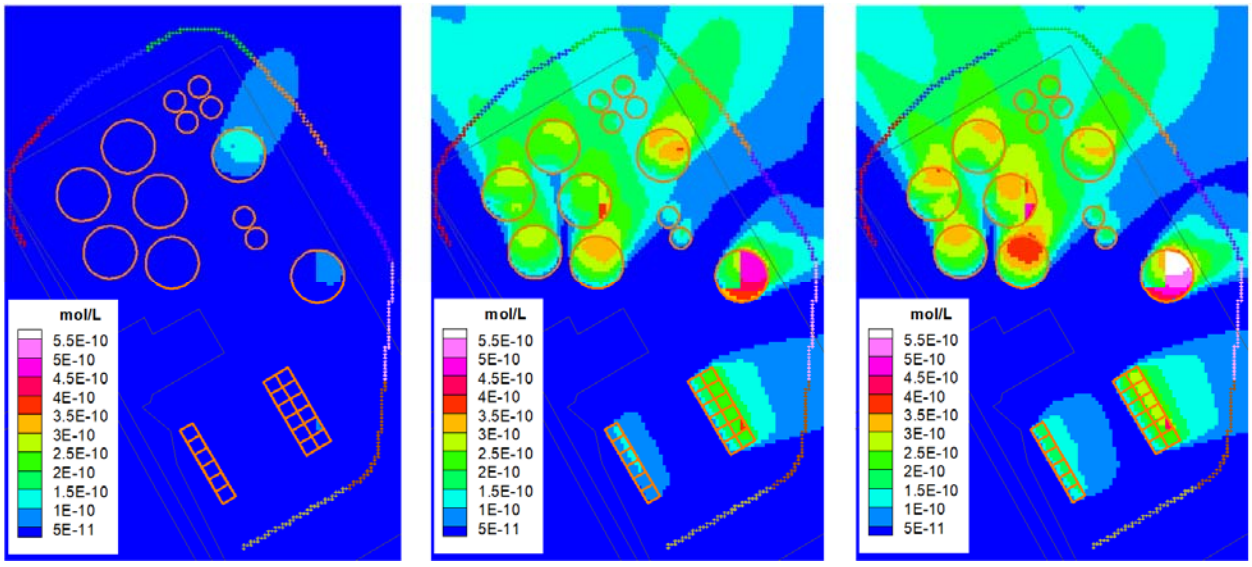

Tc-99 Plumes at 2,000 Years *Tc-99 Plumes at 5,000 Years* *Tc-99 Plumes at 10,000 Years*

5.5.1.5 MOP at 100-Meters, Ground Water Pathways Doses Over 100,000 Years

The peak ground water pathways dose was also calculated out to 100,000 years after SDF closure. This Long-Term Exploratory Period was simulated for the purpose of identifying potential risks over extremely long periods. Only the sensitivity run radionuclides (as identified in Section 5.2.4) were simulated beyond 20,000 years.

After the Performance Period, the highest doses are observed in Sector B. There are two locations along the 100-meter boundary in Sector B which may exhibit peak doses, both with very similar magnitudes. One peak occurs near the Sector A boundary and is attributed to the plumes from SDUs 11 and 12. The other peak occurs closer to the middle of Sector B and is attributed to the plumes from SDUs 6 and 8.

Figure 5.5-17 and Figure 5.5-18 show the sector-specific doses to the MOP at 100-meters for this 100,000-year, Long-Term Exploratory Period. The peak dose (approximately 1.5 mrem/yr) is an order of magnitude below the performance objective (25 mrem/yr) and occurs approximately 58,000 years after SDF closure (see Figure 5.5-19).

This peak dose is attributed to a chemical transition in the lower mud mats of the 375-foot diameter SDUs (from Oxidizing Region I to Oxidizing Region III). When this transition occurs, the K_d for iodine within the mud mat decreases by a factor of two (from 8 mL/g to 4 mL/g), effectively expelling I-129 into the soils. This increases the concentration of I-129, which contributes to a slight increase in dose (Figure 5.5-19). Shortly after the peak occurs, the inventories of I-129 from the 375-foot diameter SDUs decome depleted such that doses decrease between 60,000 years and 100,000 years after closure.

Figure 5.5-17: 100-Meter MOP Peak Ground Water Pathways Dose within 100,000 Years, Sectors A through H

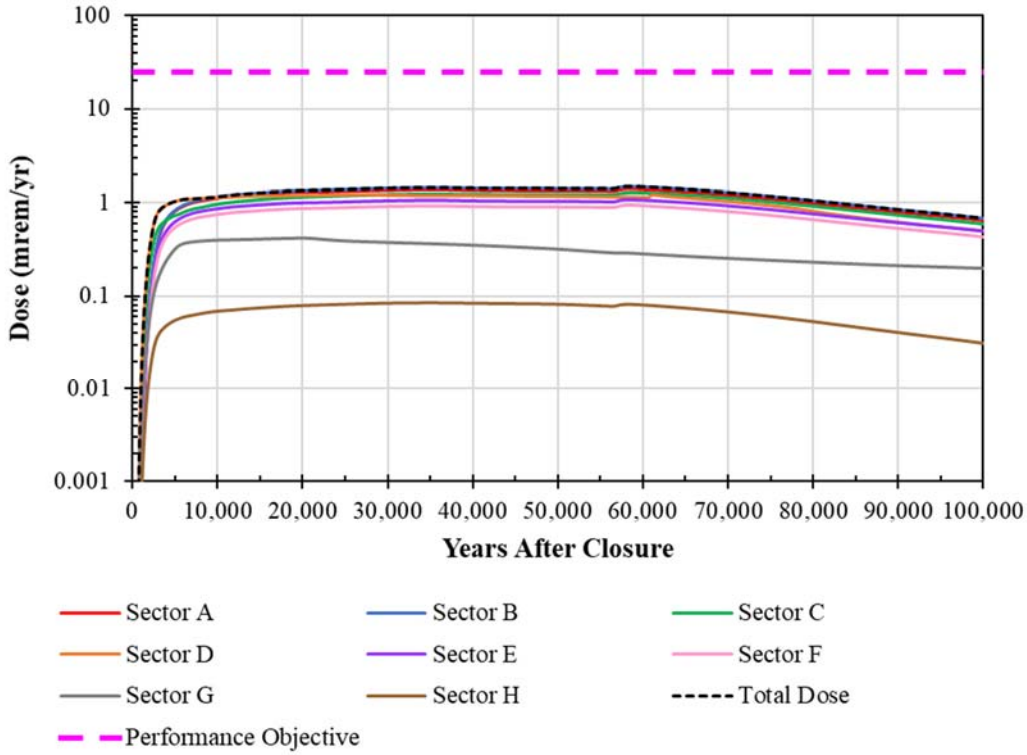

Figure 5.5-18: 100-Meter MOP Peak Ground Water Pathways Dose within 100,000 Years, Sectors A through H (Detail)

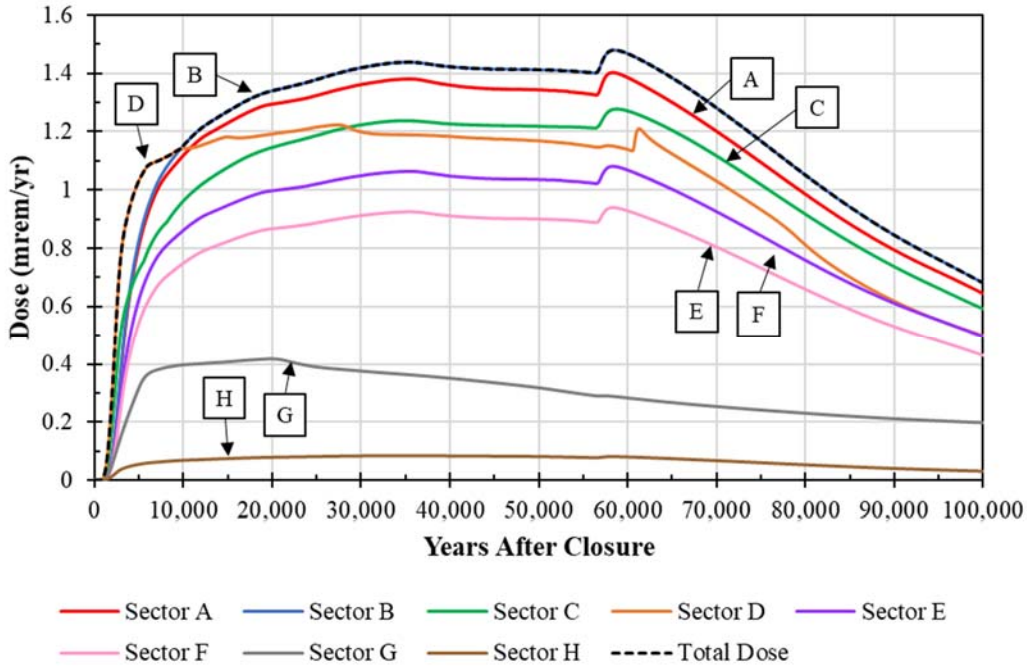

Figure 5.5-19: Radionuclide Dose Contributors to Sector B for the 100-Meter MOP Peak Ground Water Pathways Dose within 100,000 Years (Detail)

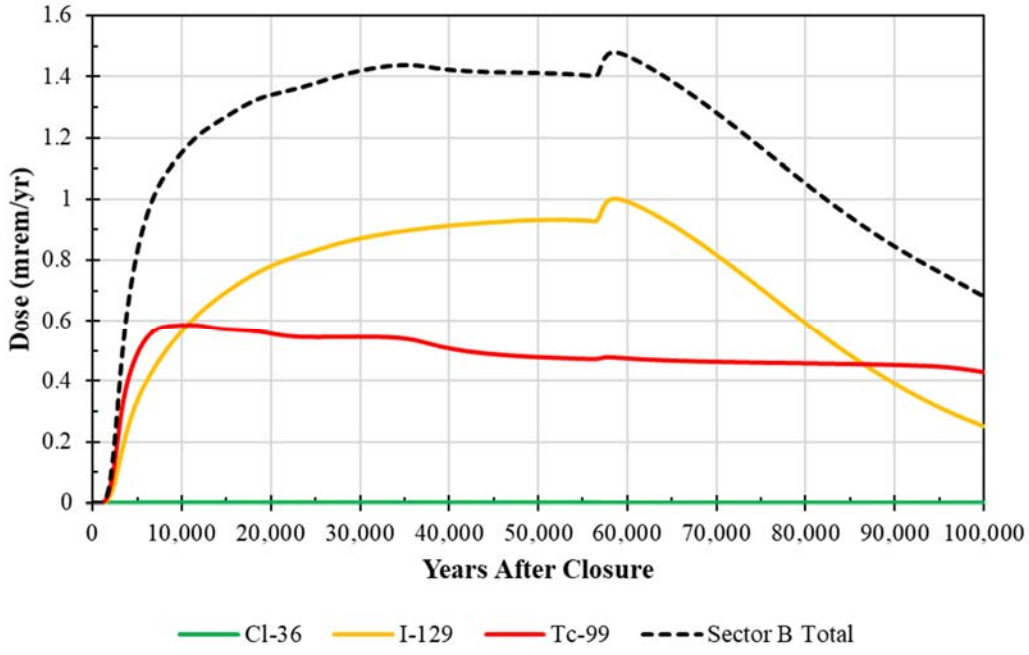

Because this evaluation only examined the sensitivity run radionuclides, an extra analysis was performed using the SDF GoldSim Model which considered all of the radionuclides in the SDF inventory. This analysis showed that following Tc-99 and I-129, the next highest dose contributors over 100,000 years were K-40 (5.2E-03 mrem/yr), Cs-135 (3.9E-03 mrem/yr), and Cl-36 (1.6E-03 mrem/yr). These were followed by Np-237 (4.9E-08 mrem/yr), Pa-231 (1.8E-08 mrem/yr), and Ac-227 (1.2E-10 mrem/yr). These results indicate that selected sensitivity run radionuclides are sufficient for evaluating risk.

5.5.2 MOP at the Seepline Ground Water Pathways Dose Results

The total dose to the MOP at the seepline (SL) assumes that the MOP uses stream water as a primary source of water for day-to-day activities (as opposed to relying on well-water as assumed for the MOP at 100-meters as described in Section 5.5.1). Because the concentrations at the SL are lower than the concentrations in the well-water along the 100-meter boundary, these doses are lower. As such, this SL scenario does not represent a compliance scenario, but is included to provide additional insights.

During the Compliance Period (i.e., the first 1,000 years after SDF closure), the MOP is assumed to use water from the MQB SL, as the doses based on the concentrations at the MQB SL are higher than those based on the UTR SL (see Figure 5.5-20). Then, once UTR SL becomes the higher SL dose contributor (at 990 years after closure), it is assumed that the MOP will relocate and make use of the water from the UTR SL (see Figure 5.5-21).

At 1,000 years after SDF closure, the peak dose is insignificant. At 10,000 years after SDF closure, the peak dose increases to approximately 0.3 mrem/yr, which is still insignificant and well below the 25 mrem/yr performance objective.

Doses along either SL (MQB or UTR) are always dominated by contributions from I-129 and Tc-99. At 1,000 years, I-129 makes up 26% of the total dose and Tc-99 makes up 74% of the total dose. At 10,000 years, I-129 makes up 51% of the total dose and Tc-99 makes up 49% of the total dose. All other radionuclide contributions were negligible relative to those of I-129 and Tc-99.

The dose pathways for the MOP at the SL are similar to those for the MOP at 100-meters, but at a lower magnitude. Water ingestion is the dominant dose pathway, making up approximately 63% of the total dose at both 1,000 years and at 10,000 years. Plant ingestion and fish ingestion are the next most important, each accounting for approximately 15% to 20% of the total dose.

Figure 5.5-20: Seepline MOP Peak Ground Water Pathways Dose within 1,000 Years

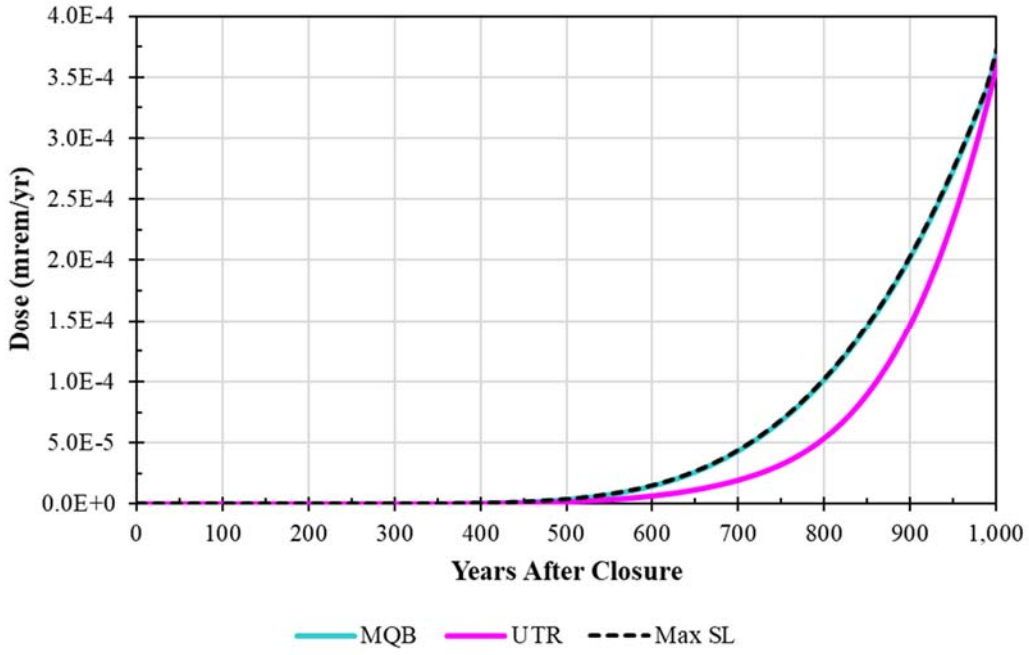

Figure 5.5-21: Seepline MOP Peak Ground Water Pathways Dose within 10,000 Years

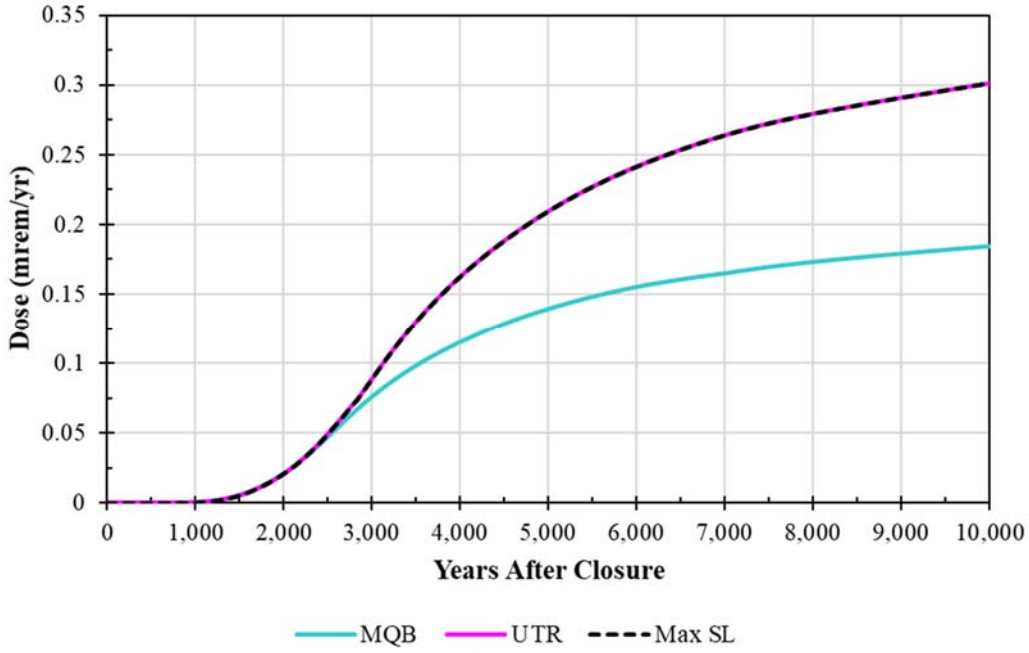

5.5.2.1 MOP at the Seepline Ground Water Pathways Dose Results Based on the Seepline Ratio

One final consideration is the SL ratio, which is a simplified approach used to efficiently account for the concentrations along the SL. The determination of the SL ratio is described in Section 5.2.3. Figure 5.5-22 shows that using the SL ratio is a reasonable approach for estimating dose contributions. Because the SL ratio is based on concentrations along the 100-meter boundary, it also shows earlier increases relative to the values from the more explicit aquifer transport modeling. Because the SL ratio yields reasonable results, it is used for all the simulations in this PA except for those within this section used to describe the SL results (i.e., Section 5.5.2): the results in Section 5.5.1, and all results presented for other modeling cases use the SL ratio rather than the maximum of the MQB or the UTR.

Figure 5.5-22: Seepline MOP Peak Ground Water Pathways Dose within 10,000 Years, Including Results Based on the SL Ratio

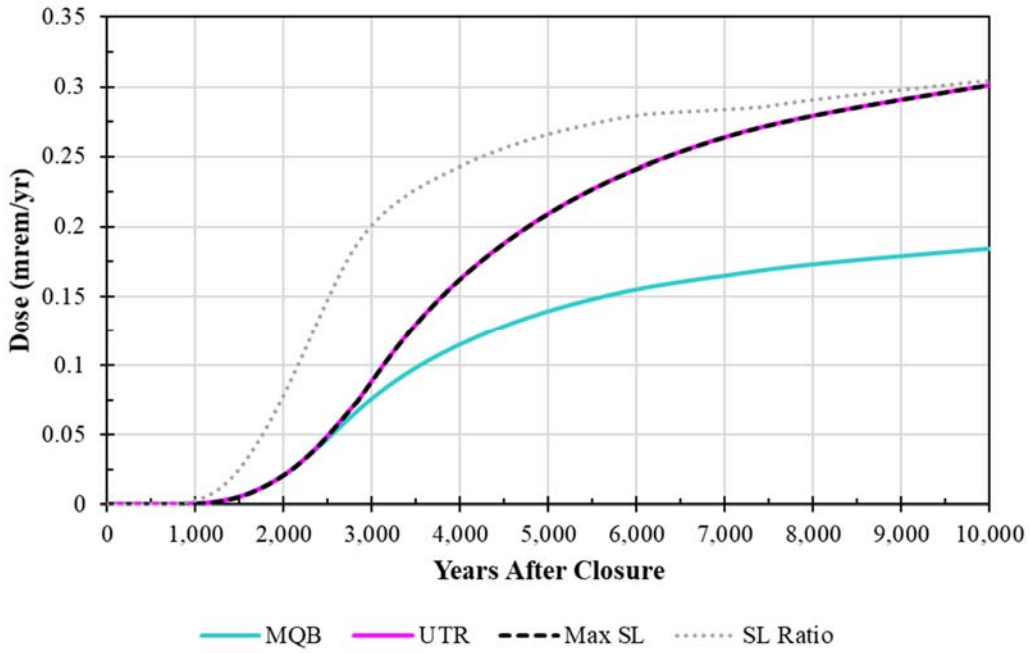

This page intentionally left blank.

5.6 GoldSim Benchmarking

The PORFLOW-developed Vadose Zone Flow Model, Vadose Zone Transport Model, and Aquifer Transport Model (collectively referred to as the SDF PORFLOW Model) are multidimensional flow and transport models designed to rigorously simulate the transport and fate of radionuclides and non-radioactive species released from the SDUs. The SDF GoldSim Model is an abstraction of the SDF PORFLOW Model and is designed to perform probabilistic uncertainty quantification and sensitivity analyses that would be prohibitive using the computationally intensive SDF PORFLOW Model.

The SDF GoldSim Model is focused on 1) reduced dimensionality and grid resolution to minimize the number of computational nodes used in numerical transport simulations, 2) adoption of PORFLOW-generated vadose zone flow fields to avoid numerical solution of the highly non-linear Richards equation, and 3) simplification of PORFLOW shrinking core models.

Spatially averaged flow rates generated from the SDF PORFLOW Model are used as input to the SDF GoldSim Model to define the influence of advection on the transport of radionuclides through a simplified assemblage of the containment features (e.g., the saltstone monolith, floor, upper mud mat, lower mud mat, wall, and HDPE/GCL liners) as well as potential release features (such as joints). While two-dimensional flow can take place within the containment structures represented by the SDF PORFLOW Model, the SDF GoldSim Model is mainly limited to one-dimensional flow through these features. Note that horizontal flow through horizontal wall joints connecting saltstone to backfill is simulated. Otherwise the horizontal migration of radionuclides within the vadose zone model is limited to diffusive transport. In the saturated zone, the complex three-dimensional PORFLOW flow fields are represented by one-dimensional flow "pipes" that were developed as abstractions of PORFLOW generated stream traces and/or tracer plumes (see Section 4.4.6). The one-dimensional GoldSim flow paths emanate from the upgradient edge of the SDU footprints with the flux, defined by the vadose zone releases, applied to the segments of the stream traces under the SDU footprints. In the saturated zone, the streamtrace lengths and particle transport times were used to determine the flow velocities from the SDU footprints to the 100-meter boundary. For a more detailed description of the abstracted model, refer to Section 4.5.

The section below describes the process used to evaluate how well the SDF GoldSim Model approximately replicates the SDF PORFLOW Model. This process is an intermodel comparison referred to as "benchmarking." The purpose of this comparison is to ensure the aptness of the abstracted model as an effective surrogate for the PORFLOW Vadose Zone Transport Model by comparing results from the complex process model (i.e., the SDF PORFLOW Model) against the results from the simplified abstraction (i.e., the SDF GoldSim Model).

Benchmarking is necessary to provide justification for the assumption that when the SDF GoldSim Model simulations are run stochastically (e.g., multi-realizations are performed to test ranges of uncertain values), the results approximate the results of the SDF PORFLOW Model for the same input combinations and reflect the influence of important processes. Specifically, deterministic bias between GoldSim and PORFLOW is ideally small relative to stochastic

uncertainty for accurate uncertainty quantification. Alternatively, if GoldSim concentration and dose predictions are consistently biased high compared to the respective PORFLOW values, then compliance with performance objectives and measures can nonetheless be established. Uncertainty quantification of PA model predictions (see Figure 5.7-6) suggests $5^{th}/95^{th}$ percentile doses around ± 500% around the median peak dose result. Therefore, GoldSim benchmarking results should lie within approximately 25% of PORFLOW results, or be biased high to support decision-making. The 25% represents approximately 2.5% of the range reflected in the 10,000 year $5^{th}/95^{th}$ percentile values as shown in Figure 5.7-6. Note that the 25% represents a guideline used here, not a hard and fast rule. For example the GoldSim and PORFLOW I-129 conceptual models differ, with PORFLOW using a more computationally intensive "shrinking core" model for generating chemical environment transition patterns (one cell at a time) and the GoldSim conceptual model assuming that larger zones are transitioned as one. For I-129, the GoldSim conceptual model will generate a spatially averaged zonal transition time. The SDF GoldSim Model is more computationally efficient but will result in larger early time releases. The lower PORFLOW Model releases are associated with a higher-K_d "rind" thickening over time around the saltstone. Because the SDF GoldSim Model is based on a more conservative conceptual model, benchmarking results where the SDF GoldSim Model peak values are greater than 25% more than the PORFLOW Model results are considered acceptable.

5.6.1 Overview of Benchmarking

In this benchmarking effort, PORFLOW/GoldSim comparisons were performed in two phases. The first phase focuses on how well the abstraction model approximates the radionuclide releases from the SDUs. Time histories of the radionuclide release rates from the vadose zone beneath the SDUs into the saturated zone are used for this comparison. The second phase focuses on how well the abstraction model approximates the radionuclide transport behavior in the saturated zone. The maximum total doses at the 100-meter compliance boundary, the sector-based (see Figure 4.4-114) total doses at the boundary, and the radionuclide-specific dose contributions are examined for this task. Because radionuclide-specific dose contributions are a function of associated ground water concentrations, time histories of radionuclide concentrations at the 100-meter compliance boundary that were used to derive the dose-contributions are presented along with the dose contributions. This benchmarking evaluation was conducted for the deterministic Compliance Case results.

The SDF GoldSim Model simulates all of the SDUs as 15 different source release locations. These are composed of nine in-place SDUs, as well as six future SDUs. The SDUs are classified by size and shape, including: the two rectangular SDUs (SDU 1 and SDU 4), six 150-foot diameter cylindrical SDUs (SDU 2A, SDU 2B, SDU 3A, SDU 3B, SDU 5A, and SDU 5B), and seven 375-foot diameter cylindrical SDUs (SDU 6, SDU 7, SDU 8, SDU 9, SDU 10, SDU 11, and SDU 12). As implemented in the SDF PORFLOW Model, the six 150-foot diameter cylindrical units are considered similar enough to be evaluated by using a single representative unit and are classified as "Type-2" SDUs. Also, as implemented in the SDF PORFLOW Model, five of the seven 375-foot diameter cylindrical units are considered similar enough to be evaluated by a representative

unit and are classified as "Type-7" SDUs. SDU 6 and SDU 9 are different enough that they are evaluated individually.

To derive the releases from specific SDUs, the SDF PORFLOW Model assigns a 1.0 Ci inventory for each radionuclide (or 1.0 kg for each non-radioactive chemical) within each simulated SDU. The releases are later scaled by the ratio of the SDU-specific inventories to the 1.0 Ci or kg inventories. The exception to this approach is Tc-99; due to solubility control on Tc, PORFLOW explicitly models the Tc-99 inventory (using the values from Section 3.3.3) in the vadose zone simulation. Note that for decay chains, the scaling method limits PORFLOW to evaluating the release of a parent species and its daughter species based on an initial inventory of a single-parent species and zero-Ci inventories of daughter species. Decay chain releases are then derived from the superposition of radionuclide specific releases from simulations for each member of a decay chain. The simplified SDF GoldSim Model includes complete SDU inventories (not including Tc-99) as initial conditions and all SDUs can be simulated in the same run.

In probabilistic mode, the SDF GoldSim Model randomly selects a set of flow fields from 54 sets of flow fields generated from PORFLOW. These flow field represents the flow conditions identified in Table 4.4-82. Within each set, there is an independent flow field for each SDU type; this data includes flow rates, SDU saturation states, chemistry transition times, Tc-99 releases from the SDUs, and time-varied diffusion coefficients.

For the benchmarking effort, a comparison of results for every radionuclide at all locations and for every flow field would be quite extensive. The benchmarking comparison selection process was devised to reduce the number of comparisons required, but still ensure that adequate model comparisons are considered.

5.6.1.1 Representative SDUs

For benchmarking purposes, four representative SDUs were selected for evaluation: SDU 1, SDU 4, SDU 2A, and SDU 7. Although SDU 6 and SDU 9 differ to some extent from the other 375-foot diameter SDUs (the Type-7 SDUs), they use the same calculation logic (with different input parameters as needed) and are therefore considered to be similar enough to the Type-7 SDUs that they are not independently benchmarked. Table 5.6-1 summarizes the selected SDUs, the rationale for their selection, and identifies sections of this document where the construction of each SDU is described.

Table 5.6-1: Summary of Representative SDUs

Representative Waste Disposal Unit	Reason for Inclusion	Section Where Described
SDU 1	Rectangular Geometry and Constructed of Six Cells	3.2.1
SDU 2A	150-Foot Diameter Cylindrical SDU	3.2.3
SDU 4	Rectangular Geometry and Constructed of Twelve Cells	3.2.2
SDU 7	375-Foot Diameter Cylindrical SDU	3.2.4

5.6.1.2 Representative Radionuclides

Of the 52 radionuclides evaluated by the SDF GoldSim Model, three (Cl-36, I-129, and Cs-135) were selected for the vadose zone benchmarking comparison. Tc-99 was not included

in the vadose zone study because the SDF GoldSim Model imports the Tc-99 "shrinking core model" results from the SDF PORFLOW Model.

For the vadose zone, evaluation of individual radionuclides is important because each radionuclide behaves differently in the engineered and natural system. Because the SDF GoldSim Model replicates the physical processes of the transport system, evaluating individual radionuclides provides validation that the different modeling components are responding appropriately. Based on saturated zone (SZ) transport results from PORFLOW, the main contributors to total dose within 20,000 years are I-129 and Tc-99. Because of their importance with regards to total dose results, PORFLOW is used to evaluate the releases of I-129 and Tc-99 using the rigorous "shrinking core model" where chemical environment transition times are evaluated on a model node-to-node basis, as opposed to transition times evaluated on a material zone basis. I-129 is representative of a radionuclide species that is only slightly subject to adsorption or dissolution-precipitation. Because I-129 is evaluated differently in the PORFLOW models, a second relatively conservative species, Cl-36, which does not use the shrinking core model in PORFLOW simulations, is also evaluated as part of the benchmarking process. Cs-135 was also chosen as a benchmarking species because it is more strongly sorbed than I-129 and Cl-36, allowing the influence of adsorption to be observed.

Because updated infiltration studies have indicated that best-estimate and compliance infiltration rates for the 2019 PA Model are orders of magnitude smaller than the values used in previous saltstone models, benchmarking of strongly sorbed species, which would have negligible release rates over the first 100,000 years, was not performed.

5.6.1.3 Representative Observation Wells

MOP Compliance Boundary

Total peak dose to the MOP along the 100-meter boundary (and along each sector) was calculated using both the SDF PORFLOW Model results and using transport results from the SDF GoldSim Model. To benchmark the SDF GoldSim Model, the two sets of dose results are compared. For a more detailed examination, the radionuclide-specific dose contributions and associated radionuclide concentrations along Sector B, Sector D, and Sector F were also compared. These comparisons focus on the dominant dose driving radionuclides (I-129 and Tc-99) and the secondary contributors (Cl-36, Cs-135, and K-40).

IHI Wells and 1-Meter Boundary

For benchmarking the IHI dose results, comparisons of dose results were performed at each of the seven IHI wells (see Figure 1.5-1). In addition, a comparison of total peak dose breakthrough curves along the 1-meter boundary (also depicted in Figure 1.5-1) was made. Note that in PORFLOW, the 1-meter boundary results are based on maximum concentrations at any depth along the 1-meter boundary. In GoldSim, the 1-meter boundary results are assumed to be based on maximum concentrations from the seven IHI wells.

5.6.2 Benchmarking of Mass Releases from SDUs

For benchmarking purposes, the Compliance Case releases (i.e., radionuclide flux at the water table) were determined using PORFLOW and GoldSim, and then these releases are compared. The Compliance Case represents the principal scenario for assessing compliance with performance objectives.

For brevity, the mass releases are presented for SDU 1, SDU 4, SDU 2A, and SDU 7. Note that the mass releases from the SDUs, as presented here, are the fluxes applied to the PORFLOW Aquifer Transport Model and the fluxes used in the SZ calculations in the GoldSim abstraction. In both models, the vadose zone calculations consider the influence of transport in the engineered barriers, as well as the partially saturated vadose zone soils immediately beneath the SDU. Note that although certain cells in the vadose zone model are saturated, the SDF GoldSim Model uses "unsaturated zone" (or UZ) in various element names within the model.

The comparison of these releases reflects differences in the construction of the two models, including the model spatial extents, and spatial discretization. The model simplifications in GoldSim are designed to provide a more computationally efficient model for the stochastic simulations for which the SDF GoldSim Model was designed. The validity of these assumptions is reflected in the benchmarking, or model-to-model, comparisons. In the following discussion, comparisons are made between PORFLOW and GoldSim. Both models assume a zero-concentration boundary condition at the interface between the vadose zone (or UZ) and the saturated zone (i.e., the water table).

In addition, for the Type 7 SDU abstraction a comparison is also made between PORFLOW and GoldSim for alternative model simulations that assume a zero concentration-gradient bottom boundary condition. A zero concentration-gradient boundary condition approximates the conditiobn where water flows out of a lysimeter and dissolved mass from the lysimeter flows undiluted into a jar or other sampling apparatus. A zero-concentration bottom boundary is analogous to water flowing into a relatively high flow aquifer (porous medium) where water at the contact between the aquifer and vadose zone is rapidly refreshed and the concentration in the aquifer is readily diluted to a very low concentration. Reality falls somewhere in-between as the water in the saturated zone would have a resultant concentration which decreases with depth. To better represent physical conditions the model would have to couple the vadose zone to the saturated zone, but that would add complexity and decrease computational efficiency. The zero-concentration bottom boundary condition was selected to generate final PA results, consistent with the PA model construction guideline of opting for simplified approaches with a bias towards higher doses when a more complex approach is not warranted.

5.6.2.1 Mass Releases from SDU 1

SDU 1 is the smaller of the two rectangular-prismatic shaped SDUs located in the southern sector of the SDF. The SDU PORFLOW Model grid and material zones used for simulating SDU 1 in the vadose zone are depicted in Figure 4.4-38 through Figure 4.4-41. Figure 5.6-1 through Figure 5.6-7 display comparison plots of the PORFLOW/GoldSim model mass release rates (in grams per year) from the vadose zone below SDU 1 into the saturated zone for the following radionuclides: Cl-36, Cs-135, and I-129, respectively.

The results are presented in both semi-log and linear plots. The results from both models are based on simulations that assume a zero-concentration bottom boundary condition. Comparing curves for similar radionuclides indicates that the SDF GoldSim Model approximates the SDF PORFLOW Model releases well for the conservative species Cl-36 and the moderately sorbed species Cs-135. For the I-129 releases, differences between the PORFLOW and GoldSim release rates are greater as discussed below.

With respect to the Cl-36 release rates, a comparison of the GoldSim and PORFLOW breakthrough curves for radionuclide releases from SDU 1 (see Figure 5.6-1 and Figure 5.6-2), shows that the SDF GoldSim Model provides an acceptable analog for the more rigorous SDF PORFLOW Model. The classification of acceptable is based on differences between the semi-log curves plotted in Figure 5.6-1, which are small, and the comparison of linear curves plotted in Figure 5.6-2, which shows a similar release pattern for the two models despite the SDF GoldSim Model having an 11% (< 25%) higher peak release rate (see Table 5.6-2). The SDU 1 Cl-36 release breakthrough curve presented in Figure 5.6-2 shows a slightly higher release rate in the first 40,000 years for the abstraction model. Although not reflected in the figure over the time span of interest, the trend of a higher release rate from the abstraction model reverses at about 65,000 years and mass balance-wise is reflected in a 13% greater cumulative release at 40,000 years, a 10% greater cumulative release at 100,000 years, and a 2% greater cumulative release at 200,000 years (Table 5.6-3). The more pronounced tail in the PORFLOW model is expected since for simplicity and efficiency the abstraction model does not include any material above the grout and any mass diffusing above that elevation will be released after the mass in the abstraction model is gone. This same assumption is assumed for all of the SDUs.

A comparison between GoldSim and PORFLOW releases of Cs-135 (see Figure 5.6-3 and Figure 5.6-4) shows that the moderate adsorption exhibited by Cs-135 delays the release. At 40,000 years the release still reflects the early (rising) portion of the breakthrough curve. The PORFLOW and GoldSim breakthrough curves show similar tendencies, but GoldSim exhibits a slightly later and steeper release-rate breakthrough curve. Comparing the peak release rates over 40,000 years for the two models, also shows a 14% higher peak for the SDF GoldSim Model (see Table 5.6-2), falling within the peak value criteria of ± 25%. Figure 5.6-5 depicts the SDU 1 Cl-36 release for first 500 years of this simulation. Comparing these figures shows that with respect to the pattern of release, the breakthrough curves for Cl-36 (Figure 5.6-5) and Cs-135 (Figure 5.6-3) show similar releases with the timing directly attributable to the greater capacity of Cs-135 to be adsorbed (see Table 4.3-5). This increased sorption of Cs-135 is reflected in the associated stretching of the breakthrough curve along the time axis (or the equivalent rescaling of the axis). The difference between the PORFLOW and GoldSim breakthrough curves in each of Figure 5.6-3, Figure 5.6-4, and Figure 5.6-5 tends to reflect a slight difference in the degree of numerical dispersion in the two models.

In PORFLOW, the release of I-129 is simulated using the "shrinking core" modeling approach which determines chemical transition timing on a node-by-node basis as opposed to a material zone specific basis (see Section 4.4.3.4.2).

Comparing the PORFLOW and GoldSim I-129 releases from SDU 1 (Figure 5.6-6 and Figure 5.6-7) shows how the use of this shrinking core model dampens the release of the I-129 compared to the GoldSim results. The PORFLOW shrinking core model produces a steadier (flatter) release pattern.

The difference between the two model results is associated with a spatial change in the chemical environment over time. In the PORFLOW Model, as the influx of acidic infiltrate reduces the pH of the pore solution in the saltstone monolith and the underlying cementitious materials, these materials transition from Reduced Region I to Reduced Region III on a cell-by-cell basis. Alternatively, within the SDF GoldSim Model this transition occurs as an instantaneous step change.

Due to this simplified approach, the SDF GoldSim Model results reflect an instantaneous increase in the iodine K_d (from 0.07 mL/g to 0.71 mL/g per Table 4.3-7) at 29,714 years after closure, while the PORFLOW Model results reflect a more gradual transition as a higher-K_d "rind" develops around the outer edges of the saltstone monolith. Note that the decrease in pH transitions fastest downwards from the top of the saltstone monolith due to the directional influence of the flow field.

Regardless of the differences between these two modeling approaches, the SDF GoldSim Model provides a reasonable approximation of the more rigorous PORFLOW Model. As shown in Figure 5.6-6 (and summarized in Table 5.6-2), the difference in peak release rates of 33% indicate that the SDF GoldSim Model represents a reasonable approximation of the simulated processes.

Figure 5.6-1: Cl-36 Release-Rate Comparison for SDU 1 Using a Zero-Concentration (Dirichlet-Type) Exit Boundary Condition (Log Scale)

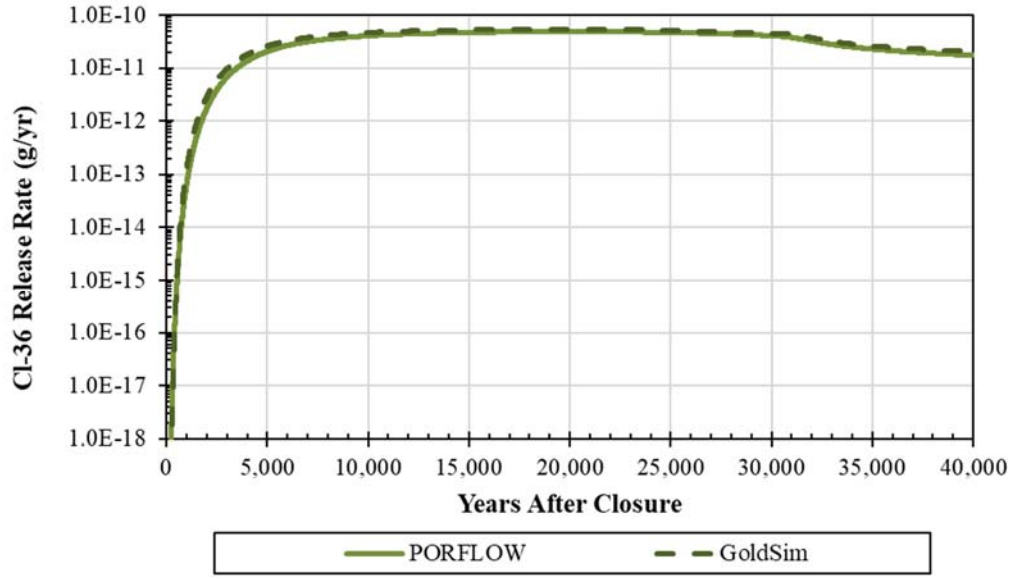

Figure 5.6-2: Cl-36 Release-Rate Comparison for SDU 1 Using a Zero-Concentration (Dirichlet-Type) Exit Boundary Condition (Linear Scale)

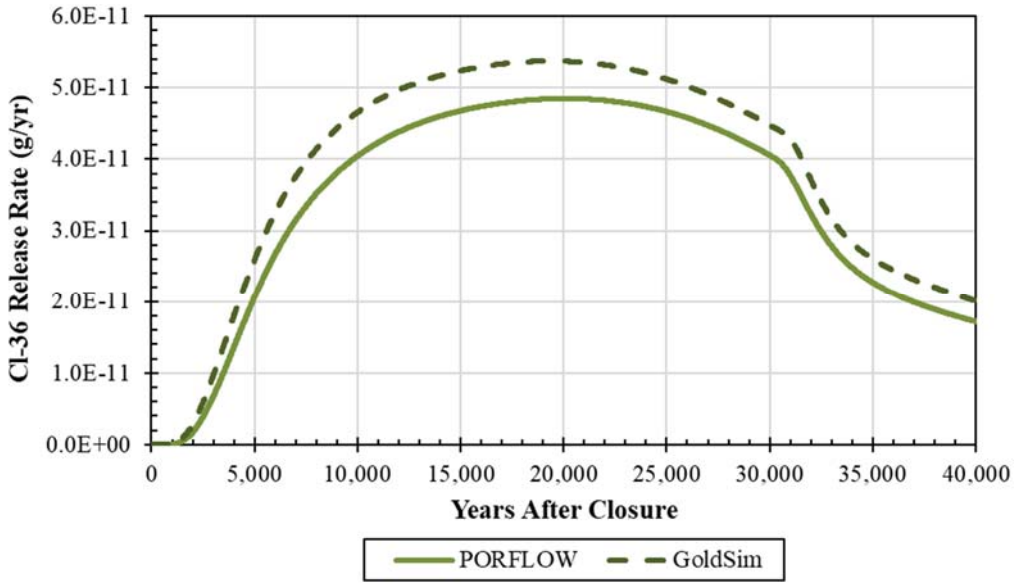

Figure 5.6-3: Cs-135 Release-Rate Comparison for SDU 1 Using a Zero-Concentration (Dirichlet-Type) Exit Boundary Condition (Log Scale)

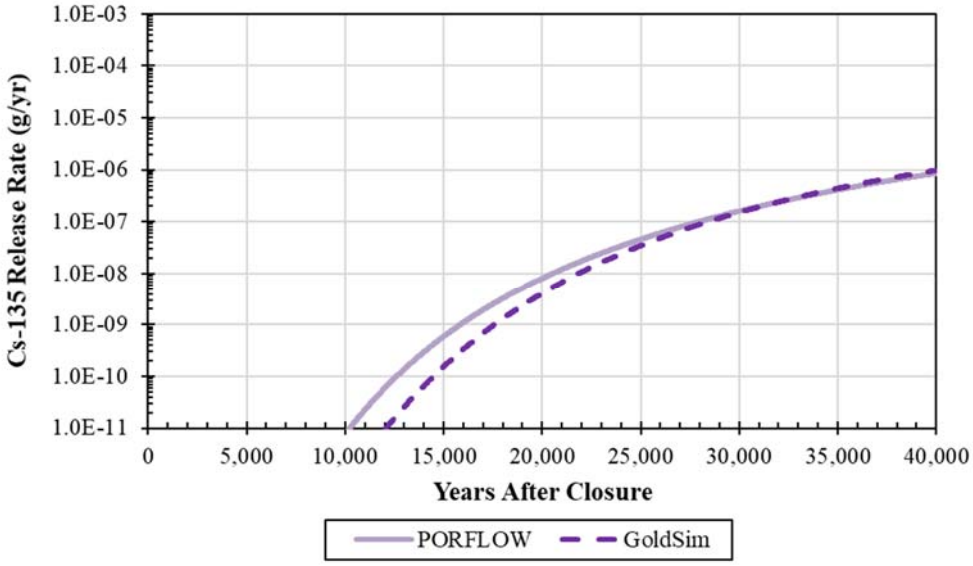

Figure 5.6-4: Cs-135 Release-Rate Comparison for SDU 1 Using a Zero-Concentration (Dirichlet-Type) Exit Boundary Condition (Linear Scale)

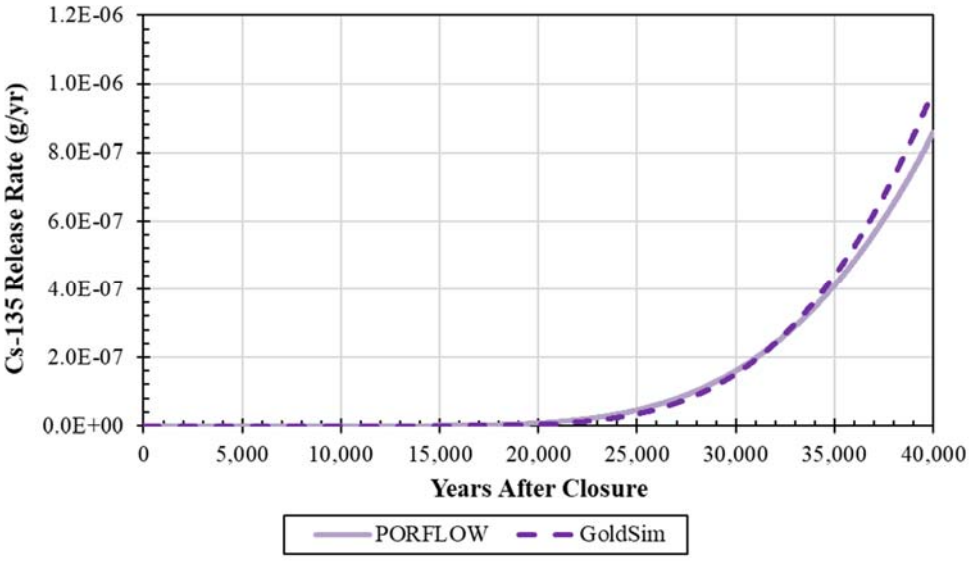

Figure 5.6-5: Cl-36 Release-Rate Comparison for SDU 1 for the First 500 Years (Log Scale)

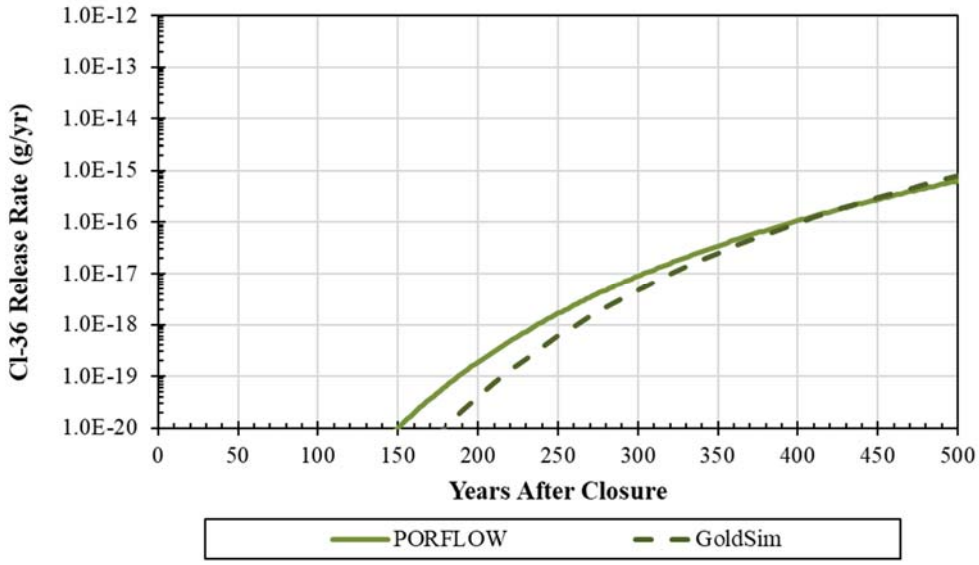

Figure 5.6-6: I-129 Release-Rate Comparison for SDU 1 Using a Zero-Concentration (Dirichlet-Type) Exit Boundary Condition (Log Scale)

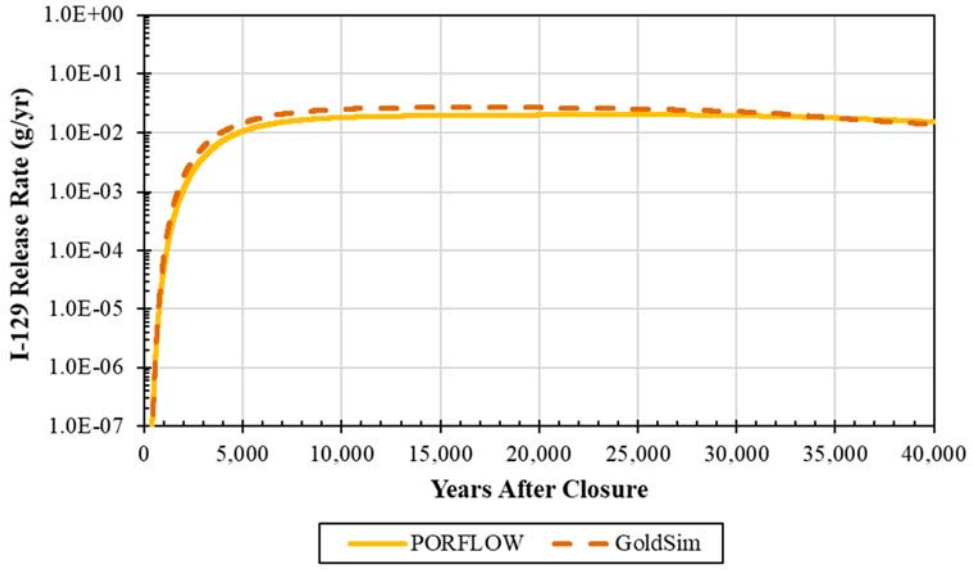

Figure 5.6-7: I-129 Release-Rate Comparison for SDU 1 Using a Zero-Concentration (Dirichlet-Type) Exit Boundary Condition (Linear Scale)

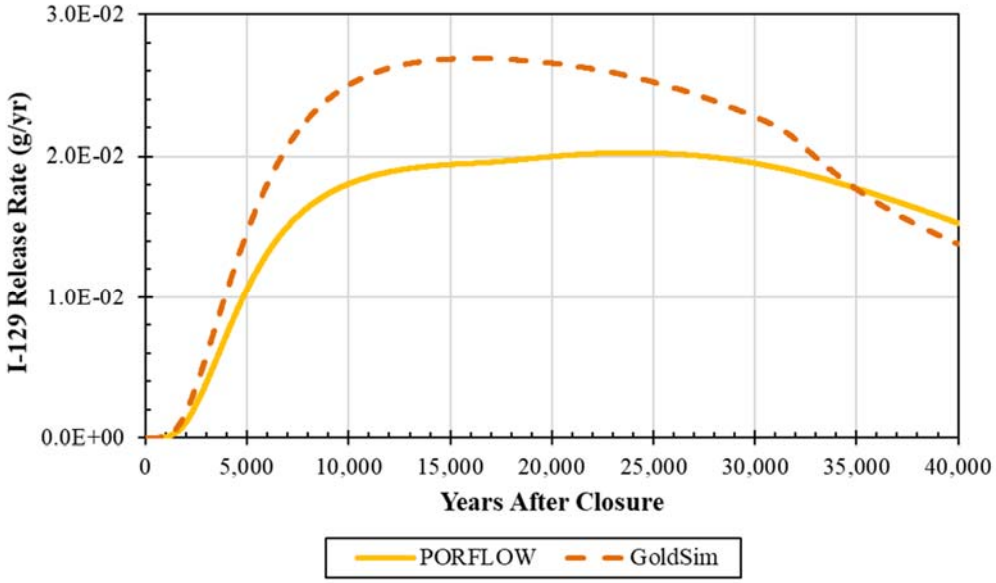

Table 5.6-2: Comparison of PORFLOW and SDF GoldSim Model Peak Release Rates for SDU 1

Radionuclide	PORFLOW Model Peak Release Rate (g/yr)	SDF GoldSim Model Peak Release Rate (g/yr)	Percent Difference
Cl-36	4.85E-11	5.37E-11	+11
Cs-135	8.57E-07	9.80E-07	+14
I-129	2.03E-02	2.69E-02	+33

Table 5.6-3: Comparison of PORFLOW and GoldSim Model Cumulative Cl-36 Releases for SDU 1

Time (yr)	PORFLOW Model Cumulative Release (g)	SDF GoldSim Model Cumulative Release (g)	Percent Difference
40,000	1.37E-06	1.55E-06	+13
100,000	1.78E-06	1.96E-06	+10
200,000	2.08E-06	2.12E-06	+2

5.6.2.2 Mass Releases from SDU 4

SDU 4 is the larger of the two rectangular-prismatic SDUs located in the southern sector of the SDF and is located closer to the 100-meter compliance boundary (in the flow direction) than SDU 1 (see Figure 4.4-114 and Figure 4.4-115). The SDF PORFLOW Model grid and material zones used in the vadose zone models are depicted in Figure 4.4-42 through Figure 4.4-45.

Figure 5.6-8 through Figure 5.6-13 display PORFLOW/GoldSim comparison plots of the mass releases (in grams per year) for the radionuclides Cl-36, Cs-135, and I-129 from the vadose zone immediately beneath SDU 4 into the saturated zone at the water table.

For SDU 4, the PORFLOW and GoldSim results for the Cl-36 releases from SDU 4 (Figure 5.6-8 and Figure 5.6-9) and the comparable releases for Cs-135 (Figure 5.6-10 and Figure 5.6-11) indicate that the SDF GoldSim Model is an acceptable surrogate for the SDF PORFLOW Model. In addition to capturing the release patterns, the benchmarking classification of acceptable is also based on a comparison of the peak dose values presented in Table 5.6-4, which shows an 11% difference between PORFLOW and GoldSim for the Cl-36 and an 11% difference for the Cs-135 over the 40,000-year simulation period.

Similarly, the model release comparison for I-129 presented in Figure 5.6-12 indicates that GoldSim produces an acceptable approximation of the SDF PORFLOW Model results. Although the GoldSim-simulated releases of I-129 have a less dispersed profile than the I-129 releases from the PORFLOW shrinking core model, the linear plot (Figure 5.6-13) still shows that GoldSim produces a conservative approximation of the more rigorous SDF PORFLOW Model. The difference in peak dose values of 46% (Table 5.6-4) also indicates that GoldSim generates a more pessimistic result. This comparison indicates that the SDF GoldSim Model can be used as a surrogate to the SDF PORFLOW Model.

Figure 5.6-8: Cl-36 Release-Rate Comparison for SDU 4 Using a Zero-Concentration (Dirichlet-Type) Exit Boundary Condition (Log Scale)

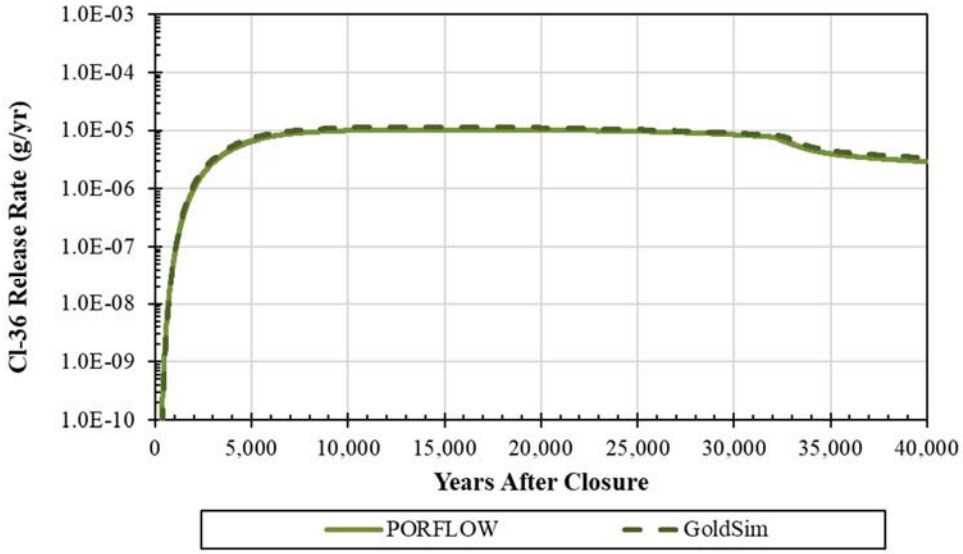

Figure 5.6-9: Cl-36 Release-Rate Comparison for SDU 4 Using a Zero-Concentration (Dirichlet-Type) Exit Boundary Condition (Linear Scale)

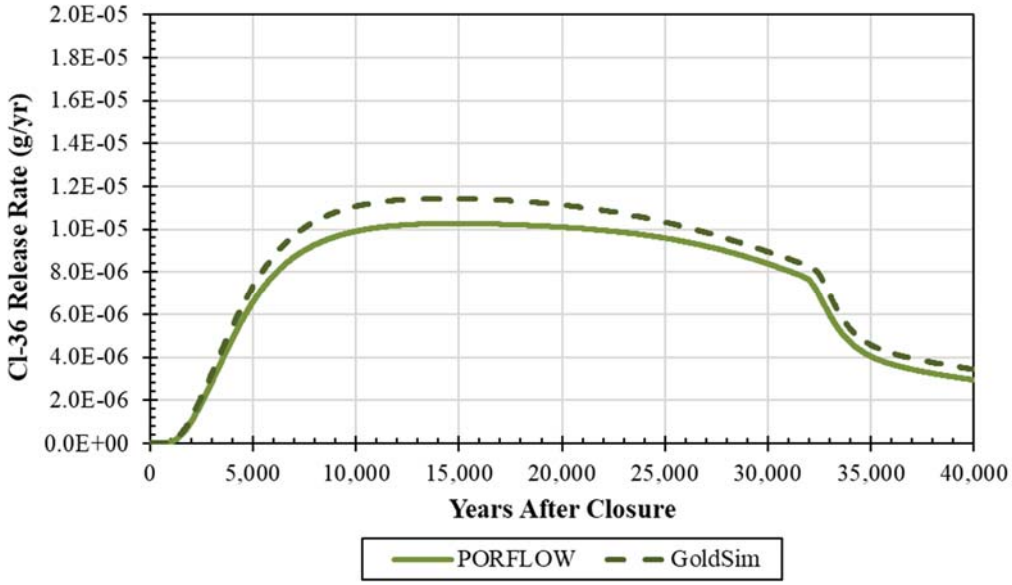

Figure 5.6-10: Cs-135 Release-Rate Comparison for SDU 4 Using a Zero-Concentration (Dirichlet-Type) Exit Boundary Condition (Log Scale)

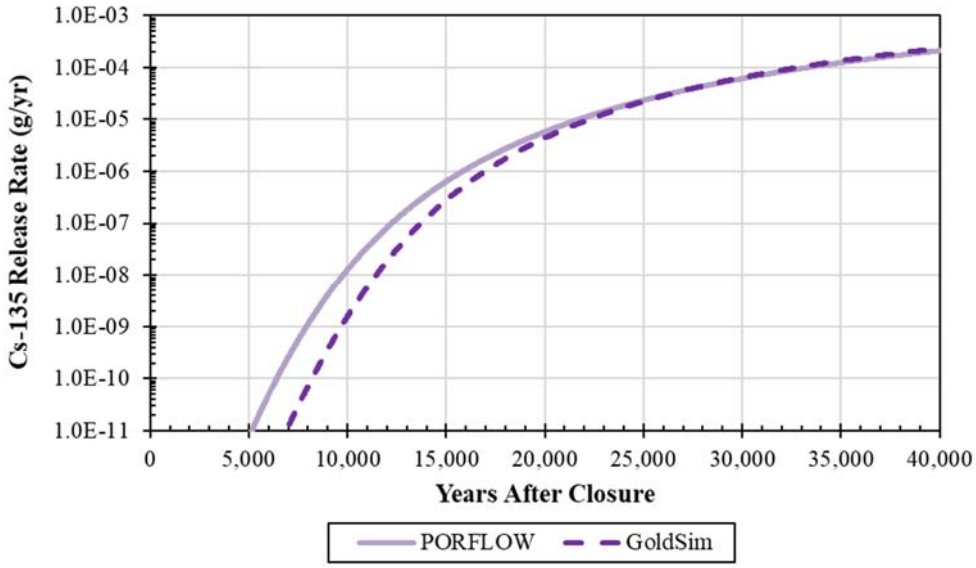

Figure 5.6-11: Cs-135 Release-Rate Comparison for SDU 4 Using a Zero-Concentration (Dirichlet-Type) Exit Boundary Condition (Linear Scale)

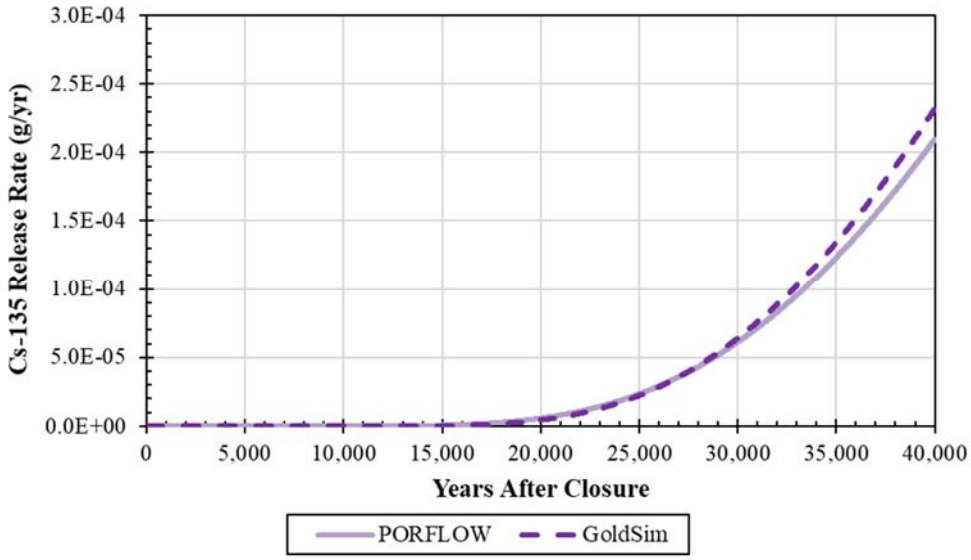

Figure 5.6-12: I-129 Release-Rate Comparison for SDU 4 Using a Zero-Concentration (Dirichlet-Type) Exit Boundary Condition (Log Scale)

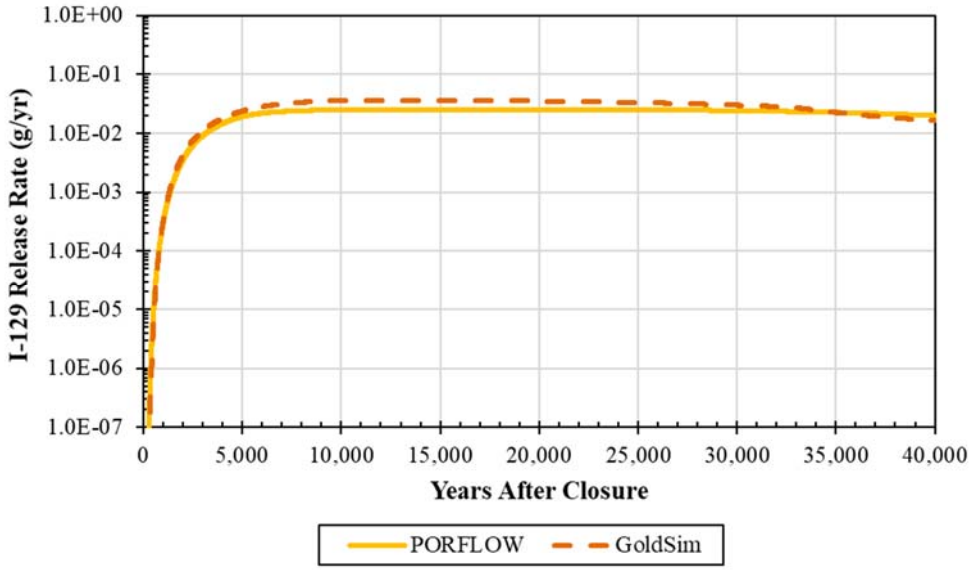

Figure 5.6-13: I-129 Release-Rate Comparison for SDU 4 Using a Zero-Concentration (Dirichlet-Type) Exit Boundary Condition (Linear Scale)

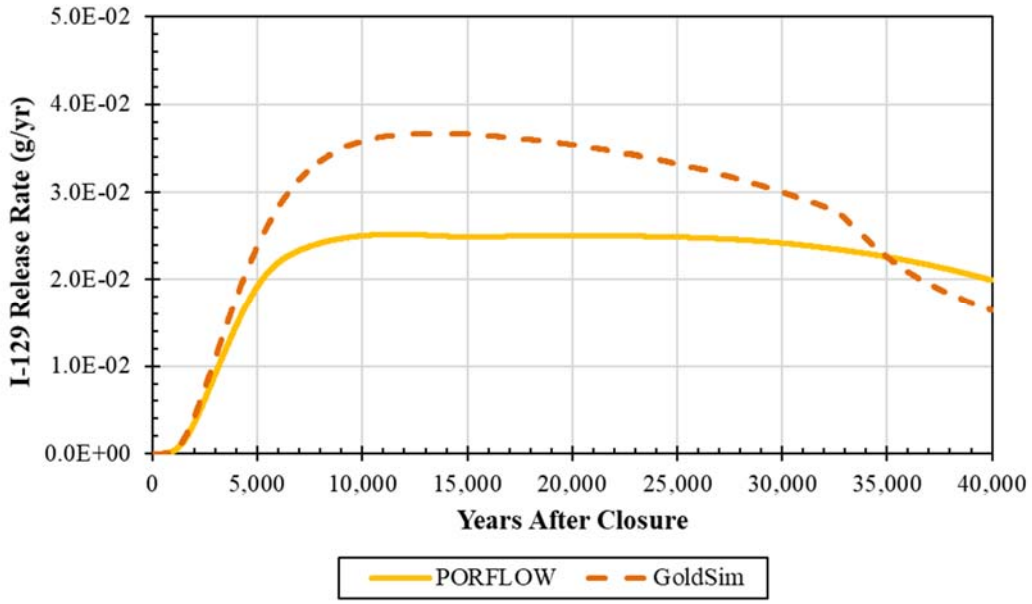

Table 5.6-4: Comparison of PORFLOW and SDF GoldSim Model Peak Release Rates for SDU 4

Radionuclide	PORFLOW Model Peak Release Rate (g/yr)	SDF GoldSim Model Peak Release Rate (g/yr)	Percent Difference
Cl-36	1.03E-05	1.14E-05	+11
Cs-135	2.10E-04	2.32E-04	+11
I-129	2.52E-02	3.67E-02	+46

5.6.2.3 Mass Releases from Type 2 SDUs

Type 2 SDUs are the 150-foot diameter cylindrical in-place disposal units: SDU 2A, SDU 2B, SDU 3A, SDU 3B, SDU 5A, and SDU 5B. In the benchmarking process, the release of radionuclides from a representative SDU (SDU 2A) is simulated using the PORFLOW Vadose Zone Transport Model and the SDF GoldSim Model abstraction, and the results of the two models are compared to evaluate how well the SDF GoldSim Model abstraction can approximate the releases generated from the more rigorous SDF PORFLOW Model. The SDF PORFLOW Model grid and material zones used in the Vadose Zone Flow Model are depicted in Figure 4.4-46 through Figure 4.4-49.

Figure 5.6-14 through Figure 5.6-19 display PORFLOW/GoldSim comparison plots of the mass releases of Cl-36, Cs-135, and I-129 (in grams per year) from the vadose zone beneath SDU 2A into the saturated zone. The releases are based on PORFLOW and GoldSim simulations that assume a zero-concentration bottom boundary condition. A comparison of the radionuclide release-rate breakthrough curves indicates that the SDF GoldSim Model provides an acceptable approximation the SDF PORFLOW Model releases from SDU 2A for the conservative species Cl-36 and for the moderately sorbed species Cs-135.

The criteria for acceptability are assessed as follows. The comparison of breakthrough curves depicts similar release patterns for each radionuclide. The similar release patterns reflect the consistency of the models' approximations of the processes controlling the releases. The peak mass release-rates over the 40,000-year simulation period differ by 11% for Cl-36 and by 6% for Cs-135 (Table 5.6-5), which is less than the 25% criterion.

Note that compared to SDU 1 and SDU 4, the SDU 2A PORFLOW and GoldSim releases of I-129 do show a larger difference in release patterns (see Figure 5.6-18 and Figure 5.6-19). The releases from GoldSim are greater at early times, reflecting differences in the transition-time models used to simulate the temporal changes in chemical environments. Specifically, the simpler SDF GoldSim Model assumes a homogeneous material zone, while the SDF PORFLOW Model applies the more refined node-by-node transitions. Because the I-129 releases between the two models do not exhibit an exceptionally large difference in peak releases (33%) as presented in Table 5.6-5 and because the GoldSim releases are higher for most of the first 28,000 years, the SDF GoldSim Model can still be considered an acceptable surrogate for the more rigorous PORFLOW model.

Figure 5.6-14: Cl-36 Release-Rate Comparison for SDU 2A Using a Zero-Concentration (Dirichlet-Type) Exit Boundary Condition (Log Scale)

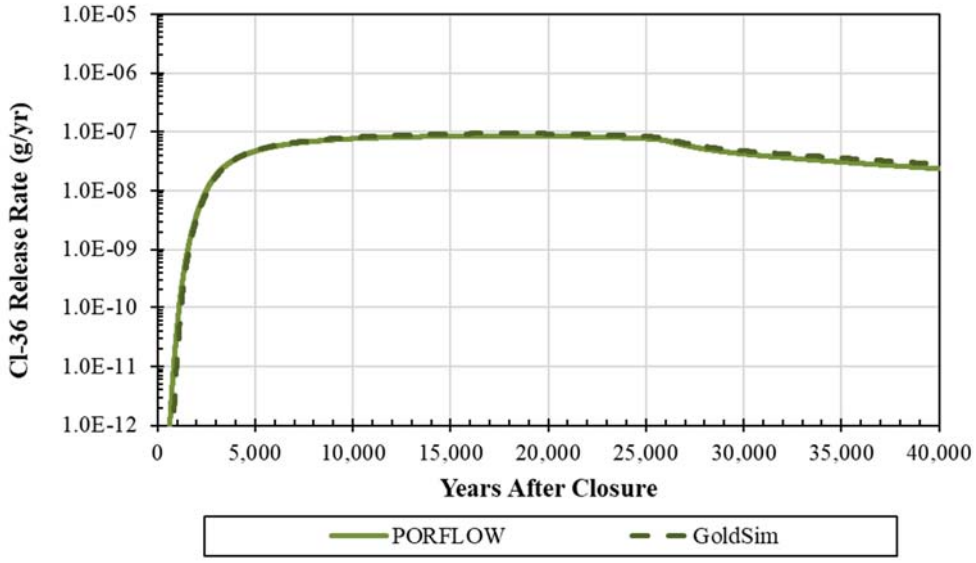

Figure 5.6-15: Cl-36 Release-Rate Comparison for SDU 2A Using a Zero-Concentration (Dirichlet-Type) Exit Boundary Condition (Linear Scale)

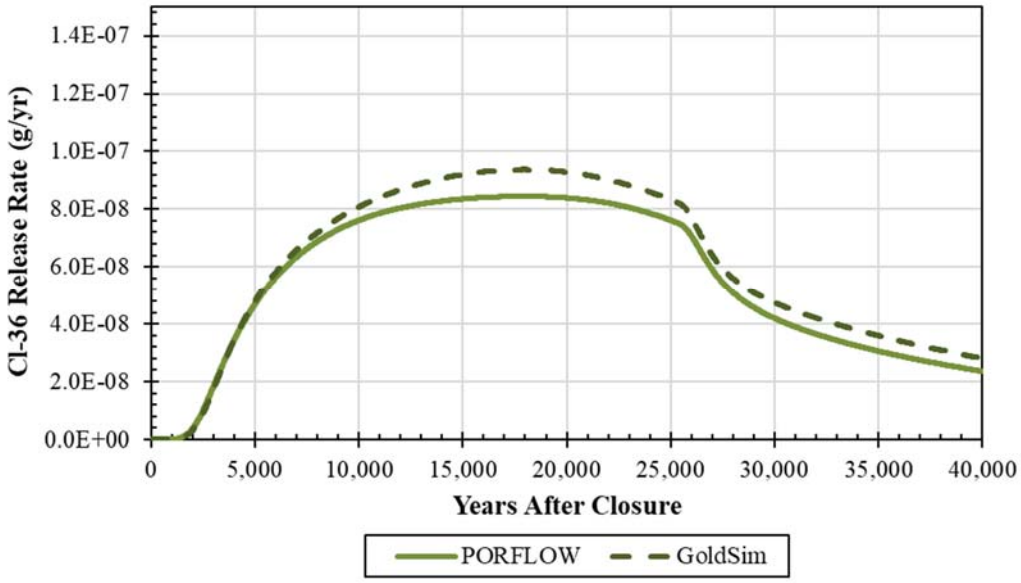

Figure 5.6-16: Cs-135 Release-Rate Comparison for SDU 2A Using a Zero-Concentration (Dirichlet-Type) Exit Boundary Condition (Log Scale)

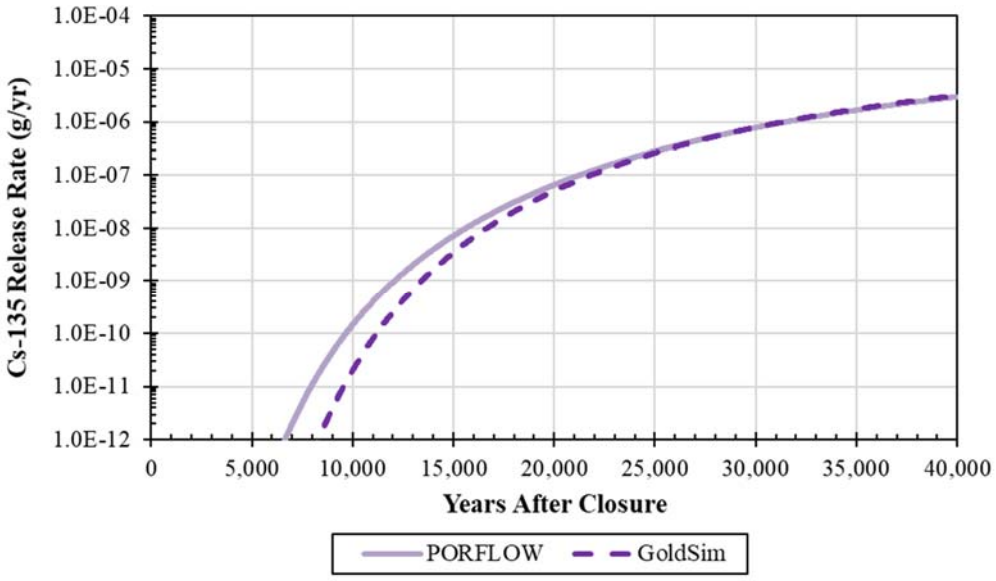

Figure 5.6-17: Cs-135 Release-Rate Comparison for SDU 2A Using a Zero-Concentration (Dirichlet-Type) Exit Boundary Condition (Linear Scale)

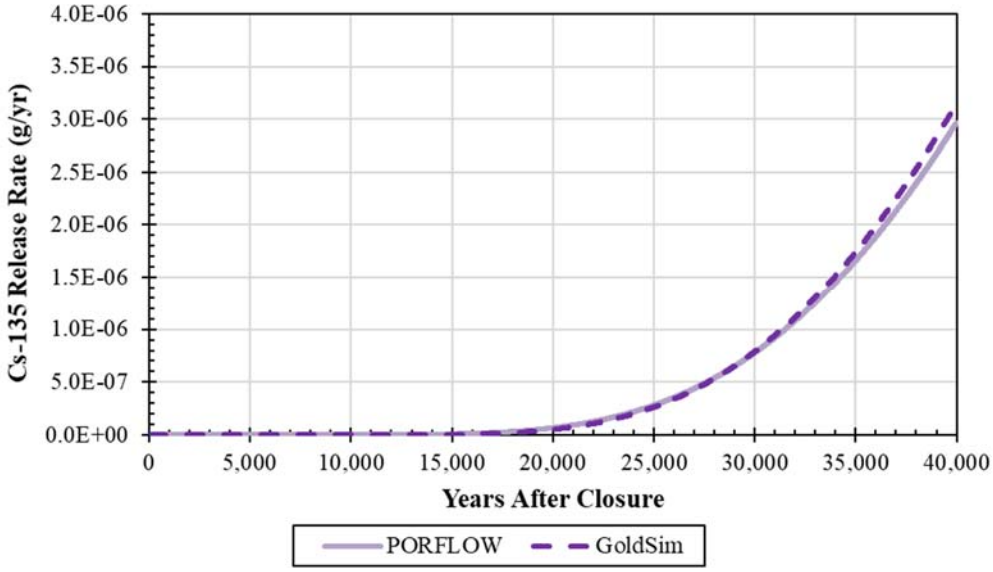

Figure 5.6-18: I-129 Release-Rate Comparison for SDU 2A Using a Zero-Concentration (Dirichlet-Type) Exit Boundary Condition (Log Scale)

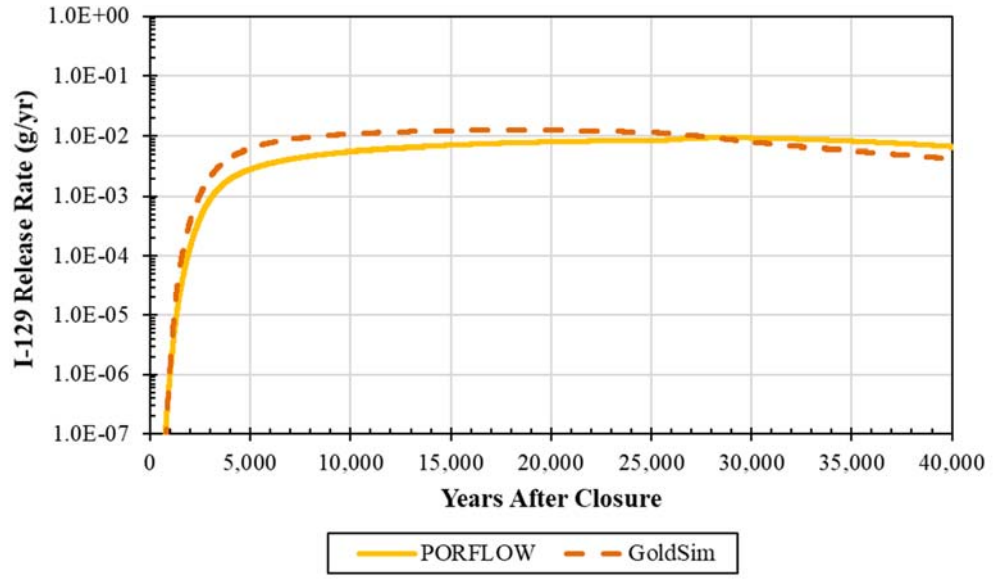

Figure 5.6-19: I-129 Release-Rate Comparison for SDU 2A Using a Zero-Concentration (Dirichlet-Type) Exit Boundary Condition (Linear Scale)

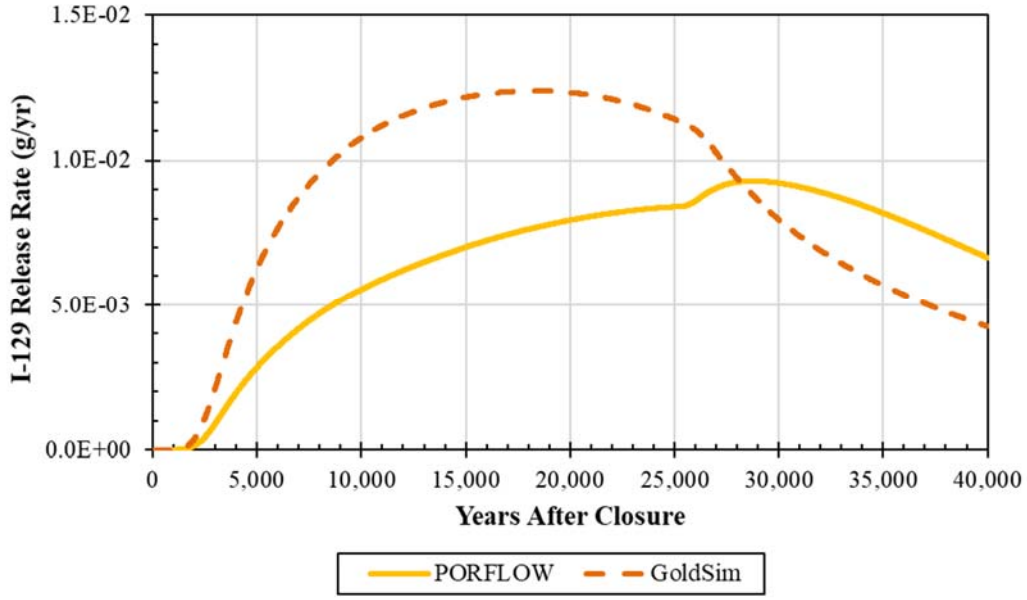

Table 5.6-5: Comparison of PORFLOW and SDF GoldSim Model Peak Release Rates Over 40,000 Years for SDU 2A

Radionuclide	PORFLOW Model Peak Release Rate (g/yr)	SDF GoldSim Model Peak Release Rate (g/yr)	Percent Difference
Cl-36	8.45E-08	9.37E-08	+11
Cs-135	2.97E-06	3.15E-06	+6
I-129	9.29E-03	1.24E-02	+33

5.6.2.4 Mass Releases from SDU 7

Type-7 SDUs are 375-foot diameter cylindrical disposal units which include SDU 7 (currently under construction) and future SDU 8, SDU 10, SDU, 11, and SDU 12. Because SDU 6 has a sloped floor but is otherwise similar in design to SDU 7, and SDU 9 which will be constructed closer to the water table (Section 4.4.4) but still has the same design as SDU 7, it is appropriate to use the result comparisons from SDU 7 as representative for all the 375-foot diameter SDUs in the benchmarking process. The SDF PORFLOW Model grid and material zones used in the vadose zone model are depicted in Figure 4.4-50 through Figure 4.4-53.

Figure 5.6-20 through Figure 5.6-25 display PORFLOW/GoldSim comparison plots of Cl-36, Cs-135, and I-129 mass releases (in grams per year) from SDU 7 into the saturated zone at the water table immediately beneath the SDU. Figure 5.6-19 through Figure 5.6-25 present Cl-36, Cs-135, and I-129 release comparisons based on PORFLOW and GoldSim simulations that assume a zero-concentration boundary condition at the bottom of the vadose zone. The breakthrough curve comparisons indicate that the SDF GoldSim Model approximates the SDF PORFLOW Model releases quite well for the conservative species,

Cl-36 (Figure 5.6-20 and Figure 5.6-21), and for the moderately sorbed species, Cs-135 (Figure 5.6-22 and Figure 5.6-23). The similarities between the two Cl-36 breakthrough curves and between the two Cs-135 breakthrough curves reflect how well GoldSim captures the processes controlling the release of Cl-36 and Cs-135 from the 375-foot diameter SDUs. A difference less than 25% is the criteria for acceptability of the SDF GoldSim Model as a surrogate to PORFLOW for radionuclides not analyzed with the shrinking core model. Table 5.6-6 shows that PORFLOW and GoldSim peak mass release-rates over the 40,000-year simulation period differ by 1% for Cl-36 and by 7% for Cs-135 constituting acceptability.

For I-129, the differences between PORFLOW and GoldSim releases (Figure 5.6-24 and Figure 5.6-25) are consistent with differences produced by the different transition-time models used to simulate temporal changes in chemical environments as previously discussed. Because the I-129 releases between the two models do not exhibit an exceptionally large difference in peak releases (31%) and the SDF GoldSim Model releases are higher for the 40,000-year simulation time (Table 5.6-6), the SDF GoldSim Model is considered to be an acceptable surrogate for the more rigorous SDF PORFLOW Model.

Prior to deciding on a final model for the PA, SDU 7 simulations were used to evaluate the most appropriate exit boundary condition to use at the water table defining the bottom of the PORFLOW and GoldSim representations of the vadose zone (Section 4.4.5.2.1). PORFLOW and GoldSim comparisons of releases based on assuming a zero-concentration (Dirichlet) bottom boundary condition versus assuming a zero concentration-gradient (Neumann) bottom boundary condition are presented in Figure 5.6-26, Figure 5.6-27, and Figure 5.6-28 for Cl-36, Cs-135, and I-129, respectively.

For this diffusion-dominated system, the comparisons of results presented in Figure 5.6-26 through Figure 5.6-28 for radionuclide specific mass releases from SDU 7 based on the zero-concentration and zero-concentration gradient boundary conditions show that the use of the zero-concentration boundary condition at the bottom of the model enhances the radionuclide release rates for all the selected radionuclides. This comparison indicates that the zero-concentration boundary condition represents a limiting condition, and the zero-concentration gradient boundary condition may underestimate the radionuclide releases in a diffusively dominated system. Peak concentration values for the simulations assuming a zero concentration-gradient boundary condition are presented in Table 5.6-7.

Figure 5.6-20: Cl-36 Release-Rate Comparison for SDU 7 Using a Zero-Concentration (Dirichlet-Type) Exit Boundary Condition (Log Scale)

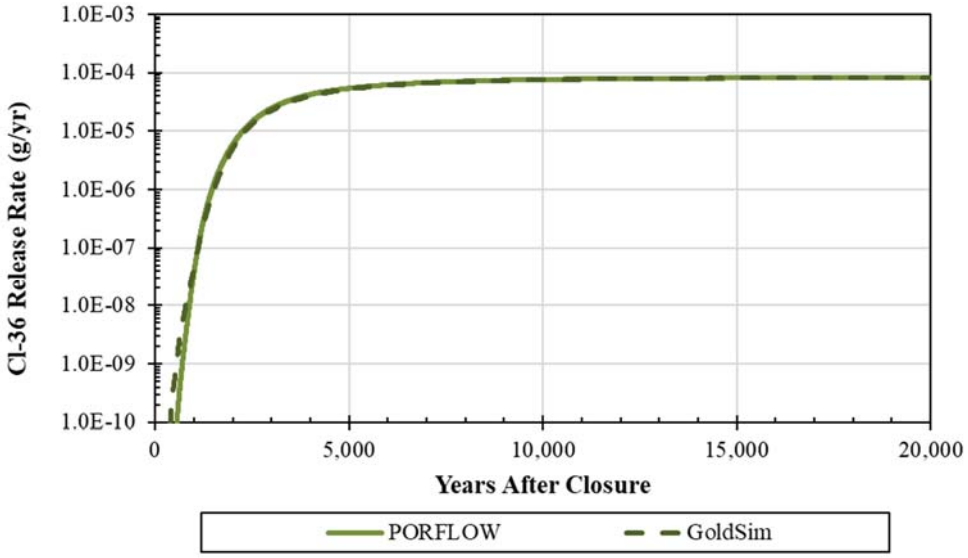

Figure 5.6-21: Cl-36 Release-Rate Comparison for SDU 7 Using a Zero-Concentration (Dirichlet-Type) Exit Boundary Condition (Linear Scale)

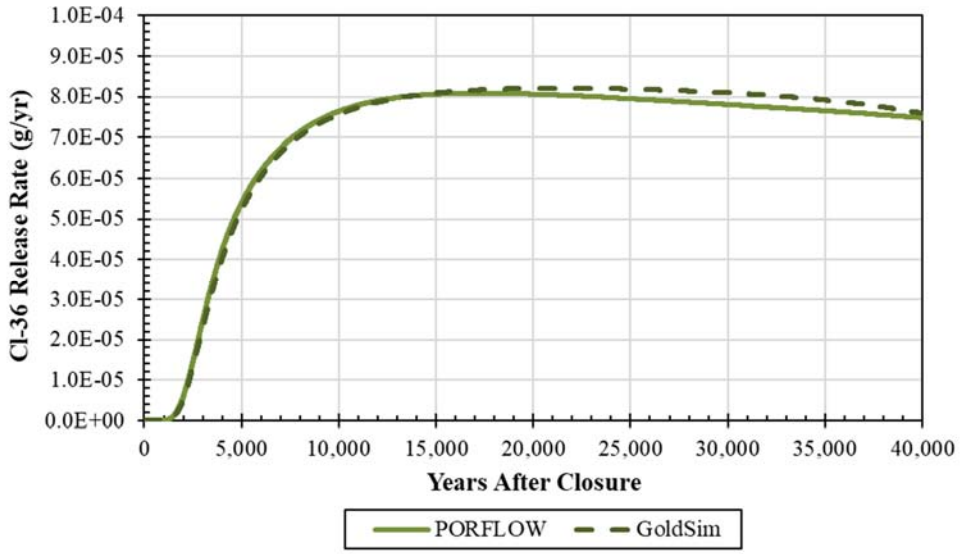

Figure 5.6-22: Cs-135 Release-Rate Comparison for SDU 7 Using a Zero-Concentration (Dirichlet-Type) Exit Boundary Condition (Log Scale)

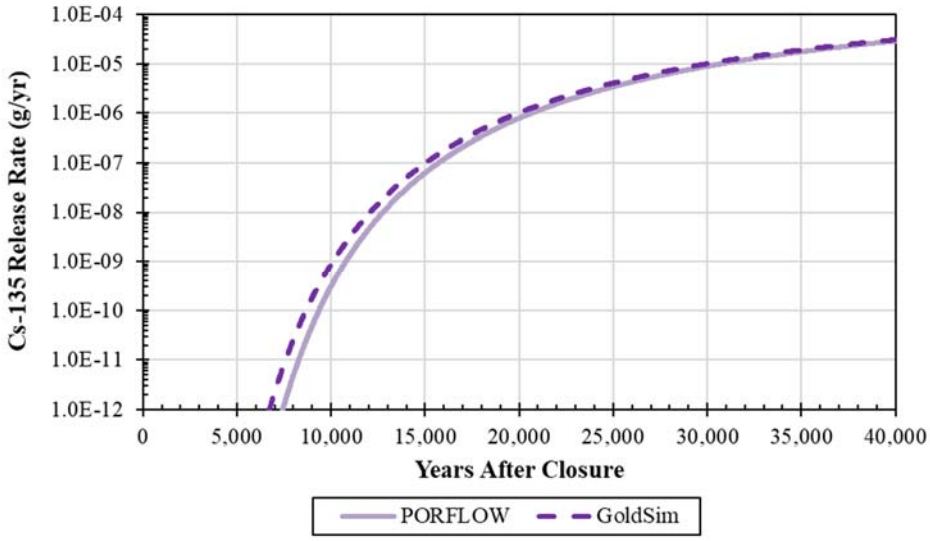

Figure 5.6-23: Cs-135 Release-Rate Comparison for SDU 7 Using a Zero-Concentration (Dirichlet-Type) Exit Boundary Condition (Linear Scale)

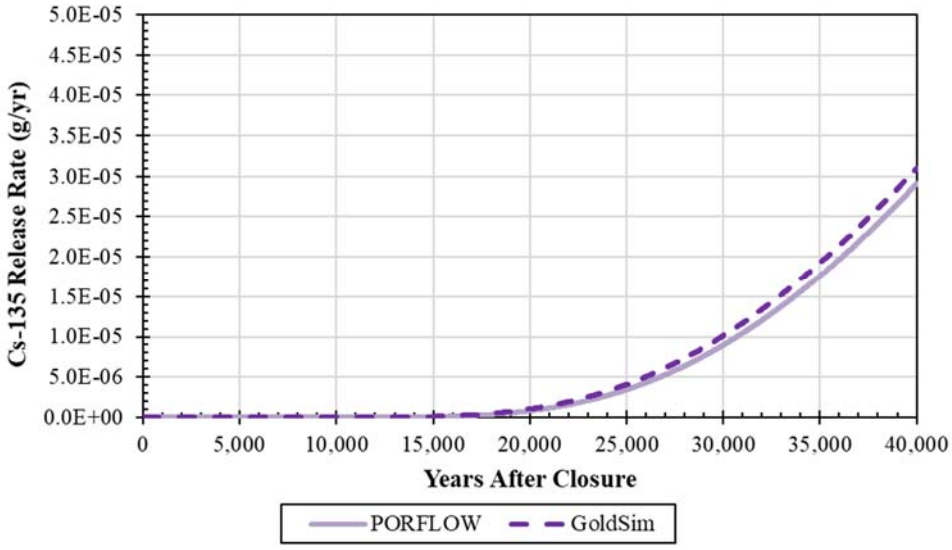

Figure 5.6-24: I-129 Release-Rate Comparison for SDU 7 Using a Zero-Concentration (Dirichlet-Type) Exit Boundary Condition (Log Scale)

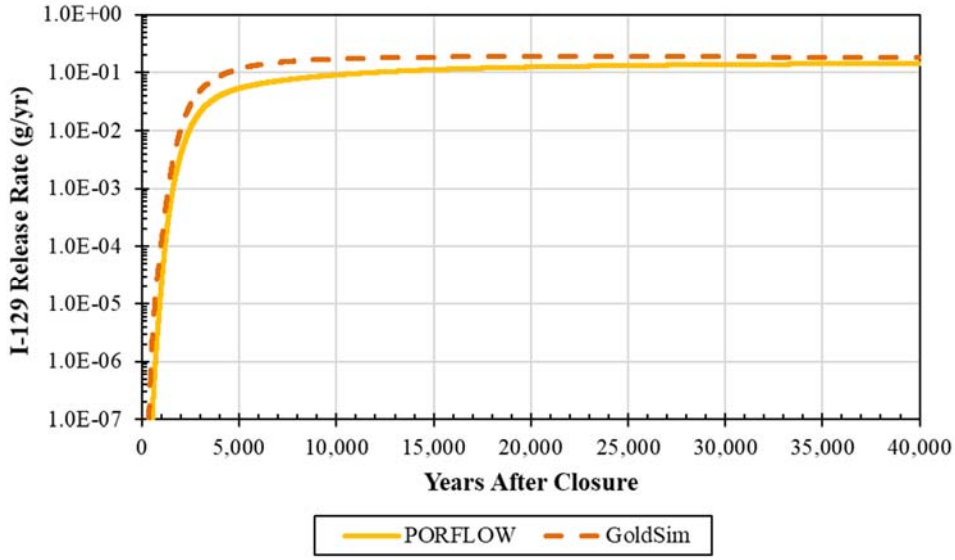

Figure 5.6-25: I-129 Release-Rate Comparison for SDU 7 Using a Zero-Concentration (Dirichlet-Type) Exit Boundary Condition (Linear Scale)

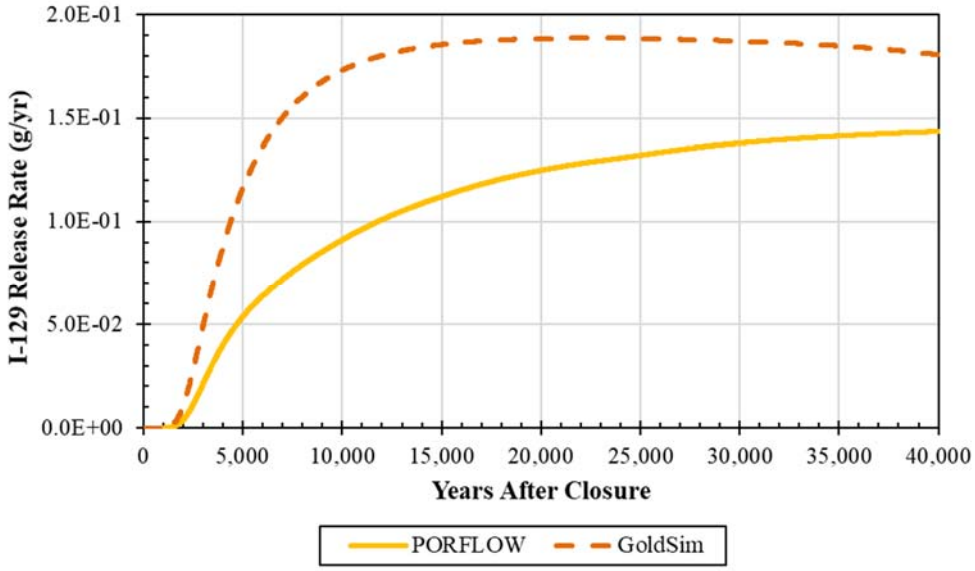

Figure 5.6-26: Cl-36 Release-Rate Comparison for SDU 7 Including Zero-Concentration and Zero Concentration-Gradient Exit Boundary Condition Breakthrough Curves (Log Scale)

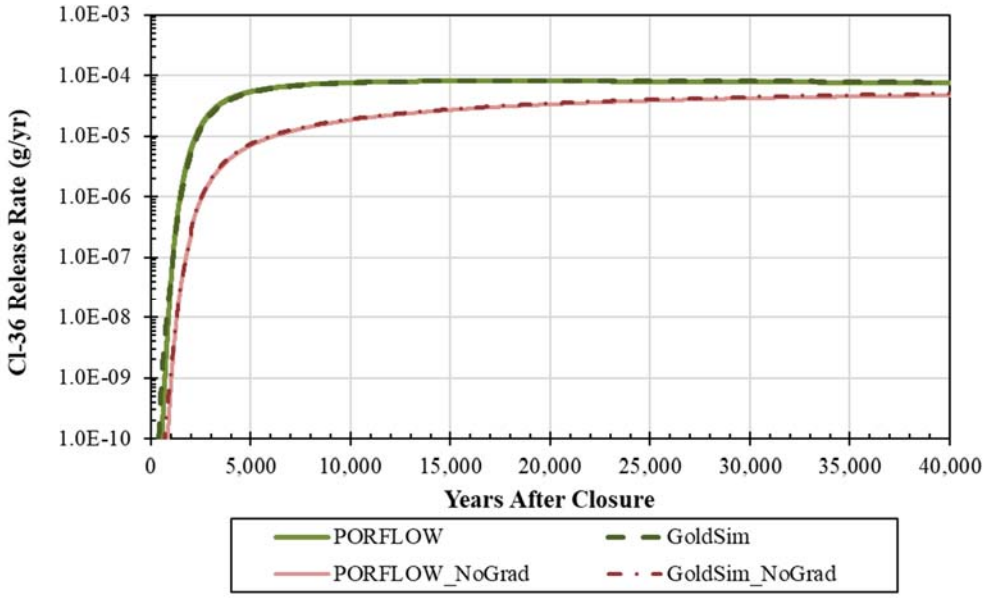

Figure 5.6-27: Cs-135 Release-Rate Comparison for SDU 7 Including Zero-Concentration and Zero Concentration-Gradient Exit Boundary Condition Breakthrough Curves (Log Scale)

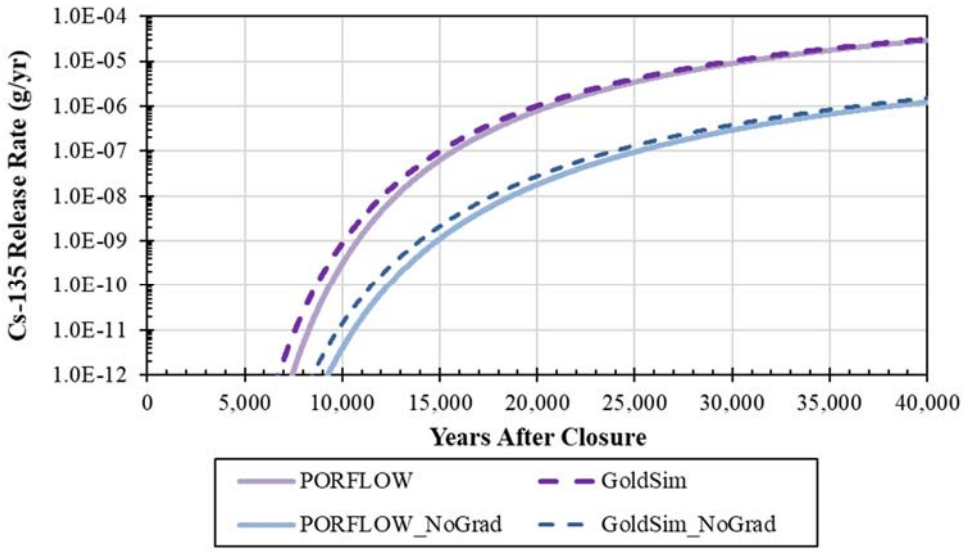

Figure 5.6-28: I-129 Release-Rate Comparison for SDU 7 Including Zero-Concentration and Zero Concentration-Gradient Exit Boundary Condition Breakthrough Curves (Log Scale)

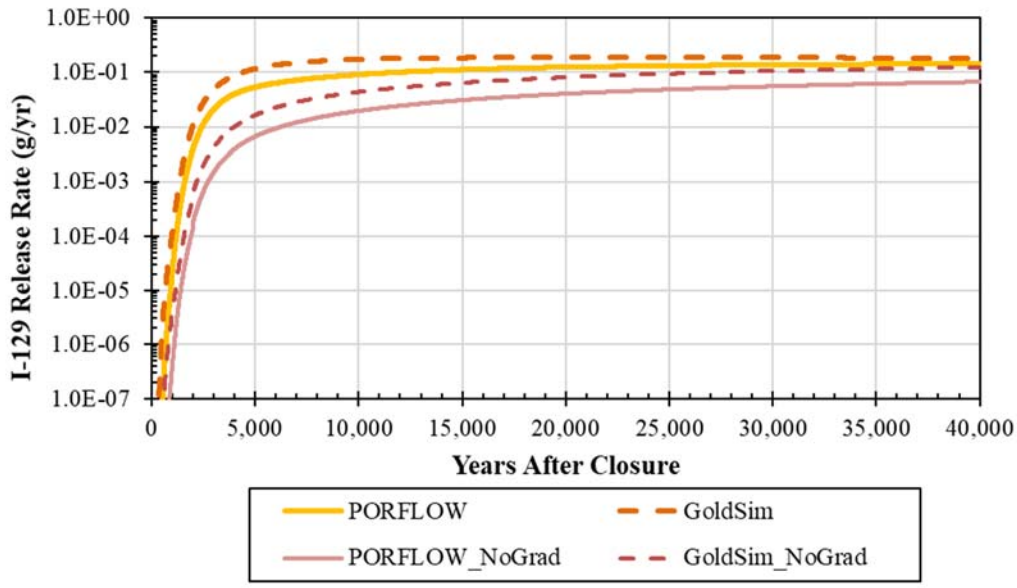

Table 5.6-6: Comparison of PORFLOW and SDF GoldSim Model Peak Release Rates from SDU 7 for Simulations Assuming a Zero-Concentration Exit Boundary Conditions

Radionuclide	PORFLOW Model Peak Release Rate (g/yr)	SDF GoldSim Model Peak Release Rate (g/yr)	Percent Difference
Cl-36	8.09E-05	8.21E-05	+1
Cs-135	2.91E-05	3.10E-05	+7
I-129	1.43E-01	1.89E-01	+31

Table 5.6-7: Comparison of PORFLOW and SDF GoldSim Model Peak Release Rates from SDU 7 for Simulations Assuming a Zero Concentration-Gradient Exit Boundary Conditions

Radionuclide	PORFLOW Model Peak Release Rate (g/yr)	SDF GoldSim Model Peak Release Rate (g/yr)	Percent Difference
Cl-36	4.67E-05	5.01E-05	+7
Cs-135	1.24E-06	1.51E-06	+22
I-129	6.68E-02	1.23E-01	+84

5.6.2.5 Benchmarking of Vadose Zone Releases for Realistic and Pessimistic Cases

To evaluate the appropriateness of the SDF GoldSim Model as an abstraction of the PORFLOW Vadose Zone Model for use with other parameter values, a set of the vadose zone releases from a subset of SDUs considered above were generated and the SDF GoldSim Model and PORFLOW Vadose Zone Transport Model results compared. To evaluate alternative model configurations, the input data for the Realistic Case and the Pessimistic Case were applied to the SDF GoldSim Model then the model results were

compared against the respective PORFLOW results. The set of releases examined included releases of Cl-36 and I-129 from SDUs 1 (a rectangular SDU) and 7 (a cylindrical SDU).

As can be seen by comparing the SDF GoldSim Model SDU 1 releases for the Realistic Case presented in Figure 5.6-29 and Figure 5.6-30 with the PORFLOW Model releases, the release patterns are similar and the abstraction model peak release rate is 46% greater than for the PORFLOW Model (see Table 5.6-8) over a simulation period of 20,000 years. The difference in peak model release rates can be associated with conservative nature of the abstraction model with respect to the PORFLOW Model where extremely low Realistic Case infiltration rates can enhance diffusion into zones above the grout not included in the abstraction model. The conservative nature of abstraction model result makes it an acceptable approximation for the PORFLOW Model even for the low-release Realistic Case.

Comparing the SDF GoldSim Model SDU 1 releases for the Pessimistic Case as presented in Figure 5.6-31 and Figure 5.6-32 with the PORFLOW Model releases, the release patterns are shown to be similar with the abstraction model peak release being 1% lower than the PORFLOW Model over a 20,000 year period (see Table 5.6-8). In conjunction with the Realistic Case and Compliance Case analyses, this comparison indicates that the abstraction model has a wide range over which it can serve as a surrogate for the PORFLOW Vadose Zone Model.

Comparing the SDF GoldSim Model SDU 7 releases for the Realistic Case presented in Figure 5.6-33 and Figure 5.6-34 with the PORFLOW Model releases found in the same figures, the release patterns are similar with the abstraction model peak release rate being 2% greater than the PORFLOW Model release rate over a period of 20,000 years (see Table 5.6-8). This indicates that the SDF GoldSim Model is an acceptable approximation for the Realistic Case.

Comparing the SDF GoldSim Model SDU 7 releases for the Pessimistic Case presented in Figure 5.6-35 and Figure 5.6-36 with the PORFLOW Model releases, the release patterns are shown to be similar with the abstraction model peak release rate being 2% lower than the PORFLOW Model release rate over a 20,000 year period (see Table 5.6-8). In conjunction with the Realistic Case and Compliance Case analyses, this comparison indicates that the abstraction model has a wide range over which it can serve as a surrogate for the PORFLOW Vadose Zone Model.

Figure 5.6-29: Cl-36 Realistic Case Release-Rate Comparison for SDU 1 Using a Zero-Concentration (Dirichlet-Type) Exit Boundary Condition (Log Scale)

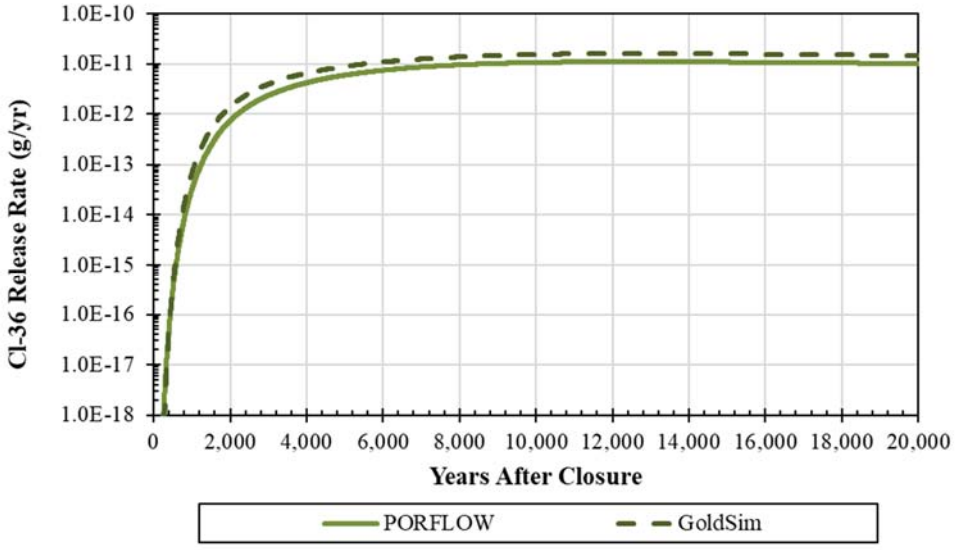

Figure 5.6-30: Cl-36 Realistic Case Release-Rate Comparison for SDU 1 Using a Zero-Concentration (Dirichlet-Type) Exit Boundary Condition (Linear Scale)

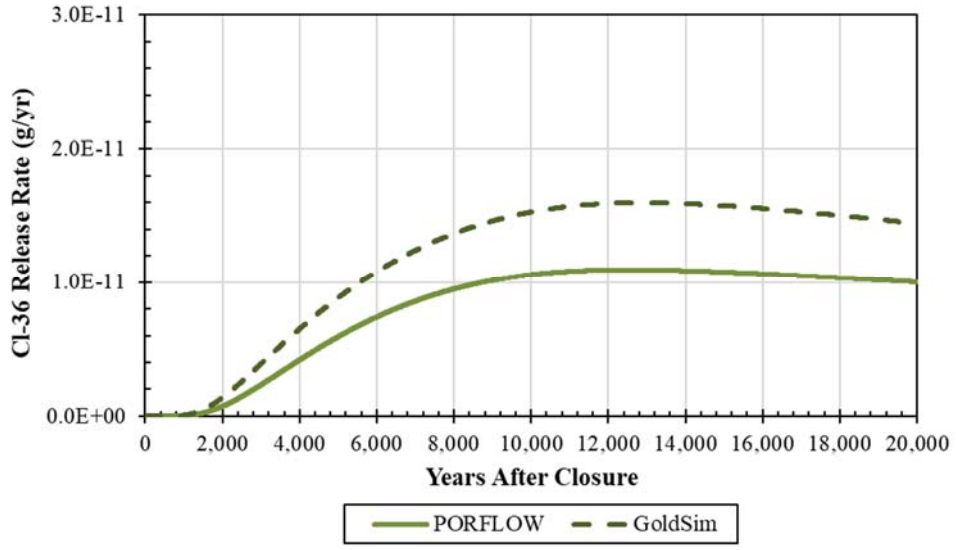

Figure 5.6-31: Cl-36 Pessimistic Case Release-Rate Comparison for SDU 1 Using a Zero-Concentration (Dirichlet-Type) Exit Boundary Condition (Log Scale)

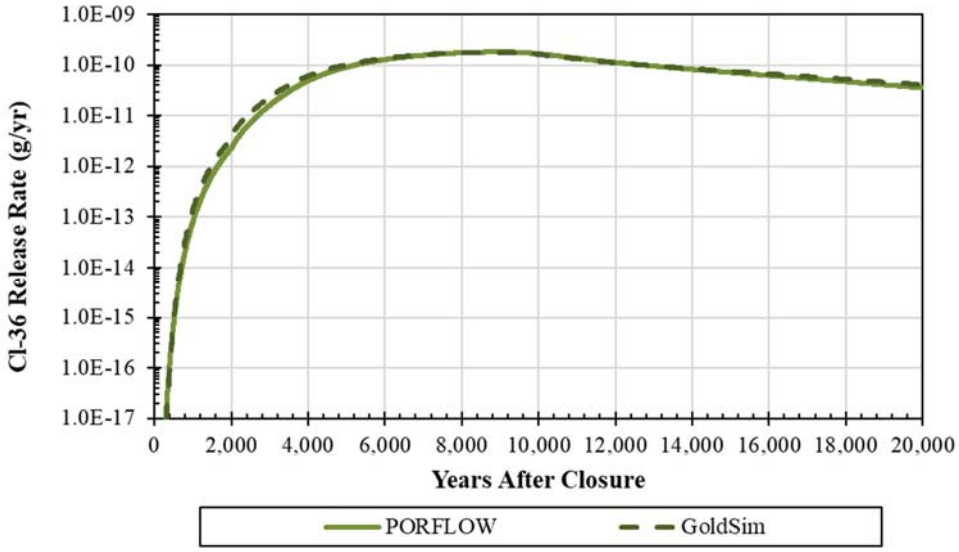

Figure 5.6-32: Cl-36 Pessimistic Case Release-Rate Comparison for SDU 1 Using a Zero-Concentration (Dirichlet-Type) Exit Boundary Condition (Linear Scale)

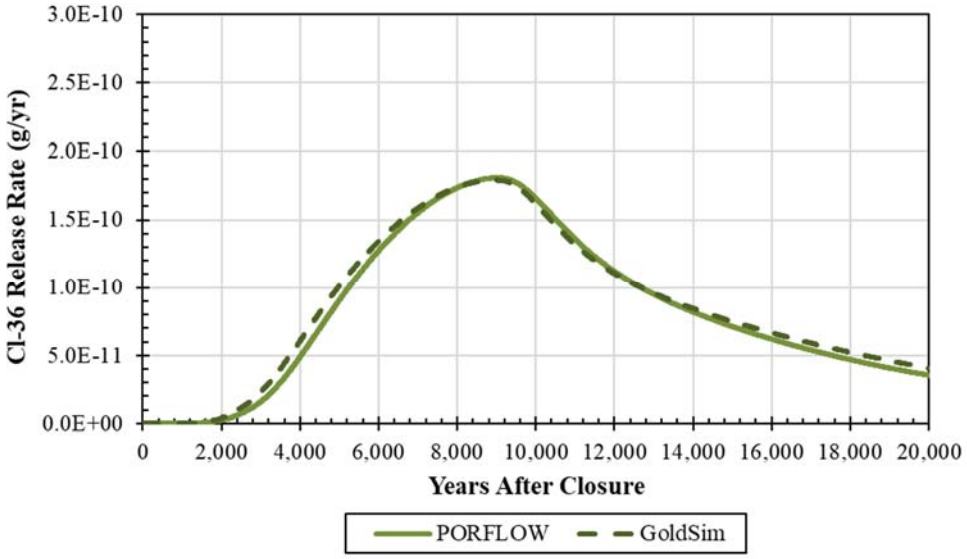

Figure 5.6-33: Cl-36 Realistic Case Release-Rate Comparison for SDU 7 Using a Zero-Concentration (Dirichlet-Type) Exit Boundary Condition (Log Scale)

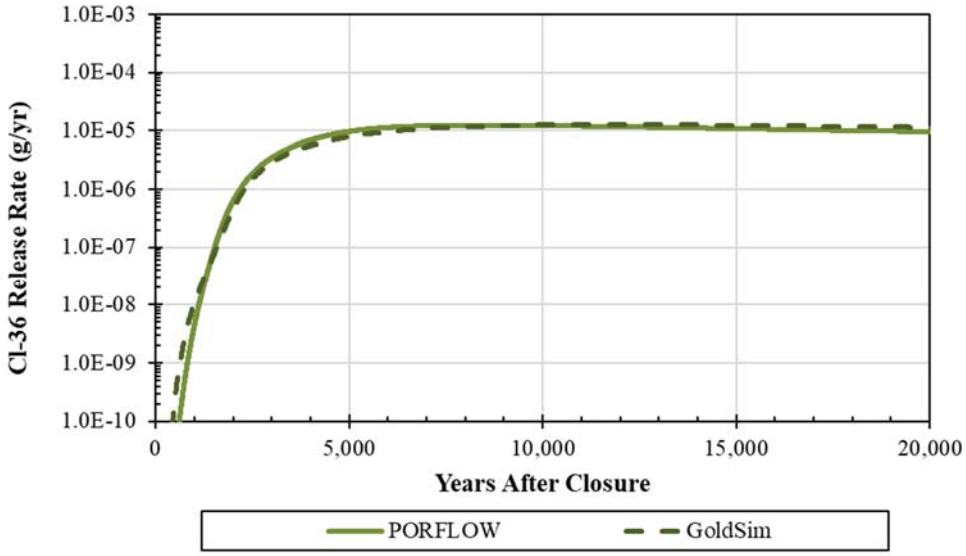

Figure 5.6-34: Cl-36 Realistic Case Release-Rate Comparison for SDU 7 Using a Zero-Concentration (Dirichlet-Type) Exit Boundary Condition (Linear Scale)

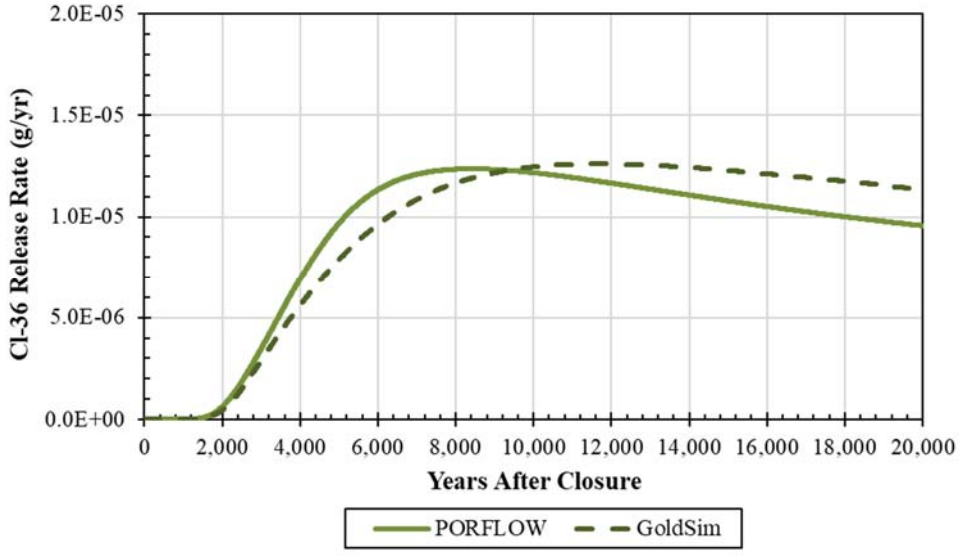

Figure 5.6-35: Cl-36 Pessimistic Case Release-Rate Comparison for SDU 7 Using a Zero-Concentration (Dirichlet-Type) Exit Boundary Condition (Log Scale)

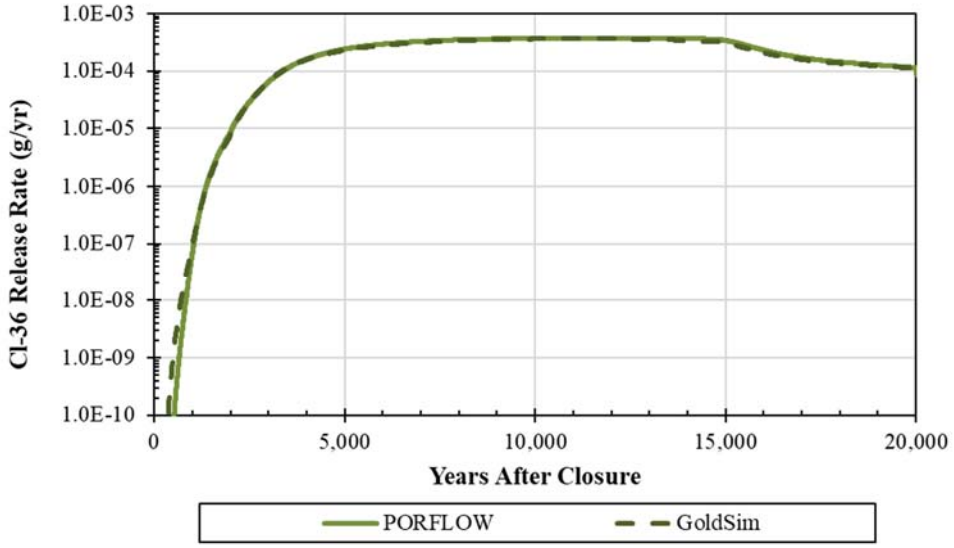

Figure 5.6-36: Cl-36 Pessimistic Case Release-Rate Comparison for SDU 7 Using a Zero-Concentration (Dirichlet-Type) Exit Boundary Condition (Linear Scale)

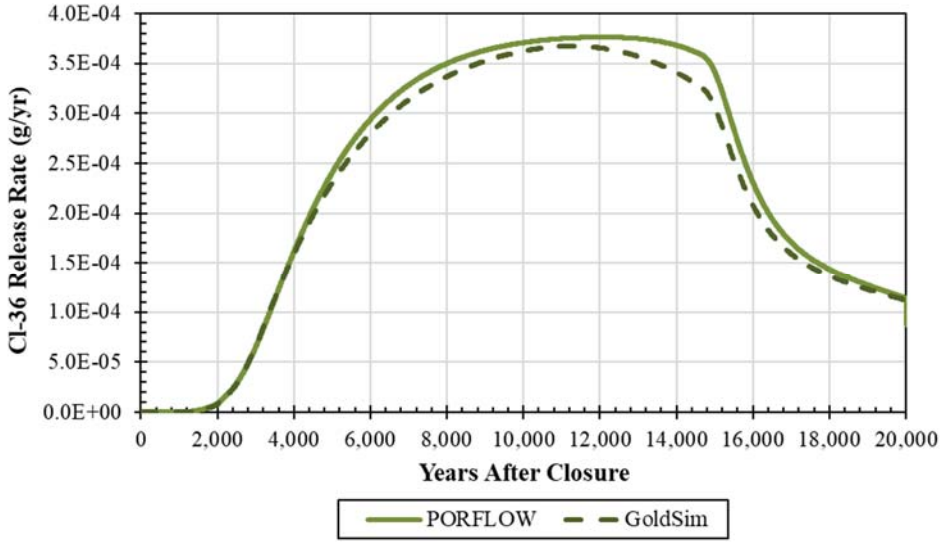

Table 5.6-8: Comparison of PORFLOW and SDF GoldSim Model Peak Cl-36 Release Rates from SDU 1 and 7 for Simulations

Case/SDU	PORFLOW Model Peak Release Rate (g/yr)	SDF GoldSim Model Peak Release Rate (g/yr)	Percent Difference
Realistic/SDU 1	1.09E-11	1.60E-11	+46
Pessimistic/SDU 1	1.24E-10	1.79E-10	-1
Realistic/SDU 7	1.24E-05	1.26E-05	+2
Pessimistic/SDU 7	3.76E-04	3.67E-04	-2

Because the I-129 conceptual models used in the PORFLOW Vadose Zone Model ("shrinking core") and the SDF GoldSim Model (zone-based chemical transition changes) are different, comparisons of I-129 releases for the Realistic and Pessimistic Cases are included. As with Cl-36, to evaluate the appropriateness of the GoldSim abstraction of the PORFLOW Vadose Zone Model for use with ranges of parameter values, a set of vadose zone releases from SDU 1 and SDU 7 were generated with the SDF GoldSim Model and PORFLOW Vadose Zone Transport Model using the input data for the Realistic Case and the Pessimistic Case then compared against the respective PORFLOW simulations. were based on the more "optimistic" Realistic Case and the more "pessimistic" Pessimistic Case input data.

As can be seen by comparing the SDF GoldSim Model SDU 1 I-129 releases for the Realistic Case presented in Figure 5.6-37 and Figure 5.6-38 with the PORFLOW Model releases, the release patterns are similar and the abstraction model peak release rate is 46% greater than the PORFLOW Model peak release rate over a 20,000 year periods (see Table 5.6-9). This indicates that the abstraction model is an acceptable approximation for the Realistic Case.

Comparing the SDF GoldSim Model SDU 1 releases for the Pessimistic Case presented in Figure 5.6-39 and Figure 5.6-40 with the PORFLOW Model releases, the release patterns are shown to be similar with the abstraction model peak release 11% higher than the PORFLOW peak release over a 20,000 year period (see Table 5.6-9). In conjunction with the Realistic Case and Compliance Case analyses, this comparison indicates that the abstraction model has a wide parameter range over which it can serve as a surrogate for the PORFLOW Vadose Zone Model.

As can be seen by comparing the SDF GoldSim Model SDU 7 releases for the Realistic Case presented in Figure 5.6-41 and Figure 5.6-42 with the PORFLOW Model releases, the release patterns are similar but the abstraction model peak release rate is 139% greater than the PORFLOW Model peak release rate over a period of 20,000 years (see Table 5.6-9). Although the abstraction release is much higher, this is to be expected for the extremely low infiltration rates used in the Realistic Case. The PORFLOW "shrinking core" model exposes the outside faces of the cylindrical SDU to more acidic infiltrate, allowing diffusion into the SDU to create an early transition from Reduced Region I to Reduced Region III conditions near the saltstone surface forming a higher-K_d saltstone "rind" which decreases the release rate from the PORFLOW model relative to the SDF GoldSim Model release rates. Because the SDF GoldSim Model K_ds transition based on instantaneous zonal changes in the chemical environment it is a highly conservative abstraction for I-129 under conditions of minimal infiltration rate. As a conservative abstraction the SDF GoldSim Model is unlikely to underestimate the I-129 releases associated within the 10,000-yeaar Performance Period and can be used as a surrogate for the PORFLOW Model.

Comparing the SDF GoldSim Model SDU 7 releases for the Pessimistic Case presented in Figure 5.6-43 and Figure 5.6-44 with the PORFLOW Model releases, the release patterns are shown to be similar and the peak release rate value generated by the SDF GoldSim Model is 17% higher over the 20,000-year simulation period (see Table 5.6-9). In

conjunction with the Realistic Case and Compliance Case analyses, this comparison indicates that the abstraction model has a wide parameter range over which it can serve as a surrogate for the PORFLOW Vadose Zone Model.

Figure 5.6-37: I-129 Realistic Case Release-Rate Comparison for SDU 1 Using a Zero-Concentration (Dirichlet-Type) Exit Boundary Condition (Log Scale)

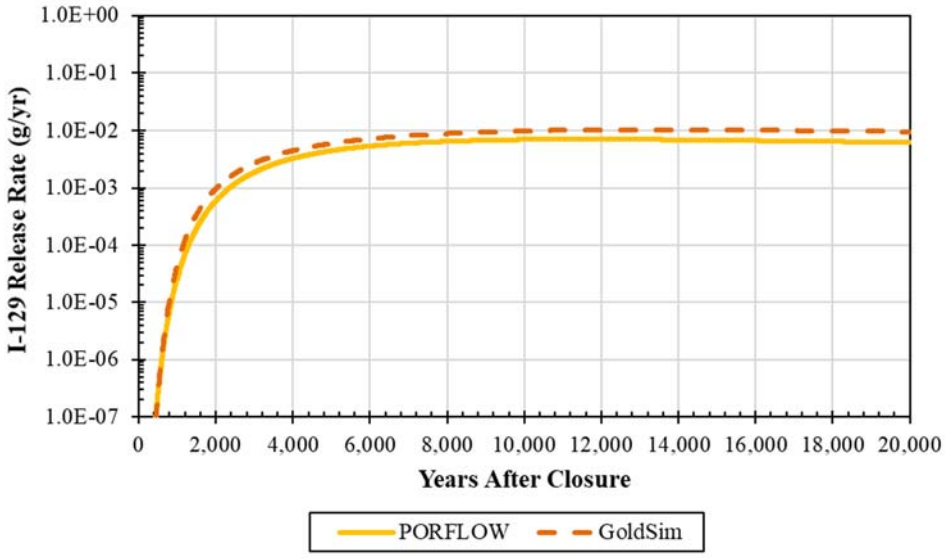

Figure 5.6-38: I-129 Realistic Case Release-Rate Comparison for SDU 1 Using a Zero-Concentration (Dirichlet-Type) Exit Boundary Condition (Linear Scale)

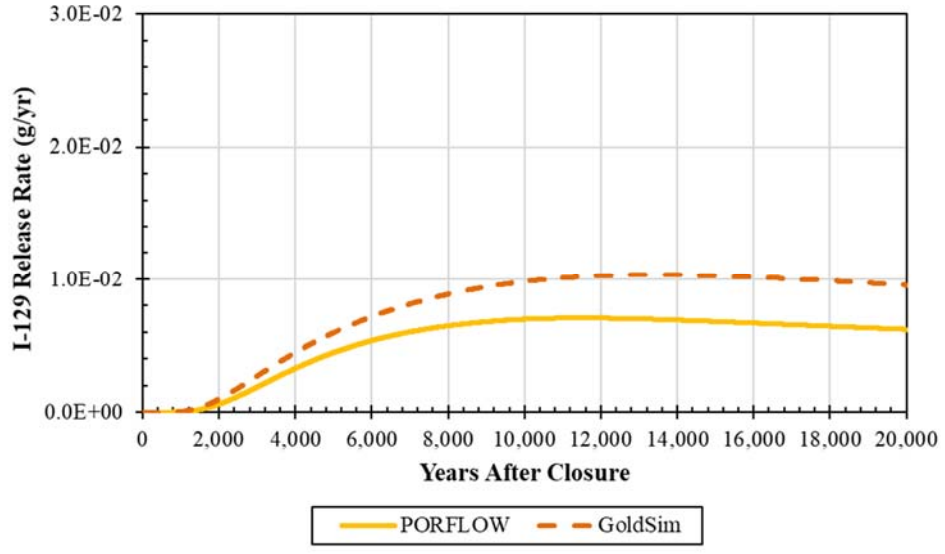

Figure 5.6-39: I-129 Pessimistic Case Release-Rate Comparison for SDU 1 Using a Zero-Concentration (Dirichlet-Type) Exit Boundary Condition (Log Scale)

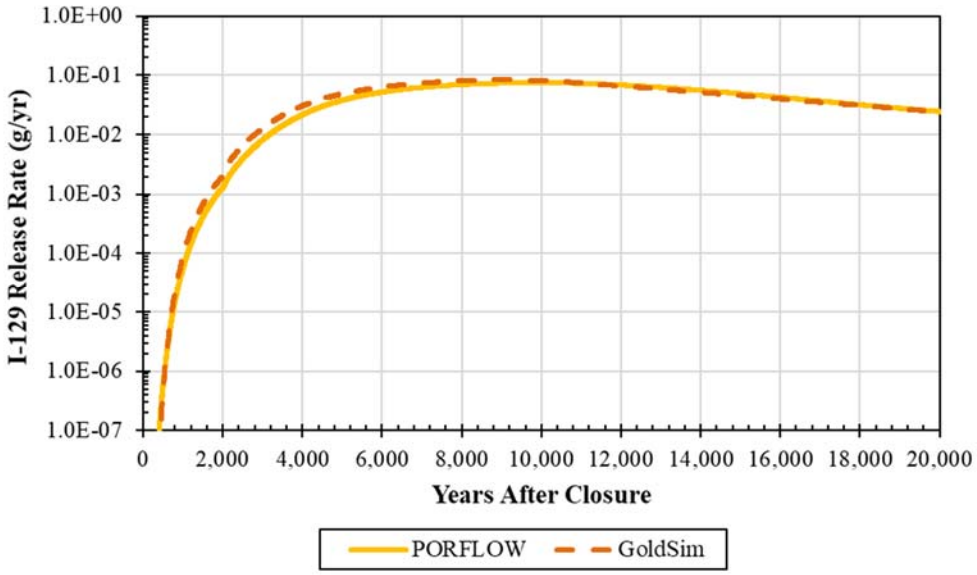

Figure 5.6-40: I-129 Pessimistic Case Release-Rate Comparison for SDU 1 Using a Zero-Concentration (Dirichlet-Type) Exit Boundary Condition (Linear Scale)

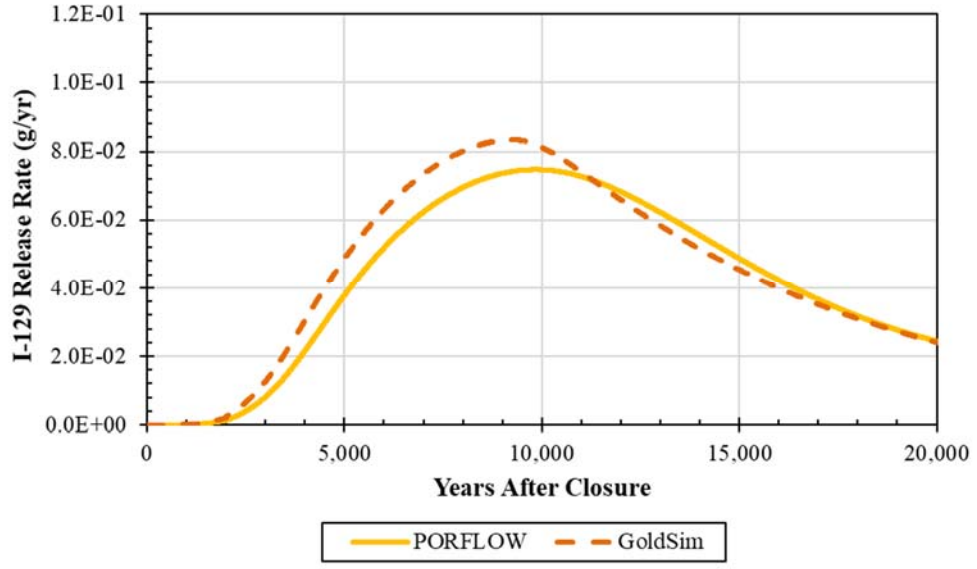

Figure 5.6-41: I-129 Realistic Case Release-Rate Comparison for SDU 7 Using a Zero-Concentration (Dirichlet-Type) Exit Boundary Condition (Log Scale)

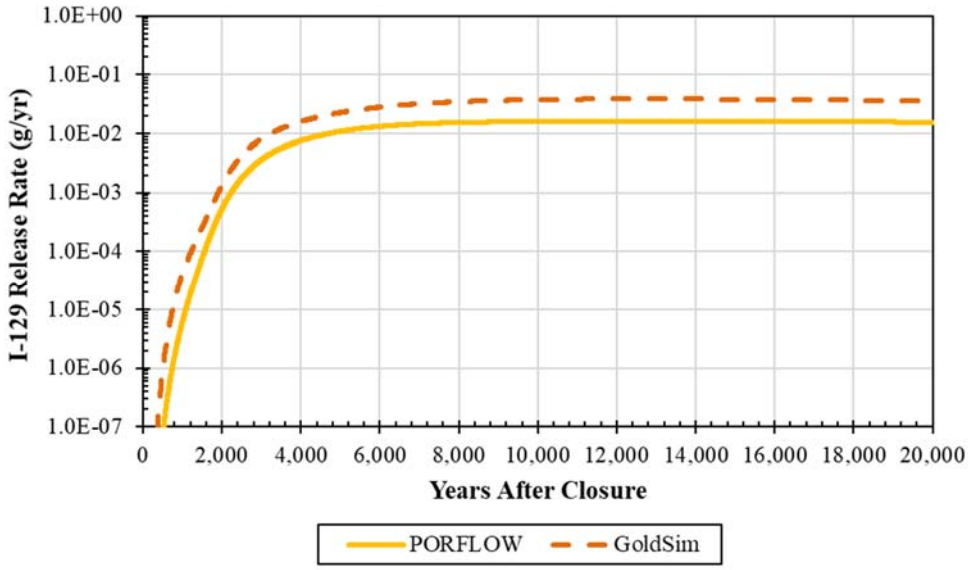

Figure 5.6-42: I-129 Realistic Case Release-Rate Comparison for SDU 7 Using a Zero-Concentration (Dirichlet-Type) Exit Boundary Condition (Linear Scale)

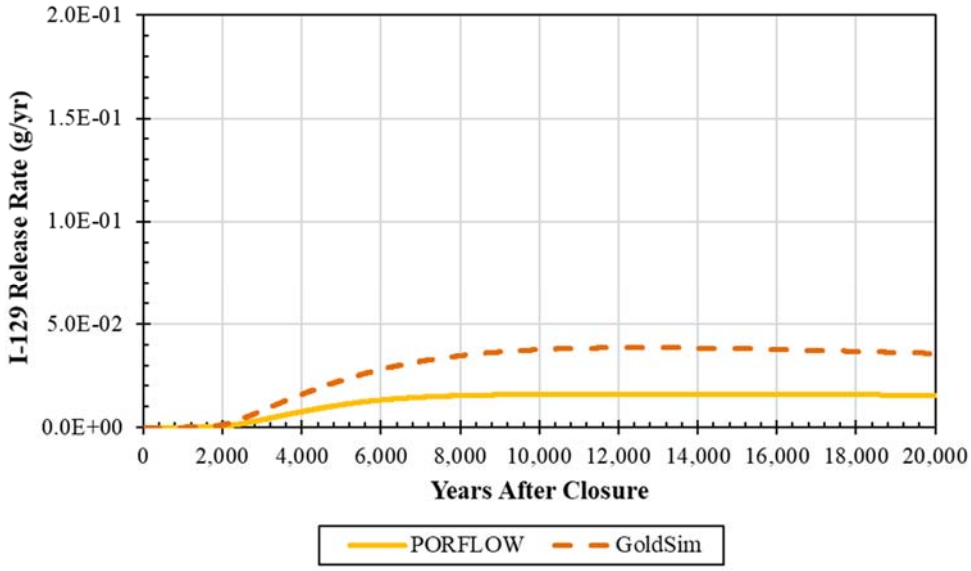

Figure 5.6-43: I-129 Pessimistic Case Release-Rate Comparison for SDU 7 Using a Zero-Concentration (Dirichlet-Type) Exit Boundary Condition (Log Scale)

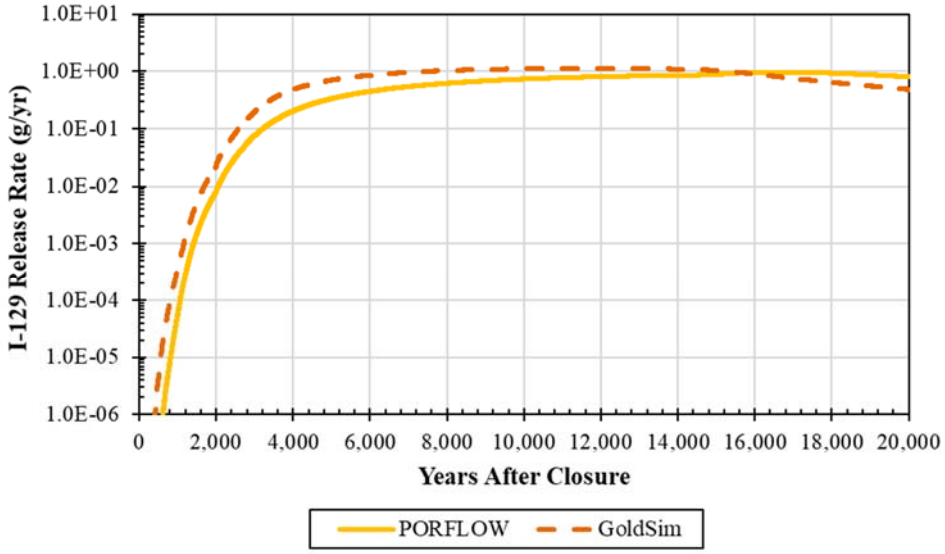

Figure 5.6-44: 1-129 Pessimistic Case Release-Rate Comparison for SDU 7 Using a Zero-Concentration (Dirichlet-Type) Exit Boundary Condition (Linear Scale)

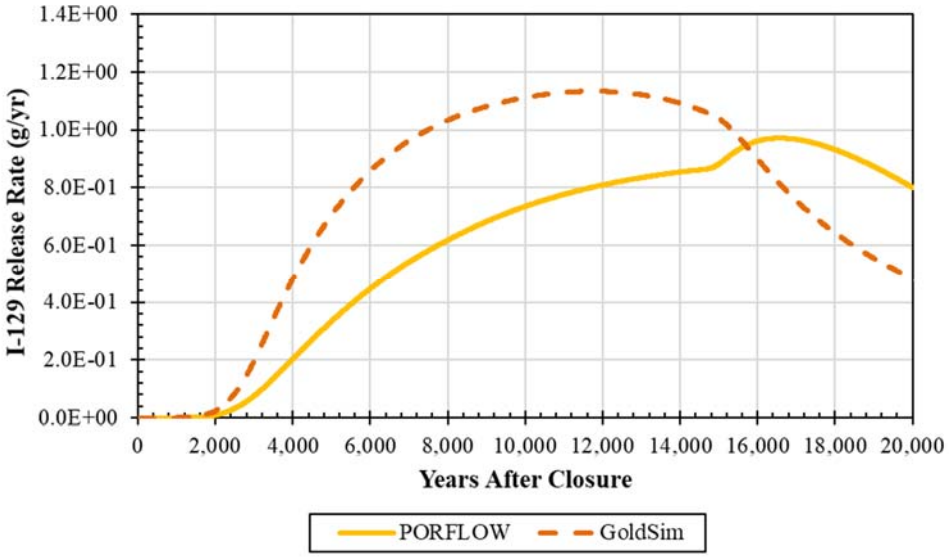

Table 5.6-9: Comparison of PORFLOW and SDF GoldSim Model Peak I-129 Rates from SDU 1 and 7 for Simulations

Case/SDU	PORFLOW Model Peak Release Rate (g/yr)	SDF GoldSim Model Peak Release Rate (g/yr)	Percent Difference
Realistic/SDU 1	7.03E-03	1.03E-02	+46
Pessimistic/SDU 1	7.48E-02	8.33E-02	+11
Realistic/SDU 7	1.61E-02	3.85E-02	+139
Pessimistic/SDU 7	9.71E-01	1.13E-00	+17

5.6.3 Benchmarking of Dose Results and Associated Radionuclide Concentrations at the 100-Meter Compliance Boundary

To evaluate the appropriateness of the SDF GoldSim Model abstraction as a surrogate for the more rigorous fully three-dimensional PORFLOW Aquifer Transport Model, a comparison (PORFLOW versus GoldSim) was made between potential doses evaluated at the 100-meter compliance boundary. Where radionuclide-specific dose contributions are discussed the associated 100-meter compliance boundary concentrations are also presented. In this study, dose comparisons are made for each sector (Sectors A through H) and for peak dose breakthrough curves representing the maximum value along the 100-meter boundary (Figure 4.4-114) at any given time.

For a detailed evaluation of model consistency, the GoldSim and PORFLOW 100-meter compliance boundary dose contributions along Sectors B, D, and F for the dominant dose-driving radionuclides (I-129 and Tc-99) and selected secondary dose contributors (Cl-36, Cs-135, and K-40) are compared. Also included are comparisons of the GoldSim and PORFLOW 100-m compliance boundary concentrations along Sectors B, D, and F for the dominant dose-driving radionuclides and the selected secondary dose contributors as an indicator of the radionuclide specific relationship between concentration and dose. The choice of Sectors B, D, and F is based on their representation of radionuclide transport controlled by the northwesterly flow under the northern assemblage of SDUs located on the western side of a ground water divide, radionuclide transport controlled by the easterly flow under the northern assembly of SDUs located on the eastern side of a ground water divide, and the maximum releases controlled by the easterly flow under the southern-sector SDUs (see Figure 4.4-114 and Figure 4.4-115).

The sector-based comparisons of 100-meter boundary doses are presented in (Figure 5.6-45 for Sectors B, D, and F, and Figure 5.6-46 for the remaining sectors). The sector-based doses from PORFLOW and GoldSim show similar trends. Note that the dose magnitude differences are associated with the differences in the vadose zone releases for I-129, and are reflected in the dose comparisons (see also Figure 5.6-7, Figure 5.6-13, Figure 5.6-19, and Figure 5.6-25). Similar trends and magnitude differences are also reflected in the maximum total peak dose results presented in Figure 5.6-47.

Comparisons of radionuclide-specific 100-meter concentration breakthrough curves for I-129, Tc-99, Cl-36, Cs-135, and K-40, and their resultant dose time-history results for Sectors B, D, and F are presented in Figure 5.6-48 through Figure 5.6-53. The radionuclide-specific concentrations for the PORFLOW and the GoldSim models are presented in Figure 5.6-48, Figure 5.6-50, and Figure 5.6-52 and the associated dose contributions are presented in Figure 5.6-49, Figure 5.6-51, and Figure 5.6-53, respectively. The results presented in Figure 5.6-48 through Figure 5.6-53 show similar trends between the two sets of model results. The differences in the magnitudes in Figure 5.6-49, Figure 5.6-51, and Figure 5.6-53 show the degree to which the I-129 and Tc-99 releases from the vadose zone control the total doses at the 100-meter boundary.

Results of special interest include the comparison between the PORFLOW and GoldSim Tc-99 concentration breakthrough curves and the Tc-99 dose contributions. Both PORFLOW and GoldSim use the same PORFLOW-generated vadose zone releases for Tc-99. Since the saturated

zone model fluxes are the same, a comparison between the PORFLOW and GoldSim 100-meter boundary dose breakthrough curves for Tc-99 provides a direct comparison for illustrating how well the SDF GoldSim Model approximates the PORFLOW Aquifer Transport Model.

As an additional check as to how well the abstracted saturated zone model can approximate the total dose results (and thus the 100-meter concentrations) generated by the more rigorous PORFLOW model, an additional set of PORFLOW Model and SDF GoldSim Model dose breakthrough curves, which neglect the I-129 dose contributions, were generated. These doses are presented for each sector and for the maximum dose for all sectors. The comparisons presented in Figure 5.6-54 (for Sectors B, D, and F) and Figure 5.6-55 (for the remaining sectors) and Figure 5.6-56 show that the saturated zone section of the SDF GoldSim Model results represent a very good approximation of the SDF PORFLOW Model results when the I-129 contributions are ignored. When limited to the Compliance Period as depicted in Figure 5.6-57, the dose breakthrough curve which is dominated by the Tc-99 release reflects how well the SDF GoldSim Model approximates the GSA Model (PORFLOW).

Figure 5.6-45: Sector-Based Dose Results for the PORFLOW and GoldSim Models, Sectors B, D, and F

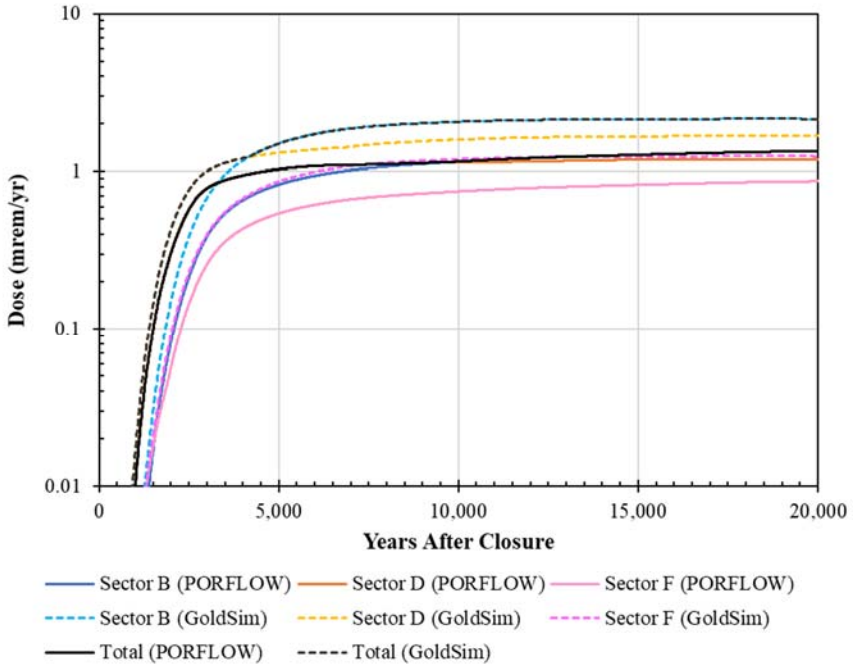

Figure 5.6-46: Sector-Based Dose Results for the PORFLOW and GoldSim Model, Sectors A, C, E, G and H

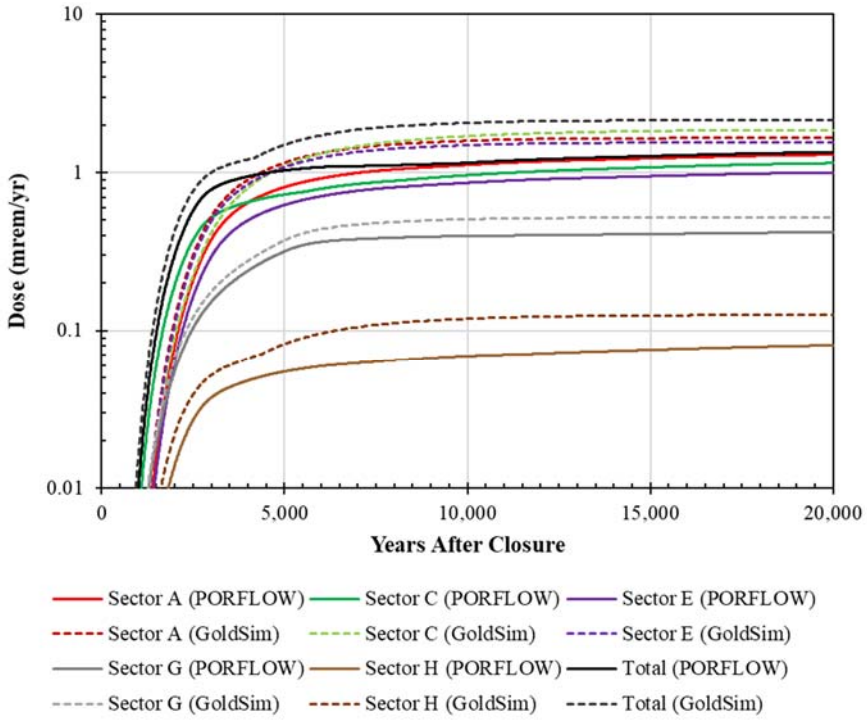

Figure 5.6-47: Maximum Dose Comparison between PORFLOW and GoldSim Model Results at the 100-Meter Compliance Boundary

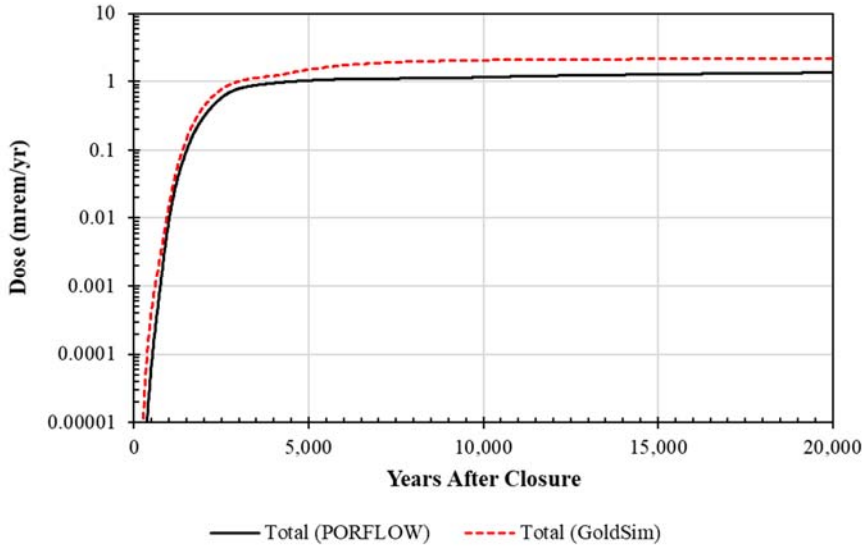

Figure 5.6-48: Radionuclide Concentration Comparison between PORFLOW and GoldSim Model Results for Sector B at the 100-Meter Compliance Boundary

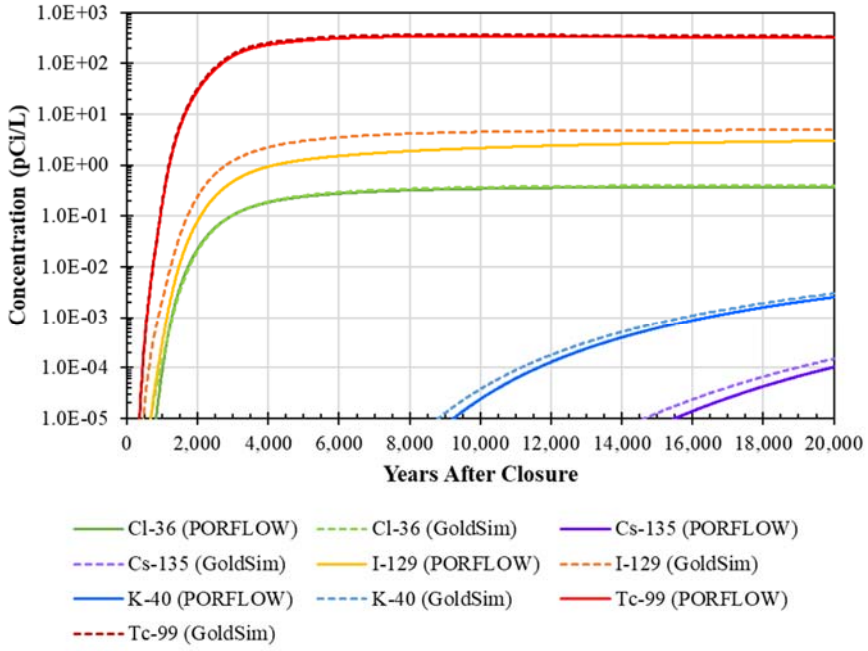

Figure 5.6-49: Radionuclide Dose Comparison between PORFLOW and GoldSim Model Results for Sector B at the 100-Meter Compliance Boundary

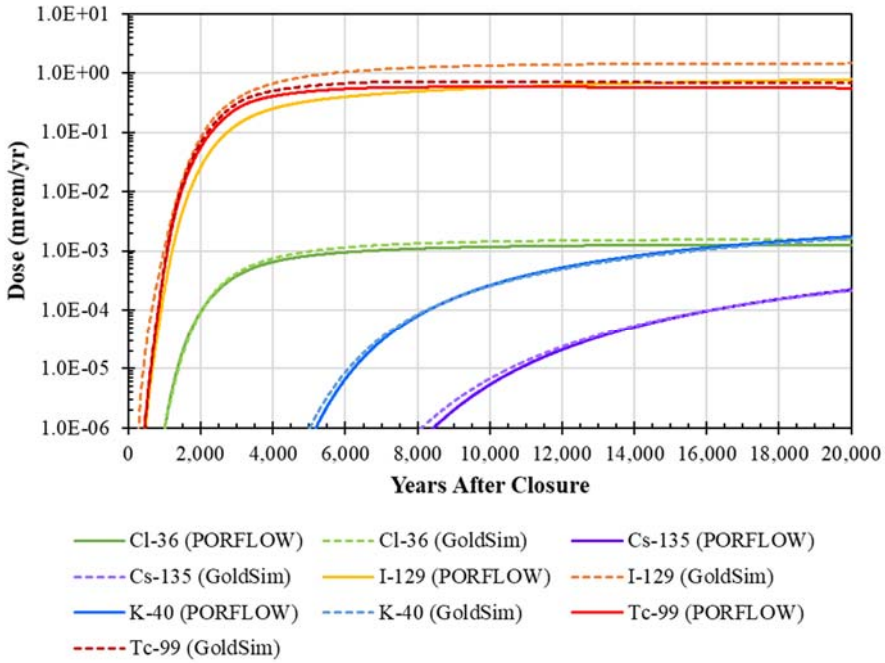

Figure 5.6-50: Radionuclide Concentration Comparison between PORFLOW and GoldSim Model Results for Sector D at the 100-Meter Compliance Boundary

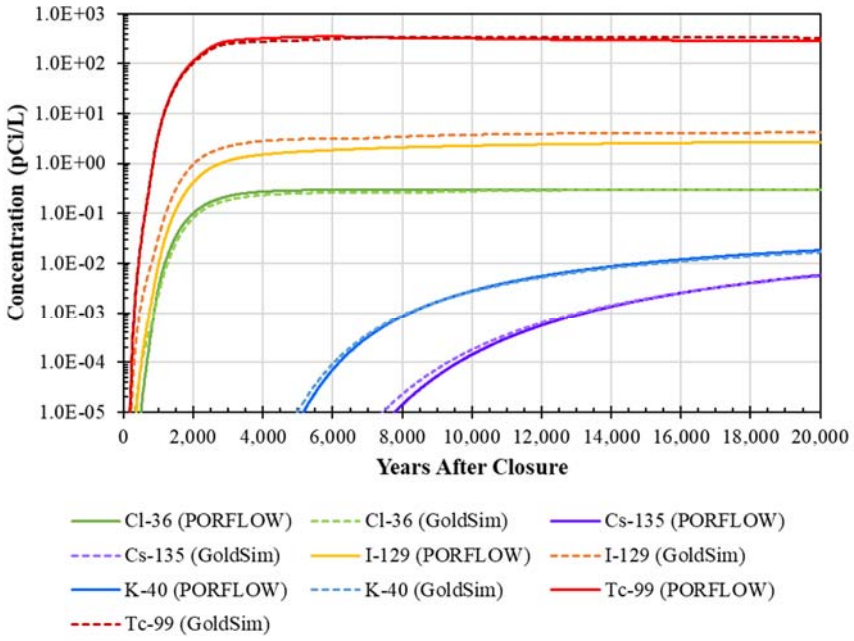

Figure 5.6-51: Radionuclide Dose Comparison between PORFLOW and GoldSim Model Results for Sector D at the 100-Meter Compliance Boundary

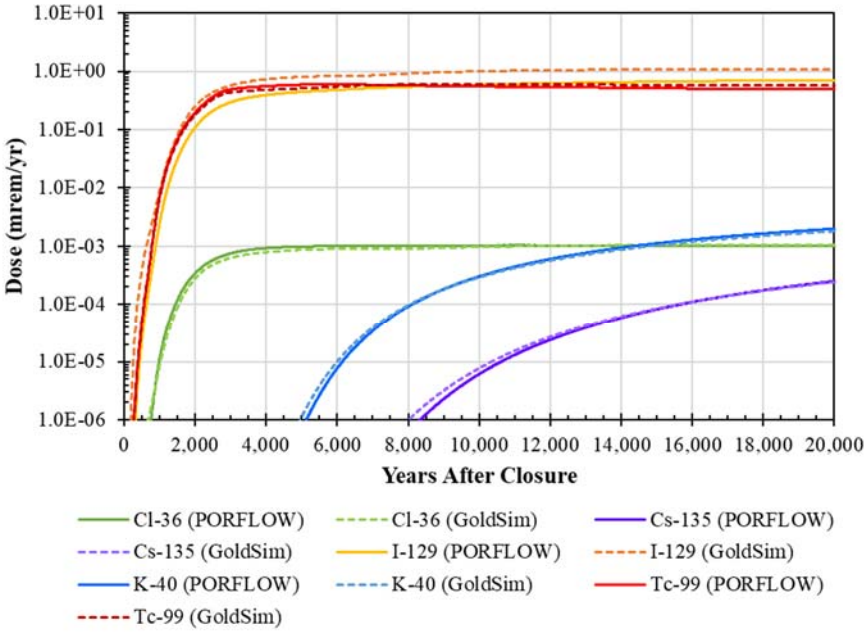

Figure 5.6-52: Radionuclide Concentration Comparison between PORFLOW and GoldSim Model Results for Sector F at the 100-Meter Compliance Boundary

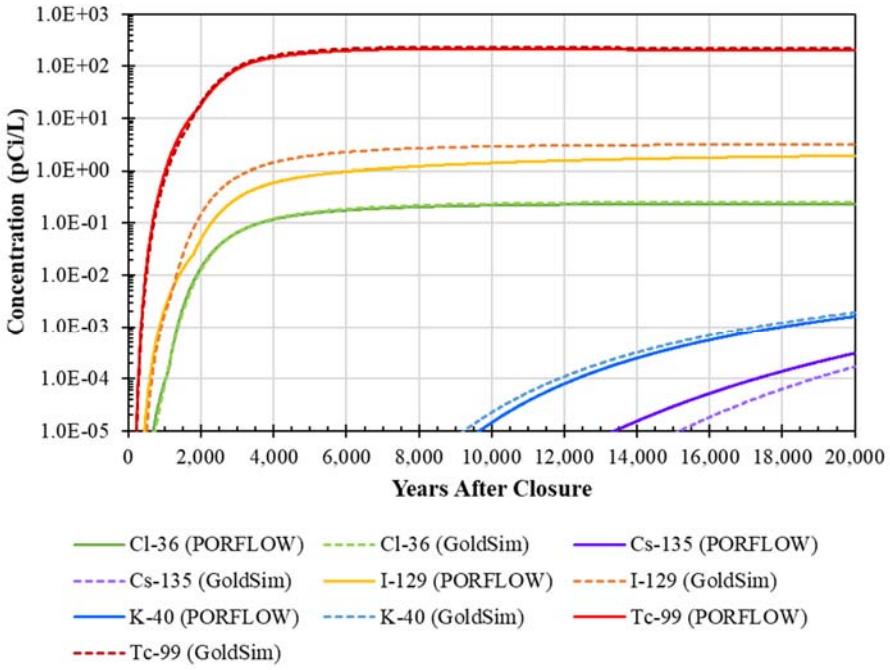

Figure 5.6-53: Radionuclide Dose Comparison between PORFLOW and GoldSim Model Results for Sector F at the 100-Meter Compliance Boundary

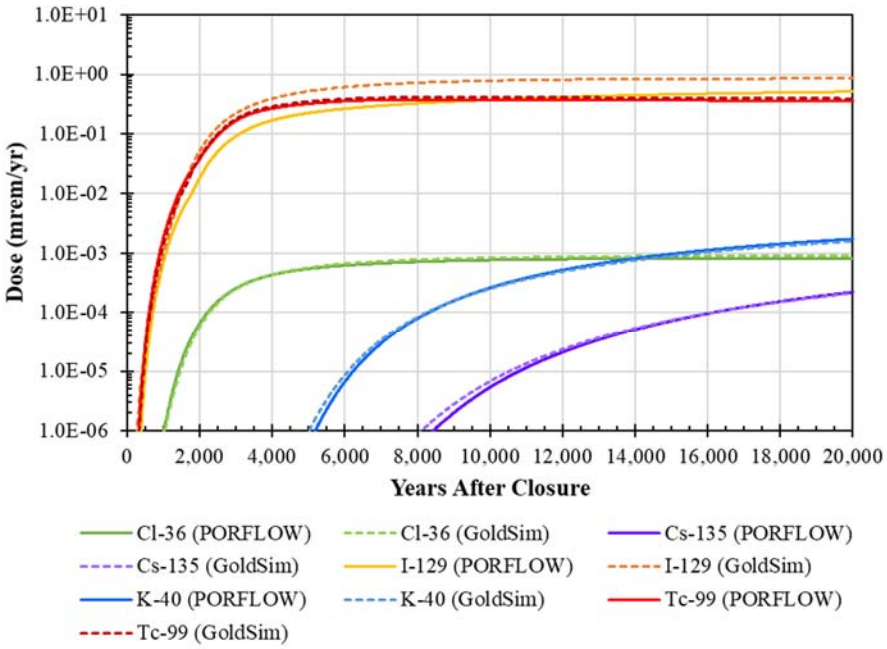

Figure 5.6-54: Sector-Based Dose Results for the PORFLOW and GoldSim Models when the I-129 Dose Contribution is Neglected, Sectors B, D, and F

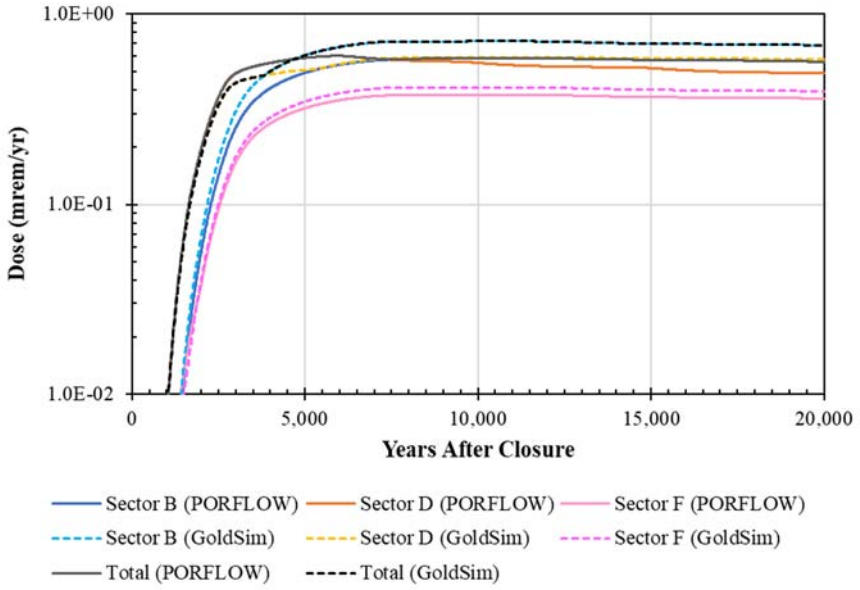

Figure 5.6-55: Sector-Based Dose Results for the PORFLOW and GoldSim Models when the I-129 Dose Contribution is Ignored, Sectors A, C, E, G and H

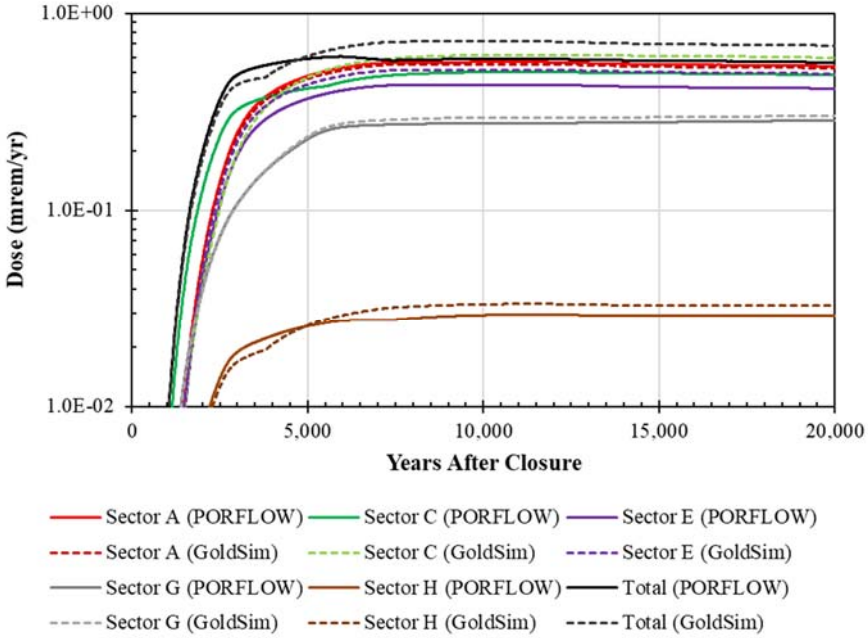

Figure 5.6-56: Maximum Dose Comparison between PORFLOW and GoldSim Model Results at the 100-Meter Compliance Boundary when the I-129 Dose Contribution is Neglected

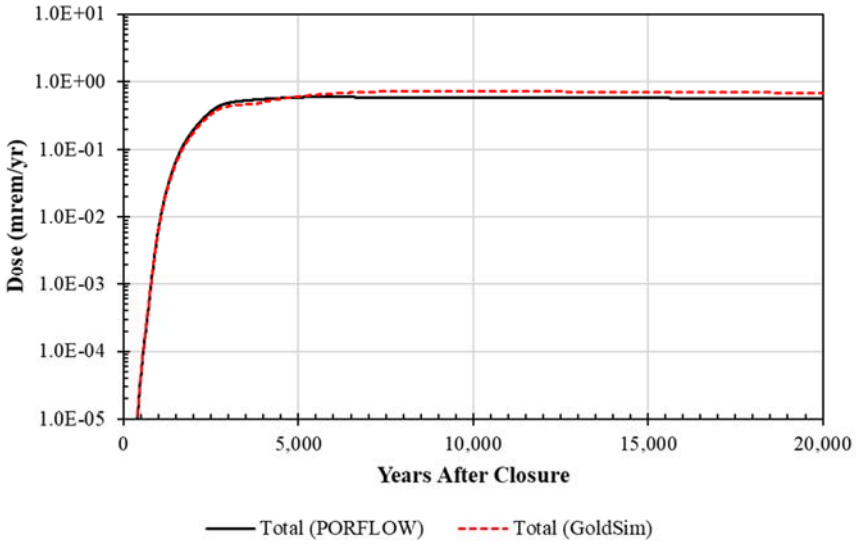

Figure 5.6-57: Maximum Compliance Period Dose Comparison between PORFLOW and GoldSim Model Results at the 100-Meter Compliance Boundary when the I-1129 Dose Contribution is Neglected

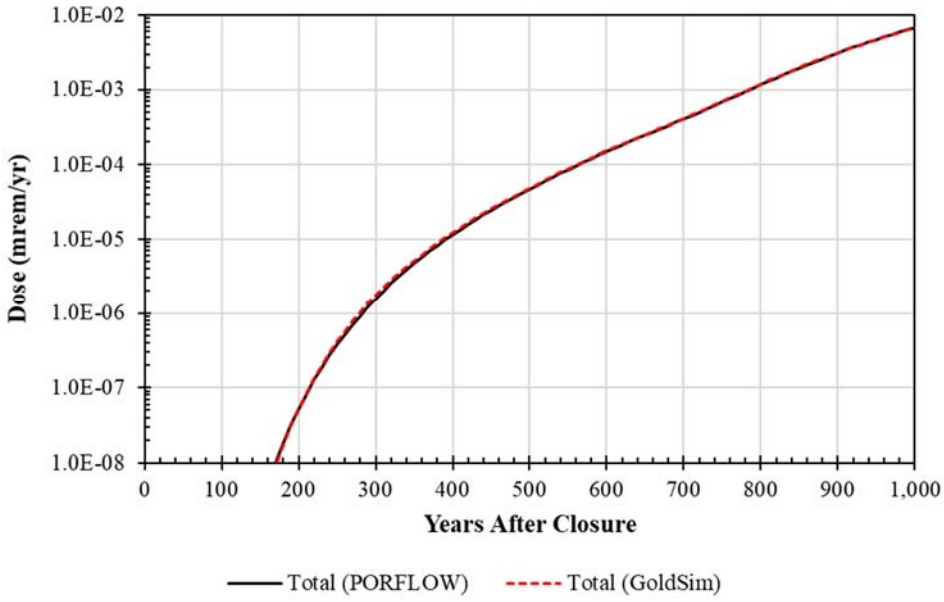

5.6.4 Benchmarking of IHI Doses at the IHI Wells and the 1-Meter Boundary

To evaluate how well the SDF GoldSim Model abstraction of the PORFLOW Model can approximate the Chronic IHI doses generated by the fully three-dimensional PORFLOW saturated zone model, a comparison was made between IHI Well and 1-meter boundary doses generated using the PORFLOW model and the SDF GoldSim Model, respectively. Note that in the IHI analysis, the proximity of the target wells and the 1-meter boundary to the source zone,

the influence of vertical mixing found in the fully three-dimensional PORFLOW model, and the placement of source nodes in different layers and materials, including the upper and lower aquifer zones of the Upper Three Runs Aquifer and the Tan Clay confining Unit between the two zones (see Figure 4.4-110), are approximated by a one-dimensional advective dispersive analytical solution that is assumed to follow a stream trace from the center of the mass release to the saturated zone. The influence of transverse dispersion is then applied to the results of the one-dimensional analysis for advective dispersive transport in a homogeneous medium using a GoldSim plume function based on Green's functions.

In this study, dose comparisons are made for each IHI well (IHI Well 1 through IHI Well 7) and for peak dose along breakthrough curves representing the maximum value along the 1-meter boundary at any given time. Note the 1-meter boundary transport calculations are handled differently in the two models with the maximum value along the boundary in the PORFLOW model represented at any given time by the highest nodal value in the vertical plane defining the boundary. In the SDF GoldSim Model, the maximum boundary value is represented by the highest value at any of the seven target IHI wells. The results presented below in Figure 5.6-58 through Figure 5.6-68 and Table 5.6-10 are based on simulations which neglect the influence of drill cuttings, generating dose contributions calculated solely from the PORFLOW-generated and SDF GoldSim Model-generated ground water concentrations.

As can be observed in Figure 5.6-58 and Figure 5.6-59 for all IHI wells and the 1-meter boundary (1-meter boundary results are also presented by themselves in Figure 5.6-60 and Figure 5.6-61), comparing PORFLOW Model and SDF GoldSim Model results indicates that the abstraction model is capable of approximating the PORFLOW Model results. Thus, the sensitivity of the modeled system to different processes can be evaluated with GoldSim despite the differences in the source geometry between the simple analytical solution used in the abstraction model and the discretized PORFLOW numerical solution (see Figure 5.6-62 through Figure 5.6-68 and Table 5.6-10).

Note there are specific IHI wells where results match quite well between the two models, such as for IHI Well 3 (Figure 5.6-64) and IHI Well 4 (Figure 5.6-65), where over 10,000 years PORFLOW generated and GoldSim generated peak doses differ by between -3% to +5% (Table 5.6-10). Other IHI observation wells such as IHI Well 1 (Figure 5.6-62), IHI Well 2 (Figure 5.6-63), IHI Well 5 (Figure 5.6-66), IHI Well 6 (Figure 5.6-67), and IHI Well 7 (Figure 5.6-68) reflect higher concentrations generated by the GoldSim Model. IHI Well 2, IHI Well 5, and IHI Well 6 range from 30% to 40% greater for the SDF GoldSim Model which is considered acceptable due to localized near-field differences (Table 5.6-10).

The saturated zone source areas for IHI Well 1 and IHI Well 7 are quite different between the two models but the SDF GoldSim Model abstraction represents the more conservative approach. IHI Well 1 is expected to show higher doses generated by the SDF GoldSim Model for three reasons: 1) the PORFLOW source configuration is more dispersed being split into two layers of nodes separated by a third layer of nodes while GoldSim has only a single source layer, 2) a superimposed plume emanating from SDU 11 will be vertically offset from the SDU 12 plume in the PORFLOW analysis, as opposed to the peak doses being assumed to be at the same level

within GoldSim, and 3) the dose-controlling I-129 releases from the SDF GoldSim Model are higher than those from the PORFLOW Model, as previously discussed. In the case of IHI Well 7 which is adjacent to SDU 10, much of the source allocation in the PORFLOW Model is initiated within a clay layer subject to lower flow rates and greater sorption (an I-129 K_d of 3 mL/g versus 1mL/g for the aquifer zones).

Figure 5.6-58: IHI Well and 1-Meter Boundary Chronic Dose Results for the PORFLOW and GoldSim Models (Log Scale)

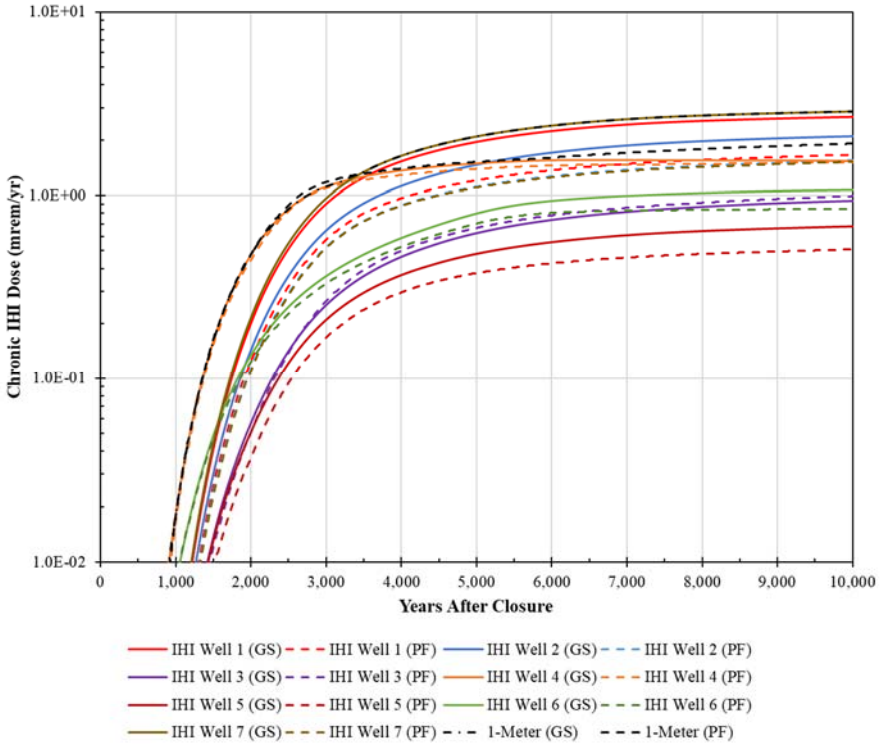

Figure 5.6-59: IHI Well and 1-Meter Boundary Chronic Dose Results for the PORFLOW and GoldSim Models (Linear Scale)

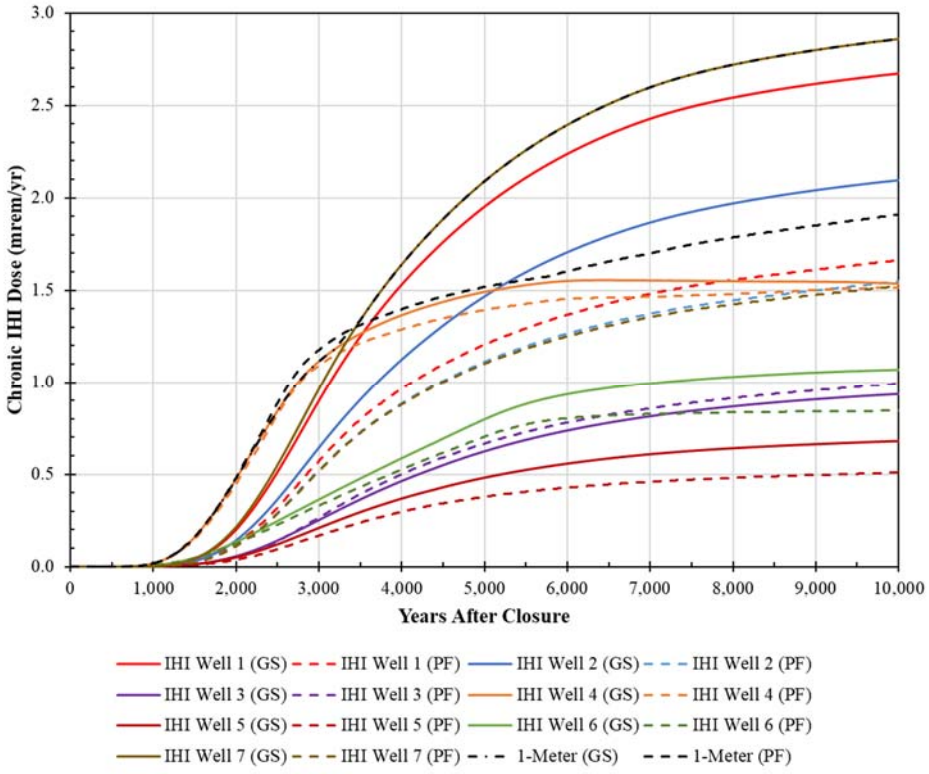

Figure 5.6-60: Chronic IHI Dose Comparison between PORFLOW and GoldSim Model Results at the 1-Meter IHI Boundary

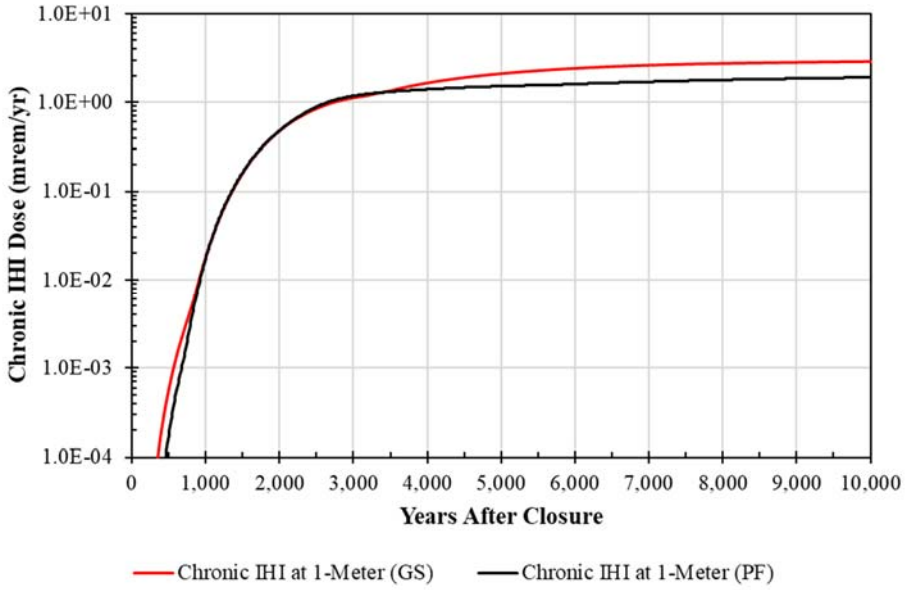

Figure 5.6-61: Chronic IHI Dose Comparison between PORFLOW and GoldSim Model Results at the 1-Meter IHI Boundary

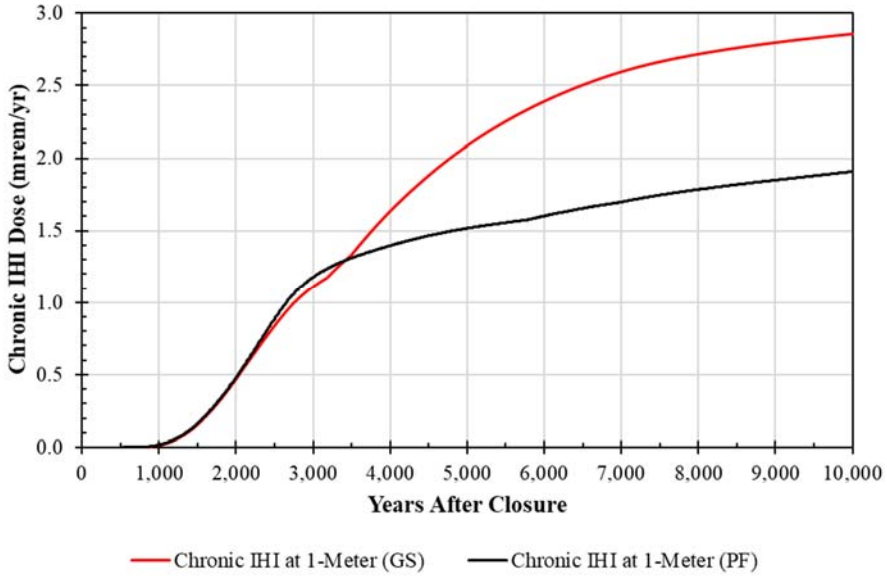

Figure 5.6-62: Chronic IHI Dose Comparison between PORFLOW and GoldSim Model Results at IHI Well 1

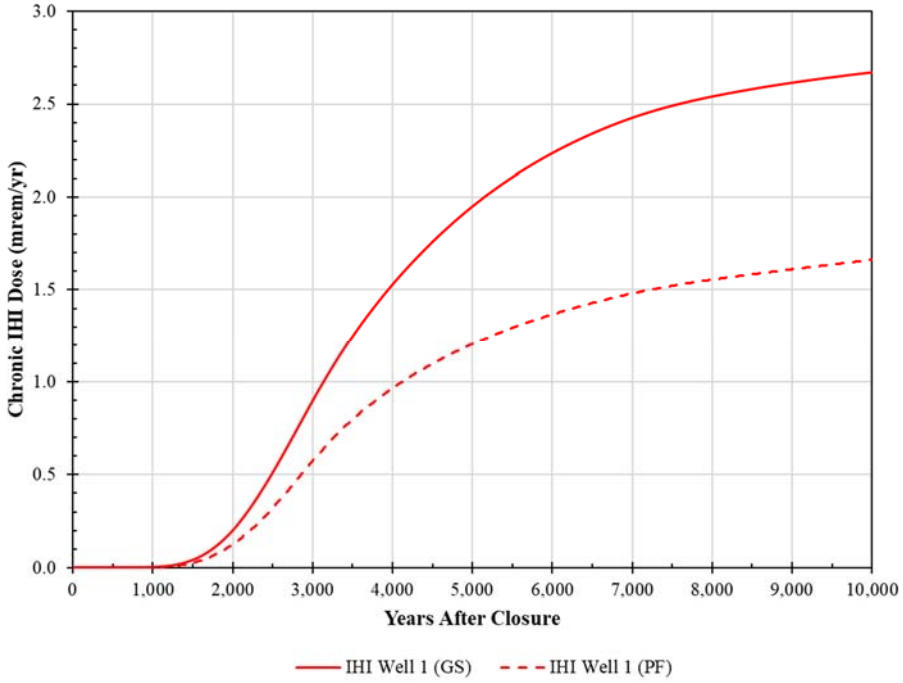

Figure 5.6-63: Chronic IHI Dose Comparison between PORFLOW and GoldSim Model Results at IHI Well 2

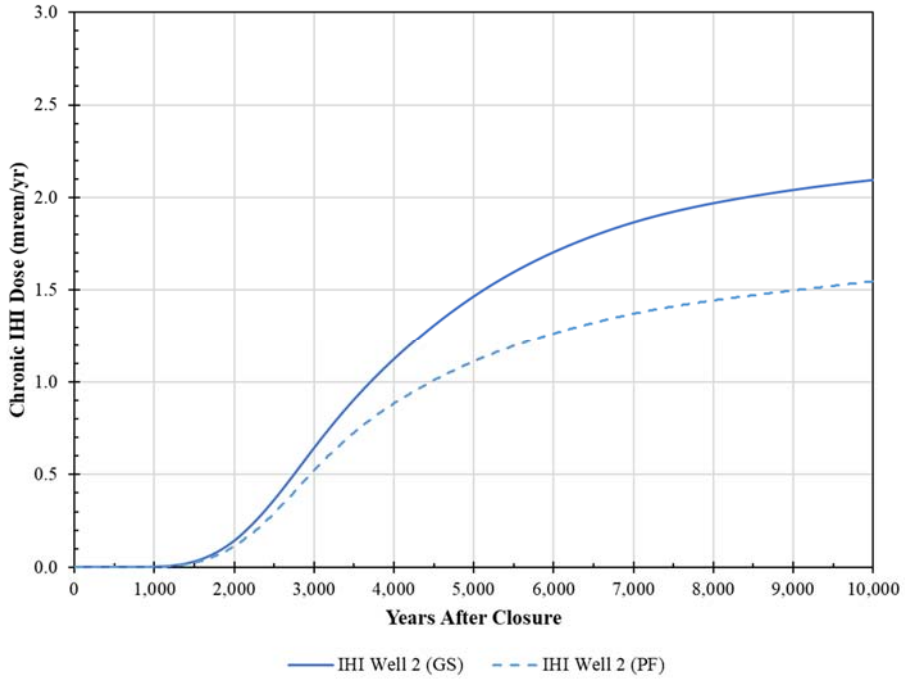

Figure 5.6-64: Chronic IHI Dose Comparison between PORFLOW and GoldSim Model Results at IHI Well 3

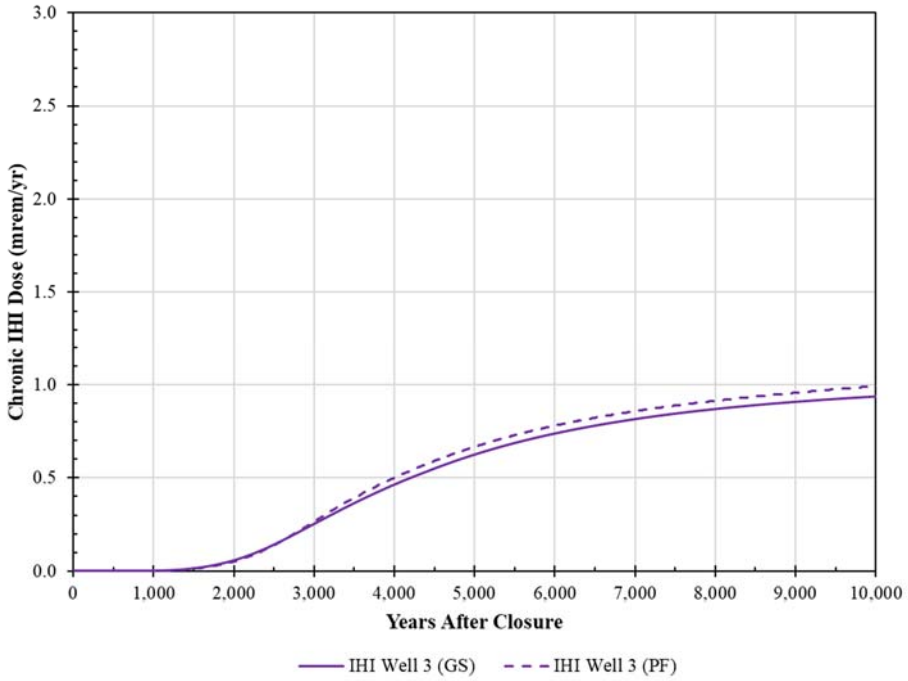

Figure 5.6-65: Chronic IHI Dose Comparison between PORFLOW and GoldSim Model Results at IHI Well 4

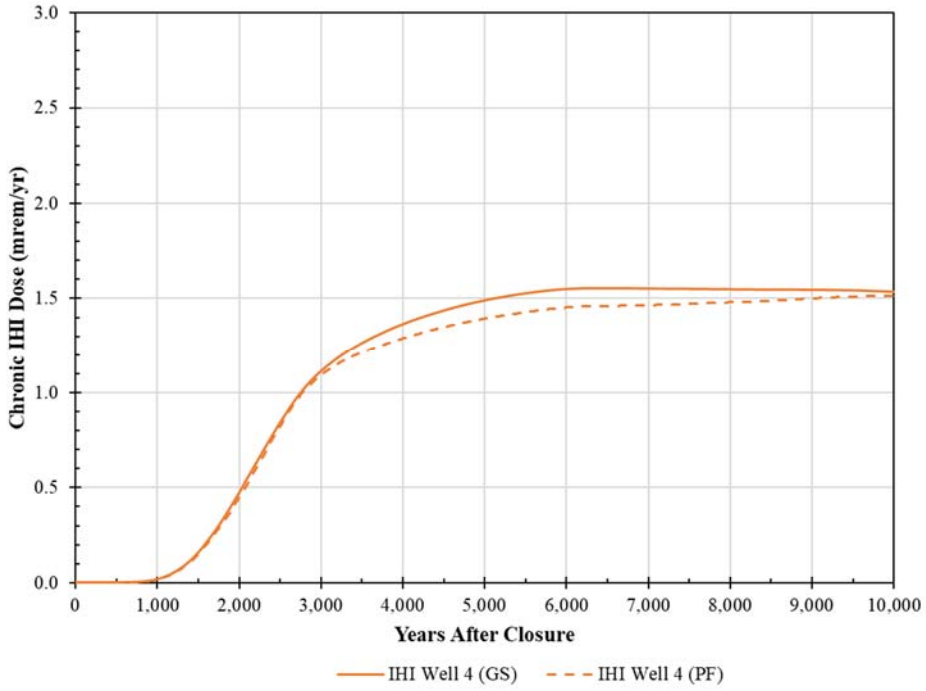

Figure 5.6-66: Chronic IHI Dose Comparison between PORFLOW and GoldSim Model Results at IHI Well 5

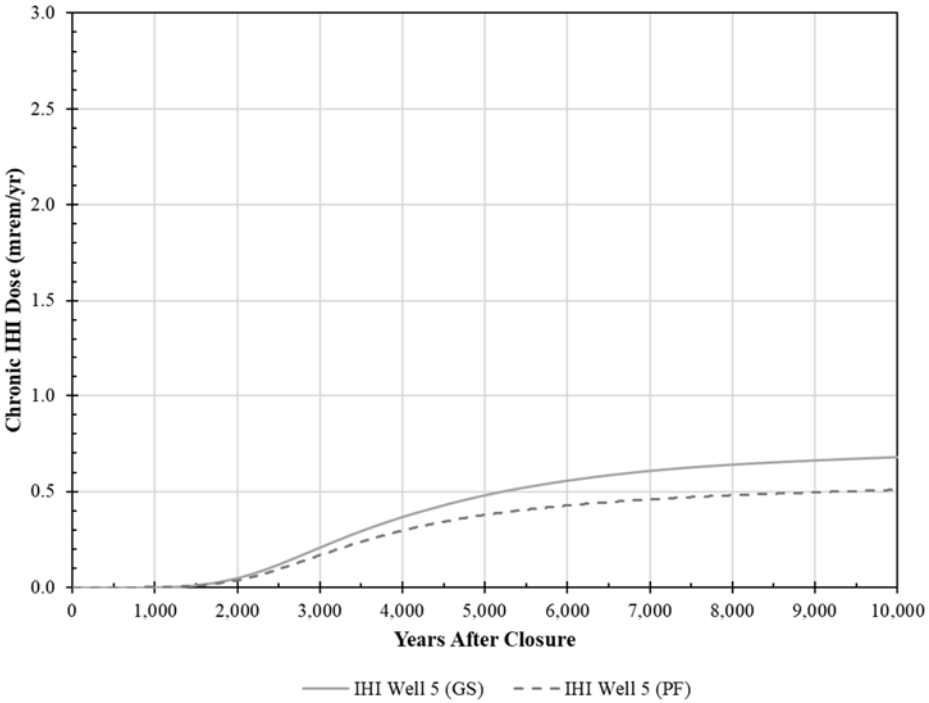

Figure 5.6-67: Chronic IHI Dose Comparison between PORFLOW and GoldSim Model Results at IHI Well 6

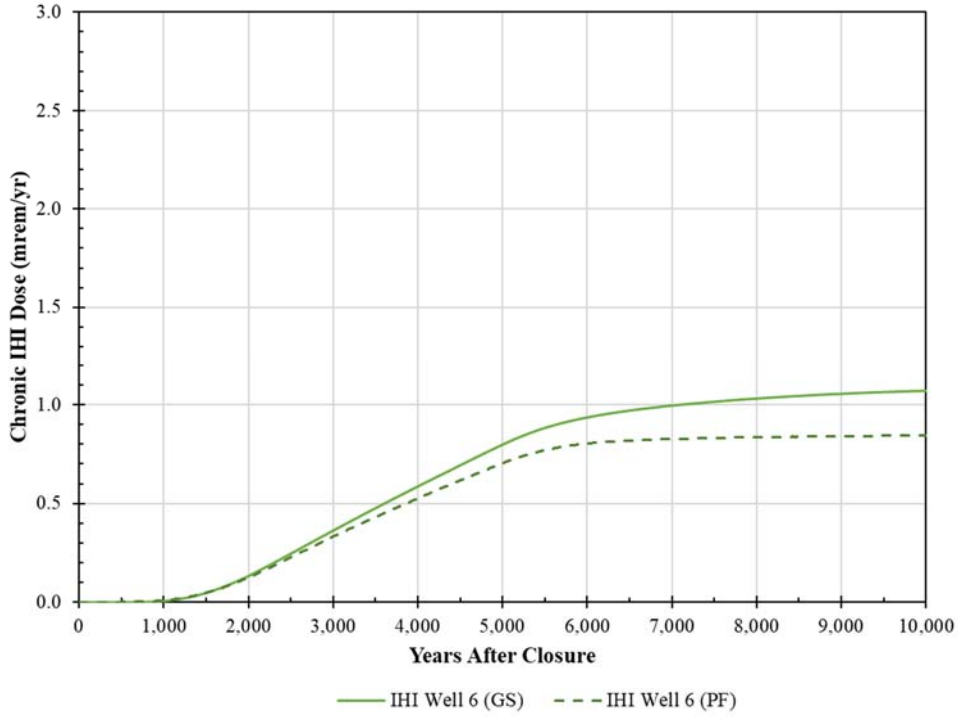

Figure 5.6-68: Chronic IHI Dose Comparison between PORFLOW and GoldSim Model Results at IHI Well 7

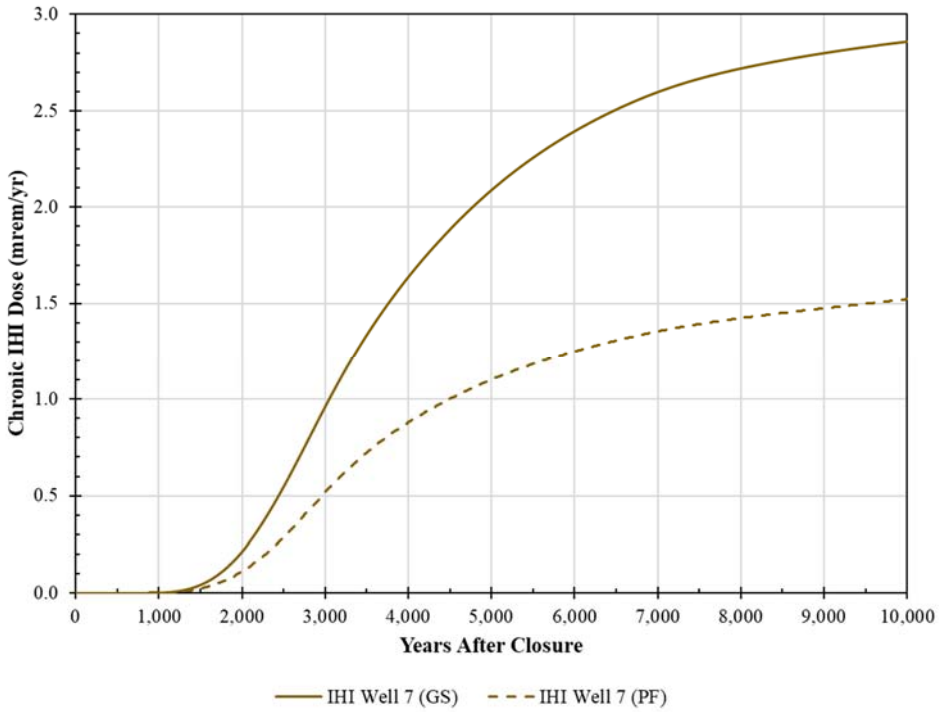

Table 5.6-10: Comparison of PORFLOW and GoldSim Model 10,000-Year Peak Doses at the IHI Wells and the 1-Meter IHI Boundary

	Peak 10,000-Year IHI Dose (mrem/yr)							
Location	**IHI Well 1**	**IHI Well 2**	**IHI Well 3**	**IHI Well 4**	**IHI Well 5**	**IHI Well 6**	**IHI Well 7**	**1-Meter**
GoldSim	2.67	2.10	0.94	1.55	0.68	1.07	2.86	2.86
PORFLOW	1.66	1.55	0.99	1.51	0.51	0.84	1.52	1.91
Percent Difference	+61%	+35%	-5%	+3%	+33%	+27%	+88%	+50%

5.6.5 Benchmarking Summary

The radionuclides used for benchmarking the SDU releases were selected based on the magnitude of their contributions to total dose in the SDF PORFLOW Model and based on their individual transport characteristics. For benchmarking of the GoldSim-based abstraction of the PORFLOW Vadose Zone Transport Model, the chosen radionuclides are either fast moving (e.g., Cl-36 and I-129 are not subject to solubility controls and are only slightly sorbed) or slower moving (e.g., Cs-135 is moderately sorbed). Because of the extremely long retarded travel times and negligible releases that would be observed in the system (see Section 5.5.1.5), highly sorbed species were not included in the benchmarking study. Verifying the transport behavior of representative radionuclides verifies by extension other radionuclides included in the inventory that have similar transport characteristics. By using the major dose contributors as indicators, confidence in the SDF GoldSim Model is established.

The results of the vadose zone benchmarking analysis show that radionuclide releases simulated by GoldSim generally match or exceed the PORFLOW peak release behavior. The analysis considered two boundary conditions for the bottom of the vadose zone when evaluating these model results: a zero-concentration boundary condition (as used for the simulations presented throughout Sections 5 and 6) and a zero-concentration gradient boundary. Both benchmarking exercises showed that SDF GoldSim Model provides an acceptable approximation of the vadose zone simulations in the SDF PORFLOW Model.

The results of the 100-meter compliance boundary dose benchmarking analysis provide validation that the SDF GoldSim Model can approximate the PORFLOW Aquifer Transport Model results. The comparison of the PORFLOW and GoldSim Tc-99 dose breakthrough curves at the 100-meter compliance boundary provides additional confidence that GoldSim does a good job of approximating the PORFLOW saturated zone transport process.

The results of the IHI dose benchmarking analysis also show that the SDF GoldSim Model adequately approximates the PORFLOW saturated zone model near-field results. The comparison of the PORFLOW and GoldSim IHI dose breakthrough curves at the seven IHI wells and at the 1-meter compliance boundary, indicate that GoldSim also does an acceptable job of approximating the PORFLOW saturated zone transport behavior in closer proximity to the SDUs, despite localized differences between the source geometry and flow field used in the two models.

5.7 Probabilistic Analysis

Uncertainty is inherent in simplified numeric models that attempt to replicate engineered or natural systems. Different types of uncertainty exist in models of complex systems: uncertainty in possible future outcomes, uncertainty in the consequences of future outcomes, and uncertainty in the parameters used as input to these models. When used in probabilistic mode, the SDF GoldSim Model is a valuable tool for assessing these uncertainties.

Using the probabilistic mode, the SDF GoldSim Model can perform the entire simulation multiple times, in which each simulation is referred to as a realization. During each realization, GoldSim randomly samples different values for those inputs that have been assigned probability distributions. These uncertainty inputs are referred to as stochastic elements. Because each realization samples a different set of input values, the output from each realization is unique. This probabilistic modeling approach is also known as the Monte Carlo Method.

As implemented in the SDF GoldSim Model, an optional Latin Hypercube Sampling (LHS) procedure is used in conjunction with the Monte Carlo Method; this GoldSim sampling approach discretizes the chosen distribution into "strata" of equal probability-space. The probability distribution for each stochastic element is divided into either 10,000 equally spaced strata or less if the number of realizations is less than 10,000. For each stochastic element, its strata are randomly shuffled and a random value is picked in turn from within each stratum. Applying the LHS method has the effect of ensuring that the probability space is uniformly spanned, which accelerates the rate of convergence (minimizing the number of realizations needed) to stabilize the probabilistic results of the Monte Carlo scheme.

Because probabilistic models vary multiple parameters simultaneously, the concurrent effects of changes in the model can be analyzed and the potential impacts can be assessed. This assessment allows for identification of parameters that are only of significance under specific conditions. The objective of the probabilistic model is to quantify parameter uncertainty explicitly (i.e., as probabilities) to bound the range of possible doses and to identify those parameters which most strongly influence doses under a variety of conditions.

Sensitivity analyses that use deterministic modeling typically only consider the effects of a single parameter, or a small number of parameters, to evaluate parametric effects in isolation. Using both probabilistic and deterministic models for sensitivity analysis versus a single approach provides additional information concerning which parameters are of most importance to the SDF PA.

As described in Section 4.5, the SDF GoldSim Model was developed using the GoldSim software program. This model facilitates the evaluation of probabilistic sensitivity analyses and the influence of parameter uncertainty on the migration of radionuclides from the SDUs to the accessible environment. The parameters selected for probabilistic evaluation were based on modeling experience and the availability of generic and site-specific data to provide a basis for parameter ranges (described in Section 5.7.1).

The SDF GoldSim Model is more computationally efficient than the Vadose Zone Transport Model (see Section 4.4.5) and the Aquifer Transport Model (see Section 4.4.6) but includes

additional calculations, such as the random sampling of stochastic parameters, which cannot be performed in PORFLOW. The SDF GoldSim Model is described in Section 4.5 and validation of the model via benchmarking is described in Section 5.6.

5.7.1 Stochastics (Uncertainty Parameters)

This section summarizes the probabilistic distributions assigned to the stochastic elements within the SDF GoldSim Model. As mentioned in Section 4.5, the SDF GoldSim Model includes seven categories of stochastic distributions:

1. Physical Property Uncertainty,
2. Inventory Uncertainty,
3. Parametric Flow Field Sampling,
4. Ground Water Hydrology Uncertainty,
5. K_d Uncertainty,
6. Technetium Solubility Uncertainty, and
7. Dose and Exposure Pathway Uncertainty.

Table 5.7-1 provides a complete listing of the stochastic elements used to evaluate uncertainty within the SDF GoldSim Model. Additional discussion of each of these stochastic categories is provided below.

Table 5.7-1: List of Stochastic Elements in the SDF GoldSim Model

Stochastic Element Name within the SDF GoldSim Model	Stochastic Category	Notes
InventoryUncert_I129_SDU[XX]	Inventory	Samples the I-129 inventory for each SDU. The "SDU[XX]" is used to indicate that there are duplicate stochastic elements within the SDF GoldSim Model (one for each SDU or SDU type).
InventoryUncert_Tc99_SDU[XX]	Inventory	Samples the Tc-99 inventory for each SDU. The "SDU[XX]" is used to indicate that there are duplicate stochastic elements within the SDF GoldSim Model (one for each SDU or SDU type).
InventoryUncertainty_SDU[XX]	Inventory	Samples the inventory for every radionuclide except I-129 and Tc-99, and for each SDU. The "SDU[XX]" is used to indicate that there are duplicate stochastic elements within the SDF GoldSim Model (one for each SDU or SDU type).
Infiltration_sample	Parametric Flow Field	Samples the infiltration rate.
Degradation_sample	Parametric Flow Field (and Physical Property)	Samples the cementitious degradation rate.
SaltstoneSatK_sample	Parametric Flow Field (and Physical Property)	Samples the initial saturated hydraulic conductivity of saltstone.
BackfillSatK_sample	Parametric Flow Field (and Physical Property)	Samples the saturated hydraulic conductivity of backfill. This parameter also influences the final (fully degraded) saturated hydraulic conductivity of cementitious material.
SatZoneDarcyVelDist	Ground Water Hydrology (and Physical Property)	Samples uncertainty of ground water flow rates (i.e., the saturated zone Darcy velocities).

Stochastic Element Name within the SDF GoldSim Model	Stochastic Category	Notes
SatThickness	Ground Water Hydrology (and Physical Property)	Samples uncertainty in the saturated zone thickness.
UzthicknessDist	Ground Water Hydrology (and Physical Property)	Samples uncertainty in the vadose zone thickness.
SDU[XX]_SatWidth	Ground Water Hydrology (and Physical Property)	Samples uncertainty in the saturated zone widths beneath each SDU. The "SDU[XX]" is used to indicate that there are duplicate stochastic elements within the SDF GoldSim Model (one for each SDU or SDU type).
Kd_Dist_Sand	K_d	Samples uncertainty in the K_d values for transport through sand. Note that this GoldSim model element is used to sample unique values for each chemical element.
Kd_Dist_Clay	K_d	Samples uncertainty in the K_d values for transport through clay. Note that this GoldSim model element is used to sample unique values for each chemical element.
Kd_Dist_SandL	K_d	Samples uncertainty in the K_d values for transport through leachate-impacted sand. Note that this GoldSim model element is used to sample unique values for each chemical element.
Kd_Dist_ClayL	K_d	Samples uncertainty in the K_d values for transport through leachate-impacted clay. Note this GoldSim model element is used to sample unique values for each chemical element.
Kd_Dist_ReI	K_d	Samples uncertainty in the K_d values for transport through Reducing Region I materials. Note that this GoldSim model element is used to sample unique values for each chemical element.
Kd_Dist_ReII	K_d	Samples uncertainty in the K_d values for transport through Reducing Region II materials. Note that this GoldSim model element is used to sample unique values for each chemical element.
Kd_Dist_ReIII	K_d	Samples uncertainty in the K_d values for transport through Reducing Region III materials. Note that this GoldSim Model element is used to sample unique values for each chemical element.
Kd_Dist_OxI	K_d	Samples uncertainty in the K_d values for transport through Oxidizing Region I materials. Note that this GoldSim model element is used to sample unique values for each chemical element.
Kd_Dist_OxII	K_d	Samples uncertainty in the K_d values for transport through Oxidizing Region II materials. Note that this GoldSim model element is used to sample unique values for each chemical element.
Kd_Dist_OxIII	K_d	Samples uncertainty in the K_d values for transport through Oxidizing Region III materials. Note that as an array element, this element is used to sample unique values for each element.

Stochastic Element Name within the SDF GoldSim Model	Stochastic Category	Notes
SaltstoneKd_Dist_Sr_RelI	K_d	Samples uncertainty in the strontium K_d for transport through Reducing Region I saltstone. Note that this is equivalent to *Kd_Dist_RelI* (which is used for sampling the strontium K_d in concrete as well as the other elements), but because strontium also has a saltstone-specific K_d (see Section 4.3.2), it is sampled independently.
SaltstoneKd_Dist_Sr_RelII	K_d	Samples uncertainty in the strontium K_d for transport through Reducing Region II saltstone. Note that this is equivalent to *Kd_Dist_RelII* (which is used for sampling the strontium K_d in concrete as well as the other elements), but because strontium also has a saltstone-specific K_d (see Section 4.3.2), it is sampled independently.
SaltstoneKd_Dist_Sr_RelIII	K_d	Samples uncertainty in the strontium K_d for transport through Reducing Region III saltstone. Note that this is equivalent to *Kd_Dist_RelIII* (which is used for sampling the strontium K_d in concrete as well as the other elements), but because strontium also has a saltstone-specific K_d (see Section 4.3.2), it is sampled independently.
SaltstoneKd_Dist_Sr_OxI	K_d	Samples uncertainty in the strontium K_d for transport through Oxidizing Region I saltstone. Note that this is equivalent to *Kd_Dist_OxI* (which is used for sampling the strontium K_d in concrete as well as the other elements), but because strontium also has a saltstone-specific K_d (see Section 4.3.2), it is sampled independently.
SaltstoneKd_Dist_Sr_OxII	K_d	Samples uncertainty in the strontium K_d for transport through Oxidizing Region II saltstone. Note that this is equivalent to *Kd_Dist_OxII* (which is used for sampling the strontium K_d in concrete as well as the other elements), but because strontium also has a saltstone-specific K_d (see Section 4.3.2), it is sampled independently.
SaltstoneKd_Dist_Sr_OxIII	K_d	Samples uncertainty in the strontium K_d for transport through Oxidizing Region III saltstone. Note that this is equivalent to *Kd_Dist_OxIII* (which is used for sampling the strontium K_d in concrete as well as the other elements), but because strontium also has a saltstone-specific K_d (see Section 4.3.2), it is sampled independently.
SaltstoneKd_Dist_Ra_RelI	K_d	Samples uncertainty in the radium K_d for transport through Reducing Region I saltstone. Note that this is equivalent to *Kd_Dist_RelI* (which is used for sampling the radium K_d in concrete as well as the other elements), but because radium also has a saltstone-specific K_d (see Section 4.3.2), it is sampled independently.
SaltstoneKd_Dist_Ra_RelII	K_d	Samples uncertainty in the radium K_d for transport through Reducing Region II saltstone. Note that this is equivalent to *Kd_Dist_RelII* (which is used for sampling the radium K_d in concrete as well as the other elements), but because radium also has a saltstone-specific K_d (see Section 4.3.2), it is sampled independently.

Stochastic Element Name within the SDF GoldSim Model	Stochastic Category	Notes
SaltstoneKd_Dist_Ra_ReIII	K_d	Samples uncertainty in the radium K_d for transport through Reducing Region III saltstone. Note that this is equivalent to *Kd_Dist_ReIII* (which is used for sampling the radium K_d in concrete as well as the other elements), but because radium also has a saltstone-specific K_d (see Section 4.3.2), it is sampled independently.
SaltstoneKd_Dist_Ra_OxI	K_d	Samples uncertainty in the radium K_d for transport through Oxidizing Region I saltstone. Note that this is equivalent to *Kd_Dist_OxI* (which is used for sampling the radium K_d in concrete as well as the other elements), but because radium also has a saltstone-specific K_d (see Section 4.3.2), it is sampled independently.
SaltstoneKd_Dist_Ra_OxII	K_d	Samples uncertainty in the radium K_d for transport through Oxidizing Region II saltstone. Note that this is equivalent to *Kd_Dist_OxII* (which is used for sampling the radium K_d in concrete as well as the other elements), but because radium also has a saltstone-specific K_d (see Section 4.3.2), it is sampled independently.
SaltstoneKd_Dist_Ra_OxIII	K_d	Samples uncertainty in the radium K_d for transport through Oxidizing Region III saltstone. Note that this is equivalent to *Kd_Dist_OxIII* (which is used for sampling the radium K_d in concrete as well as the other elements), but because radium also has a saltstone-specific K_d (see Section 4.3.2), it is sampled independently.
SaltstoneKd_Dist_I_ReI	K_d	Samples uncertainty in the iodine K_d for transport through Reducing Region I saltstone. Note that this is equivalent to *Kd_Dist_ReI* (which is used for sampling the iodine K_d in concrete as well as the other elements), but because iodine also has a saltstone-specific K_d (see Section 4.3.2), it is sampled independently.
SaltstoneKd_Dist_I_ReII	K_d	Samples uncertainty in the iodine K_d for transport through Reducing Region II saltstone. Note that this is equivalent to *Kd_Dist_ReII* (which is used for sampling the iodine K_d in concrete as well as the other elements), but because iodine also has a saltstone-specific K_d (see Section 4.3.2), it is sampled independently.
SaltstoneKd_Dist_I_ReIII	K_d	Samples uncertainty in the iodine K_d for transport through Reducing Region III saltstone. Note that this is equivalent to *Kd_Dist_ReIII* (which is used for sampling the iodine K_d in concrete as well as the other elements), but because iodine also has a saltstone-specific K_d (see Section 4.3.2), it is sampled independently.
SaltstoneKd_Iodine	K_d	Samples the selection of discrete iodine K_ds in saltstone based on Table 4.3-7.
Solubility	Tc Solubility	Samples the selection of input values for technetium solubilities based on Table 4.3-8.
UncertMultiplier_WaterUptake	Dose	Samples the uncertainty of human consumption of water.

Stochastic Element Name within the SDF GoldSim Model	Stochastic Category	Notes
UncertMultiplier_ProduceUptake	Dose	Samples the uncertainty of human consumption of produce (fruits and vegetables).
UncertMultiplier_MeatUptake	Dose	Samples the uncertainty of human consumption of meat.
UncertMultiplier_FishUptake	Dose	Samples the uncertainty of human consumption of fish.
FracLocalMeat_MOP	Dose	Samples the fraction of meat consumed by the MOP that comes from local (contaminated) sources.
FracLocalMilk_MOP	Dose	Samples the fraction of milk consumed by the MOP that comes from local (contaminated) sources.
FracLocalPoultry_MOP	Dose	Samples the fraction of poultry consumed by the MOP that comes from local (contaminated) sources.
FracLocalEgg_MOP	Dose	Samples the fraction of egg consumed by the MOP that comes from local (contaminated) sources.
FracLocalMeat_IHI	Dose	Samples the fraction of meat consumed by the IHI that comes from local (contaminated) sources.
FracLocalMilk_IHI	Dose	Samples the fraction of milk consumed by the IHI that comes from local (contaminated) sources.
FracLocalPoultry_IHI	Dose	Samples the fraction of poultry consumed by the IHI that comes from local (contaminated) sources.
FracLocalEgg_IHI	Dose	Samples the fraction of egg consumed by the IHI that comes from local (contaminated) sources.
FracLocalFished	Dose	Samples the fraction of fish consumed by the MOP and/or IHI that comes from local (contaminated) sources.
GardenSizeUncert	Dose (and Physical Property)	Samples the assumed size of the crop or garden used by the MOP or IHI.
TillDepthUncert	Dose (and Physical Property)	Samples the depth to which the crop or garden soil is tilled.
WeatheringDecayConstUncert	Dose (and Physical Property)	Samples the rate at which crops or gardens undergo weathering.
RetentionUncert	Dose (and Physical Property)	Samples uncertainty in the fraction of contaminants retained by leafy produce when irrigated.
IrrigationRateUncert	Dose (and Physical Property)	Samples the irrigation rate for crops or gardens.
CropIrrigationTimeUncert	Dose	Samples the fraction of time spent watering crops or gardens.
SoilDensityUncert	Dose (and Physical Property)	Samples uncertainty in the density of soil.
IHI_DrillEventTime_Uncert	Other	Randomly samples the time that a human intrusion occurs.

5.7.1.1 Physical Property Uncertainty

As indicated by Table 5.7-1, all of the stochastic elements which are used to vary specific physical properties within the model have been categorized into the other stochastic distribution categories. For example, the uncertainty distributions that are used to randomize the selection of the saturated hydraulic conductivities for saltstone and backfill are part of the parametric flow field sampling discussed in Section 5.7.1.3.

5.7.1.2 Inventory Uncertainty

The SDU inventories in the SDF GoldSim Model control the total amount of contaminants available for release. Section 3.3 describes the basis for estimates of the inventory values. Realistic inventory values are provided in Table 3.3-5. While the Compliance Case assumed higher inventory values to provide even greater defensibility given the uncertainty associated with the future disposal inventories, the values in Table 3.3-5 represent the best inventory estimates and are used as the base value to be multiplied by the sampled uncertainty multipliers.

The sampling distributions for the inventory uncertainty multipliers were developed based on a quantitative analysis of uncertainty in SRS Tank Farm concentration data. This quantitative analysis is described in *Recommended Implementation of Inventory Sampling Distributions for the Saltstone Disposal Facility Performance Assessment GoldSim Model* (SRR-CWDA-2018-00076). The resulting distribution recommendations, as applied to the SDF GoldSim Model, are summarized in Table 5.7-2.

Table 5.7-2: Recommended Sampling Distributions for Inventory Uncertainty

Stochastic Element Setting	I-129	Tc-99	All Other Radionuclides
Distribution Type	Log-Normal	Log-Normal	Log-Normal
Maximum (unitless multiplier)	9.78	13.71	14.4
Mean (unitless multiplier)	1.00	1.00	1.19
Standard Deviation (unitless multiplier)	0.260	0.11	3.11
Minimum (unitless multiplier)	0.079	0.13	0.10

[Source: SRR-CWDA-2018-00076]

Note that the SDF GoldSim Model is not currently setup to explicitly model the releases of Tc-99 from the SDUs. Instead, multiple Tc-99 fluxes were output from the Vadose Zone Transport Model under varying flow conditions and used as direct input to the SDF GoldSim Model. For this reason, the SDF GoldSim Model only uses the MPAD inventory values for Tc-99. These MPAD values for Tc-99 are 50% higher than the realistic values (compare Table 3.3-5 to Table 3.3-6). Regardless, stochastic elements with the recommended inventory distributions for Tc-99 have been implemented into the model in anticipation that future model development will allow for the Tc-99 releases to be explicitly simulated.

Further, any saltstone that has been disposed of into SDUs through Mrach of 2018 has already undergone characterization. There is considerably less uncertainty associated with the inventories in these SDUs; therefore, the implementation of uncertainty for SDUs 1, 2A, 2B, 3A, 4, 5A, and 5B have been assigned less uncertainty within the SDF GoldSim Model. Specifically, the standard deviations for the inventory distributions are set to ¼th the standard deviations recommended in Table 5.7-2. [SRR-CWDA-2018-00076]

Finally, it is expected that higher concentrations of I-129 will likely be associated with higher concentrations of other radionuclides. As such, it is reasonable to assume a correlation between inventory distributions within each specific SDU. Because I-129 was

expected to be the most important radionuclide relative to peak doses, the distributions for the other radionuclides were correlated to the I-129 inventory sampling with a positive correlation coefficient of 0.8. [SRR-CWDA-2018-00076]

5.7.1.3 Parametric Flow Field Sampling

This section specifically considers the uncertainty accounted for by simulating different conditions which may influence flow through the Vadose Zone. As presented in Table 4.4-82, four conditions were varied to generate 54 different parametric flow fields (Flow Cases F01 through F54). These 54 flow fields were each simulated deterministically using the PORFLOW Vadose Zone Flow Model (described in Section 4.4.4).

The four conditions that were varied are: (1) infiltration rates, (2) cementitious degradation rates, (3) the saturated hydraulic conductivity of backfill (which is also used as the final saturated hydraulic conductivities of fully degraded cementitious materials), and (4) the initial saturated hydraulic conductivity of saltstone.

The memorandum *Development of Parametric Flow Fields for the SDF PA Revision* (SRR-CWDA-2018-00061) describes the down-selection of parameters considered for generating these flow fields. A summary rationale for selecting these parameters follows:

- The infiltration rates were selected because previous modeling had demonstrated the importance of this parameter,
- The cementitious degradation rates were selected because previous modeling had demonstrated the importance of this parameter,
- The saturated hydraulic conductivities of backfill were selected because the potential impacts of this parameter had not been previously considered and it may be important given the degradation rates of the SDU concrete, and
- The initial saturated hydraulic conductivities of saltstone were selected because previous modeling had demonstrated the importance of this parameter.

Within the SDF GoldSim Model, each of these four parameters is sampled independently. Each condition has an associated stochastic element with a discrete distribution used to determine the appropriate flow field. Within the discrete distributions for each parameter, the potential conditions are assigned equal probabilities such that all 54 flow fields have an equal probability of being selected (for every 3,000 realizations, each flow field is expected to be sampled an average of 56 times). Based on the sampling of the parameters, the SDF GoldSim Model determines the associated parametric flow field and uses the flow data for that flow field. The flow data is stored in external file sets that were developed from the Vadose Zone Flow Model (PORFLOW) and called by the model using a dynamic link library (DLL).

5.7.1.4 Ground Water and Hydrology Uncertainty

With the probabilistic SDF GoldSim Model, uncertainty in the ground water flow and hydrologic processes is considered by applying distributions to the thickness of the

vadose zone, the thickness of the saturated zone, the width of the saturated zone, and the Darcy velocity of water flowing through the saturated zone.

Vadose Zone Thickness (UZThicknessDist)

The lower vadose zone in the SDF GoldSim Model retards contaminant transport with its effectiveness related to the soil K_d values and the vadose zone thickness. Table 4.3-1 shows the estimated thickness of the lower vadose zone beneath each of the disposal units. The baseline model in the SDF GoldSim Model uses the same vadose zone thicknesses for each SDU as modeled in PORFLOW (see Table 4.3-1), except for SDU 6 which assumed a slightly thicker vadose zone (43.5 ft versus 42 ft). Note that within PORFLOW the thickness of the vadose zone is 42 feet below the outer edge of the SDU; due to the sloped floor, the thickness of the vadose zone is approximately 45 feet below the center of SDU 6. Within GoldSim, 43.5 feet is used.

Based on the measured well data, all of the assumed vadose zone thicknesses are biased towards using shorter-than-expected transport distances for the vadose zone. Despite this, additional uncertainty is applied within the model; based on data provided in WSRC-TR-2005-00131, a range of ± 16.4 ft (5 m) is assumed as a reasonable variance for the vadose zone thickness beneath each disposal unit. A triangular distribution is used within the SDF GoldSim Model where the base values assigned as the mode (most likely values), the maximum value is assumed to be 16.4 ft more and the minimum value assumed to be 16.4 ft less.

Saturated Zone Thickness (SatThickness)

Mass released from the disposal units enters the saturated zone dissolved in recharge water from the vadose zone and mixes with the ground water flowing through the saturated zone. The concentrations of radionuclides at the 100-meter boundary are a direct function of the volume of water flowing through the saturated zone and the mass flux released from the vadose zone. The volume of water flowing through the saturated zone is defined as the product of the Darcy velocity and the cross-sectional area of the pipe element perpendicular to flow. The cross-sectional area of the pipe element perpendicular to flow is defined as the product of the saturated zone thickness and the saturated zone width. In the SDF GoldSim Model, the saturated zone thickness is based on a mixing zone thickness estimated from cross-sectional diagrams of results from the SDF Aquifer Transport Model via PORFLOW (see Section 4.4.6). The deterministic value and mean value for probabilistic simulations used in the model is 20 m. [SRR-CWDA-2011-00178] The distribution assigned to the saturated zone thickness is defined as a truncated normal distribution with a minimum of 12 m and a maximum of 28 m with a standard deviation of 2.78 m. [SRR-CWDA-2011-00178]

Saturated Zone Width (SDU[XX]_SatWidth)

In the SDF GoldSim Model, water leaving the vadose zone enters the saturated zone (i.e., the aquifer) as recharge and is mixed into the volume of aquifer water. The volume is determined by the flow rate and mixing volume (flow face area multiplied by the flow

velocity) in the aquifer. The flow face area is dependent on the width and thickness of the saturated zone. The width of the saturated zone is defined in the SDF GoldSim Model with the model elements: *SDU1_SatWidth* (for SDU 1), *SDU2_SatWidth* (for SDUs 2A, 2B, 3A, 3B, 5A, and 5B), *SDU4_SatWidth* (for SDU 4), *SDU6_SatWidth* (for SDU 6) and *SDU7_SatWidth* (for SDUs 7 through 12). For SDUs 1 and 4, these elements sample a uniform distribution ranging from 80% to 120% of the SDU lengths (600 ft). For the cylindrical SDUs, these elements sample a uniform distribution ranging from 80% to 120% of the SDU diameters (either 150 ft or 375 ft). This distribution are range is based on a review of data obtained from *Saltstone Disposal Facility: Determination of the Probable Maximum Water Table Elevation* (WSRC-TR-2005-00131), and engineering judgment.

Saturated Zone Darcy Velocity (SatZoneDarcyVelDist)

Ground water flow in the saturated zone is approximated as a unidirectional flow field of constant Darcy velocity. As described in Section 4.4.6, average ground water flow rates from each SDU to the 100-meter boundary were determined using two different methods (either tracer pulse figures or the streamline traces). The resulting flow rates are provided in Table 4.4-85. Within the SDF GoldSim Model, the higher flow rate is assumed as the constant Darcy velocity. Based on comparisons with the PORFLOW-generated results at the 100-meter boundary, the SDF GoldSim Model uses flow data based on the streamline traces.

Uncertainty associated with the Darcy velocity is applied with a multiplier that samples values along a truncated normal distribution with a mean of 1, an assumed standard deviation of 0.1, a minimum of 0.7, and a maximum of 1.3.

5.7.1.5 K_d Uncertainty

The cementitious material (both concrete and grout) comprising the engineered barriers and the soils that surround and underlie the SDUs have a propensity to slow the transport of certain contaminants through the environment, thus retarding their arrival to a potential receptor. The ability of the cementitious materials or soils to sorb the different radionuclides is represented using K_ds. The ability of the material to sorb the radionuclide is dependent on the chemical condition of the environment.

Table 4.3-4 and Table 4.3-5 (Section 4.3.2) show the deterministic K_d values for soils, soils impacted by reducing cement leachate, and cementitious materials. The K_d values are element dependent and vary depending on the chemical state of the system (e.g., young/old age; reducing/oxidizing regions). The basis for these deterministic values are presented in *Geochemical Data Package for Performance Assessment Calculations Related to the Savannah River Site* (SRNL-STI-2009-00473).

Uncertainty in the K_d values is addressed using a stochastic element that uses a normal distribution where the mean is equal to the deterministic (baseline) value. Although the sample distributions were assumed to be log-normal, the mean K_d is assumed to be normal based on the central limit theorem (SRNL-STI-2009-00473, Section 4.8). Table 5.7-3 provides these distributions as used in the SDF GoldSim Model for each of the materials.

Table 5.7-3: K_d Uncertainty in the SDF GoldSim Model

Material Zone	Min	Max	Normal SD
Clayey Soils[b] and Cement Leachate-Impacted Clayey Soils	0.5 × Mean[a]	1.5 × Mean	0.25 × Mean
Sandy Soils[c] and Cement Leachate-Impacted Sandy Soils	0.25 × Mean	1.75 × Mean	0.375 × Mean
Cementitious Materials [d]	0.25 × Mean	1.75 × Mean	0.375 × Mean

a Mean = mean of the normal distribution defined as the baseline value presented in Table 4.3-4 for soils and cement leachate-impacted soils, and Table 4.3-5 for cementitious materials.
b Backfill layer
c Vadose zone and saturated zone
d Concretes and saltstone

5.7.1.6 Technetium Solubility Uncertainty

Significant effort in recent years has been invested into studies to reduce the uncertainty around the solubility controls of Tc-99 within the saltstone waste form. [SREL-R-17-0005] From these efforts, improved modeling approaches have been developed to provide simulated releases that better reflect actual releases of Tc-99 from saltstone. [SRR-CWDA-2018-00046]

These improved modeling approaches added complexity to the release of Tc-99 such that it could not be directly implemented into the SDF GoldSim Model. Instead, the SDF GoldSim Model uses fluxes that were prepared using the Vadose Zone Transport Model for each of the Tc-99 flux release profiles (as recommended in Table 4.3-8) for each of the parametric flow fields (discussed in Section 5.7.1.3), and for each SDU.

Within the SDF GoldSim Model, the selection of the appropriate Tc-99 flux to "read in" from the Vadose Zone Transport Model results is based on the parametric flow field sampling and on an additional stochastic element (*Solubility*), which uses a discrete sampling distribution to select one of the technetium solubility profiles. This element assumes 25% of the distribution will select the best estimate solubility profile (as used in the Realistic Case), 50% of the distribution selects the MPAD technetium solubility profile (as used for the Compliance Case), and 25% of the distribution selects the conservative estimate technetium solubility profile (as used for the Pessimistic Case). Because the solubilities recommended in Table 4.3-8 are the same for both the MPAD inputs and the conservative estimate inputs, this assumed distribution is effectively assuming the higher solubility conditions for 75% of the realizations.

5.7.1.7 Dose Parameter Uncertainty

The dose parameter inputs described in Section 4.4.8.3 include a variety of sampling distributions, including:

- Probabilistic multipliers on the uptake of contaminated water, produce, meat, and fish (see Table 4.4-110).

- Probabilistic multipliers on the soil and crop properties such as soil densities, irrigation rates, tilling depths and the area of a garden (see Table 4.4-115 and Table 4.4-116).
- Probabilistic multipliers on the fraction of consumed foodstuffs that are assumed to be contaminated due to local productivity (see Table 4.4-118).

5.7.1.8 Other Parameter Distributions

In addition to the parameters described above, an additional stochastic element has been imposed within the SDF GoldSim Model: *IHI_DrillEventTime_Uncert*. While assuming the intrusion occurs at 100 years is defensible, it is not really indicative of expected future conditions. There is considerable uncertainty surrounding if, or when, an intrusion might occur. This element was introduced to randomly sample when the human intrusion may occur. This is applied as a uniform distribution on timing, from the beginning of the simulation (time = 0 years) to the simulation duration time. The time selected by *IHI_DrillEventTime_Uncert* is then adjusted by adding either 100 years (i.e., the institutional control period) or 500 years if the "worst case" scenario option of drilling into the SDU is selected. Note if the sum of the sampled time and either 100 years or 500 years (where applicable) is greater than the simulated duration time, drilling will not occur during the simulation.

Additionally, the assumed depth of the ground water well used by the MOP or IHI is sampled within the SDF GoldSim Model (based on the recommended distribution in Table 4.4-117), but the result from this sampling is not actually linked to the rest of the model. Instead, the deterministic value of 100 ft is assumed. This is a defensible modeling decision because a deeper well is likely to pull water from the Gordon Aquifer (or deeper), where the concentrations are lower. With respect to drill cuttings, the deeper well would also increase the volume of the drill cutting material, thus decreasing the overall contaminant concentrations of radionuclides mixed into the soil. Although the well depth distribution was developed based on actual well depth data from wells drilled in close proximity to the SDF, it is not used.

5.7.2 Probabilistic Simulations

The SDF GoldSim Model was executed to generate 3,000 independent realizations, and the collective results from these realizations are used to characterize the uncertainty manifested in the model input distributions.

The SDF GoldSim Model used to support this PA is self-contained within the GoldSim file: *SRS Saltstone v5.053.gsm*. Based on previous modeling experience, very large and complex model files with a large number of realizations can be challenging to effectively manage (e.g., computers might crash). Rather than developing a single model file with thousands of realizations, it is more efficient to develop multiple copies of the same model file, where each model file simulates 1,000 realizations each, and is assigned a unique random seed to influence the sampling. For this reason, three variations of the SDF GoldSim Model file were developed for use in the probabilistic uncertainty analysis (see Section 5.7.3) and the probabilistic sensitivity analysis (in Section 5.7.4).

Aside from the random seed used to generate the sampling distributions all three models are identical. The files used are summarized in Table 5.7-4.

Table 5.7-4: GoldSim Model Files Used in the Probabilistic Analyses

GoldSim Model Files	Number of Realizations	Random Seed (RS) for Sampling
SRS Saltstone v5.053_RS1a.gsm	1,000	1
SRS Saltstone v5.053_RS2a.gsm	1,000	2
SRS Saltstone v5.053_RS3a.gsm	1,000	3

All these realizations were performed over a span of 20,000 years (i.e., twice the Performance Period) and use 10-year timesteps.

When reviewing results from the probabilistic model, it should be noted that model uncertainty is limited by which model parameters are defined as uncertain variables (which are sampled during each realization) as opposed to those parameters defined as known quantities (i.e., input parameters that remain unchanged regardless of sampling). From the model's perspective, the definition of an input as a single value implies that the value is known perfectly. Uncertainty shown in the results do not take into account any contributions from these static (or deterministic) inputs, thereby underestimating potential uncertainty but helping identify the degree of importance of the more uncertain parameters.

5.7.2.1 Statistical Stability

A stability analysis was conducted by comparing the statistical results of the three model files from Table 5.7-4. Collectively, the results for all 3,000 realizations are used to compute the overall mean as discussed in Section 5.7.3, but by generating three independent replicates with 1,000 realizations each and using different random seeds, each set of 1,000 realizations can be used to confirm that the results are converging. Figure 5.7-1 shows the mean dose to the MOP and the 95th percentile of the dose to the MOP for the three replicates over 20,000 years. Figure 5.7-1 shows that the means from each replicate are nearly identical and the 95th precentiles only vary slightly and only after approximately 3,000 years. Therefore, the high degree of similarity among the replicates indicates that the doses are estimated with sufficient accuracy, and that a sample size of 1,000 realizations per replicate is adequate for expressing the statistical uncertainty of the simulated system.

Figure 5.7-1: Stability of Doses to the MOP Based on Comparison of Three Replicates

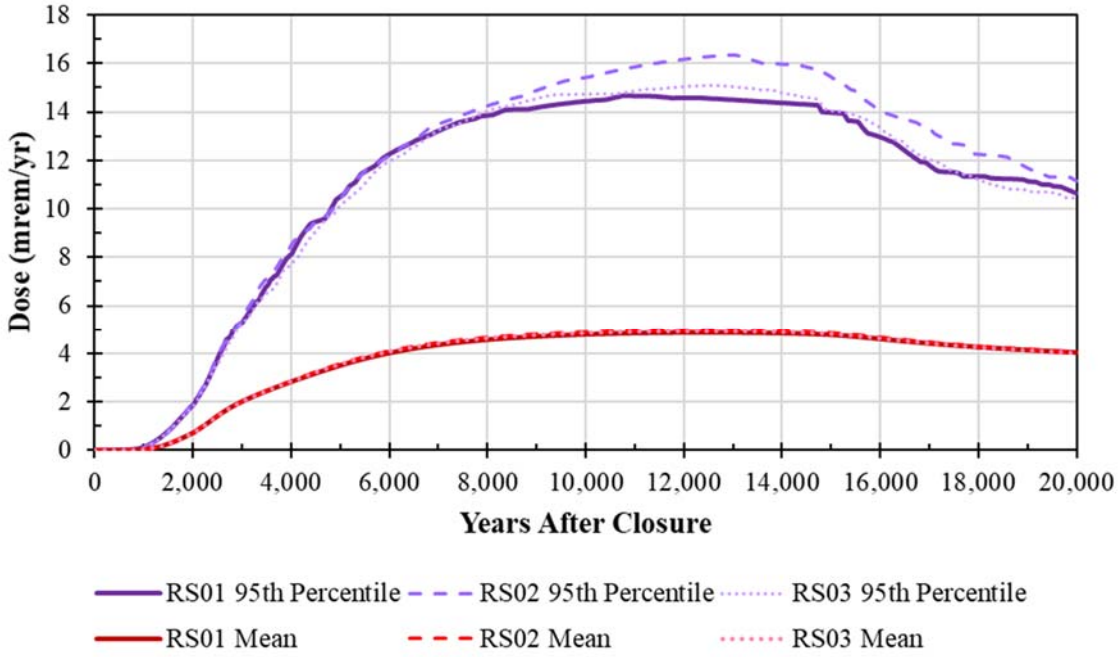

RS = Random Seed.

5.7.3 Probabilistic Uncertainty Analyses

The probabilistic results of the SDF GoldSim Model are used to characterize uncertainty manifested in the model input distributions. Collectively, the distributions of the uncertainty parameters in the SDF GoldSim Model are intended to capture the overall uncertainty in the model. The combined results from these realizations are assembled into probability distributions of possible outcomes.

The following analysis of these results is referred to as a probabilistic uncertainty analysis. These probabilistic uncertainty analyses are not intended to quantify conceptual model uncertainty or uncertainty induced by model structure. Identification of conceptual model areas of importance is primarily accomplished throughout the combined sensitivity analyses via both deterministic sensitivity cases and probabilistic sensitivity analyses.

Probabilistic uncertainty analyses are concerned with how the uncertainty in model input parameters propagate through the model to the selected model results or endpoints. These model endpoints are potential radiological doses to hypothetical human receptors. In contrast, the probabilistic sensitivity analyses (in Section 5.7.4) are focused on determining which of the many input parameters are most responsible for determining the endpoint values.

5.7.3.1 Uncertainty Analysis Summary Results

The most direct way to communicate the uncertain nature of the model results is to show graphs of certain key model endpoints. Figure 5.7-2 shows the peak doses (for the total doses to the MOP at the 100-meter well) from all 3,000 realizations. The colors of the data

points indicate the random seed (RS) of the corresponding GoldSim file (see Table 5.7-4). Note that a large number of the data points occur at 20,000 years (i.e., the end of the simulation); this indicates that peak doses for these realizations would likely occur at a point in time beyond 20,000 years. Regardless, this figure demonstrates that all three GoldSim files provides peak doses over a wide range for both timing and magnitude.

Figure 5.7-2: Peak Doses to the MOP at the 100-Meter Well from 3,000 Realizations

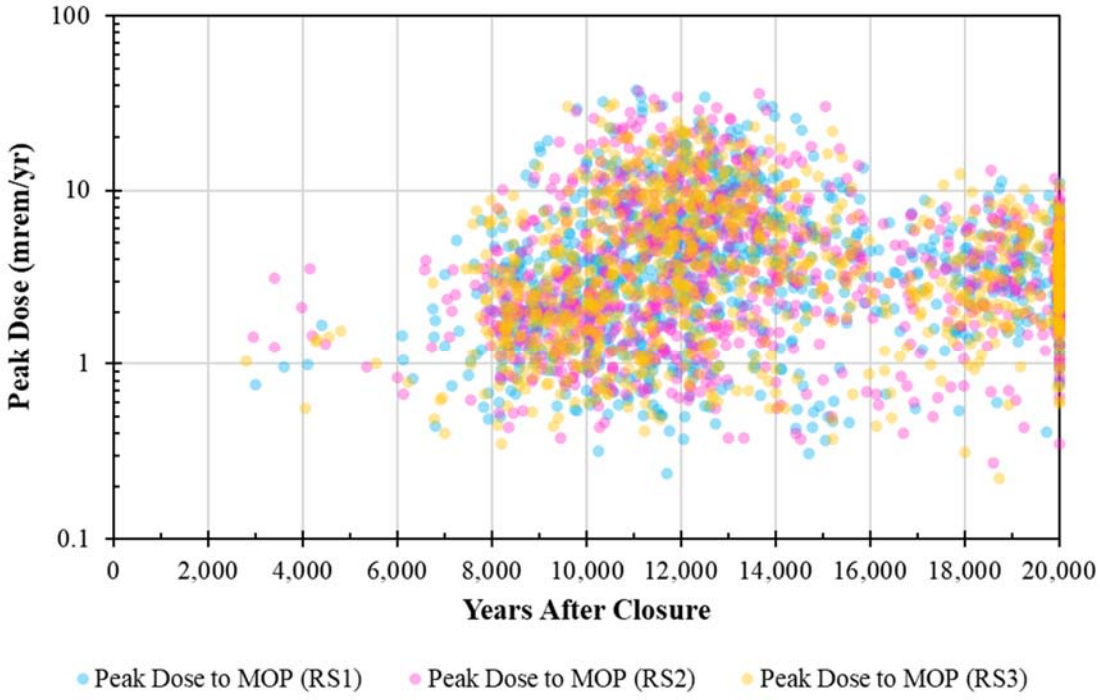

Statistics for peak dose values (e.g., mean of the peaks) are summarized in Table 5.7-5. These peak values are provided for three time periods: the Compliance Period (0 to 1,000 years after closure), the Performance Period (0 to 10,000 years after closure), and the simulated duration of the model (0 to 20,000 years after closure). For additional context, the peak dose values from the deterministic Compliance Case (see Section 5.5) and from the benchmarking analysis (see Section 5.6) are also included.

Table 5.7-5: Statistics of the Peak Doses within Any Time Period

	Dose to the MOP (mrem/yr)						
Statistic	**Total**	**Sector B**	**Sector D**	**I-129**	**Tc-99**	**Water Ingestion**	**Produce Ingestion**
Time Period	***0 to 1,000 Years (Compliance Period)***						
Mean	0.040	0.0055	0.040	0.028	0.013	0.018	0.019
95th Percentile	0.13	0.019	0.13	0.11	0.037	0.066	0.065
Median	0.022	0.0031	0.021	0.0091	0.0087	0.0072	0.011
5th Percentile	0.0040	0.00065	0.0037	0.00083	0.00085	0.00091	0.0017
Benchmarked GoldSim Model (Compliance Case)	0.016	0.0017	0.016	0.0088	0.0068	0.012	0.0028
Compliance Case (PORFLOW)	0.0094	0.00077	0.0094	0.0025	0.0069	0.0067	0.0021
Time Period	***0 to 10,000 Years (Performance Period)***						
Mean	4.8	4.8	3.7	2.8	2.1	2.0	2.5
95th Percentile	15	15	11	10	6.1	7.0	7.7
Median	3.1	3.1	2.5	1.6	1.4	1.1	1.6
5th Percentile	0.71	0.69	0.56	0.33	0.18	0.18	0.28
Benchmarked GoldSim Model (Compliance Case)	2.1	2.1	1.6	1.3	0.72	1.5	0.34
Compliance Case (PORFLOW)	1.2	1.2	1.1	0.58	0.60	0.85	0.22
Time Period	***0 to 20,000 Years (Duration of the Model)***						
Mean	5.0	4.9	3.8	3.0	2.1	2.1	2.5
95th Percentile	15	15	11	10	6.1	7.1	7.9
Median	3.3	3.2	2.6	1.8	1.4	1.1	1.6
5th Percentile	0.73	0.71	0.57	0.34	0.20	0.18	0.29
Benchmarked GoldSim Model (Compliance Case)	2.2	2.2	1.7	1.5	0.72	1.6	0.35
Compliance Case (PORFLOW)	1.3	1.3	1.2	0.78	0.60	1.0	0.24

The values presented in Table 5.7-5 do not reflect the same statistical data as the statistical values and time histories shown in the following table and figures, although these are complementary of one another. The difference between information presented in Table 5.7-5 and information below is important to understand. Table 5.7-5 shows summary statistics for peak doses achieved at *any* time within the given time frames. These are statistics of the peak dose values (e.g., mean of the peaks), regardless of when the peaks were achieved within the specific time frames. Alternatively, the information provided

below examines statistics relative to each time step and offers peak values of the statistics (e.g., peak of means).

Figure 5.7-3 illustrates the difference between the mean of the peaks and the peak of the means (i.e., the highest mean value when calculating a different mean value at each timestep). This figure also demonstrates how the mean of the peaks may exceed the peak of the means. For example, the mean of the peaks for the total dose to the MOP within 20,000 years is 5.0 mrem/yr and reflects data over the entire range of the time frame (see Table 5.7-5), whereas the peak of the means is approximately 4.9 mrem/yr and occurs at 12,450 years after closure (see Table 5.7-6).

Figure 5.7-3: Difference Between the Mean of Peaks and the Peak of Means

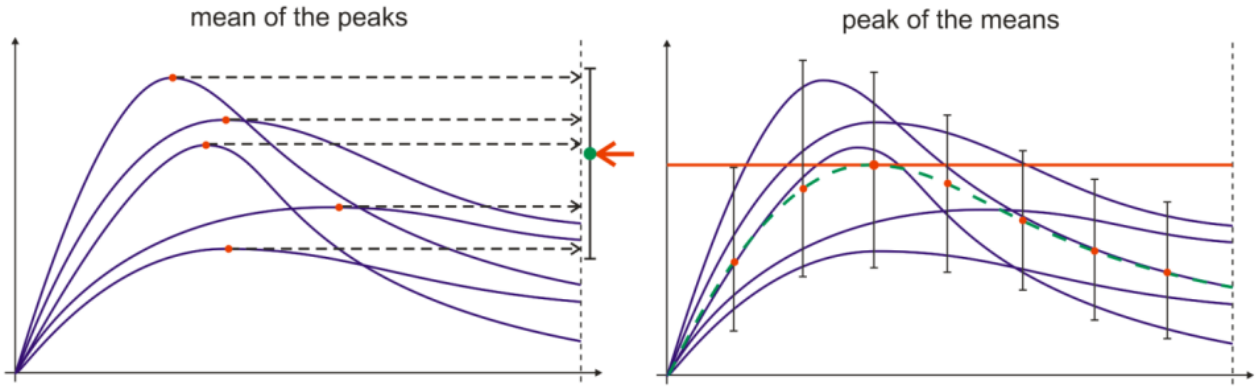

Figure 5.7-4 through Figure 5.7-6 present the statistical time histories of the total dose at any sector for the MOP at the 100-meter boundary within each of the time periods considered. In each of these figures, the 5th and 95th percentiles are significantly below and above the median values, respectively. The mean values are driven higher, approaching the 75th percentiles, by the uncertainty distributions of the modeled parameters. This indicates the model applies distributions with long tails (e.g., lognormal distributions) or extreme values are inherent in these distributions. It is somewhat expected that the mean value is higher than the median because many of the dominant distributions were established to be reasonably conservative, resulting in the distributions being skewed to the high end. This approach inflates the variance in the uncertainty analyses, resulting in a few realizations dominating the uncertainty analyses results. The intent of Section 5.7.4 is to investigate which parameters have the most impact on this aspect of the uncertainty analyses.

Table 5.7-6: Peaks of the Dose Statistics

Evaluated Endpoints	Peak of the Means		Peak of the Medians (50th Percentile)		Peak of the 95th Percentiles	
	Peak Dose (mrem/yr)	Time (yrs)	Peak Dose (mrem/yr)	Time (yrs)	Peak Dose (mrem/yr)	Time (yrs)
From 0 to 1,000 Years						
Total MOP Dose	0.040	1,000	0.022	1,000	0.13	1,000
MOP Dose at Sector B	0.0055	1,000	0.0031	1,000	0.019	1,000
MOP Dose at Sector D	0.040	1,000	0.021	1,000	0.13	1,000
Dose from I-129	0.028	1,000	0.0090	1,000	0.11	1,000
Dose from Tc-99	0.013	1,000	0.0087	1,000	0.037	1,000
Water Ingestion Dose	0.018	1,000	0.0072	1,000	0.066	1,000
Produce Ingestion Dose	0.019	1,000	0.011	1,000	0.065	1,000
From 0 to 10,000 Years						
Total MOP Dose	4.8	10,000	3.1	10,000	15	10,000
MOP Dose at Sector B	4.8	10,000	3.1	10,000	15	10,000
MOP Dose at Sector D	3.7	10,000	2.5	10,000	11	10,000
Dose from I-129	2.8	10,000	1.6	10,000	10	10,000
Dose from Tc-99	2.0	10,000	1.4	10,000	6.1	10,000
Water Ingestion Dose	2.0	10,000	1.1	10,000	7.0	10,000
Produce Ingestion Dose	2.5	10,000	1.6	10,000	7.7	10,000
From 0 to 20,000 Years						
Total MOP Dose	4.9	12,450	3.2	12,850	15	13,080
MOP Dose at Sector B	4.9	12,360	3.2	13,740	15	12,190
MOP Dose at Sector D	3.8	11,610	2.5	12,390	11	11,700
Dose from I-129	2.9	12,810	1.7	15,630	10	11,700
Dose from Tc-99	2.0	10,700	1.4	10,090	6.1	10,760
Water Ingestion Dose	2.0	12,740	1.1	12,440	7.1	13,420
Produce Ingestion Dose	2.5	12,110	1.6	10,870	7.9	12,000

Note: Comparing the peak doses from 0 to 10,000 years versus the peak doses from 0 to 20,000 years appears to yield the same peak dose values for a number of the evaluated endpoints, but at different years. If additional significant figures were provided, the peak doses occurring at later years would show slightly higher values.

Figure 5.7-4: Statistical Time History of Total MOP Doses (Any Sector) from 0 to 1,000 Years

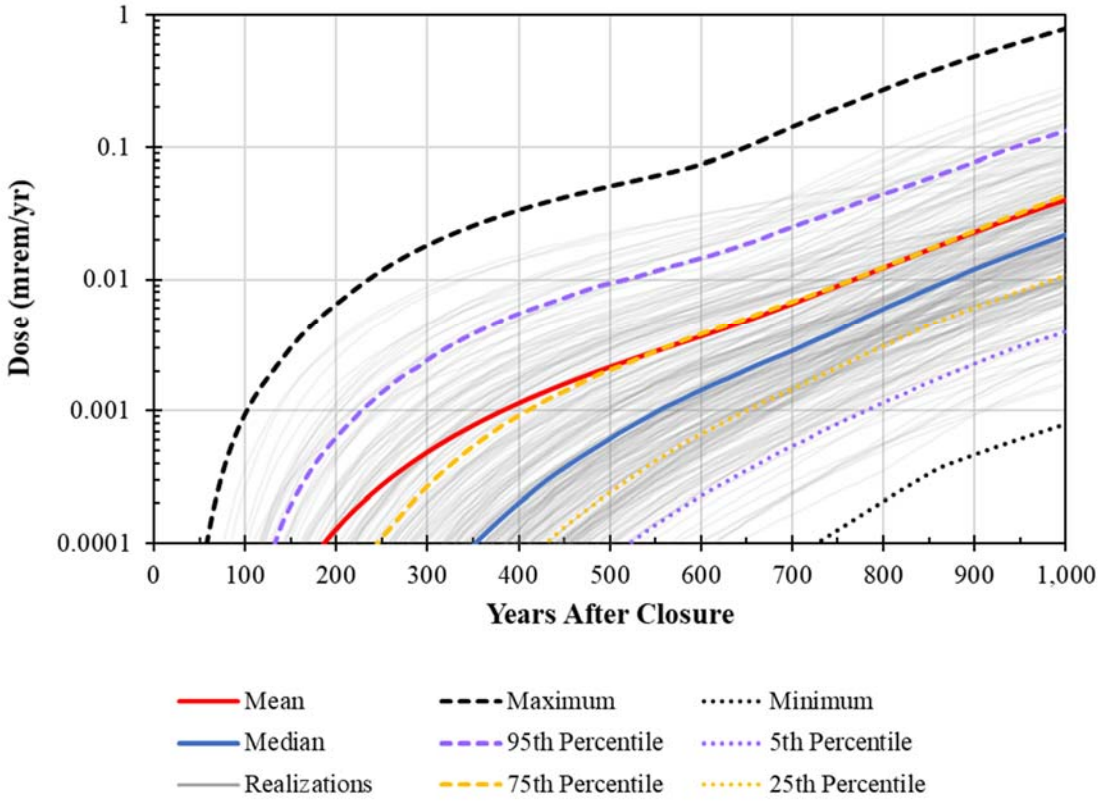

Note: For the individual realizations, only the first 245 realizations are displayed. The statistical values (e.g., Mean and Maximum) are determined using data from 3,000 individual realizations.

Figure 5.7-5: Statistical Time History of Total MOP Doses (Any Sector) from 0 to 10,000 Years

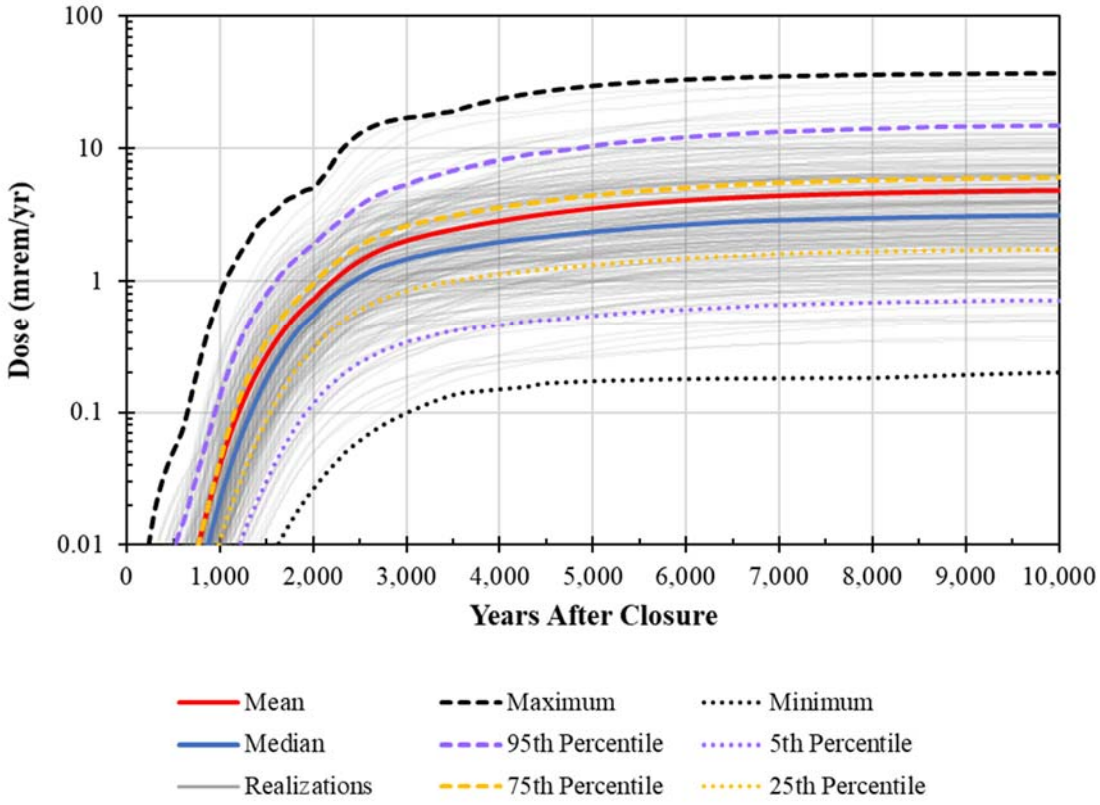

Note: For the individual realizations, only the first 245 realizations are displayed. The statistical values (e.g., Mean and Maximum) are determined using data from 3,000 individual realizations.

Figure 5.7-6: Statistical Time History of Total MOP Doses (Any Sector) from 0 to 20,000 Years

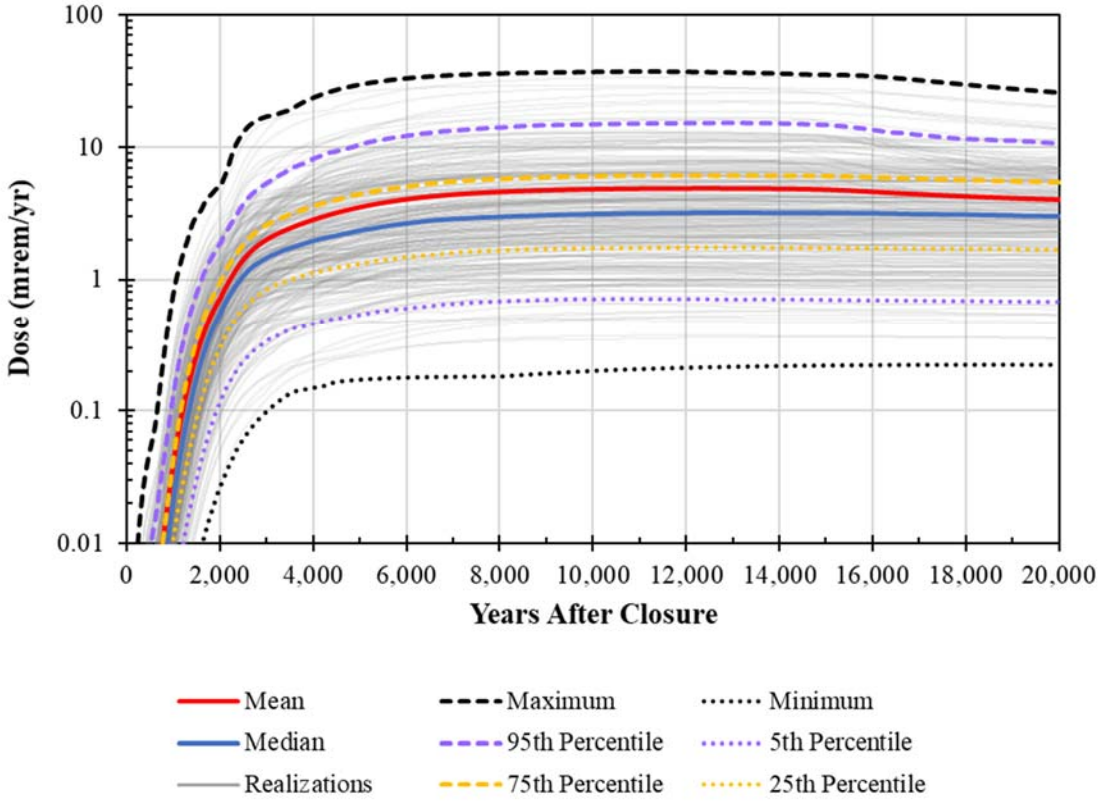

Note: For the individual realizations, only the first 245 realizations are displayed. The statistical values (e.g., Mean and Maximum) are determined using data from 3,000 individual realizations.

Figure 5.7-7 shows the mean dose to the MOP located within each of the defined SDF sectors (Sectors A through H) at any point in time for 10,000 years. Initially Sector D is likely to have the highest doses, followed by Sector B after approximately 4,000 years. This figure uses the combined results based on each of the 3,000 individual realizations.

Figure 5.7-7: Mean Doses to the MOP for Each Sector (0 to 10,000 Years)

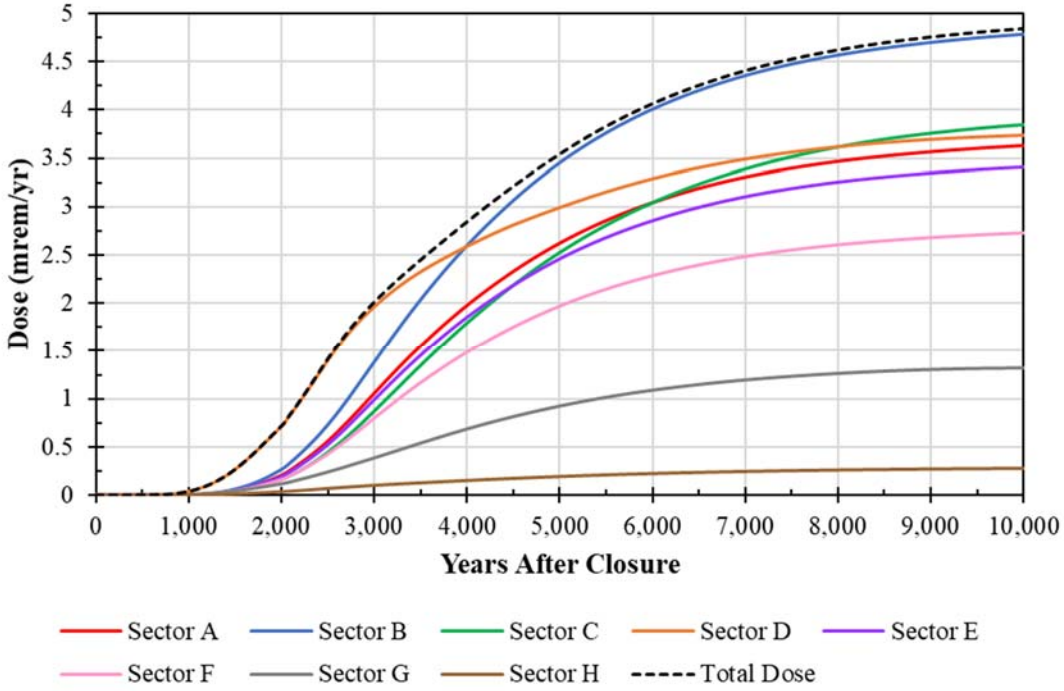

Note the mean of the total doses to the MOP is slightly higher than the mean of the highest individual sector (Figure 5.7-7). The mean of the total doses to the MOP reflects the dose from the highest sector at any given time during each realization, regardless of which sector is exhibiting this highest dose. As such, the mean of the total dose to the MOP dose is "pulled up," relative to the mean dose from each individual sector. For example, Sector B has the highest dose in most realizations, but for some realizations the highest doses occur in Sector C. We see a similar effect when observing the mean dose contributions by radionuclide (Figure 5.7-8) and by dose pathways (Figure 5.7-9).

Basing the total dose values on the highest sectors provides a comprehensive and defensible approach for considering the impacts relative to dose risk.

Figure 5.7-8: Mean Doses to the MOP for Each Radionuclide (0 to 10,000 Years)

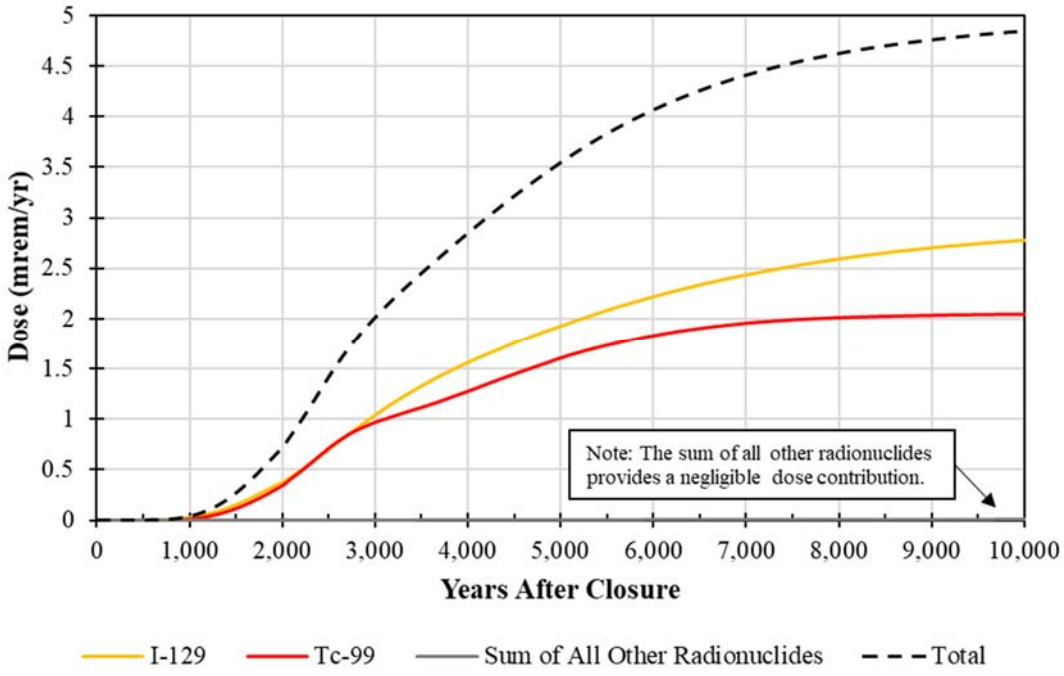

Figure 5.7-9: Mean Doses to the MOP for Each Pathway (0 to 10,000 Years)

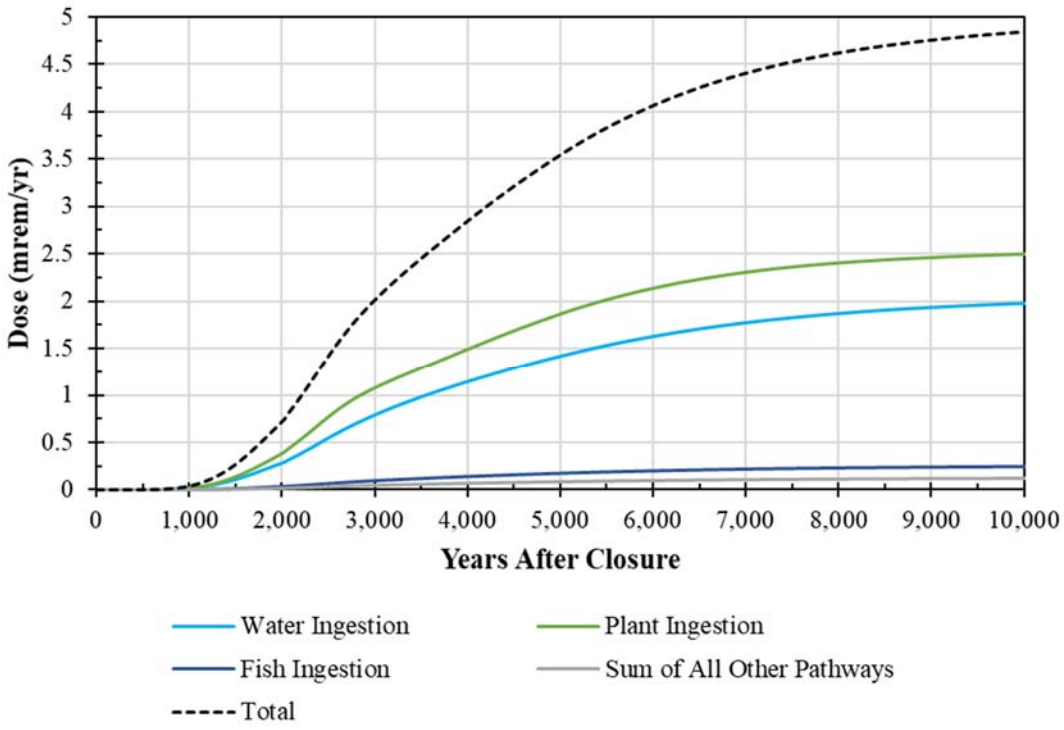

5.7.3.2 Uncertainty Analysis Insights

Based on the information presented in the uncertainty analyses section, the following general insights regarding the uncertainty analyses can be drawn.

- Within the Compliance Period, no realization exhibited a maximum peak dose that exceeded the performance objective of 25 mrem/yr.
- Peak doses within 20,000 years are not significantly higher than the peak doses within 10,000 years.
- When the full 20,000-year simulation period was considered, only 32 realizations (approximately 1% of the 3,000 realizations) exceeded the performance objective of 25 mrem/yr, and this only occurs at times that are beyond the Compliance Period.
- Of all 3,000 realizations, the highest peak dose recorded was 37 mrem/yr.
- Almost all of the realizations with peak doses that exceed 10 mrem/yr peaked between 8,000 years and 15,000 years after closure.
- The median doses are very similar to the Compliance Case results when using the SDF GoldSim Model with Compliance Case model settings. Similarly, the 5th percentile doses and the 95th percentile doses are very similar to the results from the SDF GoldSim Model with Realistic Case and Pessimistic Case model settings, respectively.

5.7.3.3 Uncertainty Analysis Realizations of Interest

This section identifies individual parameters that impact uncertainty analyses by investigating realizations that affect the overall results. Recognizing that the realizations with the highest doses to the MOP may have the most impact on the uncertainty analyses, two sets of five realizations (from any of the 3,000 realizations) were studied for this evaluation. The first set of five realizations selected for analysis were based on the peak doses within 1,000 years and the second set of five realizations were selected based on the peak doses within 10,000 years. The highest dose consequences are those that have a combination of parameters with values significantly different from what is expected (i.e., the deterministic Realistic Case values), such that when they occur concurrently they produce dose results that are higher than others. Parameters of interest are identified as having the greatest potential to influence the results.

The SDF GoldSim Model was used to generate 3,000 realizations (see Table 5.7-4). These 3,000 realizations are used to identify the five realizations with the highest peak doses within the Compliance Period (0 to 1,000 years) and within the Performance Period (0 to 10,000 years) as presented in Table 5.7-7. Equivalent results from the deterministic SDF GoldSim Model (using each of the Central Scenario model settings) is also included for comparison.

Table 5.7-7: Overview of Realizations with the Highest Peak Doses within 1,000 Years and 10,000 Years (from 3,000 Realizations)

Realization	Random Seed	Dose (mrem/yr)	Time of Peak (yr)	Sector of Peak	Radionuclide Contributors to Peak Doses	Pathway Contributors to Peak Doses
Peak Doses in 1,000 Years						
Realization #242	2[e]	0.79	1,000	D	I-129 (93%) Tc-99 (7%)	Water Ingestion (43%) Produce Ingestion (53%)
Realization #396	2[e]	0.69	1,000	D	I-129 (95%) Tc-99 (5%)	Water Ingestion (84%) Produce Ingestion (11%)
Realization #550	2[e]	0.61	1,000	D	I-129 (95%) Tc-99 (5%)	Water Ingestion (81%) Produce Ingestion (15%)
Realization #661	2[e]	0.74	1,000	D	I-129 (93%) Tc-99 (7%)	Water Ingestion (61%) Produce Ingestion (34%)
Realization #270	3[f]	0.61	1,000	D	I-129 (98%) Tc-99 (1%)	Water Ingestion (76%) Produce Ingestion (21%)
GoldSim Version of the Pessimistic Case[a]		**0.048**	1,000	D	I-129 (81%) Tc-99 (19%)	Water Ingestion (77%) Produce Ingestion (10%)
GoldSim Version of the Compliance Case[b]		**0.016**	1,000	D	I-129 (56%) Tc-99 (43%)	Water Ingestion (74%) Produce Ingestion (18%)
GoldSim Version of the Realistic Case[c]		**0.0081**	1,000	D	I-129 (23%) Tc-99 (77%)	Water Ingestion (69%) Produce Ingestion (25%)
Peak Doses in 10,000 Years						
Realization #741	1[d]	37	10,000	B	I-129 (65%) Tc-99 (35%)	Water Ingestion (37%) Produce Ingestion (55%)
Realization #780	1[d]	34	10,000	B	I-129 (58%) Tc-99 (42%)	Water Ingestion (30%) Produce Ingestion (66%)
Realization #88	2[e]	34	10,000	B	I-129 (60%) Tc-99 (40%)	Water Ingestion (22%) Produce Ingestion (75%)
Realization #547	2[e]	37	10,000	B	I-129 (52%) Tc-99 (48%)	Water Ingestion (33%) Produce Ingestion (61%)
Realization #994	2[e]	34	10,000	B	I-129 (54%) Tc-99 (46%)	Water Ingestion (24%) Produce Ingestion (74%)
GoldSim Version of the Pessimistic Case[a]		**13.5**	10,000	B	I-129 (93%) Tc-99 (7%)	Water Ingestion (78%) Produce Ingestion (8%)
GoldSim Version of the Compliance Case[b]		**2.1**	10,000	B	I-129 (65%) Tc-99 (35%)	Water Ingestion (75%) Produce Ingestion (17%)
GoldSim Version of the Realistic Case[c]		**0.92**	10,000	B	I-129 (29%) Tc-99 (71%)	Water Ingestion (70%) Produce Ingestion (14%)

a From GoldSim model file: *SRS Saltstone v5.054-GS-Defense-in-DepthCasea.gsm* (deterministic model)
b From GoldSim model file: *SRS Saltstone v5.054-GS-ComplianceCasea.gsm* (deterministic model)
c From GoldSim model file: *SRS Saltstone v5.054-GS-RealisticCasea.gsm* (deterministic model)
d From GoldSim model file: *SRS Saltstone v5.053_RS1a.gsm* (probabilistic model)
e From GoldSim model file: *SRS Saltstone v5.053_RS2a.gsm* (probabilistic model)
f From GoldSim model file: *SRS Saltstone v5.053_RS3a.gsm* (probabilistic model)

Table 5.7-7 indicates that even though the peak doses from these individual realizations are higher than those from the deterministic Central Scenario cases, the locations of the peaks (Sector D within 1,000 years and Sector B whith 10,000 years), the major radionuclide dose contributors (I-129 and Tc-99), and the major pathway contributors (water ingestion and produce ingestion) are not different from the deterministic Central Scenario cases. However, the percentages of those contributions varied.

The individual realizations are analyzed below by identifying those uncertainty parameters that have a direct impact on the magnitude or timing of the peak dose. Some initial interpretations of the deterministic model are required to do a detailed single-

realization analysis. Specifically, by identifying the individual SDUs influencing the timing and magnitude of the deterministic peak dose, the number of key uncertainty parameters can be narrowed down.

The peak doses always occur along either Sector D (within 1,000 years) or Sector B (within 10,000 years). In the SDF GoldSim Model, there are two hypothetical wells along each sector. Along Sector D, one well was placed near the centerline of the plume which emanates from SDU 9, while the other well was positioned to receive more contribution from SDU 7 releases. Due to the closer proximity of SDU 9 to the 100-meter boundary, it is expected that the peak doses in Sector D (within 1,000 years of SDF closure) are driven by the SDU 9 releases.

Along Sector B, one well is controlled by the releases from SDUs 11 and 12 while the other well is controlled by releases from SDUs 6 and 8. Based upon the plume inputs used within the SDF GoldSim Model and a qualitative investigation of the deterministic modeling results, it is expected that the first well along Sector B, driven by the releases from SDUs 11 and 12, drives the peak doses beyond 1,000 years. This is slightly different from the PORFLOW results wherein the Sector B doses are more strongly influenced by the releases from SDUs 6 and 8. Regardless, because the two sets of plumes to Sector B produce dose results that are very similar in magnitude, the two are effectively equal from a dose-risk perspective.

The analysis of individual realizations ignores any SDU-specific parameters except for those which apply specifically to SDU 9 (for the early doses) or SDUs 11 and 12 (for the later doses). Similarly, because all these realizations show I-129 and Tc-99 are always the most dominant radionuclide dose contributors, the analyses of the individual realizations ignore any element-specific or radionuclide-specific parameters except for those which apply specifically to I-129 or Tc-99.

Finally, it should be noted that contaminated produce ingestion rates presented below were post-processed from the sampling data. The values, as presented here, are calculated by multiplying the produce ingestion rate (based on the sampling distribution from Table 4.4-110) by the fraction of the ingested produce that is contaminated (which is calculated based on Eq. 4.4-247, using the respective garden size distributions). It is also noted that based on the sampling distribution for the garden size (see Table 4.4-116), Eq. 4.4-247 can result in contaminant fractions that exceed 1.0 (i.e., more than 100% percent). This is a conservatism within the model that may be conceptualized by the MOP choosing to consume additional produce when it is more abundant.

Realization #242 from Random Seed = 2

Table 5.7-7 indicates that Realization #242 (with Random Seed = 2) has a peak dose within 1,000 years that occurs in Sector D (i.e., from SDU 9 releases). The major radionuclide contributors to the peak MOP dose are I-129 (93%) and Tc-99 (7%) and the major pathway contributors are water ingestion (43%) and produce ingestion (53%). Uncertainty parameters influencing these dose contributions are identified below, along with their

respective sampled values. The equivalent deterministic (Compliance Case) value is presented within parentheses.

- Inventory multiplier for I-129 in SDU 9 = 0.98 (1.0)
- Iodine K_d in Reducing Region I Saltstone = 0.037 mL/g (0.07 mL/g)
- Iodine K_d in Reducing Region III Saltstone = 0.92 mL/g (0.71 mL/g)
- Infiltration rate selector = 2 [MPAD] (2 [MPAD])
- Initial saturated hydraulic conductivity of saltstone = 2.0E-09 cm/s (5.0E-10 cm/s)
- Vadose zone thickness for SDU 9 = 9.6 ft (23 ft)
- Saturated zone face area = 69 ft × 314 ft = 2.2E+04 ft² (2.5E+04 ft²)
  - Saturated zone thickness for the SDF = 69 ft (66 ft)
  - Saturated zone width for SDU 9 = 314 ft (375 ft)
- Water ingestion rate = 697 L/yr (505 L/yr)
- Produce ingestion rate = 442 kg/yr (207 kg/yr)
- Sampled garden size = 860 m² (100 m²)

Realization #396 from Random Seed = 2

Table 5.7-7 indicates that Realization #396 (with Random Seed = 2) has a peak dose within 1,000 years that occurs in Sector D (i.e., from SDU 9 releases). The major radionuclide contributors to the peak MOP dose are I-129 (95%) and Tc-99 (5%) and the major pathway contributors are water ingestion (84%) and produce ingestion (11%). Uncertainty parameters influencing these dose contributions are identified below, along with their respective sampled values. The equivalent deterministic (Compliance Case) value is presented within parentheses.

- Inventory multiplier for I-129 in SDU 9 = 1.01 (1.0)
- Iodine K_d in Reducing Region I Saltstone = 0.058 mL/g (0.07 mL/g)
- Iodine K_d in Reducing Region III Saltstone = 0.99 mL/g (0.71 mL/g)
- Infiltration rate selector = 2 [MPAD] (2 [MPAD])
- Initial saturated hydraulic conductivity of saltstone = 5.0E-10 cm/s (5.0E-10 cm/s)
- Vadose zone thickness for SDU 9 = 9.5 ft (23 ft)
- Saturated zone face area = 64 ft × 450 ft = 2.9E+04 ft² (2.5E+04 ft²)
  - Saturated zone thickness for the SDF = 64 ft (66 ft)
  - Saturated zone width for SDU 9 = 450 ft (375 ft)
- Water ingestion rate = 953 L/yr (505 L/yr)
- Produce ingestion rate = 95 kg/yr (207 kg/yr)
- Sampled garden size = 472 m² (100 m²)

Realization #550 from Random Seed = 2

Table 5.7-7 indicates that Realization #550 (with Random Seed = 2) has a peak dose within 1,000 years that occurs in Sector D (i.e., from SDU 9 releases). The major radionuclide contributors to the peak MOP dose are I-129 (95%) and Tc-99 (5%) and the major pathway contributors are water ingestion (81%) and produce ingestion (15%). Uncertainty parameters influencing these dose contributions are identified below, along with their

respective sampled values. The equivalent deterministic (Compliance Case) value is presented within parentheses.

- Inventory multiplier for I-129 in SDU 9 = 1.17 (1.0)
- Iodine K_d in Reducing Region I Saltstone = 0.075 mL/g (0.07 mL/g)
- Iodine K_d in Reducing Region III Saltstone = 0.71 mL/g (0.71 mL/g)
- Infiltration rate selector = 3 [conservative estimate] (2 [MPAD])
- Initial saturated hydraulic conductivity of saltstone = 5.0E-10 cm/s (5.0E-10 cm/s)
- Vadose zone thickness for SDU 9 = 11.3 ft (23 ft)
- Saturated zone face area = 83 ft × 360 ft = 3.0E+04 ft² (2.5E+04 ft²)
  - Saturated zone thickness for the SDF = 83 ft (66 ft)
  - Saturated zone width for SDU 9 = 360 ft (375 ft)
- Water ingestion rate = 956 L/yr (505 L/yr)
- Produce ingestion rate = 303 kg/yr (207 kg/yr)
- Sampled garden size = 351 m² (100 m²)

Realization #661 from Random Seed = 2

Table 5.7-7 indicates that Realization #661 (with Random Seed = 2) has a peak dose within 1,000 years that occurs in Sector D (i.e., from SDU 9 releases). The major radionuclide contributors to the peak MOP dose are I-129 (93%) and Tc-99 (7%) and the major pathway contributors are water ingestion (61%) and produce ingestion (34%). Uncertainty parameters influencing these dose contributions are identified below, along with their respective sampled values. The equivalent deterministic (Compliance Case) value is presented within parentheses.

- Inventory multiplier for I-129 in SDU 9 = 1.07 (1.0)
- Iodine K_d in Reducing Region I Saltstone = 0.099 mL/g (0.07 mL/g)
- Iodine K_d in Reducing Region III Saltstone = 0.42 mL/g (0.71 mL/g)
- Infiltration rate selector = 3 [conservative estimate] (2 [MPAD])
- Initial saturated hydraulic conductivity of saltstone = 2.0E-09 cm/s (5.0E-10 cm/s)
- Vadose zone thickness for SDU 9 = 9.3 ft (23 ft)
- Saturated zone face area = 85 ft × 370 ft = 3.1E+04 ft² (2.5E+04 ft²)
  - Saturated zone thickness for the SDF = 85 ft (66 ft)
  - Saturated zone width for SDU 9 = 370 ft (375 ft)
- Water ingestion rate = 773 L/yr (505 L/yr)
- Produce ingestion rate = 112 kg/yr (207 kg/yr)
- Sampled garden size = 772 m² (100 m²)

Realization #270 from Random Seed = 3

Table 5.7-7 indicates that Realization #270 (with Random Seed = 3) has a peak dose within 1,000 years that occurs in Sector D (i.e., from SDU 9 releases). The major radionuclide contributors to the peak MOP dose are I-129 (98%) and Tc-99 (1%) and the major pathway contributors are water ingestion (76%) and produce ingestion (21%). Uncertainty parameters influencing these dose contributions are identified below, along with their

respective sampled values. The equivalent deterministic (Compliance Case) value is presented within parentheses.

- Inventory multiplier for I-129 in SDU 9 = 1.31 (1.0)
- Iodine K_d in Reducing Region I Saltstone = 0.106 mL/g (0.07 mL/g)
- Iodine K_d in Reducing Region III Saltstone = 0.88 mL/g (0.71 mL/g)
- Infiltration rate selector = 2 [MPAD] (2 [MPAD])
- Initial saturated hydraulic conductivity of saltstone = 5.0E-10 cm/s (5.0E-10 cm/s)
- Vadose zone thickness for SDU 9 = 9.4 ft (23 ft)
- Saturated zone face area = 59 ft × 318 ft = 1.9E+04 ft² (2.5E+04 ft²)
  - Saturated zone thickness for the SDF = 59 ft (66 ft)
  - Saturated zone width for SDU 9 = 318 ft (375 ft)
- Water ingestion rate = 833 L/yr (505 L/yr)
- Produce ingestion rate = 79 kg/yr (207 kg/yr)
- Sampled garden size = 659 m² (100 m²)

Realization #741 from Random Seed = 1

Table 5.7-7 indicates that Realization #741 (with Random Seed = 1) has a peak dose within 10,000 years that occurs in Sector B (i.e., from SDU 11 and SDU 12 releases). The major radionuclide contributors to the peak MOP dose are I-129 (65%) and Tc-99 (35%) and the major pathway contributors are water ingestion (37%) and produce ingestion (55%). Uncertainty parameters influencing these dose contributions are identified below, along with their respective sampled values. The equivalent deterministic (Compliance Case) value is presented within parentheses.

- Inventory multiplier for I-129 in SDU 11 = 1.38 (1.0)
- Inventory multiplier for I-129 in SDU 12 = 1.06 (1.0)
- Iodine K_d in Reducing Region I Saltstone = 0.032 mL/g (0.07 mL/g)
- Iodine K_d in Reducing Region III Saltstone = 0.61 mL/g (0.71 mL/g)
- Infiltration rate selector = 3 [conservative estimate] (2 [MPAD])
- Initial saturated hydraulic conductivity of saltstone = 2.0E-09 cm/s (5.0E-10 cm/s)
- Vadose zone thickness for SDUs 11 and 12 = 39 ft (36 ft)
- Saturated zone face area = 49 ft × 302 ft = 1.5E+04 ft² (2.5E+04 ft²)
  - Saturated zone thickness for the SDF = 49 ft (66 ft)
  - Saturated zone width for SDUs 11 and 12 = 302 ft (375 ft)
- Water ingestion rate = 533 L/yr (505 L/yr)
- Produce ingestion rate = 74 kg/yr (207 kg/yr)
- Sampled garden size = 524 m² (100 m²)

Realization #780 from Random Seed = 1

Table 5.7-7 indicates that Realization #780 (with Random Seed = 1) has a peak dose within 10,000 years that occurs in Sector B (i.e., from SDU 11 and SDU 12 releases). The major radionuclide contributors to the peak MOP dose are I-129 (58%) and Tc-99 (42%) and the major pathway contributors are water ingestion (30%) and produce ingestion (66%).

Uncertainty parameters influencing these dose contributions are identified below, along with their respective sampled values. The equivalent deterministic (Compliance Case) value is presented within parentheses.

- Inventory multiplier for I-129 in SDU 11 = 1.05 (1.0)
- Inventory multiplier for I-129 in SDU 12 = 1.48 (1.0)
- Iodine K_d in Reducing Region I Saltstone = 0.070 mL/g (0.07 mL/g)
- Iodine K_d in Reducing Region III Saltstone = 0.49 mL/g (0.71 mL/g)
- Infiltration rate selector = 3 [conservative estimate] (2 [MPAD])
- Initial saturated hydraulic conductivity of saltstone = 2.0E-09 cm/s (5.0E-10 cm/s)
- Vadose zone thickness for SDUs 11 and 12 = 27.1 ft (36 ft)
- Saturated zone face area = 74 ft × 333 ft = 2.5E+04 ft² (2.5E+04 ft²)
  - Saturated zone thickness for the SDF = 74 ft (66 ft)
  - Saturated zone width for SDUs 11 and 12 = 333 ft (375 ft)
- Water ingestion rate = 562 L/yr (505 L/yr)
- Produce ingestion rate = 80 kg/yr (207 kg/yr)
- Sampled garden size = 741 m² (100 m²)

Realization #88 from Random Seed = 2

Table 5.7-7 indicates that Realization #88 (with Random Seed = 2) has a peak dose within 10,000 years that occurs in Sector B (i.e., from SDU 11 and SDU 12 releases). The major radionuclide contributors to the peak MOP dose are I-129 (60%) and Tc-99 (40%) and the major pathway contributors are water ingestion (22%) and produce ingestion (75%). Uncertainty parameters influencing these dose contributions are identified below, along with their respective sampled values. The equivalent deterministic (Compliance Case) value is presented within parentheses.

- Inventory multiplier for I-129 in SDU 11 = 0.70 (1.0)
- Inventory multiplier for I-129 in SDU 12 = 1.30 (1.0)
- Iodine K_d in Reducing Region I Saltstone = 0.087 mL/g (0.07 mL/g)
- Iodine K_d in Reducing Region III Saltstone = 0.76 mL/g (0.71 mL/g)
- Infiltration rate selector = 3 [conservative estimate] (2 [MPAD])
- Initial saturated hydraulic conductivity of saltstone = 2.0E-09 cm/s (5.0E-10 cm/s)
- Vadose zone thickness for SDUs 11 and 12 = 41.2 ft (36 ft)
- Saturated zone face area = 53 ft × 323 ft = 1.7E+04 ft² (2.5E+04 ft²)
  - Saturated zone thickness for the SDF = 53 ft (66 ft)
  - Saturated zone width for SDUs 11 and 12 = 323 ft (375 ft)
- Water ingestion rate = 438 L/yr (505 L/yr)
- Produce ingestion rate = 261 kg/yr (207 kg/yr)
- Sampled garden size = 738 m² (100 m²)

Realization #547 from Random Seed = 2

Table 5.7-7 indicates that Realization #547 (with Random Seed = 2) has a peak dose within 10,000 years that occurs in Sector B (i.e., from SDU 11 and SDU 12 releases). The major radionuclide contributors to the peak MOP dose is I-129 (52%) and Tc-99 (48%) and the

major pathway contributors are water ingestion (33%) and produce ingestion (61%). Uncertainty parameters influencing these dose contributions are identified below, along with their respective sampled values. The equivalent deterministic (Compliance Case) value is presented within parentheses.

- Inventory multiplier for I-129 in SDU 11 = 0.85 (1.0)
- Inventory multiplier for I-129 in SDU 12 = 0.95 (1.0)
- Iodine K_d in Reducing Region I Saltstone = 0.067 mL/g (0.07 mL/g)
- Iodine K_d in Reducing Region III Saltstone = 0.57 mL/g (0.71 mL/g)
- Infiltration rate selector = 3 [conservative estimate] (2 [MPAD])
- Initial saturated hydraulic conductivity of saltstone = 2.0E-09 cm/s (5.0E-10 cm/s)
- Vadose zone thickness for SDUs 11 and 12 = 28.8 ft (36 ft)
- Saturated zone face area = 64 ft × 320 ft = 2.0E+04 ft^2 (2.5E+04 ft^2)
  - Saturated zone thickness for the SDF = 64 ft (66 ft)
  - Saturated zone width for SDUs 11 and 12 = 320 ft (375 ft)
- Water ingestion rate = 630 L/yr (505 L/yr)
- Produce ingestion rate = 333 kg/yr (207 kg/yr)
- Sampled garden size = 757 m^2 (100 m^2)

Realization #994 from Random Seed = 2

Table 5.7-7 indicates that Realization #994 (with Random Seed = 2) has a peak dose within 10,000 years that occurs in Sector B (i.e., from SDU 11 and SDU 12 releases). The major radionuclide contributor to the peak MOP dose is I-129 (54%) and Tc-99 (46%) and the major pathway contributors are water ingestion (24%) and produce ingestion (74%). Uncertainty parameters influencing these dose contributions are identified below, along with their respective sampled values. The equivalent deterministic (Compliance Case) value is presented within parentheses.

- Inventory multiplier for I-129 in SDU 11 = 1.29 (1.0)
- Inventory multiplier for I-129 in SDU 12 = 0.97 (1.0)
- Iodine K_d in Reducing Region I Saltstone = 0.141 mL/g (0.07 mL/g)
- Iodine K_d in Reducing Region III Saltstone = 2.69 mL/g (0.71 mL/g)
- Infiltration rate selector = 3 [conservative estimate] (2 [MPAD])
- Initial saturated hydraulic conductivity of saltstone = 2.0E-09 cm/s (5.0E-10 cm/s)
- Vadose zone thickness for SDUs 11 and 12 = 31.7 ft (36 ft)
- Saturated zone face area = 76 ft × 411 ft = 3.1E+04 ft^2 (2.5E+04 ft^2)
  - Saturated zone thickness for the SDF = 76 ft (66 ft)
  - Saturated zone width for SDUs 11 and 12 = 411 ft (375 ft)
- Water ingestion rate = 624 L/yr (505 L/yr)
- Produce ingestion rate = 37 kg/yr (207 kg/yr)
- Sampled garden size = 914 m^2 (100 m^2)

5.7.3.4 Insights from the Analysis of Individual Realizations

A review of these ten realizations indicates that the parameters most significant to the highest peak doses change depending upon the time period being considered (Compliance Period versus Performance Period), as does the corresponding location (or sector) of the peak dose. Regardless of the location, a unifying theme is that all ten of these realizations sampled high water ingestion rates, indicating that uncertainty in future human behaviors has great influence on these dose results.

For the first 500 years, the infiltration rate is the same for all realizations regardless of sampling. Only after 2,000 years do the infiltration rates show significant variability between realizations. For this reason, the sampled infiltration rates are not very important during the Compliance Period (from 0 to 1,000 years), but the rates become very important for the Performance Period (from 0 to 10,000 years).

During the Compliance Period, doses along Sector D are dominant. Because Sector D is heavily influenced by SDU 9 and SDU 9 is assumed to be constructed closer to the water table, the uncertainty associated with the thickness of the vadose zone beneath SDU 9 is extremely important, as is the initial I-129 inventory (which contribute to higher dose peaks when conditions are favorable to faster releases). All five of the realizations with high doses during the Compliance Period sampled vadose zone thicknesses beneath SDU 9 with values of less than half of the 23 feet assumed for the Compliance Case. Because the flow rates are relatively low during this period, the dose results are not particularly sensitive to the initial saturated hydraulic conductivity of saltstone.

During the Performance Period, the infiltration rate is important for all sectors; all five of the realizations with high doses during the Performance Period sampled the higher infiltration rate. With the higher infiltration rate, the initial saturated hydraulic conductivity of saltstone is more important; all five of the realizations with high doses in during the Performance Period sampled an initial saturated hydraulic conductivity of saltstone of 2.0E-09 cm/s. The doses along Sector B are dominant during this period, so the inventories of I-129 in SDUs 11 and 12 can also be important.

Contrary to initial expectations, peak doses do not appear to be very sensitive to the saltstone K_d for iodine. Because the initial values are already low, all the sampled distributions around these initial values are also low.

In summary, while uncertainty is applied to many parameters, only a relatively small number of these parameters exert a significant influence on the peak doses. As such, it only takes two or three of these parameters to simultaneously sample certain values to result in higher dose peaks. Regardless, all 3,000 realizations exhibited peak doses below 25 mrem/yr within the Compliance Period and less than 2% of these realizations exceeded 25 mrem/yr beyond the Compliance Period. These results provide confidence that it would be extremely unlikely for future doses to exceed the performance objectives.

5.7.4 Probabilistic Sensitivity Analyses Using the SDF GoldSim Model

Given the uncertainties discussed in Section 5.7.3, the next step is to quantify the extent to which specific input parameters contribute to uncertainties. Even in complex models, the results are often strongly dependent on only a handful of parameters. What is important for one result (e.g., the Tc-99 concentration in well water) may be insignificant for another (e.g., the maximum dose achieved within a 10,000-year period). In fact, the maximum dose to the MOP will have different sensitivities at different times since it is influenced by temporal-spatial uncertainties. For example, dose to the MOP may be dominated by releases from SDU 9 at one time and by releases from SDU 12 at another time. Quantifying the relative importance of probabilistic model parameters is the objective of the following probabilistic sensitivity analyses.

5.7.4.1 Introduction to Probabilistic Sensitivity Analysis

Complex modeling such as the probabilistic models provides an effective tool for exploring the dynamics of systems where multiple variables interact in a nonlinear manner. The probabilistic simulation approach used in the SDF GoldSim Model propagates uncertainty regarding the independent variables (e.g., inputs such as physical soil properties or inventory) through the model to the dependent variables or predicted response (e.g., dose or concentration). One of the goals of this sensitivity analysis is to identify which independent variables have distributions that exert the greatest influence on the response.

The primary sensitivity analysis procedures used herein involve the determination and presentation of partially ranked correlation coefficients (PRCCs) and stepwise rank regression analyses.

5.7.4.1.1 Partially Ranked Correlation Coefficients

PRCCs provide a measure of the strength of the monotonic relationships between an independent variable and a specific model result after a correction has been made to remove the monotonic effects of the other independent variables in the analysis (i.e., one independent variable is analyzed at a time by isolating and ignoring the combined effects of the other independent variables). Many of the independent variables have varying effects on the results as a function of time. For such variables, the presentation of PRCCs as functions of time provides an informative display of sensitivity analysis results.

As indicated by the name, PRCCs involve the analysis of rank-transformed data. With this approach, the values for variables are replaced with their ranks and then the PRCCs are calculated with these ranks rather than with the original values for the variables. Specifically, the smallest value of a variable is given a rank of 1, the next largest value is given a rank of 2, equal observations are assigned the average of what their ranks would have been if they had not been equal, and so on up to the largest value, which is given a rank equal to the number of sample elements in use. The effect of the rank transformation is to transform monotonic relationships into linear relationships. Further, the rank transform tends to reduce the skewing

effects of outliers, which permits the regression analysis to represent the general relationships between the inputs and the specific result. Although no variable transformation is universally successful in improving the resolution of a sensitivity analysis in the presence of nonlinear relationships, the rank transformation has been found to be a broadly effective and useful means of enhancing the insights in sensitivity analyses based on partial correlation and sensitivity analyses based on stepwise regression.

The figures in Section 5.7.4.2 show the PRCCs over time, as determined using the sampling results from three sets of 1,000 realizations. Thus, at each modeled time step, there are 3,000 values for each result for which a PRCC is calculated.

Due to the large number of variables in the SDF GoldSim Model and computational limitations of analyzing such large datasets, these PRCC calculations were performed using a sub-set of the variables. For example, while the SDF GoldSim Model samples K_ds for contaminant transport in Reducing Region II cementitious materials, this chemical environment is never applicable in the current model (see discussion in Section 4.4.3); therefore, these sampled K_ds for the Reducing Region II chemical environment exhibit no impact on dose results and were screened out (i.e., not considered in these analyses). Only approximately 320 of the 410 variables were used as inputs in this analysis.

To limit the number of time-dependent PRCC curves in a given plot frame, the analysis only examined variables whose PRCCs exceed 0.25 in absolute value at some point in time. Variables with PRCCs with a smaller absolute value than 0.25 have only a limited monotonic effect on the results under consideration.

Values of PRCCs fall in the interval [−1, 1], where:

- positive PRCCs indicate that two variables tend to increase and decrease together (i.e., the independent variable has a positive effect on the dependent variable),
- negative PRCCs indicate that two variables tend to move in opposite directions (i.e., the independent variable has a negative effect on the dependent variable), and
- the absolute value of a PRCC indicate the strength of the relationship between two variables (i.e., a PRCC close to 1 in absolute value indicates a strong monotonic relationship between two variables after the removal of the monotonic effects associated with the other independent variables under consideration).

5.7.4.1.2 Stepwise Rank Regression

An alternative to the use of PRCCs is to carry out stepwise rank regressions to determine the effects of uncertain inputs on analysis results of interest. In analyses of this type, the regressions are carried out with rank-transformed variables as previously discussed rather than with the original values.

In a stepwise rank regression, the single independent variable that makes the largest contribution to the uncertainty in the dependent variable (model result) is selected in the first step. Then, at the second step, the single independent variable that, in conjunction with the first independent variable, makes the largest contribution to the uncertainty in the dependent variable is selected. This process then continues until no additional variables are found that make identifiable contributions to the uncertainty in the dependent variable; at this point, the stepwise selection process terminates. For these analyses, a significance level of $\alpha_{in} = 0.15$ is used as the criterion for entering variables into the stepwise regression and $\alpha_{out} = 0.20$ was used for dropping variables from the stepwise regression analysis. Selection of these significance levels was based on preliminary sensitivity analyses, in which it was observed that a greater value tended to introduce obviously spurious variables into the regression models. In the context of stepwise regression analysis, variable importance is indicated by the order of selection in the stepwise selection process, incremental changes in R^2 values with the successive entry of individual variables into the regression model, and the sign and size of the standardized regression coefficients in the final regression model. Because rank-transformed values were used, the standardized regression coefficients are more correctly identified as standardized rank regression coefficients (SRRCs) in the following tables.

The R^2 values correspond to the fraction of the uncertainty in the dependent variable that is accounted for by a regression model. Thus, R^2 values monotonically increase as additional variables are added to the regression model and, for a very successful regression analysis, approach 1 as additional variables are added to the model. The SRRCs provide a measure of the fractional contribution of individual independent variables to the uncertainty in the dependent variable under consideration. As with the PRCCs, a positive SRRC indicates that the independent variable and dependent variable tend to increase and decrease together, and a negative SRRC indicates that the independent variable and dependent variable tend to move in opposite directions.

As discussed above, the PRCCs are computed as a function of time. In contrast, SRRCs are computed at fixed times (i.e., for each dependent variable, the time of the peak of the means is used). These times for SRRC computation were chosen to illustrate the changes in importance of uncertain parameters over time. The same analysis times are generally used for analysis of all SDF model output variables to facilitate comparisons between the sensitivity analysis results across output variables.

Related, but not identical, information is provided by PRCCs and SRRCs. Specifically, PRCCs measure the strength of the monotonic relationship between an independent variable and a dependent variable after correcting for the effects of other independent variables, and SRRCs provide a measure of the fractional contribution of an individual independent variable to the uncertainty in the

dependent variable under consideration. Except in rare situations involving SRRCs from a regression model involving multiple correlated variables, PRCCs and SRRCs have the same sign, which indicates either a positive or a negative correlation between an input variable and an output variable. Because PRCCs are selected for display based on the maximum absolute value over time and SRRCs are computed at specific times, the selection and order of important variables indicated by PRCCs and SRRCs may be different between the two analyses.

As described in the PRCC discussion above, subsets of approximately 320 variables were used as inputs in these analyses. No-impact variables were excluded from these analyses in response to computational limitations and to reduce the occurrence of spurious correlations in the PRCC calculation results.

5.7.4.2 Probabilistic Sensitivity Analysis Results

This section presents probabilistic sensitivity analysis results for the following endpoints: total dose to the MOP at any sector, total dose to the MOP at Sector B, total dose to the MOP at Sector D, I-129 dose to the MOP at any sector, and Tc-99 dose to the MOP at any sector. Sectors B and D were selected because the peak of the mean doses from these sectors represent the highest doses during the Performance Period and during the Compliance Period, respectively (Figure 5.7-7). The dose results from I-129 and Tc-99 were chosen because they are the most dominant dose contributors (Figure 5.7-8).

Note that inclusion of data from the first 100 years results in the identification of spurious parameters. To ensure that these analyses yield the parameters with the greatest influence, the PRCC analyses only considered data from 100 years to 20,000 years. After the first 10,000 years, relatively little change was observed in the PRCC results. Therefore, all the PRCC results are displayed from 100 years to 10,000 years.

5.7.4.2.1 Sensitivity Analysis of the Total Dose to the MOP at Any Sector

The PRCCs for total dose to the MOP at any sector are depicted in Figure 5.7-10. These results show that starting at 100 years, the vadose zone thickness beneath SDU 9 (*Vadosethick_SDU9*) is initially the most dominant parameter with a strong negative correlation (PRCC = -0.97) to the total dose values. The vadose zone thickness beneath SDU 9 is assumed to be 23 feet, which is considerably less than the other SDUs that have vadose zone thicknesses that range from 36 feet to 48 feet. Despite the shorter distance, the same distributions is applied to SDU 9 as with the other SDUs (± 16.4 ft). The shorter distance from SDU 9 to the water table means that releases from SDU 9 will reach the saturated zone and the 100-meter boundary much earlier than the releases from other SDUs. The importance of this parameter diminishes over time; by approximately 5,000 years after SDF closure, its influence becomes negligible as the releases from the other SDUs begin to reach the 100-meter boundary.

Figure 5.7-10: PRCCs of the Total MOP Dose for Any Sector, Using 3,000 Realizations

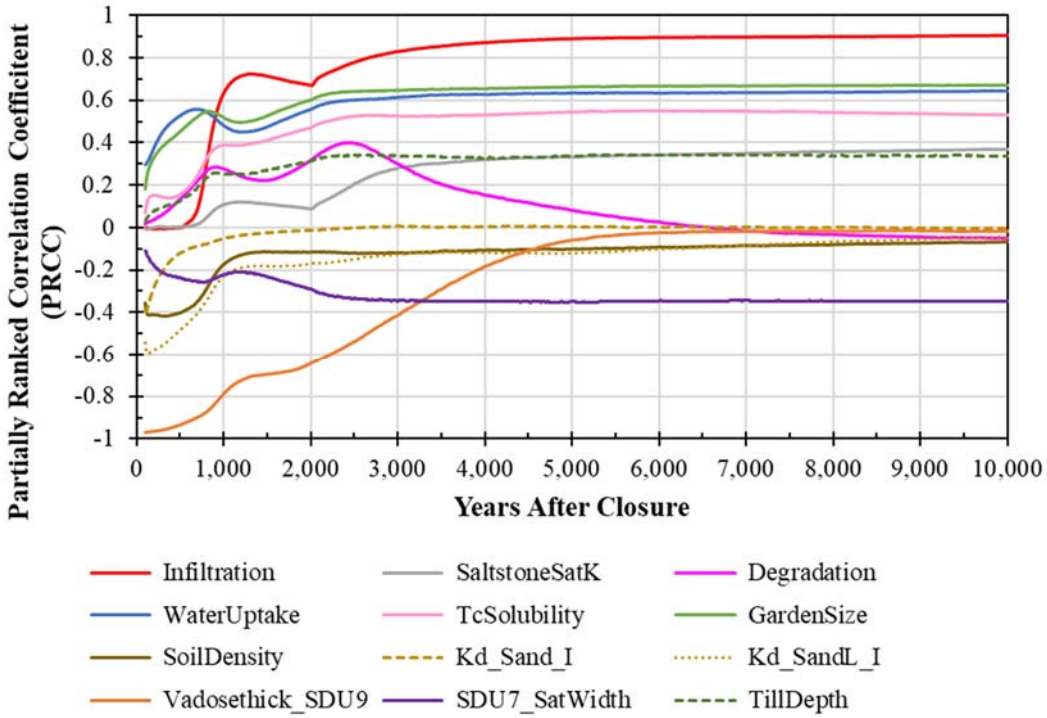

The K_d for iodine in leachate-impacted sandy soils (*Kd_SandL_I*) is important at early times with a PRCC near -0.59. The importance of this parameter diminishes significantly within the first 1,000 years.

The next most dominant parameter is the infiltration rate (*Infiltration*). Within the SDF GoldSim Model, the infiltration rate is sampled as a discrete value of 1, 2, or 3 to select the best estimate, MPAD, or conservative estimate infiltration rates (see Table 4.4-5), respectively. Initially, *Infiltration* is insignificant, then it increases in importance starting at 500 years, followed by a second increase in importance starting at 2,000 years after closure. By approximately 2,500 years after closure, *Infiltration* is the single most important parameter, based on these PRCC results. It remains the most important parameter for the duration of the simulated time.

The next most important parameters are those associated with dose: *WaterUptake* and *GardenSize* with PRCCs near 0.7. *WaterUptake* is used to sample the rate at which the MOP (or IHI) ingest contaminated water. Given the water ingestion pathway is the highest dose pathway (see Figure 5.7-9), this result is expected. The *GardenSize* parameter strongly influences the plant (or produce) ingestion pathway because it is used as an input in the calculation to determine the fraction of ingested fruits and vegetables assumed to be contaminated (see Eq. 4.4-247).

Other notable parameters are the solubility of technetium (*TcSolubility*), the saturated zone width for SDU 7 (*SDU7_SatWidth*), the initial saturated hydraulic conductivity of saltstone (*SaltstoneSatK*) and the cementitious degradation rate

(*Degradation*). Because hydraulic conductivity is only an important material property when coupled with flow, *SaltstoneSatK* is initially unimportant due to low initial infiltration rates. As the infiltration rates increase, the system gradually evolves from being a diffusion-dominated system to an advection-dominated system, such that *SaltstoneSatK* increases in importance in parallel with the increasing importance of *Infiltration*. The PRCC value for *Degradation*, on the other hand, peaks at approximately 2,500 years then gradually decreases. This behavior reflects the degradation timing of the SDU concretes as described in Section 4.4.2.

Table 5.7-8 shows the results from the stepwise regression analysis. This table only shows the first eight variables from each model as the importance of each variable quickly diminishes with each successive analysis step. In this analysis, the first four or five variables effectively dominate any influence over the dependent variable at the time analyzed. For each of the SRRC analyses, the dose results are analyzed at 1,000 and 10,000 years. These results are similar to the PRCC results.

Table 5.7-8: Top Eight SRRC Results for Total MOP Dose at Any Sector

Time = 1,000 years, Final Cumulative R^2 = 0.832			Time = 10,000 Years, Final Cumulative R^2 = 0.905		
Variable	**Cumulative R^2**	**SRRC**	**Variable**	**Cumulative R^2**	**SRRC**
Vadosethick_SDU9	0.349	-0.586	Infiltration	0.544	0.723
Infiltration	0.495	0.368	GardenSize	0.641	0.313
GardenSize	0.567	0.278	WaterUptake	0.727	0.291
WaterUptake	0.636	0.254	TcSolubility	0.774	0.216
TcSolubility	0.676	0.190	SaltstoneSatK	0.795	0.137
Degradation	0.696	0.128	SDU7_SatWidth	0.813	-0.126
SDU7_SatWidth	0.710	-0.108	TillDepth	0.828	0.126
SDU6_SatWidth	0.723	0.098	SDU6_SatWidth	0.840	0.112

5.7.4.2.2 Sensitivity Analysis of the Total Dose to the MOP at Sector B

The PRCCs for total dose to the MOP at Sector B are shown in Figure 5.7-11. As expected, these results are very similar to the total MOP results in any sector. The major difference between the PRCCs of the total MOP dose at any sector and the PRCCs of the Sector B MOP dose is in the timing and magnitude of *Vadosethick_SDU7*. Because releases from SDU 7 contribute to doses at Sector B, it makes sense for this parameter to be more important.

Also it is noted that while the releases from SDU 9 do not explicitly contribute to doses along Sector B, *Vadosethick_SDU9* still shows up as an important parameter in the early years. This is due to the application of the seepline ratio, which is used for determining the contaminant concentrations used for fish ingestion calculations (see Section 5.2.3). With the seepline ratio, the seepline concentrations are controlled by the sector that receives the highest contaminant concentrations. During the first few thousand years of the simulation, these maximum concentrations occur along Sector D, such that the early releases from SDU 9 are still important to the dose results.

Figure 5.7-11: PRCCs of the Total MOP Dose at Sector B, Using 3,000 Realizations

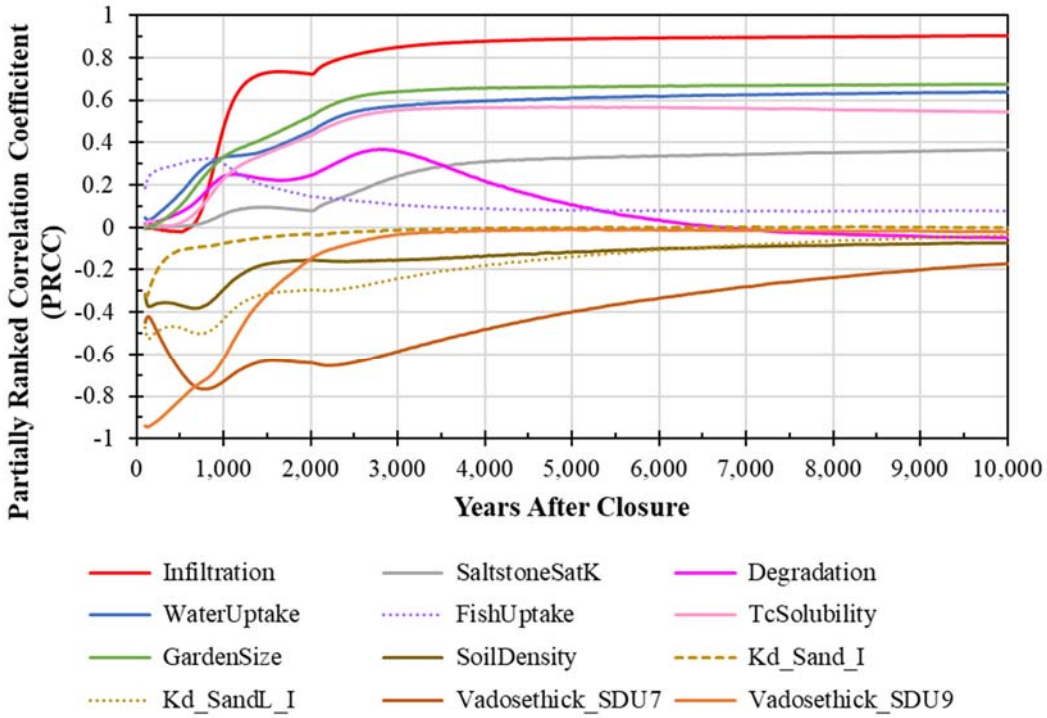

Table 5.7-9 shows the results from the stepwise regression analysis for the total doses to the MOP at Sector B. These results are similar to the equivalent results from the total MOP dose at any sector and are similar to the PRCC results.

Table 5.7-9: Top Eight SRRC Results for Total MOP Dose at Sector B

Time = 1,000 years, Final Cumulative R^2 = 0.805			Time = 10,000 Years, Final Cumulative R^2 = 0.905		
Variable	**Cumulative R^2**	**SRRC**	**Variable**	**Cumulative R^2**	**SRRC**
Vadosethick_SDU7	0.256	-0.521	Infiltration	0.536	0.719
Vadosethick_SDU9	0.413	-0.385	GardenSize	0.630	0.313
Infiltration	0.487	0.263	WaterUptake	0.717	0.285
Kd_SandL_I	0.546	-0.239	TcSolubility	0.768	0.223
WaterUptake	0.577	0.175	SaltstoneSatK	0.788	0.135
GardenSize	0.608	0.173	SDU7_SatWidth	0.808	-0.132
FishUptake	0.637	0.155	TillDepth	0.824	0.127
SoilDensity	0.657	-0.154	SDU6_SatWidth	0.838	0.120

5.7.4.2.3 Sensitivity Analysis of the Total Dose to the MOP at Sector D

The PRCCs for total dose to the MOP at Sector D are shown in Figure 5.7-12. As with the Sector B analyses, these results are very similar to the total MOP results in any sector.

Figure 5.7-12: PRCCs of the Total MOP Dose at Sector D, Using 3,000 Realizations

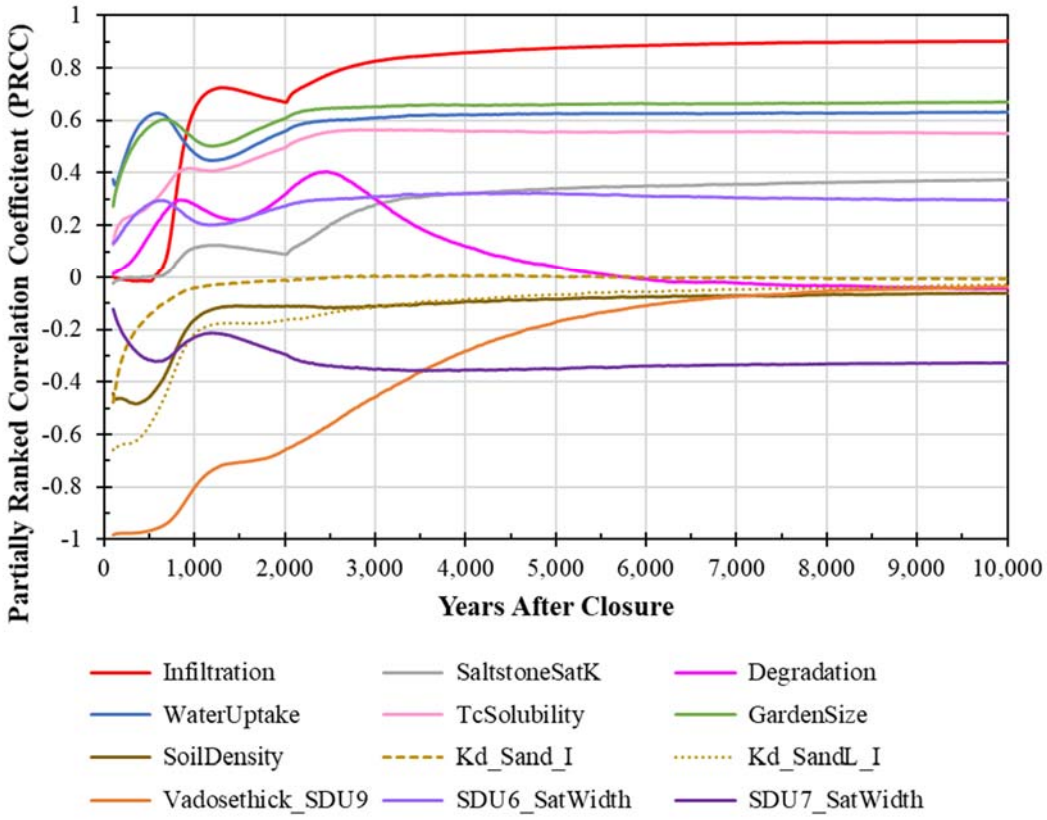

Table 5.7-10 shows the results from the stepwise regression analysis for the total doses to the MOP at Sector D. These results are similar to the equivalent results from the total MOP dose at any sector and are similar to the PRCC results.

Table 5.7-10: Top Eight SRRC Results for Total MOP Dose at Sector D

Time = 1,000 years, Final Cumulative R^2 = 0.841			Time = 10,000 Years, Final Cumulative R^2 = 0.902		
Variable	**Cumulative R^2**	**SRRC**	**Variable**	**Cumulative R^2**	**SRRC**
Vadosethick_SDU9	0.363	-0.597	Infiltration	0.532	0.718
Infiltration	0.510	0.370	GardenSize	0.626	0.316
GardenSize	0.582	0.276	WaterUptake	0.710	0.282
WaterUptake	0.645	0.240	TcSolubility	0.767	0.230
TcSolubility	0.690	0.205	SaltstoneSatK	0.788	0.142
Degradation	0.711	0.129	TillDepth	0.805	0.129
SDU7_SatWidth	0.724	-0.107	SDU7_SatWidth	0.821	-0.119
TillDepth	0.738	0.121	SDU6_SatWidth	0.833	0.108

5.7.4.2.4 Sensitivity Analysis of the I-129 Dose to the MOP at Any Sector

The PRCCs for I-129 dose to the MOP at any sector are shown in Figure 5.7-13. These results are also similar to the total MOP results in any sector. The major difference between the PRCCs of the total MOP dose at any sector and the PRCCs for the I-129 dose to the MOP at any sector is in the occurrence of the SDU 9 inventory of I-129 (*InventoryI129_SDU9*).

Figure 5.7-13: PRCCs of the I-129 Dose to the MOP at any Sector, Using 3,000 Realizations

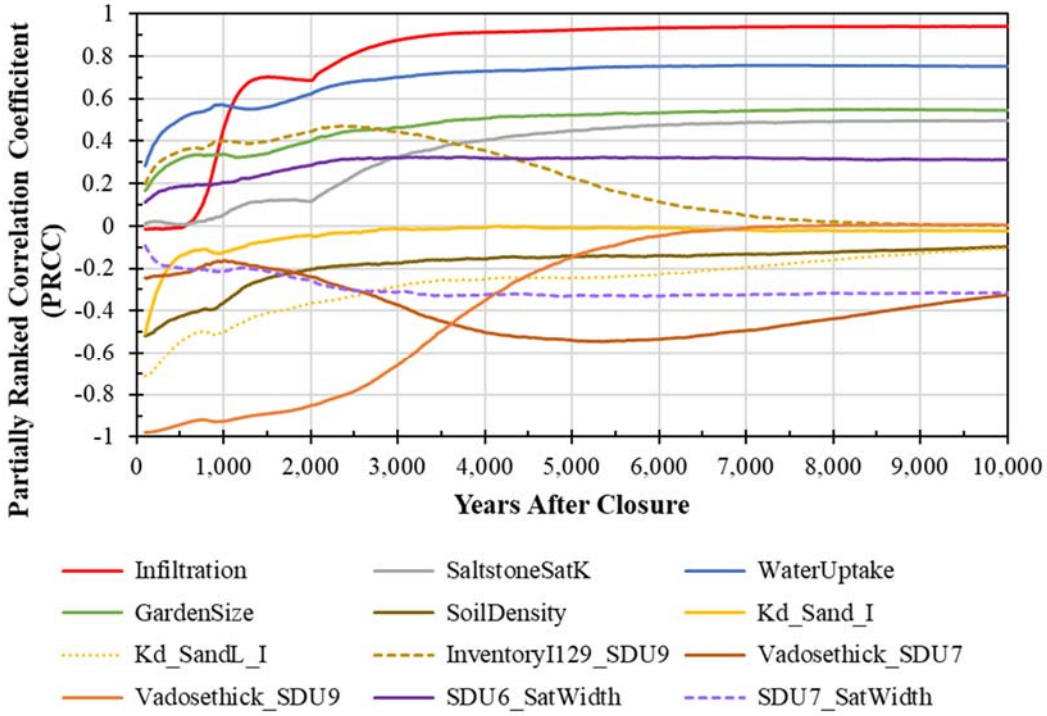

Table 5.7-11 shows the results from the stepwise regression analysis for the I-129 dose to the MOP at any sector. These results are similar to the equivalent results from the total MOP dose at any sector and are similar to the PRCC results.

Table 5.7-11: Top Eight SRRC Results for the I-129 Dose to the MOP at any Sector

Time = 1,000 years, Final Cumulative R^2 = 0.902			Time = 10,000 Years, Final Cumulative R^2 = 0.920		
Variable	**Cumulative R^2**	**SRRC**	**Variable**	**Cumulative R^2**	**SRRC**
Vadosethick_SDU9	0.697	-0.812	Infiltration	0.674	0.803
WaterUptake	0.749	0.225	WaterUptake	0.781	0.332
Kd_SandL_I	0.782	-0.194	GardenSize	0.820	0.188
Infiltration	0.815	0.168	SaltstoneSatK	0.851	0.166
InventoryI129_SDU9	0.834	0.147	SDU7_SatWidth	0.861	-0.095
SoilDensity	0.852	-0.128	Vadosethick_SDU7	0.871	-0.100
GardenSize	0.867	0.117	InventoryI129_SDU12	0.880	0.092
SDU7_SatWidth	0.872	-0.069	SDU6_SatWidth	0.889	0.095

5.7.4.2.5 Sensitivity Analysis of the Tc-99 Dose to the MOP at Any Sector

The PRCCs for the Tc-99 dose to the MOP at any sector are shown in Figure 5.7-14. These results show that a smaller number of parameters are controlling the Tc-99 dose relative to the total MOP results in any sector. As expected, the technetium solubility (*TcSolubility*) is extremely important.

Figure 5.7-14: PRCCs of the Tc-99 Dose to the MOP at any Sector, Using 3,000 Realizations

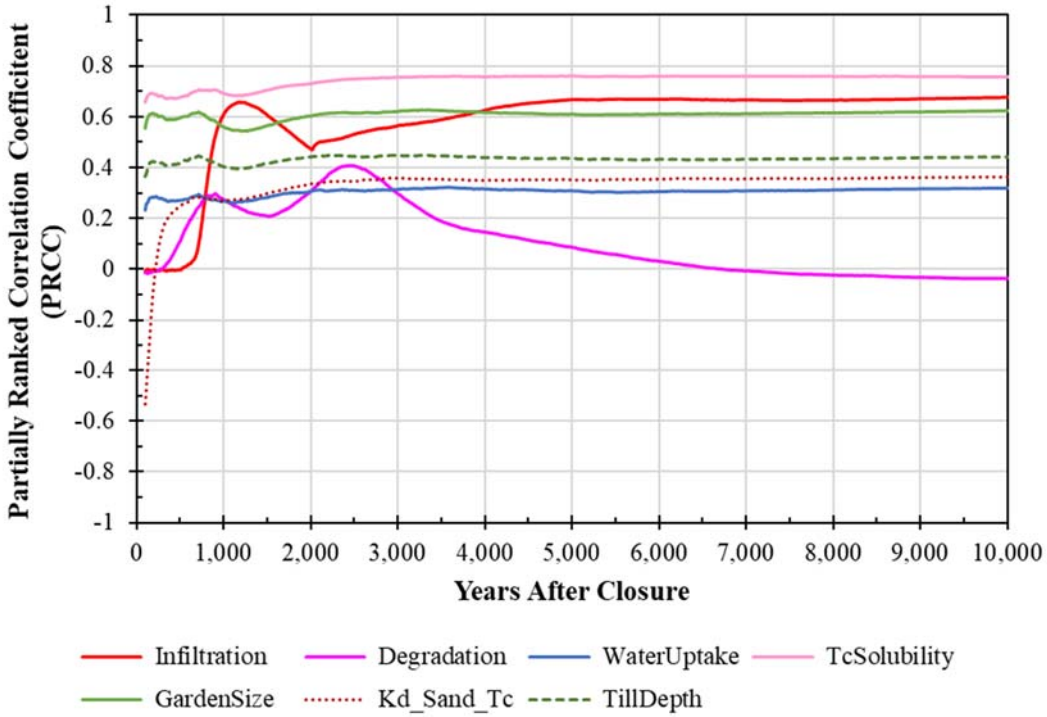

Note that unlike the previous PRCC analyses, this one shows that the *GardenSize* is more important than the *WaterUptake* parameter. This is because Tc-99 is sensitive to plant uptake, thus the uncertainty in the plant ingestion dose pathway is relatively important for Tc-99 doses.

Also note that the K_d for technetium in sandy soil has an initially negative value, but it quickly becomes positive. This is because a low sandy soil K_d will accelerate the Tc-99 transport, thus increasing the dose early on. However, in addition to transport, the sandy soil K_d also affects the soil buildup for Tc-99 such that as contaminated water is used to irrigate the crops or garden, a higher sandy soil K_d will promote the accumulation of Tc-99 within the soil, resulting in a higher plant ingestion dose.

Table 5.7-12 shows the results from the stepwise regression analysis for for the Tc-99 dose to the MOP at any sector. This SRRC analysis identified more parameters as significant compared to the PRCC analysis.

Table 5.7-12: Top Eight SRRC Results for the Tc-99 Dose to the MOP at any Sector

Time = 1,000 years, Final Cumulative R^2 = 0.730			Time = 10,000 Years, Final Cumulative R^2 = 0.784		
Variable	**Cumulative R^2**	**SRRC**	**Variable**	**Cumulative R^2**	**SRRC**
TcSolubility	0.248	0.506	TcSolubility	0.279	0.544
Infiltration	0.429	0.406	Infiltration	0.487	0.436
GardenSize	0.548	0.359	GardenSize	0.616	0.377
TillDepth	0.604	0.234	TillDepth	0.671	0.232
Kd_Sand_Tc	0.631	0.151	Kd_Sand_Tc	0.707	0.185
Degradation	0.655	0.152	WaterUptake	0.734	0.161
WaterUptake	0.678	0.148	SDU7_SatWidth	0.749	-0.125
SDU7_SatWidth	0.691	-0.111	IrrigationRate	0.760	0.097

5.7.5 Additional Analysis of Peak Doses

Figure 5.7-2 shows the peak doses over time. A number of important parameters were identified through the PRCC and SRRC analyses. This figure can be further modified based on specific sampled values from select parameters to provide additional insights of how the peak dose values are influenced.

First, it is helpful to understand where along the SDF 100-meter boundary each of these peaks occur. Figure 5.7-15 shows that during the first 5,000 years after SDF closure the peak doses only occur in Sector D (orange). After 5,000 years after closure, the peak doses predominantly occur in Sector B (blue), although Sector C (green) also sometimes provides the peak dose, especially after approximately 10,000 years. The doses in Sector C include dose contributions associated with releases from SDU 6, SDU 7, and the 150-foot diameter SDUs.

Figure 5.7-15: Peak MOP Doses within 20,000 Years, Sorted by Sector of Peak

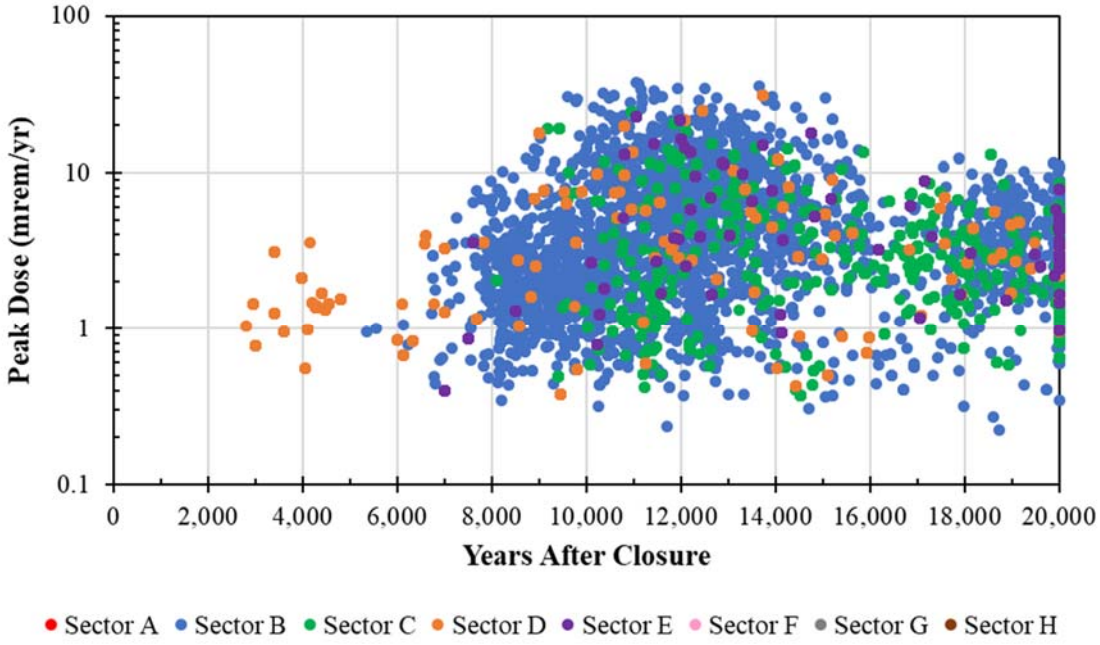

Next, Figure 5.7-16 shows the same peak doses from Figure 5.7-2, but the data points are colored as a function of the sampled infiltration rates (blue = best estimate infiltration rates, gold = MPAD infiltration rates, red = conservative estimate infiltration rates). Almost every realization with peak doses occurring within the first 6,000 years sampled the realistic (lower) infiltration rate. Under best estimate infiltration conditions, the infiltration rate does not exhibit significant changes over time; as such, an initial peak dose occurs when the initial releases reach the 100-meter boundary, then there are no specific phenomena which would result in higher peaks at later times.

Alternatively, most of the peak doses associated with the conservative (higher) infiltration rates occur between 8,000 and 16,000 years. These peak doses almost form a parabolic curve with a peak near 14,000 years, because the available inventory of I-129 would become exhausted when the conditions result in high release rates.

Figure 5.7-17 provides an alternative visual representation of these peak doses based on the statistical profiles from each set of sampled infiltration rates. Each profile is a box plot where the interfaces between the top box and bottom box represents the median value of each set of peak values, the tops and bottoms of these boxes represent the 75th percentile and the 25th percentiles of each set, respectively, and the stems (or error bars) represent the minimum and maximum values from each data set. These figures clearly demonstrate the importance of the infiltration rate relative to the magnitude of the peak doses.

Figure 5.7-16: Peak MOP Doses within 20,000 Years, Sorted by Infiltration Sampling

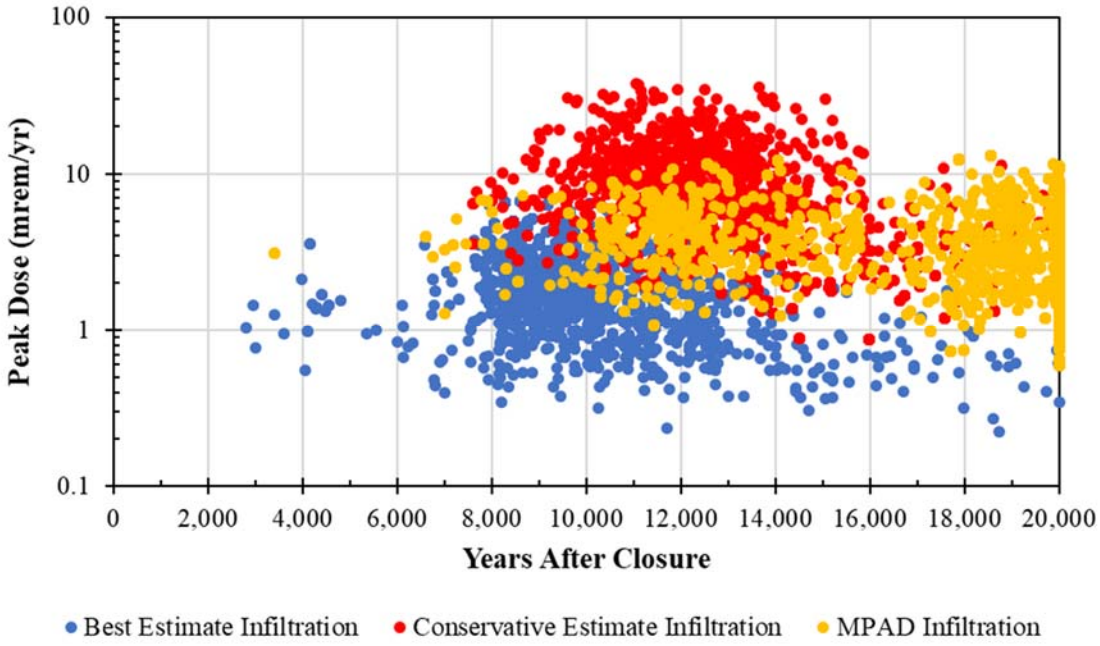

Figure 5.7-17: Box Plot of Peak MOP Doses within 20,000 Years by Infiltration Sampling

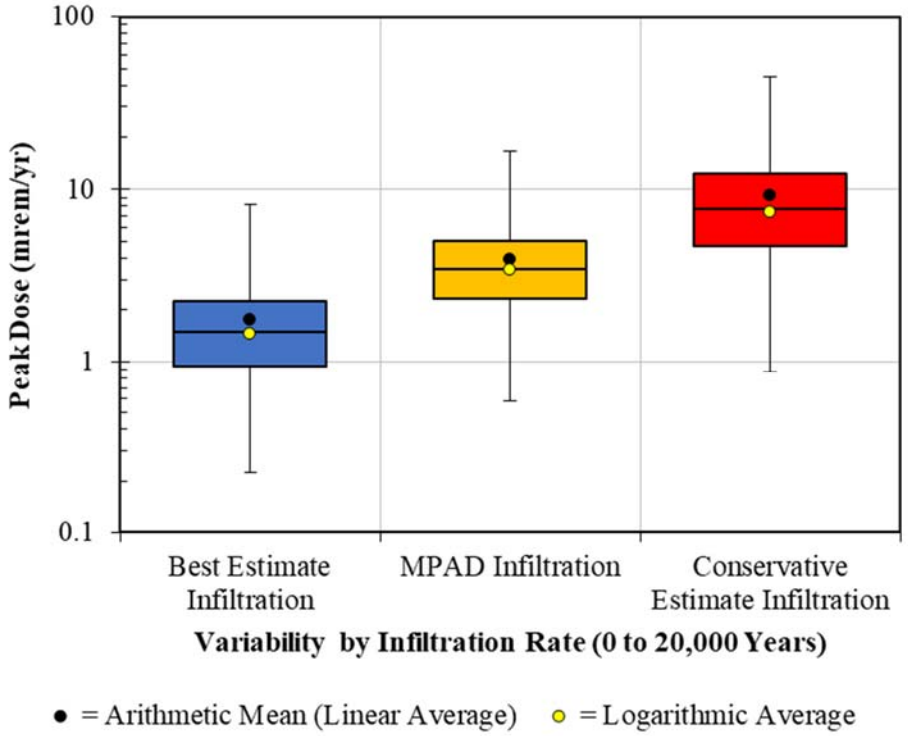

Figure 5.7-18 shows the same peak doses from Figure 5.7-2, but the data points are colored as a function of the sampled initial saturated hydraulic conductivity (K_{sat}) of saltstone (lime = 5.0E-10 cm/s and maroon = 2.0E-09 cm/s). As would be expected, when the higher K_{sat} value is sampled, the resulting doses are generally higher and earlier than when the lower K_{sat} value is sampled. Figure 5.7-19 provides the box plots for these peak doses. While not as strong an influence on the peak doses as the infiltration rates, the initial saturated hydraulic conductivity is still an important parameter.

Figure 5.7-20 shows the same peak doses from Figure 5.7-2, but the data points are colored as a function of the sampled degradation rates for cementitious materials (light blue = best estimate degradation rates, tan = MPAD degradation rates, and pink = conservative estimate degradation rates). This figure shows that the magnitude of the peak doses is not particularly sensitive to the sampled degradation rates, although it does show that the realizations with the BE degradation rates do not show any peak doses within the first 6,000 years. This indicates that while the magnitude of the peak is not affected, the degradation rates do show some influence on the timing of the peak doses.

Figure 5.7-21 provides the box plots for these peak doses which further confirms that the degradation rate has relatively little influence on the magnitudes of these peaks as all three sets of data are nearly identical in the relative magnitudes.

Finally, because the PRCC and SRRC results consistently showed that in addition to *Infiltration*, the *WaterUptake* parameter (i.e., the multiplier on the ingestion rate for drinking contaminated well water) is also important. Figure 5.7-22 is provided to illustrate how *WaterUptake* influences the peak doses. In this figure, instead of plotting the peak values as a function of time (as shown in Figure 5.7-16), the peak doses are plotted as a function of this water uptake multiplier. This figure shows that within each infiltration regime, the water uptake multiplier has a linear relationship with the magnitude of the water ingestion dose contributions, which is typically the most dominant dose pathway.

Figure 5.7-18: Peak MOP Doses within 20,000 Years, Sorted by Sampling of the Initial Saturated Hydraulic Conductivity of Saltstone

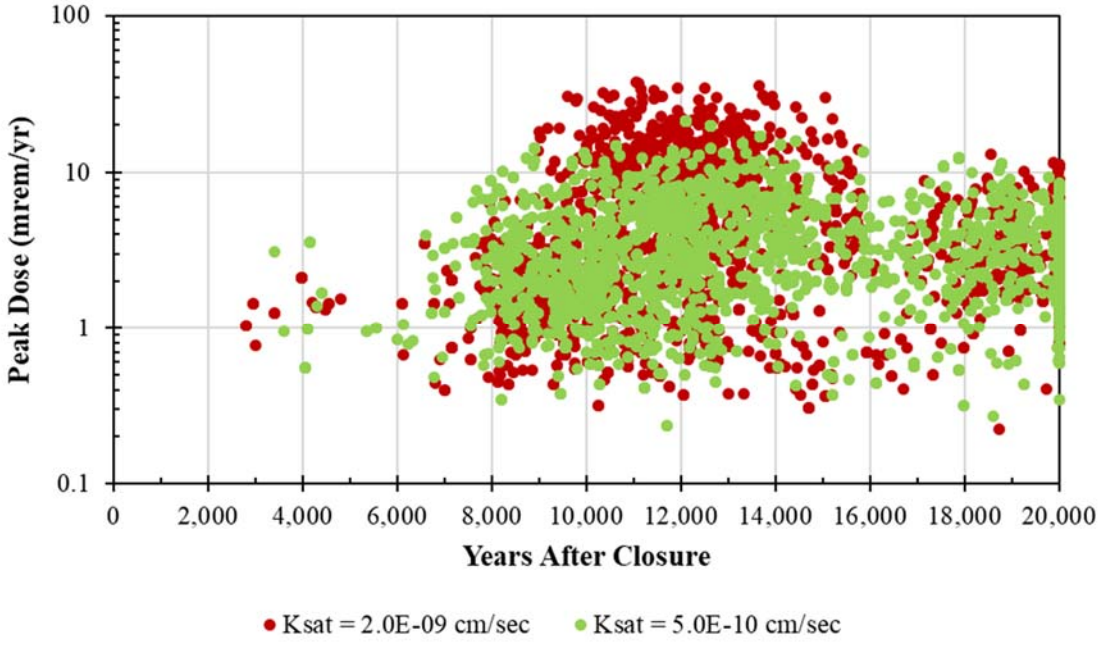

Figure 5.7-19: Box Plot of Peak MOP Doses within 20,000 Years by Sampling of the Initial Saturated Hydraulic Conductivity of Saltstone

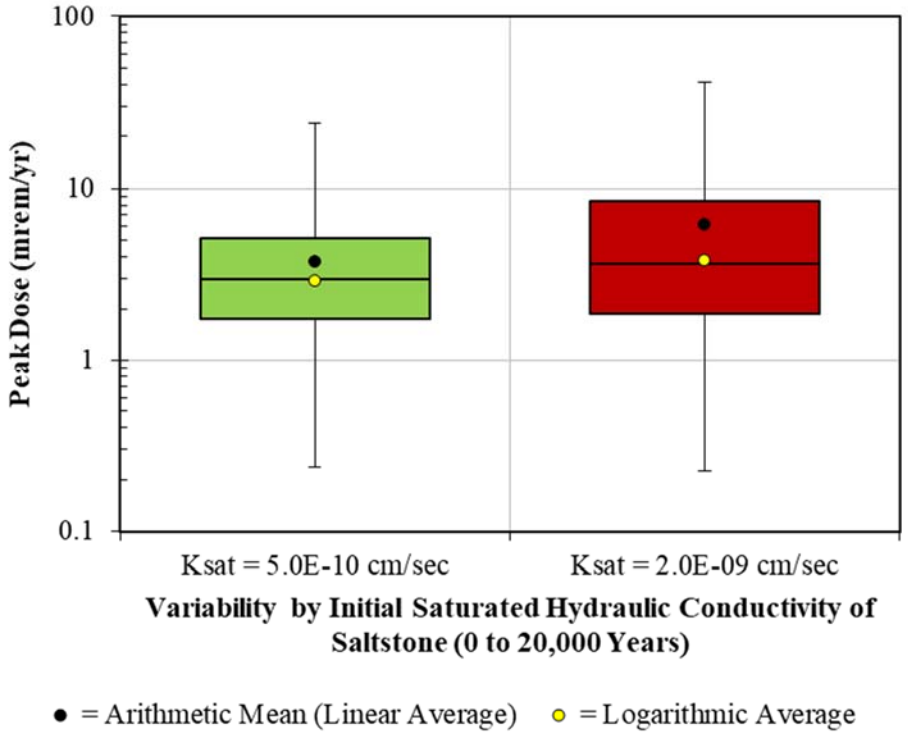

Figure 5.7-20: Peak MOP Doses within 20,000 Years, Sorted by the Sampled Degradation Rates for Cementitious Materials

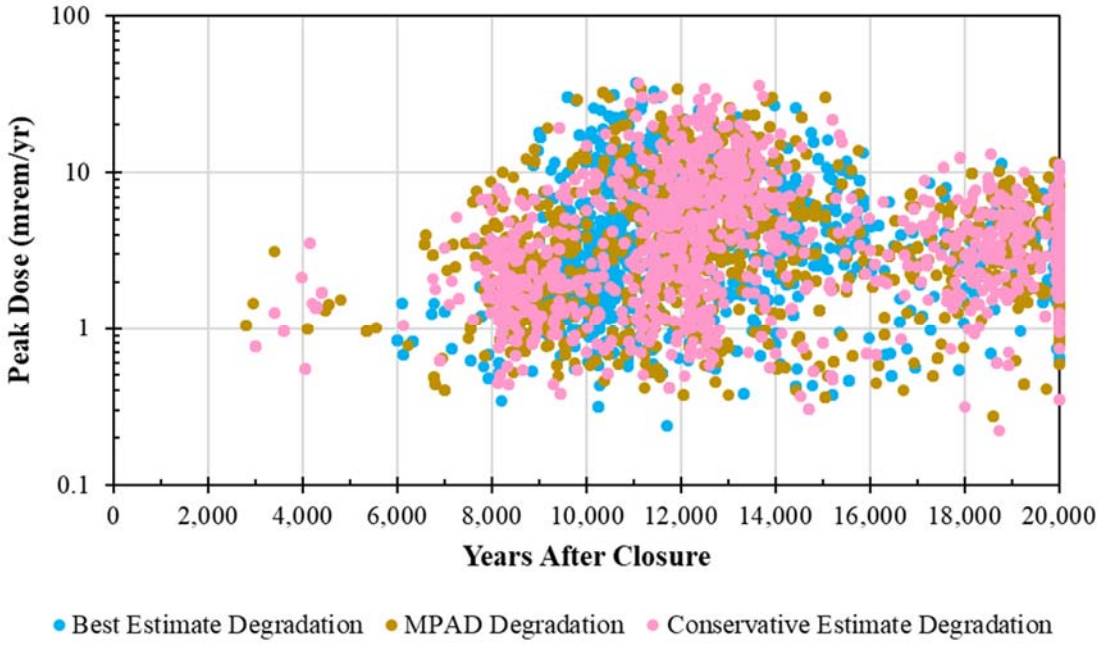

Figure 5.7-21: Box Plot of Peak MOP Doses within 20,000 Years by the Sampled Degradation Rates for Cementitious Materials

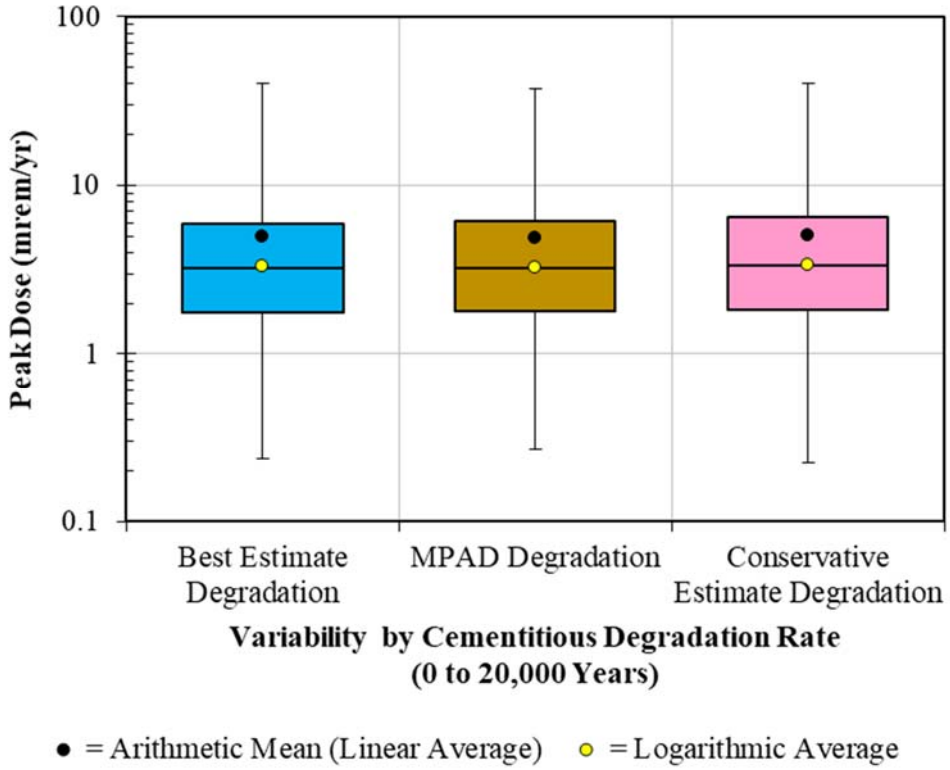

Figure 5.7-22: Peak MOP Doses within 20,000 Years, Sorted by Infiltration Sampling and Plotted as a Function of the Water Uptake Multiplier

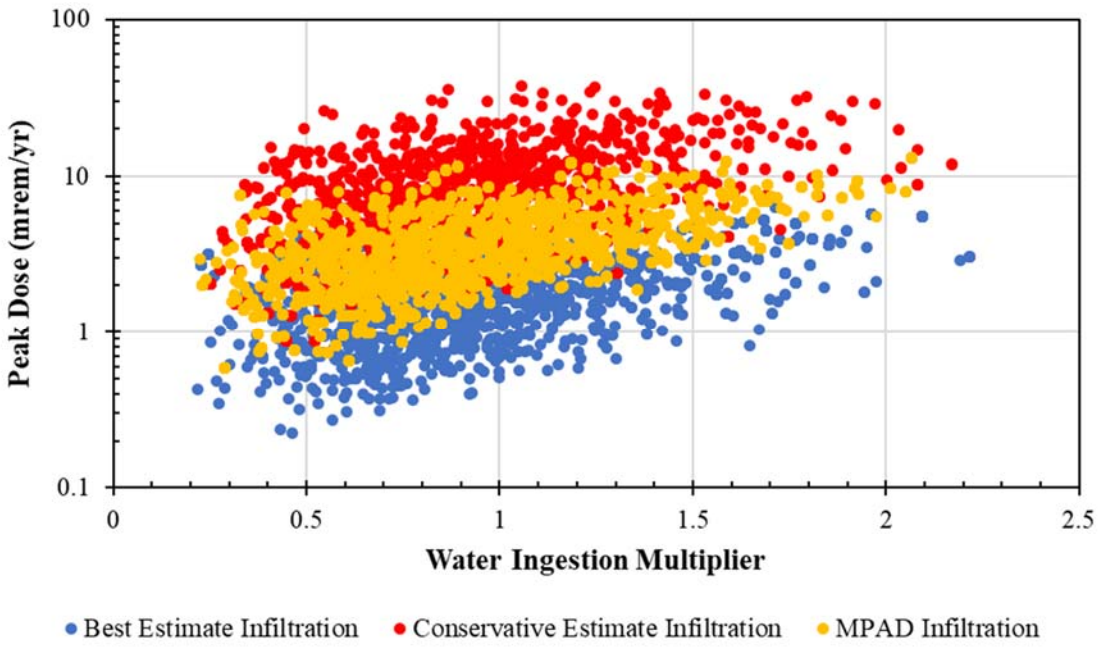

5.7.6 Summary of the SDF PA Probabilistic Sensitivity Analysis

The purpose of this section is to present general conclusions that can be made regarding the probabilistic sensitivity analyses of the SDF GoldSim Model, as presented in the previous sections. The following recurring themes appeared in these sensitivity analyses:

- The dose results range in magnitude (between the minimum and maximum doses) by approximately two orders of magnitude.
- The magnitudes of the peak doses are most strongly influenced by the infiltration rate (higher infiltration rates result in higher magnitude doses).
- The magnitude of the peak dose is also influenced by the initial saturated hydraulic conductivity of saltstone (again, higher values result in higher doses), but is less important than the infiltration rates.
- The multiplier on the rate of contaminated water ingestion also has a strong influence on the magnitude of the doses.
- The sampled garden size has an influence on the amount of contaminated produce consumed by the MOP or IHI such that larger gardens result in much greater doses via the produce ingestion dose pathway. This is attributed to a the approach used to derive the local produce fraction (see Eq. 4.4-247).
- The thicknesses of the vadose zone beneath specific SDUs has an influence on dose results. Specifically, a thin vadose zone beneath SDU 9 results in earlier and higher peak doses

during the Compliance Period (0 to 1,000 years) and a thin vadose zone beneath SDU 7 results in higher peak doses during the Performance Period (0 to 10,000 years).

- Despite I-129 being a significant dose driver, the dose results are not sensitive to any uncertainty associated with the iodine K_{ds} because all the K_d values are relatively small (i.e., very close to 0 mL/g) regardless of probabilistic sampling.

5.8 Deterministic Sensitivity Analyses

Deterministic sensitivity analyses provide insights for how varying specific parameters or modeling conditions can influence the performance of the system.

5.8.1 Central Scenario Dose Comparison

As described in Section 4.3, three sets of modeling inputs have been developed for this PA reflecting three distinct modeling philosophies:

- BE values (used to support a Realistic Case),
- MPAD values (used to support a Compliance Case), and
- CE values (used to support a Pessimistic Case).

The Compliance Case results in Section 5.5 are based on the MPAD values as described throughout Section 4.4. Table 5.8-1 summarizes some of the key differences between each of the three Central Scenario cases.

Figure 5.8-1 and Figure 5.8-2 provide a visual comparison of the dose results from each of the three Central Scenario modeling cases. These are the ground water pathways doses to the MOP at the 100-Meter well. As expected, the Pessimistic Case yields higher doses than the Compliance Case. Despite the higher dose results, the doses to the MOP remain well below the performance objective of 25 mrem/yr. However, because the doses appear to be steadily increasing over time, Figure 5.8-3 is provided to show doses over a period of time that is double the Performance Period (i.e., out to 20,000 years after SDF closure). This longer-term result shows that the Pessimistic Case peaks at approximately 16,600 years with a peak dose of 11 mrem/yr. Table 5.8-2 provides a summary of the peak doses over each of these time periods for the three Central Scenario cases.

These results demonstrate that the assumptions developed for the Compliance Case (black curves) represent a reasonable and defensible modeling approach (i.e., the assumptions in the Compliance Case result in significantly higher doses than the Realistic Case). The results from the Pessimistic Case show even when compounding multiple input assumptions all with a bias towards higher dose results, the estimated peak doses remain within the limits of the performance objectives. This provides additional confidence that uncertainties surrounding specific inputs are unlikely to result in system performance being outside the bounds of compliance.

Table 5.8-1: Key Differences Between the Central Scenario Cases

Parameter or Condition	Realistic Case	Compliance Case	Pessimistic Case	Detailed Discussion
Inventory Values	Values for future disposal were developed based on best estimates as informed by data from the Tank Farms (examples: SDF total I-129 inventory = 15.9 Ci and SDF total Tc-99 inventory = 22,400 Ci)	The best estimate values for future disposal, scaled up to reflect reasonable uncertainty assumptions (examples: SDF total I-129 inventory = 16.6 Ci and SDF total Tc-99 inventory = 33,000 Ci)	The best estimate values for future disposal, scaled up to reflect greater uncertainty assumptions (examples: SDF total I-129 inventory = 24.4 Ci and SDF total Tc-99 inventory = 35,500 Ci)	Section 3.3.3 and SRR-CWDA-2018-00041, Rev. 3
Cementitious Material Properties	In general, values were defined by the geometric mean of measured data	In general, values were defined by the arithmetic mean of measured data	In general, values were defined by the upper bounds of measured data	Section 4.3.1.2 and SRR-CWDA-2018-00004
Iodine K_d in Reducing Saltstone	Starts at 0.16 mL/g, then transitions to 2.77 mL/g	Starts at 0.07 mL/g, then transitions to 0.71 mL/g	Starts at 0.07 mL/g, then transitions to 0.71 mL/g	Section 4.3.2.1 and SRR-CWDA-2018-00045
Technetium Solubility in Reducing Saltstone	Starts at 2.0E-07 mol/L, then transitions to 7.4E-08 mol/L	Starts at 9.7E-07 mol/L, then transitions to 4.5E-07 mol/L	Starts at 9.7E-07 mol/L, then transitions to 4.5E-07 mol/L	Section 4.3.2.2 and SRR-CWDA-2018-00046
Infiltration Rates	Infiltration assumes realistic and expected future conditions	Infiltration assumes reasonable upper bound on future conditions	Assumes reasonable upper bound of future conditions plus assumes degraded GCL	Section 4.4.1 and SRR-CWDA-2018-00030
Cementitious Degradation Rates	Inputs for cementitious degradation rates based on reasonable assumptions	Inputs for cementitious degradation rates based on MPAD values	Inputs for cementitious degradation rates based on assumptions that are intentionally biased to overpredict degradation rates	Section 4.4.2 and SRNL-STI-2018-00077, Rev. 1
Reducing Capacity of Saltstone	0.65 meq e^-/g	0.50 meq e^-/g	0.35 meq e^-/g	Section 4.4.3 and SRNL-STI-2018-00586
Reducing Capacity of SDU Concrete	0.239 meq e^-/g	0.209 meq e^-/g	0.178 meq e^-/g	Section 4.4.3 and SRNL-STI-2018-00586
Pore Volume Exchanges Required for Saltstone to become Oxidizing	1,100	850	600	Section 4.4.3 and SRNL-STI-2018-00586
Human Uptake Rates (Ingestion and Inhalation)	Assumes values based on average adults (example: water ingestion = 1.23 L/day)	Assumes values based on average adults, but scaled up (where applicable) to refelect regional differences (example: water ingestion = 1.38 L/day)	Assumes values that are intentionally biased to result in higher doses (example: water ingestion = 2.0 L/day)	See Table 5.8-21

Figure 5.8-1: Dose Results from the Central Scenario Cases (Performance Period)

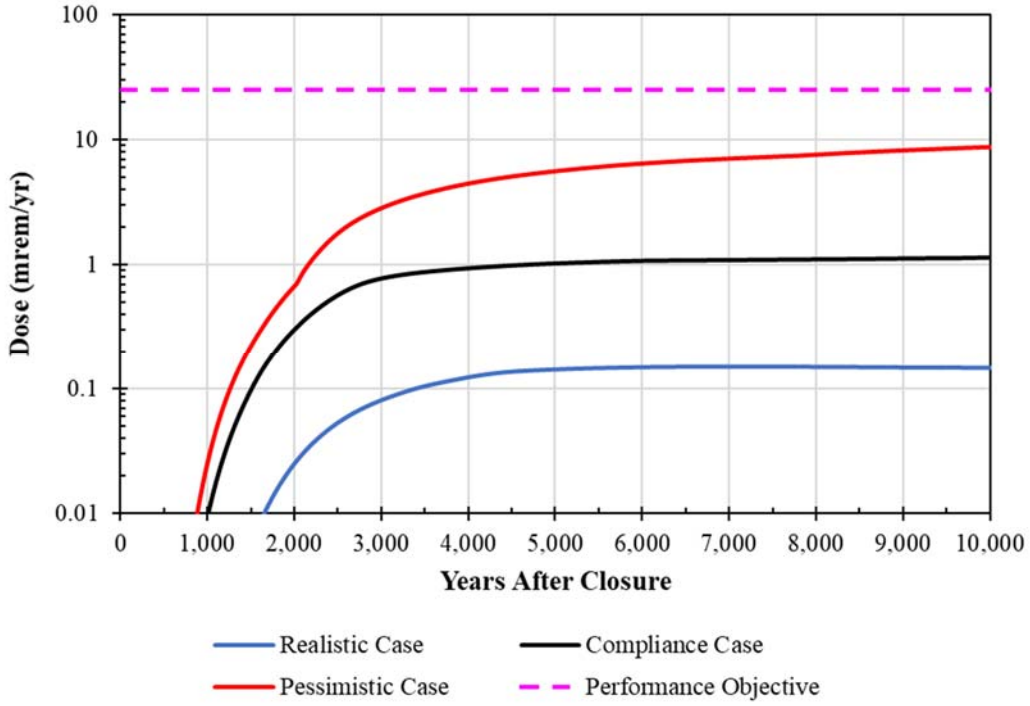

Figure 5.8-2: Dose Results from the Central Scenario Cases (Performance Period, Detail)

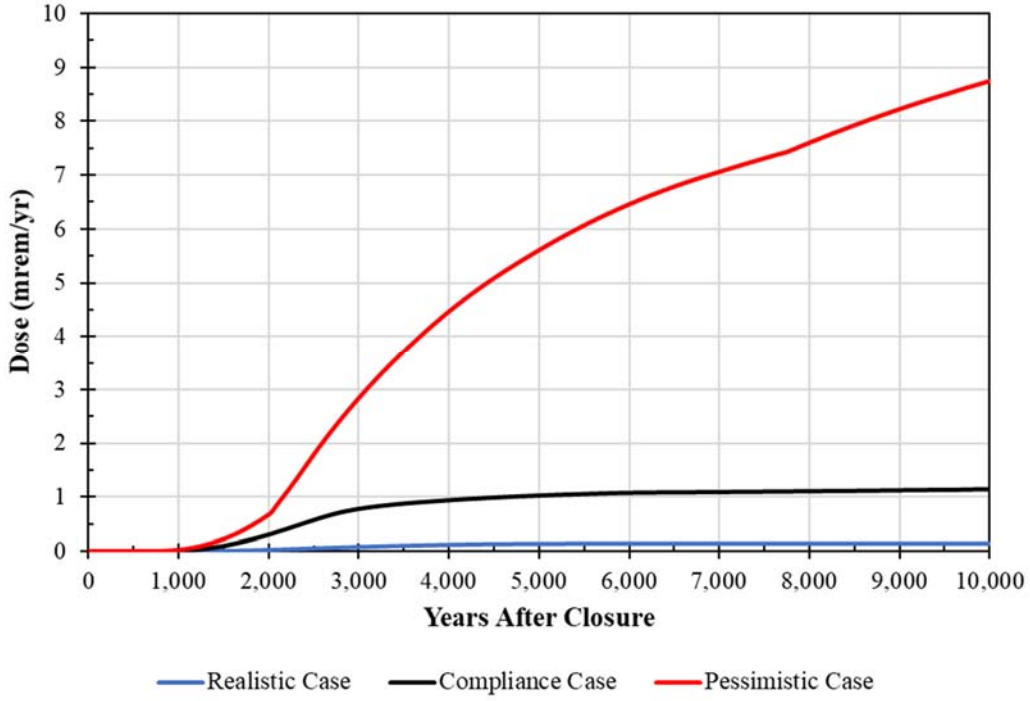

Figure 5.8-3: Dose Results from the Central Scenario Cases (Over 20,000 Years)

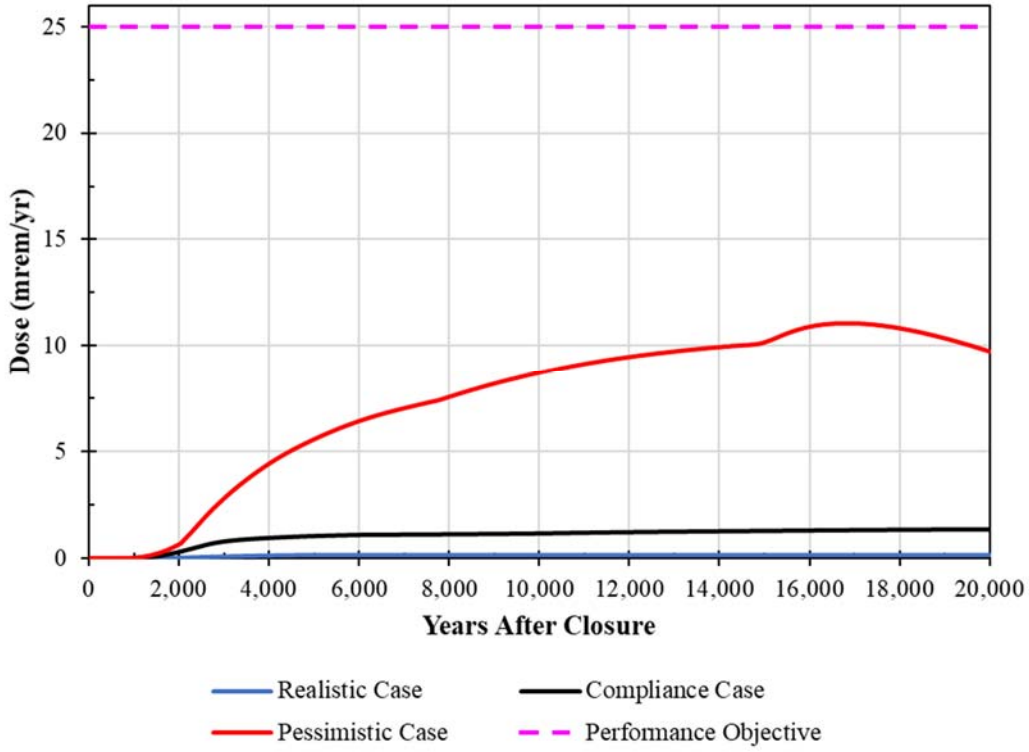

Table 5.8-2: Comparison of Central Scenario Cases, 100-Meter MOP Peak Ground Water Pathways Doses

Modeling Case	Compliance Period (0 to 1,000 Years)		Performance Period (0 to 10,000 Years)		Twice the Performance Period (0 to 20,000 Years)	
	Peak Dose (mrem/yr)	Year of Peak	Peak Dose (mrem/yr)	Year of Peak	Peak Dose (mrem/yr)	Year of Peak
Realistic Case	<0.001	1,000	0.15	7,020	0.15	7,020
Compliance Case	9.4E-03	1,000	1.2	10,000	1.3	20,000
Pessimistic Case	2.5E-02	1,000	8.7	10,000	11	16,650

A final consideration is how these three modeling cases compare to SDF GoldSim Model when using the equivalent inputs and assumptions. As described throughout Section 5.6, the SDF GoldSim Model provides relatively similar dose results to the equivalent PORFLOW modeling case when using the MPAD inputs. The largest difference in MOP dose results for the Compliance Case comparison (see Section 5.6.2.5) is that the SDF GoldSim Model produces a higher I-129 dose due to the simplification in the K_d assumptions. The comparison in Figure 5.8-4 shows that for all three Central Scenario cases, the SDF GoldSim Model provides higher doses. Inspection of the Realistic Case and Pessimistic Case results showed that, as with the Compliance Case, the largest difference was due to the higher I-129 dose contribution.

Figure 5.8-4: Comparison of Central Scenario Resulsts Using GoldSim versus PORFLOW

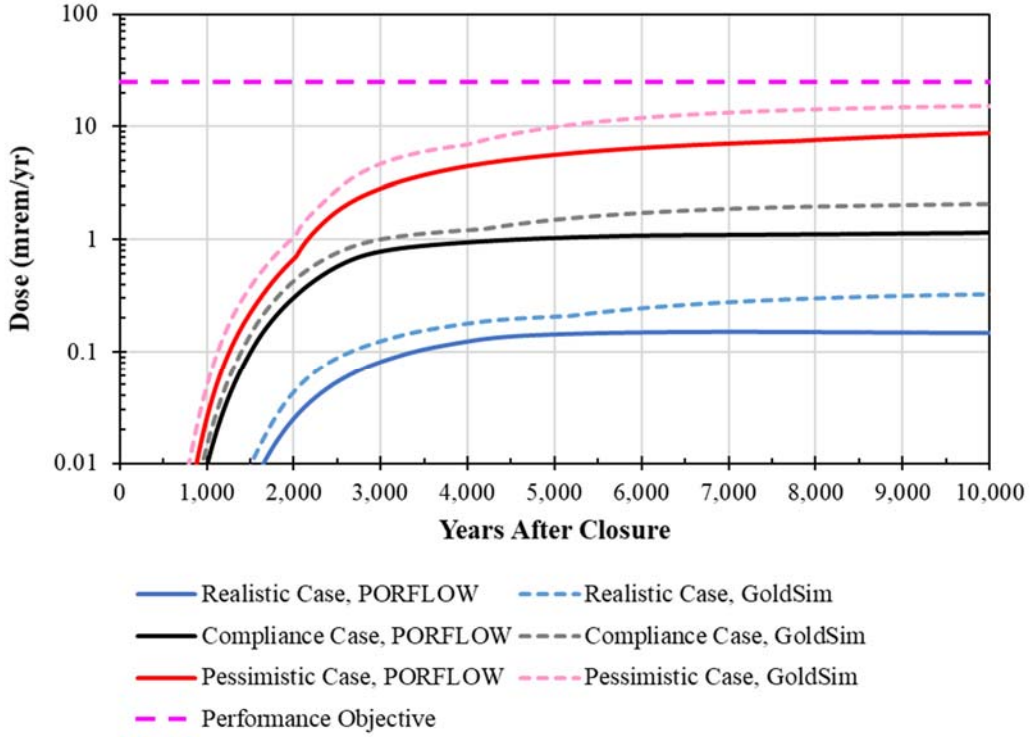

5.8.2 Closure Cap and Infiltration Rate Sensitivities

The following describes various alternative scenarios and sensitivity cases developed to better understand the uncertainties and risks that are specifically associated with the Closure Cap Model and the infiltration rates (see Section 4.4.1).

5.8.2.1 Evaluation of Central Scenario Infiltration Rates

The three Central Scenario cases are the Realistic Case, the Compliance Case, and the Pessimistic Case. These cases vary multiple parameters and conditions (see Table 5.8-1). Given these factors, assessing the relative influence of a single parameter can be challenging.

To better evaluate the influence of the infiltration rates, two alternative cases have been developed: a Low Infiltration Case and a High Infiltration Case. Both of these cases use the MPAD assumptions (as defined for the Compliance Case) for all of the inputs and settings except for the infiltration rates. For the Low Infiltration Case, the Best Estimate infiltration rates are assumed (from the Realistic Case) and for the High Infiltration Case, the Conservative Estimate infiltration rates are assumed (from the Pessimistic Case). These infiltration rates are depicted in Figure 4.4-11. In Table 4.4-82, these cases correspond to Flow Cases F09 and F45, respectively. This approach provides a more direct comparison of the influence of the assumed infiltration rates.

Figure 5.8-5 shows the resulting ground water pathways doses for these infiltration rate sensitivity cases. Table 5.8-3 summarizes the resulting peak doses.

Table 5.8-3: Comparison of Infiltration Rate Sensitivity Cases, 100-Meter MOP Peak Ground Water Pathways Doses

Modeling Case	Infiltration Rate	Compliance Period (0 to 1,000 Years)		Performance Period (0 to 10,000 Years)	
		Peak Dose (mrem/yr)	Year of Peak	Peak Dose (mrem/yr)	Year of Peak
Realistic Case	Best Estimate	<0.001	1,000	0.15	7,020
Compliance Case	Best Estimate	3.9E-03	1,000	0.62	5,030
	MPAD	9.4E-03	1,000	1.2	10,000
	Conservative Estimate	9.4E-03	1,000	2.0	10,000
Pessimistic Case	Conservative Estimate	2.5E-02	1,000	8.7	10,000

Figure 5.8-5: Dose Results from the Infiltration Rate Sensitivity Cases (Detail)

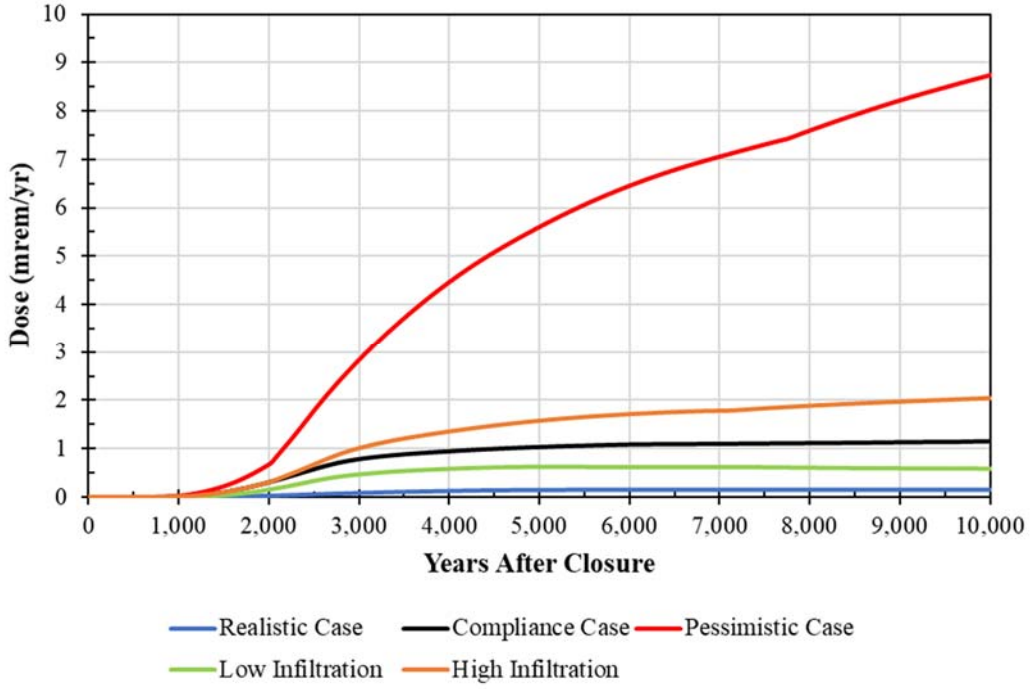

Within the Performance Period, assuming the lower infiltration rate for the Compliance Case results in a peak dose of 0.62 mrem/yr while assuming the higher infiltration rate for the Compliance Case results in a peak dose of 2.0 mrem/yr. As expected, these results are bounded by the doses from the Realistic Case and the Pessimistic Case.

5.8.2.2 Evaluation of Infiltration Rates from HELP Estimates (2008)

All three of the infiltration rates assumed for this PA (see Table 4.4-5) are considerably lower than earlier estimates. Specifically, prior to this PA the modeled infiltration rates were based on inputs developed in 2008 to support the 2009 SDF PA. The modeling performed to estimate these earlier infiltration rates was performed using the Hydrologic Evaluation of Landfill Performance (HELP) Model, software developed for the EPA. [WSRC-STI-2008-00244, SRR-CWDA-2009-00017]

As described in Section 4.4.1, the 2008 SDF HELP Model relied on different assumptions. In *Predicting Long-Term Percolation from the SDF Closure Cap* (SRRA107772-000009), Benson and Benavides explain that an improved understanding of closure cap performance has been developed based on real world observations. Given this improved understanding, some of the assumptions from the 2008 HELP Model are now considered unrealistic; thus, the Closure Cap Model for the SDF was updated (described in Section 4.4.1) and the resulting infiltration rates are lower.

Despite the lack of realism in the assumptions used for the 2008 HELP Model, understanding the relative impact from these infiltration rates can provide additional insights with respect to the risks associated with the closure cap performance. Figure 5.8-6 shows dose results from a modeling case that uses all of the same inputs and assumptions as the Compliance Case, but replaces the infiltration rates with values from the 2008 HELP Model. As expected, the higher infiltration rates result in earlier releases and higher peak doses relative to the Compliance Case. Within the Compliance Period (first 1,000 years), a peak dose of approximately 1.8 mrem/yr occurs at 1,000 years after SDF closure. Within the Performance Period (first 10,000 years), a peak dose of 12 mrem/yr occurs at approximately 2,000 years after SDF closure.

This peak dose corresponds to the degradation of the SDU concrete and the initial transport properties of I-129 and Tc-99, which promote greater mobility. As part of the shrinking core model described in Section 4.4.5, as the chemical environment in saltstone evolves, the K_d for iodine in saltstone increases by an order of magnitude (Table 4.3-7) and the solubility of technetium drops in half (see Table 4.3-8). As such, once the initial releases of I-129 and Tc-99 have occurred, the respective release rates for I-129 and Tc-99 diminish. By 10,000 years, the total dose is approximately 3.0 mrem/yr.

As part of this current PA, multiple modeling assumptions, approaches, and input values have been updated beyond just the infiltration rates. The *FY2016 Special Analysis for the Saltstone Disposal Facility at the Savannah River Site* (FY2016 SDF SA) provides the dose results from previous modeling. [SRR-CWDA-2016-00072] Comparing the FY2016 SDF SA doses against the doses shown in Figure 5.8-6 helps to illustrate the overall extent of these modeling changes.

Figure 5.8-6: Dose Results from Assuming the 2008 (SDF HELP Model) Infiltration Rates

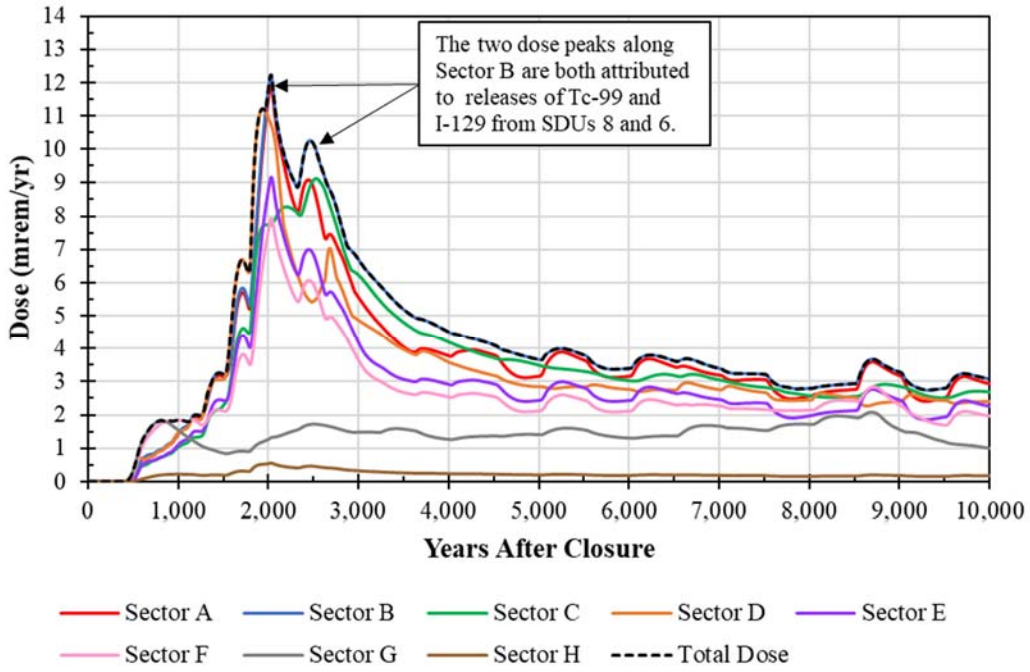

Figure 5.8-7 provides a comparison of the ground water pathways doses to the MOP at the 100-Meter well from:

1. The current Compliance Case (black curve) which assumes the MPAD infiltration rates as described in Section 4.4.1,
2. The modified Compliance Case (purple curve), as depicted in Figure 5.8-7 which assumes the infiltration rates from the 2008 HELP Model, and
3. The Evaluation Case from the FY2016 SDF SA (gray curve) which assumes the infiltration rates from the 2008 HELP Model and relied on earlier modeling assumptions, approaches, and input values.

Comparing the purple curve to the gray curve shows the relative impact from all the modeling changes excluding infiltration. Despite the earlier timing, this figure shows that if the infiltration rates had not been updated the peak dose within 10,000 years would coincidentally be similar in magnitude to the peak dose from the FY2016 SDF SA.

Figure 5.8-7: Dose Comparison for Evaluating the 2008 (HELP Model) Infiltration Rates

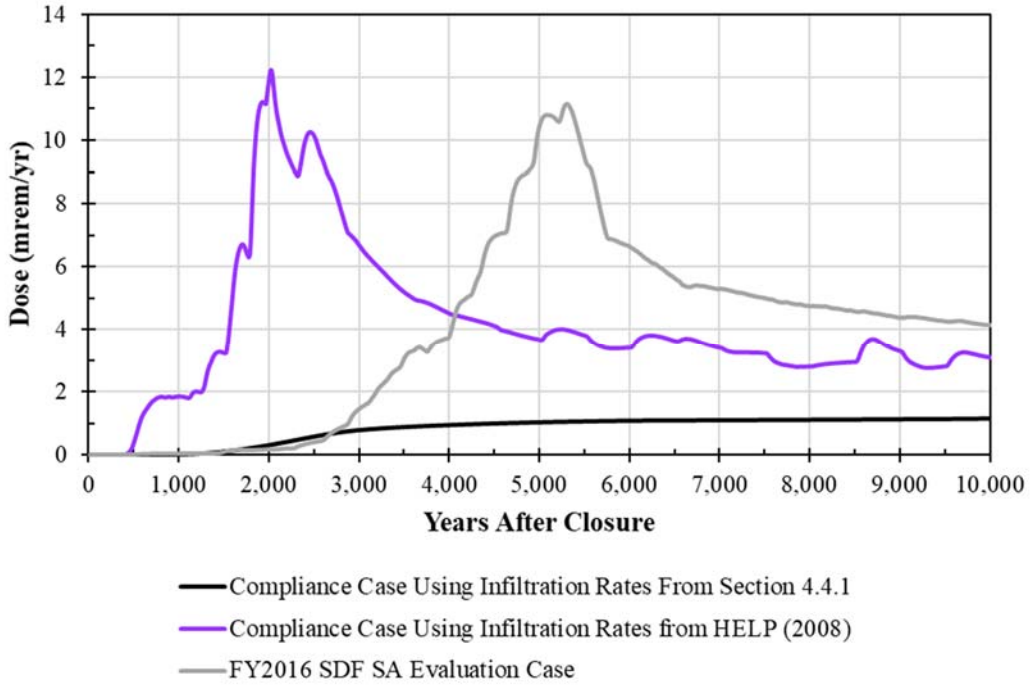

5.8.2.3 Evaluation of Alternative Infiltration Rate Based on Disappearing HDPE

The most significant difference between the 2008 HELP Model for estimating infiltration and the updated Closure Cap Model (see Section 4.4.1) is the conceptualization of the HDPE performance. In the 2008 HELP Model (WSRC-STI-2008-00244), it was assumed that HDPE holes are generated in response to embrittlement of the material after oxidation, and that the roots of pine trees would gradually penetrate through these holes, then the roots would grow, expanding the hole size, followed by decomposition of dead tree roots. As a result, the HDPE is simulated as being an ineffective barrier to flow by approximately 5,400 years after closure.

The updated closure cap model does assume that the HDPE will undergo antioxidant depletion, albeit at a slower rate than previously assumed based on recent studies; however, it is not assumed that new holes will form or that roots will penetrate through the holes. Although HDPE may become embrittled, it is not realistic for new holes to be spontaneously generated without additional external forces. The HDPE is expected to remain under constant pressure beneath a minimum of six feet of soil or earthen materials. This constant pressure is expected to provide physical stability that will prevent new holes from forming. Further, because vegetation is opportunistic (i.e., rooting structures develop by seeking out water sources that require the least amount of energy to extract) any holes that do form are unlikely to be influenced by root growth. In the unlikely event that new holes do form through the HDPE, the GCL is still expected to perform as a barrier to limit infiltration.

Existing holes (i.e., installation defects) in the HDPE are assumed to grow larger as a result of antioxidant depletion, but otherwise the HDPE is expected to remain essentially intact indefinitely. This is reasonable because the material is not expected to dissolve or otherwise cease to exist. Regardless, an alternative infiltration model has been designed to test the risk-significance of this conceptualization. For this alternative infiltration model, the performance of the closure cap is assumed to be completely dependent upon the stress crack resistance of the HDPE and applied by using the following assumptions:

- The initial infiltration rate was set to 0.13 mm/yr.
  - This is equivalent to the end state for the Compliance Case. Essentially, as a starting point, the primary degradation mechanisms from the Compliance Case (i.e., the decrease in the saturated hydraulic conductivity of the sand drainage layer at 500 years and the increase in sizes of the HDPE holes at 2,000 years) are both assumed to occur at time = 0 years.
- At 750 years, HDPE is assumed to begin losing stress crack resistance.
  - This start time is based on *Antioxidant Depletion and Service Life Prediction for HDPE Geomembranes Exposed to Low-Level Radioactive Waste Leachate* (DOI: 10.1061/(ASCE)GT.1943-5606.0001643), which predicted a minimum antioxidant depletion time of 730 years, followed by a minimum induction time of 25 years; therefore, HDPE degradation (i.e., the loss of stress crack resistance) begins at approximately 750 years (see Section 4.4.1.3.6).
- At 3,200 years, the HDPE is assumed to have lost all stress crack resistance.
  - This end time is based on *Antioxidant Depletion and Service Life Prediction for HDPE Geomembranes Exposed to Low-Level Radioactive Waste Leachate* (DOI: 10.1061/(ASCE)GT.1943-5606.0001643), which predicted 50% of stress crack resistance is lost at approximately 2,000 years (see Section 4.4.1.3.6). Based on this 50% loss of stress crack resistance from 750 years to 2,000 years, extrapolating values to 100% indicates that by approximately 3,200 the HDPE could lose 100% of stress crack resistance.
- Once all stress crack resistance is lost, the infiltration rate is assumed to be 269 mm/yr (10.6 in/yr)
  - This final condition is based on the end state from the 2008 HELP Model.
- Between 750 years and 3,200 years, the infiltration rate is assumed to increase linearly over time.
  - Note that while this assumed rate of change in the infiltration rate is similar to the rate of change from the 2008 HELP Model (WSRC-STI-2008-00244), the 2008 HELP Model was based on a series of complex assumptions about hole formation due to tree root penetrations, while this new alternative infiltration rate is based on a simple assumption that the rate of change is constant between the assumed starting and ending times.

The resulting infiltration rate is very similar to the infiltration rate for the 2008 HELP Model (Figure 5.8-8), with a higher initial value and a delay in the onset of degradation. This alternative infiltration rate is always higher than the Compliance Case rates; after the

first 1,500 years of the simulation, the alternative infiltration rate is more than three orders of magnitude higher.

Figure 5.8-8: Comparison of Alternative Infiltration Rate, 2008 (SDF HELP Model) Infiltration Rate, and the Compliance Case Infiltration Rate

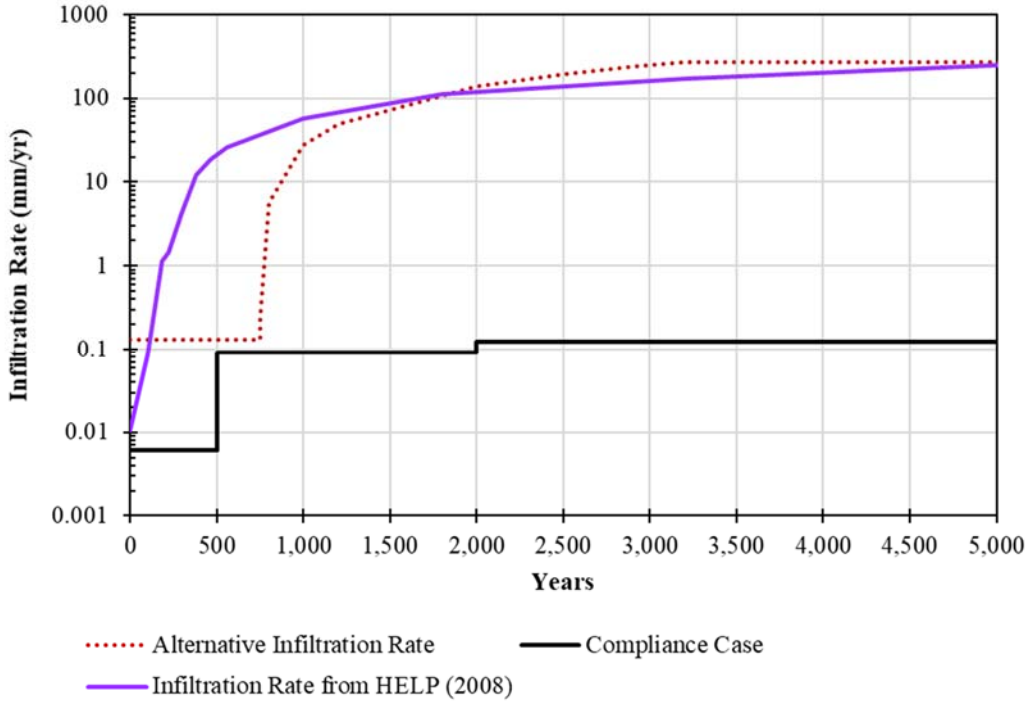

Three sensitivity cases have been developed using this alternative infiltration rate:

- The first sensitivity case (*Alternative Infiltration Case*) is completely identical to the Compliance Case with the exception of the infiltration rate.
- The second sensitivity case (*Alternative Infiltration Case w Ksat = 2.0E-09 cm/s*) is identical to the first sensitivity case but assumes a higher initial saturated hydraulic conductivity for saltstone (2.0E-09 cm/s as opposed to the Compliance Case value of 5.0E-10 cm/s).
- Finally, the third sensitivity case (*Alternative Infiltration Case w Ksat = 2.0E-09 cm/s and More HDPE Credit*) is identical to the second sensitivity case but with modifications to the rate of HDPE degradation at the SDU roof. Instead of assuming that the HDPE at the SDU roof is fully degraded at 3,200 years after closure, it is assumed to take 4,500 years for the HDPE to fully degrade, and instead of assuming that the fully degraded HDPE has backfill properties, clay properties are assumed. This third sensitivity case was designed to provide a more realistic evaluation because it is reasonable to expect that the HDPE at the SDU roof would degrade more slowly than the HDPE within the closure cap (because the HDPE at the SDU roof is buried more deeply).

Regardless, because the composite barrier is a function of the HDPE and the GCL layers, and because the GCL properties control the degraded conditions, the second and third sensitivity cases both have nearly identical material properties once the HDPE is fully degraded (Figure 5.8-9).

Figure 5.8-9: Degradation of the Composite Barrier Based on HDPE Assumptions for Selected Sensitivity Cases Using Alternative Infiltration Rates

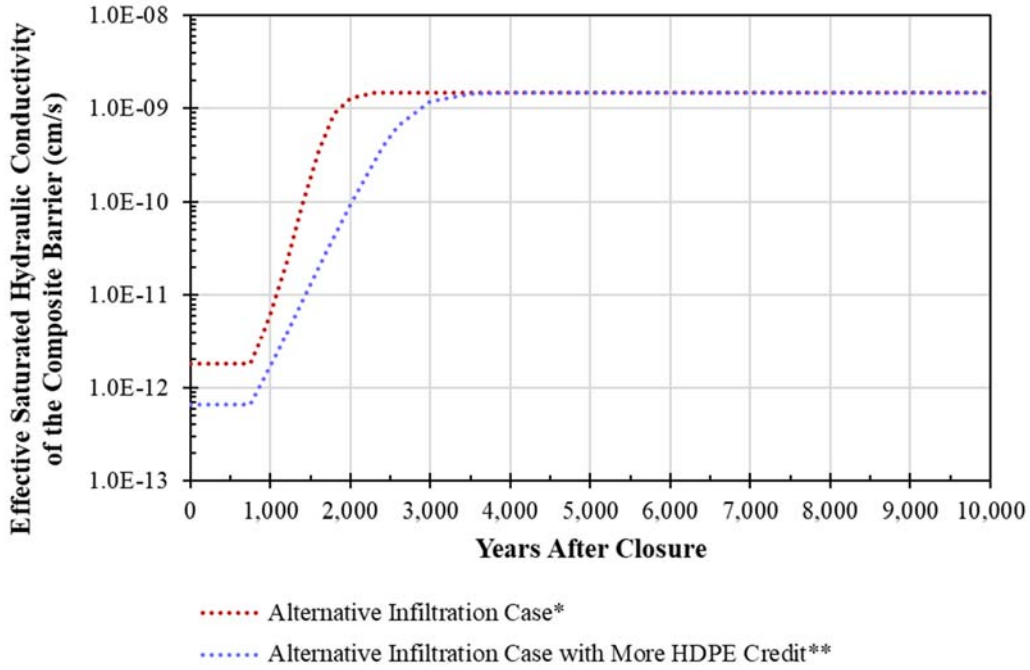

Notes: * This assumed HDPE degradation is applied to the *Alternative Infiltration Case* and the *Alternative Infiltration Case w Ksat = 2.0E-09 cm/s*.

** This assumed HDPE degradation is applied to the *Alternative Infiltration Case w Ksat = 2.0E-09 cm/s and More HDPE Credit*.

The dose results for the three sensitivity cases are shown with dotted curves in Figure 5.8-10, along with the Compliance Case (black curve) and a sensitivity case that uses all of the same assumptions as the Compliance Case but applies the infiltration rate from the Jones and Phifer 2008 HELP Model (WSRC-STI-2008-00244) (purple curve). All of these modeling cases meet performance objectives.

While assuming higher infiltration rates does increase the peak doses, the increase is not three orders of magnitude as might be expected based on the increased infiltration rate. This indicates that the dose increases do not have a direct one-to-one relationship with the magnitudes of the increases to the infiltration rates. The Alternative Infiltration Case and the Compliance Case Using Infiltration Rates from HELP (2008) both show very similar results; similarly, the Alternative Infiltration Case w Ksat = 2.0E-09 cm/s and the Alternative Infiltration Case w Ksat = 2.0E-09 cm/s and More HDPE Credit are also very similar. These comparisons indicate that under extremely high infiltration rates, the general shape and magnitude of the dose curves are controlled by the initial saturated hydraulic conductivity of saltstone and the inventories within saltstone. This insight

should be considered when making future decisions related to SDF operations (e.g., changes to WAC limits).

Figure 5.8-10: Comparison of Dose Results for Selected Sensitivity Cases Using Alternative Infiltration Rates

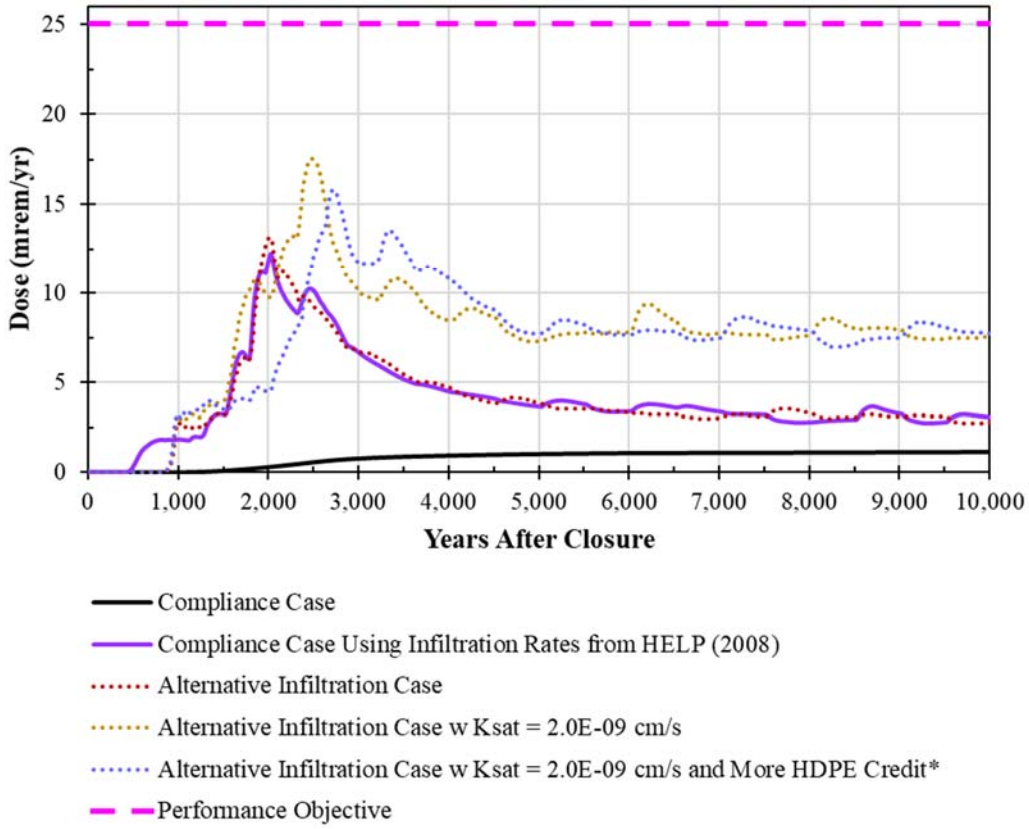

5.8.2.4 Evaluation of Soil-Only Closure Cap

The "No Closure Cap" scenario described in Section 4.6.5 was designed to non-mechanistically address the potential impacts from eight specific FEPs (SRR-CWDA-2018-00006):

- FEP 2.6.07, Erosion and Weathering;
- FEP 2.6.11, Mass Wasting;
- FEP 2.6.14, Closure Cap Performance (Differential Settlement);
- FEP 2.7.03, Cold Weather Effects;
- FEP 3.2.08, Discrete Capping of Disposal Units;
- FEP 3.8.06, Incomplete Closure;
- FEP 6.1.04, Excavating and Mining Activities; and
- FEP 6.1.06, Animal/Plant Intrusion.

The design of the closure cap has not yet been finalized; however, some form of protection for the SDUs is planned and should be expected. Regardless, because disposal at the SDF is permitted by the state as a Class Three Landfill (Permit #025500-1603), it must meet the

requirements for a Class Three Landfill as specified in SCDHEC R.61-107.19, *SWM: Solid Waste Landfills and Structural Fill*. Specifically, SCDHEC R.61-107.19, Section 258.60 specifies that a final cover system will be emplaced to minimize infiltration, with a permeability no greater than 1.0E-05 cm/s, must be at least 18 inches of earthen material, and must include an erosion control barrier.

Accordingly, the no closure cap scenario described in Section 4.6.5 is unrealistic and would provide little insight into the actual risks associated with the future performance of the system. As such, for modeling purposes, rather than simulating the system with no closure cap, a soil-only closure cap scenario is considered as a viable alternative for consideration.

This scenario is not as explicit as a no closure cap scenario with respect to addressing the effects of the FEPs listed. Table 5.8-4 lists each of the above FEPs and provides additional discussion of how these are considered or addressed via the soil-only closure cap scenario.

Table 5.8-4: FEPs Addressed via the Soil-Only Closure Cap Scenario

FEP ID	FEP Name	Discussion
2.6.07	Erosion and Weathering	Construction of a closure cap with a design that is functionally equivalent to the cap described in Section 3.2.6 is the expected final closure configuration for the SDF. Should erosion, weathering, or even mass wasting occur, it is not expected to occur on such a scale as to completely negate the performance of the closure cap. Instead, the performance of the closure cap would be partially compromised. As such, a soil-only closure cap provides a reasonable approximation for evaluating risks associated with this FEP.
2.6.11	Mass Wasting	See discussion associated with FEP 2.6.07 (above).
2.6.14	Closure Cap Performance (Differential Settlement)	All void spaces within the SDUs are expected to be filled prior to the installation of the closure cap. If any void space remains, it is expected to be negligible (although the risks associated with a collapsed roof are addressed in Section 5.8.9.3). Similarly, backfill will be used to surround the SDUs and provide support for the overlying closure cap. The backfill will be control-compacted to minimize settlement. As described in Section 3.1.4, the potential for settlement has been analyzed for extreme conditions and is expected to be less than 0.75 in to 1.25 in (depending upon the SDU). Given the geometry of each SDU, this amount of settlement is not expected to significantly influence the performance of the closure cap. Therefore, a soil-only closure cap provides a bounding approximation for evaluating risks associated with this FEP.
2.7.03	Cold Weather Effects	Because the SDUs will be buried beneath the closure cap, cold weather is not expected to impact the performance of the system. Regardless, an additional soil-only scenario has been developed which non-mechanistically accelerated the cementitious degradation rates. For this alternative scenario, the soil-only closure cap has been coupled with cementitious material properties that are assumed to degrade at a rate that is twice as fast as in the Compliance Case. It is assumed that this soil-only closure cap + accelerated degradation scenario provides a bounding approximation for evaluating actual risks associated with this FEP.

FEP ID	FEP Name	Discussion
3.2.08	Discrete Capping of Disposal Units	Each SDU is expected to be covered with the fully engineered closure cap that is functionally equivalent to the cap described in Section 3.2.6. Should the design change during the installation of the closure cap, the modified design is assumed to perform at least as well as the soil-only closure cap. Therefore, the soil-only closure cap scenario provides a bounding approximation for evaluating risks associated with this FEP.
3.8.06	Incomplete Closure	See discussion associated with FEP 3.2.08 (above).
6.1.04	Excavating and Mining Activities	The soil-only closure cap provides a non-mechanistic approach for evaluating the potential impacts from partial excavation of the closure cap.
6.1.06	Animal/Plant Intrusion	Construction of a closure cap with a design that is functionally equivalent to the cap described in Section 3.2.6 is the expected final closure configuration for the SDF. The various layers of the design are assumed to be adequate for mitigating the effects of animal and plant intrusions. Regardless, this soil-only scenario has been developed which non-mechanistically accelerated the cementitious degradation rates. For this alternative scenario, the soil-only closure cap has been coupled with cementitious material properties that are assumed to degrade at a rate that is twice as fast as in the Compliance Case. It is assumed that this soil-only closure cap + accelerated degradation scenario provides a reasonable approximation for evaluating risks associated with this FEP.

While the no closure cap scenario is unrealistic, it is noted that if no closure cap is constructed over the SDUs, the roof slope and walls would still divert nearly all incoming precipitation away from the saltstone waste form (at least until the SDU concrete is sufficiently degraded). This unrealistic scenario also has the potential for bimodal transport in which some fraction of the released contaminants may be transported via surface runoff while the remaining fraction would infiltrate into the vadose zone. This has the potential to reduce the magnitude of the peak doses depending upon the specific fractions directed along each mode of transport and upon the exposure-pathways considered.

Based on the discussions in Table 5.8-4, three modeling cases have been developed for the soil-only closure cap scenario: one that is identical to the Compliance Case except for the increased infiltration rate, one that is identical to the first case but also non-mechanistically assumes the degradation of cementitious materials occurs twice as fast, and one that is identical to the first case but also assumes that the initial saturated hydraulic conductivity of saltstone is 2.0E-09 cm/s (as opposed to the 5.0E-10 cm/s used for the Compliance Case).

These soil-only closure cap cases all assume a constant infiltration rate of 417.8 mm/yr (16.45 in/yr). This value is based on Section 6.7.3 of *Saltstone Disposal Facility Closure Cap Concept and Infiltration Estimates* (WSRC-STI-2008-00244), which states, "[t]he infiltration rate through a closure cap without the composite hydraulic barrier, lateral drainage layer, and erosion control layer of 16.45 in/yr can be used to represent the infiltration rate at complete failure of the closure cap." This value is consistent with the 400 mm/yr estimate for "deep drainage," or percolation rate, as calculated in *Predicting Long-Term Percolation from the SDF Closure Cap* (SRRA107772-000009) (see Table 4.4-3).

Figure 5.8-11 shows the dose results from the modeling case that uses all the same inputs and assumptions as the Compliance Case but replaces the infiltration rate with a constant value of 417.8 mm/yr (16.45 in/yr). Figure 5.8-12 and Figure 5.8-13 show similar dose results from the modeling cases that use all the same inputs and assumptions as the Compliance Case but replaces the infiltration rate with a constant value of 417.8 mm/yr (16.45 in/yr) and makes one additional change: the modeling case shown in Figure 5.8-12 assumes that the degradation rates for all cementitious materials are twice as fast as the rates described in Section 4.4.2, while the modeling case shown in Figure 5.8-13 assumes the initial saturated hydraulic conductivity of saltstone is 2.0E-09 cm/s (as opposed to the Compliance Case value of 5.0E-10 cm/s).

Figure 5.8-14 shows a dose comparison for these soil-only closure cap cases. As expected, the higher infiltration rates applied to these sensitivity cases all result in earlier releases with higher peak doses relative to the Compliance Case.

Figure 5.8-11: Dose Results from Assuming a Soil-Only Closure Cap

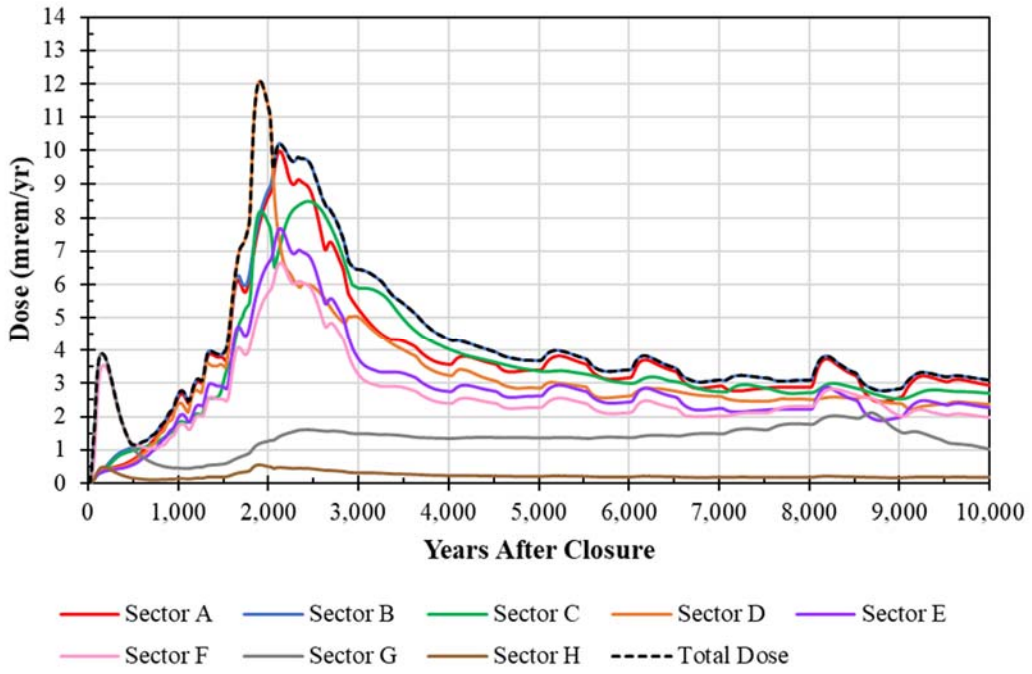

Figure 5.8-12: Dose Results from Assuming a Soil-Only Closure Cap with Accelerated (×2) Cementitious Degradation Rates

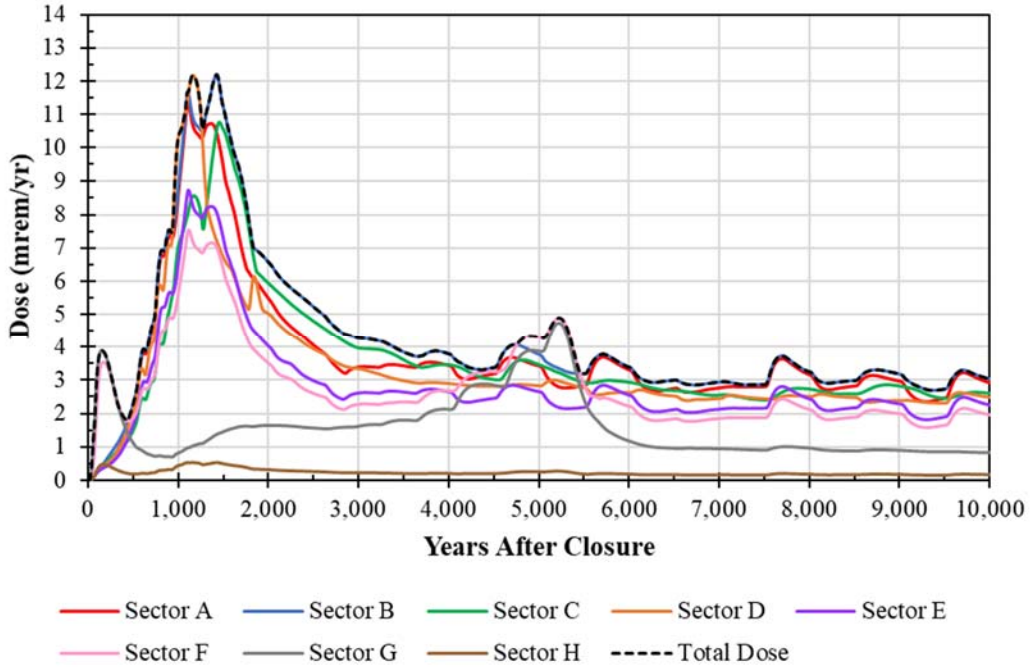

Figure 5.8-13: Dose Results from Assuming a Soil-Only Closure Cap and 2.0E-09 cm/s for the Initial Saturated Hydraulic Conductivity of Saltstone

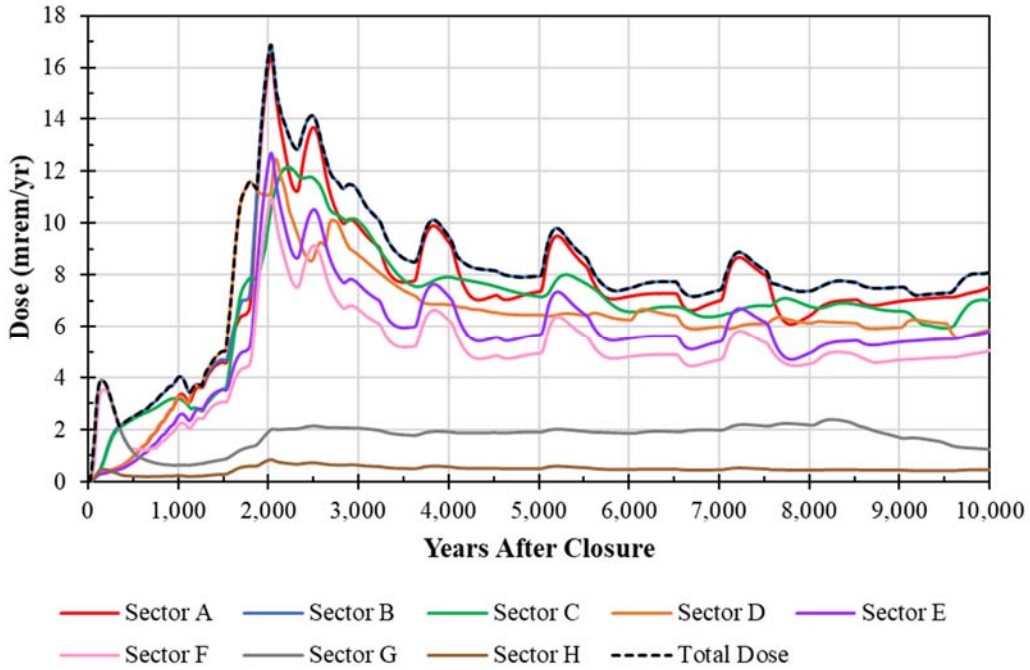

Figure 5.8-14: Dose Comparison for Evaluating the Soil-Only Closure Cap Cases

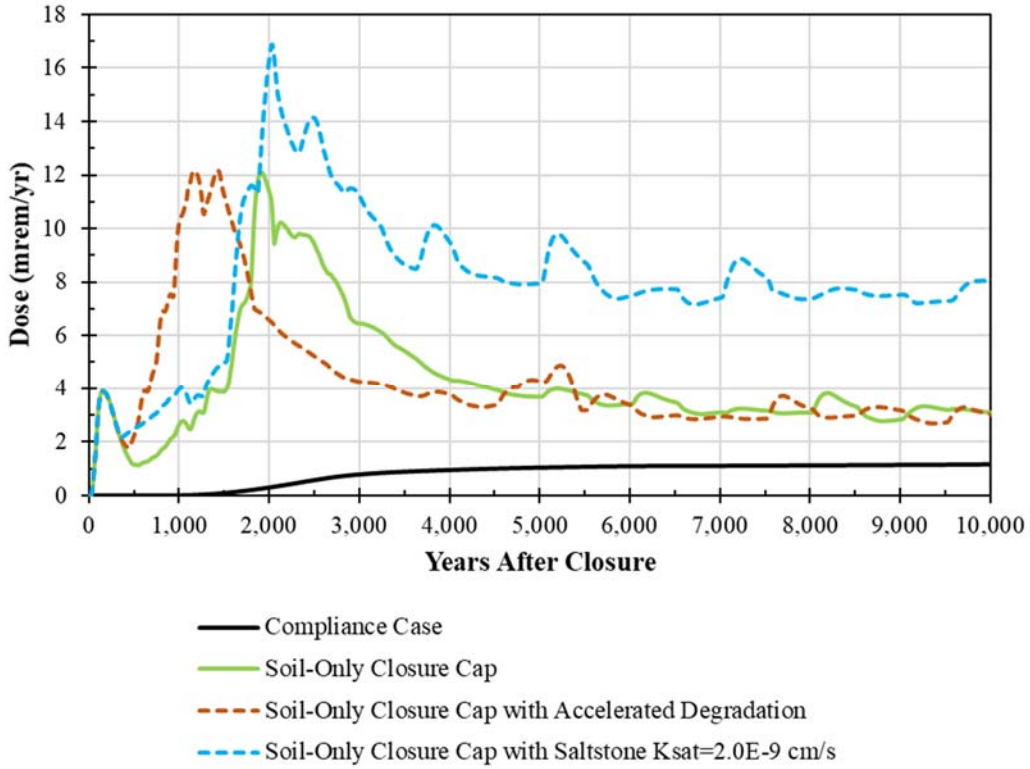

Within the Compliance Period (first 1,000 years), all three of the soil-only closure cap cases have an initial dose peak of approximately 4 mrem/yr near 150 years after SDF closure. This early peak is attributed to I-129 releases from SDUs 1 and 4 because these SDUs are assumed to have initially degraded walls (see Section 4.3.1.2).

Within the Performance Period (first 10,000 years), the soil-only closure cap case (solid green curve in Figure 5.8-14) and the case with accelerated degradation (brown dashed curve in Figure 5.8-14) both have peak doses of approximately 12 mrem/yr but with different timing (i.e., the timing of the doses from the accelerated degradation case is early enough that it impacts the 1,000-year Compliance Period). This dose peak is dominated by Tc-99 releases from the 375-foot diameter SDUs.

The soil-only closure cap case and the case with the higher initial saturated hydraulic conductivity (blue dashed curve in Figure 5.8-14) both show peaks near 2,000 years after SDF closure, but with different magnitudes. Although these peak doses are higher than the Compliance Case (black curve), they all meet the performance objectives.

Relative to the soil-only closure cap case, applying accelerated cementitious degradation rates has no impact on the magnitude of the doses, but results in an earlier dose peak. Alternatively, the increased initial saturated hydraulic conductivity has no impact on the timing of the dose peak (relative to the soil-only case) but results in a higher magnitude dose. These observations are consistent with the observation at the end of Section 5.8.2.3:

under extremely high infiltration rates, the general shape and magnitude of the dose curves are controlled by the initial saturated hydraulic conductivity of saltstone and the inventories within saltstone.

Although these results meet the performance objectives, the margin of error between the peak doses and the performance objective is limited. Given the multiple uncertainties associated with this complex system, a robust, multi-layered engineered closure cap is appropriate to provide confidence in the long-term performance of the system, assuming appropriate quality control during closure cap installation. As such, a soil-only closure cap does not reflect a realistic future condition. Any significant deviations from the current design would require additional evaluation via appropriate change control processes (e.g., Unreviewed Waste Management Question (UWMQ) Evaluation, Special Analysis, PA revision, or equivalent process).

5.8.2.5 Evaluation of Closure Cap Extent

The Vadose Zone Flow Model described in Section 4.4.4 applies a flux, or infiltration rate, along the top boundary of the vadose zone model domain. This flux is based on the results of the Closure Cap Model (Section 4.4.1.4). As a model simplification, the same flux value (from Table 4.4-5) is applied uniformly across the entire top boundary of the Vadose Zone Flow Model, effectively assuming that the engineered closure cap extends for an infinite distance beyond the edges of the SDUs; however, the designed closure cap extends a finite distance from the edges of the SDUs. Figure 4.4-2 shows that the top surface of the closure cap will extend a minimum of 50 feet from the edges of the SDUs.

While the 50-foot extent was defined as a minimum value for the top of the closure cap, a close examination of the closure cap cross sections (Figure 3.2-30 and Figure 3.2-31) show that this composite barrier typically extends much further than 50 feet and that the minimum extent of the composite barrier is approximately 75 feet. Because the flux is based on the leakage rate through this composite barrier (i.e., the HDPE and GCL layers above the lower backfill layer), this minimum extent of 75 feet beyond the edges of the SDUs provides a reasonable representation for evaluation purposes.

To evaluate the potential impacts from edge effects associated with the horizontal extent of the closure cap cover, the modeled Compliance Case conditions were modified to develop three sensitivity cases. For all three sensitivity cases, modified fluxes are applied to every SDU except for SDU 6. For SDU 6, the Compliance Case conditions are assumed because SDU 6 is surrounded by other SDUs such that it will not be impacted by edge effects.

The first two sensitivity cases (75-ft Cover Extent and 50-ft Cover Extent) apply two "zones" for defining the flux along the top boundary of the Vadose Zone Flow Model. The first zone represents the portion of the model beneath the composite barrier of the closure cap and applies the same flux as the Compliance Case. The second zone represents the portion of the model at the edge of the composite barrier of the closure cap. For this evaluation, the flux beyond the edge of the composite barrier is assumed to be 650

mm/yr; this value is higher than the natural recharge rates in the GSA, which are estimated to be between 10 in/yr (250 mm/yr) and 16 in/yr (410 mm/yr), as summarized in *Groundwater Flow Simulation of the Savannah River Site General Separations Area*. [SRNL-STI-2017-00008, Rev. 1] . The higher value is assumed to account for water that has been diverted laterally through the upper sand drainage layer. The only difference between these first two cases is the lateral extent assumed for the cover (75 feet versus 50 feet beyond each SDU).

Finally, the third sensitivity case (Retreating Cap Case) was developed as an alternative conceptual model. For this case, it is assumed that the riprap along the side slope of the closure cap fails and gradual erosion occurs along the side slope as an advancing front, and that this gradual erosion results in complete failure of the HDPE and GCL materials in the composite barrier beneath the upper sand drainage layer.

For the Retreating Cap Case, the initial conditions are the same as the 75-ft Cover Extent Case. After 100 years (i.e., the end of the Institutional Control Period), erosion of the side slope is simulated by gradually decreasing the extent of the composite barrier over time until it is completely gone. The initial flux beneath the cover is set at 0.13 mm/yr (the maximum Compliance Case value from Table 4.4-5), while the flux beyond the cover is dynamic, changing over time: it starts at 650 mm/yr (when the cover extent is 75 feet beyond the edge of the SDU), then decreases linearly to 417.8 mm/yr (once the composite barrier is completely gone). This value of 417.8 mm/yr (16.45 in/yr) is based on WSRC-STI-2008-00244, which states that an "infiltration rate through a closure cap without the composite hydraulic barrier, lateral drainage layer, and erosion control layer of 16.45 in/yr can be used to represent the infiltration rate at complete failure of the closure cap."

The rate of retreat for the composite barrier in the Retreating Cap Case is assumed to be 0.34 in/yr. This is based on modifying the inputs used in the Revised Universal Soil Loss Equation (RUSLE), Eq. 4.4-9. The modified inputs and the basis of the values used are provided in Table 5.8-5.

Before presenting the results of these sensitivity cases, it should be noted that the Vadose Zone Flow Models developed for the SDF PA are computationally efficient in that they take advantage of the symmetry in the design of the SDUs. This means that instead of simulating a full SDU, the models simulate a two-dimensional "slice" (from the center of the SDUs to 75 feet beyond the SDU walls), then extrapolates those results to generate the three-dimensional equivalent. Due to this modeling approach, the modified cover extent simulated by these sensitivity cases is applied around the entire perimeter of each SDU. This approach overestimates the potential impacts from the cover extent because, as shown in Figure 3.2-29, no SDU would be exposed to potential edge effects around its entire perimeter. The closest any SDU comes to complete perimeter exposure would be SDUs 1 and 4, which are each potentially exposed to edge effects on three sides, and SDU 10, which is potentially exposed on less than 2/3 of its circumference. The remaining SDUs have much less potential exposure to edge effects.

Table 5.8-5: Modified Erosion Estimate Parameters for RUSLE

Parameter	Short Description	Assumed Value(s)	Basis for Assumed Value(s)
R	Erosion Index	300 (100 ft • ton/acre per in/yr)	Same value used in Table 4.4-6 based on the location of the SDF.
K	Soil Erodibility Factor	0.28 (tons/acre per unit of R)	Same value used in Table 4.4-6 based on site-specific soil properties.
L	Length Factor	9.67	The length and slope factors are combined into a single parameter. The value of 9.67 was selected from Table 4-3 from USDA-HDBK-703, based on an assumed 30% surface slope and slope length of 200 feet. Note: Table 4.4-6 used 0.59.
S	Slope Factor		
C	Vegetative Cover Factor	0.1	Value assumes sparse vegetation along the side slope. This is 14 to 100 times higher than the values considered in Table 4.4-6.
P	Erosion Control Practice Factor	0.8	In Table 4.4-6 the maximum value of 1 was assumed for simplicity as this will bias the results toward a higher erosion estimate. For this analysis, the erosion control barrier and the durability of the HDPE material are credited as providing limited erosion control by assuming a value less than 1.

The overestimation of these impacts is especially exaggerated in the Retreating Cap Case, as conceptually illustrated by Figure 5.8-15. Due to the radial symmetry of the model design, once the retreat of the closure cap extends to the center of an SDU, the higher infiltration rate is effectively being applied to the entire area of the SDU and the surrounding backfill (i.e., complete failure of the cover system).

Figure 5.8-15: Conceptual Comparison of the Simulated (Radial) Cap Retreat Versus Cap Retreat as a Linear Advancing Front

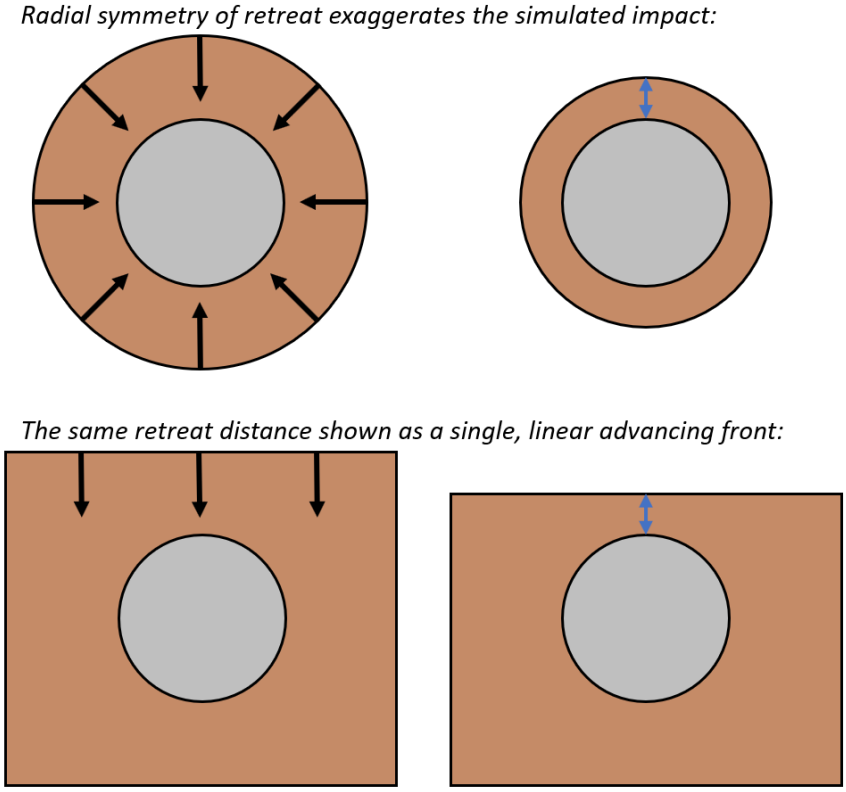

Another consideration is that these sensitivity cases assume that the increased infiltration occurs directly at the edges of the composite barrier. As shown in the cross sections in Figure 3.2-30 and Figure 3.2-31, the composite barrier extends to the side slope of the closure cap. Water shedding off the edge of the composite barrier is expected to seep out along the side slope and continue flowing away from the SDUs as surface runoff (i.e., down the side slope and into the drainage channel at the foot of the side slope). However, these sensitivity cases assume the water infiltrates into the backfill surrounding the SDUs.

Figure 5.8-16 illustrates the resulting differences in the initial saturation conditions for T = 0, showing saturation for the Compliance Case, 75-ft Cover Extent Case, and 50-ft Cover Extent Case. A brown bar has been added across the top of each cross section to illustrate the lateral extent of the composite barrier.

Using these modified fluxes, the Vadose Zone Transport Model and the Aquifer Transport Model were run using Compliance Case conditions to estimate the resulting ground water concentrations to use for determining the dose.

Figure 5.8-16: Saturation Contours at Time = 0 for 375-Foot Diameter SDUs, Based on Varied Cover Extents

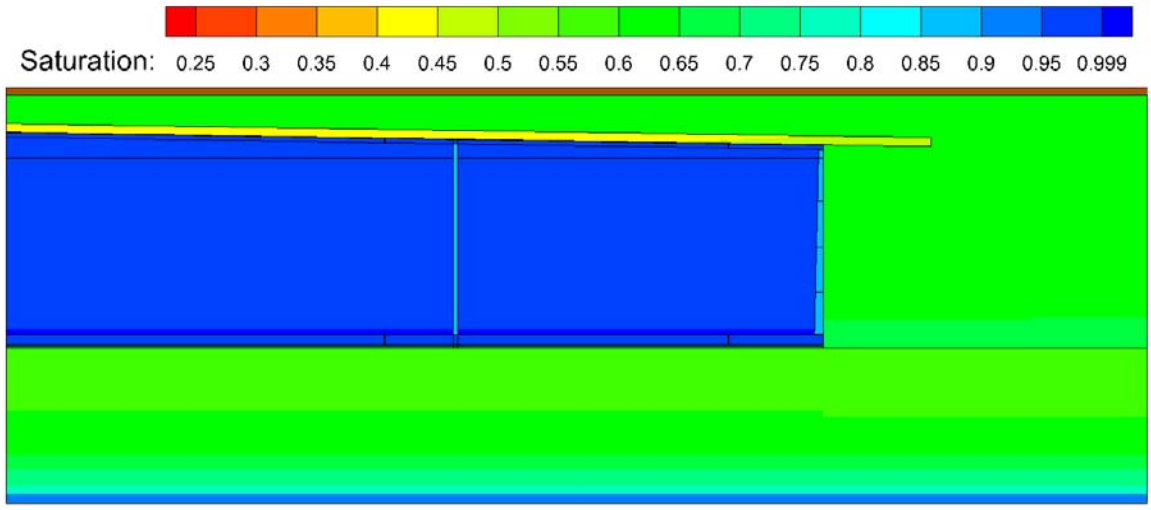

Infinite Cover Extent (Compliance Case)

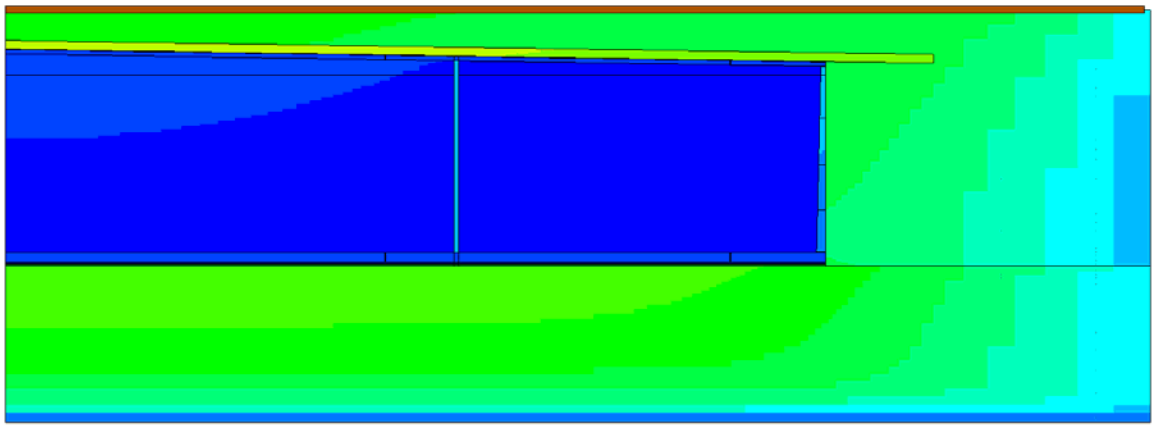

Cover Extent = 75 Feet Beyond SDU Edge

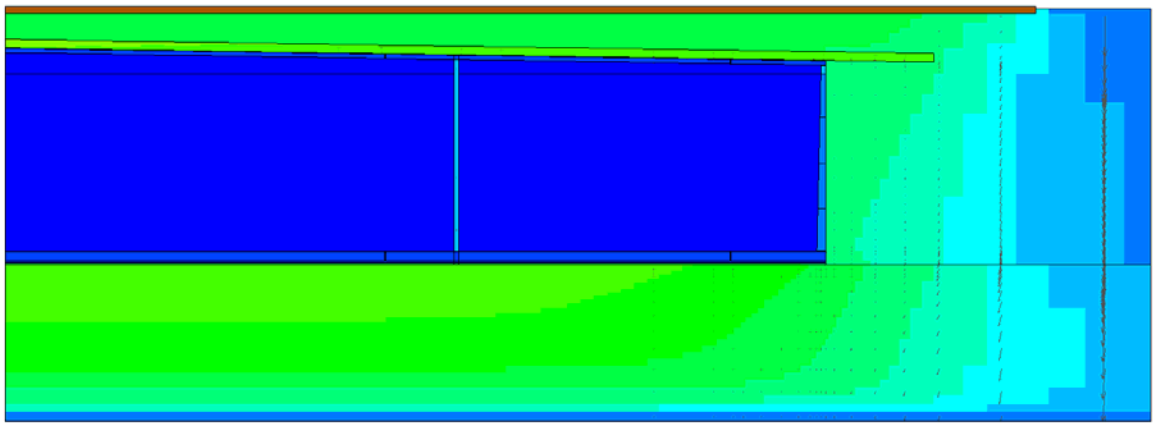

Cover Extent = 50 Feet Beyond SDU Edge

Figure 5.8-17 compares the resulting doses from the first two sensitivity cases to the Compliance Case. Given the context of the modeling approach, it is most reasonable to expect that future doses would be somewhere between the Compliance Case dose (black) and the dose from the 75-foot cover extent (blue). While the Compliance Case may be under representing dose risk due to the potential influence of edge effects, this figure demonstrates that even with an exaggerated modeling approach, the edge effects are not expected to increase doses enough to challenge the ability of the SDF to meet performance objectives.

Figure 5.8-17: Dose Results from Sensitivity Cases with 75-Foot and 50-Foot Cover Extents (Detail)

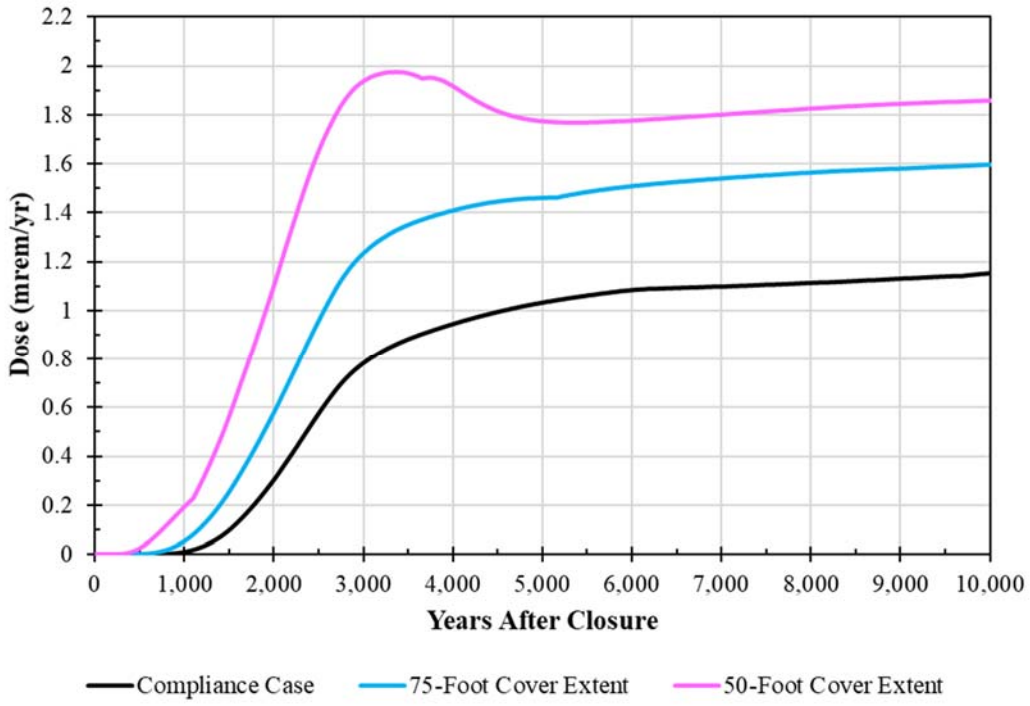

Finally, Figure 5.8-18 shows the dose results from all three modified cap extent sensitivity cases, including the Retreating Cap Case, along with the Compliance Case. As expected, the Retreating Cap Case results in a higher dose, with a peak of 9.3 mrem/yr at approximately 4,300 years after closure (Table 5.8-6). Despite assuming complete failure of the closure cap side slope and erosion of the composite barrier, the SDF is still meeting the performance objective.

Figure 5.8-18: Dose Results from All Three Sensitivity Cases with Modified Closure Cap Cover Extents

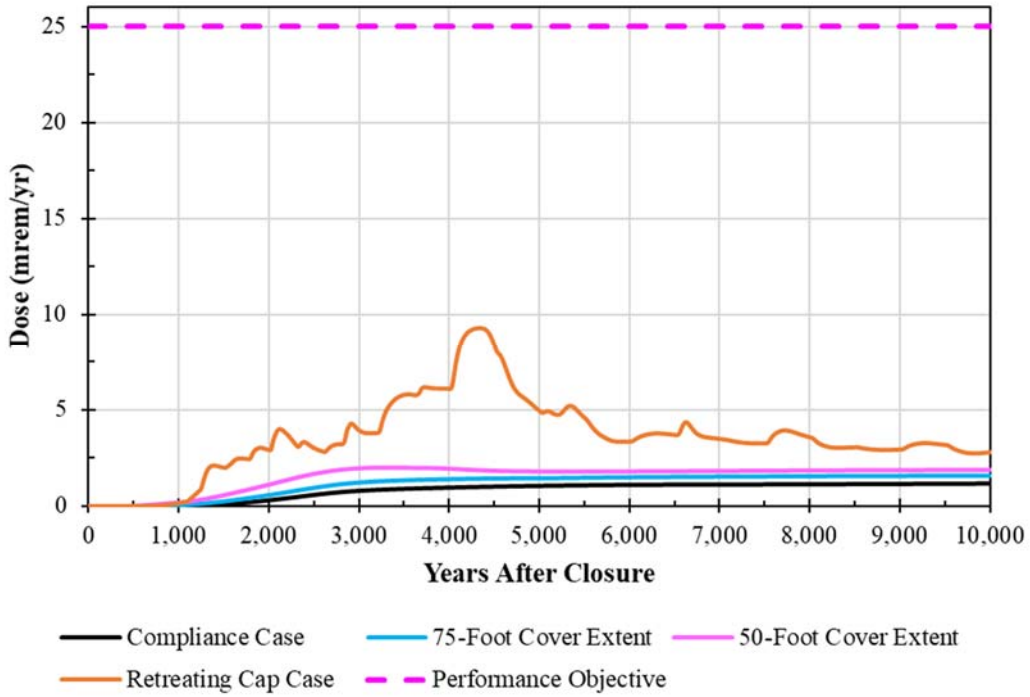

Table 5.8-6: Comparison of the 100-Meter MOP Peak Ground Water Pathways Doses Based on Modified Cover Extents

Modeling Case	Compliance Period (0 to 1,000 Years)		Performance Period (0 to 10,000 Years)	
	Peak Dose (mrem/yr)	Year of Peak	Peak Dose (mrem/yr)	Year of Peak
Compliance Case (Infinite Cover Extent)	9.4E-03	1,000	1.2	10,000
75-Foot Cover Extent Case	0.053	1,000	1.6	10,000
50-Foot Cover Extent Case	0.19	1,000	2.0	3,350
Retreating Cap Case	0.16	1,000	9.3	4,340

5.8.2.6 Evaluation of Climate Uncertainty

In the Compliance Case, it is assumed that meteorological conditions will remain approximately the same as current conditions (Section 4.6.2). As noted in Section 4.6.2, climatic records indicate climatic similarities to modern conditions over the past 8,000 years (the last half of the Holocene). Despite this relative consistency in the climate record, there is considerable debate as to the availability of moisture over the first half of the Holocene. Since long-term climate conditions remains a source of potential uncertainty, a climate-change scenario was implemented to evaluate the potential influence of rainfall change on the release and subsequent dilution of radionuclides being transported

downgradient to the 100-meter boundary where doses to the MOP are evaluated for regulatory compliance.

The "Climate Uncertainty" scenario is designed to non-mechanistically address the potential impacts from multiple FEPs, as presented in Table 5.8-7. Despite the large number of FEPs considered, it should be noted that the goal of this scenario is not to define the maximum extent of climate change that might occur at SRS, as such an exercise would be inherently uncertain, rather, the goal is to provide insights to the potential impacts associated with changes to climate conditions.

Table 5.8-7: FEPs Addressed in the Climate Uncertainty Scenario

FEP ID	FEP Name	Discussion
2.6.05	Mechanical Effects on Geologic Features	Mechanical effects on geologic features (e.g., compaction of vadose zone soils due to the overburden from the SDU and overlaying closure cap) may influence infiltration rates and assumptions related to infiltration rates.
2.6.07	Erosion and Weathering	Erosion or weathering of the closure cap or backfill may influence infiltration rates and assumptions related to infiltration rates.
2.6.11	Mass Wasting	Mass wasting of the closure cap or backfill may influence infiltration rates and assumptions related to infiltration rates.
2.6.14	Closure Cap Performance (Differential Settlement)	The closure cap may not perform as intended, which may influence infiltration rates and assumptions related to infiltration rates.
3.7.08	Swelling of Backfill and Emplacement Materials	Swelling of backfill may influence infiltration rates and assumptions related to infiltration rates.
5.1.03	Focusing of Flow Along Preferred Flow Paths (Fingers, Weeps, Faults, Fractures, etc.)	The effects of focused flow paths may be approximated by increased or decreased infiltration rates.
5.1.07	Episodic or Pulse Flow and Release	While this scenario does not explicitly address this FEP, the results from the other infiltration cases provided insights relative to risks associated with differing infiltration rates.
6.2.01	Seismicity	Significant seismic or subsidence events may disturb ground water flow patterns in ways which might be approximated by modifying infiltration rates.
6.2.03	Seismic-Induced Damage or Changes to System Components	Significant seismic or subsidence events may damage disposal units and/or disturb ground water flow patterns in ways which might be approximated by modifying infiltration rates.
6.2.04	Effects of Subsidence	Significant seismic or subsidence events may disturb ground water flow patterns in ways which might be approximated by modifying infiltration rates.
6.4.06	Movement of the Waste Form	SDU movement due to sinking, uneven swelling of backfill materials, etc. could affect closure cap performance which may be approximated by modifying infiltration rates.

[SRR-CWDA-2018-00006]

To evaluate the potential impacts from early releases, two climate change sensitivity cases were developed to reflect two potential climate scenarios: a Wetter Climate Scenario and a Drier Climate Scenario.

The SDF GoldSim Model was modified to develop these sensitivity cases, and the simulation results were compared to results from the deterministic SDF GoldSim Model

using the Compliance Case settings. The climate change sensitivity cases assume if long-term climate change impacts the SDF, it is expected to alter infiltration rates, depth to the water table, and rates of ground water flow. Table 5.8-8 provides a summary of the model changes applied. These changes are discussed below.

Table 5.8-8: Key Differences Between the Climate Uncertainty Scenario Cases

Parameter or Condition	Drier Climate	Compliance Case	Wetter Climate	References
Parametric Flow Case	Case F01 – The Best Estimate infiltration rate, cementitious degradation rate, saturated hydraulic conductivity, and initial saltstone hydraulic conductivity	Compliance Case = Parametric Flow Case F27: MPAD infiltration rate, cementitious degradation rate, saturated hydraulic conductivity, and initial saltstone hydraulic conductivity	Case F54 – The Conservative Estimate infiltration rate, cementitious degradation rate, saturated hydraulic conductivity, and initial saltstone hydraulic conductivity	Table 4.4-82
Vadose Zone Thickness Change	Increased by 7.6 feet	Unchanged	Decreased by 8 feet	SRR-CWDA-2019-00027
Saturated Zone Flow-Rate Multiplier	0.62	1	1.5	Variability based on precipitation data (Section 4.4.1.3)

To evaluate the potential influence changes in infiltration rate associated with climate variance could have on the exposure of the Compliance MOP to radionuclides, two of the 54 parametric flow cases flow fields were selected to represent variations in flow conditions due to climate change: Case F01 and Case F54. The selected flow fields are from parametric flow cases representing the Best Estimate (lowest) and Conservative estimate (highest) infiltration rates from the parametric flow cases (see Table 4.4-82). In addition to the different infiltration rates, the other parameters associated with the parametric flow cases (cementitious degradation rate, saturated hydraulic conductivity, and initial saltstone hydraulic conductivity) were also modified to capture more extreme flow conditions. This approach assumes that changing climate conditions impacts more than just the infiltration rate. In these cases, it is assumed that the best estimate flow conditions provide an approximation of a drier climate, relative to the Compliance Case, whereas the conservative estimate flow conditions provide an approximation of a wetter climate.

In the SDF GoldSim Model, the vadose zone thicknesses were assigned for each of the SDU types modeled (e.g., SDUs 1, 2, 4, 6, 7, and 9). To support the climate change sensitivity cases, these thicknesses are modified. Within the SDF GoldSim Model, the thickness of the vadose zone represents the distance from the bottom of the SDU to the water table, so modifying this value effectively redefines the water table elevation.

To support the changes to the vadose zone thickness, water level readings for SDF monitoring wells were extracted from SRS ground water monitoring data and evaluated

to determine the historical range of water table elevations from 1987 through 2015. [SRR-CWDA-2019-00027] Specifically, the variations in the vadose zone thickness are based on data from the monitoring well ZBG 2, which provided the longest range of monitoring within the SDF boundaries: water table readings for this well were compiled from 1987 through 2015 (when the well was abandoned).

The reference elevation for ZBG 2 based at the top of the monitoring well is 278.1 ft above MSL. The ground elevation at ZBG 2 is 275.8 ft above MSL. The depth to water is subtracted from the reference elevation to get the elevation of the water table in ft above MSL. The water table elevation is then subtracted from the ground elevation to get the vadose zone thickness for the respective reporting period. The vadose zone thickness for 73 sampling events (SRR-CWDA-2019-00027) were then averaged to get the average vadose zone thickness at ZBG 2 (55.4 ft), as well as providing the vadose zone maximum and minimum thicknesses (63.0 ft and 47.4 ft, respectively). Based on this data, the difference between the average and each of the minimum and maximum values was determined. The difference between the average and minimum thickness was 8 ft and the difference between the average and the maximum thickness was 7.6 ft. Based on the analysis presented in SRR-CWDA-2019-00027, it was recommended for each SDU, 8 ft be subtracted from the default (Compliance Case) vadose zone thicknesses for the wetter climate analysis and an additional value of 7.6 ft be added to the default vadose zone thickness for the drier climate analysis. Note: the saturated zone thickness was also adjusted to reflect the changes in the vadose zone thickness.

To evaluate the potential influence of changes in saturated zone flow rates, flow-rate multipliers were developed and used. The flow rate multipliers were derived based on the assumption that a change in saturated-zone flow rate could be approximated as a direct function of any change in annual rate of precipitation. To meet this end, SRS precipitation data presented in Section 4.4.1.3 were used. The data used included the mean precipitation rate, the maximum annual precipitation rate, and the minimum annual precipitation rate as recorded between 1964 and 2016. The wet climate flow rate multiplier was then assumed to be the ratio between the maximum annual precipitation rate and the mean precipitation rate (1.5 as presented in Table 5.8-8) and the dry climate flow rate multiplier was then assumed to be the ratio between the minimum annual precipitation rate and the mean precipitation rate (0.62 as presented in Table 5.8-8).

Figure 5.8-19 and Figure 5.8-20 present the resulting total doses from the climate change sensitivity models and include equivalent results from the deterministic SDF GoldSim Model using the Compliance Case settings for comparison. Both figures display the same set of dose results but Figure 5.8-19 is depicted on a semi-log scale and Figure 5.8-20 is depicted on a linear scale. The semi-log plot is a good indicator of how the wetter climate influences the timing of the dose curves, while the linear plot illustrates the relative magnitude of the change in dose based on the assumed climate change conditions.

Over the Compliance Period, the peak dose for the wetter climate case is approximately 3.7 times higher than the peak dose for the Compliance Case, and the peak dose for the Compliance Case is approximately 3.5 times higher than the peak dose for the drier

climate case (see Table 5.8-9). These peak doses occur at 1,000 years for each of the three cases over the Compliance Period.

Over the Performance Period (10,000 years), the peak dose for the wetter climate case is 2.6 times greater than for the Compliance Case, and the peak dose for the Compliance Case is 1.4 times greater than for the drier climate case (see Table 5.8-9). As presented in Table 5.8-9, these peak doses all occur at 10,000 years.

Figure 5.8-19: Comparison Between Dry Climate, Wet Climate, and Compliance Value Total Dose Results (Log Scale)

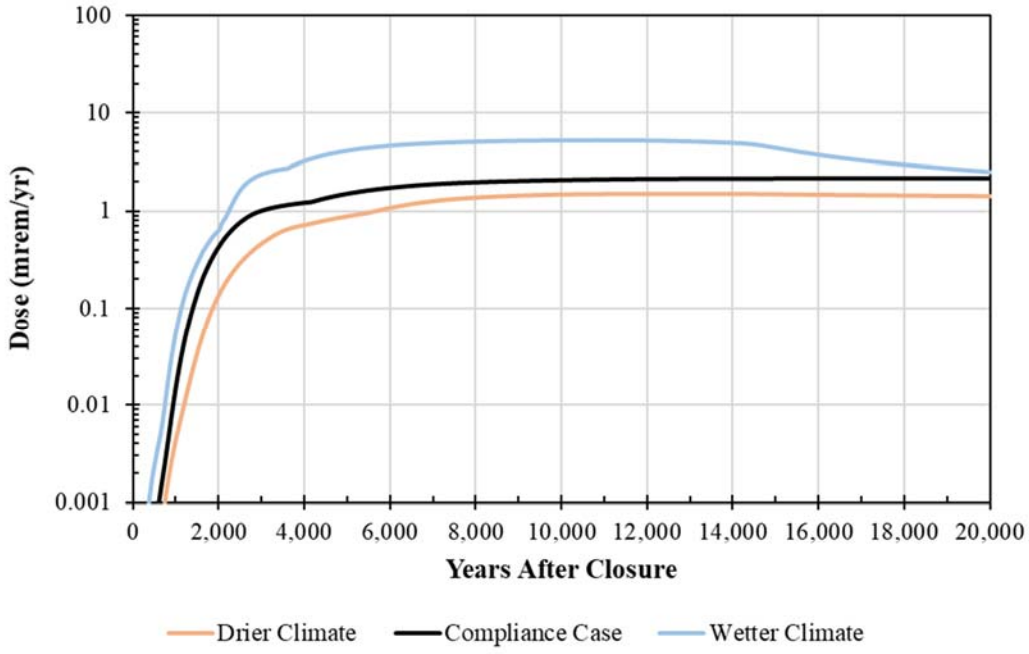

Figure 5.8-20: Comparison Between Dry Climate, Wet Climate, and Compliance Value Total Dose Results (Linear Scale)

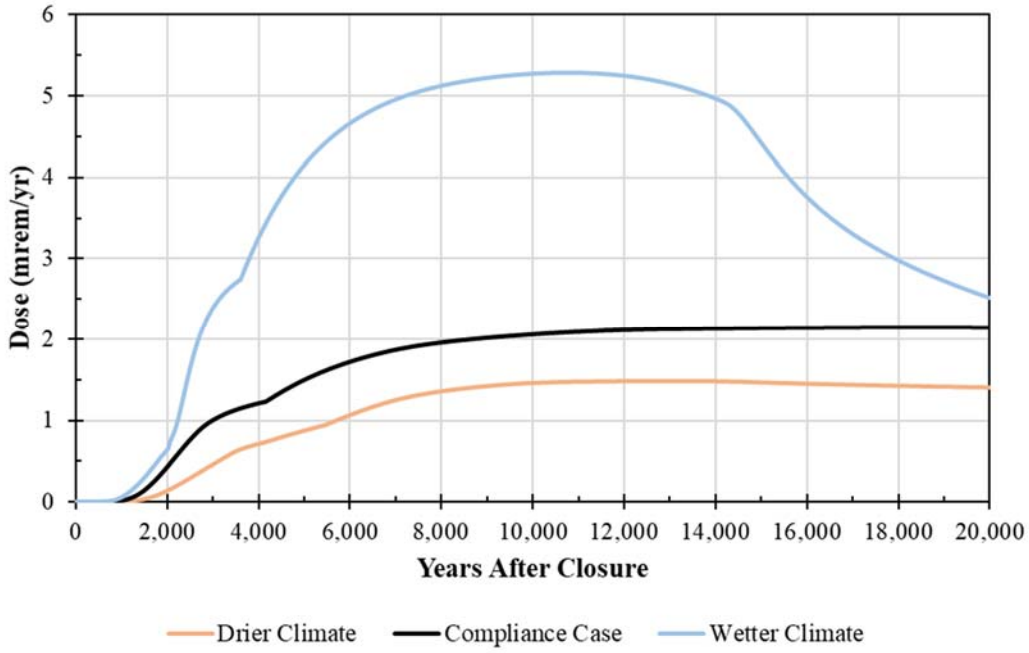

Table 5.8-9: Comparison of Climate Sensitivity Cases, 100-Meter MOP Peak Ground Water Pathways Doses Based on the SDF GoldSim Model

Modeling Case	Compliance Period (0 to 1,000 Years)		Performance Period (0 to 10,000 Years)	
	Peak Dose (mrem/yr)	Year of Peak	Peak Dose (mrem/yr)	Year of Peak
Wetter Climate Case	5.7E-02	1,000	5.3	10,000
Compliance Case	1.6E-02	1,000	2.1	10,000
Drier Climate Case	4.4E-03	1,000	1.5	10,000

5.8.3 Material Property Sensitivites

The following describes various alternative scenarios and sensitivity cases developed to better understand the uncertainties and risks that are associated with material properties (see Section 4.3.1).

5.8.3.1 Evaluation of the Saturated Hydraulic Conductivity of the Sand Drainage Layers

The final closure configuration of the SDF includes two sand drainage layers (see Figure 3.2-33). The upper lateral sand drainage layer is embedded within the closure cap (between the middle backfill layer and the composite (HDPE/GCL) barrier) and the lower lateral sand drainage layer is embedded above each SDU (between the lower backfill layer and the composite barrier above the SDU roof).

The saturated hydraulic conductivity (K_{sat}) of the sand material used within these layers is expected to exhibit some variability. To develop an understanding of the impact of this

variability, two sensitivity cases have been developed by modifying the Compliance Case. The first sensitivity case doubles the saturated hydraulic conductivity of the sand material while the second case assumes half the saturated hydraulic conductivity.

For the closure cap modeling supporting the Compliance Case, the saturated hydraulic conductivity of the sand material is specified to be at least 5.0E-02 cm/s for the first 500 years based on closure cap design specifications (SRR-CWDA-2018-00087 and WSRC-STI-2008-00244). Then, to address uncertainty in long term hydraulic performance, it is assumed that the sand drainage layers will undergo a step change at 500 years, decreasing to 1.0E-02 cm/s (SRRA107772-000009). Doubling the Compliance Case values gives 1.0E-01 cm/s and 2.0E-02 cm/s while halving the Compliance Case values gives 2.5E-02 cm/s and 5.0E-03 cm/s.

Based on the analytical solution for the leakage rate (Eq. 4.4-5 in Section 4.4.1), the saturated hydraulic conductivity of the upper lateral sand drainage layer is a key input for estimating infiltration rates. Accordingly, any assumed changes to the saturated hydraulic conductivity of the material used for the sand drainage layers will result in changes to the estimated infiltration rates. The recommended infiltration rates were calculated as described in *Recommended Percolation Rate Values to Support SDF Sensitivity Analysis of Sand Drainage Layer* (SRR-CWDA-2019-00026) and presented in Table 5.8-10.

Table 5.8-10: Recommended Infiltration Rates Based on Assumed Sand Drainage Layer Properties

Year	Sand Drainage Layer K_{sat} × 2.0		Compliance Case		Sand Drainage Layer K_{sat} × 0.5	
	Sand K_{sat} (cm/s)	Infiltration Rate (mm/yr)	Sand K_{sat} (cm/s)	Infiltration Rate (mm/yr)	Sand K_{sat} (cm/s)	Infiltration Rate (mm/yr)
0-500	1.0E-01	0.0021	5.0E-02	0.0060	2.5E-02	0.019
500-2000	2.0E-02	0.027	1.0E-02	0.091	5.0E-03	0.31
>2000		0.037		0.13		0.43

In general, doubling the saturated hydraulic conductivity of the sand material reduces the infiltration rate by approximately a factor of 3 while halving the saturated hydraulic conductivity increases the infiltration rate by approximately a factor of 3. These infiltration rates are applied to the Vadose Zone Flow Model. Then for internal consistency, the modified saturated hydraulic conductivities were also applied to the lower sand drainage layer within the Vadose Zone Flow Model and the Vadose Zone Transport Model.

Figure 5.8-21 shows these results over time and Table 5.8-11 provides a summary of the resulting peak doses. As would be expected, the respective changes to the infiltration rates facilitate a modest change to these doses. However, the influence is not directly linear: the doses did not change by a factor of 3 to reflect the change in the infiltration rate. Instead, the overall impact was less than a factor of 2.

Figure 5.8-21: Dose Results from the Sensitivity Cases that Vary the Saturated Hydraulic Conductivity of the Sand Drainage Layer Materials (Detail)

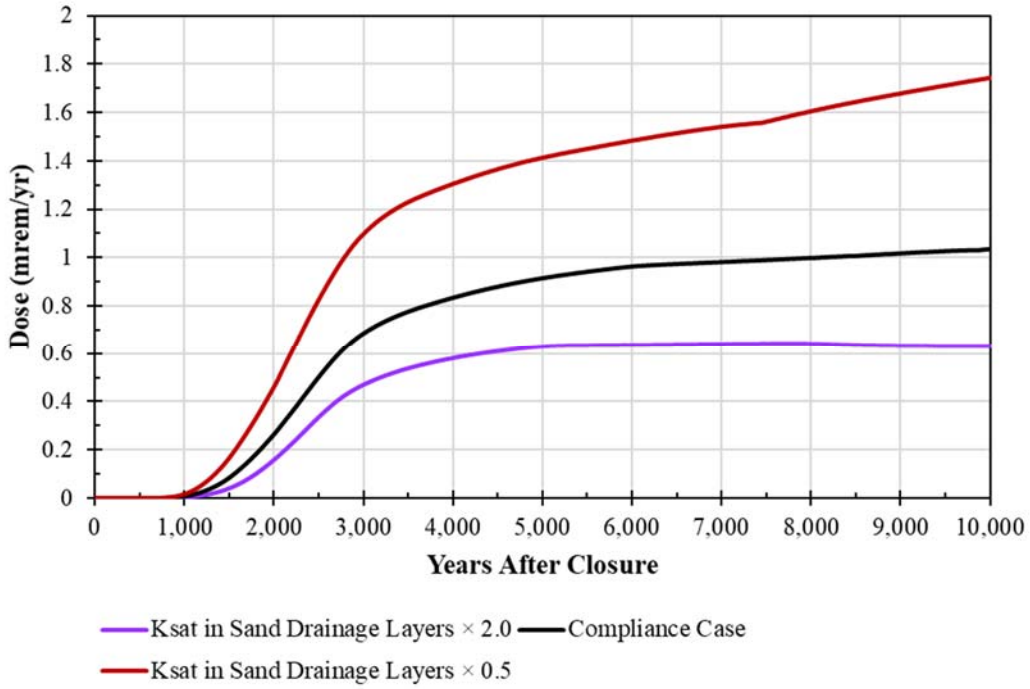

Table 5.8-11: Comparison of Sand Drainage Layer Sensitivity Cases, 100-Meter MOP Peak Ground Water Pathways Doses

Modeling Case	Compliance Period (0 to 1,000 Years)		Performance Period (0 to 10,000 Years)	
	Peak Dose (mrem/yr)	Year of Peak	Peak Dose (mrem/yr)	Year of Peak
K_{sat} in Sand Drainage Layer × 0.5	2.0E-02	1,000	1.9	10,000
Compliance Case	9.4E-03	1,000	1.2	10,000
K_{sat} in Sand Drainage Layer × 2.0	4.7E-03	1,000	0.73	10,000

5.8.3.2 *Controlled Compacted Backfill Saturated Hydraulic Conductivity Sensitivities for Vadose Zone Flow*

The assumed saturated hydraulic conductivity of the controlled compacted backfill is based on information from Section 5.3 of *Hydraulic Property Data Package for the E-Area and Z-Area Soils, Cementitious Materials, and Waste Zones*. [WSRC-STI-2006-00198] Specifically, 32 site-specific samples (from E-Area and Z-Area) were analyzed and then an "upscaling" methodology was applied to the data to include heterogeneity and spatial continuity. The result of this analysis was a recommendation of 4.1E-05 cm/s for the vertical saturated hydraulic conductivity and 7.6E-05 cm/s for the horizontal saturated hydraulic conductivity. Table 5-18 of WSRC-STI-2006-00198 also provides a summary of recommended soil properties for control compacted backfill and other soil materials.

Section 10.2 of *Engineered Covers for Waste Containment: Changes in Engineering Properties and Implications for Long-Term Performance Assessment*, Vol. 1 (NUREG/CR-7028 [ML12005A110]) makes the following recommendation:

> "The saturated hydraulic conductivity of fine-textured earthen storage and barrier layers can be assumed to range between 1×10^{-7} m/s and 5×10^{-6} m/s. This relatively narrow range of saturated hydraulic conductivities was obtained from a very broad range of as-built saturated hydraulic conductivities, which suggests that the saturated hydraulic conductivity reached an equilibrium condition during the study. Moreover, given that storage and barrier layers are constructed with fine-textured soils, saturated hydraulic conductivities higher than 5×10^{-6} m/s are unlikely unless a fundamental change in texture or mineralogy occurs during the service life of the cover. When site-specific information representing in service conditions is not available, typical conditions can be predicted using a saturated hydraulic conductivity of 5×10^{-7} m/s. Sensitivity analyses can be conducted using the aforementioned upper and lower bounds to assess the range of performance that may be encountered."

Because site-specific data is available (i.e., 4.1E-05 cm/s), rather than assuming the full range of values recommended in NUREG/CR-7028 (ML12005A110), sensitivity modeling assumes minimum and maximum values that are the geometric mean of the site-specific value (4.1E-05 cm/s), and the recommended minimum (1.0E-05 cm/s) and maximum (5.0E-04 cm/s) from NUREG/CR-7028 (ML12005A110):

- Min = GEOMEAN(4.1E-05,1.0E-05) = 2.0E-05 cm/s
- Max = GEOMEAN(4.1E-05,5.0E-04) = 1.4E-04 cm/s

When the vertical saturated hydraulic conductivity of backfill is varied in this way, it is also appropriate to vary the horizontal saturated hydraulic conductivity of backfill. Assuming a linear relationship, the horizontal saturated hydraulic conductivity is a factor of 1.85 greater than the vertical saturated hydraulic conductivity.

Table 5.8-12 summarizes these recommended K_{sat} for controlled compacted backfill used for sensitivity evaluation.

Two sensitivity cases for vadose zone flow were evaluated for varying saturated hydraulic conductivity. The High K_{sat} in Backfill Case uses all modeling parameters from the Compliance Case, only selecting the higher saturated hydraulic conductivity for controlled compacted backfill from Table 5.8-12. The Low K_{sat} Backfill Case uses all modeling parameters from the Compliance Case, only selecting the lower saturated hydraulic conductivity for controlled compacted backfill from Table 5.8-12.

Table 5.8-12: Saturated Hydraulic Conductivities for Controlled Compacted Backfill Sensitivities

Sensitivity Case	Vertical (cm/s)	Horizontal (cm/s)	PORFLOW Case Identifier
High K_{sat} in Backfill	1.4E-04	2.7E-04	CaseF29.7
Compliance Case	4.1E-05	7.6E-05	CaseCV.7
Low K_{sat} in Backfill	2.0E-05	3.8E-05	CaseF25.7

In addition to changing the hydraulic conductivity of the backfill, the corresponding moisture characteristic curves were also updated based on a technique known as "Leverett scaling" (see Eq. 4.4-105). Leverett scaling consists of adjusting the matric suction based on permeability.

When considering variability in the moisture characteristic curves, it is important to consider the conditions to which these curves are being applied. Specifically, the matric suction and the saturation conditions. At the water table (i.e., saturation = 1), the matric suction is equal to zero and increases with distance from the water table. Per Table 4.3-1, the SDU depths to the water table range from a minimum of 23 feet (for SDU 9) to a maximum of 48 feet (for SDU 1). Converted to centimeters, the minimum suction at the base of each SDU would range from 700 cm to 1500 cm. Add to this the height of each SDU and the maximum suction is expected to be only slightly higher than 2200 cm. These maximum values only occur under low saturation conditions; these values decrease as saturation in the system increases (for an example, refer to Figure 7.1-2 and Figure 7.1-3).

Figure 5.8-22 shows the resulting moisture characteristic curves considered in the backfill sensitivity cases. Note the inflection point near the suction of 30 cm; for suction heads lower than this, the lower saturated hydraulic conductivities translate to lower effective hydraulic conductivities. Alternatively, for suction heads greater than 30 cm, lower saturated hydraulic conductivities translate to slightly higher effective hydraulic conductivities.

Under these higher suctions heads, two competing processes occur: first, with lower permeabilities in the backfill, an increased volume of water flows into the SDU and saltstone (via suction) thus increasing the relative rates of contaminant releases; however, due to the lower backfill permeability, once the contaminants are released into the backfill, the rate of transport through the backfill decreases thus decreasing the relative concentrations at the water table. The net effect is that these sensitivity cases yield doses that are not significantly different from the Compliance Case.

Figure 5.8-22: Moisture Characteristic Curves for the Hydraulic Conductivity of Backfill Sensitivity Cases

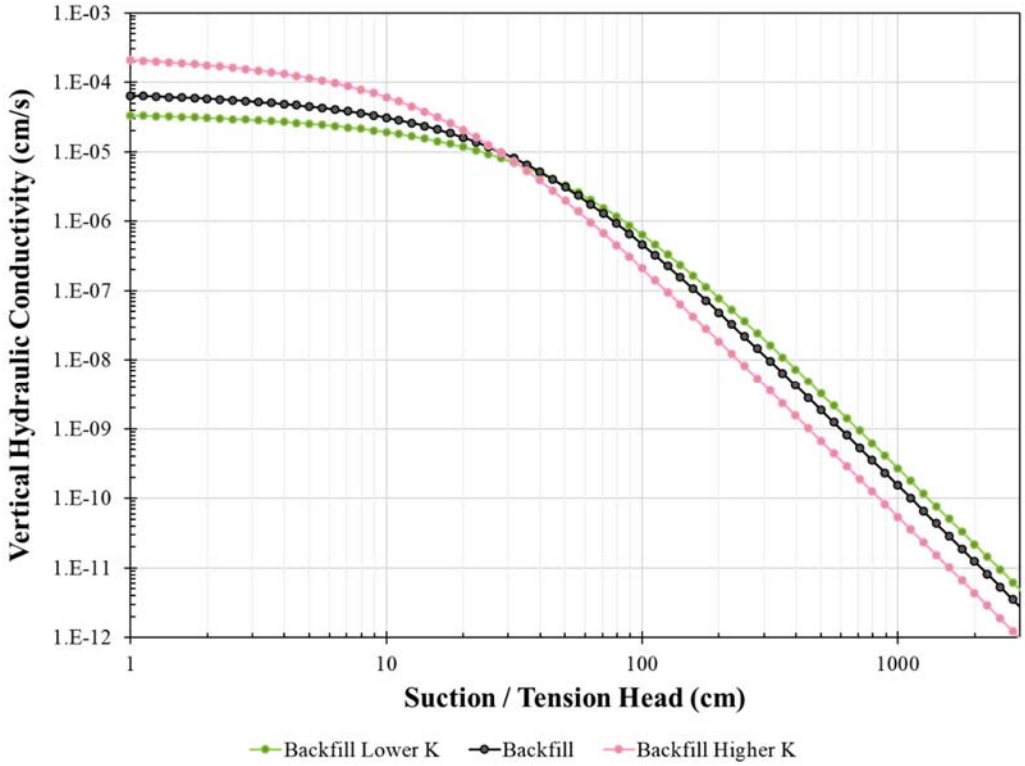

Figure 5.8-23 shows the resulting ground water pathways doses for these backfill hydraulic conductivity sensitivity cases. As indicated on Figure 5.8-23, the Compliance Case is just under 1.2 mrem/yr in 10,000 years and the maximum dose difference between the minimum and maximum backfill hydraulic conductivity is less than 0.1 mrem/yr in 10,000 years. The results of this evaluation indicate that uncertainty in the hydraulic conductivity of the controlled compacted backfill has a negligible impact on dose throughout the Performance Period.

Figure 5.8-23: Dose Results from the Backfill Hydraulic Conductivity Rate Sensitivity Cases

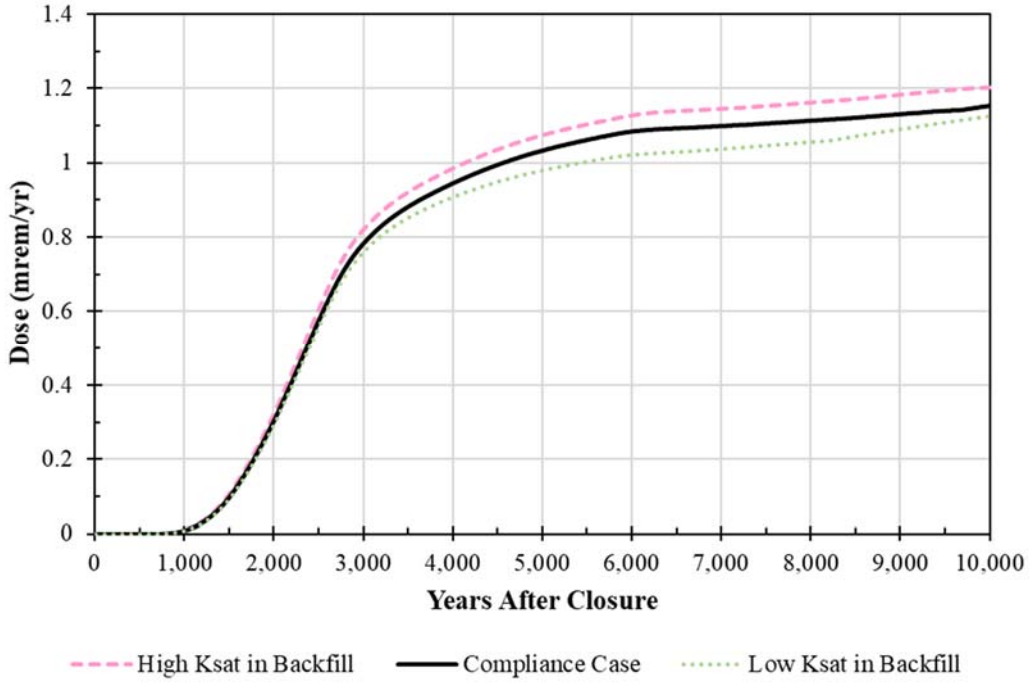

5.8.3.3 SDU Concrete Initial Hydraulic Conductivity Sensitivities

Table 4.3-3 provides a range of recommended initial saturated hydraulic conductivities for the future SDU concrete. These values were based on recent testing (0000138886-000024) using the new concrete formulation from Table 3.2-5. From these these tests, the Best Estimate value (6.4E-10 cm/s) represents the average of the last measurement from each sample, the Conservative Estimate value (9.1E-10 cm/s) represents the highest measured value, and the MPAD value (7.8E-10 cm/s) represents the average of the Best Estimate and Conservative Estimate values. [SRR-CWDA-2018-00004]

Because these values represent a relatively narrow range of recommended values, additional sensitivity models were developed to evaluate an wider range of initial saturated hydraulic conductivities for SDU concrete. Specifically, these sensitivity models considered the impacts from increasing the Best Estimate value by an order of magnitude (from 6.4E-10 cm/s to 6.4E-09 cm/s) and from decreasing by an order of magnitude (from 6.4E-10 cm/s to 6.4E-11 cm/s). This approach has the potential to create a larger operating window (for in-the-field SDU construction) should the concrete formulation need to be varied.

As a final sensitivity case, a bounding case was developed which assumed that the saturated hydraulic conductivity of the SDU concrete was nearly fully degraded, with an initial value of 1.0E-7 cm/s. This value was selected as it is the maximum permitted value for lining Class III landfills in the state of South Carolina. [SCDHEC R.61-107.19]

This sensitivity analysis uses values from the Compliance Case for all model inputs except for the initial saturated hydraulic conductivity of the SDU concrete for future SDUs (i.e., SDUs 7 through 12).

For the sensitivity cases with the initial saturated hydraulic conductivities from 6.4E-11 cm/s up to 6.4E-09 cm/s, the modeling results showed virtually no change to the doses. Even under the most bounding condition (with the initial saturated hydraulic conductivity of 1.0E-07 cm/s), the difference relative to the Compliance Case (Figure 5.8-24) was negligible. The results of this evaluation indicate that uncertainty in the initial saturated hydraulic conductivity of the SDU concrete has a negligible impact on dose throughout the Performance Period.

Because these results are somewhat counter-intuitive, Section 7.1 offers additional interpretation of how the hydraulic performance of the SDU concrete influences the overall performance of the SDF.

Figure 5.8-24: Dose Results Comparing Different SDU Concrete Hydraulic Conductivites

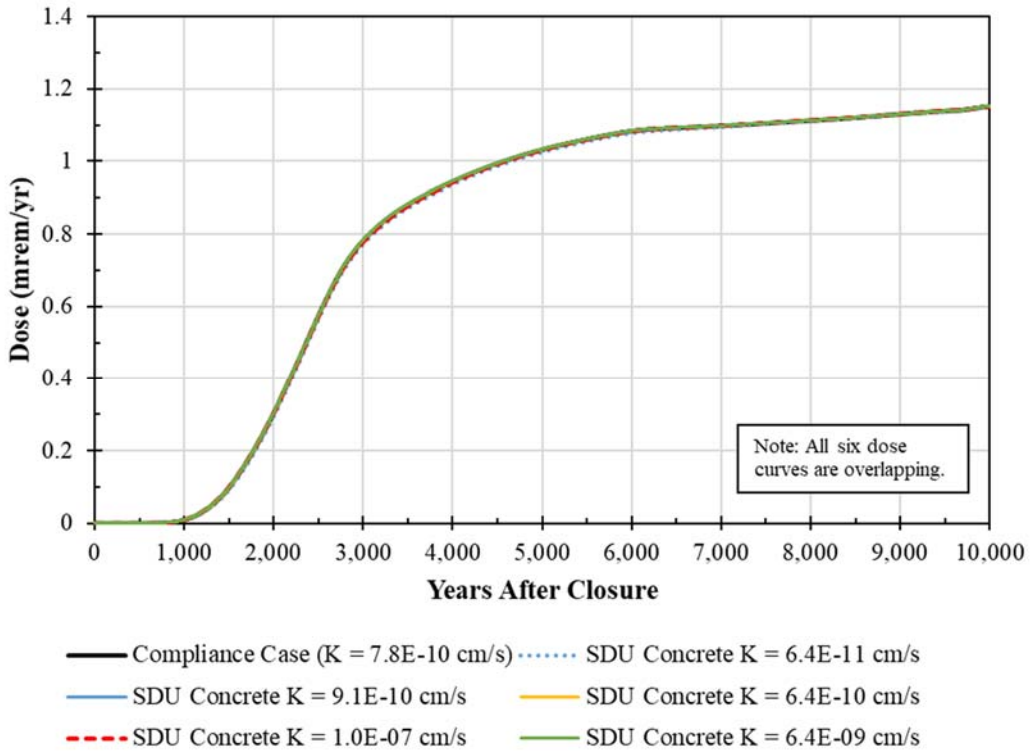

5.8.3.4 SDU Saltstone Initial Hydraulic Conductivity Sensitivities

Table 4.3-3 provides a range of recommended initial saturated hydraulic conductivities for saltstone. The recommended initial saturated hydraulic conductivity values are 1.0E-10 cm/s (Best Estimate or Realistic Value), 5.0E-10 cm/s (MPAD or Compliance Value), or 2.0E-09 cm/s (Conservative or Pessimistic Value).

To evaluate the sensitivity of varying the initial saturated hydraulic conductivity of saltstone only, a sensitivity case was developed which assumed the Compliance Case inputs and conditions, but changed the initial saturated hydraulic conductivity of saltstone from the MPAD value (5.0E-10 cm/s) to the Pessimistic value (2.0E-09 cm/s). The dose results from this sensitivity case was compared to the dose results from the Compliance Case (Figure 5.8-25).

Results show a moderate increase in the dose results over 10,000 years (the peak dose increased from 1.2 mrem/yr to 1.3 mrem/yr). Despite this moderate increase in dose, both the Compliance Case and the sensitivity case remain well below the performance objective of 25 mrem/yr in 10,000 years and the difference between the Compliance Case and the sensitivity case using the higher saturated hydraulic conductivity is relatively small (<0.2 mrem/yr). The results of this evaluation indicate that uncertainty in the initial saturated hydraulic conductivity of saltstone has a small but appreciable impact on doses within the Performance Period.

Figure 5.8-25: Dose Results Comparing the Initial Saturated Hydraulic Conductivity of Saltstone: Compliance Case Value versus Pessimistic Case Value

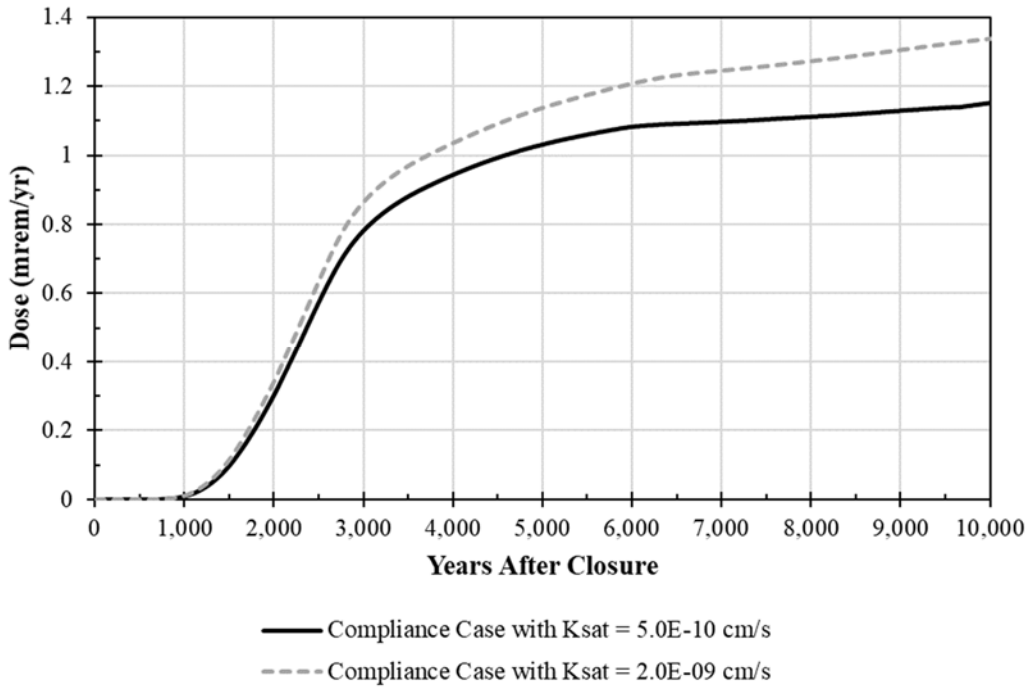

5.8.3.5 Cementitious Degradation Rate Sensitivities

The cementitious degradation modeling described in Section 4.4.2 evaluated three sets of assumed inputs: Best Estimates, Compliance Values, or Conservative Estimates. These different values were used to determine the duration of time needed for cementitious materials to progress from initial (intact or undegraded) conditions to final (fully degraded) conditions. To evaluate the individual impacts of these various cementitious degradation rates relative to the Compliance Case, two sensitivity cases were developed:

both of which assume all of the same model inputs and settings as the Compliance Case, but one case applies the cementitious degradation rates based on the best estimate assumptions and the other case applies the cementitious degradation rates based on the Conservative Estimate assumptions. The dose results are presented in Figure 5.8-26 and Figure 5.8-27.

As indicated in Figure 5.8-26, during the Compliance Period all dose results are below 0.012 mrem/yr. The case with the Conservative Estimate degradation rate has a dose that is slightly higher than the Compliance Case and the case with the best estimate degradation rate case has a dose is slightly lower than the Compliance Case.

Figure 5.8-26: Dose Results Comparing the Impacts from Select Cementitious Degradation Rates through the Compliance Period

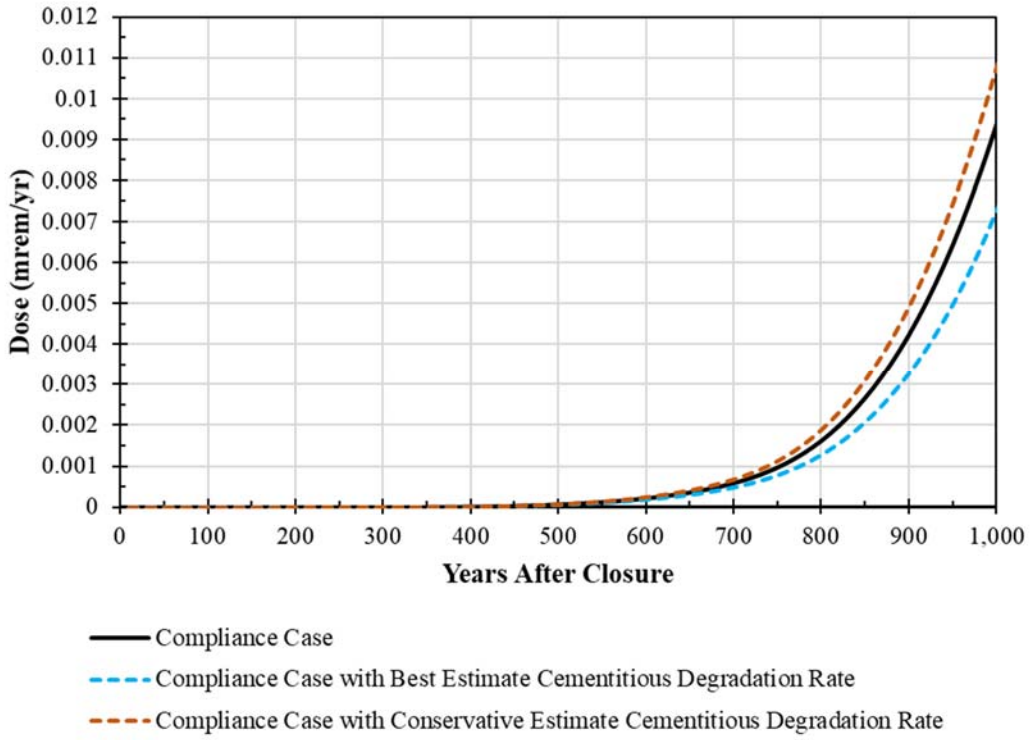

Figure 5.8-27 presents the same dose results out to 10,000 years. All of these dose results are similar in magnitude (peak doses between 1.1 mrem/yr and 1.2 mrem/yr). With faster degradation rates, the dose curve approaches the peak values earlier, but with the slower degradation rates, because it takes longer to reach approach the peak values, the saltstone retains slightly more inventory during the earlier years. As such, the slower degradation rate yields a slightly higher peak dose.

The results of this evaluation indicate that uncertainty in the degradation rates of the cementitious materials has only a slight impact on the shape of the dose curve, but does not significantly impact the timing or the magnitude of the dose results within the Performance Period.

Figure 5.8-27: Dose Results Comparing the Impacts from Select Cementitious Degradation Rates through the Performance Period

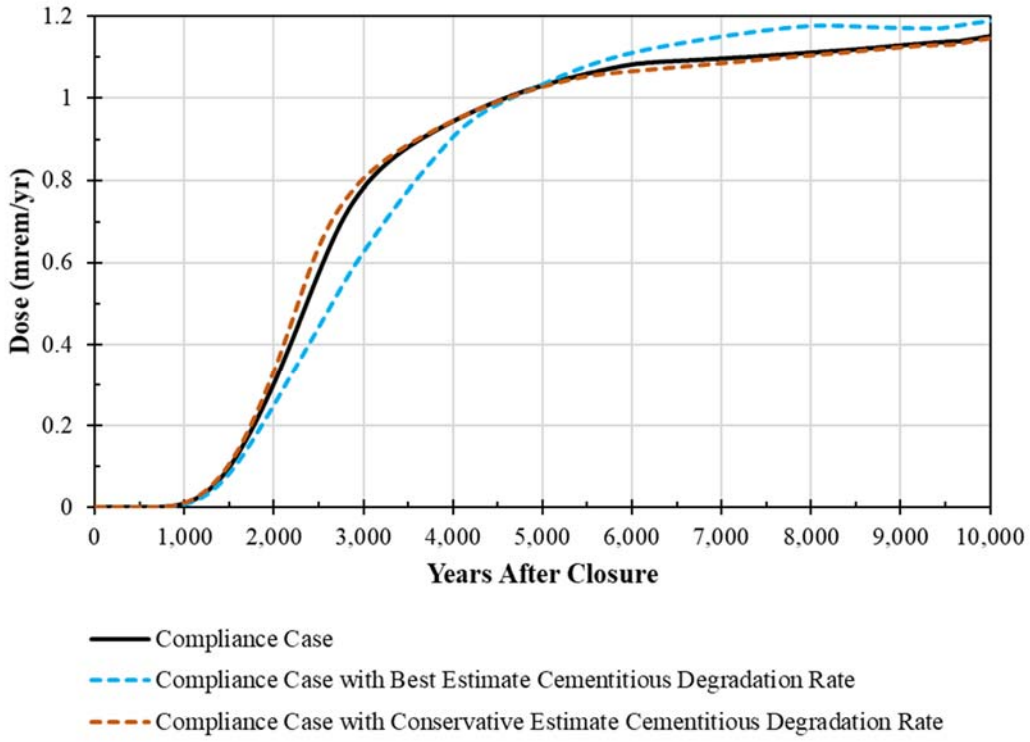

5.8.3.6 Cementitious Degradation Alternate Conductivity Averaging Rate Sensitivities

For the Central Scenario cases, degradation of the saturated hydraulic conductivity of the cementitious materials is computed using the geometric mean of the initial-intact and fully-degraded states based on a time-dependent weighting factor. In the context of a generalized power average $K_e{}^p \equiv \overline{K^p}$, geometric averaging is equivalent to $p \to 0$.

This section considers alternative averaging schemes for computing the hydraulic degradation over time. The alternatives considered are $p = +1$ (arithmetic averaging) and $p = -1$ (harmonic averaging) as described in Section 4.4.2. Parameters for these two cases were set to be the same as the Compliance Case with only the cementitious degradation rates changed.

The dose results are presented in Figure 5.8-28 and Figure 5.8-29. As shown, all of the dose results overlap: the differences between the different cases are negligible; the dose results from the sensitivity cases are virtually identical to the Compliance Case. The results of this evaluation indicate that the differences in these computational approaches for averaging the hydraulic degradation of cementitious materials has a negligible impact on the doses within the Performance Period. This is due to the influence of timing: the SDU concrete degrades relatively quickly, regardless of the computational approach for averaging, while the saltstone degrades relatively slowly. As a result, for the time periods being considered, the averaging approach is unimportant.

Figure 5.8-28: Dose Results Comparing the Impacts of Selected Computation Averaging Techniques for Hydraulic Degradation through the Compliance Period

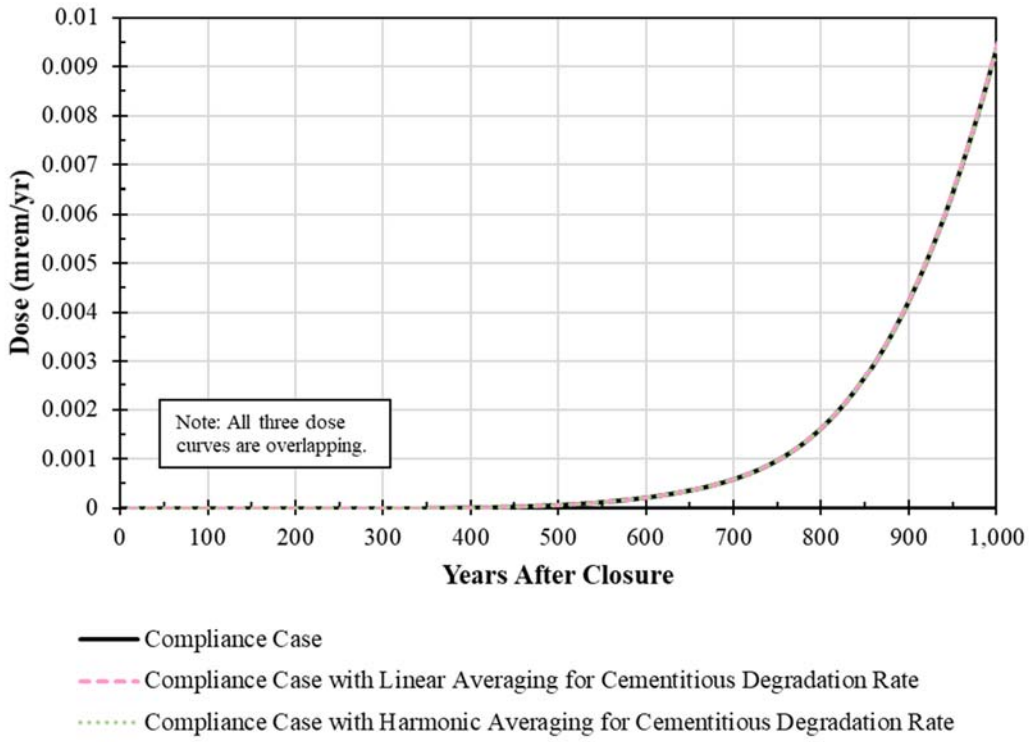

Figure 5.8-29: Dose Results Comparing the Impacts of Selected Computation Averaging Techniques for Hydraulic Degradation through the Performance Period

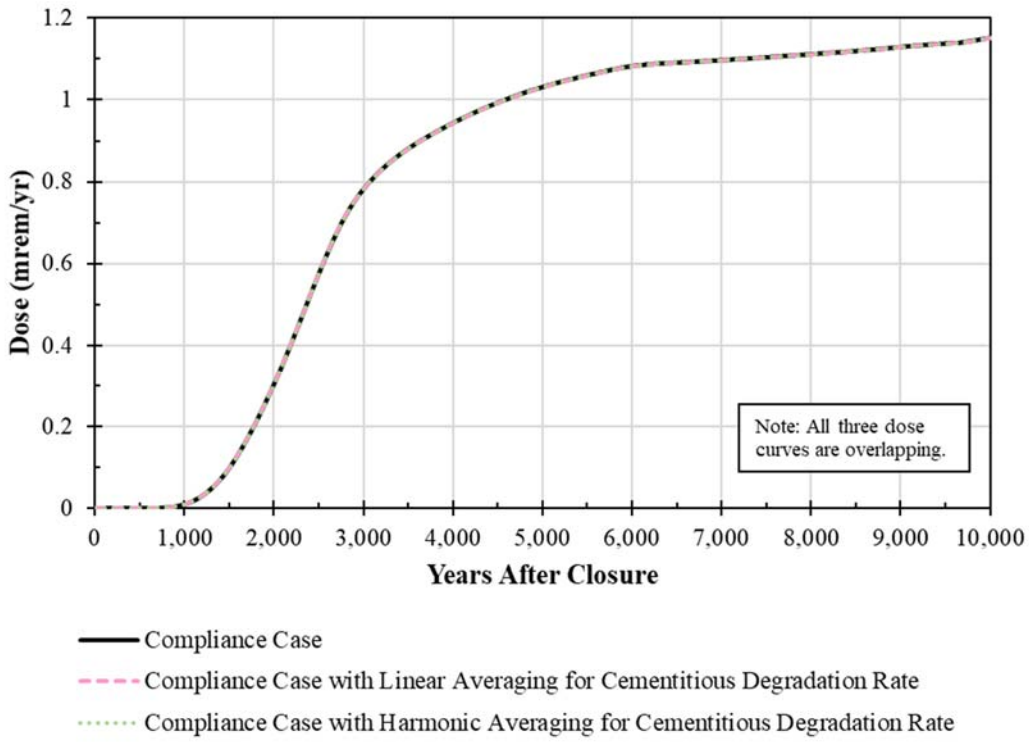

5.8.3.7 Evaluation of Stratification of Saltstone

The Stratified Saltstone Scenario described in Section 4.6.6 was designed to non-mechanistically address the potential impacts from seven specific FEPs (SRR-CWDA-2018-00006):

- FEP 3.2.04, Manufacturing and Commissioning of Components;
- FEP 3.2.10, Preparation of Cementitious Materials;
- FEP 3.3.17, Variability of Field Emplaced Saltstone;
- FEP 3.4.08, Dispersivity Inside SDUs;
- FEP 3.5.13, Dispersion of the Oxidation Front;
- FEP 3.7.09, Localized Degradation; and
- FEP 4.1.06, Waste Allocation and Emplacement.

Table 4.1-5 provides a brief description of each FEP.

As a modeling simplification, the Compliance Case (and the other modeling cases considered throughout this PA) assume that the properties of cured saltstone are homogenous because disposal operations will maintain conditions within specified bounds. However, the saltstone material properties are expected to exhibit some minor heterogeneity based on variability in the mix, changes in the waste concentrations (i.e., differing "salt batches"), and fluctuations in the temperature and humidity during the pouring and curing of fresh saltstone. Prior to curing saltstone is highly flowable, as such it is expected that any heterogeneity will be manifested as stratified layers within the saltstone as each layer is poured, as conceptually depicted in Figure 4.6-4.

For simplicity, only the 375-foot diameter SDUs (i.e., SDUs 6 through 12) are evaluated for the potential impacts of stratification. It is assumed that the smaller disposal units/cells are less likely to exhibit significant stratification. Figure 5.8-30 shows the application of stratification within the PORFLOW vadose zone models. As depicted, three distinct material property types are assumed as alternating layers throughout the saltstone waste form.

Figure 5.8-30: SDU 7 Material Zones for PORFLOW Vadose Zone Modeling, Modified to Simulate Stratified Material Properties in Saltstone

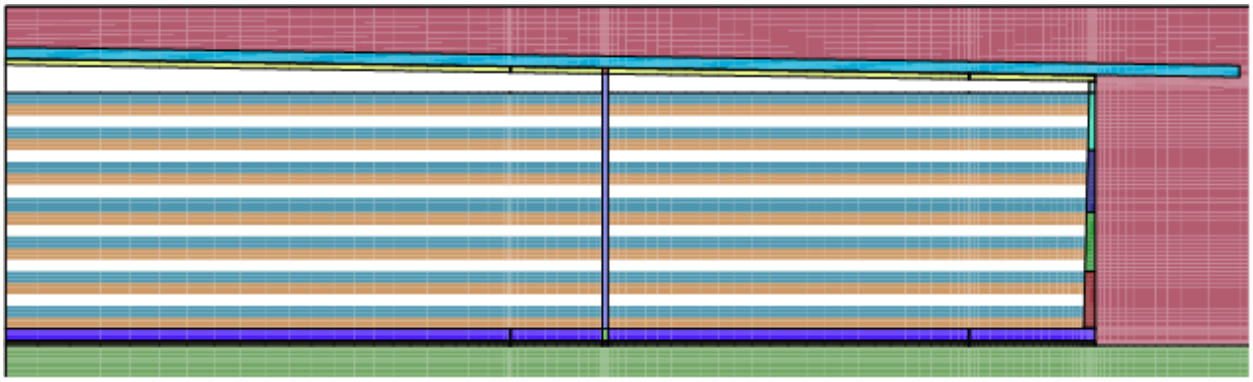

The assignments for the initial material property values for each layer are provided in Table 5.8-13. Any material properties that are not explicitly specified within Table 5.8-13 (e.g., porosity) use the same values as in the Compliance Case, as specified in Section 4.3.1. The initial saturated hydraulic conductivities and effective diffusion coefficients were selected from Table 4.3-3, the reducing capacities were selected from Table 4.3-9, the saltstone degradation timing (start and end) was selected from Table 4.4-45, and the van Genuchten shape parameter was selected from Table 4.4-81.

The last entry in Table 5.8-13 is the inventory fraction. In the Compliance Case, all contaminant inventories are distributed equally throughout the homogenous waste form (e.g., SDU 7 has 2.2 Ci of I-129). For this Stratified Saltstone Scenario, it is assumed that the layers of saltstone with an initial saturated hydraulic conductivity of 2.0E-09 cm/s has higher contaminant concentrations, so it is assigned 4/7 of the total inventory (e.g., approximately 1.26 Ci of I-129). The layers of saltstone with an initial saturated hydraulic conductivity of 1.0E-10 cm/s is assumed to have lower contaminant concentrations, so it is assigned 1/7 of the total inventory (e.g., approximately 0.31 Ci of I-129). The remaining 2/7 of the total inventory is assigned to the layers of saltstone with an initial saturated hydraulic conductivity of 5.0E-10 cm/s.

Table 5.8-13: Material Property Values Assumed for the Stratified Saltstone Scenario

Property or Condition	Units	HIGHER K	LOWER K	SALTSTONE
Initial Saturated Hydraulic Conductivity	cm/s	2.0E-09	1.0E-10	5.0E-10
Initial Effective Diffusion Coefficient	cm^2/s	3.4E-08	6.8E-09	1.3E-08
Reducing Capacity	$\mu eq\ e^-/g$	350	650	500
Degradation Timing (Start)	yr	1,371	2,306	1,552
Degradation Timing (End)	yr	2.6E+06	2.6E+08	1.7E+07
Van Genuchten shape parameter: a	unitless	4.5080e-5	1.0080e-5	2.2540e-5
Inventory Fraction	unitless	4/7	1/7	2/7

Within PORFLOW, the material type designations for each layer were labeled in reference to the initial saturated hydraulic conductivities for modified material properties:

- "SALTSTONE" is used to indicate that the values are unchanged from the MPAD (or Compliance Case) with a value of 5.0E-10 cm/s;
- "HIGHER K" is used for the teal layers which assume an initial saturated hydraulic conductivity of 2.0E-09 cm/s; and
- "LOWER K" is used for the tan layers which assume an initial saturated hydraulic conductivity of 1.0E-10 cm/s.

Note the geometric mean of these values, as applied, is slightly lower than the Compliance Case value (4.6E-10 cm/s versus 5.0E-10 cm/s).

Figure 5.8-31 shows a side-by-side comparison of the progression of I-129 concentrations within SDU 7. The left side shows the I-129 concentrations (in mol/L) from the

Compliance Case and the right side shows the I-129 concentrations for the Stratified Saltstone Scenario. Initially, the figures are notably different, but over time higher concentrations will diffuse into areas with lower concentrations such that by 10,000 years after closure, both representations are nearly identical.

Figure 5.8-31: Comparison of Evolving I-129 Concentrations between the Compliance Case and the Stratified Saltstone Scenario

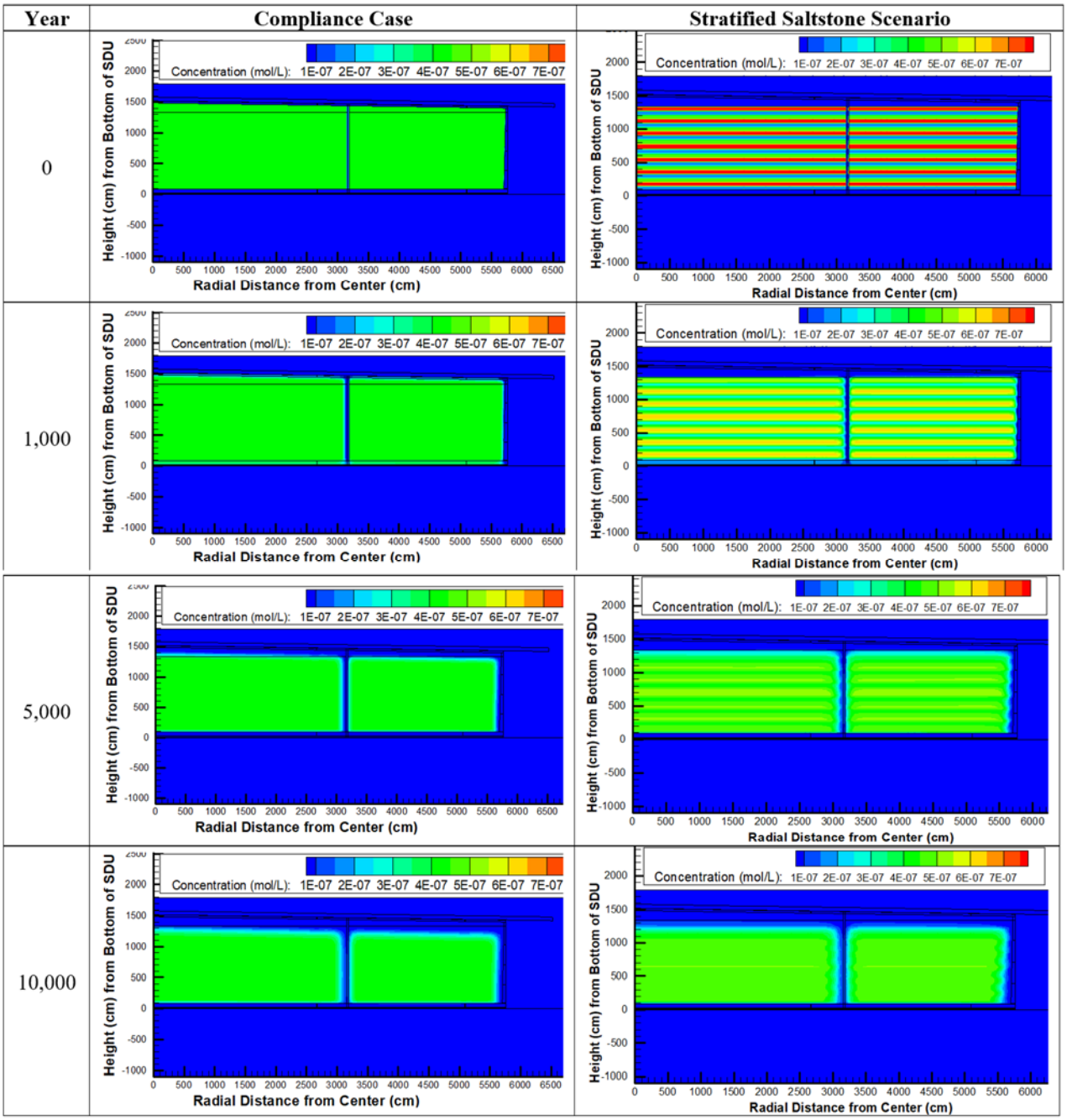

This Stratified Saltstone Scenario does not explicitly consider the influence of dispersion (FEP 3.4.08 and FEP 3.5.13). As with the Compliance Case, the Stratified Saltstone

Scenario assumes that mechanical dispersion can be neglected in the vadose zone model because the varying material properties of the cementitious materials are explicitly modeled (see Section 4.4.4). Therefore, the dispersivities were set to zero within the SDUs.

For completeness, it is important to evaluate the potential influence of dispersivity within the SDUs. To assess this, both the Compliance Case and the Stratified Saltstone Scenario were modified: the longitudinal dispersivity was set to 1 meter and the transverse dispersivity was set to 0.1 meters within saltstone. These values were selected for illustrative purposes only because actual dispersivity values within heterogeneous pours of saltstone are expected to be variable and specific to the pour conditions of each SDU. The other materials are assumed to be homogeneous and retain zero dispersivity.

Only the 375-foot diameter SDUs (i.e., SDUs 6 through 12) and only the sensitivity run radionuclides were evaluated for this analysis. Figure 5.8-32 provides the total dose to the MOP for four specific modeling cases:

- **Compliance Case** (black curve): homogenous saltstone and no dispersivity.
- **Compliance Case with Dispersivity** (green curve): homogenous saltstone but assumes 1 m longitudinal dispersivity and 0.1 m transverse dispersivity.
- **Stratified Saltstone Case** (orange curve): heterogeneous saltstone as defined in Table 5.8-13.
- **Stratified Saltstone Case with Dispersivity** (dashed curve): heterogeneous saltstone as defined in Table 5.8-13 and assumes 1 m longitudinal dispersivity and 0.1 m transverse dispersivity.

Figure 5.8-32 demonstrates that incorporating dispersivity into the model tends to accelerate releases, while stratifying the material properties tends to decelerate the releases (as controlled by the layers with the lowest saturated hydraulic conductivities). In this case, incorporating both dispersivity and stratification resulted in a slightly higher, slightly earlier dose peak. However, this case relied on simplifying assumptions with respect to the assumed dispersive lengths and the degree to which the saltstone would be stratified. Because stratification of the waste form results in doses that are lower than the Compliance Case doses, relative to peak doses within 10,000 years, the assumption that the material properties of the saltstone monolith is homogeneous is an appropriate modeling simplification.

Figure 5.8-32: Comparison of Total MOP Doses Based on Assumed Stratification and Assumed Dispersivities

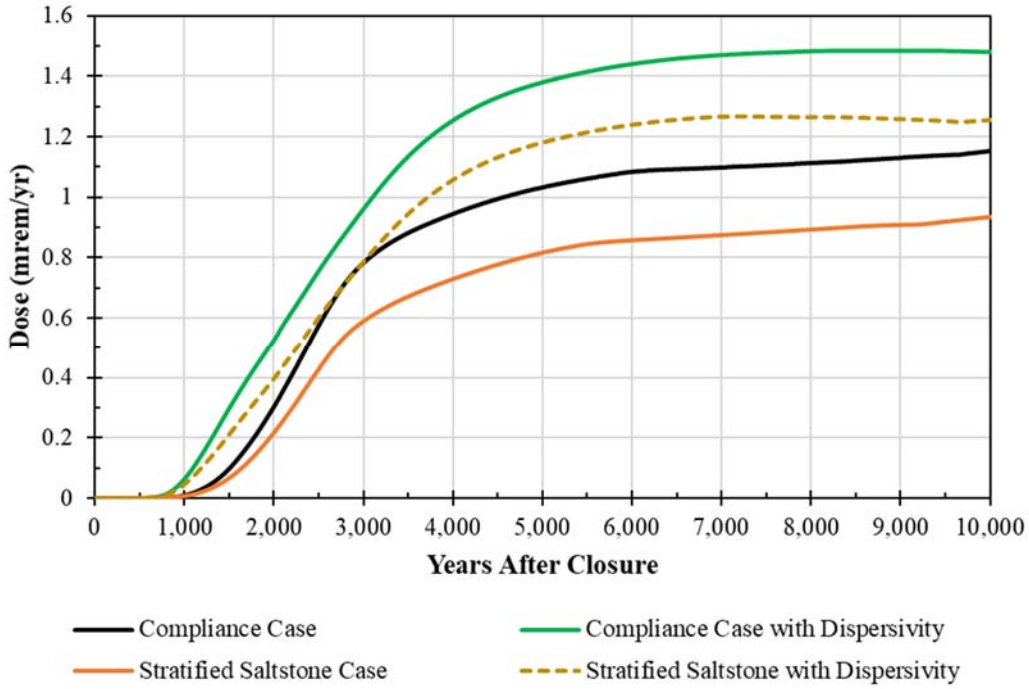

5.8.4 Contaminant Release Sensitivities

The following describes various sensitivity cases developed to better understand the uncertainties and risks that are specifically associated with the modeling assumptions applied for simulating contaminant releases (see Section 4.4.3).

5.8.4.1 Evaluation of Technetium Solubility

The shrinking-core model applied to Tc-99 transport causes saltstone solubility to decrease from 9.7E-07 to 4.5E-07 mol/L as incoming oxygen consumes the buffering capacity around the SDU periphery, and then loss of solubility control when reducing capacity is exhausted. [SRR-CWDA-2018-00046, SRNL-STI-2018-00652] These sensitivity cases simulate Tc-99 transport using a non-shrinking core model with solubility limits of 9.7E-07 and then 4.5E-07 mol/L, which are expected to approximately bracket the shrinking core model. As shown in Figure 5.8-33, the peak dose when Tc-99 solubility is fixed at 9.7 E-07 mol/L is higher than the Compliance Case, and the peak dose with the solubility at 4.5E-07 mol/L is lower, as expected. At early times, the Compliance Case flux is larger than both sensitivity cases. For the Compliance Case a fraction of the initially reducing cementitious materials becomes oxidizing and releases Tc-99 to the aqueous phase, whereas in the two non-shrinking core models the entire monolith remains in a reducing state.

Figure 5.8-33: Flux Comparison for the Sensitivity Case with a Non-Shrinking Core Tc-99 Model

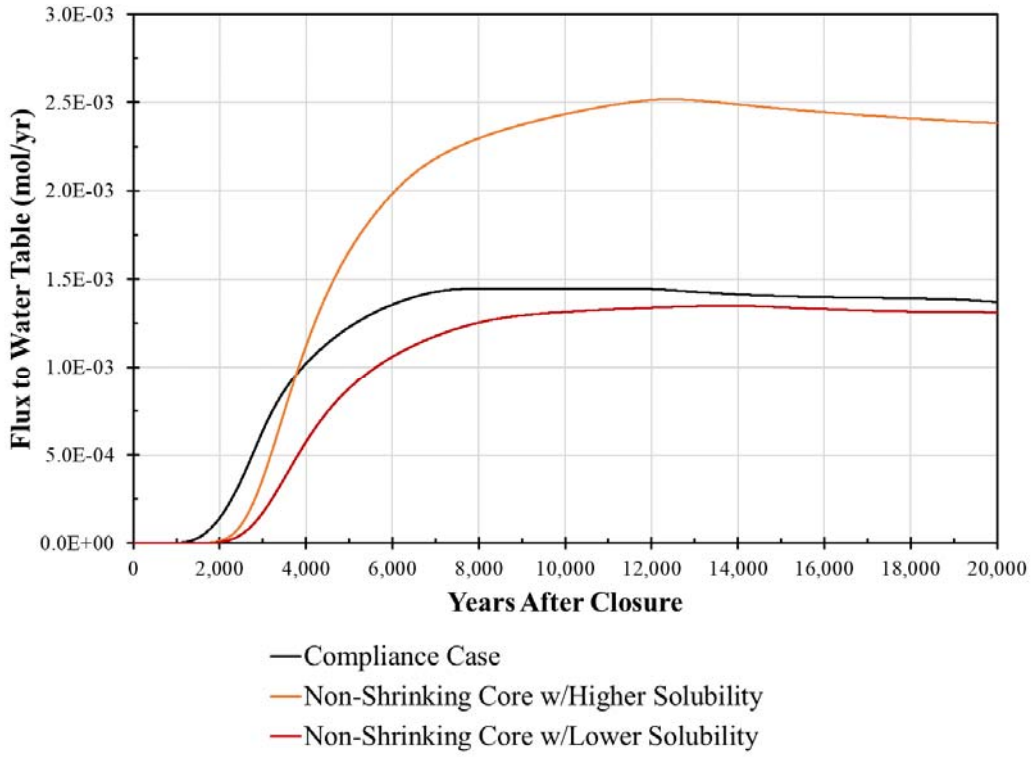

5.8.4.2 Evaluation of Iodine Partition Coefficient

The release and transport of I-129 is simulated as a function of the evolving chemical conditions in the system (see Sections 4.4.3 and 4.4.5). Table 5.8-14 provides a summary of this evolution with respect to saltstone transport based on the values provided Table 4.3-6 and the discussion of I-129 release in Section 4.4.3.

Due to the importance of I-129, relative to dose, the shrinking core modeling approach has been applied to simulate releases from saltstone. In the shrinking core model, rather than simulating the transitions from Table 5.8-14 as a function of the entire saltstone monolith, these transitions are applied on a model node-by-model node basis. With this approach, the model nodes which are subject to the more flow (e.g., near the intersection of the SDU roof and SDU walls or nearer to exposure surfaces) undergo faster transitions. This approach provides a more realistic representation of expected conditions.

Table 5.8-14: Summary of the Changing Transport Properties for I-129 in Saltstone

Transition or Condition	Resulting K_d (mL/g)	Discussion
Initial Condition (Reducing Region I)	0.07	This value is based on measured releases of I-129 (via DLM testing on a simulant core). The measured values were used as an input to a standalone GoldSim optimization model to calculate the initial K_d. [SRR-CWDA-2018-00045]
Reducing Region I → Reducing Region III	0.71	This value is based on measured releases of I-129 (via DLM testing on simulant cores). The measured values were used as an input to a standalone GoldSim optimization model to calculate the K_d. [SRR-CWDA-2018-00045] Note that the pH transition is directly from Region I to Region III as the occurrence of a Region II chemical environment is precluded by the absence of calcium hydroxide ($Ca(OH)_2$) in saltstone.
Reducing Region III → Oxidizing Region III	4.0	This value is from SRNL-STI-2009-00473 and the Eh transition (from reducing to oxidizing) is from SRNL-STI-2018-00586, which determined that this transition requires 850 pore volume exchanges for incoming oxygen to consume the reducing agents in the saltstone. Note that under Compliance Case conditions, all available I-129 is released from the saltstone before this chemical transition occurs.

A sensitivity case model has been developed to illustrate how the application of this shrinking core model influences the release and transport of I-129, relative to other modeling approaches. For this sensitivity case, all model inputs and setting are the same as the Compliance Case, but rather than using the shrinking core model, the release and transport of I-129 is simulated using the same non-shrinking core model that was applied to generic species. This approach delays the onset of the K_d transitions until the entire saltstone monolith transitions in pH or Eh. Under Compliance Case conditions, both transitions occur after 10,000 years.

Figure 5.8-34 shows fluxes of I-129 from SDU 7 to the water table based on the shrinking core modeling approach used for Compliance Case (black curve) and based on the non-shrinking core approach from this sensitivity case. As shown, the peak flux at 10,000 years increases by nearly 50% with this alternative modeling approach. The non-shrinking core model applies the lower Region I K_d to the entire monolith over 10,000 years, whereas the shrinking core model assigns the higher K_d values to outer nodes as local pH and Eh transitions occurs within 10,000 years. While the shrinking core modeling approach provides lower fluxes, it provides a better representation of the expected release and transport behavior of I-129, as informed by DLM testing.

Figure 5.8-34: Flux Comparison for the Sensitivity Case Simulating I-129 Transport with a Non-Shrinking Core Model

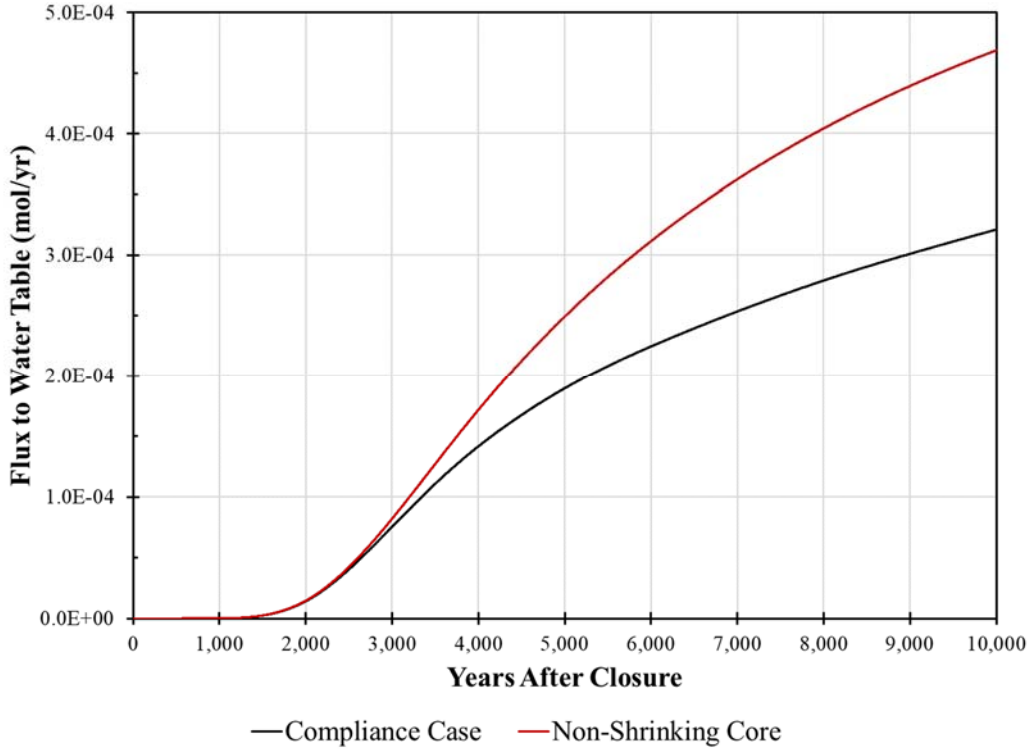

5.8.4.3 General K_d Sensitivities

Experimentally measured K_d values can vary significantly. For many of the radionuclides modeled in the Compliance Case, transport is strongly influenced by the K_d values. The following analysis uses the SDF GoldSim Model to vary the K_d values. A number of variations are applied to provide additional insights with respect to the overall influence that the K_d values have relative to the total dose to the MOP. For the values used in the Compliance Case, refer to Table 4.3-4 for soil K_ds, Table 4.3-5 for cementitious K_ds, and Table 4.3-6 for saltstone-specific K_ds.

For the first sensitivity case, every K_d value within the SDF GoldSim Model was modified uniformly, decreasing all the K_ds by a factor of 100 (All K_ds × 0.01). The resulting total dose to the MOP is shown in Figure 5.8-35.

Figure 5.8-35: Comparison of Total MOP Doses Based on Decreasing All K_ds by a Factor of 100

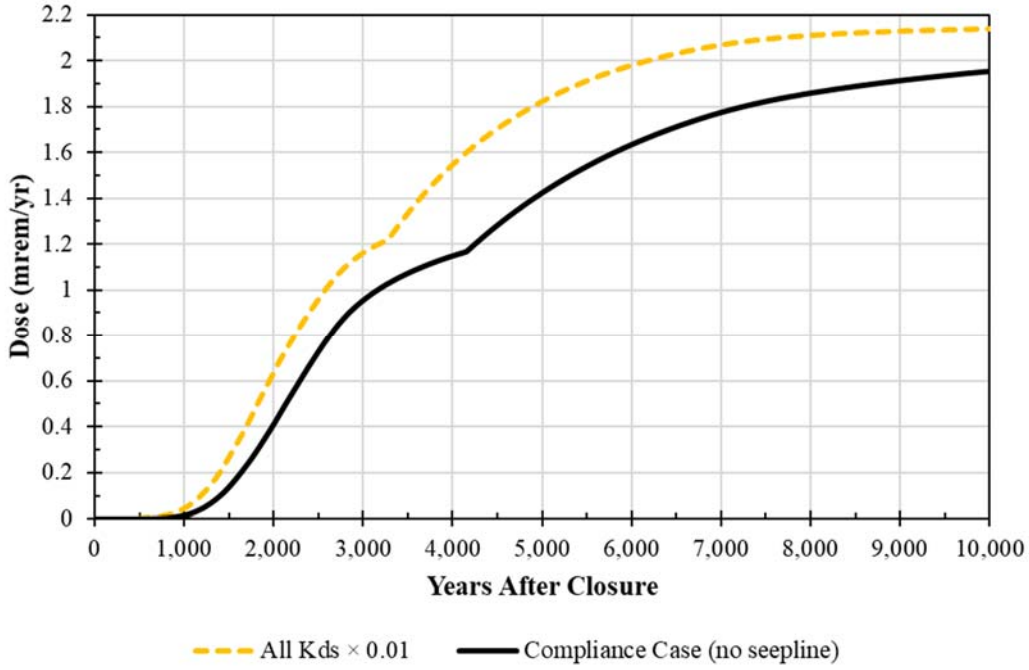

Note that because these sensitivity cases influence the soil K_ds, the assumed seepline ratio of 0.22 (see Section 5.2.3) is no longer appropriate. To simplify the comparison, the seepline ratio was set to zero for these sensitivity cases (i.e., these cases assume zero concentrations at the seepline so there is no dose contributions from fish ingestion, swimming, or boating).

Decreasing all of the K_d values in the SDF GoldSim Model by a factor of 100 results in a minor increase to the total MOP dose during the 10,000-year Performance Period: from a peak of 1.8 mrem/yr to a peak of 2.1 mrem/yr. The timing of the peak also shifted from 10,000 years to 9,920 years.

Closer inspection of this modeling case reveals that the largest relative difference to the dose contributions (albeit still negligible) were seen in Pu-239. Recent studies for the plutonium K_ds in SRS soils provide strong evidence that the plutonium K_ds used in this SDF PA are overly pessimistic (i.e., defensible). [SRRA021685-000009, SRRA021685-000010]

Ultimately, this analysis reveals that all of the K_d values used for the SDF PA would have to be incorrect by orders of magnitude in every transport media before any significant influence could be realized. This is because the total dose for the Compliance Case is currently driven by I-129 and Tc-99, which are both already assigned very small K_d values. In other words, these two radionuclides are already highly mobile and readily transported, so reducing their K_ds has a minimal impact on SDF performance.

For the next set of sensitivity cases the K_ds in select chemical environments were effectively set to zero (each sensitivity case modifies only one media/chemical environment). Specifically, values were multiplied by a very small number (1.0E-30). Five cases were developed for this set:

1. Reducing Region II K_ds × 1.0E-30 ("Re I × 1E-30"),
2. Reducing Region III K_ds × 1.0E-30 ("Re III × 1E-30"),
3. Oxidizing Region I K_ds × 1.0E-30 ("Ox I × 1E-30"),
4. Oxidizing Region III K_ds × 1.0E-30 ("Ox III × 1E-30"), and
5. All Soil K_ds × 1.0E-30 ("Soils × 1E-30").

Region II K_ds were not evaluated because these K_ds are not used. The saltstone-specific K_ds (see Table 4.3-6) were modified along with the respective cementitious materials. For the sensitivity case with the modified soil K_ds, all soils were modified, including the leachate-impacted soil K_ds.

Figure 5.8-36 illustrates the respective influence from each of the sensitivity cases except for Soils × 1E-30, which is depicted in Figure 5.8-37. While the results in Figure 5.8-36 all use the seepline ratio of 0.22, the results in Figure 5.8-37 assume zero concentrations along the seepline because this sensitivity case modifies the soil K_ds, making use of the seepline ratio an inappropriate modeling simplification. These figures show that the change to the soil K_ds had the greatest influence overall, followed by the change to the Reducing Region I K_ds. The doses from the other sensitivity cases overlap the Compliance Case dose result indicating that these changes had no noticeable impact.

Figure 5.8-36: Comparison of Total MOP Doses Based on Negating the Influence of K_ds Based on Cementitious Chemical Environments or Model Regions

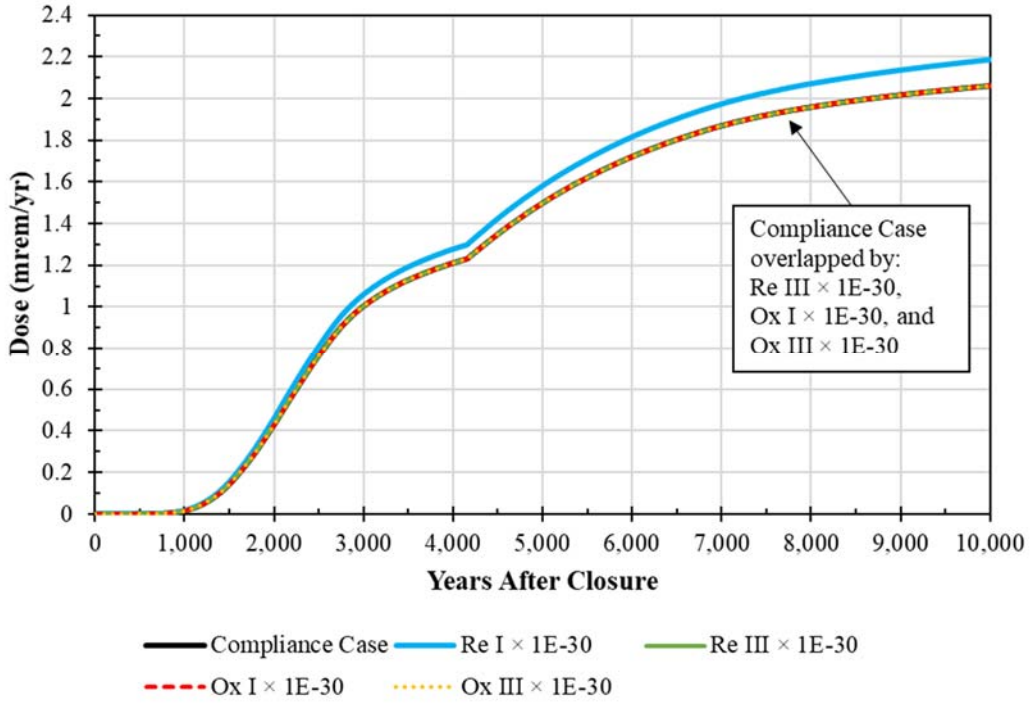

Figure 5.8-37: Comparison of Total MOP Doses Based on Negating the Influence of K_ds Based on Soils-Based Chemical Environments or Model Regions

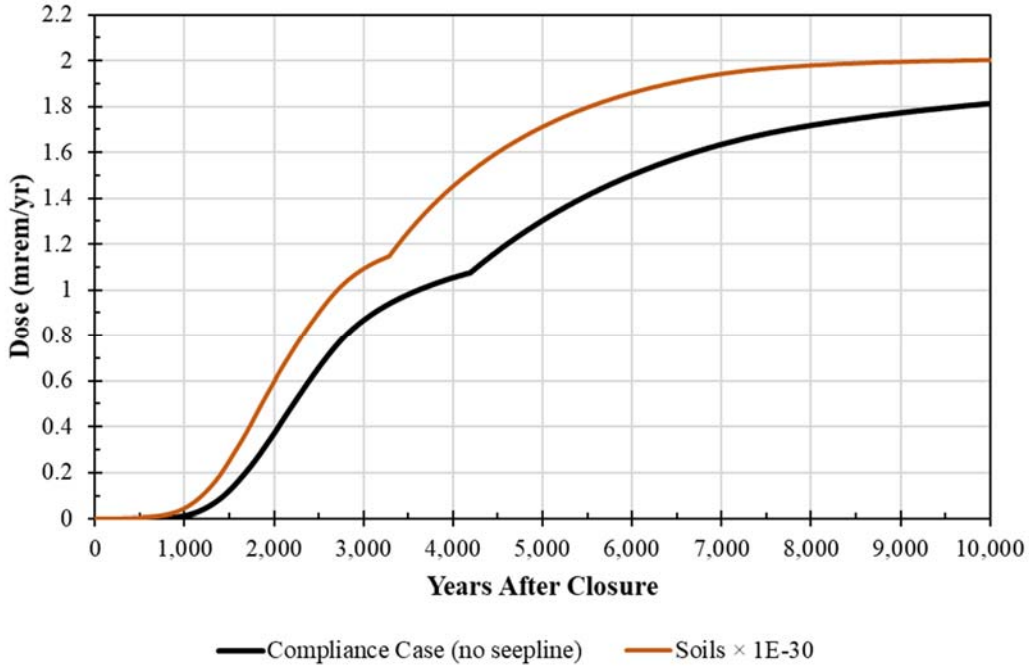

The last set of sensitivity cases evaluates the influence that K_ds have with respect to the assumed evolution of the chemical environment. As specified in Table 4.4-58, the initial chemical environment for most of the cementitious materials is assumed to be Reducing Region I. For most of these materials, the timing required to undergo any chemical transitions exceeds the Compliance Period (see Section 4.4.3). To evaluate the assumed starting chemical environment, sensitivity cases were developed which assumed the K_ds for Reducing Region I were equal to the K_ds from other chemical environments:

- Reducing Region I K_ds were set equal to Reducing Region II K_ds ("Assumes ReII"),
- Reducing Region I K_ds were set equal to Reducing Region III K_ds ("Assumes ReIII"), and
- All Reducing K_ds were set equal to the Oxidizing K_ds ("Assumes Ox").

The comparisons for this set of sensitivity cases is provided in Figure 5.8-38, which shows that the configuration selected for the Compliance Case maximizes the peak dose to the MOP within the Performance Period. This is attributed to the influence of I-129, which has lower K_ds under Compliance Case conditions.

Figure 5.8-38: Comparison of Total MOP Doses Based on Assuming K_ds from Different Cementitious Chemical Environments or Model Regions

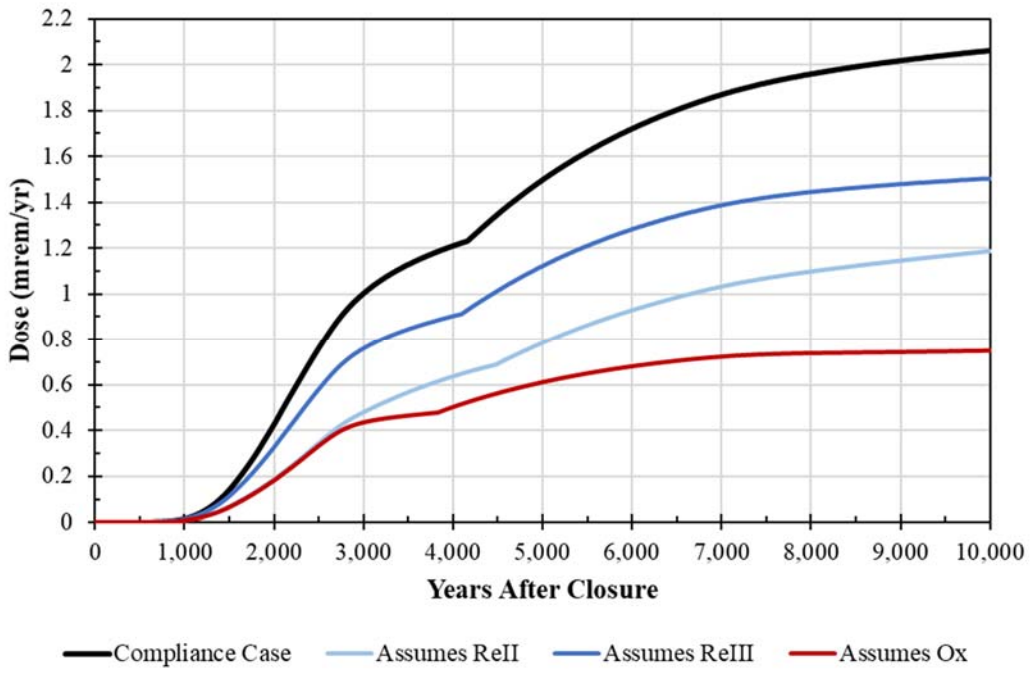

The influences of the assumed leachate-impacts on soils were also evaluated with a similar approach:

- Leachate-impacted soil K_ds (for both clays and sands) were set equal to their non-leachate-impacted counterparts ("No Leachate Impacts").
- The non-leachate-impacted soil K_ds (for both clays and soils) were set equal to their leachate-impacted counterparts ("All Leachate Impacts").

The comparisons for this final set of sensitivity cases is provided in Figure 5.8-39, which shows a minimal difference in the doses between the Compliance Case and the case that assumes all soils are leachate-impacted. Again, the configuration used for the Compliance Case maximizes the peak dose to the MOP within the Performance Period due to the influence of I-129.

Figure 5.8-39: Comparison of Total MOP Doses Based on Assuming K_ds from Different Soil-Based Chemical Environments or Model Regions

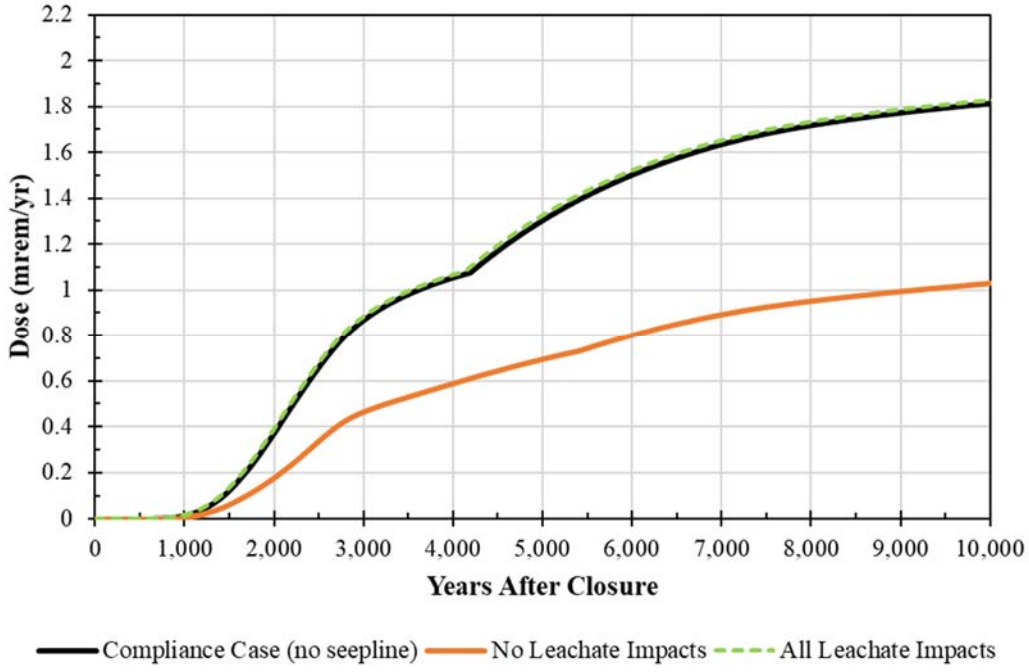

Table 5.8-15 provides a summary of each of these K_d Sensitivity Cases and the respective peak doses. These sensitivity cases demonstrate that despite the inherent uncertainty in the K_d values assumed for the PA, the risk-significance associated with this is minimal, and the modeling decisions related to the applicability of K_ds associated with specific chemical environments is defensible.

Table 5.8-15: Summary of General K_d Sensitivity Cases

Case Name	Figure(s)	Changes to K_ds	Peak Doses (mrem/yr)	
			Compliance Period (0 to 1,000 Years)	Performance Period (0 to 10,000 Years)
Cases that use the seepline ratio				
Compliance Case*	**Figure 5.8-36 and Figure 5.8-38**	**No Change**	**1.6E-02**	**2.1**
Re I × 1E-30	Figure 5.8-36	Reducing Region I K_ds × 1.0E-30	1.6E-02	2.2
Re III × 1E-30	Figure 5.8-36	Reducing Region III K_ds × 1.0E-30	1.6E-02	2.1
Ox I × 1E-30	Figure 5.8-36	Oxidizing Region I K_ds × 1.0E-30	1.6E-02	2.1
Ox III × 1E-30	Figure 5.8-36	Oxidizing Region III K_ds × 1.0E-30	1.6E-02	2.1
Assumes RelI	Figure 5.8-38	Reducing Region I K_ds = Reducing Region II K_ds	7.4E-03	1.2
Assumes RelII	Figure 5.8-38	Reducing Region I K_ds = Reducing Region III K_ds	1.2E-02	1.5
Assumes Ox	Figure 5.8-38	All Reducing Region K_ds = Oxidizing Region K_ds	6.9E-03	0.75
Cases that do not use the seepline ratio				
Compliance Case* (no seepline)	**Figure 5.8-35, Figure 5.8-37, and Figure 5.8-39**	**No Change**	**1.3E-02**	**1.8**
All K_ds × 0.01	Figure 5.8-35	All K_ds × 0.01	4.4E-02	2.1
Soils × 1E-30	Figure 5.8-37	All Soil K_ds × 1.0E-30	4.3E-02	2.0
No Leachate Impacts	Figure 5.8-39	All Leachate-Impacted Soil K_ds = Non-Leachate-Impacted Soil K_ds	6.5E-03	1.0
All Leachate Impacts	Figure 5.8-39	All Non-Leachate-Impacted Soil K_ds = Leachate-Impacted Soil K_ds	1.5E-02	1.8

* Because this is a GoldSim simulation, the peak doses are slightly different from those reported for the Compliance Case discussed in Section 5.5 which relied on PORFLOW simulations for modeling contaminant transport. Refer to the Benchmarking Analysis (Section 5.6) for graphical comparisons.

5.8.4.4 Evaluation of SDU Concrete Reducing Capacity

The SDU concrete formula contains blast furnace slag, which increases the reducing capacity of the concrete. This increased reducing capacity provides a chemical barrier to the transport of Tc-99. The reducing capacity prevents aqueous concentrations of Tc-99 from exceeding a solubility limit and incoming oxygen will consume the reducing agents until they are depleted. Because Tc-99 concentrations leaving the initially reducing saltstone are already at or below the solubility limit, the same solubility limit in concrete does not affect transport through that barrier. However, oxygen scavenging by reductants in the SDU concrete delays the oxidation of saltstone, which eventually results in the loss of solubility control. These processes may affect transport depending on total Tc-99 concentrations within the oxidized rind. Although reducing conditions delay Tc-99

transport, oxidizing conditions are preferred for I-129 retention due to a higher partition coefficient (K_d value).

To evaluate the various effects of reducing conditions in the SDU concrete, a number of simulations were performed as summarized in Table 5.8-16. In this table, settings that match the Compliance Case are shown in **black** text while settings that deviate from those of the Compliance Case are shown in red text.

Table 5.8-16: Modeling Cases to Evaluate SDU Concrete Reducing Capacity

Case		Slag in SDU Concrete?	K_dRe (mL/g)	Infiltration	Tc Solubility (mol/L)
CaseCV	Compliance Case	Yes	0.01	MPAD	9.7E-07 to 4.5E-07
CaseSA48	Compliance Case w/ no SDU Slag	No	0.01	MPAD	9.7E-07 to 4.5E-07
CaseSA49	Compliance Case K_dRe=0.5	Yes	0.5	MPAD	9.7E-07 to 4.5E-07
CaseSA50	Compliance Case w/ no SDU Slag and K_dRe=0.5	No	0.5	MPAD	9.7E-07 to 4.5E-07
CaseSA51	HELP Infil. and K_dRe=0.5	Yes	0.5	2008 HELP	9.7E-07 to 4.5E-07
CaseSA52	HELP Infil. w/ no SDU Slag and K_dRe=0.5	No	0.5	2008 HELP	9.7E-07 to 4.5E-07
CaseSA53	HELP Infil. and K_dRe=0.5 and Tc Sol = 1E-08M (CaseSA53)	Yes	0.5	2008 HELP	1.0E-08
CaseSA54	HELP Infil. w/ no SDU Slag and K_dRe=0.5 and Tc Sol = 1E-08M	No	0.5	2008 HELP	1.0E-08

K_dRe = effective K_d of technetium in the SDU concrete under reducing conditions.

Table 5.8-16 shows these modeling cases varied four parameters or settings. The first is whether slag is included in the SDU concrete formula. The next consideration was the effective K_d of technetium in the SDU concrete under reducing conditions (abbreviated as "K_dRe"). This is followed by the infiltration rate. Finally, technetium solubility was also varied to provide additional insight.

With respect to the blast furnace slag in the SDU concrete, the model changes are only applied to future SDUs (SDUs 8 through 12) because the existing SDUs all include slag. If there is blast furnace slag in the SDU concrete, the material has a reducing capacity of 2.09E-01 meq e^-/g, while concrete without the slag component is assumed to be three orders of magnitude lower (2.09E-04 meq e^-/g).

For K_dRe, Figure 4.4-85 shows in the Compliance Case the K_dRe in the SDU concrete is assumed to be 0.01 mL/g under reducing conditions, but once the material is oxidized the K_d increases to 0.5 mL/g. As with saltstone, it is expected that while the SDU concrete has reducing capacity, the mobility of the technetium within the SDU concrete will be controlled by solubility. However, because the initial concentration of Tc-99 in the SDU concrete is 0 pCi/L and the K_d for Tc-99 at concentrations below the solubility limit has not been experimentally defined, the K_dRe value of 0.01 mL/g was assumed as it is an

arbitrarily low value. Thus, when Tc-99 is transported through the oxidizing region of the SDU concrete, a higher K_d (slower transport) relative to the reducing region is applied.

Next, these modeling cases evaluated infiltration. Under higher infiltration rates, the rate of oxidation will increase. For this evaluation, the infiltration rate developed in 2008 with the HELP code (described in Section 5.8.2.2) was selected for demonstration purposes, while the Compliance Case infiltration rate is based on the MPAD results of the Closure Cap Model (see Section 4.4.1.4).

Finally, upon evaluating the other conditions (discussed below), it was determined that due to the high solubility limit, the rate of technetium transport through the SDU concrete is faster than the rate of oxidation of the SDU concrete, such that the reducing capacity had a minimal influence on technetium transport. To further evaluate, a lower technetium solubility limit was assumed (1.0E-08 mol/L) to slow the release of Tc-99.

The first sensitivity case (CaseSA48 in Table 5.8-16) assumes the SDU concrete in the future SDUs (SDUs 8 through 12) will not include any blast furnace slag. To simulate this, the much lower reducing capacity (2.09E-04 meq e^-/g) was applied to the SDU concrete. It was originally expected the lower reducing capacity would show slightly earlier releases of Tc-99; however, the comparison of the Tc-99 fluxes in Figure 5.8-40 shows the lower reducing capacity had slightly later releases.

Investigation of this modeling case revealed the later release was due to the very low effective K_d applied to technetium under reducing conditions (K_dRe of 0.01 mL/g), which was an arbitrary (and likely overly pessimistic) assumption that does not provide insight into the actual effects of changes to the reducing capacity for extremely low concentration conditions.

As with the Tc-99 fluxes in Figure 5.8-40, Figure 5.8-41 shows the fluxes for I-129 are also slower to arrive when there is no blast furnace slag in the SDU concrete. This was the expected outcome based on an in-depth literature review of iodine K_ds in cementitious materials, which indicated iodine under reducing conditions is more mobile than iodine under oxidizing conditions. [SRNL-STI-2009-00473] Accordingly, when the SDU concrete is under reducing conditions, the K_d of iodine is either 0.07 to 0.71 mL/g (depending on pH) while a K_d of 4 mL/g is applied to iodine under oxidizing conditions (see Table 4.3-5). Therefore, with respect to the iodine K_d, including the blast furnace slag in the SDU concrete provides a bias towards faster ioding transport, resulting in higher I-129 doses.

Figure 5.8-40: Comparison of Tc-99 Flux to the Water Table from SDU 8, With and Without Slag in the SDU Concrete, Based on Compliance Case Conditions

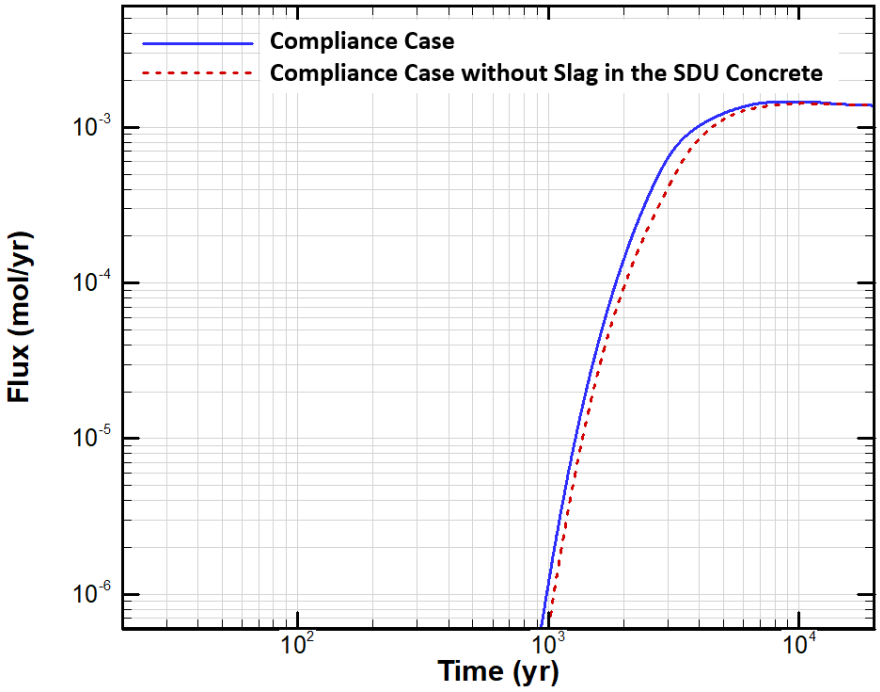

Figure 5.8-41: Comparison of I-129 Flux to the Water Table from SDU 8, With and Without Slag in the SDU Concrete, Based on Compliance Case Conditions

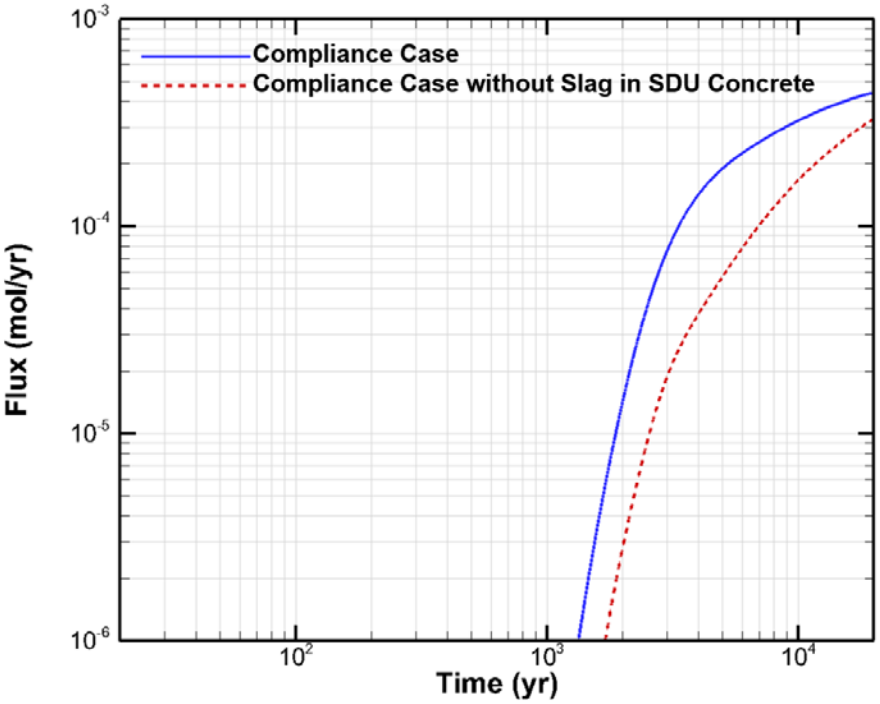

Because the Compliance Case assumed the arbitrarily low effective K_d for technetium under reducing conditions (K_dRe of 0.01 mL/g), it does not provide an adequate basis for

comparison with respect to understanding the effectiveness of the reducing capacity of the SDU concrete for inhibiting the transport of Tc-99. Therefore, a modified version of the Compliance Case was developed. For this modified version, instead of assuming an initial effective K_d for Tc-99 of 0.01 mL/g in reducing SDU concrete, the initial effective K_d was set to be equal to the K_d under oxidizing conditions (K_dRe of 0.5 mL/g).

Figure 5.8-42 shows the resulting comparison with blast furnace slag (CaseSA49 in Table 5.8-16) and without the blast furnace slag (CaseSA50 in Table 5.8-16). These two cases appear to have identical results because the depletion of Tc-99 near the outer edges of the saltstone waste form advances faster than the oxidation front passing through the SDU concrete into the saltstone. Because Tc-99 concentrations diminish to be less than the solubility limit by the time the oxidation front arrives in saltstone, the loss of solubility control does not affect Tc-99 concentrations, even though the oxidation front arrives sooner with no-slag concrete. Thus, changes to the reducing capacity of the SDU concrete have no impact on the release rates of Tc-99.

Figure 5.8-42: Comparison of Tc-99 Flux to the Water Table from SDU 8, With and Without Slag in the SDU Concrete, Based on a Minimum Effective K_d of 0.5 mL/g

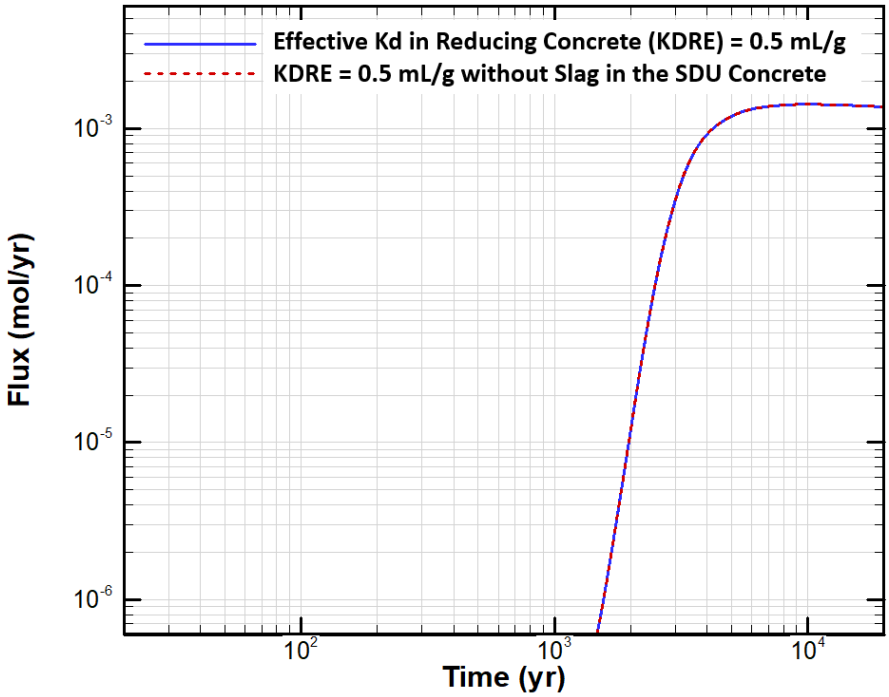

Figure 5.8-43 shows the total dose results for the first modeling cases (from Table 5.8-16), including the Compliance Case. The doses from the Compliance Case with and without slag in the SDU concrete are depicted with solid lines, while the equivalent doses from the modified cases (K_dRe of 0.5 mL/g instead of 0.01 mL/g) are depicted with dashed and dotted lines. Despite some minor differences in the timing of the breakthrough curves, these results indicate the changes in the reducing capacity of the SDU concrete has a negligible impact on the magnitude of future doses.

Figure 5.8-43: Dose Comparison of Modeling Cases With and Without Slag in SDU Concrete for SDUs 8 through 12

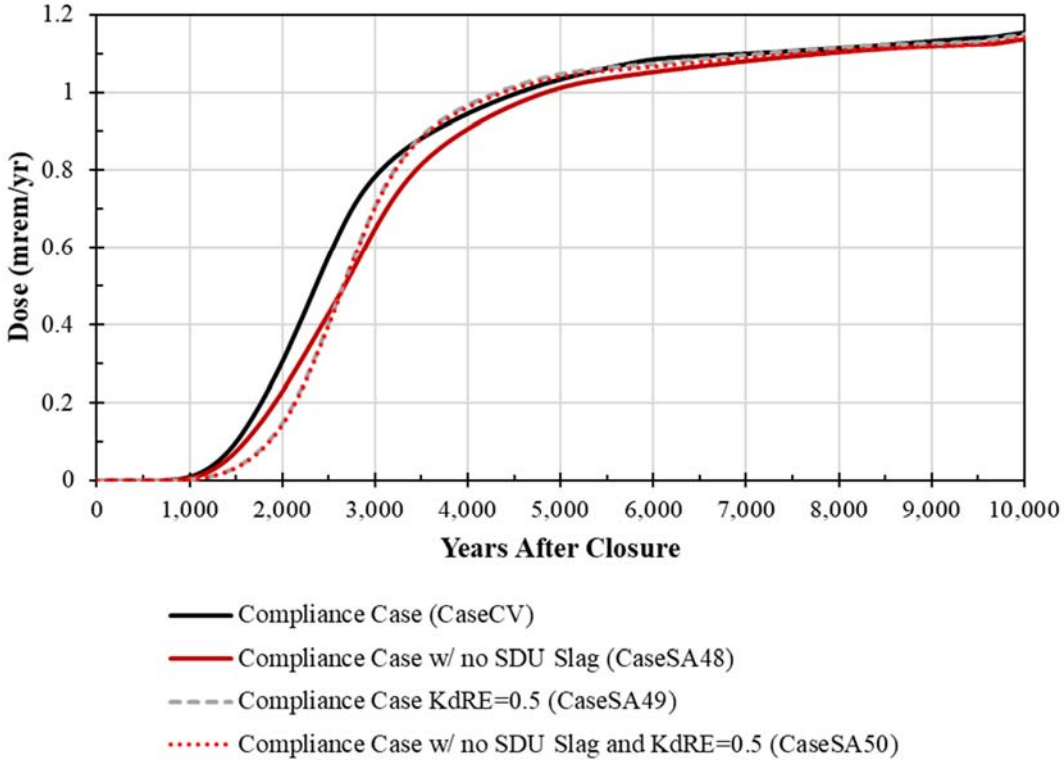

Next, the infiltration rate based on the 2008 HELP model (as described in Section 5.8.2.2) was assumed to evaluate how removing the slag from the SDU concrete might alter performance under higher infiltration rates. Starting with CaseSA49 (i.e., the modified Compliance Case with the K_dRe of 0.5 mL/g), a new case was developed by applying the higher infiltration rate from the 2008 HELP model. This case was run with and without slag in the SDU concrete (CaseSA51 and CaseSA52, respectively).

As expected, by increasing the infiltration, the magnitudes of the Tc-99 fluxes and I-129 fluxes also increased (Figure 5.8-44 and Figure 5.8-45). Despite this increased magnitude of the Tc-99 fluxes, the two cases with and without blast furnace slag in the SDU concrete both show essentially the same result. This is because the Tc-99 depletion front still moves faster than the advancing oxidation front. For the I-129 fluxes, despite the higher K_d the peak values for these two cases are also nearly identical.

Figure 5.8-44: Comparison of Tc-99 Flux to the Water Table from SDU 8, With and Without Slag in the SDU Concrete, Based on a Minimum Effective K_d of 0.5 mL/g and Higher Infiltration

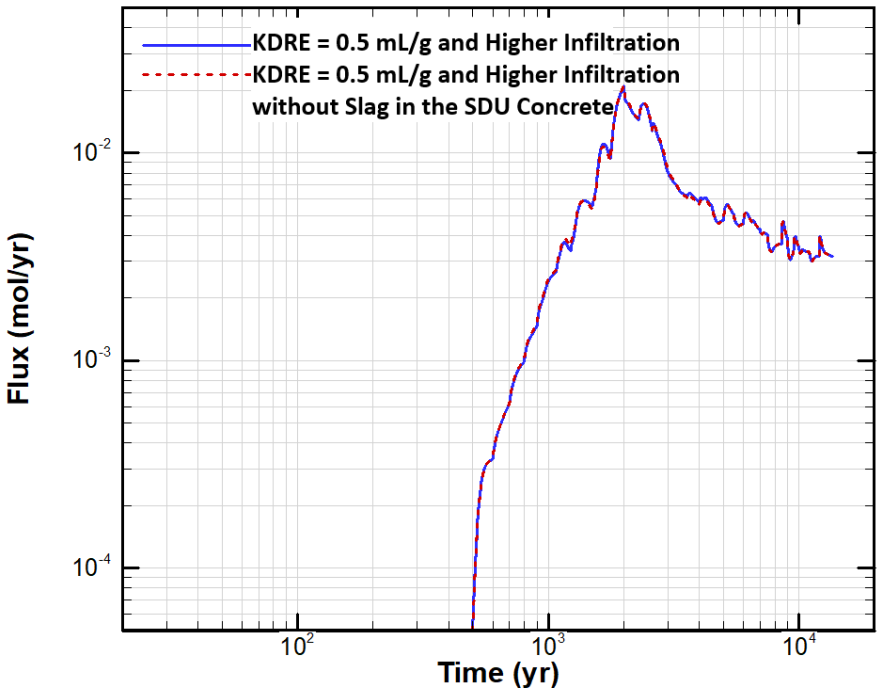

Figure 5.8-45: Comparison of I-129 Flux to the Water Table from SDU 8, With and Without Slag in the SDU Concrete, Based on a Higher Infiltration

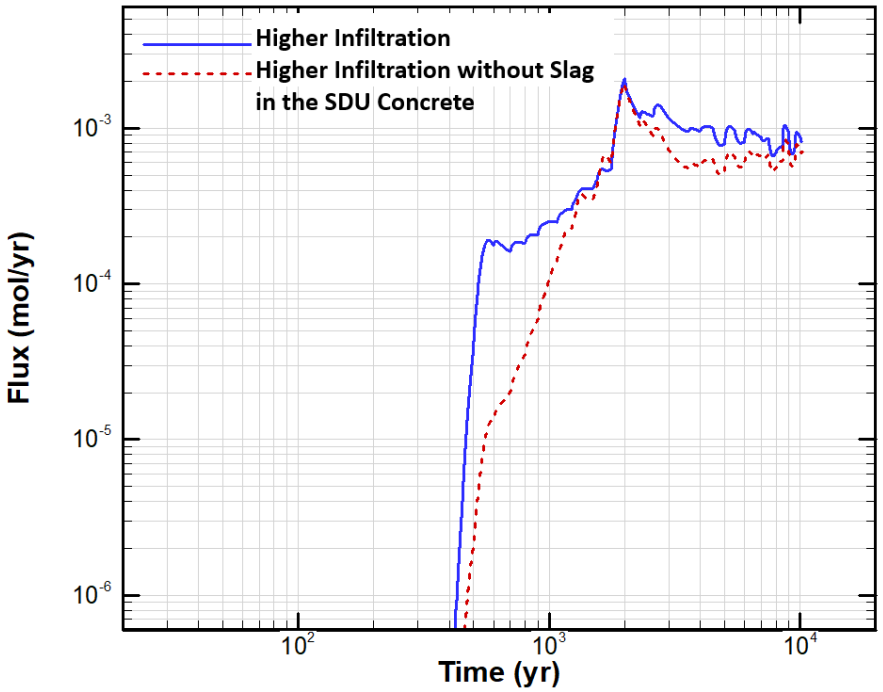

Figure 5.8-46 shows the comparison of the total dose results for CaseSA51 (blue) and CaseSA52 (orange). These doses show, even under increased infiltration, omitting the slag from the SDU concrete has a negligible impact on the dose results.

Figure 5.8-46: Dose Comparison of Modeling Cases With and Without Slag in SDU Concrete for SDUs 8 through 12, Based on Increased Infiltration

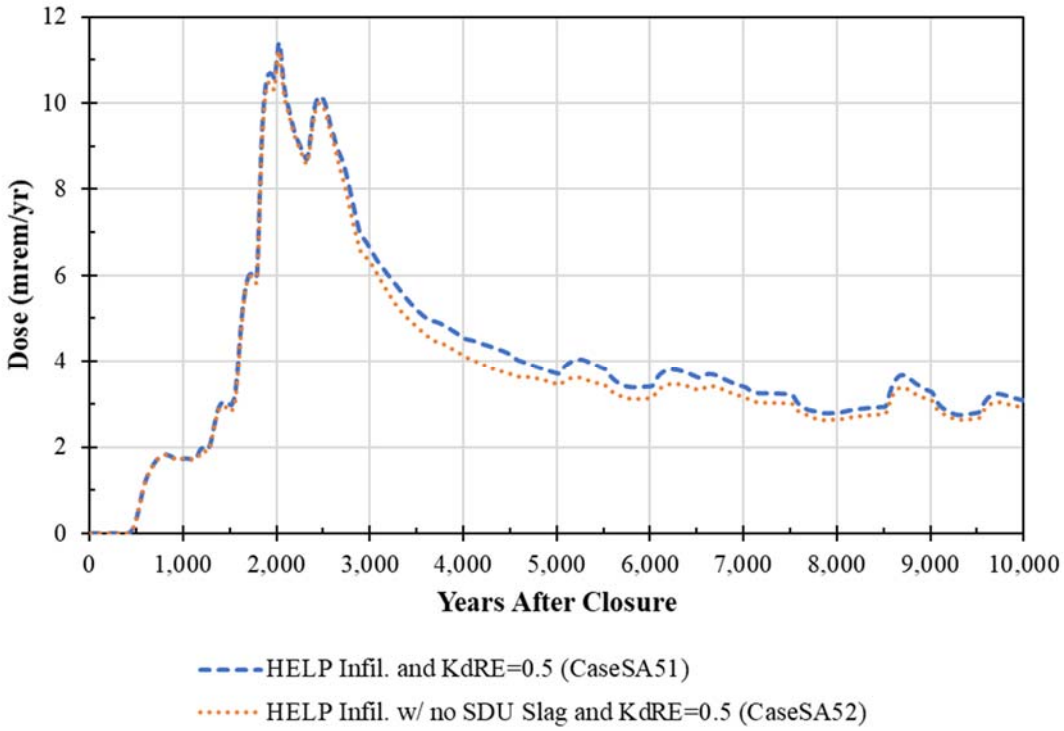

For a final comparison, the cases in Figure 5.8-46 were further modified by changing lowering solubility limit of Tc-99 to 1.0E-08 mol/L. The purpose of this change is to slow advancement of the Tc-99 depletion front. With this lower Tc-99 release rate, the differences between the results are somewhat more noticeable (see Figure 5.8-47). This demonstrates the reducing capacity of the SDU concrete only inhibits the transport of Tc-99 when the Tc-99 depletion front is slower than the oxidation front. However, DLM studies performed by SREL using the saltstone cores from SDU 2A cores indicate Tc-99 has a relatively high solubility limit and release rate. [SRRA099188-000003, SRR-CWDA-2018-00046] As such, the cases depicted in Figure 5.8-47 are not representative of expected conditions.

These sensitivity cases indicate the presence of blast furnace slag in the SDU concrete (and the associated reducing capacity) is not an effective chemical barrier for I-129 and is only effective for Tc-99 release if the solubility limit is much lower than currently expected. Therefore, the performance of the SDF is not sensitive to whether the SDU concrete includes blast furnace slag.

Figure 5.8-47: Dose Comparison of Modeling Cases With and Without Slag in SDU Concrete for SDUs 8 through 12, Based on Increased Infiltration and Lower Tc Solubility

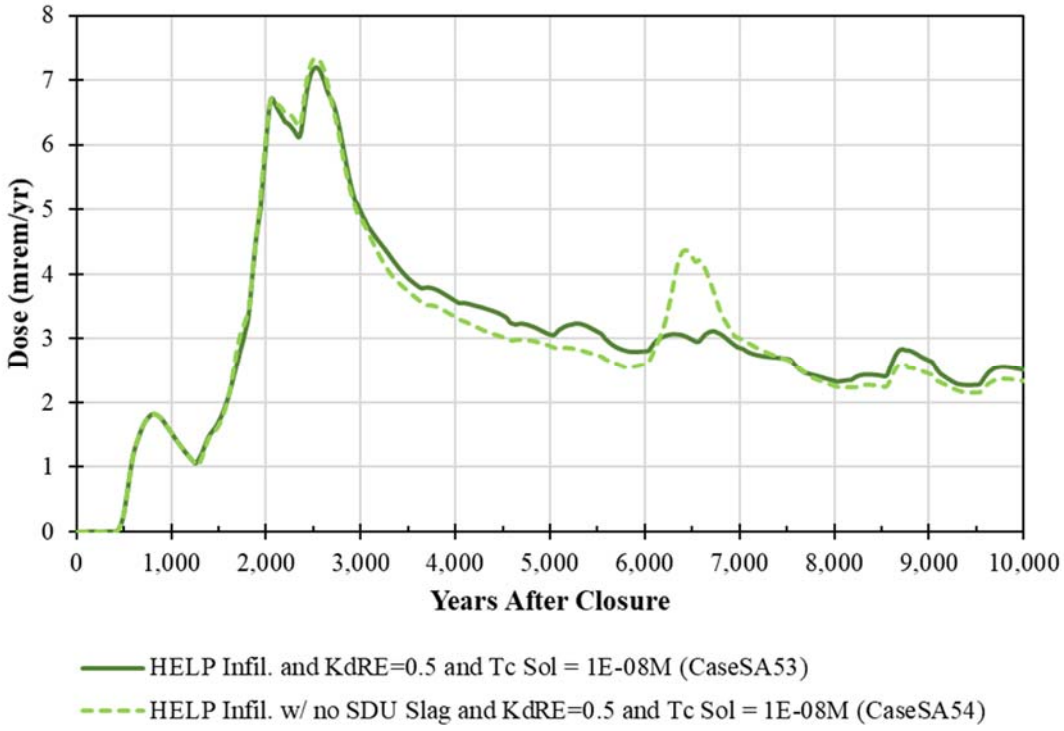

5.8.4.5 Evaluation of Saltstone Reducing Capacity

Although significant oxidation of saltstone prior to facility closure is not inferred by the data and information provided in Appendix A, pre-closure oxidation of some portion of the saltstone monolith is possible. Three sensitivity cases were performed to quantify the dose impact should the SDU concrete and a portion of the saltstone monolith be oxidized at PA time zero:

- Compliance Case + Tc K_dRe = 0.5 mL/g
- All SDU concrete and 1-foot rind of saltstone oxidized at closure
- All SDU concrete and saltstone oxidized at closure

This first case (Compliance Case + Tc K_dRe = 0.5 mL/g) is designed to be a reference case. "K_dRe" refers to the effective K_d of technetium in saltstone under reducing conditions (abbreviated as "K_dRe"). For K_dRe, Figure 4.4-85 showed that the Compliance Case assumes a K_dRe value of 0.01 mL/g under reducing conditions unless solubility controls are triggered, but once the material is oxidized the K_d increases to 0.5 mL/g (K_dOx = 0.5 mL/g). It is expected that while saltstone has reducing capacity, the mobility of the technetium within the saltstone will be initially solubility-controlled. On the other hand, reducing concrete will experience total technetium concentrations that do not trigger solubility controls because the K_d for Tc-99 at concentrations below the solubility limit has not been experimentally defined, the K_dRe value of 0.01 mL/g was assumed for the

Compliance Case as an arbitrarily low value. Thus, under low concentration conditions, this arbitrarily low K_d value results in an overestimate to Tc-99 releases. As such, this first sensitivity case (Compliance Case + Tc K_dRe = 0.5 mL/g) is designed to apply a more realistic value for K_dRe such that dose comparisons relative to the other sensitivity cases can provide a better basis for understanding.

The next sensitivity case (All SDU concrete and 1-foot rind of saltstone oxidized) assumes that all SDU concrete is fully oxidized as well as a one-foot "rind" of saltstone. This 1-foot rind is based on the data in Table A-3 of Appendix A which showed that over a 30-year pre-closure oxidation period, if the high humidity and bleed water within the SDU is ignored, a 1-foot rind of oxidation is possible. This rind is applied at the interface to the SDU roofs, at the interface to the SDU walls, and along both sides of the representative roof-support columns. Figure 5.8-48 illustrates the model setup for this sensitivity case using SDU 7, although this approach was applied to every SDU.

The third sensitivity case assumes that all cementitious materials (SDU concrete and saltstone) are all fully oxidized at time zero. This case is an extreme bounding scenario.

Figure 5.8-48: Oxidation Sensitivity Case simulation: 1-foot oxidized rind around SDU 7

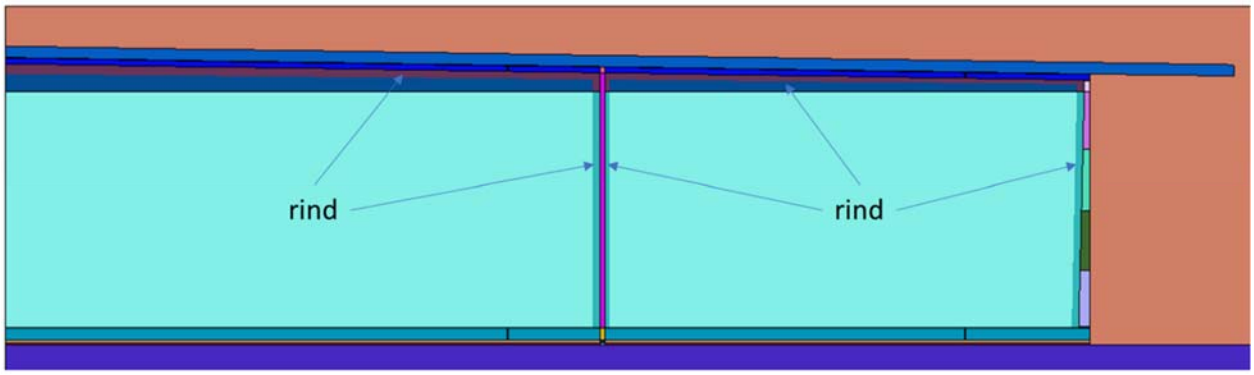

Figure 5.8-49 and Figure 5.8-50 compare Tc-99 and I-129 fluxes, respectively, again using SDU 7 as the example. Due to the transport parameters defined in Section 4.3.2, assuming pre-closure oxidation of saltstone increases the Tc-99 flux (compare Compliance Case + Tc K_dRe = 0.5 mL/g (gray) to the cases with the 1-foot oxidized rind (blue) and the fully oxidized saltstone (red) in Figure 5.8-49). Although the Tc-99 flux increases when more pre-closure oxidation is assumed, the I-129 flux decreases (compare the Compliance Case (black) to the cases with the 1-foot oxidized rind (blue) and the fully oxidized saltstone (red) in Figure 5.8-50).

Figure 5.8-49: Tc-99 Fluxes from SDU 7 for Saltstone Oxidation Sensitivity Cases

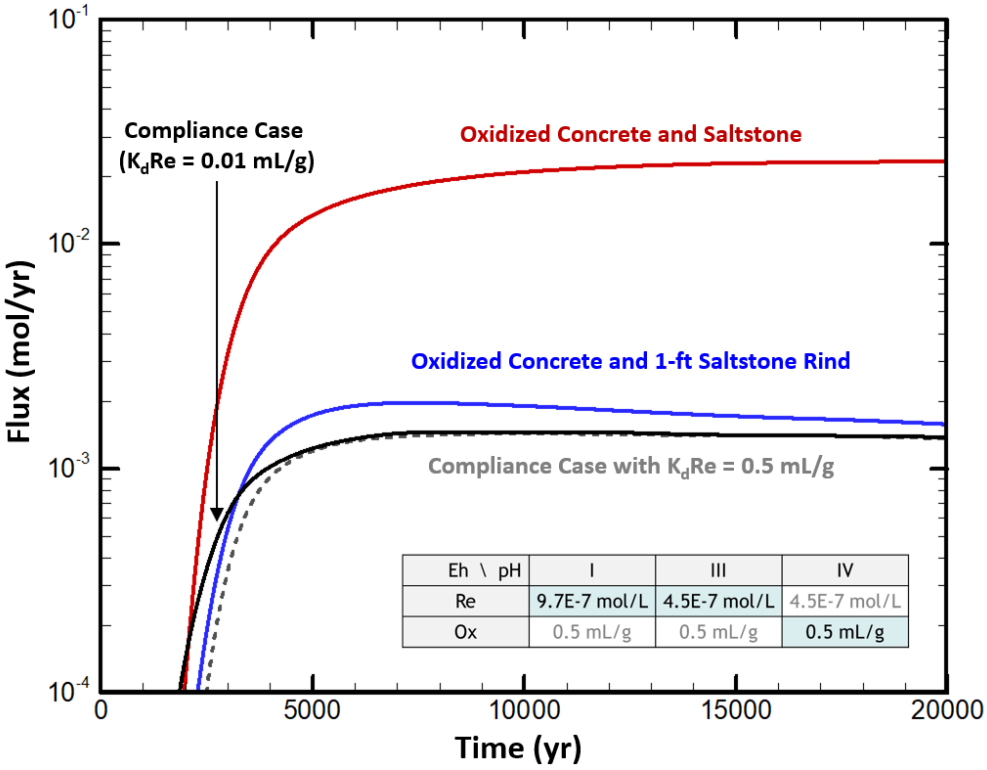

Figure 5.8-50: I-129 Fluxes from SDU 7 for Saltstone Oxidation Sensitivity Cases

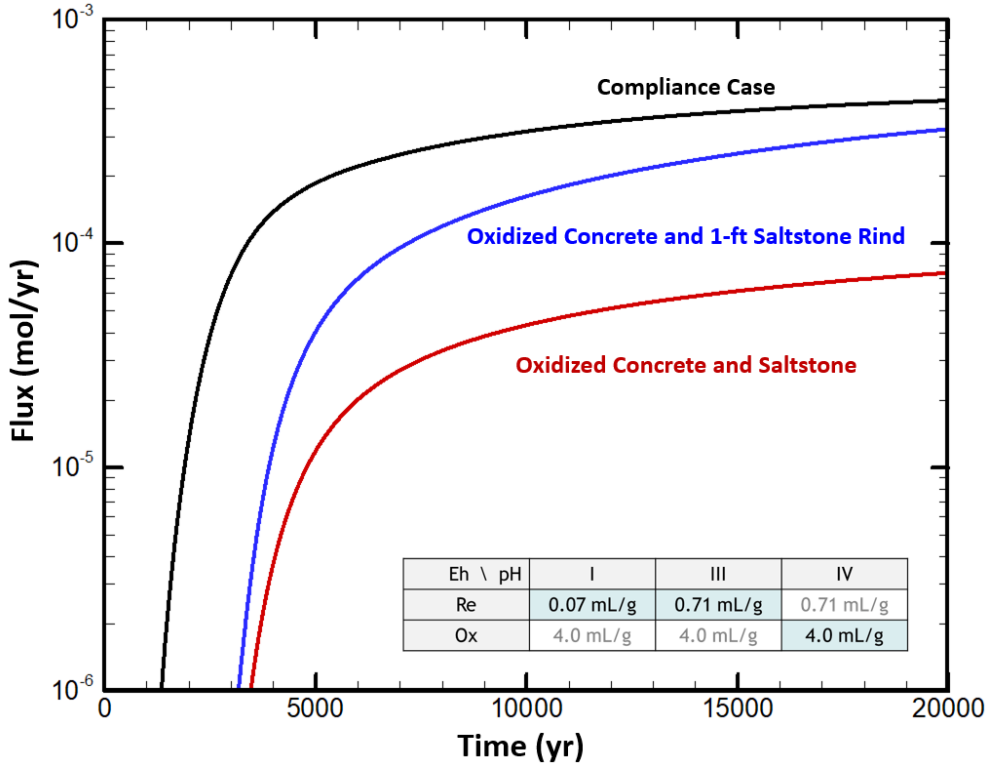

Figure 5.8-51 through Figure 5.8-53 plot the total dose results for these saltstone oxidation sensitivity cases. These dose results show that the increase to the iodine K_d under oxidizing conditions significantly offsets the effects of the increase to the technetium releases. Figure 5.8-51 shows that the Compliance Case (black), which assumes a K_dRe value of 0.01 mL/g is overpredicting the Tc-99 releases within the first 1,000 years. By applying a more reasonable 0.5 mL/g, each of the oxidation sensitivity cases show lower peak doses within the first 1,000 years, even when the entire saltstone monolith is assumed to be oxidized prior to closure.

Figure 5.8-52 shows that over a 10,000-year period, the Compliance Case, the sensitivity case with Tc K_dRe = 0.5 mL/g (gray), and the sensitivity case with the 1-foot oxidized rind (blue) all show very similar dose results indicating that the total dose results are not strongly sensitive to the potential for limited pre-closure oxidation, as is further illustrated by Figure 5.8-53. Alternatively, Figure 5.8-52 shows that the sensitivity case that assumes a fully oxidized system (red) has a higher total dose, as would be expected; however, for the first 2,000 years these doses remained below the dose results from the Compliance Case (due to the assumed value for K_dRe) and remain within 25 mrem/yr over the 10,000-year simulation. These dose results, coupled with the information provided in Appendix A, indicate that it is unlikely that the initial oxidation state of saltstone will result in doses that exceed the performance objectives.

Figure 5.8-51: Saltstone Oxidation Sensitivity Case Dose Comparisons (1,000 Years)

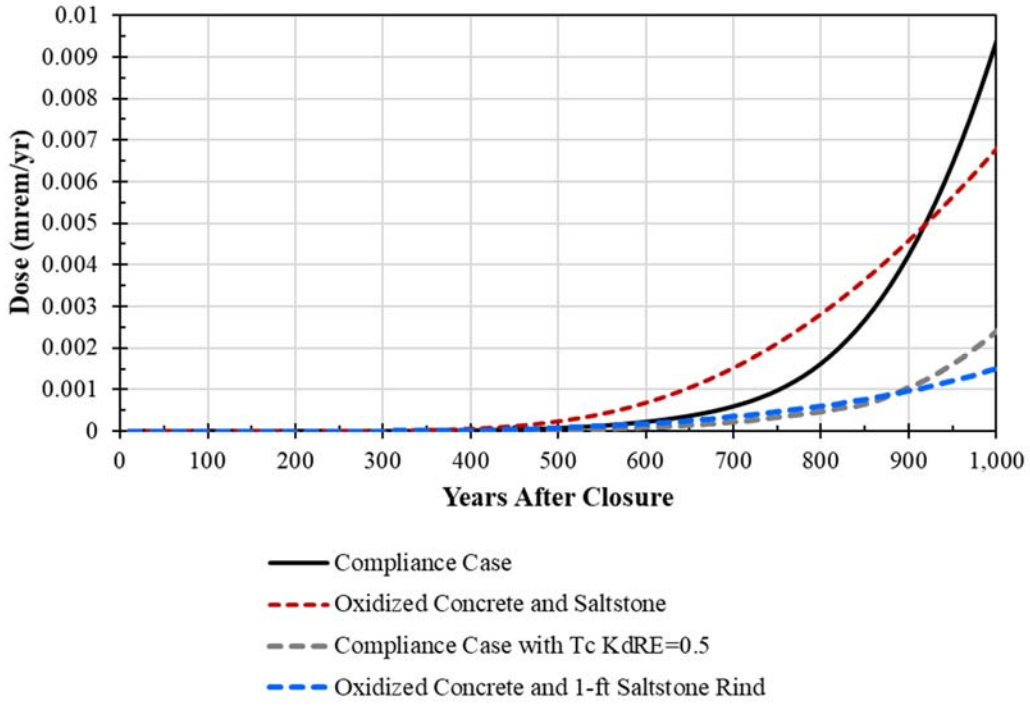

Figure 5.8-52: Saltstone Oxidation Sensitivity Case Dose Comparisons (10,000 Years)

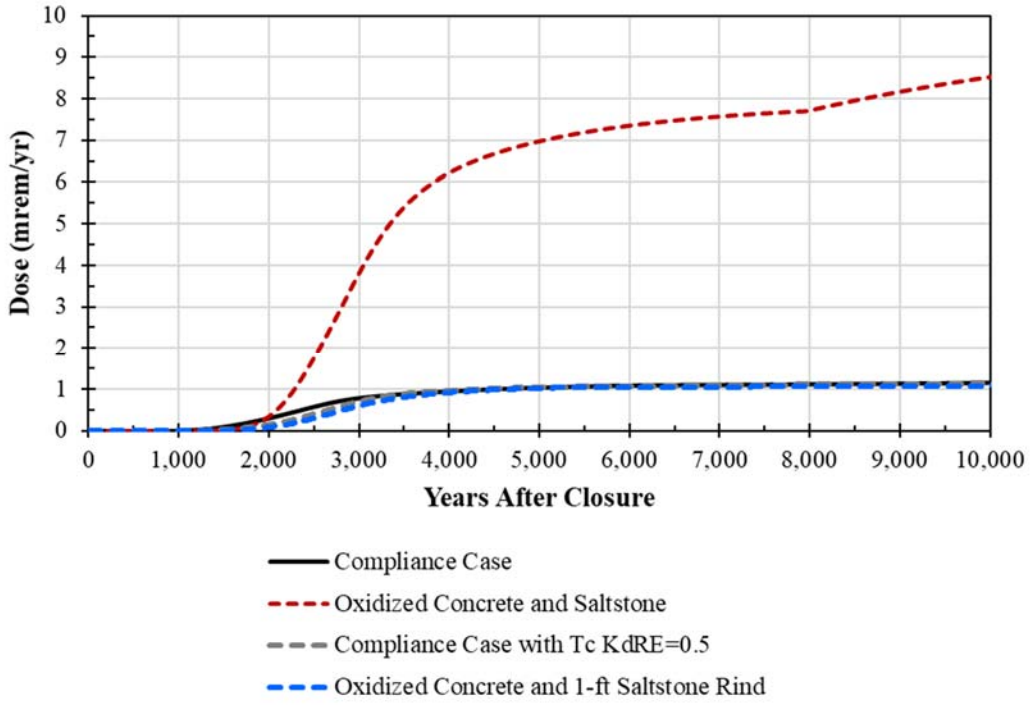

Figure 5.8-53: Saltstone Oxidation Sensitivity Case Dose Comparisons (10,000 Years), Excluding the Fully Oxidizing Saltstone Case

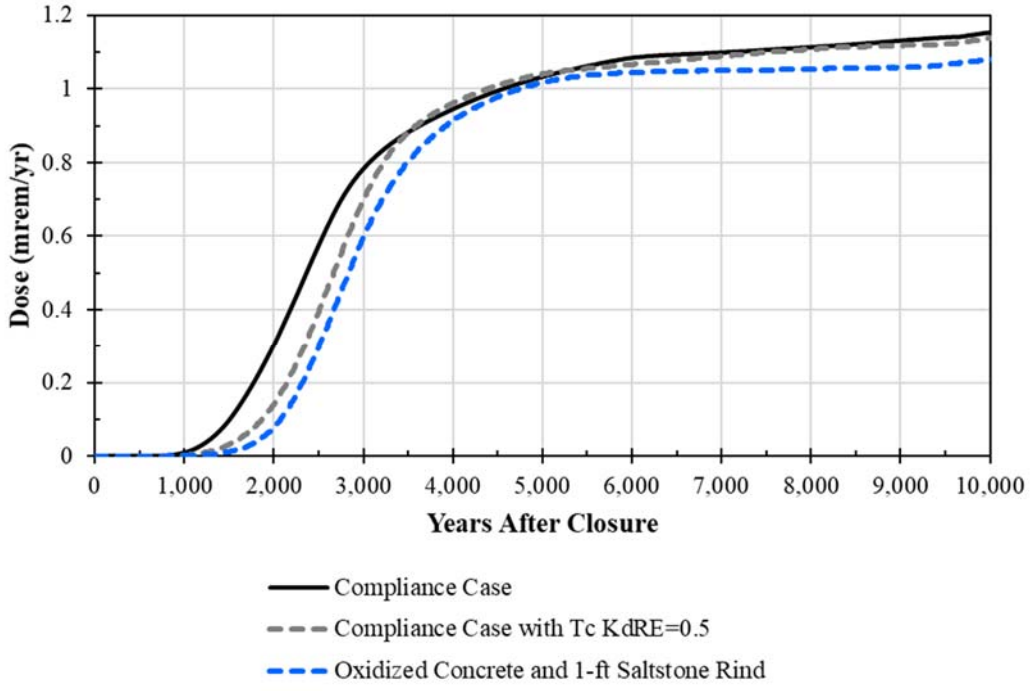

Figure 5.8-54 shows the radionuclide dose contributions from I-129 and Tc-99 for each of the modeling cases depicted in Figure 5.8-53. These results illustrate how the increased Tc-99 doses under more oxidizing conditions are being offset by the decreased I-129 doses.

Relative to the fully oxidized case, the sensitivity case with the assumed 1-foot rind of oxidizing saltstone is a far more plausible, yet still unexpected, hypothesized condition. Compared to the Compliance Case, the dose impacts of this more reasonable sensitivity case are small when compared to other uncertainties in the overall PA analysis.

Figure 5.8-54: Saltstone Oxidation Sensitivity Case Tc-99 and I-129 Dose Comparisons, Excluding the Fully Oxidizing Saltstone Case

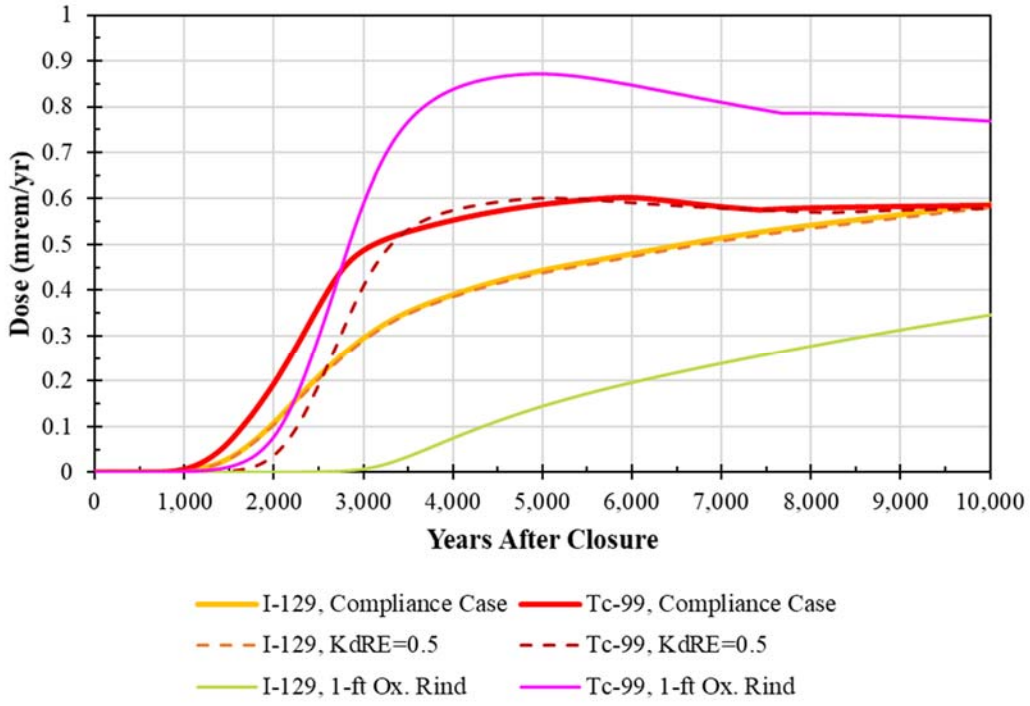

5.8.5 Inventory Sensitivities

The following describes various sensitivity cases developed to better understand the uncertainties and risks that are specifically associated with uncertainties relative to the assumed inventory values (see Section 3.3).

For additional context, the presentation of the dose results throughout this section also includes doses from the three Central Scenario cases: Realistic, Compliance, and Pessimistic Cases; however, within this section these results were all generated using the SDF GoldSim Model (in deterministic mode), as opposed to using PORFLOW. As such, the Central Scenario cases show results that vary slightly from the presentation of the results in Section 5.8.1. See Section 5.6 for a discussion of the differences between the SDF GoldSim Model and the SDF PORFLOW Model.

5.8.5.1 Central Scenario Cases Inventory Values

Sensitivity cases were developed using the Realistic (Table 3.3-5) and Pessimistic (Table 3.3-7) inventories from Section 3.3.3. Aside from changing these inventory values, these sensitivity cases assumed all the same inputs and settings as the Compliance Case to explicitly show the influence of inventory. Figure 5.8-55 shows the dose results from these inventory sensitivity cases.

Figure 5.8-55: Comparison of Dose Results Based on Central Scenario Inventory Values

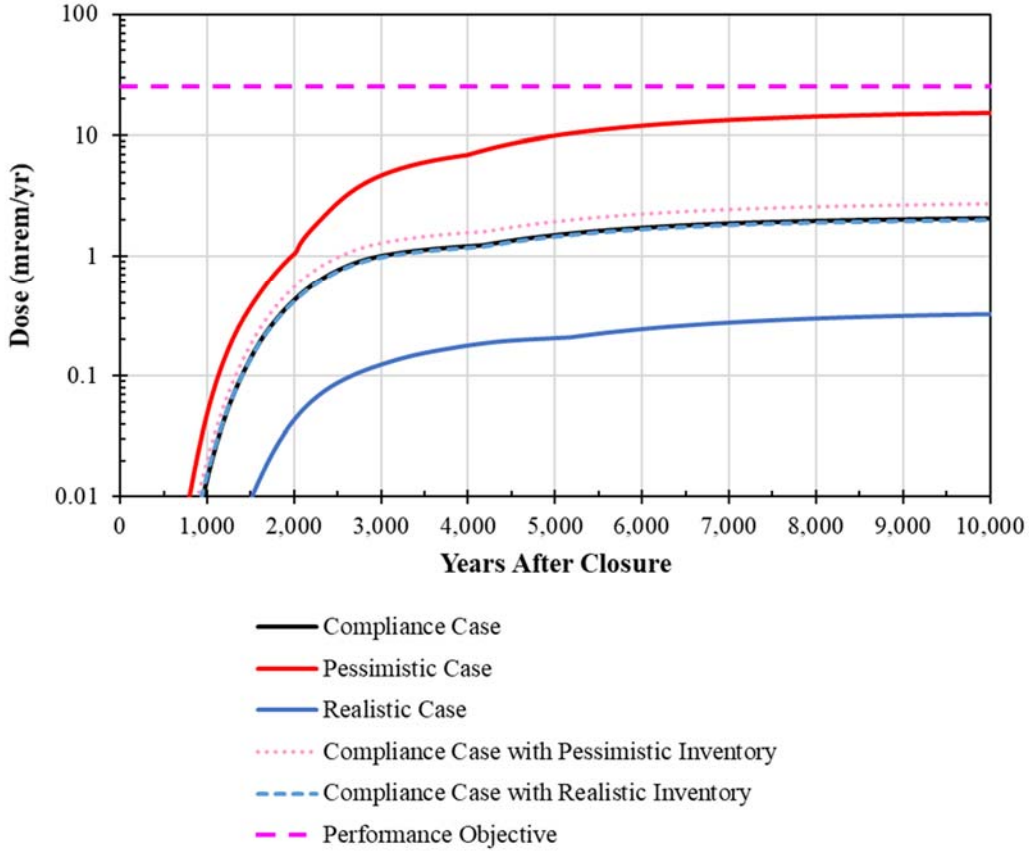

The doses resulting from the different inventories show that using the realistic inventory provides doses that are comparable to the Compliance Case, whereas using the pessimistic inventory provides doses that are 40% to 50% higher than the Compliance Case, as expected. Both of these sensitivity cases yielded dose results that are much closer to the Compliance Case than the Realistic Case and Pessimistic Case, respectively. These differences are consistent with the differences in the I-129 inventories, because I-129 is a main contributor to the SDF dose results. Comparing the I-129 inventories (see Section 3.3.3) shows relatively little difference between the Realistic and Compliance Case inventories, whereas the Pessimistic inventory is approximately 50% higher. It should also be noted that because the Tc-99 releases are solubility-limited, the release rate for Tc-99 is relatively unaffected by the inventory, as demonstrated in Section 5.8.5.4.

5.8.5.2 Preliminary System Plan I-129 Disposal Inventories

Given the importance of I-129 to the SDF dose results and to provide input to future decision making regarding the impact of disposal locations of I-129 in SDF, a sensitivity model was setup to evaluate a variation on the I-129 disposal inventory. An alternative set of SDU inventory assignments for I-129 was prepared based on a preliminary system planning estimate. This alternative set of I-129 inventories is provided in Table 5.8-17. As

a sensitivity case, these inventories replaced the Compliance Case I-129 inventories in a modeling run; the results are illustrated in Figure 5.8-56.

Table 5.8-17: Alternate I-129 Inventories

SDU	Compliance Case Inventory (Ci)	Alternate I-129 Inventory (Ci)
1	0.20	0.20
2A	0.07	0.07
2B	0.07	0.07
3A	0.19	0.19
3B	0.19	0.19
4	0.28	0.28
5A	0.14	0.14
5B	0.09	0.09
6	2.20	2.81
7	2.20	3.28
8	2.20	3.11
9	2.20	1.91
10	2.20	1.63
11	2.20	1.24
12	2.20	1.39
Total	**16.6**	**16.6**

Figure 5.8-56: Alternate I-129 Disposal Plan Dose Result

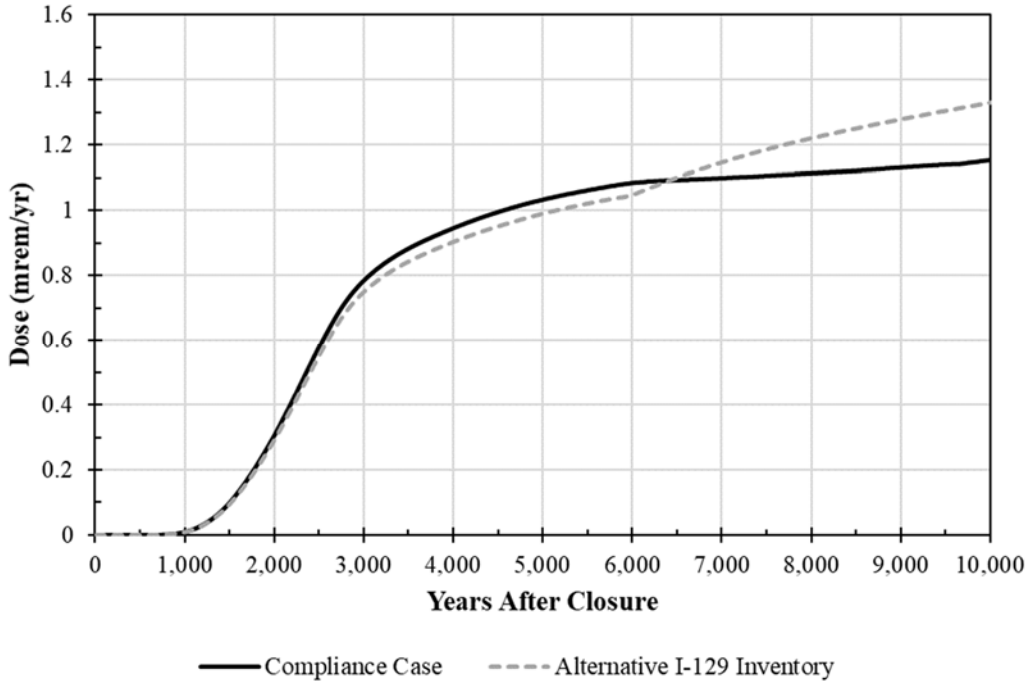

The alternative I-129 disposal inventories resulted in a slight increase to the overall dose starting at approximately 6,400 years (when Sector B overtakes Sector D as the location of the peak dose), but otherwise the differences were negligible.

5.8.5.3 Extreme Inventory Values

This section describes an evaluation of sampling distributions for stochastic sampling of inventory values for the SDF GoldSim Model. Multipliers were developed to be used with the realistic inventories to illustrate the bounding range of radionuclide inventories. [SRR-CWDA-2018-00076] Radionuclide-specific distributions were developed and normalized to the mean. A log-normal distribution around the mean was selected to represent the overall radionuclide distribution because it provided the best representation of the data sets. The recommended minimum and maximum inventory multipliers are provided in Table 5.8-18.

Table 5.8-18: Inventory Multipliers

Radionuclide	Minimum Multiplier	Maximum Multiplier
I-129	0.079	9.78
Tc-99	0.13	13.71
All other radionuclides	0.10	14.4

For the extreme inventory sensitivity cases, these multipliers were applied to the Best Estimate inventory values. Table 5.8-19 presents an example of the values considered (using I-129), although all of the radionuclide inventories were modified in a similar manner. Also note that because Tc-99 releases are not explicitly simulated within the SDF GoldSim Model, the evaluation of Tc-99 inventories was performed separately using PORFLOW, as discussed in Section 5.8.5.4.

Table 5.8-19: Example of Bounding Inventory Values: I-129

SDU	I-129 Inventory Value (Ci)		
	Minimum (Bounding)	Compliance Case	Maximum (Bounding)
1	1.6E-02	2.0E-01	2.0E+00
2A	5.8E-03	7.3E-02	7.1E-01
2B	5.4E-03	6.8E-02	6.7E-01
3A	1.5E-02	1.9E-01	1.8E+00
3B	1.4E-02	1.8E-01	1.8E+00
4	2.2E-02	2.8E-01	2.7E+00
5A	1.1E-02	1.4E-01	1.4E+00
5B	6.9E-03	8.7E-02	8.5E-01
6	1.7E-01	2.1E+00	2.1E+01
7	1.7E-01	2.1E+00	2.1E+01
8	1.7E-01	2.1E+00	2.1E+01
9	1.7E-01	2.1E+00	2.1E+01
10	1.7E-01	2.1E+00	2.1E+01
11	1.7E-01	2.1E+00	2.1E+01
12	1.7E-01	2.1E+00	2.1E+01
Total	**1.3E+00**	**1.6E+01**	**1.6E+02**

To evaluate the bounding inventory values, the Compliance Case simulations were modified to use the bouding inventories and the resulting doses were compared against the Compliance Case as shown in Figure 5.8-57.

These results are the outcome from extremely bounding inventory assumptions. The multipliers used to represent these bounding values were developed based on Tank Farm concentrations. Development of these values did not assume any credit for the effects of system planning, salt batching, or the influences of multiple lifts (or pouring campaigns) within each SDU, which would all serve to mitigate extreme variability in the SDU disposal inventories. Effectively, the maximum inventory values assume that every waste tank that feeds into future salt batches has extremely high concentrations of waste and that every lift of saltstone disposed of into every SDU will reflect these high concentrations. Realistically, the final inventory is expected to have concentrations that are closer to those of the Realistic Inventory (Table 3.3-5).

Figure 5.8-57: Dose Comparison for the Extreme Inventory Sensitivity Cases

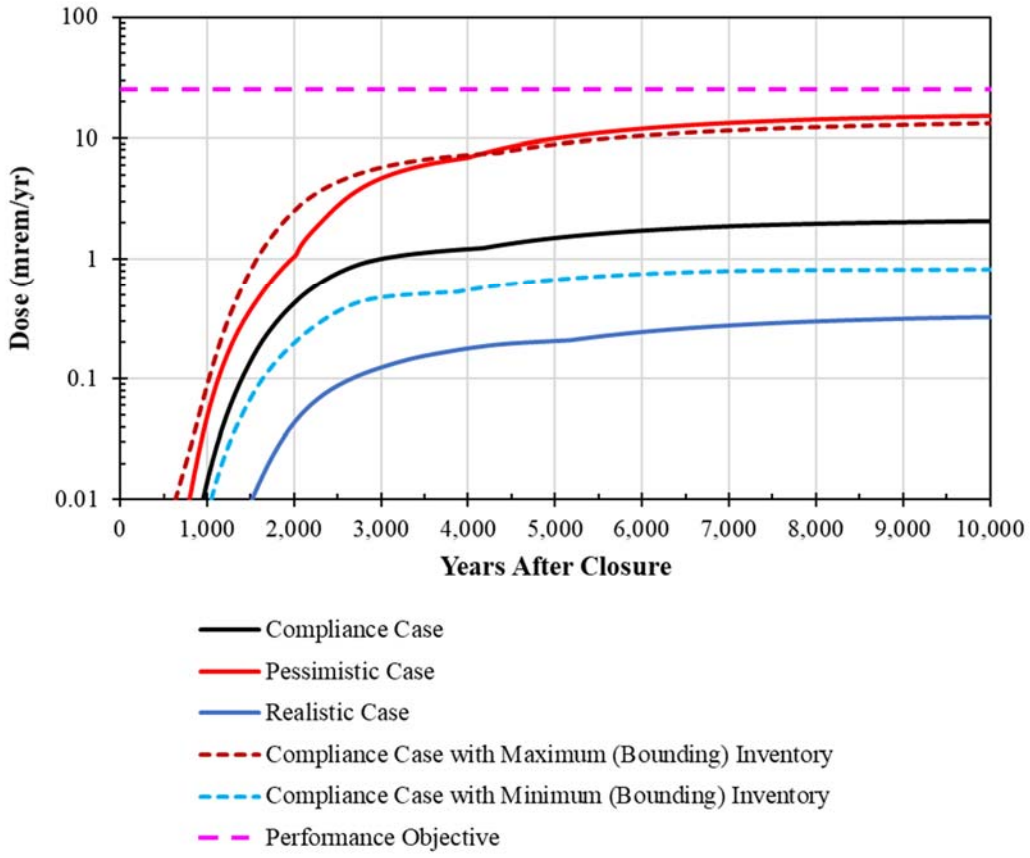

5.8.5.4 Tc-99 Inventory Sensitivities

As indicated in Sections 5.8.5.1 and 5.8.5.3, evaluations of Tc-99 inventories cannot be performed using the SDF GoldSim Model because Tc-99 releases are only simulated in PORFLOW then abstracted into GoldSim. Therefore, PORFLOW was used to generate four sensitivity cases, each using different Tc-99 inventory values (Table 5.8-20). Aside

from the Tc-99 inventory values, all these modeling cases are identical to the Compliance Case.

Table 5.8-20: Tc-99 Inventory Values (Ci) Applied for PORFLOW Inventory Sensitivity Analysis

SDU	Tc-99 Inventory Sensitivity Cases				
	Bounding LOW Inventory	Realistic Values	Compliance Case Values	Pessimistic Values	Bounding HIGH Inventory
SDU 1	4.9E+01	4.9E+01	4.9E+01	4.9E+01	4.9E+01
SDU 2A	1.1E+02	1.1E+02	1.1E+02	1.1E+02	1.1E+02
SDU 2B	1.4E+02	1.4E+02	1.4E+02	1.4E+02	1.4E+02
SDU 3A	3.3E+01	2.6E+02	3.6E+02	3.9E+02	3.5E+03
SDU 3B	3.3E+01	2.5E+02	3.8E+02	4.1E+02	3.5E+03
SDU 4	6.3E+02	6.3E+02	6.3E+02	6.3E+02	6.3E+02
SDU 5A	1.8E+02	1.8E+02	1.8E+02	1.8E+02	1.8E+02
SDU 5B	1.2E+02	1.2E+02	1.2E+02	1.2E+02	1.2E+02
SDU 6	3.9E+02	3.0E+03	4.4E+03	4.8E+03	4.1E+04
SDU 7	3.9E+02	3.0E+03	4.4E+03	4.8E+03	4.1E+04
SDU 8	3.9E+02	3.0E+03	4.4E+03	4.8E+03	4.1E+04
SDU 9	3.9E+02	3.0E+03	4.4E+03	4.8E+03	4.1E+04
SDU 10	3.9E+02	3.0E+03	4.4E+03	4.8E+03	4.1E+04
SDU 11	3.9E+02	3.0E+03	4.4E+03	4.8E+03	4.1E+04
SDU 12	3.9E+02	3.0E+03	4.4E+03	4.8E+03	4.1E+04
SDF Total	**4.0E+03**	**2.2E+04**	**3.3E+04**	**3.5E+04**	**2.9E+05**

As shown by the total values in Table 5.8-20, this analysis considered a range of Tc-99 inventories that spans nearly two orders of magnitude (from 4,000 Ci of Tc-99 to 290,000 Ci of Tc-99. However, as long as saltstone provides a reducing environment, the releases of Tc-99 will be controlled by solubility limits; therefore, as long as the concentration of Tc-99 within saltstone exceeds the solubility limit, the rate of release remains unchanged.

Due to this release behavior, the Tc-99 doses resulting from these sensitivity cases exhibit very little variability. Within 1,000 years, the differences between these doses is not discernable (Figure 5.8-58). Within 10,000 years, the differences between the doses become discernable, but demonstrate that the differences in the Tc-99 doses are not strongly sensitive to the Tc-99 inventory (Figure 5.8-59).

Figure 5.8-58: Comparison of Tc-99 Doses for the Tc-99 Inventory Sensitivity Cases within 1,000 Years

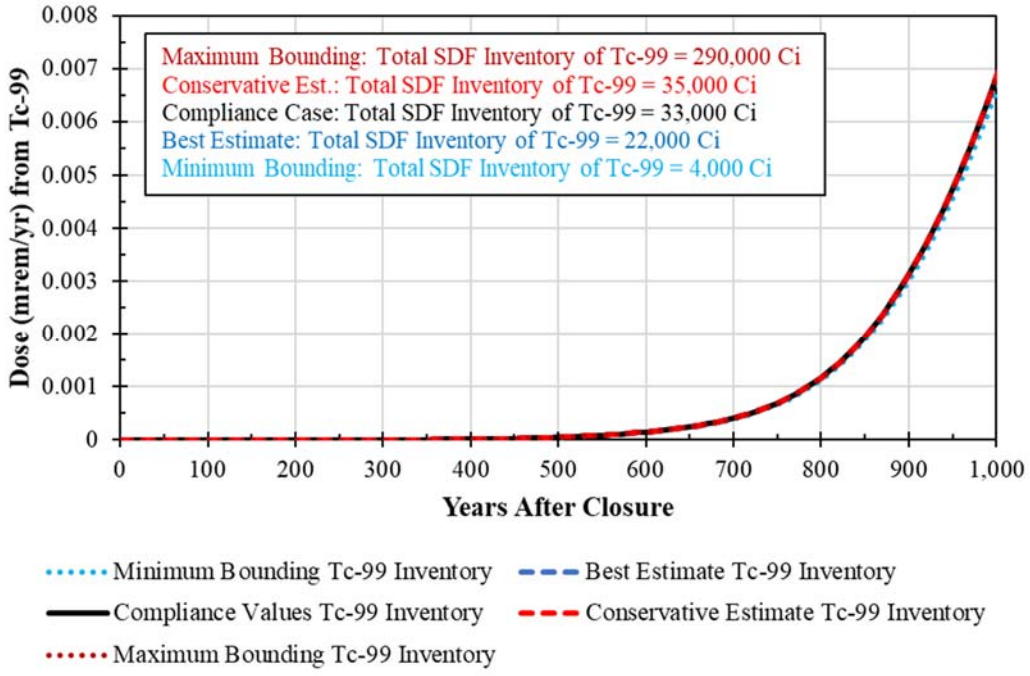

Figure 5.8-59: Comparison of Tc-99 Doses for the Tc-99 Inventory Sensitivity Cases within 10,000 Years

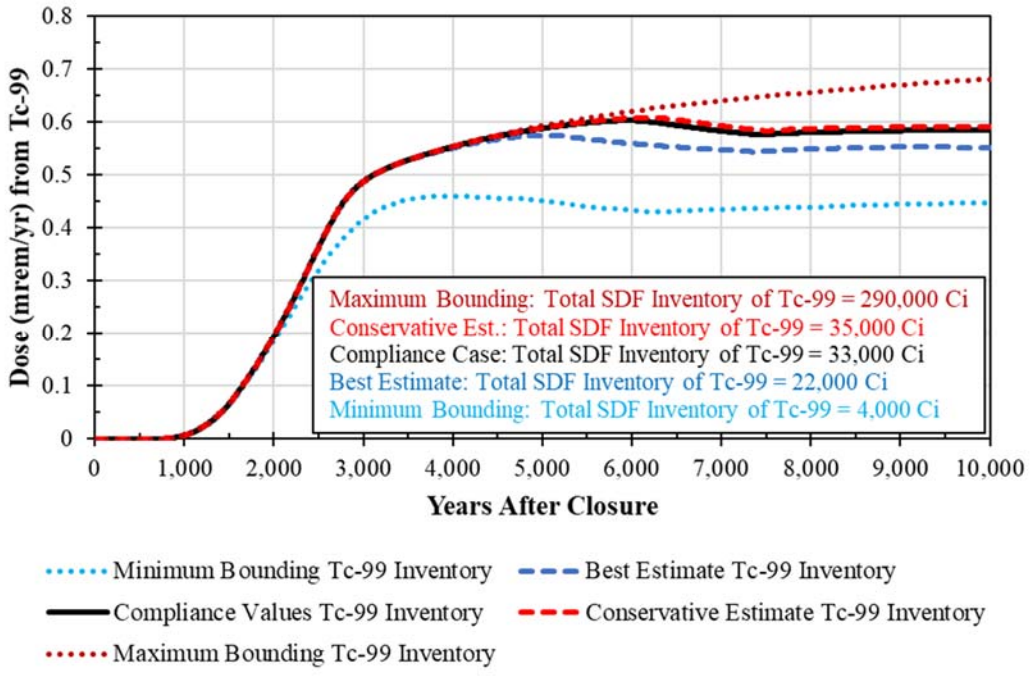

5.8.6 Dose Calculator Sensitivities

The following describes the results from sensitivity cases which vary input parameters from the dose calculations (see Section 4.4.8). These sensitivity cases were developed to better understand the uncertainties and risks that are specifically associated with the assumptions in the Dose Calculations.

5.8.6.1 Evaluation of Human Uptake Dose Parameters

To better evaluate the influence of the assumed values used for the human uptake parameters in the dose calculations, two sensitivity cases have been developed. Both cases use the ground water concentrations from the Compliance Case but for the dose calculations the values used for the human uptake parameters are based on recommended "realistic" and recommended "defense-in-depth" values (identified as "conservative" below), as described in Section 8.1 of the *Dose Calculation Methodology for Liquid Waste Performance Assessments at the Savannah River Site* (SRR-CWDA-2013-00058). Table 5.8-21 provides each of the values considered for this evaluation. In general, the realistic input values are based on an assessment of average uptake rates for adults in the United States, the recommended compliance values were scaled up to reflect local or regional variation, and the conservative values represent very conservative assumptions (e.g., the produce ingestion value is based on the 95th percentile of the adult population in the United States).

Table 5.8-21: Human Uptake Rates Evaluated

Human Uptake Parameter	Realistic Input	Recommended Compliance Input	Conservative Input	Section in Reference: SRR-CWDA-2013-00058
Water Ingestion Rate (L/yr)	448	505	731	Section 8.1.1.8
Soil and Dust Ingestion Rate (kg/yr)	1.06	1.06	1.06	Section 8.1.2
Produce Ingestion Rate (kg/yr)	199	207	546	Section 8.1.3.3
Meat Ingestion Rate (kg/yr)	62.2	68.7	151	Section 8.1.4.3
Milk Ingestion Rate (kg/yr)	67.2	75.0	201	Section 8.1.5.2
Poultry Ingestion Rate (kg/yr)	10.4	12.1	31.2	Section 8.1.6.2
Egg Ingestion Rate (kg/yr)	8.2	11.0	24.7	Section 8.1.7.2
Fish Ingestion Rate (kg/yr)	17.8	17.8	31.3	Section 8.1.8
Inhalation Rate (m^3/yr)	6,000	8,000	8,000	Section 8.1.9

Figure 5.8-60 provides a comparison of the dose results, and Figure 5.8-61 shows these same results using a linear scale. Table 5.8-22 summarizes the resulting peak doses.

Figure 5.8-60: Dose Results from the Evaluation of the Human Uptake Dose Parameters (Performance Period)

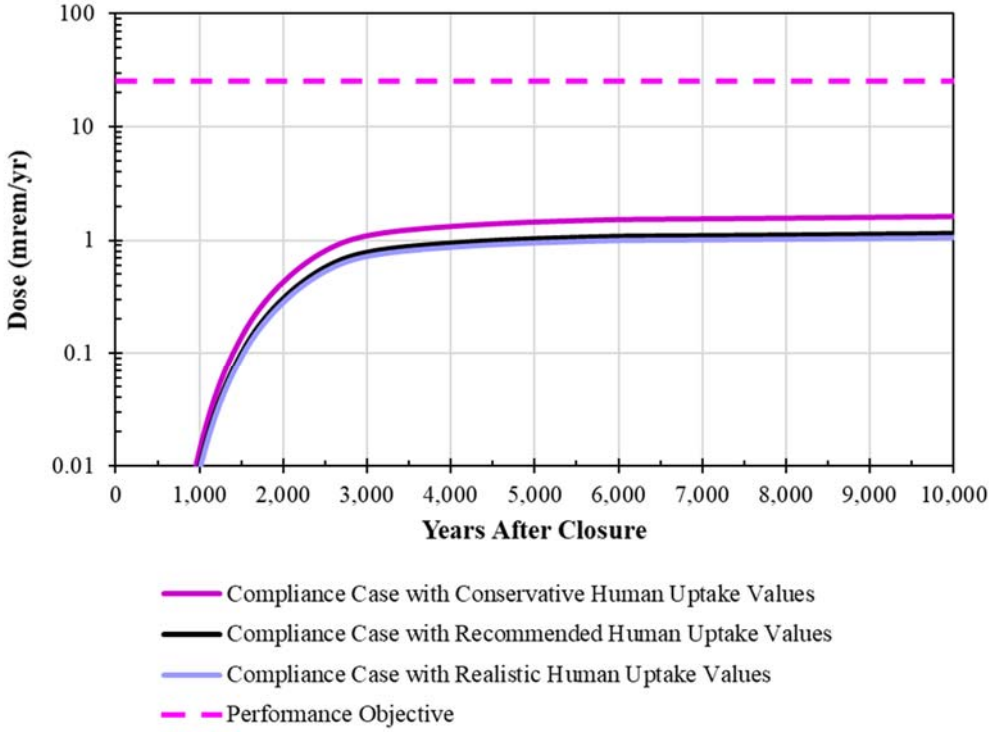

Figure 5.8-61: Dose Results from the Evaluation of the Human Uptake Dose Parameters (Performance Period, Detail)

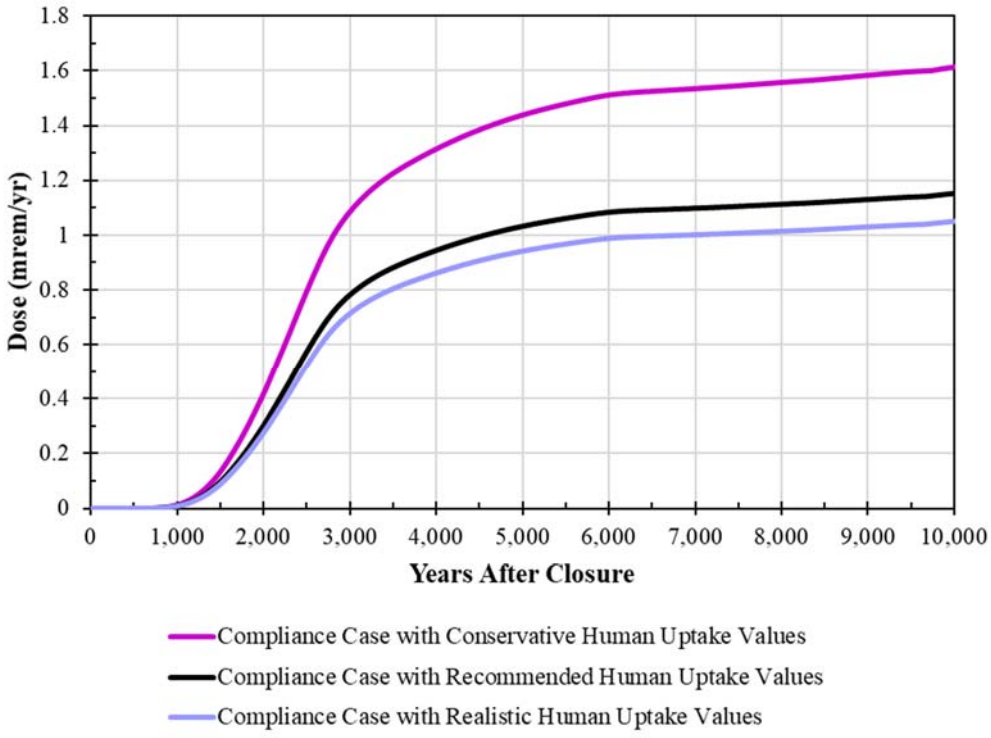

Table 5.8-22: Comparison of the 100-Meter MOP Peak Ground Water Pathways Doses Based on Varied Human Uptake Values

Modeling Case	Compliance Period (0 to 1,000 Years)		Performance Period (0 to 10,000 Years)	
	Peak Dose (mrem/yr)	Year of Peak	Peak Dose (mrem/yr)	Year of Peak
Compliance Case with Realistic Human Uptake Values	8.6E-03	1,000	1.1	10,000
Compliance Case with Recommended Human Uptake Values	9.4E-03	1,000	1.2	10,000
Compliance Case with Conservative Human Uptake Values	1.3E-02	1,000	1.6	10,000

In general, the Compliance Case (using the human uptake rates recommended for demonstrating compliance) has total doses that are approximately 10% higher than the sensitivity case using the realistic human uptake values, while the sensitivity case that uses the conservative human uptake values was 40% to 50% higher than the Compliance Case.

Because water ingestion is the dominant exposure pathway, constituting approximately 74% of the total dose to the MOP at the 100-meter well, dose results are almost linearly related to the water ingestion rates. With water ingestion, produce ingestion (13% to 21%) and fish ingestion (2% to 6%) account for almost 100% of the total dose to the MOP. The other exposure pathways have a relatively negligible influence on the total dose results.

It is also worth noting that the dose conversion factors (in Table 4.4-108), which are used to convert exposures into doses, are based on an age-weighted and gender-weighted "reference person." [SRR-CWDA-2013-00058] In other words, the development of the dose conversion factors included infants and children (i.e., individuals with less mass than adults). Despite this nuance, the assumed human uptake rates were developed based on the adult population only. Because the adult population has more mass than the "reference person," and the dose conversion factors are a function of mass, the dose calculations are inherently conservative. Similarly, it is reasonable to expect that individuals who consume more (i.e., those who would be represented by the conservative uptake rates) are likely to have more mass than average (or reference) individuals. These more massive individuals would likely require higher rates of exposure to achieve equivalent dose risks. This mitigating factor is not accounted for in any of the dose calculations. As such, the conservative uptake rates are likely bounding with respect to estimating doses.

5.8.6.2 Evaluation of Local Fraction Dose Parameters

The local fraction (or local productivity) parameters within the dose calculations (see Table 4.4-118) are used to define the fraction of food intake that is home-produced (and assumed to be contaminated), as opposed to coming from other (uncontaminated) sources. For example, although the MOP is assumed to have a farm (crops or garden), current practices indicate that only a fraction of produce consumed comes directly from

home grown sources. [SRR-CWDA-2013-00058] As such, only a fraction of the consumed produce would be contaminated.

To better evaluate the influence of the local fraction parameters in the dose calculations, two sensitivity cases have been developed. Both cases use the ground water concentrations from the Compliance Case, but for the dose calculations the values used for the local fraction parameters are all set to a value of 0 (indicating that no food comes from locally-contaminated sources) or are all set to a value of 1 (indicating that all food comes from locally-contaminated sources).

The local fraction for water ingestion was incorporated within the water uptake parameter; the uptake rate was developed using data for water ingestion from a community well rather than being developed using data for water ingestion from all sources (i.e., community well, bottled water, other wells, etc.). [SRR-CWDA-2013-00058] As such, the local fractions evaluated by these sensitivity cases did not modify the inputs related to dose from water ingestion. Therefore, these sensitivity cases provide insights that are explicitly concerned with agricultural productivity (crops and livestock):

- the fraction of total produce grown at home,
- the fraction of total terrestrial livestock meat produced at home,
- the fraction of total milk produced at home,
- the fraction of total poultry produced at home,
- the fraction of total eggs produced at home, and
- the fraction of households that fish.

Figure 5.8-62 provides a comparison of the dose results, and Figure 5.8-63 shows these same results using a linear scale. Table 5.8-23 summarizes the resulting peak doses.

In general, the Compliance Case (using the local fractions recommended for demonstrating compliance), has total doses that are approximately 30% higher than the sensitivity case that assumes no local fractions, while the sensitivity case that assumed a local fraction of 1.0 was approximately 70% higher than the Compliance Case.

When the local fractions are set to 0, water ingestion accounts for more than 99% of the total dose (the other dose contributions are from the non-ingestion pathways: external exposure and inhalation). When the local fractions are set to 1, the dose contributions from water ingestion only accounts for approximately 45% of the total dose; produce ingestion (42%) and fish ingestion (9%) account for approximately 51% of the total dose to the MOP. The other exposure pathways have a relatively negligible influence on the total dose results.

Figure 5.8-62: Dose Results from the Evaluation of the Local Fractions (Performance Period)

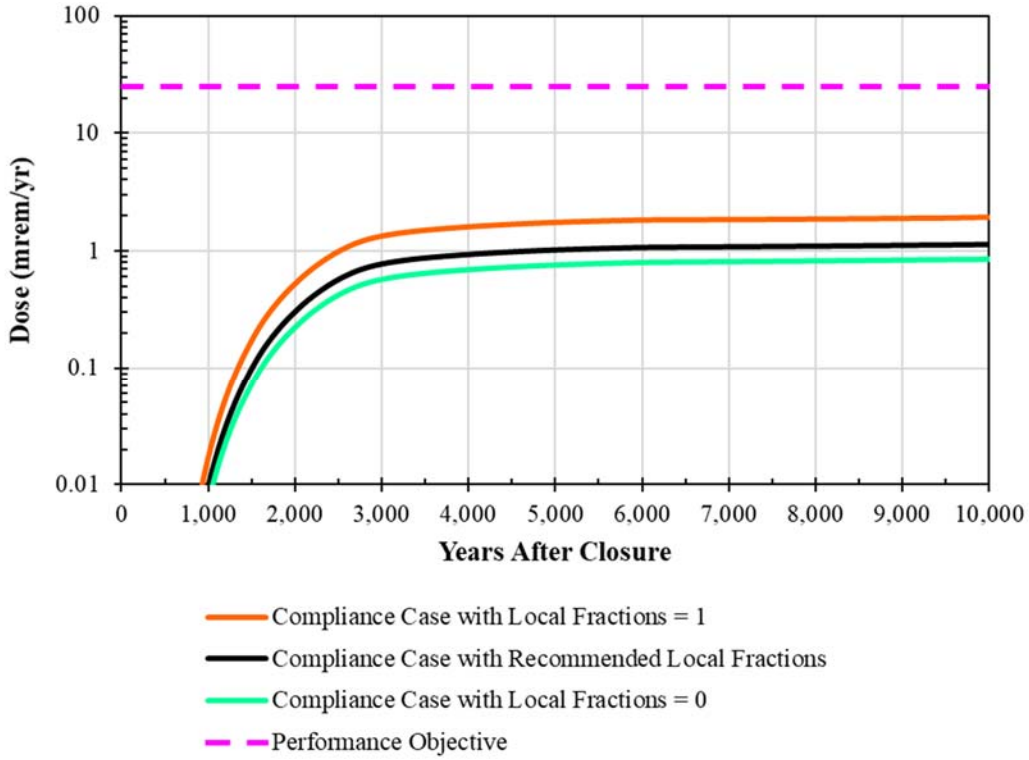

Figure 5.8-63: Dose Results from the Evaluation of the Local Fractions (Performance Period, Detail)

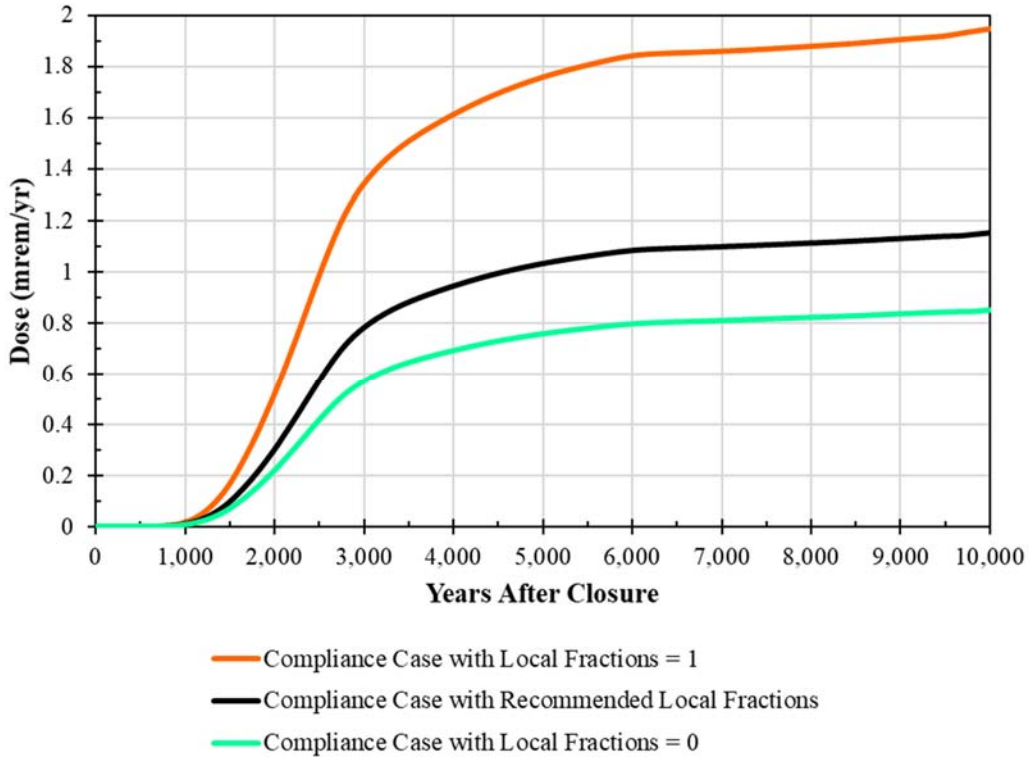

Table 5.8-23: Comparison of the 100-Meter MOP Peak Ground Water Pathways Doses Based on Varied Local Fractions

Modeling Case	Compliance Period (0 to 1,000 Years)		Performance Period (0 to 10,000 Years)	
	Peak Dose (mrem/yr)	Year of Peak	Peak Dose (mrem/yr)	Year of Peak
Compliance Case with Local Fractions = 0	6.7E-03	1,000	0.85	10,000
Compliance Case with Recommended Local Fractions	9.4E-03	1,000	1.2	10,000
Compliance Case with Local Fractions = 1	1.6E-02	1,000	1.9	10,000

5.8.6.3 Evaluation of the Garden Size Dose Parameters

In the probabilistic SDF GoldSim Model, the area of the garden is sampled with a triangular distribution that uses 100 m^2 for both the minimum and the mode and 1,000 m^2 as the maximum value (see Table 4.4-116). To better understand the dose risks associated with the garden size, a sensitivity case has been developed using this maximum value. Figure 5.8-64 provides a comparison of the dose results. Figure 5.8-65 shows these same results using a linear scale. Table 5.8-24 summarizes the resulting peak doses.

Figure 5.8-64: Dose Results from the Evaluation of the Maximum Garden Size (Performance Period)

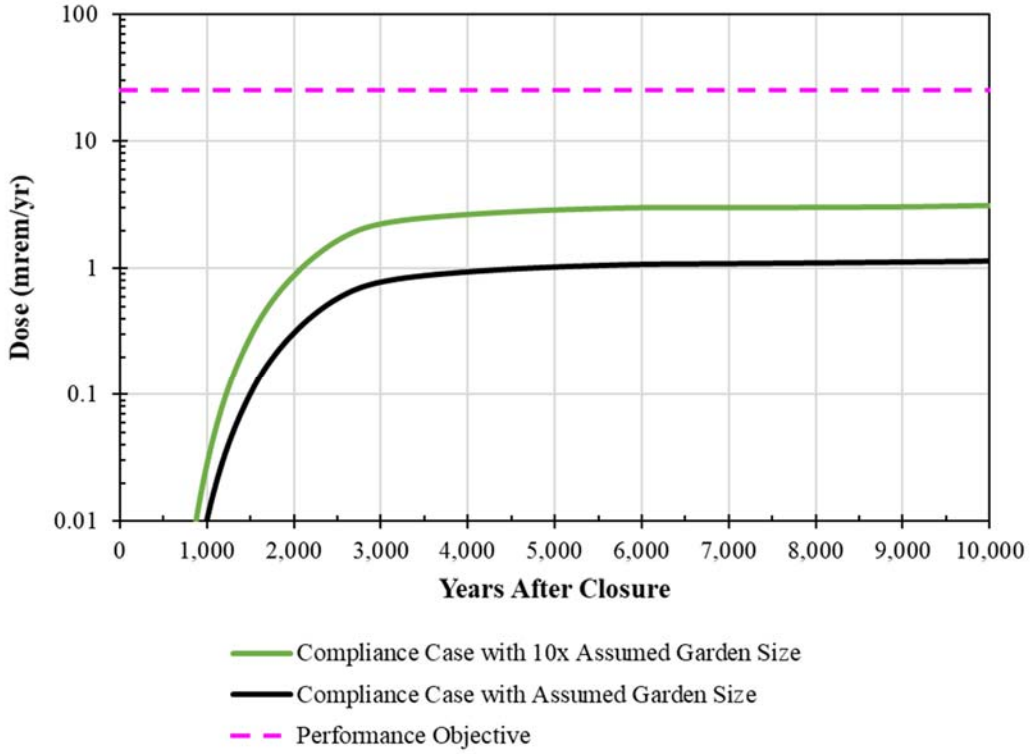

Figure 5.8-65: Dose Results from the Evaluation of the Maximum Garden Size (Performance Period, Detail)

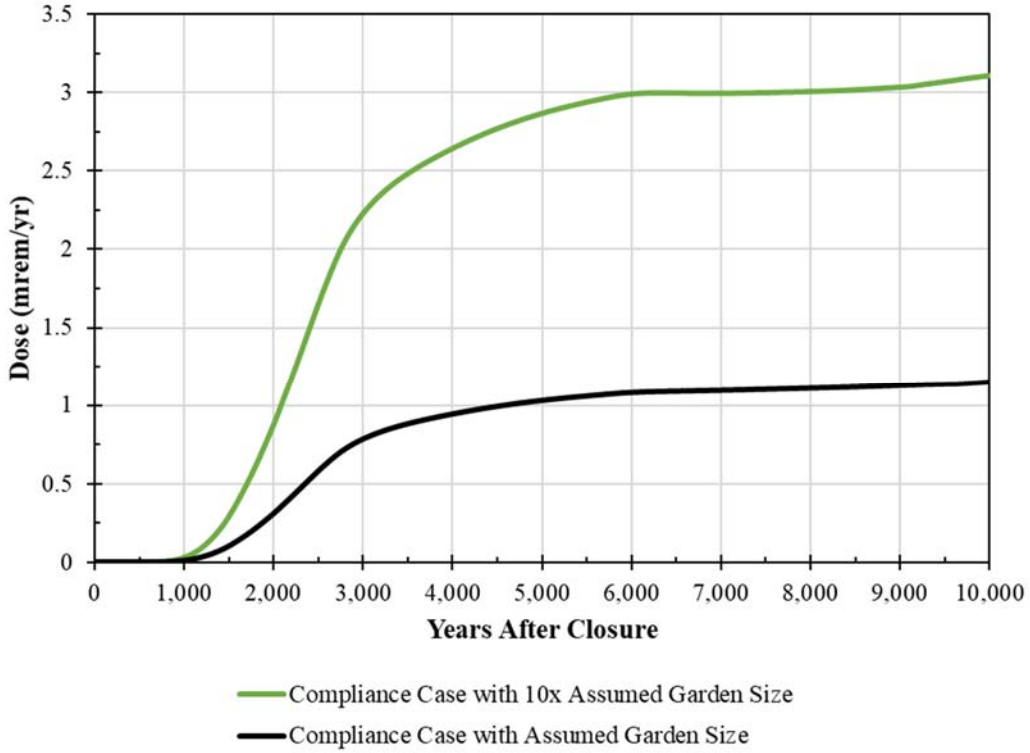

Table 5.8-24: Comparison of the 100-Meter MOP Peak Ground Water Pathways Doses Based on Using Minimum and Maximum Garden Sizes

Modeling Case	Compliance Period (0 to 1,000 Years)		Performance Period (0 to 10,000 Years)	
	Peak Dose (mrem/yr)	Year of Peak	Peak Dose (mrem/yr)	Year of Peak
Compliance Case with Recommended Garden Size (100 m²)	9.4E-03	1,000	1.2	10,000
Compliance Case with the Maximum Garden Size (1,000 m²)	2.8E-02	1,000	3.1	10,000

In general, the sensitivity case using the using the maximum garden area (1,000 m²) has total doses that are approximately 2.5 times as high as the Compliance Case (with a garden area of 100 m²). In this sensitivity case, produce ingestion (70%) surpassed water ingestion (28%) as the dominant exposure pathway.

5.8.6.4 Evaluation of K_ds Used for Soil Buildup Calculations

The dose calculations described in Section 4.4.8.2.1 include a term for soil buildup which relies on the soil K_ds to estimate contaminant concentrations that could accumulate in surface soils from successive years of irrigation (see Eq. 4.4-144 and Eq. 4.4-145). For consistency, the sandy soil K_ds defined in Table 4.3-4 are used for these equations. This consistency is a reasonable assumption because it is expected that if the contaminant is

highly mobile in subsurface conditions, it will likely continue to be highly mobile under surface conditions. Alternatively, if higher K_d values are appropriate to assume on the surface, it is likely also appropriate to assume higher K_ds for subsurface transport. Assuming the lower K_ds is generally the more defensible approach because it results in higher ground water concentrations.

Regardless, in the TER (ML121170309) for the 2009 SDF PA (SRR-CWDA-2009-00017), the NRC technical staff has noted that the K_ds that are selected to be conservative in the context of ground water transport could be non-conservative relative to the soil buildup calculations. Therefore, to evaluate this risk, inconsistent assumptions must be made with respect to the assumed K_d values. The following evaluations all use the same ground water concentrations, as calculated for the Compliance Case described in Sections 5.2 through 5.5 (i.e., the K_ds used in the ground water transport calculations are based on values from Table 4.3-4 as described in Sections 4.4.5 and 4.4.6). The only changes are the different K_d values used in the soil buildup equations within the dose calculator.

The first evaluation uses the K_d values from Table 4.3-4. This table includes four sets of K_d values: Clayey Soil K_ds, Leachate-Impacted Clayey Soil K_ds, Sandy Soil K_ds, and Leachate-Impacted Sandy Soil K_ds. Instead of defaulting to the Sandy Soil K_ds, as was done for calculating the Compliance Case doses, the maximum soil K_d values are assumed, regardless of the column in Table 4.3-4. For example, for iodine, the Sandy Soil K_d is 1.0 mL/g while the Clayey Soil K_d is 3.0 mL/g, therefore, the Clayey Soil K_d is assumed. To provide additional context, the opposite approach (i.e., using the minimum K_d values from Table 4.3-4) is also considered. Figure 5.8-66 illustrates that there is a moderate impact.

The next evaluation uses the same set of K_ds as from the first evaluation but applies a scaling factor to address the potential for uncertainty. For this evaluation, the maximum K_d values from Table 4.3-4 were increased by a factor of 5, while the minimum K_d values from Table 4.3-4 were decreased by a factor of 5. Given that site-specific surface soil K_ds are not available, this approach addresses possible uncertainties associated with these K_ds having potentially different values at the surface. As expected, Figure 5.8-67 shows that scaling the K_ds in this manner results in a larger impact to the dose.

Most of this impact is attributed to an increase in the dose contribution from Tc-99 with the higher K_ds. The increases from the other radionuclides are relatively negligible. This indicates that uncertainties associated with surface soil K_d for Tc-99 is the most risk-significant.

Figure 5.8-66: Total Dose to the MOP at 100-Meters from Using the Min/Max Recommended K_d Values in the Soil Buildup Dose Calculations (Performance Period)

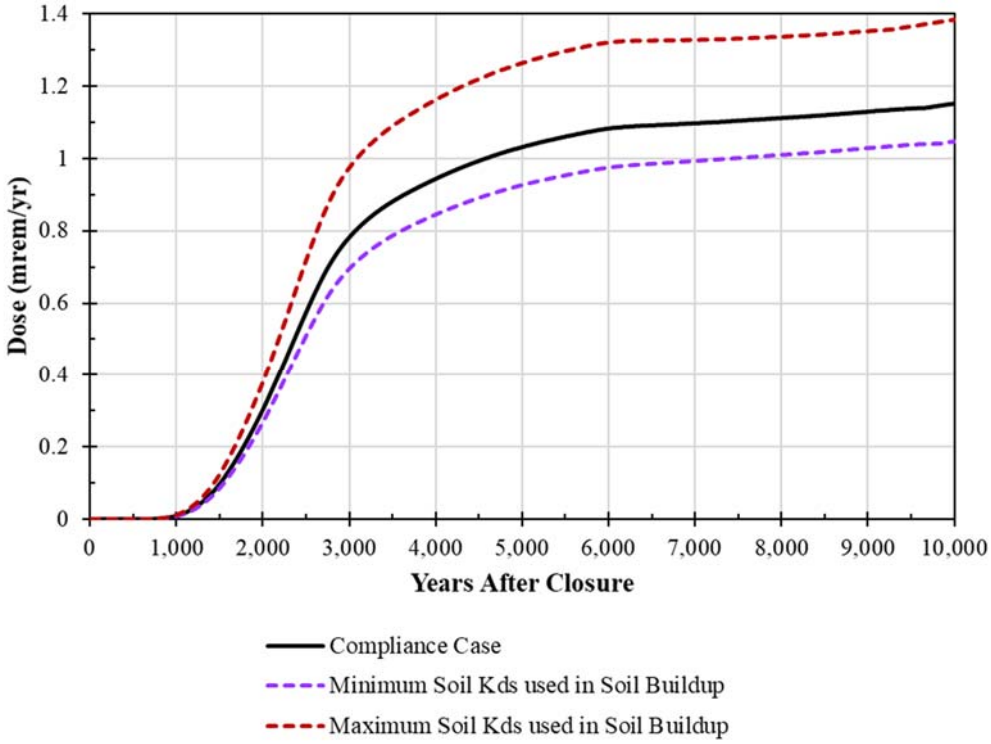

Figure 5.8-67: Total Dose to the MOP at 100-Meters from Using the Min/Max Recommended K_d Values, Modified by a Factor of 5, in the Soil Buildup Dose Calculations (Performance Period)

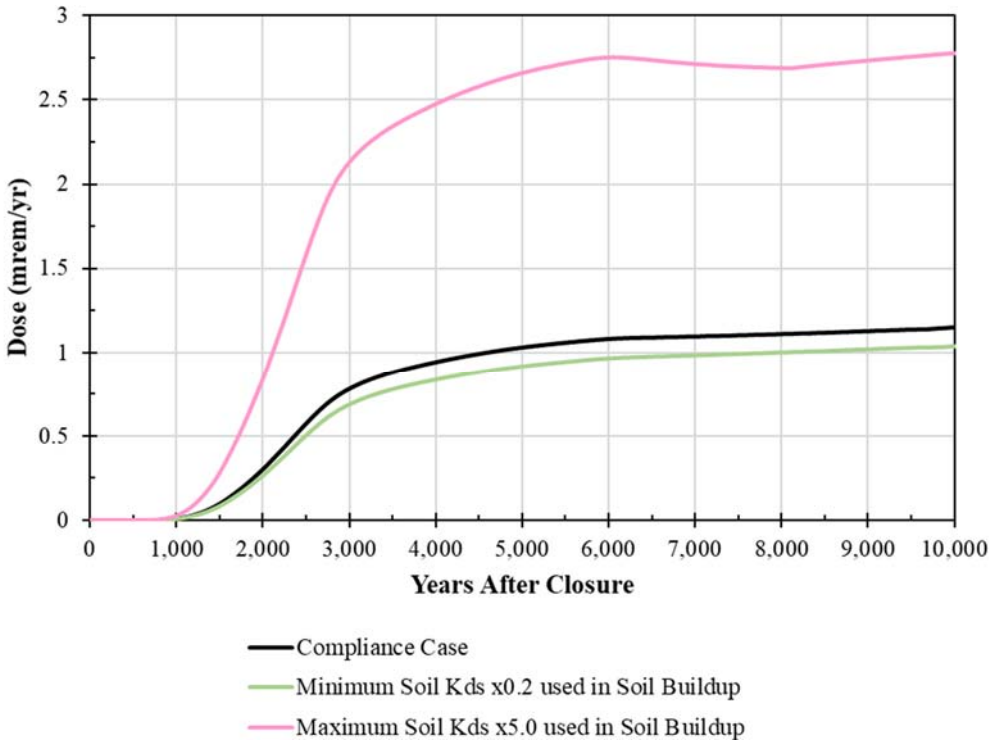

While site-specific values for surface soil K_ds are not available, surface soil K_ds for select radionuclides have been measured at other sites. As a final evaluation, the measured surface soil K_ds from the Olkiluoto site were considered as analogue values. Like the SRS, the Olkiluoto site is a humid environment with sandy and clayey soils. At both sites, the ground surface is topped by a thin layer of humus (i.e., surface material made up of decomposing organic materials). The values used for this evaluation come from *Distribution Coefficients of Caesium, Chlorine, Iodine, Niobium, Selenium and Technetium on Olkiluoto Soils* (WR-2013-68); from this report, four sets of K_d values were considered as presented in Table 5.8-25.

Table 5.8-25: Surface Soil K_ds from the Olkiluoto Site

Chemical	Reported K_d Value(s) (mL/g)				Table in WR-2013-68
	Humus, Conservative	Humus, Realistic	Top Mineral Soil, Conservative	Top Mineral Soil, Realistic	
Cesium (Cs)	100	1,000	860	5,200	Table 14
Chlorine (Cl)	0.20	1.5*	0.0	0.13	Table 15
Iodine (I)	10	460	12	32	Table 16
Niobium (Nb)	240	870	19,500**	100,000**	Table 17
Selenium (Se)	57	240	180**	250**	Table 18
Technetium (Tc)	0.0	21	0.0	0.4	Table 19

Notes: * Table 15 of WR-2013-68 actually recommends a value of 0.77 mL/g, but indicated that the higher value of 1.5 mL/g is possible if organic humus samples are included. This higher value is assumed.
** WR-2013-68 does not include "Top Mineral Soil" values for these chemicals, so these selected values are the "Intermediate Mineral Soil" values which were sampled from relatively shallow depths.

Figure 5.8-68 shows the resulting doses from assuming each set of K_d values. Note that for all other elements, the maximum recommended soil K_d was assumed. As with the previous sensitivity cases, the majority of the increase is attributed to an increase in the Tc-99 dose contribution.

Table 5.8-26 provides a summary of the peak doses associated with each of the cases evaluated.

This evaluation indicates that determining an appropriate site-specific value for the surface soil K_d for Tc-99 would reduce the risks associated with uncertainty in the soil buildup. Of all the data sets considered in this evaluation, the greatest change occurs when the "realistic humus" value from WR-2013-68 is assumed. It is worth noting that when the soil is being used for agricultural purposes, it is expected that the humus layer would be tilled into and mixed with the top mineral soil, which would mitigate the impact from these conditions (the tilling depth is assumed to the 15 cm). As such, this evaluation does not represent actual expected conditions but is only intended to provide insights relative to risk

Figure 5.8-68: Total Dose to the MOP at 100-Meters from the Evaluation Using the Olkiluoto Surface Soil K_d Values in the Soil Buildup Dose Calculations (Performance Period)

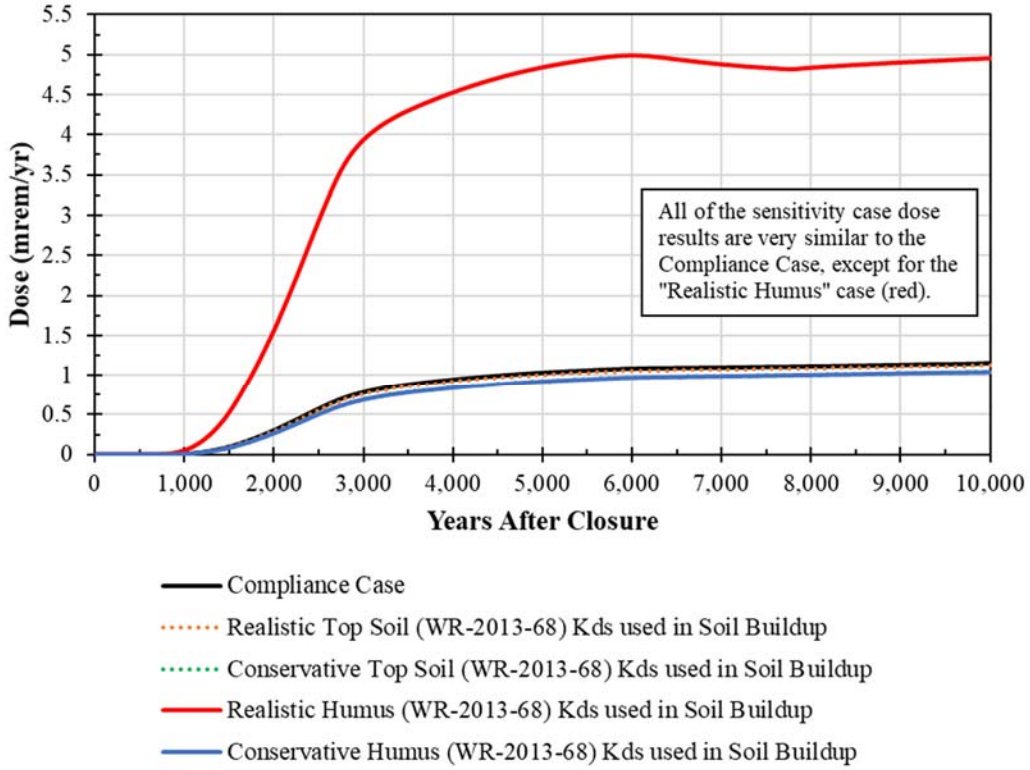

Table 5.8-26: Comparison of the 100-Meter MOP Peak Ground Water Pathways Doses Based on Various Soil Buildup K_ds

Modeling Case	Compliance Period (0 to 1,000 Years)		Performance Period (0 to 10,000 Years)	
	Peak Dose (mrem/yr)	Year of Peak	Peak Dose (mrem/yr)	Year of Peak
Compliance Case (Uses the Sandy Soil K_ds)	9.4E-03	1,000	1.2	10,000
Maximum Soil K_ds From Table 4.3-4	1.2E-02	1,000	1.4	10,000
Minimum Soil K_ds From Table 4.3-4	8.1E-03	1,000	1.0	10,000
Maximum Soil K_ds From Table 4.3-4 × 5	2.8E-02	1,000	2.8	10,000
Minimum Soil K_ds From Table 4.3-4 × 0.2	8.0E-03	1,000	1.0	10,000
Realistic Top Soil K_ds From Olkiluoto Site	9.0E-03	1,000	1.1	10,000
Conservative Top Soil K_ds From Olkiluoto Site	8.0E-03	1,000	1.0	10,000
Realistic Humus K_ds From Olkiluoto Site	5.4E-02	1,000	5.0	10,000
Conservative Humus K_ds From Olkiluoto Site	8.0E-03	1,000	1.0	10,000

5.8.7 Alternative Waste Disposal and Closure Configurations

As part of the FY2019 SDF PA evaluation, several alternative conceptual models were developed to consider potential variation in construction parameters for future 375-foot diameter SDUs, alternative closure options for SDUs 1 and 4, and for potential effects from the settlement of bags

that have already disposed of in Cells C and I of SDU 4. Each of these scenarios are discussed below.

5.8.7.1 Design Margin Case for Future 375-Foot Diameter SDUs

The design specifications for the 375-foot diameter SDUs, as assumed for modeling, are provided in Table 4.3-10, and reflect the intended design for SDU 7 and all subsequent SDUs to be constructed. As such, Compliance Case modeling assumes the SDU 7 design specifications for all future SDUs (i.e., SDUs 7, 8, 9, 10, 11, and 12). In addition to these design specifications for SDU 7, inputs for modeling the "Design Margin Case" for SDU 7 are also provided in Table 4.3-10. The Design Margin Case is an alternative modeling case that considers construction margin to ensure that if deviations from the design should occur during construction it will not adversely impact the expected performance of the SDU.

To evaluate the risks associated with design margin for future 375-foot diameter SDUs, the Design Margin Case was developed and run. This modeling case was developed using Compliance Case modeling parameters for all inputs except for those explicitly identified in Table 4.3-10. Specifically, the Design Margin Case assumes:

- The SDU concrete barriers (e.g., wall, roof, floors, etc.) are all less thick than designed,
- The SDU roof has a decreased slope (1% slope as opposed to the designed 1.5% slope),
- Increased joints through the SDU roof (3,200 linear feet of joints versus 1,220 linear feet),
- Increased joints through the SDU floor (3,200 linear feet of joints versus 1,980 linear feet), and
- No credit is assumed for repairs to the SDU walls to fill various wall form penetrations.

The Design Margin Case assumes these changes for all future SDUs.

The dose results are presented in Figure 5.8-69 and Figure 5.8-70. As indicated in Figure 5.8-69, within the Compliance Period the Design Margin Case yields doses that are higher than the Compliance Case. Despite this higher dose, the peak dose within the Compliance Period is approximately 0.15 mrem/yr, which is well below the 25 mrem/yr performance objective.

Figure 5.8-70 presents the dose results within the 10,000-year Performance Period. This figure illustrates that over longer time periods, the doses from the Design Margin Case are virtually identical in magnitude to the Compliance Case. The results of this evaluation indicate that while the timing of the releases occurs sooner, the collective conditions assumed for the alternative Design Margin Case values have a negligible impact on the magnitude of the total dose within the Performance Period.

Figure 5.8-69: Dose Results Comparing the Design Margin Case to the Compliance Case in the Compliance Period

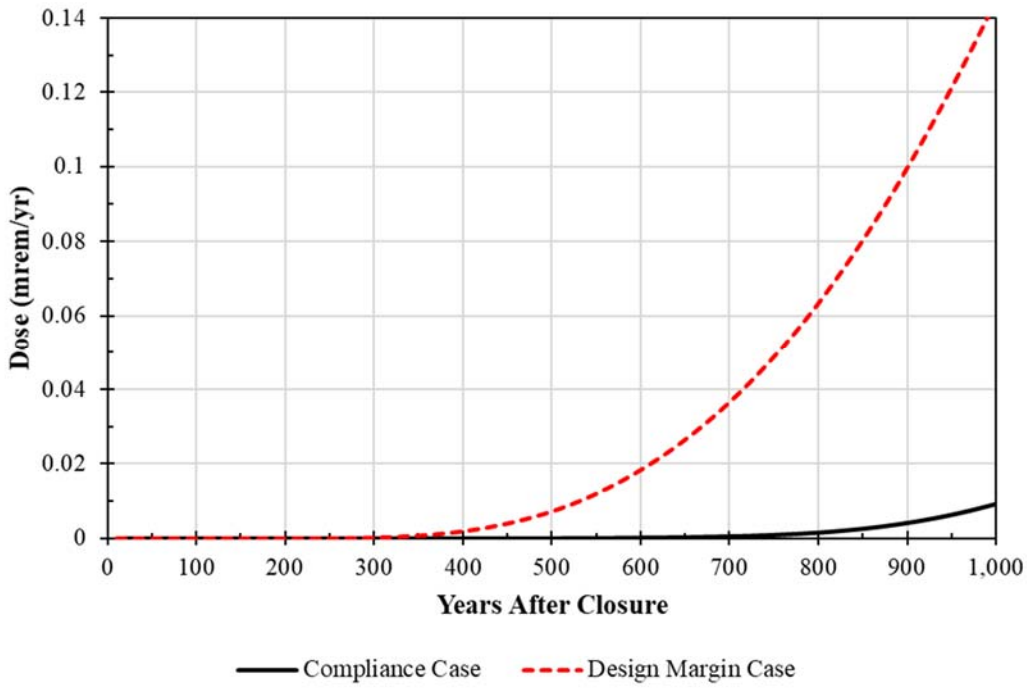

Figure 5.8-70: Dose Results Comparing the Design Margin Case to the Compliance Case in the Performance Period

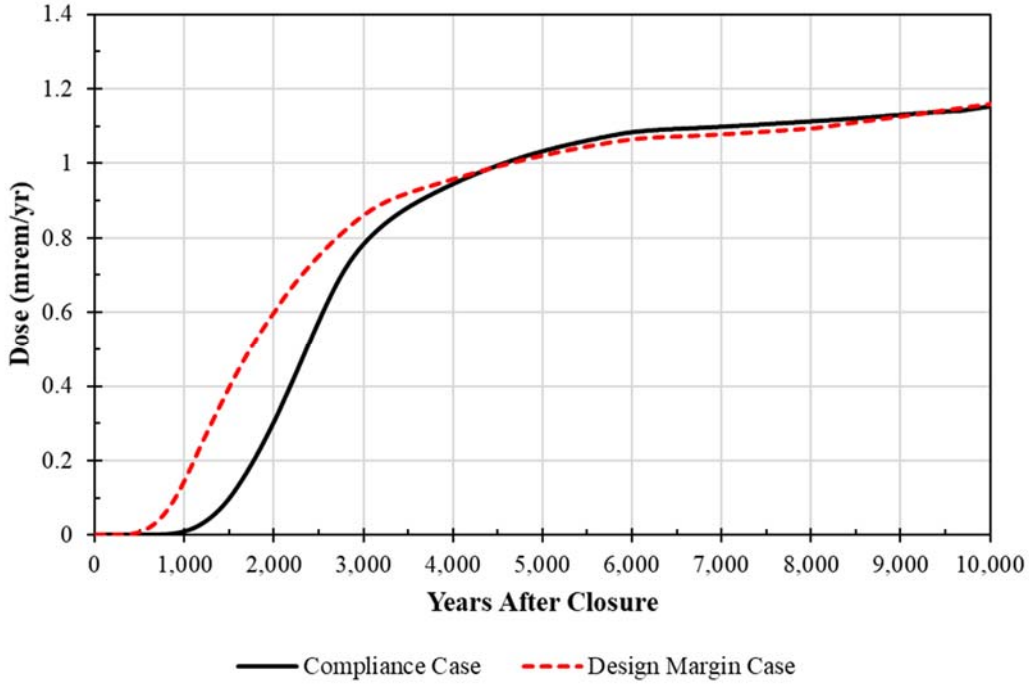

5.8.7.2 SDU 1 Soil Disposal Case

To consider a possible alternative closure configuration for the SDF, an alternative conceptual model has been developed that assumes that contaminated soils downstream of SDU 4 will be excavated and disposed of into the empty disposal cells of SDU 1. This alternative conceptual model is referred to as the Soil Disposal Case.

In April 1997, weeping was detected from Cell G of SDU 4. It is believed that rainwater accumulated in the cell prior to placement of the permanent concrete roof. Surveys of the water that leaked out were found to have a detectable level of radioactive contamination. In May 2004, contamination was found in the drainage ditch adjacent to SDU 4, Cell G. The contaminated soil was removed up to the SDU 4, Cell G wall and disposed of. [SRR-CWDA-2018-00036]

Beginning in 2007, additional wet spots were noted on the SDU 4, Cells E, F, J, and L walls. To assess any additional environmental impact from SDU 4, soil samples were collected and analyzed in 2008 to determine the nature of the chemical and radiological contamination to the surrounding soils. Soil samples were collected in two phases adjacent to SDU 4 to evaluate the distribution of contamination in soil and gravel associated with wet spots on the walls of the disposal unit. Results of the sampling indicate Cs-137 contamination in the gravel directly adjacent to the SDU. The majority of the Cs-137, which leaked onto the gravel adjacent to SDU 4, remained within 2 feet of the SDU. This indicated that contamination associated with wet spots from SDU 4 leaks was spatially limited in the surrounding soils. [SRR-CWDA-2018-00036]

In 2008, weather enclosures were constructed around various cells at SDU 4 to prevent the further vertical migration of contamination into the soils adjacent to the SDU. Troughs were also placed inside the enclosures to prevent contaminated water from reaching the surrounding soils. [SRR-CWDA-2018-00036]

SDU 1 consists of six disposal cells (Cells A through F); the first three cells (Cells A, B, and C) currently contain saltstone while the last three cells (Cells D, E, and F) are currently empty. To support the permanent closure of SDU 4, contaminated soils around SDU 4 may be excavated and disposed of. The Soil Disposal Case assumes that rather than filling the empty cells of SDU 1 with clean cap grout (as is assumed for the Compliance Case configuration), these cells will instead be used to dispose of the contaminated soils.

This evaluation is implemented on a disposal cell-by-disposal cell basis. Inventory values equal to 10% of the inventory from SDU 4 Cell G (based on SRR-CWDA-2018-00062) are assigned to the soils disposed of into SDU 1 Cells D, E, and F. Within these soil-filled disposal cells, the material properties for saltstone and clean cap grout are replaced with the material properties of backfill soil.

The MOP dose results at Sector G are presented in Figure 5.8-71 and Figure 5.8-72. Note these two figures include the results for Sector G, which is the sector that receives the most dose contribution from SDU 1 and is therefore the most impacted.

Figure 5.8-71 presents the dose results within the 1,000-year Compliance Period and shows that the Compliance Case and the Soil Disposal Case are virtually identical, with a Sector G dose of approximately 2.8E-03 mrem/yr.

Figure 5.8-72 presents the dose results within the 10,000-year Performance Period and shows that although the Soil Disposal Case shows an increase of approximately 0.04 mrem/yr in Sector G, the total dose is the same as the Compliance Case because the total dose is controlled by releases from the 375-foot diameter SDUs, which affect Sectors A through E, as aopposed to the releases from SDU 1, which affect Sectors F through H. The increase in the peak dose at Sector G is because contaminants are generally more mobile in soil than in saltstone.

The results of this evaluation indicate that replacing SDU 1 clean cap grout with contaminated soils from near SDU 4 will have a negligible impact on the overall SDF performance.

Figure 5.8-71: Sector G Dose Results Comparing the Compliance Case to the SDU 1 Soil Disposal Case in the Compliance Period

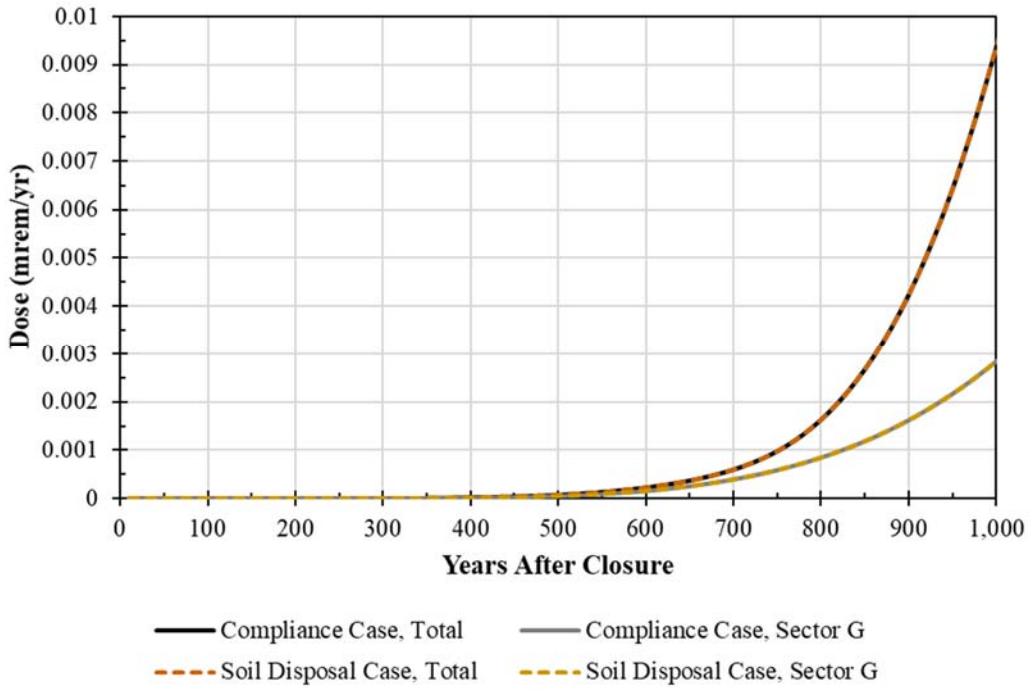

Figure 5.8-72: Sector G Dose Results Comparing the Compliance Case to the SDU 1 Soil Disposal Case in the Performance Period

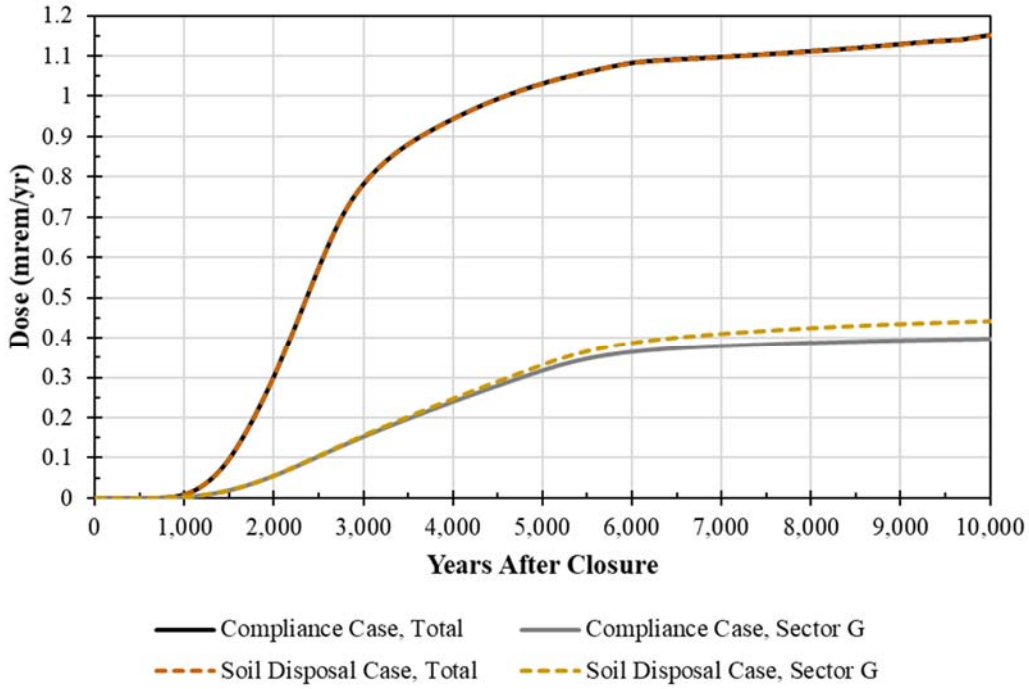

5.8.7.3 SDU 4 Waste Bags Evaluation

Currently, SDU 4 Cells C and I contain saltstone filled to heights of 15 feet and 13 feet, respectively. Piles of several hundred plastic waste bags containing contaminated grout chips have been placed on top of the saltstone in these cells (depicted in Figure 5.8-73 and Figure 5.8-74).

The plastic waste bags consist of double-bagged chips of grout and pieces of plastic, each j-sealed with black tape. Based on visual inspections, each bag is approximately 1.5 feet in diameter. The waste bags are configured in roughly half-conical piles leaning against the side of the interior wall of each of cell. Each pile is approximately 13 to 15 feet tall (reaching to within a couple of feet of the SDU roof) and approximately 12 feet in radius.

Figure 5.8-73: Waste Bags in SDU 4 Cell C

[Source: SRR-CWDA-2015-00041]

Figure 5.8-74: Waste Bags in SDU 4 Cell I

[Source: SRR-CWDA-2015-00041]

As part of the Compliance Case, clean cap grout will be added to each of the cells in SDU 4, including Cells C and I, to completely fill the cells to the roof in order to provide structural stability to support the closure cap. The Compliance Case assumes that as the clean cap grout is poured over these waste bags, the weight of the grout will adequately compress these waste bags to minimize void space and that the cured clean cap grout, coupled with the SDU roof, will provide adequate structural support to prevent collapse or settlement once the closure cap is installed. As such, the Compliance Case assumes that presence of these waste bags will have little to no impact on the performance of the post-closure system.

Regardless, an engineering evaluation was performed to determine if the presence of the waste bags in their current configuration could adversely impact the post-closure performance of the system. [K-CLC-Z-00028] Based on the assumptions used in the eingineering evaluation, it concluded that compression of the waste bags might result in settlement at the closure cap surface. Specifically, the "the maximum Closure Cap surface settlements could reasonably vary from 3 inches to 15 inches for the range of compressibility considered for the waste bags in SDU 4 Cells C and I." [K-CLC-Z-00028]

An alternative conceptual model has been developed (the SDU 4 Waste Bags Case) to provide insight to the potential impacts should compression of the waste bags occur after clean cap grouting, resulting in settlement in the overburden material. This SDU 4 Waste Bags Case assumes that no mitigation actions will be performed, and that complete compression of these waste bags does not occur until after the closure cap has been installed, resulting in a depression at the surface of the overlying closure cap. This surface depression is assumed to act as a funnel, effectively channeling water into Cells C and I.

This evaluation is implemented on a disposal cell-by-disposal cell basis for SDU 4. The infiltration rate affecting Cells C and I is set is to 269 mm/yr (10.6 in). This assumed infiltration rate is from Table 1 of the *Saltstone Disposal Facility Closure Cap Concept and Infiltration Estimates* (WSRC-STI-2008-00244), based on assuming a fully degraded closure cap. It should be noted that the more recent infiltration report, *Predicting Long-Term Percolation from the SDF Closure Cap* (SRRA107772-000009), indicates that some of the assumptions used in WSRC-STI-2008-00244 were unrealistic, thus the estimated infiltration rates were overly pessimistic. For diagnostic purposes, the assumed infiltration rate is intended to represent a bounding value.

To address how the additional influx of water into Cells C and I might affect the other Cells in SDU 4, the other cells of SDU 4 are simulated using model inputs and settings based on the Pessimistic Case (see Section 5.8.1). These changes were only applied to SDU 4; all other SDUs are modeled using Compliance Case inputs and settings.

The MOP dose results through the Performance Period are presented in Figure 5.8-75. This figure shows the total dose to the MOP from the Compliance Case, the SDU 4 Waste Bags Case. In addition to the total doses, the Sector F results are also provided because this is the sector that is most influenced by the changes to SDU 4 Cells C and I.

Figure 5.8-75: Dose Results Comparing the SDU 4 Waste Bag Case to the Compliance Case in the Performance Period

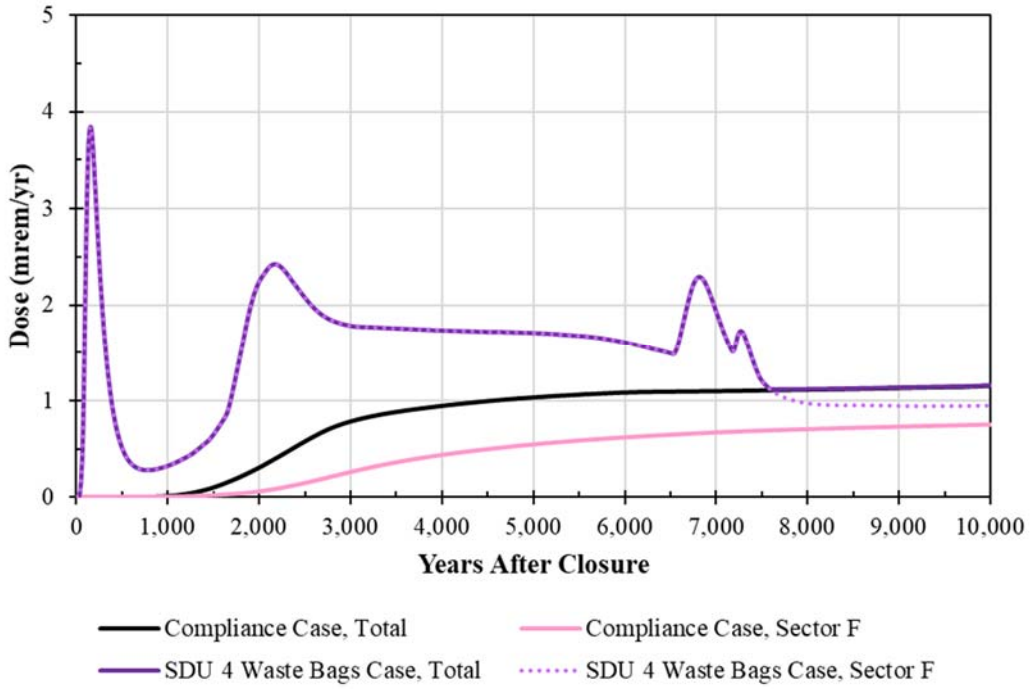

As indicated in Figure 5.8-75, the SDU 4 Waste Bags Case peaks relatively early at year 160 with a dose of 3.8 mrem/yr. While this peak is higher than the Compliance Case, it is below the performance objective of 25 mrem/yr and lower than the peak dose from the Pessimistic Case. Furthermore, the extremely high infiltration rate assumed for Cells C and I is considered bounding. It is more reasonable to expect that the potential impacts due to the compression of the waste bags would likely be minimal, with peak doses somewhere in between those of the SDU 4 Waste Bags Case and the Compliance Case. Finally, any mitigation activities prior to closure would reduce the risks associated with this scenario.

5.8.7.4 SDU 4 CLSM Closure Evaluation

Prior to closure cap emplacement, any void space remaining in the SDUs is expected to be filled in with clean cap grout. As an alternative conceptual model, the void spaces are assumed to be filled with controlled low strength material (CLSM) instead of clean cap grout for closing SDU 4. CLSM is an inexpensive, self-leveling, flowable material that is composed of sand and cement formers. [PIT-MISC-0004] SDU 4 was selected for this analysis because many of the disposal cells in SDU 4 are only partially filled (see Table 5.8-27) and no additional disposal is planned for SDU 4. As such, it is expected that any changes to the assumed fill material would be most impactful to SDU 4.

Table 5.8-27: Current Fill Heights for SDU 4

SDU 4 Disposal Cell	Fill Height (ft)
A	27 [a]
B	23.25
C [b]	15.5
D	23.75
E	21
F	22.75
G	21.5
H	9.5
I [b]	13.2
J	23.25
K	23.5
L	23.5

[Source: SRR-CWDA-2018-00062]
(a) The fill height of SDU 4 Cell A is not reflective of saltstone fill, as Cell A contains U.S. Naval fuel waste in 10,032 55-gallon drums that were disposed of in SDU 4 Cell A in 1990 and the void space surrounding the drums is filled with clean grout. SDU 4 Cell A is considered full to the height of 30 feet.
(b) Cells C and I waste bags are not included in the fill estimate.

To evaluate the impacts from using CLSM as the fill material, the SDU 4 CLSM Closure Case was developed. As shown in Table 5.8-27, the lowest fill level for saltstone in SDU 4 is currently 9.5 feet in Cell H. Based on this fill height, the SDU 4 CLSM Closure Case assumes a slightly lower fill height of 9.25 ft for all the saltstone disposal cells in SDU 4 (i.e., all except Cell A). Note that the inventory values in the disposal cells for SDU 4 remains unchanged, such that the lower fill height results in higher waste concentrations within the modeled saltstone.

The remaining volume is assumed to be filled with CLSM. For the SDU 4 CLSM Closure Case, the CLSM fill material is assumed to have the hydraulic properties of sand and no sorption (K_d = 0 mL/g). These changes were only applied to SDU 4; all other SDUs are modeled using Compliance Case inputs and settings.

The total MOP dose results and the dose results at Sector G are presented in Figure 5.8-76 and Figure 5.8-77. These two figures include the results for Sector G as this is the sector most impacted by this change to SDU 4. These figures show that the SDU 4 CLSM Closure Case results in a moderate increase to the doses at Sector G. This increase is due to the modeling assumptions applied to the model development (i.e., the lower fill height increased the waste concentrations, and the assumed hydraulic properties and zero K_d accelerated flow transport). In the absence of more applicable data, these assumptions are appropriate; however, it is reasonable to expect that using more realistic material properties to simulate the CLSM would mitigate the extent of these impacts. Regardless, the results of this evaluation indicate that filling the void space in SDU 4 with CLSM material rather than clean cap grout has a negligible impact on overall SDF performance.

Figure 5.8-76: Dose Results Comparing the Compliance Case to the SDU 4 CLSM Closure Case (Total and Sector G) in the Compliance Period

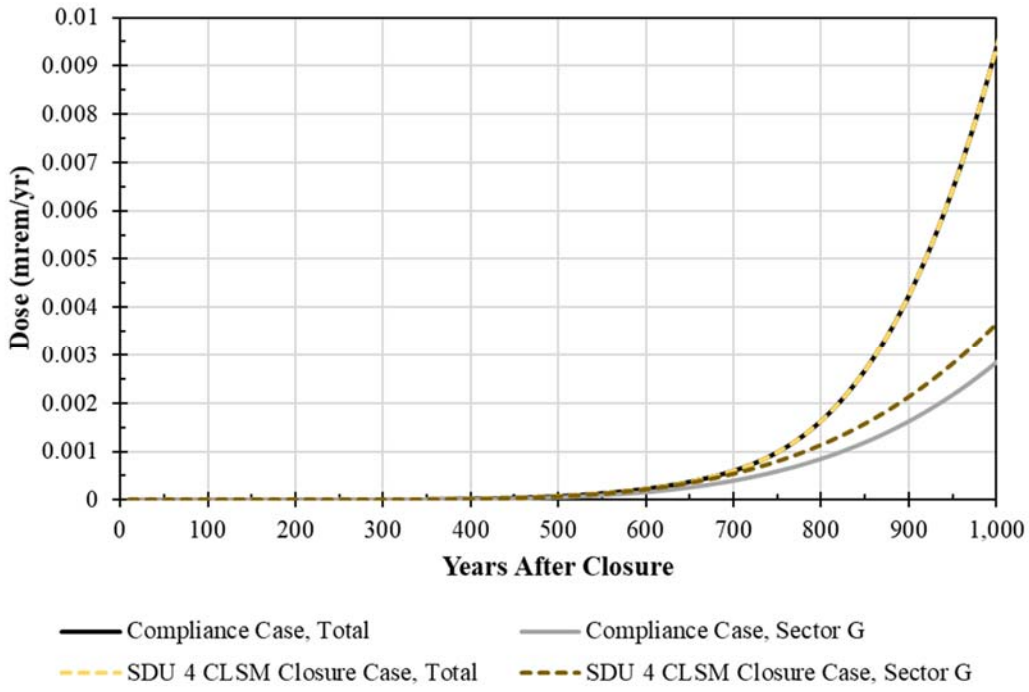

Figure 5.8-77: Dose Results Comparing the Compliance Case to the SDU 4 CLSM Closure Case (Total and Sector G) in the Performance Period

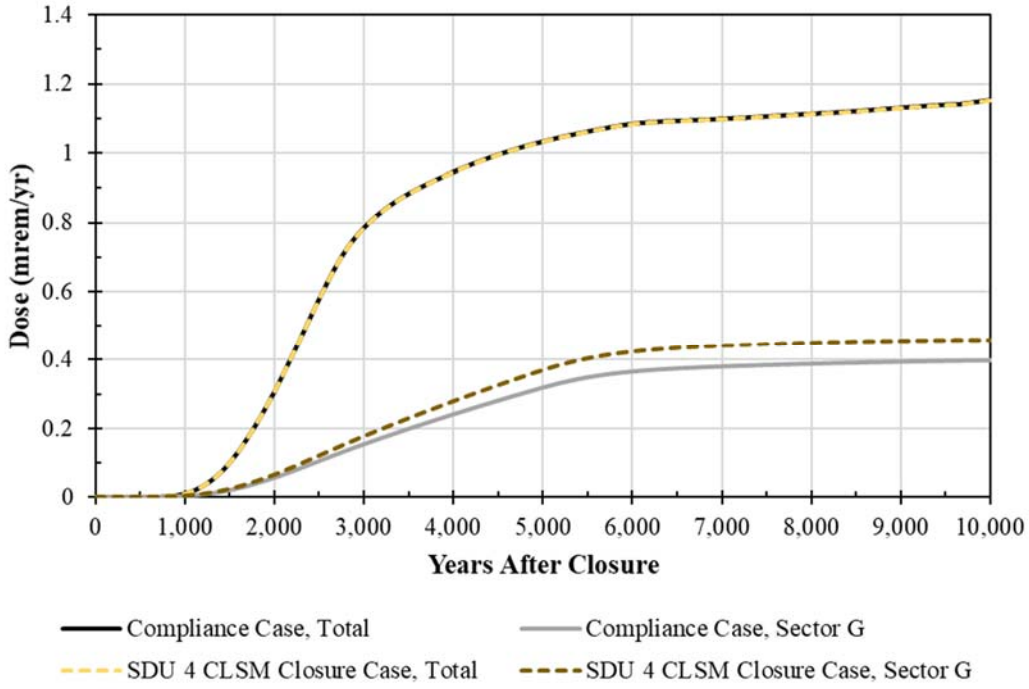

5.8.8 Flow and Transport Sensitivities

The Vadose Zone Flow and Transport models are described in Sections 4.4.4 and 4.4.5. The Aquifer Transport Model is described in Section 4.4.6. The following sensitivity cases were developed to better understand the uncertainties and risks that are specifically associated with these models.

5.8.8.1 Dose Results from Parametric Flow Cases

Alternate sensitivity cases and uncertainty analyses are used to provide additional insights into the influence of physical processes and associated parameters influencing the flow of water through SDUs and their influence on the release of radionuclides into the natural system. To meet this end, a set of parametric flow fields was developed based on various combinations of parameter settings that affect flow (Table 4.4-82), including: infiltration rates, cementitious degradation rates, backfill saturated hydraulic conductivities, and initial saltstone hydraulic conductivities.

Table 4.4-82 provides a complete list reflecting the full spectrum of flow fields that were considered. As illustrated by Figure 4.4-78, these 54 parametric flow cases can generally be organized into five groups, based on the resulting flow rates: Low, Moderate, Moderate-to-High, High, and Very High. As noted in Section 4.4.4, these groups as summarized as follows:

- The Low Group assumes the Best Estimate infiltration rate and either initial saturated hydraulic conductivity of saltstone (5.0E-10 cm/s or 2.0E-09 cm/s),
- The Moderate Group assumes the MPAD (compliance) infiltration rate and the more probable initial saturated hydraulic conductivity of saltstone (5.0E-10 cm/s),
- The Moderate-to-High Group assumes the MPAD infiltration rate and the high initial saturated hydraulic conductivity of saltstone (2.0E-09 cm/s),
- The High Group assumes the Conservative Estimate infiltration rate and the more probable initial saturated hydraulic conductivity of saltstone (5.0E-10 cm/s), and
- The Very High Group assumes the Conservative Estimate infiltration rate and the high initial saturated hydraulic conductivity of saltstone (2.0E-09 cm/s).

Figure 4.4-78 depicts the effects that this parameterization has on the volumetric flow rates through saltstone for a 375-foot diameter SDU. Within this figure, the curves were color-coded by the groupings identified above.

To better examine the influence of the parametric flow cases, representative flow cases were selected from these groups and used to develop sensitivity cases. These sensitivity cases examine the degree of influence that changes in infiltration rates, cementitious degradation rates, backfill saturated hydraulic conductivities, and initial saltstone hydraulic conductivities have on the exposures to the MOP. While the flow fields for each of these sensitivity cases were varied, all other parameters in this study are the same as used in the Compliance Case. Note that the Compliance Case uses the parametric flow case F27 data, the results for which are also included in comparison below.

The differences in infiltration rates, cementitious degradation rates, backfill saturated hydraulic conductivities, and initial saltstone hydraulic conductivities collectively influence the vadose zone flow rates, saturation levels, chemical environment transition times, and time-variant diffusion coefficients, which then influence the resulting release and transport of contaminants.

The doses to the MOP from each of these parametric flow field sensitivity cases are compared in Figure 5.8-78. This figure depicts the dose results for five parametric flow cases representing each of the flow case groupings: the Low Group (Flow Case F01), the Moderate Group (Flow Case F28), the Moderate-to-High Group (Flow Case F35), the High Group (Flow Case F45), and the Very High Group (Flow Case F54), along with the Compliance Case results (Flow Case F27). As can be seen by comparing Figure 5.8-78 with Figure 4.4-78, the different dose results tend to reflect the relative differences in volumetric flow rates.

Figure 5.8-78: Comparison of Selected Parametric Flow Case Total Dose Results with Compliance Case Dose Results

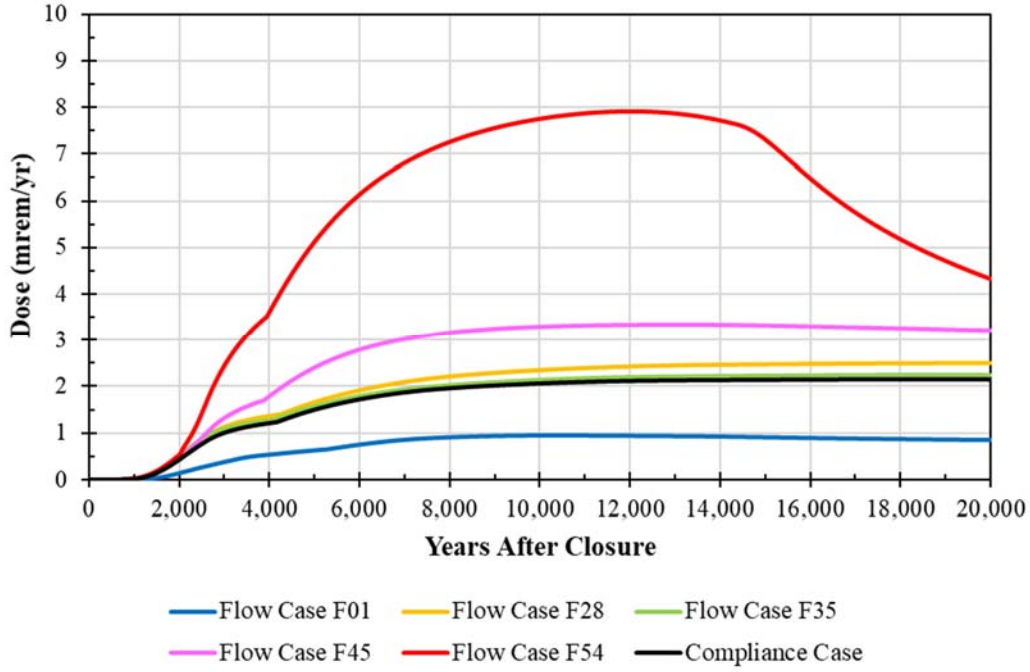

The peak doses are summarized in Table 5.8-28. Within the Compliance Period, the peak dose for the Very High Group sensitivity case (Flow Case F54) is approximately 3.6 times greater than the Low Group sensitivity case (Case F01). Within the Performance Period, the peak dose for the Very High Group sensitivity case (Case F54) is approximately 8 times greater than the Low Group sensitivity case (Case F01), but still much lower than the performance objective.

Table 5.8-28: Comparison of Parametric Flow Sensitivity Cases, for 100-Meter MOP Peak Doses Based on GoldSim 2019 PA SDF Model Simulations

Modeling Case/Group	Compliance Period (0 to 1,000 Years)		Performance Period (0 to 10,000 Years)	
	Peak Dose (mrem/yr)	Year of Peak	Peak Dose (mrem/yr)	Year of Peak
F01 (Low)	6.1E-03	1,000	0.95	10,000
F28 (Moderate)	1.8E-02	1,000	2.3	10,000
F35 (Moderate-to-High)	1.9E-02	1,000	2.1	10,000
F45 (High)	1.6E-02	1,000	3.3	10,000
F54 (Very High)	2.2E-02	1,000	7.8	10,000
F27 (Compliance Case)	1.6E-02	1,000	2.1	10,000

As would be expected based on the volumetric flow rates depicted in Figure 4.4-78, all of these cases have very similar results during the first 2,000 years of the simulation, except for the Low Group sensitivity case (Case F01) which makes use of the best estimate infiltration rate. After the first 2,000 years, the doses from the Very High Group sensitivity case (Case F54) increase to approximately 4 times greater than the doses from the Compliance Case after 10,000 years. The dose results from the Moderate Group sensitivity case (Case F28) and the Moderate-to-High Group sensitivity case (Case F35) were both similar to the doses from the Compliance Case, all three having moderate infiltration rates.

These results indicate that increases to just the initial saturated hydraulic conductivity of saltstone results in relatively small increases to the doses (Case F28 versus F27). Increases to just the infiltration more effectively increase the doses as can be seen by comparing Cases F01, F35, and F45. The significance of infiltration rate alone can also be seen by comparing Cases F28 and F54. The largest increase in dose is found between Cases F01 and F54, where Case F01 has a low initial saturated hydraulic conductivity and low infiltration rate while Case F54 has a high initial saturated hydraulic conductivity and high infiltration rate. Note that Case F54 also has a higher cementitious degradation rate than Case F01.

5.8.8.2 Evaluation of Hypothetical Fast Flow Paths

The conceptual model development report (SRR-CWDA-2018-00006) identifies several FEPs (Table 5.8-29) that could lead to fast flow paths (such as fractures or cracks) penetrating through the SDUs and through the saltstone waste form. The FEPs representing processes or mechanisms which might create such fast flow paths include seismic activity, differential settlement, material shrinkage, chemical degradation of cementitious materials, and steel corrosion. While surface cracks are likely to form in the cementitious materials, through-cracks (i.e., cracks that penetrate the full height of the SDUs) are considered unlikely and do not represent expected future conditions. Regardless, an alternative conceptual model has been developed to non-mechanistically address the potential impacts from these multiple FEPs.

Table 5.8-29: FEPs Addressed in the Fast Flow Paths through SDUs Scenario

FEP ID	FEP Name	Discussion
2.7.03	Cold Weather Effects	Cold weather effects could cause freeze/thaw damage to external surfaces. These may result in the formation of cracks which may provide fast flow paths.
3.2.09	Repairs of Construction Defects	Incomplete repair of construction defects may result in the formation of cracks which may provide fast flow paths.
3.4.05	Saturation of Fractures	Assumed cracks or fractures must account for how the presence of macro-fractures may influence water movement and saturation conditions.
3.7.02	Mechanical Degradation Mechanisms	Mechanical degradation in the form of damage to the SDU integrity may result in the formation of cracks which may provide fast flow paths.
3.7.06	Concrete Shrinkage/Expansion	Concrete shrinkage or expansion may damage the SDU integrity or may create a direct pathway from the saltstone to the soil. Both conditions may result in the formation of cracks which may provide fast flow paths.
3.7.09	Localized Degradation	Localized degradation may create a direct pathway (fast flow path) from the saltstone to the soil.
3.7.15	Waste Form (Saltstone) and Concrete (SDU) Macroscopic Fracturing	This FEP is explicitly addressed by this scenario by considering macroscopic fractures of the saltstone and SDU.
3.7.19	Site Stability	Instability of the site may result in damage to the SDUs. Such damage may result in the formation of cracks which may provide fast flow paths.
3.8.02	Void Space Formation	Void space formation may result in a collapsed roof during closure cap emplacement. This could result in the formation of cracks which may provide fast flow paths.
3.8.07	Mechanical Effects at Engineered Barrier System Component Interfaces	Mechanical damage to the SDU(s) may result in the formation of cracks which may provide fast flow paths.
5.1.03	Focusing of Flow Along Preferred Flow Paths (Fingers, Weeps, Faults, Fractures, etc.)	Focused flow along preferred flow paths may result in a direct pathway from the saltstone to the soil.
5.1.14	Deformation at Flow Interfaces	Deformation and associated influence on flow systems at joints and material interfaces may exhibit localized flow conditions which might be approximated by assuming a fast flow path.
5.3.09	Fast Transport Pathways	This FEP is explicitly addressed by this scenario by considering macroscopic fractures of the saltstone and SDU.
5.4.05	Oxidation along Fractures	Assumed cracks or fractures must account for how the presence of macro-fractures may influence oxidation conditions.
6.2.01	Seismicity	Significant seismic events may result in the formation of cracks which may provide fast flow paths.
6.2.03	Seismic-Induced Damage or Changes to System Components	Significant seismic events may result in the formation of cracks which may provide fast flow paths.
6.2.04	Effects of Subsidence	Significant subsidence events may result in the formation of cracks which may provide fast flow paths.
6.4.04	Forest/Brush Fire	A fire near the SDUs prior to emplacement of the closure cap may result in spalling (i.e., damage to the SDU concrete). Such damage may result in the formation of cracks which may provide fast flow paths.

FEP ID	FEP Name	Discussion
6.4.06	Movement of the Waste Form	Instability of the site may result in movement or damage to the SDUs. Such damage may result in the formation of cracks which may provide fast flow paths.
6.4.07	Cave-In, Collapse, or Rockfall	A collapsed roof could result in the formation of cracks which may provide fast flow paths.

[SRR-CWDA-2018-00006]

Despite the large number of FEPs considered, it should be noted that the goal of this scenario is not to explicitly simulate the presence or occurrence of each FEP, rather the goal is to provide insights to the potential impacts these FEPs may incur on the performance system. As such, these FEPs are addressed non-mechanistically through various sensitivity models developed in support of the Fast Flow Paths through SDU Scenarios:

- Partial Penetration Case, and
- Full Penetration Case.

To address the various underlying mechanisms regardless of associated probabilities, these sensitivity cases postulate modeling scenarios with partially- and fully-penetrating high-permeability pathways in the 375-foot diameter SDUs (SDUs 6, 7, 8, 9 ,10, 11, and 12), as shown in Figure 5.8-79 and Figure 5.8-80, respectively. Only the outer radius of the SDU is depicted to show fast flow path detail. The nominal spacing of fast flow paths is 3 feet (~1 meter). Like joints in the floor and roof, each aperture is 2 inches, filled with gravel material, and assigned K_d = 0 mL/g. Gravel-filled vertical seams are a modeling surrogate for a variety of potential physical features that create higher permeability pathways for infiltrating water and gas-phase oxygen, such as fractures in grout whether open or infilled with debris. Although fast flow paths occupy approximately 6% of the SDU volume, they represent much thinner physical features that occupy negligible volume or form by portions of saltstone separating. Therefore, no inventory is placed within the fast flow features at time zero.

Figure 5.8-79: Partially-Penetrating Fast Flow Paths Through 375-foot Diameter SDUs

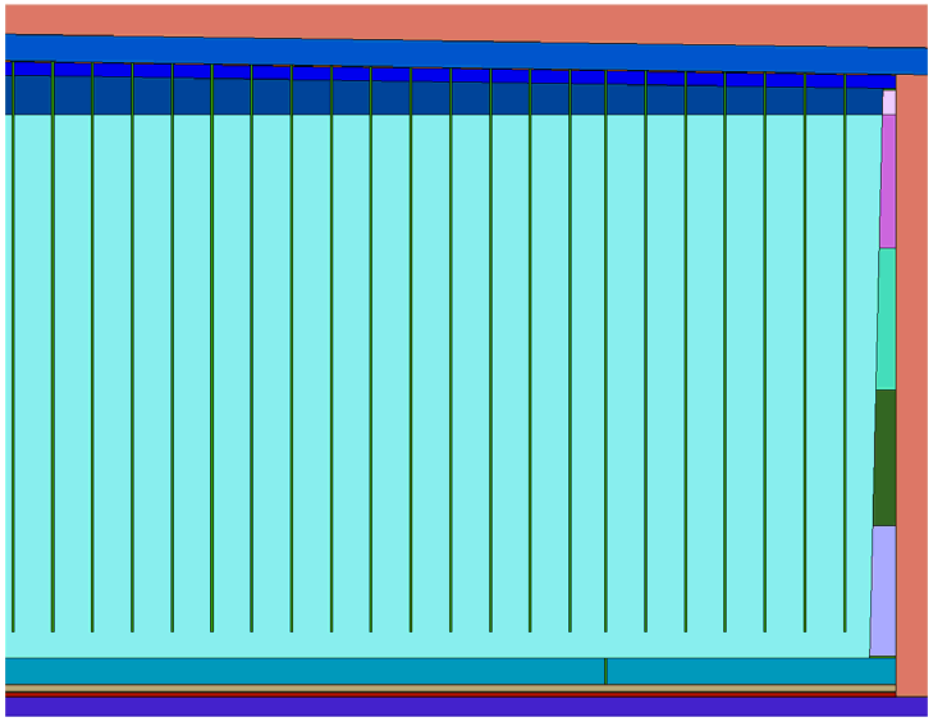

Figure 5.8-80: Fully-Penetrating Fast Flow Paths Through 375-foot Diameter SDUs

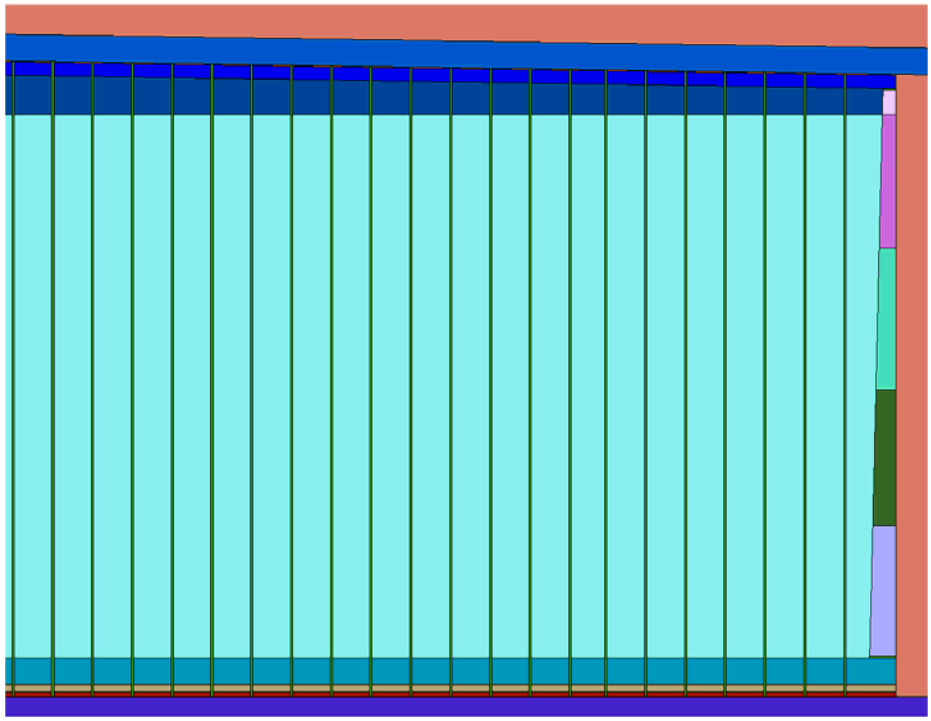

These fast flow paths are assumed to be present at the time of facility closure, even though the potential underlying physical events and mechanisms might take hundreds or thousands of years to occur or develop.

From an advective transport perspective, the significance of vertical fast flow paths is determined by the timescale for lateral diffusion into the high-permeability pathways relative to the timescale for advective transport down pathways. The timescale for lateral diffusion is

$$t_d = \frac{W^2}{D_e} \qquad \text{Eq. 5.8-1}$$

where W is the diffusion distance [cm], and D_e is the effective diffusion coefficient of saltstone [cm^2/s]. The appropriate timescale for advective transport is the "mean solute residence time" defined as

$$t_a = \frac{L}{v} \qquad \text{Eq. 5.8-2}$$

where L is the advective travel distance [cm] and $v = U/n$ is the average pore velocity [cm/s] (U = Darcy velocity, n = porosity). The average pore velocity is the rate of total flow through the system divided by total area and porosity. Thus, the mean solute residence time (t_a) is the time for solute travel through the system if the flow were uniform across intact saltstone and fast flow paths. The ratio of the longitudinal advection and lateral diffusion timescales is a nondimensional Damkohler number:

$$Da = \frac{t_a}{t_d} = \frac{LD_e}{W^2 v} \qquad \text{Eq. 5.8-3}$$

Equilibrium between a fast flow path and saltstone is expected when $Da \gg 1$. Approximate equilibrium occurs when Da is 1.0 or somewhat higher valued. Equilibrium means the solute concentrations in the fast flow path and adjoining saltstone are the same and implies fast flow paths have no effect on solute transport from saltstone. [Haggerty 2004 (DOI: 10.1029/2002WR001716), SRNL-STI-2013-00280 Section 2.6]

Table 5.8-30 presents Damkohler numbers for saltstone corresponding to several combinations of Darcy velocity and fast flow path spacing. Cells containing Da values greater than 1.0 indicate equilibrium conditions. Infiltration rates for the Compliance Value reference case and Fast Flow Path sensitivity cases range from 0.006 to 0.13 mm/yr. [SRR-CWDA-2018-00030, Table 3] Assuming cover system infiltration flows through not around the SDU, then $0.006 \le U \le 0.13$ mm/yr. For the postulated fast flow path spacing $2W$ = 3 feet ≈ 1 meter, all Damkohler numbers are well above 1.0. Therefore, the existence of fast flow paths is expected to have minimal impact on *advective* transport through SDUs.

Table 5.8-30: Damkohler Numbers for Various Combinations of Flow Rate and Fast Flow Path Spacing

Damkohler No.	Longitudinal Advection													
Da =t_a/t_d	L = 13 m	U, mm/yr:	0.01	0.02	0.05	0.1	0.2	0.5	1	2	5	10	20	50
De = 1.3E-08 cm2/s	n =0.656	t_a = nL/U (yr):	852800	426400	170560	85280	42640	17056	8528	4264	1706	853	426	171
Lateral Diffusion	$t_d = W^2/De$ (yr):													
2W = 0.1 m*	61		13985	6992	2797	1398	699	280	140	70	28	14.0	7.0	2.8
0.2 m	244		3496	1748	699	350	175	70	35	17.5	7.0	3.5	1.7	0.70
0.3 m	549		1554	777	311	155	78	31	15.5	7.8	3.1	1.55	0.78	0.31
0.5 m	1525		559	280	112	56	28	11.2	5.6	2.8	1.12	0.56	0.28	0.11
0.7 m	2988		285	143	57	29	14.3	5.7	2.9	1.43	0.57	0.29	0.14	0.057
1 m	6098		140	70	28	14.0	7.0	2.8	1.40	0.70	0.28	0.140	0.070	0.028
2 m	24392		35	17.5	7.0	3.5	1.75	0.70	0.35	0.175	0.070	0.035	0.017	0.007
3 m	54882		15.5	7.8	3.1	1.55	0.78	0.31	0.155	0.078	0.031	0.016	0.008	0.003
5 m	152451		5.6	2.8	1.12	0.56	0.28	0.112	0.056	0.028	0.011	0.006	0.003	0.001
7 m	298804		2.9	1.43	0.57	0.29	0.143	0.057	0.029	0.014	0.006	0.003	0.001	0.001
10 m	609804		1.40	0.70	0.28	0.140	0.070	0.028	0.014	0.007	0.003	0.001	0.001	0.0003
* fast flow path spacing														

Because the Compliance Case infiltration rates are very low compared to natural infiltration, diffusion is an important transport mechanism, and tends to be more dominant than advection, especially during early times. While fast flow paths are projected to have minimal effect on advection under Compliance Case infiltration rates, fast flow paths are expected to have a significant effect on diffusional releases from saltstone. One factor is greater saltstone surface area exposed to the environment. Fast flow paths increase the exposure area by approximately 12.5x. Despite the increased exposure areas, most of the exposed areas reside away from outer surfaces of the SDU, thus greatly increasing the average diffusion distance. A second factor is the absence of a concrete diffusion barrier between fast flow path surfaces and the environment.

The net effect of fast flow paths on Tc-99 and I-129 transport, which are affected by Eh and pH shrinking-core models, is not obvious. In the shrinking-core models the pH buffering capacity is low compared to the Eh reducing capacity, so the pH front advances much faster than the Eh front. The advancing pH front retards release of both species, all else being equal: for Tc-99 solubility drops from 9.7E-07 to 4.5E-07 mol/L, and for I-129 K_d increases from 0.07 to 0.71 mL/g. However, the slower advancing Eh (oxidation) front causes loss of solubility control for Tc-99, whereas I-129 K_d further increases to 4.0 mL/g. The effects noted above with respect to advection and diffusion of a general solute also affect dissolved oxygen and pH tracer ingress in the shrinking core models.

Figure 5.8-81 compares the fast flow path simulations to the Compliance Case for Cl-36 concentration at 10,000 years, and Figure 5.8-82 compares Cl-36 water table flux over time. These figures are based on releases from SDU 7 as a representative 375-foot diameter SDU. These simulations avoid the complications introduced by the Eh and pH shrinking-core models used in Tc-99 and I-129 transport. Cl-36 releases are only moderately higher than the Compliance Case because the infiltration rate is very low and diffusion distances are long for most of the fast flow path area.

Figure 5.8-81: Comparison of Cl-36 Concentration at 10,000 years for Fast Flow Path Sensitivity Cases for SDU 7

(a) Compliance Case:

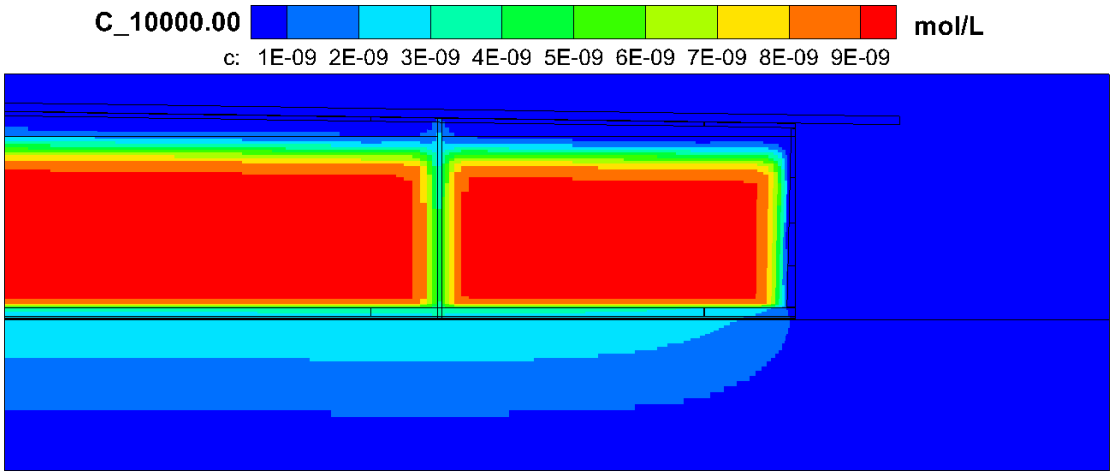

(b) Partially Penetrating Fast Flow Paths:

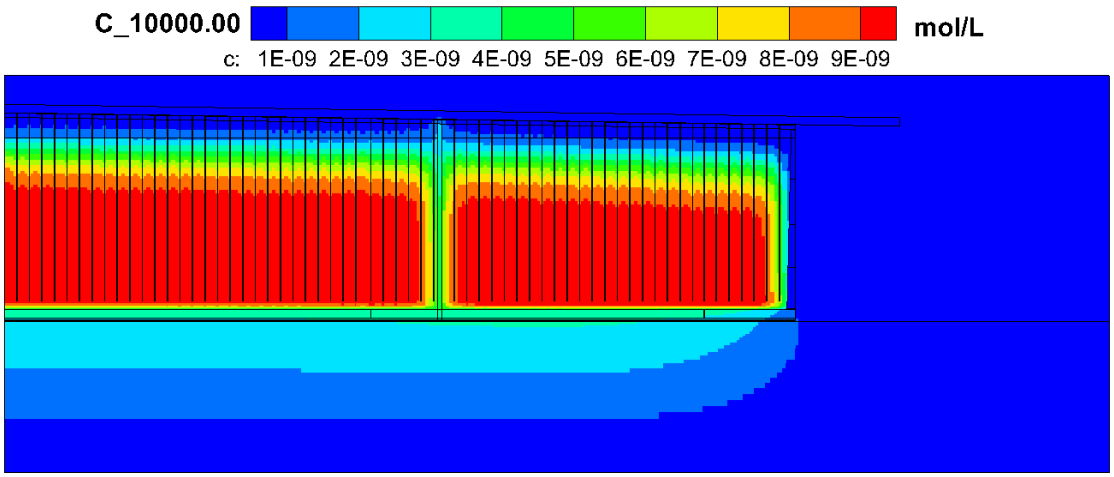

(c) Fully Penetrating Fast Flow Paths:

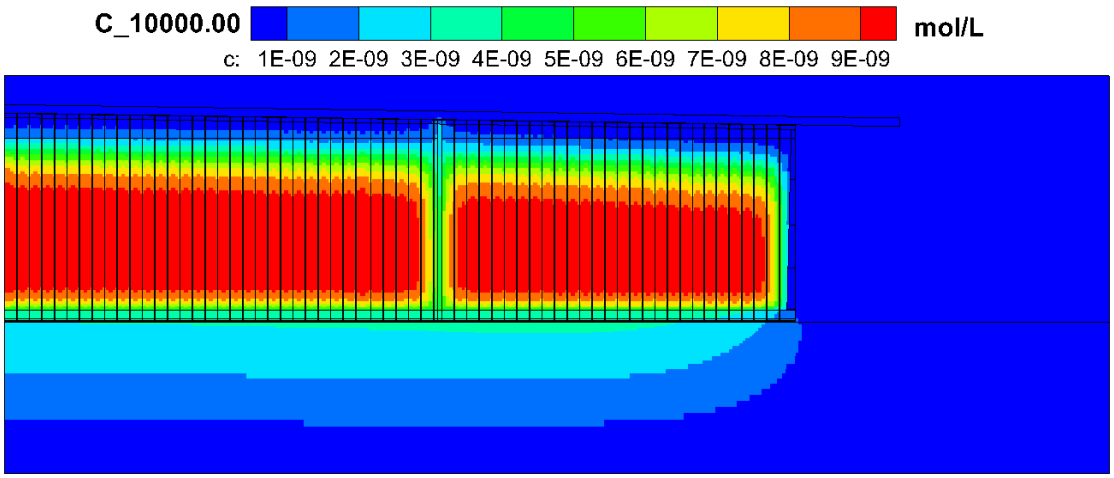

Figure 5.8-82: Comparison of Cl-36 Water Table Flux for Fast Flow Path Sensitivity Cases for SDU 7

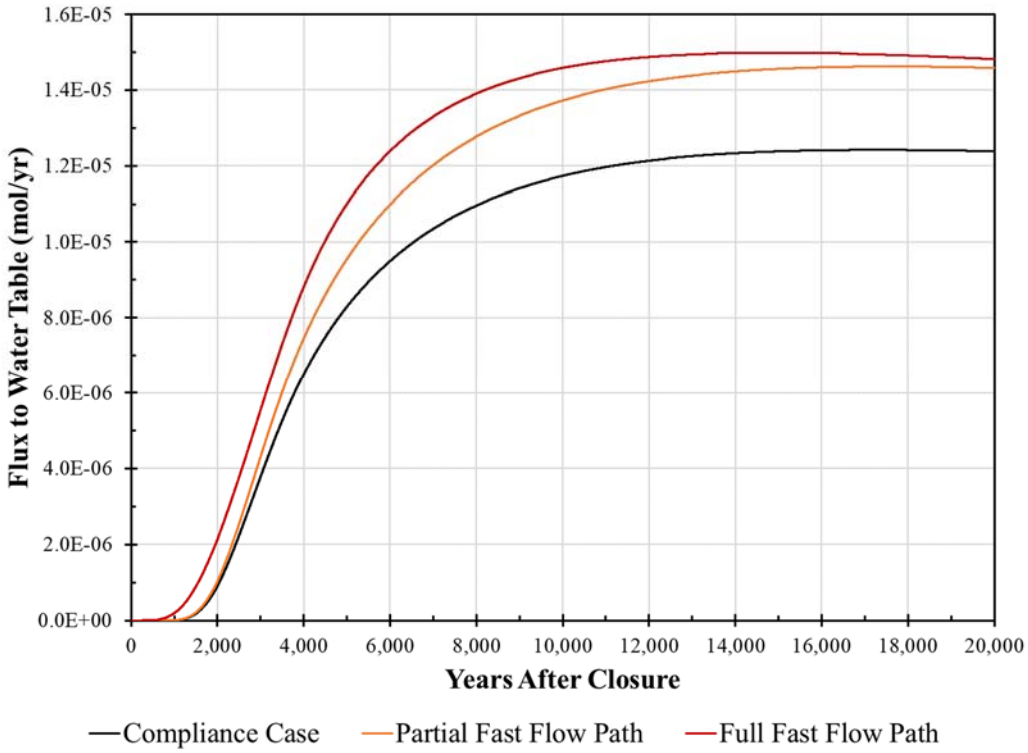

Figure 5.8-83 through Figure 5.8-85 compare I-129 concentrations at 10,000 years, and Figure 5.8-86 shows water table flux over time. These figures are based on releases from SDU 7 as a representative 375-foot diameter SDU. The net impact of fast flow paths on I-129 is also modest because of competing effects: fast flow paths expose more saltstone area to the external environment, but the ingress of the pH tracer and oxygen cause the K_d to increase from 0.07 to 0.71 or 4.0 mL/g as buffering and reduction capacity are consumed. [SRR-CWDA-2018-00045]

Figure 5.8-83: I-129 Shrinking Core Simulation at 10,000 years for the Compliance Case for SDU 7

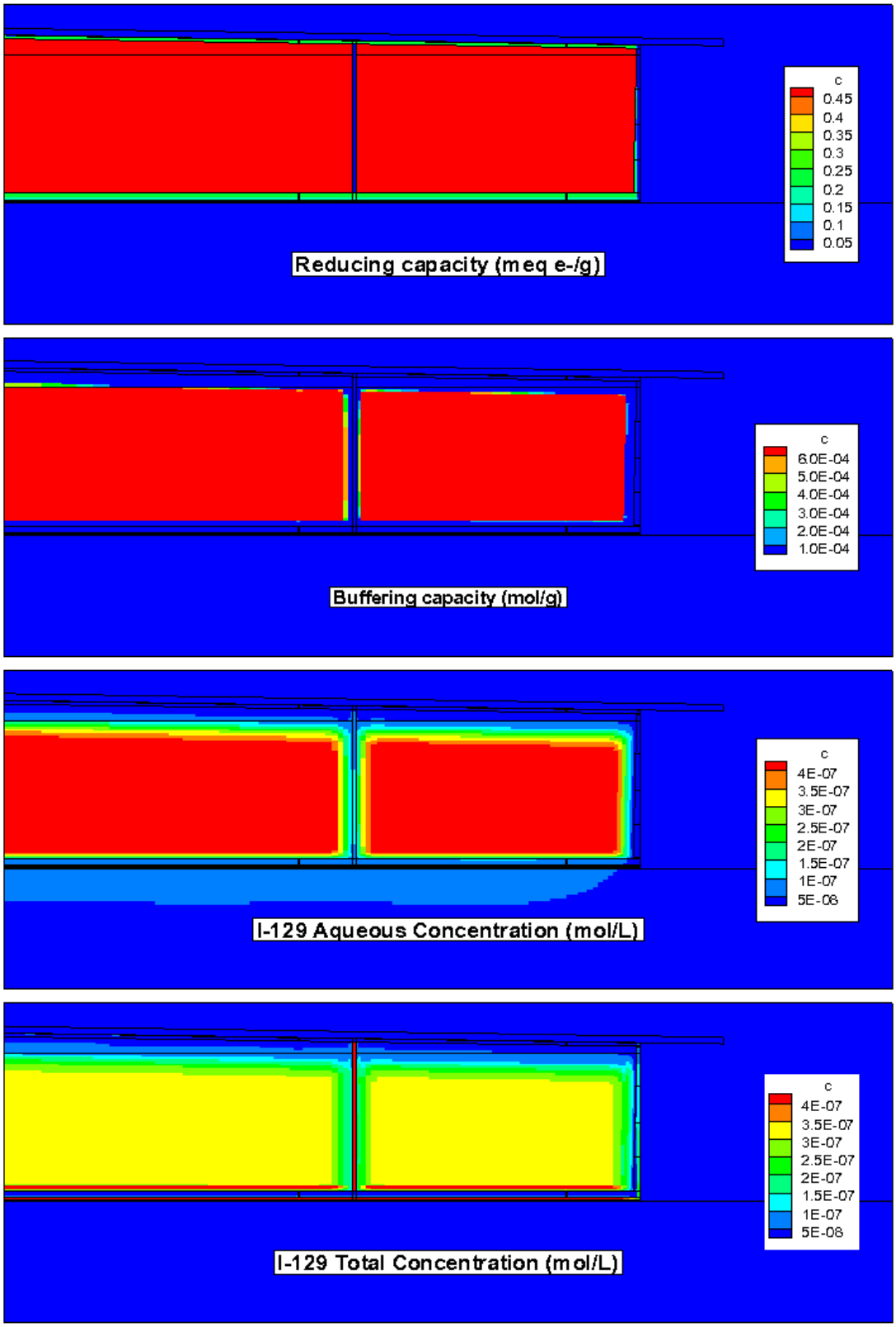

Figure 5.8-84: I-129 Shrinking Core Simulation at 10,000 years for the Partially-Penetrating Fast Flow Paths Sensitivity Case for SDU 7

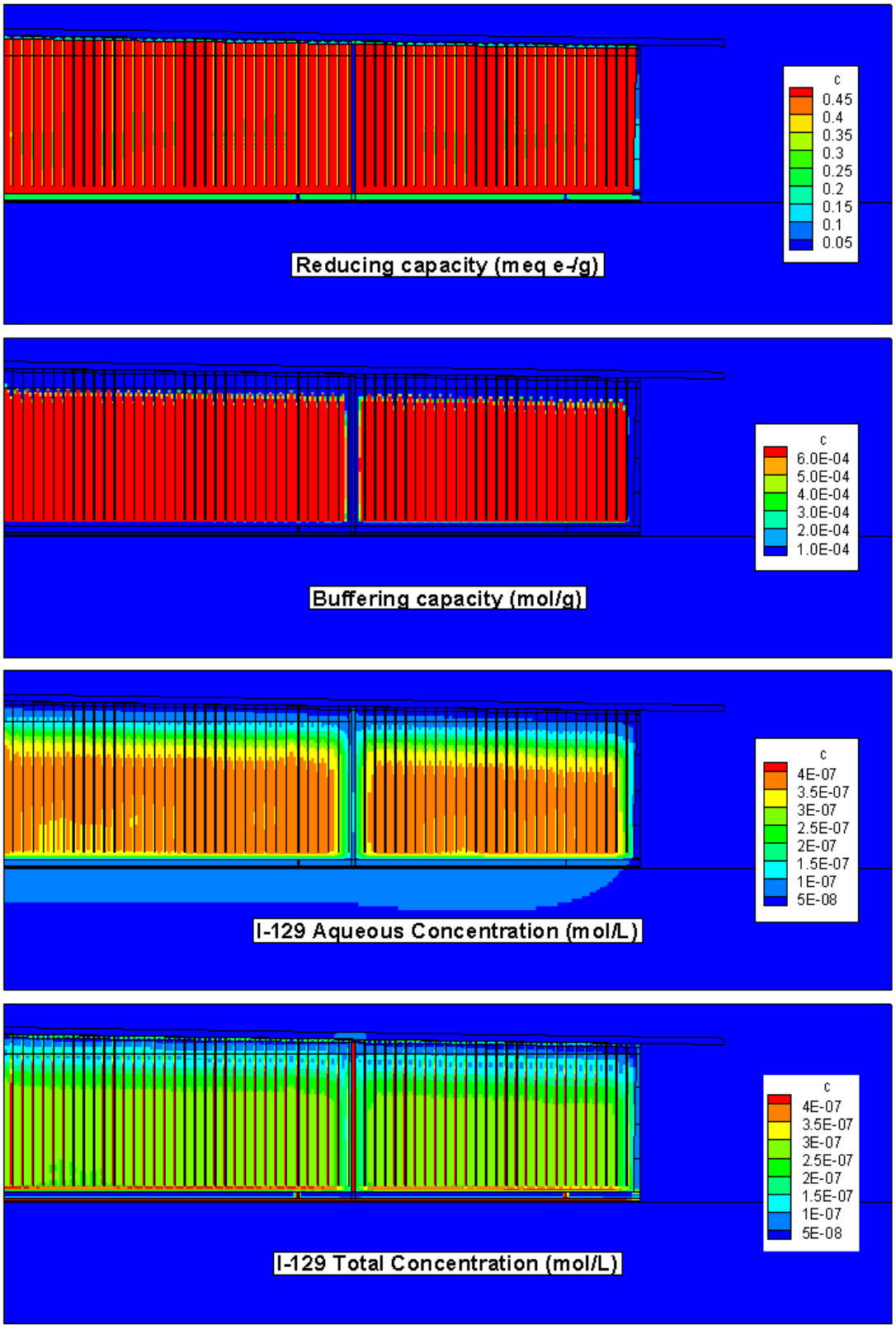

Figure 5.8-85: I-129 Shrinking Core Simulation at 10,000 years for the Fully-Penetrating Fast Flow Paths Sensitivity Case for SDU 7

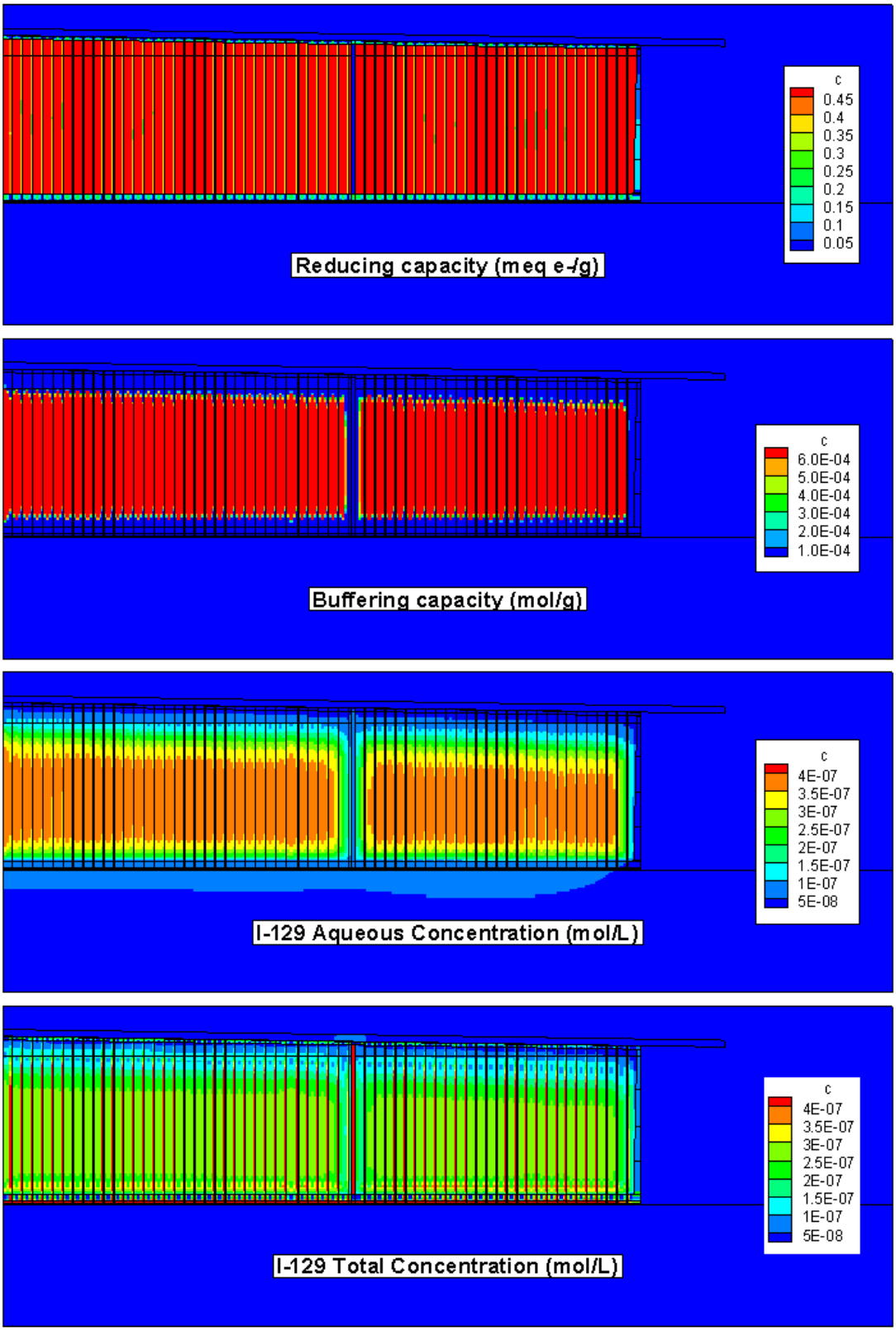

Figure 5.8-86: Comparison of I-129 Water Table Flux for Fast Flow Path Sensitivity Cases for SDU 7

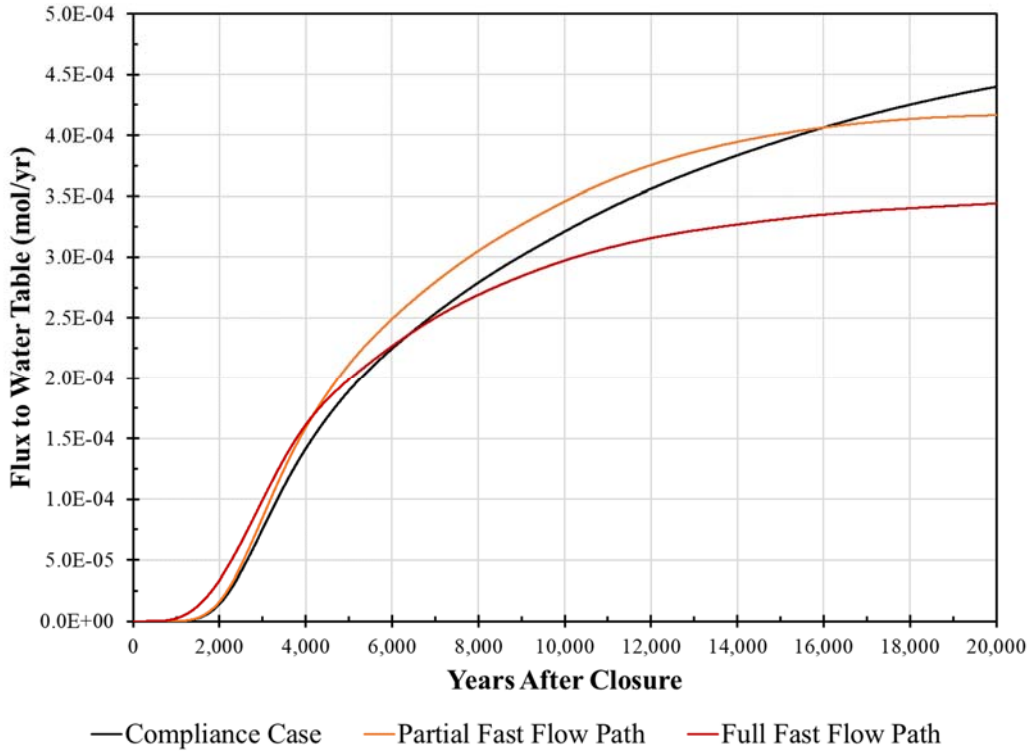

Figure 5.8-87 through Figure 5.8-89 compare Tc-99 concentrations at 10,000 years, and Figure 5.8-90 shows water table flux over time. These figures are based on releases from SDU 7 as a representative 375-foot diameter SDU. Like I-129, fast flow paths introduce competing effects: fast flow paths increase saltstone exposure to the environment and accelerate oxidation and loss of solubility control, while lower pH reduces the solubility limit under reducing conditions. However, the former two effects outweigh the latter and cause higher Tc-99 releases compared to the Compliance Case.

Figure 5.8-87: Tc-99 Shrinking Core Simulation at 10,000 years for the Compliance Case for SDU 7

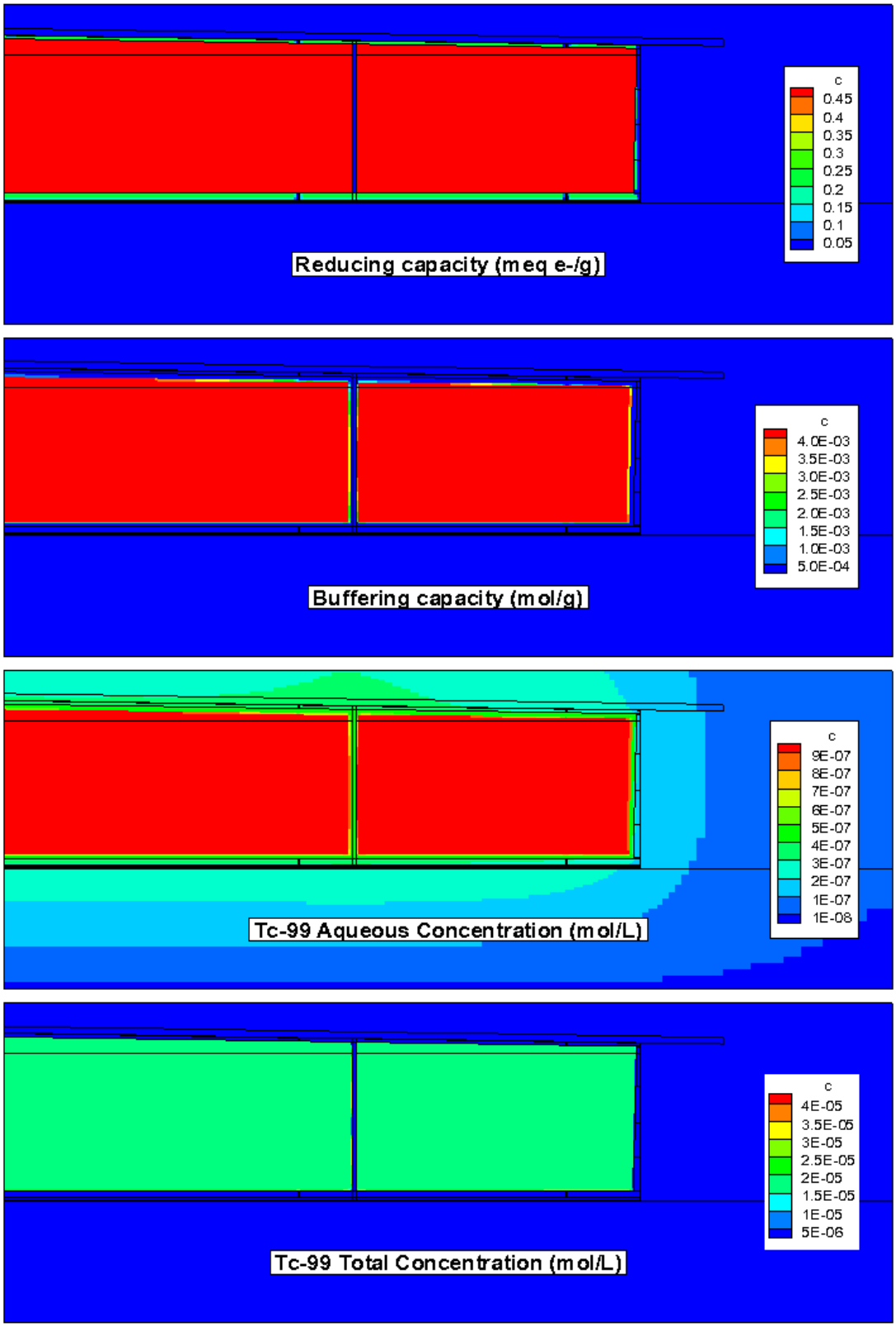

Figure 5.8-88: Tc-99 Shrinking Core Simulation at 10,000 years for the Partially-Penetrating Fast Flow Paths Sensitivity Case for SDU 7

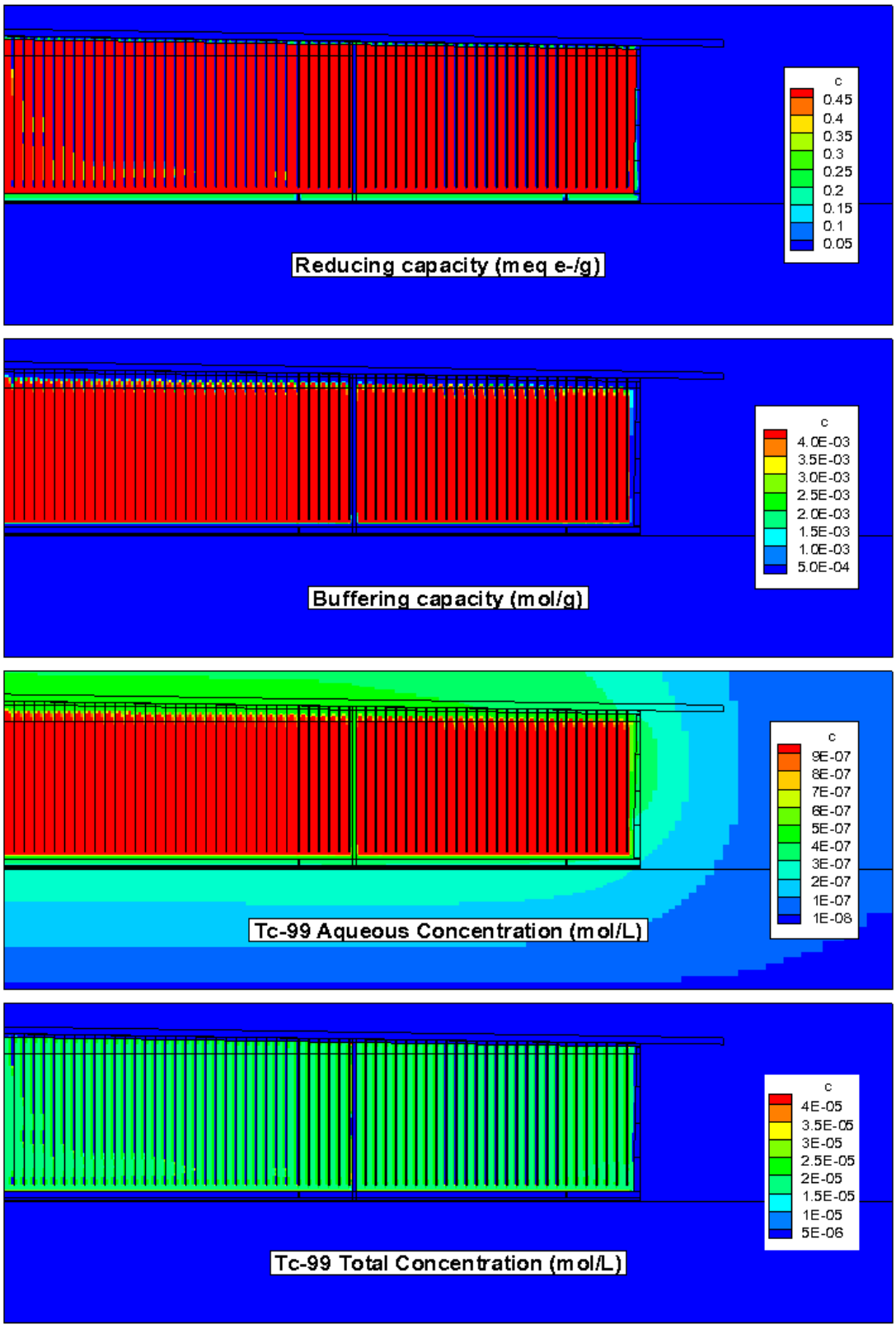

Figure 5.8-89: Tc-99 Shrinking Core Simulation at 10,000 years for the Fully-Penetrating Fast Flow Paths Sensitivity Case for SDU 7

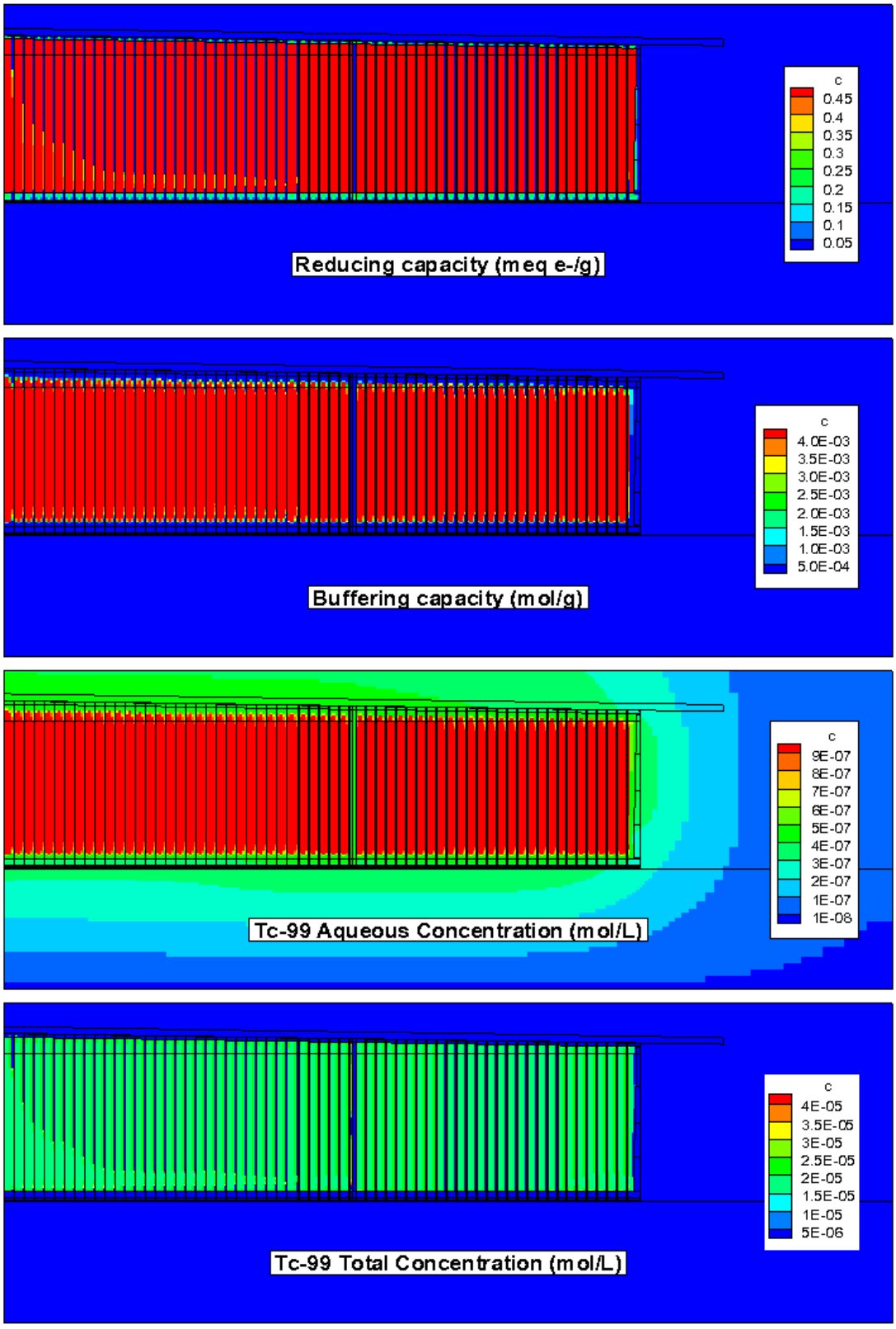

Figure 5.8-90: Comparison of Tc-99 Water Table Flux for Fast Flow Path Sensitivity Cases for SDU 7

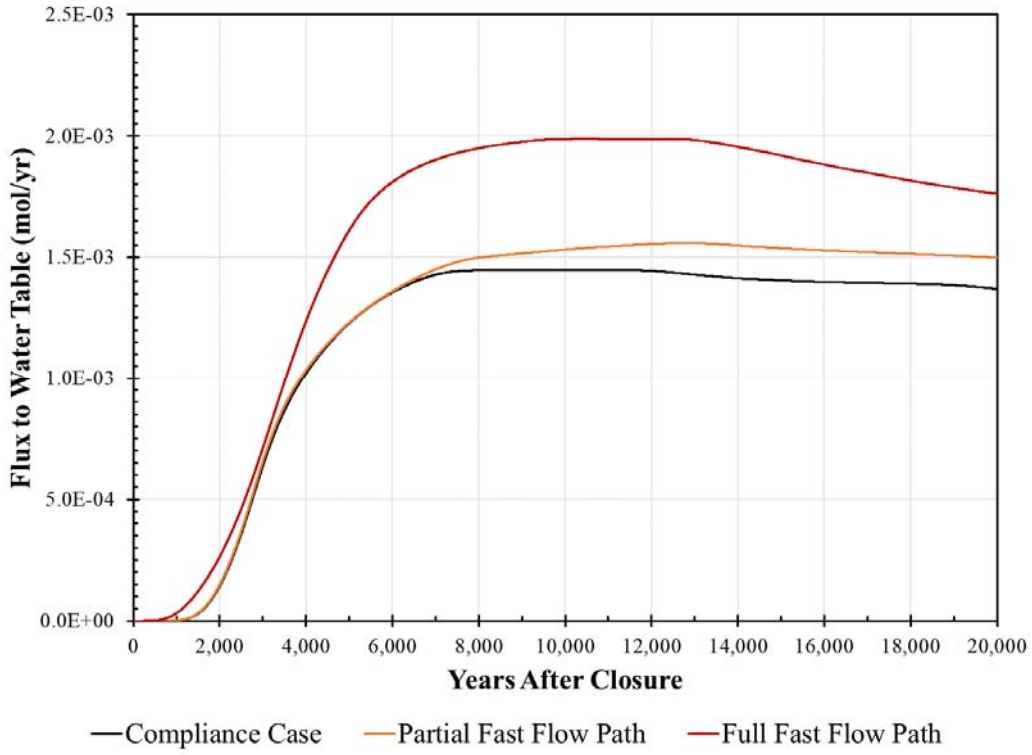

Finally, Figure 5.8-91 and Table 5.8-31 compare cumulative doses from the sensitivity run radionuclides to provide a comprehensive comparison of the combined effects relative to the Compliance Case dose results. These sensitivity cases apply the fast flow paths to every 375-foot diameter SDU (i.e., SDUs 6, 7, 8, 9 ,10, 11, and 12).

Some cracks have been observed in the exposed saltstone or the exposed clean cap grout surfaces at SDU 4. [SRNL-ESB-2008-00017, SRR-CWDA-2011-00105] Most of the cracks appeared to be minor with relatively narrow apertures. While the formation of such cracks is expected and likely, there is uncertainty as to the extent of such cracks and the timing for when future cracks will form. A detailed analysis was performed in 2003 to estimate crack formation in the saltstone disposed of at SDU 4. [T-CLC-Z-00006] This SDU 4 structural cracking analysis estimated that cracks would initially have apertures with widths of less than 0.1 inches, which is consistent with the observations at SDU 4. Over time, the cracks are expected to increase in width; by 10,000 years after closure the analysis estimated the cracks may be as wide as approximately 2.1 inches. The SDU 4 structural cracking analysis assumed intervals of 30 feet (for static settlement) and 50 feet (for dynamic settlement). The geometry for each crack was expected to be triangular (e.g., widest at the exposed surface and becoming narrower within the saltstone), thus limiting the depths of the cracks as a function of the apertures.

Figure 5.8-91: Dose Results from the Sensitivity Cases that Assume Fast Flow Paths through SDUs

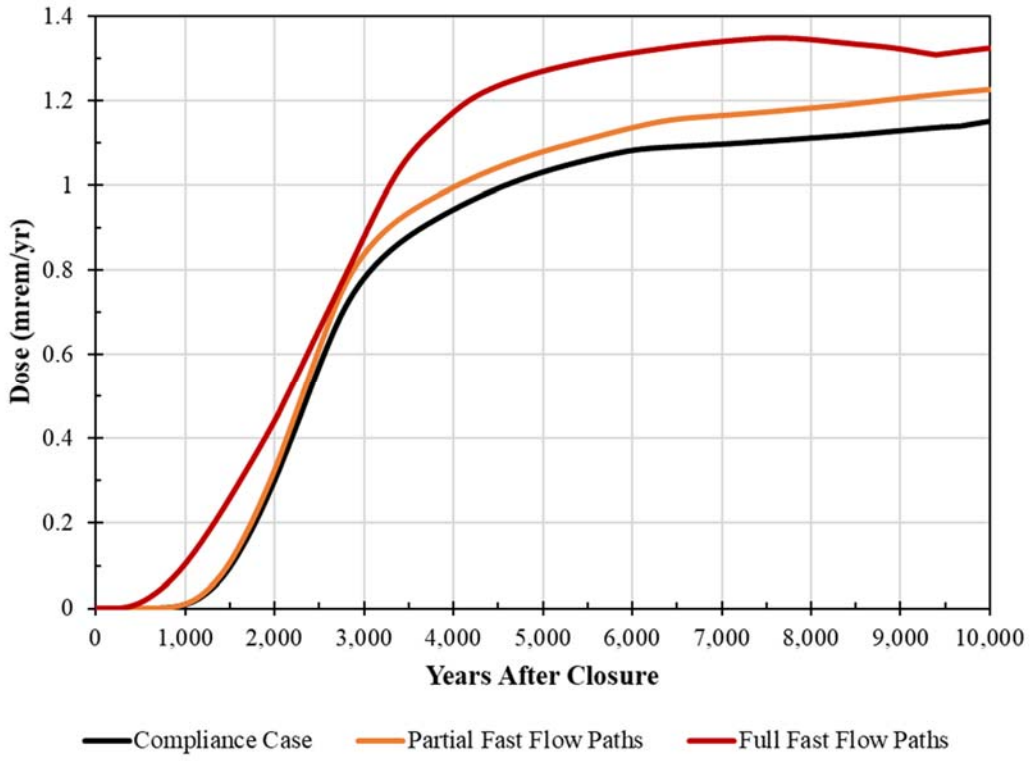

Table 5.8-31: Comparison of Sensitivity Cases that Assume Fast Flow Paths through SDUs, 100-Meter MOP Peak Ground Water Pathways Doses

Modeling Case	Compliance Period (0 to 1,000 Years)		Performance Period (0 to 10,000 Years)	
	Peak Dose (mrem/yr)	Year of Peak	Peak Dose (mrem/yr)	Year of Peak
Compliance Case	9.4E-03	1,000	1.2	10,000
Partial Fast Flow Paths	1.1E-02	1,000	1.2	10,000
Full Fast Flow Paths	1.1E-02	1,000	1.4	7,640

The modeled sensitivity cases described above did not consider cracks through all SDUs; only the 375-foot diameter SDUs were evaluated for cracks, which excludes SDU 4. Regardless, there are some general comparisons that may be made. First, the spacing intervals for the cracks in the sensitivity cases are an order of magnitude closer together (3 feet versus 30 feet), thus there are ten times more cracks. Next, the cracks are assumed to be present within the material at time = 0 and are initially 2 inches wide. Finally, both sensitivity cases extend the cracks a significant depth through the material. Therefore, within the context of the SDU 4 structural cracking analysis (T-CLC-Z-00006), the conditions assumed for these sensitivity cases are considered to be more than bounding with respect to such cracks.

Further, the complete through cracks presented in the "Full Fast Flow Paths" sensitivity case do not reflect expected future conditions. In the unlikely event that such cracks do

penetrate all the way through the SDUs, the aperture at the bottom of the cracks would still be extremely narrow such that flow would be limited. The low flow that does occur would likely facilitate self-healing of the crack as leached minerals precipitate within the cracks.

The doses from the "Partial Fast Flow Paths" sensitivity case are similar to the doses from the Compliance Case in both timing and magnitude (see Figure 5.8-90). This sensitivity case is considered a bounding representation of crack formation because the assumed cracks penetrate nearly the full height of the SDUs, have initially wide apertures, and are closely spaced. Given that this case is bounding, the similarity in the dose results indicates that the Compliance Case provides a reasonable representation of risks associated with future conditions, even though it does not explicitly include cracks.

5.8.8.3 Evaluation of Moisture Characteristic Curves and Effective Hydraulic Conductivities

Figure 4.3-3 presented the Moisture Characteristic Curves (MCCs) for cementitious materials; this figure indicates the effective hydraulic conductivity of cementitious materials decreases under higher suction heads, especially when the suction heads are much greater than 1,000 cm. Similarly, the suction heads for saltstone increase significantly when the material is not fully saturated. These relationships are described in Section 4.4.4.2.1.

While saltstone is expected to be near saturation throughout the Performance Period, it is never fully saturated. As a result, the suction head near the tops of the SDUs can exceed 1,000 cm; for SDUs 6 through 12 the suction heads exceed 2,000 cm. Therefore, the effective hydraulic conductivity of saltstone is always slightly lower than the saturated hydraulic conductivity.

To evaluate the influence of the MCCs on the effective hydraulic conductivities of the cementitious materials, a sensitivity case was developed which assumed a relative permeability of 1 for all cementitious materials. As indicated by Eq. 4.4-104, applying a relative permeability of 1 sets the effective hydraulic conductivity equal to the saturated hydraulic conductivity, thereby negating all impacts from the MCCs.

Figure 5.8-92 compares the total dose to the MOP from this sensitivity case to the Compliance Case. This figure shows the doses from both cases are the same. This is because the rate of flow entering the cementitious materials is lower than the effective hydraulic conductivities. Therefore, instead of flow being limited by the effective hydraulic conductivities, the flow rates are being limited by the availability of water entering the system. Accordingly, the use of the MCCs has no impact on the performance of the SDF.

Figure 5.8-92: Dose Results from a Sensitivity Case that Sets the Relative Permeability of the Cementitious Materials to 1

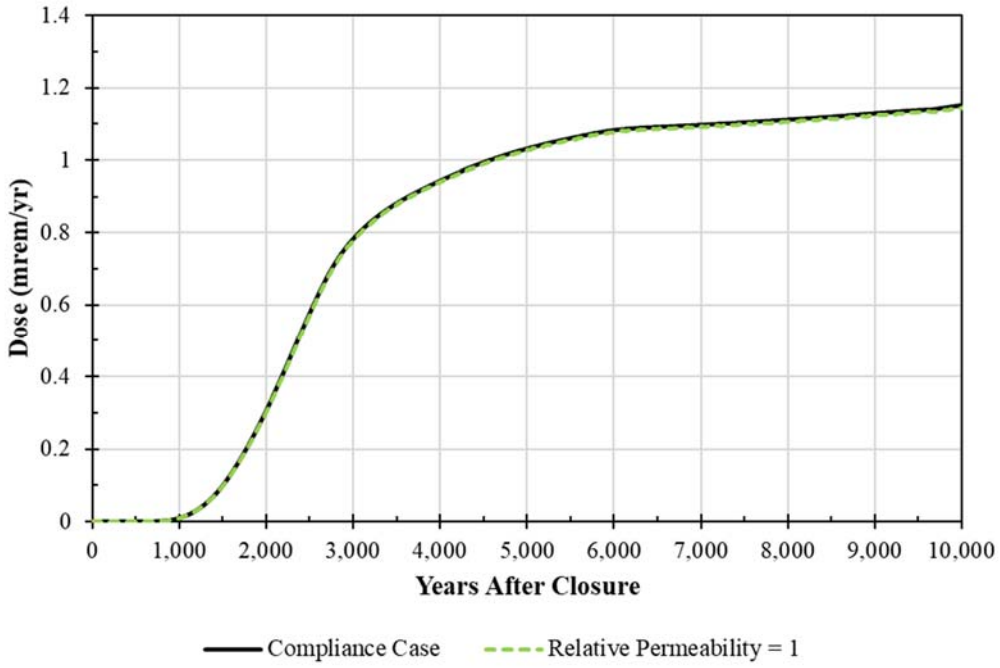

5.8.8.4 *Evaluation of Potential Impacts on Ground Water Flow Due to the Presence of the Closure Cap*

The Aquifer Transport Model described in Section 4.4.6 relies on flow data from the GSA Model. The GSA Model is a ground water flow model developed based on recent ground water behavior for the GSA, as informed by historical monitoring of well data. [SRNL-STI-2018-00643] While placing a robust closure cap over the SDF is expected to alter the ground water behavior (by reducing the localized recharge rates), the overall ground water flow conditions for the GSA are not expected to be significantly different. Regardless, to evaluate the potential impacts from the reduced recharge beneath the closure cap, two sensitivity cases have been developed by modifying the GSA Model:

(1) The first case ("Cap Recharge = 0.13 mm/yr") assumes that any water that drains off the sides of the closure cap is removed from the system via effective surface drainage or evapotranspiration. This case applies a recharge rate of 0.13 mm/yr to the area beneath the SDF closure caps to simulate the reduction in recharge. The value of 0.13 mm/yr was selected because this represents the long-term (i.e., > 2,000 years) estimate for infiltration through the closure cap under Compliance Case conditions.

(2) The second case ("Cap Recharge = 0.13 mm/yr + drainage") assumes that any water that drains off the sides of the closure cap infiltrates back into the system due to ineffective surface drainage or evapotranspiration. This case applies a recharge rate of 0.13 mm/yr to the area beneath the SDF closure caps to simulate the reduction in recharge *and* applies increased recharge to areas surrounding the perimeters of the closure cap to account for the potential influences of drainage. The increased recharge

rates (674 mm/yr around SDUs 1 and 4 and 982 mm/yr around the cylindrical SDUs) were based on water balance estimates.

For both sensitivity cases, the extent of the closure caps was set to 50 feet beyond the SDUs (note the light green boundary lines in Figure 5.8-93). Within this area, the recharge rate was set to 0.13 mm/yr. Note that the GSA Model applies a natural recharge rate throughout the GSA of approximately 380 mm/yr (15 in/yr). [SRNL-STI-2018-00643] The area for the increased recharge to account for drainage in the second sensitivity case was set to extend 250 feet beyond the cap extent (light blue boundary lines in Figure 5.8-93). The solid, pink boundary line in Figure 5.8-93 shows the 100-meter boundary and the dashed pink boundary line shows the 1-meter boundary. SDU locations are outlined in brown.

Figure 5.8-94 and Figure 5.8-95 show that the respective streamline traces are nearly identical for both cases. These figures also include the streamline traces from the GSA Model (as initially presented in Figure 4.4-115). These Compliance Case traces are shown in black to aid in comparisons. These figures indicate that the ground water flows in generally similar directions relative to the GSA Model. The most notable difference is that the streamline traces from the SDUs travel in a more northwesterly direction beneath the closure cap, with some of the streamline traces moving in the same direction for hundreds of feet before fanning out in different directions due to the influence of the local ground water divide. As a result of this shift in the direction of flow, the relative concentrations along Sector A are expected to be lower due to changes in the streamline traces from SDUs 11 and 12, while the relative concentrations in Sector C are expected to be higher due to changes in the streamline traces from SDUs 6, 7 and 8.

Close examination of the spacing between the ten-year markers (red dots) on Figure 5.8-94 and Figure 5.8-95 indicates that the reduced recharge rates have a minimal influence on the rate of ground water flow compared to the markers shown in Figure 4.4-115. In general, the markers for these sensitivity cases are spaced slightly closer together relative to the markers shown in Figure 4.4-115; this means that the ground water flow rates are slightly slower under the reduced recharge conditions.

Figure 5.8-93: Boundaries for Closure Cap Extents and Assumed Drainage Areas Considered for Modified Recharge Rate Cases

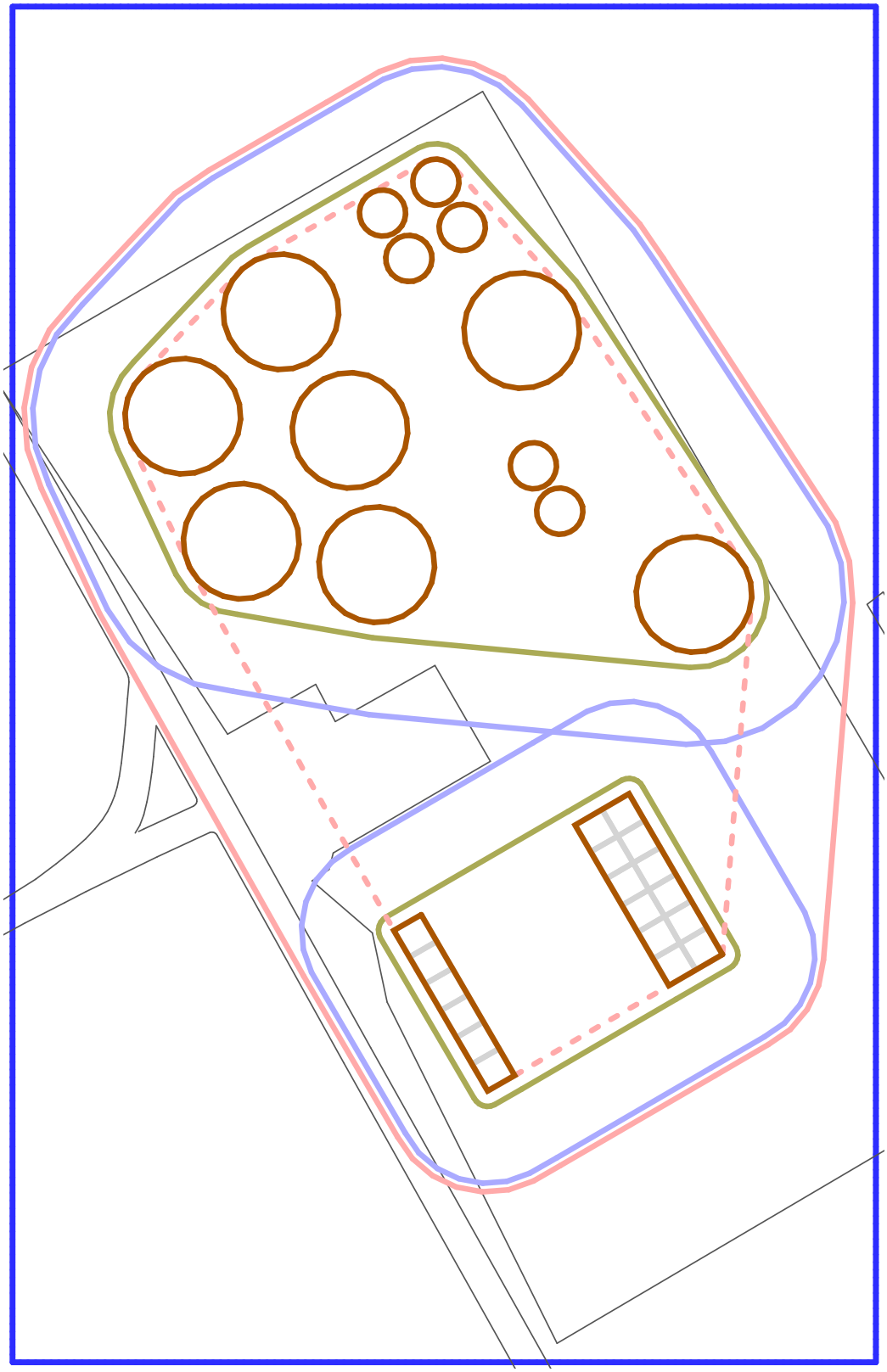

Figure 5.8-94: Streamline Traces from Each SDU for the Case that Assumes a Closure Cap Recharge Rate of 0.13 mm/yr (Blue Lines) and for the GSA Model (Black Lines)

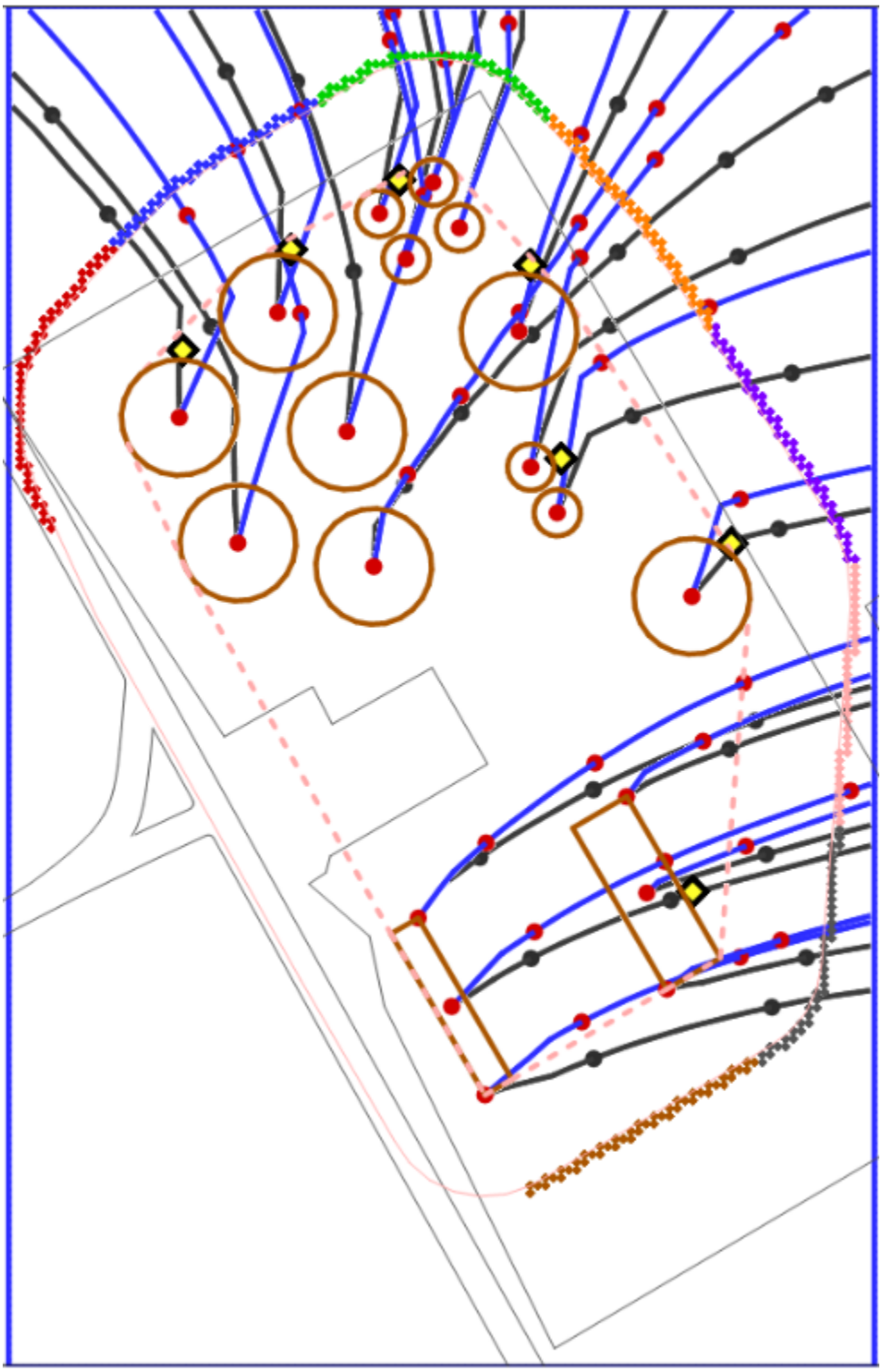

Note: Markers (red and black dots) are included to indicate ten-year travel times.

Figure 5.8-95: Streamline Traces from Each SDU for the Case that Assumes a Closure Cap Recharge Rate of 0.13 mm/yr and Includes Drainage Affects (Blue Lines) and for the GSA Model (Black Lines)

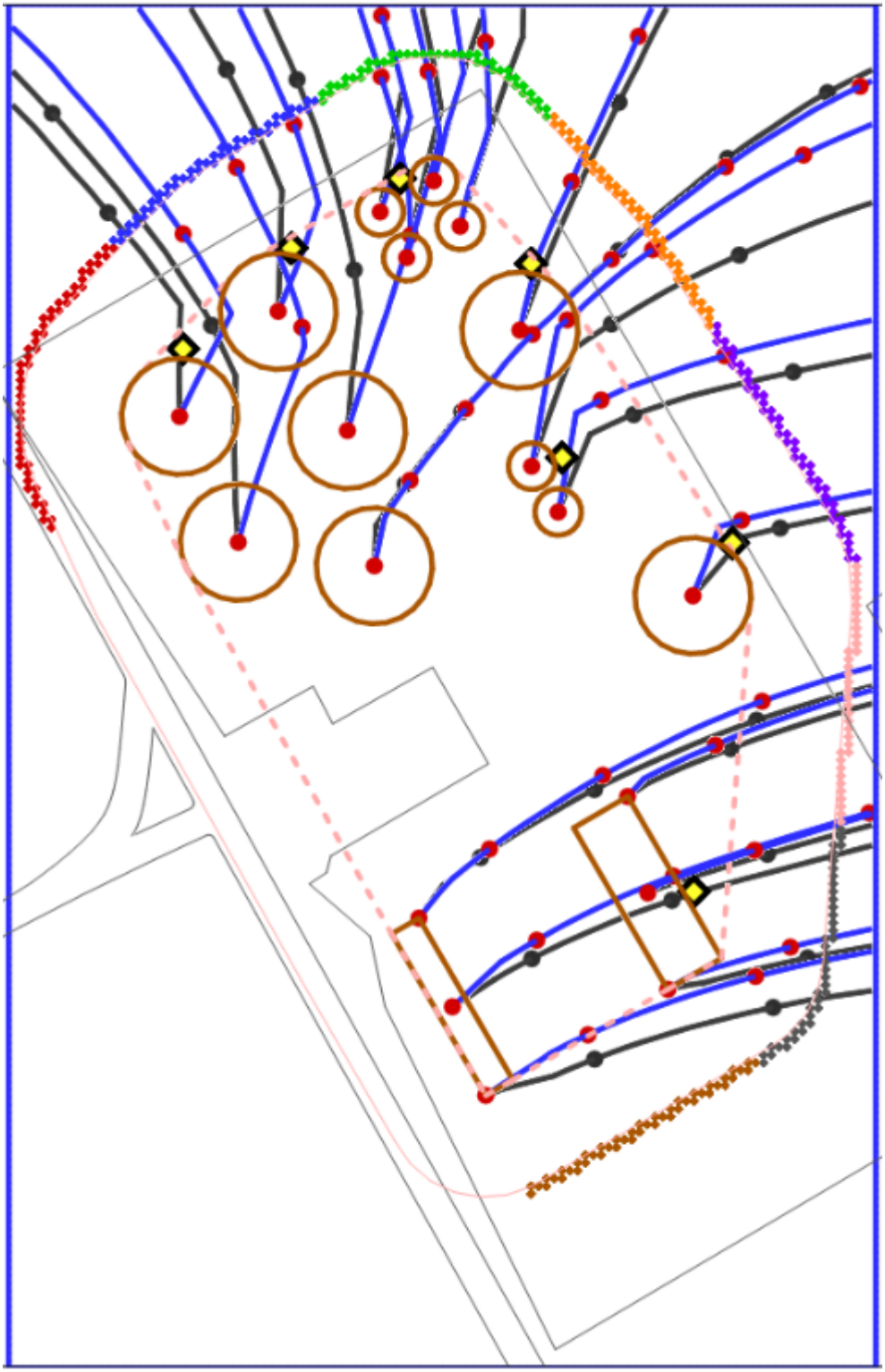

Note: Markers (red and black dots) are included to indicate ten-year travel times.

The contaminant fluxes from the Vadose Zone Transport Model (see Section 4.4.6) were input into these modified ground water flow models to estimate ground water concentrations for dose estimates. Using Compliance Case conditions, the resulting doses show that the reduced recharge rates result in a general increase to the doses when compared to the Compliance Case (see Table 5.8-32 and Figure 5.8-96).

Table 5.8-32: Comparison of the 100-Meter MOP Peak Ground Water Pathways Doses Based on Modified Recharge Rates Beneath the Closure Cap

Modeling Case	Compliance Period (0 to 1,000 Years)		Performance Period (0 to 10,000 Years)	
	Peak Dose (mrem/yr)	Year of Peak	Peak Dose (mrem/yr)	Year of Peak
Compliance Case (Natural Recharge = 380 mm/yr)	9.4E-03	1,000	1.2	10,000
Cap Recharge = 0.13 mm/yr	1.3E-02	1,000	1.8	10,000
Cap Recharge = 0.13 mm/yr + Drainage	1.2E-02	1,000	1.8	10,000

Figure 5.8-96: Dose Results from All Three Sensitivity Cases with Modified Recharge Rates Beneath the Closure Cap

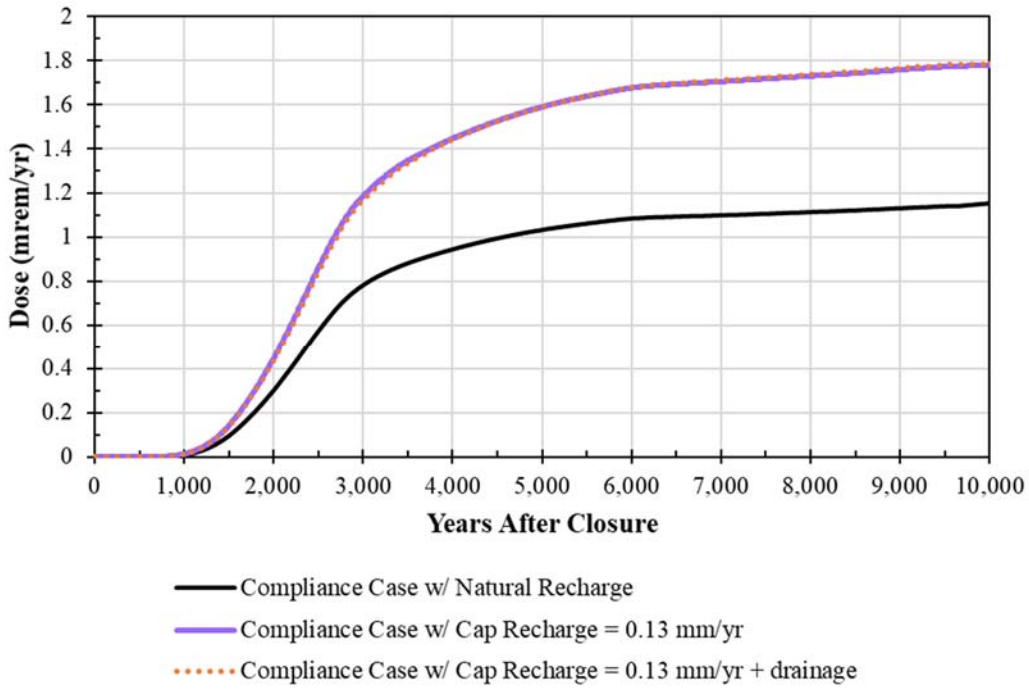

Despite the shifts in flow directions within these sensitivity cases, the doses along Sector D are still the highest sector dose within the Compliance Period; however, unlike the Compliance Case (wherein doses along Sector B eventually become higher than Sector D), these cases show that Sector D remains the highest sector throughout the Performance Period.

Both of these cases have nearly identical dose results, indicating that the peripheral drainage had a minimal influence on the ground water flow. The doses are approximately 30% higher than the Compliance Case within the Compliance Period and approximately 50% higher within the Performance Period. The increase in dose is attributed to a decrease in dilution (because there is less water in the system) and additional plume overlap (due to slight changes in flow directions), both resulting in less mixing (i.e., higher concentrations).

Regardless of these dose increases, the GSA Model has been calibrated based on measured ground water data and provides the best representation of recent conditions. Although the doses in Table 5.8-32 indicate that the presence of the closure cap will likely change these flow conditions, and these changes may increase doses, it is not possible to validate the future flow conditions simulated within these cases until the closure cap has been put in place. As such, there is uncertainty as to the actual influence that the closure cap might have on the local hydrology. Additionally, these sensitivity cases did not revise the vadose zone models to account for potential changes to the elevation in the water table as a response to the lower recharge rates. It is expected that the elevation of the water table would decrease, thus increasing the vadose zone flow and transport distances; this is likely to mitigate some of the dose impacts. Therefore, the Compliance Case is still considered an appropriate modeling case for evaluating the performance of the system.

Finally, given the importance of the closure cap as a barrier to infiltration, it is appropriate to provide additional context for the relationship between infiltration and recharge rates. If the closure cap fails to perform as designed, both the infiltration rates and the recharge rates would increase. While release and transport from the vadose zone might increase (i.e., higher concentrations), dilution within the aquifer system would also increase resulting in more mixing (i.e., lower concentrations). As such, the 30% to 50% increase in dose from these sensitivity cases cannot be extrapolated and applied to cases that assume higher-than-expected infiltration rates.

5.8.8.5 Evaluation of Well Depth and Aquifer Concentrations

This SDF PA estimates the maximum ground water concentrations based on three depth profiles: (1) the Upper Three Runs Upper Aquifer Zone (UAZ), (2) the Upper Three Runs Lower Aquifer Zone (LAZ), and (3) the Gordon Aquifer Unit (GAU). Although there is uncertainty as to how deep the MOP (or the IHI) may drill their wells for water, the simulations presented throughout this PA, including the Compliance Case, always assume that well water will be drawn from whichever depth provides the highest contaminant concentrations.

Despite this assumption, an analysis looking at thousands of wells installed at or near SRS has been performed to parameterize the uncertainties associated with well depth. [SRR-CWDA-2013-00058] The resulting well depth distribution provided in Table 4.4-117 shows that the average well depth in the vicinity of SRS is 160 feet, but is also highly variable with a minimum depth of 32 feet and a maximum depth of 990 feet. Despite this

wide range, 50% of all water wells drilled in the vicinity fall within a range of 125 feet (25th percentile depth) to 225 feet (75th percentile depth).

Based on an analysis of aquifer depths (see Table 5.6-5 of SRS-REG-2007-00002):

- Wells drilled to less than 109 feet may be assumed to be drilled into the UAZ,
- Wells drilled to depths between 109 feet and 170 feet may be assumed to be drilled into the UAZ, and
- Wells drilled to more than 170 feet may be assumed to be drilled into the GAU.

On average the height of each SDU plus the thickness of the closure cap above each SDU is approximately 60 feet; therefore, once the SDUs are constructed and filled and the closure cap is in place, the aquifer depths should be adjusted by 60 feet:

- Wells drilled to less than 169 feet may be assumed to be drilled into the UAZ,
- Wells drilled to depths between 169 feet and 230 feet may be assumed to be drilled into the UAZ, and
- Wells drilled to more than 230 feet may be assumed to be drilled into the GAU.

Based on these depths and the data for local well installations, it is estimated that drilling for water at the SDF will have a 55% chance of being installed at the depth of the UAZ, 25% in the LAZ, and 20% in the GAU.

Using the Compliance Case model, the concentrations for each depth profile yield doses as shown in Figure 5.8-97 and summarized in Table 5.8-33. As shown, the Compliance Case doses are equal to the LAZ doses because the LAZ had the highest contaminant concentrations. In addition to the doses for each depth profile, an additional dose curve (Doses Weighted by Depth Probability) shows that if the results were weighted by the probability of drilling to a specific depth, the resulting doses would be approximately 30% to 40% lower than those reported for the Compliance Case. This demonstrates that the current approach may overstate the potential dose risks by ignoring the uncertainty associated with the assumed depth of the well.

Figure 5.8-97: Comparison of Compliance Case Dose Results Based on Concentrations at Various Depths

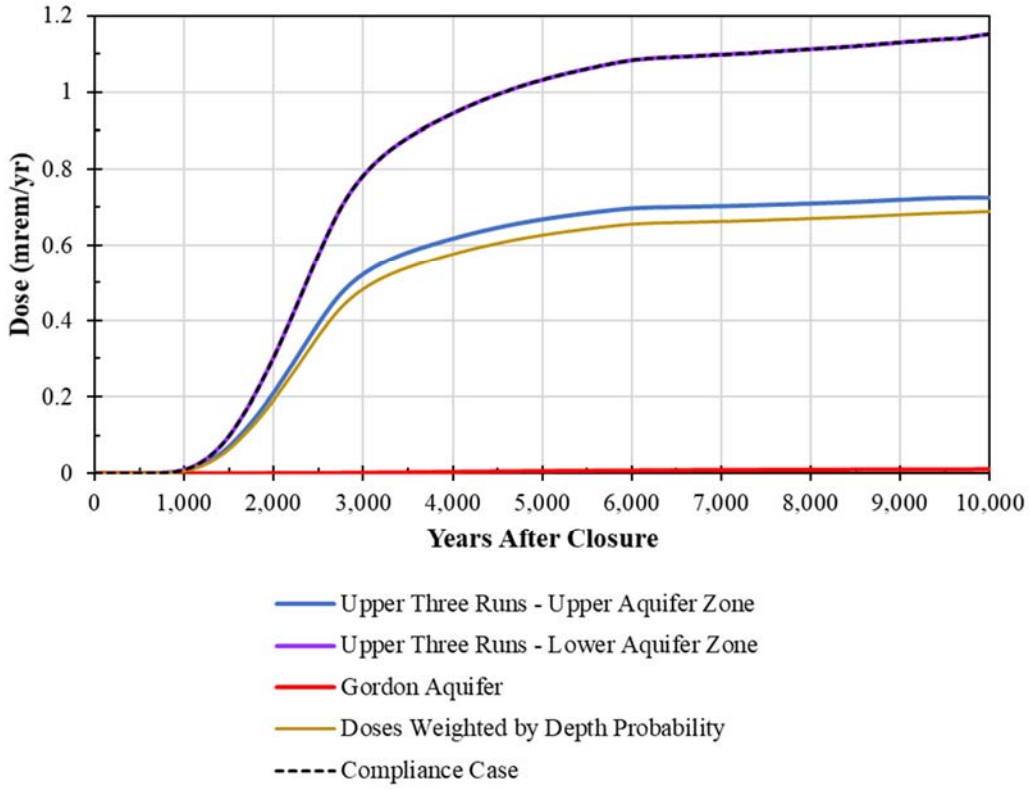

Table 5.8-33: Summary of Compliance Case Dose Results Based on Concentrations at Various Depths, 100-Meter MOP Peak Ground Water Pathways Doses

Modeling Case	Compliance Period (0 to 1,000 Years)		Performance Period (0 to 10,000 Years)	
	Peak Dose (mrem/yr)	Year of Peak	Peak Dose (mrem/yr)	Year of Peak
Upper Three Runs – Upper Aquifer Zone	7.2E-03	1,000	0.73	10,000
Upper Three Runs – Lower Aquifer Zone	9.4E-03	1,000	1.2	10,000
Gordon Aquifer Unit	1.1E-06	1,000	0.1	10,000
Doses Weighted by Depth Probability	6.3E-03	1,000	0.69	10,000
Compliance Case	9.4E-03	1,000	1.2	10,000

5.8.9 Other MOP Sensitivity Cases or Scenarios

The previous sections (Sections 5.8.1 through 5.8.8) described groups of various alternative scenarios and sensitivity cases developed to better understand the uncertainties and risks that are specifically associated with the assigned groupings. This section introduces various alternative scenarios and sensitivity cases that did not reasonable fit within any of these previous groups.

5.8.9.1 Early Release Cases

The "Early Release" scenario is designed to non-mechanistically address the potential impacts from multiple FEPs, as presented in Table 5.8-34.

Table 5.8-34: FEPs Addressed in the Early Release Scenario

FEP ID	FEP Name	Discussion
2.7.03	Cold Weather Effects	Cold weather effects could cause freeze/thaw damage to external surfaces or to transfer lines. These may result in inadvertent releases prior to emplacement of the closure cap.
3.2.04	Manufacturing and Commissioning of Components	Manufacturing defects to material used in SDU construction may result in inadvertent releases prior to emplacement of the closure cap.
3.2.05	Construction	Defects in the construction of SDUs may result in releases prior to emplacement of the closure cap.
3.2.09	Repairs of Construction Defects	Incomplete repair of construction defects may result in inadvertent releases prior to emplacement of the closure cap.
3.7.02	Mechanical Degradation Mechanisms	Mechanical degradation in the form of damage to the SDU integrity may result in inadvertent releases prior to emplacement of the closure cap.
3.7.06	Concrete Shrinkage/Expansion	Concrete shrinkage or expansion may damage the SDU integrity or may create a direct pathway from the saltstone to the soil. Both conditions may result in inadvertent releases prior to emplacement of the closure cap.
3.7.08	Swelling of Backfill and Emplacement Materials	Swelling of backfill may damage the SDU integrity, which may result in inadvertent releases prior to emplacement of the closure cap.
3.7.09	Localized Degradation	Localized degradation may create a direct pathway from the saltstone to the soil which may result in inadvertent releases prior to emplacement of the closure cap.
3.7.19	Site Stability	Instability of the site may result in damage to the SDUs. Such damage may result in inadvertent releases prior to emplacement of the closure cap.
3.8.02	Void Space Formation	Void space formation may result in a collapsed roof during closure cap emplacement. This could result in inadvertent releases shortly after emplacement of the closure cap.
3.8.07	Mechanical Effects at Engineered Barrier System Component Interfaces	Mechanical damage to the SDU(s) may result in inadvertent releases prior to emplacement of the closure cap.
5.1.03	Focusing of Flow Along Preferred Flow Paths (Fingers, Weeps, Faults, Fractures, etc.)	Focused flow may occur as a direct pathway from the saltstone to the soil and result in inadvertent releases prior to emplacement of the closure cap.
5.1.07	Episodic or Pulse Flow and Release	A significant episodic rainfall event prior to emplacement of the closure cap may result in inadvertent early releases.
5.4.06	Rinse Release	This FEP assumes early releases may occur due to unexpected contaminant release behavior.
6.2.01	Seismicity	Seismic damage to the SDU(s) may result in inadvertent releases prior to emplacement of the closure cap.
6.2.03	Seismic-Induced Damage or Changes to System Components	Seismic damage to the SDU(s) may result in inadvertent releases prior to emplacement of the closure cap.
6.2.04	Effects of Subsidence	Instability of the site may result in damage to the SDUs. Such damage may result in inadvertent releases prior to emplacement of the closure cap.
6.4.02	Flooding or Drainage System Failure	A significant flooding event prior to emplacement of the closure cap may result in inadvertent early releases.

FEP ID	FEP Name	Discussion
6.4.03	Releases Prior to Closure	This FEP assumes early releases may occur. As a sensitivity model, this scenario should consider potential dose impacts from the SDU 4 releases described in SRNL-L3200-2017-00107. Inventory estimates for soil might be informed by data found in Q-CLC-Z-00026 or in N-CLC-Z-00020.
6.4.04	Forest/Brush Fire	A fire near the SDUs prior to emplacement of the closure cap may result in spalling (i.e., damage to the SDU concrete). Such damage may result in inadvertent releases prior to emplacement of the closure cap.
6.4.06	Movement of the Waste Form	Instability of backfill material or other nearfield material may result in movement or damage to the SDUs. Such damage may result in inadvertent releases prior to emplacement of the closure cap.
6.4.07	Cave-In, Collapse, or Rockfall	A collapsed roof could result in inadvertent releases shortly after emplacement of the closure cap.

[SRR-CWDA-2018-00006]

Despite the large number of FEPs considered, it should be noted that the goal of this scenario is not to determine which events or processes could cause these early releases; rather, the goal is to assess the potential impacts associated with early releases. As such, the exact mechanisms for these releases are not explicitly considered.

To evaluate the potential impacts from early releases, two Early Release sensitivity cases were developed: Early Release Case 1 and Early Release Case 2.

To develop these early release cases, the modeling case described in Section 5.8.3.3 was used as the starting basis. This starting case assumed that the SDU concrete for the 375-foot diameter SDUs has an initial saturated hydraulic conductivity of 1.0E-07 cm/s. For evaluating risks associated with early releases, this case was modified to assume a much higher infiltration rate, albeit not as high as in the Soil-Only Closure Cap Cases (described in Section 5.8.2.4). Finally, the difference between the two early release cases is that Early Release Case 2 also assumes that part of the SDU 4 inventory is already in the soil at the time of closure. Specifically, 10% of the SDU 4 Cell G inventory is placed into the soil adjoining the base of the disposal unit. The development of this soil inventory is based on the Cell G inventory from *Saltstone Disposal Unit (SDU) 1 Cells A-C and SDU 4 Cells A-L Inventories in Support of Saltstone Disposal Facility Performance Assessment Modeling*. [SRR-CWDA-2018-00062]

Table 5.8-35 presents the assumed infiltration rate for the early release cases alongside the infiltration rates from the Compliance Case and from the Soil-Only Closure Cap Cases to provide additional context.

Table 5.8-35: Assumed Infiltration Rates for Early Release Cases

Year	Compliance Case (mm/yr)	Soil-Only Closure Cap Cases (mm/yr)	Early Release Cases (mm/yr)
0	0.0060	417.8	0.3
500	0.0060	417.8	0.3
500	0.091	417.8	6.2
2,000	0.091	417.8	6.2
>2,000	0.13	417.8	8.6

These infiltration rates are illustrated in Figure 5.8-98, which also depicts the infiltration rate from the 2008 HELP Model (labeled as "HELP (2008) Infil."). [WSRC-STI-2008-00244] The assumed infiltration rate for the early release cases does not have a supported technical basis but was arbitrarily selected to ensure that a significantly high infiltration rate was applied to ensure that early releases will occur.

Figure 5.8-98: Comparison of Assumed Infiltration Rates Used for Evaluating Early Releases

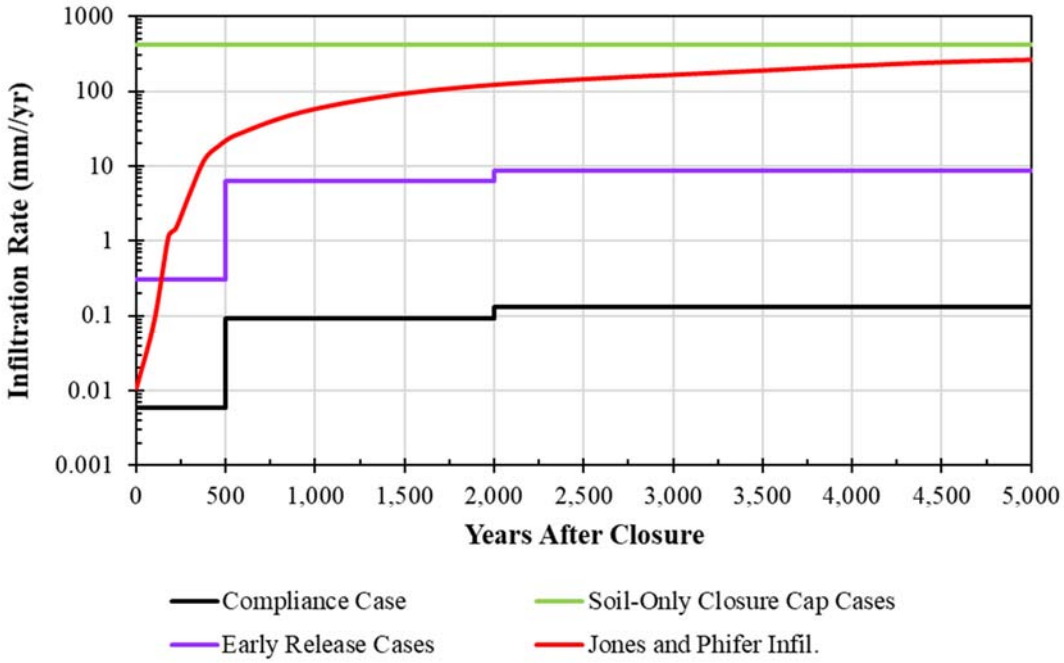

To provide further insights, multiple cases in addition to the two Early Release Cases were evaluated, as these other cases also yielded early releases. Figure 5.8-99 (log-scale) and Figure 5.8-100 (detail) present the total doses to the MOP along the 100-meter boundary for each of the cases evaluated, followed by a summary of the peak values in Table 5.8-36.

Figure 5.8-99: Dose Results from Cases Used to Evaluate Early Releases

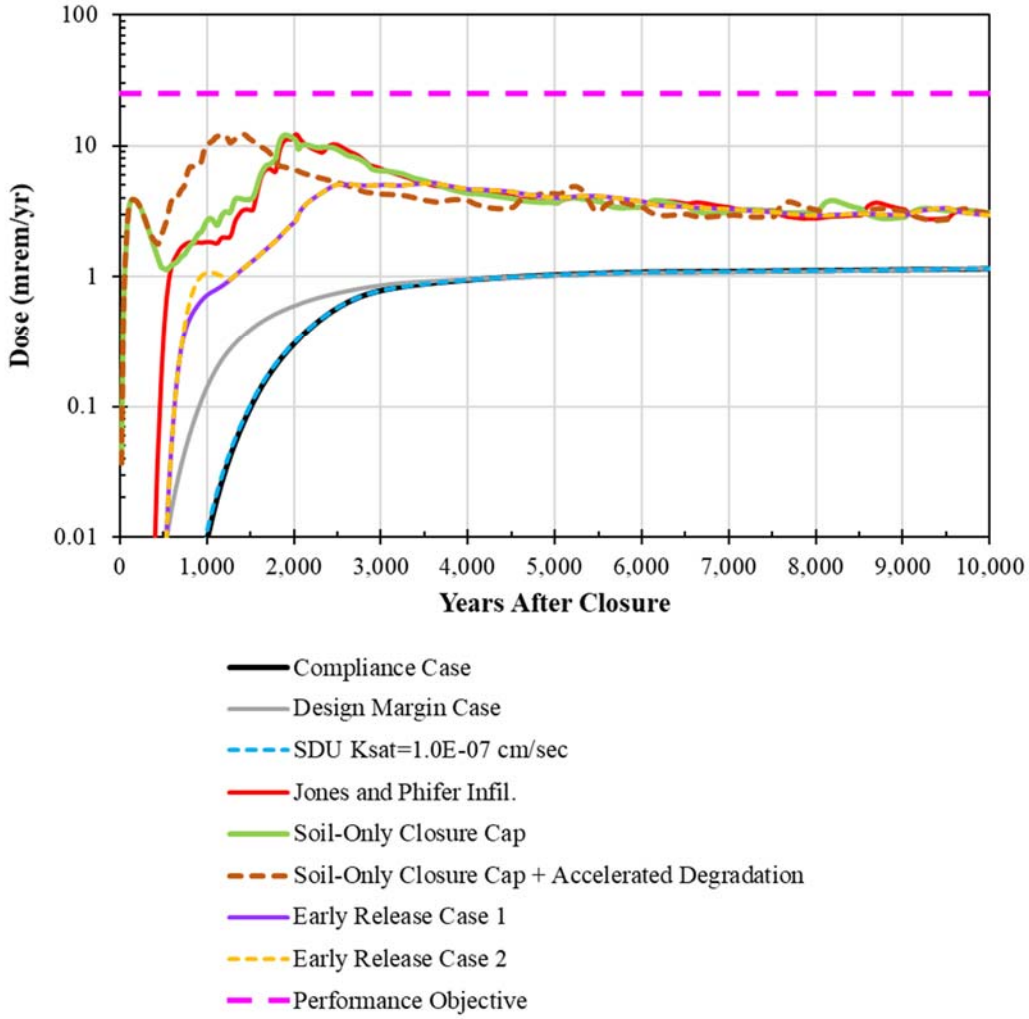

Figure 5.8-100: Dose Results from Cases Used to Evaluate Early Releases (Detail)

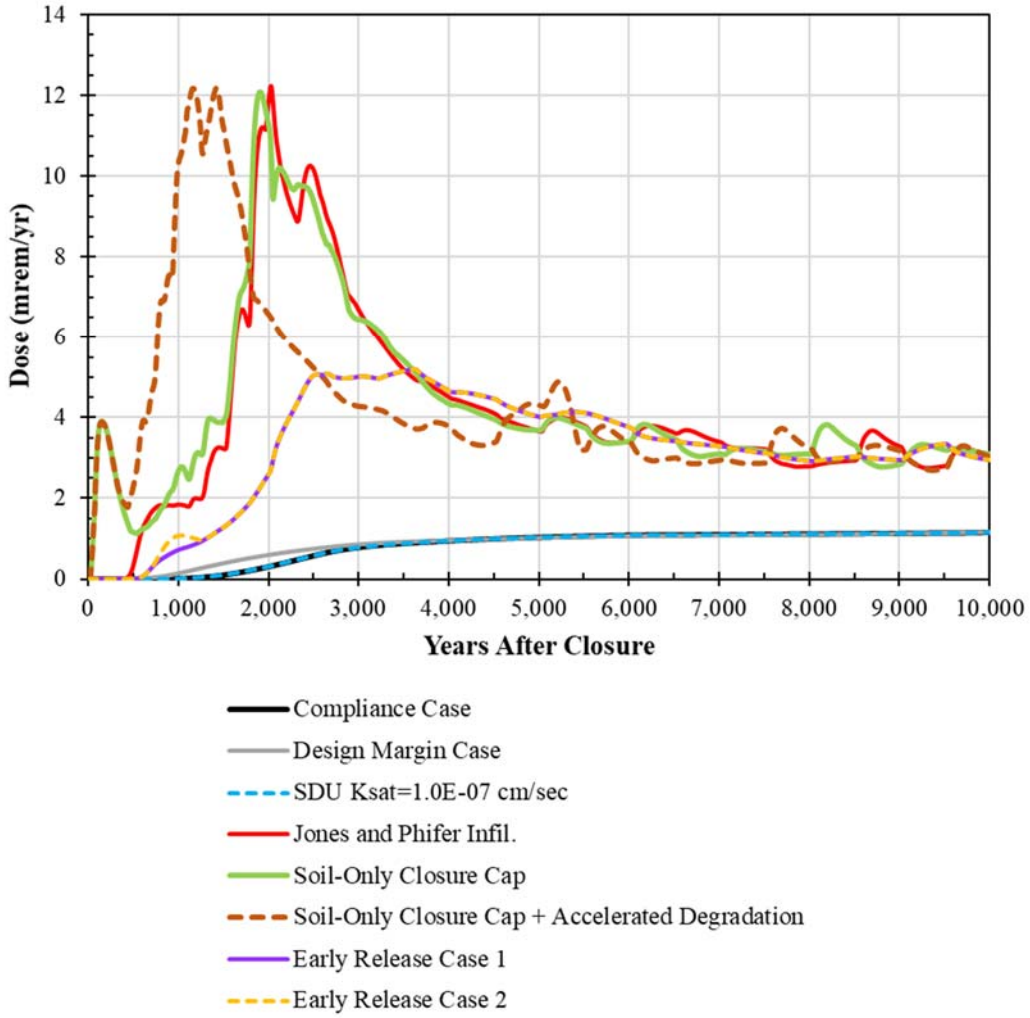

The first two cases presented (Compliance Case and the Design Margin Case) show relatively similar results. The dose from the Design Margin Case begins to climb a few hundred years earlier, but the magnitude is still low and the peak dose to the MOP within the 10,000-year Performance Period is lower than that of the Compliance Case. This indicates that construction defects may influence the timing of early doses (while the values are low), but do not have a strong influence on the magnitude of the peak doses.

The case with the initially degraded SDU concrete (SDU K_{sat} = 1.0E-07 cm/s) has even less influence as the results are nearly identical to that of the Compliance Case. This indicates that events which might damage the hydraulic integrity of the SDU concrete (e.g., freeze/thaw cycles, fires, etc.), are unlikely to have a significant impact on the overall performance of the system as modeled.

Table 5.8-36: Summary of Early Release Comparison

Modeling Case	Peak Dose (mrem/yr)		Discussion
	Compliance Period	Performance Period	
Compliance Case	9.4E-03	1.2	The Compliance Case result is provided as a basis for comparisons.
Design Margin Case	0.14	1.2	The Design Margin Case (see Section 5.8.7.1) incorporates multiple assumptions related to the geometry of the design and construction of SDUs.
SDU Ksat = 1.0E-07 cm/s	1.0E-02	1.2	This case is otherwise identical to the Compliance Case, but assumes that the initial saturated hydraulic conductivity of the SDU concrete (for the 375-foot diameter SDUs) is 1.0E-07 cm/s (see Section 5.8.3.3). The Early Release Cases are modified versions of this case.
HELP (2008) Infil.	1.8	12	This case was setup to be identical to the Compliance Case, except for assuming the infiltration rate from the 2008 HELP model (see Section 5.8.2.2).
Soil-Only Closure Cap	3.9	12	This case was setup to be identical to the Compliance Case, except for assuming a constant infiltration rate based on natural infiltration (see Section 5.8.2.4).
Soil-Only Closure Cap + Accelerated Degradation	10	12	This is the same as the "Soil-Only Closure Cap" case (green), except all cementitious materials are assumed to have a degradation rate that is twice as fast (see Section 5.8.2.4).
Early Release Case 1	0.72	5.2	This is the same as the same as the K_{sat} sensitivity case (blue), except for assuming a higher infiltration rate to specifically evaluate early releases.
Early Release Case 2	1.1	5.2	This is the same as the other Early Release Case (purple), except for assuming that 10% of the inventory for SDU 4 Cell G is already in the soils adjacent to SDU 4.

The next cases presented (HELP (2008) Infil., Soil-Only Closure Cap, and Soil-Only Closure Cap + Accelerated Degradation) were discussed in Section 5.8.2. The key observation here is that, more than any other parameter, the assumed infiltration rate has the greatest influence on results. Despite this observation, even under the bounding conditions assumed for these cases, the peak doses remain below the 25 mrem/yr performance objective.

Finally, the two early release cases (Early Release Case 1 and Early Release Case 2) assume infiltration rates that are nearly two orders of magnitude higher than the Compliance Case infiltration rate (i.e., closer to unrealistic the 2008 HELP infiltration rates, but not quite as extreme). When observed on a logarithmic scale, the assumed infiltration rate for the early release cases are approximately mid-way between the Compliance Case infiltration rate and the soil-only infiltration rate (per Figure 5.8-98) after the first 500 years. Accordingly, the resulting doses are initially (for the first 1,000 to 3,000 years) approximately mid-way between the respective cases based on these infiltration rates (see Figure 5.8-99 and Figure 5.8-100).

A final observation is that after the first few thousand years, the cases which assume high infiltration rates all reach a point where the total dose drops to less than 4 mrem/yr. This indicate that after some initial release events, the release rates for I-129 and Tc-99 become controlled by the saturated hydraulic conductivity of saltstone, which is initially the same in all these cases (i.e., starting value of 5.0E-10 cm/s).

5.8.9.2 Evaluation of the Delay Times Applied to the Onset of Cementitious Degradation of the SDU Roofs and SDU Floors

Table 4.4-39 through Table 4.4-43 indicate that the onset of carbonation and decalcification of the roofs and floors of the SDUs is delayed. This delay is imposed because the HDPE/GCL layers are credited as effective barriers to these degradation mechanisms. Due to the delayed onset, cementitious degradation takes longer than if these barriers had not been credited.

The following sensitivity case was developed to provide insight relative to the risk significance of this timing delay. First, all the delay times for the start of each degradation mechanism were set to 0 for every SDU, resulting in the following impacts for the 375-foot diameter SDUs (excluding SDU 6):

- SDU roof degradation completes at 1,203 years instead of 1,552 years.
- SDU floor degradation completes at 2,407 years instead of 2,800 years.
- Saltstone degradation begins at 1,203 years instead of 1,552 years.

The other SDUs all have similar changes to the degradation timings. Additionally, this sensitivity case assigned the material properties of sand to the HDPE/GCL material zones within the Vadose Zone Transport Model. All other modeling conditions were setup the same as the Compliance Case, including the Aquifer Transport Model and the dose calculations.

Figure 5.8-101 and Figure 5.8-102 compare the resulting doses from this sensitivity case to the doses from the Compliance Case. Although the doses within the 1,000-year Compliance Period appear to be higher, the magnitude remains orders of magnitude below the performance objective of 25 mrem/yr. Beyond the Compliance Period, the differences between these results are negligible. This indicates that the timing delays and the condition of the HDPE/GCL at theSDU roof have no significant impacts on the long-term performance of the system. This is because the HDPE/GCL at the SDU roof is a relatively thin layer and the performance of the system is diffusion controlled. Under higher flow conditions, this layer can become more important (see Section 5.8.2.3).

Figure 5.8-101: Dose Results from Sensitivity Case With No Degradation Delays (Compliance Period)

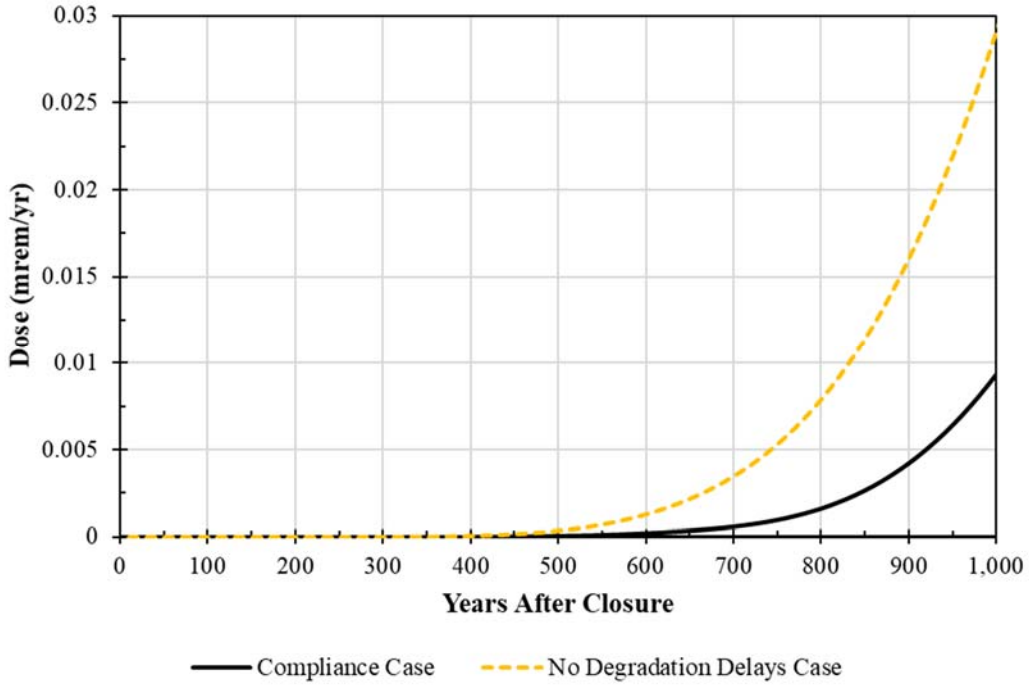

Figure 5.8-102: Dose Results from Sensitivity Case With No Degradation Delays (Performance Period)

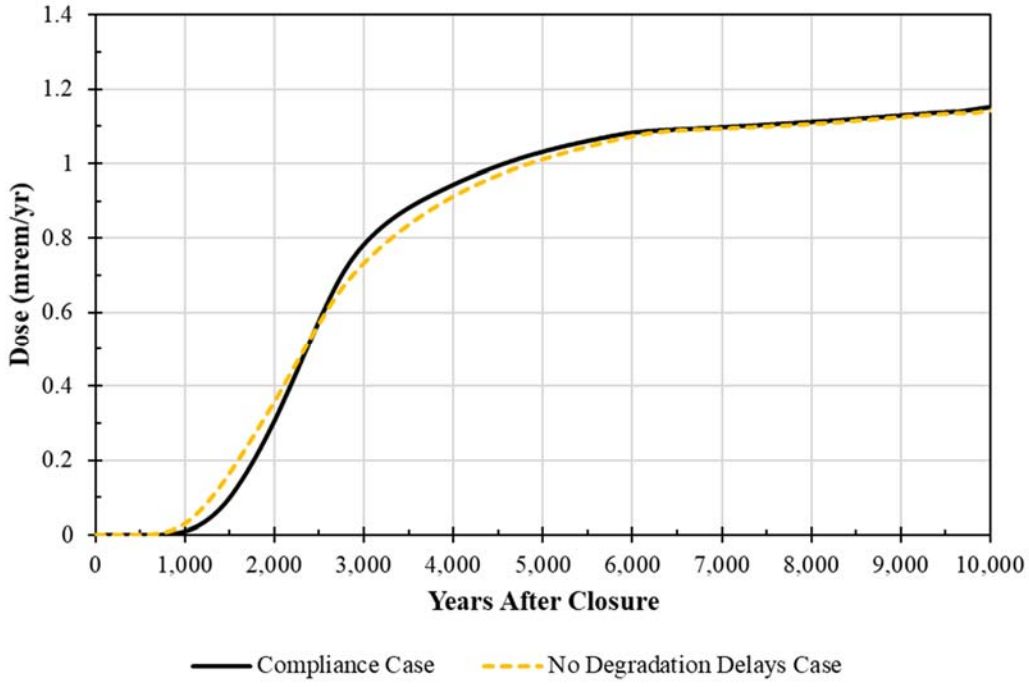

5.8.9.3 Evaluation of Collapsed SDU Roof

The conceptual model development report (SRR-CWDA-2018-00006) recommended the development of a sensitivity case to evaluate the potential impacts from a collapsed roof due to void space within the SDU. This recommendation is intended to address FEP 3.8.02 "Void Space Formation" and FEP 6.4.07 "Cave-In, Collapse or Rockfall" (see Table 4.1-5). The following describes the development and results from the Collapsed SDU Roof sensitivity case.

Conceptually, this sensitivity case assumes that a void space remains beneath the roof of each 375-foot diameter SDU (i.e., SDUs 6, 7, 8, 9, 10, 11, and 12) at the time of closure, such that roof collapses occur during installation of the closure cap. This conceptual model does not reflect expected future conditions as current plans are to completely fill any void spaces within the SDUs prior to the emplacement of the closure cap to ensure structural stability. Although sufficient void space is assumed to be present to cause roof collapse, the downward displacement of the roof is assumed to be minimal and not appreciably impact the performance of the overlying cover system. Soil deformation from localized subsidence with the SDU is assumed to spread out moving upward. The combined effect of minimal deformation within the SDU and deformation spreading is assumed to cause at most a mild depression at the ground surface and not damage cap layers.

This Collapsed SDU Roof Case is implemented via PORFLOW modeling by assigning the hydraulic properties of gravel (see Table 4.3-2) and K_d = 0 mL/g to the SDU roof and the interior volume reserved for an optional clean cap grout fill (i.e., the top 5% of the saltstone thickness at the wall). Waste inventory is placed only in the remaining volume occupied by saltstone.

Figure 5.8-103 compares dose results for the Collapsed SDU Roof sensitivity case to the Compliance Case. The peak dose is slightly higher than the Compliance Case through both the Compliance Period and Performance Period (Table 5.8-37).

Table 5.8-37: Comparison of Collapsed Roof Sensitivity Case, 100-Meter MOP Peak Ground Water Pathways Doses

Modeling Case	Compliance Period (0 to 1,000 Years)		Performance Period (0 to 10,000 Years)	
	Peak Dose (mrem/yr)	Year of Peak	Peak Dose (mrem/yr)	Year of Peak
Collapsed SDU Roof	9.4E-03	1,000	1.2	10,000
Compliance Case	1.0E-02	1,000	1.2	10,000

Figure 5.8-103: Dose Results from the Sensitivity Case that Assumes a Collapsed SDU Roof.

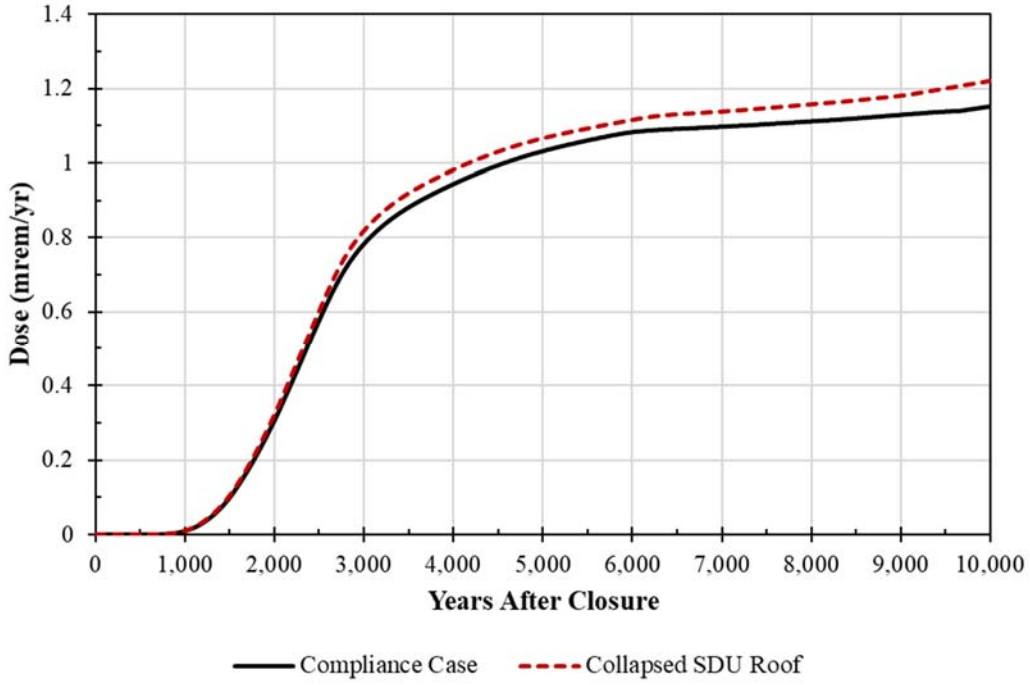

5.8.9.4 Evaluation of Perched/Pooled Water Scenarios

The conceptual model development report (SRR-CWDA-2018-00006) identifies several FEPs related to perched or pooled water (Table 5.8-38).

Table 5.8-38: FEPs Addressed in the Perched/Pooled Water Scenarios

FEP ID	FEP Name	Discussion
2.5.11	Undetected Geologic Features	This scenario assumes that there is an undetected layer of impermeable soil in the vadose zone above which infiltrating water may become trapped, forming a localized zone of perched water.
3.5.21	Pooling Water Above SDUs	This scenario assumes that the backfill material is more impermeable than currently assumed, wherein infiltrating water may become trapped along the roof the SDUs, forming a localized zone of pooled water.
5.2.09	Perched Water Develops	This scenario assumes that there is an undetected layer of impermeable soil in the vadose zone wherein infiltrating water may become trapped, forming a localized zone of perched water.
6.4.02	Flooding or Drainage System Failure	A significant flood event may result in pooled water over the SDUs. Therefore, this scenario provides insights relative to the impacts from the potential flood event.

[SRR-CWDA-2018-00006]

Based on these FEPs, two perched (pooled) water scenarios were developed:

- Pooled Water Scenario (with water potentially pooled at the SDU roof depending on infiltration rate) and

- Perched Water Scenario (with water potentially perched in the vadose zone beneath the SDU depending on infiltration rate).

It should be noted that the goal of these scenarios is not to explicitly simulate the presence or occurrence of each FEP from Table 5.8-38, rather the goal is to provide insights to the potential impacts these FEPs may incur on the performance system. As such, these FEPs are addressed non-mechanistically through the sensitivity models developed to represent these two scenarios.

Conceptually, the pooled water scenario assumes that after the SDU has been filled with saltstone, it will be surrounded with backfill prior to construction of the closure cap. It is assumed that the surface of this surrounding backfill undergoes some form of compaction or additional cover such that a region of relatively low permeability exists in the soils near the roofline of the SDU. This region of low permeability could then result in localized pooling of water in the backfill adjacent to the SDU roofline. The underlying concern addressed by this scenario is that a low-permeability layer at the SDU roofline might increase water flow through the SDU. Within PORFLOW this is implemented as a localized low-permeability feature in the backfill soil surrounding the SDU (Figure 5.8-104).

Figure 5.8-104: Placement of Low-Permeability Layer in the Sensitivity Case that Assumes Pooled Water at the SDU Roofline

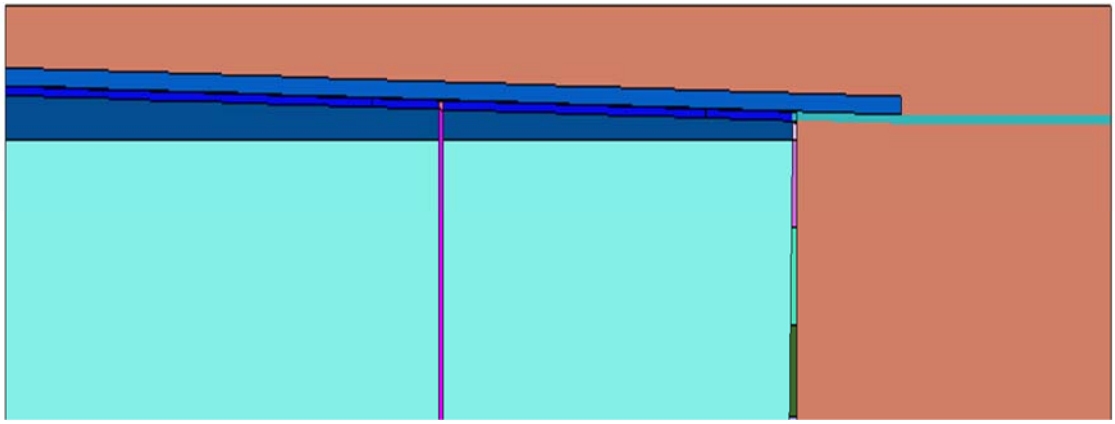

Similarly, the concept of the perched water scenario assumes that a previously unidentified layer of low permeability exists within the vadose zone, somewhere between the bottom of the SDU and the water table. The underlying concern addressed by this scenario is that perched water or a higher saturation zone atop the low-permeability layer may unduly influence transport, although it is expected that such a layer would dilute the solute concentrations and function as diffusion barrier. As with the pooled water scenario, this case is implemented within PORFLOW as a localized low-permeability feature within the vadose zone (Figure 5.8-105).

Figure 5.8-105: Placement of Low-Permeability Layer in the Sensitivity Case that Assumes Perched Water in the Vadose Zone Beneath the SDU

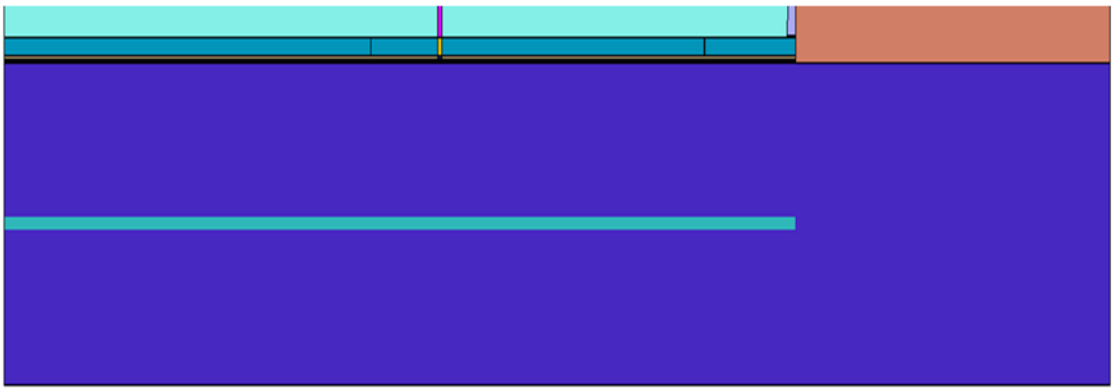

Both the pooled water and the perched water sensitivity cases were simulated in PORFLOW by introducing a 1.0E-14 cm/s layer (approximately one foot thick) at the positions indicated in Figure 5.8-104 and Figure 5.8-105, respectively. The selected hydraulic conductivity value makes each layer effectively impermeable. The effective diffusion coefficient of the layers was set at 4.0E-06 cm^2/sec (based on SRS clays per Table 5-18 of WSRC-STI-2006-00198). Also note that the layer at the SDU roofline extends into the wall to prevent water from bypassing saltstone through the degraded wall after early times. The layer below the SDU occupies the same footprint as the SDU.

Although these imposed layers assume an extremely low permeability, intermediate model results revealed that significant pooling or perching of water did not actually occur under these conditions. While the saturation levels do increase (as illustrated in Figure 5.8-106 compared to Figure 5.8-107 and Figure 5.8-108, reflecting deflection of water for 2,000+ years and lower material degradation), the higher permeability in adjacent materials allows for continuous flow such that no pooling or perching of water occurs. Regardless, the assumed 1.0E-14 cm/s is considered bounding and does alter the saturation and flow regime throughout the system, therefore these sensitivity cases still provide useful insights with respect to the behavior of the system under these alternative conceptual models.

Figure 5.8-106: Saturation at 2,000-2,300 years for the Compliance Case

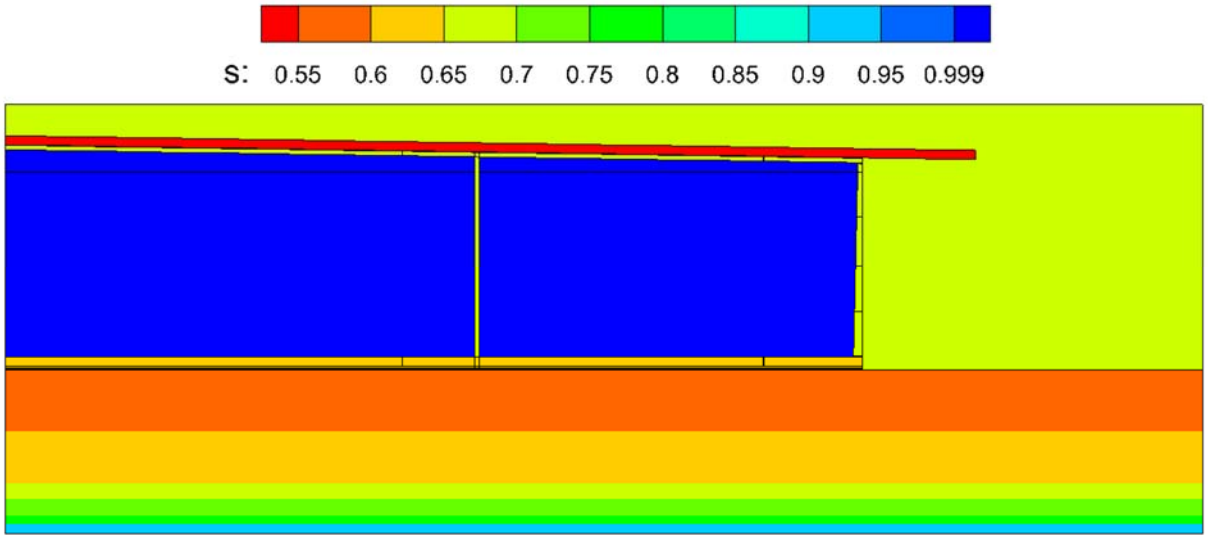

Figure 5.8-107: Saturation at 2,000-2,300 years for the Sensitivity Case that Assumes Pooled Water at the SDU Roofline

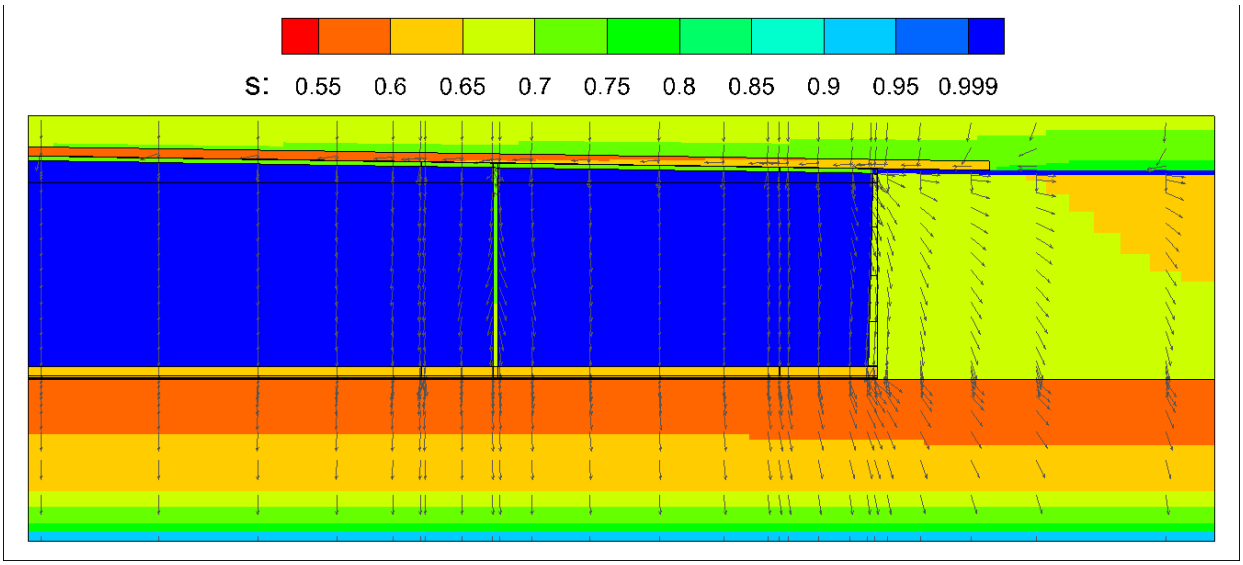

Figure 5.8-108: Saturation at 2,000-2,300 years for the Sensitivity Case that Assumes Perched in the Vadose Zone Beneath the SDU

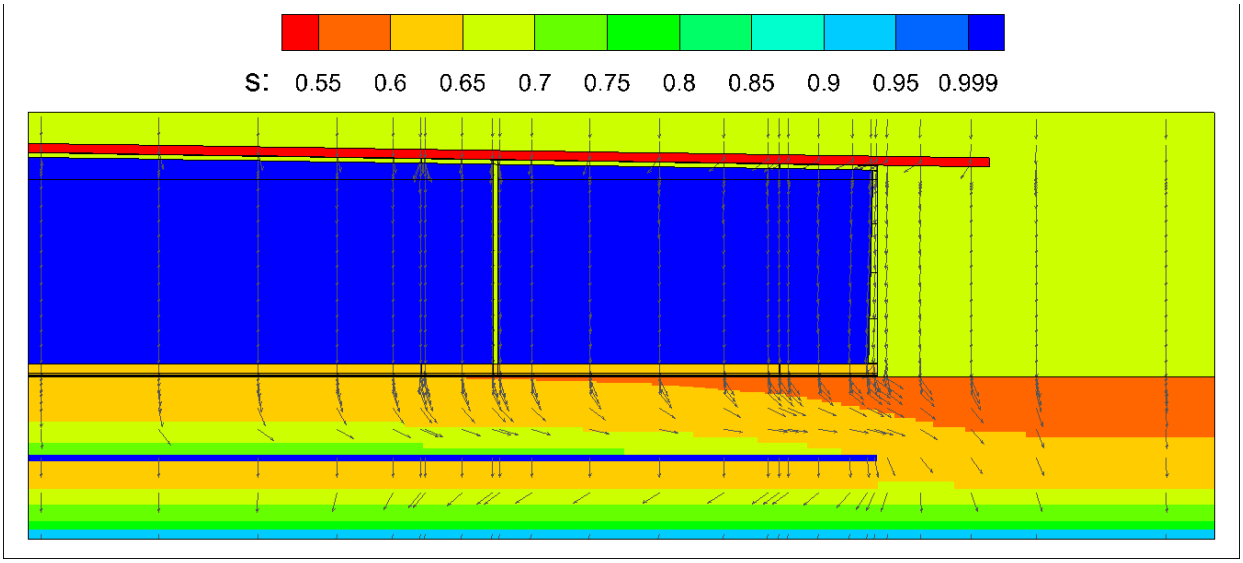

Figure 5.8-109 through Figure 5.8-111 illustrate how these simulations impact the fluxes to the water table for the sensitivity run radionuclides: Cl-36, I-129, and Tc-99. The simulation assuming a low-permeability layer at the SDU roofline (i.e., Perched Roof) forces the infiltrating water from the closure cap to pass through saltstone, increasing releases relative to the Compliance Case.

Alternatively, the simulation with a low-permeability layer beneath the SDU (Perched LVZ) leads to slightly lower releases, because the added layer functions as a diffusion barrier when compared to other lower vadose zone (LVZ) sediments (see Section 4.3.1.1 for soil properties).

These cases indicate that in the event of unexpected subsurface pooling of water at the roof-line of the SDU, there could be a slight increase to dose, while perched water within the vadose zone beneath the SDU could slightly lower doses. Regardless, the resulting doses are expected to remain below performance objectives.

Figure 5.8-109: Cl-36 Flux Comparison for the Sensitivity Cases that Assume Perched/Pooled Water

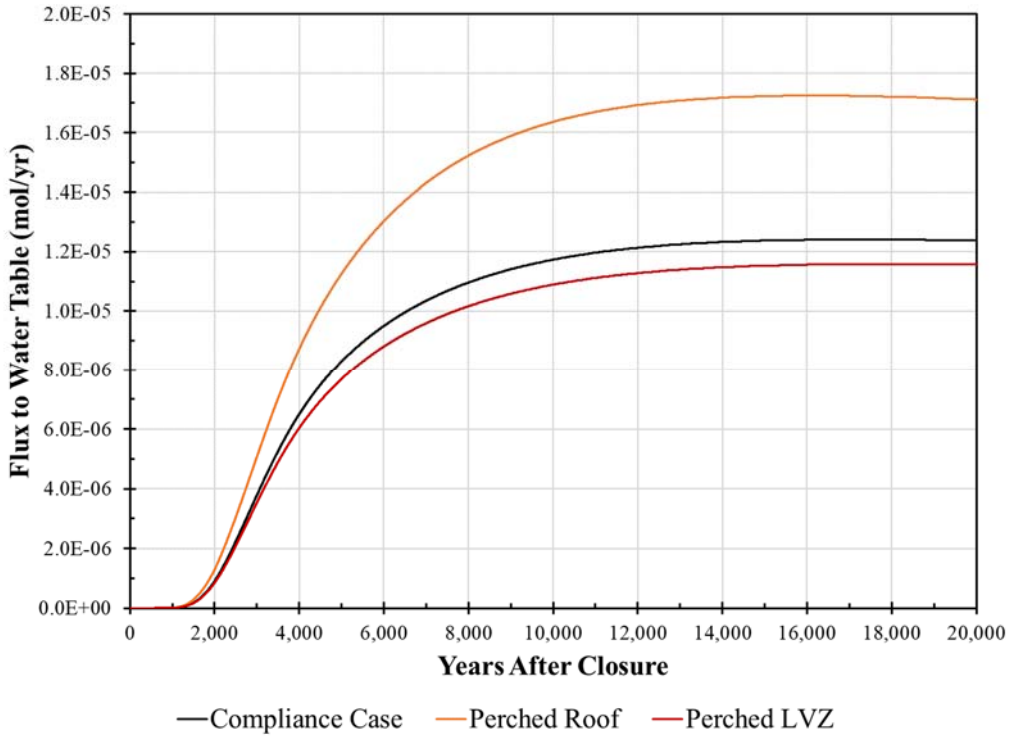

Figure 5.8-110: I-129 Flux Comparison for the Sensitivity Cases that Assume Perched/Pooled Water

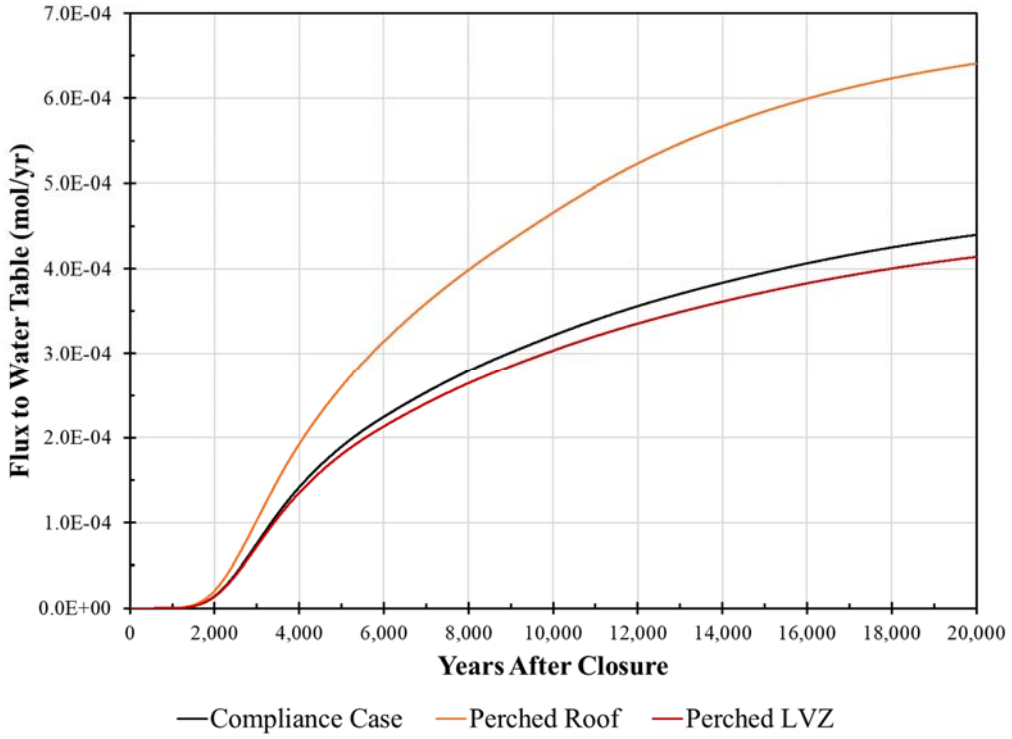

Figure 5.8-111: Tc-99 Flux Comparison for the Sensitivity Cases that Assume Perched/Pooled Water

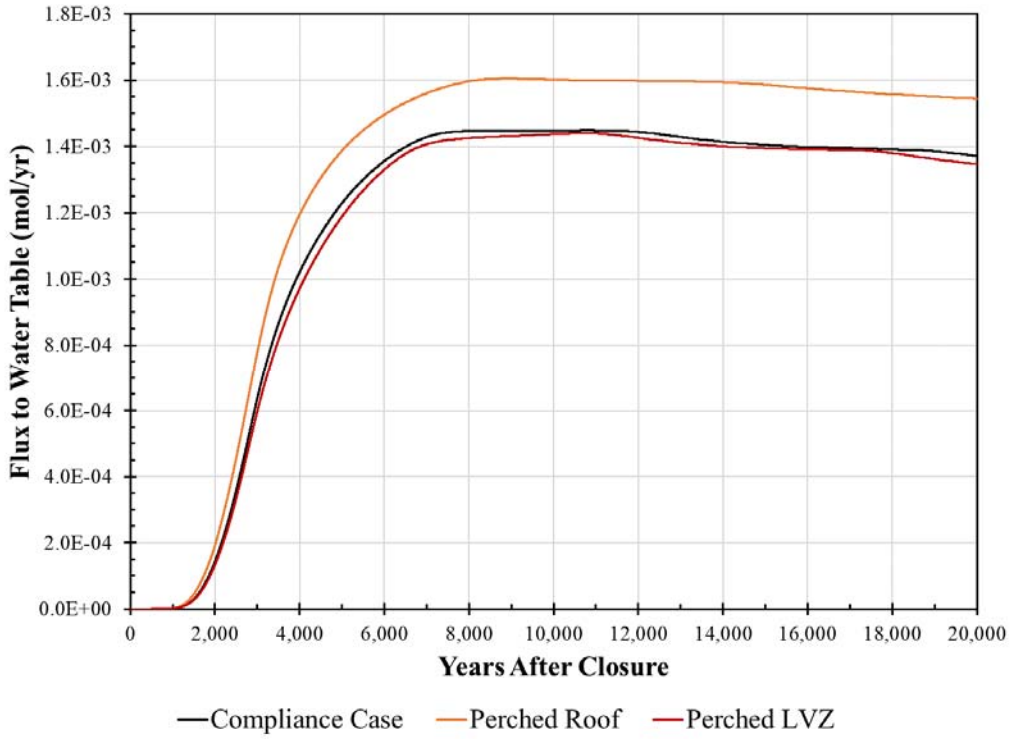

5.8.9.5 Ground Water Fast Flow Path Sensitivities

As noted in Section 4.6.4 for the Central Scenario, the hydraulic properties within specific layers of the vadose zone soils or saturated zone soils (e.g., TCCZ, LAZ, etc.) are assumed to be continuous and homogenous (within specific areas of SRS). Soft zones are subsurface regions of calcareous or clastic material with distinct material properties, which may or may not promote the formation of caverns or regions of faster flow. *A Review of Subsurface Soft Zones at Savannah River Site with Emphasis on H Area Tank Farm* (SRNL-TR-2012-00160), as discussed in Section 4.6.4, determined that:

- Soft zones beneath SRS are not cavernous voids, but are small, isolated, poorly connected, three-dimensional features filled with loose, fine-grained, water-saturated sediment.
- Despite their under-consolidated nature, soft zones have survived for a very long time and remain structurally competent in the presence of significant overburden stresses.
- Soft zones appear not to be a critical influence on either ground water flow or contaminant transport.

Given the proximity of Z-Area and the SDF to H-Area, it is reasonable to apply these conclusions to the SDF as well. Despite the conclusions from SRNL-TR-2012-00160, uncertainty regarding the presence of potential soft zones remains. To address the

potential risks associated with this uncertainty, the Fast Flow Paths through Ground Water Scenario was developed.

The Fast Flow Paths through Ground Water Scenario is designed to non-mechanistically address the potential impacts from multiple FEPs, as presented in Table 5.8-39.

Table 5.8-39: FEPs Addressed in the Fast Flow Paths through Ground Water Scenario

FEP ID	FEP Name	Discussion
2.5.08	Geologic Discontinuities and Boundary Conditions (Fractures, Faults, and Cracks)	Undetected geologic features may result in localized flow conditions which might be approximated by assuming a fast flow path through the vadose zone and the saturated zone.
2.5.10	Unconsolidated Soft Zones	Undetected geologic features, such as calcareous zones (or soft zones) may result in localized flow conditions which might be approximated by assuming a fast flow path through the vadose zone and the saturated zone.
2.5.11	Undetected Geologic Features	Undetected geologic features may result in localized flow conditions which might be approximated by assuming a fast flow path through the vadose zone and the saturated zone.
2.6.14	Closure Cap Performance (Differential Settlement)	The closure cap may not perform as intended, which may result in localized flow conditions which might be approximated by assuming a fast flow path through the vadose zone and the saturated zone.
3.7.08	Swelling of Backfill and Emplacement Materials	Swelling of backfill may result in localized flow conditions which might be approximated by assuming a fast flow path through the vadose zone.
3.7.19	Site Stability	Significant seismic or subsidence events may disturb ground water flow patterns in ways which might be approximated by assuming a fast flow path through the vadose zone and the saturated zone.
5.1.10	Alteration and Chemical Weathering Along Flow Paths	Alteration or chemical weathering, for example dissolution within calcareous zones (or soft zones), may result in localized flow conditions which might be approximated by assuming a fast flow path through the vadose zone and the saturated zone.
5.1.13	Calcareous Zone Flow	Undetected geologic features, such as calcareous zones (or soft zones) may influence localized flow conditions which might be approximated by assuming a fast flow path through the vadose zone and the saturated zone.
5.3.09	Fast Transport Pathways	This FEP is explicitly addressed by this scenario by assuming a fast flow path through the vadose zone and the saturated zone.
6.2.01	Seismicity	Significant seismic or subsidence events may disturb ground water flow patterns in ways which might be approximated by assuming a fast flow path through the vadose zone and the saturated zone.
6.2.04	Effects of Subsidence	Significant seismic or subsidence events may disturb ground water flow patterns in ways which might be approximated by assuming a fast flow path through the vadose zone and the saturated zone.
6.4.06	Movement of the Waste Form	Significant seismic or subsidence events may disturb ground water flow patterns in ways which might be approximated by assuming a fast flow path through the vadose zone and the saturated zone.

[SRR-CWDA-2018-00006]

Despite the large number of FEPs considered, it should be noted that the goal of this scenario is not to explicitly simulate the presence or occurrence of each FEP, rather the goal is to provide insights to the potential impacts these FEPs may incur on the performance system. As such, these FEPs are addressed non-mechanistically through various sensitivity models developed in support of the Fast Flow Paths through Ground Water Scenario. These models assume the presence of a soft zone:

- Soft Zone Case,
- Soft Zone Case with Full Mixing, and
- Soft Zone with lower transverse vertical dispersivity, $\alpha_v/100$.

Additionally, for comparative purposes, a modified Compliance Case was also developed:

- Compliance Case with Full Mixing.

These sensitivity cases are each described below.

Due to the expected effectiveness of the closure cap in controlling infiltration, the occurrence of a highly conductive soft zone (fast zone) is expected to have only a limited influence on doses to the MOP. This is because the limited infiltration restricts the release of moderately to highly sorbed species, and reduces the influence of very short-lived radionuclides, particularly those with half-lives shorter than the travel time from the SDUs to the 100-meter boundary. Dose contributions from I-129 and Tc-99 will continue to dominate the MOP dose as these contaminants are highly mobile in natural sediments, and long-lived. The soft zone sensitivity cases were designed to reflect the Fast Flow Paths through Ground Water Scenario and to quantify the influence of the fast zone on doses at the 100-meter boundary.

To evaluate the influence of ground water fast flow, several sensitivity cases were developed using the SDF GoldSim Model and their total dose results were compared to the results from the deterministic SDF GoldSim Model using the Compliance Case settings. Within GoldSim, the sensitivity cases were implemented by modifying the inputs to the abstraction of the Aquifer Transport Model (i.e., the simulation of the saturated zone flow and transport), as described below.

The first sensitivity case assumes that the soft zone is fully saturated, continuous, and follows a pathway with a thickness that is 10% of the saturated zone thickness (18.9 m × 10% = 1.89 m). Note that the SDF GoldSim Model assumes radionuclides do not enter the Gordon Aquifer. The SDU-specific Darcy velocities (based on Table 4.4-85) were increased by a factor of 10 within the soft zone to conserve volumetric flow rate. The mixing zone thickness, which is used to define the thickness of the source zone impacting the GoldSim pipe pathway element (refer to GTG-2017b) for saturated zone transport, was also reduced by a factor of 10 to reflect the change in ratios between the rate of infiltration (unchanged) from the vadose zone beneath the SDUs into the saturated zone and the saturated zone Darcy velocity (changed). No other parameters were changed.

The total doses to the MOP from the Soft Zone sensitivity case, depicted with a red curve, are presented in Figure 5.8-112 for the Compliance Period of 1,000 years, and Figure 5.8-113 for the duration of the simulation (20,000 years). The assumption of a continuous fast zone reduces the dose because it results in a dilution effect. As discussed later, the degree of dilution seen here is a result of assuming that the transverse vertical dispersivity in the soft zone would be the same as that used for the saturated zone under Compliance Case conditions. Since the degree of vertical mixing due to dispersion is a function of distance travelled due to advection, the radionuclides would vertically be close to fully mixed within this soft zone. Full mixing would minimize peak concentrations along the vertical axis.

A second sensitivity case (Soft Zone with Full Mixing) was developed based on the Soft Zone sensitivity case assuming the source zone thickness and soft-zone thickness are equal (vertically), such that the radionuclide concentrations are fully mixed. The total doses to the MOP for this sensitivity case are also depicted in Figure 5.8-112 and Figure 5.8-113 for comparison (blue curve). The comparison of the Soft Zone Case versus the Soft Zone Case with Full Mixing confirms that the former simulation results represent nearly complete vertical mixing.

For the Compliance Case, full vertical mixing has not been attained by the time mass reaches the 100-meter boundary, so the mass released is mixed with a lower volume of water, thus is less diluted. The third simulation (Compliance Case with Full Mixing) was developed by modifying the Compliance Case such that the source zone thickness and soft-zone thickness are equal (vertically), to better evaluate the influence of mixing.

The total doses to the MOP from the Compliance Case with Full Mixing are depicted in Figure 5.8-112 and Figure 5.8-113 (dotted purple curve). As can be seen by the similarity between the Soft Zone cases and this Compliance Case with Full Mixing, adjusted compliance model simulation results also represent total vertical mixing.

A final simulation (Soft Zone with lower transverse vertical dispersivity, $\alpha_v/100$) was performed to evaluate the relationship between the aquifer thickness and the transverse vertical dispersivity (α_v) from a different angle. In this simulation, the vertical dispersivity was decreased by a factor of 100. The factor of 100 was chosen because the vertical dispersion is a function of the square root of the distance the center of mass has travelled and the aquifer thickness was reduced by a factor of 10. Comparing this Soft Zone with $\alpha_v/100$ sensitivity case (green curve) to the Compliance Case (black curve) in Figure 5.8-112 and Figure 5.8-113 shows that the consistent scaling of geometry, flow rates, and vertical dispersivities produce similar results.

The peak doses for each of these cases are summarized in Table 5.8-40.

Figure 5.8-112: Comparison of Soft Zone Fast Flow Path Sensitivity Case Total Dose Results with Compliance Case Dose Results over 1,000 Years

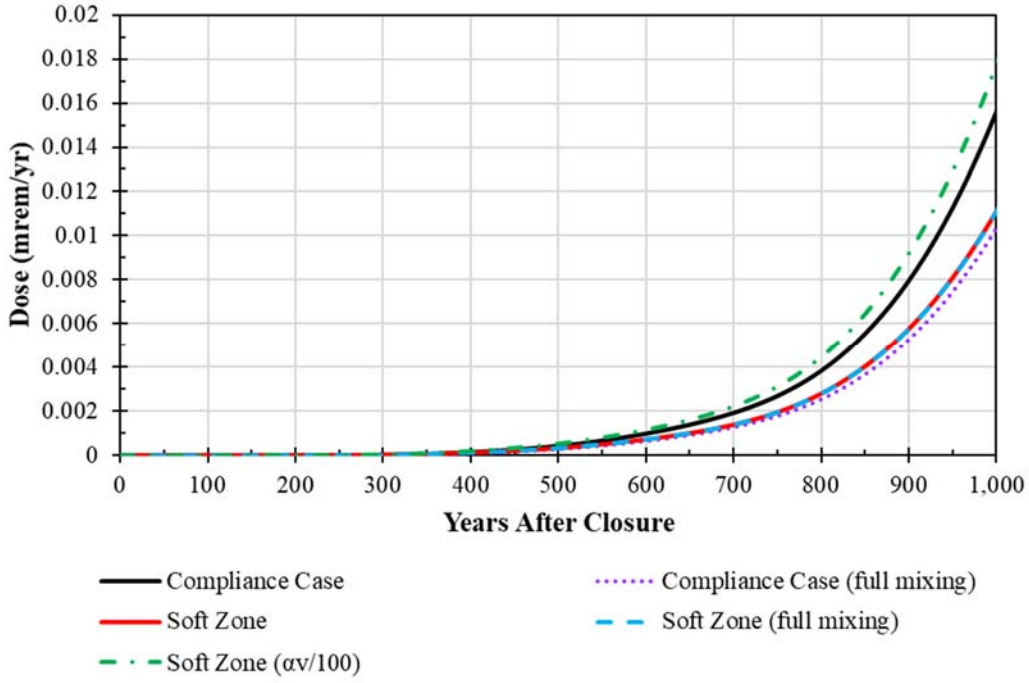

Figure 5.8-113: Comparison of Soft Zone Fast Flow Path Sensitivity Case Total Dose Results with Compliance Case Dose Results over 20,000 Years

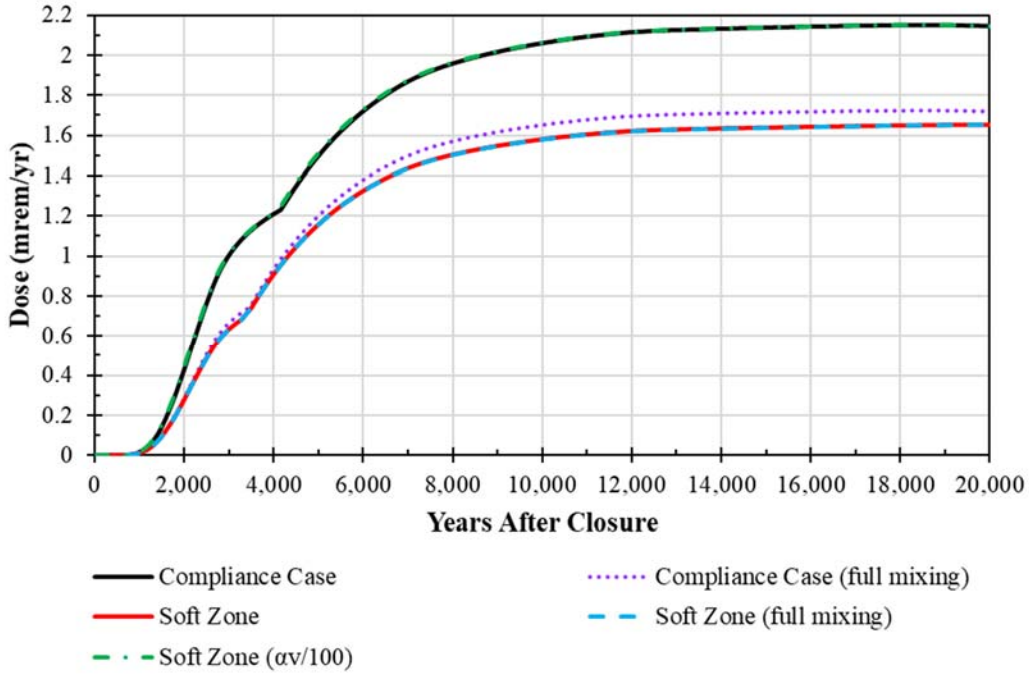

Table 5.8-40: Comparison of Soft Zone Fast Flow Path Sensitivity Case Results, for 100-Meter MOP Peak Doses Based on GoldSim 2019 PA SDF Model Simulations

Modeling Case/Group	Compliance Period (0 to 1,000 Years)		Performance Period (0 to 10,000 Years)	
	Peak Dose (mrem/yr)	Year of Peak	Peak Dose (mrem/yr)	Year of Peak
Compliance Case	1.6E-02	1,000	2.1	10,000
Compliance (Mixed)	1.0E-02	1,000	1.7	10,000
Soft Zone	1.1E-02	1,000	1.6	10,000
Soft Zone (Mixed)	1.1E-02	1,000	1.6	10,000
Soft Zone (α_V/100)	1.8E-02	1,000	2.1	10,000

5.8.9.6 Colloid Transport Case

As noted in Section 4.6.8, the Central Scenario does not explicitly address the potential for colloid formation or transport. Colloids are microscopic particles of a substance within a mixture that do not settle out of suspension. Since colloids do not settle out of suspension, they are readily transported with pore water; however, they may also be subject to filtration. Aqueous species that strongly sorb to solids (e.g., plutonium or uranium) may also sorb to these mobile colloids, resulting in a fraction migrating much faster than the remaining (retarded) mass in equilibrium with immobile solids. This phenomenon is referred to as colloid-facilitated transport.

The Colloid Transport Scenario assumes that radionuclides will contact and sorb to naturally-occurring clay colloids. The colloidal transport process is described in Section 4.6.8 and the conceptual model for this scenario is depicted in Figure 4.6-6 which illustrates the transport process associated with colloidal migration through clayey soils.

In this scenario, it is assumed that a fraction of contaminants will reversibly sorb to the colloids. For the case of colloid facilitated transport of radionuclides reversibly attached to colloids, equations for advective-dispersive transport of dissolved radionuclides in conjunction with radionuclides reversibly attached to mobile colloids are derived from the governing equations for 1) transport of the radionuclides dissolved in water and 2) transport of radionuclides sorbed to colloids suspended in water (MDL-NBS-HS-000021). The governing equation for advective-dispersive transport of dissolved radionuclides in the ground water can be written as:

$$\varphi R \frac{\partial C}{\partial t} = D \frac{\partial^2 C}{\partial x_i{}^2} - V_{Dar} \frac{\partial C}{\partial x_i} - \varphi R \lambda C \qquad \text{Eq. 5.8-4}$$

where:

φ = the effective porosity (unitless),

R = the retardation coefficient (unitless),

D = the dispersion coefficient (m^2/s),

V_{Dar} = the Darcy velocity (m/s),

λ = the decay coefficient (1/s),

C = aqueous concentration radionuclide (dissolved species mass / pore water volume, kg/m^3), and

x_i = distance in the ith-direction (m).

The governing equation for transport of radionuclides sorbed to colloids can in turn be written as:

$$\varphi R_{col}\frac{\partial C^{col}}{\partial t} = D\frac{\partial^2 C^{col}}{\partial {x_i}^2} - V_{Dar}\frac{\partial C^{col}}{\partial x_i} - \varphi R_{col}\lambda C^{col} \qquad \text{Eq. 5.8-5}$$

where:

R_{col} = the colloid retardation coefficient (unitless) and

C^{col} = colloid-bound radionuclide concentration (species mass partitioned to mobile colloids / pore water volume, kg/m^3).

Combining Eq. 5.8-4 and Eq. 5.8-5 and using the relationship:

$$K_C \equiv \frac{C^{col}}{C} \qquad \text{Eq. 5.8-6}$$

the governing equation for colloid facilitated radionuclide transport becomes:

$$\varphi\left\{\frac{R + K_C R_{col}}{1 + K_C}\right\}\frac{\partial C}{\partial t} = D\frac{\partial^2 C}{\partial {x_i}^2} - V_{Dar}\frac{\partial C}{\partial x_i} - \left\{\frac{R + K_C R_{col}}{1 + K_C}\right\}\varphi\lambda C \qquad \text{Eq. 5.8-7}$$

The governing equation for the effective retardation coefficient, R_{eff}, of colloid facilitated radionuclide transport can in turn be written as:

$$R_{eff} = \left\{\frac{R + K_C R_{col}}{1 + K_C}\right\} = 1 + \frac{K_{Deff}\rho_b}{\varphi} \qquad \text{Eq. 5.8-8}$$

where:

$K_{d,eff}$ = the effective equilibrium coefficient (MDL-NBS-HS-000021),

and:

$$\begin{aligned} K_{d,eff} &= \left(R_{eff} - 1\right)\frac{\varphi}{\rho_b} = \left\{\frac{R + R_{col}K_C}{1 + K_C} - \frac{1 + K_C}{1 + K_C}\right\}\frac{\varphi}{\rho_b} \\ &= \left\{\frac{K_d\frac{\rho_b}{\varphi} + (R_{col} - 1)K_C}{1 + K_C}\right\}\frac{\varphi}{\rho_b} \end{aligned} \qquad \text{Eq. 5.8-9}$$

Combining Eq. 5.8-7 with Eq. 5.8-8, the governing equation for colloid facilitated radionuclide transport reduces to:

$$\varphi R_{eff}\frac{\partial C}{\partial t} = D\frac{\partial^2 C}{\partial {x_i}^2} - V_{Dar}\frac{\partial C}{\partial x_i} - \varphi R_{eff}\lambda C. \qquad \text{Eq. 5.8-10}$$

The SDF GoldSim Model forr radionuclide transport can in turn be programmed to replace the saturated zone K_d vector with the $K_{d,eff}$ vector.

To evaluate the influence of the colloid facilitated transport, several GoldSim model simulations were performed and their total dose results compared to the results from the Compliance Case. The additional data needs to implement Eq. 5.8-9 included, the colloid retardation coefficient, the unitless equilibrium constant K_C, the partition coefficients for radionuclides unto the colloids, and the ground water colloid concentration.

The colloid retardation factor R^{col} was assumed to be 1 for all the simulations. This means the colloids migrate at the same rate as a non-sorbing species (tracer) and are subject to the same degree of dispersion. The unitless equilibrium constant K_C is calculated from a relationship equivalent to Eq. 5.8-6:

$$K_C = K_d^{col} C_{colloids} \qquad \text{Eq. 5.8-11}$$

where

K_d^{col} = the partition coefficient for radionuclides unto the colloids (m^3/kg) and

$C_{colloids}$ = concentration of colloids (mass of mobile colloids / volume of pore water, kg/m^3).

For these simulations, the colloids, characterized in a 1994 SRS study (Kaplan, et.al., 1994) as being composed of quartz, 2:1-clays (like hydroxy-interlayered vermiculite or mica), kaolinite, and Fe (or Fe-Ti) oxides, are assumed to be clays and therefore the clayey soils K_d values presented in Table 4.3-4 are used for K_d^{col} in Eq. 5.8-11, whereas sandy soil K_d values are used for K_d in Eq. 5.8-9. The use of clayey soil K_d values versus sandy soil K_d values results in a higher fraction of the total species concentration sorbing to mobile colloids, thus maximizing the influence of colloids. The ground water colloid concentrations were derived from the Kaplan, et.al., 1994, studies and are based on colloid diameter approximation of 0.3 μm presented in Kaplan, et.al., 1994, and a set of sampled particle concentrations ranging from 5.0E+08 to 8.0E+08 particles/liter as presented in WSRC-TR-2006-00004. Assuming the colloids are approximately spherical, a colloid diameter of 0.3 μm in conjunction with along with a particle concentration of 8.0E+008 particles/liter, and particle density of 2.65 g/cc, a base-case ground water colloid concentration was derived for use in the simulations: $C_{colloids}$ = 3E-08 g/mL = 0.03 mg/L. Because the SRS study presented in Kaplan, et.al., 1994, is based on an F-Area study performed in a low pH ground water area, the potential for differences in colloid stability where higher pH ground water occurs is possible (Takala and Manninen, 2006). Because the colloid concentrations could be higher, which would increase the influence of the colloids in colloid facilitated transport, simulations assuming 3E-07 g/mL, 3E-06 g/mL, 3E-05 g/mL, and 3E-04 g/mL colloid concentrations were also performed. These simulations are meant to be informative since there is no site-specific basis for the parameter selection. This represents a 4 order of magnitude range in colloid concentration data assumed for SRS. For a perspective on variability, the range between the median and maximum values used for the alluvium ground water colloid concentrations in the Yucca Mountain Total System Performance Assessment was between 1E-07 g/mL and 2E-04 g/mL. [MDL-NBS-HS-000021]

The first simulation was based on the 2019 SDF Compliance Case adjusted by replacing the aquifer (sandy soil) K_ds with the effective K_ds as defined in Eq. 5.8-9 based on a colloid concentration of 3E-08 g/mL. As shown in Figure 5.8-114 and Figure 5.8-115, the influence of the colloid facilitated transport on the total dose was negligible. There are two reasons that no change is perceived. The first reason is the negligible release of sorbing radionuclides over a period of 40,000 years due to the effectiveness of the engineered barrier. The second reason can be seen in Table 5.8-41 is the negligible difference between the Compliance Case sandy soil K_ds and the colloid facilitated transport effective K_ds. As noted above simulations assuming a 3E-07 g/mL, 3E-06 mg/L, 3E-05 mg/L, and 3E-04 mg/L colloid concentrations were also performed. A review of Table 5.8-41 shows that the change in K_ds used in the model are imperceptible until the colloid concentration reaches 3E-06 g/mL. Even then, the influence would be inconsequential. As the colloid concentration reaches 3E-05 g/mL the influence on K_ds for highly sorbing radionuclides such as americium and plutonium becomes consequential, especially for species where the clayey soil K_d is much greater than for the sandy soil K_d. When the colloid concentration is set to 3E-04 g/mL the influence on K_ds for highly sorbing radionuclides becomes even greater, but as shown in Figure 5.8-116 and Figure 5.8-117, the influence of the colloid facilitated transport on the total dose for this case is still negligible even when the colloid concentration is as high as 3E-04 g/mL due to the low SDU release rates.

Figure 5.8-114: Comparison of Colloid Sensitivity Case ($C_{colloids}$=3E-08 g/mL) Total Dose Results with Compliance Case Total Dose Results over 1,000 Years

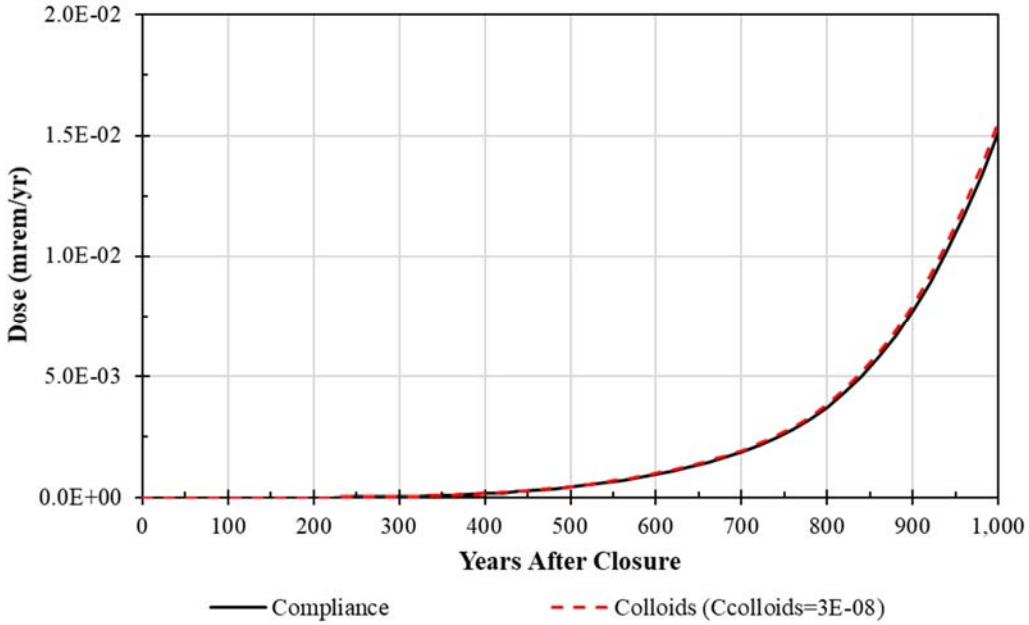

Figure 5.8-115: Comparison of Colloid Sensitivity Case ($C_{colloids}$=3E-08 g/mL) Total Dose Results with Compliance Case Total Dose Results over 40,000 Years

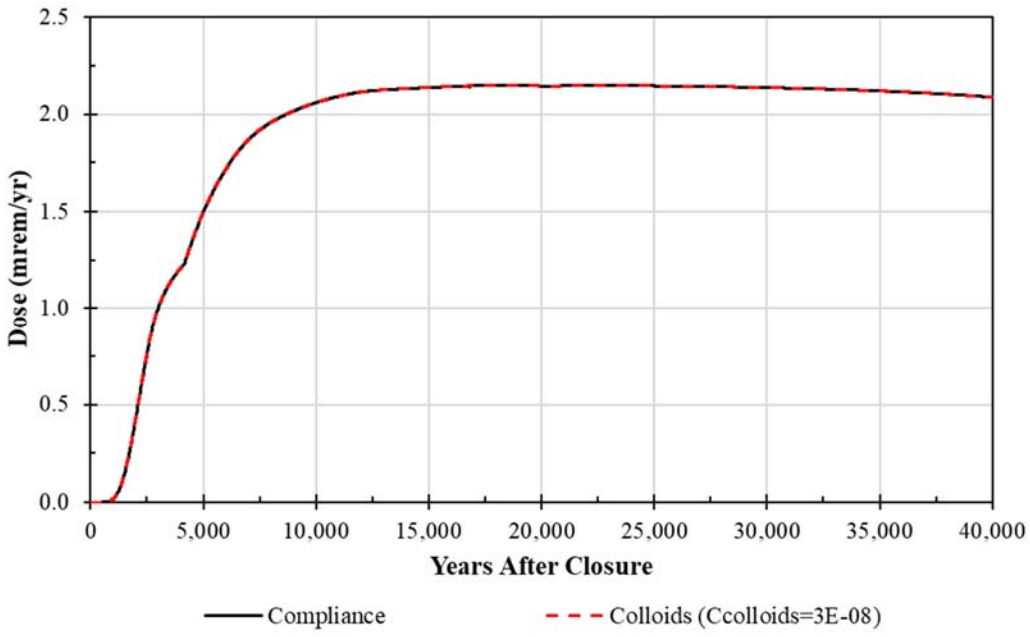

Figure 5.8-116: Comparison of Colloid Sensitivity Case ($C_{colloids}$=3E-04 g/mL) Total Dose Results with Compliance Case Total Dose Results over 1,000 Years

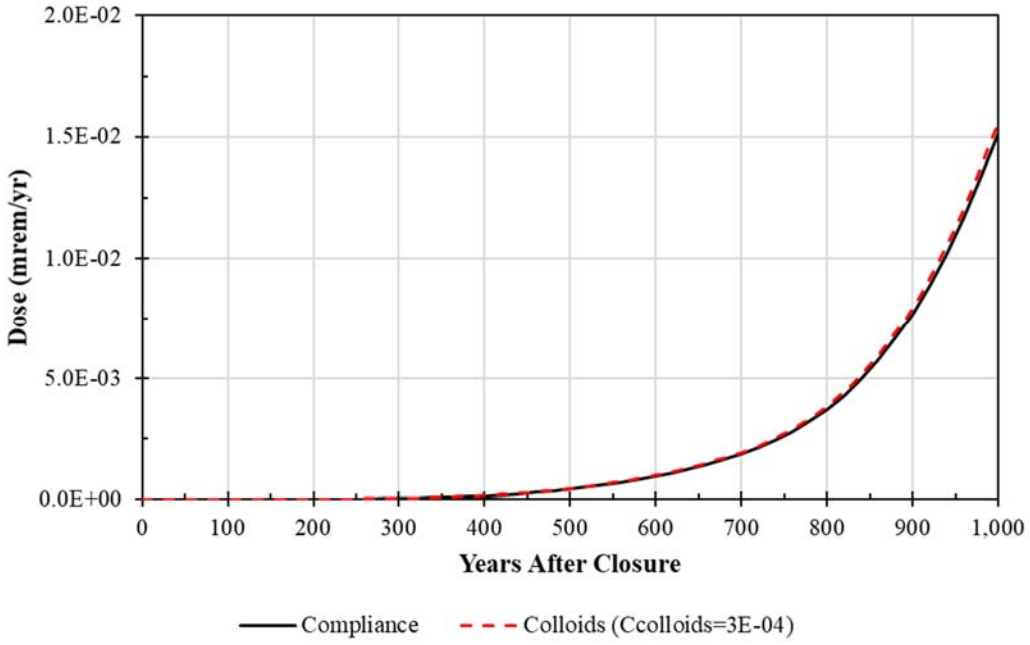

Figure 5.8-117: Comparison of Colloid Sensitivity Case ($C_{colloids}$=3E-04 g/mL) Total Dose Results with Compliance Case Total Dose Results over 40,000 Years

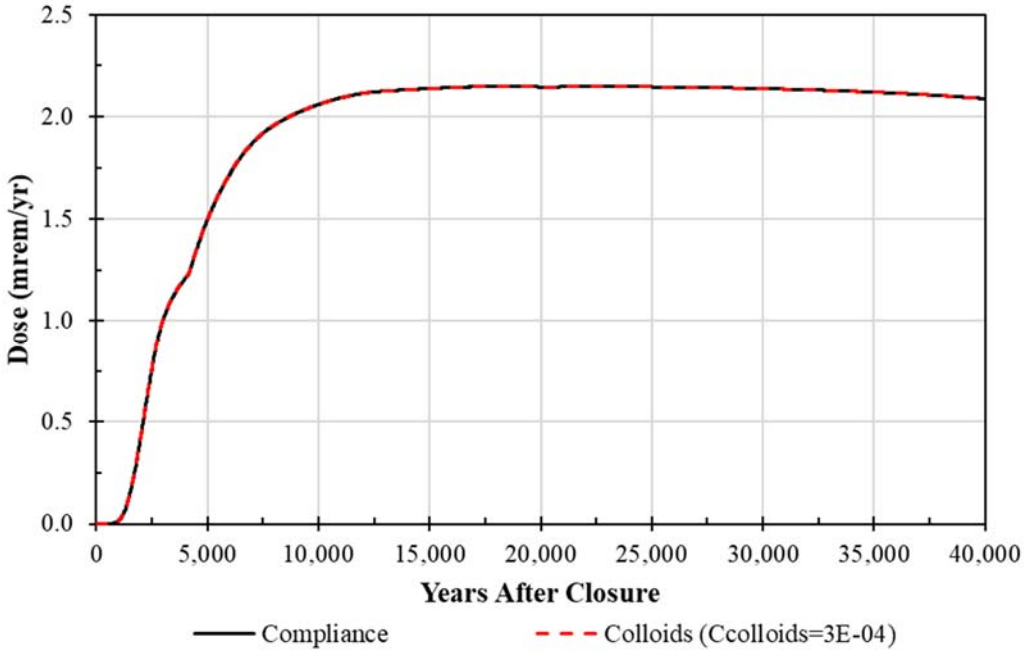

Table 5.8-41: Comparison of Effective K_ds Based on Assumed Colloid Concentrations

Radionuclide	Sandy Sediment K_d (mL/g)	Clayey Sediment K_d (mL/g)	$C_{colloids}$= 3E-08 (g/mL)	$C_{colloids}$= 3E-07 (g/mL)	$C_{colloids}$= 3E-06 (g/mL)	$C_{colloids}$= 3E-05 (g/mL)	$C_{colloids}$= 3E-04 (g/mL)
Ac-227	1000	9000	999.7	997.3	973.7	787.4	270.3
Al-26	1000	1000	1000.0	999.7	997.0	970.9	769.2
Am-241	1000	9000	999.7	997.3	973.7	787.4	270.3
Am-242m	1000	9000	999.7	997.3	973.7	787.4	270.3
Am-243	1000	9000	999.7	997.3	973.7	787.4	270.3
C-14	10	400	10.0	10.0	10.0	9.9	8.9
Cf-249	1000	9000	999.7	997.3	973.7	787.4	270.3
Cf-251	1000	9000	999.7	997.3	973.7	787.4	270.3
Cl-36	1	8	1.0	1.0	1.0	1.0	1.0
Cm-243	1000	9000	999.7	997.3	973.7	787.4	270.3
Cm-244	1000	9000	999.7	997.3	973.7	787.4	270.3
Cm-245	1000	9000	999.7	997.3	973.7	787.4	270.3
Cm-247	1000	9000	999.7	997.3	973.7	787.4	270.3
Co-60	40	100	40.0	40.0	40.0	39.9	38.8
Cs-135	10	50	10.0	10.0	10.0	10.0	9.9
Cs-137	10	50	10.0	10.0	10.0	10.0	9.9
Eu-152	1000	9000	999.7	997.3	973.7	787.4	270.3
Eu-154	1000	9000	999.7	997.3	973.7	787.4	270.3
H-3	0	0	0.0	0.0	0.0	0.0	0.0
I-129	1	3	1.0	1.0	1.0	1.0	1.0
K-40	5	30	5.0	5.0	5.0	5.0	5.0
Nb-93m	1000	1000	1000.0	999.7	997.0	970.9	769.2
Nb-94	1000	1000	1000.0	999.7	997.0	970.9	769.2
Ni-63	7	30	7.0	7.0	7.0	7.0	6.9
Np-237	3	9	3.0	3.0	3.0	3.0	3.0
Pa-231	3	9	3.0	3.0	3.0	3.0	3.0
Pb-210	2000	5000	1999.7	1997.0	1970.4	1739.1	800.0
Pt-193	7	30	7.0	7.0	7.0	7.0	6.9
Pu-238	650	6000	649.9	648.8	638.5	550.9	232.1
Pu-239	650	6000	649.9	648.8	638.5	550.9	232.1
Pu-240	650	6000	649.9	648.8	638.5	550.9	232.1
Pu-241	650	6000	649.9	648.8	638.5	550.9	232.1
Pu-242	650	6000	649.9	648.8	638.5	550.9	232.1
Pu-244	650	6000	649.9	648.8	638.5	550.9	232.1
Ra-226	30	200	30.0	30.0	30.0	29.8	28.3
Ra-228	30	200	30.0	30.0	30.0	29.8	28.3
Rn-222	0	0	0.0	0.0	0.0	0.0	0.0
Se-79	1000	1000	1000.0	999.7	997.0	970.9	769.2
Sm-151	1000	9000	999.7	997.3	973.7	787.4	270.3
Sn-126	2000	5000	1999.7	1997.0	1970.4	1739.1	800.0
Sr-90	5	20	5.0	5.0	5.0	5.0	5.0
Tc-99	0.6	1.8	0.6	0.6	0.6	0.6	0.6
Th-229	900	2000	900.0	899.5	894.6	849.1	562.5
Th-230	900	2000	900.0	899.5	894.6	849.1	562.5
Th-232	900	2000	900.0	899.5	894.6	849.1	562.5
U-232	300	400	300.0	300.0	299.6	296.4	267.9
U-233	300	400	300.0	300.0	299.6	296.4	267.9
U-234	300	400	300.0	300.0	299.6	296.4	267.9
U-235	300	400	300.0	300.0	299.6	296.4	267.9
U-236	300	400	300.0	300.0	299.6	296.4	267.9
U-238	300	400	300.0	300.0	299.6	296.4	267.9
Zr-93	900	2000	900.0	899.5	894.6	849.1	562.5

5.8.9.7 Air Pathway (Dose and Radon Release) Sensitivity Cases

Section 5.3 discusses the results of the airborne releases of radionuclides modeling. A number of assumptions were made during the development of the airborne release model. Each assumption increased the inherent uncertainty of the results. To better assess this uncertainty, a number of sensitivity cases have been developed.

The first sensitivity case considers the influence of inventory uncertainty. To assess inventory uncertainty, the inventory values based on Best Estimate (i.e., as used in the Realistic Case) and those based on Conservative Estimate (i.e., as used in the Pessimistic Case) were used. Figure 5.8-118 shows the results from running the model using Best Estimate and Conservative Estimate inventories. Note that the results are scaled to show detail at early times. Specifically, these results show peaks occurring within the 100-year institutional control period. While the different inventory assumptions do influence the magnitude of the dose results, the total air pathway dose remains negligible.

Figure 5.8-118: Air Pathways Sensitivity – Evaluation of Assumed Inventory Values

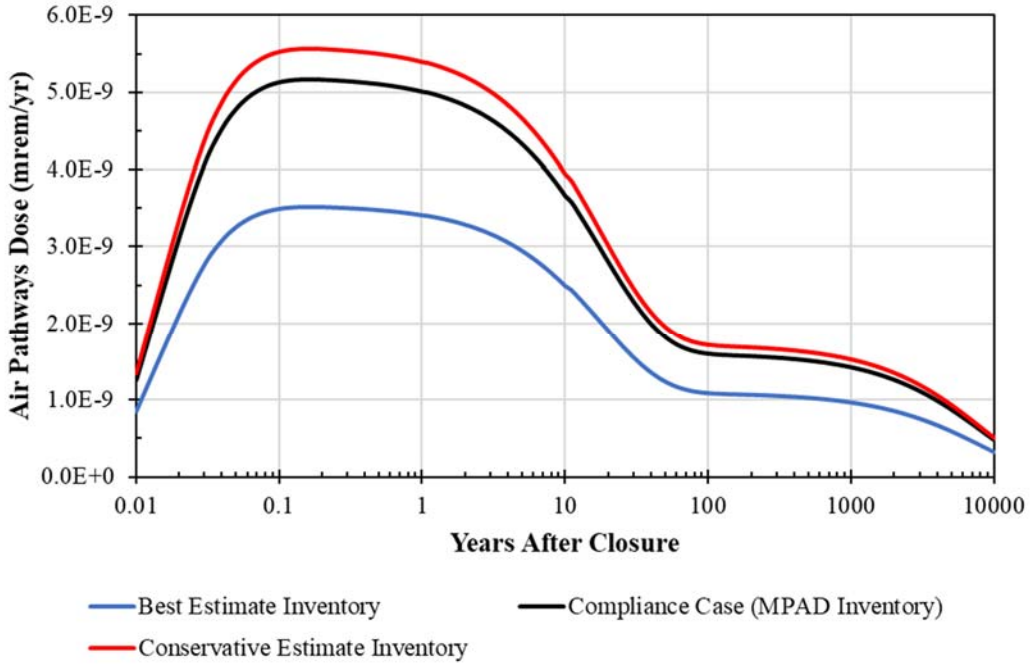

The next sensitivity case considers uncertainty relative to saturation. For Compliance Case modeling, it was assumed that all the pore spaces within the roof and in all the layers above the roof were fully desaturated. While this assumption promotes faster fluxes, it does not reflect expected saturation conditions. From the Compliance Case used for infiltration modeling (see Section 4.4.1), the MPAD saturation levels may be extracted for backfill, soils, and the erosion barrier. From the Compliance Case used for the Vadose Zone Flow Model (see Section 4.4.4), the MPAD saturation levels may be extracted for saltstone, clean cap grout, the roof, and the lower sand drainage layer. Applying these saturation levels to each of the modeled layers provides a more realistic result. This result is illustrated in Figure 5.8-119 (gold, dashed curve) and shows that after approximately 50

years, the results from the MPAD saturation case are nearly identical to that of the Compliance Case (black curve).

Figure 5.8-119 also looks at other conditions to provide additional insights. As a worst case condition for saturation, every single material (including the saltstone and clean cap layer), was assumed to be fully desaturated (dark red curve). As an intermediate case, every single material except for saltstone was assumed to be fully desaturated (light green, dashed curve). The difference between this result and the Compliance Case demonstrates the significance of saturation of the clean cap materials when all the layers above are desaturated. These desaturation conditions both result in dose peaks within the first year of the simulation of approximately 16.6 mrem/yr. While this value is exceeds the 10 mrem/yr performance objective for the air pathway dose, it does not represent realistic conditions given the amount of annual rainfall that occurs at SRS and the properties of saltstone. Further, under such dry conditions, ground water transport would be expected to decrease.

Figure 5.8-119: Air Pathways Sensitivity – Evaluation of Saturation Conditions

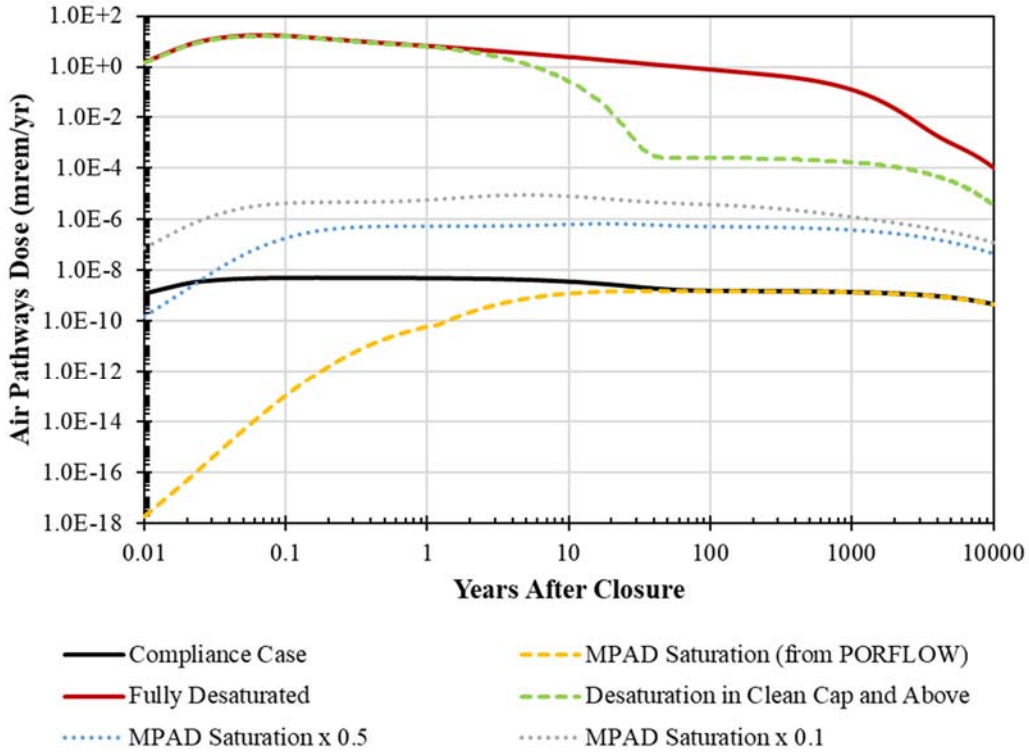

Finally, the results from two other sensitivity cases are provided in Figure 5.8-119: "MPAD Saturation × 0.5" and "MPAD Saturation × 0.1." These two cases use the MPAD saturation values but apply a multiplier to the saturation levels for every material. These results show that even if the saturation conditions within every material were simultaneously 90% drier than expected (i.e., × 0.1), the resulting air pathways dose would

peak at less than 1E-05 mrem/yr. This provides confidence that despite uncertainty, the dose contributions from airborne releases are unlikely to become significant.

The next set of sensitivity cases analyze the uncertainty associated with the Henry's Law constants. These parameters define the partitioning in the air-to-liquid phase for air transport and are based on pore water compositions. For Compliance Case modeling, the Henry's Law constants for saltstone are based on values developed based on the chemistry of saltstone (SRNL-STI-2008-00447), while the SDU concrete assume the chemical conditions for oxidizing region III and the soils assume chemical "Condition A" (SRNL-TR-2010-00096). The exception to this is radon, which always applies a derived value of 9.244E-03 mol/atm-L (SRR-CWDA-2018-00025). These conditions are described in Section 4.4.7.

There is some uncertainty associated with the chemical environments assumed for the Compliance Case. To assess the assumed values, two analyses were performed. In the first analysis, all of the cementitious materials (i.e., SDU concrete, clean cap grout, and saltstone) were assumed to have the same set of Henry's Law constants regardless of chemical environment. This assumed set of Henry's Law constants was varied for each sensitivity case. The results are shown in Figure 5.8-120. As shown, only one case yielded higher dose results than the Compliance Case: the case that assumes all cementitious materials (including saltstone) have oxidizing region III conditions (magenta curve). Because the saltstone-specific Henry's Law constants were developed based on a geochemical analysis of saltstone material, the oxidizing region III values are not appropriate to assume for saltstone and clean cap grout. Despite the variability of these dose results, the peak values are always well below the performance objectives.

Figure 5.8-121 presents the results for a similar analysis of the Henry's Law constants assumed in the soil materials. There four possible conditions: Condition A, B, C, and D for which data was developed for SRS soils (see Table 4.4-99). Figure 5.8-121 shows that all four conditions yeilded very similar results, with Condition A producing the highest fluxes. Because Condition A is assumed for the Compliance Case, there is no risk associated with this assumption.

The final sensitivity analysis performed for the air pathway doses evaluates the impact of the roof and closure cap thickness. For these sensitivity cases, the thicknesses of either the closure cap layers or the roof (or both the closure cap layers and the roof) were multiplier by a factor of 1.0E-08, resulting in materials of negligible thicknesses. As shown in Figure 5.8-122, the results of this analysis only changed the values at very, very early times and had a negligible impact on the magnitude of the dose peaks. This indicates that the material properties (i.e., saturation and Henry's Law constants) are much more important than the thicknesses of the materials.

Figure 5.8-120: Air Pathways Sensitivity – Evaluation of Henry's Law Constants for Various Cementitious Chemical Conditions

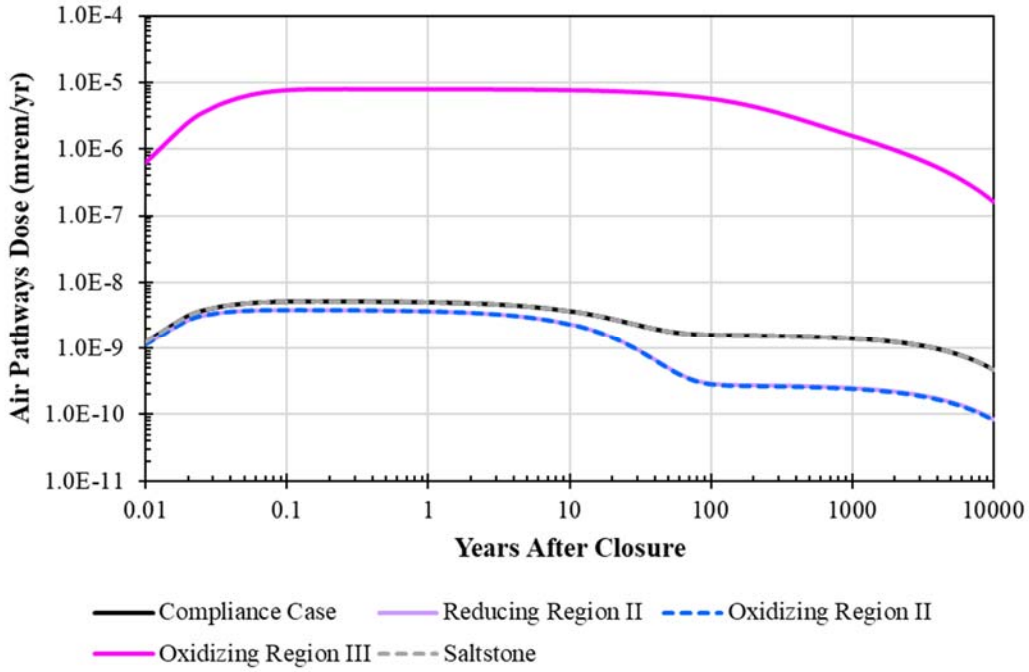

Figure 5.8-121: Air Pathways Sensitivity – Evaluation of Henry's Law Constants for Various Soil Conditions

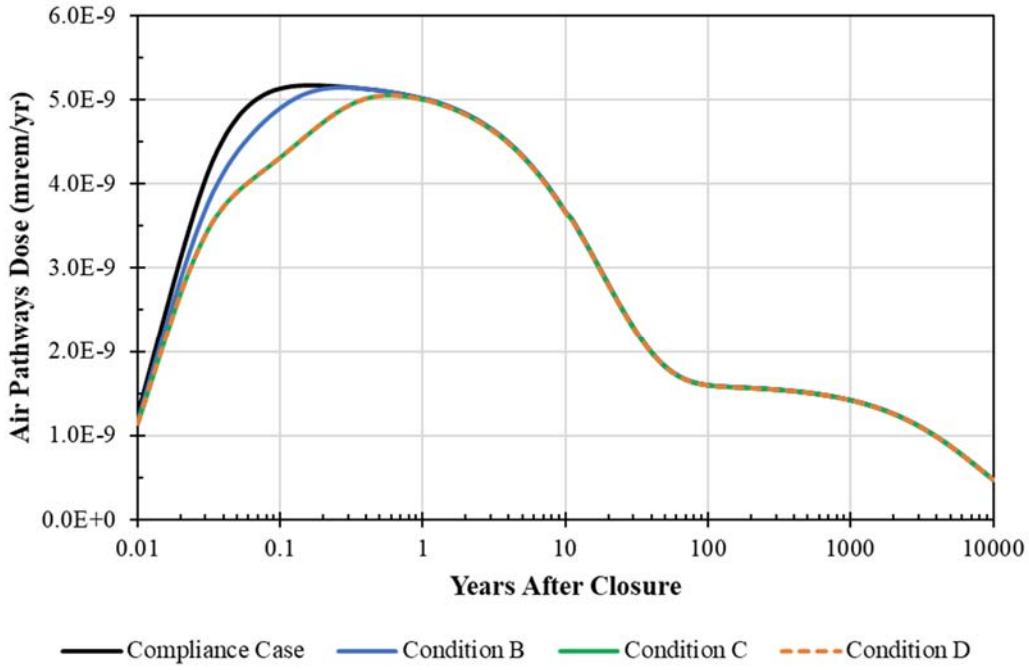

Figure 5.8-122: Air Pathways Sensitivity – Evaluation of Closure Cap and Roof Thicknesses

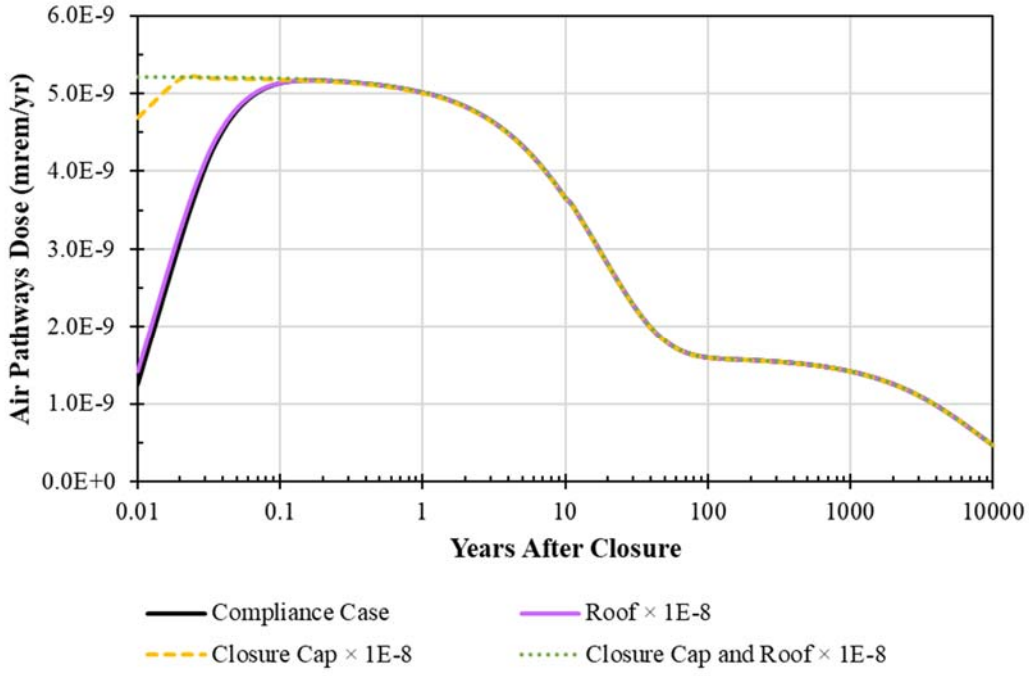

Table 5.8-42 provides a summary of the peak doses resulting from each of the air pathways sensitivity cases.

Similarly, the peak radon flux was also determined from each of the sensitivity cases, as provided in Table 5.8-43. Note that the Henry's Law Constant for radon is the same value in every sensitivity case, so the results from those sensitivity cases are identical to the Compliance Case and are not presented in this table. The highest radon flux from any of these cases was 0.03 pCi/m^2/sec, well within the performance objective of 20 pCi/m^2/sec.

Table 5.8-42: Air Pathways Sensitivities – Summary of Peak Doses

Sensitivity Cases	Compliance Period Result		Performance Period Result	
	Peak Dose (mrem/yr)	Year of Peak Dose	Peak Dose (mrem/yr)	Year of Peak Dose
Inventory Comparisons				
Realistic Inventory	3.5E-09	<1	3.5E-09	<1
Compliance Case (uses MPAD Inventory)	*5.2E-09*	*<1*	*5.2E-09*	*<1*
Pessimistic Inventory	5.6E-09	<1	5.6E-09	<1
Saturation Comparisons				
Compliance Case (Desaturated roof and above)	*5.2E-09*	*<1*	*5.2E-09*	*<1*
Desaturated in Clean Cap and Above	16.6	<1	16.6	<1
Fully Desaturated	16.6	<1	16.6	<1
MPAD Saturation (Uses modeled saturation data)	1.6E-09	38	1.6E-09	38
MPAD Saturation × 0.5	6.7E-07	18	6.7E-07	18
MPAD Saturation × 0.1	9.3E-06	4.9	9.3E-06	4.9
Henry's Law Constants for Cementitious Materials				
Compliance Case (uses saltstone values for saltstone and clean cap grout, Oxidizing Region III for SDU concrete)	*5.2E-09*	*<1*	*5.2E-09*	*<1*
Reducing Region II	3.9E-09	<1	3.9E-09	<1
Oxidizing Region II	3.9E-09	<1	3.9E-09	<1
Oxidizing Region III	8.0E-06	<1	8.0E-06	<1
Saltstone	5.2E-09	<1	5.2E-09	<1
Henry's Law Constants for Soils				
Compliance Case (uses Condition A)	*5.2E-09*	*<1*	*5.2E-09*	*<1*
Condition B	5.1E-09	<1	5.1E-09	<1
Condition C	5.1E-09	<1	5.1E-09	<1
Condition D	5.1E-09	<1	5.1E-09	<1
Layer Thickness Comparison				
Compliance Case (Full Thickness)	*5.2E-09*	*<1*	*5.2E-09*	*<1*
Closure Cap × 1.0E-08	5.2E-09	<1	5.2E-09	<1
Roof × 1.0E-08	5.2E-09	<1	5.2E-09	<1
Closure Cap and Roof × 1.0E-08	5.2E-09	<1	5.2E-09	<1

Table 5.8-43: Air Pathways Sensitivities – Peak Radon Release

Sensitivity Cases	Compliance Period Result		Performance Period Result	
	Peak Flux (pCi/m²/s)	Year of Peak Flux	Peak Flux (pCi/m²/s)	Year of Peak Flux
Inventory Comparisons				
Realistic Inventory	1.1E-05	1,000	5.0E-04	10,000
Compliance Case (uses MPAD Inventory)	*1.6E-05*	1,000	*7.3E-04*	10,000
Pessimistic Inventory	1.7E-05	1,000	7.8E-04	10,000
Saturation Comparisons				
Compliance Case (Desaturated roof and above)	*1.6E-05*	1,000	*7.3E-04*	10,000
Desaturated in Clean Cap and Above	6.6E-04	1,000	3.0E-02	10,000
Fully Desaturated	6.6E-04	1,000	3.0E-02	10,000
MPAD Saturation (Uses modeled saturation data)	2.1E-11	1,000	9.5E-10	10,000
MPAD Saturation × 0.5	5.6E-04	1,000	2.5E-02	10,000
MPAD Saturation × 0.1	6.5E-04	1,000	2.9E-02	10,000
Layer Thickness Comparison				
Compliance Case (Full Thickness)	*1.6E-05*	1,000	*7.3E-04*	10,000
Closure Cap × 1.0E-08	1.4E-04	1,000	6.4E-03	10,000
Roof × 1.0E-08	2.2E-05	1,000	1.0E-03	10,000
Closure Cap and Roof × 1.0E-08	1.8E-04	1,000	8.2E-03	10,000

5.8.9.8 Acid Rain Sensitivity

Contaminant releases from saltstone and SDU concrete are heavily dependent on the chemical environment of the pore solution (SRNL-TR-2008-00283). The Contaminant Release Model (discussed in Section 4.4.3) estimates the number of pore volume exchanges required for the pore solution chemistry to change. The pH and Eh chemical transitions for saltstone were determined using the Contaminant Release Model, which considered three different infiltrates: ground water at pH 5.4, ground water equilibrated with excess calcite at a pH of 8.04, and ground water equilibrated with excess calcium silicate hydrate (CSH) at a pH of 11.04. Note as a modeling simplification, only ground water at pH 5.4 was used for simulating SDU concrete in the Contaminant Release Model.

Results from the Contaminant Release Model revealed the fastest chemical transition times (i.e., fewest number of pore volume exchanges needed for a chemical transition to occur) are achieved for saltstone when using either the pH 5.4 ground water infiltrate or the ground water infiltrate equilibrated with excess calcite at a pH of 8.04 (Section 4.4.3). For simulations using the ground water equilibrated with excess CSH at a pH of 11.04, the number of pore volume exchanges needed for the Eh transition is slightly higher (i.e., 15 additional pore volume exchanges were needed, see Table 3.1 of SRNL-STI-2018-00586). Given this information, it is reasoned that infiltrate from acid rain with an assumed pH of 4 would not drastically change the chemical transition times for saltstone. Furthermore, it should be noted that the number of pore volumes required to transition saltstone and SDU concrete from reducing to oxidizing conditions (> 500 pore volume exchanges) per Section 4.4.3, far exceeds the number of pore volume exchanges predicted to occur within 100,000 years (see Section 7.1). Hence, even if the acid rain infiltrate did reduce the number of pore volume exchanges needed for a chemical transition to occur,

that new number is still anticipated to far exceed the number of pore volume exchanges predicted to occur within 100,000 years.

Regarding cementitious degradation, only carbonation rates are expected to be impacted by acid rain. A more acidic infiltrate will result in less carbonate present in the aqueous phase (i.e., $[H_2CO_3] + [HCO_3^-] + [CO_3^{2-}]$), which yields a lower rate constant (Eq. 4.4-13 from Section 4.4.2). The lower rate constant results in a longer time needed for the reaction front to penetrate a given depth (Eq. 4.4-17 and Eq. 4.4-18, Section 4.4.2). Hence, a lower pH infiltrate would result in longer degradation times with respect to carbonation. It should be noted in most instances, sulfate attack is the dominant degradation mechanism in SDU concrete (Section 4.4.2); therefore, slight changes in the carbonation rate constant are not expected to significantly impact cementitious degradation rates.

Based on this interpretation of the various system components and chemical conditions, which might be impacted by acid rain, the expected influence from acid rain is expected to be negligible and no explicit acid rain simulation was developed.

5.9 Updated ALARA Analysis

5.9.1 ALARA Process

The DOE As Low As Reasonably Achievable (ALARA) process helps ensure that optimization techniques will be integrated into the design and analyses of programmatic options necessary for the protection of the public and the environment in accordance with the requirements of DOE O 458.1 (*Radiation Protection of the Public and the Environment)*. As much as possible, DOE sites should consider using existing processes, programs or documentation for addressing the provisions of DOE O 458.1 in the development and implementation of the ALARA requirements. SRS has a well-documented ALARA program and processes established in company level policies and procedures. [WSRC-SA-2003-00001]

As applied by DOE, ALARA is not a level or limit to be achieved in controlling radiation exposures or doses, but rather a process used to ensure that appropriate factors are considered in making decisions that could affect protection against radiation. Under DOE O 458.1 a documented ALARA process must be implemented to optimize control and management of radiological activities so that doses to members of the public (both individual and collective) and releases to the environment are kept as low as reasonably achievable. The ALARA process must be applied to DOE activities and the design or modification of facilities that expose the public or the environment, no matter how small the dose. In all cases, the scope and detail of the ALARA analysis should be commensurate with the potential benefit of the dose reduction. [DOE-HDBK-1215-2014]

DOE O 458.1 requires that the ALARA process use a graded approach (e.g., a graded level of control and oversight) to ensure that doses to the public are low and any decisions made as a result of the process be both beneficial and cost-effective. DOE has defined the graded approach for nuclear safety management (10 CFR Part 830.3) as the process of ensuring that the level of analysis, documentation, and actions used to comply with a requirement are commensurate with:

- The relative importance to safety, safeguards, and security;
- The magnitude of any hazard involved;
- The life cycle stage of a facility;
- The programmatic mission and characteristics of a facility;
- The relative importance of radiological and non-radiological hazards; and
- Any other relevant factor.

ALARA is a self-limiting system and thus the level of analysis should be commensurate with the estimated collective dose to the exposed population; higher estimated collective doses require more rigor in the analysis. [DOE-HDBK-1215-2014] For this SDF PA, an updated ALARA Analysis was performed as appropriate (see Section 5.9.2). The updated analysis considers the relative hazards associated with the SDF as compared to other nuclear operations when considering the need for design or other modifications of disposal facilities or other closure activities.

5.9.2 ALARA Analysis

The ALARA process, as described in Section 5.9.1, should be used to optimize the disposal facility performance by applying a graded approach to optimization of the disposal system for maintaining doses to members of the public (both individual and collective) and releases to the environment as low as reasonably achievable, per DOE O 458.1 and as described in *DOE Handbook Optimizing Radiation Protection of the Public and the Environment for Use with DOE O 458.1, ALARA Requirements* (DOE-HDBK-1215-2014). This analysis should reflect a graded approach recognizing the relative hazards associated with waste disposal as compared to other nuclear operations when considering the need for design or other modifications of disposal facilities or other closure activities. [DOE-STD-5002-2017]

A review of the MOP dose results from Section 5.5 showed an insignificant dose relative to the performance objective within the Compliance Period. Examination of Table 5.5-1 shows the maximum peak dose of 8.0E-03 mrem/yr relative to the performance objective of 25 mrem/yr, more than three orders of magnitude difference.

Similarly, the total air pathway dose results in Section 5.3 showed an insignificant dose relative to the performance objectives. The air pathway dose result was 5.2E-09 mrem/yr relative to the performance objective of 25 mrem/yr and the peak radon flux was 1.6E-05 pCi/m^2/s relative to a performance objective of 20 pCi/m^2/s.

In addition, sensitivity analyses show dose results less than the performance objective within the Compliance Period. A variety of analyses were performed considering the impact of different aspects of the closure state, all of which showed dose results less than performance objectives. One sensitivity analysis of note was the variation of the infiltration rate which is controlled by the closure cap. Closure cap sensitivity analysis (Section 5.8.2.4) shows a peak of 3.8 mrem/yr (soil-only closure cap). Therefore, the impact of the closure cap design reduces the peak dose within the Compliance Period by approximately three orders of magnitude during the Compliance Period. This is a significant reduction, diminishing the resulting dose to insignificant levels.

Based on the insignificance of the dose results within the Compliance Period relative to the performance objectives, consideration of additional alternatives is expected to provide negligible benefit. Therefore, further ALARA optimization analysis is not necessary for the SDF PA.

6 RESULTS OF IHI ANALYSIS

Section 6.1 provides ground water concentration data from along the SDF 1-meter boundary and from individual Inadvertent Human Intruder (IHI) wells. These concentrations are estimated from the Aquifer Transport Model (Section 4.4.6) and are used to determine the doses to the IHI for the various IHI exposure scenarios:

- Acute IHI Well Driller (with Soil Drill Cutting Inventory) Scenario,
- Acute IHI Well Driller (with SDU Drill Cutting Inventory) Scenario,
- Chronic IHI at the 1-Meter Well Scenario (with Soil Drill Cutting Inventory),
- Chronic IHI at the 1-Meter Well Scenario (with No Drill Cutting Inventory),
- Chronic IHI at the 1-Meter Well Scenario (with SDU Drill Cutting Inventory), and
- Chronic IHI at Selected Wells Scenario (with Soil Drill Cutting Inventory).

The resulting doses from these exposure scenarios are provided in Sections 6.3, 6.4, and 6.5.

6.1 Concentrations at the SDF 1-Meter Boundary and the IHI Wells

The purpose of this section is to present the peak ground water concentrations for individual radionuclides and chemicals along the SDF 1-meter boundary and at the individual IHI wells, within 1,000 years and 10,000 years of SDF closure. The results presented here are for the Compliance Case only. The 1-meter boundary and each of the IHI wells are shown on Figure 6.1-1. The coloring of the table headings (below) correspond to IHI Well Identifiers provided in Table 6.1-1.

Table 6.1-1: Summary of Select Wells for Chronic IHI Evaluation

IHI Well Identifier	Color in Figure 6.1-1	Description of Location	Rationale for Selection
IHI Well 1	Red	Adjacent to SDU 12	Evaluate SDU 11 and SDU 12 plume overlap
IHI Well 2	Blue	Adjacent to SDU 8	Evaluate SDU 8 and SDU 6 plume overlap
IHI Well 3	Green	Adjacent to SDU 5A	Evaluate the 150-foot Diameter SDUs with SDU 6 plume overlap
IHI Well 4	Orange	Adjacent to SDU 9	Evaluate SDU 9 and SDU 7 plume overlap
IHI Well 5	Yellow	Adjacent to SDU 2A	Evaluate SDU 2A and SDU 7 plume overlap
IHI Well 6	Gray	Adjacent to SDU 4	Evaluate SDU 1 and SDU 4 plume overlap
IHI Well 7	Purple	Adjacent to SDU 10	Evaluate the unique location of SDU 10

The peak radionuclide concentrations in 1,000 years are provided in Table 6.1-2, the peak chemical concentrations in 1,000 years are provided in Table 6.1-3, the peak radionuclide concentrations in 10,000 years are provided in Table 6.1-4, and the peak chemical concentrations in 10,000 years are provided in Table 6.1-5.

These peak concentrations are compared against the applicable maximum contaminant levels (MCLs). The MCL values for beta and photon emitters are derived based on a 4 mrem/yr beta-gamma dose as described in EPA 815-R-02-001. If the sum of fractions for beta and photon emitters exceeds 1, then the beta-gamma MCL is exceeded. The peak values for all 1-meter wells and IHI wells show no radionuclides or chemicals exceed an MCL or the beta-gamma MCL fraction in 1,000 years.

Figure 6.1-1: Well Locations for the Chronic IHI at Selected Wells Scenario

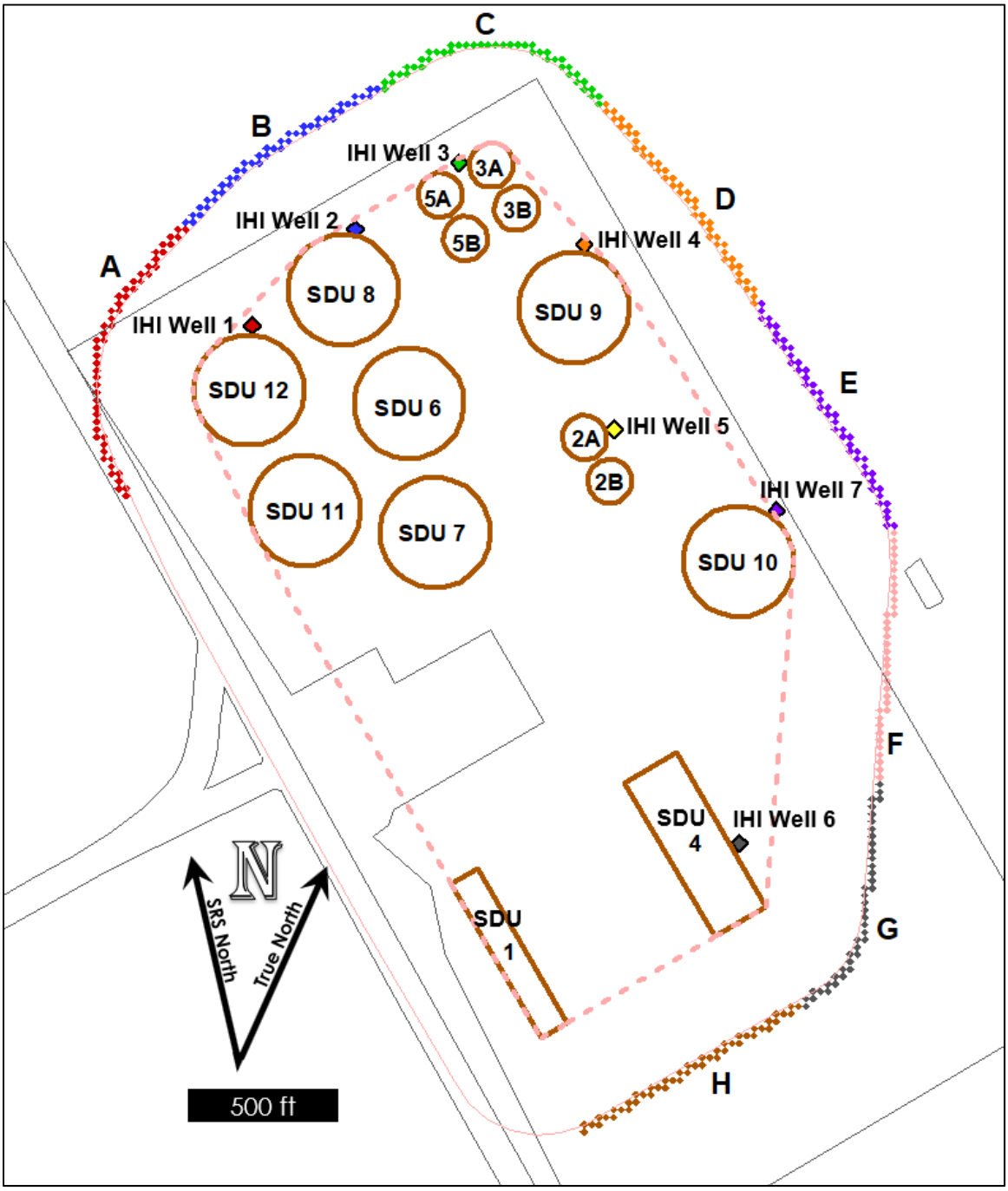

Note: The 1-meter facility boundary is indicated by pink dashed line. IHI wells are placed adjacent to and downgradient of SDUs in transport modeling.

For the 1-meter wells in 10,000 years, I-129 and NO_3 exceed their respective MCL. For I-129, the MCL of 1 pCi/L is exceeded with a peak value of 3.7 pCi/L and NO_3 exceeded the MCL of 10,000 µg/L with a peak value of 5.3E+04 µg/L. For the individual IHI wells, I-129 exceeded the MCL in IHI Wells 1, 2, 3, 4, and 6 within 10,000 years with the maximum I-129 concentrations ranging from 1.8 pCi/L to 3.2 pCi/L. NO_3 exceeded the MCL in all the IHI wells within 10,000 years, with

maximum NO_3 concentrations ranging from 2.1E+04 µg/Lto 4.6E+04 µg/L. Since these I-129 values exceed the MCL, they also cause the sum of beta-gamma MCL fractions for their respective wells to exceed 1. For I-129, the MCL of 1 pCi/L is exceeded with a peak value of 3.7 pCi/L.

The only other radionuclide that appears greater than 0.1% of its respective MCL is Tc-99 in 10,000 years. The peak value for Tc-99 in 10,000 years at the 1-meter well is 570 pCi/L (vs an MCL of 900 pCi/L).

The peak I-129 dose associated with 3.7 pCi/L (i.e., 1.1 mrem/yr) is less than the 4 millirem/year drinking water standard when calculated using an updated I-129 drinking water dose calculation methodology. This alternative methodology multiplies the peak concentration by both an updated water ingestion pathway effective dose factor (EDF) and assuming an ingestion rate of 2 liters of water consumed per day (3.7 pCi/L × 0.202 L-mrem/pCi/pCi-yr (EDF) × (2.0 L/day ÷ 1.4 L/day) = 1.1 mrem/yr). This drinking water dose calculation methodology was adapted from the alternative to the basic SCDHEC R.61-58 methodology in the *Industrial Wastewater Closure Module for Liquid Waste Tank 16H H-Area Tank Farm Savannah River Site* (SRR-CWDA-2013-00091), which received SCDHEC approval and EPA concurrence.

The drinking water standard for beta particle and photon radioactivity is specified in the *South Carolina State Primary Drinking Water Regulation* which states that "The average annual concentration of beta particle and photon radioactivity from man-made radionuclides in drinking water must not produce an annual dose equivalent to the total body or any internal organ greater than 4 millirem/year (mrem/year)." [SCDHEC R.61-58] This total body or organ dose equivalent comparison to the standard is calculated on the basis of two (2) liters per day drinking water intake. The EPA document *Radionuclides in Drinking Water: A Small Entity Compliance Guide* outlines the requirements for beta particle and photon emitters. [EPA 815-R-02-001] The Compliance Guide contains a table providing the derived concentrations (pCi/L) of beta and photon emitters in drinking water that yield an effective dose equivalent (EDE) of 4 mrem/yr as defined in the *Maximum Permissible Body Burdens and Maximum Permissible Concentrations of Radionuclides in Air and in Water for Occupational Exposure, National Bureau of Standards (NBS) Handbook 69*. [NBS Handbook 69] Rather than using the 168-hour data listed in NBS Handbook 69, the alternative drinking water dose calculation methodology presented in the *Industrial Wastewater Closure Module for Liquid Waste Tank 16H H-Area Tank Farm Savannah River Site* (SRR-CWDA-2013-00091) used the most current water ingestion pathway dose conversion factors from *Dose Calculation Methodology for Liquid Waste Performance Assessments at the Savannah River Site* (SRR-CWDA-2013-00058).

Note that these peak values are from the Compliance Case which incorporates a number of assumptions to ensure greater defensibility. The results from the Realistic Case, which is the modeling case based on best estimate assumptions, typically show concentrations for I-129 and Tc-99 that are approximately an order of magnitude lower than the results from the Compliance Case (i.e., less than the applicable MCL values). It should also be noted that these peak concentrations are from the relatively shallow LAZ. It is expected that any future wells drilled for drinking water purposes would more likely be drilled into deeper aquifer zones (e.g., the GAU), where concentrations are expected to be much lower.

Table 6.1-2: Radiological Concentrations for All Aquifers for All Wells at 1 Meter and Individual Intruder Wells in 1,000 Years

Rad	MCL (pCi/L)	All 1-Meter Wells		IHI Well 1		IHI Well 2		IHI Well 3	
		Conc. (pCi/L)	Year of Peak	Conc. (pCi/L)	Year of Peak	Conc. (pCi/L)	Year of Peak	Conc. (pCi/L)	Year of Peak
Ac-227	N/A	<1E-20	1,000	<1E-20	1,000	<1E-20	1,000	<1E-20	1,000
Al-26	N/A	<1E-20	1,000	<1E-20	1,000	<1E-20	1,000	<1E-20	1,000
Am-241	Total α	<1E-20	1,000	<1E-20	1,000	<1E-20	1,000	<1E-20	1,000
Am-242m	Total α	<1E-20	1,000	<1E-20	1,000	<1E-20	1,000	<1E-20	1,000
Am-243	Total α	<1E-20	1,000	<1E-20	1,000	<1E-20	1,000	<1E-20	1,000
C-14	2,000	<1E-20	1,000	<1E-20	1,000	<1E-20	1,000	<1E-20	1,000
Cf-249	Total α	<1E-20	1,000	<1E-20	1,000	<1E-20	1,000	<1E-20	1,000
Cf-251	Total α	<1E-20	1,000	<1E-20	1,000	<1E-20	1,000	<1E-20	1,000
Cl-36	700	6.8E-03	1,000	2.1E-04	1,000	1.9E-04	1,000	3.1E-05	1,000
Cm-243	Total α	<1E-20	580	<1E-20	1,000	<1E-20	1,000	<1E-20	1,000
Cm-244	Total α	<1E-20	360	<1E-20	1,000	<1E-20	1,000	<1E-20	990
Cm-245	Total α	<1E-20	1,000	<1E-20	1,000	<1E-20	1,000	<1E-20	1,000
Cm-247	Total α	<1E-20	1,000	<1E-20	1,000	<1E-20	1,000	<1E-20	1,000
Co-60	100	<1E-20	100	<1E-20	570	<1E-20	340	<1E-20	290
Cs-135	900	5.4E-18	1,000	<1E-20	1,000	<1E-20	1,000	<1E-20	1,000
Cs-137	200	<1E-20	590	<1E-20	1,000	<1E-20	1,000	<1E-20	1,000
Eu-152	200	<1E-20	270	<1E-20	960	<1E-20	880	<1E-20	750
Eu-154	60	<1E-20	180	<1E-20	610	<1E-20	570	<1E-20	490
H-3	20,000	2.6E-07	150	2.2E-10	210	2.0E-10	210	1.5E-11	230
I-129	1	2.0E-02	1,000	6.9E-04	1,000	6.3E-04	1,000	2.0E-04	1,000
K-40	N/A	1.1E-16	1,000	<1E-20	1,000	<1E-20	1,000	<1E-20	1,000
Nb-93m	1,000	<1E-20	1,000	<1E-20	1,000	<1E-20	1,000	<1E-20	1,000
Nb-94	N/A	<1E-20	1,000	<1E-20	1,000	<1E-20	1,000	<1E-20	1,000
Ni-63	50	<1E-20	1,000	<1E-20	1,000	<1E-20	1,000	<1E-20	1,000
Np-237	Total α	1.9E-18	1,000	<1E-20	1,000	<1E-20	1,000	<1E-20	1,000
Pa-231	Total α	<1E-20	1,000	<1E-20	1,000	<1E-20	1,000	<1E-20	1,000
Pb-210	N/A	<1E-20	1,000	<1E-20	1,000	<1E-20	1,000	<1E-20	1,000
Pt-193	3,000	<1E-20	890	<1E-20	1,000	<1E-20	1,000	<1E-20	1,000
Pu-238	Total α	<1E-20	1,000	<1E-20	1,000	<1E-20	1,000	<1E-20	1,000
Pu-239	Total α	<1E-20	1,000	<1E-20	1,000	<1E-20	1,000	<1E-20	1,000
Pu-240	Total α	<1E-20	1,000	<1E-20	1,000	<1E-20	1,000	<1E-20	1,000
Pu-241	300	<1E-20	1,000	<1E-20	1,000	<1E-20	1,000	<1E-20	1,000
Pu-242	Total α	<1E-20	1,000	<1E-20	1,000	<1E-20	1,000	<1E-20	1,000
Pu-244	Total α	<1E-20	1,000	<1E-20	1,000	<1E-20	1,000	<1E-20	1,000
Ra-226	Total α /Ra	<1E-20	1,000	<1E-20	1,000	<1E-20	1,000	<1E-20	1,000
Ra-228	Total Ra	<1E-20	1,000	<1E-20	1,000	<1E-20	1,000	<1E-20	1,000
Rn-222	N/A	<1E-20	1,000	<1E-20	1,000	<1E-20	1,000	<1E-20	1,000
Se-79	N/A	<1E-20	1,000	<1E-20	1,000	<1E-20	1,000	<1E-20	1,000
Sm-151	1,000	<1E-20	1,000	<1E-20	1,000	<1E-20	1,000	<1E-20	1,000
Sn-126	N/A	<1E-20	1,000	<1E-20	1,000	<1E-20	1,000	<1E-20	1,000
Sr-90	8	<1E-20	520	<1E-20	930	<1E-20	970	<1E-20	1,000
Tc-99	900	7.4E+00	1,000	3.6E-01	1,000	3.2E-01	1,000	1.9E-01	1,000
Th-229	Total α	<1E-20	1,000	<1E-20	1,000	<1E-20	1,000	<1E-20	1,000
Th-230	Total α	<1E-20	1,000	<1E-20	1,000	<1E-20	1,000	<1E-20	1,000
Th-232	Total α	<1E-20	1,000	<1E-20	1,000	<1E-20	1,000	<1E-20	1,000
U-232	Total U	<1E-20	1,000	<1E-20	1,000	<1E-20	1,000	<1E-20	1,000
U-233	Total U	<1E-20	1,000	<1E-20	1,000	<1E-20	1,000	<1E-20	1,000
U-234	Total U	<1E-20	1,000	<1E-20	1,000	<1E-20	1,000	<1E-20	1,000
U-235	Total U	<1E-20	1,000	<1E-20	1,000	<1E-20	1,000	<1E-20	1,000
U-236	Total U	<1E-20	1,000	<1E-20	1,000	<1E-20	1,000	<1E-20	1,000
U-238	Total U	<1E-20	1,000	<1E-20	1,000	<1E-20	1,000	<1E-20	1,000
Zr-93	2,000	<1E-20	1,000	<1E-20	1,000	<1E-20	1,000	<1E-20	1,000
Total Alpha	15	1.9E-18	1,000	<1E-20	1,000	<1E-20	1,000	<1E-20	1,000
Total Ra	5	<1E-20	1,000	<1E-20	1,000	<1E-20	1,000	<1E-20	1,000
Sum of Beta-Gamma MCL Fractions		2.8E-02	1,000	1.1E-03	1,000	9.9E-04	1,000	4.1E-04	1,000

Table 6.1-2: Radiological Concentrations for All Aquifers for All Wells at 1 Meter and Individual Intruder Wells in 1,000 Years (Continued)

Rad	MCL (pCi/L)	IHI Well 4		IHI Well 5		IHI Well 6		IHI Well 7	
		Conc. (pCi/L)	Year of Peak	Conc. (pCi/L)	Year of Peak	Conc. (pCi/L)	Year of Peak	Conc. (pCi/L)	Year of Peak
Ac-227	N/A	<1E-20	1,000	<1E-20	1,000	<1E-20	1,000	<1E-20	1,000
Al-26	N/A	<1E-20	1,000	<1E-20	1,000	<1E-20	1,000	<1E-20	1,000
Am-241	Total α	<1E-20	1,000	<1E-20	1,000	<1E-20	1,000	<1E-20	1,000
Am-242m	Total α	<1E-20	1,000	<1E-20	1,000	<1E-20	1,000	<1E-20	1,000
Am-243	Total α	<1E-20	1,000	<1E-20	1,000	<1E-20	1,000	<1E-20	1,000
C-14	2,000	<1E-20	1,000	<1E-20	1,000	<1E-20	1,000	<1E-20	1,000
Cf-249	Total α	<1E-20	1,000	<1E-20	1,000	<1E-20	1,000	<1E-20	1,000
Cf-251	Total α	<1E-20	1,000	<1E-20	1,000	<1E-20	1,000	<1E-20	1,000
Cl-36	700	6.2E-03	1,000	1.3E-05	1,000	1.7E-04	1,000	3.4E-04	1,000
Cm-243	Total α	<1E-20	1,000	<1E-20	1,000	<1E-20	1,000	<1E-20	600
Cm-244	Total α	<1E-20	1,000	<1E-20	960	<1E-20	1,000	<1E-20	370
Cm-245	Total α	<1E-20	1,000	<1E-20	1,000	<1E-20	1,000	<1E-20	1,000
Cm-247	Total α	<1E-20	1,000	<1E-20	1,000	<1E-20	1,000	<1E-20	1,000
Co-60	100	<1E-20	330	<1E-20	320	<1E-20	370	<1E-20	110
Cs-135	900	<1E-20	1,000	<1E-20	1,000	<1E-20	1,000	5.1E-18	1,000
Cs-137	200	<1E-20	1,000	<1E-20	1,000	<1E-20	870	<1E-20	600
Eu-152	200	<1E-20	830	<1E-20	730	<1E-20	850	<1E-20	280
Eu-154	60	<1E-20	540	<1E-20	480	<1E-20	550	<1E-20	180
H-3	20,000	2.3E-07	150	1.4E-11	230	1.8E-10	210	1.0E-08	150
I-129	1	1.8E-02	1,000	8.3E-05	1,000	5.7E-04	1,000	8.3E-03	1,000
K-40	N/A	2.7E-20	1,000	<1E-20	1,000	<1E-20	1,000	1.1E-16	1,000
Nb-93m	1,000	<1E-20	1,000	<1E-20	1,000	<1E-20	1,000	<1E-20	1,000
Nb-94	N/A	<1E-20	1,000	<1E-20	1,000	<1E-20	1,000	<1E-20	1,000
Ni-63	50	<1E-20	1,000	<1E-20	1,000	<1E-20	1,000	<1E-20	1,000
Np-237	Total α	<1E-20	1,000	<1E-20	1,000	<1E-20	1,000	1.9E-18	1,000
Pa-231	Total α	<1E-20	1,000	<1E-20	1,000	<1E-20	1,000	<1E-20	1,000
Pb-210	N/A	<1E-20	1,000	<1E-20	1,000	<1E-20	1,000	<1E-20	1,000
Pt-193	3,000	<1E-20	1,000	<1E-20	1,000	<1E-20	960	<1E-20	890
Pu-238	Total α	<1E-20	1,000	<1E-20	1,000	<1E-20	1,000	<1E-20	1,000
Pu-239	Total α	<1E-20	1,000	<1E-20	1,000	<1E-20	1,000	<1E-20	1,000
Pu-240	Total α	<1E-20	1,000	<1E-20	1,000	<1E-20	1,000	<1E-20	1,000
Pu-241	300	<1E-20	1,000	<1E-20	1,000	<1E-20	1,000	<1E-20	1,000
Pu-242	Total α	<1E-20	1,000	<1E-20	1,000	<1E-20	1,000	<1E-20	1,000
Pu-244	Total α	<1E-20	1,000	<1E-20	1,000	<1E-20	1,000	<1E-20	1,000
Ra-226	Total α /Ra	<1E-20	1,000	<1E-20	1,000	<1E-20	1,000	<1E-20	1,000
Ra-228	Total Ra	<1E-20	1,000	<1E-20	1,000	<1E-20	1,000	<1E-20	1,000
Rn-222	N/A	<1E-20	1,000	<1E-20	1,000	<1E-20	1,000	<1E-20	1,000
Se-79	N/A	<1E-20	1,000	<1E-20	1,000	<1E-20	1,000	<1E-20	1,000
Sm-151	1,000	<1E-20	1,000	<1E-20	1,000	<1E-20	1,000	<1E-20	1,000
Sn-126	N/A	<1E-20	1,000	<1E-20	1,000	<1E-20	1,000	<1E-20	1,000
Sr-90	8	<1E-20	1,000	<1E-20	910	<1E-20	720	<1E-20	530
Tc-99	900	6.8E+00	1,000	1.6E-01	1,000	3.0E-01	1,000	3.2E+00	1,000
Th-229	Total α	<1E-20	1,000	<1E-20	1,000	<1E-20	1,000	<1E-20	1,000
Th-230	Total α	<1E-20	1,000	<1E-20	1,000	<1E-20	1,000	<1E-20	1,000
Th-232	Total α	<1E-20	1,000	<1E-20	1,000	<1E-20	1,000	<1E-20	1,000
U-232	Total U	<1E-20	1,000	<1E-20	1,000	<1E-20	1,000	<1E-20	1,000
U-233	Total U	<1E-20	1,000	<1E-20	1,000	<1E-20	1,000	<1E-20	1,000
U-234	Total U	<1E-20	1,000	<1E-20	1,000	<1E-20	1,000	<1E-20	1,000
U-235	Total U	<1E-20	1,000	<1E-20	1,000	<1E-20	1,000	<1E-20	1,000
U-236	Total U	<1E-20	1,000	<1E-20	1,000	<1E-20	1,000	<1E-20	1,000
U-238	Total U	<1E-20	1,000	<1E-20	1,000	<1E-20	1,000	<1E-20	1,000
Zr-93	2,000	<1E-20	1,000	<1E-20	1,000	<1E-20	1,000	<1E-20	1,000
Total Alpha	15	<1E-20	1,000	<1E-20	1,000	<1E-20	1,000	1.9E-18	1,000
Total Ra	5	<1E-20	1,000	<1E-20	1,000	<1E-20	1,000	<1E-20	1,000
Sum of Beta-Gamma MCL Fractions		2.6E-02	1,000	2.6E-04	1,000	9.1E-04	1,000	1.2E-02	1,000

Table 6.1-3: Chemical Concentrations for All Aquifers for All Wells at 1 Meter and Individual Intruder Wells in 1,000 Years

Chem.	MCL (µg/L)	Conc. (µg/L)	Year of Peak	Conc. (µg/L)	Year of Peak	Conc. (µg/L)	Year of Peak	Conc. (µg/L)	Year of Peak
		All 1m Wells		IHI Well 1		IHI Well 2		IHI Well 3	
Cl^-	250,000	3.1E-01	1,000	9.7E-03	1,000	8.9E-03	1,000	1.1E-02	1,000
F^-	4,000	6.3E-01	1,000	1.9E-02	1,000	1.8E-02	1,000	4.7E-03	1,000
NO_3	10,000	2.0E+03	1,000	2.4E+02	1,000	2.2E+02	1,000	9.1E+01	1,000
NO_2	10,000	1.8E+02	1,000	2.1E+01	1,000	1.9E+01	1,000	1.4E+01	1,000
PO_4	N/A	1.3E+01	1,000	1.6E+00	1,000	1.4E+00	1,000	5.8E-01	1,000
SO_4	250,000	6.1E+01	1,000	7.2E+00	1,000	6.5E+00	1,000	3.3E+00	1,000
Al	200	<1E-20	1,000	<1E-20	1,000	<1E-20	1,000	<1E-20	1,000
Ag	100	<1E-20	1,000	<1E-20	1,000	<1E-20	1,000	<1E-20	910
As	10	<1E-20	1,000	<1E-20	1,000	<1E-20	1,000	<1E-20	1,000
B	N/A	2.5E-01	1,000	3.0E-02	1,000	2.7E-02	1,000	2.5E-02	1,000
Ba	2,000	<1E-20	1,000	<1E-20	1,000	<1E-20	1,000	<1E-20	1,000
Cd	5	<1E-20	1,000	<1E-20	1,000	<1E-20	1,000	<1E-20	1,000
Co	N/A	<1E-20	1,000	<1E-20	1,000	<1E-20	1,000	<1E-20	1,000
Cr	100	<1E-20	1,000	<1E-20	1,000	<1E-20	1,000	<1E-20	1,000
Cu	1,300	<1E-20	1,000	<1E-20	1,000	<1E-20	1,000	<1E-20	1,000
Fe	300	<1E-20	1,000	<1E-20	1,000	<1E-20	1,000	<1E-20	1,000
Hg	2	<1E-20	1,000	<1E-20	1,000	<1E-20	1,000	<1E-20	1,000
I	N/A	2.3E-05	1,000	1.5E-08	1,000	1.4E-08	1,000	8.7E-07	1,000
Mn	50	<1E-20	1,000	<1E-20	1,000	<1E-20	1,000	<1E-20	1,000
Mo	N/A	<1E-20	1,000	<1E-20	1,000	<1E-20	1,000	<1E-20	1,000
Ni	N/A	<1E-20	1,000	<1E-20	1,000	<1E-20	1,000	<1E-20	1,000
Pb	15	<1E-20	1,000	<1E-20	1,000	<1E-20	1,000	<1E-20	1,000
Se	50	<1E-20	1,000	<1E-20	1,000	<1E-20	1,000	<1E-20	1,000
Sb	6	<1E-20	1,000	<1E-20	1,000	<1E-20	1,000	<1E-20	1,000
Sr	N/A	<1E-20	1,000	<1E-20	1,000	<1E-20	1,000	<1E-20	1,000
U	30	<1E-20	1,000	<1E-20	1,000	<1E-20	1,000	<1E-20	1,000
Zn	5,000	<1E-20	1,000	<1E-20	1,000	<1E-20	1,000	<1E-20	1,000
Chem.	**MCL**	**IHI Well 4**		**IHI Well 5**		**IHI Well 6**		**IHI Well 7**	
Cl^-	250,000	2.9E-01	1,000	7.5E-03	1,000	8.0E-03	1,000	2.3E-01	1,000
F^-	4,000	5.7E-01	1,000	6.5E-03	1,000	1.6E-02	1,000	1.5E-01	1,000
NO_3	10,000	1.9E+03	1,000	5.0E+01	1,000	2.1E+02	1,000	6.0E+02	1,000
NO_2	10,000	1.7E+02	1,000	8.4E+00	1,000	1.9E+01	1,000	3.0E+01	1,000
PO_4	N/A	1.2E+01	1,000	2.6E-01	1,000	1.4E+00	1,000	1.8E+00	1,000
SO_4	250,000	5.6E+01	1,000	1.8E+00	1,000	6.3E+00	1,000	1.4E+01	1,000
Al	200	<1E-20	1,000	<1E-20	1,000	<1E-20	1,000	<1E-20	1,000
Ag	100	<1E-20	1,000	<1E-20	1,000	<1E-20	1,000	<1E-20	1,000
As	10	<1E-20	1,000	<1E-20	1,000	<1E-20	1,000	<1E-20	1,000
B	N/A	2.3E-01	1,000	2.7E-02	1,000	2.6E-02	1,000	2.1E-01	1,000
Ba	2,000	<1E-20	1,000	<1E-20	1,000	<1E-20	1,000	<1E-20	1,000
Cd	5	<1E-20	1,000	<1E-20	1,000	<1E-20	1,000	<1E-20	1,000
Co	N/A	<1E-20	1,000	<1E-20	1,000	<1E-20	1,000	<1E-20	1,000
Cr	100	<1E-20	1,000	<1E-20	1,000	<1E-20	1,000	<1E-20	1,000
Cu	1,300	<1E-20	1,000	<1E-20	1,000	<1E-20	1,000	<1E-20	1,000
Fe	300	<1E-20	1,000	<1E-20	1,000	<1E-20	990	<1E-20	1,000
Hg	2	<1E-20	1,000	<1E-20	1,000	<1E-20	1,000	<1E-20	1,000
I	N/A	3.9E-07	1,000	4.9E-07	1,000	1.4E-08	1,000	2.5E-05	1,000
Mn	50	<1E-20	1,000	<1E-20	1,000	<1E-20	1,000	<1E-20	1,000
Mo	N/A	<1E-20	1,000	<1E-20	1,000	<1E-20	1,000	<1E-20	1,000
Ni	N/A	<1E-20	1,000	<1E-20	1,000	<1E-20	1,000	<1E-20	1,000
Pb	15	<1E-20	1,000	<1E-20	1,000	<1E-20	1,000	<1E-20	1,000
Se	50	<1E-20	1,000	<1E-20	1,000	<1E-20	1,000	<1E-20	1,000
Sb	6	<1E-20	1,000	<1E-20	1,000	<1E-20	1,000	<1E-20	1,000
Sr	N/A	<1E-20	1,000	<1E-20	1,000	<1E-20	1,000	<1E-20	1,000
U	30	<1E-20	1,000	<1E-20	1,000	<1E-20	1,000	<1E-20	1,000
Zn	5,000	<1E-20	1,000	<1E-20	1,000	<1E-20	1,000	<1E-20	1,000

Table 6.1-4: Radiological Concentrations for All Aquifers for All Wells at 1 Meter and Individual Intruder Wells in 10,000 Years

Rad	MCL (pCi/L)	All 1m Wells		IHI Well 1		IHI Well 2		IHI Well 3	
		Conc. (pCi/L)	Year of Peak	Conc. (pCi/L)	Year of Peak	Conc. (pCi/L)	Year of Peak	Conc. (pCi/L)	Year of Peak
Ac-227	N/A	1.4E-12	10,000	4.8E-19	10,000	4.4E-18	10,000	<1E-20	10,000
Al-26	N/A	<1E-20	10,000	<1E-20	10,000	<1E-20	10,000	<1E-20	10,000
Am-241	Total α	<1E-20	10,000	<1E-20	10,000	<1E-20	10,000	<1E-20	10,000
Am-242m	Total α	<1E-20	2,830	<1E-20	10,000	<1E-20	8,550	<1E-20	7,460
Am-243	Total α	<1E-20	10,000	<1E-20	10,000	<1E-20	10,000	<1E-20	10,000
C-14	2,000	1.7E-18	10,000	<1E-20	10,000	<1E-20	10,000	<1E-20	10,000
Cf-249	Total α	<1E-20	6,690	<1E-20	10,000	<1E-20	10,000	<1E-20	10,000
Cf-251	Total α	<1E-20	10,000	<1E-20	10,000	<1E-20	10,000	<1E-20	10,000
Cl-36	700	5.9E-01	10,000	5.1E-01	10,000	4.7E-01	10,000	2.9E-01	10,000
Cm-243	Total α	<1E-20	580	<1E-20	2,050	<1E-20	1,680	<1E-20	1,420
Cm-244	Total α	<1E-20	360	<1E-20	1,280	<1E-20	1,150	<1E-20	990
Cm-245	Total α	<1E-20	10,000	<1E-20	10,000	<1E-20	10,000	<1E-20	10,000
Cm-247	Total α	<1E-20	10,000	<1E-20	10,000	<1E-20	10,000	<1E-20	10,000
Co-60	100	<1E-20	100	<1E-20	570	<1E-20	340	<1E-20	290
Cs-135	900	2.9E-04	10,000	5.8E-08	10,000	5.2E-08	10,000	8.7E-08	10,000
Cs-137	200	<1E-20	590	<1E-20	1,220	<1E-20	1,260	<1E-20	1,190
Eu-152	200	<1E-20	270	<1E-20	960	<1E-20	880	<1E-20	750
Eu-154	60	<1E-20	180	<1E-20	610	<1E-20	570	<1E-20	490
H-3	20,000	2.6E-07	150	2.2E-10	210	2.0E-10	210	1.5E-11	230
I-129	1	3.7E+00	10,000	3.2E+00	10,000	3.0E+00	10,000	1.8E+00	10,000
K-40	N/A	4.6E-03	10,000	4.3E-05	10,000	3.8E-05	10,000	6.0E-06	10,000
Nb-93m	1,000	<1E-20	10,000	<1E-20	10,000	<1E-20	10,000	<1E-20	10,000
Nb-94	N/A	<1E-20	10,000	<1E-20	10,000	<1E-20	10,000	<1E-20	10,000
Ni-63	50	<1E-20	1,860	<1E-20	2,660	<1E-20	2,720	<1E-20	4,050
Np-237	Total α	1.7E-08	10,000	6.5E-15	10,000	6.6E-14	10,000	3.0E-16	10,000
Pa-231	Total α	4.4E-10	10,000	1.5E-16	10,000	1.4E-15	10,000	5.4E-19	10,000
Pb-210	N/A	<1E-20	10,000	<1E-20	10,000	<1E-20	10,000	<1E-20	10,000
Pt-193	3,000	<1E-20	890	<1E-20	1,510	<1E-20	1,550	<1E-20	1,840
Pu-238	Total α	<1E-20	1,730	<1E-20	8,470	<1E-20	7,240	<1E-20	6,520
Pu-239	Total α	<1E-20	10,000	<1E-20	10,000	<1E-20	10,000	<1E-20	10,000
Pu-240	Total α	<1E-20	10,000	<1E-20	10,000	<1E-20	10,000	<1E-20	10,000
Pu-241	300	<1E-20	10,000	<1E-20	10,000	<1E-20	10,000	<1E-20	10,000
Pu-242	Total α	<1E-20	10,000	<1E-20	10,000	<1E-20	10,000	<1E-20	10,000
Pu-244	Total α	<1E-20	10,000	<1E-20	10,000	<1E-20	10,000	<1E-20	10,000
Ra-226	Total α /Ra	<1E-20	10,000	<1E-20	10,000	<1E-20	10,000	<1E-20	10,000
Ra-228	Total Ra	<1E-20	10,000	<1E-20	10,000	<1E-20	10,000	<1E-20	10,000
Rn-222	N/A	<1E-20	10,000	<1E-20	10,000	<1E-20	10,000	<1E-20	10,000
Se-79	N/A	<1E-20	10,000	<1E-20	10,000	<1E-20	10,000	<1E-20	10,000
Sm-151	1,000	<1E-20	1,780	<1E-20	7,540	<1E-20	6,380	<1E-20	5,610
Sn-126	N/A	<1E-20	10,000	<1E-20	10,000	<1E-20	10,000	<1E-20	10,000
Sr-90	8	<1E-20	520	<1E-20	930	<1E-20	970	<1E-20	1,020
Tc-99	900	5.7E+02	9,960	4.9E+02	9,640	4.6E+02	9,850	3.0E+02	9,950
Th-229	Total α	3.1E-14	10,000	<1E-20	10,000	8.6E-20	10,000	<1E-20	10,000
Th-230	Total α	<1E-20	10,000	<1E-20	10,000	<1E-20	10,000	<1E-20	10,000
Th-232	Total α	<1E-20	10,000	<1E-20	10,000	<1E-20	10,000	<1E-20	10,000
U-232	Total U	<1E-20	1,330	<1E-20	6,330	<1E-20	5,170	<1E-20	4,610
U-233	Total U	9.9E-13	10,000	3.2E-19	10,000	3.2E-18	10,000	2.7E-20	10,000
U-234	Total U	<1E-20	10,000	<1E-20	10,000	<1E-20	10,000	<1E-20	10,000
U-235	Total U	<1E-20	10,000	<1E-20	10,000	<1E-20	10,000	<1E-20	10,000
U-236	Total U	<1E-20	10,000	<1E-20	10,000	<1E-20	10,000	<1E-20	10,000
U-238	Total U	<1E-20	10,000	<1E-20	10,000	<1E-20	10,000	<1E-20	10,000
Zr-93	2,000	<1E-20	10,000	<1E-20	10,000	<1E-20	10,000	<1E-20	10,000
Total Alpha	15	1.8E-08	10,000	6.6E-15	10,000	6.8E-14	10,000	3.0E-16	10,000
Total Ra	5	<1E-20	10,000	<1E-20	10,000	<1E-20	10,000	<1E-20	10,000
Sum of Beta-Gamma MCL Fractions		4.4E+00	10,000	3.8E+00	10,000	3.5E+00	10,000	2.1E+00	10,000

Table 6.1-4: Radiological Concentrations for All Aquifers for All Wells at 1 Meter and Individual Intruder Wells in 10,000 Years (Continued)

Rad	MCL (pCi/L)	IHI Well 4		IHI Well 5		IHI Well 6		IHI Well 7	
		Conc. (pCi/L)	Year of Peak	Conc. (pCi/L)	Year of Peak	Conc. (pCi/L)	Year of Peak	Conc. (pCi/L)	Year of Peak
Ac-227	N/A	4.0E-19	10,000	2.2E-18	10,000	5.4E-18	10,000	1.5E-12	10,000
Al-26	N/A	<1E-20	10,000	<1E-20	10,000	<1E-20	10,000	<1E-20	10,000
Am-241	Total α	<1E-20	10,000	<1E-20	10,000	<1E-20	10,000	<1E-20	10,000
Am-242m	Total α	<1E-20	8,270	<1E-20	7,200	<1E-20	8,860	<1E-20	2,900
Am-243	Total α	<1E-20	10,000	<1E-20	10,000	<1E-20	10,000	<1E-20	10,000
C-14	2,000	<1E-20	10,000	<1E-20	10,000	<1E-20	10,000	1.7E-18	10,000
Cf-249	Total α	<1E-20	10,000	<1E-20	10,000	<1E-20	10,000	<1E-20	6,910
Cf-251	Total α	<1E-20	10,000	<1E-20	10,000	<1E-20	10,000	<1E-20	10,000
Cl-36	700	4.1E-01	6,860	9.3E-02	10,000	4.6E-01	10,000	5.4E-02	10,000
Cm-243	Total α	<1E-20	1,550	<1E-20	1,370	<1E-20	1,840	<1E-20	600
Cm-244	Total α	<1E-20	1,080	<1E-20	960	<1E-20	1,120	<1E-20	370
Cm-245	Total α	<1E-20	10,000	<1E-20	10,000	<1E-20	10,000	<1E-20	10,000
Cm-247	Total α	<1E-20	10,000	<1E-20	10,000	<1E-20	10,000	<1E-20	10,000
Co-60	100	<1E-20	330	<1E-20	320	<1E-20	370	<1E-20	110
Cs-135	900	2.6E-04	10,000	7.9E-08	10,000	4.7E-08	10,000	2.1E-06	10,000
Cs-137	200	<1E-20	1,230	<1E-20	1,180	<1E-20	870	<1E-20	600
Eu-152	200	<1E-20	830	<1E-20	730	<1E-20	850	<1E-20	280
Eu-154	60	<1E-20	540	<1E-20	480	<1E-20	550	<1E-20	180
H-3	20,000	2.3E-07	150	1.4E-11	230	1.8E-10	210	1.0E-08	150
I-129	1	3.1E+00	10,000	6.1E-01	10,000	2.9E+00	10,000	7.5E-01	10,000
K-40	N/A	4.3E-03	10,000	5.1E-06	10,000	3.7E-05	10,000	3.0E-06	10,000
Nb-93m	1,000	<1E-20	10,000	<1E-20	10,000	<1E-20	10,000	<1E-20	10,000
Nb-94	N/A	<1E-20	10,000	<1E-20	10,000	<1E-20	10,000	<1E-20	10,000
Ni-63	50	<1E-20	4,780	<1E-20	4,060	<1E-20	2,340	<1E-20	1,860
Np-237	Total α	4.7E-14	10,000	3.2E-14	10,000	2.2E-14	10,000	1.8E-08	10,000
Pa-231	Total α	1.3E-16	10,000	6.8E-16	10,000	1.7E-15	10,000	4.6E-10	10,000
Pb-210	N/A	<1E-20	10,000	<1E-20	10,000	<1E-20	10,000	<1E-20	10,000
Pt-193	3,000	<1E-20	1,540	<1E-20	1,430	<1E-20	1,260	<1E-20	890
Pu-238	Total α	<1E-20	7,070	<1E-20	6,360	<1E-20	5,550	<1E-20	1,780
Pu-239	Total α	<1E-20	10,000	<1E-20	10,000	<1E-20	10,000	<1E-20	10,000
Pu-240	Total α	<1E-20	10,000	<1E-20	10,000	<1E-20	10,000	<1E-20	10,000
Pu-241	300	<1E-20	10,000	<1E-20	10,000	<1E-20	10,000	<1E-20	10,000
Pu-242	Total α	<1E-20	10,000	<1E-20	10,000	<1E-20	10,000	<1E-20	10,000
Pu-244	Total α	<1E-20	10,000	<1E-20	10,000	<1E-20	10,000	<1E-20	10,000
Ra-226	Total α /Ra	<1E-20	10,000	<1E-20	10,000	<1E-20	10,000	<1E-20	10,000
Ra-228	Total Ra	<1E-20	10,000	<1E-20	10,000	<1E-20	10,000	<1E-20	10,000
Rn-222	N/A	<1E-20	10,000	<1E-20	10,000	<1E-20	10,000	<1E-20	10,000
Se-79	N/A	<1E-20	10,000	<1E-20	10,000	<1E-20	10,000	<1E-20	10,000
Sm-151	1,000	<1E-20	5,190	<1E-20	5,500	<1E-20	4,980	<1E-20	1,840
Sn-126	N/A	<1E-20	9,870	<1E-20	10,000	<1E-20	10,000	<1E-20	10,000
Sr-90	8	<1E-20	1,440	<1E-20	910	<1E-20	720	<1E-20	530
Tc-99	900	4.7E+02	5,800	1.8E+02	9,970	4.5E+02	9,700	3.6E+02	7,810
Th-229	Total α	2.5E-19	10,000	4.2E-20	10,000	3.1E-20	10,000	3.4E-14	10,000
Th-230	Total α	<1E-20	10,000	<1E-20	10,000	<1E-20	10,000	<1E-20	10,000
Th-232	Total α	<1E-20	10,000	<1E-20	10,000	<1E-20	10,000	<1E-20	10,000
U-232	Total U	<1E-20	4,920	<1E-20	4,530	<1E-20	3,800	<1E-20	1,370
U-233	Total U	5.1E-18	10,000	1.6E-18	10,000	1.1E-18	10,000	1.1E-12	10,000
U-234	Total U	<1E-20	10,000	<1E-20	10,000	<1E-20	10,000	<1E-20	10,000
U-235	Total U	<1E-20	10,000	<1E-20	10,000	<1E-20	10,000	<1E-20	10,000
U-236	Total U	<1E-20	10,000	<1E-20	10,000	<1E-20	10,000	<1E-20	10,000
U-238	Total U	<1E-20	10,000	<1E-20	10,000	<1E-20	10,000	<1E-20	10,000
Zr-93	2,000	<1E-20	10,000	<1E-20	10,000	<1E-20	10,000	<1E-20	10,000
Total Alpha	15	4.7E-14	10,000	3.3E-14	10,000	2.4E-14	10,000	1.9E-08	10,000
Total Ra	5	<1E-20	10,000	<1E-20	10,000	<1E-20	10,000	<1E-20	10,000
Sum of Beta-Gamma MCL Fractions		3.5E+00	10,000	6.8E-01	10,000	3.1E+00	10,000	8.2E-01	10,000

Table 6.1-5: Chemical Concentrations for All Aquifers for All Wells at 1 Meter and Individual Intruder Wells in 10,000 Years

Chem.	MCL (µg/L)	Conc. (µg/L)	Year of Peak	Conc. (µg/L)	Year of Peak	Conc. (µg/L)	Year of Peak	Conc. (µg/L)	Year of Peak
		All 1m Wells		IHI Well 1		IHI Well 2		IHI Well 3	
Cl^-	250,000	3.6E+01	9,990	2.4E+01	9,990	2.2E+01	9,990	2.4E+01	9,990
F^-	4,000	5.6E+01	10,000	4.8E+01	10,000	4.5E+01	10,000	2.7E+01	10,000
NO_3	10,000	5.3E+04	9,980	4.6E+04	9,970	4.3E+04	9,980	2.8E+04	9,990
NO_2	10,000	4.7E+03	9,970	4.1E+03	9,970	3.8E+03	9,990	3.3E+03	10,000
PO_4	N/A	3.5E+02	9,970	3.0E+02	9,960	2.8E+02	9,960	1.8E+02	9,970
SO_4	250,000	1.6E+03	9,950	1.4E+03	9,950	1.3E+03	9,980	8.5E+02	9,990
Al	200	<1E-20	10,000	<1E-20	10,000	<1E-20	10,000	<1E-20	10,000
Ag	100	5.0E-17	10,000	<1E-20	10,000	<1E-20	10,000	<1E-20	10,000
As	10	<1E-20	10,000	<1E-20	10,000	<1E-20	10,000	<1E-20	10,000
B	N/A	6.8E+00	9,980	5.7E+00	9,970	5.3E+00	9,990	5.7E+00	10,000
Ba	2,000	1.1E-20	10,000	<1E-20	10,000	<1E-20	10,000	<1E-20	10,000
Cd	5	1.4E-19	10,000	<1E-20	10,000	<1E-20	10,000	<1E-20	10,000
Co	N/A	<1E-20	10,000	<1E-20	10,000	<1E-20	10,000	<1E-20	10,000
Cr	100	<1E-20	10,000	<1E-20	10,000	<1E-20	10,000	<1E-20	10,000
Cu	1,300	<1E-20	10,000	<1E-20	10,000	<1E-20	10,000	<1E-20	10,000
Fe	300	<1E-20	10,000	<1E-20	10,000	<1E-20	10,000	<1E-20	10,000
Hg	2	<1E-20	10,000	<1E-20	10,000	<1E-20	10,000	<1E-20	10,000
I	N/A	7.5E-03	10,000	9.9E-05	10,000	9.1E-05	10,000	6.6E-03	10,000
Mn	50	2.1E-12	10,000	4.9E-19	10,000	4.8E-19	10,000	9.7E-15	10,000
Mo	N/A	<1E-20	10,000	<1E-20	10,000	<1E-20	10,000	<1E-20	10,000
Ni	N/A	4.0E-12	10,000	1.1E-18	10,000	1.1E-18	10,000	3.5E-13	10,000
Pb	15	<1E-20	10,000	<1E-20	10,000	<1E-20	10,000	<1E-20	10,000
Se	50	<1E-20	10,000	<1E-20	10,000	<1E-20	10,000	<1E-20	10,000
Sb	6	<1E-20	10,000	<1E-20	10,000	<1E-20	10,000	<1E-20	10,000
Sr	N/A	1.4E-13	10,000	1.5E-20	10,000	8.2E-20	10,000	<1E-20	10,000
U	30	<1E-20	10,000	<1E-20	10,000	<1E-20	10,000	<1E-20	10,000
Zn	5,000	2.7E-18	10,000	<1E-20	10,000	<1E-20	10,000	<1E-20	10,000
Chem.	**MCL**	IHI Well 4		IHI Well 5		IHI Well 6		IHI Well 7	
Cl^-	250,000	1.9E+01	7,600	1.6E+01	10,000	2.2E+01	9,990	3.8E+01	10,000
F^-	4,000	3.8E+01	8,170	1.5E+01	10,000	4.4E+01	10,000	2.3E+01	10,000
NO_3	10,000	3.5E+04	3,940	1.1E+04	9,980	4.2E+04	9,980	2.1E+04	9,950
NO_2	10,000	3.1E+03	3,970	1.9E+03	10,000	3.7E+03	9,980	1.1E+03	9,900
PO_4	N/A	2.3E+02	3,910	5.7E+01	9,990	2.8E+02	9,970	6.5E+01	9,980
SO_4	250,000	1.1E+03	3,810	3.9E+02	9,980	1.3E+03	9,950	5.0E+02	9,920
Al	200	<1E-20	10,000	<1E-20	10,000	<1E-20	10,000	<1E-20	10,000
Ag	100	<1E-20	10,000	<1E-20	10,000	<1E-20	10,000	5.3E-17	10,000
As	10	<1E-20	10,000	<1E-20	10,000	<1E-20	10,000	<1E-20	10,000
B	N/A	4.4E+00	3,910	5.9E+00	10,000	5.2E+00	9,980	7.3E+00	9,980
Ba	2,000	<1E-20	10,000	<1E-20	10,000	<1E-20	10,000	1.2E-20	10,000
Cd	5	<1E-20	10,000	<1E-20	10,000	<1E-20	10,000	1.4E-19	10,000
Co	N/A	<1E-20	10,000	<1E-20	10,000	<1E-20	10,000	<1E-20	10,000
Cr	100	<1E-20	10,000	<1E-20	10,000	<1E-20	10,000	<1E-20	10,000
Cu	1,300	<1E-20	10,000	<1E-20	10,000	<1E-20	10,000	<1E-20	10,000
Fe	300	<1E-20	10,000	<1E-20	10,000	<1E-20	10,000	<1E-20	10,000
Hg	2	<1E-20	10,000	<1E-20	10,000	<1E-20	10,000	<1E-20	10,000
I	N/A	9.3E-05	9,990	3.9E-03	10,000	9.2E-05	10,000	2.7E-03	10,000
Mn	50	1.8E-12	10,000	1.3E-14	10,000	2.3E-19	10,000	2.2E-12	10,000
Mo	N/A	<1E-20	10,000	<1E-20	10,000	<1E-20	10,000	<1E-20	10,000
Ni	N/A	3.6E-12	10,000	8.7E-14	10,000	1.5E-18	10,000	2.5E-12	10,000
Pb	15	<1E-20	10,000	<1E-20	10,000	<1E-20	10,000	<1E-20	10,000
Se	50	<1E-20	10,000	<1E-20	10,000	<1E-20	10,000	<1E-20	10,000
Sb	6	<1E-20	9,800	<1E-20	10,000	<1E-20	10,000	<1E-20	10,000
Sr	N/A	4.0E-17	10,000	6.2E-20	10,000	1.8E-18	10,000	1.4E-13	10,000
U	30	<1E-20	10,000	<1E-20	10,000	<1E-20	10,000	<1E-20	10,000
Zn	5,000	<1E-20	10,000	<1E-20	10,000	<1E-20	10,000	2.7E-18	10,000

6.2 IHI Dose Scenarios

Section 4.4.8 describes how the biotic pathways doses are calculated based on these contaminant concentrations. A complete discussion of the revised biotic pathways and related methodology is provided in *Dose Calculation Methodology for Liquid Waste Performance Assessments at the Savannah River Site* (SRR-CWDA-2013-00058).

The following provides an overview of the applicable exposure pathways for each IHI scenario and describes how the contaminant concentrations at the various points of assessment are determined for each of these exposure scenarios.

6.2.1 Acute IHI Well Driller Scenarios

For the Acute IHI Well Driller Scenarios, the human receptor is assumed to be a non-resident well driller that is exposed to direct contaminants for a brief period of time while installing a well.

The ingestion pathway is:

- Direct ingestion of contaminated drill cuttings while drilling.

The direct exposure pathway is:

- Direct exposure to contaminated drill cuttings while drilling.

The inhalation pathway is:

- Inhalation of resuspended drill cutting material while drilling.

For the Acute IHI Well Driller Scenarios, the total drill cuttings pathways dose is determined as the sum of the doses from each of these pathways. These pathways are defined in Section 4.4.8.2.

Two approaches for the Acute IHI scenario are considered, each using different assumed inventories for the drill cuttings. The first approach assumes the drill cuttings are from contaminated soils adjacent to an SDU (see Section 6.2.1.1). The second approach assumes the driller intrudes directly through the SDU roof and into the saltstone waste form (see Section 6.2.1.2). Note that this latter approach is not considered a credible IHI scenario because it requires *advertent* (i.e., purposeful) intrusion into the facility, as discussed in Section 6.2.1.2, but is provided for informational purposes. The dose results for both approaches are provided in Section 6.3.

6.2.1.1 Soil Drill Cutting Inventory for the Acute IHI Well Driller Scenario

SRS soils are generally sandy or clayey such that drillers installing wells are unlikely to penetrate through very thick layers of hardened material. Given these typical conditions, and based on current well drilling practices in the vicinity of SRS, it is expected that any driller who encounters the roof of an SDU will see unexpected materials (e.g., erosion barrier, HDPE, GCL, and the SDU roof). Because these materials are inconsistent with typical near-surface geologic conditions, the driller is likely to take up reasonable, investigative actions or would opt to relocate into softer material. Further, because local conditions are generally sandy or clayey, the standard mud rotary drilling equipment used for installing wells in the vicinity of SRS are insufficient for drilling into an SDU (i.e.,

it would be impossible to penetrate through hardened barriers such as the steel-reinforced concrete of the SDU roof without purposefully changing equipment).

As such, the most credible scenario for an inadvertent human intrusion would be a driller who misses the SDU and instead drills a well through contaminated soils adjacent to an SDU. Because this is the most credible scenario for an inadvertent human intrusion, this scenario is selected for representing compliance to performance objectives.

The estimated inventory for the soil drill cuttings assumes that the drill cuttings come from contaminated soils adjacent to the SDU. As a model simplification, the soil drill cutting inventories were developed using the peak contaminant ground water concentrations along the 1-meter boundary, as determined by the Aquifer Transport Model (see Section 6.1). From the 1-meter concentrations, the maximum concentrations were selected for each radionuclide in the Compliance Case for any time between 0 years and 20,000 years after SDF closure. This approach assumes that the timings for peak values are not relevant. Then, to ensure greater defensibility these values were scaled up by an additional factor of approximately 8 to represent a slightly closer proximity to the SDU than a single meter.

These assumed ground water concentrations for each radionuclide were then converted into a soil drill cutting inventory based on the total volume of the drill cutting material (assuming an 8-inch diameter well with a depth of 100 feet). The mass of the drill cuttings is assumed to be equivalent to an 8-inch diameter circular hole drilled from the surface of the closure cap to a depth of 100 feet (i.e., a volume of approximately one cubic meter). As a bounding assumption, the concentrations are assumed to be uniform throughout the entire 100-foot depth and throughout the entire mass of the drill cutting material. This recommended inventory is provided in Table 6.2-1.

Despite this inventory being generated from peak ground water concentrations over a 20,000-year simulation period, these values are non-mechanistically applied to this scenario at the end of the Institutional Control Period (i.e., 100 years after SDF closure).

The dose calculations for this Acute IHI scenario are defined in Section 4.4.8.2.3. For example, the effective dose factor for the ingestion of drill cuttings by the IHI driller can be determined from Eq. 4.4-200, which also identifies specific tables for each of the input values used. Section 6.3.1 provides Acute IHI doses based on this inventory approach.

Table 6.2-1: Assumed Drill Cutting Inventory for Contaminated Soil

Radionuclide	Recommended Inventory (Ci) for Soil Drill Cutting
Ac-227	7.30E-19
Al-26	3.12E-43
Am-241	5.36E-44
Am-242m	3.29E-62
Am-243	5.47E-44
C-14	3.68E-24
Cf-249	1.31E-55
Cf-251	8.00E-51
Cl-36	4.78E-09
Cm-243	3.42E-72
Cm-244	1.40E-71
Cm-245	5.01E-44
Cm-247	3.44E-44
Co-60	2.19E-64
Cs-135	7.21E-11
Cs-137	2.76E-30
Eu-152	4.19E-76
Eu-154	1.77E-77
H-3	1.97E-15
I-129	3.93E-08
K-40	2.17E-10
Nb-93m	1.73E-42
Nb-94	6.91E-40
Ni-63	2.44E-34
Np-237	4.78E-15
Pa-231	2.27E-16

Radionuclide	Recommended Inventory (Ci) for Soil Drill Cutting
Pb-210	4.36E-31
Pt-193	9.32E-40
Pu-238	3.68E-57
Pu-239	3.70E-38
Pu-240	9.86E-39
Pu-241	7.79E-44
Pu-242	4.45E-39
Pu-244	1.88E-41
Ra-226	2.92E-29
Ra-228	3.78E-45
Se-79	1.05E-36
Sm-151	6.38E-62
Sn-126	1.37E-48
Sr-90	1.40E-39
Tc-99	4.38E-06
Th-229	5.15E-20
Th-230	1.16E-39
Th-232	1.16E-46
U-232	9.41E-61
U-233	7.09E-19
U-234	1.35E-37
U-235	1.48E-39
U-236	1.41E-39
U-238	1.25E-39
Zr-93	1.91E-42

6.2.1.2 SDU Drill Cutting Inventory for the Acute IHI Well Driller Scenario

The second inventory approach (SDU drill cuttings) is not considered a credible scenario for a number of reasons. First, as a driller proceeds to drill through the closure cap, they are likely to encounter unexpected materials (e.g., erosion barrier, HDPE, GCL, and the SDU roof) that are inconsistent with typical near-surface regional geologic conditions. When they encounter these materials, future drillers are likely to take up reasonable, investigative actions. Assuming a persistent driller, they may continue all the way to the top of the SDU, but once they reach the top of the SDU, they would encounter a layer of HDPE and GCL materials, followed by the steel-reinforced concrete of the SDU roof. This steel-reinforced concrete will provide a sufficient barrier to prevent any further intrusion because standard mud rotary drills (typically used for installing wells in the area) are not designed to penetrate through very thick layers of hardened material.

However, the SDU roof will become fully hydraulically degraded over a period of a few thousand years, as shown in Table 4.4-45. This IHI scenario assumes that once completely degraded, the SDU roof no longer functions as a barrier to intrusion. Assuming the most limiting degradation times for the SDU roof (i.e., "Conservative Estimate" (or CE) in Table 4.4-45), it may be assumed that an intrusion through the SDU roof might become possible (albeit unlikely) at the following times:

- SDU 1 at 683 years,
- SDU 4 at 518 years,
- 150-foot diameter SDUs at 914 years, and
- 375-foot diameter SDUs at 1,371 years.

Once intrusion through the SDU roof occurs, the saltstone waste form will act as an additional barrier to intrusion. Saltstone is expected to remain essentially intact for tens of thousands to millions of years (see Section 4.4.2). It has material properties that are noticeably different from the local environment and it not possible to drill through it with standard mud rotary well drilling equipment. As such, an inadvertent human intrusion into the saltstone is not considered credible.

Regardless, an analysis was performed to assess the potential impacts of an *advertent* (i.e., purposeful) human intrusion scenario in which the driller notices the unusual materials but instead of investigating or relocating the well to more a favorable the site, the driller chooses to bring in additional equipment (e.g., diamond core drill bits). Note that this is not a typical practice in the SRS vicinity for installing drinking water wells or irrigation wells. Due to the assumed use of a coring drill, as opposed to using standard well drilling equipment, the drill cuttings would have a different geometry from soil drill cuttings. Instead of the drill pulling up loose soils, solid cylindrical cores would be extracted. As such, the core material would be discarded and would not be mixed into the crop or garden soil. There would, however, be a limited amount of material from along the circumference of the coring drill bit (i.e., an annular ring) where the diamond drill bit would have drilled around the core and into the saltstone. This annular ring along the circumference of the core is assumed to produce finely crushed material that may be suitable for mixing into crop or garden soil.

The calculated SDU drill cutting inventory was developed by assuming a half-inch thick ring of saltstone from around the saltstone core (the core is assumed to have a 7-inch diameter, such that surrounding it with a half-inch ring results in an 8-inch diameter hole for the water well). The height of the drill cuttings is limited to the height of the saltstone within the drilled SDU.

Because this is not considered a credible scenario, the drill cutting inventory for this scenario is based on the best estimate (or realistic) inventory assumptions. The realistic inventory values (see Table 3.3-5) for selected SDUs were divided by the volume of saltstone within the SDU to generate an estimated saltstone concentration. This concentration was then applied to the mass of the annular ring of saltstone from around the saltstone core to estimate the total inventory of the assumed drill cutting material. These inventory estimates are provided in Table 6.2-2. Section 6.3.2 provides the Acute IHI doses based on this inventory approach.

Table 6.2-2: Assumed SDU Drill Cutting Inventories (Ci) for Drilling Through Saltstone

Radionuclide	SDU 1	SDU 4	150-foot Diameter SDUs (SDU 3B)	375-foot Diameter SDUs
Ac-227	3.34E-12	6.20E-11	6.21E-12	1.24E-11
Al-26	3.43E-07	6.33E-07	1.34E-06	2.69E-06
Am-241	3.02E-09	1.40E-05	7.83E-04	1.57E-03
Am-242m	8.12E-11	1.13E-08	3.80E-07	7.59E-07
Am-243	1.85E-09	3.36E-07	3.16E-07	6.31E-07
C-14	1.72E-06	4.22E-06	2.91E-05	5.82E-05
Cf-249	1.11E-18	1.73E-07	2.44E-18	4.88E-18
Cf-251	3.98E-20	5.95E-08	8.57E-20	1.71E-19
Cl-36	1.28E-13	9.70E-09	4.95E-08	9.90E-08
Cm-243	3.84E-10	3.42E-09	1.45E-09	2.90E-09
Cm-244	1.89E-09	1.01E-05	5.63E-06	1.13E-05
Cm-245	3.55E-10	5.05E-07	4.26E-09	8.52E-09
Cm-247	2.08E-19	6.90E-08	4.39E-19	8.78E-19
Co-60	4.60E-11	3.73E-09	4.22E-07	8.44E-07
Cs-135	6.48E-08	1.12E-06	6.67E-08	1.33E-07
Cs-137	5.33E-06	7.10E-02	1.22E-02	2.45E-02
Eu-152	7.60E-10	1.80E-08	4.40E-07	8.80E-07
Eu-154	1.48E-10	4.37E-07	4.06E-06	8.12E-06
H-3	6.04E-06	7.97E-06	1.71E-04	3.41E-04
I-129	2.63E-07	1.80E-07	8.42E-07	1.68E-06
K-40	1.28E-13	9.70E-09	4.95E-08	9.90E-08
Nb-93m	9.84E-07	1.25E-03	4.88E-06	9.76E-06
Nb-94	2.65E-09	5.79E-08	7.53E-09	1.51E-08
Ni-63	1.37E-07	1.78E-06	1.10E-05	2.19E-05
Np-237	5.16E-09	3.74E-07	6.36E-07	1.27E-06
Pa-231	5.33E-12	9.89E-11	1.60E-11	3.20E-11
Pb-210	5.52E-13	2.10E-11	1.27E-12	2.54E-12
Pt-193	1.65E-06	4.44E-06	3.81E-06	7.61E-06
Pu-238	8.09E-09	1.74E-04	7.98E-03	1.60E-02
Pu-239	1.87E-08	3.80E-05	4.94E-04	9.89E-04
Pu-240	1.76E-08	4.72E-05	1.03E-04	2.06E-04
Pu-241	1.08E-08	2.34E-05	9.38E-04	1.88E-03
Pu-242	2.05E-09	2.68E-06	1.67E-07	3.33E-07
Pu-244	1.33E-11	1.09E-08	7.70E-10	1.54E-09
Ra-226	1.25E-12	5.37E-11	3.56E-12	7.12E-12
Ra-228	1.01E-11	1.36E-10	1.44E-08	2.87E-08
Se-79	4.50E-07	6.33E-06	5.02E-06	1.00E-05
Sm-151	6.25E-09	1.10E-05	2.15E-04	4.31E-04
Sn-126	1.60E-06	1.44E-06	1.95E-05	3.90E-05
Sr-90	1.28E-08	9.75E-04	2.02E-01	4.04E-01
Tc-99	6.45E-05	4.12E-04	1.19E-03	2.37E-03
Th-229	6.98E-10	2.36E-06	2.88E-09	5.76E-09
Th-230	8.48E-11	4.10E-09	2.50E-10	5.01E-10
Th-232	1.01E-11	1.36E-10	1.44E-08	2.87E-08
U-232	7.06E-10	6.31E-08	1.98E-09	3.96E-09
U-233	1.02E-07	5.75E-06	6.45E-07	1.29E-06
U-234	1.30E-07	5.83E-06	1.07E-06	2.14E-06
U-235	3.29E-09	6.08E-08	2.61E-08	5.22E-08
U-236	8.50E-09	5.42E-08	5.84E-08	1.17E-07
U-238	1.41E-08	5.15E-08	8.47E-07	1.69E-06
Zr-93	1.01E-06	5.29E-06	4.95E-06	9.90E-06

6.2.2 Chronic IHI at the 1-Meter Well Scenarios

For the Chronic IHI at the 1-Meter Well Scenarios, the human receptor is assumed to be a resident farmer that uses a well at the 1-meter SDF boundary as the primary source of water and has mixed contaminated drill cuttings into the soil of their crops. For the IHI at the 1-Meter Well Scenarios, the total ground water pathways dose is determined as the sum of the doses from each of these pathways, while the total all pathways doses is determined as the sum of total ground water pathways dose and the drill cuttings contributions. Based on the relatively low results of the air pathways dose at 100-meters (see Section 5.3), any impacts from the airborne pathways dose is expected to be negligible relative to the impacts drill cuttings and ground water concentrations and were not included in this analysis.

The ingestion pathways are:

- Direct ingestion of contaminated well water,
- Ingestion of soil that has been irrigated with the contaminated well water and mixed with contaminated drill cuttings,
- Ingestion of produce irrigated with contaminated well water and grown in soils that include the contaminated drill cuttings,
- Ingestion of meat from livestock raised with contaminated well water and fed fodder grown in soils that include the contaminated drill cuttings,
- Ingestion of milk from livestock raised with contaminated well water and fed fodder grown in soils that include the contaminated drill cuttings,
- Ingestion of poultry raised with contaminated well water and fed fodder grown in soils that include the contaminated drill cuttings,
- Ingestion of eggs from poultry raised with contaminated well water and fed fodder grown in soils that include the contaminated drill cuttings, and
- Ingestion of fish from the contaminated stream (see Section 5.4.2.2).

The direct exposure pathways are:

- Exposure to soil that has been irrigated with the contaminated well water and mixed with contaminated drill cuttings,
- Exposure to water during showers using the contaminated well water,
- Exposure to water while swimming in the contaminated stream (see Section 5.4.2.2), and
- Exposure to water while boating in the contaminated stream (see Section 5.4.2.2).

The inhalation pathways are:

- Inhalation during irrigation using the contaminated well water,
- Inhalation of dust from soil that has been irrigated with the contaminated well water and mixed with contaminated drill cuttings,
- Inhalation during showers using the contaminated well water, and
- Inhalation while swimming in the contaminated stream (see Section 5.4.2.2).

These pathways are defined in Section 4.4.8.2. For this scenario, two sources of water concentrations are assumed: the 1-meter well and the stream. These concentrations are determined as described in Section 6.2.2.1 and Section 5.4.2.2, respectively. Additionally, a drill

cutting source is also assumed (see Table 6.2-1). Dose results from the Chronic IHI at the 1-Meter Well Scenarios are presented in Section 6.4.

6.2.2.1 Ground Water Concentrations for Use in the IHI at the 1-Meter Well Scenarios

Unlike the 100-meter SDF boundary, the 1-meter SDF boundary has not been subdivided by sectors to facilitate detailed analyses (see Section 5.4.1.1). Instead, the entire 1-meter SDF boundary is treated as a single source.

Along the SDF 1-meter boundary line, there are hundreds of nodes. These nodes each represent potential points of assessment (i.e., potential 1-meter wells) for the Chronic IHI at the 1-Meter Well Scenarios. In addition to the coordinate locations for each well, these wells also have a vertical, or depth, component; the concentrations from each well could be influenced by the aquifer from which water is drawn (UAZ, LAZ, or GAU).

For the SDF dose assessments, the vertical component is simplified by using the same approach as for the 100-meter wells (i.e., assuming the highest concentration of each contaminant regardless of the depth). Similarly, the concentration of each contaminant is based on the node with the highest recorded concentration regardless of location along the boundary. Conceptually, this is equivalent to assuming that the IHI is changing well locations from year-to-year in order to maximize their exposures.

These concentration results, along with the soil drill cutting inventories from Table 6.2-1 and the seepline concentrations based on the seepline ratio (see Section 5.2.3), were then applied to the dose calculations, giving time histories for the ground water doses for the Chronic IHI at the 1-Meter Well Scenario (with Soil Drill Cutting Inventory). The dose results from this scenario are presented in Section 6.4.1. Results for alternative scenarios, using different drill cutting inventories are provided in Sections 6.4.2 and 6.4.3

6.2.3 Chronic IHI at Selected Wells Scenario

The Chronic IHI at Selected Wells Scenario is identical to the Chronic IHI at the 1-Meter Well Scenario (with Soil Drill Cutting Inventory) except that explicit nodes were selected as potential IHI well locations based on their proximity to selected SDUs and the prevailing directions of ground water flow. Table 6.1-1 provides a description for each of these IHI Wells. They are depicted in Figure 6.1-1 as colored diamonds adjacent to select SDUs.

Ground water concentrations at each of these IHI Well locations were determined. These concentrations, along with the drill cutting inventories from Table 6.2-1 and the seepline concentrations based on the seepline ratio (see Section 5.2.3), were then applied to the dose calculations, giving time histories for the ground water doses for the Chronic IHI at Selected Wells Scenario. The dose results from this scenario are presented in Section 6.5.

6.3 Acute IHI Well Driller Dose Results

For the Acute IHI Well Driller Scenario, the human receptor is assumed to be a non-resident well driller that is exposed to contaminants for a brief period of time while installing a well. Two well

drilling scenarios are considered. For demonstrating compliance with performance objectives, a reasonable scenario assumes that the well-driller intrudes into contaminated soils within the facility boundary (i.e., adjacent to the SDUs) as discussed in Section 6.3.1. Alternatively, an *advertent* (i.e., purposeful) human intruder scenario is also considered which assumes that the well-driller intrudes directly into and all the way through an SDU (see Section 6.4.1).

6.3.1 Dose Results for the Acute IHI Based on Soil Drill Cuttings

The inventory values assumed for the soil intrusion are provided in Table 6.2-1. For this scenario, it is assumed that the intrusion occurs as soon as the Institutional Control Period ends (i.e., 100 years after SDF closure). For both the Compliance Period and the Performance Period, the Acute IHI dose results were orders of magnitude lower than the performance objective (500 mrem). Figure 6.3-1 and Figure 6.3-2 provide a visual depiction of these doses over time and Table 6.3-1 summarizes the peak doses.

Figure 6.3-1: Acute IHI Dose Results within 10,000 Years

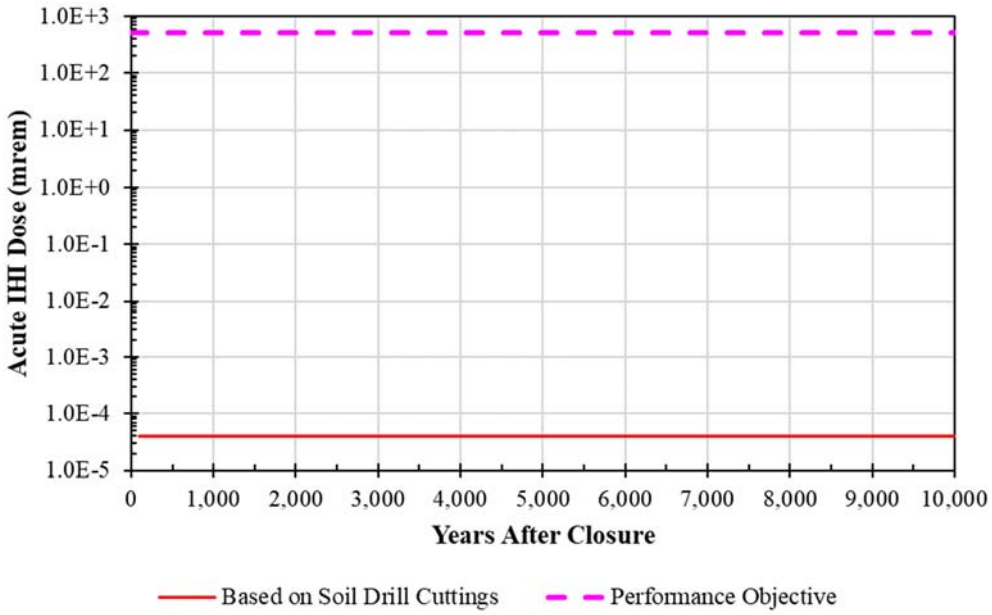

Table 6.3-1: Acute IHI Dose Results

Period	Peak Dose (mrem)	Year of Peak	Performance Objective per DOE M 435.1-1
Compliance Period (0 to 1,000 Years)	4.1E-05	100	500 mrem in 1,000 years
Performance Period (0 to 10,000 Years)	4.1E-05	100	

Analysis of these results shows that the peak of the Acute IHI dose from the soil-based drill cuttings is predominantly from I-129, with incidental ingestion of dust (e.g., contaminated soils) during drilling being the dominant exposure pathway.

Figure 6.3-2: Acute IHI Dose Results within 10,000 Years (Detail)

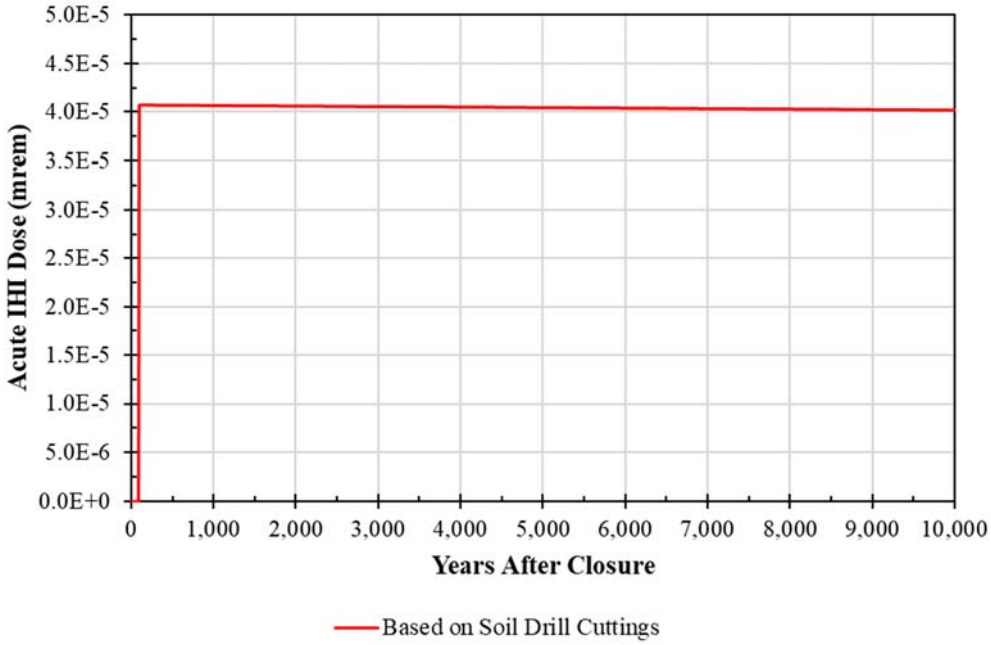

6.3.2 Alternative Dose Results for the Acute IHI Based on SDU Drill Cuttings

As was described in Section 6.2.1.2, given the material properties and current well drilling practices, any scenario which assumes that a driller would penetrate directly into an SDU is not considered a credible scenario and does not represent an expected condition. Intrusion through an SDU requires purposeful intent, thereby making it an *advertent* human intrusion as opposed to an inadvertent human intrusion. Regardless, evaluating the impact from such an event does provide valuable insights with respect to potential dose risk, but it must be noted that these results are provided for informational purposes only.

For this evaluation, the assumed time of intrusion are based on the "conservative estimate" for SDU roof degradation (see Table 4.4-45) and uses the drill cutting inventory values from Table 6.2-2. Therefore, the peak dose from drilling through an SDU is dependent upon which SDU is assumed to be the source (Figure 6.3-3). The timing of the peak always occurs at the assumed time of intrusion and all of these peak doses are below the 500 mrem performance objective for the Acute IHI dose, with the highest peak dose (2.6 mrem at approximately 1,400 years) being associated with the 375-foot diameter SDUs.

Regardless of the SDU being intruded upon, or the timing of the peak dose, the radionuclides contributing to the doses at the times of the peaks include: Pu-239, Sn-126, Pu-240, and Am-241. These radionuclides are relatively immobile such that the only way that an intruder would be subject to exposure to these would be from a direct intrusion into and through the SDU. Ingestion of dust while drilling is the predominant exposure pathway for this scenario.

Figure 6.3-3: Acute IHI Dose Results within 10,000 Years Based on Assuming Drill Cuttings from Drilling All the Way through an SDU (Detail)

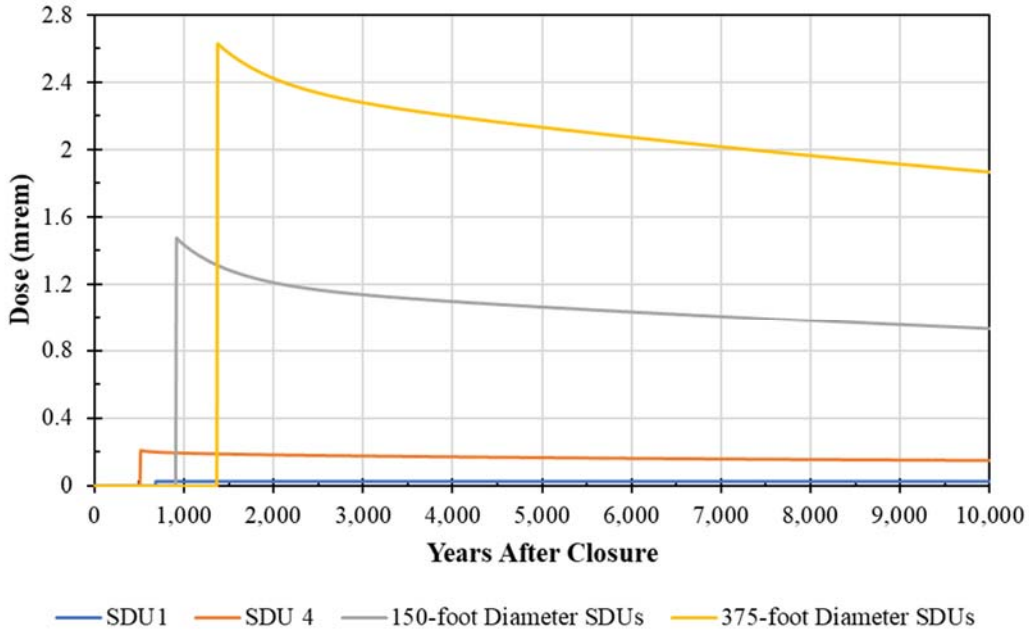

Note that prior to these postulated drilling events, the contaminants within saltstone are subject to ongoing releases and transport via diffusive and advective processes. As such, once the drilling intrusion occurs, it is expected that some of the inventory from within saltstone will have been depleted; however, the SDU drill cutting inventories in Table 6.2-2 are based on disposal values and were not modified to reflect releases prior to the intrusion. As such, these dose results overestimate the risks associated with drilling through an SDU.

6.4 Chronic IHI at the 1-Meter Well Dose Results

For the Chronic IHI at the 1-Meter Well Scenario, the human receptor is assumed to be a resident farmer that uses a well at the 1-meter SDF boundary as the primary source of water and has mixed contaminated drill cuttings into the soil of their crops.

6.4.1 Dose Results for the Chronic IHI at the 1-Meter Well Based on Soil Drill Cuttings

As with the Acute IHI Scenario, it is assumed that the intrusion occurs as soon as the Institutional Control Period ends (i.e., 100 years after SDF closure). For both the Compliance Period and the Performance Period, the Chronic IHI dose results were lower than the performance objective (100 mrem). Although these doses are relatively low, it is worth noting that the development of the assumed soil inventories (Table 6.2-1) included a number of assumptions to ensure greater defensibility. Specifically, despite the drilling event occurring 100 years after SDF closure, the drill cutting inventory for each radionuclide is based on the maximum ground water concentration over 20,000 years, then scaled to the full 100-foot height of the drill cutting volume and increased by an additional scaling factor to assume closer proximity to the SDU (see discussion in Section 6.2.1.1). Figure 6.4-1 and Figure 6.4-2 provide visual depictions of these doses over time and Table 6.4-1 summarizes the peak doses.

Figure 6.4-1: Chronic IHI at the 1-Meter Well Dose Results within 10,000 Years

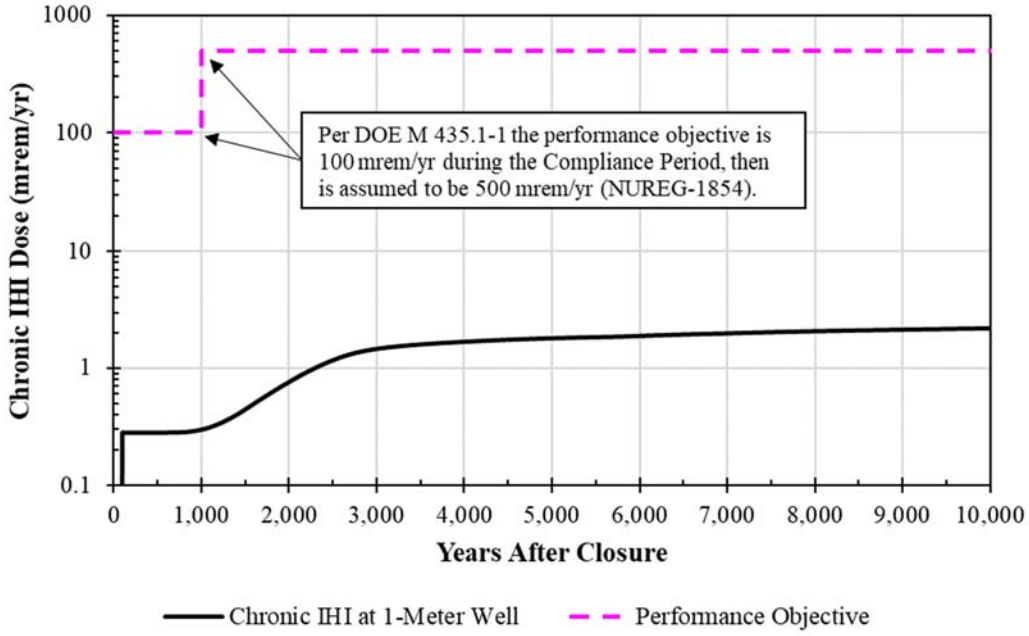

Figure 6.4-2: Chronic IHI at the 1-Meter Well Dose Results within 10,000 Years (Detail)

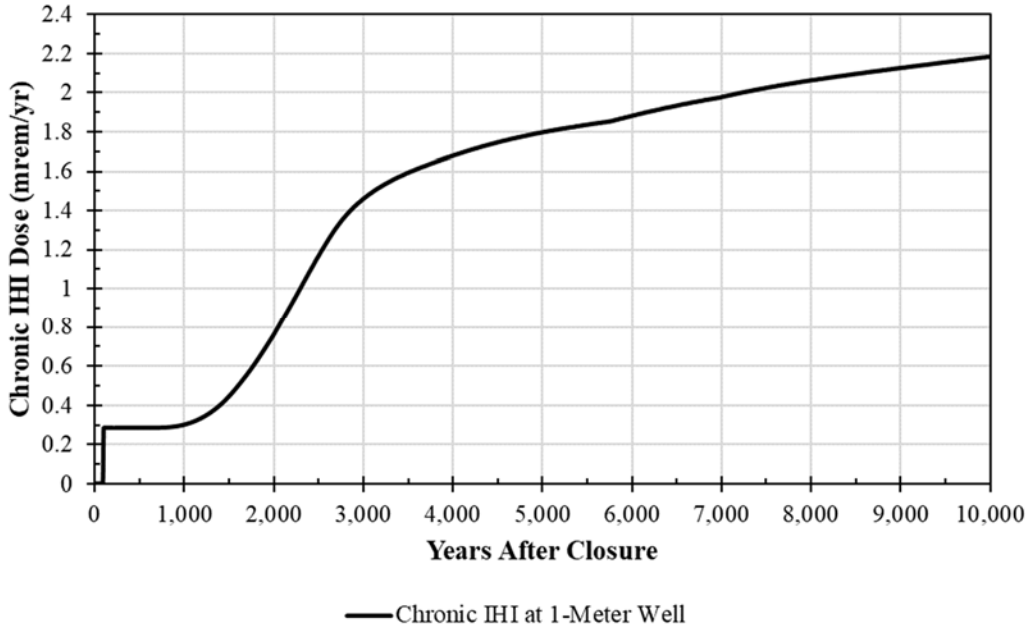

Table 6.4-1: Chronic IHI at the 1-Meter Well Dose Results

Period	Peak Dose (mrem/yr)	Year of Peak
Compliance Period (0 to 1,000 Years)	0.30	1,000
Performance Period (0 to 10,000 Years)	2.2	10,000

Analysis of these results shows that the peak of the Chronic IHI dose from the soil-based drill cuttings is predominantly from Tc-99 and I-129. At the time of the drilling event (i.e., 100 years after closure), nearly 100% of the dose contribution is from Tc-99 from the drill cuttings being mixed into the soils used for gardening. As concentrations from the 1-meter well increase over time, the doses also increase. The contributions from Tc-99 reach a peak of approximately 1.2 mrem/yr near 8,000 years after closure, but the contributions from I-129 continue to increase throughout the Performance Period. Within the Compliance Period, the primary exposure pathway is the ingestion of plants (fruits or vegetables) that are grown in a garden that is assumed to be contaminated from irrigation and from drill cuttings that are mixed into the soil. At approximately 2,000 years, the ingestion of contaminated ground water from the 1-meter well becomes the dominant exposure pathway.

6.4.2 Alternative Dose Results for the Chronic IHI at the 1-Meter Well Based on No Drill Cuttings (Ground Water Only)

Since the contaminants for the Chronic IHI scenario are introduced through both drill cuttings mixed into soils and from the use of contaminated well water from the 1-meter well, it can be difficult to evaluate the potential risks associated with these various contaminated media. To provide additional insight, an alternative scenario was developed in which only the ground water pathways are considered (i.e., no drill cuttings).

When assuming no drill cuttings, the peak dose to the Chronic IHI is less than 0.02 mrem/yr during the Compliance Period (within 1,000 years) and 1.9 mrem/yr during the Performance Period. As shown in Figure 6.4-3, the drill cuttings add approximately 0.3 mrem/yr to the Chronic IHI dose. As such, the drill cuttings account for nearly all of the risk associated with the peak during the Compliance Period, but become less risk-significant during the Performance Period as the dose contributions from the ground water concentrations increase.

Figure 6.4-3: Chronic IHI at the 1-Meter Well Dose With and Without Soil Drill Cuttings (Detail)

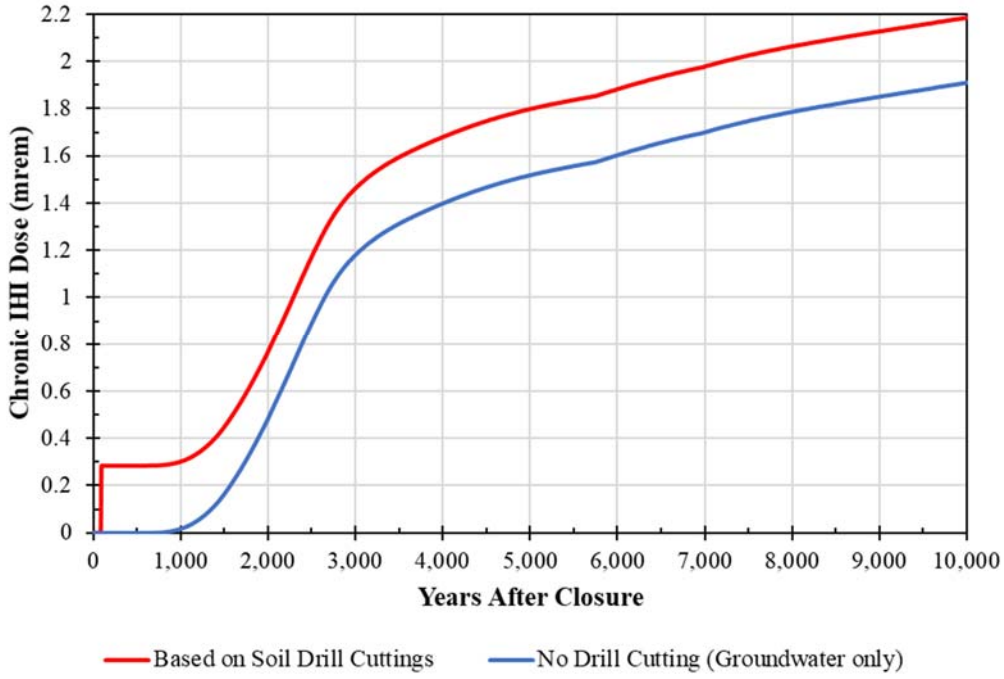

6.4.3 Alternative Dose Results for the Chronic IHI at the 1-Meter Well Based on SDU Drill Cuttings

As with the Acute IHI dose (see Section 6.3.2), a scenario that assumes that the drill cuttings come directly from drilling through an SDU (rather than soils) was also considered for the Chronic IHI doses. Again, this not considered a credible scenario and does not represent an expected condition: intrusion through an SDU requires purposeful intent, thereby making it an *advertent* human intrusion as opposed to an inadvertent human intrusion. Regardless, this scenario provides valuable insights, but it should be noted that these results are provided for informational purposes only.

As with the Acute IHI Scenario using the SDU drill cuttings, the peak dose depends on the SDU being intruded upon and the assumed timing for the intrusion. For this evaluation, the assumed timing of intrusion is based on the "conservative estimate" for SDU roof degradation (see Table 4.4-45) and uses the drill cutting inventory values from Table 6.2-2.

In this scenario, the peak dose to the Chronic IHI is 86 mrem/yr within the Compliance Period (based on the 150-foot diameter SDUs) and 170 mrem/yr within the Performance Period (based on the 375-foot diameter SDUs) as shown in Figure 6.4-4. For both of these peaks, the majority of the dose (approximately 90%) comes from Tc-99, with Pu-239 being the next highest dose contributor (approximately 5%). The primary exposure pathway is the ingestion of contaminated plants (fruits or vegetables) that are grown in a garden that is assumed to be contaminated from the drill cuttings that are mixed into the soil and irrigated with water from the 1-meter well.

As with the Acute IHI doses described in Section 6.3.2, these results are expected to overestimate the dose risk because the SDU drill cutting inventories in Table 6.2-2 are based on disposal values and were not modified to reflect any releases prior to the assumed time of intrusion.

Figure 6.4-4: Chronic IHI Dose Results within 10,000 Years Based on Assuming Drill Cuttings from Drilling All the Way through an SDU

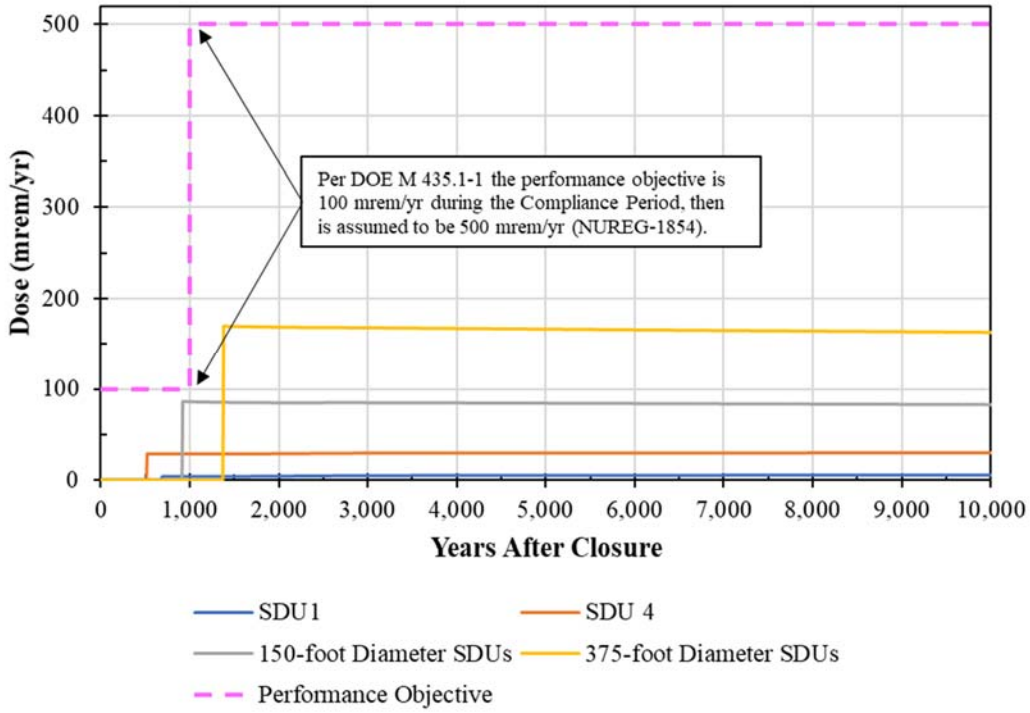

6.5 Chronic IHI at Selected Wells Dose Results Based on Soil Drill Cuttings

The Chronic IHI at Selected Wells Scenario is identical to the Chronic IHI at the 1-Meter Well Scenario (see Section 6.4) except explicit locations were selected as potential IHI well locations (see Figure 6.1-1). These locations were selected based on proximity to select SDUs and the prevailing direction of ground water flow, as described in Section 6.1.

Because the same drill cutting inventory is assumed for each of these IHI wells and the drill cutting inventory provides the dominant source for contributing the Chronic IHI dose within the Compliance Period, all seven well locations had nearly the same peak dose within the Compliance Period as from the Chronic IHI at the 1-Meter Well Scenario (0.30 mrem/yr at 1,000 years). As ground water concentrations increase, the doses at each location begin to vary. Table 6.5-1 summarizes the peak doses to the Chronic IHI, while Figure 6.5-1 provides a visual depiction of these doses over time. These values are below the performance objective of 100 mrem/yr within 1,000 years (per DOE M 435.1-1) and 500 mrem/yr beyond 1,000 years (per NUREG-1854). [ML072360184] These results indicate that the maximum concentrations along the 1-meter boundary provides the highest dose results relative to the selected IHI well locations.

Table 6.5-1: Chronic IHI at Selected Wells Dose Results

IHI Location	Compliance Period (0 to 1,000 Years)		Performance Period (0 to 10,000 Years)	
	Peak Dose (mrem/yr)	Year of Peak	Peak Dose (mrem/yr)	Year of Peak
IHI Well 1	0.28	1,000	1.9	10,000
IHI Well 2	0.28	1,000	1.8	10,000
IHI Well 3	0.28	1,000	1.3	10,000
IHI Well 4	0.30	1,000	1.8	10,000
IHI Well 5	0.28	1,000	0.78	10,000
IHI Well 6	0.29	1,000	1.1	10,000
IHI Well 7	0.28	1,000	1.8	10,000
IHI 1-Meter Wells	0.30	1,000	2.2	10,000
IHI Peak Dose	**0.30**	**1,000**	**2.2**	**10,000**

Note the colors of the row headings correspond to the IHI Well Identifiers provided in Table 6.1-1.

Figure 6.5-1: Chronic IHI Dose Results within 10,000 Years, By Location

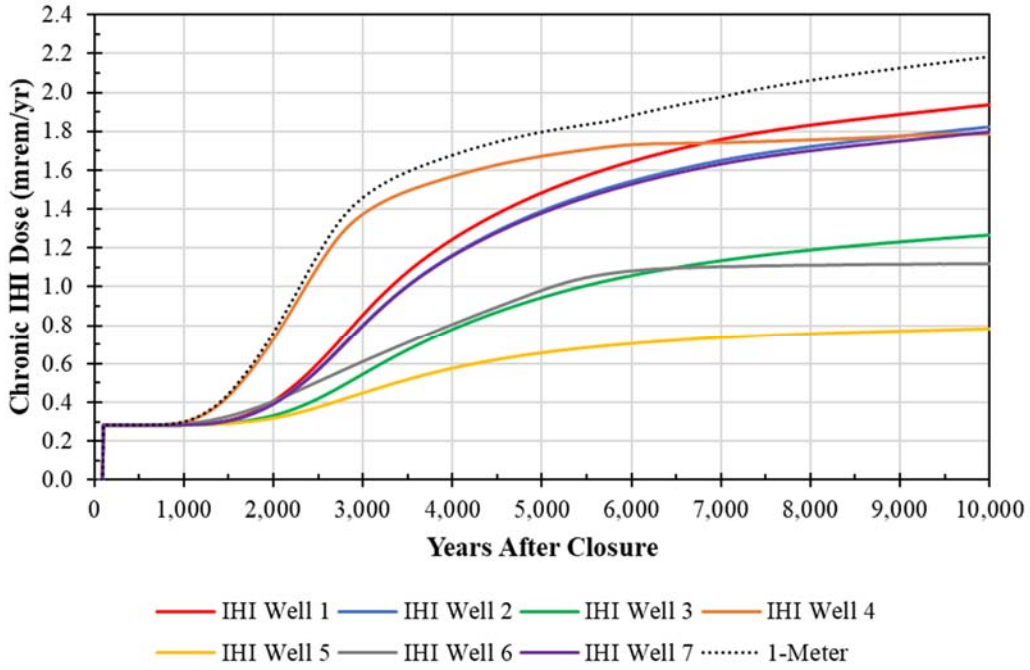

6.6 IHI Probablistic Analysis

The probabilistic analysis described in Section 5.7 focused on the results related to the doses to the MOP along the 100-meter boundary. The following analysis uses the same set of SDF GoldSim Model files from Table 5.7-4 but focuses on the doses to the Chronic IHI based on the Chronic IHI at the 1-Meter Well Scenario.

6.6.1 IHI Uncertainty Setup and Additional Considerations

The probabilistic analysis for the Chronic IHI makes a number of simplifying assumptions that require additional context to understand. The Chronic IHI at the 1-Meter Well Scenario was selected for this analysis because it is expected to be the most likely intrusion scenario. The

Chronic IHI at Selected Wells Scenario was not selected because the probability of an intrusion occurring at a single, specific point within the facility boundary is highly improbable; it is more likely that an intrusion will occur somewhere along the boundary line as opposed to one of seven single locations. Also, because the concentration results along the 1-meter boundary are almost always higher than those at the selected IHI Well locations, the Chronic IHI at the 1-Meter Well Scenario is considered to be more pessimistic when evaluating probabilistic results.

The only drill cutting inventories considered in this analysis are the soil drill cuttings. As described in Section 6.2.1.2, any scenario that assumes the driller penetrates into and all the way through an SDU does not represent a reasonable IHI scenario because it requires the IHI to exhibit purposeful intent. However, the approach used to estimate the soil drill cutting inventories in the probabilistic analysis differs from the approach described in Section 6.2.1.1. In Section 6.2.1.1, it is explained that the deterministic IHI analysis used the maximum ground water concentrations anywhere along the 1-meter boundary, for each radionuclide and from any time between 0 years and 20,000 years after SDF closure. Alternatively, for this probabilistic analysis, the contaminant concentrations in the soil drill cuttings were estimated dynamically, using the 1-meter ground water concentrations at the actual time of the drilling event. With this approach, intrusions that happen early on, before any significant releases occur, result in lower drill cutting inventories. Because this drill cutting inventory is based on a more realistic conceptual approach than those used for the deterministic modeling, the results of this analysis are expected to be more meaningful with respect to understanding risk. Regardless, this approach still assumes that the ground water concentrations are uniform throughout an entire 100-foot column of soil, and still assumes that the entire mass of the drill cutting will be mixed into the soils of the crops or gardens, so it is still expected to overestimate the doses to the IHI.

As described in Section 5.7.1.8, the timing for the intruder drilling event was set up as a uniform distribution on time. The range of this distribution was assumed to be the duration of the simulation (i.e., 0 to 20,000 years), but was then adjusted by adding 100 years to credit the institutional control period. For realizations that sample an event time greater than 19,900 years, the IHI event does not occur during the simulation. Because only a single event is assumed per realization, this distribution is equaivalent to one drilling event every 19,900 years or a frequency of occurrence of approximately 5.0E-05 per year.

If drilling into an SDU was considered a probable scenario, it would have been appropriate to delay the intiation of any such intrusion because the SDU roof is made of steel-reinforced concrete which is expected to prevent intrusions. The deterministic analysis described in Section 6.4.3 assumes that intrusion through an SDU can only occur after the SDU roof becomes fully degraded; however, as indicated by the values in Table 4.4-45, there is uncertainty associated with how long the SDU roof would take to become fully degrade.

Further, once an intrusion into an SDU is assumed, there are additional uncertainties associated with how deep the intruder might drill into the saltstone before abandoning the location and moving the well, or if they do successfully penetrate all the way though the SDU, they may proceed to drill deeper (beyond the assumed 100-foot well depth), and mix the drill cuttings with uncontaminated soils, thus reducing the contaminant concentrations within the drill cuttings.

6.6.2 IHI Uncertainty Analyses Summary Results

The most direct way to communicate the uncertain nature of the model results is to show graphs of certain key model endpoints. Figure 6.6-1 shows the peak doses for the total doses to the IHI at the 1-meter well from all 3,000 realizations. The colors of the data points indicate the random seed (RS) of the corresponding GoldSim file (see Table 5.7-4). Note that a large number of the data points occur at 20,000 years (i.e., the end of the simulation); this indicates that peak doses for these realizations would likely occur at a point in time beyond 20,000 years. Regardless, this figure shows that while all three GoldSim files provide peak doses with a wide range of variability in the timings, the magnitudes of these peak doses were relatively similar, with more than 99% of the peak doses being between 0.5 mrem/yr and 50 mrem/yr.

Figure 6.6-1: Peak Doses to the IHI at the 1-Meter Well from 3,000 Realizations

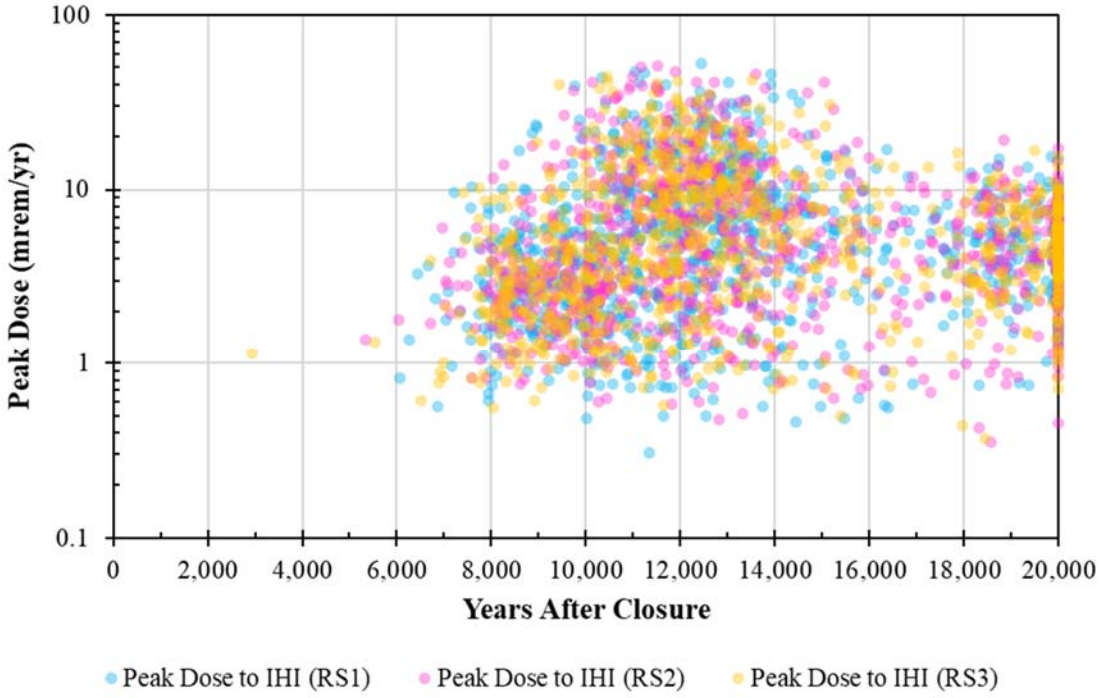

Statistics for peak values (e.g., mean of the peaks) are summarized in Table 6.6-1. These peak values are provided for three time periods: the Compliance Period (0 to 1,000 years after closure), the Performance Period (0 to 10,000 years after closure), and the simulated duration of the model (0 to 20,000 years after closure). For additional context, the peak values from the deterministic Compliance Case model (see Section 6.4) and from an SDF GoldSim Model result based on using equivalent input assumpions (see Section 6.7.1) are also included.

Table 6.6-1: Statistics of the Peak IHI Doses within Any Timestep

Statistic	Dose to the IHI at 1-Meter (mrem/yr)		
Time Period	*0 to 1,000 Years (Compliance Period)*	*0 to 10,000 (Performance Period)*	*0 to 20,000 Years (Twice the Performance Period)*
Mean	0.050	6.9	7.1
95th Percentile	0.16	21	22
Median	0.030	4.5	4.6
5th Percentile	0.0065	0.99	1.0
Benchmarked GoldSim Model (Compliance Case)	0.30	3.1	3.2
Compliance Case (PORFLOW)	0.30	2.2	2.5

The Compliance Case and the probabilistic model both handle the intrusion event in different ways. Both assume that the IHI will drill a well for water near the SDUs (or at the 1-meter boundary), and that drill cuttings from the drilling event will be mixed into the soils used for crops. However, for the deterministic Compliance Case modeling, this intrusion event is assumed to occur as soon as the Institutional Control Period ends (100 years after closure) and assumes a stylized inventory based on maximum ground water concentrations over a 20,000-year period, while the probabilistic model randomly samples timing of the IHI drilling event and uses the simulated ground water concentrations at the time of the IHI drilling event. As a result, the Compliance Case shows higher doses within the Compliance Period.

Additionally, the Compliance Case and the probabilistic model use different assumptions for determining the contaminant inventories within the drill cuttings. Within the probabilistic model, the soil inventory is calculated as a function of the 1-meter well ground water concentrations at the time of the intrusion (which makes it dependent upon the release and transport modeling), whereas the Compliance Case uses a more pessimistic assumption: it applies values that were developed based on the 20,000-year peak concentrations for every radionuclide, regardless of timing, and then scaled up by a factor of 7.79 (as described in Section 6.2.1.1). As such, the drill cuttings provide larger dose contribution for the deterministic Compliance Case, while the probabilistic results provide a more realistic representation of the risks associated with the contaminated drill cuttings.

The values presented in Table 6.6-1 do not reflect the same statistical data as the statistical values and time histories shown in the following table and figures, although these are complementary of one another. The difference between information presented in Table 6.6-1 and information below is important to understand. Table 6.6-1 shows summary statistics for peak doses achieved at *any* time within the given time frames. These are statistics of the peak values (e.g., mean of the peaks), regardless of when the peaks were achieved within the specific time frames. Alternatively, the information provided below examines statistics relative to each time step and offers peak values of the statistics (e.g., peak of mean).

Figure 5.7-3 illustrated this difference between the mean of the peaks and the peak of the means. The figure also demonstrated that the mean of the peaks can exceed the peak of the means, although in this case the statistics of the peak doses very closely reflect the peak doses of the statistics, as shown by comparing the values in Table 6.6-2 to those from Table 6.6-1.

Table 6.6-2: Peak Doses of the Statistics

Evaluated Endpoints	Peak of the Means		Peak of the Medians (50th Percentile)		Peak of the 95th Percentiles	
	Peak Dose (mrem/yr)	Time (yrs)	Peak Dose (mrem/yr)	Time (yrs)	Peak Dose (mrem/yr)	Time (yrs)
Total IHI Dose from 0 to 1,000 Years	0.050	1,000	0.030	1,000	0.16	1,000
Total IHI Dose from 0 to 10,000 Years	6.9	10,000	4.5	10,000	21	10,000
Total IHI Dose from 0 to 20,000 Years	7.0	12,420	4.6	13,590	22	11,370

Figure 6.6-2 through Figure 6.6-4 present the statistical time histories of the total dose for the Chronic IHI at the 1-meter boundary within each of the time periods considered.

Figure 6.6-2: Statistical Time History of Total IHI Doses (Any Sector) from 0 to 1,000 Years

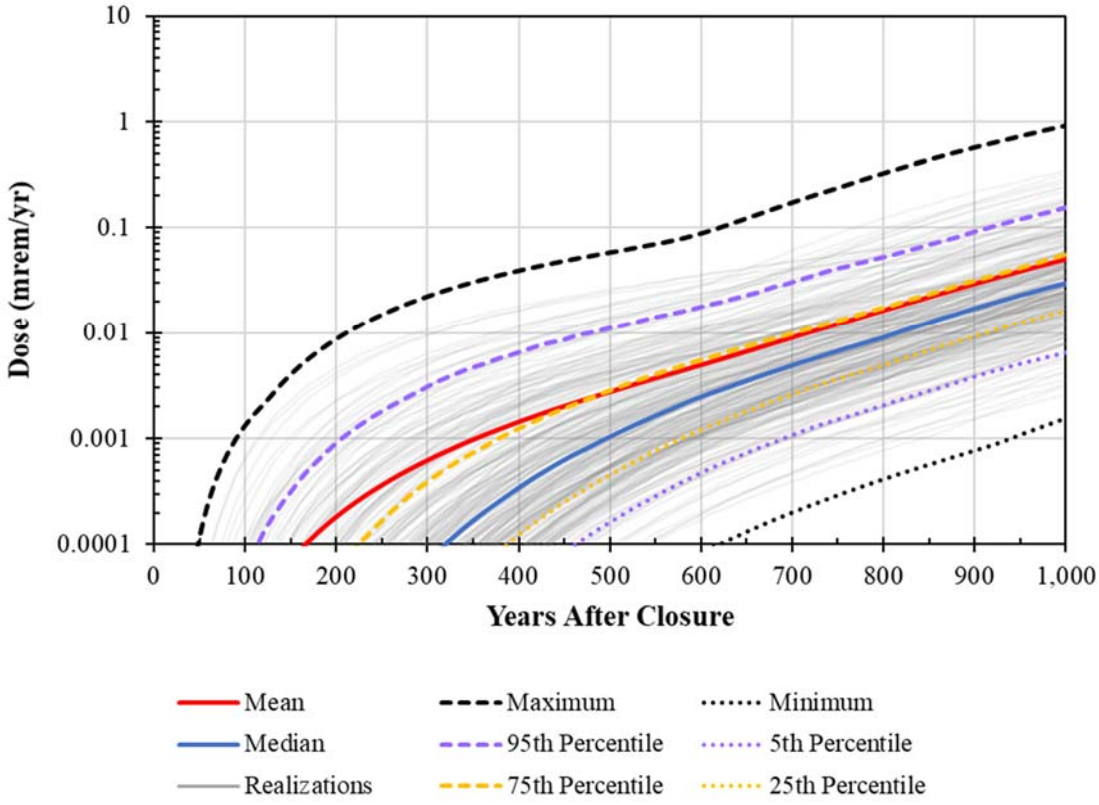

Note: For the individual realizations, only the first 245 realizations are displayed. The statistical values (e.g., Mean and Maximum) are determined using data from 3,000 individual realizations.

Figure 6.6-3: Statistical Time History of Total IHI Doses (Any Sector) from 0 to 10,000 Years

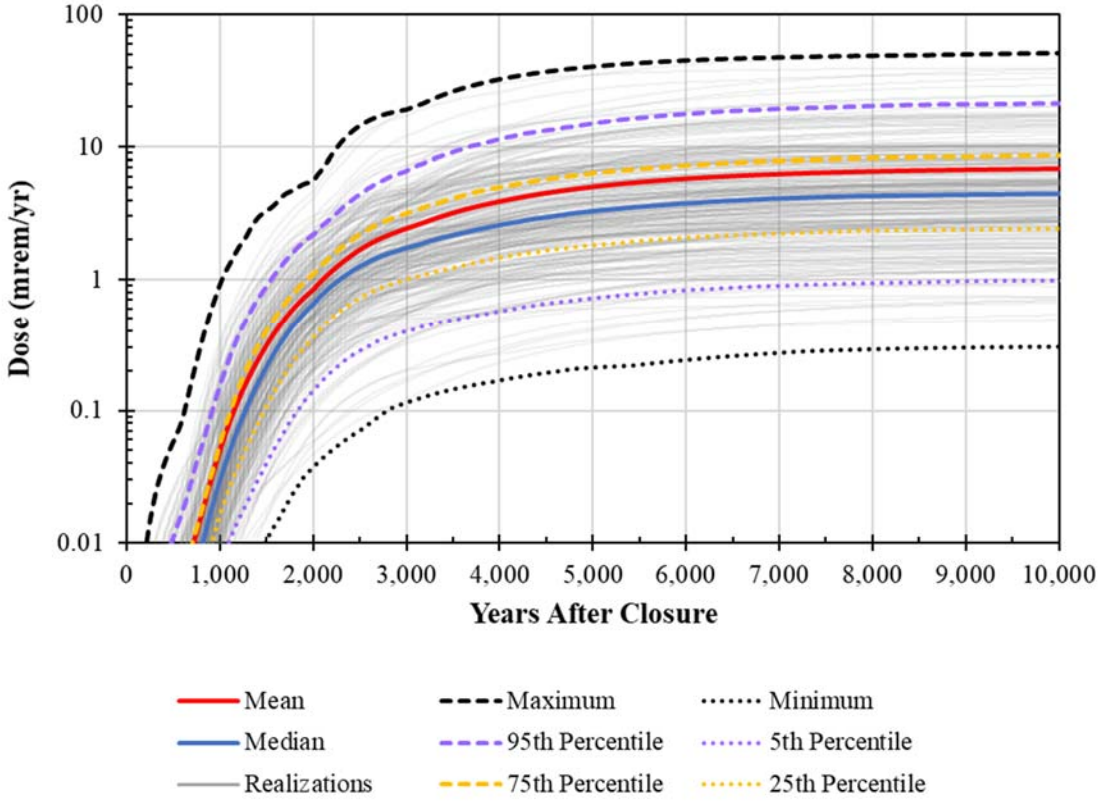

Note: For the individual realizations, only the first 245 realizations are displayed. The statistical values (e.g., Mean and Maximum) are determined using data from 3,000 individual realizations.

Figure 6.6-4: Statistical Time History of IHI Doses (Any Sector) from 0 to 20,000 Years

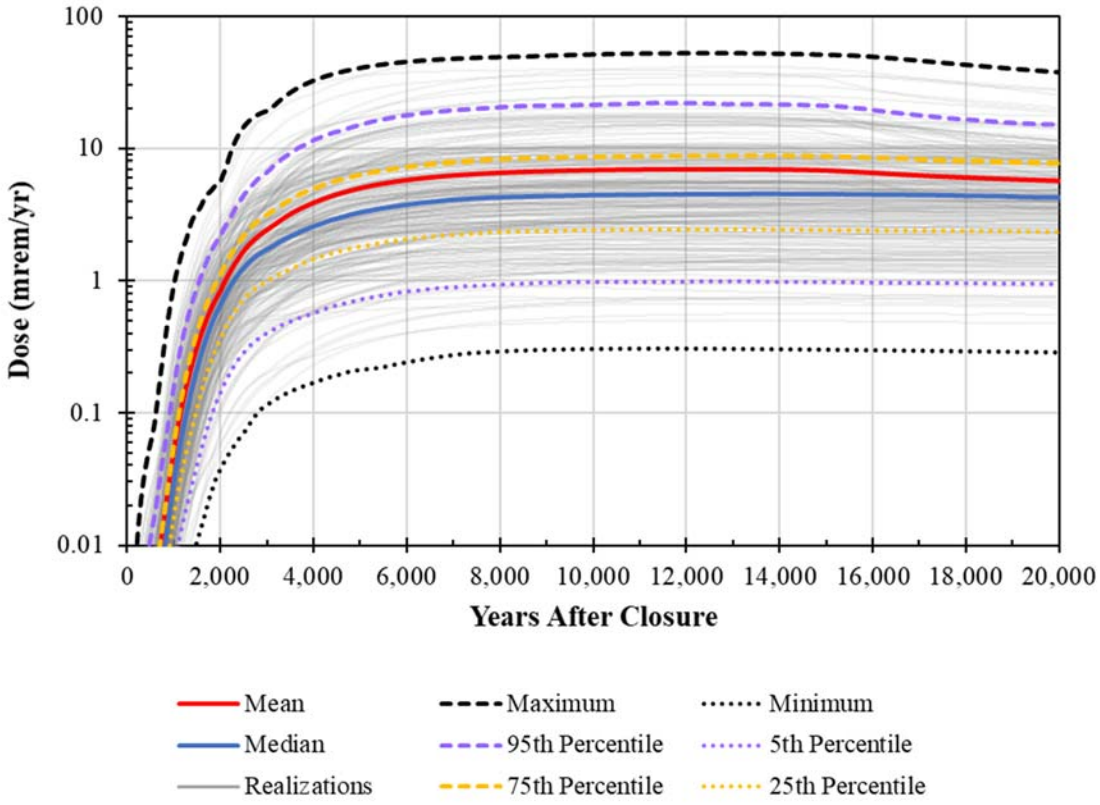

Note: For the individual realizations, only the first 245 realizations are displayed. The statistical values (e.g., Mean and Maximum) are determined using data from 3,000 individual realizations.

Figure 6.6-5 shows the mean dose to the Chronic IHI located at each of the defined IHI Wells (IHI Well 1 through 7) and the mean dose to the Chronic IHI at the 1-meter IHI boundary, at any time for 10,000 years.

Figure 6.6-5: Mean Doses to the Chronic IHI for Each IHI Well (0 to 10,000 Years)

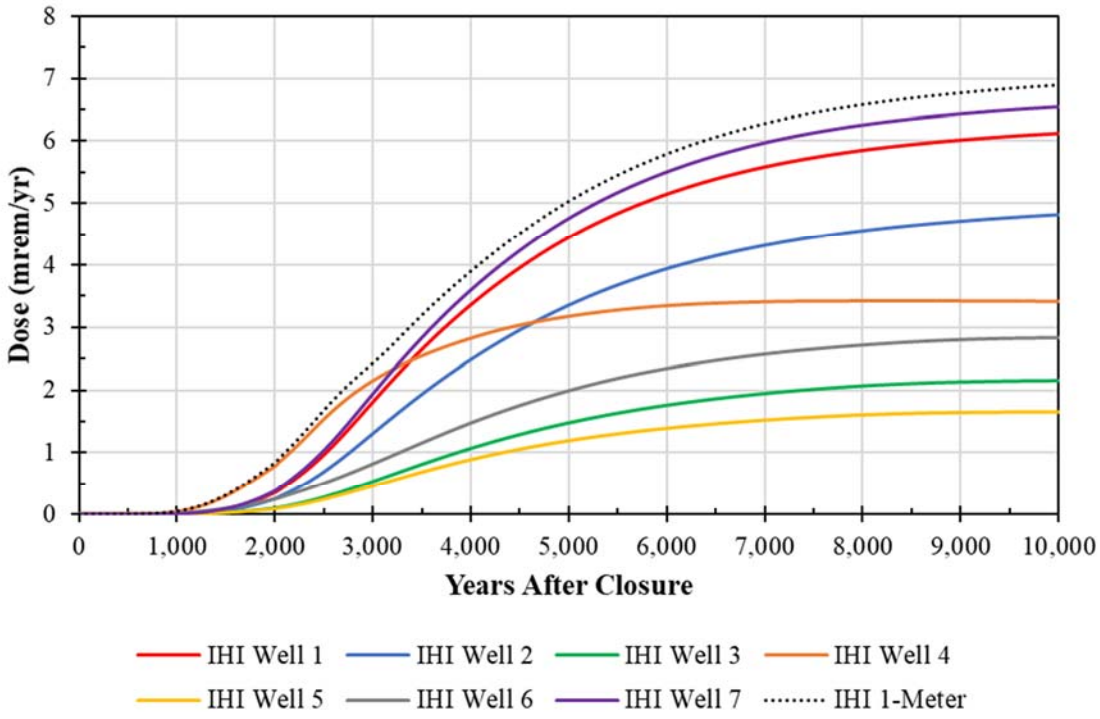

6.6.2.1 Uncertainty Analysis Insights

Based on the information presented in the uncertainty analyses section, the following general insights regarding the uncertainty analyses can be drawn.

- For all 3,000 realizations, no realization exhibited a maximum peak dose that exceeded the performance objective of 100 mrem/yr over any of the time periods considered.
- Peak doses within 20,000 years are only slightly higher than the peak doses within 10,000 years.
- The Compliance Case results are higher than the mean or median probabilistic results within the Compliance Period. The difference is attributed to the differing assumptions used for the timing of the IHI drilling event and the inventory of the drill cuttings.

6.6.3 IHI Probabilistic Analysis Results

Given the uncertainties discussed in Section 6.6.2, the next step is to quantify the extent to which specific input parameters contribute to uncertainties. Quantifying the relative importance of probabilistic model parameters is the objective of the following probabilistic sensitivity analyses. The approach is the same as the analysis of the MOP doses (from Section 5.7.4).

This section presents probabilistic sensitivity analysis results for the endpoints: total dose to the Chronic IHI along the 1-meter boundary. The inclusion of data from the first 100 years resulted in the identification of spurious parameters. To ensure that these analyses yield the parameters

with the greatest influence, the partially ranked correlation coefficients (PRCCs) analyses only considered data from 100 years to 20,000 years. As with the MOP analysis (see Section 5.7.4), PRCC results did not change much after the first 10,000 years, so the results were only displayed to 10,000 years.

6.6.3.1 Sensitivity Analysis of the Total Dose to the IHI along the 1-Meter Boundary

Figure 6.6-6 shows the PRCCs for total dose to the IHI along the 1-meter boundary. These results are similar to those for the total dose to the MOP. Initially, the vadose zone thickness beneath SDU 9 (*Vadosethick_SDU9*) is the most dominant parameter, along with soil density (*SoilDensity*). The importance of these two parameters diminishes over time. At approximately 1,000 years, the most dominant parameter becomes the infiltration rates (*Infiltration*). The assumed garden size (*GardenSize*) and the water ingestion rates (*WaterUptake*) are also consistently important.

Figure 6.6-6: PRCCs of the Total IHI Dose Along the 1-Meter Boundary, Using 3,000 Realizations

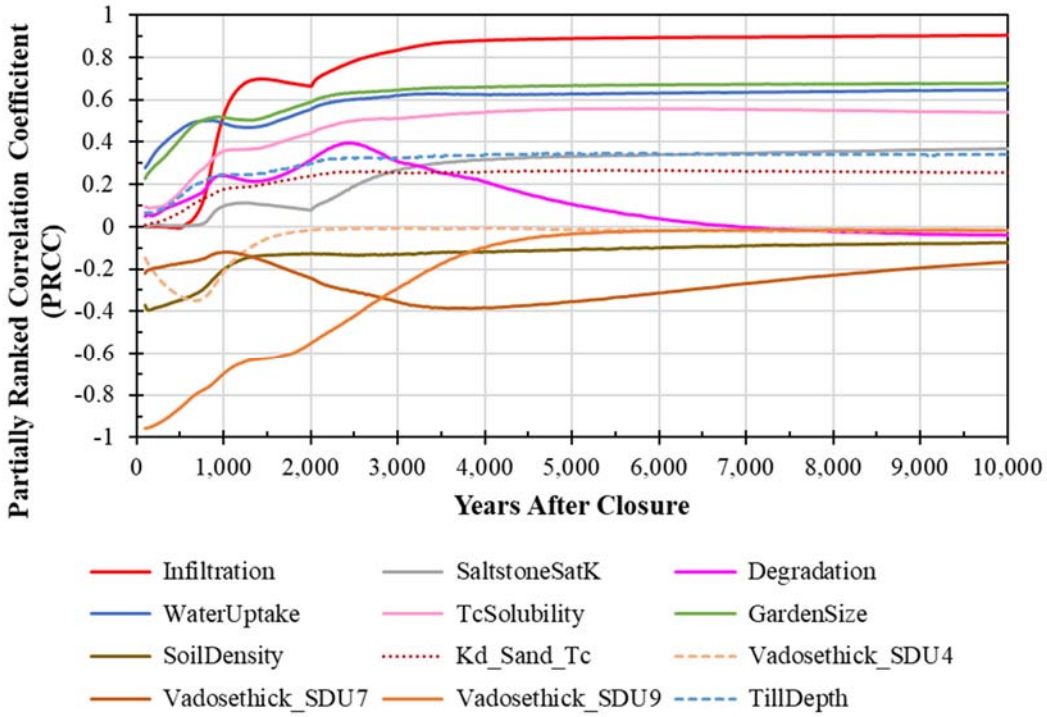

Table 6.6-3 shows the results from the stepwise regression analysis. In this analysis, the first four or five variables effectively dominate any influence over the dependent variable at the time analyzed. For each of the standardized rank regression coefficients (SRRC) analyses, the dose results are analyzed at 1,000 and 10,000 years. These results are consistent with the PRCC results.

Table 6.6-3: Top Eight SRRC Results for Total IHI Dose along the 1-Meter Boundary

Time = 1,000 years, Final Cumulative R^2 = 0.786			Time = 10,000 Years, Final Cumulative R^2 = 0.907		
Variable	**Cumulative R^2**	**SRRC**	**Variable**	**Cumulative R^2**	**SRRC**
Vadosethick_SDU9	0.262	-0.503	Infiltration	0.540	0.720
Infiltration	0.369	0.314	GardenSize	0.639	0.318
GardenSize	0.461	0.314	WaterUptake	0.725	0.291
WaterUptake	0.554	0.296	TcSolubility	0.774	0.219
TcSolubility	0.594	0.193	SaltstoneSatK	0.795	0.139
Degradation	0.613	0.121	SDU7_SatWidth	0.815	-0.133
Kd_SandL_I	0.630	-0.138	SDU6_SatWidth	0.829	0.115
TillDepth	0.646	0.134	TillDepth	0.843	0.127

6.7 Other Intruder Sensitivity Cases

Based on the analyses in Sections 6.4 and 6.5, it is apparent that additional sensitivity cases could provide more insights into the uncertainties associated with the potential doses to the IHI. These additional sensitivity cases are provided in the following sections.

6.7.1 Additional Benchmarking of the SDF GoldSim Model to Support IHI Analyses

The following sections describe IHI sensitivity cases: some of these cases rely on the use of the deterministic SDF GoldSim Model. While the benchmarking analysis (see Section 5.6.4) appropriately compared the IHI ground water modeling results from the PORFLOW simulations to the equivalent results from the GoldSim simulation, it does not include the contributions from the soil drill cuttings. As a final comparison, Figure 6.7-1 is provided to show that the application of the soil drill cutting inventories (from Table 6.2-1) affects both models in the same way. The red curve shows the SDF GoldSim Model results for the Chronic IHI dose; this curve will be used as the basis for comparison for sensitivity cases using the SDF GoldSim Model.

As noted in Section 5.6.4, dose-controlling I-129 releases from the SDF GoldSim Model are higher than those from the PORFLOW Model. Specifically, PORFLOW uses a more computationally intensive shrinking core model for generating chemical environment transition patterns (one cell at a time) and the SDF GoldSim Model assumes that larger zones (i.e., the saltstone monolith) transitions as a single unit. As such, the SDF GoldSim Model is more computationally efficient but results in larger releases within the Performance Period. Because the SDF GoldSim Model is based on a more conservative conceptual model, the results are considered acceptable.

Figure 6.7-1: Comparison of IHI 1-meter Boundary Chronic Dose Results for the PORFLOW and GoldSim Models, Including Soil Drill Cuttings

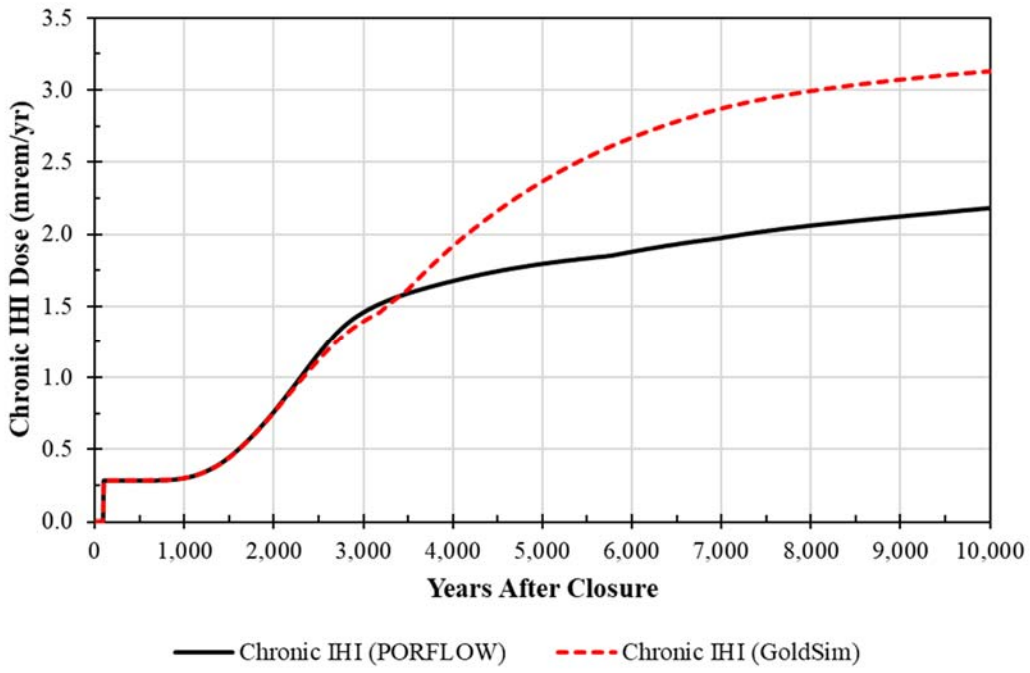

6.7.2 Evaluation of the Timing of a Soil Intrusion

The deterministic SDF GoldSim Model was used to modify the timing of the assumed IHI drilling event for multiple modeling cases. These modeling cases each assume a different time of intrusion: no intrusion, intrusion at 1,000 years, at 5,000 years, and at 10,000 years. Further, rather than using the assumed drill cutting inventories from Table 6.2-1, these sensitivity cases use the simulated ground water concentrations at the IHI 1-meter well, converted into drill cuttings.

The purpose of this set of sensitivity cases is two-fold: (1) it provides additional confirmation that the assumed drill cutting inventory from Table 6.2-1 is sufficiently bounding, and (2) it provides additional insight into how varying the timing of an intrusion event might impact the IHI results.

The results from this analysis are shown in Figure 6.7-2 and demonstrates that the assumed drill cutting inventory (i.e., the GoldSim Compliance Case) is bounding. When using an inventory based on the actual drill cuttings from the contaminated soils, the overall impact on the Chronic IHI dose is negligible, regardless of the timing of the intrusion.

Figure 6.7-2: Total Dose to the IHI Along the 1-Meter Boundary Based on the Assumed Timing of the Drilling Event (0 to 20,000 Years)

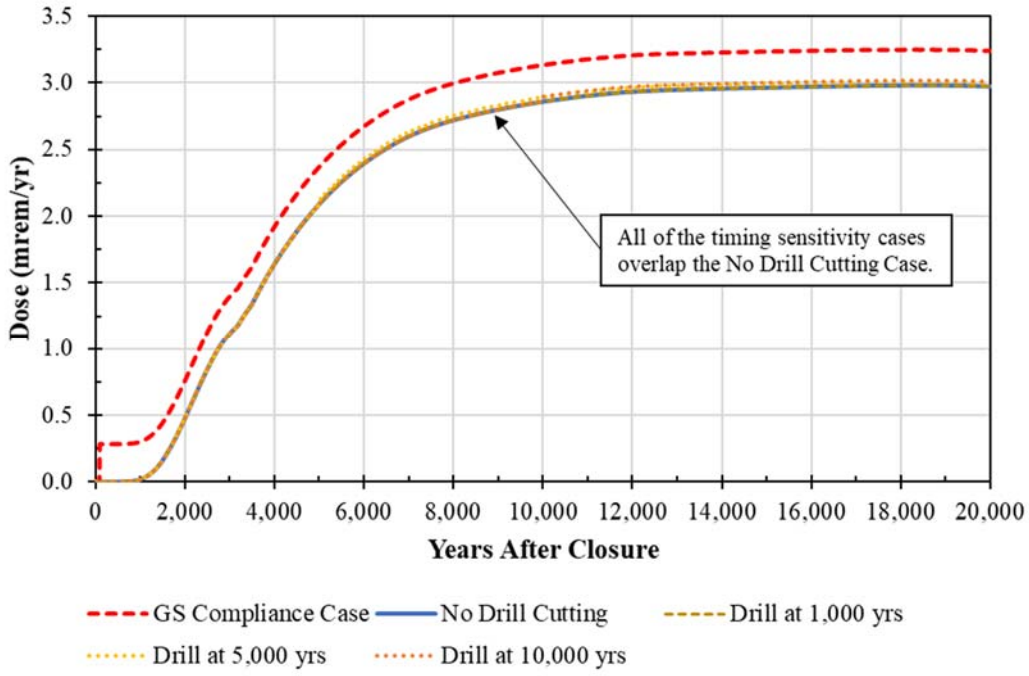

6.7.3 Evaluation of the Central Scenario IHI Doses

As described in Section 4.3, three sets of modeling inputs have been developed for this PA, reflecting three distinct modeling philosophies:

- Best estimate values (used to support a Realistic Case),
- MPAD values (used to support a Compliance Case), and
- Defensible values (used to support a Pessimistic Case).

The Compliance Case results in Sections 6.4 and 6.5 are based on the MPAD values as described throughout Section 4.4. Table 5.8-1 summarized some of the key differences between each of the three Central Scenario cases.

Figure 6.7-3 provides a visual comparison of the dose results for the Chronic IHI (using the 1-meter boundary dose) from each of the three Central Scenario modeling cases. As with the Compliance Case, these simulations used the assumed soil drill cutting inventory (from Table 6.2-1) with an intrusion event at 100 years. The ground water concentrations used in these sensitivity cases were developed using PORFLOW. The results are summarized in Table 6.7-1.

As expected, the Pessimistic Case yields higher doses than the Compliance Case. Despite the higher results, the doses to the Chronic IHI remain well below the performance objectives.

Figure 6.7-3: Chronic IHI Dose Results from the Central Scenario Cases

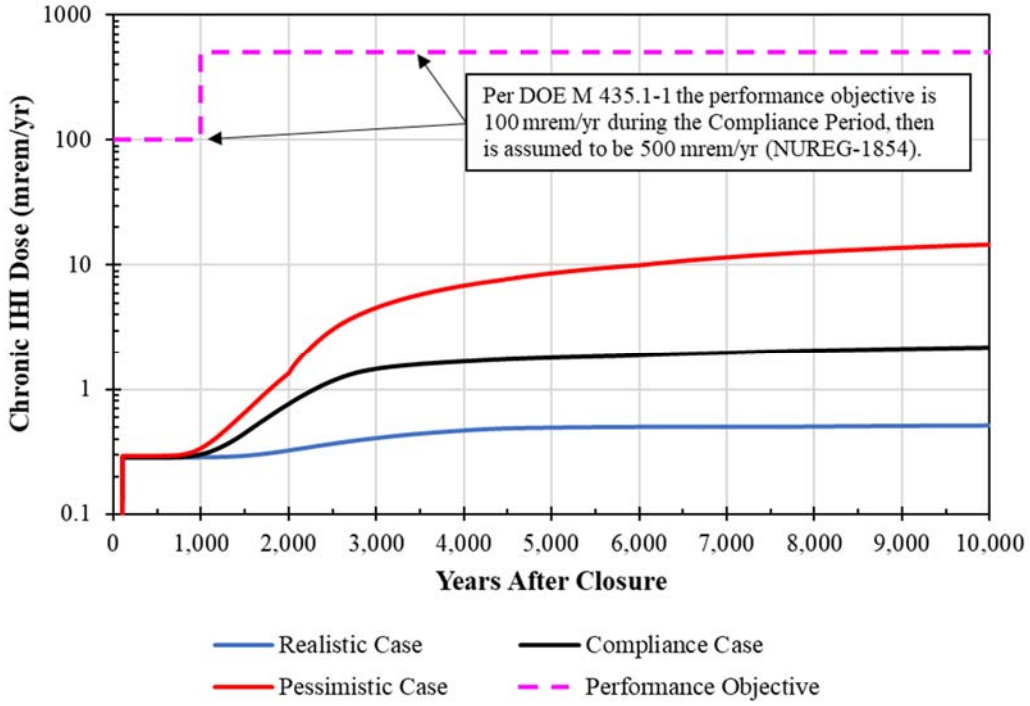

Table 6.7-1: Comparison of Central Scenario Cases, Chronic IHI Peak Ground Water Pathways Doses

Modeling Case	Compliance Period (0 to 1,000 Years)		Performance Period (0 to 10,000 Years)	
	Peak Dose (mrem/yr)	Year of Peak	Peak Dose (mrem/yr)	Year of Peak
Realistic Case	0.28	1,000	0.51	10,000
Compliance Case	0.30	1,000	2.2	10,000
Pessimistic Case	0.34	1,000	15	10,000

6.7.4 Consideration of Invertebrate Intrusion and Transport

A number of radiological sites in arid environments have asserted that ants may play a role in contaminant transport (for example, see *Biologically Induced Transport Modeling for the Clive DU PA)*. [NAC-0022_R2] While ants are present at SRS, they are not expected to play a role in contaminant transport from the SDF. The high moisture content above the impermeable HDPE layer within the closure cap is expected to create a subsurface environment that would preclude any intrusion beyond the HDPE. Further, if ant colonies do intrude beyond the closure cap (FEP 6.1.07), the Chronic IHI Scenario (see Section 6.4) may be interpreted as a non mechanistic analogue case because it assumes that the IHI is exposed to contaminated soils have been pulled up from the soils adjacent to an SDU.

7 INTERPRETATION OF RESULTS

Section 7.1 summarizes the interpretation of results presented in Sections 5 and 6. Section 7.2 provides a summary of how modeling assumptions have been applied to the SDF PA models to enhance defensibility.

7.1 Performance Assessment Results

This section provides an interpretation of the results presented in Sections 5 and 6. Sections 7.1.1 through 7.1.5 describe the processes simulated via the integrated PA system. Section 7.1.6 summarizes the dose results of the 100-meter ground water pathways. The dose to the IHI (both acute and chronic) are discussed and summarized in Section 7.1.7. Section 7.1.8 summarizes the benchmarking analysis. Finally, Section 7.1.9 summarizes the results from the probabilistic uncertainty and sensitivity analyses.

The ground water pathway dose is effectively equivalent to the all-pathways dose results, because the dose contributions from the airborne pathways are negligible, as summarized in Section 4.4.7. As such, the airborne pathways dose is not discussed further.

7.1.1 Infiltration and Flow

The primary driver for system performance is the infiltration rate entering the Vadose Zone Flow Model, which is determined by the near surface Closure Cap Model. The influence of the infiltration rate is illustrated by Figure 7.1-1 which shows the infiltration rate (blue dashed curve) superimposed over the volumetric flow rates through selected features for SDU 9 from the Vadose Zone Flow Model. The values depicted are based on the Compliance Case (or MPAD) conditions.

This discussion uses results from SDU 9 for illustrative purposes. The other 375-foot diameter SDUs (SDUs 6 through 12) all exhibit very similar behaviors. SDUs 1 and 4 and the 150-foot diameter SDUs (SDUs 2A, 2B, 3A, 3B, 5A, and 5B) are not discussed in this section because these units contain less inventory relative to the larger SDUs, so they are less risk-significant.

Figure 7.1-1 shows that aside from some minor nuances during the first 2,000 years, the volumetric flow rates controlling advective transport vary with changes in the infiltration rates. These minor nuances are associated with the degradation of the cementitious materials (i.e., SDU concrete), as discussed in Section 7.1.2. The step changes at 500 years and 2,000 years are based on the assumed timing for closure cap degradation events, as recommended by Benson and Benavides in *Predicting Long-Term Percolation from the SDF Closure Cap*. [SRRA107772-000009] Specifically, at 500 years the Compliance Case assumes that the sand drainage layer becomes less permeable. Then at 2,000 years, the Compliance Case assumes that holes in the HDPE increase in size as a result of antioxidant depletion. The basis for these assumptions is provided in SRRA107772-000009.

Figure 7.1-1: Volumetric Flow through Selected Components of SDU 9 and Infiltration Rate, Compliance Case

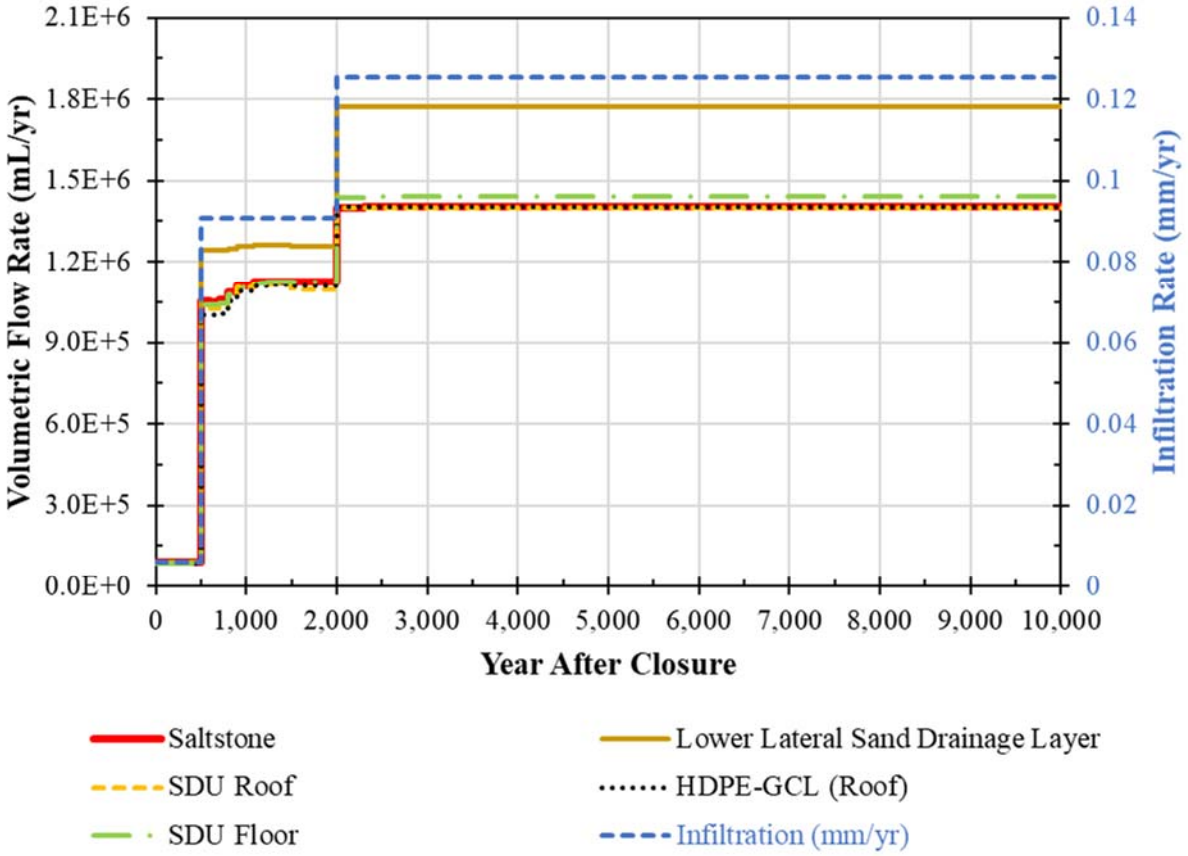

The lower lateral sand drainage layer and the HDPE above the roof were designed to promote lateral drainage so that infiltrating water would shed off the SDU roof and migrate down through the backfill. However, a different phenomenon is occurring within the Vadose Zone Flow Model for the current Compliance Case infiltration rates. Due to the much lower infiltration rates, the suction head near the top of SDU 9 is extremely high and draws moisture into the SDU (see Figure 7.1-2).

Figure 7.1-2: Cross Section of SDU 9 Showing Flow Direction and Contours to Illustrate Suction Head for Select Time Periods, Compliance Case

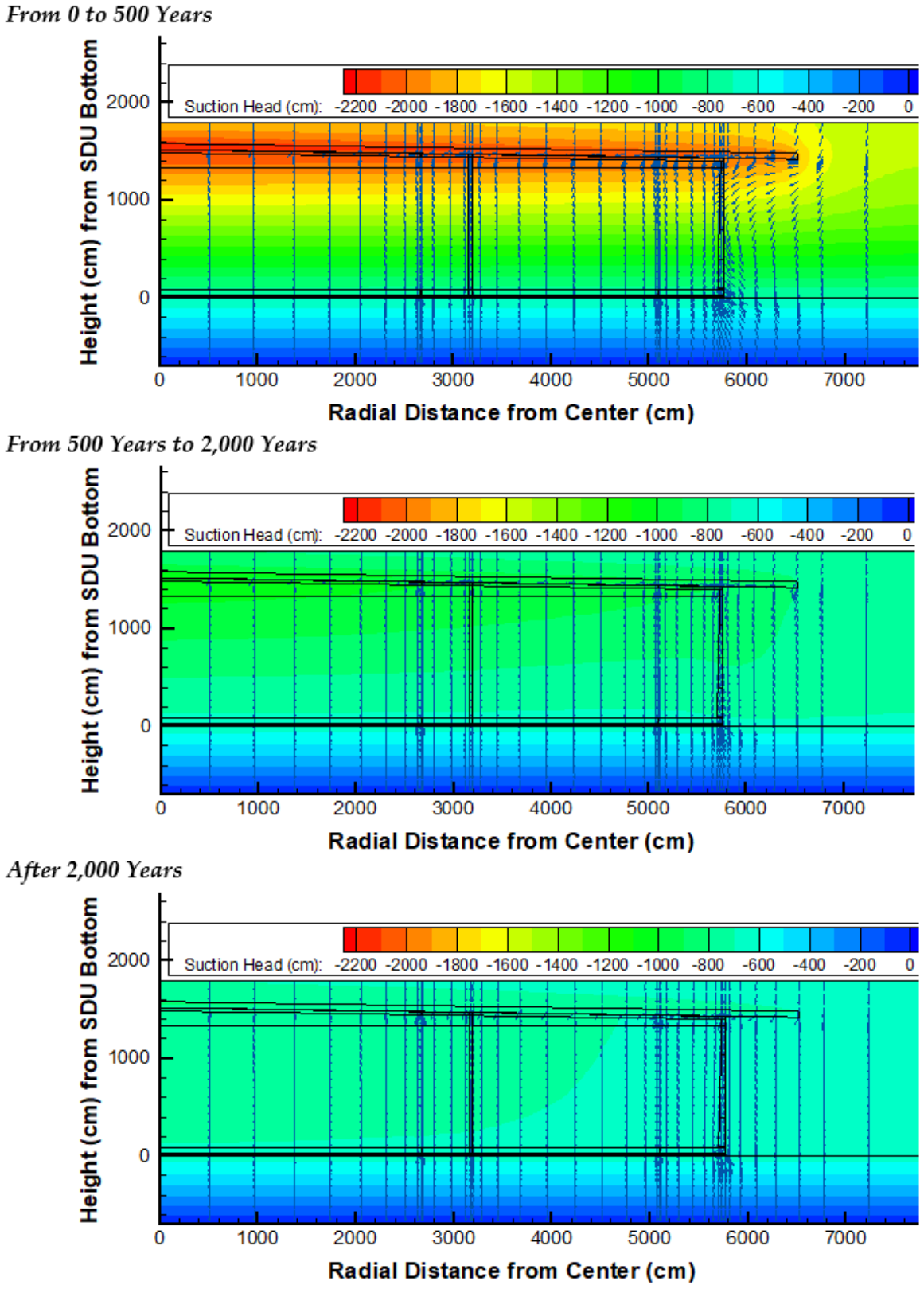

Based on the application of the moisture characteristic curves (Figure 7.1-3), this very high suction head alters the effective hydraulic conductivity of the soil materials (sand drainage layer and backfill) near the top of the SDU.

During the first 500 years, the suction head near the top of SDU 9 is approximately 2,000 cm. This drives the effective hydraulic conductivity of the soils to be lower than that of saltstone, thus creating a suction regime. This suction regime effectively pulls the moisture from the surrounding soils into the top and upper walls of the SDU and into the saltstone due to the suction gradient. This explains why Figure 7.1-1 shows that during the first 500 years, all the SDU components have identical volumetric flow rates, with nearly all infiltrating water being pulled in through the top of the SDU and expelled out at the bottom of the SDU.

Figure 7.1-3: Select Moisture Characteristic Curves and Approximate Suction Heads for Specific Time Periods at the Top of SDU 9, Compliance Case

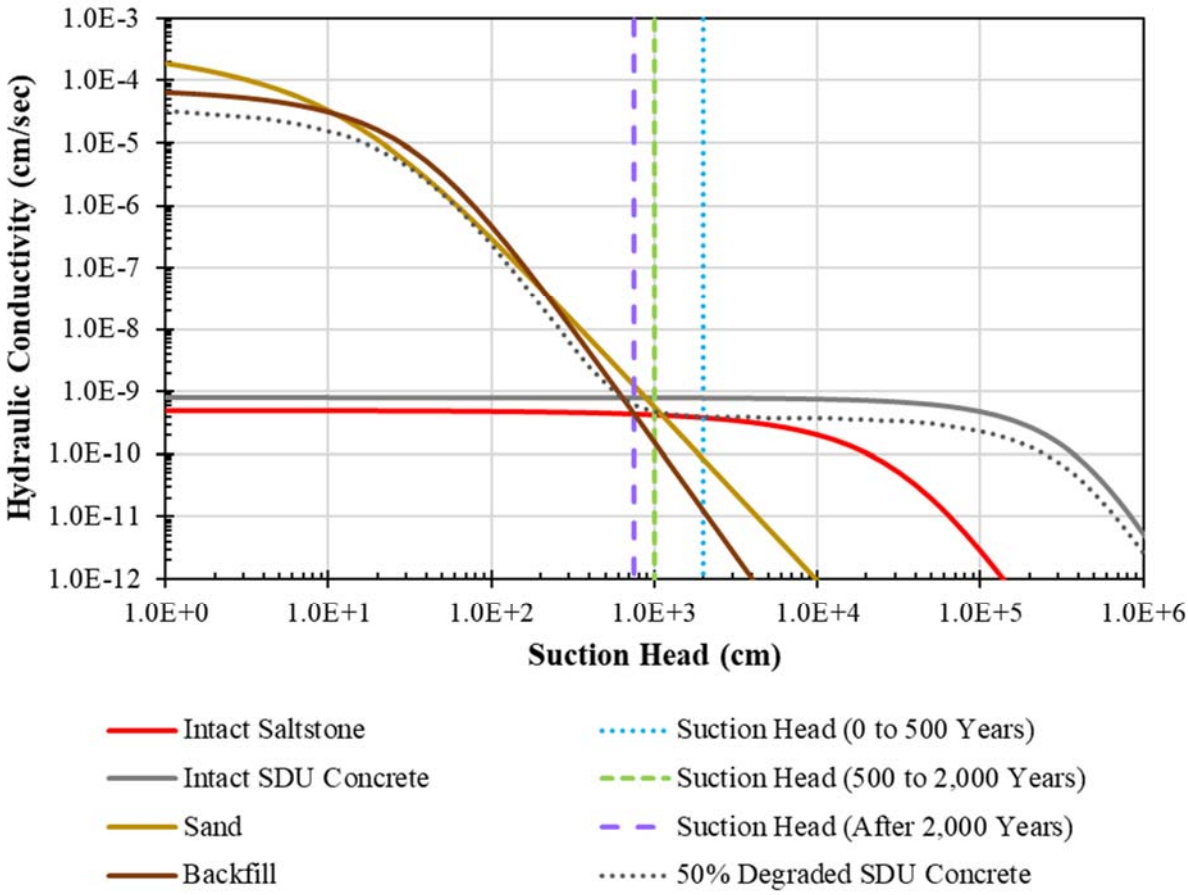

From 500 years to 2,000 years, the increased infiltration rate reduces the suction head near the top of SDU 9 (from approximately 2,000 cm to approximately 1,000 cm). This changes the suction regime slightly: the effective hydraulic conductivity of the lower lateral sand drainage layer increases to be slightly higher than saltstone, thus some infiltrating water is now draining laterally away from the SDU. Hence, Figure 7.1-1 shows a higher volumetric flow rate for the lower lateral sand drainage layer.

Finally, after 2,000 years the infiltration rate increases again, thus changing the suction near the top of SDU 9 for a second time (from approximately 1,000 cm to approximately 750 cm). Again, this increases the effective hydraulic conductivity of the soils. With this change, the backfill near the top of the SDU is approximately hydraulically equivalent to that of the saltstone. At this point, there is considerably less suction at the top of the SDU, but still enough suction to limit lateral drainage off the edge of the SDU, such that the infiltrating water continues to move in a predominantly downward direction through the top of the SDU.

Regardless of the period discussed, as water flows down through the vadose zone it approaches the water table, so the suction head approaches zero. Therefore, the influence of the suction regime diminishes with depth. With a height of 43 feet, the 375-foot diameter SDUs exhibit a large difference in the suction head between the top of the SDU and the bottom of the SDU.

7.1.2 SDU Concrete and Saltstone Degradation

The modeled degradation times for the cementitious materials of SDU 9 are summarized in Table 7.1-1 for the Compliance Case. As the table indicates, the SDU concrete degrades relatively quickly compared to saltstone. This outcome is attributed to the analytical approach for estimating the cementitious degradation timing. This analytical approach (described in Section 4.4.2), relies on conservative assumptions with respect to the availability of the various reactants and considers the combined effects of multiple phenomena to determine the most limiting degradation time scale for each cementitious material. This analytical approach is not coupled with infiltration or flow modeling.

Aside from the roof support columns (which will degrade within 100 years) and the saltstone, all the SDU features listed become fully degraded between 1,075 and 2,800 years after closure.

Essentially, the entire SDU structure is modeled as behaving hydraulically equivalent to backfill within 3,000 years. The exception is the SDU floor, which becomes hydraulically equivalent to the underlying natural soils. Despite this rapid degradation of the concrete, the saltstone within the SDU is not subject to rapid chemical degradation mechanisms such as carbonation or sulfate attack (Section 2.7.6) and therefore remains mostly intact for millions of years.

Table 7.1-1: Summary of Degradation Timing for SDU 9

Component or Feature	Time to Complete Degradation (yr)	Saturated Hydraulic Conductivity (cm/s)	
		Initial (Intact)	Final (Fully Degraded)
SDU Roof	1,552	7.8E-10	4.1E-05
SDU Column	92	5.0E-09	4.1E-05
SDU Wall 5 (top segment)	1,075	7.8E-10	4.1E-05
SDU Wall 4	1,229	7.8E-10	4.1E-05
SDU Wall 3	1,496	7.8E-10	4.1E-05
SDU Wall 2	1,767	7.8E-10	4.1E-05
SDU Wall 1 (bottom segment)	2,028	7.8E-10	4.1E-05
SDU Floor	2,800	7.8E-10	9.1E-05
Saltstone	1.7E+07	5.0E-10	4.1E-05

Note: See Section 4.4.2 for more information.

Further, due to the suction heads generated by the low infiltration rates (as discussed in Section 7.1.1), the effective hydraulic conductivity of the surrounding soils is functionally lower than the effective hydraulic conductivity of the intact SDU concrete. As a result, even before degradation occurs, the SDU concrete does not function as a hydraulic barrier. This is confirmed by the sensitivity case described in Section 5.8.3.3 which assumed an initial saturated hydraulic conductivity of 1.0E-07 cm/s for the SDU concrete but showed no appreciable change to the resulting doses.

Regardless, it is important to note that this effect is a function of the suction head generated by the low infiltration and flow rates. Under different infiltration conditions the SDU concrete properties can become much more important. For example, in the sensitivity case that assumes a soil-only closure cap with an infiltration rate of 417.8 mm/yr (discussed in Section 5.8.2.4), the suction head at the top of SDU 9 is always less than 100 cm. With a small suction head, the effective hydraulic conductivity for intact SDU concrete is orders of magnitude lower than that of the backfill or the sand drainage layer (refer to Figure 7.1-3). When there is such a large disparity between the effective hydraulic conductivity of the SDU concrete and the overlying sand drainage layer, the sand drainage layer becomes much more effective at shedding water off the top of SDU as designed.

7.1.3 Releases of I-129 and Tc-99 from Saltstone

This section focuses discussion on the release rates of I-129 and Tc-99 because all other radionuclides are shown to have a negligible impact on the SDF calculated doses. The reason that I-129 and Tc-99 dominate the SDF peak dose results is that both radionuclides are highly mobile throughout the entire chemical environment (from the saltstone waste form all the way through the saturated zone) and both have very long half-lives (~15M years and ~211,000 years, respectively). Additionally, I-129 has a relatively high dose conversion factor when ingested (see Table 4.4-108) and Tc-99 is relatively abundant within the assumed inventory (see Section 3.3.3).

Within the Vadose Zone Transport Model (Section 4.4.5), the releases of I-129 and Tc-99 are driven by both diffusion (which is independent of the infiltration and flow rates) and advection (which is controlled by infiltration and flow rates). As indicated in Section 4.4.3, considerable research has been performed to improve the overall understanding of the release rates for I-129 and Tc-99 and validate the current modeling approach. Most notably, core samples were pulled from saltstone (emplaced in SDU 2A) and researchers at SREL have been conducting Dynamic Leaching Method (DLM) tests on the saltstone cores and on laboratory-prepared simulant samples. [SRR-CWDA-2016-00051, SREL-R-17-0004, SREL-R-17-0005, SRRA099188-000003] While this research is still ongoing, the results to date have been analyzed and incorporated into modeling inputs that were developed using optimization approaches. [SRR-CWDA-2018-00045, SRR-CWDA-2018-00046]

To illustrate the progress of this research effort, the modeled releases from SDU 9 (for the Central Scenario cases) are plotted along with the laboratory measurements from the DLM tests. However, prior to discussing this comparison of simulated releases, it is important to first provide some context for the time scales being represented by the laboratory-measured pore volume exchanges. Figure 7.1-4 shows the number of cumulative pore volume exchanges based on the

volumetric flow rates through SDU 9 saltstone within the 10,000-year Performance Period. As this figure indicates, the low flow rates (as addressed in Section 7.1.1), coupled with the very large mass of the bulk saltstone within SDU 9, means that it takes a very long time for a significant number of pore volume exchanges to occur:

- Realistic Case shows 0.024 cumulative pore volume exchanges within 10,000 years,
- Compliance Case shows 0.32 cumulative pore volume exchanges within 10,000 years, and
- Pessimistic Case shows 1.3 cumulative pore volume exchanges within 10,000 years.

Because advection is so slow, diffusion is as important, or more important, to overall solute transport.

Figure 7.1-4: Cumulative Pore Volume Exchanges through SDU 9 Saltstone within the Performance Period

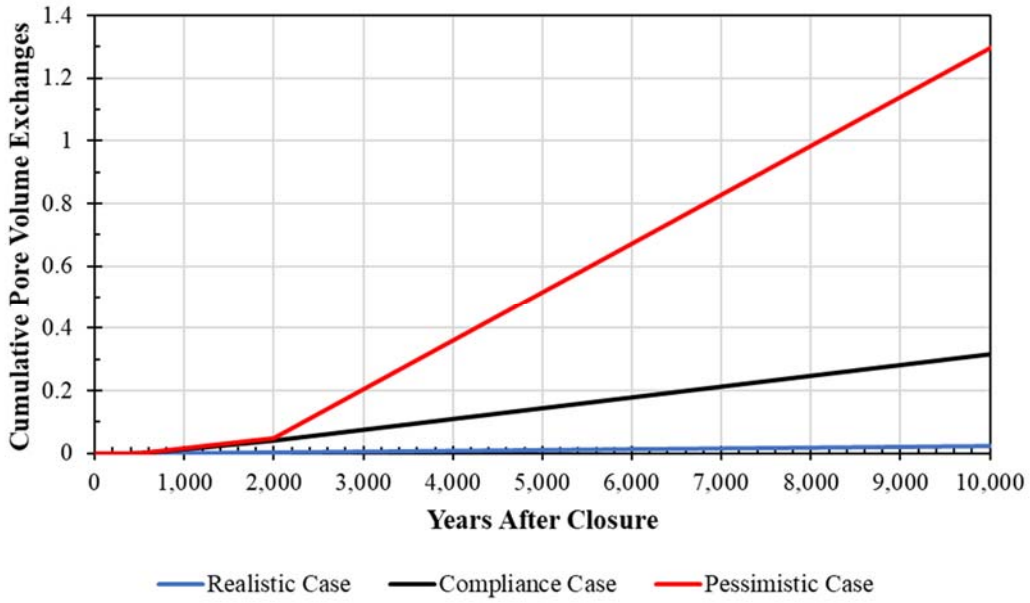

For each radionuclide (I-129 and Tc-99) two figures are provided to compare the simulated (modeled) release rates against the laboratory measurements of the DLM tests. With each pair of figures, the first figure (Figure 7.1-5) is scaled to show only the first 0.32 pore volumes to provide a comparison of the relative releases within the Performance Period, while the second figure (Figure 7.1-6) provides the results out to 3.5 cumulative pore volume exchanges, which represents approximately 130,000 years of Compliance Case performance when simulating releases from the SDU 9 saltstone. As noted above, due to diffusive releases, the model shows solute releases even under extremely low flow rates.

Further, note that the comparisons provided below tend to oversimplify the representation of the modeled transport conditions. Specifically, due to non-uniform flow conditions through the saltstone and the application of the shrinking core models (for both I-129 and Tc-99), the chemical transitions (from Region I to Region III and from reducing to oxidizing) are simulated as occurring on a node-specific basis, as opposed to occurring as a single step change for the entire saltstone monolith. The nodes that transition first are those which undergo the greatest amount

of flow. Because the first transition (from Region I to Region III) results in lower release rates for both I-129 and Tc-99, the comparisons make it appear that the models are under-estimating the rates of release. This is because the model results are depicting releases for the entire saltstone monolith wherein the greatest amount of flow occurs through regions with lower release rates. Alternatively, depictions of node-specific releases can make it appear that the models are over-estimating the rates or release.

In the first comparison (Figure 7.1-5), showing I-129 releases for 0.32 pore volume exchanges, the scale shows only a limited number of actual DLM sample measurements, so light gray lines are added to connect the data points. The figure shows that the simulated (modeled) release rates track very well with the DLM test results. Despite the differing conditions used for each of the Central Scenario cases (e.g., infiltration rates, degradation rates, etc.), for the first 0.25 pore volume exchanges all three Central Scenario cases are higher than the respective DLM test data. Within the Compliance Case, it takes approximately 8,000 years to reach 0.25 pre volume exchanges. These simulated release rates offer a very good approximation of the laboratory data.

Figure 7.1-5: Comparison of the Estimated Releases of I-129 for 0.32 Pore Volume Exchanges

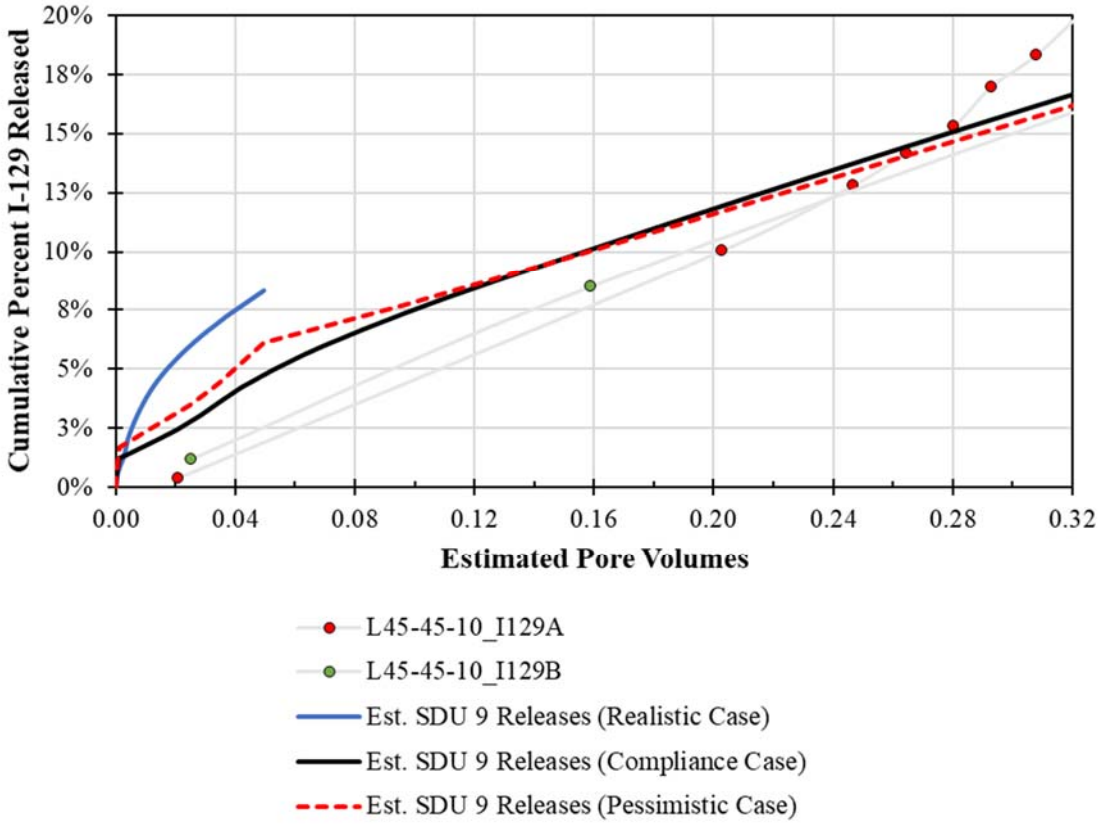

Also note that while the scale of Figure 7.1-5 is set to show approximately 10,000 years of pore volume exchanges according to the Compliance Case, the other two Central Scenario cases undergo different flow conditions such that the data for the Realistic Case ends at 0.05 pore volume exchanges, which is the full 20,000 years of the Realistic Case simulation.

The second figure (Figure 7.1-6) illustrates the longer-term comparison of the I-129 release rates. After the first 0.25 pore volume exchanges, the simulated release rates track between the two DLM samples up until approximately 1.5 pore volume exchanges (or approximately 45,000 years in the Compliance Case), at which point the release rates for the DLM samples slow down. Overall, the model provides a very good approximation of I-129 releases.

The I-129 releases for the Compliance Case (Figure 7.1-6) show the I-129 releases out to 100,000 years and for the Pessimistic Case out to 20,000 years. Although these releases occur over very long-time frames, no credit was taken for the radioactive decay of I-129, as it has a half-life that exceeds 15 million years, so the influence of decay was negligible. Regardless, both simulations released more than 95% of the total available I-129 inventory.

Figure 7.1-6: Comparison of the Estimated Releases of I-129 for 3.5 Pore Volume Exchanges

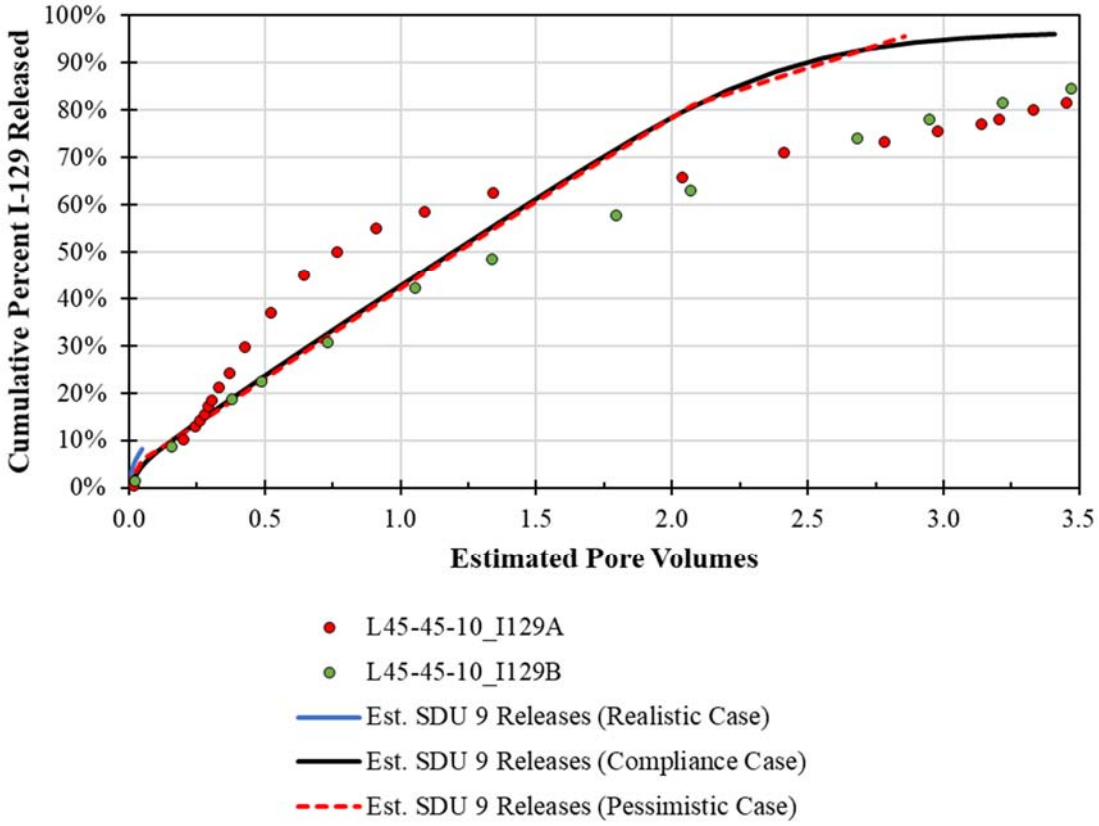

The comparisons of Tc-99 required additional setup relative to I-129. While the half-life of Tc-99 is long (approximately 211,000 years), it is not as long as I-129. Over the time-frames represented by these pore volume exchanges, the radioactive decay of Tc-99 does influence the comparison of the releases. For this reason, the modeled releases of Tc-99 have been modified to show the relative value if Tc-99 had not been subjected to radioactive decay.

Figure 7.1-7 shows the Tc-99 releases for the first 0.32 pore volume exchanges. As with I-129, the modeled releases rates of Tc-99 are higher than the respective DLM laboratory measurements,

providing confidence in the defensibility of the simulated approach with respect to the Compliance Period and the Performance Period.

Figure 7.1-8 shows that after the first 0.32 pore volume exchanges, the comparisons begin to be somewhat less favorable, as a few of the samples show release rates that appear to be higher than the Compliance Case results. However, this is not as much a difference in release rate as it is a function of the scale of the model: as the distance between the moving oxidation front and the outer edge of the saltstone material increases, the comparison appears to become less favorable. To illustrate this scaling effect, Figure 7.1-9 shows a Compliance Case result for Tc-99 released from a single PORFLOW node: the topmost, outermost saltstone node (i.e., the node that exhibits the fastest release). As presented, this node undergoes a release rate that is significantly higher than most of the saltstone monolith. More than 50% of the Tc-99 was released within the first pore volume exchange, and by 3.5 pore volume exchanges more than 60% of the Tc-99 had been released.

Regardless of the scaling, the simulated release rates generally track near the average of all five of the analyzed DLM samples, indicating that the simulated approach provides a reasonable representation of Tc-99 releases when compared to real measured releases from the DLM testing.

For context, note that Figure 7.1-8 shows the Tc-99 releases for the Compliance Case out to 100,000 years and for the Pessimistic Case out to 20,000 years. Both simulations released less than 8% of the total available Tc-99 inventory.

Figure 7.1-7: Comparison of the Estimated Releases of Tc-99 for 0.32 Pore Volume Exchanges

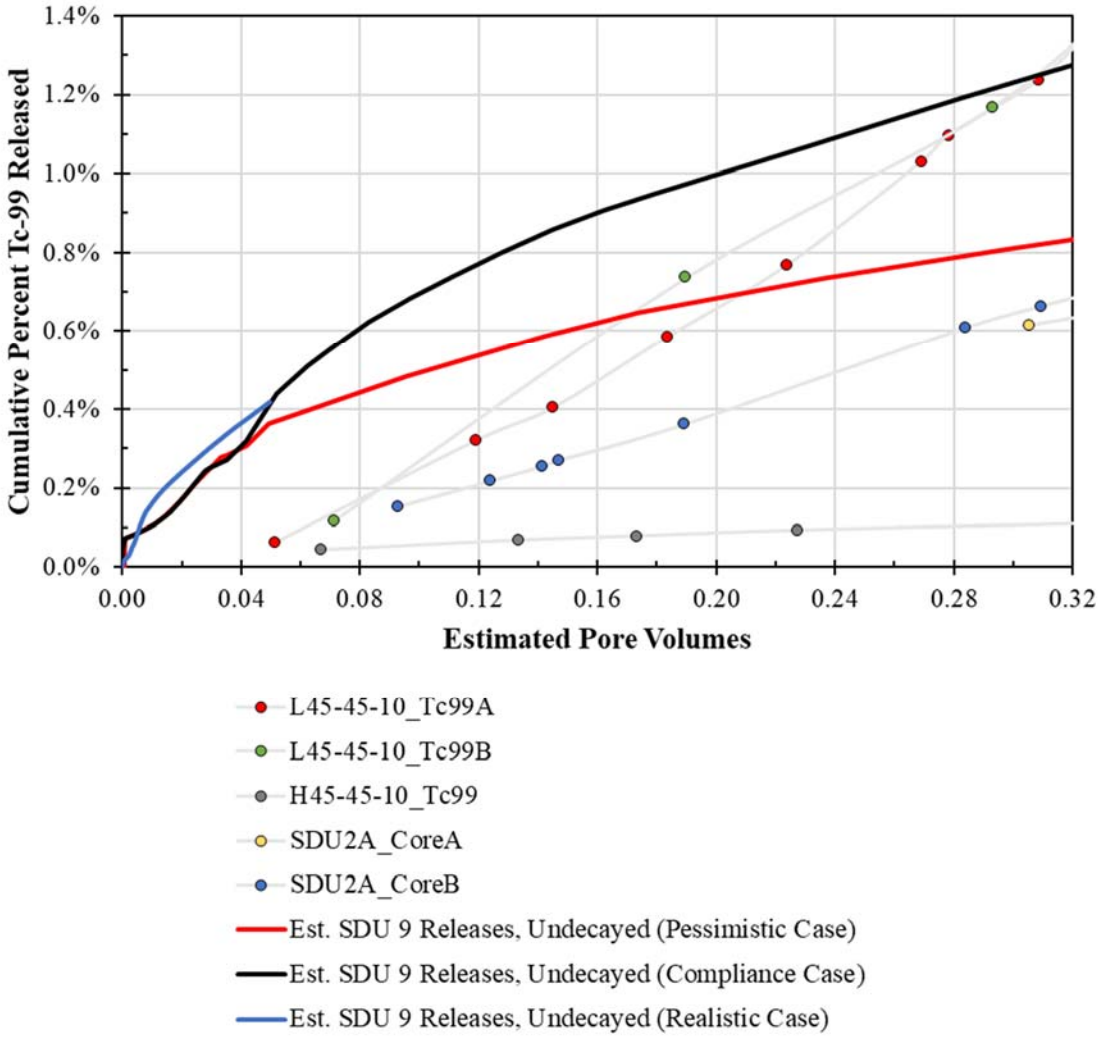

Figure 7.1-8: Comparison of the Estimated Releases of Tc-99 for 3.5 Pore Volume Exchanges

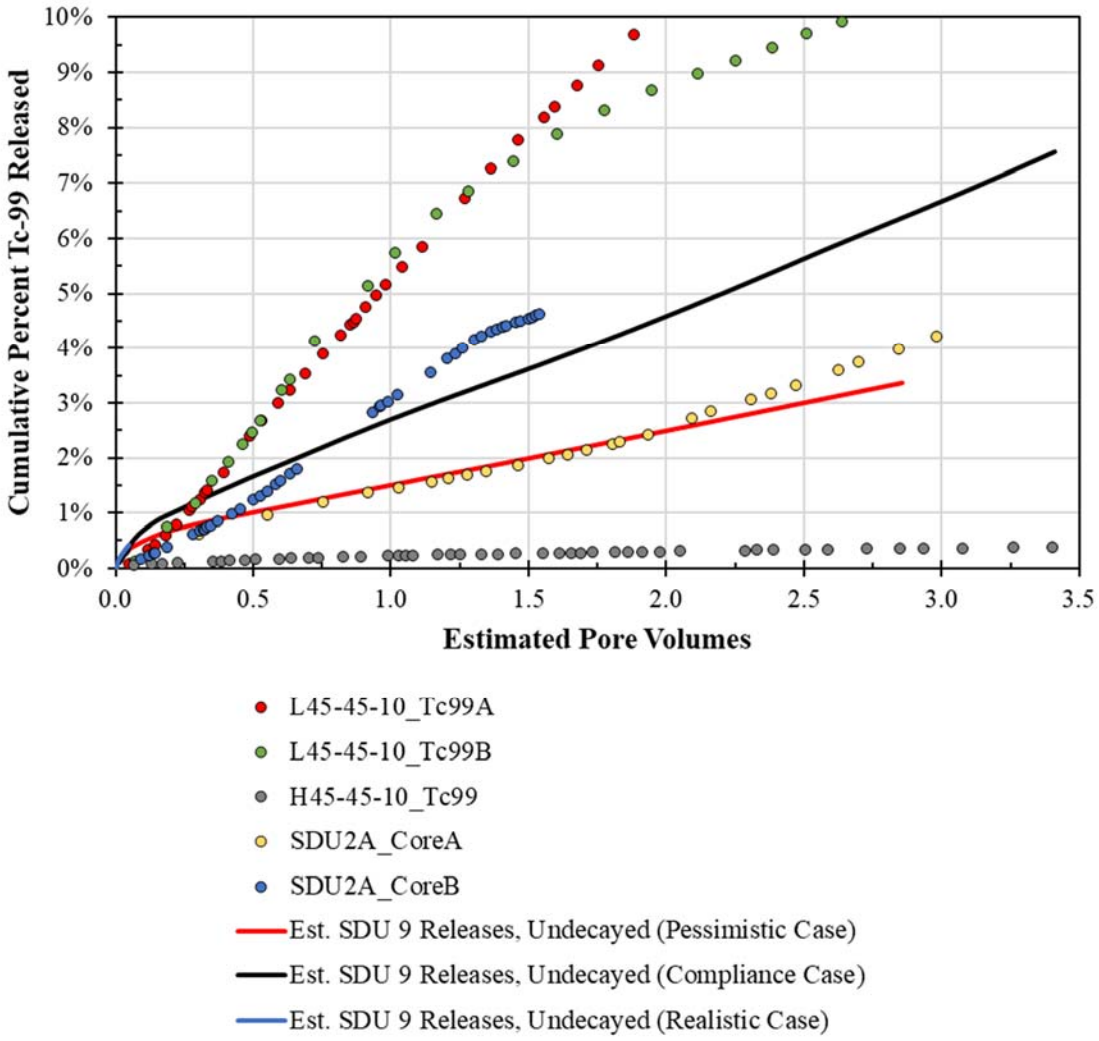

Figure 7.1-9: Estimated Releases of Tc-99 by Pore Volume Exchanges for a Single PORFLOW Node

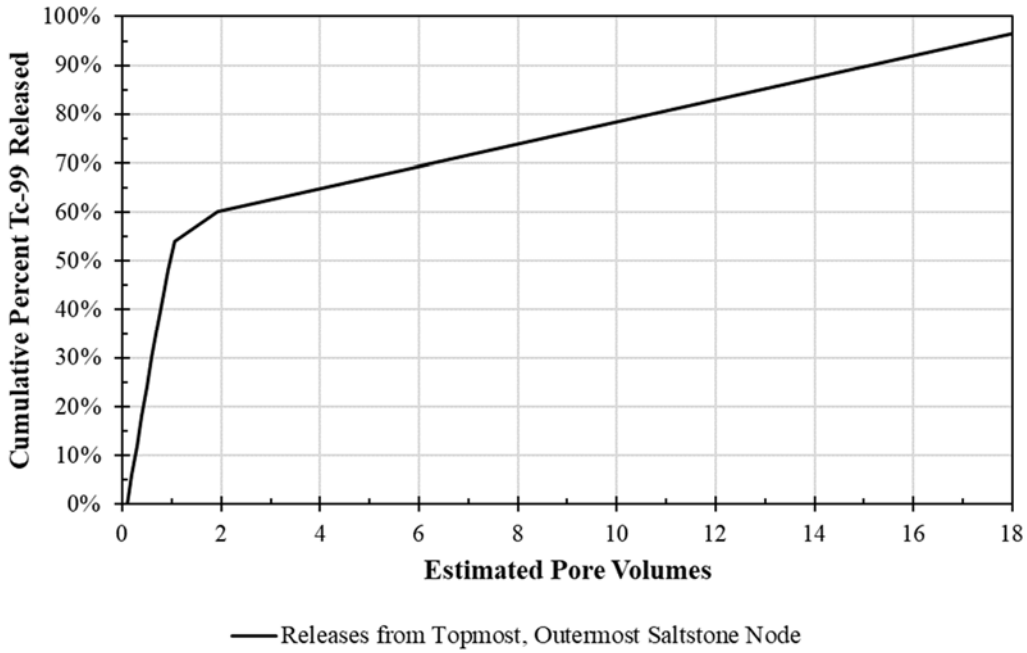

As described in Section 4.4.3, the release of Tc-99 is based on a solubility transition occurring when the pH within saltstone decreases to less than 11 (from 9.7E-07 mol/L to 4.5E-07 mol/L). Consistent with data from *Geochemical Model of Eh and pH Transitions in Pore Fluids during Saltstone and SDU Concrete Aging* (SRNL-STI-2018-00586) and *Technetium Solubility Limits for Simulating Tc-99 Releases from Saltstone SDUs* (SRR-CWDA-2018-00046), the pH transition is simulated to occur at six pore volume exchanges.

Due to the relative importance of Tc-99 and because the Tc-99 releases are dependent on this evolving chemistry, its releases are simulated using a shrinking core model. The shrinking core model tracks the pore volume exchanges explicitly for each modeling node (rather than *en masse* for the entire monolith), such that the chemical transitions occur at different times for each node. For example, in the shrinking core model the saltstone nodes along the outer edges of the saltstone monolith undergo the pH transition (from Reducing Region I to Reducing Region III) within the first few thousand years although it takes more than 60,000 years for the entire monolith to transition (per Table 4.4-62).

In addition to the advective transport, I-129 and Tc-99 are also released as a function of diffusion. Under low infiltration rates, slower flow occurs such that the relative influence of diffusion as a transport mechanism is stronger. This explains why the Realistic Case shows a higher rate of release than the Compliance Case when referenced to advective pore volume exchanges (as shown in Figure 7.1-5 and Figure 7.1-7). However, as more mass is released from the saltstone nodes, the transport distances will increase (i.e., the distances from the releasing model nodes to the boundary between the saltstone material and the SDU concrete materials). As such, under

constant flow rates the influence of diffusion will decrease over time because these transport distances will eventually exceed the diffusive distances.

7.1.4 Near Field (Vadose Zone) Transport of I-129 and Tc-99

Once released from saltstone, contaminants will be transported through the engineered SDU features (walls, floors, mud mats, etc.,), through the vadose zone soils (backfill and native soils), and into the saturated zone. As with the discussion in Section 7.1.3, this this section focuses on the transport of I-129 and Tc-99, because all other radionuclides are shown to have a negligible impact on the SDF calculated doses.

Figure 7.1-10 and Figure 7.1-11 show the cumulative release of I-129 and Tc-99, respectively, from SDU 9 saltstone to the SDU features (solid black curves), then from the SDU features to the vadose zone soils (solid brown curves), and then from the vadose zone soils to the water table (solid blue curves). The differences between the black and brown curves were used to estimate the inventories stored within the SDU materials at any given point in time (gray dashed curves) and the differences between the brown and blue curves were used to estimate the inventories stored within the vadose zone soils at any given point in time (tan dashed curves). Finally, the secondary Y-axis was used to illustrate the rate of flux from the vadose zone soils into the water table (gold curve for I-129 in Figure 7.1-10 and red curve for Tc-99 in Figure 7.1-11).

Figure 7.1-10 shows that the cumulative release curves for I-129 are nearly parallel with one another, indicating that I-129 is extremely mobile in both the SDU materials and the vadose zone soils. As such, there is relatively little change in the amount of I-129 stored within these regions over time. The flux of I-129 entering the water table initially increases, then holds steady near 2.6E-05 Ci/yr. At approximately 60,000 years it increases slightly. This corresponds with a chemical transition imposed on the soils (from leachate-impacted to non-leachate impacted). When this transition occurs, the soil K_ds for I-129 increase by a factor of three, thereby effectively reducing the storage capacity of the soils, such that some I-129 released from saltstone is held up within the SDU concrete (note the slight decrease in the cumulative release from the SDU to the vadose zone soils). However, this transition closely coincides with the depletion of the I-129 inventory, such that the flux rates and the stored inventories begin to decrease.

Figure 7.1-11 shows that Tc-99 has a more complex release profile. Specifically, after an initial increase up to approximately 3.3E-03 Ci/yr, the Tc-99 fluxes are decreasing over time. The decreases are related to the influence that the shrinking core model has on a node-by-node basis and the spatial discretization of the modeling nodes within the Vadose Zone Transport Model. Within the saltstone waste form, the releases of Tc-99 are highly localized. Initially, the technetium solubility is uniform throughout the entire saltstone monolith with a relatively high value (e.g., 9.7E-07 mol/L under Compliance Case conditions). With each successive node transition, the zone with lower solubility (e.g., 4.5E-07 mol/L) becomes larger and more impactful such that overall flux rate decreases over time. Also, as the core of reducing saltstone shrinks and increasing diffusion distances, Tc-99 solubility control under reducing conditions is lost at a slower rate over time.

Figure 7.1-10: Release and Transport of I-129 from SDU 9, Compliance Case, Performance Period (top) and Long-Term Exploratory Period (bottom)

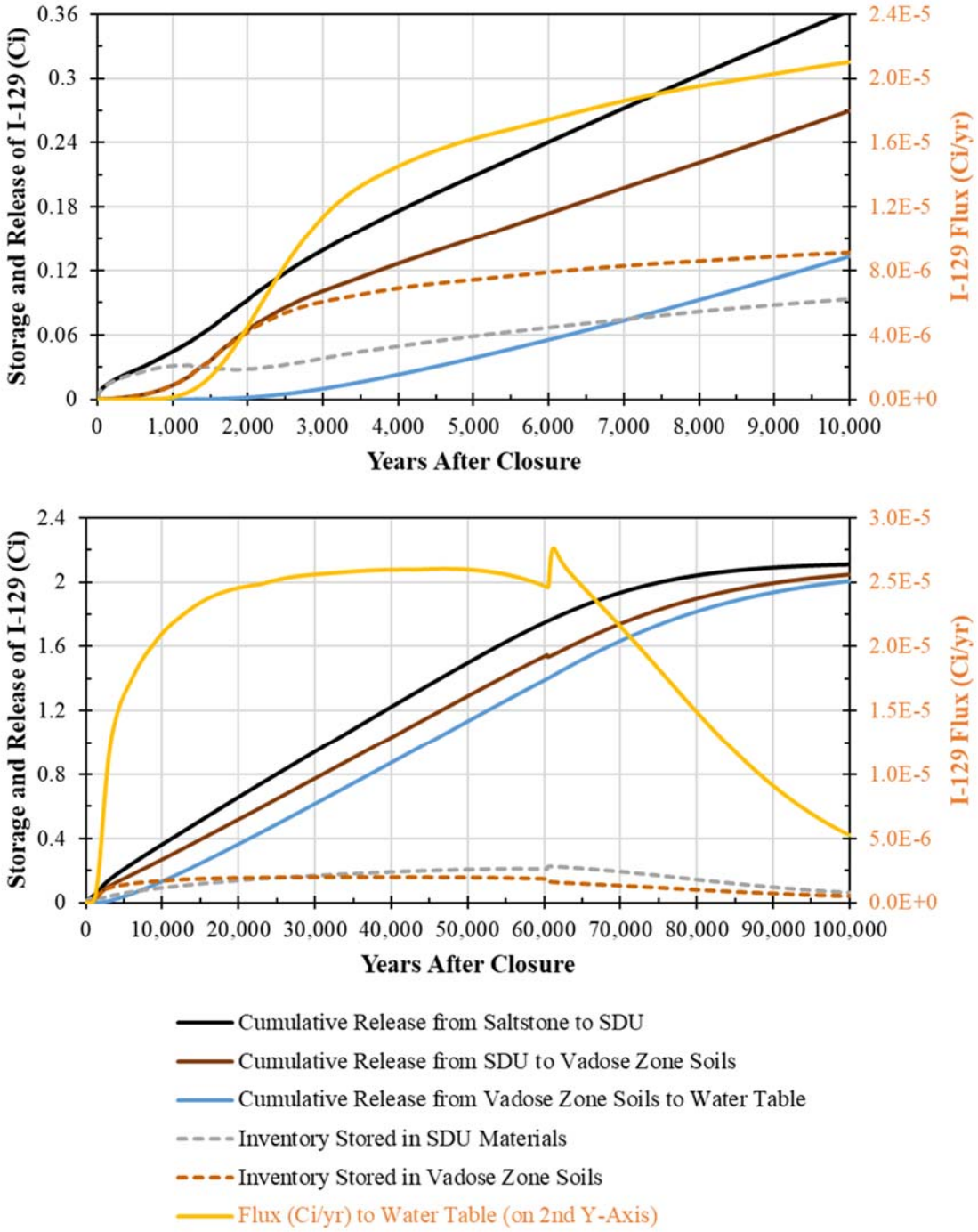

Figure 7.1-11: Release and Transport of Tc-99 from SDU 9, Compliance Case, Performance Period (top) and Long-Term Exploratory Period (bottom)

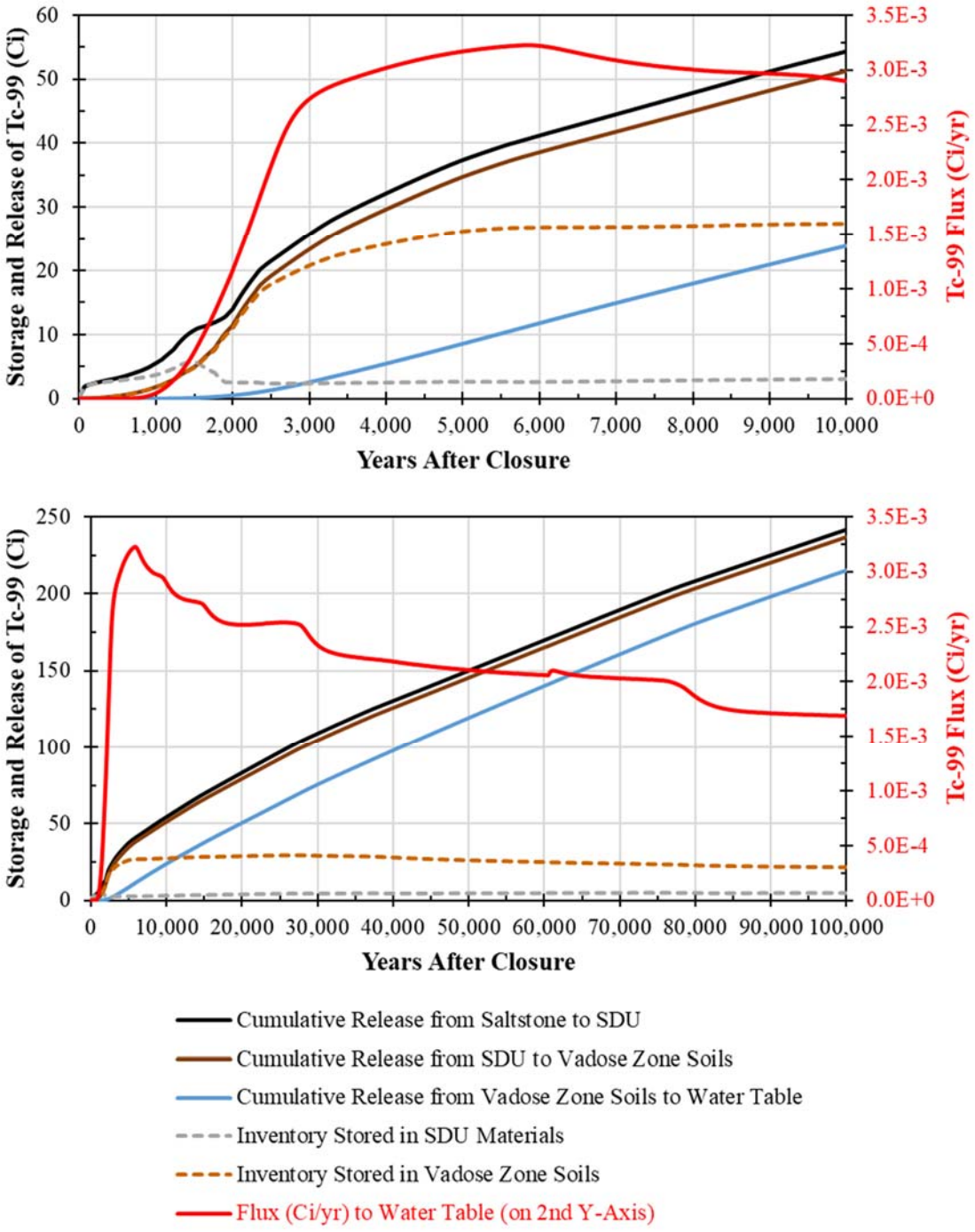

7.1.5 Far Field (Aquifer) Transport

Contaminants that reach the water table contribute to contaminant plumes in the subsurface aquifers. These plumes are transported through the saturated zone via ground water flow towards nearby streams or into deeper aquifers. Within the impacted saturated zone there are

effectively two aquifers: the relatively shallow Upper Three Runs Aquifer and the deeper Gordon Aquifer. These aquifers are separated by the Gordon Confining Unit. Due to the presence of the Tan Clay Confining Zone, the Upper Three Runs Aquifer has been subdivided into two aquifer zones: an Upper Aquifer Zone and a Lower Aquifer Zone.

The Gordon Confining Unit is relatively competent and effective at limiting the transport of contaminants into the Gordon Aquifer. Conversely, the Tan Clay Confining Zone is generally not as effective a barrier to contaminant transport due to varying thickness throughout the GSA. As such, the highest concentrations generally occur in the Lower Aquifer Zone. This observation is location-dependent, but there is generally not a large difference between the maximum concentrations in either the Upper Aquifer Zone or the Lower Aquifer Zone.

Due to the highly mobile transport properties of I-129 and Tc-99, the transport times needed for the contaminants plumes to travel from the SDU foot print to the 100-meter boundary is approximately the same as the tracer breakthrough timing provided in Table 4.4-85.

Relative to the overall performance of the system, one of the most important processes to consider is the effect of plume overlap. While the doses throughout most of the first 10,000 years are driven by the releases from SDU 9, the later doses are a function of overlapping plumes along Sector B (either from SDUs 11 and 12 overlapping or from SDUs 6 and 8 overlapping). The risks associated with these plumes are tied to the physical location/proximity of these disposal inventories and could be impacted by changes to SDU placement.

7.1.6 MOP Doses Results

Figure 7.1-12 shows the total dose to the MOP at the 100-meter boundary along Sector D for the Compliance Case (as described in Section 5.5). Sector D is selected for this discussion as it is the sector with the highest total dose throughout the Compliance Period (from 0 to 1,000 years after SDF closure) and through most of the Performance Period (from 0 to 10,000 years after SDF closure).

In this figure, the dashed black curve is the total dose to the MOP, while the orange curve shows only the dose contribution that is explicitly from SDU 9 releases. The difference between the two curves is attributed to the doses from seepline contributions (e.g., fish ingestion), which is also indirectly related to SDU 9 releases, and some plume contribution from SDU 7. The gold and red curves show the contributions to the total dose from I-129 and Tc-99, respectively. Comparing the shapes of these curves to the fluxes at the water table (Figure 7.1-10 and Figure 7.1-11) shows that these radionuclide dose contributions are effectively a function of the flux to the water table.

While Figure 7.1-12 only shows doses to Sector D (and the corresponding contribution from SDU 9), the other sectors and SDUs exhibit generally similar behaviors, albeit with some variation in the magnitude or timing.

Figure 7.1-12: Total MOP Dose and Key Radionuclide Dose Contributors at Sector D, Compliance Case

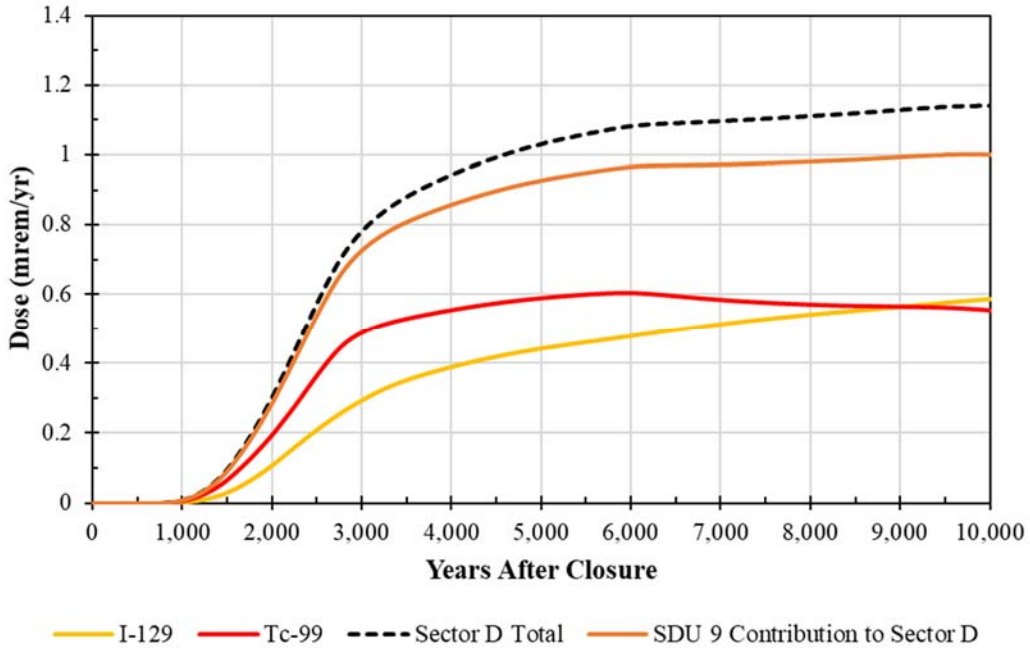

7.1.7 IHI Doses Results

As presented in Sections 6.3, the peak doses to the Acute IHI are entirely a function of the drill cutting inventory that is assumed, because this inventory controls the entire amount of exposure. The Acute IHI results indicate that performance objectives will be met.

The peak doses to the Chronic IHI are a function of both the ground water concentrations and the drill cutting inventory. For the Chronic IHI Scenario, the drill cutting inventory is assumed to be mixed into the soils that are used for raising produce and livestock. For considerations of compliance, the Chronic IHI Scenario applied a number of pessimistic assumptions when developing this drill cutting inventory (see Section 6.2). Despite these assumptions, the Chronic IHI doses remained below performance objectives. When more realistic assumptions were applied to determine the assumed contamination within the soil drill cuttings, the resulting dose was essentially the same as the dose from assuming no drill cuttings at all and was orders of magnitude below the 100 mrem/yr limit (see Section 6.6.3).

The only modeling case that showed IHI doses that exceeded performance objectives relied on unrealistic assumptions and were presented for informational purposes only.

7.1.8 Benchmarking Analysis

The two- or three-dimensional vadose zone and aquifer transport modeling that was performed in PORFLOW was abstracted into a simplified one-dimensional transport model in GoldSim for computational efficiency. This SDF GoldSim Model was developed as a tool to expedite the development of some sensitivity cases and to use for probabilistic simulations to help inform quantitative risk analyses. While both PORFLOW and GoldSim are used to simulate very similar

processes, interpretation of the results requires an understanding of how these processes are simulated differently.

The biggest difference between the two modeling approaches is the handling of I-129 releases. In the Vadose Zone Transport Model, PORFLOW applies a shrinking core model to simulate variable conditions in the transport behavior of I-129. Specifically, for the first pore volume exchange, the transport of I-129 through saltstone is based on a K_d of 0.07 mL/g; then a K_d of 0.71 mL/g is applied until the saltstone becomes oxidizing. Alternatively, the SDF GoldSim Model assumes the lower value (0.07 mL/g) for the entirety of the reducing saltstone material regardless of the estimated number of pore volume exchanges. As expected, this results in the SDF GoldSim Model showing faster (but not unreasonably faster) release rates for I-129.

The only other notable difference is that the location of the peak dose during the Performance Period is different between the two models. Based on PORFLOW, the peak dose occurs in Sector D up until the very end of the Performance Period (approximately 9,800 years after SDF closure). Alternatively, the GoldSim results show the Sector B overtakes Sector D as the dominant sector much earlier (at approximately 4,200 years after SDF closure). This is primarily due to the limited number of points of assessment evaluated (i.e., 100-meter wells) because the SDF GoldSim Model relied on simplifying assumptions when abstracting the aquifer transport model. These simplifying assumptions resulted in more plume overlap such that the SDF GoldSim Model overpredicts the doses to Sector B (see Figure 7.1-13). Regardless of the locations of the peaks, the doses in Sectors B and D are generally similar in magnitude and timing, indicating that both sectors represent a similar degree of risk relative to the total dose to the MOP.

Figure 7.1-13: MOP Dose Results Comparing PORFLOW and GoldSim at Sectors B and D

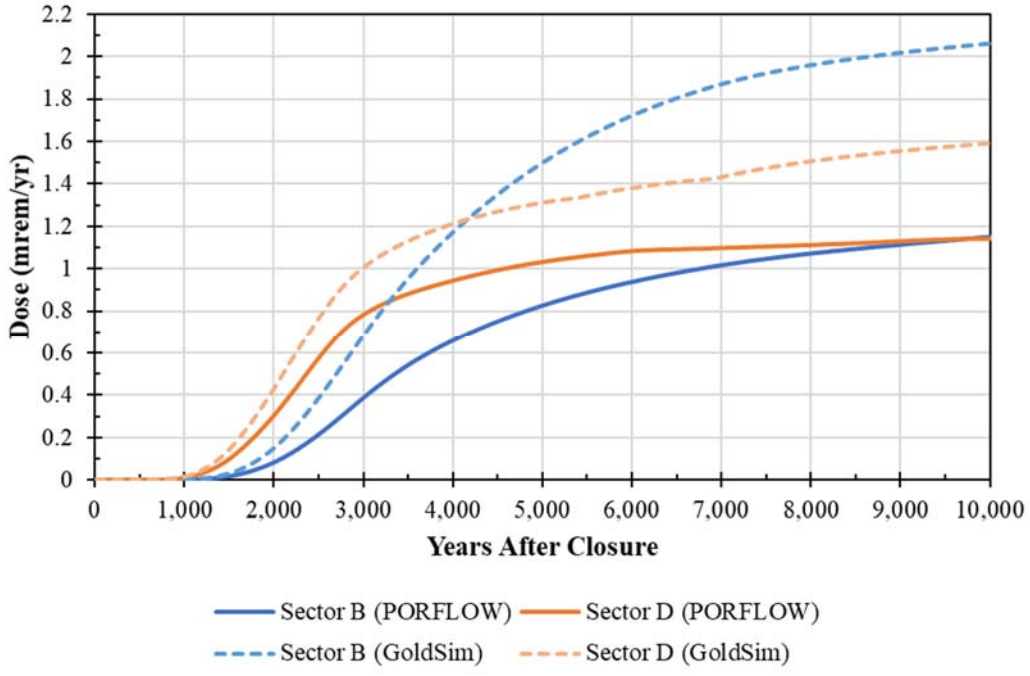

7.1.9 Probabliisitic Results

After being benchmarked to the conservatively-biased deterministic Compliance Case (developed in PORFLOW), the SDF GoldSim Model was run in "probabilistic mode" for 3,000 realizations wherein each realization sampled a different set of input values. Figure 7.1-14 shows the statistical time histories (including the mean and median doses to the MOP) for the 3,000 realizations. This figure also shows the Compliance Case doses based on PORFLOW (black curve) and from the benchmarking analysis using the SDF GoldSim Model (gray curve). This figure again illustrates that the doses from using the benchmarked SDF GoldSim Model are generally higher than the doses from the PORFLOW Compliance Case results, which are themselves biased high. It also shows that the dose results for the SDF GoldSim Model using deterministic Compliance Case settings fall between the 25th and 75th percentiles, near the median value. Over 50% of the probabilistic results are generally higher than the deterministic Compliance Case simulation, indicating that the sampling distributions likely skew towards more input selections that are biased towards generating higher dose results. However, within the Performance Period the 95th percentile peaks near 12.5 mrem/yr, indicating that it is highly unlikely that the MOP doses will exceed the performance objective of 25 mrem/yr.

Figure 7.1-14: Comparison of Deterministic Compliance Case MOP Dose Results Versus the Statistical Time Histories from 3,000 Realizations

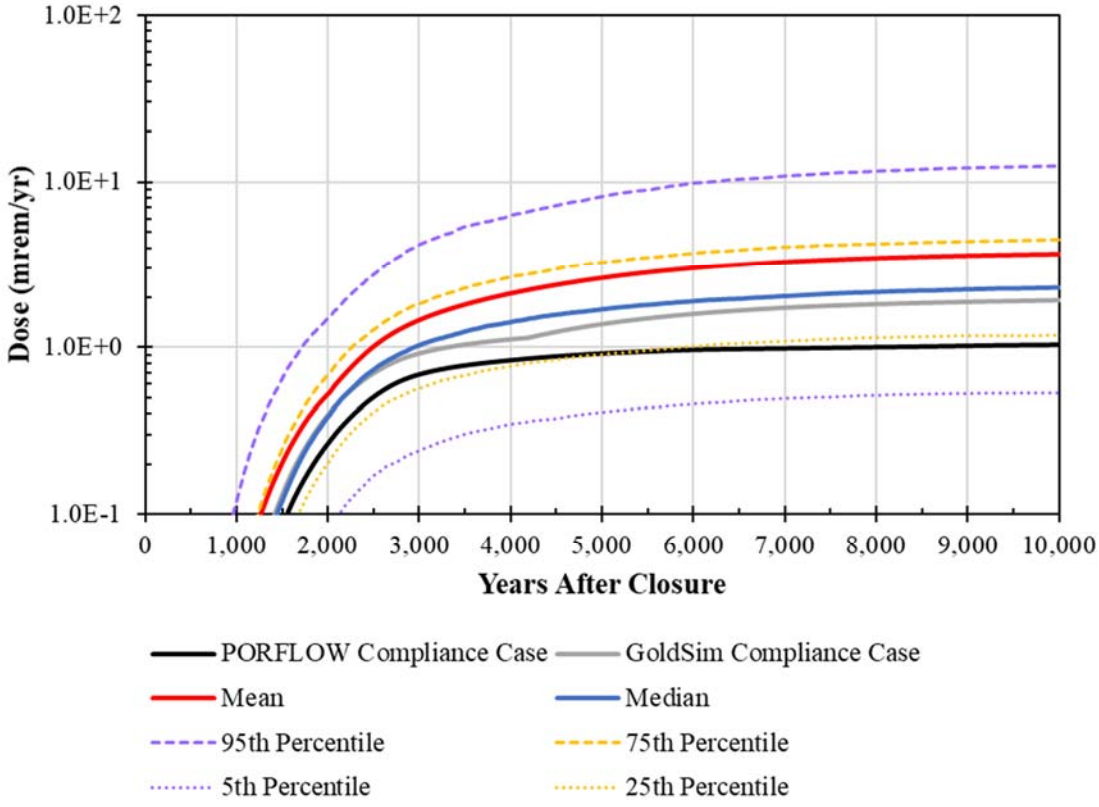

Sensitivity analysis of the probabilistic results indicated that the most important parameters influencing doses are the infiltration rate, the thickness of the vadose zone beneath SDU 9, the rate of MOP water uptake, and the assumed size of the residential garden.

7.2 Enhanced Defensibility and Risks Associated with the SDF PA

The development of the three Central Scenario cases (Realistic Case, Compliance Case, and Pessimistic Case) offers another perspective for considering the assumed inputs built in to the SDF PA models. Specifically, comparing the key differences between the Realistic Case and the Compliance Case (as provided in Table 5.8-1) offers insights into how these assumptions enhance the overall defensibility of the Compliance Case. Similarly, comparing the key differences between the Compliance Case and the Pessimistic Case (also provided in Table 5.8-1) reveals areas where additional risk might influence the Compliance Case. Ultimately, using all three Central Scenario cases (from Section 5.8.1) along with the probabilistic analysis (Section 5.7) and the other various deterministic sensitivity cases (Section 5.8) provides a comprehensive assessment of both the assumptions for enhanced defensibility and the risks associated within the SDF PA models. Even when multiple inputs are developed using assumptions with an intentional bias towards higher dose results (i.e., the Pessimistic Case), the resulting doses continue to remain below the performance objectives.

Based on the analysis of the results for the various modeling cases presented throughout Section 5, the most significant barrier with respect to overall performance is the engineered closure cap, which significantly limits infiltration. However, as indicated in Section 3.2.6.3, because the design of this closure cap is preliminary the stability calculations needed to establish erosion controls have not yet been finalized. While it is reasonable to expect that this analysis will provide sufficient design recommendations to establish passive controls to protect against significant erosion events throughout the Compliance Period and well into the Performance Period, it is acknowledged that this is a potential risk in the current Compliance Case. Due to this risk, it is recommended that decisions related to future waste disposal operations at the SDF (e.g., updates to the WAC recommendations) assume a risk-informed approach until the erosion analyses and stability calculations have been performed to support a final closure cap design.

As part of this risk-informed approach, it is prudent to evaluate cases in which the closure cap fails to perform as designed due to erosion. The sensitivity cases described throughout Section 5.8 include a plausible (albeit still unlikely) erosion scenario: the Retreating Cap Case described in Section 5.8.2.5. Although this scenario does not reflect the expected future condition of the system, it is recommended that the Retreating Cap Case be used as the basis for operational decisions to ensure that such decisions will have a robust and defensible basis.

This page intentionally left blank.

8 PERFORMANCE EVALUATION

Section 8.1 compares the Compliance Case results to the applicable performance objectives, Section 8.2 describes how the PA will be used to support future decision-making, and Section 8.3 describes future work to be done to support the maintenance of the SDF PA.

8.1 Comparison of Results to Performance Objectives

As shown in Table 8.1-1, all performance objectives for the SDF are met within the 1,000-year Compliance Period.

Table 8.1-1: Comparison of PA Results versus Performance Objectives

Performance Objectives			PA Results
DOE M 435.1-1	All Pathway MOP Dose	25 mrem/yr in 1,000 years	9.4E-03 mrem/yr
	Air Pathway MOP Dose	10 mrem/yr in 1,000 years	5.2E-09 mrem/yr
	Chronic IHI Dose	100 mrem/yr in 1,000 years	0.30 mrem/yr
	Acute IHI Dose	500 mrem/yr in 1,000 years	4.1E-05 mrem/yr
	Radon Release	20 pCi/m^2/sec in 1,000 years	1.6E-05 pCi/m^2/sec
10 CFR 61.41*	All-Pathways MOP Dose	25 mrem/yr	1.2 mrem/yr
10 CFR 61.42*	Intruder Dose	500 mrem/yr **	2.2 mrem/yr
SCDHEC R.61-58	South Carolina Ground Water Protection Standard	Concentrations below the maximum contaminant levels (MCLs) in 1,000 years	< MCLs

Notes: * Unlike the performance objectives described in DOE M 435.1-1, the performance objectives for 10 CFR 61 are not associated with a prescribed period for compliance. The doses provided for these performance objectives are based on the 10,000-year Performance Period.

** A quantitative limit is not specified. The SDF must ensure the protection of the IHI after a 100-year active institutional control period. Based on NUREG-1854 guidance, 500 mrem/yr is assumed for the performance objective. [ML072360184]

These results are based on the Compliance Case which represents a combination of the most probable and defensible assumptions. Collectively, this combination of assumptions is referred to throughout this PA as the MPAD assumptions. Even when more extreme assumptions are applied throughout the model (i.e., the Pessimistic Case), the results remained within the bounds of the performance objectives. Conversely, when the model only applied the most realistic (or best estimate) assumptions (i.e, the Realistic Case), the results were considerably lower. Understanding the context of these different sets of assumptions provides greater confidence that the results of this PA provides a reasonable expectation that waste disposal at the SDF will comply with the specified performance objectives.

Also note that although DOE M 435.1-1 specifies that the PA shall evaluate compliance out to 1,000 years after closure, all the calculations were performed to provide results over a minimum of 10,000 years after closure.

8.2 Use of Performance Assessment Results

The SDF PA is used to comply with DOE O 435.1, which requires radioactive waste to be managed in accordance with DOE M 435.1-1, *Radioactive Waste Management Manual*. Specifically, this PA was developed to meet the requirement that an assessment be prepared and maintained for DOE LLW disposed of after September 26, 1988. Additionally, this PA was developed in accordance with the DOE Standard: *Disposal Authorization Statement and Tank Closure Documentation* (DOE-STD-5002-2017). The results of this PA provide a reasonable expectation that the facility design and method of disposal will comply with the performance objectives of DOE M 435.1-1, which ensure protection of public health and the environment by limiting doses to a MOP and limiting releases of radon. The SDF PA also provides reasonable expectation that the applicable performance objectives of 10 CFR 61 will be met. This PA also assesses impacts to a hypothetical IHI and impacts to water resources.

This PA will also be used to provide input for informing the limits on the future disposal of radionuclides at the SDF. The SDF waste acceptance criteria (WAC) may be revised to ensure that waste disposal at the SDF will not jeopardize the conclusions of this PA. Similarly, as indicated in *Unreviewed Waste Management Question Requirements Document for Saltstone Facility* (SRR-CWDA-2011-00196), all revisions to the SDF WAC (X-SD-Z-00004) shall be reviewed for impacts to the PA prior to approval of the revised WAC. To support the risk-informed approach recommended in Section 7.2, although it does not reflect expected future conditions, the Retreating Cap Case described in Section 5.8.2.5 shall be the basis for technical decisions related to disposal operations, including potential changes to the WAC. Further, because no radionuclide concentrations other than I-129 are expected to challenge the PA-established WAC limits, the WAC limit for I-129 is the only WAC limit that may be modified. The limit for I-129 would not be increased by more than a factor of two. Based on the results of the Retreating Cap Case, a factor of 2 increase to the future disposal inventories of I-129 will not challenge performance objectives.

Finally, this PA will be used to inform decision-making related to operations and waste disposal at the SDF. Specifically, the information from this PA, and any maintenance activities associated with this PA (see Section 8.3), will be used as a technical basis to update the *Unreviewed Waste Management Question Requirements Document for Saltstone Facility* (SRR-CWDA-2011-00196). This requirements document is used to protect the inputs and assumptions used to develop the PA. Per the S4-ENG.46, SDF personnel will refer to the requirements document to ensure that all proposed activities or new data that may impact the PA will be appropriately evaluated.

8.3 Future Work

As required by DOE M 435.1-1, maintenance of the SDF PA will include future updates to incorporate new information, update model codes, analysis of actual disposal inventories, etc., as appropriate. Because PA results are in part, based on data that is uncertain due to use of projected

conditions over thousands of years into the future, a maintenance program has been put in place to continue to reduce uncertainty in the inputs and assumptions, providing greater confidence in the results of the analyses, and in the long-term institutional control plans for public and environmental protection. The purpose of the PA maintenance program is to confirm the continued adequacy of a PA and to increase confidence in the results of the PA. The latest version of the PA maintenance program entitled *Savannah River Site Liquid Waste Facilities Performance Assessment Maintenance Program – FY2019 Implementation Plan* (SRR-CWDA-2018-00092) was prepared in February 2019. This maintenance program plan is reviewed and updated annually.

As part of the maintenance program, the SDF PA will be reviewed as opportunities for model improvement are identified or as additional studies are conducted. Opportunities for model improvement could include such tasks as the use of improved modeling software or corrections of previously identified model irregularities (e.g., SRR-CWDA-2018-00068 identifies SDF PA irregularities having either "no impact" or a "negligible impact" that were left unmodified). As additional data become available the PA may need to be revised, and additional modeling may be required. Based on information, results, and interpretations presented in Sections 5, 6, and 7, the various areas of future work may be included in the maintenance program to facilitate discussion for improving the PA in future revisions.

Future work is also planned for continued input refinement and confirmation. For example, further work will be conducted to refine and confirm the existing radionuclide inventories that will be present in SDF at site closure. This work includes additional sampling and analyses of waste tanks that feed to the SDF. As part of input refinement and confirmation, future materials testing will be performed (e.g., validation of grout properties, site-specific soil K_d testing). This future work will consider uncertainty in material properties due to biases in testing methods including laboratory versus field experiments, as well as techniques used to measure properties (e.g., centrifuge versus flexible wall permeameter, column-based testing, and influence of cementitious material on vadose zone geochemistry). The future materials testing will concentrate on those contaminants that have been identified as having the most impact on dose results (i.e., Tc-99 and I-129).

In addition, the results of ongoing applied research, such as those from the DLM testing will be evaluated and incorporated, as necessary. The DLM testing is not expected to be completed for several years.

An engineered closure cap will be installed over the SDF as part of facility closure. The design information provided in the PA is for planning purposes, and is based on the current SDF conceptual closure cap information presented in WSRC-STI-2008-00244, SRRA107772-00009, and SRR-CWDA-2018-00087. The closure cap design will be finalized closer to the time of SDF closure, to take advantage of possible advances in materials and closure cap technology that could be used to improve the design. As a requirement for an acceptable final design, physical stability requirements will be established according to a stability analysis equivalent to that presented in Appendix A of *Saltstone Disposal Facility Closure Cap Concept and Infiltration Estimates* (WSRC-STI-2008-00244), to ensure that the closure cap will be engineered in a manner that mitigates risks associated with potential erosion or gullying events.

This page intentionally left blank.

9 QUALITY ASSURANCE

This section provides a summary of the activities performed to ensure the quality of the information throughout this PA. Section 9.1 documents how the PA inputs and data verification complies with SRS QA requirements. Section 9.2 documents how software complies with SRS QA requirements. Section 9.3 documents how computer modeling complies with SRS QA requirements.

9.1 Input and Data Quality Assurance

A quality assurance compliance document was prepared to document input data verification and technical checking of PA text, modeling files, and calculations developed in support of the FY2019 SDF PA. The report, entitled *Performance Assessment for the Saltstone Disposal Facility at the Savannah River Site: Quality Assurance Report* (SRR-CWDA-2018-00068); hereafter referred to as the QA Report, focuses on technical checking of work performed by Waste Disposal Authority (WDA) staff, as well as verification of inputs provided to WDA by organizations external to SRR, such as SRNL.

Section 2 of the QA Report describes checking and verification activities related to the development of model inputs. Sections 3 and 4 describe the checking of models developed in support of the FY2019 SDF PA. Section 5 discusses checking and verification of post-processed data and model results. Section 6 provides a summary of software QA. Section 7 sumarizes irregularities and inconsistencies identified during the preparation of this PA. Finally, Section 8 summarizes the results of these QA activities. The SRS quality assurance document used in the preparation of the FY2019 SDF PA is documented in the *Quality Assurance Management Plan* (QAMP), SRNS-RP-2008-00020 and in 1Q Manual, Procedure 2-1, *Quality Assurance Program*. Each are discussed below.

Quality Assurance Management Plan (QAMP)

The QAMP demonstrates the relationship between the QA Program, Integrated Safety Management System, and the Contractor Assurance System. The QA Program, as described in this QAMP, implements the Quality Assurance Rule (10 CFR 830 Subpart A), DOE O 414.1D, and DOE O 226.1B in accordance with the SRNS Site Standards/Requirements Identification Document that is also approved by the DOE Savannah River Office (DOE-SR) and the National Nuclear Safety Administration Savannah River Site Office. This document incorporates and satisfies the requirements of 10 CFR 830 Subpart A, DOE O 414.1D, DOE O 226.1A, and others as described.

The QAMP establishes QA requirements for conducting activities, including providing items or services that affect, or may affect, nuclear safety of facilities in a tailored manner to ensure that environmental, safety, and health risks and impacts are minimized, and that safety, reliability, products, and performance are maximized by using effective management systems.

Quality Assurance Manual 1-Q

The Quality Assurance Manual 1-Q provides the structure and procedures for achieving and verifying the SRS requirements for quality. The manual consists of a series of QA procedures that

describe applicable QA requirements. In 1Q Manual, Procedure 2-1, *Quality Assurance Program*, Section B states that the QA program has been developed to be responsive to the requirements of DOE O 414.1D, and DOE *Nuclear Safety Management*, Title 10 CFR 830, Subpart A, *Quality Assurance Requirements*. Because of the size and complexity of SRS and its varied products, services, and missions, the program has been defined in a standard framework of company policy, procedures, and instructions to be used by the implementing organizations to perform quality-related activities. [1Q Manual, Procedure 2-1]

9.2 Software Quality Assurance

Software QA is conducted in accordance with the requirements of the 1Q Manual, Procedure 20-1 through the development and execution of various software quality assurance plans (SQAPs). The SQAPs for the specific software codes used in the FY2019 SDF PA are identified in *Performance Assessment for the Saltstone Disposal Facility at the Savannah River Site: Quality Assurance Report* (SRR-CWDA-2018-00068), as well as in Section 4.2.2 of this PA.

9.3 Modeling Quality Assurance

The E7 Manual, *Conduct of Engineering Manual*, E7, Procedure 2.60, *Technical Reviews* is the QA implementing procedure for performing technical reviews. This procedure defines the processes used by SRS to verify the inputs and outputs for the different modeling codes. The end use of data drives the level of review required. Design Verification, the highest-level review, must be performed for work affecting Safety Significant/Safety Class systems. Design Check is the next lower level of review and is required for all Production Support and General Service design output documents. Because the work associated with the PA and associated documents are not associated with Safety Significant or Safety Class systems, the Design Check represents the appropriate level of rigor.

As described in Section 4.2.1.3, during a design check of the models the technical accuracy of the design document is assured by performing the following activities:

- A mathematical check, if appropriate,
- A review for correct use of technical input, including quality requirements,
- A review of the approach used and reasonableness of the output, and
- An administrative check (e.g., page numbers, format).

To perform a Design Check, the following criteria must be met:

- Cannot be a participant in the development of the portion of the document being checked,
- Must be knowledgeable in the area of the design or analysis for which they review,
- Must be capable of performing similar design or analysis activities, and
- Must have the security clearance for access to sufficient information to perform the Design Check.

Between 2002 and 2004, SRNL developed, piloted, and implemented technical review guidelines incorporating the E7 Manual, Procedure 2.60 requirements for performing Design Checks and Design Verification by document review. These guidelines also meet the requirements for review

of Type 2 Calculations contained in E7 Manual, Procedure 2.31, *Engineering Calculations*. The guidelines provide a flowchart to map the SRNL technical review process, lines of inquiry for performing reviews, a checklist for communicating instructions, and best management practices to set a benchmark for management expectations.

Documentation of the verification for the model input traced from source documents, to modeling input, and to appropriate sections within the PA has been performed and is described in *Performance Assessment for the Saltstone Disposal Facility at the Savannah River Site: Quality Assurance Report* (SRR-CWDA-2018-00068). Model inputs are implemented as components to the model files (i.e., they are "hardwired" into the models). Consequently, inputs are controlled in accordance with the QA requirements of the respective model(s) and any changes to the inputs result in a change to the model, thus requiring re-checking of the affected model file(s).

After the issuance of the QA Report, additional models were developed and checked in support of the PA. The documentation of the model checking for these additional models is documented in *Addendum to FY2019 SDF PA QA Report, SRR-CWDA-2018-00068* (SRR-CWDA-2019-00046).

This page intentionally left blank.

10 CONTRIBUTIONS

The work documented within this PA represents a culmination of years of research and modeling activities performed across disciplines and across organizations. This work could not have been accomplished without the efforts of those named below. This section is organized by Preparers (Section 10.1) to identify individuals whose work directly supported the preparation of this report, and Acknowledgements (Section 10.2) to recognize those who made significant contributions to work that supported the development of this PA.

10.1 Preparers

HOMMEL, STEVE

Waste Disposal Authority – Savannah River Remediation LLC
M.S. Information Systems, University of Phoenix
B.S. Earth Science, University of Nevada, Las Vegas

Experience: Mr. Hommel is a Principal Engineer at SRR with more than 15 years of experience working on PAs for various DOE projects. He is currently the Subject Matter Expert for the SDF PA. In his current role, he has been the lead author on multiple PA-related documents, including technical reports related to FEPs analyses, conceptual model development, dose calculations, quantitative inventory analyses, and probabilistic uncertainty analyses. In addition to technical writing, his expertise includes modeling, statistical and data analyses, and coding. Prior to coming to SRS, he used GoldSim and other quantitative tools to develop validation models for the Total System Performance Assessment for the Yucca Mountain Project.

Contributions: As the SDF PA Subject Matter Expert, Mr. Hommel served as the technical project lead for the development of the SDF PA. In this capacity, he worked closely with other team members to assign modeling tasks and to ensure writing assignments were completed in a timely manner. Mr. Hommel also prepared many of the sections of the PA. Additionally, he prepared many key references to the PA including the FEPs analysis, development of conceptual models, improvements to the dose calculations, model input development, and the interpretation of results, as well as performing the quantitative analysis of the probabilistic modeling results.

CANTRELL, BREANA

Waste Disposal Authority – Savannah River Remediation LLC
B.S. Business Management, University of South Carolina, Aiken

Experience: Ms. Cantrell serves as the WDA Administrative Assistant and provides project support in editorial processes, graphic and figure development, and development of regulatory documents.

Contributions: Ms. Cantrell tracked and maintained the status progression of the development and revision of each section of the PA. In addition, she assisted with the verification of references within the Liquid Waste Organization Document Library.

DEAN, BEN

Waste Disposal Authority – Savannah River Remediation LLC
B.S. Chemical Engineering, Clemson University

Experience: With over 21 years of experience (11 years at SRS), Mr. Dean has primarily worked with characterization of waste within the Tank Farms. He was involved with the characterization efforts for the FTF and SDF PAs. In addition, he has been involved with the current tank closure sampling process and result evaluation. The balance of experience (10 years) was spent in the chemical industry – chlor-alkali, fiberglass, and pigments – with experience in operations, commissioning, process engineering, statistics, and laboratory management.

Contributions: Mr. Dean assisted in inventory sensitivity analyses, development of the residual characterization estimates, and modifications to the air pathway model.

DIXON, DARA

Waste Disposal Authority – Savannah River Remediation LLC
M.E. Nuclear Engineering, University of South Carolina
B.S. Chemical Engineering, University of South Carolina

Experience: Ms. Dixon has 17 years of experience at SRS. During this time, her emphasis has been on chemical process development and operations for various facilities used to stabilize LLW and HLW. Ms. Dixon has spent the past five years with the WDA where she has been responsible for inventory documentation for the Tank Farm and Saltstone facilities.

Contributions: Ms. Dixon performed technical and editing reviews for various sections of the PA.

FLACH, GREGORY

Waste Disposal Authority – Savannah River Remediation LLC
Ph.D. Mechanical Engineering, North Carolina State University
M.S. Mechanical Engineering, North Carolina State University
B.S. Mechanical Engineering, University of Kentucky

Experience: Dr. Flach is an Advisory Engineer for SRR with 30 years of experience related to ground water hydrology, computational simulation, numerical code development, and DOE PAs. He has been the principal investigator on several ground water modeling studies at SRS involving regional and local scale hydrology, contaminant migration from waste sites, and evaluation of environmental cleanup alternatives. Over the last decade, his efforts have focused on subsurface flow and transport simulations supporting DOE PAs at SRS, including the SDF, FTF and HTF closures, and the E-Area Solid Low-Level Radioactive Waste Disposal Facility. Dr. Flach was awarded the DOE Secretary's Achievement Award in 2013 for his key contributions to the FTF Closure PA. His research efforts focus on dual-domain formulations of contaminant transport.

Contributions: Dr. Flach analyzed degradation of cementitious materials and led PORFLOW porous-media flow and solute transport modeling of ground water pathways.

KINARD, BROOKE

Waste Disposal Authority – Savannah River Remediation LLC
B.A. Political Science, University of South Carolina

Experience: Ms. Kinard has over five years of engineering support experience in both government and commercial nuclear sectors. In her assignment with the WDA, she is responsible for providing technical administrative support for the development and editorial process for regulatory documentation under the guidelines of the DOE and other government and state codes, regulations, and requirements.

Contributions: Ms. Kinard served as the lead technical specialist for the application of the document format and layout, editorial process, production activities, and graphic/figure development.

LAYTON, MARK

Waste Disposal Authority – Savannah River Remediation LLC
B.S. Earth Science, University of Cincinnati

Experience: Mr. Layton has over 25 years of experience at SRS in various regulatory compliance organizations. The majority of this time was spent working on HLW regulatory compliance assignments and supporting various Safety Basis activities. Mr. Layton also provided safety basis support for numerous other facilities at SRS and across the DOE complex, including Sandia, Pantex, and Oak Ridge.

Contributions: Mr. Layton assisted in the technical review of various PA sections.

LESTER, BARRY

Waste Disposal Authority – Savannah River Remediation LLC
M.S. Geology, Pennsylvania State University
B.S. Earth Science, Pennsylvania State University

Experience: Mr. Lester has over 39 years of experience working in the field of hydrogeology and the development and application of numerical and analytical ground water flow and contaminant transport codes. He is presently working in support of the SDF PA modeling efforts. Prior to coming to SRS, Mr. Lester worked for the Office of Civilian Radioactive Waste Management division where he helped develop the Yucca Mountain Total Systems Performance Analysis Model. He has also worked for the DOE Underground Test Area group developing numerical ground water flow and radionuclide transport models for the Nevada Test Site and the EPA developing analytical and numerical contaminant transport models.

Contributions: Mr. Lester is the primary developer of the GoldSim radionuclide transport models used in the stochastic transport simulations by SRR.

MANGOLD, JEREMIAH

Waste Disposal Authority – Savannah River Remediation LLC
Ph.D. Environmental Engineering, University of Texas at Austin
M.S. Environmental Engineering, Texas Tech University
B.S. Environmental Engineering, Texas Tech University

Experience: Mr. Mangold's graduate work at The University of Texas at Austin focused on environmental surface chemistry, specifically building surface complexation models to simulate contaminant sorption to iron-oxide minerals. His post-graduate work at Clemson University centered on radionuclide sorption to minerals present in proposed HLW geologic repositories at elevated temperatures and ionic strengths. He has four years of experience at SRS as a contaminant fate and transport modeler.

Contributions: Mr. Mangold worked primarily on development of the contaminant release sections of the PA and as a technical reviewer of GoldSim model files.

ROSENBERGER, KENT

Waste Disposal Authority – Savannah River Remediation LLC
B.S. Nuclear Engineering – Pennsylvania State University

Experience: Mr. Rosenberger has over 28 years of experience at SRS. He has spent the last 14 years supporting SDF and tank closure regulatory documents, including PA document development, implementation, and maintenance. He previously held positions in radiological engineering project and operations support and facility operational radiological control management. Mr. Rosenberger has considerable experience with the SRS HLW processes and facilities, in addition to experience with reactor, chemical separations, plutonium processing and storage, and laboratory facilities.

Contributions: Mr. Rosenberger provided management oversight and review.

WATKINS, DAVID

Waste Disposal Authority – Savannah River Remediation LLC
B.S. Geology – College of Charleston

Experience: Mr. Watkins has over 37 years of experience in environmental monitoring, regulatory compliance, geologic characterizations, and project management. Mr. Watkins has over 10 years of experience preparing PAs, SAs, and their supporting documents for the SRS. His various other assignments over the last 28 years at SRS have included preparing and reviewing regulatory compliance documents, including RCRA Facility Invesitgations (RFIs), Remedial Investigations, Baseline Risk Assessments, RFI Work Plans, Records of Decision, Statement of Basis/Proposed Plans, Corrective Measure Studies/Feasibility Studies, and RCRA Part B Permit Renewal Applications. Mr. Watkins has performed hydrogeologic characterizations, data compilation, and ground water monitoring for various operable units at the SRS and prepared

associated maps and reports. Additionally, he has experience in preparing and reviewing construction authorization environmental reports for commercial nuclear power plants.

Contributions: Mr. Watkins provided development of sections related to hydrogeology, demographics, radionuclide transport, and quality assurance. In addition, he assisted in the preparation and review of various other PA sections and preparation of the PA QA documents.

WOOTEN, LESLIE

Waste Disposal Authority – Savannah River Remediation LLC
M.S. Environmental Studies – College of Charleston
B.S. Environmental Engineering – Colorado State University

Experience: Ms. Wooten has over three years of engineering experience in the government nuclear sector at SRS. During her tenure at the WDA, she has been responsible for maintaining the SDF-WIDE model, annual SDF radionuclide inventory reporting, and annual SDF PA reviews, as well as developing numerous other regulatory and technical documents for SDF, FTF, and HTF.

Contributions: Ms. Wooten is the primary developer of the chemical and radiological inventory determination for PA modeling.

10.2 Acknowledgements

In addition to the preparers listed above, the SDF PA team would like to acknowledge the following individuals for their support:

J. Marie Benavides	James Dwyer	Joseph Pavletich
Craig Benson	Daniel Ferguson	Virginia Rigsby
Jeffery Bentley	J. Cameron Fields	Larry Romanowski
Thomas Brooks	Andrew Garrabrants	Paul Rutland
Kevin Brown	Thong Hang	John Seaman
William Brown	Daniel Kaplan	Roger Seitz
Timothy Coffield	Terry Killeen	Steve Simner
Dave Crowley	David Kosson	Malcolm Smith
Thomas Danielson	Matthew Kozak	Patricia Suggs
Saleigh Derico	Walt Kubilius	Steve Thomas
Bradley Dowell	Christine Langton	Aaron White

This page intentionally left blank.

11 REFERENCES

0000138886-000024, *SRNS14-022 - Test Report Z Area Type V Concrete Hydraulic Conductivity Test, Subcontract No. 0000138886, Delivery Order No. 2*, Amec Foster Wheeler, Atlanta, GA, Rev. A, September 2018.

07-ALJ-07-121-CC, *Consent Order of Dismissal*, State of South Carolina, Administrative Law Court, Columbia, SC, August 7, 2007.

10 CFR 61, *Licensing Requirements for Land Disposal of Radioactive Waste*, U.S. Nuclear Regulatory Commission, Washington DC, December 2011.

10 CFR 100, *Seismic and Geologic Siting Criteria for Nuclear Power Plants*, U.S. Nuclear Regulatory Commission, Washington DC, January 2008.

10 CFR 830, *Nuclear Safety Management*, U.S. Nuclear Regulatory Commission, Washington DC, February 2002.

10 CFR 835, *Occupational Radiation Protection*, U.S. Nuclear Regulatory Commission, Washington DC, May 2011.

1Q Manual, Procedure 2-1, *Quality Assurance Manual, Quality Assurance Program*, Savannah River Site, Aiken, SC, Rev. 14, July 2018.

1Q Manual, Procedure 20-1, *Quality Assurance Manual, Software Quality Assurance*, Savannah River Site, Aiken, SC, Rev. 19, April 2018.

40 CFR 61, Subpart H, *National Emission Standards for Hazardous Air Pollutants, Subpart H, National Emission Standards for Emissions of Radionuclides other than Radon from Department of Energy Facilities*, U.S. Nuclear Regulatory Commission, Washington DC, April 2012.

Ababou, R., and Wood, E.F., *Comment on "Effective groundwater model parameter values: influence of spatial variability of hydraulic conductivity, leakance, and recharge" by J. J. Gomez-Hernandez and S. M. Gorelick*, Water Resources Research, V.26 N.8, 1843-1846, 1990. (Copyright)

ACI 222R-01, *Protection of Metals in Concrete Against Corrosion*, ACI Committee 222, Issued 2002 (Reapproved 2010). (Copyright)

ACI 233R-17, *Guide to the Use of Slag Cement in Concrete and Mortar*, ACI Committee 233, 2017. (Copyright)

ACI 318-19, *Building Code Requirements for Structural Concrete*, ACI Committee 318, 2019. (Copyright)

ACI 350.1-2010, *Specification for Tightness Testing of Environmental Engineering Concrete Containment Structures*, American Concrete Institute, Farmington Hills, MI, January 2010. (Copyright)

ACRi-2002, *Analytic & Computational Research, Inc. PORFLOW User's Manual*, Version 5.0, Analytic and Computational Research, Inc., Bel Air, CA, Rev. 5, March 2002. (Copyright)

ACRi-2010, *ACRi Software Tools: Answer™ ◊ PORFLOW™ ◊ Tidal™, Keyword Commands*, Analytical & Computational Research, Inc., Bel Air, CA, 426p, 2010. (Copyright)

Ahmad, S., *Reinforcement Corrosion in Concrete Structures, its Monitoring and Service Life Prediction – a Review*, Cement & Concrete Composites 25:459-471, 2003. (Copyright)

Berner, U.R., *Evolution of Pore Solution Chemistry during Degradation of Cement in a Radioactive Waste Repository Environment*, Waste Management 12, 201-215, 1992. (Copyright)

Bethke, C. and Yeakel, S., *The Geochemists Workbench Release 10.0: GWB Essentials Guide*, Aqueous Solutions, LLC, Champaign, IL, December 2015. (Copyright)

Boher, C., Frizon, F., Lorente, S., and Bart, F., *Influence of the pore network on hydrogen diffusion through blended cement pastes*, Cement and Concrete Composites, Vol. 37, 30-36, 2013. (Copyright)

Brown, K.G., et.al., *Modeling Carbonation of High-Level Waste Tank Integrity and Closure. NUCPERF 2012 Conference*, Cadarache, France, November 2012. (Copyright)

Brown, K.G., et.al., *Cementitious Barriers Partnership (CBP): Training and Release of CBP Toolbox Software, Version 1.0 – 13480*, WM2013 Conference, Phoenix, AZ, February 2013. (Copyright)

Brown, K.G., et.al., *Cementitious Barriers Partnership (CBP): Using the CBP Software Toolbox to Simulate Sulfate Attack and Carbonation of Concrete Structures – 13481*, WM2013 Conference, Phoenix, AZ, February 2013. (Copyright)

Brown, K.G., and Garrabrants, A., *Predicting the Hydraulic Conductivity over Time for Degrading Saltstone Vault Concrete – Task 5 (Subcontract Number SRRA110110)*, December 2017.

B-SQP-A-00068, Dien, L., *Software Quality Assurance Plan (SQAP) for The Geochemist's Workbench*, Savannah River Site, Aiken, SC, Rev. 0, March 2015.

B-SQP-C-00002, Hommel, S.P., *Software Quality Assurance Plan for GoldSim© for Savannah River Site's Liquid Waste Program*, Savannah River Site, Aiken, SC, Rev. 3, May 2018.

B-SQP-C-00003, Lester, B.H., *Software Quality Assurance Plan for ReadPORFLOWFiles.dll for the Savannah River Site's Liquid Waste Program*, Savannah River Site, Aiken, SC, Rev. 1, June 2013.

CAP88-PC_3.0, *CAP88-PC Version 3.0 User Guide*, U.S. Environmental Protection Agency Office of Radiation and Indoor Air, Washington DC, Rev. 0, February 2013.

CAP88-PC_4.0, *CAP88-PC Version 4 Testing Report*, U.S. Environmental Protection Agency Office of Radiation and Indoor Air, Washington DC, Rev. 1, June 2013.

CBP-TR-2009-002, *Review of Mechanistic Understanding and Modeling and Uncertainty Analysis Methods for Predicting Cementitious Barrier Performance*, Cementitious Barriers Partnership, Rev. 0, November 2009.

CBP-TR-2010-007-C3, Samson, E., *Cementitious Barriers Partnership Task 7 Demonstration of STADIUM® for the Performance Assessment of Concrete Low Activity Waste Storage Structures*, Cementitious Barriers Partnership, http://cementbarriers.org, Rev. 0, 2010.

CBP-TR-2010-012-1, Arnold, J., et.al., *Characterization of Reference Materials and Related Materials for the Cementitious Barriers Partnership*, www.cementbarriers.org, December 2010.

CBP-TR-2014-005, Langton, C. A., *Technetium Oxidation in Slag-Based Sodium Salt Waste Forms Exposed to Water and Moist Hanford Soil*, Cementitious Barriers Partnership, Rev. 0, August 2014.

CBU-ENG-2003-00103, Liner, K.R., *Saltstone Vault Sheet Drain Installation*, Savannah River Site, Aiken, SC, April 2003.

CBU-PIT-2005-00146, Rosenberger, K.H., et.al., *Saltstone Performance Objective Demonstration Document*, Savannah River Site, Aiken, SC, Rev. 0, June 2005.

CBU-PIT-2005-00228, Hamm, B.A., *Savannah River Site High-Level Waste Tank Farm Closure Radionuclide Screening Process (First-Level) Development and Application*, Savannah River Site, Aiken, SC, Rev. 0, November 2006.

CMT-HTF-2017-00069, *Computer Program Modification Tracker for WCS Online*, Savannah River Site, Aiken, SC, Rev. 0, January 2018.

CRC Press, *CRC Handbook of Chemistry and Physics, 97th edition*, 2017. (Copyright)

C-CC-Z-00039, *Z-Area Saltstone Disposal Site SDU6 Tank Design Concrete Foundation Plan*, Savannah River Site, Aiken, SC, Rev. 8, November 2012.

C-CC-Z-00042, *Z-Area Saltstone Disposal Site SDU6 Tank Design Concrete Wall Column Section Details*, Savannah River Site, Aiken, SC, Rev. 10, January 2017.

C-CC-Z-00044, *Z-Area Saltstone Disposal Site SDU6 Tank Design Concrete Sections and Details*, Savannah River Site, Aiken, SC, Rev. 9, December 2015.

C-CC-Z-00049, *Z-Area Saltstone Disposal Site SDU6 Tank Design Concrete Roof Embed and Nozzle Plan*, Savannah River Site, Aiken, SC, Rev. 7, February 2017.

C-CC-Z-00059, *Z Area Saltstone Disposal Site SDU7 Tank Design Concrete Foundation Plan*, Savannah River Site, Aiken, SC, Rev. 1, April 2018.

C-CC-Z-00060, *Z Area Saltstone Disposal Facility Site SDU7 Tank Design Concrete Overall Roof Plan*, Savannah River Site, Aiken, SC, Rev. 1, April 2018.

C-CC-Z-00063, *Z Area Saltstone Disposal Facility Site SDU7 Tank Design Concrete Wall and Column Section and Details*, Savannah River Site, Aiken, SC, Rev. 2, October 2018.

C-CC-Z-00066, *Z Area Saltstone Disposal Facility Site SDU7 Tank Design Concrete Details*, Savannah River Site, Aiken, SC, Rev. 1, Jul 2018.

C-CC-Z-0010, *Saltstone Vault No. 1 Personal Protection Layers Plan, Sections and Detail*, Savannah River Site, Aiken, SC, Rev. 1, March 1995.

C-CC-Z-0012, *Saltstone Vault No. 4 Permanent Roof Plan*, Savannah River Site, Aiken, SC, Rev. 5, July 2009.

C-CC-Z-0013, *Saltstone Vault No. 4 Permanent Roof Concrete Sections and Details Sheet No. 1*, Savannah River Site, Aiken, SC, Rev. 3, July 1998.

C-CG-Z-00027, *Z-Area Saltstone Disposal Site Vault #2 Excavation and Stockpile Plan*, Savannah River Site, Aiken, SC, Rev. 2, June 2008.

C-CG-Z-00028, *Z-Area Saltstone Disposal Site Vault #2 Excavation and Stockpile Cross Sections*, Savannah River Site, Aiken, SC, Rev. 1, April 2006.

C-CG-Z-00030, *Z-Area Saltstone Site Vault #2 Finish Grading Plan*, Savannah River Site, Aiken, SC, Rev. 3, April 2006.

C-CG-Z-00048, *Z-Area Saltstone Disposal Site SDU 6 Site Preparation Excavation Grading Plan*, Savannah River Site, Aiken, SC, Rev. 2, March 2017.

C-CH-Z-00014, *Saltstone Storage Vault No. 2, Drain Water Collection System Piping Arrangement and Pipe Support*, Savannah River Site, Aiken, SC, Rev. 6, May 2009.

C-CS-Z-0002, *Saltstone Vault 4, Permanent Roof Steel Sections & Details (Sh.2)*, Savannah River Site, Aiken, SC, Rev. 2, July 1998.

C-CX-Z-0001, *Saltstone Vault #2 Site and Erosion Control Plan*, Savannah River Site, Aiken, SC, Rev. 2, April 2006.

C-CX-Z-00003, *Saltstone Disposal Site Cylindrical Disposal Cells General Arrangement Plan*, Savannah River Site, Aiken, SC, Rev. 2, October 2016.

C-CY-Z-00006, *Z Area Saltstone Disposal Site SDU6 Tank Design Civil Leakage Detection System Sections and Details*, Savannah River Site, Aiken, SC, Rev. 5, February 2017.

C-CY-Z-00011, *Z Area Saltstone Disposal Site SDU7 Tank Design Civil Leakage Detection System Sections and Details*, Savannah River Site, Aiken, SC, Rev. 1, March 2018.

C-SPP-Z-00006, Kelley, J.P., *Saltstone Vault #2 Including Excavation, Liner and Backfill*, Savannah River Site, Aiken, SC, Rev. 1, June 2008.

C-SPP-Z-00008, *Saltstone Disposal Site – SDU6 Procurement Specification*, Savannah River Site, Aiken, SC, Rev. 4, December 2014.

C-SPP-Z-00015, *Saltstone Disposal Unit 7 – SDU 7 – Procurement Specification Sheet*, Savannah River Site, Aiken, SC, Rev. 1, July 2018.

C-SPP-Z-00019, *Saltstone Disposal Unit (SDU) 8&9: GCL, HDPE Geomembrane, Specification*, Savannah River Site, Aiken, SC, Rev. 0, April 2019.

DHEC_01-23-2007, *Approval of a Modified Permit for the Savannah River Site (SRS) Z-Area Saltstone Disposal Facility ID#025500-1603,* Bureau of Land and Waste Management, South Carolina Department of Health and Environmental Control, Columbia, SC, January 2007.

DHEC_01-25-1993, *Permit to Construct, F and H-Area High-Level Radioactive Waste Tank Farms, Construction Permit #17,424-IW,* Industrial & Agricultural Wastewater Division, South Carolina Department of Health and Environmental Control, Columbia, SC, January 1993.

DHEC_02-28-1995, *Review Comments on Groundwater Monitoring Plan, dated February 15, 1995, Z-Area Saltstone Disposal Facility (IWP-217),* Bureau of Solid and Hazardous Waste Management, South Carolina Department of Health and Environmental Control, Columbia, SC, February 1995.

DHEC_04-16-1996, *Modified SRS Z-Area Industrial Solid Waste Permit, #025500-1603 (Formerly IWP-217),* Bureau of Solid and Hazardous Waste Management,South Carolina Department of Health and Environmental Control, Columbia, SC, January 1993.

DHEC_05-12-2011, *Modified Permit for the Savannah River Site (SRS) Z-Area Saltstone Disposal Facility (SDF) – Cells 3 and 5, Facility ID No. 025500-1603, Aiken County*, South Carolina Department of Health and Environmental Control, Columbia, SC, May 2011.

DHEC_09-09-2008, *Modified Permit for the Savannah River Site (SRS) Z-Area Saltstone Disposal Facility (SDF), Facility ID No. 025500-1603, Aiken County, (Class 3 Landfill Permit)*, South Carolina Department of Health and Environmental Control, Columbia, SC, September 2008.

DHEC_12-17-2012, *Modified Permit for Vault 6 in Z-Area Disposal, SRS ─ Z-Area Saltstone Facility, Facility ID No. 025500-1603, Aiken County*, South Carolina Department of Health and Environmental Control, Columbia, SC, December 2012.

DOE M 435.1-1, Chg. 2, *Radioactive Waste Management Manual*, U.S. Department of Energy, Washington DC, June 2011.

DOE O 226.1B, *Implementation of Department of Energy Oversight Policy*, U.S. Department of Energy, Washington DC, April 2011.

DOE O 414.1D, *Quality Assurance*, U.S. Department of Energy, Washington DC, April 2011.

DOE O 435.1, Chg. 1, *Radioactive Waste Management*, U.S. Department of Energy, Washington DC, August 2001.

DOE O 458.1, Chg. 3, *Radiation Protection of the Public and the Environment*, U.S. Department of Energy, Washington DC, January 2013.

DOE O 5820.2A, (Superseded) *Radioactive Waste Management*, U.S. Department of Energy, Washington DC, February 1984.

DOE Policy 450.4A, *Integrated Safety Management Policy,* U.S. Department of Energy, Washington DC, April 2011.

DOE/ID-10966, *Performance Assessment for the Tank Farm Facility at the Idaho National Engineering and Environmental Laboratory, Final*, Idaho National Laboratory, Idaho Falls, ID, Rev. 1, April 2003.

DOE_02-09-2006, *Compliance with DOE M 435.1-1 Waste Incidental to Reprocessing (WIR) Requirements and Implementation of Section 3116(a) of the National Defense Authorization Act for Fiscal Year 2005 (NDAA),* U.S. Department of Energy, Washington DC, February 2006.

DOE-EIS-0303, *High-Level Waste Tank Closure Final Environmental Impact Statement*, U.S. Department of Energy–Savannah River, Aiken, SC, May 2002.

DOE-HDBK-1215-2014, DOE Handbook, *Optimizing Radiation Protection of the Public and the Environment for Use with DOE O 458.1, ALARA Requirements*, U.S. Department of Energy, Washington DC, October 2014.

DOE-OS-2013-10-15-01, *Low Level Waste Disposal Facility Federal Review Group Review Report on the Savannah River Site Salt Waste Disposal Special Analysis to the 2009 Performance Assessment*, U.S. Department of Energy, Washington DC, October 2013.

DOE-STD-1196-2011, *DOE Standard Derived Concentration Technical Standard*, U.S. Department of Energy, Washington, DC, April 2011.

DOE-STD-5002-2017, *Disposal Authorization Statement and Tank Closure Documentation*, U.S. Department of Energy, Washington DC, May 2017.

DOI: 10.1007/s00477-003-0171-3, Sarris, T. and Paleologos, E., *Numerical investigation of the anisotropic hydraulic conductivity behavior in heterogeneous porous media*, Stochastic Environmental Research and Risk Assessment Vol. 18, Issue 3, June 2004. (Copyright)

DOI: 10.1016/j.geomorph.2008.05.024, Leigh, D.S., *Late Quaternary Climates and River Channels of the Atlantic Coastal Plain, Southeastern USA*, Geomorphology Vol. 101 (1), October 2008. (Copyright)

DOI: 10.1016/0266-1144(89)90009-5, Giroud, J.P., and Bonaparte, R., *Leakage through Liners Constructed with Geomembrane—Part I. Geomembrane Liners*, Geotextiles and Geomembranes, Vol. 8 (1), 1989. (Copyright)

DOI: 10.1016/0266-1144(89)90022-8, Giroud, J.P., and Bonaparte, R., *Leakage through Liners Constructed with Geomembrane—Part II. Composite Liners*, Geotextiles and Geomembranes, Vol. 8 (2), 1989. (Copyright)

DOI: 10.1029/2002WR001716, Haggerty, R., et.al., *What controls the apparent timescale of solute mass transfer in aquifers and soils? A comparison of diverse experimental results*, Water Resources Research, Vol. 40, 2004. (Copyright)

DOI: 10.1029/WR019i001p00161, Gelhar, L. W., and Axness, C. L., *Three-dimensional stochastic analysis of macrodispersion in aquifers*, Water Resources Research, Vol. 19, 161– 180, 1983. (Copyright)

DOI: 10.1061/(ASCE)1090-0241(2001)127:6(510), Foose, G., Benson, C., and Edil, T., *Predicting Leakage Through Composite Landfill Liners*, Journal of Geotechnical and Geoenvironmental Engineering, Vol. 127, No. 6, June 2001. (Copyright)

DOI: 10.1061/(ASCE)GT.1943-5606.0001643, Tian, K., et.al., *Antioxidant Depletion and Service Life Prediction for HDPE Geomembranes Exposed to Low-Level Radioactive Waste Leachate*, Journal of Geotechnical and Geoenvironmental Engineering, ASCE Vol. 143, No. 6, February 2017. (Copyright)

DOI: 10.1061/(ASCE)1090-0241(1998)124:6(532), Hsuan, Y.G., and Koerner, R.M., *Antioxidant depletion lifetime in high density polyethylene geomembranes*. Journal of Geotechnical and Geoenvironmental Engineering, ASCE,Vol. 124, No. 6, June 1998. (Copyright)

DOI: 10.1063/1.1749710, Huggins, M., *Molecular Constants and Potential Energy Curves for Diatomic Molecules*, The Journal of Chemical Physics, Volume 3, Issue 8, 1935. (Copyright)

DOI: 10.1093/acref/9780199204632.001.0001, Daintith, J., *A Dictionary of Chemistry*, Sixth Edition, Oxford University Press, 2008. (Copyright)

DOI: 10.1097/HP.0000000000000314, Jannik, T., et.al., *Comparison of US Environmental Protection Agency's CAP88PC Versions 3.0 and 4.0*, Health Physics, Vol. 109, Supp. 2, 2015. (Copyright)

DOI: 10.1680/gein.2004.11.1.43, Giroud, J.P., et.al., *Liquid Flow Equations for Drainage Systems Composed of Two Layers Including a Geocomposite*, Geosynthetics International, Vol. 11, No. 1, February 2004. (Copyright)

Drever, J.I., *The Geochemistry of Natural Waters, 2nd Edition*, Prentice-Hall, 1988. (Copyright)

E7 Manual, Procedure 2.31, *Conduct of Engineering and Technical Support Procedure Manual, Engineering Calculations*, Savannah River Site, Aiken, SC, Rev. 15, March 13, 2018.

E7 Manual, Procedure 2.60, *Conduct of Engineering and Technical Support Procedure Manual, Technical Reviews,* Savannah River Site, Aiken, SC, Rev. 17, August 2016.

EPA-402-R-18-001, *Federal Guidance Report No. 15: External Exposure to Radionuclides in Air, Water and Soil*, U.S. Environmental Protection Agency, Washington DC, June 2018.

EPA-600-R-090-052F, *Exposure Factors Handbook: 2011 Edition*, U.S. Environmental Protection Agency, Washington DC, September 2011.

EPA-815-R-02-001, *Radionuclides in Drinking Water: A Small Entity Compliance Guide,* U.S. Environmental Protection Agency, Washington DC, February 2002.

ESH-WPG-2006-00132, Liner, K.R., *Z-Area Industrial Solid Waste Landfill Vault Cracking*, Savannah River Site, Aiken, SC, October 2006.

Fredlund, D.G., and Rahardjo, H., *Soils Mechanics for Unsaturated Soils*, John Wiley, New York, 1993. (Copyright)

Freeze, R.A., and Cherry, J.A, *Groundwater,* Prentice-Hall, Engelwood Cliffs, NJ, 1979. (Copyright)

G-AES-S-00004, *Future Saltstone Disposal Units Siting, Systems Engineering Evaluation*, Savannah River Site, Aiken, SC, Rev. 0, June 2018.

Gelhar, L.W., et.al., *A Critical Review of Data on Field-Scale Dispersion in Aquifers Water Resources Research*, Vol. 28, No. 7, pp. 1955-1974, July 1992. (Copyright)

GTG-2018a, *GoldSim User's Guide: Probabilistic Simulation Environment*, GoldSim Technology Group LLC, Issaquah, WA, 2018. (Copyright)

GTG-2017b, *GoldSim User's Guide: GoldSim Contaminant Transport Module*, GoldSim Technology Group LLC, Issaquah, WA, February 2017. (Copyright)

Gutjahr, A.L., et.al., *Stochastic Analysis of Spatial Variability in Subsurface Flows: 2. Evaluation and Application*. Water Resour. Res., 14(5), 953–959, 1978. (Copyright)

G-ESR-Z-00018, Simner, S.P., *Proposed Simulant Salt Solution for Evaluating the Resistance of SDU Concrete to Chemical Attack*, Savannah River Site, Aiken, SC, Rev. 0, December 2015.

G-ESR-Z-00019, Thompson, J.P., *Leak Tight Liner System for Primary Containment and Chemical Resistance to the Interior of the SDU-6 Cell*, Savannah River Site, Aiken, SC, Rev. 0, June 2016.

G-SQP-A-00012, Hang, T., *PORFLOW Software Quality Assurance Plan*, Savannah River Site, Aiken, SC, Rev. 0, June 2007.

G-TAR-Z-00004, Hommel, S.P., *PORFLOW Modeling to Support an Evaluation for Alternate Future SDU Siting, Including SDU 6 As-Built Conditions, and to Envelope Potential for Construction Imperfections During Construction of Future SDUs*, Savannah River Site, Aiken, SC, Rev. 0, June 2016.

Hall, C., and Hoff, W., *Water Transport in Brick, Stone and Concrete*, Spon Press, New York, 2002. (Copyright)

HLW-SSF-TTR-2013-0021, *Liquid Waste (LW) Technical Task Request – 30 Million Gallon Saltstone Disposal Unit (SDU) PORFLOW Modeling for SDU-6 Special Analysis (SA),* Savannah River Site, Aiken, SC, Rev. 2, October 2013.

Holz, M., et.al., *Temperature-dependent Self-diffusion Coefficients of Water and Six Selected Molecular Liquids for Calibration in Accurate 1H NMR PFG Measurements*, Physical Chemistry Chemical Physics, 2: 4740–4742, 2000. (Copyright)

http://cementbarriers.org, *Cementitious Barriers Partnership*.

https://earthquake.usgs.gov, *Earthquake Hazards Program*, United States Geological Survey, Reston, VA.

https://weather.srs.gov/weather/climate_data/, Atmospheric Technologies Group, Savannah River Site, Aiken, SC.

https://www.epa.gov/ground-water-and-drinking-water/national-primary-drinking-water-regulations, U.S. Environmental Protection Agency, Washington, DC.

Hudson, M., and Barnes, G., *Yoshinogari: A Yayoi Settlement in Northern Kyushu*, Monumenta Nipponica, 46(2): 211-235, 1991. (Copyright)

IRC-1993-16, Schumann, R.R., *The Radon Emanation Coefficient: An Important Tool for Geologic Radon Potential Estimations*, The 1993 International Radon Conference, Vol. IV, pp. 40-47, 1993. (Copyright)

ISBN: 1-59726-010X, Kilgo, J.C. and Blake, J.I., *Ecology and Management of a Forested Landscape: Fifty Years on the Savannah River Site*, Island Press, Washington, D.C., June 2015. (Copyright)

ISBN: 9780486656755, Bear, J., *Dynamics of Fluids in Porous Media*, Elsevier Scientific, New York, 1972. (Reprinted by Dover, New York, 1988) (Copyright)

ISBN: 9780803145573, Daniel, D.G., and Lobo, C.L., *User's guide to ASTM specification C 94 on ready-mixed concrete. ASTM Manual Series MNL49,* ASTM International, 2005. (Copyright)

ISSN 1072-6349, Giroud, J.P., *Equations for Calculating the Rate of Liquid Migration Through Composite Liners Due to Geomembrane Defects*, Geosynthetics International, Vol. 4, No. 3-4, January 1997. (Copyright)

Kaplan, D.I., et.al., *Actinide Association with Groundwater Colloids in a Coastal Plain Aquifer*, Radiochimica Acta 66/67: 181-187, 1994. (Copyright)

K-CLC-F-00034, McHood, M.D., *Actinide Packaging and Storage Facility (APSF)*, Savannah River Site, Aiken, SC, Rev. 0, June 1998.

K-CLC-Z-00001, McHood, M.D., *Liquefaction Potential for Saltstone Disposal Facility Vault No. 4*, Savannah River Site, Aiken, SC, Rev. 0, August 2002.

K-CLC-Z-00002, *Slope Stability for the Saltstone Disposal Facility*, Savannah River Site, Aiken, SC, Rev. 1, April 2003.

K-CLC-Z-00003, Syms, F.H., *Subsurface Stratigraphy for Saltstone Vault No. 4*, Savannah River Site, Aiken, SC, Rev. 0, August 2002.

K-CLC-Z-00004, McHood, M.D., *Liquefaction Settlement for Saltstone Disposal Vault No. 4 Due to PC3 and PC4 Earthquakes*, Savannah River Site, Aiken, SC, Rev. 0, April 2003.

K-CLC-Z-00005, Syms, F.H., *Stratigraphy for the Saltstone Vault No. 2*, Savannah River Site, Aiken, SC, Rev. 0, June 2005.

K-CLC-Z-00007, Li, W.T., *Vault No. 2 Slope Stability Analysis*, Savannah River Site, Aiken, SC, Rev. 0, September 2005.

K-CLC-Z-00008, Li, W.T., *Evaluation of Test Data*, Savannah River Site, Aiken, SC, Rev. 0, January 2006.

K-CLC-Z-00009, Li, W.T., *Settlement Due to Compression of Soft Zone*, Savannah River Site, Aiken, SC, Rev. 0, March 2006.

K-CLC-Z-00010, Li, W.T., *Liquefaction Analysis for Saltstone Vault No. 2*, Savannah River Site, Aiken, SC, Rev. 0, March 2006.

K-CLC-Z-00011, Li, W.T., *Bearing Capacity and Static Settlement*, Savannah River Site, Aiken, SC, Rev. 0, April 2006.

K-CLC-Z-00012, Bennett, P.L., *Stratigraphy for Saltstone Vaults 3 and 5*, Savannah River Site, Aiken, SC, Rev. 0, July 2009.

K-CLC-Z-00013, *Test Data Evaluation for Saltstone Disposal Cells 3 and 5*, Savannah River Site, Aiken, SC, Rev. 0, July 2009.

K-CLC-Z-00014, Williams, R.J., *Bearing Capacity and Static Settlement Calculations for Saltstone Disposal Cells 3 and 5*, Savannah River Site, Aiken, SC, Rev. 0, July 2009.

K-CLC-Z-00015, Williams, R.J., *Liquefaction Analysis for Saltstone Disposal Cells 3 and 5*, Savannah River Site, Aiken, SC, Rev. 0, June 2009.

K-CLC-Z-00016, Williams, R.J., *Soft Zone Induced Settlements for Saltstone Disposal Cells 3 and 5*, Savannah River Site, Aiken, SC, Rev. 0, June 2009.

K-CLC-Z-00018, Nothdurft, D.B., *Updated SPT Liquefaction Analysis for Saltstone Disposal Unit 1*, Savannah River Site, Aiken, SC, Rev. 0, July 2010.

K-CLC-Z-00019, Geiger, A.J., *CPT-Based Liquefaction Analysis for Saltstone Vault 1*, Savannah River Site, Aiken, SC, Rev. 0, December 2010.

K-CLC-Z-00020, Nothdurft, D.B., *Stratigraphy for Saltstone Vault No. 1*, Savannah River Site, Aiken, SC, Rev. 0, January 2012.

K-CLC-Z-00021, Geiger, A.J., *Soft Zone Induced Settlements for Saltstone Vault No. 1*, Savannah River Site, Aiken, SC, Rev. 0, December 2010.

K-CLC-Z-00022, Bennett, P.L. *Stratigraphy for Saltstone Disposal Unit 6 (SDU6),* Savannah River Site, Aiken, SC, Rev. 0, March 2012.

K-CLC-Z-00023, *Soil Design Parameters for Field and Laboratory Testing for Saltstone Disposal Unit 6*, Savannah River Site, Aiken, SC, Rev. 0, March 2012.

K-CLC-Z-00024, Williams, R.J., *Bearing Capacity and Static Settlement Calculations for Saltstone Disposal Unit 6*, Savannah River Site, Aiken, SC, Rev. 0, March 2012.

K-CLC-Z-00025, Williams, R.J., *Liquefaction Analysis for Saltstone Disposal Unit 6*, Savannah River Site, Aiken, SC, Rev. 0, April 2012.

K-CLC-Z-00026, Williams, R.J., *Soft Zone Induced Settlements for Saltstone Disposal Unit 6*, Savannah River Site, Aiken, SC, Rev. 0, April 2012.

K-CLC-Z-00027, Williams, R.J., *Effect of the Saltstone Disposal Unit 6 Tank on the Static Settlement of the Commodity Bridge Foundations*, Savannah River Site, Aiken, SC, Rev. 0, August 2013.

K-CLC-Z-00028, Williams, R.J., *Evaluation on the Stability of Saltstone Disposal Facility Closure Cap System over SDU 4 with Cells C and I Containing Stacked Waste Bags*, Savannah River Site, Aiken, SC, Rev. 0, January 2015.

K-CLC-Z-00029, Bennett, P.L., *Stratigraphy for Saltstone Disposal Unit 7 (SDU 7)*, Savannah River Site, Aiken, SC, Rev. 0, October 2017.

K-CLC-Z-00031, Kyser, D.A., *Bearing Capacity and Static Settlement Calculations for Saltstone Disposal Unit 7*, Savannah River Site, Aiken, SC, Rev. 0, October 2017.

K-CLC-Z-00032, Williams, R.J., *Liquefaction Analysis for Saltstone Disposal Unit 7 (SDU 7)*, Savannah River Site, Aiken, SC, Rev. 0, October 2017.

K-CLC-Z-00033, Williams, R.J., *Soft Zone Induced Settlement for Saltstone Disposal Unit 7 (SDU 7)*, Savannah River Site, Aiken, SC, Rev. 0, October 2017.

K-ESR-G-00013, *SRS Soft Zone Initiative Historical Perspective*, Savannah River Site, Aiken, SC, Rev. 0, January 2008.

K-ESR-Z-00001, Li, W., *Saltstone Vault No. 2 Geotechnical Investigation Report*, Savannah River Site, Aiken, SC, Rev. 0, April 2006.

K-ESR-Z-00002, Williams, R.J., *Saltstone Disposal Cells No. 3 and 5 Geotechnical Investigation Report*, Savannah River Site, Aiken, SC, Rev. 0, July 2009.

K-ESR-Z-00003, Nothdurft, D.B., *Saltstone Disposal Unit No. 1 Updated Settlement Analysis*, Savannah River Site, Aiken, SC, Rev. 0, December 2010.

K-ESR-Z-00004, *Early Assessment of Geotechnical Parameters for Saltstone Disposal Unit 6 Design*, Savannah River Site, Aiken, SC, Rev. 0, December 2011.

K-ESR-Z-00005, *Saltstone Disposal Unit 6 Geotechnical Investigation Report*, Savannah River Site, Aiken, SC, Rev. 0, April 2012.

K-ESR-Z-00006, *Construction Phase Settlement Monitoring Report for Saltstone Disposal Unit 6 (SDU 6)*, Savannah River Site, Aiken, SC, Rev. 0, March 2017.

K-ESR-Z-00008, *Saltstone Disposal Unit 7 Geotechnical Investigation Report*, Savannah River Site, Aiken, SC, Rev. 0, November 2017.

K-ESR-Z-00010, *Early Assessment of Geotechnical Parameters for Saltstone Disposal Unit 9 Design*, Savannah River Site, Aiken, SC, Rev. 0, September 2018.

Leverett, M.C., *Capillary behavior in porous solids*, Transactions of the AIME (142): 159–172, 1941. (Copyright)

Levitt, M., *Concrete Materials: Problems and Solutions*, Taylor & Francis e-Library, 2003. (Copyright)

Liu Y, et.al., *Pertechnetate Immobilization in Aqueous Media with Hydrogen Sulfide under Anaerobic and Aerobic environments*, Radiochim Acta 2007, 95, 717–725. (Copyright)

Liu Y, et.al., *Potential Interferences on the Pertechnetate-Sulfide Immobilization Reaction*, Radiochim Acta 2009, 97, 33-41. (Copyright)

Lukens, et.al., *Evolution of Technetium Speciation in Reducing Grout*, Environ. Sci. Technol. 2005, 39, 8064–8070. (Copyright)

LWO-CES-2006-00010, *Savannah River Site Saltstone Disposal Facility (Vaults 1 and 4) Overview*, Savannah River Site, Aiken, SC, Rev. 0, October 2006.

LWO-SSF-2009-00001, Edwards, P., *Vault 4 Design Lessons Learned Incorporated into the Vault 2 Design*, Savannah River Site, Aiken, SC, Rev. 0, January 2009.

Matheron, G, *Ele´ments pour une The´orie des Milieux Poruex*, Masson, Paris, 1967. (Copyright)

Marrero, T.R., and Mason, E.A., *Gaseous Diffusion Coefficients. J. Phys. Chem. Ref. Data, Vol. 1, No. 1*, 1972. www.nist.gov/data/PDFfiles/jpcrd1.pdf. (Copyright)

Matschei, et.al., *The AFm Phase in Portland Cement*, Cement and Concrete Research, Vol. 37, Issue 2. pp. 118-130, http://dx.doi.org/10.1016/j.cemconres.2006.10.010. ISSN 0008-8846. February 2007. (Copyright)

MDL-NBS-HS-000021, Arnold, B.W., *Saturated Zone Flow and Transport Model Abstraction*, BSC, Las Vegas, NV, Rev. 3 (AD01 and AD02), September 2007 and January 2008.

ML022530043, (NUREG-1623), Johnson, T.L., *Design of Erosion Protection for Long-Term Stabilization*, U.S. Nuclear Regulatory Commission, Washington, DC, September 2002.

ML072360184, (NUREG-1854), *NRC Staff Guidance for Activities Related to U.S. Department of Energy Waste Determinations, Draft Final Report for Interim Use*, U.S. Nuclear Regulatory Commission, Washington, DC, August 2007.

ML092290639, (NUREG-1923), *Safety Evaluation Report for an Early Site Permit (ESP) at the Vogtle Electric Generating Plant (VEGP) ESP Site*, U.S. Nuclear Regulatory Commission, Washington, DC, July 2009.

ML100820097, *Request for Additional Information on the 2009 Performance Assessment for the Saltstone Disposal Facility at the Savannah River Site*, U.S. Nuclear Regulatory Commission, Washington DC, March 2010.

ML103400571, *Second Request for Additional Information on the 2009 Performance Assessment for the Saltstone Disposal Facility at the Savannah River Site, Docket Number PROJ0734*, U.S. Nuclear Regulatory Commission, Washington DC, December 2010.

ML12005A110, (NUREG/CR-7028), Benson, C.H., et.al., *Engineered Covers for Waste Containment: Changes in Engineering Properties and Implications for Long-Term Performance Assessment*, *Vol. 1*, U.S. Nuclear Regulatory Commission, Office of Nuclear Regulatory Research, Washington, December 2011.

ML120650576, Satorious, M., to Gilbertson, M., *Letter of Concern (Type IV) Regarding U.S. Department of Energy Disposal Activities at the Savannah River Site Saltstone Disposal Facility*, U.S. Nuclear Regulatory Commission, Washington DC, April 2012.

ML121170309, *Technical Evaluation Report For the Revised Performance Assessment for the Saltstone Disposal Facility at the Savannah River Site, South Carolina,* U.S. Nuclear Regulatory Commission, Office of Federal and State Materials and Environmental Management Programs, Washington, DC, April 2012.

ML121240822, (NUREG/CR-5542), *Models for Estimation of Service Life of Concrete Barriers in Low-Level Radioactive Waste Disposal*, U.S. Nuclear Regulatory Commission, Washington, DC, September 1990.

ML13100A113, *U.S. Nuclear Regulatory Commission Plan for Monitoring Disposal Actions Taken by the U.S. Department of Energy at the Savannah River Site Saltstone Facility in Accordance With the National Defense Authorization Act for Fiscal Year 2005*, U.S. Nuclear Regulatory Commission, Office of Federal and State Materials and Environmental Management Programs, Washington, DC, Rev. 1, September 2013.

ML14148A153, *U.S. Nuclear Regulatory Commission Staff Comments and Requests for Additional Information on the "Fiscal Year 2013 Special Analysis for the Saltstone Disposal Facility at the Savannah River Site", SRR-CWDA-2013-00062, Revision 2*, U.S. Nuclear Regulatory Commission, Washington, DC, June 2014.

ML14357A072, (NUREG-2175), Esh, D., et.al., *Guidance for Conducting Technical Analyses for 10 CFR Part 61,* U.S. Nuclear Regulatory Commission, DRAFT Final Report, October 2016.

ML15161A541, *U.S. Nuclear Regulatory Commission Staff Request for Additional Information on the "Fiscal Year 2014 Special Analysis for the Saltstone Disposal Facility at the Savannah River Site," SRR-CWDA-2014-00006, Revision 2*, U.S. Nuclear Regulatory Commission, Washington, DC, June 2015.

ML18002A545, *Technical Review: Hydraulic Performance and Erosion Control of the Planned Saltstone Disposal Facility Closure Cap and Adjacent Area (Docket No. PROJ0734)*, U.S. Nuclear Regulatory Commission, Washington, DC, January 2018.

Myer, G.E., *Analytical Methods in Conduction Heat Transfer*, McGraw-Hill, New York, 1971. (Copyright)

M-TC-Z-00008, *Saltstone Facility Disposal Unit #6 Project, Bldg. 451-006Z*, Savannah River Site, Aiken, SC, Rev. 6, June 2013.

NBS Handbook 69, *Maximum Permissible Body Burdens and Maximum Permissible Concentrations of Radionuclides in Air and in Water for Occupational Exposure, National Bureau of Standards (NBS) Handbook 69*, U.S. Department of Commerce, Washington, DC, August 1963.

NAC-0022_R2, Levitt, D., *Biologically Induced Transport Modeling for the Clive DU PA*, Neptune and Company, Inc., Los Alamos, NM, Rev. 2, November 2015.

NCRP-103, *Control of Radon in Houses*, National Council on Radiation Protection and Measurements, Bethesda, MD, January 1989. (Copyright)

NCRP-123, *Screening Models for Releases of Radionuclides to Atmosphere, Surface Water, And Ground, Volume 1 and Volume 2*, National Council on Radiation Protection and Measurements, Bethesda, MD, January 1996. (Copyright)

NCRP-160, *Ionizing Radiation Exposure of the Population of the United States (2009)*, National Council on Radiation Protection and Measurements, Bethesda, MD, March 2009. (Copyright)

NDAA_3116, *Public Law 108-375, Ronald W. Reagan National Defense Authorization Act for Fiscal Year 2005, Section 3116, Defense Site Acceleration Completion*, Accessed January 2011.

Nielson, K.K., Rogers, V.C, and Gee, G.W., *Diffusion of Radon through Soils: A Pore Distribution Model*, Soil Science Society of America, Vol. 48, 482-487, 1984. (Copyright)

NRMP-2005, *Natural Resources Management Plan (NRMP) for the Savannah River Site*, U.S. Department of Agriculture & Forestry Service, Savannah River Site, Aiken, SC, May 2005.

Ochs, et.al., *Radionuclide and Metal Sorption on Cement and Concrete*, Springer International Publishing, 2016. (Copyright)

Onitsuka, K., et.al., *Geotechnical Characteristics and Construction Methods of Voshinogari Fun-Kyu Tomb in Japan and Tu-Dun Tombs in China*, Journal of Geotechical Engineering, 736: 1-17, 2006. (Copyright)

OPS-DTZ-90-0027, Fowler, J.R., *Radionuclide Storage and Disposal in Z-Area*, Savannah River Site, Aiken, SC, Rev. 1, June 1991.

Papadakis, V.G., et.al., *A Reaction Engineering Approach to the Problem of Concrete Carbonation. AIChE Journal*, 35:1639-1650, 1989. (Copyright)

PIT-MISC-0004, *Industrial Wastewater Closure Module for the High-Level Waste Tank 17 System*, Savannah River Site, Aiken, SC, Rev. 2, August 1997.

PIT-MISC-0075, Bradbury, M.H., and Sarott, F., *Sorption Database for the Cementitious Near-Field of a L/ILW Repository for Performance Assessment*, ISSN 1019-0643, Paul Scherrer Institute, Switzerland, 1995.

PIT-MISC-0089, *Savannah River Site End State Vision*, Savannah River Site, Aiken, SC, July 2005.

PIT-MISC-0104, *Soil Survey of Savannah River Plant Area, Parts of Aiken, Barnwell, and Allendale Counties, South Carolina*, Soil Conservation Service, U.S. Department of Agriculture, Washington, DC, June 1990.

PIT-MISC-0112, Aadland, R., et.al., *Hydrogeologic Framework of West-Central South Carolina, Report 5*, South Carolina Department of Natural Resources, Columbia, SC, 1995.

PIT-MISC-0200, *Aiken County South Carolina Comprehensive Plan 2014-2024*, Aiken, SC, June 2016.

PIT-MISC-0201, *Barnwell County Comprehensive Plan*, Barnwell, SC, June 2007.

PNNL-13249, Fayer, M.J., *UNSAT-H Version 3.0: Unsaturated Soil Water and Heat Flow Model - Theory, User Manual, and Examples*, Pacific Northwest National Laboratory, Richland, WA, Rev. 0, June 2000.

Q-SQP-A-00002, Farfán, E.B., *Software Quality Assurance Plan for Environmental Dosimetry*, Savannah River Site, Aiken, SC, Rev. 2, May 2007.

Q-SQP-A-00007, *Software Quality Assurance Plan for The Geochemist's Workbench®*, Savannah River Site, Aiken, SC, Rev. 1, December 2018.

Q-SQP-G-00003, Flach, G.P., *Software Quality Assurance Plan for Aquifer Model Refinement Tool (MESH3D)*, Savannah River Site, Aiken, SC, Rev. 1, August 2012.

Rast, R., and Rinker, M.W., *Overview of Hanford Single Shell Tank (SST) Structural Integrity - 12123*, WM2012 Conference, February 2012. (Copyright)

Richards, B.G., *Measurement of Free Energy of Soil Moisture by the Psychrometric Technique Using Thermistors, in Moisture Equilibria and Moisture Changes in Soils Beneath Covered Areas: A Symposium*, p. 39-46, Butterworths, Australia, 1965. (Copyright)

Rogers, C, and Nielson, K., *Multiphase Radon Generation and Transport in Porous Materials*, Health Physics, 60. 807-15. 10.1097/00004032-199106000-00006, 1991. (Copyright)

S4 Manual, Procedure ENG.46 (S4-ENG.46), *LW Unreviewed Waste Management Question (UWMQ)*, Savannah River Site, Aiken, SC, Rev. 4, November 2018.

Sanchez-Vila, X., et.al., *A Synthesis of Approaches to Upscaling of Hydraulic Conductivities*, Water Resources Research, Vol. 31, No. 4, 867-882, 1995. (Copyright)

Sanchez-Vila, X., et.al., *Representative Hydraulic Conductivities in Saturated Groundwater Flow*, Reviews of Geophysics, 44, 1-46, 2006. (Copyright)

Sander, R., *Compilation of Henry's Law Constants (version 4.0) for Water as Solvent*, Atmos. Chem. Phys. 15, 4399–4981, 2015. (Copyright)

SCDHEC R.61-107.19, *SWM: Solid Waste Landfills and Structural Fill*, South Carolina Department of Health and Environmental Control, Columbia, SC, May 2008.

SCDHEC R.61-58, *State Primary Drinking Water Regulation,* Bureau of Water, South Carolina Department of Health and Environmental Control, Columbia, SC, September 2014.

SCDHEC R.61-67, *Standards for Wastewater Facility Construction,* South Carolina Department of Health and Environmental Control, Columbia, SC, June 2015.

SCDHEC R.61-68, *Water Classification & Standards*, South Carolina Department of Health and Environmental Control, Columbia, SC, April 2008.

SCDHEC R.61-82, *Proper Closeout of Wastewater Treatment Facilities,* South Carolina Department of Health and Environmental Control, Columbia, SC, April 1980.

SDF-IP-05, *Saltstone Disposal Facility Vault 1 Input*, Washington Savannah River Company, Rev. 0, April 2008.

SDF-IP-07, *Saltstone Disposal Facility Vault 4 Input*, Washington Savannah River Company, Rev. 0, March 2008.

Sercombe, J., Vidal, R., Gallé, C., and Adenot, F., *Experimental study of gas diffusion in cement paste,* Cement and Concrete Research, Vol. 37, 579-588, 2007. (Copyright)

SIMCO_03-01-2012, *Washington Savannah River Company Subcontract AC81850N Report – Vault Concrete Characterization*, SIMCO Technologies Inc., Quebec, Canada, March 2012.

SIMCO_06-16-2010, *Washington Savannah River Company Subcontract no. AC48992N Report; Task 6 – Characterization of a Wasteform Mixture*, SIMCO Technologies Inc., Quebec, Canada, June 2010.

SIMCO_08-31-2012, *Final Report: Comparison of Wasteform Mixtures*, SIMCO Technologies Inc., Quebec, Canada, August 2012.

SREL-R-14-0006, *Chemical and Physical Properties of Saltstone as Impacted by Curing Duration*, Savannah River Ecology Laboratory, Aiken, SC, Rev. 0, September 2014.

SREL-R-16-0003, *Contaminant Leaching from Saltstone*, Savannah River Ecology Laboratory, Aiken, SC, Rev. 0, September 2016.

SREL-R-17-0004, Seaman, J.C., and Thomas, R.J., *Impact of Cementitious Material Leachate on Iodine Partitioning*, Savannah River Ecology Laboratory, Aiken, SC, Rev. 0, September 2017.

SREL-R-17-0005, Seaman, J.C., and Coutelot, F.M., *Contaminant Leaching from Saltstone*, Savannah River Ecology Laboratory, Aiken, SC, Rev. 0, (SRRA099188-000006) September 2017.

SRNL-ESB-2007-00007, Phifer, M.A., et.al., *SRNL Vault 2 Interior Coating Performance Assessment Requirement,* Savannah River National Laboratory, Aiken, SC, April 2007

SRNL-ESB-2007-00035, Millings, M.R., et.al., *Addendum to Integrated Hydrogeological Modeling Report of the General Separations Area (GSA) (WSRC-TR-96-0399-Vol. 2, Rev.1),* Savannah River National Laboratory, Aiken, SC, October 2007.

SRNL-ESB-2008-00017, Dixon, K., *Video Survey of Saltstone Vault 4, Cell G*, Savannah River National Laboratory, Aiken, SC, April 2008.

SRNL-EST-2005-00105, Dixon, K.L., *Concrete Mixes for Saltstone Vault 4*, Savannah River National Laboratory, Aiken, SC, June 2005.

SRNL-L3100-2015-00108, Roberts, K.A., *SDU2A Core Sample Test Designation*, Savannah River National Laboratory, Aiken, SC, Rev. 0, June 2015.

SRNL-L3200-2012-00017, Millings, M.R., *Summary of Carbon Dioxide in Water Table Wells and the Vadose Zone at SRS,* Savannah River National Laboratory, Aiken, SC, May 2012.

SRNL-L3200-2012-00022, Millings, M.R., and Denham, M.E., *Background Water Table Chemistry in the General Separations Area,* Savannah River National Laboratory, Aiken, SC, August 2012.

SRNL-L3200-2013-00028, Flach, G.P., *Degradation of Cementitious Materials for Saltstone Disposal Unit No. 6,* Savannah River National Laboratory, Aiken, SC, September 2013.

SRNL-L3200-2017-00107, Flach, G.P., *Groundwater Particle Tracking and Tracer Transport Simulations Near Saltstone Disposal Unit 4 and Well ZBG-2*, Savannah River National Laboratory, Aiken, SC, September 2017.

SRNL-L3200-2018-00177, Danielson, T.L., *Design Checking of PORFLOW Modeling Supporting the Saltstone Performance Assessment*, Savannah River National Laboratory, Aiken, SC, Rev. 0, December 2018.

SRNL-RP-2017-00424, Rivera-Giboyeaux, *Savannah River Site Annual Meteorology Report for 2016*, Savannah River National Laboratory, Aiken, SC, Rev. 0, September 2017.

SRNL-STI-2008-00415, Lee, P., and Foley, T, *Air Pathway Dose Modeling for the Saltstone Disposal Facility*, Savannah River National Laboratory, Aiken, SC, Rev. 0, December 2008.

SRNL-STI-2008-00421, Dixon, K., et.al., *Hydraulic and Physical Properties of Saltstone Grouts and Vault Concretes*, Savannah River National Laboratory, Aiken, SC, Rev. 0, November 2008.

SRNL-STI-2008-00447, Dixon, K., et.al., *Air and Radon Pathway Modeling for the Saltstone Disposal Facility*, Savannah River National Laboratory, Aiken, SC, Rev. 0, December 2008.

SRNL-STI-2009-00115, Flach, G.P., et.al., *Numerical Flow and Transport Simulations Supporting the Saltstone Disposal Facility Performance Assessment*, Savannah River National Laboratory, Aiken, SC, Rev. 1, June 2009

SRNL-STI-2009-00473, Kaplan, D.I., *Geochemical Data Package for Performance Assessment Calculations Related to the Savannah River Site*, Savannah River National Laboratory, Aiken, SC, Rev. 1, July 2016.

SRNL-STI-2009-00572, Whiteside, T., et.al., *Evaluation of HELP Model Replacement Codes*, Savannah River National Laboratory, Aiken, SC, Rev. 0, July 2009.

SRNL-STI-2009-00637, Kaplan, D.I., and Roberts, K., *Reduction Capacity of Saltstone and Saltstone Components*, Savannah River National Laboratory, Aiken, SC, Rev. 0, November 2009.

SRNL-STI-2010-00035, Langton, C.A., *Chemical Degradation Assessment for the H-Area Tank Farm Concrete Tanks and Fill Grouts,* Savannah River National Laboratory, Aiken, SC, Rev. 0, January 2010.

SRNL-STI-2010-00148, Jones, W.E., et.al., *Hydrogeologic Data Summary in Support of the H-Area Tank Farm Performance Assessment*, Savannah River National Laboratory, Aiken, SC, Rev. 0, February 2010.

SRNL-STI-2010-00515, Langton, C.A., *Saltstone Characterization and Parameters for Performance Assessment Modeling*, Savannah River National Laboratory, Aiken, SC, Rev. 0, August 2010.

SRNL-STI-2010-00668, Kaplan, D.I., et.al., *Long-term Technetium Interactions with Reducing Cementitious Materials*, Savannah River National Laboratory, Aiken, SC, Rev. 0, March 2011.

SRNL-STI-2011-00661, Dixon, K., et.al., *Moisture Retention Properties of High Temperature Cure ARP/MCU Saltstone Grout*, Savannah River National Laboratory, Aiken, SC, Rev. 0, December 2011.

SRNL-STI-2012-00435, Turick, C.E., and Berry, C.J., *Review of Concrete Biodeterioration in Relation to Buried Nuclear Waste*, Savannah River National Laboratory, Aiken, SC, Rev. 0, August 2012.

SRNL-STI-2013-00118, Flach, G.P., and Smith, F.G., *Degradation of Cementitious Materials Associated with Saltstone Disposal Units*, Savannah River National Laboratory, Aiken, SC, Rev. 2, September 2014.

SRNL-STI-2013-00268, Viner B.J., *Summary of Data and Steps for Processing the 2007-2011 SRS Meteorological Database*, Savannah River National Laboratory, Aiken, SC, Rev. 0, July 2013.

SRNL-STI-2013-00280, Jordan, J.M., and Flach, G.P., *PORFLOW Modeling Supporting the FY13 Saltstone Special Analysis*, Savannah River National Laboratory, Aiken, SC, Rev. 0, May 2013.

SRNL-STI-2013-00541, Langton, C.A. and Almond, P.M., *Cast Stone Oxidation Front Evaluation: Preliminary Results for Samples Exposed to Moist Air,* Savannah River National Laboratory, Aiken, SC, Rev. 0, November 2013.

SRNL-STI-2014-00083, Flach, G.P. *PORFLOW Modeling Supporting the FY14 Saltstone Special Analysis*, Savannah River National Laboratory, Aiken, SC, Rev. 1, April 2014.

SRNL-STI-2014-00397, Langton, C., *X-ray Diffraction of Slag-based Sodium Salt Waste Forms*, Savannah River National Laboratory, Aiken, SC, Rev. 1, September 2014.

SRNL-STI-2015-00236, Flach, G.P., *Verification of Sulfate Attack Penetration Rates for Saltstone Disposal Unit Modeling*, Savannah River National Laboratory, Aiken, SC, Rev. 0, May 2015.

SRNL-STI-2016-00175, Flach, G.P., et.al., *Solid Secondary Waste Data Package Supporting Hanford Integrated Disposal Facility Performance Assessment*, Savannah River National Laboratory, Aiken, SC, Rev. 0, May 2016.

SRNL-STI-2016-00511, Hang, T., and Flach, G.P., *Evaluation Saltstone Disposal Unit 7 Floor Penetrations*, Savannah River National Laboratory, Aiken, SC, Rev. 0, September 2016.

SRNL-STI-2016-00516, Bagwell, L.A., et.al., *General Separations Area (GSA) Groundwater Flow Model Update: Hydrostratigraphic Data*, Savannah River National Laboratory, Aiken, SC, Rev. 0, February 2017.

SRNL-STI-2016-00534, Hang, T., and Flach, G.P., *Evaluation of Revised Future Saltstone Disposal Unit Locations by PORFLOW Simulations*, Savannah River National Laboratory, Aiken, SC, Rev. 0, September 2016.

SRNL-STI-2017-00008, Flach, G.P., et.al., *Groundwater Flow Simulation of the Savannah River Site General Separations Area*, Savannah River National Laboratory, Aiken, SC, Rev. 1, September 2017.

SRNL-STI-2017-00331, Dyer, J.A., *Recommended Henrys Law Constants for Non-Groundwater Pathways Models in GoldSim*, Savannah River National Laboratory, Aiken, SC, June 2017.

SRNL-STI-2018-00012, Flach, G.P., *Recommended Aquifer Grid Resolution for E-Area PA Revision Transport Simulations*, Savannah River National Laboratory, Aiken, SC, Rev. 0, January 2018.

SRNL-STI-2018-00077, Flach, G.P., *Degradation of Saltstone Disposal Unit Cementitious Materials*, Savannah River National Laboratory, Aiken, SC, Rev. 0, April 2018.

SRNL-STI-2018-00077, Flach, G.P., *Degradation of Saltstone Disposal Unit Cementitious Materials*, Savannah River National Laboratory, Aiken, SC, Rev. 1, August 2018.

SRNL-STI-2018-00275, Whiteside, T.S., *PORFLOW 6.42.9 Testing and Verification Document*, Savannah River National Laboratory, Aiken, SC, Rev. 0, June 2018.

SRNL-STI-2018-00336, Wohlwend, J.L., *Updated General Separations Areas (GSA) Groundwater Model Calibration Targets*, Savannah River National Laboratory, Aiken, SC, Rev. 0, July 2018.

SRNL-STI-2018-00586, Dyer, J., *Geochemical Model of Eh and pH Transitions in Pore Fluids during Saltstone and SDU Concrete Aging*, Savannah River National Laboratory, Aiken, SC, Rev. 0, October 2018.

SRNL-STI-2018-00624, Hamm, L.L., Aleman, S.E., Danielson, T.L., Butcher, B.T., *Special Analysis: Impact of Updated GSA Flow Model on E-Area Low-Level Waste Facility Groundwater Performance*, Savannah River National Laboratory, Aiken, SC, Rev. 0, December 2018.

SRNL-STI-2018-00643, Flach, G.P., *Updated Groundwater Flow Simulations of the Savannah River Site General Separations Area*, Savannah River National Laboratory, Aiken, SC, Rev. 0, January 2019.

SRNL-STI-2018-00652, Flach, G.P. and Hang, T., *PORFLOW Simulations Supporting the Saltstone Performance Assessment Revision*, Savannah River National Laboratory, Aiken, SC, Rev. 0, December 2018.

SRNL-TR-2008-00283, Denham, M., *Estimation of Eh and pH Transitions in Pore Fluids During Aging of Saltstone and Disposal Unit Concrete*, Savannah River National Laboratory, Aiken, SC, December 2008.

SRNL-TR-2010-00096, Denham, M., *Vapor – Aqueous Solution Partition Coefficients for Radionuclides Pertinent to High Level Waste Tank Closure,* Savannah River National Laboratory, Aiken, SC, July 2010.

SRNL-TR-2012-00160, Bagwell, L.A., *A Review of Soft Zones at Savannah River Site with Emphasis on H Area Tank Farm*, Savannah River National Laboratory, Aiken, SC, Rev. 0, July 2012.

SRNS-RP-2008-00020, *Quality Assurance Management Plan*, Savannah River Site, Aiken, SC, Rev. 9, March 2018.

SRNS-RP-2014-00537, *Savannah River Site Land Use Plan*, Savannah River Site, Aiken, SC, November 2014.

SRNS-RP-2018-00470, *Environmental Report for 2017*, Savannah River Site, Aiken, SC, Rev. 0, September 2018.

SRNS-STI-2008-00045, Kaplan, D.I., et.al., *Saltstone and Concrete Interactions with Radionuclides: Sorption (K_d), Desorption, and Reduction Capacity Measurements*, Savannah River Site, Aiken, SC, October 2008.

SRNS-STI-2012-00200, *Savannah River Environmental Report for 2011*, Savannah River Site, Aiken, SC, August 2012.

SRNS-TR-2009-00076, *Savannah River Site Groundwater Protection Program*, Savannah River Site, Aiken, SC, Rev. 1, February 2009.

SRNS-TR-2018-00099, *2017 Environmental Monitoring Program Data Report*, Savannah River Site, Aiken, SC, Rev. 0, September 2018.

SRNS-TR-2018-00149, *Z-Area Saltstone Disposal Facility Groundwater Monitoring Mid-Year Report for 2018*, Savannah River Site, Aiken, SC, Rev. 0, July 2018.

SRNS-TR-2018-00292, *Z-Area Saltstone Disposal Facility Groundwater Monitoring Report for 2018*, Savannah River Site, Aiken, SC, Rev. 0, January 2019.

SRRA021685-000009, Peruski, K., et.al., *Analysis of Plutonium Soil Concentrations in Field Lysimeter Experiments*, Clemson University, Environmental Engineering and Earth Sciences, L.G. Rich Laboratory, Anderson, SC, November 2017.

SRRA021685-000010, Peruski, K., et.al., *Analysis of Plutonium Soil Concentrations in Field Lysimeter Experiments FY18 Report,* Clemson University, Environmental Engineering and Earth Sciences, L.G. Rich Laboratory, Anderson, SC, October 2018.

SRRA099188-000003 (SREL-R-18-0004), Seaman, J.C., and Coutelot, F.M., *Technetium Solubility in Saltstone as Function of pH and Eh: Summary of Modeling Efforts*, Savannah River Ecology Laboratory, Aiken, SC, August 2018.

SRRA099188-000005 (SREL-R-18-0006), Seaman, J.C., et.al., *Contaminant Leaching from Saltstone Simulants for FY 2018*, Savannah River Ecology Laboratory, Aiken, SC, November 2018.

SRRA107772-000005, Benson, C.H., *UVA Quality Assurance Document for Research Conducted in Support of SRR*, University of Virginia School of Engineering, March 2017.

SRRA107772-000009, Benson, C.H., and Benavides, J.M., *Predicting Long-Term Percolation from the SDF Closure Cap*, Report No. GENV-18-05, University of Virginia School of Engineering, April 2018.

SRRA110110-000004, Brown, K.G., *Predicting the Hydraulic Conductivity over Time for Degrading Saltstone Vault Concrete – Task 5*, Vanderbilt University Division of Sponsored Research, December 2017

SRR-CWDA-2009-00017, *Performance Assessment for the Saltstone Disposal Facility at the Savannah River Site,* Savannah River Site, Aiken, SC, Rev. 0, October 2009.

SRR-CWDA-2009-00050, *Saltstone Disposal Facility Performance Assessment Briefing Presentation to the Nuclear Regulatory Commission*, Savannah River Site, Aiken, SC, Rev. 0, December 2009.

SRR-CWDA-2010-00023, *H-Area Tank Farm Closure Inventory for use in Performance Assessment Modeling*, Savannah River Site, Aiken, SC, Rev. 3, May 2012.

SRR-CWDA-2010-00023, *H-Area Tank Farm Closure Inventory for use in Performance Assessment Modeling*, Savannah River Site, Aiken, SC, Rev. 6, January 2016.

SRR-CWDA-2010-00033, *Comment Response Matrix for Nuclear Regulatory Commission (NRC) Requests for Additional Information (RAIs) on the Saltstone Disposal Facility Performance Assessment (SRR-CWDA-2009-00017, Revision 0, dated October 29, 2009),* Savannah River Site, Aiken, SC, Rev. 1, July 2010.

SRR-CWDA-2010-00128, *Performance Assessment for the H-Area Tank Farm at the Savannah River Site*, Savannah River Site, Aiken, SC, Rev. 1, November 2012.

SRR-CWDA-2010-00154, *Software Quality Assurance Plan (SQAP) for The Geochemist's Workbench,* Savannah River Site, Aiken, SC, Rev. 2, August 2012.

SRR-CWDA-2011-00044, *Comment Response Matrix for Nuclear Regulatory Commission RAI-2009-02 Second Request for Additional Information (RAI) on the Saltstone Disposal Facility Performance Assessment (SRR-CWDA-2009-00017, Revision 0, dated October 29, 2009),* Savannah River Site, Aiken, SC, Rev. 1, August 2011.

SRR-CWDA-2011-00054, *Comment Response Matrix for United States Nuclear Regulatory Commission Staff Comments on the Draft Basis for Section 3116 Determination and Associated Performance Assessment for the F-Tank Farm at the Savannah River Site,* Savannah River Site, Aiken, SC, Rev. 1, June 2011.

SRR-CWDA-2011-00105, Freeman, R.D., *Saltstone Disposal Facility Vault 4 Video Inspection Summary*, Savannah River Site, Aiken, SC, Rev. 0, July 2011.

SRR-CWDA-2011-00178, Lester, B.H., *Saltstone Disposal Facility Stochastic Fate and Transport Model*, Savannah River Site, Aiken, SC, Rev. 0, January 2012.

SRR-CWDA-2011-00196, *Unreviewed Waste Management Question Requirements Document for Saltstone Facility*, Savannah River Site, Aiken, SC, Rev. 8, December 2018.

SRR-CWDA-2012-00103, *Sensitivity Analysis for Disposal Operations into Saltstone Disposal Facility Vault 1, Vault 4, and SDUs 2, 3 and 5*, Savannah River Site, Aiken, SC, Rev. 1, July 2012.

SRR-CWDA-2013-00037, *Closure Plan for the Z-Area Saltstone Disposal Facility*, Savannah River Site, Aiken, SC, Rev. 1, September 2015.

SRR-CWDA-2013-00050, *Evaluation of Saltstone Disposal Structures 3A, 3B, 5A, and 5B As-Built Conditions to Support Unreviewed Waste Management Question Evaluation*, Savannah River Site, Aiken, SC, Rev. 1, June 2013.

SRR-CWDA-2013-00058, Hommel, S.P., *Dose Calculation Methodology for Liquid Waste Performance Assessments at the Savannah River Site,* Savannah River Site, Aiken, SC, Rev. 2, January 2019.

SRR-CWDA-2013-00062, *FY2013 Special Analysis for the Saltstone Disposal Facility at the Savannah River Site*, Savannah River Site, Aiken, SC, Rev. 2, October 2013.

SRR-CWDA-2013-00064, Sheppard, R.E., to Rosenberger, K.H., *PORFLOW Input to Support the Development of the SDF FY13 Special Analysis*, Savannah River Site, Aiken, SC, Rev. 1, April 2013.

SRR-CWDA-2013-00073, *Updates to the Saltstone Disposal Facility Stochastic Fate and Transport Model,* Savannah River Site, Aiken, SC, Rev. 2, August 2014.

SRR-CWDA-2013-00091, *Industrial Wastewater Closure Module for Liquid Waste Tank 16H H-Area Tank Farm Savannah River Site,* Savannah River Site, Aiken, SC, Rev. 1, April 2015.

SRR-CWDA-2014-00002, Hommel, S.P., and Watkins, D.R., *Crosswalk of Select Documents Related to the Monitoring Programs for the Saltstone Disposal Facility*, Savannah River Site, Aiken, SC, Rev. 1, February 2014.

SRR-CWDA-2014-00006, *FY2014 Special Analysis for the Saltstone Disposal Facility at the Savannah River Site*, Savannah River Site, Aiken, SC, Rev. 2, September 2014.

SRR-CWDA-2014-00059, Smith, F.M., Clendenen, G.B, and Simner, S.P., *FY2014 Saltstone Core-Drilling Mock-Up Summary*, Savannah River Site, Aiken, SC, Rev. 0, June 2014.

SRR-CWDA-2014-00099, Hommel, S.P., *Comment Response Matrix for U.S. Nuclear Regulatory Commission Staff Request for Additional Information on the Fiscal Year 2013 Special Analysis for the Saltstone Disposal Facility at the Savannah River Site*, Savannah River Site, Aiken, SC, Rev. 1, January 2015.

SRR-CWDA-2015-00003, Hommel, S.P., *Saltstone Disposal Facility Waste Inventory Disposed Estimator Model Report*, Savannah River Site, Aiken, SC, Rev. 0, January 2015.

SRR-CWDA-2015-00041, Smith, F.M., and Hommel, S.P., *Evaluation of Radioactive Waste Bags in Saltstone Disposal Unit 4, Cells C and I, to Support Unreviewed Waste Management Question Evaluation*, Savannah River Site, Aiken, SC, Rev. 1, March 2015.

SRR-CWDA-2015-00066, *Summary of Saltstone Disposal Unit Cell 2A Core Drill Activities*, Savannah River Site, Aiken, SC, Rev. 0, May 2015.

SRR-CWDA-2015-00077, *Evaluation of I-129 Concentration Data to Improve Liquid Waste Inventory Projections*, Savannah River Site, Aiken, SC, Rev. 2, February 2018.

SRR-CWDA-2015-00123, *Evaluation of Tc-99 Concentration Data to Improve Liquid Waste Inventory Projections*, Savannah River Site, Aiken, SC, Rev. 2, March 2018.

SRR-CWDA-2015-00152, *Savannah River Site Liquid Waste Facilities Performance Assessment Maintenance Program - FY2016 Implementation Plan*, Savannah River Site, Aiken, SC, Rev. 0, December 2015.

SRR-CWDA-2016-00004, Watkins, D.R., *Comment Response Matrix for U.S. Nuclear Regulatory Commission Staff Request for Additional Information on the Fiscal Year 2014 Special Analysis for the Saltstone Disposal Facility at the Savannah River Site*, Savannah River Site, Aiken, SC, Rev. 1, March 2016.

SRR-CWDA-2016-00051, Simner, S., *Property Data for Core Samples Extracted from SDU Cell 2A*, Savannah River Site, Aiken, SC, Rev. 0, April 2016.

SRR-CWDA-2016-00072, *FY2016 Special Analysis for the Saltstone Disposal Facility at the Savannah River Site*, Savannah River Site, Aiken, SC, Rev. 0, October 2016.

SRR-CWDA-2017-00019, *Updated Sorption Constants for use in Performance Assessment Modeling*, Savannah River Site, Aiken, SC, Rev. 0, February 2017.

SRR-CWDA-2017-00057, *Features, Events, and Processes for the Saltstone Disposal Facility Performance Assessment*, Savannah River Site, Aiken, SC, Rev. 0, August 2017.

SRR-CWDA-2017-00077, Hommel, S.P., *Update to the SDF Seepline Ratio Based on the GSA Update*, Savannah River Site, Aiken, SC, Rev. 1, January 2019.

SRR-CWDA-2017-00078, *FY2017 Annual Review Saltstone Disposal Facility (Z Area) Performance Assessment*, Savannah River Site, Aiken, SC, Rev. 0, January 2018.

SRR-CWDA-2018-00004, *Recommended Values for Cementitious Degradation Modeling to Support Future SDF Modeling*, Savannah River Site, Aiken, SC, Rev. 1, August 2018.

SRR-CWDA-2018-00006, *Conceptual Model Development for the Saltstone Disposal Facility Performance Assessment,* Savannah River Site, Aiken, SC, Rev. 0, May 2018.

SRR-CWDA-2018-00012, Watkins, D.R., *Additional Recommended Inputs to PORFLOW Modeling for SDU 7*, Savannah River Site, Aiken, SC, Rev. 2, August 2018.

SRR-CWDA-2018-00018, *Database Compilation of Radionuclides Standardized with Half-Lives in Seconds and Specific Activity in Ci/g*, Savannah River Site, Aiken, SC, Rev. 0, April 2018.

SRR-CWDA-2018-00025, *Air Pathway Release Model for the Saltstone Disposal Facility Performance Assessment*, Savannah River Site, Aiken, SC, Rev. 2, February 2019.

SRR-CWDA-2018-00030, *Recommended Values for Percolation Rates to Support Future SDF Modeling*, Savannah River Site, Aiken, SC, Rev. 1, November 2018.

SRR-CWDA-2018-00035, Romanowski, L.B, and Benson, C.H., *Savannah River Site Salt Waste Disposal NRC Onsite Observation Visit July 9-11, 2018*, Savannah River Site, Aiken, SC, Rev. 1, July 2018.

SRR-CWDA-2018-00036, *Evaluation of Soil and Groundwater Contamination from Saltstone Disposal Unit 4*, Savannah River Site, Aiken, SC, Rev. 0, July 2018.

SRR-CWDA-2018-00041, Dixon, K.D., *Determination of Inventory for FY2019 Performance Assessment Modeling*, Savannah River Site, Aiken, SC, Rev. 2, February 2019.

SRR-CWDA-2018-00041, Dixon, K.D., *Determination of Inventory for FY2019 Performance Assessment Modeling*, Savannah River Site, Aiken, SC, Rev. 3, July 2019.

SRR-CWDA-2018-00044, *Inventory Screening Methodology and Application to the FY2019 Saltstone Disposal Facility (SDF) Performance Assessment (PA) Inventory*, Savannah River Site, Aiken, SC, Rev. 3, February 2019.

SRR-CWDA-2018-00045, *Iodine K_ds for Simulating I-129 Releases from Saltstone SDUs*, Savannah River Site, Aiken, SC, Rev. 0, August 2018.

SRR-CWDA-2018-00046, *Technetium Solubility Limits for Simulating Tc-99 Releases from Saltstone SDUs*, Savannah River Site, Aiken, SC, Rev. 0, August 2018.

SRR-CWDA-2018-00048, *Recommended Reducing Capacity for Saltstone for the SDF PA*, Savannah River Site, Aiken, SC, Rev. 0, August 2018.

SRR-CWDA-2018-00049, *H-Canyon to Tank Farm Transfers Summary In Support of FY2019 SDF Performance Assessment Inputs and Assumptions*, Savannah River Site, Aiken, SC, Rev. 0, August 2018.

SRR-CWDA-2018-00061, Hommel, S.P., *Development of Parametric Flow Fields for the SDF PA Revision*, Savannah River Site, Aiken, SC, Rev. 0, November 2018.

SRR-CWDA-2018-00062, Wooten, L.A., *Saltstone Disposal Unit (SDU) 1 Cells A-C and SDU 4 Cells A-L Inventories in Support of Saltstone Disposal Facility Performance Assessment Modeling*, Savannah River Site, Aiken, SC, Rev. 0, October 2018.

SRR-CWDA-2018-00068, Watkins, D.R., *Performance Assessment for the Saltstone Disposal Facility at the Savannah River Site: Quality Assurance Report*, Savannah River Site, Aiken, SC, Rev. 2, January 2020.

SRR-CWDA-2018-00076, Hommel, S.P., *Recommended Implementation of Inventory Sampling Distributions for the Saltstone Disposal Facility Performance Assessment GoldSim Model*, Savannah River Site, Aiken, SC, Rev. 0, October 2018.

SRR-CWDA-2018-00087, *Saltstone Disposal Facility Closure Cap Concept Update for Large-Scale Disposal Units*, Savannah River Site, Aiken, SC, Rev. 1, April 2019.

SRR-CWDA-2018-00092, *Savannah River Site Liquid Waste Facilities Performance Assessment Maintenance Program - FY2019 Implementation Plan*, Savannah River Site, Aiken, SC, Rev. 0, February 2019.

SRR-CWDA-2019-00026, *Recommended Percolation Rate Values to Support SDF Sensitivity Analysis of Sand Drainage Layer*, Savannah River Site, Aiken, SC, Rev. 0, March 2019.

SRR-CWDA-2019-00027, Watkins, D.R., *Unsaturated Zone Thickness Variability for Supporting the Saltstone Disposal Facility PA Revision*, Savannah River Site, Aiken, SC, Rev. 0, March 2019.

SRR-CWDA-2019-00043, Flach, G.P., *PORFLOW Simulation Cases Supporting the Saltstone Disposal Facility PA Revision*, Savannah River Site, Aiken, SC, Rev. 0, May 2019.

SRR-CWDA-2019-00046, Watkins, D.R., *Addendum to FY2019 SDF PA QA Report, SRR-CWDA-2018-00068*, Savannah River Site, Aiken, SC, Rev. 3, March 2020.

SRR-CWDA-2019-00055, Hommel, S.P., *Risk Assessment of Alternative Inventory Values for Selected Radionuclides in Support of Responses to DOE-SR Comments on the SDF PA*, Savannah River Site, Aiken, SC, Rev. 0, August 2019.

SRR-CWDA-2017-00068, Mangold, J., *Evaluation of Impacts to FTF and HTF PA Doses Due to the Update of the GSA Database*, Savannah River Site, Aiken, SC, Rev. 1, September 2019.

SRR-LWP-2009-00001, *Liquid Waste System Plan*, Savannah River Site, Aiken, SC, Rev. 21, January 2019.

SRR-SDU-2011-00002, *Siting of Future Saltstone Disposal Units*, Savannah River Site, Aiken, SC, Rev. 1, June 2016.

SRR-SDU-2015-00016, *Engineering Path Forward –SDU 6 Repair and Testing*, Savannah River Site, Aiken, SC, Rev. 0, December 2015.

SRR-SDU-2016-00027, Hasan, N., et.al., *Shrinkage Evaluation of SDU 7 Type V Concrete Mixtures*, Savannah River Site, Aiken, SC, Rev. 0, February 2017.

SRR-SDU-2017-00001, *WM2017: Achieving Leak Tightness in New Savannah River Site Saltstone Disposal Units*, Savannah River Site, Aiken, SC, Rev. 0, January 2017.

SRR-SDU-2017-00003, *SDU 6 Minimum Grout Containment Capacity*, Savannah River Site, Aiken, SC, Rev. 0, February 2017.

SRR-SDU-2017-00013, Maryak, M., et.al., *Constructability Evaluation of SDU 7 Concrete Placement*, Savannah River Site, Aiken, SC, Rev. 0, May 2017.

SRR-SDU-2017-00044, *Saltstone Disposal Unit 6 SRS 1st Mega SDU*, Savannah River Site, Aiken, SC, Rev. 0, January 2018.

SRR-SPT-2013-00044, Simner, S.P., *Update of Fiscal Year 2013 Activities Related to SDU Sampling and Analysis*, Savannah River Site, Aiken, SC, Rev. 0, September 2013.

SRR-SPT-2016-00009, *Modular Caustic-Side Solvent Extraction Unit (MCU) Improved Solvent Quality and Processing Results*, Savannah River Site, Aiken, SC, Rev. 0, November 2016.

SRS-REG-2007-00002, *Performance Assessment for the F-Tank Farm at the Savannah River Site*, Savannah River Site, Aiken, SC, Rev. 1, March 2010.

Stumm, W., and Morgan, J.J., *Aquatic Chemistry: An Introduction Emphasizing Chemical Equilibria in Natural Waters*, Wiley, 1970. (Copyright)

SW24.5-2.11, *Premix Blending & Conveying System Operating Manual*, Section 2.11: Premix Blending Panel Keypad and Display Operation, Savannah River Site, Aiken, SC, Rev. 14, July 2017.

Takala, M. and Manninen, P., *Sampling and Characterisation of Groundwater Colloids at ONKALO, Olkiluoto, Finland*, Posiva WR–2006–98, 2006. (Copyright)

Therrien, R., and Sudicky, E.A., *Three-dimensional analysis of variable-saturated flow and solute transport in discrete-fractured porous media*, Journal of Contaminant Hydrology, 23, pp. 1-44, 1996. (Copyright)

Tixier, R., and Mobasher, B., *Modeling of Damage in Cement-Based Materials Subjected to External Sulfate Attack. I: Formulation*, Journal of Materials in Civil Engineering, 305-313, July/August 2003a. (Copyright)

Tixier, R., and Mobasher, B., *Modeling of Damage in Cement-Based Materials Subjected to External Sulfate Attack. II: Comparison with Experiments*, Journal of Materials in Civil Engineering, 314-322, July/August 2003b. (Copyright)

TV-0080-0041, *Part 70 Air Quality Permit,* South Carolina Department of Health and Environmental Control, Columbia, SC, Rev. 13, December 2007.

T-CLC-E-00018, Carey, S.A., *Low-Activity Waste (LAW) Vault Structural Degradation Prediction*, Savannah River Site, Rev. 1, June 2006.

T-CLC-F-00421, Carey, S.A., *Structural Assessment of F-Area Tank Farm After Final Closure*, Savannah River Site, Aiken, SC, Rev. 0, December 2007.

T-CLC-Z-00006, Peregoy, W.L., *Saltstone Vault Structural Degradation Prediction*, Savannah River Site, Aiken SC, Rev. 0, July 2003.

UCRL-ID-132088, Clodic, L., and Meike, A., *Thermodynamics of Calcium Silicate Hydrates - Development of a Database to Model Concrete Dissolution at 25ºC Using the EQ3/6 Geochemical Modeling Code*, Lawrence Livermore National Laboratory, August 1997.

USDA-HDBK-703, Rengard, K.G., et.al., *Predicting Soil Erosion by Water: A Guide to Conservation Planning with the Revised Universal Soil Loss Equation (RUSLE)*, U.S. Department of Agriculture, Tucson, AZ, 1997.

USGS OFR 2010-1059, Dart, R.L., et.al., *Earthquakes in South Carolina and Vicinity 1698-2009*, U.S. Geological Survey, Open-File Report 2010-1059, 1 Sheet, Denver, CO, September 2010.

van Genuchten, J., *A Closed-Form Equation for Predicting the Hydraulic Conductivity of Unsaturated Soils*, Soil Science America Journal, Vol. 44, No. 5, pp. 892-898, 1980. (Copyright)

VSL-14R2890-1, Papathanassiu, A., et.al., *Development of Cement-Free Saltstone Formulations Phase 2*, Vitreous State Laboratory, Washington, D.C., Rev. 0, February 2014.

W780625, *Saltstone Surface Disposal Vault Foundation and Floor Plan, Elevation and Sections*, Savannah River Site, Aiken, SC, Rev. 7, February 2004.

W828992, *Saltstone Vault 4 Plan, Sections and Details Concrete*, Savannah River Site, Aiken, SC, Rev. 3, May 2010.

W828993, *Saltstone Vault 4 Sections & Details, Concrete and Steel*, Savannah River Site, Aiken, SC, Rev. 8, May 2010.

Wang, J.S.Y., and Narasimhan, T.N., *Hydrologic Mechanisms Governing Fluid Flow in a Partially Saturated, Fractured, Porous Medium. Water Resources Research*, Vol. 21, No. 12, pp. 1861-1874, 1985. (Copyright)

WB00001K-004-G, *2.9 – MG Saltstone Tanks 2A & 2B*, Savannah River Site, Aiken, SC, Rev. F, February 2011.

WDPD-12-49, *Disposal Authorization Statement for the Savannah River Site Saltstone Disposal Facility,* U.S. Department of Energy, Washington, DC, Rev. 1, May 2012.

WDPD-12-66, *Disposal Authorization Statement for the Savannah River Site Saltstone Disposal Facility – Prestart Corrective Actions Complete,* U.S. Department of Energy, Washington, DC, July 2012.

WR-2013-68, Söderlund, M., et.al., *Distribution Coefficients of Caesium, Chlorine, Iodine, Niobium, Selenium and Technetium on Olkiluoto Soils,* University of Helsinki, Helsinki, Sweden, February 2014.

WSP-SSF-2005-00023, Liner, K.R., *Application for Modification, Z-Area Industrial Solid Waste Landfill Permit #025500-1603, Engineering Report for Vault 2 Construction*, Savannah River Site, Aiken, SC, Rev. 1, September 2007.

WSRC-IM-2004-00008, *DSA Support Document – Site Characteristics and Program Descriptions*, Savannah River Site, Aiken, SC, Rev. 1, June 2007.

WSRC-MS-2003-00617, Stevenson, D.A., et.al., *2001-2002 Upper Three Runs Sequence of Earthquakes at the SRS, South Carolina*, Savannah River Site, Aiken, SC, September 2003.

WSRC-OS-94-42, *Federal Facility Agreement for the Savannah River Site*, Savannah River Site, Aiken, SC, August 1993.

WSRC-RP-2003-00362, Kaplan, D., and Hang, T., *Estimated Duration of the Subsurface Reducing Environment Produced by the Z-Area Saltstone Disposal Facility*, Savannah River Site, Aiken, SC, Rev. 2, January 2003.

WSRC-RP-92-1360, *Radiological Performance Assessment Report for the Z-Area Saltstone Disposal Facility at the Savannah River Site*, Savannah River Site, Aiken, SC, December 1992.

WSRC-RP-94-54, Thayer, P., et.al., *Petrographic Analysis of Mixed Carbonate-Clastic Hydrostratigraphic Units in the General Separations Area*, Savannah River Site, Aiken, SC, December 1993.

WSRC-RP-98-00156, Fowler, J.R., *Addendum to the Radiological Performance Assessment for the Z-Area Saltstone Disposal Facility at the Savannah River Site*, Savannah River Site, Aiken, SC, Rev. 0, April 1998.

WSRC-SA-2003-00001, *Saltstone Facility, Documented Safety Analysis*, Savannah River Site, Aiken, SC, Rev. 15, July 2018.

WSRC-STI-2006-00198, Phifer, M.A., et.al., *Hydraulic Property Data Package for the E-Area and Z-Area Soils, Cementitious Materials, and Waste Zones*, Savannah River Site, Aiken, SC, Rev. 0, September 2006.

WSRC-STI-2007-00004, Lee, P.L., et.al., *Baseline Parameter Update for Human Health Input and Transfer Factors for Radiological Performance Assessments at the Savannah River Site*, Savannah River Site, Aiken, SC, Rev. 4, June 2008.

WSRC-STI-2007-00306, *E-Area Low-Level Waste Facility DOE 435.1 Performance Assessment*, Savannah River Site, Aiken, SC, Rev. 0, July 2008.

WSRC-STI-2007-00544, Denham, M.E., *Conceptual Model of Waste Release from the Contaminated Zone of Closed Radioactive Waste Tanks,* Savannah River Site, Aiken, SC, Rev. 2, November 2010.

WSRC-STI-2007-00607, Langton, C.A., *Chemical Degradation Assessment of Cementitious Materials for the HLW Tank Closure Project*, Savannah River Site, Aiken, SC, Rev. 0, September 2007.

WSRC-STI-2008-00244, Jones, W.E., and Phifer, M.A., *Saltstone Disposal Facility Closure Cap Concept and Infiltration Estimates*, Savannah River Site, Aiken, SC, Rev. 0, May 2008.

WSRC-TR-2000-00310, Cumbest, R.J., *Comparison of Cenozoic Faulting at the Savannah River Site to Fault Characteristics of the Atlantic Coast Fault Province: Implications for Fault Capability*, Savannah River Site, Aiken, SC, Rev. 0, November 2000.

WSRC-TR-2002-00456, Cook, J.R., et.al., *Special Analysis: Reevaluation of the Inadvertent Intruder, Groundwater, Air, and Radon Analysis for the Saltstone Disposal Facility*, Savannah River Site, Aiken, SC, Rev. 0, October 2002.

WSRC-TR-2005-00054, Sappington, F.C., et.al., *Moisture Content and Porosity of Concrete Rubble Study*, Savannah River Site, Aiken, SC, Rev. 0, October 2005.

WSRC-TR-2005-00074, Cook, J.R., et.al., *Special Analysis: Revision of Saltstone Vault 4 Disposal Limits*, Savannah River Site, Aiken, SC, Rev. 0, May 2005.

WSRC-TR-2005-00101, Phifer, M.A., et.al., *Scoping Study: High Density Polyethylene (HDPE) in Saltstone Service (U)*, Savannah River Site, Aiken, SC, Rev. 0, February 2005.

WSRC-TR-2005-00131, Hiergesell, R.A., *Saltstone Disposal Facility: Determination of the Probable Maximum Water Table Elevation*, Savannah River Site, Aiken, SC, Rev. 0, April 2005.

WSRC-TR-2005-00201, Wike, L.D., et.al., *SRS Ecology: Environmental Information Document*, Savannah River Site, Aiken, SC, March 2006.

WSRC-TR-2006-00004, Kaplan, K.I., *Geochemical Data Package for Performance Assessment Calculations Related to the Savannah River Site*, Savannah River National Laboratory, Aiken, SC, Rev. 0, February 2006.

WSRC-TR-2007-00118, Kabela, E.D., et.al., *Savannah River Site Annual Meteorology Report for 2006*, Savannah River Site, Aiken, SC, April 2007.

WSRC-TR-2008-00090, Skidmore, T.E., and Billings, K.D., *Saltstone Vault #2 Interior Lining Review*, Savannah River Site, Aiken, SC, Rev. 0, May 2008.

WSRC-TR-90-0284, Stephenson, D.E., *Review of Seismicity and Ground Motion Studies Related to the Development of Seismic Design Criteria at SRS*, Savannah River Site, Aiken, SC, August 1992.

WSRC-TR-95-0046, Denham, M.E., *SRS Geology & Hydrogeology Environmental Information Document*, Savannah River Site, Aiken, SC, June 1999.

WSRC-TR-96-0399-Vol. 1, Flach, G.P., et.al., *Integrated Hydrogeological Model of the General Separations Area, Vol. 1*, Savannah River Site, Aiken, SC, Rev. 0, August 1997.

WSRC-TR-96-0399-Vol. 2, Flach, G.P., et.al., *Integrated Hydrogeological Model of the General Separations Area, Vol. 2*, Savannah River Site, Aiken, SC, Rev. 1, April 1999.

WSRC-TR-99-00369, Chen, K.F., *Flood Hazard Recurrence Frequencies for C-, F-, E-, S-, H-, Y-, and Z-Areas*, Savannah River Site, Aiken, SC, September 1999.

WSRC-TR-99-4083, Aadland, R.K., et.al., *Significance of Soft Zone Sediments at the Savannah River Site*, Savannah River Site, Aiken, SC, Rev. 0, September 1999.

www.factfinder.census.gov, *Population Estimates*, American Fact Finder, U.S. Census Bureau, Washington, DC, accessed October 2018.

X-SD-Z-00004, *Waste Acceptance Criteria for Transfers to the Z-Area Saltstone Production Facility During Salt Disposition Integration (SDI),* Savannah River Site, Aiken, SC, Rev. 1, October 2019.

X-WCP-H-00043, *Tank 50 Waste Compliance Plan for Transfers to Saltstone During Salt Disposition Integration (SDI)*, Savannah River Site, Aiken, SC, Rev. 0, August 2019.

12 GLOSSARY

Absorption	Process in which atoms or molecules of one substance enters into another substance by penetrating its surface. This is a different process from adsorption, since molecules undergoing absorption are taken up by the volume, not by the surface (as in the case for adsorption).
Accuracy	Closeness of the result of a measurement to the true value of the quantity.
Actinide	Group of elements of atomic number 89 through 103. Laboratory analysis of actinides by alpha spectrometry generally refers to the elements plutonium, americium, uranium, and curium but may also include neptunium and thorium.
Acute Intruder	In the context of the SDF PA, an acute intruder is a person or persons who perform a well installation and unknowingly is exposed to contaminated drill cuttings brought to the surface at the time of drilling via direct external exposure, ingestion, and inhalation.
Adsorption	Process in which atoms or molecules of one substance adheres to the surface of another substance. This may result in an accumulation (or agglomeration) of particles on a surface or interface.
Advective Transport	Advective Transport is the transport of a substance (e.g., dissolved radionuclide) via bulk motion of a fluid (e.g., pore water). Advective Transport does not include transport of a substance by molecular diffusion (diffusive transport).
Air Pathway	Exposure pathway associated with radioactive material dispersed in the air in the form of dusts, fumes, particulates, mists, vapors, or gases.
ALARA	As Low As Reasonably Achievable – the policy of making every reasonable effort to maintain exposures to radiation as low as is practical consistent with the purpose for which the licensed activity is undertaken, taking into account the state of technology, the economics of improvements in relation to state of technology, the economics of improvements in relation to benefits to the public health and safety, and other societal and socioeconomic considerations.
Alternative Conceptual Model (ACM)	An alternative conceptual model is a conceptual model different from a reference conceptual model that introduces an alternative approach for addressing simulated conditions. For example, in the Central Scenario (or Base Case), it is assumed that saltstone degradation is dominated by a gradually increasing saturated hydraulic conductivity; whereas, an alternative conceptual model may assume that degradation is dominated by the formation and propagation of through-cracks. ACMs are developed based on the alternative scenarios.
Alternative Scenario (or Alternative Modeling Case)	In the context of the SDF PA, an alternative scenario is any scenario that is not the Central Scenario. Usually alternative scenarios will reflect less likely, but still plausible future evolutions of the disposal site. Alternative scenarios may include disruptive events.

Aquifer	Saturated, permeable geologic unit (water-bearing rock or soil) that can transmit significant quantities of water under ordinary hydraulic gradients. Beneath the SDF, the two primary aquifers of interest are the Upper Three Runs Aquifer (which is divided into the Upper Aquifer Zone and the Lower Aquifer Zone), and the Gordon Aquifer.
Assessment Context	The assessment context is the collection of information that provides the basis for the performance assessment. This includes the purpose for the PA, the regulatory framework, assessment end points, waste characteristics, and assessment timeframes.
Assessment Endpoints	An assessment endpoint is any analysis attribute used to assess the performance of the disposal system relative to the performance objectives. For the SDF PA, assessment endpoints typically include location endpoints (such as the buffer zone), time endpoints, and receptor endpoints (such as the member of the public) which are evaluated based on exposures (i.e., peak concentrations and peak doses).
Background Radiation	Radiation naturally occurring in the earth, fallout from nuclear weapons testing and nuclear accidents, and cosmic radiation. Generally, the lowest level of radiation obtainable within the scope of an analytical measurement, i.e., a blank sample.
Barrier	Any attribute of the disposal system and surrounding environment that acts to mitigate (reduce or delay) MOP or IHI exposure to disposed of waste.
Base Case	A historic term used within the 2009 SDF PA (SRR-CWDA-2009-00017) for the modeling case used as the basis for compliance assessment and as a basis for comparison when evaluating sensitivity case results. The Base Case model is equivalent to the Compliance Case in this updated SDF PA.
Bioaccumulation Factor	Ratio of contaminant concentration in an biological organism to concentration in an exposure medium.
Biotic Pathway	Exposure pathway via radionuclide and chemical species transfer by living components (e.g., animals, plants, or bacterial life) of an ecosystem.
Blackwater Stream	A type of river with a slow-moving channel flowing through forested swamps or wetlands, often darkly colored by tannins from decaying vegetation.
Boreholes	A hole drilled or bored into the ground, especially to locate water or to characterize subsurface conditions.
Buffer Zone	The buffer zone is a 100-meter wide band surrounding the disposal units.
Calcareous Zone	Located within the Santee Formation and the lowermost part of the overlying Dry Branch Formation, zones consist of silty and clayey fine sands, fine-grained clays, and calcareous shell fragments deposited in nearshore and inner shelf environments. Soft zones within the calcareous zones in the vicinity of the General Separations Area, which includes the SDF, are not cavernous voids, but are small, isolated, poorly connected, three-dimensional features filled with loose, fine-grained, water-saturated sediment.
Carbonation	The reaction of dissolved carbon dioxide with the hydrated phases of the cementitious materials. Carbonation lowers pH and reduces porosity.
Cementitious	Having the properties of cement.

Central Scenario	The suite of modeling cases that reflects the most likely or most expected future conditions. In this PA, the Central Scenario includes the Realistic Case, the Pessimistic Case, and the Compliance Case. These three modeling cases all use the same calculations and model design, but differ only by the assumed input values.
CERCLA	Comprehensive Environmental Response, Compensation, and Liability Act, commonly known as Superfund, enacted by Congress on December 11, 1980. This law provides for clean up of uncontrolled or abandoned hazardous-waste sites as well as accidents, spills, and other emergency releases of pollutants and contaminants into the environment. Through the Act, U.S. Environmental Protection Agency was given power to seek out those parties responsible for any release and assure their cooperation in the cleanup.
Chronic Intruder	In the context of the SDF PA, a person or persons that lives on site, consumes food crops grown and animals reared on site, and performs recreational activities on the closure site which is contaminated by both drill cuttings and irrigation well water. Exposure is by external contact, ingestion, and inhalation.
Citizens Advisory Board	The Savannah River Site Citizens Advisory Board is composed of individuals from South Carolina and Georgia. The board members are chosen to reflect the cultural diversity of the population affected by the Savannah River Site. The Board provides advice and recommendations to the U.S. Department of Energy on environmental remediation, waste management, and related issues. All meetings are open to the public and public participation is encouraged. Public comment periods are offered at various times throughout the meetings.
Clastic	A sedimentary rock texture describing rocks made of fragments of older weathered and eroded rocks.
Clean Water Act	The Clean Water Act is the cornerstone of surface water quality protection in the United States (the Act does not deal directly with ground water nor with water quantity issues). The law employs a variety of regulatory and non-regulatory tools to sharply reduce direct pollutant discharges into waterways, finance municipal wastewater treatment facilities, and manage polluted runoff.
Closure	For the purposes of SDF PA modeling, closure is assumed to be the moment when installation of the engineered closure cap is complete. Currently, closure is assumed to occur on October 1, 2037 (based on the expected completion of salt solution processing). Closure is preceded by the pre-closure operational period and is followed by the Institutional Control Period.
Colloid	A substance microscopically dispersed evenly throughout another substance. A colloidal system consists of two separate phases: a *dispersed phase* (or *internal phase*) and a *continuous phase* (or *dispersion medium*) in which the colloid is dispersed. A colloidal system may be solid, liquid, or gas. In the context of the SDF PA, microscopic solid particles dispersed in pore water.

Compliance Case	The Central Scenario modeling case that assumes input values which are designed to be a combination of the most probable and defensible (MPAD) values. Values are selected to be more defensible than those used by the Realistic Case but more reasonable than those used by the Pessimistic Case. This modeling case is intended to produces results that demonstrate reasonable expectation that performance objectives will be met thus establishing compliance.
Compliance Period	The Compliance Period is a 1,000-year period starting at the time of facility closure. SDF PA modeling results must demonstrate compliance with performance objectives within this Compliance Period. The Compliance Period includes the 100-year Institutional Control Period. The Compliance Period is preceded by the pre-closure operational period and represents the first 1,000 years of the Performance Period.
Compressive Strength	Force per unit area required to break an unconfined grout or concrete sample.
Concentration	Amount (e.g., radioactivity, mass, or moles) per unit volume of a substance.
Conceptual Model	A conceptual model is a well-defined, qualitative description of how related FEPs behave or are impacted within the bounds of a specific scenario. Conceptual models are used to inform mathematical models.
Cone Penetration Test	The cone penetration test is an in-situ testing method used to determine the geotechnical engineering properties of soils and delineate soil stratigraphy. The cone penetration test is one of the most used and accepted in-situ test methods for soil investigation. The test method consists of pushing an instrumented cone, tip first, into the ground at a controlled rate.
Confining Unit	A confining unit is an underground layer of distinctly less permeable rock or soil which bounds an aquifer. Beneath the SDF, the bottom of the Upper Aquifer Zone is confined by the Tan Clay Confining Zone, the bottom of the Lower Aquifer Zone is bound by the Gordon Confining Unit, and the bottom of the Gordon Aquifer is bound by the Crouch Branch Confining Unit.
Consumption Rates	Physical human health exposure parameters used for evaluating pathway-specific dose, e.g., volume of drinking water consumed per day.
Contaminants	For the SDF PA, a contaminant is any waste (radioactive or chemical) that may render another material (e.g., water or air) impure, harmful, or unusable when it is outside the designated disposal units.
Co-Precipitation	Co-precipitation as defined here is the incorporation of an element into the crystal structure of a solid phase that is predominantly made of other elements or the trapping of an element within the bulk mass of a phase made up of other elements, but not necessarily within the crystal lattice.
Cretaceous	The geological time period between 140 and 65 million years ago.
Curie	A unit of radioactivity; the quantity of nuclear material that has 3.7E+10 disintegrations per second.
Darcy Velocity	The volumetric rate of flow per unit of a cross-sectional area of a porous media (volumetric flux). Darcy velocity is a measure of the rate of porous medium flow.

Desorption	The opposite process to sorption, meaning detachment of one substance from another.
Deterministic	When fixed parameters are used in calculations versus a distribution of values (probabilistic).
Diffusion	Movement of contaminants from an area of higher concentration to an area of lower concentration.
Diffusion Coefficient	The rate coefficient for diffusion of molecules.
Diffusive Transport	Diffusive Transport is the net transport of a substance (e.g., dissolved radionuclide) from a region of higher concentration to one of lower concentration by molecular activity (Brownian motion) in a fluid. Diffusive transport does not include transport of a substance by bulk fluid motion (advective transport).
Dirichlet Boundary Condition	This is a condition that is applied to an ordinary or partial differential equation itself (not the derivative). For example, a zero-concentration boundary condition would be where the system's differential equation is set equal to zero.
Dispersivity	Equal to the dispersion coefficient divided by the velocity.
Distribution Coefficient (K_d)	See the entry for partition coefficient.
Dolomitic	A magnesia-rich sedimentary rock resembling limestone.
Dose	A measured quantity of a medicine, nutrient, or pathogen delivered as a unit. In the case of this PA, it primarily refers to the quantity of radionuclide exposure as it relates to long-term risk.
Dose Conversion Factor (DCF)	A factor used to convert radionuclide concentrations in environmental media to doses. Factors are used for inhalation, ingestion, immersion, and external exposure.
Dose Limits	The permissible upper bounds of radiation doses.
Effective Diffusion Coefficient (De)	The diffusion coefficient of a species through a saturated porous medium taken over the pore area of the medium through which diffusion occurs under steady-state conditions.
Erosion Barrier	The layer within a multi-part closure cap made of rock (riprap) and filler materials designed to prevent riprap movement during a probable maximum precipitation (PMP) event and therefore form a barrier to further erosion and gully formation (i.e., provide closure cap physical stability). The SDF erosion barrier will be used to maintain a minimum 10 feet of clean material above the disposal units to act as an intruder deterrent. It will also act to preclude burrowing animals from access to underlying closure cap layers. It also provides water storage for the promotion of evapotranspiration.
Escarpment	A steep slope or long cliff caused by erosion or faulting separating two level areas of differing heights.
Ettringite	Ettringite is hexacalcium aluminate trisulfate hydrate. Ettringite is found in hydrated cement as a result of the reaction of calcium aluminate with calcium sulfate.

Evaluation Case	A term used in various SDF Special Analyses (SRR-CWDA-2013-00062, SRR-CWDA-2014-00006, SRR-CWDA-2016-00072) to identify a specific modeling case used to evaluate the collective impacts to SDF performance relative to any new information. The purpose of a Special Analysis is to evaluate the potential impacts that new information may have relative to the SDF performance. The Evaluation Case incorporates model changes or updates to inputs to provide updated results which are then compared against PA model results.
Evapotranspiration	Evapotranspiration is a term used to describe the sum of direct evaporation and plant transpiration from the earth's land surface to atmosphere. Evaporation accounts for the movement of water to the air from sources such as the soil, canopy interception, and water bodies.
Event	An event is a natural or human-caused phenomenon or change that has the potential to affect the performance of the disposal system and that occurs during an interval that is short relative to the analyses timeframe. Examples of events are earthquakes, floods, storms, well drilling, and excavation.
Exposure	Being exposed to ionizing radiation or to radioactive material.
Exposure Pathway	The means by which humans are exposed to contaminants. The key exposure pathways are air and water, with most exposures via drinking water, crops, other foods, inhalation, and direct radiation.
External Dose	That portion of the dose equivalent received from radiation sources outside the body.
Facies	A distinctive sedimentary process or environment governing a rock or sedimentary deposit formation that is reflected in the rock composition, texture, age, or fossil content.
Feature	A feature is an object, structure, or characteristic that has a potential to affect the performance of the disposal system. Examples include rocks within an erosion layer of an engineered cover or a roof-support column.
Federal Facility Agreement	Agreement between U.S. Environmental Protection Agency, U.S. Department of Energy, and South Carolina Department of Health and Environmental Control that directs the comprehensive remediation of the Savannah River Site. It contains requirements for 1) site investigation and remediation of releases and potential releases of hazardous substances, and 2) interim status corrective action for releases of hazardous wastes or hazardous constituents.
FEP	A FEP is any feature, event, or process associated with a disposal system that is potentially relevant to performance. FEPs are described in the report: *Features, Events, and Processes for the Saltstone Disposal Facility Performance Assessment*. [SRR-CWDA-2017-00057]
FEPs screening	FEPs screening is the process of using established criteria to eliminate FEPs from further consideration based on potential impacts to the performance of the disposal system. The FEPs screening process is described in the report: *Features, Events, and Processes for the Saltstone Disposal Facility Performance Assessment*. [SRR-CWDA-2017-00057]
Floodplain	The area adjacent to a stream that may be submerged by floodwaters. The flat plain next to a stream built by stream deposition.

Fluoroscopy	A medical x-ray technique that obtains real-time images during a medical examination or procedure.
Fluvial	Relating to the action of a river or stream.
Flux	Strictly speaking, the rate of mass or volume flow per unit area. However, the term also commonly refers to mass or volumetric flow rate, for example, curies per year leaving the contamination zone
Fly Ash	Fly ash is a byproduct of coal burning used as a mineral admixture in cementitious materials to enhance finishing characteristics, make the mix more economical, and to improve pumping. It is finer in consistency than cement, and its particles are round. These fine particles make the mix finish easier, and pumping easier.
Gaussian plume equation	An equation that represents dispersion of a material from a release point.
General Separations Area	Central area of Savannah River Site including the heavily industrialized E, F, H, S, and Z Areas. Bounded by Upper Three Runs, Fourmile Branch and McQueen Branch.
Geosynthetic Clay Liner	A woven fabric-like material infused with (initially) dry clay primarily used for the lining of landfills. It is a kind of geomembrane and geosynthetic, which incorporates a bentonite or other clay, which has a very low hydraulic conductivity.
GoldSim	A simulation software program used in the SDF PA to dynamically model the release and transport of radioactive constituents. The fundamental output consists of predicted mass fluxes at specified locations within a system, and predicted concentrations within environmental media (e.g., ground water, soil, air).
Grainstone	A limestone-type rock composed of carbonate grains and containing less than 1% carbonate mud-sized material.
Ground Water Flow	The rate of ground water movement through the subsurface.
Grout	A cementitious mixture, sufficiently fluid, which can be pumped into equipment cavities creating a watertight bond, and increasing the strength of the existing structural foundation. Capable of slowing the vertical movement or migration of water.
Headwaters	The parts of a river furthest from the river mouth, i.e., the river source area.
Herpetofauna	Term used that refers to reptiles and amphibians, collectively.
High Density Polyethylene (HDPE) Geomembrane	A geomembrane that forms a composite hydraulic barrier in the closure cap to promote lateral drainage through the overlying lateral drainage layer and minimize infiltration to the disposal units.
Homogenous	Similar or uniform structure or composition throughout.
Human Receptor	See Receptor.
Hydraulic Communication	When ground water moves between two or more aquifers in response to pressure (head), density, or other differences, they are said to be in communication.
Hydraulic Conductivity	Property of saturated porous materials (e.g., concrete, grout, soil). Defined as the ratio of Darcy velocity to hydraulic head gradient.
Hydrographs	A graph showing the rate of surface water flow versus time past a specific point in a river or channel.

Hydrostratigraphic Unit	A geologic formation, part of a formation, or group of formations with similar hydrologic characteristics or properties related to ground water flow.
Igneous Rock	An aggregate of interlocking silicate minerals formed by cooling and solidification of magma or lava. Igneous rocks are formed by volcanic processes.
Inadvertent Human Intruder	A hypothetical future person who is a receptor (i.e., receives dose), and who is representative of average adults with reasonable adjustments to be consistent with influences based on occupation, recreation, and/or region. The Inadvertent Human Intruder is an individual who, starting at the end of the Institutional Control Period, is assumed to be located at the point of maximum exposure within the 100-meter buffer zone.
Indurated	Hard or thickened.
Infiltration	Typically, infiltration is defined as water that is absorbed by the soil at the surface, passing through the interface between the atmosphere and the ground surface. However, throughout this PA the term "infiltration" is used in the place of the term "percolation", meaning the water flux moving downward past the closure cap.
Institutional Control Period	The Institutional Control Period is a 100-year period starting at the time of closure. During this period, it is assumed that controls are in place to prevent any MOP or IHI from exposure to disposed of waste or contaminant releases. This period is based on 10 CFR 61, which requires that DOE maintains institutional control over the disposal site for a minimum of 100 years after operations are complete.
Interfluvial	The region of higher land between two rivers that are in the same drainage system.
Internal Dose	That portion of the dose equivalent received from radioactive material taken into the body.
Jurassic	The geological period between 210 and 140 million years ago.
Karst	A topography developed in some areas of limestone characterized by sinkholes, underground streams, and caverns.
Kriging	A geostatistical method for interpolating that uses distance and spatial point arrangement to predict an intermediate value between known values (points).
Lacustrine Sediments	A type of non-lithified deposit that comes from lakes, which previously occupied the area. Generally, these include fine-grained soils that have settled through the water column and accumulate on the lake bottom.
Laminae	Thin layers of sediment, usually clay, within a sedimentary rock or deposit.
Latin Hypercube Sampling	A form of sampling that can be applied to multiple variables. The method is commonly used to reduce the number or runs necessary for a Monte Carlo simulation to achieve a reasonably accurate random distribution.
Leachate	Leachate is the liquid that drains or 'leaches' from a closure system. It can contain both dissolved and suspended material.
Leaching	Leaching occurs when infiltrating water seeps into the closure system and transports contaminants out of the system.

Liquefaction	The process by which water-saturated or partially-saturated unconsolidated sediments are transformed into a substance resembling a liquid in response to an applied stress such as shaking.
Lithology	The description of rocks, especially in hand specimen and in outcrop, on the basis of such characteristics as color, mineralogic composition, and grain size.
Loam	A soil consisting of an easily crumbled mixture of varying proportions of clay, silt, and sand.
Long-Term Exploratory Period	The long-term exploratory period extends from the time of closure and continues beyond 10,000-years until peak doses are reached.
Mathematical Model	A mathematical model defines the governing equations and formulas used to abstract the conceptual models from qualitative descriptions into quantifiable calculations.
Maximum Contaminant Level (MCL)	The highest level of a contaminant allowed in drinking water by US EPA regulation under the Safe Drinking Water Act.
Mean Sea Level	The reference point used as a standard for determining terrestrial and atmospheric elevation or ocean depths and is calculated as the average of hourly tide levels measured by mechanical tide gauges over extended periods of time.
Mechanical Dispersion	The spreading of mass away from the center of mass within an advecting plume.
Member of the Public (MOP)	A hypothetical future person who is a receptor (i.e., receives dose), and who is representative of average adults with reasonable adjustments to be consistent with influences based on occupation, recreation, and/or region. The Member of the Public is an individual who, starting at the end of the Institutional Control Period, is assumed to be located at the point of maximum exposure at or outside of the 100-meter buffer zone.
Mesozoic	An area of geologic time, from the end of the Paleozoic to the beginning of the Cenozoic, or from about 225 million years to about 65 million years ago.
Microfacies	Those characteristic and distinctive aspects of a sedimentary rock reflecting the chemical, physical, and biologic features of its formation that are visible and identifiable only under the microscope.
Microsparite	A form of calcite consisting of very small carbonate (spar) crystals.
Miocene-Age	Middle of Tertiary Period, dating back 13-25 million years.
Model Abstraction	Model abstraction is the process of constructing a mathematical model based on the conceptual model. This often involves making assumptions that may reduce the complexity of a system to focus on quantifying the influence(s) of the major processes controlling the system.
Model Domain	The model domain is the area that is explicitly modeled. The SDF is not a closed system (i.e., it is exposed to external interactions which can influence performance). However, because it isn't computationally feasible to model the entire universe for the SDF PA, physical limits must be placed and the model boundary must be pre-defined.

Model Implementation	Model implementation is the application of a mathematical model. To apply a mathematical model, the equations and formulas must be combined with appropriate model inputs within a modeling software (or equivalent computational platform).
Molarity	Relating to a solution that contains *X* moles of solute per liter of solution, where *X* is a number.
Monte Carlo Method	An analytical method in which a large number of statistical realizations are simulated using randomly sampled values for each uncertain parameter distribution. All the realizations are then assembled into probability distributions of possible outcomes. This method propagates different types of uncertainty into model results, and enables easy identification of the parameters most impacting results.
Mudstone	A fine-grained sedimentary rock whose original constituents were clays or mud.
National Pollutant Discharge Elimination System	As authorized by the Clean Water Act, the National Pollutant Discharge Elimination System permit program controls water pollution by regulating point sources that discharge pollutants into waters of the United States. Point sources are discrete conveyances such as pipes or man-made ditches.
NDAA Section 3116	*Ronald W. Reagan National Defense Authorization Act (NDAA) for Fiscal Year 2005* was passed by Congress on October 9, 2004 and signed by the President on October 28, 2004. Section 3116 specifies that the term "high-level radioactive waste" does not include radioactive waste that results from reprocessing spent nuclear fuel if the Secretary of Energy determines, in consultation with the U. S. Nuclear Regulatory Commission, that the waste meets certain criteria.
Neumann Boundary Condition	This is a condition that is applied to the derivative of an ordinary or partial differential equation. For example, a zero-gradient boundary condition would be where the derivative of the system's differential equation is set equal to zero.
Occupational Exposure	The dose received by an individual in the course of employment in which the individual's assigned duties involves exposure to radiation or to radioactive material. The occupational exposure dose does not include doses received from background radiation or from any medical administration the individual has received.
Outcrop	The portion of a subsurface feature (e.g., hydrostratigraphic unit) that is visible at ground surface.
Oxidation Potential	The measure of a material's ability to oxidize or lose electrons.
Oxidized	Combined with or having undergone a chemical reaction with oxygen.
Packstone	A limestone type rock composed of carbonate grains or marine skeletal fragments containing 1% or more of carbonate mud-sized material.
Paleozoic	The geological period between 600 to 230 million years ago.
Partition Coefficient (K_d)	The quantity of a solute sorbed by a solid, per unit weight of solid, divided by the quantity of the solute dissolved in the water per unit volume of water.

Peak Ground Acceleration	A measure of earthquake acceleration on the ground expressed in g, the acceleration due to Earth's gravity, equivalent to g-force. Damage to structures can be correlated to the ground motion measured by seismic instruments.
Pedogenesis	The process of soil formation.
Percolation	The descending motion of a fluid, such as water, as it moves through a porous media (e.g., soil).
Perennial Stream	A perennial stream has flowing water year-round during a typical year. The water table is located above the stream bed for most of the year. Ground water is the primary source of water for stream flow. Run-off from rainfall is a supplemental source of water for stream flow.
Performance Objectives	Performance objectives are the requirements which must be met to establish compliance with regulations.
Performance Period	The Performance Period is an assumed 10,000-year period for evaluating long-term performance. Like the Compliance Period, the Performance Period starts at closure. The Performance Period includes the 100-year Institutional Control Period and the 1,000-year Compliance Period.
Permeability	Capability of a material to let pass other molecules or particles via a fluid pressure gradient.
Pessimistic Case	A Central Scenario modeling case that assumes input values that are intentionally biased a produce higher dose results. This modeling case is intended to provide bounding, worst-case, or pessimistic results.
Petrography	The description and systematic classification of rocks by their content and textural relationships.
Phosphatic	Pertaining to, or containing, phosphorus, phosphoric acid, or phosphates; as in phosphatic sediments.
Physiographic province	A geographic region with a characteristic type of landforms, subsurface rock types and structural elements.
Plume	A body of contaminated ground water emanating from a specific source.
Pore	One of many small openings in a solid substance of any kind that contribute to the substance's porosity (fraction of void spaces in a material).
Pore Solution	Any liquid occupying the pore space within a porous medium.
PORFLOW	A Comprehensive Fluid Dynamics simulation software program developed to accurately solve problems involving transient or steady state fluid flow, heat, salinity and mass transport in multi-phase, variably saturated, porous or fractured media with dynamic phase change. The porous/fractured media may be anisotropic and heterogeneous, arbitrary sources (e.g., wells) may be present and, chemical reactions or radioactive decay may take place. It accommodates alternate fluid and property relations and complex and arbitrary boundary conditions.
Porosity	Grout porosity is defined as the percentage of total volume of cured grout that is not occupied by the starting cementitious materials and the products that result from reaction of these cementitious materials with water. More generally, porosity is the measure of the void spaces in a material calculated as the fraction of the volume of voids over the total volume.

Potable Water	Potable water is water safe for human consumption.
Potentiometric Surface	The level to which water rises in a well. Potentiometric surface mapping depicts the elevation to which water levels will rise in wells. The maps are created by plotting elevations of the static water level and then generating contours or lines of equal elevation.
Precambrian	An informal term to include all geologic time from the beginning of the Earth to the beginning of the Cambrian period 570 million years ago.
Pre-Closure Operational Period	The pre-closure operational period is the time period of active operations at the SDF. These operations include construction of disposal units, waste form stabilization and disposal processes, and installation of the engineered closure cap. It is the only timeframe that is not explicitly included in modeling. This may also be referred to as the "disposal operations period" or the "pre-closure period."
Preliminary Remediation Goal	Health-based chemical or radionuclide concentration in an environmental media associated with a particular exposure scenario. They may be developed based on exposure scenarios evaluated prior to or as a result of a baseline risk assessment.
Probabilistic	A model that assigns a likelihood to events or data within a population, as expressed by a ranked numerical value or an estimate of best case, worst case or most likely.
Process	A process is a natural or human-caused phenomenon or change that has the potential to affect the performance of the disposal system and that occurs during all or a significant part of the analyses timeframe. Examples of processes are radionuclide transport, differential settlement, leaching, and erosion.
Progeny	Decay products or descendants of specific radionuclides.
Radiography	A medical x-ray technique assisting in medical examinations.
RCRA	The Resource Conservation and Recovery Act is the public law that creates the framework for the proper management of hazardous and nonhazardous solid waste.
Realistic Case	A Central Scenario modeling case that assumes the best estimate or most likely input values, regardless of the defensibility of these input values. This modeling case is intended to provide reasonable or realistic results.
Receptor	For this PA, a receptor is a hypothetical person who receives dose. Within this PA, two receptors are defined: the Member of the Public and the Inadvertent Human Intruder.
Recharge	The hydrologic process through which water moves downward from the surface to enter an aquifer.
Redox	Redox (shorthand for oxidation/reduction reaction) describes all chemical reactions in which atoms have their oxidation number (oxidation state) changed.
River Mile	A measure of distance in miles along a river from its mouth.

Safety Function	A safety function is defined as a function (i.e., a process or role) which must be fulfilled to contribute to long-term safety. These functions may be active or passive and may contribute to safety by any of the following means: (1) providing stability to the disposal system, (2) containing or isolating the wastes, (3) mitigating the flow of air or water through the disposal system, or (4) limiting or delaying the release and transport of contaminants. An example of a safety function would be the requirement that an engineered closure cap limit the infiltration of water into the system.
Salt (Waste)	The waste stored in SRS tanks is broadly characterized as either sludge waste or salt waste. Salt waste is soluble and is initially dissolved in the liquid waste entering a storage tank. Salt generally contains the radioactive element cesium and trace amounts of other soluble radioactive elements in the form of dissolved salts. Salt waste can be further described as being supernate (in normal solution), concentrated supernate (after evaporation has removed some of the liquid) or saltcake (previously dissolved salts that have now crystallized out of solution). A single waste tank can contain sludge, supernate, and salt cake; although an effort is made to segregate sludge and salt in different tanks.
Saltstone	The SRS waste form generated by mixing low-activity salt solution with dry chemicals (cement, slag, and fly ash) to form a homogeneous solidified grout.
Saltstone Disposal Facility (SDF)	The SDF is the area of the Savannah River Site occupied by SDUs. This area includes the SDUs and the 100-meter buffer zone, and includes the natural system (vadose zone and saturated zone) within the boundary of the facility (i.e., the 100-meter buffer zone).
Saltstone Disposal Unit (SDU)	SDUs are engineered structures used for the permanent disposal of the solidified saltstone waste form.
Saturated Zone	The saturated zone is the area below ground in which all interconnected openings within the geologic medium are completely filled with water. For the purposes of the SDF PA, the saturated zone is a natural layer of the earth wherein the top of the layer is bounded by the bottom of vadose zone (as defined by the water table), and the bottom of the layer is bounded by a confining unit. The saturated zone is fully saturated.
Scenario (or Modeling Case)	A scenario is a subset of important FEPs that are used to identify conditions or the future evolution of the disposal site. In general, a scenario can be thought of as a theme for a given model. PA documents often refer to scenarios as "modeling cases."
Sector	A subdivision of the 100-meter compliance boundary.
Sedimentary Rock	Rock that is formed by the consolidation of sediment particles or of the remains of plants and animals.
Seepline / Seepage Face	A seepage face is any area where ground water discharges to the surface. Seepline refers to the border between dry ground and a seepage face.
Sensitivity Case	Any variant of an existing modeling case or scenario used to illustrate the impact (or sensitivity) from making specific changes to the existing modeling case.

Shotcrete	Shotcrete is a cementitious material applied via pressure hoses. Shotcrete is usually concrete conveyed through a hose and pneumatically projected at high velocity onto a surface. Shotcrete undergoes placement and compaction at the same time due to the force with which it is projected from the nozzle. Shotcrete was used in the construction of SDUs.
Silica Fume	Silica fume, also known as microsilica, is a byproduct of the reduction of high-purity quartz with coke in electric arc furnaces in the production of silicon and ferrosilicon alloys. Silica fume is used as an addition in cementitious materials, generally to improve physical properties. It has been found that silica fume improves compressive strength, bond strength, and abrasion resistance. Addition of silica fume also reduces the permeability of concrete to chloride ions, which protects concrete's reinforcing steel from corrosion.
Siliceous Mudstone	A mudstone cemented by siliceous cement.
Slag	Ground blast furnace slag, or slag in short, is an ingredient of saltstone and certain SDU concrete formulations, which in addition to improving hydraulic conductivity, provides chemical reducing capacity to the mix. Slag has been shown to possess chemically reducing properties that are favorable for technetium reduction and for plutonium and selenium.
Sludge (Waste)	The waste stored in SRS tanks is broadly characterized as either sludge waste or salt waste. Sludge waste is insoluble and settles to the bottom of a waste tank, typically beneath a layer of liquid supernate. Sludge generally contains the radioactive elements strontium, plutonium, and uranium in the form of metal hydroxides. A single waste tank can contain sludge, supernate, and salt cake; although an effort is made to segregate sludge and salt in different tanks.
Slug Test	A slug test is a particular type of aquifer test where water is quickly added or removed from a ground water well, and the change in hydraulic head is monitored through time, to determine the near-well aquifer characteristics. It is a method used by hydrogeologists to determine the transmissivity and storativity of the material the well is completed in.
Solubility	The ability of a substance to dissolve in a solvent. Solubility may also refer to the measure of this ability for a particular substance in a particular solvent, equal to the quantity of substance dissolving in a fixed quantity of solvent to form a saturated solution under specified temperature and pressure. The extent of the solubility of a substance in a specific solvent is measured as the saturation concentration, where adding more solute does not increase the concentration of the solution. The extent of solubility ranges widely, from infinitely soluble, such as ethanol in water, to poorly soluble, such as silver chloride in water. The term *insoluble* is often applied to poorly or very poorly soluble compounds.
Sorption	Process by which one substance attaches to another, such as adsorption or absorption.
Source Term	The amount and type of radioactive material released into the environment.
Spalling	Destruction of a surface by frost, heat, corrosion, or mechanical causes.

Special Analysis (SA)	A DOE Order 435.1 technical document prepared to evaluate the potential impacts that new information may have relative to the SDF performance and to ensure that any requirements (or performance objectives) will continue to be met prior to making any significant changes to the design or operation of the Saltstone Disposal Facility. This typically includes updated PA-style modeling.
Stochastic (GoldSim element)	A parameter with a probabilistic distribution.
Stoichiometry	Calculation of the quantitative relationships between the amounts of reactants and products formed during a chemical reaction.
Stream Trace	Generated by PORFLOW, line represents the direction of movement of ground water plume as it flows from each of the waste tanks to hypothetical 100-meter well locations. Because the flow is also vertical through the UTR and Gordon aquifers, the actual travel distance to reach 100 meters from the SDF boundary can be greater than 100 meters.
Submodel	A submodel is any discrete model that may be used to generate intermediate modeling results for the PA. Submodels are usually associated with specific modeling software and/or specific system processes or components. For example, some of submodels generated in support of the 2009 SDF PA include the HELP Model (for infiltration rates), the Waste Release Model (for contaminant release rates, developed using The Geochemist's Workbench software), and the Vadose Zone Flow Model (for flow rates through the vadose zone, developed using PORFLOW modeling software).
System Description	The system description describes the disposal system and the natural environment of the site. At a minimum, the system description should describe the following: a) the site, b) the natural setting, c) the disposal facility, d) the interaction of the site and disposal facility, e) the waste to be disposed of including its radiological, chemical, and physical characteristics, f) processes controlling contaminant release and transport, and g) the characteristics of members of the public potentially affected by the facility.
Terrigenous sediments	Sediment derived from material eroded from the land and transported to the ocean.
The Geochemist's Workbench	The Geochemist's Workbench is a set of software tools for manipulating chemical reactions, calculating stability diagrams and the equilibrium states of natural waters, tracing reaction processes, modeling reactive transport, and plotting the results of these calculations. The package is designed for solving problems in aqueous geochemistry, including those encountered in environmental protection and remediation, the petroleum industry, and economic geology.
Thermodynamics	The science of heat and temperature and of the laws governing the conversion of heat into mechanical, electrical, or chemical energy.
Tomography	A medical x-ray technique producing a cross section through a human body.
Tortuosity	The property of a curve being tortuous (twisted, having many turns). Commonly used to describe diffusion in porous media.

Total Effective Dose Equivalent (TEDE)	The sum of the deep-dose equivalent for external exposures and the committed effective dose equivalent for internal exposures.
Tracer	A hypothetical non-sorbing, non-decaying, solute typically used to track the flow of soil moisture and/or ground water in a numerical simulation.
Triassic	The geological time-period between 248 and 213 million years ago.
Type II Concrete	Type II concrete is made using Type II cement, which is designed to have a moderate sulfate resistance. Type II concrete was used in the construction of SDUs 1 and 4 and in the lower mud mats of the 150-foot diameter cylindrical SDUs, and in both the upper and lower mud mats of the 375-foot diameter SDUs.
Type V Concrete	Type V concrete is made using Type V cement, which is designed to have a high sulfate resistance. Type V concrete was used in the construction of the 150-foot diameter cylindrical SDUs, excluding the lower mud mats, and in the construction of the 375-foot diameter SDUs, excluding both the upper and lower mud mats.
Udorthent	Areas of disturbed native soil where the upper soil material has been removed, filled, or graded; they are moderately well drained, gravelly, and sandy soil areas.
Unsaturated Zone	Typically, an unsaturated zone is a natural earthen layer with little or no saturation. Within the SDF PA, it is sometimes used in the place of the term vadose zone to indicate that the layer is not fully saturated (as opposed to the saturated zone).
Vadose Zone	For the purposes of the SDF PA, the vadose zone is a natural layer of the earth wherein the top of the layer is bounded by the ground surface, or by the bottoms of the SDUs (i.e., the bottoms of the lower mud mats) and any surrounding backfill. The bottom of the vadose zone is bounded by the water table. The vadose zone is partially saturated.
Wackestone	A limestone type rock composed of carbonate mud containing over 10% particles (carbonate grains, marine skeletal fragments) greater than 2 mm in size.
Watershed	A region or area bounded peripherally by a drainage divide and ultimately discharges captured rainfall to a particular watercourse or body of water.

APPENDIX A – Basis for Assuming Initially Reducing Conditions in Saltstone

This page intentionally left blank.

A. APPENDIX A – Basis for Assuming Initially Reducing Conditions in Saltstone

A.1 Introduction

Under post-closure conditions, saltstone is expected to be 100% liquid saturated when in equilibrium with surrounding backfilled soil (see Section 4.4.2.3.3). Because the molar concentration of dissolved oxygen at saturation is low compared to the molar concentration of O_2 in air, oxidation of saturated saltstone occurs at a very slow rate, with the rate controlled by liquid-phase diffusive and advective transport. Post-closure oxidation of saltstone is explicitly modeled in PORFLOW simulations of Tc-99 and I-129 vadose zone transport, and indirectly considered in transport simulations for the other radionuclides and chemicals. Central Scenario simulations assume saltstone occupies the interior of the SDUs as a monolith, and certain deterministic sensitivity cases consider the impact of postulated partial- and fully-penetrating fractures (see Section 5.8.8.2), which would accelerate oxidation.

Oxidation of saltstone prior to facility closure (PA time zero) is assumed to be insignificant at the facility scale. Direct and indirect information suggest the presence of high liquid saturations in saltstone under expected field conditions prior to facility closure. High liquid saturations in saltstone would preclude or minimize gas-phase oxygen ingress. Other data from studies of a saltstone-like waste form ("cast stone") that had been exposed to atmospheric conditions suggest slow oxidation rates, resulting in insignificant penetration at the facility-scale during the operational period. These expectations are supported by visual observations of cores extracted from SDU 2A, which show no distinct bands of lighter color between grout pours, which would indicate oxidation. The multiple lines of evidence supporting the assumption that there is minimal saltstone oxidation prior to facility closure are discussed in more detail below.

A.2 Saltstone Initial Saturation and Saturation Evolution

A.2.1 Water-to-Cement Ratio and Saltstone Production Facility Water Flushes

The high water-to-cementitious materials ratio of saltstone (w/c = 0.65) ensures saltstone will be fully saturated upon initial set. Although ongoing hydration reactions will consume some pore water, that loss may be replaced by excess water bleeding from subsequent pours of wet slurry. Additional water enters an SDU through periodic water flushes of the Saltstone Production Facility (SPF) hopper and transfer lines. Figure A-1 illustrates a typical series of water flushes during and after a saltstone pour. Note that the start and finish times depicted in this figure indicate times when a specific characterization sample was collected from the SPF hopper. This is described in Section 5.1.2 of *Property Data for Core Samples Extracted from SDU 2A* (SRR-CWDA-2016-00051).

Figure A-1: Periodic Water Flushes of SPF Hopper and Transfer Lines During and After a Typical Saltstone Pour

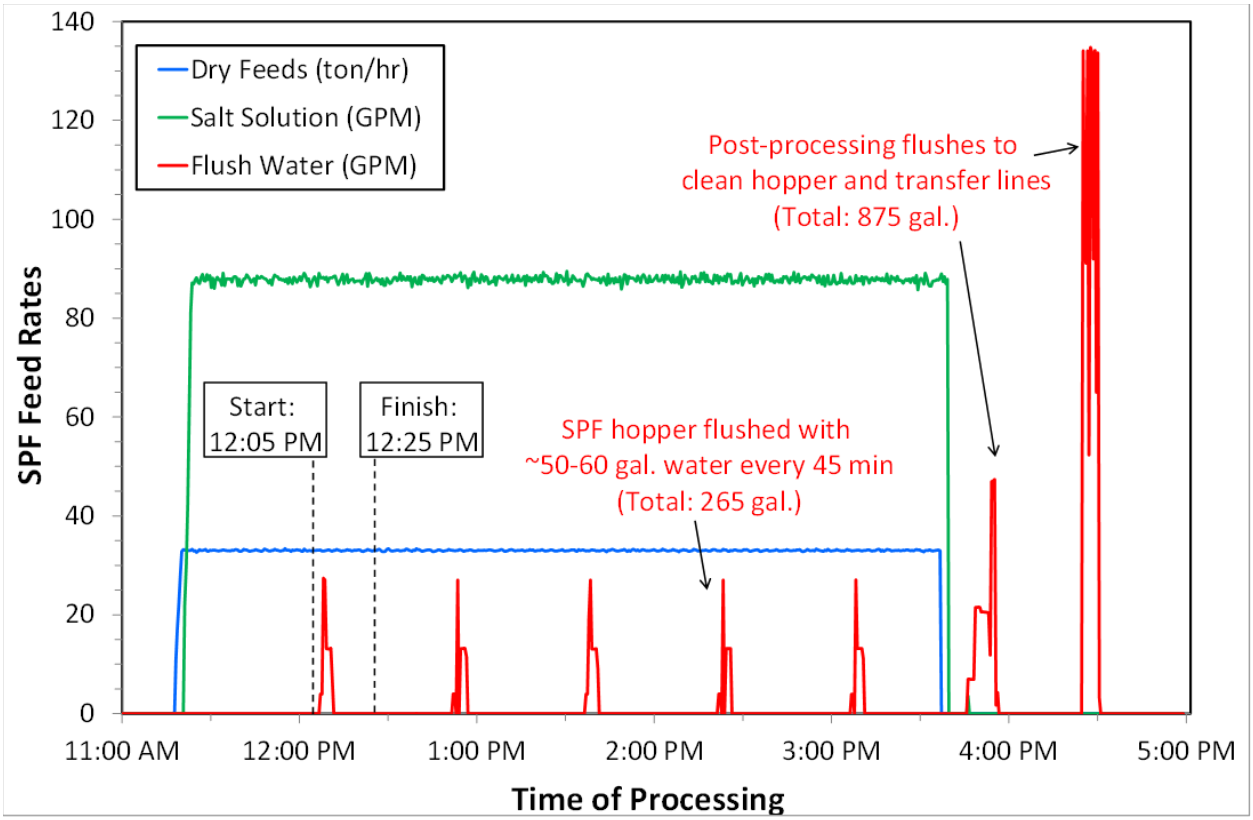

[SRR-CWDA-2016-00051]

A.2.2 Relative Humidity

Longer term, the SDU concrete enclosure will minimize saltstone moisture loss to the atmosphere. The top of the saltstone monolith will be most exposed to atmospheric conditions, but only indirectly through small vents. Measurements of the relative humidity (RH) in the air space above saltstone in SDU 2A (Figure A-2) exceeded 95% on average from late May to late June 2013 [SRR-SPT-2013-00044]. The liquid saturation state of SDU concrete and saltstone in equilibrium with RH = 95% can be estimated using the Kelvin, van't Hoff / Morse, and van Genuchten relationships. [SRNL-STI-2018-00077, Section 4.3] At RH = 95% the SDU concrete is estimated to be 99% saturated (Table A-1). Until dissolved solids leach from the saltstone pore solution, the molar concentration of ions will be very high, around 8.37 mol/L or higher. [SIMCO_08-31-2012, Table 8] A combination of capillary (small pores) and osmotic (dissolved salts) suctions will cause saltstone at equilibrium to be 100% saturated at 95% RH (Table A-1). After a sufficiently long time, when the concentration of dissolved solids approaches zero, saltstone saturation is predicted to decrease to about 83% (Table A-1, saltstone molarity = 0 mol/L).

Figure A-2: Measured Relative Humidity in SDU 2A Air Space

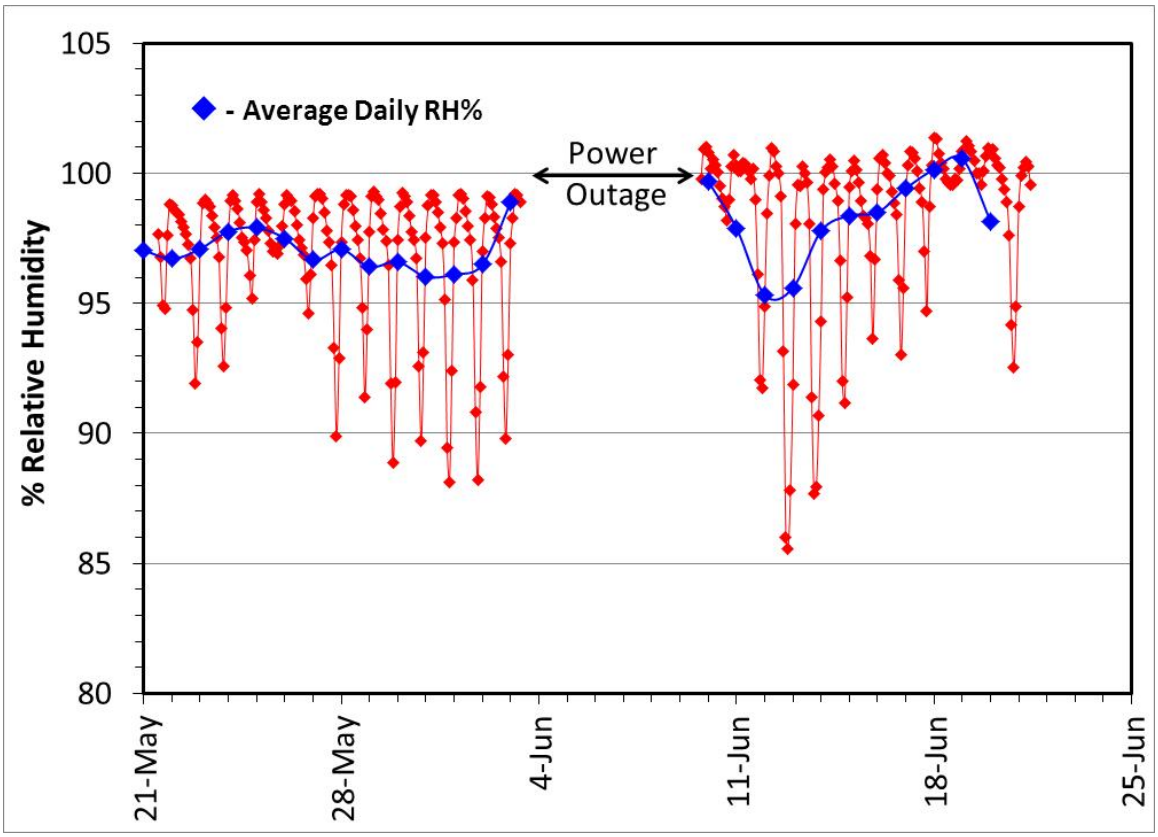

[SRR-SPT-2013-00044]

Table A-1: Saturation of Saltstone and SDU Concrete in Equilibrium with a 95% Relative Humidity Environment Using the Kelvin, van't Hoff/Morse, and van Genuchten Relationships

Parameter	Saltstone			Concrete-V2			Units
temperature, T	20	20	20	20	20	20	C
	293.15	293.15	293.15	293.15	293.15	293.15	K
relative humidity, RH	95.00%	95.00%	95.00%	95.00%	95.00%	95.00%	
saturation pressure, P_0	23.46	23.46	23.46	23.46	23.46	23.46	millibar
	2346	2346	2346	2346	2346	2346	Pa
water vapor pressure, P_v	2229	2229	2229	2229	2229	2229	Pa
gas constant, R	8.314	8.314	8.314	8.314	8.314	8.314	J/K-mol
molecular mass of water, M_w	18	18	18	18	18	18	g/mol
gravitational acceleration, g	9.81	9.81	9.81	9.81	9.81	9.81	m/s^2
density of water, ρ	998	998	998	998	998	998	kg/m^3
ρg	9790.38	9790.38	9790.38	9790.38	9790.38	9790.38	Pa/m
total suction, ψ	708	708	708	708	708	708	m
	70798	70798	70798	70798	70798	70798	cm
	6931361	6931361	6931361	6931361	6931361	6931361	Pa
	69.3	69.3	69.3	69.3	69.3	69.3	bar
van't Hoff factor, i	1	1	1	1	1	1	
molarity, M	8.37	4.185	0	0.18	0.09	0	mol/L
osmotic suction, Π	20399775	10199887	0	438705	219352	0	Pa
	2083.66	1041.83	0.00	44.81	22.40	0.00	m
	208366	104183	0	4481	2240	0	cm
	204.0	102.0	0.0	4.4	2.2	0.0	bar
capillary (matric) suction, Ψ_c	-1376	-334	708	663	686	708	m
	-137568	-33385	70798	66317	68557	70798	cm
	-13468413	-3268526	6931361	6492657	6712009	6931361	Pa
	-134.7	-32.7	69.3	64.9	67.1	69.3	bar
saturated water content, θ_s	0.58	0.58	0.58	0.1	0.1	0.1	
residual water content, θ_r	0	0	0	0	0	0	
van Genuchten (1980) α	1.008E-05	1.008E-05	1.008E-05	2.086E-06	2.086E-06	2.086E-06	1/cm
van Genuchten (1980) n	1.67131	1.67131	1.67131	1.9433	1.9433	1.9433	
m=1-1/n	0.402	0.402	0.402	0.485	0.485	0.485	
capillary suction, Ψc	-137568	-33385	70798	66317	68557	70798	cm
saturation	1.000	1.000	0.834	0.990	0.989	0.988	

A.2.3 Saturation Measurements

Non-radioactive, laboratory-scale, samples of saltstone cast for testing purposes are typically cured in a moist environment. The latter provides additional water to support ongoing hydration reactions as the material cures over extended periods (e.g. 28, 90 days). The small scale and wet curing environment tend to keep these samples in a fully saturated state that may not be representative of field conditions. However, more representative conditions occurred in meso-scale experiments conducted into FY2013 and FY2014. Simulated saltstone prepared by SRNL was poured into B-25 waste containers in daily lifts of 8-9 inches to a total height of approximately 42 inches in separate FY2013 and FY2014 mock-up tests. Cored samples were acquired after two months of monolith curing in FY2013 and at least seven months in FY2014. The FY2014 summary

report (SRR-CWDA-2014-00059) states that "B25 lid incorporated a seal to maintain a humid curing environment." Self-desiccation is possible under these curing conditions.

The gravimetric moisture content (w) of SRNL samples cored from the B-25 containers in FY2014 after approximately nine months (270 days) of curing was reported to range from 36% to 37% regardless of whether a wet- or dry-coring technique was used. [SRR-CWDA-2015-00152, page 36, SRR-CWDA-2014-00059, Section 3.10] As shown in Section A.4, the saturation state of the samples can be estimated from the equation:

$$S = \frac{w\rho_{b,dry}}{n\rho_{ps}\left(1 - \frac{M_{ds}}{M_{ps}} - w\right)} \qquad \text{Eq. A-1}$$

Where:

S = saturation,

w = gravimetric water content,

$\rho_{b,dry}$ = dry bulk density, 0.932 g/mL (SRR-CWDA-2018-00004, Table 1),

n = porosity = 0.656 (SRR-CWDA-2018-00004, Table 1),

ρ_{ps} = pore solution density, and

$\frac{M_{ds}}{M_{ps}}$ = mass fraction of dissolved solids in the solution in saltstone pores.

Based on saltstone characterization (SIMCO_08-31-2012, Table 8), the pore solution density of dissolved solids are estimated to range from 1.215 g/mL for a 28-day cure to 1.250 g/mL for a 520-day cure. Similarly, the mass fraction of dissolved solids are estimated to range from 0.287 for a 28-day cure to 0.326 for a 520-day cure. The conclusion using either set of pore solution data is $S \cong 100\%$ for w = 36%-37%, which is consistent with no difference having been observed between wet and dry coring techniques because the cores were already saturated. See Section A.4 for further information on the calculation and associated inputs.

Field samples of saltstone were cored from SDU 2A in FY2015, approximately 20 months (600 days) after placement. The average gravimetric water content of the samples, as-received by the SRNL testing laboratory, was 30.3%. [SRR-CWDA-2016-00051, Table I] For w = 0.303 the estimated average saturation of the SDU 2A samples is estimated to be 93% using Equation A-1 and the 520-day cure pore solution data. Details on this calculation are provided in Section A.4.

A.2.4 Saturation Evolution Conclusion

The saltstone water-to-cement ratio, process line flushes, RH data, and saturation measurements taken together suggest that saltstone is fully saturated upon initial set and then slowly approaches a saturation around 90% after a year or two, through self-desiccation and perhaps exposure to the atmosphere. Hydration reactions are thought to be practically complete by then so that any additional self-desiccation can be neglected compared to other uncertainties. The apparent unsaturated state of saltstone after several months of curing makes gas-phase transport of oxygen possible. The potential significance of any accelerated oxidation is assessed in the Section A.3.

A.3 Saltstone Oxidation

A.3.1 Gas-phase Intrinsic Diffusion Coefficients as a Function of Saturation

Intrinsic gas-phase diffusion coefficients are small unless liquid saturation is significantly below 100%. Figure A-3, Figure A-4, and Figure A-5 each show example of calculated and/or measured intrinsic gas-phase diffusion coefficients (D_i) for radon and hydrogen transport through porous media, primarily cementitious materials. Between 0% and approximately 60% liquid saturation, the intrinsic diffusion coefficient is observed to be roughly constant. D_i decreases orders of magnitude going from approximately 60% saturation to 100% saturation. Saltstone saturation is expected to evolve from 100% to 90% as discussed in Section A.2, resulting in minimal gas-phase oxygen transport compared to drier conditions.

Figure A-3: Intrinsic Diffusion Coefficient for Radon Gas as a Function of Average Pore Size and Moisture Saturation

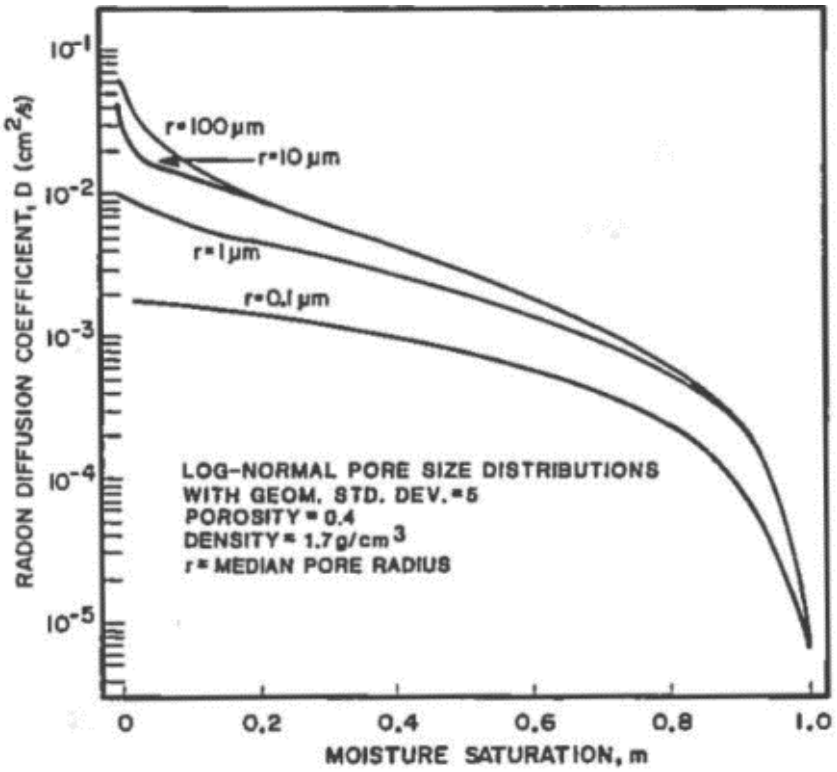

[Nielson, Rogers and Gee, 1984]

Figure A-4: Intrinsic Diffusion Coefficient for Hydrogen Gas Transport Through Selected Cementitious Materials

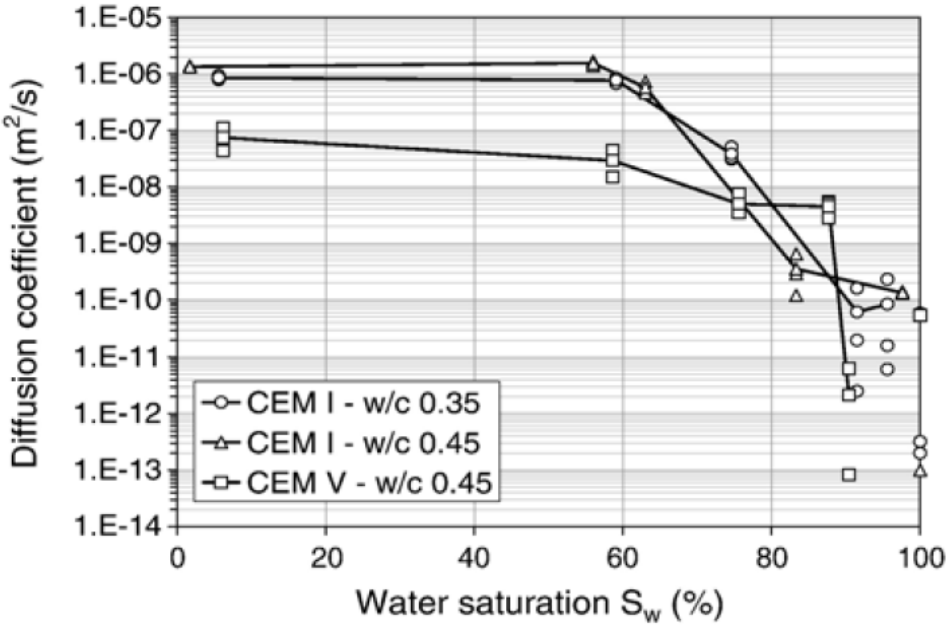

[Sercombe, *et al.*, 2007]

Figure A-5: Intrinsic Diffusion Coefficient for Hydrogen Gas Transport Through Cementitious Materials as a Function of the Water-to-Cement Ratios

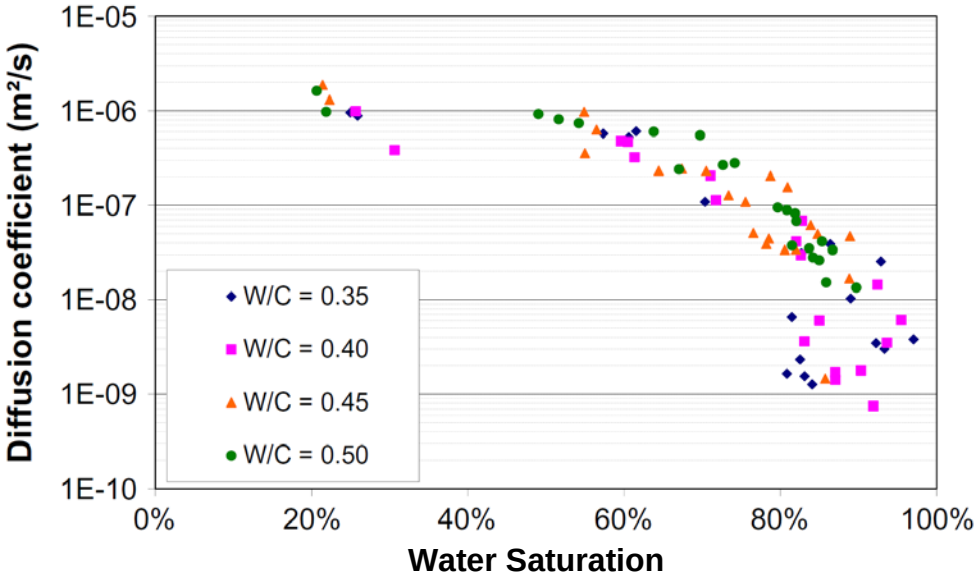

[Boher, *et al.*, 2013]

A.3.2 Oxidation Rates Under Field Conditions

The penetration depth (x) of an oxidation front controlled by diffusive transport of dissolved oxygen is a function of the liquid-phase intrinsic diffusion coefficient and other variables (SRNL-STI-2018-00077, Section 2.0):

$$x = \left[\frac{2D_i ct}{\rho_b R}\right]^{1/2} \equiv At^{1/2} \qquad \text{Eq. A-2}$$

Where:

$D_i = Sn\tau D_m$ = liquid-phase intrinsic diffusion coefficient, where

S = liquid saturation,

n = porosity,

τ= tortuosity, and

D_m = free-water molecular diffusion coefficient,

c = exposure concentration,

ρ_b = dry bulk density,

R = reduction capacity,

t = time, and

A = rate coefficient.

This expression can be generalized to the situation of combined gas and/or liquid phase transport of oxygen to the reaction front, where A is treated as an empirical constant to be estimated from a measured penetration depth x_0 and exposure time t_0:

$$A = \frac{x_0}{t_0^{1/2}} \qquad \text{Eq. A-3}$$

Penetration depth measurements for samples exposed to atmospheric conditions are available for the cast stone material (cement:slag:fly ash% = 8:47:45% per SRNL-STI-2013-00541), which is very similar to saltstone (10:45:45% per Section 3.2.5). Table A-2 summarizes observations for cast stone reported in SRNL-STI-2013-00541 and CBP-TR-2014-005. The three samples were exposed to indoor temperatures and RH and/or outdoor temperatures in a storage cooler, as noted in the table. Because the RH in these exposure environments was well below 100% (typically 65-70%), the samples were drying as the tests progressed. Ongoing hydration reactions may also have depleted pore water over time and enhanced oxygen ingress. The average penetration rate constant calculated from these tests is A = 0.065 m/√yr. Table A-3 presents projected penetration depths for saltstone using this rate constant with Equation A-2. The calculated oxidation depths are a small fraction of the 43-foot thickness of saltstone to be disposed of in SDU 7.

Table A-2: Oxidation Penetration Depths Measured for Cast Stone

Cast Stone measurements	Exposure time, *t* (d)	Penetration depth, *x* (mm)	Rate constant, *A* (m/√yr)	Exposure conditions
SRNL-STI-2013-00541, Cr spiked sample	68	35	8.1E-02	Room temperature and 65-70% RH for 63 days, followed by outdoor storage in a cooler for 68 days
SRNL-STI-2013-00541, Tc spiked sample	50	16	4.3E-02	Room temperature and humidity in a laboratory
CBP-TR-2014-005, Tc spiked sample	154	46	7.1E-02	Moist Hanford site sediment
Cast Stone average			**6.5E-02**	

Table A-3: Oxidation Penetration Depths Predicted for Saltstone

Exposure time, *t* (yr)	Penetration depth, *x* (m)	Penetration depth, *x* (ft)
0.1	0.02	0.07
0.3	0.04	0.12
1	0.07	0.21
3	0.11	0.37
10	0.21	0.67
30	0.36	1.17

A.3.3 Empirical Evidence of Oxidation: Photographic Evidence from SDU 2A Cores

Freshly placed slag cement typically takes on a "deep blue, green, or blue-green coloration" (indicating reducing conditions) that becomes "considerably lighter in color than gray portland cement … as oxidation takes place." [ACI 233R-17, Section 7.6] Figure A-6 shows an example of this phenomenon in a sample of cement-free saltstone (60% slag and 40% fly ash dry mix).

Figure A-6: Oxidation Front Penetrating a "Cement-Free" Saltstone Simulant Sample, Evident from Color Change

Photographs of saltstone cores taken from SDU 2A in spring 2015 provide an opportunity to observe any color changes that may have occurred due to oxidation. [SRNL-L3100-2015-00108] These saltstone samples (comprised of 45% slag, 45% fly ash, and 10% cement) are not as dark as the sample shown in Figure A-6 (60% slag and 40% fly ash), apparently due to their differing compositions. Although the contrast would not be as sharp, oxidized 45/45/10 saltstone would presumably still manifest itself via a notably lighter color.

Figure A-7 summarizes the relevant pouring history for SDU 2A and denotes two gaps between pours lasting four to five months. [SRR-CWDA-2015-00066] Figure A-8 through Figure A-15 identify the approximate locations of these interfaces previously expose to the air space with SDU 2A. None of these photographs show a significant color change (apart from wet versus dry surfaces) which would indicate a layer of oxidized saltstone. Presumably no significant oxidation occurred during the exposure period, or possibly any oxidized material became reduced again when covered with fresh saltstone. In either case, oxidized saltstone was not apparent at the time of coring.

Figure A-7: Partial Pouring History for SDU 2A

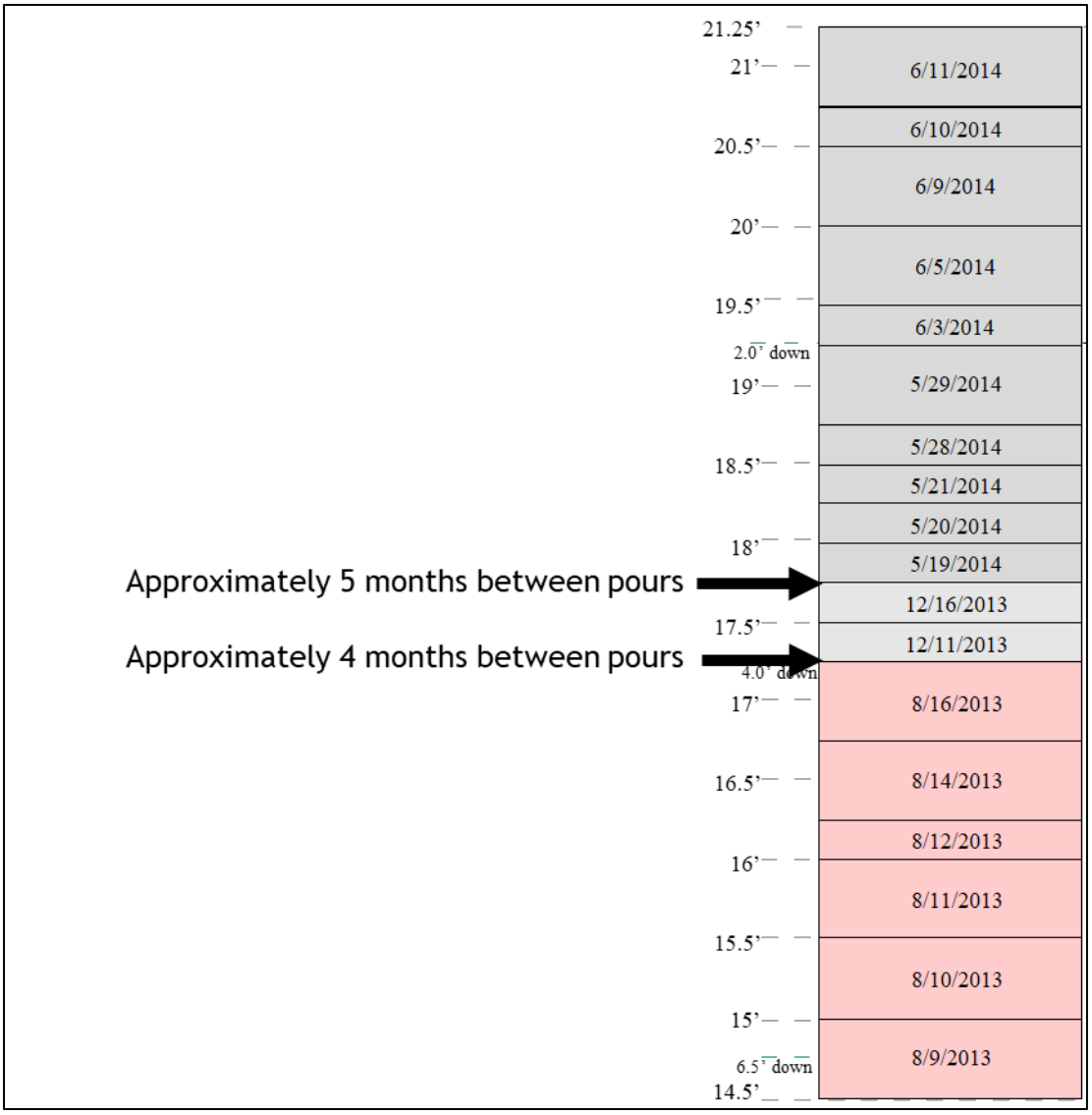

[SRR-CWDA-2015-00066, Figure 3.7-3]

Figure A-8: Photograph of Sample Core A1U

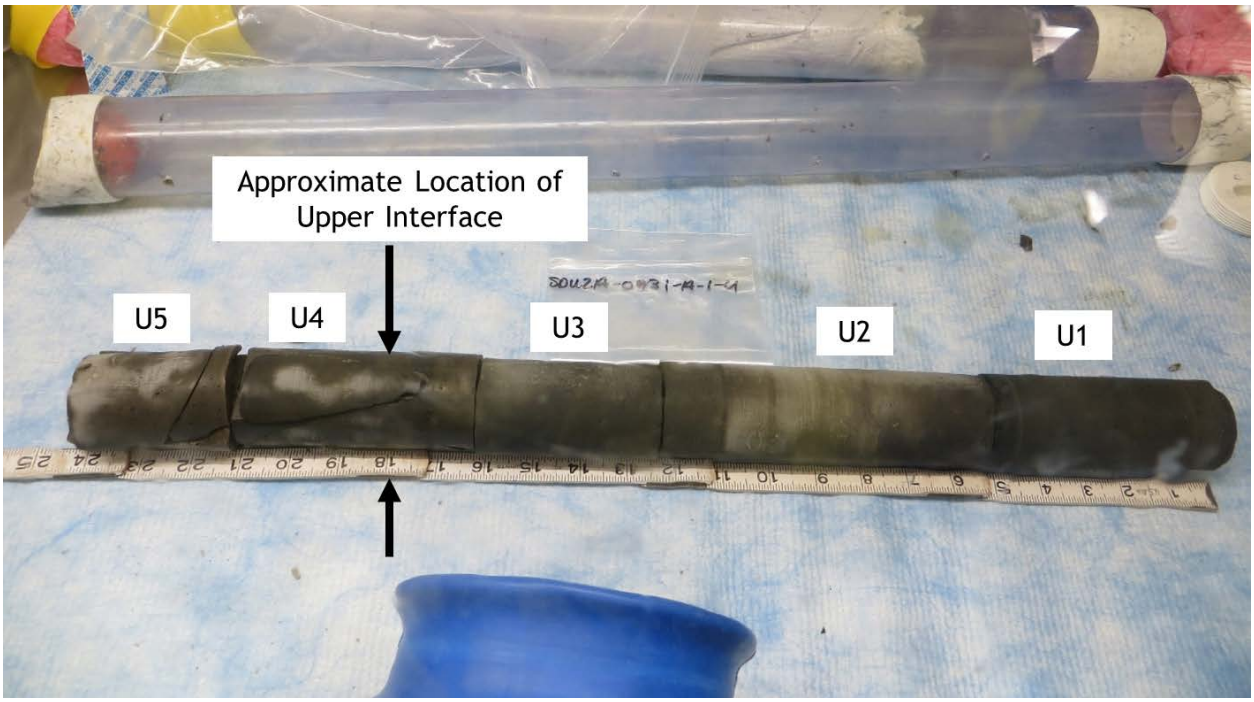

Figure A-9: Photograph of Sample Core A1U, Segment U4

Figure A-10: Photograph of Sample Core C1L

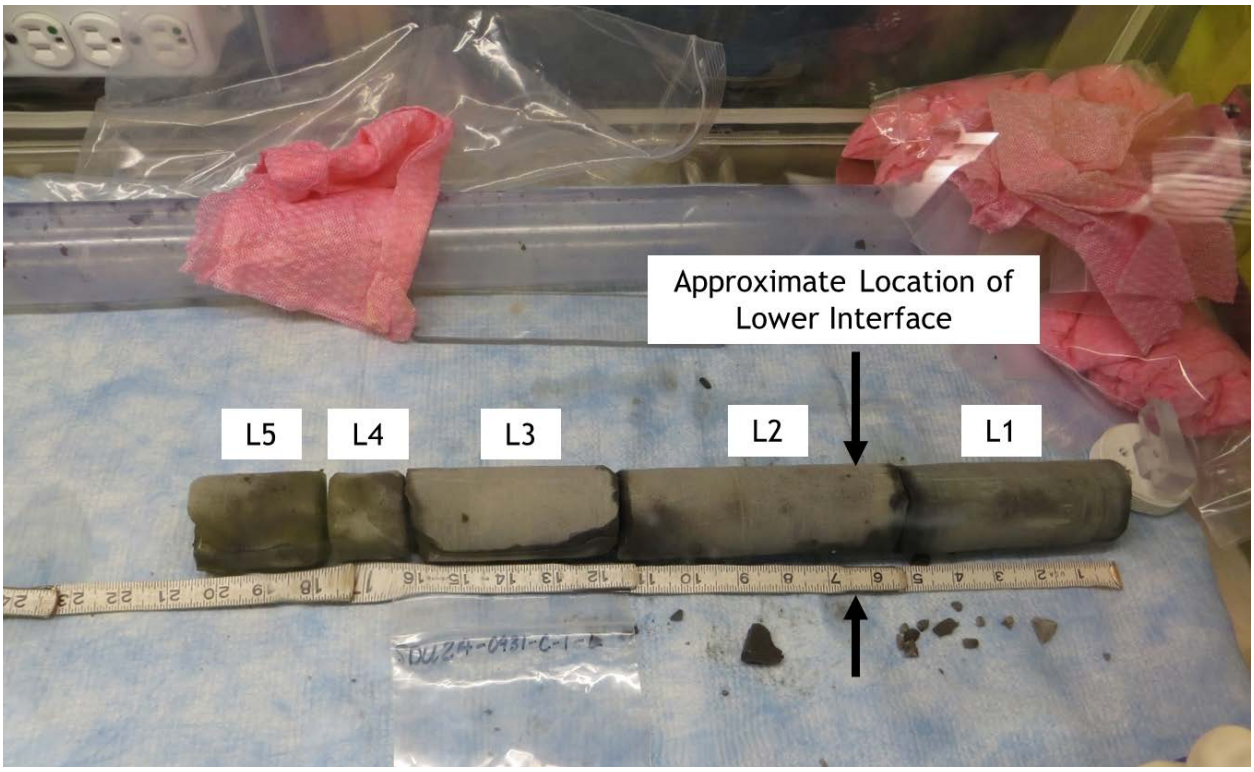

Figure A-11: Photograph of Sample Core C1L, Segment L2

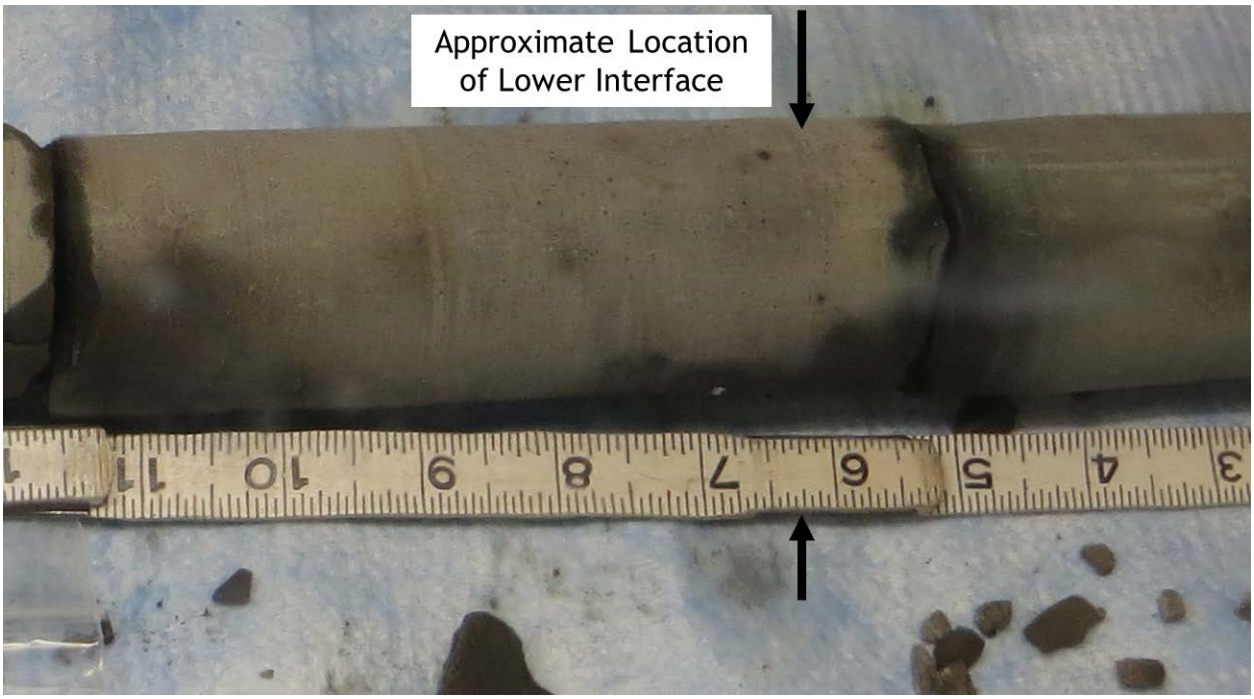

Figure A-12: Photograph of Sample Core A2U

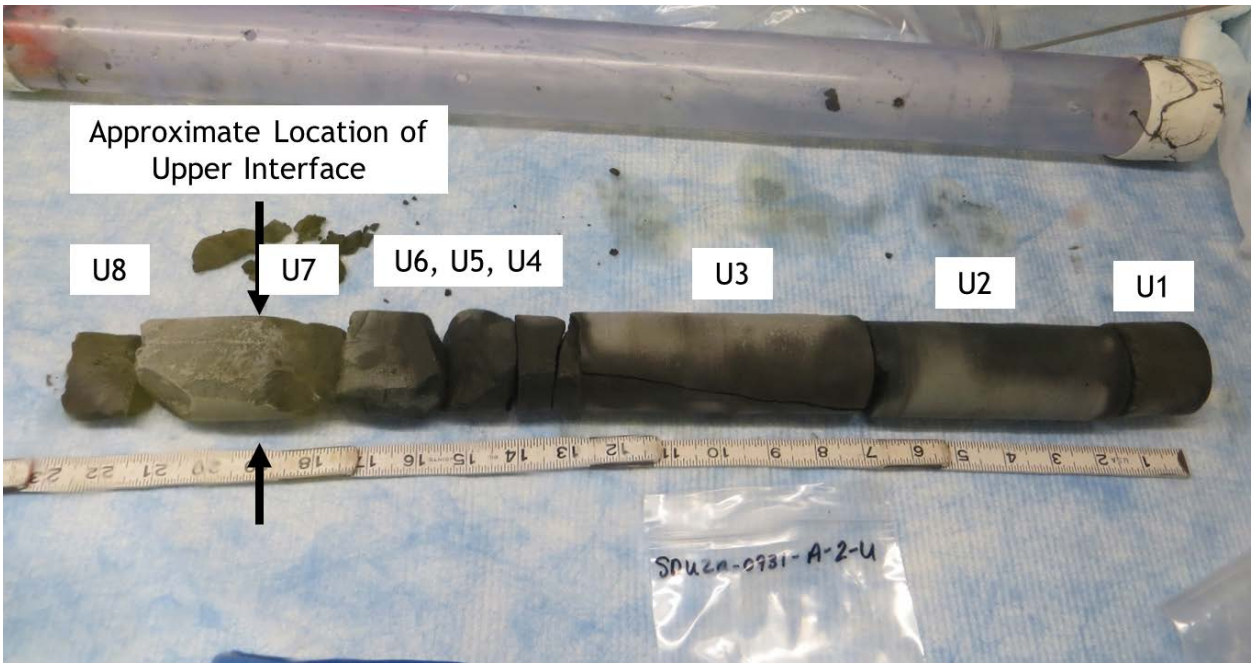

Figure A-13: Photograph of Sample Core A2U, Segment U7

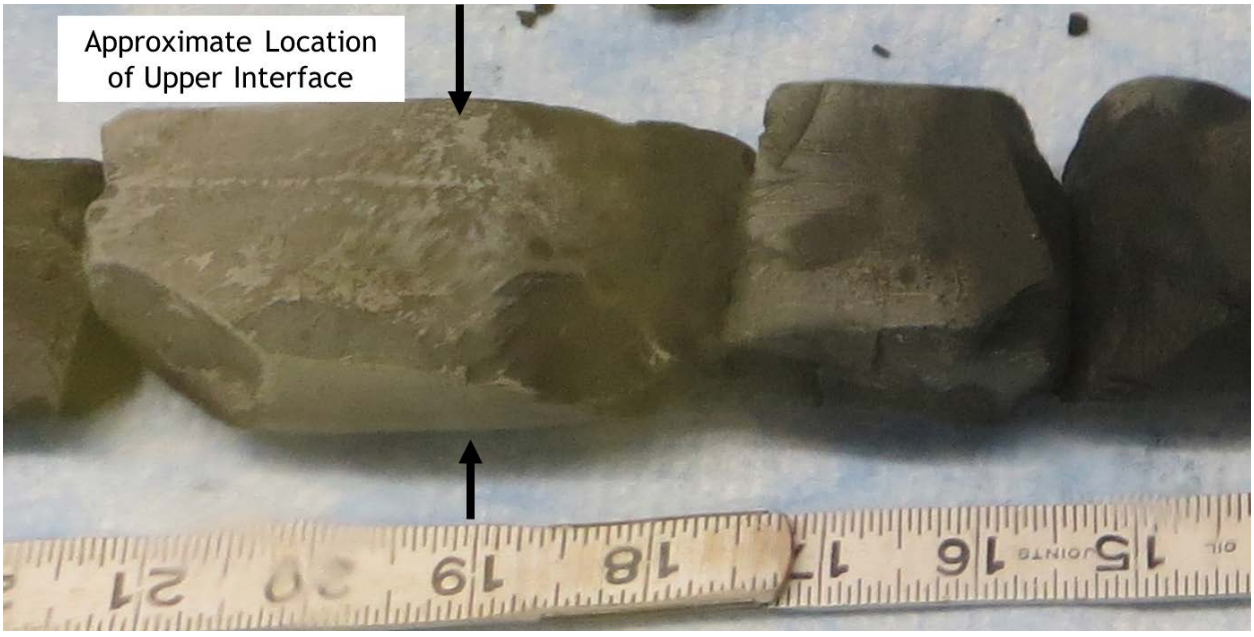

Figure A-14: Photograph of Sample Core C2U

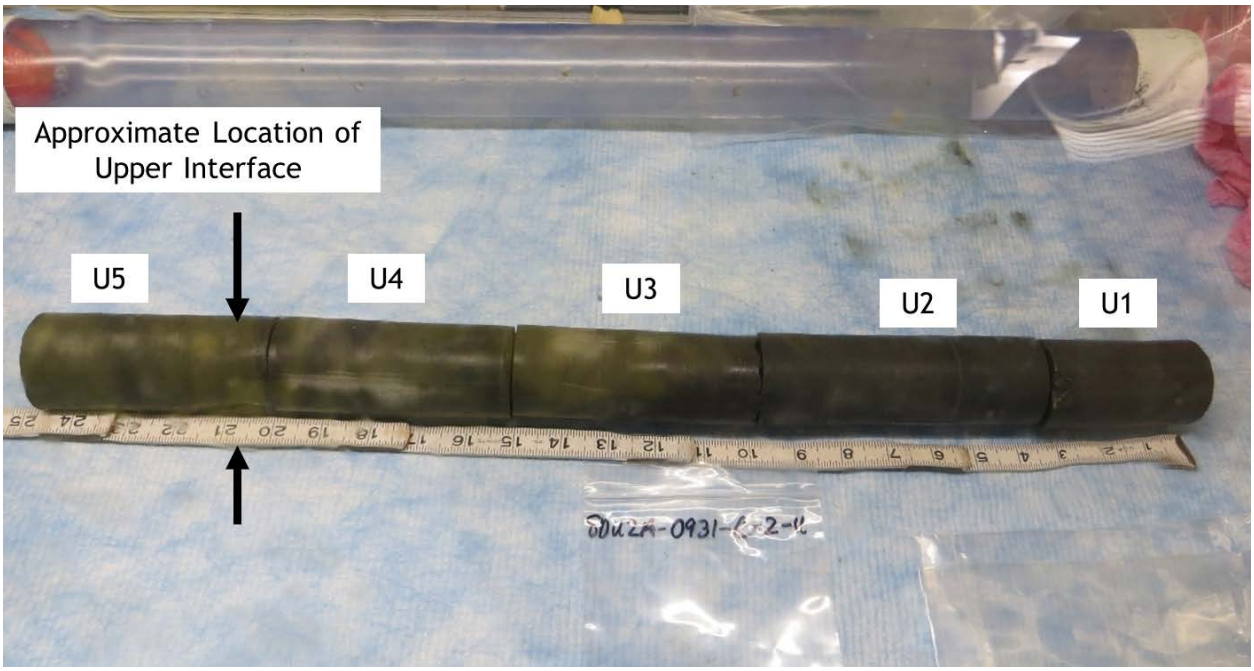

Figure A-15: Photograph of Sample Core C2U, Segment U5

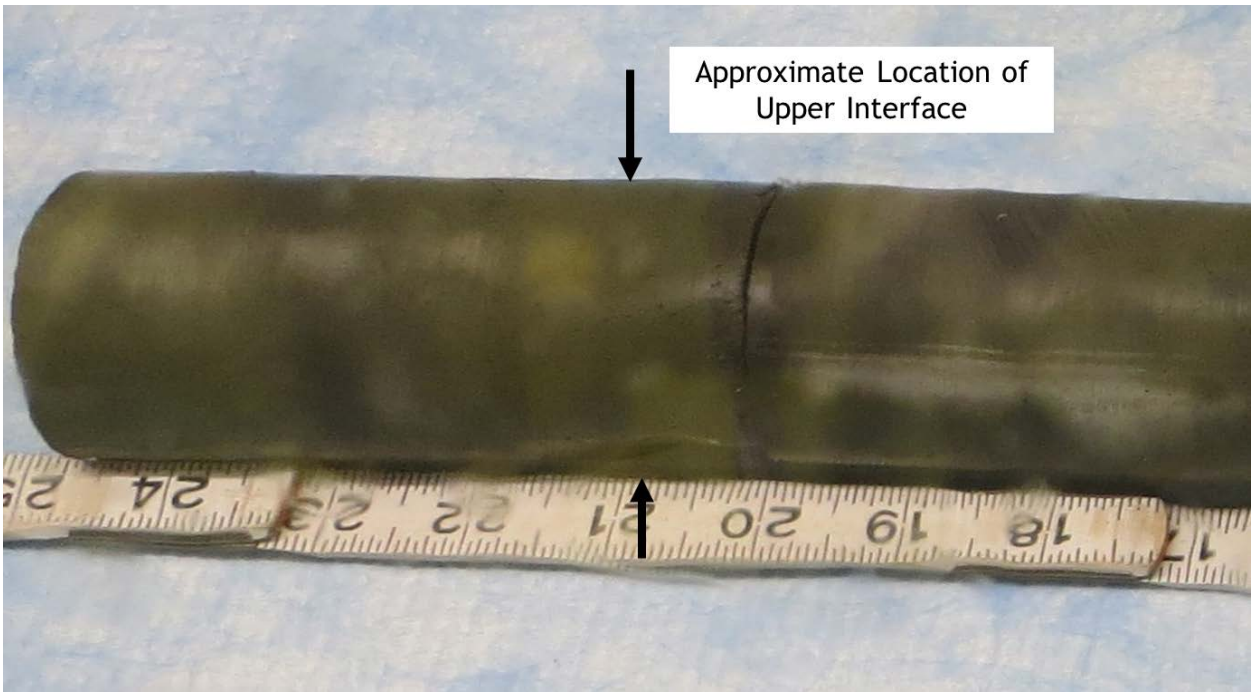

A.4 Derivation of the As-Received Saturation of Saltstone Equation (Eq. A-1)

Unsaturated saltstone is composed of skeletal solids (subscript ss), dissolved solids (subscript ds) and pure water (subscript w) composing a pore solution (subscript ps), and air (a). Letting M denote mass, gravimetric water content (w) is defined by

$$w = \frac{M_w}{M_{ss} + M_{ds} + M_w} = \frac{M_w}{M_{ss} + M_{ps}} \quad \text{Eq. A-4}$$

where the mass of air is neglected. Let V denote volume. Volumetric pore solution content is defined by

$$\theta_{ps} = \frac{V_{ps}}{V} \quad \text{Eq. A-5}$$

The mass of the pore solution is

$$M_{ps} = \rho_{ps}\theta_{ps}V \quad \text{Eq. A-6}$$

The mass of skeletal solids is

$$M_{ss} = \rho_{b,dry}V \quad \text{Eq. A-7}$$

The mass of water is

$$M_w = M_{ps} - M_{ds} = M_{ps}\left(1 - \frac{M_{ds}}{M_{ps}}\right) \quad \text{Eq. A-8}$$

Combining Equations A-6 and A-8 yields

$$M_w = \rho_{ps}\theta_{ps}V\left(1 - \frac{M_{ds}}{M_{ps}}\right) \quad \text{Eq. A-9}$$

Inserting Equations A-6, A-7, and A-9 into Equation A-4 yields

$$w = \frac{\rho_{ps}\theta_{ps}\left(1 - \frac{M_{ds}}{M_{ps}}\right)}{\rho_{b,dry} + \rho_{ps}\theta_{ps}} \quad \text{Eq. A-10}$$

or equivalently

$$w\rho_{b,dry} + w\rho_{ps}\theta_{ps} = \rho_{ps}\theta_{ps}\left(1 - \frac{M_{ds}}{M_{ps}}\right) \quad \text{Eq. A-11}$$

Solving Equation A-11 for θ_{ps} produces the expression

$$\theta_{ps} = \frac{w\rho_{b,dry}}{\rho_{ps}\left(1 - \frac{M_{ds}}{M_{ps}}\right) - w\rho_{ps}} = \frac{w\rho_{b,dry}}{\rho_{ps}\left(1 - \frac{M_{ds}}{M_{ps}} - w\right)} \quad \text{Eq. A-12}$$

Porosity is defined by

$$n = \frac{V_v}{V} \quad \text{Eq. A-13}$$

where the subscript v refers to void space. Pore solution saturation is defined by

$$S = \frac{V_{ps}}{V_v} \quad \text{Eq. A-14}$$

Thus, from Equations A-5, A-13 and A-14

$$S = \frac{\theta_{ps}}{n} \quad \text{Eq. A-15}$$

Finally, combining Equations A-12 and A-15 yields Equation A-1 as shown in Section A.2.3.

As discussed in Section A.2.3, parameters used to evaluate saturations in this analysis include: $\rho_{b,dry}$ = 0.932 g/mL (SRR-CWDA-2018-00004, Table 1), n = 0.656 (SRR-CWDA-2018-00004, Table 1), w = 0.365 on average for SRNL samples (SRR-CWDA-2014-00059, SRR-CWDA-2015-00152) and w = 0.303 on average for SDU 2A cores (SRR-CWDA-2016-00051). The pore solution density and mass fraction of dissolved solids can be estimated from SIMCO_08-31-2012 as follows.

Table A-4 and Table A-5 present pore fluid characterization data from SIMCO_08-31-2012, Table 8. The density of the solution was not stated by SIMCO but can be estimated from the SIMCO pore fluid characterization data. The pore solution is dominated by sodium nitrate/nitrite ions. Assuming the entire solution is NaNOx at the molar concentration of all anions, the solution density and mass fraction of dissolved solids can be estimated from the sodium nitrate table of data found in the *CRC Handbook of Chemistry and Physics*, 97th edition, on page 5-131. Table A-6 and Table A-7 summarize the results for the 28- and 520-day cure data from Table A-4 and Table A-5, respectively.

Table A-4: Pore Solution Characterization for Saltstone After 28-Day Cure

Ions	M	Molar Conc.	Molar Conc.	Mass Conc.
	(g/mol)	(mmol/L)	(mol/L)	(g/L)
OH-	17	383.9	0.3839	6.53
Na+	23	4144.2	4.1442	95.32
K+	39	120.5	0.1205	4.70
SO4--	96	111.7	0.1117	10.72
Ca++	40	0.1	0.0001	0.00
Cl-	35	11.9	0.0119	0.42
N as NOx-	60.4	3552.1	3.5521	214.52
CO3--	60	46.8	0.0468	2.81
Total			8.37	**335.0**
Total anions			**4.11**	
Total cations			4.26	

[SIMCO_08-31-2012, Table 8]

Table A-5: Pore Solution Characterization for Saltstone After 520-Day Cure

Ions	M	Molar Conc.	Molar Conc.	Mass Conc.
	(g/mol)	(mmol/L)	(mol/L)	(g/L)
OH-	17	90.5	0.0905	1.54
Na+	23	4784.7	4.7847	110.05
K+	39	212.3	0.2123	8.28
SO4--	96	135.3	0.1353	12.99
Ca++	40	2.4	0.0024	0.10
Cl-	35	4.7	0.0047	0.16
N as NOx-	60.4	4569.2	4.5692	275.94
CO3--	60	1.5	0.0015	0.09
Total			9.80	**409.1**
Total anions			**4.80**	
Total cations			5.00	

[SIMCO_08-31-2012, Table 8]

Table A-6: Estimated Solution Density and Solute Mass Fraction After 28-Day Cure

Parameter	Value	Units
Sodium nitrate molecular weight	85	g/mol
Sodium nitrate molar concentration	4.1	mol/L soln
Sodium nitrate density	348.5	g NaNO3/L soln
Solution density	1215	g/L soln
Water density	866.5	g H2O/L soln
Sodium nitrate mass fraction	0.287	
Sodium nitrate / water mass ratio	0.402	g NaNO3/g H2O

Table A-7: Estimated Solution Density and Solute Mass Fraction After 520-Day Cure

Parameter	Value	Units
Sodium nitrate molecular weight	85	g/mol
Sodium nitrate molar concentration	4.8	mol/L soln
Sodium nitrate density	408	g NaNO3/L soln
Solution density	1250	g/L soln
Water density	842	g H2O/L soln
Sodium nitrate mass fraction	0.326	
Sodium nitrate / water mass ratio	0.485	g NaNO3/g H2O

The cure time for the SRNL samples was approximately nine months or 270 days, which lies midway between a 28-day and 520-day cure and motivates calculations using both sets of solution chemistry data. Table A-8 and Table A-9 calculate average pore solution saturation for SRNL cores using 28-day and 520-day chemistry using the data in Table A-6 and Table A-7 for ρ_{ps} and M_{ds}/M_{ps}. The saturation results from both calculations exceed 100%, due to measurement errors and analysis approximations, and is interpreted as 100% saturation. The SDU 2A core was cured for 20 months or 600 days. Table A-10 presents the saturation calculation for the SDU 2A cores using the 520-day solution chemistry data as discussed in Section A.2.

Table A-8: Estimated Pore Solution Saturation for SRNL Cores and 28-Day Cure Solution Chemistry

Parameter	Value	Units
Porosity	0.656	mL void/mL
Dry bulk density	0.932	g/mL
Pore solution density	1.215	g/mL soln
Sodium nitrate wt%	29%	
Gravimetric water content	0.365	g H2O/mL
Pore solution volume fraction	0.804	mL soln/mL
Pore solution saturation	**1.226**	mL soln/mL void
	123%	

Table A-9: Estimated Pore Solution Saturation for SRNL Cores and 520-Day Cure Solution Chemistry

Parameter	Value	Units
Porosity	0.656	mL void/mL
Dry bulk density	0.932	g/mL
Pore solution density	1.25	g/mL soln
Sodium nitrate wt%	33%	
Gravimetric water content	0.365	g H2O/mL
Pore solution volume fraction	0.882	mL soln/mL
Pore solution saturation	**1.344**	mL soln/mL void
	134%	

Table A-10: Estimated Pore Solution Saturation For SDU 2A Cores and 520-Day Cure Solution Chemistry

Parameter	Value	Units
Porosity	0.656	mL void/mL
Dry bulk density	0.932	g/mL
Pore solution density	1.25	g/mL soln
Sodium nitrate wt%	33%	
Gravimetric water content	0.303	g H2O/mL
Pore solution volume fraction	0.610	mL soln/mL
Pore solution saturation	**0.93**	mL soln/mL void
	93%	

A.5 Appendix A References

ACI 233R-17, *Guide to the Use of Slag Cement in Concrete and Mortar*, ACI Committee 233, 2017. (Copyright)

Boher, C., Frizon, F., Lorente, S., and Bart, F., *Influence of the pore network on hydrogen diffusion through blended cement pastes*, Cement and Concrete Composites, Vol. 37, 30-36, 2013. (Copyright)

CBP-TR-2014-005, Langton, C. A., *Technetium Oxidation in Slag-Based Sodium Salt Waste Forms Exposed to Water and Moist Hanford Soil*, Cementitious Barriers Partnership, Rev. 0, August 2014.

CRC Press, *CRC Handbook of Chemistry and Physics, 97th edition*, 2017. (Copyright)

Nielson, K.K., Rogers, V.C, and Gee, G.W., *Diffusion of Radon through Soils: A Pore Distribution Model*, Soil Science Society of America, Vol. 48, 482-487, 1984. (Copyright)

Sercombe, J., Vidal, R., Gallé, C., and Adenot, F., *Experimental study of gas diffusion in cement paste,* Cement and Concrete Research, Vol. 37, 579-588, 2007. (Copyright)

SIMCO_08-31-2012, *Final Report: Comparison of Wasteform Mixtures*, SIMCO Technologies Inc., Quebec, Canada, August 2012.

SRNL-L3100-2015-00108, Roberts, K.A., *SDU2A Core Sample Test Designation*, Savannah River National Laboratory, Aiken, SC, Rev. 0, June 2015.

SRNL-STI-2013-00541, Langton, C.A. and Almond, P.M., *Cast Stone Oxidation Front Evaluation: Preliminary Results for Samples Exposed to Moist Air,* Savannah River National Laboratory, Aiken, SC, Rev. 0, November 2013.

SRNL-STI-2018-00077, Flach, G.P., *Degradation of Saltstone Disposal Unit Cementitious Materials*, Savannah River Site, Aiken, SC, Rev. 1, August 2018.

SRR-CWDA-2014-00059, Smith, F.M., Clendenen, G.B, and Simner, S.P., *FY2014 Saltstone Core-Drilling Mock-Up Summary*, Savannah River Site, Aiken, SC, Rev. 0, June 2014.

SRR-CWDA-2015-00066, *Summary of Saltstone Disposal Unit Cell 2A Core Drill Activities*, Savannah River Site, Aiken, SC, Rev. 0, May 2015.

SRR-CWDA-2015-00152, *Savannah River Site Liquid Waste Facilities Performance Assessment Maintenance Program - FY2016 Implementation Plan*, Savannah River Site, Aiken, SC, Rev. 0, December 2015.

SRR-CWDA-2016-00051, Simner, S., *Property Data for Core Samples Extracted from SDU Cell 2A*, Savannah River Site, Aiken, SC, Rev. 0, April 2016.

SRR-CWDA-2018-00004, *Recommended Values for Cementitious Degradation Modeling to Support Future SDF Modeling*, Savannah River Site, Aiken, SC, Rev. 1, August 2018.

SRR-SPT-2013-00044, Simner, S.P., *Update of Fiscal Year 2013 Activities Related to SDU Sampling and Analysis*, Savannah River Site, Aiken, SC, Rev. 0, September 2013.

APPENDIX B – Peak Groundwater Concentration Tables, Realistic Case

This page intentionally left blank.

B. APPENDIX B – Peak Groundwater Concentration Tables, Realistic Case

Appendix B presents the Realistic Case peak groundwater concentration tables for the various aquifers. Only the major radionuclides (Cl-36, I-129, and Tc-99) were included. Tables B-1, B-2, and B-3 represent the peak concentrations within 1,000 years for the Upper Three Runs – Upper Zone, Upper Three Runs – Lower Zone, and Gordon Aquifers, respectively. Tables B-4, B-5, and B-6 represent the equivalent peak concentrations within 10,000 years. Tables B-7 and B-8 represent the peak concentrations for all aquifers for all wells at 1-meter and individual IHI wells in 1,000 and 10,000 years respectively.

Table B-1: Realistic Case, Radiological Peak Concentrations along the 100-Meter Boundary for Upper Three Runs Aquifer – Upper Zone in 1,000 Years

Rad	MCL (pCi/L)	Sector A		Sector B		Sector C		Sector D	
		Conc. (pCi/L)	Year of Peak	Conc. (pCi/L)	Year of Peak	Conc. (pCi/L)	Year of Peak	Conc. (pCi/L)	Year of Peak
Cl-36	700	3.0E-06	1,000	8.0E-06	1,000	1.0E-04	1,000	2.2E-04	1,000
I-129	1	2.4E-05	1,000	6.2E-05	1,000	6.0E-04	1,000	1.3E-03	1,000
Tc-99	900	3.1E-03	1,000	8.1E-03	1,000	4.7E-02	1,000	9.8E-02	1,000
Sum of Beta-Gamma MCL Fractions		2.7E-05	1,000	7.1E-05	1,000	6.5E-04	1,000	1.4E-03	1,000
Rad	**MCL (pCi/L)**	**Sector E**		**Sector F**		**Sector G**		**Sector H**	
		Conc. (pCi/L)	Year of Peak	Conc. (pCi/L)	Year of Peak	Conc. (pCi/L)	Year of Peak	Conc. (pCi/L)	Year of Peak
Cl-36	700	6.1E-06	1,000	1.8E-05	1,000	2.9E-05	1,000	5.8E-11	1,000
I-129	1	4.8E-05	1,000	4.6E-04	1,000	7.5E-04	1,000	1.8E-05	1,000
Tc-99	900	6.4E-03	1,000	3.4E-02	1,000	5.4E-02	1,000	8.3E-04	1,000
Sum of Beta-Gamma MCL Fractions		5.5E-05	1,000	5.0E-04	1,000	8.1E-04	1,000	1.9E-05	1,000

Table B-2: Realistic Case, Radiological Peak Concentrations along the 100-Meter Boundary for Upper Three Runs Aquifer – Lower Zone in 1,000 Years

Rad	MCL (pCi/L)	Sector A		Sector B		Sector C		Sector D	
		Conc. (pCi/L)	Year of Peak	Conc. (pCi/L)	Year of Peak	Conc. (pCi/L)	Year of Peak	Conc. (pCi/L)	Year of Peak
Cl-36	700	1.2E-05	1,000	1.3E-05	1,000	1.6E-04	1,000	2.8E-04	1,000
I-129	1	9.9E-05	1,000	1.0E-04	1,000	9.9E-04	1,000	1.7E-03	1,000
Tc-99	900	1.4E-02	1,000	1.4E-02	1,000	8.1E-02	1,000	1.3E-01	1,000
Sum of Beta-Gamma MCL Fractions		1.1E-04	1,000	1.2E-04	1,000	1.1E-03	1,000	1.8E-03	1,000
Rad	**MCL (pCi/L)**	**Sector E**		**Sector F**		**Sector G**		**Sector H**	
		Conc. (pCi/L)	Year of Peak	Conc. (pCi/L)	Year of Peak	Conc. (pCi/L)	Year of Peak	Conc. (pCi/L)	Year of Peak
Cl-36	700	8.7E-06	1,000	4.4E-05	1,000	5.2E-05	1,000	3.7E-11	1,000
I-129	1	7.2E-05	1,000	1.2E-03	1,000	1.4E-03	1,000	1.6E-05	1,000
Tc-99	900	1.0E-02	1,000	9.1E-02	1,000	1.0E-01	1,000	7.4E-04	1,000
Sum of Beta-Gamma MCL Fractions		8.4E-05	1,000	1.3E-03	1,000	1.5E-03	1,000	1.7E-05	1,000

Table B-3: Realistic Case, Radiological Peak Concentrations along the 100-Meter Boundary for Gordon Aquifer in 1,000 Years

Rad	MCL (pCi/L)	Sector A		Sector B		Sector C		Sector D	
		Conc. (pCi/L)	Year of Peak	Conc. (pCi/L)	Year of Peak	Conc. (pCi/L)	Year of Peak	Conc. (pCi/L)	Year of Peak
Cl-36	700	8.8E-10	1,000	8.0E-10	1,000	6.9E-09	1,000	3.8E-09	1,000
I-129	1	3.5E-08	1,000	3.4E-08	1,000	2.2E-07	1,000	1.2E-07	1,000
Tc-99	900	1.1E-05	1,000	1.2E-05	1,000	4.2E-05	1,000	2.2E-05	1,000
Sum of Beta-Gamma MCL Fractions		4.7E-08	1,000	4.7E-08	1,000	2.7E-07	1,000	1.4E-07	1,000
Rad	**MCL (pCi/L)**	**Sector E**		**Sector F**		**Sector G**		**Sector H**	
		Conc. (pCi/L)	Year of Peak	Conc. (pCi/L)	Year of Peak	Conc. (pCi/L)	Year of Peak	Conc. (pCi/L)	Year of Peak
Cl-36	700	1.9E-11	1,000	5.2E-11	1,000	4.7E-11	1,000	<1E-20	1,000
I-129	1	8.8E-10	1,000	6.8E-09	1,000	6.7E-09	1,000	1.9E-18	1,000
Tc-99	900	2.9E-07	1,000	1.2E-06	1,000	1.0E-06	1,000	1.3E-16	1,000
Sum of Beta-Gamma MCL Fractions		1.2E-09	1,000	8.1E-09	1,000	7.8E-09	1,000	2.0E-18	1,000

Table B-4: Realistic Case, Radiological Peak Concentrations along the 100-Meter Boundary for Upper Three Runs – Upper Zone in 10,000 Years

Rad	MCL (pCi/L)	Sector A		Sector B		Sector C		Sector D	
		Conc. (pCi/L)	Year of Peak	Conc. (pCi/L)	Year of Peak	Conc. (pCi/L)	Year of Peak	Conc. (pCi/L)	Year of Peak
Cl-36	700	1.1E-02	8,310	2.9E-02	8,300	2.1E-02	5,300	4.0E-02	5,140
I-129	1	7.6E-02	10,000	2.0E-01	10,000	1.5E-01	9,980	2.8E-01	6,360
Tc-99	900	6.4E+00	10,000	1.7E+01	9,990	1.7E+01	10,000	2.1E+01	9,980
Sum of Beta-Gamma MCL Fractions		8.3E-02	10,000	2.2E-01	10,000	1.7E-01	10,000	3.0E-01	6,640
Rad	**MCL (pCi/L)**	**Sector E**		**Sector F**		**Sector G**		**Sector H**	
		Conc. (pCi/L)	Year of Peak	Conc. (pCi/L)	Year of Peak	Conc. (pCi/L)	Year of Peak	Conc. (pCi/L)	Year of Peak
Cl-36	700	2.3E-02	8,220	1.8E-03	9,970	2.6E-03	9,980	7.5E-09	10,000
I-129	1	1.6E-01	9,990	3.1E-02	9,860	4.7E-02	9,940	7.0E-03	10,000
Tc-99	900	1.3E+01	10,000	4.3E+00	9,670	6.4E+00	9,690	4.1E-01	10,000
Sum of Beta-Gamma MCL Fractions		1.7E-01	10,000	3.6E-02	9,870	5.4E-02	10,000	7.5E-03	10,000

Table B-5: Realistic Case, Radiological Peak Concentrations along the 100-Meter Boundary for Upper Three Runs – Lower Zone in 10,000 Years

Rad	MCL (pCi/L)	Sector A		Sector B		Sector C		Sector D	
		Conc. (pCi/L)	Year of Peak	Conc. (pCi/L)	Year of Peak	Conc. (pCi/L)	Year of Peak	Conc. (pCi/L)	Year of Peak
Cl-36	700	5.5E-02	8,340	5.6E-02	8,350	4.6E-02	9,660	6.1E-02	5,240
I-129	1	3.7E-01	9,990	3.8E-01	9,990	3.1E-01	10,000	4.3E-01	6,630
Tc-99	900	3.1E+01	10,000	3.4E+01	10,000	3.0E+01	10,000	3.4E+01	10,000
Sum of Beta-Gamma MCL Fractions		4.1E-01	10,000	4.2E-01	10,000	3.4E-01	10,000	4.6E-01	6,820
Rad	**MCL (pCi/L)**	**Sector E**		**Sector F**		**Sector G**		**Sector H**	
		Conc. (pCi/L)	Year of Peak	Conc. (pCi/L)	Year of Peak	Conc. (pCi/L)	Year of Peak	Conc. (pCi/L)	Year of Peak
Cl-36	700	4.1E-02	8,370	3.6E-02	8,340	5.3E-03	10,000	5.6E-09	10,000
I-129	1	2.8E-01	9,990	2.4E-01	9,980	1.2E-01	9,940	6.7E-03	10,000
Tc-99	900	2.4E+01	9,990	2.0E+01	10,000	1.4E+01	9,850	3.9E-01	10,000
Sum of Beta-Gamma MCL Fractions		3.1E-01	9,990	2.7E-01	10,000	1.4E-01	10,000	7.1E-03	10,000

Table B-6: Realistic Case, Radiological Peak Concentrations along the 100-Meter Boundary for Gordon Aquifer in 10,000 Years

Rad	MCL (pCi/L)	Sector A		Sector B		Sector C		Sector D	
		Conc. (pCi/L)	Year of Peak	Conc. (pCi/L)	Year of Peak	Conc. (pCi/L)	Year of Peak	Conc. (pCi/L)	Year of Peak
Cl-36	700	2.2E-04	10,000	4.5E-04	10,000	4.2E-04	10,000	1.3E-04	9,990
I-129	1	1.6E-03	9,990	3.4E-03	10,000	3.2E-03	10,000	1.1E-03	9,970
Tc-99	900	1.4E-01	10,000	3.2E-01	10,000	3.0E-01	10,000	1.0E-01	10,000
Sum of Beta-Gamma MCL Fractions		1.8E-03	10,000	3.8E-03	10,000	3.5E-03	10,000	1.2E-03	10,000
Rad	**MCL (pCi/L)**	**Sector E**		**Sector F**		**Sector G**		**Sector H**	
		Conc. (pCi/L)	Year of Peak	Conc. (pCi/L)	Year of Peak	Conc. (pCi/L)	Year of Peak	Conc. (pCi/L)	Year of Peak
Cl-36	700	1.0E-05	10,000	9.2E-07	10,000	3.4E-07	10,000	<1E-20	10,000
I-129	1	9.3E-05	10,000	5.9E-05	10,000	5.5E-05	10,000	4.3E-15	10,000
Tc-99	900	7.6E-03	10,000	5.1E-03	10,000	4.1E-03	10,000	2.5E-13	10,000
Sum of Beta-Gamma MCL Fractions		1.0E-04	10,000	6.5E-05	10,000	6.0E-05	10,000	4.5E-15	10,000

Table B-7: Realistic Case, Radiological Concentrations for All Aquifers for All Wells at 1 Meter and Individual Intruder Wells in 1,000 Years

Rad	MCL (pCi/L)	All 1-Meter Wells		IHI Well 1		IHI Well 2		IHI Well 3	
		Conc. (pCi/L)	Year of Peak	Conc. (pCi/L)	Year of Peak	Conc. (pCi/L)	Year of Peak	Conc. (pCi/L)	Year of Peak
Cl-36	700	5.3E-04	1,000	2.6E-05	1,000	2.4E-05	1,000	8.9E-06	1,000
I-129	1	4.1E-03	1,000	2.0E-04	1,000	1.8E-04	1,000	6.7E-05	1,000
Tc-99	900	2.9E-01	1,000	2.5E-02	1,000	2.2E-02	1,000	1.4E-02	1,000
Sum of Beta-Gamma MCL Fractions		4.4E-03	1,000	2.3E-04	1,000	2.0E-04	1,000	8.2E-05	1,000
Rad	**MCL (pCi/L)**	**IHI Well 4**		**IHI Well 5**		**IHI Well 6**		**IHI Well 7**	
		Conc. (pCi/L)	Year of Peak	Conc. (pCi/L)	Year of Peak	Conc. (pCi/L)	Year of Peak	Conc. (pCi/L)	Year of Peak
Cl-36	700	4.9E-04	1,000	2.2E-06	1,000	1.7E-04	1,000	2.2E-05	1,000
I-129	1	2.9E-03	1,000	2.9E-05	1,000	4.3E-03	1,000	1.7E-04	1,000
Tc-99	900	2.1E-01	1,000	1.2E-02	1,000	3.0E-01	1,000	2.1E-02	1,000
Sum of Beta-Gamma MCL Fractions		3.1E-03	1,000	4.2E-05	1,000	4.7E-03	1,000	1.9E-04	1,000

Table B-8: Realistic Case, Radiological Concentrations for All Aquifers for All Wells at 1 Meter and Individual Intruder Wells in 10,000 Years

Rad	MCL (pCi/L)	All 1m Wells		IHI Well 1		IHI Well 2		IHI Well 3	
		Conc. (pCi/L)	Year of Peak	Conc. (pCi/L)	Year of Peak	Conc. (pCi/L)	Year of Peak	Conc. (pCi/L)	Year of Peak
Cl-36	700	9.5E-02	8,350	8.2E-02	8,300	7.6E-02	8,470	4.7E-02	9,470
I-129	1	6.5E-01	10,000	5.7E-01	9,990	5.2E-01	9,990	3.2E-01	9,990
Tc-99	900	5.5E+01	10,000	4.7E+01	10,000	4.5E+01	10,000	3.4E+01	10,000
Sum of Beta-Gamma MCL Fractions		7.1E-01	10,000	6.2E-01	10,000	5.7E-01	10,000	3.6E-01	10,000
Rad	**MCL (pCi/L)**	**IHI Well 4**		**IHI Well 5**		**IHI Well 6**		**IHI Well 7**	
		Conc. (pCi/L)	Year of Peak	Conc. (pCi/L)	Year of Peak	Conc. (pCi/L)	Year of Peak	Conc. (pCi/L)	Year of Peak
Cl-36	700	8.4E-02	5,130	1.5E-02	8,290	1.4E-02	10,000	7.5E-02	8,320
I-129	1	5.8E-01	6,520	1.1E-01	9,980	2.5E-01	9,820	5.2E-01	10,000
Tc-99	900	4.5E+01	9,980	2.3E+01	9,980	3.4E+01	9,510	4.3E+01	10,000
Sum of Beta-Gamma MCL Fractions		6.3E-01	6,630	1.3E-01	9,980	2.9E-01	9,870	5.6E-01	10,000

This page intentionally left blank.

APPENDIX C – Peak Groundwater Concentration Tables, Pessimistic Case

This page intentionally left blank.

C. APPENDIX C – Peak Groundwater Concentration Tables, Pessimistic Case

Appendix C presents the Pessimistic Case peak groundwater concentration tables for the various aquifers. Only the major radionuclides (Cl-36, I-129, and Tc-99) were included. Tables C-1, C-2, and C-3 represent the peak concentrations within 1,000 years for the Upper Three Runs – Upper Zone, Upper Three Runs – Lower Zone, and Gordon Aquifers, respectively. Tables C-4, C-5, and C-6 represent the equivalent peak concentrations within 10,000 years. Tables C-7 and C-8 represent the peak concentrations for all aquifers for all wells at 1-meter and individual IHI wells in 1,000 and 10,000 years respectively.

Table C-1: Pessimistic Case, Radiological Peak Concentrations along the 100-Meter Boundary for Upper Three Runs Aquifer – Upper Zone in 1,000 Years

Rad	MCL (pCi/L)	Sector A		Sector B		Sector C		Sector D	
		Conc. (pCi/L)	Year of Peak	Conc. (pCi/L)	Year of Peak	Conc. (pCi/L)	Year of Peak	Conc. (pCi/L)	Year of Peak
Cl-36	700	4.1E-05	1,000	1.1E-04	1,000	2.3E-03	1,000	4.9E-03	1,000
I-129	1	2.0E-04	1,000	5.2E-04	1,000	9.3E-03	1,000	2.0E-02	1,000
Tc-99	900	7.1E-02	1,000	1.9E-01	1,000	2.4E+00	1,000	5.1E+00	1,000
Sum of Beta-Gamma MCL Fractions		2.8E-04	1,000	7.3E-04	1,000	1.2E-02	1,000	2.6E-02	1,000
Rad	**MCL (pCi/L)**	**Sector E**		**Sector F**		**Sector G**		**Sector H**	
		Conc. (pCi/L)	Year of Peak	Conc. (pCi/L)	Year of Peak	Conc. (pCi/L)	Year of Peak	Conc. (pCi/L)	Year of Peak
Cl-36	700	8.3E-05	1,000	4.9E-05	1,000	7.9E-05	1,000	1.6E-10	1,000
I-129	1	4.0E-04	1,000	1.0E-03	1,000	1.7E-03	1,000	4.0E-05	1,000
Tc-99	900	1.5E-01	1,000	5.8E-01	1,000	9.1E-01	1,000	1.0E-02	1,000
Sum of Beta-Gamma MCL Fractions		5.6E-04	1,000	1.7E-03	1,000	2.7E-03	1,000	5.1E-05	1,000

Table C-2: Pessimistic Case, Radiological Peak Concentrations along the 100-Meter Boundary for Upper Three Runs Aquifer – Lower Zone in 1,000 Years

Rad	MCL (pCi/L)	Sector A		Sector B		Sector C		Sector D	
		Conc. (pCi/L)	Year of Peak	Conc. (pCi/L)	Year of Peak	Conc. (pCi/L)	Year of Peak	Conc. (pCi/L)	Year of Peak
Cl-36	700	1.5E-04	1,000	1.6E-04	1,000	3.6E-03	1,000	6.1E-03	1,000
I-129	1	7.7E-04	1,000	8.0E-04	1,000	1.5E-02	1,000	2.5E-02	1,000
Tc-99	900	2.9E-01	1,000	3.1E-01	1,000	4.0E+00	1,000	6.7E+00	1,000
Sum of Beta-Gamma MCL Fractions		1.1E-03	1,000	1.1E-03	1,000	1.9E-02	1,000	3.3E-02	1,000
Rad	**MCL (pCi/L)**	**Sector E**		**Sector F**		**Sector G**		**Sector H**	
		Conc. (pCi/L)	Year of Peak	Conc. (pCi/L)	Year of Peak	Conc. (pCi/L)	Year of Peak	Conc. (pCi/L)	Year of Peak
Cl-36	700	1.1E-04	1,000	1.2E-04	1,000	1.4E-04	1,000	1.0E-10	1,000
I-129	1	5.4E-04	1,000	2.7E-03	1,000	3.1E-03	1,000	3.4E-05	1,000
Tc-99	900	2.1E-01	1,000	1.5E+00	1,000	1.7E+00	1,000	9.2E-03	1,000
Sum of Beta-Gamma MCL Fractions		7.8E-04	1,000	4.4E-03	1,000	5.0E-03	1,000	4.4E-05	1,000

Table C-3: Pessimistic Case, Radiological Peak Concentrations along the 100-Meter Boundary for Gordon Aquifer in 1,000 Years

Rad	MCL (pCi/L)	Sector A		Sector B		Sector C		Sector D	
		Conc. (pCi/L)	Year of Peak	Conc. (pCi/L)	Year of Peak	Conc. (pCi/L)	Year of Peak	Conc. (pCi/L)	Year of Peak
Cl-36	700	7.2E-09	1,000	6.0E-09	1,000	8.4E-08	1,000	4.7E-08	1,000
I-129	1	1.8E-07	1,000	1.7E-07	1,000	1.8E-06	1,000	1.0E-06	1,000
Tc-99	900	1.2E-04	1,000	1.3E-04	1,000	9.8E-04	1,000	5.3E-04	1,000
Sum of Beta-Gamma MCL Fractions		3.2E-07	1,000	3.2E-07	1,000	2.9E-06	1,000	1.6E-06	1,000
Rad	**MCL (pCi/L)**	**Sector E**		**Sector F**		**Sector G**		**Sector H**	
		Conc. (pCi/L)	Year of Peak	Conc. (pCi/L)	Year of Peak	Conc. (pCi/L)	Year of Peak	Conc. (pCi/L)	Year of Peak
Cl-36	700	1.5E-10	1,000	1.4E-10	1,000	1.3E-10	1,000	<1E-20	1,000
I-129	1	4.4E-09	1,000	1.6E-08	1,000	1.5E-08	1,000	4.1E-18	1,000
Tc-99	900	2.9E-06	1,000	1.8E-05	1,000	1.5E-05	1,000	1.6E-15	1,000
Sum of Beta-Gamma MCL Fractions		7.6E-09	1,000	3.6E-08	1,000	3.2E-08	1,000	5.8E-18	1,000

Table C-4: Pessimistic Case, Radiological Peak Concentrations along the 100-Meter Boundary for Upper Three Runs – Upper Zone in 10,000 Years

Rad	MCL (pCi/L)	Sector A		Sector B		Sector C		Sector D	
		Conc. (pCi/L)	Year of Peak	Conc. (pCi/L)	Year of Peak	Conc. (pCi/L)	Year of Peak	Conc. (pCi/L)	Year of Peak
Cl-36	700	3.3E-01	10,000	8.7E-01	10,000	6.2E-01	10,000	8.9E-01	8,580
I-129	1	3.5E+00	10,000	9.2E+00	10,000	6.7E+00	10,000	1.1E+01	9,980
Tc-99	900	1.7E+02	9,970	4.6E+02	9,990	4.2E+02	10,000	5.0E+02	9,080
Sum of Beta-Gamma MCL Fractions		3.7E+00	10,000	9.7E+00	10,000	7.2E+00	10,000	1.1E+01	9,980
Rad	**MCL (pCi/L)**	**Sector E**		**Sector F**		**Sector G**		**Sector H**	
		Conc. (pCi/L)	Year of Peak	Conc. (pCi/L)	Year of Peak	Conc. (pCi/L)	Year of Peak	Conc. (pCi/L)	Year of Peak
Cl-36	700	6.9E-01	10,000	3.5E-02	10,000	4.4E-02	8,150	1.3E-07	8,310
I-129	1	7.3E+00	10,000	4.1E-01	8,980	6.1E-01	8,960	7.6E-02	9,880
Tc-99	900	3.6E+02	9,980	1.4E+02	9,900	2.0E+02	9,880	1.6E+01	9,990
Sum of Beta-Gamma MCL Fractions		7.7E+00	10,000	5.6E-01	9,110	8.3E-01	9,000	9.3E-02	9,960

Table C-5: Pessimistic Case, Radiological Peak Concentrations along the 100-Meter Boundary for Upper Three Runs – Lower Zone CaseCE.8 in 10,000 Years

Rad	MCL (pCi/L)	Sector A		Sector B		Sector C		Sector D	
		Conc. (pCi/L)	Year of Peak	Conc. (pCi/L)	Year of Peak	Conc. (pCi/L)	Year of Peak	Conc. (pCi/L)	Year of Peak
Cl-36	700	1.6E+00	9,980	1.7E+00	10,000	1.4E+00	9,990	1.4E+00	8,950
I-129	1	1.7E+01	10,000	1.8E+01	10,000	1.5E+01	10,000	1.7E+01	9,990
Tc-99	900	8.6E+02	10,000	9.0E+02	10,000	7.8E+02	10,000	8.0E+02	9,210
Sum of Beta-Gamma MCL Fractions		1.8E+01	10,000	1.9E+01	10,000	1.5E+01	10,000	1.8E+01	9,990
Rad	**MCL (pCi/L)**	**Sector E**		**Sector F**		**Sector G**		**Sector H**	
		Conc. (pCi/L)	Year of Peak	Conc. (pCi/L)	Year of Peak	Conc. (pCi/L)	Year of Peak	Conc. (pCi/L)	Year of Peak
Cl-36	700	1.2E+00	9,960	1.1E+00	9,990	8.9E-02	8,160	9.4E-08	8,480
I-129	1	1.3E+01	10,000	1.1E+01	10,000	1.5E+00	9,210	7.2E-02	9,850
Tc-99	900	6.5E+02	10,000	5.6E+02	9,990	4.6E+02	9,990	1.5E+01	9,980
Sum of Beta-Gamma MCL Fractions		1.4E+01	10,000	1.2E+01	10,000	2.0E+00	9,210	8.9E-02	9,980

Table C-6: Pessimistic Case, Radiological Peak Concentrations along the 100-Meter Boundary for Gordon Aquifer in 10,000 Years

Rad	MCL (pCi/L)	Sector A		Sector B		Sector C		Sector D	
		Conc. (pCi/L)	Year of Peak	Conc. (pCi/L)	Year of Peak	Conc. (pCi/L)	Year of Peak	Conc. (pCi/L)	Year of Peak
Cl-36	700	6.2E-03	10,000	1.3E-02	10,000	1.2E-02	10,000	3.4E-03	10,000
I-129	1	7.0E-02	10,000	1.5E-01	10,000	1.4E-01	10,000	4.4E-02	10,000
Tc-99	900	3.8E+00	10,000	8.6E+00	10,000	8.0E+00	10,000	2.7E+00	9,970
Sum of Beta-Gamma MCL Fractions		7.5E-02	10,000	1.6E-01	10,000	1.5E-01	10,000	4.7E-02	10,000
Rad	**MCL (pCi/L)**	**Sector E**		**Sector F**		**Sector G**		**Sector H**	
		Conc. (pCi/L)	Year of Peak	Conc. (pCi/L)	Year of Peak	Conc. (pCi/L)	Year of Peak	Conc. (pCi/L)	Year of Peak
Cl-36	700	2.8E-04	10,000	2.5E-05	10,000	5.6E-06	10,000	1.8E-20	9,990
I-129	1	3.8E-03	10,000	6.3E-04	10,000	6.0E-04	10,000	4.6E-14	10,000
Tc-99	900	2.2E-01	10,000	1.9E-01	10,000	1.6E-01	10,000	9.7E-12	10,000
Sum of Beta-Gamma MCL Fractions		4.1E-03	10,000	8.5E-04	10,000	7.7E-04	10,000	5.7E-14	10,000

Table C-7: Pessimistic Case, Radiological Concentrations for All Aquifers for All Wells at 1 Meter and Individual Intruder Wells in 1,000 Years

Rad	MCL (pCi/L)	All 1-Meter Wells		IHI Well 1		IHI Well 2		IHI Well 3	
		Conc. (pCi/L)	Year of Peak	Conc. (pCi/L)	Year of Peak	Conc. (pCi/L)	Year of Peak	Conc. (pCi/L)	Year of Peak
Cl-36	700	1.2E-02	1,000	3.8E-04	1,000	3.5E-04	1,000	4.7E-05	1,000
I-129	1	5.1E-02	1,000	1.8E-03	1,000	1.6E-03	1,000	3.3E-04	1,000
Tc-99	900	1.2E+01	1,000	6.0E-01	1,000	5.5E-01	1,000	2.6E-01	1,000
Sum of Beta-Gamma MCL Fractions		6.5E-02	1,000	2.4E-03	1,000	2.2E-03	1,000	6.1E-04	1,000
Rad	**MCL (pCi/L)**	**IHI Well 4**		**IHI Well 5**		**IHI Well 6**		**IHI Well 7**	
		Conc. (pCi/L)	Year of Peak	Conc. (pCi/L)	Year of Peak	Conc. (pCi/L)	Year of Peak	Conc. (pCi/L)	Year of Peak
Cl-36	700	1.1E-02	1,000	2.4E-05	1,000	4.6E-04	1,000	3.2E-04	1,000
I-129	1	4.7E-02	1,000	1.4E-04	1,000	9.8E-03	1,000	1.5E-03	1,000
Tc-99	900	1.1E+01	1,000	2.1E-01	1,000	5.2E+00	1,000	5.1E-01	1,000
Sum of Beta-Gamma MCL Fractions		5.9E-02	1,000	3.7E-04	1,000	1.5E-02	1,000	2.0E-03	1,000

Table C-8: Pessimistic Case, Radiological Concentrations for All Aquifers for All Wells at 1 Meter and Individual Intruder Wells in 10,000 Years

Rad	MCL (pCi/L)	All 1m Wells		IHI Well 1		IHI Well 2		IHI Well 3	
		Conc. (pCi/L)	Year of Peak	Conc. (pCi/L)	Year of Peak	Conc. (pCi/L)	Year of Peak	Conc. (pCi/L)	Year of Peak
Cl-36	700	2.8E+00	10,000	2.5E+00	9,980	2.3E+00	9,980	1.4E+00	9,980
I-129	1	3.0E+01	10,000	2.6E+01	10,000	2.4E+01	10,000	1.5E+01	10,000
Tc-99	900	1.5E+03	9,940	1.3E+03	9,920	1.2E+03	9,990	8.2E+02	9,990
Sum of Beta-Gamma MCL Fractions		3.2E+01	10,000	2.7E+01	10,000	2.6E+01	10,000	1.6E+01	10,000
Rad	**MCL (pCi/L)**	**IHI Well 4**		**IHI Well 5**		**IHI Well 6**		**IHI Well 7**	
		Conc. (pCi/L)	Year of Peak	Conc. (pCi/L)	Year of Peak	Conc. (pCi/L)	Year of Peak	Conc. (pCi/L)	Year of Peak
Cl-36	700	1.9E+00	8,600	4.5E-01	9,990	2.4E-01	8,090	2.3E+00	9,990
I-129	1	2.3E+01	10,000	4.9E+00	10,000	3.2E+00	8,940	2.4E+01	10,000
Tc-99	900	1.1E+03	8,930	5.6E+02	9,920	1.1E+03	9,650	1.2E+03	9,930
Sum of Beta-Gamma MCL Fractions		2.4E+01	10,000	5.5E+00	10,000	4.4E+00	8,990	2.5E+01	10,000

This page intentionally left blank.